PIERS 2015 Prague

Progress In Electromagnetics Research Symposium

Abstracts

July 6–9, 2015
Prague, CZECH REPUBLIC

www.emacademy.org
www.piers.org

PIERS 2015 Prague Abstracts

Published by

The Electromagnetics Academy
777 Concord Avenue, Suite 207
Cambridge, MA 02138

www.emacademy.org
www.piers.org

ISSN: 1559-9450
ISBN: 978-1-934142-29-5

THE ELECTROMAGNETICS ACADEMY

The Progress in Electromagnetics Research Symposium (PIERS) is sponsored by The Electromagnetics Academy.

The Electromagnetics Academy is devoted to academic excellence and the advancement of research and relevant applications of the electromagnetic theory and to promoting educational objectives of the electromagnetics profession. PIERS provides an international forum for reporting progress and advances in the modern development of electromagnetic theory and its new and exciting applications.

Founded by the late Professor Jin Au Kong (1942–2008) of MIT in 1989, The Electromagnetics Academy is a non-profit organization registered in USA.

JOURNAL:
PROGRESS IN ELECTROMAGNETICS RESEARCH

Progress In Electromagnetics Research (PIER) publishes peer-reviewed original and comprehensive articles on all aspects of electromagnetic theory and applications. This is an open access, on-line journal PIER (E-ISSN 1559-8985). It has been first published as a monograph series on Electromagnetic Waves (ISSN 1070-4698) in 1989. It is freely available to all readers via the Internet.

PIER is a non-profit organization.

WWW.JPIER.ORG

Contact Email: work@jpier.org

Progress In Electromagnetics Research Symposium
July 6–9, 2015
Prague, CZECH REPUBLIC

PIERS 2015 PRAGUE ORGANIZATION

PIERS 2015 Prague General Chair

Jan Vrba, Czech Technical University in Prague, CZECH REPUBLIC

PIERS 2015 Prague Vice General Chair

Sailing He, Royal Institute of Technology, SWEDEN; JORCEP, Zhejiang University, CHINA

PIERS Chair

Leung Tsang, University of Michigan, USA

PIERS 2015 Prague Technical Program Committee Co-chairs

Kazuya Kobayashi, Chuo University, JAPAN

Qing Huo Liu, Duke University, USA

Stefan Scheel, University of Rostock, GERMANY

Ari Sihvola, Aalto University, FINLAND

Sune Svanberg, Lund University, SWEDEN

PIERS 2015 Prague Subcommittee 1
(CEM, EMC, Scattering and Electromagnetic Theory)

Weng Cho Chew, University of Illinois, USA, Lead Co-Chair
Thomas Eibert, Technische Universität München, Germany, Co-Chair
Manuel Felipe Catedra, Universidad de Alcala, Spain, Co-Chair
Levent Gurel, Bilkent University, Turkey, Co-Chair
Li Jun Jiang, The University of Hong Kong, China, Co-Chair

PIERS 2015 Prague Subcommittee 2
(Metamaterials, Plasmonics and Complex Media)

Che Ting Chan, Hong Kong University of Science and Technology, China, Co-Chair
Shuang Zhang, University of Birmingham, UK, Co-Chair
Nikolay I. Zheludev, University of Southampton, UK, Co-Chair

PIERS 2015 Prague Subcommittee 3
(Optics and Photonics)

El-Hang Lee, Fellow of Korean Academy of Science and Technology, South Korea, Lead Co-Chair
Mario Dagenais, Fellow of OSA and IEEE, University of Maryland, USA, Co-Chair
Benjamin Eggleton, Australian Laureate Fellow, University of Sydney, Australia, Co-Chair
Iam Choon Khoo, Fellow of OSA and IEEE, Pennsylvania State University, USA, Co-Chair
Ali Serpenguzel, European Local Co-Chair, Fellow of SPIE, Koc University, Turkey, Co-Chair
Katarina Svanberg, Former President of SPIE, Lund University, Sweden, Co-Chair

Gaetano Assanto	Saverio Avino	Alpan Bek	Jamal Berakdar
Elliott R. Brown	Giulio Cerullo	Jiajia Chen	Hyuck Choo
Guillermo C. del Barrio	Shane M. Eaton	Yeshaiahu Fainman	Vincenzo Giannini
Junpeng Guo	Mohammad Hafezi	Sebastian Hofferberth	Yidong Huang
Darren D. Hudson	Eli Kapon	Sergey I. Kudryashov	Xiaofeng Li
Liu Liu	David Marpaung	Riccardo Messina	Kentaro Nakamura
Sahin Kaya Ozdemir	Antonio La Porta	Sergei Popov	Roberta Ramponi
Cees Ronda	Simarjeet Singh Saini	Luca Sapienza	Mario Marques da Silva
Ilya V. Shadrivov	Xuewen Shu	Francesco Simoni	Isabelle Staude
Hon Ki Tsang	Alan X. Wang	Jinlong Wei	Kaikai Xu
Lin Yang	Weiwen Zou		

PIERS 2015 Prague Subcommittee 4
(Antennas and Microwave Technologies)

Yang Hao, Queen Mary College, University of London, UK, Lead Co-Chair
Tiejun Cui, Southeast University, China, Co-Chair
Mats Gustufsson, Lund University, Sweden, Co-Chair

PIERS 2015 Prague Subcommittee 5
(Remote Sensing, Inverse Problems, Imaging, Radar and Sensing)

Leung Tsang, University of Michigan, USA, Lead Co-Chair
Kun-Shan Chen, Institute of Remote Sensing and Digital Earth, CAS, China, Co-Chair
Xudong Chen, National University of Singapore, Singapore, Co-Chair
Simonetta Paloscia, CNR-IFAC, Italy, Co-Chair
Jianchen Shi, The Institute of Remote Sensing and Application, CAS, China, Co-Chair

PIERS 2015 Prague Local Organizing Committee: Honorary Members

Zbynek Skvor, Vice-Rector for Research of the Czech Technical University in Prague, Czech Republic
Pavel Pechac, Head of the Department of EM Field, Faculty of Electrical Engineering (FEE)
the Czech Technical University in Prague (CTU), Czech Republic
Peter Kneppo, Head of the Department of Biomedical Techniques
Faculty of Biomedical Engineering (FBME)
the Czech Technical University in Prague (CTU), Czech Republic
Pavel Fiala, Head of the Department of Theoretical and Experimental Electrical Engineering
Faculty of Electrical Engineering and Communication (FEEC)
Brno University of Technology, Czech Republic
Zbynek Raida, Director of SIX Research Centre, Brno University of Technology, Czech Republic
Eva Gescheidtova, FEEC Brno University of Technology, Czech Republic
Miloš Mazánek, FEE, Czech Technical University in Prague, Czech Republic
Stanislav Zvánovec, FEE, Czech Technical University in Prague, Czech Republic
Karel Hoffman, FEE, Czech Technical University in Prague, Czech Republic
Karel Roubik, FBME, Czech Technical University in Prague, Czech Republic
Jiri Hozman, FBME, Czech Technical University in Prague, Czech Republic
Milan Polívka, FEE, Czech Technical University in Prague, Czech Republic
Ales Prokes, SIX RC, Brno University of Technology, Czech Republic
Jiri Pokorny, Emeritus of Institute of Photonics and Electronics, CAS, Czech Republic

PIERS 2015 Prague Local Organizing Committee

David Vrba, FBME, Czech Technical University in Prague, Czech Republic
Jan Vrba, Jr., FBME, Czech Technical University in Prague, Czech Republic
Ondrej Fiser, FEE, Czech Technical University in Prague, Czech Republic
Ilja Merunka, FEE, Czech Technical University in Prague, Czech Republic
Ladislav Oppl, FEE, Czech Technical University in Prague, Czech Republic
Katerina Cervinkova, FEE, Czech Technical University in Prague, Czech Republic
Milan Kvicera, FEE, Czech Technical University in Prague, Czech Republic
Martin Haase, FEE, Czech Technical University in Prague, Czech Republic
Jaroslav Havlicek, FEE, Czech Technical University in Prague, Czech Republic
Miroslav Wiewegh, FBME, Czech Technical University in Prague, Czech Republic
Maja Shuleska, FBME, Czech Technical University in Prague, Czech Republic

PIERS 2015 PRAGUE SESSION ORGANIZERS

M. Antezza
A. Boutejdar
M. Burla
J.-D. Chai
Q. Chen
A. Costanzo
R. Dyczij-Edlinger
H. T. Ewe
K. H. Fung
M. N. Georgieva-Grosse
F. Gronwald
M. Hafezi
O. Hess
E. Kapon
V. E. Kunitsyn
J. Lettl
L. Liu
Y. Luo
R. Messina
K. Nakamura
S. Ohnuki
P. Pechac
J. Rho
S. S. Saini
Z. X. Shen
R. Solimene
S. L. Sun
I. Tsukerman
D. Vrba
Z. Wang
T. Yamasaki
J. J. Zhang
W. W. Zou

G. Assanto
E. R. Brown
M. Capek
H. S. Chen
X. D. Chen
C. De Angelis
S. M. Eaton
Y. S. Fainman
P. D. Garcia
E. Gescheidtova
B. Guizal
Z. H. Hang
S. Hofferberth
K. Kobayashi
A. La Porta
X. F. Li
L. N. Liu
Y. G. Ma
R. Mittra
D. N. Neshev
Y. Okuno
R. Pierri
J. M. Rigelsford
L. Sapienza
Y. V. Shestopalov
V. J. Sorger
T. Takenaka
S. K. Turitsyn
J. Vrba, Jr.
J. L. Wei
L. Yang
S. Zhang

A. Bek
M. Bugaj
R. Ceolato
J. J. Chen
H. Choo
G. C. Del Barrio
K. Edee
N. X. Fang
G. Genty
V. Giannini
J. P. Guo
Q. He
D. D. Hudson
J. Kracek
Y. Lai
Y. S. Li
Y. M. Liu
D. Marpaung
T. Mocek
S. Nordebo
S. K. Ozdemir
S. Popov
C. Ronda
A. Serpenguzel
J. Shibayama
I. Staude
M. R. Tripathy
V. K. Valev
A. X. Wang
M. Xia
X. Z. Ye
Y. Zhang

J. Berakdar
N. M. Bulgakova
G. Cerullo
K.-S. Chen
R. C. Conceicao
Y. Du
T. F. Eibert
M. Fleischer
G. N. Georgiev
A. A. Glazunov
M. Gustafsson
S. He
B. L. G. Jonsson
S. I. Kudryashov
M. Lapine
J. Liu
T. Low
C. F. Martino
T. Nagatsuma
M. O'Halloran
N.-C. Panoiu
R. Ramponi
D. Ronnow
I. V. Shadrivov
F. Simoni
M. Stumpf
H. K. Tsang
F. Viani
K. P. Wang
S. S. Xiao
B. L. Zhang
V. P. Zhukov

PIERS 2015 PRAGUE ORGANIZERS AND SPONSORS

- ☐ Department of EM Field, Faculty of Electrical Engineering (FEE)
  Czech Technical University in Prague
- ☐ Department of Biomedical Technique, Faculty of Biomedical Engineering (FBME)
  Czech Technical University in Prague
- ☐ Department of Theoretical and Experimental Electrical Engineering
  Faculty of Electrical Engineering and Communication, Brno University of Technology
- ☐ SIX — Research Centre of Sensor, Information and Communication System, Brno University of Technology
- ☐ EMBS Chapter of the IEEE Czechoslovakia Section
- ☐ Zhejiang University
- ☐ The Electromagnetics Academy at Zhejiang University, China
- ☐ The Electromagnetics Academy

PIERS 2015 PRAGUE EXHIBITOR

- ☐ CST-Computer Simulation Technology AG, Germany

PIERS 2015 SESSIONS

Session 1A1a
FocusSession.SC2: Planar Optics Based on Metasurfaces 1

High Efficiency Metasurface Holography

Thomas Zentgraf[1], **Holger Mühlenbernd**[1], **Guoxing Zheng**[2, 3], **Mitchell Kenney**[2], **Guixin Li**[4], **and Shuang Zhang**[2]

[1]Department of Physics, University of Paderborn, Paderborn 33098, Germany
[2]School of Physics & Astronomy, University of Birmingham, Birmingham, B15 2TT, UK
[3]School of Electronic Information, Wuhan University, Wuhan 430072, China
[4]Department of Physics, Hong Kong Baptist University, Hong Kong, China

Abstract— Plasmonic metasurfaces combine strong light-matter-interaction with high design flexibility and functionality. Here, we demonstrate the potential of ultrathin metasurfaces for use with high efficiency, high resolution holography and beam shaping. The concept is based on a topological phase change of light passing through the metasurfaces. In such a way broadband phase masks with efficiencies surpassing 80% in the visible range can be obtained.

One of the great benefits of metamaterials arises from the flexibility in engineering their optical responses to achieve control over the propagation of light to an unprecedented level. Plasmonic metasurfaces that consist only of a monolayer of planar metallic structures, have shown great promise for leveraging full control of light and low fabrication cost as they do not require complicated three-dimensional nano-fabrication techniques. One of the interesting features of metasurfaces is the capability of generating abrupt interfacial phase changes across the interface, and therefore provide a unique way of controlling the wave front locally at the subwavelength scale. Shaping the spatial phase and intensity distribution is very important for all applications that require a propagation of light, like focusing, beam shaping, and 3D image reconstruction. Recently metamaterials were used to demonstrate wave plates for generating vortex beams, ultrathin metalenses and 2D holography. However, none of these techniques has achieved a more complex functionality like reconfigurable focusing or 3D image reconstruction in the visible range. Furthermore, the achieved efficiencies at visible wavelengths were rather low, preventing the usability in many applications.

Here we will demonstrate that geometric phase metasurfaces consisting of plasmonic nanorods with spatially varying orientations are capable of generating continuous phase profiles in the subwavelength scale and therefore facilitate new perspectives in designing complicated phase-only Computer Generated Holograms for 3D image reconstruction. The design that is presented exhibits high quality holographic images with very high fidelity and a broad bandwidth of operation between 630 nm and 1050 nm. Importantly, the overall efficiency, defined as the ratio of light intensity forming the holographic image to that of the incident light, reaches 80%, greatly surpassing previously demonstrated metasurface based holograms. The metasurface holograms with their accurate phase modulation, high efficiency, and simple fabrication procedure compared to conventional multi-step phase holograms, are highly promising for various practical applications ranging from laser holographic projection to data storage and beam shaping.

Nanoantennas from the Visible to the Mid-infrared: Materials Considerations and Applications

Stefan A. Maier
Imperial College London, London, SW7 2AZ, UK

Abstract— The light harvesting properties of nanoantennas composed of different materials such as metals, semiconductors, and polar dielectrics are evaluated. A particular focus lies on applications in surface enhanced spectroscopies and optoelectronics, for frequencies spanning from the visible to the mid-infrared.

Optical nanoantennas based on metallic nanostructures enable the controlled focusing of light from the far field to highly confined volumes below the diffraction limit, and have spurred a renewed interest in the field of plasmonics [1]. Here, we present an overview over plasmonic antenna designs operating in the visible part of the spectrum, and investigate how a change in materials to hybrid structures [2], semiconductors [3], polar dielectrics [4], and anisotropic van der Waals crystals [5] enables us to overcome the disadvantages of plasmonics for certain application areas, mainly related to the associated optical losses.

Firstly, hybrid nanoantennas composed of both metallic and in this case transition metal oxides are shown to be a viable and highly efficient platform for higher harmonic generation [2]. Specifically, dipolar Au antennas with a 20 nm ITO disc in the feedback exhibit an enhancement of third harmonic generation by about six orders of magnitude.

Dielectric nanoantennas composed out of semiconductors instead of metals also enable controlled near-field localization, without heating losses and the possibility to also manipulate the magnetic field distribution in a controlled manner. We evaluate this behaviour in terms of applications in surface enhanced spectroscopies [3], and show that GaP dimers are a promising platform for low-loss, zero-heat surface enhanced Raman spectroscopy in the visible part of the spectrum.

Finally, we turn our attention to the mid-infrared part of the electromagnetic spectrum, where polar dielectrics enable nanofocusing due to the excitation of surface phonon polaritons. Specifically, nano forests composed out silicon carbide nanopillars show Purcell factors up to 107 due to the combination of low-loss phonon modes and ultra-small mode volumes. Going one step further, the combination of polar behaviour with anisotropy due to van der Waals interactions in adjacent crystal planes allows the occurrence of hyperbolicity in natural materials such as hBN [5]. This enables truly three-dimensional nanophotonic confinement (Figure), with a high promise for applications in the mid-infrared.

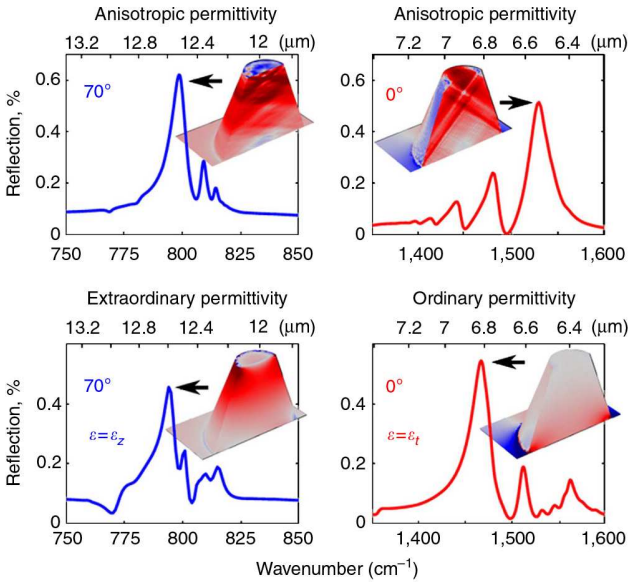

Figure 1: Comparison of field distributions in hyperbolic (top row) and isotropic conical nanoresonators [5].

REFERENCES

1. Giannini, et al., *Chemical Reviews*, Vol. 111, 3888, 2011.
2. Aouani, et al., *Nature Nanotechnology*, Vol. 9, 290, 2014.
3. Albela, et al., *ACS Photonics*, Vol. 1, 524, 2014.
4. Caldwell, et al., *Nano Letters*, Vol. 13, 3690, 2013.
5. Caldwell, et al., *Nature Communications*, Vol. 5, 5221, 2014.

Gap-plasmon Based Amplitude and Phase-gradient Metasurfaces

Sergey I. Bozhevolnyi
Department of Technology and Innovation
University of Southern Denmark, DK-5230 Odense, Denmark

Abstract— Plasmonic metasurfaces, i.e., nm-thin surface metal nanostructures with subwavelength-sized lattice units, have recently attracted considerable attention due to their abilities to efficiently control both phase and amplitude of transmitted and reflected radiation. We have recently shown that metal nanostructures, in which the top layer consists of a periodic array of nanobricks, thus supporting gap surface plasmon (GSP) resonances, offer improved control of the phase of the reflected light. At the same time, by choosing a subwavelength periodicity and weak coupling between the nanobricks and the metal underlay one can adjust the level of absorption, which is typically strong and can also be advantageously used for efficient and broadband suppression of light reflection for solar energy harvesting applications. The understanding of light reflection by arrays of GSP resonators led us to a number of potentially application-relevant developments, including the design of highly efficient and background-free (i.e., no diffraction and no scattering into other polarizations) plasmonic metasurfaces providing strong phase gradients in the reflected optical fields at the same polarization as that of the incident one. Moreover, we demonstrated also phase-gradient metasurfaces that diffract different polarizations into different directions that can be adjusted independently and exploited this approach for realization of efficient polarization-controlled coupling to surface plasmon polariton modes. Currently, following up on the recent theoretical proposal for mathematics with gradient metasurfaces [1], we develop a design strategy for independent control of phase and amplitude of the reflected radiation that is applied to realize Fourier optics based analog computing, including differentiation and integration of optical fields. Further results obtained in this direction will be presented at the conference.

REFERENCES

1. Silva, A., F. Monticone, G. Castaldi, V. Galdi, A. Alu, and N. Engheta, *Science*, Vol. 343, 160–163, 2014.

Multiple Wavefront Shaping by Spinoptical Gradient Metasurface

Erez Hasman
Micro and Nanooptics Laboratory, Faculty of Mechanical Engineering
Russell Berrie Nanotechnology Institute, Technion-Israel Institute of Technology, Haifa 32000, Israel

Abstract— Photonic gradient metasurfaces are ultrathin electromagnetic wave-molding metamaterials that provide a route for realizing flat optics. Recently, we reported on a novel class of metasurfaces — spinoptical metamaterials — which gives rise to a spin-controlled dispersion due to the optical Rashba effect. The optical spin as an additional degree of freedom offers controlled manipulation of spontaneous emission, absorption, scattering, and surface-wave excitation. Spin-symmetry breaking in nanoscale structures caused by spin-orbit interaction, leading to a new branch in optics — *spinoptics* is presented. The spin-based effects offer an unprecedented ability to control light and its polarization state in nanometer-scale optical devices, thereby facilitating a variety of applications related to nano-photonics. However, the up-to-date metasurface design, manifested by imprinting the required phase profile for a single, on-demand light manipulation functionality, is not compatible with the desired goal of multifunctional flat optics. Here, we report on a generic concept to control multifunctional optics by disordered (random) gradient metasurfaces with a custom-tailored geometric phase. This approach combines the peculiar ability of random patterns to support extraordinary information capacity, and the polarization helicity control in the geometric phase mechanism, simply implemented in a two-dimensional structured matter by imprinting optical antenna patterns. By manipulating the local orientations of the nanoantennas, we generate multiple wavefronts with different functionalities via mixed random antenna groups, where each group controls a different phase function. Disordered gradient metasurfaces broaden the applicability of flat optics as they offer all-optical manipulation by multitask wavefront shaping via a single ultrathin nanoscale photonic device.

Wavevector Selective Metasurfaces and Tunnel Vision Filters

V. A. Fedotov[1], **J. Wallauer**[2], **M. Walther**[2], **M. Perino**[1, 3], **N. Papasimakis**[1], **and N. I. Zheludev**[1, 4]

[1]Optoelectronics Research Centre and Centre for Photonic Metamaterials
University of Southampton, SO17 1BJ, UK
[2]Department of Molecular and Optical Physics, University of Freiburg, Freiburg 79104, Germany
[3]Department of Information Engineering, University of Padova, Italy
[4]Centre for Disruptive Photonic Technologies, Nanyang Technological University, 637371, Singapore

Abstract— The recent demonstration of anomalous reflection and refraction of light in optically thin two-dimensional arrays of sub-wavelength metallic scatterers (planar metamaterials or metasurfaces) has opened a new exciting chapter in photonics. Planar metamaterials can be readily fabricated using existing planar technologies and offer unprecedented flexibility in the design and control of light propagation, replacing bulk optical components and exhibiting exotic effects of asymmetric transmission and optical activity without chirality.

Here we demonstrate for the first time both computationally and experimentally that a coherent metasurface can act as a wavevector selective surface: It discriminates incident waves by the wavevector and is transparent in a very narrow range of light propagation directions thus operating as a tunnel vision filter. The filtering results in an arbitrary-shaped wavefront appearing planar as it traverses the plane of the metasurface in the absence of any active/passive spatial phase modulation or adaptive feedback.

We demonstrated the effect of wavevector filtering computationally, by simulating the propagation of spherical wavefronts through a finite-sized coherent metamaterial. It was modelled by a planar array of 14×14 identical sub-wavelength metallic resonators shaped as an asymmetrically split ring (ASR). Such a metasurface was designed to operate with no diffraction in the lower part of the terahertz spectrum, at frequencies below 0.3 THz. The spherical waves were produced by an electromagnetic point source placed close to the metasurface, at the distance equal to just one period of the ASR-array. Our findings have been fully confirmed experimentally using a metamaterial sample fabricated as the exact copy of the modelled metasurface. The transmitted wavefronts were mapped using a state-of-the-art THz-field imaging technique, which enabled accurate spatial mapping of electric-field component of the transmitted waves with the spatial resolution of 160 μm. The obtained wavefront patterns, as well as their spatial-frequency spectra, showed a very good agreement with the results of our simulations demonstrating robustness of the predicted wavevector filtering effect.

Novel Topological States in Photonics

Marin Soljacic
Department of Physics, Massachusetts Institute of Technology
Cambridge, Massachusetts 02139, USA

Abstract— Topologically non-trivial states have been raising a substantial interest in the electronics community because of their novel and unique properties. Similarly, topological states in photonics display an equally diverse range of novel and surprising phenomena. Some of our recent results in this area will be presented.

Session 1A1b
Oral Presentations for Best Student Paper Awards — SC2: Metamaterials, Plasmonics and Complex Media

Nonlocality in Discrete Metamaterials

M. A. Gorlach[1, 2] **and P. A. Belov**[1]

[1]ITMO University, Russia
[2]Belarusian State University, Belarus

Abstract— We discuss spatial dispersion effects in three-dimensional discrete metamaterials. In the present work, we consider two examples of discrete metamaterials whose behavior can not be adequately described by means of the effective medium model and where the nonlocality is important. These examples are (i) the discrete structure consisting of the uniaxial dipoles operating in the vicinity of transition from elliptic to the hyperbolic dispersion regime and (ii) the structure built from isotropic particles where anisotropy arises due to the spatial dispersion effects.

Strong spatial dispersion effects do not occur in natural materials. However, there exists a class of metamaterials where effects of spatial dispersion play an extremely important role. Therefore, it is of interest to find out what new physical effects may arise due to the nonlocality. It turns out that the use of the dyadic Green's function formalism and the discrete dipole approximation in the investigation of periodic metamaterials allows one to describe spatial dispersion effects in a rigorous and self-consistent way. We consider two examples of the discrete structures operation that can not be described properly by means of the effective medium model. The transition between elliptic and hyperbolic dispersion regime in the structure consisting of the uniaxial electric scatterers occurs when the effective permittivity calculated according to the Clausius-Mossotti formula approaches either zero or infinity. Following our recent work [1], we discuss the existence of the regime which is the transitional from elliptic to the hyperbolic dispersion (Fig. 1) and investigate the properties of the mixed dispersion regime in more detail. Moreover, possible experimental verification of the mixed dispersion regime existence is proposed.

We also discuss the anisotropy in the cubic lattice of isotropic particles that arises due to the second-order spatial dispersion effects. This feature can be easily detected plotting the system of the isofrequency contours. In the conventional isotropic medium two eigenmodes with transverse polarization correspond to the coinciding isofrequency contours. In the case of the discrete structure this degeneracy is removed and there exists a considerable difference between two transverse eigenmodes in the certain frequency range. Moreover, a longitudinal mode arises.

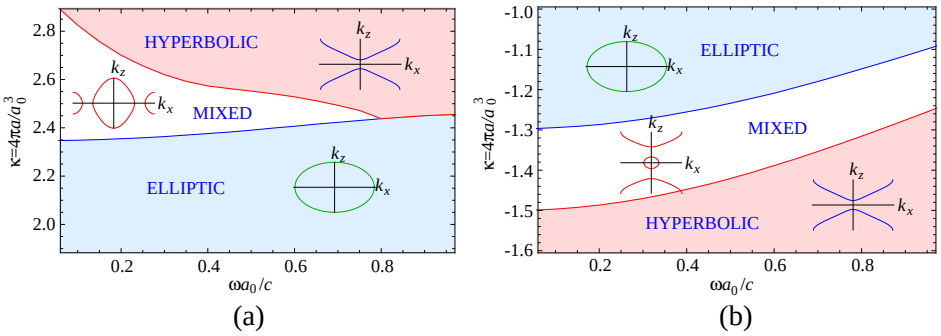

Figure 1: Different dispersion regimes in the discrete dipole structure composed of the uniaxial electric scatterers shown on "frequency-polarizability" diagram. The isofrequency contours typical for the given regime are sketched. (a) The vicinity of high ε mixed regime. (b) The vicinity of low ε mixed regime.

REFERENCES

1. Gorlach, M. A. and P. A. Belov, "Effect of spatial dispersion on the topological transition in metamaterials," *Phys. Rev. B*, Vol. 90, 115136, 2014.
2. Belov, P. A. and C. R. Simovski, "Homogenization of electromagnetic crystals formed by uniaxial resonant scatterers," *Phys. Rev. E*, Vol. 72, 026615, 2005.

Pure Electric and Magnetic Hotspots by Dielectric Cylindrical Dimers

Ali Mirzaei and Andrey Miroshnichenko
Nonlinear Physics Centre, Research School of Physics and Engineering
Australian National University, 59 Mills road, Acton, ACT 2601, Australia

Abstract— Clusters of nanoparticles have been actively studied for controlling of light [1]. Near-field enhancement of electromagnetic fields by dimers with both spherical and cylindrical geometries have also been reported [2]. These studies are mostly concentrated on plasmonic materials to achieve high field-enhancement, however plasmonic structures are associated with strong losses in metallic components, even in nonresonance regimes. In this work, we analyze dimers made of a pair of dielectric nanowires in visible wavelength range and compare them with those for similar metallic dimer nanowires, using experimental data to describe the materials. We demonstrate the enhancement of both electric and magnetic near-fields, and show that it is possible to achieve hotspots by dielectric nanowires comparable with plasmonic structures in TE polarization (magnetic field parallel to the axis of nanowires). We also show the possibility to achieving hotspots in TM polarization with dielectrics, which is not possible by using plasmonic nanowires. We demonstrate that the hotspots are not exactly in the middle of the dimers' gap. These displacements for electric and magnetic hotspots are opposite in plasmonic and dielectric dimers and lead to have both pure magnetic and pure electric hot spots close together simultaneously with dielectric nanowires [3]. Figure 1 summarizes our major results and the formation of hotspots in two polarizations.

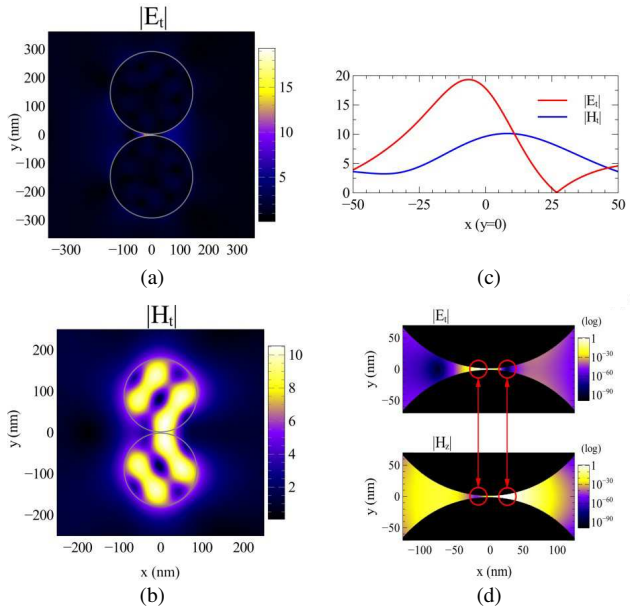

Figure 1: Dimers made by silicon nanowires, optimized for (a) electric hotspot in TE polarization and (b) magnetic hotspot in TM polarization in $\lambda = 614\,\text{nm}$, using a genetic alghorithm. (c) and (d) demonstrate that the hotspots are not exactly in the centre of dimer's gap, causing two pure magnetic and electric hotspots (related to structure in Fig. 1(a)).

REFERENCES

1. Rahmani, M., E. Yoxall, B. Hopkins, Y. Sonnefraud, Y. Kivshar, M. Hong, C. Phillips, S. A. Maier, and A. E. Miroshnichenko, "Plasmonic nanoclusters with rotational symmetry: Polarization-invariant far-field response vs changing near-field distribution," *ACS Nano*, Vol. 7, 11138–11146, 2013.
2. Esteban, R., A. G. Borisov, P. Nordlander, and J. Aizpurua, "Bridging quantum and classical plasmonics with a quantum-corrected model," *Nat. Comm.*, Vol. 3, 825, 2012.

3. Mirzaei, A. and A. E. Miroshnichenko, "Electric and magnetic hotspots in dielectric nanowire dimers," *Nanoscale*, Vol. 7, 5963–5968, 2015.

Controlled Photonic Surface Modes in 'Cholesteric Liquid Crystal — Phase Plate — Metal' Structure

M. V. Pyatnov[1], **S. Ya. Vetrov**[1, 2], **and I. V. Timofeev**[1, 2]

[1]Siberian Federal University, Krasnoyarsk 660074, Russia
[2]Kirensky Institute of Physics, Siberian Branch of the Russian Academy of Sciences
Krasnoyarsk 660036, Russia

Abstract— We demonstrated the existence of surface electromagnetic states localized in the structure of the cholesteric liquid crystal (CLC) — the phase plate — the layer of silver [1]. These states are similar to optical Tamm states (OTC). Spectral properties of such a system can be efficiently controlled due to high sensitivity of CLC structural parameters to external factors. Unlike the case with OTS observed at a photonic crystal (PC) — metal interface, it is doubtful to obtain a surface state at a CLC — metal interface under normal incidence of light. The difficulty is that Bragg reflection exists not for every arbitrary polarization. For light localization between CLC and metal to occur, we need to change the phase of the wave. To this end, between CLC and metal we introduce an anisotropic quarter-wave plate cut parallel to the optical axis and shifting the wave phase by $\pi/2$. Cholesteric molecules at the CLC — phase plate interface align along the optical axis. Fig. 1 shows individual transmission spectra of the CLC, silver film and the structure.

Light of any polarization will be localized near metal with the field intensity maximizing at the phase plate — metal layer interface. However, different degrees of ellipticity of transmitted waves and their polarization properties result in different transmission coefficients for each polarization. A possibility to control the passband position by varying the thickness of the phase plate or the CLC pitch by external fields has been demonstrated.

It was established that the transmission spectra of the propagation of light in the forward and inverse directions are different (Fig. 2). This property is inherent only in chiral environments, which include the CLC. On the basis we proposed design of the polarization optical diode based on surface photon modes. Note also that creating direct contact of the CLC with the metal is not possible. This requires the use of orientant which aligns layers of anisotropic material. Therefore orientant can simultaneously be a quarter phase plate, picking up the thickness of which it is possible to implement a localized state.

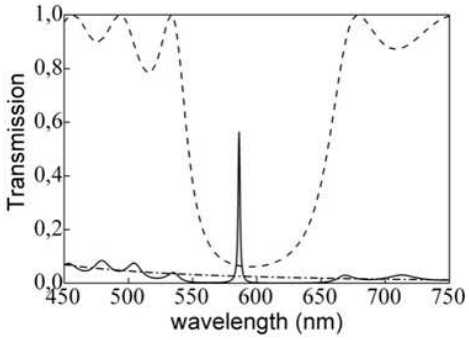

Figure 1: Transmission versus wavelength with light incidence normal to CLC (dashed line), to the silver film (dash-dotted line) and to the 'CLC — phase plate — metal' structure (solid line).

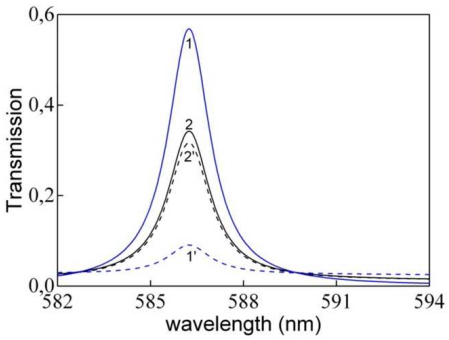

Figure 2: The transmission spectrum of the structure: 1 and 1′ for the right and left polarizations for light incident on the CLC; 2 and 2′, for the left and right polarizations of light incident on the metal.

REFERENCES

1. Vetrov, S. Ya., M. V. Pyatnov, and I. V. Timofeev, *Opt. Lett.*, Vol. 39, 2743–2746, 2014.

An Efficient and Innovative Modelisation for Nanolasers

T. Wang[1, 2], **G. P. Puccioni**[3], **and G. L. Lippi**[1, 2]

[1]Institut Non Linéaire de Nice, Université de Nice-Sophia Antipolis, France
[2]UMR 7335 CNRS, France
[3]Istituto dei Sistemi Complessi, CNR, Italy

Abstract— The current technological advances on the nanoscale have allowed for remarkable progress in the fabrication of ever smaller lasers. High promise is expected from these unusual devices, whose potential application range from on-chip integration, fast and compact data handling, inclusion on non-invasive probes, etc.. However, satisfactory modeling of the optical properties of these devices has so far proven to be quite elusive, in particular concerning their threshold and optical coherence.

Modeling approaches range from the standard rate equations, proven to present intrinsic difficulties in the characterization of threshold [1], to quantum mechanical models [2], to innovative approaches based on quantum-optical models showing non-classical statistics for few emitters [3]. Recently, we have introduced a new way of modeling lasers using a Stochastic Simulator [4] which operates on the (semiclassical) description of the physical processes which take place when lasing occurs.

We apply our model to explore the more elusive optical features of nanolasers to characterize their threshold, to infer the transition towards coherence and to predict their dynamics in the threshold region, as a function of the cavity size (quantified by the β-parameter — spontaneous emission fraction coupled into the lasing mode).

REFERENCES

1. Björk, G., A. Karlsson, and Y. Yamamoto, "Definition of a laser threshold," *Phys. Rev. A*, Vol. 50, 1675–1680, 1994.
2. Lorke, M., T. Suhr, N. Gregersen, and J. Mork, "Theory of nanolaser devices: Rate equation analysis versus microscopic theory," *Phys. Rev. B*, Vol. 87, No. 20, 205310, 2013.
3. Chow, W. W., F. Jahnke, and Ch. Gies, "Emission properties of nanolasers during the transition to lasing," *Light: Science & Applications*, Vol. 3, e201, 2014, doi:10.1038/lsa.2014.82.
4. Puccioni, G. P. and G. L. Lippi, "Stochastic simulator for modeling the transition to lasing," *Optics Express*, Vol. 23, No. 3, 2369–2374, 2015.

Session 1A2
SC2: THz Metamaterials: Fundamentals and Applications

Electromagnetic Metamaterials for Terahertz Devices

W. J. Padilla
Department of Electrical and Computer Engineering, Duke University, Durham, NC, USA

Abstract— Electromagnetic metamaterials provide unprecedented control over light matter interactions and are viable candidates for realization of devices in the terahertz frequency regime. The ability to dynamically control novel responses exhibited by electromagnetic metamaterials is a key enabling feature and further bolsters this quest. We overview our work in terahertz metamaterials and present examples of metamaterial-based systems.

The interaction of electromagnetic waves with natural materials forms the basis of many modern opto-electronic devices. At microwave and lower frequencies electrons form the basis for a myriad of devices, while at optical and infrared wavelengths, photons are the key fundamental particle utilized. However, the effectiveness of both the electron and photon is not distributed equally across the electromagnetic spectrum and both realize a diminished utility reaching a collective minimum at terahertz frequencies. Although significant effort has been exerted by scientists and engineers in search of suitable terahertz materials, all terahertz devices pale in comparison to the performance of microwave or optical components.

We present electrically controlled metamaterial modulators using both liquid crystals and semiconducting epi-layers. Our metamaterial modulators are pixelated and function as real-time tunable, spectrally sensitive spatial light modulators. We implement a terahertz optical imaging system with our metamaterial spatial light modulator and demonstrate single pixel imaging. Utilization of a technique from communication theory — called binary phase shift keying — enables complex valued masks to be displayed on our metamaterial spatial light modulator. Images are encoded with both the coefficients of the Hadamard matrix and the closely related S-matrix and both are decoded with their respective inverse matrices. The demonstrated single pixel imaging systems verify the usefulness of metamaterials and establishes a new path forward for the terahertz regime.

Electrically Driven Terahertz Metamaterial Diffraction Modulators

Hou-Tong Chen[1], **Antoinette J. Taylor**[1], **Nicholas Karl**[2], **Kimberly Reichel**[2], **Rajind Mendis**[2], **Daniel M. Mittleman**[2], **Igal Brener**[3], **Alex Benz**[3], **and John L. Reno**[3]

[1]Los Alamos National Laboratory, USA
[2]Rice University, USA
[3]Sandia National Laboratories, USA

Abstract— Teraherz (THz) waves have played an important role in both fundamental research and practical applications; however, arbitrary control of THz waves remains a significant challenge. In order to take full advantage of THz waves, there is an urgent need in developing functional THz materials to construct various kinds of THz devices and components. Metamaterials have emerged during the past few years that provide new opportunities due to the realization of tailored interactions with THz waves, which are often unavailable or very difficult to obtain from natural materials. Combining the resonant response originating from the planar metamaterial structures and tunable refractive index or conductivity of integrated functional materials, hybrid metamaterials have been developed during the past few years where the metamaterial resonances can be switched or tunable through the application of photoexcitation, temperature change, and/or voltage bias [1, 2]. Of particular interest for THz modulation are planar metamaterials that can be electrically switched [3, 4], which provides a mechanism for high-speed modulation of THz radiation relevant to practical applications, a result that is otherwise difficult to achieve. Furthermore, the metamaterial can be pixelated to enable independent control of individual pixels, forming the so-called THz spatial light modulator [5].

So far state-of-the-art demonstrations still exhibit a relatively low on/off ratio less than 10 dB [4], which may limit their applicability. In all previous works the THz modulation is attributed to the change of the direct transmission beam and, therefore, the modulation depth is limited by the transmission values of the device's ON and OFF states. In this work we present the design and experimental demonstration of an electrically switchable metamaterial diffraction grating for background-free THz modulation. We take advantage of metamaterial pixilation to form columns of electrically switchable metamaterials that are independent each other. The active metamaterial grating is created by applying the voltage bias to alternating columns, resulting in a contrast of transmission property and diffraction of the incident THz beam. The diffraction behavior disappears without the voltage bias or when a uniform voltage bias is applied to all of these columns. As such, we have created a background-free metamaterial diffraction THz modulator [6]. Experimentally, we observe that the device can function as a relatively high speed, wide-bandwidth, high-contrast THz off-axis diffraction modulator, with more than 20 dB of dynamic range.

REFERENCES

1. Chen, H.-T., J. F. O'Hara, A. K. Azad, and A. J. Taylor, *Laser Photon. Rev.*, Vol. 5, 513, 2011.
2. Chen, H.-T., *Front. Optoelectron.*, Vol. 8, 27–43, 2015.
3. Chen, H.-T., et al., *Nature*, Vol. 444, 597, 2006.
4. Chen, H.-T., et al., *Nat. Photon.*, Vol. 3, 148, 2009.
5. Chan, W. L., et al., *Appl. Phys. Lett.*, Vol. 94, 213511, 2009.
6. Karl, N., et al., *Appl. Phys. Lett.*, Vol. 104, 091115, 2014.

Full-range Gate-controlled Terahertz Phase Modulation with Graphene Metasurfaces

Ziqi Miao, **Qiong Wu**, **Xin Li**, **Qiong He**, **Kun Ding**,
Zhenghua An, **Yuanbo Zhang**, **and Lei Zhou**
State Key Laboratory of Surface Physics, Key Laboratory of Micro and Nano Photonic Structures (Ministry of Education), and Department of Physics, Fudan University, Shanghai 200438, China

Abstract— Phase modulation of electromagnetic (EM) waves plays a central role in photonics research. The ability to control the local EM phase underpins important applications such as holographic imaging, polarization manipulations, and wave-front controls [1–3]. Such phase modulation was conventionally achieved via modulating the refractive index of bulk materials. The dimension of such systems is typically on the order of wavelength, and therefore too bulky for optical integrations. Metasurfaces, ultra-thin MTMs composed of planar sub-wavelength units, were utilized to achieve phase changes covering full range of 360 degrees. However, the metasurfaces-based phase modulators currently available are mostly passive elements which cannot be tuned externally.

Here we experimentally demonstrate full-range gate-tunable THz phase modulation, realized by an ultra-thin meta-system integrating graphene and a specially designed metasurface [4]. We show that a gate bias applied on graphene through ion liquid tunes its optical conductivity, turns the coupled system from an under-damped resonator to an over-damped one, and induces drastic modulation on the phase of the reflected wave. This is in stark contrast to the two-port resonator (with both reflection and transmission channels) commonly used in previous studies, where only a small phase modulation was possible. Our findings represent a significant advance over previous attempts on photonic devices with tunable responses, and our method points to new design strategies for future active phase modulators.

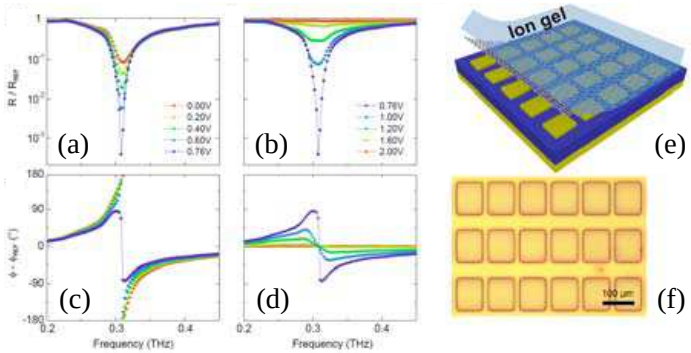

Figure 1: Experimentally measured reflectance and phase modulation and designed meta-system. (a)–(d) Dramatic phase modulation realized upon increasing the carrier concentration through gating, accompanied with a drastic change on reflection amplitude. (e) Schematics of our metasystem, a gate-controlled graphene on a reflective metasurface. (f) Macroscopic photo of our sample.

REFERENCES

1. Yu, N., et al., "Light propagation with phase discontinuities: Generalized laws of reflection and refraction," *Science*, Vol. 334, 333–337, 2011.
2. Sun, S., et al., "Gradient-index meta-surfaces as a bridge linking propagating waves and surface waves," *Nat. Mater.*, Vol. 11, 426–431, 2012.
3. Sun, S., et al., "High-efficiency broadband anomalous reflection by gradient meta-surfaces," *Nano Letters*, Vol. 12, 6223–6229, 2012.
4. Ziqi, M., et al., "Full range gate-controlled terahertz phase modulations with graphene meta-surfaces," *Cond. Mat. Mtrl. Sci.*, arXiv: 1409.6845, 2014.

Photo-generated THz Metamaterial and Metasurfaces

J. Gómez Rivas[1,2], **G. Georgiou**[1], **and A. Bhattacharya**[1]

[1]Center for Nanophotonics, FOM Institute AMOLF
Science Park 102, 1098 XG, Amsterdam, The Netherlands
[2]COBRA Research Institute, Eindhoven University of Technology
P. O. Box 513, 5600 MB Eindhoven, The Netherlands

Abstract— The versatile nature of semiconductors with a permittivity that can be controlled by the amount of free carriers, makes them excellent candidates for active metamaterials and metasurfaces. Structures made out of semiconductors can give rise to the localized resonances at THz frequencies that define the behavior of the metamaterial. The precise behavior of these structures depends on their geometry and permittivity; parameters that can be actively tuned [1, 2]. Subwavelength local field enhancements are the most relevant characteristic of localized resonances. These enhancements have triggered the interest for resonant metallic structures in sensing and spectroscopic applications.

In this contribution, we demonstrate the THz near-field enhancement in the proximity of silicon and gold resonant structures. These near fields are measured in a broadband THz time-domain near-field microscope with micro-structured photo-conductive antennas that enable the independent measurement of the two in-plane field components. The measurements clearly show the resonant response of the structures and the concomitant subwavelength field enhancement. In order to achieve a full optical control of local THz resonances, we demonstrate the feasibility of the photo-generation of resonant structures on semiconductors by shaping an optical pump beam incident on a flat GaAs layer [3]. This beam shaping has been realized with a spatial light modulator that structures the optical beam with the form of the structures. The incidence of the shaped beam on the semiconductor locally induces a metallic behaviour on the illuminated areas, with photo-excited free charges that are resonantly driven by the THz electric field. This approach provides an unprecedented flexibility in designing the far-field properties of the THz field, such as extinction and beaming [4], as well as the near field at the surface of the semiconductor. The photo-generation of metallic structures in semiconductors can be also extended to create THz waveguides [5].

REFERENCES

1. Giannini, V., et al., "Scattering efficiency and near field enhancement of active semiconductor plasmonic antennas at terahertz frequencies," *Opt. Express*, Vol. 18, 2797, 2010.
2. Berrier, A., et al., "Ultrafast active control of localized surface plasmon resonances in Si bowtie antennas," *Opt. Express*, Vol. 20, 5052, 2012.
3. Georgiou, G., et al., "Photo-generated THz antennas," *Sci. Rep.*, Vol. 4, 3584, 2014.
4. Steinbusch, T., et al., "Active terahertz beam steering by photo-generated graded index gratings in thin semiconductor films," *Opt. Express*, Vol. 22, 26559, 2014.
5. Tyagi, H., et al., "Photo-generated THz plasmonic waveguides," *J. Opt.*, Vol. 16, 094011, 2104.

A Water-based Metamaterial for Broadband and Large Tuning Perfect Absorption

W. Zhang[1], **Q. H. Song**[1], **L. B. Yan**[1], **P. C. Wu**[1, 2], **W. M. Zhu**[1], **D. T. Tsai**[2], **C. T. Chan**[3], **Z. H. Yang**[4], **R. Huang**[4], **X. Zhu**[4], **F. Capasso**[5], **and A. Q. Liu**[1]

[1]School of Electrical & Electronic Engineering, Nanyang Technological University, Singapore
[2]Department of Physics, National Taiwan University, Taiwan
[3]Department of Physics, Hong Kong Technical University, Hong Kong, China
[4]School of Electronics & Computer Engineering, Peking University, Beijing 10087, China
[5]School of Engineering and Applied Sciences, Harvard University, Cambridge, MA 02138, USA

Abstract— A perfect absorber, which fully absorbs the incoming electromagnetic (EM) wave and transfers it into other forms of energy, is intensively studied for its wide applications in energy harvesting, military defense, EM wave modulation and communications, etc.. The metamaterial, an artificial material consisting of subwavelength meta-atoms, has been designed for perfect absorption by utilizing the impedance matched meta-atoms. Although successfully demonstrated, they are usually limited in a narrow working bandwidth. The rigid structure of the design also hampersits real life applications that require all-directional absorption.

In this talk, a soft metamaterial is proposed to realize the perfect absorption in microwave regime, which can be easily deformed to face to different directions. The polymer polydimethylsiloxane (PDMS) is used as the soft substrate, which is filled with the most common material in nature, i.e., water. Due to the extremely high dielectric constant and high absorption by its polar molecules in microwave regime, water is a perfect candidate for perfect absorption. By properly patterning the PDMS channels, which are filled with water, the microwave across a wide band is well confined and fully absorbed. The perfect absorption is further manipulated in two aspects: first, the absorption band is shifted by deforming the water pattern under different inlet water pressures applied in the PDMS channel. Second, the absorption coefficient of the soft metamaterial can be effectively controlled by mixing water with other organic solvent, such as ethanol in this work. By controlling the volume ratio of the water and ethanol, the tunability from zero absorption to full absorption is realized. With the wideband and tunable capability, the proposed perfect metamaterial absorber gives a promising applications in energy harvesting, stealth system and microwave communications.

Studies of Metamaterials with Near-field Scanning Terahertz Microscopy

Xueqian Zhang[1], **Yuehong Xu**[1], **Jianqiang Gu**[1], **Zhen Tian**[1], **Chunmei Ouyang**[1], **Weili Zhang**[1, 2], **and Jiaguang Han**[1]

[1]Center for Terahertz Waves, College of Precision Instrument and Optoelectronics Engineering
Tianjin University, Tianjin 300072, China
[2]School of Electrical and Computer Engineering, Oklahoma State University
Stillwater, Oklahoma 74078, USA

Abstract— Terahertz Science and Technology has been one of the promising and active research fields, especially in military, state security and communications. From the view of current situations and tendency of terahertz science and technology, there are three major significant aspects: fundamental research, advanced technology and terahertz market. It is expected that a rapid progress will be achieved in information science, physics, astronomy, medical science, biology, and so on. The key components for terahertz include the transmitter, receiver and devices. Here we will present the recent achievements on the terahertz devices based on metamaterials, especially by using the near field technology. Although over the last decade, optical near-field technology has become an intense area of research, in the terahertz regime, this is not to be outdone. In this talk, we will give a brief discussion on the terahertz near field measurement of metamaterials based on a metal tip-terahertz system [1–3].

REFERENCES

1. Adam, A., *J. Infrated Milli. Terahz. Waves*, Vol. 32, 976, 2011.
2. Zhang, X., et al., *Adv. Materials*, Vol. 25, 4567, 2013.
3. http://terahertz.tju.edu.cn.

Heterogeneous 3D Construction of Metamaterials and Metadevices by Modular Transfer Printing

Bumki Min
Department of Mechanical Engineering, KAIST
291 Daehak-ro, Yuseong-gu, Daejeon 305-751, Republic of Korea

Abstract— Metamaterials make possible exotic control of the flow of electromagnetic waves that is ultimately impossible to achieve with naturally occurring materials. Over the past decade, the fabrication of metadevices synergistically benefitting from enhanced light-matter interaction through combining metamaterials and active functional natural materials has shown immense potential to develop highly efficient photonic devices. However, complex and heterogeneous architectures enabling diverse functionalities of metamaterials and metadevices have been challenging to realize due to the limited manufacturing capabilities of conventional fabrication methods. In this work, we report three-dimensional (3D) modular assembly based on transfer printing to construct metamaterials and metadevices with complex structural architectures for achieving on-demand photonic properties. Transfer printing-based 3D assembly provides access to the integration of dissimilar, active materials regardless of roughness and surface chemistry which is quite attractive to employ for the fabrication of metadevices exhibiting unprecedented device fidelity. The minimum repetitive process steps and rapid construction are the additional advantages of the transfer printing-based 3D modular assembly. The method presented here suggests a fascinating route to generate 2D/3D metamaterials and metadevices with heterogeneous material combination, complex device architectures, and effective functionalities for future practical use for advanced photonic applications.

Active Modulation of Terahertz Wavefront

Y. Zhang[1], **X. K. Wang**[1], **and Z. W. Xie**[2]

[1]Beijing Key Lab for Metamaterials and Devices
Key Laboratory of Terahertz Optoelectronics, Ministry of Education
Department of Physics, Capital Normal University, Beijing 100048, China
[2]Department of Physics, Harbin Institute of Technology, Harbin 150001, China

Abstract— Terahertz (THz) radiation has attracted a lot of attentions due to its fascinating potential applications. Wavefront modulation of the THz radiation will benefit the applications of THz imaging and communication. We propose a novel approach to actively modulate the wavefront of the THz radiation based on the THz hologram formed with photon-generated carriers. The diffracted THz beam will come into special amplitude and phase distribution. Experiment results demonstrate the validity of this new method.

Introduction: Terahertz (THz) imaging is one of most important applications of the THz radiation. Modulation of THz wavefront will profit the applications of THz imaging and communication. Active modulation of wavefront can help us to reduce the size of the focal point, to improve the resolution, and to achieve compressed imaging, which will greatly enhance the application of the THz technology. We adopt the photon-generated carriers to form THz holograms on the surface of a semiconductor surface, which can diffract the THz to generate the desired amplitude and phase distribution.

Basic Idea: Under the illumination of a strong light, the semiconductor will generate free carriers on its surface. These free carriers can effectively block the transmission of the THz radiation. The diffusion range of the photon-generated carriers is just few micrometers, which is much less than the wavelength of the THz radiation. Therefore, we can project a computer generated hologram (CGH) pattern on the surface of the semiconductor to generate a photo-generated carriers based THz hologram. The diffracted beam will from the special amplitude and phase distribution.

In the experiment, 100 femtosecond pulses with a 800 nm central wavelength from a Ti: sapphire regenerator amplifier are split into three beams. The control beam is utilized to construct holograms on a 500 mm thick silicon wafer, the pump beam to generate the THz radiation using a ZnTe crystal and the probe beam to detect the two-dimensional THz information. A spatial light modulator (Holoeye LC2002, resolution 800×600, pixel size $32\,\mu$m) is inserted into the control beam to excite the carrier distribution of the designed THz CGHs. In order to achieve better results, an off-line holography configuration is adopted. The THz radiation is reflected onto the silicon wafer with an incident angle of 37 degrees. Three letters C, N and U are required to be shown on the plane which is 2 cm away from the silicon wafer. The size of each letter is about $4\,\text{mm} \times 6\,\text{mm}$. The calculated CGHs are displayed on the optical SLM and projected onto the surface of the silicon wafer, respectively. The complex amplitude distribution of the THz beam on the observation plane is captured with the THz focal plane imaging system. The three letters C, N and U are clearly reconstructed. The experimental results meet the theoretical expectations quite well.

This technology can also be combined with a sub-wavelength grating to generate an arbitrary THz vector beam. The circularly polarized THz beam illuminates to a sub-wavelength ring metal grating fabricated on the high-resistance silicon substrate. Meanwhile, the projected visible light generates a photo-generated carrier THz vortex hologram on the surface of the silicon wafer. The first-order diffraction of the THz beam will form a radially polarized beam. A good match between the experiment and simulation results has been found. Furthermore, this method can work well for a broad THz band.

Conclusions: In conclusion, a scheme for generating arbitrary THz beams is exhibited. A sub-wavelength metal grating is utilized to adjust the polarization of the THz radiation. The amplitude and phase distribution of the THz beam are dynamically regulated by the THz CGH pattern formed with the photo-generated carriers. The experimental results, which correspond to the theoretical expectations well, demonstrated the effectiveness and validity of the proposed method. The proposed method may benefit to the THz sensing, THz imaging, and THz communication.

ACKNOWLEDGMENT

This work was supported by the 973 Program of China (No. 2013CBA01702), the National Natural Science Foundation of China (Nos. 91233202 and 11174211), the Program for New Century Excellent Talents in University (NCET-12-0607), the CAEP THz Science and Technology Foundation (CAEPTHZ201306), and the Scientific Research Base Development Program of the Beijing Municipal Commission of Education.

REFERENCES

1. Wang, X., Z. Xie, W. Sun, S. Feng, Y. Cui, J. Ye, and Y. Zhang, "Focusing and imaging of a virtual all-optical tunable terahertz Fresnel zone plate," *Opt. Lett.*, Vol. 38, 4731–4734, 2013.
2. Xie, Z., X. Wang, J. Ye, S. Feng, W. Sun, T. Akalin, and Y. Zhang, "Spatial terahertz modulator," Scientific Reports, Vol. 3, 3347, 2013.
3. Xie, Z., J. He, X. Wang, S. Feng, and Y. Zhang, "Generation of terahertz vector beams with a concentric ring metal grating and photo-generated carriers," *Opt. Lett.*, in press, 2015.

Metasurfaces for Terahertz Waves Polarization Control

A. V. Lavrinenko[1], **R. Malureanu**[1], **M. Zalkovskij**[1], **S. Zhukovsky**[1], **A. Andryieuski**[1], **P. U. Jepsen**[1], **D. N. Chigrin**[2], **Z. Y. Song**[3], **Q. He**[3], **and L. Zhou**[3]

[1]Department of Photonics Engineering, Technical University of Denmark
Oersteds plads, Bld. 343, Kgs. Lyngby DK-2800, Denmark
[2]RWTH Aachen University, Aachen 52074, Germany
[3]Physics Department, Fudan University, Shanghai 200433, China

Abstract— Metamaterials as the design concept and umbrella name have demonstrated a broad range of useful properties in different ranges of frequencies. The main advantage of the metamaterial-based devices is the possibility to broaden both passive and active photonic component functionalities. While in the visible, near infrared or microwave regimes these issues in principle have strong alternatives via a conventional optics or electromagnetic approaches, at terahertz (THz) frequencies metamaterials are often considered as being the unique solution for the encountered problems. Several approaches involving metamaterials-based THz components have been proposed and show good potential for applications [1, 2]. Especially fruitful appears to be two-dimensional metamaterials or metasurfaces due to fabrication simplifications and practically the same as bulk metamaterials functionalities.

In the talk we will focus on employment of THz metasurfaces as polarizers and polarization converters, absorbers and conducting layers with enhanced transmittance, dichroic and chiral reconfigurable systems, waveplates and broadband filters.

As the unified approach we employ the transmission line theory providing a needed level of the generalization. We demonstrate its applicability in optical problems by analyzing the theoretical limits of a metasurface converter with orthogonal linear eigenpolarizations that allows for linear-to-elliptical polarization transformation with any desired ellipticity and ellipse orientation. Our analysis reveals that the maximal conversion efficiency with a single metamaterial surface is 50% in transmission and up to 90% in reflection. However, a double layer transmission converter and a single layer with a metallic mirror can have 100% polarization conversion efficiency. We tested our conclusions numerically reaching the designated limits of efficiency using a simple metamaterial design and checking them against the numbers reported in literature.

The metasurfaces performance was characterized by exemplifying them with free-standing membranes patterned with a grid of air slits perforated in a uniform large area (up to several cm^2) 2 μm-thick Ni film. Depending on arrangement of both slits and their sizes different optical properties of such metasurface can be acquired. We demonstrate linear polarization filtering with the parallel slits dimmers, and more complex chiral behaviour of dimers, when non-equal slits are non-parallel. In particular, strong optical activity and circular polarization conversion are reported.

REFERENCES

1. Rahm, M., J. S. Li, and W. Padilla, *J. Infrared Millim. Terahertz Waves*, Vol. 34, 1–27, 2013.
2. Moser, H. O. and C. Rockstuhl, "3D THz metamaterials from micro/nanomanufacturing," *Laser Photon. Rev.*, Vol. 6, 219–244, 2012.

Dynamic Control of Terahertz Wave with Graphene-based Metamaterial Structures

Yin Zhang, Junming Zhao, Bo Zhu, and Yijun Feng
School of Electronic Science and Engineering, Nanjing University, Nanjing, China

Abstract— Graphene, a two-dimension material consisting of one monolayer of carbon atoms, has been recently applied in electronic and photonic devices due to its exotic properties, such as optical transparency, flexibility, high electron mobility. In addition, its sheet conductivity can be continuously tuned in a broad frequency range by shifting the electronic Fermi level via chemical or electronic doping, which enables fast electrical modulation and on-chip integration. This makes the continuous or structured graphene sheet a promising candidate for designing tunable THz metamaterial.

In this presentation, we combine the metamaterials having different unit cells of metallic resonator with the double layer graphene wires to realize several terahertz devices that could manipulate the wave propagation. Firstly, a graphene based tunable metamaterial absorber with polarization independence has been designed and analyzed. The absorption performance with a peak frequency tuning range of 15% and almost perfect peak absorption has been demonstrated by controlling the Fermi energy of the graphene that can be conveniently achieved by adjusting the bias voltage on the graphene double layers. The mechanism of the proposed absorber has been explored by a transmission line model and the tuning is explained by the variation of the effective inductance of the graphene wires under gate voltage biasing. Secondly, we propose a polarization modulation scheme of terahertz wave by applying similar polarization dependent absorbers. Through the proposed polarization modulator, it is able to electrically control the reflected wave with a linear polarization of continuously tunable azimuth angle of the major axis from 0° to 90° at the working frequency. Finally, we explore a broadband terahertz wave plate that can dynamically switch the transmission wave among left-handed circular polarization, right-handed circular polarization or linear polarization by electrically controlling the Fermi energy of graphene gratings. These design approaches enable us to electrically control the absorption spectrum and the polarization state of terahertz waves more flexibly.

ACKNOWLEDGMENT

This work is partially supported by the National Nature Science Foundation of China (61301017, 61371034, 61101011), the Key Grant Project of Ministry of Education of China (313029), the Ph.D. Programs Foundation of Ministry of Education of China (20120091110032), and partially supported by Jiangsu Key Laboratory of Advanced Techniques for Manipulating Electromagnetic Waves.

Reflective Terahertz Metamaterial Wave-plates with Ultra-wide Bandwidths

Shaojie Ma[1], **Weijie Luo**[1], **Shulin Sun**[2], **Qiong He**[1, 3], **and Lei Zhou**[1, 3]

[1]State Key Laboratory of Surface Physics and Key Laboratory of Micro and Nano Photonic Structures (Minnistry of Education), Fudan University, Shanghai 200438, China
[2]Shanghai Engineering Research Center of Ultra-Precision Optical Manufacturing, Green Photonics and Department of Optical Science and Engineering, Fudda University, Shanghai 2004333, China
[3]Collaborative Innovation Center of Advanced Microstructures, Fudan University, Shanghai 200433, China

Abstract— Full control of the polarization of Electromagnetic wave is highly desired due to a wide range of applications, like quarter wave plate or polarization convertor. Conventional methods with dichroic crystals or birefringent materials suffer the energy loss or require thick system. Recently, polarization conversion using Metamaterial has attracted much attention. Although, the wide-band reflective wave-plates based on metamaterials have been demonstrated in GHz [1], THz [2] and infrared [3] regime, the general designing principle of the polarization conversion effect is not well reported yet.

In this work [4], we firstly show a general designing principle of the meta-surface to perfectly realize the polarization conversion derived based on the Jones Matrix analysis, which lead to two type of meta-surface with different symmetry properties. Such a principle is applicable at any frequency, here we design and fabricate two terahertz samples and perform experiments to demonstrate that both can realize the half wave-plate functionality with $> 90\%$ conversion efficiency on an ultra-broad frequency interval (0.4–1.05 THz, equivalent to **∼1000% relative bandwidth**). Finally, based on similar idea, we demonstrate experimentally high efficient and ultra-board band linear-circular polarization conversion with carefully designed meta-surface.

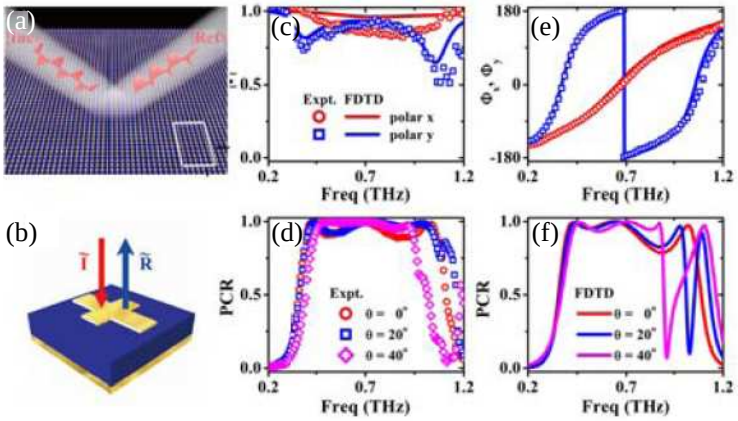

Figure 1: (a) Schematics of the high-efficient polarization conversion realized at our reflective Metasurface. (b) Geometry of the meta-actom. (c) Measured and simulated reflection coefficients and (e) phase spectra for x and y polarization. (d) Measured and (f) simulated PCR with 0°, 20° and 40° incidence.

REFERENCES

1. Hao, J., et al., "Manipulating electromagnetic wave polarizations by anisotropic metamaterials," *Phys. Rev. Lett.*, Vol. 99, 063908, 2007.
2. Grady, N. K., et al., "Terahertz metamaterials for linear polarization conversion and anomalous refraction," *Science*, Vol. 340, 1304–1307, 2013.
3. Jiang, S.-C., et al., "Controlling the polarization state of light with a dispersion-free metastructure," *Phys. Rev. X*, Vol. 4, 021026, 2014.
4. Ma, S. J., et al., "Huge-broadband reflective terahertz Metamaterial wave-plates," in Preparation.

THz Twist Polarizer Based on Supramolecular Fermat's Spiral Chiral Metamaterial

N. Yogesh, **Quanqiang Yu**, **and Zhengbiao Ouyang**
Solid State Photonics Laboratory, THz Technical Research Center
Shenzhen Key Laboratory of Micro-nano Photonic Information Technology
Key Laboratory of Optoelectronic Device and Systems of Ministry of Education and Guangdong Province
College of Electronic Science and Technology, Shenzhen University, Shenzhen 518060, China

Abstract— A THz twist polarizer formed by supramolecular Fermat's spiral chiral metamaterial (SFSCMM) is reported. Twist polarizers (TPs) are the 90° polarization rotators, in which transverse magnetic linear polarization is converted into transverse electric linear polarization and vice versa. The proposed SFSCMM consists of twisted bilayered supramolecular Fermat's spiral patterns, in which each layer is chiral in nature. The design is implemented in polyimide substrate using silver as a metal. Full-wave simulations demonstrated its function of TP, where the SFSCMM shows the zero-point ellipticity with the polarization rotation angle of 89.49° at 7.765 THz. The proposed SFSCMM has a dimension of $\lambda/1.38 \times \lambda/1.38 \times \lambda/10.3$ at the operating wavelength and can be fabricated through standard layer-by-layer method for the realization of optical logic gates and THz switches.

Session 1A3a
SC5: Imaging, Inverse Scattering and Remote Sensing 1

A Mixed Boundary through Wall Imaging Problem

Xiuzhu Ye
Beihang University, Beijing 100191, China

Abstract— The study of through wall imaging problem is of great interest in the field of security check and the anti-terrorism. In most literatures, the wall and the unknown scatterers are both assumed to be dielectric implicitly, while the problem of mixture of PEC and dielectric is not often addressed yet, which is a more commonly encountered case. Therefore, in this article, we mainly discuss the reconstruction algorithm of PEC and dielectric scatterers together under the circumstance of through wall imaging.

The T-matrix method is chosen as the modelling scheme. According to a recently published paper by the author, it is able to distinguish the PEC and dielectric scatterer simultaneously when the two kinds of scatterers coexist in the domain of interest. The optimization scheme is developed based on the subspace based optimization method, where the wall (obstacle) is considered as a known scatterer rather than part of the inhomogeneous background. Numerical results are given to show the effectiveness of the proposed algorithm.

The Lidar Sounding of the Atmosphere in St. Petersburg

Dmitry Samulenkov[1], **Maxim Sapunov**[1], **Irina Melnikova**[1], **Vladislav Donchenko**[1], **and Anatoly Kuznetsov**[2]

[1]Resource Center "Observatory for Ecological safety", Reasearch Park
St. Petersburg State University, Universitetskaya nab., 7/9, St. Petersburg 199034, Russia
[2]Russian State Hydrometeorological University, Malookhtinsky, 98, St. Petersburg 196195, Russia

Abstract— The first results of vertical profiling aerosol particles and wind parameters above the central part of St. Petersburg in day and night time are presented. Results include profiles of the extinction and backscattering coefficients, particle size distribution, depolarization rate, particle concentration and real and imagine parts of refractive index at different heights. The wind characteristics are compared with radiosounding results. Lidar sensing in the center of St. Petersburg in the daytime and nighttime and the resulting vertical profiles of variations of the atmospheric parameters of the solid dust and soot particles in the pollution header over the city accomplished to study atmospheric pollution. The analysis of the influence of profiles of wind, temperature and humidity in the atmosphere on the properties and dynamics of solids is implemented. The areas and the speed of propagation of the atmospheric contaminants on the Vasilevsky Island in St. Petersburg at different altitudes are identified. Special attention is given to space and time variations of parameters. Atmospheric pollution in the atmosphere of a big city in case of St. Petersburg is revealed. It is shown that the meteorological parameters of the atmosphere and time of day affect the dynamics of changes hats pollution over the city. Measurements of the vertical profile of velocity and wind direction in the Observatory of ecological safety, Research Park, St. Petersburg University in the center of St. Petersburg was held within a few months of 2014, the height of laser sounding of wind characteristics of up to 12 km. The results are compared with the data of radiosounding measurements of Hydrometeorological service in St. Petersburg suburb Voeikovo. The distance between the sites of measurement is 25 km. Comparison is based on the assumption of homogeneity of the wind field in this scale. In most cases showed a good coincidence of the vertical profiles of wind, obtained by both methods. However, we should identify a few measurements when the results differ sharply or at high altitudes, or, on the contrary, in the surface layer. The results of the comparison and possible explanations for differences of measured data are presented.

ACKNOWLEDGMENT

The study is in ranges of State contract No. 16.740.11.0619 of 31.05.2011 "Development of methods for studying physical processes in the formation of atmospheric pollution by smoke and smog".

Cloud Optical Parameters Retrieved from Airborne Observations

Irina Melnikova[1], **Charles K. Gatebe**[2], **and Anatoly Kuznetsov**[1]

[1]Russian State Hydrometeorological University, Malookhtinsky, 98, St. Petersburg 196195, Russia
[2]Goddard Space Flight Center, NASA, Mail Code 613.2, Greenbelt, MD 20771, USA

Abstract— Optical parameters of the extended cloudiness are retrieved from airborne observations of different kinds. Optical thickness, single scattering albedo, scattering and absorption coefficients are obtained for all available spectral channels from measurements over, under and within cloud.

Results of retrieving optical parameters of cloud atmosphere from airborne data are compared. Two airborne experiments are taken in Goddard Space Flight Center. Measurement of the diffuse solar radiance in eight spectral channels (0.340; 0.381; 0.472; 0.682; 0.870; 1.035; 1.219; 1.273 μm) at viewing zenith angles from 0° till 180° in 1° interval are accomplished above the Atlantic Ocean close to West-South Africa coast. The approach and algorithms of NASA data processing has been presented earlier.

Spectral semispherical solar irradiance in the spectral diapason 0.35–0.96 μm in 0.002 μm interval has been measured in the end of the last century in different geographical sites in ranges of international complex programs: GATE (tropical latitudes), CAENEX (mid-latitudes), POLEX (polar latitudes).

Results of solving the inverse problem of cloud optics (retrieving optical parameters of extended clouds from different observations) shows the single scattering albedo is not variable at different latitudes, but volume scattering and absorption coefficients are significantly changeable from Polar regions to Tropics. Obtained parameters (the ground albedo, optical thickness, single scattering albedo, volume scattering and absorption coefficients) provide the cloud optical model for estimation radiative divergence, heating rate and water content.

ACKNOWLEDGMENT

Russian Federal Aimed Program "Research and pedagogical personnel of innovative Russia" in 2009–2013 (contract No. P 1037 05/31/2010) on Atmospheric Physics.

State contract No. 16.740.11.0619 of 31.05.2011 "Development of methods for studying physical processes in the formation of atmospheric pollution by smoke and smog".

Agreement No. 14.B37.21.1528 from 01.10.2012 "Modeling of the formation and dynamics of fields of atmospheric aerosols result from forest fires, for operational forecasting the atmosphere pollution and studying regional climate".

An Experimental Method for Estimating the Bistatic Diffuse Scatter from Anechoic Chamber RAM

S. J. Berry and F. C. Smith
QinetiQ, Room 1146 Building A7, Cody Technology Park, Farnborough, Hampshire, GU14 0LX, UK

Abstract— Characterisation of the specular reflection coefficient of a radar absorbing material (RAM) at microwave frequencies in free space is a comparatively routine measurement, although the measurement is frequently subject to high uncertainty due to edge diffraction and/or non-plane-wave illumination by the source antenna. Less well reported is the measurement of diffuse backscatter from RAM [1, 2]. For this measurement problem the use of a bistatic antenna arrangement is preferred [3]; however, at low frequencies the method may become inaccurate due to the size of the antennas relative to the test piece and the coupling that ensues.

In this contribution, a method is described and investigated which can be used to estimate the magnitude and direction of diffuse scatter from a RAM. The method is an extension to early work in [4] and is, in principle, similar to the optically modulated scatterer method (OMS) (e.g., [5]), except that specialist equipment is not required to implement the approach. A small subwavelength metal filament held by a 50 µm dielectric cord is scanned close to the RAM test piece using a 2D planar scanning system. The total complex electric field is recorded by examining the perturbation in the signal at the port of the launching antenna; these data are then used to reconstruct the propagating angular spectrum scattered from the RAM, which contains grating lobe and diffuse scatter data. The scanning system has been combined with a Quasi-Optical (QO) antenna system which is used to create a beam of microwave radiation with planar phase fronts and an approximately 2D Gaussian intensity profile in the constant phase planes. The gain provided by the QO system in part mitigates the low dynamic range normally encountered with passive scanning systems, which occurs due to the 2-way scattering process (rather than 1-way with an active probe). A dynamic range of up to 60 dB can be achieved using the QOs and a standard bench-top vector network analyser (VNA). The QO system also alleviates the need for a high quality anechoic environment for data collection.

Verification of the technique has been performed by measuring the grating lobes scattered from an array of parallel metal rods, where good agreement is shown with theoretical data. A typical anechoic chamber RAM is then used as a test piece and the grating lobes caused by the structure have been characterised for a range of angles of incidence and frequencies. The diffuse scatter from the anechoic chamber RAM is shown to be low for high angles of incidence until the geometry of the RAM produces direct specular reflection. Unsurprisingly, the direct specular reflection occurs at an angle where the facets of the pyramidal structure are normal to the incident microwave radiation.

REFERENCES

1. Joesph, P. J., A. D. Tyson, and W. D. Burnside, "An absorber tip diffraction coefficient," *IEEE Trans. Elec. Comp.*, Vol. 36, No. 4, 372–379, 1994.
2. Dewitt, B. T. and W. D. Burnside, "Electromagnetic scattering by pyramidal and wedge absorber," *IEEE Tran. Ant. and Prop.*, Vol. 36, No. 7, 971–984, 1988.
3. Zdansky, E., J. Rahm, and A. Orbom, "Bistatic RCS measurement on different background surfaces," *FOI Tech. Rep.*, 2009.
4. Cullen, A. L. and J. C. Parr, "A new perturbation method for measuring microwave fields in free space," *Proc IEE — B: Radio and Elec. Eng.*, Vol. 102, No. 6, 836–845, 1955.
5. Hygate, G. and J. F. Nye, "Measuring microwave fields directly with an optically modulated scatterer," *Meas. Sci. Technol.*, Vol. 1, No. 8, 703, 1990.

Session 1A3b
Oral Presentations for Best Student Paper Awards — SC5: Remote Sensing, Inverse Problems, Imaging, Radar and Sensing

A 16-Element Wideband Microwave Applicator for Breast Cancer Detection Using Thermoacoustic Imaging

Hao Nan[1], **Shiyu Liu**[2], **Nemat Dolatsha**[1], **and Amin Arbabian**[1]

[1]Department of Electrical Engineering, Stanford University, USA
[2]Department of Electronic Engineering, Tsinghua University, China

Abstract— Microwave-induced thermoacoustic (TA) imaging is a hybrid technique that combines the high contrast of microwave imaging, which is based on dielectric properties of different materials, with the high resolution of ultrasound detection. When tissue absorbs the incident microwave energy, stress waves are generated due to minute thermal expansions. An ultrasound transducer array is used to detect this signal and reconstruct the target image. This technique can achieve a penetration depth in excess of 5 cm, even in dispersive tissue. Unlike CT or mammography, TA imaging has no ionization radiation hazard and can be used more frequently to detect aggressive cancer types that progress in short time spans. With all these advantages, this technique is suitable for breast cancer screening, which needs a resolution of millimeter and high contrast between cancer and benign tissues.

The conventional and the most popular way to excite the tissue sample is to employ a waveguide, which is limited in bandwidth and is usually not well matched to target for TA imaging. We design the RF applicator with a compact size and high bandwidth in the optimal frequency range for breast cancer detection. The applicator is well matched to the target with a selected matching layer. The applicator can excite tissue efficiently in the near and quasi-near field. The high bandwidth of the applicator enables the flexibility of tuning exciting microwave frequency. A 16-element phased array based on the proposed applicator is designed to help focus the input microwave energy and to control the location of high specific absorption rate (SAR) region for TA imaging. This phased array applicator system can increase local SAR by conformal focusing of the microwave energy to a local area, which directly results in a higher SNR than a uniform excitation. Tuning the phase of each element can control the location of the high SAR region. Full 3D E&M simulations demonstrate the ability to control the high SAR region across the target and over the operation bandwidth.

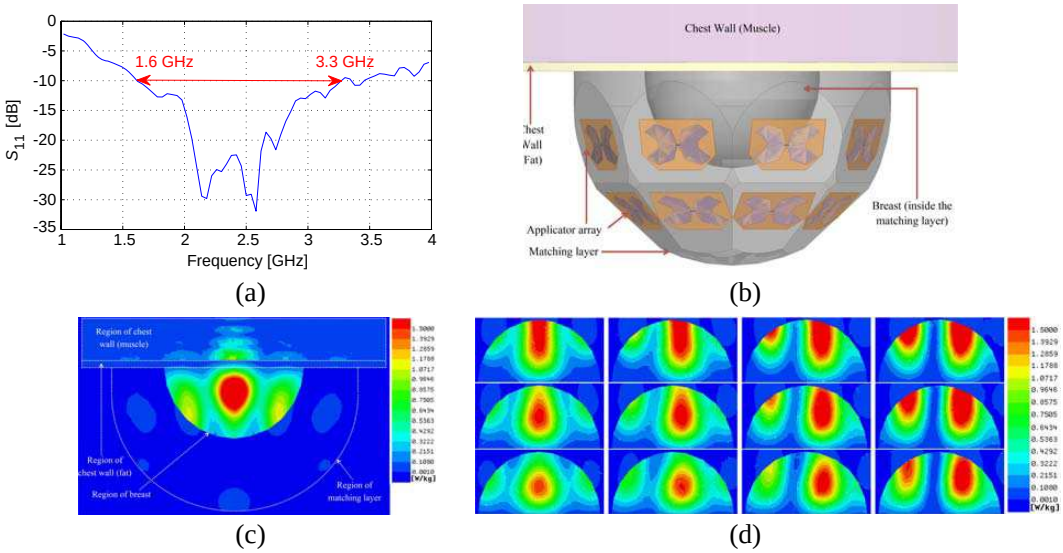

Figure 1: (a) Simulated S_{11} of the applicator. (b) Setup of the 16-element phased array applicator system. (c) Simulated SAR with same phase for each applicator. (d) Simulated SAR with tuning phase of each applicator to control the location of the high SAR region.

High Resolution Range Imaging via Model-based Compressed Sensing

V. Adler[1], **J. Moll**[2], **M. Kuhnt**[2], **B. Hils**[2], **V. Krozer**[2], **and K. Hoffmann**[1]

[1]Department of Electromagnetic Field, Faculty of Electrical Engineering, CTU in Prague, Czech Republic
[2]Department of Physics, Goethe University Frankfurt am Main, Frankfurt am Main, Germany

Abstract— This paper proposes a method for high resolution range imaging at millimeter wave frequencies (85 GHz to 100 GHz) based on model-based compressed sensing (CS). Besides a detailed description of the radar sensor, depicted in Figs. 1(a)–(b), and the theory of the underlying compressed sensing framework, the experimental setup is presented along with experimental results for one-dimensional range imaging. The measurement system is characterized by motorized reference measurements that form the dictionary matrix for the subsequent CS-processing, as well as measurements from a glass fiber reinforced polymer (GFRP) component. It is demonstrated that the proposed CS-method improves the range-resolution capabilities of conventional monostatic-radar systems that are usually based on FFT or matched filter processing. Resolution of these conventional radar systems is proportional to the inverse of its bandwidth and in our case ($BW = 15$ GHz) is approx. one centimeter. Compressed sensing results are shown in Fig. 1(c) and provide much better range resolution in the order of few micrometers, depending on the spacing of the motorized measurements, and significantly smaller sidelobes than conventional radar systems as shown in Figs. 1(d)–(e). This approach can be useful for a variety of radar applications, e.g., non-destructive material testing and precise time-of- ight measurements.

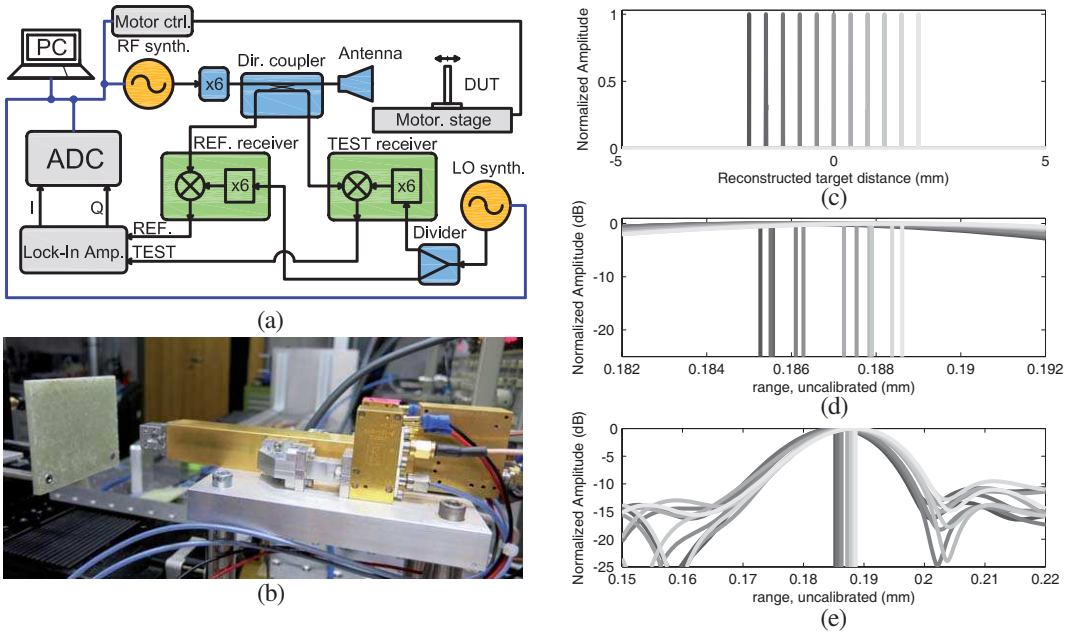

Figure 1: (a) Schematic of the radar sensor, (b) reconstructed high resolution range profiles, (c) photo of the experimental setup, (d) conventional Fourier transform to create the range profiles.

ACKNOWLEDGMENT

This research was supported by the German Aerospace Center under grant number: 50RA1326 and by the Student Grant Competition under program SGS13/198/OHK3/3T/13 of the Czech Technical University in Prague.

Fast Level Set Based Method for High Contrast Microwave Imaging

Pratik Shah and Mahta Moghaddam
Department of Electrical Engineering, University of Southern California, California, USA

Abstract— Microwave imaging has applications in through-the-wall imaging, non destructive testing, and medical imaging. The imaging problem is usually performed by formulating it using the volume integral equation. The integral equation represents the relationship between complex permittivitty and the electric field inside and outside of the inhomogeneous imaged domain. The equation is non-linear in general and common practice is to linearize by iteratively solving for the unknown complex permittivity and the field. Many numerical and experimental studies on microwave imaging have been performed, with common impediments being the inability to recover high dielectric contrasts and slow speed of computation.

For some applications, we have knowledge on what type of objects are present in the domain and their electrical properties. Although it is understood that the prior knowledge about contrasts in the imaged domain may not be very accurate or easily available, we will make the assumption that it is known to within some uncertainty. Having priors about contrasts, the microwave imaging problem essentially becomes locating the object and estimating the shape of the object. We consider an approach based on the level set method. The level set based shape recovery approaches for microwave imaging are very slow in general. The main computational burden is to estimate the adjoint field at each iteration. The adjoint operation for a linear system can be derived analytically so we explore a method, which is not based on the adjoint field evaluation. Hence, it can be very fast. The cost function is based on the variational level set functional, which regularizes the level set evolution without reinitializing it at each 'timestep'. Each iteration of the method comprises one forward solver and many iterations of the level set method. The desired results are obtained within 15 iterations of the method.

The applicability of the method is tested on synthetically generated data for a two-dimensional (2D) scenario. The data includes both lossy and lossless permittivity. The reconstructed images indicate that the method can produce accurate object localization and shape identification even for high contrast objects.

On the Connection between Jones Matrix and Sinclair Matrix

T. Dallmann and D. Heberling
Institute of High Frequency Technology, RWTH Aachen University, Germany

Abstract— The polarimetric behavior of scattering of radar targets can be described with two different 2×2 matrices: The Sinclair matrix which specifies the backscattering of a target and which is commonly used by polarimetric monostatic radar systems, and the Jones matrix which characterizes the forward scattering of a target and originates from optics [1].

Especially the decomposition of the Sinclair matrix into Huynen-Euler parameters has gained attention in some recent publications since it allows to characterize the system with so-called canonical scatterers [2, 3]. These primitives not only determine the polarization of the scatterered wave but also influence in which directions and at which frequencies the scattering occurs. Thus the Huynen-Euler parameters together with the canonical scatterers give a physical interpretation to the radar-cross section signatures of radar targets.

Unfortunately the extraction of Huynen-Euler parameters from the Sinclair matrix requires a coneigenvalue decomposition. Up to now, little research has been conducted in the field of consimilarity transformations and coneigenvalues. Some of the implications of these decompositions are therefore still unknown [5]. In contrast the Jones matrix can be decomposed with an eigenvalue decomposition. The mathematics of eigenvalues and similarity transformations are known and well understood [6].

In [4] a misleading, but simple connection between the Jones matrix J and the Sinclair matrix S was established:

$$S = AJ = \begin{bmatrix} -1 & 0 \\ 0 & 1 \end{bmatrix} J \tag{1}$$

This equation was derived for linear polarizations only. Unfortunately in some publications this connection is mistakenly emphasized as being generally valid [1]. If this would be the case, the decomposition of Sinclair matrices could be extremely simplified by transforming them to Jones matrices and performing an eigenvalue decomposition afterwards.

In this paper the following will be proved:

1. There does not exist a polarization basis-independent matrix A which allows to transform consimilar matrices S_i to similar matrices J_i for arbitrary polarization bases. This means that the transformation can generate Jones matrices with different eigenvalues even if the Sinclair matrices have the same coneigenvalues. Thus a decomposition utilizing the transformation matrix A can deliver diverging Huynen-Euler parameters in some cases.
2. If A is polarization basis-dependent then the transformation of consimilar Sinclair matrices will produce similar Jones matrices. However this means that the basis transformation connecting the Sinclair matrices must be known. In this case the transformation to Jones matrices using A is not beneficial any more.

Hence a simplification of the decomposition of Sinclair matrices as mentioned above is not possible. This emphasizes the relevance of coneigenvalue decompositions for radar polarimetry.

REFERENCES

1. Lee, J. and E. Pottier, *Polarimetric Radar Imaging: From Basics to Applications*, CRC Press, Boca Raton, 2009.
2. Dallmann, T. and D. Heberling, "Discrimination of scattering mechanisms via polarimetric rcs imaging [measurements corner]," *IEEE Antennas and Propagation Magazine*, Vol. 56, No. 3, 154–165, 2014.
3. Baird, C. S., "Design and analysis of an Euler transformation algorithm applied to full-polarimetric ISAR imagery," Ph.D. Dissertation, University of Massachusetts Lowell, Massachusetts, 2007.
4. Ulaby, F. T. and C. Elachi, *Radar Polarimetry for Geoscience Applications*, Artech House, Norwood, 1990.
5. Lüneburg, E., "Aspects of radar polarimetry," *Turk J. Elec. Engin.*, Vol. 10, No. 2, 219–243, 2002.
6. Horn, R. A. and C. R. Johnson, *Matrix Analysis*, Cambridge University Press, Cambridge, 2013.

Detection of Breast Tumors by Applying FDTD Modelling of Holographic Radar

I. L. Alborova and L. N. Anishchenko
Biomedical Engineering Department, Bauman Moscow State Technical University
5, 2d Baumanskaya str., Moscow 105005, Russia

Abstract— This paper presents the results of mathematical simulation carried out to confirm the ability of holographic radar to detect breast tumors. The simulation software used the Finite-Difference Time-Domain Method. The simulations were performed for three different scenarios: in the first model the inclusion depth under the surface was varied; for the second model two inclusions were used; while the dielectric properties of malignant tissue were modified in the third model. The model is a 3D block with dimensions $200 \times 200 \times 100$ mm, which mimicked normal breast tissue, with one or two spherical inclusion — malignant neoplasm of breast tissue. Frequency dispersion of normal and malignant tissues dielectric properties (conductivity and permittivity) was taken into account.

The results showed that differences in the dielectric properties allow to use of the radiolocation method for detecting inclusion (diameter 4 mm) on a depth up to 5 mm. The results proved that the greatest impact on the detection of inclusion has a ratio of conductivity values of normal and malignant tissues. Also the proposed method makes possible to distinguish two different objects at the distance between them of 16 mm or more, otherwise they will be identified as one inclusion.

Characterization of the Electromagnetic Propagation through Building Rubble by Means of Numerical Random Models

I. Lucresi, E. Di Giampaolo, and P. Tognolatti
Department of Industrial and Information Engineering and Economics, University of L'Aquila, Italy

Abstract— The rescue of victims buried in building rubble because of earthquakes, landslides, explosions in industrial plants or terrorist attacks, can take advantage from real-time measurements employing wireless communications devices.

Rising technologies like rescue robots, allow rubble exploration and victims localization exploiting radio signal transmissions. Moreover, radio detection of vital signs or detection of radio signals emitted by personal RF devices (e.g., cell-phone, radios, RFID, etc.) that may be close to the owner (especially in case of rescuers involved in subsequent collapses) can be very useful in post emergency operations since immediacy of action may lead to a considerable reduction in the number of victims. For these reasons communications plays a big role in this kind of systems. These operations efficacy however, is strictly related to the characteristics of propagation channel in the disaster scenario. Attenuation, multipath and noise make the radio-link weak and untrustworthy, in spite of this adequate systems can be designed if a sufficiently accurate knowledge of the features of the propagation channel is available.

This work has been developed after the earthquakes which stroked the Italian territory in the last years. The considered scenarios are then composed by rubble and debris of collapsed buildings, that is a very complex environment because of different materials, morphologies of urban fabric involved and physical characteristics of rubble and debris (i.e., shape, dimensions, humidity and level of compression), for which no general channel model exists.

In this work, in a completely new way compared to the literature, we simulate different models of rubble to evaluate phenomena of attenuation and propagation of radio signal through an extremely heterogeneous transmission medium structured in a not predictable manner.

The aim of the work is the development of a random model of the rubble that would reflect a wide range of environments, for this reason random rubble scenarios were generated and simulated through an electromagnetic tool where the transmission source is represented by a dipole antenna buried into rubble. The model involves typical materials, in established and plausible proportions, of both modern buildings (concrete, bricks and iron) and ancient ones (stones and bricks). A number of parameters characterize the model of the rubble: the degree of compression (defined as the ratio between the empty and filled spaces), the graininess (i.e., the size of the blocks of homogeneous material), the number of different materials, the dielectric properties of each material, the moisture, the thickness of the layers (one or more layers are considered). A large number of simulations have been performed for different frequencies: at 13 MHz, 432 MHz and 900 MHz. These frequencies have been chosen because they mainly concern rescue devices and are near the frequency bands of many communication services in Italy and European Countries. The study is focused on the analysis of Path Loss at different heights from the ground and for various angles of incidence of the electromagnetic wave. A statistical analysis of data are also carried out by calculating mean, standard deviation and minimum value of Path Loss for a large number of simulations.

The proposed model takes cue from a measurement campaign carried out in a number of buildings collapsed or partially destroyed in L'Aquila territory that was stroked by a severe earthquake in 2009 [1, 2].

Comparison between model results and measurement data allow us the tuning of the model parameters and is under development.

REFERENCES

1. Di Carlofelice, A., E. Di Giampaolo, M. Elaiopoulos, M. Feliziani, M. Roselli, and P. Tognolatti., "Localization of radio emitters into collapsed buildings after earthquake: Measurements of path loss and direction of arrival," *2012 International Symposium on Electromagnetic Compatibility (EMC EUROPE)*, 1, 6, Sept. 17–21, 2012
2. Di Carlofelice, A., E. Di Giampaolo, M. Feliziani, and P. Tognolatti, "Experimental characterization of electromagnetic propagation under rubble of a historic town after disaster," *IEEE Transactions on Vehicular Technology*, DOI: 10.1109/TVT.2014.2346580.

Combined Breast Microwave Imaging and Diagnosis System

B. L. Oliveira[1], **A. Shahzad**[1], **M. O'Halloran**[1],
R. C. Conceicao[2, 3], **M. Glavin**[1], **and E. Jones**[1]

[1]Electrical and Electronic Engineering, National University of Ireland Galway, Ireland
[2]Institute of Biomedical Engineering, University Oxford, United Kingdom
[3]Instituto de Biofsica e Engenharia Biomdica, FCUL, Portugal

Abstract— Several Computer-Aided Detection and Diagnosis (CAD) systems have been proposed in recent years for various breast imaging modalities, such as X-Ray Mammography, which generally involve pre-processing and segmentation of images followed by diagnosis. In the context of breast Microwave Imaging (MWI), the development of a dedicated CAD system combining features both from microwave images and recorded signals would greatly contribute to the performance of the technique in terms of specificity. In this submission, the authors focus on an improved method for automated diagnosis of breast cancer based on recorded backscattered signals.

MWI is based on the contrast between the dielectric properties of different types of breast tissue at microwave frequencies. The majority of existing studies which considered MWI of the breast have focused primarily on tumour detection, with automated tumour diagnosis seen as a secondary concern. A small number of studies have considered the use of the Radar Target Signatures (RTS) to identify tumours as benign or malignant, but it is unclear whether the performance of these algorithms can provide sufficient information in anatomically and dielectrically heterogeneous scenarios. Therefore, alternative methods need to be considered.

To address this problem, a combined breast microwave imaging and diagnosis system is proposed, where the breast images obtained using Microwave Tomography (MT) allow for the isolation of the RTS of the tumour in the recorded backscattered signals. A time-domain MT algorithm, known as Forward-Backward Time-Stepping (FBTS), is used to reconstruct the dielectric profile of the human breast, which in turn provides the location and extent of any tumour. Based on this information, a time-gating algorithm is applied to window the tumour RTS based on the average dielectric values of the breast tissues, and the round-trip distance between the antennas and the detected tumour. The estimated tumour signature is windowed from the backscattered signal with an approximate window length equal to twice the pulse width. Next, a sophisticated tumour-grading algorithm is applied to the windowed signals, which distinguishes tumours based on their level of malignancy. Since the tumour-grading algorithm processes isolated tumour signatures, rather than reflections from multiple scatterers within the breast, it can make improved judgements on the malignancy or benignancy of tumours.

The efficacy of the proposed combined breast microwave imaging and diagnosis system is benchmarked against previous studies which examined standard un-windowed microwave signals, by

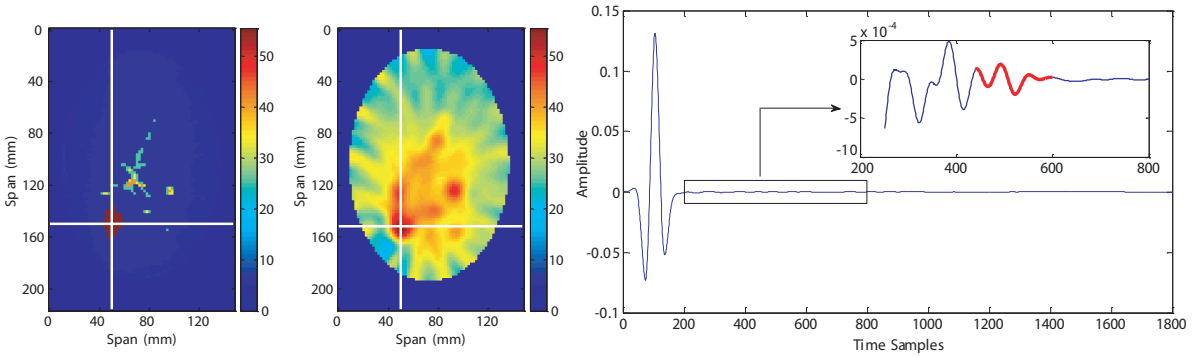

Figure 1: (a) FDTD model of a class 1 breast, with a tumour placed on the lower-outer quadrant (as identified by the cross-section of the white lines). (b) Reconstructed permittivity profile using FBTS: the tumour location is identified by thresholding the permittivity map based on dielectric properties of the tumour. (c) Backscattered signal from one of the recorded channels. The windowed tumour signature is highlighted in red.

simulating anatomically-accurate Finite Difference Time Domain (FDTD) breast and tumour models. By way of example, Fig. 1 shows a reconstructed breast image and the corresponding microwave signal, where the relevant tumour response is highlighted. Preliminary results — which will be presented in the final version of this paper — reveal an improvement in the performance of the automated diagnosis when the proposed windowing is applied to the backscattered signals, compared to the un-windowed approach. These results demonstrate the potential of windowed signatures to accurately diagnose tumour responses in high-clutter scenarios. Future work in this project includes combining the windowed tumour signatures with features extracted from the MT breast images for enhanced automated diagnosis.

Session 1A4
FocusSession.SC3: Numerical Modeling of Ultrashort Laser Pulse Propagation in Transparent Materials: Micro/nanomodification, Part 1

Pulsed Laser Modification of Transparent Dielectrics: Dynamics of Energy Absorption and Post-excitation Evolution

N. M. Bulgakova[1, 2], **V. P. Zhukov**[3, 4], **Yu. P. Meshcheryakov**[5], **and T. Mocek**[1]

[1]HiLASE Project, Institute of Physics ASCR, Na Slovance 2, Prague 18221, Czech Republic
[2]Institute of Thermophysics SB RAS, 1 Lavrentyev Ave., Novosibirsk 630090, Russia
[3]Institute of Computational Technologies SB RAS, 6 Lavrentyev Ave., Novosibirsk 630090, Russia
[4]Novosibirsk State Technical University, 20 Karl Marx Ave., Novosibirsk 630073, Russia
[5]Design and Technology Branch of Lavrentyev Institute of Hydrodynamics SB RAS
Tereshkovoi Street 29, Novosibirsk 630090, Russia

Abstract— We will present a comprehensive model to follow the details of spatiotemporal dynamics of ultrashort-laser-induced modification of a bulk glass (fused silica as an example). The model is based on two sub-models, one of which solves Maxwell's equations supplemented with the equations describing electron plasma formation and the laser-induced electric current and another one utilizes the equations of thermoelastoplastics. Spatiotemporal dynamics of laser beam propagation through the focal zone with generation of free electron plasma is analyzed for the regimes typical for nanograting formation and for creation of micro/nanobubbles. A controversial question on free electron density generated inside transparent dielectrics by ultrashort laser pulses is discussed based on the laser energy balance. The map of absorbed laser energy is used as an input for modeling the spatiotemporal dynamics of excited matter relocation and determining the final density-modulated structure that conditions refractive index change. Conclusions on the different routes of material evolution at different excitation conditions (laser beam energy, NA, pulse duration) will be made. The geometry of laser energy absorption is studied as a function of pulse duration, laser energy, and numerical aperture. The double pulse irradiation has been modeled to get insight into "exciton-seeded multiphoton ionization" [1]. Furthermore, several consecutive laser pulses have been modeled to gain a better understanding of a qualitative tendency of memory effects related to defect accumulation. Such features of laser energy coupling into the bulk glass have been revealed as asymmetry of absorption for the cylindrically-symmetric linearly-polarized beam and formation of a defect shield developing in multipulse irradiation regimes. Modeling allows foreseeing and predicting the routes of material evolution at different excitation conditions.

REFERENCES

1. Grojo, D., M. Gertsvolf, S. Lei, T. Barillot, D. M. Rayner, and P. B. Corkum, "Exciton-seeded multiphoton ionization in bulk SiO_2," *Phys. Rev. B*, Vol. 81, 212301, 2010.

Self-consistent Modeling of Photoionization for Nonlinear Ultrashort Pulse Propagation in Solids

Jeremy R. Gulley and Thomas E. Lanier
Department of Physics, Kennesaw State University, Kennesaw, GA 30144, USA

Abstract— Simulations coupling ultrashort pulse propagation with laser material interactions have traditionally contained some oversimplifications. One notable inconsistency is that propagation models, such as modified nonlinear Schrödinger equations, account for the multi-chromatic nature of ultrashort laser pulses while the ionization models they are coupled to are intrinsically monochromatic. As such, the influence of nonlinear optical behaviors such as super-continuum generation and high harmonic generation on ionization and laser-induced modifications is not well understood. Another inconsistency is the use of simplified material models (such as the Keldysh photoionization formula) that are based on physical assumptions that are not well justified in many situations. Among these are assumptions of a parabolic or Kane-type band structure, as well as effective masses and collision times chosen to fit numerical data to a particular experiment. In this work we present simulations solving the quantum semiconductor Bloch equations in a 3D quasi-momentum space and couple this model to ultrashort pulse propagation in dielectric solids. This approach self-consistently provides a quantum calculation of the photoionization yield, the photoionization current, the current from free-carriers, the generation of field harmonics, the traditional Kerr effect, and any high-order Kerr-effects without resort to a perturbative description. The material band structure is taken in the tight binding limit and is periodic in the crystal momentum space, thus ensuring a realistic treatment of Bragg reflection. The required input values for the material model include a measure of the known lattice dimensions, a band gap, and the reduced electron-hole mass at zero momentum (this value being selected to produce the known linear index of refraction in the low field limit). As the model makes no assumption about the pulse spectrum, we examine the laser-material interaction of strongly chirped pulses and multi-color multi-pulse schemes of laser-induced material modification. We then examine how a reduced laser-material model, based on this approach, may be used for multi-dimensional pulse propagation simulations.

Nonlinear Energy Deposition into Aqueous Media by Tightly Focused Laser Pulses: Tracking of Free-electron Density, Temperature Evolution, and Hydrodynamic Phenomena in a Large Range of Laser Pulse Durations and Wavelengths

Alfred Vogel, Xiao-Xuan Liang, Sebastian Freidank, and Norbert Linz
Institute of Biomedical Optics, University of Lübeck, Germany

Abstract— To date, optical breakdown modeling has mostly focused on tracking the evolution of free electron density and predicting breakdown thresholds defined by a critical free electron density. Such thresholds cannot easily be linked to experimental observations of breakdown events, which commonly rely on the detection of plasma luminescence, phase changes (leading to transient bubbles in water or permanent cavities in solids), or shock wave emission. We developed modeling tools for optical breakdown events in water, which span various phases reaching from breakdown initiation via solvated electron generation, through laser induced-plasma formation and temperature evolution in the focal spot to the later phases of cavitation bubble dynamics and shock wave emission.

The rate equation model considers the interplay of photoionization, avalanche ionization and recom-bination, traces thermalization and temperature evolution during the laser pulse, and portrays the role of thermal ionization that becomes relevant for $T > 3000\,\mathrm{K}$. Modeling of free-electron generation includes recent insights on breakdown initiation in water via solvated electron generation that were obtained by bubble threshold spectroscopy of IR nanosecond breakdown. The wavelength dependence of the breakdown threshold indicates that avalanche ionization is initiated via multiphoton excitation of valence band electrons into a solvated state at $E = 6.6\,\mathrm{eV}$ followed by up-conversion into the conduction band level that is located at $9.5\,\mathrm{eV}$ [1].

The ability of tracing the temperature evolution in the focal volume allows for a comparison with experimental data on bubble thresholds and bubble size. The model of laser-induced plasma formation is linked to a hydrodynamic model of plasma-induced pressure evolution and phase transitions that enables to trace bubble generation and dynamics as well as shock wave emission. This way, the amount of nonlinear energy deposition in transparent dielectrics and the resulting material modifications can be assessed as a function of incident laser energy. The unified model of plasma formation and bubble dynamics yields an excellent agreement with experimental results over a large range of pulse durations and wavelengths, as shown in Fig. 1.

Future challenges are to include spatio-temporal aspects of optical breakdown associated with nonlinear light propagation and with the plasma growth during the laser pulse.

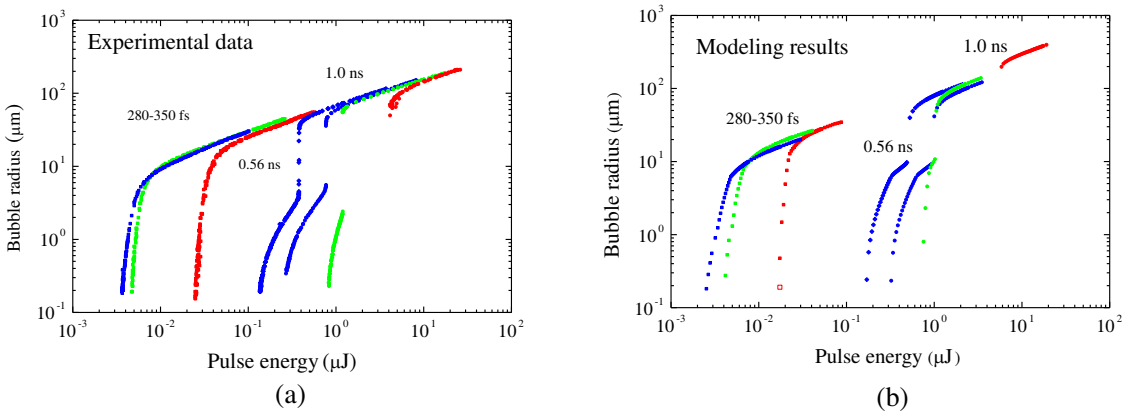

Figure 1: Maximum cavitation bubble radius in water as a function of laser pulse energy for different pulse durations and wavelengths; NA = 0.8. The colors denote the wavelengths: blue = 347 nm for fs pulses, and 355 nm for ns pulses; green = 520 nm and 532 nm, red = 1040 nm and 1064 nm. (a) Experimental data, (b) modeling results.

Multiphoton Absorption-induced Delocalization of fs Laser Pulse Energy in Si Bulk

Evgeny V. Zavedeev[1, 2], **Vitaly V. Kononenko**[1, 2], **and Vitaly I. Konov**[1, 2]

[1]Prokhorov General Physics Institute, RAS
Vavilov Str. 38, Moscow 119991, Russian Federation
[2]National Research Nuclear University MEPhI
Kashirskoye shosse 31, Moscow 115409, Russian Federation

Abstract— Modification of bulk of various transparent materials by means of writing by focused fs laser beam is well known technique nowadays. Recently, a number of experimental attempts to apply this approach to crystalline silicon were done. To our knowledge, all experiments with ultrashort pulses failed to modify deep silicon bulk. Most of them were carried out at wavelengths at which two photon absorption (2PA) occurs ($\sim$ 1120–2250 nm). Strong prefocal losses of laser energy, attributed to 2PA, and, as result, limitation of laser-induced free carrier plasma density to $\sim 10^{19}$ cm^{-3} were demonstrated [1, 2]. So the question arises: could this limitation be overcome by switching to longer wavelengths at which the number of absorbed photons increases?

The number of experiments in this field is rather poor up to now. This stimulated us to perform simulation of propagation of mid-IR fs pulse through Si bulk. We solved numerically nonlinear Schrödinger equation (NLSE) in paraxial approximation. The wavelength range in the calculations was 1200–4400 nm. The nonlinear absorption coefficients and nonlinear refractive indexes were taken from experimental works. The solutions of NLSE revealed that the prefocal depletion of the beam energy at high initial pulse energies remains strong even in 3- and 4-photon absorption cases.

Additionally, the strength of free-carrier plasma defocusing and diffraction increases with growth of wavelength, so maximum plasma density in the focus decreases. Density of absorbed energy is 2–3 orders of magnitude less then needed for melting of silicon. Thus, internal modification of c-Si structure by mid-IR fs pulses is most probably unfeasible at least at wavelengths shorter than 4400 nm.

ACKNOWLEDGMENT

Present study was supported by Russian Foundation for Basic Research (grant #14-22-02027 ofi_m).

REFERENCES

1. Zavedeev, E. V., V. V. Kononenko, V. M. Gololobov, and V. I. Konov, *Las. Phys. Lett.*, Vol. 36, No. 5, 036002, 2014.
2. Mouskeftaras, A., A. V. Rode, R. Clady, M. Sentis, O. Utéza, and D. Grojo, *Appl. Phys. Lett.*, Vol. 2014, 105, 191103.

Nonlinear Mechanisms of Light Absorption in the Laser Processing of Transparent Materials

Irina N. Zavestovskaya[1, 2]

[1]P.N. Lebedev Physical Institute of RAS, Moscow, Russia
[2]National Research Nuclear University MEPhI, Moscow, Russia

Abstract— The nonlinear mechanism of optical power consumption has been considered. This mechanism occurs in the transparency region of the solid under irradiation with ultrashort laser pulses of high-intensity.

Laser ablation under exposure to ultrashort laser pulses was shown to be a promising technique for processing and machining of transparent materials such as nitride semiconductors, sapphire, and other hard and inert materials. The clean treatment of the surface was demonstrated in contrast to the ablation with longer pulses. The typical range of treatment parameters is within the power densities of 30–50 TW/cm^2 at pulse width of $\sim$ 135 fs and wavelength of 400 nm for the process of laser ablation in GaN.

Clean pits were obtained in all experimental results under a single-shot irradiation. No signs of melting, no debris of re-deposition was found. There was no collateral damage of the not-irradiated regions as well. The results obtained testify that the femtosecond laser ablation of transparent materials keeps the chemical properties of the ablated surface unchanged.

The critical pulse energy can be compared with that in highly transparent fused silica and some other optical materials. The dependence of the laser-induced damage threshold on the energy band gap E_g was shown for several transparent materials tested under the same experimental conditions. A power function corresponds to the dependence of $E_g^{3.1}$.

The optical power consumption process leading to the laser ablation is considered theoretically. The goal is to determine the laser-induced damage threshold as a function of the material properties and laser parameters.

The effective absorption under this irradiation is estimated as $\sim 2.5 \times 10^4$ cm^{-1}, which is 20–100 times greater than the background linear absorption in GaN. This means that there is an efficient nonlinear mechanism of absorption of powerful radiation in the transparent frequency region for power densities of several TW/cm^2.

The tunneling absorption mechanism has been found to be the most efficient one for wide gap semiconductors and dielectrics processed with multi-TW/cm^2 and femtosecond laser pulses. The laser-induced damage threshold has been determined. The correlation of the threshold with the band gap is demonstrated. The threshold increases as nearly the third power of the band gap in satisfactory agreement with the experimental results.

Numerical Realizations of the Problem of Focused Laser Beam Propagation in Transparent Materials Based on Nonlinear Maxwell's Equations

V. P. Zhukov[1, 2], **N. M. Bulgakova**[3, 4], **and M. P. Fedoruk**[5]

[1]Institute of Computational Technologies SB RAS, 6 Lavrentyev Ave., Novosibirsk 630090, Russia
[2]Novosibirsk State Technical University, 20 Karl Marx Ave., Novosibirsk 630073, Russia
[3]Institute of Thermophysics SB RAS, 1 Lavrentyev Ave., Novosibirsk 630090, Russia
[4]HiLASE Centre, Institute of Physics ASCR, Za Radnicí 828, Dolní Břežany 25241, Czech Republic
[5]Novosibirsk State University, 1 Koptug Ave., Novosibirsk 630090, Russia

Abstract— We present the model describing propagation of femtosecond laser beams in transparent solids based on nonlinear Maxwell's equations supplemented by the hydrodynamics-type equations for laser-generated free electron plasma. The model takes into account linear dispersion, nonlinear Kerr effect, multiphoton and impact ionization, multiphoton light absorption. Numerically the model is realized based on Yee's FDTD scheme with the use of implicit approximation to ensure numerical stability. The scheme has been adapted for solving the specific problems under consideration and allows making sufficiently complicated simulations to be fast and accurate. Computer solution of a typical 2D problem requires around 20 hours on a usual PC without parallelization. The codes for simulations of 2D cylindrical and slab geometries as well as of 3D case for cylindrically-symmetric incoming beams have been developed. The last-mentioned code enables us to study axial symmetry violation upon laser beam propagation. The codes for cylindrical geometry require application of a specific grid to avoid the problems encountered in the calculations on the axis. This and other peculiarities will be discussed in the report.

ACKNOWLEDGMENT

This research is supported by the Russian Foundation for Basic Research (RFBR project No. 15-01-02432).

The work of M. P. Fedoruk was supported by the Russian Science Foundation (grant 14-21-00110).

Zeroth and First-order Bessel Beam Formation of Nanostructures on Thin-film Type Surfaces

Ramazan Sahin[1], **Tansu Ersoy**[1], **Ergun Simsek**[2], **and Selcuk Akturk**[1]

[1]Department of Physics, Istanbul Technical University, Istanbul 34469, Turkey
[2]George Washington University, Washington DC, 20052, USA

Abstract— We will present our recent experimental works on generation of nanometer-scale structures on various thin-film structures, using femtosecond laser beams shaped to zeroth and first order Bessel beams. The advantages of ultrashort laser pulses in materials processing and also their ability to form sub-diffraction-limit structures through nonlinear-optical processes are broadly investigated by many researchers. On the other side, the so-called diffraction-free beams also receive increasing attention due to their exotic physical behaviors such as extremely long depths of foci and self-reconstruction. Bessel beams are the most commonly used type of such beams. We show that diffraction-free beams provide significant advantages for processing of thin-layer materials, especially when high resolutions (small structures) are needed. These advantages include relaxed alignment constraints, reduced aberrations and easier scalability to shorter wavelengths. We demonstrate nanometer-scale fabrication of gold thin films and generate structures which exhibit plasmonic excitation effect. We also show that single-layer graphene can be ablated via a similar approach, although greater care is needed to avoid substrate damage. Finally, we will present ablation properties of vortex-type first order Bessel beams, on metal thin films.

Laser Energy Deposition in Glasses with Bessel Beams

A. Couairon[1], V. Jukna[1], S. Minardi[2], O. Jedrkiewicz[3], M. Selva[4], M. Lamperti[4], P. Di Trapani[4], N. Shcheblanov[5], R. Stoian[5], T. Itina[5], C. Xie[6], J. Zhang[6], J. M. Dudley[6], and F. Courvoisier[6]

[1]Centre de Physique Théorique, Ecole Polytechnique, CNRS, France
[2]Institute of Applied Physics, Friedrich-Schiller-University Jena, Germany
[3]Istituto di Fotonica e Nanotecnologie, CNR and CNISM UdR Como, Italy
[4]Dipartimento di Scienza e Alta Tecnologia, University of Insubria and CNISM UdR Como, Italy
[5]Laboratoire Hubert Curien, CNRS, Université de Lyon, France
[6]Département d'Optique P. M. Duffeux, Institut FEMTO-ST, CNRS Université de Franche-Comté, France

Abstract— I will present recent theoretical and experimental investigations on the propagation dynamics of ultrashort laser pulses focused with an axicon lens in glass, forming Bessel beams, filaments and plasma strings in the bulk of transparent solids. Numerous potential applications of bulk laser-induced plasma string range from laser micromachining to controlled temporary refractive index change or permanent damage in glasses. Recently, high angle Bessel beams delivered by femtosecond laser have been used for extremely high aspect ratio nanochannels generation and microstructuring in glass with a single laser shot. I will focus on fundamental light-matter interaction studies, devoted to the understanding of laser energy deposition in bulk glasses, with picosecond and femtosecond pulses.

I will present experiments and simulations highlighting the plasma generation dynamics and absorption when a Bessel beam of picosecond duration propagates in glass. We performed transmission measurements in the angular and wavelength domains allowing us to retrieve clear indications of the formation of the plasma in the material with a single chirped pulse playing the role of pump and probe simultaneously thanks to the spectral-temporal correspondence in the measured signal. Results showing the plasma non linear absorption effect on the trailing part of the pulse will be discussed and compared to the results of numerical simulations.

Laser propagation was modeled by a unidirectional propagation equation. Two different models were used for the matter response: (i) A classical model relies on rate equations for the generation electrons in the conduction band of the dielectric and a phenomenological Drude model for the permittivity. (ii) A computationally more expensive model but more realistic relies on a quantum- kinetic approach based on a system of Boltzmann transport equations describing electron and phonon distributions.

In the femtosecond pulse regime, we investigated numerically the propagation properties of large cone angle Bessel beams in the bulk of transparent solids and associated light-matter interaction. We compared the results to experimental results, in particular for multiple shot measurements of transmission as a function of pulse energy. Results from the classical model show that high angle Bessel beams allow the generation of a plasma channel with sub-micrometric diameter, tens of micrometers length and densities higher than the critical plasma density value. The Bessel filamentation dynamics is explained by the strong plasma absorption and is quasi-stationary. Agreement with measurements requires fine tuning of the parameters. We show that the quantum-kinetic approach is in quantitative agreement with the transmission measurements without the need for fine-tuning phenomenological parameters.

Time-resolved Modeling of Ultrafast Laser-excited Semiconductors and Dielectrics

B. Rethfeld, A. Rämer, K. Huthmacher, and N. Brouwer
Department of Physics, OPTIMAS Research Center, Technical University of Kaiserslautern, Germany

Abstract— Exciting transparent matter with an ultrashort laser pulse induces a number of processes on a broad range of timescales. We apply several different methods to describe the material's response from the initial laser absorption to the final material modification. Kinetic approaches like Boltzmann collision integrals [1] or Monte Carlo simulations of electron traces [2] are capable of following the initial excitation and the nonequilibrium electronic energy distribution. A reduction to an effective model like the multiple rate equation is possible [3]. The initial excitation and ultrafast thermalization occur on a subpicosecond timescale. The further energy dissipation can be followed by temperature-based models, which allow for additionally including the transport of particles [4]. A description of material's response with this so-called density-dependent two temperature model (nTTM) is possible up to the picosecond range [5, 6]. For the atomic movements occurring on a pico- to nanosecond range, molecular dynamic simulations are appropriate [7].

Here, we show exemplary results of these methods. In particular, we study how such processes influence each other and the further course of energy dissipation up to material modification: Electron-electron as well as electron-phonon collisions quickly lead to an isotropic momentum distribution. The particular energy distribution of the electrons might influence the propagation of the laser pulse [8]. The thermalization of laser-excited carriers to separate electron and hole temperatures occurs faster than the equilibration of the subsystem's chemical potentials. These kinetic results justify a number of assumptions made by the nTTM. However, the description of optical parameters, especially reflectivity and energy absorption, appears to be crucial for the final damage thresholds [5, 6]. The kinetics of the melting process is influenced in turn by the dependence of melting temperature on pressure known from static measurements [7].

REFERENCES

1. Brouwer, N. and B. Rethfeld, *J. Opt. Soc. Am. B*, Vol. 31, C28, 2014.
2. Huthmacher, K., et al., *Physica A*, doi 10.1016/j.physa.2015.02.031, 2015.
3. Rethfeld, B., *Phys. Rev. Lett.*, Vol. 92, 187401, 2004.
4. Van Driel, H. M., *Phys. Rev. B*, Vol. 35, 8166, 1987.
5. Rämer, A., O. Osmani, and B. Rethfeld, *J. Appl. Phys.*, Vol. 116, 053508, 2014.
6. Rämer, A. and B. Rethfeld, further presentation at *PIERS Prague*, 2015.
7. Lipp, V. P., et al., *Phys. Rev. B*, Vol. 90, 245306, 2014.
8. Gulley, J. R. and T. E. Lanier, *Phys. Rev. B*, Vol. 90, 155119, 2014.

Energy and Particle Propagation and Relaxation in Laser-excited Silicon

A. Rämer and B. Rethfeld
Department of Physics, OPTIMAS Research Center, Technical University of Kaiserslautern, Germany

Abstract— When studying the excitation of semiconductors with an ultrashort laser pulse, the evolution of the free carrier density and the subsequent transport of energy and carriers has to be treated explicitly. To that end, we apply a density-dependent two temperature description (nTTM) similar to Ref. [1] and study the influence of different modeling assumptions on the numerical result.

An 800 nm-laser pulse is absorbed in silicon via single photon and multiple photon absorption processes. Free electrons are allowed to excite further electrons-hole pairs via collisional excitation and to recombine with holes in the valence band via Auger recombination. In addition to heat transport, particle transport is considered as an ambipolar process, thus electrons and holes are assumed to move together as electrons-hole pairs. A Drude model is implemented to account for the highly transient optical parameters. The melting thresholds calculated with our model compare well with experimentally determined ones for a wide range of laser pulse durations.

Here, we study the importance of optical parameters, degeneracy and transport effects on these calculated damage thresholds. We report that the choice of the Drude collision frequency strongly influences the resulting lattice temperature and thus measurable quantities like damage thresholds [2]. Moreover, we show that it does not suffice to assume a constant carrier collision frequency at least when treating a wide range of pulse durations. In this case, a transient carrier collision frequency considering both, electron-hole and carrier-phonon collisions, has to be applied to best reproduce experimental data.

We also plan to examine the influence of laser-induced nonequilibrium in this context. The extended multiple rate equation [3] allows to study the electronic relaxation processes in laser-excited semiconductors in a simplified way. First estimations show that electron degeneracy influences the energy transfer to the lattice. These findings may have impact on the description of energy relaxation and transport in silicon.

REFERENCES

1. Van Driel, H. M., *Phys. Rev. B*, Vol. 35, 8116, 1987.
2. Rämer, A., O. Osmani, and B. Rethfeld, *J. Appl. Phys.*, Vol. 116, 053508, 2014.
3. Medvedev, N. and B. Rethfeld, *J. Appl. Phys.*, Vol. 108, 103112, 2010.

Internal Photoeffect under the Action of Ultrashort Electromagnetic Pulses: Dependence of Pulse Duration

Valery A. Astapenko and Sergey V. Sakhno
Moscow Institute of Physics and Technology (State University)
9 Institutskii lane, Dolgoprudniy, Moscow Region 141700, Russia

Abstract— The presentation is devoted to theoretical analysis of internal photoeffect induced by ultrashort electromagnetic pulses (USP). We calculated the total probability (during all time of USP action) of photo-excitation of impurity state into energy band in semiconductor matrix. The calculation based on the expression for probability of photo-induced processes derived in paper [1] in the frame of perturbation theory:

$$W = \frac{c}{(2\pi)^2} \int_0^\infty \sigma(\omega') \frac{|E(\omega')|}{\hbar\omega'} d\omega'. \quad (1)$$

here $\sigma(\omega')$ is cross-section of the impurity-band photoexcitation, $E(\omega')$ is Fourier transform of electric field strength in the pulse, c is light velocity.

In the contrast of paper [2] where only carrier distribution function in valence band was considered in the present work main attention is given to the dependence of excitation probability (W) on the pulse duration τ for various values of pulse carrier frequency (ω).

It is shown that for frequency ω smaller that the excitation threshold ($I_{\rm th}$) dependence $W(\tau)$ looks as a curve with maximum and $W(\tau \to \infty) \to 0$. On the contrary for $\hbar\omega > I_{\rm th}$ excitation probability rises with the increase of pulse duration and goes to the linear dependence at sufficiently large parameter τ.

Calculations were made in the frame of continuum model and isotropic effective mass of charge carrier with the use of cross section formula obtained in papers [3, 4].

Several types of USP are considered, namely, traditional and corrected Gaussian pulses [5], pulses with frequency chirp and also wavelet pulses with different parities.

We also calculated the spectral probability of total photo-excitation for various pulse durations and analyzed obtained spectra.

It is established that internal photoeffect induced by USP has specific features which differ from characteristics of this phenomenon under the action of long electromagnetic pulses.

REFERENCES

1. Astapenko, V. A., *Physics Letters A*, Vol. 374, 1585–1590, 2010.
2. Astapenko, V. A. and M. I. Mutafyan, *Russian Physics Journal*, Vol. 55, No. 1, Jun. 2012.
3. Chaudhuri, S., *Phys. Rev. B.*, Vol. 26, 6593, 1982.
4. Bebb, H. B., *Phys. Rev.*, Vol. 185, 1116, 1969.
5. Lin, Q., J. Zheng, and W. Becker, *Phys. Rev. Lett.*, Vol. 97, 253902, 2006.

Session 1A5
Antennas, Signals, HPEM and EMC Problems 1

High Definition Multimedia Interface in the Process of Electromagnetic Infiltration

Rafal Przesmycki
Faculty of Electronics, Military University of Technology
Gen. S. Kaliskiego 2 str., Warsaw 00-908, Poland

Abstract— The protection of information against the penetration of electromagnetic devices and electronic systems (information technology) is very important. This problem increases with ever greater use of IT equipment for the processing and transmission of information, which should not fall into the wrong hands. This is due to the fact that every electronic device is a source of undesirable (secondary) emission of electromagnetic energy induced in the surrounding area, any electrical wiring and metal structures.

When the emission undesirable signals are correlated with the non-confidential information, they can be used to reproduce the information by intelligence services. The phenomenon of the emission undesirable is called disclosing emission. The use of disclosing emission by intelligence services we call penetration or electromagnetic infiltration. Projects designed to blocking identifying systems based on disclosing emissions we call information protection against the penetration of electromagnetic emissions or safety emissions.

The article concerns problems of electromagnetic compatibility and compromising emission that is the information security. The article describes the electromagnetic channels of penetration information, and then focuses on High Definition Multimedia Interface for which shows signals of extortion used during of disclosing emission measurements. The article presents the results of compromising emissions measurements derived from High Definition Multimedia Interface. In addition, the article discusses the laboratory stand for measuring disclosing emissions.

Analze the Impact of Discretization on the Structure of the Simulation Result

Marek Bugaj and Jarosław Bugaj
Faculty of Electronics, Military University of Technology
Gen. S. Kaliskiego 2 str., Warsaw 00-908, Poland

Abstract— The demands of modern radio systems forced to look for new solutions in antenna. This requires designers conduct many tests and measurements.

Researches of antennas are a complex, time consuming and relatively expensive. In the laboratory, often we don't have possibilities to investigate the effect of the relationship between physical parameters of the antenna and its electrical parameters and radiation pattern.

The basic methods of solving complex antenna structures in the frequency domain are the method of moments and FDTD. The main condition for the correct calculation results in these numerical methods is a step structure on cell division — discretization. In the paper shows influence of discretization structure on the simulation results — VSWR, radiation patterns and impedance. The paper shows how shape of radiation patterns in discretization functions depends. It lets you see how important problem is the discrediting give correct structure.

Another equally important concern is the duration of the simulation. Simulation time depends on the degree of discretization structure. For a simple antenna structure simulation time are not too long and it does not pay to increase the size of the cell.

Directed Energy Applications to the Destruction of Informatic Devices

Rafal Przesmycki
Faculty of Electronics, Military University of Technology
Gen. S. Kaliskiego 2 str., Warsaw 00-908, Poland

Abstract— Relatively new threats for military and civil systems in the high power electromagnetic environment (HPEM) are high power microwave (HPM) sources. An attack with this kind of source is typically defined as intentional electromagnetic interference (EMI). Radiated HPEM environments which are malicious in nature can also occur at frequencies down to a few tens of MHz.

Generate an high power electromagnetic pulse in the direction of the electronic system makes electronic circuits accumulates very high voltage. This phenomenon causes damage to the circuit elements which makes the device unfit for further operation. In the case of intentional impact pulse is very important in terms of its effectiveness to generate sufficiently a strong impulse for a given frequency. The article presents an example of system for generating HPM pulse for which it can be seen that the maximum pulse is present at a frequency about 350 MHz.

The article concerns the problems of high energy electromagnetic environment. The article describes an high power electromagnetic pulse and discusses the laboratory stand for generate HPM pulses. In addition, the paper presents an analysis of possibilities of shaping the pulses spectrum generated for the destruction of IT devices, and presents the results of measurements.

Measurement of the Pulses Generated by the High Power Electromagnetic Pulse Generator

Leszek Nowosielski
Faculty of Electronics, Military University of Technology, Gen. S. Kaliskiego 2 str., Warsaw 00-908, Poland

Abstract— In the article the measurement methodology of the pulses parameters generated by the high power electromagnetic pulse generator HPEM-RF DS110 is presented. The block diagram of the meter of the pulses generated by the high power electromagnetic pulse generator is presented too. The meter of the pulses consists of: operating computer, oscilloscope with RF attenuators and sensor (AD-70D or AD-80D) with matching block. Display of data collected from sensor in the time domain occurs in the oscilloscope. Installed software of the operating computer allows, on the basis of high power pulse recorded in the time domain, to determine the frequency spectrum with the use of FFT.

In order to conduct validation of the meter of the pulses equipped with electric field sensor AD-70D and AD-80D the measuring results acquired with the use AD-70D and AD-80D are compared.

Theoretical and Experimental Analysis of the Impact of Conformal Surface on Parameters of Microstrip Antennas

Jarosław Bugaj and Marek Bugaj
Faculty of Electronics, Military University of Technology
Gen. S. Kaliskiego 2 str., Warsaw 00-908, Poland

Abstract— The article presents analysis of the impact of conformal antennas radius of curvature on their basic parameters and characteristics of radiation. In order to verify the numerical results there were built models of practically analyzed conformal antennas, their measurements were taken in anechoic chamber and compared to those of planar antennas. Numerical analysis has been carried out (for basic shapes: cylinder, sphere, toroid) using CST Studio Suite software. Analysed antennas worked within frequency range between 2200–2300 MHz and 5031–5090,6 MHz. Both ranges are used in aviation, the first one in telemetry systems, another one in Microwave Landing System (MLS).

The main reason for intensive development of conformal microstrip antennas is the fact that it is relatively easy to integrate them with the shape of the surface on which they are installed. Mainly this applies to aircraft, spacecraft, high-speed trains, rockets and missiles in which each projecting element affects adversely aerodynamics, fuel consumption, etc., while conformal antenna can be in a simple way mounted on the aircraft wings or on the outer surface of the hull.

In order to verify if numerical analysis carried out in previous chapters are correct some models of antennas were built practically and their basic parameters were measured. As part of research the following antennas were built: planar and three cylindrical antennas with radius of curvature $R = \lambda$, 2λ, 4λ.

As results from presented analysis the radius of curvature of the surface on which microstrip antenna was placed clearly affects the performance of this antenna for low values of $R < \lambda_0$. For large values of the radius of surface curvature the impact is negligibly low, for the transition areas it stays at several or ten-odd percent.

Analysis of Distinctive Features and Database Conception for Hardware Interface of It Devices in the Process of Their Identification Based on Radiated Emission

Rafal Przesmycki and Marian Wnuk
Faculty of Electronics, Military University of Technology
Gen. S. Kaliskiego 2 str., Warsaw 00-908, Poland

Abstract— Modern information technology devices emit strong disturbances, which is caused by the fact that used in casing cheap plastic does not perform the function of electromagnetic shield. Because of that the concept of electromagnetic effluents from an IT device becomes significant. Based on the analyzes and measurements we can be concluded that it is possible to identify the computer's hardware interfaces based on radiated emissions. Distinctive feature of the work of the individual interfaces is therefore the working frequency and the level of emission allowing to identification of the hardware interface.

In the article distinctive feature for modern IT equipment present on the European Union market have been presented. The collected measurement results of radiated emission generated by particular components of IT devices allowed it to build data base which could be used for identification of components characterized by too high level of radiated emission.

This paper describes the concept of building a database for IT devices in the process of identification based on radiated emissions. In addition, the article presents a similarity measure radiated emissions for each hardware interfaces of PC computer.

The Analysis of the Radius Impact on the Properties of Cylindrical Antenna with Coaxial Feed

Jarosław Bugaj and Marek Bugaj
Faculty of Electronics, Military University of Technology
Gen. S. Kaliskiego 2 str., Warsaw 00-908, Poland

Abstract— The article presents analysis of conformal multilayer antenna and array antenna with coaxial feed. The antenna has the shape of the cylinder with a radius R. It was examined an effect of change radius R on the basic operating parameters of the antenna.

Methods for modeling conformal antennas are currently developed to the extent which is sufficient to undertake a theoretical analysis of many cases of practical applications. An important direction in the development of methods for conformal antennas modeling was the extension of numerical techniques developed previously for the purposes of flat structures.

For the selected frequency range there was designed planar and cylindrical microstrip antenna with coaxial feed For conformal surface radius length was varied in the range 0.2–$50\lambda_0$. The full-wave analysis of antennas numerical parameters was carried out in CST Studio Suite.

The analysis of the tested antenna has been focused on the determination of the impact of the R-radius of the side surface of the cylinder, on which the conformal antenna have been installed, on the basic operating parameters of the antenna.

The analysis of structures of conformal antennas is a complex and complicated process. Presented analysis shows how many factors affect the final result.

Characteristics of radiation, as well as of the working bandwidth, are closely related to the value of R-radius measured on the side surface of the cylinder on which the analyzed antenna is installed (especially for low values of $R < \lambda_0$). Along with the increase in curvature of the antenna radiator (reduction in the R-radius), the radiation beam is widened, and the working bandwidth of the antenna narrows.

Implementation of Universal RF-shielded Enclosure for IT Equipment Protection

Leszek Nowosielski and Marain Wnuk
Faculty of Electronics, Military University of Technology
Gen. S. Kaliskiego 2 str., Warsaw 00-908, Poland

Abstract— In order to decrease the level of radiated emissions from information technology (IT) equipment and in order to protect the IT equipment in high level of electric field strength environment the RF shielded enclosures are needed. In the paper the implementation of universal RF shielded enclosure is presented. The description and the block diagram of the RF-shielded enclosure is presented. In the article the shielding efficiency (SE) of real RF-shielded enclosure is presented. The presented results of shielding efficiency measurements show that the level of SE is above 50 dB for radiated emissions in the frequency range from 80 MHz to 2.5 GHz. The attenuation of conducted emission is above 60 dB. The characteristics of shielding efficiency and power supply filters attenuation in frequency axis are presented too.

Furthermore the paper presents the methodology and block diagram of laboratory stand for SE measurements conducted in anechoic chamber.

The Exposure Level of High Power Microwave Pulses

Roman Kubacki and Salim Lamari
Faculty of Electronics, Military University of Technology, Warsaw, Poland

Abstract— To protect against electromagnetic radiation in the human exposure the permissive exposure limits have been recommended by the International Commission of Nonionizing Radiation Protection (ICNIRP) and Institute of Electrical and Electronics Engineers (IEEE). The maximum permissible exposure (MPE) can be based on the highest rms or peak electric or magnetic field strengths or the plane-wave equivalent power densities associated with these fields. The most authoritative exposure guidelines recommends also specific absorption rate (SAR) as a basic restrictions. The SAR is the time derivative of the incremental energy absorbed by an incremental mass contained in a volume element of given density.

Additionally, for pulsed exposures in the frequency range 0.3 to 10 GHz and for localized exposure of the head, in order to limit or avoid auditory effects caused by thermoelastic expansion, the threshold level of specific absorption (SA) is recommended.

Electromagnetic pulse-radiation emitted from High Power Microwaves (HPM) generators can also be treated as ultra-wideband (UWB) signals. The UWB signals have different forms of interaction with biological structures comparing with continuous signals because the frequency spectrum of harmonics of such radiation sometimes exceeds 500 MHz. Taking into account that the electrical properties (complex permittivity) of biological tissues change the values over such frequency range the new attempt of the permissive exposure levels should be redefined.

Electromagnetic Compatibility Studies of Selected Components for Present Day Cars

Leszek Nowosielski and Marian Wnuk
Faculty of Electronics, Military University of Technology
Gen. S. Kaliskiego 2 str., Warsaw 00-908, Poland

Abstract— A contemporary car incorporates more and more electronics. Today, each car is stuffed with integrated circuits. Some of them are responsible for correct operation of the engine, the others watchful over the security, and others yet control the equipment making travelling comfort better. The central lock, ABS, on-board computer or glasses opened electrically do not wonder anybody because today thanks to the electronics cars turn the lights and wipers themselves on, keep the driving path properly, park, and even apply brakes, when the driver will gape himself.

Although from one hand the electronics in cars yields enormous benefit, from the other hand however it is a reason for problems. From time to time they are small and irritating (glasses will not shut or ticking wipers) and another time they are so serious that immobilize the car. These statements were the basis for making emissivity measurements of one of fitting components of a modern car. Measuring circuits and positions as well as measurement results of disturbances emissions radiated and conducted from wiper motors vs. frequency were presented in the article.

Measurements of electromagnetic interference radiated emission levels of the tested motor No. 1 and motor No. 2 were done within the frequency range of 2 MHz to 1 GHz.

The metrological certification of the measurement path between the antenna and equipment for measurement data recording was done before making the measurements of radiated disturbances. In order to do so the EMC32 software application was used. The EMC32 application is used for calculating the intensity of electromagnetic field according to the dependence:

$$E = U_{wej} + T + K,$$

where:
E — electric field strength in the site of measurement antenna installation [dB(μV/m)],
U_{wej} — level of signal at the measurement receiver output [dBμV],
T — attenuation of the HF path connecting the measurement antenna with the measurement receiver input [dB],
K — antenna coefficient of measurement antenna used that takes the effective surface of the antenna into account [dB].

The results of measurements done together with their discussion will be presented in the article.

At the same time, basing on the model used for determining the signal attenuation inside the vehicle, calculations of interfering signal attenuation were done in order to check the possibility to interfere other components of the equipment.

Bandwidth Enhancement of a Microstrip Patch Antenna Using the Metamaterial Planar Periodic Structure

Salim Lamari, **Roman Kubacki**, **and Miroslaw Czyżewski**
Faculty of Electronics, Military University of Technology, Warsaw, Poland

Abstract— Today's wireless communications systems are mostly characterized by wide bandwidth, small size and profile, low cost, ... etc..

The arrival of metamaterials has injected a new breath in the design of microstrip antennas. Thanks to them, the microstrip antennas will still have good times ahead because they can improve their characteristic such as impedance bandwidth, the radiation direction, the gain, etc.. In this paper we present a wideband microstrip antenna based on the planar metamaterial concept. This later was applied to an ordinary microstrip patch antenna aiming to enhance its bandwidth. This concept consists of embedding the patch and the ground plane of an ordinary microstrip antenna with repetitive pattern, forming thus a periodic structure. The unit cell of the structure was used to model the metamaterial. Once the metamaterial property was verified by means of the dispersion diagram, the periodic structure was built upon this unit cell and applied to an ordinary rectangular microstrip patch antenna, which was designed and simulated using the CST Microwave Studio Software. To attest this approach, the design was experimentally verified by fabricating the antenna on the Rogers RT5880 substrate ($\varepsilon_r = 2.2$ and $h = 0.787\,\mathrm{mm}$). After measurements the antenna presented a $-10\,\mathrm{dB}$ impedance bandwidth more than $10\,\mathrm{GHz}$ and exceeding thus 100% fractional bandwidth. The proposed antenna can easily integer a recent wireless communication system with the above mentioned characteristics.

Session 1A6
SC4: Complex Analysis and Convex Optimization in Electromagnetics

Stored Energy and Convex Optimization

Mats Gustafsson
Department Electrical and Information Technology, Lund University, Box 118, SE-221 00 Lund, Sweden

Abstract— Convex optimization can be used to formulate and solve several fundamental problems regarding the optimal performance for small antennas [5]. The approach is based on reformulations of the antenna design problem as an easier convex optimization problem for the antenna currents, where it is used that the radiated power, stored energy, dissipated power, and radiated field are convex functions in the current density for many cases. This leads to a systematic and computational effective formulation for analysis of optimal currents and physical bounds on, e.g., $G = Q$, Q for superdirective antennas, Q for prescribed radiation patterns, antennas embedded in devices, and antennas with near field constraints [3, 5].

Accurate and efficient evaluation of the stored energy is essential for the optimization approach. The classical derivation of the stored energy is based in subtraction of the energy density related to the radiated power from the energy density [1]. This stored energy can be rewritten as a quadratic form in the current density for some antennas in free space [4, 7]. There are however cases with coordinate dependent stored energy and negative stored energy [2, 4, 8]. It is also very hard to generalize the methodology to antennas embedded in lossy media and dielectrics. Here, an alternative approach based on a state space representation is presented [6]. The state space model is constructed from a internal symmetric state space model derived from a positive real input impedance. Numerical results for antennas embedded in temporally dispersive media are presented.

REFERENCES

1. Collin, R. E. and S. Rothschild, "Evaluation of antenna Q," *IEEE Trans. Antennas Propagat.*, Vol. 12, 23–27, Jan. 1964.
2. Gustafsson, M., M. Cismasu, and B. L. G. Jonsson, "Physical bounds and optimal currents on antennas," *IEEE Trans. Antennas Propagat.*, Vol. 60, No. 6, 2672–2681, 2012.
3. Gustafsson, M., J. Friden, and D. Colombi, "Antenna current optimization for lossy media with near field constraints," *Antennas and Wireless Propagation Letters, IEEE*, 1, 2015, in press.
4. Gustafsson, M. and B. L. G. Jonsson, "Stored electromagnetic energy and antenna Q," *Progress In Electromagnetics Research*, Vol. 150, 13–27, 2015.
5. Gustafsson, M. and S. Nordebo, "Optimal antenna currents for Q, superdirectivity, and radiation patterns using convex optimization," *IEEE Trans. Antennas Propagat.*, Vol. 61, No. 3, 1109–1118, 2013.
6. Gustafsson, M., D. Tayli, and M. Cismasu, "Q factors for antennas in dispersive media," Technical Report LUTEDX/(TEAT-7232)/1–24/(2014), Lund University, Department of Electrical and Information Technology, P. O. Box 118, S-221 00 Lund, Sweden, 2014, http://www.eit.lth.se.
7. Vandenbosch, G. A. E., "Reactive energies, impedance, and Q factor of radiating structures," *IEEE Trans. Antennas Propagat.*, Vol. 58, No. 4, 1112–1127, 2010.
8. Yaghjian, A. D. and S. R. Best, "Impedance, bandwidth, and Q of antennas," *IEEE Trans. Antennas Propagat.*, Vol. 53, No. 4, 1298–1324, 2005.

Frozen and Slow Light Scattering in Photonic Crystals within a Transparency Window: A Fundamental Theorem

Aaron Welters
Florida Institute of Technology, USA

Abstract— In this talk we discuss a new theorem which has been shown to play a fundamental role in the analysis of certain electrodynamical scattering problems involving frozen and slow-light in one-dimensional photonic crystals consisting of periodic stratified layers of homogeneous passive linear media (such as anisotropic, bianistropic, or dispersive media) for frequencies in a transparency window. This theorem, related to the Bloch-Floquet theory, says that the local band structure near a stationary point of the dispersion relation (wavenumber vs. frequency) is completely determined at just the stationary point by the Jordan form of the unit cell transfer matrix and the sign characteristics with respect to the energy ux across the layers. We will elaborate on this theorem and it's proof which uses perturbation theory, linear algebra of indefinite inner product spaces, Floquet theory for periodic ordinary differential equations, complex analysis, and Herglotz function theory. A key to the result as we will show is the fact that due to the passivity and the transparency window the energy density is positive. Applications to the study of scattering in the slow light regime are emphasized.

Passive Approximation and Optimization

S. Nordebo[1], M. Gustafsson[2], and D. Sjöberg[2]

[1]Department of Physics and Electrical Engineering, Linnæus University, Sweden
[2]Department of Electrical and Information Technology, Lund University, Sweden

Abstract— An approximation problem is formulated where it is required to approximate a general "well-behaved" function on an interval of the real axis based on the set of symmetric Herglotz functions. Applications are e.g., with the optimal realizations of passive structures presented in [4].

A Herglotz function $h(\omega)$ is an analytic function with the property $\mathrm{Im}h(\omega) \geq 0$ for $\omega \in \mathbb{C}_+ = \{\omega \in \mathbb{C} | \mathrm{Im}\omega > 0\}$. It can be shown that $h(\omega)$ is a Herglotz function if and only if it can be represented as

$$h(\omega) = b_1\omega + \alpha + \int_{\mathbb{R}} \left(\frac{1}{\xi - \omega} - \frac{\xi}{1+\xi^2} \right) \mathrm{d}\beta(\xi), \tag{1}$$

where $b_1 \geq 0$, $\alpha \in \mathbb{R}$ and where $\mathrm{d}\beta(\xi)$ is a positive Borel measure with $\int_{\mathbb{R}} \mathrm{d}\beta(\xi)/(1+\xi^2) < \infty$, see, e.g., [1, 3, 5]. It is common to interpret the measure as $\mathrm{d}\beta(\xi) = \beta'(\xi)\mathrm{d}\xi = \frac{1}{\pi}\mathrm{Im}h(\xi + \mathrm{i}0)\mathrm{d}\xi$ in a distributional sense. Symmetric Herglotz functions have an even measure with $\mathrm{d}\beta(-\xi) = \mathrm{d}\beta(\xi)$ and $h(\omega) = -h^*(-\omega^*)$.

We consider general approximation problems, such as e.g.,

$$\begin{aligned} \text{minimize} \quad & \sup_{\xi \in \Omega} |h(\xi) - f(\xi)| \\ \text{subject to} \quad & f(\xi) \text{ continuous on } \Omega \\ & h(\xi) \stackrel{\text{def}}{=} h(\xi + \mathrm{i}0) \exists \text{ continuous on } \Omega \end{aligned} \tag{2}$$

where the approximation is with respect to the set of symmetric Herglotz functions $h(\omega)$ satisfying the constraints above. Here, Ω is a closed and bounded subset of $\mathbb{R}$.

It can be readily shown that (2) may have non-trivial solutions. Suppose for example that $f(\omega) = -h_0(\omega)$ is the negative of a Herglotz function $h_0(\omega)$ which is analytic in a neighbourhood of $\mathbb{C}^+ \cup \Omega$ and where $h_0(\omega) = b_1^0\omega + o(\omega)$ as $\omega \hat{\to} \infty$. It can then be shown that the following a priori lower bound holds: $\sup_{\xi\in\Omega}|h(\xi) - f(\xi)| \geq b_1^0 \frac{1}{2}|\Omega|$, see also [2].

Existence and convergence issues will be discussed regarding the approximation problem (2) and numerical examples will be presented based on convex optimization [4]. A suitable "test-problem" is to identify the Herglotz function $f(\omega) = \tan(-1/\omega)$ based on the partial knowledge $f(\xi) = \tan(-1/\xi)$ on Ω and where $f(\omega)$ is regular in a neighbourhood of $\Omega \subset \mathbb{R}$. It is noted that $\tan(-1/\omega)$ is meromorphic in $\mathbb{C}\backslash\{0\}$ and has a sequence of poles at $1/\pi(n - \frac{1}{2})$ accumulating at 0 and with residues $-1/\pi^2(n - \frac{1}{2})^2$ where $n \in \mathbb{Z}$. Mathematically, this approximation problem is trivial by analytic continuation. However, as is well known, analytic continuation may be a non-trivial task to execute numerically. Here, the example function above is considered to be as "diffcult as possible" to be represented by using a "blind" automated numerical scheme based on convex optimization.

REFERENCES

1. Akhiezer, N. I., *The Classical Moment Problem*, Oliver and Boyd, 1965.
2. Gustafsson, M. and D. Sjöberg, "Sum rules and physical bounds on passive metamaterials," *New Journal of Physics*, Vol. 12, 043046, 2010.
3. Kac, I. S. and M. G. Krein, "R-functions — Analytic functions mapping the upper halfplane into itself," *Am. Math. Soc. Transl.*, Vol. 103, No. 2, 1–18, 1974.
4. Nordebo, S., M. Gustafsson, B. Nilsson, and D. Sjöberg, "Optimal realizations of passive structures," *IEEE Trans. Antennas Propagat.*, Vol. 62, No. 9, 4686–4694, 2014.
5. Nussenzveig, H. M., *Causality and Dispersion Relations*, Academic Press, London, 1972.

Convex Optimization for Approximations of Positive Real Functions

D. Sjöberg[1] and S. Nordebo[2]

[1]Department Electrical and Information Technology, Lund University, Sweden
[2]Department Physics and Electrical Engineering, Linnaeus University, Sweden

Abstract— Passive systems are intimately connected to positive real functions. These are analytical functions $P(s)$ that map the right half complex plane $s \in \mathbb{C}^+$ to itself with the symmetry condition $P(s^*)^* = P(s)$, and can be identified with Herglotz functions, which map the upper half complex plane to itself. There is a representation theorem for these functions, stating that

$$P(s) = sC + \frac{1}{\pi}\int_{-\infty}^{\infty} \frac{s\mathrm{Re}\{P(j\xi)\}}{\xi^2 + s^2} d\xi$$

On the frequency axis $s = j\omega$, this can be used to represent the imaginary part of an arbitrary positive real function in terms of the Hilbert transform of the real part (and vice versa), $\mathrm{Im}P(j\omega) = j\omega C + \frac{1}{j\pi}\int_{-\infty}^{\infty} \frac{\mathrm{Re}\{P(j\xi)\}}{\omega - \xi} d\xi$. Allowing a pole at $\omega = 0$, and taking the symmetry of the positive real function into account, an admittance function $Y(\omega) = P(j\omega) = G(\omega) + jB(\omega)$ can be discretized as

$$\begin{aligned} G(\omega) &= G_0 + \sum_{x=0}^{N} x_n\{p(\omega/\Delta\omega - n) + p(\omega/\Delta\omega + n)\} \\ B(\omega) &= C_\omega - \frac{1}{L\omega} - \sum_{n=0}^{N} x_n\{[\mathcal{H}p](\omega/\Delta\omega - n) + [\mathcal{H}p](\omega/\Delta\omega + n)\} \end{aligned}$$

where G_0, $\{x_n\}_{n=0}^N$, C, and L^{-1} are real parameters describing the admittance function, p is a suitable basis function used for discretizing the real part $G(\omega)$, and $\mathcal{H}p$ is the Hilbert transform of this basis function. A large collection of explicit Hilbert transform pairs can be found in [1].

Using this representation, we can consider any desired target system response $Y_t(\omega)$, and study how well this can be approximated by a physical admittance $Y(\omega; x)$ represented as above, where $x = (G_0, \{x_n\}_{n=0}^N, C, L^{-1})$ are the free parameters. This can be done by formulating the convex optimization problem "minimize $\|Y(\omega; x) - Y_t(\omega)\|$", under suitable restrictions on the parameters x. For instance, a passive system is characterized by all parameters x being non-negative, and some parameters can often be restricted by known asymptotic properties of the physical situation, such as the static values of the refractive index or similar.

The linearity of the representation formula implies the optimization problem is convex, and hence is easy to solve using convex optimization [2]. Adding linear or convex constraints does not change this property. Examples where this can be applied can be found in the study of optimal absorbers, high impedance surfaces, negative refractive index, and many other circumstances [3].

REFERENCES

1. King, F. W., *Hilbert Transforms*, Vol. 2, Cambridge University Press, 2009.
2. Boyd, S. P. and L. Vandenberghe, *Convex Optimization*, Cambridge University Press, 2004.
3. Nordebo, S., M. Gustafsson, B. Nilsson, and D. Sjöberg, "Optimal realizations of passive structures," *IEEE Transactions on Antennas and Propagation*, Vol. 62, No. 9, 4686–4694, 2014.

Physical Bounds of Patch Antennas

Doruk Tayli and Mats Gustafsson
Department of Electrical and Information Technology, Lund University, Lund, Sweden

Abstract— Patch antennas are widely used since their first emergence in the 70's [1, 2]. Although there is a significant amount of literature on the subject, accurate physical bounds for patch antennas do not exist. The main reason for this is the complexity of deriving the physical bounds for horizontal currents over a ground plane.

Current optimization [3] is a technique that allows the calculation of physical bounds for antennas of any geometry. Using the method of moments to compute stored electromagnetic energy matrices [3, 4] convex optimization is applied to quadratic forms of the energies to find the optimal G/Q ratio, which is the minimal Q-factor for a specified radiation pattern. It is simple to extend this technique to antennas above infinite PEC ground planes by adding the mirror currents to the Green's function.

Here we show the G/Q bound for different patch antennas above an infinite PEC ground plane. The computed physical bounds are then verified with numerical simulations using the commercial electromagnetic software FEKO [5].

REFERENCES

1. Kumar, G. and K. P. Ray, *Broadband Microstrip Antennas*, Artech House, 2002.
2. Carver, K. R. and J. Mink, "Microstrip antenna technology," *IEEE Trans. Antennas and Propagation*, Vol. 29, No. 1, 2–24, Jan. 1981.
3. Gustafsson, M. and S. Nordebo, "Optimal antenna currents for Q, superdirectivity, and radiation patterns using convex optimization," *IEEE Trans. Antennas and Propagation*, Vol. 61, No. 3, 1109–1118, 2013.
4. Vandenbosch, G. A. E., "Reactive energies, impedance, and Q factor of radiating structures," *IEEE Trans. Antennas and Propagation*, Vol. 58, No. 4, 1112–1127, 2010.
5. Altair, S. A., Development S.A. (Pty) Ltd. Stellenbosch, "FEKO, Field computations involving bodies of arbitrary shape, Suite 7.0," 2014, https://www.feko.info/, Retrieved: 24/11/2014.

Sum Rules and Physical Bounds on Frequency Selective Structures

Andreas Ericsson and Daniel Sjöberg
Department of Electrical and Information Technology, Lund University, Box 118, Lund 221 00, Sweden

Abstract—

Introduction: A frequency selective structure is an artificial electromagnetic structure that possesses selectivity with respect to incident signals of different polarization, frequency or angle of incidence. Classical frequency selective surfaces (FSS) are commonly represented as two dimensional periodic structures of conductive elements, and the design of which is thoroughly described in [1]. There it is concluded that a smaller element size leads to an improved stability with respect to the angle of incidence. Much work has been presented the last few years where the FSS elements have an extent in the direction of propagation of the incident signal, these structures are referred to as 3D frequency selective structures [2]. It is commonly stated that the three dimensional character of these structures implies an improved stability with respect to the angle of incidence, and a better agreement between the FSS performance for TE and TM illumination.

Physical Bound on the All Spectrum Transmission: In [3] it is proven that the all spectrum transmission blockage (transmission lower than a reference level T_0) of a periodic structure is bounded by the static electric and magnetic polarizabilities $\boldsymbol{\gamma}_e$, $\boldsymbol{\gamma}_m$, which in turn are bounded by the variational expressions in [4]. If a signal is incident in the xz-plane and the polarizability dyadics have vanishing off-diagonal terms, such that $\boldsymbol{\gamma}_e = \hat{\mathbf{x}}\hat{\mathbf{x}}\gamma_{exx} + \hat{\mathbf{y}}\hat{\mathbf{y}}\gamma_{eyy} + \hat{\mathbf{z}}\hat{\mathbf{z}}\gamma_{ezz}$, $\boldsymbol{\gamma}_m = \hat{\mathbf{x}}\hat{\mathbf{x}}\gamma_{mxx} + \hat{\mathbf{y}}\hat{\mathbf{y}}\gamma_{myy} + \hat{\mathbf{z}}\hat{\mathbf{z}}\gamma_{mzz}$, the total polarizability $\gamma(\theta)$ can be introduced as

$$\gamma(\theta) = \begin{cases} \gamma_{exx}\cos^2\theta + \gamma_{ezz}\sin^2\theta + \gamma_{myy}, & \text{TM} \\ \gamma_{eyy} + \gamma_{mxx}\cos^2\theta + \gamma_{mzz}\sin^2\theta, & \text{TE.} \end{cases} \tag{1}$$

This contributes to the maximum bandwidth of the transmission blockage of the FSS through the relation

$$B\ln\left(\frac{1}{T_0}\right) \leq \frac{\pi^2\gamma(\theta)}{2A\lambda_0\cos\theta} - \left(\sqrt{n_\infty^2 - \sin^2\theta} - \cos\theta\right)\frac{\pi^2 d}{\lambda_0}, \tag{2}$$

where λ_0 is the center wavelength, $B = (\lambda_2 - \lambda_1)/\lambda_0$ is the fractional bandwidth, n_∞ is the high frequency limit refractive index and A is the unit cell area of the FSS.

Application to 3D Frequency Selective Structures: The physical bound defined in (2) has been applied to a band stop FSS design. A comparison is made between the performance of the structure as a function of the angle of incidence for TE and TM illumination, with and without vias in the direction of propagation in each element. The outcome of this type of analysis is to prove the statement that when γ_{ezz} is increased, i.e., the FSS elements have an extent in the direction of propagation, the performance of the structure is improved for oblique angles of incidence, especially with respect to TM illumination.

REFERENCES

1. Munk, B., *Frequency Selective Surfaces: Theory and Design*, John Wiley & Sons, New York, 2000.
2. Rashid, A. K., B. Li, and Z. Shen, "An overview of three-dimensional frequency-selective structures," *IEEE Antennas and Propagation Magazine*, Vol. 56, No. 3, 43–67, 2014.
3. Sjöberg, D., M. Gustafsson, and C. Larsson, "Physical bounds on the all-spectrum transmission through periodic arrays: Oblique incidence," *EPL Europhysics Letters*, Vol. 92, 34009 (6pp), 2010.
4. Sjöberg, D., "Variational principles for the static electric and magnetic polarizabilities of anisotropic media with perfect electric conductor inclusions," *J. Phys. A: Math. Theor.*, Vol. 42, 335403, 2009.

On Multidimensional Passivity in Electrodymanics

B. L. G. Jonsson
Electromagnetic Engineering Lab, School of Electrical Engineering
KTH Royal Institute of Technology, Stockholm, Sweden

Abstract— Passivity of a system in a time variable is a key ingredient in the recent derivation of several interesting bandwidth limitations results. Passivity together with linearity and time-invariance ensure that the time-Laplace transform of the system response, of the underlying physical system, is a Herglotz function. These Herglotz functions have several attractive properties working towards the goal of finding a bandwidth limitation. They include a representation theorem and certain sum-rules. Explicit examples are given in the talk. These properties have been utilized to obtain bandwidth performance bounds. In electromagnetic theory we note that the Gustafsson bound [1] for small antennas is derived this way, similarly we have Rozanovs bound [2] on absorbers and the array figure of merit [3] for array antennas over a ground plane.

The concept of passivity carry over to multi-dimensional systems in the sense of Vladimirov [4], where it is shown that equations and systems with a kernel with support in a time-like cone, e.g., the light cone, have similar attractive properties. That is the multidimensional Laplace-transform over the cone is an analytic function in a tubular neighborhood of the dual of the cone. Representation theorems for this kind of functions are also known, however with weaker properties than in the one-dimensional case.

The goal of the presentation is to compare similarities and differences between the time-passivity and the corresponding multi-dimensional passivity. We discuss here how passivity carry over to multidimensional systems and if these properties are sufficient to obtain physical bounds on multidimensional electromagnetic systems. We investigate possible candidates that might have such a physical bound, and investigate what such bounds could limit. If time permit we will also discuss matrix and operator valued convolution systems.

ACKNOWLEDGMENT

We gratefully acknowledge funding from the Swedish Foundation for Strategic Research in the grant Complex analysis and convex optimization for EM design, as well as the Next generation array antenna (NGAA) project in the Vinnova VINN Excellence Center, CASE.

REFERENCES

1. Gustafsson, M., C. Sohl, and G. Kristensson, "Physical limitations on antennas of arbitrary shape," *Proc. R. Soc. A*, Vol. 463, 2589–2607, 2007.
2. Rozanov, K. N., "Ultimate thickness to bandwidth ratio of radar absorbers," *IEEE Trans. Antennas Propagat.*, Vol. 48, No. 8, 1230–1234, 2000.
3. Jonsson, B. L. G., C. I. Kolitsidas, and N. Hussain, "Array antenna limitations," *IEEE Antenn. Wireless Propag. Lett.*, Vol. 12, 1539–1542, 2013.
4. Vladimirov, V. S., *Methods of the Theory of Generalized Functions,* Taylor & Francis, London, 2002.

Investigation and Comparison between Radiation Center and Phase Center for Canonical Antennas

Casimir Ehrenborg[1], **Jonas Fridén**[2], **and Gerhard Kristensson**[1]

[1]Department Electrical and Information Technology
Lund University, Box 118, SE-221 00 Lund, Sweden
[2]Ericsson Research, Ericsson AB, Gothenburg, Sweden

Abstract— The radiation center was introduced by Fridén and Kristensson in [1]. The need to define this parameter arose from the ambiguity of the phase center definition. The phase center is traditionally calculated by manually selecting a region in the main lobe of the radiation pattern, and minimizing the phase of the co-polarized field component. The choice of angular region to use is not obvious, and automatic calculation of beam width is hard to implement as a robust numerical algorithm. In contrast, the radiation center algorithm presented in [1] provides a unique point corresponding to the minimum of the squared angular momentum of the field.

This presentation investigates results from radiation center and phase center calculations for canonical antennas with frequencies varying inside their operational bands. The two methods are compared and evaluated against the expected phase center positions and the radiation center is investigated as a replacement parameter to the phase center. In [1] the radiation center was calculated using measured data with unknown errors in the absolute position of the antenna in the coordinate system. Therefore, in this study the concept is applied to simulated far-field patterns wherein the position of the antenna is known.

REFERENCES

1. Friden, J. and G. Kristensson, "Calculation of antenna radiation center using angular momentum," *IEEE Transactions on Antennas and Propagation*, Vol. 61, No. 12, 5923–5930, Dec. 2013.

Session 1A7
Advanced Mathematical and Computational Methods in Electromagnetic Theory and Their Applications 1

Null Space Elimination for Double-curl Operator Using Generalized Gauge Technique with Compatible Finite Element Discretization

Yan Lin Li[1], **Sheng Sun**[1], **and Weng Cho Chew**[2]

[1]Department of Electrical and Electronic Engineering, The University of Hong Kong, Hong Kong, China
[2]Department of Electrical and Computer Engineering
University of Illinois at Urbana-Champaign, Urbana, IL 61801, USA

Abstract— Recently, electromagnetics related multiphysics, such as quantum and thermal electromagnetics, have gained more and more attention in academy as well as industry. The interaction between Maxwell's equations and other equations should be considered in a consistent way. In this case, a general purpose differential electromagnetic solver is highly demanded. However, the null space of the double-curl operator has been a bottleneck in solving Maxwell's equations for magnetostatic, quasistatic, and eigenvalue problems. Based on the vector calculus language, various gauge conditions and spectral shift methods have been proposed. From the viewpoint of differential forms, these gauge/shift techniques can be unified under the same framework. Then, a compatible finite element discretization of the governing equation can be obtained in a straightforward manner.

In this work, we apply a generalized gauge condition to the variable of interest, e.g., the magnetic vector potential A or the electric field intensity E. Hence, a penalty term is enforced as a counterpart of the double-curl term. As the null space of the double-curl term belongs to the range of the penalty term, a unique solution and better convergence can be achieved. Different from the previous gauge/shift techniques, the proposed gauge condition is in a generalized form. More importantly, the penalty term can be interpreted using the concept of differential forms, which inspires compatible expansions of the primary and intermediate variables in terms of edge and nodal Whitney elements, respectively. To reduce the computational cost brought by the inverse of a mass matrix, which is involved to remove the intermediate unknowns, a nearly diagonal inverse can be constructed due to the strong localization property of the mass matrix. Finally, the condition of the matrix system is significantly improved and the sparse nature of finite element method is greatly preserved. Numerical results successfully demonstrate the stable and efficient performance of the proposed method in solving magnetostatic problems and low-frequency circuit problems.

Computing the Electric and Magnetic Green's Functions in General Gyrotropic Media

V. G. Yakhno[1] and B. Çiçek[2]

[1]Electrical and Electronics Engineering Department, Dokuz Eylul University, Turkey
[2]Graduate School of Natural and Applied Sciences, Dokuz Eylul University, Turkey

Abstract— The study of the electromagnetic fields in gyrotropic materials is an important issue of the recent electromagnetic theory [1, 2]. The electric and magnetic fluxes **D** and **B** in general gyrotropic materials have the following form

$$\mathbf{D} = \varepsilon_0 \bar{\bar{\varepsilon}} \mathbf{E}, \quad \mathbf{B} = \mu_0 \bar{\bar{\mu}} \mathbf{H},$$

where **E** and **H** are the electric and magnetic fields, respectively; positive constants ε_0 and μ_0 are defined as the permittivity and permeability of free space; the relative permittivity and permeability matrices $\bar{\bar{\varepsilon}}$ and $\bar{\bar{\mu}}$ have the following form (see, for example, [1]):

$$\bar{\bar{\varepsilon}} = \begin{pmatrix} \epsilon_{11} & \epsilon_{12} + ig_3 & \epsilon_{13} - ig_2 \\ \epsilon_{12} - ig_3 & \epsilon_{22} & \epsilon_{23} + ig_1 \\ \epsilon_{13} + ig_2 & \epsilon_{23} - ig_1 & \epsilon_{33} \end{pmatrix}, \quad \bar{\bar{\mu}} = \begin{pmatrix} \mu_{11} & \mu_{12} + ih_3 & \mu_{13} - ih_2 \\ \mu_{12} - ih_3 & \mu_{22} & \mu_{23} + ih_1 \\ \mu_{13} + ih_2 & \mu_{23} - ih_1 & \mu_{33} \end{pmatrix}.$$

The main objects of our paper are the electric and magnetic Green's functions for Maxwell's partial differential equations in the general gyrotropic media. Green's functions for equations of mathematical physics can be considered as a useful tool for different methods in the presentation of acoustic, electromagnetic, elastic and other fields, in particular, for the method of moments and boundary element method. The dyadic Green's functions for an electrically gyrotropic medium with particular form of $\bar{\bar{\varepsilon}}$ and $\bar{\bar{\mu}}$ have been derived by matrix method with dyadic decomposition in [3–5]. The time-harmonic Green's dyadics have been constructed in closed form for a particular case of homogeneous gyrotropic materials by Fourier transform approach in [6]. However, the numerical computation of the Green's functions (fundamental solutions) of Maxwell's equations in general gyro-electric materials is not known. Moreover the numerical methods for the space of tempered distributions are not developed till now. In our paper we suggest a method of an approximate (regularized) computation of the infinite-body Green's functions for the time-harmonic Maxwell's equations in the general gyrotropic media. This method is based on the Fourier transform meta-approach where the Fourier image of the Green's function is computed by some matrix transformations and symbolic computations in MATLAB. After that the inverse Fourier transform is computed in an regularized (approximate) form. The parameters of the regularization have been chosen by the comparison of the regularized Green's function with Green's function obtained by the explicit formula for the isotropic case. The approximate computation of the inverse Fourier transform has been implemented by MATLAB tools. The computational experiments are presented in the paper and confirm the robustness of the method.

REFERENCES

1. Eroglu, A., *Wave Propagation and Radiation in Gyrotropic and Anisotropic Media*, Springer, 2010.
2. Lee, J. K. and S. Y. Rhee, "Reflection and transmission of plane waves at the planar interface of a magnetically gyrotropic medium," *IEEE Geoscience and Remote Sensing Symposium*, 2005.
3. Eroglu, A. and J. K. Lee, "Dyadic Green's function for a Gyro-electric Medium," *IEEE International*, Vol. 2, 1100–1103, 2003.
4. Eroglu, A. and J. K. Lee, "Dyadic Green's function for an electrically gyrotropic medium," *Progress In Electromagnetics Research*, Vol. 58, 223–241, 2006.
5. Eroglu, A. and J. K. Lee, "Wave propagation and dispersion characteristics for a nonreciprocal electrically gyrotropic medium," *Progress In Electromagnetics Research*, Vol. 62, 237–260, 2006.
6. Olyslager, F., "Time harmonic two- and three-dimensional closed form Green's dyadic for gyrotropic, bianisotropic, and anisotropic media," *Electromagnetics, Taylor and Fracis*, Vol. 17, No. 4, 369–386, 1997.

Diverging and Converging Beam Diffraction by a Wedge. Part I: The Multipole Expansion Approach

Michael Katsav[1], **Ehud Heyman**[1], **and Ludger Klinkenbusch**[2]

[1]School of Electrical Engineering, Tel Aviv University, Tel Aviv 69978, Israel
[2]Institute of Electrical and Information Engineering
Christian-Albrechts-Universität zu Kiel, Kaiserstr. 2, D-24143 Kiel, Germany

Abstract— The complex source (CS) method provides a canonical setting for the rigorous study of beam diffraction phenomena [1, 2]. In that approach one substitutes CS coordinates into the conventional real-source Green function solution of a specific environment, thereby converting the response of that environment to a spherical wave excitation into the response due to a collimated beam-wave excitation. Physically, the extension of the real source to the CS case implies that the field in the CS case is generated by an extended source distribution in real space (a disk or a line in the 3D or 2D configurations, respectively), and that the wave-field emerges outside (i.e., causally) with respect to this source distribution [4, 5]. This implies that the field emerging from the source is diverging.

In a recent paper [3], we have used this approach for the analysis of two dimensional (2D) beam diffraction by a perfect conducting wedge as a function of the beam parameters: collimation, direction and displacement from the edge. In that paper we have compared three analytic techniques: (i) complex multipole expansion, (ii) complex Sommerfeld integral, and (iii) complex ray analysis augmented by uniform theory for complex ray diffraction. In all these solutions we used the analytical continuation of the conventional real-source Green function to CS case. However, as follows from the discussion in the previous paragraph, the field is emerging from the source distribution toward the wedge, so that the beam is diverging as it hits the wedge.

We note that in this case the incident beam converges to a complex "sink" which is located in the shadow zone of the wedge, hence a straightforward extension of the Green's function solution to CS case is not applicable. However, it has been shown recently that the complex multipole expansion can describe converging beam diffraction but only if the complex source coordinates are defined in a particular way [6]. Our goal in the present two-part paper is to explore the application of the complex multipole expansion in the cases where the incident beam is diverging or converging as it hits the wedge, and in particular find the proper definition of the complex source coordinates for the diverging or converging beam cases that yield physically meaningful solutions. In the second part of this two-part paper [7] we shall examine the validity of these solutions by comparing them to the plane wave spectrum and complex ray solutions.

REFERENCES

1. Heyman, E. and L. B. Felsen, "Gaussian beam and pulsed beam dynamics: Complex source and spectrum formulations within and beyond paraxial asymptotics," *J. Opt. Soc. Am. A*, Vol. 18, 1588–1611, 2001.
2. Green, A. C., H. L. Bertoni, and L. B. Felsen, "Properties of the shadow case by a half-screen when illuminated by a Gaussian Beam," *J. Opt. Soc. Am.*, Vol. 69, 1503–1508, 1979.
3. Katsav, M., E. Heyman, and L. Klinkenbusch, "Complex-source beam diffraction by a wedge: Exact and complex rays solutions," *IEEE Trans. Antennas Propagat.*, Vol. 62, 3731–3741, July 2014.
4. Heyman, E. and L. B. Felsen, "Complex source pulsed beam fields," *J. Opt. Soc. Am. A*, Vol. 6, 806–817, June 1989.
5. Heyman, E., V. Lomakin, and G. Kaiser, "Physical source realization of complex source pulsed beams," *J. Acoust. Soc. Am*, Vol. 107, 1880–1891, April 2000.
6. Klinkenbusch, L. and H. Bruns, "Diffraction of a uniform complex source beam by a circular cone," *International Conference on Electromagnetics in Advanced Applications (ICEAA)*, 470–472, 2014.
7. Katsav, M., E. Heyman, and L. Klinkenbusch, "Diverging and converging beam diffraction by a wedge. Part II: Plane wave spectral solutions and complex ray solutions," *Progress In Electromagnetics Research Symposium*, Prague, Czech Republic, July 6–9, 2015.

On the Theory of Transition Radiation in the Anisotropic Magneto Dielectric Plate in a Waveguide

Eduard A. Gevorkyan
Moscow State University of Economics, Statistics and Informatics
7, Nezhinskaya Str., Moscow 119501, Russia

Abstract— The transition radiation of charged particle in a regular waveguide of arbitrary cross section filled with anisotropic magneto dielectric plate of finite length is considered. It is assumed that the charged particle crosses the plate perpendicular to the waveguide axis. The wave equations and the analytical expressions for the transverse-electric (TE) field in various regions in the waveguide are obtained. Taking into account the obtained analytical expressions for TE field and using the Poynting vector the energy of transition radiation of moving particle is calculated. The case of rectangular waveguide is considered and the energy of transition radiation is analyzed in this case. The analytical expression of the transition radiation of charged particle for the case of thin plate in the waveguide (the wavelength in the plate is much grater than the length of the plate) is found. The possibility of appearance of Vavilov-Cerenkov radiation is analyzed. The conditions under which it occurs the Cerenkov radiation are found. The frequency of Cerenkov radiation is determined too.

Optical Soliton Perturbation with Semi-inverse Variational Principle

Anjan Biswas
Department of Mathematical Sciences, Delaware State University, Dover, DE 19901-2277, USA

Abstract— This talk will be on perturbed nonlinear Schrodinger's equation that models the propagation of solitons through optical fibers. The semi-inverse variational principle is employed to obtain analytical bright soliton solution in presence of several perturbation terms. This discussion will be carried out with five forms of nonlinear media. They are Kerr law, power law, parabolic law, dual-power law and log law nonlinearity. The constraint conditions (integrability criteria) will emerge for the soliton solutions to exist.

Scattering of an Obliquely Incident Electromagnetic Plane Wave by an Array of Magnetized Plasma Cylinders

V. A. Es'kin, **A. V. Ivoninsky**, **and A. V. Kudrin**
University of Nizhny Novgorod, Russia

Abstract— In recent years, the problem of electromagnetic wave scattering by arrays of gyrotropic elements has attracted increased interest. This interest is stimulated by numerous applications of the corresponding structures in, e.g., lithography, near-field microscopy, wave diagnostics of media, information processing and transmission, etc. [1–3]. Despite a significant progress in the studies of electromagnetic wave scattering by arrays of nongyrotropic elements [1], the recently obtained results for arrays of gyrotropic scatterers have revealed a variety of new interesting features [2, 3]. In particular, it has been found that the presence of gyrotropic properties in photonic crystals can significantly influence the reflection and transmission of electromagnetic waves [2]. For example, nonreciprocal properties of such crystals can be used for creating materials with one-path transmission of electromagnetic energy, as well as slow-wave systems and wideband isolators in the optical band. Moreover, it can be expected that the joint contribution of the individual and collective resonance scattering mechanisms to the diffracted field of an array containing frequency-dependent resonance elements can lead to some interesting phenomena which are yet to be determined.

It is the purpose of the present work to study the resonance scattering of an obliquely incident, linearly polarized electromagnetic plane wave by an equidistant array of parallel gyrotropic cylinders. The problem is analyzed using the scattering matrix method. As a gyrotropic medium filling the scattering elements of the array, we consider a cold collisionless magnetoplasma. The solution for the scattered field in the case of incidence at an arbitrary angle to the axes of the cylinders has been obtained. It is demonstrated that in this case, the scattered field is hybrid, i.e., the longitudinal (cylinder-aligned) components of both the electric and magnetic fields are nonzero. Analysis of the frequency dependences of the scattering coefficients of the electric- and magnetic-field components shows that near the resonant frequencies of the array, frequency ranges exist in which the absolute values of these coefficients are much smaller than the field amplitude in the incident wave. Moreover, at the resonant frequencies of the array, these coefficients vanish. Thus, the interaction of the individual and collective scattering mechanisms can lead to a significant weakening and even suppression of the scattered field. In the opposite case, the interaction of the individual and collective scattering mechanisms can lead to enhancement of the scattered field compared with the case of a single cylinder. It is shown that in the case of oblique incidence of the H-polarized wave on the array, the longitudinal component of the electric field can have, under certain conditions, a layered structure, whereas the longitudinal component of the magnetic field has a 2D-periodic chessboard-type structure.

ACKNOWLEDGMENT

This work was supported by the Russian Science Foundation (project No. 14–12–00510), the RFBR (project No. 14–01–31280), the Grant of the President of the Russian Federation (project No. MK–4688.2014.2), and the Government of the Russian Federation (contract No. 14.B25.31.0008).

REFERENCES

1. Decoopman, T., G. Tayeb, S. Enoch, D. Maystre, and B. Gralak, "Photonic crystal lens: From negative refraction and negative index to negative permittivity and permeability," *Phys. Rev. Lett.*, Vol. 97, No. 7, 073905, 2006.
2. Liu, S., W. Chen, J. Du, Z. Lin, S. T. Chui, and C. T. Chan, "Manipulating negative-refractive behavior with a magnetic field," *Phys. Rev. Lett.*, Vol. 101, No. 15, 157407, 2008.
3. He, C., M.-H. Lu, X. Heng, L. Feng, and Y.-F. Chen, "Parity-time electromagnetic diodes in a two-dimensional nonreciprocal photonic crystal," *Phys. Rev. B.*, Vol. 83, No. 7, 75117, 2011.

Theorem for the $G_1(c,n)$ Numbers

Georgi Nikolov Georgiev[1] and Mariana Nikolova Georgieva-Grosse[2]

[1]Faculty of Mathematics and Informatics
University of Veliko Tirnovo "St. St. Cyril and Methodius", Veliko Tirnovo BGC5000, Bulgaria
[2]Consulting and Researcher in Physics and Computer Sciences, Gerlingen D-70839, Germany

Abstract— The zeros of Kummer confluent hypergeometric function $\Phi(a,c;x)$ with $a=c/2-jk$ — complex, c — real, ($c\neq l$, $l=0,-1,-2,-3,\ldots$), k — real, $x=jz$, z — real, positive and $n=1,2,3,\ldots$) are of special interest in the theory of anisotropic waveguides [1–6]. Until now the attention has been the focused mainly on the positive purely imaginary zeros $\zeta_{k,n}^{(c)}$ of $\Phi(a,c;x)$ with respect to its independent variable z [2–6]. It has been established that for them it holds: $\lim\limits_{k_+\to+\infty}\zeta_{k_+,n}^{(c)}=+\infty$ and $\lim\limits_{k_-\to-\infty}\zeta_{k_-,n}^{(c)}=0$, where the subscripts "+" ("−") label quantities, corresponding to positive (negative) sign of k ($k_+>0$ and $k_-<0$) [2]. The numerical analysis has shown that if $c\neq l$ the sequences $\{K_-(c,n,k_-)\}$ and $\{M_-(c,n,k_-)\}$ ($K_-(c,n,k_-)=|k_-|\zeta_{k_-,n}^{(c)}$ and $M_-(c,n,k_-)=|a_-|\zeta_{k_-,n}^{(c)}$) are convergent provided $k_-\to-\infty$, though the multiples in the products $|k_-|\zeta_{k_-,n}^{(c)}$ and $|a_-|\zeta_{k_-,n}^{(c)}$ become infinitesimal, resp. unrestricted. They tend to finite real positive limits, called $L_1(c,n)$ numbers (denoted by $L(c,n)$, too) [2, 6–9]. The definition of the latter has been extended for $c=l$, as well. Later on a similar property of the positive purely imaginary zeros in z of certain functions, incorporating several complex confluent and possibly also a few real cylindrical functions of specially chosen parameters has been found out. The discussion has been performed in the real case, too [8–11].

Recently, an investigation of the positive purely imaginary zeros $\kappa_{z,n}^{(c)}$ in k of the Kummer function of the parameters, pointed out above has been made, assuming z as parameter. It has been observed that on condition that z diminishes, $\kappa_{z,n}^{(c)}$ grow monotonously. This hinted that the quantities $\kappa_{z,n}^{(c)}$ might possess features, resembling the ones of the zeros $\zeta_{k,n}^{(c)}$ (new families of numbers may be determined, connected with $\kappa_{z,n}^{(c)}$) [12].

In this paper the theorem for existence and for the basic properties of the $G_1(c,n)$ numbers (new real positive numbers, connected with the zeros $\kappa_{z,n}^{(c)}$ of $\Phi(a,c;x)$ in which a, c and x take the values, indicated above, is formulated and proved numerically. Its statement is accepted as a general definition of the latter. The theorem is composed of three lemmas. Lemmas 1 and 2 demonstrate the existence of quantities and determine them in case $c\neq l$ and $c=l$ (in which $\Phi(a,c;x)$ is not defined) as the limit of the infinite sequence of real positive numbers $\{R(c,n,z)\}$, ($R(c,n,z)=z\kappa_{z,n}^{(c)}$) for $z\to0$, and $\{G_1(l-\varepsilon,n)\}$ and $\{G_1(l+\varepsilon,n+1)\}$, ($\varepsilon$ — infinitesimal real positive number) for $\varepsilon\to0$, resp. Lemma 3 reveals the main features of the numbers (recurrence relation, formula for symmetry and link of some of them with the Ludolphian number). Detailed Tables and graphs illustrate the influence of parameters c and n on $G_1(c,n)$. The application of numbers in the theory of azimuthally magnetized circular ferrite waveguides, propagating normal TE_{0n} modes is demonstrated.

REFERENCES

1. Tricomi, F. G., *Funzioni Ipergeometriche Confluenti*, Edizioni Cremonese, Rome, Italy, 1954.
2. Georgiev, G. N. and M. N. Georgieva-Grosse, "A new property of the complex Kummer function and its application to waveguide propagation," *IEEE Antennas Wireless Propagation Lett.*, Vol. 2, 306–309, December 2003.
3. Georgiev, G. N. and M. N. Georgieva-Grosse, "Iterative method for differential phase shift computation in the azimuthally magnetized circular ferrite waveguide," *PIERS Online*, Vol. 6, No. 4, 365–369, 2010.
4. Georgieva-Grosse, M. N. and G. N. Georgiev, "Numerical modeling of the area of phase shifter operation of the azimuthally magnetized circular ferrite waveguide," *Proc. 6th Europ. Conf. Antennas Propagat. EuCAP 2012*, article ID P-23, 5 pages, Prague, Czech Republic, March 26–30, 2012.

5. Georgiev, G. N. and M. N. Georgieva-Grosse, "Advanced computational .methods for analysis of the circular waveguide completely filled with azimuthally magnetized ferrite: Review of recent results," *Proc. Fourteenth Int. Conf. Electromagn. Adv. Applicat. ICEAA'12*, 62–65, Cape Town, South Africa, September 2–7, 2012, (*Invited Paper* in the Special Session "Modern problems of mathematical and computational electromagnetics and their advanced applications," organized by M. N. Georgieva-Grosse and G. N. Georgiev).
6. Georgiev, G. N. and M. N. Georgieva-Grosse, "Theory of the circular waveguide completely filled with azimuthally magnetized ferrite: Review of recent results," (*Invited Paper*), *Proc. The Seventh Int. Conf. "Inverse problems: Modeling & Simulation*," Vol. 67, Ölüdeniz, Fethiye, Turkey, May 26–31, 2014.
7. Georgiev, G. N. and M. N. Georgieva-Grosse, "Theory of the $\tilde{L}_4$ numbers: Existence theorem and physical interpretation," *Proc. XXX URSI General Assembly*, article ID DP1.7, 4 pages, in CDROM, Istanbul, Turkey, August 13–20, 2011.
8. Georgiev, G. N. and M. N. Georgieva-Grosse, "Theory of the L numbers: definition, computational modeling, properties and application," *Proc. Thirteenth Int. Conf. Electromagn. Adv. Applicat. ICEAA'11*, 544–547, Turin, Italy, September 12–16, 2011, (*Invited Paper* in the Special Session "Future challenges in mathematical and computational electromagnetics and its applications," organized by G. N. Georgiev and M. N. Georgieva-Grosse).
9. Georgiev, G. N. and M. N. Georgieva-Grosse, "Theorem for the relation between the $L_1(c, n)$ and $L_2(c, \rho, n)$ numbers," *Proc. 2014 XXXI URSI GASS General Assembly and Scientific Symposium*, Vol. 2, 826–829, Beijing, China, August 16–23, 2014.
10. Georgiev, G. N. and M. N. Georgieva-Grosse, "Theory of the L numbers and its application to electromagnetism," (*Invited Paper*), *Proc. 2015 URSI Atlantic Radio Science Conference, URSI AT-RASC*, Gran Canaria, Canary Islands, Spain, May 18–22, 2015 (in print).
11. Georgiev, G. N. and M. N. Georgieva-Grosse, "Hypothesis for the identity of the $L_2(c, \rho, n)$ and $\hat{L}_2(\hat{c}, \hat{\rho}, \hat{n})$ numbers and its application in the theory of waveguides," *Progress In Electromagnetics Research Symposium Abstracts*, 805–806, Stockholm, Sweden, August 12–15, 2013; *PIERS Proceedings*, 940–945, Stockholm, Sweden, August 12–15, 2013. (in the Special Session "Advanced mathematical and computational methods in electromagnetic theory and their applications," organized by M. N. Georgieva-Grosse and G. N. Georgiev).
12. Georgieva-Grosse, M. N. and G. N. Georgiev, "Contribution to the theory of the complex Kummer function," *Proc. Sixteenth Int. Conf. Electromagn. Adv. Applicat. ICEAA'14*, 387–390, Palm Beach, Aruba, August 3–8, 2014, (*Invited Paper* in the Special Session "Challenges in mathematical and computational electromagnetics and its applications," organized by G. N. Georgiev and M. N. Georgieva-Grosse).

Diffraction Radiation Phenomena: New Methods for Physical and Engineering Analysis

Merey Sautbekova[1], **Seil Sautbekov**[1], **Yuriy Sirenko**[1, 2], **and Alexey Vertiy**[1]

[1]L. N. Gumilyov Eurasian National University, 2, Mirzoyana St., Astana 010008, Republic of Kazakhstan
[2]A. Ya. Usikov Institute of Radiophysics and Electronics, National Academy of Sciences of Ukraine
12, Academician Proskura St., Kharkov 61085, Ukraine

Abstract— Advances in electrodynamic theory of gratings play an important role in the development of topical areas of science and technology. Nowadays, optics and spectroscopy, physics and engineering of millimeter and submillimeter waves, high-power electronics, quantum radio physics and solid state physics, acoustics and resonance quasioptics benefit from methods, models and results of the grating theory both in frequency and time domains. Gratings' abilities to change their transparency over maximal limits and to transfer energy between waves propagating in different directions in a controlled manner allows much room for utilizing them as polarization and frequency filters, anti-reflection and scattering coatings, screens of various types and purposes, selective mirrors for dispersive open resonators, pattern-forming planar and cylindrical structures. One major field of application for diffraction gratings is antenna equipment, in particular, antennas operating on the effect of diffraction radiation aka diffraction antennas. When this effect occurs, an exponentially decreasing surface eigenwave of any open guiding structure (or an eigenfield of charged-particle beam in diffraction electronics) is transformed by a nearby periodic structure into a radiation field, which characteristics (directivity, energy efficiency, frequency range, scanning sector, etc.) are optimized to suit practical requirements.

In this communication, we consider in details the diffraction radiation effect, and new methods for analysis and model synthesis of diffraction antenna components and units. We presented the models making possible more detailed observations of the processes associated with near-field to far-field conversion by infinite and finite periodic structures. For the first time all these problems were considered using rigorous models exploiting exact absorbing conditions. The theoretical results have been obtained in 2-D for planar and axially-symmetrical objects. Analysis of these objects (finite and infinite gratings, planar and circular dielectric waveguides, etc.) is based on solutions of open initial boundary value problems, which computational space is truncated by exact absorbing conditions.

Inverse Spectral Theory and Kramers-Kronig Relations

G. F. Crosta
University of Milan Bicocca, Milan, Lombardy, Italy

Abstract— Inverse problems aimed at locating cracks and voids inside a dielectric medium by means of electromagnetic waves involve knowledge of transmission eigenvalues. The subject has been actively investigated by many Authors for some years and results have been presented in articles and books. Unfortunately, the frequency dependence of dielectric permittivity and magnetic permeability of the material has not been taken into account. A theorem which provides existence and asymptotic properties of real transmission eigenvalues is shown to be physically inconsistent, because it ignores the Kramers-Kronig relations.

Algebraic Regularization of Universal Functions in EM via Self-induced Hadamard Finite Parts

A. R. Baghai-Wadji
University of Cape Town, South Africa

Abstract— In boundary element method applications there are contradicting requirements which need to be accommodated skillfully in order to achieve high accuracy and high speed at the same time. Regarding acceleration of computations, it is desirable, besides parallelization and other conventional measures, to extract costly "universal" features from the computations which are common to a certain class of problems. If successful the resulting Universal Functions (UFs) can be pre-calculated and stored and referred to whenever necessary. As can be shown the introduction of UFs, however, requires additive factorization of terms, leading to high-order algebraic singularity in infrared region in spectral domain (zero and small values of the wavenumbers). Thereby, the algebraic order of the additional singularity depends on the degree of smoothness of the basis- and testing functions employed — the smoother the basis and testing functions the higher the order of singularity at the origin of the coordinate system in the spectral domain. On the other hand smooth basis- and weighting functions improve the convergence of the involved Fourier-type integrals algebraically in ultraviolet region (large values of the wavenumber in spectral domain). The main result in this contribution is the fact that all the aforementioned seemingly contradicting requirements can be reconciled naturally. The magic is done by recognizing that Hadamard finite parts appear in the introduced Universal Functions automatically, with one additional pleasant surprise: Ordinarily Hadamard finite parts technique, as the name implies, considers finite parts of infinite integrals, thus throwing away the infinities in the calculations. In the proposed procedure the infinities add up to zero exactly. Finally it should be pointed out that the Hadamard finite parts in the UFs are induced by the basis- and testing functions, thus, justifying the "self-induced" property in the title.

In an accompanying paper a second renormalization technique has been proposed which ensures exponential decay of dyadic Green's functions in ultraviolet region in spectral domain. The exponential regularization has its genesis in the construction of problem-specific Dirac delta functions, and it tempers the divergent behavior of Green's functions. In contrast the algebraic regularization, proposed in this contribution, has its origin in the smoothness properties of the chosen basis- and weighting functions. Consequently, the next logical question is whether or not the two regularization techniques, exponential and algebraic, can be combined to even further enhance the quality of our computations. The answer is unconditionally affirmative. Thus the combined exponential and algebraic regularization techniques enable ultra precise calculations of the near-fields in EM simulations while permitting the construction of Universal Functions. Furthermore, it is worth emphasizing that both regularizations techniques apply to closed-form Green's functions as well Green's functions which can be calculated only numerically. The latter property is crucially important: it enables the simulation of nanoscale devices involving complex media.

ACKNOWLEDGMENT

This work is based on the research supported in part by the National Research Foundation (UID: 93114).

REFERENCES

1. Baghai-Wadji, A. R., "D-theorem (on regularization): Green's function-induced distributed elementary sources — First kind," *Proceedings of the IEEE Antennas and Propagation Symposium*, Memphis, Mississippi, USA, 2014.
2. Baghai-Wadji, A. R., "S-theorem (on regularization): Green's function-induced distributed elementary sources — Second kind," *Proceedings of the IEEE Antennas and Propagation Symposium*, Memphis, Mississippi, USA, 2014.
3. Baghai-Wadji,A. R., "3D electrostatic charge distribution on finitely-thick bus-bars in microacoustic devices: Combined regularization in the near- and far-field," *IEEE Transactions on Ultrasonics, Ferroelectrics, and Frequency Control*, Special Issue, 2014 (invited).

On the Accuracy of Method of Moments for Solution of Full 3D Vectorial Electromagnetic Forward Scattering Problem

O. Güren[1], **M. N. Akıncı**[2], **and M. Çayören**[2]

[1]Electromagnetic Research Lab., Istanbul Technical University, Turkey
[2]Department of Electronics and Communication Engineering, Istanbul Technical University, Turkey

Abstract— In this communication, an analysis on the accuracy of the method of moments solution of full 3D vectorial electromagnetic forward scattering problem is presented. Although different mathematical techniques are developed for determination of the error rate of method of moments [1–6], this paper presents a numerical approach to this problem. In contrast to weak formulations of method of moments as in [7], we use a dyadic Green function based approach. We adopted the pulse functions as basis functions and obtained equations are weighted by the dirac-delta functions. In fact such a choice obliges us to calculate the hypersingular integrals of the components of the well known dyadic Green function. We utilize from [8] for the Cauchy principal value of these singular integrals. If the scatterer is divided into N many cells and a direct Gauss-Jordan inversion scheme is employed for the solution, then the resultant equation system requires a memory allocation of on the order of $O(N^2)$ and has a computational complexity of on the order of $O(N^3)$. To be able to decrease memory requirement to on the order of $O(N)$ and computational complexity to on the order of $O(N\log(N))$, bi-conjugate gradient method is applied instead of direct Gauss-Jordan inversion. Furthermore, the matrix multiplications are converted to spatial convolutions, which can be evaluated by the fast Fourier transform procedure. An accuracy analysis is made by comparing the simulated fields with the analytical expressions of the scattering field from a dielectric sphere. In particular, the accuracy analysis includes the following parts:

- Accuracy rate vs. the dielectric contrast between sphere and medium (Here the frequency of illumination and the size of the sphere are constant).
- Accuracy rate vs. the frequency of illumination (Here the dielectric contrast between sphere and medium and the size of the sphere are constant).
- Accuracy rate vs. the size of the sphere (Here the dielectric contrast between sphere and medium, the frequency of illumination are constant).

The results show that such an dyadic Green function based implementation of the method of moments works sufficiently well for a wide range of various parameters.

REFERENCES

1. Warnick, K. F. and W. C. Chew, "Accuracy of the method of moments for scattering by a cylinder," *IEEE Transactions on Microwave Theory and Techniques*, Vol. 48, No. 10, 1652–1660, 2000.
2. Warnick, K. F. and W. C. Chew, "Error analysis of scattering amplitudes and RCS," *IEEE Antennas and Propagation Society International Symposium*, Vol. 4, 2002.
3. Warnick, K. F. and W. C. Chew, "Error analysis of the moment method," *IEEE Antennas and Propagation Magazine*, Vol. 46, No. 6, 38–53, 2004.
4. Warnick, K. F., "An intuitive error analysis for FDTD and comparison to MoM," *IEEE Antennas and Propagation Magazine*, Vol. 47, No. 6, 111–115, 2005.
5. Hamlett, N. A. and W. Wasylkiwskyj, "A performance baseline for the convergence of electromagnetic integral-equation calculations using pulse functions," *IEEE Transactions on Antennas and Propagation*, Vol. 54, No. 5, 1523–1537, 2006.
6. Tyzhnenko, A. G. and Y. V. Ryeznik, "Estimates of accuracy and efficiency of a MoM algorithm in for 2-D screens," *Progress In Electromagnetics Research*, Vol. 71, 295–316, 2007.
7. Zwamborn, P. and P. M. Van den Berg, "The three dimensional weak form of the conjugate gradient FFT method for solving scattering problems," *IEEE Transactions on Microwave Theory and Techniques*, Vol. 40, No. 9, 1757–1766, 1992.
8. Gao, G., C. Torres-Verdin, and T. M. Habashy, "Analytical techniques to evalu- ate the integrals of 3D and 2D spatial dyadic Green's functions," *Progress In Electromagnetics Research*, Vol. 52, 47–80, 2005.

Accurate Determination of Surface Electric Fields for 2D Conformal Finite Difference Time Domain Simulations

M. C. Lin[1] and C. D. Zhou[2]

[1]Department of Electrical and Biomedical Engineering
Hanyang University, Seoul 133-791, Korea
[2]Tech-X Corporation, Boulder, CO 80303, United States

Abstract— Modeling an electromagnetic (EM) structure with curved boundaries using a conformal finite-difference time-domain (CFDTD) method retains a second order accuracy while using a staircased FDTD one only gives a first order accuracy. Although the frequencies and EM fields residing inside the spatial domain determined in the CFDTD simulation are very accurate, the calculation of surface electric fields is performed by interpolation methods, and therefore usually gives unsatisfied results. In this work, a new algorithm possibly being able to accurately determine surface electric fields near a curved surface has been developed and tested. The preliminary benchmark results show a convergence that the surface electric fields can be calculated as accurately as higher than 99% using a medium size grid in 2D. A more rigorous benchmark is used for the validation of this approach and an extension to 3D counterpart is under consideration. Accurate determination of surface electric fields in CFDTD simulations is important for a lot of research studies such as surface breakdown, field emission, plasma wall interaction and ohmic heating, etc.. Detailed algorithm and benchmark results will be presented.

ACKNOWLEDGMENT

This work was supported by the U.S. Department of Energy under Grant No. DE-SC0004436 and the research fund of Hanyang University (HY-201400000002393).

REFERENCES

1. Nieter, C. and J. R. Cary, "VORPAL: A versatile plasma simulation code," *J. Comput. Phys.*, Vol. 196, 448–473, 2004.
2. Dey, S., R. Mittra, and S. Chebolu, "A technique for implementing the FDTD algorithm on a nonorthogonal grid," *Microwave and Opt. Technol. Lett.*, Vol. 14, 213–215, 1997.
3. Dey, S. and R. Mittra, "A locally conformal finite-difference time-domain (FDTD) algorithm for modeling three-dimensional perfectly conducting objects," *IEEE Microwave and Guided Wave Lett.*, Vol. 7, 273–275, 1997.

Session 1A8
SC1: Model-order Reduction and Uncertainty Quantification

Fast Model Order Reduction Approach to Uncertainty Quantification in Electrokinetics

Lorenzo Codecasa and Luca Di Rienzo
Politecnico di Milano, Milan, Italy

Abstract— Electromagnetic computations rely on the perfect knowledge of material parameters. However, for a wide range of examples in electrical engineering, some uncertainty should be associated with that knowledge in the modeling process. In order to quantify the uncertainty of the output quantities of interest coming from the lack of knowledge of the input material parameters, the spectral stochastic finite element method, based on Polynomial Chaos Expansion (PCE), can be applied. This method, in both the intrusive and non-intrusive forms [1], allows to dramatically reduce computational time with respect to Monte Carlo (MC) method, in many electromagnetic problems. Nevertheless, in many situations, computational complexity can still be prohibitively large.

In this paper, uncertainty quantification problems due to random material parameters are considered in electrokinetics. For such problems a novel approach based on Model Order Reduction (MOR) is proposed. The starting point is an nonintrusive PCE method, in which the PCEs of variables are estimated from the solutions to the deterministic electrokinetic problems for all values of the random material parameters in a sparse grid. The main idea of the proposed algorithm is that of reducing the number of solutions of such deterministic electrokinetic problems by constructing a parametric reduced order model, which is used to approximate the solution to the deterministic electrokinetic problems. Such parametric reduced order model is tailored to approximating with chosen accuracy the deterministic elecrokinetics problems for the values of the random material parameters in the chosen sparse grid. The parametric reduced order model is generated in an efficient way by solving a reduced number of deterministic elecrokinetics problems with respect to that in the nonintrusive PCE approach. Moreover the computational cost for the solutions to the deterministic elecrokinetics problems required for constructing the parametric reduced order model is optimized by exploiting the relatedness among the solutions to the deterministic electrokinetics problems for different values of the random material parameters.

The proposed MOR approach has been validated by modeling a simplified geometry of a typical system for resistance welding [2]. In this situation the proposed MOR approach allowed to reduce the compuational time by about two orders of magnitutude with respect to that of standard nonintrusive PCE approach, maintaining the same level of accuracy. The storage requirement of the proposed approach is comparable to that for a single deterministic electrokinetics problem. The proposed approach thus seems a novel promising candidate for uncertainty quantification analysis in electrokinetics. The extension of the proposed approach to more general electromagnetic problems seems feasable and is currently under investigation.

REFERENCES

1. Xiu, D., *Numerical Methods for Stochastic Computations: A Spectral Method Approach*, Princeton University Press, 2010.
2. Codecasa, L. and L. Di Rienzo, "Stochastic finite integration technique formulation for electrokinetics," *IEEE Transactions on Magnetics*, Vol. 50, No. 2, Article 7014104, 2014.

Reduced Basis Model Reduction for Maxwell's Equations in Dispersive Media with Stochastic Coefficients

Martin Hess and Peter Benner
Max Planck Institute for Dynamics of Complex Technical Systems, Germany

Abstract— The simulation of the propagation of an electromagnetic pulse through linear, temporally dispersive media (like water) or systems (like a dielectric waveguide) is a typical problem of electromagnetics.

Consider the Maxwell-Debye model formulated in second-order form in the electric field E

$$\begin{aligned}\frac{1}{\mu_0}\nabla\times\nabla\times E+\epsilon_0\epsilon_\infty\partial_t^2 E &= f-\partial_t^2 P,\\ \partial_t P+\frac{1}{\tau}P &= \frac{\epsilon_0\left(\epsilon_s-\epsilon_\infty\right)}{\tau}E,\end{aligned}$$

with polarization P, relaxation time τ, relative permittivity at low-frequency limit ϵ_s and relative permittivity at high-frequency limit ϵ_∞, and a broadband input source f, which is modeled as a Gaussian pulse [1]. The equations are discretized with Nédélec finite elements of first order over a 2D unit square. Dirichlet zero boundary conditions (i.e., PEC, perfectly electric conducting) are imposed on all boundaries.

The model is parametrized by τ and $\Delta_\epsilon=\epsilon_s-\epsilon_\infty$, defining the 2-dimensional parameter domain D. Using a greedy sampling driven by an error indicator, we seek to generate a reduced model which accurately captures the dynamics in the parameter domain D [2]. We compare different greedy strategies and projection spaces to achieve an accurate low order model. Typically, the reduced basis model reduction reduces the model order by a factor of more than 100, while maintaining an approximation error of less than 1%. The error indicator evaluates the residual over all timesteps and finds the maximum over the parameter domain D. The maximum parameter location is then used to iteratively enrich the reduced basis space.

As an extension, we consider the parameters as random variables with an underlying distribution. We use stochastic collocation and Monte Carlo simulations to estimate the statistics of the system. This computationally expensive procedure becomes feasible by employing accurate reduced order models [3]. The statistical analysis will enable to simulate the behaviour of the electromagnetic system under uncertainties.

REFERENCES

1. Oughstun, K. E., "Electromagnetic and optical pulse propagation," *Springer Series in Optical Sciences*, 2006.
2. Rozza, G., D. B. P. Huynh, and A. T. Patera, "Reduced basis approximation and a posteriori error estimation for affinely parametrized elliptic coercive partial differential equations," *Archives of Computational Methods in Engineering*, Vol. 15, 229–275, 2008.
3. Chen, P., A. Quarteroni, and G. Rozza, "Comparison between reduced basis and stochastic collocation methods for elliptic problems," *Journal of Scientific Computing*, Vol. 59, 187–216, 2014.

Uncertainty Quantification for Complex RF-structures Using the State-space Concatenation Approach

J. Heller, **T. Flisgen**, **C. Schmidt**, **and U. van Rienen**
Institute of General Electrical Engineering, University of Rostock
Albert-Einstein-Strasse 2, Rostock 18059, Germany

Abstract— In various applications of computational engineering and accelerator physics, the computation of the electromagnetic behavior of a structure is of crucial importance for the design and operation. The electromagnetic properties of the structure depend on its geometry, which, for real-life radio-frequency (RF) structures, generally deviates from their design values due to fabrication tolerances and operation. To make assessments about the effects of such deviations as well as to employ robust optimizations, a so-called uncertainty quantification (UQ) is applied. For large and complex structures such computations are heavily demanding and cannot be carried out using standard brute-force approaches. In this paper, we propose a combination of established techniques to perform UQ for long and complex structures, where the uncertainty is located only in parts of the structure. As exemplary structure, we investigate the third-harmonic cavity, which is being used at the FLASH accelerator at DESY, assuming an uncertain geometry of the left higher-order mode coupler. The investigation is carried out using the so-called polynomial chaos expansion (gPC). For that, the repeated numerical solution of Maxwell's equations is necessary. Usually, such investigations are carried out on supercomputers or small computer clusters with heavily parallelized code. Due to the fact that maximum-performance computational infrastructure is scarce and expensive, the electromagnetic properties are being computed on standard workstation computers using a newly proposed non-overlapping domain decomposition scheme named State-Space Concatenation (SSC) which is based on model-order reduction of the decomposed segments. Using the SSC scheme has the most important advantage that only the uncertain part of the structure, in our case the left coupler, needs to be recomputed when using a non-intrusive scheme like gPC. In comparison to the huge computational demand of a straightforward simulation, the combination of uncertainty quantification and model-order reduction allows for a reasonable improvement of the computational efficiency. Both schemes can be separately applied to structures related to accelerator physics. Yet, just their combination will enable the investigation of long and complex structures beyond the scope of standard approaches.

Application of Krylov-type Parametric Model Order Reduction in Efficient Uncertainty Quantification of Electro-thermal Circuit Models

Y. Yue[1], **L. Feng**[1], **P. Meuris**[2], **W. Schoenmaker**[2], **and P. Benner**[1]

[1]Max Planck Institute for Dynamics of Complex Technical Systems
Sandtorstr. 1, Magdeburg 39106, Germany
[2]MAGWEL NV, Martelarenplein 13, Leuven B-3000, Belgium

Abstract— Electro-thermal analysis is crucial in designing systems such as power-MOS devices used in energy harvesting and RF-circuitry in wireless communication. To design systems robust to device variations due to the fabrication process, uncertainty quantification plays an important role to quantify the uncertainties of the system output propagated from the process variations. However, simulation analysis of electro-thermal systems is already computationally demanding because the mathematical model is derived from a fine 3D mesh of a multi-layered structure consisting of dielectric, vias, contacts, and metal interconnection. The computational cost of uncertainty quantification is even higher since it requires simulating the model at many parameter samples, or simulating a coupled system with a much higher dimension. To reduce the high computational cost, we use parametric model order reduction techniques, which proves to be efficient in many application fields such as circuit simulation, acoustics, and structural vibrations. A parametric model order reduction method builds a reduced model that can capture the system dynamics regardless of parameter changes within a certain range. In this work, we use a Krylov-type parametric model reduction method, whose goal is to match the (cross-)moments of the state vector, because of its modest requirements on system properties and low computational complexity. For our test case, which is a nonlinear electro-thermal system with one-way coupling from the electrical part to the thermal part, a parametric reduced model of a low order exhibits high accuracy over a very large parameter range in approximating the original high-order model. We use the parametric reduced model to accelerate two methods for uncertainty quantification, namely a Latin hypercube sampling method and a stochastic collocation method. Numerical results show that for both methods, uncertainty quantification based on a reduced model reproduces the results of that based on the original model, while leading to significant speedup compared to the latter.

Meshing Technique for Efficient Macromodel Cloning in FEM Analysis of 3D Structures

G. Fotyga, J. Grzybek, W. Dembinski, P. Bielski, and K. Nyka
Faculty of Electronics, Telecommunications and Informatics, Gdansk University of Technology, Poland

Abstract— The finite element method (FEM) is regarded as one of the most powerful and flexible numerical techniques in computational electromagnetics. However, it becomes time and memory consuming, while analyzing complex multiscale problems. We present a novel method of mesh generation, which is dedicated to analysis of microwave and photonic structures, that contain many identical elements (in terms of the geometry and the electric properties), such as: vias in SIW circuits, holes in PBG structures, tuning elements in waveguide filters, etc.. The influence of each of these elements on the electromagnetic field in the entire domain (structure) can be represented by means of the small dense FEM matrices, called macromodels (macroelements), which are obtained using the model order reduction (MOR). The proposed approach takes advantage of the fact that in the structures which contain many identical elements, one macromodel can be used to capture the electromagnetic behavior of many identical subregions. This operation is called a macromodel cloning. It requires creating an algorithm that allows for embedding one macromodel in multiple locations within the structure. The difficulty is associated with potentially nonconforming 2-D meshes on the boundaries of subregions, in which the clone of the macromodel is embedded. To overcome this problem, we developed a special tetrahedral meshing procedure, which allows one to establish an identical surface mesh on the boundaries of selected subdomains. The combination of these three techniques (3D-FEM, MOR with cloning, meshing technique) reduces the computation time and memory requirements significantly and makes it a promising method to incorporate into a CAD optimization tool.

ACKNOWLEDGMENT

This work has been financed by NCN under grant 2013/09/N/ST7/02268.

Circuit Understanding for Electromagnetics via the Reduced-basis Method

Valentín de la Rubia
Departamento de Matemática Aplicada, Universidad Politécnica de Madrid, Spain

Abstract— Finite Element Methods (FEM) have proven to be robust in solving the time-harmonic Maxwell's equations for the analysis of microwave filters and diplexers. Nowadays, microwave engineering relies on full-wave analysis not only to accurately predict the electrical behaviour prior to construction of microwave circuits, but also to actually design their electrical response. However, still we have little knowledge on how electromagnetics actually behaves, and only rather experienced microwave engineers are able to develop high-demanding specification designs. If only a link between electromagnetic phenomena and circuit behaviour were established, all our expertise in circuit theory could be used for electromagnetics. This is how microwave engineering is working nowadays, but this link is only based on approximations.

In this work, the electromagnetic behaviour in microwave filters and diplexers is described in terms of circuit theory. A transversal coupling matrix gathering all electromagnetic phenomena within a frequency band is found. As a result, further insight from the microwave point of view arises. A Finite Element Method approach is carried out for the electromagnetic analysis and a reliable reduced-order model for fast frequency sweep is proposed. The ingredients of this methodology are: 1) the use of field solutions at given frequencies as basis functions to reduce the original system, 2) adaptively choosing the field solution frequency samples, 3) evaluation of the residual error of the reduced field solution to determine the convergence of the reduced-order model in the frequency band of interest and 4) change of basis in the reduced-order model to get a transversal coupling matrix description of electromagnetics.

Once the reduced-order model is obtained, which is a reliable surrogate of the original Maxwell problem in the frequency band of interest, further manipulations are carried out to get further insight in the Maxwell problem. It is known that output ports in microwave filters and diplexers do not see individual resonators in the microwave circuit, but global eigenresonances. For the sake of circuit understanding, it is then important to force this global eigenresonance representation of the Maxwell problem.

Several microwave filters and diplexers, made up of dieletric resonators or dual-mode resonances, will illustrate the capabilities of this approach.

Robust Shape Optimization of Accelerator Magnets

O. Lass[1], **U. Römer**[2], **and S. Schöps**[3]

[1]Department of Mathematics, Technische Universität Darmstadt
Dolivostr. 15, Darmstadt 64293, Germany
[2]Institut für Theorie Elektromagnetischer Felder, Technische Universität Darmstadt
Schlossgartenstr. 8, Darmstadt 64289, Germany
[3]Graduate School of Computational Engineering, Technische Universität Darmstadt
Dolivostr. 15, Darmstadt 64293, Germany

Abstract— Bending and focusing magnets are among the most important and expensive equipment used in particle accelerators. Particle beam dynamics rely on a very high field homogeneity, that can be critically affected by uncertainties in both material and geometry. We discuss shape optimization to achieve a high field homogeneity, insensitive to stochastic influences.

In many cases the underlying field distribution can be accurately described using a magnetostatic formulation. Incorporating uncertainties results in a stochastic partial differential equation. Using the magnetic vector potential $\vec{A}$, the formulation reads as

$$\nabla \times \left(\bar{\bar{\nu}}(\omega,\vec{x})\nabla \times \vec{A}(\omega,\vec{x})\right) = \vec{J}(\vec{x}) - \nabla \times \vec{H}_c(\omega,\vec{x}), \quad \text{in } D, \tag{1}$$

$$\vec{n} \times \vec{A}(\omega,\vec{x}) = 0, \quad \text{on } \partial D. \tag{2}$$

In (1), modeling linearization, we allow for a tensor valued reluctivity $\bar{\bar{\nu}}$ and for a coercitive magnetic field strength $\vec{H}_c$. Also $\vec{J}$ refers to the source current density, $\vec{n}$ to the outer unit normal and $\omega \in \Omega$ to a random outcome. Geometric uncertainty refers to randomness in the shape of the *iron-air* interface. It is taken into account through the spatial dependency of the material. Using a truncated Karhunen-Loève or polynomial chaos expansion we obtain a finite dimensional noise representation. More precisely, for the reluctivity, we have $\bar{\bar{\nu}}(\omega,\vec{x}) \approx \bar{\bar{\nu}}_M(\vec{Y}(\omega),\vec{x})$, where $\vec{Y} \in \Gamma$ refers to an M-dimensional random vector.

The physical quantity of interest is given by the harmonic distortion factor [1]

$$Q = \sum_{i=1, i\neq N}^{K} a_i^2 + b_i^2, \tag{3}$$

where a_i and b_i refer to the skew and normal multipole coefficients, respectively, and N denotes the pole-pair number of the magnet. The multipole coefficients in turn can be seen as linear functionals of the solution.

Let $\vec{c}$ denote a set of shape parameters, e.g., the control points in a spline representation of the interface. The robust optimization problem reads

$$\vec{c}^* = \arg\min_{\vec{c}} \max_{\vec{y}\in u} Q(\vec{c},\vec{y}), \tag{4}$$

where u refers to a convex uncertainty set as given, e.g., in [2]. Solving (4) numerically can be very challenging. However, the complexity can be reduced using perturbation techniques as well as polynomial surrogate and reduced models in the stochastic and deterministic variable, respectively. These issues will be discussed and illustrated by means of numerical examples.

REFERENCES

1. Russenschuck, S., *Field Computation of Accelerator Magnets*, Wiley-VCH, 2010.
2. Ben-Tal, A. and A. Nemirovski, "Robust convex optimization," *Mathematics of Operations Research*, Vol. 23, No. 4, 769–805, 1998.

Analysis of Inhomogeneous Plane Wave Scattering from Periodic Metamaterials

S. Tooni, **T. F. Eibert**, **and L. Vietzorreck**
Lehrstuhl für Hochfrequenztechnik, Technische Universität München
Arcisstr. 21, Munich 80333, Germany

Abstract— The spectral domain analysis of periodic open metamaterial unit cells is performed by inhomogeneous plane wave excitation. The hybrid finite element boundary integral method is employed to compute the scattered field, the reflection and the transmission coefficients from unit cells. Discrete surface and complex leaky modes of the unit cells are computed from the singularities of the scattered field. The robustness of the method is demonstrated by comparing the computed results with the results from other methods.

For Sturm-Liouville problems, the Green's functions can be expanded based on constructing discrete and continuum modes [1]. Depending on the excitation methods, several procedures can be introduced to compute the eigenmodes and corresponding eigenvalues. Most of the conventional approaches are employing the singular value decomposition (SVD) of a system matrix, which is obtained from the discretization of the system operator. In open problems, usually the system matrix has a non-linear dependence on the eigenvalues. Therefore, utilizing SVD methods is not practical and non-linear optimization procedures have to be assessed. An alternative to obtain the eigenvalues and eigenmodes are excitation based methods. These methods, mathematically model the physical response of the system for excitation over a spectrum [2].

In the current paper, the method of excitation of eigensolutions in periodic structures by plane waves is investigated. Some new properties of periodic media, such as impedance boundary conditions, absorption and near-field imaging are explored based on the modal behavior of the constructing unit cells.

Green's functions of layered media are combinations of reflected and transmitted plane waves in different layers. The generalized reflection and transmission coefficients can, therefore, be considered as the desired Green's functions of these media. In periodic stratified media, while the operation frequency is enough below the cutoff of the higher order Floquet modes, the medium can be approximated as a homogeneous layered medium. However, the scattering of the field must still be computed by expansion of the scattered field based on Floquet modes. The coefficients of the fundamental Floquet mode over the open boundaries can be considered as the describing parameters of the physical properties [3].

On the one hand, complex leaky modes can be either in the fast or in the slow wave region. On the other hand, in loss less structures, complex eigenvalues exist always in conjugate pairs. In the slow wave region, all the computed eigenvalues are proper while in the fast wave region one of the poles is improper. By consideration of the radiation condition, the undesired pole can be removed from the response [4].

REFERENCES

1. Felsen, L. P. and N. Marcuvitz, *Radiation and Scattering of Waves*, Wiley-IEEE Press, 1994.
2. Reutskiy, S., "The method of external excitation for solving generalized Sturm-Liouville problems," *J. Comput. Appl. Math.*, Vol. 233, 2374–2386, 2010.
3. Tooni, S., T. F. Eibert, M. Tayarani, L. Vietzorreck, and K. Wang, "Dispersion analysis of open periodic structures using reflection pole method," *7th European Conf. Antennas Propag. (EuCAP)*, 2365–2368, Gothenburg, Sweden, April 2013.
4. Tooni, S. and T. F. Eibert, "Excitation of complex modes of periodic structures using inhomogeneous plane wave scattering in fast and slow wave regions," *IEEE Trans. Antennas Propag.*, Vol. 62, No. 12, 6290–6298, 2014.

Broadband Analysis Including Beam Steering of Phased Array Antennas by Order Reduction

O. Floch, **A. Sommer**, **O. Farle**, **and R. Dyczij-Edlinger**
Chair for Electromagnetic Theory, Saarland University, Saarbrücken D-66123, Germany

Abstract— In applications such as radar, phased antenna arrays are to be characterized over broad frequency bands and wide ranges of steering and look angles. When numerical methods, specifically the finite-element (FE) method, are used, the determination of the far-fields tends to be very time-consuming, for the following reasons: Typical antenna arrays are electrically large and consist of high numbers of radiators. Hence the resulting FE systems are of very large dimension. Furthermore, broad variations in frequency (f) and steering angles (θ_s, ϕ_s) requires the FE solution for large numbers of operating points (f, θ_s, ϕ_s), each of which has to be computed by solving the large-scale FE system. When direct solvers are no longer applicable because of their high computational complexity, one must resort to iterative techniques. In this regard, the availability of efficient preconditioners is of utmost importance. For electrically large structures, domain decomposition (DD) methods have proven to be highly effective. However, even with the aid of these techniques, solving the large-scale FE system remains a time-consuming procedure. Finally, wide variations in look angles (θ, ϕ) call for large numbers of sampling points (θ, ϕ). Each of them requires a separate near-field-to-far-field (NF-FF) transformation, for each considered operating point (f, θ_s, ϕ_s).

To reduce computational efforts, we here propose a two-step model order reduction (MOR) approach, similarly to [1, 2], but with the focus on electrically large structures: We fist construct a reduced-order model (ROM) for the near fields of the phased antenna array which is very cheap to solve at any value of the parameter triple (f, θ_s, ϕ_s). For this purpose, a multi-point MOR method with self-adaptive expansion point selection [1, 2] is employed. The second step utilizes the empirical interpolation method (EIM) [3] to construct an affine approximation to the NF-FF operator as a function of frequency and look angles. Since the EIM-based NF-FF operator is also fast to evaluate at any value of the parameter triple (f, θ, ϕ), the combination of both methods results in a highly efficient numerical model for computing the far-fields as a function of the five parameters (f, θ_s, ϕ_s, θ, ϕ). The accuracy and efficiency of the suggested two-step MOR approach is demonstrated by means of an electrically large real-world example.

REFERENCES

1. Fares, M., J. S. Hesthaven, Y. Maday, and B. Stamm, "The reduced basis method for the electric field integral equation," *J. Comput. Phys.*, Vol. 230, No. 14, 5532–5555, 2011.
2. Sommer, A., O. Farle, and R. Dyczij-Edlinger, "Efficient finite-element computation of far-fields of phased arrays by order reduction," *COMPEL*, Vol. 32, No. 5, 1721–1734, 2013.
3. Barrault, M., Y. Maday, N. C. Nguyen, and A. T. Patera, "An 'empirical interpolation' method: Application to efficient reduced-basis discretization of partial differential equations," *C. R. Math. Acad. Sci. Paris*, Vol. 339, No. 9, 1721–1734, 2013.

Session 1A9
SC1: Electromagnetic Field Transformations for Measurements and Simulations

Spherical-multipole Based Near-to-near and Near-to-far Field Transformations

L. Klinkenbusch
Kiel University, Germany

Abstract— Spherical-multipole expansions have been employed in the context of near-to-far field transformations from antenna near-field measurements in the frequency domain [1] and (less often) in the time domain [2]. Since these approaches (among others) exploit the orthogonality of the spherical modes the scanning process has to be performed on a spherical surface. Spherical-multipole expansions can also be used for conveniently describing the electromagnetic field outside of the solution domain for numerical methods via a spherical-multipole interface [3]. In that case the radiating structure is replaced by a certain number of elementary (Hertz and Fitzgerald) dipoles located on a Huygens surface which completely encloses all radiating elements but otherwise can have an arbitrary form. The multipole expansion of the field of a dipole is known analytically in the frequency domain, and a linear superposition (summation) leads to the total frequency-domain spherical-multipole expansion of the electromagnetic field valid outside of a minimum sphere containing all sources. By means of the analytically known Fourier Transform of the spherical Bessel function of the first kind,the far-field approximation of that spherical-multipole expansion can be transformed into the time domain [4]. Furthermore a finite expansion of the spherical Hankel function yields the opportunity to recursively derive the time-domain spherical-multipole expansion in the near-field from that one valid in the far field, and hence to perform a systematic time-domain near-to-near field transformation [5]. Finally, the field information is non-redundantly stored in a discrete set of time-domain spherical-multipole amplitudes and ready for an arbitrary post-processing.

Besides a brief review of these methods and corresponding new numerical results the paper focuses on the validity of the reconstructed electromagnetic fields in the near of the Huygens surface.

REFERENCES

1. Hansen, J. E., *Spherical Near-field Antenna Measurements*, Peter Peregrinus Ltd., London, 1988.
2. Hansen, T. B., "Formulation of spherical near-field scanning for electromagnetic fields in the time domain," *IEEE Trans. on Antennas and Propagation*, Vol. 45, No. 4, 620–630, 1997.
3. Klinkenbusch, L., "A spherical-multipole interface for numerical methods in electromagnetic field theory," *Proc. of the Latsis Symposium on Computational Electromagnetics*, 242–247, Zürich, 1995.
4. Adam, J., L. Klinkenbusch, M. Mextorf, and R. Knoechel, "Numerical multipole analysis of ultra-wideband antennas," *IEEE Trans. on Antennas and Propagation*, Vol. 58, No. 12, 3847–3855, 2010.
5. Klinkenbusch, L., "Time domain near-field to near-field transformation using a spherical-multipole approach," *Radio Science*, Vol. 46, RS0E17, doi:10.1029/2011RS004670, 2011.

Comparison and Application of Different Echo Reduction Techniques in Antenna Measurement

Manuel Sierra Castañer[1], **Javier García-Gasco Trujillo**[2], **Pilar González Blanco**[1], **Manuel López Morales**[1], **Francesco Saccardi**[3], **and Lars J. Foged**[3]

[1]Universidad Politécnica de Madrid, Spain
[2]SES Engineering, Spain
[3]Microwave Vision, Italy

Abstract— During the last years, different methods for improving the quality of the antenna measurements results have been developed, in particular for echo reduction. This paper is a common research work between Universidad Politécnica de Madrid and Microwave Vision Group whose objective is the comparison of different echo reduction techniques in order to be able to explore the advantages of each one in antenna measurements applications. In particular, these techniques are specially important for outdoor antenna measurement systems, for systems as the StarLab (where the measurement equipment is placed without full coverage of absorbing material) or for measurements at lower frequencies where the performance of the absorbing material is not good enough. These techniques are based on spatial filtering, modal filtering and time gating techniques. The paper analyzes different approaches: in particular for spatial filtering, holographic techniques [1] and source reconstruction based on integral equations [2] are analyzed. In the first case, the field is back propagated to a large planar surface containing the antenna under test, and the fields out of the antenna area are filtered out. The main advantage is the very small time required for the transformation, while the disadvantages are focused on the specific applications for planar antennas and the need of geometrical information to improve the results. The second algorithm, based on source reconstruction using integral equation (in particular the authors analyzed MVG INSIGHT© algorithm). The main disadvantage is the time consumption, although the results are better accurate than the previous one. In the case of modal filtering, there are different approaches, with similar theoretical basis. This paper uses the approach included in MV-Echo© [3] for the cancellation of the echos based on the spherical modes decomposition of the radiated field. The last group of algorithms are based on time filtering. In particular FFT [4], Matrix Pencil method [5] and non uniform DFT are used. In all the cases, the results are similar. The first algortihm requires uniformly frequency spaced samples (not always available) but it is faster. In these three cases, the main disadvantage is the number of frequencies (and step) required for having a good echo reduction. The different algorithms have been applied to the measurement of a dipole antenna (SD1900) in the MVI StarLab System. Results show that depending on the angular range of the pattern the improvements are better or worst using any of the methods. Results will be shown in the final paper or presentation.

REFERENCES

1. Cano-Fácila, F. J., S. Burgos, F. Martín, and M. Sierra-Castañer, "New reflection suppression method in antenna measurement systems based on diagnostic techniques," *IEEE Transactions on Antennas and Propagation*, Vol. 59, No. 3, 941–949, Mar. 2011.
2. Quijano, J. L. A., L. Scialacqua, J. Zackrisson, L. J. Foged, M. Sabbadini, and G. Vecchi, "Suppression of undesired radiated fields based on equivalent currents reconstruction from measured data," *IEEE Antennas and Wireless Propagation Letters*, Vol. 10, 2011.
3. MV-Echo Software, Microwave Vision Group, www.microwavevision.com.
4. Aubin, J., M. Winebrand, R. Soerens, and V. Vinogradov, "Accurate near-field measurements using time-gating," *Antennas Measurement Techniques Association Annual Symposium Proceedings*, 362–365, Nov. 2007.
5. Adve, R. S., T. K. Sarkar, O. M. C. Pereira-Filho, and S. M. Rao, "Extrapolation of time-domain responses from three-dimensional conducting objects utilizing the matrix pencil technique," *IEEE Transactions on Antennas and Propagation*, Vol. 45, No. 1, 147–156, Jan. 1997.

Electromagnetic Field Transformations with Spectral Field Representations on the Ewald Sphere

T. F. Eibert, **E. Kılıç**, **C. Lopez**,
R. A. M. Mauermayer, **O. Neitz**, **and G. Schnattinger**
Lehrstuhl für Hochfrequenztechnik, Technische Universität München, Munich, Germany

Abstract— Electromagnetic field transformations are of increasing importance for achieving improved insight into field measurements and into simulations. Spectral field representations utilizing propagating plane wave expansions on the Ewald sphere provide for extremely flexible field transformations without compromising the efficiency of a fast transformation approach. The transformations can be set up with various equivalent sources representations and for arbitrary measurement locations, where the measurements can be collected with arbitrary measurement probes. The paper presents an overview of hierarchical propagating plane wave based field transformations and discusses various transformation results from the fields of near-field far-field transformations for antennas, antenna diagnostics and imaging as well as from the solution of nonlinear inverse problems.

Electromagnetic field transformations have been developed to high sophistication in the field of near-field antenna measurements [1], where focus is, however, mostly on the common measurement configurations (spherical, planar, cylindrical) with regular sampling. Inspired from the new possibilities achieved in the numerical solution of integral equations, a series of propagating plane wave based field transformation algorithms have been designed and realized over the past years [2, 3], which provide for excellent flexibility without compromising the efficiency known from so-called fast algorithms. With this flexibility, there is also a chance to establish novel measurement approaches and it will become possible to seamlessly merge simulated and measured field data in a common framework. The hierarchical propagating plane wave based algorithms have become very mature over the past years and many of their properties have been investigated [4–7]. In this contribution, we review important properties of the hierarchical propagating plane wave based algorithms and we will discuss novel achievements and applications in the fields of near-field far-field transformations, antenna diagnostics and broadband imaging, as well as of the solution of nonlinear inverse problems, e.g., nonlinear inverse medium problems or phaseless near-field far-field transformations.

REFERENCES

1. Yaghjian, A. D., "An overview of near-field antenna measurements," *IEEE Trans. on Antennas and Propag.*, Vol. 34, No. 1, 30–45, 1986.
2. Schmidt, C. H. and T. F. Eibert, "Multilevel plane wave based near-field far-field transformation for electrically large antennas in free-space or above material halfspace," *IEEE Trans. on Antennas and Propag.*, Vol. 57, No. 5, 1382–1390, 2009.
3. Eibert, T. F., Ismatullah, E. Kaliyaperumal, and C. H. Schmidt, "Inverse equivalent surface current method with hierarchical higher order basis functions, full probe correction and multilevel fast multipole acceleration (Invited Paper)," *Progress In Electromagnetics Research*, Vol. 106, 377–394, 2010.
4. Schnattinger, G. and T. F. Eibert, "Solution to the full vectorial 3D inverse source problem by multi-level fast multipole method inspired hierarchical disaggregation," *IEEE Trans. on Antennas and Propag.*, Vol. 60, No. 7, 3325–3335, 2012.
5. Qureshi, M. A., C. H. Schmidt, and T. F. Eibert, "Efficient near-field far-field transformation for nonredundant sampling representation on arbitrary surfaces in near-field antenna measurements," *IEEE Trans. on Antennas and Propag.*, Vol. 61, No. 4, 2025–2033, 2013.
6. Kılıç, E. and T. F. Eibert, "An inverse scattering technique based on finite element — Boundary integral method," *Progress In Electromagnetics Research Symposium Abstracts*, 777, Stockholm, Sweden, Aug. 12–15, 2013.
7. Qureshi, M. A., C. H. Schmidt, and T. F. Eibert, "Near-field error analysis for arbitrary scanning grids using fast irregular antenna field transformation algorithm," *Progress In Electromagnetics Research B*, Vol. 48, 197–220, 2013.

Full-sphere Radiation Pattern Measurement of 3D Antennas Using a Compact Planar Very-near-field Scanner

Kasra Payandehjoo and Ruska Patton
EMSCAN Corp., Calgary, AB, Canada

Abstract— Far-field test facilities for antenna pattern measurements are often very large, costly, and slow. An alternative to direct far-field measurement exists based on near-field scanning and near-field to far-field transformations. The compact size of these near-field measurement systems allows for integration of measurement probes in planar [1], circular [2], and other array configurations to reduce the required movements of the antenna-under-test (AUT) and hence the measurement time. Planar very-near-field scanning has already been successfully commercialized for small antennas with an array of 1600 H-field probes printed on a 45 cm by 45 cm printed circuit board [1]. Radiation pattern in a hemisphere is predicted in a matter of a few seconds using plane wave spectrum expansions. The accuracy of these far-field patterns however, degrades as the "apparent antenna dimension"-to-"scanner aperture" ratio increases. Hence, a single planar scan fails to accurately predict the pattern of 3D antennas that have high profiles relative to the dimensions of the scanner. Alternatively, multiple planar scans that close the measurement surface around the antenna can improve pattern accuracy [3]. As suggested in [3], a cubic measurement surface composed of 6 planar scans is considered herein. Phase coherence between the six measurements is crucial and is ensured by feeding a sample of the input signal to the scanner via a power divider. For fast far-field predictions, measured fields on each face are independently transformed to far-field in a matter of a few seconds. Subsequently, the far-field contributions of different faces are superimposed after proper coordinate translation/rotation.

This works investigates the optimum setup required for accurate radiation pattern measurement of high profile antennas. It is concluded that different box dimensions are required at different frequency bands. A 40 cm × 40 cm × 40 cm box provides good far-field results below 1GHz whereas a smaller 20 cm × 20 cm × 20 cm box is required at higher frequencies. Two test fixtures are prototyped to facilitate movements of the AUT for all 6 measurements. The rather large height-to-scan-area ratio in these setups leads to two spurious artifacts; first, the consequent large truncation error results in ripples in the radiation pattern. A raised cosine window with a quadratic phase window is optimized for elimination of these pattern ripples. Secondly, the large separation of the AUT above the scanner results in inaccurate far-field phase of a single scan beyond the solid angle formed between AUT and the corresponding face [4]. At each point in the far-field, before superimposing the contributing fields, the phase of the fields are corrected according to the phase of the field that is most accurate at that point. Figure 1(a) depicts the near-fields of a 900 Hz antenna measured on faces of a 40 cm × 40 cm × 40 cm box. Only the magnitude of H_x is shown in Figure 1(a). The predicted far-field pattern of Figure 1(b) is in good agreement with chamber measurements.

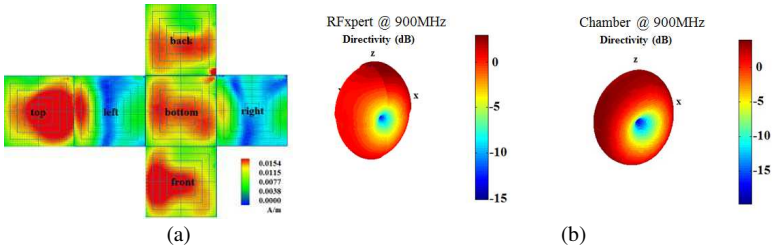

(a) (b)

Figure 1: (a) Measured $|H_x|$ on a box at 900 MHz. (b) Far-field patterns from RFxpert and chamber.

REFERENCES

1. http://www.emscan.com/downloads/RFxpert/Brochure_Datasheet/RFX2-Datasheet-v1.pdf.
2. http://www.satimo.com/sites/www.satimo.com/files/StarLab_2014_bd_0.pdf.
3. Gregson, S., C. Parini, and J. McCormick, "Full sphere far-field antenna patterns obtained using a small planar scanner and a poly-planar measurement technique," *28th Annual meeting on Antenna Measurement Techniques Association (AMTA 2006)*, 447–451, August 2006.

4. Payandehjoo, K. and R. Patton, "De-embedding the effect of a printed array of probes on planar very-near-field measurements," *2014 IEEE Conference on Antenna Measurements & Applications (CAMA)*, 1, 4, November 16–19, 2014.

Parametric Near-field-to-far-field Transformation by Precomputed Empirical-interpolation Patches

A. Sommer, **O. Floch**, **O. Farle**, **and R. Dyczij-Edlinger**
Chair for Electromagnetic Theory, Saarland University, Saarbrücken D-66123, Germany

Abstract— Using conventional finite-element (FE) methods, the broadband analysis of antenna arrays and the resulting farfields tends to be computationally demanding, because the FE systems are of large size and need to be solved at a high number of frequency points.

Methods of order-reduction provide an attractive alternative. They need some extra time to construct a reduced-order model (ROM), but the ROM itself is so cheap to solve that evaluation time is usually dominated by the costs of the nearfield-to-farfield (NF-FF) transformation. To improve runtimes even further, it was suggested in [1, 2] to replace the steps of field reconstruction on the Huygens surface and subsequent NF-FF transformation by a procedure that computes the farfields directly from the ROM. For this purpose, an affine approximation to the NF-FF operator is constructed by the empirical interpolation method (EIM) [3]. The suggested approach greatly accelerates the *online* computation of antenna patterns, at the price of increased *offline* time, for constructing the model.

In a previous paper, the authors proposed a subdomain approach on the Huygens surface that allows to restict the EIM domain to a small number of reference surfaces. Since the subface areas are much smaller than that the entire Huygens surface, the offline part of the EIM is performed much more efficiently. Still, the EIM offline step is not cheap and needs to be done for every antenna structure anew.

The present work shows that the offline part of the EIM may be computed upfront, without reference to a specific FE model. The resulting data structures are stored as templates which may be incorporated into ROMs later on, by cheap scaling and compression steps. The proposed method computes an affine approximation to the NF-FF operator for the Huygens surface similarly [4] and supports fast online computation of antenna patterns as a function of frequency and observation angles.

REFERENCES

1. Fares, M., J. S. Hesthaven, Y. Maday, and B. Stamm, "The reduced basis method for the electric field integral equation," *J. Comput. Phys.*, Vol. 230, No. 14, 5532–5555, 2011.
2. Sommer, A., O. Farle, and R. Dyczij-Edlinger, "Efficient finite-element computation of far-fields of phased arrays by order reduction," *COMPEL*, Vol. 32, No. 5, 1721–1734, 2013.
3. Barrault, M., Y. Maday, N. C. Nguyen, and A. T. Patera, "An 'empirical interpolation' method: Application to efficient reduced-basis discretization of partial differential equations," *C. R. Math. Acad. Sci. Paris*, Vol. 339, No. 9, 1721–1734, 2013.
4. Sommer, A., O. Floch, O. Farle, R. Baltes, and R. Dyczij-Edlinger, "An efficient parametric near-field-to-far-field transformation technique," *Proceedings of the 2013 International Conference on Electromagnetics in Advanced Applications*, 332–335, Torino, Italy, Sep. 2013.

Electromagnetic Scattering-matrix Theories Based on Plane Waves and Complex-source Beams

T. B. Hansen
Seknion Inc., Boxford, Massachusetts, USA

Abstract— Plane waves and complex-source beams constitute complete sets of basis functions for electromagnetic fields in homogeneous source-free regions. From the completeness of these basis functions, one can derive exact scattering-matrix theories of antennas and antenna-antenna interactions, which lead to efficient computation schemes for electromagnetic field transformations in both near and far-field regions.

This presentation discusses two such theories for time-harmonic fields in three dimensions: (i) a plane-wave theory with a directional spectrum that is obtained through a complex-source point substitution procedure, and (ii) a complex-source beam theory based on a beam expansion of spherical multipole fields. The plane-wave basis functions have sources of infinite extent whereas the complex-source beams have sources of finite extent. Hence, the two types of expansions are distinctly different in many ways.

Scattering matrices for plane-wave expansions, which determine the plane-wave spectrum of the scattered field of an object due to an incoming plane wave, are readily available. The analogous scattering matrices based on complex-source beams will be derived from Waterman's T matrices. These scattering matrices determine the beam weights for the scattered field in terms of the output of elementary beam-receivers, which sample the incident field at complex points in space.

With the scattering matrices based on the complex-source beams, the scattering computation is performed by integrating over radiating and receiving-beam directions. Expansions based on plane waves and complex-source beams each have their advantages and disadvantages as will be illustrated through numerical examples involving near-field scanning and scattering. The two scattering-matrix formulations will also be compared with Kerns plane-wave theory.

Metamaterials for Microwave Radomes: An Overview

E. Özis[1], A. V. Osipov[1], and T. F. Eibert[2]

[1]German Aerospace Center (DLR), Microwaves and Radar Institute, Oberpfaffenhofen, Germany
[2]Lehrstuhl für Hochfrequenztechnik, Technische Universität München, Munich, Germany

Abstract— Metamaterials have a great potential for designing improved and novel antenna components and systems, including substrates, feed networks, phased array antennas and antenna radomes [1]. In radome applications, metamaterials can enable such features as improved transmission over a broader range of antenna scan angles, reconfigurable pass and reject frequency bands, polarization transformations, one-way transmission and switchability.

A radome is a cover protecting an antenna from a hostile environment (wind, rain, ice, heat, aerodynamic drag, electromagnetic interference, etc.). From the electromagnetic point of view the ideal radome should be fully transparent, non-refractive and lossless, in order not to distort the fields traveling from and to the covered antenna. In practice, however, the choice of the shape and material of the radome is typically determined by the application so that the radomes are often curved structures made from ceramics and composites with high values of permittivity, which results in a degraded performance of the antenna [2, 3].

Furthermore, in modern applications it is often desirable to make the radome impenetrable outside the operating frequency band to reduce interference with other antennas that can be maintained on the same platform. This and many other features are hardly possible with conventional materials, but can be achieved with metamaterials.

Metamaterials are artificial structures that involve variously shaped, typically metallic, inclusions placed in a substrate material and organized in periodic arrays, e.g., [4, 5]. In contrast to frequency selective surfaces, the size of the unit cells is much smaller than the wavelength so that metamaterial structures appear as effectively homogeneous with effective values of such electromagnetic parameters as permittivity, permeability, losses, reflection and transmission coefficients. By choosing the shape, orientation and size of the inclusions and the size of the unit cells, the effective parameters can be tailored to the desired values. A new kind of metamaterial structures, the so-called meta-sheets, which are quasi two-dimensional structures involving just a single layer of inclusions in an electrically thin substrate, is particularly promising for radome applications since meta-sheets permit eliminating reflection while controlling transmission [6–8]. Metamaterial layers can be added to existing radomes not only to correct the distortions but also to enable new features, like non-reciprocal transmission [9] or frequency- and polarization-selective behavior.

The purpose of this paper is to give an overview of applications of metamaterials to microwave radomes. This paper reviews the available literature, reports relevant applications and illustrates them by examples.

REFERENCES

1. Anand, M., "Applications of metamaterials in antenna engineering," *International Journal of Technical Research and Applications*, Vol. 2, No. 1, 49–52, 2014.
2. Balanis, C. A., *Modern Antenna Handbook*, Wiley, 2008.
3. Kozakoff, D. J., *Analysis of Radome-Enclosed Antennas*, Artech House, 2010.
4. Engheta, N. and R. W. Ziolkowski, *Metamaterials: Physics and Engineering Explorations*, Wiley-IEEE Press, 2006.
5. Capolino, F., ed., *Metamaterials Handbook*, Taylor & Francis, 2009.
6. Niemi, T., A. Karilainen, and S. Tretyakov, "Synthesis of polarization transformers," *IEEE Trans. Antennas Propag.*, Vol. 61, No. 6, 3102–3111, 2013.
7. Pfeiffer, C. and A. Grbic, "Metamaterial Huygens surfaces: Tailoring wave fronts with reflectionless sheets," *Phys. Rev. Lett.*, Vol. 110, No. 19, 197401, 2013.
8. Selvanayagam, M. and G. V. Eleftheriades, "Discontinuous electromagnetic fields using orthogonal electric and magnetic currents for wavefront manipulation," *Opt. Exp.*, Vol. 21, No. 12, 14409–14429, 2013.
9. Radi, Y., V. S. Asadchy, and S. A. Tretyakov, "One-way transparent sheets," *Phys. Rev. B*, Vol. 89, No. 7, 075109, 2014.

Session 1A10
FocusSession.SC3: Advances in Optical Networking

Programmable Optical Signal Transmission and Processing for Flexible Optical Networks

Ming Tang[1], **Zhenhua Feng**[1], **Ruoxu Wang**[1], **Songnian Fu**[1], **and Perry Ping Shum**[2]

[1]Next Generation Internet Access National Engineering Lab (NGIA)
School of Optical and Electronic Information
Huazhong University of Science and Technology, Wuhan, China
[2]Photonics Centre of Excellence, School of Electrical and Electronic Engineering
Nanyang Technological University, 50 Nanyang Avenue, Singapore

Abstract— The technologies incorporating optical fibers and smart optical fiber based devices are essential for future flexible all-optical network to enhance the transmission capacity and processing efficiency. We will demonstrate our works in this presentation about flex-grid tunable optical filter, flexible wavelength selective filter, space-wavelength division flexible optical transmission and all-optical fiber based signal processing in spectral or temporal domains.

Flow Aggregation and Migration Scheme Based on Real-time Monitoring for Time-varying Traffic in Optical Networks

Yuan Wen, Wei Guo, and Weisheng Hu
State Key Laboratory of Advanced Optical Communication Systems and Networks
Shanghai Jiao Tong University, China

Abstract— Nowadays, the transport network is experiencing a challenge of bulky data transfer for large-scale applications, such as E-science computing, data center data back-ups and cloud services [1]. When these applications require high transmission rate (e.g., 10 GE or more), a lightpath with guaranteed bandwidth provided by optical circuit-switched networks becomes an effective solution to meet application performance requirements, such as bit rate, packet loss and latency. However, the bandwidth of a lightpath is often underutilized. A major reason is that flows generated by applications may have a time-varying bandwidth demands, typically, higher traffic volume during daytime and lower traffic volume at night. If a lightpath is dedicatedly used by a flow, this may lead to bandwidth resource waste when flow rate becomes low.

In order to make better utilization of bandwidth resources, we proposed a flow aggregation method implemented by an extended SDN controller [2]. This method is to aggregate multiple fine-granularity flows into a lightpath, whose bandwidth resources have not been fully utilized. In this way, these flows can share the same lightpath and lightpath bandwidth utilization increases. However, the transmission rates of flows vary frequently over time. If the total transmission rate of the flows exceeds the bandwidth of the lightpath, packet loss will occur and transmission quality of flows will degrade.

In this paper, we propose a flow aggregation and migration scheme (AM) based on real-time monitoring to improve bandwidth utilization while guaranteeing transmission performance of the entire network. Our method is to aggregate some fine-granularity flows (with low-priority) into a lightpath with spare bandwidth resources. To guarantee transmission performance, the low-priority flows will be migrated into another lightpath when bandwidth resources of the original lightpath are used up. Since flow migration needs time, we set a threshold to control the maximal load in the lightpath. Once the overall flow rate exceeds the threshold (but still less than the bandwidth of the lightpath), flow migration will be executed to reduce packet loss. Due to the flexible programmability of SDN controller to flow, we can easily complete the flow aggregation and ow migration. We have tested the performance of our extended controller on our testbed. Experimental results show that our extended controller can migrate a flow from one lightpath into another in 2 seconds, with no influence on data transmission delay and packet loss of the original flow (with high-priority). In addition, we can reduce the packet loss of low-priority flows by reducing the threshold. We also conduct simulations, which illustrate that our AM scheme improves the lightpath bandwidth utilization and reduces the blocking rate.

REFERENCES

1. Larry, S., "The OptIPuter and its applications," *LEOSST*, 151–152, 2009.
2. Guo, W. B., Wang, Y. Jin, et al., "Joint optimization of transmission performance and bandwidth utilization based on software defined network," *Optical Fiber Communications Conference and Exhibition (OFC)*, 1–3, 2014.

Experimental Demonstration of 100-Gb/s TWDM-PON

Lilin Yi, **Zhengxuan Li**, **Xiaodong Wang**, **and Weisheng Hu**
The State Key Lab of Advanced Optical Communication Systems and Networks
Shanghai Jiao Tong University, Shanghai 200240, China

Abstract— With the wide spreading of internet-based services such as online video, cloud computing, etc., demands on the capacity of optical access network is growing continuously. Time and wavelength division multiplexed passive optical network (TWDM-PON) based solution for next generation PON stage 2 (NG-PON2) is being discussed and will come to a conclusion in the near future. A lot of 40-Gb/s TWDM-PON system demonstrations have been reported, providing a variety of technical candidates for practical applications [1–3]. However, for further capacity upgrade, e.g., 100-Gb/s TWDM-PON, the technical proposal is still open for discussion, where cost-effective transmitter with 25-Gb/s capacity is a key component. Some research institutions are making efforts to increase the modulation bandwidth of both external modulators [4] and directly modulated distributed-feedback lasers (DFBs) [5]. On the other side, advanced modulation formats with high spectral efficiency have been proposed to realize high data rate modulation on bandwidth-limited transmitters. A 4×25 Gb/s four-level pulse amplitude (4-PAM) modulation using 10-GHz devices have been demonstrated [6]. Besides, a symmetric 100-Gb/s TWDM-PON, where double sideband (DSB) orthogonal frequency division multiplexing (OFDM) was used in both upstream and downstream directions has been presented [7]. However, high sampling rate ADC/DAC are required in these systems which increases the difficulty and cost for real-time signal processing.

In this paper, we present 25-Gb/s operation of a commercial 10-GHz directly modulated DFB laser (DML) and PIN. Non-return to zero on-off-keying (NRZ-OOK) instead of advanced modulation format is used, which significantly simplifies the digital signal processing (DSP) module. In order to increase the modulation bandwidth, we employ a delay interferometer (DI) following the DML to equalize the modulation response. Simultaneously, the DI narrows the optical spectrum of the directly modulated signal and realizes chirp and dispersion management during fiber transmission. As a result, 40-km standard single mode fiber (SSMF) transmission is demonstrated with bit error ratio (BER) lower than 1×10^{-3}, which provides a cost-effective solution for 4×25-Gb/s TWDM-PON systems.

REFERENCES

1. Ma, Y., et al., "Demonstration of a 40 Gb/s time and wavelength division multiplexed passive optical network prototype system," *Proc. OFC 2012*, Paper PDP5D.7, 2012.
2. Yeh, C. H., et al., "Using OOK modulation for symmetric 40-Gb/s long-reach time sharing passive optical networks," *IEEE Photon. Technol. Lett.*, Vol. 22, 619–621, 2010.
3. Yi, L., et al., "Symmetric 40-Gb/s TWDM-PON with 39-dB power budget," *IEEE Photon. Technol. Lett.*, Vol. 25, 644–646, 2013.
4. De Valicourt, G., et al., "A 20 Gbit/s directly modulated hybrid III-V/Si laser tunable over 12 wavelengths for short-reach access network," *Proc. ECOC 2014*, Paper Tu.3.2, 2014.
5. Hasebe, K., et al., "50-Gbit/s operation of lateral pin diode structure electro-absorption modulator integrated DFB laser," *Proc. ECOC 2014*, Paper Mo.4.4.2, 2014.
6. Zhang, H., et al., "30 km downstream transmission using 4×25 Gb/s 4-PAM modulation with commercial 10 Gbps TOSA and ROSA for 100 Gb/s-PON," *Proc. OFC 2014*, Paper M2I.3, 2014.
7. Luo, Y., et al., "Symmetric 100-Gb/s TWDM-PON with DSB OFDM modulation," *Proc. OFC 2014*, Paper W2A.61, 2014.

Advancements in Next Generation Broadband Optical Access Networks

Cedric F. Lam
Google, USA

Abstract— The Internet has become an indispensible part of our modern society. Development in broadband access networks are directly connected with economic growth and prosperity of societies. Companies are foraying into new technologies for next generation broadband systems. In this talk, we review the challenges and advancements in next generation broadband optical access network developments.

Impact of Protection to Converged Access Networks Planning in Rural Areas

Carmen Mas Machuca[1] **and Ana Muñoz Díaz**[1, 2]

[1]Technical University of Munich, Germany
[2]Technical University of Madrid, Spain

Abstract— Network operators are reluctant to offer broadband access in rural areas due to the high investments and limited revenues. Protection in those areas is even more critical and hence, not yet considered by operators. One alternative to decrease costs in rural areas is the use of new architectures such as Hybrid Passive Optical Network (HPON). These architectures offer several advantages not only from the longer reach and higher client count, but for the possibility of offering different bandwidth per end point. The recently proposed HPON architecture could be used to offer more bandwidth to the base stations (10 Gbps) and less bandwidth to residential users (300–500 Mbps). Recent work has presented a detailed framework that using real building and street data provided by OpenStreetMap allows computing the fiber layout for different access architectures and splitting ratios. The approach aims at minimizing the duct length, since costs associated to ducts and trenching have been shown to be cost drivers in access deployment. This framework has been applied in rural areas to compare the infrastructure required for a disjoint versus a joint planning. Savings depend on the building density, area size and the interBS distance. The new contribution of this paper is focused on the analysis of the cost impact of BS protection. The required availability is obtained when protection of feeder fiber and distribution fiber is guaranteed. The investment and extra fiber and duct infrastructure required for two protection schemes are compared with the unprotected scenario. The cost increase is shown to be relatively low compared with the unprotected solution.

Experimental Evaluation of Noise Impairments in Unrepeated Distributed Raman Amplified DP-16QAM SSMF Links

Xiaodan Pang[1], **Oskars Ozolins**[1], **Atalla El-Taher**[2], **Richard Schatz**[3], **Gunnar Jacobsen**[1], **Sergei Popov**[3], **and Sergey Sergeyev**[2]

[1]Network and Transmission Laboratory, Acreo AB, Kista SE-164 25, Sweden
[2]Aston University, Birmingham B4 7ET, UK
[3]Optics Division, Royal Institute of Technology (KTH)
Electrum 229, Kista SE-164 40, Sweden

Abstract— Unrepeated fiber transmissions over hundreds of kilometers span with advanced modulation formats and DSP-based coherent detection schemes are considered as a potential candidate to meet the distance and capacity requirements in certain application scenarios where render amplification sites between terminals are impractical due to geographic, commercial or security constrains [1]. Distributed Raman fiber amplifier (DFRA) ensuring a relatively constant power distribution of the optical signals along links can effectively improve the system OSNR and fiber nonlinearity tolerance, therefore is widely adopted in unrepeated transmission solutions. To date, unrepeated transmissions of 30 Gbaud DP-QPSK over 444 km [2], single and dual carrier 28 Gbaud DP-16QAM over 240 km [3, 4] have been demonstrated by using Raman amplification with large effective area fibers (LEAF). In this paper we report on a systematic experimental characterization of both the amplitude and phase impairments of the received signal induced by a bidirectional Raman pump at 1455 nm with an evaluation of the coherent transmission performances of a 28 Gbaud DP-16QAM signal in a standard single mode fiber (SSMF). The Raman induced amplitude and phase noise on the received 1550 nm signal is directly measured and the discussions around the operational rules and limitations are presented considering the inter-relation between pump power, signal OSNR and induced noise. Furthermore, performances of different carrier phase recovery algorithms, including decision-directed phase-locked-loop (DDPLL) [5], blind phase search (BPS) [6] and a two-stage QPSK partitioning [7] with variable filtering implementations in the DSP routine are investigated taking into account the specific noise profile of the received signal.

ACKNOWLEDGMENT

This work was supported by EU project GRIFFON, gr. No. 324391; project ICONE, gr. No. 608099. The equipment was funded by Knut and Alice Wallenberg foundation.

REFERENCES

1. *Applications for Distributed Raman Amplification*, Finisar White Paper, 2012.
2. Chang, D., et al., "8 × 120 Gb/s unrepeatered transmission over 444 km (76.6 dB) using distributed raman amplification and ROPA without discrete amplification," *ECOC 2011*, Tu.3.B.2, 2011.
3. Oda, S., et al., "80 × 224 Gb/s unrepeated transmission over 240 km of Large-Aeff pure silica core fibre without remote optical pre-amplifier," *ECOC 2011*, Th.13.C.7, 2011.
4. Meloni, G., et al., "Unrepeated link distance increase for 448 Gb/s channel transmission by using large core area," *OECC 2013*, TuR1-2, 2013.
5. Borkowski, R., et al., "Anatomy of a digital coherent receiver," *IEICE Trans. Commun.*, E97.B, 1528–1536, 2014.
6. Pfau, T., et al., "Hardware-efficient coherent digital receiver concept with feedforward carrier recovery for M-QAM constellations," *J. Lightw. Technol.*, Vol. 27, 989–999, 2009.
7. Zhong, K. P., et al., "Linewidth-tolerant and low-complexity two-stage carrier phase estimation based on modified QPSK partitioning for dual-polarization 16-QAM systems," *J. Lightw. Technol.*, Vol. 31, 50–57, 2013.

System Aspects of 400 Gigabit Ethernet Links Using Advanced Modulation Formats

J. L. Wei[1], **R. V. Penty**[2], **I. H. White**[2], **and H. Griesser**[3]

[1]ADVA Optical Networking SE, Märzenquelle 1-3, Meiningen, Germany
[2]Centre for Photonic Systems, Electrical Engineering Division, Engineering Department
University of Cambridge, 9 JJ Thomson Avenue, Cambridge CB3 0FA, UK
[3]ADVA Optical Networking SE, Campus Martinsried
Fraunhoferstraße 9a, Martinsried/Munich 82152, Germany

Abstract— Today's Internet data traffic has exceeded 1 Zettabyte and continues to grow exponentially. By 2016, 90% of the global Internet/IP wide area network (WAN) traffic passes through data centers. This requires big data centers to handle the massive data traffic based on high speed optical data links. Considering the high volume of such short haul data links and optical transceivers in data centers, cost- and energy-efficiency is the critical consideration for implementations. As a response, the IEEE 802.3 created the IEEE P802.3bs 400 GbE Task Force on May 2014 and agreed objectives for both single-mode fiber (SMF) and multimode fiber (MMF) links. The distances considered include 100 m over MMF, 500 m, 2 km and 10 km over SMF. For such applications, conventional non-return-to-zero (NRZ) becomes very demanding on the transceiver bandwidth. Alternatively, advanced modulation formats with high spectral efficiency are promising solutions to achieve high data rate by using relatively less advanced components. The 400 GbE Task Force is still open to the choice of modulation format and number of wavelengths per fibre, four-level pulse amplitude modulation (PAM4) with eight wavelengths at 50 Gb/s as well as PAM4 and orthogonal frequency division multiplexing (OFDM) with four wavelengths at 100 Gb/s per wavelength dominate the debate. I addition to PAM and OFDM, there have been high speed short reach optical links demonstrated by using other advanced modulation formats such as duobinary, carrierless amplitude and phase (CAP) modulation, and quadrature amplitude modulation (QAM). This paper aims to review a wide range of implementation options for 400 Gigabit Ethernet using advanced modulation formats that have arisen in recent years. Simulations are provided to compare the system optical link power budget over both directly modulated laser and externally modulated laser based SMF links.

Programmable Photonics in Data Centers: Architectures and Algorithms

Carla Raffaelli
DEI, University of Bologna, Italy

Abstract— The recent evolution of the Internet is characterized by the need to dynamically share physical resources like storage, computing capacity and networks themselves, thus enabling modern applications, like social networking, cloud computing, video streaming and others to efficiently perform their service.

Data centers are emerging as aggregates of increasingly powerful physical facilities which generate high amount of traffic and consume high power, accordingly. In spite of the continue increase of peak performance, the allowable power consumption is required to increase at a much slower rate [1].

As a consequence, data center interconnection design will result one of the most challenging networking problem in the next future which can be solved in a massive adoption of new technological solutions, possibly based on silicon integrated photonics.

On the network service side, the evolving characteristics of content providers call for enhanced dynamic network reconfiguration capability. Emerging photonic technology can provide interconnection at extremely high rates with enhanced flexibility in spectrum sharing [2]. At the same time network control and management technologies should be able to exploit this flexibility in relation to cloud-based application dynamics.

Solutions based on combinations of Network Function Virtualization (NFV) and Software Defined Networking (SDN) can achieve the extreme flexibility required to support current and future development of cloud computing paradigms. Programmable features of emerging photonic technology can be fruitfully exploited in this context thus defining new roles and chances for optical interconnection both in capacity exploitation and energy efficiency perspective [3]. In any case the joint deployment of photonics and SDN to fulfill future dynamic network requirements, needs algorithms and architectures to harmonize and optimize several functionalities [4], which are addressed in this presentation.

The application of standard protocols like Open Flow must be studied to map network management functionalities on programmable photonics. Different approaches can be adopted based on protocol extensions or on protocol compliance. Architectures and algorithms to support the management of flexible grid channels are here considered through possible virtualization of photonic network elements based on emerging SDN protocols. Solutions to optimize the usage of wavelength channels will be also discussed in terms of procedures and performance.

REFERENCES

1. Gringeri, S., et al., "Technologies and protocols for data center and cloud networking," *IEEE Comunications Magazine*, Vol. 51, No. 9, 24–31, 2013
2. Orlandi, P., et al., "Reconfigurable silicon filter with continuous bandwidth tunability," *Journal Optics Letters*, Vol. 37, No. 17, 3669–3671,2012
3. Channegowda, M., et al., "Software-defined optical networks technology and infrastructure: Enabling software-defined optical network operations," *J. Opt. Commun. Netw.*, Vol. 5, No. 10, A274–A282, 2013
4. Raffaelli, C., et al., "SDN-controlled flexible-grid optical switch," *Proceedings EUCNC 2014*, Bologna, Italy, 2014.

Session 1A11
FocusSession.SC1: Casimir Effect and Heat Transfer 1

Experimental Study of Near-field Radiative Heat Transport

B. Song[1], **K. Kim**[1], **Y. Ganjeh**[1], **S. Sadat**[1], **W. Lee**[1], **W. Jeong**[1], **D. R. Thompson**[1], **A. R. Fiorino**[1], **V. Fernández-Hurtado**[2], **J. Feist**[2], **F. J. García Vidal**[2], **J. C. Cuevas**[2], **P. Reddy**[1], **and E. Meyhofer**[1]

[1]Department of Mechanical Engineering, University of Michigan, Ann Arbor 48109, USA
[2]Departamento de Física Teórica de la Materia Condensada and Condensed Matter Physics Center (IFIMAC), Universidad Autnoma de Madrid, Madrid 28049, Spain

Abstract— Near-field radiative heat transfer (NFRHT) has attracted considerable attention recently, with orders-of-magnitude heat transfer enhancement already demonstrated between bulk materials. Using custom-built experimental platforms we conducted experimental studies in the sphere-plate configuration and tip-plate configuration to probe NFRHT in the 30 nm–10 micron range and 1 nm–10 nm ranges, respectively. In our sphere-plate study, we systematically investigated the effect of film thickness on NFRHT. By studying thermal radiation between a hot silica microsphere and thin silica films of varying thicknesses (50 nm to 3 microns) as a function of gap size (30 nm to 10 microns), we found substantial enhancements in heat transport properties due to near-field effects, even for the thinnest films when the gaps size was comparable to the film thickness [1]. Further, we find that at larger separations (∼1 micron), the thicker films show substantially larger near-field enhancement than thinner films. These results provide first direct evidence of a distance-dependent penetration depth in thin films. In our experiments leveraging the tip-plate configuration we sought to understand NFRHT in the extreme near-field regime (gaps of 1–10 nm) using atomic force microscope (AFM)-based scanning probes with integrated nanoscale thermocouples, which were coated with dielectrics (SiO_2 or SiN_x) and metals (Au, Pt). Our measurements [2] of heat transport between the scanning probes and a flat substrate coated with dielectrics/metals, performed in an ultra-high vacuum environment, suggest that heat transport is dramatically enhanced in the near-field. This measured enhancement in heat flows was found to be in good agreement with computational predictions — thus establishing the validity of using fluctuational electrodynamics in modeling near-field heat transport even at single-digit nanometer separations.

REFERENCES

1. Song, B., Y. Ganjeh, S. Sadat, D. Thompson, A. Fiorino, V. Fernández-Hurtado, J. Feist, F. J. García-Vidal, J. C. Cuevas, P. Reddy, and E. Meyhofer, to Appear in *Nature Nanotechnology*, 2015.
2. Kim, K., V. Fernández-Hurtado, B. Song, W. Lee, W. Jeong, J. Feist, F. J. García-Vidal, J. C. Cuevas, E. Meyhofer, and P. Reddy, in Preparation.

Near-field Radiative Heat Transfer: Testing Fluctuational Electrodynamics at the Nanoscale

J. C. Cuevas[1], **V. Fernández-Hurtado**[1], **J. Feist**[1], **F. J. Garcia-Vidal**[1], **B. Song**[2], **Y. Ganjeh**[2], **S. Sadat**[2], **D. Thompson**[2], **A. Fiorino**[2], **K. Kim**[2], **W. Lee**[2], **W. Jeong**[2], **E. Meyhofer**[2], **and P. Reddy**[2]

[1]Departamento de Física Teórica de la Materia Condensada and Condensed Matter Physics Center (IFIMAC), Universidad Autónoma de Madrid, Madrid 28049, Spain
[2]Department of Mechanical Engineering, University of Michigan, Ann Arbor 48109, USA

Abstract— Radiative heat transfer between objects at different temperatures is of fundamental importance in applications such as energy conversion, thermal management, lithography, data storage, and thermal microscopy [1, 2]. It was predicted long ago that when the separation between objects is smaller than the thermal wavelength, which is of the order of 10 µm at room temperature, the radiative heat transfer can be greatly enhanced due to the contribution of evanescent waves (or photon tunneling) [3]. In recent years, different experimental studies have confirmed this long-standing theoretical prediction. However, in spite of this progress, there are still many basic open questions in the context of near-field radiative heat transfer (NFRHT). Thus for instance, recent experiments exploring the radiative thermal transport in nanometric gaps have seriously questioned the validity of fluctuational electrodynamics [4], which is presently the standard theory for the description of NFRHT. In this talk, I will review our recent theoretical and experiment efforts to shed new light on this fundamental problem. In particular, I will discuss the following two basic issues. The first one concerns the NFRHT using polar dielectric thin films. In this case, I will show how fluctuational electrodynamics naturally accounts for the enhancement of NFRHT reported in very recent experiments, where it has been shown that polar dielectric films as thin as 50 nm can exhibit NFRHT enhancements comparable to those of bulk samples when the gaps are smaller than the film thickness [5]. In the second part of the talk, I will address the issue of radiative heat transfer in the extreme near-field regime when objects are separated by nanometer-size distances. In particular, I will present a very detailed comparison of novel NFRHT experiments performed with scanning thermal probes with state-of-the-art simulations based on the fluctuating-surface-current formulation of the heat transfer problem [6]. The ensemble of our results clearly show that fluctuational electrodynamics provides an adequate description of the NFRHT between both metals and dielectrics all the way down to nanometer-size gaps [7].

REFERENCES

1. Basu, S., Z. M. Zhang, and C. J. Fu, *Int. J. Energy Res.*, Vol. 33, 1203, 2009.
2. Cahill, D. G., et al., *Appl. Phys. Rev.*, Vol. 1, 011305, 2014.
3. Polder, D. and M. Van Hove, *Phys. Rev. B*, Vol. 4, 3303, 1971.
4. Worbes, L., D. Hellmann, and A. Kittel, *Phys. Rev. Lett.*, Vol. 110, 134302, 2013.
5. Song, B., Y. Ganjeh, S. Sadat, D. Thompson, A. Fiorino, V. Fernández-Hurtado, J. Feist, F. J. García-Vidal, J. C. Cuevas, P. Reddy, and E. Meyhofer, *Nature Nanotechnology*, to appear, 2015.
6. Rodriguez, A. W., M. T. H. Reid, and S. G. Johnson, *Phys. Rev. B*, Vol. 88, 054305, 2013.
7. Kim, K., V. Fernández-Hurtado, B. Song, W. Lee, W. Jeong, J. Feist, F. J. García-Vidal, J. C. Cuevas, E. Meyhofer, and P. Reddy, in preparation.

Optical Thermotronics

P. Ben-Abdallah[1] and Svend-Age Biehs[2]

[1]Laboratoire Charles Fabry, UMR 8501, Institut d'Optique, CNRS, Université Paris-Sud 11
2, Avenue Augustin Fresnel, 91127 Palaiseau Cedex, France
[2]Institut für Physik, Carl von Ossietzky Universität, D-26111 Oldenburg, Germany

Abstract— The control of electric current in solids is at the origin of the modern electronics which has revolutionized our daily lifes. The concept of diodes, transistors and memories respectively introduced by Braun [1] in 1846, Williams and Kilburn [2] in 1946 and by Bardeen and Brattain [3] in 1948 are undoubtedly the corner stones of almost all modern systems of information treatment. Such elementary devices allow for rectifying, switching, modulating and even amplifying the electric current and allow for storing bits of information. Thermal analogs of such devices which make possible the control of heat flow are not as widespread today. In 2000s Baowen Li et al. have proposed thermal counterparts of transistors [4] and memories [5] using phononic circuits made with interconnected solid segments. However, this technology suffers from some weakness (slow operating speed, presence of Kapitza resistance which strongly reduced the magnitude of heat flux) of fundamental nature which intrinsically limit its performances. In this work we discuss the feasability for a contactless technology [6–8] for the thermal management based on photonics analogs of classical diodes, transistors and volatile memories.

REFERENCES

1. Braun, F., *Annalen der Physik und Chemie*, Vol. 153, 556, 1874.
2. Kilburn, T., *From Cathode Ray Tube to Ferranti Mark I*, Resurrection (The Computer Conservation Society), Vol. 1, No. 2, 1990.
3. Bardeen, J. and W. H. Brattain, *Phys. Rev.*, Vol. 74, 230, 1948.
4. Li, B., L. Wang, and G. Casati, *Appl. Phys. Lett.*, Vol. 88, 143501, 2006.
5. Wang, L. and B. Li, *Phys. Rev. Lett.*, Vol. 101, 267203, 2008.
6. Ben-Abdallah, P. and S.-A. Biehs, *Appl. Phys. Lett.*, Vol. 103, 191907, 2013.
7. Ben-Abdallah, P. and S.-A. Biehs, *Phys. Rev. Lett.*, Vol. 112, 044301, 2014.
8. Kubytskyi, V., S.-A. Biehs, and P. Ben-Abdallah, *Phys. Rev. Lett.*, Vol. 113, 074301, 2014.

Radiative Heat Transfer in 2D Dirac Materials

D. A. R. Dalvit[1], **P. Rodriguez-López**[2], **and W.-K. Tse**[1]

[1]Theoretical Division, MS B213, Los Alamos National Laboratory, Los Alamos, NM 87545, USA
[2]Laboratoire de Physique Théorique et Modèles Statistiques
CNRS UMR 8626, Bât. 100, Université Paris-Sud, Orsay Cedex 91405, France

Abstract— We compute the radiative heat transfer between two sheets of 2D Dirac materials, including topological Chern insulators and graphene, within the local optics approximation. We derive both numerically and analytically the short-distance asymptotics of the near-field heat transfer in these systems, and show that it scales as the inverse of the distance between the two sheets. We discuss the limitations to the validity of this scaling law imposed by spatial dispersion in 2D Dirac materials.

Probing the Casimir Force with Optical Tweezers

Diney S. Ether, Jr.[1], **Luis Pires**[1], **Yareni Ayala**[1], **Felipe S. da Rosa**[1], **Stefan Umrath**[2], **Gert-Ludwig Ingold**[2], **Nathan Viana**[1], **H. Moysés Nussenzveig**[1], **and Paulo A. Maia Neto**[1]

[1]Instituto de Física UFRJ, Brazil
[2]Institut für Physik, Universität Augsburg, Germany

Abstract— Optical tweezers (OT) are single-beam laser traps for neutral particles, usually applied to dielectric microspheres immersed in a fluid. The stiffness is proportional to the trapping beam power, and hence can be tuned to very small values, allowing one to measure femtonewton forces, once the device is carefully calibrated [1, 2]. In this work, we employ OT to measure the Casimir (or retarded van der Waals) force between polystyrene beads in a fluid, for distances between 50 and 500 nanometers. The spherical beads have diameters ranging from 3 to 7 micrometers. This configuration is well beyond the validity of the commonly employed [3, 4] Proximity Force (or Derjaguin) approximation (PFA), thus revealing unprecedented features of the Casimir interaction. For the comparison with experimental data, we compute the Casimir force using the scattering approach [5] applied to the spherical geometry [6]. We also present experimental results for the total force between a mercury microdroplet and a polystyrene bead immersed in ethanol, with similar distances and diameters.

REFERENCES

1. Dutra, R. S., N. B. Viana, P. A. Maia Neto, and H. M. Nussenzveig, "Absolute calibration of optical tweezers including aberrations," *Appl. Phys. Lett.*, Vol. 100, 131115, 2012.
2. Dutra, R. S., N. B. Viana, P. A. Maia Neto, and H. M. Nussenzveig, "Absolute calibration of forces in optical tweezers," *Phys. Rev. A*, Vol. 90, 013825, 2014.
3. Krause, D. E., R. S. Decca, D. Lopez, and E. Fischbach, "Experimental investigation of the casimir force beyond the proximity-force approximation," *Phys. Rev. Lett.*, Vol. 98, 050403, 2007.
4. Munday, J. N. and F. Capasso, "Precision measurement of the Casimir-Lifshitz force in a fluid," *Phys. Rev. A*, Vol. 75, 060102(R), 2007.
5. Lambrecht, A., P. A. Maia Neto, and S. Reynaud, "The Casimir effect within scattering theory," *New J. Phys.*, Vol. 8, 243, 2006.
6. Emig, T., N. Graham, R. L. Jaffe, and M. Kardar, "Casimir forces between arbitrary compact objects," *Phys. Rev. Lett.*, Vol. 99, 170403, 2007.

Experimental Determination of the Thermal Dependence of the Casimir Interaction

Ricardo S. Decca
Department of Physics, Indiana University-Purdue University Indianapolis
Bldg LD154, 402 N. Blackford St., Indianapolis, IN 46202, USA

Abstract— In this talk we will present recent developments using a rotating engineered sample made out of Au and Ni sectors buried under a thin Au layer of thickness t. This approach follows the proposal made by G. Bimonte [1]. The rotating disc is placed in close proximity to either a Ni or Au covered sapphire sphere, which in turn is glued to a highly sensitive MEMS force transducer. The thermal noise of the apparatus is $\sim 3\,\mathrm{fN/Hz^{1/2}}$. Measurements with a sensitivity of 0.3 fN with integration times of the order of 1000 s have been performed. The collection of measurements for different configurations, different values of t and measurements with separations between the sphere and the disc between 200 to 1000 nm allows to distinguish between different potential explanations for the thermal effect of the Casimir interaction. A Drude model where thermal fluctuations in the magnetic contribution from Ni is taken into account is excluded. The plasma model, however, still appears to be consistent with the data.

Systematic effects arising from the experimental implementation, as well as a description of the sample characterization that was performed will be presented.

REFERENCES

1. Bimonte, G., *Phys. Rev. Lett.*, Vol. 112, 240401, 2014.

The Role of the Casimir-Polder Potential in the Development of Atom Chips That Incorporate Quantum Electronic Components

T. M. Fromhold[1], **B. Kaczmarek**[1], **T. E. Judd**[1], **P. Krüger**[1], **G. Sinuco-León**[1, 2], **F. Wang**[1], **and N. Welch**[1]

[1]Midlands Ultracold Atom Research Centre, School of Physics and Astronomy
University of Nottingham, Nottingham NG7 2RD, UK
[2]Department of Physics and Astronomy, University of Sussex
Falmer, Brighton, BN1 9QH, United Kingdom

Abstract— In this talk I will consider the importance of tailoring the Casimir-Polder potential in order to develop atom chips that use quantum electronic components to control nearby ultracold atom clouds. In particular, I will consider the potential advantages of using quantum electronic components to trap, manipulate, and electrically image the ultracold atom clouds. Conversely, I will also consider how the cold atom clouds can be used to provide functional imaging of the electronic systems.

I will present calculations which predict that current through quantum electronic components fabricated within a two-dimensional electron gas (2DEG) in semiconductor heterostructures [1, 2] can trap ultracold atoms $\sim 200\,\mathrm{nm}$ away, with orders of magnitude less spatial and temporal noise than for metal trapping wires. This noise reduction, combined with low Casimir-Polder attraction [2], may enable the creation of hybrid atom chip structures, which exploit small changes in the conductance of quantum electronic devices to control the trapped atoms. For example, activating a single quantized conductance channel in a quantum point contact can split a Bose-Einstein (BEC) for atom interferometry [1, 3]. In turn, the BEC offers unique imaging of quantum devices and transport in heterostructures.

REFERENCES

1. Sinuco-León, G. B. Kaczmarek, P. Krüger, and T. M. Fromhold, *Phys. Rev. A*, Vol. 83, 021401(R), 2011.
2. Judd, T. E., R. G. Scott, A. M. Martin, B. Kaczmarek, and T. M. Fromhold, *New J. Phys.*, Vol. 13, 083020, 2011.
3. Montgomery, T. W. A., W. Li, and T. M. Fromhold, *Phys. Rev. Lett.*, Vol. 111, 105302, 2013.

Molecular Matter-wave Diffraction at Ultra-thin Gratings: The Role of the Van Der Waals Interactions

Christian Brand[1], **Michele Sclafani**[1, 2], **Christian Knobloch**[1], **Yigal Lilach**[3], **Thomas Juffmann**[1, 4], **Jani Kotakoski**[1], **Clemens Mangler**[1], **Andreas Winter**[5], **Andrey Turchanin**[5, 6], **Jannik Meyer**[1], **Ori Cheshnovsky**[3, 7], **and Markus Arndt**[1]

[1]Faculty of Physics, University of Vienna, VCQ, QuNaBioS, Boltzmanngasse 5, A-1090 Vienna, Austria
[2]ICFO — Institut de Ciènces Fotòniques, 08860 Castelldefels, Barcelona, Spain
[3]The Center for Nanosciences and Nanotechnology, Tel Aviv University, Israel
[4]Physics Department, Stanford University, 382 Via Pueblo Mall, Stanford, CA 94305-4060, USA
[5]Faculty of Physics, University of Bielefeld, Universitätsstr. 25, D-33615 Bielefeld, Germany
[6]Institute of Physical Chemistry, Friedrich Schiller University Jena, Lessingstr. 10, D-07743 Jena, Germany
[7]The Raymond and Beverly Faculty of Exact Sciences, School of Chemistry
Tel Aviv University, Tel Aviv 69978, Israel

Abstract— Matter-wave interferometry has become an essential tool for precision measurements of physical constants and phenomena like for instance the fine structure constant, and gravity and its curvature [1, 2]. Modern atom interferometers achieve this feat by making use of near-resonant light gratings to realize large angle beam splitters [3]. However, these schemes often necessitate closed optical transitions, which are not available in complex molecules.

Material gratings have the advantage that they are universally applicable, as the diffraction mechanism is independent of the particles' properties. They have been demonstrated for atoms [4], molecules [5] and clusters [6]. However, they may also imprint substantial van der Waals phase shifts upon the polarizable particle during the diffraction process. For large masses this attractive interaction may even prevent the molecules from traversing the grating.

We have addressed this problem by reducing the grating's width to its ultimate natural limit: A single sheet of atoms. Single-layer and bilayer graphene, carbon nanoscrolls as well as $a1$ nm thin carbonaceous biphenyl membrane are compared with regard to their suitability for diffracting large organic molecules. The population of different diffraction allows us characterize the electrical interaction between the polarizable molecules and the nanomasks We observe a minimal van der Waals interaction for single layer graphene. This paves the way for new quantum experiments with material gratings.

REFERENCES

1. Cronin, A. D., J. Schmiedmayer, and D. E. Pritchard, "Optics and interferometry with atoms and molecules," *Reviews of Modern Physics*, Vol. 81, 1051–1129, 2009.
2. Rosi, G., et al., "Measurement of the gravity-field curvature by atom interferometry," *Physical Review Letters*, Vol. 114, 013001, 2015.
3. Chiow, S.-W., T. Kovachy, H.-C. Chien, and M. A. Kasevich, "102 hk large area atom interferometers," *Physical Review Letters*, Vol. 107, 130403, 2011.
4. Keith, D. W., M. L. Schattenburg, H. I. Smith, and D. E. Pritchard, "Diffraction of atoms by a transmission grating," *Physical Review Letters*, Vol. 61, 1580–1583, 1988.
5. Arndt, M., et al., "Wave-particle duality of C60 molecules," *Nature*, Vol. 401, 680–682, 1999.
6. Schöllkopf, W. and J. P. Toennies, "Nondestructive mass selection of small van der waals clusters," *Science*, Vol. 266, 1345–1348, doi:10.1126/science.266.5189.1345, 1994.

Weak Thermal Contact is Not Universal for Work Extraction

H. Wilming, R. Gallego, and J. Eisert
Dahlem Center for Complex Quantum Systems, Freie Universität Berlin, Berlin 14195, Germany

Abstract— The free energy difference limits the amount of work that can be extracted on average using heat baths of fixed temperature from a system out of thermal equilibrium. This bound can be saturated by protocols putting the system and a bath into weak thermal contact (WTC), i.e., bringing the system into a Gibbs state at the bath's temperature. In this sense, WTC is universal for work extraction — a notion that can be made precise in a variety of operational frameworks. In this work, we introduce the study of work-extraction protocols under restrictions encountered in realistic devices at the nano-scale. We consider limitations on the maximum energies in the system and on the local structure of many-body Hamiltonians. Remarkably, we find that WTC then loses its universality. We do so by proving a general bound for the extractable work in such restricted scenarios. This is used to prove a gap between the work the can be extracted with WTC and with more general operations. Our work highlights the relevance of operational frameworks such as those of thermal operations and Gibbs preserving maps, as they can improve the performance of thermal machines. Furthermore, it provides a unifying framework of incorporating natural restrictions in quantum thermodynamics.

Thermodynamics with Superconducting Circuits

B. Huard
Ecole Normale Supérieure, CNRS, Paris, France

Abstract— In this talk, we will discuss an elementary thermal machine able to cool down or heat up a superconducting quantum bit. We have realized such a machine using superconducting circuits in two protocols. First, by measurement based feedback, a macroscopic observer acquires information about the quantum system and reacts on it. Second, by reservoir engineering, the entropy of the qubit is transferred to a cavity mode and towards a cold reservoir. We will discuss how these protocols relate to Maxwell demons.

Session 1A12
SC3: Nanophotonics Light-trapping and Photodetection. Parts I and II

Semiconductor Nanowires: Emitting and Receiving Nanoantennas

D. R. Abujetas[1], **R. Paniagua-Domínguez**[1], **A. D. van Dam**[2], **G. Grzela**[2], **J. Gómez Rivas**[2], **and J. A. Sánchez-Gil**[1]

[1]Instituto de Estructura de la Materia, Consejo Superior de Investigaciones Científicas (IEM-CSIC)
Serrano 121, 28006 Madrid, Spain
[2]Center for Nanophotonics, FOM-Institute AMOLF, c/o Philips Research Labs
High-Tech Campus 4, 5656 AE Eindhoven, The Netherlands

Abstract— The shape and dimensions of semiconductor nanowires are responsible for the strong polarization anisotropy in their emission and absorption. The diameter of nanowires (comparable to the wavelength of visible light) leads to optical resonances, which can be described by Mie scattering theory or by coupling to guided modes in a cylindrical geometry. Based on this behavior, it is also expected a strong angular dependence of the emission and absorption by individual nanowires. The directional optical response of nanowires is a fundamental property that depends on the material, geometry and dimensions of the nanostructures and that needs to be considered in the design of nanowire LEDs and solar cells [1, 2].

In this contribution, we investigate photoluminescence and absorption from finite semiconductor NWs, theoretically and experimentally (Fourier microscopy) demonstrating their behavior as efficient optical nanoantennas [3–5]. Directional emission of polarized light is governed by the material and also by the NW geometry and dimensions, which determine the Fabry-Perot-like guided/leaky mode resonances [3]. We have indeed developed a simple model based on 1D line currents induced by leaky/guide modes that fully describes the physical mechanisms underlying nanowire photoluminescence [4]. Conversely, light absorption at finite semiconductor NWs has been also addressed, showing that, apart from the expected impact on absorption of Mie resonances at normal incidence, leaky/guided modes play a relevant role at grazing incidence [5]. Our results demonstrate that semiconductor nanowires can be described as linear nanoantennas which can efficiently emit and absorb electromagnetic radiation in defined directions, shedding light onto the nano-optics underlying NW photon sources and photodetectors.

ACKNOWLEDGMENT

The authors acknowledge the Spanish "Ministerio de Economía y Competitividad" for financial support through the Consolider-Ingenio project EMET (CSD2008-00066), and NANOPLAS + (FIS2012-31070); and also the Dutch FOM research program, financially supported by the NWO and part of an industrial partnership program between Philips and FOM.

REFERENCES

1. Cao, L., J. S. White, J.-S. Park, J. A. Schuller, B. M. Clemens, and M. L. Brongersma, *Nature Materials*, Vol. 8, 643, 2009.
2. Claudon, J., N. Gregersen, P. Lalanne, and J.-M. Gérard, *Chem. Phys. Chem.*, Vol. 14, 2393, 2013.
3. Grzela, G., R. Paniagua-Domínguez, T. Barten, Y. Fontana, J. A. Sánchez-Gil, and J. Gómez Rivas, *Nano Lett.*, Vol. 12, 5481, 2012.
4. Paniagua-Domínguez, R., G. Grzela, J. Gómez Rivas, and J. A. Sánchez-Gil, *Nanoscale*, Vol. 5, 10582, 2013.
5. Grzela, G., R. Paniagua-Domínguez, T. Barten, Y. Fontana, J. A. Sánchez-Gil, and J. Gómez Rivas, *Nano Lett.*, Vol. 14, 3227, 2014.

Plasmonic Core-shell Nanoparticles Boosting the Power Conversion Efficiency of Dye-sensitized Solar Cells

Dang Yuan Lei[1, 2]

[1]Department of Applied Physics, the Hong Kong Polytechnic University, Hong Kong, China
[2]Shenzhen Research Institute, the Hong Kong Polytechnic University, Shenzhen, China

Abstract— Plasmonics has been widely demonstrated to be an efficient means to improve the power conversion efficiency of dye-sensitized solar cells (DSSCs). The proposed enhancement mechanisms mainly include nanoparticle scattering-induced increased light absorption path, plasmonic near-field-enhanced absorption of both semiconductors and dyes, and transfer of plasmonic hot electrons from metals to semiconductors at the metal-semiconductor Schottky junction. However, a decreased efficiency has also been observed in other studies with inclusion of metal nanoparticles, and attributed to the reduced surface area of the underlying semiconductor in direct contact with the absorbing dyes, Forster-type energy transfer from the semiconductor or from the dyes to the metallic nanoparticles, and the electron trapping at the metal surface. These controversial results have made plasmon-enhanced DSSCs an open study. To clarify these disagreements, we will present a systematic study on the plasmonic effects in the power conversion efficiency of DSSCs by using metallic core-dielectric shell nanoparticles with adjustable shell thickness. This is because the respective contribution from each of the aforementioned mechanisms strongly depends on the distance between the metal nanoparticle and the semiconductor. For example, since the plasmonic near-field amplitude exponentially decays from the nanoparticle surface, it is expected that the plasmon-enhanced absorption of both semiconductors and dyes will decrease with increasing the dielectric shell thickness. On the other hand, the dielectric shell on the metal nanoparticle can also rule out the possibility of electron trapping at the metal surface, thus clarifying the negative contribution by inclusion of metal nanoparticles in DSSCs. Specifically, we will investigate the power conversion efficiency as a function of the shell thickness varying from 0 to 20 nm, aiming at providing a complete scenario of the contribution channels and their respective dominant ranges.

Theoretical Description of Novel Applications of Nano-plasmonics in Super-resolution Microscopy

Y. Sivan
Unit of Electro-optics Engineering, Ben-Gurion University, Israel

Abstract— We study various applications of metal nanoparticles and metal patterned surfaces in microscopy, including super-resolution techniques in live-cell imaging as well as in inorganic systems.

The field of nanoplasmonics has attracted a lot of interest over the last few decades due to a wide variety of applications in many fields. Here we focus on the theoretical description of various novel applications of metal nanoparticles in super-resolution microscopy, including Stimulated emission depletion (STED) microscopy and saturated excitation (SAX) microscopy. We show the importance of a detailed account of the temporal and temperature dependence of the optical and thermodynamic properties of the medium in order to interpret correctly the images; in live-cell imaging, this is also necessary in order to avoid damage to the cells.

We further discuss the relevance of these considerations to photothermal imaging, where the generated heat modifies the optical properties of the medium, hence, is detectable with a variety of interferometric techniques and the extension of these ideas to 2D imaging, namely, to imaging in a close proximity to a metal patterned surface, a configuration which is very popular among bio-chemists and cell biologists. This is done partially in order to allow for effective removal of the generated heat in the metal. We describe the challenges on the way to achieve super-resolution in these two configurations.

Finally, we establish links to the novel application of refractory (high temperature) plasmonics.

Optical and Electrical Design of Novel Photodetectors Based on Hot-electron Collection

Yaohui Zhan, Xiaofeng Li, Shaolong Wu, and Kai Wu
School of Optoelectronic Information Science and Engineering, Soochow University, China

Abstract— Conventional photodetectors are mostly propelled by p-n junctions, where the detection wavelength is constrained by the band-gap width. Here we present some novel designs on metal/insulator/metal, which shows strong detection tunability without such a material constraint. The proposed hot-electron devices exhibits superior optical and electrical advantages, i.e., optically the proposed design leads to a strong asymmetrical photoabsorption and results in a high unidirectional photocurrent, as desired by the hot-electron collection; electrically the hot-electrons are generated in the region very close to the barrier, facilitating the electrical transport.

Plasmonic Properties of Ion-shaped Nanoparticles

Giancarlo Rizza
Laboratoire des Solides Irradiés (LSI) , Ecole Polytechnique
UMR 7642 CEA/DSM/IRAMIS, CNRS, Palaiseau Cedex 91128, France

Abstract— In the last years, ion-shaping technique has been proposed as an innovative and powerful tool to sculpt the matter at the nanometer scale [1–3]. Its importance relays in its unique capability to control both the morphology and the spatial orientation of metallic nanoparticles embedded within an amorphous host matrix. For example, spherical nanoparticles embedded within a dielectric matrix can be shaped into a nanowires along the ion-beam, Fig. 1(a). However, more complex shapes can also be obtained, e.g., a solid sphere with two arms. or onion-like NPs (prolate hollow NPs and prolate silica@metal nanoshell), Fig. 1(b). Consequently, ion-shaping technique can be seen as a novel route for downscaling the engineering of embedded NPs with a precision that is barely reachable with standard techniques, Fig. 1(c).

In the first part of this talk the fabrication of a model system and the potentialities offered by the ion-shaping technique will be reviewed. In particular, a model system is composed of nearly monodisperse metallic nanoparticles (NPs) (8–100 nm) confined between two silica. We show that the ion-shaping is not limited to the transformation into prolate nanorods and/or nanowires, but that depending on the initial size of the NPs, several new classes of ion-shaped NPs can also be obtained: i) facetted-like NPs, ii) nanowires growing from a facetted core or iii) chromosome-like NPs. In parallel, the evolution of the temperature profile within the nanoparticle is simulated by implementing the thermal-spike model for three-dimensional anisotropic and composite media [4]. In this way, a clear correlation is found between the fraction of the nanoparticle that is molten (vaporized) and the deformation path followed by the nanoparticles during the irradiation. This allows the construction of a size-vs-shape diagram relating the initial nanoparticle size to its final morphology. This diagram is used to give a rational description of the ion-beam shaping process for all the nanoparticle dimensions [5].

Besides the fundamental aspects related to the ion-matter interaction, ion-shaping can also be used to give new insights into the plasmonic properties of metallic nanorods and nanowires. Here, Electron Energy Loss Spectroscopy (EELS) is used to study Localized Surface Plasmon Resonances (LPSR) in ion-shaped metallic nanoparticles with a nanometer-scale spatial resolution [6]. LSPR are generated through electron excitation is a Scanning Transmission Electron Microscope (STEM), equipped with a High Angle Annular Dark Field (HAADF) detector. As the NPs are continuously deformed under irradiation, we investigate the LPSRs dependance on

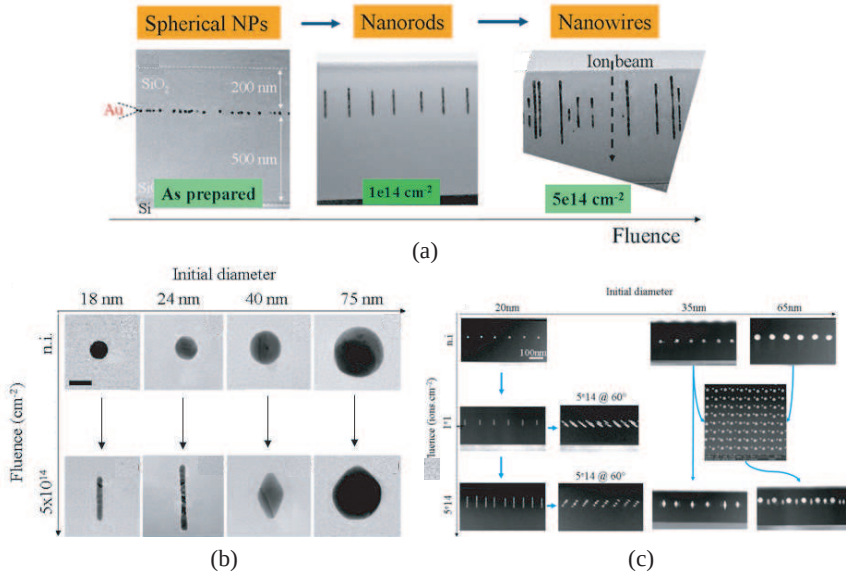

Figure 1: (a) irradiation-induced ion-shaping of Au NPs embedded within a SiO_2 matrix. (b) Relationship between initial NP size and final morphology. (c) Ion-shaped plasmonic crystals.

both the geometry and aspect ratio of the nanostructure. Finally, optical spectra are simulated using a specifically developed Auxiliary Differential Equations-Finite Difference Time Domain (ADE-FTDT) code [7], whereas EELS spectra and maps are simulated using the MNPBEM toolbox [8].

This work demonstrates the possibility to use ion irradiation as tool for the controllable fabrication of a whole family of plasmonic nanostructures with topologically tunable optical properties. These ion-beam shaped composite media have potential applications spanning from plasmonic photovoltaics, to bio-sensing, SERS and SEIRA spectroscopies.

REFERENCES

1. Dawi, E. A., G. Rizza, M. P. Mink, A. M. Vredenberg, and F. H. P. M. Habraken, *J. Appl. Phys.*, Vol. 105, 074305, 2009.
2. Rizza, G., E. A. Dawi, A. M. Vredenberg, and I. Monnet, *Appl. Phys. Lett.*, Vol. 95, 043105, 2009.
3. Ridgway, M. C., R. Giulian, D. J. Sprouster, P. Kluth, L. L. Araujo, D. J. Llewellyn, A. P. Byrne, F. Kremer, P. F. P. Fichtner, G. Rizza, H. Amekura, and M. Toulemonde, *Phys. Rev. Lett.*, Vol. 106, 095505, 2011.
4. Dufour, C., V. Khomenkov, G. Rizza, and M. Toulemonde, *J. Phys. D Appl. Phys.*, Vol. 45, 065302, 2012.
5. Rizza, G., P. E. Coulon, V. Khomenkov, C. Dufour, I. Monnet, M. Toulemonde, S. Perruchas, T. Gacoin, D. Mailly, X. Lafosse, C. Ulysse, and E. A. Dawi, *Phys. Rev. B*, Vol. 86, 035450, 2012.
6. Nelayah, J., M. Kociak, O. Stephan, F. J. Garcia de Abajo, M. Tencé, L. Henrad, D. Taverna, I. Pastoriza-Santos, L. Liz-Marzàn, and C. Colliex, *Nature Physics*, Vol. 2, 348, 2007.
7. Fafin, A., J. Cardin, and C. Dufour, *Optics Express*, Vol. 21, 24171, 2013.
8. Hohenester, U., *Comp. Phys. Comm.*, Vol. 185, 1177, 2014.

Magnetic Field Modification of Optical Magnetic Dipoles

G. Armelles, B. Caballero, A. Cebollada, A. Garcia-Martin, and D. Meneses-Rodríguez
IMM — Instituto de Microelectrónica de Madrid (CNM-CSIC)
Isaac Newton 8, PTM, Tres Cantos, Madrid E-28760, Spain

Abstract— Exploring and acting on the magnetic component of the electromagnetic field (optical magnetic field) in plasmonic nanostructures and metamaterials allows extending the control of light matter interaction, not only via the excitation of electric dipoles, but also through magnetic dipoles [1]. Many of the systems considered to study these effects make use of Babinet's principle, which deals with the complementarity of the optical response of structurally complementary systems. An archetype of complementary systems is that which relates metallic disks (electric dipole) with holes (magnetic dipole) in a metallic film [2, 3].

Here we demonstrate magnetic field modulation of the magnetic dipolar moment characteristic of resonant nanoholes in a thin metallic magnetoplasmonic film [4]. This effect is due to the magnetic field action on the electric currents induced around the hole and responsible for the existence of the magnetic dipole. This is experimentally shown by determining the contribution of holes to the Magneto Optical activity of a perforated magnetoplasmonic film, and comparing it with its Babinet inverted system: the contribution of disks to the MO activity of a layer of magnetoplasmonic disks on a substrate. Both, holes and disks, have mirror imaged MO spectral dependencies. This complementarity of the MO activity in structurally complementary systems may be considered as the equivalent to Babinet's principle in magnetooptics and proofs magnetic field effects on optical magnetic dipoles in the visible.

REFERENCES

1. Burresi, M., et al., *Science*, Vol. 326, 550, 2009.
2. Bethe, H. A., *Phys. Rev.*, Vol. 66, 163, 1944.
3. García de Abajo, F. J., J. J. Sáenz, I. Campillo, and J. S. Dolado, *Opt. Expr.*, Vol. 14, 7, 2006.
4. Armelles, G., B. Caballero, A. Cebollada, A. Garcia-Martin, and D. Meneses-Rodríguez, *Nano Lett.*, 2015.

Engineering of Single Nanowires for Broadband and Efficient Optical Absorption and Photoconversion

Zhenhai Yang[1, 2], **Aixue Shang**[1, 2], **Shaolong Wu**[1, 2], **Yaohui Zhan**[1, 2], **Dang Yuan Lei**[3, 4], **and Xiaofeng Li**[1, 2]

[1]College of Physics, Optoelectronics and Energy & Collaborative Innovation Center of Suzhou Nano Science and Technology
Soochow University, Suzhou 215006, China
[2]Key Lab of Advanced Optical Manufacturing Technologies of Jiangsu Province & Key Lab of Modern Optical Technologies of Education Ministry of China
Soochow University, Suzhou 215006, China
[3]Department of Applied Physics, The Hong Kong Polytechnic University, Hong Kong, China
[4]Shenzhen Research Institute, The Hong Kong Polytechnic University, Shenzhen 518057, China

Abstract— Single semiconductor nanowires enable a diverse range of applications in sensing, photodetection, and photovoltaics. Such devices allow versatile designs on the cross-sectional configuration for controlling and optimizing the optical and electrical response. Although antenna effect is present in these devices, contributing improved absorption, a convincingly high absorption in a broad spectral band has seldom been realized.

We performed a series of numerical studies on properly design of the cross-sectional morphology for the photovoltaic single nanowires, with considering both optical absorption as well as the detailed carrier transport in the compact cells. Circular, square and crescent-deformed single nanowires are studied by examining the absorption spectra, internal cavity resonances, external quantum efficiency, current-voltage characteristics, etc., enabling a complete performance evaluation on the the designed single nanowire solar cells. For example, our study shows that the photocurrent density of the crescent-deformed single-nanowire solar cell can be improved by over 45%; under assistance of a metallic back reflector the photocurrent enhancement ratio can be up to 66.2% without taking into account the material reduction. We have also performed an extensive electrical investigation on the electrical optimization of single-nanowire solar cells.

Nanomolecular Mechanisms for Enhancing Light Capture in Silicon

Tom Markvart[1], **Nick Alderman**[1, 2], **Lefteris Danos**[3], **Liping Fang**[1], **and Thomas Parel**[1]

[1]Solar Energy Laboratory, University of Southampton, Highfield, Southampton SO17 1BJ, UK
[2]Department of Chemistry, University of Ottawa, Ontario, Canada
[3]Department of Chemistry, University of Lancaster, Lancaster, UK

Abstract— Efficient capture of sunlight remains one of the great challenges to photovoltaics today. This is particularly so for the dominant photovoltaic material — crystalline silicon — which, as an indirect gap semiconductor, needs several hundred micrometers thickness for efficient operation. This paper will review the principal concepts that are currently being considered to enhance light capture by the solar cell. We shall, in particular, compare and contrast two main lines of thought that underpin the current status of the field. The first, based on thermodynamics, makes use of light trapping where photon path within a structure is extended by virtue of a stochastic photons distribution inside a dielectric/weakly absorbing semiconductor. The second approach rests on the use of sub-wavelength or nano-scale structures which allow the possibility of electromagnetic energy injection into very thin semiconductor layers, by direct interaction with the trapped modes or via the near field of an intermediate dipole absorber or scatterer.

The use of light trapping to enhance current generation in silicon solar cells can be traced to the COMSAT "black cell" in the 1970's, with a surface texture in the form of etched pyramids [1]. A theoretical explanation which gives the limit to light trapping in thermodynamic terms soon followed [2] but the origins of the fundamental ideas are much older, and date back to Planck's celebrated papers that marked the beginning of the quantum theory [3]. This approach has more recently been revisited and combined with the frequency management of light, more usually encountered in the so-called fluorescent concentrators/collectors [4, 5]. If combined with simple photonics this thermodynamic "squeezing" of light can produce devices which can concentrate diffuse light and operate with photon collection efficiency in excess of 90%. A similar structure (the "photonic bandgap solar cell") can be optimised for light trapping, and the resulting energy conversion efficiency can match (or even slightly exceed) the efficiency of an ideal (thick) crystalline silicon solar cell.

We shall then take a look at photon management at the "nanoscale". Particular attention will be paid to two principal mechanisms for the generation of electron-hole pairs in a very thin layer of weakly-absorbing semiconductor such as silicon, via the excitation of molecules near the surface:

(i) Photon tunnelling between an excited molecular state and the trapped modes inside the semiconductor layer, mediated by the evanescent field;
(ii) Interaction between the near field of the molecular dipole and the transition dipole moment of the electron transition between the valence and conduction band of the semiconductor. Similar to Förster's resonance dipole interaction between molecules [6], this mechanism parallels the energy collection by light harvesting in the photosynthetic unit [7–9].

REFERENCES

1. Haynos, J., J. Allison, R. Arndt, and A. Meulenberg, *Proc. Int. Conf. on Photovoltaic Power Generation*, 487, Hamburg, 1974.
2. Tiedje. T., E. Yablonovitch, G. D. Cody, and B. G. Brooks, "Limiting efficiency of silicon solar cells," *IEEE Trans. Electron Devices*, Vol. 31, 711, 1984.
3. Planck, M., *The Theory of Heat Radiation*, Dover, 1991.
4. Kittidachachan, P., L. Danos, T. J. J. Meyer, N. Alderman, and T. Markvart, "Photon collection efficiency of fluorescent solar collectors," *Chimia*, Vol. 61, 780, 2007.
5. Markvart, T., L. Danos, L. Fang, T. Parel, and N. Soleimani, "Photon frequency management for trapping and concentration of sunlight," *RSC Adv.*, Vol. 2, 3173, 2012.
6. Förster, Th., "Zwischenmoleculare Energiewanderung und Fluoreszenz," *Ann. Physik*, Vol. 2, 55, 1948.
7. Danos, L. and T. Markvart, "Excitation energy transfer rate from Langmuir Blodgett (LB) dye monolayers to silicon: Effect of aggregate formation," *Chem. Phys. Lett.*, Vol. 49, 194, 2010.
8. Danos, L., R. Greef, and T. Markvart, "Efficient fluorescence quenching near crystalline silicon from Langmuir-Blodgett dye films," *Thin Solid Films*, Vol. 516, 7251, 2008.
9. Alderman, N., et al., to be published.

Research and Design of Photonic Devices Based on Optical Tamm Plasmon

Wei-Li Zhang, Fen Wang, and Yun-Jiang Rao
Key Laboratory of Optical Fiber Sensing & Communications (Education Ministry of China)
University of Electronic Science & Technology of China, China

Abstract— As a special type of surface plasmon (SP), optical Tamm plasmon (OTP) can be excited directly by TE or TM polarized light without any additional operations, even at the status of normal incidence. Usually, OTP can be observed at the interface of metal and distributed Bragg reflector (DBR), showing stronger light-trapping ability than SP. Taking advantages of all these characteristics, many photonic devices based on OTP have been reported, such as optical switch, laser, and perfect absorber, which opens a new way for the realization of all-optical integrated photonic circuits.

Firstly, an all-optical bistable switching is proposed through sandwiching a Kerr medium in the metal-DBR structure. We realize the clockwise (anticlockwise) bistability by varying the intensity (angle) of the external optical injection. This structure is also proved to be polarization sensitive, showing lower switching threshold in TM-polarized injection than TE.

Based on the above bistable structure, we add an additional DBR in the metal side and realized low-threshold all-optical bistable logic control. Control (i.e., pump) and controlled (i.e., probe) light are chosen near two OTP, respectively. Intensity and injection angle of pump light can induce bistable effect with low threshold because of the enhanced Kerr nonlinearity. Meanwhile, the probe changes correspondingly with the pump.

Besides the above-mentioned applications, optical sensing using OTP is also supposed to be a promising way to enhance sensing performance. We use a high-refractive-index-contrast optical Tamm plasmon (OTP) structure, i.e., an air/dielectric alternate-layered DBR coated with metal. In the reflection spectrum of the structure, a dip related to the formation of OTP appears. Wavelength and reflectivity of this dip are sensitive to variation of ambient refractive index. Thus refractive index sensing can be achieved by wavelength or intensity interrogation. In addition, metal thickness, injection angle and polarization can be adjusted according to the detailed sensing requirement.

Proximity Effect Assisted Absorption Enhancement in Thin Film with Locally Clustered Nanoholes

Shaolong Wu, Xiaofeng Li, Yaohui Zhan, and Cheng Zhang
College of Physics, Optoelectronics and Energy & Collaborative Innovation Center of Suzhou Nano Science and Technology, Soochow University, Suzhou 215006, China

Abstract— Periodically structuring the photoactive material in micro/nano-scale has been extensively employed for high-efficiency light harvesting; however, the clustering effect is usually encountered in fabrication process and thus believed to be harmful. This study indicates that the controlled clustering effect can be useful for substantially improving the light-trapping characteristics of a thin film. For a 100-nm-thick amorphous silicon film, the optimal nanohole-clustering design is able to double the integrated optical absorption over solar spectrum, compared to the planar counterpart, as well as shows much improved optical performance than that of the unclustered setup. The behind physical reasons are intensively explored/discussed in terms of mode analysis, dispersion relation, power and electric profiles. As a conclusion, the improved and wide-angle light-trapping capability of NH-clustered thin film relative to the periodic counterpart is ascribed to a combination of more available modes, higher input coupling efficiency, and higher density of photon states. We believe that the information contained would attract a wide interest in nanotechnology and solar energy utilizations (e.g., photovoltaic and photocatalytic devices) since it enables efficient photo-conversion devices based on semiconductors with low optical-absorption coefficients and short minority-carrier diffusion lengths.

Optical Resonance Analysis in Dielectric-film Supporting Metallic Gratings and the Infrared Perfect Optical Absorption Design

Zhiqiang Guan and Hongxing Xu
Center for Nanoscience and Nanotechnology, School of Physics and Technology
Wuhan University, Wuhan 430072, China

Abstract— Optical responses of dielectric-film supporting metallic grating structures are analyzed by coupled-mode analysis within single-mode approximation. Two kinds of resonances are found in the optical spectra. One is reflection deep which is also well known as extraordinary optical transmission (EOT). The other resonance is transmission null which is a new resonance and is introduced by the dielectric film. The two resonance conditions are analyzed by multiple interface scattering coefficients and their direct relation with two different phase matching conditions are revealed. The waveguide modes in dielectric films, surface plasmon polaritons on interfaces, and metal slit Fabry-Parot modes are shown to contribute to these resonances, as seen from the dispersion plots and electromagnetic field distributions. By simultaneously satisfying reflection deep and transmission null, perfect optical absorption (POA) in infrared wavelength is predicted. The POA devices show a wide range tunable POA wavelength together with very high quality factors. Benefit from phase matching analysis, three simple analytical formulas are derived for POA device design. A practical device fabrication scheme is also proposed. Thus our findings will find important applications for enhanced light-matter interactions, such as nonlinear optics, optical cavities and optoelectronics.

Session 1A13
FocusSession.SC3: Solid-state Quantum Photonics 1

Polariton Condensates in Complex Potential Landscapes

C. Schneider[1], **K. Winkler**[1], **A. Schade**[1], **R. Dall**[2], **M. Amthor**[1], **E. A. Ostrovskaya**[2], **M. Kamp**[1], **and S. Höfling**[1,3]

[1]Technische Physik, University of Würzburg, 97074 Würzburg, Germany
[2]Nonlinear Physics Centre and AMPL, Research School of Physics and Engineering
The Australian National University, Canberra, ACT 0200, Australia
[3]SUPA, School of Physics and Astronomy, University of St. Andrews, St. Andrews KY16 9SS, UK

Abstract— Exciton polaritons are an ideal system to study collective behavior of macroscopic coherent quantum states in a solid state environment as they facilitate condensation into a single energy state at rather high temperatures, even under non-equilibrium conditions [1]. The properties of polaritons can be engineered by manipulating either the excitonic or photonic part of the composite particles. Nanotechnology allows defining potentials which can be arranged in almost arbitrary landscapes. This triggered the effort to engineer polaritonic integrated circuits by tailoring their flow on a chip, and furthermore makes polaritons promising candidates for solid state quantum emulation [2]. An ideal trapping technique for the implementation of polariton quantum emulation architectures should combine the following features: (i) deep and tunable confinement on a single site; (ii) controllable inter-site coupling; (iii) surface recombination effects from etching the active medium should be fully avoided.

Deep and flexible confinement of polaritons has been demonstrated in locally elongated microcavity structures [3, 4], however the technological difficulties have prevented the observation of polariton condensation phenomena under non-resonant pumping in such devices.

Here, we exploit this technology that enables deep tunable trapping in any 2D geometry without compromising any of the favorable polariton characteristics. Attractive polariton potentials are generated by local elongations of the microcavity that can be defined by standard lithography (Fig. 1(a)). The optical confinement in such buried traps indeed can exceed several meVs, facilitating strong localization of polaritons in single sites. We observe condensation of polaritons in such mesas, study the directed flow of polaritons into such traps and furthermore demonstrate the successful formation of polariton bands separated by well-defined energy gaps in a square lattice geometry (Fig. 1(b)). Under high power injection, we observe the formation of a polariton condensate in the energy gap at the M-Point of the Brillouin zone, which indicates the existence of a localized gap state.

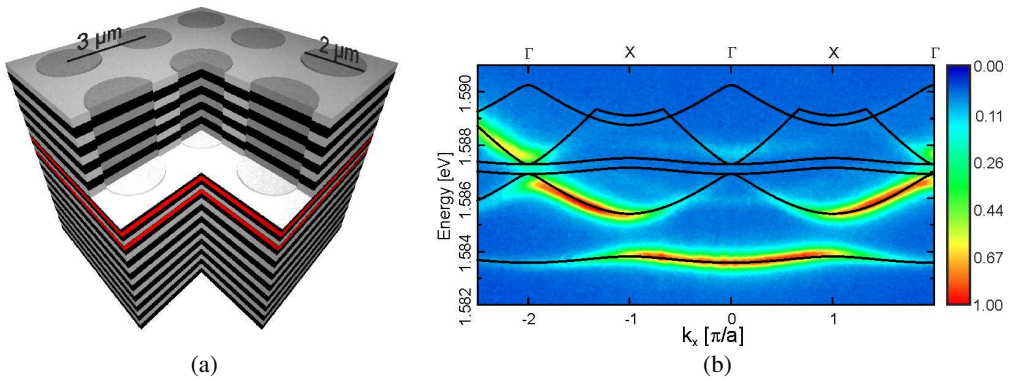

(a) (b)

Figure 1: (a) Layer sequence of our polariton lattice. Confinement is accomplished by the locally elongated cavity. (b) Polariton band structure in the square lattice (experiment and theory).

REFERENCES

1. Kasprzak, J., et al., *Nature*, Vol. 443, 409–414, 2006.
2. Kim, N. Y., et al., *Physics of Quantum Fluids*, 157–175, Springer Berlin, Heidelberg, 2013.
3. El Daif, O., et al., *Applied Physics Letters*, Vol. 88, 061105 2006.
4. Winkler, K., et al., *Applied Physics Letters*, 102.4 041101, 2013.

Light-matter Interaction of a Many-body System in Solid State: Resonance Fluorescence of the Two Dimensional Electron Gas

Nathan Shammah and Simone de Liberato
School of Physics and Astronomy, University of Southampton, Southampton SO17 1BJ, UK

Abstract— In 1969 Mollow predicted that when a two level quantum system is strongly pumped near its resonance, it reemits light not only at the resonance frequency but also at two satellite frequencies. The prediction of this nonlinear phenomenon is a major result of quantum optics theory. Part of its beauty resides in the fact that it could be tested in very different solid-state systems that fit into the two-level-system and dipole-interaction approximation.

From this premise, we extend the description of resonance fluorescence to a solid-state system in which the electron gas is confined in two dimensions. This system can be implemented in a doped semiconductor quantum well, in which the electronic excitations are intersubband transitions. This is an attractive system for the generation of terahertz radiation, which currently poses a technological challenge. As transitions occur between parallel subbands, their bare absorption line is very thin (down to a few meV). When the system is strongly pumped, each electron cycles between the two subbands, similarly to what occurs in a collection of independent two level systems. For this reason driven intersubband transitions have been described in terms of dressed states of artificial atoms in solid state.

We show that this picture, while useful to describe the collective Rabi oscillations, is broken when the system couples with the free electromagnetic field. The unbound nature of intersubband transitions allows processes between different electron states. We develop a general many-body theory that can be used to describe the resonance fluorescence of this and similar systems. Due to the many-body nature of this system, several interaction processes must be accounted for, notably also electron interference effects that lead to the enhancement of the central peak of photon emission. This mechanism is controlled by the coherence of the two-dimensional electron gas, as explored analytically and numerically. This mechanism thus hints at the intriguing possibilities of mapping the coherence of the two-dimensional electron gas onto photon emission profile. Constraints on the characteristics of a suitable realization in solid state will be discussed.

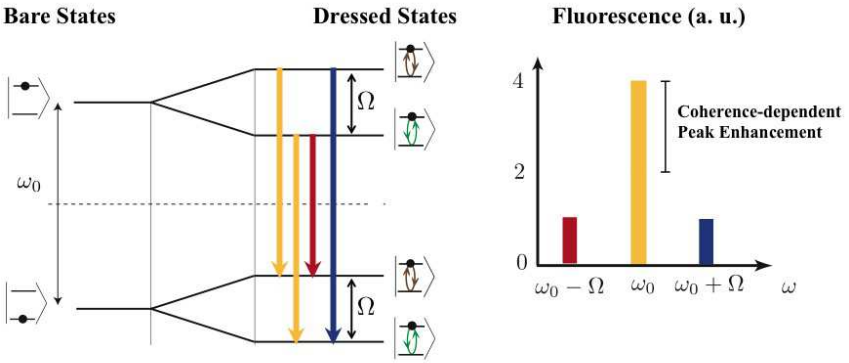

Figure 1: Energy levels and transitions leading to the Mollow triplet explained in terms of dressed states. In this system many-body effects lead to a different fluorescence profile.

REFERENCES

1. Mollow, B. R., *Phys. Rev.*, Vol. 188, 1969, 1969.
2. Xu, X., et al., *Science*, Vol. 317, 198, 2007.
3. De Liberato, S. and C. Ciuti, *Phys. Rev. Lett.*, Vol. 110, 133603, 2013.
4. Shammah, N., S. De Liberato, and C. C. Phillips, *Phys. Rev. B*, Vol. 89, 235309, 2014.
5. He, Y., et al., *Phys. Rev. Lett.*, Vol. 114, 097402, 2015.

Probing Emitter-cavity Dressed States through Environmental Transitions

Ahsan Nazir
School of Physics & Astronomy, Photon Science Institute
The University of Manchester, Alan Turing Building, Oxford Road, Manchester M13 9PL, UK

Abstract— In this talk I shall show that emitter-cavity dressed states may be probed through interactions with a thermal environment in solid-state cavity QED systems. This is true even in regimes that can be described semiclassically in the absence of such an environment, for example when the emitter-cavity coupling strength is dominated by cavity losses. For this experimentally relevant case, I shall outline how bath-induced dressed state transitions lead to asymmetries in the cavity emission properties, which are absent otherwise. This behaviour is attributed to the quantum nature of the environment and its resulting sensitivity to the joint eigenstructure of the cavity and emitter. This heralds a failure of the semiclassical approach, and challenges the notion that coupling to a thermal bath supports a more classical description of the system. Bath-induced asymmetries also persist over wider regions of parameter space, including the Fano and quantum strong coupling regimes.

Two-color Second-order Correlations and Pulsed Resonance Fluorescence Spectrum of the Light Scattered by a Quantum Dot

K. Konthasinghe, **M. Peiris**, **B. Petrak**, **and A. Muller**
University of South Florida, Tampa, FL, USA

Abstract— The theoretical prediction and experimental measurement of the spectrum of the light resonantly scattered by a two-level atom remains one of the major achievements in quantum optics. Under monochromatic excitation, the resonance fluorescence spectrum evolves from a sharply peaked line (coherently scattered light) into the characteristic Mollow triplet (incoherently scattered light) as the magnitude of the external field is increased [1]. Today, this evolution is also well-documented in other two-level quantum systems, such as quantum dots (QDs). Within the monolithic support of a semiconductor chip, a resonantly driven two-level QD may be used for emerging applications in quantum information science, for example as a source of single photons with tailored properties. However, despite much progress in recent years in this direction, the conventional approach to investigating this system still typically resorts to ordinary first or second order correlations of light scattered under monochromatic excitation.

Here we report recent measurements that go beyond basic photon correlation spectroscopy of a quantum dot under monochromatic laser excitation. First, we report the measurement of the resonance fluorescence spectrum under pulsed excitation. Although one might expect pulsed excitation to simply give rise to a broadened version of the Mollow triplet, our measurements reveal a rich spectrum with a shape strongly dependent upon the laser pulse width and laser intensity. Secondary sidebands emerge as the light-matter interaction evolves beyond saturation, i.e., when the Rabi frequency exceeds the decoherence rate. At the same time, pulsed-area dependent Rabi oscillations develop, with a different evolution for coherently and incoherently scattered light [2]. Second, we describe experiments in which the light scattered by the QD under resonant excitation is being spectrally filtered. Using tunable spectral filters in front of the detectors of a Hanbury-Brown-Twiss type arrangement provides access to a color-resolved two-photon spectroscopy of the scattered light. By scanning the filter frequencies and recording the detector coincidence rate, a two-photon spectrum (TPS) — recently introduced theoretically by del Valle et al. [3] — can be reconstructed experimentally for the first time. The TPS captures previously obscured features of the cascaded emission involved in the scattering process, such as "leapfrog" transitions proceeding via virtual intermediate states. Our measurements further reveal that the underlying correlated photon pair-emission violates classical inequalities such as the Cauchy-Schwartz criterium [4].

ACKNOWLEDGMENT

The authors acknowledge financial support from the National Science Foundation (NSF grant No. 1254324).

REFERENCES

1. Mollow, B. R., "Power spectrum of light scattered by two-level systems," *Phys. Rev.*, Vol. 188, No. 1969, 1969.
2. Konthasinghe, K., M. Peiris, and A. Muller, "Resonant light scattering of a laser frequency COMB by a quantum dot," *Phys. Rev. A*, Vol. 90, No. 023810, 2014.
3. Del Valle, E., A. Gonzalez-Tudela, F. P. Laussy, C. Tejedor, and M. J. Hartmann, "Theory of frequency-filtered and time-resolved N-photon correlations," *Phys. Rev. Lett.*, Vol. 109, No. 183601, 2012.
4. Peiris, M., B. Petrak, K. Yu. Y. Konthasinghe, Z. C. Niu, and A. Muller, "Two-color photon correlations of the light scattered by a quantum dot," arXiv:1501.00898v1, 2015.

Decoherence of Semiconductor Quantum Dots Coupled to Micro and Nanocavities

Jesper Mork, **Dara McCutcheon**, **Anders Nysteen**, **and Niels Gregersen**
DTU Fotonik, Department of Photonics Engineering
Technical University of Denmark, Kgs. Lyngby DK-2800, Denmark

Abstract— A semiconductor quantum dot embedded in a micropillar or photonic crystal cavity is a promising system for realizing solid-state sources that emit on-demand indistinguishable single-photons. Such sources are considered important for the development of quantum computers. However, phonons in the solid-state environment perturb the quantum dot energy levels, leading to decoherence and jeopardizing the indistinguishability of subsequently emitted photons. In the talk we will discuss how the characteristic parameters characterizing the coupled system, like cavity quality factor and cavity-dot coupling strength, affect the rate of decoherence and the indistinguishability. It turns out that differences between phonon emission and phonon absorption probabilities lead to a "coloured" reservoir, where non-Markovian effects are important. Thus, simple approaches, where the dephasing is described by the common Lindblad-approach, fail in predicting how the indistinguishability depends on the characteristic parameters of the coupled system. Possibilities for reducing the rate of decoherence will be discussed.

Nanophotonic Design for Bright Single-photon Sources Based on Single Quantum Dots

M. Davanço[1], **Jin Liu**[1, 2], **L. Sapienza**[1, 2, 3], **A. Badolato**[4], **and K. Srinivasan**[1]

[1]Center for Nanoscale Science and Technology
National Institute of Standards and Technology, Gaithersburg, MD 20899-6203, USA
[2]Maryland NanoCenter, University of Maryland, College Park, MD 20742, USA
[3]School of Physics and Astronomy, University of Southampton, Southampton SO17 1BJ, United Kingdom
[4]Department of Physics and Astronomy, University of Rochester, Rochester, NY 14627, USA

Abstract— Nanophotonic design can be effectively employed to engineer the radiative properties of single solid-state quantum emitters, allowing significant modification of the spontaneous emission rate, as well as spatial emission patterns. Such characteristics can be harnessed to create a variety of important devices for photonic quantum information, ranging from strongly coupled cavity quantum-electrodynamic systems to bright single-photon sources, with optimized efficiency and performance. In particular, single photon source brightness is crucial in many proposed applications, and for that single InAs quantum dots (QDs) grown epitaxially in GaAs constitute a particularly promising technology: the short QD radiative lifetimes and narrow linewidths allow for bright and pure emission, and the availability of mature device fabrication technology allows the creation of scalable nanophotonic structures with maximized efficiency.

Here, we describe design and performance of bright single-photon sources based on individual epitaxially grown InAs quantum dots embedded in GaAs-based nanophotonic geometries which can be produced via standard III-V fabrication processes. Two different types of geometries will be covered (Fig. 1), predicted and verified to provide a moderate enhancement of spontaneous emission rate and allow spectrally broad and efficient single-photon extraction and coupling respectively into free-space or guided collection optics. Our design process involves extensive use of finite-difference time domain and frequency-domain finite element-based simulations and allows optimization and assessment of Purcell enhancement factor, mode volume, and, importantly, the efficiency with which the emitted radiation can be funnelled into collection optics. The importance of dipole location within the nanophotonic structure will be illustrated. Lastly, the potential for the incorporation of nanophotonic structures with embedded single quantum dots within hybrid, III-V/silicon photonic circuits will also be discussed.

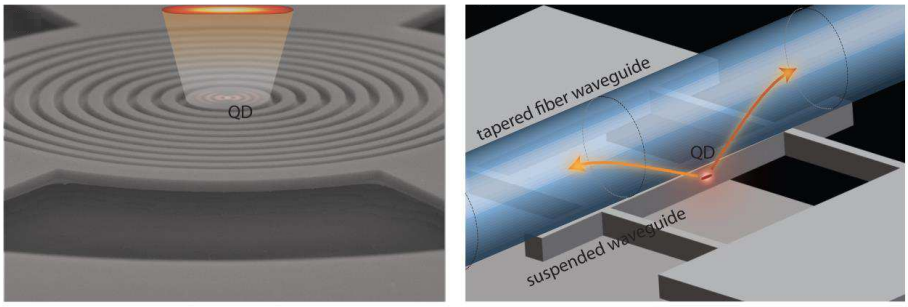

Figure 1: Nanophotonic geometries for high-brightness single-photon sources: (a) 'bullseye' cavity; (b) directional coupler formed between suspended nanowaveguide and tapered optical fiber waveguide.

High-performance Single-quantum Dot Nanophotonic Devices through Photoluminescence Imaging

K. Srinivasan[1], **M. Davanço**[1], **A. Badolato**[4], **and L. Sapienza**[1, 2, 3]

[1]Center for Nanoscale Science and Technology
National Institute of Standards and Technology, Gaithersburg, MD 20899-6203, USA
[2]Maryland NanoCenter, University of Maryland, College Park, MD 20742, USA
[3]School of Physics and Astronomy, University of Southampton
Southampton SO17 1BJ, United Kingdom
[4]Department of Physics and Astronomy, University of Rochester, Rochester, NY 14627, USA

Abstract— Epitaxially-grown InAs/GaAs quantum dots are promising semiconductor quantum emitters for a variety of photonic quantum information processing applications. Their usefulness for applications such as single-photon sources is significantly increased when they are embedded in a controlled photonic environment that enables, for example, strong radiative rate enhancement (the Purcell effect) and near-unity collection into a desirable optical channel, such as a single mode optical fiber. However, the self-assembly process by which InAs/GaAs quantum dots are commonly grown results in an essentially random spatial distribution of quantum dots within the plane of the wafer, presenting a challenge in the creation of such high performance quantum nanophotonic devices. In particular, the desired photonic environments are often creating using nanophotonic geometries in which confined optical fields significantly vary over length scales of $\approx 100\,\mathrm{nm}$. Therefore, optimally performing geometries will often require knowledge of the quantum dot location prior to device fabrication.

Here, we present one approach to quantum dot location, utilizing a novel two-color photoluminescence imaging technique. We locate single InAs/GaAs quantum dots with respect to alignment features with an average (minimum) positioning uncertainty of $< 30\,\mathrm{nm}$ ($< 10\,\mathrm{nm}$). We combine this position data with spectroscopic information provided by the same microscopy setup and use calibrated device fabrication processes to create quantum-dot single-photon sources based on optimally located quantum dots. These sources are simultaneously bright (collection efficiency as high as 48.5% $\pm$5% into a 0.4 numerical aperture lens), pure (multiphoton probability $< 1\%$ at the highest collection efficiency), and Purcell-enhanced ($\approx 3\times$ Purcell factor). We will conclude our presentation by discussing new developments on the positioning technique and its application to various device geometries.

Advances in Quantum Dot Cavity Quantum Electrodynamics Using Photonic Crystal Structures

Satoshi Iwamoto[1, 2], **Yasutomo Ota**[2], **Shun Takahashi**[2], **and Yasuhiko Arakawa**[1, 2]

[1]Institute of Industrial Science, The University of Tokyo, Japan
[2]Institute for Nano Quantum Information Electronics, The University of Tokyo
4-6-1 Komaba, Meguro-ku, Tokyo 153-8505, Japan

Abstract— Photonic crystal (PhC) structures embedding semiconductor quantum dots (QDs) form a fascinating platform for investigating solid-state cavity quantum electrodynamics (CQED) and its applications. Various CQED phenomena including vacuum Rabi splitting, Purcell enhancement of spontaneous emission rate, single photon tunneling and so on, have been observed in PhC nanocavities coupled with a single QD. However, some interesting aspects, which could deepen our understanding and be applicable to various nanophtonic devices, has not been revealed yet. QD-PhC coupled systems with higher quality and novel techniques/structures enable to tackle such unexplored physics in QD-CQED systems.

In this presentation, we will discuss our resent experimental progresses on QD-CQED systems with PhC structures. We first discuss the figure of merit of QD-CQED systems, g/κ, where g is the QDcavity coupling strength and κ is the cavity decay rate. Using a high-Q H0-type PhC nancavity, we achieved the largest g/κ ever reported in QD-CQED systems. This is an important step for diving into deeper strong coupling regime, where more quantum characteristics of the systems are available. We will also report a novel spectroscopic study measuring the direct spontaneous emission form a QD strongly coupled with a PhC nanocavity.

In addition to PhC nanocavities, engineered electromagnetic vacuum field in defectless PhCs provides another tool to tailor the light emission properties of QDs in the structures. In the presentation, we will briefly touch the possibility to enhance the circularly polarized light emission from QDs due to the increased density of states of circularly polarized photons in chiral 3D PhCs.

ACKNOWLEDGMENT

This work is supported in part by the Project for Developing Innovation Systems, MEXT, Japan and NEDO.

Engineering Collective Quantum Effects with Solid-state Nanostructures in Cavities

E. M. Gauger
Institute of Photonics and Quantum Sciences, Heriot-Watt University, UK

Abstract— Placing multiple optically active quantum systems in a common light field can give rise to profound non-classical phenomena. A signature example of such an effect is superradiance, where constructive interference leads to a pulse of light that is being emitted faster and more intense than is possible classically [1]. Combining this well-studied many-body effect with advances in cavity QED, super- (and subradiant) behaviour has recently been observed for pairs of superconducting qubits [2], atoms [3], and ions [4] interacting with a common cavity mode.

In this theoretical presentation, we will consider systems comprising several quantum nanostructures, which are not only collectively coupled to a structured electromagnetic environment, but which in addition also experience mutual pairwise interactions as well as the influence of their condensed matter host environment. Their mutual interactions may be — but do not need to be — naturally present (e.g., mediated by the vacuum light field or a common cavity mode), or they could be engineered in a different fashion.

Traditionally considered detrimental, we will show that when harnessed in the right way, these additional interactions become an asset for unlocking light absorption beyond what is possible classically. Suitably engineered systems can support one or more of several distinct effects contributing to enhanced photon absorption efficiencies: inverting superradiance, breaking detailed balance, und optical ratcheting. Potential practical applications of these effects include improved photon detectors [5] and light harvesting devices [6].

Interestingly — and unlike for observing superradiance — for these purposes, small numbers of quantum absorbers may be sufficient or even advantageous. Since the required levels of control over the geometrical arrangement of the nanostructures and their dissipative processes are within the current state-of-the-art, near future experimental verification of these effects may be possible.

REFERENCES

1. Dicke, R. H., "Coherence in spontaneous radiation processes," *Phys. Rev.*, Vol. 93, No. 99, 1954.
2. Van Loo, A. F., et al., "Photon-mediated interactions between distant artificial atoms," *Science*, Vol. 342, No. 1494, 2013.
3. Reimann, R., et al., "Cavity-modified collective rayleigh scattering of two atoms," *Phys. Rev. Lett.*, Vol. 114, No. 023601, 2015.
4. Casabone, B., et al., "Enhanced quantum interface with collective ion-cavity coupling," *Phys. Rev. Lett.*, Vol. 114, No. 023602, 2015.
5. Higgins, K. D. B., et al, "Superabsorption of light via quantum engineering," *Nature Communications*, Vol. 5, No. 4705, 2014.
6. Higgins, K. D. B., B. W. Lovett, and E. M. Gauger, manuscript in preparation, 2015.

Session 1A14
FocusSession.SC2: PT Symmetry, Reciprocity, Nonlinear Phenomena

Whispering-gallery-mode Optical Resonators around an Exceptional Point

B. Peng[1], **Ş. K. Özdemir**[1], **S. Rotter**[2], **H. Yilmaz**[1], **M. Liertzer**[2], **F. Monifi**[1], **C. M. Bender**[3], **F. Nori**[4, 5], **and L. Yang**[1]

[1]Department of Electrical and Systems Engineering, Washington University, St. Louis, MO 63130, USA
[2]Institute for Theoretical Physics, Vienna University of Technology, Vienna A-1040, Austria
[3]Department of Physics, Washington University, St. Louis, MO 63130, USA
[4]Center for Emergent Matter Science, RIKEN, Wako-shi, Saitama 351-0198, Japan
[5]Physics Department, University of Michigan, Ann Arbor, Michigan 48109-1040, USA

Abstract— I will report our experiments on unconventional control of light flow in high-quality whisperinggallery-mode (WGM) resonators around an exceptional point (EP), which is characterized by the coalescence of the eigenvalues and eigenstates of a system. The presence of an EP affects the system significantly, leading to nontrivial physics with interesting counterintuitive features. In the experiment, we show that when the resonator system is operated in the vicinity of an EP, the effect of loss could be reversed. Specifically, we demonstrate that the lasing power increases with increasing the loss introduced to the system.

Wave Propagation in the Presence of Parity-Time Symmetry: Examples from Integrated Optics and Electronics

T. Kottos
Department of Physics, Wesleyan University, CT-06457, USA

Abstract— In recent years, research have focused their efforts in manipulating absorption, and via a judicious design that involves the combination of delicately balanced amplification and absorption mechanisms, to achieve new classes of synthetic structures with altogether new physical behavior and novel functionality. This idea can potentially have a vast range of applicability to wave systems, ranging from optical structured materials, to electronics and antenna arrays. In fact, optical and electronic synthetic structures, which incorporate gain and loss mechanisms such that they are invariant under space-time reflection, have been reported over the last years, showing intriguing functionality. These systems are currently known as Parity-Time symmetric systems.

In this talk we will review our recent efforts on PT-symmetric wave propagation. Using integrated photonics and electronics as a playfields we show how one can construct new circuitry designs that allow for asymmetric wave transport due to interplay of the novel properties of PT-symmetry and non-linearity or gyrotropic elements. Finally we will demonstrate a non-reciprocal dynamics occurring in a new type of PT-symmetric lattices that emerges in the presence of periodic driving.

Constant-intensity Waves in Non-hermitian Optical Systems

K. G. Makris[1, 2], **Z. H. Musslimani**[3], **A. Brandstötter**[1], **P. Ambichl**[1], **D. N. Christodoulides**[4], **and S. Rotter**[1]

[1]Vienna University of Technology (TU Wien), Vienna A-1040, Austria
[2]Princeton University, Princeton, NJ 08544, USA
[3]Florida State University, Tallahassee, FL 32306, USA
[4]CREOL, University of Central Florida, Orlando, FL 32816, USA

Abstract— Recent years have witnessed an intense research activity in theoretical and experimental studies of non-hermitian effects in photonics. This activity was partially initiated by the recent introduction of the concept of PT-symmetry [1] in the framework of optics [2], and its subsequent experimental observation [3]. In this context of open photonic systems, we now demonstrate for the first time the existence of so-called "constant-intensity waves" (or CI-waves) [4], which can evolve with constant intensity in the presence of inhomogeneous gain-loss media — a property known so far only for plane waves in free space. We show here that quite in contrast to the conventional paradigm of hermitian optics, such CI-waves can even exist in strongly scattering cavities and resonators when these are composed of components with gain or loss that satisfy certain relationships in terms of the real and imaginary part of the underlying refractive index. We derive these relationships analytically for such CI-states in one-dimensional Fabry-Perot cavities and in the particularly counter-intuitive case of disordered resonators. The existence of such novel waves allows us also to study for the first time the modulation instability of constant wave solutions in optical complex potentials. In particular, for a general class of non-Hermitian potentials we can derive analytical constant intensity solutions valid for any sign of the Kerr nonlinearity. In the self-focusing regime, these waves are always unstable, while in the defocusing case the instability appears for specific perturbation Bloch momenta values. In both regimes, the CI-waves break up into filaments following a complex nonlinear evolution pattern.

REFERENCES

1. Bender, C. M. and S. Boettcher, "Real spectra in non-hermitian hamiltonians having PT symmetry," *Phys. Rev. Lett.*, Vol. 80, 5243, 1998.
2. Makris, K. G., R. El-Ganainy, D. N. Christodoulides, and Z. H. Musslimani, "Beam dynamics in PT symmetric optical lattices," *Phys. Rev. Lett.*, Vol. 100, 103904, 2008.
3. Rüter, C. E., K. G. Makris, R. El-Ganainy, D. N. Christodoulides, M. Segev, and D. Kip, "Observation of parity-time symmetry in optics," *Nat. Phys.*, Vol. 6, 192, 2010.
4. Makris, K. G., Z. H. Musslimani, D. N. Christodoulides, and S. Rotter, "Constant intensity waves and their modulation instabilities in non-hermitian potentials," Submitted, 2014.

Non-Hermitian Supersymmetric Photonic Structures

R. El-Ganainy
Department of Physics, Michigan Technological University, Houghton, Michigan 49931, USA

Abstract— Parity time reversal (PT) symmetry has been a subject of intense investigations for the last few years [1]. PT symmetric photonic structures represent a sub-class of non-Hermitian photonic arrangements and they exhibit a wealth of intriguing effects such as power oscillations, asymmetric transport dynamics and spontaneous symmetry breaking [2]. On the other hand, the notion of discrete supersymmetry (SUSY) has been only recently introduced to the research field of optics [3, 4].

Here we show that combining non-Hermiticity and supersymmetry can be employed to engineer the complex spectrum of photonic structures and we discuss how to utilize this concept to solve a long standing problem, namely that of building single mode laser arrays that exhibit a regular temporal behavior [5].

In particular, starting from a cavity array that contains N lasing elements, we construct its partner array by using discrete supersymmetry. By introducing an evanescent coupling between the two arrays, we show how the quality factors of the supermodes can be tuned at will through a precise control of the optical loss of the superpartner structure.

We investigate the lasing onset of these configurations under different conditions and we show that single-transverse mode operation can be achieved either by introducing nonuniform optical losses to the superpartner array or by applying selective pumping to the main structure [6].

We discuss the robustness of these arrangements against disorder and nonlinear effects and we show that the laser array can function in the single mode regime within a wide range of physical parameters. Finally, methods to extend these design concepts for two dimensional planar structures are also presented.

REFERENCES

1. Bender, C. M. and S. Boettcher, *Phys. Rev. Lett.*, Vol. 80, 5243, 1998.
2. Ruter, C. E., K. G. Makris, R. El-Ganainy, D. N. Christodoulides, M. Segev, and D. Kip, *Nature Physics*, Vol. 6, 192, 2010.
3. Miri, M. A., M. Heinrich, R. El-Ganainy, and D. N. Christodoulides, *Phys. Rev. Lett.*, Vol. 110, 233902, 2013.
4. Heinrich, M., M. A. Miri, S. Stützer, R. El-Ganainy, S. Nolte, A. Szameit, and D. N. Christodoulides, *Nature Communications*, Vol. 5, 3698, 2014.
5. Wang, S. S. and H. G. Winful, *Appl. Phys. Lett.*, Vol. 52, 1774, 1988.
6. El-Ganainy, R., L. Ge, and D. N. Christodoulides, arXiv: 1501.02972, 2015.

Local Symmetry Induced Structures in Wave Scattering Systems

P. A. Kalozoumis[1], **C. Morfonios**[2], **F. K. Diakonos**[1], **and P. Schmelcher**[2]

[1]Department of Physics, University of Athens, Athens GR-15771, Greece
[2]Zentrum für Optische Quantentechnologien, Universität Hamburg
Luruper Chaussee 149, Hamburg 22761, Germany

Abstract— Symmetries constitute one of Physics' corner stones as they possess a central role in the theoretical treatment of physical systems. The usual pathway, which is based on the global validity of a symmetry transformation is an idealized scenario, not adequate in most cases for the description of realistic physical systems. On the other hand, in a multitude of complex systems, like large molecules [1] and quasicrystals [2], these symmetries appear broken and manifest locally in restricted spatial domains. Moreover, technological advances often require such symmetries to be present by design in application-oriented, tailored structures as photonic multilayered devices [3], quantum superlattices [4] or acoustic waveguides [5]. Focusing on broken global symmetries — namely, inversion, translation and PT-symmetry — locally retained in one-dimensional scattering setups, we find a class of symmetry-induced, invariant currents which provide a systematic pathway towards discrete symmetry breaking. In a fundamental level, these currents, viewed as remnants of the corresponding broken global symmetry, allow for the generalization of the well-known Bloch and parity theorems through an appurtenant mapping relation [6].

Additionally, we develop a local symmetry-based construction scheme which utilizes the simultaneous decomposition of a setup in non-overlapping reflection symmetric parts for the design of complex wave mechanical devices with intriguing wave control properties [7, 8]. Setups with such decomposition properties constitute a new class of materials referent as *completely locally symmetric* (CLS) [6]. The fact that this scheme lies on very general symmetry arguments, combined with the Helmholtz-Schrödinger isomorphism, provide a unified framework applicable to quantum, optical and acoustic systems, notwithstanding their essential differences. Employing aperiodic photonic multilayers, we implement the aforementioned design technique and we find how local reflection symmetries are utilized for the manifestation of perfect transmission resonances at preselected frequencies [8]. Subsequently, by considering optical systems with PT-symmetry we show that the symmetry-induced invariant indicates the broken PT-symmetric phase and acts as the natural order parameter for the system, permitting the full determination of the corresponding phase diagram for any incoming scattering state [9]. Finally, recent and successful experimental results performed in acoustic waveguides [10] pave the way towards the design of specialized filtering devices with possible control of wave localization.

ACKNOWLEDGMENT

P. A. Kalozoumis acknowledges support from IKY Fellowships of Excellence for Postdoctoral Research in Greece — Siemens Program.

REFERENCES

1. Grzeskowiak, K., et al., *Biochemistry*, Vol. 32, 8923, 1993.
2. Widom, M., D. P. Deng, and C. L. Henley, *Phys. Rev. Lett.*, Vol. 63, 310, 1989.
3. Macia, E., *Rep. Prog. Phys.*, Vol. 69, 397, 2006.
4. Peng, R. W., X. Q. Huang, F. Qiu, Mu Wang, A. Hu, S. S. Jiang, and M. Mazzer, *Appl. Phys. Lett.*, Vol. 80, 3063, 2002.
5. Hladky-Hennion, A. C., J. O. Vasseur, S. Degraeve, C. Granger, and M. de Billy, *J. Appl. Phys.*, Vol. 113, 154901, 2013.
6. Kalozoumis, P. A., C. Morfonios, F. K. Diakonos, and P. Schmelcher, *Phys. Rev. Lett.*, Vol. 113, 050403, 2014.
7. Kalozoumis, P. A., C. Morfonios, F. K. Diakonos, and P. Schmelcher, *Phys. Rev. A*, Vol. 87, 032113, 2013.
8. Kalozoumis, P. A., C. Morfonios, N. Palaiodimopoulos, F. K. Diakonos, and P. Schmelcher, *Phys. Rev. A*, Vol. 88, 033857, 2013.
9. Kalozoumis, P. A., G. Pappas, F. K. Diakonos, and P. Schmelcher, *Phys. Rev. A*, Vol. 90, No. 4, 043809, 2014.
10. Kalozoumis, P. A., O. Richoux, F. K. Diakonos, G. Theocharis, and P. Schmelcher, Submitted for Publication.

Dissipation-induced Super Scattering from PT-synthetic Plasmonic Metafilms

Simin Feng
Naval Surface Warfare Center Dahlgren Division, Virginia, USA

Abstract— Parity-time (PT) synthetic materials represent a new class of metamaterials with novel electromagnetic properties arising from a delicate balance between loss and gain elements. Interaction between loss and gain media can lead to surprising electromagnetic properties which cannot be fund in nature. Except for compensating loss with gain, active plasmonic materials offer an ideal platform for studying non-Hermitian Hamiltonian in the electromagnetic domain at the subwavelength scale. Currently, most studies on the PT-symmetric structures use analytical models based on either one dimensional scalar Helmholtz equation or two dimensional scalar paraxial wave equation. For plasmonic metamaterials having subwavelength "meta-atom" as resonators, above analytical descriptions are not applicable. In this paper, by recasting Maxwell's equations in a Schrödinger-type form, we numerically investigate electromagnetic properties of a PT-synthetic plasmonic metafilm composed of a planar array of coupled PT-symmetric dimers embedded in a metallic substrate. We found that the extraordinary transmission and reflection of a finite bandwidth can occur at the same wavelength when the electromagnetic wave is incident on the PT-synthetic metafilm. Remarkably, this phenomenon disappears if the metallic substrate is lossless while keeping other parameters unchanged. When the metafilm is adjusted to the vicinity of a spectral singularity, tuning the substrate dissipation to a critical value can lead to supper scattering in stark contrast to what would be expected in conventional systems. This phenomenon implies that strong coherent radiation may be able to generate from a cavity having gain elements by tuning cavity dissipation to a critical value.

PT and RT Symmetries in Non-reciprocal Periodic Photonic Systems

Jin Wang[1], **Hui Yuan Dong**[2], **C. W. Ling**[3], **C. T. Chan**[4], **and Kin Hung Fung**[3]

[1]Department of Physics, Southeast University, Nanjing, China
[2]School of Science, Nanjing University of Posts and Telecommunications, Nanjing, China
[3]Department of Applied Physics, The Hong Kong Polytechnic University, Hong Kong, China
[4]Department of Physics, Hong Kong University of Science and Technology, Hong Kong, China

Abstract— We use simple examples to illustrate the roles of PT symmetry and RT symmetry in phenomena associated with non-reciprocal dispersion. In the first example, we present a one-way surface mode in a PT symmetric magnetized photonic system at "effective" mu close to zero. The new mode is non-propagating and purely magnetic when the system is infinite while it becomes propagating in the finite case. One-way optical tunneling is supported in oblique-incidence configuration. In the finite-slab case, the radiative mode supports non-reciprocal unidirectional beam shift at normal incidence. The PT symmetry provides exceptional point and high transmission. In the second example, we show that a magnetized diatomic chain of plasmonic nanoparticles can support a non-reciprocal dispersion, only when the RT symmetry is broken. Plasmonic optical isolation can be achieved in such a simple non-chiral and translationally periodic structure.

Electromagnetic Scattering Properties of Topological Insulators

Lixin Ge[1], **Dezhuan Han**[2], **and Jian Zi**[1]

[1]Key Laboratory of Micro and Nano Photonic Structures (MOE)
Key Laboratory of Surface Physics, Department of Physics, Fudan University, Shanghai 200433, China
[2]Department of Applied Physics, Chongqing University, Chongqing 400044, China

Abstract— Topological insulators (TIs) exhibit many exotic properties. In particular, a topological magneto-electric (TME) effect, quantized in units of the fine structure constant α, exists in TIs. As is known, the constitutive relations for bi-isotropic media are:

$$\begin{aligned}\mathbf{D} &= \varepsilon_0\varepsilon\mathbf{E} + (\chi + i\kappa)\sqrt{\varepsilon_0\mu_0}\,\mathbf{H} \\ \mathbf{B} &= \mu_0\mu\mathbf{H} + (\chi - i\kappa)\sqrt{\varepsilon_0\mu_0}\,\mathbf{E},\end{aligned}$$

where κ and χ are the chirality and magneto-electric parameters, respectively. The medium with $\chi \neq 0$ is non-reciprocal and named Tellegen medium. TIs are a kind of Tellegen medium in which χ is contributed from surface Hall currents and quantized in units of α. We theoretically study the scattering properties of electromagnetic waves by TI cylinders and spheres. Compared with ordinary dielectrics, the electromagnetic scattering of TIs shows many unusual features due to the TME effect. For TI cylinders, the topological quantization can be determined simply by measuring the electric-field components of scattered waves in the far field at two scattering angles. This could also offer a way to measure the fine structure constant. Moreover, in certain configurations, the bulk scattering can be suppressed leading to strong backward scattering in both Rayleigh and Mie scattering regimes due to the TME effect. At anti-resonance frequencies, an interesting filed trapping phenomenon is found which is absent in conventional dielectric cylinders. For TI spheres, enhanced backward scattering and field trapping effect at anti-resonances are also investigated.

REFERENCES

1. Qi, X. L., T. L. Hughes, and S. C. Zhang, "Topological field theory of time reversal invariant insulators," *Phys. Rev. B*, Vol. 78, 195424, 2008.
2. Ge, L. X., T. R. Zhan, D. Z. Han, X. H. Liu, and J. Zi, "Unusual electromagnetic scattering by cylinders of topological insulator," *Opt. Express*, Vol. 22, 30833–30842, 2014.
3. Ge, L. X., T. R. Zhan, D. Z. Han, X. H. Liu, and J. Zi, "Determination of the quantized topological magneto-electric effect in topological insulators from Rayleigh scattering," *Sci. Rep.*, Vol. 5, 7948, 2015.

Four-port THz Circulator Based on One-way Magnetoplasmonic Cavity

Kexin Liu[1, 2] **and Sailing He**[1, 2]

[1]Department of Electromagnetic Engineering, School of Electrical Engineering
Royal Institute of Technology, Stockholm S-100 44, Sweden
[2]Centre for Optical and Electromagnetic Research
State Key Laboratory of Modern Optical Instrumentation
Zhejiang University, Hangzhou, China

Abstract— In recent years, research on plasmonics in THz spectral range has progressed rapidly due to its important potential in spectroscopy, imaging and integrated circuits. Many THz plasmonic components and waveguides are based on surface plasmons or spoof surface plasmons on semiconductor or metal surface. When the metals and semiconductors are under external static magnetic field in the Voigt configuration, the surface plasmons could only propagate in one direction in a certain frequency regime, which is called one-way surface magnetoplasmons [1, 2]. This effect could be used to design nonreciprocal devices such as isolators (to prevent unwanted reverse propagation of wave) and circulators in THz frequencies.

Here we introduce a one-way magnetoplasmonic cavity to construct a Four-port THz circulator. The cavity is a semiconductor disk which supports magnetoplasmons at the boundary. The magnetoplasmons circulate around the cavity in one-direction, clockwise or anticlockwise, depending on the direction of the applied magnetic field. The cavity couples with two parallel waveguides. Because of the unidirectional property of the magnetoplasmons, the coupling efficiency is different for the guiding wave from different ports. As shown in the following figure, assuming that the magnetoplasmons circulate around the cavity anticlockwise (blue line), the guiding wave from Port 1 cannot couple with the one-way magnetoplasmonic cavity, as direction of their wave vectors are opposite, and thus the wave exports at Port 2 (red line). While, the guiding wave from Port 2 can couple with the cavity and export at Port 3 (green line). For the same reason, the wave from Port 3 exports at Port 4 and the wave from Port 4 couples out at Port 1. The above four-port circulator is analyzed by the coupled-mode theory and demonstrated by numerical simulation.

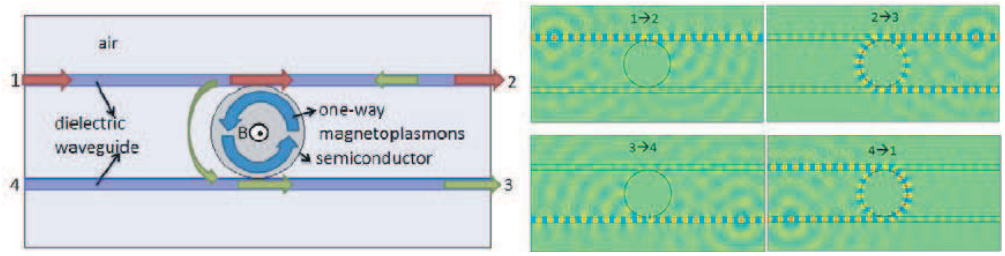

REFERENCES

1. Yu, Z., G. Veronis, Z. Wang, and S. Fan, "One-way electromagnetic waveguide formed at the interface between a plasmonic metal under a static magnetic field and a photonic crystal," *Physical Review Letters*, Vol. 100, No. 2, 023902, 2008.
2. Hu, B., Q. J. Wang, and Y. Zhang, "Broadly tunable one-way terahertz plasmonic waveguide based on nonreciprocal surface magneto plasmons," *Optics Letters*, Vol. 37, No. 11, 1895–1897, 2012.

Tunable Nonlinear Parity-time-symmetric Defect Modes with an Atomic Cell

Chao Hang[1], **Dmitry A. Zezyulin**[2], **Vladimir V. Konotop**[2], **and Guoxiang Huang**[1]

[1]State Key Laboratory of Precision Spectroscopy and Department of Physics
East China Normal University, Shanghai 200062, China
[2]Centro de Física Teórica e Computacional and Departamento de Física, Faculdade de Ciências
Universidade de Lisboa, Instituto para Investigação Interdisciplinar
Avenida Professor Gama Pinto 2, Lisboa 1649-003, Portugal

Abstract— We propose a scheme of creating a tunable highly nonlinear defect in a one-dimensional photonic crystal. The defect consists of an atomic cell filled in with two isotopes of three-level atoms. The probe-field refractive index of the defect can be made parity-time (PT) symmetric, which is achieved by proper combination of a control field and of Stark shifts induced by a far-off-resonance field. In the PT-symmetric system, families of stable nonlinear defect modes can be formed by the probe field.

REFERENCES

1. *Opt. Lett.*, Vol. 38, 4033, 2013.
2. *Opt. Lett.*, Vol. 39, 5387–5390, 2014.

Theoretical Study of Infinite-lifetime Guided Modes inside the Light Cone

Xingwei Gao[1], **Chia Wei Hsu**[2], **Marin Soljacic**[2], **and Hongsheng Chen**[1, 2]

[1]The Electromagnetics Academy at Zhejiang University, Zhejiang University, Hangzhou 310027, China
[2]Department of Physics, Massachusetts Institute of Technology, Cambridge, Massachusetts 02139, USA

Abstract— Normally, guided modes only exist below the light line, where fields are confined in the higher-index region due to total internal reflection. However, a photonic-crystal waveguide allows for guided modes above the light line [1]. These modes, instead of being leaky, can have infinite lifetimes. By using mode expansion method with structural symmetry, we theoretically studied this phenomenon in a 2D layered waveguide. The absence of radiation loss is explained by an edge cancellation among transmitted fields from multiple eigenmodes inside the photonic crystal waveguide.

REFERENCES

1. Hsu, C. W., B. Zhen, J. Lee, et al., *Nature*, Vol. 499, No. 7457, 188–191, 2013.

Session 1A0
Poster Session 1

Mode Suppression for Microdisk Laser with Cylindrical Metallic Nanoparticle

J. Y. Hsing, T. E. Tzeng, and T. S. Lay
Department of Electrical Engineering, Graduate Institute of Optoelectronic Engineering
National Chung Hsing University, Taichung, Taiwan

Abstract— We have fabricated microdisk laser with a cylindrical gold-germanium (AuGe) nanoparticle on the microdisk cavity, and measured the lasing spectra at 80 K. The microdisk cavity has a diameter near at 3.5 μm. The cylindrical metallic nanoparticle is placed close to the rim of the microdisk. The diameter and thickness of cylindrical AuGe nanoparticle are 230 nm and 50 nm, respectively. The gain material is InGaAs quantum dots (QDs) grown on (001) n^+-GaAs substrate by molecular beam epitaxy. The wafer structure consists of 1 μm AlGaAs sacrifice layer and InGaAs QDs active layer. The emission properties for the microdisk lasers were investigated at $T = 80$ K by optical pumping under pulse condition with duty cycle 1.5% and pulse width 30 ns. Fig. 1(a) illustrate the top view of SEM image for microdisk cavity without cylindrical AuGe nanoparticle, and the lasing spectrum. The lasing peaks are designated to whisper gallery modes (WGMs) obtained by simulation, as shown in Fig. 1(b). Fig. 2(a) shows the SEM image for the microdisk cavity with cylindrical AuGe nanoparticle, and the corresponding lasing spectrum which exhibits a blue-shift emission to a strong 1st-order WGM with $m = 24$ of wavelength near 1000 nm. Fig. 2(b) shows the simulated lasing spectrum of the microdisk with AuGe nanoparticle. The adding of AuGe nanoparticle to the microdisk eliminates the $M_{1,22}$, $M_{1,21}$ WGMs at longer wavelength, and enhance the $M_{1,24}$.

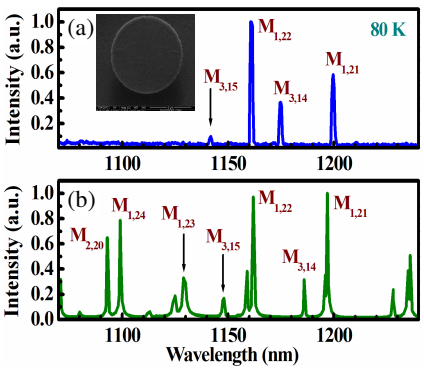

Figure 1: Microdisk laser without cylindrical AuGe nanoparticle.

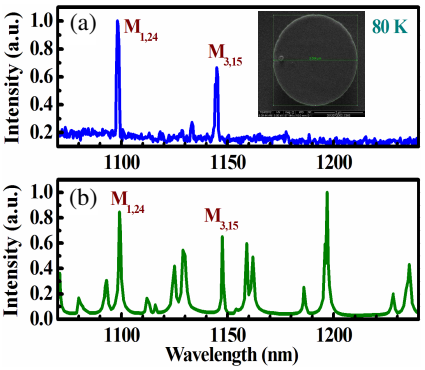

Figure 2: Microdisk laser with cylindrical AuGe nanoparticle.

LTE Baseband DSP/FPGA for Beamspace MIMO RF Antenna

Uooyeol Yoon and Dang-Oh Kim
Wireless Power Transfer Research Center
KAIST (Korea Advanced Institute of Science and Technology), Daejeon, Republic of Korea

Abstract— As the MIMO processing gets popular in LTE wireless mobile communication, the number of RF chains of eNodeB for MIMO processing gets increased, which results in the increase of cost and the volume of eNodeB base-station. In order to solve this problem, the Beam-space MIMO RF Antenna has been proposed. The advantage of Beam-space MIMO RF Antenna is to reduce the RF chain which results in the cost reduction of LTE RF module. In order to support Beam-space MIMO RF Antenna, the LTE baseband signal from LTE modem should be modified. This modification includes the matrix computation which is hard to be performed by FPGA. From this observation, authors have implemented baseband algorithm in DSP processor which enables the complex matrix computation efficiently. The requirement of DSP processing is 300 Mbps in 33 MHz band which supports 4 streams. While DSP processor is very efficient for the matrix computation, there should be interface module between baseband DSP and the impedance loading module for Beam-space MIMO RF Antenna. Authors have implemented this interface module with FPGA. The interface between DSP processor and FPGA has been implemented PCIe (PCI Express) to support high-speed serial IO. The integration system has been designed with LTE modem that supports 4×4 MIMO. The testing of full integration system consists of baseband DSP, FPGA, LTE modem and Beam-space MIMO RF Antenna module. Various spectrum analyzers have been used to validate the design of Beam-space MIMO RF baseband system during the test procedure.

Dynamical and Stochastic Approach to Non-linear Polarization Optics

Satoshi Tuchida and Hiroshi Kuratsuji
Department of Physics, Ritsumeikan University-BKC, Kusatsu City 525-8577, Shiga, Japan

Abstract— The polarization characterizes the light propagation in anisotropic materials. The polarized state is orthogonal to traveling direction and is described by two component (complex) wave function. What we are going to develop is concerning the dynamical as well as stochastic aspect for the polarized light transmitting the non-linear media. The central concept of our attempt is the non-linear birefringence (NLBR). The NLBR is realized for the two component non-linear Schrödinger equation (NLSE). Let $\psi(\mathbf{x}, z)$ be the polarized wave. The variable z is the coordinate of propagation direction, and the $\mathbf{x}$ is that of polarized plane. We put ansatz: $\psi = (\psi_1\ \psi_2) = (a(z)\ b(z))\, F(\mathbf{x})$, where $F(\mathbf{x})$ is the single component scalar wave which is given as the "soliton" solution of NLSE, and $(a(z), b(z))$ may be called *profile* function. We define the action function as : $S = \int \psi^* \left(i\lambda \frac{\partial}{\partial z} - \mathcal{H}\right) \psi d\mathbf{x} dz$, where λ is the wave length for traveling wave, and $\mathcal{H}$ is the Hamiltonian which includes effect of NLBR, and is written by 2×2 matrix. By using the action principle, we derive the coupled equation for profile function, which can be reduced to the equation of motion for the Stokes parameter. The next problem takes into account of randomness contained in the birefringence media, together with the effect of dissipation. Then we get the Langevin equation for the Stokes parameter. From this equation, we can derive the Fokker-Planck (FP) equation for the probability distribution with respect to the Stokes parameter. In order to get the FP equation, we employ the technique of functional path integral. We analyze the FP equation, for some specific cases.

Calculations of Inductance and Induced EMF in a Planar Pickup Coil

G. A. Topasna and D. M. Topasna
Department of Physics and Astronomy, Virginia Military Institute, Lexington, VA, USA

Abstract— We present derivations of the equations and numerical solutions for the inductance and induced EMF in a rectangular pickup loop in the presence of a current-carrying short straight wire. We explore three orientations of the loop with respect to the wire: in the plane of the wire with one edge of the loop parallel to the wire, in the plane of the wire with one edge of the loop at an arbitrary angle to the wire, and with the loop at an arbitrary angle in three-space with respect to the wire. Solutions in closed-form are presented for the simple cases. This work has applications related to pickup coils in general.

Time Delay Module Design, Simulation and Synthesis Based on FPGA for Dielectric Dispersion Logging

Changqi Yang, **Simin Liu**, **Liuyi Yang**, **and Cheng Yang**
School of Science, Xi'an Shiyou University, Xi'an 710065, China

Abstract— A few years ago, a kind of dielectric scanning imaging logging instrument emerged in the foreign markets. That instrument scanned the earth at different frequency electromagnetic wave. It can measure the dielectric constant at different frequencies of the layer. There is not any similar instrument developed at home. Xi'an Shiyou University has launched a project to develop a comparable instrument. This paper introduces the basic principle of dielectric dispersion logging. A general layout is given for the dielectric dispersion logging. The time delay module is simulated and synthesized based on FPGA. This laid the foundation for the development of comparable instruments gradually.

Geometry and Its Physical Meaning

S. L. Vesely[1] and A. A. Vesely[2]

[1]I.T.B. — C.N.R., Italy
[2]Via L. Anelli 13, Milano, Italy

Abstract— The physical meaning of geometry has been evolving during several centuries, bringing about salient epistemological changes. Maxwell developed his theory based on Faraday's experiments, so as to overcome the concept of action-at-a-distance while also attributing a physical meaning to space.[1] At a time when it was generally agreed that geometry can depict objective relations in the physical space, Klein conceived a mathematically rigorous *geometric model* of Maxwell's equations in a vacuum. He showed that those equations are invariant under projective transformations of the linear complex of lines,[2] where a line is represented by six Cartesian coordinates E_x, E_y, E_z, B_x, B_y, B_z. That model complies with the principle of relativity, according to the Erlangen program.[3] Unlike vector spaces, the *null system* requires neither a definition of orthogonality nor one of volume, thus, as a model, it is more general. Einstein discarded Klein's proposal because one of the invariant transformations of the projective group — the inversion — is not compatible with the convention of using measuring-rods and clocks.[4] He considered that operational convention irrefutable because Mach, in his influential critical account of the science of mechanics, stressed that mathematical idealizations should manifest the role of physical experiences in the development of a geometry for technical and scientific purposes. Mach criticized two of Newton's assertions in particular, 1) the existence of the extent,[5] and 2) the identification of physical space and Euclidean geometry.[6] To overcome those problems, he tried to imbue geometry with experimental contents by establishing statics anew, on the basis of *geometric constructions*, and then deriving mechanics from statics.

From Mach's critics, Einstein inferred geometrical properties have to be independent of a coordinate system in order to bear a physical meaning. Subsequently,[7] he conceived the extent as an effect of geometrizable forces. However, the purpose of having the whole of physics agree on a shared conception of geometry[8] met some difficulties. While Einstein requires to unambiguously identify geometric quantities with their corresponding "elements of reality", quantum mechanics must ascribe a physical meaning to the square of the wave function, which supplants the single outcome.[9] There are two main interpretations, the ontic one, which ascribes to objects the properties measured by the wave function, and the epistemic one, which focuses on the physically relevant information that that function conveys. In either case, the implied geometrical space is strikingly different from Minkowski's. At that point, the best option was Hilbert's suggestion to discriminate between the validity of logical deductions and their truth, and to treat in the same manner as geometry — by means of axioms — those physical sciences in which mathematics plays an important part. After that move, geometry turns back into just a logical development, deprived of any intuitive association with physical space. The ontic interpretation of quantum mechanics deals with the truth of the undefined elements and relations. Information theories applied to telecommunications and information-based complexity theories draw rather from the epistemic interpretation.

[1]Maxwell considered aether accessible to physical testing. At his time, geometrical space was considered homogeneous and isotropic.

[2]A complex of lines is an aggregate of lines of the projective space, defined by a single relation. Möbius' null system, which represents forces and momenta equated to zero, is an example of a linear complex of lines (because the defining relation is linear). To define one ruled quadric three relations are necessary.

[3]For both Einstein and Klein, the *transformations of space* are associated to physical laws. The principle of relativity is the first postulate of special relativity, whereby physical laws must be the same in every inertial frame of reference. The second postulate states the invariance of speed of light. In order to satisfy the second postulate, Klein introduced a metrical hypercone in addition to the null system.

[4]Framing physics in space and time is traced back to Aristotle.

[5]Newton calls Aristotle's absolute space *Sensorium Dei*, meaning that the extent is an attribute of God.

[6]Euclid set geometry apart from the cosmology of his time.

[7]In general relativity, the operational definition of rods-and-clock measure is replaced with the hypothesis that dynamics determines the intrinsic space-time curvature. Thus, space-time, rather than being "empty", is endowed with a geometric structure. The original formulation of that hypothesis is due to Helmholtz, according to whom potential results from kinetic energy of cyclic motions.

[8]The shared conception is Hamiltonian geometry. It can account also for non-homogeneous/anisotropic coordinates, needed for quantum magnitudes such as spin.

[9]The single-outcome expectation would interpret a prediction like "A half of these students will pass the exam" as a half of each student, unless 1/2 is interpreted as the likelihood that a student passes.

After recalling the above, the full paper endeavors to illustrate the scope of projective geometry as a hypothetical-deductive system. Our goal is to also use it to model the extent and compare on a common basis graphic constructions, optical perception, and image reconstruction techniques in other frequency ranges. For modeling the extent, the use of construction tools is inherent in synthetic geometry. Straightedge-and-compass figures of Euclidean geometry are conceptually different from straightedge-only constructions of projective geometry, and cannot be reduced to one another in general. We'll restrict ourselves to showing the impact that a switch from analytic to synthetic geometry may imply on the means used to relate geometrically based pictorial display and mathematical analysis. In particular, the points that are to be tackled in order to have Klein's geometric model of Maxwell equations also cover sampling, transforming and interpreting received signals that can be presented as images.

Efficient Analysis of EM Scattering from Rotating Structures Using a Fast Iterative Physical Optics Method

E. Pascual, G. Gutierrez, and F. J. Jimenez
EMC & MW Department, AIRBUS DS, Spain

Abstract— Analysis of the electromagnetic fields scattering from rotating structures such as aerogenerators, aircraft propellers, turbojets and turbofans, helicopter rotors, etc. has an increased interest due to the influence in civil and military radars efficiency and in radiation characteristics of on-board antennas. Doppler effects and spatial modulations can degrade the performances of radars and antennas. To predict accurately the scattering is necessary to compute the interaction of EM fields with the rotating and fixed parts and the interaction of scattered fields from one part with the others for each relative position between them taking into account also the different electromagnetic material properties. In the case of complex rotating structures such as turbofans or turbojets with hundreds of blades rotating at different speeds and directions, it is necessary to analyze efficiently thousands of relative positions in order to obtain useful results. An Iterative Physical Optics method (IPO) [1, 2] accelerated by a fast Far Field Approximation (FFA) [3] has been developed in such a way that the computation time is reduced by means of a multilevel FFA, a preprocessing of the parameters that are invariant with the rotations, a fast calculation of the rotation transformations of the parameters affected by the movement and a parallelization schema based on FORTRAN co-arrays. Cross comparison with Multilevel Fast Multipole Method results of several test cases shows an excellent agreement at a much lower computational cost. Complex cases such as time-variant radar cross section of an aircraft with four rotating propellers have also been computed in affordable time.

REFERENCES

1. Obelleiro, F., J. L. Rodriguez, and R. J. Burkholder, "An iterative physical optics approach for analyzing the electromagnetic scattering by large open-ended cavities," *IEEE Trans. Antennas and Propagation*, Vol. 43, No. 4, 356–361, 1995.
2. Burkholder, R. J., Ç. Tokgoz, C. J. Reddy, and P. H. Pathak, "Iterative physical optics: Its not just for cavities anymore," *Proc. IEEE Antennas and Propag. Soc. Int. Symp.*, Vol. 1A, 18–21, 2005.
3. Lu, C. C. and W. C. Chew, "Fast far-field approximation for calculating the RCS of large objects," *Microwave Opt. Tech. Lett.*, Vol. 8, No. 5, 238–241, 1995.

On the Impact of Dissipation on Dispersion Interactions between Two Atoms

P. Barcellona and S. Y. Buhmann
University of Freiburg, Germany

Abstract— We consider the interaction between two neutral, ground-state atoms in the presence of an arbitrary arrangement of dispersing and absorbing magnetodielectric bodies by means of a dynamical approach. Our result differs from the previous ones obtained with time-independent perturbation theory because it accounts for the influence of dissipation via the atomic decay rates. Modern measurements of Casimir force seems to indicate an agreement with plasma model instead of Drude model [1]. This has lead to heated debates, because the latter is more a more realistic description of matter. Our new result can explain the agreement with the plasma model for the zero-temperature case. Further investigations will be needed in order to include finite temperature and many-body interactions.

We also consider the interaction between a ground-state atom and an excited atom. There are discordant results in the literature for the retarded potential: one oscillating [2–4] and one monotonous [5–7]. Our dynamical result uniquely leads to the oscillating result when taking into account the decay rates. The result seems go into the same line with recent measurements of the Casimir force between an excited barium ion and a mirror [8, 9].

REFERENCES

1. Decca, R. S., D. Lpez, E. Fischbach, G. L. Klimchitskaya, D. E. Krause, and V. M. Mostepanenko, *Phys. Rev. D*, Vol. 75, 07710, 2007.
2. Gomberoff, L., R. R. McLone, and E. A. Power, *J. Chem. Phys.*, Vol. 44, 4148, 1966.
3. McLone, R. R. and E. A. Power, *Proc. R. Soc. Lond. Ser. A*, Vol. 286, 573, 1965.
4. Philpott, M. R., *Proc. Phys. Soc. Lond.*, Vol. 87, 619, 1966.
5. Power, E. A. and T. Thirunamachandran, *Phys. Rev. A*, Vol. 51, 3660, 1995.
6. Power, E. A. and T. Thirunamachandran, *Chem. Phys.*, Vol. 171, 1, 1993.
7. Power, E. A. and T. Thirunamachandran, *Phys. Rev. A*, Vol. 47, 2539, 1993.
8. Wilson, M. A., P. Bushev, J. Eschner, F. Schmidt-Kaler, C. Becher, R. Blatt, and U. Dorner, *Phys. Rev. Lett.*, Vol. 91, 213602, 2003.
9. Bushev, P., A. Wilson, J. Eschner, C. Raab, F. Schmidt-Kaler, C. Becher, and R. Blatt, *Phys. Rev. Lett.*, Vol. 92, 223602, 2004.

Modeling the Scattering by Small Holes

R. Solimene, **P. Piccolo**, **and R. Pierri**
Dipartimento di Ingegneria Industriale e dell'Informazione, Seconda Università degli studi di Napoli, Italy

Abstract— The scattering by a hole within a perfect electric conducing (PEC) plane is a classical electromagnetic problem.

As is well known, the scattering by an aperture can be formulated as the solution of an integral equation where the unknown aperture electric field (or equivalently the magnetic source) once the incident field is known.

When the aperture becomes a hole, which is small in terms of the wavelength the Bethe diffraction theory [1] or the low frequency approximation (Stevenson's series first term) [2] can be invoked to approximate the mentioned integral equation. This allows getting analytical results for simple hole's shape, for example, in the case of circular hole. For such a case the analytical results are compared with numerical simulation obtained by a commercial FDTD forward solver. It is shown that the low-frequency approximation fits numerical simulations better than the Bethe theory does in near zone. However, Bethe theory works fairly well in predicting the radiated field (far-zone) and allows to more easily considering the role of the incident field polarization and the hole's shape. To this end, the case of an elliptical shaped hole with incident field having different polarizations is considered and compared with simulations.

Finally, also the case of a hole made over the faces of a rectangular waveguide in different point is analyzed.

REFERENCES

1. Bethe, H. A., "Theory of diffraction by small holes," *Physical Review*, Vol. 66, 163–182, 1944.
2. Butler, C. M., Y. Rahamat-Sami, and R. Mittra, "Electromagnetic penetration through apertures in conducting surfaces," *IEEE Transactions on Antennas and Propagation*, Vol. 26, 82–93, 1978.
3. Stevenson, A. F., "Solution of electromagnetic scattering problems as power series in the ratio (dimension of scatter)/wavelength," *J. Appl. Phys.*, Vol. 24, No. 9, 1134–1142, 1953.

Compact Circularly Polarized RFID Tag Antenna with an Embedded L-shaped Feedline for Metallic Objects

Cheng Liu, **Zhibin He**, **Hui Liu**, **Yoichi Okuno**, **and Sailing He**
Centre for Optical and Electromagnetic Research, Academy of Advanced Optoelectronics
South China Normal University, Guangzhou, China

Abstract— An ultra-high frequency (UHF) passive radio frequency identification (RFID) tag antenna with circular polarization for metallic objects is proposed. Using a novel and embedded L shape microstrip line to feed, a good performance of impedance matching is achieved. The proposed antenna can cover the whole operating frequency of UHF RFID system from 860 MHz to 960 MHz. The 3-dB circular polarization bandwidth is 7 MHz (from 916 to 923 MHz). The optimized antenna has a high gain of −5.5 dBi in 0 degree direction. The main parameters of the antenna are also discussed.

Microwave Dielectric Properties of $BiNbO_4$ Ceramics

C. S. Ferreira, **M. P. F. Graça**, **T. Santos**, **and L. C. Costa**
I3N and Physics Department, University of Aveiro, Aveiro 3810-193, Portugal

Abstract— $BiNbO_4$ is a dielectric material that presents high dielectric constant,at microwave frequencies. In this work, $BiNbO_4$ ceramics were prepared by the solid state reaction, and the as-prepared samples were treated at temperatures between 600 and 1200°C. The samples structure was analyzed by X-Ray Diffraction and the morphology was studied using Scanning Electron Microscopy.

For the microwave dielectric measurements, a resonant cavity operating at 2.7 GHz, in the TE_{105} mode, was used. The electromagnetic fields, inside the cavity, without and with the cylindrical sample were simulated using the COMSOL Multiphysics software.

The low-perturbation resonance cavity method has been used in order to calculate the dielectric properties of the ceramic material. In this technique, we measured the shift in the cavity resonant frequency, Δf, caused by the insertion of the sample inside the cavity, which can be related to the real part of the complex permittivity, ε', and the change in the inverse of the quality factor of the cavity, $\Delta(1/Q)$, which is related with the imaginary part, ε''. The relations are simple when we consider only the first-order perturbation in the electric field caused by the sample.

The samples heat treated at temperatures above 800°C present the $BiNbO_4$ crystal phase, being also the predominant phase on the samples treated above 950°C. The samples treated below 900°C present the $Bi_5Nb_3O_{15}$ phase, which seems to be responsible for the highest dielectric constant values observed at room temperature. The dielectric losses of all samples are always lower than 10^{-4}.

Measurement and Uncertainty Analysis of Free-space Antenna Factors of a Log-periodic Antenna with Bow-tie Element Using Time-domain and Pulse Compression Technique

Satoru Kurokawa, **Masanobu Hirose**, **and Michitaka Ameya**
National Metrology Institute of Japan
National Institute of Advanced Industrial Science and Technology of Japan, Japan

Abstract— We propose a method for evaluating the free-space antenna factor of a log-periodic dipole antenna with bow-tie element (Bi-log antenna) using a time-domain and pulse compression technique. The proposed method enables the direct wave to be isolated from reflected waves on the ground plane of an open-area test site (OATS) and evaluation of the free-space antenna factor.

In a measurement, two antennas are held on masts at a height of 8 m above the ground and are separated by 10 m. The direct wave is separated using a Wiener filter obtained from frequency-domain data at 3 m antenna separation. The proposed method can completely separate the direct wave from other waves from the ground plane of an OATS. The expanded uncertainty ($k = 2$) of Bi-log antenna was estimated to be 0.4 dB over the frequency range from 30 MHz to 1000 MHz.

Chaos Generation Utilizing Optically Square-wave-injected Semiconductor Lasers

Chen-Wei Fu, **Shao-Wei Peng**, **and Yu-Shan Juan**
Department of Photonics Engineering, Yuan Ze University
No. 135, Yuandong Rd., Zhongli Dist., Taoyuan City 32003, Taiwan

Abstract— Benefiting from a non-zero value of the linewidth enhancement factor which leads to a variety of dynamics different from any other lasers, the broad bandwidth of chaos can be easily generated. There are several applications in chaotic laser, such as broadband random-bit generation, ranging, and secured communications. In the past two decays, most studies of the chaos generations focused on the nonlinear dynamics of the traditional continuous wave (cw) injection and dynamical pulse and sine wave injection. In this work, we study chaos generation utilizing an optically square-wave-injected semiconductor laser with tunable duty cycle. By injecting a slave laser with periodic optical square-wave at specific parameters, chaos oscillation and chaos pulsing can be generated individually. Compared with continuous wave injection with the same injected conditions, the chaos oscillation generated by square-wave injection shows larger bandwidth and more complex behaviors. Furthermore, if the operating variables are adjusted to the center of the chaos area in the dynamical mapping, the waveforms of power spectra of the generated chaos are much smoother and broader. In this paper, the distribution map of chaos oscillation and pulsing oscillation are investigated. When the duty cycle is operated at high level, chaos oscillation is observed. On the other hand, if we operate the condition at high repetition rate and strong injection strength, the nonlinear dynamics is driven into the chaos pulsing states and the bandwidth of chaos pulsing is two times larger than chaos oscillation which is operated in week injection strength. The three parameters, duty cycle, repetition rate and injection strength, all play important roles in chaos generation utilizing optical square-wave injection system.

Coupling between Double Split Ring Resonators and Complementary Split Ring Resonators

Yu-Zhan Lin and Watson Kuo
Department of Physics, National Chung Hsing University, Taichung 402, Taiwan

Abstract— In this work we study the coupling between double split ring resonators (DSRRs) and complementary split ring resonators (CSRRs) by experiment and simulation. As a planar resonator, DSRR is frequently used in building most planar left-handed material. For our study, the resonators have resonance frequency between 3 GHz and 4 GHz. We study inter-resonator coupling in two ways: For the first study, two DSRRs were placed on the same plane with various center-to-center distance and different orientations. We found that the difference of their resonance frequencies increases when center-to-center distance decreases, featuring the coupling between two resonators. When the gaps of outer ring are face-to-face, the coupling is stronger. The difference can vary as large as 0.11 GHz. Secondly, we studied the coupling of a DSRR and a CSRR when they are respectively placed on upper and lower planes of a printed circuit board. Their resonance frequencies f_D (DSRR) and f_C (CSRR) were monitored when center-to-center distance were continuously changed by using a home-made moving stage. We found that shift of f_D is greatest when center-to-center distance is roughly the resonator's radius, $R = 3.9$ mm. Moreover, frequency difference of two resonators f_D-f_C decreases when center-to-center distance reduces, with a maximum change of 0.1 GHz, a phenomenon opposite to coupled DSRR case.

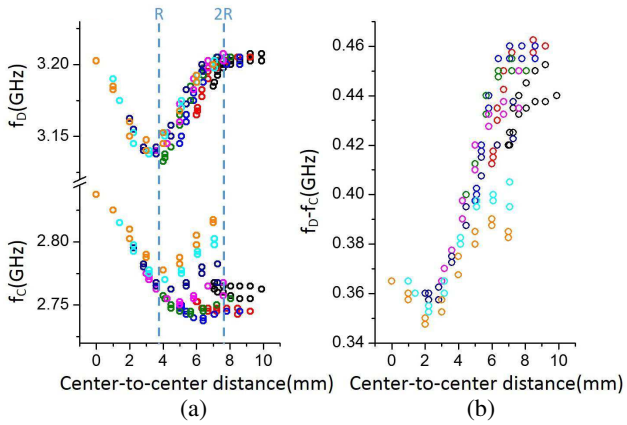

Figure 1: The measurement of inter-resonator coupling between DSRR and CSRR. (a) Resonance frequency of DSRR and CSRR as a function of center-to-center distance. (b) Frequency difference, f_D-f_C reduces as center-to-center distance reduces.

Photonic Band Structure and Field Distribution for TE Polarization. High Plasmon Concentration in the Corners of Metallic Rods of a 2D Photonic Crystal

D. M. Calvo-Velasco and N. Porras-Montenegro
Departamento de Física, Universidad del Valle, A. A. 25.360, Cali, Colombia

Abstract— In recent years the study of photonic crystals (PCs) and their optical properties, aroused the interest of the scientific community, thanks to the discovery of the photonic band gaps present in these structures, that is, frequency ranges where the propagation of the electromagnetic field is prohibited, allowing the development of new technologies. PCs are an arrangement of materials with different refraction index, which allow light behaviors not present in the bulk materials. The photonic band structure (PBS) and the band gaps in the PCs depend on the difference between the refractive index of the components of the PC, their geometry disposition, and the filling fraction. The different studies on this structures rangs from multiple slabs of different materials for 1D systems up to 3D structures, including fractal disposition of a dielectric material in air in a limited region of the space. Also, some studies are related to defects which modify the translation symmetry of the PC allowing the existence of high localized modes used in the construction of wave guides.

In this work we calculated the photonic band structure (PBS) of a square 2D photonic crystal (PC) made of square metallic rods embedded in air, considering a Drude type dielectric function without loss for different values of the rod plasma frequency, ω_p. The PBS was calculated for TE polarization in the Γ-X direction using the revised plane wave method (RPWM), considering the Li's rules for the product of two periodic functions. We found that the PBS presents at bands below and above the frequency value $\omega_p/\sqrt{2}$, and by calculating the distribution of $|H_z|^2$ in the crystal unit cell we found that these bands are related with the existence of plasmon-polaritons in the surface of the rods, as it has been discussed and published in previous works. Besides these findings, in this work we also present the distribution of $|E|^2$, but in this case the square shape of the metallic rods contributes to a high field concentration close to their corners. For frequencies around ω_p, we found that the magnetic field presents a distribution which does not change in passing from the metallic regime to the dielectric one, being not the case of the electric field, which is distributed only inside the rods for frequencies below ω_p and in the whole unit cell above this frequency.

Unidirectional Nanoantenna for Second-harmonic Generation

X. Y. Z. Xiong, L. J. Jiang, W. E. I. Sha, Y. H. Lo, and Yan Lin Li
Department of EEE, The University of Hong Kong, Hong Kong, China

Abstract— Due to symmetry breaking at surface and plasmonic enhancement, second-harmonic generation (SHG) from centro symmetric metal nanoparticles has a bright outlook for nanoscale sensing and detection applications. While SHG were greatly enhanced by well-engineered nanostructures, a directional (or angular) control of second harmonic (SH) radiation, which is highly important to far-field detection of nonlinear signals, has not been explored yet. In this work, a unidirectional nanoantenna is designed tore direct radiated SH wave and separate it from incident wave spectrally and spatially. To solve challenging issues in the modeling of the nanoantenna system, SH nonlinearity is described by equivalent nonlinear current sheets on the surface of metal nanoparticles. Then, the nanoantenna is simulated and optimized by the surface integral equation (or boundary element) method based on equivalent principles. A modified PMCHWT formulation is solved iteratively to capture the mutual coupling between fundamental and SH fields. As a result, the modeling of SHG is not restricted by the undepleted-pump approximation. Compared to other simulation approaches, the proposed method is efficient with a surface discretization; and could employ experimentally tabulated linear susceptibility and nonlinear surface susceptibility tensor of metals directly.

The SH radiation from a plasmonic small sphere with a plane wave excitation can be modeled by the emission from an induced electric dipole and an induced electric quadruple. According to the selection rule, the SH radiation is strictly zero along the incident direction. However, SH radiation always shows a double-side scattering feature due to mirror symmetry along the radiation directions. In the designed nanoantenna, two passive dielectric nanospheres functioned respectively as a director and reflector are employed to break the mirror symmetry. By tuning the size of dielectric spheres and sphere-sphere spacing, interference and retardation effects between multiple spheres could be fully controlled, which leads to the unidirectional scattering of SH waves at a desired wavelength. The work paves a new way to far-field detection and sensing of nonlinear signals.

The Dispersion Properties of Three-dimensional Magnetized Plasma Photonic Crystals as the Mixed Polarized Waves Considered

Hai-Feng Zhang[1, 2], **Yi-Bing Lin**[2], **Yu-Qing Chen**[2], **and Guo-Wen Ding**[1]

[1]College of Electronic and Information Engineering
Nanjing University of Aeronautics and Astronautics, Nanjing 210016, China
[2]Nanjing Artillery Academy, Nanjing 211132, China

Abstract— In this paper, the dispersion properties of three-dimensional (3D) magnetized plasma photonic crystals (MPPCs) with face-centered-cubic lattices are theoretically investigated based on the modified plane wave expansion method, in which the homogeneous magnetized plasma spheres are immersed in the homogeneous and isotropic dielectric background, as the mixed polarized waves and magneto-optical Faraday effects are considered. The more general case has been studied, and PBG of such MPPCs is not only for the left and right circular polarized waves but also for the mixed polarized waves. The equations for calculating the PBG for all of the electromagnetic waves in such 3D MPPCs also are theoretically deduced. Theoretical computing results show that one PBG and two flatbands regions can be observed. Compared to the conventional dielectric-air photonic crystals with similar structure, the larger PBG can be obtained in such 3D MPPCs. However, the narrower PBG can be achieved compared to the PBG for the right circular polarized (RCP) wave, but the larger upper edge frequency of flatbands region can be obtained.

Zn Concentration, Shape and Size Effects on the Band Structure of Photonic Crystals Based on Ferrofluids with ($Co_{1-x}Zn_xFe_2O_4$) Nanoparticles

Luz E. González and N. Porras-Montenegro
Departamento de Física, Universidad del Valle, A.A. 25360, Cali, Colombia

Abstract— In this work using the transfer matrix technique we study the Zn concentration and shape effects on the band structure of a 1D photonic crystal, made of alternating layers of air and a ferrofluid containing ($Co_{1-x}Zn_xFe_2O_4$) nanoparticles, coated by oleic acid suspended in ethanol. For the three-phase mixture we have based our study on the Maxwell-Garnett theory for two confocal inclusion phases contained in a background representing the third phase. We found that the photonic band structure (PBS) is shifted to higher frequencies with the increasing of the Zn concentration and with ferrofluids containing ellipsoidal instead of spherical nanoparticles. However, the difference in the shifting of the PBS due to oblate or prolate ellipsoidal nanoparticles, is negligible. The effects of the Zn concentration, the width of the ferrofluid and air layers, as well as their dielectric constant on the PBS, allow us to propose photonic quantum wells by means of which we can have very well defined frequency regions to transmit or reflect electromagnetic waves to be used in technological applications. Taking into account that there have been several experimental reports showing that an external magnetic field applied perpendicular to the plane of the ferrofluid organize the nanoparticles in parallel rods to form a hexagonal 2D photonic crystal, we also extended our study to these kind of photonic crystals considering the effect of dispersive dielectric response, dissipation effects, as well as the influence of the applied magnetic field by using the Finite-Difference Time Domain. We hope our results can be taken into account for future understanding of the optical response of these systems to be used in technological applications.

Porphyrinic Photosensitizers for Biology and Medicine

Sergey I. Gorelov[1], **Marina V. Dobrun**[1], **Antonina V. Dadeko**[2, 3], **Tatyana K. Krisko**[2], **Tatyana D. Muravieva**[2], **Andrey M. Starodubtsev**[2], **and Ivan M. Kislyakov**[3]

[1]Sokolov Clinical Hospital No. 122, Saint-Petersburg 194291, Russia
[2]S. I. Vavilov State Optical Institute, Saint-Petersburg 199053, Russia
[3]ITMO University, Saint-Petersburg 197101, Russia

Abstract— Porphyrin-based substances are modern materials applied in the design of preparations for for photodiagnosis and photodynamic therapy of cancer [1]. The wide interest to their study is drawn by its low toxicity and selectivity to accumulation in tumor tissues. At that, the photodiagnosis task requires pronounced photoluminescent property of porphyrins whereas the photodynamic therapy applications are based on their high efficiency as regards to photosensibilization of reactive oxygen species, and especially of singlet oxygen.

We report on study of three water-soluble forms of porphyrins as the photosensitizing objects: 1) chlorine E6 salt with N-methyl-D-glucamine as the dye composition of Photoditasin preparation; 2) coproporphyrin III tetrapotasssium salt, the base of preparation Coproporphyrin III; 3) 2, 4-di-(alpha-methoxyethyl)-deuteroporphyrin IX disodium salt, known as the Dimegin photosensitizer. The first preparation is already widely applied in clinical practice for photodiagnosis and photodynamic therapy. The second one was developed and manufactured by Elest JSC (Saint-Petersburg, Russia) and its optical properties were studied last few years [2].

Coproporphyrine III and Dimegin preparations can be promising drugs for medical purposes, due to their high solubility in water and low rat intravenous toxicity (240 ± 16 mg/kg for Dimegin as has been found in St. Petersburg Research Institute of Toxicology) and 2400 ± 120 mg/kg for Coproporphyrine III [3]).

Here, we experimentally show a high singlet oxygen photosensibilization ability of these species. The process of singlet oxygen generation and its quantum yield for each of the photosensitizers was studied in phosphate buffer. The singlet oxygen production was measured by two chemical trap methods. The first one was based on the simultaneous application of L-histidine and p-nitrosodimethylaniline, while another one used L-tryptophan.

Dimegin showed the greatest singlet oxygen quantum yield (ca. 0.8) compared to other dyes. The quantum yields for Photoditasin and Coproporphyrin III were found to be 0.6 and 0.37 correspondingly. It was note that biological media possess a significant effect on the singlet oxygen generation property. For example, 0.1% ovalbumin addition led to reduction of Photoditasin and Coproporphyrin III singlet oxygen photosensibilization efficiency in 3 and 2 times correspondingly.

The comparative study performed corroborates high perspectives of Dimegin preparation for photodynamic cure.

REFERENCES

1. Josefsen, L. B. and R. W. Boyle, *Theranostics*, Vol. 2, No. 9, 916, 2012.
2. Poltavskaya, O. G., G. V. Barabanschikova, M. A. Malkov, V. Ya. Bykhovsky, and O. A. Lukina, "The arthrobacter globiformis bacterial strain — Producer of coproporphyrine III and the method of coproporphyrine III preparation," RF Patent # 2078138, priority from 22.11.1993.
3. Belousova, I. M., M. V. Dobrun, L. V. Galebskaya, S. I. Gorelov, K. I. M. islyakov, S. E. Kolbasov, A. V. Kris'ko, T. K. Kris'ko, M. A. Malkov, T. D. Murav'eva, and N. N. Petrishchev, *Proc. of SPIE*, Vol. 7822, 78220W, 2010.

Analysis on the Aperture Averaging Weight Factor for Equidistant Dual-aperture Receiver

Changqi Yang and Simin Liu
School of Science, Xi'an Shiyou University, Xi'an 710065, China

Abstract— Free-space optical communication receiver aperture is usually a single circular aperture. When the aperture size is large, its cost will be high. This paper proposes a new receiver aperture structure: equidistant dual-aperture receiver. The authors analyze its performance. Aperture Averaging Weight Factors of the two kinds of receiver structures are compared. The analysis results show that: Equidistant dual-aperture receiver can obviously decrease the Aperture Averaging Weight Factor, and reduce the optical scintillation.

Trend Technology's Theory Model and Experiment Verification for Atmospheric Optical Scintillation

Changqi Yang
School of Science, Xi'an Shiyou University, Xi'an 710065, China

Abstract— Trend technology's theoretical model for atmospheric optical scintillation is establishes in this paper. For many years, people have always thought that atmospheric optics is completely random. In the previous paper, the author has used several experiments to overturn the traditional view. In this paper, the author will put forward a model to explain the author's point of view theoretically. It will demonstrate the process how does the optical scintillation evolve according to the trend. In this paper, the author will give the second batch of the experimental data to verify the theory model.

Zn-diffusion 850 nm VCSEL with Stable Single Mode Operation and 21 GHz Bandwidth

Fang-I. Lai[1], **Dan-Hua Hsieh**[2], **Jin-Wei Shi**[3], **and Hao-Chung Kuo**[2]

[1]Department of Photonic Engineering, Yuan Ze University, Taoyung, Taiwan
[2]Department of Photonic & Institute of Electro-Optical Engineering
National Chiao Tung University, Hsinchu, Taiwan
[3]Department of Electrical Engineering, National Central University, Taoyuan, Taiwan

Abstract— The vertical-cavity surface-emitting laser (VCSEL) had been an attractive light source for the fiber-optical communication due to its high bandwidth, low cost and high reliability. Until now, most VCSELs are used in short-haul optical link, which usually transfer data through multimode fiber and the distance is shorter than 2 km. To reach the longer transfer distance, significant effort had been paid on the development of high power single-transverse mode VCSELs. In this study, we demonstrate stable pure single-mode operation by using selective Zn-diffusion technique to suppress the lasing of high order mode. The effect of Zn-diffusion is also investigated via simulation. Here the commercial software of Photonic Integrated Circuit Simulator in 3D (PICS3D) is conducted to simulate the device character, which is developed by Crosslight corp. The simulator is based on the nonlinear Newton-Raphson method. All the equations involved in the calculation are discretized on the grids within target devices self-consistently. Because of the mutual interaction between optical, electrical and thermal occurs within VCSEL devices. All these effects are taken into consider during the simulation. To obtain a good result, the key factor to discretize the mesh distribution is based on the box method. The target VCSEL structure consist three GaAs/$Al_{0.3}Ga_{0.7}As$ MQWs sandwiched by 35-pair n-type and 22-pair p-type DBR. An oxide layer is placed above the MQWs for the current and optical confinement. Zn-diffused region is formed in p-DBR to provide a high order mode stopper. The calculation results show that, except for the fundamental mode, almost all high order modes are stopped by Zn-diffusion region due to the high free-carrier-absorption and the decreased reflectivity of p-DBR, the only observable high order mode is the first high order mode, which has a large overlap between the mode profile and Zn-diffusion region. Finally, the fabricated device shows stable single mode operation over all bias point ($1 \sim 5$ mA), which is consistent with the simulation result. And the maximum bandwidth exceeds 20 GHz as bias current over 2 mA.

Electromagnetic Simulation of Coupled Silicon and Diamond Microdisks and Slab Waveguides in the Mid-infrared

Muhammad Rehan Chaudhry[1], **Zeeshan Rashid**[1], **Yiğit Uysallı**[2], **Adnan Kurt**[3], **Ulaş Sabahattin Gökay**[1], **and Ali Serpengüzel**[1]

[1]Microphotonics Research Laboratory, Department of Physics
Koç University, Rumelifeneri Yolu, Sarıyer, Istanbul 34450, Turkey
[2]Department of Physics, Middle East Technical University, Ankara 06531, Turkey
[3]Teknofil Limited, Vişne 2 Mahallesi, 3. Cadde
Market Blok No. 8, Zekeriyaköy, Sarıyer, Istanbul 34450, Turkey

Abstract— Electromagnetic numerical studies of silicon and diamond microdisks coupled with silicon and diamond slab waveguides are performed in the CO_2 laser emission region in the mid-infrared. Microdisk is the 2D analog of the microsphere and the slab waveguide is the 2D analog of the rectangular optical waveguide. The evanescent coupling between the waveguide and the microdisk results in efficient pumping of the whispering gallery modes of the microdisk. On-resonant and off-resonant studies are performed by tuning the laser wavelength to the microdisk whispering gallery modes.

Global Simulation for Quantum Cascade Lasers Subjected to External Optical Injection

Yohei Sakasegawa[1], **Shingo Saito**[1], **Norihiko Sekine**[1], **Akifumi Kasamatsu**[1], **Masaaki Ashida**[2], **and Iwao Hosako**[1]

[1]National Institute for Information and Communications Technology, Japan
[2]Graduate School of Engineering Science, Osaka University, Japan

Abstract— Recently, the use of the terahertz (THz) frequency band for wireless communication has attracted considerable attention. In this context, the development of modulation schemes for solid-state THz sources such as THz-quantum cascades lasers (THz-QCLs) has become a very important technological issue. However, in contrast to the several investigations being carried out on radio-frequency (and thus electrical) modulation of THz-QCLs, the optical modulation of THz-QCLs is at an early stage of development. In the optical scheme, amplitude or spectral changes of the QCL arise from photon-generated electrons (holes) in the conduction (valence) band of the devices, which trigger on various modulation mechanisms, such as the change in the intersubband laser gain [1], additional mirror loss induced by free carrier plasma, or even heating of the device in the limit of high intensity excitation ($> \mu$J/pulse) [2]. Up to now, one obvious problem in the optical modulation is that these coexisting and interacting relaxation processes leads to a complexity in relating certain output behavior to the specific processes in a decomposed or integrated manner.

In this paper, we report a global simulation scheme for QCLs subjected to the optical pulse injection, allowing us to reproduce the optically induced amplitude change in the QCL over a wide range of injection power. Our scheme consists of the heat equation and the three-level rate equation. Here, the internal parameters (e.g., electron temperature, scattering times, and hence internal gain) are treated as spatiotemporal, evaluated on the basis of the temperature distribution of the device, and by substituting these parameters into the rate equation photon number is obtained, which is then converted into the output power using the reflectivity of the illuminated facet (time dependent). The simulation results are in good agreement with our previous measurements [2].

REFERENCES

1. Sekine, N. and I. Hosako, *Appl. Phys. Lett.*, Vol. 95, 201106, 2009.
2. Sakasegawa, Y., S. Saito, N. Sekine, A. Kasamatsu, M. Ashida, and I. Hosako, submitted.

A Photonic QPSK Modulator Aimed at Space Applications

J. Panasiewicz[1, 2], D. M. S. Morais[2], and G. M. Pacheco[2]

[1]National Institute for Space Research, Brazil
[2]Aeronautics Technical Institute, Brazil

Abstract— This paper addresses the subject of the satellite payload signal transmission and the digital-microwave link. Usually, the carrier modulation data transmitter (DT) employs in-phase (I) and quadrature-phase (Q) processing to achieve phase shift keying (M-PSK). Typically, this I/Q processing is obtained by multiplying a low-frequency reference signal. Such systems usually have many stages of multipliers, amplifiers and filters. As a result, the microwave transmitter is complicated, bulky and costly. The results presented are based on a photonic circuit that achieves QPSK modulation directly at the microwave frequency carrier. The QPSK modulation was performed using a carrier frequency of 2 GHz and 2 Mbps I/Q signal from a pattern generator using a photonic circuit with a pair of Mach-Zehnder optical modulators arranged in a parallel configuration. The source of the photonic circuit is a DFB diode laser with a wavelength equal to 1550 nm. The modulated optical signal direct detection comes from an InGaAs photo detector. The optical modulator circuit output can be directly connected to the high power amplifier (HPA) and the transmission antenna. The resulting system enables one to achieve a microwave data transmitter with a reduced mass and volume, further lowering power consumption. These achievements are very important for spacecraft engineering teams during the conception of the satellite payloads when starting a new satellite project. Gamma radiation and thermal effects of the space environment are also discussed.

Ultra-porous Aluminium Oxides for GHz and THz Components

O. Stepanenko[1], **A. Tartari**[2], **M. Amamra**[3], **T. H. N. Nguyen**[3], **M. Piat**[2], **A. Kanaev**[3], **and G. Leo**[1]

[1]Université Paris Diderot, MPQ, CNRS-UMR 7162, Case courrier 7021, 75205 Paris Cedex 13, France
[2]Université Paris Diderot, APC, CNRS-UMR 7164, Case courrier 7021, 75205 Paris Cedex 13, France
[3]Université Paris 13, LSPM, CNRS UPR 3407, 99 Avenue J.-B. Clément, Villetaneuse 93430, France

Abstract— We report on the experimental study of ultra-porous alumina (UPA) [1], which is a promising low-κ dielectric material for GHz wideband antennas. The UPA samples are fabricated by oxidation of laminated metallic aluminium through a mercury film at room temperature [2], which leads to the formation of a nano-porous monolith of up to 99% porosity. Since the UPA monolith is extremely fragile at this stage, spectroscopic measurements were carried out after annealing at temperatures 870 and 1300°C, milling to a powder, and compaction under pressure to form rigid tablet samples. Some of UPA samples are also treated in trimethylethoxysilane (TMES) vapour. In this case, an additional annealing decomposes TMES molecules, resulting in a silica film covering the UPA nanofibres and mechanically reinforcing the samples.

The electromagnetic characterization consisted in the measurement of the S-matrix parameters of our ultra-low-ε UPAs substrates. Our setup relies on a Vector Network Analyzer (VNA) with 8–19 GHz generation and multiplication stages up to the THz range. Different fabrication conditions have been comparatively studied in the 150 GHz range, the VNA enabling us to retrieve the complex permittivity $\varepsilon(1 - j\tan\delta)$ of the material. While we measured an interestingly low refractive index $\sqrt{\varepsilon} \approx 1.1$, the loss tangent ($\tan\delta \approx 10^{-2}$) is still one-order-of-magnitude higher than the typical values of commercially available antenna substrates. However we are confident that such losses can be strongly reduced by the fabrication process optimization that is currently under way.

While we presently focus on the 110–170 GHz range because of its importance in the research on the cosmic microwave background, UPAs can also be interesting for higher frequencies in the THz range, once their hydrophilic nature will be properly dealt with. In this case, beyond their potential use in patch antennas, UPA might also become competitive with currently available THz optical components, whose spectral ranges are sometimes limited. In this respect, the potential of creating refractive index gradients through thermally induced UPA density gradients might also lead the way to fancy optical components like THz Luneburg lenses [3]. In the low-microwave range, an approximate version of these lenses (manufactured by assembling concentric, homogeneous dielectric shells with different ε) is widely used for radio communications in the X-band between 12 and 16 GHz, as well as in the military field. [4] UPA-based Luneburg lenses would of course be very interesting in the THz domain, where implementing the above piecewise-constant radial permittivity seems impractical.

REFERENCES

1. Wislicenus, H., *Zeitschrift Chemie Industrie Kolloide*, Vol. 2, XI–XX, 1908.
2. Vignes, J.-L., C. Frappart, T. di Costanzo, J.-C. Rouchaud, L. Mazerolles, and D. Michel, "Ultraporous monoliths of alumina prepared at room temperature by aluminium oxidation," *J. Mater. Sci.*, Vol. 43, 1234, 2008.
3. Luneburg, C. R., *Mathematical Theory of Optics*, Brown University Press, 1944.
4. Caille, G., et al., www.radar-reflector.com.

Optoelectronic Applications of Sapphire Microspheres

Muhammad Zakwan, Muhammad Sohail Anwar,
Syed Sultan Shah Bukhari, Ulaş Sabahattin Gökay, and Ali Serpengüzel
Microphotonics Research Laboratory, Department of Physics, Koç University
Rumelifeneri Yolu, Sarıyer, Istanbul 34450, Turkey

Abstract— The sphere with its highly symmetric geometrical shape enhances the efficiency of optical effects with its high quality factor morphology dependent resonances (MDRs). We report here on numerical studies of elastic light scattering in a sapphire microdisk coupled to slab waveguides, i.e., the 2D analog of a microsphere coupled to the 2D analog of an optical waveguide. The numerical electromagnetic simulations for the surface electric field strength are performed at 800 nm. The experimental elastic light scattering measurements are also proposed in the near-infrared from sapphire microspheres. 800 nm operation with sapphire microspheres is suitable for local area networks (LANs) applications such as channel dropping, filtering, switching, modulation, and monitoring.

Silicon Microspheres in Metrology

Muhammad Hamza Humayun, **Farhan Azeem**, **Imran Khan**,
Ulaş Sabahattin Gökay, **and Ali Serpengüzel**
Microphotonics Research Laboratory, Department of Physics, Koç University
Rumelifeneri Yolu, Sarıyer, Istanbul 34450, Turkey

Abstract— The Système International unit of mass is the kilogram. The present definition of the kg is based on a prototype dating back to 1880s. New approaches to define the unit of mass are being investigated. Avogadro Project uses 10 cm diameter single crystal silicon spheres. The technique commonly observed to measure the radius of the silicon sphere is optical interferometry. Here, we propose an alternate method of measuring the diameter of the single crystal silicon sphere using near-infrared spectroscopy. We demonstrate our approach by numerically simulating the electromagnetic coupling of a silicon microdisk of radius 5 μm to an optical waveguide of width 0.5 μm, thereby approximating the coupling of a microsphere to a rectangular optical waveguide. It might be possible to have a precise technique for determining the radius of the sphere, which can be used for the definition of the kilogram.

A 10 Gbps, Wide Dynamic Range CMOS Optical Receiver

Sheng-Hua Lai and Wei-Zen Chen
Department of Electronics Engineering, National Chiao-Tung University, Hsinchu, Taiwan

Abstract— This paper describes the design of a 10 Gbps, high sensitivity and wide dynamic range optical receiver is TSMC 40 nm CMOS technology. Typically, a high sensitivity optical receiver is achieved by utilizing a core voltage amplifier with a large shunt-shunt feedback resistor, so as to diminish the input referred noise current. The voltage amplifier's 3 dB bandwidth should be at least $\sqrt{2}$ times the overall TIA bandwidth (ω_{TIA}), while its gain should be sufficiently high (> 15 dB) to tolerate the parasitic capacitance of PD. Thus shunt-peaking inductors in general are required for bandwidth enhancement in the core amplifier design under the constraint of low supply voltage in the nano meter CMOS technology. On the other hand, the feedback resistor should be tunable to accommodate wide dynamic range input signal. However, it may suffer from phase margin degradation under the low gain mode, and results in significant gain peaking. To overcome the aforementioned issues, the proposed TIA is composed of dual path nested feedback loop architecture. In addition to an outer passive feedback loop that determines the TIA gain, an inner active feedback loop in the core amplifier is incorporated for bandwidth enhancement. Thus no peaking inductors are required for a small form factor. By monitoring TIA's output with an automatic gain controlled circuit, the core amplifiers voltage gain is adjusted in conjunction with the feedback resistor, so as to maintain a relatively constant damping factor and alleviate gain peaking. The TIA is integrated with a 2 stage post limiting amplifier, and the circuit performance is demonstrated by integrating a photo detector with a responsivity of 0.65 A/W. Experimental results show that it has a maximum conversion gain of 86 dBΩ while tolerating input power level from -15 dBm to 0 dBm. The measured bit error rate is less than 10^{-12}. The total power dissipation is 17.3 mW from 1.2 V supply. Chip area is 0.628 mm $\times$ 0.53 mm^2.

Light Out Coupling Efficiency of Top-emitting Organic Light Emitting Diode

Dong Bin Yeo, Woo Young Kim, Chang-Bum Moon, and Chul Gyu Jhun
School of Green Energy & Semiconductor Engineering
Hoseo University, Asan, Chungnam 336-795, Korea

Abstract— We theoretically study the light out coupling efficiency of the top-emitting OLED with inverted structure. The dipole mode is used analyzing the light out coupling efficiency of the top emitting OLED. With this process, we can analyze the out coupling efficiency with respect to the location of the emitting dipole from the cathode.

Organic light emitting diode (OLED) is considered as the next-generation display technology owing to its superior performance such as fast response, wide viewing angle, and high contrast ratio [1–4]. The response time is a few tens of microseconds. The viewing angle is over 170°. The contrast ratio is over 70,000 for all viewing angle. However, the out coupling efficiency is limited to about 20% due to the total reflection caused by the organic layer and glass. In this paper, we analyze the light out coupling efficiency of the OLED for the high efficiency.

The analysis of light out coupling efficiency must consider near field. The traditional approach for such device simulation is known as the dipole model [5]. Our simulations about the out coupling efficiency are also based on this model, in which, the dipole source takes the form of a forced damped harmonic oscillation. Using the dipole model and considering the surface plasmon resonance effects, the power dissipation of the top-emitting OLEDs was calculated. The light out coupling efficiency of the top-emitting OLED was analyzed with respect to the location of the emitting dipole from the cathode.

REFERENCES

1. Yang, L., P. Wu, B. Huang, and P. Gu, *Chin. Opt. Lett.*, Vol. 2, 299, 2004.
2. Huang, S., Z. Ye, J. Lu, Y. Su, C. Chen, and G. He, *Chin. Opt. Lett.*, Vol. 11, 062302, 2013.
3. Geffroy, B., P. L. Roy, and C. Prat, *Polym. Int.*, Vol. 55, 572, 2006.
4. Tsujimura, T., W. Zhu, S. Mizukoshi, N. Mori, K. Miwa, S. Ono, Y. Maekawa, K. Kawabe, and M. Kohno, *Proc. of SID*, Vol. 38, 84, 2007.
5. Barnes, W. L., *J. Mod. Opt.*, Vol. 45, 661, 1998.

Monolithic Integration of GaN-based Light-emitting Diodes and Metal-oxide-semiconductor Field-effect Transistors

Ya-Ju Lee[1], **Zu-Po Yang**[2], **Pin-Guang Chen**[1, 3], **Yung-An Hsieh**[1], **Yung-Chi Yao**[1], **Ming-Han Liao**[3], **Min-Hung Lee**[1], **Mei-Tan Wang**[4], **and Jung-Min Hwang**[4]

[1]Institute of Electro-Optical Science and Technology, National Taiwan Normal University
88, Sec.4, Ting-Chou Road, Taipei 116, Taiwan
[2]Institute of Photonic System, National Chiao-Tung University
301, Gaofa 3rd Road, Tainan 711, Taiwan
[3]Department of Mechanical Engineering, 1, Sec. 4, Roosevelt Road, Taipei 106, Taiwan
[4]Green Energy and Environment Research Laboratories, Solid-State Lighting Systems Department
Industrial Technology Research Institute (ITRI), Hsinchu 310, Taiwan

Abstract— In this work, we have demonstrated a monolithic integration of optoelectronic (LED) and electronic (MOSFET) devices in the GaN-based platform by using standard semiconductor-manufacturing technologies. The fabricated monolithically integrated LED/MOSFET device exhibits a maximum output current of $I_{DS} = 1050\,\mathrm{mA/mm}$ and a peak transconductance of $G_m = 368\,\mathrm{mS/mm}$. The LED exhibits a well rectifying behavior with a slightly high turn-on voltage of 5.32 V, mainly due to the un-optimized condition of p-contact metal. Most importantly, the monolithically integrated LED/MOSFET device exhibits good gate controllability in the LED's light output power, and hence is viable and highly promising for a broad range of applications.

ACKNOWLEDGMENT

The authors gratefully acknowledge financial support from the Ministry of Science and Technology in Taiwan (contract No. MOST 103-2112-M-003-008-MY3) and from the Bureau of Energy, Ministry of Economic Affairs in Taiwan.

Comparison of the Two Rapid Measurement Methods for Circular-cut Far-field Patterns of Elongated Base-station Antennas — Kim Method and Evans-Vilenko Method

Masanobu Hirose and Kurokawa Satoru
National Institute of Advanced Industrial Science and Technology, NMIJm, Japan

Abstract— For wireless mobile communications, the base-station antennas are indispensable equipment and the rapid as well as accurate measurements of the far-field patterns are one of the critical issues in the mass productions.

Many base-station antennas have elongated structures and the far-field patterns have narrow tilted beams along the longitudinal direction. To obtain the far-field patterns along the direction rapidly, 1-D linear near-field scanning methods and the Evans-Vilenko method (a circular scanning in the Fresnel region) are relatively well-known. Whereas the 1-D linear near-field scanning cannot make it possible to obtain the circular-cut far-field patterns in the narrow beam cut-plane, the Evans-Vilenko method can realize to obtain the circular-cut patterns from the measurement on a circle in the Fresnel region.

We show a superior candidate (Kim method) for the rapid as well as accurate measurement methods suitable to obtain the circular-cut patterns of the elongated base-station antennas. The Kim method is derived from the formula of the cylindrical near-field scanning method and the equation of the near-field to far-field transformation is the same as that of the cylindrical near-field scanning method except a factor. Therefore the same algorithm of the cylindrical near-field scanning method can be used without performing the Fourier transform along the z direction.

In the Kim method and the Evans-Vilenko method, we measure the s_{21} between two antennas (the base-station antenna and a probe) on a circle of a finite radius in the Fresnel region and calculate the far-field patterns in the plane including the circle.

For elongated base-station antennas, we show that the Kim method is superior to the Evans-Vilenko method with respect to the errors after the near-field to far-field transformation at the radius that is shorter than a few parts in a ten or a hundred of the well-known far-field distance.

Resonance in Rectangular Microstrip Structure Loaded with a Thin Omega Medium Layer in the Substrate

R. Lech, **A. Kusiek**, **W. Marynowski**, **and J. Mazur**
Faculty of Electronics, Telecommunications and Informatics
Gdansk University of Technology, Gdansk 80-233, Poland

Abstract— The resonant frequency problem of a microstrip patch has been extensively studied. In literature one can find the configurations of microstrip patches located on planar substrate with superstrate layer [1], microstrip patches located on single [2] or multilayer substrate covering conducting circular cylinder and loaded with superstrate layers [3], or located on elliptic cylinder [4, 5]. For electrically small structures the analysis is commonly carried out by solving the electric field integral equation with the method of moments.

Electromagnetic properties of the complex, chiral or pseudochiral materials, have also gained considerable attention in the literature [6]. The chiral material consists of small wire helixes inserted into the host medium, whereas the pseudochiral material contains Ω-shaped microstructures in which both the loop and stamps lie in the same plane. The induced electric and magnetic field polarizations in Ω element of the pseudochiral medium are perpendicular to each other, while in chiral medium they are parallel. The chiral medium exhibits optical activity that refers to the rotation of the polarization plane, while in the Ω medium the field displacement phenomenon occurs. Introducing Ω particles into the substrate layer results in a notable field displacement due to the pseudochirality properties of the particles, which in turn affects the resonant frequency of the structure.

The complex resonant frequency of a rectangular microstrip structure with substrate layer containing a thin Ω medium layer is studied here. The investigation is performed by using a full-wave analysis and Galerkin's moment method. To simplify the analysis approximate continuity conditions modeling a thin Ω layer are introduced [6]. The numerical results for the effect of Ω medium layer location in the substrate on the complex resonant frequency of the rectangular microstrip structure are presented.

ACKNOWLEDGMENT

This work was supported from sources of National Science Center under grant decision No. DEC-2013/11/B/ST7/04309.

REFERENCES

1. Row, J.-S. and K.-L. Wong, "Resonance in a superstrate-loaded rectangular microstrip structure," *IEEE Trans. Microw. Theory Techn.*, Vol. 41, No. 8, 1349–1355, Aug. 1993.
2. Ali, S. M., et al., "Resonance in cylindrical-rectangular and wraparound microstrip structures," *IEEE Trans. Microw. Theory Techn.*, Vol. 37, No. 11, 1773–1783, Nov. 1989.
3. Lech, R., et al., "An analysis of probe-fed rectangular patch antennas with multilayer and multipatch configurations on cylindrical surfaces," *IEEE Trans. Antennas Propag.*, Vol. 62, No. 6, 2935–2945, Jun. 2014.
4. Angiulli, G., G. Amendola, and G. Di Massa, "Radiation from dielectric coated elliptic conducting cylinder by assigned electric current distribution," *Progress In Electromagnetics Research*, Vol. 57, 131–150, 2006.
5. Lech, R., et al., "An analysis of elliptical-rectangular multipatch structure on dielectric-coated confocal and nonconfocal elliptic cylinders," *IEEE Trans. Antennas Propag.*, Vol. 63, No. 1, 97–105, Jan. 2015.
6. Mazur, J. and D. Pietrzak, "Field displacement phenomenon in a rectangular waveguide containing a thin plate of Ω medium," *IEEE Microwave and Guided Wave Letters*, Vol. 6, No. 1, 34–36, Jan. 1996.

A Moment-method Analysis of a Thin-wire Chireix-coil Antenna

A. A. Ayorinde[1], **S. A. Adekola**[1, 2], **and A. Ike Mowete**[1]

[1]Department of Electrical and Electronics Engineering
Faculty of Engineering, University of Lagos, Nigeria
[2]Department of Electrical and Electronics Engineering
Niger Delta University, Wilberforce Island, Yenegoa, Nigeria

Abstract— Using a moment-method solution technique in an Electric-Field Integral Equation (EFIE) formulation approach, this presentation examines certain performance characteristics of the electrically thin-wire variety of the Chireix-coil antenna, whose geometry as defined by Kraus (1998) is given by $C_\lambda = \sqrt{1 + 2S_\lambda}$, where the parameters ($C_\lambda$, S_λ), respectively symbolize helix circumference and turn spacing, measured in units of wavelength at the operating frequency.

Computational results obtained for the Chirac coil with 4-, 6-, 8-, and 10-turns suggest that the maximum value of magnitude of current distributed along the axis of the antenna is more or less independent of number of antenna turns. And the results also indicate that when S_λ is less than 0.9 the radiation field (E_ϑ, E_φ) patterns on the azimuthal plane consist of two diametrically oppositely directed majors; which degenerate into four distinct lobes (with relative maxima along $\varphi = 0°$, $90°$, $180°$, and $270°$ axes) for values of S_λ in excess of 1.0.

A particularly remarkable feature of these radiation field pattern characteristics is that they appear to be independent of the number of coil turns.

REFERENCES

1. Kraus, J. D., *Antennas*, 2nd Edition, McGraw-Hill Inc., USA, 1988.

A Frequency Reconfigurable PIFA Design for Wireless Communication Applications

S. C. Basaran and E. Dokuzlar
Department of Electrical-Electronics Engineering
Akdeniz University, Antalya 07058, Turkey

Abstract— In order to sustain the enormous bandwidth and multi-functionality requirements of modern wireless communication technologies, wideband reconfigurable antenna designs have attracted considerable attention in recent years. Compared to conventional wideband antennas that can cover multiple communications bands, reconfigurable antennas provide much needed agility to dynamically tune into sub-bands for improved noise, crosstalk, and jamming suppression without using external filters, thus also reducing the size, cost, and power requirements of wireless mobile devices.

In this paper, we propose a novel frequency reconfigurable PIFA design based on printed split-ring elements. The proposed design with novel configuration is depicted in Fig. 1. As seen, the antenna is fabricated on the Rogers RO3006(tm) substrate with 0.64 mm thickness and dielectric constant of $\varepsilon_r = 6.15$. The radiating top plate consists of two concentric split-ring elements and six metallic loadings (s_1–s_6) appropriately placed between the rings. The antenna height is 10 mm, and the space between the top plate and the substrate is filled with air. The shorting plate has dimensions of 3 mm, and the feed plate has dimensions of 7 mm. The shorting plate is placed under the top corner of the top plate. The horizontal distance between shorting and feed plates is 22 mm. The proposed antenna is fed by a current-probe placed in the feeding plate in the simulations. In addition, a conductive switch, implemented as a small metallic pad in the numerical design, is integrated into a straight patch and inner split-ring element. Computed return loss characteristic of the proposed antenna is shown in Fig. 1 for the two states of the switch (SW). When the switch is in OFF state, a dual band operation at 1.8 GHz and 3.5 GHz is achieved. On the other hand, when the switch is the ON state, the antenna provides a dual band performance at 1.7 GHz and 5.2 GHz, respectively. In the full paper, the details of design steps will be discussed, and also the related pattern/gain characteristics will be presented.

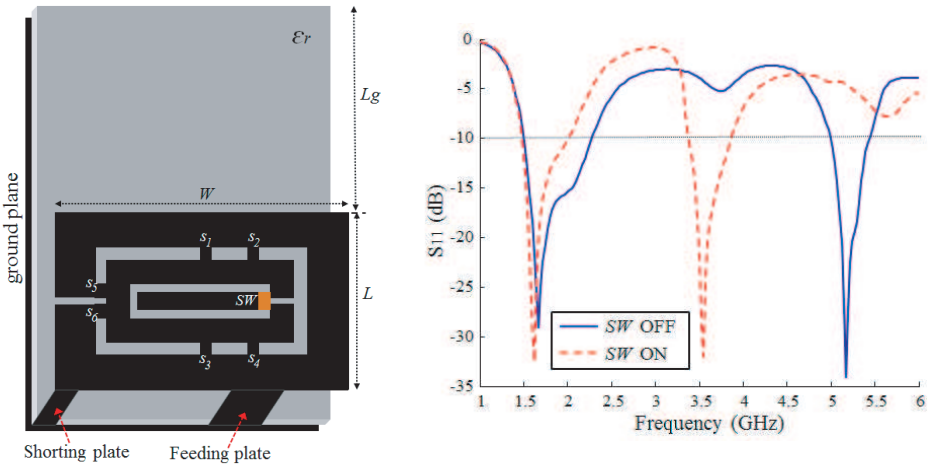

Figure 1: Proposed frequency reconfigurable PIFA design and its frequency response: ($W = 40$, $L = 20$, $L_g = 40$ (all in mm), $\varepsilon_r = 6.15$).

An Accurate Technique to Model the Substrate of Wearable Textile Antennas

Ghufran M. Hatem, **Ali J. Salim**, **and Jawad K. Ali**
Microwave Research Group, Department of Electrical Engineering, University of Technology, Iraq

Abstract— The utilization of wearable textiles in the antennas has shown a dramatic increase due to the recent challenges imposed on wireless devices to be miniaturized. For RFID purposes, a wearable antenna is meant to be a part of the clothing used. This includes tracking and navigation, mobile computing and public safety applications. Investigating the wearable textile antennas reported in the literature, it has been noted that when modeling the antenna using the commercially available EM simulators, the substrate (textile) has been dealt with as a solid homogenous material. This is fact is not the case, since the textile as a substrate is composed of woven threads (fibers). As a result, this adds some inaccuracy when comparing the simulated results with measured ones. In this paper, the textile antenna material, as a substrate, has been modeled in a way closer to the real practice. It has been modeled as horizontal and vertical fibers with different thread levels. A case study, representing a wearable textile antenna structure, has been investigated and the relevant textile material is being modeled using the proposed modeling technique. Simulation results of the antenna return loss responses using the proposed modeling technique; have shown to be more accurate than those obtained using the conventional modelling technique in that they are more close to measured results relevant to the antennas involved in the case study.

A CMOS I/Q Up-conversion Mixer and a Power Pre-amplifier for UHF RFID Reader Systems

C. C. Zhang[1, 2], **L. S. Gao**[1, 2], **C. H. Dong**[1, 2], **Y. F. Guo**[1, 2], **D. B. Wang**[1, 2], **and Y. Zhang**[1, 2]

[1]Jiangsu Provincial Engineering Laboratory of RF Integration and Micro-assembly
Nanjing University of Posts and Telecommunications, Nanjing 210023, China
[2]College of Electronics Science & Engineering
Nanjing University of Posts and Telecommunications, Nanjing 210023, China

Abstract— A high gain, high linearity, low noise I/Q up-conversion mixer and a programmable gain power pre-amplifier are designed in a standard 0.18 µm CMOS process, which are both the critical building blocks in a transmitter for UHF RFID reader systems. To comply with the system specifications, both low noise figure (NF) and high LO-IF isolation for the up-conversion mixer are required, so the I/Q mixer topology based on two coupled double-balanced Gilbert cells is applied. Besides, other techniques such as the pseudo-differential structure and the active load are also used to improve its linearity, gain, etc.. As for the power pre-amplifier, a programmable gain fully differential cascode configuration is employed to satisfy the emission spectrum requirements from various application environments. A 3-bit control word is used to switch the three parallel trans-conductance transistors in each side to change the output power flexibly. And the source inductance negative feedback technique is adopted to achieve a good trade-off among noise matching, impedance matching, linearity and gain. From a single 1.8 V power supply, simulation results show that the up-conversion mixer has a total conversion gain of 4 dB, an input 1 dB compression point ($IP_{1\,dB}$) of 4.84 dBm, and an input NF of less than 20.9 dB. The power pre-amplifier has an output 1 dB compression point ($OP_{1\,dB}$) of better than 2.8 dBm, a gain of above 7 dB, and a good input impedance matching.

A UHF RFID Reader Receiver SoC in 0.18 μm CMOS Technology

C. C. Zhang[1, 2], **Y. Q. Qian**[1, 2], **J. Zhao**[1, 2], **Y. Zhang**[1, 2], **D. B. Wang**[1, 2], **and Y. F. Guo**[1, 2]

[1]Jiangsu Provincial Engineering Laboratory of RF Integration and Micro-assembly
Nanjing University of Posts and Telecommunications, Nanjing 210023, China
[2]College of Electronics Science & Engineering
Nanjing University of Posts and Telecommunications, Nanjing 210023, China

Abstract— A fully-integrated single-chip receiver for an 860-960MHz UHF RFID reader is designed in 0.18 μm CMOS technology. It is mainly composed of an RF front-end, a DC offset cancellation (DCOC) block, and an analog baseband. The RF front-end consists of a double-mode low noise amplifier (LNA) and an I/Q mixer. The LNA can operate under two different modes, which correspond to the listen-before-talk (LBT) and the normal mode specified by UHF RFID protocols, respectively. The common-gate structure and the dynamic current injection technique are used for the mixer to achieve high linearity and low $1/f$ noise. The analog baseband comprises a programmable gain amplifier (PGA) and a low-pass filter (LPF). The opamp-based PGA is composed of a fine gain stage with a gain step of 1 dB, and a coarse gain stage with three fixed gain, corresponding to 6 dB, 12 dB and 24 dB, respectively. The LPF is a fourth-order Butterworth active RC one, whose bandwidth can be adjusted between 480 kHz and 1.68 MHz. Simulation results show that the receiver achieves $P_{1\,dB}$ of -2.1 dB in LBT mode and sensitivity of -88 dBm in normal mode, with power dissipation of 95.72 mW from a 1.8 V power supply.

Compact Substrate Integrated Waveguide BPF for Wideband Communication Applications

Aya N. Alkhafaji[1], **Ali J. Salim**[2], **and Jawad K. Ali**[2]

[1]Department of Electrical Engineering, University of Technology, Baghdad, Iraq
[2]Microwave Research Group, Department of Electrical Engineering
University of Technology, Baghdad, Iraq

Abstract— A new compact substrate integrated waveguide (SIW) bandpass filter (BPF) is presented in this paper as a candidate for use in wide bandwidth X-band applications. The proposed filter is constructed by embedding two semi-circular slots have been in the SIW structure from the input and the output sides. The simulation and performance evaluation of the proposed filter have been carried out using Microwave Studio Suite of Computer Simulation Technology CST. A parametric study reveals that the insertion of these slots has successfully led to the compact size and the wide bandwidth. The cavity dimensions are $13.6 \times 10.6\,\mathrm{mm}^2$ while the overall filter dimensions are $28.5 \times 16\,\mathrm{mm}^2$ using a substrate with relative permittivity of 2.2 and thickness of 0.245 mm. The resulting filter exhibits a return loss less than $-15\,\mathrm{dB}$ and insertion loss approaching to 0 dB over the passband. The proposed filter offers a $-3\,\mathrm{dB}$ fractional bandwidth of about 68.4% centered at 11.7 GHz. The compact size offered by this filter makes it a suitable for use in designing microwave and millimeter-wave circuits.

Investigations of Elliptical Ferrite Coupled Line Junction

A. Kusiek, W. Marynowski, and J. Mazur
Faculty of Electronics, Telecommunications and Informatics
Gdansk University of Technology, Gdansk 80-233, Poland

Abstract— Nonreciprocal devices have been extensively used in modern microwave and millimeter wave system. Recently, the longitudinally magnetized ferrite coupled strip- or slotlines [1, 2] are being developed and employed to realize integrated nonreciprocal devices. Significant interest in these devices results from their advantages, which are weak biasing magnetic field and wide operation bandwidth.

So far, studies concerning FCL devices have been focused mainly on structures realized in planar line technology. Such structures allow one to obtain fully integrated FCL devices. However, the main drawback is high level of insertion losses occurring in the ferrite material [3]. The promising results concerning losses reduction were obtained for cylindrical ferrite coupled line (CFCL) junction [4, 5]. In such configuration strong gyromagnetic coupling occurs which is a result of high magnetic field concentration in the ferrite medium. This makes possible to design shorter ferrite junctions ensuring lower insertion losses in comparison to planar ones. However, in the experiment the narrow operation bandwidth was observed for fabricated nonreciprocal devices utilizing such junctions [4, 5].

In this paper the elliptical ferrite coupled line (EFCL) junction is proposed. In the analysis the hybrid technique combining spectral-domain approach (SDA) with coupled-mode method (CMM) is applied. In this approach the SDA is applied to determine the propagation coefficients and field distributions of fundamental modes propagated in the dielectric basis guide. The basis guide has the same cross-section as EFCL where instead of ferrite the dielectric material with the same permittivity is utilized. Then utilizing CMM the gyromagnetic coefficient, dispersion characteristics of ferrite coupled lines and scattering matrix of EFCL junction are determined.

ACKNOWLEDGMENT

This work was supported from sources of National Science Center under grant decision No. DEC-2013/11/B/ST7/04309.

REFERENCES

1. Cao, M. and R. Pietig, "Ferrite coupled-line circulator with reduced length," *IEEE Transactions on Microwave Theory and Techniques*, Vol. 53, No. 8, 2572–2579, August 2005.
2. Yang, L.-Y. and K. Xie, "Design and measurement of nonuniform ferrite coupled line circulator," *Journal of Electromagnetic Waves and Applications*, Vol. 25, No. 1, 131–145, 2011.
3. Marynowski, W. and P. Kowalczyk, "Analysis of magnetic losses in ferrite coupled lines using SDA and hybrid root finding algorithm," *Progress In Electromagnetics Research Symposium Abstracts*, 635, Taipei, March 25–28, 2013.
4. Kusiek, A., W. Marynowski, and J. Mazur, "Investigations of nonreciprocal devices employing cylindrical ferrite coupled line junction," *Journal of Electromagnetic Waves and Applications*, Vol. 26, No. 13, 1685–1693, 2012.
5. Kusiek, A., W. Marynowski, and J. Mazur, "Investigations of four-port circulator utilizing cylin- drical ferrite coupled line junction," *Progress In Electromagnetics Research*, Vol. 134, 379–395, 2013.

Wave Properties of the Rectangular Waveguide Loaded with Thin Pseudochiral Medium Layer

W. Marynowski, **A. Kusiek**, **R. Lech**, **and J. Mazur**
Faculty of Electronics, Telecommunications and Informatics
Gdansk University of Technology, Gdansk 80-233, Poland

Abstract— One of the artificial materials is a pseudochiral medium firstly introduced by Saadoun and Engheta [1]. Due to its interesting features it is still in the area of researchers' interest [2–8]. The possible applications of this medium in the novel devices operating at microwave and millimeter-wave frequency ranges have been recently published in literature. Both the waveguide devices and the planar integrated structures were proposed and studied [1, 4]. The typical pseudochiral material is composed of Omega shaped microstructures where loops and stamps lie in the same plane. In such structure the field displacement phenomenon occurs [3] which is similar to the one obtained for transversely magnetized ferrite materials, except nonreciprocity [9].

In this paper a rectangular waveguide loaded with thin pseudochiral medium layer is investigated. The considered waveguide structure is composed of dielectric layer with thin omega medium layer placed on one side and the metallic strips on the other side. Based on the mode-matching method the mathematical model of the electromagnetic wave propagation in the investigated guide is derived. To simplify the analysis the approximate continuity condition are used in the modeling of the Omega medium [5]. With the use of the derived model the wave parameters, such as propagation coefficients and field distributions, are obtained. The different configurations regarding material parameters, dimensions and Omega medium layer location are considered. In comparison to the isotropic guide (without the thin Omega medium layer) for the investigated structure only the small differences in the propagation coefficients are observed. However, due to the presence of omega medium, the strong field displacement phenomenon occurs in the structure.

ACKNOWLEDGMENT

This work was supported from sources of National Science Center under grant decision No. DEC-2013/11/B/ST7/04309.

REFERENCES

1. Mamdouh, M., I. Saadoun, and N. Engheta, "A reciprocal phase shifter using novel pseudochiral or omega medium," *Microwave and Optical Technology Letters*, Vol. 5, No. 4, 184–188, 1992.
2. Tretyakov, S. A. and A. A. Sochava, "Proposed composite material for nonreflecting shields and antenna radomes," *Electronics Letters*, Vol. 29, No. 12, 1048–1049, Jun. 1993.
3. Tretyakov, S. A., "Thin pseudochiral layers: Approximate boundary conditions and potential applications," *Microwave and Optical Technology Letters*, Vol. 6, No. 2, 112–115, 1993.
4. Toscano, A. and L. Vegni, "Novel characteristics of radiation patterns of a pseudochiral point-source antenna," *Microwave and Optical Technology Letters*, Vol. 7, No. 5, 247–250, 1994.
5. Mazur, J. and D. Pietrzak, "Field displacement phenomenon in a rectangular waveguide contain- ing a thin plate of omega; medium," *IEEE Microwave and Guided Wave Letters*, Vol. 6, No. 1, 34–36, Jan. 1996.
6. Dorko, K. and J. Mazur, "Characterization of rectangular waveguide with a pseudochiral/spl omega/slab," *IEEE Microwave and Wireless Components Letters*, Vol. 12, No. 12, 482–484, Dec. 2002.
7. Matos, S. A., C. R. Paiva, and A. M. Barbosa, "Surface and proper leaky-modes in a lossless grounded pseudochiral omega slab," *Microwave and Optical Technology Letters*, Vol. 50, No. 3, 814–818, 2008.
8. Ardakani, H. H., J. Rashed-Mohassel, A. A. Jahromi, and M. K. Amirhosseini, "Propagation characteristics of pseudochiral microstrip lines," *IEEE Transactions on Microwave Theory and Techniques*, Vol. 58, No. 12, 3409–3416, Dec. 2010.
9. Baden Fuller, A. J., *Ferrites at Microwave Frequencies*, Peter Peregrinus Ltd., London, UK, 1986.

A Diplexer with a Dual-mode Resonant Junction

Eugene Ogbodo, Yi Wang, and Predrag Rapajic
Department of Electronic, Electrical and Computer Engineering
University of Greenwich, Kent, ME4 4TB, UK

Abstract— Microwave diplexers are used in communication systems to connect two channels operating at different frequencies to a common antenna port. A conventional diplexer is made up of two channel filters which are connected to a signal distribution network. Such a network usually contains a transmission-line based junction or a circulator [1]. In the past few years, a new diplexing configuration based on resonant junctions has attracted a lot of attention. Different circuit techniques have been used. For instance, in [2] two novel multiplexer topologies based on all-resonator structures were reported at X-band using waveguide technology. In [3], an FDD diplexer that integrates a T-shaped resonator and two sets of square open-loop resonators was developed. In [4], a compact diplexer was proposed and designed using an SIR resonator which acted as a common resonator.

In this work, a miniaturised and novel diplexer has been proposed and designed using hairpin resonator filters of 3.39 GHz and 4.39 GHz with a 4% fractional bandwidth each, linked together using a perturbed patch resonator. Each of the filters was individually designed using a three-pole structure and fed using proximity coupling. In order to achieve a diplexer, the two filters were joined together and here the novelty behind this proposal comes to light. A patch resonator structure, resonating at the overall central frequency of the two filters were designed and perturbed into a dual-mode to resonate at the centre frequencies of the two individual filters. The perturbed patch resonator was then used to replace the first hairpin resonator and the input feed line of each filter. Here the patch resonator acts as a common resonator linking both filters as well as a frequency selective splitter. This idea used, led to the miniaturisation of the structure from a total of six resonators to five resonators and without using any transmission-line based signal distribution network for matching. The CST EM wave simulator was employed in this design. Rogers 3010 substrate was used with a thickness of 1.27 mm, relative permittivity of 10.8 and loss tangent of 0.0035.

REFERENCES

1. Skaik, T., "Synthesis of coupled resonator circuits with multiple outputs using coupling matrix optimization," Ph.D. Thesis, University of Birmingham, 2011.
2. Shang, X., Y. Wang, X. Wenlin, and M. J. Lancaster, "Novel multiplexer topologies based on all-resonator structures," *IEEE Trans. Microwave Theory and Techniques*, Vol. 61, No. 11, 3838–3845, 2013.
3. Chuang, M. L. and M. T. Wu, "Microstrip diplexer design ussing common T-shaped resonator," *IEEE Microwave and Wireless Components Letters*, Vol. 21, No. 11, 583–585, Nov. 2011.
4. Chen, C. F., T. Y. Huang, C. P. Chou, and R. B. Wu, "Microstrip diplexers with common resonator sections for compact size, but high isolation," *IEEE Transactions on Microwave Theory and Techniques*, Vol. 54, No. 5, May 2006.

A Compact Dual-band Bandstop Filter Based on Fractal Microstrip Resonators

Hayder S. Ahmed, **Ali J. Salim**, **and Jawad K. Ali**
Microwave Research Group, Department of Electrical Engineering, University of Technology, Iraq

Abstract— Fractal geometries are found attractive to designers seeking for compact size microwave circuits and antennas. In this paper, Peano fractal based open-loop resonators are adopted to design dual-band microstrip band-stop filters (PSFs). The suggested filter structure is essentially based on that of the conventional open-loop rectangular microstrip resonators. The resonators of the proposed PSF structure are made in the form of Peano fractal geometry with different iteration levels. Many filters have been modeled and their performances have been evaluated using a commercially available full-wave electromagnetic simulator. Each of the modeled filter structures contains two pairs of open loop fractal based resonators with different iteration levels. The lower frequency band-stop performance is attributed to the resonators with higher iteration level, while the higher frequency band-stop performance is due to the resonators with lower iteration level. Simulation results for the proposed microstrip filters are shown to confirm the validity to realize compact dual-band narrow-stopband microstrip filters. A comparative study implies that higher size reduction of the realized filter has taken place as the iteration level of the fractal microstrip open-loop resonators becomes higher. The results presented show that the fractal based resonators can be used to construct compact narrow-stopband filters suitable for a wide variety of the recently available communication applications.

Development of High Stretchable Devices Material for the Wearable Electronics

Se-Hoon Park, **Dong Su Kim**, **and Jong-In Ryu**
System Packaging Research Center, Korea Electronics Technology Institute
#68 Yatap-dong, Bundang-gu, Seongnam-si, Gyeonggi-do 463-816, Korea

Abstract— Recently, IoT (internet of things) technology has strong demands for the wearable devices for the communications between mans and machines. Thus, the needs for wireless rechargeable devices which has a high efficiency will be continuously increased due to a convenience. Because a part of human body is normally deformed up to approximately 30%, wearable material also should be elongated to at least 30% and the flexible devices should provide comfortable fits to human body. When we consider these things, flexible material must have a proper modulus, high elongation and function of 3D forming. In this work, new flexible material and stretchable antenna were developed for the near field data transaction and wireless recharge for wearable devices. Flexible epoxy film was fabricated by casting epoxy resin on coper foil. In order to increase flexibility and stretchability of the film, alkoxy silane modified epoxy, phenol-novolac epoxy and half-ester modified acid anhydride were synthesized. The elongation, tensile modulus and tensile stress of flexible film showed 110%, 1 Gpa, 16 MPa respectively (see Fig. 1). Furthermore the flexible film had elastic restoring force. After it was elongated to plastic deformation region, its length was restored to a degree of 101.5% by itself compared to original length at room temperature (see Fig. 2). After fabricating flexible film, a type of inductor antenna was realized and evaluated by embedding 32 μm thick Cu pattern into polymer layer to reduce total thickness and increase flexibility. The pre-formed thick Cu pattern was transferred to the flexible films for embedding patterns and inductor pattern was interconnected through vias. The new flexible antenna has 150% thicker Cu pattern, lower electrical resistance, 10% lower thickness and 1.5 times higher Q factors than commercialized products.

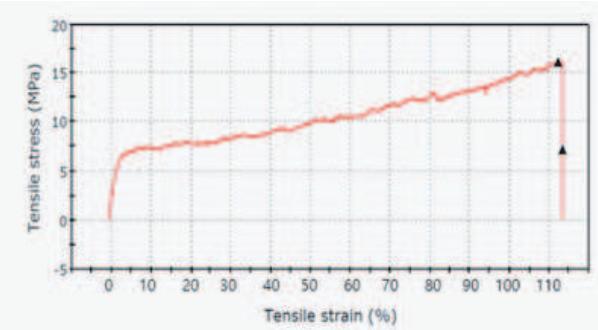

Figure 1: Tensile strain and stress test results of flexible film.

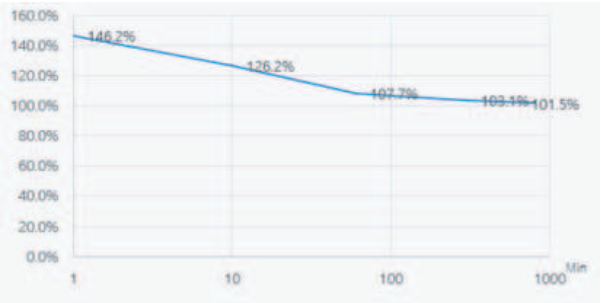

Figure 2: Restoration measurement after 60% elongation at RT.

Design of Evaluation Board with a Built-in 25 Gb/s PRBS Source for Testing High-frequency Probe

Wei Wang, **Hong-Lu Lin**, **Jau-Ji Jou**, **Yaw-Dong Wu**, **and Tien-Tsorng Shih**
Department of Electronic Engineering, National Kaohsiung University of Applied Sciences
415 Chien Kung Road, Sanmin District, Kaohsiung 80778, Taiwan

Abstract— There are more and more internet applications, such as internet TV, multimedia network, online games, social networking sites and cloud computing. We need to decrease the time of the data processing and increase the quality of the data transmission. For higher data rate applications, the 40/100 Gigabit Ethernet (GbE) standards was proposed in 2010. The 100 GBase can use four parallel 25 Gb/s channels to achieve the transmission rate. Therefore, the performance of the high data rate products, modules, devices, or testing kits need be measured over 25 GHz frequency range. The time domain measurement of high-speed signal needs generally an expensive pattern generator to provide a pseudo-random binary sequence (PRBS) signal.

In this paper, an evaluation board with a built-in 25 Gb/s PRBS source was developed for testing high frequency probe in time domain. The high frequency probes in semiconducting testing field are one of convincing contact elements selections. A commercial clock-data-recovery (CDR) chip was used to design the PRBS source. Some printed circuit board (PCB) layout techniques were used to design the 25 Gb/s evaluation board. The differential traces were designed to reduce noise interference, and the length of signal traces was short as possible for improving the transmission bandwidth. The dielectric material of our PCB used Rogers 4350B with dielectric constant 3.66. Special K connectors with 40 GHz bandwidth were used in signal input and output interfaces. The advantages of our 25 Gb/s evaluation board for testing high frequency probe have low cost, small size, and light weight.

The Optimized Electrode between a SMPM Connector and a Microstrip for High Frequency Applications

Cheng-Ying Wu, **Hong-Lu Lin**, **Jau-Ji Jou**, **Yaw-Dong Wu**, **and Tien-Tsorng Shih**
Department of Electronic Engineering, National Kaohsiung University of Applied Sciences
Kaohsiung, No. 415 Chien Kung Road, Kaohsiung City, Taiwan

Abstract— Due to the advent of the cloud computing, a high data rate transmission is greatly demand. The data traffic between servers inside a data center becomes busy. According to the requirement of a 100 GBASE Ethernet, the transmitted data rate of a single channel is 25-Gb/s and the aggregated data rate is 100-Gb/s by adopting 4-channel transmission simultaneously. The testing setup and connection for a 100-Gb/s environment is very essential. Signal integrity and impedance match are key points in designing either the transmission line on a printed circuit board (PCB) and the connector. Usually, a k-type connector is generally adopting and soldering with PCB. However, the size for a k-type connector is large, and makes a difficulty in minimizing the length of a microstrip of a PCB. A long trace of microstripe limits the transmission bandwidth. In this research, a smaller and cheaper novel Subminiature Modular Plug-in Mini (SMPM) connector has been used to replace a K-type connector. The SMPM connector is installed on the top of PCB and soldering with an electrode to reduce the trace of a microstrip and to maintain the high frequency performance. Three designs of the PCB electrode have been simulated and verified experimentally. The optimized impedance mismatch of the soldering point between a SMPM connector and the PCB electrode is controlled within a range of ±2-Ohm. The 3-dB bandwidth of the whole setup including two SMPM connectors and a 2.5-cm long microstrip is above 25-GHz. This optimization can be used in designing high-speed PCB for the application of 100 GBASE Ethernet.

High Frequency Performance Comparison among Three Kinds of Board to Wire Connectors

Ruei-Nian Wang, **Li-Wei Chen**, **Jau-Ji Jou**, **Yaw-Dong Wu**, **and Tien-Tsorng Shih**
Department of Electronic Engineering, National Kaohsiung University of Applied Sciences
Kaohsiung No. 415 Chien Kung Road, Kaohsiung City, Taiwan

Abstract— In recent years, due to the vigorous develop of information and communication technology, it makes the popularization of the internet broadband applications, such as bandwidth internet games, online teaching platform, network conference, and cloud applications. The 100 Gigabit Ethernet can use four parallel 25 Gb/s channels to achieve the transmission rate. Therefore, the bandwidth of the related device, module, equipment, and network must increase to near 25 GHz. For the high-speed modules, the signal integrity and impedance match between the printed circuit board (PCB) and connector have to be investigated.

In this paper, we analyze and compare the properties of three kinds of high frequency board to wire connectors which are subminiature modular plug-in mini (SMPM) connector, vertical K-type connector, and horizontal K-type connector. The S-parameters of these connectors were simulated through the High Frequency Structure Simulator (HFSS) software. Using these connectors, three kinds of evaluation boards (EVB) were designed for measuring the high frequency performance of the connectors. The impedances of these EVBs were measured through the time domain reflector (TDR), and the S-parameters were also measured and verified through the network analyzer. The insertion loss from PCB sheet material or connector can be distinguished through the different length EVBs. The bandwidth of the SMPM connector is about 20 GHz, the bandwidth of the vertical K-type connector is about 24 GHz, and the bandwidth of the horizontal K-type connector is above 25 GHz. The board to wire horizontal K-type connector is more suitable than the other two connectors for 25 Gb/s transmission applications.

Seasonal and Temporal Variation of GPS Phase Fluctuations at High Latitude under Low Solar Activity

Chien-Chih Lee[1], **Wei-Sheng Chen**[1], **and Fang-Dar Chu**[2]

[1]General Education Center, Chien Hsin University of Science and Technology
No. 229, Jianxing Rd., Zhongli City, Taoyuan County 32097, Taiwan
[2]National Standard Time and Frequency Lab of Telecommunication Laboratories
Chunghwa Telecom Co. Ltd., No. 99, Dianyan Rd., Yangmei City, Taoyuan County 32601, Taiwan

Abstract— This study investigates GPS (Global Positioning System) phase fluctuations over the high latitude site, Tromsø, Norway (69.66°N, 18.94°E, MLAT 66.75°N) during the low solar activity year 2007. In this study, the phase-fluctuation index Fp is used to characterize GPS phase fluctuations. Investigations include the seasonal and the temporal variation of Fp, the correlation between Fp and Kp, and the comparisons between Fp and the ionospheric electron density. The objects are to show the general variation of GPS phase fluctuations and the variation of the ionospheric electron density when irregularities occur. The results are that the active GPS phase fluctuations (Fp $\geq$ 50) occur frequently in all months; the highly active GPS phase fluctuations (Fp $\geq$ 200) prefer to occur in the equinox months; the occurrence of Fp $\geq$ 50 and Fp $\geq$ 200 both concentrate in the 18–03 LT period. These indicate that the active GPS phase fluctuations results from particle precipitation. Moreover, the temporal variation of Fp consists with that of scintillations in published papers but the seasonal variation does not. Regarding Kp, it shows positive correlations to Fp, which links the intensity of GPS phase fluctuations to the geomagnetic activity. Finally, the comparisons show that Fp $\geq$ 50 occurs when the E region density is quickly increasing or the E region density structure is extending up. This implies that GPS phase fluctuations are activated when intense particle precipitation is proceeding. Moreover, irregularities distribute from the E to the F region. The results of this study demonstrate the effective application of GPS phase fluctuations to space weather.

An Investigation of Equatorial Ionospheric Irregularities under Solar Maximum in the 24th Solar Cycle in Middle and East Africa Using GPS

Fang-Dar Chu[1], **Wei-Sheng Chen**[2], **and Chien-Chih Lee**[2]

[1]National Standard Time and Frequency Laboratory, Chunghwa Telecom Co., Ltd., Taiwan
[2]General Education Center, Chien Hsin University of Science and Technology, Taiwan

Abstract— Ionospheric irregularities exert scintillations on electromagnetic waves when the waves pass through them. So they are interesting for satellite signal propagation in the ionosphere at the magnetic equator and low latitudes. The global navigation satellite system (GNSS) observations recorded at ground-based tracking sites have been a convenient database for investigating ionospheric irregularities. The irregularities over Africa during solar maximum years of 2013–2014 in the 24th solar cycle were investigated by employing the Global Positioning System (GPS), which is a GNSS system. Six African GPS tracking sites of the International GNSS Service (IGS) network were adopted in this study. First three sites were located at low latitudes close to the geomagnetic equator, in Middle and East Africa from the coast of Atlantic Ocean to that of Indian Ocean. The other three were located at midlatitudes and at about the same longitudes as the aforementioned low-latitude sites. Equatorial irregularities were characterized by hourly GPS phase-fluctuation index. This index categorized irregularities into three levels: they are background, moderate, and strong irregularities. The important climatological results have been obtained as followings. First: The equinoctial irregularity occurrence rates over the three low-latitude sites decreased slowly from Middle to East Africa (94%, 89%, 83% and 87%, 73%, 64% for moderate and strong irregularities, respectively). Likewise, the June solstitial rates also decreased similarly (90%, 88%, 74% and 67%, 58%, 37%). However, the December solstitial rates decreased faster (55%, 24%, 28% and 26%, 10%, 7%). Thus, the equinoctial and June solstitial occurrence rates were also high in East Africa (83% and 64%; 74% and 37%), while the December solstitial one was low (only 28% and 7%). Second: Although moderate and strong irregularities occurred very frequently over the low latitude sites (e.g., 94% and 87%), they over the three midlatitude sites all were nearly at the background level (i.e., nearly 0% and 0%). This indicates the irregularities did indeed come from the equator. Third: Although the equinoctial irregularities were dominant, the June solstitial irregularities also occurred frequently and their occurrence rates were comparable to the equinoctial ones, especially in Middle Africa. As for the December solstitial irregularities, they were obviously of minor importance compared to both the equinoctial and June solstitial ones. The prominent June solstitial rates in Middle Africa may be due to the northward shifted geomagnetic equator (located in the northern hemisphere) and small declination angles.

Assessment of the Forest Disturbances Rate Caused by Windthrow Using Remote Sensing Techniques

Paula Furtuna[1], **I. Haidu**[2], **I. H. Holobaca**[1], **M. Alexe**[1], **Cristina Rosca**[1], **and D. Petrea**[1]

[1]Faculty of Geography, "Babes Bolyai" University, Cluj Napoca, Romania
[2]Laboratoire LOTERR, Université de Lorraine, France

Abstract— Change detection using multi-temporal satellite images data is an important domain with various applications in forestry and can allow an evaluation of areas extended to the same spatial temporal scale. The focus of the study is to assess the changes occurring after catastrophic wind events using Landsat time series data. Estimates of disturbance rates are derived using 8 sample selected across the Apuseni Mountains during 2000–2014 periods. Multi-temporal analysis on annual basis has detected the patterns of the changing forest ecosystem and the trends that are occurring and give more accurate results. The satellite images have been calibrated and the root mean square error has been made. The satellite images preprocessing is made in order to transform the DN values into the surface reflectance. The approach requires images during the peak growing season. Local knowledge and available ancillary data about windthrow occurrence are required in order to fully understand the nature of these trends. The statistical algorithms are applied to characterize the magnitude of the disturbance. We found evidence of systematic change in the forest ecosystem of the Apuseni Mountains by analyzing multi-temporal surface data. The accuracy of forest disturbance detection diminishes with the decrease of the temporal resolution. Therefore, the approach described in this paper demonstrates that the Landsat time series data can be used operationally for assessing forest cover changes analysis after a windthrow occurrence across a large area.

Monitoring Land Use Change in South-west Romania Using Multi-temporal Landsat Remote Sensing Imagery

Cristina Rosca[1], **I. Holobaca**[1], **M. Alexe**[1], **D. Petrea**[1], **Paula Furtuna**[1], **and I. Haidu**[2]

[1]Faculty of Geography, Babeş-Bolyai University, Cluj-Napoca, Romania
[2]Laboratoire LOTERR, Université de Lorraine, Ile du Saulcy, Metz 57000, France

Abstract— Early detection of changes in land use is especially important in environments with fragile ecological equilibrium, such as those affected by drought or soil with a sandy texture. In this article we use remote sensing techniques integrated into a surface analysis to identify areas of nuts plantation, that have been deforested. Nut plantation, with an area of 50 hectares is situated in the south-west of Romania, in the field of sand dunes Dabuleni. According to Research Development Center for Agricultural Plants on Sandsăbuleni, at locality level area occupied with sand is: Calarasi — 6.800 ha, Dăbuleni — 10.300 ha, Bechet — 5.900 ha. Deforestation the nuts plantation occured gradually, beginning in the fall of 2012 and ending in the fall of 2013. The six curtains (plots) have been cut gradually, but deforestation occurred by pruning of the tree branches, subsequently tree trunks. We have been used multitemporale satellite data, Landsat (TM and OLI) covering the period 1987–2014. In order to ensure comparability of data, was chosen July, because it was in full vegetation season , the crowning is very developed. Deforested areas were detected by calculating NDVI and the use of thresholds. The changes were highlighted using the Erdas change detection module. The surface analysis has indicated an increase of deforested areas, so if the area occupied in July 1987 with rare vegetation (low pixel) was 15.05 ha, in July 2014 the affected area amounts to 42.7 ha out of 50 ha. The results show that the method used has proved to be useful in detecting precise and rapid environmental changes.

Looking for a Biophysical Approach to Early Stages of Chronic Kidney Disease

Alberto Foletti[1, 2] **and Mario Cozzolino**[3]

[1]Institute of Translational Pharmacology, National Research Council-CNR, Rome, Italy
[2]Clinical Biophysics International Research Group, Lugano, Switzerland
[3]Department of Health Sciences, University of Milan, Italy

Abstract— Chronic Kidney Disease (CKD) and its subsequent complications and consequences are an increasing concern in general population. A biophysical integrated approach in early stages of CKD was investigated in 30 patients with a 12-month follow-up. A clinical approach based on the use of an electro medical device (Medselect 729) was employed following previous reports as well as the procedure of electromagnetic information transfer through aqueous systems. Interestingly, we observed a significant increase in the estimated glomerular filtration rate (eGFR) according to CKD-EPI formula (+11.57 ml/min; +18.43%, $p < 0.0001$). Beside further studies are certainly recommended, a biophysical integrated approach in the management of early stages of Chronic Kidney Disease seems feasible, effective, and promising.

REFERENCES

1. Baron, P., G. Bucci, A. Rinaudo, R. Rocco, E. Sclauzero, and A. Foletti, "System information therapy in the management of pain: A pilot study," *PIERS Proceedings*, 1698–1702, Stockholm, August 12–15, 2013.
2. Bókkon, I., A. Erdöfi-Szabó, A. Till, et al., "EMOST: Elimination of chronic constipation and diarrhea by low-frequency and intensity electromagnetic fields," *Electromagn. Biol. Med.*, Vol. 33, No. 1, 68–74, 2014.
3. Cueto-Manzano, A. M., L. Cortés-Sanabria, H. R. Martínez-Ramírez, E. Rojas-Campos, B. Gómez-Navarro, and M. Castillero-Manzano, "Prevalence of chronic kidney disease in an adult population," *Arch. Med. Res.*, pii: S0188-4409(14)00130-1, 2014.
4. Foletti, A., M. Ledda, E. D'Emilia, S. Grimaldi, and A. Lisi, "Experimental finding on the electromagnetic information transfer of specific molecular signals mediated through aqueous system on two human cellular models," *J. Altern Complement Med.*, Vol. 18, No. 3, 258–261, 2012.
5. Foletti, A., S. Grimaldi, A. Lisi, M. Ledda, and A. R. Liboff, "Bioelectromagnetic medicine: The role of resonance signaling," *Electromagn. Biol. Med.*, Vol. 32, No. 4, 484–499, 2013.
6. Foletti, A. and M. Cozzolino, "A biophysical integrated approach to autoimmune nephrotic syndrome: case report," *Recenti. Prog. Med.*, Vol. 104, No. 9, 488–489, Article in Italian, 2013.
7. Mitchell, T., N. Hadlow, and A. Chakera, "The impact of routine reporting of estimated glomerular filtration rate using the CKD-EPI formula in a community population: A cross-sectional cohort study," *Nephrology*, Carlton, May 30, 2014. doi:10.1111/nep.12283. [Epub ahead of print] PubMed PMID: 24888643.
8. Nitta, K., K. Okada, M. Yanai, and S. Takahashi, "Aging and chronic kidney disease," *Kidney Blood Press Res.*, Vol. 38, No. 1, 109–120, 2013.

Steps towards a Biophysical Approach to Refractory Gynecological Infections

Ida Ferrara[1] **and Alberto Foletti**[1, 2]

[1]Clinical Biophysics International Research Group, Lugano, Switzerland
[2]Institute of Translational Pharmacology, National Research Council-CNR, Rome, Italy

Abstract— Refractory gynecological infections are often very difficult to treat. The need for new strategies of their management is therefore continuously increasing. Some researchers have recently pointed up that microorganisms could emit specific electromagnetic signals. Moreover electromagnetic signals could be able to yield response from immune system. The aim of this study was to assess the possibility to employ electromagnetic signals from swabs of refractory gynecological infections to rise a response of the immune system able to erase them. Twenty-two consecutive patients with refractory gynecological infections, since at least 3 months, participate into this study employing an electro medical device(Med Matrix) to perform the electromagnetic information delivery procedure. Vaginal swab was picked up for microbiological assessment at baseline and after 7 days. Out of 22 swabs performed 15 were positive for microbiological assessment at baseline. Out of the 15 positive at baseline only 2 were still positive after one week of biophysical treatment ($p < 0.0031$). Biophysical treatment of refractory gynecological infections seems to be an useful and promising second line clinical tool.

REFERENCES

1. Foletti, A., S. Grimaldi, A. Lisi, M. Ledda, and A. R. Liboff, "Bioelectromagnetic medicine: The role of resonance signaling," *Electromagn. Biol. Med.*, Vol. 32, No. 4, 484–499, 2013.
2. Foletti, A., P. Baron, E. Sclauzero, G. Bucci, A. Rinaudo, and R. Rocco, "Assessment of biophysical therapy in the management of pain in current medical practice compared with ibuprofen and placebo: A pilot study," *J. Biol. Regul. Homeostat Agents*, Vol. 28, No. 3, 431–439, 2014.
3. Foletti, A., M. Ledda, S. Piccirillo, S. Grimaldi, and A. Lisi, "Electromagnetic information delivery as a new tool in translational medicine," *Int. J. Clin. Exp. Med.*, Vol. 7, No. 9, 2550–2556, 2014.
4. Inhan-Garip, A., B. Aksu, Z. Akan, D. Akakin, A. N. Ozaydin, and T. San, "Effect of extremely low frequency electromagnetic fields on growth rate and morphology of bacteria," *International Journal of Radiation Biology*, Vol. 87, No. 12, 1155–1161, 2011.
5. Herrmann, E. and M. Galle, "Retrospective surgery study of the therapeutic effectiveness of the MORA bioresonance therapy with conventional therapy resistant patients suffering from allergies, pain and infection diseases," *Eur. J. Integrative Med.*, Vol. 2, No. 4, 257–258, 2010.
6. Jerman, I., R. Ruźic, R. Krašovec, M. Škarja, and L. Mogilnicki, "Electrical transfer of molecule information into water, its storage, and bioeffects on plants and bacteria," *Electromagn. Biol. Med.*, Vol. 24, No. 3, 341–353, 2005.
7. Jerman, I., M. Berden, and R. Ruźic, "Biological influence of ultraweak supposedly EM radiation from organisms mediated through water," *Electro and Magnetobiology*, Vol. 15, No. 3, 229–244, 1996.
8. Liboff, A. R., "Electromagnetic vaccination," *Med. Hypotheses*, Vol. 79, No. 3, 331–333, 2012.

The Characteristics of Current-gated Single Electron Transistors

W. C. Chien[1], C. Y. Hong[2], C. S. Wu[2], and Watson Kuo[1]

[1]Department of Physics, National Chung Hsing University, Taichung 402, Taiwan
[2]Department of Physics, National Changhua University of Education, Changhua 500, Taiwan

Abstract— Superconducting single-electron transistors (SETs) with a gating junction are experimentally studied. Because of its large impedance, a one-dimensional Josephson junction array on the same chip is used for constant current gating. We experimentally studied the current-voltage characteristics of SETs under the constant current gating via a tunnel junction. The results can be compared with those obtained by using constant voltage gating through a tunnel junction. The SET current varies when one changes gating current, giving a current on-off ratio more than 1000 near zero voltage bias. The highest current gain of our current-gated SET was 16 dB when biased at the threshold of quasi-particle tunneling process.

Reliability Verification of Printed Electronics Type FPCB Used in NFC Antenna

Soon-Mi Hwang[1], **Kwan-Hun Lee**[1], **and Jin-Sung Lee**[2]

[1]Korea Electronics Technology Institute (KETI), South Korea
[2]Dreamtech Co. Ltd., South Korea

Abstract— Printed circuit board (PCB) is the carrier of electronic components which is widely used in many fields such as airborne electronic equipment [1]. Among the several types of PCB, Flexible printed circuit boards (FPCB) is being used extensively in current electronics devices because of their excellent flexibility, light weight, and reduced thickness [2].

There are two types depending on the production process FPCB; etching type and printed electronics type. Printed electronics refer to the printing of electronic circuitry on a common media such as paper, plastic, or textile. The conductive materials are available in liquid and paste forms, and can be applied using ink jetting and screen printing respectively. Printed electronics are portable, thin, tiny and suitable for customized applications such as smart labels, animated posters, and active clothing. Printed electronics is being regarded as the second coming of the semiconductor industry because it can significantly reduce their cycle times and cost structure [3].

FPCB for NFC antenna and wearable system is used in a variety of environments, and 'product reliability' is important as much as the function of each part. But so far, there is no validation for the product reliability. This thesis verified reliability of printed electronics type FPCB used in NFC antenna through environmental stress tests.

An environment test was carried out according to standard of FPCB used in NFC antenna. Seven kinds of test (; High temperature test, Low temperature test, Thermal Shock test, High temperature and humidity test, Salt test, Bending test, Electrostatic test) were carried out. The test items for performance verification were electric resistance, Inductance, Insulation resistance. High temperature test was carried out during the 120 hours in the $(85 \pm 2°\mathrm{C})$. Low temperature test was carried out during the 120 hours in the $(-40 \pm 2°\mathrm{C})$. Thermal Shock test was carried out in high temperature $(85 \pm 2°\mathrm{C})$, low temperature $(-40 \pm 2°\mathrm{C})$ and run for 30 cycles. High temperature and humidity test carried out 120 hours in conditions of $(85 \pm 2°\mathrm{C})/(85 \pm 3)\%$R.H. Salt test carried out 48 hours in conditions of $5\%/(35 \pm 2°\mathrm{C})$. ESD test was carried out according to IEC61000-4-2 and bending test was carried out 10 times, a 180-degree angle. As a result, we knew that environmental immunity levels.

After the environment test, the failed samples were carefully examined with Environmental Scanning Electron Microscope (ESEM) and 2D X-ray. Analysis result, the major failure stress and failure mechanism of the electronics type FPCB were confirmed.

REFERENCES

1. Dehri, M. E., "The effect of relative humidity on the atmospheric corrosion of defective organic coating material: An EIS study with a new approach," *Corrosion Science*, Vol. 42, No. 6, 969–978, 2000.
2. Nathan, A. and B. R. Chalamala, "Special issue on flexible electronics technology, Part 1: Systems and applications," *Proceedings of the IEEE*, Vol. 93, No. 7, 1235–1238, July 2007.
3. Salam, B. and B. K. Lok, "Solderability and reliability of printed electronics," *International Symposium on the Physical and Failure Analysis of Integrated Circuits*, 1–4, July 7–11, 2008.

High Temperature Accelerated Test of Tower Mounted Amplifier (TMA) Module Used in 4G Communication

Soon-Mi Hwang, Chul-Hee Kim, and Kwan-Hun Lee
Korea Electronics Technology Institute (KETI), Korea

Abstract— Tower Mounted Amplifier (TMA) is normally used to improve cell coverage, capacity and quality of a wireless communication system. [1]. TMA is used to expand signal coverage through enhancing the uplink receiving sensitivity in the area where call drops and handoff failure happen frequently. Improved receiving sensitivity at base station, TMA also helps to improve signal quality, enhance voice clarity and increase data transmission speed. Usually TMA is installed near to transmit and receive antenna at the top of a cell tower [2]. In general, TMA module is exposed to the outside, it should be guaranteed sufficient immunity for a variety of environmental stresses that can occur in the Outdoor. One of the major failures stresses of the TMA is high-temperature. In this paper, high-temperature degradation of TMA was studied through the accelerated test.

Accelerated test is the basis of the conventional reliability test to inspect the product's reliability during a short period of time. The basic thought of accelerated test is to obtain more failure data within less time via stresses which is higher than normal condition, i.e., accelerated stress, on the premise of keeping the consistency of degradation or failure mechanism. Thus we can inspect the product's reliability after obtaining the parameter under accelerated condition [3]. Accelerated test is a powerful and effective approach to evaluate the high reliability and long life products. At the accelerated life test, by revealing the relationship between life of products and sentimental stress under the consistency of degradation failure mechanism at accelerated stress, it can predict the product's real life from the life data obtained under the high stress environment.

High temperature accelerated test was conducted in four harsh conditions (130°C, 125°C, 120°C, 100°C) over 400 hours. Real-time measurement system (measuring Insertion Loss, Return Loss, Gain, Current) of was used to determine the failure of product.

After the high temperature accelerated tests, we analyzed fail samples using optical microscope and FIB (Focused Ion Beam). Failure of TMA in high-temperature environments is breakdown of the internal amplifier chip.

Test results are analyzed using commercially available reliability software. (Weibull++, ALTA) As a result, The Weibull is suitable for distribution of TMA's lifetime. And temperature coefficient of TMA is 342 if the using temperature is 33.5°C and test temperature is 70°C.

REFERENCES

1. Razif, A. R. A. and M. Benyazwar, "Performance analysis of uplink WCDMA tower mounted amplifier," *RF and Microwave Conference*, 80–24, Oct. 5–6, 2004.
2. Lee, H.-K., C. S. King, H.-M. Fuad, and C. K. Chong, "A low noise figure high linearity balanced amplifier module for cellular band base station's tower mounted amplifier application using E-mode pHEMT technology," *Asia-Pacific Microwave Conference*, 1–4, Dec. 16–20, 2008.
3. Liu, Y., Z. Yang, H. Ju, and L. Gan, "Electronic products accelerated testing system design and implementation," *IEEE Conference on Prognostics and System Health Management (PHM)*, 1–5, May 23–25, 2012.

FEM Evaluation of the Novel Cardiac Defibrillation Electrode Placement

Elham Khosrowshahli[1] and Aleksandar Jeremic[2]

[1]School of Biomedical Engineering, McMaster University, Canada
[2]Department of Electrical and Computer Engineering, McMaster University, Canada

Abstract— Defibrillation is a common process in treatment of patients with certain cardiac dysfunctions like ventricular fibrillation and ventricular tachycardia. Different external defibrillation systems use two electrodes to create an electric path in torso to pass current through it, and consequently through heart to regain normal hear beat. Amount of current delivered to heart is an important factor in successful defibrillation and its amplitude (and hence the outcome) is determined by the impedance seen by the defibrillator. In order to gain higher current in the heart, this impedance should be minimized. Reducing the impedance between skin and electrode by the application of proper gels is one of the methods to reduce the total impedance seen by defibrillator. One significant component of this impedance is transthoracic impedance, which is the impedance of current path between two points on the skin under electrodes on the chest. It is not easy to determine the current path in torso because of the internal organs with complicated shapes and diverse electrical properties which results in highly inhomogeneous medium and therefore complex current profile in torso. As it has been shown in electric circuit theory, one of the ways to decrease the impedance would be connecting a parallel impedance to the existing one. Using this rule, if an electric path is added to the conventional defibrillation system, transthoracic impedance can be reduced to attain higher current in torso. To implement this idea, a third electrode is added to the existing defibrillation electrode configuration. Adding this electrode creates parallel paths for current in torso in addition to the existing path. This leads to smaller impedance seen by defibrillator and achieving the desired defibrillation current with lower voltage and power levels of defibrillator. This can decrease size and increase lifetime of batteries of automated and wearable cardiac defibrillators and hence lead to lighter and more efficient systems. To verify the new method, a Finite Element model of torso is developed, and different conventional and novel electrode placements are simulated and total current delivered to heart is obtained when the new electrode is added in different positions. Outcomes show that although the amount of current increase is different, larger current is delivered to myocardium when the system of three electrodes is used in comparison to the conventional system when the same voltage is applied to both versions.

Conductivity Estimation of Breast Cancer Using Stochastic Optimization

A. Jeremic[1] and E. Khosrowshahli[2]

[1]Department of Electrical and Computer Engineering, McMaster University, Canada
[2]School of Biomedical Engineering, McMaster University, Canada

Abstract— According to Canadian Cancer Society, breast cancer is the most frequently diagnosed cancer in women with over 23,400 new cases expected in 2011. Although mammography is extremely important diagnostic technique, it suffers from some limitations such as false negative and positive results and using ionizing radiation. The number of false positives is rather significant in the case of so called dense breasts in which healthy tissue may be mistaken for malignant. Microwave imaging has been recently proposed as an additional medical imaging technique which can potentially overcome some of the shortcomings of the mammography. From the physical point of view this can be represented as a propagation in the medium that contains scatterers. Due to the fact that malignant tissue has larger conductivity the measurements obtained by receiving array of antennas will be different in the presence of scatterers. Most of the image reconstruction techniques minimize a particular cost function where the number of unknowns is much larger than the number of available measurements which requires an additional constraint. In this paper we propose a simplified parametric model which enables detection and estimation of tumors. Previously, we proposed a maximum-likelihood based method which estimates the unknown parameters by minimizing the residual error vector. However we have recently demonstrated that the detection performance can be significantly improved if classical sample covariance estimate is replaced by a structured covariance estimate. In this paper we develop a finite-element model and apply newly proposed weighted Frechet mean estimation to determine the unknown conductivity.

2D and 3D Durable Phantoms for Verification of Capabilities of Microwave Tomography and Hyperthermia Systems

M. Wiewegh, P. Spurny, J. Vrba, Jr., and D. Vrba
Faculty of Biomedical Engineering, Czech Technical University in Prague, Czech Republic

Abstract— In this paper, seven different durable phantoms for verification of imaging and heating capabilities of developed microwave tomography and microwave hyperthermia system respectively were developed. The phantoms are based on silicone-graphite powder mixtures.

For microwave tomography systems two 2D cylindrical phantoms as well as two 3D phantoms with simplified shape of a breast were developed. Both types of phantoms consist of a layer of skin-mimicking outer layer and the inner space mimics healthy breast tissue. Tumors are modeled with cylindrical and spherical inclusions in 2D and 3D phantoms, respectively.

For hyperthermia 3D phantoms were developed. For superficial hyperthermia one phantom is homogeneous and mimics muscle tissue and two are heterogeneous with three layers mimicking skin, fat and muscle tissue. One of the heterogeneous phantoms consists of a spherical tumor as well.

Prior to phantom manufacturing, all materials mimicking different biological tissues were prepared and their dielectric properties were measured using an open-ended coaxial probe.

A proper volumetric ratio of graphite powder and silicon was tested. By manufacturing of the phantoms part of the material used for phantoms was used for creation of homogeneous samples and were characterized separately.

ACKNOWLEDGMENT

This research has been supported by the research program of the Czech Science Foundation (GACR) of the Czech Republic, Project No. 14-00386P Study of Thermal and Nonthermal Effects of High-Power EM Field on Structure of Matter.

Numerical Modeling of rTMS with High-resolution Head Phantoms

M. Shuleska and J. Vrba, Jr.
Faculty of Biomedical Engineering, Czech Technical University in Prague, Czech Republic

Abstract— One of the common issues of orofacial pain treatment using transcranial stimulations (TSs) is that the stimulations are applied by MDs based solely on their knowledge and experience and there is no mean to measure exact location, level and extent of the stimulation. The main aim of a planned project is, by means of patient-specific numerical simulations, to further improve current understanding of TSs as well as to investigate new possibilities how to improve their efficacy in pain treatment. Repetitive transcranial magnetic stimulation (rTMS) is relatively new, and most promising, type of method used in pain treatments. It belongs in non-invasive and painless brain cortex stimulation using magnetic fields. The rTSM neuromodulation method is using coils that are positioned on the surface of the head's patient. This method is inducing electrical current impulse in the human brain and causing an increase in the brain activity. The latest studies showed that this method has the ability to cause changes in the central nervous system on a cellular level. Therapeutic effect of the rTMS was confirmed in mental disorders such as depression, hallucination, schizophrenia and post-traumatic stress. This stimulation method was also used in patients with neurological disorder, patients with Parkinson's disease, epilepsy or functional disorders after a stroke. The main focus of this paper is, based on results of numerical simulations, to find extent, location and intensity of the stimulation process for particular patients. Finding out these quantities is accomplished through the following stages: creation of a patient specific numerical model by segmentation of the patient's MRI images, creating numerical model of stimulation device both in SEMCAD X and performance of numerical simulation and evaluation of results. The developed methodology, presented in this paper, will be used in future clinical studies with the aim of improving treatment efficiency.

ACKNOWLEDGMENT

This research has been supported by the research program of the Czech Science Foundation (GACR) of the Czech Republic, Project No. 14-00386P Study of Thermal and Nonthermal Effects of High-Power EM Field on Structure of Matter.

Segmentation of Brain MR Images

M. Shuleska and D. Vrba
Faculty of Biomedical Engineering, Czech Technical University in Prague, Czech Republic

Abstract— One of the common issues of orofacial pain treatment using transcranial stimulations (TSs) is that the stimulations are applied by MDs based solely on their knowledge and experience and there is no mean to measure exact location, level and extent of the stimulation. The main aim of a planned project is, by means of patient-specific numerical simulations, to further improve current understanding of TSs as well as to investigate new possibilities how to improve their efficacy in pain treatment. This paper focuses on different aspects of the segmentation process of magnetic resonance images (MRI), of a human head, using a specialized segmentation program — iSeg. The proper segmentation of human head is a challenging task and is of crucial importance for planned numerical analysis. Availability of suitable (in terms of used MRI parameters) and high resolution MRI of each patient is essential part of the segmentation. The signal weighting (T1, T2, PD) and sequences parameters (TR, TE) of MRI are therefore discussed as well. The segmentation creates three-dimensional (3D) unstructured triangulated surface objects representing gray matter (GM), white matter (WM), the cerebrospinal fluid (CSF), skull, skin and various parts of the head. These surfaces define different domains in a 3D numerical model which can be imported into special programs for numerical simulation on electromagnetic field and develop and explore diverse medical situations. In our case the numerical models are imported in well-proven commercial simulation tool SEMCAD X, where numerical simulations are performed and evaluated.

ACKNOWLEDGMENT

This research has been supported by the research program of the Czech Science Foundation (GACR) of the Czech Republic, Project No. 13-29857P Human Body Interactions with EM Field Radiated by Metamaterial Structures.

EM Exposure System with Well Defined Dosimetry

J. Vrba[1], **L. Vísek**[1], **L. Oppl**[1], **D. Vrba**[2], **J. Vrba, Jr.**[2], **F. Vožeh**[3], **J. Barcal**[3], **and L. Vannucci**[4]

[1]Department of EM Field, Faculty of Electrical Engineering
Czech Technical University in Prague, Prague, Czech Republic
[2]Department of Biomedical Technique, Faculty of Biomedical Engineering
Czech Technical University in Prague, Kladno, Czech Republic
[3]Department of Patophysiology, Medical Faculty in Pilsen
Charles University in Prague, Pilsen, Czech Republic
[4]Institute of Microbiology, Czech Academy of Sciences, Prague, Czech Republic

Abstract— The whole-body exposure system for unrestrained mice was designed in order to analyze the influence of electromagnetic field. The setup operating at 900 MHz was designed with respect to induced uniform field, external radiation elimination, absorbed power determination, sufficient space for mice movement together with even mice exposure and costs. The main aim of this paper is to assure that the dosimetry results reached by computer simulations can be used for determination of absorbed power in the unrestrained mouse. The whole-body exposure chamber with anatomical mouse model was simulated by two different numerical methods: finite-difference-time-domain method (FDTD) and Finite Integration Technique (FIT) and its dosimetry results were compared by computed SAR values. In our contribution we will describe our first results dealing with observed biological effects of EM field, obtained by real exposures of experimental animals.

Numerical Modeling of Dielectric Properties of Silicon Phantoms for Microwave Imaging and Hyperthermia

P. Spurny, J. Vrba, Jr., D. Vrba, and M. Wiewegh
Faculty of Biomedical Engineering, Czech Technical University in Prague, Czech Republic

Abstract— Silicon-graphite powder mixtures with different silicon-graphite powder volumetric ratios were considered as composite material for preparation of solid and durable phantoms. The phantoms were intended for testing of microwave imaging as well as microwave hyperthermia systems. Several samples of these composites were prepared and dielectric properties were measured. The full desired range of dielectric properties of biological tissues were not achieved so far. A 3D concept for the numerical estimation of effective dielectric properties of oil and water emulsions with random droplet distribution was presented in the previous paper. Here this concept was adapted for estimation of effective dielectric properties of silicon-graphite powder mixtures. Geometry of powder particles as well as of the silicon-graphite powder mixtures were optically inspected and used in generation of the numerical models. The adapted concept can be described as follows. A MATLAB script automatically generates a random mixture of impenetrable graphite particles randomly placed in a cubic computational domain. The script assigns a proper boundary conditions to every face located on the outer walls of the computational domain as well as the corresponding dielectric parameters to each subdomain. The script also controls frequency of applied electric field and it also starts the quasi-static electric COMSOL Multiphysics simulation and evaluation of volume integrals (in COMSOL Multiphysics). It subsequently evaluates the effective dielectric properties. For each frequency and volumetric ratio up to ten simulations with independently generated random geometry were performed and statistical quantities, e.g., mean values and standard deviations, were computed. The results of the numerical simulations were compared to data estimated using different two mixing formulas as well as measured data. The main goal is to validate the numerical concept and use it subsequently to numerically test different components to be used for preparation of durable phantoms.

ACKNOWLEDGMENT

This research has been supported by the research program of the Czech Science Foundation (GACR) of the Czech Republic, Project No. 14-00386P Study of Thermal and Nonthermal Effects of High-Power EM Field on Structure of Matter.

Tunable Polarization Rotator in Bilayered Metamaterial

Zui Tao, Xiang Wan, Bai Cao Pan, and Tie Jun Cui
State Key Laboratory of MWs, Southeast University, Nanjing 210096, China

Abstract— Polarization is one of the most important factors which conveys valuable information for electromagnetic signal processing. Polarization conversion dichroism can lead to an asymmetric transmission (AT) phenomenon, which was discovered in planar chiral metamaterial patterns from microwave to optical frequencies. The AT phenomenon is that a specific polarized electromagnetic can pass through a material from forth to back, but it can't pass back in the same polarization. To get the diodelike AT phenomenon, simple structure and high polarization conversion efficiency polarization rotators are desirable needed. Mostly we need three layered metallic patterns to get a relatively broad work band, but sometimes bilayered polarization rotator is also needed for its simple structure. Although many polarization rotators are reported before, they are mostly designed for a specific function, which mean that they can't satisfy the demand of intelligent control, as the environment changing. To get multi-functional polarization rotator, we designed a newly tunable bilayered metamaterial in this paper, which consists of a two layered polarization rotator and an active diode. The two layered polarizations rotator has simple structure and can provide high polarization conversion efficiency in around 8 GHz. The simulation results show that the performance of the asymmetric metamaterial can be controlled by the voltage of the active diode to work in different situations for linearly polarization waves. When the state of active diode is on, the metamaterial can fulfill AT phenomenon in one polarization, but can be regarded as a reflection plate in the other polarization. However, it is a reflection plate in both two polarizations when the state of active diode is off.

Simulation and Analysis of Radio Wave Propagation Characteristics of Typical Outdoor Environment

Yong Li[1], **Feng Chen**[2], **and Yuan-Jian Liu**[2]

[1]Zhongxing Limited Corporation of Telecommunications, China
[2]College of Electronic Science and Engineering
Nanjing University of Posts and Telecommunications, Nanjing 210003, China

Abstract— As the rapidly development of the mobile communication technology in recent years, predicting the propagation characteristics for urban area has become an important subject. In this paper, the propagation characteristics of typical outdoor environment at 3.5 GHz are simulated and analyzed by using the method of SBR (Shooting and bounding ray tracing). And it is achieved agreement by a comparison of simulated results and results in the literature, so the correctness of the method has been validated. Some propagation parameters are obtained in the simulation, such as the 3-D received power, RMS (Root Mean Square) delay spread, direction of arrival, Doppler shift and so on. These propagation parameters under LOS (Line-of-sight) and NLOS (None-line-of-sight) have been compared in this paper. The study can avoid time-consuming, laborious and the larger cost of testing and analyze radio wave propagation in urban micro-cellular environment by computer simulation. In the typical outdoor environment, the delay spread of the mobile station in NLOS is significantly higher than that in LOS. So the signal quality is poor, and results in the inter-symbol interference. The direct path is in a dominant role in outdoor street environment of radio wave propagation. As the transmitter leave away, the receiver power will reduce. But due to the reflection and diffraction paths, street power distribution has ups and downs, and the received power does not completely depend on the distance between the transmitting and receiving antennas. When the receiver is mainly located in NLOS environment and the transmitter is fixed, the variation of the radio wave propagation Doppler frequency in outdoor micro-cell environment is large. The contrast analysis of the above results provides the theoretical foundation for outdoor micro-cell at 3.5 GHz radio wave communication system, and benefits the base station planning and optimization of urban micro-cellular environment.

Mutual Coupling Evaluation within Waveguide Slotted Antennas

Giovanni Leone and Domenico Russo
Dipartimento di Ingegneria Industriale e dell'Informazione
Seconda Università degli Studi di Napoli, Italy

Abstract— Phased arrays made of a very large number of slot antennas find still appealing applications because of their mechanical advantages. A full wave complete analysis is prevented by the very large electrical dimension of the array. Accurate radiation performance predictions require to consider both internal and external mutual coupling effects between slots of different sizes. These effects can be decoupled by introducing a generalized admittance matrix (GAM) approach. Hereafter, by assuming that slots are embedded within an infinite PEC plane and that tangential fields are expanded under modal expansions of rectangular waveguides over each slot, the external GAM is computed in closed form. It connects the expansion coefficients of the tangential magnetic field over the slots to the ones of the tangential electric field. In principle, a generic element of the matrix requires the numerical evaluation of a quadruple integral. In this paper a cancellation approach is used to remove the singularity of the Green's function and the order of integration is reduced by a suitable changes of variables. In this way self and mutual admittances can be estimated by computing double integrals. By a further approximation mutual admittance elements can be reduced to a single integrals saving computational time and resources. Results of such approach are finally compared with the ones provided by a commercial numerical simulation tool showing good agreement. The approach allows to appreciate the role of the number of expansion modes and the distances between the slots on the accuracy of the array radiation pattern prediction.

Chaotic Low-frequency Fluctuations of the Laser Radiation Emitted by a Diode Laser Working at Currents above the Laser Threshold

I. R. Andrei[1], **A. Baleanu**[2], **and M. L. Pascu**[1, 2]

[1]National Institute for Laser, Plasma and Radiation Physics, Magurele, Romania
[2]Faculty of Physics, University of Bucharest, Magurele, Romania

Abstract— A complex chaotic behavior can be found in nonlinear dynamics of a semiconductor laser under optical feedback provided by an external reflector. When an external cavity is coupled, the laser system switches to an oscillating state; it follows a chaotic trace. The amplitude of the induced chaotic "noise" seems to be important, depending on the feedback intensity which is between 1% and 10% of laser emission power. One of the most studied issues on the chaotic dynamics is the low-frequency fluctuations (LFF) regime which occurs at laser operation near the lasing threshold and behaves as a cyclic dropout almost to zero of the output light beam intensity.

The chaotic behavior of the semiconductor laser emission with external feedback is influenced by laser parameters. Optical feedback intensity, injection current and diode temperature greatly influence the chaotic system evolution.

In this paper an extensive analysis of phenomena observed in the laser emission of an external cavity — semiconductor laser (ECSL) system operating in the low-frequency fluctuations regime has been carried out. We present data about the stability of the LFF chaotic dynamics regimes of a semiconductor laser (AlGaInP Fabry-Perot semiconductor lasers) for different sets of experimental parameters. The injection current during the measurements was adjusted at values near and over the threshold current corresponding to different set temperatures.

LFF regimes were obtained at current values over the threshold current, but only in certain conditions which depend of the intrinsic properties of the active region, respectively at currents where there is instability of mode-hopping type in the laser emission dynamics without feedback. The values of parameters for such regimes can only be determined experimentally, but the high temperatures favor the stability of the LFF regime. Also, the amount of feedback intensity must be of the same order of magnitude as at the operation at threshold current.

ACKNOWLEDGMENT

This work was supported by the Romanian ANCS/CNDI-UEFISCDI program, projects PN-II-ID-PCE-2011-3-0922 and NUCLEU program, project LAPLAS 3-PN09 39.

An Adaptive Spectroellipsometric Technology for the Diagnosis of Water Ecosystems

F. A. Mkrtchyan, **V. F. Krapivin**, **and V. V. Klimov**
Institute of Radioengineering & Electronics RAS
1 Vvedensky Sq., Fryazino, Moscow reg. 141190, Russia

Abstract— Design and development of methods spectroellipsometry and creation on their basis of a multi-channel polarization-optical devices is regarded as one of the most important stages of the study of water systems in real time. The efficiency for solving multi-parameter problems to a large extent depends on the sensitivity and accuracy of the instruments, their high speed measurements, the possibility of using a wide spectral range. Spectral measurements in aqueous media provide an informative basis for the use of modern detection and classification of pollutants that environment.

In this paper we developed a multi-channel information-measuring system (Adaptive Spektroellipsometric Identifier) for the control of water pollution, based on the combined use of methods spectroellipsometry, learning algorithms, classification and identification. The system differs from existing foreign spectroellipsometric devices using a new method of ellipsometric measurements, the original element base polarization optics and complex mathematical approach to assessing the quality of a water body subjected to anthropogenic influence. The system has the functions of learning recognition and classification of aquatic pollutants. The system allows to realize the function of prediction and decision making for the detection of contaminants in water, detect oil slick and determine their parameters; thickness, the location of the source of contamination, time of occurrence.

ACKNOWLEDGMENT

The reported study was partially supported by RFBR, research project No. 13-07-00146.

The Experimental, Frequency-selective Evaluation of the Pattern of Environmental Radiofrequency Electromagnetic Radiation in Ground and Underground Public Transport Infrastructure in Warszawa

Krzysztof Gryz, Jolanta Karpowicz, and Wiesław Leszko
Central Institute for Labour Protection — National Research Institute (CIOP-PIB)
Czerniakowska 16, Warszawa 00-701, Poland

Abstract— In the city over the million of population, the significant percentage of it is travelling at least 1–2 hours daily by public transport, such as buses, trams, metro. During the drive they are exposed to a specific combination of radiofrequency electromagnetic radiation, emitted by various wireless communications systems (e.g., antennas of mobile phones base transceiver stations and handsets used by passengers, internet public access, etc., and emitters are located in various distances, including very short one — e.g., of mobile handsets of other passengers or base station antennas located inside underground metro. The investigations of radiofrequency environmental electromagnetic radiation inside ground (busses and trams) and underground (metro) public transport infrastructure were performed in Warszawa (capital city of Poland). The frequency-selective exposimeters of electric field strength were used to register a set of exposimetric profiles of exposure of passengers and public transport workers (excluding drivers). The statistical parameters of registered exposure were analysed, with attention to the day-time of measurement, kind of transport and city location (downtown, residential areas) — calculated for each frequency range and for total value (representing wide-band result of complex exposure).

Investigations shown the statistically significant differences in sup-groups of registered exposimetric profiles. It was shown that for the users or workers of public transport infrastructure, the exposure during daily trip to work/school and back home may be a dominating component of the life exposure. In conclusion it is therefore recommended to pay attention on the daily travels habits of any subject of epidemiological studies related to radiofrequency radiation health outcome (e.g., studies related to IARC classification of radiofrequency radiation in the group of possible carcinogenic environmental factors). It was also found that investigated exposure is significantly lower (of an order of a fraction of V/m in the mean value and a several V/m in the maximum value) than international exposure limits (of an order of 50 V/m in the radiofrequency band).

ACKNOWLEDGMENT

Research supported — within the scope of state services — by the Ministry of Labour and Social Policy, Poland (2014–2016) — within the National Programme "Improvement of safety and working conditions" (2.Z.29). The CIOP-PIB is the Programme's main co-ordinator.

Experimental Analysis by Dual Characterization of Near Field Impact on Humans Level of Occupational Exposure to 30–110 MHz Radiation

Simona Miclaus[1], **Jolanta Karpowicz**[2], **and Paul Bechet**[1]

[1]Department of Technicals Sciences, "Nicolae Balcescu" Land Forces Academy, Sibiu, Romania
[2]Laboratory of Electromagnetic Hazards
Central Institute for Labour Protection-National Research Institute (CIOP-PIB), Warszawa, Poland

Abstract— In the frequency range 30–110 MHz, which is the band of interest in present paper, the induced current in body limbs is regulated in guidelines for limiting human exposure to radiofrequency fields because of the limbs thermal load caused by exposure. The safety limits are set to $I_{limit1} = 45\,\text{mA}$ — for general public and $I_{limit2} = 100\,\text{mA}$ — for occupational exposure (averaged over a six-minutes periods). They supplement the safety levels set for both electric and magnetic field strengths of unperturbed fields where anyone may be present. Practically, the characterization of an occupational exposure situation may be complete by including limb currents evaluation instead of thermal effects numerical calculations. In references presently available, just scarce approaches exist that follow experimentally the simultaneous determination of both indicators, in real exposure conditions. In addition, characterization of near field and mainly its reactive region — presenting steep gradients — from the perspective of occupational exposure assessment, remains a complex task.

Present work analysed individual exposition in a group of 15 human volunteers being placed in the reactive near field of a biconical antenna (2 m distance) fed by continuos wave and input powers levels similar to that used by military radiocommunication equipment in the HF band. The variables of the experiment were: a) intrinsec: the person's position and posture (sitting, standing up facing the antenna, standing up lateral) and contact with the floor (type of shoes sole); b) extrinsec: frequency (three values were used: 30, 70 and 110 MHz), input power level (low and medium) and antenna polarization (horizontal and vertical). Incident field stregth (omnidirectional) in a fixed position was measured by an electric-field sensor while induced current in the feet of the human was determined by using an ankle fastened clamp-on current meter.

Descriptive statistics applied on experimental results showed: 1. Frequency and posture are the most sensitive parameters relating to induced currents for the same polarization. 2. Grounding/shoe sole type is not so important in near-field exposure level determination. 3. No correlations were obtained between induced currents and subjective parameters — height, weight, BMI, water content, fat content. 4. Strong correlations were obtained between induced currents at different frequencies but only for postures presenting high area of received field (in both standing postures, but not in sitting posture — this conducts to the idea of a body shape efficiency factor). 5. High correlation coefficients were obtained between induced currents and incident E-field strength for the same posture for all three frequencies, indicating that E-field level can be a proper predictor of induced current levels for the same polarization and same posture in the reactive near field. 6. Average height of volunteers presented a resonance at 70 MHz which is approx. 40% of the wavelength in free space (the ground was low conductive).

Wideband Dual-mode Dielectric Waveguide with Applications in Millimeter-wave Interconnects and Wireless Links

Nemat Dolatsha and Amin Arbabian
Center of Integrated Systems (CIS), EE Department, Stanford University, Stanford, CA, USA

Abstract— With the exponential growth in data traffic arising from new subscriptions and emerging web and mobile applications, there is a significant need for efficient and extremely high throughput wired and wireless links that can provide similar gains in network capacity at all levels. A substantial improvement in bandwidth and energy efficiency is required. Thanks to the recent progress in developing efficient CMOS transceivers, a relatively large bandwidth is now available at millimeter/sub-millimeter waves. The available large bandwidth can be still boosted by deploying multi-mode excitation of waveguide interconnects and antennas. Here, the challenge is the efficient excitation of appropriate modes.

To this aim, recently, we have proposed an all-electrical, low-cost and easy-to-package structure based on mm-wave dielectric waveguides for high-throughput interconnects [see Fig. 1(a)]. Use of mm-wave dielectric waveguides addresses the low-loss transmission requirement and leads to high energy-efficiency especially for short to medium range applications. A planar feed structure excites two *polarization-orthogonal* modes of a rectangular dielectric waveguide, namely the E_x^{11} and E_y^{11} modes. A printed electric dipole (in x direction) placed on top of the waveguide simply launches the E_x^{11} mode (with electric field in x direction) into the waveguide. The E_y^{11} mode is coupled into the waveguide using a printed slot dipole placed on the bottom side of the waveguide. In the current paper, to simplify the implementation, the feed structure is modified and both mode couplers are mounted on the single side of the waveguide. Due to difficulties in together integration of electric dipole and slot dipole on a single side, the slot dipole is replaced by a planar horn-like structure realized in a substrate-integrated waveguide (SIW) [see Fig. 1(b)]. The upper metal plate of the SIW structure is extended to serve a reflector for the electric dipole. Its lower metal plate is truncated after the *metal wall* to efficiently couple SIW fields into the E_y^{11} mode (with y polarization electric field) into the dielectric waveguide. The coupling efficiency of better than 4 dB over a wide frequency range from 60 GHz to 90 GHz is shown in Fig. 1(c). The isolation to the unwanted mode is better than 35 dB for both mode couplers. In practice, the electric dipole and the SIW feed will be connected to transceivers using appropriate microstrip transitions printed on the upper RO3003 dielectric. The complete feed network input return loss, transmission and isolation of modes in the back-to-back structure with a polyethylene dielectric

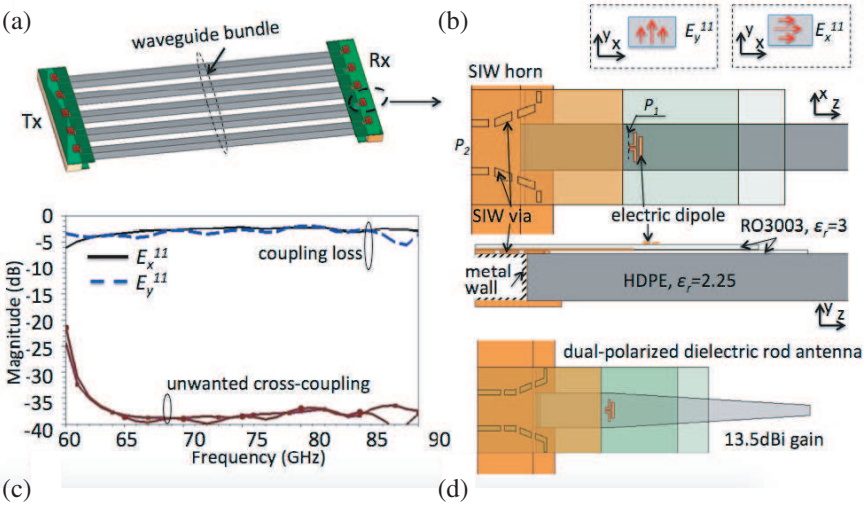

Figure 1: (a) Conceptual schematic of the proposed multi-mode dielectric waveguide for high throughput wireline links, (b) top view and side view of the planar multimode excitation structure, electric dipole for E_x^{11} mode and the SIW horn for the E_y^{11} mode (p_1 and p_2 shows the excitation points of electric dipole and the SIW horn structure), (c) coupling efficiency and mode isolation between launched modes, (d) high gain dual-polarized dielectric rod antenna fed by the proposed planar excitation structure.

waveguide in between will be discussed in the full-paper. The proposed feed structure is also used for dual polarization excitation of a high gain dielectric rod antenna (Fig. 1(d)). This doubles the available capacity of the single rod antenna. Simulations show gains of better than 13 dBi for each of polarizations at the center frequency of 75 GHz.

Some Results of Troposphere Mesoscale Fluctuation Analysis in City by Using Network of GPS-GLONASS Receivers

V. E. Khutorov, **G. M. Teptin**, **and O. G. Khutorova**
Kazan Federal University, Russia

Abstract— In this paper we show results of troposphere fluctuation analysis and its influence on radiowaves refractive index variations. For comparison of inhomogeneous impurities structure we used electromagnetic waves refraction index data which don't depend on impurity but depend on atmospheric parameters only. Our main object of investigation is a mesoscale process in troposphere. These processes have size from 1 km to 1000 km and time frames around few hours. This task requires system with good temporal and spatial resolution. We can estimate space structure of atmospheric parameters, using the data from network based on Global Navigation System receivers.

On the stage of the calculation of the tropospheric delay measurements were divided into two samples in the first included delay calculated for radiopaths passing over the town. In the second sample included radiopaths going out of town. Compared diurnal variation of the structure function zenith tropospheric delay resulting from these two samples.

We used structure function to estimate characteristics of impurities and refraction index fluctuation. Structure function is a basic characteristic of process with random increments. Physically, structure function is a square of fluctuation of investigated parameter. Function shows the contribution of the processes of the defined scale in the total variance of the fluctuations.

It is shown that remote sensing signals, of GLONASS and GPS satellites passed though troposphere, measured by a network of receivers, allows us to study the quantitative characteristics of inhomogeneities of the refractive index dm radio waves at different heights of the troposphere, in particular, the horizontal structure functions of the index of refraction and troposphere delay of signals, including their diurnal variations. Comparison of results obtained in the data of independent ground-based measurements of the structural function of the refraction index and high-altitude radiosonde measurements showed good agreement. The results obtained in this paper do not contradict the previously known publications.

Development of Wireless Power Induction Cooker Using Magnetic Induction-based Technology

Wonho Jang[1], **Seonghun Lee**[2], **Jeongsug Yeom**[3], **Byungduk Min**[4], **Goonyeon Kim**[1], **and Sangho Choi**[1]

[1]Electromagnetic Wave Technology Institute of RAPA, Seoul, Korea
[2]Creative Innovation Center of LGE, Seoul, Korea
[3]Komatech, Seoul, Korea
[4]R&D Department of Green Power, Suwon, Korea

Abstract— Tightly coupled (TC) wireless power transmission offers higher power transmission and higher efficiency of power transmission compared to the loosely coupled technology which is magnetic resonance-based technology. We develop wireless power cooker using magnetic induction-based technology which means tightly coupled technology. The cooker has over 90% dc-to-dc power transmission efficiency and transmits high power up to 2.4 kW. We used 20 kHz frequency to resonate between transmission coil and reception coil.

Introduction: Wireless power transfer (WPT) systems are becoming ubiquitous with applications in powering smartphones, transportation and a range of kitchen appliance devices such as induction cooker.

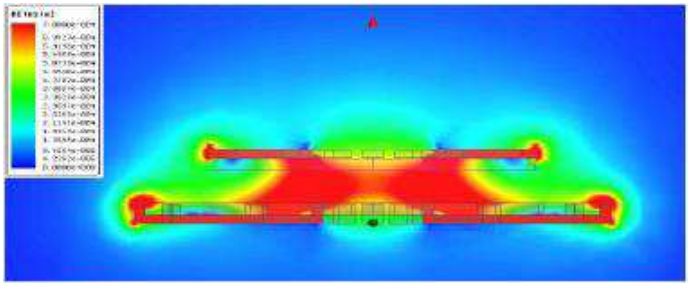

Figure 1: Coil shielding part simulation by Maxwell.

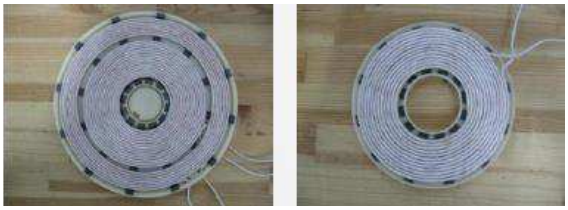

Figure 2: Transmission and reception resonators.

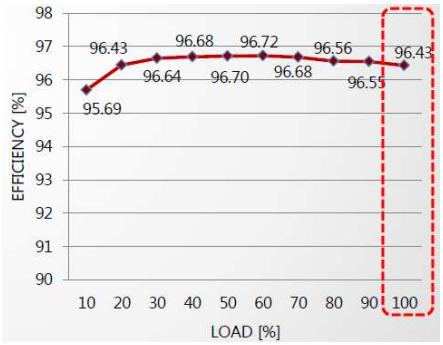

Figure 3: Power transmission efficiency graph.

Weight Reduction Structure for Wireless Charging Vehicle

Hyung-Wook Shim, Dang-Oh Kim, Jong-Woo Kim, and Dong-Ho Cho
Korea Advanced Institute of Science and Technology, South Korea

Abstract— For replacing fossil fuel to eco-friendly resources, many types of transportation have been introduced in our life. Wireless charging transportation (WCT) such as electric vehicle and bus is one of the transportation developed in KAIST (Korea Advanced In Science and Technology) since 2009. Although it have a few hinders regarding power, transfer efficiency and heavy cost, it is obvious that WCT will bring out ripple effect in transportation trend for convenient charging and various applications. To develop performance of WCT at the level of commercialization, it is essential to achieve acceptable power transfer efficiency. Moreover, according to the limitation of battery capacity, the alternative solution about the increasing mileage should be needed. Despite an advanced technology such as magnetic shaping technology and the massive capacity battery have been introduced recently, the effective and fundamental solution is a weight reduction structure. If the lighter structure is installed, suppose that has as same power efficiency as before, it is possible to increase driving distance or room for battery. However, there are two important issues of weight reduction. First, maintain the power transfer efficiency. Second, maintain the strength of system structure. That is, as mentioned above, it is the key to design of lighter charging system without fluctuation of efficiency and strength. Therefore, the research regarding these issues should be carried on. Connected to upper states, in this paper, the weight reduction wireless charging system for a railroad is suggested to promote eco-friendly rail system. Since, it is used the diffraction property of electromagnetic fields, it shows prominent performance with little power efficiency drop and strength.

A New UWB Antenna with Unidirectional Radiation

Mingjian Li, Kwai-Man Luk, and Yue Zhao
Electronic Engineering Department, City University of Hong Kong
83 Tat Chee Avenue, Kowloon, Hong Kong SAR, China

Abstract— A new ultra-wideband antenna with unidirectional radiation pattern is proposed. The antenna is based on the model of magneto-electric dipole and excited by utilizing a new pair of differential feeds to provide an ultra-wideband impedance matching. Besides, a rectangular box-shaped reflector is employed to reduce the back radiation and the fluctuation of the antenna gain. Experimentally, an antenna prototype was fabricated and tested. The proposed antenna exhibits an impedance bandwidth of over 130% covering the whole UWB spectrum. The antenna gain varies between 7.16 and 14.1 dBi. More importantly, this antenna radiates unidirectionally with low cross polarization and low back radiation over the operating frequency range.

Miniaturized Transmitter in Digital Modulation System with Non-constant Envelope for VHF Band

Heon-Kook Kwon, Sung Jun Lee, Byung-Su Kang, and Bong-Hyuk Park
Electronics and Telecommunications Research Institute (ETRI), Korea

Abstract— In this paper, compact transmitter included power amplifier linearization in digital modulation with non-constant envelope for VHF band using cartesian feedback loop is presented. The digital modulation (QPSK/16-QAM/64-QAM) signal is non-constant envelope with constant peak to average power ratio. Digital modulation signal is used when linearized PA is 64-QAM, 70 ksps symbol rate, 0.35 of roll-off factor, and 7.5 dB PAPR. We used the Mitsubishi's Silicon power module, RA60H1317M1A, as a results, obtained an Adjacent Channel Power Ratio(ACPR) of less than −72 dBc, Error Vector Magnitude (EVM) of 2.8% at +39 dBm in VHF band. This technique is utilized to achieve miniaturization of transmitter with high linearity.

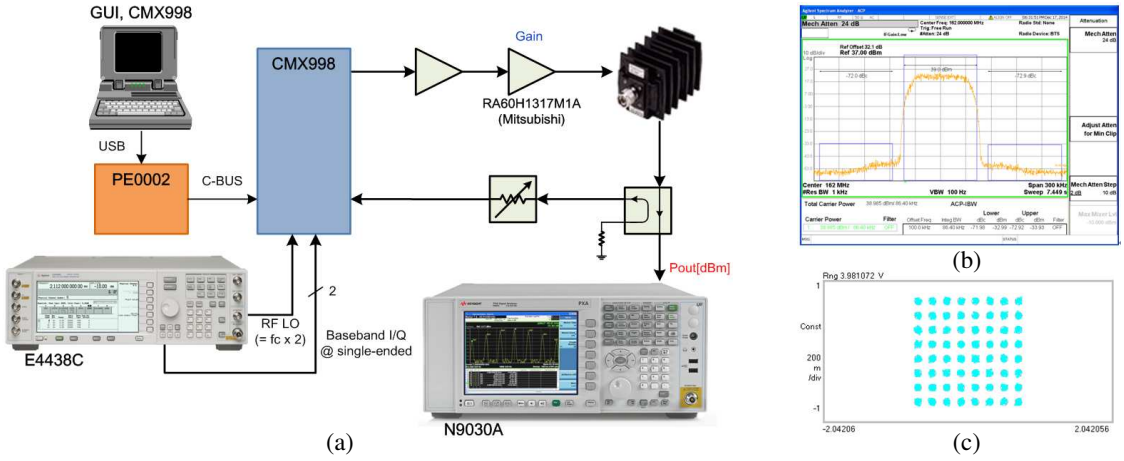

Figure 1: Test configuration and results for linearization of the power amplifier. (a) Test configuration. (b) ACPR. (c) Constellation

ACKNOWLEDGMENT

This research was supported by 'The Cross-Ministry Giga KOREA Project' of the Ministry of Science, ICT and Future Planning, Korea [GK14N0100, 5G mobile communication system development based on mmWave].

REFERENCES

1. Narendra, K., L. Anand, P. Sangaran, S. Anbalagan, and G. Boeck, "RF power amplifier with cartesian feedback for TETRA modulation," *ICECS*, 262–265, Dec. 11–14, 2007.
2. White Paper, "TETRA enhanced data services on TETRA 1 hardware," CML Microsystems, Feb. 2010.

Session 1P1
FocusSession.SC2: Nonlocal and Spatially Dispersive Electromagnetic Media

Nanophotonics in Material-systems of Large Sizes

Marin Soljacic
Department of Physics, Massachusetts Institute of Technology
Cambridge, Massachusetts 02139, USA

Abstract— Recent nano-fabrication developments enabled implementation of many nanophotonic techniques to macroscopic scales, which is crucial for many applications of interest (e.g., energy conversion, displays, lighting). Some exciting new opportunities in this area will be presented.

Photonic Hypercrystals

E. E. Narimanov
Purdue University, USA

Abstract— We describe a new class of artificial optical media — the photonic hyper-crystals. These hyperbolic metamaterials with a periodic spatial variation of dielectric permittivity on a subwavelength scale, combine the features of optical metamaterials and photonics crystals within the same medium.

Metamaterials [1] and photonic crystals [2] currently represent the two primary paradigms for new optical materials. An artificial medium for electromagnetic applications generally relies on either the effect of a subwavelength pattern that changes the average electromagnetic response of the medium, or on Bragg scattering of light due to a periodic variation that is comparable to the wavelength. Due to this inherent scale separation, the corresponding metamaterial and photonic crystal concepts are generally considered mutually exclusive within the same environment.

The situation is however dramatically different in the case of hyperbolic metamaterials [3], where the opposite signs of the dielectric permittivity components in two orthogonal directions ($\epsilon_n \epsilon_\tau < 0$) lead to a hyperbolic dispersion of TM-polarized propagating waves

$$\frac{k_\tau^2}{\epsilon_n} + \frac{k_n^2}{\epsilon_\tau} = \frac{\omega^2}{c^2}, \tag{1}$$

with the wave numbers unlimited by the frequency. As a result, a periodic variation in the dielectric permittivity, regardless of how small is its period, will necessarily cause Bragg scattering of these high-k waves, leading to the formation of photonic bandgaps in both the wavenumber and the frequency domains.

The resulting hyper-crystals [5] — the hyperbolic metamaterials with a periodic spatial variation of dielectric permittivity on a subwavelength scale — bring a broad range of the physical phenomena from the field of photonic crystals to the metamaterial realm, leading to an unprecedented degree of control of light propagation in this new class of optical media.

ACKNOWLEDGMENT

This work was partially supported by NSF Center for Photonic and Multiscale Nanomaterials, ARO MURI and Gordon and Betty Moore Foundation.

REFERENCES

1. Cai, W. and V. Shalaev, *Optical Metamaterials*, Springer, New York, 2010.
2. Joannopoulos, J. D., et al., *Photonic Crystals: Molding the Flow of Light*, Princeton University Press, Princeton, 2008.
3. Jacob, Z., L. V. Alekseyev, and E. Narimanov, *Optical Hyperlens: Far-field Imaging beyond the Diffraction Limit*, Vol. 14, 8247, 2006.
4. Hoffman A. J., et al., "Negative refraction in semiconductor metamaterials," *Nature Materials*, Vol. 6, 948, 2007.
5. Narimanov, E., "Photonic hypercrystals," *Phys. Rev. X*, Vol. 4, 041014, 2014.

Investigation of the Permittivities of Metal Films at Nanometer Scales

Haoliang Qian, Yuzhe Xiao, Dominic Lepage, and Zhaowei Liu
Department of Electrical and Computer Engineering
University of California, San Diego, 9500 Gilman Drive, La Jolla, California 92093-0407, USA

Abstract— With the development of nano-fabrication techniques, the dimensions of the plasmonic device have been shrunk into the nanometer scales. To understand the physics in such small plasmonic devices, the quantum confinement effects need to be considered. Here we choose the ultra-thin metal film as a platform to study this effect. We focus on their optical properties by studying the reflection and transmission of gold thin films with thickness varying from 30 nm to 2.5 nm. A theoretical model based on the self-consistence solution of Schrodinger equation and Poisson equation is proposed. According to this model, the transmission of a few nanometer gold film increases with increasing incident wavelength, which is completely different to the predictions based on Drude model and nonlocal model. We fabricated a series of ultra-thin gold films and ellipsometry results agree well with our theoretical model.

Ultra-transparency Induced by Spatial Dispersions

Jie Luo[1], **Yuting Yang**[1], **Weixin Lu**[1], **Zhongqi Yao**[1],
Zhi Hong Hang[1], **C. T. Chan**[2], **and Yun Lai**[1]

[1]College of Physics
Optoelectronics and Energy & Collaborative Innovation Center of Suzhou Nano Science and Technology
Soochow University, Suzhou 215006, China
[2]Department of Physics and Institute for Advanced Study
Hong Kong University of Science and Technology, Clear Water Bay, Hong Kong, China

Abstract— Transparencyis usually not perfect in nature. Reflection of light on the surface of transparent materials such as glass is usually small but inevitable, except for transverse magnetic (TM) polarization and a single incident angle called the Brewster's angle. Light of any other incident angles or of transverse electric (TE) polarization willbe partly or totally reflected due to impedance mismatch. Based on the principle of destructive interference, most anti-reflection coatings have been widely applied to reduce reflection but only for light at normal incidence.Wide-angle and even omni-directional non-reflection and total transmission, which we denote as ultra-transparency, is really difficult if not impossible.

In this work, we propose a possible solution to ultra-transparency by going beyond the framework of local photonic media by incorporating spatial dispersions, in which $\boldsymbol{\varepsilon}(\omega, \mathbf{k})$ and $\boldsymbol{\mu}(\omega, \mathbf{k})$ are not only dependent on the angular frequency ω, but also on the wave vector $\mathbf{k}$. We find that the Brewster's angle can thus be expanded from a single one to a wide range of angles, leading to the property of wide-angle and even omnidirectional non-reflection and total transmission. By designing pure dielectric photonic crystals with a shifted elliptical dispersion, we numerically and experimentally demonstrated such an ultra-transparency effect. This new type of photonic media, with the new degree of freedom of spatial dispersion introduced, opens possibilities to novel optical designs.

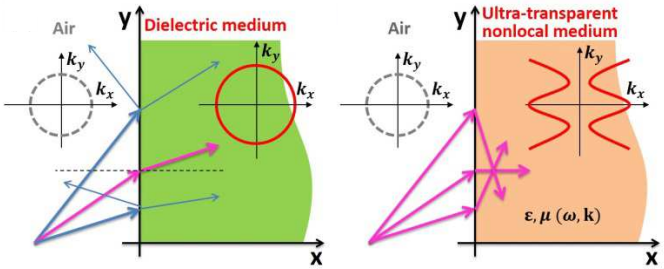

Figure 1: Illustration of reflection and transmission on the surfaces of dielectric and ultra-transparent spatially dispersive photonic media.

Dislocated Double-layer Metal Gratings as an Efficient Unidirectional Coupler

Yang Shen and Chongjun Jin
State Key Laboratory of Optoelectronic Materials and Technologies
School of Physics and Engineering, Sun Yat-sen University, Guangzhou 510275, China

Abstract— We propose and demonstrate a dislocated double-layer metal grating structure, which operates as a unidirectional coupler capable of launching surface plasmon polaritons (SPPs) in a desired direction under normal illumination. The structure consists of a slanted dielectric grating sandwiched between two gold gratings, as a result, the upper gold grating has a latitudinal relative displacement to the lower one. Numerical simulations show that a grating structure with 7 periods can convert 49% of normally incident light into surface plasmons, with a contrast ratio of 78 between the powers of the surface plasmons launched in two opposite directions. We explain the unidirectional coupling phenomenon by the dislocation-induced interference of the diffracted waves from the upper and lower gold gratings. Furthermore, we developed a simple and cost-effective technique to fabricate the structure via tilted two-beam interference lithography and subsequent shadow deposition of gold. The experimental results demonstrate a coupling efficiency of 36% and a contrast ratio of 43. The relatively simple periodic nature of our structure lends itself to large-scale low-cost fabrication and simple theoretical analysis. Also, unlike the previous unidirectional couplers based on aperiodic structures, the design parameters of our unidirectional coupler can be determined analytically. Therefore, this structure can be an important component for surface-plasmon-based nanophotonic circuits, by providing an efficient interface between free-space and surface plasmon waves.

Bridging Classical and Quantum Optics

Yu Luo
School of Electrical and Electronic Engineering
Nanyang Technological University, Nanyang Avenue 639798, Singapore

Abstract— The miniaturization trend in experimental nano-optics is currently approaching the subnanometer regime, where the quantum effect plays a key role. On the one hand, the classical macroscopic electromagnetism cannot describe the quantum nature of electrons. On the other hand, previous full-quantum approaches demand high computational resources, preventing their applicability to realistic nanophotonic devices. In this talk, I will introduce a multiscale model able to describe realistic nanophotonic systems in the quantum regime. I will show how to connect the quantum simulation and the classical electromagnetic method at the mesoscopic scale through an appropriate modification to the local dielectric function at critical geometrical features. Our approach incorporates radiative, nonlocal, and quantum tunnelling effects, and thus can be applied to design large-scale plasmonic systems with Angstrom-sized geometrical features. As an example, I will show how to use this model to design super-resolution imaging system able to resolve sub-10-nm objects.

Manipulating of the Surface State between a Photonic Crystal and a Metasurface

Qiang Wang[1], **Meng Xiao**[2], **Hui Liu**[1],
Shining Zhu[1], **and C. T. Chan**[2]

[1]School of Physics, Nanjing University, Nanjing 210093, China
[2]Department of Physics, The Hong Kong University of Science and Technology
Clear Water Bay, Hong Kong, China

Abstract— A surface state is introduced between a photonic crystal and a metasurface. The surface state is excited when the reflection phase matching condition is satisfied. The reflection phase of metasurface can be tuned by changing the structural parameter. The resonance properties of surface state can be manipulated in the process. Field enhancement induced by the surface state will have important applications in nonlinear and quantum optics.

Probing Spatial Nonlocality Effects in Plasmonic Nanostructures with Surface-enhanced Raman Scattering Spectroscopy

Dang Yuan Lei[1, 2]

[1]Department of Applied Physics, The Hong Kong Polytechnic University, Hong Kong, China
[2]Shenzhen Research Institute, The Hong Kong Polytechnic University, Shenzhen, China

Abstract— Spatial nonlocality effects, arising from atomic interactions and electron-electron repulsion, are recently believed to set the ultimate limits of plasmonic near-field enhancements in metallic nanostructures with critical dimensions on the order of a few nanometers or less [1, 2]. In a different context, surface-enhanced Raman scattering (SERS) spectroscopy has become a versatile vibrational spectroscopic technique with a number of applications in the chemical, material and, in particular, life sciences in the last decades. In this talk, I will show our recent work on the use of SERS spectroscopy for probing the spatial nonlocality effect in rough metal films with controlled surface roughness [3]. Our results reveal that this quantum mechanical effect on the metal dielectric response of metal has to be taken into account for more accurate prediction of the SERS enhancement at large surface roughness. Our current work focuses on the SERS spectroscopy of both spatial nonlocality and quantum tunneling effects in metal nanoparticle dimers with tunable interparticle distance down to sub-nanometer scales which are prepared by a sophisticated layer-by-layer self-assembly method [4].

REFERENCES

1. Ciracì, C., et al., *Science*, Vol. 337, 1072, 2012.
2. Mortensen, N. A., S. Raza, M. Wubs, T. Søndergaard, and S. I. Bozhevolnyi, *Nat. Commun.*, Vol. 5, 3809, 2014.
3. Zhao, Y., X. Liu, D. Y. Lei, and Y. Chai, *Nanoscale*, Vol. 6, 1311, 2014.
4. Yu, X., et al., *Nano Today*, Vol. 8, 480, 2013.

Ultrathin Planar Optical Devices with Unusual Functionalities

Xianzhong Chen[1], **Dandan Wen**[1], **Fuyong Yue**[1], **and Ming Chen**[2]

[1]Institute of Photonics & Quantum Sciences, School of Engineering and Physical Sciences
Heriot-Watt University, Edinburgh, EH14 4AS, UK
[2]Guangxi Experiment Center of Information Science
Guilin University of Electronic Technology, Guilin 541004, China

Abstract— Miniaturization and integration are two continuing trends in the production of photonic devices. Metamaterials, the artificial materials, whose optical properties are determined by their geometrical structures instead of their constituent material composition, have opened new avenues in the manipulation of the light propagation. Metasurfaces, the emerging field of metamaterials, which consist of a single layer of artificial "atoms" have captured the attention of the scientific community over the past several years. At the interface of a metasurface, wave front shaping is accomplished within a distance much smaller than the wavelength of light beam, thus providing new opportunity to develop ultrathin devices that are easy to integrate into compact platforms. This technique does not require complicated three-dimensional nano-fabrication techniques but can provide full control of light propagation, which promises a whole variety of amazing applications, e.g., quarter-wave plates, spin-hall effect of light, and spin controlled photonics. In this talk, we are going talk our recent work in developing new ultrathin optical devices with unusual functionalities, including metasurface for characterization of light polarization, longitudinal multi-foci metalens for circularly polarized light and high efficiency functionality-switchable devices. Full and arbitrary phase control is achieved without extra look-up table or phase accumulation along an optical path. New ultrathin optical devices with unusual functionalities will be demonstrated. These findings are still under investigation and promise new exciting applications.

Multirefringence Phenomena in Plasmonic Multilayers

A. A. Orlov[1], **S. V. Zhukovsky**[1, 2],
P. M. Voroshilov[1], **A. S. Shalin**[1], **and P. A. Belov**[1]

[1]ITMO University, Kronverksky pr. 49, St. Petersburg 197101, Russia
[2]DTU Fotonik Technical University of Denmark
Ørsteds Pl. 343, Kongens Lyngby DK-2800, Denmark

Abstract— We show that a light beam incident on a multiperiodic plasmonic multilayer, which is different from a conventional periodic multilayer in that its unit cell is composed of more than two layers, undergoes unusual refraction. Namely, splitting of the incident beam into more than two refracted beams having the same polarization is numerically observed.

Plasmonic multilayers can be used to manipulate light in various ways and at different scales down to the nanoscale [1]. They are also known to exhibit strong spatial dispersion and thus to demonstrate novel electromagnetic phenomena. In this talk we study refraction of macroscopic beams at the interface between an ambient dielectric and a plasmonic multilayer.

In particular, complicated plasmonic layered structures involving more than two different kinds of metal and dielectric layers, so that the unit cell of the structure is composed of four rather than two layers [2], are especially worth considering. Due to their inherent strong optical nonlocality, such structures have a multi-band plasmonic wave dispersion relation, so that several waves with the same frequency but different wave vectors can propagate simultaneously. This in turn gives rise to multirefringence phenomena, occurring when all these waves are excited simultaneously by an externally incident light beam (Fig. 1). This effect is distinct from trirefringence in photonic crystals, which occurs due to extreme polarization mixing arising from the structure patterning [3].

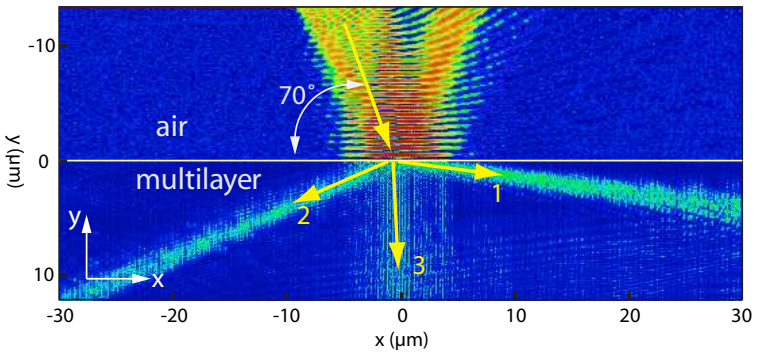

Figure 1: Numerically simulated field distribution ($|H|^2$) of a TM-polarized light beam impinging on an air/multilayer interface. Splitting into three refracted beams is observed.

ACKNOWLEDGMENT

This work was supported by Russian Fund for Basic Research within the project No. 14-02-31720.

REFERENCES

1. Orlov, A. A., I. V. Iorsh, S. V. Zhukovsky, and P. A. Belov, "Controlling light with plasmonic multilayers," *Photon. Nanostruct. Fundam. Appl.*, Vol. 12, 213, 2014.
2. Orlov, A. A., A. K. Krylova, S. V. Zhukovsky, V. E. Babicheva, and P. A. Belov, "Multiperiodicity in plasmonic multilayers: General description and diversity of topologies," *Phys. Rev. A*, Vol. 90, 013812, 2014.
3. Netti, M. C., A. Harris, J. J. Baumber, D. M. Whittaker, M. B. D. Charlton, M. E. Zooroob, and G. J. Parker, "Optical trirefringence in photonic crystal waveguides," *Phys. Rev. Lett.*, Vol. 86, 1526, 2001.

Plasmonic Waveguide Array: Simulating Topological Photonic States and Massless Dirac Fermion

Tao Li, **Yiming Pan**, **Q. Q. Cheng**, **B. B. Xu**, **and S. N. Zhu**
National Laboratory of Solid State Microstructures
College of Engineering and Applied Sciences, Nanjing University, Nanjing 210093, China

Abstract— Topological phases have been successfully extended to the optical system, which gives rise to the novel optical phenomena (e.g., one-way optical propagations and robustness against scattering from defects in two-dimensional (2D) photonic crystals) [1]. Recently, the optical mimics of the 1D topological Su-Schrieffer-Heeger (SSH) model [2] were investigated in systems [3, 4]. However, the light diffraction in waveguide array, as an important simulator for the condensed matter physics, has not yet been demonstrated within such a 1D topological system. In this work [5], we proposed and demonstrated, a topologically protected plasmonic interface mode in metallic ridge waveguide array based on the SSH model. Here, we investigate the surface plasmon propagations in PWAs with two kinds of kinked defects, where the immunity against structural disorders is mainly discussed. It is well demonstrated that one of the interface modes is immune to the structural disorder and nanofabrication errors, while another kinked defect cannot support such an optical mode. Furthermore, due to the convenience in modulating the coupling coefficient in the ridge waveguide array, it is possible to construct an alternating positive and negative couplings in such a binary PWAs. From this point, we successfully find appropriate parameters to model a linear dispersive photonic energy band with a Dirac point [6, 7]. In this system the CMT equation is analog to the massless Dirac equation, so that we can use this PWA to simulate the massless Dirac Fermion. It is really realized by our COMSOL simulation, that a bidirectional non-dispersive SPP propagations in the PWA.

REFERENCES

1. Lu, L., J. D. Joannopoulos, and M. Soljačić, "Topological photonics," *Nat. Photonics*, Vol. 8, 821–829, 2014.
2. Su, W. P., J. R. Schrieffer, and A. J. Heeger, "Solitons in polyaeetylene," *Phys. Rev. Lett.*, Vol. 42, 1698, 1979.
3. Atala, M., et al., "Direct measurement of the Zak phase in topological Bloch bands," *Nat. Phys.*, Vol. 9, 795–800, 2013.
4. Kitagawa, T., et al., "Observation of topologically protected bound states in photonic quantum walks," *Nat. Commun.*, Vol. 3, 882, 2012.
5. Pan, Y., et al., "Topologically protected interface mode in plasmonic waveguide arrays," 2014, Submitted.
6. Zeuner, J. M., et al., "Optical analogues for massless dirac particles and conical diffraction in one dimension," *Phys. Rev. Lett.*, Vol. 109, 023602, 2012.
7. Nam, S. H., A. J. Taylor, and A. Efimov, "Diabolical point and conical-like diffraction in periodic plasmonic nanostructures," *Opt. Express*, Vol. 18, 10120–10126, 2010.

Nonlocal Effective Medium Theory and Its Relation with Zak Phase in Two-dimensional Photonic Crystals

Meng Xiao, **Xueqin Huang**, **Anan Fang**, **Z. Q. Zhang**, **and C. T. Chan**
Department of Physics and Institute for Advanced Study,
The Hong Kong University of Science and Technology, Clear Water Bay, Hong Kong, China

Abstract— We build a nonlocal effective medium theory (EMT) for a two-dimensional (2D) photonic crystal (PC) comprising a square lattice of dielectric cylinders with the incident electric field polarized along the axis of the cylinders. In particular, we discuss the feasibility of constructing an EMT for the case where the effective wave vector is far away from the center of Brillouin Zone (BZ). When the k-vector is away from the center of BZ, the optical response of the PC is necessarily anisotropic, implying that effective medium description becomes inevitability angle dependent, or in other words, nonlocal. While traditional EMT is only good near the zone center, we extend the effective range by including nonlocal effect. We employ the layer-by-layer scattering method as well as the parameter retrieval method to analytically obtain the effective impedance (Z_{eff}) and the effective refractive index (n_{eff}).

The obtained Z_{eff} is purely real for the pass band and purely imaginary in band gaps. While Z_{eff} is a function of frequency, sgn[Im(Z_{eff})] is a constant for all the frequencies inside a band gap, which means that we can classify the band gaps using sgn[Im(Z_{eff})]. We further prove that the sgn[Im(Z_{eff})] of each gap is related to the summation of Zak phases of all the bands below this gap. The relationship between the value of Zak phase and the symmetries of the band edge states is well studied, and the latter ones can be predicted with the group theory, which means we can obtain the sgn[Im(Z_{eff})] from symmetry argument with little effort.

With the sgn[Im(Z_{eff})] of each gap determined, we can predict the existence of interface state between two different systems. For example, we can explain why there is usually no surface state on the boundary of typical fully gapped PCs. Our non-local EMT also allows us to quantitatively predict the dispersion of surface states between different PCs for surface wave vectors that are well beyond the zone center.

Conditions for Negative Refraction and Negative Refractive Index in Lossy Media

Liming Ji and Vasundara V. Varadan
Microwave and Optics Laboratory of Imaging and Characterization, Department of Electrical Engineering
University of Arkansas, 700 W. Research Center Blvd., Fayetteville, Arkansas 72701, USA

Abstract— Negative refractive index (NRI) has been reported to be the requirement for negative refraction of waves (NRW) in lossless, isotropic electromagnetic media. Metamaterials have been used to create effective media with NRI by exciting plasmon-like resonances. In reality, there are no lossless metamaterials. For example, metamaterials composed of Split Ring Resonators (SRR) show significant loss at the SRR resonance frequency. It has been pointed out by other authors that in lossy media, NRI does not result in NRW. In this paper, we present a comprehensive list of conditions on material properties that are required for NRW to occur in lossy media.

Beginning with a straightforward derivation of refraction of obliquely incident waves from free space into a lossy, isotropic medium characterized by complex dielectric permittivity $\varepsilon'+\mathrm{j}\varepsilon''$ and complex magnetic permeability $\mu'+\mathrm{j}\mu''$. The angles for phase refraction and energy refraction are one and the same for waves travelling across lossless media. It is understood that they are different in lossy media. NRI is required for negative phase refraction but is not a requirement for negative energy refraction in lossy media. Since actual metamaterials are lossy and experiments measure the angle of refracted power flow into such materials, conditions need to be derived for this to occur in lossy media. Our derivation shows that certain parameter combinations of the complex permittivity and permeability and the conditions are polarization dependent. Negative permittivity is a requirement for TM polarization and negative permeability is a requirement for TE polarization in order for NRW to occur in lossy media. A complete table of conditions on the complex permittivity and permeability will be presented for TE and TM polarizations for both NRI and NRW. The amount of loss, that is the values of ε'' and μ'' also determine whether NRW will occur. These results are new.

We have tried to prove these conditions experimentally. However, our results depend on a big assumption, that our SRR metamaterial samples are isotropic, at least in the direction of wave propagation. In reality, there are no manmade metamaterials that are isotropic at the resonance frequency. In order to provide some guidance for designing and fabricating metamaterials, an assumption of isotropy in the direction of wave propagation is justifiable. Material samples with negative permittivity, permeability and NRI were constructed using periodically spaced Cu SRRs, Cu wires and a combination of SRRs and wires. The samples were characterized in a free space measurement system. There are three scenarios for wave refraction based on our derivation: a) simultaneous negative energy refraction and negative phase refraction; b) simultaneous positive energy refraction and negative phase refraction and c) simultaneous negative energy refraction and positive phase refraction. We will present experimental results for the three cases.

Spatially Dispersive Inhomogeneous Dielectric Wire Media with Periodic Structure

J. Gratus[1, 3], **R. Letizia**[2, 3], **and M. McCormack**[1]

[1]Physics Department, Lancaster University, LA1 4YB, UK
[2]Engineering Department, Lancaster University, LA1 4YW, UK
[3]Cockcroft Institute of Accelerator Science, Darsbury WA4 4AD, UK

Abstract— Spatially dispersive electromagnetic media are considered where the parameters defining the permittivity relation vary periodically [1]. This contrasts with most theoretical articles which consider inhomogeneous spatially dispersive media, where the inhomogeneity is restricted to looking at two homogeneous media which are connected and investigating the corresponding additional boundary conditions.

The use of a spatially dispersive inhomogeneous medium enables one to shape the propagation modes, extending the possibilities from the usual sinusoidal shape. This may have a number of advantages. For example in an accelerating drift tube, one could flatten the mode shape to enable higher acceleration for a given peak field. By contrast in signal transmission one may desire a higher peak for a given total energy.

In order to construct an inhomogeneous spatially dispersive medium it is necessary to consider a medium where the permittivity and permeability depend on both the wave vector $\mathbf{k}$ and the position $\mathbf{x}$ within the unit cell, i.e., $\tilde{\epsilon}(\omega, \mathbf{k}, \mathbf{x})$ and $\tilde{\mu}(\omega, \mathbf{k}, \mathbf{x})$. In order to make sense of the arguments of $\tilde{\epsilon}(\omega, \mathbf{k}, \mathbf{x})$ we no longer interpret $\tilde{\epsilon}(\omega, \mathbf{k}, \mathbf{x})$ as the Fourier transform of the permittivity response function $\epsilon(t, \mathbf{x})$ but in terms of a differential equation.

Maxwell's equations then give rise to a difference equation corresponding to the Floquet modes. Two methods are given for solving this equation and numerical method and an approximate solution, which are valid when the inhomogeneity is small. In the latter case the set of approximate solutions is calculated.

A new feature arises when considering spatially dispersive media, that is the existence of coupled modes. These change the frequency and the shape of the mode.

A medium which is both inhomogeneous and spatially dispersive is an inhomogeneous wire media. This is constructed from a grid of parallel wires with diameters which change sinusoidally as one goes along them. This can be used to the shaping of the propagation modes. The modelling of such a structure may be done using a standard 3D FDTD EM solver (which does not include spatial dispersion). However it is much quicker to model it in terms of a 1-dimensional spatially dispersive medium. The results of the two methods are compared.

REFERENCES

1. Gratus, J. and M. McCormack, "Spatially dispersive inhomogeneous electromagnetic media with periodic structure," *J. Optics*, Vol. 17, No. 2, 025105–025115, 2015.

Local Field Effects and Spatial Dispersion of Dielectric Permittivity

A. A. Tishchenko
National Research Nuclear University "MEPhI", Moscow, Russia

Abstract— Local field, i.e., the average acting field in system of many particles, is known to differ from average macroscopic field. This fact is well known in optics, spectroscopy and indeed in all branches of electrodynamics. For example, the Clausius-Mossotti relations join the microscopic and macroscopic properties of a substance and they are well known and widely used in the optics, spectroscopy of condensed media and many other fields of physics. Usually, these relations take into account only frequency dispersion, not the spatial one. The effects of frequency and spatial dispersions are caused by the nonlocal properties of response functions in time and in space, correspondingly.

In natural materials effects of frequency dispersion are usually much more considerable than that of spatial dispersion and only in special cases like electrons in plasma spatial dispersion plays vital part. But sometimes, despite their smallness, the latter may play a vital part. For example, one should take the spatial dispersion of dielectric function into account to describe the gyrotropy (natural optical activity) of some materials, optical anisotropy of nongyrotropic cubic crystals, and so on [1]. The spatial dispersion of dielectric function may change the number of the roots of the dispersion equation. Therefore, taking into account of the spatial dispersion may give us the additional, new types of electromagnetic waves, which are absent in the medium without spatial dispersion [2]. For example, spatial dispersion can be very important for artificial structures, like photonic crystals or metamaterials.

In this work proceeding from local field theory we demonstrate that spatial dispersion of permittivity can be caused not only by effects of moving electrons — as it takes place in plasma and so on — but directly by the structure of the material. At example of Clausius-Mossotti relations we show this for 3D material; in case of 2D-structure (monolayer of particles with arbitrary dielectric properties) we manage to improve our previous results [3] and get the relations with spatial dispersion. The analytical properties of responses functions are discussed. There are two of responses functions that are obtained: the one describing the response of the monolayer to the field of external sources, and the second one describing the response to the field of eigenmodes. Our results for 3D and 2D systems are valid not only for materials and artificial structures consisting of dielectric particles, but also for metal ones, including nanoparticles.

REFERENCES

1. Agranovich, V. M. and V. L. Ginzburg, *Spatial Dispersion in Crystal Optics and the Theory of Excitons*, Wiley-Interscience, New York, 1966.
2. Ryazanov, M. I., *Electrodynamics of Condensed Matter*, Nauka, Moscow, 1984 (in Russian).
3. Ryazanov, M. I. and A. A. Tishchenko, "Clausius-mossotti-type relation for planar monolayers," *JETP*, Vol. 103, 539, 2006.

Session 1P2
SC3: Nanoscale Platforms for Molecular Sensing

Recent Progress in Nanoscale Sensing Using Surface-enhanced Raman Scattering

Kenneth B. Crozier
The University of Melbourne, Australia

Abstract— This presentation reviews recent work by the author and his research group on plasmonic structures for surface-enhanced Raman scattering.

Plasmonic dimers, consisting of two closely spaced metallic nanoparticles, represent a highly effective means for achieving very strong electromagnetic (EM) enhancement for suface-enhanced Raman scattering (SERS). It was recently suggested that quantum effects start to play a significant role for gaps $< 10\,\mathrm{nm}$ [1, 2]. We review work [3] in which we fabricate dimers in a highly controllable manner using electron-beam lithography, perform SERS, and correlate the results with transmission electron microscope (TEM) images of the dimers. We show that quantum mechanical tunneling across the gaps limits the enhancement in SERS.

We furthermore review our recent work [4] in which we demonstrate a micro-patterned silicon structure that enables the preparation of a SERS substrate and pre-concentration of the analyte molecules. The structure is designed to produce a hydrophobicity gradient. As a result, a water droplet placed on it will remain centred on the structure as it dries, enabling delivery of materials to its center. The structure is therefore referred to as a superhydrophobic bull's-eye. A water droplet containing gold colloids placed on it dries to produce a cluster at the bull's-eye center. A second water droplet placed on it, this time containing analyte molecules, dries such that the molecules are delivered to the gold colloid cluster. We demonstrate the detection of molecules at low concentrations (Rhodamine 6G at $10^{-15}\,\mathrm{M}$) from small droplets.

REFERENCES

1. Ciraci, C., et al., "Probing the ultimate limits of plasmonic enhancement," *Science*, Vol. 337, 1072, 2012.
2. Savage, K. J., et al., "Revealing the quantum regime in tunneling plasmonics," *Nature*, Vol. 491, 574, 2012.
3. Zhu, W. and K. B. Crozier, "Quantum mechanical limit to plasmonic enhacement as observed by surface-enhanced Raman scattering," *Nature Communications*, Vol. 5, 5228, 2014.
4. Song, W., D. Psaltis, and K. B. Crozier, "Superhydrophpbic bull's-eye for surface-enhanced Raman scattering," *Lab Chip*, Vol. 14, 3907, 2014.

Hot Spots of Plasmonic Nanostructures and Their Spectroscopic Potential for Molecular Probing at the Nanoscale and at the Single Molecule Level

Katrin Kneipp[1], **Harald Kneipp**[1], **and Janina Kneipp**[2]

[1]Department of Physics, Danmarks Tekniske Universitet DTU, Lyngby 2800, Denmark
[2]Department of Chemistry, Humboldt Universität zu Berlin, Berlin 12489, Germany

Abstract— Frequencies of collective oscillations of the free electrons in metal nanostructures, called surface plasmons, fall in the optical range of the electromagnetic spectrum. Resonances between light and the surface plasmons result in enhanced local optical fields in the vicinity of metal nanostructures including also dramatic changes of field intensities within a few nanometers and the formation of so-called "hot spots". Hot spots open up exciting capabilities in optical spectroscopy by enhancing weak spectroscopic signals ("surface-enhanced spectroscopy") and by limiting probed volumes to (sub) nm dimensions.

Surface enhanced Raman scattering (SERS) is a prominent example to demonstrate the power of spectroscopy performed in hot spots. Moreover, Raman spectroscopy is of particular interest since spectroscopic observation of vibrational modes provides a non-invasive key to the molecular structure of matter. Raman spectra measured in hot spots can provide molecular structural information of a single individual molecule. At the same time, spectroscopic signals collected from a single molecules deliver sensitive information on the optical field at the location of the molecule.

We discuss recent developments for studying plasmonic metal nanostructures and related local optical fields as well as spectroscopic capabilities of these local fields. We start with considering Raman experiments using one- and two-photon excitation. Complementary to photons, we discuss Electron-energy-loss spectroscopy (EELS) as an emerging novel characterization tool for plasmonic structures which can provide high spatial resolution at the subnanometer scale. The complementary use of photons and electrons enables us to access a new level of information by combining the high energy selectivity of laser radiation with the atomic scale spatial resolution of electron microscopy.

New capabilities to characterize plasmonic properties become of particular interest for structures where quantum effects play a role, such as metal nanoaggregates with atomic scale interparticle gaps. Interestingly, such structures at the transition from the classical to the quantum regime seem to provide the hottest hot spots.

We discuss the unique potential of SERS performed in these hottest spots for chemical probing and sensing.

REFERENCES

1. Kneipp, K., H. Kneipp, and J. Kneipp, *Chemical Science*, 2015, DOI: 10.1039/C4SC03508A.

Development of Electrically Driven Plasmonic Nanoparticles Sensors and Investigation of Their Stability

Andre Dathe[1], **Uwe Hübner**[2], **Mario Ziegler**[2], **Jacqueline Jatschka**[1], **Mattias Thiele**[1], **Pavel Kliuiev**[1], **Andrea Csaki**[1], **Ondrej Stranik**[1], **and Wolfgang Fritzsche**[1]

[1]Department of Nano Biophotonic, Leibniz Institute of Photonic Technology (IPHT)
Albert-Einstein-Str. 9, Jena 07745, Germany
[2]Department of Quantum Detection, Leibniz Institute of Photonic Technology (IPHT)
Albert-Einstein-Str. 9, Jena 07745, Germany

Abstract— Surface Plasmon Resonance (SPR) in metallic nanostructures is an optical effect, which can be exploited for the detection of small molecules. The current research aims for the development of nanostructures with high detection sensitivity and their easy implementation into a sensing schema. There is a broad range of metallic nanostructures supporting different SPR modes, and nanostructures can be even geometrically combined leading to the creation of new hybridised SPR modes. Most commonly, either spherical metal nanoparticles supporting localised surface plasmon resonances or thin metal layers supporting propagating plasmon resonances are implemented in bio-sensing.

In our study, we investigated the properties of a hybridised SPR mode (gap modes GM) created by the placement of metallic nanoparticles onto metallic layers and its use as a sensitive sensor. The spectral characteristic of these GM are highly sensitive on the nanoparticle substrate separation, which makes it an attractive sensing mechanism. We experimentally observed the creation of the GM for nanoparticle-substrate separation smaller then 10 nm and measured the effectivity of the excitation depending on the illumination conditions.

As a contrary to the commonly used far field light excitation of the SPR modes, an innovative way of electrically driven excitation of the GM was applied. Due to the planar geometry of the metallic layer, it was possible to extend this single metallic layer structure into metal-insulator-semiconductor (MIS) structure. The tunnelling current passing through such MIS structure generates supported SPR modes, which can be then scattered by the GM. This concept was experimentally confirmed. The MIS structures with tunnelling junctions were lithographically produced prior to electrical and optical characterization. We showed that the spectral emission is changed when the MIS structure also supports the GM. This was achieved by placing metal nanoparticle onto the upper metallic layer.

In such a scheme also other than spherical gold nanostructure supporting localised SPR can be used, which has a potential advantage in a stronger and spectrally shifted resonances. However, the stability of these nanostructures for further use has to be considered. In the remaining part of the talk, the stability issue of the triangular shaped silver nanoparticles is discussed. We were able to experimentally follow the degradation of such nanoparticles under ambient conditions in real time. Using atomic force microscopy and optical spectroscopy we observed that an anisotropic corrosion, that is starting from the tips of the nanoparticles.

Silicon Nanostructuring for SERS Applications and Hybrid Infrared Light Sensing Devices

V. Derek[1], **L. Mikac**[1], **E. D. Głowacki**[2], **N. S. Sariciftci**[2], **C. D'Andrea**[3], **P. G. Gucciardi**[3], **S. Trusso**[3], **A. Foti**[3], **and M. Ivanda**[1]

[1]Center of Excellence for Advanced Materials and Sensing Devices
Ruder Bošković Institute, Bijenička c. 54, Zagreb, Croatia
[2]Linz Institute for Organic Solar Cells (LIOS)/Institute of Physical Chemistry
Johannes Kepler University Linz, Altenbergerstraβe 69, Linz 4040, Austria
[3]CNR IPCF, Istituto per i Processi Chimico-Fisici, Viale F. Stagno D'Alcontres 37, I-98156, Messina, Italy

Abstract— Inorganic semiconductor materials have for a long time been a standard member of electronic devices ecosystem, with silicon being the material of choice for most applications. Introducing structuring in silicon has proven to be advantageous for its many properties and applications. Introduction of silver nanocrystals in the porous silicon is promising for Surface Enhanced Raman Sppectroscopy (SERS). Heterojunction interfaces between organic and structured silicon substrate in devices show promise in using the advantages of both materials simultaneously. Here we present the results on preparation of stable and uniform SERS solid substrates using macroporous silicon (pSi) with deposited silver and gold and on the devices based on heterojunctions of porous silicon formed by anodisation in HF-based electrolytes and organic thin films formed by vacuum evaporation. Macroporous silicon is produced by anodisation of p-type silicon in hydrofluoric acid. The as prepared pSi is then used as a template for Ag and Au depositions. The noble metals were deposited in three different ways: by immersion in silver nitrate solution, by drop-casting silver colloidal solution and by pulsed laser ablation (PLA). Substrates obtained by different deposition processes are evaluated for SERS efficiency using methylene blue and rhodamine 6G at 514.5, 633 and 785 nm. Substrate concentrations detected in most of the cases were in the nanomolar range suggesting that it may be possible to detect lower analyte concentrations when using porous instead of crystal silicon template. For inorganic part of the heterojuction we choose porous silicon due to its compatibility to established CMOS technology and its enormous surface area being presented to thin organic films. For organic part of the junction we investigated the applicability of various organic semiconductor thin films for optoelectronic and biosensing applications. Our porous silicon-based devices show in optical response and moderate sensitivity in infrared spectral region.

Surface Enhanced Raman and Fluorescence Spectroscopies

P. M. Adam
Laboratoire de Nanotechnologie et d'Instrumentation Optique (LNIO)
Institut Charles Delaunay, Université de Technologie de Troyes, UMR 6281
12 rue Marie Curie, BP 2060, Troyes Cedex 10010, France

Abstract— Plasmonics is a field connected to optics dealing with the properties and applications of surface plasmons which are modes of metal dielectric interfaces. Nanoplasmonics concerns the excitation, manipulation and detection of the surface plasmons at the nanometric scale. It has highly potential applications for ultrasensitive biochemical sensing. Surface enhanced spectroscopies are the ultimate sensor tools as they can reach single molecule sensitivity. We will present in this paper our latest results towards the realization of highly controllable and reproducible nanoplasmonics substrates.

Plasmonics is a now well established field finding numerous applications in pharmacology, biology, optoelectronics and metamaterials among others. For the sensitive detection of molecules or markers Surface Enhanced Spectroscopies are well widespread [1]. Among them, Surface Enhanced Raman Spectroscopy (SERS) and Metal Enhanced Fluorescence (MEF) or Surface Enhanced Fluorescence (SEF), are the most used for applications. Both these enhanced spectroscopies are based on local field enhancement entailed in the near vicinity of metallic nanoparticles when Surface Plasmon oscillations are driven for a specific optical wavelength. SERS can achieve single molecule detection when two or more metallic nanoparticles are near-field coupled, resulting in enhancements ranging between 8 and 10 orders of magnitude, even if absolute magnitude of enhancement is still a subject of debate. However, these particular SERS substrates are difficult to reproduce.

Less enhancement is obtained with MEF/SEF but usually the intrinsic fluorescence cross section of a molecule is 14 orders of magnitude more important than that of its Raman cross-section. In MEF/SEF one has to take into account the finite lifetime of the excited levels of the molecule of interest, which results in quantum yield modifications in the presence of the metallic nanoparticles. Quantum yield can be enhanced or even reduced, leading in the latter case to a competition with local field excitation enhancement and thus the possibility of quenched fluorescence of the emitters.

This contribution will show the ties between SERS, MEF and sensors in the light of recent works done in the LNIO laboratory [2, 3].

REFERENCES

1. Kosuda, K. M., J. M. Bingham, K. L. Wustholz, and R. P. Van Duyne, *Handbook Nanoscale Optics and Electronics,* Chapter 10, G. Wiederrecht, Ed., Elsevier, Amsterdam, 2010.
2. Rumyantseva,A., S. Kostcheev, P. M. Adam, S. V. Gaponenko, S. V. Vaschenko, O. S. Kulakovich, A. A. Ramanenka, D. Guzatov, D. Korbutyak, V. Dzhagan, A. Stroyuk, and V. Shvalagin, *ACS Nano*, Vol. 7, No. 4, 3420–3426, 2013.
3. Viste, P., J. Plain, R. Jaffiol, A. Vial, P.-M. Adam, and P. Royer, *ACS Nano*, Vol. 4, 759, 2010.

Core/Shell Dielectric Colloids and Metal/Dielectric Nanostructures: Multi-purpose Platforms for Advanced Diagnostics of Chemical Reactions

I. Alessandri[1], **N. Bontempi**[1], **L. Carletti**[2], **and C. De Angelis**[2]

[1]INSTM and Chemistry for Technologies Laboratory, Mechanical and Industrial Engineering Department University of Brescia, via Branze, 38, Brescia 25123, Italy
[2]Department of Information Engineering, University of Brescia, via Branze, 38, Brescia 25123, Italy

Abstract— Core/shell nanostructures are intensively investigated for broadband light trapping and management, because they can play as optical cavities and directly take advantage of morphology dependent resonances. The same properties can be exploited in imaging and vibrational spectroscopy (Raman, IR), in order to enhance their analytical sensitivity [1–3]. Moreover, the synergistic combination of plasmonic nanoantennas with dielectric core/shell colloids allowed for fabricating near-field optical light concentrators, which are very efficient in stimulating photon-driven processes at metal-semiconductor interfaces and show an impressive decrease in degradation time (minutes instead of hours) of organic pollutants [4].

This presentation will review some applications of core/shell light nanoconcentrators as non-plasmonic Raman enhancers, which have been used to investigate biochemical reactions in aqueous environment, and their coupling to plasmonic nanoantennas for promoting and *in-situ* monitoring light-assisted chemical reactions [1–6]. Using both approximated analytical models and full wave numerical simulations, the role of morphology dependent optical resonances in driving the spectral response of different systems will be discussed also taking into account the nonlinear properties of the metallic nanostructures [7, 8].

REFERENCES

1. Alessandri, I., "Enhancing Raman scattering without plasmons: Unprecedented sensitivity achieved by TiO_2 shell-based resonators," *Journal of the American Chemical Society*, Vol. 135, No. 15, 5541–5544, 2013.
2. Alessandri, I., N. Bontempi, and L. E. Depero, "Colloidal lenses as universal Raman scattering enhancers," *RSC Advances*, Vol. 4, 38152–38158, 2014.
3. Alessandri, I. and L. E. Depero, "All-oxide Raman-active traps for light and matter: Probing redox homeostasis model reactions in aqueous environment," *Small*, Vol. 10, 1294–1298, 2014.
4. Bontempi, N., M. Salmistraro, M. Ferroni, L. E. Depero, and I. Alessandri, "Probing the spatial extension of light trapping-induced enhanced Raman scattering in high-density Si nanowire arrays," *Nanotechnology*, Vol. 25, 465705, 2014.
5. Salmistraro, M., A. Schwartzberg, W. Bao, L. E. Depero, A. Weber-Bargioni, S. Cabrini, and I. Alessandri, "Triggering and monitoring plasmon enhanced reactions by optical nanoantennas coupled to photocatalytic beads," *Small*, Vol. 9, 3301–3307, 2013.
6. Sinha, G., L. E. Depero, and I. Alessandri, "Recyclable SERS substrates based on Au-coated nanorods," *ACS-Applied Materials and Interfaces*, Vol. 3, No. 7, 2557–2563, 2011.
7. Celebrano, M., et al., "Mode-matching in multiresonant plasmonic nanoantennas for enhanced second harmonic generation," *Nature Nanotechnology*, in Press.
8. De Ceglia, D., M. A. Vincenti, C. De Angelis, A. Locatelli, J. W. Haus, and M. Scalora, "Role of antenna modes and field enhancement in second harmonic generation from dipole nanoantennas," *Optics Express*, Vol. 2, 1715–1729, 2015.

Plasmonics on Waferscale

Uwe Hübner[1], **Thomas Mayerhöfer**[1], **Richard Knipper**[1, 2], **Dana Cialla-May**[1, 2], **Karina Weber**[1, 2], **and Jürgen Popp**[1, 2]

[1]Leibniz Institute of Photonics Technology (IPHT)
Albert-Einstein-Strasse 9, Jena 07745, Germany
[2]Institute of Physical Chemistry and Abbe Center of Photonics
Friedrich-Schiller-University Jena, Helmholtzweg 4, Jena 07743, Germany

Abstract— Plasmonic substrates for surface enhanced vibrational spectroscopy (i.e., SERS or SEIRA), which use strong local electric field enhancement, are currently being developed for chemical and bio-sensing application fields. These artificial nanomaterials are constructed of millions of very small metallic pattern with typical feature sizes down to $\lambda/10$ and layered dielectric thin films. To test the substrates a sufficiently large number of test samples are needed. In addition, for future applications the fabrication of such nanomaterials over large areas, with a few million nanostructures per mm^2 presents a major challenge for the top-down lithography not at least due to frequently changing layouts.

In this work we present our unique e-beam lithography with Character Projection (CP) which is a promising technique for the fast fabrication of complex nanomaterials and optical metamaterials on wafer scale areas. Compared to the serial working standard e-beam lithography the Character Projection lithography operate in a partially parallel processing exposure mode which offers a significant advantage in writing speed by factors > 100 compared to the relative fast Variable Shaped Beam mode (VSB) [1, 2] and it opens the way for the fabrication of devices with large areas which are impossible to realize with SEM based Gaussian electron beam-writers often used in R&D. For example, the exposure times for a metamaterial accounts for nearly 1 year for the Gaussian-mode, whereas 2.4 h for the VSB-mode and only 1.4 min for the CP-mode are needed! Due to the enormous write time reduction also the pattern quality and the pattern homogeneity on large areas are improved significantly [3].

This write time reduction together with a high flexibility in terms of pattern diversity was achieved by the implementation of a computer controlled aperture stage with a multi-stencil diaphragm array in our SB350 OS Variable Shaped e-beam system (from Vistec Electron Beam GmbH Jena) [2]. More than 2000 different aperture geometries (= characters) can be addressed within one exposure job. The types of available pattern include various 1D-gratings with pitches down to 100 nm and with different angles of orientation, 2D-gratings and also patterns with geometries which are hard to approximate by geometrical primitives like circular dots and dot arrays, spirals, split-rings, rhombus, rod shape and bow-ties (Fig. 1). All these shapes can be combined and aligned to realize even more complex layouts.

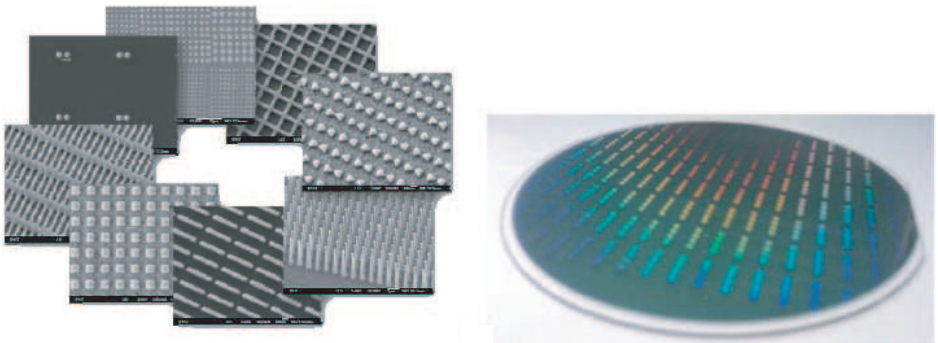

(a) (b)

Figure 1: (a) Examples for different nanogratings and metamaterials, fabricated by means of the Character Projection (CP) mode. (b) A 100 mm-wafer with nanogratings. In CP-mode, the e-beam writing time for this wafer is only 1.5 hours.

ACKNOWLEDGMENT

Funding of the research projects 'QuantiSERS' and 'JBCI 2.0' within the framework 'Unternehmen Region — InnoProfile Transfer', the project 'PhoNa' within the framework 'Spitzenforschung und Innovation in den NeuenLändern' from the Federal Ministry of Education and Research, Germany (BMBF) and EFRE is gratefully acknowledged. Further the research project "FastTB" was supported by the Thüringer Aufbaubank.

REFERENCES

1. Kley, E.-B., *Proc. SPIE*, Vol. 8352, 83520M, 2012.
2. Zeitner, U. D., et al., *Proc. SPIE*, Vol. 8974, 89740G, 2014.
3. Hübner, U., et al., *Proc. SPIE*, Vol. 9231, 92310E, 2014.

Transfer-printing-based Fabrication of 3-dimensional Plasmonic Superlattice Nanostructures for Surface-enhanced Raman Spectroscopy Analyses

Jae Won Jeong and Yeon Sik Jung
Department of Materials Science and Engineering
Korea Advanced Institute of Science and Technology (KAIST)
291 Daehak-ro, Yuseong-gu, Daejeon 305-701, Republic of Korea

Abstract— Three-dimensional (3D) plasmonic nanostructures for surface-enhanced Raman spectroscopy analyses (SERS) have recently attracted much attention due to their superior signal enhancement capability compared to two-dimensional nanostructures. However, the controlled fabrication of ultrafine 3D super-structures that can maximize SERS hotspots is not straightforward. This talk will present the use of a solvent-assisted nanotransfer printing (S-nTP) technique for the 3D stacking of plasmonic nanostructures in a fast and convenient manner. General nanotransfer printing (nTP) technology offers outstanding simplicity and throughput in the fabrication of transistors, metamaterials, epidermal sensors, and other emerging devices. Nevertheless, the development of a large-area sub-50 nm nTP process has been hindered by fundamental reliability issues in the replication of high-resolution templates and in the release of generated nanostructures. In contrast, our S-nTP is based on high-fidelity replication of ultrahigh-resolution (8–20 nm scale) patterns using a dual-functional polymer thin film and solvent-assisted release of such nanostructures. We show how the signal intensity can be maximized with the choice of nanoscale geometries and the number of stacks. Based on the same principle, facile printing of plasmonic nanostructures for non-destructive and rapid surface-enhanced Raman spectroscopy (SERS) analyses can also be achieved. The utilization of S-nTP can significantly enhance the analysis throughput of SERS by decreasing the analysis preparation time for the formation of plasmonic nanostructures on analytes. As another example of a near-term application, this talk will also demonstrate that Ag nanowires printed on the inner surface of a vial glass can enhance SERS signals, enabling direct and convenient detection of molecules dispersed in a solution at an extremely low concentration.

Silver Nanowires as Efficient Sensing Platforms

Sebastian Mackowski
Institute of Physics, Faculty of Physics, Astronomy and Informatics
Nicolaus Copernicus University, Torun, Poland

Abstract— Silver nanowires are unique metallic nanostructures, which on the one hand are characterized with strong plasmon resonance, while on the other, can be imaged using standard fluorescence microscope. With appropriate surface functionalization both aspects of silver nanowires can be efficiently explored for sensing biomolecules. Chlorophyll-containing biomolecules, which participate in photosynthesis, exhibit strongly enhanced fluorescence upon conjugation with silver nanowires. In addition to intensity increase, the emission of chlorophylls is decaying much faster pointing towards radiative rate increase upon coupling with plasmon excitations. However, for large proteins, where coupling with plasmon excitations in silver nanowires is much weaker and induces at most minute changes in their spectral properties, silver nanowires play a role of geometrical constrain. In other words, through proper functionalization of the surface of silver nanowires, fluorescent biomolecules can be attached to them and their position can be precisely determined. Both these approaches can be combined for real-time observation of attachment and glowing of properly designed structures, also at a single molecule level.

Additional features of potential sensing platforms composed of silver nanowires can be introduced by covering them with graphene or its derivatives. Recent results of these experiments will be presented.

ACKNOWLEDGMENT

Research was supported by the DEC-2013/10/E/ST3/00034 project from the National Research Center of Poland and by the National Research and Development Center(NCBiR) under Grant ORGANOMET No. PBS2/A5/40/2014.

REFERENCES

1. Olejnik, M., et al., *Applied Physics Letters*, Vol. 102, 083703/1–5, 2013.
2. Kowalska, D., et al., *The Scientific World Journal,*, Vol. 2013, 670412/1–12, 2013.
3. Wiwatowski, K., et al., submitted
4. Twardowska, M., et al., submitted
5. Twardowska, M., et al., *Applied Physics Letters*, Vol. 104, 093103/1–5, 2014.

Linear and Non-linear Optical Properties of Bi-metallic Heterodimers

A.-L. Baudrion[1], **J. Wang**[1,2], **A. Horrer**[3], **D. Gollmer**[3], **A. Horneber**[2], **M. Fleischer**[3], **D. Zhang**[2], **and P.-M. Adam**[1]

[1]Laboratoire de Nanotechnologie et d'Instrumentation Optique
Institut Charles Delaunay, UMR CNRS 6281, Université de Technologie de Troyes, France
[2]Institute of Physical and Theoretical Chemistry, University of Tuebingen, Germany
[3]Institute for Applied Physics, University of Tuebingen, Germany

Abstract— Metal nanoparticles have attracted great scientific and technological interest in biomolecular detection and clinical diagnostic application due to their specific physical and chemical characteristics. Several reported experimental results illustrated that nanomaterial based non-linear optics assay can be used for monitoring chemical processes, biological and chemical toxins with excellent sensitivity and selectivity [1–4]. Linear optical properties and plasmon resonances of metallic nanoparticles or nano-antennas are well described in the literature by extinction and/or scattering spectroscopies and by radiation patterns in direct or in Fourier space. However, much less is known on their non-linear optical properties, and in the role of plasmon resonances in the enhancement of these effects. Two-photon luminescence (TPL) and second harmonic generation (SHG) both are prominent examples of non linear effects observed on metallic nanoparticles. In this study, we focused on the linear and non linear optical characterization of Au-Al heterodimers (Fig. 1). These dimers have been fabricated by a two-step electron-beam lithography process and the diameters of the Au and Al nanoparticles have been independently varied, as for the gap distance. The linear optical properties (single dimer scattering spectra) and the non-linear optical properties (SHG images and TPL spectra) have been compared to understand the main physical phenomena involved.

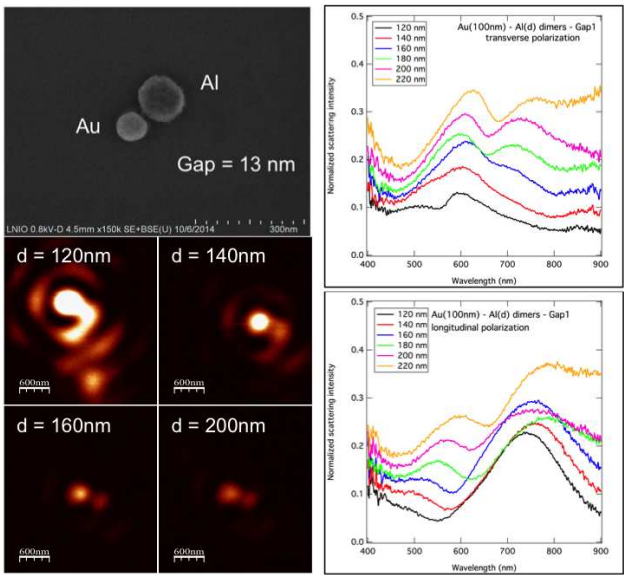

Figure 1: Linear and non linear optical characterization of single dimers composed by a 100 nm diameter Au nanoparticle and varying diameter Al nanoparticles.

REFERENCES

1. Kim, Y., R. C. Johnson, and J. T. Hupp, *Nano Lett.*, Vol. 1, 165, 2001.
2. Russier-Antoine, I., E. Benichou, G. Bachelier, C. Jonin, and P. F. Brevet, *J. Phys. Chem. C*, Vol. 111, 9044, 2007.
3. Darbha, G. K., U. S. Rai, A. K. Singh, and P. C. Ray, *Chem. Eur. J.*, Vol. 14, 3896–3903, 2008.
4. Griffin, J., A. K. Singh, D. Senapati, E. Lee, K. Gaylor, J. Jones-Boone, and P. C. Ray, *Small*, Vol. 5, 839, 2009.

Enhancing the Interaction of Light and Matter Using Photonic Nanostructures

S. Götzinger
Max Planck Institute for the Science of Light (MPL) and
Friedrich Alexander University Erlangen-Nürnberg, Erlangen 91058, Germany

Abstract— Clever methods to enhance the interaction of light and matter are at the heart of ultra-sensitive optical sensing. Prominent approaches are based on large field enhancements inside optical cavities or in the close vicinity of metallic nanostructures supporting plasmonic resonances. The latter can show extremely large enhancement factors [1]. Their performance is, however, strongly dependent on the exact shape of the structure. I will report on the controlled fabrication of gold nanocones using focused ion beam milling. The precision of the fabrication procedure allows us to control the plasmon resonance of the nanocones. Theoretical investigations predict an enhancement of the spontaneous emission rate of a single emitter by several hundred times. I will show an experiment where we could indeed observe a factor of about 340 in the spontaneous emission rate enhancement of a single colloidal semiconductor quantum dot [3]. In the second part of the talk I will report on an ultrasmall scannable Fabry-Perot microcavity with a mode volume of $0.5\lambda^3$ [4, 5]. The cavity is made of a gold coated curved micromirror fabricated on a silicon cantilever using focused ion beam milling and a planar distributed Bragg reflector. By scanning the curved gold mirror across the planar mirror we detect 80 nm gold nanoparticles by measuring the change in the cavity finesse This type of cavity is attractive for a number of studies ranging from sensing to quantum optics.

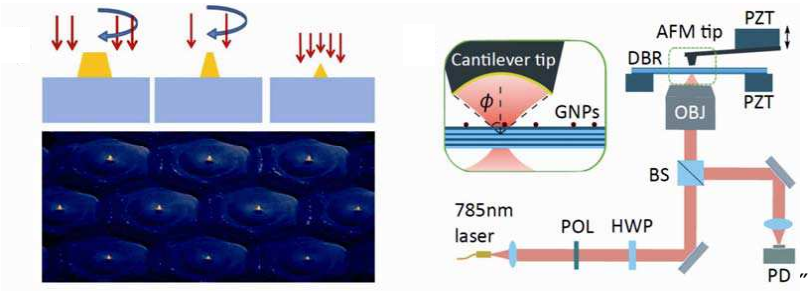

(a) (b)

Figure 1: (a) Fabrication of gold nanocones with controlled shape using focused ion beam milling. After a first course etching of the gold, we shape the cones with a fine etching step and a final polishing. (b) Schematics of the scanning microcavity setup. OBJ: microscope objective; BS: beam splitter; HWP: half-wave plate; POL: linear polarizer; PD: photodiode; GNP: gold nanoparticle.

REFERENCES

1. Lee, K.-G., H. Eghlidi, X.-W. Chen, A. Renn, S. Götzinger, and V. Sandoghdar, "Spontaneous emission enhancement of a single molecule by a double-sphere nanoantenna across an interface," *Optics Express*, Vol. 20, 23331, 2012.
2. Hoffmann, B., S. Vassant, X.-W. Chen, S. Götzinger, V. Sandoghdar, and S. Christiansen, "Fabrication and characterization of plasmonicnanocone antennas for strong optical field enhancement," 2015, submitted.
3. Vassant, S., B. Hoffmann, K. Matsuzaki, S. Christiansen, S. Götzinger, and V. Sandoghdar, 2015, in preparation.
4. Toninelli, C., Y. Delley, T. Stoeferle, A. Renn, S. Goetzinger, and V. Sandoghdar, "A scanning microcavity for in situ control of single-molecule emission," *App. Phys. Lett.*, Vol. 97, 021107, 2010.
5. Kelkar, H., D. Wang, D. Martin-Cano, B. Hoffmann, S. Christiansen, S. Götzinger, and V. Sandoghdar, "A sub-λ^3-volume cantilever-based Fabry-Pérot cavity," 2015, submitted, arXiv: 1502.02736v1.

Air Quality Monitoring by Using One Dimensional Nanomaterial Based Gas Sensors

Inkyu Park
Department of Mechanical Engineering, Korea Advanced Institute of Science and Technology, South Korea

Abstract— Recently, the interest and importance in environmental monitoring, especially real-time tracking of air quality are dramatically rising. With the advent of manufacturing industry, the sources for harmful gaseous species such as nitrogen dioxide (NO_2), carbon monoxide (CO), hydrogen (H_2), hydrogen sulfide (H_2S), hydrocarbon (HC), volatile organic compounds (VOC) are continuously increasing. Although there already exist engineering systems that can provide accurate measurement of critical air quality factors, they are heavy, expensive and require high maintenance costs. Therefore, ultra-compact, inexpensive, yet high quality gas sensors based on integrated semiconductor chip should be developed for personalized, localized and real-time environmental monitoring for individual users. In this talk, we will introduce our effort to develop highly integrated gas sensors enabled by one dimensional (1D) nanostructures (e.g., nanorods, nanowires and nanotubes) of functional sensing materials such as silicon (Si), metal and metal oxides. 1D nanostructures provide high sensitivity and fast response due to high surface to volume ratio, chemical reactivity and electrical sensitivity. Here is the list of different 1D nanostructure-based gas sensors that we will discuss: (1) top-down fabricated silicon nanowires for H_2 gas detection: silicon nanowires that are fabricated by photolithography or electron beam lithography processes and functionalized with catalytic metal nanoparticles can provide high sensitivity and fast response to H_2 gas. Furthermore, self-heating provides higher selectivity to H_2 in the background of humidity (H_2O) or CO gases; (2) template synthesized metallic nanotubes for room temperature H_2 gas detection: multimetallic nanotubes can be easily fabricated by wet chemical process along hydrothermally synthesized zinc oxide (ZnO) nanowires and can be used for highly sensitive H_2 gas detection, (3) metal oxide nanostructures for multi-component gas detection: multiplexed array of heterogeneous metal oxide nanomaterials can be synthesized by focused energy field (FEF) method in liquid precursor environment and can be used for multi-component (e.g. NO_2 and CO) gas detection. We believe that these sensors will be very useful component for smart mobile telecommunication platforms (e.g., smartphone, table PC or handheld accessories) and wearable electronics systems.

Nanoscale Energy Transfer Sensing

Jana B. Nieder
INL — International Iberian Nanotechnology Laboratory
Av. Mestre Jose Veiga, Braga 4715-330, Portugal

Abstract— Advanced fluorescence spectroscopy with single molecule sensitivity can be used to unravel details of excitation energy transfer on the nanoscale.

Time-dependent single-molecule spectroscopy at low temperatures was used to study the emission of different pigments being part of a photosynthetic light harvesting system. Correlation analysis of the various emission contributions of such time resolved spectra revealed multiple and interchangeable excitation energy transfer pathways in individual photosynthetic complexes [1].

Besides high-resolution low temperature single molecule spectroscopy, a more recent experimental technique based on ultrafast femtosecond pulse shaping excitation with single complex fluorescence emission read out [2] prove to be suited to unravel the quantum coherent nature of energy transfer in individual light-harvesting complexes. This study was performed on a highly symmetric light harvesting system, with two main absorption bands, which can individually be addressed with resonant pulses with defined phase relations.

To this end we developed a pulse compression and characterization technique with simultaneous femtosecond and nanometer sensitivity based on the second harmonic signal generated from nonlinear nanoparticles positioned in the focus of the microscope objective used for single molecule studies [3].

In this contribution we will describe the application of low temperature and ultrafast pulse shaping single molecule spectroscopy techniques to study energy transfer characteristics of photosynthetic pigment protein complexes and we will additionally present the sensitivity of such techniques to study the effects of plasmonic interaction [4]. Enhanced knowledge of (plasmonic) metal interaction effects bears the opportunities of advanced molecular sensing and new approaches for real time live cell super resolution microscopy as recently demonstrated by Chizhik et al. [5], such concepts will be discussed.

ACKNOWLEDGMENT

In this contribution on nanoscale energy transfer I will present works developed mainly in the single molecule research groups of Prof. Robert Bittl at Freie Universitaet Berlin, Germany and of Prof. Niek van Hulst at ICFO — The Institute of Photonic Sciences in Barcelona, Spain with funding via the Cluster of Excellence UniCat and support via the advanced ERC grant NanoAnntennas awarded to Prof. Niek van Hulst.

REFERENCES

1. Brecht, M., V. Radics, J. B. Nieder, and R. Bittl, "Protein dynamics-induced variation of excitation energy transfer pathways," *Proc. Natl. Acad. Sci.*, Vol. 106, No. 29, 11857–11861, 2009.
2. Hildner, R., D. Brinks, J. B. Nieder, R. J. Cogdell, and N. F. Van Hulst, "Quantum coherent energy transfer over varying pathways in single light-harvesting complexes," *Science*, Vol. 340, No. 6139, 1448–1451, 2013.
3. Accanto, N., J. B. Nieder, L. Piatkowski, M. Castro-Lopez, F. Pastorelli, D. Brinks, and N. F. Van Hulst, "Phase control of femtosecond pulses on the nanoscale using second harmonic nanoparticles," *Light: Science & Applications*, Vol. 3, No. 1, e143, 2014.
4. Nieder, J. B., R. Bittl, and M. Brecht, "Fluorescence studies into the effect of plasmonic interactions on protein function," *Angw. E. Chem. Int. Ed.*, Vol. 49, No. 52, 10217–10220, 2010.
5. Chizhik, A. I., J. Rother, I. Gregor, A. Janshoff, and J. Enderlein, "Metal-induced energy transfer for live cell nanoscopy," *Nature Phot.*, Vol. 8, 124–127, 2014.

Silver Capped Silicon Nanopillars as Surface Enhanced Raman Spectroscopy Substrates

Kaiyu Wu, **Michael Stenbæk Schmidt**, **Tomas Rindzevicius**, **and Anja Boisen**
Department of Micro- and Nanotechnology, Technical University of Denmark
Ørsteds Plads, Building 345B, Kgs. Lyngby 2800, Denmark

Abstract— In order to achieve widespread use in practical applications, a Surface-enhanced Raman Scattering (SERS) substrate should possess (i) a compatibility with high volume manufacturing process flows (ii) high and reproducible enhancement factors (EF), i.e., enhancement uniformity, over large surface areas and (iii) a tunable localized surface plasmon resonance (LSPR) wavelength over a broad spectral region. Using a novel lithography free reactive ion etch process, we fabricate wafer-scale silicon nanopillars with a high aspect ratio and subsequently coat them with silver by electron beam evaporation [1] to form plasmon supporting structures. The fabricated pillars (Fig. 1(a)) are flexible and will lean towards their nearest neighbors as the deposited analyte solution evaporates, creating self-assembled SERS hot spots at which the analyte molecules are exactly located. The fabrication method has been optimized with an emphasis on improving the SERS signal-to-noise ratio, to realize molecular detection at ultra-low concentrations [2]. The employed etching process is wafer-scale, and since it does not require any lithographic step, is fast and repeatable, thus allowing the produced substrates to be used as cheap and expendable consumables. Additionally, the produced substrate exhibits a highly uniform EF across a large area (Fig. 1(b)). It also displays a broad LSPR band (Fig. 1(c)), enabling SERS sensing at various excitation wavelengths. In the hot-spots in-between the pillars, strong localized fields are generated by the hybridized LSPR modes and the cavity LSPR mode (Fig. 1(d)). This presentation will highlight the key features of this SERS substrate and give examples of sensing applications.

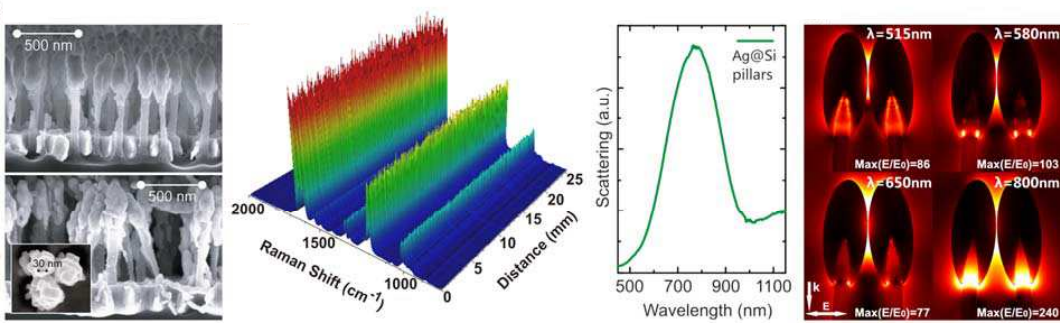

(a) (b) (c) (d)

Figure 1: (a) SEM images of the Ag@Si nanopillars before (above) and after leaning (below), (b) mapped SERS spectra of 10 mM trans-1,2-bis (4-pyridyl) ethylene in ethanol solution under 780 nm excitations, (c) measured scattering spectrum of the Ag@Si nanopillar substrate, (d) simulated cross-sectional electric field EF distributions for a dimer of Ag@Si nanopillars at different excitation wavelengths.

REFERENCES

1. Schmidt, M. S., J. Hübner, and A. Boisen, *Adv. Mater.*, Vol. 24, No. 10, OP11–OP18, 2012.
2. Wu, K., T. Rindzevicius, M. S. Schmidt, K. B. Mogensen, A. Hakonen, and A. Boisen, *J. Phys. Chem. C*, Vol. 119, 2053–2062, 2015.
3. Yang, J., M. Palla, F. G. Bosco, T. Rindzevicius, T. S. Alstrøm, M. S. Schmidt, A. Boisen, J. Ju, and Q. Lin, *ACS Nano*, Vol. 7, No. 6, 5350–5359, 2013.

3D Metamaterials and Plasmonic Nanostructures for Sensing Applications

Minkyung Kim[1] **and Junsuk Rho**[1, 2]

[1]Department of Mechanical Engineering
Pohang University of Science and Technology (POSTECH), Pohang, Korea
[2]Department of Chemical Engineering
Pohang University of Science and Technology (POSTECH), Pohang, Korea

Abstract— Metamaterials, artificially structured nanomaterials, have enabled unprecedented phenomena such as negative refraction. In this abstract, I will discuss recent development of hierarchical fabrication techniques for three-dimensional metamaterial and plasmonic structures based on ultra-accurate and precise electron-beam lithography overlay. The examples include 3D bulk negative index metamaterials, chiral metamaterials in optical frequencies and so on. Also, quick discussion about plasmonic sensing in complex nanostructures will be followed. This unique technique will provide the opportunity to achieve true isotropic metamaterials and the bulk properties induced from the metamaterials.

REFERENCES

1. Zhang, S., J. Rho, et al., "Photoinduced handedness switching in terahertz metamolecules," *Nature Communications*, Vol. 3, 946, 2012.
2. Dong, Z. G., J. Rho, et al., "Optical toroidal dipolar response by an asymmetric double-bar metamaterials," *Applied Physics Letters*, Vol. 101, 144105, 2012.
3. Kante, B., et al., "Symmetry breaking and optical negative index of closed nanorings," *Nature Communications*, Vol. 3, 1180, 2013.
4. O'Brien, K., J. Rho, et al., "Ultrafast acousto plasmonic control and sensing in complex nanostructures," *Nature Communications*, Vol. 5, 4042, 2014.
5. Rho, J., et al., "One-way transmission in optical isolator made by stacked metamaterials," in preparation.
6. Rho, J., et al., "Electron-beam lithography overlayed 3D chiral metamaterials in optical frequencies," in preparation.

Session 1P3
FocusSession.SC5: Imaging, Inverse Scattering and Remote Sensing 2

Source Reconstruction from Near- and Far-field Data with Antenna and Radome Applications

Mats Gustafsson
Department of Electrical and Information Technology
Lund University, Box 118, Lund SE-221 00, Sweden

Abstract— Electromagnetic problems are often analyzed using numerical solutions of the Maxwell's equations. In addition to being fast and cost effective, these solutions are useful for our understanding of the interaction between electromagnetic fields and devices through visualization of currents and fields. Although the numerical solutions are indispensable, they must be supplemented by measurements, where the radiated field is measured in the far-field or in the non-reactive near field. This provides valuable information but does not visualize the interaction between the device and the electromagnetic fields in the same way as a numerical simulation.

Visualization is much harder in measurement situations where we are restricted to far-field data or near-fields on a circumscribing structure. The near fields and sources are reconstructed from the measurements of the fields outside the object or volume of interest. This reconstruction is performed as the solution of an inverse source problem. This inverse problem is ill-posed and the solution requires regularization. Here, we review the theory of inverse source problems, non-uniqueness, and regularization. We present formulations based on equivalent currents using integral equations and integral representations for planar, spherical, body of revolution, and general geometries. The results are compared with analytic results for spherical and cylindrical structures. Source reconstruction is useful in applications such as non-destructive testing of antennas and radomes [1–7]. We illustrate how they can be used in antenna and radome diagnostics to, for example, image the radome thickness.

REFERENCES

1. Alvarez, Y., F. Las-Heras, and M. R. Pino, "Reconstruction of equivalent currents distribution over arbitrary three-dimensional surfaces based on integral equation algorithms," *IEEE Trans. Antennas Propagat.*, Vol. 55, No. 12, 3460–3468, 2007.
2. Cappellin, C., A. Frandsen, and O. Breinbjerg, "Application of the SWE-to-PWE antenna diagnostics technique to an offset reflector antenna," *IEEE Antennas and Propagation Magazine*, Vol. 50, No. 5, 204–213, 2008.
3. Eibert, T. F. and C. H. Schmidt, "Multilevel fast multipole accelerated inverse equivalent current method employing Rao-Wilton-Glisson discretization of electric and magnetic surface currents," *IEEE Trans. Antennas Propagat.*, Vol. 57, No. 4, 1178–1185, 2009.
4. Jörgensen, E., D. W. Hess, P. Meincke, O. Borries, C. Cappellin, and J. Fordham, "Antenna diagnostics on planar arrays using a 3D source reconstruction technique and spherical near-field measurements," *IEEE Proceedings of the 6th European Conference on Antennas and Propagation (EUCAP)*, 2547–2550, 2012.
5. Persson, K. and M. Gustafsson, "Reconstruction of equivalent currents using a near-field data transformation — With radome applications," *Progress In Electromagnetics Research*, Vol. 54, 179–198, 2005.
6. Persson, K., M. Gustafsson, G. Kristensson, and B. Widenberg, "Source reconstruction by far-field data for imaging of defects in frequency selective radomes," *IEEE Antennas and Wireless Propagation Letters*, Vol. 12, 480–483, 2013.
7. Persson, K., M. Gustafsson, G. Kristensson, and B. Widenberg, "Radome diagnostics — Source reconstruction of phase objects with an equivalent currents approach," *IEEE Trans. Antennas Propagat.*, Vol. 62, No. 4, 2014.

Reconstruction of 3D Anisotropic Magnetodielectric Objects with the Mixed Order BCGS-FFT and DBIM

Zhiru Yu and Qing Huo Liu
Duke University, Durham, NC, USA

Abstract— Although inverse scattering problems for isotropic materials have seen widespread applications in recent year, little has been done so far for objects that are anisotropic and magnetic. The inverse scattering problem for reconstructing anisotropic magnetodielectric material distributions is investigated in this work. Similar to isotropic media, this inverse scattering problem formulated by the integral equations is generally nonlinear. To solve the nonlinear problem efficiently, Chew et al. proposes the born iterative method (BIM) and distorted born iterative method (DBIM), where the true total fields inside objects are approximated by the total fields calculated from estimated material properties in the previous step. Therefore, material properties are updated by solving a linear problem in each iteration. However, the forward scattering problem has to be solved in each iteration, which can be time consuming and requires a lot of computational resources. Several fast methods for solving integral equations are available; nevertheless most of them are not appropriately formulated for anisotropic magnetodielectric objects.

This work proposes a mixed order BCGS-FFT method based DBIM to solve the inverse scattering problems for anisotropic magnetodielectric objects. The forward scattering problem is formulated by the combined field volume integral equations (CFVIE). Volume equivalent theorem is chosen because it is flexible in handling inhomogeneous anisotropic objects. The CFVIE is solved by a fast frequency domain solver called the mixed order BCGS-FFT method. The mixed order BCGS-FFT method expands the electric and magnetic ux densities ($\mathbf{D}$ and $\mathbf{B}$) with first order divergence conforming basis functions and expands the magnetic and electric vector potentials ($\mathbf{A}$ and $\mathbf{F}$) with second order curl conforming basis functions. The benefits of the mixed type and mixed order basis functions are two folded: 1. It can account for correct boundary conditions for both the ux densities and the vector potentials so that the calculated results are more accurate. Thus, objects with higher contrasts can be handled. 2. The mixed order basis functions formulation avoids zero terms caused by the divergence or curl operations on the vector potentials in the weak form integral equations. Therefore both dielectric and magnetic contrasts can be taken into account with higher order basis functions. This means magnetodielectric objects can be handled. The inverse problem is solved by the DBIM method. Reformulation of the DBIM to incorporate inhomogeneous anisotropic objects is shown in this work. Examples are given to demonstrate the performance of the mixed order BCGS-FFT based DBIM on anisotropic magnetodielectric objects. Discussions are also given on the key factors that might affect the performance of this method.

Efficient Imaging of Dielectric Targets Based on Contrast Source Inversion Method

S. C. Yan, C. X. Yang, J. Zhang, and M. S. Tong
Department of Electronic Science and Technology
Tongji University, 4800 Cao'an Road, Shanghai 201804, China

Abstract— Solving inverse scattering problems is challenging because the involved governing equations are nonlinear and the solutions are inherently nonunique. This is particularly true when measuring conditions are unfavorable and diverse scattering data are not available. Usually, the inverse problems are solved by linearizing governing equations and gradually minimizing the mismatch between calculated data and measured data in an iterative scheme. In the integral equation approach (IEA) for reconstructing dielectric objects, there are forward scattering integral equation (FSIE) and inverse scattering integral equation (ISIE) and traditionally we need to alternatively solve them in the context of Born iterative method (BIM) or its variations. The solution of permittivity from the ISIE can reveal the profile of unknown object in the imaging domain.

In this work, we use the contrast source inversion method (CSIM) to reconstruct the dielectric objects for the application in target recognition and atmosphere or space sensing. In such an application, the details of object are not important but obtaining a sufficient observation or measurement to the object may be difficult. The CSIM is motivated by and similar to the modified gradient method (MGM), but it updates the contrast source and contrast simultaneously instead of the field and contrast. The CSIM can avoid the direct solution of FSIE because it defines a cost functional including mismatches or errors from both the FSIE and ISIE and update them together. Compared with the MGM, the CSIM is more computationally efficient and also requires less measurement data. This is particularly desirable when we consider the reconstruction with a poor measurement condition which may be encountered in many applications. Numerical examples for reconstructing typical dielectric objects under a limited view are presented and good images can be observed.

Inverse Scattering Approach without Information on Incident Field Using Gradient-based Optimization Method

Takashi Takenaka[1], **Toshifumi Moriyama**[1], **Toshiyuki Tanaka**[1], **and Zhi Qi Meng**[2]

[1]Graduate School of Engineering, Nagasaki University, Nagasaki 852-8521, Japan
[2]Faculty of Engineering, Fukuoka University, Fukuoka 814-0180, Japan

Abstract— Inverse scattering analysis generally assumes the knowledge of the incident field in a region of interest (ROI) as well as on a measurement surface. In some measurement situations, the transmitting antenna producing an incident field is placed close to the ROI. This causes antenna characteristics to change due to the coupling with the ROI. This characteristics change makes it difficult to know the incident field generated by the antenna accurately. In our previous work [1], we have proposed an inverse scattering approach based on the field equivalence principle which does not require the knowledge of the incident field and applied it to a nondestructive testing problem to detect homogeneous defects by a genetic algorithm (GA). GAs are not appropriate optimization techniques for estimating a large number of unknowns such as electrical parameter distributions of an inhomogeneous object.

In this paper, we apply a gradient-based optimization method to our inverse scattering approach for imaging an inhomogeneous object. In [1], we have shown that the inverse scattering problem can be reduced to an optimization problem where the following functional of the parameters $\mathbf{p} = [\varepsilon_r(\mathbf{r}),\ \mu_r(\mathbf{r}),\ \eta\sigma(\mathbf{r})]$ is to be minimized:

$$Q(\mathbf{p}) = \sum_{m=1}^{M} \int_0^{cT} \int_{\Omega_e} \left|\mathbf{v}_m^{eq}(\mathbf{p};\mathbf{r},t)\right|^2 d\mathbf{r}d(ct) \tag{1}$$

where Ω_e is the region exterior to the measurement surface S and T is the measurement time. The total field $\mathbf{v}_m^{eq}(\mathbf{p};\ \mathbf{r},t)$ is the solution of the equivalent problem for the object with estimated parameters $\mathbf{p}$ under the mth illumination. The quantities c and η are the light speed and the intrinsic impedance of the background, respectively. We minimize the functional (1) by a gradient method. The Fréchet differential of (1) is represented as an inner product of a parameter variation $\delta\mathbf{p}$ and the gradient $\mathbf{g}(\mathbf{r}) = [g_\varepsilon(\mathbf{r}),\ g_\mu(\mathbf{r}),\ g_\sigma(\mathbf{r})]$. Due to space limitations, only the expression of g_ε is shown:

$$g_\varepsilon(\mathbf{p};\mathbf{r}) = \sum_{m=1}^{M} \int_0^{cT} \mathbf{u}_m^e(\mathbf{p};\mathbf{r},t) \cdot \frac{\partial \mathbf{E}_m^{eq}(\mathbf{p};\mathbf{r},t)}{\partial(ct)} d(ct) \tag{2}$$

where $\mathbf{E}_m^{eq}(\mathbf{p};\ \mathbf{r},\ t)$ and $\mathbf{u}_m^e(\mathbf{p};\ \mathbf{r},\ t)$ are, respectively the electric components of the total field and the adjoint field under the mth illumination for the object with an estimated parameter $\mathbf{p}$. Numerical simulations were carried out using the conjugate gradient algorithm for minimizing the cost functional and the results indicate the effectiveness of the method.

REFERENCES

1. Takenaka, T. and T. Moriyama, "Inverse scattering approach based on the field equivalence principle: Inversion without a priori information on incident fields," *Optics Letters*, Vol. 37, 3432–3434, Aug. 2012.

Application of Domain Decomposition Techniques to Quantitative Inverse Scattering Problems

I. Voznyuk, **A. Litman**, **and H. Tortel**
CNRS, Centrale Marseille, Institut Fresnel UMR 7249, Aix-Marseille Université, 13013 Marseille, France

Abstract— Often, inverse scattering schemes are based on iterative techniques which require to call a forward solver at each iteration. This forward solver must simulate in an efficient way the scattered field associated to the predicted permittivity map provided at that specific iteration. It must also take into account the environment in the vicinity of the object (rough surface, medias with complex shapes) .... Moreover, this forward solver is also exploited to estimate efficiently the various gradients which are necessary to compute the descent direction updates. Indeed, due to the reciprocity properties of the wave equations, it is possible to directly provide close-form expressions of these gradients by means of a point-by-point complex multiplication of the electromagnetic field and of a so-called ajoint field.

Various works take profit of the finite element method in order to solve inverse problems in different scientific domains, such as in optical imaging, electroencephalography imaging, electro-cardiographic imaging, and, of coarse, in microwave imaging. Thanks to its flexibility and its capabilities of managing complex geometrical configurations, this type of modelling scheme is more than appropriate to tackle biomedical and non-destructive testing applications.

Nevertheless, the numerical resolution of the Helmholtz equation in heterogeneous media at high wave number is a challenging problem for the classical finite element method. A way to overcome these difficulties is to apply a domain decomposition (DDM) technique. The principal idea of DDM is to split the entire computational domain into smaller non-overlapping sub-domains and to solve a sequence of similar sub-problems on these sub-domains. Among a variety of DDMS, the Finite-Element Tearing and Interconnecting (FETI) method and its electromagnetic counter part, the Finite-Element Tearing and Interconnecting-Dual Primal Electromagnetic methods (FETI-DPEM) are shown to be powerful techniques with an excellent scalability. In this method the computationnal problem is divided into non overlapping subdomains in order to construct and solve an equivalent reduced-order interface problem. The solution inside each subdomain can then be evaluated independently by imposing knwon mixed boundary conditions at the internal interfaces between subdomains. We will present in this talk the combination and the optimization of this direct solver in a Newton-type minimization scheme and inversion results obtained from 3D experimental datas will be displayed.

Virtual Experiments for the Solution of Inverse Scattering Problems

M. Bevacqua[1], **L. Crocco**[2], **L. Di Donato**[3], **and T. Isernia**[1]

[1]DIIES, University 'Mediterranea' of Reggio Calabria, Italy
[2]IREA, CNR, Naples, Italy
[3]DIEEI, University of Catania, Catania, Italy

Abstract— Inverse scattering is an active area of research in applied electromagnetics, due to its relevance to many applications ranging from sub-surface prospections to biomedical diagnostics or safety and security surveying operations. Unfortunately, the non-linearity and ill-posedness of the inverse scattering problem [1] make the development of effective and reliable solution methods a still open and challenging task.

The *virtual* experiments framework [2–6], is an emerging paradigm that has been conceived to smartly cope with these fundamental difficulties. The basic idea is to exploit the linearity of the scattering phenomena to recombine the available scattering experiments into new, "virtual" ones, without performing additional measurements. The main advantage is that properly designed virtual experiments allow to enforce some properties of the field or, equivalently, of the contrast source, which in turn can be helpful to reduce the difficulty of the problem. For example, by enforcing focused fields or contrast sources, it is possible to estimate the contrast of non-weak targets within a linear inversion framework or even to retrieve the unknown contrast solving a set of algebraic equations (see [2–6]).

The contribution will review the basics of the virtual experiments concept, describe the simple but powerful inversion techniques that can be derived from it and address the many future methodological developments that can steam from this emerging paradigm.

REFERENCES

1. Colton, D. and R. Kress, *Inverse Acoustic and Electromagnetic Scattering Theory,* Springer-Verlag, Berlin, Germany, 1992.
2. Crocco, L., I. Catapano, L. Di Donato, and T. Isernia, "The linear sampling method as a way for quantitative inverse scattering," *IEEE Trans. Antennas Propag.*, Vol. 4, No. 60, 1844–1853, 2012.
3. Crocco, L., I. Catapano, L. Di Donato, and T. Isernia, "Enhancing the factorization method relying on its physical meaning," *2013 7th European Conference on Antennas and Propagation (EuCAP)*, 70–71, Apr. 8–12, 2013.
4. Bevacqua, M., L. Crocco, L. Di Donato, and T. Isernia, "An algebraic solution method for nonlinear inverse scattering," *IEEE Trans. Antennas Propag.*, Vol. 63, No. 2, 2015, in Print.
5. Di Donato, L., M. Bevacqua, L. Crocco, and T. Isernia, "Inverse scattering via virtual experiments and contrast source regularization," *IEEE Trans. Antennas Propag.*, Vol. 63, No. 4, 2015, in Print.
6. Bevacqua, M., L. Crocco, L. Di Donato, and T. Isernia, "Microwave imaging of non weak targets via compressive sensing and virtual experiments," *IEEE Antennas Wireless Propag. Lett.*, Vol. 13, 1–4, 2014.

On Constructing Globally Convergent Algorithms: Applications to GPR and Marine CSEM Sounding

A. Timonov
University of South Carolina Upstate, USA

Abstract— The challenging problem of constructing the globally convergent algorithms for electromagnetic sounding is addressed. The traditional numerical techniques, such as the gradient or Newton like methods, require an initial approximation in a sufficiently small neighborhood of the true solution. On the other hand, the global optimization algorithms are extremely time-consuming and heuristic. In the last decade the so-called convexification method was proposed by Klibanov and Timonov. Later, some modifications of this method were developed by Klibanov and Beilina. Being a special form of the Carleman-weighted nonlinear least squares, the method allows for constructing some iterative algorithms that do not require the proximity of an initial approximation to the true solution. However, being approximate by its nature, the method provides convergence to an approximation of the true solution. The main challenge is constructing algorithms that guarantee the maximum closeness of the approximate solutions to the true one. In this talk we present two such algorithms. The main distinctive feature of the first algorithm is the refinement procedure, in which we search for a better approximation performing matching the interior field generated by the iterative solution by the solutions of the forward problem in the region of interest. In the second algorithm the Tikhonov's regularizing functional is used in combination with the alternating split Bregman algorithm. The computational effectiveness of the proposed algorithms is demonstrated in some numerical experiments with the inverse models of GPR and marine CSEM sounding of layered media. The latter has become significant only in the last decade due to the growing interest to hydrocarbon deposits on a shelf, as well as to the rapid development of technologies used in marine geophysics.

Modeling of Random Media for Controlled Light Scattering

Olga Korotkova
Department of Physics, University of Miami, USA

Abstract— We propose a new method for modeling of scattering from weakly random, statistically stationary media based on manipulation of the two-point correlation function of its scattering potential (CFSP) for generating of the scattered far-fields with prescribed intensity distributions. This method is based on the fact that the far-field intensity distribution is the 3D Fourier transform of the CFSP calculated at the momentum transfer vectors. We illustrate that regardless of the size, the geometrical shape and the boundary profile of the scatterer, the scattered average intensity distribution can be tuned solely by prescribing the CFSP.

In particular we introduce mathematical models for the CFSP that lead to scattered fields with flat circular, ring-like and flat rectangular-like average intensity distribution. Without loss of generality we always assume a spherically symmetric particle, employing either solid-sphere or soft-sphere (Gaussian) functions for the average refractive index distribution. Our mathematical modeling of the CFSP involves 3D multi-Gaussian families of functions that may have circular, cylindrical and Cartesian symmetry. Such families are the sums of Gaussian functions with different heights and widths with alternating signs. The 1D, 2D and 3D multi-Gaussian functions have been previously employed in optics for different purposes, such as the control of the aperture functions, the modeling of the radiation field correlation function, the intensity shaping, etc.. They allow designing of the distributions (of scattered intensity in our case) ranging from soft (Gaussian) for the single term in summation to square-pulse like for the number of terms approaching infinity. We also investigate under which conditions the component of the CFSP along the axis of scattering does not influence the scattered distribution.

After outlining the scalar treatment valid for a single scatterer and the incident plane wave, we also discuss the extension of the theory to particulate collections, other incident waveforms and electromagnetic treatment. In the latter case the polarization properties of the far field, such as degree of polarization and the parameters of the polarization ellipse can be adjusted at will.

Demonstration of Radiative and Inductive Couplings of Traveling Wave to a Phantom in a Small-bore 16.4 T MRI

Alexey Tonyushkin[1], **Patrick Bluem**[2], **Dinesh Deelchand**[3], **Gregor Adriany**[3], **Pierre-Francois Van de Moortele**[3], **Zoya Popovic**[2], **and Andrew J. M. Kiruluta**[1]

[1]Radiology Department, Massachusetts General Hospital
Harvard Medical School, Boston, MA, United States
[2]Electrical Engineering Department
University of Colorado, Boulder, CO, United States
[3]Center for Magnetic Resonance Research
University of Minnesota Medical School, MN, United States

Abstract—

Introduction: At ultra high field strength propagating RF field effects emerge [1] making traditional MRI less effective for achieving ultimate SNR [2]. To date few systems have been adopted to demonstrate traveling wave MRI (TW-MRI), among these preclinical human scanners (7 T, 9.4 T) [3, 4] and research small bore systems (16 T, 21.1 T) [5, 6]. Whole body scanners correspond to above cut-off cylindrical waveguides with one or two TW modes propagating in the unloaded bore. On the contrary, most of the small-bore research as well as clinical (< 4 T) systems correspond to below cut-off undermoded waveguides that require special high dielectric inserts [7] or coaxial transmission lines [8] for mode propagation. Hence, the TW excitation methods vary in such systems; for example, the typical RF probes for preclinical TW-MRI are patch antennas or other electric dipole probes in a radiative wave regime [9]. In undermoded waveguides it is much more difficult to excite TW due to relatively large free-space wavelength that makes regular patch antennas impractical. Therefore, previous demonstrations of TW-MRI at below cut-off were limited to loop-coils that inductively couple to long (few wavelengths) dielectric inserts that limits SNR. Here, we demonstrate a new TW coupling mechanism that involves a specially designed patch antenna and a metal waveguide and compare its performance to that with an inductive TW coupling using loop-coil.

Methods: The system of interest is 16.4 T (Varian) horizontal bore small animal NMR imaging system with a bore diameter of 26 cm (~ 12 cm with gradient insert) and the resonance frequency of 698 MHz ($\lambda = 43$ cm). The typical setup with inductive coil coupling consists of a dielectric waveguide made of an acrylic tube ($L = 34$ cm, $D = 9$ cm) and filled with deionized water or saline ($\varepsilon_r = 80$) and a simple transmit-receive loop-coil ($D = 8$ cm) placed at the edge of the tube. The orientation of the loop with respect to the edge of the tube (vertical or horizontal planes) defines the specific single or multiple modes excitation in the dielectric tube. A second setup uses a circular patch probe antenna (ground plane diameter 20 cm, patch diameter 7 cm, Fig. 1(c)) that provides circular polarization with a single coaxial feed and a crossed-slot polarizer in the patch ground plane [10]. The measured match to the 50-Ω feed of the patch inside the bore is $|S_{11}| = -20$ dB. A cylindrical array of 3-cm wide longitudinal strips 2-m long and 12 cm in diameter is inserted in the bore with a goal of modifying the travelling-wave mode content in the gradient coil region. The patch probe is placed 5 cm from the edge of the bore at the start of the strip cylinder. The MR images were obtained with a GRE sequence: FOV = 20×20 cm, TR/TE = 275 ms/2.1 ms, slice thickness of 1 mm for both axial and coronal slices. In addition to GRE we used SE imaging with: TR/TE = 1 s/20 ms, FOV = 20×20 cm, matrix = 256×128, slice thickness of 2 mm, 0.8 mm gap, 10 slices. We carried out simulations of the modes inside the dielectric guide using FEM E&M solver COMSOL Multiphysics (Burlington, MA).

Results and Discussions: For comparison study of the two excitation methods: by loop-coil and patch probe. We placed the loop-coil vertically (coaxially) (Fig. 2) and horizontally (Fig. 3) at the edge of the dielectric guide. These two arrangements allow excitation of a various modes, as predicted by the corresponding simulations: TE01 (Fig. 2), and mixture of TE11 and TM11 (Fig. 3(a)) that matches mode population by the patch probe (Fig. 3(b)). The patch probe excitation efficiency is maximal when it is placed close to the gradient coil section and couples TW from the air region into the dielectric phantom (Fig. 1), providing the best SNR (Fig. 3(b)). The nulls on z-axis (sagittal slices) correspond to the standing waves of various modes due to reflection from the far end of the dielectric guide. The high spatial frequency fringes and edge brightening correspond to artifacts due to unencoded volume of the dielectric guide that extends beyond the gradient insert. Apart from the artifacts the modes structure between the radiative

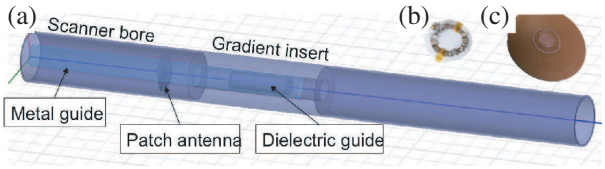

Figure 1: Experimental setup: (a) scheme of the scanner with patch antenna inside the larger bore, dielectric guide, and optional metal guide; (b) loop-coil; (c) patch antenna.

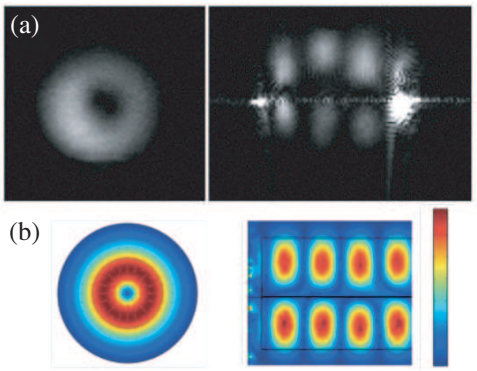

Figure 2: MR images for loop-coil, (a) B_1 modes simulations, (b) the colorbar represents relative B_1 field strength (left column — axial, right column — sagittal slices).

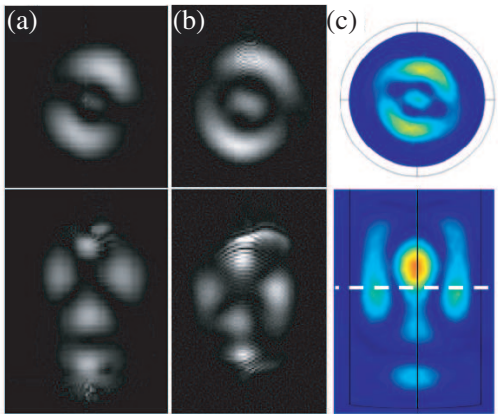

Figure 3: MR images for (a) loop-coil, (b) patch probe excitations; (c) B_1 modes simulations, dashed line indicates axial slice position (top row — axial, bottom row — sagittal slices).

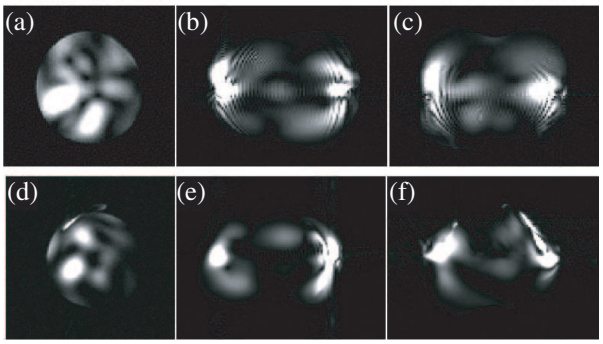

Figure 4: (a)–(c) GRE and (d)–(f) SE MR images obtained in dielectric guide with patch antenna and metal guide excitation: (a), (d) axial, (b), (e) coronal, and (c), (f) sagittal slices.

and inductive couplings looks similar with comparable SNR. For the next step, we used the patch probe antenna placed at the entrance of the optional 2-m long copper strip guide enclosing the dielectric guide. Although the guide diameter of a metal guide is too small implying the TW are below cut-off, we found this system to provide seven time higher SNR (Fig. 4) as compared to the patch probe without the strip cylinder (Fig. 3(b)). The axially oriented strips provide a frequency-dependent anisotropic surface impedance which modifies the modal content, and in addition to the presence of the high-permittivity dielectric cylinder, allows for travelling wave propagation. Such high SNR allowed us to utilize SE sequence (Figs. 4(d)–(f)). Another feature of the new probe system is the presence of higher order modes that could potentially be used for B_1 field shimming.

Conclusion: We have demonstrated new TW excitation schemes that involves a loop-coil or patch antenna and an optional metal guide that provides coupling to a phantom via far-field. The combined patch probe is robust and does not require extensive tuning inside the scanner. The excitation scheme provides high order modes that potentially could be used for B_1 field shaping for homogeneity improvement. The experimental method is scalable to the other MRI systems with below cut-off conditions such as clinical scanners.

REFERENCES

1. Kiruluta, A., *JMR*, Vol. 182, 308–314, 2006.
2. Lattanzi, R. and D. K. Sodickson, *MRM*, Vol. 68, 286–304, 2012.
3. Brunner, D. O., et al., *Nature*, Vol. 457, 994–999, 2009.

4. Geschewski, F. H., et al., *MRM*, Vol. 69, 1805–1812, 2013.
5. Tonyushkin, A., et al., *Proc. ENC*, Vol. 53, 2012.
6. Tonyushkin, A., et al., *Proc. ISMRM*, Vol. 20, #22, 2012.
7. Tonyushkin, A., et al., *Proc. ISMRM*, Vol. 20, #3995, 2012.
8. Tang, J. A., et al., *A. Con. in Mag. Res. A*, Vol. 38A, 253–267, 2011.
9. Raaijmakers, A. J. E., et al., *MRM*, Vol. 66, 1488–1497, 2011.
10. Biao, X. L. and M. J. Ammann, *IET Electronic Lett.*, Vol. 42, No. 4, Feb. 2006.

Raw Data Generation of Maritime Scenes Using MOCEM V4 and PHYS-IQ V1

Christian Cochin[1], **Jean-Christophe Louvigne**[1], **and Julien Houssay**[2]

[1]DGA MI, French MoD, Bruz, France
[2]Corentin LE BARBU, Nicolas Pinel, Goulven Monnier Alyotech, Rennes, France

Abstract— Since years, DGA MI — expertise center of French MoD develops simulation tools for SAR surveillance applications. These tools have now capabilities of raw data generation and therefore can be used for many other applications that their first purpose of simulation. The GPU computing has recently opens news efficient ways for raw data simulation. For advanced processing and new imagery modes (SAR/ISAR with or without use of CS technics), the simulation of realistic raw data is crucial. In this paper we'll illustrate the possible use of the tools in the context of maritime applications.

We'd like to focus on opportunities offered by this set of tools, part of the French DGA simulator SIROS — **S**imulation toolset for **I**magery **R**adar and **O**cean **S**urveillance —, for studies and for tuning processing.

For maritime scenes, we have to take into account:

- For the target, realistic 3D ship models with Electromagnetic (EM) materials, inertial ship motions.
- For the sea clutter, it is essential to deal with the grazing angle challenge or effects associated to High sea states (shadows, sea spikes, heavy tail distributions).
- We have also to consider interactions that include coupling effects, wakes ...

MOCEM V4 has been shown in conferences and detailed in several publications. But MOCVIEW has been newly developed in order to generate raw data. PHYS_IQ is also a new tool dedicated tool to create raw data of a dynamic sea. We will illustrate possible combinations and configurations of the tools to several needs and uses. We'd like also to focus how methods and time computation can be adjusted to the user's needs, including precision and phenomena taken into account to limit computation time. We will illustrate the tools capabilities in the field of polarimetry, interferometry, multi-channel, in addition to high resolution in range and all the dynamic aspects, associated to a radar acquisition of a complex and dynamic maritime scene.

The problem of the maritime scenes is the variety of parameters concerning the target, the environment, the radar mode. To deal this that, it is essential to create number of cases to test and tune a new processing or radar mode. The availability of efficient and realistic tools is a real opportunity to prepare experimental modes and develop new detection technics and imagery products.

Figure 1: Military ship.

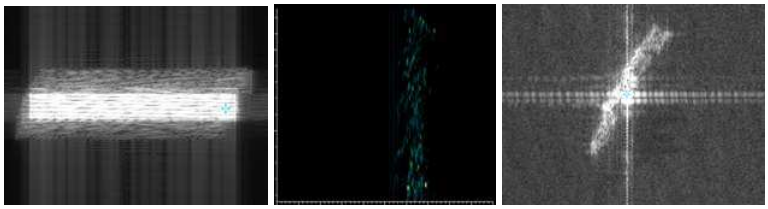

Figure 2: Target & clutter raw data, focused image of the ship.

Remote Sensing of Ionospheric Disturbances Caused by Exhaust Jets of the 'Progress' Cargo Spacecraft

V. V. Khakhinov, **B. G. Shpynev**, **V. P. Lebedev**, **D. S. Kushnarev**, **and S. S. Alsatkin**
Institute of Solar-Terrestrial Physics SB RAS
Lermontov st. 126a, P/O Box 291, Irkutsk 664033, Russia

Abstract— This paper presents results of active space experiment "Radar-Progress" conducted by FSUE Central Research Institute of Machine Building (TsNIIMash), Rocket and Space Corporation Energia, and Institute of Solar-Terrestrial Physics of Siberian Branch of Russian Academy of Sciences (ISTP SB RAS). More than 80 sessions were conducted in 2007–2014. The experiment is aimed at studying parameters of ionospheric disturbances generated by exhaust jets of propulsion devices of the Progress cargo spacecraft. The following ISTP SB RAS ground-based facilities for remote sensing of the ionosphere are used: Irkutsk Incoherent Scatter Radar. The experiment sessions were carried out under different helio- and geophysical conditions, given various directions of the jet efflux and duration of operation of different propulsion devices. Space-time characteristics of ionospheric irregularities were assessed. The dependence of observability of irregularities on height, direction of jet efflux and exhaust amounts was examined too.

Two Dimensional Inverse Scattering Problems with Four Different Boundary Conditions

Xudong Chen[1], **Rencheng Song**[2], **and Xiuzhu Ye**[3]

[1]Department of Electrical and Computer Engineering, National University of Singapore, Singapore
[2]Halliburton, Singapore
[3]Department of Electrical and Computer Engineering, Beihang University, Beijing, China

Abstract— This paper deals with a special inverse scattering problem, where four different boundary conditions, i.e., Dirichlet, Neumann, impedance, and transmission boundary, simultaneously exist. We present a general inversion method to simultaneously reconstruct scatterers with four different boundary conditions without prior information on their locations, shapes, or types of boundary condition. In the forward problem, the scattering of mixed scatterers is modeled by the T-matrix method, where the scattered field is expanded in multipole radiation series. Regardless of the type of boundary condition, the multipole expansion of scattered field is always applicable, and thus it provides a unified framework for representing the four different boundary conditions. The unknowns in the inverse problem are T-matrix coefficients, and the first step of the inversion solver is to reconstruct the T-matrix coefficients. The objective function considered in the inverse problem is solved by a subspace-based optimization method. In the second step of inversion, the types of boundary conditions of scatterers are inferred from the T-matrix coefficients.

Numerical Simulation of Aquifer Detection Using Low Frequency Pulsed Radar

K. van den Doel[1] and M. Robinson[2]

[1]University of British Columbia, Vancouver, Canada
[2]Adrok Ltd., Edinburgh, United Kingdom

Abstract— We describe two numerical models of the detection of aquifers under limestone using low frequency pulsed radar which we use for experimental design, depth range estimations, and testing data analysis methods. The first model implements a 1D FDTD scheme for Maxwell's equations coupled to a ground model incorporating dielectric permittivity, conductivity, and a Debye polarization model. The material parameters of the model were obtained from in situ measurements through limestone pillars performed underground in a mine [2]. The input to the simulation is the measured output of a low frequency pulsed radar system manufactured by Adrok Ltd. The complicated radar pulse produced by the transmitter contains frequencies from 3 to 65 MHz and the low frequency component allows for deep penetration in suitable materials, see for example [1], where a similar simulation for deep surface probing on Mars is described.

The simulated pulse propagates through the limestone with a relative permittivity avaraging $\epsilon_r = 6$ and is re ected by an aquifer which we model as a layer with $\epsilon_r = 40$. After reflecting off the wet layer the pulse travels back up and is measured on the surface as a time domain trace. Synthetic noise calibrated to match measurements from the actual equipment is added to the computed result. In normal operation mode (STARE), 8000 traces are stacked, and the reflection is detected from the data using either visual identification of the return or, when the return signal is very weak, by analysing the correlations between stacked traces. Results indicate the aquifer is detectable up to about 350 m depth and that extending the range to 500 m depth is achievable by increasing the stacking by a factor 25. Detecting a reflection from 650 m would require stacking 2000×8000 traces, and down to 800 m would require 100000×8000 traces. Assuming a trace length of 20 µs, suitable for detecting reflections up to 1km for $\epsilon_r \leq 9$, the latter would require a theoretical minimum acquisition time of about 5 hours, which is probably close to what is practical.

In order to convert the reflection time of the pulse to depth we need to know the velocity which is governed by the relative permittivity ϵ. In some practical applications this may be known from geology, but if it is not it can be obtained from a WARR scan, where measurements are taken with transmitter and receiver at increasing separations and using a normal moveout method or a velocity spectrum (as used in seismic) to estimate velocity and ϵ_r. Because of the high frequency components in the pulse and the high accuracy required of the FDTD simulator (due to the large dynamic range that needs to be simulated) the required grid spacing is about 5 cm and large computational resources would be required for a full 2D FDTD simulation which is why we model the WARR scan with a raytracing method. Simulated data is rendered by propagating the measured input pulse through all rays that reach the surface using computed re ection/transmission coefficients and an attenuation filter derived from the FDFT model. The ground is modeled as a layer with mean $\epsilon_r = 6$ with random fluctuations with standard deviation 0.5 at intervals which are distributed exponentially with a mean of 5 m. This models irregularities and causes complicated backscatter similar to what is observed in practice. From a velocity spectrum analysis (suitably modified to incorporate radar specific losses) it appears that the velocity can be estimated from the backscatter up to about 150 m down and from the stronger aquifer re ection at 350 m with about 5% accuracy leading to a similar accuracy in depth estimation.

REFERENCES

1. Ciarletti, V., B. Martinat, A. Reineix, J. J. Berthelier, and R. Ney, "Numerical simulation of the operation of the gpr experiment on netlander," *Journal of Geophysical Research*, Vol. 108, No. E4, 8028, 2003, Doi: 10.1029/2002JE00186.
2. Van den Doel, K., J. Jansen, M. Robinson, G. C. Stove, and G. D. C. Stove, "Ground penetrating abilities of broadband pulsed radar in the 1–70 MHz range," *SEG Technical Program Expanded Abstracts 2014*, 1770–1774, Denver, 2014.

Session 1P4a
SC3: Laser Writing of Optical Waveguides and Optical Components in Novel Materials

Expanding the Parameter Space in Optimizing Ultrafast Laser Written Structures for Photonics Device Applications

T. Toney Fernandez, J Siegel, and J Solis
Grupo de Procesado por Láser, Instituto de Optica
Consejo Superior de Investigaciones Científicas (CSIC), Madrid, Spain

Abstract— An ultrafast laser irradiation based optical micropipette is proposed, able to manipulateand control the laserinduced plasma distributions and — as a consequence — ionmigration, net refractive index change and aspect ratio of the induced structures.

Production of micrometer to nanometer scale structures isone of the major strengths of ultrafast laser-based micromachining. Short pulse duration leading to heat accumulation rather than heat diffusion help induce much smaller structures. When combined with complementary strategies, such as slit shaping of the laser beam and the use of high repetition rates, extraordinary results can be obtained. Applied to direct writing of optical waveguides, we have recently found a counterintuitive result in a study operating at 500 kHz repetition rate, leading to a reduction of the aspect ratio of the waveguide cross section to almost 4 times that of a structure written at low repetition rate (1 kHz). Adjoining this approach with the control of ion migration in the laser excited volume, we propose a novel light based tool — an optical micropipette. By means of simple shaping techniques of the focal volume a strong control can be exerted on the shape of the laser-induced plasma distribution, directly controlling ion migrating mechanisms, achievable refractive index change and the area/aspect ratio of the written structure. It appears that multivalent ions migrate towards regions which feature a higher density in the final structure, whereas monovalent ions migrate towards the rarefied zones. The behavior of multivalent ions could be classified in two regimes, where light elements (atomic weight $< 31u$, observed in a lanthanum aluminium phosphate glass doped with Erbium and Ytterbium, Figure (a1) and heavy elements (Figure (a2)) play the role of densification. The migration directions of such group of ions with respect to the laser propagation direction can be inverted (Figures (b1) and (b2)) by inducing strong positive or negative spherical aberration in the beam, effectively inverting the laser-induced plasma distribution. Figures (c) and (d) show the effect of slit shaping in two different glasses with two different laser writing parameters. (c1) (no slit) and (c2) (1.4 mm slit) are single scan waveguides produced inside a phosphate glass. (d1) and (d2) are multiscan waveguides produced inside a Borosilicate glass.

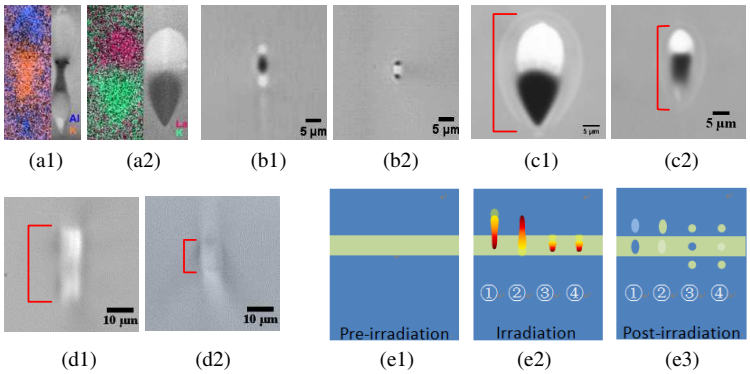

Figure 1: (a1) demonstrate the cross migration between (a1) and K, where as (a2) shows cross migration of La and K. Figures (a), (b) and (c) are structures produced inside a phosphate glass using 500 kHz, (b1) written with 0.68 NA objective, 260 mW, 80 µm/s at a depth of 100 µm. (b2) 0.85 NA aberration-corrected objective, 100 mW, 100 µm/s at a depth of 100 µm. (c1) and (c2) written with 500 kHz, 0.68 NA without (395 mW) and with slit (365 mW, 1.4 mm), respectively. (d1) and (d2) are structures written with and without slit (2 mm), respectively using the following parameters: 500 kHz, 0.4 NA objective, 140 mW, 1 mm/s and at a depth of 100 µm. In all cases the laser is incident from the top. (e1) Sample before irradiation, Green layer could be an implanted region or a sandwich region, (e2) four possible laser induced plasma scenarios and (e3) their possible finalresult.

Combining these effects, we propose that an optical micropipette could be designed to relocate/remap/transfer ions from an area of interest to another. A proper tuning of laser fluence, spherical aberration and slit shaping offers a good control of the type and direction of migrating ions. Four possible potential application scenarios are sketched in Figure (e).

REFERENCES

1. Toney Fernandez, T., J. Siegel, J. Hoyo, B. Sotillo, P. Fernandez, and J. Solis, "Controlling plasma distributions as driving forces for ion migration during fs laser writing," *Journal of Physics D: Applied Physics*, Vol. 48, 155101, 2015.
2. Toney Fernandez, T., B. Sotillo, J. del Hoyo, J. A. Valles, R. Martinez Vazquez, P. Fernandez, and J. Solis, "Dual regimes of ion migration in high repetition rate femtosecond laser inscribed waveguides," *IE3 Phothon. Tech Lett.*, in press, 2015.

Flexible Photonic Components in Silica Glass Fabricated by Ultrafast Laser Direct Writing

Sheng Huang[1], **Mingshan Li**[1], **Sean M. Garner**[2], **Ming-Jun Li**[2], **and Kevin P. Chen**[1]

[1]Department of Electrical and Computer Engineering
University of Pittsburgh, USA
[2]Corning Incorporated, One Riverfront Plaza
Corning, New York 14831, USA

Abstract— Flexible glass is a brand new class of glass materials that is attracting widespread interest from industry and research groups. Designed as substrates for flexible electronics and display applications, this new type of glass substrate exhibits remarkable mechanic flexibility. Compared with flexible polymer substrates, flexible glass materials show superior thermal capability, dimensional stability, surface quality, barrier properties, hermiticity, and durability beyond the fundamental limitations of polymeric substrates.

From an optical perspective, propagation loss in the flexible glass substrates could also be substantially lower than the polymer materials currently used to build flexible photonic circuits. In this paper, we present three-dimensional photonic devices and sensors written in flexible Corning® Willow® Glass and other glass substrates. Using the ultrafast laser direct writing technique, low-cost and highly symmetrical optical waveguides were fabricated in flexible glass with thicknesses between 25 µm and 100 µm. The waveguide propagation loss at 1550-nm is between 0.11 dB/cm and 0.25 dB/cm, and birefringence of waveguides is less than 0.5×10^{-6}. The flexible waveguide devices exhibit excellent thermal stability when heated above 450°C. Using laser assisted etching, we discuss possibility of flexible lab-on-chip opto-fluidic devices and their applications for bio- and –chemical sensing. By laser inscribing waveguide Bragg grating at different depths of glass substrates on and off neutral planes inside the flexible glass substrates, we demonstrate smart optical sensors that can perform simultaneous measurements of temperature, axial strain, and magnitude and directions of bending. This paper presents new possibilities to develop smart flexible sensors that are environmentally robust using glass substrates.

Realization of Birefringent Nanogratings in Various Glasses

S. Richter[1], **F. Zimmermann**[1], **A. Tünnermann**[1, 2], **and S. Nolte**[1, 2]

[1]Institute of Applied Physics, Abbe Center of Photonics, Friedrich-Schiller-Universität Jena, Germany
[2]Fraunhofer Institute of Applied Optics and Precision Engineering, Jena, Germany

Abstract— One of the most fascinating effects of the irradiation of glasses with ultrashort laser pulses is the formation of birefringent domains [1]. This birefringence is due to periodic nanostructures, so-called nanogratings, whose orientation is perpendicular to the laser polarization [1, 2]. Nanogratings in fused silica consist of small anisotropic cavities with a size of several tens of nm [2]. The arrangement of these cavities forms a grating structure with a period smaller than the wavelength of the incident laser pulses. The anisotropic structure of the modified material results in form birefringence which can be used to realize polarization sensitive optical devices such as waveplates, zone plates or polarization converters [2].

So far, it was assumed that nanogratings can be induced only in pure fused silica or slightly doped silica glasses. We report on the ultrashort pulse laser induced formation of birefringent structures in the volume of different glasses: Borofloat 33, BK7 and ULE [3]. We conducted an intensive study to analyze the formation process and structure of these birefringent structures using polarization contrast microscopy, Focussed Ion Beam milling, Small Angle X-Ray Scattering and Raman spectroscopy. Thus, we could prove that the birefringence is induced by nanopores in these glasses, too. In addition, the retardance achieved in ULE is even slightly higher than in fused silica facilitating the realization of photonic devices with tailored birefringent domains in isotropic host materials.

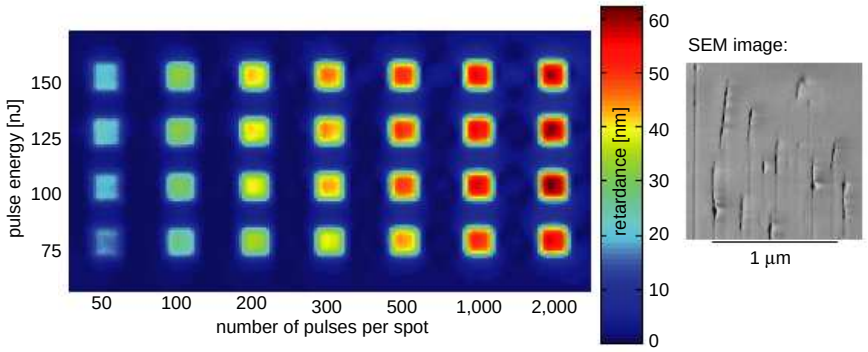

Figure 1: Retardance of laser induced nanogratings in ULE for different irradiation parameters. On the right, an SEM image of the induced modification is shown. Here, a Focussed Ion Beam was used to dissect the sample and expose the nanopores.

REFERENCES

1. Kazansky, P. G., H. Inouye, T. Mitsuyu, K. Miura, J. Qiu, and K. Hirao, "Anomalous anisotropic light scattering in Ge-doped silica glass," *Phys. Rev. Lett.*, Vol. 82, No. 10, 2199–2202, 1999.
2. Richter, S., A. Plech, M. Steinert, M. Heinrich, S. Döring, F. Zimmermann, U. Peschel, E. B. Kley, A. Tünnermann, and S. Nolte, "On the fundamental structure of femtosecond laser-induced nanogratings," *Laser Photon. Rev.*, Vol. 6, No. 6, 787–792, 2012.
3. Richter, S., C. Miese, S. Döring, F. Zimmermann, M. J. Withford, A. Tünnermann, and S. Nolte, "Laser induced nanogratings beyond fused silica — Periodic nanostructures in borosilicate glasses and ULE," *Opt. Mater. Express*, Vol. 3, No. 8, 1161–1166, 2013.

3D Laser Sub-μm Structuring for Novel Near- and Mid-IR Photonics: Recent Advances in SiO_2, $LiNbO_3$ and YAG Processing

A. Ródenas, **J. Martínez**, **H. D. Nguyen**, **and F. Díaz**
Departamento de Química Física e Inorgánica, Universitat Rovira i Virgili, Tarragona 43007, Spain

Abstract— Mid-infrared photonics are rapidly emerging as a powerful technology platform for the biomedical and chemical fields. Mid-infrared spectroscopy takes advantage of the unique fingerprints of inorganic/organic molecular bonds for identifying chemical compounds, biological tissues, cells or biofluids. From the device engineering point of view, having an optically resonant medium close to the anomalous dispersion regime also allows for designing novel robust sensing schemes where different photonic building blocks such as optical waveguides, photonic crystals or fluidic pores, can be interconnected to monolithically operate across infrared resonant ranges to perform fast sensing functions. In this talk I will present recent efforts on 3D micro- and nano-structuring techniques focused on achieving these infrared photonic elements embedded in industrially relevant optical materials like electro-optic lithium niobate, yttrium aluminum garnet (YAG) laser crystals, or the ubiquitous fused silica glass. I will present results on: (i) a laser micro-manufactured glass fibre-interconnected infrared sensor tuned to monitor water-ice transitions with fast response, which has applications in the aircraft industry (for monitoring ice formation on the wings or inside kerosene tanks), or in the pharmaceutical and food industries for freeze-drying (lyophilization) control processes; (ii) on micro-stress engineering and analysis of mid-infrared waveguide structures in lithium niobate circuits for propagation and bend loss minimization; and (iii) on the sub-micron resolution 3D structuring of YAG crystals towards interconnected waveguides and photonic crystals, as well as for enabling novel sensing schemes on sub-wavelength structures for light guiding and optofluidic device engineering.

Femtosecond Laser Micro Fabricated Structures for Lab on Chip Applications

Surya S. K. Guduru[1, 2], **Francesco Scotognella**[2], **Luigino Criante**[1], **Rebeca Martinez Vazquez**[3], **Roberta Ramponi**[3], **and Krishna Vishnubhatla**[1]

[1]Center for Nano Science and Technology@PoliMi
Istituto Italiano di Tecnologia, Via Giovanni Pascoli, 70/3, Milan 20133, Italy
[2]Dipartimento di Fisica, Politecnico di Milano, Piazza Leonardo da Vinci 32, Milan 20133, Italy
[3]Istituto di Fotonica e Nanotecnologie — CNR, Piazza Leonardo da Vinci 32, Milan 20133, Italy

Abstract— Femtosecond laser micromachining (FLM) is a very versatile 3D micro-fabrication techniques. Tightly focused femtosecond laser pulses can be viewed as a pen for fabricating such devices in both transparent and opaque materials [1]. This technique can be exploited for creating complex micro architectures in an integrated lab-on-chip device [2, 3].

Motivation: Here in this work we envisage the demonstration of wavelength selective light harvesting in a fully integrated opto-fluidic chip configuration. Creating such an integrated many functionalities in one device creates possibilities for high sensitivity sensing applications. The idea is to excite the analyte inside a microchannel and try to collect the fluorescence from them in a wavelength selective manner. The schematic of the idea is given in Fig. 1(a).

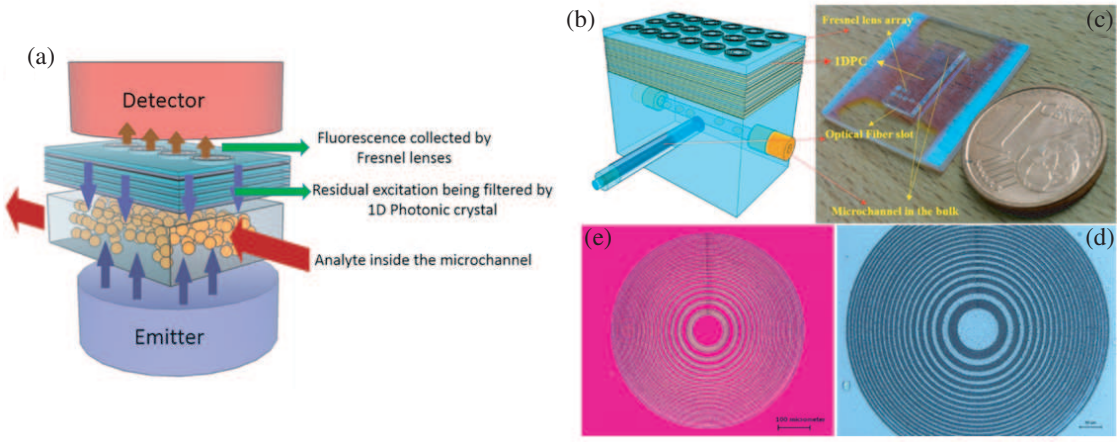

Figure 1: (a) Schematic of the motivation of the work. (b), (c) The schematic of the chip and picture of the actual chip in fused silica substrate. (d), (e) Images of the Fresnel lens in reflection and transmission respectively.

Experimental: The chip contains a 1D photonic crystal (1DPC) as one of its components. The 1DPC is customized in the fabrication stage to reflect the excitation wavelength of the dye. While we fabricate binary Fresnel lenses which are designed to focus the fluorescence of the dye. In essence the device as a whole acts a wavelength selective light harvesting device [4]. For the purpose of demonstrating the principle we conceived the fabrication of such a chip in two different configurations. One chip in PMMA substrate with microchannels on the surface while the other chip in fused silica substrate with microchannels sub-surface. In the former we have the 1DPC fabricated by spin coating alternating layers of two different polymers with a refractive index contrast, while in the latter we create the 1DPC using inorganic materials with a refractive index contrast. Fig. 1(a) is the schematic of the motivation of the work while 1(b) & 1(c) the schematic of the chip and picture of the actual chip in fused silica substrate. (d) & (e) Images of the Fresnel lens in reflection and transmission respectively. Creation of such devices is a very strong demonstration of the capability of micro-fabrication by FLM in creating prototypes in lab on chip specific applications.

REFERENCES

1. Vishnubhatla, K. C., et al., "Shape control of microchannels fabricated in fused silica by femtosecond laser irradiation and chemical etching," *Optics Express*, Vol. 17, 8685, 2009.

2. Gattass, R. R., et al., "Femtosecond laser micromachining in transparent materials," *Nature Photonics*, Vol. 2, 219–225, 2008.
3. Vázquez, R. M., et al., "Fabrication of binary Fresnel lenses in PMMA by femtosecond laser surface ablation," *Optics Express*, Vol. 19, No. 12, 11597, 2011.
4. Guduru, S. S. K., et al., "Fresnel lenses fabricated by femtosecond laser micromachining on polymer one-dimensional photonic crystal," *Opt. Eng.*, Vol. 53, No. 7, 071813, 2014.

Ultrafast Laser Plasma Implantation — A New Approach to Active and Passive Integrated Optics

Gin Jose[1], **Jayakrishnan Chandrappan**[1], **Matthew Murray**[1], **Tarun Kakkar**[1], **D. P. Steenson**[2], **and Animesh Jha**[1]

[1]Institute for Materials Research, School of Chemical and Process Engineering
University of Leeds, Leeds LS29JT, UK
[2]Institute of Microwave and Photonics, School of Electronic and Electrical Engineering
University of Leeds, Leeds LS29JT, UK

Abstract— The simultaneous implantation of multiple, atomically dissimilar ions into silica glass is achieved using ultrafast laser processing for fabricating rectangular and step index optical waveguides. The high refractive index contrast ($> 10\%$) waveguides in silica with and without rare earth co-doping allows us to engineer novel integrated optic waveguide devices with small footprints that facilitate the realisation of high density data optical interconnects Precise engineering of the waveguide parameters are obtained by tuning the process parameters like femto second laser energy and target glass compositions. Record levels of doping concentrations and fluorescent life-times without rare earth segregation can be achieved with the ultrafast laser plasma implantation (ULPI) process. The multi-ion doping adopted in this process helps to maintain the large distance between the Er^{3+}-ions, essential for lowering the concentration quenching at higher doping concentrations. For an Er^{3+}-ion doped waveguide the absorption and emission cross sections at 1534 nm are estimated as $3 \times 10^{-22}\,\mathrm{cm}^2$ with a measured fluorescence lifetime of 129 ms. The 1 mm thick substrates with the planar waveguides on it were measured to have a high optical transparency of 95% and the waveguide propagation losses are $< 0.5\,\mathrm{dB/cm}$ at 1550 nm. Selective doping and un-doped regions are achieved with masked implantation approach in the same substrate with a good control over the step index waveguide formation. The proposed approach can support the mass manufacturing of photonic integrated circuits in a CMOS foundry line. Further this method can be extended for engineering the optical devices and sensors with hybrid integration of silica, silicon, metal and polymer materials.

Laser Fabrication in Diamond for Photonic Applications

Patrick Salter, **Bangshan Sun**, **and Martin Booth**
Department of Engineering Science
University of Oxford, Parks Road, Oxford OX1 3PJ, UK

Abstract— Diamond's remarkable characteristics make it a promising medium for many optical devices, since it is ideal for structures allowing light manipulation on small scales across a broad spectrum. Other advantages include a high degree of biocompatibility, rendering it useful in biological studies. Colourcentres formed by inclusions or vacancies in diamond's crystal structure are being used as tools in quantum optics, opening up numerous possible applications of quantum-enhanced technologies. Recent breakthroughs in the manufacture of affordable high-grade synthetic diamond substrates are fuelling interest for such photonic applications in diamond.

Laser fabrication offers many potential advantages over traditional methods used for diamond processing. For the first time truly 3D structures embedded in the diamond can become a reality. However, this can only be made possible through the compensation of the optical aberrations induced when focussing inside the diamond. Diamond has a high refractive index meaning the spherical aberrations generated at high numerical aperture are particularly pronounced. To this end, adaptive optic elements are used during the machining to remove the depth-dependent aberration and create high resolution uniform features deep into the diamond.

When the laser is focused into the diamond, the electric field is sufficiently strong at the focus for non-linear absorption leading to breakdown of the diamond lattice and the formation of a graphitic phase. By tracing the diamond through the laser focus, continuous graphitic wires may be machined within the diamond bulk. The microwires, with lateral dimensions as low as 400 nm, can be fabricated to follow any three dimensional path within the diamond. Properties and applications of the embedded graphitic microwires will be discussed.

Surface laser processing of bulk single crystal diamond will also be demonstrated for the manufacture of optical elements. Diamond optics are temperature-insensitive, can withstand high power radiation and thus have wide applications. Using fine control over the incident laser fluence, it is possible to operate in the "nano-ablation" regime to give control over the surface topology whilst maintaining optical quality.

3D Printed Optical Components

M. Thiel
Nanoscribe GmbH, Eggenstein-Leopoldshafen, Germany

Abstract— We present our recent progress in fabricating high-quality optical components by additive manufacturing based on multiphoton polymerization.

Fabrication of high-quality optics: In the last decade, additive manufacturing based on multiphoton polymerization has set new standards for three-dimensional (3D) microfabrication [1–3]. Due to its sub-micrometer spatial resolution, the technique also allows for the fabrication of high-quality optical elements [4]. Here, we present our efforts to standardize 3D manufacturing based on multiphoton polymerization for optical applications.

High-speed fabrication is enabled by a set of pivoted galvomirrors insuring highest spatial resolution (printer is commercial available [3]). To enlarge the patterning volume, we employ stage stitching allowing for the fabrication of highly complex photonic structures on areas in the cm^2 range on arbitrary substrates. We follow a standardized workflow for digital production using typical CAD data of 3D printers. To demonstrate the validity of our approach, we fabricate and characterize (i) diffractive optical surfaces (DOEs), (ii) 3D photonic crystals, and (iii) microoptics. As an example for integrated optics, we finally present the concept of optical wirebonds (iv).

Additive manufacturing based on multiphoton polymerization allows for sub-100 nm feature sizes, i.e., printing of DOEs becomes possible. We show examples of photonic color materials [5] which are built up by 10s of millions of nanodots on reflective silicon substrates. We also fabricate and characterize transmissive DOEs and phasemasks. 3D photonic crystals are well-studied optical materials that, e.g., may exhibit a complete photonic band gap for sufficiently high refractive index contrast of the constituent material. To tune the Bragg reflection bands to optical frequencies, rod spacings of a few hundred nanometers are necessary, i.e., highest accuracy of the fabrication process is required. We demonstrate the fabrication of woodpile photonic crystals and of chiral photonic crystals. Next, we demonstrate 3D free-form microoptics. The geometrical parameters of the unitcells (e.g., pyramids and hemispheres) are in the 10 micrometer range. To validate the optical properties of the fabricated structures we use laser diodes at green and red wavelengths in a forward-scattering setup. Qualitative agreement between approximate calculations and experiments is good. Finally, we explain the concept of photonic wire bonds that allow on-chip optical communication due to their waveguiding properties.

Conclusion: In conclusion, we have demonstrated high-speed 3D printing of microoptics. We have fabricated and characterized a couple of examples showing the versatility of the additive manufacturing method. We argue that the technique opens new routes for free-form optics that are not accessible with other fabrication techniques.

ACKNOWLEDGMENT

We acknowledge financial support of Bundesministerium fuer Bildung und Forschung (BMBF) in the context of photonic wirebonding (www.phoibos.de).

REFERENCES

1. Kawata, S., "Finer features for functional microdevices," *Nature*, Vol. 412, 697, 2001.
2. Malinauskas, M., "Ultrafast laser nanostructuring of photopolymers," *Physics Reports*, Vol. 533, 1, 2013.
3. www.nanoscribe.de.
4. Wu, D., "High numerical aperture microlens arrays of close packing," *Appl. Phys. Lett.*, Vol. 97, 031109, 2010.
5. Kumar, K., "Printing colour at the optical diffraction limit," *Nature Nanotech.*, Vol. 7, 557, 2012.

Session 1P4b
SC2: Manipulating Light-matter Interaction by Plasmonics 1

Dielectric Platforms for Surface Enhanced Spectroscopies

Stefan A. Maier
Imperial College London, London, SW7 2AZ, UK

Abstract— Plasmonic nanostructures serve as the main backbone of surface enhanced sensing methodologies, yet the associated optical losses lead to localized heating as well as quenching of molecules, complicating their use for enhancement of fluorescent emission. Additionally, conventional plasmonic materials are limited to operation in the visible part of the spectrum. We will elucidate how nanostructures consisting of conventional and polar dielectrics can be employed as a highly promising alternative platform.

Dielectric nanostructures can sustain scattering resonances due to both electric and magnetic Mie modes. We have recently predicted high enhanced local electromagnetic field hot spots in dielectric nanoantenna dimers [1], with the hallmark of spot sizes comparable to those achievable with plasmonic antennas, but with lower optical losses. Here, we will present first experimental evidence for both fluorescence and Raman enhancement in dielectric nanoantennas, including a direct determination of localized heating, and compare to conventional Au dimer antennas. The second part of the talk will focus on the mid-infrared regime of the electromagnetic spectrum, outlining possibilities for surface enhanced infrared absorption spectroscopy based on polar [2] and hyperbolic [3] dielectrics.

REFERENCES

1. Albela, et al., *ACS Photonics*, Vol. 1, 524, 2014.
2. Caldwell, et al., *Nano Letters*, Vol. 13, 3690, 2013.
3. Caldwell, et al., *Nature Communications*, Vol. 5, 5221, 2014.

Active Tuning of Light-graphene Interactions

Sanshui Xiao[1, 2]

[1]Department of Photonics Engineering
Technical University of Denmark, Kongens Lyngby DK-2800, Denmark
[2]Centre for Nanostructured Graphene (CNG)
Technical University of Denmark, Kongens Lyngby DK-2800, Denmark

Abstract— Graphene opens up for novel optoelectronic applications thanks to its high carrier mobility, ultra-large absorption bandwidth, and extremely fast material response. In particular, the opportunity to control optoelectronic properties through Fermi-level tuning enables electrooptical modulation, optical-optical switching, and other optoelectronics applications. Except for the statistic gating and chemical doping, the Fermi level of graphene can also be optically tuned. With the aid of external optical pumping, electrons can be excited in the substrate, then move to the graphene layer, leading to the electrical doping in graphene. In this talk, I will firstly discuss how the graphene property changes when applying the optical pumping with different incident power. Then I will discuss graphene-silicon microring devices with having a high modulation depth and with a relatively low bias voltage. Finally, I will discuss a novel hybrid graphenemetal system for studying light-matter interactions with gold-void nanostructures exhibiting resonances in the visible range. The hybrid system is further explored for sensing of Rhodamine 6G molecules with respect to the strong surface-enhanced Raman scattering.

Electron Tunneling in Plasmonic Nanogaps Explored Using the Self-consistent Hydrodynamic Model

G. Toscano[1], **A. Kwiatkowski**[1], **J. Straubel**[1], **and C. Rockstuhl**[1, 2]

[1]Institute of Theoretical Solid State Physics
Karlsruhe Institute of Technology (KIT), Karlsruhe D-76131, Germany
[2]Institute of Nanotechnology
Karlsruhe Institute of Technology (KIT), Eggenstein-Leopoldshafen D-76021, Germany

Abstract— The optical response of coupled metallic nanoparticles in the tunneling regime is strongly affected by non-local screening and electron spill-out effects, which originate from the quantum nature of the electron-electron interaction. Under such extreme coupling conditions, classical electrodynamics breaks down and quantum mechanical ab-initio methods must be employed to describe the electron tunneling across sub-nanometric gaps [1]. However, these methods are critically limited with respect to the number of considered atoms. Currently, such ab-initio methods cannot be applied to realistically sized nanoparticles. Orbital-Free Density Functional methods are preferred to describe such realistic systems, since they do not calculate single-particle orbitals, but employ effective energy functionals which approximate the full quantum calculations [2]. We propose here to use our recently developed Self-Consisted Hydrodynamic Model (SC-HDM) to explore the electron tunneling in tiny gaps between plasmonic nanoparticles of arbitrary shape [3]. The SC-HDM is an orbital-free method thas has proven to accurately describe the plasmonic response of isolated metallic nanoparticles. We will present selected results for a dimer of sodium spheres and benchmark them against the results obtained with more refined TD-DFT calculations. Finally, we will compare the performances of our SC-HDM with those of a quantum-corrected method (QCM) for electron tunneling proposed by Esteban et al. [4].

REFERENCES

1. Teperik, T. V., P. Nordlander, J. Aizpurua, and A. G. Borisov, "Quantum effects and nonlocality in strongly coupled plasmonic nanowire dimers," *Optics Express*, Vol. 21, 27306, 2013.
2. Neuhauser, D., S. Pistinner, A. Coomar, X. Zhang, and G. Lu, "Dynamic kinetic energy potential for orbital-free density functional theory," *J. Phys. Chem. C*, Vol. 134, 144101, 2011.
3. Toscano, G., C. Rockstuhl, F. Evers, H. Xu, N. A. Mortensen, and M. Wubs, "Self-consistent hydro-dynamic approach to nanoplasmonics: Resonance shifts and spill-out effects," arXiv:1408.5862.
4. Esteban, R., A. G. Borisov, P. Nordlander, and J. Aizpurua, "Bridging quantum and classical plasmonics with a quantum-corrected model," *Nat. Commun.*, Vol. 3, 825, 2012.

Quantifying the Field Enhancement Spectra of Individual Nanoantennas Using Single Quantum Dots

Jianwei Tang[1] **and Sailing He**[1, 2]

[1]Centre for Optical and Electromagnetic Research
JORCEP [Sino-Sweden Joint Research Center of Photonics]
Zhejiang Provincial Key Laboratory for Sensing Technologies, Zhejiang University
East Building No. 5, Zijingang Campus, Zhejiang University, Hangzhou 310058, China
[2]Department of Electromagnetic Engineering, Royal Institute of Technology, Stockholm 10044, Sweden

Abstract— Nanoantennas have become an enabling technique in the field of nanophotonics, owing to their great capabilities of strongly enhancing light-matter interactions by concentrating light energy into highly condensed plasmonic hot spots, and of effectively modifying quantum emissions by providing large local densities of photon states. Theoretical and numerical tools are rich for design and analysis of nanoantennas, whereas experimental techniques are very limited for revealing comprehensive near field properties. Here we proposed an experimental method to quantify the field enhancement spectra of individual nanoantennas by quantitatively detecting the modified fluorescence of single quantum dots in the hot spots. The fluorescence modification of a single quantum dot by the nanoantenna is the combined effect of both the absorption enhancement and the emission modification. By pumping the single quantum dot towards its saturation, the absorption enhancement effect was ruled out in the detected emission modification, and the emission modification was obtained. Then by pumping the single quantum dots at different wavelengths (thanks to the broad absorption spectra of semiconductor quantum dots) in the linear pumping region, we obtained the absorption enhancement factors at different wavelength to build the absorption enhancement spectrum, which was taken as the field enhancement spectrum of the nanoantenna at the specific point defined by the single quantum dot's position coordinates. In our preliminary experiment, single quantum dots were fixed on the substrate surface while the antennas were assembled by moving chemically synthesized plasmonic nanoparticles to around the single quantum dots. Further development of this technique is to stabilize a single quantum dot at a scanning nanoscale tip so that 3D mapping of field enhancement spectra can be performed.

Revealing a Symmetry Class of Periodic Gratings Using Transformation Optics

Matthias Kraft[1], **Yu Luo**[2], **and John B. Pendry**[1]

[1]Blackett Laboratory, Imperial College London, SW7 2AZ, UK
[2]Nanyang Technological University, Singapore

Abstract— Symmetries are omnipresent in physics. However, sometimes they are hidden from plain sight. Transformation optics can help us to reveal those symmetries, which are not obvious at first sight. In a recent paper [1], we showed how a hidden spherically rotational symmetry of spheroids, can be used to classify their plasmon eigenstates and calculate their optical properties. Here, we present some new results extending this approach to treat other systems. Specifically, we study two-dimensional periodic gratings.

We present a novel transformation mapping a simple slab to a periodic grating. Since the spectrum of a nano-particle is conserved under conformal mappings in the quasi-static limit, the grating derives its spectrum from the simple slab system. An interesting result on its own, it becomes even more intriguing. Because the transformation from the slab to the grating contains two free parameters, we can modulate the grating's depth and periodicity. However, since all gratings are derived from the same slab, they all inherit the slab's spectrum. Thus a whole symmetry class is revealed through a single transformation, as all gratings within that class derive their spectral properties from the symmetry of the slab.

With the spectral properties and eigenstates of the grating known, we calculate the optical properties of the grating under plane wave illumination. Results for the reflection, transmission and absorption spectra are compared to COMSOL simulations and very good agreement is found between analytics and simulations. Finally, we model the grating as a metamaterial and discuss the limitations of our analytical approach, such as its inability to predict the bi-anisotropic coupling parameter for very strongly modulated gratings.

REFERENCES

1. Kraft, M., J. B. Pendry, S. A. Maier, and Y. Luo, "Transformation optics and hidden symmetries," *Phys. Rev. B*, Vol. 89, 245125, 2014.

Defect Tolerance and the Effect of Structural Inhomogeneity in Plasmonic DNA-nanoparticle Superlattices

Michael B. Ross[1], **Jessie C. Ku**[2], **Chad A. Mirkin**[1, 2], **and George C. Schatz**[1]

[1]Department of Chemistry, Northwestern University
2145 Sheridan Rd., Evanston, IL 60208, USA
[2]Department of Materials Science, Northwestern University
2220 Campus Drive, Evanston, IL 60208, USA

Abstract— Bottom up assemblies of plasmonic nanoparticles exhibit unique optical effects such as tunable reflection, optical cavity modes, and tunable photonic resonances. However, because all bottom-up assemblies use chemically synthesized nanoparticles, which are not uniform in size and shape, nanoparticle assemblies incorporate various inhomogeneities including defects, grain boundaries, and vacancies. Here, we use the comparison of detailed simulations with experiment to explore the effect of structural inhomogeneity on the optical response in DNA-nanoparticle superlattices. In particular, we explore the effect of background environment, nanoparticle polydispersities ($> 10\%$) and variation in nanoparticle placement ($\sim 5\%$). We identify that at volume fractions less than 20% Au, the optical response is robust to defects and inhomogeneity in the superlattice. However, at elevated volume fractions (20 and 25%), structures built using different sized plasmonic nanoparticles (10, 20 and 40 nm diameter) each exhibit distinct far-field extinction and near-field properties. As such, these structures are beyond that which can be described as an effective medium; that is, the properties of these superlattices are sensitive to the fine structure of the nanoparticle lattice. Moreover, the incorporation of experimentally informed inhomogeneity in these higher volume fraction superlattices exhibit distinct variation in far-field extinction and inconsistent electric field intensities throughout the lattice, in contrast with those systems with less than 20% Au. The variation between randomly generated superlattices is more pronounced for higher volume fractions (closer nanoparticle spacings) due to stronger plasmonic coupling between particles. In turn, these data have important implications for building consistent and scalable nanomaterial architectures where reproducibility and sample-to-sample variation remains a challenge.

Sub-wavelength Magnetic Field Enhancement via Fano Coil-type Resonances

S. Panaro[1], **A. Nazir**[1], **R. Proietti Zaccaria**[1], **C. Liberale**[1,2], **F. De Angelis**[1], **and A. Toma**[1]

[1]Istituto Italiano di Tecnologia, via Morego 30, I-16163 Genova, Italy
[2]BESE Division, KAUST, King Abdullah University of Science and Technology
Thuwal 23955-6900, Kingdom of Saudi Arabia

Abstract— In the last decade, several efforts have been spent in the investigation of the "artificial magnetism". Structures able to locally modify the magnetic susceptibility present unique properties with applications in super-lensing [1], cloaking [2] and spintronics [3]. Within this context, the study on split-ring resonators has provided one of the first proof-of-concepts for this phenomenon.

In concomitance, plasmonic nano-assemblies have been deeply studied for the high field enhancement properties which they exhibit in the visible/near-infrared range [4]. In particular, the employment of *symmetry breaking* [5] approaches on plasmonic oligomers in strong coupling condition, has revealed the arising of Fano-like interferential features. The extraordinary enhancement properties presented by these sub-wavelength systems result from the hybridization of strongly radiative *bright* modes and low-loss *dark* modes [6]. In the last years, the exploitation of these concepts on circulating plasmonic currents has produced magnetic-like Fano resonances at optical frequencies [7].

Here, we apply a symmetry breaking process on a strongly coupled nanodisk trimer, inducing a radical modification in the optical response of the plasmonic system. In particular, the gradual increasing of the upper disk diameter (see panel (a), from bottom to top) promotes the arising of a pronounced Fano-like extinction dip inside the broad trimer spectrum (see spectra evolution in panel (b)). The magnetic character of the Fano resonance is confirmed by the near-field analysis inside the trimer gap region (see panel (c)). For small upper disk diameters (panel (a)), the local magnetic field enhancement is around the unity (black dots in panel (c)) and the associated plasmonic currents are in phase (see (i) inset of panel (c)). However, beyond a diameter size threshold (around 250 nm), the magnetic enhancement in Fano resonance condition presents a steady increase towards a factor around 10. The arising of a magnetic hot-spot (see (iii) inset of panel (c)) inside the gap region is attributed to the mutual de-phasing of the localized surface plasmons supported by the three disks. In Fano resonance condition indeed the strongly coupled plasmonic currents undergo a re-arrangement which results in a coil-type plasmonic mode within

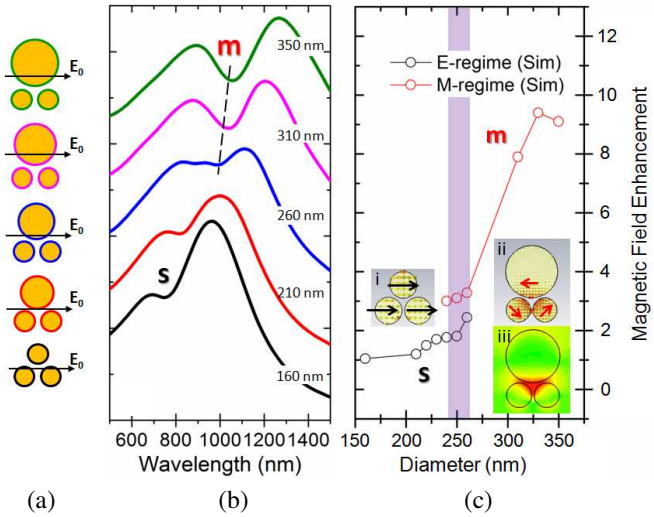

Figure 1: Panel (a) Sketches reporting the morphological symmetry breaking on nanodisk trimer. Panel (b) Simulated extinction efficiency spectra of nanodisk trimer for increasing upper disk diameter. Panel (c) Simulated magnetic field enhancement associated to the triemr gap region, as a function of the upper disk diameter.

the gap region (see (ii) inset of panel (c)). Gold trimer arrays have been fabricated by electron beam lithography and optically characterized by far-field spectroscopy, observing the occurrence of the coil-type Fano resonance in the visible/near-IR range.

The intense magnetic hot-spots generated in Fano resonance condition promote arrays of strongly coupled disk trimers as feasible plasmonic platforms for a wide variety of nano-photonic applications. In fact, the possibility to enhance the optical magnetic fields in sub-wavelength regime, opens fascinating scenarios in high-resolution imaging, bio-sensing and enhanced nonlinear optical spectroscopy.

REFERENCES

1. Fang, N., et al., "Sub diffraction-limited optical imaging with a silver superlens," *Science*, Vol. 308, No. 5721, 534–537, 2005.
2. Pendry J. B., et al., "Controlling electromagnetic fields," *Science*, Vol. 312, No. 5781, 1780–1782, 2006.
3. Kampfrath, T., et al., "Terahertz spin current pulses controlled by magnetic heterostructures," *Nat. Nanotechnol.*, Vol. 8, No. 4, 256–260, 2013.
4. Lassiter J. B., et al., "Fano resonances in plasmonic nanoclusters: Geometrical and chemical tunability," *Nano Lett.*, Vol. 10, 3184–3189, 2010.
5. Panaro S., et al., "Dark to bright mode conversion on dipolar nanoantennas: A symmetry-breaking approach," *ACS Photon.*, Vol. 1, 310–314, 2014.
6. Lassiter J. B., et al., "Designing and deconstructing the Fano lineshape in plasmonic nanoclusters," *Nano Lett.*, Vol. 12, 1058–1062, 2012.
7. Nazir A., et al., "Fano coil-type resonance for magnetic hot-spot generation," *Nano Lett.*, Vol. 14, No. 6, 3166–3171, 2014.

Plasmonic Optical Binary Storage Based on Nematic Liquid Crystal Layers

Mahmoud A. Elrabiaey[1], **Nihal F. F. Areed**[1, 2], **and Salah. S. A. Obayya**[1]

[1]Centre for Photonics and Smart Materials, Zewail City of Science and Technology, Gizza, Egypt
[2]Faculty of Engineering, Mansoura University, Mansoura, Egypt

Abstract— A novel design for an easily and compact integrated optical 2-bit binary storage is presented and analysed using 2D-finite difference time domain (2D-FDTD) method. The proposed structure utilizes silver sheet with two nano-holes and two nematic liquid crystal (NLC) layers of type E_7. The suggested device can be used to store the visible light beam to one of the two holes based on the biasing states of the two NLC layers. The suggested device offers absorption efficiency and crosstalk of 0.4 and 13 dB, respectively. In addition the reported structure opens-up the revenue to build optical n-bit binary storage through the use of appropriately positioned n metallic nano holes and n NLC layers.

Design and Numerical Results: In this paper, a combination of plasmonic holes and NLC layers has been investigated using 2D FDTD [1] to realize optical 2-bit binary storage. Figure 1 shows the proposed optical device that consists of two nano-holes each of 20 nm width which are drilled in silver sheet of thickness 200 nm. The silver sheet is sandwiched between layers of silicon compositions and coplanar two NLC layers. The confining to the required nano-hole is mainly depending on the equivalent permittivity upon this hole which can be easily controlled through the tuning of NLC layers. In this way, we have 3 states for the proposed 2-bit binary storage which are "10", "01" and "11". In the 1st storage state "10", NLC_1 is biased while NLC_2 is unbiased. In this case, the light will be confined around $hole_1$. In the 2nd state "01", NLC_1 is unbiased while NLC_2 is biased. Therefore, the light will be confined around $hole_2$. Finally, in the 3rd storage state the two NLC layers are biased, and then the light will be confined and distributed equally among the two holes. The pre-recorded information can be retrieved by near field spectroscopic optical detection method [2]. Figure 2 shows the calculated absorption power efficiency (η) around the two holes for the 1st storage state. It is evident from the figure that the majority of the absorbed light with $\lambda = 722$ nm is confined around $hole_1$ where the magnitudes of the η_{hole1} and η_{hole2} are equal to 0.406 and 0.02, respectively. Figure 2 shows the steady state electric field distribution along xy plane for the 1st state. The shown distribution clearly agrees with the behaviour of the calculated absorbed efficiency.

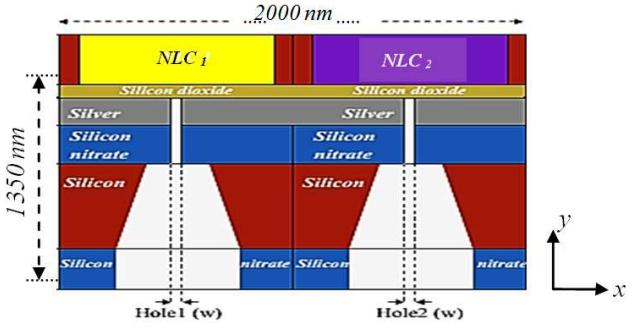

Figure 1: Proposed 2 bit binary storage.

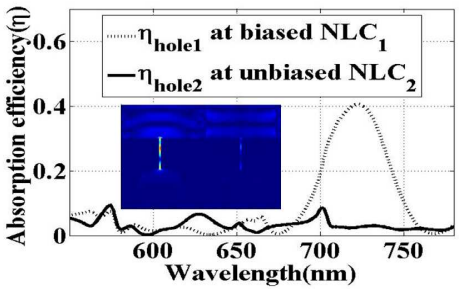

Figure 2: Absorption efficiency for the first storage state.

REFERENCES

1. www.lumerical.com.
2. Mansuripur, M., A. Zakharian, A. Lesuffieur, S. Hyun, R. Jones, N. Lindquist, H. Im, A. Kobyakov, and J. Moloney "Plasmonic nano-structures for optical data storage," *J. Opt. Exp.*, Vol. 17, 14001–14014, 2009.

Quantifying Light-matter Interaction in Plasmonic Nanogaps

Shunping Zhang[1] **and Hongxing Xu**[1, 2]

[1]Center for Nanoscience and Nanotechnology, School of Physics and Technology
Wuhan University, Wuhan 430072, China
[2]Institute for Advanced Studies, Wuhan University, Wuhan 430072, China

Abstract— Plasmonic nanogaps serve as a perfect configuration for light concentration owing to the extreme localization of surface plasmons [1]. Nanogaps in different type of neighboring metallic structures are widely exploited, e.g., for surface enhanced Raman spectroscopy [2]. However, the plasmon resonances and the field enhancement depend sensitively on the gap distance, the geometry of the nanoparticle etc.. Therefore, a controlled nanogap is highly demanded to quantify the light-matter interaction inside the gap, such as changing the gap distance in situ [3]. Here, we used a nanoparticle over mirror to obtain stable SERS enhancement, quantify the gap dependence [4] and push the limit into atomic thin nanogap [5].

REFERENCES

1. Moskovits, M., *Rev. Mod. Phys.*, Vol. 57, 783, 1985.
2. Xu, H. X., E. J. Bjerneld, M. Käll, et al., *Phys. Rev. Lett.*, Vol. 83, 4357, 1999.
3. Alexander, K. D., K. Skinner, S. P. Zhang, et al., *Nano Lett.*, Vol. 10, 4488, 2010.
4. Mubeen, S., S. P. Zhang, N. Kim, et al., *Nano Lett.*, Vol. 12, 2088, 2012.
5. Zhang, S. P., et al., manuscript in preparation.

Session 1P5a
Antennas, Signals, HPEM and EMC Problems 2

Prediction of Signal Fadings in Air Radio Communications

Leszek Nowosielski and Marain Wnuk
Faculty of Electronics, Military University of Technology
Gen. S. Kaliskiego 2 str., Warsaw 00-908, Poland

Abstract— Radio in aviation plays very important role. It allows to communicate the pilot with the fly control tower in order to provide security in the air as well as good coordination of air operations. Within the VHF, the frequency band of mobile radio communication air service is in the range of 118.000 MHz to 136.975 MHz. It is divided into channels with the spacing of 25 kHz, what gives 720 channels in the whole frequency band. Radio telephones used in this communications employ amplitude modulation (AM). The resistance to Doppler effect is the only, but also the most important argument speaking for using it. When a plane is flying it cause considerable voice distortions. There, in the article, the analysis of the fading deepness of the signal at the receiving antenna input of the aircraft flying in the air space between the repeater station and a power line were presented as well as it was determined if the level of fadings generated by signal reflections from power columns has destructive effects to the quality of radio link used.

To this purpose, the analysis of the terrain between the repeater station and individual power columns was carried out. Basing on the analysis results it could be accepted that the propagation of the radio link at the sector of the ray reflected, i.e., the repeater station antenna, reflecting surface of particular power columns and receiving antenna installed on the plane, can be modeled using the free space propagation model.

The signal level R at the input of receiving antenna installed on-board of the plane depends on the level and phase of the direct ray signal Ray_1 as well as the level and phase of the component being the sum of the rays Ray_2 reflected from the power columns. The signal level R can be calculated from the dependence:

$$R = Ray_1 + Ray_2$$

The computer simulation was done of effects of the rays reflected from particular power columns present in the antennas beam to the signal level R. The reflecting coefficient was defined as the ratio of metal surface area exposed directly to the influence of the incident electromagnetic wave, being a part of the spherical area sector comprising the angular range of the azimuth and elevation corresponding, to the segment of power line operated by one power column to the total surface area of the spherical sector comprising the angular range of the azimuth and elevation corresponding to the segment of power line operated by one power column.

In order to evaluate effects of particular power columns to the radio communication quality, the signal level R coming to the receiving antenna installed on-board of the plane with taking into account the level and phase of the direct ray signal Ray_1 as well as the level and phase of the ray signal Ray_2 reflected from a given power column. It allowed to determine deepness values of fadings at the input of the receiving antenna installed on the aircraft created by the effects of amplitude and phase of the direct ray Ray_1 and reflected one Ray_2. Basing on this, it can be stated that the coefficient of signal reflection from metal structure of particular power columns has the deciding effect to the fading deepness of the signal at the input of the receiving antenna.

The Reflectivity of the Ni-Zn Ferrite Tiles in the Microwave Frequency Range

Roman Kubacki
Faculty of Electronics, Military University of Technology, Warsaw, Poland

Abstract— To obtain high shielding performance for suppressing the radio frequency reflections inside the anechoic chamber the broadband absorptive materials with low level of reflection coefficient is necessary. Ferrites are the most commonly used materials as a kind of electromagnetic wave absorber. In this study the electromagnetic properties of commercially available Ni-Zn ferrite, were investigated. Typically this material is used as metal-backed absorber. The principle of the metal-backed microwave absorber is to make use of the reflection reduction by impedance matching. The impedance matching condition depends on the values of the absorber electromagnetic parameters. The permittivity and permeability of Ni-Zn ferrite tiles were measured using Hewlett-Packard Vector Network Analyzer (VNA) with a synthesized sweep oscillator and an S-parameter test set. Material parameters of the complex permeability and permittivity were calculated from the measured S parameters using the Reflection/Transmission Nicolson-Ross model.

The reflection coefficient expressed in dB can be given as:

$$L_R = 20\log(\Gamma)$$

where:

$$\Gamma = \frac{\sqrt{\mu}\tanh(\gamma d) - \sqrt{\varepsilon}}{\sqrt{\mu}\tanh(\gamma d) + \sqrt{\varepsilon}}$$

γ and d are: propagation constant and the thickness of the ferrite tile, respectively.

Modelling of the Angle of Arrival Scattering Using the Von Mises Function for Compatibility Analysis

Leszek Nowosielski, **Marian Wnuk**, **Jan M. Kelner**, **and Cezary Ziółkowski**
Faculty of Electronics, Military University of Technology
Gen. S. Kaliskiego 2 Str., Warsaw 00-908, Poland

Abstract— A designing and building of sector antenna systems in the modern wireless communication systems require an analysis of a cross-sectors electromagnetic compatibility. This is due to the occurrence of the angular dispersion of the received signal. It is result of the multipath phenomena. This problem is particularly important in the urban environment.

To analyse the angle of arrival (AOA) are used two model types: the probability density function (PDF) of AOA and the power azimuth spectrum (PAS). PDF of AOA models are theoretical. In contrast, PAS models are practical, because the PAS characteristics are determined on the basis of measurements. PAS and PDF of AOA models can be divided into two main groups, i.e., theoretical geometric and empirical models. The empirical models, e.g., the Gaussian and Laplacian models, use the well-known functions (distributions) for modelling the statistical properties of AOA. Physical interpretation of such models is difficult, however, these functions fit well PAS characteristics obtained in the real environment.

This paper presents an empirical model based on the von Mises distribution. This model allows a varied shapes of AOA distribution. If model parameter equal to zero then this distribution is uniform that is often used for modelling of the local isotropic scattering. If the von Mises parameter tends to infinity then distribution has the high concentration and small variance like the Dirac delta. The fit of the von Mises model to empirical PAS is presented in figures. Results of measurements taken from the open literature are used as reference data. Authors present brief characteristics of measurement scenarios. Accuracy assessment of the fit of the proposed model and empirical data is shown. The least square error and the rms angle spread are used as evaluation criteria.

The rms delay spread is used to classify the type of propagation environment. An example of such classification is presented in COST 207. This parameter can be determined based on the power delay profile (PDP) or the power delay spectrum (PDS). The relationship between the rms delay spread and the rms angle spread obtained on the basis of the empirical PAS and von Mises model is presented. Methodology of the von Mises model parameter selection depending on the environment type is based on the obtained relationship. As a result, the proposed model can be applied to the channel modelling for the various scenarios and propagation conditions.

Influence of the Environment on the Cross-sector Compatibility in Wireless Access System

Leszek Nowosielski, **Cezary Ziółkowski**, **and Jan M. Kelner**
Faculty of Electronics, Military University of Technology
gen. Sylwestra Kaliskiego St. No. 2, Warsaw 00-908, Poland

Abstract— Multipath of the wave propagation is the phenomenon that plays a dominant role in formation of internal disturbances in radio systems. This phenomenon significantly limits the possibilities of signal transmission in wireless systems. To increase the capacity of access system, the spatial sectorisation of areas that are supported by the access base station (BS), is used. The multipath phenomenon that occurs in urban area, is the cause of the signal power permeation to neighbouring sectors. It is reason the occurrence of additional disturbances in access neighbouring sectors. This phenomenon is especially important in the case of mobile object (mobile station MS) location near the border of neighbouring sectors. In wireless access systems, the effect of the phenomenon is important for the implementation handover procedure.

This paper is devoted the evaluation of power permeation to BS from MS that is in neighbouring sector. The basis for the analysis is power azimuth spectrum (PAS) that describes the angle distribution of signal power at the input of the receiver. For different tapes of environments, these characteristics are differentiated. The results of the numerous measurements show that with the increase of the environment urbanization degree, the angular dispersion of the received signal is increased. From among the many models, the von Mises function is used as PAS model. Influence of the environment differentiation on PAS is taken into account by the adaptive selection of van Mises parameter. The model validation is made on the basis of the results that are obtained for five measurement scenarios taken from open literature. As criterion of model validation, the least square error (LSE) minimization is used. The characteristic that shows the functional relationship of permeation power and location angle of MS with respect to BS of neighbouring sector is the analysis result presented in the paper. The obtained characteristic is the basis for the evaluation of the disturbance power level that originates from the neighbouring sectors of the wireless access system.

Mobile Recorder for Electrical Activity of the Heart

M. Bernat and Z. Piotrowski
Faculty of Electronics, Military University of Technology, Warsaw, Poland

Abstract— The presented study is dedicated to a mobile recorder designed to keep log of electric activity of the heart and incorporated into the expert system developed to detect fatigue status of a patient. The newly designed recorder has a modular structure and its enclosure houses two double-sided printed circuit boards (PCBs), separately for the analog part (BtECG) and the digital one (BtECGradio).

The analog module is responsible for measurement of electric signals received from the patient's body with their further amplification, filtration and conversion to digital form. In addition, in comprises a source of stabilized voltage(s) for both analog and digital circuits. The digital module receives binary data, extracts its useful portion, carries out formatting of the data to form of frames required for RF communication according to the Bluetooth standard and enables wireless communication with a collaborating unit.

The analog subassembly is meant to record electric potentials within the range from 0.2 to 2 mV and owing to the high level of the CMRR factor it substantially eliminates the common-mode signals. Furthermore, it enables two-stage amplification, filtration of high-frequency interferences, high-pass filtration and active, five-staged low-pass filtration.

The digital module of the recorder enables RF data transmission according to the Bluetooth v.4.0 standard, communication with a host unit with use of the UART and SPI interfaces (reading of RF packages from the CPU module) as well as communication with a host unit with use of the Full Speed USB 2.0 (BGAPI) protocol. Its power consumption is ultra low and the communication sessions is controlled by a microprocessor of the 8051 architecture. The digital module also enables the user to embed own application and to debug them via the CC Debugger Connector link.

The base chip for development of the digital module is the BLE112 Bluetooth Smart module from Bluegiga.

Implementation of a Steganographic Algorithm in an Internet VoIP Phone

Damian Bachmat and Zbigniew Piotrowski
Faculty of Electronics, Military University of Technology
Gen. S. Kaliskiego 2 Str., Warsaw 00-908, Poland

Abstract— The paper describes implementation of the steganographic method based on the least significant bits (LSB) in a program Internet phone VoIP. In the developed program Internet phone VoIP a library PJSIP has been used. Selected technology — LSB is characterized by easiness of implementation and high data rate and perceptual transparency of a signal with embedded steganographic sequence. In case of the LSB method a change in the least significant bits in a datagram takes place after quantizer of an analog-digital converter circuit. This solution enabled simple implementation of the embedding algorithm by modification of a source code of a codec G.711. The way of the method implementation protects data from errors since mechanisms of the error control and correction of the RTP protocol monitored correctness of sent data. One of the advantages of the method is the fact that for determined number of the least significant bits it does not cause an audible speech degradation and therefore, modified speech signal is perceptually transparent for a subscriber at the receiver side. The paper includes results of tests of developed steganographic phone, among others, subjective audible tests based on signal fidelity estimation standard — ITU-R BS 1116-1, tests of minimal, required time of transmission and integrity tests of steganographic sequence.

Multimedia Filter for Data Hiding Counteraction

Zbigniew Piotrowski
Faculty of Electronics, Military University of Technology
Gen. S. Kaliskiego 2 str., Warsaw 00-908, Poland

Abstract— Data hiding methods are realised in the form of steganographic communication channels and in the form of digital content labelled with watermark while employing as the carrying layer among the others: speech signal, audio, video and photos. Detection of the fact of additional data hiding is hindered among the others because of constantly improved and increasingly advanced methods for embedding and extraction of hidden data. In the article there is presented the concept of the program container based on which the filtration of the above-mentioned signals is carried out in order to remove the hidden data. The purpose of multimedia filter action is to remove from the original signal (carrier) the hidden data or its significant degradation, but in such manner that the original signal itself is not degraded significantly.

Session 1P5b
Antenna Theory and Radiation 1

Printable Interdigitated Ferroelectric Varactors for Reconfigurable Antennas

Mahdi Haghzadeh, **Craig Armiento**, **and Alkim Akyurtlu**
Department of Electrical and Computer Engineering, Raytheon UMass Lowell Research Center
University of Massachusetts Lowell, Lowell, MA 01854, USA

Abstract— In this work we propose, analyze and implement a novel printable varactor based on barium strontium titanate (BST)/polymer composite filled interdigitated capacitors (IDCs). The model of the BST material filled IDC was simulated by CST Microwave Studio and compared with a conventional model of IDC on BST thick film in terms of capacitance value and tunability. Ferroelectric varactors are of special interest for RF and microwave applications due to their higher performance, and reduced power consumption, size and cost. Among various ferroelectric materials, Barium Strontium Titanate ($Ba_xSr_{1-x}Ti$, or BST), a perovskite-type compound, is the material of choice since it is the most studied composition for microwave applications, and its Curie temperature is controllable by Ba content and is below room temperature for $x < 0.7$. Therefore, it is in the paraelectric phase at room temperature and has a high dielectric constant, high tunability, low loss tangent, and high switching speed. In addition, its relative permittivity is decreased in a nonlinear fashion with no hysteresis when a bias voltage is applied across it. BST-based varactors are usually used in a coplanar-plate design called Interdigitated Capacitor (IDC), where plates are placed on top of a thick or thin film of BST, and are interdigitated in order to increase the capacitance per unit area. From the printed electronics perspective, utilizing thick or thin films of BST are impractical since processing BST films require very high sintering temperatures (above 850°C) and they are brittle in nature, thus failing to be compatible with flexible substrates. One promising solution to this critical problem may be a BST/polymer composite made by suspending micro- or nano-BST particles in a polymer matrix. Such a solution is a compromise between the processing flexibility of a polymer and the desired ferroelectric properties of BST. The fabrication and material properties of many BST/polymer composites have been reported using various polymers such as silicon-rubber, epoxy resin, polymethylmethacrylate (PMMA), polyphenylene sulfide (PPS), cyclic olefin copolymer (COC), and polypropylene-graft-poly(styrene-stat-divinylbenzene) (ER). The multi-phase, solvent-based composite was made by mixing nanoparticles of BST, 4-tert-butycatechol (BTC) as a dispersant, and thermoplastic cyclic olefin copolymer (COC) in toluene. This resulted in developing a nano-BST ink to be used for ferroelectric dielectric printing purposes. A coplanar waveguide (CPW)-based test structure was used to enable GSG probe based RF measurements of IDCs. Plates of IDCs as well as the CPW test structure were printed on 5 mil Kapton sheets by Optomec Aerosol Jet printer using nano-silver ink. BST/polymer composites were printed by Sonoplot printer using the nano-BST ink between and on the IDC fingers. RF measurements were performed to gain insight into the dielectric properties of the printed composites.

A Dualband Circularly Polarized Rectangular Dielectric Resonator Antenna with L-shaped Slots on the Ground

Yuxiang Sun, **Kwok Wa Leung**, **and Wei Wei Li**
Department of Electronic Engineering and State Key Laboratory of Millimeter-Waves
City University of Hong Kong, Hong Kong SAR, China

Abstract— This paper presents a dualband circularly polarized (CP) rectangular dielectric resonator (DR) antenna (DRA). Its fundamental TE_{111} mode and higher-order TE_{113} mode are excited simultaneously to obtain two working bands. The dimensions of the dual-band DRA are calculated by solving simplified formulas of the dual-mode rectangular DRA. To generate circularly polarized fields, two asymmetric diagonal L-shaped slots are etched on the ground plane to excite two degenerate orthogonal modes in each band, giving a CP dualband antenna. For demonstration, a dual-band dual-sense CP antenna working in GPS L1 band (1.575 GHz) and 2.4 GHz WLAN band are designed using ANSYS HFSS. Its reflection coefficient, axial ratio (AR), antenna gain, and radiation pattern are studied. The antenna radiates right- and left-hand circularly polarized fields in the lower and upper bands, respectively.

Bidirectional Dielectric Resonator Antenna Using Slotted Ground Structure

Nan Yang, Kwok Wa Leung, and Wei Wei Li
State Key Laboratory of Millimeter Waves, Department of Electronic Engineering
City University of Hong Kong, Hong Kong SAR, China

Abstract— A bidirectional cylindrical dielectric resonator antenna (DRA) is proposed in this paper. The DRA operating in its fundamental $TM_{01\delta}$ mode is fed by an axial coaxial probe protruded from a circular ground, which has the same radius of the DRA. Two slots are fabricated on the ground to obtain a bidirectional radiation pattern. It was found that the measured gain on the azimuth plane is 3.75 dBi and −10.16 dBi in the main-lobe and side-lobe directions, repsectively.

Impact of Bending on the Performance of Circularly Polarized Wearable Antenna

Muhammad Rizwan, **Lauri Sydänheimo**, **and Leena Ukkonen**
Department of Electronics and Communications Engineering
Tampere University of Technology, Tampere, Finland

Abstract— Wearable electronic devices are becoming a part of human clothing for applications such as sensing, navigation and health monitoring. Textile antennas are a strong candidate for transceiver node in wearable applications due to their flexibility and low cost. In wearable systems, flat surfaces are not always available so the antenna should be able to retain its performance in bent conditions. This paper analyses the effects of bending on the performance of a circularly polarized textile antenna. The antenna under test is fabricated on thin denim substrate and operates for Industrial, Scientific and Medical (ISM) band and Wireless Body Area Network (WBAN) applications at 2.45 GHz. Copper tape with thickness 0.25 mm is used as the conductive material for the patch and the ground plane on denim substrate. Rectangular slot along diagonal axes at the center of the circular patch is used for achieving circular polarization at 2.45 GHz while bandwidth enhancement is done by using partial and slotted ground plane. The measured operating frequency range of antenna spans from 2.42 GHz to 2.58 GHz with gain of 2.25 dB at 2.45 GHz. Bending in both xz and yz plane is done by placing the antenna on cylinders with different radii (50 mm and 75 mm) and then analyzing the effects on return loss, bandwidth, axial ratio and radiation characteristics. Fabricated antenna shows good conformity between simulated and measured results. A set of comparative results of antenna in free space and bending conditions are discussed to validate the operability of antenna with bending in different planes. In future, the performance of antenna can be analyzed on different body parts like arms and legs etc. to validate its operability for BAN applications in vicinity of human body.

Design and Optimization of Miniaturized Dual-band Implantable Antenna for MICS and ISM Bands

Muhammad Ali Babar Abbasi, Salman Arain, Photos Vryonides, and Symeon Nikolaou
Department of Electrical Engineering, Frederick University, Nicosia, Cyprus

Abstract— This work discusses the design method towards the implementation of a compact, stacked, implantable antenna for biotelemetry applications. The proposed antenna consists of three stacked layers, printed on high permittivity grounded substrate, namely, Roger's RO3210. The bottom layer of the antenna above the ground plane, contains a meandered structure with a symmetrically placed T-shaped slot. The middle layer consists of two U-shaped radiators and on the top layer, an M-shaped metallic segment is added to enhance the radiation efficiency of the antenna. The bottom and the middle layers are excited at the top right corner with an extended coaxial feed. A via connecting the top with the middle layer of the antenna, at top left corner, opposite to the coax feed corner, enables symmetrical virtual feeding for the middle layer. Two vias, placed at right and left bottom corners, additionally connect the middle with the top layer of the stacked antenna. These three stacked layers, consist a symmetrical closed loop structure resonating on its fundamental resonant mode, at 402 MHz, for the Medical Implant Communication Service (MICS) band. A shifted higher order mode of the same closed loop structure, along with the two radiating U-shaped coupled resonators on the middle layer and the M-shaped resonator on the top layer, enables wide band operation, at 2.45 GHz, for the industrial, scientific, and medical (ISM) band.

To resolve the constraints associated with implanting an antenna in human body that usually results in detuning and impedance mismatch, the antenna's most important radiating sections were thoroughly investigated. A fully parameterized solution is proposed that makes the antenna a good candidate for a device implanted at different areas of the human body with potentially different electric properties with consequently different detuning effect. For further investigation, the particle swarm algorithm was implemented to optimize the antenna's performance while operating inside a compact, $23 \times 23 \times 5\,\text{mm}^3$ block of human skin equivalent phantom. The simulated performance of the proposed prototype antenna, indicates that it can be used for either in vitro or in vivo operations. Finally, the small size of the proposed antenna ($18 \times 15 \times 2\,\text{mm}^3$) is compared favorably against the sizes of previously reported antennas, operating in both MICS and ISM bands.

Session 1P6
Advances in Diffraction Gratings Theories

A Comparison of Numerical Modal Methods for Lamellar Gratings

G. Granet[1, 2] **and C. S. Lavranos**[3]

[1]Institut Pascal, Clermont Universités, Université Blaise Pascal
BP 10448, Clermont-Ferrand F-63000, France
[2]CNRS UMR 6602, IP, Aubière F-63177, France
[3]Department of Electrical & Computer Engineering
Democritus University of Thrace, Xanthi, Greece

Abstract— There are many methods for analysing diffraction gratings and other periodic structures. When the structure is invariant along one axis, modal methods not only allow to calculate the electromagnetic field but have also the advantage to easily give insight into the physical phenomena. Lamellar gratings are the most simple structures that can be analyzed with a modal method. Since the dielectric constant depends only on one spatial coordinate, it is possible to expand the electromagnetic field in the grating region in terms of the eigenfunctions of the Helmholtz equation.

Modal methods include analytical modal method [1] in which the only numerical parameters-the eigenvalues-are obtained as the zeros of a transcendental equation, the Fourier modal method [2] and many other variants based on finite differences [3], polynomials [4], and B spline expansions [5], and also the pseudo-spectral modal method [6].

Among the above methods, the Fourier modal method is certainly the most popular and has been intensively researched which has lead to dramatic improvements. Its main drawback is that discontinuous fields are represented using a finite number of Fourier coefficients, which leads to the unavoidable Gibbs' phenomenon. One of the main reasons why convergence rates are so different from a given implementation of the method to another lies in the treatment of the discontinuities of the electromagnetic field at the interface between different dielectrics or metals. This is particularly true when materials with negative permittivity or permeability are involved.

The goal of our presentation is to make a fair comparison of the various numerical modal methods in terms of accuracy and speed of convergence for dielectric and metallic lamellar gratings.

REFERENCES

1. Botten, L. C., M. S. Craig, R. C. McPhedran, J. L. Adams, and J. R. Andrewartha, "The dielectric lamellar grating," *Opt. Acta*, Vol. 28, 413–428, 1981.
2. Moharam, M. G. and T. K. Gaylord, "Diffraction analysis of dielectric surface-relief gratings," *J. Opt. Soc. Am.*, Vol. 72, 1385–1392, 1982.
3. Lalanne, P. and J.-P. Hugonin, "Numerical performance of finite-difference modal methods for the electromagnetic analysis of one-dimensional lamellar gratings," *J. Opt. Soc. Am. A*, Vol. 17, 1033–1042, 2000.
4. Morf, R. H., "Exponentially convergent and numerically efficient solution of Maxwell's equations for lamellar gratings," *J. Opt. Soc. Am. A*, Vol. 12, 1043–1056, 1995.
5. Armeanu, A. M., M. K. Edee, G. Granet, and P. Schiavone, "Modal method based on spline expansion for the electromagnetic analysis of the lamellar grating," *Progress In Electromagnetics Research*, Vol. 106, 243–261, 2010.
6. Song, D., L. Yuan, and Y. Y. Lu, "Fourier-matching pseudospectral modal method for diffraction gratings," *J. Opt. Soc. Am. A*, Vol. 28, 613–620, 2011.

Hypersingularity of Transverse Electric Field at Sharp Edges: A Case Study of a Special Lamellar Grating

Lifeng Li
Department of Precision Instrument, Tsinghua University, Beijing 100084, China

Abstract— After half century of research the rigorous electromagnetic theory of gratings has been developed to an advanced level so that to date many theoretical theories exist, including the integral methods, the differential methods, the modal methods, the coordinate transformation method, the finite difference time domain method, and the finite element method, and most practical grating problems can be solved by one or more of the numerical methods based on the theoretical theories. However, some old challenges remain and some new challenges have appeared. The advent of plasmonics and metamaterials research has brought about the necessity of studying electromagnetic wave guiding and scattering by structures consisting of lossless metals (media of negative permittivities). In particular, it was recently noted that when a grating contains sharp edges formed by a lossless metal surrounded by some lossless dielectrics, the transverse magnetic grating diffraction problem cannot be solved by any existing numerical method, if the permittivity ratios of the media fall in certain ranges. While the root cause of the problem has been clearly identified as the excitation of hypersingular surface modes at the sharp edges, many questions remain unanswered: Is hypersingularity physical? If yes, why do all well-established numerical method fall to work, and how to solve the diffraction problem when hypersingularity is excited? If no, how to solve a practical problem that is nearly hypersingular? Is the hypersingular diffraction problem well-defined? If no, can we impose additional conditions to make it well-defined?

In this work, I perform a case study on the diffraction of a transverse magnetic incident plane wave by a lossless metallic lamellar grating. The theoretical analysis is carried out in the framework of the exact modal method. The diffraction problem is made as simple as possible so that the mathematical steps leading to the expression of the diffraction amplitudes are the fewest. It is hoped that this research may shed some light on the numerical divergence due to hypersingularity.

Gegenbauer Polynomial Expansion Applied to Crossed Binary Gratings

B. Guizal[1], **K. Edee**[2], **and J. P. Plumey**[2]

[1]Laboratoire Charles Coulomb, UMR 5221 du CNRS, University Montpellier 2, France
[2]Universit Blaise Pascal, Institut Pascal, BP 10448, F-63000 Clermont-Ferrand, France

Abstract— We present the modal method based on Gegenbauer polynomials (MMGE) as applied to crossed binary gratings [1]. We use the version of the MMGE that incorporates boundary conditions into the definition of a new basis of polynomial functions, that are adapted to the boundary value problem of interest. We will discuss the performances of this approach against the famous Fourier Modal Method (FMM) [2] eventually equipped with the Adaptive Spatial Resolution Concept (ASR) [3] and illustrate that on the extraordinary optical transmission phenomenon [4, 5].

REFERENCES

1. Edee, K. and J. P. Plumey, *JOSA A*, Vol 32, No. 3, 402, 2015.
2. Li, L., *JOSA A*, Vol 14, No. 10, 2758, 1997.
3. Granet, G. and J. P. Plumey, *J. Opt. A: Pure Appl. Opt.*, Vol. 4, S145, 2002.
4. Moreau, A., G. Granet, F. Baida, and D. Van Labeke, *Opt. Express*, Vol 11, No. 10, 1131, 2003.
5. Van Labeke, D., D. Gerard, B. Guizal, F. Baida, and L. Li, *Opt. Express*, Vol 14, No. 25, 11945, 2006.

Impact of Surface Backward Waves on Radiation Suppression and Enhancement. Periodic Interface of Metamaterial

G. Granet[1], **P. Melezhik**[2], **A. Poyedinchuk**[2],
S. Sautbekov[3], **Y. Sirenko**[2, 3], **and N. Yashina**[2]

[1]Universite Blaise Pascal, Av. des Landais, Clermont-Ferrand 24, 63177, France
[2]A. Ya. Usikov Institute of Radiophysics and Electronics of National Academy of Sciences of Ukraine
12, Ak. Proskury St., Kharkov 61085, Ukraine
[3]L. N. Gumilyov Eurasian National University
2, Mirzoyana St., Astana 010000, Republic of Kazakhstan

Abstract— The fundamental and most useful electromagnetic quality of diffraction gratings is the ability to operate as frequency selective structure (FSS) [1, 2]. Various materials have been used for construction FSS for solving different optical and electromagnetic tasks [3, 4]. The modern advanced technologies facilitated the production of artificial materials with diverse astonishing electromagnetic features. Among them there are materials with extraordinary dispersive properties with constitutive parameters varying within rather narrow frequency range from negative values (of considerable magnitude) to conventional domain of positively valued constitutive parameters.

Combination of dispersive materials and geometrical periodicity, characteristic to diffraction gratings, open new possibilities for construction FSS having pronounced electrically and geometrically controlled dispersive features.

In present communication we discuss the scattering of inhomogeneous electromagnetic wave by periodic interface (with determined arbitrary profile) of dispersive medium that is certain artificial material with already defined dispersion relation describing constitutive parameters. Our study is based on accurate solution to boundary value problem [2] and robust numerical algorithm which efficiency ensure reliable, extensive, profound simulation of complicated scattering processes. The main attention here is concentrated on the study of regularities and mechanism of scattered electromagnetic field enchantment and suppression; the transformation of the energy of incident electromagnetic field into the energy of the eigen surface waves and investigation of their nature in the case of artificial media with various dispersion properties.

As an example we present in Fig. 1 the total energy $W_T(k)$ of scattered field inside the media, characterized by the Drude law $\varepsilon(k) = 1 - \frac{k_\varepsilon^2}{k(k+i\nu_\varepsilon)}$; $\mu(k) = 1 - \frac{k_\mu^2}{k(k+i\nu_\mu)}$, for lossless media $\nu_\varepsilon \cong 0$; $\nu_\mu \cong 0$ with $k_\varepsilon = 0.1$; $k_\mu = 1$, k is dimensionless frequency parameter, $\beta = \nu/c$, ν is normal to the interface corrugation railings component of phase velocity of incident wave.

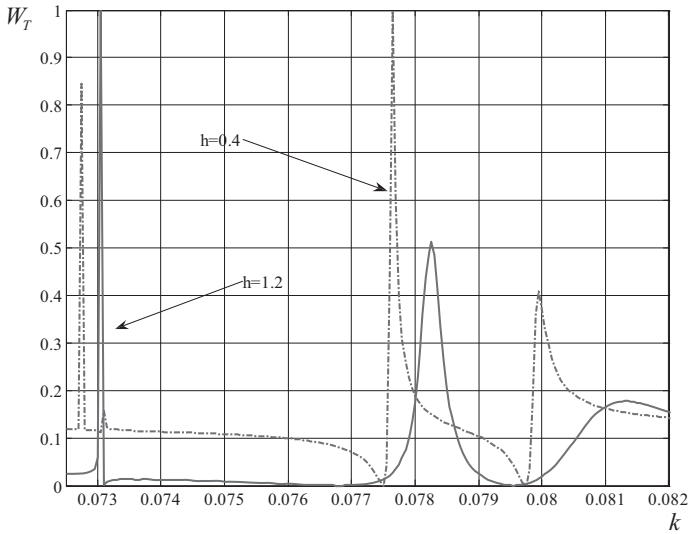

Figure 1.

Interface period is chosen equal to 2π, h is a depth of grooves. For the case illustrated by Fig. 1 within frequency range of interest the propagating harmonics in the space above the corrugated interface of artificial medium are forbidden. The energy may be carried only by harmonics inside the medium. In Fig. 1 we can see the pronounced resonant enhancement of the energy of the field excited inside material, but also the regions of nearly complete suppression of $W_T(k)$ within certain intervals of k. The larger h, the wider k interval. Such suppression of the scattered field appears due to the transformation of electromagnetic field of incident wave into the energy of eigen surface waves. The described situation exists in the case of double negative media and under conditions of coincidence of phase velocity of incident wave β with phase velocity of certain backward surface waves.

REFERENCES

1. Petit, R., *Electromagnetic Theory of Gratings*, Springer, New York, 1980.
2. Sirenko, Y. K. and S. Strom, *Modern Theory of Gratings. Resonant Scattering: Analysis Techniques and Phenomena*, Springer, New York, 2010.
3. Zouhdi, S., A. Sihvola, and A. P. Vinogradov, *Metamaterials and Plasmonics: Fundamentals, Modelling, Applications*, Springer, Dordrecht, 2009.
4. Engheta, N. and R. W. Ziolkowski, *Metamaterials: Physics and Engineering Explorations*, Wiley-IEEE Press, 2006.

Local Transformation Leading to an Efficient Fourier Modal Method for Perfectly Conducting Gratings

Agnès Maurel[1], **Simon Félix**[2], **and Jean-François Mercier**[3]

[1]Institut Langevin, CNRS, ESPCI ParisTech, 1 rue Jussieu, Paris 75005, France
[2]LAUM, CNRS, Université du Maine, avenue Olivier Messiaen, Le Mans 72085, France
[3]CNRS, ENSTA ParisTech, INRIA, 828 boulevard des Maréchaux, Palaiseau 91762, France

Abstract— We present an efficient Fourier modal method for the wave scattering by perfectly conducting gratings (in the two polarizations). The method uses a geometrical transformation, similar to the one used in the C-method [1, 2], which transforms the grating surface into a at surface (Fig. 1(a)), thus avoiding to question the Rayleigh hypothesis. In addition, we use a geometrical, or optical, transformation which only affects a bounded inner region and naturally matches the outer region; this allows to apply a simple criterion to select the ingoing and outgoing waves. Otherwise, our proposed numerical scheme is similar to the Fourier Modal Method and it can be straightforwardly implemented.

A noticeable improvement of the presented method concerns the convergence, which is often not quantitatively reported in the literature. For penetrable gratings, the wavefield has a discontinuous gradient, which limits the convergence of the method to a power law $N^{-3/2}$, N being the truncation order of the Fourier series [3]. If the limit of perfectly conducting grating is considered, the error in the Fourier method is known to increase but the convergence in terms of power law is the same. Here, these limiting cases are directly treated as impenetrable gratings and this modifies drastically the convergence. Indeed, our geometrical transformation leads to a modified wave equation in a continuously varying medium, with space-dependent coefficients having the same regularity than the groove profile. For smooth profiles (described by a function of class C^∞), this produces a convergence with exponential rate, much better than the usual power laws. More results can be found in [4].

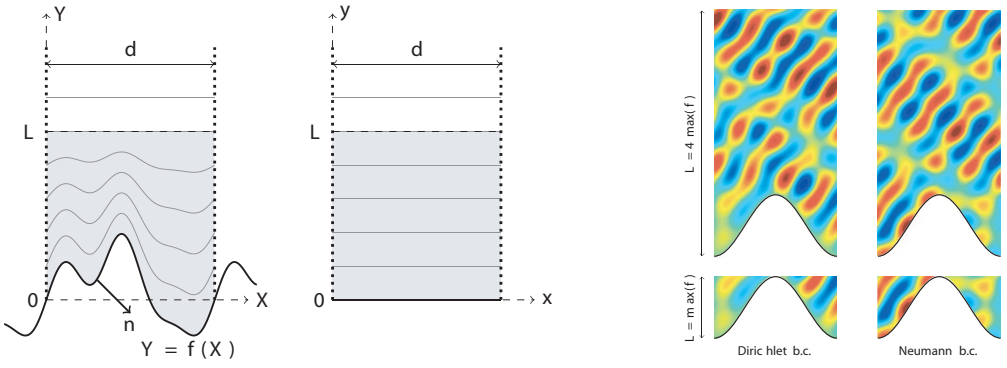

(a) (b)

Figure 1: (a) real $(X; Y)$ space and transformed $(x; y)$ space (after transformation). (b) Examples of wave field computed for warring transformed regions, in Dirichlet and Neumann conditions.

REFERENCES

1. Chandezon, J., G. Raoult, and D. Maystre, *J. Opt.*, Vol. 11, No. 4, 235–241, 1980.
2. Li, L., G. Granet, J. P. Plumey, and J. Chandezon, *Pure Appl. Opt.*, Vol. 5, No. 2, 141–146, 1996.
3. Maurel, A., J.-F. Mercier, and S. Félix, *J. Acoust. Soc. Am.*, Vol. 135, No. 1, 165–174, 2014.
4. Félix, S., A. Maurel, and J. F. Mercier, *JOSA A*, Vol. 31, No. 10, 2249–2255, 2014.

Vertical Mode Expansion Method for Applications in Plasmonics

Hualiang Shi and Ya Yan Lu
Department of Mathematics, City University of Hong Kong, Hong Kong, China

Abstract— Structures in plasmonics, such as metallic films with holes and metallic nanoparticles on a substrate, are often multiply-layered. A layered structure is a 1D structure for which the material properties depend only on one spatial variable z (assuming z is in the "vertical" direction). A multiply-layered structure is a 3D structure with a number of cylindrical regions where the material properties depend only on z in each region. General numerical methods can be used to analyze the scattering of light by a 3D multiply-layered structure, but it is possible to develop more efficient special methods. For structures involving circular cylinders, an efficient numerical method has been developed based on 1D vertical mode expansions and 2D horizontal cylindrical wave expansions [1–3]. In this paper, we consider multiply-layered structures where the cylindrical regions have arbitrary cross sections. An efficient method is developed by combining 1D vertical mode expansions and 2D boundary integral equations.

The vertical mode expansion process gives rise to a 2D Helmholtz equation for each mode. For each of these 2D equations, we calculate the so-called Neumann-to-Dirichlet (NtD) operator using a boundary integral equation (BIE) method. The BIEs are discretizd by Alpert's hybrid Gauss-trapezoidal quadrature rule. Notice that the NtD operators are calculated independent of each other. They are used to set up the final linear system of equations by matching tangential field components on the vertical walls of the cylindrical regions. We illustrate our method using examples in plasmonics.

REFERENCES

1. Boscolo, S. and M. Midrio, "Three-dimensional multiple-scattering technique for the analysis of photonic-crystal slabs," *J. Lightwave Technol.*, Vol. 22, 2778–2786, 2004.
2. Yuan, L. and Y. Y. Lu, "Dirichlet-to-Neumann map method for analyzing hole arrays in a slab," *J. Opt. Soc. Am. B*, Vol. 27, 2568–2579, 2010.
3. Lu, X., H. Shi, and Y. Y. Lu, "Vertical mode expansion method for transmission of light through a single circular hole in a slab," *J. Opt. Soc. Am. A*, Vol. 31, 293–300, 2014.
4. Alpert, B. K., "Hybrid Gauss-trapezoidal quadrature rules," *SIAM J. Sci. Comput.*, Vol. 20, 1551–1584, 1999.

Simulating the Linear and Nonlinear Response of 1D Nanostructures under a Focused Beam with a B-spline Modal Method

Patrick Bouchon[1, 2] and Patrick Bouchon[1]

[1]The French Aerospace Lab., ONERA, Palaiseau 91761, France
[2]Laboratoire de Photonique et Nanostructures, CNRS, Marcoussis 91460, France

Abstract— Focusing the light onto nanostructures thanks to spherical lenses is a first step to enhance the field, and is widely used in applications, in particular for enhancing non-linear effects like the second harmonic generation.

Nonetheless, the electromagnetic response of such nanostructures, which have subwavelength patterns, to a focused beam can not be described by the simple ray tracing formalism. Here, we present a method to compute the response to a focused beam, based on the B-spline modal method [1], which is known to be fast thanks to a non-uniform mesh and sparse matrices. The eigenmodes are computed in each layer for both polarizations in conical mounting, and are then combined for the computation of scattering matrices. The simulation of a gaussian focused beam is obtained thanks to a truncated decomposition on plane waves computed on a single period, which limits the computation burden [2].

Eventually, we develop a formalism to compute the second harmonic field under the undepleted pump approximation. The nonlinear polarization induced by a fundamental plane wave or a focused beam generates a source term at the doubled frequency. The latter is divided into a finite number of sub-sources and the second harmonic field is subsequently computed by integration of these subsources contributions [3].

REFERENCES

1. Bouchon, P., et al., *J. Opt. Soc. Am. A*, Vol. 27, 696, 2010.
2. Chevalier, P., et al., *J. Opt. Soc. Am. A*, Vol. 31, 1692, 2014.
3. Heron, S., et al., *J. Opt. Soc. Am. B*, Vol. 32, 275, 2015.

Asymmetric Reciprocal Transmission through Double Metallic Gratings

M. Stolarek[1], **D. Yavorskiy**[1], **J. Łusakowski**[1], **C. Zapata-Rodríguez**[2], **and R. Kotyński**[1]

[1]Faculty of Physics, University of Warsaw, Pasteura 7, Warsaw 02-093, Poland
[2]Department of Optics, University of Valencia, Dr. Moliner 50, Burjassot 46100, Spain

Abstract— In this paper we analyse the propagation of sub-terahertz electromagnetic waves through double metallic gratings (DMG) with sub-wavelength slits. We demonstrate theoretically and experimentally the possibility of achieving directional transmission of electromagnetic radiation through the DMG structure in a planar geometry — for the TM polarisation, and in the cylindrical geometry — for the radially polarised field.

We optimise the overall system parameters in terms of the transmission efficiency, contrast and spectral range. The modelling is based on the finite-difference-time-domain method.

We provide structure parameters leading to the transmission of more than 50% and to a high transmission contrast in opposite directions for the wavelength range from 2.5 to 4 mm. The reciprocity of the system is maintained, and we prove that the unidirectional transmission in the zeroth diffraction order is not possible, therefore we do not classify our arrangement as an optical isolator [1]. In the planar geometry, the transmitted radiation propagates in the -1 and $+1$ diffraction orders. An analogues cylindrical grating led us to the design of an unidirectional diffractive lens [2]. The experimental set-up for the latter geometry requires to illuminate the structure with radial polarisation, which is obtained like in Ref. [3] by converting from the linear polarisation with modal selection in a tapered waveguide combined with the use of a discontinuous wave-retarder. A Gunn diode operating at 3 mm is used as the radiation source for both geometries. We have reached a good agreement between the experimental and modelling results.

REFERENCES

1. Stolarek, M., D. Yavorskiy, R. Kotyński, C. Z. Rodriguez, J. Łusakowski, and T. Szoplik, "Asymmetric transmission of terahertz radiation through a double grating," *Opt. Lett.*, Vol. 38, 839–841, 2013.
2. Yavorskiy, D., M. Stolarek, J. Łusakowski, and R. Kotyński, "Asymmetric transmission of radially polarized THz radiation through a double circular grating," *Opt. Express*, Vol. 22, 30547–30552, 2014.
3. Grosjean, T., F. Baida, R. Adam, J.-P. Guillet, L. Billot, P. Nouvel, J. Torres, A. Penarier, D. Charraut, and L. Chusseau, "Linear to radial polarization conversion in the THz domain using a passive system," *Opt. Express*, Vol. 16, 18895–18909, 2008.

Electromagnetic Methods for Some Gratings with Extreme Opto-geometrical Parameters

Evgeny Popov, Nadège Rassem, Yoann Brulé, Boris Gralak
Guillaume Demesy, and Anne-Laure Fehrembah
Aix-Marseille Université, Centrale Marseille, Institut Fresnel, CNRS UMR 7249, Marseille, France

Abstract— Several different electromagnetic spectral methods for modelling light diffraction by single or periodically arranged dielectric or metallic objects are compared in studying three systems having extreme optogeometrical parameters. The first system represents a three-segment dielectric diffraction grating having 1D periodicity, the middle segment is a resonant subwavelength grating acting as a narrow-band resonant reflection filter, the two outmost segments consist of Bragg grating used to reflect back the waveguide mode of the middle section. The entire length of the system contains several hundreds of wavelengths, and we demonstrate the capacity of two rigorous electromagnetic methods to correctly model the diffraction properties of the system, namely the Fourier modal method, and the Coupled dipole method. The results show an extreme flattening of the dispersion curve of the waveguide mode that can be explained by using a four-wave coupled mode approximate theory.

The second system represents a 2D grating made of arrays of metallic cones on a metallic substrate. The diffraction by the grating is modelled using the Coordinate transformation (C-) method and the Finite element method, and the results show a giant (10 000 fold) enhancement of the field intensity, compared to the incident field intensity.

The third example consists of a 1D echelette metallic grating made of negative-permittivity materials having simple- or hyper-singularity. We show the possibility of two electromagnetic methods (Integral method and C-method) to correctly predict the diffraction properties, when rounding of the corners is used. In the case of hypersingularity, the field varies with an increasing frequency and amplitude, as the radius of rounding is reduces, confirming the analytical theoretical predictions.

We compare the relative computation times for the different methods and they show similar duration for identical structures.

A New Approach to Diffraction in Volume Gratings and Holograms

David Brotherton-Ratcliffe
Centre for Ultra-realistic Imaging, Applied Science, Computing & Engineering,
Glyndŵr University, Mold Road, Wrexham, Wales LL1 2AW, UK

Abstract— Coupled wave theory has historically been successfully used to provide various analytic theories of optical diffraction in volume phase gratings. Here we develop a different approach based on a decomposition of the permittivity profile of the grating into an infinite array of infinitesimal discontinuities or step functions. By considering the corresponding elementary Fresnel solutions from each discontinuity, a first-order set of coupled partial differential equations can be derived, which are then solved in a rotated frame of reference to give analytical expressions for the diffraction efficiency of the general slanted grating at arbitrary angle of incidence. The underlying differential equations derived from the approach are a rigorous representation of Maxwell's equations for the case of the unslanted grating and few assumptions are required to provide highly accurate solutions for harmonic or quasi-harmonic permittivity distributions, even at large grating slant.

The method can be applied to either reflection or transmission geometry, although it is most accurate in the case of the reflection grating. It can also been extended to include finite absorption in phase gratings and to treat the cases of absorption and mixed absorption-phase gratings. It can also treat multi-chromatic gratings, spatially multiplexed gratings and holograms. Finally it can be used to provide accurate analytic expressions for gratings with variable fringe contrast profiles.

Comparison with rigorous numerical computations of Maxwell's equations show that the approach works somewhat better than simple coupled wave theory for most reflection gratings, whereas the coupled wave approach appears a little better in describing the transmission geometry.

The approach appears to offer a general approximate method for the analysis of electromagnetic, acoustic and other types of diffraction occurring in harmonic or quasi-harmonic structures.

Curvilinear Coordinate Generalized Source Method for Corrugated Gratings with Sharp Edges

A. A. Shcherbakov[1] and A. V. Tishchenko[2]

[1]Moscow Institute of Physics and Technology, Russia
[2]University of Lyon, France

Abstract— In this work we continue development of the fast and efficient methods for grating diffraction calculation. Recently we have proposed an extension [1, 2] of the previously developed Generalized Source Method [3]. The key novelty consisted in formulating the method in curvilinear coordinate system and introducing a concept of the generalized metric sources. Both standard and curvilinear formulations of the GSM were shown to possess near to linear numerical complexity and computer memory consumption relative to the number of Fourier orders. This allows for outperforming conventional Fourier space modal methods including the FMM and the C-method. Current talk will include a discussion of application of the curvilinear GSM to gratings with sharp edges, supported with demonstration of relevant numerical behavior. Treatment of sharp grating edges within the scope of the curvilinear GSM is done in a way similar to the treatment of continuous and discontinuous field components relative to grating corrugation interface (the analogous implementation for the C-method can be found in [4]).

The novel method reveals much better efficiency with respect to the standard GSM in modeling metallic gratings with complicated profiles.

REFERENCES

1. Shcherbakov, A. A. and A. V. Tishchenko, "Efficient curvilinear coordinate method for grating diffraction simulation," *Opt. Express*, Vol. 21, 25236–25247, 2013.
2. Shcherbakov, A. A. and A. V. Tishchenko, "Fast and efficient modeling of metallic gratings diffraction with metric sources," *EOSAM 2014*, Berlin, Germany, September 15–19, 2014.
3. Shcherbakov, A. A. and A. V. Tishchenko, "New fast and memory-sparing method for rigorous electromagnetic analysis of 2D periodic dielectric structures," *JQSRT*, Vol. 113, 158–171, 2012.
4. Li, L. and J. Chandezon, "Improvement of the coordinate transformation method for surface-relief gratings with sharp edges," *J. Opt. Soc. Am. A*, Vol. 13, 2247–2255, 1996.

Casimir-Lifshitz Force out of Thermal Equilibrium between Dielectric Gratings

Antonio Noto[1, 2], **Riccardo Messina**[1], **Brahim Guizal**[1], **and Mauro Antezza**[1, 3]

[1]Laboratoire Charles Coulomb (L2C), UMR 5221 CNRS, Université de Montpellier, Montpellier, France
[2]Dipartimento di Fisica e Chimica, Università degli Studi di Palermo and CNISM, Palermo, Italy
[3]Institut Universitaire de France, France

Abstract— We calculate the Casimir-Lifshitz pressure between two different 1D dielectric lamellar gratings in a system out of thermal equilibrium where the two gratings have different temperatures and are immersed in an environment having a third temperature. The calculation of the pressure is based on the scattering formalism and the needed scattering operators are deduced using the Fourier Modal Method. The behavior of the pressure is studied in detail varying many parameters of the system like the three temperatures involved as well as the geometrical parameters of the two gratings (period, filling factor, corrugation depth). We show that the interplay between non-equilibrium effects and geometrical periodicity offers a rich scenario for the manipulation of the force. In particular, we find regimes where the force can be strongly reduced close to zero for large ranges of temperatures. Moreover, a repulsive pressure can be obtained (purely non-equilibrium effect), whose features can be tuned by varying the temperatures as well as the several geometrical parameters associated with each grating. Remarkably, the transition distance between attraction and repulsion can be decreased with respect to the known case of two slabs, allowing one to obtain transition distances as low as 2.5 μm and implying an experimental interest for the observation of repulsion.

REFERENCES

1. Noto, A., R. Messina, B. Guizal, and M. Antezza, *Physical Review A*, Vol. 90, No. 022120, 2014.

Analytical Regularization Method for Wave Diffraction by Grating of Resonant Cylindrical Screens

Yury A. Tuchkin, **Ali Şanlı**, **Emrah Sever**, **and Fatih Dikmen**
Electronics Engineering Department, Gebze Technical University, Kocaeli, Turkey

Abstract— The subject of our investigation is numerical modeling of diffraction by one-dimensionally periodical gratings formed by unclosed cylindrical screens of arbitrary smooth profiles, namely construction of numerically stable and efficient algorithm for solving the correspondent diffraction boundary value problems (BVP). The approach we suggest is based on Analytical Regularization Method (ARM) for such a class of BVPs. It essentially enforces the ideas and methods of [1–6]. We start with classic reducing of the problem to integral (or differential-integral) equation following with necessity from well-known Green's formulae technique. Integral equations such appearing are ones of the first kind in space $L_2(S)$, where S is a periodic set of closed or unclosed boundaries or contours of the obstacle. In particular, the Dirichlet BVP leads to the following integral equation $\int_S J(p)G(q,p)dS = u^i(q)$, $q \in S$. ARM principal idea is *analytical* (in closed form) construction of two-sided regularizer, i.e., a pair (R, L) of two invertible (possibly on corresponding dense sets only) operators R and L, such that $LAR = I + H$, where A is the operator of the BVP, I is the identity and H is a compact operators. Having such regularizer, one can reduce equation $Ax = b$ of the first kind to equation $(I + H)y = Lb$, y, $Lb \in l_2$ with new unknown $y = Rx$. The advantages of the equations of the second kind over ones of the first kind are well known.

Essential part of our approach plays algorithm of fast summation of the series representing Green's function for periodic gratings in the form $G_{gr}(q;\chi,\varphi) = (4\pi i)^{-1}\Sigma_{n=-\infty}^{\infty}\exp(\varphi_n x_q + \Gamma_n|y_q|)/\Gamma_n$, where $q(x_q, y_q) \in R^2$, $\varphi_n = n+\varphi$ and $\Gamma_n = (\chi^2 - \varphi_n^2)^{1/2}$ with $\mathrm{Re}(\Gamma_n) \geq 0$, $\mathrm{Im}(\Gamma_n) \geq 0$. The very slow convergence of this series is accelerated by means of rather sophisticated version of Kummer acceleration, which is essentially enforced in comparison with [2, 4].

REFERENCES

1. Tuchkin, Yu. A., "Wave scattering by unclosed cylindrical screen of arbitrary profile with Dirichlet boundary condition," *Soviet Physics Doclady*, Vol. 12, 1027–1030, 1985 (English translation from Russian).
2. Krutin, Yu. I., Yu. A. Tuchkin, and V. P. Shestopalov, "Regularization of boundary value problem of wave diffraction by grating which formed by rods of arbitrary profile with Dirichlet boundary condition," *USSR Computational Mathematics and Mathematical Physics*, Vol. 31, No. 6, 60–69, 1991 (English translation from Russian).
3. Poyedinchuk, A. Ye., Yu. A. Tuchkin, and V. P. Shestopalov, "New numerical-analytical methods in diffraction theory," *Mathematical and Computer Modeling*, Vol. 32, 1029–1046, 2000.
4. Shestopalov, V. P., Yu. A. Tuchkin, A. Ye. Poyedinchuk, and Yu. K. Sirenko, *New Methods for Solving Direct and Inverse Problems of Diffraction Theory. Part 1: Analytical Regularization of Boundary Value Problems of Electromagnetics*, "Osnova" Publishing House, Kharkov, 1997 (in Russian).
5. Chandezon, J., G. Granet, P. N. Melezhik, A. Ye. Poyedinchuk, Yu. K. Sirenko, D. Sjoberg, S. Strom, Yu. A. Tuchkin, and N. P. Yashina, *Modern Theory of Gratings. Resonant Scattering: Analysis Techniques and Phenomena*, 390, Springer, 2010.
6. Panin, S. B., B. Turetken, A. Ye. Poyedinchuk, and Yu. A. Tuchkin, "Diffraction from a grating on a chiral medium: Application of analytical regularization method," *Progress In Electromagnetics Research B*, Vol. 59, 19–29, 2014.

Session 1P7
Advanced Mathematical and Computational Methods in Electromagnetic Theory and Their Applications 2

Regular Coulomb Wave Function Method for Analysis of the Azimuthally Magnetized Circular Ferrite Waveguides

Mariana Nikolova Georgieva-Grosse[1] **and Georgi Nikolov Georgiev**[2]

[1]Consulting and Researcher in Physics and Computer Sciences, Gerlingen D-70839, Germany
[2]Faculty of Mathematics and Informatics
University of Veliko Tirnovo "St. St. Cyril and Methodius", Veliko Tirnovo BG-5000, Bulgaria

Abstract— The solution of the problems for normal TE_{0n} modes propagation in the circular waveguides, containing coaxially positioned ferrite cylinder or toroid of azimuthal magnetization faces serious obstacles of mathematical nature [1–12]. To overcome them different techniques have been proposed, allowing to reveal various aspects of microwave filed-anisotropic medium interaction: *i*) Bolle-Heller functions [1], *ii*) transverse network representation [2], *iii*) perturbation techniques [3], *iv*) variational calculus [4], *v*) confluent hypergeometric functions [6–10], *vi*) Coulomb wave functions [5, 11].

This paper presents the method of regular Coulomb wave function, applied to the problem for propagation of normal TE_{0n} modes along the circular waveguide, entirely filled with azimuthally magnetized ferrite. The magnetically dependent second-order ordinary differential equation for the H_z — component is reduced to the Coulomb wave equation [13, 14]. To apply the Coulomb wave functions $F_L(\eta, \rho)$ and $G_L(\eta, \rho)$ [13, 14] in the theory of waveguides, is an original idea by Georgiev and Georgieva [5, 11]. It is based on the Thompson and Barnett's proposal [15] to extend the definition of these functions, initailly introduced for real $\rho > 0$, real η and integer $L \geq 0$, for ρ, η and L — all complex, employing their link with the confluent hypergeometric functions [13, 14]. In contrast to Thompson and Barnett [15] who considered the computation of $F_L(\eta, \rho)$ and $G_L(\eta, \rho)$ through the latter, it is suggested to harness the representation of $F_L(\eta, \rho)$ in the Abramowitz form [14] and it is proved numerically that the same is applicable when L is a positive or negative factional number, as well. Here the regular Coulomb function is considered solely, since propagation in a single-connected waveguide cross-section is discussed. It is shown that the original series for $F_L(\eta, \rho)$ is much more rapidly convergent in the case mentioned and is preferable in the calculations. Graphs are depicted, showing the variation of the generalized function with ρ, provided $L = \pm 0.5$ and $\eta = 0$, ± 1, ± 5 and ± 10. A numerical investigation of dependence $F_L(\eta, \rho)$ on ρ is performed, too for the aforesaid values of L and $\eta = \pm\rho/2$. Tables of the zeros $o^L_{\eta,n}$ of $F_L(\eta, \rho)$ are also compiled. The phase characteristics, differential phase shift and the borderlines of the area of phase shifter operation of the configuration are computed through sophisticated iterative techniques and debated.

REFERENCES

1. Bolle, D. M. and G. S. Heller, "Theoretical considerations on the use of circularly symmetric *TE* modes for digital ferrite phase shifters," *IEEE Trans. Microwave Theory Tech.*, Vol. 13, No. 4, 421–426, Jul. 1965, See also D. M. Bolle, and N. Mohsenian, Correction, *IEEE Trans. Microwave Theory Tech.*, Vol. 34, No. 4, 427, Apr. 1986.
2. Clarricoats, P. J. B. and A. D. Olver, "Propagation in anisotropic radially stratified circular waveguides," *Electron. Lett.*, Vol. 2, No. 1, 37–38, Jan. 1966.
3. Eaves, R. E. and D. M. Bolle, "Perturbation theoretic calculations of differential phase shifts in ferrite-loaded circularly cylindrical waveguides in the TE_{01} mode," *Electron. Lett.*, Vol. 2, No. 7, 275–277, Jul. 1966.
4. Lindell, I. V., "Variational methods for nonstandard eigenvalue problems in waveguide and resonator analysis," *IEEE Trans. Microwave Theory Tech.*, Vol. 30, No. 8, 1194–1204, Aug. 1982.
5. Georgiev, G. N. and M. N. Georgieva, "On several new applications of Coulomb wave functions," *Proc. 1994 Int. Conf. Comput. Electromagn. Its Appl. ICCEA' 94*, 163–166, Beijing, China, 1994.
6. Georgiev, G. N. and M. N. Georgieva-Grosse, "Analysis of the differential phase shift in the circular ferrite-dielectric waveguide with azimuthal magnetization," *Proc. 2010 IEEE AP-S Int. Symp. on Antennas Propagat. & CNC-USNC/URSI Radio Science Meeting*, Paper 330.9, CDROM, Toronto, ON, Canada, Jul. 11–17, 2010.

7. Georgiev, G. N. and M. N. Georgieva-Grosse, "On the confluent hypergeometric functions and their application: Basic elements of the Tricomi theory. Case of waveguide propagation," *Telecommunications and Radioengineering*, Vol. 71, No. 3, 209–216, 2012.
8. Georgieva-Grosse, M. N. and G. N. Georgiev, "Assumptions on the characteristic parameter of the coaxial ferrite waveguide phase shifter and its application," *Proc. Fourteenth Int. Conf. Electromagn. Adv. Applicat. ICEAA' 12*, 1129–1132, Invited Paper in the Special Session "Advanced 2 Applications of the Mathematical and Computational Electromagnetics," Organized by G. N. Georgiev and M. N. Georgieva-Grosse, Cape Town, South Africa, Sep. 2–7, 2012.
9. Georgieva-Grosse, M. N. and G. N. Georgiev, "Iterative method for analysis of the differential phase shift in an azimuthally magnetized circular ferrite-dielectric waveguide," *Proc. 2013 Int. Symp. Electromagn. Theory, URSI-EMTS 2013*, 763–766, Hiroshima, Japan, May 20–24, 2013.
10. Georgiev, G. N. and M. N. Georgieva-Grosse, "Theorem for the relation between the $L_1(c, n)$ and $L_2(c, \rho, n)$ numbers," *Proc. 2014 XXXI URSI GASS General Assembly and Scientific Symposium*, Vol. 2, 826–829, Beijing, China, Aug. 16–23, 2014.
11. Georgiev, G. N. and M. N. Georgieva-Grosse, "Circular waveguide, completely filled with azimuthally magnetized ferrite," Chapter in *Wave Propagation*, L. Rocha and G. Mateus, Eds., 161–196, Academy Publish, Cheyenne, Wyoming, USA, 2014.
12. Georgiev, G. N. and M. N. Georgieva-Grosse, "Cut-off characteristics of the normal TE_{0n} modes in the circular waveguide with a dielectric cylinder and an azimuthally magnetized ferrite toroid," *Proc. 2015 IEEE AP-S Int. Symp. on Antennas Propagat. & URSI CNC/USNC Radio Science Meeting*, Vancouver, BC, Canada, Jul. 19–25, 2015, in Print.
13. Curtis, A. R., *Coulomb Wave Functions*, Computational Center of the Academy of Sciences of USSR, Moscow, USSR, 1969 (in Russian).
14. Abramowitz, M. and Stegun, I., Eds., *Handbook of Mathematical Functions with Formulas, Graphs and Mathematical Tables, (Applied Mathematics Series 55),* National Bureau of Standards, Washington, DC, 1964.
15. Thompson, I. J. and A. R. Barnett, "Coulomb and Bessel functions of complex arguments and order," *J. Comput. Phys.*, Vol. 64, 490–509, 1986.

A Generalized Drude Model for Time-domain Simulations of Ferromagnetic Metals in Plasmonics

C. Wolff[1] **and K. Busch**[2, 3]

[1]School of Mathematical Sciences, University of Technology, Sydney (UTS), NSW 2007, Australia
[2]Institut für Physik, AG Theoretische Optik & Photonik
Humboldt-Universität zu Berlin, Newtonstraße 15, Berlin 12489, Germany
[3]Max Born Institute, Max-Born-Straße 2A, Berlin 12489, Germany

Abstract— Time-domain simulation techniques such as the finite-difference time domain method (FDTD) or the Discontinuous Galerkin time domain method (DGTD) are a key tool to investigating the broad-band and potentially the nonlinear response of plasmonic and other nano-optical structures. Within these method, the commonly used noble metals such as silver and gold are usually represented by a Drude model for the conduction electrons with additional Lorentz poles to account for inter-band transitions. However, this fails for non-noble transition metals, especially for the ferromagnetic metals iron, nickel and cobalt, which have recently gained some interest because their magneto-optic Kerr effect might provide an effective way to control the propagation of surface plasmons.

The failure of the common Drude-Lorentz description is due to the high degree of electron-electron correlation in ferromagnets and manifests itself in a different frequency dependence of the material loss compared to the conventional Drude model. We derive a generalized Drude model which includes the effect of such correlations to leading order. To this end, we introduce one new fit parameter that reflects the degree of correlation inside the electron system. In combination with two Lorentz poles, our model results in a very good reproduction of the experimentally measured permittivity of iron, nickel and cobalt into the ultra-violet.

The resulting equations can be easily formulated as auxiliary differential equations of very similar numerical effort compared to the conventional Drude-Lorentz. Additionally, we present an efficient way to include magneto-optic properties into time-domain frameworks by adding the Lorenz force to any polarization current. This avoids dispersive anisotropic material parameters, which lead to considerable overhead in FDTD simulations and pose serious problems to the formulation of DGTD. We check our implementation of the generalized Drude-Lorentz model including the magneto-optic terms against analytical expressions. Furthermore, we compare our method to numerical frequency-domain results and experimental data from the literature.

Undersampling to Regularize the Source Reconstruction Problem for an Electric Point Source

S. G. Sen
Electrical Electronics Engineering Department, Ataturk University, Turkey

Abstract— In this article, a source reconstruction problem is solved by sampling the tangential components of the electric field of an electric point source on the surface of a hemisphere the center of which is the location of the point source. The source reconstruction is performed by sampling the electric field at five different sampling rates. One of the sampling rate corresponds to the Nyquist rate, two of them are oversampling rates and the rest are undersampling rates. The problem is discretized into a matrix equation which is solved iteratively. For each of the solution iterate, the field components are reconstructed and the error with respect to the original fields are computed. It is shown that the error made is approximately the same for all the sampling rates. In addition, the fields are reconstructed on hemispheres outside the sampling hemisphere. The error made in this reconstruction is calculated and shown to be not too much varying among the five different sampling rates. By means of these two field reconstruction demonstrations, it is proven that the oversampling and Nyquist rate sampling do in fact provide redundant information for the source reconstruction since the oversampling and the Nyquist rate sampling do not increase the accuracy of the reconstructed fields. The current reconstruction is also made using the lowest sampling rate and it is indicated that the reconstructed current is close to the original current although the sampling rate is lowest. As a result, it is determined that undersampling regularizes the reconstruction problem by deleting the redundant information due to higher rate sampling.

A Novel Computational Method for Calculating Electrostatic Capacity and Screening in Conducting Objects of Arbitrary Shape

Beatriz A. Pazmiño Betancourt[1, 2] **and Jack F. Douglas**[1]

[1]Materials Science and Engineering Laboratory, NIST, Gaithersburg, MD 20879, USA
[2]Physics Department, Wesleyan University, Middletown, CT 06459, USA

Abstract— The calculation of the electrostatic capacity of an object relative to an electrode at infinity, the self-capacitance, involves the solution of Laplace's equation with a Dirichlet boundary condition. Although this problem is well known and well posed, its explicit analytic solution is notoriously difficult. Solution for even a cube is apparently impossible and there are only a handful of particle shapes that allow for exact solution. Finite element and boundary element methods are useful, but these methods are computational expensive and convergence problems exist when the shape of the object is irregular. Meshing in these calculations can be very time consuming and difficult to implement at all in some cases. We really need a versatile and accurate method suitable for particles having any shape. There has been recent progress in solving this type of problem by probabilistic potential theory where the solution is obtained numerically through path-integral sampling [PRE 64 061401], an approach that exploits a fundamental connection between long random walk paths and Laplace's equation. There is another probabilistic method to determining capacity using an ergodic theorem of Spitzer [Z. Wahr 3, 110]. This method consists on considering the volume swept out by a Brownian particle ('Wiener sausage') divided by the mean square displacement of the particle, a quantity that is proportional to the objects self-capacitance for objects having any shape. We use this formal mathematical construct to implement a simple computational algorithm for calculating capacity. This novel computational method takes advantage of current GPU technology which makes the computation rather fast. Capacity estimates obtained by this method are compared with estimates obtained by other methods. As a non-trivial application, we show that the minimization of the capacity of spherical objects and the electrostatic screening transition of spheres can be understood in a simple geometrical way form the shapes of Wiener sausages created by particles having different shapes. Thus, our method allows not only to determine the self-capacitance, put provides great practical intuition of understanding into how particle shape influences capacity. We also summarize many applications of capacity in applications outside the field of electrostatics.

Sparse Tensor Approximation for Uncertainty Quantification on 2D Periodic Gratings

G. Silva and C. Jerez-Hanckes
School of Engineering, Pontificia Universidad Católica de Chile, Santiago, Chile

Abstract— Grating structures have been considered in many applications, such as spectroscopy and energy conversion devices. Exhaustive theoretical and numerical analyses have been performed in order to design gratings optimally. However, real-life manufacturing processes can create random variations on the surface that greatly influence the properties of the gratings. In this work, we implement a numerical algorithm based on the Boundary Element Method (BEM) for randomly perturbed ideal surfaces, considering one dimensional gratings with Gaussian rough surfaces and satisfying Dirichlet boundary conditions. We calculate first and second statistical moments of the scattered field with a sparse tensorization and a discretization based on wavelets. Calculations are provided for different geometries and angles of incidence and show that our method converges significantly faster than taking Monte-Carlo (MC) simulations for BEM.

REFERENCES

1. Garcia, N. and E. Stoll, "Monte Carlo calculation for electromagnetic-wave scattering from random rough surfaces," *Phys. Rev. Lett.*, Vol. 52, No. 20, 1798–1801, 1984.
2. Harbrecht, H., R. Schneider, and C. Schwab, "Sparse second moment analysis for elliptic problems in stochastic domains," *Numer. Math.*, Vol. 39, No. 3, 385–414, 2008.
3. Bruno, O. P. and M. C. Haslam, "Dfficient high-order evaluation of scattering by periodic surfaces: Vector-parametric gratings and geometric singularities," *Waves in Random and Complex Media*, Vol. 20, No. 4, 530–550, 2010.
4. Bruno, O. P. and M. C. Haslam, "Dfficient high-order evaluation of scattering by periodic surfaces: Deep gratings, high frequencies, and glancing incidences," *J. Opt. Soc. Am. A*, Vol. 26, No. 3, 658–668, 2009.
5. Steinbach, O., *Numerical Approximation Methods for Elliptic Boundary Value Problems*, 390, Springer, New York, 2008.

Cascades of π Circuits Modeled by Independent Matrix Equations for Each Infinitesimal Unit

A. J. Prado[1], **L. S. Lessa**[2], **R. C. Monzani**[3], **L. F. Bovolato**[2], **J. Pissolato Filho**[3], **E. Assunção**[2], **and M. C. M. Teixeira**[2]

[1]Telecommunication Engineering Department, Campus of S. J. Boa Vista
Univ. Estadual Paulista — UNESP, Brazil
[2]Electrical Engineering Department, Campus of Ilha Solteira
Universidade Estadual Paulista — UNESP, Brazil
[3]Electrical Engineering Department
The State University of Campinas — UNICAMP, Brazil

Abstract— A modified numeric procedure is applied to analyse the application of π circuits for representing distributed parameters. Numeric oscillations, which are associated usually with digital simulations associated with π circuits, are decreased. It is shown that these numeric oscillations, or Gibb's oscillations, are not related only to the mentioned associations. They are created by the application of the specific numeric integration methods for solving linear systems that describe the associations of π circuits. If the state equations are determined for each π circuit, then the proposed changes of the numeric routine for solving systems with π circuits lead to results with little influence on the numerical oscillations. This is confirmed using comparisons with results obtained from the Laplace transform and ATP software.

Searching for a simple representation of the cascade of π circuits, each unit is modelled individually. The influence of adjacent π circuit units are included by the differential relations among the state variables. Thus, the Gibb's oscillations are decreased significantly. Therefore, the limit for the increase in the number of π circuits is related to the best accuracy attained by the modified numeric routine for specific values of the applied parameters. The proposed numeric routine is more accurate than the numeric routine based on the application of only one matrix for representing the dynamics of π circuits. The results of the modified numeric routine are very close to those obtained using the Laplace transform method and ATP software.

The Exact Absorbing Conditions Method. Open Electrodynamic Structures

Merey Sautbekova[1], **Seil Sautbekov**[1], **Yuriy Sirenko**[1, 2], **and Alexey Vertiy**[1]

[1]L. N. Gumilyov Eurasian National University, 2, Mirzoyana St., Astana 010008, Republic of Kazakhstan
[2]A. Ya. Usikov Institute of Radiophysics and Electronics, National Academy of Sciences of Ukraine
12, Academician Proskura St., Kharkov 61085, Ukraine

Abstract— Exact absorbing conditions (EAC) are used in computational electrodynamics of nonsine waves for truncating the domain of computation when replacing the original open initial boundary value problem by a modified problem formulated in a bounded domain. In the opening sections of our communication we construct EAC as applied to the analysis of axially-symmetrical electrodynamic structures illuminated by the symmetrical pulsed TE- and TM-waves and prove the equivalency of the original (open) and modified (closed) initial boundary value problems. We present here the following results: The EAC for virtual boundaries in a cross-section of regular circular and coaxial waveguides and for an artificial spherical boundary in free space; the transport operators relating the near-zone and far-zone fields generated by compact waveguide inhomogeneities and obstacles in free space. We also prove the unique solvability of the modified closed problem and its equivalency to the initial open problem and solve the problem of extended and remote sources of pulsed waves giving grounds for rigorous theoretical justification of the EAC-method.

In the next sections, omitting technical details, we construct EAC as applied to the analysis of plane (2-D) electrodynamic structures illuminated by pulsed E- and H-polarized waves and EAC for 3-D vector initial boundary value problems describing spatial-temporal electromagnetic field transformations in open waveguide and compact resonators. Closing section is devoted to enhancement of efficiency of computation of the analytical results obtained in the previous sections.

The efficient limitation of the computational domain in open initial boundary value problems (i.e., the problems whose domain of analysis is infinite in one or more directions) is a vital issue in computational electrodynamics as well as in other physical disciplines using mathematical simulation and numerical experiments. Most of the well-known and extensively used heuristic and approximate solutions to this problem are based on the so-called absorbing boundary conditions (ABC) and perfectly matched layers (PML). The use of various modifications and improving techniques for respective methods yield good results in various specific physical situations. However, it appears that for certain problems associated with the resonant wave scattering, the numerical implementation of these methods may cause unpredictable growth of the computational error for large observation times.

The method utilizing the exact absorbing conditions for the artificial boundaries that truncate an unbounded domain of computation is outnumbered by the classical approximate approaches. However, the carefully computed testing data as well as a series of physical and applied results obtained with the help of this method, show its evident potential, especially, for obtaining reliable numerical data on space-time and space-frequency electromagnetic field transformations in open waveguide, periodic, and compact resonators.

Combining Boundary Element and Reduced Basis Methods for Fast Electromagnetic Field Computations

Yating Shi, **Xiuguo Chen**, **Chuanwei Zhang**, **Hao Jiang**, **Haiqing Wei**, **and Shiyuan Liu**
State Key Laboratory of Digital Manufacturing Equipment and Technology
Huazhong University of Science and Technology, Wuhan 430074, China

Abstract— Fast and efficient modeling of electromagnetic fields is highly desirable in the design, optimization, and optical measurement of nanostructures as one needs to repeatedly evaluate the distribution of electromagnetic field under variations of the frequency, the incident angle of the incident wave, and the nanostructure geometric parameters. Many numerical methods, such as the finite element method (FEM), the finite-difference time-domain method (FDTD), or the boundary element method (BEM) [1] have been proposed to simulate the electromagnetic fields scattered from aperiodic nanostructures. However, these numerical methods are quite computationally expensive. Recently, a numerical technique called the reduced basis method (RBM) has shown great potential in rapidly solving variable partial differential equations [2, 3] and has been widely applied in areas ranging from mechanics [4], fluid dynamics [5], to electromagnetics [6, 7]. In this work we focus on rapid and accurate calculations of electromagnetic scattering over dielectric nanostructures with varying parameters including the frequency, the incident angle, and the nanostructure geometric parameters. For solving problems with multiple homogeneous domains separated by predetermined boundaries, the BEM is probably the best candidate because it assigns and limits the unknown variables only on the boundaries. When further combined with the RBM, the enhanced performance can be expected for applications involving repeated calculations of electromagnetic scattering over an object which consists of multiple homogeneous regions separated by variable boundaries. In our combined BEM-RBM approach, we firstly select a number of so-called snapshots from the space of variable parameters, and establish offline a reduced basis space from BEM solutions corresponding to the snapshot parameters. By means of projecting both the electromagnetic field vectors and the BEM operators to the reduced basis space, the computationally large linear system of BEM is converted to a much smaller system that can be solved rapidly. The key to such a reduction is the affine decomposition of the BEM operator which divides the whole computation into a parameter-dependent time-consuming offline part and a parameter-independent computationally rapid online part. In this work, we will use the empirical interpolation method (EIM) to realize such affine decomposition. By varying the geometric parameters of the nanostructure, we are able to identify an affine mapping from a predetermined reference configuration to other actual configurations. Such mapping converts computation based on the actual configurations to the reference configuration, and hence avoids repeated meshing for different configurations. Practical numerical simulation shows that the efficiency of this BEM-RBM method is several ten times higher than that of the traditional BEM method.

REFERENCES

1. Chew, W. C., J. M. Jin, E. Michielssen, et al., *Fast and Efficient Algorithms in Computational Electromagnetics*, Artech House Publishers, 2001.
2. Prud'homme, C., Y. Maday, A. T. Patera, et al., "Reliable real-time solution of parametrized partial differential equations: Reduced-basis output bound methods," *J. Fluid Eng.-T ASME*, Vol. 124, 70–80, 2002.
3. Rozza, G., D. B. P. Huynh, and A. T. Patera, "Reduced basis approximation and a posteriori error estimation for affinely parametrized elliptic coercive partial differential equations," *Arch. Comput. Method E*, Vol. 15, 229–275, 2008.
4. Milani, R., A. Quarteroni, and G. Rozza, "Reduced basis method for linear elasticity problems with many parameters," *Comput. Methods Appl. Mech. Engrg.*, Vol. 197, 4812–4829, 2008.
5. Quarteroni, A. and G. Rozza, "Numerical solution of parametrized Navier-Stokes equations by reduced basis methods," *Numerical methods for PDEs*, Vol. 23, 923–948, 2007.
6. Hess, M. W. and P. Benner, "Fast evaluation of time-harmonic Maxwell's equations using the reduced basis method," *IEEE T. Microw. Theory*, Vol. 61, 2265–2274, 2013.
7. Fares, M., J. S. Hesthaven, Y. Maday, et al., "The reduced basis method for the electric field integral equation," *J. Comput. Phys.*, Vol. 230, 5532–5555, 2011.

Whistler Modes Guided by Enhanced Density Ducts in a Nonresonant Magnetoplasma

O. M. Ostafiychuk, **V. A. Es'kin**, **and A. V. Kudrin**
University of Nizhny Novgorod, Russia

Abstract— We consider axisymmetric waves guided by a cylindrical duct with enhanced plasma density in a magnetoplasma in the nonresonant region of the whistler frequency range. The overwhelming majority of theoretical studies on the subject deal with waves guided by density ducts in the resonant region of this range, which lies above the lower hybrid frequency and is characterized by the presence of an unbounded branch of the whistler-mode refractive index surface [1–3]. As to the whistler waves in the range below the lower hybrid frequency, when the magnetoplasma is nonresonant and the whistler-mode refractive index surface is closed, their guided propagation in density ducts has received little attention in the literature. Note that the interest in the behavior of whistler waves in the nonresonant magnetoplasma was stimulated in the past decade by experimental studies aimed at developing efficient methods of wave excitation in the indicated frequency interval [4].

We first consider a sharp-walled uniform cylindrical duct aligned with an external static magnetic field and surrounded by a homogeneous background plasma. Satisfying the continuity conditions for the tangential electric- and magnetic-field components at the duct surface, we obtain the dispersion relation that allows determining the propagation constants of the guided whistler modes. It is established that in the chosen frequency region, eigenmodes exist only in ducts with enhanced density. It is demonstrated that such eigenmodes allow a simplified description which significantly facilitates analysis of the features of their guided propagation. The description is based on that the corresponding modes have quasi-TE polarization. Using this fact, we have derived an approximate dispersion relation which gives mode propagation constants that are almost identical to those obtained from a rigorous dispersion relation. Then we analyze the propagation of axisymmetric whistler eigenmodes guided by a smooth-walled enhanced density duct in a nonresonant magnetoplasma. The possibility of a simplified description of these modes due to the extremely small value of the longitudinal component of their electric field inside and outside the duct has been demonstrated as well. It is shown that in this case, analytical results for the propagation constants and field structures of the eigenmodes can be obtained under certain conditions. The developed simplified description of the studied modes can assist in analysis of the features of their excitation by electromagnetic sources.

ACKNOWLEDGMENT

This work was supported by the Russian Science Foundation (project No. 14-12-00510), the RFBR (project No. 14-01-31280), the Grant of the President of the Russian Federation (project No. MK-4688.2014.2), and the Government of the Russian Federation (contract No. 11.G34.31.0048).

REFERENCES

1. Zaboronkova, T. M., A. V. Kudrin, M. Yu. Lyakh, and L. L. Popova, "Nonsymmetric whistler waves guided by cylindrical ducts with enhanced plasma density," *Radiophys. Quantum. Electron.*, Vol. 45, No. 10, 764–783, 2002.
2. Es'kin, V. A., T. M. Zaboronkova, and A. V. Kudrin, "Whistler waves guided by ducts with enhanced density in a collisional magnetoplasma," *Radiophys. Quantum Electron.*, Vol. 51, No. 1, 28–44, 2008.
3. Bakharev, P. V., T. M. Zaboronkova, A. V. Kudrin, and C. Krafft, "Whistler waves guided by density depletion ducts in a magnetoplasma," *Plasma Phys. Rep.*, Vol. 36, No. 11, 919–930, 2010.
4. Karavaev, A. V., N. A. Gumerov, K. Papadopoulos, X. Shao, A. S. Sharma, W. Gekelman, A. Gigliotti, P. Pribyl, and S. Vincena, "Generation of whistler waves by a rotating magnetic field source," *Phys. Plasmas*, Vol. 17, No. 1, 012102, 2010.

Application and Efficient Evaluation of Half-line Source Potentials and Their Derivatives

F. Turker Celepcikay[1], **D. R. Wilton**[2], **and D. R. Jackson**[2]

[1]Electrical and Electronics Engineering, Turgut Ozal University, Ankara, Turkey
[2]Applied Electromagnetics Group, Department of Electrical and Computer Engineering
University of Houston Houston, TX 77204-4005, USA

Abstract— Recently, in many applications including microwaves, optics, metamaterials and nanostructures, one- or two-dimensional periodic structures in layered media are being utilized. For this reason, the fast and accurate evaluation of periodic mixed-potential Green's functions in layered-media has become a very important problem. A typical strategy for acceleration involves identifying and removing the asymptotic terms in the spectral sums that correspond to a periodic array of point sources in an infinite homogeneous medium. The removed terms are added back to the spectral sums after utilizing the Ewald transformation which results in a Gaussian decay. This extraction not only accelerates the convergence of the spectral sum, but also creates a "regularized" Green's function that is much smoother as a function of spatial coordinates, and hence is much easier to interpolate.

For some of the dyadic and scalar components of the Green's function the asymptotic extractions from the spectral sums correspond in the spatial domain to an infinite periodic array of half-line sources in a homogenous medium. The potentials from these sources may also be regularized within a unit cell by removing the contributions from the individual (non-periodic) half-line sources located at the corners of the unit cell. Another interpolation can then be applied to the "regularized extracted potential". Based on recent analysis, a speed-up factor of over 20 is observed when using interpolation, for which the major cost is the evaluation of the singular terms including the potential of the half-line source. Therefore, an efficient evaluation of the scalar Green's function (potential) due to a single half-line source is a key element in the efficient calculation of the periodic layered-media Green's function.

The half-line source is shown in Fig. 1, where it is assumed that the tip of the source is at $z = 0$. This potential depends only on two variables, $k\rho$ and kz, where $k = 2\pi/\lambda$, i.e., on the electrical distances from the source axis and source tip, respectively, as illustrated in Fig. 1.

The potential is given exactly as

$$G_z = \int_z^\infty \frac{e^{-jkR}}{4\pi R} dz'' = \int_0^\infty \frac{e^{-jkR}}{4\pi R} dz'' - \int_0^z \frac{e^{-jkR}}{4\pi R} dz'' = \frac{1}{8j} H_0^{(2)}(k\rho) - \int_0^z \frac{e^{-jkR}}{4\pi R} dz''. \qquad (1)$$

where $R = \sqrt{\rho^2 + (z - z')^2}$ and $z'' = z - z'$.

Methods and Results: The potential the half-line source expressed in Eq. (1) can be efficiently evaluated in various ways, with the efficiency of the method depending on the location of the observation point. In this research, we examine several different methods, and find that each one is more efficient than the others in a certain region of the (ρ, z) plane.

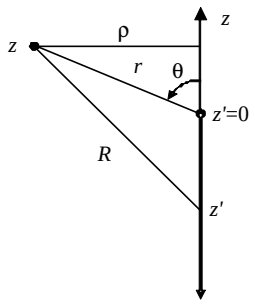

Figure 1: Half-line source that lies along the negative z axis, with the relevant coordinate system and geometrical parameters defined.

Hybrid TEM Wave Radiation from a Coaxial Waveguide with a Semi-infinite PEC Outer Cylinder and an Infinite Inner Cylinder Loaded with Partial Impedance

Kutlu Karayahşi[1], **İsmail H. Tayyar**[2], **and Arif Dolma**[3]

[1]Electrical & Electronics Engineering Department, Okan University
Tuzla Campus, Akfirat, Tuzla, Istanbul 34959, Turkey
[2]Mechatronic Engineering Department, Engineering Faculty
Karabük University, Balıklarkayası, Mevkii, Karabük, TR 78050, Turkey
[3]Electronics & Communications Engineering Department, KOU Engineering Faculty
Kocaeli University, Building B, Umuttepe Campus Kocaeli, TR 41380, Turkey

Abstract— The geometry of the problem is depicted in Fig. 1. The system consists of two coaxial cylinders the inner of which is infinite and has piecewise surface impedance while the outer cylinder is infinitely thin, semi-infinite and has a perfect electrical conductor surface. An incident TM_{00} (Hybrid TEM) mode travelling in the positive z direction is confined between the inner and the outer cylinders. The dimensions of the structure are chosen to satisfy the condition that only the dominant mode propagates inside the waveguide. The radius of the inner cylinder is a while the radius of the outer cylinder is b. For the sake of generality we assume that the sureface impedances of the inner cylinder where $z < 0$ and $z > 0$ are different from each other and denoted by $Z_1 = \eta_1 Z_0$ and $Z_2 = \eta_2 Z_0$, respectively, with Z_0 being the characteristic impedance of the free space. The aim of this work is to determine the effect of the relative surface impedances and the radii of the cylinders on the reflection coefficient and the radiated field. Being a very good model for long monopole antennas or traveling wave antennas, it important to analyze such structures.

The problem has been defined as a Wiener-Hopf equation by applying Fourier transformation to the scattered field and to the boundary conditions. The scattered field inside the waveguide has been expanded to series in terms of waveguide modes and the solution of the problem has been obtained by using the continuity conditions for the electromagnetic fields and transforming the problem into three sets of infinite algebraic equations containing three sets of infinite constants. The effects of the geometrical parameters and the impedances of the waveguide to the radiated field and the reflection coefficient has been observed.

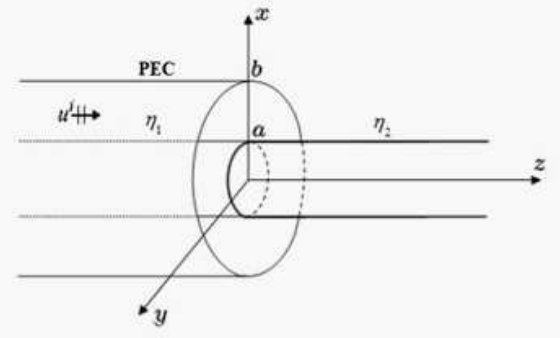

Figure 1: Geometry of the problem.

One Way Speed of Light and Why Nothing Can Be Faster Than Light

V. N. Matveev and O. V. Matvejev
Homo Sapiens Publishers, Vilnius, Lithuania

Abstract— Einstein's theory of clock synchronization is based on an arbitrary assumption of the equality of the speed of light in opposite directions and on experimental data on the constancy of the average speed of light on the way "there and back". All experiments to measure the speed of light were conducted by measuring it with just one clock and calculating the time of signal propagation on the way to the reflector and back. All methods, including the method of astronomical observations used by Roemer, yield an average value of the speed of light in opposite directions.

Brillouin wrote: "... the rule says that signals propagating from east to west and from west to east have the same speeds, whereas Michelson's experiment only allows measuring the simple average of these two speeds ...".

Does it mean that the speed of light from west to east or reverse cannot be measured at all?

The fact that such measurement is possible and that it does not require prior synchronization of two spatially separated clocks may be deduced from the following.

Let us imagine that a short-wave radar is stationed close to the city of Quito, sending a narrow-angle signal in the east direction. Let us also imagine that all over the equator line a great number of reflectors are stationed in such a way that any of the adjacent reflectors is within the field of vision from another. Let the reflectors deflect the radar signal emitted in Quito in such a way that it, propagating zigzag-wise near the Earth's surface, circles the Earth along the equator, coming back to the radar in Quito from the west.

Knowing the length of the zigzag line along which the radar signal propagates and the time needed for signal to circle the Earth, an operator of a radio relay station can calculate the propagation speed of the signal circling the Earth from east to west or reverse. These speeds will not be identical to the constant C.

It is known that the velocities of material bodies cannot achieve the speed of light in a vacuum. Why does the speed of light, being finite, behave as if it is infinite and is therefore unattainable for materials bodies?

In our presentation a possible cause of the finiteness of the velocity of tangible objects is demonstrated without reference to the provisions of the special theory of relativity. A condition is formulated on the basis of which the assumption of the movement of tangible objects at any prescribed velocities proves to be self-contradictory in instances when the prescribed velocities of the objects exceed a certain value.

This condition consists of the presence of interaction signals and carrier particles in material bodies that are propagated at a velocity greater than any prescribed velocity of the material bodies. The condition does not contain a limitation of the velocity of tangible objects, but also does not contradict it. The condition is as follows: *"Massles signals and particles that are always present in material objects are propagated at a velocity, V, that is unattainable for physical objects and particles that do have mass, continuously initiate interactions and processes in these bodies".*

Experimental and Numerical Analyses of Leakage Flux Distribution in Core-type Voltage Transformers

Fevzi Kentli[1], **İsmail Bozkurt**[2], **and Nevzat Onat**[2]

[1]Faculty of Technology, Marmara University, Turkey
[2]Vocational School of Technical Studies, Marmara University, Turkey

Abstract— Recognition of the flux distribution in machines is required for three reasons: 1) for measurement of the inductances, 2) for measurements of the forces applied to the coils, and 3) for measurements of the additional losses that occur in the coils and steel parts. The analog form can be used to determine the flux distribution in the machines and the magnitudes related to the magnetic field. However, numerical methods for measuring these factors are desirable, as analog methods are difficult and inefficient. Today, several methods are used for field analysis. The finite different (FDM) and the finite element (FEM) methods are two of the main methods used in this area. This study is based on the leakage magnetic flux analysis of a core type transformer. The distributions obtained experimentally were verified with two-dimensional FDM and FEM calculation results to verify them. A special test assembly for obtaining actual measurements at different heights was installed. The experiment set included a voltage transformer and measurement coils that were used to determine leakage flux distribution around a transformer iron leg. With the solution of the matrix created by measuring the induced voltage, polynomial mathematical equations were obtained. The flux values were then calculated in accordance with the numerical methods. In order to compare the results, plotting of the flux distribution was the best solution, and for this purpose, the total flux lines were determined. In addition, the difference between the smallest and largest value of the vector potential was also determined. The voltage (potential difference) vector was calculated by dividing the difference between the flux lines. In the last step, the equipotential points were determined by adding to the minimum potential value. This process was repeated using eight different heights on the leg, and the two-dimensional coordinates of the equipotential point were determined at each height. By combining the same valuable points, flux distribution was obtained graphically. Finally, fluxes were drawn in line with the measurement and calculation results and were compared with each other. As a result, the leakage flux distribution of the voltage transformer was obtained, and it was observed that the FEM model succeeded in calculating closer values to the measurement results. According to the study results, the use of measurements from several points taken by means of magnetic field probes in the FEM model provides sufficient accuracy solutions. The degree of the polynomial used in the FEM method will increase the accuracy rate. By increasing the degree of the polynomial used in the FEM method, more accurate results can be achieved.

Session 1P8
SC2: Recent Advances of Metamaterials for Novel Electromagnetic and Photonic Devices 1

Redshifting Silver Glare: Nanoparticle Morphology and Plasmonic Resonances

A. Sihvola[1], **P. Ylä-Oijala**[1], **D. C. Tzarouchis**[1], **O. Vartia**[2], **A. Seppälä**[2], **E. Haimi**[3], **and T. Ala-Nissilä**[4]

[1]Department of Radio Science and Engineering, Aalto University, Espoo, Finland
[2]Department of Energy Technology, Aalto University, Espoo, Finland
[3]Department of Materials Science and Engineering, Aalto University, Espoo, Finland
[4]Department of Applied Physics, Aalto University, Espoo, Finland

Abstract— Progress in present-day electromagnetics research happens very much on boundaries where other disciplines are encountered. Metamaterials, nano-optics, and plasmonics are some of the domains into which many classical electromagnetics experts focus their interest these days. Indeed, with traditional Maxwell-based mathematics and computational tools it is possible to analyze and understand very much of the fascinating physical phenomena that take place when light and electromagnetic radiation interacts with complex nanomaterial structures.

Volume plasmons in metals are oscillations of the electron cloud. The boundaries in discrete particles constrain these oscillations, resulting into various modes of localized particle plasmons [1]. In this presentation, we discuss the varieties how the properties of plasmonic resonances depend on the morphological and topological features of nanoparticles. It turns out that using fairly simple quasistatic analysis of the electric field interaction with a particle inclusion [2] whose dielectric function follows a Drude model, the main resonant features of these particles can be predicted satisfactorily for particles below 30 nm size. The material used in computations is silver [3], and the interesting physics happens within the optical wavelengths. Among these effects are redshifting (and sometimes also blue-shifting) of resonances, variation in their magnitudes, and differences in the behavior of scattering, absorption, and extinction efficiencies when the shape, structure, and dielectric contrast against environment varies. It is to be noted that the region of validity is of course bounded also from below: the classical description fails when the particle size goes down to a few nanometers where quantum effects can no longer be neglected.

For the analysis of larger and complex-form composite scatterers, we use other computational tools capable of full-wave simulation: surface- and volume-integral-equation, and discrete-dipole approximation based codes. This research is a result of the EXPECTS project within the framework of Aalto Energy Efficiency Research Programme.

REFERENCES

1. Maier, S. A., *Plasmonics: Fundamentals and Applications,* Springer, 2007.
2. Sihvola, A., *Electromagnetic Mixing Formulas and Applications,* IEE, London, 1999.
3. Johnson, P. B. and R. W. Christy, "Optical constants of noble metals," *Physical Review B*, Vol. 6, 4370–4379, 1972.

Structured Metals Transparency for Ultrabroadband Electromagnetic Waves and Acoustic Waves

Ru-Wen Peng, **Ren-Hao Fan**, **Dong-Xiang Qi**, **Xiao-Ping Ren**, **and Mu Wang**
National Laboratory of Solid State Microstructures, Department of Physics
Nanjing University, Nanjing 210093, China

Abstract— In this talk, we present our recent work on making structured metals transparency for ultrabroadband electromagnetic waves and acoustic waves via surface excitations. First, we show that periodic, quasiperiodic, and disordered metallic gratings can become transparent and completely antireflective for extremely broadband electromagnetic waves at oblique incidence. Second, we significantly develop oblique metal gratings transparent for broadband electromagnetic waves (including optical waves and terahertz ones) under normal incidence. In the third, we present that the principles of broadband transparency for structured metals can be extended from one-dimensional metallic gratings to two-dimensional cases. Moreover, similar phenomena are found in sonic artificially metallic structures, which present the transparency for broadband acoustic waves. These investigations provide guidelines to develop novel broadband metamaterials, and have potential applications on transparent conducting panels, antireflective conducting solar cells, broadband acoustic imaging and sensing, and so on.

REFERENCES

1. Ren, X. P., R. H. Fan, R. W. Peng, X. R. Huang, D. H. Xu, Y. Zhou, and M. Wang, "Non-periodic metallic gratings transparent for broadband terahertz waves," *Phys. Rev. B*, Vol. 91, 045111, 2015.
2. Qi, D. X., Y. Q. Deng, D. H. Xu, R. H. Fan, R. W. Peng, Z. G. Chen, M. H. Lu, X. R. Huang, and Mu Wang, "Broadband enhanced transmission of acoustic waves through serrated metal gratings," *Appl. Phys. Lett.*, Vol. 106, 011906, 2015.
3. Fan, R. H., R. W. Peng, X. R. Huang, and M. Wang, "Making structured metals transparent for ultrabroadband electromagnetic waves and acoustic waves," *Annals of Physics*, 2015, DOI :10.1016/j.aop.2014.12.029.
4. Fan, R. H., J. Li, R. W. Peng, X. R. Huang, D. X. Qi, D. H. Xu, X. P. Ren, and M. Wang, "Oblique metal gratings transparent for broadband terahertz waves," *Appl. Phys. Lett.*, Vol. 102, 171904, 2013.
5. Fan, R. H., L. H. Zhu, R. W. Peng, X. R. Huang, D. X. Qi, X. P. Ren, Q. Hu, and M. Wang, "Broadband antireflection and light-trapping enhancement of plasmonic solar cells," *Phys. Rev. B*, Vol. 87, 195444, 2013.
6. Qi, D.-X., R.-H. Fan, R.-W. Peng, X.-R. Huang, M.-H. Lu, X. Ni, Q. Hu, and M. Wang, "Multiple-band transmission of acoustic wave through metallic gratings," *Appl. Phys. Lett.*, Vol. 101, 061912, 2012.
7. Huang, X.-R., R.-W. Peng, and R.-H. Fan, "Making metals transparent for white light by spoof surface plasmons," *Phys. Rev. Lett.*, Vol. 105, 243901, 2010.
8. Fan, R. H., R.-W. Peng, X.-R. Huang, J. Li, Y. Liu, Q. Hu , M. Wang, and X. Zhang, "Transparent metals for ultrabroadband electromagnetic waves," *Advanced Materials*, Vol. 24, 1980, 2012.

Properties of Optical Cavities Made of Metamaterials

Haitao Jiang, Yunhui Li, and Hong Chen
School of Physics, Tongji University, Shanghai 200092, China

Abstract— Metamaterials with engineered permittivity ε and permeability μ have attracted people's great interest due to their unique electromagnetic (EM) properties. In this talk we will discuss our recent studies on properties of optical cavities made of metamaterialssuch as the artificial medium with zero index (ZI) and with special dispersion coming from the classical analog of the electromagnetic induced transparency (EIT) phenomenon. It is known that an optical cavity is one of basic devices for light manipulation and novel properties are required for modern applications. For example, requirement of strong coupling in cavity quantum optics need to put a quantum dot right at the cavity field peak, which is very challenging for a cavity made of ordinary optical materials because of inhomogeneous distribution of the cavity field. To overcome this difficulty, we propose to get uniform field distribution in a cavity made of ZI metamaterilas, then realize experimentally position-independent quantum optics phenomenon such as Rabi splitting. On the other hand, in some applications, one needs an optical cavity with both high quality factor (Q) and high transmittance (T). In a conventional cavity, stronger confinement of the cavity field can boost Q, at the cost of T decreasing as stronger scattering loss is involved. To reduce scattering loss, a cavity made of an EIT-like metamaterial is introduced, where Q is enhanced by the mechanism of special EIT dispersion, instead of confinement effect. Enhancement of Q while keeping T unchanged is illustrated experimentally.

Effective Medium Approach to Compute Optical Stress

Wujiong Sun[1, 2], **Jack Ng**[3], **Lei Zhou**[2], **and C. T. Chan**[1, 4]

[1]Department of Physics, Hong Kong University of Science and Technology, Hong Kong, China
[2]Department of Physics, Fudan University, Shanghai, China
[3]Department of Physics and Institute of Computational and Theoretical Studies
Hong Kong Baptist University, Hong Kong, China
[4]Institute for Advanced Studies, Hong Kong University of Science and Technology, Hong Kong, China

Abstract— Light can exert a force on material objects, which may be computed by a surface integral of the Maxwell stress tensor over a surface that encloses the entire object. However, it is also highly desirable to know the optical stress (e.g., to deform a cell). In principles, the stress can be given by the divergence of the stress tensor. Unfortunately, there are still controversies in what is the appropriate stress tensor inside a medium.

Consider an artificial effective medium, for example, consisting of a periodic or random array of dielectric cylinders with sub-wavelength cylinder size and lattice constant. The stress will be calculated by two methods. The first method is a rigorous but slow microscopic approach where the stress is defined as the force per unit area, and the force can be computed by Maxwell stress tensor. The second method is a very efficient effective medium approach where the cylinder array is treated as an effectively homogeneous medium and the stress for that effectively homogeneous medium is calculated directly using the divergence of three commonly employed stress tensors. It turns out that only the stress tensor derived from free energy, which takes into account the electrostriction, gives consistently correct results. In other words, MST and its "macroscopic generalization" have failed.

Situations other than dielectric cylinders will also be discussed. More examples with different composition and lattice structures will be considered.

Slowing Microwaves with Deeply Subwavelength 3D Printed Metamaterial Waveguides

N. Kaina[1], **A. Causier**[2], **M. Fink**[1], **T. Berthelot**[2], **and G. Lerosey**[1]

[1]Institut Langevin, ESPCI Paris Tech, France
[2]CEA Saclay, IRAMIS, NIMBE, LICSEN, UMR 3685, F-91191 Gif sur Yvette, France

Abstract— We study resonant wire media that are scaled at very subwavelength scales. We show that introducing local defects permits to guide the waves with a transverse confinement of the order of one period in any direction, independently of the spatial organization of the medium. We prove that the propagation within these waveguides exhibit a very low group velocity that can be tuned by modifying the geometrical and frequency parameters of the neighboring wires. We present simulation and experimental results of 3D printed polymer copper coated waveguides.

Slowing down the waves is one stake of time-signal processing, signal energy compressing, wave-matter interaction enhancements and device miniaturization. This can be achieved using strong material dispersion, for example very high index media, or with engineered systems such as photonic crystals waveguides (PCW) or coupled resonator optical waveguides (CROWS). If those are valid solutions for optical signals, photonic crystal based systems become very bulky for microwaves and telecommunication signals. In previous work [1], we demonstrated that is was possible to steer waves at scales independent of the wavelength in a deeply subwavelength wire-medium metamaterial by locally introducing defects whose frequency lie in the hybridization bandgap of the metamaterial. Whithin those waveguides, the wave tunnels from one defect to its neighbour thus providing a very low group velocity propagation as in photonic crystals. Contrarily to PCWs however, our waveguides can have arbitrarily small transverse dimensions, solely limited by the size the wires.

Using the 3D printing technology along with chemical copper plating process we were able to fabricate waveguides embedded in a wire medium with periodicities down to 2 mm ($\lambda_0/30$ at 5 GHz). We first show that our waveguides can exhibit an almost 0 dB transmission provided that an appropriate feeding is used. We then investigate the influence of the surrounding medium on the group velocity of a pulse propagating in the waveguide and as well as the shape of the dispersion relation within the transmission band (Fig. 1). We especially experimentally demonstrate that by decimating the medium density by a factor 3.5, the group index can be tuned from $n_g = 65$ up to $n_g = 230$.

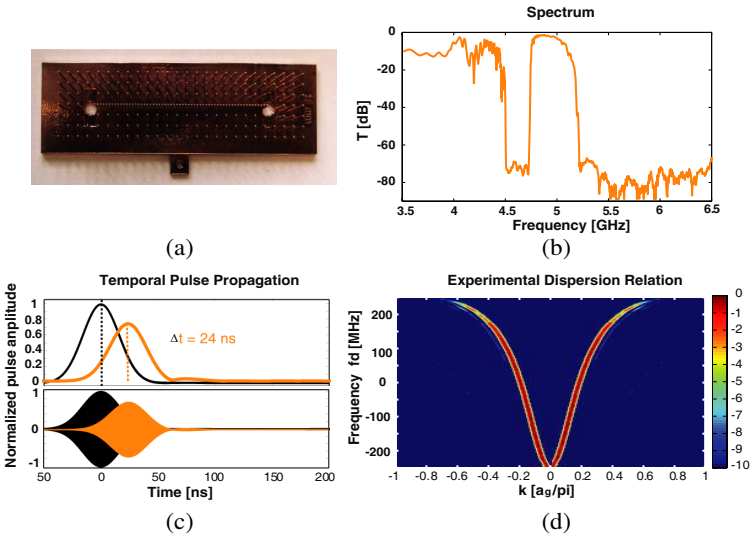

Figure 1: (a) 3D printed copper coated metamaterial waveguide. (b) Experimental spectral transmission (dB). (c) Temporal pulse emitted (black) and recieved after propagation (orange). (d) Experimental dispersion relation in the waveguiding transmission band.

We believe that our deeply subwavelength slow propagation waveguides in the microwave frequencies are promising candidates for the miniaturization of delay lines, filters, multiplexers as well as for more fondamental wave-matter enhancement studies.

REFERENCES

1. Lemoult, F., N. Kaina, M. Fink, and G. Lerosey, *Nature Physics*, Vol. 9, 5560, 2013.

Optical Gravitational Collimation and Observation of Einstein's Rings

Chong Sheng[1], **Rivka Bekenstein**[2], **Hui Liu**[1], **Shining Zhu**[1], **and Mordechai Segev**[2]

[1]School of Physics, Nanjing University, 210093, China
[2]Physics Department and Solid State Institute, Technion, Haifa 32000, Israel

Abstract— Light beams propagate along shortest paths by the Fermat principle, diffracting and broadening as described by the proper wave equation. The behavior of electromagnetic waves in static curved space is exactly analogues to that in inhomogeneous media, were the change in refractive index plays the role of the curvature. The space curvature affects the trajectories and the diffraction rate of light beams causing a unique behavior which can be emulated in an optical system by engineering the optical properties of a material. Here we experimentally demonstrate collimation of a beam in homogenous media for an order of magnitude more than the diffraction length, created after passing through a predesigned refractive index. The refractive index profile is analogues to a curvature of some massive star enabling observation of Einstein's Rings caused by the gravitational lensing as predicted by Einstein in 1936.

Effective Model for Plasmonic Coupling: Theory and Experiments

Meng Qiu, **Bin Xi**, **Shiyi Xiao**, **Hao Xu**, **Shulin Sun**, **Qiong He**, **and Lei Zhou**
State Key Laboratory of Surface Physics and Key Laboratory of Micro and Nano Photonic Structures
Fudan University, Shanghai, China

Abstract— Plasmonic couplings between nanoparticles generate fascinating physical phenomena, which can be utilized to realize certain applications [1, 2]. However, theoretical understandings on such problems are relatively behind experimental developments. Most theoretical efforts are based full wave simulations, which are not only computational complicated but also physically less transparent [3]. A complete effective model accounting for both electric and magnetic dipole terms in plasmonic nanoparticles, derived from a rigorous ground, is highly desired and is the key motivation of present work [4].

Based on the generalized tight-binding method for dispersive photonic media [5] and a multiple-expansion technique, we derived an analytical model for plasmonic coupling coefficient $t_{1,2}$ between two NPs, which includes all interacting terms between electric and magnetic dipoles of the NPs,

$$t_{1,2} = t_{pp} + t_{pp}^{rad} + t_{pm} + t_{mm} \tag{1}$$

where

$$t_{pp} = (f_0/8\pi\varepsilon_0 \langle\Phi|\Phi\rangle) \cdot \left[\vec{p}_1^{\,*} \cdot \vec{p}_2 - 3\left(\vec{p}_1^{\,*} \cdot \hat{d}\right)\left(\vec{p}_2 \cdot \hat{d}\right)\right]/d^3 \tag{2}$$

and

$$t_{mm} = (f_0\mu_0/8\pi \langle\Phi|\Phi\rangle) \cdot \left[\vec{m}_1^{\,*} \cdot \vec{m}_2 - 3\left(\vec{m}_1^{\,*} \cdot \hat{d}\right)\left(\vec{m}_2 \cdot \hat{d}\right)\right]/d^3 \tag{3}$$

are the standard dipolar interactions between electric and magnetic dipoles in different NPs.

$$t_{pp}^{rad} = -\left(f_0 \;/\; 16\pi\varepsilon_0 \langle\Phi|\Phi\rangle\right) \cdot (kd)^2 \cdot \left[\vec{p}_1^{\,*} \cdot \vec{p}_2 + \left(\vec{p}_1^{\,*} \cdot \hat{d}\right)\left(\vec{p}_2 \cdot \hat{d}\right)\right]/d^3 \tag{4}$$

is the electric dipolar interaction contributed from radiation effect.

$$t_{pm} = i\,(f_0/8\pi\varepsilon_0 c \langle\Phi|\Phi\rangle) \cdot kd \cdot \vec{p}_1^{\,*} \cdot \left(\vec{m}_2 \times \hat{d}\right)/d^3 \tag{5}$$

describes the interaction between electric and magnetic dipoles [4].

We performed extensive full-wave simulations [4] on particular plasmonic coupled systems to verify the effective model presented in Eqs. (1)–(5). Computations [4] show that our effective model can well describe the plasmonic coupling behaviors in general cases. In particular, when the NP is large enough so that a quasi-static approximation is no longer valid, one has to take the radiation correction term t_{pp}^{rad} into account (see Figs. 1(e)–(f)) to reasonably describe the plasmonic coupling behaviors, and the EM cross-interaction term t_{pm} is crucial to explain an intriguing mode-sequence reversal effect discovered in a particular coupled NP systems. In addition, we found that the coupling strength between certain plasmonic nanoparticles can be tuned through varying the orientations of NPs, leading to interesting phenomena such as ultra-slow-wave plasmon propagation. These intriguing phenomena have been experimentally verified in the microwave regime using split-ring-based resonators (see Fig. 1(i)) [6], and we will describe our latest THz experiments in the conference.

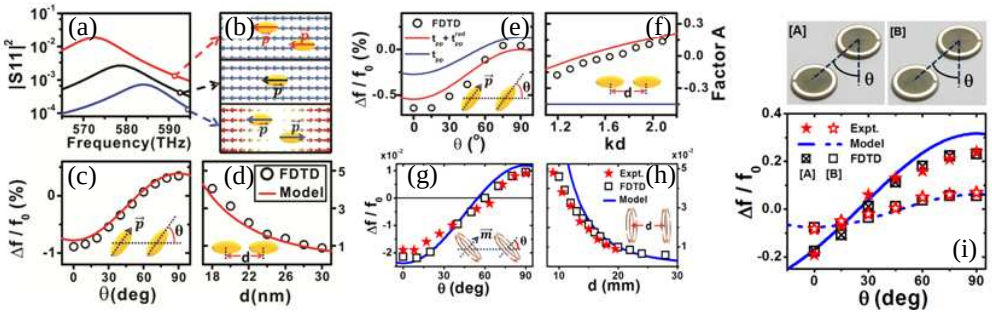

Figure 1: Simulation method to detect (a)–(b) the "Dark mode", and (c)–(i) comparisons between FDTD simulations, microwave experiments, and the effect model in different coupled systems.

REFERENCES

1. Rycenga, M., C. M. Cobley, J. Zeng, W. Li, C. H. Moran, Q. Zhang, D. Qin, and Y. Xia, *Chemical Reviews*, Vol. 111, 3669, 2011.
2. Halas, N. J., S. Lal, W. S. Chang, S. Link, and P. Nordlander, *Chemical Reviews*, Vol. 111, 3913, 2011.
3. Zuloaga, J., E. Prodan, and P. Nordlander, *Nano Letters*, Vol. 9, 887, 2009.
4. Xi, B., M. Qiu, S. Xiao, H. Xu, and L. Zhou, *Physical Review B*, Vol. 89, 035110, 2014.
5. Xi, B., H. Xu, S. Xiao, and L. Zhou, *Physical Review B*, Vol. 83, 165115, 2011.
6. Qiu, M., S. Xiao, Q. He, S. Sun, and L. Zhou, *Optics Letters*, Vol. 40, 272, 2015.

Multi-layer Transmission of Spoof Surface Plasmon Polaritons

Bai Cao Pan, **Zui Tao**, **and Tie Jun Cui**
State Key Laboratory of Millimetre Waves, School of Information Science and Engineering
Southeast University, Nanjing 210096, China

Abstract— Spoof surface plasmon polaritons (SSPPs) show a low-pass transmission property with a remarkable stop frequency due to the asymptotic property of the dispersion relationship. A series of SSPPs waveguides and their applications have been reported such as high efficiency transmission, ultra-thin waveguides and active device researches. However, in order to show more potential in combining with the traditional integrated circuits and achieve new-type plasmonic circuits, the SSPPs signal needs to be transmitted between multiple layers efficiently. Here, we propose a method to transmit such surface modes from one side of the substrate to the other side efficiently. In our design, a metallic hole in layed inside the substrate is used to connect the traditional corrugated metallic strip waveguide on both sides of the substrate. The metallic hole could provide a decoupling effect near the transition parts between the two waveguide on different sides since the electromagnetic field distribution is remained. The simulation results show that our design could transmit the SSPPs wave from the top layer of the medium to the bottom layer without significant loss. On the other hand, through the modulation of the position of the metallic hole, a series of absorption peaks during the transmission frequency band appears because of the coupling in the superposition section of the two waveguides. It's simulated that such design could provide a broadband high-efficient multi-layer transmission with a controllable absorption and such absorption is only related to the superposition area of the corrugated metallic strip. Based on our design, SSPPs with ultra-short wavelength and high-confinement property are able to play a more important role in the plasmonic integrated circuits.

Electromagnetic Metamaterial Absorbers for High Temperature Applications

Wei Li[1], **Yi Wang**[1], **Urcan Guler**[2], **Wei Wang**[1], **Tianlong Wu**[1] **and Jianguo Guan**[1]

[1]State Key Laboratory of Advanced Technology for Materials Synthesis and Processing
Wuhan University of Technology, Wuhan 430070, China
[2]School of Electrical & Computer Engineering and Birck Nanotechnology Center
Purdue University, West State Street, West Lafayette 47907, USA

Abstract— Electromagnetic metamaterial absorbers exhibit distinct absorbing properties compared to the traditional electormagnetic absorbers, such as thin thickness, adjustable or even real-time controllable absorption, and circumstance responsible absorption [1]. These properties endow the metamaterials with important applications in sensing, stealth, electromagnetic compatibility and communications [2]. However, existing metamaterial absorbers are nearly all designed for room temperatures since they are mostly made of heat-vulnerable polymer dielectrics and low-melting-point metals such as copper, silver and gold.Those metamterials will be distructed or work improperly at temperatures no higher than 1000°C, which restricts their high temperature applications [3]. However, few research efforts are made on refractory metamaterials till now [4].

As a meaningful start, we reported a refractory metamaterial optical absorber for high temperature of more than 1000°C in solar thermophotovotaics. The broadband and polarization independent metamaterial absorber uses a plasmonic material of Titanium Nitride (TiN) instead of traditional noble metals. We measured an absorption of more than 95% in average over the entire visible spectrum (400–800 nm). The high temperature stability of the metamaterial is demonstrated experimentally. Our investigation suggests that TiN, which exhibits lower plasmonic resonant frequency and higher thermal stability than noble metals, and merges the benefits of better impedance match from bulk plasmon and losses caused by localized surface plasmon, is more favorable in broadband optical absorption.

In microwave regime, we proposed a rafractory metamaterial made of titanium boride (TiB_2) and alumina (Al_2O_3). Without the help of plasmonic resonance, the metamaterial absorber achieved a nearly perfect absorption through standing wave resonance at X band with a thickness of less than 1 mm at 1000°C. The absorption changes from around 40% to 99% with temperature rising from room temperature to 800°C. These features enable the metamaterial to be used in temperature sensing and hyper sonic aircraft stealth applications.

These two works extended the metamaterial research to high temperature and opened a path to the application of ultrathin broadband absorbers in various high temperature applications sincluding solar thermophotovoltaics (STPV).

REFERENCES

1. Turpin, J. P., J. A. Bossard, K. L. Morgan, D. H. Werner, P. L. Werner, *Int. J. Antenn. Propag.*, Vol. 2014, 18, 2014.
2. Watts, C. M., X. Liu, and J. Padilla, *Adv. Mater.*, Vol. 24, OP98, 2012.
3. Guler, U., A. Boltasseva, and V. M. Shalaev, *Science*, Vol. 344, 263, 2014.
4. Li, W., U. Guler, N. Kinsey, G. V. Naik, A. Boltasseva, J. Guan, V. M. Shalaev, and A. V. Kildishev, *Adv. Mater.*, Vol. 26, 7959, 2014.

Enhancement of Polarizabilities of Cylinders with Cylinder-slab Resonances

Meng Xiao[1], **Xueqin Huang**[1], **H. Liu**[1, 2], **and C. T. Chan**[1]

[1]Department of Physics and Institute for Advanced Study
The Hong Kong University of Science and Technology, Clear Water Bay, Hong Kong, China
[2]National Laboratory of Solid State Microstructures & Department of Physics
Nanjing University, Nanjing 210093, China

Abstract— If an object is very small in size compared with the wavelength of light, it does not scatter light efficiently. It is hence difficult to detect a very small object with light. Meanwhile, a superlens type metamaterial slab is impedance matched with background, so it is also difficult to detect with light. However, the effective polarizability of a small cylinder can be greatly enhanced by coupling it with a superlens type metamaterial slab and this is shownusing analytic theory as well as full wave numerical calculations. This kind of enhancement is not due to the individual resonance of the metamaterial slab, nor due to that of the object, but is caused by a collective resonant mode of the cylinder and the slab. The enhancement ratio is limited by factors such as the absorption of the metamaterial slab and the cylinder, and the radius of the cylinder relative to the wavelength of light. The condition of this hybrid resonance mode is derived using an analytic model where we only consider the monopole moment of the cylinder. The analytically derived condition is confirmed with full wave simulations. We find that this type of particle-slab resonance is actually closely related to the reverse effect known in the literature as "cloaking by anomalous resonance" which can make a small cylinder undetectable. We also show that the enhancement of effective polarizability of the cylinder can lead to strongly enhanced electromagnetic forces that can be attractive or repulsive, depending on the material properties of the cylinder.As the force enhancement is quite strong (four orders of magnitude) at the resonance condition, the system can behave as a light-enabled "force shield", where the energy barrier as the particle approach (or recede from) the slab is significant.

Quantum Dot Optical Frequency Comb Laser (QD-FCL) for Simultaneous Multiple-wavelength Peak Generation

Naokatsu Yamamoto, Kouichi Akahane, Toshimasa Umezawa, and Tetsuya Kawanishi
National Institute of Information and Communications Technology
4-2-1 Nukui-Kita, Koganei, Tokyo 184-8795, Japan

Abstract— High-capacity and high-speed photonic networking and device technologies are essential for constructing advanced metro/access network systems. Additionally, radio-over-fiber (RoF) systems and short-reach interconnections and/or data center networks require a large number of channels for their many port-to-port connections. Solutions that satisfy these requirements incorporate two technical components to increase the operational optical frequency range: alternative wavebands and ultrabroadband photonic devices and materials. As an alternative waveband application, we have proposed the use of T and O bands (T band: 1000–1260 nm; O band: 1260–1360 nm) because large optical frequency resources (> 70 THz) can be employed to obtain many wavelength channels in these wavebands. A semiconductor quantum dot (QD) structure is a potential candidate as an optical gain material for high-performance and ultrabroadband photonic ICT devices. The QD nanostructures also have interesting optical gain properties based on the discrete energy state of carriers, which are confined in the QDs, as shown in Fig. 1(a). By using these discrete optical gain properties of QDs, we successfully developed a QD optical frequency comb laser (QD-FCL) as a novel functional wavelength division multiplexing (WDM) light source, as shown in Fig. 1(b), for stable generation of multiple-wavelength peaks from single and compact QD gain chips. Fig. 1(c) shows typical multiple-wavelength peak generation in the T + O band with a stable optical power characteristic. It is clearly demonstrated that five-wavelength peaks can be obtained from a single QD device. We also successfully demonstrated error-free optical data transmissions using the developed QD-FCL as a multiple-wavelength optical carrier generator.

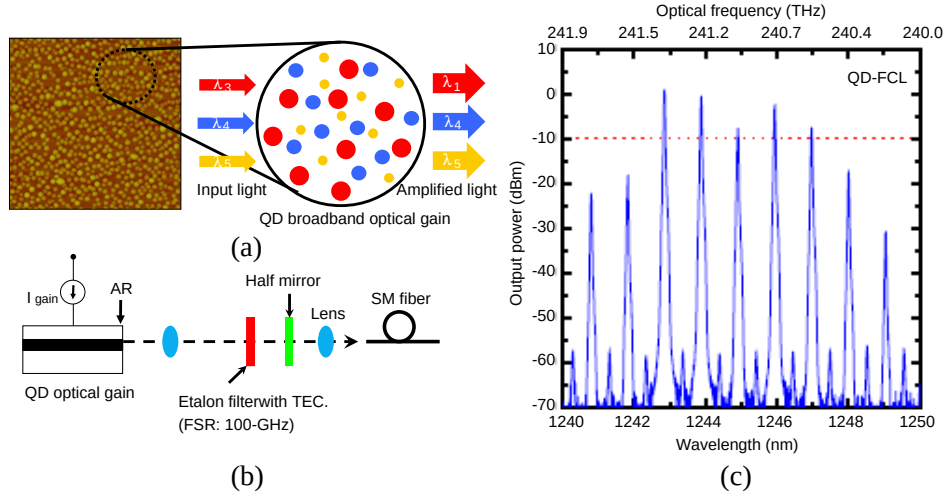

Figure 1: (a) Atomic force microscope image of the InAs/InGaAs QD structure (1 μm^2) using the SSNS technique, and schematic of discrete optical gain properties of QDs for each wavelength. (b) Optical setup of the QD-FCL using an external-cavity structure. (c) Stable multiple-wavelength peak generation using the QD-FCL device.

ACKNOWLEDGMENT

This study was conducted as part of a research project supported by the Japanese Government funding for "R&D to Expand Radio Frequency Resources" by the Ministry of Internal Affairs and Communications.

Broadband High Efficiency Asymmetric Transmission of Achiral Metamaterials

Jinwei Shi, Dahe Liu, and Wenjun Fan
Applied Optics Beijing Area Major Laboratory, Department of Physics
Beijing Normal University, Beijing 100875, China

Abstract— Asymmetric transmission (AT) effect has attracted great interest in recent years, due to its potential application in integrated photonics from GHz to optical frequency. To realize AT effect, numerous metamaterials have been proposed, mainly based on the chirality of the structure. In this paper, we demonstrate that achiral metamaterials can also have AT effect. Furthermore, it is shown that modal conversion is more essential than chirality to achieve AT effect. In particular, we have proposed a mirror symmetric metamaterial with broadband high efficiency AT effect for circular polarization wave operating at THz region. With further optimization of the unit cell, $> 80\%$ of the central frequency bandwidth and average 74.05 (maximum 150) transmission ratio can be obtained. The idea demonstrated here can also be applied to other frequency regions and the development of linear polarization devices.

Analysis of EM Shielding Effectiveness of CNT Films Based on TEM Cell Electric and Magnetic Coupling Fields

Jung-Yeol Park[1], **Jin-A Choi**[1], **Jae-Kyung Wee**[1], **Inchae Song**[1], **and Soon-Il Yeo**[2]

[1]School of Electronic Engineering, Soongsil University, Korea
[2]Electronics and Telecommunications Research Institute, Korea

Abstract— In this paper, we evaluated the electromagnetic (EM) shielding effectivenesses (SEs) on various CNT-based films which are prepared with deposits densities and thicknesses of the carbon nanotubes (CNTs) films. The test environment based on a TEM cell is adapted for a comparison of the standard ASTM test and the near-field test using electric and magnetic coupling fields and differences of CNT films' SEs on electric field and magnetic field according to near end or far-end tests by the rotations of a microstrip patch antenna as a DUT. In addition, the effect of CNT's composites and their film thickness on the SEs are investigated with TEM cell electric and magnetic field coupling to the DUT.

Figure 1 shows the test environment and measured EM SEs according to composites and thicknesses of CNT films. The antenna as an EM source is devised with a 2-layers PCB and the test repeats four times in the 0, 90, 180, and 270 degrees. The SEs are calculated with the equations as follows, $\mathrm{SE}\,[\mathrm{dB}] = P_1\,[\mathrm{dBm}] - P_2\,[\mathrm{dBm}]$ where P_1 and P_2 mean the transmitted power without and with that of CNT-film shielding, respectively. Measured SEs shows that EM powers are more reduced with increasing CNT composites than film thickness. Also a comparison of the standard ASTM test and the near-field test at the antenna rotation of 90 degree shows similar measured results. The tests with 0 or 180 degrees, however, show the different results between those of ASTM tests and the near-field test. The measured SEs of CNT films at 0 and 180 degrees are very lower levels than those of 90 and 270 degrees because the eddy currents on CNT films give the additional magnetic coupling effect. The 4 rotated test results can be explained as CNT films don't effectively prevent magnetic fields but CNT films can reduce electric fields. Also, the SE characteristics of CNT films are changed according to CNT composites and maximized SE peak points moves low frequency to high frequency as the CNT composites are increasing. The SE levels are changed, but the maximized SE peak doesn't change according to thicknesses of CNT films.

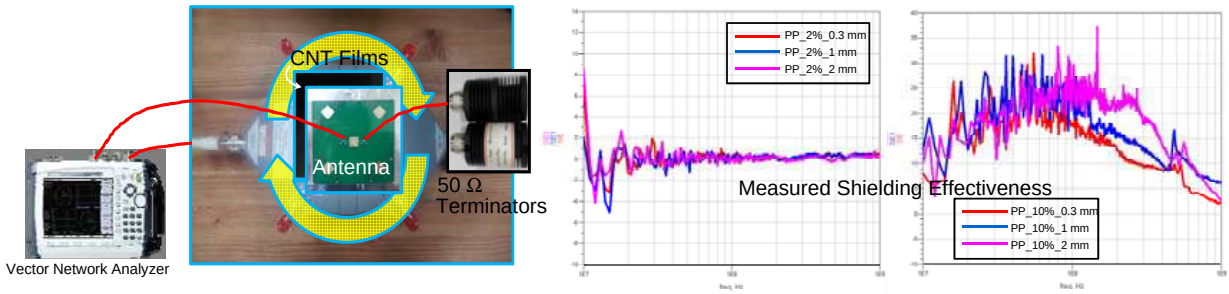

Figure 1: Test Environrmnt and measured EM SEs according to densities and thicknesses of CNT films at antenna rotation of 90 degree..

Manipulating Electromagnetic Waves Based on Magnetic Plasmonic Gradient Metasurface

Shiyang Liu[1], **Huajin Chen**[2], **Zhifang Lin**[3], **and C. T. Chan**[4]

[1]College of Mathematics Physics and Information Engineering
Institute of Information Optics, Zhejiang Normal University, Jinhua, Zhejiang 321004, China
[2]State Key Laboratory of Surface Physics (SKLSP) and Department of Physics
Fudan University, Shanghai 200433, China
[3]Key Laboratory of Micro and Nano Photonic structures (Ministry of Education)
Fudan University, Shanghai 200433, China
[4]Department of Physics, The Hong Kong University of Science and Technology
Clear Water Bay, Hong Kong, China

Abstract— Molding the electromagnetic features of spatially propagating waves or the propagating surface waves is considerable important due to its significant importance for scientific exploration and technological advancement. Photonic crystals and metamaterials are the typical candidates to tailor the photonic dispersions by introducing, respectively, the wavelength-scale periodic structures and the subwavelength resonant building blocks. A great quantity of exotic phenomena and potential applications are realized based on the concept of photnic crystals and metamaterials. Nonetheless, due to the size mismatch of the photonic crystals based circuits and the electronic integrated circuits, an inevitable deficiency comes into appearance for the integration compatibility of photonics and electronics. Although metamaterials can manipulate photons at subwavelength scale, the loss is still an inherent disadvantage owing to the resonating nature of the building blocks.

The recent emerging "flat optics" offers an alternative way in engineering optical components, which is capable of circumventing the essential issues obstructing the development of PCs and metamaterials such as strong loss, high cost, and even integration compatibility. It enables full control of the electromagnetic waves via engineering the amplitude, phase, and polarization of photons. In this presentation, we provide a newly designed gradient metasurface made of ferrite materials, quite different from the previous design with dielectric and metallic composite structures. Due to the time reversal symmetry breaking nature of the magnetic system under an external magnetic field, unidirectional magnetic surface plasmon can be excited, resulting in the construction of gradient magnetic plasmonic metasurfaces (GMPMS). We demonstrate that a remarkably enhanced unidirectional coupling of a Gaussian beam to the GMPMS with the coupling efficiency about 80 percent can be realized. The underlying physics lies in that the dispersion features can be tailored by optimizing the gradient of the GMPMSs, which strongly reinforces the interaction between the photons and GMPMSs, resulting in the excitation of unidirectionally guided edge states.

Thermal Imaging of RF Induced Heat Loss in a Microwave Metamaterial Absorber

K. Ozden[1], **O. M. Yucedag**[2], **A. Ozer**[2], **H. Bayrak**[2], **H. Isik**[3], **and H. Kocer**[2]

[1]Defense Sciences Institute, Turkish Military Academy Ankara, Turkey
[2]Department of Electrical Engineering, Turkish Military Academy Ankara, Turkey
[3]Department of Mechanical Engineering, Turkish Military Academy Ankara, Turkey

Abstract— Metamaterial absorbers (MAs) play an important role in stealth technology in microwave bands. Although MAs absorbs incident RF power, they usually convert it into the heat which might be a disadvantage for counter-measurement against remote thermal imaging systems. In this study, we present the design, simulation, fabrication and RF/thermal imaging measurement of a narrowband MA absorber in the microwave region. MA consists of a two dimensional periodic array of a well-known metallic split ring resonator (SRR) and a ground plane separated by a dielectric layer. It is found that the RF simulation results are in good agreement with the measurements such that near-perfect absorption occurs at 4.75 GHz when the incident electric field vector is perpendicular to the SRR gaps. On the other hand, near-zero absorption is obtained when the incident electric field vector is parallel to the gaps. Thermal imaging of these two cases are carried out using a commercial thermal imager which has a longwave infrared sensor between 8–12 μm wavelengths. Surface temperature map of the MA are extracted from the recorded thermal images of the MA at these two cases. It is shown that a slight temperature difference happens with respect to the ambient temperature for the MA of the near-perfect absorption whereas the MA of the near-zero absorption has zero temperature difference. Physical mechanisms of the RF absorption and the RF induced heat loss are explained using further electromagnetic numerical simulations and heat transfer model. Results are going to be presented and discussed in the conference paper.

Plasmonic Switches

J. Leuthold, **A. Emboras**, **W. Heni**, **C. Hoessbacher**, **C. Haffner**, **Y. Salamin**, **P. Ma**, **Y. Fedoryshyn**, **and Christian Hafner**
Institute of Electromagnetic Fields (IEF), ETH Zurich, Zurich 8092, Switzerland

Abstract— Plasmonic modulators and switches have attracted considerable attention because they offer ultra-compact size in the order of a few micrometers, high speed with bandwidths in the order of THz and potentially low power consumption in the order of a few fJ/bit. However, the debate as of which concept is most efficient is ongoing and it ultimately might depend on the application as of what concept might be most advantageous. In this review we shed light on some of the recent findings and try to categorize the various mechanisms.

An ideal optical switch should feature a small footprint, offer high speed operation and operate with the least possible power consumption. However, to this day, optical switches have relatively large footprints compared to λ and are not really power efficient nor can they achieve THz bandwidths.

More recently, plasmonics has emerged as a potential solution to some of those issues [1–10]. Plasmonic waves can be confined to sub $100\,\mathrm{nm}^2$ dimensions, which offers a way to build devices with footprints of $\mu\mathrm{m}^2$ and to take advantage of strong nonlinearities that are a direct consequence of the ultra-compact confinement. More recently the first high-speed plasmonic devices have emerged [11, 12].

In this paper we review waveguide structures and concepts to build optical modulators. We will discuss plasmonic devices based on the thermo-plasmonic effect [1], the free carrier dispersion effect [8, 13, 14], the Pockels effect [11, 12, 15], the phase-change effect [16–18] and the electro-chemical metallization effect [19, 20]. We will then compare them with respect to speed, power efficiency and footprint.

REFERENCES

1. Nikolajsen, T., K. Leosson, and S. I. Bozhevolnyi, "Surface plasmon polariton based modulators and switches operating at telecom wavelengths," *Applied Physics Letters*, Vol. 85, 5833–5835, 2004.
2. Krasavin, A. V., A. V. Zayats, and N. I. Zheludev, "Active control of surface plasmon-polariton waves," *Journal of Optics A: Pure and Applied Optics*, Vol. 7, S85, 2005.
3. Ozbay, E., "Plasmonics: merging photonics and electronics at nanoscale dimensions," *Science (New York, N.Y.)*, Vol. 311, 189–193, 2006.
4. Dionne, J. A., L. A. Sweatlock, H. A. Atwater, and A. Polman, "Plasmon slot waveguides: Towards chip-scale propagation with subwavelength-scale localization," *Physical Review B*, Vol. 73, 035407, 2006.
5. Cai, W., J. S. White, and M. L. Brongersma, "Compact, high-speed and power-efficient electrooptic plasmonic modulators," *Nano letters*, Vol. 9, 4403–4411, 2009.
6. MacDonald, K. F., Z. L. Samson, M. I. Stockman, and N. I. Zheludev, "Ultrafast active plasmonics," *Nat Photon*, Vol. 3, 55–58, 2009.
7. Knight, M. W., H. Sobhani, P. Nordlander, and N. J. Halas, "Photodetection with Active Optical Antennas," *Science (New York, N.Y.)*, Vol. 332, 702–704, 2011.
8. Sorger, V. J., N. D. Lanzillotti-Kimuara, R.-M. Ma, and X. Zhang, "Ultra-compact silicon nanophotonic modulator with broadband response," *Nanophotonics*, Vol. 1, 17–22, 2012.
9. Leuthold, J., C. Hoessbacher, S. Muehlbrandt, A. Melikyan, M. Kohl, C. Koos, W. Freude, V. Dolores-Calzadilla, M. Smit, I. Suarez, J. Martínez-Pastor, E. P. Fitrakis, and I. Tomkos, "Plasmonic Communications: Light on a Wire," *Opt. Photon. News*, Vol. 24, 28–35, 2013.
10. Babicheva, V. E., N. Kinsey, G. V. Naik, M. Ferrera, A. V. Lavrinenko, V. M. Shalaev, and A. Boltasseva, "Towards CMOS-compatible nanophotonics: Ultra-compact modulators using alternative plasmonic materials," *Optics Express*, Vol. 21, 27326–27337, 2013.
11. Melikyan, A., L. Alloatti, A. Muslija, D. Hillerkuss, P. C. Schindler, J. Li, R. Palmer, D. Korn, S. Muehlbrandt, D. Van Thourhout, B. Chen, R. Dinu, M. Sommer, C. Koos, M. Kohl, W. Freude, and J. Leuthold, "High-speed plasmonic phase modulators," *Nature Photonics*, Vol. 8, 229–233, 2014.

12. Haffner, C., D. Elder, B. Baeuerle, A. Emboras, A. Josten, F. Ducry, M. Kohl, L. Dalton, D. Hillerkuss, C. Hafner, and J. Leuthold, "High-speed plasmonic Mach-Zehnder modulator in a waveguide," *in European Conference on Optical Communication, ECOC*, PD.2.6, Cannes, France, 2014.
13. Dionne, J. A., K. Diest, L. A. Sweatlock, and H. A. Atwater, "PlasMOStor: A metal-oxide-si field effect plasmonic modulator," *Nano Letters*, Vol. 9, 897–902, 2009.
14. Melikyan, A., N. Lindenmann, S. Walheim, P. M. Leufke, S. Ulrich, J. Ye, P. Vincze, H. Hahn, T. Schimmel, C. Koos, W. Freude, and J. Leuthold, "Surface plasmon polariton absorption modulator," *Optics Express*, Vol. 19, 8855–8869, 2011.
15. Randhawa, S., S. Lachèze, J. Renger, A. Bouhelier, R. E. de Lamaestre, A. Dereux, and R. Quidant, "Performance of electro-optical plasmonic ring resonators at telecom wavelengths," *Optics Express*, Vol. 20, 2354–2362, 2012.
16. Briggs, R. M., I. M. Pryce, and H. A. Atwater, "Compact silicon photonic waveguide modulator based on the vanadium dioxide metal-insulator phase transition," *Optics Express*, Vol. 18, 11192–11201, 2010.
17. Kiouseloglou, A., G. Navarro, V. Sousa, A. Persico, A. Roule, A. Cabrini, G. Torelli, S. Maitrejean, G. Reimbold, B. De Salvo, F. Clermidy, and L. Perniola, "A novel programming technique to boost low-resistance state performance in Ge-Rich GST phase change memory," *IEEE Transactions on Electron Devices*, Vol. 61, 1246–1254, 2014.
18. Perniola, L., V. Sousa, A. Fantini, E. Arbaoui, A. Bastard, M. Armand, A. Fargeix, C. Jahan, J. F. Nodin, A. Persico, D. Blachier, A. Toffoli, S. Loubriat, E. Gourvest, G. B. Beneventi, H. Feldis, S. Maitrejean, S. Lhostis, A. Roule, O. Cueto, G. Reimbold, L. Poupinet, T. Billon, B. De Salvo, D. Bensahel, P. Mazoyer, R. Annunziata, P. Zuliani, and F. Boulanger, "Electrical behavior of phase-change memory cells based on GeTe," *Electron Device Letters, IEEE*, Vol. 31, 488–490, 2010.
19. Emboras, A., I. Goykhman, B. Desiatov, N. Mazurski, L. Stern, J. Shappir, and U. Levy, "Nanoscale plasmonic memristor with optical readout functionality," *Nano letters*, Vol. 13, 6151–6155, 2013.
20. Hoessbacher, C., Y. Fedoryshyn, A. Emboras, A. Melikyan, M. Kohl, D. Hillerkuss, C. Hafner, and J. Leuthold, "The plasmonic memristor: A latching optical switch," *Optica*, Vol. 1, 198–202, 2014.

Electromagnetically Induced Transparency Analogy of Metamaterial

Fuli Zhang, **Xuan He**, **and Yuancheng Fan**
Key Laboratory of Space Applied Physics and Chemistry
Ministry of Education and School of Science
Northwestern Polytechnical University, Xi'an 710072, China

Abstract— Recent research reveals that elaborately controlling microstructure coupling effect between neighboring elements enables metamaterial to exhibit not only frequency shift but also an analogy of electromagnetically induced transparency (EIT) of classical quantum effect of atomic system. To resemble classical quantum behaviour, various metamaterial based approaches including "trapped mode" and destructive interference between bright and dark (superradiant or subradiant) resonators were developed.

In the first part, we investigated coupling effect of asymmetric SRR metamaterial dimer whose elements differ from magnetic resonance frequency. An electromagnetically induced transparency (EIT)-like transmission spectrum with one transparency peak located between two dips is observed. Due to interplaying effect between asymmetric SRRs, a steep normal phase occurs, resulting in an enhancement of group delay with respect to SRR alone. Furthermore, local field demonstrates a suppressed mode formed by opposite local magnetic dipoles of two SRRs can explain the underlying physics.

To produce different dissipation loss between magnetic resonance elements, barium strontium titanate (BST) and calcium titanate ($CaTiO_3$) are chosen as the bright and dark EIT resonators, respectively, due to their different intrinsic dielectric loss. Under incident magnetic field excitation, dielectric metamaterial exhibits an EIT-type transparency window which is accompanied by abrupt change of transmission phase.

At last, instead of electromagnetically induced transparency, analogy effect of electromagnetically induced absorption (EIA) will be addressed. An EIA effect is observed inside a metal/dielectric hybrid microstructure. Meanwhile, an enhanced group delay of more than 20 ns for X band is verified experimentally and numerically.

ACKNOWLEDGMENT

This work was funded from National Natural Science Foundation of China (Grant Nos. 11372248, and 61101044), National High Technology Research and Development Program of China (863 Program) (Grant No. 2012AA030403), Aeronautical Science Foundation of China (Grant No. 20120153-001), and NPU Aoxiang Star Project.

REFERENCES

1. Fedotov, V. A., M. Rose, S. L. Prosvirnin, N. Papasimakis, and N. I. Zheludev, "Sharp trapped-mode resonances in planar metamaterials with a broken structural symmetry," *Phys. Rev. Lett.*, Vol. 99, 147401, 2007.
2. Papasimakis, N., V. A. Fedotov, N. I. Zheludev, and S. L. Prosvirnin, "Metamaterial analog of electromagnetically induced transparency," *Phys. Rev. Lett.*, Vol. 101, 253903, 2008.
3. Singh, R., I. A. I. Al-Naib, M. Koch, and W. Zhang, "Sharp Fano resonances in THz metamaterials," *Opt. Express*, Vol. 19, 6312, 2011.
4. Singh, R., I. A. I. Al-Naib, Y. Yang, D. Roy Chowdhury, W. Cao, C. Rockstuhl, T. Ozaki, R. Morandotti, and W. Zhang, "Observing metamaterial induced transparency in individual Fano resonators with broken symmetry," *Appl. Phys. Lett.*, Vol. 99, 201107, 2011.
5. Zhang, S., D. A. Genov, Y. Wang, M. Liu, and X. Zhang, "Plasmon-induced transparency in metamaterials," *Phys. Rev. Lett.*, Vol. 101, 047401, 2008.
6. Tassin, P., L. Zhang, R. Zhao, A. Jain, T. Koschny, and C. M. Soukoulis, "Electromagnetically induced transparency and absorption in metamaterials: The radiating two-oscillator model and its experimental confirmation," *Phys. Rev. Lett.*, Vol. 109, 187401, 2012.
7. Zhang, F., X. Huang, Q. Zhao, L. Chen, Y. Wang, Q. Li, X. He, C. Li, and K. Chen, "Fano resonance of an asymmetric dielectric wire pair," *Appl. Phys. Lett.*, Vol. 105, 172901, 2014.
8. Zhang, F., L. Chen, Y. Wang, Q. Zhao, X. He, and K. Chen, "Thermally tunable electric Mie resonance of dielectric cut-wire type metamaterial," *Opt. Express*, Vol. 22, 24908–24913, 2014.

9. Zhang, F., Q. Zhao, C. Lan, X. He, W. Zhang, J. Zhou, and K. Qiu, "Magnetically coupled electromagnetically induced transparency analogy of dielectric metamaterial," *Appl. Phys. Lett.*, Vol. 104, 131907, 2014.
10. Zhang, F., X. He, X. Zhou, Y. Zhou, S. An, G. Yu, and L. Pang, "Large group index induced by asymmetric split ring resonator dimer," *Appl. Phys. Lett.*, Vol. 103, 221904, 2013.
11. Zhang, F., Q. Zhao, J. Zhou, and S. Wang, "Polarization and incidence insensitive dielectric electromagnetically induced transparency metamaterial," *Opt. Express*, Vol. 21, 19675, 2013.

Session 1P9
Analog & RF Circuits and Systems for Emerging Applications

Analog Multiplexer with an Improved High Linearity Bootstrapped Switch for Multi-channel Neural Signal Recording

Feng Yuan[1], **Zhi-Gong Wang**[2], **Xiao-Ying Lü**[2], **and Yu-Feng Guo**[1]

[1]College of Electronic Science and Engineering
Nanjing University of Posts and Telecommunications, Nanjing 210023, China
[2]Southeast University, Nanjing, China

Abstract— The acquisition of neural signals has received significant interest from the neuroscience research community very recently. Usually, the micro-electrode array is used to acquire electric signals from neurons and transmits them to multichannel micro-electronic recording systems for amplify, filter, and digitization. Since the number of the electrodes should be affirmatively much larger than the number of recording channels, the multiplexer is necessary in such systems. An analog integrated multiplexer and a bootstrapped switch as an indispensable element for the input analog interface of multi-channel neural signal recording system in a 0.5 μm CMOS process is presented in this situation. Considerable attention is paid to low distortion performance of the multiplexer as it is the importance part delivering the amplified neural signals to the analog to digital converters. However, most switches suffer from the distortion of passing signals from the non-ideality of the MOS transistor. Bootstrapped switch is attractive as a circuit technique to alleviate the poor conduction and varying on-resistance of many traditional switches such as single MOS transistor switch or complementary MOS transistors pair switch. In this article, the bootstrapped switch is improved to suit the specific environment, which satisfies the requirements of constant clock feed-through, constant charge injection, and compensation for body-effect. Meanwhile, the switch remains the practicability for less increase in complexity. An exemplary 4-channels analog multiplexer is constructed based on the proposed bootstrapped switch for verifying the effectiveness of the optimization. Analysis and discussion follows the simulation results, which show a higher linearity comparing the proposed switch to the conventional bootstrapped switches.

A 2 GSps 8 bit Folding & Interpolation ADC in 90 nm CMOS Technology

Yi Zhang[1, 2], **Qiao Meng**[3], **Debo Wang**[1, 2], **Changchun Zhang**[1, 2], **and Yufeng Guo**[1, 2]

[1]Jiangsu Provincial Engineering Laboratory of RF Integration & Micropackaging, Nanjing, China
[2]College of Electronics Science and Engineering
Nanjing University of Posts and Telecommunications, Nanjing, China
[3]Institute of RF- & OE-ICs, Southeast University, Nanjing, China

Abstract— High-speed (GSps), medium-resolution (6∼8 b) analog-to-digital converters (ADCs) are essential in realizing multi-Gbps communication systems. They are also required in some other applications, including radar, satellite, and test instruments. However, increased devices mismatch, decreased supply voltage prevent current GSps single-channel CMOS converters from being extended to 8-bit. Flash- and folding-ADCs are the primary candidates for GSps applications due to high conversion speed and low latency. As the flash architecture requires $2^N - 1$ comparators for N bits of resolution, resulting in area and power costs, folding-ADC becomes the best choice as it can simplify the circuit while maintaining the same conversion speed as flash.

A single channel 2 GSps, 8 bit folding and interpolation (F&I) ADC with digital assisted calibration designed in TSMC 90 nm CMOS technology was presented in this paper. The ADC utilized cascaded folding architecture, which incorporated an additional inter-stage sample-and-hold amplifier between the folding circuits to enhance the quantization time. A pipelined track-and-hold amplifier (THA) with bootstrapped switch was taken as the front-end THA. To improve the stability of THA's hold-mode voltage, the sub-threshold charging problem was found and the improved pre-amplifier was taken instead of the normal one. The foreground digital assisted calibration was also employed in this design to correct the error of zero-crossing point, thus to improve the linearity of the ADC. Chip area of the whole ADC including all pads is 930 µm × 930 µm. Post simulation results demonstrate that under a single supply of 1.2 Volts, the ADC costumes 210 mW. For the clock of 2 GHz, the signal to noise and distortion ratio (SNDR) is 45.93 dB for Nyquist input signal frequency.

10 bit 100 MS/s SAR ADC with Reduced Loop Delay

Dong Li[1], **Qiao Meng**[1], **Linfeng Wang**[1], **Yi Zhang**[2], **and Wenwei He**[1]

[1]Institute of RF- & OE-ICs, Southeast University, Nanjing, China
[2]College of Electronics Science and Engineering
Nanjing University of Posts and Telecommunications, Nanjing, China

Abstract— This paper proposes a novel logic control scheme to reduce successive approximation (SA) loop delay of the successive approximation register (SAR) analog-to-digital (ADC). The propagation delay in the SA loop is one of the dominant speed limiting factors, it can be reduced to improve the conversion operation of the SAR ADC. The key path of the SA loop is from the start of the comparison to the completely settlement of the DAC. In the proposed SAR ADC, the regeneration of the comparator and the operation of the shift register and the switch-driving register (SDR) are simultaneous. When the comparator control clock (CLKC) triggers the comparator to be in regeneration phase, it also triggers the shift register to generate multi-phase clocks for SDR. Then the SDR is turned on. Thus, the comparison results of the comparator are directly transmitted to determine charging or discharging the DAC capacitor array before the next comparison without waiting for the completion of the comparison. Compared with the conventional SAR ADC, the valid signal of the proposed technique is only used to pull-down the corresponding-phase clock to low and is not in the key timing path. So the propagation delay of the key path of the SA loop is shortened in the proposed SAR ADC. In addition, a novel SDR is proposed to further improve the conversion speed. The input of the SDR is the output of the comparator. During the sample phase of the DAC, the output of the SDR is reset to low. The proposed SAR ADC is realized in 90 nm CMOS process. With the proposed logic control scheme and SDR, the proposed SAR ADC achieves high conversion rate, low power, leading to SNDR of 59 dB and SFDR of 72.6 dB at 100 MS/s with 49.7 MHz input. The figure-of-merit (FoM) is 39.1 fJ/conversion-rate at 100 MS/s with a power consumption of 2.87 mW.

High Speed Pipelined ADC Uses Loading-balanced Architecture

Linfeng Wang[1], **Qiao Meng**[1], **Dong Li**[1], **Yi Zhang**[2], **and Wenwei He**[1]

[1]Institute of RF- & OE-ICs, Southeast University, Nanjing, China
[2]College of Electronics Science and Engineering
Nanjing University of Posts and Telecommunications, Nanjing, China

Abstract— Applications such as wireless sensor networks, image recognition and medical instrumentation require high-speed high resolution and low power consumption analog to digital converters (ADCs). Moreover the trend of system on a chip (SoC) based on advanced VLSI technology requires lower power consumption. Pipelined ADC has been widely used in these fields because it achieves a good compromise between speed, accuracy and power consumption. Pipelined ADC also has the advantage of much wider effective-bandwidth performance, because it can realize single-path sampling of the signal.

Because the speed and resolution of the pipelined ADC is in proportional to the hardware cost and power consumption, so many circuit techniques such as sample-and-hold Amplifier (SHA)-less front end, op-amp sharing, capacitor sharing and scaling down capacitor values through the pipeline have been developed in order to reduce the power consumption.

In this work, a prototype of 10 bit 200 MS/s pipelined ADC with loading-balance architecture is developed, the circuit consists of eight 1.5 bit stages and a 2 bit backend flash. It uses one op-amp less than the traditional ADC for using SHA-less architecture. The number of op-amp is reduced from 8 to 4 for op-amp sharing technique is used, the capacitor load of the first stage is reduced equal to the second stage for capacitor sharing technique, the non-standard inter-stage gain makes the feedback factor of the first stage increased equal to the second stage. So the load of op-amp shared by the first two stages is balanced. The load capacitor and feedback factor of the third and fourth stage are the same. The fifth to eight stage is the same as the third and fourth stage. From the system view, all the loads of the OTAs shared are balanced. The design power optimized.

The ADC is implemented in TSMC 0.18 μm 1P6M CMOS process. The power voltage is 1.8 V, The simulation results show 57.7 dB SNDR and 61.13 dB SFDR, ENOB = 9.3 with an 98 MHz input operating at a 200 MS/s sampling rate, the power consumption is 152 mV, the layout area is 1.2 mm × 1.2 mm.

A 30-GHz Low Phase Noise LC VCO and Frequency Divider in 90-nm CMOS Technology

Junliang Wang, **Zhigong Wang**, **Jian Xu**, **and Yan Wen**
Institute of RF- & OE-ICs, Southeast University, Sipailou 2, Nanjing 210096, China

Abstract— The large wide bandwidth around microwave frequency for high transmission data rate of multi gigabit per second is very attractive in both academic and industry. In China, the $59 \sim 64$ GHz frequency band was assigned for these applications, and recently a 45-GHz band of Q-band was developed to support both long-range and short range high data rate wireless communications. More and more up-coming frequency bands are posing the urgent needs and challenges of microwave chip designing.

In a typical double-conversion low intermediate frequency receiver architecture for the 45-GHz applications, considering a first intermediate frequency (IF) of 15 GHz and a low second intermediate frequency, two local oscillator (LO) signals can be generated by a 30-GHz LC voltage control oscillator (LC-VCO) and its divided-by-two frequency divider. This paper presents the design of a 30-GHz narrow-band VCO and its high speed divider using a standard 90-nm CMOS process. Two drain resistors are adopted in the VCO to suppress the flicker noise up-conversion.

For the 30-GHz LC-VCO, a single PMOS cross-coupled architecture is implemented. To suppress the flicker noise up-conversion, two small resistors are inserted in series to the drain of the cross-coupled MOSFETs. This method avoids the degradation of the start-up margin which is the start-up transconductance of the MOSFET, and makes the circuit reach remarkable phase noise suppression. Two sets of varators with different DC biasing are adopted in the VCO to make the K_{VCO} more linear. The simulated tuning range of the VCO covers from 28.7 to 32.4 GHz in four tuning curves. The simulated output phase noise at offsets of 10 kHz, 100 kHz and 1 MHz is -50, -78, and -104 dBc/Hz, respectively. The power consumption of the VCO is 9 mW under a 1.2 V power supply.

A current mode logic (CML) divide-by-two module is designed to operate at 28 to 32 GHz. The tail current is removed to make sure the divider can work under a 1.2 V power supply. The simulated operating range of the divider covers from 22 to 40 GHz and the self-resonant frequency is set to 32 GHz.

The layout area of the proposed schematics is $609 \times 497\,\mu\mathrm{m}^2$. The VCO operates at the supply voltage of 1.2 V and consumed an average current of 7.5 mA and the divider consumed an average current of 3.3 mA under the same supply voltage.

The paper is organized as follows: Section 1 is the introduction of the recent development of microwave wireless communications. Section 2 presents the VCO architecture and the phase noise enhanced technology. The CML based divider structure and its operation are describe in Section 3. Simulation results and conclusion are provided in Sections 4, 5, along with a comparison of the presented work with other recent works.

A 45-GHz CMOS Low-power LNA Using Active Feedback

Li Ma, **Zhigong Wang**, **Jian Xu**, **and Xixi Chen**
Institution of RF-&OE-ICs, Southeast University, Sipailou 2, Nanjing 210096, China

Abstract— In recent years, millimeter-wave (MMW) circuits have been studied widely for its capability of high data rate communication. Q-LINKPAN which has been included in IEEE 802.11aj (45 GHz) Task Group is a newly proposed communication standard working within the 40∼50 GHz. A low noise amplifier (LNA) that provides good noise performance, good matching and enough gain is necessary in MMW receiver.

The development of deep submicrometer CMOS process makes it possible to implement a CMOS MMW LNA. Therefore, a 45 GHz low power MMW low noise amplifier (LNA) using a 40-nm CMOS process is presented in this paper. The resistive feedback and active feedback structures are widely used in wideband LNA. The transconductance of the transistor in resistive feedback LNA is restricted to 20 mS which is not large enough for better noise performance. So the active feedback structure for excellent input matching is adopted in the first stage of the proposed 3-stage LNA. The output matching employs an L-type matching network and a cascode structure is adopted in the third stage for better reverse isolation.

Simulations have been carried out using Cadence Spectre®. It shows that both S_{11} and S_{22} are less than −18 dB at 45 GHz. The die area of the layout is 0.78 mm × 0.7 mm. The LNA consumes 18.7 mW under a 1.1-V voltage supply, achieving an maximum S_{21} of 17.9 dB through the −3 dB frequency band of 41.5∼49 GHz. Compared to several recently published MMW LNAs, this work consumes the least power. The minimum NF is 5.7 dB at 42.5 GHz. The simulation results show that the proposed LNA is promising for the Q-LINKPAN application.

Microwave-rectification RFI Response in MOSFET Valid in All Operation Regions

Clovis Pouant[1, 2], **Jérémy Raoult**[2], **Patrick Hoffmann**[1], **and Sylvie Jarrix**[2]

[1]CEA, DAM, GRAMAT, Gramat F-46500, France
[2]Institut d'Electronique du Sud (IES), Université de Montpellier II
860 rue de St Priest, 34097, Montpellier cedex 5, France

Abstract— When Radio Frequency (RF) interference is superimposed at the terminals of the Metal Oxide Semiconductor (MOS) transistor, various susceptibility effects take place depending on RF power level, frequency and the operation region of the transistor. Due to the nonlinearity of the MOS current-voltage characteristics, RF excitations cause distorted drain current waveform which leads to a bias point shift. This modification of the average of the drain current called the rectification effect is discussed. An analytic formulation of the bias point shift has initially been proposed by Richardson, but only for a saturation region of the transistor. This paper presents a global study of the rectification effect for all transistor regions of inversion (saturation, nonsaturation and linear).

Traditionally, the semi-empiric modeling procedure is based on a one variable Taylor series expansion of the gate voltage-drain current characteristic $I_D = f(V_{GS})$, when the transistor is in the saturated operating mode. If a microwave voltage is applied at the gate there is a small increase in drain current. In this operating mode the increase in drain current is proportional to the variation in transconductance with gate voltage, and the square of the microwave voltage amplitude. The average of the drain current is given by: $\Delta I_D = \frac{V_{GS}^2}{4} \frac{\partial g_m}{\partial V_{GS}}$.

When the transistor is in the nonsaturation and linear operating modes, a one variable Taylor series expansion is not enough to predict the drain current rectification. The output conductance becomes an important nonlinear source and must be included in the calculation of the rectified current. So we use a two variables Taylor series expansion of the gate voltage-drain current and the drain voltage-drain current characteristics $I_D = f(V_{GS}, V_{DS})$. In these operating modes if a microwave voltage is applied at the gate there is a small decrease in drain current and its average value can be expressed as: $\Delta I_D = \frac{V_{GS}^2}{4} \frac{\partial g_m}{\partial V_{GS}} + \frac{V_{DS}^2}{4} \frac{\partial g_d}{\partial V_{GS}} + \frac{1}{2} V_{GS} V_{DS} g_{md} \cos\varphi$. The transconductance, the conductance and the cross terms were extracted experimentally from the characteristics $I_D = f(V_{GS})$ and $I_D = f(V_{DS})$. The derivatives of these terms are then computed numerically. Our semi-empiric model which predicts the average drain current under RFI (Radio Frequency Interference) takes into account of the transconductance and conductance nonlinearity. In fact in the linear or nonsaturation regions of the transistor, the conductance can vary strongly with bias voltages (V_{GS}, V_{DS}). Our model is limited by the RF voltage amplitude applied at the gate and the frequency of the RFI. Experiments on a commercial MOS transistor have been conducted. Drain current shifts in all transistor regions of inversion have been measured and calculated. Theirs comparisons have shown a very good agreement until RF voltage amplitudes about 4 V and RFI frequencies of 500 MHz.

Finally this model could be used to predict effects of high-power microwave (HPM) coupling on digital MOS circuit.

A Broadband E-band Vertical Transition from Substrate Integrated Waveguide to Rectangular Waveguide

Elnaz Abaei[1] and Alireza Shamsafar[2]

[1]Facultad de Informatica y Electronica
Escuela Superior Politécnica de Chimborazo, Riobamba, Ecuador
[2]Dipartimento di Ingegneria Informatica Modellistica, Elettronica e Sistemistica
Università della Calabria, Rende, CS 87036, Italy

Abstract— In this paper, a compact wideband vertical transition from substrate integrated waveguide (SIW) to WR12 rectangular waveguide at E-band (77 GHz) is presented. SIW, as a planar and low profile type of waveguide, has received much attention in recent years and various kinds of microwave and millimeter-wave integrated circuits such as antenna, couplers and filters have been realized in this structure. The advantages of SIW are low-loss, low radiation, low profile, simple fabrication, small size, and compactness compared to standard air filled waveguide. However, classical waveguide (RWG), which has better power handling compared with SIW techniques, is still an important transmission line in microwave and millimeter wave circuit design, and a large number of commercial and existing products are in waveguide format. Moreover, RWD is especially more suitable for building complicated 3D feeding structure and is more rigid. So, it is necessary to develop various kind of transition between planar SIW and rectangular waveguides.

In the vertical transition which is designed in this work, a rectangular cavity resonator with closely metalized via holes is used to connect the SIW and WR12 waveguide. The energy between SIW and RW12 is coupled through the slot window etched on the board wall of the rectangular SIW cavity resonator. In this transition, the substrate of SIW can be easily surface-mounted to the standard flange of the waveguide; so the proposed component has a simple mechanical alignment. Moreover, the proposed SIW to RW transition can be easily realized and integrated with standard double-sided PCB technologies.

Commercial full-wave HFSS software is used for the design and simulation. The simulation results of designed transition show that the return loss remain below than −10 dB from 72 GHz to 83 GHz (more than 12%) while this value decrease to below than −15 dB from 73 GHz to 82 GHz. Insertion loss on the frequency band is always higher than −1.5 dB, which shows good electromagnetic power coupling from SIW to WR12. The simplicity and compact size of the designed transition is attractive for development of millimeter- wave circuits and measurements.

Development of a Radio Interferometer Operating at 12 GHz for Education and Research

Junghwan Han[1], **Bangwon Lee**[2], **Bi-Ho Jang**[3], **In-Woo Han**[3], **Sang-Eun Jung**[4], **Ji-Sung Ha**[4], **Seung-Soo Hong**[4], **Min-Ho Ka**[1], **and Yong-Sun Park**[2]

[1]School of Integrated Technology, Yonsei University, Korea
[2]Department of Physics and Astronomy, Seoul National University, Korea
[3]Korea Astronomy & Space Science Institute, Korea
[4]National Youth Space Center, Korea

Abstract— A radio interferometer system operating at 12 GHz for educations and possibly for research is developed. The commercial components are usually used for satisfying a low cost strategy, and the driving system is made to resist the strong wind, because the installation site is located near the seaside. The interferometer system consists of three off-axis parabola antennas, whose diameter is 1.8 m. The baselines between antennas are about 4 m, 19 m, and 20 m, so about 4' resolution can be acquired. The baseline vectors are accurately measured by using a theodolite, a light wave distance measurement, and GPS (Global Positioning System). The center frequency of the receivers is 12.177 GHz, and the bandwidth is 6 MHz. The receiver is able to observe the methanol line (12.178 GHz) and continuum from the Sun, the Moon, and the Galactic plane. The signals of each receiver are sampled and quantized by the AD convertor, and then software correlation is conducted with the developed parallel process program. The used libraries for software correlation are Fastest Fourier Transform in the West (FFTW), CompuScope Software Development Kit (SDK) of Gage Instrument, and Open Multi-Processing (OpenMP). We succeeded in finding fringes toward the Sun, Moon, Crab Nebula, and Cassiopeia A. By using a Nobeyama solar radio image taken at 17 GHz with a bright spot at the center of solar disk, we tried to calibrate uncertainties involving signal cable length, but it was found to be only partially successful. In order to make images of celestial objects, more careful treatment seems necessary with the use of phase calibrators or with a method similar to self-calibration without the phase calibrator.

ACKNOWLEDGMENT

This research was supported by the National Youth Space Center, Korea.

REFERENCES

1. Oppenheim, A. V., A. S. Willsky, and S. Hamid, *Signals and Systems*, 2nd Edition, Prentice Hall, 2000.
2. Park, Y.-S., et al., "Development of semi-VLBI system and observation of sun at 21 cm," *JKAS*, Vol. 39, No. 51, 2006.
3. Park, Y.-S., et al., "Development of a toy interferometer for education and observation of sun at 21 cm," *JKAS*, Vol. 41, No. 77, 2008.
4. Taylor, G. B., C. L. Carilli, and R. A. Perley, "Synthesis imaging in radio astronomy II," *Astronomical Society of the Pacific Conference Series*, Vol. 180, 2007.
5. Wilson, T. L., K. Rohlfs, and S. Huttemeister, *Tools of Radio Astronomy*, 5th Edition, Spring, 2009.

A Varactor-based Tunable Microstrip Band Pass Filter

M. Y. Abou Shahine[1], **M. Al-Husseini**[2], **Y. Nasser**[1], **and K. Y. Kabalan**[1]

[1]American University of Beirut, Beirut 1107 2020, Lebanon
[2]Lebanese Center for Studies and Research, Beirut 2030 8303, Lebanon

Abstract— Broadband wireless access communication systems are undergoing a rapid expanding growth. Such systems employ RF filters in their transceivers. Therefore, there is an increasing demand for low cost and compact size filters. Tunability of these filters is a required feature in these multi-standard communication systems, as it allows them to tune to several frequencies and operate for different applications.

A simple tunable microstrip band pass filter is presented in this paper. The basic configuration of this filter is shown in Fig. 1. A simple microstrip line is designed on a 40 mm × 20 mm Rogers RO3203 substrate with dielectric constant of 3.02 and thickness $h = 1.6$ mm over a full ground plane. The filter is based on a T-shaped slot incorporated in the microstrip line between a pair of gaps. The slot itself has bandstop characteristics, but the two gaps which act as capacitors transform the bandstop into bandpass operation. The designed filter operates in the frequency band from 1.8 to 3 GHz. Frequency tunability is obtained by inserting a varactor in the design as indicated in Fig. 1 and modifying its capacitance using the shown DC bias lines. The size of the varactor is compatible with the design and its capacitance ranges between 0.6 and 71 pF.

Figure 2 shows the reflection coefficient plots for different capacitance values of the varactor. As shown, frequency tunability is achieved and the filter can operate on different frequencies in the 1.8–3 GHz band corresponding to different applications such as LTE, UMTS, WiFi, and others. Detailed and verified results will be included in the full paper.

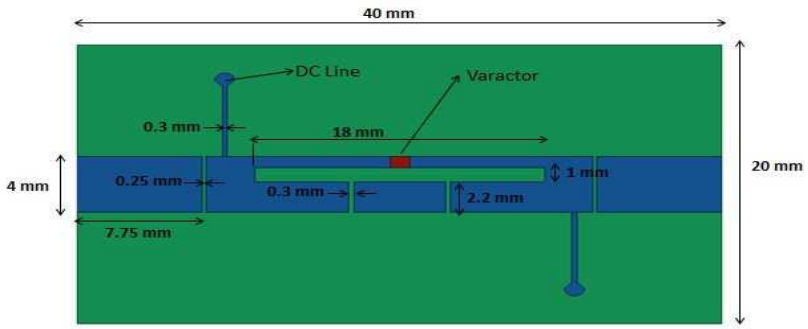

Figure 1: Microstrip filter configuration.

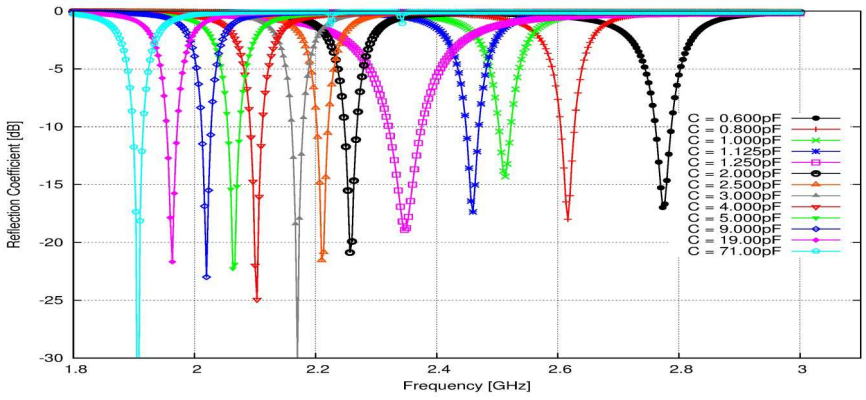

Figure 2: Simulated reflection coefficients for different capacitance values.

A Simple Digital Predistortion Architecture for Beamforming Transmitter

Yasushi Yamao[1], **Toshiki Hamanaka**[1], **Yuelin Ma**[1], **Koki Tanji**[2], **and Eiichiro Otobe**[2]

[1]The University of Electro-Communications, Japan
[2]Samsung R & D Institute, Japan

Abstract— Beamforming (BF) signal transmission using SHF band is a promising scheme for enhancing the bandwidth and capacity of 5G mobile communications. Since antenna elements are smaller for SHF, a BF antenna can be composed of a large number of antenna elements. Although it realizes high performance, the same numbers of power amplifiers (PAs) are necessary. In order to suppress outband radiation caused by nonlinear distortion of PAs, a digital predistortion (DPD) technique should be employed. This paper proposes a simple DPD architecture for beamforming transmitters that uses only one common digital predistorter for multiple PAs. Fig. 1 shows the proposed DPD architecture. The predistorter output is divided into necessary numbers for beam forming and they are modulated by different phases and then input to PAs. The multiple feedback paths from PA outputs are combined after removing the phase shifts for beam forming and then digitized by single analog-digital converter (ADC). The concern about the architecture is sensitivity against deviations of PA nonlinearity characteristics. The following Saleh's PA behavior model has been employed for analyzing this issue.

$$y = \frac{ax}{\sqrt{1+b|x|^2}} \exp\left(j\frac{c|x|^2}{\sqrt{1+d|x|^2}}\right) \tag{1}$$

By shifting parameters *a, b, c, d* in the model, sensitivity of the proposed DPD architecture has been simulated. Fig. 2 shows AM-AM conversion characteristics of four antenna BF transmitter when the linear gain parameter *a* is deviated among four PAs. With the DPD, AM-AM characteristics for all PAs are successfully linearized. On the other hand, when the phase conversion

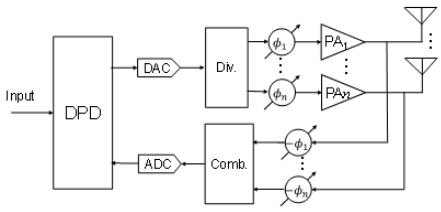

Figure 1: Proposed BF DPD architecture.

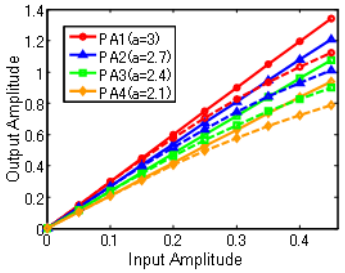

Figure 2: Input/output conversion characteristics when the linear gain has a deviation.

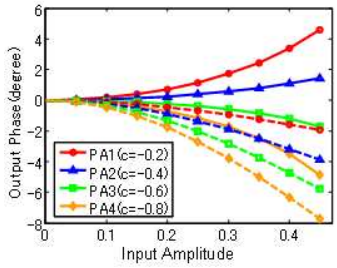

Figure 3: Input/output conversion characteristics when the phase shift gain has a deviation.

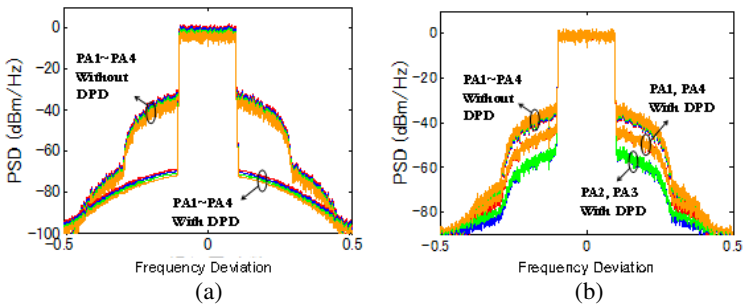

Figure 4: PA output spectra with deviation of PA parameter for (a) linear gain deviation, (b) phase shift gain deviation.

gain parameter c is deviated, only the average phase shift among four PAs is compensated as shown in Fig. 3. The corresponding power spectra output from PAs are presented in Figs. 4(a) and (b). Outband radiation is perfectly suppressed when the parameter a is deviated. However, outband radiation is not perfect when the parameter c is deviated.

In conclusion, the proposed DPD architecture is effective to linearize BF transmitter with reduced circuit size and cost, while the deviation of AM-PM conversion characteristics for PAs needs to be controlled.

An Optimized Opamp-sharing in 2nd Order ΔΣ Modulator Based on Changing the Stages Output Capacitance Timing Strategy

M. Sabaghi[1], **M. Dashtbayazi**[2], **and S. Marjani**[1, 2]

[1]Laser and Optics Research School
Nuclear Science and Technology Research Institute (NSTRI), Tehran, Iran
[2]Department of Electrical Engineering, Ferdowsi University of Mashhad, Mashhad, Iran

Abstract—

Application of ΔΣ Modulators in Power Electronics: An application of delta-sigma modulators is the Control loop of the DC-DC Switching Converters that tabernacle with PWM generators and decreases the ripple and noise of the DC-DC converters [1].

The Proposed Opamp-sharing Idea: In this paper, an opamp-sharing technic discussed that made the delta-sigma modulator with two loop-filters and one opamp. In this structure, the opamp moved from stage1 (loop filter1) to stage2 (loop filter2) and conversely. Furthermore one opamp saved that causes power dissipation and area is minimized by factor2. In phase1, opamp presented in the integrator1 (stage1) and in phase2, the opamp presented in other integrator. In the loop filter1, noise once shaped and in loop filter2, noise twice shaped than the stage2 requires fewer output capacitance in the switch capacitor integrator structure and it must have been less pulse-width (i.e., phase2 pulse-width according to Fig. 1) rather than stage1. Therefore, the sampling frequency is maximized and the harmonic distortion is minimized with this technic. Since the pulse-width designed according to integrator output capacitance and opamp conditions in two stages not changed, the harmonic distortion is minimized.

According to Fig. 1, the pulse-width dedicated to stage2 is less than stage1 and the phases are madding from the clock signal with very high frequency rather than two phases.

The proposed integrator structure shown in Fig. 2. In this structure, the opamp only required in one phase and it can move to other stages. According to Fig. 2 based on [2], in the phase Φ_{1a}, the integrator sampled the input signal on the sampling capacitor (C_S) and in the phase Φ_{1b}, the integrator transfer the electric load from sampling capacitor to integrator capacitor (C_f) and conversely. Therefore the opamp not require been in the integrator structure at phase2 and moved to other integrator.

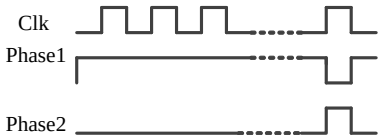

Figure 1: Proposed switch-capacitor delta-sigma modulator timing diagram.

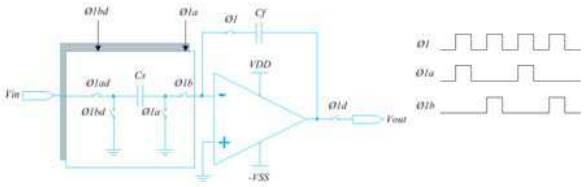

Figure 2: Proposed switch-capacitor integrator in phase1 (Φ_1).

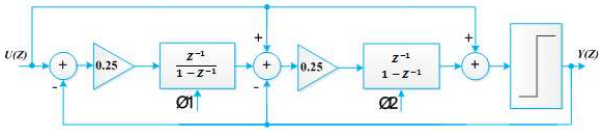

Figure 3: Proposed 2nd order delta-sigma modulator block diagram.

Table 1: Simulation results for the proposed 2nd order ΔΣ at 1.2 v power supply.

f_{BW} (Hz)	SNDR(dB)	Power (μw)	FoM (fJ/s-c)
10 k	80.7	69.2	392.2

Table 2: Simulation results for the proposed 2nd order $\Delta\Sigma$ at different process corners.

Parameters	$\boldsymbol{T \cdot T}$	$\boldsymbol{S \cdot S}$	$\boldsymbol{S \cdot F}$	$\boldsymbol{F \cdot S}$	$\boldsymbol{F \cdot F}$
f_{BW} (Hz)	10 k	10 k	10 k	10 k	10 k
SNDR (dB)	80.66	81.85	78.70	80.21	78.23
ENOB (bit)	13.11	13.30	12.78	13.03	12.70
FoM (fJ/s-c)	392.25	295.79	540.16	385.39	648.44

Simulation Results: In this paper, the proposed block diagram in Fig. 3 is simulated. According to Fig. 3, the opamp has been in stage1 at phase1 (Φ_1) and the opamp has been in the other stage at phase2 (Φ_2). The output capacitance of the stage1 is about six times than stage2. Therefore, the pulse-width for stage1 is about six times other stage.

The Proposed idea simulated at the 130 nm CMOS model and the simulation results presented at the Table 1. Also, Table 2 shows the simulation results in the process corners.

REFERENCES

1. Alghamdi, M. K. and A. A. Hamoui, "A spurious-free switching buck converter using a delta-sigma modulation controller with a scalable sampling frequency," *IEEE J. Solid-State Circuits*, Vol. 47, 841–851, Feb. 2012.
2. Perez, A. P., E. Bonizzoni, and F. Maloberti, "A 84 dB SNDR 100 kHz bandwidth low-power single OP-AMP third-order $\Delta\Sigma$ modulator consuming 140 µW," *IEEE ISSCC Dig. Tech. Papers*, 478–480, Feb. 2011.

A 4 MHz-10-GHz, 10-ps/dec Dynamic Comparator Using Negative Resistance Combined with CMOS Input Pair

M. Dashtbayazi[1], **S. Marjani**[1, 2], **and M. Sabaghi**[2]

[1]Department of Electrical Engineering, Ferdowsi University of Mashhad, Mashhad, Iran
[2]Laser and Optics Research School
Nuclear Science and Technology Research Institute (NSTRI), Tehran, Iran

Abstract—

Application of Comparator in Power Electronics:

An application of comparators is in the Control loop of the DC-DC Switching Converters. In the loop of DC-DC Switching Converters, PWM generators uses comparator that compare Triangular wave with the difference DC-DC output voltage and reference voltage.

Proposed Dynamic Comparator:

A. Structure:

The comparator is consists of two parts that namely pre-amplifier and latch These parts operate in the same phase. Therefore, comparator can pull the latch. The pre-amplifier output nodes up to the power supply voltage level in the second phase. Also in this phase, the comparator offset can be cancelled [1, 2]. Consequently in this paper, the comparator offset effect has not been considered. Fig. 1 shows the Schematics of circuit diagram that has been used in simulations and has been obtained from [3] with adding Q2 and Q4, thus a dual rail pre-amplifier is achieved. Two CMOS inverters have been used to supply capacitive loads for decreasing the loading effect on the comparator output. The comparator consumes dynamic power Because the comparator consists of dynamic latch and pre-amplifier [4].

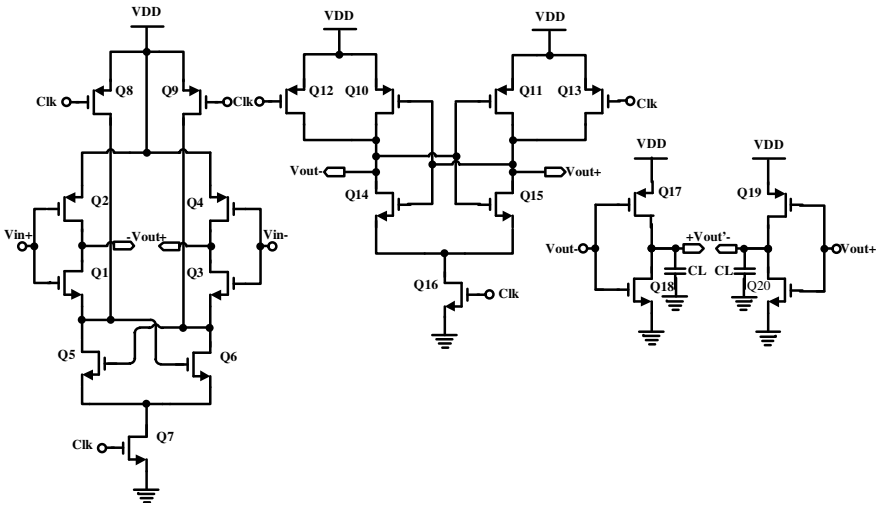

Figure 1: Schematics of the dynamic comparator and CMOS inverters.

B. Transient Behavior:

Figure 2 shows the sketch map of the transient behavior of the dynamic comparator in the comparison phase. By the switching transistors Q8, Q9, Q12, and Q13 during the reset phase, the output terminals and the drain side voltages of Q5 and Q6 are all pulled high to VDD, respectively. The comparison phase begins by turning on the two tail transistors Q7 and Q16. Therefore, the CMOS input stage transfers the differential small signal to the cross coupled stage. When the input common mode is lower than the Q1 or Q3 threshold voltage, Q2, Q4 are activating. Therefore, the dual-rail differential input obtain since they are supplies the preamplifier output. Based on [5], the comparison transition can be divided into phase 1 to phase 3. During the phase 1, the output terminals are pulled down by two tail transistors Q7 and Q16. Until one of the two output terminal voltages decreases to (V_{DD}-V_{thp}), the p-channel transistors Q10 and Q11

remain cut-off. When the cross-coupled stage composed from Q1, Q3, Q5 and Q6 cannot start, the Q2 and Q4 activate. Therefore, the speed of proposed idea is more than paper [3]. In order to enhance the voltage difference between the output terminals, the cross-coupled inverters provide strong positive feedback in the phase 2. The transition state changes from phase 2 into phase 3 when one of the transistors Q14 and Q15 is cut-off. There is no static power dissipation since the current flows through these n-channel MOSFETs stop automatically after the transition.

Therefore, the strong positive feedback provided by these two cross-coupled inverters separates the output voltages. Against paper [3], this design aren't use from p-wells, thus the cost of comparator chip is lower.

C. Simulation Results:

In this paper, the proposed comparator (Fig. 1) is simulated and for simulation reliability, the Post-Layout Simulation (PLS) for layouts in the Fig. 3 is adopted.

The Proposed idea simulated at the 180 nm CMOS model. The post-layout simulation results versus Sampling Frequency presented at the Table 1.

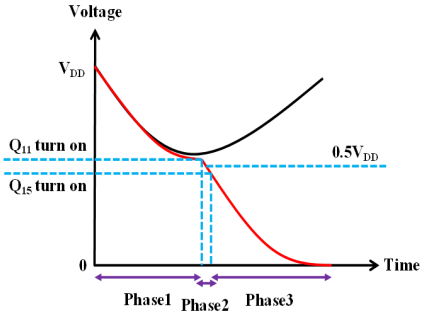

Figure 2: The sketch map for the transition behavior of the dynamic comparator.

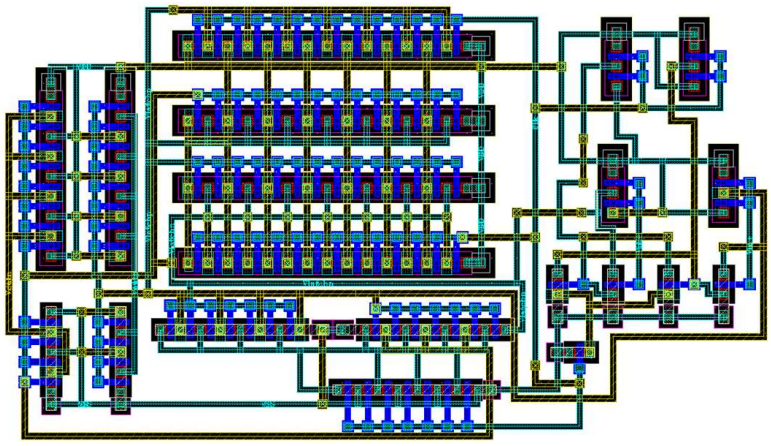

Figure 3: Layouts of the dynamic comparator and CMOS inverters.

Table 1: Post-layout simulation results of the proposed comparator versus sampling frequency.

Sampling Frequency (GHz)	**0.004**	**0.01**	**0.1**	**1**	**5**	**10**
Resolution (mv)*	27	24	25	27	700	700
Power Supply (v)**	0.4	0.45	0.55	0.8	1.05	1.8
Power Consumption (μw)***	0.835	2.07	20.7	204.6	795.6	964

*Resolution calculated at 1.8 V DC power supply.

**Power supply calculated for maximum resolution.

***Power consumption calculated at maximum resolution and 1.8 V DC power supply.

REFERENCES

1. Chan, C. H., et al., "A voltage-controlled capacitance offset calibration technique for high resolution dynamic comparator," *International SoC Des. Conf.*, 392–395, Nov. 2009.
2. Xu, Y., et al., "Offset-corrected 5 GHz CMOS dynamic comparator using bulk voltage trimming: Design and analysis," *IEEE New Circuits Syst. Conf.*, 277–280, Jun. 2011.
3. Chen, B. W., et al., "A 3-GHz, 22-ps/dec dynamic comparator using negative resistance combined with input pair," *IEEE Asia-Pacific Conf. Circuits Syst.*, 648–651, Dec. 2010.
4. Liu, C. C., et al., "A 10-bit 50-MS/s SAR ADC with a monotonic capacitor switching procedure," *IEEE J. Solid-State Circuits*, Vol. 45, 731–740, Mar. 2010.
5. Wicht, B., T. Nirschl, and D. Schmitt-Landsiedel, "Yield and speed optimization of a latch-type voltage sense amplifier," *IEEE J. Solid-State Circuits*, Vol. 39, 1148–1158, Jun. 2004.

Session 1P10
Chiral and Nonlinear Metasurfaces

Theoretical and Experimental Study of Tunneling-induced Optoelectronic Effects in Plasmonic Nanoantennas with Ultra-narrow Gaps

R. Esteban and J. Aizpurua
Donostia International Physics Center DIPC and Materials Physics Center CSIC-UPV/EHU
Paseo Manuel de Lardizabal 4, 20018 Donostia-San Sebastián, Spain

Abstract— Coulomb coupling between two or more metallic nanoparticles separated by a narrow gap introduces great possibilities to tune and optimize the optical response of the whole system. When the distance between the different elements of such an optical nanoantenna becomes nanometric or even subnanometric, however, the well-understood classical behavior is modified by quantum effects [1–3] such as nonlocal correlations of the electron gas, the spill-out of the electrons at the metal interface and the electron tunneling current across the gap. In the case of small systems, these effects can be studied within Time-Dependent Density Functional Theory (TDDFT). We recently developed a Quantum Corrected Model (QCM) that allows treating quantum effects also in large systems [4].

Using TDDFT and the QCM, together with experimental results for subnanometric gaps, we demonstrate and analyze how electron tunneling can completely modify the optical response of a plasmonic system, an optoelectronic effect occurring at extreme fast speed and in a nanometric volume [2, 4, 5]. For gaps limited by spherical surfaces, the charge transfer due to tunneling leads, already before contact is established, to a gradual transition from the Bonding Modes to the Charge Transfer Plasmons, strongly modifying the far field response. The charge transfer also quenches strongly the local fields at the gap. Electron tunneling alters the optical response of modes of both electric and magnetic nature. The latter has not been studied in the context of quantum effects.

We discuss these effects for two different experimental systems for which subnanometric gaps are well controlled (Figure 1). Furthermore, we demonstrate that the morphology of the gaps needs to be considered to understand the effect of tunneling on the optical response [6]. Notably, while quenching of the near fields at the gap appears to be a general trend, our calculations for flat gaps defined by two large planar surfaces predict the inhibition of tunneling-induced optical far-field effects, in contrast to the results of spherical gap terminations. This difference between flat and spherical gaps can be critical when trying to identify quantum effects from the experimental far-field response. Our study thus demonstrates the intriguing properties of plasmonic systems at the limit, with potential future applications in nanooptics and optoelectronics.

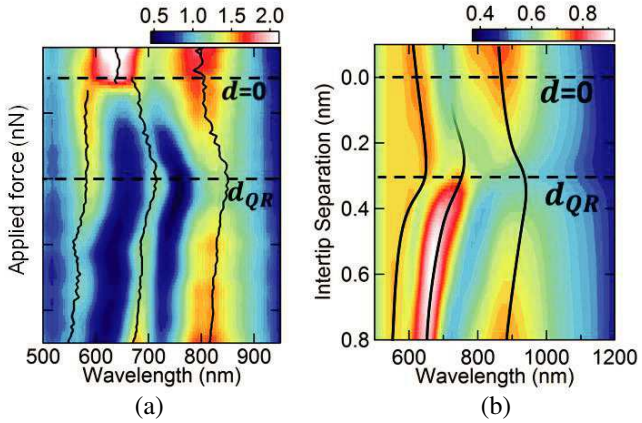

Figure 1: (a) Experimental and (b) QCM-based theoretical far field spectra [5] of two approaching tips (bottom to top), showing a similar modal evolution distances $d_{QR} > 0$ where tunneling becomes important.

REFERENCES

1. Zuloaga, J., E. Prodan, and P. Nordlander, *Nano Letters*, Vol. 9, 887–891, 2009.

2. Scholl, J. A., A. García-Etxarri, A. L. Koh, and J. A. Dionne, *Nano Letters*, Vol. 13, 564–569, 2013.
3. Esteban, R., A. Zugarramurdi, P. Zhang, et al., *Faraday Discussions*, 10.1039/C4FD00196F
4. Esteban, R., A. G. Borisov, P. Nordlander and J. Aizpurua, *Nat. Commun.*, Vol. 3, 825, 2012.
5. Savage, K. J., M. M. Hawkeye, R. Esteban, et al., *Nature*, Vol. 491, 574–577, 2012.
6. Esteban, R., G. Aguirregabiria, A. G. Borisov, et al., *ACS Photonics*, 10.1021/ph5004016.

Binary Mixtures of Chiral Gases

C. Presilla[1, 2] **and G. Jona-Lasinio**[1, 2]

[1]Sapienza Università di Roma, Italy
[2]Istituto Nazionale di Fisica Nucleare, Italy

Abstract— According to quantum mechanics chiral molecules, that is molecules that rotate the polarization of light, should not exist. The simplest molecules which can be chiral have four or more atoms with two arrangements of minimal potential energy that are equivalent up to a parity operation. Chiral molecules correspond to states localized in one potential energy minimum and can not be stationary states of the Schrödinger equation. A possible solution of the paradox can be founded on the idea of spontaneous symmetry breaking. This idea was behind work we did previously involving a localization phase transition: at low pressure the molecules are delocalized between the two minima of the potential energy while at higher pressure they become localized in one minimum due to the intermolecular dipole-dipole interactions. Evidence for such a transition is provided by measurements of the inversion spectrum of ammonia and deuterated ammonia at different pressures. A previously proposed model gives a satisfactory account of the empirical results without free parameters. In the present paper, we extend this model to gas mixtures. The main results are as follows.

i. Also in the case of mixtures there is a quantum phase transition between a delocalized (or achiral, or nonpolar) phase and a localized (or chiral, or polar) phase. At fixed temperature, the crossover between the two phases is determined by a properly defined critical pressure.

ii. We derive formulas expressing the critical pressure of the mixture in terms of the doublet splittings of the isolated chiral molecules and of the fraction of the constituents. Different formulas are derived for mixtures made up of one chiral species and several non polar gases or several chiral species. In both cases, the inverse critical pressure of the mixture is the fraction-weighted average of the inverse critical pressures of its components.

iii. We derive formulas giving the dependence of the inversion frequencies on the pressure. These results are susceptible to experimental tests.

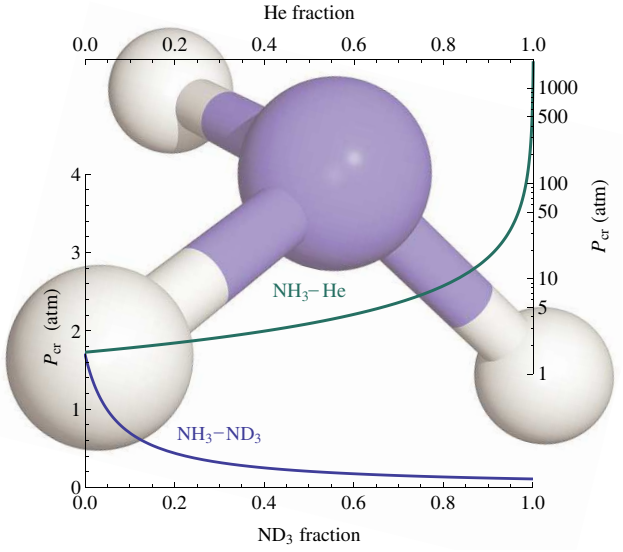

On the Application of Group Theory to Understand the Optical Response of a Chiral Nanostructured Surface

Xuezhi Zheng[1], **Guy A. E. Vandenbosch**[1], **and Victor V. Moshchalkov**[2]

[1]Department of Electric Engineering (ESAT-TELEMIC), KU Leuven, Belgium
[2]Institute for Nanoscale Physics and Chemistry (INPAC), KU Leuven, Belgium

Abstract— Symmetry holds a prominent position in defining the electromagnetic response of a chiral nanostructured metasurface [1, 2]. In this talk, we base our discussion [3] on a powerful mathematical tool, group representation theory [4], and combine it with the eigenvalue problem of Volumetric Integral Equations (VIE) [5] that models the light-nanoantenna interaction. We illustrate how the symmetry allows or forbids the coupling between the metasurface's eigenmodes and an incident left/right polarized light and, which leads to so-called circular dichroism (CD). Further, the effects of symmetry on the energetic coupling (i.e., interference) between the eigenmodes will be discussed. Specifically, we start our demonstration with a metasurface whose unit cell is a symmetric cross (which has a D_2 group, See Fig. 1(a)). Then, the mirror symmetry of the cross is removed to form two chiral structures with different handedness (See Figs. 1(b)–(c)). The eigenmodes of the above structures are extracted with their mutual coupling and their coupling to left/right circularly polarized light discussed in detail. We believe that the present work enhances the fundamental understanding of the modes in a chiral metasurface and thus allows the engineering of a metasurface's spectrum.

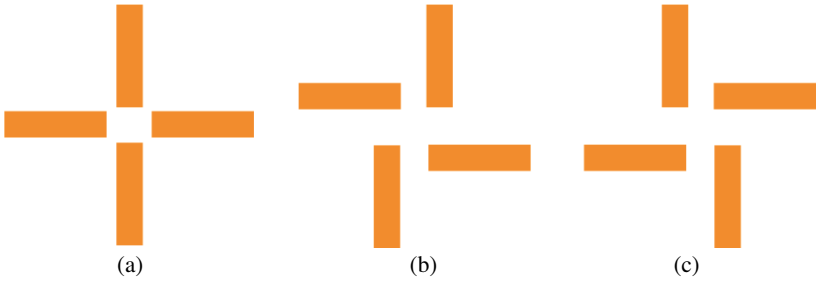

Figure 1: Illustration of the topologies studied in this talk (a) symmetric cross and crosses with (b) left- and (c) right-handedness.

REFERENCES

1. Valev, V. K., D. Denkova, X. Zheng, A. I. Kuznetsov, C. Reinhardt, B. N. Chichkov, G. Tsutsumanova, E. J. Osley, V. Petkov, B. De Clercq, A. V. Silhanek, Y. Jeyaram, V. Volskiy, P. A. Warburton, G. A. E. Vandenbosch, S. Russev, O. A. Aktsipetrov, M. Ameloot, V. V. Moshchalkov, and T. Verbiest, "Plasmon-enhanced sub-wavelength laser ablation: Plasmonic nanojets," *Adv. Mater.*, Vol. 24, OP29–OP35, 2012.
2. Valev, V. K., J. J. Baumberg, B. De Clecq, N. Braz, X. Zheng, E. J. Osley, S. Vandendriessche, M. Hojeij, C. Blejean, W. Libaers, J. Mertns, C. G. Biris, V. Volskiy, M. Ameloot, Y. Ekinci, G. A. E. Vandenbosch, P. A. Warburton, V. V. Moshchalkov, N. C. Panoiu, and T. Verbiest, "Nonlinear superchiral meta-surfaces: Tuning chirality and disentangling non-reciprocity at the nanoscale," *Adv. Mater.*, Vol. 26, 4074–4081, 2014.
3. Zheng, X., N. Verellen, D. Vercruysse, V. Volskiy, P. Van Dorpe, G. A. E. Vandenbosch, and V. V. Moshchalkov, "On the use of group theory in understanding the optical response of a nanoantenna," *IEEE Trans. on Antennas and Propag.*, DOI 10.1109/TAP.2015.2400471, 2015.
4. Tinkham, M., *Group Theory and Quantum Mechanics*, McGraw-Hill, New York, 1964.
5. Sancer, M. I., K. Sertel, J. L. Volakis, and P. Van Alstine, "On volume integral equations," *IEEE Trans. on Antennas and Propag.*, Vol. 54, 1488–1495, 2006.

Boundary Integral Operators in Linear and Nonlinear Nano-optics

Jouni Mäkitalo[1], **Saku Suuriniemi**[2], **Godofredo Bautista**[1], **Robert Czaplicki**[1], **Mikko J. Huttunen**[1], **and Martti Kauranen**[1]

[1]Department of Physics, Tampere University of Technology
P. O. Box 692, Tampere FI-33101, Finland
[2]Department of Electrical Engineering, Tampere University of Technology
P. O. Box 692, Tampere FI-33101, Finland

Abstract— The development of precise nanofabrication methods has enabled the study and engineering of the optical properties of nanostructured media, i.e., optical metamaterials, which may display unconventional properties, such as negative index of refraction. The properties often arise from the geometry of the nanostructure rather than the atomistic composition.

Noble metal nanoparticles display resonances of the electron gas. These, so-called plasmon resonances, can enhance the local electric field near the surface of a particle, which can then amplify nonlinear optical effects, such as second-harmonic generation (SHG). Consequently, nonlinear optical metamaterials hold promise for many practical applications.

As the fabrication of nanostructures is slow and expensive, there is a call for accurate and versatile numerical simulation of their electromagnetic response. For plasmonic materials, this can be especially demanding due to the presence of resonances. Frequency-domain boundary element method (BEM), especially the Poggio-Miller-Chang-Harrington-Wu-Tsai formulation (PMCHWT) with vector basis functions, has been found suitable for such demands [1]. We have extended the PMCHWT BEM for the modeling of surface SHG in the undepleted-pump approximation from individual plasmonic particles [2] and it has been further extended by others for the modeling of periodic structures [3] and the nonlocal bulk response [4].

One advantage of the use of BEM in frequency domain is that the use of focused Gaussian beams with unconventional polarization states is straight-forward. We have developed algorithms for the fast simulation of scanning a focused beam over a nanoparticle while collecting the SHG in reflection by the focusing lens [5, 6]. We have also recently shown that the modeling of SHG from a periodic metasurface by BEM yields unprecedented agreement with measurements, thus validating the method in practice [7]. Our recent work also details how geometrical symmetry can be utilized in BEM to decrease the memory requirements and computation time for both linear and weak nonlinear response [8].

In addition to modeling the response of a nanostructure to an incident field, it is often of interest to understand the possible outcomes of the system without the specification of an incident field; the resonances and modes are properties of the structure. We have proposed an approch based on boundary integral operators for the characterization of resonances and the study of eigenmodes in the time-harmonic setting [9]. The modes are defined over the compact surface of the scatterer, thus avoiding many inconveniences associated with direct analysis of Maxwell's partial differential equations. We show that the approach is fully compatible with the Mie theory for spheres and with a previously studied quasistatic limit. We also calculated the complex resonance frequencies and eigenmodes of structures that are elementary, but comparable in size to the vacuum wavelength.

REFERENCES

1. Kern, A. M. and O. J. F. Martin, *J. Opt. Soc. Am. A*, Vol. 26, 732–740, 2009.
2. Mäkitalo, J., S. Suuriniemi, and M. Kauranen, *Opt. Express*, Vol. 19, 23386–23399, 2011.
3. Butet, J., et al., *J. Opt. Soc. Am. B*, Vol. 30, 2970–2979, 2013.
4. Forestiere, C., A. Capretti, and G. Miano, *J. Opt. Soc. Am. B*, Vol. 30, 2355–2364, 2013.
5. Bautista, G., et al., *Nano Lett.*, Vol. 12, 3207–3212, 2012.
6. Huttunen, M. J., et al., *Opt. Lett.*, Vol. 39, 3686–3689, 2014.
7. Czaplicki, R., et al., *Nano Lett.*, Vol. 15, 530–534, 2015.
8. Mäkitalo, J., S. Suuriniemi, and M. Kauranen, *J. Opt. Soc. Am. A*, Vol. 31, 2821–2832, 2014.
9. Mäkitalo, J., S. Suuriniemi, and M. Kauranen, *Phys. Rev. B*, Vol. 89, 165429, 2014.

Effective Dielectric Tensor of Optically Thick Chiral Composite Layers

A. A. Shcherbakov[1], **A. A. Ushkov**[1], **and A. V. Tishchenko**[2]

[1]Moscow Institute of Physics and Technology, Russia
[2]University of Lyon, France

Abstract— Composite 2D and 3D periodic media are promising candidates for replacing natural materials since they provide benefits of engineering specific macroscopic anisotropic properties. Currently there exist reliable technological methods of fabrication and characterization of complex 2D and 3D periodic chiral artificial structures at macroscale [1]. These methods should be supported by powerful computational techniques being are able to predict and optimize artificial media optical properties, and there is still a need in research towards better numerical methods.

In this work we continue development of a method for composite 3D protonic crystal homogenization [2]. The method is based on the Fourier space formulation of the Maxwell's equations with source terms. Being reduced to a linear algebraic equation system they provide a response to a given excitation that can be found in linear time relative to the total number of Fourier harmonics. An efficient resonant analysis of the obtained response provides propagation constants and propagating mode amplitudes with quite high accuracy.

First part of the talk will cover the formulation of the method with correct treatment of the electromagnetic boundary conditions in the Fourier space, which results in the following linear equations system for electromagnetic response:

$$\mathbf{E} = \left[\frac{\varepsilon_b}{\varepsilon}\right]\left(\left[\frac{\varepsilon_b}{\varepsilon}\right] - \mathrm{K}\left\{\left(\left[\frac{\varepsilon}{\varepsilon_b}\right] - \mathrm{I}\right)\left[\frac{\varepsilon_b}{\varepsilon}\right] + \left(1 - \left[\frac{\varepsilon}{\varepsilon_b}\right]\left[\frac{\varepsilon_b}{\varepsilon}\right]\right)\Gamma\right\}\right)^{-1}\mathbf{E}^{inc}$$

where $\mathbf{E}$ is unknown vector of the electric field components Fourier images, $\mathbf{E}^{inc}$ is the corresponding excitation vector; matrices $[\varepsilon/\varepsilon_b]$ and $[\varepsilon_b/\varepsilon]$ are the Fourier matrices of microscopic dielectric permittivity and inverse permittivity in a protonic crystal unit cell with ε_b being some constant; matrix K is composed of spatial wavevector components; and matrix Γ contains spatial Fourier images of normal vector components to microscopic interfaces between different media provided that normal vector functions are appropriately continued to a whole unit cell. Second part of the talk will include demonstration of the method numerical behavior as well as examples of chiral composite layers simulation.

REFERENCES

1. Valev, V. K., J. J. Baumberg, C. Sibilia, and T. Verbiest, "Chirality and chiroptical effects in plasmonic nanostructures: Fundamentals, recent progress, and outlook," *Adv. Mater.*, Vol. 25, 2517–2534, 2013.
2. Shcherbakov, A. A. and A. V. Tishchenko, "3D periodic dielectric composite homogenization based on the generalized source method," arXiv preprint arXiv:1501.01752, 2015.

Phase Matching Opportunities with Hyperbolic Dispersion

C. Duncan[1], **L. Perret**[1], **S. Palomba**[1], **B. T. Kuhlmey**[1], **C. Martijn de Sterke**[1], **and M. Lapine**[2]

[1]School of Physics, University of Sydney, NSW 2006, Australia
[2]School of Mathematical Sciences, University of Technology Sydney, NSW 2007, Australia

Abstract— Nonlinear frequency conversion is in the core of the modern world of nonlinear optics. For efficient generation of harmonics, phase matching conditions must be satisfied, to ensure constructive interferences of the generated signal over the entire interaction length. So far, three main techniques were employed to achieve phase matching: one is the use of birefringence, when, e.g., an ordinary wave at fundamental frequency and an extraordinary wave at second harmonic have the same refractive index. This option, however, is only available for a limited range of nonlinear crystals. The other technique relies on periodic poling of nonlinear crystal, which is also not universally available. More recently, the advent of metamaterials enabled dispersion engineering, such as for bi-resonant systems, however this track is barely suitable at optical frequencies. We propose to make use of hyperbolic dispersion, which recently became accessible in layered metal-dielectric metamaterials (Fig. 1). Hyperbolic media support, in principle, arbitrary k-vectors, promising novel opportunities for phase matching. Taking second harmonic generation as an example, we systematically analyse all the possible combinations of the dispersion types at the two relevant frequencies, and find several configurations appropriate for nonconventional phase matching (Fig. 2). We analyse the arising possibilities with the available material parameters, and point out some specific examples, presenting a parametric analysis on the range of fill fractions, incident angles and frequencies (Fig. 3). Importantly, this novel approach yields a possibility to run phase-matched nonlinear processes with materials where conventional birefringent phase matching is not available. With the rapid progress in fabrication techniques for hyperbolic metamaterials, we trust the proposed approach will be soon available for practical applications.

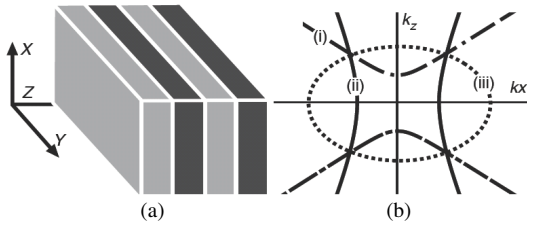

Figure 1: (a) Schematic of the considered structure; (b) normal surfaces showing: (i) NS hyperbolic, (ii) EW hyperbolic; (iii) elliptical.

Case	FF	SH
(a)	EW	EW
(b)	EW	elliptical
(c)	EW	NS
(d)	NS	NS

Figure 2: The four different configuration which are appropriate for phase matching in layered.

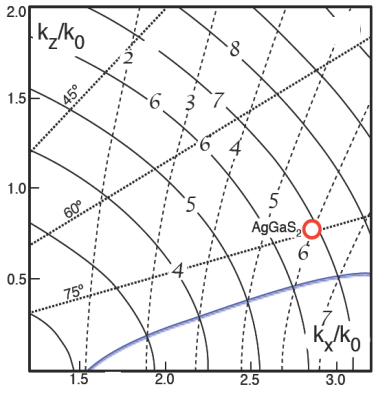

Figure 3: Fundamental frequency (1064 nm) and second harmonic normal surfaces in k-space. Dashed and solid curve correspond to constant values of the dielectric permittivity at FF and SH. An example solution using $AgGas_2$ is shown by the red circle.

A New Type of Optical Activity in a Toroidal Metamaterial

T. A. Raybould[1], **V. A. Fedotov**[1], **N. Papasimakis**[1], **I. Youngs**[2], **W. T. Chen**[3], **D. P. Tsai**[3], **and N. I. Zheludev**[1, 4]

[1]Optoelectronics Research Centre and Centre for Photonic Metamaterials
University of Southampton, SO171BJ, UK
[2]DSTL, Salisbury, UK
[3]Department of Physics
National Taiwan University, Taipei 10617, Taiwan
[4]Centre for Disruptive Photonic Technologies
Nanyang Technological University, Singapore

Abstract— Optical activity is a phenomenon which is widely observed across both natural and artificially chiral structures. Microscopically, the presence of optical activity in a system is conventionally understood in terms of the coupling of excited, co-aligned electric and magnetic dipoles [1]. Whilst combinations of electric dipoles with higher-order multipoles can also contribute to optical activity, such effects are frequently considered to be negligible. Metamaterial engineering however, allows for the design of structures where conventional microscopic multipole responses are suppressed in favour of more unusual excitations, including the elusive toroidal dipole.

First considered by Zel'dovich in 1958 [2], the toroidal dipole has recently been identified as an integral component in the excitations of metamaterial structures [3]. As the toroidal dipole radiates as an electric multipole [4], it is anticipated that it could contribute to optical activity in the same manner as an electric dipole. Here, we report on the first observation of optical activity in a structurally-chiral metamaterial that cannot be attributed to conventional multipoles, and can only be accounted for by the inclusion of the toroidal dipole in the multipole expansion.

The metamaterial unit cell studied consists of four split-ring resonators embedded in a low-loss dielectric, with the unit cells arranged such that the material has a structural chirality. The metamaterial is studied experimentally in a microwave chamber and computationally using a commerical Maxwell's equation solver. By extracting the microscopic multipole response, we confirm that at resonance a non-negligible toroidal dipole is excited and contributes to the observed circular dichroism in the metamaterial's transmission spectrum. This is corroborated by an examination of the material's polarisation eigenstates and how they vary upon removal of multipole excitations from the metamaterial's response.

ACKNOWLEDGMENT

The authors acknowledge support from DSTL, the Engineering and Physical Sciences Council, U.K. and the Leverhulme Trust.

REFERENCES

1. Barron, L. D., *Molecular Light Scattering and Optical Activity*, Cambridge Univ. Press, Cambridge, U.K., 1982.
2. Zel'dovich, I. B., "Electromagnetic interaction with parity violation," *Sov. Phys. JETP*, Vol. 6, 1184–1186, 1958.
3. Kaelberer, T., et al., "Toroidal dipolar response in a metamaterial," *Science*, Vol. 330, 1510–1512, 1986.
4. Dubovik, V. M. and V. V. Tugushev, "Toroid moments in electrodynamics and solid-state physics," *Phys. Rep.*, Vol. 187, 145–202, 1990.

Natural Chiral Photonic Structures: Morphology, Self-assembly and Optical Properties

Silvia Vignolini
Department of Chemistry, University of Cambridge, Cambridge, UK

Abstract— Nature provides a multitude of nanostructures that have been finely tuned by natural selection and produce structural coloration that play a role in many biological functions such as mating, signalling or camouflage [1–3]. A recurring design that is found both in the animal and plant kingdoms is the helicoidal structure, i.e., a multi-layer structure where adjacent layers rotate along a helical screw [4], see Figure 1(a).

Examples of such structures have been found in different plant tissues [5], in algae, and also in fish and insects. Two example of photonic chiral structures in insect and plants are reported in Figures 1(b) and (c), respectively.

In this talk I will review some example of chiral structures in nature, their optical response. I will discusses on how their common morphology suggests convergent evolution of optimized, left-handed multilayered structure. Finally, I will present a bio-inspired approach to replicate such chiral optical response found in natural structures, using the same materials as nature: cellulose [4, 5].

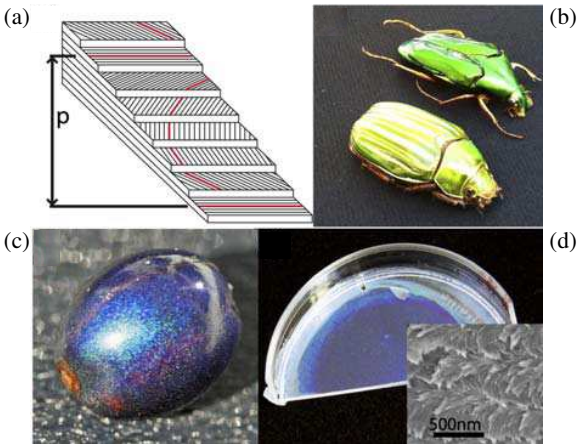

Figure 1: (a) Schematic diagram showing a wedge of a left-handed helicoid structures (adapted from [2]). (b), (c) Picture of beetle and *Pollia* fruit, respectively. (d) Camera picture of cellulose structurally coloured film obtained by cellulose nanocrystals self assembly, in the inset a cross sectional SEM of the structure, showing the twisting of the nanocrystals.

REFERENCES

1. Kinoshita, S., *Structural Colors in the Realm of Nature*, World Scientific Publishing Company, 2008.
2. Wilts, B. D., H. M. Whitney, B. J. Glover, U. Steiner, and S. Vignolini, "Natural helicoidal structures: morphology, self-assembly and optical properties," *Materials Today: Proceedings*, Vol. 1, 177–185, 2014.
3. Vignolini, S., P. J. Rudall, A. V. Rowland, A. Reed, E. Moyroud, R. B. Faden, J. J. Baumberg, B. J. Glover, and U. Steiner, "Pointillist structural color in Pollia fruit," *PNAS*, Vol. 109, 15712–15715, 2012.
4. Dumanli, A. G., H. van der Kooij, G. Kamita, E. Reisner, J. J. Baumberg, U. Steiner, and S. Vignolini, "Digital color in cellulose nanocrystal films," *ACS Appl Mater Interfaces*, Vol. 6, 12302, 2014.
5. Dumanli, A. G., G. Kamita, J. Landman, H. van der Kooij, B. J. Glover, J. J. Baumberg, U. Steiner, and S. Vignolini, "Controlled bio-inspired self-assembly of cellulose-based chiral reflectors," *Adv. Opt. Mat.*, Vol. 2, 646, 2014.

Chiral Reflectors of Circularly-polarised Light in Scarab Beetles of the Genus *Chrysina*

Ewan D. Finlayson, Luke T. McDonald, and Pete Vukusic
Department of Physics and Astronomy, University of Exeter, EX4 4QL, UK

Abstract— Certain species of jewel scarab beetle of the genus *Chrysina* exhibit a highly-reflective vivid metallic appearance to the human eye. This specular reflectance is accompanied by the anomalous preservation of the handedness of circularly polarised (CP) light upon reflection. Both of these properties result from the elaborate lamellar structure of the insect cuticle, in which planes of anisotropic chitin-based microfibrils are orientated parallel to the surface and are assembled such that their azimuth rotates continuously through the outer exocuticle layer The resulting helicoidal construction forms a chiral dielectric multilayer optical reflector. In this work we study natural structures that achieve broadband CP reflectance of silver or gold appearance by means of their helicoidal pitch being chirped. The CP-specific reflectance magnitudes of the insect elytra are measured experimentally at normal incidence for human-visible and near-infrared wavelengths. A scattering matrix technique based on the Berreman 4×4 matrix method for simulating anisotropic multilayers is used to model the optical behaviour. The model is informed by the experimental quantification of the physical dimensions of the chiral multilayer configurations using transmission electron microscopy (TEM) performed on the specimens, while refractive index values are selected from the literature. The origin of the broadband reflectance is elucidated by the simulations in terms of the role of the helicoidal pitch distribution and its arrangement in forming the chirped multilayer reflector. A quantitative comparison is made between the simulations and the reflectance measurements in order to gauge the applicability of the selected refractive index data to the species studied. The future goal of the realisation of novel optical devices containing synthetic biomimetic analogues of these natural structures is served by the development of an understanding of the observed optical behaviour.

REFERENCES

1. Vukusic, P. and J. R. Sambles, "Photonic structures in biology," *Nature*, Vol. 424, 852–855, 2003.
2. Pye, J. D., "The distribution of circularly polarized light reflection in the Scarabaeoidea (Coleoptera)," *Biol. J. Linn. Soc.*, Vol. 100, 585–596, 2010.
3. Caveney, S., "Cuticle reflectivity and optical activity in scarab beetles: The role of uric acid," *Proc. R. Soc. Lond. B*, Vol. 178, 205–225, 1971.
4. Berreman, D. W., "Optics in stratified and anisotropic media: 4×4-matrix formulation," *J. Opt. Soc. Am.*, Vol. 62, 502–510, 1972.
5. Jewell, S. A., P. Vukusic, and N. W. Roberts, "Circularly polarized colour reflection from helicoidal structures in the beetle *Plusiotis boucardi*," *New J. Phys.*, Vol. 9, 1–10, 2007.

Giant Broadband Chiral Response in Three-dimensional Shell-like Plasmonic Nanostructures

Dang Yuan Lei[1, 2]

[1]Department of Applied Physics, the Hong Kong Polytechnic University, Hong Kong, China
[2]Shenzhen Research Institute, the Hong Kong Polytechnic University, Shenzhen, China

Abstract— Continuous breaking of the mirror symmetry in a symmetric metal nanoshell can result in the formation of a new class of three-dimensional shell-like chiral structures (SLCSs). Here we demonstrate a record chiral response from a large-area plasmonic SLCS sample prepared through a two-step glancing angle deposition of different metals on a self-assembled microsphere array. A circular dichroism signal, defined as the ratio of the transmission intensity difference and sum of the right- and left-circularly polarized lights, of ~ 0.4 and a chiral parameter of $k_{\text{chiral}} > 0.09$ are achieved over the whole visible spectral range. Full-wave electromagnetic simulations reveal that the giant broadband chiroptical effect results from the weighted average of chirality over many microscopic domains in the plasmonic SLCS samples and the removal of the disorder arrangement of the microsphere array in long range.

Surface Enhanced Raman Scattering Induced by Periodic Gratings with Random Gold Particles

Chongjun Jin
State Key Laboratory of Optoelectronic Materials and Technologies
School of Physics and Engineering, Sun Yat-Sen University, Guangzhou 510275, China

Abstract— Raman scattering is the fingerprint of a molecular, which is very important for identifying the composition of materials, especially in polymer, food and biological sciences. However, the signal of the Raman scattering is very weak. Fortunately, the signal of the Raman can be enhanced by the metal nanoparticles and nanostructures, such as gold and silver nano particles. This enhanced Raman scattering is named as Surface enhanced Raman scattering (SERS). SERS has enormous applications in many areas of chemical and biological sensing, including single molecule detection, non-intrusive study of reaction dynamics, and identification of trace amounts of dangerous chemical species in foods. In the presentation, we propose a novel method to increase the signal of SERS via periodic grating with random gold particles. The experimental results show that, compared with the random gold particles on a flat surface, if the particles are sprayed on the periodic gratings, the signal of SERS will be further increased by a factor of over 10. We also explain this phenomenon via FDTD simulation and the interaction of different resonant modes.

Chiral Metasurfaces

Hyeon-Ho Jeong[1], **Sahand Eslami**[1, 2], **Insook Kim**[1, 2], **Johannes Sachs**[2], **Mariana Alarcon-Correa**[1, 2], **Tung-Chun Lee**[1], **John G. Gibbs**[1], **Dhruv P. Singh**[1], **Andrew G. Mark**[1], **and Peer Fischer**[1, 2]

[1]Max Planck Institute for Intelligent Systems
Heisenbergstrasse 3, Stuttgart 70569, Germany
[2]Institute for Physical Chemistry, University of Stuttgart
Pfaffenwaldring 55, Stuttgart 70569, Germany

Abstract— Two dimensional chiral surfaces exhibit interesting polarization properties and can, by virtue of their additional symmetry-breaking, give rise to additional second harmonic generation signals. Here, we describe arrays of chiral nanostructures that form metasurfaces with dense sub-wavelength features, which can simultaneously exhibit multiple properties, including plasmonic enhancement and very strong optical activities. These chiral metasurfaces are based on a parallel fabrication scheme we have recently developed that allows shape-control at the nanoscale [1]. We have grown arrays of chiral helices that predominately contain silver, gold, copper, or oxides to name but a few of the materials. However, it is also possible to grow hybrid structures as well as alloys or magnetic materials. The scalability of the technique is unique as it permits the rapid structuring of nanophotonic elements at the wafer-scale.

Chiroptical responses in transmission (optical rotation) and absorption (circular dichroism) are typically small effects. The chiroptical signal may be enhanced using amplification schemes, including weak value amplification [2], or by increasing the multipolar light-matter interaction itself. The latter is possible when the chiral object has a size that approaches the wavelength of light. Since we can fabricate structures that are of a similar length-scale as the wavelength of visible light, whilst being small enough to minimize scattering, large chiroptical signals can be recorded even in films that are only about a 100nm thick [1]. We show chiroptical measurements conducted on transparent substrates of wafer-scale metasurfaces [3–5]. In addition it is possible to study the same chiral nanostructures as a colloidal suspension, a "metafluid". Dynamic alignment of the chiral nanocolloids permits spectral discrimination between those effects that arise in the chiral signal due to their orientation on a chiral metasurface and those that arise in the isotropic state.

REFERENCES

1. Mark, A. G., J. G. Gibbs, T.-C. Lee, and P. Fischer, *Nat. Mater.*, Vol. 12, 802, 2013.
2. Pfeifer, M. and P. Fischer, *Opt. Express*, Vol. 19, 16508, 2011.
3. Gibbs, J. G., A. G. Mark, T.-C. Lee, S. Eslami, D. Schamel, and P. Fischer, *Nanoscale*, Vol. 6, 9457, 2014.
4. Gibbs, J. G., A. G. Mark, S. Eslami, and P. Fischer, *Appl. Phys. Lett.*, Vol. 103, 213101-1–213101-4, 2013.
5. Eslami, S. J. G. Gibbs, Y. Rechkemmer, J. van Slageren, M. Alarcón-Correa, T.-C. Lee, A. G. Mark, G. L. J. A. Rikken, and P. Fischer, *ACS Photonics*, Vol. 1, 1231–1236, 2014.

Polariton Lasing in Hybrid Organic-inorganic Microvavity

G. Paschos[5], **N. Somaschi**[1, 2], **G. Christmann**[1], **D. Coles**[3], **D. G. Lidzey**[3], **Z. Hatzopoulos**[1, 4], **P. G. Lagoudakis** [2], **S. I. Tsintzos**[1], **and P. G. Savvidis**[1, 5]

[1]Institute of Electronic Structure & Laser-FORTH, P. O. Box 1527, Heraklion 71110, Greece
[2]Department of Physics and Astronomy, University of Southampton, Southampton SO17 1BJ, UK
[3]Department of Physics and Astronomy, University of Sheffield, Sheffield S37RH, UK
[4]Department of Physics, University of Crete, Heraklion 71300, Greece
[5]Department of Materials Science and Technology, University of Crete, Heraklion 71300, Greece

Abstract— Cavity polaritons are formed when a confined optical mode within a high Q cavity strongly couples with exciton within the same cavity. A reversible exchange of energy between excitons and photons results in new allowed energy eigenstates of the system manifesting as a mixture of the uncoupled photon and exciton energies while exhibiting an anticrossing at the point of exciton-photon resonance. Strong coupling regime has been observed in microcavity structures incorporating both inorganic quantum wells (QWs) as well as organic materials such as J-aggregates, molecular crystals and polymers [1].

In this work we study hybrid exciton-polaritons that arise from mixing of two different organic-inorganic excitonic species with the resonant photon mode [2]. A planar microcavity structure consists of GaAs QWs and Jaggregate molecular dye assembled together in a multi-layered stack to form the active region. Angle-resolved photoluminescence at 80 K, when the system is excited almost-resonantly by a low repetition laser pulse at 780 nm reveals clear anticrossing. The complete structure containing both species exhibits large Rabi splitting of ∼68 meV shown in Figure 1(a), consistent with the presence of large oscillator strength J-aggregate Frenkel excitons. The measured polariton dispersion relations can be fitted well using coupled harmonic oscillator model in which both Wannier-Mott and Frenkel excitons couple to cavity photon. Furthermore, through power dependent measurements we demonstrate for the first time strong nonlinear emission and onset of hybrid polariton lasing regime with simultaneous line narrowing and interaction induced energy blueshift shown in Figure 1(b).

Such hybrid excitonic system presents an ideal playground for engineering nonlinear interactions and at the same time offers concrete possibilities for optoelectronics application. For example, laser diode designs combining high electrical conductivity of inorganic semiconductors with exciton robustness of organic compounds to maintain strong coupling regime at room temperature could provide efficient means to achieve electrically pumped organic polariton lasers.

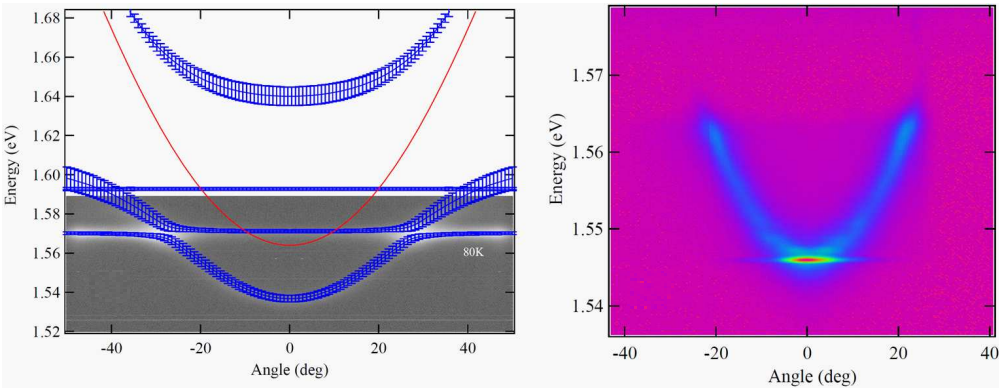

Figure 1: PL images recorded with Fourier plane projection technic. In Figure 1(a), clear polariton dispersion is revealed at 80 K while in Figure 1(b), clear polariton lasing obtained in similar detuning at 20 K.

REFERENCES

1. Lidzey, D. G., et al., "Strong exciton-photon coupling in an organic semiconductor microcavity," *Nature*, Vol. 395, 53, 1998.

2. Agranovich, V. M., H. Benisty, and C. Weisbuch "Organic and inorganic quantum wells in a microcavity: Frenkel-Wannier-Mott excitons hybridization and energy transformation," *Solid State Communications*, Vol. 102, 631–636, 1997.

Local Optical Activity in Metal Nanostructures Visualized by Near-field Circular Dichroism Microscopy

Hiromi Okamoto
Institute for Molecular Science, Myodaiji, Okazaki, Aichi 444-8585, Japan

Abstract— Confinement and enhancement of optical fields due to plasmons in metal nanostructures have great potentials in high-sensitivity spectroscopy, enhanced photochemical reactions, and so forth. In the past decade, our research group has made efforts to visualize the nanoscale optical fields in the periphery of the nanostructures, based on near-field optical imaging [1, 2]. Recently, optical activities of chiral nanostructures and chiral optical fields in the periphery of metal nanostructures have attracted attention of researchers. We are extending the near-field imaging study of nanoscale optical fields to local chiral optical fields generated by metal nanostructures [2].

For this purpose, we developed a near-field circular dichroism (CD) microscope [3]. The sample was irradiated by light for observation, which was modulated between left- and right-handed circular polarizations. The response field near the metal structure was picked up by an apertured near-field probe, and the CD signal was obtained by lock-in detection of the response field intensity, to construct the sub-wavelength CD image.

We prepared two-dimensional chiral gold nanostructures such as "S" and its enantiomeric mirrored structure, and recorded the CD images [3, 4]. Even though the far-field CD signal at the same observation wavelength was found to be small (10^{-3} level in absorbance unit) for this sample, *large local CD signal (10^{-1} level) was observed* on the nanostructure. The CD signals were not uniform in the nanostructures and CD signals of both positive and negative signs were observed at the same time in single nanostructures. An average of the local CD signal over the nanostructure yields a CD signal level similar to that observed with macroscopic CD measurements. This finding implies that metal nanostructures in general give locally enhanced CD signals even if they do not show strong optical activity macroscopically. In fact, we found that *even highly symmetric gold nanorectangles, which gave null macroscopic CD, showed strong local CD signals* [5]. This result is important in view of the selection rule of CD measurements of materials. The conventional macroscopic CD selection rule that only chiral materials are CD active is no longer valid for the local optical activity, because it reflects the *local symmetry* of the material.

To get information on the origin of local optical activity, we prepared a series of gold nanostructures composed of two "C" structures with various distances between their ends (it corresponds to "S" at zero distance between the two partial structures), and measured the near-field CD images [6]. The local CD signal at the connecting region of the associating structure was enhanced when the two partial structures were close enough (approx. 300 nm or less), and connection of the two partial structures was not necessary to get locally enhanced CD. This indicates that *the local CD of the two-dimensional metal nanostructure originates mainly from long-range electromagnetic interaction* and not from electronic exchange between the partial structures.

The method proposed here and the information obtained may serve as a basis for design and control of chiral optical fields, which is indispensable to applications of chiral fields to analytical purposes, optical devices, and so forth.

ACKNOWLEDGMENT

The author is grateful to the collaborators who contributed to this work, in particular, Drs. T. Narushima, Y. Nishiyama, Mr. S. Hashiyada, Ms. A. Ishikawa, and Prof. K. Imura.

REFERENCES

1. Okamoto, H. and K. Imura, *J. Phys. Chem. Lett.*, Vol. 4, 2230–2241, 2013.
2. Okamoto, H., T. Narushima, Y. Nishiyama, and K. Imura, *Phys. Chem. Chem. Phys.*, 2015, in press.
3. Narushima, T. and H. Okamoto, *Phys. Chem. Chem. Phys.*, Vol. 15, 13805–13809, 2013.
4. Narushima, T. and H. Okamoto, *J. Phys. Chem. C*, Vol. 117, 23964–23969, 2013.
5. Hashiyada, S., T. Narushima, and H. Okamoto, *J. Phys. Chem. C*, Vol. 118, 22229–22233, 2014.
6. Narushima, T., S. Hashiyada, and H. Okamoto, *ACS Photonics*, Vol. 1, 732–738, 2014.

Session 1P11
FocusSession.SC1: Casimir Effect and Heat Transfer 2

Transport and Harvesting of Excitons Mediated by Strong Coupling

Johannes Feist[1], **Carlos Gonzalez-Ballestero**[1],
Esteban Moreno[1], **and Francisco J. Garcia-Vidal**[1, 2]

[1]Departamento de Física Teórica de la Materia Condensada and Condensed Matter Physics Center (IFIMAC), Universidad Autónoma de Madrid, Madrid, Spain
[2]Donostia International Physics Center (DIPC)
Donostia/San Sebastian, Spain

Abstract— The transport of excitons (bound electron-hole pairs) is a fundamental process that plays a crucial rule both in natural phenomena such as photosynthesis, where energy has to be transported to a reaction center, and in artificial devices such as organic solar cells, whose power conversion efficiency can be improved significantly when the exciton diffusion length is increased. Similarly, excitons can play an important role in heat transport, and understanding and manipulating their role has possible applications ranging from thermoelectric effects to heat-voltage converters, nanoscale refrigerators, and even thermal logic gates. However, most systems composed of organic molecules are disordered and possess relatively large dissipation and dephasing rates, such that exciton transport typically is inefficient.

Very recently, an increase of the *electrical* conductance of an organic material was shown under strong coupling of the excitons to a cavity mode [1]. Strong coupling is achieved when the energy exchange rate between exciton and electromagnetic field modes becomes faster than the decay and decoherence rates of either constituent. Inspired by this result, we demonstrate that exciton conductance in organic materials can be enhanced by several orders of magnitude when the molecules are strongly coupled to an electromagnetic mode. Using a 1D model system, we show how the formation of a collective strongly coupled mode (a polariton) allows excitons to bypass the disordered array of molecules and jump directly from one end of the structure to the other [2].

We furthermore show that by designing the electric field profile of the electromagnetic mode that provides the strong coupling, the transport properties can be tuned to achieve exciton harvesting and funneling, i.e., to guide excitons from a collection area to a specific location. We demonstrate this effect using the localized plasmon resonances of a single metallic nanosphere and a three-sphere structure. The latter provides pronounced *hot spots* where the electric field is strongly concentrated. We show that excitons are efficiently transported between these hot spots, bypassing the rest of the system.

REFERENCES

1. Orgiu, E., J. George, J. Hutchison, E. Devaux, J. F. Dayen, B. Doudin, F. Stellacci, C. Genet, P. Samorì, and T. W. Ebbesen, arXiv:1409.1900, 2014.
2. Feist, J. and F. J. Garcia-Vidal, *Phys. Rev. Lett.*, in press, arXiv:1409.2514, 2014.

Thermally-activated Non-local Amplification in Quantum Excitation Transport

Bruno Leggio[1], **Riccardo Messina**[1], **and Mauro Antezza**[1, 2]

[1]Laboratoire Charles Coulomb
UMR 5221 Université de Montpellier and CNRS, Montpellier F-34095, France
[2]Institut Universitaire de France, 103 Boulevard Saint-Michel, Paris F-75005, France

Abstract— We study energy transport efficiency in 2-D and 3-D configurations of two-level atoms (real or artificial ones). We show that, if the atomic system is embedded in a common blackbody radiation, the transport efficiency can be greatly increased with respect to the case $T = 0$. To understand this phenomenon we exploited the exact knowledge of field self-correlations, and showed that excitations can travel along the atomic system due to two alternative physical effects: in addition to the standard excitation hopping thanks to the atomic dipole interactions, atoms can affect each other's internal energy also by collective dissipation induced by non-local self-correlations of the electromagnetic field. This latter term has been neglected in previous phenomenological approaches since its effect has been assumed to be negligible. Although this assumption is well justified for regular systems where the hopping dominates, it breaks down in more general, non-regular configurations. By using a fully microscopic analysis of atomic dynamics, we show that these non-local terms, triggered by the thermal noise induced by the blackbody radiation, play a fundamental role in atomic energy transport. This generates a counter-intuitive temperature-dependence of the transport efficiency, which does not monotonically decrease as in the case of pure hopping, and gets instead amplified in a certain range of temperatures. By this effect excitations can travel along paths where hopping is forbidden with efficiencies remarkably higher than 100%.

Photonic Heat Transfer and Electronic Cooling in Hybrid Superconducting Nanostructures

H. Courtois[1], **C. B. Winkelmann**[1], **and F. W. J. Hekking**[2]

[1]Institut Néel, CNRS and Université Grenoble Alpes, Grenoble, France
[2]LPMMC, CNRS and Université Grenoble Alpes, Grenoble, France

Abstract— Electron thermodynamics at the nano-scale is a fast developing topic, in particular in superconductor-based hybrid devices. For instance, a simple Normal metal-Insulator-Superconductor (NIS) tunnel junction, when biased at a voltage just below the energy gap of the superconductor, enables only electrons with a higher energy to flow through. This selective evaporation process makes the normal metal electronic population as a whole to cool down. Electronic cooling is limited by electron-phonon coupling in the normal metal and by heat conduction. In a superconductor, electrons are paired into Cooper pairs so the electron-phonon coupling is vanishing, just as the electronic heat conductance. Therefore, only photons contribute to the heat conduction at very low temperature.

With a good matching between source and drain, the conductance of a superconducting transmission line is equal to the thermal conductance quantum: $K_Q = k_B^2 T\pi/6$ hbar. An inductance can also be present in some realistic configurations, due to the wiring geometry. We investigate the photonic heat transfer through a reactive impedance, i.e., a linear coupling circuit that contains a capacitor, an inductance, a resonant circuit or a transmission line. We follow a simple circuit approach, valid at low temperatures when the relevant photons have wavelengths larger than the size of the typical circuit element. The metallic parts can then be treated as lumped elements characterized by an electrical impedance. We present a quantitative analysis, enabling us to establish design rules for useful devices, including phonon thermometers or electron coolers. The photonic channel for heat transfer can in principle couple metallic systems that are galvanically isolated, e.g., through a capacitor. This effect can be detrimental when one wants to maintain two electronic populations at different quasi-equilibrium temperatures, but also beneficial in several cases.

Optomechanics at Microwave Frequencies: Mechanical Resonators Coupled to Microwave Cavities and Superconducting Qubits

J.-M. Pirkkalainen[1], **S. U. Cho**[2], **F. Massel**[3], **J. Tuorila**[4], **T. T. Heikkilä**[3], **P. J. Hakonen**[2], **and M. A. Sillanpää**[1]

[1]Department of Applied Physics, School of Science
Aalto University, P. O. Box 11100, Aalto FI-00076, Finland
[2]O. V. Lounasmaa Laboratory, Low Temperature Laboratory
Aalto University, P. O. Box 15100, Aalto FI-00076, Finland
[3]Department of Physics, University of Jyväskylä, P. O. Box 35 (YFL), Jyväskylä FI-40014, Finland
[4]Department of Physics, University of Oulu, FI-90014, Finland

Abstract— Micromechanical resonators affected by radiation pressure forces allow to address fundamental questions on quantum properties of mechanical objects, or, to explore quantum limits in measurement and amplification. A new setup for the purpose is an on-chip microwave cavity coupled to a mechanical resonator (Fig. 1(a)). Under blue sideband irradiation, we demonstrate the possibility of building a mechanical microwave amplifier [1], with noise properties approaching the quantum regime. On the red sideband side, we show how one can couple mechanical resonators via the cavity bus, while simultaneously cooling the mechanical modes very close to the ground state of motion [2]. A recent development in linear optomechanics is the coupling of graphene membranes to microwave-frequency cavities. Here, we observe radiation pressure back-action on the motion of graphene.

One can add intriguing features to the basic optomechanics setup by including a superconducting qubit made with Josephson junctions. The nonlinearity of the two-level system allows for much more rich physics than is possible with linear cavities. We have realized a superconducting transmon qubit interacting with a micromechanical resonator [3]. We operate the qubit in the circuit cavity quantum electrodynamics (circuit QED) architecture, where the qubit is coupled also to a microwave cavity. Hence, the combined setup represents an artificial atom coupled to two different cavities (Fig. 1(b)). We measure the phonon Stark shift, splitting of the qubit spectral line into motional sidebands, and coherent sideband Rabi oscillations. Another motivation the tripartite system owes from the challenges to increase the single-quantum coupling strength to exceed the cavity dissipation rate. Motivated by this goal, we present a new design of the circuit optomechanical experiment, where the on-chip microwave cavity includes a Josephson charge qubit [4]. The cavity is coupled to a micromechanical resonator whose motion is visible as charge, and hence affects the cavity frequency. This way we were able to boost the coupling in the setup by six orders of magnitude up to the MHz regime.

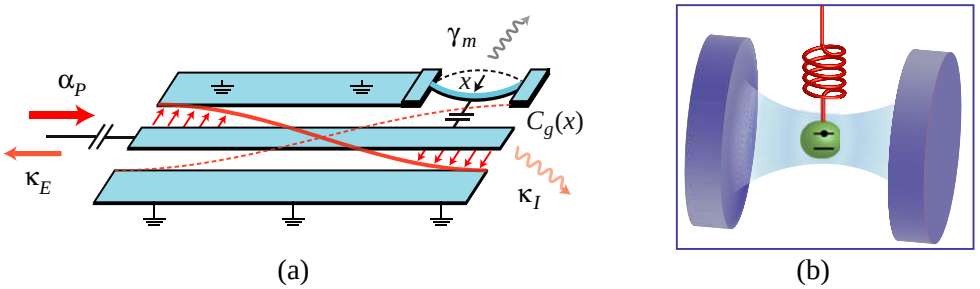

Figure 1: (a) A microwave resonator can be coupled capacitively to an arbitrary number of mechanical resonators. (b) Idea of introducing nonlinearity in optomechanics. Inside the cavity (blue) there is a quantum two-level system (green) which is mechanically compliant (red).

REFERENCES

1. Massel, F., et al., *Nature*, Vol. 480, 351, 2011.
2. Massel, F., et al., *Nature Communications*, Vol. 3, 987, 2012.
3. Pirkkalainen, J. M., et al., *Nature*, Vol. 494, 211, 2013.
4. Heikkilä, T. T., et al., *Phys. Rev. Lett.*, Vol. 112, 203603, 2014.

Light-matter Interface for Probing Quantum Gases

Gabriele De Chiara
Queen's University Belfast, UK

Abstract— I propose a scheme to probe many-body quantum states of ultracold gases using a light-matter interface based on the quantum Faraday effect. The polarisation fluctuations of light interacting with an atomic ensemble or atoms in optical lattices bear signatures of the many-body state. These fluctuations, observed with a quantum non-demolition measurement, allow one to reconstruct the phase diagram of a variety of Bose-Hubbard and spin models. In particular, I show how the critical point of the Mott insulator to superfluid phase transition can be accurately extracted from the light measurement [1]. Moreover, I propose a scheme, based on the same interface, to measure work and heat fluctuation relations, including the famous Jarzynski equality in ultracold quantum gases. This result opens the way to the exploration of mesoscopic quantum thermodynamics with cold atoms towards the realisation of quantum engines [2].

REFERENCES

1. Rogers, B., M. Paternostro, J. F. Sherson, and G. De Chiara, "Characterization of Bose-Hubbard models with quantum non-demolition measurements," *Phys. Rev. A*, to appear, 2014.
2. De Chiara, G., A. J. Roncaglia, and J. P. Paz, *New J. Phys.*, Vol. 17, 035004, 2015.

Thermal Emission by a Subwavelength Aperture

K. Joulain, **Y. Ezzahri**, **and J. Drevillon**
Institut Pprime, CNRS, Université de Poiters, ENSMA, Poitiers, France

Abstract— We calculate, by means of fluctuational electrodynamics, the thermal emission of an aperture filled by vacuum or a material at temperature T. We show that thermal emission is very different whether the aperture size is large or small compared to the thermal wavelength. Subwavelength apertures filled with vacuum (subwavelength blackbody) have their thermal emission strongly decreased compared to classical blackbodies. A simple expression of their emissivity can be calculated and their total emittance scales as T^6 instead of T^4 for large apertures. Subwavelength apertures filled with an opaque material have generally a similar behavior. However, if the material support surface waves or exhibit resonances, thermally excited evanescent resonant modes are scattered by the aperture. In this case, the thermal emission tends to be monochromatic and is strongly enhanced in comparison to the Planck theory. We think this behavior could open the way to very useful applications such as very narrowband passive source.

Thermal Emission of a Hyperbolic Blackbody

Svend-Age Biehs[1], **Slawa Lang**[2], **Alexander Yu. Petrov**[2], **Manfred Eich**[2], **and Philippe Ben-Abdallah**[3]

[1]Institut für Physik, Carl von Ossietzky Universität, D-26111 Oldenburg, Germany
[2]Institute of Optical and Electronic Materials
Hamburg University of Technology, 21073 Hamburg, Germany
[3]Laboratoire Charles Fabry, UMR 8501, Institut d'Optique, CNRS
Université Paris-Sud 11, 2, Avenue Augustin Fresnel, 91127 Palaiseau Cedex, France

Abstract— The blackbody theory of Planck [1] is revisited in the case of thermal electromagnetic fields inside uniaxial anisotropic media in thermal equilibrium with a heat bath using the fluctuation dissipation theorem [2, 3]. When these media are hyperbolic, we show that the spectral energy density of these fields radically differs from that predicted by Planck's blackbody theory. We demonstrate that the maximum of their spectral energy density is shifted towards frequencies smaller than Wien's frequency making these media look colder than classical blackbodies for a given temperature. Finally, using Rytov's fluctuational electrodynamics we derive Stefan-Boltzmann's law for hyperbolic media which becomes a quadratic function of the heat bath temperature. We discuss direct consequences for heat transport through vacuum [4] and through a hyperbolic medium [5].

REFERENCES

1. Planck, M., *Ann. Phys.*, Vol. 309, 553, 1901.
2. Agarwal, G. S., *Phys. Rev. A*, Vol. 11, 230, 1975.
3. Eckhardt, W., *Opt. Commun.*, Vol. 27, 299, 1978.
4. Biehs, S.-A., M. Tschikin, and P. Ben-Abdallah, *Phys. Rev. Lett.*, Vol. 109, 104301, 2012.
5. Liu, J. and E. E. Narimanov, *Phys. Rev. B*, Vol. 91, 041403(R), 2015.

Measurements of the Heat Transfer in Near Field Regime

J. Chevrier and P. J. van Zwol
Institut Néel, CNRS and Universite Joseph Fourier Grenoble
BP 166 38042, Grenoble Cedex 9, France

Abstract— Heat can be exchanged between two surfaces through emission and absorption of thermal radiation. For distances smaller than the peak wavelength of the black body spectrum, radiative heat transfer can be increased by the contribution of evanescent waves. This contribution can be viewed as energy tunnelling through the gap between the surfaces. On the basis of results published in [1], we shall here present a detailed quantitative comparison between theory and experiments in the nanometre range. We shall describe an experimental setup that allows measurement of conductance for gaps varying between 30 nm and 2.5 µm. We shall then show how the systematic use of this machine has enabled us to measure the heat transfer in near field regime for different materials including VO2 which presents a prototypical metal insulator transition. Further we have investigated the change of the near field contribution to heat transfer when one surface is covered with graphene. Indeed owing to its two dimensional electronic structure, graphene exhibits many unique properties. One of them is a wave vector and temperature dependent plasmon in the infrared range. Theory predicts that due to these plasmons, graphene can be used as a universal material to enhance nanoscale radiative heat exchange for any dielectric substrate. Based on [2], we shall report on radiative heat transfer experiments between SiC and a SiO_2 sphere which have non matching phonon polariton frequencies, and thus only weakly exchange heat in near field. Heat flux contribution of graphene epitaxially grown on SiC will be shown to dominate at short distances. The influence of plasmons on radiative heat transfer is further supported with measurements for doped silicon. These results highlight graphene's strong potential in photonic near field and energy conversion devices.

REFERENCES

1. Rousseau, E., A. Siria, G. Jourdan, S. Volz, F. Comin, J. Chevrier, and J.-J. Greffet, *Nat. Photonics*, Vol. 3, 514, 2009.
2. Van Zwol, P. J., S. Thiele, C. Berger, W. A. de Heer, and J. Chevrier, *Phys. Rev. Lett.*, Vol. 109, 264301, 2012.

Experiments on Giant Radiative Heat Flux at the Nanometer Scale

A. Kittel, K. Kloppstech, N. Könne, L. Worbes, and D. Hellmann
Institute of Physics, Carl-von-Ossietzky University of Oldenburg, D-26111 Oldenburg, Germany

Abstract— We report on a precise *in situ* procedure to calibrate the heat flux sensor of a near-field scanning thermal microscope. This calibration procedure is based on modulation technique and utilizes a hot wire method to build a metrologically accessible and controllable heat reservoir. This reservoir is coupled thermally via near-field interactions to our probe exactly in the same way as it is coupled in a actual measurement. Thus the sensor's conversion relation can be precisely determined which is the thermopower, generated in the sensor's coaxial thermocouple, in dependence on the thermal flux from reservoir through the sensor. The achieved accuracy is about 8%. With such a calibrated sensor we perform quantitative measurements of the heat flux between a gold coated near-field scanning thermal microscope tip and a planar gold sample at nanometer distances across a vacuum gap. We find an extraordinary large heat flux which is more than five orders of magnitude larger than black-body radiation and three orders of magnitude larger than the values predicted by conventional theory of fluctuational electrodynamics often used to describe near field effects of heat transfer. Furthermore, experiments show that this heat transfer can be drastically influenced by a thin layer of material on the surface. The findings demand modified, or even new models to describe the heat transfer across a vacuum gap at nanometer distances.

Casimir Actuation of MEMS between Real Materials

G. Palasantzas, M. Sedighi, W. H. Broer, V. B. Svetovoy, and J. Knoester
Zernike Institute for Advanced Materials, University of Groningen, Nijenborgh 4, The Netherlands

Abstract— Using the measured optical response and surface roughness topography as inputs, we perform realistic calculations of the combined effect of Casimir and electrostatic forces on the actuation dynamics of micro/nanoelectromechanical systems (MEMS/NEMS) using as input optical properties and surface roughness. Our findings play a principal role for the stability of micro/nanodevices such as vibration sensors, switches, and other related device architectures operating at distances below 200 nm. In contrast with the expectations, roughness can influence MEMS dynamics, even at distances between bodies significantly larger than the root-mean-square roughness. This effect is associated with statistically rare high asperities that can be locally close to the point of contact. It is found that even though surface roughness appears to have a detrimental effect on the availability of stable equilibria, it ensures that those equilibria can be reached more easily than in the case of flat surfaces. Moreover, it appears that surface roughness can suppress chaotic behavior towards stiction. In addition, the dependence of the Casimir force on the frequency dependent dielectric functions of interacting materials makes it possible to tailor the actuation dynamics of microactuators. The Casimir force is largest for metallic interacting systems due to the high absorption of conduction electrons in the far-infrared range. For less conductive systems, such as phase change materials or conductive silicon carbide, the reduced force offers the advantage of increased stable operation of MEMS devices against pull-in instabilities that lead to unwanted stiction. Bifurcation analysis with phase portraits has been used to compare the sensitivity of a model actuator when the optical properties are altered. Finally, computations using the Drude-Plasma models to model low optical frequencies show differencies that are strongly minimized for weakly conductive systems as are the doped insulators making actuation modeling more certain to predict.

Reducing the Casimir Force

S. A. R. Horsley and T. G. Philbin
Department of Physics and Astronomy, University of Exeter, Exeter, UK

Abstract— A considerable body of research has demonstrated that the Casimir force can be engineered to some extend. Theoretical and experimental work has shown that the choice of materials and the geometry of material samples can have a significant effect on the magnitude, and even the direction, of the Casimir force. This work has implications for future engineering on nanometre scales where the Casimir effect can play a significant role. Here we report on a theoretical study of artificially engineered non-reflecting coatings as a method of reducing the Casmir force. The use of artificial materials in Casimir manipulation has been limited by the need for broadband functioning, which is impossible with many designs based on "meta-atoms". The coatings we consider are inhomogeneous with specially chosen dispersion and absorption, but they do not have a "meta-atom" structure and can function as desired over a broad range of frequencies.

Photonic Forces on Magneto-dielectric Nanoparticles at Optical Wavelengths with Random Fields. Creating Optical Analogous of Van der Waals and Casimir Interactions and Beyond: Their Control and Design through the Spectrum and Spatial Coherence

Manuel Nieto Vesperinas[1] **and Juan Miguel Auñón**[2]

[1]Instituto de Ciencia de Materiales de Madrid, Consejo Superior de Investigaciones Científicas
Campus de Cantoblanco, Madrid 28049, Spain
[2]School of Physics and Astronomy, University of St. Andrews, North Haugh, Fife KY16, 9SS, Scotland

Abstract— At selected wavelengths, (visible and near-infrared), the Planck energy of optically produced random light is equivalent to that of the vacuum fluctuations; thus employing a quasi-monochromatic optical source, the forces on nanoparticles may be made analogous to Casimir-Polder and Van der Waals interactions.

We show how for some wavelengths, the contribution of the particle induced magnetic dipole predominates over that of the electric one, and how when Kerker conditions hold, (see [1] and references therein), the magnetic dipole can cancel to the purely dipole force, the interference being responsible for the mechanical action on the particle.

We derive new power-laws for the induced dipole forces. Further, we show how controlling the optical spectrum shape and bandwidth, as well as the degree of coherence of the emitted fields, one can tailor at will the electric and/or magnetic, conservative or non conservative, attractive or repulsive, nature of these forces, as well as their magnitude.

REFERENCES

1. Auñón, J. M., C. W. Qiu, and M. Nieto-Vesperinas, "Tailoring photonic forces on a magnetodielectric nanoparticle with a fluctuating optical source," *Phys. Rev. A*, Vol. 88, 043817, 2013.

Fluctuation Induced Effects in Nanostructures

Lilia M. Woods
Department of Physics, University of South Florida
Tampa, Florida 33620, USA

Abstract— Fluctuations of observables can give rise to many types of interactions. Dipolar fluctuations are responsible for Casimir forces, which are of great importance for the operation of micro-machines and the stability of inert materials composites. Nanostructured materials, such as graphitic systems, offer a great opportunity to study such effects and discover unique functionalities. Near-field radiation, which can be characterized as Casimir-like phenomenon between systems at temperature gradient, is of particular relevance in graphene systems. In this presentation, we review how the thermo-plasmons tunability can be utilized in order to take advantage of the graphene transverse electric mode. Utilizing this phenomenon, one is able to find new ways for radiation control and probe the relaxation scattering times in graphene. In addition to dipolar fluctuations, charge fluctuations can also be responsible for Casimir-like forces. We show that such effects are of relevance to capacitor systems especially when nanostructured materials are involved. Our theory, which utilizes the quantum capacitance concept, demonstrates novel pathways for probing quantum mechanical and thermal fluctuations effects in materials with reduced dimensions.

ACKNOWLEDGMENT

Financial support from DOE-DE-FGE02-06ER46297 is acknowledged.

Probing the Surface with Atoms

Ron Folman
Ben-Gurion University of the Negev, Israel

Abstract— As cold atoms are brought evermore closer to surfaces, they open a wide variety of possibilities of probing the surface. In this talk I will review past realizations of such experiments around the world, and the possibilities made available in the near future for probing the CP force, Johnson noise, the hypothesized short range fifth force, plasmons, and other surface effects.

Dispersion Interactions with Long-time Tails or Beyond Local Equilibrium

C. Henkel
Institute of Physics and Astronomy, University of Potsdam, Germany

Abstract— Dispersion forces out of thermal equilibrium can be understood as the rectification of electromagnetic fluctuations that arise from spatially separated sources (bodies). The forces are often observed on time scales much longer than the characteristic periods of thermal or zero-point radiation fields. Such a separation of time scales is a strong motivation for approximate treatments, assuming that the electromagnetic response of a body to an incident field is fast or that thermalization takes place rapidly. Many applications of radiative energy transfer on the nano-scale build on this picture (light harvesting, enhanced near-field heat transfer etc.).

The purpose of this contribution is twofold. (1) We take up the problem of the response time of the electromagnetic field or of a polarizable object in the extreme quantum limit (zero temperature). One finds in some cases correlation functions of the zero-point fields that are long range in time ('fat tails'), in distinction to the more familiar response (Green) functions. We discuss the relevance of these tails by focusing on a simple example: the electromagnetic drag force on a small polarizable particle (quantum friction). The corresponding field theory of photons and a few-level atom has been analyzed with the help of perturbation theory in Refs. [1, 2].

(2) A fictitious conversation is engaged to scratch for the foundations of dispersion forces in *local* thermodynamic equilibrium (LTE). Our focus is on suitable validity criteria and on potential observations that would illustrate non-LTE physics. As a concrete example, we address radiative heat transport across the interface between two transparent dielectrics, as discussed in Refs. [3–6].

ACKNOWLEDGMENT

I thank B. Budaev, S. Buhmann, D. Dalvit, F. Intravaia, V. Mkrtchian, G. Pieplow, and S. Scheel for instructive discussions and collaboration at various stages.

REFERENCES

1. Barton, G., "On van der Waals friction. II: Between atom and half-space," *New J. Phys.*, Vol. 12, 113045, 2010.
2. Intravaia, F., V. E. Mkrtchian, S. Y. Buhmann, S. Scheel, D. A. R. Dalvit, and C. Henkel, "Friction forces on atoms after acceleration," submitted to *J. Phys. Condens. Matt.*, 2014.
3. Levin, M. L., V. G. Polevoi, and S. M. Rytov, "Contribution to the theory of heat exchange due to a uctuating electromagnetic field," *Sov. Phys. JETP*, Vol. 52, 1054, 1980.
4. Pan, J. L., "Radiative transfer over small distances from a heated metal," *Opt. Lett.*, Vol. 25, 369, 2000.
5. Budaev, B. V. and D. B. Bogy, "On the role of acoustic waves (phonons) in equilibrium heat exchange across a vacuum gap," *Appl. Phys. Lett.*, Vol. 99, 053109, 2011.
6. Ezzahri, Y. and K. Joulain, "Vacuum-induced phonon transfer between two solid dielectric materials: Illustrating the case of Casimir force coupling," *Phys. Rev. B*, Vol. 90, 115433, 2014.

The Coherent Effects of the Casimir-Polder Interaction on Driven Atoms and the Quasi-resonant Van Der Waals Interaction between Non-identical Atoms

Manuel Donaire and Astrid Lambrecht
Laboratoire Kastler-Brossel, UPMC-Sorbonnes Universités, CNRS, ENS-PSL Research University
Collège de France, 4, Place Jussieu, F-75252 Paris, France

Abstract— In this talk we address several aspects of the Casimir-Polder (CP) and van der Waals (vdW) interactions which need a time-dependent approach. In the first part of this talk we will show that the CP interaction of an atom with a material surface may give rise to a renormalisation of the Rabi frequency of the atom when the atom is driven under the action of two Raman lasers [1]. Likewise, CP-induced Rabi oscillations may generate between two Zeeman sub-levels of a free atom in the vicinity of a reflecting surface [2].

In the second part of this talk we will present the vdW interaction between two non-identical atoms, one of which is prepared in an excited state [3]. Finally, we will give results for the quantum friction which an excited atom experiences as it moves at constant velocity parallel to a dilute atomic surface.

REFERENCES

1. Donaire, M. and A. Lambrecht, "On the coherent effect of vacuum fluctuations on driven atoms," arXiv:1504.05066, 2015.
2. M. Donaire, M.-P. Gorza, A. Maury, R. Guérout, and A. Lambrecht, "Casimir-Polder induced Rabi oscillations," *EPL*, Vol. 109, 24003, 2015.
3. M. Donaire, R. Guérout, and A. Lambrecht, "Quasi-resonant van der Waals interaction between non-identical atoms," arXiv:1503.06743, 2015.

Session 1P12
SC1&3: Design and Simulation of Electromagnetic and Optical Devices

Calculation of Gain in a Lossy Medium

Takuichi Hirano, Jiro Hirokawa, and Makoto Ando
Tokyo Institute of Technology, Japan

Abstract— Characterization of propagation in a lossy medium is demanded in applications like ground penetrating radar (GPR), ultra wideband (UWB) radar for cancer detection and so on (see Fig. 1). This paper presents extension of Friis transmission equation [1] from a lossless medium to a lossy one.

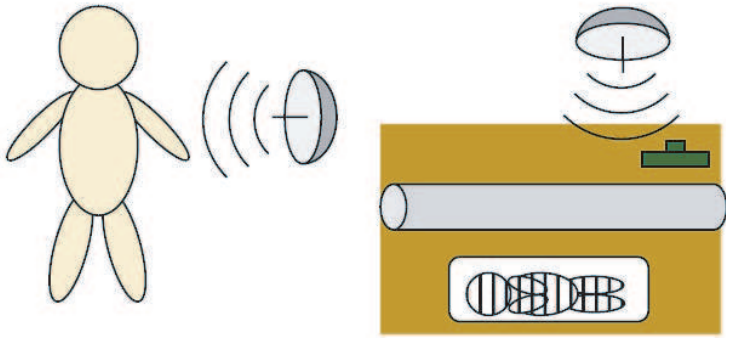

(a) (b)

Figure 1: Friis transmission equation in a lossy medium. (a) UWB radar. (b) GPR.

When two antennas #1 and #2 are separately placed with distance r in a lossy medium as shown in Fig. 1, the extended Friis transmission equation becomes

$$\frac{P_r}{P_t} = G_1 G_2 \left(\frac{\lambda}{4\pi r}\right)^2 \exp(-2\alpha r) \tag{1}$$

where G_1 and G_2 are gains of the antenna #1 and #2, respectively. The $\lambda = 2\pi/\beta$ is the wavelength which is calculated from the phase constant β in the lossy medium. The α is the attenuation constant of the lossy medium. The factor $\exp(-2\alpha r)$ represents attenuation in the lossy medium, which does not appear in the conventional Friis transmission equation.

The authors developed the gain measurement algorithm [2], averaging method for the shortened far-field gain measurement technique, which is applicable for measurement and simulation.

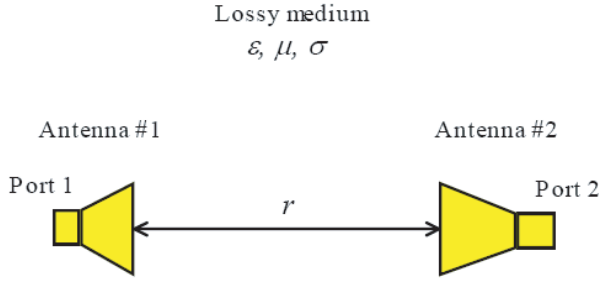

Figure 2: Friis transmission equation in a lossy medium.

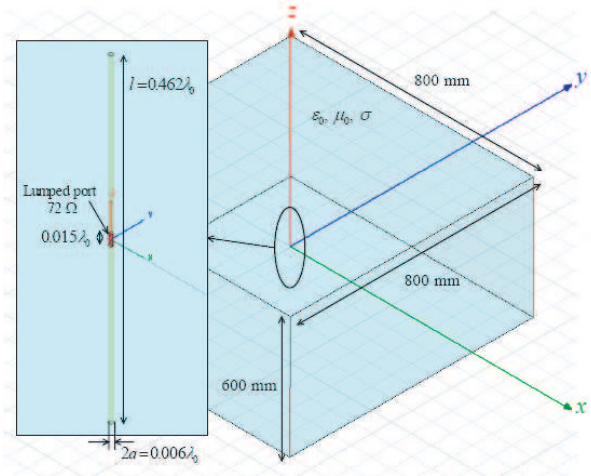

Figure 3: Simulation model of a half-wavelength dipole antenna.

For verification of the extended Friis transmission equation [1], the gain of a half-wavelength dipole antenna in a lossy medium is analyzed. Fig. 3 shows a simulation model of a half-wavelength dipole antenna. Ansys HFSS Ver.11 is used for the simulation. Table 1 shows calculated gain of the dipole antenna for several conductivities σ. The method in [2, 3] are used for the analysis of gain. The gain decreases as the conductivity σ increases. The result is verified by the simulation with two dipole antennas. Transmission coefficient S_{21} agrees well each other by that obtained by Eq. (1) ($P_r/P_t = |S_{21}|^2$).

Table 1: Calculated gain.

σ (S/m)	Gain (dBi)
0	2.22
0.001	2.08
0.01	0.86

REFERENCES

1. Friis, H. T., "A note on a simple transmission formula," *Proc. of the IRE*, Vol. 34, No. 5, 254–256, May 1946.
2. Hirano, T., et al., "Errors in shortened far-field gain measurement due to mutual coupling," *IEEE Transactions on Antennas and Propagation*, Vol. 62, No. 10, 5386–5388, Oct. 2014.
3. Hirano, T., et al., "Measurement technique for gain and distance and numerical simulation with a dipole antenna," *Proc. of IEEE AP-S International Symposium*, Session 116.3, Memphis, TN, USA, Jul. 2014.

A Novel Ka-band Spatial Combiner Amplifier: Global Design and Modeling

Alberto Leggieri[1], **Davide Passi**[1], **Franco Di Paolo**[1], **Marco Bartocci**[2], **Antonio Tafuto**[2], **and Antonio Manna**[2]

[1]Department of Electronic Engineering, University of Rome Tor Vergata, Rome, Italy
[2]Elettronica SpA, Via Tiburtina Valeria Km. 13, Rome 7-00100, Italy

Abstract— This article describes the complete design of high performances Ka-Band small size Spatial Power Combiner (SPC) Amplifier. Several multiple physics aspects are treated in the proposed study as electromagnetic behavior and thermo-mechanical features, in order to drive the active devices at full power. The combiner consists of quadruple Fin lines to microstrip (FLuS) (Figure 1) transitions inserted into a WR28 waveguide T-junction (Figure 2). In this structure, 16 Monolithic Microwave Integrated Circuit (MMIC) Solid State Power Amplifiers (SSPA's) are integrated.

When devices operate in high efficiency regime, thermal expansion of materials may induce significant stresses and strains with consequent displacement of the guiding and combining structures, resulting in an undesired modification of the electromagnetic behavior of the device. For this reason, thermal exposition has been controlled by an opportune heat-sinker subjected to a cooling air flow (Figure 3).

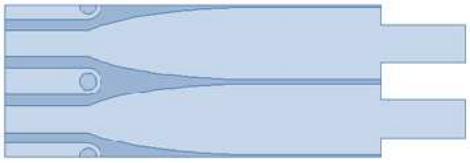

Figure 1: Quadruple FLuS employing the innovative dielectric Parallel QWT.

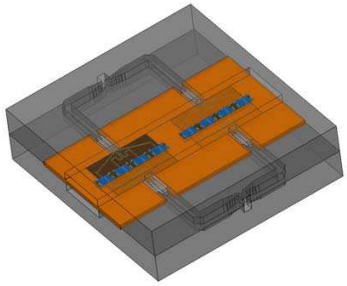

Figure 2: The complete Ka-band SPC Amplifier.

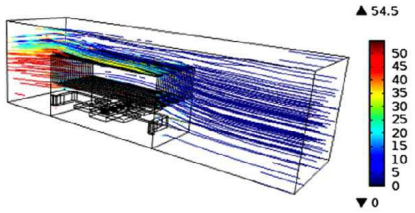

Figure 3: SPC subjected to the cooling airflow with temperature distribution (°C). Since the device has two symmetry planes, only a quarter of the SPC structure has been employed for the modeling by introducing opportune boundary conditions.

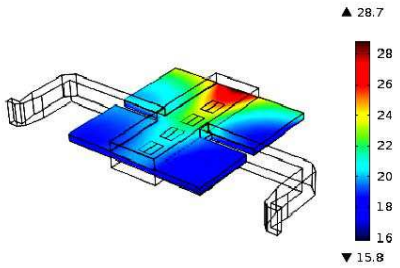

Figure 4: Maximum displacement on MMIC and carrier (μm). Thermal expansion induces a maximum displacement of 28.7 μm on the carrier.

Thermodynamic and Fluid-Dynamic analysis coupled to structural mechanics computation have been employed in order to study the effect of these critical factors. A main design has been followed by FEM simulation using Ansys-Ansoft HFSS and Comsol Multiphysics.

Scattering parameters, stresses and strains have been computed together with the temperature and airflow distributions. While operating at maximum power, the transistors present a maximum displacement of 28.7 μm (Figure 4) caused by the thermal expansion of the material due to a

channel temperature of 125°C (Figure 5). In such condition, a mean insertion loss of 2 dB for the passive SPC is achieved with a return loss better the 10 dB in the 31–37 GHz bandwidth (Figure 6).

In order to allow for the heat dissipation without mismatch between coefficients of thermal expansion (CTE) for GaAs and conductors, MMIC's are brazed onto CuMo heat spreader and the whole assembly is brazed onto copper carriers.

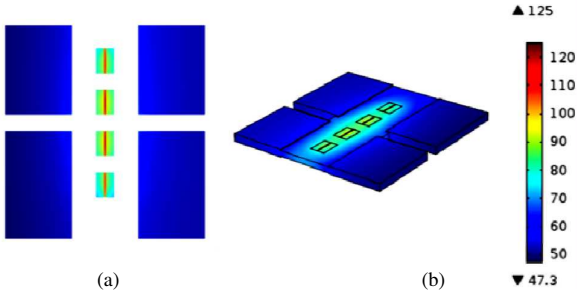

Figure 5: Temperature distribution (°C) on carrier and MMIC in (a) plane section and (b) 3D view. When the active devices operate at full power, the channels reach a maximum temperature of 125°C (below maximum rating).

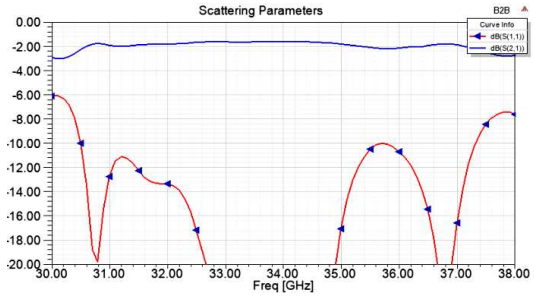

Figure 6: SPC insertion loss and return loss in dB.

Analysis of Bandpass Filters Consisting of Air Holes in Post-wall Waveguides

Ken'ichiro Yashiro[1] and Ning Guan[2]

[1]Chiba University, 1-33, Yayoi-cho, Inage-ku, Chiba 263-8522, Japan
[2]Fujikura Ltd., 1440, Matsuzaki, Sakura 285-8550, Japan

Abstract— A post wall waveguide is a promising candidate for the development of low cost circuits in the millimetre-wave region. The post wall waveguide consists of metallized dielectric substrate and arrays of metallic posts. If some air holes are set up in the post-wall waveguige, they have a filtering function. It is prospected to fabricate air holes easier than post-wall waveguide itself.

In this paper, we analyse the air-hole bandpass filter shown in Fig. 1. To do so, we developed the technique based on the method of moments. In order to treat the penetrating circular cylinders such as dielectric cylinders in the same way as perfect conductive cylinders, we assume the equivalent surface currents on the surface of each cylinder. By using Green function, that is a Hankel function of 0-th order, the scattered fields are given in the integral form in terms of the equivalent surface currents. The surface current density on each cylinder is expanded into a series of global basis functions in the local polar coordinate system. The global basis functions were used to reduce the number of unknowns per cylinder and the necessary computer memory is also reduced. The integrals for the scattered fields are calculated analyticaly by using Graf's addition theorem. We introduce the surface impedance so that the boudary condition is imposed at the surfaces of all of cylinders in the unified manner, Furthermore, the Galerkin method was used to obtain a sytem of linear equations. That is, the global basis functions were also used as weighting functions. When the field point and the source point locate on the different cylinders, the Graf's addition theorem was used again to evaluate the elements of the coefficient matrix analytically.

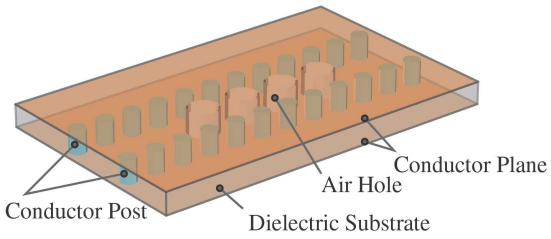

Figure 1: Air-holes in post-wall waveguide.

Several filters with the different number of air holes were analyzed and the frequency characteristics of them will be given. Furthermore, the electric field distributions are given for both cases of passband and stopband.

Bending-loss Improvement of Subwavelength Grating Waveguides by Using a Modified Structure

Hung-Hsuan Chen and Chin-Ping Yu
Department of Photonics, National Sun Yat-Sen University, Kaohsiung 80424, Taiwan

Abstract— Silicon on insulator (SOI) structures with high index contrast can efficiently reduce the device sizes to realize highly integrated optical circuits. However, due to their high confinement of lightwave, optical devices based on SOI structures suffer serious scattering losses resulted from the rough surfaces. In addition, the coupling effects and sensing abilities of SOI devices are relatively small due to only a few light field extended into the cladding regions. Recently, subwavelength grating (SWG) waveguides formed by periodically interlacing silicon segments at the subwavelength scale have been proposed to guide light in the SOI structures with larger extended filed in the cladding regions. In addition, it has been demonstrated that the propagation loss of SWG waveguides can be as low as 2.1 dB/cm for their delocalized mode field can reduce the scattering losses caused by the roughness of the vertical walls. However, the delocalization of mode filed in SWG waveguides may result in high bending losses, which limits the applications of SWG waveguides. In this study, we propose a modified bending SWG waveguide to reduce the bending losses. Along the bending, the rectangular segments are replaced by trapezoid segments with their bases are a and m, respectively. The numerical results obtained ny a 2-D finite element method (FEM) demonstrate that the larger base m can concentrate more field along the inner side of bending to prevent radiation losses as light propagates along the bending waveguide. We will also discuss the bending losses of our modified bending SWG waveguide for variant bending radii to help the development of optical devices based on SWGs.

Power Evaluation of a Metal Disc-shaped Terahertz Surface Wave Splitter

J. Shibayama, **D. Kusunoki**, **J. Yamauchi**, **and H. Nakano**
Faculty of Science and Engineering, Hosei University, Tokyo 184-8584, Japan

Abstract— Surface plasmon polaritons (SPPs) propagate along a metal-insulator interface at optical frequencies. At terahertz (THz) frequencies, however, SPPs cannot be supported along the metal-dielectric interface owing to negligible penetration of the electromagnetic fields. This is because THz frequencies are far below the plasma frequency of metal. Note, at THz frequencies, that spoof SPPs are supported on a metal surface with an array of holes, the sizes of which are much smaller than the THz wavelength [1]. For spoof SPP waves, bi- and multi-directional frequency splitters consisting of metal gratings with finite thickness have been studied numerically and experimentally [2]. The grating structures have also been investigated for slow wave devices [3].

Very recently, we have proposed novel splitters consisting of metal discs with a center hole and radially placed gratings [4, 5]. It has been shown that the discs act as frequency splitters at two, three and four frequencies. However, we have not evaluated the power propagating in each direction. In this presentation, we calculate the power based on the Poynting vector to investigate the splitting characteristics in detail. In addition, we illustrate the spoof SPP waves propagating along the disc, paying attention to the frequency splitting behavior.

REFERENCES

1. Maier, S. A., S. R. Andrews, L. Martín-Moreno, and F. J. García-Vidal, "Terahertz surface plasmon-polariton propagation and focusing on periodically corrugated metal wires," *Phys. Rev. Lett.*, Vol. 97, No. 17, 176805-1–4, 2006.
2. Zhou, Y. J., Q. Jiang, and T. J. Cui, "Bidirectional surface wave splitters excited by a cylindrical wire," *Opt. Exp.*, Vol. 19, No. 6, 5260–5267, 2011.
3. Gan, Q., Z. Fu, Y. J. Ding, and F. J. Bartoli, "Ultrawide-bandwidth slow-light system based on THz plasmonic graded metallic grating structures," *Phys. Rev. Lett.*, Vol. 100, No. 25, 256803-1–4, 2008.
4. Shibayama, J., J. Yamauchi, and H. Nakano, "Metal disc-type splitter with radially placed gratings for terahertz surface waves," *Electron. Lett.*, Vol. 51, No. 4, 352–353, 2015.
5. Inside view, "Surface plasmon polariton propagation properties can be used to split terahertz surface waves in multiple directions with metal disc-shaped devices," *Electron. Lett.*, Vol. 51, No. 4, 302, 2015.

Formation of One-dimensional Image by Pulsed Light Diffraction on Running Sound Wave

Victor Petrov[1] **and Roman Kijan**[2]

[1]St.-Petersburg Politechnical University, St.-Petersburg, Russia
[2]Laser Zentrum Hannover e.V., Hannover, Germany

Abstract— The advanced system for formation of a TV image on a projection screen is an acoustooptic system that relies on the principle of exposure of the entire TV 1D image by one laser radiation pulse and further deflection of 1D images across the frame will be presented. A general solution of the integral equation for a diffracted field for the case of wide-band anisotropic light diffraction by a slow shear elastic wave near the optical axis of an acoustooptic modulator (AOM) made from a crystal of paratellurite TeO_2 was found by us. We will discuss the solution for the diffracted field and consider the problem of formation of the image of an amplitude-modulated 1D image that fills the AOM aperture on the projection screen. For the practical realization a light source, a copper-vapor laser with wavelength $\lambda_0 = 0.5106\,\mu$m and generation pulse duration $\tau_0 = 10\,$ns was used.

In the approximation of a low diffraction efficiency, a two-dimensional field distribution in the (+1)st diffraction order in the focal plane of the input cylindrical lens and also time-average distribution of intensity of light from a pulsed coherent source in the image plane have been calculated. Calculations of the modulation-transfer function of the acoustooptic system for the 1D image formation including a pulsed copper-vapor laser and AOM from a paratellurite crystal (TeO_2) for different light pulse durations, carrier frequencies of ultrasound, acoustooptic interaction lengths, and also cones of angles of light incidence on the AOM in the plane orthogonal to the scattering plane have been carried out.

Numerical calculations have shown that an increase in the light pulse duration leads to a decrease in the contrast in transfer of amplitude-modulated signals at high frequencies. An increase in the contrast at high frequencies results from a decrease in the piezotransducer width and decrease in the carrier frequency of ultrasound. It approaches the frequency of two-phonon interaction.

It has been shown that in the case of incidence of a plane light wave on the input cylindrical lens, a dip of intensity associated with specific features of interference of diffracted elliptically-polarized light beams that propagate at different angles $\pm\alpha_0$ to the optical axis of the gyrotropic TeO_2 crystal is observed at the centre of the light intensity distribution along the y coordinate. When a light beam with angular divergence is incident on the input lens, the dip in the transverse distribution of intensity becomes less pronounced.

Requirements to the choice of the parameters of the optical components and AOM for the used geometry have been formulated.

Multi-physics Simulation for Evaluating High-density Magnetic Recording Methods

S. Ohnuki, **Y. Takano**, **A. Kuma**, **K. Tatsuzawa**,
Y. Ashizawa, **K. Nakagawa**, **and A. Tsukamoto**
College of Science and Technology, Nihon University
1-8-14 Surugadai, Kanda, Chiyoda-ku, Tokyo 101-8308, Japan

Abstract— High-density magnetic recording is an indispensable technology to develop storage devices for current big data demand. Some kinds of energy-assisted schemes using recording media with high magnetic anisotropy have become recent trend. In this presentation, we will discuss magnetization reversal process of high anisotropy recording media using micromagnetic and electromagnetic simulation and numerically verify a high-density recording method with assisted microwave irradiation. To evaluate exchange and magnetic dipole interactions efficiently, a fast computational method will be proposed and the effect of assisted microwave will be clarified.

We will also discuss another novel method, all-optical magnetic switching (AOS) with circularly polarized light, which has been recently discovered by one of the authors [1]. To localize the polarized light for triggering AOS beyond the diffraction limit, the higher density over 2 Tbit/inch^2 can be achieved [2–4]. Using FDTD electromagnetic simulation with the auxiliary motion equation of electrons, robust and efficient plasmonic antennas to generate the localized light will be designed. The surfaces of antennas are assumed to be perturbed considering nano-fabrication process. Characteristics of antennas are evaluated in terms of the Stokes parameters.

REFERENCES

1. Stanciu, C. D., F. Hansteen, A. V. Kimel, A. Kirilyuk, A. Tsukamoto, A. Itoh, and Th. Rasing, *Phys. Rev. Lett.*, Vol. 99, 047601-1–047601-4, Jul. 2007.
2. Nakagawa, K., Y. Ashizawa, S. Ohnuki, A. Itoh, and A. Tsukamoto, *J. Appl. Phys.*, Vol. 109, No. 7, 07B735-1–07B735-3, Apr. 2011.
3. Kishimoto, S., S. Ohnuki, Y. Ashizawa, K. Nakagawa, and W. C. Chew, "Time domain analysis of nanoscale electromagnetic problems by a boundary integral equation method with fast inverse laplace transform," *Journal of Electromagnetic Waves and Applications*, Vol. 26, Nos. 8–9, 997–1006, Jul. 2012.
4. Ohnuki, S., T. Kato, Y. Takano, Y. Ashizawa, and K. Nakagawa, *Radio Science*, Vol. 50, No. 1, 29–40, 2015.

Surface Plasmon Resonances in Cylindrical Periodic Nanocylinders System

Vakhtang Jandieri[1, 2], **Kiyotoshi Yasumoto**[3], **and Jaromir Pistora**[1]

[1]Nanotechnology Centre, VSB — Technical University of Ostrava
17. listopadu 15, 708 33 Ostrava, Poruba, Czech Republic
[2]Department of Electrical and Computer Engineering, Free University of Tbilisi
Tbilisi 0179, Republic of Georgia
[3]College of Information Science and Technology, Nanjing Forestry University, Nanjing 210037, China

Abstract— Interaction of light with the metallic nanostructures and nanoparticles gives rise to various unique and surprising effects in photonics and optoelectronics [1]. The surface plasmons characterize the unique response in collective motions of electrons on a metal-dielectric interface, which is allowed when the permittivity of the metal is negative for the wavelength of excitation. Recently, much attention has been paid to the light scattering from *metal-dielectric* layered structures, because of their novel applications in sensors, super-scattering and invisible cloaking. Surface plasmons are accompanied by localized enhancement of the electromagnetic field. This leads to developing metallic nanostructures that can control light at the nanoscale in direct analogy to traditional optical components such as lens, mirrors and waveguides. Many of these applications rely on a planar geometry in practice.

An alternative of the planar configuration is a cylindrical configuration. In this regard, in the manuscript we investigate the light scattering by metal (silver)-coated dielectric nanocylinders periodically distributed along the cylindrical surface. The rigorous formulation uses T-matrix of a circular scatterer in isolation and it is taking into account all cylindrical Floquet modes and their interactions through the scattering between the nanocylinders periodically distributed along the circular ring [2]. The structure is under our interest from the viewpoint of its practical applications as plasmonic waveguides, plasmonic lasers and plasmonic ring resonators.

We investigate up to four metal (silver)-coated dielectric nanocylinders periodically located along the circular ring in a free space. Firstly, the scattering and absorption cross sections of three and four metal (silver)-coated nanocylinders are studied at various distances between the nanocylinders keeping their radii the same. The resonances appearing in the short wavelength region correspond to the plasmon resonances of metal-coated nanocylinders in isolation and the resonance wavelengths does not change by changing the separation distance between the nanocylinders. The spectral responses show some interesting profile characterizing the cylindrical configuration of the nanocylinders. When a separation distance between the nanocylinders is small (the nanocylinders are located very close, but not touching each other), there appear resonance peaks in the long wavelength region for both scattering and absorption cross sections. These resonances are characterized as the resonances intrinsic to the cylindrically periodic system. Other resonances appearing in the intermediate wavelength region describe the resonant coupling of the surface plasmon fields in the multiple nanocylinders systems.

Based on the analyses of the spectral responses, the near field distributions are calculated at the particular wavelengths corresponding to the resonance wavelengths. A deep physical insight is given to **a)** enhancement of the near fields at the inner (metal-dielectric) and outer (metal-free space) interfaces (corresponding to the resonances in the short wavelength region); **b)** localization of the excited field in the gap region between the nanocylinders through the coupled plasmon resonance (corresponding to the resonances in the intermediate wavelength region); **c)** strong confinement of the field inside the cylindrical structure (corresponding to the resonances in the long wavelength region). The latter uniquely characterizes the cylindrical configuration of the nanocylinders.

REFERENCES

1. Berini, P., "Long-range surface plasmon polaritons," *Advances in Optics and Photonics*, Vol. 1, 484, 2009.
2. Jandieri, V., K. Yasumoto, and Y. Liu, "Directivity of radiation of a dipole source coupled to cylindrical electromagnetic bandgap structures," *J. Opt. Soc. Am. B*, Vol. 29, 2622, 2012.

Comparative Study on Boundary Conditions for Terminating Photonic Crystal Waveguides

Zhen Hu[1] and Ya Yan Lu[2]

[1]Department of Mathematics, Hohai University, Nanjing, China
[2]Department of Mathematics, City University of Hong Kong, Hong Kong, China

Abstract— Photonic crystal (PhC) devices often use PhC waveguides as input and output ports. These periodic waveguides create a significant problem for numerical simulations of PhC devices, since they cannot be easily truncated to obtain a finite computation domain. The perfectly matched layer (PML) technique is extremely powerful for truncating unbounded homogeneous media in numerical simulations of waves [1], and it has been tried on PhC waveguides [2], but it fails to accurately simulate outgoing Bloch modes in PhC waveguides [3]. On the other hand, it is possible to numerically calculate a rigorous boundary condition for terminating a PhC waveguide. Joly et al. first applied the so-called limiting absorption principle [4] to calculate such a boundary condition. We have used Bloch mode expansions to find the same boundary condition [5]. The rigorous boundary condition can be used arbitrarily close to the main part of the device, but it is nonlocal, and is rather expensive for slab-based PhC devices. In [6], we developed a simpler and approximate boundary condition that models the outgoing Bloch modes accurately, but assumes that the evanescent modes and other radiating field can be ignored. In this paper, we compare different methods for truncating PhC waveguides, analyze the limitations of various methods in terms of accuracy or computational cost. The results are illustrated by numerical examples.

REFERENCES

1. Berenger, J., "A perfectly matched layer for the absorption of electromagnetic waves," *J. Comput. Phys.*, Vol. 114, 185–200, 1994.
2. Koshiba, M., Y. Tsuji, and S. Sasaki, "High-performance absorbing boundary conditions for photonic crystal waveguide simulations," *IEEE Micr. and Wireless Comp. Lett.*, Vol. 11, 152–154, 2001.
3. Oskooi, A. F., L. Zhang, Y. Avniel, and S. G. Johnson, "The failure of perfectly matched layers, and towards their redemption by adiabatic absorbers," *Optics Express*, Vol. 16, 11376–11392, 2008.
4. Joly, P., J.-R. Li, and S. Fliss, "Exact boundary conditions for periodic waveguides containing a local perturbation," *Commun. Comput. Phys.*, Vol. 1, 945–973, 2006.
5. Hu, Z. and Y. Y. Lu, "Efficient analysis of photonic crystal devices by Dirichlet-to-Neumann maps," *Optics Express*, Vol. 16, 17383–17399, 2008.
6. Hu, Z. and Y. Y. Lu, "A simple boundary condition for terminating photonic crystal waveguides," *Journal of the Optical Society of America B*, Vol. 29, 1356–1360, 2012.

Study on Polarization Splitter and Converter Using Square Lattice Elliptical-hole Core Circular-hole Holey Fibers

Zejun Zhang[1], **Yasuhide Tsuji**[1], **and Masashi Eguchi**[2]

[1]Division of Information and Electronic Engineering
Muroran Institute of Technology, Muroran 050-8585, Japan
[2]Department of Photonics System Technology
Chitose Institute of Science and Technology, Chitose 066-8655, Japan

Abstract— Recently, the importance of silicon photonic integrated circuits has been widely recognized, especially in silicon-on-insulator (SOI) platform due to its advantage of hight-index-contrast and CMOS-compatible processing. However, the polarization dependent characteristics limit the application of silicon photonics devices. To overcome this problem, polarization diversity scheme is often used, where polarization converters (PCs) are the fundamental components. Photonic crystal fibers (PCFs), also known as holey fibers (HFs), which consisting of single material with periodical array of air holes around the fiber core, have attracted a lot of attention in the last two decades due to their flexible structure and the special properties that cannot be obtained by the conventional fibers. In recent years, elliptical-hole core circular-hole holey fiber (EC-CHF), a novel single-polarized holey fiber with a core filled with elliptical-holes, has been proposed for achieving the single polarization transmission easily [1]. In this research, we propose a novel PC using square lattice EC-CHFs with a short conversion length and a simple structure distribution. In addition, we combine the PC with a polarization splitter which we have proposed [2] to achieve the polarization separation and conversion at the same time.

In this research, we introduced elliptical-holes whose major axis rotated 45° counterclockwise against x-axis into the core region to achieve the polarization conversion. The ellipticity is set to $d_{\mathrm{major}}/d_{\mathrm{minor}} = 2$, and the holes in cladding is circular air holes. Since the large birefringence can be realized in the core region by using ellipses, our proposed PC has a short conversion length which consists of only two kinds of air holes. The air hole size dependence of conversion length has been discussed by using full-vector finite-element method (FV-FEM). From the analysis results, we note that if the diameter of cladding hole is set to be a constant, the conversion length has a minimum value with the variation of ellipses in core region. The shortest conversion length can be up to 31.7 μm. The propagation behaviors by using full-vector finite-element beam propagation method (FEBPM) shown that an x-polarized incident light can be completely converted into a y-polarized light through our proposed PC. Moreover, we demonstrated that the polarization splitter in [2] can completely divide an arbitrarily polarized light beam into two orthogonal polarization states based on square lattice EC-CHFs. In the future, we consider a kind of polarization splitter and converter based on square lattice EC-CHFs to achieve the polarization separation and conversion at the same time.

REFERENCES

1. Eguchi, M. and Y. Tsuji, "Design of single-polarization elliptical-hole core circular-hole holey fiber with zero dispersion at 1.55 μm," *J. Opt. Soc. Am. B*, Vol. 25, No. 10, 1690–1701, Oct. 2008.
2. Zhang, Z., Y. Tsuji, and M. Eguchi, "Study on crosstalk-free polarization splitter with ellipticalhole core circular-hole holey fibers," *J. Lightwave Technol.*, Vol. 32, No. 23, 3956–3962, Dec. 2014.

Broadband Line Imaging with Subwavelength Resolution Using Plasmonic Waveguides

Nina Podoliak[1], **Peter Horak**[1], **Jord C. Prangsma**[2], **and Pepijn W. H. Pinkse**[2]

[1]Optoelectronics Research Centre, University of Southampton, Southampton SO17 1BJ, United Kingdom
[2]MESA+ Institute for Nanotechnology, University of Twente
P. O. Box 217, 7500 AE Enschede, The Netherlands

Abstract— In this paper we design a high-resolution line imaging device allowing for broadband operation at near-infrared wavelengths ranging from 1 µm to 2 µm utilizing the advantage of subwavelength light confinement in plasmonic waveguides. The device consists of an array of air-guided plasmonic waveguides in gold with fanned-out geometry (see Fig. 1(a)) [1]. In the main part of the device the separation between waveguides increases gradually from the input towards the output. High resolution is achieved on the input side by tapering down the periodicity between channels to 150 nm, while simultaneously maintaining propagation losses of a few dB. The proposed design also minimizes optical cross-coupling between waveguides; each channel thus transmits optical fields independently allowing for high signal-to-noise ratio imaging. At the low-resolution side properly tailored output couplers are designed to enhance optical coupling to free space. This is also shown to be an effective method to reduce back reflection, thus minimizing Fabry-Pérot effects in the waveguides and allowing for broadband operation.

The imaging capacity of the device is demonstrated using finite-element simulations (see Fig. 1(a)). The numerical model shows that up to 90% of the light from two closely spaced point dipole emitters can be coupled into the corresponding waveguides on the high-resolution side and can be transmitted to the low-resolution side with moderate losses and low cross talk. Thus, two point dipole sources separated by 150 nm can be effectively distinguished by such a device. Moreover, consistent operation in the whole wavelength range from approximately 1 µm to above 2 µm is demonstrated. Fig. 1(b) shows total losses of each channel calculated for a set of wavelengths. At wavelengths near 1 µm the loss increase is caused by gold material absorption, while at wavelengths above 2 µm cross-coupling between channels limits the device performance. For the proposed device dimensions (shown in the inset in Fig. 1(b)), the array can contain up to 19 channels, which is limited by cross-coupling and losses caused by sharp channel bending.

Exhibiting large coupling efficiency and moderate transmission losses, the device allows for imaging of weak sources with a resolution of 150 nm over a broad bandwidth in the near-infrared range. This device can be effectively applied as a high-resolution linear image detector or, by operating in the reverse, for high-resolution optical writing.

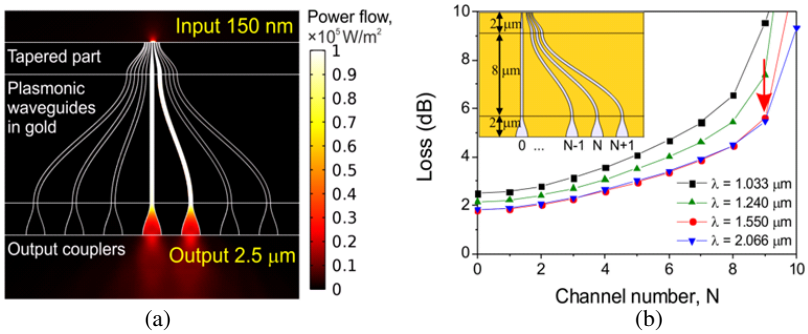

Figure 1: (a) Optical power flow inside the plasmonic waveguides excited by two incoherent point dipole sources emitting at 1.55 µm and separated by 150 nm. (b) Propagating loss of each channel for wavelengths between 1 µm and 2 µm. Inset shows the device dimensions.

REFERENCES

1. Podoliak, N., P. Horak, J. C. Prangsma, and P. W. H. Pinkse, *IEEE J. Quantum Electron.*, Vol. 51, 7200114, 2015.

Surface Plasmon Resonance Sensing in the THz Regime

J. Shibayama, **K. Shimizu**, **J. Yamauchi**, **and H. Nakano**
Faculty of Science and Engineering, Hosei University, Tokyo 184-8584, Japan

Abstract— The characteristics of surface plasmon polaritons (SPPs) are quite sensitive to the property of a dielectric material on a thin metal layer. Using these characteristics, surface plasmon resonance (SPR) sensors have widely been investigated [1] and already been made available commercially. Note that the SPPs are excited along a metal-dielectric interface at optical frequencies. On the other hand, at terahertz (THz) frequencies, InSb exhibits a negative permittivity as in metal at optical frequencies. In addition, an interesting feature of InSb is its permittivity varying with temperature. Recently, THz plasmonic filters and lenses consisting of InSb have been studied theoretically [2–4].

In this article, we investigate an SPR waveguide sensor with InSb at THz frequencies. The dispersion of InSb is efficiently taken into account using the frequency-dependent FDTD method based on the trapezoidal recursive convolution technique [5]. It is shown that the sensor exhibits an SPR response versus THz frequency, the peak frequency of which is around 1 THz. We also calculate the SPR curves with varying temperature, showing a possibility of realizing an SPR sensor in the THz regime.

REFERENCES

1. Shibayama, J., "Three-dimensional numerical investigation of an improved surface plasmon resonance waveguide sensor," *IEEE Photon. Technol. Lett.*, Vol. 22, No. 9, 643–645, 2010.
2. Tao, J., B. Hu, X. Y. He, and Q. J. Wang, "Tunable subwavelength terahertz plasmonic stub waveguide filters," *IEEE Trans. Nanotech.*, Vol. 12, No. 6, 1191–1197, 2013.
3. Shibayama, J., Y. Wada, J. Yamauchi, and H. Nakano, "Application of the explicit and implicit FDTD methods to the analysis of a terahertz plasmonic grating," *Progress In Electromagnetics Research Symposium Abstracts*, 1904, Guangzhou, China, August 25–28, 2014.
4. Chen, M. K., Y. C. Chang, C. E. Yang, Y. Guo, J. Mazurowski, S. Yin, P. Ruffin, C. Brantley, E. Edwards, and C. Luo, "Tunable terahertz plasmonic lenses based on semiconductor microslits," *Microw. Opt. Tech. Lett.*, Vol. 52, No. 4, 979–981, 2010.
5. Shibayama, J., R. Ando, A. Nomura, J. Yamauchi, and H. Nakano, "Simple trapezoidal recursive convolution technique for the frequency-dependent FDTD analysis of a Drude-Lorentz model," *IEEE Photon. Technol. Lett.*, Vol. 21, No. 2, 100–102, 2009.

RF Design of Input Cavity Structure of a Low Frequency, High Average Power IOT

Meenu Kaushik[1, 2] **and L. M. Joshi**[1, 2]

[1]CSIR-Central Electronics Engineering Research Institute (CEERI), Pilani, Rajasthan, India
[2]Academy of Scientific and Innovative Research (AcSIR), New Delhi, India

Abstract— Inductive Output Tube (IOT) is a vacuum electron tube device capable of amplifying RF power with very good efficiency. The major components of an IOT are electron gun, input/output cavities, input/output couplers, focussing magnet and collector.

IOT has been extensively used in TV services as UHF transmitters to amplify both audio and video signals. Its power gain, high efficiency and long life make it suitable for this application. Besides that, this tube has been proving its capability and reliability in scientific areas like in high energy particle accelerators and fusion plasma heating purposes.

The paper will present the RF design of input cavity of a low frequency IOT carried out at CSIR-CEERI. It is an important component of the device. The cavity should be smartly positioned so that the cathode-grid gap plays the role of cavity drift gap and contributes to the interaction between electron beam (emitting from the electron gun) and the input RF signal (applied at the cathode-grid gap). One key issue is that the cavity operates in grounded mode and in this case, the inner wall of the cavity is connected to the cathode and grid, having high negative potentials, hence proper isolation of the input circuit is mandatory for its successful operation. The simulation of the cavity has been carried out in CST and MAGIC2D codes. The CAD drawings have been prepared and the cavity structure has been fabricated. The details of design approach using CAD tools and cold test results shall be presented in this paper.

REFERENCES

1. Kowalczyk, R. D., "Input circuit for a wideband IOT," L-3 Communications Electron Devices, USA, IEEE, 2007.
2. McGinnis, D. and M. Lindroos, "The European spallation source," *2013 IEEE 14th International Vacuum Electronics Conference (IVEC)*, 21–23, Paris, May 2013.

Session 1P13a
FocusSession.SC3: Solid-state Quantum Photonics 2

Quantum Optics with Solid-state Spins and Photons

Mete Atatüre
Cavendish Laboratory, University of Cambridge, JJ Thomson Avenue, Cambridge CB3 0HE, UK

Abstract— Spins confined in solids, such as quantum dots and atomic impurities provide interesting and rich physical systems. Their inherently mesoscopic nature leads to a multitude of interesting interaction mechanisms of confined spins with the solid state environment of spins, charges, vibrations and light. Implementing a high level of control on these constituents and their interactions with each other creates exciting opportunities for realizing stationary and flying qubits within the context of spin-based quantum information science. I will provide a snapshot of the progress and challenges for optically interconnected spins, as well as first steps towards hybrid distributed quantum networks involving other physical systems.

A Spin-photon Interface in the Solid State

J. Demory[1], **C. Arnold**[1], **V. Loo**[1], **A. Lemaître**[1], **I. Sagnes**[1], **M. Glazov**[2], **O. Krebs**[1], **P. Voisin**[1], **P. Senellart**[1], **and L. Lanco**[1, 3]

[1]Laboratoire de Photonique et de Nanostructures, CNRS, Marcoussis 91460, France
[2]Ioffe Physical-Technical Institute of the RAS, St-Petersburg 194021, Russia
[3]Département de Physique, Université Paris Diderot, Paris 7, Paris 75205, France

Abstract— A quantum-dot (QD) strongly-coupled to a cavity mode is an extremely sensitive device whose optical properties can be controlled with single incident photons. A key requirement in this context is the fabrication of state-of-the-art cavity-QED devices using micropillars: indeed, pillar cavities can demonstrate a maximized light-matter interaction (thanks to deterministic coupling techniques [1]) together with high coupling efficiencies and quality factors [2]. The optical properties of these devices can then be probed using high-resolution resonant spectroscopy techniques [3], and be exploited for various applications such as few-photon optical nonlinearity [4] or optical nanosensing [5].

In this presentation, we will focus on the development of a cavity-based spin-photon interface [6], making use of the rotation of optical polarization (Faraday or Kerr rotation) induced by a single spin in a cavity-QED device. This approach allows interfacing the spin with a photon generated by an external source, thus opening new possibilities in quantum optics. Up to now, however, Faraday/Kerr rotations induced by a single spin were reported only recently, with rotation angles in the few 10^{-3} degrees range.

Here, thanks to the cavity-QED enhancement of the spin-photon interaction, we report a huge amplification of the spin-photon interaction. As illustrated in Fig. 1(a), the reflected probe beam polarization is rotated clockwise or counter-clockwise depending on the spin state. Fig. 1(b) shows the Kerr rotation angle as a function of the probe energy: a macroscopic Kerr rotation of $\pm 6°$ (depending on the spin state) is demonstrated for the reflected probe beam, three orders of magnitude higher than the previous state of art [6].

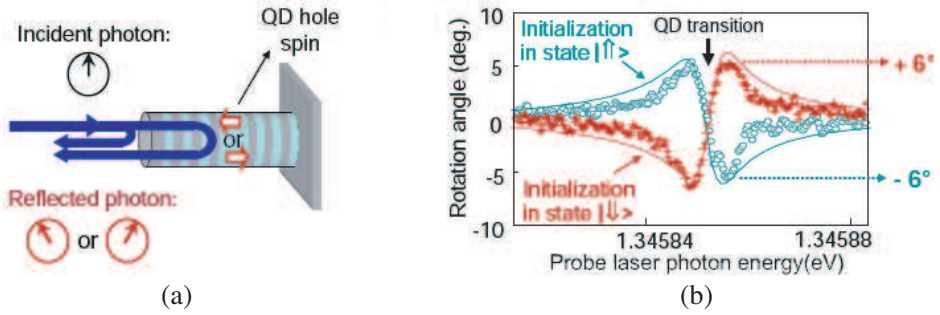

Figure 1: (a) Spin-dependent polarization rotation for the reflected probe beam. (b) Demonstration of giant Kerr rotation induced by a single spin. The spin state is pumped in the up or down state by a resonant pump beam, and a spin-dependent Kerr rotation up to $\pm 6°$ is observed.

In addition, cavity-QED calculations allow us to predict that an optimized device will be able to act as a spin-photon entangler with a unity-fidelity. It will also be possible to perform a perfect quantum non demolition measurement, projecting the spin qubit on either its up or down state, using a single photon detected by a photon counter. This novel way of interfacing a flying qubit and a solid-state quantum memory opens the road for a wide range of applications for quantum information processing and long-distance quantum communication.

REFERENCES

1. Dousse, A., L. Lanco, J. Suffczynski, E. Semenova, A. Miard, A. Lemaître, I. Sagnes, C. Roblin, J. Bloch, and P. Senellart, "Controlled lightmatter coupling for a single quantum dot embedded in a pillar microcavity using optical lithography," *Phys. Rev. Lett.*, Vol. 101, 267404, 2008.
2. Arnold, C., V. Loo, A. Lemaître, I. Sagnes, O. Krebs, P. Voisin, P. Senellart, and L. Lanco, "Optical bistability in a quantum dots/micropillar device with a quality factor exceeding 200 000," *Appl. Phys. Lett.*, Vol. 100, 111111, 2012.

3. Loo, V., L. Lanco, A. Lemaître, I. Sagnes, O. Krebs, P. Voisin, and P. Senellart, "Quantum dot-cavity strong-coupling regime measured through coherent reflection spectroscopy in a very high-Q micropillar," *Appl. Phys. Lett.*, Vol. 97, 241110, 2010.
4. Loo, V., C. Arnold, O. Gazzano, A. Lemaître, I. Sagnes, O. Krebs, P. Voisin, P. Senellart, and L. Lanco, "Optical nonlinearity for few-photon pulses on a quantum dot-pillar cavity device," *Phys. Rev. Lett.*, Vol. 109, 166806, 2012.
5. Arnold, C., V. Loo, A. Lemaître, I. Sagnes, O. Krebs, P. Voisin, P. Senellart, and L. Lanco, "Cavity-enhanced real-time monitoring of singlecharge jumps at the microsecond time scale," *Phys. Rev. X*, Vol. 4, 021004, 2014.
6. Arnold, C., J. Demory, V. Loo, A. Lemaître, I. Sagnes, M. Glazov, O. Krebs, P. Voisin, P. Senellart, and L. Lanco, "Macroscopic rotation of photon polarization induced by a single spin," *Nature Communications*, Vol. 6, 6236, 2015.

Nitrogen-vacancy Defects in Diamond Coupled to Open Microcavities — Towards an Efficient Spin-photon Interface

S. Johnson, Y. C. Chen, L. Weng, P. R. Dolan, A. A. P. Trichet, and J. M. Smith
Department of Materials, University of Oxford, Oxford OX1 3PH, UK

Abstract— The realisation of an efficient spin-photon interface using the negatively charged nitrogen-vacancy centre (NV-) in diamond requires the resonant coupling of the zero phonon line (ZPL) of the centre to an optical microcavity [1]. The cavity serves to encourage emission into the ZPL in preference to the phonon sidebands, and potentially also to increase the homogeneous linewidth via a reduction of the lifetime (the Purcell effect) thus assisting in the generation of indistinguishable photons. Cavity coupling thus has potential to improve by orders of magnitude the speed with which entanglement can be created between spatially remote NV-centres [2], and to enable other mechanisms for realising spin-photon interfaces via non-demolition measurements [3]. Some previous demonstrations of ZPL coupling have been reported in monolithic cavities [4–6], but it is difficult to achieve optimal positioning of the emitter and resonant tuning in these structures.

Here we report on the coupling of ZPLs of single NV-centres to open microcavities at low temperature. The NV-centres are in nanodiamond produced by high pressure high temperature methods, while the open cavity is of a plano-concave design with the concave mirror substrate produced by the focused ion beam milling method [7]. The cavity has a mode volume around $2\,\mu m^3$ and a quality factor of about 1000. The cavity mirrors are mounted on piezoelectric actuators that enable tuning of the cavity mode wavelength and positioning of the nanodiamond in the confined cavity mode *in-situ*, whilst cooled to 77 K. We use registration marks on the planar mirror (onto which the nanodiamond is spin cast), to enable characterisation and recording of the positions of nanodiamonds of interest so that direct comparison can be made between the free-space and cavity-coupled behaviour of the same NV-centre, giving a direct measure of the effect of the cavity.

We will present data showing the change in fluorescence properties (spectrum, lifetime) as the cavity mode is tuned through resonance with an NV-centre ZPL. A significant enhancement of the emission into the cavity mode is observed on resonance. The ZPL is increased by about a factor of 10 relative to free-space emission as a result of the cavity coupling, so that it constitutes almost half of the total fluorescence and up to 15,000 photon counts/s on the detector. We will discuss the outlook for further enhancements and the prospects for realising a highly efficient quantum interface between the NV-spin state and an optical photon.

REFERENCES

1. Benjamin, S. C., B. W. Lovett, and J. M. Smith "Prospects for measurement-based quantum computing using solid state spins," *Laser & Photon. Rev.*, Vol. 3, 556, 2009.
2. Bernien, H., B. Hensen, W. Pfaff, G. Koolstra, M. S. Blok, L. Robledo, T. H. Taminiau, M. Markham, D. J. Twitchen, L. Childress, and R. Hanson, *Nature*, Vol. 497, 86, 2013.
3. Hu, C. Y., A. Young, J. L. O'Brien, W. J. Munro, and J. G. Rarity, *Phys. Rev. B*, Vol. 78, 085307, 2008.
4. Faraon, A., P. E. Barclay, C. Santori, K.-M. C. Fu, and R. G. Beausoleil, *Nature Photon.*, Vol. 5, 301, 2011.
5. Faraon, A., C. Santori, Z. Huang, V. M. Acosta, and R. G. Beausoleil, *Phys. Rev. Lett.*, Vol. 109, 033604, 2012.
6. Li, L., T. Schröder,, E. H. Chen, M. Walsh, I. Bayn, J. Goldstein, O. Gaathon, M. E. Trusheim, M. Lu, J. Mower, M. Cotlet, M. L. Markham, D. J. Twitchen, and D. Englund, *Nature Commun.*, Vol. 6, 6173, 2015.
7. Dolan, P. R., G. M. Hughes, F. Grazioso, B. R. Patton, and J. M. Smith, *Optics Lett.*, Vol. 35, 3556, 2010.

NV Center Dynamics in the Vicinity of a Metallic Mirror

Alexander Huck[1], **Niels M. Israelsen**[1], **Shailesh Kumar**[1, 2], **Jonas S. Neergaard-Nielsen**[1], **and Ulrik L. Andersen**[1]

[1]Department of Physics
Technical University of Denmark, Fysikvej, Kgs. Lyngby 2800, Denmark
[2]Institute of Technology and Innovation
University of Southern Denmark, Campusvej 55, Odense 5230, Denmark

Abstract— The spontaneous emission rate of an emitter depends on the local photonic environment and can strongly be modified when the emitter is placed in the vicinity of a planar reflecting interface such as a silver mirror. By recording the spontaneous emission rate as function of the emitter mirror distance, information on the decay rate modification can be used, for instance, to determine the emitters dipole orientation, its intrinsic quantum efficiency, and to reveal higher order transition moments.

In this contribution we report on modifications of the spontaneous emission rate of nitrogen vacancy (NV) centers embedded in diamond crystals and placed in the vicinity of a planar silver mirror. The silver mirror was prepared on the end facet of a cleaved optical fiber and mounted on a piezo stage. At room temperature the emission spectrum of NV centers is characterized by a zero phonon line at 637 nm and a red shifted broad phonon sideband centered around 700 nm with a bandwidth of approximately 150 nm. When recording the decay rate as a function of NV center mirror distance we only observe small spontaneous emission rate modifications. These small modification we associate with the NV centers broad emission spectrum and averaging over the entire bandwidth. In contrast to the total decay rate, the broad emission spectrum is strongly modified in the vicinity of the mirror. To model our findings we use a rate equation approach taking into account scattering of photons on the broad phonon spectrum associated with the diamond lattice.

Infrared Counting and Imaging at Single-photon Frontier with Superconducting Nanowires

Alessandro Casaburi
University of Glasgow, UK

Abstract— Advances in materials growth and nanopatterning have enabled the creation of a new class of ultra-sensitive optical detector: the superconducting nanowire single-photon detector (SNSPD) [1]. These devices offer exquisite sensitivity and low noise at infrared wavelengths, far outperforming off-the-shelf alternatives such as semiconductor avalanche photodiodes and photomultiplier tubes [2]. The potential of SNSPDs has been demonstrated in a range of important scientific applications, including quantum cryptography [3], remote sensing [4] and laser-based cancer treatment [5]. Our efforts are focussed on the development of next generation SNSPDs employing state-of-the-art nanofabrication techniques, sensor configurations and innovative materials.We will review the results obtained with these innovative sensors in the recent years and describe how these devices can be modified to satisfy the stringent requirements of future applications. In this work, we will give a short overview on our recent results concerning direct detection of singlet oxygen luminescence [6], fibre Raman temperature sensing [7, 8] time-of-flight depth imaging [9]. We will also present results on the realization and characterization of a 2×2 SNSPDs array [10] to scale up the sensitive area of the detector at $60 \times 60\,\mu m^2$ for multimode fibre optical coupling on the perspectives for next future applications.

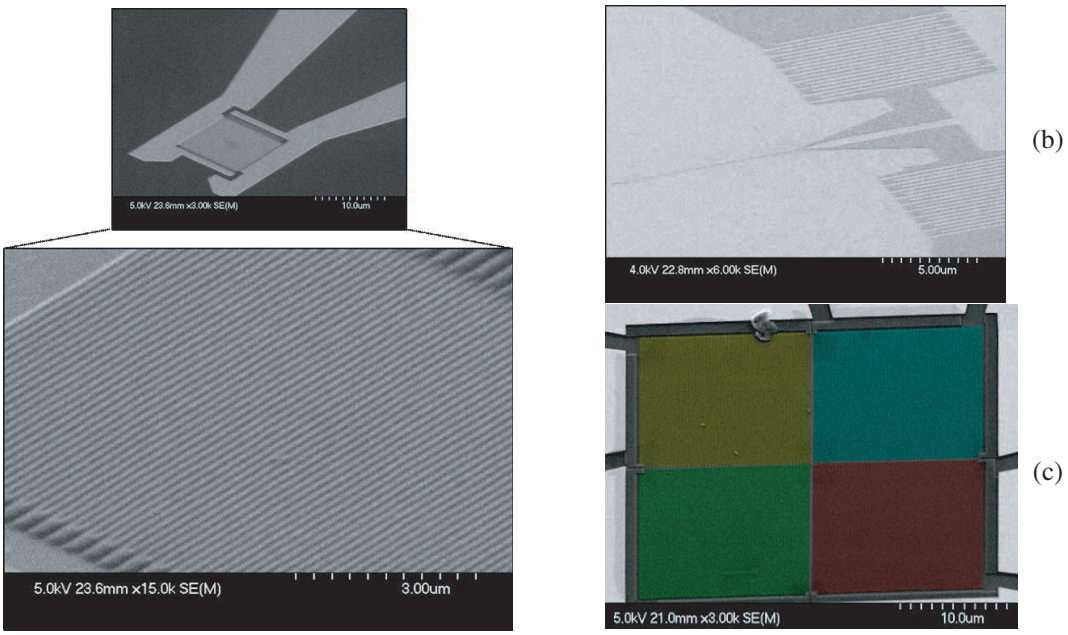

Figure 1: Next generation Superconducting Nanowire Single Photon Detectors (SNSPDs) under development at the University of Glasgow, UK. (a) Meander type single pixel (10 micrometre width) SNSPD. (b) Waveguide integrated SNSPD concept. (c) 2×2 SNSPD array ($30 \times 30\,\mu m^2$).

REFERENCES

1. Natarajan,C. M., et al., *Supercond. Sci. and Technol.*, Vol. 25, 063001, 2012.
2. Hadfield, R. H., *Nature Photonics*, Vol. 3, 696, 2009.
3. Takesue, H., et al., *Nature Photonics*, Vol. 1, 343, 2007.
4. Tanner, M. G., et al., *Applied Physics Letters*, Vol. 99, 201110, 2011.
5. Gemmell, N. R., et al., *Optics Express*, Vol. 21, 5005, 2013.
6. Gemmell, N. R., et al., *Optics Express*, Vol. 21, 5005–5013, 2013.

7. Tanner, M. G., et al., *Applied Physics Letters*, Vol. 99, 201110, 2011.
8. Dyer, S. D., et al., *Optics Express*, Vol. 20, 3456, 2012.
9. McCarthy, A., et al., *Optics Express*, Vol. 21, 8904–8915, 2013.
10. Casaburi, A., et al., *IEEE Xpl., Photonics Technologies, Proc. Fotonica AIET Italian Conference*, 2014, DOI: 10.1109/Fotonica.2014.6843851.

Experimental Demonstration of Chiral Light-mater Interaction: Towards On-chip Non-reciprocal Photonic Elements and Quantum-information Processing

I. Söllner[1], S. Mahmoodian[1], S. Lindskov Hansen[1], L. Midolo[1], A. Javadi[1], G. Kiršanskė[1], T. Pregnolato[1], H. El-Ella[1], E. H. Lee[2], J. D. Song[2], S. Stobbe[1], and P. Lodahl[1]

[1]Niels Bohr Institute, University of Copenhagen
Blegdamsvej 17, Copenhagen DK-2100, Denmark
[2]Center for Opto-Electronic Convergence Systems
Korea Institute of Science and Technology, Seoul 136-791, Korea

Abstract— Quantum dots (QDs) in photonic nanostructures open a promising route towards realizing all-solid-state scalable quantum networks for quantum-information processing [1]. In such networks single photons will serve as ying qubits, while the internal spin state of a single electron or hole trapped in the QD serves as the stationary qubit. For this vision to be realized it is necessary to create a spin-photon interface such that different spin states within quantum dots interact with orthogonal optical modes with near-unity efficiency. We have recently shown that photonic crystal waveguides (PCW) allow near-unity coupling efficiency, $\beta \sim 1$, with an embedded quantum dot [2]. However, interfacing different QD spin states with orthogonal modes with near-unity efficiency remains a challenge [3]. Here we show that by manipulating the geometry of a conventional PCW, we can design a new waveguide whose modes have a broadband in-plane circular polarization. Due to time reversal symmetry, $\mathbf{E}_{-\mathbf{k}}(\mathbf{r}) = \mathbf{E}^*_{\mathbf{k}}(\mathbf{r})$, and thus counter-propagating modes have orthogonal circular polarizations in this new design. In an external magnetic field, applied along the QD-growth direction, QDs have two orthogonal transition dipole moments with opposite circular polarizations. As illustrated schematically in Fig. 1(a) orthogonal circular dipoles couple to counter-propagating modes in the above discussed PCW, thus exhibiting *chiral light-matter interaction*. We demonstrate this experimentally in Fig. 1(b) where the emission spectra are simultaneously recorded from the two opposite ends of the waveguide. The QD emission is highly directional as can be seen by the two orthogonal transition dipoles, $QD_{+/-}$, coupling almost exclusively to counter-propagating modes [4]. We extract the average directionality factor, $F_{dir} = 91\%$. This quanties the likelihood that the emission from a given circular dipole into the waveguide, propagates into the direction indicated in the schematic of Fig. 1(a).

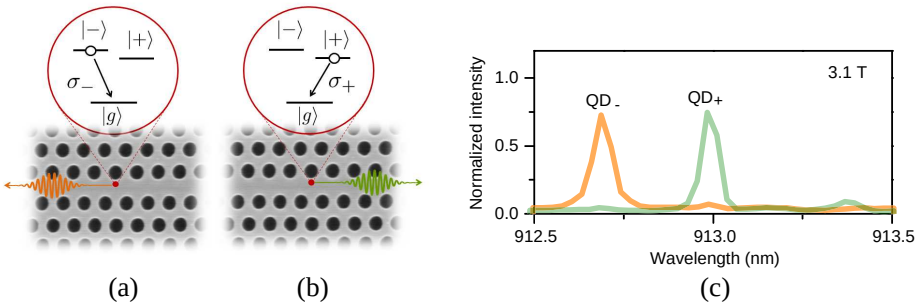

Figure 1: (a) Illustration of directional photon emission where the propagation direction of the single photon depends on the rotation direction of the circular transition dipole. The level structure of the quantum dot is shown schematically and the position of the quantum dot is indicated by the red spot. Single photons emitted from (a) the σ_--transition only couple to the left-propagating (orange) mode whereas photons emitted from (b) state σ_+-transition only couple to the right-propagating (green) mode. (c) Experimental verication of the directional photon emission [4]. The QD in this structure has highly directional emission as can be seen by QD_- and QD_+ coupling almost exclusively to counter-propagating modes, indicated by the two different colors.

Perhaps the most exciting aspect of the chiral light-matter interaction relates to the single photons scattering properties. The transmission coefficient for on-resonant narrowband photons is [5]

$$t_0 = 1 - 2\beta_{dir}, \tag{1}$$

where $\beta_{dir} = F_{dir}\beta$ is the fraction of photons channelled into the directional mode of interest, as opposed to all other modes. For $\beta_{dir} \to 1$, Eq. (1) implies a large transmission amplitude and a π phase shift, for a photon propagating to the left and on resonance with the σ_--transition, cf. Fig. 1(a). However, when reversing the propagation direction of the photon it does not interact with the emitter. This forms the basis of non-reciprocal photonic elements with applications in on-chip quantum information processing [4].

REFERENCES

1. Lodahl, P., S. Mahmoodian, and S. Stobbe, arXiv: 1312.1079, to Appear in *Rev. Mod. Phys.*, 2015.
2. Arcari, M., et al., *PRL*, Vol. 113, 093603, 2014.
3. Luxmoore, I. J., et al., *PRL*, Vol. 110, 037402, 2013.
4. Söllner, I., et al., *Quantum Physics*, arXiv: 1406.4295, 2014.
5. Fan, S., S. E. Kocabaş, and J. T. Shen, *PRA*, Vol. 82, 063821, 2010.

Session 1P13b
FocusSession.SC3: High-capacity Optical Communication: Systems, Algorithms, Components 1

Tunable Narrow-linewidth Photonic Microwave Oscillators Using Optically Injected Semiconductor Lasers at Period-one Dynamics

Yu-Han Hung[1] **and Sheng-Kwang Hwang**[1, 2]

[1]Department of Photonics, National Cheng Kung University, Tainan, Taiwan
[2]Advanced Optoelectronic Technology Center, National Cheng Kung University, Tainan, Taiwan

Abstract— Period-one (P1) dynamics excited in an optically injected semiconductor laser have been widely investigated not only for academic interest in understanding nonlinear dynamics but also for practical interest for novel technological applications. Thanks to the self-sustained microwave oscillation of the laser intensity, P1 dynamics can be applied for photonic microwave generation. While the microwave frequency can be broadly tuned from a few to tens and even hundreds of gigahertz by simply adjusting the optical injection power and frequency, optical single-sideband modulation is so feasible as to mitigate microwave power fading over fiber distribution. However, owing to the inartistic laser noise, the linewidth of the photodetected microwaves is typically on the order of tens to hundreds of megahertz. To stabilize the photodetected microwaves, several stabilization schemes have been proposed, including direct modulation, optoelectronic feedback, and optical feedback. However, these proposed schemes suffer from either device bandwidth restriction or significant frequency jitter, limiting respectively the highest lockable microwave frequency, up to 25 GHz, or the lowest stabilized microwave linewidth, down to the order of kilohertz only. In this study, we propose to use modulation sideband injection locking scheme to stabilize the P1 dynamics. A 3-dB linewidth of 1 Hz is experimentally demonstrated for microwave generation up to 32 GHz using an electronic microwave reference at a small fraction, such as one-eights, of the generated microwave frequency. A higherfrequency microwave generation is feasible, such as 100 GHz or more, using devices of higher bandwidth.

Optical Fibre Limits: An Approach Using ASE Channel Estimation

N. Mac Suibhne, **M. E. McCarthy**, **S. T. Le**,
S. Sygletos, **F. M. Ferreira**, **and A. D. Ellis**
Aston Institute of Photonics Technologies, Aston University, Birmingham, B4 7ET, UK

Abstract— In this talk we investigate the usage of spectrally shaped amplified spontaneous emission (ASE) in order to emulate highly dispersed wavelength division multiplexed (WDM) signals in an optical transmission system. Such a technique offers various simplifications to large scale WDM experiments. Not only does it offer a reduction in transmitter complexity, removing the need for multiple source lasers, it potentially reduces the test and measurement complexity by requiring only the centre channel of a WDM system to be measured in order to estimate WDM worst case performance.

The use of ASE as a test and measurement tool is well established in optical communication systems and several measurement techniques will be discussed [1, 2]. One of the most prevalent uses of ASE is in the measurement of receiver sensitivity where ASE is introduced in order to degrade the optical signal to noise ratio (OSNR) and measure the resulting bit error rate (BER) at the receiver. From an analytical point of view noise has been used to emulate system performance, the Gaussian Noise model is used as an estimate of highly dispersed signals and has had considerable interest [3]. The work to be presented here extends the use of ASE by using it as a metric to emulate highly dispersed WDM signals and in the process reduce WDM transmitter complexity and receiver measurement time in a lab environment. Results thus far have indicated [2] that such a transmitter configuration is consistent with an AWGN model for transmission, with modulation format complexity and nonlinearities playing a key role in estimating the performance of systems utilising the ASE channel emulation technique. We conclude this work by investigating techniques capable of characterising the nonlinear and damage limits of optical fibres and the resultant information capacity limits.

REFERENCES

1. McCarthy, M. E., N. Mac Suibhne, S. T. Le, P. Harper, and A. D. Ellis, "High spectral efficiency transmission emulation for non-linear transmission performance estimation for high order modulation formats," *2014 European Conference on IEEE Optical Communication (ECOC)*, 2014.
2. Ellis, A., N. Mac Suibhne, F. Gunning, and S. Sygletos, "Expressions for the nonlinear transmission performance of multi-mode optical fiber," *Opt. Express*, Vol. 21, 22834–22846, 2013.
3. Vacondio, F., O. Rival, C. Simonneau, E. Grellier, A. Bononi, L. Lorcy, J. Antona, and S. Bigo, "On nonlinear distortions of highly dispersive optical coherent systems," *Opt. Express*, Vol. 20, 1022–1032, 2012.

Impact of Phase Noise in High Capacity Optical Coherent Transmission Systems

Gunnar Jacobsen[1] **and Sergei Popov**[2]

[1]Acreo Swedish ICT, Box 1070, Kista SE-16425, Sweden
[2]Royal Institue of Technology, Stockholm SE-16440, Sweden

Abstract— Laser phase noise from the transmitter and Local Oscillator lasers strongly limits the performance of high capacity, high constellation coherent optical transmission systems. Using Digital Signal Processing techniques it is possible to mitigate the influence with specific form of the DSP for different modulation formats. In this paper we will present a number of possible mitigation techniques, applicable for such modulation schemes as N-level PSK and N-level QAM. It will specifically be shown that the circular QAM configuration has inherent significant added phase noise tolerance compared to the classical square configuration. The research has also been performed considering the so-called Equalization Enhanced Phase Noise, which appears as an added phase noise based impairment for coherent transmission systems with optically induced dispersion and digital (electrical) dispersion compensation. A novel understanding of the origin of EEPN and of straightforward mitigation techniques will be presented.

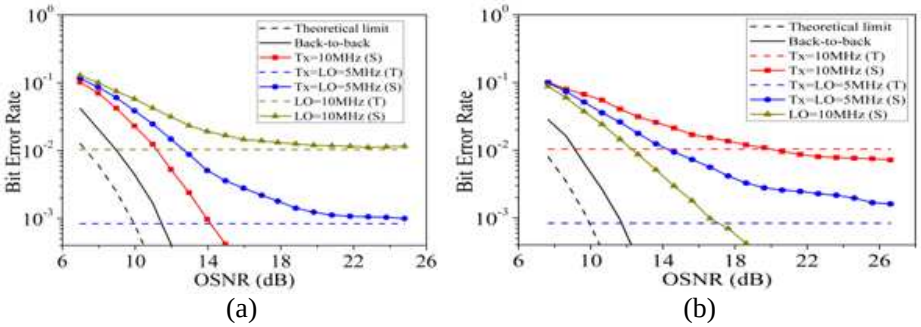

Figure 1: Bit Error Rate versus OSNR for a 28 GS/s DQPSK transmission system with (a) post- and (b) pre-compensation of chromatic dispersion influence (see [1, 2]). The transmission distance is 2000 km. It is observed that the phase noise influence of Tx and LO lasers is reversed for the pre- and post-compensation cases.

ACKNOWLEDGMENT

This work was supported by EU project GRIFFON, gr. # 324391 and the EU project ICONE, gr. # 608099.

REFERENCES

1. Jacobsen, G., M. S. Lidón, T. Xu, S. Popov, A. T. Friberg, and Y. Zhang, "Influence of pre- and post-compensation of chromatic dispersion on equalization enhanced phase noise in coherent multilevel systems," *Journal of Optical Communications*, Vol. 32, 257–261, September 2011.
2. Xu, T., G. Jacobsen, S. Popov, J. Li, A. T. Friberg, and Y. Zhang, "Analytical estimation of phase noise influence in coherent transmission system with digital dispersion equalization," *Optics Express*, vol. 19, 7756–7768, April 2011.

Higher-order Raman Amplification for Unrepeatered and Long-haul Super-channel Transmission

J. D. Ania-Castañón, G. Rizzelli, M. Camarasa-Gómez, and D. Hernangómez-Pérez
Instituto de Óptica "Daza de Valdés", IO-CSIC, Serrano 121, Madrid 28006, Spain

Abstract— Over the past 5 years, coherent super-channel transmission has become a comercial possibility, with companies announcing Tb/s capabilities and spectral efficiencies as high as 3.4 b/s/Hz [1]. In this context, distributed Raman amplification, and in particular higher-order solutions such as those based ultralong Raman fiber lasers [2], have shown great promise for super-channel communications, demonstrating full compatibility with super-channel techniques such Nyquist-WDM both in long-haul and unrepeatered schemes [3]. Still, the optimal amplification scheme configuration can be expected to depend strongly on the particular choice of super-channel implementation, desired system capacity, fiber base and distance requirements. In this paper we explore these and other dependencies for the optimal design of amplification solutions for super-channel transmission systems.

REFERENCES

1. See solutions, for example, from Infinera Corporation, http://www.infinera.com/go/super-channels/index.php, or Coriant, http://www.coriant.com/company/press_release.asp?id=1139.
2. Ania-Castañón, J. D., T. J. Ellingham, R. Ibbotson, X. Chen, L. Zhang, and S. K. Turitsyn, "Ultralong raman fiber lasers as virtually lossless optical media," *Phys. Rev. Lett.*, 96, 023902, 2006.
3. Rosa, P., et al., "Nyquist-WDM PDM-QPSK transmission over SMF-28 fibre using URFL amplification," *Proceedings of ICTON 2014*, Graz, Germany, 2014.

Channel Model and Lower Capacity Bound for the Transmission Based on Nonlinear Fourier Transform (Invited)

J. E. Prilepsky[1], **S. A. Derevyanko**[2], **and S. K. Turitsyn**[1]

[1]Aston Institute of Photonic Technologies, Aston University, Birmingham B4 7ET, UK
[2]Department of Physics of Complex Systems, Weizmann Institute of Science, Rehovot 76100, Israel

Abstract— The integrability of the nonlinear Schrödinger equation (NLSE) by the inverse scattering transform shown in a seminal work [1] gave an interesting opportunity to treat the corresponding nonlinear channel similar to a linear one by using the nonlinear Fourier transform. Integrability of the NLSE is in the background of the old idea of eigenvalue communications [2] that was resurrected in recent works [3–7]. In [6, 7] the new method for the coherent optical transmission employing the continuous nonlinear spectral data — nonlinear inverse synthesis — was introduced. It assumes the modulation and detection of data using directly the continuous part of nonlinear spectrum associated with an integrable transmission channel (the NLSE in the case considered). Although such a transmission method is inherently free from nonlinear impairments, the noisy signal corruptions, arising due to the amplifier spontaneous emission, inevitably degrade the optical system performance. We study properties of the noise-corrupted channel model in the nonlinear spectral domain attributed to NLSE. We derive the general stochastic equations governing the signal evolution inside the nonlinear spectral domain and elucidate the properties of the emerging nonlinear spectral noise using well-established methods of perturbation theory based on inverse scattering transform [8]. It is shown that in the presence of small noise the communication channel in the nonlinear domain is the additive Gaussian channel with memory and signal-dependent correlation matrix. We demonstrate that the effective spectral noise acquires "colouring", its autocorrelation function becomes slow decaying and non-diagonal as a function of "frequencies", and the noise loses its circular symmetry, becoming elliptically polarized. Then we derive a low bound for the spectral efficiency for such a channel. Our main result is that by using the nonlinear spectral techniques one can significantly increase the achievable spectral efficiency compared to the currently available methods [9].

REFERENCES

1. Zakharov, V. E. and A. B. Shabat, *Sov. Phys. JETP*, Vol. 34, 62–69, 1972.
2. Hasegawa, A. and T. Nyu, *J. Lightwave Technol.*, Vol. 11, 395–399, 1993.
3. Yousefi, M. I. and F. R. Kschischang, *IEEE Trans. Inf. Theory*, Vol. 60, 4312–4328, 2014.
4. Yousefi, M. I. and F. R. Kschischang, *IEEE Trans. Inf. Theory*, Vol. 60, 4329–4345 2014.
5. Yousefi, M. I. and F. R. Kschischang, *IEEE Trans. Inf. Theory*, Vol. 60, 4346–4369, 2014.
6. Prilepsky, J. E., S. A. Derevyanko, K. J. Blow, I. Gabitov, and S. K. Turitsyn, *Phys. Rev. Lett.*, Vol. 113, 013901, 2014.
7. Le, S. T., J. E. Prilepsky, and S. K. Turitsyn, *Opt. Express*, Vol. 22, 26720–26741, 2014.
8. Kaup, D. J. and A. C. Newell, *Proc. R. Soc. Lond. A*, Vol. 361, 413–446, 1978.
9. Essiambre, R.-J., G. Kramer, P. J. Winzer, G. J. Foschini, and B. Goebel, *J. Lightwave Technol.*, Vol. 28, 662–701, 2010.

Transoceanic Fibre-optic System Capacity with Electrical Power Constraints

Steve Desbruslais
Xtera Communications Ltd., UK

Abstract— Recent progress in maximising submarine optical fibre transmission capacity has benefited from significant gains using advanced coding techniques and coherent detection. The methods have not only allowed a dramatic increase in system capacity, but have enabled these gains to be made with little effect on the power requirements of the submarine plant. But now that these methodologies have been pushed close to their limit and demand is still increasing, we have to face the inevitable tenet that increasing transmission capacity requires an increase in total signal power. Each channel will have a modulation format dependent signal power requirement and so the more channels we implement, the greater the total optical power requirement will be. We can increase the system bandwidth, the number of transmission modes per fibre, the number of cores per fibre or else the number of fibres. We can also trade signal power with the type of modulation format. But no matter which of these methods we use the total signal power must inevitably increase. There is a direct relationship between the optical signal power and the electrical power required to generate it at the output of each repeater. But it is clear that we cannot increase the power delivered to the submarine plant without limit. The two approaches we can use to overcome this difficulty are to seek savings in energy conversion efficiency and seek improvements to the way the electrical power is delivered. Here we consider the latter.

We consider methods for maximizing the transmission capacity that is achievable in a system of given length subject to the constraints inherent in the powering of submarine repeaters. The way the power is distributed has a large bearing on the efficiency with which the available power can be utilised. Nevertheless, we come to the conclusion that the ultimate limits to long distance submarine transmission capacity are not optical nonlinearities or any other optical phenomena but rather electrical power constraints.

Machine Learning Approaches for Nonlinearity Mitigation and Component Characterization

D. Zibar and M. Piels
DTU Fotonik, Technical University of Denmark, Kgs. Lyngby DK-2800, Denmark

Abstract— Machine learning is an area of intelligent signal processing which uses advanced statistical and probabilistic methods to identify, learn, and track patterns about the underlying system from measured/observed data. The area of machine learning has, so far, had a great impact on our modern society. The Google search engine, for example, uses machine learning to predict the notably nonlinear behavior of internet users. There is a good reason to expect that machine learning can have similar impact on optical fibre communication. In this paper, we link powerful methods used in machine learning community to the future challenges in optical communication. Moreover, methods from machine learning can be used to learn the impairments from the observed data and built a probabilistic model of the impairment. One of the tools that we will consider in this paper is Bayesian filtering and parameter estimation using expectation maximization algorithm. Bayesian filtering allows for tracking of time-varying parameters such as amplitude and phase noise as well as self- and -cross phase modulation. The expectation maximization algorithm allows for maximum likelihood estimation of constant parameters. A significant advantage of Bayesian filtering is that it can be applied to nonlinear systems and account for non-white and also non-Gaussian noise. We will demonstrate how Bayesian filtering in combination with expectation maximization can be used for optical fibre channel nonlinearity mitigation and component characterization. Three special cases of Bayesian filtering are considered: particle filtering, extended Kalman filter (EKF) and extended Kalman smoother (EKS).

Predicting System Performance — An Art or Playing the Lottery?

André Richter and Hadrien Louchet
VPI Photonics, Carnotstrasse 6, Berlin 10587, Germany

Abstract— For many years, modeling and numerical simulation play an important role for characterizing equipment and dimensioning performance limitations of high-speed optical transmission systems. We try nothing less but to emulate in a computer environment what will happen in real life under real-world conditions, evaluate the performance of alternating transmission methods and corresponding technologies, and based on that make strategic decisions about the way to move forward.

How can modeling and numerical simulation actually address this challenging demand? Foremost, a good understanding of all relevant effects influencing the information transmission — from the initial digital (or analog) source to the corresponding sink — is required. If this is known and interactions are understood, one needs to determine, what it takes to emulate these effects realistically in a modeling environment and to obtain reliable measures predicting system performance. So, one needs to determine the required level of modeling abstraction as well as efficient and accurate means for implementing the emulation process.

Clearly, extensive numerical simulations should go hand-in-hand with equipment and system characterizations, and laboratory or field transmission experiments. Where possible, experimental data, either pre-recorded or measured live during simulation, can be integrated with numerical studies in order to deliver realistic and reliable performance predictions.

What characteristics should be evaluated in order to be able to draw the right conclusions? The range of options is large: optical spectra and required OSNR, (time-dependent) statistics of eye openings and constellation diagrams, symbol or bit error ratios, Q factor and EVM, or mutual information? And then, how should those characteristics be calculated/estimated/displayed?

When reviewing the evolution of technology over the past years, we see that the perspective changed significantly about what are important limitations and how should they be evaluated. Up to the end of the last century (dense) WDM transmission of $N \times 10\,\mathrm{Gbit/s}$ channels over dispersion-managed fiber links using OOK-based NRZ or (chirped) RZ modulation and direct detection receivers represented state-of-the-art. Optical loss and noise, CD and Kerr nonlinearities represented the main limiting effects. Soon after, channel rates of 40 Gbit/s using DPSK and later DQPSK modulation combined with balanced detection became popular. With this, limitations due to PMD and nonlinear phase noise became important. A few years later efficient means for IQ-modulation have been introduced and coherent optical detection has been rediscovered, which allowed using spectrally efficient modulation formats and moving key functionality for pulse shaping and mitigation of limiting performance effects to then available high-speed electronics. Nowadays, we develop systems with channel rates of 400 Gbit/s and more using many different types of single- or multi-carrier based two-dimensional and coded modulation formats, sophisticated multi-stage DSP and soft-decision FEC algorithms.

These developments made the task of reliably predicting system performance using modeling and numerical simulation a lot more challenging. With this paper we discuss numerical techniques for estimating the signal performance for high-speed optical transmission systems. We illustrate how the perspective about 'good methods' and 'reliable criterions' changed over the years with the advancement of technology. Further we highlight major challenges for estimating signal performance in today's transmission systems and discuss techniques to overcome them.

Interleaving to Reduce Code Overhead in DQPSK Systems

M. Y. Leong[1, 2], **K. J. Larsen**[3], **S. Popov**[2],
G. Jacobsen[1, 2], **D. Zibar**[3], **and S. Sergeyev**[4]

[1]Acreo Swedish ICT, Sweden
[2]KTH Royal Institute of Technology, Sweden
[3]Technical University of Denmark (DTU), Denmark
[4]Aston University, United Kingdom

Abstract— A method for selecting interleavers and BCH codes for systems with cycle slips.

Recently, both phase noise and Gaussian noise are considered in code design [1–3]. However, codes in [3] have high overheads due to correlation. We use interleaving to reduce overhead.

We add an interleaver of length L code blocks with $n_{B,S}$ bits/block after the Bose-Chaudhuri-Hocquenghem (BCH) encoder in [3]. It reorders the bits using randomly-generated permutations. A deinterleaver before the BCH decoder restores the bit order. We fit the probability density function (PDF) $\Pr(Y_G = y_G,\, Y_C = y_C)$ as in [3]. Let the random variable (RV) Y_A represent the number of bit errors in a code block, $\Pr(Y_A = y_A) = \sum_{(y_G,y_C):2y_G+y_C=y_A} \Pr(Y_G = y_G,\, Y_C = y_C)$. Let Y_L represent the number of bit errors in L blocks. $\Pr(Y_L = y_L)$ is the L-fold convolution of $\Pr(Y_A = y_A)$. After deinterleaving, the y_L bit errors are distributed randomly over L blocks. Let the RV Z_ℓ represent the number of bit errors in the ℓ-th block. $\Pr(Z_\ell = z_\ell | Y_L = y_L) = \binom{y_L}{z_\ell} (1/L)^{z_\ell} (1 - 1/L)^{y_L - z_\ell}$ if $z_\ell \le y_L$, and 0 otherwise. The PDF of Z_ℓ is $\Pr(Z_\ell = z_\ell) = \sum_{y_L=0}^{\infty} \Pr(Z_\ell = z_\ell | Y_L = y_L) \Pr(Y_L = y_L)$. A code corrects up to τ bit errors. Let X_ℓ be a RV that is 1 if $\tau + 1 \le Z_\ell \le \tau + 3$, and 0 otherwise. Let $X = \sum_{\ell=1}^{L} X_\ell$. The expectation of X is $E[X] = L \cdot \Pr(\tau + 1 \le Z_\ell \le \tau + 3)$. Post-forward error correction (FEC) bit error rate (BER) $P_{\text{post}} \approx [(\tau + 1)/n_{B,S}] \cdot \Pr(\tau + 1 \le Z_\ell \le \tau + 3)$. Suitable interleavers and codes are the combinations of $n_{B,S}$, τ, and L that meet a target post-FEC BER.

As an example, a 28 Gbaud system optimized for linewidth < 100 kHz uses a 41-tap moving average filter for Viterbi-Viterbi [4]. We assume the worst-case "poor phase estimate (PE)" curve has linewidth 25.2 MHz. Simulations use VPI [5]. Our interleaver-code combinations achieve 2 × BER target (Fig. 1).

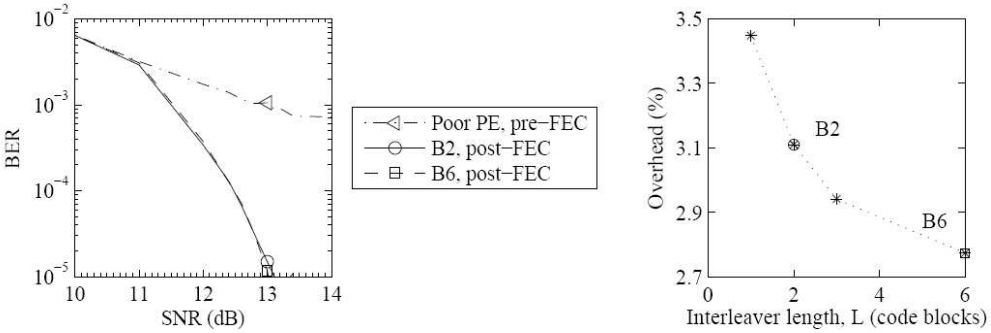

(a) (b)

Figure 1: (a) BER vs. signal-to-noise ratio (SNR). We design interleaver-code combinations for "poor phase estimate (PE) pre-FEC" triangle (◁). In post-FEC simulations, B2 is BCH(8190,7943) with $L = 2$, and B6 is BCH(8190,7969) with $L = 6$. Pre-FEC BER is calculated on 10^6 bits, and post-FEC BER on 10^7 post-FEC bits. (b) Trade-off for ◁ in (a). Interleaver delay is proportional to L. Interleaver-code combinations for target post-FEC BER 10^{-5} are marked with a star (∗). B2 and B6 are simulated in (a).

ACKNOWLEDGMENT

This work was supported by EU project GRIFFON (No. 324391) and ICONE (No. 608099), and by Vetenskapsrådet (No. 0379801).

REFERENCES

1. Schmalen, L., "A low-complexity LDPC coding scheme for channels with phase slips," *J. Lightw. Technol.*, in print.
2. Koike-Akino, T., et al., "Cycle slip-mitigating turbo demodulation in LDPC-coded coherent optical communications," *Proc. OFC*, M3A.3, Mar. 2014.
3. Leong, M. Y., et al., "Dimensioning BCH codes for coherent DQPSK systems with laser phase noise and cycle slips," *J. Lightw. Technol.*, Vol. 32, No. 21, 4048–4052, Nov. 2014.
4. Leong, M. Y., et al., "Interleavers and BCH codes for coherent DQPSK systems with laser phase noise," *IEEE Photon. Technol. Lett.*, in print.
5. www.vpiphotonics.com.

Polarization Sensitivity Mitigation for AM-CO-OFDMA PON Uplink Transmission

S. M. Jung, **K. H. Mun**, **and S. K. Han**
Department of Electrical and Electronic Engineering, Yonsei University
50 Yonsei-ro, Seodaemun-Gu, Seoul, Korea

Abstract— In the optical coherent detection, the basic detection process is optical beating between the optical field of uplink signal and optical field of the local oscillator (LO) laser at the receiver. This detection provides the phase diversity and polarization diversity which lead to high spectral efficiency with higher order modulation. During this optical beating process, the polarization states between the signal optical fields and optical field of LO has very important relationship. Because the LO optical field and signal fields are divided as X-polarization components and Y-polarization components relative to the fiducial polarization axis, each polarization components beats each other during the photo detection process and generate the electrical signal for each polarization. But, in the multiple access system, the polarization diversity could cause serious issue. In the adatively modulated coherent optical orthogonal freuqency division multiple access (AM-CO-OFDMA) passive optical network (PON) system, the multiple access function is easly achieved just by dividing subcarrier subbands of its signal frame. However, the received uplink optical fields of ONUs could not have same polarization states each other because of its different transmission path and responses of the devices in the link. These variously polarized optical fields lead to reduce SNR after photo-detection and crosstalk between the multiple access user signals. In this work, we proposed a mitigating technique for the polarization mismatch of the uplink optical fields in the coherent AMO-OFDMA-PON. By using the trigonometric features of polarization states, we experimentally demonstrated stable transmission performance of uplink multiple access.

Optically Controlled Triple Notched UWB Antenna

Heba Zakaria[1], **Moataza Hindy**[2], **and Adel El-Henawi**[1]

[1]Faculty of Engineering, Ain Shams University, Cairo, Egypt
[2]Electronics Research Institute, Cairo, Egypt

Abstract— A new printed reconfigurable ultra-wideband (UWB) antenna was designed on a 35×28 mm FR4 substrate with relative dielectric constant of 4.6 and thickness of 1.5 mm. This design proposes triple narrow notched bands at center frequencies 3.5 GHz "WIMAX", 5.5 GHz "WLAN" and 8.4 GHz (7.4 GHz WPAN and 7.15–9 GHz) [1, 2]. The coplanar fed microstrip UWB antenna is shown in Fig. 1(a) while Fig. 1(b) illustrates the optically controlled design. The proposed UWB can work at eight modes using controlling switches ON and OFF. The optical switches are made by placing $0.5\,\text{mm} \times 0.5\,\text{mm}$ silicon wafers over the slots of the resonator. When laser is applied the switches are in the ON state (as shown in Table 1) the notches disappear and the antenna operates in full ultra wideband frequency range. In case, all diodes are OFF all the notches are activated. Moreover, the average gain of this antenna is 5.5 dBi and UWB ranges from 3 to 11 GHz. The antenna was simulated, fabricated, and measured results well agree with the simulation.

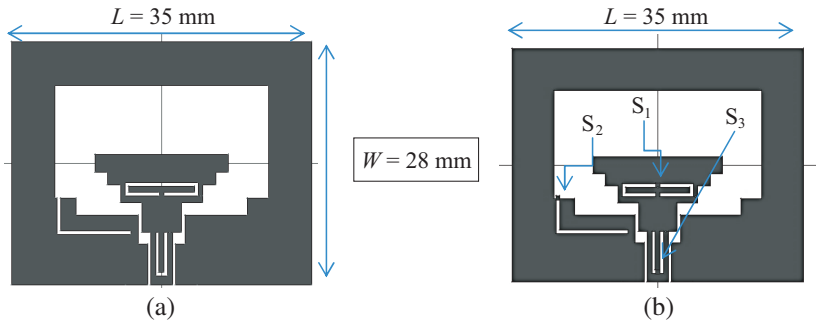

Figure 1. The geometry of the proposed ultra wideband antenna. (a) The origin design, (b) UWB antenna without 3 switches.

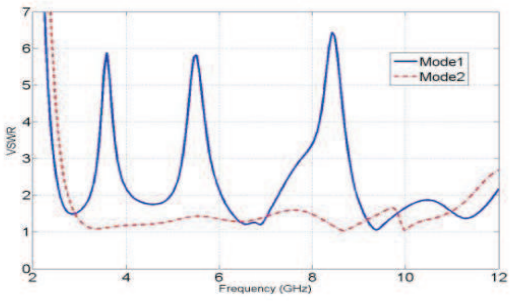

Figure 2. VSWR of UWB antenna made1 UWB "case1" mode2 "case2" UWB from 2.8 to 11.8 GHz.

case	Notched Band	S_1	S_2	S_3
1	3.5 & 5.5 & 8.5 GHz	OFF	OFF	OFF
2	None	ON	ON	ON
3	3.5 GHz	ON	OFF	ON
4	5.5 GHz	OFF	ON	ON
5	8.5 GHz	ON	ON	OFF
6	3.5 & 5.5 GHz	OFF	OFF	ON
7	3.5 & 8.5 GHz	ON	OFF	OFF
8	5.5 & 8.5 GHz	OFF	ON	OFF

Table 1.

REFERENCES

1. Mehranpour, M., J. Nourinia, Ch. Ghobadi, and M. Ojaroudi, "Dual band-notched square monopole antenna for ultra-wideband applications," *IEEE Antennas Wireless Propag. Lett.*, Vol. 11, 172–175, 2012.
2. Flemish, J. R. and R. L. Haupt, "Optimization of a photonically controlled microwave switch and attenuator," *IEEE Transactionsons on Microwave Theory and Techniques*, Vol. 58, No. 10, 2582–2588, 2010.

Session 1P14a
SC3: Silicon Photonic Integration and Devices for Optical Communications and Interconnects

Silicon Photonics at the University of Southampton

D. J. Thomson[1], K. Li[2], F. Y. Gardes[1], Y. Hu[1,3], M. Nedeljkovic[1], C. Littlejohns[1], R. Topley[1], A. Z. Khokhar[1], S. Stanković[1], J. Soler Penades[1], C. J. Mitchell[1], S. A. Reynolds[1], G. Z. Mashanovich[1], P. R. Wilson[2], and G. T. Reed[1]

[1]Optoelectronics Research Centre, University of Southampton
Highfield, Southampton, Hampshire SO17 1BJ, United Kingdom
[2]School of Electronics and Computer Science, University of Southampton
Highfield, Southampton, Hampshire SO17 1BJ, United Kingdom
[3]Caliopa, Technologiepark 19, Zwijnaarde 9052, Belgium

Abstract— Over the past decade silicon photonics has gone through a period of rapid technological advancement coinciding with significant research effort worldwide from both academia and industry. Motivations for silicon photonics are the potential for low cost manufacture of photonic integrated circuits (PICs) and the prospects for photonic-electronic convergence. Several of the building blocks required to produce high PICs in silicon have been demonstrated from high speed optical modulators and detectors to filters, multiplexers and hybrid laser sources. The Silicon Photonics Group at Southampton University has been active across a breadth of activities within the field. In this talk an overview will be given of recent research efforts and results of the group.

Previously we have demonstrated optical modulators based on carrier depletion operating up to speeds of 50 Gbit/s. Devices such also need high speed electronic amplifiers in order to drive them with the required voltage levels. We have recently been working on the heterogeneous integration of CMOS electronic drivers with silicon optical modulators based on wire bonding. A fully integrated silicon photonics data link operating up to 10 Gbit/s has been demonstrated

We have shown that coarse wavelength division multiplexers (CWDM) based upon angled multimode interference (AMMI) structures can be advantageous in terms of fabrication simplicity and tolerance to fabrication variations. Recently we have demonstrated a bi-directional AMMI structure which results in two CWDM devices that share the same multimode region. Almost identical spectral responses are obtained from the two devices. This can be highly advantageous in applications where two (DE)MUX structures are required with matching spectral responses for example in polarisation diversity based receivers. We have also recently demonstrated a 50 Gbit/s four channel receiver based on the integration of an AMMI and germanium based photodetectors.

Wafer scale testing of PICs is essential in mass-production to ensure high yield is achieved and fabrication costs are minimised. To date few solutions have offered an efficient scheme which allows testing of individual components within an optical circuit. In our work we demonstrate a solution to this based on grating couplers formed by selective ion implantation induced amorphisation of silicon. Respectable coupling efficiencies have been achieved and it has also been shown that the amorphous silicon can be recrystallized through localised laser annealing and as a result the coupling gratings are erased.

Another area of research we have been highly active in is the use of silicon waveguides at mid-infrared wavelengths. We have demonstrated a range of waveguides and photonic components at different wavelengths beyond those traditionally used for telecommunications.

Athermal CMOS-compatible Silicon Photonics for Computing and Networking Applications

S. J. Ben Yoo
Department of Electrical and Computer Engineering, University of California, Davis, USA

Abstract— We will discuss athermal CMOS-compatible silicon photonic integrated systems designed for computer interconnects and networking applications. In particular, we will discuss CMOS-compatible athermal silicon photonic waveguides that can be building blocks for athermal modulators, lasers, and multiplexer/demultiplexers necessary for practical and scalable computing and networking systems. We will first discuss the design and fabrication processes utilizing a titanium dioxide overcladding layer on silicon photonics where full compatibility with CMOS fabrication steps have been implemented. Then, we will discuss an example of fabricated silicon photonic resonant ring modulators for athermal operations at 1550 nm and 1310 nm, respectively. We will follow up by discussing athermal silicon-photonic RFPhotonic lattice filters, arrayed grating waveguide mux and demuxes, and DBR gratings for InP/Si hybrid lasers, all designed and fabricated for large-scale integrated athermal silicon photonic systems on a die. Finally, we will discuss athermal silicon photonic optical-arbitrary waveform generation and measurement (OAWG and OAWM) system on chip for elastic optical networking applications, and prospects for future computing and networking systems.

Quantum Dot Lasers for Silicon Photonics

Yasuhiko Arakawa
Institute for Nano Quantum Information Electronics, The University of Tokyo
4-6-1 Koamaba, Meguro-ku, Tokyo 153-8505, Japan

Abstract— We discuss our recent advances in quantum dot lasers [1] for silicon photonics. High temperature stability and high feedback-noise tolerance due to small α-parameter of the quantum dot lasers are unique features for application to silicon optical interposers. High-temperature operation of silicon optical interposers showing the bandwidth-density of 15 Tbps/cm^2 up to 125 C was successfully demonstrated by integrating quantum dot lasers with flip-chip bonding method [2]. High performance operation of the quantum dot lasers on silicon by wafer-bonding technique was also examined [3, 4].

ACKNOWLEDGMENT

This works is supported by FIRST program, NEDO, and the Project for Developing Innovation Systems, MEXT, Japan.

REFERENCES

1. Arakawa, Y. and H. Sakaki, *Appl. Phys. Lett.*, Vol. 40, 939, 1982.
2. Urino, Y., Y. Arakawa, et al., *IEEE J. of Lightwave Tech.*, Vol. 3, 1223, 2015.
3. Tanabe, K., T. Rae, K. Watanabe, and Y. Arakawa, *Appl. Phys. Express*, Vol. 6, 82703, 2013.
4. Jhang, Y., K. Tanabe, S. Iwamoto, and Y. Arakawa, *IEEE*, Vol. 27, 875, 2015.

Recent Advances in Carbon Nanotube Photonics on Silicon Platform

A. Noury[1,6], **E. Durán-Valdeiglesias**[1], **W. Zhang**[1], **F. Sarti**[2,3], **C. Alonso-Ramos**[1], **F. La China**[2,3], **H. C. Hoang**[1], **X. Le Roux**[1], **H. Yang**[5], **E. Cassan**[1], **N. Izard**[1,7], **A. Filoramo**[4], **V. Bezugly**[5], **M. Gurioli**[2,3], **and L. Vivien**[1]

[1]Inst. Elect Fondamentale (IEF), CNRS UMR 8622, Université Paris 11, Orsay F-91405, France
[2]Department of Physics, University of Florence, Sesto Fiorentino (FI) 50019, Italy
[3]European Laboratory for Non-linear Spectroscopy, Sesto Fiorentino (FI) 50019, Italy
[4]CEA Saclay, IRAMIS, NIMBE (UMR 3685), LICSEN, Bat. 125, Gif-sur-Yvette F-91191, France
[5]Institute for Materials Science, Technische Universitaet Dresden, Dresden, Germany
[6]ICFO-Institut de Ciencies Fotoniques, Mediterranean Technology Park
Castelldefels, Barcelona 08860, Spain
[7]Laboratoire Charles Coulomb, CNRS-UMR 5221, Univ. Montpellier, Montpellier 34095, France

Abstract— Silicon is now considered as a material of choice for photonic applications including optical interconnects and telecommunications. These applications are mainly based on the use of optoelectronic devices (i.e., light sources/modulators/detectors) operating in the telecom wavelength range. Even if the development of silicon photonics was impressive in terms of device demonstrations, the integration of all the photonic building blocks is considered to remain as challenging due to the diversity of needed materials (Si for modulator, Ge for detector and III–V semiconductors for laser sources). The integration of all these materials on silicon is technically possible, but as different and sometimes non-compatible processes are used, the resulting scheme is not cost-effective, and consequently reduces the use of silicon photonics for a broad application domain.

The use of carbon nanotubes (CNT) as active materials for the development of all optoelectronic devices on silicon could overcome this integration issue. Indeed, carbon nanotubes exhibit the major optical properties to emit, modulate and detect light in the telecom wavelength range and can be integrated into the Si photonics platform.

In this context, we will present recent advances in CNT integration in silicon waveguides and in optical resonators. Several waveguide geometries including strip waveguides, slot waveguides, micro-disk and photonic crystal cavities have been studied and analyzed to enhance the optical interaction between the optical mode guided in the silicon structures and carbon nanotubes deposited on the top.

Subwavelength Grating Filters in Silicon Photonics

Lawrence R. Chen
Department of Electrical and Computer Engineering
McGill University, Montreal, QC H3A 0E9, Canada

Abstract— There is an increasing need for integrated solutions in optical communications interconnections, and sensing applications. In the past few years, a variety of active and passive devices as well as integrated subsystems in CMOS-compatible silicon photonics platforms have been realized. One specific structure that has attracted considerable interest is the subwavelength grating (SWG). An SWG is based on a periodic arrangement between two different materials with a period much smaller than the wavelength of the light. SWG waveguides have the potential for low loss and provide significant flexibility in tailoring the effective index. Indeed, a number of SWG-based building blocks in silicon-on-insulator (SOI) have been developed, including waveguide crossings, bends, couplers, mode transformers, polarization converters, and modulators. In this paper, we review recent progress on developing SWG filters based on ring resonators as well as Bragg structures. We compare the performance of conventional ring vs. racetrack resonator designs and discuss applications in sensing. We also describe narrowband reflection filters based on interleaving two SWG waveguides to create a periodic variation in refractive index, i.e., a Bragg grating. These filters add significantly to the SWG 'toolbox' and should enable the development of more complex wavelength selective devices with enhanced functionality, e.g., optical add/drop multiplexers.

Silicon Photonics for Data Center Networking Applications

Yung Jui Chen, **Chun Yen Chen**, **and Cheng Yu Wang**
Department of Photonics, National Sun Yat-Sen University, Kaohsiung 804, Taiwan

Abstract— Data center, a new concept of warehouse scale computing, offers economic and efficient solutions to the rapid expanding Internet applications. If Internet is a human body, data centers are the organs of the body. Currently, data center is one of the most rapid growth areas in information technology. The servers and storage devices in a data center are connected by clos switches built by high radix switch chips. As the number and speed of the servers and storage devices grow, the electronic clos switch fabric can no long keep up with the networking demand. One of the possible solutions of this data center network bottleneck is to utilize optical technology — a hybrid optoelectronic switch system. In this talk we will describe the concept of a WDM based wavelength switch solution based on silicon photonics platform. Issues and challenges of developing this novel data center networking system will be discussed.

Session 1P14b
FocusSession.SC3: Nonlinear Optics: Novel Phenomena, Materials and Applications 1

Photonic Topological Insulators

Mordechai Segev[1], **Mikael C. Rechtsman**[1], **Yonatan Plotnik**[1], **Yaakov Lumer**[1], **Miguel A. Bandres**[1], **Julia M. Zeuner**[2], **and Alexander Szameit**[2]

[1]Department of Physics and Solid State Institute
Technion — Israel Institute of Technology, Haifa 32000, Israel
[2]Institute of Applied Physics, Abbe Center of Photonics
Friedrich-Schiller-Universität Jena, Max-Wien-Platz 1, 07743 Jena, Germany

Abstract— The recent experiments on photonic topological insulators signified a new direction. The progress on experiments and theory in this area will be reviewed, with an emphasis on universal ideas common to optics, cold atoms and quantum systems.

The discovery of topological insulators relying on spin-orbit coupling in condensed matter systems has created much interest in various fields, including in photonics. In two-dimensional electronic systems, topological insulators are insulating materials in the bulk, but conduct electric current on their edges such that the current is completely immune to scattering. However, demonstrating such effects in optics poses a major challenge because photons are bosons, which fundamentally do not exhibit fermionic spin-orbit interactions (i.e., Kramer's theorem). At microwave frequencies, topological insulators have been proposed [1, 2] and demonstrated [3] in magneto-optic materials, relying on strong magnetic response to provide topological protection against backscattering — in the spirit of the quantum Hall effect. However, at optical frequencies the magneto-optic response is extremely weak, hence a photonic topological insulator would have to rely on some other property. Indeed, numerous theoretical proposals have been made for photonic topological insulators [4–8], but their first observation [9], made by our group, relied on a different idea: Floquet topological insulators [10, 11]. Later that year, another group reported imaging of topological edge states in silicon photonics [12, 13]. These experiments have generated much follow up: predictions of nonlinear waves [14]; and of storage and release of information in such systems [15]. The purpose of this talk is to review this recent progress, discuss new conceptual ideas, and suggest applications.

REFERENCES

1. Haldane, F. D. M. and S. Raghu, *Phys. Rev. Lett.*, Vol. 100, 013904, 2008.
2. Wang, Z., Y. Chong, J. D. Joannopoulos, and M. Soljacic, *Phys. Rev. Lett.*, Vol. 100, 013905, 2008.
3. Wang, Z., Y. Chong, J. D. Joannopoulos, and M. Soljacic, *Nature*, Vol. 461, 772, 2009.
4. Koch, J., A. A. Houck, K. L. Hur, and S. M. Girvin, *Phys. Rev. A*, Vol. 82, 043811, 2010.
5. Umucalılarm, R. O. and I. Carusotto, *Phys. Rev. A*, Vol. 84, 043804, 2011.
6. Hafuzi, M., E. A. Demler, M. D. Lukin, and J. M. Taylor, *Nat. Phys.*, Vol. 7, 907, 2011.
7. Fang, K., Z. Yu, and S. Fan, *Nat. Photonics*, Vol. 6, 782, 2012.
8. Khanikaev, A. B., et al., *Nat. Mater.*, Vol. 12, 233, 2013.
9. Rechtsman, M. C., J. M. Zeuner, Y. Plotnik, Y. Lumer, D. Podolsky, F. Dreisow, S. Nolte, M. Segev, and A. Szameit, *Nature*, Vol. 496, 196, 2013.
10. Lindner, N. H., G. Refael, and V. Galitski, *Nat. Phys.*, Vol. 7, 490, 2011.
11. Kitagawa, T., E. Berg, M. Rudner, and E. Demler, *Phys. Rev. B*, Vol. 82, 235114, 2010.
12. Hafuzi, M., S. Mittal, J. Fan, A. Migdall, and J. M. Taylor, *Nat. Photonics*, Vol. 7, 1001, 2013.
13. Mittal, S., J. Fan, A. Migdall, J. M. Taylor, and M. Hafuzi, *Phys. Rev. Lett.*, Vol. 113, 087403, 2014.
14. Lumer, Y., Y. Plotnik, M. C. Rechtsman, and M. Segev, *Phys. Rev. Lett.*, Vol. 111, 243905, 2013.
15. Bandres, M. A., M. C. Rechtsman, A. Szameit, and M. Segev, *CLEO*, 2014.

Enhancing and Inhibiting Stimulated Brillouin Scattering in Photonic Integrated Circuits

Benjamin J. Eggleton
Centre for Ultrahigh Bandwidth Devices for Optical Systems (CUDOS)
Institute of Photonics and Optical Science (IPOS), School of Physics
University of Sydney, NSW 2006, Australia

Abstract— On-chip nonlinear optics is a thriving research field, which creates transformative opportunities for manipulating classical or quantum signals in small-footprint integrated devices. Since the length scales are short, nonlinear interactions need to be enhanced by exploiting materials with large nonlinearity in combination with high-Q resonators or slow-light structures. Here, we exploit the frequency dependence of the optical density-of-states near the edge of a photonic-bandgap to selectively enhance or inhibit nonlinear interactions on a chip. We demonstrate this concept for one of the strongest nonlinear effects, stimulated Brillouin scattering using a narrow-band one-dimensional photonic-bandgap structure: a Bragg grating. The stimluated-Brillouin scattering enhancement enables the generation of a 15-line Brillouin frequency comb. In the inhibition case, we achieve stimulated Brillouin scattering free operation at a power level twice the threshold.

Evolutionary Photonics: From Black-body Lasers to Ultrafast Subwavelength Rogue Waves in Photonic Seas

Andrea Fratalocchi
PRIMALIGHT, Faculty of Electrical Engineering, Applied Mathematics and Computational Science
King Abdullah University of Science and Technology (KAUST)
Thuwal 23955-6900, Saudi Arabia

Abstract— Chaos and disorder are often perceived as detrimental effects, which are typically unwanted in man-made applications due to their unpredictable character. Millions of year of evolution of natural systems, however, enabled pathways where these effects are exploited constructively and efficiently. In this invited talk, I will summarize my research activity in the field of evolutionary photonics, where I developed new types of applications that leverage on different aspects of chaos and randomness. I will begin my talk by discussing a new mechanism of energy harvesting, based on the unpredictable motion of light rays in chaotic cavities, and that is able to dramatically enhance the trapping performances of micro and nanoscaled systems [1, 2]. By using this technology, we are developing new applications in the field of solar cells [3], extreme localization of light [4], and new concepts in laser devices [5]. The traditional design of a laser exploits a cavity with single or multiple resonant modes, and their coherent amplification in a feedback structure. Following an evolutionary approach, we demonstrated a system where lasing does not result from a cavity or a resonance. In particular, we considered the possibility to achieve lasing from a black-body material. We fabricate the latter by combining a biomimetic approach with transformation optics. Measurements in the visible between 200 nm to 800 nm under isotropic illumination angles show that this material has a flat absorption $> 98\%$, behaving like an almost ideal back-body. In performing light emission experiments, we diluted a standard dye inside the black-body metamaterial, and then illuminate the system by a pulsed laser operating at 532 nm, characterized by a repetition rate 10 Hz and pulse duration 10 ns. We selected Rhodamine B (RhB) as a gain material, with fluorescence peak at 625 nm. We observed a strong emission peak that from an initial fluorescent emission 60 nm wide, creates an almost monochromatic line with 5 nm bandwidth. Further theory showed that such regime is the characteristic emission of the system, which occurs by a new mechanism of light "condensation" that coherently gathers all energy from the amplifier, confining it to a single frequency.

REFERENCES

1. Liu, C., A. Di Falco, D. Molinari, Y. Khan, B. S. Ooi, T. F. Krauss, and A. Fratalocchi, *Nat. Photon*, Vol. 7, 473, 2013.
2. Fratalocchi, A., "Chaotic energy harvesting," *Nat. Nanotech.*, Vol. 10, 11, 2015.
3. Labelle, A. J., et al., "Colloidal quantum dot solar cells exploiting a hierarchical structure," *Nano Lett.*, to appear.
4. Liu, C., R. E. C. van der Wel, N. Rotenberg, L. Kuipers, T. F. Krauss, A. Di Falco, and A. Fratalocchi, "Triggering extreme events at the nanoscale in photonic seas," *Nature Phys.*, 2015, to appear.
5. Huang, J., C. Liu, Y. Zhu, S. Masala, H. Yu, and A. Fratalocchi, "Black-body metamaterials," 2015, submitted.

Soliton Explosions in Normal Dispersion Fibre Lasers

Antoine F. J. Runge, Neil G. R. Broderick, and Miro Erkintalo
Dodd-Walls Centre for Photonic and Quantum Technologies, Department of Physics
The University of Auckland, Private Bag 92019, Auckland 1142, New Zealand

Abstract— Mode-locked fiber lasers can be host to numerous exotic dissipative structures, and they have thus become ideal testbeds for the exploration of complex dissipative dynamics [1]. Among all such dynamics, soliton explosions display perhaps the most astonishing characteristics. In this regime, a *quasi*-stable dissipative soliton circulates in the laser cavity for a number of roundtrips, but then suddenly undergoes an abrupt structural collapse. Remarkably, after a few roundtrips the collapsed pulse self-recovers and returns back to its initial form [2]. However, the extreme transient nature of the explosions makes them difficult to capture in laboratory measurements. In fact, so far only one observation has been reported, in a solid-state Ti : Sapphire laser [3]. Here we report on the first observation of soliton explosions in a *mode-locked fiber laser*. We also show that explosions manifest themselves in the time-domain as abrupt, measurable temporal shifts of the pulse train.

The laser used in our experiment is an all-normal dispersion, all-PM-fiber device that is passively mode-locked using a nonlinear amplifying loop mirror. Depending on the pump power, the laser can sustain either stable or noise-like operation. By carefully adjusting the pump power to lie in between these two regimes, we observe a new mode of operation. It is in this transition regime that soliton explosions occur, as shown in Fig. 1(a). Here we plot the shot-to-shot spectra of 100 consecutive pulses emitted by the laser, recorded in real time. When an explosion occurs, the broad spectrum of the quasi-stable dissipative soliton collapses into a much narrower profile with larger amplitude, but after a few roundtrips returns back to its previous state. This is further highlighted in Fig. 1(b), where we show four consecutive spectra around a particular explosion event. Time domain measurements are shown in Fig. 1(c). We find that each explosion event gives rise to an abrupt temporal jump in the output pulse train: the pulse completes a cavity roundtrip approximately 40 ps later than in the quasistable regime.

We will present numerical simulations demonstrating how these explosions are generated by gain competition between an already existing pulse and a new one that grows parasitically on the shoulder of the first. These results demonstrate the universal nature of explosions in dissipative systems such as mode-locked lasers and should help to illuminate complicated dynamics elsewhere.

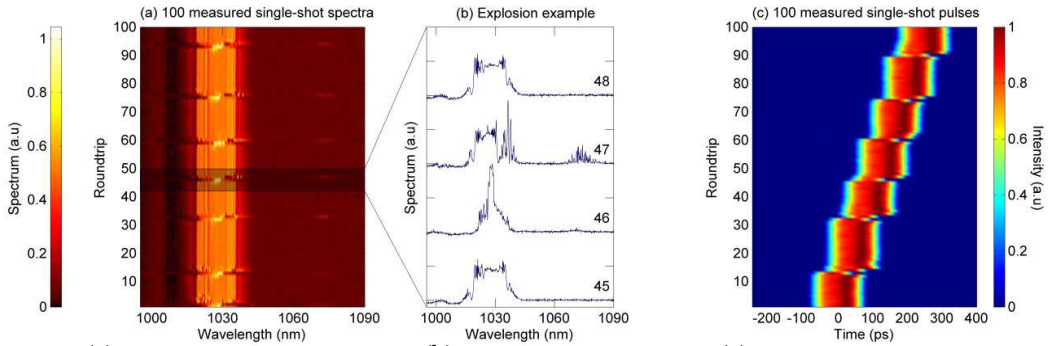

Figure 1: (a) Experimentally measured single-shot spectra of 100 consecutive pulses with the laser operating in the transition regime. (b) Example spectra at indicated roundtrip numbers around a particular explosion event. (c) Experimentally measured temporal evolution relative to the average roundtrip time over 100 roundtrips.

REFERENCES

1. Grelu, P. and N. Akhmediev, "Dissipative solitons for mode-locked lasers," *Nat. Photonics*, Vol. 6, 84–92, 2012.
2. Soto-Crespo, J. M., N. Akhmediev, and A. Ankiewicz, "Pulsating, creeping, and erupting solitons in dissipative systems," *Phy. Rev. Lett.*, Vol. 85, 2937–2940, 2000.

3. Cundiff, S. T., J. M. Soto-Crespo, and N. Akhmediev, "Experimental evidence for soliton explosions," *Phy. Rev. Lett.*, Vol. 88, 073903, 2002.

Interplay between Raman and Plasma Effects in Gas-filled Hollow-core Photonic Crystal Fibers

Fabio Biancalana
School of Engineering and Physical Sciences, Heriot-Watt University, EH14 4AS Edinburgh, UK

Abstract— Hollow-core photonic crystal fibers (HC-PCFs) with Kagome-style cladding structure have granted strong guided interactions between light and gaseous media over relatively-long propagation distances with low transmission losses and pressure-tunable dispersion in the visible region [1]. Stimulated Raman scattering processes in gases are characterized by having a very long molecular coherence relaxation time, of the order of hundreds of picoseconds or more. In this work, we analyze the propagation of two non-overlapped pulses, temporally separated by a delay smaller than the relaxation times, in HC-PCFs filled with Raman-active gases. The leading pulse is an ultrashort strong 'pump' fundamental soliton with a temporal width shorter than the Raman oscillation period of the gas, while the trailing pulse is a weak 'probe' pulse with negligible nonlinearity. The pump induces a lagging sinusoidal temporal modulation of the medium refractive index, which has been observed experimentally [2], due to Raman polarization. This soliton is uniformly accelerated with acceleration g_1 as a result of its Raman-induced spectral redshift. In the reference frame of soliton, we have found that the probe governing equation is the exact analogue of the time-dependent Schrödinger equation of an electron in a periodic crystal in the presence of an external electric field [3]. In our case, we deal with a spatially dependent Schrödinger equation of a single particle 'probe' in an induced temporal crystal by the accelerated pump.

Consider the propagation of an ultrashort soliton in a H_2-filled HC-PCF. Exciting the rotational Raman shift frequency δ in the fiber via this soliton will induce a long-lived trailing temporal periodic crystal with a lattice constant $\Lambda = 56.7\,\text{fs}$. In the absence of the applied force, the solutions are the Bloch modes, while in the presence of the applied force, the periodic potential is tilted, and the eigenstates of the system are the Wannier functions portrayed as a 2D color plot in Fig. 1(a), where the horizontal axis is the time and the vertical axis is the corresponding eigenvalue. After an eigenvalue step $g_1\Lambda$ the eigenstates are repeated, but shifted by Λ, forming the Wannier-Stark ladder. Each potential minimum allows a single localized state with weak tails. A large number of delocalized modes with long and strong tails exist in between. An

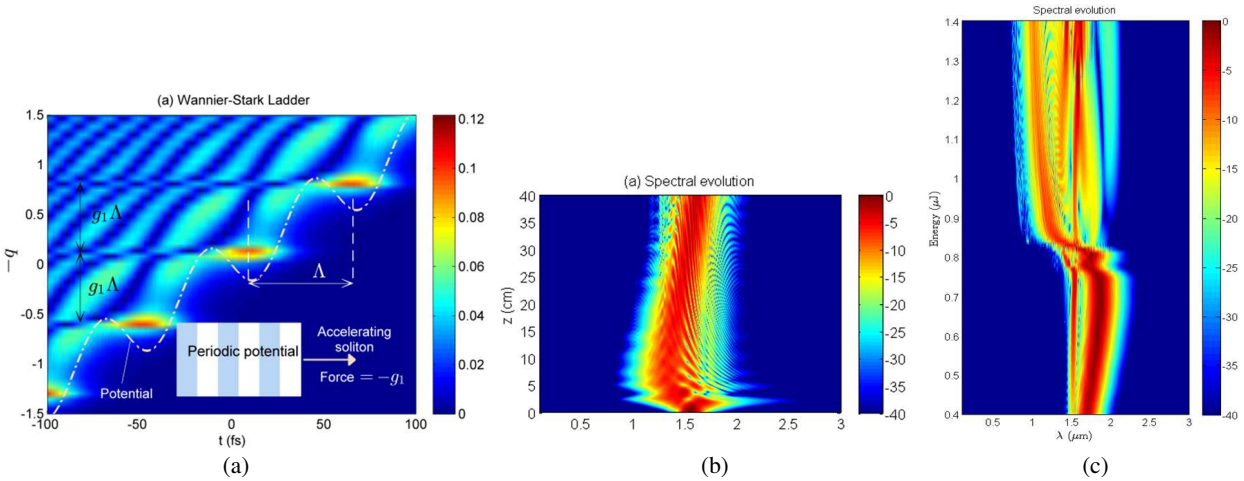

Figure 1: (a) A fundamental pump soliton with central wavelength 1064 nm, and full width at half maximum (FWHM) 15 fs is propagating in a H_2-filled HC-PCF that has a flat-to-flat core diameter 18 μm, gas pressure 7 bar, and rotational Raman frequency $\omega_R = 17.6\,\text{THz}$. (a) A portion of the absolute eigenstates of the Raman-induced temporal periodic crystal with a lattice constant $\Lambda = 56.7\,\text{fs}$ in the presence of a force with magnitude $g_1 = 0.1408$ in the positive-delay direction. The vertical axis represents the corresponding eigenvalues $-q$. The dotted-dashed line is the tilted potential. (b) Control over the Raman coherence wave in presence of Raman and plasma effects, and (c) control over the pulse spectrum due to the interplay between Raman and plasma effects as a function of pump energy.

arbitrary weak probe following the soliton will be decomposed into these Wannier modes. The evolution of a delayed probe is depicted in Fig. 2(b). Due to beating between similar eigenstates in different potential wells, Bloch oscillations arise with a period 34.7 cm. After each half of this period, an accelerated radiation to the left due to Zener tunneling is also emitted. The Zener tunneling is dominant over the Bloch oscillations, because the potential wells are relatively far from each other, hence, the overlapping between the localized modes are small.

When the intensity of light overcomes a certain threshold, the gas becomes ionized and generates an electron plasma, which in turn will influence nonlinearly the pulse. This leads to a soliton self-frequency *blueshift* and can be used to push energy into the blue part of the spectrum. We discuss the interplay between the Raman effect and the plasma effect, which leads to a very interesting control of the temporal and spectral domain of the pulse. Our novel theories on these two combined effects reveal all the main ingredient of supercontinuum generation in Raman- and plasma-active gases.

REFERENCES

1. Travers, J. C., W. Chang, J. Nold, N. Y. Joly, and P. St. J. Russell, "Ultrafast nonlinear optics in gas-filled hollow-core photonic crystal fibers," *J. Opt. Soc. Am. B*, Vol. 28, A11–A26, 2011.
2. Korn, G., O. Dühr, and A. Nazarkin, "Observation of raman self-conversion of fs-pulse frequency due to impulsive excitation of molecular vibrations," *Phys. Rev. Lett.*, Vol. 81, 1215, 1998.
3. Saleh, M. F., A. Armaroli, T. X. Tran, A. Marini, F. Belli, A. Abdolvand, and F. Biancalana, "Temporal condensed matter physics in gas-filled photonic crystal fibers," ArXiv 1412.0988, 2014.

Multicomponent Rogue Waves

A. B. Aceves[1], **F. Baronio**[2], **M. Conforti**[3], **A. Degasperis**[4], **B. Frisquet**[5], **B. Kibler**[5], **S. Lombardo**[6], **G. Millot**[5], **Ph. Morin**[5], **and S. Wabnitz**[2]

[1]Southern Methodist University, USA
[2]University of Brescia, Italy
[3]Lille University, France
[4]University of Rome I, Italy
[5]University of Bourgogne, France
[6]Northumbria University, UK

Abstract— Rogue or extreme waves have been extensively investigated in recent years in various application contexts, ranging from oceanography to nonlinear optics. A new frontier in the study of rogue waves is provided by multi-component wave systems, where the transfer of energy among the various components of a vector field may lead to novel and unexpected complex phenomena. In this presentation we discuss our recent advances in the theory and experiments on multi-component rogue waves, with a special focus on the case of vector propagation in randomly birefringent optical fibers, and in periodic Bragg gratings. Polarization coupling in telecommunication fibers is described by the vector nonlinear Schröinger equation or Manakov system. We have found a new class of coupled wave rogue wave solutions in both the anomalous and in the normal dispersion regime of the fiber. We have experimentally demonstrated the generation of black vector rogue waves by using standard telecom components. Pulse propagation in periodic fiber Bragg gratings is described by a variant of the massive Thirring model. We recently found the rational rogue wave solution of the massive Thirring model, which may open the way for the observation of rogue waves in periodic optical media, in oceans with a periodic bottom, as well as in relativistic fields.

Non-instantaneous Polarization Decay in Resonant Dielectrics

J. Hyyti[1,2], **M. Hofmann**[3], **S. Birkholz**[1], **M. Bock**[1], **S. K. Das**[1,4], **R. Grunwald**[1], **M. Hoffman**[5], **T. Nagy**[5,6], **A. Demircan**[6], **M. Jupé**[7], **D. Ristau**[7], **U. Morgner**[5,7], **C. Brée**[3], **M. Woerner**[1], **T. Elsaesser**[1], **and G. Steinmeyer**[1]

[1]Max-Born-Institut für Nichtlineare Optik und Kurzzeitspektroskopie, Berlin 12489, Germany
[2]Optoelectronics Research Centre, Tampere University of Technology, Tampere 33720, Finland
[3]Weierstrass Institute for Applied Analysis and Stochastics, Berlin 10117, Germany
[4]Department of Physics, School of Applied Sciences
Campus 3, KIIT University, Bhubaneswar 751024, India
[5]Institut für Quantenoptik, Leibniz-Universität Hannover, Hannover 30167, Germany
[6]Laser-Laboratorium Göttingen e.V., Göttingen 37077, Germany
[7]Laser Zentrum Hannover e.V., Hannover 30419, Germany

Abstract— We experimentally demonstrate and theoretically analyze the appearance of a lasting polarization response in a dielectric material. This previously unreported finding stems from a resonance condition of the third harmonic of the input light with the bandgap of the material. Polarization decay times up to 7 fs are observed for an effect that has previously always been considered to be unmeasurably fast.

Introduction: Third-order optical nonlinearities are extensively utilized in generation and characterization of ultrashort optical pulses, e.g., for frequency-resolved optical gating (FROG), which can be based on a variety of $\chi^{(3)}$ effects. FROG intrinsically relies on the instantaneity of the polarization response. Here we demonstrate that resonant third harmonic excitation in a dielectric medium may exhibit a surprisingly slow polarization decay, with a relaxation time constant that exceeds the duration of the shortest pulses generated to date.

Results: We used a collinear variant of third harmonic FROG (THFROG) [1] to characterize 7.5 fs Ti:sapphire laser pulses. Employing an identical THFROG setup, we focus either onto a TiO_2 half-wave layer or onto an uncoated SiO_2 substrate. From the recorded THG spectrum, we retrieve the intensity profiles [2] and observe that the pulse appears significantly broadened in TiO_2 relative to the measurement in SiO_2, despite of an otherwise identical setup. Deconvolution with a single-sided exponential kernel then allows determining a polarization lifetime $\tau_{\mathrm{pol}} = 6.5\,\mathrm{fs}$. For deeper understanding of this surprising effect, we solved the time-dependent Schrödinger equation (TDSE) for the parameters of the two dielectrica, which clearly identifies a resonance condition as responsible for the lasting response in TiO_2. Using the same deconvolution approach on the TDSE data, a time constant of 8 fs is reproduced in our theoretical treatment. Furthermore, extraction of the fundamental polarization reveals a similar lasting response also for self-refraction.

Conclusions: In conclusion, our results indicate a surprisingly slow few-femtosecond polarization decay of dielectrics in case of resonant excitation of the third harmonic. This previously unreported affect may impact $\chi^{(3)}$ based characterization methods, in particular at short visible or ultraviolet wavelengths [3]. Moreover, similar effects in the Kerr response may also limit the efficiency of few-cycle pulse generation schemes when they are based on self-refraction. Resolution of the measured $\approx 7\,\mathrm{fs}$ time constants is among the fastest ever reported effects at near-visible wavelengths, demonstrating the remarkable capability of FROG of resolving the temporal dynamics of nonlinear processes at the few-cycle scale.

REFERENCES

1. Das, S. K., et al., "Highly efficient THG in TiO_2 nanolayers for third-order pulse characterization," *Opt. Express*, Vol. 19, 16985–16995, 2011.
2. Stibenz, G. and G. Steinmeyer, "Interferometric frequency-resolved optical gating," *Opt. Express*, Vol. 13, 2617–2626, 2005.
3. Hofmann, M., et al., "Non-instantaneous polarization dynamics in dielectric media," *Optica*, accepted for publication, 2015.

Session 1P15a
Oral Presentations for Best Student Paper Awards — SC3: Optics and Photonics

F-band Millimeter-wave Signal Generation for Wireless Link Data Transmission Using On-chip Photonic Integrated Dual-wavelength Sources

Robinson Guzman[1], **Guillermo Carpintero**[1], **Carlos Gordon**[1], **Katarzyna Lawniczak**[2], **and Xaveer Leijtens**[2]

[1]Tecnología Electrónica, Universidad Carlos III de Madrid, Leganés, Madrid, Spain
[2]Photonic Integration, Technical University of Eindhoven, Eindhoven, The Netherlands

Abstract— The upper millimeter-wave band (> 60 GHz) signals generation used for either broadband wireless or wired communications links has recently become a very attractive field having a significant interest among diverse groups comprising broadcasters, enterprise users, astronomy, security, defense issues and others; due to all the potential applications which they can be used for. However, generation of these signals is not possible by conventional techniques due to electronic limitations [1], so new devices and techniques are needed. Between the possible millimeter-wave signal generation sources are Photonic Integrated Circuits (PIC) which have a key advantage enabling the integration of multiple photonic building blocks within a single chip to develop compact systems with increased functionality and performance [2] Eliminating the need to fiber couple these photonic building blocks has a huge impact on the cost and component footprint.

Photonic integration allows us to develop compact and cost efficient transmitters, generating the wireless carrier frequency at the remote location where the antenna is to be located. There are several photonic techniques that are available for this task, and some photonic integration advances have already been reported [3]. Here, we shall present a photonic source for millimeter-waves signal generation using on-chip photonic dual-wavelength sources based on arrayed waveguide grating (AWG) using Multimode Interference reflectors (MIR). Furthermore, this paper presents our progress in F-band wireless link system technologies that contribute to extending the transmission distance of the wireless links.

REFERENCES

1. Nagatsuma, T., et al., "Photonic generation of millimeter and terahertz waves and its applications," *Applied Electromagnetics and Communications*, Vol. 1, No. 4, 24–26, 2007.
2. Smit, M., X. Leijtens, E. Bente, J. Van der Tol, H. Ambrosius, D. Robbins, M. Wale, N. Grote, and M. Schell, "Generic foundry model for InP-based photonics" *IET Optoelectronics*, 187, 2011.
3. Nagatsuma, T., S. Horiguchi, Y. Minamikata, Y. Yoshimizu, S. Hisatake, S. Kuwano, N. Yoshimoto, J. Terada, and H. Takahashi, "Terahertz wireless communications based on photonics technologies," *Opt. Express*, Vol. 21, 23736, 2013.

Design and Simulation of Ultra-compact 25-Gbit/s Directly-modulated V-cavity Tunable Laser at 1310-nm Band

Lingxuan Lan, **Lin Wu**, **and Jian-Jun He**
Center for Integrated Optoelectronics
State Key Laboratory of Modern Optical Instrumentation
Department of Optical Engineering, Zhejiang University, Hangzhou 310027, China

Abstract— Tunable semiconductor lasers have been intensively studied for next-generation optical networks. Besides their use for source sparing with the advantages of reduced inventory and cost, they are also the key components for wavelength-agile access and communication between data centers. However, tunable lasers based on grating or MEMS structure are expensive for the need of complex fabrication process and complicated tuning algorithm.

In this paper, we design and investigate a high-speed directly-modulated tunable V-cavity laser working at 1310-nm band, which is based on AlGaInAs multiple-quantum-wells. The V-cavity laser is ultra-compact with device size of only 300 μm × 200 μm, and it does not require grating and multiple epitaxial regrowth. This structure consists of a channel selector cavity and a reference cavity with different optical path lengths, which are coupled by a reflective 2 × 2 half-wave coupler.

By employing the time-domain traveling-wave method, the static and dynamic performances of the V-cavity laser are investigated. 21 × 200 GHz tuning with ∼ 40 dB side-mode suppression ratio is achieved by simple single-electrode-control using carrier injection effect, when the lengths of the channel selector cavity and reference cavity are 220 and 210 μm, respectively. The layer structure and ridge waveguide are optimized to obtain a mode confinement factor of 0.16 for better performance. Small signal response simulation is carried out by an impulse current injection with a fast Fourier transform algorithm, and the simulated 3-dB bandwidth is 29.9 GHz when the coupler electrode is biased at 70 mA. Moreover, 10 Gbit/s and 25 Gbit/s direct modulations are demonstrated with clear eye-opening. The corresponding extinction ratio is about 8 dB when the injection current is 100 mA and 40 mA for "1" and "0", respectively. Error-free 10-km single-mode fiber transmission is also obtained.

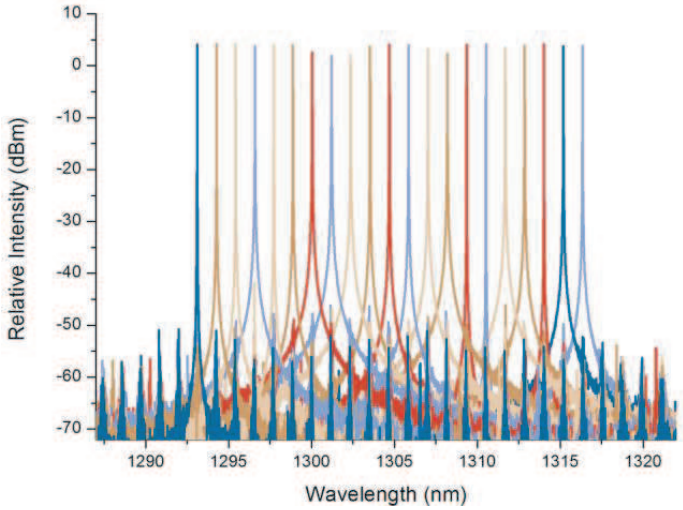

Self-homodyne Detection in Optical Coherent Transmission Using Extracted Carrier as the Local Oscillator by Saturated SOA

K. H. Mun, **S. M. Jung**, **and S. K. Han**
Department of Electrical and Electronic Engineering
Yonsei University, 50 Yonsei-ro, Seodaemun-Gu, Seoul, Korea

Abstract— In the homodyne coherent detection, the wavelength of local oscillator at the receiver should be same as the transmitted signal; otherwise, carrier frequency offset (CFO) noise occur and it makes system performance worse. Therefore, in the homodyne system, a technique which tunes the wavelength of LO to the signal and stabilizes the wavelength is required, such as optical frequency locked loop (OFLL), or it is required to compensate CFO using DSP. On the other hand, in case of the self-homodyne detection, the techniques are not required because LO light which originates the signal source is transmitted from transmitter. However, the conventional self-homodyne detection requires another single mode fiber or multi-core fiber for transmission of LO light, so this is inefficient in terms of cost and system realization. In this paper, we proposed a self-homodyne coherent detection technique using extracted carrier from the received optical signal as LO by saturated semiconductor optical amplifier (SOA). Saturated SOA has data erasing characteristic, so LO light can be extracted from the received optical signal by erasing modulated data of optical signal. In the proposed scheme, there is no CFO because LO light originating from the received signal has a totally same wavelength with the signal; thus, expensive OFLL or complex CFO compensation algorithm can be avoided and also colorless operation is possible. In addition, there is no additional requirement of optical fiber for LO light transmission, so it is cost efficient. The test bed has been set up and the feasibility was experimentally demonstrated.

THz Oscillations in DNA Monomers, Dimers and Trimers

K. Lambropoulos, **K. Kaklamanis**, **G. Georgiadis**, **M. Theodorakou**,
M. Chatzieleftheriou, **A. Morphis**, **M. Tassi**, **and C. Simserides**
Faculty of Physics, Department of Solid State Physics
National and Kapodistrian University of Athens
Panepistimiopolis, GR-15784 Zografos, Athens, Greece

Abstract— We study [1–3] charge transfer in DNA monomers, dimers and trimers (monomer is one base-pair) with a tight binding approach (I) at the base-pair level using the relevant on-site energies of the base-pairs and the hopping parameters between successive base-pairs or (II) at the single-base level using the relevant on-site energies of the bases and the hopping parameters between neighboring bases. The parameters can be found in Refs. [1, 4]. We solve numerically a system of (I) N or (II) $2N$ coupled differential equations with the eigenvalue method, determining the temporal and spatial evolution of electrons or holes along a N base-pair DNA segment [1–3]. With the approach (I), we predict electron or hole oscillations in DNA dimers [1, 2] with frequency in the range $f \approx 0.25$–$100\,\mathrm{THz}$ (period $T \approx 10$–$4000\,\mathrm{fs}$), i.e., mainly in the mid- and far-infrared with wavelengths $\lambda \approx 3$–$1200\,\mu\mathrm{m}$ [2]. The efficiency of charge transfer between the two monomers which constitute the dimer is described with the maximum transfer percentage p and the pure maximum transfer rate pf. For dimers made of identical monomers $p = 1$, but for dimers made of different monomers $p < 1$. For trimers made of identical monomers the carrier oscillates periodically with $f \approx 0.5$–$33\,\mathrm{THz}$ ($T \approx 30$–$2000\,\mathrm{fs}$) [2]; for 0 times crosswise purines $p = 1$, for 1 or 2 times crosswise purines $p < 1$. For trimers made of different monomers the carrier movement may be non-periodic [1, 2]. The method can be applied to polymers, too [1, 3] allowing us to evaluate the extent at which a DNA segment can serve as an efficient medium for charge transfer. With the approach (II) we investigate carrier oscillations in DNA monomers and dimers. This (II) approach allows us to examine the system in higher detail; the results agree in a coarse frame with the results of approach (I). Calculations based (III) on Real-Time Time-Dependent Density Functional Theory (RT-TDDFT) for the adenine-thymine and the guanine-cytosine base-pairs are under way; here we present our first results. Similar THz oscillations within smaller systems, e.g., p-nitroaniline and FTC chromophore [5], zinc porphyrin and green fluorescent protein chromophores and adenine-thymine base-pair [6] have been presented in the literature. Applying our methods (I) and (II) in the A-T monomer we get a period of oscillations in agreement with the prediction of that much more computationally complex technique [6]. Hence, the simpler approaches (I) and (II) catch the key phenomenon, while, we can easily treat dimers, trimers, tetramers [7] etc. and polymers, something exceptionally time-demanding for the approach (III). Our results show that a non conventional source or receiver of THz and above THz electromagnetic radiation can be envisaged.

REFERENCES

1. Simserides, C., "A systematic study of electron or hole transfer along DNA dimers, trimers and polymers," *Chem. Phys.*, Vol. 440, 31–41, 2014.
2. Lambropoulos, K., K. Kaklamanis, G. Georgiadis, and C. Simserides, "THz and above THz electron or hole oscillations in DNA dimers and trimers," *Ann. Phys.*, Vol. 526, 249–258, Berlin, 2014.
3. Lambropoulos, K., K. Kaklamanis, G. Georgiadis, M. Theodorakou, M. Chatzieleftheriou, M. Tassi, A. Morphis, and C. Simserides, in Preparation.
4. Hawke, L. G. D., G. Kalosakas, and C. Simserides, "Electronic parameters for charge transfer along DNA," *Eur. Phys. J. E*, Vol. 32, 291–305, 2010; "Erratum to: Electronic parameters for charge transfer along DNA," *Eur. Phys. J. E*, Vol. 34, 118, 2011.
5. Takimoto, Y., F. D. Vila, and J. J. Rehr, "Real-time time-dependent density functional theory approach for frequency-dependent nonlinear optical response in photonic molecules," *J. Chem. Phys.*, Vol. 127, 154114, 2007.
6. Lopata, K. and N. Govind, "Modeling fast electron dynamics with real-time time-dependent density functional theory: Application to small molecules and chromophores," *J. Chem. Theory Comput.*, Vol. 7, 1344–1355, 2011.
7. Lambropoulos, K., "Charge transfer in small DNA segments: Description at the base-pair level," Diploma Thesis, National and Kapodistrian University of Athens, Greece, 2014.

Formation of Caustics by Refraction of Structured Laser Radiation in the Diffusive Layer of Liquid

A. V. Vedyashkina, I. L. Raskovskaya, and I. N. Pavlov
V. A. Fabrikant Physics Department, National Research University
"Moscow Power Engineering Institute", Moscow 111250, Russia

Abstract— Nowadays research of optically inhomogeneous media represent great scientific interest. In such media the refractive index is not the same in any point and light passes due to refraction not rectilinearly.

It is often important to know what occurs when two or more mediums with different physical characteristics contact each other, how the refractive index of liquid changes by heating or cooling objects inside it.

One method of researching optically inhomogeneous mediums is the method of the laser refractography. It is based on the phenomenon of refraction of structured laser radiation (SLR) in optically inhomogeneous media and registration of its form deviations with the digital video camera [1].

In this paper we consider case when optical inhomogeneity created by diffusion. The diffusive layer of liquid appears near interface of two liquid mediums with various refraction indexes. Refraction index of more solid liquid is n_1, less solid $-n_2(n_1 > n_2)$. The model of diffusive layer we will describe with special exponential model [2].

In this paper two types of structured laser radiation are considered: laser plane and cylindrical beam. When probing of the medium by radiation of these types caustics appear. Caustic is the envelope of light rays. In this method, it is a special line or special surface near which the intensity of light field increases sharply [3]. It is presented experimental and computer 3D-visualization of dynamics of caustics' formation when changing parameters of inhomogeneity and laser radiation. It is shown how position and shape of caustic's surface can changes by variation different parameters such as angle of SLR incidence, size of cylindrical beam, gradient of refraction index, etc.. Fig. 1 shows experimental setup for registration 3D-refractogram of cylindrical beam in diffusive layer.

It is very important to know the area of caustics' occurrence that allows optimizing experiments. At the consideration experimental refractogram, which was made in diffusive layer, it is possible to analyze how can mediums diffuse each other and estimate gradient of refraction index.

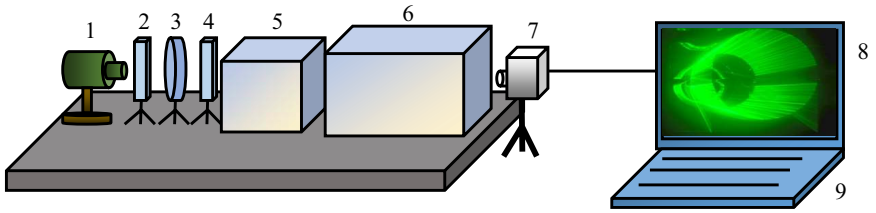

1 – laser, 2, 4 – lenses, 3 – DOE, 5 – cuvette with diffusive layer of liquid, 6 – cuvette with scattering particles in water, 7 – digital camera, 8 – 3D-refractogram, 9 – PC

Figure 1: Experimental setup.

REFERENCES

1. Rinkevichyus, B. S., O. A. Evtikhieva, and I. L. Raskovskaya, *Laser Refractography*, Springer, New York, 2011.
2. Vedyashkina, A. V., "Computer modeling of optical rays' refraction in inhomogeneous mediums," *Journal of Beijing Institute of Technology*, Vol. 22, No. 1, 71–76, 2013.
3. Vedyashkina, A. V., I. N. Pavlov, I. L. Raskovskaya, and B. S. Rinkevichyus, "Experimental and computer 3D-visualization's dynamics of optical caustics in inhomogeneous mediums," *Proceedings of 16 International Symposium on Flow Visualization*, report ISFV16-1178, 2014.

Self-organizing And Filamentary Behaviour in Broad-area Lasers

A. V. Pakhomov[1, 2], **A. A. Krents**[1, 2], **D. A. Anchikov**[1], **and N. E. Molevich**[1, 2]

[1]Department of Physics, Samara State Aerospace University, Samara, Russia
[2]Theoretical Sector, Lebedev Physical Institute of Russian Academy of Sciences
Samara Branch, Samara, Russia

Abstract— Broad-area lasers are often necessary for high-power laser applications since increasing of transverse sizes of pumping region entails increasing the output power. However, for pumping levels well above the lasing threshold broad-area lasers exhibit complicated spatio-temporal dynamics. This is caused by the development of steady lasing instabilities that turn to be especially complex in broad-area lasers as transverse space-coupling processes and corresponding nonlinearities become involved. As a result related laser operation leads to degradation of brightness of these devices and coherence reduction of emitted beam.

In presented work we report on detailed investigation of spatio-temporal instabilities emergence for steady stationary operation in broad-area lasers. Our analysis was based on Maxwell-Bloch equations for frequency detuned cavity along with transversely distributed two-level lasing media. Performed analytical investigations together with numerical modeling demonstrated several separable dynamical regimes depending on ratios between active media and cavity parameters. Principally, it allowed distinguishing filamentary instability from pattern forming instability.

Filamentary behaviour is shown to emerge for incoherent light-media interaction when medium polarization instantaneously follows the intracavity field. This dynamical regime is found to be induced by modulation-type instability and is accompanied with both temporal and spatial nonregular dynamics. Filamentation can be often explained by strong gain-index coupling or by influence of self-focusing nonlinearity in the case of strongly nonlinear regimes. Our results show possibility of such dynamics in active system for even low electromagnetic field intensity just above the threshold. Therefore we expect this instability to be one of the possible routes to filamentation and light threads formation when extending the transverse section in many active optical systems like broad-area semiconductor lasers and amplifiers.

Pattern formation is found to evolve for coherent light-media interaction according to another scenario. This type of behaviour arises when steady lasing becomes unstable in favor of self-oscillating operation and it is in turn supplemented by instability against small spatio-temporal perturbations with finite wavelength. A number of spontaneously forming regular patterns was observed in this case like standing autowaves and spiral patterns. Self-organizing can eventually lead to either stationary or oscillating inhomogeneous intensity profile. Main principles and formation concepts of these optical patterns in the transverse section of the broad-area laser emission were elaborated.

Hydrogen and Humidity Sensing Based on WGMs of Elastic Polymer Optical Microresonators

M. Eryürek[1], **Y. Karadag**[2], **S. Anand**[1], **N. Kılınç**[3], **A. Kiraz**[1]

[1]Department of Physics, Koç University, Rumelifeneri Yolu, Sarıyer, İstanbul 34450, Turkey
[2]Department of Physics, Marmara University, Göztepe, İstanbul 34722, Turkey
[3]Department of Mechatronics Engineering, Niğde University, Niğde 51245, Turkey

Abstract— Hydrogen gas is an attractive energy source because of its energy conversion efficiency. However, the lower flammable limit of hydrogen gas is 4% in the air at room temperature. In addition, hydrogen storage is difficult because of its small molecular volume. Therefore selective detection of small concentrations of hydrogen gas at room temperature with a quick response is crucial for the public health and the safety of property. In this work, we propose a hydrogen gas sensor based on polymer optical microdisk resonators fabricated using standard UV photolithography. The sensing mechanism relies on the shift of optical whispering gallery modes (WGMs) due to the size change of the resonator which is induced by the volume expansion of a palladium layer coated on the resonator. These resonators and the waveguides are fabricated using SU-8 photoresist on a thick-oxide Si wafer substrate. A tunable laser (1500–1630 nm) is coupled to the waveguide using end-face coupling method. When the transmission spectrum is measured, transmission dips are observed revealing WGMs. A maximum quality factor of 2000 is measured which can be improved by either controlling the waveguide-resonator separation to obtain critical coupling or by fabricating much smoother microdisk resonators to decrease the scattering loss.

Palladium (Pd) layer is coated on these resonators for hydrogen sensing experiments. A lower detection limit of 0.3% is recorded in nitrogen environment. These sensor devices can reversibly respond hydrogen concentrations up to 1.5%. After 1.5% the sensor devices suffer from irreversible changes because of a phase transition in palladium. This phase transition can be delayed to higher hydrogen concentrations by using palladium alloys instead of Pd.

Hydrogen sensing performance of these sensor devices also tested under humid conditions. At room temperature and under 100% relative humidity the sensor did not respond to 0.5% hydrogen. However at 50% relative humidity, 0.5% hydrogen was successfully detected which is important in terms of practical applications.

Session 1P15b
Oral Presentations for Best Student Paper Awards — SC4: Antennas and Microwave Technologies

Electron Beam Detection by Induced Resonance in Cylindrical Cavity

Alberto Leggieri[1, 2], **Davide Passi**[1], **Franco Di Paolo**[1], **Giuseppe Felici**[2], **Alessia Ciccotelli**[2], **Silvia De Stefano**[2], **and Filippo Marangoni**[2]

[1]Dipartimento di Ingegneria Elettronica, Università degli Studi di Roma "Tor Vergata", Roma, Italy
[2]S.I.T., Sordina IORT Technologies S.p.A., Aprilia, Italy

Abstract— An investigation on the power energy injection in a resonator by electron stream is reported in this paper, by documenting the power transfer between the electron current to a resonant system. The beam current emitted by an electron linear accelerator (LINAC) has been monitored through a particular radiation detector. This device was developed for the dose measurements of a Medical Linear LINAC where monitoring system are required for the real time control of the dose delivered to the patient [1–4]. The power transfer has been observed employing the relation of interaction of the LINAC beam current with a passive resonant cavity [5] placed at the output interface of the accelerator. The LINAC beam current have a bunched form. The spectral content is a line at the accelerating pulsation $\omega_0 = 2\pi f$ and whole-number harmonics [4]. The beam has been used to induce TM_{010} mode oscillations in a cylindrical cavity at the frequency f [6]. The current drives the cavity in resonance and the energy exchange is heavily regulated by the transit time factor T [7] and the coupling factor k [8]. A magnetic loop antenna is inserted in the cavity in order to perceive the magnetic flux at the TM_{010} resonance. A voltage induced on the terminals of the magnetic loop is forwarded to an envelope detector through a coaxial transmission line loaded (Fig. 1). The envelope detector shows a matched impedance to the loop-cavity system where a certain amount of power is dissipated. The cavity modeling has been performed on POISSON SUPERFISH and the whole system consisting of the cavity and the magnetic loop has been optimized and finally simulated on HFSS version 15 of ANSYS

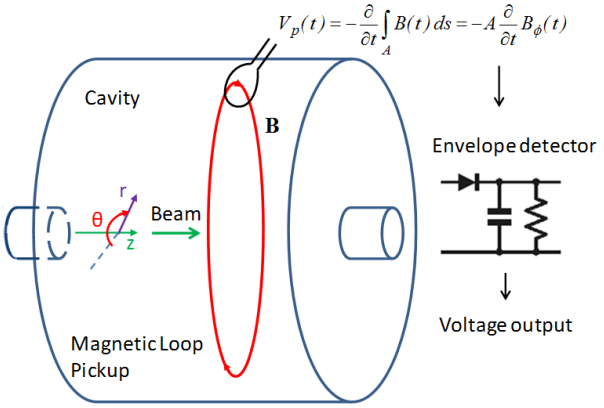

Figure 1: Block diagram of the operative principle.

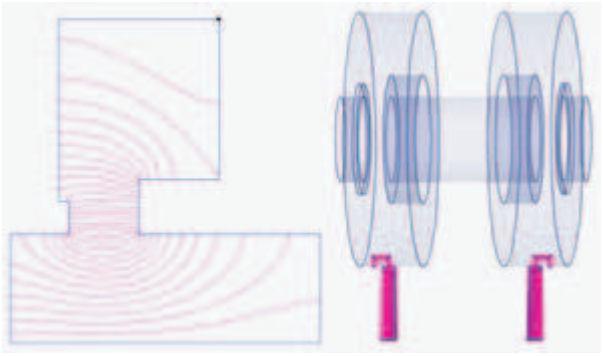

(a) (b)

Figure 2: (a) Field profile of a quarter of the re-entrant cavity modeled in POISSON SUPERFISH and (b) the whole cavity-loop system in ANSYS-ANSOFT HFSS 3D model.

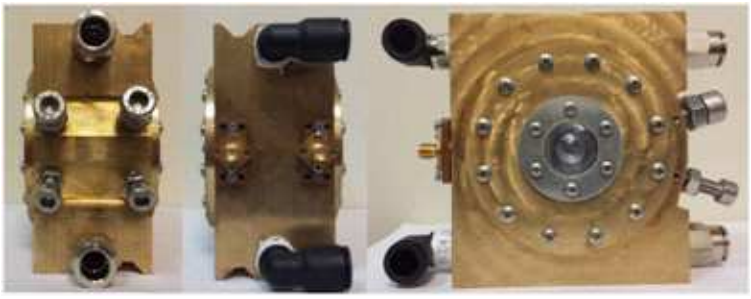

Figure 3: Prototype of the proposed detector in main profile views.

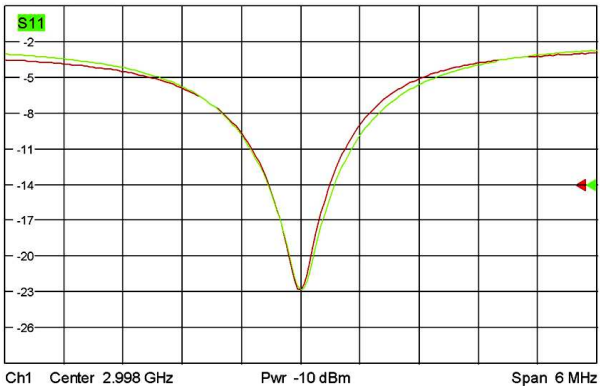

Figure 4: Measured scattering reflection parameters.

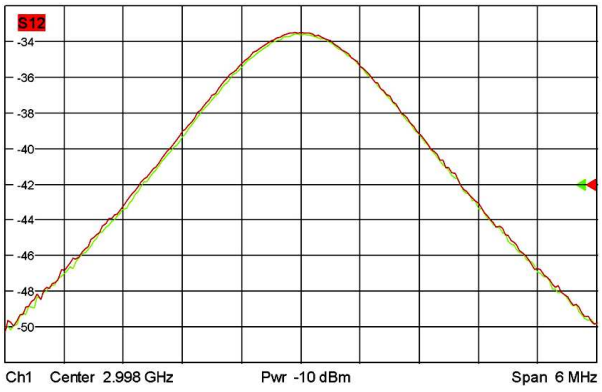

Figure 5: Measured scattering transmission parameters.

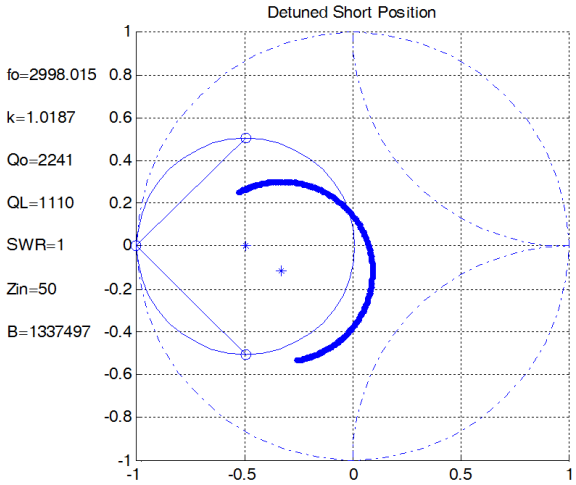

Figure 6: Detuned short position elaboration for coupling analysis.

(Fig. 2). A prototype has been fabricated (Fig. 3) and tested through VNA cold measurements and by shooting a beam current in the while cavity observing the output voltage. The input characteristic of the cavity system have been measured showing a quality factor $Q_0 = 2.24 \cdot 10^3$, a Return Loss of 23 dB a cross talk of -34 dB and a Coupling Factor $k = 1.019$, (Figs. 4–6). The output voltage has been digitalized by a microcontroller, obtaining numerical values. The system has been calibrated by relating the radiation dose, measured by a certified electrometer, to this digital output, yielding the monitor units [1]. The linearity of the monitor units for different values of accumulated dose, have allowed to employ this system for the real time measurements of ionizing radiation emitted by a medical LINAC [1–3].

Low-loss Millimeter-wave Phase Shifters Based on Mechanical Reconfiguration

P. Romano[1], **O. Araromi**[2], **S. Rosset**[2],
J. Perruisseau-Carrier[3], **H. Shea**[2], **and J. R. Mosig**[1]

[1]Laboratory of Electromagnetics and Acoustics (LEMA)
École Polytechnique Fédérale de Lausanne (EPFL), Switzerland
[2]Microsystems for Space Technologies Laboratory
École Polytechnique Fédérale de Lausanne (EPFL), Switzerland
[3]Deceased. Adaptive MicroNano Wave Systems
École Polytechnique Fédérale de Lausanne (EPFL), Switzerland

Abstract— We propose the analysis, design, and implementation of mechanically reconfigurable true-time delay (TTD) phase shifters using micro-fabricated actuators at millimeter-waves (MMW). TTD phase shifters are key building blocks in many array antenna systems, including wideband beamsquint-free scanning arrays.

Reconfigurable phase shifters are critical components in modern communications and remote sensing systems at MMW. In general, advanced reconfiguration capabilities are increasingly required to dynamically update antenna characteristics, such as coverage, polarization or operating frequency. Different technologies are currently available for the implementation of tunable phase shifters, including semiconductors, RF-MEMS, Liquid Crystal, ferroelectrics. However, a common feature to all these technologies is the significant increased loss, complexity and cost with regard to non-reconfigurable devices. In this context, low-loss reconfigurability, complexity and cost are driving factors in the choice of a given technology and can constitute major limitations to future development of MMW antenna devices.

The proposed mechanical tuning allows to achieve phase shift reconfiguration with very low losses. Variable phase shift is in fact obtained modifying the physical geometry of the device in order to affect the propagation constant of a transmission line (TL) section, thus providing TTD. Using micro-actuators, this can be done by changing the geometry of the device, in order to modify the effective permittivity of the equivalent TL. Such an approach allows to completely isolate the actuation part from the electromagnetic (EM) active area, thereby achieving reconfiguration with losses comparable to the device fixed counterpart.

In particular, the preliminary design and performance of three different reconfigurable concepts operating at Ka-band is presented. The design of one concept has been further optimized to be manufactured and tested. The proposed concepts can be potentially implemented using different technologies for mechanical reconfiguration. For instance electrostatic, magnetic, piezoelectric or electroactive polymers actuators could be integrated to implement the final device. Here dielectric electroactive polymer (DEAP) actuators are used to reconfigure the phase shifter concept that has been successfully manufactured and tested. The fabricated phase shifter provides a maximum analog phase range (i.e., between maximum and minimum displacement) of around 180° at 30 GHz with extremely low losses. The insertion loss is in fact always lower than 1.6 dB with an average value of 0.83 dB over the total frequency range. The return loss is always better than 11 dB, which means good matching for all the phase shifting states in the whole 10 GHz (25–35 GHz) bandwidth. The low-loss phase shift reconfiguration demonstrated by experimental results allows state-of-the-art performance in terms of the most important figure of merit for TTD phase shifters, namely, the phase-shift/loss ratio. Indeed, a mean value of 235°/dB is achieved at 35 GHz.

Tunable Periodic Deflector Structure Based on Ferroelectric Materials

R. A. Platonov[1], **A. G. Altynnikov**[1], **I. V. Kotelnikov**[1], **A. B. Kozyrev**[1], **V. N. Osadchy**[1], **and A. G. Chernokalov**[2]

[1]Saint Petersburg Electrotechnical University "LETI", Russian Federation
[2]Limited Liability Company Samsung Research Center, Russia Federation

Abstract— In recent years electrically tunable lenses (ETL) (so called deflectors) for microwave (MW) frequencies range becomes powerful beam-forming platform that combines the best features of MW aperture antennas and phase array antennas. This approach allows the radical decrease of MW losses and greatly simplified design due to absent of dividers and intrinsic feeder lines. There are two branches for design development of ETL: (i) array lenses (AL) based on lumped elements ($L \ll \lambda$, where L is a scale of element sizes, λ — wave length) [1–4]; (ii) lenses consist of distributed elements ($L \geq \lambda/4$), based on material with nonlinear properties in electro-magnetic field.

In a set of works the ferroelectric (FE) elements are proposed to be used as a base of tunable lenses [5–7]. Ferroelectrics of BSTO type ($Ba_xSr_{1-x}TiO_3$) in paraelectric state are promising materials for this application due to no frequency dispersion of dielectric constant (ε) up to 100 GHz and the suitable tunability of ε under electrical control field. Operating principle of such lenses is based on the variation of phase shift of signal propagated through ferroelectric material due to the change of its dielectric constant by control voltage. These tunable lenses are characterized by simplicity of construction and the absence of discrete (lumped) elements that allows to use them in a wide frequency range.

In this paper the electrically tunable lens based on periodical multilayer ferroelectric structure FE/LD/FE/LD/FE (LD — linear dielectric) with transparent for MW electrodes between layers is presented. Control voltage applied to the FE ceramic leads to the change of FE layers permittivity and, as consequence, to the change of the wave impedance and the delay time across the periodical structure for MW signal. Formation of dielectric permittivity gradient along the plane of FE layers allows to deflect phase front of the plane wave propagated through the structure. The use of periodical structure allows to decrease the control voltages value and to increase the scan angle in comparison with non periodical analogues. The main parameters of device (scan angle ~ 20 deg.; bandwidth ~ 1 GHz) were obtained by modeling and were confirmed by experimental testing of antenna prototype at frequency ~ 30 GHz.

REFERENCES

1. Clemente, A., L. Dussopt, R. Saileau, P. Porier, et al., "Wideband 400-element electronically reconfigurable transmitarray in X band," *IEEE Trans. Antennas Propag.*, Vol. 61, 5017–5027, Oct. 2013.
2. Lau, J. Y. and S. V. Hum, "A planar reconfigurable aperture with lens and reflectarray modes of operation," *IEEE Trans. Microw. Theory Tech.*, Vol. 58, 3547–3555, Dec. 2010.
3. Boccia, L., I. Russo, G. Amendola, and G. Massa, "Multilayer antenna-filter antenna for beam-steeringtransmit-array applications," *IEEE Trans. Microw. Theory Tech.*, Vol. 60, 2287–2300, Jul. 2012.
4. Abbaspour-Tamijani, A., K. Sarabandi, and G. M. Rebeiz, "A millimetre-wave bandpass filter–lens array," *IET Microw. Antenna P.*, Vol. 1, No. 2, 388–395, Apr. 2007.
5. Wames, R. E., W. F. Hall, W. W. Hall, and T. C. Lim, "Monolithic, voltage controlled, phased array," U.S. Patent 4 323 901, Apr. 6, 1982.
6. Cherman, V., P. Fihol, S. Gevorgian, et al., "Ferroelectric lens," U.S. Patent 0 237 322, Sep. 24, 2009.
7. Jaganmohan, B. L., "Voltage controlled ferroelectric lens phased array," U.S. Patent 5 729 239, Mar. 17, 1998.

Point-to-point Radio Link Variation at E-band and Its Effect on Antenna Design

A. N. H. Al-Rawi, **A. Dubok**, **M. H. A. J. Herben**, **and A. B. Smolders**
Electromagnetics Group, Department of Electrical Engineering
Eindhoven University of Technology, The Netherlands

Abstract— Radio propagation will strongly influence the design of the antenna and front-end components of E-band point-to-point communication systems. Based on the ITU rain model, the rain attenuation is estimated in a statistical sense and it is concluded that for backhaul links of 1–10 km, antennas with a gain of 49.5 dBi are required. Moreover, depolarization can be a limiting factor for backhaul systems that are employing orthogonal polarization in order to improve capacity. Antenna mast movement becomes a relevant problem due to the narrow beamwidth of the high gain antennas, which is around 0.7°. We propose to implement a focal plane array as feed for the parabolic reflector antenna. This is to tackle the mast movement by electronic beam steering and to increase EIRP by increasing the number of active antenna elements, and to assist the mechanical alignment during installation.

60 GHz Antenna on Metallic Nanowired Membrane Substrate

L. G. Gomes[1], **M. V. Pelegrini**[1], **P. Ferrari**[2], **G. P. Rehder**[1], **and A. L. C. Serrano**[1]

[1]Laboratory of Microelectronics, University of São Paulo, Brazil
[2]IMEP-LAHC, Grenoble University, France

Abstract— Given the large number of wireless communication protocols functioning at microwave frequencies (0.9 GHz to 30 GHz) and the need for higher data transfer rates, interest on the millimeter wave frequency range (30 GHz to 300 GHz) has increased in both academic and industrial communities. However, integration of the millimeter-sized antenna with the micrometer-sized transceiver circuit proves to be problematic due to the high cost per square millimeter even in low-cost CMOS technologies. Several antennas have been presented in the literature at millimeter frequencies (DOI 10.1109/APS.2011.5996530, 10.1109/IEEE-IWS.2013.6616744, 10.1109/APS.2014.6904381), but only a few uses a patch topology with easy fabrication.

This work presents for the first time an antenna operating at millimeter wave frequencies, at 60 GHz using the novel low-cost Metallic nanowire Membrane substrate (MnM-substrate) (DOI 10.1109/TMTT.2014.2366108). The MnM-substrate consists of a 50-µm-thick-nanoporous-alumina-membrane filled with copper nanowires, a copper ground plane on its underside connecting all the nanowires and a silicon dioxide layer on its upper side, shown in Fig. 1.

On the top of the dielectric layer, the antenna is defined. When the membrane is filled with metal nanowires, the slow wave effect appears, confining the electrical field inside the oxide layer (Serrano, et al., 2014). Although the slow-wave effect reduces the size of the devices, it is inconvenient for the antenna, which needs to irradiate the electrical field. Thus, there are no nanowires below the antenna region, only the alumina membrane. The proposed antenna is a rectangular patch fed through a reentrant line stub transformer in order to match the 50 ohms characteristic impedance of the feed line. The feed line width at 60 GHz is close to the width of the antenna patch, degrading the antenna efficiency. Therefore, the nanowires are grown below the feed line to reduce its width. Since a patch antenna needs a thicker substrate to radiate properly it was necessary to thicken the membrane, which was done via stacking three rectangular membrane pieces on a copper-covered silicon base in order to meet the 200 µm designed thickness and guarantee ground plane continuity, as shown in Fig. 2.

The antenna was simulated in HFSS, Ansys, in order to evaluate its performance. The EM simulation of the patch antenna showed a maximum gain of 4.5 dB and return loss better than −20 dB at 60 GHz. Antenna dimensions are 750 µm × 730 µm. Although the lower gain comparing to the ones presented in the literatura, the area is highly reduced, since substrate electrical permittivity is higher (9.8 for alumina and 2.2 to 1 in onther antennas). It has been concluded that the nanowire substrate is adequate for antenna manufacturing and operation, being cheap, easy to manufacture and allowing high performance antennas to be designed. Measurements are currently in progress.

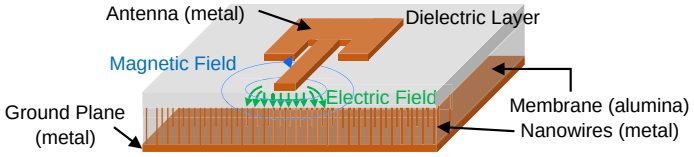

Figure 1: MnM substrate.

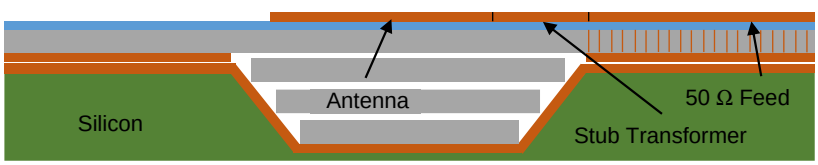

Figure 2: Cross-section af the antenna substrate assembly.

Analysis of Sampling Grids for Spherical Near-field Antenna Measurements

R. Cornelius and D. Heberling
Institute of High Frequency Technology, RWTH Aachen University, Germany

Abstract— Spherical near-field antenna measurements are commonly used to characterize an antenna under test (AUT). Therefore the electromagnetic field is measured on a closed surface around the antenna and transformed to the far-field by a near-field to far-field transformation.

The most popular transformation algorithm first calculates a spherical mode spectrum using Fourier transforms [1]. From this mode spectrum the far-field is derived. Due to the Fourier transform the transformation algorithm is very fast and efficient but requires equiangular sampling in spherical coordinates. Consequently the sampling point density is high at the poles and low at the equator. According to the number of unknown spherical modes the sphere is therefore oversampled approximately by a factor of two and this oversampling increases the measurement time. This is disadvantageous since long measurement times are a general drawback of near-field measurement systems. In order to improve the measurement speed more efficient sampling grids may be used at the expense of different and/or more complex transformation algorithms. Reformulating the transmission equation in [1] in matrix form as used for truncation error reduction in [2] is a very simple and straightforward approach. Alternatively, algorithms for general purpose presented in [3, 4] could be used. Furthermore, near-field interpolation methods could be utilized to determine the near-field on an equiangular grid [5]. Besides the larger flexibility new algorithms provide additional features like higher order probe correction, possibility of different measurement distances and position correction. Due to the technical progress in computer technology the transformation time is usually negligible compared to the measurement time and therefore a less important factor. Although new algorithms have been verified by simulations and measurements, a comprehensive investigation of different sampling grids is still missing. So far only little attention has been paid to the minimal number of required near-field samples and their distribution over the sphere. This distribution is a very important factor for the measurement time due to different capabilities of different positioning systems (e.g., roll-over-azimuth, robot arm).

In the paper we will present different sampling grids, evaluate the required hardware and the complexity of the grids. Besides the location of the sampling points the polarization will be investigated. The near-field to far-field transformation algorithm used is based on matrix inversion and calculation of the spherical modes. Therefore the condition number of the grids will be evaluated and compared. Simulations and measurements will be performed and analyzed for all grids. Finally the required relative measurement time and accuracy will be specified for the different sampling grids. It will be highlighted that the measurement speed can be increased significantly compared to equiangular sampling.

REFERENCES

1. Hansen, J. E., *Spherical Near-field Antenna Measurements*, Peter Peregrinus Ltd., United Kingdom, 1988.
2. Wittmann, R. C., C. F. Stubenrauch, and M. H. Francis, "Spherical scanning measurements using truncated data sets," *Proceedings of the 24th AMTA Annual Meeting & Symposium*, Nov. 2002.
3. Sarkar, T. and A. Taaghol, "Near-field to near/far-field transformation for arbitrary near-field geometry utilizing an equivalent current and MoM," *IEEE Trans. Antennas Propag.*, Vol. 47, No. 3, 566–573, 1999.
4. Schmidt, C., M. Leibfritz, and T. Eibert, "Fully probe-corrected nearfield far-field transformation employing plane wave expansion and diagonal translation operators," *IEEE Trans. Antennas Propag.*, Vol. 56, No. 3, 737–746, 2008.
5. Bucci, O. M., C. Gennarelli, and F. D'Agostino, "A new and efficient NF-FF transformation with spherical spiral scanning," *Proceedings of IEEE Antennas and Propagation Society International Symposium*, Jul. 2001.

A Dual V-band Push-push VCO Using the 0.18 μm CMOS Process Technology

Yu-Hsin Chang and Yen-Chung Chiang
National Chung Hsing University, Taiwan

Abstract— In this paper, a dual-band push-push voltage-controlled oscillator implemented in the 0.18-μm CMOS process for V-band applications is presented. By using a forth order resonance network composed of symmetric inductors and varactors and a push-push topology, the oscillation frequencies of the proposed circuit can be switched with only one control signal between two bands. And the second order harmonic is extracted from the central taps of inductors to achieve the frequencies of two V-band operations. The tuning ranges of the proposed voltage-controlled oscillator are from 67.78 to 69.42 GHz and from 52.2 to 54.7 GHz, respectively. The measured phase noise at 1 MHz frequency offset are −86.4 dBc/Hz and −90.5 dBc/Hz for 69.42 GHz and 54.7 GHz output frequencies, while the corresponding phase noises at 10 MHz frequency offset are −108.4 dBc/Hz and −112 dBc/Hz, respectively. The core circuit consumes a 12.96 mW dc power from a 1.8-V supply.

Spatial Power Combiner Technology

Davide Passi[1], **Alberto Leggieri**[1], **Franco Di Paolo**[1], **Antonio Tafuto**[2], **and Marco Bartocci**[2]

[1]University of Roma "Tor Vergata", Via del Politecnico 1, Roma 00133, Italy
[2]Elettronica SpA, Via Tiburtina Valeria Km 13.7, Roma 00100, Italy

Abstract— This article describes the spatial power combining techniques dealing with the state of the art of Spatial Power Combiners (SPC) considering recent developments. A brand-new splitting scheme is proposed where different types of SPC are grouped according to the space where power combining and splitting occur. This paper should provide compendium knowledge for SPC design and selection of the opportune SPC basing on the target application.

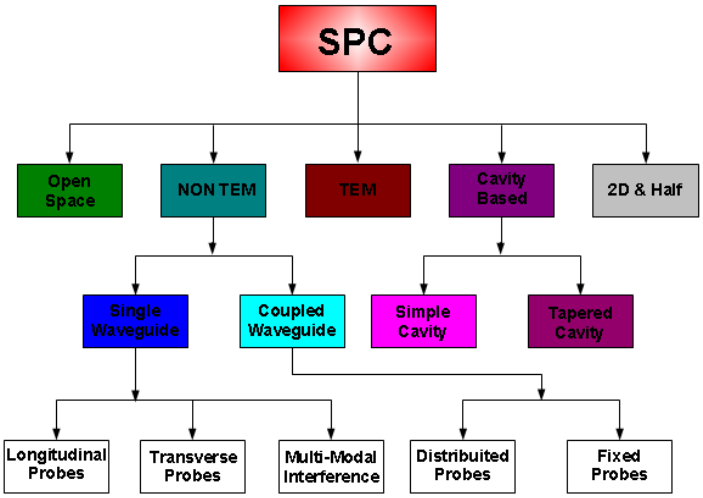

Figure 1: New splitting scheme.

The fundamental SPC Amplifier's concept is to provide a large power value with minimum losses. For this aim, SPC has several characteristics that make it unique and innovative. First one is that the electromagnetic energy coming from input is divided as much as possible in the space, without using transmission lines, and it is sent to many SSPA. After amplified energy is collected, it is sent to output port without using transmission lines. Another common feature of SPC is the presence of probes, antennas or transitions to collect the spatial RF energy and send it to a two wired transmission line. The system's quality is usually determined from its efficiency. In SPC technology efficiency can be defined basing on the portion of power sent to the active devices respect to the amount of power provided at the input port, such as it quantifies the capability of the combiner to intercept incoming energy and distribute it to N energy dividing/combining internal ports.

There are TEM and NON TEM spatial combiners, cavity based, open space and 2D&Half ones.

Non TEM SPC use waveguides to confine RF electromagnetic energy and they can be completely closed or slotted to couple energy to another slotted waveguide. This type is composed by three families: the single waveguide family, with longitudinal probes and transverse probes, the coupled waveguides and the multimodal interference families.

Then RF probes can be realized in several technologies, as monopoles, dipoles, patches or slots or combinations among them. In many other cases Fin Line transition are realized, especially when wide band applications are needed.

Two examples taken by our design experience are going to show: an X band and Ka band SPC.

Single waveguide with transverse probes and amplifiers is named Grid Amplifier. The basic concept in SPC Grid Amplifiers is to intercept the incoming signal with a defined polarization, amplify it with the active device and then send the amplified signal using the orthogonal polarization respect the incoming one.

A different type of SPC is the Multimodal Interference SPC, uses the interferences among many propagating modes in an overmoded waveguide. This multimodal interference effect is also named "Talbot's effect".

The Coupled Waveguides SPC use two waveguides connected between them through two wires transmission lines, so it is possible to insert amplifying active devices between these two waveguides.

Coupled Waveguides SPC are divided in two subgroups, the distributed probes group and fixed group of probes. In the first case, probes are located along the waveguide, while in the second case probes are located just near the shortest wall of the waveguide.

TEM SPC use TEM transmission lines to confine RF electromagnetic energy. The simplest and well known TEM structure is the coaxial transmission line, here there are going to illustrate two versions, the classic circular and the square one.

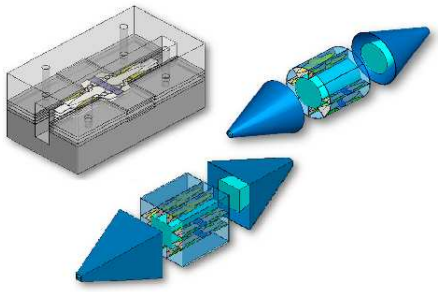

Figure 2: Non TEM and TEM SPC.

Cavity Based SPC use a closed cavity excited by an input port, and the output ports are realized inserting probes inside such cavity.

This family consists of two different groups and differing from the modality of input port coupling with the cavity: if the coupling is made through a conical transmission line the SPC is named in literature as Conical Transmission Line, otherwise it is named Simple Cavity SPC.

Their efficiency is very high due to the fact that they use closed cavities and thus energy is well confined inside it.

Open Space SPC use amplifiers connected to probes placed in an open space environment. Usually lens are used to focus the beam to and from grid amplifier.

2D&Half SPC, that are two dimensions and half SPC, remember SIW technology (Substrate Integrated Waveguide) or micro open space SPC.

Session 1P0
Poster Session 2

Time-domain Beam Propagation Method Based on Gradient Smoothing Technique for Dispersive Materials

Khaled S. R. Atia[1], **A. M. Heikal**[2], **and S. S. A. Obayya**[1]

[1]Center for Photonics and Smart Material, Zewail City of Science and Technology, Egypt
[2]Department of Electronics and Communication Engineer, Mansoura University, Egypt

Abstract— In this paper, a novel finite element time domain beam propagation method based on gradient smoothing technique. The proposed method is described for the analysis of dispersive materials. It is more accurate and stable than the conventional finite element time domain.

Introduction: The previously introduced time domain beam propagation method [1] uses a second order triangular element. However, the first order triangular element (T3) is often preferable because of its computational efficiency. A smoothed bilinear form for Galerkin formulation has been introduced [2] to improve T3 accuracy. This paper adopts the smoothed bilinear form to analyse the dispersive materials in time domain.

Formulation: We consider a TE wave equation and a plasma model under slowly varying envelop approximation. After Applying Galerkin procedure, The Shape function derivative is then replaced by the smoothed derivative as follows,

$$\nabla N(x,y) = \frac{1}{A_s} \oint_{\Gamma_s} N(x,y) d\Gamma_s, \tag{1}$$

where $N(x,y)$ is the first order shape function, A_s is the area of smoothing domain, Γ_s is the boundary of the smoothing domain. The smoothing domain is constructed by simply connect the centroid of the element by the two end points of each edge.

Results: The proposed method is tested by computing the reflection and transmission of a 20 mm slab of dispersive material. The dispersive material has a plasma frequency and a damping frequency equal 28.7 GHz and 20 GHz, respectively. An excellent agreement between the reflection and transmission obtained by the presented method and the analytical solution can be noticed from Fig. 1.

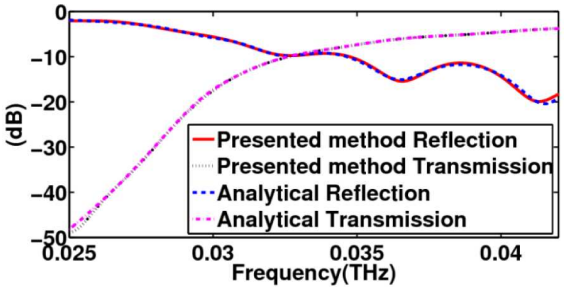

Figure 1: Reflection and transmission calculated using the proposed method and the analytical solution.

REFERENCES

1. Koshiba, M., Y. Tsuji, and M. Hikari, "Time-domain beam propagation method and its application to photonic crystal circuits," *Journal of Lightwave Technology*, Vol. 18, No. 1, 102–110, 2000.
2. Liu, G. R., "A Generalized gradient smoothing technique and the smoothed bilinear form for galerkin formulation of a wide class of computational methods," *J. Comput. Methods*, 2008.

Statistical Models of Noise Distribution in Broadband PLC Networks

A. M. Nyete, **T. J. O. Afullo**, **and I. E. Davidson**
HVDC/Smart Grid Research Centre, Discipline of Electrical, Electronic and Computer Engineering
University of KwaZulu-Natal, Durban, South Africa

Abstract— The recent advancements in digital communication techniques have seen renewed interest in the possible utilization of the traditional power grid for the provision of broadband data and voice services. However, the power line communication (PLC) channel (the power network), presents a very challenging environment for communication purposes. This is due to the fact that severe noise and distortion effects are inherent in the medium. But, if these noise and distortion effects can be effectively analyzed and modeled, then the resulting models can be utilized in the optimal or sub-optimal design of a digital communication system for PLC applications. In this paper, frequency domain noise measurements done in broadband indoor PLC networks are presented. The measurement results obtained are then modeled using the alpha stable distribution, motivated by the flexibility of the distribution as a modeling tool and the fact that the measured noise distribution is heavily tailed and skewed.

Localized Surface Plasmon Enhancement of Photoluminescence Signal from Thin Silicon Nanocrystal Film

A. Marinins[1], **S. A. Dyakov**[1], **G. S. Lobov**[1], **D. M. Zhigunov**[2], **M. Yan**[1], **S. Popov**[1], **and M. Qiu**[1, 3]

[1]School of Information and Communication Technology, KTH Royal Institute of Technology Stockholm, Kista 164 40, Sweden
[2]Faculty of Physics, Lomonosov Moscow State University, Moscow 1199991, Russia
[3]State Key Laboratory of Modern Optical Instrumentation
Department of Optical Engineering, Zhejiang University, Hangzhou 3100027, China

Abstract— Silicon nanocrystals embedded into SiO_2 matrix possess promising luminescence properties and are a subject of interest for integrated photonics applications [1]. Compatibility with standard CMOS fabrication technologies is a significant advantage. Though, luminescence energy output does not exceed several percent from pump source energy in silicon nanocrystals thin films. One of the ideas to solve this problem is to incorporate plasmonic metal nanostructures on top of Si NC matrix. Metal nanostructures are supposed to induce localized surface plasmons (LSP) which interact with silicon nanocrystals and enhance their light emissivity. Strong near-field coupling between nanocrystals and metal nanostructures is needed in order to reach noticeable luminescence improvement. Also, periodicity and geometry of metal nanostructures play a significant role in luminescence output signal. Another thing to study are quasi-guided modes in layer with silicon nanocrystals.

The scope of this work is to study the interaction between localized surface plasmons, induced by light incident on metal nanostructures, and silicon nanocrystals in SiO_2 thin film. Mathematical simulations were run in order to estimate metal nanostructure geometry which supports resonant interaction with poossibly higher luminescence output. LSP main parameters were characterized with angle-resolved reflectance spectroscopy. The influence of metal nanostructure geometry and silicon nanocrystalline film composition on emissivity was investigated with photoluminescence measurements.

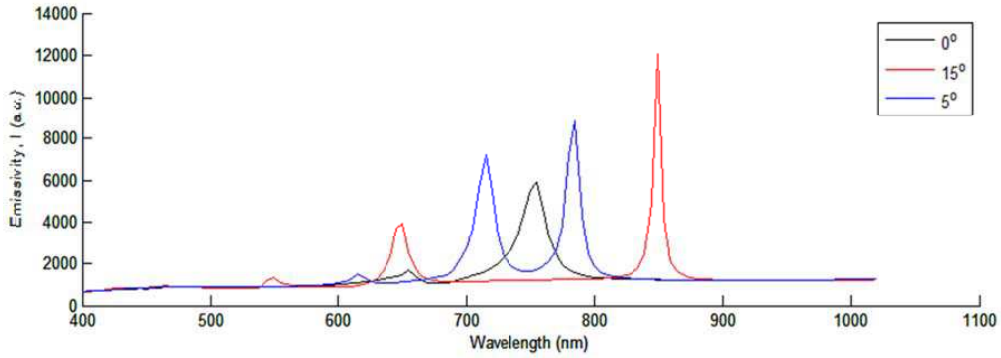

Figure 1: Emissivity spectra calculated for Si NC thin film with gold grating on top (100 nm stripe width, 450 nm period) for 0°, 5° and 15° collection angles.

REFERENCES

1. Gusev, O. B., A. N. Poddubny, A. A. Prokofiev, and I. N. Yassievich, "Light emission from silicon nanocrystals," *Semiconductors*, Vol. 47, No. 22, 183–202, 2013.

Discovery of Ionospheric 'Hubble' Frequency Shifts and Impact on Gravity Wave Detection and the Age of the Universe?

Michael J. Underhill
Underhill Research Ltd, Lingfield, UK

Abstract— Measurements have been made with resolutions of a few milli-Herz of the spectra of various carrier frequencies from 100 kHz to 25 MHz propagated by the Ionosphere. Ionospheric propagation of the various world-wide Standard Frequency signal sources at 10 MHz has been found to be of particular interest. Some new physical effects have been discovered from extensive measurements. New concepts, processes and theory have been derived from analysis of these measurements and what has been observed so far [1–5].

In Figure 1 first note the persistent lower trace which is about 10 Hz below the exact (1 in 10^9) 10 MHz of the several worldwide sources all transmitting at that frequency. Also note that the bandwidth of this signal is $<\sim 20$ mHz implying a Q of $> 5 \times 10^8$. Again note there can be two overlapping components in the lower trace, on steady and the other oscillating in frequency by up to ± 500 mHz or occasionally more. These new discoveries are in need of an explanation, which will be provided in the full paper and which is based on references [1, 2, 5] expanded further. This can be said to be a 'Hubble shift' as it is to a lower frequency. But it is not a simple Hubble shift as there are other mechanisms at work [1, 2].

Secondly note the partially repeating 'diurnal' variations particularly in the upper less shifted trace. Shifts and spreading of carrier energy of up to a few Hz are visible on a daily basis. The magnitude and duration cannot be explained as Doppler shifts, since they would imply physically impossible movements of the ionosphere. The proposal is that such variations may reflect variations in gravitational potential. In effect gravity waves may be being detected? Direct EM wave detection of gravity waves may be possible?

Thirdly these observed and measureable effects imply that the astronomical Hubble shift is not a 'receding universe' Doppler frequency shift proportional to distance. But it may be a progressive reduction in photon or light-wave energy and frequency exponentially proportional to distance. This contradicts the view that the 'Big-Bang' age of the Universe is 13.8 billion years?

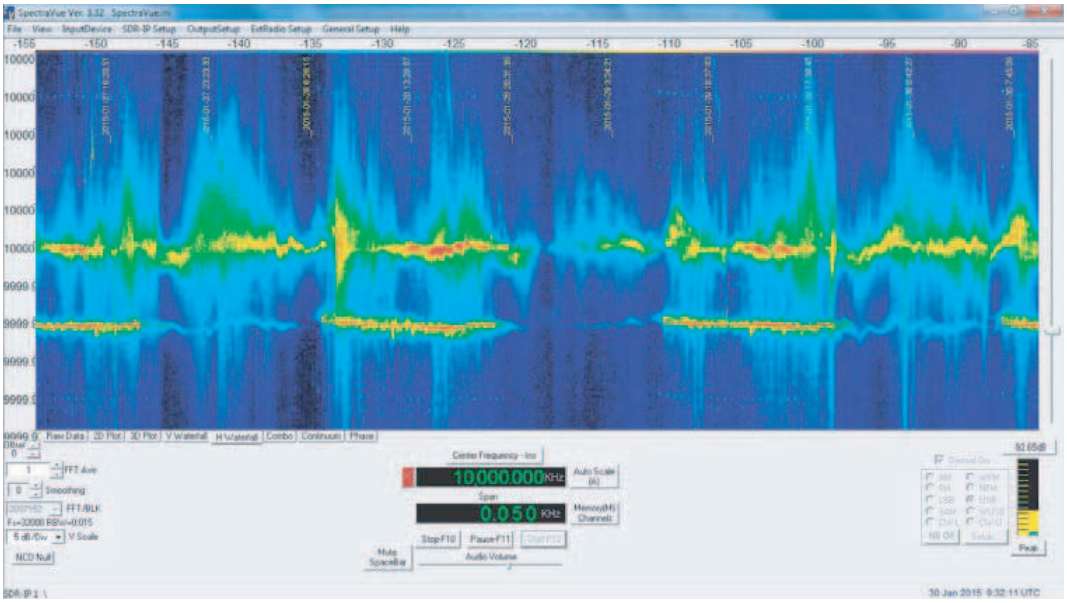

Figure 1: Three day (to Jan. 01, 2015) right to left waterfall record of 50 Hz bandwidth at 10 MHz of mixture of carriers from WWV Fort Collins USA (4700 mile NW path), BPM China (5200 miles NE path), PPE Rio de Janeiro, Brazil (5700 miles SW), WWVH Kekaha, Hawaii (7200 miles NNW). From RF Space SDR-IP receiver using SpectraVue software with 15 mHz resolution. Antenna is 83 m perimeter horizontal loop, 15 m height in Ling field (30 km south of London) UK.

REFERENCES

1. Underhill, M. J., "Coupling theory for fluctuating spurs in oscillators," *Proceedings, 2014 IEEE Int. Frequency Control Symp.*, 1–5, Taipei, Taiwan, May 19–22, 2014.
2. Underhill, M. J., "Discovery and theory of small antenna near-field dissipation and frequency conversion with implications for antenna efficiency, beverage antenna noise reduction, Maxwell's equations and the Chu criterion," *PIERS Proceedings*, 1780–1784, Guangzhou, Aug. 25–28, 2014.
3. Underhill, M. J., "Discovery of persistent ionospheric frequency shifts of a few Herz and impact on time and frequency transfer," submitted to *IFCS-EFTF 2015*, Denver, Colorado, Apr. 12–16, 2015.
4. Underhill, M. J., "SDR and self-focusing radar techniques for milliherz measurement of multi-component phase noise spectra?," submitted to *IFCS-EFTF 2015*, Denver, Colorado, Apr. 12–16, 2015.
5. Underhill, M. J., "A physical model of electro-magnetism for a theory of everything," *PIERS Online*, Vol. 7, No. 2, 196–200, 2011.

High Quality InAlAs on InP for High Sensitivity Photodiodes

D. V. Dmitriev, A. M. Gilinsky, A. I. Toropov, E. V. Fedosenko, and K. S. Zhuravlev
Rzhanov Institute of Semiconductor Physics, The Siberian Branch of the Russian Academy of Sciences
pr. Ac. Lavrentieva, 13, Novosibirsk 630090, Russia

Abstract— For creation of high-sensitivity high frequency (HF) photodetectors for use in telecom, spectroscopy, remote sensing and quantum informatics applications the utilization of InAlAs/InGaAs heterostructures grown on InP has been proposed. A reduced noise level and a better temperature stability of avalanche multiplication were predicted for the InAlAs-based structures. However, it was shown that a high dark count rate, being at least 2–3 orders of magnitude greater than that of InGaAs/InP diodes, is observed in such structures. Some of the reports have attributed the high dark count rates to tunneling currents in the InAlAs layer, possibly via deep levels in the material. Thus, the realization of the predicted advantages of InAlAs/InGaAs/InP structures requires optimization of the heterostructure growth technology and, first of all, of the InAlAs layer aimed at obtaining a low concentration of deep levels and therefore a better multiplying layer.

The epitaxial structures were grown using molecular beam epitaxy (MBE) technique in a Riber-32P and Compact-21 machines on (100)InP substrates. The quality of the layers was attested using in situ reflection high-energy electron diffraction (RHEED) and ex situ techniques: atomic force and electron beam microscopies, double-crystal x-ray diffraction and optical characterization by low-temperature photoluminescence.

We have studied the influence of the InP substrate temperature and V/III flux ratio on the crystalline and optical properties of $In_{0.52}Al_{0.48}As$ layers. These investigations show that we have achieved a substantial improvement in the quality of MBE $In_{0.52}Al_{0.48}As$ grown at a high substrate temperature of 520°C and a V/III flux ratio greater than 10.

Finite Element Analysis of Separation Force on Non-ferrous Metals Induced by Eddy Current Separator

Ahmet Fenercioğlu and Hamit Barutcu
Department of Mechatronics Engineering, Gaziosmanpaşa University, Tokat 60250, Turkey

Abstract— Finite element analysis (FEA) of the eddy current separator (ECS) that can separate non-ferrous metals from waste via the eddy current method have been carried out in this study. The forces induced in the non-ferrous metals to be separated by the magnetic drum determining the performance of the separator have been analyzed according to certain variables. These variables are drum speed, air gap between the material and the magnet pole, material sizes, magnet height and the type of material. The resultant force has been estimated according to these variables. The increase of drum speed, decrease of the air gap, increase of the separated metal dimensions and the high conductivity of material increase the separation force. The ECS design is determined according to the analytic equalities has been verified by these analyses.

An Easy Way to Obtain the Extinction Cross Section of Radiation Propagating in a Medium with Nonspherical Particles

Piero Bruscaglioni
University of Florence, Italy

Abstract— Radiation beams propagating in ma medium with non-spherical particles receive different attenuation according to their polarization. The effect is due to different values of the extinction cross section $\sigma\varepsilon$.

The explicit values of the latter can be obtained by considering the four f_{mn} parameters of the scattering matrix.

Then a simple method to obtain $\sigma\varepsilon$ is based on considering a distribution of equal particles along a plane normal to the direction of the propagating field.

This avoids the complexity of mixing the geometries of a planar incident wave and of a spherical scattered wave. The procedure considers a plane wave incident normally on a uniform plane distribution of equal non-spherical particles with equal orientation of their axes. By applying the principle of stationary phase one obtains a scattered plane wave which proceeds in the same direction of the incident one. Interference produces a reduction of the intensity of the incident plane wave.

The reduction of the power density of the incident wave is proportional to the planar density of the spherical scatterers. Thus one derives the extinction cross section C_{ext} of one scatterer.

By indicating as f_{11}, f_{12}, f_{21}, f_{22} the elements of the forward scattering amplitude matrix $\mathbf{J}$.

The explicit form of the derived C_{ext} then is

$$C_{ext} = (4\pi/k)\mathrm{Im}\left(f_{11}|ax|^2 + f_{12}ax\,ay + f_{21}ax\,ay^* + f_{22}|ay|^2\right)$$

with the incident electric field propagating in the z direction given as

$$E(ax\ \mathbf{i} + ay\ \mathbf{j}) \text{ with } |ax|^2 + |ay|^2 = 1,$$

Equation (2) is equivalent to Equation (31) of Ref. [1] where C_{ext} is given in terms of the extinction matrix elements K_{11}, K_{12}, K_{13}, K_{14}, on turn related to the S_{mn} elements of the forward scattering matrix given in the form presented in that reference.

The two polarization modes of radiation propagating with no polarization change in a medium with non-spherical particles can then be easily obtained, by considering the f_{mn} parameters, and by imposing that the scattered field in the forward direction maintains the ratio between the field components normal to the propagation direction.

By considering simple cases of incident radiation with different polarization, simple examples of polarization change during propagation of radiation will be showed.

REFERENCES

1. Mischenko, M., J. Hovenier, and L. Travis, *Light Scattering by Nonspherical Particles*, Academic Press.

Numerical Estimation of Muscle Conductivity in Terms of Human Body Internal Resistance

Hiroo Tarao[1], **Katsuaki Aga**[1], **Olenxandr Okun**[2], **and Leena Korpinen**[3]

[1]National Institute of Technology, Kagawa College, Japan
[2]National Technical University, Ukraine
[3]Tampere University of Technology, Finland

Abstract— Numerically-anatomical human models have been often used for wide band frequency electromagnetic dosimetry. For the dosimetry calculation, furthermore, typical dielectric properties such as conductivity and permittivity have been used for tissues that are assigned to each voxel of the human models. In our previous study, calculated results of human body internal resistances between hand and foot were two times larger than measured results (500–700 Ω). One possible explanation for this is that there are few voxels assigned as blood, having relatively higher conductivity, because of the limitation that blood vessels with a diameter of less than 2 mm could not be included in the model. Human body impedance is given as internal impedance combined in series with skin impedance. At low frequency, the resistive components of internal impedance are more dominant than capacitive components, and skin impedance changes greatly depending on contact area and surface wetness. Hence, we focus on internal resistances at 60 Hz in the study, ignoring skin impedance and capacitive components of internal impedance. Therefore, with consideration for the fact that conductive currents in a body flow mostly through muscle, and the assumption that conductivities of blood and extracellular fluid should be mixed into the muscle conductivity, we calculate human body internal resistances between the left hand and left foot in the present paper, with changing muscle conductivity: 0.35–2.0 S/m. Here, 0.35 S/m for muscle, 0.7 S/m for blood, and 2.0 S/m for extracellular fluid have been used as the typical conductivity values at 60 Hz. It is found for both absolute values and relative scale that the newly calculated internal resistances with muscle conductivity of 0.8–1.0 S/m are much closer to measured values. In contrast, the internal resistances did not vary when conductivity values of other tissues which distribute through the body, such as adipose tissues and bones, are changed.

Quantum Friction in Different Regimes

J. Klatt[1], **S. Y. Buhmann**[1] **D. Dalvit**[2]

[1]University of Freiburg, Germany
[2]Los Alamos National Laboratory, USA

Abstract— Quantum friction is the velocity-dependent force between two polarizable objects in relative motion, resulting from field-fluctuation mediated transfer of energy and momentum between them. Due to its short-ranged nature it has proven difficult to observe experimentally.

Theoretical attempts to determine the precise velocity-dependence of the quantum drag experienced by a polarizable atom moving parallel to a surface arrive at contradicting results. Scheel [1] and Barton [2] predict a force linear in relative velocity v the former using the quantum regression theorem (QRT) and the latter employing time-dependent perturbation theory. Intravaia [3], however, predicts a v^3 power-law starting from a non-equilibrium fluctuation-dissipation theorem (NFDT).

The main difference brought along by either relying on a quantum regression or a non-equilibrium fluctuation-dissipation theorem, is the long-time behavior of correlations of the type $\langle d(t)d(t')\rangle$, where d is the atomic dipole operator. The former approach means assuming that these correlations decay exponentially, whereas the latter approach means acknowledging a power-law behavior of that decay for very large times. We want to find a general form of $\langle d(t)d(t')\rangle$ in order to see which assumption is proper in which regimes and where exactly the transition takes place.

REFERENCES

1. Scheel, S. and S. Y. Buhmann, *Phys. Rev. A*, Vol. 80, 2009.
2. Barton, G., *New J. Phys.*, Vol. 12, 2010.
3. Intravaia, F., et al., *Phys. Rev. A*, Vol. 89, 2014.

A Necessary Condition for Application of Topological Derivative in Limited-aperture Inverse Scattering Problem

C. Y. Ahn[1], K. Jeon[1], Y.-K. Ma[2], and W.-K. Park[3]

[1]National Institute for Mathematical Sciences, Daejeon 305-811, Korea
[2]Department of Applied Mathematics, Kongju National University, Chungcheongnam-do 314-701, Korea
[3]Department of Mathematics, Kookmin University, Seoul 136-702, Korea

Abstract— Throughout various works, topological derivative-based non-iterative imaging algorithm has demonstrated its applicability in full- and limited-aperture inverse scattering problems. However, most of researches have considered full-aperture problem. So, in the limited-aperture inverse problem, this applicability has been relied through the results of numerical simulations, and the reason behind this applicability has not been theoretically explained. Motivated from this, we consider the topological derivative for imaging of arc-like perfectly conducting crack for Transverse Magnetic (TM) polarization case in limited-aperture inverse scattering problem, and correspondingly explore a necessary condition of application. This is based on the relationship between topological derivative imaging function and infinite series of Bessel functions of integer order of the first kind. This relationship leads us explored necessary condition is highly depending on the shape of unknown crack. Numerical results are demonstrated in order to support our explore.

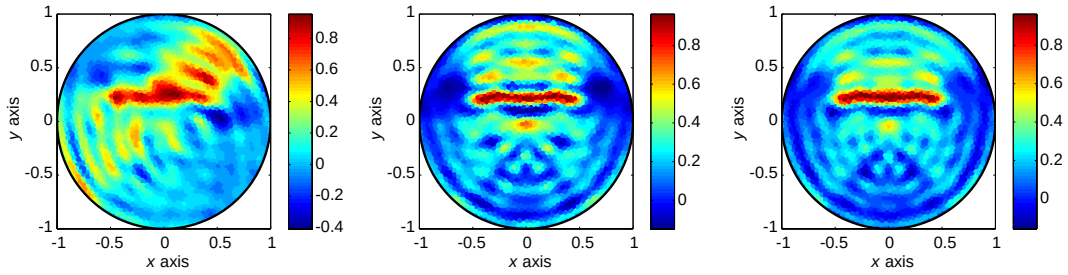

Figure 1: Imaging results via topological derivative with various settings of incident directions.

REFERENCES

1. Ahn, C. Y., K. Jeon, M.-K. Ma, and W.-K. Park, "A study on the topological derivative-based imaging of thin electromagnetic inhomogeneities in limited-aperture problem," *Inverse Problems*, Vol. 30, 105004, 2014.
2. Ma, Y.-K., P. S. Kim, and W.-K. Park, "Analysis of topological derivative function for a fast electromagnetic imaging of perfectly conducing cracks," *Progress In Electromagnetics Research*, Vol. 122, 311–325, 2012.
3. Park, W.-K., "Multi-frequency topological derivative for approximate shape acquisition of curve-like thin electromagnetic inhomogeneities," *J. Math. Anal. Appl.*, Vol. 404, 501–518, 2013.
4. Park, W.-K., "Topological derivative strategy for one-step iteration imaging of arbitrary shaped thin, curve-like electromagnetic inclusions," *J. Comput. Phys.*, Vol. 231, 1426–1439, 2012.

Subspace Migration for Imaging of Thin Electromagnetic Inhomogeneities without Shape Information

W.-K. Park
Department of Mathematics, Kookmin University, Seoul 136-702, Korea

Abstract— Subspace migration is a stable and effective non-iterative imaging technique in inverse scattering problem. But, for a successful application of imaging of thin electromagnetic inhomogeneities, *a priori* information of tangential and normal directions to unknown targets must be considered beforehand. Without this consideration, one cannot obtain good results via subspace migration. Due to this reason, various test vectors are applied to the subspace migration and select a vector which maximize the value of imaging functional. However, this requires large computational costs and sometimes the results are poor. Motivated this fact, we consider the structure of single- and multi-frequency subspace migration without any shape information of of unknown targets and explore its certain properties.

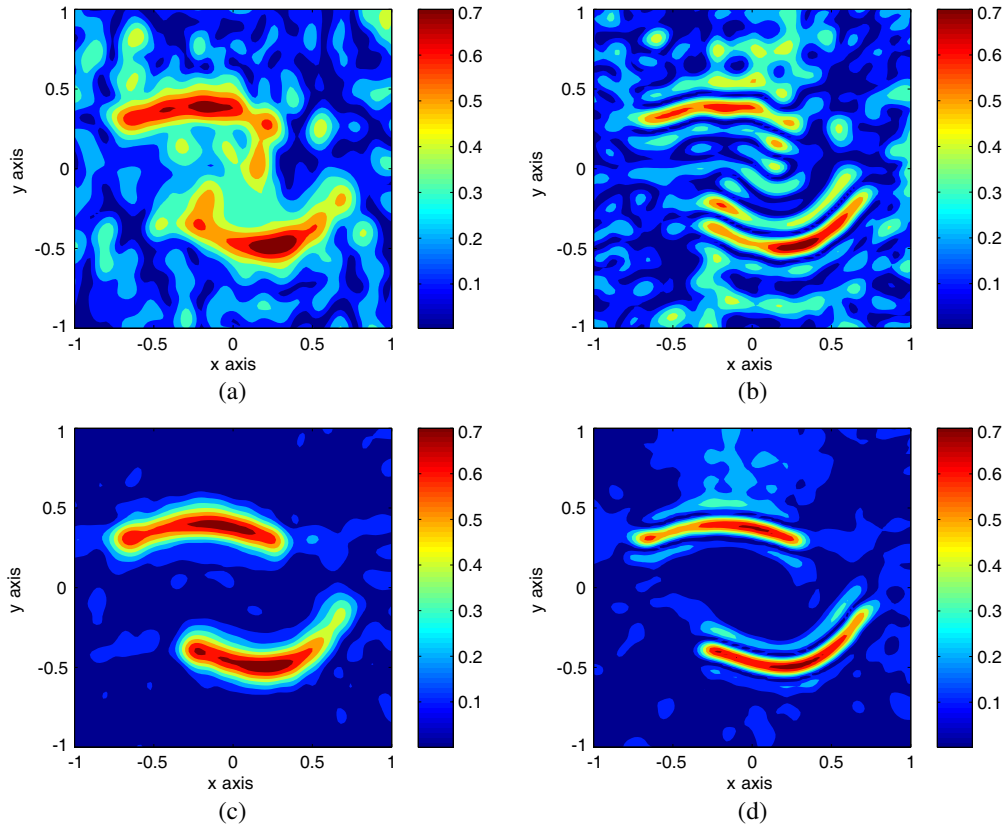

Figure 1: Imaging results via single- and multi-frequency (subspace migration with (left column) and without (right column) consideration of shape of thin inclusion. (a) Single-frequency, (b) single-frequency, (c) multi-frequency, (d) multi-frequency.

REFERENCES

1. Park, W.-K., "Analysis of a multi-frequency electromagnetic imaging functional for thin, crack-like electromagnetic inclusions," *Appl. Numer. Math.*, Vol. 77, 31–42, 2014.
2. Park, W.-K., "Multi-frequency subspace migration for imaging of perfectly conducting, arc-like cracks in full- and limited-view inverse scattering problems," *J. Comput. Phys.*, Vol. 283, 52–80, 2015.

Analysis of Matching Media Effect on Microwave Brain Stroke Imaging via a Spherically Symmetrical Head Model

E. Bilgin, **A. Aygun**, **A. Yapar**, **and I. Akduman**
Electrical and Electronics Engineering Faculty, Istanbul Technical University, Istanbul, Turkey

Abstract— The objective of this study is to analyse the effectiveness of the microwave imaging in detecting stroke areas in the human brain. Microwave tomography can represent an alternative to commonly used imaging techniques such as computerized tomography or magnetic resonance imaging [1]. The researches on the subject are motivated by the need to make continuous control of the patient's state possible [2]. Since non-hazardous and portable imaging systems can be designed using microwave technology, an imaging tool operating on microwave frequency would be suitable for long term monitoring [1, 2].

Microwave imaging techniques rely on the difference in the electromagnetic properties between healthy tissues and stroke areas in the brain [1]. This difference results in a variation in the scattered field when the head region is excited by an external source operating in the microwave frequencies. Therefore, it is of crucial importance to maximize the penetration of the electromagnetic field into the inner parts of the human brain where the strokes occur. To this end, a matching medium with suitable electromagnetic parameters can be used. The effect of the matching medium is usually assessed by using 2-D head models [1, 2]. However 3-D models can provide a more realistic structure to test both the relevancy of using a matching medium, and the effectiveness of microwave imaging techniques in general.

In this work, a four layered piecewise homogeneous sphere has been used as a head model. In order to assess the feasibility of the microwave imaging techniques, the related three dimensional scattering problem must be solved. However, given the high contrast values of the brain tissues, the solution of the 3-D scattering problem by classical techniques, such as method of moments, is a computationally expensive procedure. Therefore, in this study the problem has been transformed into a one dimensional form by taking advantage of the spherical symmetry [3]. As an alternative method, the dyadic Green's function related to the layered spherical structures has been used to verify the results [4]. After solving the scattering problem, the effect of the matching medium on the field distribution in each layer has been analysed via both methods. Also, by modelling the stroke area by an internal source, the possibility of brain stroke detection through microwave imaging has been assessed.

REFERENCES

1. Scapaticci, R., L. Di Donato, I. Catapano, and L. Crocco, "A feasibility study on microwave imaging for brain stroke monitoring," *Progress In Electromagnetics Research B*, Vol. 40, 305–324, 2012.
2. Semenov, S. Y. and D. R. Corfield, "Microwave tomography for brain imaging: Feasibility assessment for stroke detection," *Intl. J. Antennas Propag.*, Vol. 2008, 1–8, 2008.
3. Bilgin, E. and A. Yapar, "Electromagnetic scattering by radially inhomogeneous dielectric spheres," *IEEE Trans. Antennas Propag.*, Under Review.
4. Li, L. W., P. S. Kooi, M. S. Leong, and T. S. Yeo, "Electromagnetic dyadic Green's function in spherically multilayered media," *IEEE Trans. Microw Theory Tech.*, Vol. 42, 2302–2310, 1994.

Field Invariants, Amplitude Mapping, and Perfect Transmission in Media with Local Symmetries

C. Morfonios[1], **P. A. Kalozoumis**[2], **P. Schmelcher**[1], **and F. K. Diakonos**[2]

[1]Centre for Optical Quantum Technologies, Hamburg University, Germany
[2]Department of Physics, Athens University, Greece

Abstract— A theoretical approach for generic wave propagation in systems with local spatial symmetries is developed and applied. The concept of local symmetry refers to the presence of subsystems which obey certain symmetries while the total system is non-symmetric under the same transformations. Groups of neighboring subsystems may form additional local symmetries, emergent at a larger scale, leading to the notion of different local symmetry decompositions of a composite setup. Local mirror and translation symmetries are here shown to yield invariant quantities that characterize wave propagation in one effective dimension. The symmetry-induced spatial invariants map the wave amplitude between symmetry-related points and thereby enable a generalization of the parity and Bloch theorems to the case of broken global symmetry.

The novel theoretical framework applies generically to wave propagation in continuous or discrete media, with particular relevance for the field of micro- and nanophotonics where wave localization and transmission control are desired for devices with flexibility in setup geometry. Indeed, such designed systems are usually decomposable into locally symmetric pieces; representative examples are photonic crystal structures and dielectric multilayer systems, where pioneering applicational aspects combine with fundamental theoretical investigations. Also structurally complex photonic setups with long-range aperiodic order or even partially disordered systems feature inherent local symmetries and thereby encompass corresponding field invariants.

As an application to photonic multilayer systems with local mirror symmetries, the approach is used to classify light scattering modes according to the symmetry decomposition of the field profile. In particular, the spatial distribution of perfectly transmitting resonance (PTR) states is shown to follow the underlying local symmetries when the derived local invariants align along the medium of propagation. This connects the occurrence of PTRs to the corresponding spatial structure of the amplitude in an unambiguous manner based on symmetry principles. Further, the simultaneous presence of different local symmetry decompositions in a given device is exploited to develop a construction scheme for the design of multiple PTRs at prescribed wave frequencies.

The connection of wave transmission properties and amplitude distribution to the local symmetry structure of the medium of propagation opens the perspective for novel types of optical device designs. More generically, the proposed local symmetry approach may lead to a deeper understanding of signal response and wave localization phenomena in media with order on multiple scales.

High Resolution Ka-band Backscattering Measurement of Deciduous and Coniferous Tree

Wei-An Chuang[1], **Hsuan Ren**[1, 2], **Kuan-Liang Chen**[1], **and Jhih-Syuan Huang**[1]

[1]Institute of Space Science, National Central University, Taiwan
[2]Center for Space and Remote Sensing Research, National Central University, Taiwan

Abstract— In this paper, we present high resolution Ka-band backscattering measurement of deciduous and coniferous tree on National Central University (NCU) campus for ground-truth validation in vegetation monitoring. The coherent radar system, designed and configured based on a vector network analyzer N5245A PNA-X (10 MHz–50 GHz) is operated in a continuous-wave mode, was used to generate the transmitting signal and to detect scattered signals both in amplitude and phase for VV, HH, HV polarizations at incidence angles between 30 and 80 degrees. In measuring process, the radar system has typical trace of the frequency ranges from 28 to 38 GHz of the received power for a given footprint of tree canopy. For this ultrawide bandwidth, the wind-induced Doppler effects can be ignored. By this feature, the propagating depth through the tree can also be precisely determined so that the effective propagation constant and attenuation factor can be estimated. A reference measurement was taken at normal incidence using a conducting sphere as a calibration target, showed that the measurement capabilities of this system are satisfactory. The calibration was conducted both in anechoic chamber and in-situ measurements. Ensemble average of 2000 samples was taken to estimate the mean return power and later by inverting the radar equation to obtain the backscattering coefficient as functions of frequencies and incident angles are then estimated. To simplify the matrix inversion, a narrow beam is realized with dish antenna. Based on the measured results, backscattering characteristics and statistical properties were analyzed for the cases of deciduous (banyan) and coniferous (pine) trees.

To obtain backscattering coefficient for tree canopy, measuring system was mounted on the top of a 15 m-height roof. From this platform, the radar had an unobstructed view of the selected tree targets. The banyan and pine trees were substantially larger than the footprint of Radar with 2.6-degree antenna beamwidth. Target trees were selected where adjacent unwanted scatters (ground and tree) could be conveniently rejected by range gating in time domain. In the proposed study, frequency, polarization, incident angle, and canopy parameters are the primary factors affecting backscattering properties. The results indicated that cross-polarized returns generally presents higher dynamic ranges over the frequency and angular behavior. At Ka band, its wavelength (1.1 cm$\sim$0.7 cm) is much smaller than leaves and branches. For banyan tree, leaf stems constitute a very small proportion of the target areas, and the corresponding return signal may be reasonably ignored. However, leaf stems of the pine trees constitute a larger portion of the beam areas. The contributions from multiple backscattering are larger than those of banyan trees.

Investigation of Switched Reluctance Machine for EV Propulsion Unit with Torque Smoothening Strategy

M. Ruba and D. Fodorean
Department of Electrical Machines and Drives
Technical University of Cluj-Napoca, Cluj-Napoca, Romania

Abstract— The paper deals with the investigation of a 30 kW switched reluctance machine (SRM) designed to be used in the automotive industry, as propulsion unit for electrical vehicles (EV). The paper details the most important steps when designing such an electrical machine, and validates the structure using advanced co-simulation techniques, coupling finite element analysis software (Cedrat Flux2D) with software used to implement the controller (Matlab/Simulink). As the advantages of the SRM are known, its main drawback, the torque ripples, are reduced as much as possible using a dedicated control strategy, the direct instantaneous torque control (DITC). The solution offered by the paper highlights the possibility of using a cheap, reliable and robust electrical machine for propulsion unit.

Introduction: As already stated in the abstract, in the past years, many studies revealed the considerable advantages of the SRM against the other electrical machines, such as simplicity in design and building, low cost, simple control, robust and reliable operation, etc. [1–4]. Considering all these, implementing this machine as propulsion unit in EVs became a challenge that worth to be investigated. The increased torque ripples that are present when phase commutation occurs, makes the machine impossible to be used with its natural control strategy. However using special control strategies, this problem can be completely solved.

The SRM in Study: The design of the SRM is focused on the torque production with regards to the total volume of the machine. Hence, proper sizing of the machine will reach the optimal dimensions in order to achieve the required mechanical power. The developed torque is computed function of the machine's main dimensions, of the current and the number of turns per phase:

$$T_{SRM} = (N_f \cdot I)^2 \cdot \frac{D_g - g_x}{2} \cdot \mu_0 \cdot \frac{l_s}{2 \cdot g_x} \tag{1}$$

In Fig. 1, the preliminary validation of the SR machine in study is highlighted. As it can be seen, it develops the required torque but whit the already mentioned ripples. For the final paper, the DITC method will be implemented to prove that the machine can reach linear torque characteristic.

Conclusions: The paper will present a complex study for design, analysis and wise control of the SRM in order to place it in the field of traction motor for EV industry.

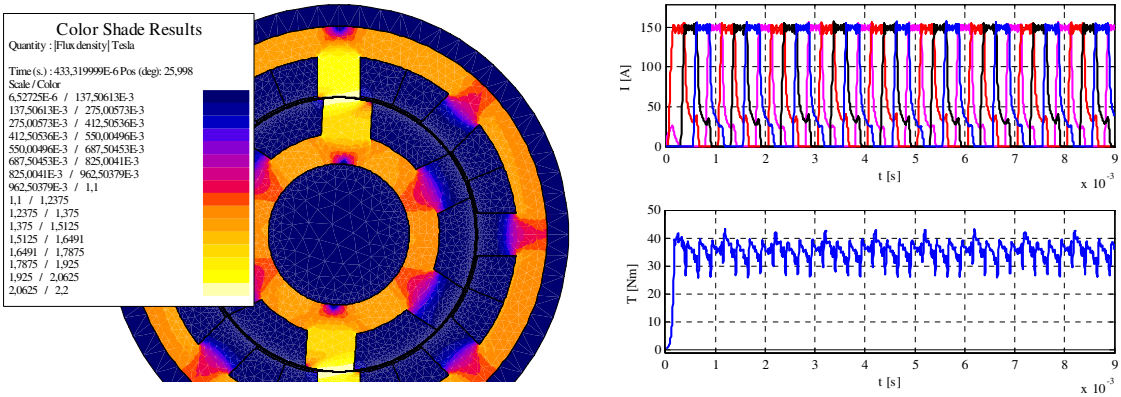

Figure 1: The FEA model and the currents and torque developed with simple hysteresis controller.

ACKNOWLEDGMENT

This work was supported by a grant of the Romanian National Authority for Scientific Research, CNDI-UEFISCDI, project number PCCA191/2012.

REFERENCES

1. Hannoun, H., M. Hilairet, and C. Machand, "Comparison of instantaneous and average torque control for a switched reluctance motor," *IEEE, SA Treci Conferinta Din Care Provine*, data, plus paginile.
2. Ruba, M. and D. Fodorean, "Design, analysis and torque control of low voltage high current SRM for small automotive applications," *Proceedings of EuroCon 2013*, 1499–1503, Zagreb, Croatia, July 1–4, 2013.
3. Vol. 57, No. 9, 2988–2997, September 2010.
4. Matyas, A. R., K. A. Biro, and D. Fodorean, "Multi-phase synchronous motor solution for steering applications," *Progress In Electromagnetics Research*, Vol. 131, 63–80, September 2012.

Achieving Tunable Mode Splitter and Omnidirectional Absorber by Semiconductor Photonic Crystal

Guo-Wen Ding[1], **Shao-Bin Liu**[1], **Hai-Feng Zhang**[1, 2], **Xiang-Kun Kong**[1], **Bo-Ri Bian**[1], **and Hai-Ming Li**[1]

[1]College of Electronic and Information Engineering
Nanjing University of Aeronautics and Astronautics, Nanjing 210016, China
[2]Nanjing Artillery Academy, Nanjing 211132, China

Abstract— In this paper, the properties of one-dimensional (1D) photonic crystals (PCs) composed of the semiconductor (GaAs) and dielectric layers are theoretically investigated by the transfer matrix method (TMM). The absorption of semiconductor layers is investigated theoretically. Due to the magneto-optical Voigt effect, the dielectric constant of the semiconductor is modified differently in different modes and frequency ranges. If the frequency range of the incident wave is larger than the plasma frequency, TE and TM modes of the incident wave will be absorbed in a wide incident angle. TM wave will be absorbed but TE wave will be reflected while the frequency range is less than the plasma frequency. The absorption of semiconductor can also be tuned by varying the external magnetic filed. The proposed PCs have a reconfigurable application to design a tunable omnidirectional absorber and mode splitter at same time.

Tunable Electromagnetically Induced Transparency Like Transmission in Graphene Metamaterials with Indirect Coupling

Guo-Wen Ding[1], **Shao-Bin Liu**[1], **Hai-Feng Zhang**[1, 2], **Xiang-Kun Kong**[1], **Bo-Rui Bian**[1], **and Hai-Ming Li**[1]

[1]College of Electronic and Information Engineering
Nanjing University of Aeronautics and Astronautics, Nanjing 210016, China
[2]Nanjing Artillery Academy, Nanjing 211132, China

Abstract— Novel graphene-based metamaterials with tunable electromagnetically induced transparency (EIT)-like transmission are numerically studied in this paper. The designed structures consist of a graphene layer composed of coupled cut-wire pairs printed on a substrate. The simulation confirms that an EIT-like transparency phenomenon occurs in the metamaterial owing to indirect coupling and the proposed structure can be used in terahertz frequency range. More importantly, the transparency windows for the structures with indirect coupling can be dynamically controlled over a broad frequency range by varying the Fermi energy levels of the graphene layer (through electrostatic gating). The proposed metamaterial structures offer additional opportunities to design novel applications such as active plasmonic switching and optical sensing.

Cylindrical Metasurface Absorber Using Home Inkjet Printing System

Hyung Ki Kim and Sungjoon Lim
School of Electrical and Electronic Engineering, Chung-Ang University
221 Heukseok-dong, Dongjak-gu, Seoul 156-756, Republic of Korea

Abstract— A novel cylindrical metasurface absorber will be presented. The proposed metasurface absorber is inkjet-printed on a flexible polymer film using a commercial EPSON WF-7011 home printer as shown in the following figure. A silver nanoparticle ink is used for conductive patterns. The unit cell of the metasurface is designed with a modified Jerusalem-cross ring resonator. The absorber's flexibility and absorption performance are demonstrated by measuring the absorption ratio after coating the proposed absorber on a cylindrical object with a radius of 4.56 cm. An absorption rate exceeding 99% is achieved at 9.21 GHz for both flat and cylindrical surfaces. In addition, the cylindrical model attains an absorption rate higher than 96% for all polarization angles, and a high absorption rate of 95% is preserved until the incident angle is less than 30°.

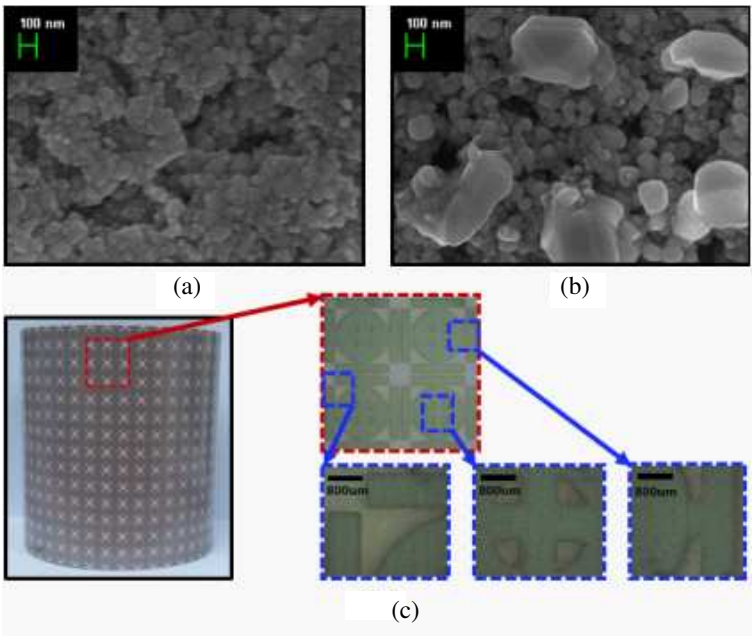

Figure 1: SEM images (a) before sintering and (b) after sintering; (c) the fabricated sample absorber coated on a PET cylinder and a microphotograph of the sample absorber.

ACKNOWLEDGMENT

This work was supported by the National Research Foundation of Korea (NRF) grant funded by the Korea government (MSIP) (No. 2014R1A2A1A11050010).

Reversal of Microwave Propagation Nonreciprocity in Metastructures by Voltage Application under Ferromagnetic Resonance Excitation near Resonance of Dipole or Chiral Elements

G. A. Kraftmakher, V. S. Butylkin, and Yu. N. Kazantsev
Kotelnikov Institute of Radioengineering & Electronics, RAS, Russia

Abstract— In recent years, there has been increasing interest in the study of metamaterials containing resonant conductive elements, of nonreciprocal metamaterials, containing combination of ferrite and resonance elements, with tunable or switchable characteristics for development of microwave devices such as filters, nonreciprocal isolators and circulators. The emphasis is novel functionality as the fast electric control of amplitude-frequency characteristics in comparison with traditional magnetic control of ferrite by external static magnetic field. In the case of magnetic control time switching is not so fast because one depends on not fast complex processes of magnetization and remagnetization as a result of which reversal of sense of spins precession occurs.

At present there are also ideas about artificial Faraday rotation in magnetless metamaterials without gyrotropic component.

In real microwave devices and under consideration nonreciprocal effect is due to the ferromagnetic resonance (FMR). In this case circular or elliptical polarization of microwave magnetic field h is necessary. Waveguide nonreciprocal devices contain transversely magnetized ferrite plate at distance of $\pm\lambda/8$ from the side wall in a rectangular waveguide, where polarization of microwave magnetic field is circular. In the case of metastructures necessary h-field is formed by the grating of resonant elements at frequencies near their resonance. Besides metastructures show amplification and possibility of electric control of nonreciprocity [1].

In this paper electrically controlled reversing the sign of the nonreciprocity of microwave propagation is proposed and confirmed by direct experimental proofs on ferrite plate/varactor-loaded dipoles metastructures placed along rectangular waveguide axis in the presence of static magnetic field H. Dipoles of various shapes (butterfly, loop, snake, double split rings) with different type-varactors have been investigated. In Figs. 1(a), (b) we see photos of metastructure ferrite plate/varactor-loaded split Butterfly dipole (a) and ferrite plate/varactor-loaded double split rings (b). The nonreciprocity δ is defined without reversal of the propagation direction (single-channel measurements). In this case nonreciprocity δ (dB) is defined as the difference between transmission coefficients $T = |S_{21}|^2$ corresponding to the opposite direction of magnetization, when senses of h-field rotation are the same but senses of spin precession are opposite, $\delta\,(\mathrm{dB}) = T(H_-) - T(H_+)$. H_+ and H_- correspond to opposite directions of the external transverse applied field H and provide opposite senses of spins precession. Results of measurements contain dependences of δ on frequency at different bias conditions. It has been shown that inversion of the nonreciprocity sign occurs by the application of a bias voltage to a varactor in order to provide jump of resonance frequency of a dipole through the ferromagnetic resonance frequency as a result of which reversal of sense of rotating elliptically polarized h-field takes place.

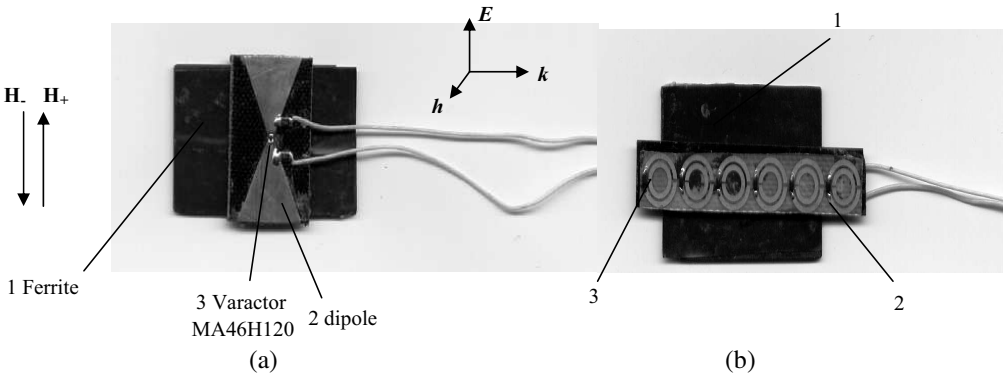

REFERENCES

1. Kraftmakher, G. A., V. S. Butylkin, and Yu. N. Kazantsev, *Tech. Phys. Lett.*, Vol. 39, No. 6, 505–508, 2013, http://dx.doi.org: 10.1134/S1063785013060060.

Millimeter-wave Metamaterial Antenna in Standard CMOS Technology

Kazuki Hiraishi, **Takehiro Kawauchi**, **and Eiichi Sano**
Research Center for Integrated Quantum Electronics, Hokkaido University, Japan

Abstract— The crowded bands of 2.4 and 5 GHz will push the operation bands of wireless communication systems to the millimeter (MM)-wave region (e.g., 60 GHz). Reduced sizes of antennas in the MM-wave region enable them to be monolithically integrated with CMOS RF and baseband circuits. However, the low-resistivity ($\sim 10\,\Omega$cm) Si substrates commonly used in standard CMOS processes degrade the antenna gain. The antenna gain at 60 GHz remains below -10 dBi in standard CMOS technology [1]. Thus, an ingenious development is needed to increase the gains of antennas fabricated on low-resistivity Si substrates. A metamaterial-based antenna, such as a composite right-/left-handed (CRLH) antenna, has a reduced size [2], which results in reduced loss in the metal wire in the antenna. The antenna size in standard CMOS technology can be further reduced by using small-size lumped elements such as metal-insulator-metal (MIM) capacitors for the metamaterial components. In this study, a CRLH monopole antenna was designed and fabricated in 0.18 µm CMOS with six metal layers. The series capacitances for the left-handed (LH) mode were composed of the MIM structure between the 5th and 6th metal layers while the shunt inductors in the LH mode and the shunt capacitances/series inductances in the right-handed (RH) mode were composed of the 6th metal layer. The CRLH unit cell was 300×420 µm. Two unit cells were used to construct the monopole antenna. The designed CRLH monopole antenna had LH and RH radiation modes at 41 and 65 GHz, respectively. The fabricated antenna was measured on wafer by using a network analyzer, RF probe, and a horn antenna. The gain of the CRLH monopole antenna was calibrated by comparing the transmission (S_{21}) measured between the CRLH monopole and horn antennas with that measured between two horn antennas. The measured gains of the CRLH monopole antenna were -5.8 dBi in RH mode and -14.4 dBi in LH mode. A conventional slot antenna using the 6th metal layer was also designed and fabricated for comparison purposes. Its measured gain was -20 dBi at 60 GHz. These results clearly demonstrate the advantage of the CRLH monopole antenna. Further increase in the gain can be achieved by optimizing the component values in the CRLH antenna.

REFERENCES

1. Chuang, H.-R., et al., *IEEE Trans. Electron Devices*, Vol. 58, No. 7, 1837–1845, 2011.
2. Takahagi, K., et al., *Electron. Lett.*, Vol. 48, No. 16, 971–972, 2012.

3D Emission Profiles of Disk-limacon-coupled Resonators

Jakob Kreismann[1], **Martina Hentschel**[1], **and Stefan Sinzinger**[2]

[1]Group for Theoretical Physics II/Computational Physics, Institute for Physics
Technische Universität Ilmenau, Ilmenau, Germany
[2]Group Technische Optik, Department of Mechanical Engineering
Technische Universität Ilmenau, Ilmenau, Germany

Abstract— Microcavity lasers made of dielectric disk-shaped resonators with sizes in the micrometer range have gained a lot of interest in recent years. A drawback of pure disk resonators for microlaser applications is their isotropic light output. To overcome this problem, deformed cavities were proposed such as limacon-shaped resonators which display directional light emission attractive for microcavity lasers.

In this work we study the coupling of a disk resonator to a limacon-shaped cavity using three dimensional FDTD wave-calculations. For this purpose a limacon resonator is placed on top of a disk resonator, a whispering gallery mode with high Q-factor is excited inside the disk resonator and its coupling into the limacon cavity is analyzed for different geometric configurations.

Furthermore we investigate the directional light emission and its tuning in such microcavity arrangements. In detail we calculate a full three dimensional emission profile with respect to the limacon cavity size and its position on the disk resonator. Thus we obtain the direction of light output in 3D and its benefit for microcavity laser applications.

Reliability Study on LED Packages Using Real-time Monitoring of Internal Quantum Efficiency

Byungjin Ma and Kwan-Hun Lee
Reliability Research Center, Korea Electronics Technology Institute, Korea

Abstract— It is very important to know the effect of the reliability of semiconductor LED chip on the LED packages. But it has been impossible to estimate the LED chip's effect on the total optical degradation of the LED packages quantitatively.

We have already proposed a new method for the internal quantum efficiency (IQE), used to investigate the mechanism of an optical degradation of the LED packages, which is based on the precise measurement of electrical, optical and thermal properties and a computational fluidic dynamic simulation [1]. IQE can be driven as a function of the junction temperatures and the optical output powers of LED packages. This IQE model is basically based on energy conservation.

We implemented our IQE testing algorithm into a real-time reliability tester for LED packages. Not only the electrical and optical properties but also the junction temperature and the internal quantum efficiency can be monitored at any time we want to measure.

Furthermore, we carried out a 2,500 hour lifetime test at 85° as shown in Fig. 1. Although there was an about 10% optical degradation after 2,500 hour aging time, there was no evidence of the IQE degradation of GaN LED chip. Thus, we could separate the effect of the LED chip on total optical degradation of the LED package for the first time. And we could conclude that a main origin of the optical degradation of the LED package affecting the lifetime of the LED packages is not from the LED chip but from other component materials in our LED packages.

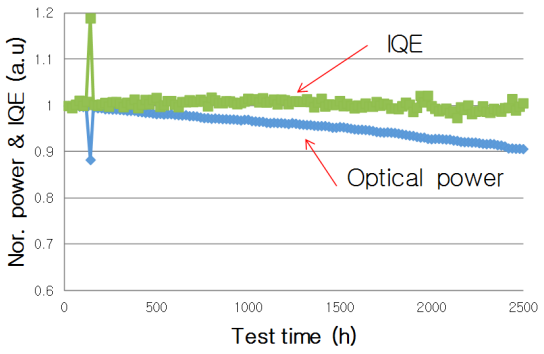

Figure 1: Relative optical output power and IQE monitored during a 2,500 hours lifetime test.

REFERENCES

1. Ma, B. and K. Lee, *IWN*, TuP-PR-68, 2012.

Performance Comparison of InGaN LEDs Containing V-and U-shaped Quantum Wells with and without Electron Blocking Layer and Emitting in the 400–500 nm Range

Abdelmajid Salhi, **Mohammad Alanzi**, **and Bandar Alonazi**
National Center for Nanotechnology, King Abdulaziz City for Science and Technology (KACST)
Riyadh 11442-6086, Kingdom of Saudi Arabia (KSA)

Abstract— The solid state device, such as light emitting diode (LED) is one of the best candidates to substitute the conventional incandescent and fluorescent lamps [1, 2] due to many advantages, e.g., compact size, low power consumption and long lifetime [3, 4]. However, the optical performance of III-nitride LEDs still suffers from poor light emission as a result of different mechanisms including: electron current leakage as a result of piezoelectric effect [5], non-radiative recombination in the wells due to the Auger recombination [6] and limited injection efficiency of holes [7].

In this paper, we report on the performance comparison between v-shaped quantum well (VSQW) and u-shaped quantum well (USQW) light emitting diodes with and without electron blocking layer emitting in a wide wavelength range from 400 nm to 500 nm. The physical reasons for improving the efficiency of VSQW LEDs compared to USQW LED structure are analyzed numerically using the commercial software APSYS (Advanced physical model of semiconductor devices) [8].

The simulation results showed that the devices containing VSQW have superior performance in terms of optical power and internal quantum efficiency droop compared to the devices containing USQW. The optical power of the LEDs containing USQW increases gradually and reaches a maximum at 460 nm, however the optical power of the LEDs with VSQW improves gradually and the maximum is obtained in a window from 420 to 436 nm as a result of radiative recombination enhancement. The simulation results suggest that the higher performance of the VSQW is a result of piezoelectric field reduction and an enhancement of electron and hole wavefunctions overlap.

The incorporation of the electron blocking layer in the case of VSQW structure improves the performance only for wavelength shorter than 436 nm and it's useless for $\lambda \geq 440$ nm. However in the case of USQW LEDs, the electron blocking layer is necessary to improve the efficiency as long as $\lambda \leq 470$ nm. This suggests that the VSQW design is a better choice for implementing InGaN LEDs compared to USQW design.

REFERENCES

1. Schubert, E. F. and J. K. Kim, "Solid state light sources getting smart," *Science*, Vol. 308, 1274-1278, 2005.
2. Pimputkar, S., J. Speck, S. P. Denbaars and S. Nakamura, "Prospects for LED lighting," *Nature Photonics*, Vol. 3, 180–182, 2009.
3. Lee, S. N., H. S. Paek, H. Kim, T. Jang and Y. Park, "Monolithic InGaN-based white light-emitting diodes with blue, green and amber emissions," *Appl. Phys. Lett.*, Vol. 92, 081107-1–081107-03, 2008.
4. Huang, C. F., C. F. Lu, T. Y. Tang, J. J. Huang, and C. C. Yang, "Phosphor-free white-light light-emitting diode of weakly carrier-density-dependent spectrum with prestrained growth of InGaN/GaNquantum wells," *Appl. Phys. Lett.*, Vol. 90, 151122-1–151122-3, 2007.
5. Rozhansky, I. V. and D. A. Zakheim, "Analysis of process limiting quantum efficiency of AlGaInN LEDs at high pumping," *Phys. Stat. Sol. A*, Vol. 96, 227–230, 2007.
6. David, A. and M. J. Grundmann, "Droop in InGaN light-emitting diodes: A differential carrier lifetime analysis," *Appl. Phys. Lett.*, Vol. 204, 103504, 2010.
7. Rozhansky, I. V. and D. A. Zakheim, "Analysis of the causes of the decrease of in the electroluminescence efficiency of AlGaInN light emitting diode heterostructures at high pumping density," *Semiconductors*, Vol. 40, No. 7, 839–845, 2006.
8. APSYS by Crosslight Software Inc., Burnaby, Canada, [online]. Available: http://www.crosslight.com.

Enhanced Group Velocity Characteristics of a ENG Cladded Metamaterial Loaded Helical Guide

D. K. Sharma and S. K. Pathak
Microwave and ECE Diagnostic Division, Institute for Plasma Research, Gandhinagar, India

Abstract— In recent years much attention have been given towards slow wave structures [2, 3] for the dynamical control of EM wave velocity and power flow for numerous engineering applications in microwave to optical frequency spectrum [1].

In this paper, we propose, an ENG Cladded Metamaterial Loaded Helical (CMLHG) Waveguide, as shown in Fig. 1, to achieve enhance slow wave in THz spectrum. Both analytical as well as numerical computation has been reported to characterize the dispersion behavior. It is observed that the waveguide supports forward wave (FW) mode having parallel phase and group velocities over a wide bandwidth with an enhanced slow wave characteristics. A comparative study of slow wave behavior has been done between the ENG CMLHG waveguide and two other cases — (i) when helix is in free space and (ii) when helix is cladded with DPS material and loaded with metamaterial, as shown in Fig. 2. It is found that present structure provides almost 4 times lesser group velocity in comparison to the helix in free space. Engineering design feasibility of manufacturing these types of waveguides are also discussed and reported.

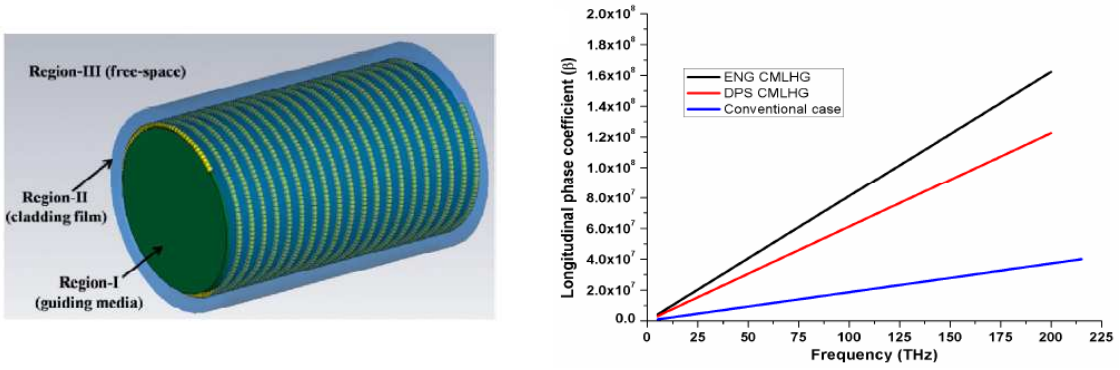

(a) (b)

Figure 1: (a) Cladded metamaterial loaded helical guide (CMLHG) structure. (b) Dispersion characteristic (β vs frequency) is plotted for different cases (i) conventional case, helical guide in free-space (ii) helix is cladded with DPS material and loaded with metamaterial and (iii) ENG CMLHG waveguide represents in blue, red and black color respectively.

REFERENCES

1. Salvatore, S., B. D. F. Casse, W. Lu, and S. Sridhar, *Appl. Phys. Lett.*, Vol. 98, 171907, 2011.
2. Erfaninia, H. and A. Rostami, *Optik*, Vol. 124, 1230, 2013.
3. Shadrivov, I. V., A. A. Sukhorukov, and Y. S. Kivshar, *Phy. Review E*, Vol. 67, 057602, 2003.

Optical Heterodyning in Microwave Photonic Receiving Channel

Victor V. Kulagin[1, 2, 3], **Vladimir A. Cherepenin**[2], **and Victor V. Valuev**[2, 3]

[1]Sternberg Astronomical Institute of Moscow State University
Universitetsky prosp. 13, Moscow 119992, Russia
[2]Kotel'nikov Institute of Radio-engineering and Electronics of RAS, Moscow, Russia
[3]Joint Stock Company "RTI", Russia

Abstract— Direct analog-to-digital conversion of microwave signals with subsequent digital processing looks very attractive for microwave receivers due to clear structure and minimal number of steps for analog signal transformation. However, microwave frequencies require photonic analog-to-digital converters (ADCs) which can provide now 5–6 effective bits only. At the same time, in many practical applications, it is necessary to receive a signal with a relatively small bandwidth and carrier frequencies of tens of gigahertz. In particular, such microwave signals with a pronounced carrier frequency are widely used in radar systems. In this situation, a microwave signal can be first converted to intermediate frequency using photonic heterodyning and then digitized with a relatively slow electronic ADC. In a sense, this approach corresponds to the usual methods of microwave signals processing using electronic devices when the received signal is frequency down converted.

The key point for building a photonic receiver is the development of an optoelectronic circuit for converting the microwave signal to an intermediate or low (envelope) frequencies [1–3]. We consider a microwave photonic receiver comprising a continuous wave (cw) laser together with amplitude modulators and narrow band optical filters. An amplitude modulation of the cw optical carrier with microwave signal results in creation of the signal sidebands. Then, the optical carrier and one of the sidebands can be suppressed using optical band-pass filter based on, e.g., microresonators or fiber Bragg gratings. To create an optical reference signal necessary for heterodyning, part of the laser beam is modulated by the second amplitude modulator with a microwave signal whose frequency is close to the microwave carrier frequency. Then this part of the laser beam is also filtered to suppress the optical carrier and the same side band. After that, two optical signals containing radar signal and radar carrier can be mixed at a photodetector and digitized with a slow electronic ADC.

Performance capabilities of the microwave receiving channel with optical heterodyning are estimated analytically. Different modes of receiving channel operation are discussed and optimal parameters are derived. It is shown that homodyne as well as heterodyne methods for transformation of the spectrum of the input microwave signal to the low frequency region can be used and linearity of the transformation for these methods is studied. Also, the regime of the optical carrier suppression in modulators is considered. In this case, it is not necessary to use narrow-band optical filters in the scheme. For the photonic receiver using modern optical elements the signal-to-noise ratio at the output can reach 60–70 dB and more that corresponds to 9–11 effective bits in the digitized signal with the carrier frequency of tens of gigahertz and the frequency bandwidth of 100 MHz and more.

REFERENCES

1. Hossein-Zadeh, M. and A. F. J. Levi, "Self-homodyne photonic microwave receiver architecture based on optical modulation and filtering," *Microwave and Optical Technol. Lett.*, Vol. 50, No. 2, 345–350, 2008.
2. Hossein-Zadeh, M., "Photonic microwave receivers based on high-Q optical resonance," *Laser Resonators, Microresonators, and Beam Control XIV*, Alexis V. Kudryashov, Alan H. Paxton, Vladimir S. Ilchenko, Lutz Aschke, Kunihiko Washio, Eds., *Proc. of SPIE*, Vol. 8236, 82360T, 2012.
3. Ridgway, R. W., C. L. Dohrman, and J. A. Conway, "Microwave photonics programs at DARPA," *J. of Lightwave Technol.*, Vol. 32, 3428–3439, 2014.

Influence of Optical Fiber Dispersion on Mamyshev Type Regenerator Performance

Piyush Baypajee, Jurgis Porins, and Andis Supe
Institute of Telecommunications, Riga Technical University, Azenes st. 16/20, Riga, Latvia

Abstract— Optical signal degrades considerably during propagation in the telecommunications fiber line. It is caused by many factors: fiber attenuation, dispersion (group-velocity dispersion, material dispersion, waveguide and polarization mode dispersion) that broadens the pulses, accumulated amplified spontaneous emission that is a broadband noise source induced mostly by amplifiers and, of course, different nonlinear optical effects. Distortions induced by optical fiber nonlinearity actually can be the most significant and the most difficult avoidable, especially in the high data rate multichannel transmission, used in dense wavelength division multiplexed systems. Nonlinear effects cause the undesired crosstalk between adjacent transmission channels as well as new harmonic generation in the signal frequency bandwidth. Such distortions cannot be filtered out, therefore optical signal regeneration is needed especially in a long haul transmission systems.

In this research we present results from the study on optical signal regeneration by using Mamyshev type regenerator and its dependence on fiber dispersion. Fiber dispersion is a very important parameter in the regeneration process since it influences the self-phase modulation nonlinear effect. This effect in turn provides the signal quality improvement by ensuring different transfer functions for useful signal and noise. Setup of investigated regenerator consists of a high power erbium doped fiber amplifier, highly nonlinear fiber and an optical bandpass filter that is slightly shifted away from the signal central frequency. Signal used for regeneration was an on-off keying return-to-zero code manipulated 40 Gbit/s pulse sequence covered with white noise. We have performed simulations and experimental characterization of regenerator by obtaining it's transfer function and output optical signal to noise ratio for different optical filters and fiber dispersion coefficients.

Characteristics of Femtosecond Pulse in Silicon Nanowire Embedded Photonic Crystal Fiber: Variational Approach

K. Senthilnathan[1], **E. Gunasundari**[1], **Abdosllam M. Abobaker**[2], **S. Sivabalan**[3], **K. Nakkeeran**[4], **and P. Ramesh Babu**[1]

[1]Photonics, Nuclear and Medical Physics Division, School of Advanced Sciences
VIT University, Vellore 632 014, India
[2]Department of Communications Engineering, College of Electronic Technology, Bani Walid, Libya
[3]School of Electrical Engineering, VIT University, Vellore 632 014, India
[4]School of Engineering, University of Aberdeen, Aberdeen AB24 3UE, UK

Abstract— Waveguides with sub-wavelength dimensions known as photonic nanowires are among the most attractive optical structures for ultrafast nonlinear optics. Due to their small sizes, nanowire exhibits tight optical confinement, large effective nonlinearity and strong waveguide dispersion. Nanowires are fabricated from different materials such as silica, silicon, etc.. Silicon has excellent transmission properties compared to silica and hence, would require relatively lesser input power for the desired nonlinear applications. The silicon photonics has become the current topic of research as the silicon waveguides. Such a dielectric waveguide of sub-wavelength diameter upon being embedded into the photonic crystal fiber called photonic crystal fiber nanowire (PCF-NW) results in enhanced optical properties and the same has subsequently been demonstrated. From the literature, it is very clear that the small core silicon nanowire embedded photonic crystal fiber (SN-PCF) structures has been a good candidate for nonlinear applications such as soliton-effect pulse compression and supercontinuum generation In this paper, we investigate the propagation characteristics of femtosecond pulses using the proposed SN-PCF. The pulse propagation in SN-PCF is governed by the well known higher order nonlinear Schrödinger (HNLS) equation. Using variational analysis, we study the propagation characteristics of an hyperbolic secant pulse, namely, pulse amplitude, temporal position, width, chirp, frequency and phase.

Theoretical model: The pulse parameter equations in SN-PCF are given by:

$$
\begin{aligned}
\dot{x}_1 &= -2\Gamma x_1^3\left[\frac{1}{\pi^2}+\frac{1}{3}\right]+\frac{\beta_2}{2}x_1x_4+\frac{\beta_3}{2}x_1x_4x_5-\frac{\beta x_1^5x_3\sigma}{6h\nu_0A_{eff}^2}-\frac{\alpha}{2}x_1\\
\dot{x}_2 &= \beta_2x_5+\frac{\beta_3}{6}\left[\frac{1}{x_3^2}+\frac{x_4^2x_3^2\pi^2}{4}+3x_5^2\right]+\gamma_sx_1^2\\
\dot{x}_3 &= \frac{4\Gamma x_1^2x_3}{\pi^2}-\beta_2x_3x_4-\beta_3x_3x_4x_5\\
\dot{x}_4 &= \beta_2\left[x_4^2-\frac{4}{x_3^4\pi^2}\right]+\beta_3x_5\left[x_4^2-\frac{4}{x_3^4\pi^2}\right]-\frac{4\gamma x_1^2}{x_3^2\pi^2}-\frac{4\gamma_sx_1^2x_5}{x_3^2\pi^2}\\
\dot{x}_5 &= \frac{-2\gamma_sx_1^3x_4}{3}-\frac{8\gamma_R}{15}\frac{x_1^3}{x_3^2}\\
\dot{x}_6 &= \beta_2\left[\frac{1}{3x_3^2}-\frac{x_5^2}{2}\right]-\frac{\beta_3}{3}x_5\left[x_5^2-\frac{1}{2x_3^2}\right]-\frac{\beta_3}{24}x_3^2x_4^2x_5\pi^2+\frac{5}{6}\gamma x_1^2-\frac{1}{6}\gamma_Sx_1^2x_5
\end{aligned}
$$

A Novel Improvement Technique Using a Commercially Available Phosphorescent White LED for High Speed Visible Light Transmission Systems

Nobuhiro Fujimoto and Daiki Nakamura
Kinki University, Japan

Abstract— The white light emitting diodes (LEDs) have been dramatically developed. In specially, a low-cost phosphorescent white LED that consists of a phosphor layer and a blue LED is expected to replace incandescent or fluorescent lights in offices, homes, cars, and traffic lights. According to these backgrounds, visible light communication (VLC) system using white LEDs is one of promising infrastructure for Ubiquitous Network. In the network, they are used for both illumination and wireless data transmission.

There are many approaches to realize high-speed VLC system. A phosphorescent white LED especially is difficult to modulate at high-speed. A 230 Mbit/s on-off-keying (OOK)-NRZ-based transmission experiment [1] was demonstrated with a phosphorescent white LED. However, this experiment required filtering the low-speed phosphorescent component to increase the bandwidth of the VLC system. Then, owing to the insertion of a lossy and expense blue optical filter, its transmittable distance is decreased and its total cost is increased.

Here, we propose the two improvement techniques to realize a long distance and low-cost high-speed VLC system using a phosphorescent white LED without a blue filter. Fig. 1(a) shows a frequency response of a phosphorescent white LED (LED Engin, LZ1-10CW00). It consists of a frequency response of a phosphor layer and that of a blue LED. That response of the phosphor layer has a greater gain than that of the blue LED. Our first proposed technique focuses on a frequency response of a phosphorescent white LED to get a longer transmission distance by adding a pre-emphasis circuit for a LED driver [2] without a blue filter. Fig. 1(b) shows the improved 3 dB down frequency from 2.3 MHz to 41.9 MHz keeping a flat gain of 24 dB. On the contrary, the blue LED has a higher 3 dB down frequency than that of the phosphor layer. The second proposed technique focuses on the frequency response of a blue LED to get a higher transmission speed by adding a pre-emphasis for a LED driver and a post-equalizing circuit for a receiver circuit without a blue filter. Fig. 1(c) shows the improved 3 dB down frequency from 2.3 MHz to 82.8 MHz having a little lower flat gain of 20 dB. And the measured bit error rate characteristics are shown in Fig. 1(d). For example, it is confirmed a 100 Mbit/s error-free operation with a bit-error ratio of less than 10^{-7} at a longer distance between a LED and a Si-PIN-PD of 66 cm by the 1st proposed technique than that of the 2nd technique. And we have

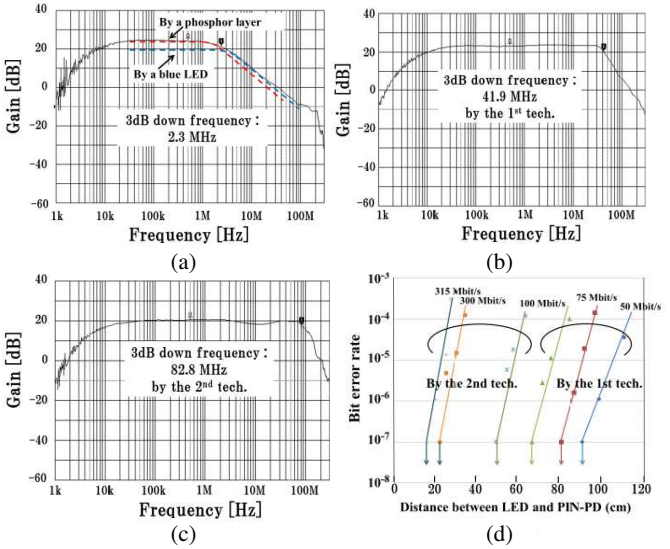

Figure 1: Measured results of a proposed high-speed visible light communication system. (a) Frequency response of a phosphorescent white LED. (b) Improved response by the first technique. (c) Improved response by the second technique. (d) Bit error rate characteristics of the system.

first confirmed the maximum transmission speed of 315 Mbit/s error-free operation by the 2nd proposed technique. This 315 Mbit/s operating speed of a simple OOK-NRZ based modulation using a single commercially available phosphorescent LED is a world record. These experimental results show that our proposed techniques are suitable for simple, low-cost, and high-speed VLC systems.

REFERENCES

1. Vucic, J., et al., "230 Mbit/s via a wireless visible-light link based on OOK modulation of phosphorescent white LEDs," *Proc. OFC/NFOEC'2010*, OThH3, 2010.
2. Fujimoto, N., et al., "614 Mbit/s OOK-based transmission by the Duobinary technique using a single commercially available visible LED for high-speed visible light communications," *Proc. ECOC'2012*, P4.03, 2012.

Optical WDM-PON Access System with Shared Light Source

Sandis Spolitis, **Lilita Gegere**, **Anita Alsevska**,
Ilja Trifonovs, **Jurgis Porins**, **and Vjaceslavs Bobrovs**
Institute of Telecommunications, Riga Technical University, Riga, Latvia

Abstract— We report on 16-channel wavelength division multiplexed passive optical network (WDM PON) with shared amplified spontaneous emission (ASE) light source, which is spectrum sliced by an arrayed waveguide grating (AWG), see Figure 1. In this research ASE source is generated by two cascaded erbium doped fiber amplifiers which parameters were manipulated in such a way obtaining flat spectrum in wavelength range from 1545.32 nm to 1558.98 nm (C-band). It must be mentioned, that spectrum slicing technique is one of available techniques in WDM-PON systems in order to reduce cost of components and simplify the architecture of PON network.

Investigated optical transmission system can be considered as energy efficient and cost effective in the way that single seed light source (ASE) is shared among many users instead of using individual light source for each user, for example, distributed feedback lasers or vertical-cavity surface-emitting lasers. After ASE slicing operation slices are modulated by an optical modulator (electro-absorption modulator or Mach-Zehnder modulator), multiplexed by second AWG, transmitted over standard single mode fiber transmission line, demultiplexed and received by optical receivers located in user premises. In this research, we propose 16-channel spectrum sliced optical access system based on ITU T G.694.1 DWDM frequency grid. Proposed solution shows good performance (bit error ratio BER $< 10^{-10}$) and is capable to provide data transmission at least over 20 km long fiber span with data transmission speed up to 10 Gbit/s per channel, that fit the needs of next generation passive optical networks (NG-PON).

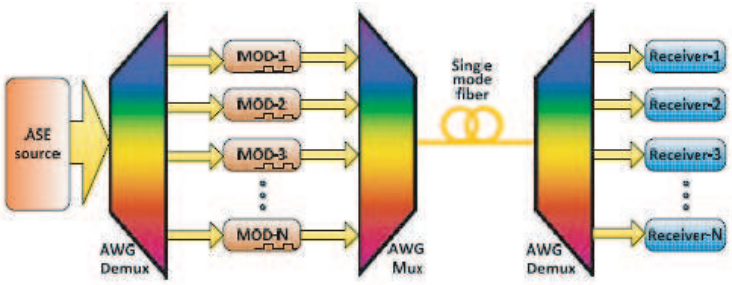

Figure 1: Operational principle of WDM PON transmission system with single light source.

Estimation of EDFA Performance in 40 Gbit/s 8 Channel DWDM Transmission System

Ingrida Lavrinovica, Jurgis Porins, and Girts Ivanovs
Institute of Telecommunications, Riga Technical University, Azenes st.16/20, Riga LV-1048, Latvia

Abstract— Erbium Doped Fiber Amplifier (EDFA) obtained a wide range of applications in research and commercial applications in optical fiber communication systems. It has been considered as an attractive solution because of several major advantages — immunity to cross talk among wavelength multiplexed channels, insensitivity to light polarization state, high energy efficiency (> 50%) and time constant enough to cover modulation noises, which is suitable solution for the simultaneous amplification of all dense wavelength division multiplexing (DWDM) channels. However, the presence of amplified spontaneous emission (ASE) limits the peak gain. EDFA gain spectrum is wavelength dependent and it applies as SNR differential between channels after passing through a cascade of EDFA. Number of cascaded amplifiers is limited by the noise accumulation [1, 2].

In this research the performance of an EDFA in a 40 Gbit/s 8 channel DWDM transmission system with NRZ-OOK modulation format and 100 GHz channel spacing was investigated. The experimental part was focused on optimization of EDFA parameters. Experimental measurement scheme is shown in the Fig. 1.

Optimal length depends on doping level and pump power, therefore different doped fiber lengths (10 m, 15 m, 20 m, 25 m, and 30 m) and excitation source power (200 mW, 300 mW, 400 mW, 500 mW) were used in order to reach the highest amplification value.

The obtained results have shown that at the pump power of 400 mW and 500 mW EDFA has already reached its saturation regime and gain is almost constant: 41–42 dB. The highest gain of 43 dB was gotif doped fiber length is chosen to 30 m. In order to reach higher gain values-longer fibers and more powerful excitation sources should be used.

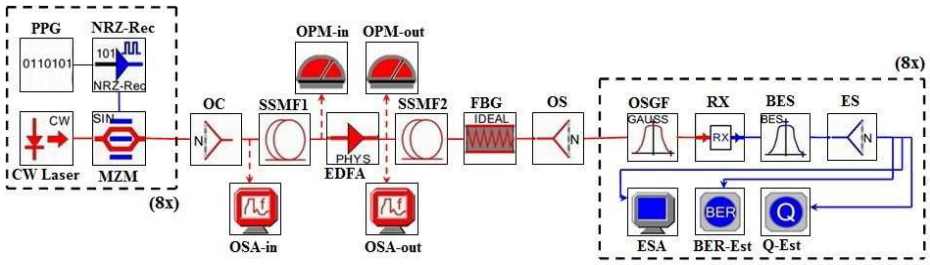

Figure 1: The experimental setup used for investigating the DWDM transmission.

REFERENCES

1. Kim, H. K., S. Y. Park, D. H. Lee, and C. S. Park, "Design and control of gain flattened erbium doped fiber amplifier for WDM application," *ETRI Journal*, Vol. 20, No. 1, 28–38, 1998.
2. Bobrovs, V., S. Berezins, and S. Olonkins, "EDFA operating parameter research and its application in WDM transmission systems," *Latvian Journal of Physics and Technical Sciences*, Vol. 6, 1, 2012.

Bidirectional Radio-on-Fiber Transport Systems Using Fiber Nonlinearity and Injection Locked Technique

W. S. Tsai and G. C. Lin
Department of Electrical Engineering, Ming Chi University of Technology, Taiwan

Abstract— We propose a novel bidirectional transmission system based on stimulated Brillouin scattering (SBS) effect and injection locked distributed-feedback (DFB) laser to achieve optical single sideband (OSSB) modulation for downlink transmission. For uplink transmission, we reuse transmitting light by phase modulation (PM) to avoid signal interference each other in bidirectional transport. After 25 km single mode fiber (SMF) transmission, we can observe the sideband power ratio (SBPR) $>$ 15 dB for downlink transmission and system's power penalty is $<$ 2.8 dB. Good performances for bit error rate (BER) analysis are observed in our proposed bidirectional transmission system.

Transponder and 3R Regenerator Impact on Energy per Bit and Optical Bandwidth Required for Data Transmission over 10-40-100 Gbps Mixed-line Rate WDM Links

Aleksjes Udalcovs and Vjaceslavs Bobrovs
Institute of Telecommunications, Riga Technical University, Riga, Latvia

Abstract— Although the mixed-line rate (MLR) design of wavelength division multiplexing (WDM) optical networks has proved itself as a cost-efficient solution for dealing with the heterogeneity of continuously growing traffic demands, however some MLR configurations might not be the best in term of energy consumption per bit (or power efficiency in W/bps) required accumulating the aggregated traffic. In general, power efficiency of MLR solutions depends on the number of factors, such as power consumption of transponders and 3R regenerators, number of the 10 Gbps, 40 Gbps, and 100 Gbps wavelengths, and the overall transmission distance. Depending on the configuration and the link length the MLR-based WDM system could outperform some of the 10 Gbps, 40 Gbps and 100 Gbps single-line rate (SLR) solutions or not. Therefore, it is important to use the proper criteria (e.g., transponder's or regenerator's power consumption; spectral efficiency which could be achieved with a particular modulation format; optical bandwidth required for the wavelength allocation in a transmission spectra) for choosing the number of different wavelengths. Hence, in this paper we aim at exploring the impact of transponders and 3R (re-timing, re-shaping, re-amplification) power consumption on the transmission's power efficiency for the set of link's lengths and on the optical bandwidth required for the allocation of the wavelength channels.

Diffraction Effects on a Dual External Cavity Tunable Laser ECTL Source

Ahmed Fawzy[1], **Osama Elghandour**[2], **and Hesham F. A. Hamed**[1]

[1]Electrical Engineering Department, Faculty of Engineering, Minia University, Minia, Egypt
[2]Electronics and Communications Engineering Department, Faculty of Engineering
Helwan University, Cairo, Egypt

Abstract— Fabrication of mirrors by using Deep Reactive Ion Etching DRIE technology allowed for production of monolithically integrated chip that contains mirrors, actuators and laser on the same die. These configurations has great importance in optoelectronics. There are many characteristics required in tunable laser also such as wide wavelength tuning, high tuning speed and minturize the device dimensions. Wide tuning range improve suitability for all practical application. New effects appear due to miniaturization of External Cavity Tunable Laser ECTL source. Diffraction effect is the important one. So in this paper presents the diffraction effects on the performance of an dual external cavity tunable laser source, whose external cavities are constructed by micro electro mechanical systems (MEMS). One of the main problems in these structures is the optical diffraction as the emitting surface of the laser diode is usually quite limited in the transverse directions. The emitted beam diffracts rapidly in the air and only a small amount of light is coupled back to the source that usually limits the tuning range of the source. We use flat mirror in our model. Device characteristics such as tuning range ($\lambda_m ax$–$\lambda_m in$), wavelength shift and sensitivity are evaluated. New expression are used and multiple reflection inside external cavities are considered. The simulation results have shown that single external cavity has limited tuning range. It is shown that multiple reflection has significant effect in our model. To get a better engineering for the dual ECTL dimensions, diffraction effects must be taken into account.

Measurement and Prediction of Non-scaling Differences between Thermal and Radiation Efficiencies of Various Antennas

Michael J. Underhill
Underhill Research Ltd., Lingfield, UK

Abstract— A previous paper put forward an explanation and theory for the significant differences found between thermal and radiation efficiencies particularly of small antennas [1]. The important discovery reported in [1] is that the 'missing' RF power is converted to a combination of broadband 'white noise' and enhanced 'spurious' sidebands. This paper reports comparative field strength measurements of the gains and associated radiation efficiencies of various types of small and large monopoles, dipoles and loop antennas, both tuned and untuned. Figure 1 shows some of the antennas measured with the MiniVNA Tiny (f) which can be used to measure and compare antenna gains and directivities at different frequencies between 1 and 1500 MHz. The coaxial cable choke balun (e) used to feed the antennas above 50 MHz is also shown. All the antennas tested have thermal efficiencies better than 95% to 98% so that gain is < 0.2 dB less than directivity.

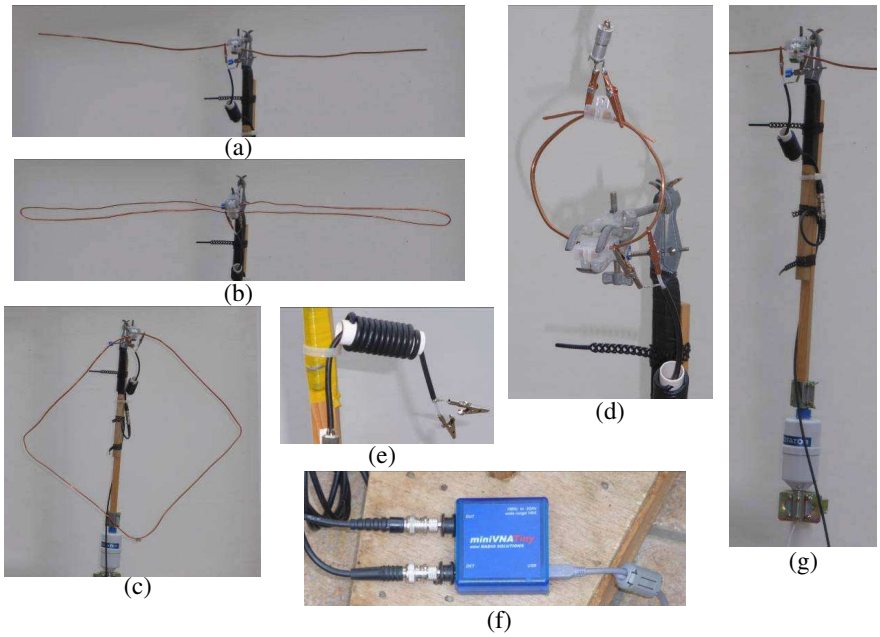

Figure 1: (a) 106 cm half-wave dipole. (b) 109 cm half-wave folded dipole. (c) 220 cm full-wave perimeter loop. (d) 10 to 20 cm adjustable diameter tuned loop with 'gamma-match' feed. (e) Choke balun feed used on all the VHF/UHF test antennas. (MRS Radio Solutions MiniVNA Tiny used for gain and antenna impedance measurements from 1 MHz to 1.5 GHz. (g) Antenna rotator for pattern measurements.

Notable results so far (with more to follow in full paper and presentation) are:

1. Full-wave perimeter loop (c) gain is ~ 4.5 dB greater than half-wave folded dipole (b) gain. Measured and computed directivities are < 1 dB different. (Measured at ~ 140 MHz.)
2. Minimum radiation efficient size of a small tuned loop (d) empirically is $\propto 1/f^{1/2}$ between 2 and 200 MHz. *Thus efficient small tuned loops do not scale conventionally, size with wavelength.*
3. The radiation efficient diameter D_e of a tuned loop is reduced as the square root of the tuned loop Q thus $D_e \propto 1/Q^{1/2}$.

REFERENCES

1. Underhill, M. J., "Wideband small loop-monopole HF transmitting antenna with implications for Maxwell's Equations and the Chu criterion," *PIERS Proceedings*, 764–768, Taipei, March 25–28, 2013.
2. Underhill, M. J., "Discovery and theory of small antenna near-field dissipation and frequency conversion with implications for antenna efficiency, beverage antenna noise reduction, Maxwell's equations and the Chu criterion," *PIERS Proceedings*, 1780–1784, Guangzhou, August 25–28, 2014.

A Generalized Vector-potential Integral Formulation for the Paraboloidal Reflector Antenna

F. O. Okewole[1], **S. A. Adekola**[1, 2], **and A. Ike Mowete**[1]

[1]Department of Electrical and Electronics Engineering, Faculty of Engineering
University of Lagos, Lagos, Nigeria
[2]Department of Electrical and Electronics Engineering
Niger Delta University, Wilberforce Island, Yenegoa, Nigeria

Abstract— This paper develops a generalized vector magnetic potential integral formulation for the paraboloidal reflector antenna, using the elliptic paraboloid geometry as basis. First, parametric expressions informed by the problem geometry are specified for the conventional 'field' and 'source' points, and the ellipse's major and minor axes are described by a common expression, also based on the geometry. When the expressions are utilized in the integral equation for the vector magnetic potential for the problem, and following the usual 'magnitude' and 'phase' approximations, an expression for the radiation field, which may be described as a general expression for certain special cases, emerges. It is shown for example, that when the ellipse's eccentricity is set to zero to prescribe the circular paraboloid, the corresponding expression for the radiation agrees with those available in the open literature [1, 2]. A moment-method solution of the associated radiation field's integro-differential equation is also presented in the paper.

REFERENCES

1. Salman, O. I., A. S. Tahir, and A. A. Al-Hilo, "Theoretical analysis of the radiation fields of parabolic reflector antenna fed by circular shaped microstrip antennas," *Basrah Journal of Science (A)*, Vol. 30, No. 2, 30–43, 2012.
2. Maclean, T. S. M., *Principles of Antennas*, Cambridge University Press, New York, 1986.

A Compact Dual-band Balanced Slot Antenna for LTE Applications

I. T. E. Elfergani[1], **Abubakar Sadiq Hussaini**[1, 3, 4], **Jonathan Rodriguez**[1, 2], **and R. A. Abd-Alhameed**[3]

[1]Instituto de Telecomunicações, Aveiro, Portugal
[2]Universidade de Aveiro, Portugal
[3]Radio Frequency, Antennas, Propagation and Computational Electromagnetics Research Group
School of Electrical Engineering and Computer Sciences, University of Bradford, Bradford, BD7 1DP, UK
[4]School of Information Technology & Communications, American University of Nigeria, Nigeria

Abstract— The new technology in wireless communication has brought a lot of portable devices in the future, such as a mobile phone that will possess Long Term Evolution (LTE) function for the voices and data transmissions [1]. Conventionally, the unbalanced planar inverted F antenna (PIFA) is one of the most popular candidates for compact internalized antennas for mobile handsets due to its unique characteristic that makes it suitable for use in portable wireless device especially on mobile handsets. However, PIFAs use the ground plane as a part of the radiator, enabling very small antennas to achieve adequate gain and bandwidth [2]. Therefore, radiating currents are induced on both the ground plane and the antenna element, resulting in currents flowing on the human body, which degrade the performance of the antenna's radiation characteristics and introduce losses and uncertainty in its matching [3].

To solve these problems, a balanced structure is introduced to not only to eliminate such constraints but also to avoid the degradation of antenna performance in aforementioned unbalanced antennas. In this kind of antennas, currents cancel the effect of each other, the current flows only on the antenna element and not on the ground plane. Therefore, the coupling between the antenna and the user's body will be neglected when the mobile is held by its user which leads in no effect on the performance of the antenna. Lately, several mobile antennas with the balanced technique have proved the enhanced stability of antenna performance, compared to the unbalanced type especially when the handset is positioned in a close vicinity to the human head and/or hand [4, 5]. However, these balanced antennas are not capable to meet the frequency bands of LTE. Thus, the proposed work has been investigated to offer a low profile antenna for Long Term Evolution (LTE) applications at 700 MHz and 2600 MHz bands using the balanced antenna concept.

The proposed antenna will be implemented based on built-in planar dipoles with two folded slot arms structure. Fig. 1 shows the geometry of the balanced antenna for a mobile phone. The antenna was designed first and then was mounted 4 mm on top of a finite ground plane with dimension of $100 \times 50\,\text{mm}^2$ which acts as the mobile handset chassis or what today we would identify as the ground plane of a practical mobile phone handset, as seen in Fig. 1. The dimensions of the proposed antenna geometry were found comparable to the practical handset size as illustrated in Fig. 1. The slot has a uniform width of 2 mm. The antenna was constructed from a copper sheet with thickness of 0.15 mm. The objective of the embedded slot was to tune the radiator structure to resonate at our targeted bands of LTE 700/2600 MHz. This was achieved through multiple simulated attempts, by conducting several modification of the authors' previous

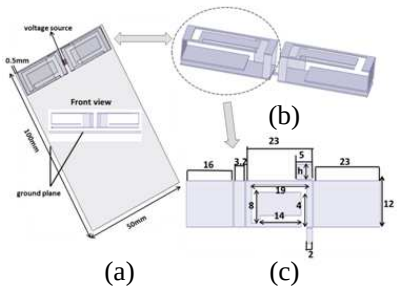

Figure 1: Basic antenna structure; (a) 3D, (b) folded slotted arms, (c) unfolded slotted arm, dimensions in mm.

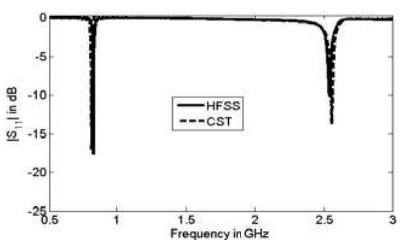

Figure 2: Reflection coefficient of folded arms slotted proposed antenna.

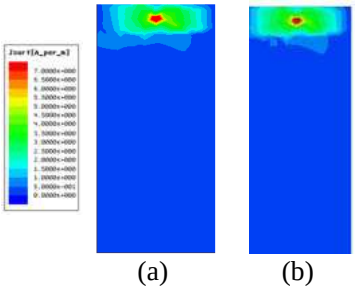

Figure 3: Surface current distributions for the proposed balanced antenna at (a) 700 MHz, (b) 2600 MHz.

work in [5] to move toward the desired outcome of developing highly compact and dual-band antenna for use in LTE applications. It is obvious that the S_{11} of proposed antenna generated by HFSS agrees well with the one obtained from the CST as shown in Fig. 2. The analysis of the current surface on the ground plane of the proposed antenna was studied using the EM simulator at the 700 MHz and 2600 MHz, i.e., the targeted frequencies within this work as shown in Fig. 3. One can clearly note that, most of the current is induced exactly underneath the two folded slotted arms at both resonant frequencies while it is more or less vanished on the rest of the ground plane in which proves the concept of balanced antenna whereby it reduces the coupling between the handset and the user's hand.

REFERENCES

1. Kumar, N. and G. Saini, "A novel low profile planar inverted-F antenna (PIFA) for mobile handsets," *International Journal of Scientific and Research Publications*, Vol. 3, No. 3, Mar. 2013.
2. Elfergani, I., A. S. Hussaini, J. Rodriguez, C. H. See, and R. Abd-Alhameed, "Wideband tunable PIFA antenna with loaded slot structure for mobile handset and LTE applications," *Radioengineering*, Vol. 23, No. 1, 345–355, Apr. 2014.
3. Abd-Alhameed, R. A., P. S. Excell, R. A. K. Khalil, and J. Mustafa, "SAR and radiation performance of balanced and unbalanced mobile antennas using a hybrid computational electromagnetics formulation," *IEE Proceedings — Science, Measurement and Technology Special Issue on Computational Electromagnetics*, Vol. 151, 440–444, 2004.
4. Sasaki, D., et al., "A planar folded dipole antenna for mobile handset," *IEEE Interanational Workshop on Antenna Technology*, 133–136, Mar. 2005.
5. Alhaddad, A. G., R. A. Abd-Alhameed, D. Zhou, I. T. E. Elfergani, C. H. See, P. S. Excell, and M. S. Bin-Melha, "Low profile balanced handset antenna with dual-arm structure for WLAN application," *IET Microwaves, Antennas and Propagation*, Vol. 5, 1045–1053, 2011.

Novel Quadrifilar Helical Antenna for RFID Applications Using Genetic Algorithms

M. O. Akinsolu[1], **A. Ali**[1], **A. Atojok**[1], **E. Ibrahim**[1, 2], **I. T. E. Elfergani**[3], **R. A. Abd-Alhameed**[1], **Abubakar Sadiq Hussaini**[1, 3, 5], **J. M. Noras**[1], **and Jonathan Rodriguez**[3, 4]

[1]University of Bradford, Bradford, West Yorkshire, BD7 1DP, UK
[2]College of Electronic Technology Bani Walid, Libya
[3]Instituto de Telecomunicacoes, Aveiro, Portugal
[4]Universidade de Aveiro, Portugal
[5]School of Information Technology & Communications, American University of Nigeria, Nigeria

Abstract— Antennas constitute a very important part of Radio Frequency Identification (RFID) systems. Coming in various forms and types, they are usually designed and intended to ensure maximum effective and efficient communication links between tags or transponders and their associated readers or interrogators. One of the primary challenges in the design and development of antennas in RFID applications as it is in other wireless applications is having an antenna with optimised parametric features that are desirable and in consonance with laid down specifications and functional requirements. These parametric features include but are not limited to: profile, gain, directivity, bandwidth and polarisation.

Radio Frequency Identification (RFID) systems which connote the physical interaction between a tag and a reader for automatic identification operate within the global bandwidth of (860–960) MHz as specified by the International Standards Organisation (ISO). It should also be noted the RFID systems function adopting a non-contact application of radio-frequency does not require a line-of-sight channels. Thus, in order to optimise an RFID system, the orientation of the tags and associated readers must be fully established through the polarisation characteristics of their corresponding antennas. RFID tags are often designed to have linearly polarised dipoles. Consequently, their orientation in a typical RFID system is not always predictable.

The quadrifilar helical antenna (QHA) has been identified by previous works as a suitable antenna for tag reading in RFID and other wireless applications, due to its ability to give circular polarisation over a wide angular area [1, 2]. Another excellent property of QHAs in terms of the symmetry of their geometry is their ability to give a cardioid-shaped radiation pattern regardless of the axial length and diameter. It has also been established that the inherent cardioid-shaped radiation patterns of QHAs can be made conical by extending the resonant fractional turns of the QHA to an integral number for improved characteristics [2]. Consequent to the aforementioned, a novel compact QHA was designed and optimised over a perfect ground to function optimally within the RFID global bandwidth of (860–960) MHz. The novel QHA antenna is named linearly-shifted quadrifilar helical antenna (LSQHA) because its elements are linearly-shifted and made compact as revealed in Fig. 1(b). With reference to its helical elements and as can be observed, the proposed LSQHA design does not take the form of the conventional QHA. Specifying a finite ground and feeding of the LSQHA via an integrated feed network is proposed, to avoid the intricacy and losses associated with multiple feed points of a centre feed. At the risk of repetition, the

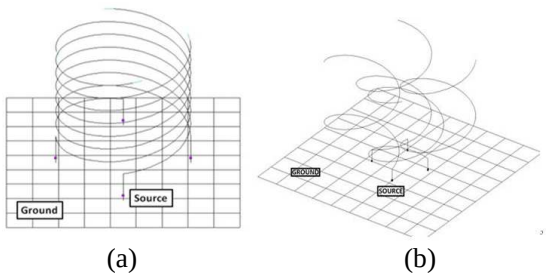

(a) (b)

Figure 1: Antenna configurations examined: (a) QHA; (b) LSQHA.

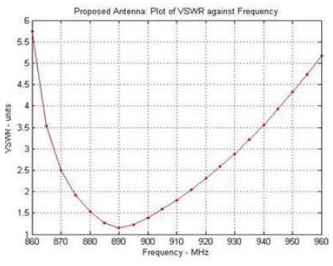

Figure 2: Computed VSWR for the proposed LSQHA.

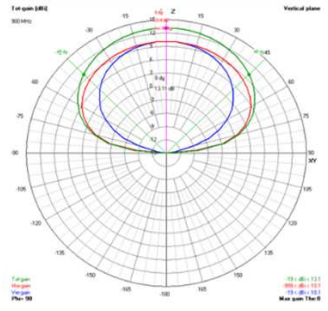

Figure 3: Computed gain radiation patterns of the proposed antenna for one vertical cut plane.

novel antenna structure is achieved by linearly-shifting the helical elements of the conventional QHA by 90° using a defined phase quadrature distance. This design is expected to reduce the axial length and overall volumetric equivalent of the LSQHA, while retaining good axial ratio, high power gain and wide beamwidth coverage.

REFERENCES

1. Zhou, D., R. A. Abd-Alhameed, C. H. See, P. S. Excell, and E. A. Amushan, "Design of quadrifilar helical and spiral antennas in the presence of satellite-mobile handsets using genetic algorithms," *First European Conference on Antennas and Propagation, EuCAP 2006*, 1–5, 2006.
2. Zhou, D., S. Gao, R. A. Abd-Alhameed, C. Zhang, M. S. Alkhambashi, and J. D. Xu, "Design and optimisation of compact hybrid quadrifilar helical-spiral antenna in GPS applications using genetic algorithm," *2012 6th European Conference ont Antennas and Propagation (EUCAP)*, 1–4, 2012.

Circularly Polarized Crossed Bowtie Dipole Radiator with a Half-wavelength-thick Partially Reflecting Surface

Huy Hung Tran[1], **Ikmo Park**[1], **and Hanjo Lim**[2]

[1]Department of Electrical and Computer Engineering
Ajou University, Suwon, Republic of Korea
[2]CINAP, Institute for Basic Science (IBS), Department of Energy Science
Sungkyunkwan University, Suwon, Republic of Korea

Abstract— The gain of a radiator can be improved by placing a partially reflecting surface (PRS) at an appropriate distance from the ground plane. The maximum radiation in the broadside direction occurs when the reflectivity of a PRS is maximized, and a cavity structure achieves in-phase electromagnetic wave transmission. The main characteristics of the antenna, such as the impedance and gain bandwidths, and radiation patterns are determined by the properties of the radiator and PRS. It is well-known that the PRS should be placed at a half-wavelength distance from the ground plane for optimum performance, and the maximum gain increase is accompanied by a decrease in the operation bandwidth. Therefore, it is very difficult to achieve both gain and bandwidth enhancement at the same time.

Recently, a method for using multiple dielectric slabs to form multiple PRSs has been proposed. This method uses several superstrates to create multiple resonances with multiple cavities, and achieved a broad 3-dB gain bandwidth. However, the design of the PRSs with multiple dielectric slabs requires a complicated optimization process. Even though a wide gain bandwidth can be achieved with multiple dielectric slabs, the size of the antennas is large, and there may have fabrication difficulties.

In this paper, a high-gain circularized polarized bowtie crossed dipole with wideband characteristics is proposed. A planar conducting screen acting as the ground plane is placed behind a crossed bowtie dipole radiator and a reflecting screen acting as a superstrate is placed in front of the radiator. The antenna employing a half-wavelength-thick PRS achieves wide reflection coefficient, axial ratio (AR), as well as gain bandwidths. The final design with an overall size of $80 \times 80 \times 28.35\,\text{mm}^3$ yielded a -10-dB impedance bandwidth of 40% (5.6–8.4 GHz), a 3-dB AR bandwidth of 25.6% (6.3–8.15 GHz), a 3-dB gain bandwidth of 42.7% (5.7–8.8 GHz).

A Bandwidth Enhanced Compact Circularly Polarized Crossed Dipole Antenna Loaded with a Parasitic Element

Son Xuat Ta and Ikmo Park
Department of Electrical and Computer Engineering
Ajou University, Suwon, Republic of Korea

Abstract— In this paper, a compact circularly polarized (CP) crossed dipole antenna loaded with a parasitic element is proposed for use in GPS L1 (1.575 GHz) and GLONASS L1 (1.605 GHz) bands. The dual-band operation is obtained by combing two CP bands; one from the crossed dipole driver and other from the parasitic element. A meander line and an arrowhead shaped ending were utilized to achieve a compact size in both driver and parasitic elements. The antenna was demonstrated to be well matched to a 50-Ω coaxial line without any matching network and to have reasonably high radiation efficiency. The antenna was characterized using a finite-element method-based full-wave electromagnetic solver, Ansoft HFSS. Both crossed dipole and parasitic elements were designed on a Rogers RT/Duroid 5880 substrate with a permittivity of 2.2, a thickness of 0.508 mm, and a loss tangent of 0.0009.

The final design with an overall size of 38 mm×38 mm×1.016 mm yields a −10-dB $|S_{11}|$ bandwidth of 1.505–1.695 GHz and a 3-dB axial ratio bandwidth of 1.555–1.635 GHz with two CP center frequencies at 1.575 GHz (AR = 1.0 dB) and 1.605 GHz (AR = 0.9 dB). The antenna radiated a bi-directional electromagnetic wave at both bands; it radiated a right-hand circular polarization wave at the broadside direction whereas it radiated left-hand circular polarization wave at the back direction. Additionally, the antenna yielded gains of 1.45 and 1.78 dBic, and radiation efficiencies of 88.3% and 93.5% for the lower and upper bands, respectively. With compact size, good impedance matching, and good CP radiation, the proposed antenna can be widely used in GPS and GLONASS applications.

A Compact Tri-band Monopole Antenna with Multiple Meander Lines for WLAN and WiMAX Communication Applications

Xinbo Liu, Yingsong Li, and Wenhua Yu
College of Information and Communications Engineering
Harbin Engineering University, Harbin, China

Abstract— In this paper, a compact tri-band monopole antenna with three meander lines is proposed and investigated for wireless local area networks (WLANs) and worldwide interoperability for microwave access (WiMAX) system applications. The designed tri-band antenna is realized by using three meander line structures that are connected to the 50-Ohm microstrip feed signal strip line to generate the desired triple resonance frequencies. By adjusting the dimensions of the proposed three meander lines, the expected resonant frequencies can be tuned for WLAN and WiMAX communication applications. The experimental results demonstrate that the optimized tri-band monopole antenna can give three impedance bandwidth for $S_{11} \leqslant -10\,\mathrm{dB}$ of 160 MHz (2.39–2.55 GHz), 450 MHz (3.30–3.75 GHz) and 730 MHz (5.14–5.87 GHz), which can be applied to cover both 2.4/5.2/5.8-GHz WLAN bands and 3.5/5.5-GHz WiMAX bands. Furthermore, omnidirectional radiation patterns and stable gains can be achieved, which make the designed tri-band monopole antenna promising for integrating into modern portable devices.

Efficient 2D Simulation Model for the Analysis and Optimal Design of DNP-NMR Solenoid Coils

Alexandros I. Dimitriadis[1], **Murari Soundararajan**[1], **Dongyoung Yoon**[1], **Alessandro Macor**[2], **and Jean-Philippe Ansermet**[1]

[1]Institute of Condensed Matter Physics
École Polytechnique Fédérale de Lausanne (EPFL), Switzerland
[2]Institute of Condensed Matter Physics
École Polytechnique Fédérale de Lausanne (EPFL) & SWISSto12 S.A., Switzerland

Abstract— Nuclear magnetic resonance (NMR) spectroscopy is a broadly used research technique that exploits the magnetic properties of atomic nuclei with non-zero spin in order to determine the physical and/or chemical properties of the molecules in which they are contained. Specifically, it can provide detailed information regarding the structure, dynamics, reaction state, and chemical environment of the molecules, while its spectra are (at least for small molecules) well-resolved, analytically tractable and highly predictable. However, NMR has fundamental sensitivity limitations, as a consequence of the small energy difference between nuclear spin states. This drawback has always restricted its application to complex structures, like large biomolecules (proteins, nucleic acids etc.).

Dynamic nuclear polarization (DNP) has emerged as a widely applicable technique to improve the sensitivity of NMR experiments (involving RF currents in the region of few hundreds of MHz) by transferring the relatively large polarization of electron spins to bulk nuclei, a process which requires the excitation of electron paramagnetic resonance (EPR) transitions with high-power millimeter-wave (MMW) radiation. The result is a significant enhancement of the original NMR signal, thus leading to an important reduction of the corresponding spectrum acquisition times. Such experiments have been made possible in the past few years due to the development of stable, high-power gyrotrons as MMW sources and low-loss waveguides which transfer the power to the sample. DNP enhancement values depend on a number of factors, but most importantly on the intensity of the MMW magnetic field, which is oscillating in resonance with the electron spins, throughout the sample.

In this paper, we develop a 2D simulation model in order to analyze the MMW performance of a typical NMR solenoid coil operating at cryogenic temperatures. The structure is approximated by a single unit cell — corresponding to one turn of the coil — together with appropriate periodic boundary conditions, while a plane wave with the proper electric field polarization is considered for the MMW excitation. Then, this model is succesfully utilized to examine the reflection/transmission characteristics of the coil, visualize the field distributions, estimate and maximize the average magnetic field in the sample region and, hence, optimize the geometry of the device in a very fast and convenient way. The results of our analysis show very good agreement with those of a more realistic — yet computentionally intensive — 3D model of the same setup, while our conclusions can serve as the basis for the development of more advanced NMR coils, which can deal efficiently with the crucial issue of sample heating. All simulations are performed with the RF module of COMSOL Multiphysics, a simulation package based on the Finite Element Method (FEM).

Low-cost Implementation of a Waveguide-based Microwave Filter in Substrate Integrated Waveguide (SIW) Technology

A. Coves[1], **Á. A. San Blas**[1], **S. Marini**[2], **G. Torregrosa**[1], **E. Bronchalo**[1], **and A. Martellosio**[3]

[1]Departamento de Ingeniería de Comunicaciones, Universidad Miguel Hernández de Elche, Spain
[2]Departamento de Física, Ingeniería de Sistemas y Teoría de la Señal
I.U. Física Aplicada a las Ciencias y las Tecnologías, Universidad de Alicante, Spain.
[3]Department of Electrical, Computer and Biomedical Engineering, University of Pavia, Italy.

Abstract— The increasingly known transmission line called SIW (Substrate Integrated Waveguide) [1, 2] is a low-cost realization of the traditional rectangular waveguide, taking the advantages of planar lines for easy integration with other circuits, and low radiation losses of waveguides. Furthermore, this new technology has been used for making a large number of microwave devices such as filters, antennas, multiplexers, etc. [3–5].

This paper presents the design and practical implementation of a waveguide-based microwave filter in Substrate Integrated Waveguide technology. The use of SIW technology for implementing waveguide filters makes the presented design specially aimed for being used in undergraduate courses related to microwave engineering and filter designing. Their low cost and easiness from the filter fabrication point of view allows their use in microwave laboratory courses where students can implement their own theoretical filter designs and measure their frequency response.

The requiring mechanics in the manufacturing of microwave filters in waveguide technology (both rectangular and circular) makes its use practically unfeasible in academic laboratories for various reasons (cost, high frequency operation ...), despite the abundant literature dealing on waveguide filters implementation [6]. For this reason, a practical design example of a waveguide iris filter using the impedance inverter model is proposed in this paper for academic laboratories, using SIW technology. This is a low cost and easy to manufacture technology. The overall process includes the design of the ideal band-pass prototype filter using the impedance inverter and its implementation in an inductive iris-coupled waveguide filter, by using a developed electromagnetic simulator based on the mode-matching technique [7]. Finally, the equivalent filter in SIW technology is obtained and optimized by using HFSS simulator [8]. Since the response of the designed filter is going to be measured using a vector network analyzer, a SIW to microstrip transition is designed at both ends of the filter, at which ends are connected SMA connectors.

ACKNOWLEDGMENT

This work was supported by the Ministerio de Economía y Competitividad, Spanish Government, under the coordinated project TEC2013-47037-C5-4-R.

REFERENCES

1. Deslandes, D. and K. Wu, "Design consideration and performance analysis of substrate integrated waveguide components," *32nd European Microwave Conference Proceedings*, Vol. 2, 881–884, Sep. 2002.
2. Cassivi, Y., L. Perregrini, P. Arcioni, M. Bressan, K. Wu, and G. Conciauro, "Dispersion characteristics of substrate integrated rectangular waveguide," *IEEE Microw. Wirel. Compon. Lett.*, Vol. 12, No. 9, 333–335, Sep. 2002.
3. Yan, L., W. Hong, G. Hua, J. Chen, K. Wu, and T. J. Cui, "Simulation and experiment on SIW slot array antennas," *IEEE Microw. Wirel. Compon. Lett.*, Vol. 14, No. 9, 446–448, Sep. 2004.
4. Chen, X. P., K. Wu, and Z. L. Li, "Dual-band and triple-band substrate integrated waveguide filters with Chebyshev and quasielliptic responses," *IEEE Trans. Microw. Theory Tech.*, Vol. 55, No. 12, 2569–2578, Sep. 2007.
5. Bozzi, M., A. Georgiadis, and K. Wu, "Review of substrate integrated waveguide (SIW) circuits and antennas," *IET Microw. Antennas Propagat.*, Vol. 5, No. 8, 909–920, Jun. 2011.
6. Cameron, R. J., C. M. Kudsia, and R. R. Mansour, *Microwave Filters for Communication Systems: Fundamentals, Design, and Applications*, Wiley, 2007.
7. Valero, N. C., *Análisis Multimodal de Discontinuidades en Guía Rectangular Mediante la Técnica de Adaptación Modal*, Final Project, Universidad Miguel Hernández de Elche, 2005.
8. HFSS: 3D Full-wave Electromagnetic Field Simulation, Available: http://www.ansoft.com/products/hf/hfss, 2007.

A Broadband GaN Power Amplifier Using Thin-film Integrated Passive Device Technology

Dongsu Kim[1], **Sung Jin Ahn**[1, 2], **Jong-Min Yook**[1], **Jong-In Ryu**[1], **Jong-Gwan Yook**[2], **and Junchul Kim**[1]

[1]Packaging Research Center, Korea Electronics Technology Institute, Korea
[2]Electrical and Electronic Engineering, Yonsei University, Korea

Abstract— In this paper, we propose an RLC matched GaN HEMT broadband power amplifier using silicon-based integrated passive device (IPD) technology. For broadband operation, the RLC type bridged-T all-pass network is used at the input matching network [1]. The initial values are calculated by a formula from the reference [1] with an input capacitance (C_{gs}) of the GaN HEMT. Based on the calculated values, the proposed power amplifier is designed and optimized to obtain broadband characteristics. Also, the LC ladder-typed topology is employed at the output matching network, as shown in Figure 1.

The X-band power amplifier was implemented using thin-film IPD technology, as shown in Figure 2. The passive elements at the input and output matching networks were implemented using metal-insulator-metal (MIM) capacitors, spiral inductors, and thin-film resistors. The GaN HEMT and two matching networks were attached using high-K conductive epoxy and interconnect between them was done by wire bonding. This approach provides several key properties such as high integration, which is very close to MMIC dimension, high design flexibility, low cost by standard silicon technology, and so on. The measured impedance contours of the fabricated matching networks are shown in Figure 2. The dimension of the input and output matching networks is 1.4 mm × 1.2 mm and 2.2 mm × 1.6 mm, respectively. The thickness of the matching networks is only 0.15 mm. A more than 1.5-GHz bandwidth with an output power of 37 dBm at X-band can be obtained by this input RLC matched network and output LC ladder-type topology.

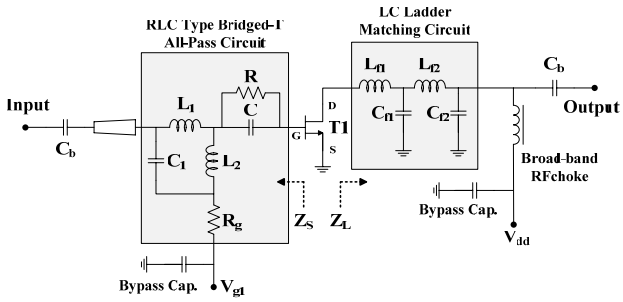

Figure 1: Schematic of the broadband power amplifier.

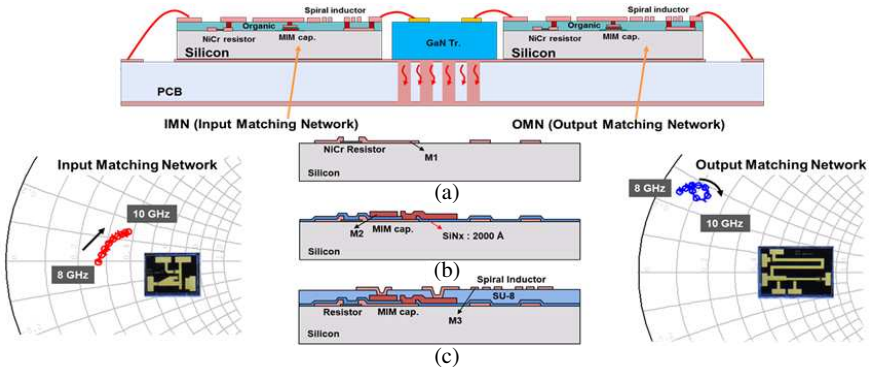

Figure 2: Proposed power amplifier structure, process and measured impedances.

REFERENCES

1. Ikalainen, P. K., "An RLC matching network and application in 1–20 GHz monolithic amplifier," *IEEE MTT-S Int. Microw. Symp. Digest*, 1115–1118, June 1989.

Band-pass Filter Based on Magnetoelectric Composite at Electromechanical Resonance

A. S. Tatarenko, **R. V. Petrov**, **V. M. Petrov**, **and M. I. Bichurin**
Novgorod State University, Russian Federation

Abstract— Ferrite-piezoelectric layered structures are known to be magnetoelectric (ME) due to interaction of ferrite magnetization and piezoelectric polarization via elastic deformations [1]. The applicability of ME composites for signal processing devices, such as phase shifters and filterswas reported recently [2]. The present paper focuses on the ferrite-piezoelectric bilayer based LF-band filter performance. This structure enables one to control the filter characteristics in a wide range of input signal amplitude by means of bias magnetic field.

The filter considered consisted of a ferrite-piezoelectric bilayer placed into a solenoid. Bias magnetic field up to 2000 Oe was generated by an electromagnet. DC magnetic field H is necessary to provide non-zero piezomagnetic coefficient for magnetic layer and obtain the resonant characteristics. The ferrite-piezoelectric bilayer was formed by single-crystal $Zn_{0.2}Ni_{0.8}Fe_2O_4$ (NZFO) and piezoelectric lead zirconate-titanate (PZT). PZT and NZFO had dimensions of $24 \times 24 \times 2\,\mathrm{mm}^3$ and $30 \times 20 \times 2.25\,\mathrm{mm}^3$, correspondingly. Electrodes were placed on lateral surfaces of piezoelectric layer to measure the output voltage across the piezoelectric layer. Bilayer geometry corresponded to electromechanical resonance (EMR) frequency of 86 kHz. The measurements were carried out with Agilent DSO-X 2002A oscilloscope.

The resonance pick at frequency of 86.8 kHz corresponds to the longitudinal mode of EMR and has the bandwidth of 2 kHz. The output voltage was equal to 2.53 V at zero bias magnetic field and input ac voltage of 10 V. The output voltage increased to 12.62 V at dc magnetic field of 170 Oe and input ac voltage of 0.714 V. The resonance value of ME voltage coefficient equaled 0.47 V/(cm·Oe). Thus, the proposed filter design enables one to achieve the peak transmission coefficientregulation of 10 dB. The obtained results can be further used in practical applications.

ACKNOWLEDGMENT

The research was supported by a grant of government task from the Ministry of Education and Science of Russian Federation.

REFERENCES

1. Bichurin, M., V. Petrov, R. Petrov, and S. Priya, "Electromechanical resonance in magnetoelectric composites: Direct and inverse effect," *Solid State Phenomena*, Vol. 189, 129–143, 2012.
2. Bichurin, M. I., R. V. Petrov, and V. M. Petrov, "Magnetoelectric effect at thickness shear mode in ferrite-piezoelectric bilayer," *Appl. Phys. Lett.*, Vol. 103, 092902, 2013.

Silicon Carbide MEMS Based Tunable Resonator Filters

B. Sviličić[1, 2], E. Mastropaolo[1], and R. Cheung[1]

[1]Scottish Microelectronics Centre, University of Edinburgh, Edinburgh, United Kingdom
[2]Faculty of Maritime Studies, University of Rijeka, Rijeka, Croatia

Abstract— Micro-electro-mechanical system (MEMS) resonators have emerged as a potential candidate technology for implementation of high-Q tunable filters that are able to solve power consumption and miniaturization issues [1]. Electrically tunable filters with a wide operational range are crucial elements in both multiband communication systems and wideband tracking receivers because they have the ability to replace filter banks [2]. Silicon carbide (SiC), due to its excellent electrical, mechanical and chemical properties, is one of the most promising materials for high efficiency MEMS resonators [3].

Recently, we have demonstrated a silicon carbide MEMS based resonator filter that is actuated electrothermally and sensed piezoelectrically [4]. Electrothermal technique for induction of mechanical vibrations has been attracting increasing attention as a means of allowing simple fabrication process, low actuation voltages, impedance matching and effective frequency tuning. Piezoelectric transduction allows active generation of electrical potential in response to an applied mechanical stress (no bias voltage source is needed), and it enables stronger electromechanical coupling and simpler fabrication process compared to the electrostatic transduction.

In this work, we present a two-port SiC MEMS resonator device electrothermally actuated with u-shaped designed electrode in order to provide tunable filter function with wide operation range (Figure 1). Two-port transmission frequency response measurements have shown that, by increasing the DC bias of the actuating voltage from 3 to 7 V, the operating frequency of a 1.4 MHz device can be adjusted up to 31%. Details of the design, fabrication processes and measurement setup will be presented. Moreover, the origin of resonant frequency change induced by tuning DC voltage will be studied.

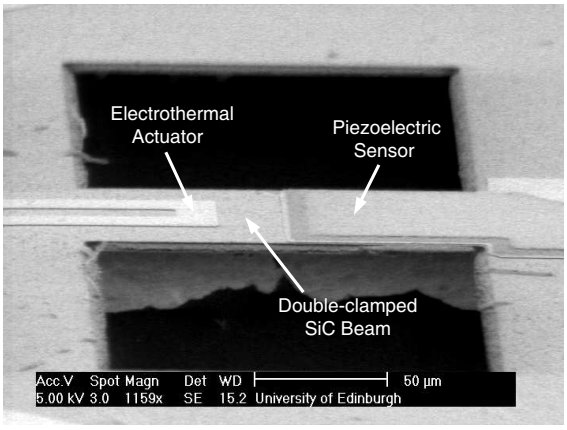

Figure 1: SEM of the fabricated resonator with the electrothermal actuator (input port) and piezoelectric sensor (output port) placed on the top of SiC double-clamped beam.

ACKNOWLEDGMENT

B. Sviličić acknowledges financial support of Croatian Science Foundation and University of Rijeka.

REFERENCES

1. Van Beek, T. M. and R. Puers, *J. Micromech. Microeng.*, Vol. 22, 013001–35, 2012.
2. Mansour, M. M., H. Fengxi, S. Fouladi, W. D. Yan, and M. Nasr, *IEEE Microw. Mag.*, Vol. 15, 70–83, 2014.
3. Sarro, P. M., *Sens. and Act. A*, Vol. 82, 210–218, 2000.
4. Sviličić, B., E. Mastropaolo, B. Flynn, and R. Cheung, *IEEE Electron Device Lett.*, Vol. 33, 278–280, 2012.

Yagi Rectenna Application to Increase the Battery Lifetime of Sensor Nodes

R. Fernández-García and I. Gil
Departmentof Electronic Engineering, Universitat Politècnica de Catalunya
08222 Colom 1, Terrassa, Spain

Abstract— In the last years a massive increase of the use of wireless communications has been produced in industrial and domestic applications. Specifically, one of the latest applications of the wireless communication is the Wireless Sensor Networks (WSNs) [1]. The WSNs consist of small communication nodes. These nodes contain a sensing part, a microcontroller, communication components and power supply (typically a battery). Moreover, these nodes should fulfil restrictions of low-cost and low-power consumption to guarantee its usefulness. In this sense, the RF energy-harvesting technology [2] can help to increase the battery lifetime of sensor nodes and, in some cases, even to avoid using the battery. The main RF energy harvesting element is the rectenna, which consists of an antenna plus a rectifier to convert the RF signal to DC voltage.

In this work, a Yagi rectenna to harvest the RF energy of the GSM system at 1.8 GHz is proposed. The rectenna has been designed by means of the commercial *Keysight Advance Design System* (ADS) software. Fig. 1 shows the proposed Yagi antenna implemented of commercial FR4 substrate (dielectric constant $\varepsilon_r = 4.6$, thickness $h = 1.53\,\text{mm}$). Fig. 2 plots the simulated return loss, bandwidth of 250 MHz (1700 MHz to 1950 MHz) it is observed at $S_{11} = -10\,\text{dB}$ with antenna gain from 4.5 dBi to 7 dBi (5.78 dBi at 1.8 GHz). At 1800 MHz the antenna input impedance corresponds to 62.74+j6.31 Ω. Fig. 3 shows a voltage double RF-DC converted base on HSMS-286c Schottkydiodes. Note that in order to design correctly the matching network between antenna and RF-DC converter the parasitic impedance of diode packed SOT-323 has

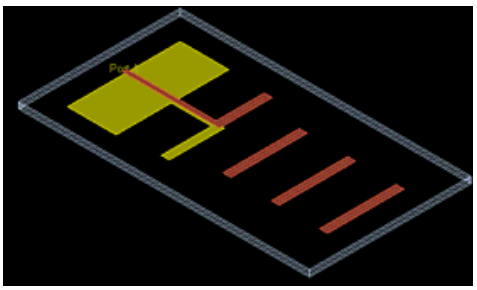

Figure 1: Antenna return loss.

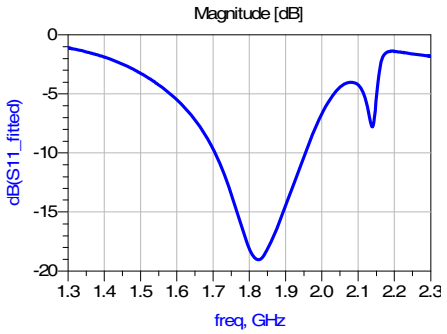

Figure 2: Antenna return loss.

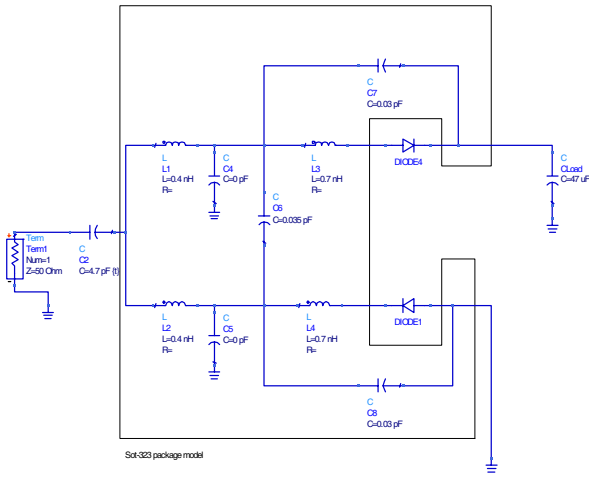

Figure 3: RF-DC converter.

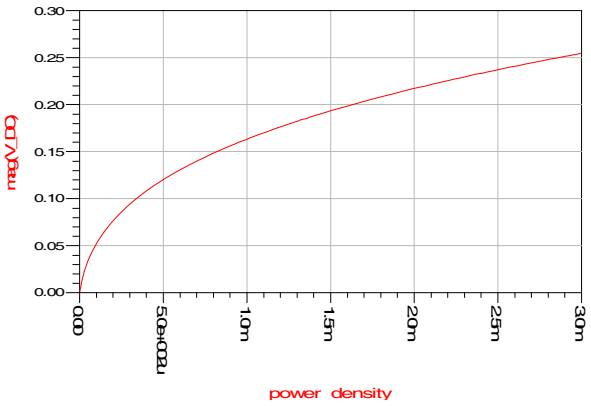

Figure 4: Output voltage versus power density (mW/m^2).

been included. The RF-DC converter input impedance at 1.8 GHz is $2.01-\mathrm{j}\,224.16\,\Omega$. Therefore,a LC matching network with 20 nH and 8.2 pF is used. In Fig. 4 the dependence of DC voltage with the RF power density of the designed antenna at 1.8 GHz is drawn, 200 $\mathrm{mV_{DC}}$ are obtained for a power density of 1.5 $\mathrm{mW/m^2}$.

ACKNOWLEDGMENT

This work was supported by the Spanish Government-MINECO under Project TEC2013-41996-R and AGAUR 2014 SGR 375.

REFERENCES

1. Baronti, P., P. Pillai, V. W. C. Chook, S. Chessa, A. Gotta, and Y. F. Hu, "Wireless sensor networks: A survey on the state of the art and the 802.15.4 and ZigBee standards," *Comput. Commun.*, Vol. 30, No. 7, 1655–1695, May 2007.
2. Kim, S., R. Vyas, J. Bito, K. Niotaki, A. Collado, A. Georgiadis, and M. M. Tentzeris, "Ambient RF energy-harvesting technologies for self-sustainable standalone wireless sensor platforms," *Proc. IEEE*, Vol. 102, No. 11, 1649–1666, Nov. 2014.

A Model-free Method for Real-time High Precision Carrier Phase Observation

Tianyi Zhang, Qiao Meng, Quantao Yu, Jifei Tang, and Wei Liu
Institution of RF-&OE-ICs, Southeast University, Sipailou 2, Nanjing 210096, China

Abstract— Carrier phase observation is a ranging method with high accuracy that used in various applications including radar ranging, satellite orbits determination, high precise relative GPS positioning and mobile communication location system. It achieves the radial distance between target and receiver by measuring and tracking the changes to the carrier phase. Relative velocity could be obtained from instantaneous frequency (IF).

Carrier signal of target in motion is a typical nonstationary signal and its model is difficult to determine. This paper describes a model-free method of obtaining total phase and IF of carrier signal in real-time with high resolution. The estimation of signal model is unnecessary, which reduces the computation and complexity. Frequency rate, initial frequency and fractional phase are estimated using de-chirp algorithm in fixed short-time interval called integral time. The de-chirp algorithm is based on ambiguity function (AF) and high resolution frequency estimator is used. Total phase are calculated and filtered by Savitzky-Golay smoothing filter to reducing measure noise. Meanwhile, instantaneous frequency with better accuracy could be obtained by deriving the smoothed total phase which can also be implemented by a FIR filter like Savitzky-Golay filter. The degree of polynomial used to design smoothing filter should be chosen cautiously and the integral time should be designed wisely. This method is adapted to be implemented using hardware.

Monte-Carlo simulation using polynomial phase signal (PPS) model with additive white Gauss noise (AWGN) shows the validity of the method. The simulation results also indicate that the proposed approach could obtain accuracy total phase and IF at low signal-to-noise ratio (SNR).

Real-time Processing Technique for Panoramic Infrared Imaging System

G. Sun, G. Li, W. H. Wang, X. L. Fan, and Z. P. Chen
Science and Technology on Automatic Target Recognition Laboratory
National University of Defense Technology, Changsha 410073, China

Abstract— High-resolution, multi-pixels and large view field infrared detector is an important research direction that would improve the detection capability of infrared imaging alarm system. However, along with the aggrandizement of view field, especially for the omnidirectional search system of surrounding-view infrared imaging, the background composition of the infrared image is very complicated, and the difficulty of target detection increases correspondingly, at the same time, the data quantity of infrared image in large view field also increases rapidly. This makes the traditional spatial filtering methods those based on pixel operation or transform process methods meaningless when processing the infrared image under large view field, besides that the real-time performance and engineering realization also face more rigorous challenge.

Panoramic infrared imaging system (PIIS) based on the 1152×6 long linear array long-wave detector is introduced. Due to the real-time processing and high-speed data transfer demanding, we propose a high-performance processing platform based on field programmable gate array (FPGA) + multicore digital signal processor (DSP) architecture. To reduce the platform's power consumption, dynamic power monitoring technology is used to provide variable core voltage management for DSP. Then mapping an application to the platform is illustrated, which is guided by parallel-task segmentation mechanism of multi cores system. We show that, the designed platform with the optimization strategies achieves powerful capabilities of data throughput and processing performance.

Monitoring for Resonant Mode of High-way System at Impulsive Impact

Shigehisa Nakamura
Kyoto University, Japan

Abstract— This note concerns on monitoring for a resonant mode of a high-way system at an impulsive impact. This work might be helpful for elementary finding of a key to show an advanced techniques at design, constructing, and maintaining of the life line systems which should be in a resonant mode for safety of public use even under any severe seismic condition on the surface of the earth.

Examples of Electromagnetic Field Sources in an Indoor Distribution Substation

Rauno Pääkkönen[1], **Marko Lundström**[2], **Jari Mustaparta**[3], **and Leena Korpinen**[1]

[1]Tampere University of Technology, Tampere, Finland
[2]Tampereen Sähköverkko Oy, Tampere, Finland
[3]Turku Energia Sähköverkot Oy, Turku, Finland

Abstract— In indoor distribution substations, there are typically extremely low frequency (ELF) electric and magnetic field sources, e.g., transformers and cables. However, nowadays there can also be smart meters or collector meters. These smart meters most often send information or communicate using either a radio frequency (800–3000 MHz) aerial signal to masts or a 50–100 kHz electromagnetic field signal via cables. The aim of this paper was to present example measurements of electromagnetic field exposure to sources in an indoor distribution substation. We used the magnetic field meter MFM 3000 by Combinova, with a separate probe version, video recording with RMS values, and spectrum (Samsung smart phone type Samsung Galaxy S III), the Narda EMR-300 with probe T-33C, and a Holaday 3603 VLF Survey meter. We performed measurements at three places. Place A was near the fuse panel, where we made measurements with (1) frequency bandwidth 40 kHz–100 kHz (57 measurements) and (2) 5 Hz–100 kHz (62 measurements). Place B was on the surface of the collector meter (15 measurements), Place C was near the antenna of the collector meter (7 measurements) and Place D on the surface of the antenna (24 measurements). In Place A, using the bandwidth (1) we got eleven values, which varied from 0.011–0.039 μT, other values were 0.0038–0.0052 μT. The source of those values can be the collector meter, which signals via cables. Using the bandwidth (2), the magnetic fields were 67–74 μT. In Place B, the magnetic fields varied from 0.022 to 0.083 μT, and the frequency bandwidth was 40 kHz–100 kHz. In Place C, the radio frequency maximum field was 1.0 W/m^2, and in Place D, it was 1.8 W/m^2. To evaluate the possible effects of electromagnetic fields, it is possible to use guidelines of the International Commission on Non-ionizing Radiation Protection (ICNIRP), and measured values were below guidelines. In the final paper, we will present more details of the measurement results.

Emission of Smart Meter Electric Fields (50–100 kHz) in Finland

Rauno Pääkkönen[1], **Marko Lundström**[2], **Jari Mustaparta**[3], **and Leena Korpinen**[1]

[1]Tampere University of Technology, Tampere, Finland
[2]Tampereen Sähköverkko Oy, Tampere, Finland
[3]Turku Energia Sähköverkot Oy, Turku, Finland

Abstract— Discussion of the possible health effects of electromagnetic field (EMF) exposure caused by smart meters has become livelier as the use of smart meters has increased, for example, in Finland. The International Commission on Non-ionizing Radiation Protection (ICNIRP) has published guidelines, which are possible to use to evaluate EMF exposure. The aim of this paper was to present example measurements of electric field exposure to smart meters for cable-transmitted (50–100 kHz) signal emissions. We used the directional electric field meter Holaday 3603. The measurement distance was at the surface of the meter because the values were so small, it was not possible to get values from other distances. The operator of a utility company remotely read the smart meters when we measured electric fields. Altogether, we measured 27 smart meters, which used Power Line Communication (PLC). Meters used plan and lon protocols. The highest electric field was 5.2 V/m, which is only 6% of the recommended public exposure limit according to the ICNIRP guidelines. However, the smart meter readings were very short (about 20 s); therefore, the possible exposure time is also very short. This is important to take into account when we analyze the measurement results and compare to guidelines. Based on our measurements, it is possible to conclude that there is no specific need to improve the sheltering of the meters from the public or to measure electromagnetic field emissions from smart meters. In the final paper, we will present more examples and details of the measurement results.

Smart Receiver for Multi-antenna Transmitters with Constellation Shaping

Paulo Montezuma[1, 2, 3], **Sara Ribeiro**[1], **Mario Marques da Silva**[2, 4], **and Rui Dinis**[1, 2]

[1]DEE, FCT Universidade Nova de Lisboa, Portugal
[2]IT, Instituto de Telecomunicações, Av. Rovisco Pais, Lisboa, Portugal
[3]Uninova, Instituto de Desenvolvimento de Novas Tecnologias, Quinta da Torre, Caparica, Portugal
[4]Universidade Autonoma de Lisboa, Portugal

Abstract— Power and bandwidth constrains in wireless communications systems can be mitigated by MIMO (Multiple-input multiple-output) systems. Still, high spectral efficiency is only attainable by multilevel constellations that may impose restrictions on power amplification, since efficiency in power amplification usually implies that amplifiers must operate in non-linear zone or near saturation. Thus, constant or quasi constant envelope signals are needed. This problem can be overpassed by a transmitter structure with a power efficient amplification stage where multilevel constellations are decomposed on M BPSK (Bi-Phase Shift Keying) sub constellations, which are amplified and transmitted independently by an antenna. Being uncorrelated the BPSK components, instead changes on radiation pattern there is a constellation shaping which optimizes the transmitted constellation only on the desired direction. This means, that we have directivity at information level, i.e., at the transmitted constellation. This directivity depends on the coefficient values associated to the set of M BPSK components and the constellation's shaping changes dynamically with changes on these coefficients or errors due to phase imbalances. Consequently, this transmitter has inherent security since the transmitted constellation is only optimized in the desired direction. Under these conditions, the receiver must know the set of constellation's coefficients g_i, $i = 1, \ldots, M$, associated to each BPSK component and the array phase configuration used by the transmitter, otherwise the received constellation suffers a uncompensated nonlinear distortion due to phase rotations of components associated to each amplification branch (it should be noted that these phase imbalances also change the distances between constellation's symbols which has impact on system performance).

Therefore, for successful data reception it becomes crucial a smart receiver based on an algorithm that estimates the set of coefficients used at the transmitter. We propose a "smart receiver" using an algorithm that can estimate the set of coefficients applied in constellation shaping introduced at the transmitter. Simulation results show that the good performance is attainable by the proposed receiver and corresponding algorithm, even when the directivity increases with the number of BPSK components used in the decomposition of the multilevel constellation.

Impact of Aeronautical Mobile Telemetry System on MFCN SDL Operating Co-channel in Frequency Band 1452–1492 MHz

M. Zilinskas[1], **E. Stankevicius**[2], **and S. Oberauskas**[3]

[1]Vilnius University, Sauletekio al. 9, Vilnius LT-10222, Lithuania
[2]Vilnius Gediminas Technical University, Sauletekio al. 11, Vilnius LT-10223, Lithuania
[3]Communications Regulatory Authority of the Republic of Lithuania
Algirdo str. 27A, Vilnius LT-03219, Lithuania

Abstract— This paper presents the co-channel compatibility analysis between International Mobile Telecommunications (IMT) system and Aeronautical Mobile Telemetry (AMT) system in the frequency band 1452–1492 MHz.

There is a growing mobile technology development and increasing demand for radio frequencies to mobile services. Broadband mobile communications systems (e.g., LTE) are developing at staggering rates. Companies have the resources to expand their mobile networks, but it becomes increasingly difficult to avoid interference between adjacent stations due to ever growing density of all other applications. Mobile operators always search for new possible frequency bands to expand their networks.

World Radiocommunication Conference in 2012 (WRC-12) approved Resolution COM6/6 which contains the agenda for next conference in 2015 (WRC-15). Under agenda item 1.1 additional frequency bands for IMT systems could be identified. For this purpose it is proposed to considered frequency bands 1429–1452 MHz, 1452–1492 MHz, 1492–1518 MHz and 1518–1525 MHz as possible candidate bands.

Frequency band 1452–1492 MHz is attractive for communications due to the qualified radio propagation conditions. The usage of this frequency band for IMT system enables Mobile/Fixed Communications Networks (MFCN) to provide additional Supplemental Downlink (SDL) which will increase downlink throughput to carry more data. However this band is already used by other technologies such as radio relay links, broadcasting networks and aeronautical networks. Nevertheless this frequency band is also allocated to mobile (except aeronautical mobile) service on a primary basis in Radio Regulations, however co-channel and adjacent channel electromagnetic compatibility have to be evaluated in order to identify possible harmful interference from currently existing services Electromagnetic compatibility between AMT and IMT is one of the most sensitive issues regarding the decision to designate this band to Mobile Services.

Frequency band in consideration for IMT identification is proposed only for downlink communication component hence in order to protect IMT system the study scenario will be limited to the case where only IMT user equipment (UE) receivers experiences the interference from telemetry system.

This paper compares two possible ways to evaluate the electromagnetic compatibility in co-channel operation between UE receivers of IMT system and airborne transmitters of AMT system based on Minimum Coupling Loss method and statistical Monte-Carlo method. The results show that the compatibility is feasible in particular configuration of mobile networks.

The Influence of Atmospheric Radio Refractivity on the WiMAX Signal Level in the Areas of Weak Coverage

M. Zilinskas[1, 2], **M. Tamosiunaite**[3], **S. Tamosiunas**[2], **M. Tamosiuniene**[3], **and E. Stankevicius**[4]

[1]Department of Radio Communication
Communications Regulatory Authority of the Republic of Lithuania, Vilnius, Lithuania
[2]Faculty of Physics, Vilnius University, Vilnius, Lithuania
[3]Center for Physical Sciences and Technology, Vilnius, Lithuania
[4]Vilnius Gediminas Technical University, Vilnius, Lithuania

Abstract— Radio refractivity of the atmosphere, N, is an important parameter in design of telecommunication systems. Gradient of N determines the curvature radius of the propagation path. Variations of N-value might influence propagation path and quality of the signal. The method for determination of N-value has been proposed by International Telecommunication Union (ITU). In the ITU method, the data of air temperature, pressure, and relative humidity are used.

As it was already emphasized in some papers, various phenomena in the radio wave propagation such as ducting, scintillation, radar acquisition, refraction and fading of electromagnetic waves are due to refractivity variations in the troposphere. Atmospheric refractivity consists of two parts — a dry term and a wet term. Therefore, the influence of weather conditions is significant.

Lithuania is situated in the intermediate zone between maritime Western Europe, continental Eastern Europe and Asia climates. Lithuania, being in the transitional geography zone from the Baltic Sea climate to Atlantic and continentals East Europe climate, distinguishes by variable humid climate. Therefore, it is very important to examine the meteorological impact on variation of the N-value, and reliability of the wireless networks, as well.

The data of measurements are presented. Reliability of the fourth generation wireless network (WiMAX technology) has been investigated. The power level of the received signal was continuously measured and compared to the calculated values of atmospheric radio refractivity. It was examined if changes of signal level and variations of the N-value occur at the same time. N-values were calculated using measured values of air temperature, pressure, and relative humidity. The long-term measurements were carried out at the same time and place. The experiment was carried out in an area of weak coverage.

It was concluded that in the areas of weak coverage WiMAX signals are strongly influenced by variations of the atmospheric radio refractivity.

Evaluation of LTE 700 and DVB-T Electromagnetic Compatibility in Adjacent Frequency Bands

G. Ancans[1], **E. Stankevicius**[2], **V. Bobrovs**[1], **and S. Paulikas**[2]

[1]Institute of Telecommunications, Riga Technical University, Azenes St. 12-201, Riga LV-1048, Latvia
[2]Vilnius Gediminas Technical University, Sauletekio al. 11, Vilnius LT-10223, Lithuania

Abstract— The 2012 World Radiocommunication Conference allocated the 694–790 MHz (700 MHz) band for the mobile service on a co-primary basis with other services in Region 1 (Europe, Africa, the Middle East). However, countries of Region 1 will also be able to continue the use of these frequencies for their digital terrestrial television services, if necessary. This allocation will be effective immediately after the WRC-15. The objective of this paper is to assess the electromagnetic compatibility of Digital Video Broadcasting-Terrestrial (DVB-T) operating below 694 MHz and mobile broadband (LTE) operating in 700 MHz band. The study contains an assumption of a preferred frequency division duplex (FDD) channelling arrangement which contains confined 2×30 MHz block: 703–733 MHz (uplink) and 758–788 MHz (downlink). The model consists of two elements, a LTE network and a DVB-T system. An adjacent channel scenario was analyzed in this paper: possible impact of LTE user equipment (uplink) to DVB-T receiver. The Minimum Coupling Loss method and Monte Carlo simulation within SEAMCAT software was used for interference analysis. The Minimum Coupling Loss method was chosen to calculate worst case (most conservative scenario) in order to understand most critical points of these two systems. The Monte Carlo simulations show more relaxed electromagnetic compatibility scenario. During simulations more appropriate propagation model was used (Recommendation ITU-R P.1546), which allows to analyse also non line of sight radio propagation conditions. The results obtained provide the minimum coupling distance required between LTE and DVB-T in the 700 MHz band to maintain the necessary performance level of the DVB-T system.

Möbius Strip with Back-to-back CPW Transmission Line: Simulation and Microwave Characterization

M. Sabrera and L. C. Kretly
Department of Communication, DECOM, University of Campinas, UNICAMP
Campinas, State of Sao Paulo, Brazil

Abstract— The objective of this work is to investigate special EM behavior of the Möbius Strip devices using simulation and measurements. This kind of device exhibit a series of interesting phenomenon not totally determined but, with practical applications. This work presents some insight into these behaviors by EM simulations using the method FIT, Finite Integration Technique adopted by some commercial software packages. The Möbius strip used in microwave band can exhibit a series of phenomenon, depending on the layout and engraved lines on it. The Möbius strip can emulate an infinite transmission line characteristics capable of retaining a large bandwidth frequencies, special resonators, and in a stritu sensu antenna or radiators. The Möbius strip is a one-sided non-orientable surface with Euler characteristic $\chi = 0$. Topologically, the Möbius strip can be defined as the square $[0, 1] \times [0, 1]$ with its top and bottom sides identified by the relation $(x, 0) \sim (1 - x, 1)$ for $0 \leq x \leq 1$. See Figure 1(a).

One of the most critical challenge related to the Möbius strip is how excite the device by means a connection to the generator. This problem was investigated by simulation and measurements with a VNA — Vector Network Analyser. Several Möbius strip devices were made with different length. A more sophisticated device based on Möbius strip topology is the CPW Back-to-Back Möbius Strip shown in Figure 1(a). Due to this special topology, antenna with Möbius strip configuration, if properly bisected could presents approximately the double of electrical length when compared with conventional ring radiators. This could improve, for example, miniaturization of RFID antennas. Several devices were simulated, fabricated and measured showing EM behavior as depicted in Figure 1(b).

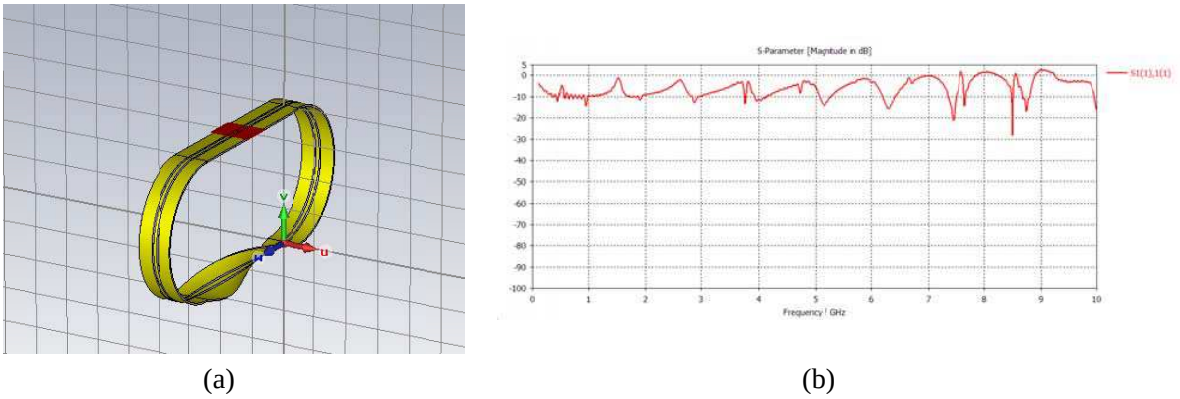

(a) (b)

Figure 1: (a) Back-to-back CPW Möbius strip — B2B CPW-MS and (b) insertion loss results.

Fabrication of a Novel Radial-firing Optical Fiber Probe Using Electric Arc-discharge Process

Seung Ho Lee[1], **Yong-Tak Ryu**[2], **Dong Hoon Son**[1], **Seongmook Jeong**[1], **Youngwoong Kim**[1], **Seongmin Ju**[1], **Bok Hyeon Kim**[3], **and Won-Taek Han**[1]

[1]Department of Physics and Photon Science, School of Information and Communications
Gwangju Institute of Science and Technology (GIST)
123 Cheomdan-gwagiro, Buk-Gu, Gwangju, Republic of Korea
[2]Department of Physics, GIST College, Gwangju Institute of Science and Technology
123 Cheomdan-gwagiro, Buk-Gu, Gwangju, Republic of Korea
[3]Advanced Photonics Research Institute, Gwangju Institute of Science and Technology
123 Cheomdan-gwagiro, Buk-Gu, Gwangju, Republic of Korea

Abstract— Optical fiber-based endoscopic laser technologies have been widely used for operation of the several minimally invasive medical surgeries such as prostatectomy, lithotripsy, varicose vein surgery, herniated disk surgery in modern medicine [1–4]. Recently, in addition to a frontal-firing optical fiber, a laterally light-emitting fiber probe has been required for more accurate medical operation. However, the several established methods to fabricate the lateral-firing configuration cannot be easily implemented due to complication of the fabrication process [3, 5].

In this study, we demonstrated a novel radial-firing optical fiber probe having capability of the side angle upto 87° to the direction of the fiber. The present radial-firing optical fiber probe was quite simply fabricated by electric arc-discharge process using a commercially available fusion splicer. A conventional optical fiber was spliced with a hollow optical fiber and then an intagliated conical shaped fiber region was formed by the gradual collapse of the cavity of the hollow fiber by discharging electric arcs of the fusion splicer. Then the end-face of the hollow optical fiber tip was arc-discharged again to form an air pocket, resulting in the uniform radial-firing of a laser beam ($\lambda = 632.8\,\text{nm}$) with the side angle upto 87°.

ACKNOWLEDGMENT

This work was partially supported by the Advanced Technology Radiation Laboratory of the Korea Atomic Energy Research Institute, the New Growth Engine Industry Project of the Ministry of Trade, Industry and Energy, the Basic Science Research Program through the National Research Foundation of Korea (NRF) funded by the Ministry of Education (No. 2013R1A1A2063250), the Brain Korea-21 Plus Information Technology Project through a grant provided by the Gwangju Institute of Science and Technology, South Korea.

REFERENCES

1. Bown, S. G., "Phototherapy of tumors," *World J. Surg.*, Vol. 7, 700–709, 1983.
2. Katzir, A., *Laser and Optical Fiber in Medicine*, Academic Press Inc., 1993.
3. Van Swol, C. F. P., R. M. Verdaasdonk, R. J. van Vliet, D. G. Molenaar, and T. A. Boon, "Side-firing devices for laser prostatectomy," *World. J. Urol.*, Vol. 13, 88–93, 1994.
4. Kim, J. K., J. W. Choi, A. Schwuchow, H. Bartelt, T.-H. Kim, W. J. Choi, J. Y. Kim, D. U. Kim, S. Y. Ryu, G. H. Kim, I.-H. Kim, and K. S. Chang, "Multidirectional illuminating optical fiber tip on beam expanding coreless silica fiber," *IEEE Photon. Technol. Lett.*, Vol. 25, No. 24, 2431–2434, 2013.
5. Sohn, I. B., Y. S. Kim, Y. C, Noh, I. W. Lee, J. K. Kim, and H. Lee, "Femtosecond laser and arc discharge induced microstructuring on optical fiber tip for the multidirectional firing," *Opt. Express*, Vol. 18, No. 19, 19755–19760, 2010.

Weak Extremely Low Frequency Magnetic Field is Likely to Trigger the Frequency Dependent Activation of Motility Mechanism

Xia Wu[1, 2], **Juan Du**[1], **Weitao Song**[1], **Sanjun Zhang**[2], **Shude Chen**[1], **and Ruohong Xia**[1, 2]

[1]Physics Department, East China Normal University, Shanghai, China
[2]State Key Lab of Precision Spectroscopy, East China Normal University, Shanghai, China

Abstract—

Background: The epidermal growth factor receptor (EGFR) is implicated in cytoskeleton kinetics and cell migration. EGFR oligomerization initiates its activationclosely relative to the actin cytoskeleton assembly (ACA). Our previous work has shown that a weak 50 Hz magnetic field (MF) induced EGFR clustering *in vivo* and *in vitro* and activated its downstream motility pathways, resulting in a weak actin-cytoskeleton and provoking the cell migration in several cell lines, suggests that the 50 Hz MF may enhance interactions among EGFRs and depressed the ACA.

Methods: Immunofluorescence and fluorescence resonance energy transfer (FRET) were used to inspect the MF effects on the ACA through exerting EGFR clustering under 0.4 mT, 50 Hz MF, and the field frequency dependent effect on the ACA under 0.4 mT MF of 35, 50, 70, 110, and 140 Hz at the protein/cell levels.

Results: Similar to EGF stimulation, the 50 Hz MF obviously enhanced the FRET signals among the EGFRs and declined the donor dye fluorescent intensity *in/ex vivo*, and induced the cellular EGFR clustering in FL, PC12, and CHL cell lines; however, significantly depressed both the ACA in cells and the FRET signal among actins. Furthermore, the ACA in FL cells were mostly depressed under both 50 Hz and 110 Hz MF exposures, not the other frequencies. These MF-induced EGFR-clustering/actin-cytoskeleton-depolymerization were obviously inhibited by a EGFR tyrosine inhibitor PD151015 (PD); Hill Plot of EGFR vs. [PD] found that the MF partially ease the PD inhibition, with increased K_d and IC_{50} values.

Conclusion: These results strongly suggest that the MF enhances the EGFR monomer clustering and eases the PD inhibition, but interrupts the actin assembly mechanism similar to EGF stimulation, possibly in a MF frequency dependent way.

Microwave Magnetoelectric Isolator-attenuator Based on Coplanar Line

A. S. Tatarenko, D. V. Lavrentieva, M. I. Bichurin, and D. V. Kovalenko
Novgorod State University, Veliky Novgorod 173003, Russia

Abstract— An electrically controlled magnetoelectric (ME) microwave isolator-attenuator based on layered ferrite-piezoelectric structure formed on a coplanar waveguide is considered. The simulations of different structures of coplanar devices are made for selecting of optimal waveguide and resonator characteristics.

The task of matching the microwave power source to the load is achieved by using nonreciprocal properties of ferrites. However, the non-reciprocal ferrite devices control the parameters realized by magnetic system, so these devices have low speed of operation, high power consumption and cannot be manufactured by integrated technology. ME non-reciprocal device can obviate the existing disadvantage of ferrite devices [1].

The difference between the ferrite devices and proposed ME nonreciprocal devices is to replace the ferrite resonator with magnetic control system by ME resonator and system of electrodes connected to the source of the control voltage.

Here we discuss the microwave isolator-attenuator. The basic design of ME isolator-attenuator is coplanar waveguide and ME resonators which have rectangular (or disks) composite samples based on lead zirconate titanate (PZT) — ittrium iron garnet (YIG). The permanent magnet creates a required magnetizing field in the area of ME resonator. The control voltage is applied to the electrodes.

The principle of operation of the isolator-attenuator based on microwave ME effect, is to shift the ferromagnetic resonance line under the influence of an electric field. ME layered structure in this case plays the role of a resonator. Shift of magnetic resonance line at applied an electric field is defined as $\delta H_E = AE$, where A is magnetoelectric coefficient; E is applied DC electric field.

The simulation of coplanar isolator-attenuator was made. That allows to get the selection of waveguide substrate parameters and the shape of ferrite and piezoelectric. For experimental verification of the simulations the coplanar device model was made. The ME resonator are based on layered structure of YIG with dimensions $13 \times 4 \times 0.9$ mm and PZT with dimensions $15 \times 4 \times 0.5$ mm. The coplanar waveguide has next parameters: the width of the gap $S = 3$ mm; distance between slits $W = 2$ mm; substrate thickness $h = 2$ mm; dielectric permittivity of substrate $\varepsilon = 10$. Isolation ratio was 20 dB. At applied an electric field $E = 10$ kV/cm, the shift of the resonance line corresponded 30 MHz.

To decrease the control voltage and the increase the valve ratio is necessary to reduce the thickness of the piezoelectric, and hence the thickness of the ferrite.

The use of ME structures in the resonant microwave devices allows electrical control of their parameters and opens promising opportunities of the new devices for functional electronics.

ACKNOWLEDGMENT

The research was supported by a grant of government task from the Ministry of Education and Science of Russian Federation.

REFERENCES

1. Tatarenko, A. S. and M. I. Bichurin, "Microwave magnetoelectric devices," *Advances in Condensed Matter Physics*, Vol. 2012, 10p, 2012.

Modeling of Microwave Magnetoelectric Devices

A. S. Tatarenko and M. I. Bichurin
Novgorod State University, Veliky Novgorod 173003, Russia

Abstract— Computation, design and manufacturing technology of nonreciprocal microwave devices intended for application in receiving-transmitting modules of antenna array have a great interest in current time. Problems, which appear in design of integrated devices, and combine properties of several microwave signal-processing devices, are analyzed. The possibility for the development of a complex approach to designing and manufacturing of nonreciprocal microwave devices with improved radio-engineering characteristics is shown. The main directions for further research based on the use of modern computer design programs.

Currently, a large development have program High Frequency System Simulator (HFSS) of company AnSoft, which is designed for the analysis of three-dimensional microwave structures, including antennas and non-reciprocal devices containing ferrites and ferroelectrics. Electromagnetic simulation in HFSS is based on the use of the finite element method (Finite Element Method, FEM).

Passive microwave devices are units made of segments of transmission lines. In the microwave range used microstrip line, coplanar line and slot line. The microstrip lines most widely used [1]. However, at creating a non-reciprocal devices using ferrites it requires the microwave field of circular polarization. In microstrip line this region is absent and need additional elements, for example in the form of stubs to create area of circular polarization. From this point of view, the slot and coplanar line are of interest, because they contain the area of circular polarization. Also, all conductors at these types of lines are disposed on one substrate surface. The design of these lines is convenient for parallel connection of various lumped elements, including active semiconductor devices. The structure of the microwave field in the slot line and coplanar waveguide is significantly different from the structure of the wave field in microstrip line. If the area of the circular polarization of the magnetic field contains transversely magnetized ferrite, it is possible to create a non-reciprocal device.

The use of modern simulation software allows the fast design of various types of non-reciprocal microwave devices. We conducted a simulation of various types of non-reciprocal magnetoelectric devices based on slot and coplanar lines by using HFSS. A comparison with similar devices based on the microstrip line is made.

For example, the simulation of ME coplanar isolator-attenuator was made. That simulation allow to get the selection of waveguide substrate parameters and the shape of ferrite and piezoelectric. The ME resonator based on layered structure of YIG and PZT was used.

To decrease the control voltage and the increase the valve ratio it is necessary to reduce the thickness of the piezoelectric, and hence the thickness of the ferrite.

The use of computer simulation for ME structures in the non-reciprocal microwave devices opens promising opportunities for the creation of the new devices.

ACKNOWLEDGMENT

The research was supported by a grant of government task from the Ministry of Education and Science of Russian Federation.

REFERENCES

1. Bichurin, M. I., V. M. Petrov, R. V. Petrov, G. N. Kapralov, F. I. Bukashev, A. Y. Smirnov, and A. S. Tatarenko, "Magnetoelectric microwave devices," *Ferroelectrics*, Vol. 280, 213–220, 2002.

Equalization of EDFA Gain Spectrum and Increase of OSNR through Introducing a Hybrid Raman-EDFA Solution

S. Olonkins, **I. Lyashuk**, **V. Bobrovs**, **and G. Ivanovs**
Institute of Telecommunications, Riga Technical University, Azenes st. 16, Riga LV-1048, Latvia

Abstract— The main goal of this paper is to demonstrate the advantages of a hybrid Raman-EDFA optical signal amplification solution over the use of conventional EDFA amplifiers. To achieve this goal a simulation model of a 16 channel 10 Gbps DWDM transmission system with transmission distance of 180 km and an EDFA in-line amplifier, placed 30 km away from the receiver end, was introduced. The most promising solution of hybrid amplification is supplementing the existing discrete amplifier with a distributed Raman amplifier, as it not only can broaden and equalize the gain spectrum, but it also can increase the optical signal-to-noise ratio of the signal at the output of the amplifier and can provide higher level of amplification. The EDFA in-line amplifier was re-configured and supplemented with a distributed Raman amplifier with counter-propagating pumping. While configuring the hybrid amplifier the authors focus their attention on equalizing the gain spectrum in the wavelength region used for transmission of the 16 channels, and on obtaining higher values of optical signal-to-noise ratio for all channels. Simultaneously it was required to provide the level of amplification, which was required to ensure bit error rate below the 10^{-12} threshold in all channels. For the solution based on the single EDFA amplifier the gain for all channels has varied from 38 dB to 39.5 dB, but the hybrid amplifier has provided 38.4 ± 0.05 dB, therefore, the gain difference between the 16 channels was reduced from 1.5 dB to 0.1 dB. The obtained results have shown, that the implementation of the hybrid solution has allowed to increase the optical single-to-noise ratio by at least 1.7 dB in all of the channels.

Beam-footprint Detection for Non-cooperative Spaceborne/Airborne Bistatic SAR

Feifei Yan, **Wenge Chang**, **and Xiangyang Li**
College of Electronic Science and Engineering
National University of Defense Technology, Changsha, Hunan 410073, China

Abstract— In this paper, we consider non-cooperative bistatic SAR using aircraft as receiver and spaceborne radar as illuminating of opportunity. As there is no synchronization link between the transmitter and receiver, the transmitter beam-footprint should be detected in real time to realize beam synchronization. Theoretical analysis shows that the signal-to-noise ratio (SNR) of the reflected echoes from the observational area is too low to use the conventional detect method of linear frequency modulation (LFM) signal. According to the cross-correlation between the echoes of adjacent pulse repetition frequency (PRF) and M-out-of-N (M/N) detection, a beam footprint detection method is proposed in this paper. This method can realizethe accumulation of the signal energy and enormously improve the SNR of scene raw data. Therefore, it can be used for transmitter beam-footprint detection in real time.

The proposed method consists of the following two main steps:

1. Cross-correlation and CFAR detection. Since the observational area between the adjacent PRF is almost the same, so the adjacent backscattering echoes have high correlation. As noises between the adjacent PRF are irrelevant, there will be a peak value in cross-correlation result. So CFAR detection can be realized to determine whether signal exists. When transmitter and receiver achieve swath overlap of beam-footprint, the number of backscattering target is very large. Then peak value of cross-correlation result will be highly increased. So the performance of signal detection will be highly improved.

2. M/N detection. The cross-correlation result between the adjacent echoes cannot determine whether the received signal is LFM echo arisen from the spaceborne radar. As the signal bandwidth of the spaceborne radar can be get from the direct path signal, then M/N detection is performed after noncoherent integration to distinguish received signal between LFM signal and other signal in frequency domain. The proposed detection method can realize the accumulation of signal energy and enormously improve the performance of backscattering echo detection method.

Monte-Carlo simulation is carried out to test the performance of the proposed detection method. Simulation results show that the proposed method is superiority over the conventional detection method; meanwhile, the detection performance is gradually improved with the increase number of noncoherent integration. **Simulation results show that when the overlap between the beam footprints of the transmitter and receiver exceeds 10%, and the noncoherent integration numbers exceed 30**, the backscattering echo can be stably detected by the proposed method.

We also use raw data of one monostatic SAR to test the propose detection method equivalently. Monostatic SAR can be equivalently seen as the beam footprint overlap is 100% in bistatic SAR. Three kinds of scene echo are chosen to test the proposed method. The number of noncoherent integration is 30. Cross-correlation results show that there is an obvious peak value in cross-correation result, which is suitable for CFAR detection. At the same time, the bandwidth of noncoherent integration result is coincide with the bandwidth of the transmitter. The detection probability of homogeneous scene is slightly higher than heterogeneous scene; meanwhile, as the beam footprint overlap of monostatic SAR is 100%, so the detection probability is very high.

Studies of the RF Energy Delivery Mechanism and Its Reformation in the Low Pressure ICP Discharge

A. F. Piskunkov and V. A. Riaby
Research Institute of Applied Mechanics and Electrodynamics of the Moscow Aviation Institute (National Research University), Moscow, Russia

Abstract— The model of a cylindrical inductively coupled plasma (ICP) discharge based on movable current layers travelling towards the axis of discharge space from the steady-state skin sheath at the external plasma boundary has been proposed. Current layers act like magnetic electrostatic traps catching electrons with small pinch-angles that are responsible for gas atom ionization. Movement of the layers induces electric field excites currents. At the optimal driving frequency magnetic field of a definite sign fills all discharge space during current half-period in the process of convective diffusion and eventually it is replaced by the field of opposite sign. Ohmic losses in the current layers are compensated by annihilation of magnetic field. The layers are formed by the Hall Effect while their boundary areas are shaped in a forceless magnetic field. They have form of one-turn spirals and their pairs are short-circuited in the edge plasma areas.

Concentration of trapped layer particles is determined from the equation for trapped electrons entering and leaving the layer by way of single-shot Coulomb collisions at the pinch-angle.

Discharge power loss, ion energy price and electron temperature are calculated at different argon pressures for the discharge chamber of 35 cm external radius. Comparison with published experimental data showed that the proposed model satisfactorily describes the main ICP discharge characteristics.

Single Feed Dualband Miniaturized E-shaped/U-slot Patch Antenna

N. P. Yadav[1] **and M. R. Tripathy**[2]

[1]School of Electronic Engineering and Optoelectronic Technology
Nanjing University of Science and Technology, 210094, China
[2]Department of Electronics and Communication Engineering
Amity School of Engineering and Technology
Amity University Uttar Pradesh, Noida 201313, India

Abstract— This letter presents the design of dual band microstrip patch antenna. This antenna is with single layer E-shaped patch loaded by two U slots. The −10 dB return loss impedance bandwidths of 2.26% and 1.91% are realized at center frequencies of 10.94 GHz and 13.06 GHz, with gains of 9.12 dBi and 8.54 dBi respectively. The radiation patterns are also presented. Compared with the published results of the similar scenario, in this design the size is reduced. The design guidelines are provided.

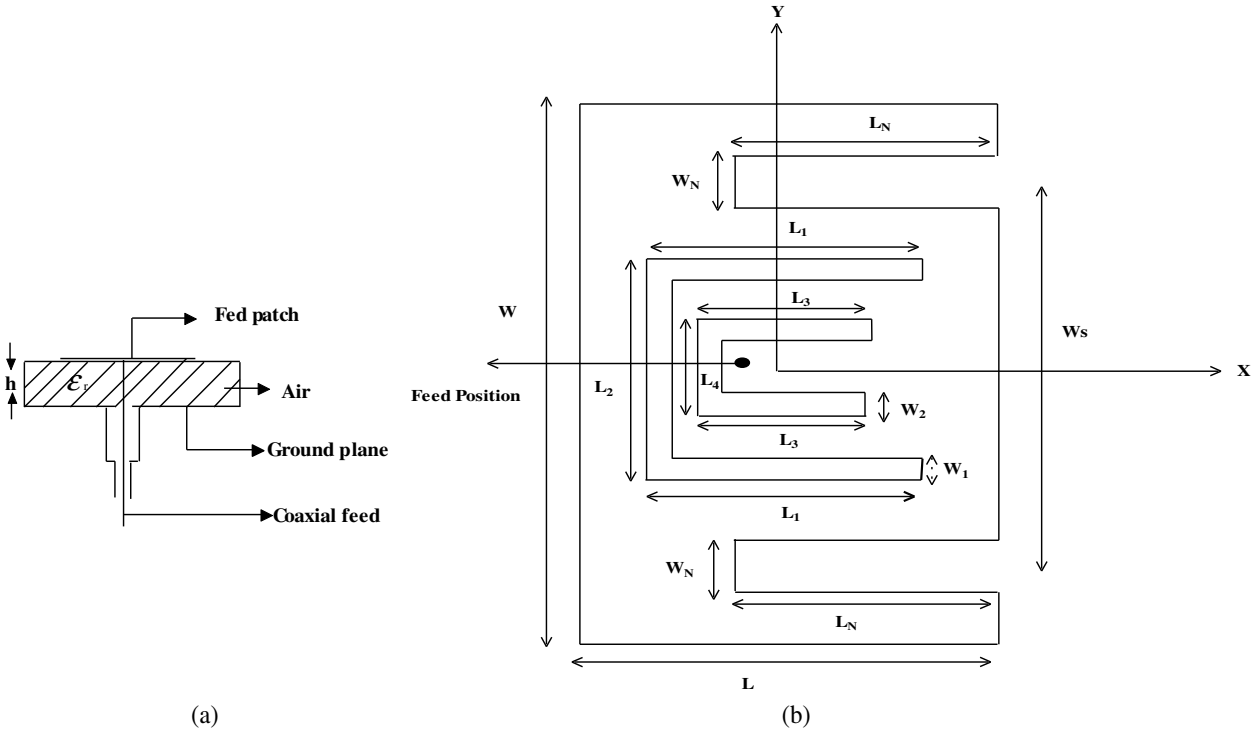

Figure 1: (a) Top view and (b) side view geometry of the proposed antenna.

Simulation and Study of the Effects of EM Radiations on Cantilever Beams with RF Functionality

Kshitij Chopra, **Preeti Singh**, **Kritika Nigam**, **Malay Ranjan Tripathy**, **and Sujata Pandey**
Department of Electronics and Communication, Amity School of Engineering and Technology
Amity University, Uttar Pradesh, Noida, India

Abstract— Wireless technology is an indispensable part of modern lifestyle. The exponential increase in the use of wireless transmission in varied forms of gadgetry has posed a grave interest in RF functionality producing circuits and systems. The most prominent and promising solution the wireless transmission and microwaves technology have been through RF MEMS, they produce radio-frequency through resonating cantilevers.

RF MEMS are Microelectromechanical devices that produce radio waves for wireless transmission and other applications, these are quintessential in modern circuitry for providing RF functionality. The MEMS devices are fabricated using SiO_2 and Si_3N_4 along with other insulators. The electrostatic charging in these materials poses a challenge to reliability and performance of MEMS devices. Also, the irradiation due to Electromagnetic waves contributes significantly to this phenomenon.

The semiconductor when subjected to irradiations produces electrostatic charge that may get absorbed and hence produce a charging in the device that can alter the dynamic behavior of the device. This effect is profound when the devices are exposed to ionizing radiations.

This paper is a study of the behavior of the cantilever beams under the influence of Electromagnetic Radiation/ionizing radiation and its effect on the working and efficiency of RF MEMS especially for medical devices where RF MEMS components are used. Also, the sensitivity of RF MEMS devices towards electromagnetic irradiation is studied. Varied irradiations were studied

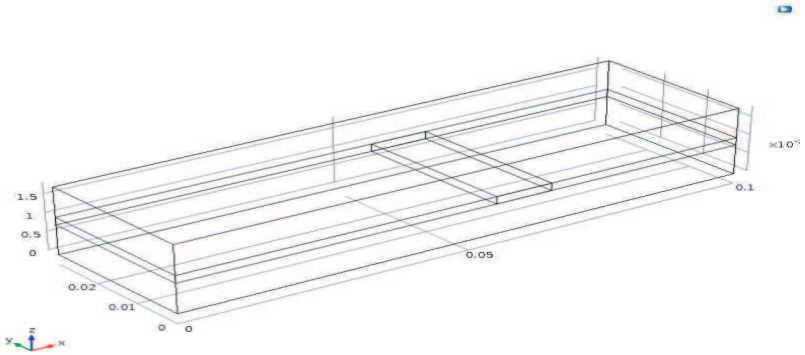

Figure 1: Test structure.

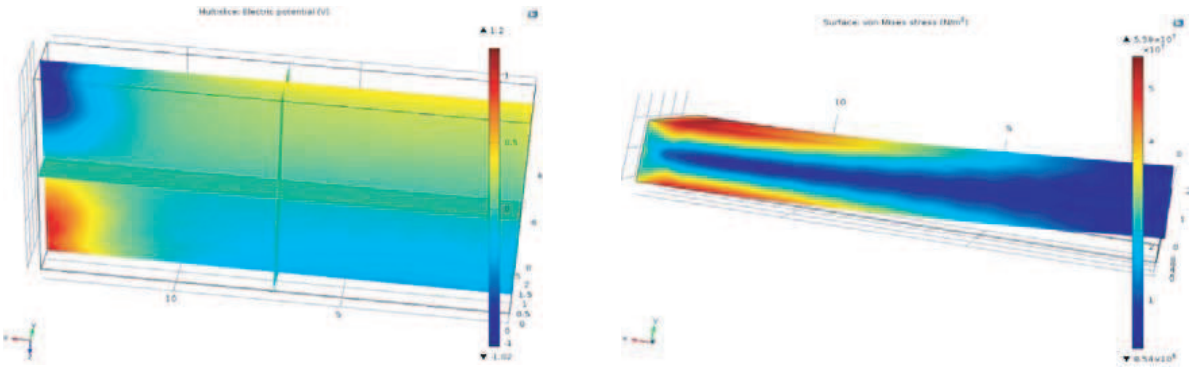

(a) (b)

Figure 2: (a) Voltage distribution across the whole structure. (b) Displacement.

and their effects on the materials were recorded through simulations using multiphysics simulation software.

Figure 1 shows the part of resonator which is in the shape of cantilever and was tested for the material properties. Different Piezoelectric materials were used for testing the structure. Figures 2(a) and (b) show voltage distribution and displacement produced across the whole test structure.

It was observed that the behavior of the RF MEMS devices changes drastically with the change in type of different piezoelectric materials used. In the present case Zinc Oxide, Lead Zirconate Titanate (PZT-2) and Quartz were used. The effect of EM radiations were also evlauted.

REFERENCES

1. Santos, H. J. D. L., *RF MEMS Circuit Design for Wireless Communications*, Artech House, Micro Electro Mechanical System Library, 2002.
2. Rebeiz, G. M., *RF MEMS Theory, Design, and Technology*, Wiley, 2003.
3. Arevalo, A. and I. G. Foulds, "Parametric study of polyimide-lead zirconate titanate thin film cantilevers for transducers applications," *Proceedings of 2013 COMSOL Conference in Rotterdam*, 2013.
4. He, C., M. E. Kiziroglou, D. C. Yates, and E. M. Yeatman, "A MEMS self powered sensor and RF transmission platform for WSN nodes," *IEEE Sensors Journal*, Vol. 12, 3437–3445, 2011.
5. Jeon, Y. B., R. Sood, J.-H. Jeong, and S.-G. Kim, "MEMS poer generator with traverse mode thin film PZT," *Sensors and Actuators A*, Vol. 122, No. 1, 16–22, 2005.
6. Naduvinamani, S. N., B. G. Paramatti, and S. V. Kalalbandi, "Simulation of cantilever based RF-MEMS switch using coventware," *World Journal of Science and Technology*, Vol. 1, No. 8, 149–153, 2011.
7. Huang, Y., "Energy harvesting using RF MEMS," *Proceedings 60th Electronic Components and Technology Conference (ECTC), 2010*, 1353–1358, Jun. 1, 2010.
8. Contreras, A., et al., "A Ku-band RF MEMS frequency reconfigurable multimodal band pass filter," *International Journal of Microwave and Wireless Technology*, 277–285, Cambridge Press, Jun. 3, 2014.
9. Chopra, K., K. Nigam, and S. Pandey, "A method for harvesting energy using piezoelectric transducers," *Applied Mechnics and Materials*, Vol. 727–728, 607–611, 2015.

Performances Evaluation of a Magnetic Gear with High Transmission Ratio Used for High Speed Applications

D. Fodorean[1], **C. Irimia**[2], **and P. Minciunescu**[3]

[1]Technical University of Cluj-Napoca, Romania
[2]Siemens Industry Software, Romania
[3]ICPE SA, Romania

Abstract— The paper presents a study of a magnetic gear used for high speed applications, and its performances are analytically and numerically evaluated.

The advantages of the magnetic gear (MG) are clear: There is no need for lubrication, no local heat (and losses) due to teeth contact and no risk for teeth breaking. Moreover, a MG offers a higher range of use since for high transmission ratio there is no need to link 2, 3 or more gears together; thus, globally, the efficiency and power density are improved. Besides, with a specific configuration of the MG is possible to obtain smooth mechanical characteristics — i.e., torque and speed.

The attention of the designer, when dealing with a MG, is focused on the used materials, especially the permanent magnets and the active steel. Here, several rear-earth and non-rear-earth materials will be evaluated for the excitation of the MG, as well as different steel materials and sheets thickness. Different magnetization variants will be evaluated too. It is clear that the main loss component is in the active iron, but for high speed applications the mechanical loss component cannot be neglected. All these elements will be investigated by looking also at the torque wave characteristic, which should be as smooth as possible. Thus, we will have a complete picture of the efficiency and performances of the proposed high transmission ratio MG, used for high speed applications.

The main data of the application under study are: 22 kW for the output power, input speed is 26'000 r/min and the output speed is 1625 r/min, meaning that the transmission ratio is 1/16.

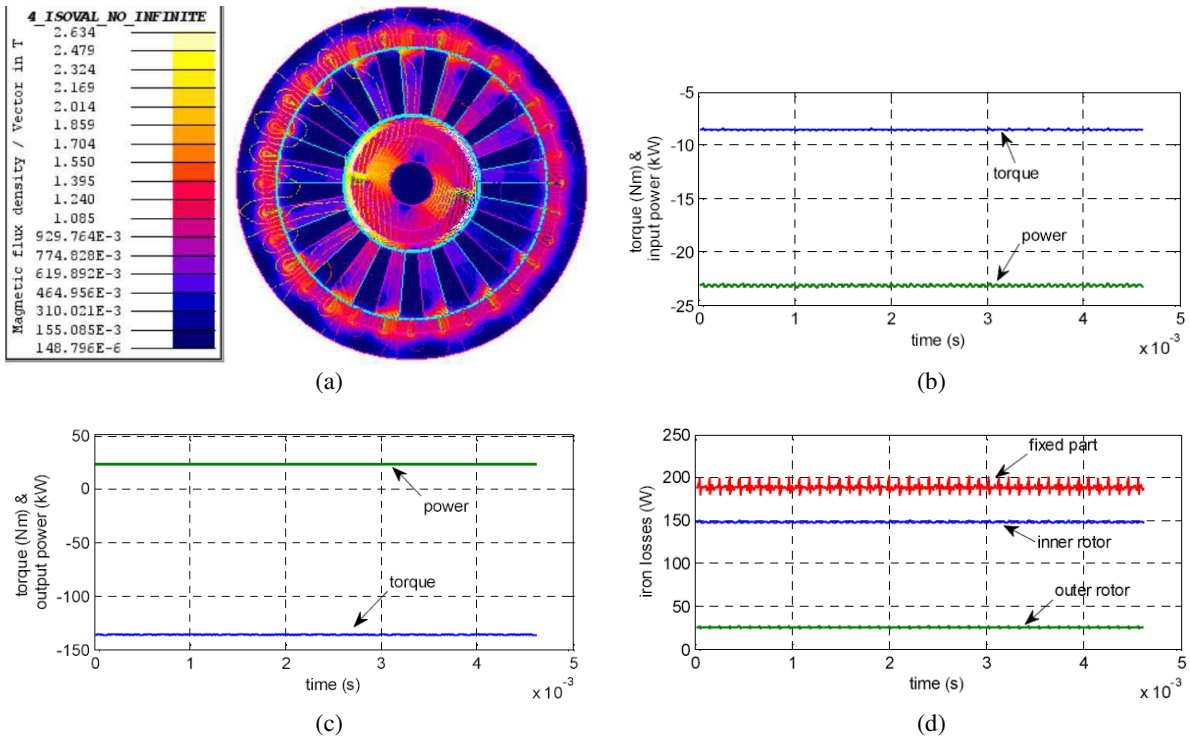

Figure 1: (a) The field and flux density distribution in the active parts of the MG; (b) input torque and power; (c) output torque and power; (d) iron losses in the MGs active parts.

Preliminary results of the numerically analyzed MG are presented in Fig. 1. Here, the flux density distribution, the input & output power and the iron losses are presented. It worth notice that

the input power is negative, since the inner rotor (high speed one) receives, externally, the input torque. On the other hand, the output power is positive since the outer rotor (low speed one) rotates in oposite direction. Very smooth mechanical characteristics are obtained with this MG configuration. Also, the iron loss level is low: the inner rotor, outer rotor and fixed part poles iron losses are plotted in Fig. 1. *More results and conclusions will be presented in the final paper.*

ACKNOWLEDGMENT

This work was supported by a grant of the Romanian National Authority for Scientific Research, CNDI-UEFISCDI, project number PCCA191/2012.

Visible Light Communication between Moving Objects Using a Camera Receiver

Jiri Libich[1], **Stanislav Zvanovec**[1], **and Zabih Ghassemlooy**[2]

[1]Department of Electromagnetic Field
Czech Technical University in Prague, Prague 166 27, Czech Republic
[2]OCR Group, Northumbria University, Newcastle-upon-Tyne NE1 8ST, UK

Abstract— Visible light communication (VLC) has attracted attention of many researchers in the last years. New technology enables to use light emitting diodes (LED) as light sources in many applications from illumination of rooms, street lighting to car lights and many more. These light sources are characterized mostly by their lower power consumption, relatively higher energy efficiency, switching capability and much wider bandwidth compared to incandescent bulbs. Hence LEDs are suitable not only for illumination but also for data transmission as well as localization [1–3].

Typical communications scenario involves a data source, driver, transmitter, detector, transimpedance amplifier and decision circuit. This arrangement is not suitable for communication where both objects can move and the setting of the system needs rapid adaptability in time. Camera based receiver can capture the entire scene present in its field of view and acquire the information data by means of image sequence processing. This dual purpose detection technique also offers a unique feature, the multiple input and multiple output (MIMO) capability supporting multitude of sources simultaneously. Nowadays, almost every smartphone and many new cars come with a camera which can be also used for data communication. However, camera based communication offers a low data rate because of the low frame rate of standard low cost cameras. Thus, it makes them attractive for car-to-car communications, financial transaction, low data rate navigation, and low content advertisement etc..

This paper aims to experimentally demonstrate the concept of VLC communications with the camera as a receiver (see in Fig. 1). The transmitter is composed of white LEDs that are intensity modulated. At the receiver the output of the camera is processed using Matlab to extract the data information from the captured image. The system performance is validated in terms of the bit error rate performance under the degraded channel conditions and for a number of LED configurations.

Figure 1: Arrangement of the measurement.

REFERENCES

1. Wu, Z., J. Chau, and T. Little, "Modelling and designing of a new indoor free space visible light communication system," *16th European Conference on Networks and Optical Communications (NOC)*, 72–75, July 20–22, 2011.
2. Okada, H., S. Misawa, T. Yamazato, T. Fujii, and T. Yendo, "Channel information estimation for error correcting code in road-to-vehicle visible light communication systems," *IEEE 5th International Symposium on Wireless Vehicular Communications (WiVeC)*, 1–5, June 2–3, 2013.
3. Trong-Hop, D., H. Junho, and Y. Myungsik, "TDoA based indoor visible light positioning systems," *Fifth International Conference on Ubiquitous and Future Networks (ICUFN)*, 456–458, July 2–5, 2013.

An Efficient Progressive Phase Distribution Consideration of Reflectarray Antennas

M. Y. Ismail and M. Inam
Wireless and Radio Science Center (WARAS)
Universiti Tun Hussein Onn Malaysia, Batu Pahat, Johor, Malaysia

Abstract— Reflectarray is a high gain antenna which combines the unique features of a flat reflector and an array of microstrip patch elements printed on a thin dielectric substrate. It is illuminated using a primary feed horn placed at a particular distance from the array. The reflectarray exhibits a number of significant advantages over conventional parabolic reflector and phased array antennas such as easy deployability, lower manufacturing cost, scannable beam, and surface mountability with lower mass and volume. Due to these growing numbers of advantages, reflectarray has been considered as a potential alternative to the parabolic reflector and phased array antennas.

The most important aspect of reflectarray antenna design is the design of printed microstrip elements which can be used for the performance appraisal of the antenna. The individual elements of the periodic array have to be designed with progressive phase distribution so that the spherical beam from the horn antenna can be converted into a planar wavefront. The required reflection phase values from individual elements of an array also depend on the location of the feed horn. For proper phase requirements, different techniques such as, identical patches of variable-length stubs, square patches of variable sizes, identical planar elements of variable rotation and identical rectangular patches with different types of slot configurations have been used. All these phasing techniques increase the possibility of reflectarrays to become an alternative option to the parabolic reflectors. However one of the main concerns of a reflectarray antenna is its limited bandwidth performance as compared to the parabolic reflector antennas. Different configurations have been proposed by researchers in the past few years for the bandwidth improvement of reflectarray antennas but considerable efforts are still required to improve the bandwidth performance of reflectarrays.

This paper provides a novel and efficient procedure for the X-band reflectarray antenna design emphasizing on the progressive phase distribution which is required to achieve the planar wave in front of antenna aperture. Detailed theoretical procedure has been provided with mathematical modeling of the required reflection phase from each of the individual reflectarray elements. The importance of material properties in reflectarray antenna design has been highlighted and different novel design configurations has been proposed for the unit cell reflectarray elements. Scattering parameter measurements and simulated results provide a very close agreement for different slot embedded designs proposed in this work. Two different configurations of mixed rectangular and circular slots embedded patch elements have been investigated. The variation in width of slot in the case of three rectangular slot patch configuration, the measured reflection loss varied from 2.89 dB to 5.60 dB while in the case of mixed rectangular and circular slot configurations, measured reflection loss is varied from 7.90 dB to 5.60 dB by varying the radius of circular slot. Moreover a maximum frequency variation of 2.58 GHz and a dynamic phase range of 345° with the variation in slot dimensions have also been demonstrated.

Problems of Statistical Decisions for Remote Monitoring of the Environment

F. A. Mkrtchyan
Institute of Radioengineering and Electronics, RAS
Vvedensky sq. 1, Fryazino, Moscow Region, Russia

Abstract— In connection with technical progress and growth of the population of a planet the anthropogenic stress on biosphere sharply amplifies. Therefore the role of remote monitoring allowing sharply raises to receive an estimation and the forecast of anthropogenic changes, to reveal sources of influence and the reasons of these changes. Modern scientific and technical level gives sufficient means for remote monitoring.

The basic sense of the concept of remote monitoring consists in connection in system of means of data gathering, methods of their processing, mathematical models of natural objects, computer implementers of algorithms and models with a wide spectrum of service maintenance at visualization of results of monitoring. Now wide development in the world is received by multichannel monitoring systems of remote basing. These systems occupy an important place for the study of sea surface.

The technique of detection offered in given work and identification of the abnormal phenomena in the water environment (microwave and optical) combines presence with application of possibilities of remote measurements algorithmic and the software, allowing to solve measurement and detection problems in real time. The effective decision of these problems is impossible without wide introduction in practice of researches of the automated systems of gathering, storage and data processing on the basis of modern computer systems with application of technology of open systems. Already created methods and algorithms possess ability to overcome such difficulties, as scantiness and not stationarity information, presence small statistically non-uniform samples.

It is obvious that complex research of the given land and remote measurements can raise reliability of estimations of parameters of natural systems and solve a problem of planning of these measurements. Application of means of remote monitoring in many cases is connected with acceptance of the statistical decision on presence on a surveyed part of studied space of this or that phenomenon. One of features of conditions of gathering of the information for such decision is the impossibility of reception statistical samples great volumes. Therefore working out and research of optimum algorithms of distinction of the casual signals characterized by samples of the limited volume, in the conditions of parametrical aprioristic indefinite are necessary.

One of the important features for the detection and classification of phenomena on the sea surface of the sea is a "spottiness" of the sea surface. Therefore the study of the statistical characteristics of "spottiness" is important. In this paper the analysis of the statistical characteristics of "spottiness" for certain areas of the Atlantic, Pacific and Arctic oceans. These statistical characteristics were determined for the most informative thresholds.

ACKNOWLEDGMENT

The reported study was partially supported by RFBR, research project No. 13-07-00146a.

Simulation Evaluation of the IEEE 802.11ac ad-hoc Network for Voice Communication in Emergency Scenario

J. Jarmakiewicz, K. Maślanka, and K. Parobczak
Military University of Technology in Warsaw, Poland

Abstract— The paper presents simulation study of a voice communication system consisting of mobile nodes during crisis situation scenario. Nodes' network interfaces work in compliance with the IEEE 802.11ac standard in ad-hoc mode, while smartphone devices operate under control of the Google Inc. Android operating system.

Overview of current Wi-Fi techniques was described, with respect to current mobile market shares and an indication of further standard evolution. Limitations of the current Wi-Fi ad-hoc mode implementation in the Android operating system were addressed, with emphasis on ongoing research projects oriented toward overcoming specific wireless communication protocols restrictions: the Wi-Fi Peer-to-Peer extension and a multi-hop transmission. Studies of power management issues were conducted, with particular attention to sustain reliable conditions in case of multiple "exposed" and "hidden" terminals phenomenon.

An evaluation of network efficiency with Voice over IP service activity during an emergency scenario was performed in a simulation environment. Lack of cellular connectivity, no external power access and no special communication equipment availability during rescue operation were assumed. About 50 smartphone mobile nodes, randomly placed across a 150-meters radius area, participate in voice-data exchange, with possibility to relay frames through one intermediate node (two-hop transmission mode) or through two or more intermediate nodes (multi-hop transmission mode).

Obtained results show insignificant impact of service realization on network resources utilization, low maximum end-to-end packet delivery delay and jitter values during continuous telephone conversations. Thus, described assessment shows high degree of IEEE 802.11ac ad-hoc network applicability in scope of basic voice communication service realization, in case of absence of usually ubiquitous cellular infrastructure, when only typical communication equipment is available. Future works are focused on implementation of developed custom software solutions in order to confirm obtained results in laboratory conditions.

Improvement of the Radiated Immunity Test Using a Broadband Signal

Hongsik Keum[1], **Gunsuk Yoo**[1], **Jungyu Yang**[2], **and Heung-Gyoon Ryu**[3]

[1]Electromagnetic Wave Technology Institute, RAPA, South Korea
[2]Department of Radio Environment Safety, Radio Research Agency, South Korea
[3]Department of Electronic Engineering, Chungbuk National University, South Korea

Abstract— In this paper, we have investigated improvement of the radiated immunity test using a broadband signals. We have analyzed the recent standardization activity related with radiated immunity test based on IEC 61000-4-3 and have proposed a new test method using digitally modulated broadband signals to improve the testing time and frequency step. The possibility of this new test method has been practically verified through a radiated immunity test on GTEM cell. The results show that the devices were influenced same or much more by digital modulation signal than by AM or PM signal. It shows that we can use the broadband signal for a radiated immunity test and it is possible to improve the RS test using new method.

Study of a Wide-band Strip Line Couplers' Susceptibility Based on the Number of Transmission Lines with Non-uniform Impedances

Javad Soleiman Meiguni and Ehsan Faalpour
Faculty of Electrical and Computer Engineering, Semnan University, Semnan, Iran

Abstract— Hybrids and couplers are commonly used in the microwave applications as very important elements. These elements are made of various forms and used at the specific applications. The strip line structure is one of the cheap structures for couplers and hybrid's design due to their less radiation loss and interference on the micro strip. Presented is a wideband stripline directional coupler which is of interest in any measurement application. The susceptibility parameter of this coupler at 2–6 GHz band, have been reported based on the number of transmission line with non-uniform impedances.

Fluctuations of GPS-derived Atmospheric Integral Water Vapor versus Ground Meteoparameters Variability

O. G. Khutorova, **G. M. Teptin**, **V. E. Khutorov**, **V. V. Kalinnikov**, **and A. A. Jouravlev**
Kazan federal University, Russia

Abstract— Water vapor is one of the most important constituents of the troposphere which effects the weather in various ways. Water vapor is a greenhouse gas. Over the past decades, considerable progress has been made in satellite navigation systems monitoring technology, which is significantly increasing the atmospheric information. The integral water vapour (IWV) is an important parameter of the atmosphere and directly or indirectly reflects the weather processes and variations.

This paper presents a hardware and software complex for continuous measurements and prediction of atmospheric thermodynamics. The main part is a network of ground-based spatially separated GPS-GLONASS receivers, which allows the remote sensing zenith tropospheric delay one per second. The network of weather stations measure meteorological parameters at the same points synchronously and allows determining the integrated humidity. Comparing the results with remote sensing data of weather stations, radiosonde and reanalysis showed good agreement. GPS-Derived integral water vapor shows the mesoscale spatial and temporal fluctuations and its seasonal variability. Variations of atmospheric integral water vapor were found. Greatest intensity as mesoscale and diurnal IWV variations observed in summer and the minimum — in the winter. Intensity IWV fluctuations in the summer is 21% higher, and in winter 13% less than in other seasons. A relationship with the fields of humidity and pressure fields of wind speed is found.

ACKNOWLEDGMENT

This work is supported by Russian foundation on basic research (No. 13-05-97054).

Steady-state Analysis of Permanent Magnet Synchronous Machine for Integrated Starter-alternator Applications

Florin Jurca and Daniel Fodorean
Department of Electrical Machines and Drives, Technical University of Cluj-Napoca, Romania

Abstract— Due to their high efficiency and reliability, permanent magnet synchronous machine became more and more used in the automotive applications in the last decade. There are two main reasons for this trend: the reduction of the fuel consumption and the increase of the travel comfort. In this study we consider the approach of the electromagnetic design of a special topology of permanent synchronous machine (radial flux machine with outer rotor) suited for automotive applications.

A preliminary design procedure will be presented and its results will be used in order to perform a numerical analysis using finite element method in order to analyze the performances of the machine: magnetic field density, saturation level, torque, distribution of magnetic flux density in the air-gap. Starter-alternator applications require operation at high speed in the generator regime. This is a sensitive issue for any type of electrical machine, since by increasing the frequency the iron losses increase considerably with a negative effect on efficiency value. In order to reduce these effects we consider the possibility to use various materials capable of operating at high frequencies. The main drawback of the permanent magnet synchronous machine (PMSM) is the price of rare earth permanent magnet. In this context it is necessary to investigate for this type of machine the use of new types of advanced materials in the construction of magnetic core in order to maintain a low cost for PMSM construction at high energy efficiency and the use of considerably weaker permanent magnets than those of rare earth type.

The thermal behavior is another problem in the automotive application. For this machine we have developed a thermal model in order to study the thermal stresses as a consequence of the level of losses (iron, copper), in conditions of high temperatures of ambience for the vehicles with internal combustion engine.

REFERENCES

1. Cai, W., "Comparison and review of electrical machine for integrate starter-alternator applications," *Industry Applications Society Annual Meeting (IAS), IEEE*, 386–393, 2004.
2. Barcaro, M., A. Alberti, L. Faggion, M. Sgarbossa, D. Pr'e M, and N. Binachi, "Expereimental tests on a 12-slot 8-pole integrated starter-alternator," *Proceedings of the 2008 International Conference on Electrical Machines*, 1–6, 2008.

Prediction of Temperature and Stress in a Multi-stage Depressed Collector under Different Enviornmental Conditions

Vishant Gahlaut[1] and Sanjay Kumar Ghosh[2]

[1]Department of Physics, Banasthali University, Banasthali, Rajasthan, India
[2]CSIR-Central Electronics Engineering Research Institute (CEERI), Pilani, Rajasthan, India

Abstract— Increasing requirement of traveling-wave tubes (TWTs) with miniature size, less weight, high efficiency, high power, high gain, etc., increases complexity of packaging for thermal modeling. Specially, high power TWTs has to have very good heat dissipation from its sub-assemblies, specially, from the collector where the spent beam is collected (Figure 1) [1]. Moreover, collector, may be, conduction and or radiation cooled, should have metallic jacket or packaging such that weight should be less with efficient cooling which is very much important for TWTs is to be used for space applications. In this paper authors have temperature distribution and stress developed, during operation, in a multi-stage depressed collector for typical space applications.

In this paper, temperature distribution in different electrodes has also been studied under different environmental conditions. However, under the extreme condition, say, at 80°C, the temperature in all the collector electrodes in much more compare to other two conditions and which needs to be proper packaging of the TWT. Moreover, expansion of electrodes and stress developed at different braze joints have also been studied. Heat dissipation, expansion and stresses developed among the collector electrodes in a typical MDC, under different environmental conditions, under development for space applications. Present study has been made using COSMOS which provides one screen solution for thermal, stress, frequency and harmonic analysis. It has post processing options to give the results as per convenience. 3-D model of the complex geometry with symmetric is constructed in Solid Works [2] and imported in COSMOS finite element analysis (FEA) [3].

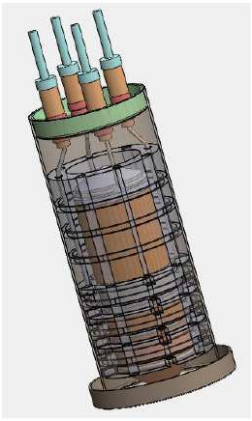

Figure 1: Schematic view of four-stage MDC.

REFERENCES

1. Yao, L. M., Z. H. Yang, B. Li, L. Liao, B. Q. Zeng, and X. F. Zhu, "Thermal analysis of novel helix TWTs," *IEEE Tran. on ED*, Vol. 6, 139–140, 2006.
2. SolidWorks Manual online tutorial professional 2009 SP3.0.
3. COSMOS Manual online tutorial professional 2009 SP3.0.

Study on Thermal-mechanical Issues of Co-axial Interaction Cavity for High Power Gyrotron

Vishant Gahlaut[1], **A. R. Choudhary**[2], **and S. K. Ghosh**[2]

[1]Department of Physics, Banasthali University, Banasthali, Rajasthan, India
[2]CSIR-Central Electronics Engineering Research Institute (CEERI), Pilani, Rajasthan, India

Abstract— The fast wave microwave tube, gyrotron, as a source of high-power microwave radiation, plays an important role in controlled thermonuclear fusion energy research and is found to be an efficient tool for heating of magnetically confined fusion plasmas (electron cyclotron resonance heating), to drive a noninductive plasma current Electron Cyclotron Current Drive (ECCD) and to suppress instabilities in the plasma [1]. As this device deals with very high thermal loading hence, efficient thermal management of gyrotron and its constituent parts is very important.

In this manuscript thermal-mechanical analysis of co-axial interaction cavity operating in $TE_{22,8}$ mode has been presented using the ANSYS code. The analysis of temperature built in the cavity and the study of its structural deformation has been carried out in order to address the thermal and mechanical issue which arises due to the heat dissipation at the cavity wall. In the interaction cavity, some amount of RF power is lost due to the finite electrical conductivity of material (called as ohmic wall loss). The ohmic wall loss for the above mentioned operating mode has been calculated. A 3-D interaction cavity with and without grooves has been modelled in ANSYS Workbench 10.0. In the simulation, the conduction mechanism is applied to transfer the heat from inner wall to outer wall of the interaction cavity whereas from outer wall to the coolant, convection mechanism is applied. The DI water (288K) has been used as a coolant. Iterating repeatedly, the heat film coefficient, the hydraulic diameter and the water flow rate have been optimized. Figure 1 shows the 3D cross sectional view of the co-axial cavity with radial grooved for the above mentioned optimized values of the thermal parameters.

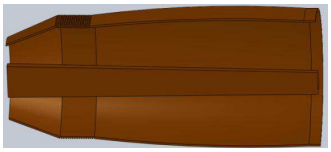

Figure 1: Cross-sectional view of co-axial cavity.

REFERENCES

1. Choudhury, A. R., S. Kern, and M. Thumm, "Study of dynamicafter cavity interaction in gyrotrons, part I: Adiabatic approximation," *IEEE Transactions on Electron Devices*, Vol. 62, No. 1, 184–191, Jan. 2015.

Erbium-doped Fiber Laser with Distributed Feedback from a Fiber Grating Array

Xinyong Dong[1, 2, 3], **Junwei Yuan**[3], **Lei Zhu**[3], **Perry Ping Shum**[2, 4], **and Haibin Su**[1, 2]

[1]School of Materials Science and Engineering, Nanyang Technological University, Singapore
[2]CINTRA, Research Techno Plaza, 50 Nanyang Drive, Singapore
[3]Institute of Optoelectronic Technology, China Jiliang University, Hangzhou, China
[4]School of Electrical & Electronic Engineering, Nanyang Technological University, Singapore

Abstract— An erbium-doped fiber laser with low coherence, low threshold, high efficiency and narrow linewidth is demonstrated for the first time based on distributed feedback from a fiber Bragg grating (FBG) array. The FBG array contains tens of FBGs with identical Bragg wavelength but very weak reflectivity of ∼1‰, inscribed along a normal single-mode fiber with random separations. Low pump threshold power of 3 mW and high slope efficiency of 24% are achieved, which are comparable with that of normal erbium-doped fiber lasers but much better than that of conventional random fiber lasers based on distributed Rayleigh scattering.

Antenna Factor Measurements for Electrically Small Antennas Immersed in a Lossy Medium

R. Mouthaan and B. Loader
National Physical Laboratory, UK

Abstract— Wireless body area networks are increasingly being leveraged to try to provide telemedicine solutions to contemporary healthcare problems. Applications include heart rate monitors, accelerometers and temperature sensors, whereas implanted technologies include pacemakers, glucose sensors and insulin pumps. Both body-mounted nodes and the implanted nodes present measurement challenges when the antenna and communication link are considered. It is important to simulate the presence of the body by or around the antenna when trying to characterise its resonant frequency, bandwidth, channel performance or radiation pattern. This is done using a phantom with similar permittivity ϵ and conductivity σ to the human body. Measuring the antenna factor of an implanted antenna presents further challenges, and these shall be discussed and addressed.

The antenna factor of an antenna is defined as the electric field required to induce a unit voltage across the terminals of the antenna. The antenna factor is a function of the design of the antenna and also of the properties of the surrounding medium. In the case of a lossy medium such as a phantom it can be difficult to correct the free-space properties to obtain an accurate description of how the antenna would behave once immersed. Instead, an antenna intended for use inside a lossy medium must be directly calibrated inside the medium.

A standard field method using a matched waveguide system (Fig. 1) is proposed here. Exciting the input port of the waveguide with a known voltage allows the electric field induced inside the liquid to be calculated. The antenna under test can then be introduced into the known field and the antenna factor calculated from the voltage induced across the terminals of the antenna. Using a network analyser allows the antenna factor of the antenna under test to be measured across the entire waveguide band. The described system operates in the 490 MHz to 750 MHz range, but the relevant theory can be applied to different waveguide sizes.

An electrically small dipole antenna is used as a test antenna for which the antenna factor is measured at a number of heights inside the liquid section of the waveguide. The antenna factor is calculated by taking a weighted average of the individually measured antenna factors. The weighting factors used are based on the uncertainties associated with each individual measurement. The approaches used to calculate both the uncertainties associated with the individually measured antenna factors and the uncertainty associated with the average antenna factor shall also be presented.

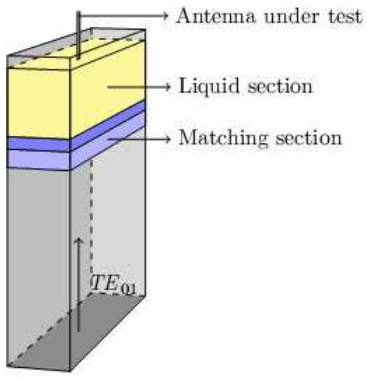

Figure 1: Schematic of the waveguide system.

ACKNOWLEDGMENT

The authors would like to acknowledge funding from the UK's National Measurement System.

Session 2A1
FocusSession.SC4: Optimal Antennas

Analysis of Optimized Embedded Antennas Using Radiation and Energy Storage Modes

K. R. Schab and J. T. Bernhard
University of Illinois at Urbana-Champaign, USA

Abstract— In many wireless devices, antennas occupy small volumes embedded within a larger device volume also containing circuit boards, screen components, batteries, and other antennas. These are frequently referred to as embedded antennas and often analyzed as electrically small antennas mounted on or near other conducting scatterers. Several approaches have been taken to incorporate contemporary electromagnetic theory (such as source-based Q calculations and characteristic modes) into the optimized design of such antennas. Many of these techniques are based heavily on the use of method of moments solvers. As such, a common step in many analyses is subdomain reduction, by which a fixed component of the system (e.g., a circuit board acting as a finite ground plane) is modeled as a distributed load on the antenna being optimized. In this way the order of computation can be greatly reduced by removing the need to reanalyze the ground plane during each iteration. However, this reduction also removes the intuition and potential design improvements to be gained by leveraging the innate properties of the chassis or finite ground plane.

In this presentation, we present the analysis of electrically small antennas and finite ground planes using radiation and energy storage modes derived from method of moments based radiation and energy storage operators. We discuss and give examples of using these modes in the analysis of single embedded antennas and multiband, collocated multi-antenna systems produced by various optimization methods. In particular, we use these modes to understand the role of finite ground planes and other internal scatterers in designing for parameters such as reactive current localization, pattern diversity, and pattern reconfigurability. We then propose methods to efficiently specify such properties as additional costs in optimization routines for antenna design.

A Universal Method for the Design of Antenna Arrays

Geyi Wen
Research Center of Applied Electromagnetics
Nanjing University of Information Science and Technolgy, Nanjing 210044, China

Abstract— The major target of antenna designs for telecommunication systems is to achieve maximum possible power transfer between the transmitting antenna and receiving antenna in the systems. For this reason, the power transmission coefficient between two antennas, which is defined as the ratio of the recived power to the transmitting power, can be used as a performance index or a target function for antenna designs. In this presentation, we demonste how the power transmission coefficient may be used to design antenna arrays in complicated envirionments for various purposes, such as beam steering, energy focusing, patten systhesis etc.. The design process is based on the optimization of the power transmission coefficient betwee the antenna arrays to be desgined and a testing antenna introduced in the desired direction in which radiation must be enhanced. The power transmission coefficient may be expressed as a Rayleigh quotient, by extremizing which an eigenvalue equation can be obtained. The solution of the eigenvalue equation gives the optimized distribution of excitations for the antenna arrays in the specified direcition. The optimized distribution may be realized by various feeding techniques. A number of design examples for various applications are expouned to illustrate the design procedure.

Optimal Array Antennas for Mask-constrained Shaped Beams: A Review

T. Isernia and A. F. Morabito
DIIES, University 'Mediterranea' of Reggio Calabria, Italy

Abstract— A huge amount of synthesis problems could be defined for arrays according to the degrees of freedom one has at his/her disposal (excitations, locations, excitations and locations, and so forth) and to the kind of pattern one wants to realize (pencil, difference, shaped, reconfigurable) [1]. In all cases, one is interested in a kind of 'optimal' synthesis, which means to optimize some performance parameters for given resources (and constraints) or, vice versa, to minimize the resources, e.g., the number of elements, for given radiation performances and constraints.

In order to enlarge the degrees of freedom available to the designer, specifications in terms of a 'mask' for the power pattern have to be preferred to the pursuit of a fixed (field or power) nominal pattern.

In [2, 3] it has been shown that the optimal synthesis of a mask-constrained shaped beam by means of a uniformly-spaced array can be conveniently tackled in terms of a linear programming problem (establishing the feasibility of the given problem) followed by a factorization allowing to determine all the possible solutions to the given problem.

Recent extensions of the basic theory include a class of planar arrays [4] as well as the synthesis of circularly symmetric planar apertures radiating shaped beams [5]. Interestingly, the capability to get all the different solutions has allowed establishing a new framework for the optimal synthesis of reconfigurable arrays [6], as well as to choose particularly convenient reference solutions for the case where locations and excitation phases (rather than the complex excitations) are the degrees of freedom of the synthesis problem [7].

Contribution will briefly discuss basics, relevance (per se as well as for creating reference solutions for more cumbersome synthesis problems), and possible extensions of the results above.

REFERENCES

1. www.lemma.unirc.it.
2. Isernia, T., "Problemi di sintesi in potenza: Criteri di esistenza e nuove strategie," *Atti Riunione Nazionale di Elettromagnetismo*, Applicato, Cesena, 1994.
3. Isernia, T., O. M. Bucci, and N. Fiorentino, "Shaped beam antenna synthesis problems: Feasibility criteria and new strategies," *Journal of Electromagnetic Waves and Applications*, Vol. 12, No. 1, 103–138, 1998.
4. Morabito, A. F., A. R. Laganà, and T. Isernia, "On the optimal synthesis of ring-symmetric shaped patterns by means of uniformly spaced planar arrays," *Progress In Electromagnetics Research B*, Vol. 20, 33–48, 2010.
5. Bucci, O. M., T. Isernia, and A. F. Morabito, "Optimal synthesis of circular symmetric shaped beams," *IEEE Trans. on Antennas and Propagation*, 2014.
6. Morabito, A. F., A. Massa, P. Rocca, and T. Isernia, "An effective approach to the synthesis of phase only reconfigurable linear arrays," *IEEE Trans. on Antennas and Propagation*, 2012.
7. Bucci, O. M., T. Isernia, and A. F. Morabito, "An effective deterministic procedure for the synthesis of shaped beams by means of uniform amplitude linear sparse arrays," *IEEE Trans. on Antennas and Propagation*, 2013.

Antenna Q and D/Q Bounds for Small Antennas with Electric and Magnetic Sources

B. L. G. Jonsson[1] and M. Gustafsson[2]

[1]Electromagnetic Engineering Lab, School of Electrical Engineering
KTH Royal Institute of Technology, Stockholm, Sweden
[2]Department of Electrical and Information Technology, Lund University, Lund, Sweden

Abstract— Small antennas are today an essential part of data and voice communication and they appear in, e.g., cellular phones, computers, watches, clothes and shoes. Often there are constraints on the physical size of these antennas, and worse they are also often electrically small. The smallness is known to limit the available matching bandwidth of the antennas. It is therefore interesting to examine the essential elements in this type of bandwidth limitations.

The physical bounds on bandwidth of small antennas have had some recent development. It was shown in [1], that passivity as a system property yields on set of bandwidth limitations on the absorption cross-section. For small antennas with separate resonances this bound can be expressed in terms of the partial directivity over the antenna quality factor, D/Q.

The classical Chu-bound for antennas bounded by a sphere use both electric and magnetic sources. An alternative approach to passivity based bandwidth bounds is to dene a stored energy for small antennas [2]. Using such an approach it is possible to obtain bandwidth limitations on the antenna Q and on D/Q. In our recent paper [3], we proposed a method of how to include both electric and magnetic sources in the bounds on antenna Q. In the present paper we compare optimal D/Q with optimal antenna Q in the presence of both electric and magnetic sources. Each of these problems results in explicit optimization problems, which strongly depend on the enclosing geometry of the antenna and the choice of sources in the domain of the antenna. The D/Q optimization is a convex problem, and the optimal Q-problem is an eigenvalue problem. Analytical and numerical solutions are shown.

ACKNOWLEDGMENT

We gratefully acknowledge funding from the Swedish Foundation for Strategic Research in the grant Complex analysis and convex optimization for EM design, as well as the Next generation array antenna (NGAA) project in the Vinnova VINN Excellence Center, CASE.

REFERENCES

1. Gustafsson, M., C. Sohl, and G. Kristensson, "Physical limitations on antennas of arbitrary shape," *Proc. R. Soc. A*, Vol. 463, 2589–2607, 2007.
2. Vandenbosch, G. A. E., "Reactive energies, impedance, and Q factor of radiating structures," *IEEE Trans. Antennas Propagat.*, Vol. 58, No. 4, 1112–1127, 2010.
3. Gustafsson, M. and B. L. G. Jonsson, "Stored energies in electric and magnetic current densities for small antennas," *ArXiv Physics e-prints*, arXiv: 1410.8704, 2014.

Topology Optimization of Wideband Directive Antennas

Emadeldeen Hassan[1], **Daniel Noreland**[1], **Robin Augustine**[2], **Eddie Wadbro**[1], **and Martin Berggren**[1]

[1]Department of Computing Science, Umeå University, Umeå SE-901 87, Sweden
[2]Ångström Laboratory, Department of Engineering Sciences, Uppsala University, Sweden

Abstract— There is a growing interest in using microwave detection and imaging systems, especially for medical applications. Wideband directive antennas are key elements for such systems to function efficiently. There are only few antenna types that are characterized as being wideband and directive. One example is the famous Vivaldi antenna introduced by Gibson [1]. These antennas can be described with a small number of parameters, which limits the possibility to find satisfactory designs by optimizing only these parameters.

On the other hand, topology optimization techniques allow parameter-free optimization to the whole layout of a device hosted in a given design domain. In other words, to optimize a specific objective function, topology optimization techniques decide on each point in a given design domain whether to hold void or a predefined material. Topology optimization was first introduced for structural optimization [2]. Recently, the approach has been extended to design various antenna types [3–5].

Here, we present a topology optimization approach to design, from scratch, wideband directive antennas for the purpose of near-field sensing. The antenna design is formulated as an optimization problem with the objective to maximize the coupling coefficient between two neighbouring antennas separated by a specific distance, and also to minimize the reflection coefficient of each antenna. We use the FDTD method to numerically solve the 3D Maxwell's equations and the design variables are the local conductivity at each Yee edge in a given design domain. Design problems with more than 100,000 design variables are solved, in less than 200 iterations, by using a gradient-based optimization method. The objective function gradient is computed based on solutions to an adjoint-field problem, which is also a FDTD discretization of Maxwell's equations but with a different excitation. For any number of design variables, the objective function gradient can be computed with only two FDTD simulations. The optimization problem is solved iteratively through solutions to a series of subproblems, in which the design variables are updated by using the globally convergent version of Svanberg's Method of Moving Asymptotes [6].

By using this approach to design planar antennas, we obtain novel antenna topologies that show wideband directivity and matching over more than two octaves. When used to detect a nearby phantom, experimental and simulation results show that the optimized antennas give more than 400% improvement in signal strength compared to a standard wideband antenna with comparable size.

REFERENCES

1. Gibson, P., "The Vivaldi aerial," *9th European Microwave Conference, 1979*, 101–105, Sep. 1979.
2. Bendsoe, M. P. and O. Sigmund, *Topology Optimization. Theory, Methods, and Applications*, Springer, 2003.
3. Erentok, A. and O. Sigmund, "Topology optimization of sub-wavelength antennas," *IEEE Trans. Antennas Propag.*, Vol. 59, No. 1, 58–69, Jan. 2011.
4. Hassan, E., E. Wadbro, and M. Berggren, "Topology optimization of metallic antennas," *IEEE Trans. Antennas Propag.*, Vol. 62, No. 5, 2488–2500, May 2014.
5. Hassan, E., E. Wadbro, and M. Berggren, "Patch and ground plane design of microstrip antennas by material distribution topology optimization," *Progress In Electromagnetics Research B*, Vol. 59, 89–102, 2014.
6. Svanberg, K., "A class of globally convergent optimization methods based on conservative convex separable approximations," *SIAM J. Optim.*, Vol. 12, No. 2, 555–573, 2002.

Investigation of the Optimal Matching Impedance for Finite Array Antennas

S. Shi and B. L. G. Jonsson
Electromagnetic Engineering Lab, School of Electrical Engineering
KTH Royal Institute of Technology, Teknikringen 33, Stockholm 114 28, Sweden

Abstract— The growth of data rates for communication demands a more efficient use of the bandwidth spectra, and also of a higher lateral concentration and flexibility of the coverage. One solution to these problems is to use array antennas in base-station applications. Such arrays should be efficient preferably optimally efficient both from an environmental point of view and in their use of the available spectrum. Optimality on matching bandwidth for small antennas has recently became better understood with the Gustafsson bound [1]. However, for array antennas many optimality questions remain open. A recent result here was the array figure of merit [2].

In this paper we investigate the behavior of the matching impedance for finite array antennas. The goal is to absorb as much power as possible of the incoming waves. The absorption cross section of an array is limited over any frequency range, as is shown by the sum rule for extinction [1].

Here we use CST Microwave Studio to simulate the arrays and their extinction and absorption cross sections. The results are validated by a comparison with the result in [3, 4]. We examine several antenna elements, their array, on its influence on the absorbed power and associated optimal matching resistance. Since the absorbed power over a frequency interval is bounded, there is an optimal resistive matching. We use here the same resistance on all elements, as a simplification. We explore the properties of the best resistive matching as a function of element number, element shape and array configuration.

REFERENCES

1. Gustafsson, M., C. Sohl, and G. Kristensson, "Physical limitations on antennas of arbitrary shape," *Proceedings of the Royal Society of London A: Mathematical, Physical and Engineering Sciences*, Vol. 463, No. 2086, 2589–2607, The Royal Society, UK, October 2007.
2. Jonsson, B. L. G., C. I. Kolitsidas, and N. Hussain, "Array antenna limitations," *IEEE Antennas and Wireless Propagation Letters*, Vol. 12, 1539–1542, 2013.
3. Jonsson, B. L. G. and M. Gustafsson, "Limitations on the effective area and bandwidth product for array antennas," *International Symposium on Electromagnetic Theory*, 711–714, 2010.
4. Gustafsson, M., M. Cismasu, and B. L. G. Jonsson, "Physical bounds and optimal currents on antennas," *IEEE Transactions on Antennas and Propagation*, Vol. 60, No. 6, 2672–2681, 2012.

Antenna Current Optimization and Optimal Antennas

Mats Gustafsson
Department Electrical and Information Technology, Lund University, Box 118, SE-221 00 Lund, Sweden

Abstract— Design of small antennas is challenging because fundamental physics constrains the antenna performance [2, 11]. Physical bounds provide basic restrictions on the antenna performance solely expressed in the available antenna design space. Here, an overview of antenna current optimization for physical bounds and antenna optimization is presented [3, 7]. Physical bounds are presented for antennas in free space, antennas integrated in metallic structured, and antennas embedded in lossy dispersive media. The physical bounds are compared with numerical data for several antennas.

Several proposals for the definition and interpretation of stored energy have been presented the last years [1, 4–6, 9, 10]. Here, the stored energy is derived from a state space representation generalizing previous expressions to more general cases [8]. The stored energy expressions are also used for antenna optimization and several antenna designs are presented.

REFERENCES

1. Capek, M., L. Jelinek, P. Hazdra, and J. Eichler, "The measurable Q factor and observable energies of radiating structures," *IEEE Trans. Antennas Propagat.*, Vol. 62, No. 1, 311–318, Jan 2014.
2. Chu, L. J., "Physical limitations of omnidirectional antennas," *J. Appl. Phys.*, Vol. 19, 1163–1175, 1948.
3. Cismasu, M. and M. Gustafsson, "Antenna bandwidth optimization with single frequency simulation," *IEEE Trans. Antennas Propagat.*, Vol. 62, No. 3, 1304–1311, 2014.
4. Geyi, W., "A method for the evaluation of small antenna Q," *IEEE Trans. Antennas Propagat.*, Vol. 51, No. 8, 2124–2129, 2003.
5. Geyi, W., "On stored energies and radiation Q," arXiv preprint arXiv:1403.3129, 2014.
6. Gustafsson, M. and B. L. G. Jonsson, "Antenna Q and stored energy expressed in the fields, currents, and input impedance," *IEEE Trans. Antennas Propagat.*, Vol. 63, No. 1, 240–249, 2015.
7. Gustafsson, M. and S. Nordebo, "Optimal antenna currents for Q, superdirectivity, and radiation patterns using convex optimization," *IEEE Trans. Antennas Propagat.*, Vol. 61, No. 3, 1109–1118, 2013.
8. Gustafsson, M., D. Tayli, and M. Cismasu, "Q factors for antennas in dispersive media," Technical Report LUTEDX/(TEAT-7232)/1–24/(2014), Lund University, Department of Electrical and Information Technology, P. O. Box 118, S-221 00 Lund, Sweden, 2014, http://www.eit.lth.se.
9. Vandenbosch, G. A. E., "Reactive energies, impedance, and Q factor of radiating structures," *IEEE Trans. Antennas Propagat.*, Vol. 58, No. 4, 1112–1127, 2010.
10. Vandenbosch, G. A. E., "Radiators in time domain, part II: Finite pulses, sinusoidal regime and Q factor," *IEEE Trans. Antennas Propagat.*, Vol. 61, No. 8, 4004–4012, 2013.
11. Volakis, J., C. C. Chen, and K. Fujimoto, *Small Antennas: Miniaturization Techniques & Applications*, McGraw-Hill, New York, 2010.

High Gain Printed Monopole Arrays for Wireless Applications

M. Farran[1], **S. Boscolo**[2], **D. Modotto**[1], **A. Locatelli**[1],
A. D. Capobianco[3], **M. Midrio**[2], **and V. Ferrari**[1]

[1]Dipartimento di Ingegneria dell'Informazione, Università degli Studi di Brescia, Italy
[2]Dipartimento di Ingegneria Elettrica, Gestionale e Meccanica, Università degli Studi di Udine, Italy
[3]Dipartimento di Ingegneria dell'Informazione, Università degli Studi di Padova, Italy

Abstract— Linear monopole arrays are extensively used in many antenna systems due to their simplicity, low cost, polarization purity, reasonable bandwidth, and power handling capability.

In this work we show a novel antenna array design in which $N+1$ parasitic monopoles, properly placed in a linear array of N active elements, allow a broadside radiation reaching a gain value close to that one of a standard $2N+1$ active element array. For each active element we place symmetrically on both sides of the monopole (at a distance of $\lambda/4$) two parasitic metallic strips which are protrusions of the ground plane. Since currents in active and parasitic radiating elements are required to oscillate in phase, meandered lines are inserted between the feeding microstrips and the active monopoles: in such a way, the correct phase lag for the currents in the elements is obtained.

The uniqueness of this design is due to its simple feeding network since a balun section is not necessary: for a $2N+1$ array only N elements will be fed reducing the problem of spurious radiation and losses. The N active elements, the meanders and the feeding network can be fabricated on the front of a standard FR4 substrate, whereas the ground plane and the parasitic elements are fabricated on the back of the same substrate (see Figure 1). We present two designs of broadside array working in the wireless local area network (WLAN) band around 2.4 GHz. The microstrip arrays composed of 5×1 and 9×1 linear monopoles with their feeding network have been simulated by using CST. In order to obtain a unidirectional pattern, a metallic plane reflector is placed at a distance of $\lambda/4$ from the array board: predicted gain (11 dB for 5×1 linear array and 15 dB for 9×1 linear array) and bandwidth (around 400 MHz) are larger than for conventional microstrip patch arrays (having similar board dimensions). The proposed antenna arrays are also compact: the size of a 9×1 array working at 2.4 GHz is $27\times9\times3.2$ cm as in Figure 1, where 3.2 cm is the distance between the array board and the reflecting plane.

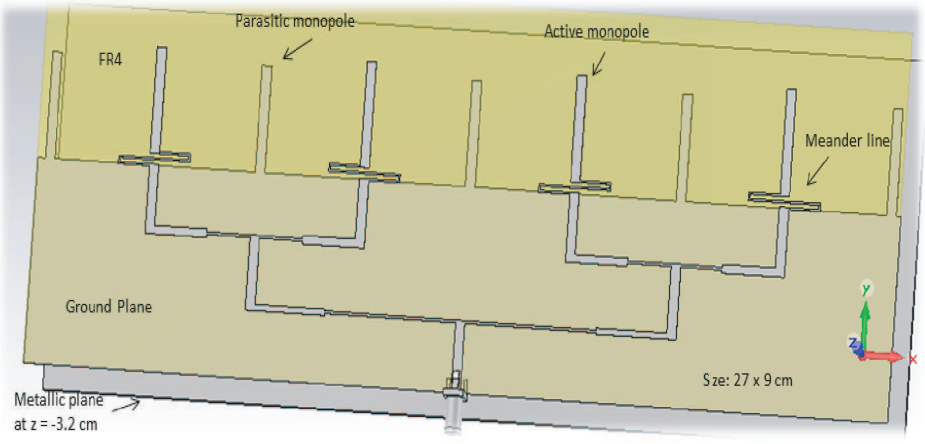

Figure 1: 9×1 monopole linear array.

Technology Advances in GNSS High Precision Positioning Antennas

D. V. Tatarnikov
Topcon Positioning Systems, Russia

Abstract— Currently, typical error of differential positioning with the Global Navigation Satellite Systems (GNSS) is of the order of 1–2 cm in real time. In open sky environments, multipath reflections from the earth surface are recognized to be the largest error source. With the GNSS signals below the ambient noise floor, antennas employed for positioning are to accommodate the signals with the smallest possible losses and to possess the decreased gain in directions below the local horizon to mitigate the reflections. Three types of antennas are currently in use: compact rover antennas, field base station antennas and reference station antennas. Novel developments in regards to these types are discussed in the paper.

To achieve 10–12% bandwidth in the Lower GNSS band and 4–6% in the Upper band for patch antenna stacks, artificial dielectric substrates are employed in the form of dense grids of metal elements. Homogenization techniques to estimate the effective dielectric constant of the structures have been discussed in the paper. Antenna design examples are also presented. One of novel antenna types is a compact end-fire helix antenna with the size of the order of a quarter-wavelength; it allows a 15 dB multipath suppression in the direction downwards.

Field base station antennas are to provide with improved precision in practical environments; besides mitigation of the reflections, antennas are to have the decreased field intensity in the near field region underneath. A novel antenna with a semi-transparent ground plane combined with an artificial magnetic conductor structure has been designed and developed. For practical applications such an antenna ensures the phase center stability in vertical coordinate on the level of 1 mm.

Convex impedance ground plane reference station antenna is to provide with multipath suppression typical for the common choke ring structures along with the improved gain for low elevated satellites; the surface impedance is provided by a grid of straight pins. The internal volume of the antenna allows accommodating high-Q cavity filters for interference protection.

Antennas with a cutoff pattern are to provide improved multipath suppression starting from low elevations. The purpose of their development is to achieve the mm-level precision of positioning in real time. Thus far, the antennas are known to be spacious in the wavelength scale. New results for large impedance ground plane antennas are presented. There is also given a discussion of potentials to achieve the cutoff pattern in the antennas of practical size.

Travelling Wave Antennas with Semitransparent Surfaces for Forming a Cutoff Pattern

D. V. Tatarnikov and I. M. Chernetsky
Topcon Positioning Systems, Moscow, Russia

Abstract— Antennas with a cutoff pattern are of special interest to various applications, in particular, to high-precision positioning with the Global Navigation Satellite Systems (GNSS). Since ground reflections are the largest error source, antennas with a cutoff pattern allow approaching millimeter-level precision of real-time positioning.

Solutions known so far involve structures of 10–15 wavelengths span. Such are a vertical array antenna of [1] or a large impedance ground plane antenna of [2]. However it has been found out that by employing semi-transparent surfaces with pure reactive grid impedance a travelling-wave antenna with the size of about 1.5 wavelengths would serve the purpose. Thus, systems with millimeter-level precision in real time would be considered as practical. The relevant discussion and results achieved is a purpose of the paper.

An electromagnetic model of a parallel-plate waveguide with semi-transparent endings has been developed. By means of optimization techniques it has been shown that if the endings are of about 1.5 wavelengths span, then grid impedance varying along the endings could be synthesized such that a cutoff pattern would be achieved along with the proper return loss levels.

Quadrifilar helix antenna has been chosen as a principle for practical implementation. The antenna has lumped impedances embedded into the strip conductors. Antenna forms a homogeneous pattern within the top semi-sphere with about 20 dB drop of the gain while crossing the local horizon. A proper functionality within the bandwidth of about 10% has been achieved.

Precision of GNSS positioning in open-field environment has been evaluated. RMS of the error in real time was found to be below 1 mm.

REFERENCES

1. Lopez, A. R., "GPS landing system reference antenna," *IEEE AP Magazine*, Vol. 52 No. 1, 104–111, 2010.
2. Tatarnikov, D. and A. Astakhov, "Large impedance ground plane antennas for MM-accuracy of GNSS positioning in real time," *PIERS Proceedings*, 1825–1829, Stokholm, Sweden, August 12–15, 2013.

Parametric Analysis and Optimisation of a 8–18 GHz Quad-ridged Horn Antenna

Deniz Bolukbas[1, 2] **and Ali Ziya Ozer**[2]

[1]Department of Electrical and Electronics Engineering, Okan University, Istanbul, Turkey
[2]Electromagnetic Design and Analysis Team, Figes A.S., Pendik, Tuzla, Turkey

Abstract— In this paper, parametric analysis and optimization of a 8–18 GHz ultra wide band (UWB) quad-ridged horn (QRH) antenna is presented. As an initial configuration a horn antenna is designed with boxed dimensions of $5.4 \times 5.4 \times 8$ cm as defined in [1]. The gain of the antenna varies between 10 dBi–13 dBi over the entire bandwidth. To analyze these effects the parametric analysis simulations are performed with HFSS.

Introduction: Horn antennas can be used as a feed and provide high gain, relatively wide bandwidth. In this paper, the parametric analysis and optimization of a QRH antenna is presented. A QRH antenna is designed based on the design explained in [1]. The dimensions of the antenna are described in Figure 1. The physical sizes of the antenna are given in Table 1. The horn fed by coaxial cable.

The gain of QRH antenna is presented in Figure 2. In 8–18 GHz frequency band, the gain varies between 10 to 13 dBi.

The outer dimensions A_1 and B_1 is selected to be equal and the gain patterns for five cases are given for 8 GHz and 18 GHz at Figure 2 respectively.

This analysis is repeated while $A_1 = 5.6$ cm and constant, B_1 is varying from 2.6 cm to 8.6 cm. The numerical values of gain are presented at Table 2.

Table 1: The physical sizes of QRH antenna for initial configuration.

Parameter	*Length (mm)*	*Parameter*	*Length (mm)*
A	1.6	L_1	4
B	1.6	L_2	4
A_1	5.6	d	0.3
B_1	5.6	w	0.14

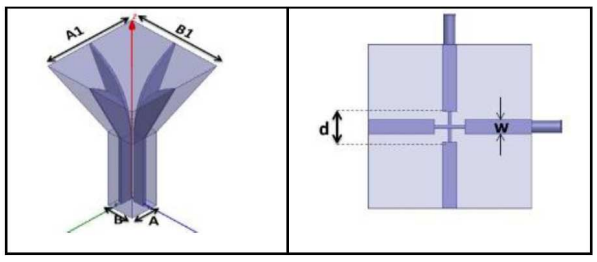

Figure 1: The description of horn antenna's dimensions.

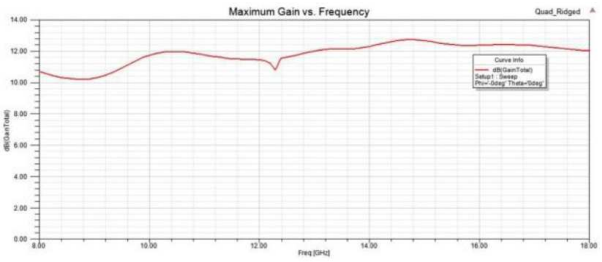

Figure 2: The gain of QRH antenna at 8–18 GHz.

Table 2: Gain vs dimensions for $A_1 = 5.6$ cm.

	Freq [GHz]	B1=2.6cm	B1=4.1cm	B1=5.6cm	B1=7.1cm	B1=8.6cm
1	8.00	9.37	10.83	10.76	9.91	9.21
2	10.00	10.22	10.87	11.84	10.63	10.80
3	12.00	10.54	11.52	11.57	11.65	10.80
4	14.00	10.52	12.46	12.34	11.40	11.01
5	16.00	11.79	13.15	12.42	11.52	12.24
6	18.00	12.62	13.06	12.08	12.33	12.01

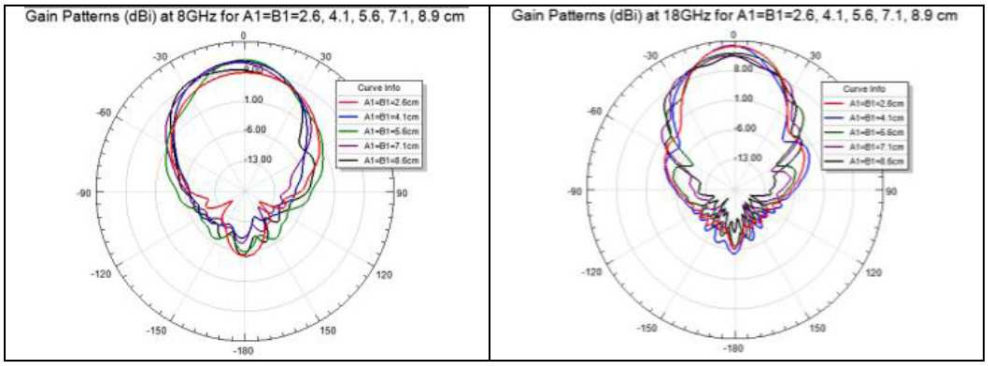

Figure 3: Gain pattern for (a) 8 GHz, (b) 18 GHz.

In this case to obtain the maximum gain, B_1 can be selected around 5.6 cm, while A_1 is constant. The parametric analysis are performed also for d and w parameters as they were described at Figure 1.

Conclusion: In this paper, the quad ridged horn antenna design is performed, parametric analysis are simulated and the results are presented. The simulation tools are very useful for this kind of parametric analysis. With the help of such tools the best performance of the antenna can be achieved.

REFERENCES

1. Dehdasht-Heydari, R., H. R. Hassani, and A. R. Mallahzadeh, "Quad ridged horn antenna for UWB applications," *Progress In Electromagnetics Research*, Vol. 79, 23–38, 2008.

Session 2A2
FocusSession.SC3: Optical Properties of Resonant Dielectric and Plasmonic Nanostructures 1

Si Nanoparticles with Optical Resonances for Dielectric Photonics

Andrey B. Evlyukhin, Urs Zywietz, Carsten Reinhardt, and Boris N. Chichkov
Laser Zentrum Hannover e.V., Hollerithalle 8, D-30419 Hannover, Germany

Abstract— Strong resonant light scattering by Si nanoparticles is experimentally and theoretically demonstrated, revealing pronounced resonances in the visible spectral range associated with the excitation of magnetic and electric modes in these nanoparticles. In this work we discuss the origin of the magnetic dipole resonance in dielectric nanoparticles. Our consideration is based on the approach of quasi-static electromagnetic field and Mie theory.

Theoretical and experimental results concerning the resonant optical properties of differently shaped Si nanoparticles are presented. The role of magnetic and electric modes in the scattering optical spectra is clarified. A new theoretical approach allowing multipole analysis of light scattering by arbitrary-shaped nanoparticles located on flat substrate surface is demonstrated. This approach is applied to investigations of light and surface plasmon polariton (SPP) scattering by Si nanoparticle structures. It is shown how the particle resonant magnetic mode can affect spatial distribution of the scattered SPPs and light. Applications of Si nanoparticles for realization of nanoantennas and metametrials will be discussed.

Interrogating Nanoparticles with Focused Doughnuts

T. A. Raybould[1], **V. A. Fedotov**[1], **N. Papasimakis**[1], **I. Youngs**[2], **and N. I. Zheludev**[1, 3]

[1]Optoelectronics Research Centre and Centre for Photonic Metamaterials
University of Southampton, SO171BJ, UK
[2]DSTL, Salisbury, UK
[3]Centre for Disruptive Photonic Technologies
Nanyang Technological University, Singapore

Abstract— The propagation of electromagnetic radiation in free-space is described by the source-free Maxwells equations. In contrast to conventional solutions such as infinite-energy plane waves and Gaussian pulses, there exists a family of exact solutions which represent localised transmission of finite electromagnetic energy [1]. One such solution is known as the Focused Doughnut (FD) pulse a peculiar single-cycle electromagnetic perturbation with a unique toroidal field topology and 3-dimensional, polynomial energy localisation [2]. Here, for the first time we present a comprehensive study of the FD pulse: we investigate the propagation dynamics and interactions of these complex electromagnetic pulses with homogeneous and structured media.

The FD pulse exhibits a number of intriguing properties. Its purely single-cycle nature results in an ultra-broadband frequency spectrum and a well defined spatial-chirp. In fact, the spatial dependence of the pulse is inseparable from its temporal dependence. In addition, the toroidal topology of the pulse gives rise to significant longitudinal field components at the pulse that hold potential for particle acceleration applications [2]. Although the FD pulse has remained a theoretical curiosity since its first prediction, successful experimental realisation could lead to its use in a variety of settings, such as microscopy, communications, directed energy transfer, spectroscopy, and particle trapping and acceleration. Further interest in the FD pulse stems from the burgeoning field of toroidal electrodynamics, owing to the topological similarities between the FD pulse and the near-field configuration of the toroidal dipole excitation [3].

The intriguing light-matter interactions of the FD pulse are examined from several perspectives. We present a full evaluation of the transformations the FD pulse undergoes due to interactions with dielectric and metallic interfaces. This has revealed the unusual behaviour of both the TE and TM pulses under reflection, with respect to the reversal of the azimuthal and radial field components. Furthermore, the interactions of FDs with small dielectric and plasmonic particles are considered, where the broadband nature and complex field topology of the pulses is expected to play a significant role in mode excitation. Recent work has demonstrated broad modal excitation within the nanostructures and distinct differences between the interaction with TE and TM pulses. Possible experimental realisations of these complex electromagnetic perturbations resulting from the theoretical/computational treatment presented here will be discussed.

ACKNOWLEDGMENT

The authors acknowledge support from DSTL, the Engineering and Physical Sciences Council, U.K. and the Leverhulme Trust.

REFERENCES

1. Ziolkowski, R., "Localised transmission of electromagnetic energy," *Phys. Rev. A*, Vol. 39, 2005–2033, 1989.
2. Hellwarth, R. W. and P. Nouchi, "Focused one-cycle electromagnetic pulses," *Phys. Rev. E*, Vol. 54, 889–895, 1996.
3. Kaelberer, T., et al., "Toroidal dipolar response in a metamaterial," *Science*, Vol. 330, 1510–1512, 2010.

Dielectric Mie Antennas

N. Bonod
Aix Marseille Université, CNRS, Centrale Marseille, Institut Fresnel UMR 7249, Marseille 13013, France

Abstract— Dielectric antennas are composed of subwavelength sized particles that feature electric and magnetic Mie resonances. These antennas can be used to enhance at subwavelength scales either the electric or the magnetic field counterparts, to accelerate the spontaneous emission or to shape the emission pattern of light emitters.

Introduction: The interplay between electric and magnetic resonances in dielectric resonators offers novel opportunities to control the light scattering. In particular, when coupling Mie resonators to a dipolar source, the excitation of both electric and magnetic dipoles (or multipoles) permits to achieve very high gain in directivity [1]. It can be also proved that by tuning the emission frequency, light can be emitted either toward the forward or the backward direction [1, 2]. Interestingly, the presence of magnetic modes can lead to strong magnetic Purcell factors [3]. In the case of lanthanide ions that feature electric and magnetic transitions, enhancing preferentially the magnetic Purcell factors could promote a magnetic transition. Reciprocally, when illuminated from far field, dielectric antennas can strongly enhance the magnetic field, without enhancing the electric field counterpart [4].

Fabrication: The development of fabrication methods of Mie antennas made of semi-conductors is very challenging. Recently, we followed a bottom-up strategy to fabricate over wafer scales monocrystaline Si-based resonators. The technique is based on the dewetting of thin silicon layers over silica at high temperature. The dewetting can be spontaneous, assisted by electron-beam lithography or by FIB to fabricate individual resonators or oligomers. This technique is well adapted to large samples since the time process does not depend on the size of the sample.

Theory: Silicon mie antennas are very promising to design light cavities. In this context, it is important to quantify the Purcell factor silicon particles doped with quantum emitters. For that purpose, we derived the effective volumes as a function of the normal modes of the Mie resonator. It is seen that when Mie resonators are doped with electric dipolar emitters, the electric modes provide stronger Purcell factors than the magnetic ones [6].

REFERENCES

1. Rolly, B., B. Stout, and N. Bonod, "Boosting the directivity of optical antennas with magnetic and electric dipolar resonant particles," *Opt. Express*, 20376–20386, 2012.
2. Rolly, B., J. M. Geffrin, R. Abdeddaim, and N. Bonod, "Controllable emission of a dipolar source coupled with a magneto-dielectric resonant subwavelength scatterer," *Sci. Rep.*, Vol. 3, 3063, 2013.
3. Rolly, B., B. Bebey, S. Bidault, B. Stout, and N. Bonod, "Promoting magnetic dipolar transition in trivalent lanthanide ions with lossless Mie resonances," *Phys. Rev. B.*, Vol. 245432, 2012.
4. Boudarham, G., R. Abdeddaim, and N. Bonod, "Enhancing the magnetic field intensity with a dielectric gap antenna," *Appl. Phys. Lett.*, Vol. 104, 021117, 2014.
5. Abbarchi, M., et al., "Wafer scale formation of monocrystalline silicon-based Mie resonators via SOI dewetting," *ACS Nano*, Vol. 8, 11181–11190, 2014.
6. Zambrana-Puyalto, X. and N. Bonod, "Purcell factor of dielectric Mie resonators featuring electric and magnetic resonances," arXiv:1501.07452, 2015.

Low Loss Non-plasmonic Nanoantennas for Surface-Enhanced Spectroscopy and Fluorescence

P. Albella[1], **M. Caldarola**[2], **E. Cortés**[1], **M. Rahmani**[1], **T. Roschuk**[1], **G. Grinblat**[2], **A. V. Bragas**[2], **and S. A. Maier**[1]

[1]The Blackett Laboratory, Department of Physics, Imperial College London, London SW7 2AZ, UK
[2]Laboratorio de Electrónica Cuántica, Departamento de Física, FCEN
Universidad de Buenos Aires, IFIBA Conicet, Argentina

Abstract— Plasmonic structures enable control and manipulation of light at the nanoscale, allowing for strong enhancements of the electric field for interactions with molecules and materials in their vicinity [1]. Unfortunately, these large enhancements come with the cost of high optical losses due to absorption in the metal, severely limiting some real-world applications. Specifically, localized heating strongly limits the total power that can be delivered to a nanoscale field hot spot before the nanostructure melts and reshapes, affecting their suitability for applications such as lighting and photonic modulation [2]. Moreover, the emission properties of molecules placed near the nanoantennas, can also be modified by this local heating [3]. Here we present a method to overcome these heating issues via the realization of a novel nanophotonic platform based on the low absorption dielectric nanostructures (silicon, germanium or gallium phosphide) that we theoretically proposed in [4, 5] to form efficient non-plasmonic nanoantennas with ultra-low light-into-heat conversion. We show that silicon-based nanoantennas produce both high surface enhanced fluorescence (SEF) and good surface enhanced Raman scattering (SERS), while at the same time producing a negligible temperature increase in their hot spots and surrounding environments compared to gold [6].

REFERENCES

1. Bharadwaj, P., B. Deutsch, and L. Novotny, "Optical antennas," *Advances in Optics and Photonics*, Vol. 1, No. 3, 438, 2009.
2. Kuhlicke, A., S. Schietinger, C. Matyssek, K. Busch, and O. Benson, "In situ observation of plasmon tuning in a single gold nanoparticle during controlled melting," *Nano Letters*, Vol. 13, No. 5, 2041–2046, 2013.
3. Mahmoudi, M., et al., "Variation of protein corona composition of gold nanoparticles following plasmonic heating," *Nano Letters*, Vol. 14, No. 1, 6–12, 2013.
4. Albella, P., M. A. Poyli, M. K. Schmidt, S. A. Maier, F. Moreno, J. J. Saenz, and J. Aizpurua, "Low-loss electric and magnetic field-enhanced spectroscopy with subwavelength silicon dimers," *Journal of Physical Chemistry C*, Vol. 117, 13573–13584, 2013.
5. Albella, P., R. Alcaraz de la Osa, F. Moreno, and S. A. Maier, "Electric and magnetic field enhancement with ultralow heat radiation dielectric nanoantennas: Considerations for surface-enhanced spectroscopies," *ACS Photonics*, Vol. 1, No. 6, 524–529, 2014.
6. Caldarola, M., P. Albella, E. Cortés, M. Rahmani, T. Roschuk, G. Grinblat, A. V. Bragas, and S. A. Maier, "Non-plasmonic nanoantennas for surface enhanced spectroscopies with ultra-low heat conversion," (Submitted).

Magnetic and Electric Hotspots with Silicon Nanodimers

R. M. Bakker[1], **D. Permyakov**[2], **Ye F. Yu**[1], **D. Markovich**[2], **R. Paniagua-Dominguez**[1], **L. Gonzaga**[1], **A. Samusev**[2], **Y. Kivshar**[2, 3], **B. Lukyanchuk**[1], **and A. I. Kuznetsov**[1]

[1]Data Storage Institute, A*STAR, 5 Engineering Drive 1, 117608, Singapore
[2]ITMO University, St. Petersburg 197101, Russia
[3]Nonlinear Physics Centre, Australian National University, Canberra, ACT 0200, Australia

Abstract— High refractive index dielectric nanoparticles have risen to prominence in the nanophotonics toolkit for control of light in the near-field [1–3]. Compared to metallic nanostructures employed in plasmonics, the near-fields in dielectric nanostructures immediately adjacent to the particles are less intense but can have larger far-field scattering cross sections [4]. Dielectric nanoparticles can reduce quenching and provide higher quantum efficiency of localized emitters than plasmonic structures that can be important for engineering emission at the subwavelength scale [4].

We present for the first time to our knowledge the experimental evidence of near-field enhancement of the magnetic fields with silicon resonant nanodimers at visible frequencies. The response of the system has been studied as a function of wavelength, polarization, and gap [5]. Theory and numerical simulations predict that such a structure should have a strong magnetic response [4, 5]. The near-field measurements show a very good correlation with the simulations. When the simulated near-fields are broken down into their components, it is confirmed that the resonance measured in the near-field is strongly magnetic in nature, for both polarizations.

Additionally, we have conducted a complete analysis of the modes excited inside the dielectric nanodimer system by means of the multipole decomposition. This analysis reveals the excitation of a toroidal dipole moment which interferes with the Cartesian electric dipole moment resulting in a dip in the total electric dipole radiation. This is the first reporting of toroidal dipole excitation in dielectric nanodimer antennas. The dimer system is the basic building block for many nanophotonics systems. The results demonstrated in this paper lay the groundwork for future engineering of the magnetic field response at optical frequencies with high-index dielectric nanostructures for the ultimate control on the subwavelength scale.

REFERENCES

1. Kuznetsov, A. I., A. E. Miroshnichenko, Y. H. Fu, J. B. Zhang, and B. Luk'yanchuk, "Magnetic light," *Sci. Rep.*, Vol. 2, 492, July 2012.
2. Evlyukhin, A. B., S. M. Novikov, U. Zywietz, R. L. Eriksen, C. Reinhardt, S. I. Bozhevolnyi, and B. N. Chichkov, "Demonstration of magnetic dipole resonances of dielectric nanospheres in the visible region," *Nano Letters*, Vol. 12, No. 7, 3749–3755, 2012.
3. Krasnok, A. E., P. A. Belov, A. E. Miroshnichenko, A. I. Kuznetsov, B. S. Lukyanchuk, and Y. S. Kivshar, "All-dielectric optical nanoantennas," *Progress in Compact Antennas*, 143–172, Huitema, L., Eds. InTech, New York, 2014.
4. Albella, P., M. A. Poyli, M. K. Schmidt, S. A. Maier, F. Moreno, J. J. Senz, and J. Aizpurua, "Low-loss electric and magnetic field-enhanced spectroscopy with subwavelength silicon dimers," *J. Phys. Chem. C*, Vol. 117, 13573–13584, 2013.
5. Bakker, R. M., D. Permyakov, Y. F. Yu, D. Markovich, R. Paniagua-Domínguez, L. Gonzaga, A. Samusev, Y. S. Kivshar, B. Lukyanchuk, and A. I. Kuznetsov, "Magnetic and electric hotspots with silicon nanodimers," *Nano Letters*, 2015, doi:10.1021/acs.nanolett.5b00128.

Dual and Chiral Dielectric Scatterers for Optical Activity in General Directions

I. Fernandez-Corbaton[1], M. Fruhnert[2], and C. Rockstuhl[2]

[1]Institute of Nanotechnology, Karlsruhe Institute of Technology, Germany
[2]Institut für Theoretische Festkörperphysik, Karlsruhe Institute of Technology, Germany

Abstract— We demonstrate a route to design structures exhibiting optical activity in general scattering directions. When the structure is illuminated from an arbitrary direction, the polarization of the field measured in another arbitrary direction is a rotated version of the incident polarization. The angle of rotation depends on both incident and scattered directions. The design guidelines are based on two necessary conditions for optical activity: Lack of spatial inversion symmetries, and helicity preservation, i.e., zero coupling between the states of opposite polarization handedness of the incident and scattered plane waves [1]. In forward scattering, helicity preservation can be achieved by geometrical means: Scatterers with discrete rotational symmetry with degree equal to or higher than 3 preserve plane wave polarization handedness. In an arbitrary scattering direction, helicity preservation is achieved by scatterers with electromagnetic duality symmetry [2]. While materials meeting the exact duality condition are usually not available, it is possible to purposefully design electromagnetically small scatterers to show approximately dual behavior [3–5]. Particles with such properties have attracted attention, particularly in the context of zero backscattering and the Kerker conditions [3, 4, 6, 7]. We show that approximately dual symmetric structures can be built using small dielectric spheres whose dipolar response is dual symmetric. We show that a chiral arrangement of such spheres exhibits optical activity in general scattering directions. In our work, the electromagnetic responses of the designed structure is calculated through rigorous techniques which allow to compute its scattering matrices to an arbitrary multipolar order [8], and renders our analysis and conclusions valid up to the approximations inherent in the macroscopic Maxwell's equations. We believe that the consideration of the electromagnetic duality symmetry is a valuable addition to the research in optical activity, to both its fundamental and practical sides.

REFERENCES

1. Fernandez-Corbaton, I., X. Vidal, N. Tischler, and G. Molina-Terriza, "Necessary symmetry conditions for the rotation of light," *J. Chem. Phys.*, Vol. 138, No. 21, 214311-1–214311-7, Jun. 2013.
2. Fernandez-Corbaton, I., X. Zambrana-Puyalto, N. Tischler, X. Vidal, M. L. Juan, and G. Molina-Terriza, "Electromagnetic duality symmetry and helicity conservation for the macroscopic maxwell's equations," *Phys. Rev. Lett.*, Vol. 111, No. 6, 060401, Aug. 2013.
3. Gerin, J. M., B. García-Cámara, R. Gómez-Medina, P. Albella, L. S. Froufe-Pérez, C. Eyraud, A. Litman, R. Vaillon, F. González, M. Nieto-Vesperinas, J. J. Sáenz, and F. Moreno, "Magnetic and electric coherence in forward-and back-scattered electromagnetic waves by a single dielectric subwavelength sphere," *Nat. Commun.*, Vol. 3, 1171, Nov. 2012.
4. Person, S., M. Jain, Z. Lapin, J. J. Sáenz, G. Wicks, and L. Novotny, "Demonstration of zero optical backscattering from single nanoparticles," *Nano Lett.*, Vol. 13, No. 4, 1806–1809, 2013.
5. Zambrana-Puyalto, X., X. Vidal, M. L. Juan, and G. Molina-Terriza, "Dual and anti-dual modes in dielectric spheres," *Opt. Express*, Vol. 21, No. 15, 17520–17530, Jul. 2013.
6. Staude, I., A. E. Miroshnichenko, M. Decker, N. T. Fofang, S. Liu, E. Gonzales, J. Dominguez, T. S. Luk, D. N. Neshev, I. Brener, and Y. Kivshar, "Tailoring directional scattering through magnetic and electric resonances in subwavelength silicon nanodisks," *ACS Nano*, Vol. 7, No. 9, 78247832, 2013, PMID: 23952969.
7. Liu, W., A. E. Miroshnichenko, D. N. Neshev, and Y. S. Kivshar, "Broadband unidirectional scattering by magneto-electric core-shell nanoparticles," *ACS Nano*, Vol. 6, No. 6, 5489–5497, 2012.
8. Fruhnert, M., S. Mühlig, F. Lederer, and C. Rockstuhl, "Towards negative index self-assembled metamaterials," *Phys. Rev. B*, Vol. 89, 075408, Feb. 2014.

Refractory Plasmonics for Harsh Environment

U. Guler[1], J. Liu[2], H. Eragamreddy[2], A. V. Kildishev[2], A. Boltasseva[2], and V. M. Shalaev[2]

[1]Nano-Meta Technologies Inc., 1281 Win Hentschel Boulevard, West Lafayette, IN 47906, USA
[2]School of Electrical & Computer Engineering and Birck Nanotechnology Center
Purdue University, West Lafayette, IN 47907, USA

Abstract— Plasmonic materials and their response to electromagnetic radiation has been a hot topic over the last decades mostly because of the exciting properties and useful functionalities arising from the interaction of electrons with light. The deviation from bulk material properties dramatically increases as the lengths in one or more dimensions become sub-wavelength. Moreover, once the material properties change with downsizing to the nanometer scale the structures get more vulnerable against the environmental effects such as temperature, mechanical stress and contaminants Changes in thermal, mechanical, and chemical properties of the material result in reduced durability of the elements. Increased surface to volume ratio leads to corrosion due to enhanced chemical interaction with the surrounding medium, melting point depression and deformation. The problem gets more serious due to the softness and solubility of noble metals which otherwise could've been able to provide desired plasmonic properties in the visible and near infrared regions of the spectrum.

Although the initial stages of research on plasmonics was focused on noble metals, it has been evident that a richer pool of materials would be required in order to cover the needs of a wide variety of proposed applications. Harsh environmental factors such as high temperatures, aggressive chemistry, and extreme local forces require harder plasmonic materials. Transition metal nitrides are well known for their refractory properties and they are used in a wide variety of industries where hard surface coatings are required in order to enhance material durability. Recent advances in the development of high quality thin films of transition metal nitrides resulted in improved optical properties and enabled the use of nitrides as refractory plasmonic materials. Exhibiting plasmonic properties in the visible and near infrared regions of the electromagnetic spectrum, transition metal nitrides allow the use of plasmonic components, which would otherwise suffer from extreme local thermal and chemical properties, in emerging technologies.

Plasmonic components based on refractory materials will be discussed in this talk. Spectrally selective refractory metamaterial absorbers and emitters for solar energy harvesting, spectral manipulation, and optical sensing will be introduced. Use of transition metal nitrides as near field transducer for light confinement applications such as heat assisted magnetic recording will be discussed. Photothermal properties of titanium nitride colloidal solutions with plasmonic dipolar resonance in the biological transparency window will be presented.

Measuring Chromatic Aberration in Imaging Systems Using Plasmonic Nano-particles

Sylvain D. Gennaro, **Tyler R. Roschuk**, **Stefan A. Maier**, **and Rupert F. Oulton**
The Blackett Laboratory, Department of Physics, Imperial College London, London SW7 2AZ, UK

Abstract— We demonstrate a method to measure chromatic aberrations of microscope objectives with metallic nano-particles using incoherent white light. Extinction spectra are recorded while scanning a single nano-particle through a lens's focal plane. We show a direct correlation between the focal wavelength and the longitudinal chromatic focal shift through analysis of the variations between scanned extinction spectra at each scan position and peak extinction over the entire scan. The method has been tested on achromat and apochromat objectives using aluminum nano-particles.

Chromatic aberration in optical systems arises from the wavelength dependence of a glass's refractive index. Polychromatic rays incident upon an optical surface are refracted at slightly different angles and in traversing an optical system follow distinct paths creating images displaced according to colour. Despite the capability to correct chromatic aberration in individual lens components, its accumulation within imaging systems is difficult to assess. While longitudinal chromatic aberration is readily measured with interferometry, less elaborate methods are attractive for their ease of use and low cost. These involve measuring transmission spectra through a pinhole or optical fibre placed at the focus. Unfortunately, the sensitivity of these techniques diminishes rapidly with aperture size limiting their usefulness, especially in high magnification imaging [1]. This limitation can be circumvented by applying Babinet's principle. In a chromatic aberration measurement, we can consider replacing the aperture with a scattering object and measuring extinction instead of transmission. Although Rayleigh scattering by small particles suggests this approach has a similar limitation to Bethe's, it has been shown that dipole scattering in a focused beam allows near perfect extinction [2, 3]. Metallic nano-particles are particularly attractive dipole scatterers as they support surface plasmon resonances that provide strong extinction cross sections in the visible spectral range. Moreover, due to the fast radiative rates and electronic damping in metallic nano-particles, extinction spectra can be octave spanning enabling assessment of chromatic focal shift across the entire visible spectrum in a single measurement. We retrieve the longitudinal chromatic focal shift of high numerical aperture (NA) achromatic (not shown here) and apochromatic (See Fig. 2) corrected microscope objectives from the extinction spectra of metallic nanoparticles placed within the focal plane. We show that the technique is accurate even for the finest measurements on high NA objectives with apochromatic correction. The method enables rapid assessment of the chromatic aberration of any microscopy system since it uses incoherent illumination and is straightforward to implement.

REFERENCES

1. Bethe, H., "Theory of diffraction by small holes," *Phys. Rev.*, Vol. 66, 163–182, 1944.
2. Zumofen, G., N. Mojarad, V. Sandoghdar, and M. Agio, "Perfect reflection of light by an oscillating dipole," *Phys. Rev. Lett.*, Vol. 101, 1–4, 2008.
3. Gennaro, S. D., Y. Sonnefraud, N. Verellen, P. Van Dorpe, V. V. Moshchalkov, S. A. Maier, and R. F. Oulton, "Spectral interferometric microscopy reveals absorption by individual optical nanoantennas from extinction phase," *Nat. Commun.*, Vol. 5, 3748, 2014.

A Study in Asymmetry: Resonances in Arrays of Asymmetric Disc Dimers

Alastair D. Humphrey, **Nina Meinzer**, **and William L. Barnes**
School of Physics and Astronomy, University of Exeter
Stocker Road, Exeter EX4 4QL, United Kingdom

Abstract— Symmetry is one of the most fundamental concepts in nature. From elementary particles to complex protein molecules it impacts on the properties of a physical entity and on the interaction with its environment. In photonics, for example, the symmetry of a system determines if and how strongly it couples to an electro-magnetic field. In the specific case of a symmetric plasmonic antenna, which can support several multipolar eigenmodes only modes with a non-vanishing net dipole moment can couple to a normally-incident plane wave; all other modes are non-radiating, or *dark*, meaning that although the antenna can support these modes they cannot be observed under the given conditions. However, one can render such modes *grey*, i.e., weakly radiating, by symmetry breaking, either by deviating from normal incidence and thus lowering the symmetry of the excitation or by introducing an asymmetry to the antenna itself. There has recently been significant interest in *grey* modes because their small net dipole moment results in narrow spectral features with high quality factors, which are desirable for many applications.

In this paper we study the resonance behaviour of asymmetric disc dimers (ADD), both as individual dimer structures and within periodic arrays, ranging from the non-diffractive metamaterial regime to the diffractive case, where they exhibit interesting surface-lattice resonances (SLR), which are very narrow and appear as a double resonance for the right excitation conditions. We discuss the ADD resonances in all three regimes (single dimers, non-diffractive, diffractive) both experimentally and with additional data from numerical modelling but we focus specifically on the SLR of asymmetric dimers, for which we have also modified a previous analytical model to incorporate the effect of an asymmetric two-element base.

Field Enhancement in Rhodium Tripod Stars and Dimers

R. Alcaraz de la Osa[1], **J. M. Sanz**[1], **A. I. Barreda**[1], **J. M. Saiz**[1], **F. González**[1], **H. O. Everitt**[2], **and F. Moreno**[1]

[1]University of Cantabria, Spain
[2]Duke University, USA

Abstract— During the last two decades, local field enhancements produced by metal nanoparticles have been widely investigated in the visible range for common metals like gold and silver. Interest in extending nanoplasmonics into the ultraviolet (UV) spectral region has grown in the past few years [1]. Very recently, the UV plasmonic properties of Rh tripod stars have been examined, by means of surface-enhanced Raman spectroscopy, surface-enhanced fluorescence, and photo-induced degradation [2]. These findings confirmed the exciting potential of Rh nanostructures for UV plasmonic and photocatalytic applications.

In this research, we report results of our numerical study of the plasmonic properties of isolated Rh tripod stars and dimers. We explore the role of the geometry, shape, angle of incidence and polarization of the incident radiation on the performance and generation of localized surface plasmon resonances in the UV, as well as, the possibility of generating hot spots with nanoparticle aggregates for applications in SERS experiments.

Figure 1 shows a near field intensity map of a tripod star dimer with their points confronted and separated by a given gap distance. The dimer is illuminated under normal incidence with the electric field parallel to the line connecting the dimers. The inset shows spectra of the electric field intensity averaged over the dimer's surface and the absorption efficiency.

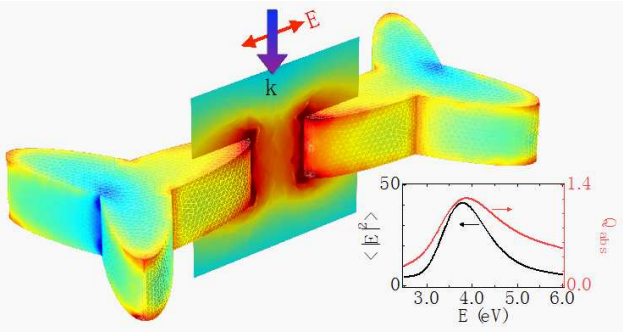

Figure 1: Near field intensity map of a tripod star dimer illuminated under normal incidence with the electric field parallel to the line connecting the dimers. The inset shows spectra of the electric field intensity averaged over the dimer's surface $\langle|\mathbf{E}|^2\rangle$ and the absorption efficiency Q_{abs}.

REFERENCES

1. Sanz, J. M., et al., "UV plasmonic behavior of various metal nanoparticles in the near-and far-field regimes: Geometry and substrate effects," *The Journal of Physical Chemistry C*, Vol. 117, No. 38, 19606–19615, 2013.
2. Watson, A. M., et al., "Rhodium nanoparticles for ultraviolet plasmonics," *Nano Lett.*, 2015, DOI: 10.1021/nl5040623.

Optical Spectroscopy Study of Colloidal Gold Nanorods

N. Zabala[1, 2], L. Bergamini[1, 2], F. J. Recio[3, 4], A. Ayuela[2], A. Rivacoba[2, 5], P. Crespo[3], P. M. Echenique[2, 5], and A. Hernando[3]

[1]Department of Electricity and Electronics, FCT-ZTF
University of the Basque Country UPV-EHU, Bilbao, Spain
[2]Materials Physics Center CFM
CSIC-UPV/EHU and Donostia International Physics Center, DIPC, San Sebastian, Spain
[3]Instituto de Magnetismo Aplicado, UCM-CSIC-ADIF, and Departamento Física de Materiales
Universidad Complutense, Madrid, Spain
[4]Departamento de Química de los Materiales, Fac. de Química y Biología
Universidad de Santiago de Chile, Santiago, Chile
[5]Departamento de Física de Materiales, Fac. de Química, UPV-EHU, San Sebastian, Spain

Abstract— We report results on the optical absorption of thin gold nanorods (NRs) produced with a seed-mediated growth method followed by a filtering process [1]. Gold NRs are obtained with different aspect ratios and lengths covering the range between tenths to a few hundred of nanometers. Because of our interest in medical applications, these nanostructures are dispersed in colloidal solutions, so that molecules are bound to their surfaces and keep them partially separated. We use well-known solvents: first a CTAB aqueous solution, where gold NRs of different sizes are grown from Au NP seeds, and then a thiolate solution. Nanorod samples of different lengths are characterized using HRTEM and UV-Vis-NIR spectroscopy.

The study focuses on the long NR samples ($L > 100\,\mathrm{nm}$) obtained after filtering. One of the main challenges concerning the characterization of their optical response is to understand the origin of the different peaks in the absorption spectra, in particular a main peak that appears about 960 nm for several solvents, and their evolution with the Au NR colloidal concentration.

A theoretical analysis is performed by using the boundary element method (BEM) to solve the full electrodynamical problem and obtain the extinction cross section and near field distributions around the NRs. In the case of the thiolate solution the main peak of the long NR sample, which is attributed to the $n = 3$ antenna mode, is split when the surface of the NRs is chemically modified due to the thiolate coverage around their surface. The use of a dielectric model which incorporates parameters based on ab-initio calculations of thiolate-gold cluster surfaces allows us to explain the trends observed in the spectra recorded for the self-assembled thiolate functionalized gold NRs.

REFERENCES

1. Recio, F. J., N. Zabala, A. Rivacoba, P. Crespo, A. Ayuela, P. M. Echenique, and A. Hernando, "Optical resonances of colloidal gold nanorods: From seeds to chemically thiolated long nanorods," *J. Chem. Phys. C*, Vol. 119, 7856–7864, 2015.

Session 2A3
FocusSession.SC3: Single Photonics: Integrated Optics for On-chip Manipulation of Single Photons

Second-order Correlations of the Nonclassical Light from a Single Quantum-dot State

G. S. Solomon[1, 2], **T. Thomay**[1, 3, 4], **E. B. Flagg**[1, 5], **E. Goldschmidt**[1], **V. Loo**[1], **O. Gazzano**[1], **A. Migdall**[1, 2], **and S.V. Polyakov**[1, 2]

[1]Joint Quantum Institute, National Institute of Standard & Technology, and University of Maryland
100 Bureau Drive, Gaithersburg, MD 20899, USA
[2]National Institute of Standard & Technology, Gaithersburg, MD, USA
[3]Institute for Research in Electronics and Applied Physics
University of Maryland, College Park, MD 20742, USA
[4]Department of Electrical Engineering, SUNY Buffalo, NY, USA
[5]Department of Physics & Astronomy, West Virginia University, Morgantown, WV, USA

Abstract— Second-order correlations are an essential tool in characterizing the nature of light. The second-order autocorrelation is important in distinguishing between classical and quantum light sources, and of particular importance here, the single-photon purity. The second-order cross-correlation offers insight into the indistinguishability properties of the light. As technology improves and material system change, these measurements naturally evolve. Here we discuss one or two evolutions in these techniques.

In typical second-order correlations ($g^{(2)}$) measurements, a time invariant emission process is assumed, where the optical field properties depend only on the time difference of the two photon detections, not when the detections occur. This has been robustly applied to atomic and parametric down-conversion systems for several decades, but it assumes there are no time dynamics in the system. For solid-states sources, such as quantum dots, where resonant excitation of a state is not always necessary and coupling to environmental reservoirs is likely, there are time-dependent processes, and new second-order correlation tools are needed. We demonstrate timeresolved $g^{(2)}$ measurements of the photons emitted from a single exciton in an InAs quantum dot in a GaAs/AlAs planar microcavity. These measurements shows the dynamics of a nonclassical optical field, quantifying single-photon purity and coherence as a function of when in the excitation-decay cycle of the QD a photon is detected. The results offer an optimization scheme by selecting detection regions. Time permitting, we will discuss more efficient and practical second-order measurement variations and protocols.

Quantum Dots in Photonic Wires: Highly Efficient Single Photon Sources for Free-space and On-chip Applications

J. M. Gérard[1], **J. Claudon**[1], **P. Stepanov**[1], **M. Munsch**[1], **T. Jakubczik**[1], **E. Peinke**[1], **J. Bleuse**[1], **N. Gregersen**[2], **J. Mørk**[2], **X. Zang**[3], **and P. Lalanne**[3]

[1]CEA-CNRS-UJF Joint Group "Nanophysique et Semiconducteurs"
CEA, INAC, SP2M, Grenoble 38054, France
[2]DTU Fotonik, Technical University of Denmark, DK-2800 Kongens Lyngby, Denmark
[3]LP2N, Institut d'Optique d'Aquitaine, U. Bordeaux, CNRS, 33405 Talence, Cedex, France

Abstract— Optimizing the coupling between a localized quantum emitter and a single-mode optical channel represents a powerful route to realise bright sources of non-classical light states. Reversibly, the efficient absorption of a photon impinging on the emitter is key to realise a spin-photon interface, the node of future quantum networks

Besides optical microcavities [1], photonic wires are very attractive in this context [2, 3]. We introduce the Photonic Trumpet [4], formed by a high-index single-mode waveguide and a conical tapering. Nearly perfect single mode emission, low-divergence Gaussian radiation pattern, linear polarization control and high efficiency single photon emission (> 0.75 photon per pulse) are reported for a single quantum dot embedded in a Photonic Trumpet. We also demonstrate a broadband tuning of the emission wavelength without efficiency loss using strain-effects. More generally, this novel photonic microstructure appears as a very promising platform to explore the unique optical properties of "one-dimensional atoms" [5] and hybrid optomechanical systems where the interaction between the two-level quantum system and mechanical modes is mediated by strain [6].

Finally, we will also report experimental work on QDs embedded in ridge waveguides on a chip, showing efficient control over QD spontaneous emission, which is promising in view of the integration of efficient QD single photon sources on photonic integrated circuits [7].

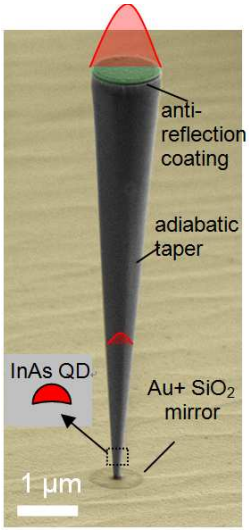

Figure 1: Colorized scanning electron micrograph of a GaAs photonic trumpet (from [3]).

REFERENCES

1. Gérard, J. M., et al., *Phys. Rev. Lett.*, Vol. 81, 1110, 1998.
2. Friedler, et al., *Opt. Exp.*, Vol. 17, 2095, 2009.
3. Claudon, et al., *Nat. Phot.*, Vol. 4, 174, 2010.
4. Munsch, M., et al., *Phys. Rev. Lett.*, Vol. 110, 177402, 2013; and Vol. 111, 239902(E), 2013.
5. Valente, D., et al., *New J. Phys.*, Vol. 14, 083029, 2012; *Phys. Rev. A*, Vol. 86, 022333, 2012.
6. Yeo, I., et al., *Nature Nanotechnology*, Vol. 9, 106, 2014.
7. Stepanov, P., et al., *Appl. Phys. Lett.*, Vol. 106, 041112, 2015.

Quantum Optics in One-dimensional Photonic Reservoirs

I. Söllner and P. Lodahl
Niels Bohr Institute, University of Copenhagen, Denmark

Abstract— Here we review the recent experimental progress on the use of quantum dots coupled to photonic-crystal waveguides [1]. We show that single photons can be channeled into the waveguide with an efficiency exceeding 98% [2], constituting an almost ideal 1D artificial-atom. In such a system a single quantum dot couples exclusive to a 1D photonic reservoir, enabling the experimental demonstration of dipole-induced transparency and strong quantum-dot-mediated photon-photon interaction. Furthermore, we discuss how chiral photon-emission can be achieved in specifically engineered waveguides and present experimental results showing that the directionality of single-photon emission in such waveguides exceeds 90% [3]. Finally, we discuss the prospects of scaling the platform to larger quantum architectures for applications in quantum-information processing, such as efficient photon sorting [4] and a deterministic CNOT gate for photons [3].

REFERENCES

1. Lodahl, P., S. Mahmoodian, and S. Stobbe, "Interfacing single photons and single quantum dots with photonic nanostructures," *Rev. Mod. Phys.*, arXiv: 2013.1312.1079, 2014.
2. Arcari, M., I. Söllner, A. Javadi, S. Lindskov Hansen, S. Mahmoodian, J. Liu, H. Thyrrestrup, E. H. Lee, J. D. Song, S. Stobbe, and P. Lodahl, "Near-unity coupling efficiency of a quantum emitter to a photonic-crystal waveguide," *Physical Review Letters*, Vol. 113, 093603, 2014.
3. Söllner, I., S. Mahmoodian, S. Lindskov Hansen, L. Midolo, A. Javadi, G. Kiršanskė, T. Pregnolato, H. El-Ella, E. H. Lee, J. D. Song, S. Stobbe, and P. Lodahl, "Deterministic photon-emitter coupling in chiral photonic circuits," *Quantum Physics*, arXiv: 1406.4295, 2014.
4. Ralph, T. C., I. Söllner, S. Mahmoodian, A. G. White, and P. Lodahl, "Photon sorting, efficient Bell measurements and a deterministic CZ gate using a passive two-level nonlinearity," *Quantum Physics*, arXiv: 1502.04261, 2015.

Design and Simulations of Highly Efficient Single-photon Sources

N. Gregersen, J. R. de Lasson, and J. Mørk
DTU Fotonik, Department of Photonics Engineering, Technical University of Denmark, Denmark

Abstract— The realization of the highly-efficient single-photon source represents not only an experimental, but also a numerical challenge. We will present the theory of the waveguide QED approach, the design challenges and the current limitations. Additionally, the important numerical challenges in the simulations of sources with in-plane emission will be discussed.

Introduction: Within optical quantum information processing, deterministic generation of single indistinguishable photons on demand is a key functionality. An optically or electrically excited quantum emitter, e.g., a semiconductor quantum dot, embedded inside a solid-state semiconductor host material represents an attractive platform for such a single-photon source. However, for an emitter in bulk material, the symmetry of the system leads to a collection efficiency of only 1–2%, and efficient light extraction thus poses a major challenge in single-photon source engineering [1].

Several approaches have been proposed to control the light emission and ensure an efficient coupling to the collection optics. Within waveguide quantum electrodynamics, the quantum dot is placed inside a waveguide. By carefully tailoring the waveguide dimensions, the relative coupling of the spontaneous emission (SE) to the fundamental waveguide mode, known as the SE β factor, can reach 0.95 in uniform GaAs waveguides. This high β is obtained thanks to a suppression of the SE contribution to radiation modes due a screening effect [2]. Furthermore, in photonic crystal waveguides the β additionally benefits from increased SE into the fundamental mode near the band edge, thus enabling an experimentally measured β above 0.98 [3].

Such near-unity coupling to a waveguide relies critically on correct engineering of the dimensions, which in turn requires accurate numerical simulation of SE in the considered waveguide. This simulation represents an extremely demanding task. Whereas determination of the SE contribution to the fundamental mode is straightforward, the contribution to the radiation modes must be evaluated for a waveguide placed in an open system. The difficulty lies in that most computational methods require that the computational domain be limited to fit in memory, leading to parasitic reflections from the surrounding wall. Here, an absorbing boundary condition can be employed to reduce the influence of the size of the computational domain, and to compute the correct SE contribution the absorbing boundary condition must perfectly mimic the open geometry system.

State-of-the-art methods to compute the SE will be discussed with emphasis on the influence of the size of the computational domain. We will show that proper convergence towards an open boundary limit is generally not obtained, representing a major numerical challenge in optical engineering of high-efficiency single-photon sources.

ACKNOWLEDGMENT

This work was funded by project SIQUTE (contract EXL02) [4] of the European Metrology Research Programme (EMRP). The EMRP is jointly funded by the EMRP participating countries within EURAMET and the European Union. Additionally, support from the Villum Foundation via the VKR Centre of Excellence NATEC is gratefully acknowledged.

REFERENCES

1. Gregersen, N., P. Kaer, and J. Mørk, "Modeling and design of high-efficiency single-photon sources," *IEEE J. Sel. Top. Quantum Electron*, Vol. 19, 9000516, 2013.
2. Bleuse, J., J. Claudon, M. Creasey, N. S. Malik, J. M. Gérard, I. Maksymov, J. P. Hugonin, and P. Lalanne, "Inhibition, enhancement and control of spontaneous emission in pohotonic nanowires," *Phys. Rev. Lett.*, Vol. 106, 103601, 2011.
3. Arcari, M., I. Söllner, A. Javadi, S. L. Hansen, S. Mahmoodian, J. Liu, H. Thyrrestrup, E. H. Lee, J. D. Song, S. Stobbe, and P. Lodahl, "Near-unity coupling efficiency of a quantum emitter to a photonic crystal waveguide," *Phys. Rev. Lett.*, Vol. 113, 093603, 2014.
4. http://www.ptb.de/emrp/siqute-home.html.

Design of Slow and Fast Light Photonic Crystal Waveguides for Single-photon Emission Using a Bloch Mode Expansion Technique

J. R. de Lasson[1, 2], B. Rigal[2], E. Kapon[2], J. Mørk[1], and N. Gregersen[1]

[1]DTU Fotonik, Department of Photonics Engineering, Technical University of Denmark, Denmark
[2]Laboratory of Physics of Nanostructures, École Polytechnique Fédérale de Lausanne, Switzerland

Abstract— We design slow and fast light photonic crystal waveguides for single-photon emission using a Bloch mode expansion and scattering matrix technique. We propose slow light designs that increase the group index-waveguide mode volume ratio for larger Purcell enhancement, and address efficient slow-to-fast-light waveguide coupling.

Introduction: In the quest to realize quantum information technology and quantum computers, development of efficient and deterministic single-photon sources is an important step on the way. Single-photon emission occurs from quantum emitters, like atoms or quantum dots, via spontaneous emission that inherently is a non-deterministic process. To obtain a deterministic single-photon source, the spontaneous emission must be controlled, which is typically achieved by placing the quantum emitter in a suitably designed photonic environment; both resonant systems (cavities) and broadband structures (waveguides) have been proposed [1]. In cavity systems, matching of the spectrally narrow emitter and cavity is required, while waveguides relax this requirement due to their broadband nature. For on-chip emission and detection of single-photons, planar integration is necessary, and for this purpose semiconductor photonic crystal (PhC) membranes constitute a flexible and versatile platform. Theoretical efforts [2] and experimental demonstration [3] of single-photon emission in PhC waveguides have been reported.

In this contribution, we employ the Bloch mode expansion technique [4] for engineering of PhC waveguide modes as well as of quantum dot light emission. With this technique, one spatial direction is treated analytically, which makes it highly suitable for long structures like waveguide based single-photon sources, in contrast to spatial discretization methods as FDTD and FEM. In addition, direct access to scattering matrices [5] makes the optimization of multi-section structures particularly transparent, for example when interfacing slow and fast light waveguides in a PhC waveguide based single-photon source.

Specifically, we address the designs of slow and fast light PhC waveguides that serve the purposes of enhancing light-matter interactions and photon transport, respectively. In the former, much attention has been paid to increasing the Purcell factor via large group indices, while little has been said about designs that minimize the waveguide mode volume [2]. We propose designs that simultaneously provide large group indices and small mode volumes, and furthermore propose efficient transmission from slow to fast light PhC waveguides, needed for efficient routing of singly emitted photons to collection optics.

REFERENCES

1. Gregersen, N., P. Kaer, and J. Mørk, "Modeling and design of high-efficiency single-photon sources," *IEEE J. Sel. Top. Quantum Electron.*, Vol. 19, 9000516–9000516, 2013.
2. Manga Rao, V. S. C. and S. Hughes, "Single quantum-dot purcell factor and β factor in a photonic crystal waveguide," *Phys. Rev. B*, Vol. 75, 205437, 2007.
3. Arcari, M., I. Söllner, A. Javadi, S. Lindskov Hansen, S. Mahmoodian, J. Liu, H. Thyrrestrup, E. H. Lee, J. D. Song, S. Stobbe, and P. Lodahl, "Near-unity coupling efficiency of a quantum emitter to a photonic crystal waveguide," *Phys. Rev. Lett.*, Vol. 113, 093603, 2014.
4. Lecamp, G., J. P. Hugonin, and P. Lalanne, "Theoretical and computational concepts for periodic optical waveguides," *Opt. Express*, Vol. 15, 11042–11060, 2007.
5. Li, L., "Formulation and comparison of two recursive matrix algorithms for modeling layered diffraction gratings," *J. Opt. Soc. Am. A*, Vol. 13, 1024–1035, 1996.

Tuning Solid-state Single-photon Sources into Resonance with Each Other

M. Petruzzella[1], **T. Xia**[1], **F. Pagliano**[1], **S. Birindelli**[1], **L. Midolo**[1], **Z. Zobenica**[1], **L. H. Li**[2], **E. H. Linfield**[2], **and A. Fiore**[1]

[1]COBRA Research Institute, Eindhoven University of Technology
P. O. Box 513, Eindhoven NL-5600MB, The Netherlands
[2]School of Electronic and Electrical Engineering
University of Leeds, Leeds LS2 9JT, United Kingdom

Abstract— Single quantum emitters embedded in semiconductor nanocavities represents a key building block for the generation and manipulation of non-classical light in envisioned quantum photonic circuits. In the past decade, the monolithic integration of quantum dots (QDs) with photonic crystals has been successfully adopted to demonstrate the basic cavity quantum electrodynamics (c-QED) phenomena ranging from non-linearities arising in the strong coupling regime [1] to the static and dynamic [2, 3] control of the spontaneous emission process. Nevertheless, the integration and interconnection of multiple c-QED nodes pose the major limitation to the number of qubits that can be generated within the same chip. One of the leading experimental challenges in this context resides in the spectral matching of several cavity-emitter systems. Indeed, for scalable and indistinguishable single-photons, tuning the energy of both emitters and cavities is crucial in order to overcome the inhomogeneous broadening of self-assembled QDs and the energy spread in the cavity resonance caused by unavoidable fabrication imperfections. Here we report the energy control over a full cavity-emitter node, consisting of Stark-tunable QDs coupled to electromechanically reconfigurable double-membrane photonic crystal cavity [4]. The all-electrical wavelength-tuning of the emitter over 7.5 nm as well as an 8.5 nm mode shift are demonstrated on the same device. Furthermore, by bringing a tunable single excitonic line into resonance with a tunable cavity mode, we demonstrated a ten-fold Purcell-enhancement of its spontaneous emission rate at two distinct wavelengths [5]. Finally, we discuss the integration of this fully-tunable architecture with ridge waveguides, needed to build a low-loss photonic channel between several solid-state qubits.

REFERENCES

1. Buckley, S., et al., *Rep. Prog. Phys.*, Vol. 75, 126503, 2012.
2. Jin, C., et al., *Nat. Nanotechnol.*, Vol. 9, 886, 2014.
3. Pagliano, F., et al., *Nat. Commun.*, Vol. 5, 5786, 2014.
4. Midolo, L., et al., *Appl. Phys. Lett.*, Vol. 101, 091106, 2012.
5. Petruzzella, M., et al., in Preparation, 2015.

Integration of Site-controlled Quantum Dots with Photonic Crystal Cavities and Waveguides

Eli Kapon
Laboratory of Physics of Nanostructures, Ecole Polytechnique Fédérale de Lausanne (EPFL), Switzerland

Abstract— Integration of semiconductor quantum dots (QDs) with photonic cavities and waveguides is useful for studying the fundamentals of light-matter interaction as well as for applications such as quantum light sources, quantum information processing and low power consumption lasers for optical interconnects. Recent progress in the realization of QD systems with good control over dot position and optical spectra opens new possibilities for on-chip generation, detection and manipulation of single photons. Here we review such progress achieved with pyramidal QDs epitaxially grown on pre-patterned substrates. The site-controlled InGaAs/GaAs QDs are grown by metallorganic vapor phase epitaxy on (111)B GaAs "membrane" substrates pre-patterned with arrays of inverted pyramids of different configurations [1, 2]. This QD system exhibits excellent site control, inhomogeneous broadening as small as < 2 meV, reproducible QD exciton spectra [3], and high in-plane QD symmetry [4] essential for emission of entangled photons. Photonic crystal (PhC) cavities and waveguides are designed and fabricated on top of the QD arrays with the aid of alignment marks by electron beam lithography. Spatial alignment accuracy of better than 50 nm and QD-cavity energy matching of better than few-meV can be achieved with this approach. The integrated QD systems allow observation of QD-cavity coupling free of spurious multi-excitonic effects, mediated only by phonon exchange [5]. Experiments and modeling yield insight into the role of pure QD depahsing in the weak-coupling regime [6]. Coupling of several QDs to the same cavity mode is evidenced by the co-polarization of the QD emission with the related PhC cavity modes [7]. Integration of pyramidal QDs with PhC cavities for few-QD lasers and with PhC waveguides for multiplexing single photon sources will be discussed.

REFERENCES

1. Hartmann, A., et al., *Appl. Phys. Lett.*, Vol. 73, 2322, 1998.
2. Felici, M., et al., *Small*, Vol. 5, 938, 2009.
3. Jarlov, C., et al., *Appl. Phys. Lett.*, Vol. 101, 191101, 2012.
4. Dupertuis, M.-A., et al., *Phys. Rev. Lett.*, Vol. 107, 127403, 2011.
5. Calic, M., et al., *Phys. Rev. Lett.*, Vol. 106, 227401, 2011.
6. Jarlov, C., et al., in preparation.
7. Lyasota, A., et al., *J. Crystal Growth*, Vol. 414, 192, 2015.

Integration of Site-controlled Quantum Dots in a Photonic Molecule

B. Rigal, **C. Jarlov**, **B. Dwir**, **A. Rudra**, **P. Gallo**, **M. Calic**, **A. Lyasota**, **and E. Kapon**
Ecole Polytechnique Fédérale de Lausanne, Lausanne CH-1015, Switzerland

Abstract— Since the seminal proposal of Feynman in 1981 [1], different well-controlled quantum computing systems suitable for solving complex quantum physics problems have been proposed [2]. A promising implementation of quantum simulators would be an array of quantum dots (QDs) interacting through the optical modes of an array of coupled photonic cavities [3]. Construction of such systems requires strict position and spectral control of the QD systems involved as well as avoiding mode localization due to optical disorder. Here, we present the fabrication and optical study of a system composed of two InGaAs/GaAs pyramidal QDs [4] deterministically integrated in two coupled photonic crystal membrane cavities ("photonic molecule") (Figure 1(a)). A statistical analysis of the energy splitting between the symmetric and antisymmetric modes of the fabricated photonic molecules evidenced strong inter-cavity coupling, indicating delocalisation of the supermodes across both cavities. Scanning micro photoluminescence (PL) spectroscopy based on the high reproducibility of the QD emission spectra allowed identification of the spectral features of each QD (Figure 1(b), X_i and XX_i denote exciton and bi-exciton of dot i.) The simultaneous weak coupling of both QDs to the delocalized cavity supermode is demonstrated thanks to the Purcell effect inducing a vertical co-polarization of these otherwise unpolarized lines (Figure 1(c)). This demonstrates the versatility and scalability of pyramidal site controlled QDs for integration with nano-photonic elements.

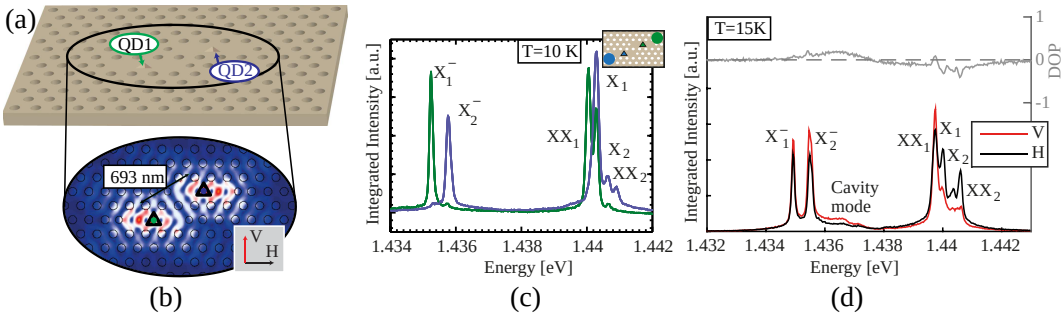

Figure 1: (a) 3D geometry of the sample, (b) calculated near field of the antibonding photonic supermode, (c) PL spectra of QD emission for two different excitation positions (see inset), identifying the features of each QD, (d) vertically and orthogonally polarized PL spectra and degree of linear polarization (DOP) showing copolarization of QD lines and cavity emission (excitation power: 200 μW).

REFERENCES

1. Feynman, R. P., "Simulating physics with computers," *Int. J. Theor. Phys.*, Vol. 21, 467–488, 1982.
2. Brown, K. L., W. J. Munro, and V. M. Kendon, "Using quantum computers for quantum simulation," *Entropy*, Vol. 12, 2268–2307, 2010.
3. Greentree, A. D., C. Tahan, J. H. Cole, and L. C. Hollenberg, "Quantum phase transitions of light," *Nat. Phys.*, Vol. 2, 856–861, 2006.
4. Gallo, P., et al., "Integration of site-controlled pyramidal quantum dots and photonic crystal membrane cavities," *Appl. Phys. Lett.*, Vol. 92, 263101–263101, 2008.

Quantum Dot Integrated in Photonics Crystal Nanocavity for Single Dot Photonics

Yasuhiko Arakawa[1, 2], **Yasutomo Ota**[1], **Vincent Elfving**[2], **Kenji Kamide**[1], **Mark Holmes**[1], **and Satoshi Iwamoto**[1, 2]

[1]Institute for Nano Quantum Information Electronics, The University of Tokyo
4-6-1 Koamaba, Meguro-ku, Tokyo 153-8505, Japan
[2]Institute of Industrial Science, The University of Tokyo
4-6-1 Koamaba, Meguro-ku, Tokyo 153-8505, Japan

Abstract— Progress in quantum dot integrated in photonics crystal nanocavity for single dot photonics are discussed. The presentation includes experimental and theoretical discussion on single dot lasers with a high-Q photonic crystal nanocavity. Moreover, spontaneous two photon emission controlled with the high-Q nanocavity is demonstrated. Finally, single photon emission from a nanowire quantum dot at room temperature is also discussed.

ACKNOWLEDGMENT

This works is supported by the Project for Developing Innovation Systems, MEXT and NEDO Project, Japan.

REFERENCES

1. Arakawa, Y. and H. Sakaki, *Appl. Phys. Lett.*, Vol. 40, 939, 1982.
2. Urino, Y., Y. Arakawa, et al., *IEEE J. of Lightwave Tech.*, Vol. 3, 1223, 2015.
3. Tanabe, K., T. Rae, K. Watanabe, and Y. Arakawa, *Appl. Phys. Express*, Vol. 6, 82703, 2013.
4. Jhang, Y., K. Tanabe, S. Iwamoto, and Y. Arakawa, *IEEE Photonics Technology Letters*, Vol. 27, 875, 2015.

On-chip Quantum Optics Using Electrically Contacted Quantum Dot Micropillars

P. Munnelly[1], **T. Heindel**[1], **M. M. Karow**[1], **E. Stock**[1], **M. Kamp**[2], **S. Höfling**[2], **C. Schneider**[2], **and S. Reitzenstein**[1]

[1]Institut für Festkörperphysik, Technische Universität Berlin, Berlin, Germany
[2]Technische Physik, Universität Würzburg, Würzburg, Germany

Abstract— The prospect of studying quantum optics effects in the solid state and the development of quantum light sources for applications in the field of quantum communication has triggered enormous efforts in the fabrication of micro- and nanocavity systems with embedded quantum dots (QDs). These structures exploit cavity quantum electrodynamics (cQED) effects and can act as efficient non-classical light sources and as high-β microlasers. Their further development towards applications in quantum technology focusses on the realization of triggered sources of indistinguishable photons and efficient schemes for electrical pumping. Combining these two goals has turned out to be highly challenging because a high degree of indistinguishability requires resonant excitation schemes while electrical pumping using pin-diode structures is intrinsically non-resonant. To tackle this issue we propose an on-chip quantum optics concept where an integrated microlaser resonantly excites a QD-micropillar cavity acting as non-classical light source. As such, our approach combines two very active but so far independent routes of cQED, namely high-β lasing and single QD light-matter interaction at the quantum in a novel, integrated device concept.

The on-chip device concept is illustrated in Fig. 1(a) and relies on the opportunity that micropillar cavities allow for the localization of vertically emitting modes and laterally emitting whispering gallery modes (WGMs). We take advantage of this unique opportunity provided by the micropillar geometry to utilize an electrically pumped WGM micropillar as in-plane laser source. Here, the integrated WGM microlaser resonantly excites a peripheral QD-micropillar. This specific configuration allows us to demonstrate for the first time on-chip quantum optics experiments in the cQED regime by applying an integrated coherent light source (cf. Fig. 1(b)) [1]. Moreover, we apply pulsed electrical excitation of the integrated microlaser (cf. Fig. 1(c)) to demonstrate electrically triggered emission of non-classical light from the peripheral micropillar [2].

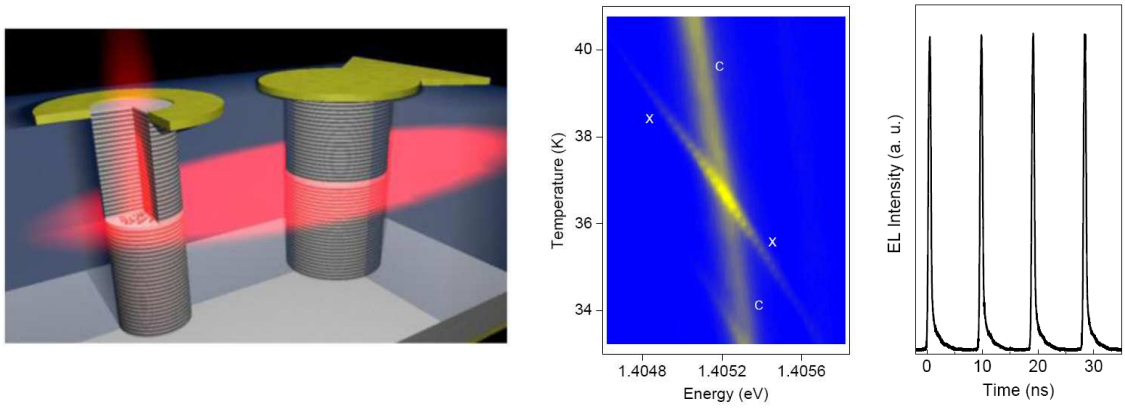

(a) (b) (c)

Figure 1: (a) Schematic view of device design for on-chip quantum optics. The WGM laser (right) resonantly excites a peripheral micropillar cavity (left) acting as non-classical light source. (b) Demonstration of Purcell enhancement of a QD-micropillar under resonant pumping via an electrically driven internal WGM microlaser. (c) Pulsed emission of light from a integrated WGM laser at a repetition rate of 107 MHz.

REFERENCES

1. Stock, E., et al., *Adv. Mater.*, Vol. 25, 707, 2013.
2. Munnelly, P., et al., submitted.

Deterministic Coupling of Multiple Quantum Dots to Selected Modes of a Photonic Crystal Cavity

A. Lyasota, C. Jarlov, B. Dwir, A. Rudra, P. Gallo, and E. Kapon
Ecole Polytechnique Fédérale de Lausanne, Lausanne CH-1015, Switzerland

Abstract— Quantum information science relies on the possibility to transfer information between qubits or quantum memories with photons. Advances have been made recently in this direction in atomic systems [1], however the need for scalability and on-chip integration makes semiconductor systems better candidates. In this abstract, we present the integration of up to four site-controlled semiconductor quantum dots (QDs) in linear photonic crystal (PhC) cavities, and demonstrate the coupling of each QD to the same cavity mode. This is an important step towards the observation of collective effects in few quantum dot systems, such as QD-based nanolasers [2].

We rely on the site-controlled nature of InGaAs pyramidal QDs [3] to ensure a finite overlap of the QD dipoles with the cavity mode field pattern. Furthermore, the high spectral uniformity of these QDs (∼5 meV) is in the range of phonon-mediated coupling interactions [4], ensuring a finite spectral coupling between each QD and a selected cavity mode. We use the QD-cavity coupling signatures already observed in systems comprising of a single QD coupled to a PhC cavity, which include the co-polarization of the excitonic lines with the cavity and off-resonant cavity emission (Figure 1(a)), to investigate the coupling of up to four different QDs to the same cavity mode. QDs are identified by monitoring the intensities of the excitonic spectral features while changing the position of the excitation spot (Figure 1(b)). These excitonic features are indicated in the photoluminescence spectrum displayed in Figure 1(c). The cavity peak was identified by performing polarization resolved photoluminescence measurements while varying the sample temperature. The upper panel of Figure 1(c) shows the degree of linear polarization of the photoluminescence (DOLP). All the QD features, initially unpolarized, have a positive DOLP in the presence of the cavity mode, proving the simultaneous coupling of each QD to the cavity mode.

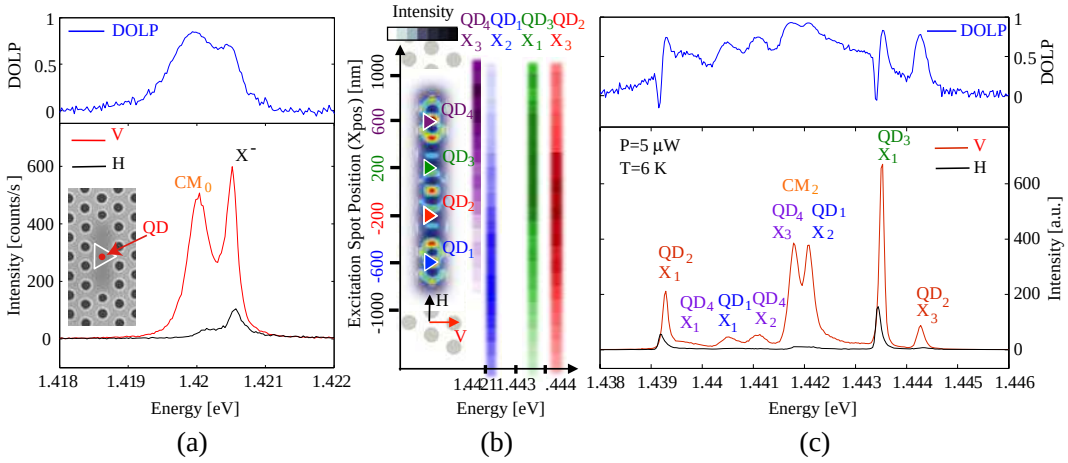

Figure 1: (a) Spectrum of a single QD coupled to the mode of a PhC cavity (see inset for design); upper panel: degree of linear polarization. (b) Design showing the nominal position of the four QDs in the L7 PhC cavity. The intensity of four QD features as a function of the excitation spot position is shown to illustrate how the lines were identified. (c) Spectrum of a four QD structure. The upper panel shows the degree of linear polarization of the luminescence.

REFERENCES

1. Casabone, B., *Phys. Rev. Lett.*, Vol. 114, 023602, 2015.
2. Nomura, M., et al., *Nature*, Vol. 6, 279, 2010.
3. Felici, M., *Small*, Vol. 5, No. 8, 938–943, 2009.
4. Calic, M., *Phys. Rev. Lett.*, Vol. 106, 227402, 2011.

Hybrid Approaches for Single Photon Collection: Diamond Defect Centers on Fibers, Chips, and Polymer Photonic Structures

Oliver Benson
Nano-Optics, Humboldt-University Berlin, Germany

Abstract— Single photon emitters are a key element for future integrated quantum optical technology. Until today many different realizations have been demonstrated, for example single molecules, semiconductor quantum dots or color defect centers. Requirements for scalable applications are reliable integration into other optical elements, stability and room-temperature operation.

Very promising quantum emitters fulfilling all these constraints are defect centers in diamond, and among them the most prominent ones, the nitrogen vacancy (NV) and the silicon vacancy (SiV) center. However, compared to the well-established semiconductor technology micro- or nanointegration and fabrication are still challenging. For this reason a hybrid approach seems promising, where diamond-based single photon emitters are integrated on a different material platform.

In this presentation we present two approaches. One utilizes optical fibers where single photons from color defect centers in nanodiamonds are collected with high efficiency by near-field coupling [1, 2]. Assembly and experimental challenges will be discussed.

In another approach we use direct laser writing to fabricate various light collecting microstructures, such as waveguides, modified lenses or microresonators around pre-characterized nanodiamonds containing single defect centers. We discuss the potential of this technique to realize almost arbitrary three-dimensional architectures, which can be aligned on-demand with respect to several single photon emitters.

REFERENCES

1. Albrecht, R., A. Bommer, C. Pauly, F. Mücklich, A. W. Schell, P. Engel, T. Schröder, O. Benson, J. Reichel, and C. Becher, *Appl. Phys. Lett.*, Vol. 105, 073113, 2014.
2. Liebermeister, L., F. Petersen, A. V. Münchow, D. Burchardt, J. Hermelbracht, T. Tashima, A. W. Schell, O. Benson, T. Meinhardt, A. Krueger, A. Stiebeiner, A. Rauschenbeutel, H. Weinfurter, and M. Weber, *Appl. Phys. Lett.*, Vol. 105104, 031101, 2014.
3. Schell, A. W., H. Takashima, S. Kamioka, Y. Oe, M. Fujiwara, O. Benson, and S. Takeuchi, *Scientific Rep.*, accepted.
4. Schell, A. W., J. Kaschke, J. Fischer, R. Henze, J. Wolters, M. Wegener, and O. Benson, *Scientific Rep.*, Vol. 3, 1577, 2013.
5. Schell, A. W., T. Neumer, Q. Shi, J. Kaschke, J. Fischer, M. Wegener, and O. Benson, *Appl. Phys. Lett.*, Vol. 105, 231117, 2014.
6. Schell, A. W., T. Neumer, and O. Benson, *Opt. Lett.*, Vol. 39, 4639, 2014.

Session 2A4
SC2: Manipulating Light-matter Interaction by Plasmonics 2

Coupling of NV Centers in Nanodiamonds to Plasmonic Waveguides

Sergey I. Bozhevolnyi
Department of Technology and Innovation
University of Southern Denmark, Odense DK-5230, Denmark

Abstract— Surface plasmon (SP) modes supported by various dielectric-metal waveguide configurations facilitate ultra-strong (subwavelength) confinement of electromagnetic fields, enabling miniaturization of photonic circuits and also strongly enhancing interaction of emitters with these modes. The latter feature has important implications in quantum optics, sensing and lab-on-a-chip applications. Here we report experimental investigations of local SP excitation by nitrogen vacancy (NV) centers in individual nanodiamonds (NDs) incorporated into different waveguide configurations. First, we studied the excitation of SPs at a silver-air interface using ND fluorescence. In this case, NDs acted as both a source and a scatterer for propagating SPs. Fluorescence spectra measured from the illuminated ND and from the ND scatterer exhibited significant difference originating from the wavelength-dependent SP propagation loss. We have further studied the SP excitation in waveguiding structures such as dielectric-loaded SP polariton waveguides (DLSPPWs) and V-grooves. Fabricated DLSPPWs were terminated with diffraction gratings that out-coupled fluorescence excited by an illuminated ND and guided as the DLSPPW modes. V-groove geometry is one of the most promising plasmonic waveguide configurations for efficient coupling to quantum emitters. We present fluorescence images, featuring NV centers in one (or several) ND located near the center of the V-groove and coupled to channel SP modes propagating towards terminations shaped as nano-mirrors. Also, in these cases, the local SP excitation by NV fluorescence was evidenced not only by the images obtained but also by the correspondently recorded fluorescence spectra. In parallel, life-time measurements indicate that NDs containing multiple NV centers result in different life-time characteristics for different radiation channels, contrasting the free radiation channel against channels of SP excitation. While we continue further experiments with NDs containing multiple NV-centers studying their spectral and life-time characteristics, we intend in the nearest future to extend our investigations to SP excitation with single NV centers and present the corresponding results at the conference.

Exciton Emission from Plasmonic Metal/Organic Multishell Semiconductor Nanowires

Masoud Kaveh[1], **Ondrej Dyck**[2], **Gerd Duscher**[2],
Qiang Gao[3], **Chennupati Jagadish**[3], **and Hans-Peter Wagner**[1]

[1]Department of Physics, University of Cincinnati
345 Clifton Court, Cincinnati, OH 45221, USA
[2]Department of Materials Science and Engineering, University of Tennessee
421 Ferris Hall, Knoxville, TN 37996, USA
[3]Department of Electronic Materials Engineering, Research School of Physics and Engineering
Australian National University, Canberra ACT 0200, Australia

Abstract— We investigate the emission of excitons in bare and coated plasmonic metal/organic wurtzite/zincblende (WZ/ZB) InP and zincblende AlGaAs/GaAs shell-core nanowires (NWs) by intensity- and temperature-dependent time-integrated (TI) and time-resolved (TR) photoluminescence (PL). The $\sim$ 100 nm diameter III-V NWs were grown using the Au catalyzed vapor-liquid-solid method. The plasmonic InP NWs were coated with a 20 nm thick Alq_3 interlayer and a $Mg_{0.9}$:$Ag_{0.1}$ metal cluster top layer with nominal metal film thicknesses ranging from 10 to 20 nm by organic molecular beam deposition (OMBD). The AlGaAs/GaAs NWs were coated with a 10 nm thick gold film and various Alq_3 spacer thicknesses by OMBD.

Figure 1 shows the PL spectra from uncoated and coated InP NWs at 20 K. The incident excitation intensity was 40 W/cm^2. The red line shows the spectrum of bare InP NWs revealing two strong emission bands at $\sim$ 1.48 and $\sim$ 1.44 eV. These bands, which are separated by the LO-phonon energy, are attributed to nonthermalized weakly and deeply localized indirect WZ/ZB excitons due to randomly distributed short WZ and ZB segments within the NW. The PL yield of both bands increases by a factor of nearly 4 when the InP NWs are covered with an Alq_3 layer (see blue line) which is attributed to surface charge passivation. When the Alq_3 coated InP NWs are subsequently covered with a nominally 15 nm thick Mg:Ag layer, the PL yield of the weakly and strongly localized indirect WZ/ZB exciton bands is reduced by a factor of $\sim$ 20 and $\sim$ 10, respectively, compared to the Alq_3 coated sample, shown by the black line in Fig. 1. Increasing the nominal thickness of the deposited metal to 40 nm further reduces the PL intensity by a factor of 2 (dashed black line). The PL intensity quenching of the indirect WZ/ZB emission is attributed to Förster energy-transfer from mobile or weakly trapped indirect excitons to plasmon oscillations in the Mg:Ag clusters. TR PL investigations on uncoated and plasmonic InP NW support this interpretation revealing the shortest lifetime of weakly localized indirect excitons in metal coated InP NWs while the dynamics of strongly localized indirect WZ/ZB excitons is less affected.

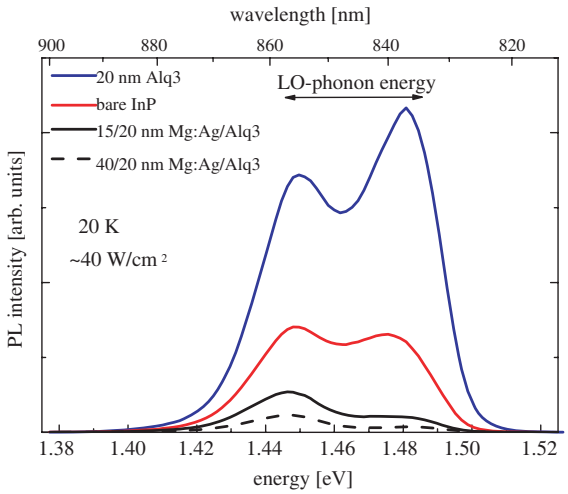

Figure 1: Photoluminescence spectra of bare, Alq_3 coated and plasmonic InP nanowires as labelled at 20 K. The excitation intensity of the He-Ne laser was 40 W/cm^2 for all NW ensembles.

Intensity-dependent PL spectra of zincblende AlGaAs/GaAs NWs show a strong and weak emission band at 1.515 and 1.47 eV at 15 K, which are attributed to the GaAs exciton transition and to an impurity related luminescence, respectively. Plasmonic AlGaAs/GaAs NWs with a ~ 10 nm thick Au coating but without Alq_3 spacer layer reveal a significant reduction of the PL intensity for both emission bands compared with the uncoated NW sample. Plasmonic NW samples with the same nominal Au coverage and an additional Alq_3 interlayer of 5 or 10 nm thickness show a noticeably stronger PL intensity which increases with rising Alq_3 spacer thickness. The observed behaviour suggests that again Förster energy-transfer from free GaAs excitons to plasmon oscillations in the gold film is mainly responsible for the PL quenching.

Controlled energy-transfer from NW excitons to plasmons in the deposited metal has the potential to compensate for metal losses in novel plasmonic devices.

Plasmonics towards the Industry: Sensing, Structural Colors and Solar Light Management

B. Gallinet
CSEM SA, CSEM Muttenz, Switzerland

Abstract— Metallic nanostructures interact strongly with light through surface plasmon modes and many application fields have been proposed during the past decade, including light harvesting to sensing and structural colors. However, their implementation for the industry requires the development of up scalable and cost effective manufacturing processes. The fabrication at wafer scale of plasmonic nanostructures and metamaterials using nano imprint lithography is reported. After structuring, one or several evaporations of various plasmonic materials are performed with a tilt angle with respect to the substrate, which increases the light interactions with the different metallic layers as well as enlarges the design possibilities. A step and repeat process is used to increase further the area of nanostructured surface. The measured optical properties of the fabricated structures show a very good agreement compared to numerical calculations using the rigorous coupled wave analysis and the surface integral method. These numerical calculations together which structural characterization, increase the process control and enable the design of the nanostructures for specific applications. In particular, nanostructures with a shape similar to split ring resonators and which support high order plasmonic modes showing Fano resonances are shown to be promising for sensing applications. Another kind of plasmonic substrates is reported, which shows unique color effects with a large palette of colorations. With a specific design, the structural colors are associated with a strong interaction between the polarizations which increases the complexity of the color effect rendered to the user. Finally, the potential of plasmonic nanostructures for the management of solar light is discussed.

Theory of Localized Plasmons for Multiple Metal Nanostructures

Masakazu Ichikawa
Department of Applied Physics, Graduate School of Engineering
The University of Tokyo, Japan

Abstract— Many theoretical studies of the localized plasmons in metal nanostructures have been reported until now [1]. We have also reported a theory of localized plasmons for metal nanostructures in random-phase approximation (RPA) [2] and have recently developed it to consider the retardation of the electromagnetic potentials [3]. In this presentation, a theory of localized plasmons in multiple metal nanostructures is reported, which is the development of the previous ones.

Considering the retardation of the scalar potentials and the local electron density $n(\mathbf{r})$, an effective scalar potential $\varphi_{\mathit{eff}}(\mathbf{r}, \omega)$ and an external scalar potential $\varphi_{ext}(\mathbf{r}, \omega)$ satisfy the following equation in the RPA at high-frequency condition (plasmon frequency region) [3]:

$$\varphi_{\mathit{eff}}(\mathbf{r}, \omega) = \varphi_{ext}(\mathbf{r}, \omega) + \int d\mathbf{r}_1 G_0(\mathbf{r} - \mathbf{r}_1, \omega)\, \rho(\mathbf{r}_1, \omega),$$
$$\because\ \rho(\mathbf{r}_1, \omega) \equiv -\frac{e^2}{m_e \omega^2} \nabla_1 \cdot [n(\mathbf{r}_1)\, \nabla_1 \varphi_{\mathit{eff}}(\mathbf{r}_1, \omega)], \tag{1}$$

where $G_0(\mathbf{r} - \mathbf{r}_1, \omega)$ is the retarded Green's function that satisfies the following Helmholtz equation.

$$\left(\nabla_{\mathbf{r}}^2 + \omega^2/c^2\right) G_0(\mathbf{r} - \mathbf{r}_1, \omega) = -4\pi\delta(\mathbf{r} - \mathbf{r}_1), \quad G_0(\mathbf{r} - \mathbf{r}_1, \omega) = \exp(i\omega/c \cdot |\mathbf{r} - \mathbf{r}_1|) / |\mathbf{r} - \mathbf{r}_1|.$$

$\rho(\mathbf{r}_1, \omega)$ in Eq. (1) is the induced electric charge density by the localized plasmon excitation. The local electron density $n(\mathbf{r})$ is expressed by $n(\mathbf{r}) = \sum_n n_0(\mathbf{r} - \mathbf{R}_n)$ for multiple metal nanostructures where $\mathbf{R}_n$ is the position of the each nanostructure. When the quasi-static approximation is used, neglecting the retardation ($c \to \infty$), the localized plasmon excitations in multiple metal nanospheres can be analytically studied. When the electron density is assumed to have a step function shape at the nanosphere surface ($r = a$), Eq. (1) can be analytically solved by using the normalized spherical harmonics and the following determinant equation is derived to calculate the localized surface plasmon frequency:

$$\det\left[\left(\omega^2 - \frac{\omega_p^2 l}{2l+1}\right)\delta_{ll'}\delta_{mm'}\delta_{ns} - \frac{\omega_p^2 l' a^{l'+1}}{(2l'+1)} B_{lm;\,l'm'}(\mathbf{R}_n - \mathbf{R}_s,\, a)(1 - \delta_{ns})\right] = 0,$$
$$\because\ B_{lm;\,l'm'}(\mathbf{R}_n - \mathbf{R}_s,\, a) = \int d\Omega_{\mathbf{r}} \left.\frac{Y_{lm}^*(\mathbf{r})\, Y_{l'm'}(\mathbf{r} + \mathbf{R}_s - \mathbf{R}_n)}{|\mathbf{r} + \mathbf{R}_s - \mathbf{R}_n|^{l'+1}}\right|_{|\mathbf{r}|=a}, \tag{2}$$

where $\delta_{ll'}$ etc. are the Kronecker's delta functions, ω_p is the bulk plasmon frequency, $\Omega_{\mathbf{r}}$ is the solid angle for $\mathbf{r}$ at $|\mathbf{r}| = a$, Y_{lm}^* and $Y_{l'm'}$ are the normalized spherical harmonics, and $\mathbf{R}_n$, $\mathbf{R}_s$ are the central positions of the metal nanospheres. The first term of Eq. (2) gives the surface plasmon frequency $\omega = \omega_p\sqrt{l/(2l+1)}$ for the individual nanosphere and the second term gives the frequency shift caused by the interaction between the multiple nanospheres. The calculation for the nanosphere dimer gives the red frequency shift that is proportional to $-(a/|\mathbf{R}_s - \mathbf{R}_n|)^2$ in the dipole approximation ($l = l' = 1$). The property of the red shift coincides with that of other studies [1, 4]. We also report the light emission from the nanosphere dimer, a formula of the localized plasmons for the periodic metal nanostructures using the Bloch's theorem and a method to consider the retardation of the scalar potentials using the structural Green's function method [5].

REFERENCES

1. García de Abajo, F. J., *Rev. Mod. Phys.*, Vol. 82, 209, 2010.
2. Ichikawa, M., *J. Phys. Soc. Jpn.*, Vol. 80, 044606, 2011.
3. Ichikawa, M., *e-J. Surf. Sci. Nanotech.*, Vol. 12, 431, 2014.
4. Scholl, J. A., et al., *Nano Lett.*, Vol. 13, 564, 2013.
5. Kohn, W. and N. Rostoker, *Phys. Rev.*, Vol. 94, 1111, 1954.

Van der Waals Interaction between Plasmonic Particles with Diminutive Geometric Features: A Transformation Optics Approach

Yu Luo[1], **Rong Kuo Zhao**[2], **and J. B. Pendry**[3]

[1]School of Electrical and Electronic Engineering
Nanyang Technological University, Nanyang Avenue 639798, Singapore
[2]NSF Nano-scale Science and Engineering Center, 3112 Etcheverry Hall
University of California, Berkeley, California 94720, USA
[2]The Blackett Laboratory, Department of Physics
Imperial College London, London SW72AZ, UK

Abstract— Understanding the van der Waals interaction between plasmonic particles with diminutive geometric features is paramount to many microelectromechanical applications. However, modelling of this type is widely acknowledged as a difficult task because the plasmon modes supported by these systems are difficult to describe with traditional electromagnetic methods. In this talk, I will describe an efficient and accurate approach based on transformation optics [1] to investigate three-dimensional (3D) sharp plasmonic particles. This approach enables us to transform an apparently unsymmetrical plasmonic system to a more symmetrical partner with an identical spectrum and through which the electromagnetic properties can be classified and calculated analytically. For a pair of plasmonic tips and the tip-plane coupled system, we present details of this technique and discuss the characteristics of the plasmon modes and van der Waals forces [2]. The results are compared with the sphere-sphere and sphere-plane configurations [3, 4]. A deviation is observed for tips with a small cone angle.

REFERENCES

1. Pendry, J. B., Y. Luo, and R. K. Zhao, "Transforming the optical landscape," Submitted to *Science*.
2. Luo, Y., R. K. Zhao, and J. B. Pendry, "Van der Waals interactions between plasmonic nanotips," in Preparation.
3. Pendry, J. B., A. I. Fernandez-Dominguez, Y. Luo, and R. K. Zhao, "Capturing photons with transformation optics," *Nature Physics*, Vol. 9, 518–522, 2013.
4. Zhao, R. K., Y. Luo, A. I. Fernandez-Dominguez, and J. B. Pendry, "Description of van der Waals interactions using transformation optics," *Phys. Rev. Lett.*, Vol. 111, 033602, 2013.

Plasmonic and Metamaterial Band Theory: Fundamentals and Applications

Aaswath Raman, **Wonseok Shin**, **and Shanhui Fan**
Ginzton Laboratory, Stanford University, Stanford, CA, USA

Abstract— The past two decades have been extraordinary advances in the study and understanding of nanoscale photonic structures such as photonic crystals, plasmonic structures and metamaterials. As researchers have sought to fully characterize and explore the physical phenomena possessed by such nanophotonic structures, it has become increasingly necessary to understand how such structures behave over a broad range of frequencies. It is both of intrinsic and applied interest to develop an analytical, physical framework capable of describing the electromagnetic modes of all plasmonic and metamaterial systems in a general way: a plasmonic and metamaterial band theory.

The need to accurately calculate the eigen modes and band structures of such periodic structures numerically, and place analytic constraints on the modes of plasmonic systems whose constituent materials are typically dispersive and metallic, motivates the development of a rigorous plasmonic band theory. Beyond band structure computation, the development of a plasmonic band theory would also allow one to fully study and characterize important plasmonic/metamaterial device applications. In particular, there has been substantial recent interest in using plasmonic structures for active devices and sensing. Finally, the development of device applications is ultimately contingent on basic physical limits related to the use of dispersive materials such as metals in these systems. Understanding limits on the modal loss introduced by these metals is of vital importance.

In our work, we introduce a rigorous metamaterial band theory. We first demonstrate that the band structure of dispersive photonic crystals, plasmonic structures and optical metamaterials, in general, can be obtained by solving a standard matrix eigenvalue problem. In the case where the material can be approximated as lossless, the eigenvalue problem is Hermitian, which directly leads to an orthogonality-condition for modes at different frequencies. We next implement the band theory numerically using a finite difference scheme and demonstrate its effectiveness. We further build upon the band theory to construct a plasmonic perturbation theory that can generally treat the effect of small changes in any system parameter, whether geometric or material. In particular, we use the perturbation theory to predict modal frequency shifts due to changes in the dielectric constants of dispersive systems involving both metals and dielectrics. Finally, we prove rigorously that, for any electromagnetic mode of a plasmonic metamaterial structure, there exists an upper bound on its material loss rate. When the plasmonic material is described by a multi-pole Lorentz model, the upper bound is a frequency dependent weighted-average of the damping rates of the oscillators that underlie the poles. We validate this proof by full-field simulations of a variety of systems including periodic arrays of slot antennas.

Characteristics of Guided Modes in Plasmonic Metal/Aluminumquinoline Multilayer Waveguides

Niranjala Wickremasinghe[1], **Jonathan Thompson**[1], **Xiaosheng Wang**[1], **Heidrun Schmitzer**[2], **and Hans-Peter Wagner**[1]

[1]Department of Physics, University of Cincinnati, 345 Clifton Court, Cincinnati, OH 45221, USA
[2]Department of Physics, Xavier University, 3800 Victory Parkway, Cincinnati, OH 45207, USA

Abstract— We investigated the mode properties of planar plasmonic aluminum-quinoline (Alq_3) multilayer waveguides which have one single or three equally spaced nanometer-thin $Alq_3Mg_{0.9}$:$Ag_{0.1}$ composite metal-island layers in or near the center. The waveguides were grown by organic molecular beam deposition (OMBD) on 0.5 mm thick amorphous Pyrex® substrates at room temperature. An alloy of 90% Mg and 10% Ag ($Mg_{0.9}$:$Ag_{0.1}$) was used for the metal layers. Atomic force microscopy (AFM) on similarly thin Mg:Ag layers showed that the metal was deposited as clusters with layer filling factors ranging from 0.7 to 0.9.

Three of the $\sim$ 2.0 µm thick Alq_3 films had one single centered Mg:Ag layer each, nominal thickness of 8, 10 and 15 nm, respectively. In addition, a $\sim$ 2.0 µm thick stack of four Alq_3 layers (thickness of each: 500 nm) and three embedded Mg:Ag layers (thickness of each: 10 nm) was grown. Deviations from the nominal total growth thicknesses of the deposited films were determined using a profilometer prior to the optical investigation and were considered in the data evaluation. We used the m-line technique at a wavelength of 633 nm to investigate the effect of the inserted composite metal cluster layer(s) on the effective refractive indices n_{eff} of TM and TE modes and compared the results with a pure Alq_3 waveguide as reference. The effective refractive indices n_{eff} and field distributions of each mode were also calculated with a multilayer waveguide model.

We find that the effective refractive indices n_{eff} increase with the thickness of the inserted metal layer for odd TM modes, because these modes have an antinode at the position of the metal layer. Since even TM modes have a node at the metal layer, their refractive indices n_{eff} remain nearly unchanged. In TE modes, the metal layer forces a local minimum in the electric field distribution at the position of the metal film. The resulting field distribution of odd TE modes, which should have an antinode at the position of the composite metal layer, thus becomes similar to the field distribution of the adjacent next higher even TE mode (see Figure 1). This leads to lower effective refractive indices n_{eff} for odd TE modes compared to the pure Alq_3 reference. Even TE modes, which have a node at the location of the inserted metal film, have similar n_{eff} values as the pure Alq_3 reference. Accordingly, the metal resistivity losses are highest for odd TE modes, while they are less for even TE modes.

Our investigations suggest that strategically placed composite dielectric-metal or continous metal layers could be used to selectively increase the effective refractive indices of specific TM or TE modes, while at the same time decreasing the n_{eff} value of others. It is also possible to excite and/or attenuate certain TM or TE modes in a controlled way: This way mode selective attenuaters could be realized by inserting metal stripes into a dielectric waveguide during growth.

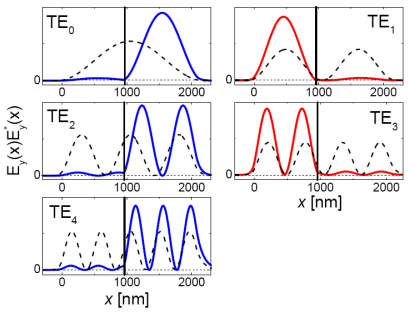

Figure 1: Calculated squared electric field distribution of guided TE modes in a plasmonic Alq_3 waveguide with a nominal 15 nm thick single Mg:Ag metal layer. The vertical line indicates the position of the composite metal layer with respect to the air/Alq_3 interface at $x = 0$. Calculated field distributions of TE modes in a pure Alq_3 reference waveguide are given as dashed lines.

Nanoantennas with Dual-wavelength Plasmonic Hotspots

Juan Xia[1] **and Sailing He**[1, 2]

[1]Centre for Optical and Electromagnetic Research
JORCEP [Sino-Sweden Joint Research Center of Photonics]
Zhejiang Provincial Key Laboratory for Sensing Technologies, Zhejiang University
East Building No. 5, Zijingang Campus, Zhejiang University, Hangzhou 310058, China
[2]Department of Electromagnetic Engineering, Royal Institute of Technology, Stockholm 10044, Sweden

Abstract— Plasmonic nanoantennas create strongly enhanced local fields when pumped resonantly as well as provide highly increased local densities of photon states. By coupling quantum emitters such as quantum dots, fluorescent molecules or atoms to specially designed nanoantennas, large fluorescence enhancement and effective emission control can be realized. Generally, the emission spectra of quantum emitters are different from their absorption analogues, which means, if we want to boost the absorption and control the emission simultaneously, at least two plasmonic resonances are needed for nanoantennas, one at the excitation wavelength and the other at the emission wavelength. Here we designed a novel nanoantenna with a dual-wavelength hotspot, which could be viewed as a combination of two different gap antennas and is featured by two different resonances sharing one plasmonic hotspot at the same gap region. One of the resonances at shorter wavelength is expected to be used for excitation enhancement, while the other one at longer wavelength used for emission control due to modified radiative decay rate. Another remarkable advantage of this nanoantenna is that by adjusting its shape (each gap antenna's arm length, width, orientation, etc.), each resonance's wavelength can be tuned separately. Finite-difference time-domain simulations (FDTD Solutions, Lumerical) of the antenna-emitter system were performed. For fabrication, chemically synthesized plasmonic nanoparticles were accurately moved and assembled by using an AFM tip to form this antenna. Finally, we used dark field scattering spectroscopy to characterize this dual-wavelength nanoantenna. This presented nanoantenna is a highly promising means for emission control of single quantum emitters.

Hydrodynamic Model for Nonlinear Plasmonics: From Nonlinear Mode Coupling to Supercontimuum Generation

Alexey V. Krasavin[1], **Pavel Ginzburg**[1,2], **Paulina Segovia**[1], **Giuseppe Marino**[1], **Gregory A. Wurtz**[1], **and Anatoly V. Zayats**[1]

[1]Department of Physics, King's College London, London WC2R 2LS, United Kingdom
[2]School of Electrical Engineering, Tel Aviv University, Ramat Aviv, Tel Aviv 69978, Israel

Abstract— The electromagnetic response of a free-electron gas leads to the inherent nonlinear optical behaviour of nanostructured plasmonic materials enabled through both strong local field enhancements and complex collective electron dynamics [1]. In this presentation, we will overview our recent results on implementation of the hydrodynamic model for conduction electrons to describe a broad range of nonlinear effects in metallic nanostructures. It will be started with an illustrative hydrodynamic analytical approach, defining the nonlinear coupling of the plasmonic modes in metallic nanoparticles, particularly revealing an important role of the resonance symmetries [2]. In the further development, we will report our very recent numerical time-domain implementation of the hydrodynamic model, which enables non-perturbative studies of nonlinear coherent interactions between light and plasmonic nanostructures without any simplifications [3]. The effects originating from the convective acceleration, the magnetic contribution of the Lorenz force, the quantum electron pressure, as well as the presence of the nanostructure's boundaries are taken into account leading to the appearance of second, third and higher harmonics in the scattering field of a metallic nanorod (Fig. 1) [2]. We will also report supercontinuum generation in resonantly-tuned metallic nanospirals originating from the nonlocal effects [3]. The proposed time-domain method enables one to obtain a universal, self-consistent numerical solution free from any approximations, enabling investigations of nonlinear optical interactions with arbitrary shaped optical pulses, in contrast to the generally employed plane-wave CW pump assumption, opening unique opportunities to approach realistic experimental scenarios.

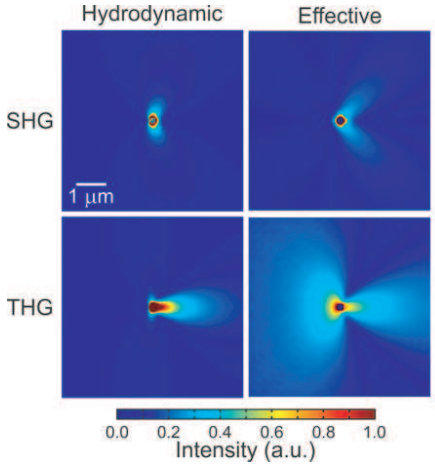

Figure 1: Comparison of SHG and THG scattering fieldmaps obtained using hydrodynamic and phenomenological effective models.

REFERENCES

1. Kauranen, M. and A. V. Zayats, "Nonlinear plasmonics," *Nature Phot.*, Vol. 6, 737–748, 2012.
2. Ginzburg, P., A. Krasavin, Y. Sonnefraud, A. Murphy, R. J. Pollard, S. A. Maier, and A. V. Zayats, "Nonlinearly coupled localized plasmon resonances: Resonant second-harmonic generation," *Phys. Rev. B*, Vol. 86, 085422, 2012.
3. Ginzburg, P., A. V. Krasavin, G. A. Wurtz, and A. V. Zayats, "Nonperturbative hydrodynamic model for multiple harmonics generation in metallic nanostructures," *ACS Photonics*, Vol. 2, 8–13, 2015.

Three Dimensional Orientation and Rotation of Nanostructures Using Optical Torques

T. V. Raziman and Olivier J. F. Martin
Nanophotonics and Metrology Laboratory
Swiss Federal Institute of Technology Lausanne (EPFL), Lausanne-1015, Switzerland

Abstract— Light carries linear and angular momenta, and can impart these to nanoparticles, exerting optical forces and torques on them. The field of optical nanomanipulation has grown tremendously in the recent years, and the ability to trap nanoparticles and rotate and orient them in desired ways promises many practical applications. Here, we present a study on how optical torques can be used to orient plasmonic nanoparticles in desired directions as well as continuously rotate them about an axis. The electromagnetic response of plasmonic particles is simulated using the surface integral equation (SIE) method, and optical forces and torques are evaluated by integrating the Maxwell's stress tensor from the SIE surface currents directly.

A linearly polarised plane wave can exert a restoring torque on nanoparticles, orienting them both in the direction of propagation and perpendicular to it. We analyse how the restoring torques in the two directions can help achieve full three-dimensional orientation of particles. We find the equilibrium orientations of the particles and analyse how angular displacements away from these orientations tend to result in a stabilising or destabilising torque on them, making them orientations of stable and unstable equilibria, respectively.

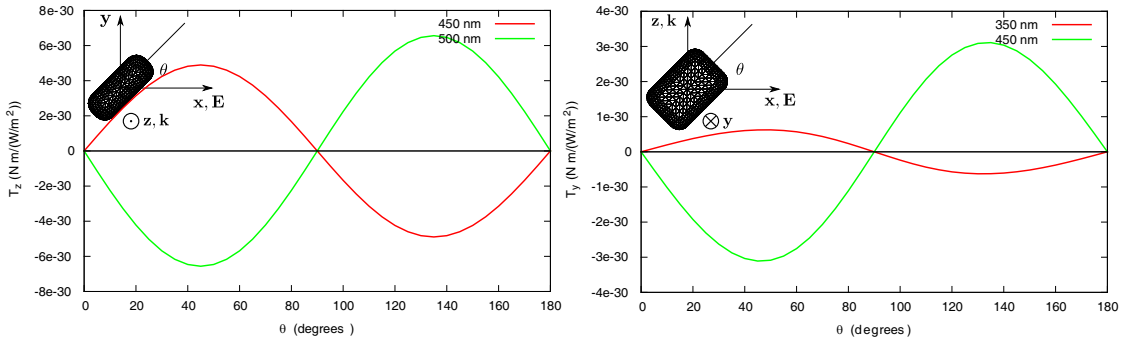

Figure 1: Optical torques on a silver cuboid ($L_x = 100\,\text{nm}$, $L_y = 40$ nm, $L_z = 70\,\text{nm}$) due to an x-polarised plane wave propagating in the z direction when given an angular displacement θ about (a) z axis and (b) y axis

As an example, consider the torques on a silver cuboid given an angular displacement about the z and y axes. For displacement about the z axis, as shown in Fig. 1(a), both $\theta = 0°$ and $\theta = 90°$ are equilibrium positions for both incident wavelengths of 450 nm and 500 nm. At 450 nm, a small displacement from 90° results in a restoring torque. As a result, the particle executes oscillations about 90°, and would settle to the equilibrium position in the presence of damping. On the other hand, displacement from 0° causes the particle to continue rotating in the same direction making it unstable. The opposite behaviour is seen at 500 nm with the stable equilibrium now occurring at 0°. A similar switch of stable equilibrium orientation is seen for displacement about the y axis as well, as seen in Fig. 1(b). We analyse the switching of the stable orientation as a function of wavelength, and explain the features in terms of the modes of the system. In addition, we show how circularly polarised waves can be used to continuously rotate nanoparticles.

Suppression of Light Scattering with ENZ-metamaterials

Alexander S. Shalin[1, 2, 3], **Pavel A. Belov**[1], **and Yuri S. Kivshar**[1, 4]

[1]ITMO University, St. Petersburg 197101, Russia
[2]Kotel'nikov Institute of Radio Engineering and Electronics of RAS, Ulyanovsk 432011, Russia
[3]Ulyanovsk StateUniversity, Ulyanovsk 432017, Russia
[4]Nonlinear Physics Center, Australian National University, Canberra ACT 0200, Australia

Abstract— Nearly perfect concealing of arbitrary objects in hyperbolic metamaterial acting as an alignment-free cloak is proposed. The scattering suppression relies on the combination of normal and additional modes simultaneously existing in a spatially dispersive material.

Suppression of scattering in a specifically design material environment leads to reduced detectability of objects, and may, ultimately, result in "invisiblity" if the scattering is absent. The concept of 'cloaking' was introduced in [1, 2] and gained considerable attention due to continuous demand to achieve invisibility for radar waves [3] and visible light [4, 5]. The general approaches for cloaking rely either on transformation optics concepts [1] or conformal optical mapping of complex electromagnetic potentials [2]. While the former generally results in the requirements of highly anisotropic (and sometimes singular) electric and magnetic susceptibilities of a medium of a cloak, the latter approach requires a position-dependent refractive index variation but is restricted for two-dimensional geometries by its nature.

Here we demonstrate cloaking of arbitrary shaped and arbitrary (not necessarily subwavelength) sized objects placed inside a layered metal-dielectric metamaterial. We show that a metamaterial realization has major influence on the cloaking phenomenon since the electromagnetic response of those plasmonic multilayers is substantially affected by spatial dispersion effects [6]. Investigation of the exact numerical model, taking into account material losses and finite dimensions of the metamaterial realization, shows the possibility of nearly perfect cloaking of arbitrary shaped bodies with the minimal variations of the phase front of the transmitted/reflected optical wave and highly suppressed scattering. Analysing the dipolar emission inside spatially dispersive layerd metamaterial by considering its spatial dispersion (Fig. 1(a)), we show that in contrary to the free space scenario the radiation patterns have flat uniform wavefronts (Fig. 1(b)). Beeing the 0-order approximation in the scattering analysis, the dipole paves a way for investigation more complex geometries. Figs. 1(c), (d) show the electromagnetic scattering in the empty cloak and the one with an object inside. The similarity between transmitted wave fronts verifies the validity of the general concept.

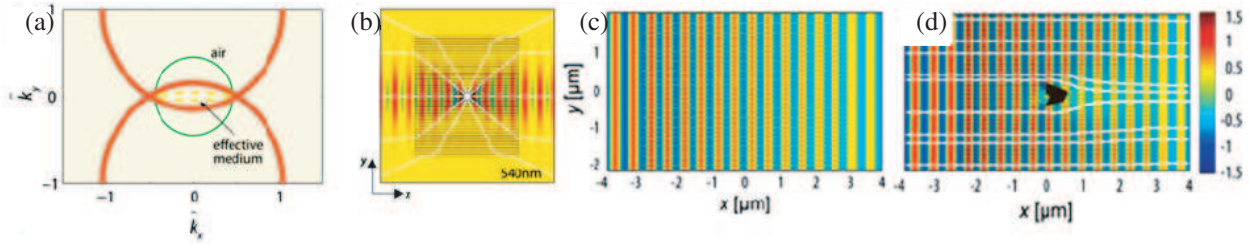

Figure 1: (a) Isofrequency contours for multilayered metamaterial (100 nm air and 20 nm Au) at $\lambda = 540$ nm. Red curves show propagation modes: (bright) main, (pale) additional. Green circle represents light cone in air. Yellow — isofrequency contours, simulated in the effective medium theory. (b) The electric field (y-component) distributions of the radiating y-polarized dipole situated in the centre of the metamaterial block of 15×4 μm size at the wavelength corresponding to the isofrequency contours in (a). Wave numbers k_x and k_y are normalized to the Brillouin zone boundaries $\pi/(d_a + d_g)$. White lines represent the power flow. (c) Electric field (y-component) distributions for the plane wave illuminating the empty cloak. (d) PEC object (larger than the wavelength) of an arbitrary shape inside the cloak.

In addition, the nearly perfect operation for 2D objects has been shown to be preserved for relatively long (longer than the wavelength) 3D arbitrary shaped objects. Moreover, other cloaking scenarios, interplay between local and nonlocal metamaterial dispersion, comprehensive analytical theory will be presented. The proposed type of cloaking may find use not only in the conventional concealing applications but also serve as a platform for 'cloaked detectors' schemes [7] where bulk and alignment free cloaks may significantly reduce the complexity of the realisation.

REFERENCES

1. Pendry, J. B., D. Schurig, and D. R. Smith, *Science*, Vol. 312, 1780, 2006.
2. Leonhardt, U., *Science*, Vol. 312, 1777, 2006.
3. Schurig, D., J. J. Mock, B. J. Justice, S. A. Cummer, J. B. Pendry, A. F. Starr, and D. R. Smith, *Science*, Vol. 314, 977, 2006.
4. Valentine, J., J. Li, T. Zentgraf, G. Bartal, and X. Zhang, *Nature Materials*, Vol. 8, 568, 2009.
5. Cai, W., U. K. Chettiar, A. V. Kildishev, and V. M. Shalaev, *Nature Photon.*, Vol. 1, 224, 2007.
6. Orlov, A. A., S. V. Zhukovsky, I. V. Iorsh, and P. A. Belov, *Photonics and Nanostructures*, Vol. 12, 213, 2014.
7. Fan, P., U. Chettiar, L. Cao, F. Afshinmanesh, N. Engheta, and M. Brongersma, *Nature Photon.*, Vol. 6, 380, 2012.

Session 2A5
SC3: Ultra-thin Metal-dielectric Structured Surfaces and Thin Films for Antireflection, Light Trapping, and Perfect Absorption 1

Perfect Optical Absorbtion to Achieve High Efficiency of Photon-to-heat Conversion with a Multi-layered Metal/Dielectric Film Structure in the Solar Radiation Region

M. H. Liu[1], E. T. Hu[1], Y. Yao[1], K. Y. Zang[1], N. He[2], J. Li[1], Y. X. Zheng[1], S. Y. Wang[1], Y. M. Yang[1], O. Yoshie[2], Y. P. Lee[3], C. Z. Wang[4], D. W. Lynch[4], X. X. Liu[5], J. J. Zheng[5], W. Wei[5], and L. Y. Chen[1]

[1]Department of Opt. Sci. & Eng., Fudan University, Shanghai, China
[2]Graduate School of IPS, Waseda University, Fukuoka, Japan
[3]Department of Phy., Hanyang University, Seoul, Korea
[4]Department of Phy., Iowa State University, Ames, Iowa, USA
[5]School of Opto-Elec. Eng., Nanjing University of Post and Telecom., China

Abstract— In order to overcome the physical limits, the ways to realize high efficiencies close to the theoretical limit for solar-to-heat conversion in the solar radiation region have been studied. In terms of numerical calculations based on the spectral properties of multilayer stacks with different metal/dielectric materials and film thickness, the optical properties and thermal stability of a typical 6-layered metal/dielectric film structure are investigated in this work. A high optical absorption average of $> 98\%$ is achieved in the broad spectral range of 250–1200 nm with experiment results, in good agreement with our simulated results. The samples have a typical layered structure of: SiO_2(57.3 nm)/Ti(5.7 nm)/SiO_2(67.1 nm)/Ti(11.6 nm)/SiO_2(51.4 nm)/Cu($>$ 100 nm), deposited on optically polished Si or K9-glass substrates by magnetron sputtering. The sample of the 6-layered metal/dielectric film structure has an AM1.5G solar absorptance of 95.5% with the features of low thermal emittance of 0.136 at 700 K and good thermal stability, and will be potentially suitable for practical application in high-efficiency solar absorber devices in many fields.

Guided-mode Resonant Nanophotonic Devices: Physics, Design, Fabrication, and Characterization

Robert Magnusson, **Jae Woong Yoon**, **Manoj Niraula**, **and Kyu Jin Lee**
Department of Electrical Engineering, University of Texas — Arlington
Arlington, Texas 76019, USA

Abstract— Many innovative device concepts in nanoplasmonics and nanophotonics rely on intricate resonance effects generated with nanopatterned films. As incident light couples to the film, attendant resonance effects impose diverse spectral signatures on the output light. The guided-mode resonance (GMR) concept refers to quasi-guided, or leaky, waveguide modes induced in periodic layers. Whereas the fundamental GMR occurs in any diffraction regime, subwavelength architectures enable the most useful spectra. Even though these effects have been known for a long time, new attributes and application possibilities continue to appear. Wide parametric design spaces allow precise control of light amplitude, phase, polarization, near-field intensity, and light distribution on surfaces as well as within the device volume. The output spectra can be retrieved in either transmission or reflection. Applications such as laser mirrors, multiparametric biosensors, solar-cell absorption enhancement, tunable filters, narrowband nanoelectromechanical display pixels, nonlinear conversion, surface-enhanced Raman spectroscopy, slow-light control, leaky-mode nanoplasmonics, resonant Rayleigh reflectors, and many others have been suggested in the past.

In this paper, we review the physics of GMR device operation, illustrate their design with rigorous methods, discuss fabrication processes, and present results of physical and spectral characterization. We indicate the application potential of this field, discuss some past device examples, and provide new and emerging aspects. In particular, we present new wideband resonant reflectors designed with gratings in which the grating ridges are matched to an identical material thereby eliminating local reflections and phase changes. This critical interface therefore possesses zero refractive-index contrast; hence we call them "zero-contrast gratings." For simple gratings with two-part periods, we show that zero-contrast grating reflectors outperform comparable high-contrast grating reflectors with nearly 700-nm bandwidth achieved at 99% reflectance. We introduce a new class of reflectors and polarizers fashioned with dielectric nanowire grids that are mostly empty space. We provide computed results predicting high reflection and attendant polarization extinction in multiple spectral regions. Experimental results with Si nanowire grids yield ∼200-nm-wide band of total reflection for one polarization state and free transmission of the orthogonal state. Finally, resonance elements functioning as simultaneous spatial and spectral filters are introduced and substantiated with computed and experimental results that are in excellent agreement.

Tunable Graphene Absorber in the Visible Region Based on Plasmonic Metamaterials

Jinfeng Zhu[1], **Yijun Cai**[1], **Yanqiang Bai**[1], **and Qing Huo Liu**[2]

[1]Institute of Electromagnetics and Acoustics, Department of Electronic Science
Xiamen University, Xiamen 361005, China
[2]Department of Electrical and Computer Engineering, Duke University, Durham, NC 27708, USA

Abstract— Manipulation and enhancement of light absorption in graphene is a significant issue for applications of graphene-based optoelectronic devices. In order to achieve this purpose in the visible region, we have proposed a novel optical absorber for graphene inspired by the design principles of plasmonic perfect absorbers. Based on the design principles of metamaterial ideal absorbers, the reflectance and transmittance of the artificial structure must reach the minimum, which is determined by the match of wave impedance between air and the artificial medium. In an metal-dielectric-metal structure, there is no transmittance, and its reflectionless property depends on the electromagnetic coupling induced by a gap-plasmon guided mode, which is influenced by the size and separation period of metal nanoribbon, loss in the metal, and effects of dielectric spacers. Therefore, with regard to these factors, we investigate the optical absorption enhancing mechanism of single and multilayer graphene, and discuss the light manipulation approaches in the proposed nanostructure. The result shows the absorption spectra of graphene is sensitive to the polarization of incident light but almost independent of the incident angle. Furthermore, the peak position and bandwidth of graphene absorption spectra are tunable in a wide wavelength range through a specific structural configuration. The research reveals the potential implementation of plasmonic perfect absorbers for graphene absorption in novel nanophotonic devices, and provides a guide to design related nanostructures and devices.

Enhanced Linear and Nonlinear Behaviors of Graphene under Localized Surface Plasmon Resonances: Analyses with Boundary-integral Spectral Element Method

Jun Niu[1], **Ma Luo**[2], **and Qing Huo Liu**[1]

[1]Duke University, USA
[2]Wave Computation Technologies, Inc., USA

Abstract— Graphene has been considered as a promising alternative for silicon in the next generation advanced optoelectronic devices. Over the past few years, a considerable number of optoelectronic devices have been demonstrated based on graphene's linear optical performance. However, despite its outstanding quantum efficiency and fast carrier mobility, graphene's application in several categories of designs is still challenging. When designing graphene-based photodetectors around visible spectra, two typical limitations need to be overcome: The 2.3% optical absorption of floating single-atom layer graphene is poor for photo-responsivity. Additionally, graphene shows a considerably at absorption in the visible to near-infrared spectra, and thus does not provide a frequency selectivity.

As another crucial property, graphene's nonlinear optical behavior is also under intensive theoretical and experimental studies. Recent investigations show that single layer graphene's third-order nonlinear optical response is particularly strong. Previous four wave mixing experiment shows that the effective third-order susceptibility is in the order of $|\chi^{(3)}| \sim 10^{-15}\,\mathrm{m}^2/\mathrm{V}^2$. Moreover, although the centrosymmetric structure of graphene theoretically forbids the emission of second harmonic generation, this symmetry can be broken by its adjacent materials. However, few tools are available for numerically analyzing these interesting nonlinear phenomena within relatively complex designs.

In this work, effective light absorption engineering of graphene around visible spectrum by localized surface plasmon resonances (LSPR) is first proposed. Based on boundary-integral spectral element method (BI-SEM), we theoretically investigate the strategy of incorporating periodic gold nanoparticle (NP) cluster arrays with Bragg reflectors into the prototypes of graphene-based photodetectors. Numerical simulation shows that the proposed structures can effectively engineer the light absorption in graphene by tuning plasmon resonances. In the spectra of 300 nm to 1000 nm, a maximum light absorption of 67.54% is observed inside a graphene layer, while it is 41% within the visible spectra.

In the meantime, while the photo-responsivity can be improved via LSPR by confining a significant amount of energy inside the graphene layer, graphene's nonlinear optical field generation can also be dramatically enhanced. To study this interesting nonlinear interaction, we further investigated graphene's nonlinear performance with accurate numerical analysis. Based on BI-SEM, the optical fields at fundamental frequency and high order harmonic frequency are solved iteratively. For a complete nonlinear optical evaluation, both the backward and forward exiting power and the stored energy of the nonlinear fields are provided. With the spectral accuracy of BI-SEM, the proposed numerical method is able to solve the optical fields accurately with a relatively high convergence rate. Meanwhile, the flexibility of spectral element method also makes this scheme suitable for the simulation of more complex optoelectronic designs.

Strong Light-matter Interaction in Nano- and Micro-scale Heterostructures

B. S. Simpkins
Chemistry Division, Naval Research Laboratory, Washington, DC 20375, USA

Abstract— Inducing strong interactions between light and matter is at the heart of technologies such as photovoltaics, sensing, analytic spectroscopies, optical computing, and photo-catalysis for energy production or pollutant remediation. In this discussion, we review our efforts to design and probe (i) collective resonances and field distributions associated with visible and near-IR antenna arrays, (ii) strong polaritonic coupling between a Fabry-Perot cavity and molecular vibrational modes, and (iv) symmetryforbidden modes in loaded hybrid nanogap antennas.

We will first discuss cooperative effects in nano- and micro-scale resonators where we find universal coupling behaviors when data is scaled by antenna length and substrate index. In addition to the oftdescribed *radiative* to *evanescent* transition, a transition to a third regime, termed here as *near-field* coupling, is observed in which the extension of the resonant mode beyond the physical antenna end overlaps that of its neighbor. Arrays were integrated with an active dielectric layer in periodic square arrays of gold nano-squares patterned atop an aluminum nitride thin film on a gold substrate. The metal-insulator-metal metamaterial surfaces exhibit several strong absorption bands that correlate well with numerical simulations and are attributed to a grating-coupled transverse-electric slab-waveguide mode and a transverse-magnetic surface-plasmon polariton mode.

Next, we examine coherent coupling between an optical-transition and confined optical mode, which, when sufficiently strong, gives rise to new modes separated by the vacuum Rabi splitting. Such systems have been investigated for electronic-state transitions, however, only very recently have vibrational transitions been considered. Here, we bring strong polaritonic-coupling in cavities from the visible into the infrared where a new range of static and dynamic *vibrational* processes await investigation. We have experimentally and numerically described coupling between a Fabry-Perot cavity and carbonyl stretch ($\sim 1730\,\mathrm{cm}^{-1}$) in poly-methylmethacrylate. As is requisite for "strong coupling", the measured vacuum Rabi splitting of $132\,\mathrm{cm}^{-1}$ is much larger than the full width of the cavity ($34\,\mathrm{cm}^{-1}$) and the inhomogeneously broadened carbonyl-stretch ($24\,\mathrm{cm}^{-1}$). Agreement with classical theories provides evidence that the mixedstates are relatively immune to inhomogeneous broadening. Next, we investigate strong and weak coupling regimes through examination of cavities loaded with varying concentrations of urethane and demonstrate coupling to liquids using the C-O stretching band ($\sim 1985\,\mathrm{cm}^{-1}$) of $Mo(CO)_6$ in an aqueous solution.

Finally, we note that theoretical work has identified a new type of hybrid nanoresonator akin to a loaded-gap antenna, wherein the gap between two collinearly aligned metal nanorods is filled with active dielectric material. The gap optical load has a profound impact on resonances supported by such a "nanogap" antenna, and thus provides opportunity for (i) active modulation of the antenna resonance and (ii) delivery of substantial energy to the gap material. To this end, we have produced and characterized such nanostructures. In addition to conventional transverse and longitudinal resonances, these loaded nanogap antennas support a unique symmetry-forbidden gap-localized transverse mode arising from the splitting of degenerate transverse modes located on the two gap faces. This previously unobserved mode is strong (E^2 enhanced ~ 20), tightly localized in the nanoscopic ($\sim 30\,\mathrm{nm}$ separation) gap region, and is shown to red-shift with decreased gap size and increased gap dielectric constant. In fact, the mode is highly suppressed in air-gapped structures which may explain its absence from the literature to date. Understanding the complex modal structure supported on hybrid nanosystems is necessary to enable the multi-functional components many seek.

THz Characterization of ITO Films on p-Si Substrates

E. R. Brown[1], **W.-D. Zhang**[1], **H. Chen**[2], **and G. T. Mearini**[2]

[1]Department of Physics and Electrical Engineering
Wright State University, Dayton, OH 45435, USA
[2]Genvac Aerospace, Inc., 110 Alpha Park, Cleveland, OH 44143, USA

Abstract— This paper reports broadband THz transmission measurements and modeling of indium-tin-oxide (ITO) thin films on low-doped p-Si (CMOS-grade) substrates. ITO has long been of interest as a transparent ohmic-contact (TOC) material for infrared detectors and other optical applications. In recent years the ITO TOC has migrated into the THz region, along with interesting metamaterial-based component research. A key feature of ITO is that its bulk conductivity is in the semi-metallic range, $\sigma \approx 10^5$ S/m, compared to $\sigma > 10^7$ S/m in common (transition) metals, so that sheet resistances of around 377 Ω/sq can be obtained with thin-film thicknesses of ∼100 nm instead of the few-nm required of transition metals. However, the electrical properties of ITO depend on several material characteristics, such as the stoichiometry, and the effect on GHz-to-THz (RF) electrical conductivity is not well understood. In this study, two ITO films having thickness of 50 (#1) and 100 nm (#2), and DC sheet conductance 260 Ω/sq (3.85 mS/sq) and 56 Ω/sq (17.9 mS/sq), respectively, were deposited by ion-beam-assisted sputtering, and the THz conductivity was measured between 0.1 and 1.2 THz using a frequency-domain photomixing spectrometer. Fig. 1(a) shows the experimental configuration and (b) shows the transmission-line model used for analysis. Fig. 2 shows the modeled transmittance parametrized by the RF sheet conductance. The experimental transmission for film #2 is plotted in Fig. 3(a),

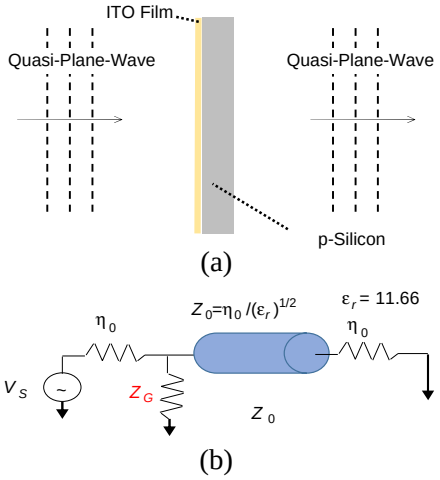

Figure 1.

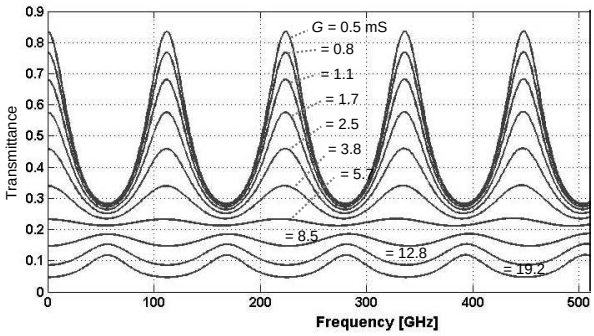

Figure 2.

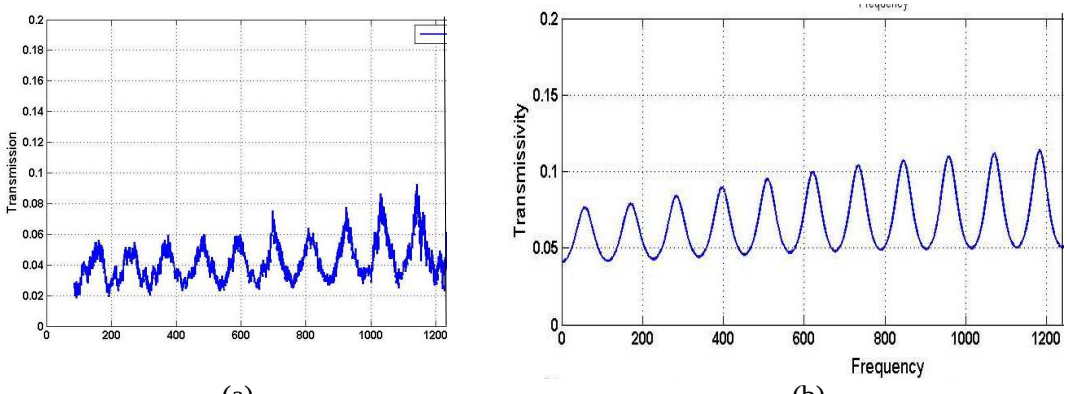

Figure 3.

and the modeled transmission in (b), calculated for the real part of the THz conductance equal to the DC value and the imaginary part dependent upon a Drudian scattering time of 3 fs. The experimental curve is considerably lower than the modeled, but most of the discrepancy can be explained by free-carrier absorption in the p-substrate. Similar agreement was obtained for film #1, suggesting that the Drude model is accurate in the ITO, at least up to 1.2 THz.

Nano-gap Induced Multi-resonant Metamaterials in the Visible and the Near IR

O. J. Glembocki[1], **S. M. Prokes**[1], **A. Giles**[2], **J. D. Caldwell**[1], **R. A. Flynn**[1], **A. Makinen**[1], **and N. Sharac**[3]

[1]US Naval Research Lab, USA
[2]NRC Post, USA
[3]University of California at Irvine, USA

Abstract— Metamaterials have been of significant interest for nearly two decades for use in subwavelength light confinement and manipulation. Plasmonics allows for high field *E-M* field confinement through localized surface plasmons (LSP's) around well-defined geometric structures made of coinage metals. In addition, it is possible to create traveling modes using surface plasmon polaritons (SPP's) by using thin metal films. An area of high interest and common to both LSP's and SPP's involves the use of narrow gaps to induce light confinement. Recent work using Ag films deposited by atomic layer deposition have shown that the structural form of the Ag has a mosaic like pattern that is characterized by Ag islands that are separated by uniform gaps that are 4–6 nm wide and extend throughout the film thickness. These gaps have been shown to have very high fields with well-defined optical resonances in the visible, despite being randomly distributed. In addition, it has been shown that ALD-Ag can be deposited onto other geometries that would be used in plasmonics and yield dual resonant metamaterials. This form of Ag allows us to understand the impact of periodicity on light confinement in gap based metamaterials. Toward this end, we have used both theory and experiments, with lithographically patterned Au gratings with narrow gaps that would resemble a periodic version of ALD Ag. These structures allow us to have fine control over the resonances that is not possible in ALD Ag and to serve as a periodic model for the ALD-Ag geometry. Optically, they exhibit well defined resonances that can be impacted by the structure of the unit cell and the substrate that they are placed on. The high fidelity of the resonances enable us to more calculate the band structure and density of states of the system. The calculations show that gap based metamaterials have both localized and traveling modes. The localized modes have high densities of states and thus can survive randomization and still maintain a resonance. Simulations are then extended to ALD Ag using gap based model, such as rings of air embedded in Ag (coaxial). The results are similar to the model systems and indicate that a simple model of ALD-Ag as a periodic array of coaxial spoof material is accurate because of the low impact of randomization on the fundamental mode in periodic arrays of gaps. The results for both systems show high field localization and potential for applications where high light confinement is small regions is required. We will discuss the possible use of these structures for energy harvesting and other applications that require high light confinement in thin films.

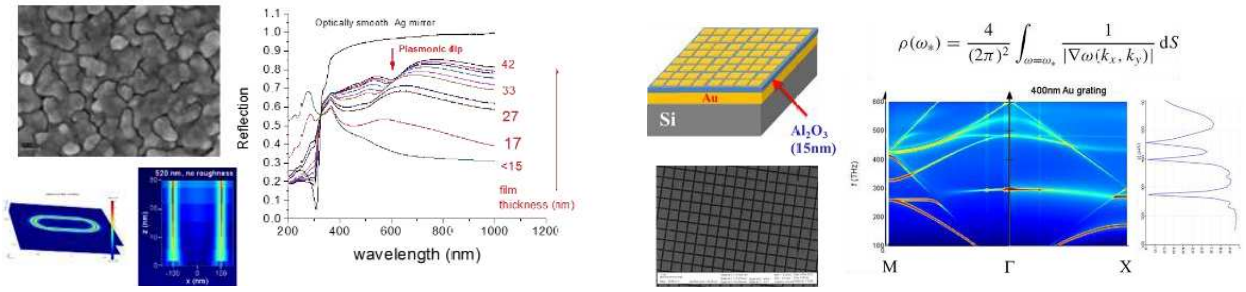

Coupled Resonator Mediated Transmission of Light through Sub-wavelength Holes for Multispectral Imaging Applications

W. R. Buchwald and K. C. Kerby-Patel
University of Massachusetts Boston, USA

Abstract— The transmission of light through arrays of sub-wavelength holes in an optically thick metallic film is in general explained by the excitation of surface plasmon modes at the incident dielectric/metal interface allowing propagation of energy through the holes and into the far field via scattering. This effect is known to produce transmission resonances at wavelengths longer than what would be expected by simply considering classical electromagnetic waveguide theory In this work, it is shown through numeric simulation of 3 μm square holes, with an array period of 6 μm, that the addition of a 2.4 μm square metallic resonator, centered within the sub-wavelength hole, shifts the characteristic resonant frequency to longer wavelengths. In addition, a substantial reduction in resonance line-width is observed when a thick (3 μm) background metal and a thin (100 nm) resonator metal are used. Investigated over the wavelength range of 2 to 14 μm, full-width half-max values of 2.1 μm are observed for the thin background metal case, which produced a characteristic resonance at a wavelength of 9.7 μm. Increasing the Au background metal thickness to 3 μm shifted the transmission resonance to 8.7 μm along with a significant reduction in full-width half-max to 0.322 μm. By adjusting the period and resonator dimensions tuning of distinct spectral bands over the 7.0 μm to 14.0 μm range are achieved as a function of in-plane surface dimensions. Such engineered films are being investigated for use in multispectral imaging spectroscopic systems whereby a distinct spectral line could be allocated to each pixel of a LWIR imaging array enabling the direct detection and identification of certain pathogens or adverse chemical compounds in real time at video frame rates impacting cancer diagnosis and treatment as well as providing front line defense capability for homeland security applications.

Harmonic Double-resonance Cones in Hyperbolic Metamaterials

Domenico de Ceglia[1], **Maria Antonietta Vincenti**[1], **Salvatore Campione**[2, 3], **Filippo Capolino**[2], **Joseph W. Haus**[4], **and Michael Scalora**[5]

[1]National Research Council-AMRDEC
Charles M. Bowden Research Laboratory, Redstone Arsenal, AL 35898, USA
[2]Department of Electrical Engineering and Computer Science
University of California Irvine, California 92697, USA
[3]Center for Integrated Nanotechnologies (CINT), Sandia National Laboratories, P. O. Box 5800, Albuquerque, NM 87185, USA
[4]Electro-Optics Program, University of Dayton, 300 College Park, Dayton, Ohio 45469, USA
[5]Charles M. Bowden Research Laboratory, AMRDEC, U.S. Army RDECOM
Redstone Arsenal, Alabama 35898, USA

Abstract— The formation of double-resonance cones in nonlinear media with hyperbolic dispersion is discussed. We show that an electric dipole near the surface of the medium generates harmonic signals that propagate into two distinct volume plasmon-polaritons. We identify a harmonic component that propagates within its own peculiar resonance cone and a phase-locked, harmonic signal that is trapped under the pump's resonance cone. The large material anisotropy induces a significant angular divergence between the two volume plasmon-polaritons, which makes these structures suitable for subwavelength harmonic imaging microscopy. The effect is shown in a metamaterial made by a stack of metal-dielectric layers with subwavelength thicknesses. We use the Bloch theory to highlight the differences between double-resonance cones achievable with homogeneous hyperbolic media and those formed in discrete hyperbolic metamaterials.

MM-wave-to-THz Modulation with Graphene-oxide-silicon Etalon Structures

W.-D. Zhang[1], **P. H. Q. Pham**[2], **E. R. Brown**[1], **and P. J. Burke**[2]

[1]Department of Physics and Electrical Engineering
Wright State University, Dayton, OH 45435, USA
[2]Department of Electrical and Computer Engineering
University of California, Irvine 92697, USA

Abstract— This paper reports a millimeter-wave (MMW) amplitude modulator based on a graphene-oxide-silicon etalon structure. The device consists of an oxide-pre-coated high-resistivity silicon substrate with a monolayer graphene film sitting on top of the oxide. The structure is fabricated as a graphene-channel field-effect transistor (GFET) with source and drain contacts deposited on the graphene, and a gate contact on the opposite side of the silicon (backgate). Gate bias voltage changes the graphene sheet conductance which then modifies the transmission of radiation propagating perpendicular to the substrate. The transmission spectrum displays Fabry-Perot resonant peaks located at integer multiples of $f_0 = c/2nL = 112\,\text{GHz}$ where $L = 392\,\mu\text{m}$ is the silicon thickness, and $n = 3.41$ is its refractive index. A plane-wave transmission line model is used to predict the transmission as a function of graphene sheet conductance, and a large change of transmission (i.e., depth-of-modulation) is found to occur for incident frequency at or near the resonant peaks, i.e., 112 GHz, 224 GHz, etc.. The depth-of-modulation can reach $\approx 11\,\text{dB}$ if the sheet conductance is varied from 0.1 mS to 5.5 mS (Fig. 1, 112 and 224 GHz are overlapped). To test the performance, $\sim 1 \times 1\,\text{cm}$ graphene films were grown by

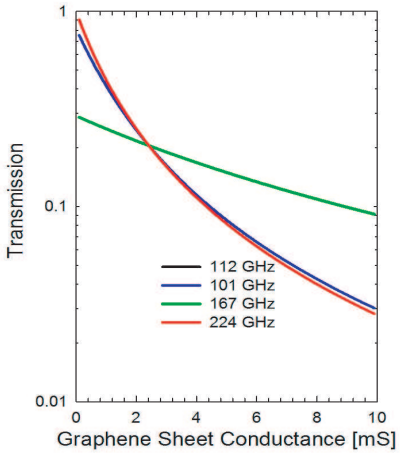

Figure 1.

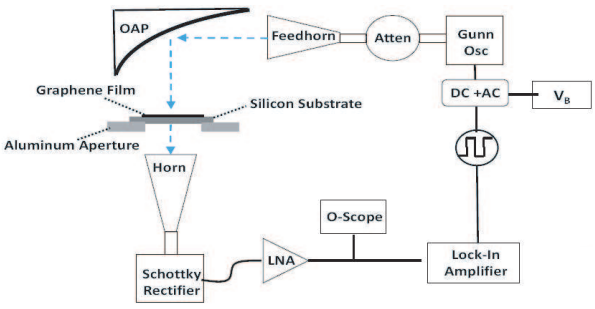

Figure 2.

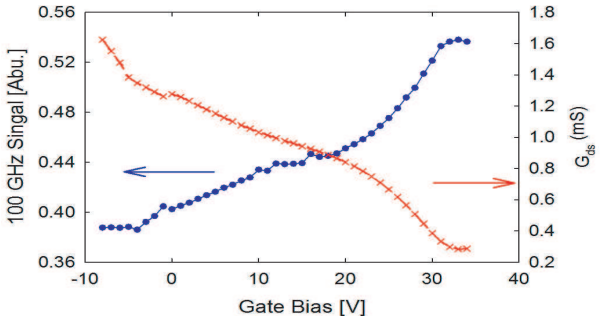

Figure 3.

CVD and transferred from copper to silicon through a polymethylmethacrylate (PMMA) "fishing" procedure. The experimental setup included a 101 GHz waveguide-mounted Gunn-oscillator as the source, and a Schottky-rectifier together with mode-matched feedhorn as the receiver (Fig. 2). The output signal from the Schottky rectifier is coupled to a 1000x-gain low-noise voltage amplifier. The model predicts good depth-of-modulation at 101 GHz, just slightly weaker than the maximum at 112 GHz (Fig. 1). This was tested experimentally (Fig. 3), where the depth-of-modulation was measured to be ~ 1.3 dB when the gate bias was varied from -4 V to $+34$ V. However, this is less than the predicted value — ~ 3.1 dB — calculated using the sheet-conductance change from 0.4 mS to 1.6 mS (Fig. 3). The discrepancy is attributed to inaccuracy of the transmission line model, which assumes a TEM mode radiation, while the experimental MMW beam is actually Gaussian. Nevertheless, there is room for improvement toward a practical MMW transmission amplitude modulator, approaching 10-dB depth-of-modulation, by obtaining greater change in the graphene sheet conductance with gate voltage, which may require a top gate rather than the backgate used here.

Session 2A6a
SC3: Nonlinear Optical Fibers for Sensing and Signal Processing

Distributed Brillouin Sensing Using Plastic Optical Fibers

Yosuke Mizuno, **Neisei Hayashi**, **and Kentaro Nakamura**
Tokyo Institute of Technology, Yokohama 226-8503, Japan

Abstract— Plastic optical fibers (POFs) can withstand large strain of up to several tens of percent and are regarded as one of the most promising candidates for the development of flexible fiber-optic sensors. We here provide an overview of the characterization of Brillouin scattering in POFs and its application to distributed large-strain sensing with a "memory" function. First, we review the first observation of Brillouin scattering in POFs at 1.55 μm, clarifying its fundamental properties, including a Brillouin gain coefficient, Brillouin threshold power, Brillouin frequency shift (BFS), and the BFS dependences on strain (relatively small strain and large strain) and temperature. These results indicate that Brillouin scattering in PFGI-POFs could be used to develop high-sensitivity temperature sensors and large-strain sensors. We also have a look at a new phenomenon named "BFS hopping", with which the BFS abruptly changes from 2.7 GHz to 3.2 GHz by applying large strain of up to 60% to POFs. It is shown that, after this effect, the BFS in POFs becomes more sensitive to temperature change and less sensitive to strain. Finally, we present our latest results on distributed strain and temperature sensing with a centimeter-order spatial resolution in a POF based on correlation-based technique. A 10-cm-long heated section of a 1.3-m-long POF is successfully detected with a theoretical spatial resolution of 7.4 cm and a sampling rate of 3.3 Hz (per measured point). We also discuss the influence of the POF characteristics (including BFS, Brillouin bandwidth, propagation loss, etc.) on the sensing performance.

Advances in Optical Fiber Reflectometry for Optical Access Network Diagnostics and Distributed Sensing

Xinyu Fan, **Qingwen Liu**, **Jiangbing Du**, **Lin Ma**, **and Zuyuan He**
State Key Laboratory of Advanced Optical Communication Systems and Networks
Shanghai Jiao Tong University, Shanghai 200240, China

Abstract— In this talk we will present the advances in research and development (R&D) activities of optical reflectometry in our laboratory.

A prototype ofphase-sensitive coherent optical time domain reflectometry (ϕ-COTDR) was developedfor the purpose of distributed vibration measurement. The performance is reported with the results of laboratorial tests and field tests. The frequency response of our prototype is 200 Hz at a measurement range of 40 km, and 1 kHz at a measurement range of 8 km. This prototype is believed to be eligible as being used as an important part of distributed vibration measurement applications such as a fiber fence security monitoring system, and a pipeline warning system.

Time-gated optical frequency domain reflectometry (TG-OFDR)is developed for the purpose of optical access network diagnostics. With the advantage of fully utilizing the frequency tuning range of the source and overcoming the spatial resolution degradation in long FUT, a spatial resolution of 2 m over a whole measurement range of 55 km was successfully obtained with a very simple scheme. We are now in the progress of developing it to a prototype for fault detection after the splitter of passive optical network (PON) scheme.

For high-spatial-resolution application, a broadly linearly-swept optical source based on optical comb and nonlinear fiber-optics is developed for being used in an OFDR scheme. With the high order sideband sweeping together with a four-wave mixing (FWM) phenomena to broaden the frequency sweep span 22-times, a spatial resolution of 0.75 cm is obtained with an original sweep span of only 638 MHz.

With the progress of the above introduced R&D activities of optical fiber reflectometry in our laboratory, we are trying to push the cutting-edge technologies be widely used in the industry.

Photonic Arbitrary Waveform Generation Using Optical Pulse Synthesizer and Its Applications

Ken Kashiwagi[1] **and Takashi Kurokawa**[1, 2]

[1]Tokyo University of Agriculture and Technology, Tokyo 184-8588, Japan
[2]National Astronomical Observatory of Japan, Tokyo 181-8588, Japan

Abstract— An optical frequency comb (OFC) is a light source whose spectral modes are equally spaced and is the topic of Nobel Prize in physics in 2005. Precise control of its spectral mode frequencies lead to diverse applications; distance measurement, profilometry, spectroscopy and optical frequency standard. A major generation technique propagates an intense pulse from a femto-second fiber laser through a highly-nonlinear fiber for spectral broadening. This approach can yield a broad spectrum, which typically has narrow mode spacing in an order from 10 to 100 MHz. On the contrary, the OFC with a mode spacing in a gigahertz range, which we call "multi-gighertz comb (MGC)", has advantages over the narrow-spacing OFC that each comb lines has higher powers and can be separated by gratings. We have studied optical pulse synthesis at high repetition rates using an MGC as a light source and an optical pulse synthesizer (OPS) as a device for frequency domain modulation onto the MGC. The OPS contains the all elements for the optical pulse synthesis on a single chip; an arrayed waveguide grating and multiple intensity and phase modulators. First, we introduce the pulse synthesis technique using the OPS and a variety of synthesized pulse waveforms. We demonstrate the generation of not only common types of pulses, Gaussian and sech^2 pulses, but also special types of pulses, parabolic, dark-soliton, and saw-tooth pulses. The synthesized pulses are used as a pump to induce optical nonlinearity in highly nonlinear fibers for signal processing and spectral broadening. Finally, we present our recent experimental results of ultra-fast wavelength conversion using a saw-tooth pulse for optical communication signals and a broadband MGC generation for an optical frequency calibrator of a spectrograph for an extra-solar planet finder.

High Sensitive Ammonia Gas Sensor Based on Graphene Coated Microfiber

Xiaohui Sun[1, 2], **Qizhen Sun**[1, 2], **Si Zhu**[1],
Ye Yuan[1], **Zhao Huang**[1], **Xin Liu**[1], **and Deming Liu**[1, 2]

[1]School of Optical and Electronic Information
Huazhong University of Science and Technology, Wuhan, Hubei 430074, China
[2]National Engineering Laboratory for Next Generation Internet Access System
Huazhong University of Science and Technology, Wuhan, Hubei 430074, China

Abstract— Ammonia is a kind of common poisonous gas in the atmosphere, thus ammonia gas sensor has a great demand in the fields of agriculture, chemical industry, medicine, etc.. The reported detection principles are mostly based on the electrochemical effect. However, miniaturized and electrical magnetic immune ammonia gas sensors become more and more important for severe environment.

Micro/nanofiber (MNF) featured with small size, tight optical confinement, low optical loss and large evanescent field transmission, is suitable for subminiature and passive photonic devices. In this paper, we propose an all-fiber miniature ammonia gas sensor based on graphene coated microfiber (GCMNF). Benefitting from the super-large specific surface area and fast electron transfer rate of graphene, the electrical properties and refractive index of graphene can be changed along with the number of ammonia molecules, leading to the variation of the transmission power of the GCMNF.

The graphene can be effectively coated onto the microfiber by light induced deposition which allows an interaction between graphene and the evanescent field of microfiber. Firstly, the graphene solution is confected by mixing 2 mg reduced graphene oxide powder with 20 ml anhydrous ethanol with a concentration of 0.1 mg/ml and then dispersed by an ultrasonic cleaner for 60 mins. Secondly, by using the flame-heating and taper-drawing technology, the microfiber with the waist diameter of $\sim 5\,\mu$m and the length of 10 mm is fabricated from a standard single mode fiber (SMF). Finally, make the microfiber dangle in the V groove and drip several drops of graphene dispersion until the microfiber is immersed into it. The light from high power EDFA is injected into the microfiber, and then the graphene particles start to be deposited onto the microfiber by thermal swirl and convection. Until the power remains unchanged, the ethanol evaporates completely. Consequently, the graphene coating process is finished. Before and after the deposition, we alternately use alcohol and deionized water to clean the microfiber many times to get rid of the dust and non-uniformly deposited graphene.

For the experimental demonstration of ammonia gas sensing, the GCMNF is fixed in the air chamber. Broadband light source injects into the GCMNF and the transmission intensity is detected by the optical power meter. Under the nitrogen atmosphere, the concentration of NH_3 injected into the chamber is changed from 0 ppm to 500 ppm by accurate control of the flow meter. We repeat the measurements for concentration rising and falling process, respectively. Experimental results indicate that the response time of GCMNF to NH_3 is only millisecond, and the sensitivity of the ammonia concentration is about 0.1352 dB/100 ppm through linear fitting of the experiment data. By employing the power meter with high resolution of 0.001 dB, high detection resolution of 0.74 ppm can be obtained. Furthermore, the sensitivity can be improved by decreasing the thickness of the coated graphene as well as the selective materials doping.

High Resolution Demodulation Platform for Large Capacity Hybrid WDM/FDM Microstructures Sensing System Assisted by Tunable FP Filter

Fan Ai[1, 2], **Qizhen Sun**[1, 2, 3], **Jianwei Cheng**[1, 2], **and Deming Liu**[1, 2]

[1]School of Optical and Electronic Information
Huazhong University of Science and Technology, Wuhan, Hubei 430074, China
[2]National Engineering Laboratory for Next Generation Internet Access System
Huazhong University of Science and Technology, Wuhan, Hubei 430074, China
[3]Aston Institute of Photonic Technologies, Aston University, Birmingham, B4 7ET, UK

Abstract— To increase the capacity of FBG sensing units in one single fiber, many methods have been taken to encode the FBGs such as the WDM, TDM, SDM schemes. In our previous work, we have reported a hybrid WDM/FDM sensing system by employing the simultaneous wavelength and frequency encoded microstructures as the sensing units along the fiber. The microstructure is composed of a pair of identical weak FBGs with certain spacing, resulting in the central wavelength of the FBG as the wavelength encoder and the cavity length of the FBG based Fabry-Perot Interferometer (FPI) related to the frequency encoder. However, the sensing system requires high resolution wavelength and frequency demodulation from the complex reflected spectrum, which the industrial optical spectrum analyzer cannot realize.

In this paper, we propose and demonstrate a flexible and high resolution demodulation platform for the hybrid WDM/FDM microstructures based on a tunable FP filter. The demodulation platform is constructed by an ASE light source, a circulator, a tunable FP filter, a photo detector, a NI FPGA card, a NI 16 bit AD/DA card and driving circuit for FP filter. The FPGA card is used to produce the driving signal of the tunable FP filter, and the driving circuit is employed to ensure steady output of the filter. The photo detector and the AD/DA card are adopted to gather the light signal reflected from the sensing units along the fiber. The transmission spectrum of the filter is very small, just like a delta function in wavelength domain. When the optical signal reflected from the fiber transmits through the FP filter, the output spectrum will be the convolution of the spectrum to be measured and the delta function. The tunable filter is driven by a ladder rising signal produced by the FPGA card, of which the central wavelength is determined by the driving voltage. Owing to the high resolution of AD/DA card, the step voltage of the driving signal is small enough to achieve high wavelength resolution. The light intensity data is collected during one step duration at a very high sampling speed and then is averaged to eliminate the perturbation of the filter and the detector noise. By recording the acquisition time, the light intensity data corresponding to the wavelength will be obtained, and then the full spectrum of signal reflected from all the sensing units along the fiber could be demodulated. Through wavelength grouping, spectrum FFT transformation, frequency filtering, and reverse FFT transformation, the spectrum of each microstructure can be separately demodulated. In order to accurately track the wavelength shift larger than one fringe in the interference pattern, we propose the curve fitting algorithm to get the envelope of it and then the wavelength shift of the envelope is considered to revise the wavelength shift of the interference fringe.

In order to test the performance of the demodulation platform, 16 microstructures of 4 WDM and 4 FDM are applied for experiment. The results demonstrate that each optical spectrum of the 16 sensing units can be extracted and retrieved separately, with a very high resolution up to 2.5 pm ranging from 1500 nm to 1590 nm at the high demodulation speed of 800 Hz. Due to the improvement in the wavelength resolution of the demodulation system, the capacity of the sensing units in one single fiber could be significantly enhanced.

Microfiber Resonators for Photonic Filtering and Sensing

Qizhen Sun[1, 2, 3], **Zhilin Xu**[1, 2], **Weihua Jia**[1, 2], **Haipeng Luo**[1, 2], **Yiyang Luo**[1, 2], **Deming Liu**[1, 2], **and Lin Zhang**[3]

[1]School of Optical and Electronic Information
Huazhong University of Science and Technology, Wuhan, Hubei 430074, China
[2]National Engineering Laboratory for Next Generation Internet Access System
Huazhong University of Science and Technology, Wuhan, Hubei 430074, China
[3]Aston Institute of Photonic Technologies, Aston University, Birmingham B4 7ET, UK

Abstract— Due to the promising properties of compact size, tight confinement, large evanescent field, high nonlinear effect and low transmission loss, optical microfibers have been emerging as a novel platform for exploring fiber-optic devices on micro-scale. In this paper, our recent progress in theory, fabrication of microfiber resonators and their applications in photonic filtering, lasing and sensing are discussed. Firstly, we present the microfiber based Fabry-Parot resonator, whose spectral filtering is composed of the interference fringes induced by multi-beam interference and reflection spectrum envelope induced by FBGs. The applications for tunable microwave generation and dual-parameters sensing are experimentally demonstrated. Secondly, we propose the "8" shaped resonator consisting of two microfiber Sagnac loop mirrors as the reflectors and a section of microfiber as the cavity. Owing to the high coupling efficiency induced by the large evanescent field of the microfiber, a broadband comb filtering spectrum with high extinction ratio and flat amplitude can be obtained, which has been applied in fiber ring laser to generate tunable multiwavelength lasing with high channel count. Finally, a compact tunable comb filter based on cascaded microfiber knot resonators (CMKRs) is designed, theoretically analyzed and fabricated by "Drawing-Knotting-Assembling (DKA)" technique On account of the Vernier effect, FSR broader than 63.682 nm and the Q value larger than 10^6 can be expected. In addition, sensitivity of 6523 nm/RIU and detection resolution up to 1.533×10^{-7} RIU for refractive index detection are realized, which can be widely used for chemical and biological detection, etc..

Session 2A6b
SC3: Ultrafast Fiber Lasers

Precision Metrology with Frequency Combs over the Air: Time/Frequency Transfer and Spectroscopy

Nathan R. Newbury
National Institute of Standards and Technology, 325 Broadway, Boulder, CO 80305, USA

Abstract— The coherence, frequency accuracy, and broad optical bandwidth of frequency combs have enabled applications ranging from supporting optical clocks, to time/frequency metrology, to microwave generation, to precision molecular spectroscopy and beyond [1–4]. I will focus on two very different applications that both rely on frequency combs to provide higher precision and accuracy than conventional methods. Both applications require the use of two or more frequency combs and ultimately require operation outside the laboratory. Such applications are only possible with the continued evoluation of fiber-based frequency combs [5].

First, I will discuss coherent dual-comb spectroscopy. In dual-comb spectroscopy, the complex linear response of a sample is probed at each tooth of the frequency comb via massively parallel multi-heterodyne detection. In particular, we are focus on the use of dual-comb spectroscopy for atmospheric sensing over open air paths. Dual-comb spectroscopy (DCS) offers several favorable characteristics for intermediate-path sensing, including a coherent, collimated light source capable of traversing long path lengths (0.1–10 km), and simultaneous broad spectral coverage with extremely high resolution to enable coverage of the absorbing wavelength regions of several species with negligible instrument-derived distortion to the absorption spectrum. I will discuss a recent demonstration of the use of DCS for simultaneous, quantitative measurements of several greenhouse gas absorbers over a 2-km path above the NIST Boulder campus using near-infrared (1.5–1.7 μm) frequency combs.

The second application supports state-of-the-art optical clocks or oscillators, which have reached remarkable levels of stability and accuracy [6–9]. We have developed a technique to allow for comparison of two such optical clocks over a free-space link. This method essentially follows the conventional two-way time-frequency (TWTFT) technique but implemented in the optical domain rather than the rf domain. Through the two-way exchange of coherent optical pulse trains over turbulent, but nevertheless reciprocal, free-space links, one can completely cancel any timing noise associated with turbulence. Recent experiments conducted over a turbulent, 4-km free space link at the NIST Boulder campus have verified the low residual instability and high accuracy possible with this method [10]. With further development, this approach should enable the synchronization of two distant optical locks. This free-space approach can supplement current fiber-optic based approaches in situations when the remote clock is not located at the end of a deployed fiber link. In the future, such techniques might also support the use of optical clocks in satellite platforms.[1]

REFERENCES

1. Hall, J. L., *Rev. Mod. Phys.*, Vol. 78, 1279, 2006.
2. Hänsch, T. W., *Rev. Mod. Phys.*, Vol. 78, 1297, 2006.
3. Newbury, N. R., *Nature Photon.*, Vol. 5, 186, 2011.
4. Diddams, S. A., *J. Opt. Soc. Am. B*, Vol. 27, B51, 2010.
5. Sinclair, L. C., et al., *Opt. Express*, Vol. 22, 6996, 2014.
6. Rosenband, T., et al., *Science*, Vol. 319, 1808, 2008.
7. Bloom, B. J., et al., *Nature*, Vol. 506, 71, 2014.
8. Hinkley, N., et al., *Science*, Vol. 341, 1215, 2013.
9. Katori, H., *Nature Photon*, Vol. 5, 203, 2011.
10. Giorgetta, F. R., et al., *Nature Photon*, Vol. 7, 434, 2013.

Advances in Passively Mode-locked All Normal Dispersion Fibre Lasers

Patrick G. Bowen[1], **Harman Singh**[1], **Antoine F. J. Runge**[1], **Neil G. R. Broderick**[1], **Miro Erkintalo**[1], **John Harvey**[1, 2], **Richard Provo**[2], **and Claude Aguergaray**[3]

[1]Dodd-Walls Centre for Photonic and Quantum Technologies, Department of Physics
The University of Auckland, Private Bag 92019, Auckland 1142, New Zealand
[2]Southern Photonics, Level 4, 49 Symonds St, Auckland 1010, New Zealand
[3]Alphanov, IOA, Rue François Mitterrand, Talence 33400, France

Abstract— In the last decade, research in high energy, short duration, pulsed fibre laser systems has yielded significant advances that have allowed fibre laser systems to compete with more established solid state lasers [1, 2]. Users of these products look for a number of qualities. High energy and short pulse duration are fundamentally important. Other design objectives include beam quality, wall plug efficiency, and thermal stability. We have recently demonstrated robust, passively mode-locked fibre laser designs that achieve these goals [3]. These devices use nonlinear amplifying loop mirrors (NALMs) for mode-locking, which allows for integrated all-fibre, all-polarisation maintaining (PM) cavity configurations that are inherently stable against environmental perturbations.

Here we report on our latest achievements in this area focussing on the excellent long term stability and adaptability of these sources. Fig. 1 shows our basic design fabricated using all-normal dispersion fibres and also equally import all-PM fibres making for a environmentally robust system. Our initial cavity worked at 1030 nm but we have also managed through appropriate choice of components, to obtain operation at 1060 nm.

A typical output spectrum is shown in Fig. 1(a). The pulses have a spectral bandwidth of about 3 nm, 0.34 nJ energy and a temporal duration of 5.8 ps. Using an external grating-pair compressor, we obtained comparatively clean pulses with 360 fs duration (FWHM) [see Fig. 1(b)]. The final figure in Fig. 1 shows the spectrum of our 1030 nm laser after over a period of 500 on-off cycles demonstrating both that it self-starts 100% of the time and that the resulting pulses are extremely reproducible.

We will discuss other extensions to our basic design allowing increased power, shorter pulses, altered repetition rate and operating wavelength etc.. These results emphasise the flexibility of our design and highlight what can be achieved using an all-fibre approach. Lastly we will discuss plans to further amplify these pulses to the multi-Watt level suitable for a range of industrial applications.

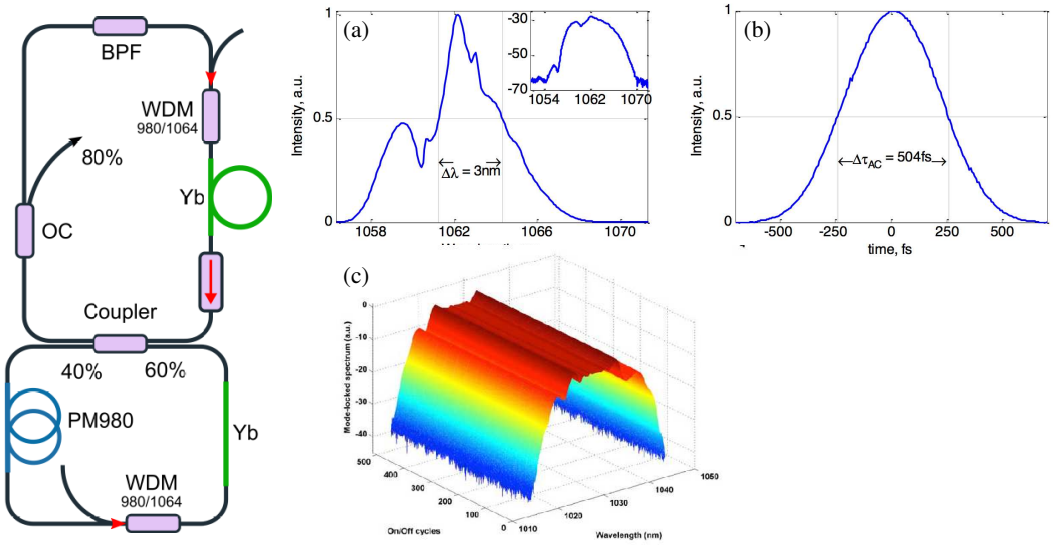

Figure 1: Schematic diagram of laser cavity. (a) Output spectrum in linear and (inset) logarithmic scale. (b) Autocorrelation after recompression. (c) Long term reliability test for 1030 nm laser.

REFERENCES

1. Shiner, B., "The fibre laser: Delivering power," *Nature Photonics*, Vol. 4, 290, 2010.
2. Fermann, M. E. and I. Hartl, "Ultrafast fibre lasers," *Nature Photon.*, Vol. 7, 868–874, 2013.
3. Aguergaray, C., R. Hawker, A. F. J. Runge, M. Erkintalo, and N. G. R. Broderick, "120 fs, 4.2 nJ pulses from an all-normal-dispersion, polarization-maintaining, fiber laser," *Applied Physics Letters*, Vol. 103, 121111, 2013.

Thulium Doped Fibers and Components for Fiber Lasers at around 2 µm

Pavel Peterka[1], **Pavel Honzátko**[1], **Ivan Kašík**[1], **Jan Tarka**[2], **Grzegorz Sobon**[2], **and Jaroslaw Sotor**[2]

[1]Institute of Photonics and Electronics, The Czech Academy of Sciences, Prague, Czech Republic
[2]Wroclaw University of Technology, Wroclaw, Poland

Abstract— Thulium-doped fiber lasers are becoming attractive laser sources in the spectral region around 2 µm with applications in material processing, biological imaging, atmospheric transmission and LIDAR for pollution monitoring. Among other applications belong pumping of solid state lasers (crystals, holmium-doped fiber), spectroscopy and efficient generation of super-continuum in the mid-IR range. Thulium fiber lasers operating at wavelengths around 2 micrometers are coherent light sources with a high slope efficiency reaching 70% and thus they are challenging the well-established ytterbium-doped fiber lasers operating at around 1 micrometer. Two-micrometer radiation sources have many advantages over the one-micrometer sources, e.g., better eye-safety, relaxed non-linear limits and often more efficient material processing.

In this paper we will review our recent progress in developing thulium-doped fibers. The fiber preforms were prepared by the modified chemical vapor deposition and solution doping techniques. Several approaches have been investigated in order to modify the the local environment of rare- earth ions in silica and to increase the quantum conversion efficiency of 3F4 level (upper level of the 2 µm transition) in thulium-doped silica fibers. We will review also the components for fiber lasers at around 2 micrometer that are based on fused biconical taper process. Several applications in fiber- based devices will be presented, namely in monolithic configuration of the laser cavity and broad band amplified spontaneous emission sources. Special attention will be given to the mode-locked femtosecond fiber laser with graphene-based saturable absorber.

ACKNOWLEDGMENT

The research was supported by the Czech Science Foundation, under project No. 14-35256S and by the European Action COST MP1401 "Advanced Fibre Laser and Coherent Source as tools for Society, Manufacturing and Lifescience".

Stretched-pulse Operation of an All-fiber Thulium/Holmium Doped Fiber Laser

Brian R. Washburn
Department of Physics, Kansas State University, 119 Cardwell Hall, Manhattan, KS 66506, USA

Abstract— Thulium/holmium doped fibers are promising gain sources for fiber based lasers in the near-infrared at 2 µm [1]. The combination of high gain and wide gain bandwidth (1.7–2.1 µm) make Tm/Ho doped fibers an attractive source for the production of femtosecond duration, high peak power pulses. Recently, we have demonstrated solitonic [2] and stretched-pulse [3] operation of a mode-locked thulium/holmium doped fiber laser. Positive net-cavity dispersion was obtained using a high numerical aperture fiber in the laser cavity that exhibits normal group-velocity dispersion [4, 5]. The laser dynamics as a function of the net cavity dispersion was experimentally observed. We clearly observe the transition from stretched-pulse to solitonic operation as the length of high numerical aperture fiber was reduced. The optimized laser bandwidth was 30 nm centered at 1.94 µm with a corresponding pulse duration of 450 fs. High numerical aperture fibers can be also used to simultaneously compensate both the second and third-order dispersion allowing for even shorter pulses to be generated.

One motivation for developing mode-locked Tm/Ho lasers is the generation mid-infrared (3–10 µm) ultrashort pulses and frequency combs. Mid-infrared laser sources have long been sought after for many important applications such as medical diagnostics, molecular identification, or gas monitoring. Furthermore, due to the success of using direct frequency comb-based spectroscopy in the visible and near-infrared [6] there is a strong desire to push phase-stabilized frequency combs to the mid-infrared to cover molecular fingerprint region from 2.5 µm to 12 µm. These applications will require robust and portable systems so fiber lasers are a better choice than their solid-state counterparts. Unfortunately, the strong mid-infrared absorption of fused silica fibers and the limited available of non-silica based gain fibers make it difficult produced mid-infrared pulses directly from a fiber laser. An alternative method is use a low mid-infrared loss, nonlinear fiber to extend the wavelength a pulsed near-infrared fiber laser to the mid-infrared. Chalcogenide or fluoride glass fibers could be used since they have low mid-infrared loss and high nonlinearity. Here, we investigate using the mode-locked Tm/Ho doped fiber laser to generate short, mid-infrared pulses and the possibility of using this laser as a source for a mid-infrared frequency comb. High peak power pulses produced by the Tm/Ho doped fiber laser will seed nonlinear spectral broadening in a ZBLAN fiber. By solving the nonlinear Schrödinger equation we demonstrate that the Raman soliton formation produce power-tunable, nearly transform-limited pulses centered in the mid-infrared.

REFERENCES

1. Nelson, L. E., E. P. Ippen, and H. A. Haus, "Broadly tunable sub-500 fs pulses from an additive mode-locked thulium-doped fiber ring laser," *Appl. Phys. Lett.*, Vol. 67, 19–21, 1995.
2. Kadel, R. and B. R. Washburn, "All-fiber passively mode-locked thuliun/holmium laser with two center wavelengths," *Appl. Opt.*, Vol. 51, 6465–6470, 2012.
3. Kadel, R. and B. R. Washburn, "Stretched-pulse and solitonic operation of an all-fiber thulium/holmium-doped fiber laser," *Appl. Opt.*, Vol. 54, 746–750, 2015.
4. Liu, H., L. Kieu, S. Lefrancois, W. H. Renninger, A. Chong, and F. W. Wise, "TM fiber laser mode-locked at large normal dispersion," *Proceeding of Conference on Lasers and Electro-Optics*, Paper CMK1, 2011.
5. Haxsen, F., D. Wandt, U. Morgner, J. Neumann, and D. Kracht, "Monotonically chirped pulse evolution in an ultrashort pulse thulium-doped fiber laser," *Opt. Lett.*, Vol. 37, 1014–1016, 2012.
6. Thorpe, M. J. and J. Ye, "Cavity-enhanced direct comb spectroscopy," *Appl. Phys. B*, Vol. 91, 397–414, 2008.

500 fs Pulses from a 3 µm Mode-locked Fiber Laser

T. Hu[1], **S. D. Jackson**[2], **and D. D. Hudson**[1]

[1]Centre for Ultrahigh bandwidth Devices for Optical Systems (CUDOS)
Institute of Photonics and Optical Science, School of Physics
The University of Sydney, NSW 2006, Australia
[2]MQ Photonics, Department of Engineering, Macquarie University, New South Wales 2109, Australia

Abstract— Ultrafast mode-locked fiber lasers, owing to their high peak power and short pulse widths, have driven applications in imaging, industrial machining and nonlinear optics. Taking these systems to the mid-infrared wavelengths (2–20 µm) allows access to other fields such as sensing and frequency comb based metrology, due to molecules absorbing light strongly at these wavelengths. However the performance of mode-locked fiber lasers in the mid-infrared has been limited with no demonstration of femtosecond scale pulses, and little evidence for a direct pulse measurement [1, 2]. At best an intensity autocorrelation of a 6 ps pulse was measured [3], but it did not reveal the true pulse shape or any phase information. Here we demonstrate the first modelocked fiber laser operating at wavelengths > 2.1 µm, producing 497 fs pulses with a peak power of 6.4 kW, with the electric field completely characterized using a Frequency Resolved Optical Gating (FROG) technique. This marks the first femtosecond-level fiber laser in the mid-infrared and highlights fluoride lasers as a strong candidate for ultra-fast mid-infrared sources.

This fiber laser was mode-locked by the use of nonlinear polarisation rotation (NPR) inside the ZBLAN fiber. The cavity (Fig. 1(a)) consisted of 3 µm of erbium doped ZBLAN fiber (7 mol.%) operating in a ring cavity, consisting of polarisation optics to act as an effective saturable absorber for mode-locking. NPR modelocking was achieved in the standard way [4] where a train of pulses was produced at 56.7 MHz, having a strong rf-beat signal with a signal to noise ratio of 73 dB. In order to unambiguously characterise the pulses we built a FROG measurement system based on the second harmonic generation from the mode-locked pulses through a $AgGaS_2$ crystal. By spectrally resolving the frequency-doubled light a spectrogram was constructed (Fig. 1(b)). Using standard algorithms the complete temporal and spectral fields were retrieved (Figs. 1(d), (e)), which revealed a pulse width of 497 fs and a calculated peak power of 6.4 kW. The retrieved spectrogram was in good agreement with the measured (Fig. 1(c)) as described by the low FROG algorithm error of 1.8×10^{-4}. Not only was this the shortest pulse produced from these fiber lasers, it was also the first ambiguity-free measurement of the pulses that retrieved the phase information, revealing characteristics such as pulse chirp. These fluoride fibre lasers will be one of the key sources of ultrafast mid-infrared laser radiation.

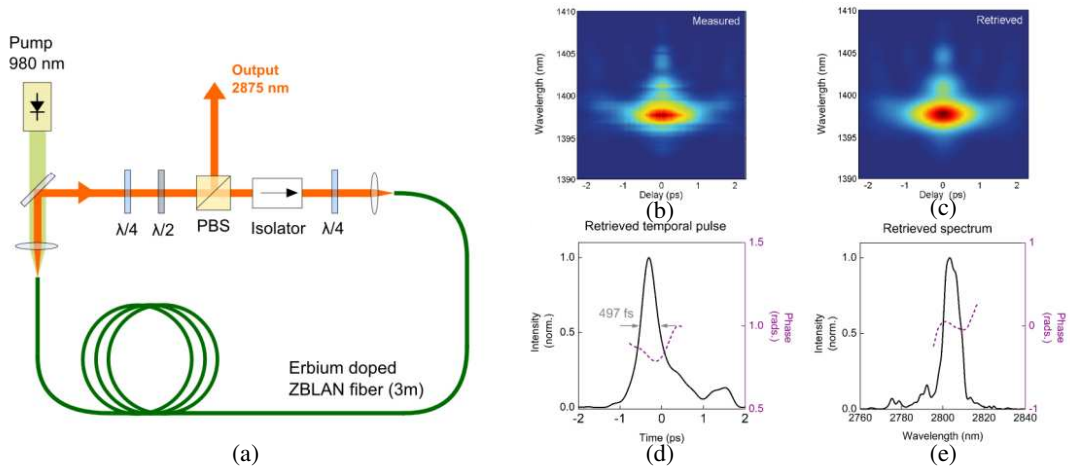

Figure 1: (a) Schematic of NPR based mode-locked laser at 2.8 µm. Laser operates in a ring configuration with polarising optics to create the NPR mode-locking. (b) Measured spectrogram of mode-locked pulses for the FROG analysis. (c) Retrieved spectrum from FROG algorithm. (d) Retrieved temporal pulse with a FWHM of 497 fs. (e) Retrieved spectrum and spectral phase.

REFERENCES

1. Haboucha, A., V. Fortin, M. Bernier, J. Genest, Y. Messaddeq, and R. V Allée, "Fiber Bragg grating stabilization of a passively mode-locked 2.8 µm Er^{3+}:fluoride glass fiber laser," *Opt. Lett.*, Vol. 39, 3294–3297, 2014.
2. Wei, C., X. Zhu, R. A. Norwood, and N. Peyghambarian, "Passively continuous-wave mode-locked Er^{3+}-doped ZBLAN fiber laser at 2.8 µm," *Opt. Lett.*, Vol. 37, 3849–3851, 2012.
3. Hu, T., D. D. Hudson, and S. D. Jackson, "Stable, self-starting, passively mode-locked fiber ring laser of the 3 µm class," *Opt. Lett.*, Vol. 39, 2133–2136, 2014.
4. Ma, D., Y. Cai, C. Zhou, W. Zong, L. Chen, and Z. Zhang, "37.4 fs pulse generation in an Er:fiber laser," *Opt. Lett.*, Vol. 35, 2858–2860, 2010.

SiGe Nonlinear Mid-infrared Integrated Photonics

L. Carletti[1], P. Ma[2], Y. Yu[2], B. Luther-Davies[2], S. Madden[2], D. Hudson[3], D. J. Moss[4], M. Brun[5], S. Ortiz[5], S. Nicoletti[5], P. Labeye[5], S. Nicoletti[5], R. Orobtchouk[1], C. Monat[1], and C. Grillet[1]

[1]Ecole Centrale de Lyon, Institut des Nanotechnologies de Lyon
University of Lyon, 36 Avenue Guy de Collongue, Ecully 69134, France
[2]CUDOS, Laser Physics Centre
Australian National University, Canberra, ACT 0100, Australia
[3]CUDOS, School of Physics, University of Sydney, NSW 2006, Australia
[4]School of Electrical and Computer Engineering
Royal Melbourne Institute of Technology, Victoria 3001, Australia
[5]CEA-Leti MINATEC Campus, 17 rue des Martyrs, 38054, GRENOBLE Cedex 9, France

Abstract— We report nonlinear measurements of SiGe waveguides in the mid-IR performed in the picosecond and femtosecond regime and compare the results to numerical calculations. Nonlinear properties of SiGe waveguides in the mid-IR are extracted. We discuss the potential of SiGe alloys to become the platform of choice for nonlinear Mid-infrared integrated photonics (for operation between 2 and 12 µm).

The interest in expanding the spectral window of operation of group IV photonics towards the mid-infrared (mid-IR), which corresponds to wavelengths between 2 and 12 µm, is rapidly growing. The strong appeal of this particular spectral range derives from a vast range of potential applications such as chemical and biological sensing, active imaging, tissue ablation, secure free-space communication, and multiwavelength light sources [1, 2]. The mid-IR region has also been welcomed as a promising future regime for silicon based nonlinear photonic devices. The nonlinear loss phenomenon of two-photon absorption, that limits nonlinear optical applications in the near-infrared region, vanishes at these wavelengths [2, 3], thus opening the door to photonic devices with new capabilities such as parametric waveguide amplifiers with positive net gain [4]. However, it has recently [5], been shown that, under some experimental conditions, e.g., using picosecond pulses, nonlinear losses in the mid-IR can still be significant. The free carriers generated by multi-photon absorption can have a strong impact through free-carrier absorption (FCA) and thus limit some applications for which a strong nonlinear response is required, as for example supercontinuum generation [5].

The silicon-on-insulator (SOI) material platform has attracted significant interest to implement on-chip integrated waveguides operating in the mid-IR thanks to the possibility of a CMOS compatible fabrication process. However, the increasing absorption of the silica cladding layer of the SOI at wavelengths longer than 3.5 µm may limit the useful wavelength range of this material platform. It is therefore crucial to explore other material platforms. In this context, SiGe alloys on Si are seen as an attractive alternative platform to SOI for applications in the mid-IR due to their expected lower propagation losses and higher nonlinear response [6, 7].

Recently [8, 9], we reported SiGe/Si waveguides with propagation losses as low as 0.5 dB/cm at a wavelength of 4.75 µm. Here, in collaboration with CEA-LETI, RMIT Melbourne and the laser physics center of ANU Canberra we experimentally investigate the nonlinear response of these SiGe waveguides in the mid-IR including nonlinear transmission and self-phase modulation (SPM) using picosecond and femtosecond optical pulses centered at wavelengths between 3 and 5 µm [10].

REFERENCES

1. Soref, R., "Mid-infrared photonics in silicon and germanium," *Nat. Photonics*, Vol. 4, 495, 2010.
2. Jalali, B., "Silicon photonics: Nonlinear optics in the mid-infrared," *Nat. Photonics*, Vol. 4, 506, 2010.
3. Leuthold, J., et al., "Nonlinear silicon photonics," *Nat. Photonics*, Vol. 4, 535, 2010.
4. Liu, X., et al., "Mid-infrared optical parametric amplifier using silicon nanophotonic waveguides," *Nat. Photonics*, Vol. 4, 557, 2010.
5. Gai, X., et al., "Nonlinear absorption and refraction in crystalline silicon in the mid-infrared," *Laser & Photonics Reviews*, Vol. 7, 1054, 2013.

6. Hon, N. K., et al., "The third-order nonlinear optical coefficients of Si, Ge, and SiGe in the midwave and longwave infrared," *J. App. Phys.*, Vol. 110, 011301, 2011.
7. Hammani, K., et al., "Optical properties of silicon germanium waveguides at telecommunication wavelengths," *Opt. Express*, Vol. 21, 16690–16701, 2013.
8. Grillet, C., et al., "Low loss SiGe waveguides in the MID-IR," *Micro- and Nano-Photonics, CLEO®/Europe-IQEC 2013*, Munich, Germany, 2013.
9. Brun, M., et al., "Low loss SiGe graded index waveguides for mid-IR applications," *Opt. Express*, Vol. 22, 508, 2014.
10. Carletti, L., et al., "Nonlinear optical response of low loss silicon germanium waveguides in the mid-infrared," submitted to *Opt. Express*.

Session 2A7
Advanced Mathematical and Computational Methods in Electromagnetic Theory and Their Applications 3

Diverging and Converging Beam Diffraction by a Wedge. Part II: Plane Wave Spectral Solutions and Complex Ray Solutions

M. Katsav[1], **E. Heyman**[1], **and L. Klinkenbusch**[2]

[1]School of Electrical Engineering, Tel Aviv University, Tel Aviv 69978, Israel
[2]Institute of Electrical and Information Engineering, Christian-Albrechts-Universität zu Kiel
Kaiserstr. 2, Kiel D-24143, Germany

Abstract— This two-part paper is concerned with calculating the diffraction of a two dimensional (2D) beam by a perfect conducting wedge. Specifically, we are interested in the case where the incident beam is converging as it hits the wedge. In a recent paper [1], we have used the complex source (CS) method to analyze the problem of beam diffraction by a wedge, but as discussed in Part I of this paper [3], the solution in [1] applies only for the case where the incident beam is diverging as it hits the wedge.

Following [2], we have explored in Part I [3] the application of the CS approach to the case where the incident beam is converging as it hits the wedge. We have utilized the multipole expansion of the conventional Green's function and have shown that it can be extended to the address the converging beam case but only if the CS coordinates are defined in a particular way. Specifically, we have determined the proper value of the CS coordinates for the diverging or for the converging beam cases so that the complex multipole expansion yields physically meaningful solutions.

In the present paper we establish the validity of the results in [3] by comparing them to solutions obtained via two alternative approaches: a plane wave spectrum approach and a complex ray tracing approach. In the former, the field of the incident converging beam is synthesized using the CS approach in conjunction with the plane-wave spectral analysis, and the diffracted field is then calculated using a multipole expansion approach. The exact solution obtained via this spectral technique is then compared with an asymptotic solution obtained via CR tracing augmented with nonuniform/uniform complex ray diffraction. The CR solution includes also selection rules that delineate the CR lit and shadow zones for the diverging or converging beam cases.

REFERENCES

1. Katsav, E. H. and L. Klinkenbusch, "Complex-source beam diffraction by a wedge: Exact and complex rays solutions," *IEEE Trans. Antennas Propagat.*, Vol. 62, 3731–3741, July 2014.
2. Klinkenbusch, L. and H. Bruns, "Diffraction of a uniform complex source beam by a circular cone," *International Conference on Electromagnetics in Advanced Applications (ICEAA)*, 470–472, 2014.
3. Katsav, M., E. Heyman, and L. Klinkenbusch, "Diverging and converging beam diffraction by a wedge. Part I: The multipole expansion approach," *Progress In Electromagnetics Research Symposium*, Prague, Czech Republic, July 6–9, 2015.

Phase Behaviour of an Azimuthally Magnetized Two-layered Ferrite-dielectric Circular Waveguide

Mariana Nikolova Georgieva-Grosse[1] and Georgi Nikolov Georgiev[2]

[1]Consulting and Researcher in Physics and Computer Sciences
Gerlingen D-70839, Germany
[2]Faculty of Mathematics and Informatics
University of Veliko Tirnovo "St. St. Cyril and Methodius", Veliko Tirnovo BG-5000, Bulgaria

Abstract— The circular waveguides, entirely or partially filled with ferrite of azimuthal magnetization are apt for the development of nonreciprocal digital phase shifters, operating in the normal TE_{01} mode, since they can provide differential phase shift when switching the remanent magnetization of their anisotropic load between its two stable states [1–13]. For certain combinations of parameters the multilayered ferrite-dielectric structures could afford an increased value of this important quantity [1, 2, 4–6, 8, 13]. Due to the complexity of the tasks, however, still the phase behaviour of these configurations is not sufficiently clarified.

This purpose of this paper is the calculation and investigation of the phase characteristics of a two-layered circular waveguide, containing a coaxially positioned azimuthally magnetized ferrite cylinder, surrounded with an isotropic dielectric toroid, in contact with the transmission line wall that supports normal TE_{0n} modes. The boundary-value problem approach is employed. The complex Kummer confluent hypergeometric and the real Bessel and Neumann functions [14, 15] are accepted as wave functions for propagation in the ferrite and dielectric medium, resp. A procedure is worked out, making use of the numerically found purely imaginary roots of characteristic equation of the structure, yielding the aforesaid characteristics for both signs of ferrite magnetization in normalized form. In view of the great number of parameters involved, to facilitate the examination, the relative permittivities of both strata are assumed equal. A family of phase pictures of the geometry is computed and presented as a function of the ferrite cylinder to waveguide radius ratio ρ. As expected, the phase behaviour of the structure under study is much more complicated than those of the circular and coaxial waveguides filled with ferrite solely [7, 12]. Particularly, for both signs of off-diagonal ferrite tensor element α envelope lines exist at which the phase characteristics terminate. Hence, in contrast to the simpler ferrite configurations [7, 12], the propagation may occur in bounded frequency bands both for $\alpha < 0$ and $\alpha > 0$. This is a results of the appearance of the $L_{\pm}$ numbers, linked with the roots of characteristic equation [16]. For all values of ratio ρ the curves for negative lie above those for positive magnetization. For the pertinent normalized phase constants $\bar{\beta}_-$ and $\bar{\beta}_+$, answering to chosen normalized guide radius $\bar{r}_0$ and $|\alpha|$ ($|\alpha| < 1$), it holds $\bar{\beta}_- > \bar{\beta}_+$. The structure may produce positive differential phase shift $\Delta\bar{\beta} = \bar{\beta}_- - \bar{\beta}_+$ in a wide area of change of both $\bar{r}_0$ and $|\alpha|$. There are values of the latter, however, for which no $\Delta\bar{\beta}$ is provided. To the left of cutoff there is a backward-wave region where $\Delta\bar{\beta}_-$ is a double-valued function of $\bar{r}_0$ [9]. For certain values of parameters a magnetically controlled cutoff exists.

REFERENCES

1. Clarricoats, P. J. B. and A. D. Olver, "Propagation in anisotropic radially stratified circular waveguides," *Electron. Lett.*, Vol. 2, 37–38, Jan. 1966.
2. Baden-Fuller, A. J., *Ferrites at Microwave Frequencies*, IEE Electromagnetic Waves Series 23, Peter Peregrinus, London, UK, 1987.
3. Che, W., E. K. Yung, and J. Wen, "Cutoff characteristics of modes in a circular waveguide filled with microwave ferrite," *Journal of Electromagnetic Waves and Applications*, Vol. 16, No. 8, 1103–1118, 2002.
4. Georgiev, G. N. and M. N. Georgieva-Grosse, "Phase behaviour of a two-layered circular ferrite-dielectric waveguide with azimuthal magnetization," *Progress In Electromagnetics Research Symposium Abstracts*, 742, Moscow, Russia, Aug. 18–21, 2009; *PIERS Proceedings*, 1473–1477, Moscow, Russia, Aug. 18–21, 2009.
5. Georgiev, G. N. and M. N. Georgieva-Grosse, "Effect of the dielectric filling on the phase behaviour of the circular waveguide with azimuthally magnetized ferrite toroid and dielectric cylinder," *Proc. Asia-Pacific Microwave Conf. APMC-2009*, 870–873, Singapore, Dec. 7–10, 2009.

6. Georgiev, G. N. and M. N. Georgieva-Grosse, "Impact of the material properties on the phase characteristics of a two-layered ferrite-dielectric circular waveguide," *Proc. 32nd ESA Antenna Worksh. on Antennas for Space Applicat., ESA/ESTEC*, 270–276, Noordwijk, The Netherlands, Oct. 5–8, 2010.
7. Georgieva-Grosse, M. N. and G. N. Georgiev, "Transmission properties of the circular waveguide, containing an azimuthally magnetized ferrite toroid and a dielectric cylinder," *Proc. 5th Europ. Conf. Antennas Propagat. EuCAP 2011*, 1870–1874, Rome, Italy, Apr. 11–15, 2011.
8. Georgiev, G. N. and M. N. Georgieva-Grosse, "Propagation in the circular waveguide, containing an azimuthally magnetized ferrite cylinder and a dielectric toroid," *Proc. 6th Europ. Conf. Antennas Propagat. EuCAP 2012*, 5 pages, Prague, Czech Republic, article ID P-75, Mar. 26–30, 2012.
9. Georgieva-Grosse, M. N. and G. N. Georgiev, "Cut-off characteristics of the normal TE_{0n} modes in the circular waveguides, containing azimuthally magnetized ferrite," *Proc. Fourteenth Int. Conf. Electromagn. Adv. Applicat. ICEAA'12*, 1194–1197, Cape Town, South Africa, Sep. 2–7, 2012, (Invited Paper in the Special Session "Advanced applications of the mathematical and computational electromagnetics," organized by G. N. Georgiev and M. N. Georgieva-Grosse).
10. Georgieva-Grosse, M. N. and G. N. Georgiev, "Advanced iterative methods for exact computation of the differential phase shift in the circular waveguide, completely filled with azimuthally magnetized ferrite: Review of recent results," *Proc. Sixteenth Int. Conf. Electromagn. Adv. Applicat. ICEAA'14*, 1290–1293, Palm Beach, Aruba, Aug. 3–8, 2014, (Invited Paper in the Special Session "Challenges in mathematical and computational electromagnetics and its applications," organized by G. N. Georgiev, and M. N. Georgieva-Grosse).
11. Georgieva-Grosse, M. N. and G. N. Georgiev, "On an application of the hypothesis for the identity of the $L_2(c, \rho, n)$ and $\hat{L}_2(\hat{c}, \hat{\rho}, \hat{n})$ numbers and its application in the theory of waveguides," *Progress In Electromagnetics Research Symposium Abstracts*, 1218–1219, Guangzhou, China, Aug. 25–28, 2014; *PIERS Proceedings*, 1739–1744, Guangzhou, China, Aug. 25–28, 2014, (in the Special Session "Advanced mathematical and computational methods in electromagnetic theory and their applications," organized by G. N. Georgiev and M. N. Georgieva-Grosse).
12. Georgiev, G. N. and M. N. Georgieva-Grosse, "Circular waveguide, completely filled with azimuthally magnetized ferrite," *Chapter in Wave Propagation*, 161–196, L. Rocha and G. Mateus (Eds.), Academy Publish, Cheyenne, Wyoming, USA, 2014.
13. Georgieva-Grosse, M. N. and G. N. Georgiev, "Phase characteristics of the circular waveguide with an azimuthally magnetized ferrite cylinder and a dielectric toroid," *Proc. 2015 IEEE AP-S Int. Symp. on Antennas Propagat. & URSI CNC/USNC Radio Science Meeting*, Vancouver, BC, Canada, Jul. 19–25, 2015, in print.
14. Tricomi, F. G., *Funzioni Ipergeometriche Confluenti*, Edizioni Cremonese, Rome, Italy, 1954.
15. Abramowitz, M. and I. Stegun, Eds., *Handbook of Mathematical Functions with Formulas, Graphs and Mathematical Tables. Applied Mathematics Series 55*, National Bureau of Standards, Washington, D.C., 1964.
16. Georgiev, G. N. and M. N. Georgieva-Grosse, (Invited Paper), "Theory of the L numbers and its application to electromagnetism," *Proc. 2015 URSI Atlantic Radio Science Conference URSI AT-RASC 2015*, Gran Canaria, Canary Islands, Spain, May 18–22, 2015, in print.

A Nonlinear Boundary Condition for Continuum Models of Biomolecular Electrostatics

J. P. Bardhan[1], **D. A. Tejani**[1], **N. S. Wieckowski**[1], **A. Ramaswamy**[1], **and M. G. Knepley**[2]

[1]Northeastern University, Boston, MA, USA
[2]University of Chicago, Chicago, IL, USA

Abstract— Understanding the behavior of biomolecules such as proteins requires understanding the critical influence of the surrounding fluid (solvent) environment — water with mobile salt ions such as sodium. Unfortunately, for many studies, fully atomistic simulations of biomolecules, surrounded by thousands of water molecules and ions are too computationally slow. Continuum-solvent models based on macroscopic dielectric theory (e.g., the Poisson equation) are popular alternatives, but their simplicity fails to capture well-known phenomena of functional significance. For example, standard theories predict that electrostatic response is symmetric with respect to the sign of an atomic charge, even though response is in fact strongly asymmetric if the charge is near the biomolecule surface. In this work, we present an asymmetric continuum theory that captures the essential physical mechanism — the finite size of solvent atoms — using a nonlinear boundary condition (NLBC) at the dielectric interface between the biomolecule and solvent. Numerical calculations using boundary-integral methods demonstrate that the new NLBC model reproduces a wide range of results computed by more realistic, and expensive, all-atom molecular-dynamics (MD) simulations in explicit water. We discuss model extensions such as modeling dilute-electrolyte solvents with Debye-Huckel theory (the linearized Poisson-Boltzmann equation) and opportunities for the electromagnetics community to contribute to research in this important area of molecular nanoscience and engineering.

ACKNOWLEDGMENT

MGK was partially supported by the U.S. Department of Energy, Office of Science, Advanced Scientific Computing Research, under Contract DE-AC02-06CH11357, and also NSF Grant OCI-1147680. JPB has been supported in part by the National Institute of General Medical Sciences (NIGMS) of the National Institutes of Health (NIH) under award number R21GM102642.

Metamaterials for Medical Implants to Enhance Compatibility with Magnetic Resonance Imaging (MRI)

Giorgio Bonmassar
Harvard Medical School, AA. Martinos Center, Massachusetts General Hospital
Building 149, 13th Street, Charlestown, MA 02129, USA

Abstract— Pacemakers, spinal cord stimulators, cochlear implants, and deep brain stimulators (DBS) and other electrical implants are becoming increasingly available as a treatment option to patients suffering from a wide range of diseases. Despite their remarkable success, one of the significant limitations of these medical devices is the limited compatibility with magnetic resonance imaging (MRI), which a standard diagnostic tool in medicine. A major concern when performing MRI examinations in patients with electrically conductive implants is the increase in induced currents ("antenna effect") along conductive leads in the body that are exposed to the radiofrequency (RF) waves of the MRI. The increase in current flow into the tissue at the point of contact with the lead (i.e., the electrodes), causing a large amount of RF energy to be absorbed in the tissue, which in turn causes surges in temperatures that can lead to serious injury [1, 2]. In this work we present a design based on metamaterials to decreases the antenna performance and the induced currents along the wire. The new implant exposed to an RF field can be represented with a hybrid model composed of an antenna attached to a transmission line, which consists of resistive traces with sharp changes in conductivity to maximize reflections, followed by a load such as an electrode connected to the tissue. According to our model [3], the equivalent antenna (i.e., the entire metamaterial) receives the electromagnetic field and injects it into the first port (i.e., layer) with impedance Z_1 of such a network. A portion of the power transmitted to the first port of the metamaterial lead is reflected back as a result of an impedance mismatch between the first port and the antenna, while a remaining portion is supplied to the second layer of the metamaterial lead. The impedance of this second port is intentionally mismatched to reflect the greatest amount of power back to the implantable pulse generator (IPG) or pacemaker and away from the electrode that is in contact with the tissue.

In the case of our metamaterial, we will present solutions to the following Pocklington's integral equation:

$$\begin{aligned} &\int_0^{L_2} I(z)\left(\frac{\boldsymbol{\partial}^2}{\boldsymbol{\partial}\mathbf{z}^2}+k^2\right)\frac{e^{-jkR}}{R}dz' + \int_{L_2}^{L_1+L_2} I(z)\left(\frac{\boldsymbol{\partial}^2}{\boldsymbol{\partial}\mathbf{z}^2}+k^2\right)\frac{e^{-jkR}}{R}dz' \\ =\ & -j\omega\varepsilon_w(z)\left(\|\mathbf{E}_{\mathbf{B}_1}(\mathbf{z})\| - \frac{I(z)}{L_w(z)\sigma_w(z)}\right) \end{aligned} \tag{1}$$

where $\sigma_w(z)$, $\varepsilon_w(z)$ and $L_w(z)$ are respectively equal to σ_1, ε_1 and L_1 when $L_2 \geq z \geq L_1 + L_2$ and equal to σ_2, ε_2 and L_2 when $z < L_2$. The solution $I(z)$ represents the current density field inside our lead implant, with the specific design goal to decrease the antenna performance and the induced currents along the wire. The analytic solution was compared to the numerical solution and confirmed that the metamaterial produced a lower inductance, which corresponded to a shorter equivalent antenna length and lower induced currents.

REFERENCES

1. Guy, A., "Biophysics-energy absorption and distribution," *AGARD Lecture Series, Radiation Hazards (Non-ionizing Radiations-Biological Effects and Safety Considerations*, 78, 1975.
2. Angelone, L., et al., "Analysis of the role of lead resistivity in specific absorption rate for deep brain stimulator leads at 3 T MRI," *IEEE Trans. Med. Imaging*, Vol. 29, No. 4, 1029–1038, 2010.
3. Bonmassar, G., "Resistive tapered stripline (RTS) in electroencephalogram recordings during MRI," *IEEE Trans. on Microw. Theory and Tech.*, Vol. 52, No. 8, 1992–1998, 2004.

Coherent Helical Undulator Radiation in Resistive Waveguide

M. Ivanyan, T. Vardanyan, A. Tsakanian, and V. Tsakanov
CANDLE Synchrotron Research Institute, Yerevan 0040, Armenia

Abstract— The circular polarized intense radiation produced in helical undulators of advanced synchrotron light sources and free electron laser has an essential value for structural biology and molecular biophysics studies. The properties of the undulator radiation in free space and in the perfectly conducting walls waveguides have been extensively studied during the last decade. An important feature of the undulator radiation in waveguide is the radiation discrete spectrum conditioned by the excited waveguide modes. Actually, the waveguide modifies the continious spectrum of undulator radiation into a number of sharp peaks, each corresponding to an excited waveguide mode. The selected modes can be enhanced by proper choice of the undulator and waveguide parameters thus improving the undulator radiation source performance. However, in a real finite conductinmg wall metallic waveguide the properties of the radiation are changed due to boundary impedance.

In this paper, the helical undulator radiation in circular waveguide with finite conducting walls in surface impedance boundary conditions is studied. The solution of Maxwell equations are searching by the help of Fourier transformation of source and radiation fields and their expansion into modes of the resistive circular waveguide with impedance boundary conditions. The dispersion relations for the waveguide eigenvalues are given and the unknown amplitudes are determined using the orthogonality of the modes in impedance boundary condition approximation. The explicit forms of the point-charge longitudinal and transverse wake functions along the helical orbit are obtained. For the charge longitudinal distribution the particles within the bunch interact with the radiated electromagnetic fields that can be evaluated in terms of the wake potentials. The low frequency part of the wakefields formes the coherent part of the radiation, while the high frequency part leads to energy modulation within the bunch. The beam coherent radiation and particle energy modulation for various charge distributions are studied using the longitudinal wake function. An impact of the waveguide walls finite condcutivity to the helical undulator radiation performance is analysed.

High-power Short Pulse Compression: New Methods for Physical and Engineering Analysis

Merey Sautbekova[1], **Seil Sautbekov**[1], **Yuriy Sirenko**[1, 2], **and Alexey Vertiy**[1]

[1]L. N. Gumilyov Eurasian National University, 2, Mirzoyana St., Astana 010008, Republic of Kazakhstan
[2]A. Ya. Usikov Institute of Radiophysics and Electronics, National Academy of Sciences of Ukraine
12, Academician Proskura St., Kharkov 61085, Ukraine

Abstract— One section in the book [1] is devoted to the model synthesis of resonant quasi-optical devices. An approach developed therein, has been originally described in [2] as applied to microwave energy compressors. The approach includes the following steps: estimation of the functional capabilities of isolated components, matching these capabilities with the functionality of the unit as a whole, construction of the corresponding mathematical model, electrodynamic analysis and synthesis of the unit and its components with due regard for optimization of the designed device. Mathematically, we deal here, as a rule, with open boundary value or initial boundary value problems, i.e., the problems whose domain of analysis is infinite in one or more directions. An efficient technique combining the time-domain and frequency-domain methods has been proposed to solve this kind of problems. The basic idea was to use the so-called exact absorbing conditions (EAC) in the finite-difference or finite-element algorithms and to invoke the analytical results obtained from the time-domain analysis of open resonators. These rigorous methods allow one to analyze the corresponding initial boundary value problems in bounded spatial domains and for long time intervals and to obtain reliable numerical data describing the transient processes under resonant conditions.

It is these methods that are best suited for reliable and precise analysis of the energy storage process in an active compressor, which is a high-Q resonant system excited by long quasi-monochromatic pulses, as well as of resonant and distributed energy switches. We have also proposed to apply this technique to the study of the compression of frequency-modulated pulses propagating long distances in the dispersive guiding structures like passive compressors. The proposed algorithms are based on exact analytical representations for the so-called 'transport operators' — diagonal convolution operators in the space of evolutionary bases of signals. The use of the FFT (fast Fourier transform) accelerated schemes is of great aid in their numerical realization.

The developed methods and algorithms have been implemented in the special-purpose software packages for 2-D (and partially — for 3-D) simulation and analysis of energy compressors and resonant radiators of high-power short radio pulses with arbitrary types of (i) cross-uniform regular waveguides for passive compression, (ii) storage units (waveguide and open resonators with metal, semitransparent, and frequency-selective mirrors), and (iii) switches (distributed grating-type switches for compressors on multimode waveguides and for resonant radiators, interference and resonant switches for compressors with single-mode output waveguides) for active compression.

Our approach as applied to formation and radiation of high-power short radio pulses we discuss in detail in this communication. We consider briefly the models that have been employed in the numerical experiments based on the EAC method too. Detailed discussion of these models and certain associated analytical results can be found in [1, 3].

REFERENCES

1. Sirenko, Y. K., S. Strom, and N. P. Yashina, *Modeling and Analysis of Transient Processes in Open Resonant Structures, New Methods and Techniques*, Springer, New York, 2007.
2. Kuzmitchev, I. K., P. M. Melezhyk, V. L. Pazynin, K. Y. Sirenko, Y. K. Sirenko, O. S. Shafalyuk, and L. G. Velychko, "Model synthesis of energy compressors," *Radiofizika I Elektronika*, Vol. 13, No. 2, 166–172, 2008.
3. Kravchenko, V. F., Y. K. Sirenko, and K. Y. Sirenko, *Electromagnetic Wave Transformation and Radiation by the Open Resonant Structures, Modelling and Analysis of Transient and Steady-State Processes*, Fizmathlit, Moscow, 2011 (in Russian).

Multi-objective Optimization Applied to RF and Photonic Components

Jogender Nagar, **Douglas H. Werner**, **and Pingjuan L. Werner**
Department of Electrical Engineering
The Pennsylvania State University, University Park, PA 16802, USA

Abstract— This study shows the potential of multi-objective optimization in the design of RF and photonic components. Multi-objective optimizers provide a visualization of the trade-offs between multiple conflicting objectives, allowing the designer to choose between a set of quasi-optimal solutions. Robustness and convergence efficiency are crucial for these optimizers to have real-world applications. In this study, three unique multi-objective algorithms will be compared in the analysis of a variety of RF and photonic components, including a microstrip patch and optical lens.

Introduction: Single-objective genetic algorithms have long been a critical tool in the design and analysis of electromagnetic components [1]. Real-world designs often have a large number of conflicting trade-offs, most notably performance vs. cost. The traditional single-objective approach requires the designer to make assumptions about the best way to combine these objectives, and the result is a single solution. In contrast, multi-objective optimizers require no assumptions and provide the designer with a set of solutions highlighting the design trade-offs involved [2]. This gives the designer an insight into the underlying physics of the problem, and provides them with the flexibility to choose the best design for a given application.

Multi-objective Optimization Applied to Electromagnetism: Electromagnetic simulations often require a large amount of time, making the convergence efficiency and parallelization of an optimization algorithm critical to its feasibility for real-world design applications. In addition, the cost functions are often noisy and extremely sensitive to the design parameters, making robustness another critical factor. Many unique algorithms have been proposed for multi-objective optimization, notably BORG [3], MOCMA [4] and MOEAD [5]. The convergence efficiency, ease of parallelization and sensitivity to parameters are compared for a variety of difficult problems, including an aperture-coupled stacked microstrip patch and GRIN lens.

Conclusion: Multi-objective optimizers provide a new design paradigm which has the potential to give RF and photonics designers a great degree of flexibility and insight. A study of these optimizers shows very promising results, but room for improvement as well.

REFERENCES

1. Haupt, R. L. and D. H. Werner, *Genetic Algorithms in Electromagnetics*, Wiley-IEEE Press, 2007.
2. Deb, K., *Multi-objective Optimization Using Evolutionary Algorithms*, Wiley, 2001.
3. Hadka, D. and P. Reed, "Borg: An auto-adaptive many-objective evolutionary computing framework," *Evolutionary Computation*, Vol. 21, No. 2, 231–259, 2012, DOI:10.1162/EVCO.a.00075.
4. Igel, C., N. Hansen, and S. Roth, "Covariance matrix adaptation for multi-objective optimization," *Evolutionary Computing*, Vol. 15, No. 1, 1–28, 2007.
5. Zhang, Q. and H. Li, "MOEA/D: A multiobjective evolutionary algorithm based on decomposition," *IEEE Transactions on Evolutionary Computation*, Vol. 11, No. 6, 712–731, Dec. 2007.

Concerning the Circular- and Square-loop Antennas Mounted over a Ground Plane of Finite Extent

A. A. Ayorinde[1], **S. A. Adekola**[1, 2], **and A. Ike Mowete**[1]

[1]Department of Electrical and Electronics Engineering
Faculty of Engineering, University of Lagos, Lagos, Nigeria
[2]Department of Electrical and Electronics Engineering
Niger Delta University, Wilberforce Island, Yenegoa, Nigeria

Abstract— As a natural sequel to an earlier presentation [1], which compared the performance features of equal perimeter circular- and square-loop antennas located over finite ground planes, this paper, using the same formulation, examines the same performance characteristics, but this time, with the antennas being of equal cross-sectional areas; and with loop heights varying between 0.05λ and 1.00λ at the operating (center) frequency of 1.25 GHz. Computational results for the antennas' input characteristics reveal that whereas they share virtually identical input resistance profiles, input reactance for the square loop has values that are in general, lower than those for the circular loop, for the entire range of 'height above ground plane' considered. Results for the E- and H-plane radiation field patterns indicate that when the loops are located at heights beyond 0.3λ above the finite ground plane, the front lobes become distorted; an observation supported by the profiles of the forward directive gain, which display the 'notch filter response' behavior. Furthermore, the results suggest that acceptable front-to-back ratio performance can only be maintained if loop heights above the ground plane are kept below 0.3λ.

REFERENCES

1. Ayorinde, A. A., S. A. Adekola, and A. I. Mowete, "Performance characteristics of loop antennas above a ground plane of finite extent," *PIERS Proceedings*, 769–744, Taipei, March 25–28, 2013.

Integrated Matrix-form of the Boundary Conditions for Electromagnetic Field in Anisotropic Media

Bing Zhou[1] **and Graham Heinson**[2]

[1]Department of Geosciences, The Petroleum Institute, Abu Dhabi, UAE
[2]Geology & Geophysics, The University of Adelaide, Australia

Abstract— Boundary conditions of electromagnetic fields at the interface between two media are generally expressed as two separate equations:

$$(\mathbf{F}^+ - \mathbf{F}^-) \times \mathbf{n} = \mathbf{0}, \qquad (\boldsymbol{\alpha}^+ \cdot \mathbf{F}^+ - \boldsymbol{\alpha}^- \cdot \mathbf{F}^-) \cdot \mathbf{n} = -\Delta I^{\pm}. \tag{1}$$

Here $\mathbf{F} \in \{\mathbf{E}, \mathbf{H}\}$ stands for electromagnetic field intensity, $\boldsymbol{\alpha} \in \{\boldsymbol{\sigma} + i\omega\boldsymbol{\varepsilon}, \boldsymbol{\mu}\}$ defines physical properties of the media, $\Delta I^{\pm} \in \{\Delta J^{\pm}, \Delta M^{\pm}\}$ is the net electromagnetic current on the interface and $\hat{\mathbf{n}}$ is the interface normal. Eq. (1) shows that the boundary values $\mathbf{F}^{\pm}$ at a contact of two anisotropic media become the two implicit functions of the interface normal ($\mathbf{n}$) and tensors of electric permittivity ($\boldsymbol{\varepsilon}$), conductivity ($\boldsymbol{\sigma}$) and magnetic permeability ($\boldsymbol{\mu}$). This paper demonstrates that the two separate and implicit boundary equations can be combined as the following integrated explicit matrix-form

$$\mathbf{F}^{\mp} = \mathbf{C}_{\boldsymbol{\alpha}}^{\mp}\mathbf{F}^{\mp} + \left(\Delta I^{\mp}/\Delta_{\boldsymbol{\alpha}}^{\pm}\right)\mathbf{n}, \tag{2}$$

where the matrix have either the normal version

$$\left(\mathbf{C}_{\boldsymbol{\alpha}}^{\mp}\right)_{ij} = \delta_{ij} + n_i n_k \left(\alpha_{kj}^{\mp} - \alpha_{kj}^{\mp}\right)/\Delta_{\boldsymbol{\alpha}}^{\mp}, \qquad \Delta_{\boldsymbol{\alpha}}^{\mp} = n_i \alpha_{ij} n_j. \tag{3}$$

or tangential version

$$\left(\mathbf{C}_{\boldsymbol{\alpha}}^{\mp}\right)_{ij} = \tau_{1i}\tau_{1j} + \tau_{2i}\tau_{2j} + n_i \left[Q_1\left(\boldsymbol{\alpha}^{\mp}\right) n_j + Q_2\left(\boldsymbol{\alpha}^{\mp}\right)\tau_{1j} + Q_3\left(\boldsymbol{\alpha}^{\mp}\right)\tau_{2j}\right], \tag{4}$$

where

$$Q_1\left(\boldsymbol{\alpha}^{\mp}\right) = \Delta_{\boldsymbol{\alpha}}^{\mp}/\Delta_{\boldsymbol{\alpha}}^{\pm}, \quad Q_2\left(\boldsymbol{\alpha}^{\mp}\right) = n_i\left(\alpha_{ij}^{\mp} - \alpha_{ij}^{\pm}\right)\tau_{1j}/\Delta_{\boldsymbol{\alpha}}^{\pm}, \quad Q_3\left(\boldsymbol{\alpha}^{\mp}\right) = n_i\left(\alpha_{ij}^{\mp} - \alpha_{ij}^{\pm}\right)\tau_{2j}/\Delta_{\boldsymbol{\alpha}}^{\pm}. \tag{5}$$

Here $\{\boldsymbol{\tau}_1, \boldsymbol{\tau}_2\}$ are two perpendicular tangential vectors of the interface. Eq. (2) reveals that the boundary values of electromagnetic fields are linked by a 3×3 boundary matrix which depends on the interface topography $\{\mathbf{n}, \boldsymbol{\tau}_1, \boldsymbol{\tau}_2\}$ and the model property tensors $\{\boldsymbol{\sigma}, \boldsymbol{\varepsilon}, \boldsymbol{\mu}\}$. In addition, we demonstrate the mathematical equivalency of these different versions, as well as their synthetic examples of a hill and a ridge model in geo-electromagnetic analysis, and we highlight their advantage of being a simpler and more straightforward method of applying electromagnetic boundary conditions.

Session 2A8
SC2: Recent Advances of Metamaterials for Novel Electromagnetic and Photonic Devices 2

Optimization of Metamaterials for Microwave Devices

B. Vial and Y. Hao
School of Electronic Engineering and Computer Science, Queen Mary University of London
London E1 4NS, UK

Abstract— We report the design of an all-dielectric cloaking device using topology optimization and provide a quantitative assessment of its performances in the microwave regime. The physical mechanism leading to the cloaking effect is investigated through a modal analysis. We also discuss potential improvements and applications of optimization methods, including bandwidth enhancement and dispersion engineering.

Optimization Technique Applied to Cloak Design: Invisibility cloaks obtained analytically by Transformation Optics (TO, [1]) require extreme material properties (anisotropic, spatially varying permittivity and permeability). Such complex properties are not available in nature and have been achieved based on the use of metamaterials with microstructure much smaller than the wavelength. Those devices rely on resonances with narrow-band and lossy response and are difficult to realize in practice, which calls for other approaches for invisibility cloaks.

Recently, gradient-based topology optimization have been proposed to realize all-dielectric cloaks with low index contrast [2, 3]. We apply this idea to the design of a cloak made of ABS ($\varepsilon = 2.69 - 0.02i$) for TE polarization working at 10 GHz. It is designed to cloak an ABS dielectric cylinder of radius $r = \lambda$. The results are presented together with a quantitative analysis of the performances of the cloak [4]. In addition, we study the cloaking mechanism through modal analysis, and show that it is different from the one at stake in TO-based cloaks.

We finally discuss potential improvements the optimization technique, and its potential applications such as bandwidth enhancement, angular tolerance and dispersion engineering.

ACKNOWLEDGMENT

This work was funded by the Engineering and Physical Sciences Research Council (EPSRC), UK under a Programme Grant (EP/I034548/1) The Quest for Ultimate Electromagnetics using Spatial Transformations (QUEST).

REFERENCES

1. Pendry, J. B., D. Schurig, and D. R. Smith, "Controlling electromagnetic fields," *Appl. Phys. Lett.*, Vol. 98, No. 021112, 2006.
2. Andkjr, J. and O. Sigmund, "Topology optimized low-contrast all-dielectric optical cloak," *Science*, Vol. 312, No. 5781, 1780–1782, 2011.
3. Lan, L., F. Sun, Y. Liu, C. K. Ong, and Y. Ma, "Experimentally demonstrated a unidirectional electromagnetic cloak designed by topology optimization," *Appl. Phys. Lett.*, Vol. 103, No. 121113, 2013.
4. Bao, D., R. C. Mitchell-Thomas, K. Z. Rajab, and Y. Hao, "Quantitative study of two experimental demonstrations of a carpet cloak," *IEEE Antennas Wireless Propag. Lett.*, Vol. 12, 206–209, 2013.

Broadband Microwave Absorber Utilizing Metamaterial and Magnetic Absorbing Material

Tianlong Wu, **Wei Li**, **Jin Yang**, **Wei Wang**, **and Jianguo Guan**
State Key Laboratory of Advanced Technology for Materials Synthesis and Processing
Wuhan University of Technology, Wuhan 430070, China

Abstract— The bandwidth of microwave absorbing materials is important for the practical applications [1]. However, the traditional magnetic absorbing materials (MAMs) cannot simultaneously show high magnetic loss and good impedance matching in the whole frequency range of 2–18 GHz because of the magnetic resonance nature and Snoek's limit [2]. On the other hand, it is also hard for metamaterial absorbers (MAs) to achieve a wide absorption bandwidth because of the resonant absorption nature. In this presentation, by combing the broadband absorption property of the MAMs in high frequency and easily adjustable advantages of the MAs, we proposed a two-layer hybrid absorber that the top layer of the non-planar MA stands on the bottom layer of the MAM. In this bilayer hybrid absorber, the MA layer offers strong absorption for low frequency waves while allowing high frequency waves to propagate through without reflection. The bottom MAM layer then strongly absorbs the high frequency EM waves. Through combining different functionalities into the composite design, a broadband, high efficiency, light-weight, and easily tunable absorber is obtained [3]. To further broaden the absorbing bandwidth and reduce the thickness, we then advanced a crisscross two-layer composite absorber by two identical polarization sensitive MAs. The lower frequency is firstly absorbed by the bottom layer MA as TE absorbing mode and the higher frequency is consumed by the top layer MA as TM absorbing mode. Consequently, the total reflection is reduced (less than 10%) in a wide frequency range as broad as 3–40 GHz. In our works, a simple patterning method is also proposed to drastically broaden the absorption bandwidth of a conventional MAM. In such a patterned absorber, the broadband strong absorption is mainly originated from the simultaneous incorporation of $\lambda/4$ resonances and edge diffraction effects. Simulated and experimental results reveal an ultra-broadband microwave absorber with more than 90% absorption in the frequency range of 4–40 GHz which has a thin thickness of 3.7 mm [4]. Besides, we have designed a bran-new planar composite absorber by embedding metamaterial (MM) in the MAM. By optimizing the structure and shape of the MM to eliminate or weaken the coupling effect between the MM and the MAM. So the composite absorber possess flexible and adjustable characteristics of the MM at low frequencies, while retaining the broadband absorbing in high frequencies of the MAM. Significantly, the thickness of this planar composite design is much smaller than the multilayer configuration to broad the absorbing band. So, integrating MM with MAM reveal a promising and flexible method to greatly extend or control the absorption bandwidth of absorbers. By changing the properties of the MM and the magnetic MAM as well as their arrangement, more electromagnetic hybrid absorbers can be made to accommodate diverse intended applications.

REFERENCES

1. Tong, G. X., J. H. Yuan, J. Ma, J. G. Guan, W. H. Wu, L. C. Li, and R. Qiao, *Materials Chemistry and Physics*, Vol. 129, No. 3, 1189, 2011.
2. Acher, O. and S. Dubourg, *Phys. Rev. B*, Vol. 77, 104440, 2008.
3. Li, W., T. L. Wu, W. Wang, J. G. Guan, and P. C. Zhai, *Applied Physics Letters*, Vol. 104, No. 2, 2014.
4. Li, W., T. L. Wu, W. Wang, P. C. Zhai, and J. G. Guan, *Journal of Applied Physics*, Vol. 116, No. 4, 2014.

A Sharp Bending Device for Broadband Electromagnetic Waves

Youming Zhang[1] **and Baile Zhang**[1, 2]

[1]Division of Physics and Applied Physics, School of Physical and Mathematical Sciences
Nanyang Technological University, Singapore 637371, Singapore
[2]Centre for Disruptive Photonic Technologies
Nanyang Technological University, Singapore 637371, Singapore

Abstract— We demonstrate the condition of unitary transmission between uniaxial epsilon-near-infinity (ENI) media with double infinite components. We propose that broadband uniaxial ENI metamaterials at microwave frequencies can be realized by alternatively stacking thin metallic plates and air. Making use of the unitary-transmission condition and broadband ENI metamaterials, a sharp bending device in rectangular waveguide working for broadband electromagnetic waves is demonstrated.

Self-guided One-way EM Wave by Chain of Gyro-magnetic Rods

Rui-Xin Wu, **Zhen Li**, **Qing-Bo Li**, **and Yin Poo**
School of Electronic Science and Engineering
Nanjing University, Nanjing 210093, China

Abstract— Magnetic photonic crystals (MPCs) are of great interest in recent years for their many unique characteristics, which will lead to great potential applications in microwave and optics engineering. One-way self-guided propagation for which electromagnetic waves are guided along the edge of the MPC without any other cladings [1], is one of the most attractive characteristics of magnetic photonic crystals. Most of the one-way self-guided transmission is based on MPC slabs made of gyro-magnetic rod array [1–3]. The underline mechanisms are topological electromagnetic (EM) edge states [2], or magnetic surface plasmon (MSP) resonance [3].

As the edge stats is localized on the interface of MPC, we will show here that even for a single layer of gyro-magnetic rods, i.e., a chain of rods, can support self-guided one-way propagation of EM waves. We investigate two types of rod chain: one is of zigzag form, another has straight-line one. The variation of band structures from MPC to rod-chains proves the existence of edge modes in gyro-magnetic rod-chains. Both simulated and measured results show that the two forms of rodchain have broadband frequency range of one-way transportation that is robust to the wave channel bending.

The rod-chain configuration provide a new way to the applications of one-way waveguides, which has deep sub-wavelength transverse dimension and very flexible to form arbitrary shapes of oneway waveguide. An example is given. These characteristics make the rod-chain very attractive for practical applications.

ACKNOWLEDGMENT

This work was supported by the NSFC (6130106, 61271080 and 61071007) and RFDP (20110091110030). R. X. W. thanks partial support from STP of Jiangsu Province (BK2012722).

REFERENCES

1. Poo, Y., R. X. Wu, Z. F. Lin, Y. Yang, and C. T. Chan, "Experimental realization of self-guiding unidirectional electromagnetic edge states," *Phys. Rev. Lett.*, Vol. 106, 093903, 2011.
2. Wang, Z., Y. Chong, J. D. Joannopoulos, and M. Soljacic, "Observation of unidirectional backscattering-immune topological electromagnetic states," *Nature*, Vol. 461, 772, 2009.
3. Liu, S. Y., W. L. Lu, Z. F. Lin, and S. T. Chui, "Molding reflection from metamaterials based on magnetic surface plasmons," *Phys. Rev. B*, Vol. 84, 045425, 2011.

Hyperbolic Polaritons for Near-field Optical Imaging

Lian Shen, **Zuojia Wang**, **and Hongsheng Chen**
The Electromagnetics Academy at Zhejiang University, Zhejiang University, Hangzhou 310027, China

Abstract— We study the behavior of hyperbolic polaritons — an alternative form of light propagation with effective wavelength that is much shorter than $\lambda_0/2n$ — in hyperbolic materials. We find that the wave vector refraction of hyperbolic polaritons at different hyperbolic medium interface obeys the Snell's law which is an effective way to manipulate waves at deep subwavelength scale. In particular, we develop a bilayer lens by combining Type I and Type II hyperbolic materials with proper thickness for realizing near-field imaging. Such approach constitutes a further important step towards practical applications of optical imaging.

Broadband Focusing: On-chip Demultiplexers for SPPs and Guided Modes

Tao Li, **L. Li**, **Q. Q. Cheng**, **and S. N. Zhu**
National Laboratory of Solid State Microstructures
College of Engineering and Applied Sciences, Nanjing University, Nanjing, 210093, China

Abstract— Recent advances have pushed the optical design from the macro scale to micro/nano scales, in order to meet the requirement of compact photonic integration. One of the important techniques in optical intercommunication is the wavelength division multiplexing (WDM), by which the information carried by the optical signal can be multiplexed with large capacity. Plasmonics does provide such a solution in routing the optical field in very compact area, and great successes have been achieved in manipulating the surface plasmon polariton (SPP) field. Among them, SPP focusing is a basic and useful function that can be adopted to many nanophotonic devices. Here, I would introduce a recently developed in-plane Bragg diffraction method in manipulating the SPP beam [1, 2], by which a broadband SPP focusing was successful achieved [3]. Taking good usage of the broadband focusing, a plasmonic WDM was proposed and realized with a typical wavelength resolution about 12 nm. Although this resolution is not very good, this device has a relative bandwidth (more than 100 nm) and compact footprint. More importantly, this method provides people a new and general method in steering the SPP and guided modes. As consequences, it is extended to manipulate the guided modes in metal/insulator/insulator hybrid waveguides. According to different mode indices (as well as propagation wave numbers), multi-modes of a same free spaces wavelength (633 nm) inside the hybrid waveguide were clearly separated by this focusing design [4]. Therefore, an compact mode division mulitiplexer (MDM) was achieved. From another viewpoint, both the WDM for SPPs and MDM for guided modes, can regarded as the integrated spectrometers, which are very important components in the on-chip integration for the photonic sensing and detection.

REFERENCES

1. Li, L., T. Li, S. M. Wang, C. Zhang, and S. N. Zhu, "Plasmonic airy beam generated by in-plane diffraction," *Phys. Rev. Lett.*, Vol. 107, 126804, 2011.
2. Li, L., T. Li, S. M. Wang, and S. N. Zhu, "Collimated plasmon beam: Nondiffracting versus linearly focused," *Phys. Rev. Lett.*, Vol. 110, 046807, 2013.
3. Li, L., T. Li, S. M. Wang, S. N. Zhu, and X. Zhang, "Broad band focusing and demultiplexing of in-plane propagating surface plasmons," *Nano Lett.*, Vol. 11, 4357, 2011.
4. Cheng, Q. Q., T. Li, L. Li, S. M. Wang, and S. N. Zhu, "Mode division multiplexing in a polymer-loaded plasmonic planar waveguide," *Opt. Lett.*, Vol. 39, 3900, 2014.

Performance Comparison of Phase-corrected and Classical 1D Electromagnetic Band Gap Resonator Antennas

Basit Ali Zeb, **Muhammad Usman Afzal**, **and Karu P. Esselle**
Centre for Electromagnetic and Antenna Engineering
Department of Engineering, Macquarie University, Sydney, Australia

Abstract— Electromagnetic band gap resonator antennas (ERA), also known as Fabry-Perot cavity antennas or 2D Leaky-Wave antennas, are planar high-gain antennas that employ a resonant cavity formed between a partially reflecting superstructure (PRS) and a fully reflecting ground plane. The cavity is fed by a small less-directive antenna. Since the pioneering work of Von Trentini in 1956 [1], several research groups have investigated techniques to improve the performance figures of ERAs such as antenna bandwidth, peak directivity/gain, sidelobe levels and aperture efficiency. Our recent investigations indicated that many ERAs have non-uniform aperture phase distributions, or phase errors, which can be a limitation in achieving the optimal antenna performance. This motivated us to correct these phase errors [2] to achieve nearly uniform aperture phase distribution, and hence to significantly increase the antenna performance, particularly directivity and sidelobe levels. In this paper, we present a qualitative comparison of one phase-corrected ERA and a classical ERA with the help of full-wave numerical simulations in CST MWS. The antenna configurations are shown in Fig. 1. For this study, we used a simple probe-fed microstrip patch as the feed antenna. The example phase-corrected ERA utilises an all-dielectric phase correcting structure (PCS) [2] placed on top of the base ERA, which itself has one unprinted quarter-guided-wavelength-thick superstrate layer placed half a wavelength distance above the PEC ground. The classical ERA consists of a 1D EBG structure [3] (also known as a Bragg reflector), i.e., a stack of identical dielectric slabs (two or more) placed quarter of a wavelength distance apart with alternate layers of low and high permittivity material (air-dielectric-air). The key results and performance parameters are compared in Table 1. A 9.4 dB increase in antenna directivity, lower sidelobe levels and better aperture efficiency are achieved for ERA with PCS over the classical 1D ERA with one slab. The phase-corrected ERA is suitable for wideband applications that require directivity greater than 20 dB. For very narrowband applications, classical 1D ERA with 3 slabs is suitable.

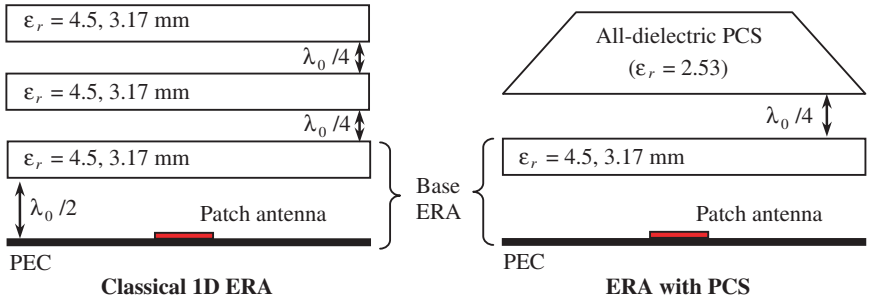

Figure 1: Configurations of the two ERAs under study.

Table 1: Performance comparison of two different ERAs. Design frequency is $f_0 = 11.1$ GHz.

		Classical 1D ERA					ERA with PCS
		1 Slab	2 Slabs	3 Slabs	4 Slabs	5 Slabs	
Peak Directivity (dBi)		12.5	20.8	24.3	22.6	18.3	21.9
3 dB Directivity Bandwidth (%)		11.2	3.1	2	1.2	0.8	8
Sidelobe level (dB)	*E*-plane	−9.8	−16.1	−20.0	−13.7	−10	−16
	H-plane	−19.2	−24	−20.2	−13.7	−9	−20
3 dB Beamwidth (deg)	*E*-plane	34.2	12.3	9.6	10.2	11	13.9
	H-plane	35.4	11.9	9.9	9.8	10.1	13.6
Aperture Efficiency (%)		4	23	44	44	11	28
Total Antenna Height (mm)		∼ 16	∼ 27	∼ 37	∼ 47	∼ 57	∼ 60

REFERENCES

1. Trentini, G. V., "Partially reflecting sheet arrays," *IRE Trans. Antennas Propag.*, Vol. 4, 666–671, 1956.
2. Afzal, M. U., K. P. Esselle, and B. A. Zeb, "Dielectric phase correcting structures for electromagnetic band gap resonator antennas," *IEEE Trans. Antennas Propag.*, 2015, accepted for publication.
3. Weily, A. R., K. P. Esselle, T. S. Bird, and B. C. Sanders, "High-gain 1D EBG resonator antenna," *Microw. Opt. Lett.*, Vol. 47, No. 2, 107–114, 2005.

Electrical-optical Converter Using Electric-field-coupled Metamaterial Antennas on Electro-optic Modulator

Y. N. Wijayanto[1, 2], **A. Kanno**[1], **S. Nakajima**[1], **P. Daud**[2], **D. Mahmudin**[2], **and T. Kawanishi**[1, 3]

[1]National Institute of Information and Communication Technology (NICT), Japan
[2]Indonesian Institute of Sciences (LIPI), Indonesia
[3]Waseda University, Japan

Abstract— Wireless microwave technology with large bandwidth are always required in high-capacity communication, precise measurement, and high-resolution radar. The large bandwidth can be achieved by use of wireless microwave in high-operational frequency such as millimeter-wave or terra-hertz bands. Additionally, there are availability spectrum of the millimeter-wave/terra-hertz bands and promising to open for new advanced applications. However, the bands have large propagation loss in the air and metal cables. The drawback can be compensated for by adopting radio-over-fiber (ROF) technology, where the wireless microwave is modulated to lightwave and propagated through low loss optical fibers. Furthermore, the large area can be covered by installing small wireless cells with optical fiber connection. Therefore, a converter from electrical and optical signals is required in the high-speed ROF technology. The electrical-optical converter can be composed of microwave antennas and optical modulators. Recently, microstrip patch antennas and electro-optic (EO) modulator using planar structures were developed for microwave/millimeter-wave bands. The antenna size becomes very small for high operational frequency. Precise tuning is also required for effective resonance. Therefore, a new device structure are investigated for high operational frequency.

In this paper, we propose a new electrical-optical converter using electric-field-coupled (ELC) metamaterial antennas on an EO modulator for wireless millimeter-wave/terra-hertz applications. By irradiation wireless millimeter-wave/terra-hertz signals, strong millimeter-wave/terra-hertz electric field can be induced on the ELC metamaterial antennas. The induced millimeter-wave/terra-hertz electric field can be used for EO modulation when a lightwave propagates into an optical waveguide located under regions of the induced wave/terra-hertz electric field. The proposed device has compact structure and passive operation with no external electrical power supply. Analysis in microwave and optical modulation of the proposed electrical-optical converter and its fabrication process in experiment are discussed and reported in detail for operational frequency of 100 GHz.

Broadband Perfect Absorption of Ultrathin Conductive Films

Sucheng Li, Weixin Lu, and Bo Hou
College of Physics, Optoelectronics and Energy
Collaborative Innovation Center of Suzhou Nano Science and Technology
Soochow University, 1 Shizi Street, Suzhou 215006, China

Abstract— Absorption of microwave by metallic conductors is typically inefficient, albeit naturally broadband, due to the huge impedance mismatch between metal and free space. Reducing metal to ultrathin profile may improve the absorption efficiency, but is still bounded by a maximal 50% limit induced by the field continuity. Here, we experimentally show that broadband, perfect (100%) absorption of microwave can be realized in a single layer of ultrathin conductive film when it is illuminated coherently by two oppositely incident beams. Inheriting the intrinsic broadband feature of metal, the complete absorption is frequency-independent in the spectrum which spans 6–18 GHz in our microwave experiments and may range from kilohertz to gigahertz frequencies in theory. Remarkably, it occurs in films with thicknesses that are at the extreme subwavelength scales, $\sim \lambda/10000$ or less.

Furthermore, the coherent illumination ($\Delta\varphi = 0$) requires a zero-path-delay interferometer for the two counter-propagating coherent beams. The critical interfering condition guarantees a constructive interference of the electric fields and simultaneously a destructive one of the magnetic fields at the film position at every frequency, which eliminates the dispersive coupling in conventional interfering absorber designs and can be equivalently regarded as a frequency-independent magnetic boundary.

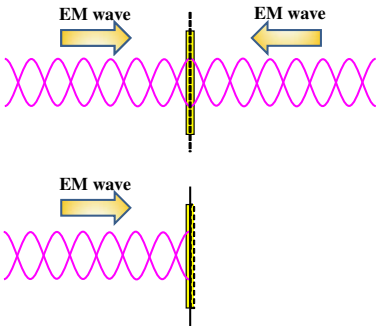

(a)

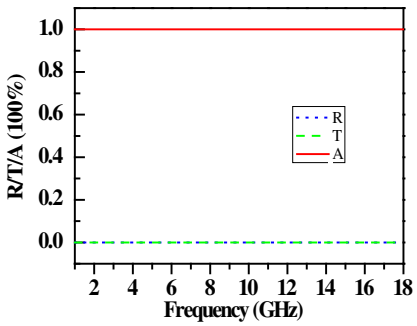

(b)

REFERENCES

1. Li, S. C., et al., "Broadband perfect absorption of ultrathin conductive films with coherent illumination: Super performance of electromagnetic absorption," http://arxiv.org/abs/1406.1847.
2. Li, S. C., et al. "An equivalent realization of coherent perfect absorption under single beam illumination," *Scientific Reports*, Vol. 4, 7369, 2014.

Negative Refraction of Natural Composite Based on Graphene Barium Ferrite

Karen Oganisian and Wieslaw Strek
Institute of Low Temperature and Structure Research Polish Academy of Science
Okolna 2, Wroclaw 50-244, Poland

Abstract— In recent decades an interest with the negative refraction materials (metamaterials) increased due to their exotic features such as reversed geometrical optics, Doppler shifts, Cerenkov radiation etc.. There are many different classes of metamaterials but one feature is common for all of them — they have an artificial origin. The natural negative refraction materials may solve the main problem of their fabrication. Here we present the possibility to obtain negative refraction in natural physic-chemical synthesis of graphene ferrite composition which can be simply applied in industrial scale.

The structure, dc magnetic and electromagnetic properties of graphene barium hexoferrite-$BaFe_{12}O_{19}$ obtained by a hot pressing were examined by X-ray diffraction, scanning electron microscopy, dc magnetization and the capacitance and inductance measurements in the frequency range between 10 and 1 GHz.

It was found that the graphene plates were stacked parallel to each other forming the dense layered quasi-2D percolated structure along the samples as result of high pressure treatment. The barium ferrite nanoparticles were inhomogeneously distributed in graphene host. The dc magnetization loop was characterized by conventional ferromagnetic ordering with relatively high coercivity and remanence. In turn, electromagnetic investigations revealed electric and magnetic resonances near 500 MHz and 100 MHz, respectively. The resonances were accompanied by changes of the sign of permittivity and permeability. Moreover the region with simultaneously negative ε' and μ' was extended up to several GHz.

The observed resonances may be associated to the pressed graphene features because both such resonances were detected in the pure graphene samples. Recently we have observed the strong electric resonance in pure graphene samples that may be explained by the creation of 2D plasmons due to strong coupling between a quasi-2D structure of graphene and perpendicular oriented TE mode of incident wave. Such a strong interaction may arise from the modification of Fermi energy in graphene by an external electromagnetic field. On the other hand it also can be related to Drude relaxation on graphene plates.

However, in pure graphene, magnetic resonance do not change the sign of permeability. Whereas in graphene ferrite composition, magnetic impurities reduce permeability "background" due to barium ferrite ferromagnetic resonance which appears at lower frequencies. Therefore even weak magnetic resonance of graphene may changes the sign of permeability to negative.

Following well known definition the refractive index $n = \sqrt{\varepsilon\mu}$ is negative when the real parts of ε and μ are negative simultaneously in the overlapped frequency range. Thus, it was found that the refraction of graphene ferrite nanocomposite was negative from 500 MHz up to several GHz.

In summary the nanocomposite of graphene barium ferrite obtained by a hot pressing revealed both negative permittivity and permeability in the overlapped frequency range suggesting on negative refraction in the broad frequency region from 500 MHz up to several GHz.

Session 2A9
Bioelectromagetics

Study of Change in Enzymatic Reaction under Radiowaves/Microwaves on Lactic Acid Dehydrogenase and Catalase at 2.1, 2.3 and 2.6 GHz

Sohni Jain[1], **Vuk Vojisavljevic**[1], **and Elena Pirogova**[1, 2]

[1]School of Electrical and Computer Engineering, RMIT University, Melbourne, Australia
[2]Health Innovation Research Institute, RMIT University, Victoria, Australia

Abstract— In modern life, global population is continuously exposed to electromagnetic radiation emitted by mobile phones, computers, radars, smart meters and medical technology equipment etc. In the last 10 years, use of mobile phone worldwide has increased by almost 200% resulting in 4.65 billion users in 2014. This rate is further increasing at approximately 5% annually [1]. Because mobile phone use is so widespread, public concerns about the possible health effects of mobile phones receive a lot of coverage in the media. Intensive international research has found no conclusive or convincing evidence that mobile phones are damaging to health in the short or long term. However, in May 2011, the World Health Organization (WHO) classified RF radiation as 'possibly carcinogenic for humans, based on an increased risk for glioma, a type of brain cancer' [3].

There is an increasing need to study and evaluate the impact of weak RF at cellular and molecular levels. Recent reports confirm that even weak RF induces modulating effects on various biological systems [2, 3]. This study aims to improve our understanding of impact of low power RF radiation (4G mobile network frequencies) on enzymatic reactions. The selected enzymes play crucial roles in the biological processes. L-Lactic dehydrogenase is extensively present in blood cells and heart muscles, and is a marker of common injuries and disease. Catalase enzyme can be found in all living organisms, it is important for protecting a cell from oxidative damage by reactive oxygen species (ROS). This *in vitro* study evaluates the effects of low power RF on kinetics of LDH and Catalase enzymes irradiated at the frequencies of 2.1, 2.3, and 2.6 GHz and two powers of 17 and −10 dBm using the commercial Transverse Electro-Magnetic (TEM) cell. The experimental findings reveal that RF exposures at the particular studied parameters can induce changes in the enzymes' kinetics, which in turn lead to modulation of rate of change in corresponding reactions these enzymes catalyze. The results of experimental evaluation are presented and discussed in the paper. This study will contribute towards identifying guidelines for safety measures of RF exposures.

REFERENCES

1. Australian Communications and Media Authority (ACMA), Communications report, 2012–13.
2. World Health Organisation (WHO), "Electromagnetic fields and public health: Mobile telephones and their base stations," June 2011, Available from: http://www.who.int/ mediacentre/factsheets/fs193/en.
3. Volkow, N. D., D. Tomasi, G. J. Wang, et al., "Effects of cell phone radiofrequency signal exposure on brain glucose metabolism," *JAMA*, Vol. 305, No. 8, 808–813, 2011.

Electromagnetic Activity of Living Cells and Cancer

Jiří Pokorný[1], **Jan Vrba**[2], **Jan Pokorný**[3, 4], **Jitka Kobilková**[5], **David Vrba**[6], **and Jan Vrba, Jr.**[6]

[1]Institute of Photonics and Electronics, ASCR, Prague, Czech Republic
[2]Faculty of Electrical Engineering, Department of EMG Field
Czech Technical University in Prague, Prague, Czech Republic
[3]Institute of Physics, ASCR, Prague, Czech Republic
[4]Department of Materials Science and Engineering, The University of Sheffield, UK
[5]Department of Gynaecology and Obstetrics
Ist Medical Faculty, Charles University, Prague, Czech Republic
[6]Department of Biomedical Technique, Faculty of Biomedical Engineering
Czech Technical University in Prague, Kladno, Czech Republic

Abstract— Energy supply to a biological system excites and sustains a state far from thermodynamic equilibrium which is a basic condition of life. Distribution of charges in biological molecules and structures and exceptional electric polarity of biological objects suggest excitation of coherent electromagnetic field (EMG) generated by polar vibrations [2]. Microtubules in the cytoskeleton of the living cell are the generating structures [5]. Resonant frequencies of individual microtubules were recently investigated in a systematic fashion in the frequency range from 1 kHz to 20 GHz. Two frequency bands were disclosed: One band has resonant frequencies 10–30 MHz, the other 100–200 MHz. Generation of EMG is conditioned by electric polarity, nonlinearity of vibrations, and energy supply to microtubules. Mitochondria provide energy supply, establish a strong static electric field and ordered water around them resulting in low damping of oscillations [3]. Energy of the generated EMG is transformed into physical forces and useful work for biological needs and provides interactions, transport, organization, synchronization of dynamic processes and information transfer. The brain activity, central control function, instinct of self-preservation, and consciousness are assumed to depend on electrodynamic processes, mainly of quantum nature.

Basic items of biological electromagnetic activity were formulated in the form of postulates to set up a solid foundation for further theoretical and experimental studies in a new interdisciplinary field–physical biology [6]. First postulates concern existence of the endogenous coherent electromagnetic field, generating structure, and supporting organelles: The field is generated by microtubules, which are nonlinear oscillating structures, and the supporting organelles are mitochondria. Other postulates describe function of the electrodynamic field in biological cells and the brain. The last postulate concerns pathological states of the electrodynamic field, in particular, in cancer development. Therefore, cancer process is a pathological state of disturbed energy processing system including generation of the EMG [4]. Besides postulated functions the generated electrodynamic field should carry out other essential functions of life.

Cancer is a pathological breakdown of coherent energy states in living cells, in particular, of generated electromagnetic field. After mutation of genome the power plants of the cell, mitochondria, are attacked. Oxidative metabolism is deformed by closing the sugar way. This link of cancer transformation was discovered by O. Warburg [7]. As a result of this link damping of the electric polar vibrations and electromagnetic field is increased. Due to damping coherence of oscillations is diminished and in the phenotype of the Warburg effect (the reverse Warburg effect) the power of the electromagnetic field decreased (increased), and frequency of oscillations increased (decreased) with respect to healthy cells in the tissue. Due to frequency changes interaction between healthy and cancer cells are not attractive [1]. The cancer cells perform invasive motion into their surroundings and then initiate metastastic process. The main part of the cancer process is of physical nature. The transformation pathway of cancer will be shown.

REFERENCES

1. Fröhlich, H., *IEEE Trans. MTT*, Vol. 26, 613–617, 1978.
2. Fröhlich, H., *Adv. Electron. Electron Phys.*, Vol. 53, 85–152, 1980.
3. Pokorný, J., *AIP Advances*, Vol. 2, 011207, 2012.
4. Pokorný, J., et al., *Eur. J. Oncology*, Vol. 17, 23–36, 2012.
5. Pokorný, J., et al., *Sci. World J.*, Vol. 2013, Article ID 195028, 11, 2013.
6. Pokorný, J., et al., *Integr. Biol.*, Vol. 5, 1438–1446, December 2013.
7. Warburg, O., et al. *Biochem Z*, Vol. 152, 309–344, 1924.

Effects of Weak 7 MHz Magnetic Fields on Reactive Oxygen Species *in vitro*

Robert J. Usselman[1], **Pablo Castello**[2], **and Carlos F. Martino**[3]

[1]Electromagnetics Division
National Institute of Standards and Technology, Boulder, CO 80305, USA
[2]Instituto de Química y Fisicoquímica Biológicas
Universidad de Buenos Aires, Buenos Aires, Argentina
[3]Biomedical Engineering Department
Florida Institute of Technology, Melbourne, FL 32901, USA

Abstract— The effects of weak magnetic fields on the production of reactive oxygen species from (ROS) intracellular superoxide ($O_2^{\bullet -}$) and extracellular hydrogen peroxide (H_2O_2) were investigated *in vitro* with rat pulmonary arterial smooth muscle cells (rPASMC). We observe a decrease in $O_2^{\bullet -}$ and an increase in H_2O_2 concentrations in the presence of a 7 MHz radio frequency (RF) at 10 μT_{RMS} and static 45 μT magnetic fields. We propose that $O_2^{\bullet -}$ and H_2O_2 production in metabolic processes occur through singlet-triplet modulation of semiquinone flavin ($FADH^{\bullet}$) enzymes and $O_2^{\bullet -}$ spin-correlated radical pairs. Spin-radical pair products are modulated by the 7 MHz RF magnetic fields that presumably decouple flavin hyperfine interactions during spin coherence. RF flavin hyperfine decoupling results in an increase of H_2O_2 singlet state products, which creates cellular oxidative stress and acts as a secondary messenger that affects cellular proliferation. This study demonstrates the interplay between $O_2^{\bullet -}$ and H_2O_2 production when influenced by RF magnetic fields and underscores the subtle effects of low-frequency magnetic fields on oxidative metabolism, ROS signaling, and cellular growth.

Principles and Methods of EMF Safety Maintenance by Individual Protective Means

I. V. Bukhtiyarov, N. B. Rubtsova, S. Yu. Perov, O. V. Belaya, and T. A. Kravtsova
FSBSI "Research Institute of Occupational Health", Moscow, Russian Federation

Abstract— According the principles of electromagnetic safety one of way of this problem solving is protective mean use. There are 2 main directions of protective means: collective and individual. Collective protective means in dependence of EMF frequency range decrease EMF value by means of EMF reflection or absorption. Individual protective means (protective suits) use as a rule in cases of static electric field, power frequency (50/60 Hz) electric field and radiofrequency (RF) EMF occupational exposure. The methods of these protective suits testing are developed in different countries. Great difficulties are connected with correct evaluation of RF EMF individual protective means protective characteristics.

There is presented the method of RF EMF protective suit (PS) safety properties evaluation. Safety properties of modern PS are based on EMF reflection, which ensures shielding effect. PS is made of electro-conductive materials; all elements are connected to produce a "cover" around a human body, which allows reducing the EMF values to permissible levels.

The testing of protective suit is carried out by special setup use. EMF are emitted by means of RF generator connected with antenna through amplifier. Special setup includes human body phantom (head, trunk and extremities) and measuring probe connected to personal computer by optic fiber. Phantom is placed in spatially homogeneous EMF for all body parts. EMF measurement is carried out in three control points (head, breast and groin) at fixed distances from RF EMF source in two phantom positions: in front and back to the RF EMF source (with and without PS).

The results obtained by suggested approach allow determining PS protection level (in dB), and develop recommendations for construction upgrade.

Furthermore, the obtained data of shielding effectiveness suggest that there is the relationship between protective properties and RF EMF values. Proposed method of PS shielding effectiveness evaluation can help analyze those relationship in future studies.

Experimental Study of Digital Enhanced Cordless Telecommunication Devices Electromagnetic Field Possible Hazard Health Effects

N. B. Rubtsova, S. Yu. Perov, O. V. Belaya, and E. V. Bogacheva
FSBSI "Research Institute of Occupational Health", Moscow, Russian Federation

Abstract— Radiofrequency electromagnetic field (RF EMF) wireless personal telecommunication devices may be the reason of increased adverse human health effects. The most of recent studies analyze the possible health hazards of cellular phone EMF only.

The goal of research was to investigate the Digital Enhanced Cordless Telecommunication (DECT) EMF biological effects to animal behavior and reproduction function. EMF exposure parameters: frequency 1890 MHz, continuous wave (CW), power density 250 $\mu W/cm^2$ (exposure time 2 hours/day; 5 days/week; 4 weeks) and 500 $\mu W/cm^2$ (3 hours/day; 5 days/week; 4 weeks). The objects: white rats male (190–210 and 340–360 g). Each exposed group had sham exposure. The evaluated parameters: weight (body, spleen, adrenal glands, testis), behavioral parameters (open filed test), the function of reproduction system (epididymis sperm count, sperm osmotic resistance).

Exposure value 500 $\mu W/cm^2$: significant decrease of rats' behavioral parameters after 5 days; decrease of behavioral parameters, sperm osmotic resistance, spleen and testis weights after 10 days; decrease of sperm osmotic resistance and body weight after 20 days. Exposure value 250 $\mu W/cm^2$: significant decrease of rats' sperm osmotic resistance after 20 days of exposure and after 2 postexposure weeks, as well as significant decrease of adrenal glands weight and epididymis sperm count after 2 postexposure weeks.

There were carried out the simulation EMF exposure experiment. The simulation helps to find the dependency interrelation between power density, power exposure and specific absorption rates.

The results showed that exposure to CW EMF at 1890 MHz with 500 and 250 $\mu W/cm^2$ may lead to adverse health effects on reproductive system of male rats; and using of DECT devices may be evaluated as possible human health risk factor.

Numerical Field Calculations for Assessment of Electric Field Strength Arising in Human Body Tissues Caused by Magnetic Field Exposure

Reinhard Doebbelin, Stefan Foerster, Lars Middelstaedt, and Andreas Lindemann
Otto-von-Guericke-University Magdeburg, Germany

Abstract— Application of high currents in industrial processes is accompanied by intense magnetic fields in the vicinity of such equipment and so in the workplace area of operators.

The International Commission on Non-Ionizing Radiation Protection (ICNIRP) is a respected institution which has been engaged in analysis of human field exposure and definition of limit values for a lot of years. Considering the guidelines concerning the limitation of exposure to time-varying fields published by ICNIRP in 1998 and 2010, the EU issued a directive on the minimum health and safety requirements regarding the exposure of workers to the risks arising from electromagnetic fields (EMF) in 2013. According to these rules, limits exist for parameters of the in-situ electric field (named basic restrictions/exposure limit values) and for affecting (external) electric and magnetic fields (named reference levels/action levels). Compliance of an exposure situation with the limits for the affecting field can be checked by means of measurements. However, the limits for the electric field arising in relevant tissues of the human body represent the, in the end, decisive criterion for the field exposure assessment. The reference levels for the external field were derived from the basic restrictions in a relatively conservative way. Therefore, especially in technological high-current applications, it can be useful to perform a field exposure assessment considering compliance with the basic restrictions. Nowadays, the determination of the in-situ electric field strength occurring in the body tissues can be done by means of numerical field calculations using appropriate software and an anatomically-based human body model including the required characteristics of the body tissues. Such numerical field calculations were carried out for exposure situations at resistance welding equipment using high-amperage welding currents in the kA range. An example of the modelled arrangements is depicted in Fig. 1. By means of the applied simulation program *EMPIRE XCcel*$^{\text{TM}}$. the simulation space including the magnetic-field generating welding circuit, the human body model (model *Duke* of the *Virtual Family*, established by IT'IS Foundation, Zurich, Switzerland) and air is discretized into cells in the form of cuboids. The mentioned simulation software uses the finite differences time domain technique to solve the Maxwell equations. This way, the field parameters of all cells are updated at each time step and finally the resulting electric field strength values in all relevant regions of the body model and the corresponding tissues are determined. This is illustrated in

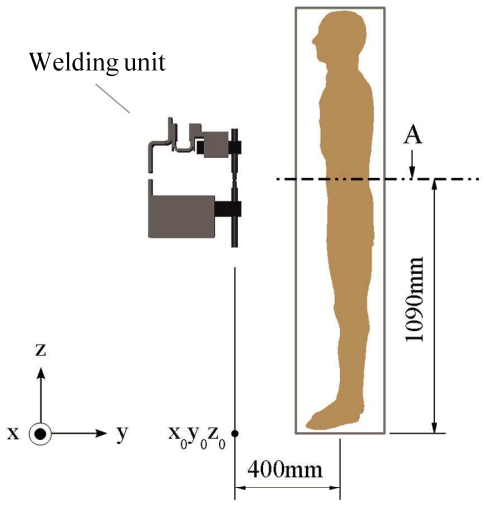

Figure 1: Example for positioning of the human body model in front of the welding circuit of resistance welding equipment.

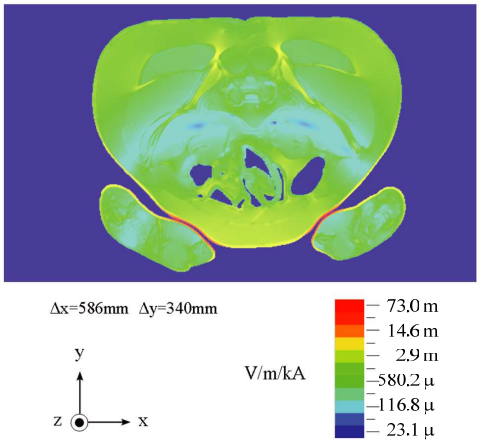

Figure 2: Distribution of electric field strength in sectional plane A of the body model indicated in Fig. 1, frequency 50 Hz.

Fig. 2 by means of a sectional view (field strength values normalized to a welding current of 1 kA).

Details of the field calculation procedure and arising possibilities to assess exposure situations occurring in industrial praxis shall be illustrated in the paper.

ACKNOWLEDGMENT

The research project IGF 16776 BR of the Research Association for Welding and Allied Processes of the DVS, Düsseldorf, Germany, was promoted via the AiF (Federation of Industrial Research Associations) in the framework of the Program for Promotion of Industrial Collaborative Research and Development of the German Federal Ministry for Economic Affairs and Technology based on an enactment of the German Bundestag (the Parliament of the Federal Republic of Germany).

Stochastic Approach for EM Modelling of Suspended Bacterial Cells with Non-uniform Geometry and Orientation Distribution

Dominique Rauly[1], **Eric Chamberod**[2], **Pascal Xavier**[1], **Jean M. F. Martins**[3], **Jean Angelidis**[4], **and Hakima Belbachir**[5]

[1]IMEP-LAHC, UMR 5130 CNRS/INPG/UJF, MINATEC, BP 257, 38016 Grenoble Cedex 1, France
[2]IUT Grenoble, Joseph Fourier University
51 rue de la Papeterie, Domaine Universitaire, BP 67, 38 402 St Martin d'Hères, France
[3]LTHE UMR 5564, Grenoble University — CNRS INSU — G-INP IRD
70, rue de la physique, Domaine Universitaire, BP 53, 38041 Grenoble Cedex 09, France
[4]LEAS, ZA La Batie 175 Allée de Champrond, St Ismier 38330, France
[5]HBA BIOTECH SA, 2 r Ancien Champ de Mars, Grenoble 38000, France

Abstract—

Introduction: Interactions between electromagnetic (EM) fields or currents and living cells constitute a recurrent subject of interest for several decades, and their effects have been profusely discussed [1], especially for the frequency bands currently encountered in everyday life of humans. In a more restrictive domain, large number of studies have been done, focused on EM modelling of a bacteria medium, in order to predict the EM field penetration and inner induced currents in living microorganisms. Relevant information to be collected deals with level and frequency of the EM signal that may affect the development of the considered cells. The former because non-thermal effects are nowadays suspected to exist, altering cell's metabolism, the latter because it is well known that the spectral response of the living cell impedance exhibits some dispersion in relation with cell membrane behaviour and shield effects [2].

It appears that these parameters may be strongly sensitive to shape, dimensions and orientation of bacterial cells in relation to the applied electric field orientation. The present paper aims to examine this problem and brings a streamlined lighting. This is done through the elaboration of a simplified equivalent electric circuit, supported by a prior COMSOL^{TM} analysis and a stochastic approach.

Analysis: The bacterium selected to test our approach is *Escherichia coli* DH5α. A first model, suitable for the required level of resolution, may be a 2 ± 1 µm long and 0.5 ± 0.2 µm wide cylinder filled with physiological fluid and surrounded by a dielectric membrane of thickness 50 nm. The medium is considered also as a physiological fluid. Figure 1 shows the COMSOL^{TM} model, with possible orientations for the external applied electric field, assuming that the field is provided through the application of an AC voltage between two plane parallel electrodes. A simplified equivalent circuit, similar to those explicited in the literature [2], can then be extracted from COMSOL^{TM} computation, where capacitance and resistor values depend on size and orientation (Figure 2). Next, the equivalent circuit for the overall medium, containing the suspended bacterial cells, is deduced, taking into account the concentration and the orientation of bacteria, as well as the electrodes/medium interface.

Results: As an example of interesting result, Figure 3 shows the admittance of a bacterium longitudinally oriented with the electric field. It reveals the well-known shield effect at lower frequencies. The final paper will relate other relevant parameters as inner current in the micro-organism. Variations according to the size and orientation of bacteria will be detailed for both uniform and non-uniform media, supported by a stochastic analysis.

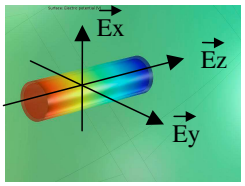

Figure 1: COMSOL^{TM} Model of E. Coli.

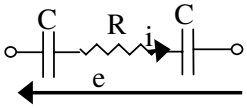

Figure 2: Equivalent circuit for one bacterium, to be inserted in the overall circuit representing the bacterial medium. C and R values are orientation-dependent.

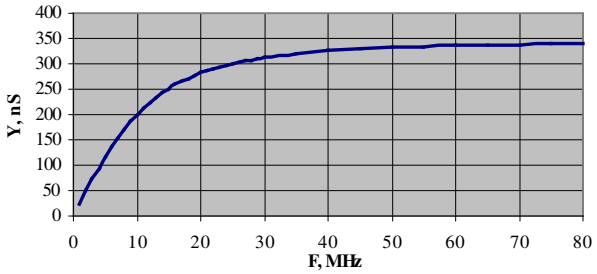

Figure 3: Frequency behaviour of the admittance of E. Coli.

REFERENCES

1. Cifra, M., J. Z. Fields, and A. Farhadi, "Electromagnetic cellular interactions," *Progr. in Biophys. & Molec. Biology*, Vol. 105, 223–246, 2011.
2. Kell, D. B. and C. M. Harris, "Dielectric spectroscopy and membrane organization," *Jal. of Bioelectricity*, Vol. 4, No. 2, 317–348, 1985.

Assessment of Specific Absorption Rate and Temperature Increase in Anatomical Sheep Models due to a 3 T MRI Body Coil

Tahir Malas[1], **Hamza Ergüder**[1], **Samat Turdumamatov**[1], **Muhammed Ergül**[1], **Ceylin Gamze Sünger**[1], **Havva Sümeyye Türker**[1], **and Çağdaş Oto**[2]

[1]Department of Electrical and Electronic Engineering, Turgut Özal University, Turkey
[2]Faculty of Veterinary Medicine, Department of Anatomy, Ankara University, Turkey

Abstract— With the development of high field magnetic resonance imaging (MRI) scanners ($\geq$ 3 T), there has been a concern about possible heating effects of radio-frequency (RF) coils used in MRI. To ensure RF safety, International Electrotechnical Commission set limits both for the whole body specific absorption rate (SAR) and local SAR. In a clinical MRI scan, however, only whole-body SAR is controlled. Full-wave electromagnetic simulations with anatomic models reveal that it is possible to highly exceed local SAR limits even if whole-body SAR is kept below the specified limits. Moreover, such worrisome results are also obtained for 1.5 T scanners which have been used for about 30 years with no known incidents of hazards due to excessive heating.

To be able to explain such a dilemma, we aim to compare simulations with experimental findings. For this purpose, we obtained whole body MRI scans of a sheep and constructed its anatomical models using Mimics software. The resolution of the image set obtained using T1 weighting is 1.56 mm $\times$ 1.56 mm $\times$ 1.56 mm. For the part including brain and neck, we segmented skin, fat, brain, bone, muscle tissues, and air. We used cavity fill, multiple slice edit, extrude, and boolean operations for some tissues but most of the time manual segmentation is required particularly to differentiate air and bone since their gray-scale colors are quite close to each other. After obtaining 3D model, we performed further validation to correct erroneous segmented slices. We also performed smoothing and wrapping processes to In Figure 1, we depict a sagittal slice of the original MR image, a partial model constructed using skin, fat, and muscle tissues, and a more detailed anatomical model consisting of six tissues. Simulations pertaining to SAR and temperature increase of these models will be obtained from the Sim4Life software and will be contrasted to experimental results.

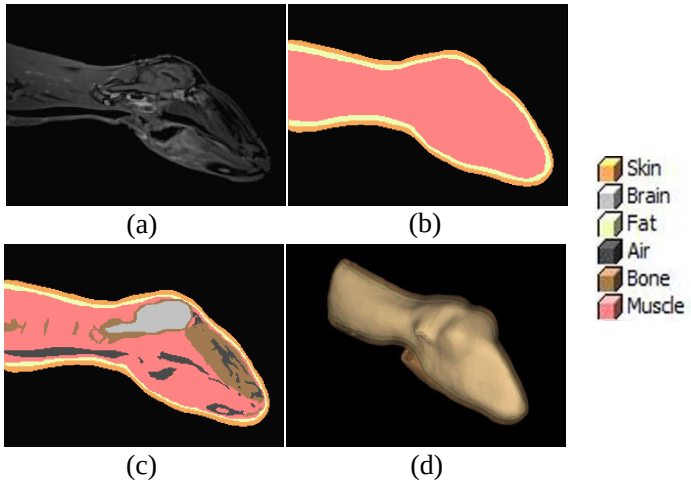

Figure 1: The process of constructing the anatomical model of a sheep: (a) Sagittal MR image, (b) partial model consisting of skin, fat, and soft tissue (muscle), (c) more detailed model with six tissues, and (d) 3D image of the anatomical model.

ACKNOWLEDGMENT

This work was supported by the Scientific and Technical Research Council of Turkey (TUBITAK) under research grant 113E187.

The Use of Quasi-phantom Measurements for Characterization of Vertigo Hazards Caused by Static Magnetic Fields Exposure of Magnetic Resonance Workers

Jolanta Karpowicz
Central Institute for Labour Protection, National Research Institute (CIOP-PIB)
Czerniakowska 16, Warszawa 00-701, Poland

Abstract— There are many reports from workers involve in various activities near magnets of magnetic resonance scanners (radiographers, nurses, technicians, cleaners, etc.) that during activities near or inside magnet tube they experienced vertigo, sometimes strong enough to significantly disturb their work. In 2014 International Commission on Non-ionizing Radiation Protection (ICNIRP) published guidelines for limiting exposure to electric fields induced by movement of the human body in static magnetic field and by time-varying magnetic fields below 1 Hz — in order to prevent vertigo and phosfenes. The ICNIRPs reference level to protect against effects in peripheral nervous system due to movement in static magnetic field and due to time-varying magnetic field of 0–1 Hz exposure is 2700 mT/s (2.7 T/s), and basic restriction was set at 2,000 mT (2 T). It triggered scientific debate if such measures of exposure hazards are sufficient, because magneto-mechanical interaction with the exposed body is not reflected in mentioned limits.

The aim of presented studies was to characterize the vertigo hazards near magnetic resonance scanners by expanded set of exposure parameters (including phenomenon of induced electric field and magneto-mechanical interaction mechanism). The 3-axis Hall probe connected to the pocket data logger was used in quasi-phantom measurements near 1.0; 1.5 and 3.0 T scanners. The significant differences in the exposure parameters between components of various polarization in magnetic field affecting worker (vertical, sagital, transverse). The new approach developed to characterize complex pattern of exposure may help to understand better what mechanism of interaction between static magnetic field and human body play dominating role in vertigo developing.

ACKNOWLEDGMENT

Research within the statutory activity of the CIOP-PIB (II-33), supported by the Ministry of Science and Higher Education, Poland (2014–2015).

Geographical Distribution of Childhood Acute Leukaemia in the Metropolitan Area of Guadalajara, Mexico and Its Correlation with the Wireless and High Voltage Network

Leonardo Soto Sumuano[1, 2], **Carlos Ruiz Chavez**[3], **Alberto Tlacuilo-Parra**[1], **Roberto Garibaldi Covarrubias**[4], **Hugo Romo Rubio**[4, 5], **Mijail Suarez Arredondo**[1], **and Jesus Arriaga Dávila**[1]

[1]Medical Research Division, UMAE Hospital de Pediatria CMNO, IMSS, Guadalajara, Mexico
[2]Information Systems Department, CUCEA, University of Guadalajara, Zapopan, Mexico
[3]Independent Consultant in Information Technologies, Guadalajara, Mexico
[4]Pediatric Hematology and Oncology Department
UMAE Hospital de Pediatria CMNO, IMSS, Guadalajara, Mexico
[5]Pediatric Hematology and Oncology Department
Nuevo Hospital Civil de Guadalajara, OPD, Guadalajara, Mexico

Abstract— This first study conducted by the University of Guadalajara, the Pediatric National Social Security Medical Center, the Hospital Civil de Guadalajara and the General Hospital of Guadalajara, shows the geographical and temporal distribution of 274 cases of children suffering from Leukemia in 6 municipalities in the metropolitan area of Guadalajara (2014). In Mexico, geographical information systems (GIS) have been rarely implemented to monitor spatial assessments of leukemia. We present an analysis of the spatial distribution of acute leukemia among children from 0 to 16 years of age in the metropolitan zone of Guadalajara, Mexico using individual case Hospital data from the three main hospital facilities attending this population.

Methods: Using the approach of spatial epidemiology DBSCAN and 1-dist, cases of leukemia obtained from the databases of hospitals resulted in "clusters" or groups of cases/100,000 inhabitants. Cancer cases were grouped according to an internationally recognized morphology-based.

Results: The results shows 24 cases/100,000 inhabitants for leukemia (acute lymphoblastic leukemia) LLA and 4.4 cases/100,000 inhabitants for leukemia AML (acute myeloid leukemia). These results were outside of international references. The values are usually 3–5 cases/100,000 for LLA and 0.8 cases/100,000 for AML.

Conclusions: Although the etiology of most childhood leukemias is unknown, there is a significant correlation between spatial disease cluster with an unusual elevated disease incidence rate and the high voltage distribution network and the wireless communication network. Studies in the literature have focused on childhood leukemia because of its relative large incidence among children compared with other malignant disease, its apparent tendency to cluster, and the public concern over locally elevated leukemia incidence.

Experimental Assessment of Influence Factors of Body Shadow Effect in Dosimetry Measurements in Indoor Enclosures

S. de Miguel-Bilbao[1], **J. Roldán**[2], **J. Blas**[3], **and V. Ramos**[1]

[1]Health Institute Carlos III, Telemedicine and e-Health Research Unit, Madrid, Spain
[2]Health Institute Carlos III, National Center for Environmental Health, Madrid, Spain
[3]Department of Signal Theory, Communications and Telematic Engineering
University of Valladolid, Valladolid, Spain

Abstract— The use of wireless systems, such as WLAN spreading to a wide range of sectors, ranging from domestic households, to administrative as well as industrial and healthcare environments, with a broad and transverse application scope. The number of personal devices that operate in the frequency band of 2.4 GHz is spreading in enclosed environments. Personal exposure meters (PEMs) are used for measuring exposure to electromagnetic fields (EMF), and are typically worn by the user during the measurement campaigns. The immediate proximity of the user underestimates EMF exposure levels in the registered data. This alteration is known as body shadow effect (BSE). Regulations about the protection of human exposure to non-ionizing radiation provide thresholds to assure the health and protection of the human beings. These thresholds have been fixed taking into account unperturbed data provided by scientific studies, so these thresholds must be compared with objective and undisturbed data. This study describes the procedure of design of an experimental protocol of measurement of the E-field levels in indoor enclosures to avoid the influence of the BSE. The designed protocol isolates the treatment of the BSE from other intrinsic uncertainties of the exposure assessment from WLAN devices, such as the discontinuous transmission. The quantification of this uncertainty is performed by the duty factor, defined as the relation between the effective information transmission and the total duration of the transmission. Simulations have been performed means of a software prediction tool in order to estimate the measured E-field levels obtained with the designed experimental method.

Session 2A10
Electromagnetic Scattering by Random Media and Rough Surfaces

Measuring the Optical Extinction of Aerosol Particles with Digital Holography

Matthew J. Berg, Nava R. Subedi, and Perter A. Anderson
Department of Physics & Astronomy, Mississippi State University
355 Lee Blvd., Mississippi State, MS 39762, USA

Abstract— This work will present a new technique to measure an aerosol particle's extinction cross section. The concept relies on digital holography, where the interference pattern of a particle's scattered and incident light is recorded optoelectronically to yield a digital hologram. Much information about a particle's physical character can be extracted from such holograms. For example, a silhouette-like image of the particle can be obtained via a simple Fourier-transform-based operation. This talk will show how the digital hologram can also yield the value of the extinction cross section for single and multiple nonspherical particles. Given the simplicity of the measurements involved, such capability could have important applications to quantify extinction by complex-shaped aerosol particles, such as mineral dust, and could do so *in situ*.

Analysis of Layered Dielectric Capped Wedge for RCS Reduction

Hulya Ozturk[1] and Korkut Yegin[2]

[1]Department of Mathematics, Gebze Technical University, Kocaeli 41400, Turkey
[2]Electrical and Electronics Engineering Department, Ege University, Izmir 35100, Turkey

Abstract— Conducting wedge is a canonical structure in electromagnetic scattering problems. Applications of scattering from wedge geometries range from reflector designs to aerial vehicles. Due to wide range of applications, plane wave scattering due to a wedge shape has been studied extensively in the past. However, wedge capped with dielectric layers with the intention of RCS reduction has been overlooked. We first took a canonical wedge infinite in z-direction (longitudinal) and covered this wedge with dielectric layers of varying thicknesses and dielectric properties including conductive loss. Then, scalar Helmholtz equation in two dimensions is formulated for each solution region and a matrix of unknown coefficients are arrived at for problem solution. For different wedge shapes and dielectric layer properties, corresponding RCS values are computed in one- and two-dimension. We observed that if certain conditions are met, RCS can be reduced from that of uncovered perfect electric conductor wedge. We also formulated the RCS reduction as a single objective optimization problem to observe the interdependence of wedge parameters to RCS values. Since wedge shapes are particularly useful in unmanned aerial vehicles, airplanes, and missile structures, the analysis which was carried in two-dimensions (infinite in longitudinal direction), is further expanded for simplistic shapes in three dimensions using computer-aided electromagnetic scattering programs. These numerical solvers also permit solutions for coated wedge geometries where it is possible to compare the effectiveness of coating to dielectric capped wedge configurations. Both analytical and simulated results will be presented in detail to express the degree of agreement and to validate the proposed concept on 3D shapes.

REFERENCES

1. Redadaa, S., A. Boualleg, N. Merabtine, and M. Benslama, "Radar cross section study from wave scattering structures," *Semiconductor Physics, Quantum Electronics & Optoelectronics*, Vol. 9, No. 4, 71–76, 2006.
2. Bowman, J. J., T. B. A. Senior, and P. L. E. Uslenghi, *Electromagnetic and Acoustic Scattering by Simple Shapes*, Hemsisphere Publishing, NY, 1987.

A Perturbative Solution to Plane Wave Scattering from a Rough Dielectric Cylinder

Rahul Trivedi and Uday K. Khankhoje
Department of Electrical Engineering, Indian Institute of Technology Delhi, New Delhi, India

Abstract— Scattering of electromagnetic waves by vegetation such as tree trunks, branches and leaves is a significant contributor to radar scattering. At low microwave frequencies, modelling the tree trunk as a smooth cylinder is usually sufficient to accurately capture it's effect on the incident radiation. However, at higher frequencies, the surface roughness begins to play an increasingly important role in the scattering properties of the tree trunk. Numerical methods such as the integral equation method can be used to compute the scattered fields for a rough cylinder, however, their use is limited by the large computation time involved.

We present a second order perturbative analysis of scattering of a plane electromagnetic wave from a stochastically rough cylinder. The rough cylinder surface is described by a stochastic process, $h(\phi, z)$, which denotes the radial distance of a point on the rough surface at azimuthal coordinate ϕ and z-coordinate z from the mean smooth cylinder of radius a. We analytically solve Maxwell's equations to obtain a perturbative expression to second order for the scattered fields:

$$\begin{aligned}\mathbf{E}^{sca}(\mathbf{r}) \;=\; \mathbf{E}_0^{sca}(\mathbf{r}) + \sum_{m=-\infty}^{\infty} \int_{-\infty}^{\infty} \alpha_m(\mathbf{r};k)\tilde{h}_m\left(k - k_0\cos\alpha\right) dk \\ + \sum_{m=-\infty}^{\infty}\sum_{p=\infty}^{\infty} \int_{-\infty}^{\infty}\int_{-\infty}^{\infty} \beta_{m,p}(\mathbf{r};k,k')\tilde{h}_m\left(k' - k_0\cos\alpha\right)\tilde{h}_p\left(k - k'\right) dkdk' \qquad (1)\end{aligned}$$

where $\tilde{h}_n(k) = \frac{1}{4\pi^2}\int_{-\infty}^{\infty}\int_0^{2\pi} h(\phi,z)\exp(-j(n\phi+kz))d\phi dk$, the incident field is assumed to propagate along $\mathbf{k}_i = k_0(\hat{z}\cos\alpha + \hat{x}\sin\alpha)$, and $\mathbf{E}_0^{sca}(\mathbf{r})$ is the scattered field due to a *smooth* cylinder of radius a. Closed form expressions for the functions $\alpha_m(\mathbf{r};k)$ and $\beta_{m,p}(\mathbf{r};k,k')$ are derived from the Maxwell's equations and the boundary conditions at the rough cylinder surface. Clearly, Eq. (1) can be used to evaluate the ensemble average of the scattered field and other derived quantities (such as the scattering cross section), if the autocorrelation function of the random process $R(\phi,z) = \overline{h(\Phi,Z)h(\Phi+\phi,Z+z)}$ is known. Our method therefore allows the direct calculation of the statistical properties of the scattered fields in terms of the statistical properties of the rough cylinder surface, significantly reducing the computational time involved as compared to the other numerical methods that can be employed for analysing the same problem.

We also investigate the validity of our analysis by numerically comparing it with a method-of-moments based solution of the same problem. For simplicity, we assume that the cylinder surface is only *azimuthally* rough, i.e., $h(\phi,z)$ is independent of z, and that it is exponentially correlated:

$$R(\phi) = \overline{h(\Phi)h(\Phi+\phi)} = h_0^2\exp\left(-|\phi|/\phi_0\right)\forall\in(-\pi,\pi] \qquad (2)$$

h_0 being the root mean square roughness and $l = a\phi_0$ being the correlation length of the rough surface. This numerical validation gives us a region of validity in terms of bounds on h_0 and l within which the perturbative solution is sufficient to describe the scattered fields due to the rough cylinder.

Multispectral Light Scattering Imaging and Multivariate Analysis of Airborne Particulates

Stephen Holler[1], **Charles Skelsey**[2], **and Stephen D. Fuerstenau**[3]

[1]Department of Physics & Engineering Physics
Fordham University, 441 East Fordham Road, Bronx, NY 10458, USA
[2]Fordham University, 441 East Fordham Road, Bronx, NY 10458, USA
[3]SDF Consulting San Mateo, CA, USA

Abstract— Light scattering patterns from non-spherical particles and aggregates exhibit complex structure that is only revealed when observing in two angular dimensions. However, due to the varied shape and packing of such aerosols, the rich structure in the two-dimensional angular optical scattering (TAOS) pattern varies from particle to particle. We examine two-dimensional light scattering patterns obtained at multiple wavelengths using a single CCD camera with minimal cross talk between channels. The integration of the approach with a single CCD camera assures that data is acquired within the same solid angle and orientation. Since the optical size of the scattering particle is inversely proportional to the illuminating wavelength, the spectrally resolved scattering information provides characteristic information about the airborne particles simultaneously in two different scaling regimes. The simultaneous acquisition of data from airborne particulate matter at two different wavelengths allows for additional degrees of freedom in the analysis and characterization of the aerosols. Whereas our previous multivariate analyses of aerosol particles has relied solely on spatial frequency components, our present approach attempts to incorporate the relative symmetry of the particle-detector system while extracting information content from both spectral channels. In addition to single channel data, this current approach also examines relative metrics. Consequently, we have begun to employ multivariate techniques based on novel morphological descriptors in order to classify "unknown" particles within a database of TAOS patterns from known aerosols utilizing both spectral and spatial information acquired. A comparison is made among several different classification metrics, all of which show improved classification capabilities relative to our previous approaches.

Evaluation of the Angular Spectrum of Scattered High Frequency Radio Waves in the Anisotropic Collision Magnetized Ionospheric Plasma

G. V. Jandieri[1], Zh. M. Diasamidze[2], M. R. Diasamidze[3], and I. Nemsadze[4]

[1]Special Department, Georgian Technical University, Georgia
[2]Physics Department, Batumi Shota Rustaveli State University, Georgia
[3]Department of Exact and Natural Sciences, Batumi State Maritime Academy, Georgia
[4]Physics Department, Batumi Shota Rustaveli State University, Georgia

Abstract— This paper represents incline incidence of high-frequency radio wave on the magnetized collision ionospheric plasma slab in the ray (-optics) approximation taking into account boundary conditions using the Snell's low. Fourth order dispersion equation is derived for the mean field of scattered radio waves including components of the second rank dielectric permittivity tensor of the magnetized plasma. Set of stochastic differential equations is obtained for the fluctuating electric field vector. Second order statistical moments of the phase and amplitude fluctuations of high-frequency electromagnetic waves are investigated taking into account both electron density and external magnetic field fluctuations. Polarization effects for the ordinary and extraordinary waves are taken into account. The obtained results are valid for arbitrary correlation functions of fluctuating plasma parameters in the near and far zones from a slab. The influences of both anisotropy factor and angle of inclination of prolate irregularities with respect to the external magnetic field on the statistical characteristics of scattered radio waves: Stokes parameters, broadening of the spatial spectrum of scattered radiation, displacement of its maximum, angle of arrivals in the principle and perpendicular planes are investigated analytically and numerically for both anisotropic Gaussian and power law spectral functions characterizing electron density fluctuations on different ionospheric layers. Interaction effect of waves is considered on the basis of the dispersion equation at different angles of incidence on plasma slab. Phase portraits of the correlation functions of the amplitude and phase fluctuations were constructed for different spatial parameters characterizing given problem taking into account external magnetic field fluctuations. Numerical calculations were carried out at different distances between observation points and parameters characterizing anisotropic irregularities having different characteristic spatial scales. The obtained results are of interest and will have application in satellite communication and ionospheric monitoring stimulating investigation of ionospheric irregularities.

Stochastic Geometry for Electromagnetic Scattering Modeling

Frédéric Gruy
Ecole Nationale Supérieure des Mines
158 Cours Fauriel, 42023 Saint-Etienne, Cedex 2, France

Abstract— Electromagnetic scattering by particles consisting in a homogeneous material has been studied a lot by means of Maxwell equations that are numerically solved. Solutions depend on the morphology of the particles; the morphology of the particle is revealed at the boundary conditions. In the case of a homogeneous material a relationship between the scattering properties, the optical indices of the material and the surface characteristics can be expected. The need of fast calculations is important for industrial applications, even if the accuracy is lower. Fitting the accuracy of the calculation with the accuracy of the measurement is sufficient. Moreover the use of relevant descriptors for the particle geometry can simplify the correspondence between optical and geometrical properties. In the past some optical approximations have been developed for the calculations for soft materials, e.g. Rayleigh-Debye-Gans approximation for small particles, Van de Hulst approximation for large particles. In these cases phase function and scattering cross section explicitly contain geometrical parameters like the distance between two points inside the particle, the chord length, etc.. On the other hand Fraunhoffer diffraction for large and optically hard particles is often related to the projected area of the particle. As a consequence there may exist a relationship between the optical properties and the statistical distribution of such geometrical parameters. In this sense the chord length distribution (CLD) seems to be a good candidate to optically describe a particle. This paper:

- reminds how the optical properties are related to these distributions,
- presents the way to estimate the distributions,
- presents some examples of distributions (for spheres, ellipsoids, cylinders, facetted crystals),
- reminds some mathematical properties of these distributions,
- presents some rules to reconstruct rapidly the CLD for convex particles,
- compares the exact and approximated calculations of the scattering cross section.

Plasmons and Charge Noise at Composite Surfaces

C. Henkel[1] and B. Horovitz[2]

[1]Institute of Physics and Astronomy, University of Potsdam, Germany
[2]Department of Physics, Ben Gurion University, Beer Sheva, Israel

Abstract— We discuss the scattering of photons, plasmons, and electrons at a rough metallic surface. Our motivation are experiments with surfaces that are not perfectly characterized, covered with adsorbates or hosting localized charge states. For example, the randomly varying work function (patch potentials) of an amorphous metal actually shows fluctuations; these can be measured in the MHz band with charged particle traps at sub-millimeter distances. Our goal is to develop a microscopic model and to identify strategies to reduce this noise. Another experimental signature is the dispersion of the surface plasmon resonance at large parallel momentum. It is well known since the work of Feibelman [1] that the slope of the dispersion relation is sensitive to the response of the electron density in the near-surface region.

Our model builds upon previous work on a kinetic theory where bulk and surface electrons are coupled via non-specular scattering at a rough surface [2]. We use the relevant conservation laws for hydrodynamic fields (density, current) to complement material relations in the bulk with boundary conditions. This yields, for example, a modified dispersion relation for surface plasmon polaritons. The electromagnetic response problem for fields incident upon the surface is solved and yields electric and magnetic fluctuation spectra in conjunction with the fluctuation — dissipation relation [3]. We analyze in particular the average Lorentz force in a high-density conductor that may give a significant temperature dependent correction to the work function. The goal is to establish the spectral density of the thermal Lorentz force and to compare with frequency- and temperature-dependent data for surface charge noise from miniature ion traps.

ACKNOWLEDGMENT

This work is supported by the DIP programme of the *Deutsche Forschungsgemeinschaft* within the project "IANV Hybrids".

REFERENCES

1. Feibelman, P. J., "Surface electromagnetic fields," *Progr. Surf. Sci.*, Vol. 12, 287–408, 1982.
2. Horovitz, B. and C. Henkel, "Surface plasmons at composite surfaces with diffusive charges," *Europhys. Lett.*, Vol. 97, 57010, 2012.
3. Henkel, C. and B. Horovitz, "Noise from metallic surfaces: Effects of charge diffusion," *Phys. Rev. A*, Vol. 78, 042902, 2008.

Resonant Electromagnetic Scattering in Anisotropic Layered Media with Random Fabrication Errors

Emily A. McHenry
Mathematics Department, Louisiana State University, Baton Rouge, Louisiana

Abstract— The excitation of an electromagnetic guided mode (occurring at a frequency embedded in the continuous spectrum of the underlying Maxwell operator) of a slab structure by an exterior source field elicits anomalous scattering behavior, particularly resonant field amplification and sharp variations in energy transmission and reflection across the slab (known as Fano resonance). This resonance phenomena is utilized by optical devices that require the precise tuning of the width and central frequency of a resonance, including lasers, filters, and light-emitting diodes. However, these characteristics are sensitive to random fabrication errors that occur during the production process. In this talk, we will quantify quantify the sensitivity of resonant characteristics to these material imperfections.

In [4] a slab structure that supports a spectrally embedded guided mode was constructed using the properties of anisotropic layered media. Into this regime, we introduce random perturbations of the dielectric and magnetic tensors ϵ and μ across the slab; the random perturbations are controlled by a small parameter σ:

$$\begin{aligned}\epsilon(z) &= \epsilon_0(z) + \sigma\xi(z)\\ \mu(z) &= \mu_0(z) + \sigma\eta(z),\end{aligned}$$

where ξ and η are random variable matrices. The effect of the random perturbations on the resonant characteristics of the slab is analyzed through the poles of the scattering matrix $\tilde{S} = (TP_- - P_+)^{-1}$, where $P_\pm$ are the projections in $\mathbb{C}^4$ onto the two-dimensional rightward $(+)$ and leftward $(-)$ Bloch modes of the ambient (nonrandom) medium. Representing the scattering matrix in this way, the random variation of a pole is obtained through perturbation analysis of the analytic eigenvalue $\lambda(\boldsymbol{\kappa}_\parallel, \omega)$ of the matrix $(T_0(I + \sigma M))P_- - P_+$, where $T_0(I + \sigma M)$ denotes the transfer matrix T up to the first order in σ.

The transmission and reflection coefficients are obtained by projecting the scattering matrix to the propagating harmonics of the ambient medium. The result has the form

$$S(\boldsymbol{\kappa}_\parallel, \omega; \sigma) = \frac{1}{\lambda(\boldsymbol{\kappa}_\parallel, \omega; \sigma)} \begin{bmatrix} b_1(\boldsymbol{\kappa}_\parallel, \omega; \sigma) & a_2(\boldsymbol{\kappa}_\parallel, \omega; \sigma) \\ a_1(\boldsymbol{\kappa}_\parallel, \omega; \sigma) & b_2(\boldsymbol{\kappa}_\parallel, \omega; \sigma) \end{bmatrix}.$$

The eigenvalue λ, reflectances a_j, and transmittances b_j vanish simultaneously at the guided mode point $(\boldsymbol{\kappa}_\parallel^0, \omega^0; 0)$. A rigorous description of transmission anomalies in the nonrandom lossless case is given in [1–3]. We will extend this analysis to establish the properties of transmission anomalies as random variables, particularly the mean and variance of the heights and locations of the sharp peaks and dips in the Fano lineshape.

REFERENCES

1. Ptitsyna, N. and S. P. Shipman, "A lattice model for resonance in open periodic waveguides," *Discret. Contin. Dyn. S*, Vol. 5, No. 5, 2012.
2. Shipman, S. P., "Resonant scattering by open periodic waveguides," *E-book Progress in Computational Physics*, Vol. 1, Bentham Science Publishers, 2010.
3. Shipman, S. P. and S. Venakides, "Resonance and bound states in photonic crystal slabs," *SIAM J. Appl. Math.*, Vol. 72, No. 1, 216–239, 2012.
4. Shipman, S. P. and A. T. Welters, "Resonant electromagnetic scattering in anisotropic layered media,". *J. Math. Phys.*, Vol. 54, No. 10, 103511-1-40, 2013.

Patterning Highly Oriented Pyrolytic Graphite for Efficient Broad-band Absorption

Julian Evans, **Yaoran Sun**, **and Sailing He**
Center for Optical and Electromagnetic Research, Zhejiang University, China

Abstract— Highly absorbing materials have many applications in astronomical observation, photothermal solar light harvesting, and thermal photonic devices. Many groups use vertical aligned carbon nanotubes to create such materials, which require complicated growth processes and large thicknesses. Highly Oriented Pyrolytic Graphite (HOPG) can be structured using ICP-etching to produce significantly thinner, more robust materials that have potentially comparable performance for a variety of applications. In this talk I will describe a method using gold nanoparticle masks to produce 400 nm tall nanocone structures that allow for broadband absorption of greater than 95% for wavelengths ranging from 400 nm–1600 nm. The density and size of nanocones can be easily tuned by varying the density of nanoparticle masks and etching conditions. Using polyethylene glycol capped spheres, we've achieved nearly complete coverage of the surface with the nanocone structures through a simple spin coating process. Computer simulations indicate that surface coverage and height are the critical parameters for achieving high absorptivity and that the overall pattern of nanocone arrangement and polydispersity are less critical in material performance.

A Study of Periodic Multilayered Structure in Fractional Dimension Space and Euclidian Space

M. J. Mughal[1] and Safiullah Khan[2]

[1]COMSATS Institute of Information Technology, Islamabad, Pakistan
[2]Ghulam Ishaq Khan Institute of Engineering Sciences and Technology, Topi 23640, Pakistan

Abstract— In this paper, Transfer Matrix Method and modified Maxwell equations are used to find the general expressions for reflection and transmission coefficients of periodic multilayered structure. The structure is placed in D dimension space where D is integer for Euclidean space and non-integer for Fractional space. Characteristics of these structure are studied when an electromagnetic wave strikes on it at both normal and oblique incident angle. The final expressions are the function of frequency, dimension and incident angle. Numerical results for multilayered periodic strong chiral — strong chiral structure are presented. This study provides motivation to investigate the electromagnetic waves propagation in multilayered structures at fractional boundaries.

Summary: Advances in the metamaterials (MTM) has significantly attracted the attention of researchers. Multilayered structures composed of composite materials are being widely used in applications such as antenna designing, lens designing, frequency selective surfaces etc. [1–3]. Since, metallic structures have losses associated with it, metamaterial structures are used to achieve desirable outcomes. Until recently, frequency, incident angle and constitutive parameters behaviour were studied but with the introduction of fractional calculus, effect of dimension can also be studied. Irregular surfaces, porous media, and complex structures can be modelled with fractional calculus [4].

In this paper strong chiral — strong chiral multilayered structure placed in D dimension space is presented for analysis as shown in Figure 1. The general incident, reflected and transmitted fields are [4],

$$\mathbf{E}_i = \left[E_{i\parallel}\left(\hat{x}\cos\theta_i + \hat{z}\sin\theta_i\right) + E_{i\perp}\hat{y}\right] e^{-jk_F(-x\sin\theta_i)}(k_F z\cos\theta_i)^n \left[H_n^{(2)}(k_F z\cos\theta_i)\right], \tag{1}$$

$$\mathbf{H}_i = \frac{1}{\eta}\left[E_{i\parallel}\hat{y} - E_{i\perp}\left(\hat{x}\cos\theta_i + \hat{z}\sin\theta_i\right)\right] e^{-jk_F(-x\sin\theta_i)}(k_F z\cos\theta_i)^{nh} \left[H_{nh}^{(2)}(k_F z\cos\theta_i)\right], \tag{2}$$

$$\mathbf{E}_r = \left[E_{r\parallel}\left(\hat{x}\cos\theta_r - \hat{z}\sin\theta_r\right) + E_{r\perp}\hat{y}\right] e^{-jk_F(-x\sin\theta_r)}(k_F z\cos\theta_r)^n \left[H_n^{(1)}(k_F z\cos\theta_r)\right], \tag{3}$$

$$\mathbf{H}_r = \frac{1}{\eta}\left[-E_{r\parallel}\hat{y} + E_{r\perp}\left(\hat{x}\cos\theta_r - \hat{z}\sin\theta_r\right)\right] e^{-jk_F(-x\sin\theta_r)}(k_F z\cos\theta_r)^{nh} \left[H_{nh}^{(1)}(k_F z\cos\theta_r)\right], \tag{4}$$

$$\mathbf{E}_t = \left[E_{t\parallel}\left(\hat{x}\cos\theta_t - \hat{z}\sin\theta_t\right) + E_{t\perp}\hat{y}\right] e^{-jk_F(-x\sin\theta_t)}(k_F z\cos\theta_t)^n \left[H_n^{(2)}(k_F z\cos\theta_t)\right], \tag{5}$$

$$\mathbf{H}_t = \frac{1}{\eta}\left[E_{t\parallel}\hat{y} + E_{t\perp}\left(\hat{x}\cos\theta_t + \hat{z}\sin\theta_t\right)\right] e^{-jk_F(-x\sin\theta_t)}(k_F z\cos\theta_t)^{nh} \left[H_{nh}^{(2)}(k_F z\cos\theta_t)\right] \tag{6}$$

where $n = \frac{|3-D|}{2}$ and $nh = \frac{|D-1|}{2}$. Hankel function of the second kind and Hankel function of the first kind represents the forward travelling wave and backward travelling wave respectively. Transfer Matrix Method (TMM) is applied on Equations (1)–(6) and electric and magnetic field expressions for strong chiral medium, to compute field expressions on either side of the structure. The final expression is of the following form,

$$\begin{bmatrix} E_{i\parallel} \\ E_{i\perp} \\ E_{r\parallel} \\ E_{r\perp} \end{bmatrix} = [T] \begin{bmatrix} E_{t\parallel} \\ E_{t\perp} \end{bmatrix} \tag{7}$$

$$[T] = \begin{bmatrix} a_{11} & a_{12} \\ a_{21} & a_{22} \\ a_{31} & a_{32} \\ a_{41} & a_{42} \end{bmatrix} = [M_1][P_A][T_1]^m[M_2] \tag{8}$$

$$[T_1] = [M_{AB}][P_B][M_{BA}][P_A] \tag{9}$$

where $[T]$ is the transfer matrix and it relates the field on either side of the structure. Figures 2 and 3 show the reflectance at normal and oblique incidences, respectively (for simplicity only reflectance is shown here).

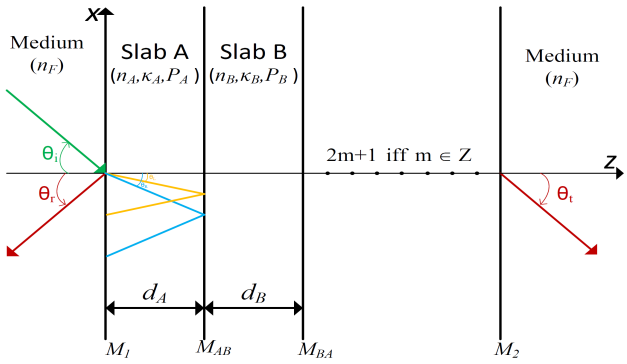

Figure 1: Five layered metmaterial structure placed in D dimension space.

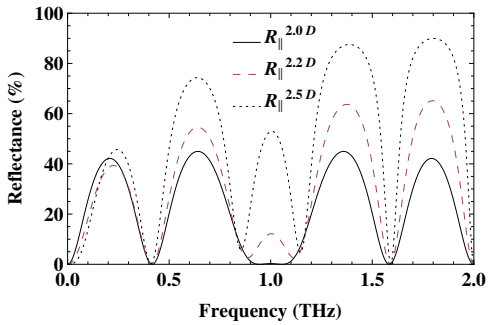

Figure 2: Reflectance for five layered SC-SC structure. $n_A = 0.8$, $n_B = 0.6$, $\kappa_A = 1.2$, $\kappa_B = 1.0$, $|n_A|d_A = |n_B|d_B = \lambda_0/4$, $\theta_i = 0°$.

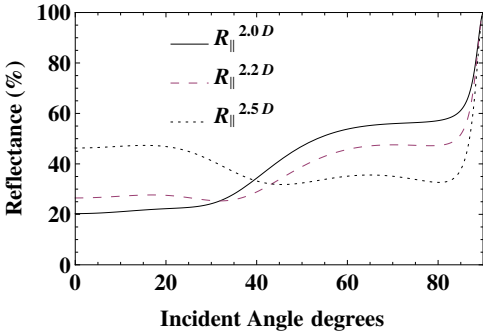

Figure 3: Reflectance for five layered SC-SC structure. $n_A = 0.8$, $n_B = 0.6$, $\kappa_A = 1.2$, $\kappa_B = 1.0$, $|n_A|d_A = |n_B|d_B = \lambda_0/4$, $f/f_0 = 0.5$.

REFERENCES

1. Liu, C. H. and N. Behdad, "Tunneling and filtering characteristics of cascaded-negative metamaterial layers sandwiched by double-positive layers," *Journal of Applied Physics*, Vol. 111, 014906, 2012.
2. Sabah, C. and H. G. Roskos, "Design of a terahertz polarization rotator based on a periodic sequence of chiral-metamaterial and dielectric slabs," *Progress In Electromagnetics Research*, Vol. 124, 301–314, 2012.
3. Oraizi, H. and M. Afsahi, "Design of metamaterial multilayer structures as frequency selective surfaces," *Progress In Electromagnetics Research C*, Vol. 6, 115–126, 2009.
4. Zubair, M., M. J. Mughal, and Q. A. Naqvi, *Electromagnetic Fields and Waves in Fractional Dimensional Space*, 1st Edition, Springer, 2012.

Session 2A11
FocusSession.SC1: Casimir Effect and Heat Transfer 3

Quantum Thermodynamics: An Information Theoretical Viewpoint

Mauro Paternostro
Centre for Theoretical Atomic, Molecular, and Optical Physics
School of Mathematics and Physics, Queen's University Belfast, BT71 NN, Belfast, UK

Abstract— Thermodynamics is one of the pillars of physical, chemical and biological sciences. It is able to predict the occurrence and efficiency of complex chemical reactions and biological processes. In physics, the conduction of heat across a medium or the concept of the arrow of time are formulated thermodynamically. In information theory, the definitions of information and entropy are given in thermodynamical terms. Even more, the tightness of the link between information and thermodynamics can be deduced from the thermodynamic interpretation of the landmark embodied by Landauers erasure principle, Jaynes principle of maximum entropy, or the exorcism of Maxwell's demon operated using information theoretical tools. Another example is the analysis of the spectrum of blackbody radiation made by Planck, which triggered the quantum mechanical revolution. However, science and technology have evolved immensely from the early days of the quantum era, allowing us to witness quantum effects that could only be dreamed of decades ago. Our capabilities to control and guide processes at the microscopic scale has reached outstanding levels of dexterity. Yet, a series of tantalising questions arise: what happens to the principles of thermodynamics when we deal with the quick dynamics of small quantum systems brought dramatically out of equilibrium? Can we formulate in a thermodynamical way the working principles of quantum devices designed to perform transformations analogous to "canonical" thermo-machines? In this talk I will present a framework that is able to show the emergence of thermodynamics out of genuinely quantum processes enforced in quantum many- body systems, thus establishing a tight link between thermodynamics and quantum critical phenomena. I will discuss how work can be extracted from intricate (mesoscopic) quantum motors to ensure engines performances overcoming any classical counterpart and suggest tantalising connections between the irreversible quantum entropy produced across a process and the establishment of quantum correlations among the constituents of a quantum device.

Steady Many-body Entanglement Induced by an out of Thermal Equilibrium Environment

Bruno Bellomo[1, 2] **and Mauro Antezza**[2, 3]

[1]Observatoire des Sciences de l'Univers THETA, Institut UTINAM, UMR CNRS 6213
Université de Franche-Comté, Besançon F-25010, France
[2]Laboratoire Charles Coulomb (L2C), UMR 5221 CNRS, Université de Montpellier, Montpellier, France
[3]Institut Universitaire de France, 103, bd Saint-Michel F-75005 Paris, France

Abstract— This work concerns the manipulation of quantum systems by engineering the properties of the environment they interact with. It is based on recent studies regarding the properties of the radiation field produced in a given configuration when macroscopic bodies are kept at different temperatures [1]. Indeed, it has been shown that the interaction of small atomic systems (one or two atoms) with a field produced in a configuration kept out of thermal equilibrium may permit a strong manipulation of the atomic dynamics [2–5].

Here we study an ensemble of more than two two-level quantum systems (qubits) interacting with a common electromagnetic field in proximity of a dielectric slab whose temperature is held different from that of some far surrounding walls (see Fig. 1). We show that the dissipative dynamics of the qubits driven by this stationary and out of thermal equilibrium (OTE) field, allows the production of steady many-body entangled states, differently from the case at thermal equilibrium where steady states are always non-entangled. By studying up to ten qubits, we point out the role of symmetry in the entanglement production, which is exalted in the case of permutationally invariant configurations. In the case of three qubits, we find a strong dependence of tripartite entanglement on the spatial disposition of the qubits, and in the case of six qubits, we find several highly entangled bipartitions where entanglement can, remarkably, survive for large qubit-qubit distances up to 100 µm [6].

Our analysis points out the potentialities of rich yet simple configurations involving macroscopic bodies held at different temperature, which are within experimental reach. They may permit the production and manipulation of steady multipartite entanglement, resistant for large inter-qubits distances, offering then new tools possibly exploitable for quantum computational tasks. All this is obtained without any further external actions on the qubits, being the result of the qubits dissipative dynamics itself. These protocols are then intrinsically robust to environmental effects and do not need of initializing the total system in a given configuration.

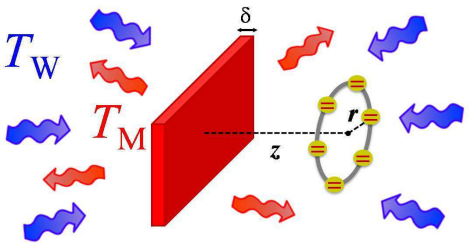

Figure 1: Several qubits close to a slab at temperature T_M different from the temperature of some far surrounding walls, T_W.

REFERENCES

1. Messina, R. and M. Antezza, *Phys. Rev. A*, Vol. 84, 042102, 2011; *Europhys. Lett.*, Vol. 95, 61002, 2011.
2. Bellomo, B., R. Messina, and M. Antezza, *Europhys. Lett.*, Vol. 100, 20006, 2012.
3. Bellomo, B., R. Messina, D. Felbacq, and M. Antezza, *Phys. Rev. A*, Vol. 87, 012101, 2013.
4. Bellomo, B. and M. Antezza, *Europhys. Lett.*, Vol. 104, 10006, 2013; *New J. Phys.*, Vol. 15, 113052, 2013.
5. Leggio, B., B. Bellomo, and M. Antezza, *Phys. Rev. A*, Vol. 91, 012117, 2015.
6. Bellomo, B. and M. Antezza, arXiv: 1409.7178, 2014.

Tightening the Second Law of Thermodynamics for Restricted Baths

Karen V. Hovhannisyan, Martí Perarnau-Llobet, and Paul Skrzypczyk
ICFO-Institut de Ciencies Fotoniques, Mediterranean Technology Park
Castelldefels, Barcelona 08860, Spain

Abstract— The most operationally meaningful formulation of the second law of thermodynamics is the so called maximum work principle: The maximal work one can extract from a system attached to a bath is given by the difference of initial and final free energies of the system. The law is universal: It does not depend on the details of the bath. Yet, while working with small systems, we face different kinds of limitations connected to the fact that the bath is not infinite or it cannot be engineered to have correct macroscopic spectrum, etc.. A fundamental question then would be whether one can put additional limitations on the extractable work which will respect the new constraints but will still be independent on the other details of the bath. In case of fixed dimensionality of the Hilbert space of the bath we find general dimensionality-dependent bounds on the corrections to free energy difference formula. We further study another kind of limitation where it is not the dimensionality that is bounded but the fine tuning in the bath. We do so by considering an ensemble of identical spins as a bath. There we prove that the lack of fine tuning is compensated by taking the continuum limit and we find the scaling of the corresponding correction term. The role of correlations built up between the system and the bath and within the bath is also studied.

Finite Temperature Reservoir Engineering and Entanglement Dynamics

S. Fedortchenko[1], **A. Keller**[2], **T. Coudreau**[1], **and P. Milman**[1]

[1]Laboratoire Matériaux et Phénomènes Quantiques, Sorbonne Paris Cité
Université Paris Diderot, CNRS UMR 7162, Paris 75013, France
[2]Université Paris-Sud 11, Institut des Sciences Moléculaires d'Orsay (CNRS)
Bâtiment 350, Campus d'Orsay, 91405 Orsay Cedex, France

Abstract— For the vast majority of experimentally controllable and measurable quantum systems, interaction with the environment leads to a decoherence process that rapidly and irreversibly destroys the quantum properties of the studied system. Decoherence impedes the large scale applications of quantum mechanics, as quantum information and quantum metrology. Such unavoidable coupling between a system and an inaccessible environment privileges so-called pointer states. When interaction with the reservoir prevails over the system's free Hamiltonian, the specific properties of the system — environment coupling determine the steady, or more stable states of the considered system. Decoherence owes its bad reputation to the fact that, for experimentally relevant situations, these steady states usually do not display nonclassical properties. However, quantum reservoir engineering showed that decoherence can be rendered compatible with the preservation of quantum properties. Indeed, by judiciously engineering the effects of exotic system — reservoir couplings, quantum states with useful quantum properties, such as entanglement or quantum coherence, can turn out to be the steady states of the decoherence process. Reservoir engineering can be used to protect interesting quantum states from decoherence, even in the case where a "natural" reservoir is present. As a matter of fact, an engineered reservoir can dominate a system's dynamics, turning the total system's steady state arbitrarily close to its own steady state, that can be controllably chosen.

The experimental implementation of reservoir engineering became achievable with the rapid technological development of quantum devices. Recent experimental results demonstrate the production of steady maximally entangled states through controlled dissipation in trapped ions and superconducting systems. Most theoretical proposals and experimental realizations are focused on engineering zero temperature reservoirs, since they can lead to the production and protection of pure states.

The steady state of a finite temperature reservoir is mixed. Finite temperature reservoir engineering can lead to the production and protection of mixed states with interesting entanglement properties, a problem that remains unexploited in the literature. Nevertheless, there are a number of interesting and unusual entanglement properties that engineered thermal reservoir can help to reveal and fully exploit for applications. One example is thermal entangled states, states that are separable at zero temperature, but entangled at finite temperature. They are the eigenstates of a strongly interacting spin system coupled to a reservoir that, due to the strongly interacting Hamiltonian, is non-local, i.e., it acts in many spins at the same time. Experimental observation of thermal entanglement is possible in strongly interacting many body systems. However, in such systems, entanglement cannot be extracted and used as a resource for quantum based protocols. Moreover, the system-reservoir Hamiltonian is fixed by the specific material under study, and cannot be engineered and controlled.

In the present contribution, we provide theoretical proposals leading to finite temperature reservoir engineering which are well adapted to the state-of-the art of different set-ups successfully used to demonstrate quantum protocols. We detail these ideas for a trapped ion systems. Extending the proposed ideas to other set-ups, as superconducting qubits and photons, is also possible, but will not be detailed here.

The Best Quantum Thermoelectric at Finite Power Output

Robert S. Whitney
Laboratoire de Physique et Modélisation des Milieux Condensés (UMR 5493)
Université Grenoble 1 and CNRS, Maison des Magistères, BP 166, Grenoble 38042, France

Abstract— Carnot efficiency is only achievable at zero power output. We ask what is the maximum efficiency at some given finite power output. It appears that this question is ill-defined in classical thermodynamics, but can be answered with a quantum theory.

We use the Landauer-Buttiker scattering theory to find this maximum efficiency for heat engines and refrigerators made of thermoelectric quantum systems. We initially find the exact maximum efficiency for two-terminal systems without energy relaxation [1]. We then use phenomenological models to explore whether this maximum can be exceeded by two-terminal systems with relaxation [2], or by three-terminal systems. We have not yet found a system which can exceed the maximum efficiency given in Ref. [1], although open questions remain.

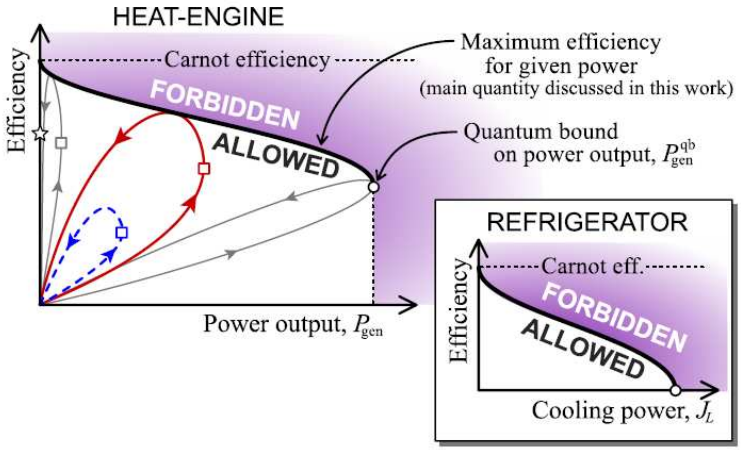

Figure 1: Taken from Ref. [2]. The thick black curves are qualitative sketches of the maximum efficiency as a function of heat-engine power output (main plot), or refrigerator cooling power (inset), with the shaded regions being forbidden. The colored loops (red, grey and blue) are sketches of the efficiency versus power of *individual* heat-engines as we increase the load resistance.

REFERENCES

1. Whitney, R. S., *Phys. Rev. Lett.*, Vol. 112, 130601, 2014.
2. Whitney, R. S., arXiv:1408.3348.

Non-adiabaticity and Irreversible Entropy Production

F. Plastina
Dipartimento Fisica, Universita' della Calabria, Arcavacata di Rende (CS) 87036, Italy

Abstract— The out-of-equilibrium thermodynamic properties of closed quantum systems driven by a change in a control parameter and undergoing a unitary transformation have been the subject of an intense research activity. We study the work actually done on the system and compare it with the adiabatic one, that would be performed following an ideal adiabatic protocol. The non-adiabatic part of the work, usually called *inner friction*, can be used to reveal irreversibility in the process and it is intimately linked to the non-equilibrium entropy production. Indeed, it is related to the heat exchanged in a specific thermalization process that would occur after the end of the adiabatic transformation, and it can be expressed as the relative entropy between the actual state of the system and the ideal equilibrium one. Furthermore, it is associated to a specific fluctuation relation for the entropy production, which allows the inner friction to be expressed in terms of its cumulants. We apply this formalism to various cases of experimental relevance, including a qubit and an harmonic oscillator. In such cases, we show explicitly that the inner friction is linked to the speed at which the thermodynamic transformation is performed and to the diabatic transitions that occur in the system.

REFERENCES

1. Plastina, F., et al., *Phys. Rev. Lett.*, Vol. 113, 260601, 2014.

Critical Casimir Forces

S. Dietrich[1, 2]

[1]Max Planck Institut für Intelligente Systeme, Germany
[2]Institut für Theoretische Physik IV, Universität Stuttgart, Germany

Abstract— Long-ranged correlations in a fluid near its critical point lead to clearly identifiable effective forces acting on confining walls. The corresponding universal scaling functions are discussed for different boundary conditions and geometries. The theoretical predictions are compared with high precision experimental data for He^4 and He^3/He^4 wetting films near the superfluid phase transition as well as with synchrotron scattering data from classical binary liquid mixtures. Direct measurements and applications for colloidal suspensions are discussed.

Critical Casimir Forces & Many-body Effects

Andrea Gambassi
SISSA — International School for Advanced Studies and INFN
via Bonomea 265, Trieste 34136, Italy

Abstract— In 1948, Hendrik Casimir predicted that two uncharged conducting surfaces in vacuum attract each other due to the quantum fluctuations of the electromagnetic field which are spatially confined by these surfaces. The classical analogue of this effect was theoretically investigated by Michael Fisher and Pierre-Gilles de Gennes in 1978 and it originates from the confinement of thermal fluctuations in fluids near continuous phase transitions, such as the demixing of a mixture of two liquids. The equilibrium force of these fluctuations — the so-called critical Casimir force — has been recently measured and it can be harnessed for controlling soft matter and colloids at the micrometer scale. Due to its very same nature, this force is non-additive and therefore many-body effects have to be expected. In the talk I will discuss the current status of their investigation.

Photonic Control of Thermal Emission for Radiative Cooling

Aaswath Raman, **Linxiao Zhu**, **and Shanhui Fan**
Ginzton Laboratory, Stanford University, Stanford, CA, USA

Abstract— From a thermodynamic standpoint, one can improve the efficiency of any energy conversion process by having access to both a higher-temperature heat source and a lower-temperature sink. While the Sun has been actively exploited as a renewable source of the former, relatively little work has gone into exploiting a lower-temperature sink that we have access to radiatively: the cold of outer space. At its highest level our work shows how a photonic approach to control far-field thermal radiation can allow us to efficiently exploit the 'heat sink' of the universe at all hours of the day to improve energy efficiency and conversion processes.

From a practical point of view, cooling is a significant end-use of energy globally and a major driver of peak electricity demand. At night, electricity-free cooling below ambient air temperature has been demonstrated using a technique known as radiative cooling or night-sky cooling, where one uses a device exposed to the sky to radiatively emit heat to outer space through a transparency window in the atmosphere between 8–13 μm. Peak cooling demand however occurs during the daytime. Daytime radiative cooling below ambient under direct sunlight has not previously been achieved because sky access during the day results in heating of the radiative cooler by the sun.

In this talk, we will discuss how a photonic approach to the control of far-field thermal emission from a surface is both formally necessary for optimal radiative cooling, and enables new technological possibilities. We first introduce the theoretical requirements necessary for daytime radiative cooling and derive the upper bound of performance possible by a thermal emitter. This bound is constrained by the second law of thermodynamics and is only attainable using a selective emitter. We show moreover that the optimal selective emitter for radiative cooling varies as a function of the operating temperature below ambient.

We then present results of the first experimental demonstration of daytime radiative cooling, where we achieve a temperature of nearly 5°C below the ambient air temperature under direct sunlight. Using a thermal photonic approach, we design and fabricate an integrated photonic solar reflector and thermal emitter consisting of 7 layers of HfO_2 and SiO_2 that reflects 97% of incident sunlight while emitting strongly and selectively in the mid–infrared atmospheric transparency window. Even when exposed to direct solar irradiance of greater than $850\,W/m^2$ on a rooftop, the photonic radiative cooler achieves an average of 4.9°C below ambient air temperature over, and has a cooling power of $40.1\,W/m^2$ at ambient.

Finally, we will discuss both the theory behind, and an experimental demonstration of, a photonic approach to passively maintain solar cells at lower temperatures through radiative cooling, while maintaining their solar absorption.

Heat Transfer and Thermodynamics of Thermal Radiation in the Near and Far Fields

Gang Chen, **Vazrik Chiloyan**, **Poetro L. Sambegoro**, **Jonathan K. Tong**, **Yi Huang**, **Wei-Chun Hsu**, **and Svetlana V. Boriskina**
Department of Mechanical Engineering
Massachusetts Institute of Technology Cambridge, MA 02139, USA

Abstract— This talk will discuss two aspects of thermal radiation. One is on the limit of radiative heat transfer in the near fields. When the spacing between two surfaces is less than the dominant wavelength of thermal radiation, heat transfer between the two surfaces can significantly exceed the blackbody limit. In the past, we have demonstrated experimentally that near-field thermal radiation can far-exceed the far-field blackbody limit and the experimental results are in agreement with the Rytov's fluctuating electrodynamics description. However, in the limit when two surfaces are in contact, heat transfer is described in terms of heat conduction and phonon transport. We develop an approach using lattice dynamics and the microscopic Maxwell equations to bridge the theories of conduction and radiation. We will also update recent experiments on near field heat transfer between different materials. We will then move on to discuss next the thermodynamics of thermal radiation, focusing on entropy of thermal radiation and its consequences on the limits of various energy conversion processes, and the extraction of the near field thermal radiation to the far field.

ACKNOWLEDGMENT

This work is supported by DOE BES (DE-FG02-02ER45977) and DOE EFRC (Grant No. DE-SC0001299).

Session 2A12a
SC4: Novel Frequency Selective Structures

Double-layered Frequency Selective Surface with Quasi-elliptic Bandstop Filtering Response

Hui Jiang[1], **Bo Li**[1], **Zhongxiang Shen**[2], **and Yiming Tang**[1]

[1]School of Electronic Science and Engineering
Nanjing University of Posts and Telecommunications, Nanjing, Jiangsu 210003, China
[2]School of Electrical and Electronic Engineering
Nanyang Technological University, 50 Nanyang Avenue, 639798, Singapore

Abstract— A frequency selective surface (FSS) usually operates as a spatial filter for the incoming electromagnetic waves with different operating frequencies, polarizations, and incident angles [1]. Based on its special characteristics, an FSS are widely used in applications of target invisibility and interference reduction [2, 3]. It is highly desirable that an FSS can achieve high performance (such as high selectivity and wide stopband characteristics) with simple fabrication process. Although most of single-layered FSSs have simple topologies and can be easily fabricated, it is very difficult for a single-layered FSS to realize high selectivity and wide stopband characteristics [4, 5]. On the other hand, three-dimensional (3D) frequency selective structures can achieve the above mentioned high performance [6, 7]. However, the fabrication process will be complex due to their complicated topologies.

In this work, a double-layered FSS with quasi-elliptic bandstop filtering response is presented. The proposed FSS consists of two cross dipole arrays printed on both sides of a substrate respectively and a number of via holes connecting these cross dipoles, as shown in Fig. 1. With appropriately tuning the locations of the via holes and the length ratios of the dipoles and via holes, a wideband bandstop filtering response can be obtained, as shown in Fig. 2. Furthermore, two transmission zeros and two transmission poles are achieved in the operating frequency band, thus resulting in high selectivity. Moreover, the present structure has simple topology and can be easily fabricated with high accuracy. Experimental verifications will be carried out in the near future.

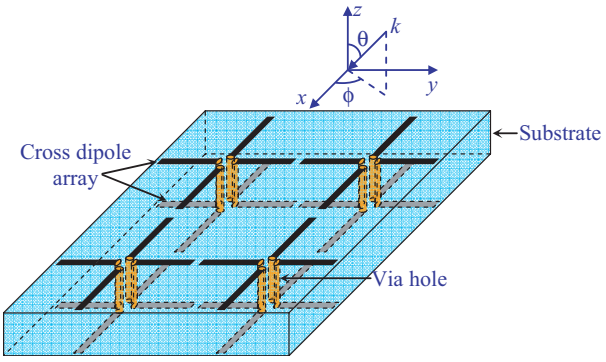

Figure 1: Perspective view of the designed bandstop FSS.

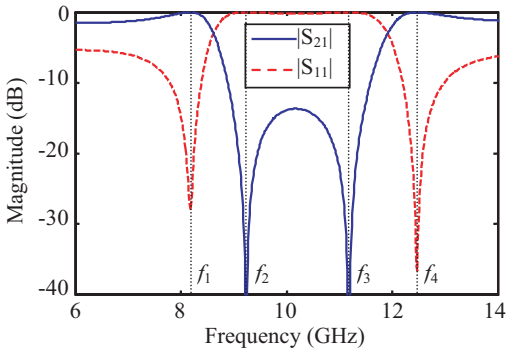

Figure 2: Simulated S-parameter results of the designed bandstop FSS.

REFERENCES

1. Munk, B. A., *Frequency Selective Surfaces: Theory and Design*, John Wiley & Sons Inc., 2000.
2. Costa, F. and A. Monorchio, "A frequency selective radome with wideband absorbing properties," *IEEE Trans. Antennas Propag.*, Vol. 60, No. 6, 2740–2747, 2012.
3. Syed, I. S., Y. Ranga, L. Matekovits, K. P. Esselle, and S. G. Hay, "A single-layer frequency-selective surface for ultrawideband electromagnetic shielding," *IEEE Trans. Electromagnetic Compatibility*, Vol. 56, No. 6, 1404-1411, 2014.
4. Liu, H. L., K. L. Ford, and R. J. Langley, "Design methodology for a miniaturized frequency selective surface using lumped reactive components," *IEEE Trans. Antennas Propag.*, Vol. 57, No. 9, 2732–2738, 2009.

5. Yang, G., T. Zhang, W. Li, and Q. Wu, "A novel stable miniaturized frequency selective surface," *IEEE Antennas Wireless Propag. Lett.*, Vol. 9, 1018–1021, 2010.
6. Huang, X., C. Yang, Z. Lu, and P. Liu, "A novel frequency selective structure with quasi-elliptic bandpass response," *IEEE Antennas Wireless Propag. Lett.*, Vol. 11, 1497–1500, 2012.
7. Li, B. and Z. Shen, "Angular-stable and polarization-independent frequency selective structure with high selectivity," *Appl. Phys. Lett.*, Vol. 103, No. 17, 171607, 2013.

Some Novel Applications of Frequency Selective Surfaces (FSSs)

Raj Mittra
EMC Laboratories, Pennsylvania State and Central Florida Universities, USA

Abstract— Frequency Selective Surfaces find a wide variety of applications as components in electromagnetic devices, as for instance in high-performance radomes and frequency re-use systems for satellite communications, among others. In this paper we will discuss two other uses of FSSs, namely as screens for mobile phones that are designed to mitigate the SAR (Specific Absorption Rate) problem in mobile phones, and as substrates or superstrates for off-the-shelf dielectric materials to alter their permittivities to desired values specified by the user.

The SAR problem stems from the fact that a large share ($\sim 80\%$) of the RF power radiated by cellphone antennas end up being absorbed by the human head when the phone operates close to a human head, as it typically does in normal use. Attempts to reduce the radiation in the back direction of the phone, where the hea is typically located, have not been very successful to-date. The paper will describe, as one of the novel applications of the FSS, how we can selectively reduce the SAR at higher end of the frequency spectrum covered by cellphones designed for 4G and LTE frequency bands — where it is most needed because it exceeds the threshold deignated by the FCC at higher frquencies.

Next the paper will discuss another non-traditional application of the "FSS-type" screens. In this application the FSSs-type screens are printed on off-the shelf dielectric materials to tweak their permittivity values to those specified by the user, but are unavailable from a vendor for such materials. Such materials are often called for in the design of low profile lenses and in broadband reflectarrays. We will describe how the FSS-type screen is used to artificially synthesize dielectric materials for the applications mentioned above, as well as for other antenna applications.

Before closing we mention that FSSs used for the two applications mentioned above are often referred to as Metamateials, which we believe is a misnomer. In any case, we employ the reflection the reflection and transmission characteristics of the FSS screen for our purposes, and we neither evaluate nor utilize the effective medium properties of the FSSs we employ in our designs.

An Active Mono-layer Phase Switched Screen

Jonathan M. Rigelsford and Radhwan J. Mahmoud
Department of Electronic & Electrical Engineering
The University of Sheffield, Mappin Street, Sheffield S1 3JD, United Kingdom

Abstract— The classical single layer phase-switched screen (PSS) described by Chambers and Tennant [1] was designed as a radar absorbent material that can attenuate the incident waves. Their design comprises an active frequency selective (FSS) layer suspended above a conducting ground plane. The phase shift is achieved by switching the FSS between its transmissive and reflective states.

In this work we present an active mono layer PSS in which the conducting ground plane has been removed, additionally allowing it to perform as a conventional FSS. An advantage of this design is that the mono-layer PSS is thinner than conventional designs and can be designed to have some level of optical transparency. A section of the active mono-layer PSS is illustrated in Figure 1. It consists of two dimensional arrays of rectangular metallic patches that have a length of L and a width of W. Each strip is horizontally separated with its adjacent one by a distance of d and connected via PIN diodes on short interconnecting arms. The rectangular patches are vertically separated from each other by 1 mm and are electrically connected using capacitors. The PIN diodes are reverse biased by applying voltage at each end of the horizontal arrays.

When diodes are switched ON, they will short the patches together and make the surface has low impedance and the layer will act as a reflector. However, when they are OFF, they will isolate the strips from each other which will cause the surface to have high impedance. At the operational frequency, both switching cases have the same magnitude of reflection coefficients but a negative phase to the other. By switching the diodes rapidly and periodically with a switching frequency (f_s) between these two impedance states, binary phase modulation to the incident signal will be performed with reallocation of its energy out of its band acting as an absorber.

Figure 2 shows reflection and transmission results for a mono-layer PSS designed to operate at 2.7 GHz. At this frequency it can be seen that the state of the PIN diodes (ON — low impedance,

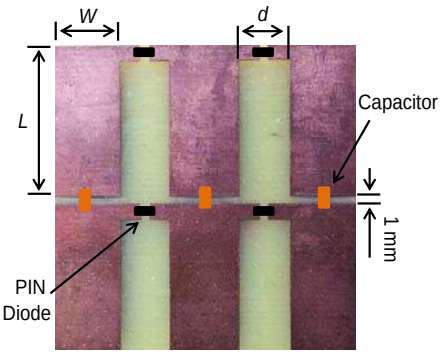

Figure 1: A section of the active mono-layer PSS prototype.

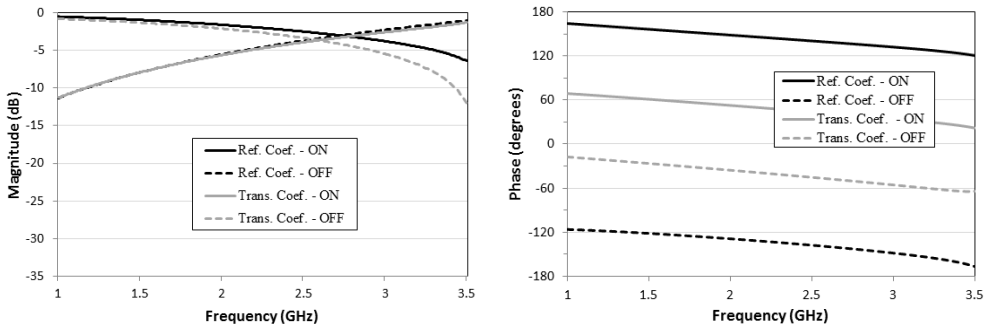

Figure 2: A section of the active mono-layer PSS prototype.

or OFF — high impedance) has minimal effect on the magnitude of the reflection and transmission coefficient. In this case (Figure 2(a)) all four parameters are approximately -3 dB and so the mono-layer acts purely as a PSS and is neither preferentially reflective nor transmissive. Out of the frequency band of operation, the surface can be switched between reflective or transmissive states. Figure 2(b) shows that a phase difference of 90° can be achieved between the two switching states for both the reflection phase and transmission phase.

The full paper will demonstrate further results and performance analysis of the designed mono-layer PSS

REFERENCES

1. Chambers, B. and A. Tennant, "The phase-switched screen," *IEEE Antennas and Propagation Magazine*, Vol. 46, No. 6, December 2004.

A Multilayer Meander Line Structure for Dual Band Orthogonal Circular Polarization Selectivity

D. Sjöberg
Department Electrical and Information Technology, Lund University, Sweden

Abstract— In the context of multiple beam antennas for the emerging broadband satellite market, accurate control of circular polarization is of interest. In order to efficiently reject out-of-band signals, a combination of orthogonal polarizations and different frequencies are employed in a four-color scheme to cover the earth surface. A desirable component in this kind of system is a dual band circular polarization structure [1], the function of which is to reflect one handedness of polarization at frequency f_1, and transmit the other polarization. At another frequency f_2, the operation should be switched. The ratio f_2/f_1 should typically be in the order of 1.5–2.

Such a structure can be realized by a multilayer meander line concept as presented in [2]. The concept is based on consecutive meander line sheets, rotated with respect to each other corresponding to their separation in the normal direction. For a nominal wavelength $\lambda_1 = c/f_1$ and sheet spacing d, this means each sheet is rotated clockwise by an angle φ_1 determined by $\varphi_1/2\pi = d/\lambda_1$, leading to re ection of right hand circular polarization (RHCP). This leads to an interesting harmonic at a wavelength $\lambda_2 = c/f_2$: when $\varphi_2 = \pi - \varphi_1 = 2\pi(d/\lambda_2)$, the structure is rotated counter-clockwise resulting in re ection of LHCP. This provides the dual band operation of the structure.

In the presentation I will give examples of such designs, explaining how the number of layers and other geometrical parameters affect the performance of the design, measured in terms of return loss, insertion loss, and axial ratios around or less than 1 dB. The conceptual harmonic property deduced in the previous paragraph will be shown to produce a viable design after applying some full-wave optimization.

REFERENCES

1. Fonseca, N. J. and C. Mangenot, "Low-profile polarizing surface with dual-band operation in orthogonal polarizations for broadband satellite applications," *IEEE 2014 8th European Conference on Antennas and Propagation (EuCAP)*, 471–475, 2014.
2. Sjöberg, D. and A. Ericsson, "A multi layer meander line circular polarization selective structure (MLML-CPSS)," *IEEE 2014 8th European Conference on Antennas and Propagation (EuCAP)*, 464–468, 2014.

A New Frequency Selective Surface Geometry Design at the Unlicensed 2.4 GHz and 5.8 GHz ISM Bands

Mesut Kartal[1] and Bora Döken[2]

[1]Department of Electronics and Communications Engineering
Istanbul Technical University, Maslak, Istanbul 34469, Turkey
[2]Vocational School, Istanbul Technical University, Maslak, Istanbul 34469, Turkey

Abstract— The usage of wireless devices within buildings at ISM bands is growing rapidly in recent years. Mutual interferences within the adjacent wireless devices degrade the system performances. Securing personal data is also becoming another important problem between the adjacent devices. Transforming existing building walls to a band stop frequency selective surface can an efficient solution for such problems. This work is proposed to design band stop frequency selective surface for interference mitigation and network security within the buildings in the unlicensed 2.4 GHz and 5.8 GHz ISM bands.

Frequency selective surfaces (FSS) are periodic structures which have filter characteristics depending upon their geometries when interacting with electromagnetic waves. Band stop FSSs and their isolation capabilities have been investigated by different researchers for WLAN security and interference mitigation in indoor environment. According to given results, FSSs are capable of providing radio isolation of minimum 10 dB between the two adjacent rooms at both ISM bands. These researches also showed that wireless signals in indoor environment have a wide range of incidence angles. Although the 2.45 GHz and 5.8 GHz ISM bands have been investigated sufficiently for FSS designs, there are not many works in the literature which stops the both ISM bands at the same time. In this work, an attenuation of 10 dB on the transmission (S_{21}) parameter is desired for 2.4 GHz and 5.8 GHz ISM bands while providing maximum transparency at broadcast frequencies for wide range of oblique incidence angles and for all polarizations.

One of the most important factors influencing the response of FSS is the periodic element geometries, geometrical and electrical parameters of these geometries and the gaps between these periodic elements. Unit cell dimensions and the gaps between the unit cells should be small in terms of the wavelength of the resonance frequency to avoid earlier onset of grating lobes and greater variation of the first resonant frequency with angle of incidence. Meandering of the excited metal patch is used to reduce unit cell sizes in our work. The advantages of fractal geometries and convoluting the array elements are being taken.

Simulation and optimization processes are performed by Ansoft HFSS software. Equivalent circuit (EC) models of these FSSs geometries are used to define the relationship between the geometrical parameters of the periodic elements and their frequency responses.

In this work band stop FSS is designed for interference mitigation and network security within the buildings in the unlicensed 2.4 GHz and 5.4 GHz ISM bands. To achieve a stable frequency response for wider oblique incidence of angles a new element geometry is introduced. Satisfying results are obtained for oblique incidence angels from normal to 70° for all polarizations. Achieved attenuation levels are below −20 dB for TE and TM polarizations and for all incidence angles. Besides, the thickness of this structure is 1 mm which gives the possibility of using this design as a structural surface material for blocking ISN signals.

In-building Propagation Control Using Passive Elements Installed in a Corridor

Christopher J. Davenport and Jonathan M. Rigelsford
Department of Electronic & Electrical Engineering
The University of Sheffield, Mappin Street, Sheffield S1 3JD, United Kingdom

Abstract— The use of comb reflection frequency selective surfaces (CR-FSS) to reduce specular scatters and re-direct signal in alternate directions has previously been researched [1]. Although work has been done to understand how the scattering characteristics change relative to incidence angle [2], the application of such surfaces in in-building simulations has not been discussed. The research summarised in this paper discusses the design of a CR-FSS for installation in a building corridor to electromagnetically separate two rooms, reducing the signal-to-noise (SNR) ratio and the potential for co-channel interference at 2.4 and 5 GHz, commonly used frequencies for Wi-Fi transmissions

An initial design study using CST Microwave Studio is conducted to understand the performance of the CR-FSS (Fig. 1) for various angles of incidence and both TE and TM polarisations. The period, height, and thickness parameters are optimised so both TE and TM bands overlap, as shown in Fig. 2. Harmonics in the 5 GHz region can be utilised to reduce specular scatter in this Wi-Fi band also. Further simulations are completed to understand the variation of the response with respect to angle of incidence.

Finally, the surface is applied to an in-building scenario where comparisons at different frequencies are observed. Cumulative distribution function (CDF) plots are used to quantify the differences between a normal building, and a building with the CR-FSS installed. Reductions of E-field level in the required areas will mean that co-channel interference is reduced and thus the SNR of these areas is also increased.

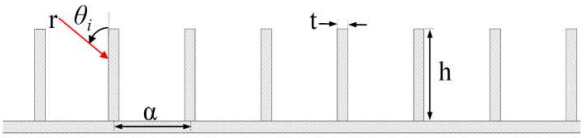

Figure 1: The CR-FSS structure optimised at 2.4 GHz with parameters: height, $h = 70$ mm, period, $\alpha = 80$ mm, $t = 4$ mm.

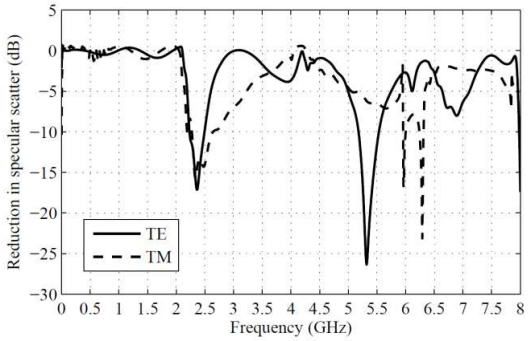

Figure 2: Frequency characteristics of the 2.4 GHz optimised CR-FSS at $\theta_i = 50°$.

REFERENCES

1. Davenport, C. J. and J. M. Rigelsford, "Design of comb reflection frequency selective surface for interference reduction in building corridors," *Electronics Lett.*, Vol. 49, No. 23, 1478–1479, 2013.
2. Davenport, C. J. and J. M. Rigelsford, "Specular reflection reduction using periodic frequency selective surfaces," *IEEE Trans. Antennas Propag.*, Vol. 62, No. 9, 4518–4527, 2014.

Session 2A12b
FocusSession.SC5: SAR Systems and Technology

Radar Response of Soil Moisture from ALOS-2 SAR

Yuan Liu[1], **Kun-Shan Chen**[2], **Zhao-Liang Li**[1], **and Yu Liu**[2]

[1]ICube, UdS, CNRS, Bld Sebastien Brant, CS10413, 67412 Illkirch, France
[2]Institute of Remote Sensing and Digital Earth, Chinese Academy of Sciences, Beijing, 100101, China

Abstract— The objective of this study is to analyze the radar response of soil moisture and to develop a method for retrieving soil moisture using ALOS-2 data based on the advanced integral equation method (AIEM) model which was proved to be one of the most valid surface microwave scattering models. However, retrieval of soil moisture from SAR data is not straightforward as it may seem, for it is profoundly affected by numerous factors such as surface roughness, vegetation cover, and soil texture, to certain extent depending upon the probing wavelength. The AIEM model was used to simulate the radar scattering characteristics of the soil surface to analyze the coupling effects of the surface parameters including the root mean squared (rms) height, correlation length, soil moisture as well as the radar system parameters including the incident angle and polarization. For ALOS-2 SAR, four components decomposition method by Yamaguchi was first applied to decompose the total response into volume, surface, double bounce, and helix scattering components, from which the sensitivity of soil moisture scattering response due to polarimetric properties was investigated. Yellow River delta, one of the largest deltas in China formed by the silts from the Yellow River in Shandong province, was selected as test site. Influence of radiometric quality including speckle and calibration accuracy will be discussed in regard of soil moisture.

Electronic Counter-countermeasures in Bistatic Radars

Faran Awais Butt[1], **Ijaz Haider Naqvi**[2], **and Madiha Jalil**[3]

[1]University of Management and Technology (UMT), Lahore, Pakistan
[2]Lahore University of Management Sciences (LUMS), Lahore, Pakistan
[3]University of Engineering and Technology (UET), Lahore, Pakistan

Abstract— Bistatic configuration of radars has become a topic of great interest for Electronic counter-countermeasures designers. The paper emphasized the need for bringing about a trend of employing bistatic radars in place of traditional monostatic radars which are no more useful under the hostile environment that is created by the electronic counter measures effect. It has been shown that noise and deception jamming can be countered using bistatic configuration of the radar system. Moreover, low observability of the target threat can also be dealt with using this.

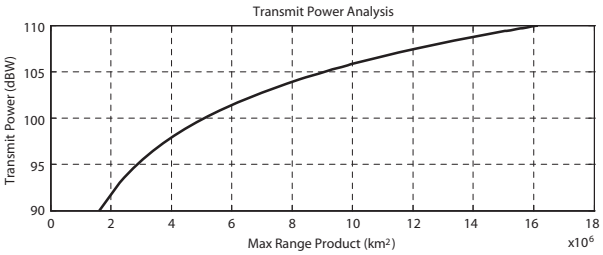

Figure 1: Transmit power analysis for bistatic angle of 10 degrees and RCS of 20 dBsm.

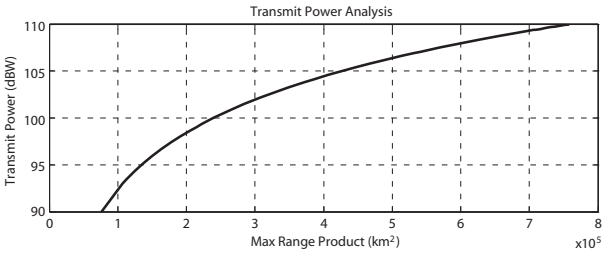

Figure 2: Transmit power analysis for bistatic angle of 20 degrees and RCS of 10 dBsm.

Figures 3 and 4 show the signal to noise ratio analysis of bistatic radar corresponding to max range product. From these figures, it can be concluded that if the bistatic angle is increased, the corresponding SNR is reduced. The bistatic angle, i.e., positioning of transmitter and receiver has a big role to play in the overall working of the system.

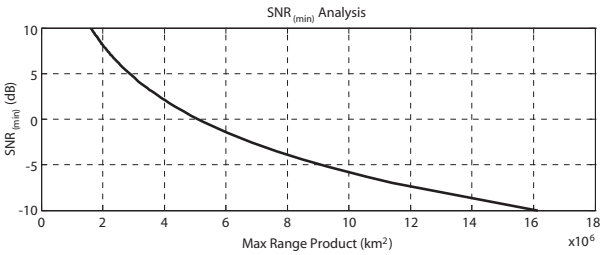

Figure 3: SNR analysis where angle is 10 and RCS of the target is 20 dBsm.

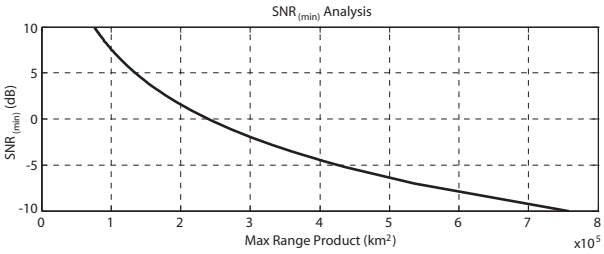

Figure 4: SNR analysis where angle is 20 and RCS of the target is 10 dBsm.

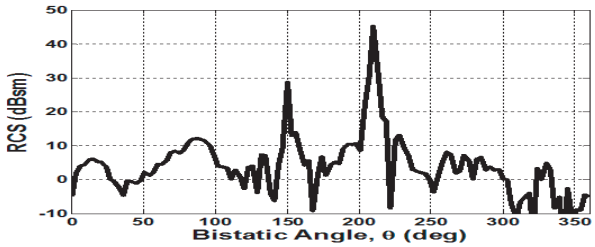

Figure 5: RCS vs. bistatic angle.

The paper has shown the advantages that the radar designers can exploit from a bistatic radar approach, courtesy of the geo placement of the distant receiver. Similarly bistatic approach

allows simultaneous accomplishment of ECCM techniques which improves the probability of detection. Bistatic radars can also give the liberty to designers of employing MIMO functionality by making an intelligent transceiver system on both the sites. Low observable stealthy targets which scatter the incoming transmitted wave in various directions can be best dealt with if there is a corresponding receiver or a transceiver system in best probable direction. Moreover for such targets, there is a range of aspect angles which can be exploited by using bistatic system. In addition to this, jammers which target the antenna sight of the radar for a typical monostatic system, no longer remains effective if there is a receiver at a distant sight.

Polarimetric SAR Simulations of Bare Soil and Vegetated Surfaces Using Scattering and Coherency Matrix from 3-D Numerical Solutions of Maxwell Equation (NMM3D)

Tien-Hao Liao[1], **Kuan-Liang Chen**[2], **Leung Tsang**[3], **and Hsuan Ren**[2]

[1]Department of Electrical Engineering, University of Washington, Seattle, USA
[2]Institute of Space Sciences, National Central University, Jhongli, Taiwan
[3]Department of Electrical Engineering and Computer Science, University of Michigan, Ann Arbor, USA

Abstract— Polarimetric synthetic aperture radar (PolSAR) images have been widely studied to classify target and retrieve target information in microwave remote sensing. Scattering matrices ($S_{VV}, S_{HH}, S_{VH}, S_{HV}$) calculated from numerical 3D solutions of Maxwell equations (NMM3D) have been shown to be capable of simulating polarimetric SAR signature of bare soil at L-band [1]. In this paper, we made two extensions to the previous work . 1) We extend Pol-SAR simulations of scattering matrices of bare soil up to C-band, and 2) we simulate the Pol-SAR signature of coherency matrices for vegetated surface.

For polarimetric signatures of bare soil at C-band, results of scattering matrices from NMM3D are computed. Comparisons are made with theoretical speckle distributions, including amplitude, phase difference, and amplitude ratio. Surface roughness dependence with entropy, anisotropy, and alpha angle from the ensemble average of coherency matrix. We calculate polarimetric statistics of rough surface at C-band (5.4 GHz) with 40 degree incidence. Surface rms heights are from $1 \sim 4$ cm ($ks = 1.13 \sim 4.52$) with correlation length to rms height equal to 15 and the dielectric constant is $9 + 2.5i$.

Using distorted born approximation in conjunction with NMM3D we compute the coherency matrix for vegetated surface. Averages are taken to compute the coherency matrix of volume scattering and double bounce. These are then combined with the NMM3D coherency matrix. The following shows examples of terms from coherency matrix of volume scattering and double bounce. α and β stand for orientation of vegetation which will be averaged out to give ensembled results for coherency matrix. The scattering matrix elements for surface scattering with attenuation, rough surface under vegetation (RV), is also shown.

$$\begin{aligned}
\left\langle S_{vv}^{vol} S_{hh}^{vol^*} \right\rangle &= n_0 A d \frac{1 - e^{-d[-i2(Re(k_{ivz}) - Re(k_{ihz})) + Im(k_{ivz}) + Im(k_{ihz})]}}{-i2(Re(k_{ivz}) - Re(k_{ihz})) + Im(k_{ivz}) + Im(k_{ihz})} \\
&\quad \langle f_{vv}(\theta_s, \phi_s; \pi - \theta_i, \phi_i) f_{hh}^*(\theta_s, \phi_s; \pi - \theta_i, \phi_i) \rangle_{\alpha,\beta} \\
\left\langle S_{vv}^{DB} S_{hh}^{DB^*} \right\rangle &= n_0 A d \left[R_v(\theta_i) e^{2ik_{ivz}d} R_h^*(\theta_i) e^{2ik_{ihz}^* d} \right] \\
&\quad \langle f_{vv}(\pi - \theta_s, \phi_s; \pi - \theta_i, \phi_i) f_{hh}^*(\pi - \theta_s, \phi_s; \pi - \theta_i, \phi_i) \rangle_{\alpha,\beta} \\
S_{hv}^{RV} &= e^{ik_{ihz}d} e^{ik_{ivz}d} S_{hv}^R \\
S_{vv}^{RV} &= e^{ik_{ivz}d} e^{ik_{ivz}d} S_{vv}^R \\
S_{vh}^{RV} &= e^{ik_{ivz}d} e^{ik_{ihz}d} S_{vh}^R \\
S_{hh}^{RV} &= e^{ik_{ihz}d} e^{ik_{ihz}d} S_{hh}^R
\end{aligned}$$

REFERENCES

1. Chen, K.-S., L. Tsang, K.-L. Chen, T.-H. Liao, and J.-S. Lee, "Polarimetric simulations of SAR at L-band over bare soil using scattering matrices of random rough surfaces from numerical three-dimensional solutions of Maxwell equations," *IEEE Transactions on, Geoscience and Remote Sensing*, Vol. 52, No. 11, 7048–7058, 2014.

Towards a Fully Coherent Snowpack Scattering Model Based on Numerical Simulation of Maxwell's Equation Using Bicontinuous Media and Half Space Green's Function

Shurun Tan[1], **Xiaolan Xu**[2], **and Leung Tsang**[1]

[1]Radiation Laboratory, Department of Electrical Engineering and Computer Science
The University of Michigan, Ann Arbor, MI 48109-2122, USA
[2]Jet Propulsion Laboratory, M/S 300-233, Pasadena, CA 91109, USA

Abstract— Wave propagation and scattering inside dense media such as snow has been extensively studied with the partially coherent approach of dense media radiative transfer (DMRT). In DMRT, one accounts for the coherent wave interaction only within few wavelengths as represented by phase matrix. Multiple volume scattering beyond a few wavelengths and volume-surface interactions are included through the radiative transfer theory by propagating the specific intensity. Such approach ignores the cyclical terms in Feynman diagram which give rise to the characteristic phenomenon of backscattering enhancement in active remote sensing [1]. On the other hand, the backscattering enhancement is inherent in the fully coherent approach. The fully coherent approach can also be applied to coherent radar observations such as interferometric and tomographic applications by simulations of the scattering matrices of the snowpack.

In this paper, we calculate the scattering matrix of the terrestrial snowpack over a flat ground by solving Maxwell's equations directly. The snow microstructure is represented by the bicontinuous media as a continuous representation of interfaces within a two-phase medium [2, 3]. The bicontinuous media could be quantified in terms of correlation function and specific surface area (SSA), and could be compared to field measurements of snow grain size distribution and SSA [4–6]. The effects of the ground are modeled by the half space Green's function. The dyadic half space Green's function is decomposed into a primary component of the free space Green's function and a response component expressed as Sommerfeld integrals. The kernel of the response part depends only on two independent variable, viz. the horizontal displacement between the field point and source point, and the sum of the offset of the field point and source point above the bottom interface. Lookup tables are built to expedite the evaluation of half space Green's function. The volume integral equation is then solved by the discrete dipole approximation (DDA). The matrix vector multiplication is accelerated by FFT taking advantage of the symmetry of both parts of the Green's function [2, 7].

The computation domain in this study is significantly increased. It increases from a ~ 8 cubic wavelengths cube size as used in the phase matrix calculations [1–6], to a much larger size in the calculation of the scattering matrix of a snowpack. The high computation demand is carried out by using parallel computing on high performance computing clusters.

The scattering matrix of the snowpack is computed for each realization. The statistical distribution property of the scattering matrix and backscatter are then computed using Monte Carlo simulations. The results of the snowpack backscattering and bistatic scattering coefficients are compared with the results of the DMRT approach with or without cyclical corrections [1].

REFERENCES

1. Tan, S., W. Chang, L. Tsang, J. Lemmetyinen, and M. Proksch, "Modeling both active and passive microwave remote sensing of snow using dense media radiative transfer (DMRT) theory with multiple scattering and backscattering enhancement," *IEEE Journal of Selected Topics in Applied Earth Observations and Remote Sensing*, 2014, submitted for review.
2. Ding, K.-H., X. Xu, and L. Tsang, "Electromagnetic scattering by bicontinuous random microstructures with discrete permittivities," *IEEE Transactions on Geoscience and Remote Sensing*, Vol. 48, No. 8, 3139–3151, 2010.
3. Xu, X., L. Tsang, and S. Yueh, "Electromagnetic models of co/cross polarization of bicontinuous/DMRT in radar remote sensing of terrestrial snow at X- and Ku-band for CoReH$_2$O and SCLP Applications," *IEEE Journal of Selected Topics in Applied Earth Observations and Remote Sensing*, Vol. 5, No. 3, 1024–1032, 2012.
4. Chang, W., S. Tan, J. Lemmetyinen, L. Tsang, X. Xu, and S. H. Yueh, "Dense media radiative transfer applied to SnowScat and SnowSAR," *IEEE Journal of Selected Topics in Applied Earth Observations and Remote Sensing*, Vol. 7, No. 9, 3811–3825, 2014.

5. Chang, W., K.-H. Ding, L. Tsang, and X. Xu, "Microwave scattering and medium characterization for terrestrial snow with QCA-Mie and bicontinuous models: Comparison studies," submitted to *IEEE Transactions on Geoscience and Remote Sensing*, 2014.
6. Chang, W., *Electromagnetic Scattering of Dense Media with Application to Active and Passive Microwave Remote Sensing of Terrestrial Snow*, University of Washington, Ph.D. Thesis, 2014.
7. Cui, T. J. and W. C. Chew, "Fast algorithm for electromagnetic scattering by buried 3-D dielectric objects of large size," *IEEE Transactions on Geoscience and Remote Sensing*, Vol. 37, No. 5, 2597–2608, 1999.

Session 2A13a
FocusSession.SC3: High-capacity Optical Communication: Systems, Algorithms, Components 2

All-optical Mitigation of Non-linear Gain in SOA

Cristiano De Mello Gallep[1], **Peterson Rocha**[2], **and Evandro Conforti**[2]

[1]School of Technology — FT, University of Campinas, Brazil
[2]Fac. Electrical and Computing Eng. — FEEC, University of Campinas, Brazil

Abstract— The intrinsic non-linear gain of semiconductor optical amplifier is mitigated in a simple all-optical scheme that enables transparent, quasi-linear response. Operation with advanced modulation formats such as n-PSK and n-QAM, presented good performance for access networks (< 30 km) up to 5 WDM channels.

The always increasing demand of high speed services have pushed for the new generation of optical carriers employed in long haul links, with 100 Gbit/s to 400 Gbit/s capacity per lambda [1]. Up to Terabit/s transmission can be accomplished in supper channel configurations [CPQd^2]. The more efficient use of spectra is achieved by multi-level modulation formats and optical polarization multiplexing, with addition of high speed digital signal processing to enable coherent detection and error correction, usually with base-rate of 25 Gbaud/s. These high capacity channels will run over fiber links together with carriers of the past generations — 40 Gbit/s (PSK) and 10 Gbit/s (OOK), that are simpler to generate and detect, and will continue to be used for small-metro and access networks for some time. With maturity of low-cost Tx/Rx for coherent detection, this technology tends to push over access network, with link solutions at lower rates, as 20 G and 10 Gbaud/s.

The semiconductor optical amplifier (SOA) is a noisy, non-linear device that can be employed to compensate splitting/switching losses, and other minor attenuation in the last-mile links, and also to detect and remodulate carriers in PON schemes [3]. The SOA is an attractive solution for integration and reduction of costs. But its small carrier lifetime — in nano-second range, and high non-linear gain index, make the use of SOA a trick problem: gain saturation can easily lead to cross-talk, and even single channel operation can suffer, by self-phase modulation. In multilevel formats such (D)QPSK and n-QAM, different amplitude transitions induce different phase delay, in non-linear response that impacts over the constellation diagrams as non-linear phase rotation — the n-point star rotates un-equally and single spots turn to arches, even connecting to of them. So, used as it is, SOA is not compatible with the new high capacity channels.

To solve the non-linear gain of SOA we proposed a new, all-optical regeneration scheme based on a second SOA working as non-linear absorber, in such a way that the two SOA give a reasonable gain (> 20 dB) with small phase distortion. The technique may mitigate non-linear phase noise up to 50%, even for multi-channel operation, and can still be an attractive solution for medium and small fiber links working with both old and new modulation schemes.

ACKNOWLEDGMENT

Authors are thankful to FAPEPS/PADTEC (#07/56024-4), CNPQ/FOTONICOM (574017/2008-9) and CAPES.

REFERENCES

1. Porto da Silva, E., et al., "Spectrally-efficient 448-Gb/s dual-carrier PDM-16QAM channel in a 75-GHz grid," *OFC*, JTh2A, 2013, DOI: 10.1364/NFOEC.2013.JTh2A.39.
2. Carvalho, L. H. H., et al., "Transmission of a DAC-Free 1.12-Tb/s Superchannel with 6-b/s/Hz over 1000 km with Hybrid Raman-EDFA Amplification and 10 Cascaded 175-GHz Flexible ROADMs," *ECOC*, 2013, DOI: 10.1049/cp.2013.1624.
3. Guo, G. and A. V. Tran, "Demonstration of 40-Gb/s WDM-PON system using SOA-REAM and equalization," *Photonics Techn. Lett.*, 951–953, 2012, DOI: 10.1109/LPT.2012.2190051.

The Nonlinear Fiber-optic Channel: Modeling and Achievable Information Rate

E. Forestieri and M. Secondini
TeCIP Institute, Scuola Superiore Sant'Anna, Italy

Abstract— The evaluation of channel capacity in nonlinear fiber-optic systems is still an open issue. The main difficulty is due to the unavailability of an exact and mathematically tractable channel model. In fact, most of the results obtained so far either refer to highly simplified models or provide loose bounds to the capacity. A useful and practical approach to lower bound the capacity is that of evaluating the achievable information rate for an arbitrarily fixed input distribution (modulation format) and a suboptimal decoder optimized for an approximate version of the channel (mismatched decoding). In this context, the capacity problem can be seen as a joint optimization of the achievable information rate over both the input distribution and the channel model.

According to the popular Gaussian noise (GN) model, nonlinearity is simply modeled as additive white Gaussian noise: it cannot be compensated for, but it can be easily accounted for in the evaluation of channel capacity, leading to the conclusion that capacity vanishes at high powers. This result, however, is not supported by theory and is contradicted by some counter examples. Though it is now clear that the GN model has some limitations, it is still unclear whether these limitations are only of theoretical interest or do have a practical value.

After properly defining the fiber-optic channel — indeed, not a trivial task due to its highly nonlinear nature — and reviewing the main characteristics of the GN model, we consider a few alternative models and discuss their suitability for system design and performance evaluation. The choice of the right model depends on the problem at hand: while numerical methods, such as the split-step Fourier method, are suitable for compensating deterministic nonlinearity through the back-propagation technique, analytical approximations — based, for instance, on perturbation methods or Volterra series expansion — are more suitable for modeling stochastic effects such as signal noise-interaction and inter-channel nonlinearity. Finally, an exact analytical model, accounting only for dispersion and nonlinearity, can be obtained by employing the inverse scattering (nonlinear Fourier) transform. It is still unclear, however, whether this approach is competitive with the split-step Fourier method in terms of computational complexity and whether it can be used for modeling stochastic nonlinear effects.

By employing the aforementioned models, it is possible to show that the optimum modulation and detection strategies differ from those designed according to the GN model and typically used in fiber-optic systems. Therefore, in the second part of the talk, we consider different modulation and detection schemes aimed at providing higher robustness to nonlinear effects and investigate their actual advantage over GN-model-based strategies in terms of achievable information rate. Depending on the considered scenario, a non-negligible improvement is achieved. However, at high powers, the gap between lower and upper bounds to channel capacity remains large and does not allow to establish whether capacity is bounded or not. Possible directions for reducing the gap are finally discussed.

Flex-grid All-optical Interconnect Supporting Transparent Multi-hop Connection in Data Centers

Yuanyuan Hong[1], **Xuezhi Hong**[2], **Sailing He**[1, 3], **and Jiajia Chen**[3]

[1]Center for Optical and Electromagnetic Research
Zhejiang University, Hangzhou 310058, China
[2]ZJU-SCNU Joint Research Center of Photonics
South China Normal University, Guangzhou 510006, China
[3]School of Information and Communication Technology
KTH Royal Institute of Technology, Kista 16443, Sweden

Abstract— The demand of higher capacity and lower power consumption in data centers makes optical interconnects become an attracting solution. Many existing optical switching schemes [1, 2] employ optical-electrical-optical (O-E-O) conversion for multi-hop connections and hence have relatively low power efficiency. In this paper, a novel flex-grid all-optical interconnect architecture is proposed for data centers. All-optical interconnects between servers in different racks are realized with an optical switch matrix and flex-grid WSSs. Transparent multi-hop connections can be implemented by using optical bypass rather than going through O-E-O conversion. Compared with the O-E-O based multi-hop scheme, a higher energy efficiency is achieved with the proposed one. By employing flex-grid WSSs and advanced modulation formats, the elastic spectrum allocation [3] can be achieved, which greatly improves the resource utilization and scalability. Transmission performance evaluation has been carried out to verify the feasibility of our scheme.

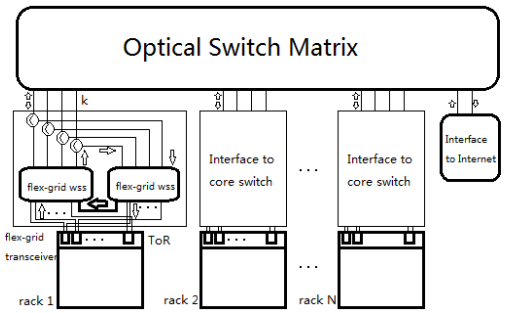

Figure 1: Proposed flex-grid all-optical Interconnect supporting transparent multi-hop connections in data centers.

ACKNOWLEDGMENT

The work described in this paper was carried out with the support by the projects titled "Enabling Scalable and Sustainable Data Center Networks", funded by Swedish Foundation of Strategic Research, and "Towards Flexible and Energy-Efficient Datacentre Networks", funded by Swedish Research Council.

REFERENCES

1. Chen, K., et al., "OSA: An optical switching architecture for data center networks with unprecedented flexibility," *IEEE/ACM Transactions on Networking*, Vol. 22, 498–511, Apr. 2014.
2. Liu, L., et al., "Design and performance evaluation of an OpenFlow-based control plane for software defined elastic optical networks with direct detection optical OFDM (DDO-OFDM) transmission," *Optical Express*, Vol. 22, 30–40, Jan. 2014.
3. Christodoulopoulos, K., et al., "Elastic bandwidth allocation in flexible OFDM-based optical networks," *Journal of Lightwave Technology*, Vol. 29, 1354–1366, May 2011.

Session 2A13b
SC3: Near-field Optics: Light-matter Interaction Inside a Wavelength Volume 1

Strong Quadrupole Light-molecule Interaction and the Dipole-quadrupole Theory of Surface Enhanced Spectroscopy

V. P. Chelibanov[1] and A. M. Polubotko[2]

[1]State University of Information Technologies, Mechanics and Optics
Kronverkskii 49, Saint Petersburg 197101, Russia
[2]A.F. Ioffe Physico-Technical Institute, Russian Academy of Sciences
Politechnicheskaya 26, Saint Petersburg 194021, Russia

Abstract— Surface Enhanced spectroscopy is associated with such optical processes as Surface Enhance Raman scattering (SERS), Surface Enhanced Hyper Raman scattering (SEHRS) and Surface Enhanced Infrared absorption (SEIRA). The essence of these effects is that the cross-sections of these processes increase strongly for molecules adsorbed near rough metal surfaces and the enhancement can achieve huge values. For example for SERS it is 10^6, for SEHRS — 10^{12} and for SEIRA — 10^2–10^3. From our point of view these effects are associated with very strong dipole and especially quadrupole light-molecule interactions, arising in surface fields strongly varying in space near rough metal surfaces [1]. As can be shown the electric field near the roughness with a very large curvature enhances very strongly. Therefore there is the enhancement of both of the electric field and its derivatives in such regions and the dipole and quadrupole light-molecule interactions increase very strong. In order to check the validity of this mechanism one can analyze the spectra of the above processes in symmetrical molecules. The major regularity of these spectra is appearance of forbidden lines in molecules with sufficiently high symmetry. In SERS these lines are caused by the vibrations transforming after a irreducible representation, which describes transformational properties of the d_z moment which is perpendicular to the surface, while in SEHRS and SEIRA spectra they are the lines, caused by the totally symmetric vibrations transforming after a unit irreducible representation of the molecule symmetry group. Analysis of the surface enhanced spectra of various symmetrical molecules such as ethylene, benzene, 1,3,5 trideutereobenzene, hexafluorobenzene, 1,3,5 trifluorobenzene in SERS, ethylene in SEIRA and pyrazine and phenazine in SEHRS, reveals existence of such lines and another regularities of the enhance spectra that strongly support our theory of the surface enhanced processes

REFERENCES

1. Polubotko, A. M., *The Dipole-Quadrupole Theory of Surface Enhanced Raman Scattering*, Nova Science Publishing Ltd., New York, 2009.

Femtosecond-scale Polarization Fluctuations of Light Measured by Two-photon Absorption

A. Shevchenko[1], **M. Roussey**[2], **A. T. Friberg**[2], **and T. Setälä**[2]

[1]Department of Applied Physics, Aalto University, Aalto FI-00076, Finland
[2]Institute of Photonics, University of Eastern Finland, Joensuu FI-80101, Finland

Abstract— Most natural and artificial light sources radiate unpolarized or partially polarized light, and the degree of polarization measures the time-averaged fraction of the polarized part. However, two optical fields can possess the same degrees of polarization, but their polarization fluctuations can have different speeds. Previously, to be able to characterize the polarization dynamics, we have proposed a certain polarization-correlation function $\gamma(\tau)$. It is equal to a statistically averaged fraction of the field intensity that at some delayed instant of time $t + \tau$ remains in the original polarization state of time t [1–3]. The maximum value of this function is $\gamma(0) = 1$. A particular value of τ at which $\gamma(\tau)$ decreases, say, to $1/2$ determines a time interval τ_p within which, on average, the field polarization remains essentially unchanged. Hence, the time τ_p can be called the polarization time.

In this work we introduce a method to experimentally investigate the dynamics of ultrafast polarization fluctuations and measure the polarization time τ_p of optical beams. The method is based on second-order interference and two-photon absorption in a semiconductor photo-multiplier tube. It is independent of the polarization fluctuation statistics and can be used regardless of the origin of the fluctuations. In the experiments, we use a Michelson-type interferometer with a polarizer and a quarter-wave plate inserted in each of its arms. The wave plates and the polarizers allow us to select the polarization components of interest from the incident light beam. The photomultiplier is used at the interferometer's output as a counter of photon pairs. It operates in the two-photon absorption regime at the wavelengths from 900 to 1800 nm. The time resolution of the measurements is limited by the lifetime of the virtual state via which the photon pairs are absorbed. For our detector, it is on the order of 1 fs. We have applied the technique to an unpolarized amplified spontaneous emission of an erbium-doped fiber amplifier (the peak wavelength is 1530 nm and the bandwidth is about 40 nm) and to a beam obtained by superimposing two independent single-longitudinal-mode laser beams operating at 1525 nm and 1615 nm wavelengths. The polarization time for the first source was measured to be 115 fs and for the second one 15 fs. The beams can therefore be considered as polarized within the propagation distance of 35 μm for the first and 4.5 μm for the second light source.

REFERENCES

1. Setälä, T., A. Shevchenko, M. Kaivola, and A. T. Friberg, "Polarization time and length for random optical beams," *Phys. Rev. A*, Vol. 78, 033817, 2008.
2. Shevchenko, A., T. Setälä, M. Kaivola, and A. T. Friberg, "Characterization of polarization fluctuations in random electromagnetic beams," *New J. Phys.*, Vol. 11, 073004, 2009.
3. Voipio, T., T. Setälä, A. Shevchenko, and A. T. Friberg, "Polarization dynamics and polarization time of random three-dimensional electromagnetic fields," *Phys. Rev. A*, Vol. 82, 063807, 2010.

Ultrasensitive Label-free Biosensor Based on Photonic Crystal Surface Waves: A Tool to Study Dynamics of Receptor-ligand Interactions with Living Bacteria and Cells

Ekaterina Rostova, **Sergey Sekatskii**, **and Giovanni Dietler**
Laboratory of Physics of Living Matter, EPFL, Lausanne, Switzerland

Abstract— Although different types of optical biosensors are widely used to study kinetics of biomolecular interactions among a variety of macromolecules including antibodies, enzymes, hormones, low-molecular-weight molecules, toxins, cancer markers, drugs, etc., large biological objects with highly inhomogeneous refractive index such as cell suspensions impose significant difficulties.

A surface wave is an electromagnetic wave propagating along an optical interface, strongly confined there, and decaying exponentially away from the interface. In the utilized biosensor [1] such an interface is formed between a functionalized photonic crystal chip and a suspension of a biological sample under investigation. Angular interrogation of the surface wave resonance is used to detect changes in the thickness of an adsorbed layer, while an additional detection of the critical angle of total internal refection provides independent data on the liquid refraction index, see Fig. 1. Besides segregation of surface and volume effects, the exploitation of a photonic crystal supporting long-range surface waves enables to achieve mass sensitivity at the level of $0.3\,\mathrm{pg/mm^2}$ and refraction index (RI) sensitivity at the level of $10^{-7}\,\mathrm{RIU/Hz^{1/2}}$.

Another characteristic feature of this biosensor is large, in the order of $1\,\mu\mathrm{m}$, surface wave penetration depth into an external medium, which enables to study not only binding kinetics of interactions between macromolecules, but also with such large objects as viruses, bacteria, and cell organells. Here we report the first steps in this direction. We elaborated a chitosan-based protocol of surface modification of the sensor chip enabling to produce sufficiently dense and homogeneous (mono)layers of live *E. Coli* bacteria (see Fig. 1). The attached bacteria have been exploited as a target to study binding kinetics of different ligands onto a bacterial surface.

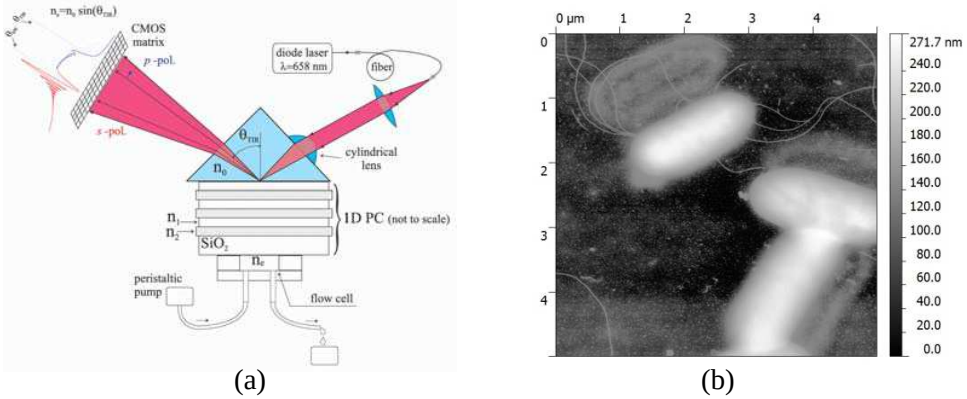

(a) (b)

Figure 1: (a) Schematic of the biosensor. (b) AFM image of a (mono)layer of *E. Coli* bacteria used as an immobilized target in the sensor.

REFERENCES

1. Konopsky, V. N., et al., *Sensors*, Vol. 13, 2566, 2013.

Nanoplasmonics for Control over Localized Emission and Heat Generation

Stefan A. Maier
Imperial College London, London SW7 2AZ, UK

Abstract— Metallic nanostructures allow for the generation of spatially structured optical near-fields and near-field gradients, and have been heavily employed in surface-enhanced sensing and spectroscopies. Here we will present two new studies, namely control over quantum dot emission in extended hot spots of ring nanocavities, and the controlled heating of a solid state nanopore for molecular translocation studies.

Via engineering the photonic density of state on the nanoscale, metallic nanostructures allow the modification of the radiative properties of nanoscale emitters such as molecules and quantum dots. We will present a study of a hybrid quantum dot — plasmonic system with the hallmark of a spatially extended hot spot, based on ring nanocavities. Controlled placement of quantum dots via a dual-step electron beam lithography process allows high control over their radiative properties [1], and we will discuss extensions of this system towards higher field enhancement and more complex multi-emitter systems.

The second part of the talk will focus on controlled heating of a solid state nanopore [2] used for studies of molecular translocation. Localized heating at the nanopore centre occurs via controlled surface plasmon focusing based on a bull's eye geometry (see Figure 1). Changes in ionic conductivity directly allow for the assessment of local temperature in the pore region, in good agreement with full-field electrodynamic simulations.

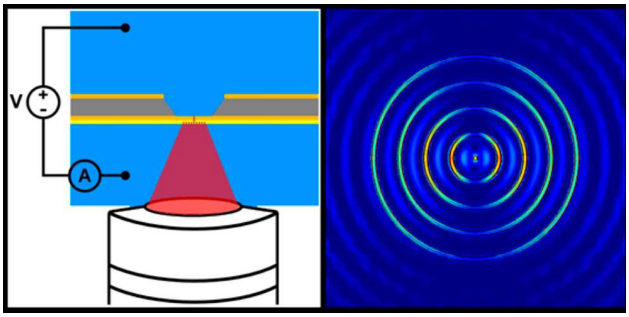

Figure 1: Localized plasmonic heat generation in a solid state nanopore [2].

REFERENCES

1. Rakovich, et al., *ACS Nano*, 2015, Doi: 10.1021/nn506433e.
2. Crick, C. R., et al., *Nano Letters*, Vol. 15, 553, 2015.

Near Field Investigation of Bloch Surface Based Platform for 2D Integrated Optics

R. Dubey, **E. Barakat**, **and H. P. Herzig**
Optics & Photonics Technology Laboratory (OPT)
École Polytechnique Fédérale de Lausanne (EPFL), Switzerland

Abstract— Dielectric multilayers sustaining Bloch surface waves (BSWs) are considered as a novel platform for two dimensional (2D) integrated optics. The dielectric platform is exploited to manipulate surface waves by patterning 2D dielectric optical components on top of it. BSW shows a potential of higher propagation length and large resonance strength because of low loss characteristics of dielectric materials. Taking the advantage of high field confinement on the surface, the platform has also applications in sensing.

In order to excite a BSW, momentum of incoming beam should match with the momentum of the BSW. Therefore, we use Total internal reflection configuration for this purpose, which consists of BK7-glass prism. The schematic of the configuration and the platform is presented in Figure 1. New design of multilayer platform consists of periodic stacks of alternative SiO_2 and Si_3N_4 layers. It has been fabricated to work around the wavelengths of 1.5 µm.

In this paper, we study the key parameters, propagation length and the effective refractive index (n_{eff}), of BSW. They play an important role in characterizing losses associated with the multilayer platform and propagation of surface modes. Effective refractive index contrast (Δn) is introduced by depositing an additional layer of high refractive index material on the top of platform. It is basically the difference between n_{eff} of additional layer and platform. It plays a key role in determining the optical properties of the 2D surface photonic devices and hence their capability to manipulate the BSW most essentially. High refractive index materials, as an active material to pattern 2D optical elements on the top of the platform, have been investigated in near field and far field. These material include titanium dioxide (TiO_2), for the time being, and Graphene.

We obtained propagation length of around 2 mm for 15 nm thickness of additional TiO_2 layer with the aid of multi-heterodyne scanning near-field optical microscopy (MH-SNOM). It is around 25 times longer compare to the recently obtained "Long-Range SPPs" studied by Lin et al. [1]. We achieved Δn of around 0.2 measured in the far field with 100 nm thickness of TiO_2. It is around 3.5 times higher than the Δn obtained for same thickness of Photoresist [2].

In near future, we aim to characterize different optical components on the top of multilayer platform with the aid of MH-SNOM, for example, Ring resonators and Interferometers for the time being.

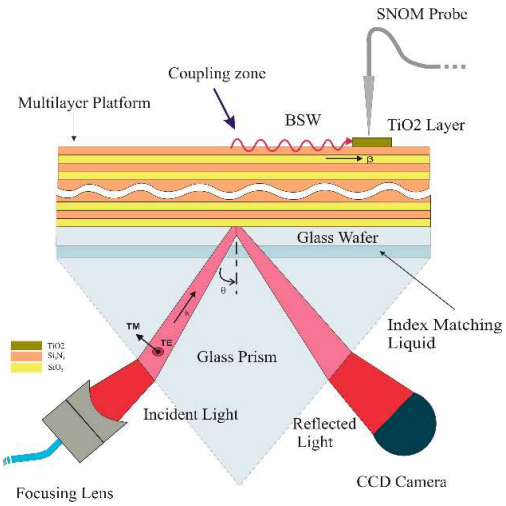

Figure 1: Total internal reflection configuration using BK7-glass prism to excite BSW.

REFERENCES

1. Lin, J., et al., *Physical Review Letters*, Vol. 109, 093904, Aug. 2012.
2. Yu, L., et al., *Light: Science & Applications*, Vol. 3, Jan. 2014.

3-nm-resolution Optical Imaging Based on Plasmonically-excited Near-field to Near-field Coupling and Scanning Optical Microscopy

Toshihiko Nakata[1] **and Takehiro Tachizaki**[2]

[1]Yokohama Research Laboratory, Hitachi, Ltd., Yokohama 244-0817, Japan
[2]Department of Optical and Imaging Science & Technology, Tokai University, Hiratsuka 259-1292, Japan

Abstract— Near-field scanning optical microscopy is expected to overcome the diffraction limit, realizing a spatial resolution far beyond the wavelength of light. However, the spatial resolution, image contrast, and imaging repeatability obtainable using conventional aperture or apertureless probes do not currently satisfy the requirements for research or engineering applications. Here, we describe an optical imaging technique based on plasmonically-excited near-field to near-field coupling that has the potential to achieve a resolution of a few nanometers. Far-field near-infrared light is focused on the front edge of an Au-coated tetrahedral Si tip on the free end of a Si cantilever used as a plasmon waveguide (Fig. 1(a)). By coupling the scattered light to the Au wedge, the far-field light is converted into propagating plasmons that generate an optical near field at the top of the Si tip used as an excitation source (Fig. 1(b)). The excitation near field is coupled to a wear-resistant multiwalled carbon nanotube with a sharpened end, attached to the top of the Si tip (Fig. 2). This nanotube is used as both an optical nanoantenna and nanoprobe. The electric field is concentrated at the 4-nm-diameter conical end of the nanoprobe, so that it generates a second optical near field with the same spot size as the nanoprobe tip (Fig. 1(c)). By scanning the near-field probe spot over the sample surface, this plasmon-excitation cascaded-near-field coupling technique can achieve extremely high-resolution optical imaging. At a wavelength of 850 nm, an ultrahigh spatial resolution of less than 3 nm was achieved for a cross-sectional Au/SiO_2 superlattice sample (Fig. 3).

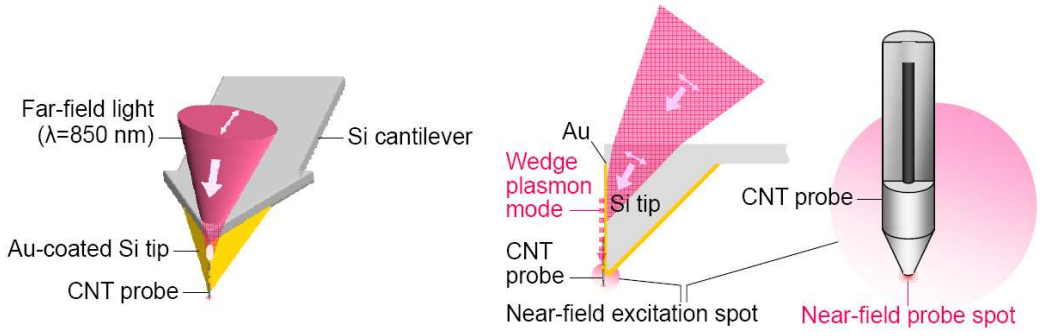

Figure 1: CNT probe coupled with plasmon waveguide. (a) Plasmon waveguide. (b) Excitation of wedge plasmon mode. (c) Generation of near-field probe spot.

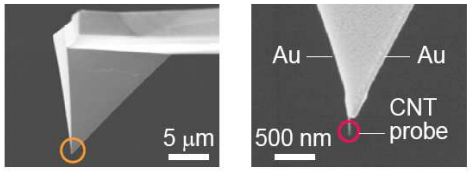

Figure 2: SEM images of CNT probe coupled with plasmon waveguide. (a) Si cantilever. (b) CNT probe fixed on Au-coated Si tip.

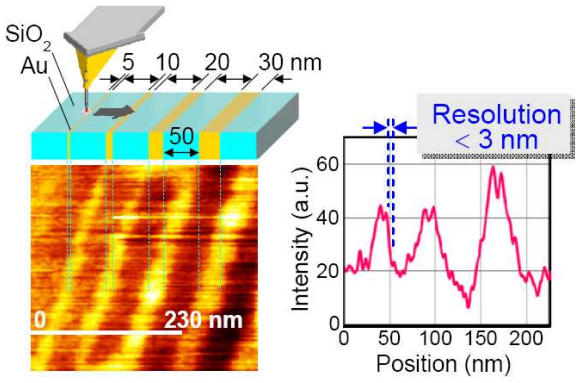

Figure 3: Near-field imaging of Au/SiO_2 superlattice sample. (a) Sample structure and near-field image. (b) Intensity profile along the white line in (a).

Interaction of Optical Beams with Spatially Dispersive Optical Nanomaterials

A. Shevchenko, **V. Kivijärvi**, **M. Nyman**, **P. Grahn**, **A. Karrila**, **and M. Kaivola**
Department of Applied Physics, Aalto University, P. O. Box 13500, FI-00076 Aalto, Finland

Abstract— Optical nanomaterials are artificial or natural materials which contain nanoscale-size structural units. Optical waves interacting with such materials are not Bragg-diffracted, since the material's unit cells are small compared to the light wavelength. The waves can therefore be considered as interacting with a homogeneous medium that has designable macroscopic characteristics.

At visible-light frequencies, nanomaterials with non-trivial and relatively large structural units (say, $> 50\,\mathrm{nm}$) are spatially dispersive, as a result of non-negligible excitation of higher-order electromagnetic multipoles in the unit cells [1]. Hence, the effective refractive index (n) and wave impedance (Z) evaluated or measured for any plane wave interacting with the material will depend not only on the polarization, but also on the direction of propagation of the wave [2, 3]. Since optical beams are composed of intercorrelated plane waves, spatial dispersion will necessarily affect the beam propagation characteristics in such nanomaterials [4].

In this work we introduce a proper theoretical basis for treating the interaction of optical beams with spatially dispersive optical nanomaterials. The method is based on a vector form of the angular-spectrum representation and a technique to evaluate the parameters n and Z for any required direction of plane-wave propagation. The parameters are retrieved from numerically evaluated transmission and reflection matrices that take into account possible changes of polarization of each plane-wave component upon interaction with nanomaterial layers. We apply the method to several particular examples and demonstrate (1) unexpected changes of light polarization in an anisotropic nanomaterial, (2) unidirectional diffraction-free propagation of optical beams in a designed spatially dispersive nanomaterial, and (3) spatial filtering of a focused optical beam by a flat nanomaterial slab.

REFERENCES

1. Grahn, P., A. Shevchenko, and M. Kaivola, "Electromagnetic multipole theory for optical nanomaterials," *New J. Phys.*, Vol. 14, 093033, 2012.
2. Grahn, P., A. Shevchenko, and M. Kaivola, "Theoretical description of bifacial optical nanomaterials," *Opt. Express*, Vol. 21, 23471, 2013.
3. Grahn, P., A. Shevchenko, and M. Kaivola, "Interferometric description of optical metamaterials," *New J. Phys.*, Vol. 15, 113044, 2013.
4. Shevchenko, A., P. Grahn, V. Kivijärvi, M. Nyman, and M. Kaivola, "Spatially dispersive functional optical metamaterials," *J. Nanophoton.*, Vol. 9, 093097, 2015.

Session 2A14
FocusSession.SC3: Nonlinear Optics: Novel Phenomena, Materials and Applications 2

Twin-beam Optical Parametric Generation and Cascaded Processes in Hexagonally Poled Nonlinear Lattices

Katia Gallo[1], **Martin Levenius**[1], **and Matteo Conforti**[2]

[1]KTH — Royal Institute of Technology, School of Engineering Sciences, SE-106 91 Stockholm, Sweden
[2]PhLAM/IRCICA, CNRS-Universite Lille 1, UMR 8523/USR 3380, F-59655 Villeneuve d'Ascq, France

Abstract— We review recent experimental and theoretical progress in the study of optical parametric generation and cascaded frequency up conversion in two-dimensional purely nonlinear lattices, relying on acoherent coupling of multiple resonances in the quadratic lattice.

Since their original proposal [1], two dimensional (2D) nonlinear photonic crystals in periodically poled materials have been the subject of a number of experimental and theoretical investigations, exploring the enhanced possibilities to engineer the nonlinear dynamics of quadratic interactions afforded in such structures [2, 3]. Most of the studies have concerned frequency up-conversion, until the recent demonstration of twin-beam optical parametric generation (TB-OPG) in 2D hexagonally poled crystals [4, 5].

TB-OPG experiments in hexagonally poled MgO:$LiTaO_3$ lattices demonstrated enhanced parametric gains as well as a rich spectral and angular response underpinned bythe coherent coupling of concurrent nonlinear processes throughshared signal or idlermodes. They provided evidence forrich interaction scenarios, generating multiple outputs in the infrared as well in the visible and encompassing also self-phase modulation and cascaded upconversion processes arising from the interplay of multiple lattice resonances.A good agreement was found with a simple model involving the cross-seeding of two non-collinear OPG processes via a common signal (idler), while the development of advanced ad-hoc simulation tools enabled to fully account for the complex nonlinear dynamics in the 2D lattices and faithfully reproduce the rich spectral-angular response seen in the experiments [6].

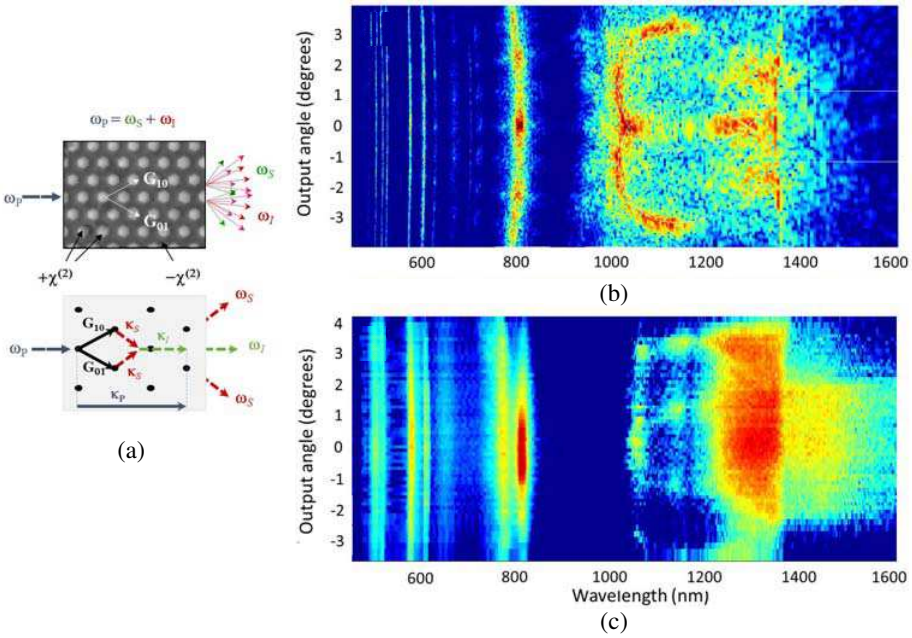

Figure 1: (a) Twin-beam parametric generation in a hexagonal nonlinear lattice. Spectral and angular mappings of the response in the visible and near infrared obtained in: (b) simulations and (c) experiments with a pump at $\sim 800\,\mathrm{nm}$.

REFERENCES

1. Berger, V., "Nonlinear photonic crystals," *Phys. Rev. Lett.*, Vol. 81, 4136, 1998.

2. Broderick, N. G., G. W. Ross, H. L. Offerhaus, D. J. Richardson, and D. C. Hanna, "Hexagonallypoled lithium niobate: A two-dimensionalnonlinearphotoniccrystal," *Phys. Rev. Lett.*, Vol. 84, 4345, 2000.
3. Gallo, K., A. Pasquazi, S. Stivala, and G. Assanto, "Parametricsolitons in two-dimensionallattices of purelynonlinearorigin," *Phys. Rev. Lett.*, Vol. 100, 053901, 2008.
4. Gallo, K., M. Levenius, F. Laurell, and V. Pasiskevicius, "Twin-beamopticalparametricgeneration in $\chi^{(2)}$ nonlinearphotoniccrystals", *Appl. Phys. Lett.*, Vol. 98, 161113, 2011.
5. Levenius, M., V. Pasiskevicius, and K. Gallo, "Angular degrees of freedom in twin-beam parametric downconversion," *Appl. Phys. Lett.*, Vol. 101, 121114, 2012.
6. Conforti, M., F. Baronio, M. Levenius, and K. Gallo, "Broadband parametric processes in $\chi^{(2)}$ nonlinear photonic crystals," *Opt. Lett.* , Vol. 39, 3457, 2014.

Optical Properties of Chalcogenide Microstructured Optical Fibers

Johann Troles[1], **Laurent Brilland**[3], **Celine Caillaud**[1], **David Mechin**[3], **Jean-Luc Adam**[1], **and Gilles Renversez**[2]

[1]Equipe Verres et Céramiques, UMR-CNRS 6226, Institut des Sciences Chimiques de Rennes
Université de Rennes 1, 35042 Rennes Cedex, France
[2]Aix Marseille Université, CNRS, Ecole Centrale Marseille
Institut Fresnel, UMR 7249, Marseille 13013, France
[3]Perfos R&D, Platform of Photonics Bretagne, Lannion, France

Abstract— Compared to oxide based glasses, vitreous materials composed of chalcogen elements (S, Se, Te) show large transparency windows in the infrared. Indeed, chalcogenide glasses can be transparent from the visible up to 12–15 µm, depending on their compositions. In addition, chalcogenide glasses contain large polarisable atoms and external lone electron pairs which induce exceptional non-linear properties. Consequently, the non-linear properties can be 100 or 1000 times as high as the non-linearity of silica. An original way to obtain single-mode fibers is to design microstructured optical fibers (MOFs). These fibers present unique optical properties thanks to the high degree of freedom in the design of their geometrical structure. Our group has prepared various chalcogenide MOFs operating in the IR range in order to associate the high non-linear properties of these glasses and the original MOF properties. Indeed, chalcogenide MOFs might lead to new devices with unique optical properties in the mid-infrared domain like multimode or endlessly single-mode transmission of light, small or large mode area fibers, non-linear properties for wavelength conversion or generation of supercontinuum sources. Optical fiber sensors for the mid-IR region between 2 and 14 µm are another promising area of applications. The IR signatures of most molecules, including biomolecules, are located in this spectral domain, which allows in situ, non-invasive and real-time detection of gaz or organics molecules.

Playing Billiard in Laser Micro-cavities: A Test-bed for Semi-classical Physics

Joseph Zyss, Clément Lafargue, Stefan Bittner, and Mélanie Lebental
Laboratoire de Photonique Quantique et Moléculaire
Institut d'Alembert, Ecole Normale Supérieure de Cachan, France

Abstract— The generic "billiard problem" is a well-known paradigm of nonlinear mathematical physics, which connects to deep issues in quantum and wave physics all the way to quantum chaos. It can be implemented in mechanics, optics or electromagnetism, either in classical or quantum mechanics, depending on experimental configurations and on the billiard length-scale. The elusive borders between wave and geometric optics on the one hand, and between quantum and classical mechanics on the other, exhibit deep analogies which can be both addressed in actual billiard-like physical systems. We will show the relevance in this context of micro-billiard shaped lasers [1–4], thanks to new experimental and technological advances in the realm of polymer based photonics at micron and submicron scales. In such configurations, confinement of light in resonators can be considered by analogy with that of a quantum particle in a well (the 2-D quantum or wave billiard). Spatially distributed modes can be connected to classical orbits within the frame of semiclassical physics approximations, by use of a celebrated "trace theorem", herein generalized to open and chaotic cavities. A beneficial feature of dielectric cavities, in contrast with their more investigated metallised contour counterparts, is the ability for the electromagnetic wave to spread-out of the cavity by refraction, diffraction, evanescent tunnelling or a combination of these, allowing to simplify the otherwise hidden physics and eventually lending itself to sensor applications. However, such "open cavities" are more challenging from a theoretical and modelling point of view, giving raise to non-Hermitian operators and imaginary eigenvalues accounting for a finite modal excitation life-time in lossy cavities. Analytical solutions such as available for the metallized 2-D rectangle are not valid for the equivalent open structures which demand to resort either to full fledged solutions of the Maxwell-Helmholtz equations with continuity conditions on the contour, or to application of semi-classical orbit methods. We will show consistence between those two avenues and experimental findings. Particular attention will be paid to recent advances: systematic investigations of triangular cavities [5] and extension to 3-D micro-billiards [6]. The role of contour singularities will be evidenced and the related diffractive orbits evidenced. The technological precision required for such studies is reached by advanced e-beam patterning methods applied to dye-doped polymer structures, down to the required nanoscale precision.

Our investigations illustrate an approach whereby, contrary to the more academic pathway from upstream mathematical predictions down to experimental applications, experimental findings may help provide guidelines towards otherwise elusive mathematical problems, such as the diffraction of light by a dielectric prism that the lasing property allows to illuminate from its inside.

REFERENCES

1. Lebental, M., J. S. Lauret, J. Zyss, C. Schmidt, and E. Bogomolny, "Directional emission of stadium shaped micro-lasers," *Phys. Rev. A*, Vol. 75, 033806, 2007.
2. Lebental, M., N. Djellali, C. Arnaud, J.-S. Lauret, J. Zyss, R. Dubertrand, C. Schmit, and E. Bougomolny, "Inferring periodic orbits from spectra of shaped micro-lasers," *Phys Rev. A*, Vol. 76, 023830, 2007.
3. Lebental, M., E. Bogomolny, and J. Zyss, "Organic micro-lasers: A new avenue onto wave chaos physics," *Practical Applications of Microresonnators in Optics and Photonics*, Chapter 6, 317–353, A. Matsko, ed., CRC Press, Boca Raton, 2009.
4. Bogomolny, E., N. Djellali, R. Dubertrand, I. Gozhyk, M. Lebental, C. Schmit, C. Ulysse, and J. Zyss, "Trace formula for dielectric cavities. II. Regular, pseudointegrable, and chaotic examples," *Phys. Rev. E*, Vol. 83, 036208, 2011.
5. Lafargue, C., M. Lebental, A. Grigis, C. Ulysse, I. Gozhyk, N. Djellali, J. Zyss, and S. Bittner, "Localized lasing modes of triangular organic microlasers," *Phys. Rev. E*, Vol. 90, 052922, 2014.
6. Chen, V. W., N. Sobeshchuk, C. Lafargue, E. S. Mansfield, J. Yom, L. R. Johnstone, J. M. Hales, S. Bittner, S. Charpignon, D. Ulbricht, J. Lautru, I. Denisyuk, J. Zyss, J. W. Perry, and M. Lebental, "Three-dimensional organic microlasers with low lasing thresholds fabricated by multiphoton and UV lithography," *Optics Express*, Vol. 22, No. 10, 12316–12326, 2014.

Liquid Crystals for Nonlinear Optics with Femtoseconds — CW Lasers

I. C. Khoo
Electrical Engineering Department, Pennsylvania State University, University Park, PA 16802, USA

Abstract— A critical analysis of various all major mechanisms for optical nonlinearities of nematic as well as Blue-Phase liquid crystals is presented, along with feasibility demonstrations of femtoseconds pulse compression, all-optical switching with nanoseconds — CW laser and tuning/modulations of micro- or nano-photonic structures [1–3]. Specifically, we will delve into individual molecular electronic nonlinearities with femtoseconds [4] response speed as well as slower (nanoseconds-milliseconds) collective molecular responses such as laser induced crystalline axis rotation, lattice reorientation and distortion, c.f. Fig. 1. The merits and limitation of nematics are discussed together with some recent results with Blue Phase liquid crystals that could circumvent some of the limitations.

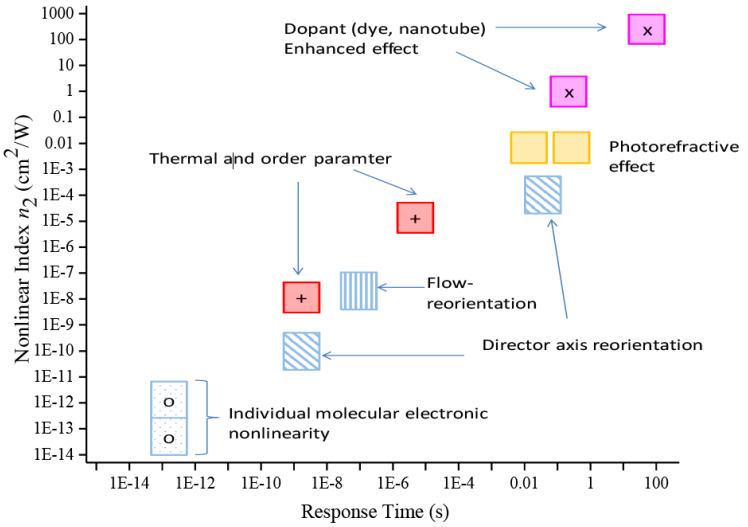

Figure 1: Nonlinear index coefficients and response speed of some exemplary nonlinear optical mechanisms in NLC.

REFERENCES

1. Khoo, I. C., "Nonlinear optics of liquid crystalline materials," Physics Report, Vol. 471, 221–267, 2009.
2. Khoo, I. C., "Nonlinear optics, active plasmonic and tunable metamaterials with liquid crystals," *Progress in Quantum Electronics*, Vol. 38, No. 2, 77–117, 2014.
3. Khoo, I. C., "DC field-assisted grating formation and nonlinear diffractions in methyl-red dye-doped blue phase liquid crystals," *Optics Letters*, Vol. 40, 60–63, 2015.
4. Song, L., S. Fu, Y. Liu, J. Zhou, V. G. Chigrinov, and I. C. Khoo, "Direct femtosecond pulse compression with miniature-sized Bragg cholesteric liquid crystal," *Optics Letters*, Vol. 38, 5040–5042, 2013.

Nonlinear Optical Imaging with Unconventional Light Fields

Godofredo Bautista, Mikko J. Huttunen, Jouni Mäkitalo, and Martti Kauranen
Department of Physics, Tampere University of Technology, P. O. Box 692, FI-33101 Tampere, Finland

Abstract— Nonlinear optical (NLO) microscopy, which embraces all imaging techniques that endow contrast based on nonlinear optics, has allowed unprecedented characterization of natural and artificial materials. Most past works, however, utilized linear, elliptical or circular polarization, where the state of polarization (SOP) is uniform across the beam cross-section. Recently, there has been a renewed interest in the unique focusing properties of beams that exhibit rotationally symmetric SOPs, and their novel imaging applications [1]. For example, when azimuthal and radial polarizations are focused, the intensity distributions of their transverse electric-field components preserve the doughnut-shaped intensity patterns and corresponding polarizations. However, when all the electric-field components are accounted for, the radial polarization exhibits a Gaussian-like intensity distribution due to the presence of a strong electric-field component along the beam axis, usually referred to as the longitudinal component.

In this talk, we show that NLO microscopy techniques equipped with unconventional polarizations provide completely unique capabilities in the characterization of the structural properties of three-dimensional nano-objects such as nanocones and nanowires, at microscopic resolution [2–5].

Our samples consist of either metal nanocones or semiconductor nanowires. For sample characterization, we used a custom-built point-scanning NLO microscope powered by a femtosecond laser (wavelength 1060 nm, pulse duration 200 fs, repetition rate 82 MHz). Upon routine beam cleaning, we directed the excitation beam onto the sample using a strainfree microscope objective (numerical aperture 0.8). We collected the respective NLO signals in reflection and/or transmission using photomultiplier tubes equipped with appropriate dichroic and optical filters. To generate azimuthal or radial polarizations, we used a polarization mode converter (ARCoptix).

We found that the introduction of azimuthal and radial polarizations in second- and third-harmonic generation microscopy allows us to directly determine the orientation and anisotropy of individual nanocones and nanowires. In essence, any deviation of the image pattern can be correlated with subtle structural features of the nano-objects.

REFERENCES

1. Zhan, Q., *Adv. Opt. Photon.*, Vol. 1, 1–57, 2009.
2. Bautista, G., et al., *Nano Lett.*, Vol. 12, 3207–3212, 2012.
3. Bautista, G., et al., *Opt. Express*, Vol. 21, 21918–21923, 2013.
4. Huttunen, M. J., et al., *Opt. Lett.*, Vol. 39, 3686–3689, 2014.
5. Bautista, G., et al., submitted.

Beam Bistability in Nematic Soft Matter

A. Piccardi[1], **A. Alberucci**[1,2], **N. Kravets**[1], **O. Buchnev**[3], **M. Kaczmarek**[3], **and G. Assanto**[1,2]

[1]NooEL, Nonlinear Optics and Opto-Electronics Lab, University "Roma Tre", 00146 Rome, Italy
[2]Optics Laboratory, Department of Physics, Tampere University of Technology, Tampere 33101, Finland
[3]Zepler Institute, University of Southampton, Southampton SO17 1BJ, UK

Abstract— We investigate optical bistability with diffracting and self-trapped beams in nematic liquid crystals. We demonstrate the coexistence of dispersive and solitary beams in an interval of $\approx 2\,\mathrm{mW}$. Bistability stems from the reorientational response in the presence of a threshold.

Optical bistability is a classic topic in nonlinear optics [1]. Two key ingredients for bistability are a nonlinear response and a feedback mechanism. Nematic liquid crystals (NLC) are birefringent dielectrics featuring a large reorientational nonlinearity, the latter based on molecule rotation in the presence of electric fields [2]. When launching a bell-shaped (extraordinary polarized) light beam, the molecular (angular) distribution becomes inhomogeneous: The beam itself defines a transverse gradient of the refractive index, leading to self-focusing at high enough powers [3]. When the molecules at rest are perpendicular to the beam electric field, this reorientation undergoes the so-called optical Freedericksz threshold (OFT), with threshold power depending on the beam width. Thus self-focusing, altering the beam size, changes the OFT threshold and can leads to a hysteretic behavior versus input beam power. Starting from a diffracting beam and increasing the excitation, above the OFT nonlinear reorientation takes place until a self-confined beam — a nematicon — is formed. Such self-localization in turn lowers the OFT below the initial value, so that when reducing the power the spatial soliton is supported at powers smaller than initially required for its formation.

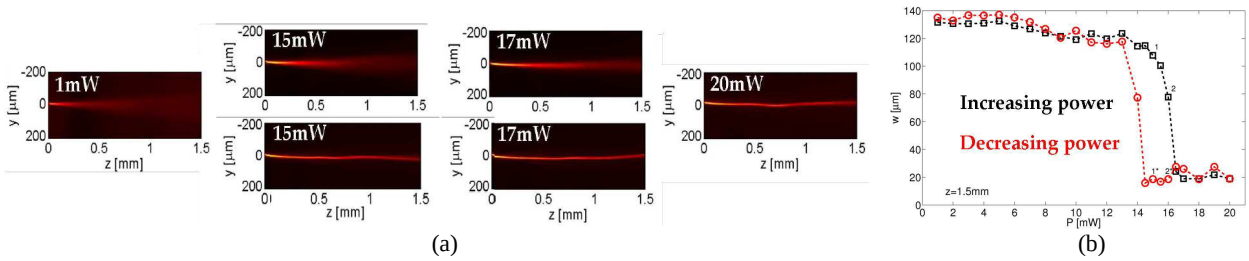

(a) (b)

Figure 1: (a) Acquired images of beam propagation for increasing (top, left to right) and decreasing (bottom, right to left) power. (b) Beam width vs power along a cycle. Hysteresis is observed between 15 and 17 mW.

We launched a $2\,\mu\mathrm{m}$ wide beam at $\lambda = 1064\,\mathrm{nm}$, with linear polarization perpendicular to the NLC optic axis, thus enabling the OFT. At low power the beam diffractes as reorientation did not occur. Self-confinement was observed from $P = 17\,\mathrm{mW}$, leading to a solitary wave. When power was then diminished, the nematicon was maintained down to $P = 15\,\mathrm{mW}$: The system exhibited a hysteresis loop about 2 mW wide, with the two stable states associated to dispersive and localized wavepackets, respectively [4]. The observed bistable behavior stems from the inherent feedback provided by the reorientational nonlinearity between the beam profile and the self-focusing threshold, in agreement with Kaplan's recipe [5] despite the observation of only one soliton state.

REFERENCES

1. Gibbs, H., *Optical Bistability: Controlling Light With Light*, Academic Press, San Diego, 1985.
2. Khoo, I. C., *Liquid Crystals*, Wiley, New York, 1995.
3. Peccianti, M. and G. Assanto, "Nematicons," Phys. Rep., Vol. 516, 147, 2012.
4. Kravets, N., et al., "Bistability with optical beams propagating in a reorientational medium," *Phys. Rev. Lett.*, Vol. 113, 023901, 2014.
5. Kaplan, A. E., "Bistable solitons," *Phys. Rev. Lett.*, Vol. 55, 1291, 1985.

Enhanced Nonlinear Interaction in a Silicon Microcavity under Coherent Control

S. Serna[1,2], **J. Oden**[1], **M. Hanna**[1], **C. Caer**[2], **X. Le Roux**[2], **C. Sauvan**[1], **P. Delaye**[1], **E. Cassan**[2], **and N. Dubreuil**[1]

[1]Laboratoire Charles Fabry, Institut d'Optique, CNRS
Université Paris-Sud 11, 2 Avenue Augustin Fresnel, Palaiseau Cedex 91127, France
[2]Institut d'Electronique Fondamentale, Université Paris-Sud 11
CNRS UMR 8622, Bat. 220, Orsay Cedex 91405, France

Abstract— The strong light confinement achieved in photonic crystal microcavities allows the enhancement of light-matter interactions and the reduction of the energy required to control nonlinear optical devices, like for instance low energy optical switches operating under the control of a resonant pulse. Although nonlinear refractive effects assist the switching operation, the imparted frequency shift dynamics of the cavity resonance tends to limit the coupling efficiency of the control pulse. As a result, the cavity enhancement effect is not maintained for the entire pulse duration, even if the latter is longer than the cavity photon lifetime.

To overcome this problem, a technique inspired by the coherent control of molecular and atomic systems [1] has been implemented to enhance the nonlinear behaviour of silicon-based optical resonators. In a silicon cavity, the optical resonance mainly experiences a frequency blue-shift driven by the refractive index variation induced by the free carriers generated by two-photon absorption (TPA). By delaying the blue spectral components, under a tailored linearly chirped pulse, we show that the benefit of light localization can be maintained throughout the pulsed excitation despite the cavity resonance dynamic frequency shift. This approach has only been theoretically investigated [2–4].

The fabricated cavity whose the SEM picture is presented in Fig. 1(b) has a mode volume of $0.8(\lambda/n)^3$. It exhibits a linear transmission spectrum, shown in Fig. 1(c) (grey line $\times 12$), with a narrow peak at 1578.8 nm. The measured linewidth of 0.3 nm corresponds to a quality factor $Q = 5260$ and a cavity photon lifetime equal to 4.4 ps. Optical pulses delivered by a mode-locked Erbium doped fibre laser are sent through a grating based pulse stretcher, which delimitates the spectral linewidth to 6.5 nm (spectrum shown by the black dashed-line in Fig. 1(c)) and introduces an adjustable 2nd order dispersion coefficient $\phi^{(2)}$. For $\phi^{(2)} = 0\,\mathrm{ps}^2$, the measured auto-correlation pulse duration is 2 ps.

The transmission spectra achieved with two opposite chirps + and $-1.6\,\mathrm{ps}^2$, both coinciding to a pulse duration (5.7 ps) longer than the cavity photon lifetime are shown in Fig. 1(c). Compared with the $-1.6\,\mathrm{ps}^2$ chirped pulses (green curve), the transmission spectrum for $\phi^{(2)} = +1.6\,\mathrm{ps}^2$ (red curve) leads to a broader transmitted spectrum, which almost matches the input pulse bandwidth. The increase by a factor 2 of the blue shift, achieved with the red curve of Fig. 1(c), means that TPA generated carrier density is twice higher and proves an enhanced nonlinear interaction in the silicon material thanks to the coherent excitation of the cavity. A coupled mode theory model that includes all the silicon nonlinearities has been implemented and the results are in good agreement with the experimental results.

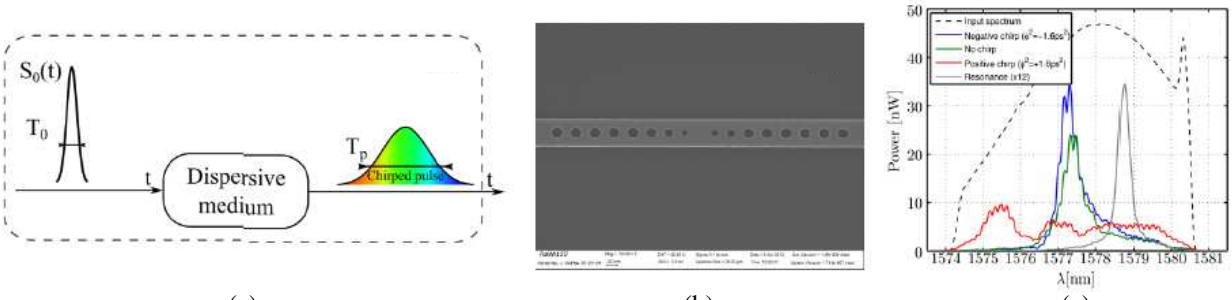

(a) (b) (c)

Figure 1: (a) Scheme of the chirped pulsed excitation used to excite the microcavity, (b) SEM view of the tapered nanobeam Silicon microcavity and (c) spectra of the input pulse (dashed), linear resonance (grey $\times 12$) and nonlinear transmitted spectra at 3 pJ incident energy for various chirps.

REFERENCES

1. Weiner, A. M., "Femtosecond pulse shaping using spatial light modulators," *Rev. Sci. Instrum.*, Vol. 71, 1929, 2000.
2. Sandhu, S., M. Povinelli, and S. Fan, "Enhancing optical switching with coherent control," *App. Phys. Lett.*, Vol. 96, 231108, 2010.
3. Kristensen, P. T., M. Heuck, and J. Mørk, "Optimal switching using coherent control," *App. Phys. Lett.*, Vol. 102, 041107, 2013.
4. Oden, J., S. Trebaol, P. Delaye, and N. Dubreuil, "Coherent excitation of a nonlinear microcavity," *J. Europ. Opt. Soc. Rap. Public.*, Vol. 8, 13046, 2013.

Integrating Single Photon Sources and High-efficiency, Low Dark Count Single Photon Detectors Using Photonic Crystal Microcavities in Silicon-on-insulator Waveguides

Ellen N. Schelew, **Mohsen K. Akhlaghi**, **and Jeff F. Young**
Department of Physics and Astronomy, University of British Columbia, Vancouver V6T 1Z1, Canada

Abstract— Scalable photonic quantum technologies are sought after for applications in quantum communication, computing and sensing. One promising approach involves integrating key components, including single photon sources, single photon detectors, and conventional optical components like beamsplitters and filters, in planar lightwave circuits. Silicon-on-insulator (SOI) is an attractive host-material, as it benefits from ongoing advances in classical integrated silicon photonic technologies. Recent progress has been made towards realizing both single photon sources and detectors for wavelengths near 1550 nm. We describe a photon pair source integrated with a superconducting nanowire single photon detector, to form a heralded single photon source in SOI. The photon pairs are generated through a third order nonlinear process — Spontaneous Four-Wave Mixing (SFWM) — in a planar two-dimensional photonic crystal (2D PC) triple-cavity system engineered to resonantly enhance the nonlinear interaction, and strategically filter generated photons into a single output waveguide. This design improves on previously reported 'photonic molecule' designs by taking advantage of the high Q modes, and flexible waveguide and cavity coupling schemes, supported by 2D PCs. We also report on our novel approach to single photon detection in SOI which employs a superconducting nanowire lying on the surface of a 1D PC nanobeam cavity designed for coherent perfect absorption (CPA) of photons. While many competing designs require a large volume of superconducting material to achieve high-efficiency absorption, in the CPA implementation, a short (8.5 μm long) and narrow ($8 \times 35\,\mathrm{nm}^2$) nanowire achieves near unity quantum efficiency, together with a low dark count rate (< 0.1 Hz) and favorable speed and timing accuracy at 2 K.

ACKNOWLEDGMENT

We gratefully acknowledge financial support from the Canadian Institute of Advanced Research, and the Natural Sciences and Engineering Research Council, including the Silicon Electronic-Photonic Integrated Circuits (Si-EPIC) CREATE Program. We would also like to acknowledge Lumerical Solutions Inc. and CMC Microsystems.

First-principle Models of Light-matter Interactions for Large-scale Computer Simulations in Extreme Nonlinear Optics

M. Kolesik[1, 2]

[1]College of Optical Sciences, The University of Arizona, Tucson, USA
[2]Arizona Center for Mathematical Sciences, University of Arizona, Tucson, USA

Abstract— Computer simulations in modern nonlinear optics need to has to address two basic issues. The first is a transformation of the Maxwell equations into a one-way pulse propagation system. The second issue is the implementation of a light-mater interaction model that is based on first principles, and is sufficiently effective computationally to allow realistic simulations. White the first issue has been successfully addressed in the form of pulse-propagation equations, the second is still a subject of intense research work. I will describe a novel approach to nonlinear medium modeling that is based on metastable electronic quantum states. Rather than the stationary quantum states, i.e., eigen-states of the given Hamiltonian, the meta-stable electronic states provide a most natural tool to describe the dynamics in strong optical fields. They possess the properties of both bound and continuum-energy wavefunctions, and exhibit non-perturbative response to the driving optical field. As such they allow to construct an extremely economic implementation of a nonlinear medium model; I will demonstrate that even the lowest-order approximation can provide semi-quantitative results. The rest of this talk will briefly discuss the mathematical aspects of the method, describe numerical methods to obtain necessary characteristics of the metastable quantum states, and demonstrate that the framework makes it possible to perform large-scale simulations of the coupled Maxwell-Schrödinger system. The method is most suitable for high-intensity nonlinear optics which often deals with regimes in which both bound and free electronic states contribute to the medium response.

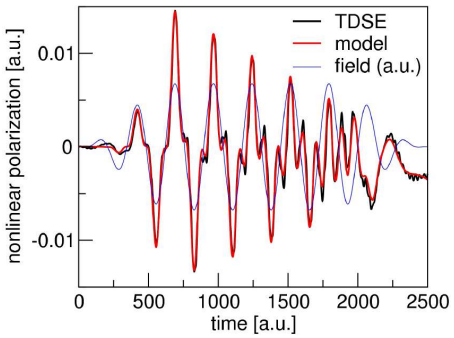

Figure 1: Illustration of the metastable electronic state approach for calculation of the nonlinear polarization and ionization induced by a strong optical pulse (arbitrarily scaled electric field is shown as the blue line). The black line shows the numerically exact solution obtained from the time-domain simulation of the Schrödinger equation. The red line represents the result obtained with the new method: It shows the nonlinear response, i.e., the atom dipole moment, obtained from a single resonance state, combined with the current induced by ionized electrons. In this example, the atom response is initially dominated by the self-focusing (optical Kerr) effect, while at later times, de-focusing effects of freed electrons prevail. Similarly accurate results are obtained across a wide range of regimes.

Instabilites and Rogue Waves in Optics

G. Genty
Optics Laboratory, Tampere University of Technology, Tampere FI-33101, Finland

Abstract— The emergence of high amplitude events that occur with low probability has been observed in many physical systems. Ocean rogue waves that emerge unexpectedly from the sea with massive destructive power is the most striking example of extreme events. Recently, the observation of extreme events in optical systems has attracted significant attention with the possibility, for the first time, to study in real time the dynamics of extreme-value phenomena. More specifically, a wide range of studies have shown how extreme spatio-temporal localization of light waves can occur in various optical systems including the nonlinear growth of a weak perturbation present on top of a plane wave or the generation of short pulses in laser cavities. Common features to many (although not all) of the systems where extreme localization has been observed in optics is the presence of noise and nonlinearity in the system. In this context, the nonlinear Schrodinger equation (NLS) describing nonlinear waves localization dynamics in weakly nonlinear media plays a particular role and it has been extensively studied in various contexts in nonlinear science [1, 2]. A particular class of solutions of the NLS that possess extreme localization characteristics are the solitons on finite background which have been proposed as a possible mechanism underlying the formation of extreme amplitude waves on the surface of the ocean [3, 4]. In an optical context, these structures have been shown to emerge spontaneously in noise-seeded modulation instability and play a central role in the observation of extreme events in optical fibers.

Here, we review the recent progress on extreme events in optics with particular emphasis on optical fiber systems. Experiments and modelling of localization dynamics are constantly providing new insights into how noise drives the dynamics of nonlinear optical systems. As research continues to progress in this field, it is likely that the noise properties in a wide range of optical systems may find analogies with areas of physics other than oceanography, allowing the use of a convenient optical testbed with which to study a wide range of different physical processes.

REFERENCES

1. Akhmediev, N. and N. Ankiewicz, *Solitons, Nonlinear Pulses and Beams*, Chapman and Hall, London, 1997.
2. Dauxois, T. and M. Peyrard, *Physics of Solitons*, Cambridge University Press, Cambridge, 2006.
3. Zakharov, V. E., A. I. Dyachenko, and A. O. Prokofiev, "Freak waves as nonlinear stage of Stokes wave modulation instability," *Eur. J. Mech. B — Fluids*, Vol. 5, 677–692, 2006.
4. Shrira, V. I. and Y. V. Geogjaev, "What make the Peregrine soliton so special as a prototype of freak waves?" *J. Eng. Math.*, Vol. 67, 11–22, 2010.

Session 2A15a
Oral Presentations for Best Student Paper Awards — SC1: CEM, EMC, Scattering & EM Theory

Effective Lennard-Jones Parameters for CO_2-CO_2 Dispersion Interactions in Water and near Amorphous Silica-water Interfaces

P. Thiyam[1], **O. I. Malyi**[2], **C. Persson**[1, 2, 3], **S. Y. Buhmann**[4, 5], **D. F. Parsons**[6], **and M. Boström**[2]

[1]Department of Materials Science and Engineering
Royal Institute of Technology, SE-100 44 Stockholm, Sweden
[2]Centre for Materials Science and Nanotechnology
University of Oslo, P. O. Box 1048, Blindern, NO-0316 Oslo, Norway
[3]Department of Physics, University of Oslo, P. O. Box 1048, Blindern, NO-0316 Oslo, Norway
[4]Physikalisches Institut, Albert-Ludwigs-Universität Freiburg
Hermann-Herder-Str. 3, 79104 Freiburg, Germany
[5]Freiburg Institute for Advanced Studies, Albert-Ludwigs-Universität Freiburg
Albertstraβe 19, 79104 Freiburg, Germany
[6]School of Engineering and IT, Murdoch University, 90 South St, Murdoch, WA 6150, Australia

Abstract— Tight rocks may provide most of the world's future fossil energy. New production methods that allow hydrocarbons to be produced directly from tight source rocks such as shale gas and shale oil systems have changed the world's energy outlook. We are now at a stage where the technology for recovery of gas by CO_2 injection has advanced beyond our scientific understanding of the underlying processes. Much fundamental research focuses on molecular physisorption/chemisorption and meso-scale transport processes in nanostructured shales. The aim of such research is to understand carbon dioxide (CO_2)-methane (CH_4) conversion processes and trends of adsorption of CO_2 in model porous media and hydrofractured shale [1]. Standard simulation parameters on modeling near interfaces are based on intermolecular forces in bulk media. Using the formalism of Sambale et al. [2], we demonstrate that the attractive part of the Lennard-Jones parameters of intermolecular interaction in bulk media, i.e., the van der Waals parameter C_6 ($U_{vdW} = -C_6/\rho^6$) where ρ is the distance between the two molecules, is strongly modified by the presence of surfaces. We explore the retarded van der Waals interaction of two CO_2 molecules near an amorphous SiO_2-water interface and near a vapor-water interface. Different models for effective polarizabilities in water [3] and the corresponding dispersion forces between dissolved molecules are explored in bulk water and near interfaces. The interaction energy depends on the surface material, polarizability model of the molecule used and the relative orientation of the molecules near the interface, and shows considerable deviation from intermolecular interaction in the absence of surfaces. The dielectric properties of amorphous SiO_2 are computed using density functional theory (DFT) and Born-Oppenheimer molecular dynamics (BOMD).

REFERENCES

1. Boström, M., M. Dou, P. Thiyam, D. F. Parsons, O. I. Malyi, and C. Persson, *Phys. Rev. B*, Vol. 91, 075403, 2015.
2. Sambale, A., D.-G. Welsch, H. T. Dung, and S. Y. Buhmann, *Phys. Rev. A*, Vol. 79, 022903, 2009.
3. Sambale, A., S. Y. Buhmann, D.-G. Welsch, and M. S. Tomas, *Phys. Rev. A*, Vol. 75, 042109, 2007.

The C-method as an Initial Value Problem: Application to Multilayer Gratings

Cihui Pan[1, 2, 3], **Richard Dusséaux**[1], **and Nahid Emad**[2, 3]

[1]Laboratoire LATMOS, 11 Boulevard d'Alembert, Guyancourt 78280, France
[2]Laboratoire PRiSM, 45 avenue des Etats-Unis, Versailles 78035, France
[3]Laboratoire Maison de la Simulation, Bâtiment 565, Gif-sur-Yvette Cedex 91191, France

Abstract— We study our approach of the C-method [1, 2] as an initial value problem for the efficient calculation of the N-dimensional scattering matrix of a grating. We apply this method to multilayer gratings with an arbitrary number of interfaces. The interfaces can have different functional form and amplitude and can be parallel or not.

For each interface separating two homogeneous media, we consider two horizontal planes above and below the interface, and define a coordinate system such that the interface and both horizontal planes correspond to coordinate surfaces. Inside the area delimited by the two horizontal planes, the Maxwell's equations lead to an initial value problem which can be solved with initial conditions satisfying the boundary conditions. Outside this area, the fields are represented by Rayleigh expansion. The scattering matrix between two consecutive media is obtained by using continuity relations between different components of fields on the horizontal planes [3].

We consider a $n+1$ layer diffraction grating, thus there are n interfaces separating the layers. From the uppermost to downmost, these layers are composed of medium 1 to medium $n+1$. Each medium has a constant optical index. Thus we can calculate the scattering matrix $S_{1,2}$ which associate the incoming and outcoming waves from medium 1 and 2. Then we collect all the scattering matrix of adjacent medium, $S_{i,i+1}, i = 1, \ldots, n$ and obtain the global matrix $S_{1,n+1}$ by combination of elementary matrices $S_{i,i+1}, i = 1, \ldots, n$.

The proposed method gives the efficiencies with a good accuracy. Experiments are performed on a three layer grating with interfaces described by Trigonometric functions. We also study the anomalies of coated dielectric gratings [4].

REFERENCES

1. Chandezon, J., D. Maystre, and G. Gaoult "A new theoretical method for diffraction gratings and its numerical application," *J. Optics*, Vol. 11, 235–241, Paris, 1980.
2. Li, L. and J. Chandezon, "Improvement of the coordinate transformation method for surface-relief gratings with sharp edges," *JOSA A*, Vol. 13, 2247–2255, 1996.
3. Pan, C., R. Dusséaux, M. Fall, and N. Emad, "Curvilinear coordinate method as an initial value problem: application to gratings," *JOSA A*, Vol. 32, No. 1, 143–149, 2015.
4. Popov, E., L. Mashev, and D. Maystre, "Theoretical study of the anomalies of coated dielectric gratings," *Optica Acta*, Vol. 33, No. 5, 607–619, 1986.

Efficient Numerical Solution for Time-domain Volume Integral Equations

J. Zhang and M. S. Tong
Department of Electronic Science and Technology
Tongji University, 4800 Cao'an Road, Shanghai 201804, China

Abstract— Integral equation approach is widely used for solving electromagnetic (EM) problems. For inhomogeneous penetrable structures, the volume integral equations (VIEs) are indispensable, and furthermore the time-domain version (TDVIEs) should be applied when a transient interaction with the structures exists. The TDVIEs are usually solved by combining the method of moments (MoM) with a well-designed basis function like the Schaubert-Wilton-Glisson (SWG) basis function in spatial domain and a march-on-in-time (MOT) scheme in temporal domain. The MoM requires conforming meshes in geometric discretization and also needs to perform two-fold integrations in evaluating matrix elements, resulting in certain inconvenience. On the other hand, the MOT has a well-known stability problem which has not been fully solved yet although various improvements were proposed.

In this work, we propose a different scheme to solve the TDVIEs for transient EM problems with penetrable objects. Unlike the conventional approach, the Nyström method is used in the spatial domain while the MoM with Laguerre basis and testing functions is employed in the temporal domain. The Nyström method uses a point-matching procedure to discretize integral equations and does not use any basis and testing functions so that the implementation can be simplified. Also, the method does not require conforming meshes and can endure low-quality meshes, leading to much convenience in geometric discretization. In temporal domain, the expansion of Laguerre basis function can naturally enforce the causality and also the Galerkin's testing procedure can fully solve the numerical stability problem in a march-on-in-degree (MOD) manner, so it is very suitable to solve transient problems. Numerical examples for transient EM scattering by a dielectric cube are presented and the merits of proposed approach has been demonstrated.

Analysis of EM Emission Characteristics by Arbitrarily Oriented Microstrip Lines Based on TEM Cell Electric and Magnetic Coupling Fields

Jung-Yeol Park[1], **Jin-A. Choi**[1], **Jae-Kyung Wee**[1], **In-Chae Song**[1], **Boo-Gyoun Kim**[1], **Hyok Lee**[2], **and Seung-Real Ryu**[2]

[1]School of Electronics, Soongsil University, Korea
[2]Korea Automotive Technology Institute, Korea

Abstract— In this paper, we analyze the electromagnetic (EM) emission characteristics of the arbitrarily oriented microstrip lines and PCB board makes it possible to predict the radiation characteristics by using a library of normalized line modeling. Figure 1(a) shows the test environment on various microstrip lines which are prepared to consider with thickness, length and current direction. The measurement method based on a transverse electromagnetic (TEM) cell rotates DUT. The test results by using a vector network analyzer (VNA) is different from that of direction DUT. The coupling factor by the direction of the DUT are all affected by the electric field. But the magnetic field is affected in different ways between TEM cell and DUT. In the Figure 1(b), when the DUT direction of a 180 degree (far end), the magnetic field is cancelled between DUT and Septum of TEM cell. And when the DUT direction 90, 270 degree magnetic fields are same results because magnetic fields are that it does not affect.

The method of lines (MoL) is used to calculate the capacitance matrix with the measured S_{12} of microstrip lines. Some simulations such as HFSS and ADS are carried out in order to improve the accuracies of extracting capacitances and inductances. For accurate coupling factors, the measured and simulated E and H powers on TEM cell as shown in Figure 1(b) are used for coupling capacitance and an inductance. A library based on the well-proven line parameters is established for evaluating a real PCB EMC including the accurate coupling factor models. In addition, the prepared library will be applied to evaluate its accuracy where the simulated EMIs will be compared with measurements of their EMIs predicted from those generated from line patterns on the tested PCB board as shown in Figure 1(c).

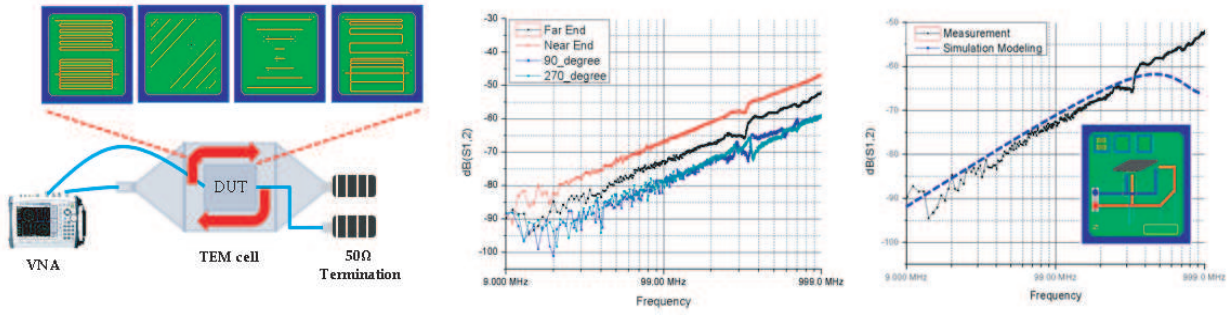

(a) (b) (c)

Figure 1: (a) Test Environrmnt and measured EM emission according to arbitrarily oriented of microstrip lines at DUT rotations of 0, 90, 180, 270 degree, (b) coupling factors by direction of DUT, (c) applied modeling library in PCB board.

Algebraic Function Approximation for Eigenvalue Problem in Rectangular Waveguide Partially Filled with Transversely Magnetized Ferrite

Oguzhan Demiryurek[1] and Namık Yener[2]

[1]Technical Education Faculty, Kocaeli University, Izmit, Kocaeli 41380, Turkey
[2]Technology Faculty, Kocaeli University, Izmit, Kocaeli 41380, Turkey

Abstract— In this work, a lossless and closed rectangular waveguide partially filled with a slab of transversely magnetized ferrite without assuming vanishing of the derivative in the direction of the dc biasing field, has been analyzed using Method of Moment (MoM). Generally, there are basically three types of modes in the waveguide: propagating, evanescent and complex modes. To support evanescent mode, the waveguide must be bidirectional. But a rectangular waveguide filled with a slab of ferrite transversely magnetized is not bidirectional, if there exists no symmetry with respect to the rotation by π about an axis perpendicular to propagation direction. So such a waveguide does not support the evanescent waves. Propagation constant is complex or pure imaginary. Our waveguide is filled with a transversely magnetized gyrotropic medium and does not satisfy the condition of symmetry with respect to the rotation by π about an axis perpendicular to propagation direction. So it is not bidirectional and hence does not support evanescent modes. Results of the MoM are consistent with this situation. In a lossless and closed rectangular waveguide partially filled with a slab of transversely magnetized ferrite Maxwell's equations, consisting of partial differential equations, are transformed into an infinite linear algebraic equation system by application of the Galerkin version of Moment method. As the result of algebraic operations, from the transmission line equations a quadratic eigenvalue problem is obtained whose eigenvalue corresponds to the propagation constant. The determinant of the coefficient matrix of the quadratic eigenvalue problem is a monic polynomial of the propagation constant whose coefficients are rational functions of the complex frequency. If the polynomial is set equal to zero and is multiplied by the common denominator of the coefficients, an algebraic equation is obtained. The roots of this equation are the propagation constants. In this work as the contribution, using algebraic function theory the solution of the algebraic equation (propagation constant) for the waveguide filled with transversely magnetized ferrite medium, is expressed by means of a Puiseux series in the neighborhood of the algebraic branch point. Puiseux series coefficients are solved using transmission line equations and the propagation constant is computed from this series expansion. Puiseux series results are compared and found to conform with MoM results and the exact solution.

The Transmittance of Electromagnetic Waves and Field Correlations in Multilayered Microspheres with Quasi-periodic Structures

M. Nájera-Villeda and G. Burlak
Centro de Investigación en Ingeniería y Ciencias Aplicadas
Universidad Autónoma del Estado de Morelos, Cuernavaca, Mor., México

Abstract— The dielectric spheres have a complex spectrum of electromagnetic eigenoscillations with low Q-quality factor because of the power leakage in outer space. The case of the compound structure: the dielectric sphere coated by an alternative stack, is richer. The Q-factor of such oscillations strongly depends on the properties of the stack. It has a large value in the frequency regions of high reflectivity, and beyond these regions Q remains small. The combination of factors makes a variety of optical properties of microspheres with a multilayer stack. Particularly, a system of this type can serve as a symmetrical spherical photonic band gap structure (PGC), which has strong selection transmittance properties, and can arrange photon emitting nanoscale.

Researched the transfer matrix approach and the Green function technique we numerically study the electromagnetic properties (narrow peak positions) of the transmission spectra for microspheres coated by a multilayered stack with the generalized Cantor and Pascal structure (fractal). Quasi-periodic design structures allow obtaining the photonic band gaps in the field radiation. The location of light in disordered systems offers range of applications in optoelectronic applications.

In a microsphere, only narrow resonance spectrum (eigenfrequencies) peaks can be observed in the frequency spectrum of radiation. We show that the wave phase interference in such a fractal pattern leads to formation of very narrow electromagnetic transmittance resonances that can be used in modern optoelectronics.

It is of great interest investigate how a stack is modified with a quasi-periodic spherical structure, the working frequency spectrum numerically in sequence Pascal and Cantor set in a microsphere SI and SiO_2 multilayer. To do that we explore the transmission spectra and frequency resonances of such structures deposited on surface of a dielectric microsphere. Besides we calculate the structure of the field correlations in such a multilayered microsphere with incorporated nanoemitters. It is well-known that due to the fluctuation-dissipation theorem the correlation function of the photon states in the absorbing environment for temperature T and frequency ω can be written with the help of the macroscopic Green function (GF) as follows $\langle \mathbf{E}(r)\mathbf{E}(r')\rangle_\omega = \frac{\hbar\omega^2}{c^2}\coth(\frac{\hbar\omega}{2T})\mathrm{Im}(\mathbf{G}(r, r', \omega))$. For our purposes it is sufficient to give more attention to the imaginary part of GF to study a specific interaction between the field resonances in points r and r'. Figure below displays the results of such simulation of $\mathrm{Im}(G)$ in the radial section of a coated microsphere.

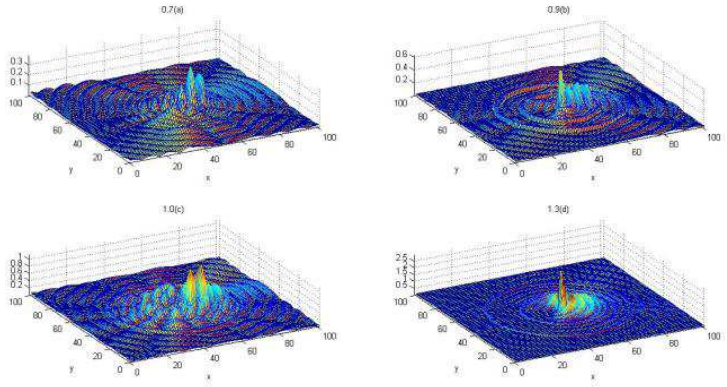

Such study allows using the multilayered microsphere to effective management of the photon properties in modern informational industry.

Evaluation of Power Transistors Figure of Merit for Hard Switching Commutation Mode through Experimental Analysis

Michal Frivaldsky, **Pavol Spanik**, **Boris Kozacek**, **and Marek Piri**
Faculty of Electrical Engineering, Department of Mechatronics and Electronics
University of Zilina, Univerzitna 1, Zilina 010 26, Slovak Republic

Abstract— Nowadays demand for efficiency and high density of electronic device is high. Therefore, great emphasis is placed on the properties of electronic components such as diodes, transistors, transformers and more. Hence the scientific discipline was created Figure of Merit (FOM) which is dealing with this issue.

The proposed article will deal about the analysis of FOM of several power MOSFETs, whereby main parameters are taken into consideration for calculation purposes. In order to verify faithfulness of FOM, the parametrical simulation analysis of hard-switching commutation mode for given parameters of target application (front-end converters) will be done. Consequently, experimental measurements for determination of switching as well as conduction losses of selected transistors will be performed. The aim of simulation and experimental analysis of commutation process shall be confirmation of the accuracy of simulation models due to fact that simulation analysis can be very useful during investigation of set of suitable transistors for improvement of the qualitative indicators (rapid prototyping) of switched mode power supplies (efficiency, power density, hold-up time etc.. . .).

Almost simulation analysis represents time-consuming process for evaluation of transistor switching performance. Therefore various FOM methodologies will be described taking into account main parameters for the FOM evaluation (transistor parasites, gate charge, switching frequency, parameters of target application, e.g., voltage — current ratings). Comparisons between the amount of transistor's losses and its FOM indicator will be provided.

FoM Evaluation for Power MOSFET Transistors: The development of switching power supply significantly moved forward. Requested parameters of switched mode power supplies (SMPS) are reduction of the size and reduction of power losses (increase of efficiency). In this article we decided to analyze several methods of FOM for the power MOSFET transistors. These methods are:

- Switching FOM
- Conduction FOM
- Detailed FOM
- Johnson FOM

Selected transistors for FOM evaluation as well as for simulation and experimental analysis of hard-switching commutation mode are CoolMOS IPW60R165CP, CoolMOS, SPP20N60C3 and MOSFET IRF840. The last mentioned device represents older technology of MOSFET transistors, whereby CoolMOS transistors exhibits currently best in class performance for power applications (for example solar inverters, renewable energy, telecom/servers, front-end converters etc.. . .).

The simulation and experimental analysis as well as FOM evaluation will be made parametrically, i.e., in dependency on the parameters that are influencing hard-switching commutation mode in the most manners (switching frequency, load current).

Session 2A0
Poster Session 3

A Hybrid Trefftz Finite Element Analysis of Eigen-modes Propagating in a Holey Fiber

Yoshihito Morita, Shingo Sato, and Koji Hasegawa
Muroran Institure of Technology, Japan

Abstract— Hybrid Trefftz finite element method (HTFEM) is developed for a fast eigen-mode solver of electromagnetic waveguides with symmetric cross-sections such as photonic crystal fibers and micro-structured optical fibers. HTFEM divides the cross-sections of waveguides into Trefftz finite elements (TFEs) whose interpolation functions are fundamental solutions of vector wave equations of electric fields in infinite spaces and conventional vector finite elements (VFEs) with polynomial interpolation functions. Numerical dispersion of TFEs, therefore, is expected lower than VFE dispersion in the same element size. But complex element shape of TFEs requires more computational cost than simple element shape, HTFEs are suitable for modeling homogeneous disc and complementary disk parts of the waveguide cross-sections such as the fiber cores and jackets of holey fibers, and the remaining ring parts which include holes of the holey fibers should be divided by VFEs.

We had demonstrated advantages of HTFEM over conventional FE method with VFEs and perfect matched layers by analysis of holey fibers with six air holes: (1) HTFEM computation time of the whole cross-section of the holey fiber is shorter than the conventional FE analysis of a quarter of the cross-section at the same accuracy of the propagation constant, (2) HTFEM can analyze a quarter of the cross-section of the holey fiber under symmetric or asymmetric electric field conditions on the symmetric boundaries, and HTFEM can compute the eigen-modes faster and more accurately than the conventional FE method under the same number of total unknowns. When we compute specified eigen-modes, analysis of the whole cross-section or a quarter of the cross-section gives the propagation constants of the required eigen-modes and other eigen-modes that we should discard by inspecting the symmetry of electric field distributions.

To compute only specified eigen-modes, in this paper, we presented an HTFEM with electric field distributions restricted to the specified symmetry. We confirmed the validity of the modified HTFEs from the numerical results of a holey fiber with six air holes. The method ensures to compute only specified eigen-modes and needs no distinction by the distribution of the electric fields.

Using Microwave Radiation for Porcelain Tableware Sintering

T. Santos[1, 4], **L. Hennetier**[2], **V. A. F. Costa**[3], **and L. C. Costa**[1]

[1]Department of Physics and I3N, University of Aveiro, Aveiro 3810-193, Portugal
[2]Technological Center for Ceramic and Glass Industries, Coimbra 3025-307, Portugal
[3]Department of Mechanical Engineering, University of Aveiro, Aveiro 3810-193, Portugal
[4]CICECO, University of Aveiro, Aveiro 3810-193, Portugal

Abstract— This work presents an improved microwave multimode cavity developed for the sintering of porcelain tableware. It includes 6 magnetrons operating at 1 kW with a nominal frequency of 2.45 GHz. The way as the electromagnetic field propagates and is absorbed by the materials is very important for the control of the heating process. For a better understanding of the process, the distribution of the electromagnetic field inside the cavity was calculated using COMSOL Multiphysics software, with different magnetron configurations and sample positions. The improved automated control system comprises the usage of a pyrometer that allows the analyses of the thermal delay between the temperature given by a thermocouple and the real temperature in the material. The tip of the thermocouple lies fairly close to the material sample, approximately 1 cm from its surface, and for the maximum temperature its reading is nearly 35°C lower than the temperature measured by the pyrometer. Although this difference is not very high, it is significant to produce the bloating phenomenon. The best porcelain characteristics were achieved for sintering temperatures around 1355°C, in accordance with the industrial practice effective porcelain temperature. We exclude the existence of the so-called non-thermal microwave effect in the microwave porcelain tableware sintering.

The pyrometer was been calibrated with the thermocouple used in the experiments to guarantee the correct measurements. The calibration was been made in a conventional electric oven. Some physical properties such as the rupture energy, impact resistance and porosity of the obtained porcelain have been measured and compared with those of similar porcelain pieces obtained by conventional methods. The improved microwave oven allows a better temperature measurement, with a faster sintering (and thus higher production rates) with the same quality standards than the conventional sintered porcelain.

Design of Complex Metal-dielectric Diffraction Gratings

Alexander Lerer[1], **Stepan Vyhlidka**[2, 3], **Galina Kalinchenko**[2], **Daniel Kramer**[2], **and Bedrich Rus**[2]

[1]Physics Department of Southern Federal University
Zorge St. 5, Rostov-na-Donu 344090, Russia
[2]ELI Beamlines, Fyzikální Ústav AV ČR, v.v.i.
Na Slovance 2, 182 21 Praha 8, Czech Republic
[3]Faculty of Mathematics and Physics, Charles University, Ke Karlovu 3, Prague 2, 121 16, Czech Republic

Abstract— Mathematical and computational methods in electromagnetic theory have been attracting an increasing attention of scientific community because of recent progress in integrated photonics, metamaterials and laser optics. Better understanding of light diffraction and propagation ensures effective design of nanoscale structures. To proof a design accuracy, the same object needs to be simulated by different methods.

The majority of mathematical methods for calculation of electromagnetic fields can be split in two groups. The first group — the methods based on direct solution of wave equations with defined boundary conditions — includes finite-difference time-domain, the finite element method, and the finite integration technique. In the second group of methods, the boundary problem is reduced to the solution of integrals, the integral-differential, pairs of integrals, and pairs of sum equations. The advantage of the first group of methods is their versatility. Their disadvantages are high requirements for a computer processing power, long calculation time, the need to digitize not only the scattering object, but also the space around the scatterer, and difficulties with simulations of small-scale elements. In addition, there is a problem with satisfaction of boundary conditions for radiation to open space. For the second group of methods these problems do not exist. The choice of the integral equation (IE) type is defined by the structure of the object under investigation. Therefore, the methods based on the IE solution are not as universal as the methods in the first group, but computer programs based on them work several orders of magnitude faster. Here we compare the results obtained by commercial numerical software and self-developed analytical method.

A Volume Integral Equation (VIE) Method was developed to simulate optical wave diffraction on metal-dielectric one and two dimensional diffraction gratings based on flat multilayered structures with regular inhomogeneity in each layer. Exact solution of the equation is obtained with the Galerkin method, taking into account the complex dielectric permittivity of metals and semiconductors in optical range. The Method is applicable for s and p polarized waves.

As examples of photonic crystals we simulated sieve-looking diffraction grating placed on multilayer dielectric substrate and metal forest-looking grating placed on multilayer dielectric substrate. Dispersion characteristics with windows of opacity are found out. The results are compared to the simulations done by commercial numerical software Ansoft HFSS. Also VIE Method was applied for a design of broad-band multilayer reflective diffraction gratings for compression of high-energy ultra-short laser pulses Tolerances for groove depth and angle of incidence are estimated, optimal duty-cycle parameters are found out. Electric field distribution inside of the gratings is also numerically studied. The results were compared to the simulations by numerical Fourier Modal Method in LightTrans Virtual Lab. The methods show excellent agreement.

Comparative Study of Different Dielectric Function Fitting Model for Gold, Silver, Copper, Aluminum in Visible Bandwidth by Using PSO

Dong Liu[1, 2] and Krzysztof A. Michalski[2]

[1]School of Electrical Engineering
Southwest Jiaotong University, Chengdu 610031, China
[2]Departmentof Electrical and Computer Engineering
Texas A&M University, College station, TX 77840, USA

Abstract— FDTD is one of the most common choice used in optical device simulation. In FDTD, the dielectric value of dispersive material in a continuous frequency range must be known. Because the dielectric value are measured by experiment at discrete frequency, we need to use dielectric function fitting to find an expansion to fit the tabulated dielectric constant in a wide frequency range. There are several dielectric model widely used in FDTD method, such as Debye, Drude, Lorentz, Complex-conjugate pole-residue pair, Citical points, Rational-Fraction and Partial-Fraction models. In these models, the parameters corresponding to different material are different and unknown, so we need to use a certain method to find the suitable parameters for each material. In fact, the process of finding the suitable model parameters for selected material can be seem as a optimization problem, so the optimization algorithms is naturally used. Many local and global optimization algorithms are adopt in dielectric function fitting, such as Nelder-Mean algorithm (NM), Levenberg-Marquardt algorithm (LM), Simulated Annealing algorithm (SA), Genetic Algorithm (GA), Particle Swarm Optimization (PSO), etc.. In our work, we use PSO to optimize the parameters of different dielectric model for several common materials, such as gold, silver, copper and aluminum. The frequency range of model fitting is the visible bandwidth. The accuracy of different model with different orders on different materials are compared, and the computational time costs are also compared. For optimization algorithms, the fitness function is very important. There are several fitness functions used in dielectric function fitting and the different fitness may get different parameters with different accuracy. In this paper, we also discussed the different fitness function used by optimization algorithms and recommended a appropriate fitness function for all selected materials.

In Re Electric Switching Sense of Microwave Magnetic Field Rotation near Varactor-loaded Dipole Excited by a Plane Wave

Valery Butylkin[1, 2], **Galina Kraftmakher**[1], **and Yuri Kazantsev**[1]

[1]Kotelnikov Institute of Radioengineering & Electronics RAS, Moscow, Russia
[2]Moscow Institute of Physics & Technology, State University, Dolgoprudnyi, Russia

Abstract— It is theoretically investigated movement of the microwave magnetic field near dipole, which is excited by a plane electromagnetic wave. The total magnetic field $\vec{H}$ being the superposition of incident and scattered fields of waves is under consideration. Until now a superposition of the incident and scattered fields near dipole has been not treated because, probably, dipoles were used generally as elements of antennas and the emphasis was radiant properties. But in recent years, there has been increasing interest in studies of metastructures on basis of resonant dipoles. As an example, one can point to nonreciprocal metamaterials, containing combination of ferrite and dipole elements [1]. These metamaterials are of interest for development of microwave devices such as filters, nonreciprocal isolators and circulators. In this case microwave nonreciprocity is due to different absorption of waves whose sense of rotation of magnetic field $\vec{H}$ coincides with sense of precession of the ferrite spins, and waves possessing the opposite sense of magnetic field rotation. That is why it is important to study properties of the microwave magnetic field in the neighborhood of the dipole. In this paper it has been shown that projections of the field $\vec{H}$ of electromagnetic wave near dipole satisfy canonical ellipse equation (in general case). This field rotates in one direction at frequencies above dipole resonance (DR) and in the opposite direction below the DR. Besides senses of rotation are opposite on opposite sides of the dipole (on the right or on the left of the dipole). Fig. 1 presents time-dependent normalized magnetic field $\vec{h}(t) = \vec{H}/H_{x0}^{inc} = \vec{e}_x h_x + \vec{e}_y h_y = \vec{e}_x \cos\omega t + \vec{e}_y g\cos(\omega t + \alpha)$. Here: $\vec{e}_j$ are the orts; $g = Z_0 l^2/4\pi Z a^2$; $\alpha = \tan^{-1}[(1-\omega^2/\omega_0^2)/\omega RC]$; Z and Z_0 are impedances of the equivalent oscillator simulating the dipole and of free space; capacity C, inductance L, and resistance R of the equivalent oscillator; $\omega_0 = (LC)^{-1/2}$ and ω are the dipole resonant frequency and the wave frequency; l and a are the dipole's length and distance between the dipole and ferrite. Parameters: $\alpha = \pi/4$, $g = 1$ and 0.5.

One can see that left-handed h-field takes place at frequencies $\omega > \omega_0$ while right-handed h-field corresponds to $\omega < \omega_0$. When dipole break is loaded with varactor one can change the capacity C by application of bias voltage to varactor. It results tuning the DR. Electrically tunable DR can provide controlled sense of rotating magnetic field and, in the end, switchable nonreciprocity in metastructures ferrite/varactor loaded dipole.

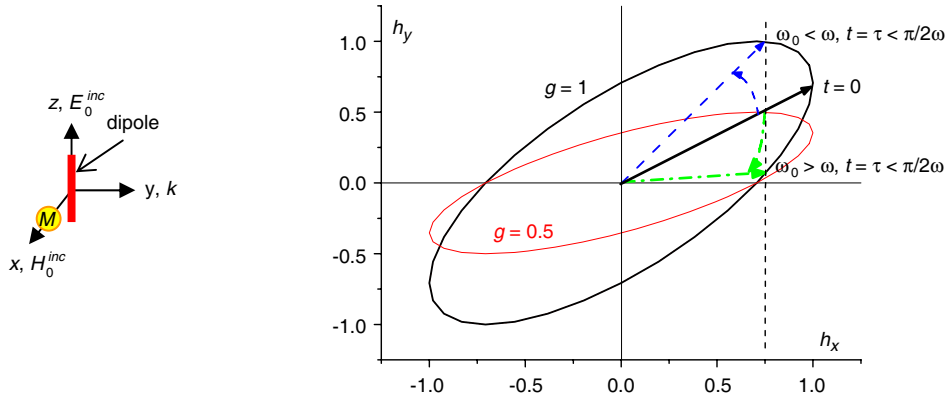

Figure 1: Disposition of dipole and ferrite with respect to incident wave and movement of normalized total microwave magnetic field h. M denotes point of location of ferrite, k, E_0^{inc}, H_0^{inc} are wave, electric and magnetic vectors of incident wave. Straight arrows depicts field h in instants of time $t = 0$ (black) and $t = \tau < \pi/2\omega$ (color). Bent arrows point sense of rotation of h. Blue lines correspond to $\omega_0 < \omega$. Green lines correspond to $\omega_0 > \omega$.

REFERENCES

1. Butylkin, V. S., G. A. Kraftmakher, and V. P. Mal'tsev, *J. Commun. Technol. Electron.*, Vol. 54, 1124–1135, 2009, http://dx.doi.org: 10.1134/S1064226909100039.

Analysis of EMG Waves from a Pulse Source

R. Kadlec, D. Nešpor, P. Fiala, and E. Gescheidtová
Department of Theoretical and Experimental Electrical Engineering
Brno University of Technology, Technická 3082/12, Brno 616 00, Czech Republic

Abstract— The authors report on an analysis of conditions on the boundary between layers having varied electromagnetic properties. The research is performed using consistent theoretical derivation of analytical formulas, and the underlying problem is considered also in view of multiple boundaries, including the effect of the propagation of electromagnetic waves exhibiting different instantaneous speed.

The paper includes a theoretical analysis and references to the generated algorithms. The main algorithm was assembled to enable simple evaluation of all components of the electromagnetic field in relation to the speed of the wave propagation in a heterogeneous environment. The proposed algorithms are compared by means of different numerical methods for the modelling of electromagnetic waves on the boundary between materials; moreover, electromagnetic field components in common points of the model are also subject to comparison.

The article describes the obstacles in comparison of different principles based analyses. Thus, analysis using numerical modelling performed via the wave equation in the ANSYS and the applied methods in the Matlab program.

When in conjunction with tools facilitating the analysis of material response to the source of a continuous signal, the algorithms constitute a supplementary instrument for the design of a layered material. Such design enables the realization of, for example, recoilless plane, recoilless transition between different types of environment, and filters for both optical and radio frequencies. This phenomenon occurs in metamaterials.

ACKNOWLEDGMENT

Research described in this paper was financed by the National Sustainability Program under grant LO1401, by the Czech Science Foundation under grant No. GA15-08803S, a project of the BUT science fund, No. FEKT-S-14-2545, and a project from the Education for Competitiveness Operative Programme, No. CZ.1.07.2.3.00.20.0175 (Electro-researcher). For the research, infrastructure of the SIX Center was used.

Propagation of Fluorescence Radiation through μ-capillary Holes of Glass Micro-channel Plate

Mikhail Mazuritskiy[1], **Alexander Lerer**[1], **Alexander Ezovtsov**[1], **and Galina Kalinchenko**[2]

[1]Physics Department, Southern Federal University, Zorge St. 5, Rostov-na-Donu 344090, Russia
[2]ELI Beamlines, Fyzikální ústav AV ČR, v.v.i. Na Slovance 2, 182 21 Praha 8, Czech Republic

Abstract— Propagation of X-rays through microcapillaries is of great interest due to the high efficiency of radiation transportation by holes of microcapillaries, and, as a consequence, due to the possibility for creation of new optical elements conditioning the X-ray beams. In addition to the high practical importance, capillary optical systems represent a fine tool for studying fundamental features of radiation dispersion by a surface.

Diffraction phenomena at the entrance of a hollow x-ray waveguide with real and imaginary parts of permittivity (absorption by dielectric cladding layers) are investigated using the model (approximation) of transmission layer on the surface of microchannels. It is shown that the wave penetrating through cladding material substantially modifies the wave field near the waveguide surface. It results in a significant increase of total energy flux inside guiding layer and leads to additional spatial modulation of the electromagnetic field.

In this work, the features of soft X-ray fluorescence spectra of radiation propagating inside microchannel plates have been analyzed in the framework of wave approximation. X-ray and fluorescence yield due to the grazing incidence reflection phenomenon have been investigated with respect to the geometry of channel walls. We discussed experimental spectra collected at the exit of microcapillaries under total x-ray reflection condition and supported them with theoretical calculations taking into account a surface transition layer at sample surface. Also, we have presented results on X-ray transmission through microcapillary structures, aimed at the Research & Development of dedicated optics working in "water window" spectral region (energy 100–600 eV). Have been studied spectroscopic features of **phenomenon of interaction of channeling radiation with unoccupied electronic states**. In the future it may allow to identify optimal transport conditions for the fluorescence radiation excited inside of microcapillary structures. The fluorescence transport conditions optimization is very important for improvement of X-ray focusing properties and, in principle, for delivery of high flux density on a sub-micrometer area of sample.

Diffraction by Arbitrary-angled Dielectric Wedges: Closed Form High-Frequency Solutions

M. Frongillo[1], **G. Gennarelli**[2], **and G. Riccio**[1]

[1]D.I.E.M., University of Salerno, Via Giovanni Paolo II 132, Fisciano (SA) 84084, Italy
[2]Institute for Electromagnetic Sensing of the Environment, National Research Council
Via Diocleziano 328, Naples 80124, Italy

Abstract— The canonical problem involving the electromagnetic field evaluation inside and outside an arbitrary-angled dielectric wedge illuminated by an incident plane wave is here addressed in the frequency domain. The use of numerical techniques represents a possible solution, but they become very expensive at high-frequency, where asymptotic methods based on ray-tracing are more efficient. Accordingly, it is valuable to have efficient solutions for the diffracted field able to compensate for the discontinuities at the Geometrical Optics (GO) boundaries related to the incident, reflected and transmitted fields in the observation regions. Uniform Asymptotic Physical Optics (UAPO) solutions were proposed in explicit closed form for evaluating the field diffracted by right-, obtuse- and acute-angled lossless dielectric wedges in the inner and outer regions [1–3]. They were able to compensate the GO discontinuities and resulted easy to handle since expressed in terms of the GO response of the structure and the transition function of the Uniform Theory of Diffraction (UTD) [4]. On the other hand, the use of a PO approximation implies inaccuracies when operating at grazing incidence and in correspondence of the dielectric interfaces.

Note that the diffraction problem concerning an acute-angled wedge was limited in [3] to a specific case of plane wave incidence.

This contribution is devoted to extend the previous analysis to all possible cases of plane wave incidence and to provide generalized UAPO solutions, which can be applied to the diffraction by a wedge with arbitrary apex angle. Such solutions include those proposed in [1–3] as particular cases and are obtained accounting for the equivalent electric and magnetic PO current densities on the internal and external faces of the wedge. Multiple internal reflections and external transmissions are considered for their explicit evaluation varying direction and polarization of the incident plane wave. Numerical tests confirm the effectiveness of the proposed UAPO solutions for the field diffracted in the dielectric wedge-shaped region and the surrounding free-space.

REFERENCES

1. Gennarelli, G. and G. Riccio, "A uniform asymptotic solution for diffraction by a right-angled dielectric wedge," *IEEE Trans. Antennas Propagat.*, Vol. 59, No. 3, 898–903, 2011.
2. Gennarelli, G. and G. Riccio, "Plane-wave diffraction by an obtuse-angled dielectric wedge," *J. Opt. Soc. Am. A*, Vol. 28, 627–632, 2011.
3. Gennarelli, G., M. Frongillo, and G. Riccio, "High-frequency evaluation of the field inside and outside an acute-angled dielectric wedge," *IEEE Trans. Antennas Propagat.*, Vol. 63, No. 1, 374–378, 2015.
4. Kouyoumjian, R. G. and P. H. Pathak, "A uniform geometrical theory of diffraction for an edge in a perfectly conducting surface," *Proc. of IEEE*, Vol. 62, 1448–1461, 1974.

Analysis and Design of a Wideband Low Phase Noise LC VCO

Xuemei Lei, Jianxin Zhang, and Jing Shi
College of Electronic Information Engineering
Inner Mongolia University, Daxuexilu, Hohhot 010010, China

Abstract— In this paper, a LC voltage-controlled oscillator (LC-VCO) design optimization methodology based on switchable capacitor array is presented. The study of the compromises between phase noise and tuning range permits optimization of the design for given specifications. According to analytical phase noise models and tuning range, it allow to get a design space map where the design tradeoffs are easily identified. The proposed VCO is designed with the proposed methodology and implemented in SMIC's 0.18-µm RF CMOS technology and the chip area is 650 µm × 500 µm including the test buffer circuit and the pads. Simulation results show that its tuning range is 36.4%, from 4.5 to 6.5 GHz The simulating phase noise is −112.8 dBc/Hz at 1 MHz offset from the 6.5 GHz carrier. The maximum average power consumption of the core part is 6.47 mW at 1.8 V power supply.

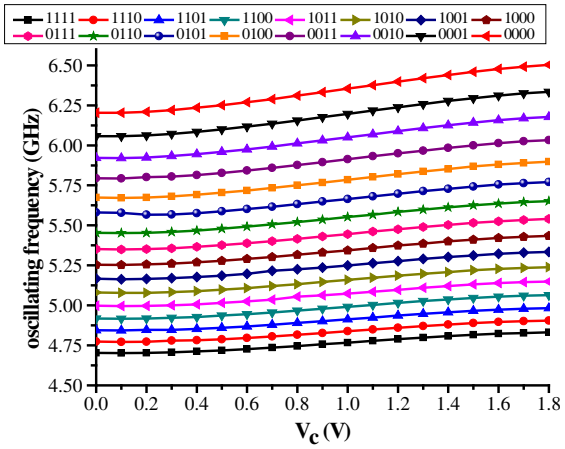

Figure 1: The simulated f-V curve of the proposed VCO.

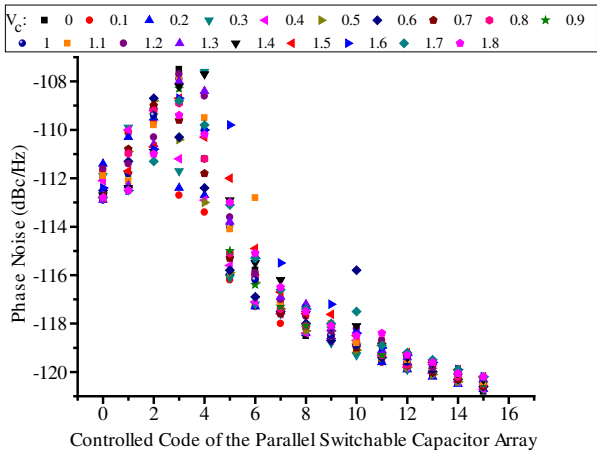

Figure 2: Simulated phase noise of the proposed VCO in different controlled code and different controlled voltage at 1 MHz offset.

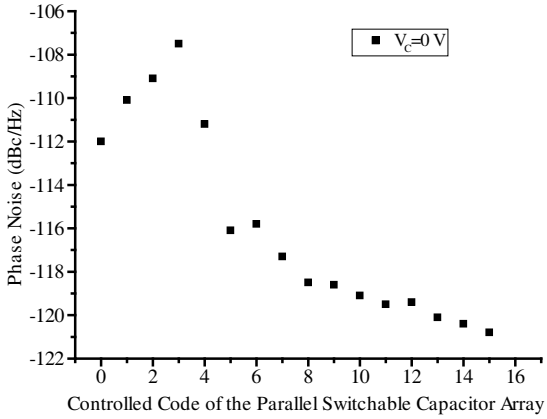

Figure 3: Simulated phase noise of the proposed VCO in different controlled code at 1 MHz offset.

Visualization of Electromagnetic Environment in Magnetic Confinement Fusion Test Facilities

Y. Kamimura[1], **S. Nakayama**[1], **and M. Tanaka**[2]

[1]Utsunomiya University, Japan
[2]National Instutute for Fusion Science, Japan

Abstract— The purpose of this study is to investigate the time varying (random and intermittent) properties of the leakage electromagnetic field that has specific broadband characteristics in the magnetic confinement fusion test facilities, and to establish worker's safety management method for particular leakage electromagnetic field (EMF) exposure. This study paid attention to the power supply room of coils and the surround of power amplifiers of ion cyclotron range of frequencies (ICRF) for plasma heating where workers may approach comparatively easily and the leakage EMF are generated. The visualization of the leakage EMF (i.e., EMF distribution measurement) has been performed using a position tracking device with IR camera of Wii-remote.

In the surrounding of the power amplifier for ICRF plasma heating, the visualization system for time varying leakage EMF distribution that had been developed recently is used [1]. In this system, two electric field meters (EMR-20 and EMR-300, Narda S.T.S.) are used. One field meter that adhered an IR marker has measured the E-field strength distribution. Another is fixed to a comparatively strong position of E-field for obtaining the time variance. The E-field strength distribution corresponding to the peak of the time-variance is obtained based on the measurement results of both meters. The leakage E-field that we measured was, however, very weak, and we can say that it hardly has potential hazard.

In the experiment in the coil power supply room, the compliance of the protection guidelines in the passage between power supply units was visualized and evaluated by the visualization system for low frequency leakage magnetic field distribution with magnetic field meter (ELT-400, Narda S.T.S.) [2, 3]. As a result, though the results of the instrument in accordance with the ICNIRP guidelines 1998 exceeded the reference level at the passage entrance between power supply units, the results by the instrument in accordance with the ICNIRP guidelines 2010 did not exceed it except the interior of the passage.

At present, the leakage EMF that exceeded the protection guideline has not been observed around the devices of ICRF plasma heating. It is confirmed that the visualization system for the low frequency magnetic field distribution can easily distinguish the compliance of protection guidelines of the leakage magnetic field in the power supply room of coils.

REFERENCES

1. Sato, K., S. Nakayama, and Y. Kamimura, "A measuring method for time-varying EM field distributions," *AP-RASC'13*, Taipei, Taiwan, EK-2, September 2013.
2. Sato, K., H. Kawata, Y. Kashimura, and Y. Kamimura, "A measurement of ELF field distributions by using freehand scanning method by Wiimote," *EMC Europe 2012*, P3-1:5, Roma, Italy, 2012.
3. Sato, K. and Y. Kamimura, "Measurement and visualization of EMF distributions," *J. Plasma Fusion Res.*, Vol. 88, No. 8, 432–436, 2012 (in Japanese).

Adaptive Beam-forming Optimization Based Hybrid PSOGSA Algorithm for Smart Antennas Systems

Ahmed Magdy[1], **Osama M. El-Ghandour**[2], **and Hesham F. A. Hamed**[1]

[1]Department of Electrical Engineering, Minia University, Minia, Egypt
[2]Department of Electronics, Communications, and Computer Engineering
Helwan University, Cairo, Egypt

Abstract— Adaptive beam-forming capabilities for smart antenna arrays are nowadays used in different applications such as suppression and reduction of interference in wireless mobile communication, besides its effects on the overall quality of service. Several optimization techniques are considered in the previous literature to deal with Adaptive beam-forming for smart antennas. Particle Swarm Optimization (PSO), Central Force Optimization (CFO), Bacterial Swarm Optimization (BSO), and Gravitational Search Algorithm (GSA) are well known Global optimization techniques that are based on a nature-inspired heuristic. Recently hybrid PSOGSA technique was proposed and showed better performance than standard PSO and GSA in terms of computational speed.

In this paper, a novel algorithm that is based on the hybrid PSOGSA technique is developed for optimal beam-forming using ULA and UCA. The goal is to maximize the beam of the radiation pattern towards the intended user or Signal of Interest (SOI) and minimize the beam of the radiation pattern towards Signal Not of Interest (SNOI) based on controlling the complex weights (phase) of ULA or UCA.

Simulation results prove the directed power in terms of normalized array factor toward the intended direction (SOI) using UCA is better than ULA by approximately more than 6 dB, 3.5 dB, and 1.5 dB for different cases, on the other hand, directed null to SNOI better than ULA by approximately 35 dB, 5 dB and 14 dB for several cases. In addition, simulations of beam-forming showed accurate results even for a big set of simultaneously incident signals. It is found that hybrid PSOGSA is more attractive for beam-forming applications and better than GSA with approximately -3 dB in average besides it was demonstrated that hybrid PSOGSA achieves fast and robust global convergence over GSA.

Semiconductor Temperature Tunable Metameterial for Terahertz Applications

K. L. Koshelev[1, 2, 3] **and A. A. Bogdanov**[2, 3, 4]

[1]Saint-Petersburg State Polytechnical University, St. Petersburg 195251, Russian Federation
[2]ITMO University, St. Petersburg 197101, Russian Federation
[3]Ioffe Institute, St. Petersburg 194021, Russian Federation
[4]The Academic University, St. Petersburg 194021, Russian Federation

Abstract— We introduce a new model of homogeneous temperature tunable THz metamaterial with controllable frequency range of hyperbolic dispersion based on semiconductor superlattice with doped quantum wells. We propose a method of thermal manipulating the shape of equal frequency surface in k-space. We discuss the phenomenon of permittivity tensor signature changing which results in transition from dielectric to hyperbolic regime of the material.

Hyperbolic metamaterials (HMMs) are one of the most developing branch of modern optics [1, 2]. HMMs represent uniaxial crystals. Dielectric function of uniaxial crystals is described by tensor with two different components corresponding to the directions along ($\varepsilon_{||}$) and across ($\varepsilon_{\perp}$) the optical axe.

Depending on the signs of these components, crystal represents a dielectric media ($\varepsilon_{\perp} > 0$, $\varepsilon_{||} > 0$), metal ($\varepsilon_{\perp} < 0$, $\varepsilon_{||} < 0$) or hyperbolic metamaterial ($\varepsilon_{\perp}\varepsilon_{||} < 0$). HMM's unique properties stem from the equal frequency surface of extraordinary waves.

We propose a new model of ultra homogeneous temperature tunable THz metamaterial based on semiconductor superlattice (SL) with doped quantum wells. Efficiency of thermal tunability is a result of high sensitivity of semiconductor conductivity to the temperature. Under term "ultra homogeneous" we mean that SL has tunnel transparent barriers and thickness of the wells is so small that that Drude-Lorentz model is inapplicable for a single layer. Here we use more accurate approach for dielectric function considering energy spectrum of carriers modified by SL potential and carrier distribution function. We show that away from interband transition and reststrahlen band each permittivity tensor component has Drude-Lorentz dispersion with modified plasma frequency:

$$\Omega_{\alpha}^2 = \frac{4\pi e^2}{\varepsilon_{\infty}} \frac{2}{(2\pi\hbar)^3} \iiint f(E,\mu,T) \frac{\partial^2 E}{\partial p_{\alpha}^2} d^3p, \quad \alpha = \perp, \| . \tag{1}$$

Here E is energy of carriers which depends on the momentum $\mathbf{p}$, $f(E,\mu,T)$ is the Fermi-Dirac distribution function, μ is the chemical potential, T is the temperature and ε_{∞} is a permittivity of the lattice without free carriers.

Tunability mechanism in proposed metamaterials is the following. Free carrier concentration and, therefore, plasma frequency of semiconductors is sensitive to the temperature in contrast to dielectrics and metals. Implementation of SL in semiconductors makes carrier spectrum and plasma frequency anisotropic. So, in SL we can distinguish plasma frequency along ($\Omega_{\|}$) and across ($\Omega_{\perp}$) the optical axis. Permittivity tensor signature and, therefore, optical properties of SL depends on the relation between frequency of the electromagnetic wave ω and plasma frequencies $\Omega_{\perp,\|}$. There are three cases corresponding to the different signatures of permittivity tensor: (i) dielectric case if $\omega > \Omega_{\perp,\|}$; (ii) hyperbolic case if ω is between $\Omega_{\perp}$ and $\Omega_{\|}$; (iii) metallic case if $\omega < \Omega_{\perp,\|}$. At fixed ω transition from one to another case can be realized by the manipulation with plasma frequencies which are easily controlled by thermal excitation.

REFERENCES

1. Poddubny, A., et al., "Hyperbolic metamaterials," *Nature Photonics*, Vol. 7, 948–957, 2013.
2. Noginov, M., et al., "Focus issue: Hyperbolic metamaterials," *Opt. Express*, Vol. 21, 14895–14897, 2013.

One-way Helical Electromagnetic Wave Propagation Supported by Magnetized Plasma

Biao Yang[1], **Mark Lawrence**[1], **Wenlong Gao**[1, 2], **Qinghua Guo**[1, 3], **and Shuang Zhang**[1]

[1]School of Physics and Astronomy
University of Birmingham, Birmingham B15 2TT, United Kingdom
[2]State Key Laboratory of Precision Measuring Technology and Instruments
Tianjin University, Tianjin 300072, China
[3]MOE Key Laboratory of Weak-Light Nonlinear Photonics
School of Physics, Nankai University, Tianjin 300071, China

Abstract— In this paper we reveal the presence of photonic one-way helical surface states in a simple natural system — magnetized plasma. The application of an external magnetic field to a bulk plasma body not only breaks time-reversal-symmetry but also leads to separation of Equi-Frequency Contour surfaces (EFCs) to form topologically nontrivial gaps in k space. Interestingly, these EFCs support topologically protected surface states. We numerically investigate an interface between magnetized plasma, using a realistic model for parameter dispersion, and vacuum, to confirm the existence of one-way scatter-immune helical surface states. Unlike previous proposals for achieving photonic one-way propagation, our scheme does not require the use of artificial structures and should therefore be simple to implement experimentally.

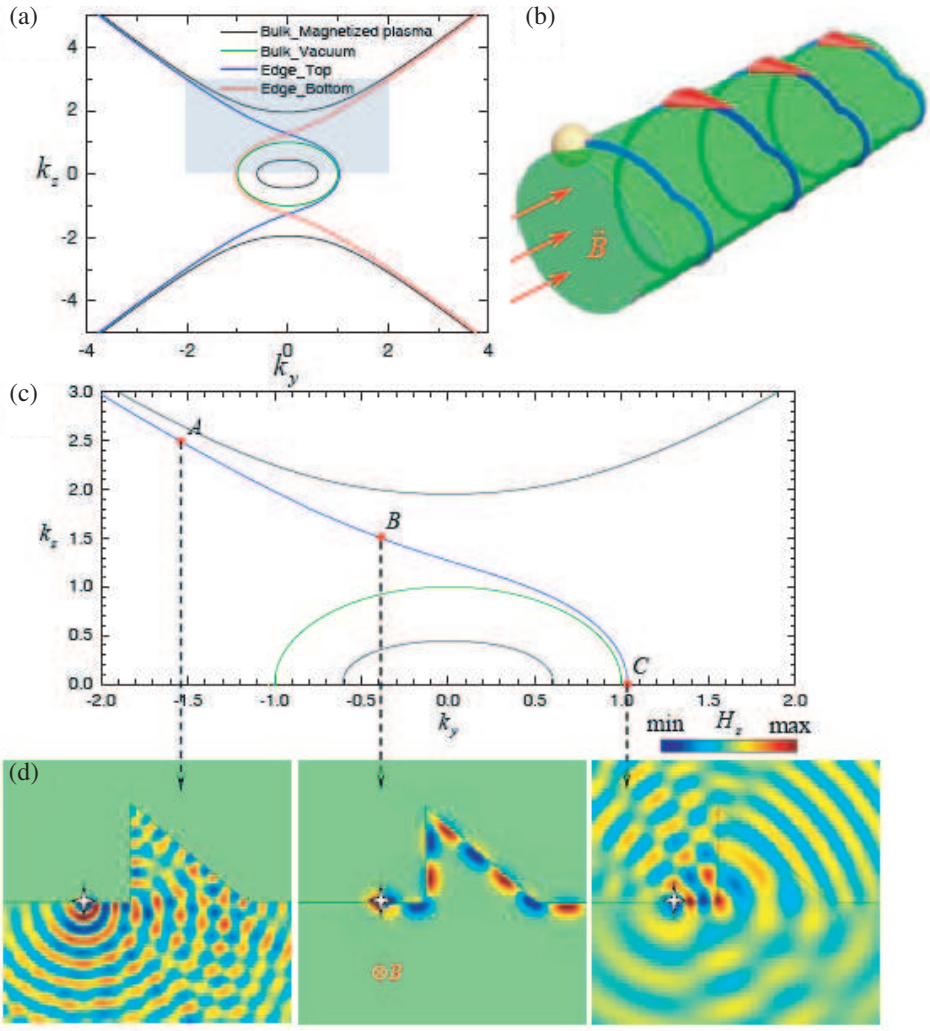

This immunity to backscattering has been confirmed using full wave simulations shown in Fig. 1(d) in which a right moving surface wave propagates seamlessly around a sharp defect. The simulation is performed in the x-y plane for three different propagation constants k_z in the shadow area as indicated by 'A', 'B' and 'C' in Fig. 1(c). For point 'A' and 'C', since they are not located in the gap region, the electromagnetic wave can be scattered into the bulk states by z-invariant scatterers. On the other hand, at point 'B' where k_z is in the middle of the gap, the surface wave is immune from scattering by the sharp edges, and therefore the numerical simulation confirms that it is a topologically nontrivial surface state. As expected, when the direction of the magnetic field is flipped, the propagation of the surface wave is also switched to the opposite direction. This may enable topological surface states with dynamically reconfigurable properties.

The Properties of Surface Plasmon Polaritons at Linearly Graded Interfaces

Dalibor Blažek[1, 2, 3], **Michael Čada**[1, 2], **and Jaromír Pištora**[1, 3]

[1]Nanotechnology Centre, VŠB — Technical University of Ostrava
17. listopadu 15., Ostrava-Poruba 708 33, Czech Republic
[2]Department of Electrical and Computer Engineering
Dalhousie University, Halifax B3H 4R2, Canada
[3]IT4 Innovations National Supercomputing Center, VŠB — TU Ostrava
17. listopadu 15., Ostrava-Poruba 708 33, Czech Republic

Abstract— Plasmonic structures are a promising solution for overcoming the diffraction limit of light and for developing novel integrated optics devices. The advantage of using semiconductors is the possibility of tuning the semiconductor properties by changing the composition and doping of a given material. The inhomogeneous structures can be prepared.

New results are reported on investigation of dispersion curves for surface plasmon polaritons (SPPs) at an inhomogenously doped semiconductor/dielectric interface whereby the dielectric is represented by the same undoped semiconductor. The doped semiconductor is described by its frequency-dependent permittivity that varies with the depth. It is shown that a transition layer (TL) with a linear change in carrier concentration supports one branch dispersion curve regardless of the TL thickness. The obtained dispersion curves reach a maximum at a finite frequency depending on the TL thickness, and subsequently asymptotically approach the zero frequency in the shortwave limit. Therefore two surface plasmon modes are supported at a given frequency: a long-wave mode with a positive group velocity and a short-wave mode with a negative group velocity. It is shown that the conventional dispersion relation for SPPs at a TL with a zero thickness is an asymptotic solution, and the convergence of real dispersion curves is point-wise instead of an expected uniform convergence.

One stationary SPP exists for each thickness of TL. However, these modes differ in their potential for coupling with external source of light. Large modal index bandwidth is necessary to be able to couple practically to the slow light mode and also to enable the efficient energy accumulation without spatial spreading. It may be concluded that the narrow TL supports stationary SPPs with better MIB, but very short wavelengths [1].

REFERENCES

1. Blazek, D., M. Cada, and J. Pistora, *Optics Express*, Vol. 23, No. 5, 6264–6276, 2015.

Noise Spectroscopy Tests in the Analysis of Materials and Periodic Material Structures

Z. Szabo[1], **P. Drexler**[1], **J. Seginak**[1], **D. Nešpor**[1], **M. Steinbauer**[1], **P. Marcoň**[1], **and P. Fiala**[2]

[1]Department of Theoretical and Experimental Electrical Engineering
Technicka 12, Brno 616 00, Czech Republic
[2]SIX VUT v Brně, Technická 12, Brno 616 00, Czech Republic

Abstract— The authors discuss the application of broadband noise signal in the research of periodic structures and present the basic testing related to the described problem. The aim is to find a metrological method utilizable for the investigation of metamaterials in the frequency range between 100 MHz and 10 GHz; this paper therefore characterizes the design of a suitable measuring technique based on noise spectroscopy and introduces the first tests conducted on a periodic structure (metamaterial). In this context, the applied equipment is also shown to complement the underlying analysis.

REFERENCES

1. Maslovski, S., S. Tretyakov, and P. Alitalo, "Near-field enhancement and imaging in double planar polariton-resonant structures," *J. Appl. Phys.*, Vol. 96, 1293, 2004.
2. Freire, M. and R. Marques, "Near-field imaging in the megahertz range by strongly coupled magnetoinductive surfaces: Experiment and ab initio analysis," *J. Appl. Phys.*, Vol. 100, 063105, 2006.
3. Machac, J., P. Protiva, and J. Zehentner, "Isotropic epsilon-negative particles," *2007 IEEE MTT-S Int. Microwave Symp. Dig.*, 1831–1834, Honolulu, USA, Jun. 2007.
4. Protiva, P., J. Mrkvica, and J. Macháč, "Universal generator of ultra-wideband pulses," *Radioengineering*, Vol. 17, No. 4, 74–79, 2008.
5. Oppenheim, A. V., R. W. Schafer, and J. R. Buck, *Discrete-time Signal Processing,* Prentice Hall, Upper Saddle River, NJ, 1999, ISBN: 0-13-754920-2.
6. Brigham, E. O., *The Fast Fourier Transform,* Prentice-Hall, New York, 2002.
7. Addisson, P. S., *The Illustrated Wavelet Transform Handbook,* 400, Institute of Physics Publishing, Bristol, 2002.
8. Bell, B. M. and D. B. Percival, "A two step Burg algorithm," *IEEE Transactions on Signal Processing*, Vol. 39, No. 1, 1991.

Supercontinuum Generation in a Silicon Nanowire Embedded Photonic Crystal Fiber

E. Gunasundari[1], **Abdosllam M. Abobaker**[2], **K. Senthilnathan**[1], **S. Sivabalan**[3], **K. Nakkeeran**[4], **and P. Ramesh Babu**[1]

[1]Photonics, Nuclear and Medical Physics Division
School of Advanced Sciences, VIT University, Vellore 632 014, India
[2]Department of Communications Engineering, College of Electronic Technology, Bani Walid, Libya
[3]School of Electrical Engineering, VIT University, Vellore 632 014, India
[4]School of Engineering, University of Aberdeen, Aberdeen AB24 3UE, UK

Abstract— The supercontinuum generation in photonic crystal fibers (PCFs) has been a topic of intense research ever since it was reported by Ranka et al.. To generate the supercontinuum (SC), the medium should at least exhibit a flat low anomalous dispersion with a small third order dispersion or zero dispersion. It is obvious that the PCFs operating near a zero dispersion wavelength (ZDW) with higher nonlinearity do not demand large input power for generating the SC. In addition, these desired conditions help smoothen the power spectra of SC. Therefore, highly nonlinear dispersion flattened PCF turns out to be the right candidate for generating SC. Nowadays, the generation of SC in photonic nanowire (PN) with sub-wavelength diameter has attracted significant interest due to its unique properties. Such a dielectric waveguide with a nanocore diameter possesses a tight mode confinement and as a result, it exhibits appreciable group velocity dispersion and nonlinearity. Very recently, a new fiber called nanowire embedded photonic crystal fiber has been introduced by exploiting the optical properties of both PN and PCF. Such a photonic device is termed as photonic crystal fiber nanowire (PCF-NW). This kind of small core PCF has been a good candidate for nonlinear applications such as soliton-effect pulse compression and SC generation In this paper, we demonstrate the supercontinuum generation in a silicon nanowire embedded photonic crystal fiber (SN-PCF) using fully-vectorial finite element method. The variation of supercontinuum is investigated by changing the fiber length, pump peak power and pump wavelength. The proposed fiber exhibits broad spectrum of more than 2200 nm within 2 mm length of fiber for peak power of 500 W of input pulse.

Design of the proposed SN-PCF and evolution of supercontinuum within a 2 mm length of SN-PCF:

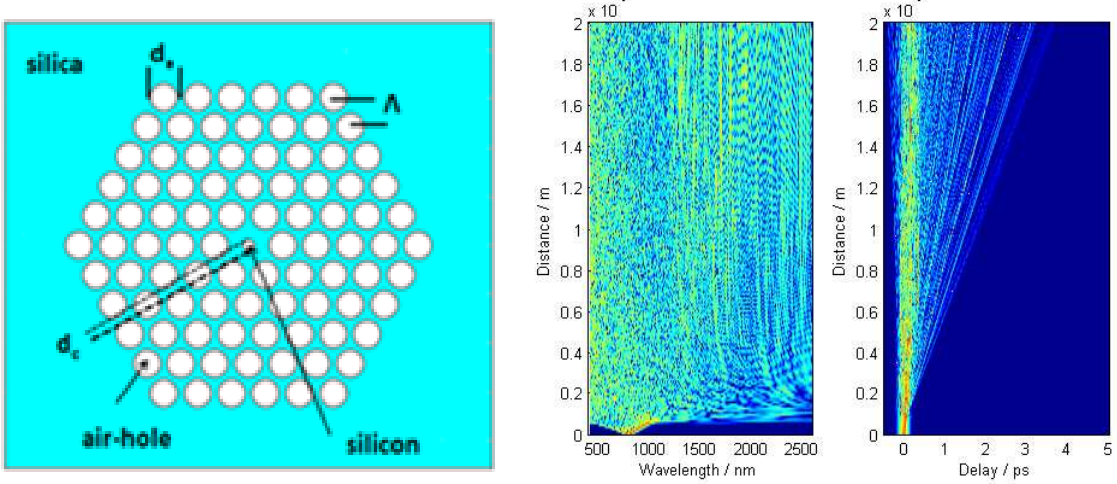

Temperature Dependence of the Equilibrium Distance in Plane-parallel Thin Films at Thermal Equilibrium

V. Esteso, S. Carretero-Palacios, and H. Míguez
Instituto de Ciencia de Materiales de Sevilla, Consejo Superior de Investigaciones Científicas
Universidad de Sevilla, Sevilla 41092, Spain

Abstract— The Casimir force, which is especially intense between materials with separation distances at the nanoscale, may be attractive or repulsive depending on the geometry, temperature and the optical properties of the materials involved [1]. By a proper choice of a set of materials and slab thicknesses, this force gives rise to nanolevitation phenomena when the gravity force is taken into account at thermal equilibrium in planar geometries mediated by fluids [2, 3]. For a given geometry, the equilibrium separation can be adjusted by fine tuning of the volume occupied by each material in systems containing thin films, bilayers, or composite matrices with small inclusions inside. In addition, the equilibrium distance depends on the temperature through the Casimir force [2].

In this work we show that temperature dependence of the Casimir force is related to the difference between the static dielectric constants ε_0 of materials involved in the system. We analyse the temperature dependence of the Casimir force in terms of the transverse electric (TE) and transverse magnetic (TM) modes for realistic plane-parallel systems that show nanolevitation phenomena at thermal equilibrium. These systems consist of a thin film of Teflon, silica or polystyrene immersed in glycerol over a silicon substrate. Since the magnetic permittivity (which defines the TE modes) for all the materials considered is assumed to be unit at all frequencies, the largest variations with temperature come from the TM modes. Moreover, by splitting these contributions into two terms, that at zero frequency and that at non-zero frequencies, we prove that the main contribution to the temperature changes of the Casimir force is related to the term at zero frequency, which explicitly depends on the static dielectric constant ε_0 (see Fig. 1). Therefore the dependence of the equilibrium separation (and thus, of the Casimir force) with temperature can be controlled through the relation of ε_0 between materials.

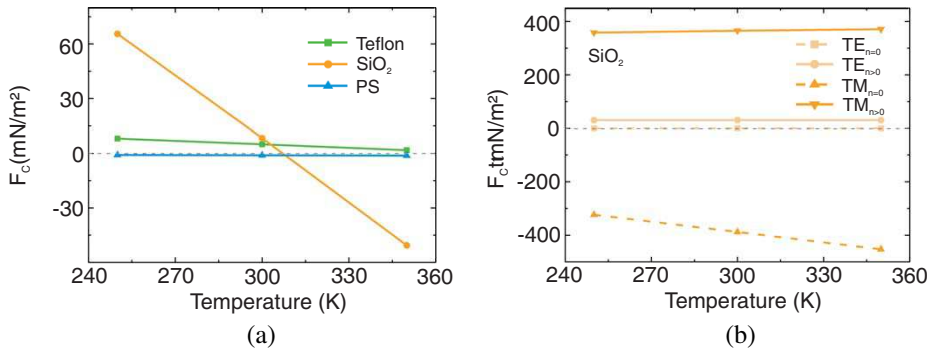

Figure 1: (a) Casimir force as a function of temperature for Teflon, silica (SiO_2) and polystyrene (PS) thin films of 500 nm thickness, at equilibrium distances 175, 60 and 450 nm, respectively, at $T = 300$ K, immersed in glycerol over a silicon substrate. (b) For a thin film of 500 nm of SiO_2, TE and TM contributions to the Casimir force for zero frequency ($n = 0$) and non-zero frequencies ($n > 0$).

REFERENCES

1. Lifshitz, E., *Sov. Phys. JETP*, Vol. 2, No. 1, 73–83, 1956.
2. Esteso, V., S. Carretero-Palacios, and H. Miguez, *J. Phys. Chem. C*, doi:10.1021/jp511851z.
3. Maofeng D., F. Lou, M. Boström, I. Brevik, and C. Persson, *Phys. Rev. B*, Vol. 89, 201407, 2014.

Dispersion Characteristics of Zinc Oxide Nanorods Organaized in Two-dimensional Uniform Arrays

A. M. Lerer[1], **P. E. Timoshenko**[1, 2], **G. A. Kalinchenko**[3], **E. M. Kaidashev**[2], **and A. S. Puzanov**[1]

[1]Physics Department, Southern Federal University, Russia
[2]Laboratory of Nanomaterials, Southern Federal University, Russia
[3]ELI-Beamlines, Czech Republic

Abstract— The propagation of electromagnetic waves in two-dimensional uniform arrays of zinc oxide (ZnO) nanorods of various diameters coated with a thin metal layer was studied by separation of variables method in cylindrical coordinates. The numerical results for single optical waveguide and two-dimensional array of waveguides are discussed in this paper. The dispersion of the dielectric constants of ZnO and metals are taken into account in the model because, as it is known, metals at optical wavelengths have a finite complex permittivity. The accuracy of results shown in this paper are ensured by comparison with results obtained by finite element method implemented in commercial software COMSOL Multiphysics, which is highly demanding to computing resources and slower than proposed method. As the advantages of finite element method may be distinguished its conservativeness, absolute stability, the possibility of constructing a finite-element approximations on unstructured grids, and calculating electrodynamic parameters of devices with complicated geometries. The dispersion characteristics calculated by finite element method are in good agreement with the results obtained by our method over all optical range and have minor deviations for the wavelength range close to the critical wavelength. Resonances located at the amplitude-frequency characteristics of optical nanoantennas may be interpreted as resonances of circular bilayer nanowaveguide segments with the ZnO core covered with thin metal shell. In this regard it is of interest to investigate the range of the optical characteristics of similar waveguides. The results may also be used to predict the resonant wavelength of two-dimensional periodic arrays of ZnO nanorods coated with a thin metal layer and grown on a dielectric substrate.

Dynamical Evolution of the Laser Linewidth at Switch-on

G. P. Puccioni[1], **N. Dokhane**[2], **and G. L. Lippi**[3, 4]

[1]Istituto dei Sistemi Complessi, CNR, Italy
[2]Department of Physics, Faculty of Science, University of M'Hamed Bougara, Algeria
[3]Institut Non Linéaire de Nice, Université de Nice-Sophia Antipolis, France
[4]UMR 7335 CNRS, France

Abstract— Experimentally, the laser response is measured by following the time evolution of the light output by a laser, whether this operates in a single- or multimode regime. Frequency-selective detection is obviously possible, but typically cumbersome and avoided when several modes are simultaneously present. Integrated spectral features are easier to implement, as they do not require the simultaneous operation of independent fast detection over several wavelengths, but can result from the simple integration (e.g., on a CCD) obtained from a dispersive device (e.g., a grating). Traditional, rate-equation-based modelling of multimode semiconductor lasers coupling the modal intensities to the carrier reservoir have hinted to the presence of pronounced oscillations accompanied by slower modal relaxations [1].

We analyse the dynamical buildup of the laser intensity starting far below threshold and ending well above threshold. The total intensity quickly grows to the well-known peak and rapidly relaxes in oscillatory fashion towards its equilibrium value, accompanied by the quadrature oscillations of the carrier density. The individual modal intensities, however, display a much slower evolution which gives rise to a very slow convergence of the spectral distribution, which — as is well-known — differs strongly below and above threshold [2].

Our analysis illustrates the evolution between the two spectral distributions [3] thus showing how modulation schemes successfully applied to single mode lasers [4, 5] also improve the transient dynmaics in multimode devices [6], as experimentally verified [7].

REFERENCES

1. Marcuse, D. and T. P. Lee, *IEEE J. Quantum Electron.*, Vol. 19, 1397, 1983.
2. Dokhane, N., G. P. Puccioni, and G. L. Lippi, "Slow dynamics in semiconductor multi-longitudinal-mode laser transients governed by a master mode," *Phys. Rev. A*, Vol. 85, 043823, 2012.
3. Puccioni, G. P. and G. L. Lippi, "Fast dynamics and spectral properties of a multilongitudinal-mode semiconductor laser: Evolution of an ensemble of driven, globally coupled nonlinear modes," *Physics Optics*, arXiv:1401.4947v1, 2014.
4. Dokhane, N. and G. L. Lippi, "Improved direct modulation technique for faster switching of diode lasers," *IEE Proc. — Optoelectron.*, Vol. 149, 7, 2002.
5. Dokhane, N. and G. L. Lippi, "Erratum," *IEE Proc. — Optoelectron.*, Vol. 150, 278, 2003.
6. Dokhane, N., "Amélioration de la modulation logique directe des diodes laser par la technique de l'espace des phases," Ph.D. Thesis, Université de Nice-Sophia Antipolis, France, 2000 (in French).
7. Hachair, X., S. Barland, J. R. Tredicce, and G. L. Lippi, "Optimization of the switch-on and switch-off transition in a commercial laser," *Appl. Opt.*, Vol. 44, 4761, 2005.

Free-running Semiconductor Laser Dynamics: The Role of the Phase Instability

L. Gil[1, 2] **and G. L. Lippi**[1, 2]

[1]Institut Non Linéaire de Nice, Université de Nice Sophia Antipolis, France
[2]CNRS, UMR 7335, 1361 Route des Lucioles, 06560 Valbonne, France

Abstract— An unusual kind of spontaneous, multimode dynamics near the threshold of a semiconductor laser has been reported approximately a decade ago [1–4]. In some devices, it is characterized by a (nearly) constant total intensity, accompanied by regular modal jumps in orderly progression from the shortest to the longest wavelength of the lasing interval, followed by a jump to the shortest wavelength and cyclical repetition over the whole spectral interval at a constant, slow frequency (typically two to three orders of magnitudes slower than the intrinsic time scales) [2, 3]. Less regular behaviour is observed in all devices [1–4], including irregular, but not entirely stochastic, jumps and a residual modulation of the total intensity. The latter remains small compared to the modulation depth for each individual mode.

A heuristic interpretation of these observations was proposed on the basis of two completely opposing assumptions: A deterministic one, where the lasing modes are coupled either through Four-Wave-Mixing [1–4], Cross-Modulation or Self-Modulation [5]; or a stochastic one where noise is projected onto the ensemble of modes [6]. Curiously, both approaches produce predictions in qualitative agreement with the observations, thus hinting at the fact that the physics underlying this phenomenon must run deeper.

Performing a new derivation of the basic semiconductor laser equations [7], without ressorting to the usual approximations, and employing codimension 2 bifurcation theory, we obtain a new model for the laser dynamics near threshold which, without the need for introducing a projection onto cavity modes, shows the existence of a phase instability [8]. Its features are those of the well-known Benjamin-Feir instability of hydrodynamics and reconcile the deterministic description with an apparently stochastic one, where the role of noise is played by the underlying turbulence.

REFERENCES

1. Yamada, M., W. Ishimori, H. Sakaguchi, and M. Ahmed, "Time-dependent measurement of the mode-competition phenomena among longitudinal modes in long-wavelength lasers," *J. Quantum Electron.*, Vol. 39, 1548, 2003.
2. Yacomotti, A., L. Furfaro, X. Hachair, F. Pedaci, M. Giudici, J. R. Tredicce, J. Javaloyes, S. Balle, E. Viktorov, and P. Mandel, "Dynamics of multimode semiconductor lasers," *Phys. Rev. A*, Vol. 69, 053816, 2004.
3. Furfaro, L., F. Pedaci, M. Giudici, X. Hachair, J. R. Tredicce, and S. Balle, "Mode-switching in semiconductor lasers," *J. Quantum Electron.*, Vol. 40, 1365, 2004.
4. Tanguy, Y., J. Houlihan, G. Huyet, E. A. Viktorov, and P. Mandel, "Synchronization and clustering in a multimode quantum dot laser," *Phys. Rev. Lett.*, Vol. 96, 053902, 2006.
5. Ahmed, M., "Numerical characterization of intensity and frequency fluctuations associated with mode hopping and single-mode jittering in semiconductor lasers," *Physica (Amsterdam)*, Vol. 176D, 212, 2003.
6. Ahmed, M. and M. Yamada, "Influence of instantaneous mode competition on the dynamics of semiconductor lasers," *IEEE J. Quantum Electron.*, Vol. 38, 682, 2002.
7. Gil, L. and G. L. Lippi, "Phase instabilities in semiconductor lasers: A codimension-2 analysis," *Phys. Rev. A*, Vol. 90, 053838, 2014.
8. Gil, L. and G. L. Lippi, "Phase instability in semiconductor lasers," *Phys. Rev. Lett.*, Vol. 113, 213902, 2014.

Terahertz Photoluminescence of Lithium Doped Silicon at Band-to-band Optical Exitation

A. V. Andrianov[1], **A. O. Zakharín**[1], **R. Kh. Zhukavin**[2], **V. N. Shastin**[2], **and N. V. Abrosimov**[3]

[1]A.F. Ioffe Physical Technical Institute, RAS, St. Petersburg 194021, Russia
[2]Institute of Physics of Microstructures, RAS, Nizhniy Novgorod 603600, Russia
[3]Leibniz Institute for Crystal Growth, Berlin 12489, Germany

Abstract— A relativity simple and cost effective terahertz (THz) emitter can be realized on the base of optical transition between the levels of shallow impurities in semiconductors. Intracenter THz radiative transition takes place during the energy relaxation of nonequilibrium carriers created in allowed band at the impact ionization of impurities by electric field [1, 2] or at the photoionization of impurity centers by infrared laser radiation [3]. Recently we showed experimentally that intracenter THz radiative transition can appear under interband optical excitation of semiconductors doped with shallow impurities centers [4, 5]. Development of THz emitter based on silicon can allow direct integration of it with silicon electronic.

Here we report on the observation of intense THz emission under the interband photoexcitation of Si(Li) at low temperatures. The experiments were curried out on the float-zone n-Si samples doped with Li during the growth with the concentration $N_D - N_A \sim 1 \times 10^{16}\,\mathrm{cm}^{-3}$. The photoexcitation was provided by a 660 nm line of a continuous wave semiconducting laser with a maximal output power of 45 mW. Laser radiation modulated at a frequency of 75 Hz with a mechanical chopper was transmitted through a series of small diaphragms and filters, preventing penetration of the laser thermal background into the experimental setup, and then focused onto the sample surface to 2 mm spot size. The spectra were measured using a step-scan Fourier spectrometer at $T = 5\,\mathrm{K}$. The THz signal was detected using a liquid helium cooled Si-bolometer and a lock-in amplifier.

The THz PL is attributed to radiative capture of nonequilibrium carriers by charged impurity centers. These charged centers appear in the crystal due to the impurity-assisted electron-hole recombination at low temperatures. Intracenter optical transitions give the main contribution to the THz emission. THz photoluminescence (PL) spectra contain lines related to optical transition from first excited donor levels to ground state of Li donor. The observed experimental regularities will be presented and discussed.

ACKNOWLEDGMENT

This work was partly supported by Russian Found for Basic Research and Special Programs of Russian Academy of Science (RAS).

REFERENCES

1. Koenig, S. H. and R. D. Brown, *Phys. Rev. Lett.*, Vol. 4, 170, 1960.
2. Andrianov, V., A. O. Zakharín, I. N. Yassievich, and N. N. Zinovév, *JETP Lett.*, Vol. 79, 365, 2004.
3. Pavlov, S. G., R. K. Zhukavin, E. E. Orlova, et al., *Phys. Rev. Lett.*, Vol. 84, 5220, 2000.
4. Andrianov, A. V., A. O. Zakharín, Yu. L. Ivanov, and M. S. Kipa, *JETP Lett.*, Vol. 91, 96, 2010.
5. Zakharín, A. O., A. V. Andrianov, A. Yu. Egorov, et al., *Appl. Phys. Lett.*, Vol. 96, 211118, 2010.

The Effect of UV Laser Irradiation and Thermal Treatment on the Luminescent Properties of Silver-containing Glasses

V. S. Leonteva, **D. A. Klyukin**, **A. I. Sidorov**, **A. I. Ignatiev**, **and N. V. Nikonorov**
ITMO University, Russia

Abstract— The aim of this work is the investigation of transformations of silver in silver-containing silicate glasses under the influence of UV laser irradiation and thermal treatment and of the influence of this transformation on luminescent properties of glasses.

The glasses of the system Na_2O-ZnO-Al_2O_3-SiO_2-NaF-NaCl with addition of Ag_2O and Sb_2O_3 were synthesized in the ITMO University. The measured glass transition temperature was $T_g = 494°C$. It was shown in [1] that such glasses contain the charged silver molecular clusters (MCs) which have a very weak visible luminescence. For laser irradiation we used third harmonic pulses of YAG : Nd (Lotis TII) with $\lambda = 355\,\text{nm}$, $\tau = 5\,\text{ns}$, $E = 2.7\,\text{mJ/cm}^2$ and $f = 10\,\text{Hz}$. The laser irradiation led to the color changes in the irradiated zone and to the orange luminescence appearance under excitation by $\lambda = 400\,\text{nm}$ (Fig. 1(a)). This effect is caused by the photoionization of glass matrix by laser radiation, by trapping of free electrons by charged silver MCs and their transformation to the neutral ones.

The thermal treatment experiments were performed at temperatures below and above T_g. The thermal treatment below T_g led to the increase of the luminescence intensity (Fig. 1(b)). This effect can be explained by the increase of the concentration of neutral silver MCs as a result of trapping electrons from charged defects of glass net and Sb ions. The thermal treatment above T_g led to the decrease of luminescence intensity in the center if irradiated zone (Fig. 1(c)), because of the formation of silver nanoparticles there. The observed effects are confirmed by the optical absorption and luminescence spectra measurements.

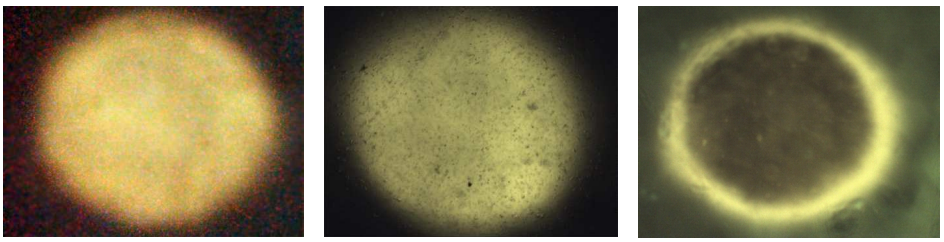

Figure 1: Luminescence of silver doped glass (a) after laser irradiation, (b) after thermal treatment below T_g, and (c) after thermal treatment above T_g. Excitation wavelength is 400 nm.

REFERENCES

1. Dubrovin, V. D., A. I. Ignatiev, N. V. Nikonorov, A. I. Sidorov, T. A. Shakhverdov, and D. S. Agafonova, *Optical Materials*, Vol. 36, 753–759, 2014.

Transmission Properties of THz Silicon Photonic Crystal Fiber

Abdosllam M. Abobaker[1], E. Gunasundari[2], K. Senthilnathan[2], S. Sivabalan[3], K. Nakkeeran[4], and P. Ramesh Babu[2]

[1]Department of Communications Engineering, College of Electronic Technology, Bani Walid, Libya
[2]Photonics, Nuclear and Medical Physics Division, School of Advanced Sciences
VIT University, Vellore 632 014, India
[3]School of Electrical Engineering, VIT University, Vellore 632 014, India
[4]School of Engineering, University of Aberdeen, Aberdeen AB24 3UE, UK

Abstract— Nowadays, the terahertz (THz) regime finds numerous applications in various important fields such as imaging, astronomy, communications, pharmaceutical quality control and security-sensitive areas, namely, monitoring drugs, explosives or weapons in a non-destructive manner and complex biological systems. In general, designing THz waveguides with low loss are essential for the successful implementation of THz systems. THz radiation lies between electronic and optical region in the electromagnetic spectrum with range of frequencies from 300 GHz to 10 THz. To date, most of the THz systems rely on free space propagation due to the virtual absence of low-loss waveguides at THz frequencies. In general, plastic, metallic ribbon waveguides and polymer PCF have demonstrated the THz guidance. These THz waveguides were fabricated by the drill and draw or stack and fuse technology.

In this paper, we design a novel photonic crystal fiber using finite element method which acts as a THz silicon waveguide. Here, the core is made of silicon material and the teflon is used in the cladding region wherein the air-holes are arranged in a triangular pattern. It is known that the silicon has excellent transmission properties compared to other guiding materials. It is known that the nonlinear index coefficient, n_2, of silicon is about 200 times larger than that of silica. The refractive index of silicon (around 3.5) is much larger than that of air which ensures a much tighter light confinement. Therefore, we study the important transmission properties, namely, group velocity dispersion, absorption coefficient, effective mode area and effective nonlinearity by varying the core diameter ($d_c = 0.6$, 0.75 and 0.9 mm) and distance between two consecutive air-holes, pitch ($\Lambda = 2$, 2.5 and 3 mm) for a wide range of frequency from 0.5 to 10 THz. The proposed THz silicon PCF exhibits three zero dispersions at 1.75, 4.8 and 7.8 THz frequencies and also report a low absorption coefficient of 10^{-4} cm^{-1} in the broad frequency region (2.5 to 10 THz). Further, we obtain a large mode area of 325000 μm^2 at 0.5 THz frequency for the core diameter of 0.9 mm and the pitch of 3 mm. These results show that the proposed THz silicon PCF would turn out to be a good candidate for THz waveguide compared to other plastic THz waveguides.

Design of the proposed SN-PCF and variations of dispersion with respect to frequency:

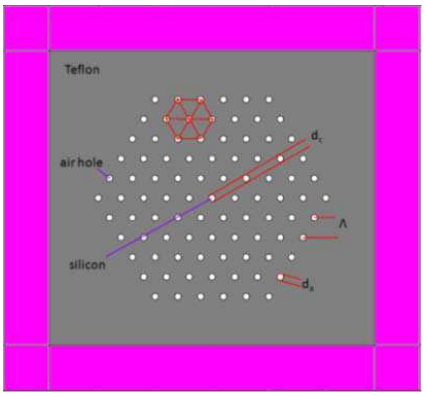

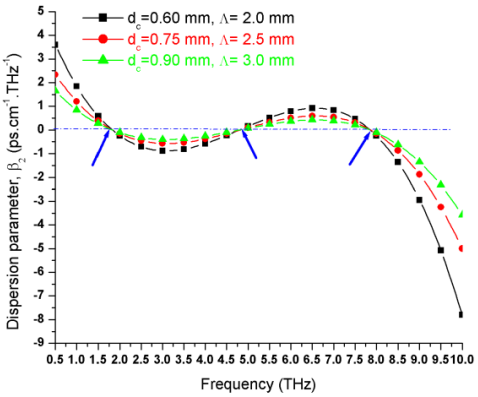

Minimally Invasive W-band Microwave Imaging

No-Weon Kang, Young-Pyo Hong, and Dong-Joon Lee
Center for Electromagnetic Wave, Korea Research Institute of Standards and Science
267 Gajeong-Ro, Yuseong-gu, Daejeon 305-340, Korea

Abstract— We present a minimally invasive microwave imaging technique for analyses of W-band transmission lines. Due to the high-frequency nature of the W-band (75 GHz–110 GHz), its power delivery generally requires millimeter-scale transmission lines. The industry-standard waveguide and co-axial schemes use WR-10 and 1.0 mm cable adaptors, as shown in Fig. 1(a). The physical dimensions of WR-10 are 2.54 mm × 1.27 mm, and 1 mm represents the outer conductor diameter of a coax adaptor. Owing to the minute embodiments of W-band mating components, mechanical precision of these components is crucial to determine the component grades. Their mating performances are usually evaluated by checking the field-transfer characteristic between mating ports. For a better characterization, it is desirable to measure the confined electric fields of each component directly, but this has not been feasible due to the finite areas of W-band components. To address this challenge, we have developed an extremely minute fiber-coupled optical probe for millimeter-wave sensing [1, 2]. The probe consists of an electro-optic wafer; its size is small enough to be directly mounted onto a bare fiber faucet. In addition, the wafer is virtually transparent to both millimeter-wave and near-infrared spectra. This probing scheme is a feasible solution to realize minimally invasive W-band imaging with (sub-) millimeter spatial resolutions. For instance, Fig. 1(a) shows the open ends of WR-10 and 1 mm-coax male connector. The minute fiber-coupled probe travels over the open ends on the x-y plane. The probe is sensitive to only certain directions, and we set it to measure the y-direction of the electric field. The field distribution, measured ∼0.3 mm above the metallic surface for the waveguide and connector, is shown in Fig. 1(b) and in the simulation illustrated in Fig. 1(c). We are currently working on imaging for on-wafer millimeter-wave calibration substrates. The field distribution over a co-planar waveguide which is launched by a 150-μm-pitch GSG probe is to be provided in a conference presentation.

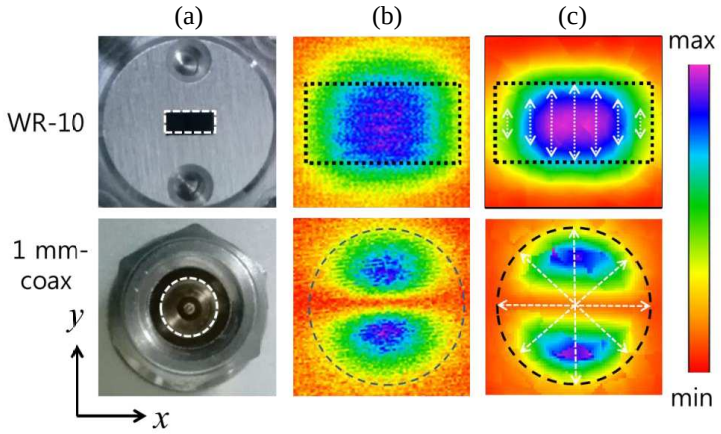

Figure 1: (a) Photograph of the W-band waveguide and coax adaptor, (b) measured electric field distribution at 94 GHz, (c) simulated electric field distribution at 94 GHz; most fields are concentrated within the dotted boundary.

REFERENCES

1. Lee, D. J., J. Y. Kwon, and N. W. Kang, "An optical-fiber-scale electro-optic probe for minimally invasive high-frequency field sensing," *Optics Express*, Vol. 16, No. 26, 21587–21597, 2014.
2. Lee, D. J., J. Y. Kwon, and N. W. Kang, "Field analysis of electro-optic probes for minimally invasive microwave sampling," *Optics Express*, Vol. 22, No. 3, 2897–2909, 2014.

Phase-stabilized Microwave Imaging Using Dual Electro-optic Probes

Young-Pyo Hong, No-Weon Kang, and Dong-Joon Lee
Center for Electromagnetic Wave, Korea Research Institute of Standards and Science
267 Gajeong-Ro, Yuseong-gu, Daejeon 305-340, Korea

Abstract— A highly stabilized electro-optic (EO) sensing technique for phase measurements in electric fields in a high-frequency transmission line is presented. For EO applications, a femtosecond mode-lock laser can be an effective source of microwave photonics, generating extremely high-order harmonics in its pulse repetition frequency [1]. These harmonic components can be utilized as a local oscillator (LO) to down-convert the radio frequency (RF) from a tested microwave device to an intermediate frequency (IF). The electromagnetic quality — especially the phase — associated with RF and LO processes directly affects that of the IF signal. The phase stability levels of both RF signals and LO signals tend to degrade rapidly at higher frequencies. The overall instability of the phase information associated with RF and LO processes can be monitored by coupling each LO and RF component with directional couplers with down-conversion to IF with a mixer [2]. However, this technique ultimately requires expensive microwave components for applications at higher frequencies. Here, we present a fairly simple and effective photonics-based technique which uses two probes to compensate for the phase drift which often occurs in high-frequency electro-optic sensing. In Fig. 1(a), one EO probe is positioned at a fixed position where strong electric fields are formed over a CPW line, while the other EO probe travels over the line on a programmed x-y plane. Both probes concurrently experience the overall phase drift associated with the unstable nature of W-band RF and LO sources. However, such phase instability can be corrected by subtracting the phases of each probe. This correction can be realized during scanning so as to provide phase-stabilized EO sensing for high-frequency microwave imaging. Figures 1(c) and (d) show electric field images of the amplitude and phase for an open-terminated CPW line at 220 GHz. A detailed experimental demonstration of the phase-stabilized imaging technique is to be provided at a conference.

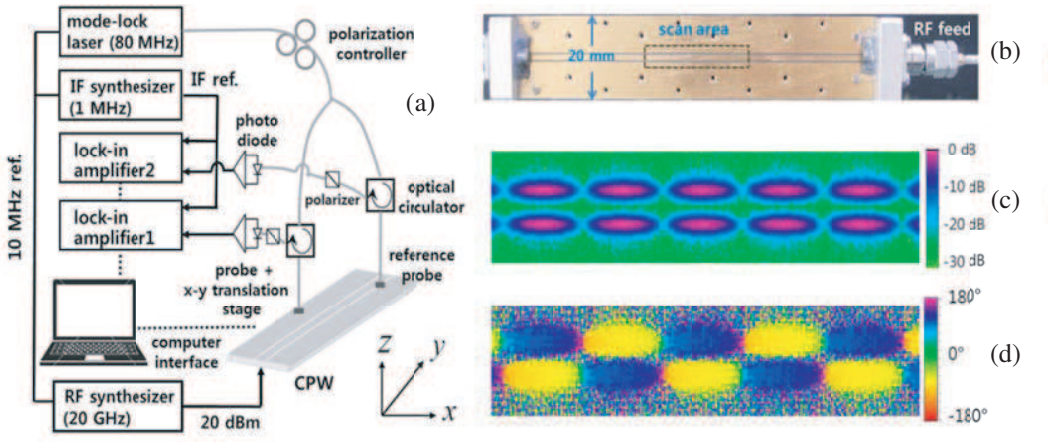

Figure 1: (a) Phase-stabilized EO imaging system, (b) CPW line for 20 GHz imaging, (c) amplitude of E-fields, (d) stabilized-phase of E-fields.

REFERENCES

1. Yang, K., L. P. B. Katehi, and J. F. Whitaker, "Electro-optic field mapping system utilizing external gallium arsenide probes," *Applied Physics Letters*, Vol. 77, No. 4, 486–488, July 2000.
2. Lee, D. J., J. Y. Kwon, N. W. Kang, J. G. Lee, aand J. F. Whitaker, "Vector-stabilized reactive near-field imaging system," *IEEE Trans. Instrumentation and Measurement*, Vol. 60. No. 7, 2702–2708, 2011.

Field-calibrated Electro-optic W-band Power Sensor

Dong-Joon Lee, **Young-Pyo Hong**, **No-Weon Kang**, **and Jae-Yong Kwon**
Center for Electromagnetic Wave, Korea Research Institute of Standards and Science
267 Gajeong-Ro, Yuseong-gu, Daejeon 305-340, Korea

Abstract— We present a photonic-assisted microwave power sensor for W-band applications. For the evaluation of W-band (75 GHz–110 GHz) power delivery, a commercial power sensor with WR-10 waveguide is a widely used solution. However, most W-band power sensors show relatively limited sensing capability; their typical maximum power handling level is ∼20 dBm with ∼40 dB dynamic range. One solution to enhance the dynamic range of a sensor is employing a photonic technology. Electro-optic (EO) sensors have served as a good alternative for microwave field sensors. The EO sensors can be fabricated in an extremely minute scheme and they can be readily coupled with an optical fiber [1]. For instance, an optical fiber-scale EO sensor is shown in Fig. 1(b). The fiber is embedded along a 0.2 mm groove at one side on a narrow wall of WR-10 aperture. The sensor tip is placed in the center of the aperture where the electric field intensity is the strongest for TE_{10} mode of rectangular waveguides. We terminated this open-end with a WR-10 power sensor as shown in Fig. 1(a). The W-band power, delivered through a WR-10 waveguide, is read through a power meter. Knowing the power levels, the electric field intensity, where the EO sensor is located, can be attained analytically. The calculated electric field strength with respect to the power in the waveguide is shown in Fig. 1(c) with a dashed line. On the other hand, the EO sensors can measure millimeter-wave electric fields associated with a femtosecond laser which is electrically synchronized with microwave sources. By virtue of such laser-electronics synchronization, the EO sensors can interact with both optical and electronic units and yield microwave signals in terms of modulated light. The data points in Fig. 1(c) are the sensor signals with respect to the power in the waveguide at 94 GHz. These values are in arbitrary unit but can be calibrated in an absolute unit. The EO sensor shows excellent linearity up to 20 dBm level as in Fig. 1(c). Because the sensor's all-dielectric embodiment, its high field sensing capability is known as ∼ MV/m scale [2]. We believe this kind of photonicCassisted power sensor would show at least 80 dB of dynamic range. We are currently trying to enhance the sensor's capability. The improved data set is to be provided at a conference presentation.

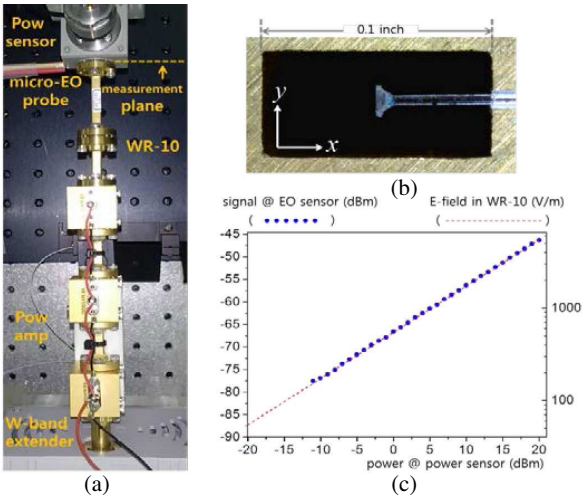

Figure 1: (a) Photonic-assisted W-band waveguide power measurement system, (b) field sensing geometry with a minute EO sensor, (c) field-calibrated performance of an EO sensor at 94 GHz.

REFERENCES

1. Lee, D. J., J. Y. Kwon, Y. P. Hong, and J. A. Jargon, "Photonic-assisted endoscopic analysis of W-band waveguide," *IEEE Photonics Society Annual Meeting*, San Diego, USA, Oct. 2014.
2. Lee, D. J., J. Y. Kwon, N. W. Kang, and J. F. Whitaker, "Calibrated 100 dB dynamic range electro-optic sensor for high power applications," *Optics Express*, Vol. 18, No. 19, 14437–14450, Jul. 2011.

Broadband Tunable Terahertz Metamaterial with Photoinduced Vanadium Dioxide Film

Shen Qiao and Yaxin Zhang
Terahertz Science Cooperative Innovation Center
University of Electronic Science and Technology of China, Chengdu 610054, China

Abstract— The composite structure of metamaterial and vanadium dioxide film is a novel way to realized active terahertz device within specific frequency band. By designing the resonant structure of metamaterial, there will be different frequency response in the applied spectrum. The vanadium dioxide is a reversible phase transition material due to its insulator-metal transition at a critical temperature or enough light intensity. Applying the photoinduced characteristics of vanadium dioxide, a dynamic resonant terahertz functional device is suggested to realize the ultrafast external spatial terahertz wave modulator. This paper carried out a broadband terahertz modulator at 0.21–0.53 THz with more than 80% modulation depth in typical frequency. In this modulator, the vanadium dioxide film is deposited on silicon substrate using sol-gel method. Then a dual-resonance metamaterial is patterned on the vanadium dioxide film using photo etching technology. Simulation results show that this dual-resonance metamaterial is a band-pass frequency selective surface with tunable band width by changing the dimensions of the split gaps and each resonance peak have its own resonant mode with different circular current. In the static test, the characteristics of the structure spectrum are performed using terahertz time-domain spectroscopy with different incident laser powers on the surface of this device. The transmission of the broadband spectrum is decreasing linearly with the increasing leaser power. The dynamic experimental result illustrate that this device realizes up to 1 MHz amplitude modulation by utilizing a 0.34 THz CW terahertz source. The simulation and experimental results show that this work may have many potential use in the design of modulators, switches, sensors, detectors and so on.

Generation Method for Bandwidth-limited Terahertz Pulses by Spectral Synthesis of Optical Comb Generated by a MZM-based Flat Comb Generator

Isao Morohashi, Takahide Sakamoto, Norihiko Sekine, Tetsuya Kawanishi, Akifumi Kasamatsu, and Iwao Hosako
National Institute of Information and Communications Technology
4-2-1 Nukui-Kitamachi, Koganei, Tokyo 184-8795, Japan

Abstract— Terahertz (THz) time-domain spectroscopy (TDS) is a powerful tool for characterization of material properties. In general THz-TDS is performed using broadband THz pulses covering up to tens of terahertz generated by ultrashort optical pulses. However, in many cases, the frequency range of interest is relatively narrow, while the high dynamic range and the high frequency resolution are required. Bandwidth-limitation of THz pulses has an advantage in terms of the power modal density. In this presentation, we propose a generation method for bandwidth-limited THz pulses by using a Mach-Zehnder-modulator-based flat comb generator (MZ-FCG).

Our approach to bandwidth-limited THz pulse generation is based on the photomixing technique, in which a single-mode and a pulsed signal are mixed on a photomixer. Picosecond pulse trains generated by the MZ-FCG are halved by an optical splitter. They are launched into optical bandpass filters (BPFs), respectively. One BPF extracts a mode (single-tone), and the other BPF extracts several modes (multi-tone), which is a pulse train elongated from the original pulse in pulsewidth. By mixing them, the optical pulse trains are down-converted to THz pulse trains. The envelope of the optical pulses is preserved to THz pulses. The carrier frequency is corresponds to the frequency difference between the center frequencies of the filters, and the pulsewidth is proportional to the bandwidth of the multi-tone signal. Merits of our system are tunability of both the center frequency and the bandwidth (pulsewidth) of the THz pulses by changing the center frequency and the pass-bandwidth of the BPF, respectively. A typical bandwidth of the comb signal is several hundred gigahertzes, so that THz pulses with the center frequency of several hundred can be generated by the MZ-FCG.

The MZ-FCG, which is composed of a dual-drive-type MZM is driven by two RF signals, converted a cw light to a flat comb. By driving the MZ-FCG with 10 GHz signals, optical combs with mode spacing of 10 GHz and the 10 dB-reduction bandwidth of 330 GHz were generated. By chirp compensation using an SMF with a length of 1.1 km, the comb signal was converted to a 2.85 ps pulse train.

The optical combs were halved by an optical splitter; one is launched into a tunable bandpass filter (TBPF1) and extracted a single-tone signal from the comb. The other is launched into another TBPF (TBPF2), and an extracted multi-tone signal. The filtered signals were coupled by another coupler, and THz pulses were measured by the OSO with the temporal resolution of 1.1 ps. As a result, THz pulse trains were successfully observed. By tuning the center frequency and pass-bandwidth of TBPF2, tunabilities on frequency and bandwidth were also demonstrated.

Collapse of Nonlinear Terahertz Pulses in n-InSb

C. Castrejon-Martinez, V. Grimalsky, S. Koshevaya, and J. Escobedo-Alatorre
CIICAp, Autonomous University of State Morelos (UAEM)
Av. Universidad 1001, Cuernavaca, ZP 62209, Mor., Mexico

Abstract— The radiation of the terahertz (THz) range $f = 100\,\text{GHz}$–$30\,\text{THz}$ is used in spectroscopy, medicine, scanning, and environmental science. The interaction of THz radiation with narrow-gap semiconductors like n-InSb, n-InAs, and low dimensional structures is of great interest, because it gives a possibility to create both active and passive electromagnetic and electronic devices.

In the report there are investigated nonlinear electrodynamic phenomena in a volume narrow-gap semiconductor n-InSb $f \sim 1$–$5\,\text{THz}$. The nonlinearity of electron gas due to the Kane dispersion law is dominating here. The equation for the amplitude, which is slowly varying with respect to time only, has been derived. The dependence of the wave amplitude on the longitudinal coordinate z and the transverse one ρ is arbitrary. The saturation of nonlinearity is taken into account. Under a propagation of THz transverse limited electromagnetic pulses through the structure intrinsic InSb-n-InSb-intrinsic InSb with the electron nonlinearity both the longitudinal and transverse focusing occurs. This leads to the spatiotempotal collapse, or the formation of the electromagnetic wave bullets from the input pulses. The influences of the wave dissipation and the saturation of nonlinearity on the nonlinear wave dynamics are important. The optimum conditions for realizing wave collapse have been obtained for the carrier frequencies, transverse sizes of the input pulses, the input intensities, and the wave dissipation. A comparison with the layered structures that include the 2D graphene sheets or thin n-InSb layers jointly with linear dielectric ones is given.

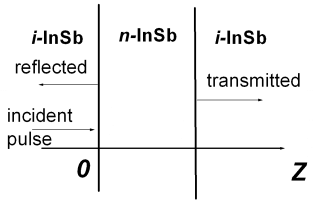

Figure 1: Geometry of the problem.

A Novel Dual-band Dielectric Resonator Antenna for WLAN Applications

Jwo-Shiun Sun, Chi-Yeh Kan, Hung-Wen Liu, Guan-Pu Pan, and Tsung-Lin Li
Department of Electronic Engineering, National Taipei University of Technology, Taipei, Taiwan

Abstract— A novel dual-band dual-polarized dielectric resonator antenna (DRA) is proposed to utilize a T-shaped slot with high isolation between two input ports to reduce the coupling effect between the excited modes. The proposed DRA offers measured impedance bandwidth for WLAN-802.11b (2400–2484 MHz) and WLAN-802.11a (5725–5825 MHz) applications with the peak gain 5–8.65 dBi. Simulated results of the return loss, isolation and gain of the DRA get fairly good agreement with those experimental ones.

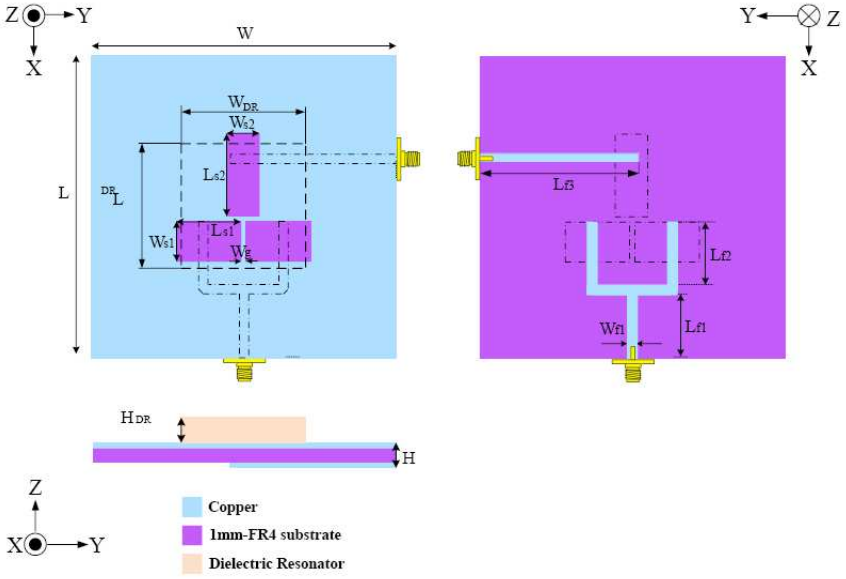

Triple-band MIMO Antenna with Proximity Coupling Radiators

Jwo-Shiun Sun[1], **Chi-Yeh Kang**[1], **Han-Sheng Fang**[1], **Po-Yen Lin**[1], **and Ching-Song Chuang**[2]

[1]Department of Electronic Engineering, National Taipei University of Technology, Taipei, Taiwan
[2]Department of Electronic Engineering, Lunghwa University of Science and Technology, Taoyuan, Taiwan

Abstract— This paper presents a triple-band mobile wireless MIMO antenna that meets GSM900/1800 and LTE2600 bands protocols. The antenna element is designed with three individual resonant Planar Inverted-L Antennas (PILs) with proximity coupling structures. The highest band is generated by the inverted-L structure fed by a transmission line, and the other two bands are produced by two meander lines, for which one is a coupling PIL construction for the lowest band and a parasitic element is located on the backside of the circuit board for the middle band. The MIMO antenna consists of two symmetric antennas with edge-to-edge separation of nearly one-tenth wavelength of the lowest band. The rectangular slot on the ground plane is implemented to enhance the isolation for the highest band, and the winded microstrip line inserting in the rectangular slot serves the purpose of isolation for the lowest band. Good isolation in middle band is achieved by its tilt unsymmetrical radiation pattern. The MIMO antenna measurement results show good impedance matching with low mutual coupling. The Envelope Correlation Coefficient is calculated to verify that the proposed antenna is suitable for wireless mobile applications.

A Planar Dual-band Antenna for WLAN MIMO Application

Li Ju Chen and K. H. Lin
National Sun Yat-Sen University, Kaohsiung, Taiwan

Abstract— A Multiple Input Multiple Output (MIMO) system has been one of the most promising wireless technologies for broadband communication systems. A planar dual-band antenna for WLAN MIMO application is proposed. The proposed antenna covers two operation frequencies at 2.4 GHz–2.5 GHz and 5.15 GHz–5.85 GHz for WLAM applications. To have good isolation between the antennas is difficult due to both strongly coupled between two and coupling currents of the surface in the ground plane. The mutual coupling increases the envelope correlation of the two ports and reduces the radiation efficiency.

The configuration of the proposed MIMO antenna was presented in Fig. 1. The MIMO antenna has two planar pitch antennas with slot on the top side and a notch filter on the bottom side. Fig. 1(a) shows the top view of the antenna and Fig. 1 (b) shows the bottom view of the antenna. The proposed antenna was implemented on the single layer FR4 substrate with a volume of 50 mm × 35 mm × 0.8 mm and relative permittivity of 4.4. Two symmetry antennas are placed at the top edge of the system ground. The dimension for the antenna is 17.5 mm × 14.5 mm. The dimension parameter is shown in Fig. 1 as well. The width of the feed line is 2.2 mm and the length of feeding line is 18 mm.

In order to improve the isolation at the lower band, a notch filter with meander line design was added at the bottom side. The dimensions of the notch filter are shown in Fig. 1(b). The simulation result of return loss (S_{11}) and isolation (S_{21}) were shown in Fig. 2. The return loss for proposed antenna covers 2.4 GHz–2.5 GHz and 5.15–5.85 GHz. The return loss is below −10 dB at two operation bands. The proposed MIMO antenna has the isolation of about 16 dB at the lower band and over 15 dB at the upper band. The proposed antenna provides two pass bands for dual-band application and also has good isolation between two single antennas for MIMO application.

Figure 1: The proposed design of dual-band antenna for MIMO application. (a) Top view. (b) Bottom view.

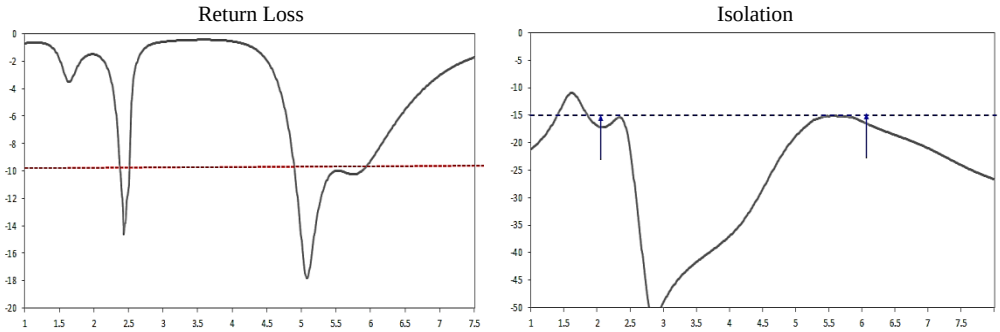

Figure 2: The simulation result for return loss and isolation.

Resonant Antenna Design Employing Equivalent Circuit Mode

Cheng-Nan Hu, Siam-Chen Huang, Jhih-Neng Yang, and Jen-Kai Hong
School of Communication Engineering, Oriental Institute of Technology, New Taipei 22061, Taiwan

Abstract— Utilization of the equivalent circuit model has shown more time-effective for designing RF circuits and antennas rather than Electromagnetic fields analysis. This study investigates equivalent circuit perspective on designing the resonant antenna. An equivalent π-network circuit is firstly proposed and de-embedded by using even-odd mode analysis to approach the electromagnetic fields coupling of a closely coupled two-element diversity antenna. Thus, the improvement on the isolation between antennae can be straightforward achieved by employing resonant and absorption method. Numerical and experimental study are presented herein.

Flexible PIFA Antenna Design for Wireless Sensor Networks in Wearable Healthcare Applications

I. Gil and R. Fernández-García
Departmentof Electronic Engineering
Universitat Politècnica de Catalunya, 08222 Colom 1, Terrassa, Spain

Abstract— In recent years, the Wireless Sensor Networks (WSNs) [1] have emerged as a communication technology to address applications such as healthcare monitoring, environmental sensing, industrial monitoring, etc.The WSNs consist of small communication nodes containing a sensing part, a microcontroller, communication components and a battery. Wearable WSN healthcare applications require compact size and optimized radiation patterns [2] and, therefore, antenna design play a fundamental role incustomized designs.The planar inverted-F antenna (PIFA) is a common antenna for portable devices because of its excellent balance between low-profile, low-cost and performance [3].

In this work an optimized PIFA including the textile and human skin effects has been designed, simulated and characterized for wearable WSN healthcare applications. The proposed PIFA has been designed by means of the commercial *Keysight Advanced Design Systems and Momentum* software.Fig. 1(a) shows the proposed substrate based on the implementation of the flexible PIFA in the commercial Pyralux (dielectric constant $\varepsilon_{rP} = 4.6$, thickness $h_P = 50\,\mu\text{m}$). A textile layer ($\varepsilon_{rT} = 2$, $h_T = 1\,\text{mm}$) has also been considered to emulate the outfit impact on the antenna. Finally, the human skin has been included as the lowest layer in the substrate ($\varepsilon_{rS} = 39$, $h_S = 1.5\,\text{mm}$) [4]. The antenna has been designed to operate under the Bluetooth 4 standard (2400–2483.5 MHz). The optimized PIFA ($20 \times 26\,\text{mm}^2$) considering the overall substrate is illustrated in Fig. 1(b). The antenna return losses (S_{11}) for several steps with regard to the optimization design process are depicted in Fig. 1(c). An original PIFA meandered antenna has been designed at the operation frequency in Pyralux substrate. Obviously, the introduction of the textile and skin layers increases the overall dielectric constant and, therefore, a reduction in the radiation frequency is expected. The redesigned antenna performance correspond to 300 MHz bandwidth at $S_{11} = -10\,\text{dB}$ and a maximum return losses of $-18\,\text{dB}$.

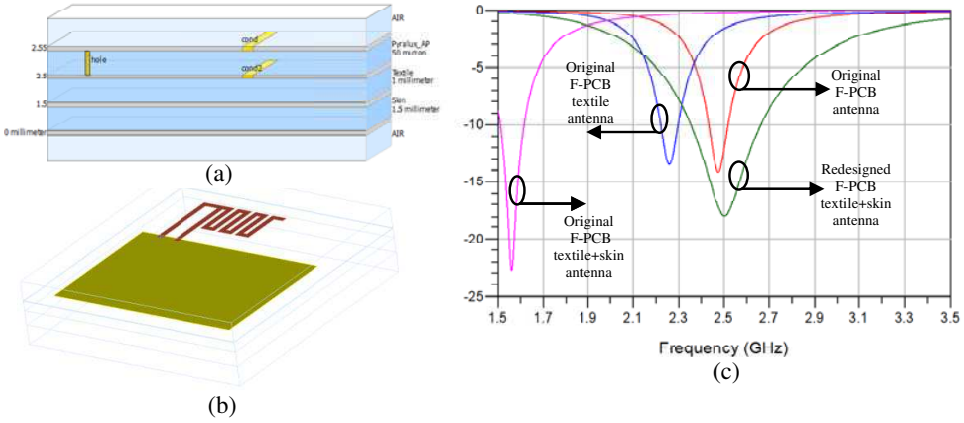

Figure 1: (a) Antenna return losses. (b) Substrate including F-PCB, textile and skin effects. (c) Redesigned PIFA antenna.

ACKNOWLEDGMENT

This work was supported by the Spanish Government-MINECO under Project TEC2013-41996-R and AGAUR 2014 SGR 375.

REFERENCES

1. Akyildiz, I. F., T. Melodia, and K. R. Chowdury, "Wireless multimedia sensor networks: A survey," *IEEE Wireless Communications*, Vol. 14, No. 6, 32, 39, December 2007.
2. Kan, Y.-C. and C.-K. Chen, "Analysis of the inverted-F antennas integrated on the displacement detector for wireless sensor network applications," *Asia Pacific Microwave Conference*, 1849–1851, 2009.

3. Wong, K. L., *Planar Antennas for Wireless Communications*, John Wiley & Sons Inc., 2003.
4. Shrestha, S., M. Agarwal, P. Ghane, and K. Varahramyan, "Flexible microstrip antenna for skin contact application," *International Journal of Antennas and Propagation*, Vol. 2012, 1–5, June 2012.

Dual-band Printed Antenna for WLAN Applications

Lanchao Zhang, **Tao Jiang**, **and Yingsong Li**
College of Information and Communication Engineering, Harbin Engineering University
Harbin 150001, China

Abstract— A dual-band printed antenna for wireless local area networks (WLAN) applications is presented in this paper. The proposed antenna is printed on a FR4-epoxy substrate with a dielectric constant of 4.3 and an overall size of $40 \times 40 \times 1.6\,\mathrm{mm}^3$. The antenna consists of two strips which locate at the top and bottom sides of the substrate respectively. The top one is fed by a $50\,\Omega$ microstrip line directly, and operates in 5.8 GHz band. The bottom is fed by the coupling current and operates in 2.4 GHz band. The two strips have overlapping parts in space, which have a good effect on improving impedance matching and expanding the bandwidth. Good return loss is achieved, higher than 25 dB in the low frequency band and 20 dB in the high frequency band respectively. It is shown that the proposed antenna is suitable for WLAN applications.

Compact Reconfigurable Antenna Design Based on Variable Capacitive Loading

Youngkyu Kim[1], **Seok-Jae Lee**[1], **Jongsik Lim**[1], **Dal Ahn**[1], **Jin-Ho Ahn**[2], **Seung-Hwan Lee**[3], **and Sang-Min Han**[1]

[1]Soonchunhyang University, Asan, Chungnam 336-745, Republic of Korea
[2]Hoseo University, Asan, Chungnam 336-795, Republic of Korea
[3]Electronic Telecommunication Research Institute (ETRI), Daejeon 305-700, Republic of Korea

Abstract— A planar frequency reconfigurable antenna is proposed with variable capacitors. The proposed one is designed of a planar monopole antenna with a controllable load as shown in Fig. 1. Resonant frequencies are adjusted by variable capacitive loading of a varactor diode [1]. To achieve compact design, the monopole is designed with meander shape, while the bias circuit isolates between RF and DC paths. For the performance analysis, the equivalent circuit has been constructed with a variable capacitor using the Agilent ADS [2]. In addition, electromagnetic (EM) simulation is conducted using the ANSYS HFSS. The proposed antenna has been implemented on an epoxy substrate with a size of $32 \times 35 \times 1\,\text{mm}^3$. The implemented frequency variable monopole antenna has been verified by comparing prototypes with designed capacitors and ones with biased varactor diodes. The experimental results show expected resonant frequencies corresponding to loading capacitors as shown in Fig. 2. Moreover, the measured radiation patterns keep almost the same shape and performance for variable resonances. The proposed antenna has presented the resonant frequency variations from 2.25 GHz to 2.42 GHz.

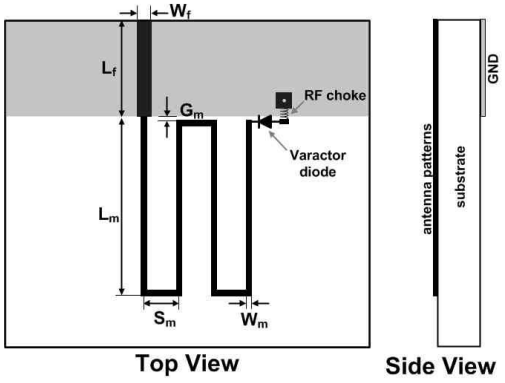

Figure 1: Proposed antenna configuration.

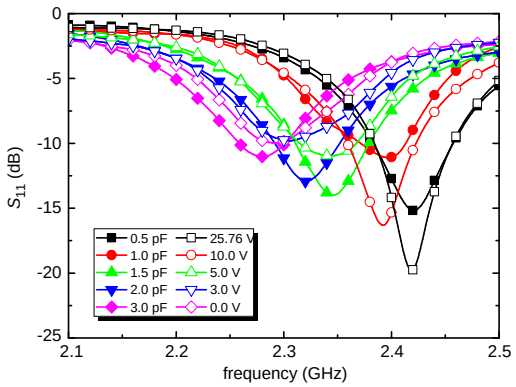

Figure 2: Freq. reconfigurability for variable loads.

REFERENCES

1. Yang, S.-L. S., et al., "Frequency reconfigurable U-slot microstrip patch antenna," *IEEE Antennas Wireless Propag. Lett.*, Vol. 7, 127–129, Jul. 2008.
2. Hosono, R., et al., "An equivalent circuit model for meander-line monopole antenna attached to metallic plate," *Proc. Int. Symp. Antennas Propag.*, 1421–1424, Nov. 2012.

Unequal Power Divider Using Series RC Circuit for Improved Isolation

Young Kim[1], **Seok-Hyun Sim**[1], **and Young-Chul Yoon**[2]

[1]Kumoh National Institute of Technology, Republic of Korea
[2]Catholic Kwandong University, Republic of Korea

Abstract— This paper presents a high dividing ratio unequal power divider with improved isolation using a series RC circuit. To improve isolation, we used an isolation component composed of a series resistor and capacitor circuit. This circuit is placed at an arbitrary position in the quarter-wave transmission line to achieve power division. In addition, to achieve a high dividing ratio, the low impedance line is composed of a capacitive loaded transmission line with slow-wave characteristics. To validate the performance of the proposed unequal power divider, we simulated and fabricated the unequal power divider for an operating frequency of 1 GHz. The experimental results are in good agreement with the simulated results.

Microwave Amplifier Design for Solid State Radar Transceivers at X-band

T. J. Korfiati[1], E. A. Karagianni[2], Ch. N. Vazouras[2], Ch. C. Lessi[1], and N. K. Uzunoglu[3]

[1]Department of Informatics and Telecommunications
National and Kapodistian University of Athens, Panepistimioupoli, Athens 15784, Greece
[2]Department of Naval Sciences, Hellenic Naval Academy
Hatzikyriakou Avenue, Piraeus 18539, Greece
[3]Department Division of Information Transmission Systems and Material Technology School of Electrical and Computer Engineering National Technical University of Athens
Zografou Campus Heroon Polytechniou 9, Zografou 15780, Greece

Abstract— The next generation of military, civilian, and commercial radar transmitters (T/R) would rely on various distributed architectures employing solid state power amplifiers (SSPA) using gallium nitride (GaN) device technology that promise to play an important role. These devices can support systems with higher sensitivity, increased detection range and improved reliability with lower cost and weight. The GaN Monolithic Microwave Integrated T/R Circuit (MMIC) enables improved resolution and DC power distribution efficiency in Radar Systems. The first challenge for the T/R module that is presented in this paper is fitting all the components in a package designing a suitable amplifier. The analytical structure followed to create amplifier bias circuits is presented in this paper. A discrete GaN on SiC HEMT was used. Incorporating matching circuits to bias circuits, various simulations are extracted to find what bias circuits do not affect the overall behavior of the amplifier. Simulation results show good matching $S_{11} = -12.2\,\text{dB}$, $S_{22} = -14\,\text{dB}$ and a gain value at 15.4 dB, almost the maximum supported. With new values S parameters resulting from the design of this circuit, $K = 1.3$ and $D < 1$ which mean that the circuit is stable. In this paper, the single stage X-band amplifier design which uses only one MMIC amplifier has an excellent performance at 10 GHz and can be utilized in Solid State T/R module for advanced Phased Array Radar Systems.

Microwave Dielectric Properties of $(Bi_{1-x}Eu_x)NbO_4$ Ceramics

S. Devesa, **M. P. Graça**, **and L. C. Costa**
I3N and Physics Department, University of Aveiro, Aveiro 3810-193, Portugal

Abstract— Bismuth-based dielectric ceramics are well known as low-firing materials and have been studied for applications as multilayer capacitors. Various attempts have been undertaken to improve the dielectric properties of $BiNbO_4$, such as the addition of oxides or the substitution of bismuth by lanthanides.

In this work, $(Bi_{1-x}Eu_x)NbO_4$ ($x = 0.00$, 0.05, 0.10, 0.20 and 0.50) samples were prepared using the sol-gel method through the citrate route.

The solution was dried at 400°C for 48 h to evaporate the solvent and the obtained powders were thermally analyzed by differential thermal analysis.

The fine particles were pressed into cylinders and then treated at six different temperatures, between 400 and 1150°C, using a dwell time of 4 h, with a heating rate of 5°C/min. This heat treatments were performed in agreement with the differential thermal analysis results.

The structure was studied by X-ray diffraction and the morphology by scanning electron microscopy.

The measurement of the complex permittivity was made using the small perturbation theory, with a cavity operating in TE_{01n} mode, at resonant frequency of 2.7 GHz.

In this method, the resonance peak frequency and the quality factor of the cavity, with and without a sample, can be used to obtain the complex dielectric permittivity of the material. We measured the shift in the resonant frequency of the cavity, Δf, caused by the insertion of the sample, which can be related to the real part of the complex permittivity, ε', and the change in the inverse of the quality factor of the cavity, $\Delta(1/Q)$, which gives the imaginary part, ε''.

The inclusion of europium allowed an increase of the complex permittivity and a decrease of the dielectric losses.

THz Generation of Bloch Oscillators from SiC Structures due to Strong Electric Fields

V. I. Sankin, A. V. Andrianov, A. G. Petrov,
S. S. Nagalyuk, P. P. Shkrebiy, and A. O. Zachar'in
Ioffe Institute, 26 Politekhnicheskaya, St. Petersburg 194021, Russia

Abstract— In this work the experimental and theoretical studies of the THz electroluminescence (EL) were carried out on SiC natural superlattices (NSL) structures of 4H-SiC, 6H-SiC and 8H-SiC polytypes [1] at $T = 5$–10 K. Figures 1(a), 1(b), 1(c) show typical THz EL spectra for the 8H-, 6H- and 4H-structures. The results of experimental measurements can be summarized as follows: i) When electric field applied to natural SL exceeds certain threshold value single THz emission line appears in the spectra. The frequencies of these lines demonstrate increasing linear dependence on applied voltage. An integrated THz emission is linearly polarized along an axis of natural SL with polarization degree above 50%. For the polytypes 8H-, 6H-, 4H-SiC threshold electric fields required for observation of THz emission are 50, 85 and 170 kV/cm respectively. The current through the structure is proportional to a voltage in the degree 5/2 [2]. The THz emission peaks for hexagonal polytype family 8H-SiC, 6H-SiC, and 4H-SiC are located in accordance with increasing of the miniband width value [2]. These results are the first unambiguously demonstration of the Bloch Oscillation regime. ii) As is seen, new emission line at about 12.5–13 meV appears at higher electric fields and currents in the spectrum of the THz emission from 8H-, 6H- and possibly from 4H-SiC structures. We attribute this line to electron optical transitions between several Wannier-Stark ladders in the slightly higher second minimum due to current injection from n^{++}-n^{-} junction of n^{++}-n^{-}-n^{+} structure to this minimum. The THz emission power about 40 μW is a well basis for development of electrically tuned emitters with frequency 1.2–3 THz.

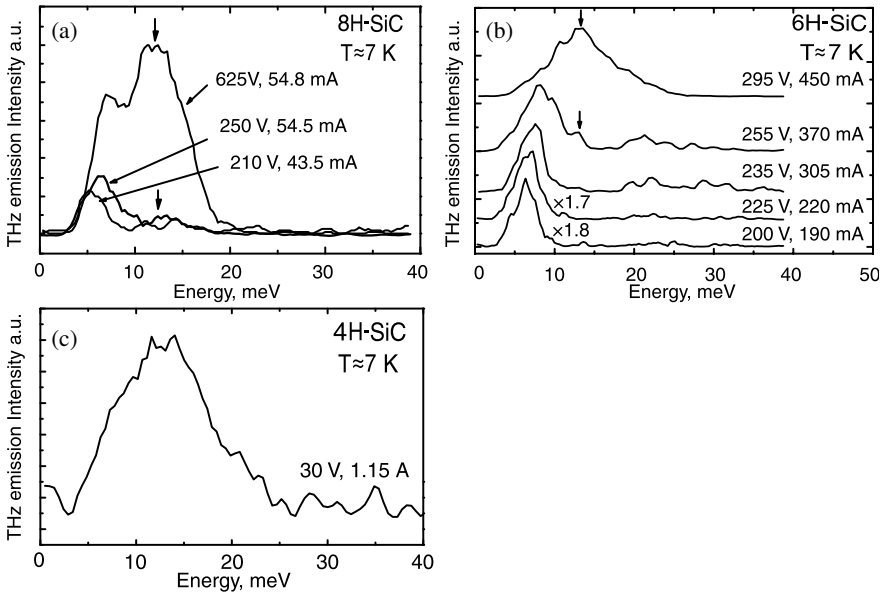

Figure 1: THz EL spectra of the structure with NSL (a) 8H-SiC, (b) 6H-SiC, (c) 4H-SiC.

REFERENCES

1. Verma, A. R. and P. Krishna, *Polymorphism and Polytypism in Crystals*, Wiley, New York, 1966.
2. Sankin, V. I., et al., *Appl. Phys. Lett.*, Vol. 100, 111109, 2012.

Electromagnetic Emission Analysis of a Multiband EMI Filter Based on Sub-wavelength Resonators

J. M. Ruiz[1], **I. Gil**[2], **and M. Morata**[1]

[1]Escuela Universitaria Salesiana de Sarriá, Psg. Sant Joan Bosco 74, Barcelona, E-08017, Spain
[2]Department of Electronics Engineering, UPC Barcelona Tech, Colom 1, Terrassa, E-08222, Spain

Abstract— The increasing pollution of the electromagnetic emissions requires the design of electronic systems which are immune to electromagnetic interferences (EMI) and, more specifically, to radiofrequency interference (RFI). Recent developed solutions in order to reduce the cost and dimensions of conventional EMI filters consisting of strategies based on sub-wavelength resonator have been proposed [1]. However, these structures can provoke electromagnetic emissions that can affect to the nearly electrical components. This fact is especially critical in small electronic devices where analogue, digital and RF signals coexist in a reduced area, such as wireless sensor networks motes. In order to determine if metamaterial resonators can be used as EMI filter on these small electronic devices, in this paper the electromagnetic emission of sub-wavelength EMI filter based on SRR and CSRR resonator has been analysed by means of near E and H fields simulation with the FDTD SEMCAD [2] software. Fig. 1 shows the designed filter [3]. The target bands are 900 MHz (RFID UHF), 1.8 GHz (GSM) and 2.4 GHz (ISM, Instrumentation, Scientific and Medical). A 3-stages/5-stages rejection band filter was designed and fabricated in a PCB. The preliminary simulation results (Fig. 2) show that the more significant emissions take place at higher frequencies, the 1.8 GHz GSM band and ISM band (2.4 GHz) and are located at the resonators' surface.

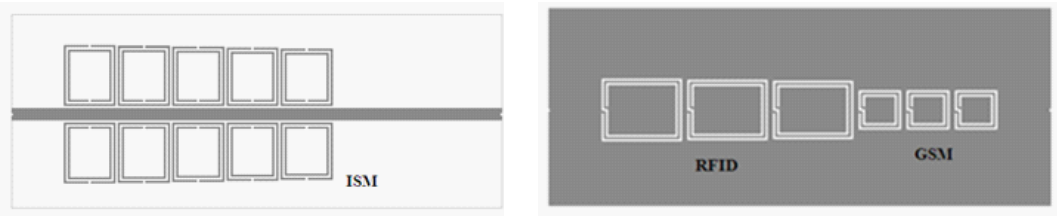

(a) (b)

Figure 1: Topology of the designed multiband microstrip EMI filter. (a) Top layer with microstrip line and the SRRs designed at 2.4 GHz. (b) Bottom layer with CSRs etched in the ground metal tuned at 900 MHz and 1.8 GHz, respectively. Metallization zones are depicted in grey.

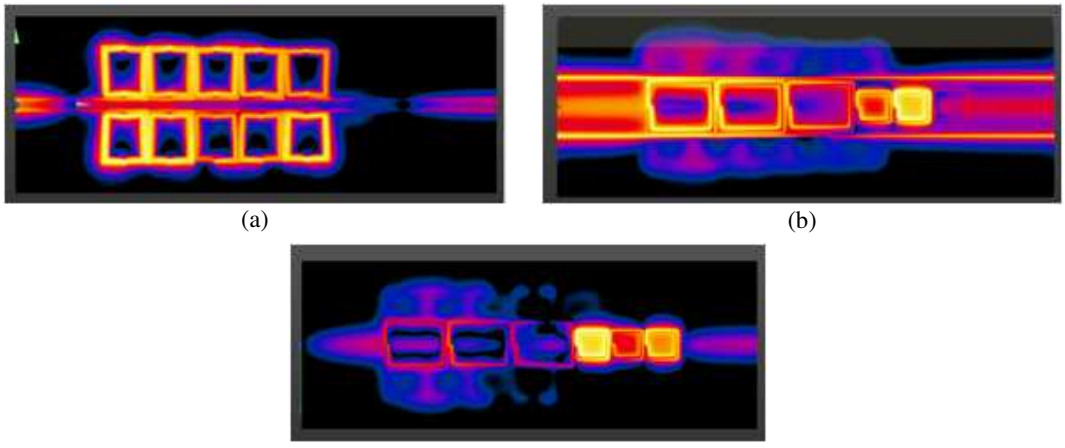

(a) (b)

(c)

Figure 2: RMS values of the near electric field (E) at (a) 2.4 GHz, (b) 0.9 GHz, and (c) 1.8 GHz.

REFERENCES

1. Pérez, D., I. Gil, J. Gago, R. Fernández-garcía, J. Balcells, S. Member, D. González, N. Berbel, and J. Mon, "Reduction of electromagnetic interference susceptibility in small-signal analog circuits using complementary split-ring resonators," Vol. 2, No. 2, 240–247, 2012.
2. "SEMCAD," Schmid & Partner Engineering AG (SPEAG).
3. Gil, I., R. Fernández, J. Gago, and J. Balcells, "Multiband EMI filter based on metamaterials," *IEICE Electron. Express*, Vol. 7, No. 9, 563–568, May 2010.

Overhead and Cable Transmission Lines Magnetic Fields: Standardization, Estimation, and Design

N. B. Rubtsova and A. Yu. Tokarskiy
FSBSI "Research Institute of Occupational Health", Moscow, Russian Federation

Abstract— Main principles of power frequency (50/60 Hz) magnetic field (MF) occupational and general public safety are analyzed taking into account international approach to maximum permissible levels achieving.

Overhead and cable power transmission lines magnetic field strength estimation algorithm is presented. Example of 500 kV overhead transmission line power frequency MF strength distribution is presented in comparison with 500 kV cable transmission line MF distributions. Cable transmission line (CL) MF distribution considered on the example of two 500 kV CL parallel circuits alive to the same electric bus. According with the problem of general public electromagnetic safety maintenance is suggested the optimal circuits' arrangement with changed order of the phases that allow reducing the 50 Hz MF values to maximal permissible levels (hygienic standards of general public exposure).

It is shown that multiphase sources create the field of elliptic polarization, which most root-mean square strength value is on the ellipse major axis, whereas result values calculation by components with Pythagorean Theorem use lead to errors with the increase of real value to 41%. By the example of 500 kV lines is shown the differences between results of the applied calculation methods. For 500 kV cable lines the ways of MF value decrease to permissible levels under different kinds of it lying are examined.

In addition it is shown that muff coupling use with cables and muffs locations in the corners of equilateral triangle under correctly changed order of the phases as well as slight increase of cable depth gives the possibility to avoid the ferromagnetic screens arrangement, and to cut costs.

Electromagnetic Compatibility of Contactless Power Transfer Modeled in FEM Analysis Software

R. Fajtl and K. Buhr
Department of Electric Drives and Traction, Faculty of Electrical Engineering
Czech Technical University in Prague, Technická 2, 166 27 Prague 6, Czech Republic

Abstract— This paper deals with electromagnetic compatibility of Contactless power transfer (CPT) and its effects on the surrounding electric devices. In the first part of this paper there are mentioned mathematical equations which describe basic parameters of CPT. Most of these equations feature the CPT transformer which is the main part of CPT.

CPT operates at high frequency which causes growth of reactance value. With increasing value of reactance the efficiency of CPT highly decreases. In the second part of the paper are listed four basic electric circuits using capacitors to compensate reactive power and increase the efficiency of CPT. This part also shows basic equations describing parameters of compensated CPT such as efficiency, operational frequency and others.

The third section of this work is about creating a model of CPT transformer in a multiphysics FEM software. From analysis of the model of CPT transformer in this multiphysics software the basic parameters of electromagnetic field is derived. Layout of electromagnetic field is shown and described in this part.

The last part of this paper is about valorization of electromagnetic field and its effects on the CPT device and its surroundings. Electromagnetic compatibility of any electric device has to be explored because it may cause serious hazards to others electric devices. Operation of CPT can disrupt functionality of electric devices such as pacemaker, security electronics and others electric devices in its surroundings.

The whole paper is about basic principles of CPT functions and its effects on its surroundings. It shows layout of electromagnetic field of the CPT and it deals with possible interference with other electric devices.

Parallel Imaging Based on Multicore DSP for FMCW SAR

Chengfei Gu, **Wenge Chang**, **and Xiangyang Li**
College of Electronic Science and Engineering
National University of Defense Technology, Changsha, Hunan 410073, China

Abstract— The combination of frequency modulated continuous wave (FMCW) and synthetic aperture radar (SAR), which leading to compact structure and high resolution imaging sensor, has been a hot spot in recent SAR research. Predictably, FMCW SAR will have enormous potential application in remote sensing and mapping, whereas the main challenge of this light-duty and high-resolution sensor is the realization of real-time imaging, which limited to restricted load and time-consuming autofocus processing. A Ku-band FMCW SAR system is demonstrated which has the capability of real-time processing with the application of single high-performance multi-core DSP. The navigational data of platform movement, which particularly used for high precision motion compensation, is accurately measured by GPS and accelerometer. Furthermore, to realize the real-time processing, an effective parallel processing approach based on multicore DSP is presented in detail, also the time consumption of key steps are minutely listed. To verify the capability of real-time processing, an automobile experiment is campaigned, which has equipped a FMCW SAR system on the top of the car. The obtained results of real-time processing and post-processing are presented and compared, processed with 35 cm and 25 cm resolution, respectively.

The main content of this paper is organized as follows briefly.

1. The selection of imaging algorithm and motion compensation strategy are presented for FMCW SAR real-time processing.

2. Section 2 depicts the processing flow of real-time imaging, also the time consumptions are minutely listed. Fig. 1 shows the data flow of real-time processing.

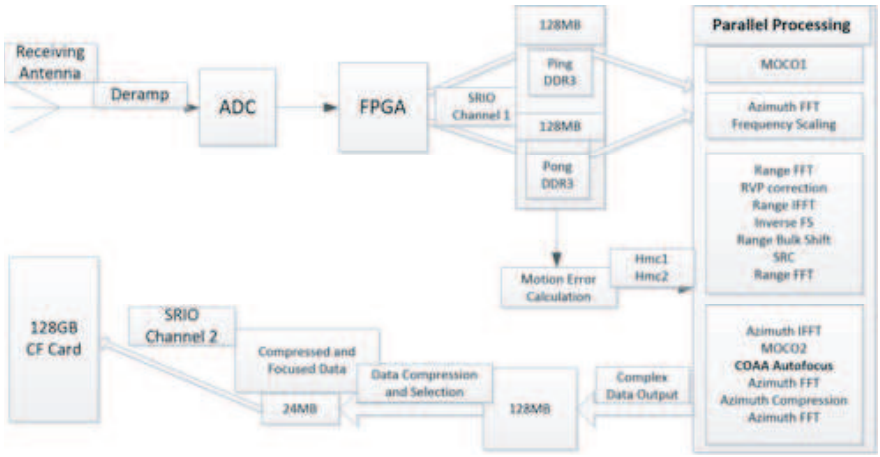

Figure 1: Data flow of real-time processing.

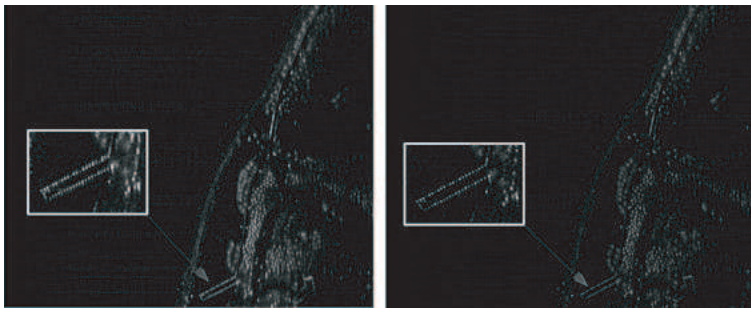

(a) (b)

Figure 2: Comparison of (a) real-time processed and (b) post-processed images.

3. In Section 3, the results of real-time and post processing are presented and compared, also the image performance for corner reflecters is analyzed in detail. The SAR images of the real-time processing and the post-processing are shown in Fig. 2 for resolution comparison.

4. Section 4 gives the conclusion of this paper.

A compact real-time processing SAR sensor is presented in this paper. On the foundation of this compact SAR system, the FSA which also contains high precision motion compensation and time-consuming COAA autofocus processing is efficiently realized in parallel with a single eight-core DSP. Furthermore, both the real-time processed result and the post-processed result of experiment are presented and compared, also the performance of SAR images are analyzed in detail.

Monitoring of Buoyancy Effects to Structures by Tsunami Water after Heavy Seismic Shocks

Shigehisa Nakamura
Kyoto University, Japan

Abstract— This work concerns on monitoring of structures under heavy seismic shocks. The author concentrates his interest to introduce some typical problems of structures. Specific references are found in the coastal zones at the event of the 201l Earthquake in the northwestern Pacific. It is discussed what could be the key in order to realizing the hazardous damages of the structures especially in the coastal zones.

Monitoring of Orographic Patterns in Relation to Tsunami Earthquake

Shigehisa Nakamura
Kyoto University, Japan

Abstract— This work is a note to problems on monitoring of orographic processes in relation to tsunami earthquake on the planet earth. The author is now in need to see a problem of a orographic patterns on the earth. For his convenience, Global orographic patterns are studied. The orographic patterns found in the geological surveys are selected as references. In a scope of any electromagnetics scope, it has been hard to consider any application can be effective for orography in the past. Now, the author has to notice about application of electromagnetic techniques for orography.

Reconstruction Algorithm through Laplacian Image in X-Ray Differential Phase-Contrast Computed Tomography

Tetsuya Yuasa[1], **Naoki Sunaguchi**[2], **and Masami Ando**[3]

[1]Yamagata University, Japan
[2]Gunma University, Japan
[3]Tokyo University of Science, Japan

Abstract— Phase-contrast CT reproduces a three-dimensional (3D) distribution of refractive indices in biological soft tissue with high contrast, and provides pathology and physiology with important information concerning biological soft tissues, e.g., breast cancer tissues. Typically, phase-contrast CT imaging system acquires the derivative of projections required for reconstruction. Then, a refraction-contrast CT image is reconstructed from the differential projections by convolving them with a signum function (i.e., $\mathrm{sgn}(\xi) = 1$ for $\xi \geq 0$, -1 for $\xi < 0$) and then applying a filtered backprojection (FBP) method. As, originally, FBP is an algorithm derived from a continuous model, the CT measurement must satisfy the sampling theorem for obtaining an artifact-free image. That is, $N_p \approx 2/\pi \cdot N_b$, where N_b and N_p are the number of bins in a single projection and of projections, respectively. When the number of detective elements in the horizontal direction of the two dimensional detector is assumed to 4000, the required number of projections is, indeed, 2500. In addition, due to the low photon count efficiency of the system, the x-ray exposure time to acquire a single projection is relatively long compared with the conventional CT. Therefore, use of FBP is disadvantage in terms of measurement time.

For this problem, we devised a novel reconstruction scheme for reduction of the number of projections to be measured. First, we obtain the second derivatives of the projections by numerically differentiating the differential projection measured. Then, we reconstruct the Laplacian of refractive-index image to be reconstructed from the second derivative projections using algebraic reconstruction technique with total variation regularization. Finally, we obtain the refractive-index image by solving the Poisson equation with the reconstructed Laplacian image being a source. In this presentation, we theoretically prove the reconstruction algorithm, and show its efficacy by demonstrating the experimental data.

An Efficient Approach of Lengthening Battery Age and Working Hours through Redistributing Battery Packs

L. Chen[1], **X. H. Feng**[1], **G. C. Wan**[2], **and M. S. Tong**[2]

[1]School of Electrical and Electronic Engineering, Shanghai Institute of Technology, Shanghai, China
[2]Department of Electronic Science and Technology, Tongji University, Shanghai, China

Abstract— The smart power management devices have wide applications in electric vehicles and energy storage systems. For the sake of facilitating battery management, individual batteries are generally grouped to form battery packs by serial and parallel connections and a complete power supply system consists of the battery packs in serial and parallel connections. Initially, the performance of each individual battery which constitutes battery packs is different and the difference between individual batteries will be gradually enlarged during the use of batteries, resulting in a significant degradation of the battery packs' performance. Because the released maximum power by a power supply system is determined by the minimum-power battery pack and the minimum-power battery pack will be seriously harmed if it continuously discharges and we must stop its discharging process. Similarly, if the maximum-power battery pack has a full charge, we must stop its further charge to prevent it from being harmed. When the difference of performance between battery packs is magnified, the working hours of power supply system will sharply reduce and the age of batteries will also be shortened greatly.

In this paper, we fully investigate a set of lithium-iron-phosphate batteries and propose an efficient approach for lengthening the working hours and age of the batteries by redistributing battery packs. The approach analyzes the data about the state of charge (SOC) and voltage of battery packs and then quantifies the level of their inconsistency between battery packs. The redistribution of battery packs will be automatically managed according to the level of inconsistency and we have designed a smart electronic device for controlling the process. The experimental tests show that the approach can significantly lengthen the working hours and age of the batteries. We will show the details of design and testing results in the presentation.

An Accurate Estimation for the State of Health of Lithium-ion Batteries by Using Fuzzy Logic System

L. Chen[1], **F. Q. Xiong**[1], **G. C. Wan**[2], **and M. S. Tong**[2]

[1]School of Electrical and Electronic Engineering, Shanghai Institute of Technology, Shanghai, China
[2]Department of Electronic Science and Technology, Tongji University, Shanghai, China

Abstract— Lithium-ion batteries have been widely used as a power source for electric vehicles and their performance significantly impacts the operation of electric vehicles. The state of health (SOH) and state of charge (SOC) are the two important indexes reflecting the state of batteries. However, the study on the SOH has not received a sufficient attention compared with the study for the SOC and there has not been a mature estimation method for the SOH. As the battery management system of electric vehicles gets constantly improved, seeking an accurate estimation method for the SOH of lithium-ion batteries has become more and more important. The SOH estimation belongs to a nonlinear problem which requires a highly accurate solution and the traditional linear estimation methods cannot meet the estimation requirements. The lack of accurate estimation for the SOH has seriously affected the practical applications of lithium-ion battery packs and it is very imperative to find a good solution.

In this paper, we propose an equivalent circuit model to accurately estimate the SOH for lithium-ion batteries. The residual capacity and equivalent DC resistance of the lithium-ion batteries under different SOHs can be easily obtained by charging and discharging experiments for the batteries and their relationships to the SOHs can be figured out to define the corresponding fuzzy rule table. Also, the static estimation and dynamic estimation are combined together so that the system reliability and the estimation accuracy can be improved. The simulated results show that the scheme can remarkably enhance the estimation accuracy for the SOH of lithium-ion batteries. We will show the details of the scheme and testing results in the presentation.

Estimation of Equivalent Model Parameters for $LiFeO_4$ Batteries Based on Particle Swarm Optimization

L. Chen[1], **T. Geng**[1], **Q. Zhang**[1], **G. C. Wan**[2], **C. H. Jiang**[2], **and M. S. Tong**[2]

[1]School of Electrical and Electronic Engingeering, Shanghai Institute of Technology, Shanghai, China
[2]Department of Electronic Science and Technology, Tongji University, Shanghai, China

Abstract— Power batteries are very important components in electric vehicles and they have a significant impact on the performance and security of a whole vehicleTo ensure the safe and reliable operation of batteries,designing an optimal battery management system (BMS) is very essentialThe BMS manages the batteries based on their states and instructions from a vehicle management system (VMS)The voltage, current, and temperature of batteries can be measured directly by sensors while other parameters such as the state of charge (SOC) has to be estimated indirectly by certain algorithms which usually rely on the battery model and its parametersThe battery model and parameters are essential because they form the basis of loop simulations for hardware and SOC estimation, and also provide a reference for the control of BMS

In this paper, we propose a unified form of equivalent circuit model for $LiFeO_4$ batteries based on the analysis of similarity between the internal mechanism and external characteristic of a chemical power source. A two-order equivalent circuit of $LiFeO_4$ batteries is built and their resistance and capacity are estimated with a least square method (LSM) and particle swarm optimization (PSO). By comparing the results from different estimation methods, we find that the relationship between the SOC and the electric motive force (EMF) or EMF-SOC can be significantly affected by the temperature. We also build a BP neural network in which the EMF and temperature are taken as inputs while the SOC works as an output and the results are used to estimate the SOC. The simulated and experimental results show that the proposed estimation method can accurately estimate the SOC for$LiFeO_4$ batteries.

Noncoherent Detection for Multi-hop Amplify-and-forward-based Multi-branch Cooperative Diversity Systems

Minghe Mao[1], **Ning Cao**[1], **Yunfei Chen**[1, 2], **and Haobing Chu**[3]

[1]School of Computer and Information, Hohai University, Nanjing 210098, China
[2]School of Engineering, University of Warwick, Coventry CV4 7AL, UK
[3]School of Engineering, UBC Okanagan, Kelowna, BC V1V 1V7, Canada

Abstract— Since the actual distribution of the received signals in multi-hop amplify-and-forward (AF) relaying transmission is no longer Gaussian, which is caused by the multiplication of fading gains and noise, a new fitted distribution named as logistic distribution is used to derive a novel noncoherent detector based on the maximum likelihood (ML) method. In order to get better performance of the receiver, one or more multi-hop AF links are added to form a multi-branch cooperative diversity system. Therefore, at the destination, combining method is applied to combine several signals together to obtain better diversity gains. Numerical results show that the new detector based on the logistic distribution outperforms the conventional energy detector. Also, it is shown that the performance of receiver is significantly improved when combining method is applied in the multi-branch cooperative diversity system especially when the number of branches increases.

Preliminary Numerical Results: Figure 1 shows the preliminary results for this work. Assume that, the number of hops is 5. Compared with the conventional energy detection on single branch, the new detector based on logistic fitting distribution has better bit-error-rate (BER) performance. One sees that the BER of the new detector can further decrease when the number of combined branches increases and the maximum ratio combining method is applied.

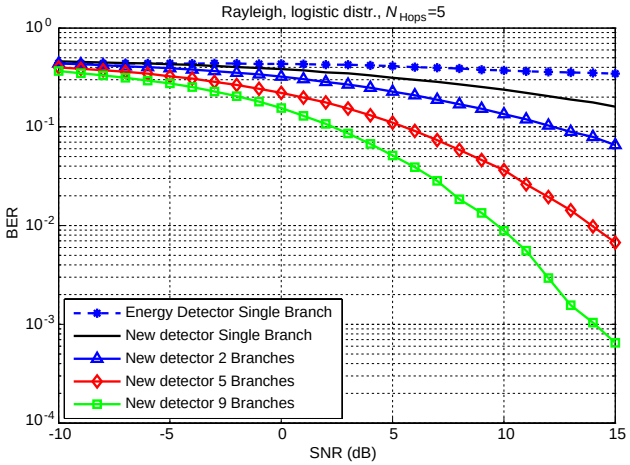

Figure 1: BER vs. SNR, new detector using logistic fitting parameters for combining different numbers of branches (single, $M = 2$, $M = 5$, $M = 9$), compared with the conventional energy detection on single branch with 5 hops AF relaying.

A New Design of High-speed Decimal Direct Digital Frequency Synthesizer

Guochun Wan, **Gui Zhu Yin**, **Jie Zhang**, **and Mei Song Tong**
Department of Electronic Science and Technology
Tongji University, 4800 Cao'an Road, Shanghai 201804, China

Abstract— Direct digital synthesizer (DDS) has been widely used in wireless communications due to its convenience and high frequency resolution. Although the resolution of the current design has been high, the binary operation phase accumulation restricts the minimum resolution of the DDS which is only $1/2^M$, where M is the number of accumulator bits, and this cannot meet a special output frequency requirement. In some applications, for example, in the terminal of very long baseline interferometry (VLBI) technology, more precise frequency signal is needed to adjust the received microwave signal. To satisfy this demand, the mixture of decimal and binary operation is used to enhance the DDS minimum frequency resolution to $1/(2^M 10^N)$, where M is the number of binary bits and N is the number of decimal bits.

The original DDS adopts a binary algorithm which limits the output frequency resolution in some cases and cannot switch the frequency and phase quickly. To solve this problem, the high-speed decimal DDS was proposed to replace the original DDS algorithm by using the mixture of decimal and binary algorithms and pipelined segment accumulator to realize the phase accumulation. It also uses a look-up table (LUT) to achieve a fast waveform output so that a high-speed and high-resolution performance can be achieved. We implement the new DDS design with VHDL language and its good performance has been demonstrated by simulations.

Coverage Impact for Data Traffic Profiling in WCDMA Networks

Karolis Žvinys, Darius Guršnys, and Evaldas Stankevičius
Department of Telecommunication Engineering
Vilnius Gediminas Technical University, Lithuania

Abstract— A packet data traffic volume and a packet switch related services climb upward in UMTS networks. Nowadays UTRAN is a key data carrier in mobile communications, while other generation networks are still implemented. Even serving a huge amount of customers and processing an enormous traffic quantity it is still required to ensure a sufficient quality of service (QoS) level. With rapid development of mobile networks, operators need to continually focus on quality. Quality of service (QoS) is a comprehensive reflection of the service capability of a WCDMA system. It defines how satisfied the users are with the services received from cellular networks. Therefore, the improvement of efficiency for provided services has become a major concern for operators.

One of the way to maintain differentiated services (DiffServ) for the large number of satisfied users is QoS management. Basically QoS can be managed for the main four UMTS traffic classes: conversational, streaming, interactive and background.

According to these classes three different user groups (Gold, Silver, Copper) are distinguished, which are formed by combining several network parameters related to QoS assurance. In such a way customers can be controlled in cellular networks providing them prioritized services. However could we already assume that the prioritization of individual user will ensure guaranteed priority service anytime and anywhere?

The goal of this study is to discover an impact for users received data services with individual QoS based on uneven network conditions. Therefore the study investigates three differently profiled customers which belong to background WCDMA traffic class. Main focus is paid for customers achieved uplink and downlink throughput evaluation regarding to variable radio network environment. Data transfer rate measurements are carried out in a commercial mobile network on heavy loaded cells in order to reach the results closest to reality. To draw an impact of radio conditions variation, a radio signal strength changes gradually for a user with a higher priority. The performance of the user experience is analyzed by the metrics of data rate and channel quality. Received benefits of the user service satisfaction related to radio environment changes is provided graphically. The drawbacks of prioritization the customers in cellular networks are introduced in the work also. On this study user profile QoS management over CN and UTRAN network has been applied only. It means that QoS profiling over Iub/Iur links was not involved into consideration.

The investigation process consists of analysis of related works on Section 2. Section 3 provides a determination of user profiles. The rest part of research presents the obtained results on Sections 4, 5 and 6. This includes NodeB selection, HSDPA and HSUPA users profiling topics. Finally conclusions are introduced in Chapter 7.

A Nyström-based Approach for Solving Time-domain Magnetic Field Integral Equation

W. J. Chen, **G. C. Wan**, **J. Zhang**, **and M. S. Tong**
Department of Electronic Science and Technology
Tongji University, 4800 Cao'an Road, Shanghai 201804, China

Abstract— Transient electromagnetic (EM) problems can be formulated by a time-domain integral equation approach. For conducting or homogeneously penetrable objects, the time-domain surface integral equations (TDSIEs) including the time-domain electric field integral equation (TDEFIE), time-domain magnetic field integral equation (TDMFIE), or their combination can be applied. Traditionally, the TDSIEs are solved by the method of moments (MoM) in spatial domain and a march-on in time (MOT) scheme in temporal domain. The MoM requires a well-designed basis function like the Rao-Wilton-Glisson (RWG) basis function which needs conforming triangular meshes in geometric discretization and double surface integrations in evaluating matrix elements. The MOT scheme, on the other hand, suffers from a late-time instability problem although some improved versions have been proposed in recent years. The instability and accuracy are still dependent upon the choice of time step.

In this work, we propose a hybrid scheme to solve the TDMFIE for transient scattering problems by conducting objects. Compared with the TDEFIE, the TDMFIE is thought of little more difficult to solve due to the nature of its integral kernel. We use the Nyström method to discretize the spatial domain while employ the MoM with Laguerre basis and testing functions to discretize the temporal domain for the TDMFIE. The merits of Nyström method in spatial domain includes the simple mechanism of implementation, removal of basis and testing functions, and allowance of using nonconforming meshes. Although the method requires an efficient treatment for hypersingular integrals, we have developed a robust technique to handle them. The time-domain MoM (TDMoM) with Laguerre basis and testing functions is superior to the MOT because the Laguerre function can naturally enforce the causality and also the Galerkin's testing scheme can fully eliminate the numerical instability with a march-on-in-degree (MOD) procedure. A numerical example for EM scattering by a conducting cylinder is presented to illustrate the scheme and its robustness has been verified.

A Hybrid Scheme for Solving Transient Electromagnetic Problems with Conductors

W. J. Chen, **G. C. Wan**, **J. Zhang**, **and M. S. Tong**
Department of Electronic Science and Technology
Tongji University, 4800 Cao'an Road, Shanghai 201804, China

Abstract— Solving transient electromagnetic (EM) problems is essential in many applications such as the design of radar cross section of aircrafts and design of some antennas or microwave circuits. The problems are usually of broadband, nonlinear, and time-varying characteristics and can only be described by time-domain governing equations. Although time-domain differential equations can be used to solving the problems, the time-domain integral equations (TDIEs) may be preferred in many situations due to their unique merits. The TDIEs could be in different forms and they are electric field integral equation (EFIE), magnetic field integral equation (MFIE), and combined field integral equation (CFIE), in a time-domain form, if objects are conducting or homogeneously penetrable.

Those TDIEs are usually solved by combining the method of moments (MoM) in spatial domain and a march-on-in-time (MoT) scheme in temporal domain. The MoM requires a well-designed basis function like the divergence-conforming Rao-Wilton-Glisson (RWG) basis function or curl-conforming edge basis function, resulting in an inconvenient implementation. On the other hand, the MoT scheme is conventionally inefficient and inherently unstable due to the low- and high-frequency modes of creeping into the solution. The late-time instability of MoT has not been fully solved albeit many improved versions have been developed in recent years.

We propose a novel hybrid scheme to efficiently solve the time-domain EFIE for transient EM problems with conductors. The Nyström method instead of the traditional MoM is used in spatial domain while the MoM instead of the conventional MoT is employed in temporal domain. The benefits of Nyström method in spatial domain include the simple mechanism of implementation, removal of basis and testing functions, and allowance of using nonconforming and low-quality meshes. In time domain, we use the MoM with Laguerre basis and testing functions which was proposed by Jung et al. and it is superior to the MoT scheme because the Laguerre function can naturally enforce the causality. Using a Galerkin's testing, we can eliminate the numerical instability through a march-on-in-degree (MoD) procedure. We present a numerical example to demonstrate the hybrid scheme and its robustness has been observed.

Influences of High Relative Humidity on Extremely Low Frequency Electric Field Measurements

Leena Korpinen[1], **Hiroo Tarao**[1, 2], **Rauno Pääkkönen**[1], **Oleksandr Okun**[3, 4], **and Lauri Sydänheimo**[1]

[1]Tampere University of Technology, Tampere, Finland
[2]Department of Electrical and Computer Engineering
Kagawa National College of Technology, Kagawa, Japan
[3]LLC Soyuzenergoproekt, Kharkiv, Ukraine
[4]Department of Electrical Energy
National Technical University "Kharkiv Polytechnic Institute", Kharkiv, Ukraine

Abstract— An earlier study indicated that humidity can influence electric field measurement results; thus, it is important to take into account when these results will be compared to the values given in different exposure safety guidelines (e.g., the International Commission on Non-Ionizing Radiation Protection (ICNIRP) or Directive 2013/35/EU of the European Parliament and of the Council on the minimum health and safety requirements regarding the exposure of workers to the risks arising from physical agents (electromagnetic fields). The aim of the study was to investigate extremely low frequency (ELF) electric field measurements in a climate room when the electric field meters were in a high-humidity environment before the measurements. We used the commercial three-axis meters EFA-3 and EFA-300, which contained a bandwidth ranging from 5 Hz to 2 kHz. We employed two methods: (1) the sensor was placed on a tripod; and (2) the sensor was fixed using a plastic clamp and was suspended by three fishing lines. With Method 1 (with both meters), the first experiment period included 7 measurements, when the relative humidity was 75% and temperature varied from 1°C to 25°C and the electric fields varied from 1 kV/m to 25 kV/m. Then, the meter measurements took over 3 hours, exposing it to humidity varying from 79% to 95%. Then, the second measurement period began. With Method 2, the protocol was similar; however, the time that the meters endured high humidity was over 5 hours. In the first periods of Method 1, the maximum percentage error was 5.6%, and in Method 2, it was 11.9%. In the second period, the maximum percentage errors were 14.5% (Method 1) and 24.4% (Method 2). We evaluated only two sensor types because there are a limited number of commercial sensors available for electric field measurements. Therefore, our material is quite limited. In conclusion, it can be stated that in the future it is important to also take humidity into account before the measurement period, not only during electric field measurements.

Examples of Variation in Measured ELF Electric Fields under 400 kV Power Lines

Leena Korpinen[1], **Rauno Pääkkönen**[1], **Hiroo Tarao**[1, 2], **Oleksandr Okun**[3, 4], **and Lauri Sydänheimo**[1]

[1]Tampere University of Technology, Tampere, Finland
[2]Department of Electrical and Computer Engineering
Kagawa National College of Technology, Kagawa, Japan
[3]LLC Soyuzenergoproekt, Kharkiv, Ukraine
[4]Department of Electrical Energy
National Technical University "Kharkiv Polytechnic Institute", Kharkiv, Ukraine

Abstract— The physiological effects and public exposures of electromagnetic fields have been studied at Tampere University of Technology (TUT). Parts of the earlier projects have also measured the electric fields in the same place under 400 kV power lines. The aim of the work was to investigate how the measured ELF electric fields fluctuate in the same measurement place when humidity varied. When we compare the measured values to the recommendations (e.g., guidelines of the International Commission on Non-Ionizing Radiation Protection (ICNIRP) or Directive 2013/35/EU), it is important to know how humidity influences the measured results. During three days, the electric field measurements were performed at three places near 400 kV power lines in Finland. The electric field strength was measured with two 3-axis commercial electric meters: EFA-3 meter (accuracy ±5%, RMS) and EFA-300 meter (accuracy ±3%, RMS). In Place A, nine electric field measurements were performed; in Place B, five measurements were performed; and in place C, two measurements performed. In place A, the electric fields varied from 6.8 to 12.5 kV/m when relative humidity was from 70.5% to 86%. In place B, the electric fields were 5.1–8.2 kV/m when relative humidity ranged from 67% to 76 %, and in place C, the electric field was 0.90–0.92 kV/m when humidity was 68–76%. The measured electric fields varied significantly. For example, in place A the lowest electric field (6.8 kV/m, relative humidity 70.5%) was only 54% of the maximum value (12.5 kV/m, relative humidity 86.0%). In the example, the difference in relative humidity was 15.5%. The measurement material is quite limited; however, it is possible to find examples where the measured electric fields were quite different, when the humidity also varied. In the future, humidity is important to take account in electric field measurements.

Possible Methods for Limiting Exposure to the Electric Fields of High Voltage Power Lines on Active Implantable Medical Devices in the Human Body

Oleksandr Okun[1, 2], **Leena Korpinen**[3], **and Lauri Sydänheimo**[3]

[1]LLC Soyuzenergoproekt, Kharkiv, Ukraine
[2]Department of Electrical Energy
National Technical University "Kharkiv Polytechnic Institute", Kharkiv, Ukraine
[3]Department of Electronics and Communications Engineering
Tampere University of Technology, Tampere, Finland

Abstract— According to earlier studies, the electric field (EF) under a 400 kV power line in some conditions may disturb active implantable medical devices (cardiac pacemakers, implantable cardioverter defibrillator, and others) in the human body and affect their functioning. Therefore, it is reasonable to consider possible ways to limit the impact of EF on medical devices. One of the known methods of limiting EF intensity under power lines without changing the design of lines is to plant trees and shrubs under the power lines. The second simplest method of limiting the field intensity of transmission lines is to install grounded wires (shields) under lines' wires. In this case, the induced charges on grounded wires partially compensate for the EF produced by line wires and limit the field intensity. It is economically feasible to connect shields under the line wires to a voltage source and thus ensure the effective utilization of the cross section. It is clear that the potential of each lower wire for the shielding effect must be the opposite of the upper wire potential. In this case, as with the grounded wires, the charge on the lower wire has the opposite sign to the charge on the corresponding wire. However, the presence of potential on the lower shield wire increases the charge and, consequently, the shielding effect. The aim of the study is to consider the shielding effect of additional wires (with and without voltage) to reduce the EF intensity under high voltage power lines. The field intensity under power lines at the height above the ground level in this case is calculated by geometrically summing the fields generated by each conductor and its image separately. The charges on grounded and line conductors are determined by solving the system of Maxwell's potential equations. In the final paper, more details of the study will be presented. Examples will be shown of the results of calculating the EF generated under a 400 kV power line with additional shielding wires. The shielding effectiveness and the possibility of its application will also be estimated.

Negative Permeability from Random Particle Composites

Shahid Hussain
Smart Technologies Group, QinetiQ Limited
Cody Technology Park, Farnborough, Hampshire, GU14 0LX, UK

Abstract— Artificial media, such as those composed of periodically-spaced wires for negative permittivity and split ring resonators for negative permeability have been extensively investigated for negative refractive index (NRI) applications [1, 2]. This paper introduces an alternative method for producing negative permeability: granular (or particulate) composites incorporating magnetic fillers.

Artificial media, such as split-ring resonators, are designed to produce a magnetic resonance feature, which results in negative permeability over a narrow frequency range about the resonance frequency. The position of the feature is dependent upon the size of the inclusion. The material in this case is anisotropic, such that the feature is only observable when the materials are orientated in a specific direction relative to the applied field. A similar resonance can be generated in magnetic granular (particulate) materials: ferromagnetic resonance from the natural spin resonance of particles.

Although the theoretical resonance profiles in granular composites shows the permeability dipping to negative values, this is rarely observed experimentally due to resonance damping effects. Results are presented for carbonyl iron in spherical form and in flake form, dispersed in insulating host matrices. The two particle shapes show different permeability performance, with the magnetic flakes producing a negative contribution. This is attributed to the stronger coupling with the magnetic field resulting from the high aspect ratio of the flakes. The accompanying ferromagnetic resonance is strong enough to overcome the effects of damping and produce negative permeability. The size of random particle composites is not dictated by the wavelength of the applied field, so the materials are potentially much thinner than other, more traditional artificial composites at microwave frequencies.

Programmable Fiber-based in-band OSNR Monitoring for Flexgrid Coherent Optical Communication System

Ruoxu Wang[1], **Liangjun Zhang**[1], **Ming Tang**[1], **Zhenhua Feng**[1], **Rui Lin**[2], **Songnian Fu**[1], **and Perry Ping Shum**[3]

[1]Next Generation Internet Access National Engineering Lab (NGIA)
School of Optical and Electronic Information
Huazhong University of Science and Technology, Wuhan 430074, China
[2]School of Information and Communication Technology
The Royal Institute of Technology (KTH), Electrum 229, Kista 164 40, Sweden
[3]Photonics Centre of Excellence, School of Electrical and Electronic Engineering
Nanyang Technological University, Singapore 637553, Singapore

Abstract— With the rapid development of ultra-dense large capacity coherent WDM optical communication networks, the monitoring of in-band optical signal-to-noise ratio (OSNR) plays an essential role to ensure signal qualities. Different from the classic polarization-nulling method, we proposed and experimentally demonstrated a novel fiber-based programmable in-band OSNR monitoring method for flexgrid coherent transmission system, the OSNR monitor is based on linearly chirped fiber Bragg grating (LCFBG) and commercial thermal print head (TPH). For the coherent communication system, when the output power of the pre-amplifier at the receiving terminal is constant, degraded OSNR leads to decreased signal power and elevated ASE noise. Therefore, if the central spectrum (signal and in-band noise) is filtered by an ultra-narrow bandwidth optical filter, the output optical power is in proportional to the OSNR value, the influence of the filtered in-band ASE noise will be negligible with relatively high OSNR and the ultra-narrow bandpass filter is the key element for this technique. Based on the thermo-optic effect of the LCFBG, we used the in-house developed driver circuits and a LabVIEW based software to implement a programmable ultra-narrow passband optical filter for OSNR monitoring. Linear monitoring range of 9–27 dB OSNR values with wavelength ranging from 1530.6 to 1538 nm is achieved. The OSNR monitor has advantages of low cost, low insertion loss, large wavelength tunability and compatible with current optical fiber communication system.

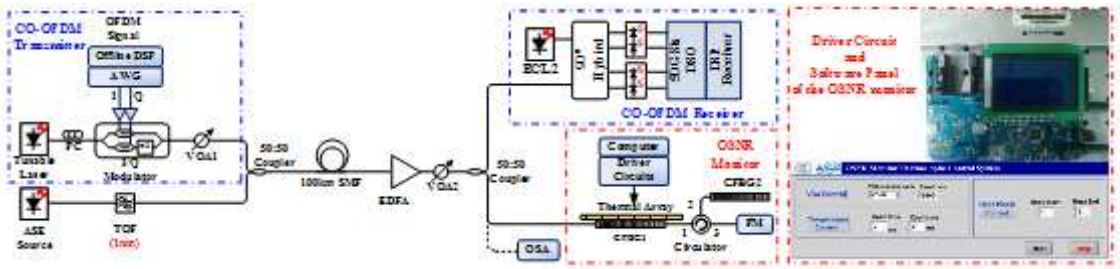

Figure 1.

The Study of Structure (XRD) and Optics (PL) and Magnetism (SQUID and ESR) Based on Undoped GaMnN Grown by MBE

J. W. Lee[1], **Yoon Shon**[1], **N. G. Subramaniam**[1], **T. W. Kang**[1], **C. S. Park**[2], **E. K. Kim**[2], **J. D. Song**[3], **and H. C. Koo**[4, 5]

[1]Quantum-Functional Semiconductor Research Center
Dongguk University, Seoul 100-715, Republic of Korea
[2]Quantum-Function Spinics Laboratory, Department of Physics
Hanyang University, Seoul 133-791, Republic of Korea
[3]Center for Spintronics Research, Korea Institute of Science and Technology
Seoul 136-791, Republic of Korea
[4]Spin Convergence Research Center, Korea Institute of Science and Technology
Seoul 136-791, Republic of Korea
[5]KU-KIST Graduate School of Converging Science and Technology, Korea University
Seoul 136-701, Republic of Korea

Abstract— GaN:Mn epilayers were grown on Al_2O_3 substrate uisng MBE. XRD data showed two phase; intrinsic GaMnN and precipitates including MnGa and MnN. PL transitions (e, Mn) and (D, Mn) related to Mn were remarkably activated. The clear ferromagnetic hysteresis loops were obtained in both samples, which means a good formation of ferromagnetic coupling. The M-T curves revealed two Tc of $140 \sim 170$ K which is originated to intrinsic GaMnN and above 300 K which is originated to precipitates MnGa and MnN. These results agree with the results of XRD and PL. In order to reconfirm the magnetic property, ESR was performed. The samples clearly display the magnetic resonance at around 200–400 mT. ESR data depicted the shift of H_{center} (i.e., $\Delta H_{\text{center}} = 337 - H_{\text{center}}$ [mT]) is greater than 20 mT for samples, and the appearance of H_{center} with positive ΔH_{center} is indicative of the samples having obvious ferromagnetism. The incorporated Mn ions are in a 2+ ionic state (i.e., Mn^{2+}) because Mn^{2+} with the spin state of $S = 5/2$ typically exhibits a magnetic resonance with $g \approx 2$ when Mn was doped in semiconductors. The trend of XRD and PL results totally coincides with that of the results of SQUID and ESR.

Laser Sensor for Monitoring Methane Emission in the Arctic Permafrost

A. S. Grishkanich[1], **S. V. Kascheev**[1], **V. V. Elizarov**[1], **I. S. Sidorov**[2], **and A. P. Zhevlakov**[1]

[1]National Research University of Informational Technologies, Mechanics and Optics
Saint-Petersburg, Russia
[2]University of Eastern Finland, Kuopio, Finland

Abstract— Over the past 100 years, the rate of the temperature change in the Arctic increased almost twice compared to the average rate of warming on the Earth. The advantages of laser sensor for monitoring of methane from the permafrost are to create an alternative to the conventional visual monitoring and sampling, which are more expensive and inefficient in the Arctic. We developed Raman laser sensor for monitoring of methane emissions from the permafrost. The laser sensor is based on Nd: YAG laser (266 nm, 50 mJ, 5 ns, 100 Hz) and hyperspectral resolution detection system for resolving the isotopic shifts in the Stokes spectra.

Over the past 100 years, the rate of the temperature change in the Arctic increased almost twice compared to the average rate of warming on the Earth. Preliminary estimations predict the fast and wide degradation of permafrost across the Arctic by the year 2100. Deconservation of 0.1% of the organic carbon from the upper 100 m layer of permafrost (about 10,000 Gt of carbon in the form of CH_4) may double the atmospheric methane with radiation activity about 20 times higher than that of CO_2.

The advantages of Raman laser sensor for monitoring of methane from the permafrost are to create an alternative to the conventional visual monitoring and sampling, which are more expensive and inefficient in the Arctic.

CH_4 frequency spectra are characterized by isotopic shifts, depend on the isotopic mass (and neutrons) and can be extremely fine. For example, C^{14} shifts from the relatively stable C^{12} by only $12.4 \cdot 10^{-3}\,\mathrm{cm}^{-1}$ and hyper/ultraspectral ($\lambda/\Delta\lambda \gg 100$) resolution measurements required for their identification. Hyperspectral resolution helps to avoid the overlapping of spectral lines, resolves the isotopic shifts in the Stokes spectra, and allows determine the isotopic composition. C^{14}/C^{12} ratio of the composition identifies the source of the carbon emission (permafrost or oil deposits).

We developed on-board Raman laser sensor which allows methane pockets detection, and classifies parameters (C^{14}/C^{12} ratio) of the permafrost anomalies. The laser sensor is based on Nd: YAG laser (266 nm, 50 mJ, 5 ns, 100 Hz) and hyperspectral resolution detection system for resolving the isotopic shifts in the Stokes spectra.

Dual Source Railway Vehicles

T. Lelek, V. Schejbal, and O. Sadilek
Department of Electrical and Electronic Engineering and Signaling in Transport Jan Perner Transport Faculty, Studentska 95, Pardubice 532 10, Czech Republic

Abstract— The paper will deal with research activities about technical aspects of dual source railway vehicles (DSRV) on the Czech railway traffic system. The thought vehicle uses for powered traction equipment the catenary and traction battery system. The battery system design is based on the traction and vehicular simulations.

The discussion about decrease of using fossils fuels is today more serious than last years. That problem is correlating with finding the alternative energy sources. The problems around of the electric car revolution in connection with energy sources has solved in the book Energy myths and realities from V. Smil. The publication has concluded that contemporary transmission system is not ready for age of the clear electric transport means. Therefore the first rational step lays in the expanding hybrid transport means for railway and road transport. It will help to progressive transition to independent traction vehicles and prepare national transmission systems for high energy flows. Presently the professional society explores possibilities of use electric independent vehicles.

The multisource railway vehicles are solving at the Department of Electrical and Electronic Engineering and Signaling in Transport. Research activities are focused on the traction and propulsion computer simulations and on the real measurement of the experimental vehicle. The paper will discuss a design of dual source railway vehicle with the trolley collector and the battery. At first the paper will deal with basic concept of DSRV, next step will be ideological proposal design of battery system, simulations of traction motors efficiency and final simulation of specific track with price calculations. It is expected that this vehicle will be operating in the Czech district.

The designed vehicle has a lot of advantages unlike conventional one. Among these advantages we might include operation in a short section without an electric line, elimination of combustion engine, using a principle of regenerative braking and recharging battery under catenary. Recharging in a station is not necessary. This realities lead to more effective vehicle using.

Design of Slot Plannar Applicator for Local Thermotherapy

Jaroslav Vorlicek[1], **Ladislav Oppl**[2], **and Jan Vrba**[2]

[1]Faculty of Biomedical Engineering, Department of Biomedical Technology
Czech Technical University in Prague, Technicka 2, Prague, Czech Republic
[2]Faculty of Electrical Engineering, Department of Electromagnetic Field
Czech Technical University in Prague, Technicka 2, Prague, Czech Republic

Abstract— Microwave thermotherapy is form of treatment which profits from effect affiliated with higher than common temperatures in biological tissue, such as higher blood flow and thus improved oxygenation and faster cell metabolism. From these effects we profit both in rehabilitation applications and above all in adjuvant cancer treatment. It's well known fact, that hyperthermia used in combination with conventional oncological methods significantly improves results.

The aim of this work was to design and construct a suitable planar slot applicator for microwave thermotherapy. Planar slot applicator is very good solution for superficial treatment, but can also be used for intracavitary treatment, as it can be manufactured from elastic materials. As resonant structure the slot applicator poses very good solution for energy transfer to biological tissue. Crucial for it's function is optimal impedance matching between applicator itself and treated tissue to ensure that all the energy radiated from antenna aperture is delivered to treated area. To allow applicator operate in unshielded room, we set its working frequency to 434 MHz, which is designated for biomedical and industrial use.

To design and simulate optimal resonant structure we used CST MICROWAVE STUDIO software suite. The aperture dimensions were set to 45 mm × 45 mm. After the optimal solution was found, applicator was made by the same technique as printed circuit board to evaluate its real behavior on phantom. As biological tissue phantom we chose agar model as one the best models of muscular tissue, or generally tissue with high water content. To simulate dielectric properties of real biological tissue, we added to agar 3 g of salt (NaCl). Measurement of scattering parameters was performed on vector analyzer Agilent E5071C.

To analyze how heat is distributed in tissue model was used thermal analyzer FLIR P25. After $t = 300$ s of heating was phantom evaluated with thermal analyzer from above a then immediately cut in pieces to see heat distribution inside.

By analyzing realized applicator was confirmed, that the lowest energy loss is indeed on frequency 434 MHz. So that makes our applicator perfect for furthermore clinical testing. To prevent creating hotspots applicator should be always equipped with water bolus.

Our slot applicator is suitable for use in biomedical applications in human medicine, preferably for cancer treatment, as it is capable delivering high amounts of energy to target tissue.

Array of Spiral Applicators for Local Thermotherapy

Jaroslav Vorlicek[1], **Ladislav Oppl**[2], **and Jan Vrba**[3]
[1]Faculty of Biomedical Engineering, Department of Biomedical Technology
Czech Technical University in Prague, Technicka 2, Prague, Czech Republic
[2]Faculty of Electrical Engineering, Department of Electromagnetic Field
Czech Technical University in Prague, Technicka 2, Prague, Czech Republic

Abstract— Hyperthermia, also called thermotherapy, is a type of cancer treatment in which body tissue is exposed to high temperatures (up to 43°C). It has been shown that high temperatures can damage and kill cancer cells, usually with lower injury to normal tissues. Damaging proteins and structures within cells is causing death of cancer cells by damaging proteins and their inner structures.

Hyperthermia is often used with other forms of cancer therapy, such as chemotherapy and radiation therapy. Hyperthermia may make some cancer cells more sensitive to radiation or harm other cancer cells that radiation cannot damage and it can also enhance the effects of certain cytostatics.

There are two main streams in hyperthermia thermotherapy depending on the area of the human body where the heat was applied. Thus, we have a local hyperthermia application and a whole body application.

In local hyperthermia, heat is applied to a small area, such as a tumor, using techniques that deliver energy to heat the tumor. Different types of energy may be used in this case including radiofrequency, microwave, or ultrasound.

Depending on the tumor location, there are several approaches to local hyperthermia: External approaches are used to treat tumors in superficial area, which means that the tumors are not more than 30 mm below the skin. External applicators are often positioned around or near the appropriate region, and energy is focused on the tumor.

Two-wire Archimedean spiral applicator configurations, when properly excited, have been shown to be circularly polarized radiators with wide broadband characteristic with respect not only to input impedance but also to radiation pattern. In practice, the configuration is excited from a transmission line connected to the center terminals of the configuration.

Such energized two-wire Archimedean spiral radiates a broad circularly polarized beam to each side of the spiral. Each radiated beam is normal to the plane of the spiral Accordingly, the radiated beams are identical except that the rotational sense of polarization of the radiated field on one side is the opposite of that on the other.

In most applications it is desirable that the spiral radiate to one side this is accomplished by appropriately backing the spiral on one side by a ground plane.

The matrix composition of the two-wire Archimedean spiral applicators is a very useful when we want to irradiate the larger area, which can be useful for example treating the tumors in thoracic region, e.g..

Our main aim was to discuss the array of four of the two-wire Archimedean spiral applicators. From the results based on the simulations in simulator of electromagnetic field we assume that this setup is the most suitable applicator for the superficial thermotherapy covering the largest area of tissue. Effective field size of the single applicator is 63%. The measured impedance matching to the biological tissue is less than −10 dB. When composed together in the shape of five spiral applicators, this setup is capable of effectively heating the superficially located tumors.

Development of Applicator for Microwave Hyperthermia System for Treatment of Mice

D. Vrba[1], **J. Vrba, Jr.**[1], **M. Wiewegh**[1], **M. Bursik**[1], **and J. Vrba**[2]

[1]Faculty of Biomedical Engineering, Czech Technical University in Prague, Czech Republic
[2]Faculty of Electrical Engineering, Czech Technical University in Prague, Czech Republic

Abstract— A microwave hyperthermia treatment of mice is planned within the research project "Utilization of novel mouse strains for investigation of the natural killer cell regulatory role in development and therapy of cancer" supported by Czech Scientific Foundation.

For this purpose a microwave exposure chamber working at 434 MHz was designed and its configuration was optimized in numerical simulator in terms of SAR and temperature distributions created by electromagnetic waves irradiated by the applicator in a numerical mouse model. The considered mouse model is a high resolution anatomical model depicted in Fig. 1. The mouse model was created by IT'IS Foundation, Switzerland and consists of 50 different tissues. To every tissue dielectric and thermal material properties were assigned from IT'IS Foundation biological tissue material properties database. A numerical model of the exposure chamber was created in the SEMCAD X and the mouse model was imported to the numerical model as well. Such overall numerical model allowed estimation of 3D distribution of the power loss density as well as computation of temperature 3D distribution in a treated mouse. Even effect of blood flow on the 3D temperature distribution was taken into account. The chamber was integrated to an available clinical hyperthermia system ALBA ON 4000, ALBA Hyperthermia System, Italy. The exposure chamber consists of two radiating structures (LC resonators) and the exposed mouse is located between them in a well-defined position. Advantage of using the ALBA 4000 is that the system already includes all necessary components such as microwave power generator, water bolus, minimal invasive temperature sensors and control unit and allows performance of well controlled hyperthermia treatments of mice. Preliminary experimental validations of performance of the exposure chamber integrated into ALBA 4000 on agar mouse phantoms were performed and are discussed here.

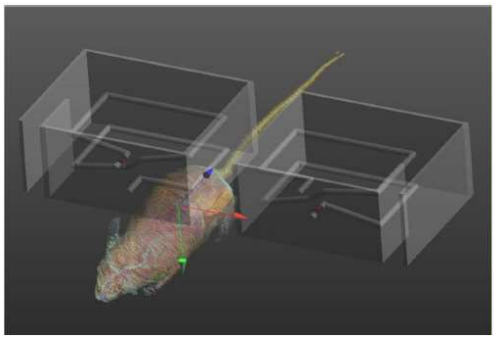

Figure 1: Numerical model of the applicator and mouse.

ACKNOWLEDGMENT

This research has been supported by the research program of the Czech Science Foundation (GACR) of the Czech Republic, Project No. 14-10100S Utilization of novel mouse strains for investigation of the NK cell regulatory role in development and therapy of cancer.

Numerical Study of System Requirements for Microwave Hyperthermia Treatment of Breast

D. Vrba[1], **O. Fiser**[2], **I. Merunka**[2], **M. Polacek**[1], **and J. Vrba, Jr.**[1]

[1]Faculty of Biomedical Engineering, Czech Technical University in Prague, Czech Republic
[2]Faculty of Electrical Engineering, Czech Technical University in Prague, Czech Republic

Abstract— In this paper a numerical study of requirements on microwave components for breast microwave hyperthermia is performed. The main goal is to find information about ranges of system settings in terms of phases and powers of each channel for different parameters as working frequencies of the system, positions and sizes of tumors. This information will be used for specification of microwave components needed for system implementation. In this study, 8 balanced antipodal Vivaldi antennas, developed originally for microwave imaging, in the field of microwave hyperthermia for breast cancer treatment are used as radiating elements. The working frequencies considered here are 915, 1400 and 2450 MHz. Ability of the system to effectively focus electromagnetic power into a tumor region within a numerical breast phantom is investigated using numerical simulations of SAR and temperature distributions created by an electromagnetic waves irradiated by the system. A commercial full-wave electromagnetic numerical simulation tool SEMCAD X with a built-in thermal solver is used for this task. A simple homogeneous breast phantom with a skin layer considered here was adopted from [1]. For the purpose of this study, a spherical tumor of diameter $d = 10$; 20 and 30 [mm] is virtually placed into the breast phantom at one quarter, one half and three quarters of the breast radius (out of the longitudinal axis). Average value of relative permittivity ε_r and equivalent conductivity σ_e of the healthy breast tissue as well as of the malignant tumor tissue were adopted from [2]. Statistical evaluation of achieved results will be performed as well as discussed.

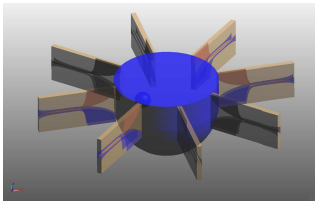

Figure 1: Schematic of 8-antenna configuration around the homogeneous breast phantom.

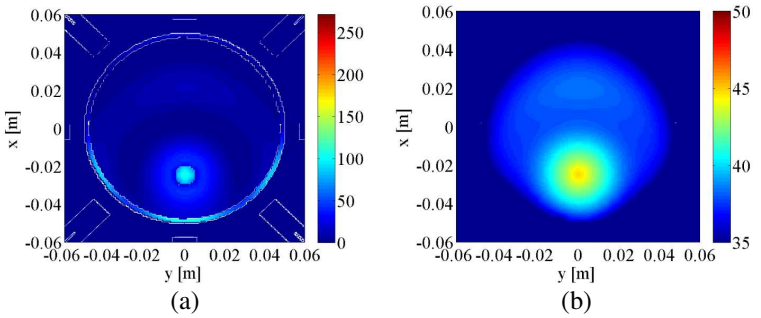

Figure 2: Optimized SAR distribution for 8-antenna configuration in the (a) numerical phantom at 1400 MHz and (b) corresponding temperature distribution, respectively.

ACKNOWLEDGMENT

This research has been supported by the research program of the Czech Science Foundation (GACR) of the Czech Republic, Project No. 13- 29857P Human Body Interactions with EM Field Radiated by Metamaterial Structures.

REFERENCES

1. Davis, S., H. Tandradinata, S. Hagness, and B. Van Veen, "Ultrawideband microwave breast cancer detection: a detection-theoretic approach using the generalized likelihood ratio test," *IEEE Transactions on Biomedical Engineering*, Vol. 52, No. 7, 1237–1250, 2005.
2. Li, X. and S. Hagness, "A confocal microwave imaging algorithm for breast cancer detection," *IEEE Microwave and Wireless Components Letters*, Vol. 11, No. 3, 130–132, 2001.

A Miniaturized Single Balanced Mixer for UWB Applications

Wahab Mohyuddin, **Dong Sik Woo**, **Byung Gil Choi**,
Hyun Chul Choi, **and Kang Wook Kim**
School of Electronics Engineering, Kyungpook National University
Sankyuk-dong, Buk-gu, Daegu 702-701, South Korea

Abstract— Microwave mixers perform the frequency conversion of electromagnetic signals and their operating principle is mostly based on the nonlinear behavior provided by the diodes or the transistors. The frequency translation is significant in numerous modern microwave systems applications ranging from radar and radio astronomy to microwave instruments and biological sensing. The selection of mixer's topology is based on its required performance. Transistor mixers are typically used in several applications where cost is the main driver rather than performance of the mixer. However, Schottky diode mixers utilizing hybrid couplers as their balun are used almost exclusively for the more challenging and high performance applications. For a diode mixer, the bandwidth limitation of the balun limits the overall performance of the mixer, which inspired the recent studies on design of wideband mixer topologies based on various types of baluns.

A new design of miniaturized single balanced diode mixer that comprises of a ring coupler as balun is presented in this paper for ultra wideband microwave applications. The ring structure of proposed mixer utilizes a pair of ultra wideband phase inverted transitions. To design analogous in-phase and inverted-phase transitions of ring coupler, consecutive transitions from parallel stripline to coplanar waveguide to parallel stripline are utilized. However, in order to interface ring coupler with diodes and to feed RF and LO signals, additional parallel stripline to microstrip line transition is introduced The diode matching circuit is designed after studying the nonlinear behavior and embedded impedance of diodes in nonlinear circuit simulator. Finally, the IF signal is extracted through external low pass filter. A favorable 3.1 to 10.6 GHz ultra wideband mixer performance has been achieved by optimizing the diode matching circuit with ring coupler. The proposed mixer exhibits flat conversion loss, good inter-port isolation of more than 20 dB, and compact size of 30% of the conventional ring mixer. The measured results show a conversion loss of 7.5 dB over 3.1 to 10.6 GHz ultra-wideband range of frequencies and also covers the IF frequency range of DC to 1 GHz. For optimal system performance, the proposed mixer can preferably be desirable for the high volume applications of UWB.

A Broadband Equiangular Spiral Antenna for UWB Ground Penetrating Radar (GPR) Applications

Dong Sik Woo, **Wahab Mohyuddin**, **Sung Kyun Kim**,
Hyun-Chul Choi, **and Kang Wook Kim**
School of Electronics Engineering, Kyungpook National University, Daegu, South Korea

Abstract— A design and its experimental result of a broadband equiangular spiral antenna for ultra-wideband (UWB) ground penetrating radar (GPR) applications are presented. Ultra-wideband antennas are one of the most critical parts of broadband GPR system. Dispersive or non-dispersive antennas have been commonly used for GPR systems, such as monopole, dipole or Bow-tie antenna, TEM horn antenna, Vivaldi or tapered slot antenna (TSA), and equiangular spiral antenna. The proposed antenna, which is fed by a vertically connected planar-type microstrip-to-coplanar stripline (CPS) balun, has ultra-wideband characteristics of the inherent equiangular spiral antenna. The curved microstrip-to-CPS balun transforms a unbalanced 50 Ω to a balanced 110 Ω of CPS impedance. The two conductors of the CPS strips are connected to the two arm radiators by utilizing vertical CPS substrate at the center. The spiral radiator consists of two identical arms which are shifted by 180° with respect to each other. The overall design of the spiral antenna is simply done by connecting between separately designed microstrip-to-CPS balun and two-arm equiangular spiral radiator. The calculated phase imbalance of the balun at feeding point was within 8° for whole frequency band. The implemented equiangular spiral antenna demonstrates wideband performance for frequency ranges from 2.9 to 12 GHz with the gain of 2.7 to 5.3 dB. The axial ratio is within 3 dB and the half-power beamwidth (HPBW) is more than 70°. Simulated radiation efficiency is about 90%. Good agreement was achieved between the simulations and the experimental results. This antenna can be widely applied to various UWB and GPR system applications.

Simulation on Power Handling Enhancement for the Ohmic Contact RF MEMS Switch with Micro-spring Structure

Zhuhao Gong, **Huiliang Liu**, **and Zewen Liu**
Institute of Microelectronics, Tsinghua University, Beijing 100084, China

Abstract— This paper presents a RF MEMS (Radio Frequency Micro-electro-mechanical System) switch which is capable of handling high power. By optimizing the design of its contact configuration and cantilever structure, the RF current distribution becomes more uniform through each contact of the multi-contact switch. The novel design of micro-spring cantilever structure also ensures a good contact between the contacts and top electrode when the switch is in the "on" state. The simulation results demonstrate the RF MEMS switch has excellent microwave performance: insertion loss < 0.15 dB, return loss > 31.6 dB and isolation > 14.5 dB from DC to 40 GHz as well as the ability of handling 3.1 W RF power which means a 300% improvement in power handling capability compared with traditional cantilever switch.

To be specific, the mechanical and electromechanical performances are simulated using CoventorWare to compare the traditional cantilever switch with the proposed micro-spring cantilever switch in the 2×2 contact configuration. The result shows the advantage of micro-spring cantilever structure in providing a good contact interface with multiple contacts. Fig. 1 shows the simulated S-parameters of the original switch and the proposed switch by full-wave EM simulator-Ansoft HFSS as well as the measured S-parameters of the original switch which implies a good consistence with the simulated results. To analyze the RF current distribution through each contact, the maximum RF current density through each contact in different contact configurations is simulated, as shown in Fig. 2. Simulation results demonstrate that the adoption of optimized 2×2 contact array ensures a more even current distribution between each contact in high frequency and therefore greatly improves its power-handling capability.

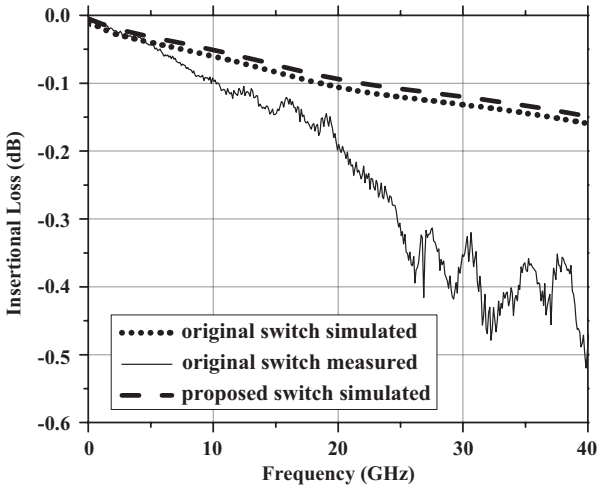

Figure 1: Simulated and measured S-parameters of the original switch and the proposed switch.

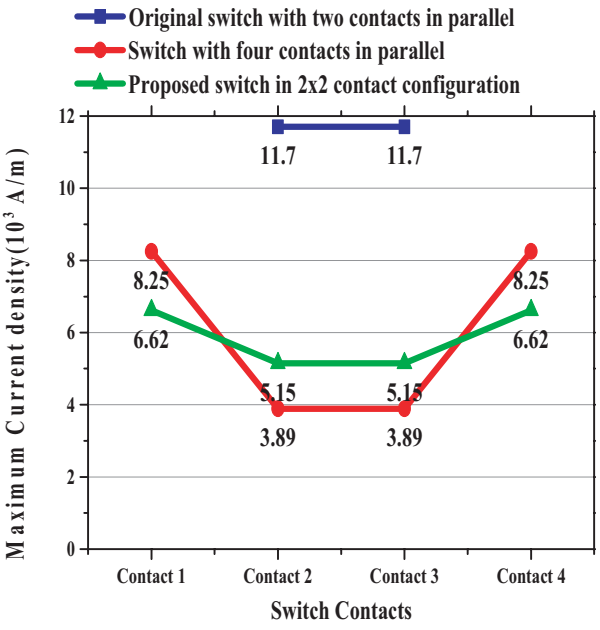

Figure 2: HFSS simulations of current distribution for different switches with 1 W input signal at 10 GHz.

Evaluation of Electromagnetic Interference Emitted from Compact Fluorescent Lamps According to CISPR-15

A. Kocakusak[1], **M. Cakır**[1, 2], **S. Yalcın**[3], **S. Ozen**[1], **and S. Helhel**[1]

[1]Electrical & Electronics Engineering Department, Akdeniz University, Antalya 07058, Turkey
[2]Electrical & Electronics Engineering Department, Bayburt University, Bayburt, Turkey
[3]Electrical & Electronics Engineering Department, Suleyman Demirel University, Isparta, Turkey

Abstract— Today, energy saving has become increasingly important and use of compact fluorescent lamps (CFL) has become widespread in structures such as shopping malls, offices, factories, hotels, houses, schools, hospitals and so on in order to provide more efficient lighting and conserve electrical energy. There are many commercial brands on the market. In recent years, electromagnetic interferences (EMI) problems induced by CFLs are investigated. In this study, EMI emitted by CFLs has been investigated in accordance with CISPR-15 which is an international standard.

It has been known that transmission emissions of lamps with different trademarks are also different; some of them don't provide the requirements of CISPR-15 standards and act as contaminants in the electric supply system. As an example of the analysis conducted, considering the limit, which is 66 dBμV, of CISPR-15 at 166.216 kHz frequency; it has been seen that the effect of CFL produced by Company A at 166.216 kHz frequency is 81.56 dBμV, whereas the effect of CFL produced by Company B at 166.216 kHz frequency is 50 dBμV, respectively.

In this case, the suitable filter was designed within scope of the study in order to prevent and minimize the risks created by commonly used brands in terms of energy quality, EMI and health; and solutions were presented to suppress CFL-induced noise transmitted to the electric grid.

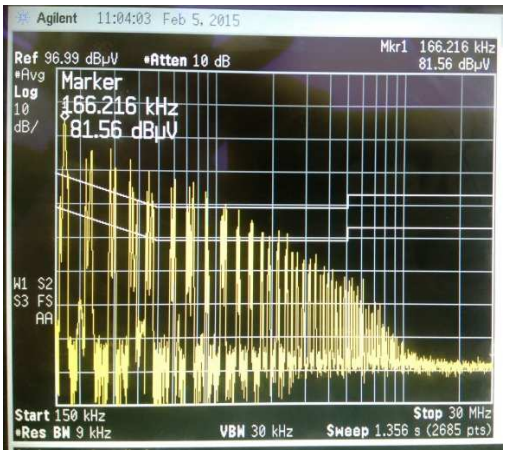

Figure 1: Interference values of CFL of A.

Analysis of the SMOS, MODIS and GCOM-W1 Data during the Growing Season in the Southern Part of the Western Siberia

P. P. Bobrov, A. S. Lapina, and A. S. Yashchenko
Omsk State Pedagogical University, Omsk, Russia

Abstract— The microwave emission of the soil covered with vegetation mainly depends on the following parameters: soil moisture and water content in the vegetation, temperature of the surface , and soil roughness. The SMOS Soil Moisture Retrieval Algorithm estimates vegetation attenuation (optical depth) at L-band by MODIS data (LAI and NDVI) using semi-empirical equations [1]. However, MODIS data that refer to the territory of the SMOS footprint often include cloudy areas. It makes difficulties in using optical sensor data.

This paper presents an analysis of the SMOS level 2 optical depth data, normalized microwave polarization difference index (MPDI), microwave vegetation index (MVI) derived from GCOM-W1 data and optical vegetation indexes (LAI and NDVI). We found that dependence between the data sets is determined by the type of surface. The best correlation for any type of the surface is between the optical and microwave indexes calculated according to the GCOM-W1 data. Among them, the best dependence was observed for indexes (MVI and MDPI) calculated according to the data at 6.9 and 10.7 GHz for the forest-steppe zone. It was also found that relationship between the optical depth (SMOS Level 2) and LAI, NDVI for any type of surface is very weak.

We also compared LAI and NDVI with ground-based measurements of the vegetation water content (VWC) taken from the southern part forest-steppe and steppe zone. The relation between them was extremely low. However the dependency between VWC and MDPI at frequencies of 18 GHz 23 GHz was significantly better.

Thus, GCOM-W1 data in frequency band can be used to retrieve the state of vegetation canopy instead of the MODIS data.

REFERENCES

1. Kerr, Y. H., P. Waldteufel, P. Richaume, J.-P. Wigneron, et al., "The SMOS soil moisture retrieval algorithm," *IEEE Trans. 2012*, Vol. GRS-50, No. 5, 1384, 2012.

A Spread Spectrum Clock Generator Using Discontinuous Modulation Technique for Reduction of Time Interval Errors

Taiming Piao, **Jae-Kyung Wee**, **Inchae Song**, **and Boo-Gyoun Kim**
School of Electronic Engineering, Soongsil University, Seoul, Korea

Abstract— spectrum clock generator with a low maximum time interval error (MTIE) and low electromagnetic interference (EMI). The proposed circuitry was fabricated with 0.35 µm CMOS process and operated with 3.3 V supply voltage at the average center frequency of 100 MHz. The measured results showed the MTIE of 11.59 ns with the EMI reduction of 14.57 dBm.

Multi-wavelength Erbium-doped Fiber Laser Based on Distributed Rayleigh Scattering Feedback

Lulu Wang[1, 2, 3], **Xinyong Dong**[1, 3, 4], **Perry Ping Shum**[2, 3], **and Haibin Su**[3, 4]

[1]Institute of Optoelectronic Technology, China Jiliang University, Hangzhou, China
[2]School of Electrical & Electronic Engineering, Nanyang Technological University, Singapore
[3]CINTRA, Research Techno Plaza, 50 Nanyang Drive, Singapore
[4]School of Materials Science and Engineering, Nanyang Technological University, Singapore

Abstract— A multi-wavelength erbium-doped fiber (EDF) laser based on random distributed feedback through backward Rayleigh scattering in a 20-km-long single-mode fiber and a polarization-maintaining fiber loop mirror (PMF-LM) is demonstrated. 7 lasing lines with wavelength spacing of 0.8 nm is obtained at room temperature. Due to the half-opened laser cavity design and the efficient gain from the pumped EDF, the measured threshold power is only 20 mW, and the pump efficiency is up to 14%.

Analysis of the Induction Motor Drive Predictive Control Method and Its Comparison with the Fundamental Direct Torque Control Method

Jiri Lettl and Pavel Karlovsky
Faculty of Electrical Engineering, Department of Electric Drives and Traction
Czech Technical University in Prague, Technicka 2, 166 27, Prague 6, Czech Republic

Abstract— Thanks to their simplicity, low price and high reliability, induction motor drives are one of the most common in many applications nowadays. Many ways of their control strategies have been developed since launching of mass production of the modern semiconductor devices of high power at high switching frequency. These methods include not only standard frequency control but also modern techniques of field oriented control or direct torque control.

The fundamental direct torque control method of induction motor drive, using two hysteresis controllers to maintain the asked stator flux amplitude and generated torque values, is simple and efficient, however, in some applications relatively high torque ripple can be seen as its disadvantage. That is why various modifications of the method, such as direct torque control with space vector modulation, multilevel inverter application or some forms of predictive algorithms have been performed reduce the torque ripple.

The paper presents suggested predictive direct torque control method of induction motor drive based on predicting the most suitable inverter output voltage vector for the next control step. The prediction calculation is proceeding from torque and stator flux reference values, motor parameters, and actual values estimated from voltage and current measurements. In the paper theoretical analysis of the method is performed, mathematical description of the system is created and the functionality of the proposed control algorithm is verified both by simulation in MatLab/Simulink environment and by measurement on the real induction motor drive. Comparison of the designed predictive control method with the fundamental direct torque control method developed by Takahashi is presented, too.

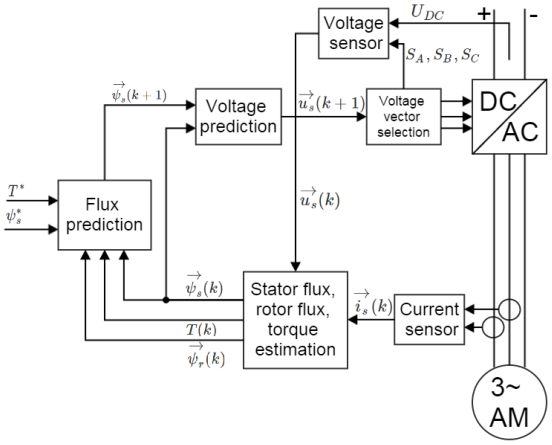

Figure 1: Block diagram of the proposed predictive direct torque control method.

Effect of Neutral Grounding Methods on the Earth Fault Characteristics

Abdallah R. Al-Zyoud[1], **A. Alwadie**[2], **A. Elmitwally**[2], **and Abdallah Basheer**[3]

[1]Electrical Engineering Department, Albalqa Applied University, Jordan
[2]Electrical Engineering Department, Najran University, Saudi Arabia
[3]National Electrical Power Company, Jordan

Abstract— Medium voltage (MV) distribution systems use different methods for grounding the neutral point. Influences of these grounding methods on the single line to ground (SLG) fault characteristics are discussed in this paper. Jordanian MV network is used as a case study. The network has both underground cables and overhead lines. Simulation models are implemented in both MATLAB®/SIMULINK®, and DigSilent/Power Factory® softwares. The models allow detailed investigation of the different fault factors and grounding methods. Results are obtained to evaluate the impact of each grounding method on the SLG fault features. Isolated neutral, solid grounding, resistance grounding and Petersen coil (Arc suppression coil) grounding are compared for different fault locations, fault incidence angles, and fault resistances. Current and voltage waveforms, as well as symmetrical components are used to describe the fault case.

Wheel Speed Measurement of Traction Locomotive under Wheel Slip Conditions

O. Zoubek, P. Pichlík, and J. Zděnek
Czech Technical University in Prague, Czech Republic

Abstract— Wheel speed of heavy freight train locomotive under non-ideal traction conditions was measured with very high resolution and fine precision. Many authors published papers in this area over a past century, but only recent advance in information technology enabled measurement in such extent and resolution at the same time.

Most modern locomotives have the speed sensor coupled with the traction motor. Unlike many other authors doing research in area of wheel-slip, the wheel speed was measured directly on the wheel, not indirectly on the traction motor. This allowed to directly observe the wheel speed without requirement to implement motor — wheel model, which can carry inaccuracies.

Thanks to an independent method of determining train speed using sensitive GPS receiver, wheel slip speeds were accurately identified regardless of synchronous slip phenomenon.

Despite adhesion theory, three types of operation were identified: Stable traction with negligible slip without oscillations, semi-stable traction with evident slip and oscillations and prominent wheel slip. As the wheel speed was measured directly on the wheel, a much larger oscillations than ever published were revealed. The source of the oscillations is discussed.

A simple MATLAB model of rotational masses was constructed and tuned to match the measurements. Eigenvalues and eigenvectors of the model are discussed. The rotational masses model is completed with adhesion model to perform simulations. The simulation results are presented with comparison to the results of the measurements.

Electric Vehicle Drive Control Based on GPS and GSM Path Parameters

T. Haubert, Z. Čeřovský, P. Mindl, and P. Mňuk
Department of Electric Drives and Traction, Faculty of Electrical Engineering
Czech Technical University in Prague, Technická 2, 166 27, Prague 6, Czech Republic

Abstract— Minimizing of energy consumption is important task which is solved at all vehicles. In the case of electric vehicles (EV), energy stored on board in chemical accumulators must be used very effectively. For this purposes mathematical model of EV and real journey data used for energy consumption calculation must be used. On the basis of journey regime optimization lower energy consumption will be achieved.

Optimal journey regime is calculated by means of known road data, obtained by means of GPS and GSM navigation system. From the road horizontal and vertical data basic route elements are calculated. Basic route elements are compared with needed torque, generated by driver's pedal. All this information's are processed, optimized, and needed mechanical torque is transmitted to the control unit of electric drive.

For model implementation the dSpace DS1103 has been used. The DS1103 dSpace platform is used as a simulator of the electric vehicle in laboratory and it is used for HIL (Hardware In the Loop) tests. The DS1103 device is covered in the AutoBox with Ethernet communication interface and Autoboot option enabling usage of Compact Flash card. The complete EV mathematical model is loaded in DS1103 device.

For laboratory verification special testing bench has been built. Testing bench consists of permanent magnet synchronous motor, power inverter and power sources. The load is substituted by the dynamometer. Both machines are controlled by master controller. Hardware structure of the laboratory stand is depicted on Fig. 1. In the first step journey simulation required torque of EV drive in the single path elements has been calculated. Real path data obtained within the journey were generated by means of GPS and GSM mobil-phone and stored in the memory.

Stored data were used as EV simulation model input data. Then for needed driving torque, actual power and consumed energy are calculated. With respect to the obtained results optimized path elements strategy calculation has been developed.

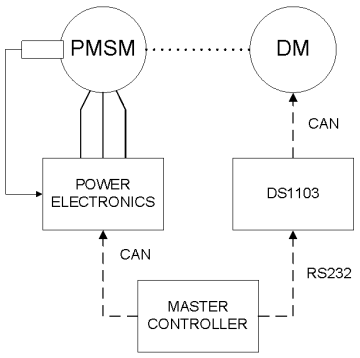

Figure 1: Hardware structure of the laboratory stand.

A Novel Ultrathin CdS/CdTe Solar Cell with Conversion Efficiency of 31.2% for Nano-area Application

M. Sabaghi[1], **A. Majdabadi**[1], **S. Khosroabadi**[2], **and S. Marjani**[1, 3]

[1]Laser and Optics Research School
Nuclear Science and Technology Research Institute (NSTRI), Tehran, Iran
[2]Department of Electrical Engineering, Imam Reza International University, Mashhad, Iran
[3]Department of Electrical Engineering, Ferdowsi University of Mashhad, Mashhad, Iran

Abstract— Due to limited availability and the rising price, the layer thickness reduction of solar cells is an attractive prospect. In this paper, we investigated a thin high efficiency structure of CdTe solar cells for nano-area application The proposed structure, achieved by rotating 90° in the base line structure, suggests high efficiency due to high current density. The proposed structure showed acceptable efficiency which is quite noteworthy in reducing the amount of material used and associated losses. The result showed a considerable improvement over the 15% efficiency of the reference sample. Under global AM 1.5 conditions, the designed cell had a V_{oc} of 866 mV, a J_{sc} of 74.84 mA/cm^2, and a FF of 48.2%, corresponding to a conversion efficiency of 31.2%.

The starting point of this work was the baseline case as reported in [1, 2]. In brief, the CdTe device model in the base line case consists of a 4 µm-thick CdTe absorber layer, a 100-nm thick CdS window layer, and a 500-nm-thick SnO_2 buffer layer. At the next step, this structure was modified by rotating 90° of the structure without dimension variation. Figure 1 illustrates the CdTe baseline case structure and the modified structures investigated in this study. The proposed structure has many advantages such as high photogeneration and low recombination rate. The J_{sc} of the cell can be improved by reducing the carrier recombination losses at the back contact or increasing the photogeneration rate in the absorber layer. Because the light inters to layers independently, the photogeneration rate is high in each layer. Figure 2 shows the comparison the photogeneration rate between conventional and proposed structure.

In addition, using less semiconductor material by thin cells is one of the main goals of today's solar cell research. Also, the thinning will reduce the recombination loss as well as lower production time and the energy need to produce solar cells. Consequently, all of these factors will decrease the production cost. Hence, it is possible to reduce the dimension of proposed structure considerably and achieve better base line results, simultaneously. Figure 3 shows the current-voltage and power-voltage curves for comparison with the base line case. As it is shown in Figure 3, the conversion efficiency can be increased to 31.2% mostly due to improvement of J_{sc} compared to the base line case. Although FF is smaller than base line case because of the high difference between J_{sc} and maximum current of the cell, the important parameters of the solar cell are much more than base line case.

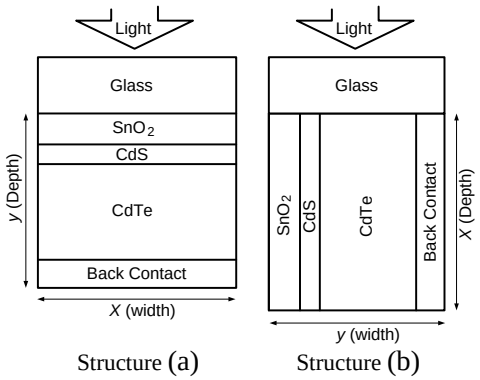

Figure 1: Structures of the CdTe solar cells: (a) baseline case structure and (b) modified cell structure for higher efficiency.

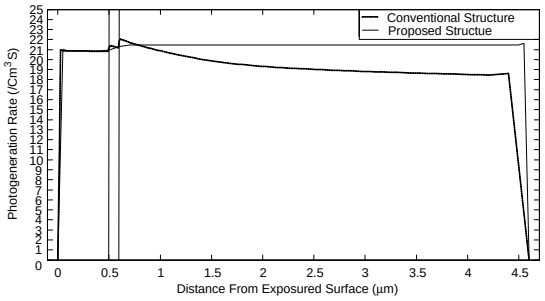

Figure 2: Photogeneration rate for the conventional and proposed structure.

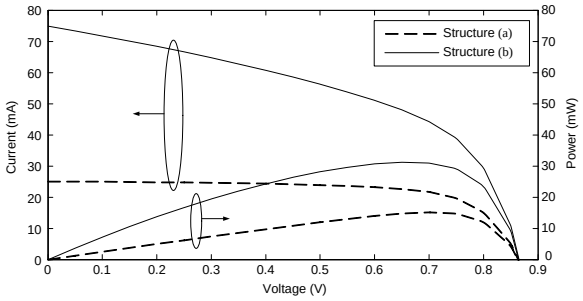

Figure 3: Characteristics of the (a) baseline case structure and (b) modified cell structure for higher efficiency.

REFERENCES

1. Khosroabadi, S. and S. H. Keshmiri, "Design of a high efficiency ultrathin CdS/CdTe solar cell using back surface field and backside distributed Bragg reflector," *Opt. Express*, Vol. 22, A921–A929, 2014.
2. Khosroabadi, S., S. H. Keshmiri, and S. Marjani, "Design of a high efficiency Cds/Cdte solar cell with optimized step doping, film thickness, and carrier lifetime of the absorption laye," *Journal of the European Optical Society*, Vol. 9, 14052-1–14052-6, 2014.

Session 2P1
FocusSession.SC2: Planar Optics Based on Metasurfaces 2

Metasurfaces' Solutions for Polarization Spectroscopy, Optical Activity, Colored Phase Holograms and Compact Nano-cavities

Vladimir M. Shalaev, **Amr M. Shaltout**, **Jingjing Liu**,
Sajid Choudhury, **Alexandra Boltasseva**, **and Alexander V. Kildishev**
Birck Nanotechnology Center, School of Electrical and Computer Engineering
Purdue University, West Lafayette, IN 47907, USA

Abstract— Tremendous efforts have been done over the last decade to produce 3D optical metamaterials that transcend properties of natural materials. However, the realization of the hoped-for 3D devices is challenged by large absorptive losses and complex and cost-ineffective fabrication. Metasurfaces have been introduced to overcome these two major challenges. They provide simple, compact and power efficient solutions to problems of immense importance. In our work, we use metasurfaces to obtain circular dichroism (CD) spectrometer, polarization rotator, color hologram, and subwavelength nano-cavities.

CD spectrometers are typically used to sense chiral molecules which are highly recurrent in biological structures and organic compounds. These spectrometers measure the differential absorption between circular polarizations of light (or different spins). A typical CD spectrometer takes sequential measurements of spin components which require complex hardware for switching laser source and managing data acquisition. Instead, we implement a metasurface that employs photonic spin Hall Effect to spatially separate spectra of different spins. This is a real-time CD spectrometer, and the smallest to our knowledge. Applications include bio-sensing, DNA structural analysis and stereochemistry.

We also used metasurfaces to perform optical rotation of linearly polarized light — used in secure quantum communications. Using natural materials will necessitate a long optical path to accumulate the differential phase-shift between spin components required for optical rotation. Ultrathin metasurfaces have shown the ability to split these components, and introduce the required phase-shift through a single deep-subwavelength layer.

Another metasurface generates a polychromatic holographic image with a broadband white source. This is done by using nano-slit antennas that can simultaneously control phase and wavelength of transmission. Antennae size controls wavelength (color), while antennae orientation manipulates Pancharatnam-Berry phase allowing for concurrent generation of arbitrary RGB images.

In addition to previous applications, we design subwavelength Fabry-Pérot cavities by replacing conventional mirrors with reflecting metasurfaces that introduce arbitrary phase-shifts compensating for reduced accumulated phase through the ultra-small cavity. 100-nm cavities showed resonance in the range (0.6–1.1 μm). Applications include nano-lasers, spontaneous emission enhancement (Purcell effect) and single photon sources.

Metasurfaces have proven to be applied efficiently to the areas of bio-medical optics, coherent optics, optical imaging and quantum nanophotonics, and many other applications are yet to be explored.

Controlling the Polarization State of Light with Metastructures

Mu Wang, **Shang-Chi Jiang**, **Xiang Xiong**, **Ren-Hao Fan**, **and Ru-Wen Peng**
National Laboratory of Solid State Microstructures and School of Physics
Nanjing University, Nanjing 210093, China

Abstract— In this talk, we present our recent work on controlling the polarization state of light with metastructures. First, we illustrate an approach to tune efficiently the phase difference of light in two orthogonal directions by controlling the time retardation with a microstructured surface. Second, we demonstrate the general mechanism to construct the dispersion-free metastructure, in which the intrinsic dispersion of the metallic structures is perfectly cancelled out by the thickness-dependent dispersion of the dielectric spacing layer. By selecting the structural parameters, the polarization state of light can be freely tuned across a broad frequency range, and all of the polarization states on the Poincaré sphere can be realized dispersion free. Third, we present a freely tunable polarization rotator for broadband terahertz waves using a metastructure, which can conveniently rotate the polarization of a linearly polarized terahertz wave to any desired direction with nearly perfect conversion efficiency. The investigations provide some guidelines to control the polarization state of light at subwavelength scale.

REFERENCES

1. Jiang, S. C., X. Xiong, Y. S. Hu, Y. H. Hu, G. B. Ma, R. W. Peng, C. Sun, and Mu Wang, "Controlling the polarization state of light with a dispersion-free metastructure," *Phys. Rev. X*, Vol. 4, 021026, 2014.
2. Jiang, S. C., X. Xiong, P. Sarriugarte, S. W. Jiang, X. B. Yin, Y. Wang, R. W. Peng, D. Wu, R. Hillenbrand, X. Zhang, and M. Wang, "Tuning the polarization state of light via time retardation with a microstructured surface," *Phys. Rev. B*, Vol. 88, 161104(R), 2013.
3. Xiong, X., Y. S. Hu, S. C. Jiang, Y. H. Hu, R. H. Fan, G. B. Ma, D. J. Shu, R. W. Peng, and M. Wang, "Metallic stereostructured layer: An approach for broadband polarization state manipulation," *Appl. Phys. Lett.*, Vol. 105, 201105, 2014.
4. Fan, R. H., Y. Zhou, X. P. Ren, R. W. Peng, S. C. Jiang, D. H. Xu, X. Xiong, X. R. Huang, and M. Wang "Freely tunable broadband polarization rotator for terahertz waves," *Advanced Materials*, 2014, DOI: 10.1002/adma.201404981.

Manipulating Surface Waves by Metasurfaces

Luigi La Spada and Yang Hao
Queen Mary, University of London, United Kingdom

Abstract— Surface waves on dissimilar interfaces have been extensively studied during the years [1]. Controlling these surface waves is of great interest in several new areas of technology including applications for surface wave suppression [2], improved antenna performances [3], wireless communication technologies, microwave circuits [4] and military applications among the others. In this regard, the properties of these surface waves supported on thin structured surfaces, known as metasurfaces, have been recently studied. In particular, a family of surface waves may be supported by pillar or crossed slit structures [5]. TM surface modes associated with a square array of metal patches on a dielectric coated ground plane and a "mushroom" metasurface were shown in [6]. By engineering the dimensions of metasurface elements across the array, the phase velocity of the surface mode can be controlled [7], and the propagation of the surface mode manipulated. Unfortunately, all such methods are highly dispersive, intrinsically narrow-band, lossy and anisotropic. The objective of this paper is to present a new metasurface-based design for surface waves manipulation.

The proposed structure consists of a metallic object, hidden underneath a dielectric structure above a ground plane, surrounded by a planar metasurface-based structure. This work has been divided into two main parts. The first part deals with the analytical formulation and the design of surface wave cloak. The second part will examine the simulation results of the proposed structure in the frequency range 8–10 GHz. The most significant findings from this study is that the proposed structure is polarization independent (it works for any impinging wave polarization: TE and TM), has wide-band and multi-band behaviour and it is easy to fabricate.

REFERENCES

1. Polo, J. A., T. G. Mackay, and A. Lakhtakia, *Electromagnetic Surface Waves: A Modern Perspective*, Elsevier, 2013.
2. Feresidis, A. P., G. Apostolopoulos, N. Serfas, and J. C. Vardaxoglou, "Closely coupled metallodielectric electromagnetic band-gap structures formed by double-layer dipole and tripole arrays," *IEEE Transactions on Antennas and Propagation*, Vol. 52, 1149–1158, 2004.
3. Wang, S., A. P. Feresidis, G. Goussetis, and J. C. Vardaxoglou, "Low profile resonant cavity antenna with artificial magnetic conductor ground plane," *Electronics Letters*, Vol. 40, 405–406, 2004.
4. Yang, F., Y. Rahmat-Sammi, and A. Kishk, "Novel surface wave antennas for wireless communications," *IEEE Antennas Propagation Symp. (APS)*, 2005.
5. Shi, H., C. Wang, C. Du, X. Luo, X. Dong, and H. Gao, "Beam manipulating by metallic nano-slits with variant widths," *Opt. Express*, Vol. 13, 6815–6820, 2005.
6. Yakovlev, A. B., M. G. Silveirinha, O. Luukkonen, C. R. Simovski, I. S. Nefedov, and S. A. Tretyakov, "Characterization of surface-wave and leaky-wave propagation on wire-medium slabs and mushroom structures based on local and nonlocal homogenization models," *IEEE Transactions on Microwave Theory and Techniques*, Vol. 57, 2700–2714, 2009.
7. Maci, S., G. Minatti, M. Casaletti, and M. Bosiljevac, "Metasurfing: Addressing waves on impenetrable metasurfaces," *IEEE Antennas and Wireless Propagation Letters*, Vol. 10, 1499–1502, 2011.

Extremely Confined Gap Surface-plasmon Modes in Metallic Metasurfaces Probed by Electron Energy-loss Spectroscopy (EELS)

Nicolas Stenger[1, 2]

[1]Department of Photonics Engineering, Technical University of Denmark
DK-2800 Kgs, Lyngby, Denmark
[2]Center for Nanostructured Graphene (CNG), Technical University of Denmark
DK-2800 Kgs, Lyngby, Denmark

Abstract— Applying EELS to ultra-sharp convex grooves in gold, we directly probe extremely confined gap surface-plasmon (GSP) modes excited by swift electrons in nanometer-wide gaps, down to approximately 5 nm.

We report an experimental study of GSPs in ultra-sharp gold convex nanogrooves using EELS [1]. The geometry of these nanogrooves is characterized by gradual and relatively slow variations in the gap width when moving deeper inside a groove. This means that the groove GSP modes can be considered as being formed by local metal-insulatormetal (MIM) GSP modes (that is, by GSP modes supported by constant-gap MIM configurations) that are weighted accordingly, a representation which is widely used in integrated optics and plasmonics for effective-index approximation. In EELS experiments (Fig. 1), the strongly confined electrical fields of moving electrons excite thereby local MIM GSP modes, corresponding to the position of the electron beam inside the groove. Note that a sample should necessarily be thin along the groove (Fig. 1) in order to be transparent for an electron beam, but not too thin with respect to the GSP wavelength. Overall, the considered groove geometry is ideal for studying MIM GSP modes, as the width of the insulating layer (gap size) decreases as the position of the electron probe is moved down the nanogroove, thus allowing us to map the evolution of MIM GSP modes for varying gap size in a single groove. We intentionally propagate the electron beam along the axis of the groove within the mirror-symmetry plane (yz plane, cf. Fig. 1) in order to allow for probing of modes near the groove bottom and to study the optically dark modes. We verify experimentally the existence of the MIM GSP mode in the crevice of the groove, i.e., at extremely narrow gaps of only 5 nm.

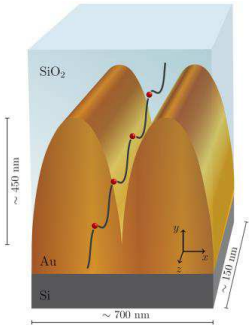

Figure 1: Artistic impression of the gold nanogroove studied in this work, with the electron probe moving parallel to groove axis. The groove is filled with silicon dioxide and the substrate is silicon. The groove height, depth and periodicity are approximately 450 nm, 150 nm and 350 nm, respectively.

REFERENCES

1. Raza, S., N. Stenger, A. Pors, T. Holmgaard, S. Kadkhodazadeh, J. B. Wagner, K. Pedersen, M. Wubs, S. I. Bozhevolnyi, and N. A. Mortensen, " Extremely confined gap surface-plasmon modes excited by electrons," *Nature Commun.*, Vol. 5, 4125, 2014.

Highly Efficient Decoupling-free Surface Plasmon Meta-couplers

Wujiong Sun[1], **Qiong He**[1, 2], **Shulin Sun**[3], **and Lei Zhou**[1, 2]

[1]State Key Laboratory of Surface Physics
Key Laboratory of Micro and Nano Photonic Structures (Ministry of Education)
Fudan University, Shanghai 200438, China
[2]Collaborative Innovation Center of Advanced Microstructures, Fudan University, Shanghai 200433, China
[3]Shanghai Engineering Research Center of Ultra-Precision Optical Manufacturing, Green Photonics
Department of Optical Science and Engineering, Fudan University, Shanghai 200433, China

Abstract— Surface plasmon polaritons (SPPs) have recently found numerous applications in photonics, but traditional devices to excite them (such as grating and prism couplers) all suffer inherent low-efficiency issues, since the generated SPPs can decouple back to free space and the reflection at the device surface can never be avoided. Here, based on a transparent gradient metasurface, we propose a new SPP-excitation scheme and numerically demonstrate that it exhibits inherently high efficiency (94%), since the designed meta-coupler kills both the decoupling and the reflection at its surface. As a proof of concept, we fabricate a meta-coupler in the microwave regime, and combine near- and far-field experiments to demonstrate that the achieved SPP-excitation efficiency reaches 75%, which is several times higher than all other available devices. Our findings can inspire the designs and realizations of high-performance plasmonic devices to harvest light-matter interactions.

Meta-line and Meta-surface for Cloaking

Hong Chen Chu, **Jie Luo**, **and Yun Lai**
Optoelectronics and Energy & Collaborative Innovation Center of Suzhou Nano Science and Technology, College of Physics, Soochow University, Suzhou 215006, China

Abstract— Meta-surface has not only shown extraordinary ability to control the reflection and refraction of waves [1], but also the ability to change propagating waves into surface waves along the surface [2].

Here, we investigate the 1D counterpart of a meta-surface: meta-line, i.e., a one-dimensional structure with gradually changing parameters [3]. Our study shows that such a line is also capable of converting incident propagating waves into guided localized waves along the line. In such a way, propagating waves in space can be collected at a high efficiency.

The other topic that we investigate is the application of meta-surface for cloaking.

REFERENCES

1. Yu, N. F., et al., *Science*, Vol. 334, 333, 2011.
2. Sun, S. L., et al., *Nature Materials*, Vol. 11, 426, 2012.
3. Chu, H. C., J. Luo, and Y. Lai, to be Submitted.

Few-layer Metasurfaces for High Efficiency Linear Polarization Conversion and toward Planar Flat Optics

Hou-Tong Chen, **Nathaniel K. Grady**, **Jane E. Heyes**, **Dibakar Roy Chowdhury**, **Yong Zeng**, **Matthew T. Reiten**, **Abul K. Azad**, **Diego A. R. Dalvit**, **and Antoinette J. Taylor**
Los Alamos National Laboratory, USA

Abstract— The properties of metamaterials are determined by their structures rather than the materials being used. They enable electromagnetic functionalities by design, which are applicable to the entire electromagnetic spectrum from microwave to visible. Bulk metamaterials often suffer from high resonant losses and three-dimensional fabrication challenges, particularly when approaching the optical frequency regime where metals become lossy and structural dimensions are on the micro- or nano-scale. Single layer planar metamaterials — metasurfaces — are relative easy to fabricate using modern micro- and nano-fabrication technologies, and at the same time minimize their losses. However, their interactions with electromagnetic waves are limited, resulting moderate device performance and insufficient for many real world applications.

When a few layers of metasurfaces are added together and separated by subwavelength dielectric spacers, the overall response could be dramatically different from the simple addition of individual metasurface layers. Taking advantage of the tailored resonance (dispersion) and anisotropic response, we achieve few-layer terahertz (THz) metamaterials for efficient linear polarization conversion over a broad bandwidth more than two octave [1]. The few-layer THz metamaterials consist of two orthogonal metal gratings and an array of subwavelength anisotropic metal resonators in between, which are separated by polyimide spacer. Similar to the metasurface structures previously demonstrated [2], the phase of the cross-polarized waves depends on the geometry and dimensions of the resonators being used, spanning the entire 2π range. This enables the creation of spatial phase profile for arbitrary wavefront shaping. For instance, a thin-film-like flat metamaterial with appropriately arranged resonators can deflect the transmission waves to a specific frequency-dependent angle, a function could be otherwise only accomplished using a bulk prism. Other flat optics can be designed using the demonstrated few-layer metamaterials, for instance, for beam focusing/collimation.

REFERENCES

1. Grady, N. K., J. E. Heyes, D. Roy Chowdhury, Y. Zeng, M. T. Reiten, A. K. Azad, A. J. Taylor, D. A. R. Dalvit, and H.-T. Chen, "Terahertz metamaterials for linear polarization conversion and anomalous refraction," *Science*, Vol. 340, 1304, 2013.
2. Yu, N. F., P. Genevet, M. A. Kats, F. Aieta, J. P. Tetienne, F. Capasso, and Z. Gaburro, "Light propagation with phase discontinuities: Generalized laws of reflection and refraction," *Science*, Vol. 334, 333, 2011.

High-performance Reflective Focusing of Terahertz Beams Using Holographic Metasurfaces

S. A. Kuznetsov[1, 2, 3], **M. A. Astafev**[1], **M. Beruete**[4], **M. Navarro-Cía**[5, 6, 7], **and A. V. Arzhannikov**[1, 2]

[1]Novosibirsk State University, Pirogova St. 2, Novosibirsk 630090, Russia
[2]Budker Institute of Nuclear Physics SB RAS, Lavrentiev Ave. 11, Novosibirsk 630090, Russia
[3]Institute of Semiconductor Physics SB RAS, Novosibirsk Branch "TDIAM"
Lavrentiev Ave. 2/1, Novosibirsk 630090, Russia
[4]Antennas Group — TERALAB, Universidad Pública de Navarra, Pamplona 31006, Spain
[5]Optical and Semiconductor Devices Group, Department of Electrical and Electronic Engineering
Imperial College London, SW7 2BT, London, UK
[6]Centre for Plasmonics and Metamaterials, Imperial College London, London SW7 2AZ, UK
[7]Centre for Terahertz Science and Engineering, Imperial College London, London SW7 2AZ, UK

Abstract— The terahertz (THz) band of the electromagnetic spectrum is conveniently sandwiched between the microwave and infrared regions that allows one to combine both optical and microwave techniques in THz instrumentation and to synthesize unique instrumental solutions. Such a synthesis is proven to be very effective when planar metallized microstructures of subwavelength topology, commonly referred to as frequency selective surfaces (FSSs) or measurfaces (metaFSS), are used for manipulating amplitude, polarization and phase characteristics of quasi-optical THz beams. In microwave engineering, the phase control is of great importance in the technology of low-profile reflectarray antennas, whose conventional design implies exploiting a grounded-dielectric-slab-backed FSS with spatial-depended reflection phase. Transferred to the THz band, this approach is estimated to be promising for beam-shaping and beam-focusing techniques as it allows creating purely flat, thin and lightweight reflectors capable of properly manipulating the wavefront through the control of the FSS unit cell geometry. Due to relative simplicity in photolithographic fabrication, such kind of reflectors serve as an attractive alternative to the conventional diffractive optical elements (DOEs) based on cost-consuming structures with profiled surfaces.

In this contribution we demonstrate feasibility for high performance reflective focusing of THz beams using flat DOEs based on metaFSS-inspired holographic reflectarrays (HRAs), whose design is accomplished using a combined technique involving:

a) a computer-generated holography method to synthesize an appropriate distribution of the reflection phase $\varphi_{\mathrm{HRA}}(x, y)$ over the metasurface;

b) a full-wave-electromagnetic-analysis-based method to control the complex reflectance ρ_{HRA} (x, y) of the HRA at any local point (x, y) of its surface via proper morphing the metaFSS unit cells geometry from metallic patches to U-shaped and split-ring resonator elements.

We present the experimental results of testing different planar focusing devices designed with the aforementioned technique and optimized for the operation frequency of 0.35 THz. The devices are implemented on basis of polypropylene substrates with the thickness of 190 μm and provide radiation focusing into simple and sophisticated shapes including single and multiple spots, as well as Latin letters. The overall diffraction efficiency up to 80% is demonstrated that outperforms similar characteristics of many metaFSS-based analogues working at THz frequencies.

ACKNOWLEDGMENT

This work is supported by the Ministry of Education and Science of the Russian Federation under the State Assignment Contract #3002 (technological implementation and experimental testing) and the Russian Science Foundation under the Project 14-12-01037 (full-wave electromagnetic simulations).

Plasmonic Metalens Lithography Far beyond the Near Field Diffraction Limit

Xiangang Luo, **Changtao Wang**, **Zeyu Zhao**, **Yanqin Wang**,
Na Yao, **Ping Gao**, **and Yunfei Luo**
State Key Lab of Optical Technologies on Nano-fabrication and Micro-engineering
Institute of Optics and Electronics, Chinese Academy of Sciences, P. O. Box 350, Chengdu 610209, China

Abstract— Near-field imaging optics, including scanning near-field optical microscope, near field proximity lithography and super lens, have always been suffering from the issue of near field diffraction limit, which implies that the obtainable resolution is strongly dependent on the light wavelength and the distance between objects and lens or fiber tip's apex. This results in great troubles in practical applications, like the physical abrasion of near field mask patterns. A method of plasmonic metalens going far beyond the near field diffraction limit was proposed and demonstrated experimentally in our recent investigations. The plasmonic metalens is composed of silver-photoresist-silver structure and applied with high numerical aperture off-axis photons illumination and surface plasmons illumination, generated by hyperbolic metamaterial of multiple metal-dielectric films. The air working distance between mask patterns and metalens could be significantly elongated far beyond of the near field diffraction limit, benefitting from sub-diffraction imaging information enhancement due to the cavity metalens structure and the shift of Fourier components of nano patterns. As examples, nano patterns of half pitch 60 nm are successfully resolved with 365 nm light wavelength and 100 nm air gap distance, about four times that in conventional near-field imaging or superlens scheme. Much Deeper subwavelength resolution with half pitch 4× nm, 3× nm and 2× nm are demonstrated theoretically and experimentally as well. The method is believed to significantly improve the compatibility of plasmonic lithography application as a cost effective, nano-fabrication way.

Transparent Conducting Oxides as Plasmonic Component in Near Infrared

J. Kim[1], **N. Kinsey**[1], **A. Dutta**[1], **M. Ferrera**[1,2], **C. De Vault**[3], **I. Kitamura**[1], **A. V. Kildishev**[1], **V. M. Shalaev**[1], **and A. Boltasseva**[1]

[1]School of Electrical & Computer Engineering and Birck Nanotechnology Center, Purdue University
1205 West State Street, West Lafayette, IN 47907, USA
[2]School of Engineering and Physical Sciences, Heriot-Watt University
David Brewster Building, Edinburgh, Scotland EH14 4AS, UK
[3]Department of Physics, Purdue University, 512 Northwestern Ave, West Lafayette, IN, 47907, USA

Abstract— Research on alternative plasmonic materials is becoming an important step to improve the performance of plasmonic and nanophotonic devices for many applications. Our study focuses on transparent conducting oxides which have great potential for enabling high performance, tunable, semiconductor compatible plasmonic devices.

The development of new plasmonic materials enables novel optical devices, and they in turn assist in the progress of optical communications. As a result of the significant attention in searching for alternative materials, transparent conducting oxides (TCOs) have been proposed as promising plasmonic compounds in near infrared (NIR) regime, especially at telecommunication wavelengths [1]. They are eminently practical materials because they are CMOS-compatible, can be grown on many different types of substrates, patterned by standard fabrication procedures, and integrated with many other standard technologies. In addition, like any other semiconductor, the optical properties of TCOs can be tuned by changing the carrier concentration/doping. Thus, TCOs form an obvious choice as alternative plasmonic materials in the NIR.

In our studies, we have demonstrated that simple TCO structures patterned by electron beam lithography support strong plasmonic resonances in the NIR, and such resonances are easily adjustable with post processing such as thermal annealing [2]. These characteristics of TCOs provide the capability to design essential optical components for nanophotonic systems. For example, we recently demonstrated a TCO based metasurface which functions as a quarter wave plate with a 200 nm bandwidth at the 1.55 μm wavelength [3].

TCOs can be used not only as an alternative to metal, but also as epsilon near zero (ENZ) materials since they naturally offer ENZ properties in the NIR regime. From our recent study of the behavior of nanoantennae sitting upon a TCO substrate, we found that TCOs can be a potential optical insulating media in nanophotonic systems due to the high impedance of TCOs at the ENZ frequency.

In addition, the optical properties of TCOs can be varied by optical or electrical means. Current research is focused on studying the ultrafast carrier dynamics in doped zinc oxide films using transient pump-probe spectroscopy. We have shown that CMOScompatible doped zinc oxide films can achieve a 40% change in reflection (30% in transmission) with ultrafast dynamics (< 1 ps) under a small fluence of $3\,\mathrm{mJ/cm^2}$. Consequently, TCOs are shown to be extremely flexible materials, enabling fascinating physics and unique devices for applications in the NIR regime.

ACKNOWLEDGMENT

This work was supported by ONR MURI N00014-10-1-0942.

REFERENCES

1. Boltasseva, A. and H. Atwater, *Science*, Vol. 331, No. 6015, 290–291, 2011.
2. Kim, J., et al., *IEEE Journal of Selected Topics in Quantum Electronics*, Vol. 19, 4601907–4601907, 2013.
3. Kim, J., et al., *CLEO: QELS_Fundamental Science. Optical Society of America*, 2014.

Photonic Spin Hall Effect with Nearly 100% Efficiency

Weijie Luo[1], **Shiyi Xiao**[1], **Qiong He**[1, 2], **Shulin Sun**[3], **and Lei Zhou**[1, 2]

[1]State Key Laboratory of Surface Physics
Key Laboratory of Micro and Nano Photonic Structures (Ministry of Education)
Fudan University, Shanghai 200438, China
[2]Collaborative Innovation Center of Advanced Microstructures
Fudan University, Shanghai 200433, China
[3]Shanghai Engineering Research Center of Ultra-Precision Optical Manufacturing, Green Photonics
Department of Optical Science and Engineering, Fudan University, Shanghai 200433, China

Abstract— Photonic spin hall effect (PSHE), that spin-polarized photons can be laterally separated in transportation, gains increasing attention from both science and technology, but available mechanisms either require bulky systems or exhibit very low efficiencies. Here we demonstrate that a giant PSHE with $\sim$ 100% efficiency can be realized at certain meta-surfaces with deep-subwavelength thicknesses. Based on rigorous Jones-Matrix analysis, we establish a general criterion to design meta-surfaces that can realize 100%-efficiency PSHE. The criterion is approachable from two distinct routes at general frequencies. As a demonstration, two microwave meta-surfaces are fabricated and then experimentally characterized, both showing $\sim$ 90% efficiencies for the PSHE. Our findings pave the road for many exciting applications based on high-efficiency manipulations of photon spins, with a polarization detector experimentally demonstrated here as an example.

Control of Ultrafast Coherent Nonlinear Response of Plasmonic Metasurfaces

Giovanni Sartorello[1], **Nicolas Olivier**[1], **Jingjing Zhang**[1,2], **Weisheng Yue**[3], **Alexey Krasavin**[1], **Pavel Ginzburg**[1], **Grégory Wurtz**[1], **and Anatoly Zayats**[1]

[1]King's College London, UK
[2]Technical University of Denmark, Denmark
[3]King Abdullah University of Science and Technology, Saudi Arabia

Abstract— Nonlinear phenomena are widely studied in nano-optics, and are often implemented in synergy with plasmonic effects to provide strong field enhancement. Research on arrays of plasmonic nanostructures can form the basis for the development of efficient, active metasurfaces with designed coherent and ultrafast optical functionalities. These can be useful in applications requiring for example frequency conversion or efficient integrated quantum sources. This work is developed within this context and aimed at gaining the understanding necessary to develop coherent nonlinear metasurfaces rationally.

The unit cell of the metasurface we study (Fig. 1(a)) is a 30 nm high Au cut disc. It is designed to support plasmonic resonances at both fundamental and harmonic frequencies. The extinction spectrum (Fig. 1(b)) exhibits a Fano resonance in the visible and a magnetic dipole resonance in the near-IR, both optically active due to the presence of the slit [1] and at the basis of the strong coherent response of the metasurface.

We experimentally study and discuss the dispersion of both second and third-order nonlinear processes produced by this structure with a particular focus on the mechanisms enabling their optically-controlled modulation at the sub-picosecond time scale. The experiments, including pump-probe spectroscopy, are rationalized using theoretical considerations and numerical computations.

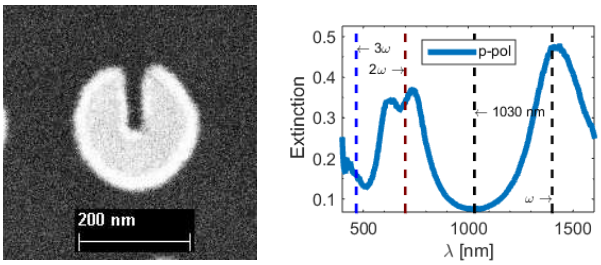

(a) (b)

Figure 1: (a) SEM image of split Au nanodisk. (b) Extinction spectrum.

Figure 2: Two-colour pump-controlled nonlinear Fourier response spectrum of a plasmonic resonator array (emission angle v. wavelength). "SHG" and "THG" mean second and third-harmonic generation respectively. SFG indicates sum-frequency generation and FWM four-wave mixing.

REFERENCES

1. Klein, M. W., M. Wegener, N. Feth, and S. Linden, "Experiments on second-and third-harmonic generation from magnetic metamaterials," *Opt. Express*, Vol. 15, No. 8, 5238–5247, 2007.

Polarization Measurement Method Based on Metasurface

Dandan Wen[1], **Fuyong Yue**[1], **Santosh Kumar**[1], **Yong Ma**[1], **Ming Chen**[1, 2], **Ximing Ren**[1], **Peter E. Kremer**[1], **Brian D. Gerardot**[1], **Mohammad R. Taghizadeh**[1], **Gerald S. Buller**[1], **and Xianzhong Chen**[1]

[1]Institute of Photonics and Quantum Sciences, School of Engineering and Physical Sciences
Heriot-Watt University, Edinburgh, EH14 4AS, UK
[2]Guangxi Experiment Center of Information Science
Guilin University of Electronic Technology, Guilin 541004, China

Abstract— Polarization is one of the fundamental properties of electromagnetic radiation. Based on the measurement and interpretation of the polarization of light waves, polarimetry has found its applications in many areas of science and technology, ranging from ellipsometry, remote sensing to polarization light scattering and ophthalmic polarimetry. Although the traditional measurement systems bring distinguished functionality in measuring speed and accuracy, their applications are still limited due to the various polarization elements and complicated data processing system adopted, which result in large volume and high cost. What's more, the miniaturization of measurement systems currently used to characterize the polarization state of light is limited by the bulky optical components used such as polarizers and waveplates. We propose and experimentally demonstrate a simple and compact approach to characterize the polarization state of light using an ultrathin (40 nm) gradient metasurface. A completely polarized light beam is decomposed into a left circularly polarized (LCP) beam and a right circularly polarized (RCP) beam, which are steered in two directions by the metasurface consisting of nanorods with spatially varying orientations. By measuring the intensities of the refracted light spots, the ellipticity and handedness of various incident polarization states are characterized at a range of wavelengths and used to determine the polarization information of the incident beam. Interestingly, since the refracted LCP and RCP light diverge naturally from each other, the metasurface can also be used as a circular polarization beam splitter, whose split angle is determined by controlling the spatial distribution of the nanorods in the metasurface.

Waveform-selective Metasurfaces to Distinguish Different Waves at the Same Frequency

H. Wakatsuchi[1, 2]

[1]Center for Young Innovative Researchers, Nagoya Institute of Technology, Japan
[2]Department of Electrical and Electronic Engineering, Nagoya Institute of Technology, Japan

Abstract— In general the responses of materials to an electromagnetic wave depend on the composite molecules and incoming frequency. Although the advent of metamaterials [1, 2] allowed us to obtain electromagnetic properties independent of composite molecules, still none of materials has permitted sensing different waves at the same frequency unless they had nonlinearity [3]. However, such nonlinearity was controlled by the magnitude of the incoming wave or bias. Recently we have reported circuit-based metasurfaces composed of circuit components including schottky diodes, capacitors, inductors and resistors. These metasurfaces allowed us to distinguish different surface waves even at the same frequency in response to their waveforms or pulse widths [4–7]. In this paper we demonstrate that such a new capability termed *waveform selectivity* is not limited to surface waves but can be applied to controlling different types of incoming waves including free space waves normal to the metasurfaces. The metasurfaces demonstrated here are composed of periodically deployed square patches, ground plane, and dielectric spacer (Rogers3003). In each gap between square patches, a set of four diodes is deployed to play a role of a diode bridge and to convert the incoming frequency component to zero frequency. This frequency conversion is used together with the time domain response of capacitors or inductors deployed inside diode bridges, which ends up with sensing specific waveforms even at the same frequency. Under these circumstances, capacitor-based metasurfaces more effectively absorb short pulses, while inductor-based metasurfaces absorb longer pulses or continuous waves. The use of such waveform-selective metasurfaces gives us a new capability to control electromagnetic properties and thus is expected to develop new kinds of microwave applications and technologies, e.g., waveform-selective wireless communications [8].

ACKNOWLEDGMENT

This work was in part supported by the Japan Science and Technology Agency under Funds for the Development of Human Resources in Science and Technology, Ministry of Internal Affairs and Communications under Strategic Information and Communications R&D Promotion Programme, Japan Society for the Promotion of Science under Grant-in-Aid for Challenging Exploratory Research 26630175, the Murata Science Foundation, Tatematsu Foundation, the Telecommunications Advancement Foundation, the Hori Sciences and Arts Foundation, and Toukai Foundation for Technology.

REFERENCES

1. Smith, D. R., W. J. Padilla, D. C. Vier, S. C. Nemat-Nasser, and S. Schultz, "Composite medium with simultaneously negative permeability and permittivity," *Phys. Rev. Lett.*, Vol. 84, 4184–4187, 2000.
2. Sievenpiper, D., L. Zhang, R. F. J. Broas, N. G. Alexópolous, and E. Yablonovitch, "High-impedance electromagnetic surfaces with a forbidden frequency band," *IEEE Trans. Microw. Theory Tech.*, Vol. 47, 2059–2074, 1999.
3. Chen, H., W. J. Padilla, J. M. O. Zide, A. C. Gossard, A. J. Taylor, and R. D. Averitt, "Active terahertz metamaterial devices," *Nature*, Vol. 444, 597–600, 2006.
4. Wakatsuchi, H., S. Kim, J. J. Rushton, and D. F. Sievenpiper, "Waveform-dependent absorbing metasurfaces," *Phys. Rev. Lett.*, Vol. 111, 245501, 2013.
5. Wakatsuchi, H., J. J. Rushton, J. Lee, F. Gao, M. Jacob, S. Kim, and D. F. Sievenpiper, "Experimental demonstration of nonlinear waveform-dependent metasurface absorber with pulsed signals," *Electron. Lett.*, Vol. 49, 1530–1531, 2013.
6. Wakatsuchi, H., D. Anzai, J. J. Rushton, F. Gao, S. Kim, and D. F. Sievenpiper, "Waveform selectivity at the same frequency," arXiv:1412.6308, 2014.
7. Eleftheriades, G. V., "Electronics: Protecting the weak from the strong," *Nature*, Vol. 505, 490–491, 2014.

Session 2P2a
Nonlinear Plasmonics

Optimization of Second Harmonic Generation in Plasmonic Nanostructures by Mode Matching

Gabriel D. Bernasconi, Jérémy Butet, and Olivier J. F. Martin
Nanophotonics and Metrology Laboratory (NAM)
Swiss Federal Institute of Technology Lausanne (EPFL), Lausanne 1015, Switzerland

Abstract— In the dipolar approximation, second harmonic generation (SHG) is forbidden in the bulk of centrosymmetric nanostructures (such as gold) but can arise at the interface thanks to the breaking of inversion symmetry. As a consequence, SHG is an appropriate tool to acquire information about nanostructures surfaces. In this presentation, we will show that SHG can also provide information on the underlying modes supported by a given structure. Furthermore, a combination of modes at the fundamental frequency can generate a SH wave supported by modes that cannot be excited at the fundamental frequency, the so-called dark modes. This optical nonlinear process can then be used to measure the radiation pattern of those dark modes. When the fundamental frequency matches a resonance of the structure, the high field enhancement will yield a high SHG. Additionally, if the SH frequency matches another higher frequency mode, the SH emission will be stronger and thus more easily measurable. Hence, being able to optimize the structure so that both SHG and fundamental frequencies match resonant modes is very useful for practical applications.

Using a surface integral equation method (SIE) to describe 3D nanostructures, we study the behavior of the eigenvalues of the corresponding matrix $\mathbf{M}(\omega)$ where ω is the frequency. First we consider the equation relating the surface currents j_{surf} to the excitation field E_{inc}

$$\mathbf{M}(\omega) j_{surf} = E_{inc}. \tag{1}$$

Then, by setting the incident field E_{inc} to zero, we can find the (non-trivial) solutions that don't need any external excitations to exist. This is done by re-writing Equation (1) as

$$\mathbf{M}(\omega) V_i = \lambda_i V_i = 0. \tag{2}$$

Looking for the frequencies ω where one of the eigenvalue λ_i of $\mathbf{M}(\omega)$ tends to zero, it is possible to find the eigenmodes. The frequency ω thus corresponds to the resonant frequency, and the eigenvector V_i associated to the current distribution (and so to the charge distribution) corresponds to the eigenmode. By scanning the complex frequency plane, we can find the multiple resonances supported by a given nanostructure.

This approach is especially interesting since dark modes cannot be found by considering a plane wave excitation. Indeed, the scattering spectrum can be used as prior knowledge of the resonant frequency (both its real and imaginary parts, the latter being related to the losses and the width of the resonance) at which the bright modes can be excited. Having the mode structure in mind allows optimizing the geometry in order to reach the most efficient SHG at the nanoscale, as will be demonstrated with different experimental configurations.

Linear and Nonlinear Spectral Signatures of Surface Plasmon Polaritons

S. A. Ponomarenko, L. Wang, and F. Che
Department of Electrical and Computer Engineering, Dalhousie University, Halifax, NS, B3J 2X4, Canada

Abstract— We explore spectral behavior of the fundamental and sum-frequency fields generated in thin metal films upon reflection of polychromatic light and elucidate a surface plasmon polariton role therein.

The field of plasmonics has lately experienced a truly explosive growth [1]. Much research in plasmonics has so far been focused on linear light-matter interaction modalities [2], owning largely to the success of plasmonic-based sensors as a powerful tool for probing surfaces [3]. However, resonantly enhanced local electric fields bring about pronounced enhancement of nonlinear responses of plasmonic materials as well [1].

Although the vast majority of work in plasmonics deals with quasi-monochromatic light, there has been growing interest in spectral signatures of plasmon enhanced electromagnetic fields. In particular, the linear optical response of homogenous [4] and inhomogeneous — periodic or random [5] — plasmonic nanostructures, probed with broadband light beams, has been recently examined. However, to the best of our knowledge, plasmon-enhanced *nonlinear* optical processes, excited by polychromatic light sources, have not yet been studied. In this context, it is especially instructive to learn whether plasmon polaritons, excited on the surface of a conducting material or nanostructure, leave any signatures in the far-field spectra of generated second-order nonlinear waves. The affirmative answer to this question can trigger new developments in surface nonlinear spectroscopy, microscopy, and surface morphology studies.

In this work, we investigate the spectral behavior of the fundamental and sum-frequency waves in the surface SFG from a thin metal film with the polychromatic (pulsed) incident light. The wide bandwidth of the source makes it possible to realize SFG with a single source: any pair of monochromatic components within the source spectrum gives rise to a sum-frequency wave through the surface SFG process. We assume a wellcollimated broadband light source such that its output can be treated as a plane wave. The source plane wave is assumed to be incident on a thin metal film, arranged in the Kretchmann configuration at a plasmon coupling angle.

For symmetric source spectra in the Kretchmann geometry, one would expect the SFG spectrum to peak at half the carrier wavelength of the source. We show, however, that at the incidence angle corresponding to light coupling to the SPP, the reflected sum-frequency wave (SFW) spectrum gets blue-shifted from the expected maximum whereas the reflected fundamental wave has a spectral hole at the carrier frequency. We further demonstrate that the magnitude of the effect depends on the bandwidth of the source spectrum and the incidence angle: The shifts of SFW spectra become more pronounced as the source bandwidth increases, while at a certain angle a spectral switch is observed. Also, as the incidence angle deviates from the plasmon coupling angle, all spectral changes disappear. The appearance of large SFW spectral shifts and switches can serve as an unambiguous plasmon signature in nonlinear surface spectroscopy.

REFERENCES

1. Stockman, M. I., "Nanoplasmonics: past, present, and glimpse into future," *Opt. Express*, Vol. 19, 22029–22106, 2011.
2. Novotny, L. and B. Hechi, *Principles of Nano-Optics*, Cambridge University, Cambridge, 2006.
3. Homola, J., S. S. Yee, and G. Gauglitz, "Surface plasmon resonance sersors: Review," *Sensors and Actuators B*, Vol. 54, 3–15, 1999.
4. Lan, T.-H., Y.-K. Chyng, J. Li, and C.-H. Tien, "Plasmonic rainbow rings induced by white radial polarization," *Opt. Lett.*, Vol. 37, 1205–1207, 2012.
5. Nishijima, Y., L. Roza, and S. Juodkazis, "Surface plasmon resonances in periodic and random patterns of gold nano-disks for broadband light harvesting," *Opt. Express*, Vol. 20, 11466–11477, 2012.

Metallic Nanocones as Nonlinear Optical Point Light Sources

Monika Fleischer[1], **Dominik A. Gollmer**[1], **Philipp Reichenbach**[2], **Anke Horneber**[3], **Andreas Hille**[2], **Josip Mihaljevic**[3], **Christian Schäfer**[1], **Alfred J. Meixner**[3], **Dai Zhang**[3], **Dieter P. Kern**[1], **and Lukas M. Eng**[2]

[1]Institute for Applied Physics, Eberhard Karls University Tuebingen, Germany
[2]Institute of Applied Photophysics, Technische Universität Dresden, Germany
[3]Institute of Physical and Theoretical Chemistry, Eberhard Karls University Tuebingen, Germany

Abstract— The search for time-stable and tunable point light sources with ultra-small dimensions constitutes a challenging task since the early days of nano-optics. Quantum dots, single molecules, or NV-centers in nano-diamonds may manifest ultimately small point light sources. Nevertheless, many such emitters suffer from blinking or photo-bleaching. In contrast, plasmonic nanostructures or pointed metal tips exhibit more stability even when illuminated with focused laser beams for strong field enhancement. In particular nonlinear effects such as second-harmonic generation (SHG) may benefit greatly from the strong and highly localized near-fields.

Using specially developed techniques, we fabricate plasmonic nanocones from thin films of different metals on glass/ITO and on silicon [1]. The cones with a tip radius down to less than 10 nm act as optical antennas [2, 3]. The external electric field is concentrated near the cone tip, leading to a narrow region of high near-field enhancement, which can be employed for SHG as well as tip-enhanced Raman spectroscopy [4] or molecule sensing [5, 6]. The geometry of the metallic nanocones breaks the centro-symmetry, thus providing stronger second-harmonic polarizability along the direction of symmetry-breaking, and concentrates the field energy via both plasmon oscillations and the lightning-rod effect into the cone tip. We demonstrate that plasmonic nanocones can act as nonlinear optical point-like sources for spectrally narrow second harmonic generation and a spectrally broad two-photon photoluminescence signal when excited by near-infrared femto-second laser pulses [7]. The nonlinear emission from cones of four different sizes is observed in two different setups (top and bottom illumination). Either the tip of the nanocones or the cone base is predominantly excited depending on the polarization of the excitation and of the respective plasmon resonance frequencies of the two modes. By size variation and choice of the illumination, the tip-to-base-edge ratio of the emission can be optimized. Such nanocones can thus potentially be used as nonlinear single point light sources for scanning near-field probing or lab-on-chip sensor applications.

REFERENCES

1. Fleischer, M., et al., *Nanotechnology*, Vol. 21, 065301, 2010.
2. Fleischer, M., et al., *Appl. Phys. Lett.*, Vol. 93, 111114, 2008.
3. Schäfer, C., et al., *Nanoscale*, Vol. 5, 7861, 2013.
4. Fleischer, M., et al., *ACS Nano*, Vol. 5, 2570, 2011.
5. Horrer, A., et al., *Small*, Vol. 9, 3987, 2013.
6. Schäfer, C., et al., *Lab Chip*, Vol. 15, 1066, 2015.
7. Reichenbach, P., et al., *Opt. Exp.*, Vol. 22, 15484, 2012.

Nonlinear Conversion of Continuous Wave Light by Fano Resonant All-plasmonic and Molecular-plasmonic Hybrid Nanostructures

Musa Kurtulus Abak[1, 2], Bilge Can Yildiz Karakul[2, 3], Mehmet Emre Tasgin[4], Ljiljana Fruk[5], Marco Lazzarino[6], and Alpan Bek[2, 3]

[1]Micro and Nanotechnology Program, Middle East Technical University, Ankara, Turkey
[2]Center for Solar Energy Research and Applications (GÜNAM)
Middle East Technical University, Ankara, Turkey
[3]Physics Department, Middle East Technical University, Ankara, Turkey
[4]Institute of Nuclear Sciences, Hacettepe University, Ankara, Turkey
[5]DFG-Centre for Functional Nanostructures
Karlsruhe Institute of Technology, Karlsruhe, Germany
[6]CNR-IOM, Area Science Park, Trieste, Italy

Abstract— Finding a possibility to control the activation of a single molecule is interesting since it paves the way to realize logic devices as small as molecules. This can be achieved by carefully designed devices which can interface a single molecule and interact with it at the same size scale. Such devices can be of electrical, magnetic or optical origin [1] and may induce changes in the properties of a single or few molecules which can act as switching registers for data processing or data storage at the nanometer scale. Electrical devices at the single molecule size level include break-junctions, scanning tunneling junctions and molecular landers. Optical devices that can interface a single molecule among an ensemble of many molecules are yet lacking. The main difficulty lies in the diffraction limit of practically $\sim$ 150–180 nm focal size for a wavelength of 600 nm light. Compared to a few nm sizes of individual molecules, unambiguous activation of single molecules by means of absorption of light can only be possible for a device prepared from a sparse ensemble of molecules. Thanks to advancement in near-field optical instrumentation technology this main difficulty can be circumvented as the near-field light intensities typically have a very strong nonlinear dependence on distance (from $\sim r^3$ to $\sim r^6$). Strongly confined, highly intense fields of light called "hot spots," can be achieved by engineering the nanoscale environment of a single molecule. By utilizing plasmonic resonances of nanoscale metal structures, such spots can be arranged to occupy from a few down to a single molecule. Nevertheless in these schemes, a broad far-field background component of the activation wavelength is inevitably superposed on to the near-field of the nanoparticles. This imposes limitations on single molecule activation experiments to be performed with high fidelity.

In this study we propose a method which is feasible for deterministic activation of few molecules. We demonstrate effective background-free continuous wave nonlinear optical excitation of enhanced yellow fluorescent protein molecules that are sandwiched between asymmetrically constructed plasmonic gold nanoparticle clusters [2]. We observe that infrared photons are converted to visible photons through efficient plasmonic second harmonic generation. Our theoretical model and simulations demonstrate that nonlinear conversion of continuous wave light becomes possible by Fano resonance in the nonlinear response. We show that nonlinearity enhancement of plasmonic nanostructures via coupled quantum mechanical oscillators such as molecules can be several orders larger as compared to their classical counterparts [3, 4]. Our numerical simulations demonstrate that observation of second harmonic generation with continuous wave laser becomes possible owing to the cooperative action of conversion enhancement through Fano resonance, hybridization in the plasmon absorption spectrum and the size asymmetry of nanoparticle dimers.

We further investigate the Fano resonances in intrinsic nonlinear optical response of single or coupled metal nanoparticles. We show that Fano resonance conditions can be tuned to enhance nonlinear optical conversion. When a bare metal nanoparticle is coupled with a plasmonic nonlinear converter, second harmonic generation can be enhanced by several orders of magnitude. This phenomenon emerges due to path interference effects. It is shown that second harmonic generation enhancement in hybrid structures can be obtained even in the absence of coupled quantum emitters [5]. This is an important simplification for facilitating the use of purely metal nanoparticles with appropriate functionality.

REFERENCES

1. Browne, W. R. and B. L. Feringa, *Annu. Rev. Phys. Chem.*, Vol. 60, 407–428, 2009.

2. Salakhutdinov, I., D. Kendziora, M. K. Abak, D. Turkpence, L. Piantanida, L. Fruk, M. E. Tasgin, M. Lazzarino, and A. Bek, Preprint at http://arxiv.org/abs/1402.5244v2, 2014.
3. Türkpence, D., G. B. Akguc, A. Bek, and M. E. Tasgin, *J. Opt.*, Vol. 16, 105009, 2014.
4. Tasgin, M. E., Preprint at http://arxiv.org/abs/1404.3901, 2014.
5. Yildiz, B. C., M. E. Tasgin, M. K. Abak, S. Coskun, H. E. Unalan, and A. Bek, Preprint at http://arxiv.org/abs/1412.0238, 2014.

Resonantly Enhanced Nonlinear Toroidal Moments in Plasmonic Metamaterials

D. Timbrell[1], **N. Braz**[2], **M. Weismann**[1, 3], **P. A. Warburton**[2], **and N. C. Panoiu**[1]

[1]Department of Electronic and Electrical Engineering, University College London
Torrington Place, London, WC1E 7JE, United Kingdom
[2]London Centre of Nanotechnology, University College London, London, WC1H, 0AH, United Kingdom
[3]Photon Design Ltd, 34 Leopold Street, Oxford OX4 1TW, United Kingdom

Abstract— We theoretically and computationally demonstrate that a plasmonic metamaterial containing split-ring resonators exhibits a strong toroidal resonance at the second harmonic (SH). The electric dipole, magnetic dipole, electric quadrupole, and toroidal dipole determined by the charge and current distributions at the SH are determined by firstly calculating the electric field at the fundamental frequency (FF) and, subsequently, the corresponding nonlinear polarization (nonlinear currents) induced by the FF field. In addition, the total transmission, reflection and absorption spectra for this structure, both at the FF and SH, are presented and the connection between the spectral features of these optical coefficients and those of the electromagnetic multipoles are discussed.

Toroidal dipoles, first discovered by Zel'dovich in 1957, are formed when the magnetic dipoles of a system form a closed loop, all pointing in the toroidal direction. Although it is often neglected due to its small contribution, this dipole moment can, in a similar fashion to the other electromagnetic moments, be considered as a source term of a multipolar expansion of charge and current distributions. In this work, four gold split-ring resonators embedded in a dielectric background constitute the basis for our metamaterial. In order to induce a resonant electromagnetic response in each ring, the incident light impinges at an angle of 45° with respect to the planes of the rings. The electromagnetic interactions of our metamaterial with the incident light were simulated at the FF using the rigorous coupled-wave analysis method whereas the optical response at the SH was analyzed using a nonlinear version of the generalized source method. In particular, after parameters were enhanced to ensure a strong resonance we computed the spectral dependence of the total reflection, transmission, and absorption coefficients from 2 μm to 4 μm, a resonance being apparent at $\lambda = 2.5\,\mu\text{m}$.

The generated polarization at the SH, which induces the nonlinear toroidal dipole, is a result of a nonlinear optical process occurring primarily at the surface of the metallic rings embedded in the dielectric background. As every electromagnetic moment is dependent upon the nonlinear polarization (or equivalently, via the continuity equation, the corresponding current density), this physical quantity must be calculated in order to fully analyze the multipole moments. To this end, the unit cell of our metamaterial was covered by a three-dimensional computational grid, with the electric field being calculated for every grid point. This field at the FF was then used to calculate the distribution of the nonlinear polarization, which was subsequently employed to compute the nonlinear electric dipole, magnetic dipole, electric quadrupole, and toroidal dipole.

Surface Polaritons in a Negative-index Metamaterial with Active Raman Gain

Chaohua Tan[1] and Guoxiang Huang[2]

[1]State Key Laboratory of Precision Spectroscopy and Department of Physics
East China Normal University, Shanghai 200062, China
[2]ECNU-NYU Joint Physics Research Institute at NYU-Shanghai, Shanghai 200062, China

Abstract— We propose a scheme to realize stable propagation of linear and nonlinear surface polaritons (SPs) by placing a N-type four-level quantum emitters at the interface between a dielectric and a negative-index metamaterial (NIMM). We show that in linear propagation regime SPs can acquire an active Raman gain (ARG) from a pump field and a gain doublet appears in the gain spectrum of a signal field induced by the quantum interference effect from a control field. The ARG can be used not only to completely compensate the Ohmic loss in the NIMM but also to acquire a superluminal group velocity for the SPs. We also show that in the nonlinear propagation regime a huge enhancement of the Kerr nonlinearity of the SPs can be obtained. As a result, ARG-assisted $(1+1)$- and $(2+1)$-dimensional superluminal surface polaritonic solitons with extremely low generation power may be produced based on the strong confinement of the electric field at the dielectric-NIMM interface.

REFERENCES

1. *Phys. Rev. A*, Vol. 89, 033860, 2014.
2. *Phys. Rev. A*, Vol. 91, 023803, 2015.

Session 2P2b
FocusSession.SC2: Plasmonic Nanolasing

Plasmonic Stopped-light Nanolasing

Ortwin Hess
The Blackett Laboratory, Department of Physics, Imperial College London
Prince Consort Road, London SW7 2AZ, United Kingdom

Abstract— Every Laser has two vital components: a (laser) again material and a light-feedback mechanism. In normal lasers feedback is provided by placing the gain material between mirrors — i.e., inside a cavity. Going beyond traditional cavity-concepts, recently conceived nanolasers employ plasmonic resonances for feedback, allowing them to concentrate light into mode volumes that are no longer limited by diffraction [1]. The use of localized surface plasmon resonances as cold-cavity modes, however, is only one route to lasing on subwavelength scales. Lasing, in fact, does not require modes predefined by geometry but merely a feedback mechanism [2].

Here we demonstrate that the concept of dispersion-less stopped-light [3] allows by combination of nanoplasmonics with quantum gain materials [4] *stopped-light lasing* in hybrid nanoplasmonic heterostructures.

In a stopped-light laser, photons are trapped and amplified in space just at the point of their emission. It will be discussed that, at the stopped-light point, a stable lasing mode can form over a finite region of gain material due to the arising local (cavity-free) feedback in the form of a sub-wavelength optical vortex.

The remarkable spatio-temporal dynamics of nanoplasmonic stopped-light lasing is studied on the basis of a Maxwell-Bloch Langevin approach [4]. Moreover, a new rate-equation framework is shown to grasp the particular physics of stopped-light lasing involving [4]. The observed high-β characteristics and picosecond relaxation oscillations of cavity-free stopped-light lasing can potentially allow for the design of thresholdless plasmonic laser diodes that can be modulated with THz speeds.

REFERENCES

1. Hess, O. and K. L. Tsakmakidis, *Science*, Vol. 339, 654, 2013.
2. Hamm, J. M. and O. Hess, *Science*, Vol. 340, 1298, 2013.
3. Tsakmakidis, K. L., T. W. Pickering, J. M. Hamm, A. F. Page, and O. Hess, *Phy. Rev. Lett.*, Vol. 112, 167401, 2014.
4. Pickering, T., J. M. Hamm, A. F. Page, S. Wuestner, and O. Hess, *Nature Communications*, Vol. 5, 4971, 2014.

Metal Nanoantennas: Nonlinear Response and Enhanced Light-matter Interaction

Rudolf Bratschitsch
Institute of Physics, University of Mnster, Münster D-48149, Germany

Abstract— Metal nanoantennas have been demonstrated to work as optical analogues to their well-known counterparts at radio and microwave frequencies. We investigate the nonlinear optical properties of these plasmonic nanosystems. Using few-cycle femtosecond light pulses for excitation we find strong third harmonic generation from single nanoantennas and study the emission characteristics of the created harmonics [1, 2]. Nanoantennas are also well suited to enhance the light-matter interaction. We couple nanoantennas to atomically thin semiconductors and present the exceptional optical properties of this hybrid system [3].

REFERENCES

1. Hanke, T., et al., *Phys. Rev. Lett.*, Vol. 103, 257404, 2009.
2. Hanke, T., et al., *Nano Lett.*, Vol. 12, 992, 2012.
3. Kern, J., et al., Submitted.

Ultrafast Plasmonic Lasers at the Surface Plasmon Frequency

Themistoklis P. H. Sidiropoulos[1], **Robert Röder**[2], **Sebastian Geburt**[2], **Ortwin Hess**[1], **Stefan A. Maier**[1], **Carsten Ronning**[2], **and Rupert F. Oulton**[1]

[1]Imperial College London, Prince Consort Road, UK-SW7 2BZ London, UK
[2]University of Jena, Max-Wien-Platz 1, D-07743 Jena, Germany

Abstract— Light-matter interactions are generally slow as the wavelengths of optical and electronic states differ greatly. Surface plasmon polaritons, the electromagnetic excitations at metal-dielectric interfaces, have generated significant interest because their spatial scale is decoupled from the vacuum wavelength, promising accelerated light-matter interactions. In principle, the acceleration of the dynamics in recently demonstrated surface plasmon lasers [1] can also be achieved [2]. In this talk, we report the observation of sub picosecond pulses from plasmonic zinc oxide (ZnO) nanowire lasers [3]. Operating at room temperature, ZnO excitons lie near the SPP frequency in such silver-based plasmonic lasers, leading to accelerated spontaneous recombination, gain switching, and gain recovery compared to conventional non-plasmonic ZnO nanowire lasers.

The plasmonic lasers consist of ZnO nanowires separated from a Silver substrate by a thin 10 nm LiF gap layer in a so-called hybrid geometry. The nanowires were optically pumped (150 fs pulses @ 800 KHz) at 355 nm and their emission was monitored spectrally at room temperature. Evidence for the lasing of plasmonic modes arises from a range of tests including emission polarization, reduced cut-off diameter where laser action ceases as well as temporal dynamics.

We have measured the temporal characteristics of these plasmonic lasers using a novel double-pump approach that exploits the natural non-linearity of the laser itself to expose its own dynamics. We find that gain recovery times in the very smallest diameter lasers occurs on ~ 1 ps time scales (Fig. 1(b)). Furthermore,we see extremely strong acceleration of the optical processes with decreasing nanowire diameter for plasmonic lasers consistent with increasing mode confinement. Nanowires without a metal substrate however, become slower with decreasing nanowire diameter, which we attribute to the loss of mode confinement.

Our study shows that plasmon pulses can be as fast as gain the thermalization process of excitons in ZnO (< 800 fs), which seems to preclude lasing in the thinnest and fastest devices (diameter < 120 nm). The capability to combine surface plasmon localization with ultra fast amplification provides the means for generating extremely intense optical fields with applications in sensing, non-linear optical switching, as well as potentially in the physics of strong field phenomena.

REFERENCES

1. Oulton, R. F., *Mater. Today*, Vol. 15, 592–600, 2012.
2. Altug, H., et al., *Nat. Phys.*, Vol. 2, 484–488, 2006.
3. Sidiropoulos, T., et al., *Nat. Phys.*, Vol. 10, 870–875, 2014.

Investigation of Superradiant Surface Plasmon Mode Generated in Ag Slit Array/InGaAsP at Room Temperature

Kwang Jun Ahn[1], **Seung-Hyun Kim**[2], **and Ki-Ju Yee**[2]

[1]Department of Energy Systems Research & Department of Physics
Ajou University, Suwon 443-749, Korea
[2]Department of Physics, Chungnam National University, Daejeon 305-764, Korea

Abstract— A well-known method to generate surface plasmon (SP) is the SP amplification by stimulated emission (SPASER) [1]. Similar to conventional lasers for generating coherent photons, the operation of SPASERs is also accomplished by stimulated emission of excited light emitters.

In this study, we generated SP radiation with a completely different approach. A strong burst of the SP mode was created by a cooperative radiation process called superradiance (SR) [2]. Fluctuating electromagnetic fields resulting from highly excited light emitters and their reabsorption by the emitters build a phase-locked macroscopic polarization as a source of the SR. In Fig. 1(a) we schematically illustrate our sample structure. A 100 nm-thick silver slit array was fabricated on a 700 nm-thick InGaAsP bulk semiconductor grown on an InP substrate. The sample was optically pumped by a femtosecond pulse laser at a center wave length of 800 nm, and time-resolved emission from samples was measured by using frequency up-conversion technique. By varying the slit period Λ, the fill factor FF (the ratio of the slit width to the period), and temperature we were able to control the emission wavelength in a 400 nm-wide telecommunication band ($\lambda \sim 1.5\,\mu$m) at room temperature. Furthermore, our samples with $\Lambda > 430$ nm support for the simultaneous generation of the SP and a pure photonic (waveguide) mode (WG). Even though the SP mode has larger losses than the WG mode does, we experimentally and theoretically found that the SP mode overwhelms the WG one in a high excitation regime (Fig. (b)) on account of the enhanced dipole moment of the gain medium due to its mirror image. We expect that our new SP source can be applied for optical information processing as a mesoscopic quantum light source and investigating cooperative interaction of bosons in solid state many-body system.

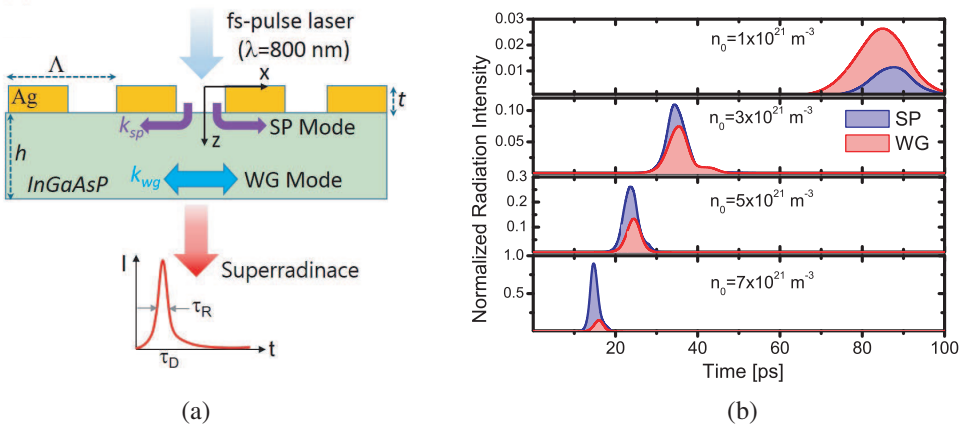

Figure 1: (a) Schematic illustration of the sample structure. (b) Simulated superradiant pulse profile of surface plasmon (SP) and waveguide (WG) modes depending on the excited carrier density (n_0) at $T = 300$ K.

Influence of Gold Nanoparticles on the Lasing Properties of Rh6G-PMMA Material

E. Vasileva, **A. Marinins**, **F. Ye**, **S. Popov**, **and M. Toprak**
School of Information and Communication Technology
KTH Royal Institute of Technology, Stockholm, Kista 164 40, Sweden

Abstract— Surface plasmons is a hot topic in the scientific world due to effect of local field enhancement. At the same time, continual research progress is ongoing in the laser industry. New materials are tested in order to create new laser types and to improve performances of the existing ones. In this study, two main trends of the research were combined to get the maximum benefits from both of them. In this paper, we analyze the influence of localized surface plasmons existing on the Au nanoparticles (NP) on the properties of dye molecules Rh6G in PMMA.

There are permanent debates about either localized surface plasmons produce quenching or enhancement of photoluminescence of the active media [1, 2]. In order to clarify the situation, Au NPs were placed in the matrix of Rh6G in PMMA. The size of the NPs was chosen in such a way that localized surface plasmon resonance band overlaps with absorption band of the laser medium. We found that the presence of Au nanoparticles caused several effects. The first one is the change of radiation and non-radiation rates in comparison with the pure samples of Rh6G in PMMA. The second one is the absorption efficiency of the doped samples was significantly increased in comparison to the undoped ones (Fig. 1). The third one is the influence of the gold concentration on the emission properties of the material. The varying stripe line method [3] used in our experiments showed exponential growth of the emission intensity depending on the distance light traveled inside the media symbolizes existence of optical gain. This dependence changes its behavior at the certain length where the lasing threshold occurs, that corresponds to the theory [4]. The measured emission spectra show the existence of the random laser (Fig. 2). At high concentration of Au NPs, the quenching of the luminescence by NPs introduces losses exceeding the amplification value that leads to the drop of optical gain and, consequently, stimulated emission. Energy transfer between dye molecules and Au NPs was shifted towards to NPs what caused strong quenching of luminescence. However the previous research done for the liquid solution of Rh6G in ethanol with Au NPs showed the possibility of the optical gain enhancement [5]. Therefore, optimized concentrations ratio between the dye molecules and nanoparticles has to be established. Also we surmise that the metal nanoparticles cause the temperature redistribution inside the material under pumping that influences on the optical gain value and leads to refractive index anisotropy.

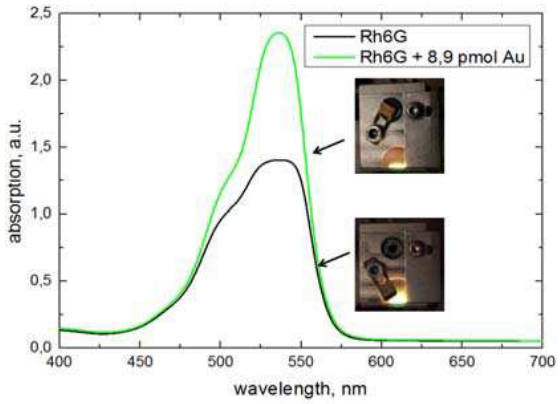

Figure 1: Absorption spectra for the sample of Rh6G with/without Au NPs. Inset: the photo of the samples.

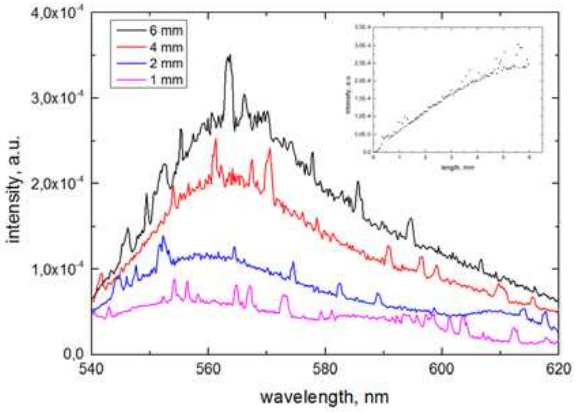

Figure 2: Measured emission spectra at different distances light traveled inside the media. Inset: Dependence of emission intensity at 575 nm wavelength from the length.

REFERENCES

1. Soller, T., et al., "Radiative and nonradiative rates of phosphors attached to gold nanoparticles," *Nano Lett.*, Vol. 7, 1941–1946, 2007.

2. Zakiah, W., et al., "Plasmonics enhancement of gain in random lasers," *Proceeding on Optoelectronics Communication Conference and Australian Conference Optical Fibre Technology*, July 6–10, 2014
3. Shaklee, K. L., et al., "Optical gain in semiconductors," *Journal of Luminescence*, Vol. 7, 284–309, 1973.
4. Zaitsev,O. and L. Deych, "Recent developments in the theory of multimode random lasers," *J. Opt.*, Vol. 12, 2010.
5. Dong, L., et al., "Lasing from water solution of Rhodamine 6G/gold nanoparticles: Impact of SiO_2-coating On Metal Surface," *IEEE Journal of Quantum Electronics*, Vol. 48, No. 9, 2012.

Magneto-optical Intensity Effects in Active Magneto-plasmonic Structures

Olga Borovkova[1], **Andrey Kalish**[1], **Petr Vetoshko**[1], **Vladimir Belotelov**[1], **Igor I. Syvorotka**[2], **Igor M. Syvorotka**[2], **and A. Luchechko**[3]

[1]Russian Quantum Center, Skolkovo, Russia
[2]Institute of Materials, SRC "Carat", Lviv, Ukraine
[3]Ivan Franko National University of Lviv, 107 Tarnavskogo Str., Lviv 79017, Ukraine

Abstract— Magnetic effects find their applications in modern data recording, storage and readout devices, optical isolators and etc.. In particular, modern hard disks use magnetic effects in ferromagnetic layers separated by thin layer of nonmagnetic dielectric. Direction of magnetization in domains of ferromagnetic layers encodes storage information. Thus, novel methods of the magnetization control and the enhancement of magnetic effects are required for the further development of technology. An employment of magneto-optical (MO) effects seems to be a very promising approach. MO effects mean that the magnetization of material essentially depends on the intensity and polarization of the light passing through the material. We are focused on the intensity MO effects like transverse magneto-optical Kerr effect (TMOKE). Such effects can be significantly enhanced by the excitation of surface plasmon-polaritons (SPPs) at the surface of ferromagnetic dielectric. In Ref. [1] it was investigated the influence of SPPs propagating along the interface of ferromagnetic dielectric film and the nanoscaled grating of noble metal on the TMOKE. SPPs increase the interaction area of light beam and magnetic material, and therefore enhance the MO effect in both reflected and transmitted light.

However, it is well-known that SPPs dissipate their energy through the interaction with metal that limits their propagation length. In our structure ferromagnetic material containing iron ions contributes additional losses. Thus, the problem of loss compensation and amplification of SPPs is crucial for the further enhancement of the MO effect.

Loss compensation and amplification of surface plasmon-polaritons have been investigated deeply in active nonmagnetic materials, like dye solution, or PMMA doped by quantum dots, etc. (see review [2]). Amplified spontaneous emission of surface plasmon polaritons can be observed at the interface with a resonant amplifying medium. In our work we consider a ferromagnetic film doped by Cr ions or ions of rear-earth elements, like Yb, Er, Nd. We address a magnetoplasmonic crystal of one dimensional gold grating deposited on the doped iron garnet grown on top of the non-magnetic gadolinium gallium garnet substrate. Transmittance and reflectance spectra and enhancement of magnetooptical effects were demonstrated on the value of the gain parameter and on the geometrical parameters of the magnetoplasmonic crystal and type of the dopants. Experimental observation of this phenomenon is discussed.

ACKNOWLEDGMENT

The work is supported by the Russian Foundation for Basic Research (projects Nos. 13-02-01122, 14-02-01012).

REFERENCES

1. Belotelov, V. I., et al., *Nature Nanotech.*, Vol. 6, 370–376, 2011.
2. Berini, P. and I. De Leon, *Nature Photon.*, Vol. 6, 16–24, 2012.

Classical Spaser

V. G. Bordo
Nanosyd, Mads Clausen Institute, University of Southern Denmark, Denmark

Abstract— A spaser is a hybrid plasmonic device which generates coherent surface plasmon polaritons (SPPs). The underlying mechanism of its operation is stimulated emission which occurs under an intensive optical or electrical pumping of a gain medium incorporated into the plasmonic structure. There is, however, a fundamental question: Is stimulated emission the only way to achieve an avalanche of SPPs?

In this talk, a principally new avenue to SPP generation will be considered. It is based on the utilization of a feedback mechanism which exists for an oscillating dipole moment in close vicinity (within a wavelength) from a reflecting surface. Such a dipole is driven by its own reflected field that modifies essentially its dynamics [1]. In particular, its damping constant is renormalized in accordance with the imaginary part of the reflected field at the dipole position. In the case where the latter quantity is negative the reflected field performs a positive work on the dipole oscillations thus providing a positive feedback. If an ensemble of dipoles is located nearby a surface their mutual interaction mediated by the reflected field can cause a collective polarization instability which is accompanied by lasing in the system [2]. This effect can occur, in principle, in any subwavelength structures. In the case of a dipole in/at a metal cavity the dipole field launches SPP modes acting back on the dipole polarization and thus establishing a feedback loop which can lead to self-excitation of surface plasmons (SESP). The considered mechanism is an essentially classical effect. It does not imply stimulated emission in the structure and hence does not require a population inversion in the dipole.

A possible implementation of the SESP effect in the cavity formed by a nanogap between two metals will be discussed in this talk. It is assumed that the gap material contains polarizable inclusions with resonance frequency being in the SPP frequency band. Basing on the dyadic Green's function of the structure, the equations for the SPP mode field in the cavity are investigated. It is shown that under certain conditions the field becomes unstable that leads to its self-excitation. The threshold criterion for self-excitation as well as the frequency of self-oscillation are derived in an analytical form. Calculations are carried out for a dielectric slab containing metal nanoparticles enclosed between Ag, Au and Cu surfaces.

REFERENCES

1. Chance, R. R., A. Prock, and R. Silbey, "Lifetime of an emitting molecule near a partially reflecting surface," *J. Chem. Phys.*, Vol. 60, No. 7, 2744–2748, 1974.
2. Bordo, V. G., "Lasing in nanowires: Ab initio semiclassical model," *Phys. Rev. A*, Vol. 88, No. 1, 013803-1–7, 2013.

Session 2P3
SC3: Advanced Optofluidics: Optical Control and Photonics in Microfluidics

Chiral Optofluidics

R. J. Hernández[1], **A. Mazzulla**[1], **P. Pagliusi**[1, 2], **C. Provenzano**[2], **M. G. Donato**[3], **O. Maragò**[3], **D. Kasyanyuk**[4], **Yu. Reznikov**[4], **and G. Cipparrone**[1, 2]

[1]Licryl Lab, CNR-IMIP, Rende, CS 87036, Italy
[2]Physics Department, University of Calabria, Rende, CS 87036, Italy
[3]UOS Messina, CNR-IPCF, Messina 98158, Italy,
[4]Institute of Physics, National Academy of Sciences of Ukraine, pr. Nauky 46, Kyiv 03028, Ukraine

Abstract— Chirality in soft matter is emerging as a tool to address innovative concepts in materials science, colloidal systems, optical and photonics devices, optomechanics, optofluidics etc..

Two examples are presented; the first one refers to chiral optofluidics devices and the second one to optofluidics strategies for nanoparticles assembling and manipulation.

We investigate the optical forces and torques on spherical polymeric particles with chiral arrangement of the inner structure consisting of supramolecular helices (left or right-handed). The methodological approach used for micro-particles preparation is such that the helical arrangement self-organizes in precursor cholesteric liquid crystal droplets by proper selection of a chiral dopant. The helical pitch is adjusted from nanometre to micrometre range by means of the dopant concentration. The helicoidal arrangement can leads to a shell structure of the refractive index and to a selective Bragg phenomenon that makes them to behave as chiral spherical reflectors for light propagating along the helical axis and wavelength within the stop band. The circularly polarized light component having the same handedness of the chiral arrangement is reflected leaving its spin state unchanged. On the contrary, the light having opposite handedness is transmitted unaffected. The sign and strength of the optical force depend on the particles reflectance. Moreover, in contrast to conventional reflecting particles, these chiral particles can be set in rotation because of the transfer of spin angular momentum. We investigate the tunability and the coupling of the optical forces and torques by controlling the amount of the reflected light. Several approaches have been adopted: particle size, optical tweezers wavelength position within the stop band and light ellipticity. Chirality-controlled optical trapping and manipulation opens novel strategies for optomechanics and optical sorting.

We exploit chiral photosensitive materials to move nanoparticles-charged disclination lines in anisotropic chiral fluids. We demonstrate the ability to trap nanoparticles and to manipulate them at large range by low power incoherent light. The chirality is introduced at two levels, by the boundary architectures and by a photosensitive chiral dopant. The first permits to design the topological defects templates, the second to move nanoparticles-charged disclination lines without disrupting them. Full reconfigurability and time stability make this strategy attractive for future developments and practical applications.

ACKNOWLEDGMENT

We acknowledge the MPNS COST Action 1205 "Advances in Optofluidics: Integration of Optical Control and Photonics with Microfluidics" for supporting these activities.

Optofluidics for Energy Applications

Demetri Psaltis
Ecole Polytechnique Federale de Lausanne (EPFL), Lausanne 1028, Switzerland

Abstract— We will describe applications of microfluidics and optofluidics for energy conversion and storage. Specifically we will discuss the role of optofluidics for solar energy harvesting and also methods for water splitting to generate and store hydrogen.

Optofluidic Nanoparticle and Biomolecule Manipulation and Sorting

A. Q. Liu
School of Electrical & Electronic Engineering
Nanyang Technological University, Singapore 639798, Singapore

Abstract— Microfluidics represent the science and technology that process or manipulate small amount of fluids (10^{-9} to 10^{-18} liters) with dimensions of tens to hundreds of micrometers in microfluidic chip. Optofluidics or micro-opto-fluidic-systems (MOFS) aim at manipulating light and fluid at microscale and exploiting their interaction to create highly versatile devices that is significant scientific and interests in many areas. The novelties of the optofluidics are twofold. First, fluids can be used to carry substances to be analyzed in highly sensitive optical microdevices. Second, fluids can also be exploited to control optical microdevices, making them tunable, reconfigurable and adaptive. It is a new breakthrough research area that can provide new solutions and opportunities for a wide range of traditional photonic devices allowing tuning and reconfiguration at the micrometer scale using microfluidic manipulation. This new innovation allows scientists and researchers to tackle many classical problems with new tools and new research ideas.

Among many novel innovations have been demonstrated, such as liquid-liquid waveguide, liquid lens, liquid bubbles grating and microfluidic waveguide laser etc., the manipulation and sorting of a small size of particle and molecule with dimensions of tens to hundreds of nanometers in a microfluidic chip is one of the most significant research approaches. In this talk, light is shaped effectively to generate distinctive interference patterns in the optofluidic chip, which can be used to sort and assemble biological samples. For example, the optical field can be switched from the Bessel profile for particle sorting to various discrete interference patterns for particle assembly.

REFERENCES

1. Liu, A. Q., H. J. Huang, L. K. Chin, Y. F. Yu, and X. C. Li, "Label-free detection with micro-opto-fluidic systems (MOFS): A review," *Anal. Bioanal. Chem.*, Vol. 391, 2443–2452, 2008.
2. Chin, L. K., A. Q. Liu, Y. C. Soh, C. S. Lim, and C. L. Lin, "A reconfigurable optofluidic Michelson interferometer using tunable droplet grating," *Lab on a Chip*, Vol. 10, 1072–1078, 2010.
3. Ando, K., A. Q. Liu, and C. D. Ohl, "Homogeneous nucleation water microfluidic channels," *Physical Review Letters*, Vol. 109, 044501, 2012.
4. Yang, Y., A. Q. Liu, L. K. Chin, X. M. Zhang, D. P. Tsai, C. L. Lin, C. Lu, G. P. Wang, and N. I. Zheludev, "Optofluidic waveguide as a transformation optics device for lightwave bending and manipulation," *Nature Communications*, Vol. 3, 651, 2012.
5. Zhu, W. M., A. Q. Liu, T. Bourouina, D. P. Tsai, J. H. Teng, X. H. Zhang, G. Q. Lo, D. L. Kwong, and N. I. Zheludev, "Microelectromechanical maltese-cross metamaterial with tunable terahertz anisotropy," *Nature Communications*, Vol. 3, 1274, 2012.
6. Chong, W. H., L. K. Chin, R. L. S. Tan, H. Wang, A. Q. Liu, and H. Chen, "Stirring in suspension: Nanometer-sized magnetic stir bars," *Angewandte Chemie Inter. Edit.*, 2013, DOI: 10.1002/anie.201303249.

Light-induced Bulk Flows

Jean-Pierre Delville, **Hamza Chraibi**, **David Riviere**, **and Ulysse Delabre**
Université of Bordeaux, CNRS, LOMA, UMR 5798, Talence F-33400, France

Abstract— Light waves exchange momentum with or transfer energy to matter. A force density results from this interaction whenever photon momentum undergoes a modification in amplitude and/or in direction. This force produces bulk flows in liquids. Flows may also result from the light energy deposited in the liquid. Here we aim at reviewing the different origins of this opto-hydrodynamics. On the one hand, an incident beam may lose forward momentum during its propagation by photon absorption in absorbing liquids or by elastic scattering in transparent turbid liquids. As a consequence, momentum conservation produces a density force within the fluid along the propagation axis and triggers centro-symmetric flows. This density force is proportional to the wave momentum nI/c, the so-called radiation pressure (where n is the index of refraction, I the beam intensity and c the light celerity), and to the beam attenuation $(-1/I)dI/dz$ represented by either the absorption or the turbidity. On the other hand, an incident beam may lose energy due to optical absorption. Energy deposition heats the liquid which in turn produces a pressure gradient that induces bulk convection. These bulk flows can be characterized by Particle Imaging Velocimetry or by the stresses they may produce on a liquid interface. Finally, a tangential shear stress can be triggered by interfacial tension gradients at the interface between two fluids, thus setting up Marangoni flows on both sides of the interface. These gradients of interfacial tension may be triggered optically by light-induced concentration (soluto-capillarity) or thermal (thermo-capillarity) gradient at the interface. Optocapillary flows can as well be characterized Particle Imaging Velocimetry or by the interface deformation resulting from the induced flows. These different ways to drive microflows prove to be a nice and accurate alternative to actuate bulk liquids by light in a contactless manner for optofluidic applications.

Liquid Crystal Photonics

Igor Muševič[1, 2]

[1]Jozef Stefan Institute, Jamova 39, SI-1000 Ljubljana, Slovenia
[2]Faculty of Mathematics and Physics, University of Ljubljana
Jadranska 19, SI-1000, Ljubljana, Slovenia

Abstract— When liquid crystals are dispersed in an immiscible fluid, microdroplets of liquid crystal [1] are spontaneously formed in a fraction of a second. They have optically anisotropic internal structure, which is determined by the ordering of liquid crystal molecules at the interface. Spherical droplets of a nematic liquid crystal can function as whispering-gallery-mode microresonators [2] with an unprecedented width of wavelength tunability by an electric field. WGM pulsed lasing in dye-doped nematic microdroplets is sensitive to strain, temperature and presence of molecules [3, 4] that change molecular orientation at the interface. Omnidirectional 3D lasing was demonstrated in droplets of chiral liquid crystals that form 3D Bragg-onion resonators [5, 6]. We showed that anisotropic and topologically nontrivial fibres could be self-assembled from smectic liquid crystals [7], which could support Laguerre-Gaussian modes. We present recent progress in this field, including electric tuning of 3D lasing, resonant transport of light between waveguides and liquid crystal resonators [8].

REFERENCES

1. Poulin, P., H. Stark, T. C. Lubensky, and D. A. Weitz, *Science*, Vol. 275, 1770, 1997.
2. Humar, M., M. Ravnik, S. Pajk, and I. Muševič, *Nat. Photonics*, Vol. 3, 595–600, 2009.
3. Muševič, I. and M. Humar, *Proceedings of SPIE*, Vol. 7955, 795509-1–795509-8, 2011.
4. Humar, M. and I. Muševič, *Optics Express*, Vol. 19, 19836–19844, 2011.
5. Humar, M. and I. Muševič, *Optics Express*, Vol. 18, 26995–27003, 2010.
6. Cipparrone, G., A. Mazzulla, A. Pane, R. J. Hernandez, and R. Bartolino, *Adv. Mat.*, Vol. 23, 5773–5778, 2011.
7. Peddireddy, K., V. S. R. Jampani, S. Thutupalli, S. Herminghaus, Ch. Bahr, and I. Muševič, *Opt. Express*, Vol. 21, 30233–30242, 2013.
8. Jampani, V. S. R., M. Humar, and I. Muševič, *Optics Express*, Vol. 21, 20506–20516, 2013.

Organic Dye DFB Laser Sensor Arrays for Image Refractometry

Christoph Vannahme, **Kristian Tølbøl Sørensen**, **Petur Gordon Hermannsson**, **Martin Dufva**, **and Anders Kristensen**
DTU Nanotech, Technical University of Denmark, Kongens Lyngby 2800, Denmark

Abstract— This paper describes the design, fabrication, and experimental validation of optically pumped, solid state organic dye distributed feedback (DFB) laser intra-cavity sensor arrays. The DFB dye lasers are low-cost and highly sensitive refractive index sensors. The lasers are fabricated by UV-nanoimprint lithography into Pyrromethene doped Ormocomp thin films on glass, and the surface refractive index sensitivity is enhanced by a factor of up to five by subsequent deposition of a thin titanium dioxide (TiO_2) waveguiding layer. The multiple wavelength laser arrays presented here enable high frame-rate and highly sensitive imaging of refractive index changes on a $2 \times 2\,\mathrm{mm}^2$ surface, without moving parts, providing a detection limit of $8 \cdot 10^{-6}$ RIU in combination with spatial resolution of 25 µm. The omission of moving parts in the setup improves the robustness of the imaging system and allows a very high frame rate of up to 12 Hz, limited by the CCD camera. The laser sensor arrays are applied for visualizing and studying the dynamics of dissolution, mixing, and biological processes without the need for labeling. The unique multi-wavelength DFB laser structure comprises several areas with different grating periods. Imaging in two dimensions of space is enabled by analyzing laser light from all areas in parallel with an imaging spectrometer. With this multi-resonance imaging refractometry method, the spatial position in one direction is identified from the horizontal, i.e., spectral position of the multiple laser lines which is obtained from the spectrometer CCD array. The orthogonal spatial position is obtained from the vertical spatial position on the spectrometer CCD array as in established spatially resolved spectroscopy. Here, the imaging technique is demonstrated by monitoring the motion of small sucrose molecules upon dissolution of solid sucrose in water.

Light at Work: Optical Delivery, Sorting and Self-assembly of Microobjects

P. Zemánek, **O. Brzobohatý**, **P. Jákl**, **L. Chvátal**, **S. Simpson**, **and M. Šiler**
Institute of Scientific Instruments of the ASCR, v.v.i.
Královopolská 147, Brno 612 64, Czech Republic

Abstract— Illumination of a colloidal suspension by laser beams leads to a force interaction between the light and microobjects. Spatially structured illumination of microobjects enables their sorting according to their sizes, shapes or composition, delivery by the principles of optical "tractor" beam or conveyor belt, self-arrangement into structures kept together by the scattered light. Recent results and applications of this topic will be presented.

Introduction: A single tightly focused laser beam, referred to as the optical tweezers represents now the most famous optical micromanipulation tool. However, since this invention more complex spatial distributions of laser beams can be dynamically generated using spatial light modulators. If more particles are illuminated at the same time, they interact with each other by scattered light and so called optical binding occurs. It results in formation of stable structures composed of microparticles kept together by light. Optical forces acting upon objects depend on particles properties and can be effectively used for separation of different components of heterogeneous suspensions or even optically self-arranged structures [1].

Conclusion: Several examples of optical sorting of microobjects in traveling interference patterns will be presented. We also explain the principle of optical "tractor" beam and its utilization for particles delivery, separation (see Fig. 1) and self-arrangement of optically bound structures.

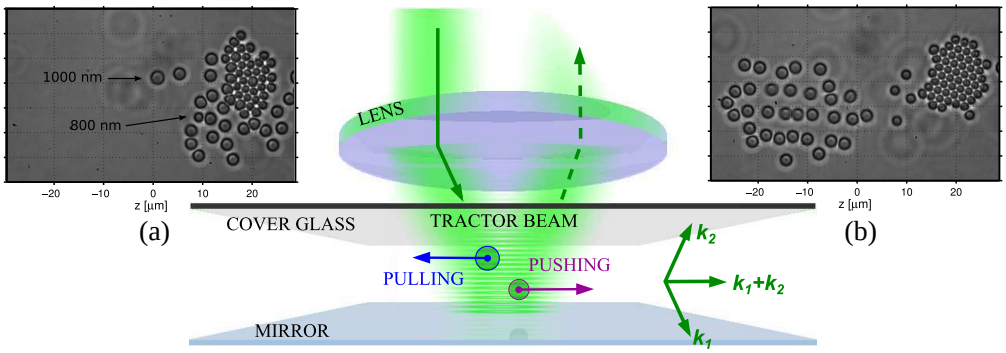

Figure 1: Geometry of the "tractor" beam experiment. Larger particle scatter light differently than a smaller particle and thus moves in opposite direction. Images show separation of polystyrene particles of radii 400 nm and 500 nm using the same geometry by switching the polarization of the beam from (a) p to (b) s polarization.

ACKNOWLEDGMENT

The authors acknowledge support from the Czech Science Foundation (14-36681G, 14-16195S), Ministry of Education, Youth and Sports of the Czech Republic (LO1212, LD14069) together with the European Commission (CZ.1.05/2.1.00/01.0017).

REFERENCES

1. Brzobohatý, O., V. Karásek, M. Šiler, L. Chvátal, T. Čizmár, and P. Zemánek, "Experimental demonstration of optical transport, sorting and self-arrangement using a 'tractor beam'," *Nature Phot.*, Vol. 7, No. 2, 123–127, 2013.

A Nanophotonic Platform for High-throughput Precision Single Biomolecule Manipulation

Michelle D. Wang
Department of Physics, Laboratory of Atomic and Solid State Physics, Howard Hughes Medical Institute
Cornell University, Ithaca, New York 14853, USA

Abstract— Optical trapping has been proven to be a powerful manipulation and measurement technique widely used in the biological and materials sciences. A prominent example of the application of optical trapping techniques is in the study of single biological molecules, in which the mechanical behavior of a molecule can be investigated. These techniques make it possible to disrupt protein complexes with piconewton forces and track motor proteins with nanometer and millisecond resolution. However, conventional optical trapping instruments are only capable of manipulating one molecule at a time, which limits their throughput. Miniaturizing optical trap instruments onto optofluidic platforms holds promise for high-throughput lab-on-a-chip applications. We have been developing novel nanophotonic platforms for precision manipulation and measurements of a bio-molecular array. In addition to on-chip optical trapping, we demonstrate that such a platform can be integrated with fluorescence and laminar flow cells, substantially enhancing its utility. We anticipate that this approach will make single molecule measurements broadly available.

Localized Fluorescence Enhancement with Gold-coated Microtools

Pál Ormos, Badri L. Aekbote, Gaszton Vizsnyiczai, and Lóránd Kelemen
Institute of Biophysics, Biological Research Centre, Temesvári krt. 62, Szeged, Hungary

Abstract— There is an increasing interest in functionalized complex microstructures for micro- and nanotechnology applications in biology. Particularly in imaging, metal-enhanced fluorescence (MEF), achieved by microscopic surfaces coated with metal nanoparticles (NPs) or films has been applied recently on cells observing otherwise weakly detectable signals [1, 2]. We introduce the combination of microstructures made of SU-8 photoresist by two-photon polymerization and gold nanoparticles or thin gold layers as fluorescence signal enhancers. The polymer microstructures serve as platforms and can be tailor made into any shape with sub-diffraction resolution required by the actual application. We coated these platforms either with 80 nm gold nanoparticles (NP) at various surface density [3] or sputtered gold layers of high reflectivity. We demonstrated localized MEF by NP-coated microstructures equipped with tips of 250 nm radius of curvature that provided enhancement factor of more than 3. The NP-mediated enhancement factor was as high as 6 over areas of several square-micrometers when flat microstructures without tips were used. We attributed the enhancement effect to reflection of the excitation and emitted light, what is demonstrated with the use of tilted polymer platforms. According to this observation, highly reflecting gold thin films were also used for coating and provided enhancement up to 8.

The coated microtools are further developedfor optical tweezers actuation.These microtools can be held and positioned in holographic optical tweezers. This gives the possibility of targeted local fluorescentenhancement at desired locations.

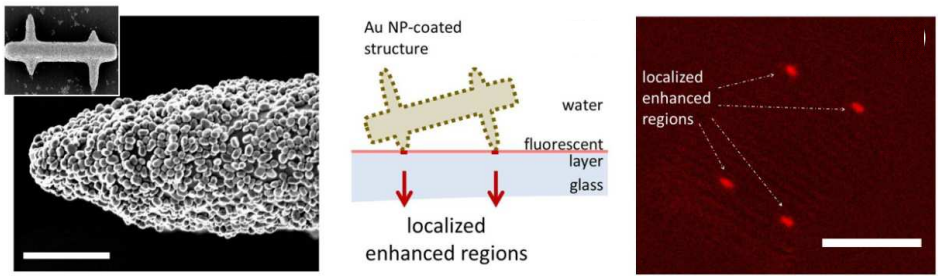

(a) (b) (c)

Figure 1: Fluorescence enhancement with a tipped SU-8 microstructure coated with Au nanoparticles. (a) The Au-coated tip region of the microstructure (insert: the entire structure). Scale bar: 1 µm. (b) Scheme of the microstructure arrangement over a fluorescent layer showing the enhanced regions. (c) Confocal fluorescence image of the achieved enhancement. Enhancement factor in this case is ~ 3.2.

REFERENCES

1. Gartia, M. R., A. Hsiao, M. Sivaguru, Y. Chen, and G. L. Liu, "Enhanced 3D fluorescence live cell imaging on nanoplasmonic substrate," *Nanotechnology*, Vol. 22, 365203–365214, 2011.
2. Le Moal, E., E. Fort,S. Lévêque-Fort, A. Janin, H. Murata, F. P. Cordelières, M.-P. Fontaine-Aupart, and C. Ricolleau, "Mirror slides for high-sensitivity cell and tissuefluorescence imaging,"*J. Biomed. Opt.*, Vol.12, 024030, 2007.
3. Aekbote, B. L., J. Jacak, G. J Schütz, E. Csányi, Z. Szegletes, P. Ormos, and L. Kelemen, "Aminosilane-based functionalization of two-photon polymerized 3D SU-8 microstructures," *Eur. Polym. J.*, Vol.48, 1745–1754, 2012.

Lab on a Chip Integrated Light Source: The Femto-laser Direct Writing Design for a New Fabrication Route

S. Lo Turco[1, 2], S. Bonfadini[1], R. Ramponi[1, 2, 3], D. E. Lucchetta[4], P. Spegni[4], F. Simoni[4], and L. Criante[1, 4]

[1]Center for Nano Science and Technology@PoliMi, Istituto Italiano di Tecnologia
Via Giovanni Pascoli, 70/3, Milan 20133, Italy
[2]Dipartimento di Fisica, Politecnico di Milano
Piazza Leonardo da Vinci 32, Milan 20133, Italy
[3]Istituto di Fotonica e Nanotecnologie — CNR
Piazza Leonardo da Vinci 32, Milan 20133, Italy
[4]Dipartimento SIMAU, Università Politecnica delle Marche
Via Brecce Bianche, Ancona 60131, Italy

Abstract— The development of simple and low-cost miniaturized fabrication methods has been very important for the advancement of microfluidics technology. Despite recent advances in the lab on a chip samples, in particular for biomedical applications, the increasing need of high sensitivity and performance of the devices is not yet satisfied. The fulfillment of these requirements makes necessary the fabrication of complex 3D fluidic structures that allow analysis of physico-chemical properties of micro amount of sample by optical techniques. This involves being able to achieve levels of integration and control of photonic signals not yet reached in the advanced opto-fluidics platform. With the aim of designing a way to integrate optical signal in lab on a chip systems, an investigation on novel optofluidic laser microcavities has been performed in view of getting tuning capability exploiting by liquid crystal orientational properties.

Although planar micro-fabrication approach based on photolithography is well established and is suitable for surface micro-fabrication, multilayer and multistep processes, including stacking and bonding of different substrates, are required to form true three-dimensional (3D) microstructures. An innovative, simple and maskless technique is the femtosecond laser micromachining, which allows a 3D fast prototyping thanks to its inherent ability to fabricate buried microstructures. Taking advantage from ultrashort-pulse laser, it is possible to realize surface (ablation) or internal (nanocracks) modification of the transparent materials or a high localized photo-polymerization of sensitive polymeric materials, in the focus of the laser beam. Since both the microfluidic channels and waveguides in glass can be fabricated by the same tool on the same substrate, it is easy to create integrated and vibration-free optofluidic devices. After the volume laser irradiation, the optofluidic circuit is obtained by chemical etching removing the laser modified areas.

Taking advantage from this new fabrication technique, different geometries of the laser cavity with excellent flexibility can be fabricated. Many geometries has been fabricated and investigated although the digging out of two empty "basins" located close to the dye recirculation microchannel has been the basic configuration. Covering their side walls with a thin film of conductive ink, two broadband micro reflectors have been recorded (one partially and the other fully reflective). Exploiting the potential of inkjet printing technology, the micro mirrors are also electrodes allowing the tuning of the stimulated light emission by control the alignment of the liquid crystal in the microchannel. A fine control of reflectivity from 30% to 100% has been achieved, even in useful no-planar geometries (curved mirrors). A selective microlaser wavelength imprinting Bragg reflectors into two empty "basins" previously filled with the photopolymerizable mixture can be obtained exploiting the full potential of holography. Either way an integrated broad band fibers optic completes the microcircuit design in order to outcouple the emitted light.

Optofluidic Platforms for Miniaturized Biomedical Analysis Systems

C. Karnutsch[1,2], **C. Prokop**[1,2], **Crispin Szydzik**[2], **Khashayar Koshmanesh**[2], **and Arnan Mitchell**[2]

[1]Institute for Optofluidics and Nanophotonics (IONAS)
Karlsruhe University of Applied Sciences, Karlsruhe 76133, Germany
[2]Microplatforms Research Group, School of Electrical and Computer Engineering
RMIT University, GPO Box 2476, Melbourne VIC 3001, Australia

Abstract— Polymers are a popular material platform for low-cost, mass-producible optofluidic sensing applications. However, due to the low refractive index contrast between various polymer materials, the efficiency of such devices is often limited. The most elegant way to achieve maximum refractive index contrast, not only in polymer photonic devices, is to use air as cladding layers. We exploit a novel polymer-onto-polymer lamination method that enables air-suspended polymer photonic devices and the merging of microfluidic channels and photonic functionalities in one layer. Polymer films with thicknesses down to single-mode condition for waveguided light can be transferred onto microchannels of several hundred microns in width and centimeters of length by using a simple PDMS stamp. This allows firstly to achieve highly efficient polymer grating couplers due to the high refractive index contrast and secondly the embedded microchannel can be exploited for transporting analytes. Combining a microchannel for fluid handling with photonic structures enables research towards a large range of applications, such as optofluidics, biosensing, biomedical analysis, environmental investigations and renewable energy. Here, we report on the modeling, progress towards experimental realization and characterization of air-suspended photonic structures (such as grating couplers) as well as a resulting optofluidic refractive index sensor.

Furthermore, in the context of biomedical analysis, absorption spectroscopy-based portable blood analysis systems are highly desirable for improved patient care. In this regard, air-suspended polymer integrated circuits — consisting of input and output grating couplers and a waveguide that is probing an embedded analyte channel (see Fig. 1) — are a promising platform.

Apart from the actual sensing device, many biomedical analysis methods require blood plasma as an analyte. Typically, this blood plasma is obtained through centrifugation of relatively large volumes of blood in a central lab. This method is not practical for mobile point-of-care devices, therefore an effective miniaturized method of plasma extraction is required to enable portable lab-on-a-chip based point-of-care devices.

In this contribution, we also report on a new method of blood plasma extraction that fulfils the requirements for a mobile point-of-care blood analysis device. This system is enabled by repulsive dielectrophoresis forces actively unblocking a cross flow filter.

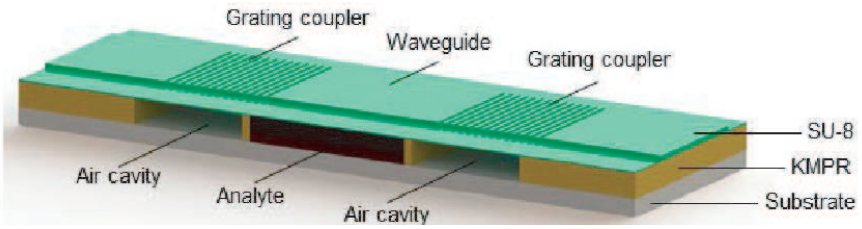

Figure 1: Vision of an optofluidic biosensor exploiting air-suspended grating couplers for light coupling and an embedded microchannel to transport an analyte sample.

Optofluidic Devices and Platforms for Sensing Applications

G. Testa, **G. Persichetti**, **I. A. Grimaldi**, **and R. Bernini**
Istituto per il Rilevamento Elettromagnetico dell'Ambiente
Consiglio Nazionale delle Ricerche (IREA-CNR), Via Diocleziano 328, Naples 80124, Italy

Abstract— Optofluidics is an emerging research field that combines the advantages of microfluidics and optics on the same platform towards highly functional and compact devices. This approach offers innovative design in order to increase performances and optical functionalities of sensing devices. In particular, the possibility to use a fluid as an optical material and guiding light through it offers very interesting solutions enabling unprecedented sensitivity and limit-of-detection.

In this work we present the design, fabrication and characterizations of optofluidics devices and microsystems for sensing applications that ranges from biosensing to environmental monitoring.

The confinement properties and the strong light matter interaction between light and fluids occurring in optofluidics waveguides, like Antiresonant Reflecting Optical Waveguide (ARROW) or liquid jet waveguide, have been exploited to realize simple but effective and sensitive microfluidic sensors. The use of optofluidic waveguides for spectroscopy methods like absorption, fluorescence, Raman is illustrated showing that the optofluidic approach permits to overcome the sensitivity problems related to the reduced the interaction length of light with fluid due to device miniaturization. Besides the use of the waveguides itself as optofluidic sensor, we show that more sophisticated devices can be realized by using liquid core ARROWs. In particular, we demonstrate that single mode ARROWs provide the opportunity to implement sensor devices which make uses of interferometric phenomena that are very attractive for sensing applications as they combine high sensitivity with compactness and low-production cost. We show that, despite ARROWs are leaky waveguides high performance liquid core Mach-Zehnder interferometers (MZI) and Ring resonator could be realized.

Finally we demonstrate the possibility to combine solid core with liquid core ARROWs and microfluidic devices in a single sensing platform. This represents a significant step towards an effective realization of chip scale integrated system. The integration of planar optofluidic components with microfluidic tools at the chip scale represents the future trend of sensing systems for point-of care diagnosis or in situ monitoring. Increasing the synergy between these technologies can lead to highly reliable and portable systems.

A Tunable Nano-optofluidic Polymer Filter Based on Guided-mode Resonance

Guohui Xiao and Chongjun Jin
State Key Laboratory of Optoelectronic Materials and Technologies
School of Physics and Engineering, Sun Yat-sen University, Guangzhou 510275, China

Abstract— Optical filters with reconfigurable spectral properties are highly desirable in a wide range of applications. We propose and experimentally demonstrate a tunable nano-optofluidic polymer guided-mode resonance (PGMR) filter. The device is composed of a periodic grating sandwiched between a high index waveguide layer and a low index capping layer, which integrates nano-fluidic channel arrays and PGMR filter elegantly. A finite difference time domain (FDTD) methods is employed to understand the spectral properties and determine appropriate device parameters. We fabricate the polymer guided-mode resonance filter with a method combining two-beam interference lithography, floating nanofilm transfer and thermal bonding techniques. Experimental results show that our tunable nano-optofluidic PGMR filters can provide a broad spectral tuning range (13.181 nm), a narrow bandwidth ($<$ 2.504 nm), and a high reflection efficiency ($>$ 85%) in the visible region. Such nano-optofluidic PGMR filters are highly compatible with existing nano/microfluidic technologies and would be valuable for the integrated flexible optical system.

Single Microbial Cell Manipulation in a Three Dimensional Microfluidic Chip

A. Keloth[1], **L. Paterson**[1], **G. H. Markx**[1], **and A. K. Kar**[2]

[1]Institute of Biological Chemistry, Biophysics and Bioengineering
School of Engineering and Physical Sciences, Heriot Watt University, Edinburgh EH14 4AS, UK
[2]Institute of Photonics and Quantum Sciences, School of Engineering and Physical Sciences
Heriot Watt University, Edinburgh EH14 4AS, UK

Abstract— Novel microfluidic devices with integrated optical waveguides can be used to enable sorting, culture and testing of cells from very small volumes of biological samples [1]. Controlled flow and optical manipulation of cells within a femtosecond laser machined and chemically etched microchannel using optical scattering force has been demonstrated in our previous work [2] and by others [3].

In this paper we present the design and fabrication of a three dimensional microfluidic device fabricated using femtosecond laser micromachining combined with selective chemical etching. We use the device to focus microbes in a hydrodynamic flow and then use optical scattering forces to deflect single cells from the flow for downstream analysis and culture of the isolated cells. Taking advantage of method simplicity and three dimensional capability of femtosecond laser micromachining, 3-dimensional microfluidic structures that are capable of implementing hydrodynamic focusing were fabricated in a fused silica substrate. Hydrodynamic flow focusing inside the microfluidic channel enables the sample to be focused into a narrow stream and has been previously demonstrated by others within a cell counter device [4]. The three dimensional hydrodynamic focusing capability of our device was demonstrated by focusing dye, polystyrene beads of 7 micrometre diameter and 2 micrometre diameter and a range of biological cells (bacteria, yeast, microalgae cells) inside the microfluidic channel. Waveguides were integrated into the device to provide an optical scattering force to deflect cells into a side channel. Our experimental results highlight the potential for single cell isolation by integrating 3-dimensional hydrodynamic focusing of samples and the deflection of cells within a femtosecond laser micromachined and chemically etched device.

REFERENCES

1. Choudhury, D., W. T. Ramsay, R. Kiss, N. A. Willoughby, L. Paterson, and A. K. Kar, "A 3D mammalian cell separator biochip," *Lab Chip*, Vol. 12, 948–953, 2012.
2. Keloth, A., L. Paterson, G. H. Markx, and A. K. Kar, "Three-dimensional optofluidic device for isolating microbes," *Proc. of SPIE*, Vol. 9320, 93200Z, 2015.
3. Bragheri, F., P. Minzioni, R. Martinez Vazquez, N. Bellini, P. Paiè, C. Mondello, R. Ramponi, I. Cristiani, and R. Osellame, "Optofluidic integrated cell sorter fabricated by femtosecond lasers," *Lab Chip*, Vol. 12, 3779–3784 2012.
4. Paiè, P., F. Bragheri, R. M. Vazquez, and R. Osellame, "Straightforward 3D hydrodynamic focusing in femtosecond laser fabricated microfluidic channels," *Lab Chip*, Vol. 14, 1826–1833, 2014.

Light Moves Macro-objects

D. E. Lucchetta[1], **F. Simoni**[1], **L. Nucara**[2, 3], **and R. Castagna**[1]

[1]Dipartimento SIMAU, Università Politecnica delle Marche, Via Brecce Bianche, Ancona 60131, Italy
[2]The BioRobotics Institute, Scuola Superiore Sant'Anna
Viale Rinaldo Piaggio 34, Pontedera, PI 56025, Italy
[3]Center for Micro-BioRobotics@SSSA, Istituto Italiano di Tecnologia
Viale Rinaldo Piaggio 34, Pontedera, PI 56025, Italy

Abstract— Conversion of photons energy into mechanical work usually requires intermediate, energy-expensive steps, which make not convenient the use of light to generate work. In order to bypass these steps, different approaches have been proposed. Here we focus on light-induced gradients of surface tension to generate motion of small objects floating on supporting fluids. These phenomena fall into the general framework of the Marangoni effect [1]. It has been shown how a composite object made by poly-dimethyl-siloxane and carbon nano-tubes can be easily moved on the fluid surface driven by light absorption by using IR radiation [2]. Other approaches concern the possibility of moving micro-droplets of oil in micro-channels by light induced-pH gradients [3] or through a photo induced cis-trans isomerization effect [4]. In this work we present a simpler complementary approach to the problem based on the possibility of generating objects motion and to control in real time their trajectories on any supporting fluid. We use low power visible light to induce motion of any floating objects. An object able to absorb the impinging radiation can be asymmetrically heated and moved on the liquid surface whereas transparent objects can be moved by a suitable doping of the supporting fluid and irradiating the fluid surface near the floating object. Light-induced displacement versus time of the floating object has been recorded on different supporting fluids as function of the dopant concentrations and impinging light intensities.

REFERENCES

1. Marangoni, C., *Il Nuovo Cimento*, Vol. 2, Nos. V–VI, 239–273, 1872.
2. Okawa, D., S. J. Pastine, A. Zettl, and J. M. J. Fréchet, *J. Am. Chem. Soc.*, Vol. 131, No. 15, 5396–5398, 2009.
3. Florea, L., K. Wagner, P. Wagner, G. G. Wallace, F. Benito-Lopez, D. L. Officer, and D. Diamond, *Adv. Mat.*, 2014, Doi: 10.1002/adma.201403007.
4. Diguet, A., R.-M. Guillermic, N. Magome, A. Saint-Jalmes, Y. Chen, K. Yoshikawa, and D. Baigle, *Angew. Chem. Int. Ed.*, Vol. 48, 9281–9284, 2009.

Session 2P4
FocusSession.SC2&3: Scalable and Hierarchical Nanofabrication for Deep Sub-wavelength Nanophotonics

Atomic Layer Lithography for High-throughput Fabrication of Sub-10-nm Plasmonic Gap Arrays

Xiaoshu Chen, **Hyeong-Ryeol Park**, **Daehan Yoo**, **and Sang-Hyun Oh**
Department of Electrical and Computer Engineering
University of Minnesota, Minneapolis, MN 55455, USA

Abstract— The research field of nanoplasmonics has progressed along with advances in nanofabrication technologies. This presentation will focus on the development of a new technique to create ultra-thin nanogaps in metal films using atomic layer deposition (ALD). ALD has been widely used for conformal coating of metal oxides on a wide variety of surfaces. Recent work demonstrated a new scheme to transform sub-nanometer thickness control of ALD into sub-nanometer patterning resolution. Using this technique, called atomic layer lithography, it is now possible to create plasmonic nanogaps that are sub-1-nm in width but as long as 1 cm. These high-aspect-ratio nanogap structures can exhibit a series of strong optical resonances, which can be utilized for sensing and spectroscopy in broad frequency ranges. Some applications of these ALD-patterned nanogap structures will be demonstrated.

Plasmonic Optical Transformer as Scanning Probe Microscopy: Status and Perspectives

Aleksandr Polyakov, **Mauro Melli**, **Wei Bao**, **Alexander Weber-Bargioni**, **P. James Schuck**, **and Stefano Cabrini**
Molecular Foundry, LBNL, One Cyclotron Road, Berkeley, CA, USA

Abstract— The expansion of nanoscale optics and nanofabrication capabilities has generated a variety of scanning probe geometries that yield spatial resolution below 10 nm. Efficient conversion of photonic to plasmonic energy is important for nano-optical applications, particularly imaging and spectroscopy. Recently a new generation of photonic/plasmonic transducers has been fabricated on top of an optical fiber combining the concepts of optical transformer and adiabatical compression to be used as optical near field scanning probes. Those devices, called the 'campanile' probes [1], have been developed that overcomes many shortcomings of previous near-field probes by efficiently merging broadband field enhancement with bidirectional coupling of far- to near field electromagnetic modes. Field confinement, enhancement, and polarization near the apex of the probe are evaluated relative to local fields created by conical tapered tips in vacuum and in tip-substrate gap mode [2]. Campanile design has similar field enhancement and bandwidth capabilities as those of ultra-sharp metallized tips, but without the substrate and sample restrictions inherent in the tip-surface gap mode operation often required by those tips.

We will present a physical model for coupling far-field radiation to plasmonic modes on the surface of a scanning probe [3], and propose a scheme for extending the working distance of such a probe. In a subsurface application, an optical transformer at the tip of a probe can be coupled to a remote near-field antenna placed inside the sample at a distance away from the surface, expanding the effective working distance up to 100 nm.

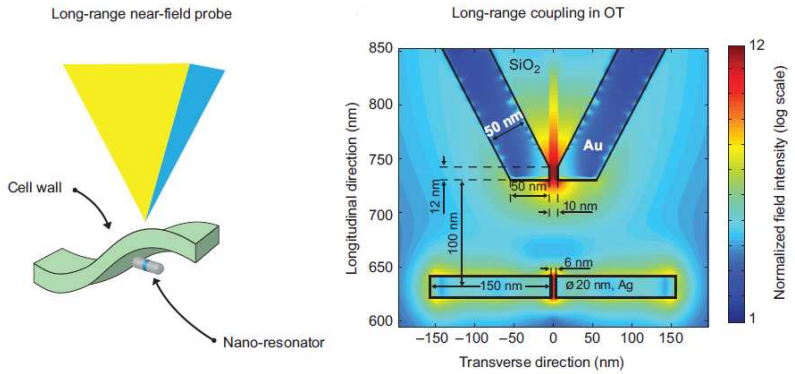

(a) (b)

Figure 1: (a) The effective working distance of a near-field probe can extended beyond the typical 3 nm by placing a resonator some distance away from the apex of the OT. (b) In this configuration, the electric field couples between the probe and the resonator establishing an efficient channel for locally exciting the sample at the location of the resonator hotspot and collecting the resulting signal from it. OT, optical transformer.

REFERENCES

1. Bao, W., M. Melli, N. Caselli, F. Riboli, D. S. Wiersma, M. Staffaroni, H. Choo, D. F. Ogletree, S. Aloni, J. Bokor, S. Cabrini, F. Intonti, M. B. Salmeron, E. Yablonovitch, P. J. Schuck, and A. Weber-Bargioni, "Mapping local charge recombination heterogeneity by multidimensional nanospectroscopic imaging," *Science*, Vol. 338, No. 6112, 1317–1321, 7 December 2012.
2. Bao, W., M. Staffaroni, J. Bokor, M. B. Salmeron, E. Yablonovitch, S. Cabrini, A. Weber-Bargioni, and P. J. Schuck, "Plasmonic near-field probes: a comparison of the campanile geometry with other sharp tips," *Optics Express*, Vol. 21, No. 7, 8166–8176, 2013.
3. Polyakov, A., M. Melli, G. Cantarella, A. Weber-Bargioni, P. J. Schuck, and S. Cabrini, "Coupling model for an extended-range plasmonic optical transformer scanning probe," *Light: Science & Applications*, Vol. 3, e195, 2014.

Quantum-dot Plasmonics

David J. Norris
Optical Materials Engineering Laboratory, ETH Zurich
Leonhardstrasse 21, Zurich 8092, Switzerland

Abstract— Quantum optics involves the coupling of quantum emitters to their electromagnetic environment. Because this coupling is related to the concentration of the optical field, it is typically constrained by the diffraction limit of light. One way to circumvent this is by moving to quantum plasmonics, which uses surface plasmon polaritons (SPPs) instead of photons. SPPs are surface waves that arise from the coupling of photons to electronic oscillations. They allow light to be concentrated well below the diffraction limit. However, despite this capability, quantum plasmonics has not yet been thoroughly exploited. This can be attributed to challenges in fabricating high-quality systems that combine robust efficient emitters with well-defined plasmonic structures. To address this, we have recently fabricated quantum-plasmonic systems that consist of active colloidal quantum dots precisely placed in the mode of a passive plasmonic resonance. Since material quality is critical, we optimized both the active and passive components. For the active part, quantum dots were synthesized with stable fluorescence quantum yields above 90%. For the passive part, finite-element simulations were used to identify suitable structures. These were then fabricated by combining template stripping with a cryogenic deposition process to yield ultrasmooth silver patterns with previously unattainable performance. Countable numbers of quantum dots were placed into the plasmonic modes of these structures with nanometer precision using an electrohydrodynamic printing technique. The result is an ideal system for exploring fundamental physics in quantum plasmonics.

DNA-based Functional Plasmonic Particle Assemblies

Tim Liedl
Physics, Ludwig-Maximilians-University of Munich, Munich, Germany

Abstract— We use the DNA origami method [1] for the fabrication of functional self-assembled nanoscopic objects and materials [2]. In DNA origami, a virus-based 8 kilobase-long DNA single-strand is folded into shape with the help of ~ 200 synthetic oligonucleotides. The resulting DNA nanostructures can be designed to adopt any two- and three-dimensional shape. By offering attachment sites for active nano-components on these DNA objects, we have realized complex and nanometer-precise assemblies of organic fluorophores as well as of fluorescent and plasmonic nanoparticles.

With this method in hand we are able to build plasmonic metamolecules that freely float in solution and exhibit striking optical properties such as switchable optical activity in the visible range [3, 4]. The metamolecules can also be tethered to surfaces to be operated by external stimuli [5]. The observed circular dichroism signals are reversible and in very good agreement with plasmonic dipole theory.

We are currently also exploring the possibility to create defined electric and magnetic responses at visible wavelengths with DNA-based plasmonic arrangements of sub-wavelengths sizes. By, e.g., positioning 40 nm gold particles in rings with a diameter of 65 nm we were recently able to observe signatures of magnetic resonances in such ring structures at the red end of the optical spectrum [6].

REFERENCES

1. Rothemund, P. W. K., "Folding DNA to create nanoscale shapes and patterns," *Nature*, Vol. 440, 207, 2006.
2. Seeman, N. C., "Nanomaterials based on DNA," *Annu. Rev. Biochem.*, Vol. 79, 12.1, 2010.
3. Kuzyk, A., et al., "DNA-based self-assembly of chiral plasmonic nanostructures with tailored optical response," *Nature*, Vol. 483, 311, 2012.
4. Kuzyk, A., et al., "Reconfigurable 3D plasmonic metamolecules," *Nat. Mat.*, Vol. 13, 862, 2014.
5. Schreiber, R., et al., "Chiral plasmonic DNA nanostructures with switchable circular dichroism," *Nat. Comm.*, 2013, doi:10.1038/ncomms3948.
6. Roller, E. M., et al., "DNA-assembled nanoparticle rings exhibit electric and magnetic resonances at visible frequencies," *Nano Lett.*, 2015, DOI: 10.1021/nl5046473.

Crystal Growth Methods as a Tool for Manufacturing Metamaterials and Plasmonic Materials

D. A. Pawlak[1, 2], **M. Gajc**[1], **K. Sadecka**[1], **P. Osewski**[1], **A. Klos**[1], **Emilija Petronijevic**[3], **Alessandro Belardini**[3], **Grigore Leahu**[3], **and C. Sibilia**[3]

[1]Institute of Electronic Materials Technology (ITME), ul. Wólczyńska 133, Warsaw 01-919, Poland
[2]Centre of New Technologies University of Warsaw, ul. Banacha 2C, Warsaw 02-097, Poland
[3]Dipartimento di Scienze di Base e Applicate per l'Ingegneria
Sapienza Università di Roma, via A. Scarpa 14, Rome 00161, Italy

Abstract— We report on developments in fabricating nano and micro-structured volumetric plasmonic materials and metamaterials utilizing crystal growth techniques based on directional solidification and crystallization as the micro-pulling down method. Two types of materials will be discussed: (i) based on directional solidification of eutectic composites [1–3], and (ii) directional solidification of dielectrics nonchemically doped with functional nanoparticles [4, 5].

It has been shown that with self-organization mechanism during the eutectic crystallization the various shapes pertinent to metamaterials can be obtained as the 'split-ring resonator' geometry [1], rodlike structures which can be used as hyperbolic metamaterials, or for subwavlength transmission of electromagnetic waves [2, 6, 7], eutectic-based nanoplasmonic materials have been demonstrated for the first time [8], as well as anomalous transmission and enhanced second harmonic generation has been demonstrated [9].

On the other hand the novel method developed by us called NanoParticles Direct Doping, NPDD, enables doping dielectric matrices with various nanoparticles of various size, shape and chemical composition as well as various additional elements as rare earths [3].

The developments in this field will be reported.

ACKNOWLEDGMENT

The authors thank the National Science Centre of Poland MAESTRO Grant No. 2011/02/A/ST5/00471 and HARMONIA Grant, AFOSR Award No. FA9550-14-1-0061.

REFERENCES

1. Pawlak, D. A., S. Turczynski, M. Gajc, K. Kolodziejak, R. Diduszko, K. Rozniatowski, J. Smalc, and I. Vendik, "How far are we from making metamaterials by self-organization? The microstructure of highly anisotropic particles with an SRR-like geometry," *Adv. Funct. Mat.*, Vol. 20, 1116–1124, 2010.
2. Pawlak, D. A., K. Kolodziejak, S. Turczynski, J. Kisielewski, K. Rozniatowski, R. Diduszko, M. Kaczkan, and M. Malinowski, "Self-organized, rodlike, micrometer-scale microstructure of $Tb_3Sc_2Al_3O_{12}$-$TbScO_3$:Pr eutectic," *Chem. Mat.*, Vol. 18, 2450–2457, 2006.
3. Pawlak, D. A., "Self-organized structures for metamaterials," *Handbook of Artificial Materials*, Editor in Chief: F. Capolino, ISBN10: 1420054236, Taylor & Francis, 2009.
4. Gajc, M., B. H. Surma, A. Klos, K. Sadecka, K. Orlinski, A. E. Nikolaenko, and K. Zdunek, "Nanoparticle direct doping: Novel method for manufacturing three-dimensional bulk plasmonic nanocomposites," *Adv. Funct. Mat.*, Vol. 23, 3443–3451, 2013.
5. www.itmeteam.pl, attractive demonstration of the dichroic effect in volumetric nanoplasmonic material obtained by the NPDD method.
6. Myroshnychenko, V., A. Stefanski, A. Manjavacas, M. Kafesaki, R. I. Merino, V. M. Orera, D. A. Pawlak, and F. J. Garcia de Abajo, "Interacting plasmon and phonon polaritons in aligned nano- and microwires," *Opt. Express*, Vol. 20, 10879–10887, 2012.
7. Massaouti, M., A. A. Basharin, M. Kafesaki, M. F. Acosta, R. I. Merino, V. M. Orera, E. N. Economou, C. M. Soukoulis, S. Tzortzakis, "Eutectic epsilon-near-zero metamaterial terahertz waveguides," *Optics Letters*, Vol. 38, 1140–1142, 2013.
8. Sadecka, K., M. Gajc, K. Orlinski, H. B. Surma, A. Klos, I. Jozwik-Biala, K. Sobczak, P. Dluzewski, J. Toudert, and D. A. Pawlak, "When eutectics meet plasmonics: Nanoplasmonic, volumetric, self-organized, silver-based eutectic," *Advanced Optical Materials*, published online, Dec. 16, 2014.
9. to be published.

Nanofabrication Approaches for Plasmonic Nanoantenna Design

Simon Dickreuter[1], **Emre Gürdal**[1], **Dominik Gollmer**[1], **Andreas Horrer**[1], **Dieter Kern**[1], **and Monika Fleischer**[2]

[1]Institute for Applied Physics, Auf der Morgenstelle 10, Tuebingen 72076, Germany
[2]Institute for Applied Physics, Eberhard Karls University, Tuebingen, Germany

Abstract— Metallic nanoparticles are under intense investigation as optical antennas for the local enhancement of electromagnetic fields,both in fundamental studies of light-matter interaction and for applications such as biosensors or opto-electronic devices.

Electron beam lithography is typically the method of choice for fabricating individual antenna shapes with high flexibility. Different approaches include standard lift-off processes as well as etch-mask transfer into a continuous metal layer [1, 2]. By varying the geometric parameters the plasmon resonance frequencies of the nanoantennas can be tuned over a wide range [3]. In order to maintain the high resolution and flexibility of e-beam lithography while simultaneously increasing the throughput of nanostructure fabrication, stamps can be patterned by e-beam lithography, where the patterns are subsequently transferred onto a substrate by nanoimprint. For device applications with following layer deposition it may be beneficial that the surface remains planar, such that the nanoantennas can be embedded into the surface [4]. In an alternative approach, nanosphere lithography can be applied for structuring larger areas in a parallel process, where the self-assembly of polystyrene spheres allows for patterning optical antennas with hexagonal or honeycomb order, using either mono or double layers of nanospheres as evaporation or etch masks [5].

Moving from top-down fabricated metal antennas to the flexible approach of self-assembled metal nanostructures, colloidal particles can be prepared in considerable quantities and purchased commercially. Such size-selected metal particles exhibit clear plasmonic resonances. The resonance properties strongly depend on the order and distribution of the nanoparticles, since coupling and grating effects can have a strong influence. In a fully self-assembled approach, diblock copolymers are applied to a substrate. Distinct patterns with dimensions pre-determined by the copolymer will formunder suitable treatment. After selective removal of one of the diblock components a surface topography emerges, which can serve as a template for ordering colloidal particles at defined distances. In a hierarchical approach combining e-beam lithography with capillary self-assembly of colloidal particles, oligomers containing a fixed number of colloids assemble in hole patterns created by e-beam lithography and development. Such oligomers of nanoantennas may provide coupling across narrow gaps, and offer antenna assemblies with distinct optical properties depending on the plasmonic modes of the individual particles, the morphology of the oligomer, and the respective excitation.

In this presentation different techniques, serial vs. parallel and individual vs. scalable, will be shown in their application for the fabrication of optical nanoantennas together with the scattering, extinction or Raman spectra of the resulting antenna structures.

REFERENCES

1. Fleischer, M., et al., *Nanotechnology*, Vol. 21, 065301, 2010.
2. Fleischer, M., et al., *Appl. Phys. Lett.*, Vol. 93, 111114, 2008.
3. Schäfer, C., et al., *Nanoscale*, Vol. 5, 786, 2013.
4. Gollmer, D. A., et al., *Microelectron. Eng.*, Vol. 119, 122, 2014.
5. Horrer, A., et al., *Small*, Vol. 9, 3987, 2013.

Fabrication of Three-dimensional Metamaterials

Takuo Tanaka[1, 2]

[1]RIKEN Metamaterials Laboratory and Innovative Photon Manipulation Research Team, Japan
[2]Tokyo Institute of Technology, Japan

Abstract— Metamaterials is man-made materials using sub-wavelength resonant structures and have introduced a new paradigm to create unprecedented optical properties. Since the resonant element of metamaterial such as a split-ring resonator (SRR) is an analog of antenna and there is no ideal antenna that has isotropic radiation properties, the optical responses of metamaterials are inevitably anisotropic. In order to realize isotropic responses of metamaterials, three-dimensional symmetric alignment of metamaterial elements is employed at microwave frequencies, but in the optical regime, such isotropic metamaterials are still challenge due to the limitation of three-dimensional micro/nanofabrication. To this end, we present the first experimental realization of an isotropic metamaterial using fourfold-symmetric configuration of metallic nanostructures. Mass-productive formation of the assembled stereo-structures was achieved by a metal-stress driven self-folding method. Transmission spectrum of this three-dimensional metamaterial shows unambiguous isotropic characteristics for any lateral rotation, polarization, and incident angle up to 40°. The corresponding numerical simulations well re-produced the experimental results, revealing that the interplay of electric and magnetic interactions of the three-dimensional metamaterial structure plays a crucial role for the bi-anisotropic responses and it creates effective refractive index of 0.35, which is smaller than that of vacuum, at 32.8 THz. We anticipate our technique to be a breakthrough for introducing the concepts of metamaterials to real-components.

Three-dimensionally Structured Optical Metamaterials via Holographic Lithography and Eutectic Solidification

Paul V. Braun
Department of Materials Science and Engineering, University of Illinois at Urbana-Champaign
1304 West Green St., Urbana, Illinois 61801, USA

Abstract— Over the past few decades, three-dimensional structures have been widely proposed as a path to enhance light-matter interactions in devices such as solar cells and LEDs. While the sophistication of self and directed-assembly approaches for functional photonic structures has increased dramatically, application of these structures has remained elusive, in part because real structures almost always contain finite defect densities and cannot be produced from materials with the appropriate optical properties. We have now made considerable strides in integration of metallic and non-metallic material into ultra-low defect density three-dimensionally structured optical materials (e.g., epitaxially grown single crystal GaAs). We accomplish this by applying unique template-based and post-synthetic materials transformations in conjunction with powerful computational design tools. Our materials toobox now includes metals (e.g., Al and Ag), single crystal semiconductors (GaAs, GaP, and Cu_2O), and materials with variable refractive indexes (e.g., porous Si). We are particularly intrigued by the possibility of ultra-large volume processing strategies for the formation of deterministically structured materials, and have found eutectic solidification, in conjunction with a template which provides a structural driving force to limit the defect density in the material to be quite promising. Via eutectic solidification, dielectric structures with characteristic length scales as small at 100 nm have been formed in large volumes of material.

Wafer-scale 3D Nanofabrication for Sub-wavelength Nanophotonics

Peer Fischer[1, 2]

[1]Max Planck Institute for Intelligent Systems, Heisenbergstrasse 3, Stuttgart 70569, Germany
[2]Institute for Physical Chemistry, University of Stuttgart
Pfaffenwaldring 55, Stuttgart 70569, Germany

Abstract— We have recently developed a fast, parallel growth method that permits the fabrication of large arrays of nanostructures with control over their size, spacing and material composition [1]. Plasmonic metals such as silver, copper, or gold can be grown pure, or as alloys, or in combination with other materials, such as oxides, conducting or magnetic materials. The method allows us to grow structures that are of interest to nanophotonics at the wafer-scale on a large range of substrates, including transparent substrates. Several hundred billion nanostructures cover a wafer, where they form thin films with remarkable properties [2–4]. It is also possible to remove the nanostructures from the substrate and suspended them in solution, where they can form stable nanocolloidal solutions [1]. We have recently used the fabrication method to grow chiral plasmonically-active nanohelices, as small as 90 nm with two turns, that show record optical activities [2, 3]. Combination with magnetic materials can be used to grow hybrid plasmonic-ferromagnetic nanohelices [4]. We have demonstrated a resolution of 10 nm in the growth of the hybrid structures.

The growth method consists of a combination of block-copolymer micellar nanolithography (BCML) [5] with shadow growth physical vapor deposition (GLAD) [6]. First, a substrate which may be transparent, flexible, or (semi)conducting is patterned with an array of hexagonally close-packed gold (Ag or Pt) nanodots by spin-coating via block-coplymer micellar nanolithography [5]. In a subsequent plasma step the organic polymer is removed and the metal salt is reduced to a metal nanoparticle. The nanoseed are generally too small to show a plasmonic resonance (and hence field enhancement). However, a subsequent shadow growth step (glancing angle deposition) together with substrate manipulation and cooling [1] allows us to increase the size of the nanoseeds and to give them a 3D shape, including a helical shape. The nanoparticles' size, material composition and size can be tuned [1]. It is possible to grow high-density plasmonic nanodot arrays whose size and spectral response is tuned to different regions in the UV, visible, or NIR spectrum. Examples will be presented.

REFERENCES

1. Mark, A. G., J. G. Gibbs, T.-C. Lee, and P. Fischer, *Nat. Mater.*, Vol. 12, 802, 2013.
2. Gibbs, J. G., A. G. Mark, T.-C. Lee, S. Eslami, D. Schamel, and P. Fischer, *Nanoscale*, Vol. 6, 9457, 2014.
3. J. G. Gibbs, A. G. Mark, S. Eslami, and P. Fischer, *Appl. Phys. Lett.*, Vol. 103, 213101-4, 2013.
4. Eslami, S., J. G. Gibbs, Y. Rechkemmer, J. Van Slageren, M. Alarcón-Correa, T.-C. Lee, A. G Mark, G. L. J. A. Rikken, and P. Fischer, *ACS Photonics*, Vol. 1, 1231–1236, 2014.
5. Hawkeye, M. M. and M. J. Brett, *J. Vac. Sci. Technol. A*, Vol. 25, 1317–1335, 2007.
6. Glass, R., M. Möller, and J. P. Spatz, *Nanotechnology*, Vol. 14, 1153–1160, 2003.

Nanofabrication of 3 Dimensional Taper Structures for Nanofocusing Purposes

Junlong Kou, **Zheng Li**, **and Hyuck Choo**
Electrical Engineering, Division of Engineering and Applied Science
California Institute of Technology, Pasadena, CA, USA

Abstract— We have demonstrated experimentally a highly efficient on-chip three-dimensional (3D) linearly tapered metal-insulator-metal (MIM) nanoplasmonic photon compressor (3D NPC) with a final aperture size of $14 \times 80\,\mathrm{nm}^2$. An optimized and linearly tapered MIM gap plasmon waveguide could theoretically reduce the excessive losses that would occur during nanofocusing processes. This nanofocusing concept has existed for some time, yet researchers had difficulty in realizing structures based on the concept because precisely fabricating the nanoscale waveguides that taper in three dimensions had been very challenging. In simulation study, this approach could enable nanofocusing into a $2 \times 5\,\mathrm{nm}^2$ area with the coupling loss and maximum E^2 enhancement of 2.5 dB and 3.0×10^4, respectively. We fabricated the 3D NPC on a chip employing electron beaminduced deposition and demonstrated its highly localized light confinement using a twophoton photoluminescence (TPPL) technique. From the TPPL measurements, we experimentally estimated an intensity enhancement of 400 within a $14 \times 80\,\mathrm{nm}^2$ crosssectional area and a coupling efficiency of -1.3 dB (or 74% transmittance).

Extremely Long Nanochannel Arrays Realized by PnP

Junyong Park, **Changui Ahn**, **Kisun Kim**, **Jerome K. Hyun**, **and Seokwoo Jeon**
Graphene Resarech Center, KINC
Department of Materials Science and Engineering, KAIST, Daejeon, Republic of Korea

Abstract— The realization of high resolution, large area nanopatterning has been demonstrated from numerous methods. Above all, Proximity field nanoPatterning (PnP) is a unique three dimensional (3D) patterning methods using optical interference from conformal phase masks that contact directly on top of the surface of photosensitive materials. The contact allows incomparable stability in the size of pattering area, resolution, and reproducibility. Extending the thickness and structural degree of freedom of patterned structure are essential topics of current research in my group. In this presentation, in-depth study of the influence of phase and diffraction on 3D Talbot image formed from binary phase masks is explained for achieving rational design of 3D nanopatterns, especially in the regime where the grating periodicity is close to the wavelength and where scalar treatments fail to accurately capture the phase optics. The ability to precisely control diffraction and interference in this regime is illustrated by tuning the grating height in the phase mask up to values that exceed a full phase cycle. Based on these understanding, two examples of unusual pattering will ensure the robustness of PnP. One is large area patterning of three-dimensional (3D) nano-architectures that serve as sacrificial templates for the realization of highly stretchable materials by infiltrating various materials, especially poly (dimethylsiloxane) (PDMS) in this work. The 3D networked PDMS enables 62% enhancement of stretchability compared to the constituent solid film. The 3D structural PDMS has stretched up to $\sim$ 225% at optimized elastic modulus and thickness. A stretchable conductor, which contain liquid metal inside the porous network of the 3D PDMS, show extremely high electrical conductivity of 24,100 S cm^{-1} at 220% strain with god cyclic properties. The other is extremely long ($>$ cm) nanochannel arrays ($>$ 30 by 30,000 in cross-section) whose hole size could be well below 100 nm. Those nanochannels can promise new applications in the field of nanofluidics and optical components in display.

Scalability of 3D Micro-printing: Issues in Diffraction Limited Parallel Writing

Erik Waller[1] **and Georg von Freymann**[1, 2]

[1]Department of Physics and Research Center OPTIMAS
University of Kaiserslautern, Kaiserslautern 67663, Germany
[2]Fraunhofer Institute for Physical Measurement Techniques (IPM)
Kaiserslautern 67663, Germany

Abstract— Direct Laser Writing, or in more modern terms three-dimensional micro printing, has seen a tremendous development during recent years. While it took up to several ten minutes to write one single photonic crystal roughly one decade ago [1], today many samples are fabricated in the same time. Micro-printed three-dimensional samples range from a few cubic micrometers to several cubic millimeters, covering more than two orders of magnitude in dimension with one single technique, allowing for hierarchical structures to be realized. Even larger structures just seem a matter of further increased writing speed. One possible avenue is parallelization of the writing process by generating multiple foci using spatial light modulators [2, 3].

Along these lines we find that closely spaced features vary in size depending on the order they are written. At first sight this is surprising as all foci are generated with same intensity and shape, but a closer look reveals that today's high writing speeds initiate features on a timescale smaller or comparable to the time needed to finalize the polymerization process. This could provide us with detailed knowledge about the different physical mechanisms driving this so-called proximity-effect and their relative strength.

We present simultaneous multi-foci exposures to study photoresist-specific polymerization processes. We generate different focus patterns, allowing to precisely tuning timing and spacing between different features. These patterns are calculated such that different physical mechanisms leading to the proximity-effect may be separated and characterized in their time and spatial dependence. Numerical modeling of the processes shows good agreement with our experimental observations.

REFERENCES

1. Deubel, M., et al., "Direct laser writing of three-dimensional photonic-crystal templates for telecommunications," *Nature Materials*, Vol. 3, 444, 2004.
2. Waller, E., et al., "Active aberration- and point-spread-function control in direct laser writing," *Optics Express*, Vol. 20, 24949, 2012.
3. Waller, E., et al., "Multi foci with diffraction limited resolution," *Optics Express*, Vol. 21, 21708, 2013.

Formulating Nanostructures to More Scalable and Functional Architectures via Assembling Hierarchical Hybrids and Adopting Continuous Nanomanufacturing Methods

Jong G. Ok
Department of Mechanical and Automotive Engineering
Seoul National University of Science and Technology, Seoul, Korea

Abstract— Recently there has been increasing interest in micro- and nano-scale materials, structures, and phenomena from both academia and industry. Many diverse fields including optoelectronics, photonics, bioengineering, and energy conversion have all shown significant increases in utilization of, and demand for, micro/nano-scale features. To meet this demand, more scalable, practical, and efficient methodologies for small-scale architecturing are called for. This talk will discuss these issues while focusing on two main topics: (1) how complementary micro- and nanoscale structures and materials can be hierarchically assembled into more functional hybrid architectures; and (2) how these nanoarchitectures can be engineered in a continuous manner towards commercially-feasible scales.

In part one of this talk, carbon nanotubes, graphene, and metal oxide nanowires (NWs) will be considered as small-scale building blocks. Assembling these complementary functional components, three-dimensional (3D) hybrid nanoarchitectures comprising ZnO and VOx NWs hierarchically integrated with CNT constructs will be demonstrated for advanced energy applications based on photonic and electrochemical conversion.

In the second part, a series of continuous and high-throughput micro/nano-manufacturing techniques will be presented based around roll-to-roll (R2R) lithography as well as seamless and template-free nanopatterning, along with direct photonic applications. R2R nanoimprint lithography (R2R NIL) and Photo Roll Lithography (PRL) will exhibit the scalable nanofabrication of various sub-wavelength-scale features by combining NIL and photolithography with continuous rolling principle. Further, the seamless nanopatterning enabled by continuous inscribing of a cleaved grating mold edge on a polymer substrate will be demonstrated, which will be followed by the template-free nanopattering via vibrational indentation of a simple flat edge over a softer substrate.

Moving forward, we will discuss how nanomaterials/nanostructures and nanopatterning methodologies can be mingled with each other towards more scalable and multidimensional nanoarchitectures. For instance, the mechanically-rolled 2D CNT sheets will be introduced for direct fabrication of NW/CNT hybrid thin-film devices. Then we will demonstrate PRL-fabricated metal mesh patterns can be incorporated to the transparent graphene films for flexible nanoelectronics. It will also be presented various 2D micro/nanopatterns can be continuously fabricated by sequential 1D patterning strokes enabled by nanoinscribing and vibrational indentation.

High-contrast Sensing Using Hyperbolic Metamaterials and Plasmonic Cavity Resonators

H. J. Lezec[1], **T. Xu**[1, 2], **A. K. Agrawal**[1, 2], **and W. Zhu**[1, 2]

[1]Center for Nanoscale Science and Technology
National Institute of Standards and Technology, Gaithersburg, MD, USA
[2]Maryland Nanocenter, University of Maryland, College Park, MD, USA

Abstract— Hyperbolic metamaterials, a class of artificially engineered materials with a highly anisotropic permittivity response originating from opposite signs of the principal components of the electric tensor, have attracted significant interest in recent years due to their ability to manipulate the propagation light in exotic ways [1]. Such materials enable distinctive optical phenomena such as negative refraction, super-resolution imaging, and enhanced spontaneous emission.

Here we exploit the hyperbolic iso-frequency characteristic of a planar type-II HMM (composed of a template-stripped [2] stack of alternating, 25-nm-thick, sputtered films of Ag and SiO_2) to achieve high-sensitivity proximity detection of nanoparticles in transmission. The iso-frequency surface of the HMM is unique in that propagation of light over the entire visible-range is allowed only for electromagnetic modes having tangential spatial frequencies k_x exceeding the free-space wavevector k_0 by over a factor of two [3, 4]. Due to its high sensitivity to nanoparticles in deep-subwavelength proximity to a surface, achieved without the use of dark-field optics, this HMM-based device hints at promising applications in bio-chemical sensing, particle tracking and contamination analysis.

High-contrast refractive-index-change sensors consisting of ultra-high quality factor open-cavity resonators for surface-plasmon polaritons will also be discussed. The resonator structures, fabricated using a combination of template stripping [2] and focused-ion-beam milling, are designed to overcome the intrinsically short plasmon lifetimes which typically limit the sensing performance of plasmonic systems strongly coupled to free space, such as sub-wavelength hole arrays in metal films.

REFERENCES

1. Poddubny, A., et al., "Hyperbolic metamaterials," *Nat. Photon.*, Vol. 7, 958–957, 2013.
2. Nagpal, P., et al., "Ultrasmooth patterned metals for plasmonics and metamaterials," *Science*, Vol. 325, No. 5940, 594–597, 2009.
3. Tumkur, T. U., et al., "Control of reflectance and transmittance in scattering and curvilinear hyperbolic metamaterials," *Appl. Phys. Lett.*, Vol. 101, 091105, 2012.
4. Xu, T., H. J Lezec, et al., "Visible-frequency asymmetric transmission devices incorporating a hyperbolic metamaterial," *Nat. Comm.*, Vol. 5, No. 4141, doi:10.1038/ncomms5141, 2014.

Fabrication of a Nanoscale Plasmonic Fishnet Structure for the Enhancement of Absorption in Thin Film Solar Cells

Sayan Seal, **Vinay Budhraja**, **Liming Ji**, **and Vasundara V. Varadan**
Department of Electrical Engineering, University of Arkansas, USA

Abstract— Incorporating plasmonic structures in the back spacer layer of thin film solar cells (TFSC's) is an efficient way to increase the yield. The incoming light is scattered into the absorber layer and light is also trapped by total internal reflection from the top of the absorber layer. This light trapping results in increased efficiency and hence we can extract more power from the cell. The plasmonic fishnet structure is one such geometry using which this effect can be realized. Numerical simulations have shown the ability of these structures to bring about an enhancement in the short circuit current density of TFSCs. The fishnet should be designed to operate at wavelengths near the band gap of amorphous silicon, which is the absorber material in the TFSC. At these wavelengths, the absorption of light in amorphous Si is extremely low. We show that light absorption in the a-Si absorber layer is enhanced by a factor of 10.6 at the design wavelength of 690 nm due to the presence of the fishnet structure. Furthermore, the total absorption over all wavelengths was increased by a factor of 3.2. The short circuit current densityof the TFSC was increased by 30% as a result of including the fishnet. No deterioration at lower wavelengths occurred unlike what happens with plasmonic particulate structures.

This paper presents the fabrication process of the fishnet structure. A fishnet structure made of silver was fabricated using a combination of electron beam lithography and thermal evaporation. A complete TFSC was fabricated using PECVD to deposit a-Si on the fishnet structure. In effect, the fishnet was placed in the back spacer layer preventing shadowing effects. The final structure optically resembled a TFSC in all respects except that there were no doped layers. The fishnet structure is essentially a mesh of linewidth 100 nm, and a thickness of 20 nm. The process for fabricating such a fine structure is challenging, especially if a repeatable process is desired. The adhesion of this structure to the substrate is also a matter of concern since there is more processing that follows the fabrication of the fishnet. The procedures leading up to the establishment of a repeatable process for the fabrication of the fishnet structure will be presented. The designed solar cell was optically characterized using spectroscopic ellipsometry. The measured results were in agreement with those predicted by full wave electromagnetic simulations.

Session 2P5a
Light Carrying Orbital Angular Momentum: Theory and Applications

Magneto-optics with Light Carrying Orbital Angular Momentum

Thomas Bose[1], **Roy W. Chantrell**[1], **and Jamal Berakdar**[2]

[1]University of York, York, UK
[2]Martin-Luther-University, Halle, Germany

Abstract— The design and fabrication of ever smaller and faster magnetic devices for data storage, sensorics and information processing necessitates the development of efficient tools to control the dynamic behavior of the magnetization. In particular, femtosecond laser-induced magnetic excitations, originating in thermal and non-thermal effects, were demonstrated for magnetic systems [1, 2]. A key element in the underlying mechanism in this case is the material spin-orbit interaction that facilitates the coupling of the electric field component of the laser to the magnetic degrees of freedom of the material under study. A more general approach is to structure the laser beam. For this purpose we demonstrate here the potential of optical vortices, i.e., laser beams designed as to carry transferrable orbital angular momentum (OAM) in addition to the light polarization (associated with the photon spin) [3–5].

We predict a non-thermal magneto-optical effect for magnetic insulators subject to intense light carrying orbital angular momentum (OAM) [6]. Using a classical approach to second harmonic generation in non-linear media with specific symmetry properties we find a significant nonlinear contribution to the local magnetic field triggered by light with OAM. The resulting magnetic field originates from the displacement of electrons driven by the electric field (with amplitude E_0) of the spatially inhomogeneous optical pulse, modeled here as a Laguerre-Gaussian beam carrying OAM. In particular, the symmetry properties of the irradiated magnet allow for magnetic field responses which are second-order ($\sim E_0^2$) and fourth-order ($\sim E_0^4$) in electric-field strength and have opposite signs. For sufficiently high laser intensities, the terms $\sim E_0^4$ dominate and generate magnetic field strengths which can be as large as several Tesla. Moreover, changing the OAM of the laser beam is shown to determine the direction of the total light-induced magnetic field, which is further utilized to study theoretically the non-thermally induced magnetization dynamics. Pump-probe experiments [2] may be used to verify the effect.

REFERENCES

1. Stöhr, J. and H. C. Siegmann, *Magnetism — From Fundamentals to Nanoscale Dynamics*, Springer, Berlin, 2006.
2. Kirilyuk, A., A. V. Kimel, and T. Rasing, "Ultrafast optical manipulation of magnetic order," *Rev. Mod. Phys.*, Vol. 82, 2731–2784, 2010.
3. Allen, L., M. W. Beijersbergen, R. J. C. Spreeuw, and J. P. Woerdman, "Orbital angular momentum of light and the transformation of Laguerre-Gaussian laser modes," *Phys. Rev. A*, Vol. 45, 8185–8189, 1992.
4. Allen, L., M. J. Padgett, and M. Babiker, "The orbital angular momentum of light," *Prog. Opt.*, Vol. 39, 291–372, 1999.
5. Molina-Terriza, G., J. P. Torres, and L. Torner, "Twisted photons," *Nat. Phys.*, Vol. 3, 305–310, 2007.
6. Bose, T. and J. Berakdar, "Nonlinear magneto-optical response to light carrying orbital angular momentum," *J. Optics*, Vol. 16, 125201, 2014.

Illumination of Optical Vortices Forms Chiral Nanostructures

Takashige Omatsu
Graduate School of Advanced Integration Science, Chiba University
1-33 Yayoi-cho, Inage-ku, Chiba 263-8522, Japan

Abstract— Optical vortices, e.g., the Laguerre-Gaussian modes, have been widely investigated in various fields, such as optical telecommunications, and super resolution microscopes, because they have unique properties, such as annular intensity profiles due to a phase singularity. They also carry an orbital angular momentum characterized by an integer (a topological charge) due to the helical wavefronts and a spin angular momentum associated with a helical electric field.

Their orbital and spin angular momenta, causing orbital motion of submicron particles in optical tweezers, will have the potential to control the dynamics of compositional elements (a melted matter or a vaporized matter) produced by irradiation of laser pulses. However, there is no reports concerning the angular momentum effects of optical vortices on the laser ablation, so far.

In recent years, we and our co-workers have found that the optical vortices enable us to twist an irradiated material through an ablation process, so as to form chiral nanostructures. The resulting nanostructures show the chilarity (twisted direction) determined by the sign (handedness) of the the optical vortices. Such chiral nanostructures will have the potential to open the door to a variety of research opportunities, such as micro-electro mechanical systems, planar metamaterials, chiral selective nanoscale imaging systems and chemical reactions on plasmonic nanostructures.

In this paper, we present the state of art of the chiral nanostructures fabrication based on illumination of the optical vortices. The chiral metal nanoneedles with a twisted conical surface had a minimum tip curvature of $< 40\,\mathrm{nm}$ ($< 1/25$ of the laser wavelength (1064 nm)).

Such chiral metal nanoneedle formation can be understood as follows. The metal melted by irradiation of the optical vortex pulse then receives the total angular momentum from the optical vortices, to rotate azimuthally around the dark core of the optical vortices. Subsequently, the melted metal is directed and confined in the dark core (stable equilibrium position) by the optical scattering force, so as to establish the chiral nanostructures.

We also address chiral azo-polymeric materials formed by the illumination of green optical vortices. The irradiation of a green optical vortex makes the softer cis azo-polymer arising from trans-cis photo-isomerization of the azo-polymer. Subsequently, the cis azo-polymer is forced to revolve in a clockwise (or counter-clockwise) direction owing to the total angular momentum transfer, and it is directed toward the dark core of the optical vortices owing to the mass transport driving force, resulting in the chiral surface relief formation.

REFERENCES

1. Hamazaki, J., R. Morita, K. Chujo, Y. Kobayashi, S. Tanda, and T. Omatsu, "Optical-vortex laser ablation," *Opt. Express*, Vol. 18, 2144–2151, 2010.
2. Omatsu, T., K. Chujo, K. Miyamoto, M. Okida, K. Nakamura, N. Aoki, and R. Morita, "Metal microneedle fabrication using twisted light with spin," *Opt. Express*, Vol. 18, 17967–17973, 2010.
3. Toyoda, K., K. Miyamoto, N. Aoki, R. Morita, and T. Omatsu, "Using optical vortex to control the chirality of twisted metal nanostructures," *Nano Lett.*, Vol. 12, 3645–3649, 2012.
4. Toyoda, K., F. Takahashi, S. Takizawa, Y. Tokizane, K. Miyamoto, R. Morita, and T. Omatsu, "Transfer of light helicity to nanostructures," *Phys. Rev. Lett.*, Vol. 110, No. 14, 143603, 2013.
5. Watabe, M., G. Juman, K. Miyamoto, and T. Omatsu, "Light induced conch-shaped relief in an azo-polymer film," *Sci. Rep.*, Vol. 4, 4281, 2014.

Highly Efficient Torque Extraction from Light Using a Bilayer Structure

Xiao Li[1], **Jun Chen**[1, 2], **Liyong Cui**[1], **Neng Wang**[1, 3], **Zhifang Lin**[4], **and Jack Ng**[1, 5]

[1]Department of Physics, Hong Kong Baptist University, Hong Kong, China
[2]Department of Physics, Shanxi University, Shanxi, China
[3]Department of Physics, Fudan University, Shanghai 200433, China
[4]State Key Laboratory Surface Physics (SKLSP), Department of Physics
Fudan University, Shanghai 200433, China
[5]Institute of Computational and Theoretical Studies
Hong Kong Baptist University, Kowloon Tong, Hong Kong, China

Abstract— Angular momentum transfers between light and material object induces optical torque. In 1936, Beth measured the optical torque acting on a centimeter sized birefringent plate using circularly polarized light. Here, we showed that a pair of parallel birefringent slabs not only preserve the magnitude of the torque and the broadband nature of the birefringence, but also shows up novel effects that a single plate can never achieve. Examples include, but not limited to, a large torque beyond the limit of a single plate, controllable counter or parallel rotation of the two plates, and a high torque extraction rate from light.

To zeroth order, the plates convert the polarization of the light, and receiving a torque in response. Multiple scattering between the plates further opens up additional possibilities. We optimize and engineer the structure for better torque extraction by introducing a dielectric (e.g., oil) between the plates (to enhance counter rotation), fine tuning the light frequency, and using different birefringent refractive indices (to enhance the torque).

We then turn our attention to bilayer plasmonic particle clusters. In addition to the functionalities stated above, the hybridized modes of the plasmonic particles enabled strong counter rotation that is an order of magnitude stronger than the single layer torque. Another disadvantage of a single resonance plasmonic structure is its reliance on large extinction cross section, which requires the particle to be isolated. In contrast, the bilayer structures allows strong torque with high torque per unit extinction cross section, allowing a very high efficiency in torque extraction from light.

Extreme Nonlinear Optical Processes with Beams Carrying Orbital Angular Momentum

C. Kern[1], **M. Zürch**[1], **P. Hansinger**[1], **A. Dreischuh**[2], **and Ch. Spielmann**[1, 3]

[1]Institute of Optics and Quantum Electronics
2Abbe Center of Photonics Friedrich-Schiller-University Jena, Max-Wien-Platz 1, D-07743 Jena, Germany
[2]Department of Quantum Electronics, Faculty of Physics, Sofia University
5, J. Bourchier Blvd, BG-1164 Sofia, Bulgaria
[3]Helmholtzinstitut Jena, Helmholtzweg 4, D-07743 Jena, Germany

Abstract— Light beams carrying an isolated point singularity with a screw-type phase distribution are called an optical vortex (OV). The fact that in free space the Poynting vector of the beam gives the momentum flow leads to an orbital angular momentum (OAM) of the photons in such a singular beam, independent on the spin angular momentun [1] There are many applications of optical OAM shown in literature that would benefit from the availability of optical vortex beams in all spectral regions. For example it was shown that transitions forbidden by selection rules in dipole approximation appear allowed when using photons with the additional degree of freedom of optical OAM [2]. However, the common techniques of producing new light frequencies by nonlinear optical processes seem problematic in conserving the optical vortex when the nonlinearity becomes large. We show that with the extremely nonlinear process of High Harmonic Generation (HHG) it is possible to transfer OVs from the near-infrared to the extreme ultraviolet (XUV) [3] at wavelengths down to $\sim 30\,\mathrm{nm}$. The observed XUV light was examined spatially and spectrally. The spatial profile showed the expected singular behavior, a dark region in the centre. A phase feature that showed a shift of π on opposing sides of the beam profile was found with a wavefront splitting technique. A screw-like phase evolution around the profile was also verified by employing a Hartmann type measurement. The generated spectrum revealed that in all Harmonic orders an OV was present. The profile however looked the same in all orders, indicating identical topological charge, which runs counterintuitive to the assumption that the phase of $\exp(-il\varphi)$ is multiplied by the order of the nonlinearity.

REFERENCES

1. Allen, L., et al., "Orbital angular-momentum of light and the transformation of Laguerre-Gaussian laser modes," *Phys. Rev. A*, Vol. 45, No. 11, 8185, 1992.
2. Picón, A., et al., "Transferring orbital and spin angular momenta of light to atoms," *New J. Phys.*, Vol. 12, 083053, 2010.
3. Zürch, M., et al., "Strong-field physics with singular light beams," *Nature Physics*, Vol. 8, No. 10, 743, 2012.

Space-time Mapping of Variable Vortex Pulses

Martin Bock, **Thomas Elsaesser**, **and Ruediger Grunwald**
Max-Born-Institute for Nonlinear Optics and Short-Pulse Spectroscopy, Germany

Abstract— The adaptive generation and diagnostics of ultrashort coherent light pulses carrying an extrinsic orbital angular momentum enables to exploit specific degrees of freedom for applications like plasmonics, communication or materials processing. We report on recent experiments in which few-cycle vortex pulses were simultaneously shaped and detected by a tandem of sequentially arranged liquid-crystal-on-silicon (LCoS) spatial light modulators (SLMs) [1]. The pulses to be shaped were emitted by a Ti : sapphire laser oscillator. Because of the significant coupling between spatial and temporal features, the pulse characterization in few-cycle range is non-trivial and requires a resolution in time and space. In the shaping part of the setup, variable phase patterns like single or arrayed spiral phase plates are programmed into the phase map of a HoloEye SLM. The detection part works as a second order wavefront autocorrelator. It combines (i) the spatial resolution and robustness of a reconfigurable, SLM-based Shack-Hartmann sensor with programmable axicons, (ii) the high time-resolution of a Michelson interferometer, (iii) a nonlinear conversion in a thin (10 µm) BBO crystal, and (iv) the high quantum efficiency of an EMCCD camera. The detailed analysis of the twisted Shack-Hartmann patterns reveals the vortex structure and indicates the tunable topological charge. Together with the spatially resolved nonlinear autocorrelation, one obtains also the relative pulse front travel time map. The results enable to reconsider the concepts of optical propagation for vortex pulses and related types of structured beams.

Generation of Twisted Light via Metallic Nanospirals

A. Sprafke[1], **R. Kamrla**[1], **R. B. Wehrspohn**[1, 2], and **J. Berakdar**[1]

[1]Institute of Physics, Martin Luther University Halle-Wittenberg, Halle 06120, Germany
[2]Fraunhofer Institute for Mechanics of Material IWMH, Halle 06120, Germany

Abstract— Light can carry an orbital angular momentum (OAM). Light with OAM exhibits a corkscrew-like rotation of the maximum of the electric field around the axis of propagation. Therefore, such light is also called twisted light. Twisted light has been suggested for a number of applications, e.g., for optical tweezers to trap and rotate microparticles, atoms, molecules, and Bose-Einstein-condensates, for light-control of magnetic fields as well as for novel approaches for photovoltaics. The amount of OAM is experimentally tunable. Hence, the use of twisted light is particularly interesting for strongly enhanced data transmission rates. Light beams carrying no OAM are commonly converted into twisted light beams by either a macroscopic spiral phase plate, a holographic grating, a spatial light modulator, or by mode conversion inside a laser resonator. It was shown recently that twisted light can transfer its OAM to metal surfaces and transform planar metal surfaces into chiral nano needles. In this work, we numerically and theoretically investigate the reverse problem: Can a chiral metallic structure, such as a metal spiral that has feature sizes in the range of the wavelength, transform plane waves into structured light beams carrying OAM? We show that light reflected by small metal spirals indeed carries OAM provided that the geometrical properties of the spiral, such as height to wavelength ratio, or spiral turns per wavelength, are properly adjusted. Furthermore, we discuss the robustness of our suggested system, e.g., with regard to the angle of incidence, spiral size, and generated beam size and divergence. These finding are important in so far, as they suggests a new route to transfer locally and temporally angular momentum, e.g., by depositing the metal nanospiral on the tip of a scanning tunneling microscope which is irradiated by a Gaussian laser beam. Such a device offers qualitatively new possibilities to explore the local dynamics of spin and/or orbitally ordered matter.

Nonlinear Vortex Light Beams Resistant to Dissipation

Miguel A. Porras[1] **and Carlos Ruiz-Jiménez**[2]

[1]Complex Systems Group, Technical University of Madrid, Rios Rosas 21, Madrid 28003, Spain
[2]Complex Systems Group, Technical University of Madrid, Ciudad Universitaria s/n, Madrid 28040, Spain

Abstract— The research on light beams carrying orbital angular momentum, and in particular those with screw topological wave front dislocations or vortices, was initially focused on Laguerre-Gauss beams, but quickly spread to other vortex beams, many of them endowed by the property of being non-diffracting, as high-order Bessel beams in the linear regime of propagation, vortex solitons in transparent nonlinear media, and dissipative solitons in media with gain and losses. In this work we describe a novel class of vortex beams that we have called nonlinear vortex Bessel beams with the unique feature that can propagate without any change, including any attenuation, while continuously dissipating energy and orbital angular momentum in the host medium via multiphoton absorption. This "self-healing" property makes these beams particularly attractive in applications requiring optical pumping of angular momentum. Nonlinear vortex Bessel beams are easily generated in practice from standard axicon-generated high-order Bessel beams. Recent studies in the highly nonlinear regime indicate that they are also involved in a new type of light filamentation with tubular geometry. Contrary to many vortex solitons, nonlinear vortex Bessel beams do not require Kerr-type nonlinearities to exist, but only nonlinear absorption, and therefore are not affected by Kerr-induced instabilities.

Controlling Atomic Transparency with Structured Light

S. Franke-Arnold[1], **N. Radwell**[1], **T. W. Clark**[1], **B. Piccirillol**[2], **and S. M. Barnett**[1]

[1]University of Glasgow, SUPA, UK
[2]Universitá di Napoli Federico II, Italy

Abstract— Electromagnetically induced transparency (EIT) is a curious but well-established effect that can drastically change the optical response of an atomic medium. Atoms can become transparent to a resonant probe laser if they are simultaneously exposed to a suitable control light beam. Here we show that the opacity of atoms can vary across the beam profile, dictated by the local phase and polarisation of the light [1]. We use a single probe beam with an azimuthally varying polarisation and phase structure, generated by a q-plate [2]. Its right and left polarisation components, which carry opposite orbital angular momenta, provide the probe and control beam for the EIT transition. We measure the transmission of our structured light beam through cold rubidium atoms and observe an azimuthal variation of the absorption profile, with alternating regions of transparency and opacity.

Conventional EIT systems do not exhibit phase sensitivity. We show, however, that a weak transverse magnetic field closes the EIT transitions, thereby generating phase dependent dark states [3] which in turn lead to phase dependent transparency, in agreement with our measurements.

Tailored spatial atomic dark states could provide a potentially robust storage mechanism, offering an alternative to coherence based quantum memories [4].

REFERENCES

1. Radwell, N., et al., "Spatially dependent electromagnetically induced transparency," arXiv:1412.1275 [physics.atom-ph], 2014.
2. Piccirillo, B., et al., "Photon spin-to-orbital angular momentum conversion via an electrically tunable q-plate ," *Appl. Phys. Lett.*, Vol. 97, 241104, 2010.
3. Buckle, S., et al.,, "Atomic Interferometers: Phase dependence in multi-level atomic transitions," *Opt. Acta*, Vol. 33, 1129, 1986.
4. Nicolas, A., et al.,, "A quantum memory for orbital angular momentum photonic qubits," *Nat. Photonics*, Vol. 8, 1234, 2014.

Spontaneous Formation of Square Optical Vortex Lattice in a Transverse Section of Broad-area Laser

A. A. Krents[1, 2], **A. V. Pakhomov**[1, 2], **D. A. Anchikov**[1], **and N. E. Molevich**[1, 2]

[1]Samara State Aerospace University, Samara 443086, Russia
[2]Lebedev Physical Institute, Samara 443011, Russia

Abstract— The paper studies the spontaneous formation of square optical vortex lattice (SVL) in broad-area lasers theoretically. The possible motion of vortices is also studied. The nonlinear interaction of numerous transverse modes in broad-area lasers can lead to the spontaneous formation of complex spatiotemporal optical structures including the SVL. The SVL is experimentally observed in the Nd:YVO_4 laser, in a broad-area CO_2 laser operating at a single longitudinal mode, in the solid-state laser with optical pumping on a chip $LiNdP_4O_{12}$, in a Na_2 laser, in the vertical cavity surface emitting laser.

We studied the formation of SVL both analytically and numerically using the full Maxwell-Bloch model:

$$dE/dt=\sigma\,(P-E)+ia\Delta E;\; dP/dt=-\,(1+i\delta)\,P+DE;\; dD/dt=-\gamma[D-r+0.5\,(E^*P+EP^*)],\quad (1)$$

where Δ is the transverse two-dimensional Laplace operator, E, P are, respectively, the dimensionless electric field and polarization amplitudes, D is the dimensionless population inversion. σ, γ are the dimensionless electric field and inversion decay rates, respectively, r is the pump parameter, δ is the detuning.

In case $\delta > 0$, we have shown analytically that the SVL is solution of the full Maxwell-Bloch model. Also, the SVL solution was found numerically (Fig. 1). For numerical simulation of Equation (1), we used the split step Fourier method. Random initial conditions were used. A distance between neighbor vortices was calculated analytically: $d = \pi\sqrt{a/\delta}$. This value is in a good agreement with our numerical results.

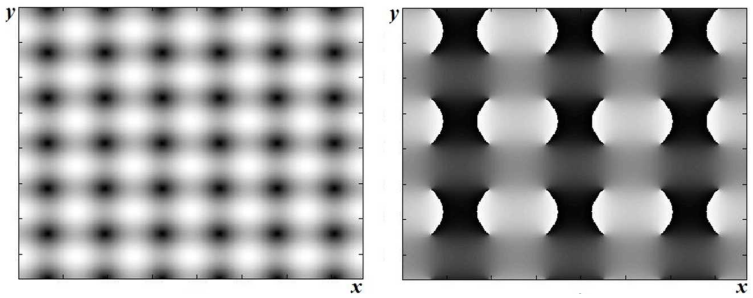

Figure 1: Stationary square vortex lattice: (a) Intensity distribution and (b) phase distribution.

By increasing the pump parameter r, the SVL becomes unstable. Each vortex oscillates around the steady state. The frequency of vortex oscillations is calculated analytically: $\omega = \delta/(\sigma + 1)$. This value is in a good agreement with our numerical results.

Superpositions of Three-dimensional Diffraction-free Asymmetrical Bessel Beams

A. A. Kovalev, V. V. Kotlyar, and A. P. Porfirev
Image Processing Systems Institute of the Russian Academy of Sciences, Russia

Abstract— We considered physical properties of superpositions of the diffraction-free asymmetrical Bessel beams. These beams differ from a conventional symmetrical Bessel beams by arbitrary complex shifts along both the Cartesian coordinates. The intensity distribution of the asymmetrical Bessel beam has a form of a crescent. We derived an equation, which allows to obtain from the values of the complex shifts the position of the n-fold phase singularity of the beam (n is the topological charge, the order of the Bessel function), as well as orientation angle of the crescent on the diffraction pattern.

Using representation of the complex amplitude via the angular spectrum of plane waves, a general analytical expression was derived for the orbital angular momentum (OAM) of the superposition of a finite number of the asymmetrical Bessel beams, each of them having its own complex shifts along the Cartesian coordinates (although the topological charge of the beams in superposition supposed to be the same).

Using the obtained expression for the OAM, we proved that the beam, composed of arbitrary number of the same-order symmetrical Bessel beams located at the arbitrary points in space, has the OAM equal to the topological charge of each beam.

Using the same equation, we considered the OAM of the beams composed of three or four asymmetrical Bessel beams located at the vertices of the equilateral triangle (triple beams) or the square (quadruple beams). For triple beams, we obtained a closed-form expression for the OAM without any integrals and series. For both triple and quadruple beams, we obtained the condition when the OAM is equal to the topological charge of each constituent beam (like is the case for the conventional Bessel beams). For example, we calculated the intensity distribution of quadruple beams with their pattern composed of the light square instead of the circle. Such beam consists of four 5-order Bessel beams and the OAM of the superposition is also equal to 5.

We also showed that the diffraction pattern of a superposition of the infinite number of the symmetrical Bessel beams with their centers located on a circle coincides with the diffraction pattern of one Bessel beam located at the center of the circle.

Session 2P5b
SC3: Ultra-thin Metal-dielectric Structured Surfaces and Thin Films for Antireflection, Light Trapping, and Perfect Absorption 2

Metasurface Optical Antireflection Coating

Boyang Zhang[1], **Joshua Hendrickson**[2], **Nima Nader**[2, 3], **Hou-Tong Chen**[4], **and Junpeng Guo**[1]

[1]Department of Electrical and Computer Engineering, University of Alabama in Huntsville
Huntsville, Alabama 35899, USA
[2]Sensors Directorate, US Air Force Research Laboratory
Wright Patterson AFB, Ohio 45433, USA
[3]Solid State Scientific Corporation, Nashua, New Hampshire 03060, USA
[4]Center for Integrated Nanotechnologies, Los Alamos National Laboratory
Los Alamos, New Mexico 87545, USA

Abstract— Light reflection at the boundary of two different media is one of the fundamental phenomena in optics, and optical antireflection is desirable in many optical systems such as cameras, telescopes, displays, and solar cells. Traditionally, optical antireflection has been accomplished using single- or multiple-layer dielectric films and graded index surface relief structures. However, these approaches either impose strict requirements on the refractive index matching or involve complicated fabrication processes that are difficulty for device integration. Here we report a demonstration of a new strategy of antireflection coating employing metasurfaces with designer surface optical properties in the mid-wave infrared. Our results show that the metasurface antireflection coating can completely eliminate optical reflection and enhance light transmission over a broad spectral bandand a wide range of incidence angle.

Structured Conductive Zinc Oxide for Mid-IR Perfect Light Trapping

Joshua R. Hendrickson[1], **Shivashankar R. Vangala**[1, 2], **Nima Nader**[1, 2], **Kevin D. Leedy**[1], **Junpeng Guo**[3], **and Justin W. Cleary**[1]

[1]Air Force Research Laboratory, Sensors Directorate, Wright Patterson AFB, OH 45433, USA
[2]Solid State Scientific Corporation, Nashua, NH 03060, USA
[3]Department of Electrical and Computer Engineering
University of Alabama in Huntsville, Huntsville, AL 35899, USA

Abstract— Plasmonic assisted mid-infrared (MIR) light trapping using 1D grating microstructures patterned in gallium doped ZnO films is investigated. The resonant absorption due to the excitation of surface plasmon polaritons in the highly conductive ZnO film can be controlled with a proper choice of grating period and film thickness. Lumerical finite-difference time-domain (FDTD) simulations show resonant modes resulting in close to 100% light trapping observed as reflection dips in the 4–8 µm wavelength regime. Experimental demonstrations of the perfect trapping is accomplished using a 1.3 µm thick Ga doped ZnO film deposited on high resistivity Si substrate by pulsed laser deposition. The achieved film was nominally $Zn_{0.974}Ga_{0.026}O$ with a doping level of $\sim 10^{21}\,cm^{-3}$ as determined by IR ellipsometry. The 1D grating structures of different periods are fabricated using standard photolithography followed by reactive ion etching. When comparing experimental resonant reflection dips with FDTD simulations, unanticipated low-wavelength roll-offs where found. Films that had undergone the etch processing where again characterized via IR ellipsometry and notably showed a decreasingly negative permittivity versus the un-etched counterpart. Analysis via further simulations shows the etch has the effect of making a thin layer on top of the structure less metallic which is likely due to a local annealing process. Incorporating a thin layer over the entire structure in the simulation using the less metallic optical constants then gives a good qualitative fit to experimental light trapping resonances. By tuning the grating parameters these perfect light trapping device structures could easily be extended to the long wavelength IR in the range of 8 to 12 microns. Such structures have potential uses in IR sensing and filter applications.

Broadband Metamaterial Absorber Based on Multiple Resonances of Fundamental and Second Harmonics

Chang Long, **Sheng Yin**, **Wei Li**, **Wei Wang**, **and Jianguo Guan**
State Key Laboratory of Advanced Technology for Materials Synthesis and Processing
Wuhan University of Technology, Wuhan 430070, China

Abstract— Metamaterial absorbers (MMAs) may show perfect absorption and adjustable absorption frequency from microwave to visible light band by simply tuning the parameters of the artificial structured unit cells. However, the absorption bandwidth is usually so narrow that the practical applications are strongly limited.

In this work, we design an ultra-broadband, thin-thickness metamaterial absorber by alternatively assembling two different sized quadrangular frustum pyramids containing multiplexed resonance cavities in a backplane metal. Unlike the traditional methods that simply mix resonances by horizontal or vertical integration [1, 2], we make full use of both fundamental (TE/M_{10}) and second order harmonics (TE/M_{21}) of the structure. The modes of the resonance are verified by square waveguide theory [3] and simulated electromagnetic field distribution. By arranging big pyramids in the "white blank" of the chessboard, TE/M_{21} modes are enhanced because of the unevenness of the units. Meanwhile, TE/M_{10} modes remain the same though the other half of the chessboard are empty. So dual-band absorption are obtained. The gap of the two bands is connected by the TE/M_{10} modes of the small pyramids and a broadband absorption are acquired when they are arranged in the "black blank" of the chessboard.

Above all, the fundamental and second order harmonics of the multiplexed resonance cavities are both excited in this design, so that the MMA shows $\geq 90\%$ absorption in the whole 6.8–18 GHz range, triple bandwidth of that based on the single sized counterpart at the same total thickness (h) of 4.36 mm. Though the MMA are not strictly symmetrical, it is still insensitive to the polarization. The as-proposed design idea is flexible, and can be manipulated to meet the absorbing requirements in other frequency by simply changing the characteristic dimension of the MMAs. The design strategy provides a novel route to exponentially extend the absorption bandwidth of MMAs without increasing h.

REFERENCES

1. Ding, F., Y. Cui, X. Ge, Y. Jin, and S. He, *Appl. Phys. Lett.*, Vol. 100, 103506, 2012.
2. He, S., F. Ding, L. Mo, and F. Bao, *Progress In Electromagnetics Research*, Vol. 147, 69–79, 2014.
3. Pozar, D. M., *Microwave Engineering*, John Wiley & Sons, 2009.

Thin Film Dielectric Gradient Optical Structures for Space Photonics

O. Volpian[1], **A. Kuzmichev**[2], **G. Ermakov**[1], **Yu. Obod**[1], **N. Silin**[3], **and S. Shkatula**[1]

[1]Scientific-Manufacturing Enterprise "Fotron-Auto Ltd.", Moscow, Russia
[2]National Technical University "Kiev Polytechnical Institute", Kiev, Ukraine
[3]Far Eastern Federal University, Vladivostok, Russia

Abstract— Optical devices and photonics, in general, play an important role in space and aviation technology. The basis for many devices is layered interference systems and huge challenge is to ensure resistance and spectral characteristics stability of the interference systems against action of the cosmic environment factors, including intermittent high-intensity heating and deep cooling, and of the factors related to the functioning of spacecraft (in particular, laser radiation with high power density ($W > 10^9\,\mathrm{W/cm^2}$ and plasma). Authors' experience in the design and manufacture of precision optical coatings and lasers shows that these problems can be solved by use of gradient optical structures instead of the conventional multilayer interference systems with an abrupt change in the refractive index at the boundaries of each layer.

Design, technological aspects and test results of gradient optical coatings for space and aviation photonics are considered in the contribution. The magnetron sputtering facilities for deposition of the dielectric coatings with gradient/nanogradient of refraction index $\mathrm{grad}_z\ n(z)$ along light direction **z** has been designed and built. The sputtering unit contains two magnetrons with metal sputtered targets. The programmable movement of substrates over the magnetrons allows obtaining the desired composition variation and refraction index profile of coating material along **z**. The pulse mid-frequency mode of magnetron discharge provides stable deposition process in reactive gas medium ($Ar + O_2$ is used). An oxygen activator is used for better oxygenation of the deposited material. The special facilities for testing the manufactured optical structures in situ also has been designed and built. The gradient structures with different refraction index profile (simple "one-periodical", multi-periodical, rugate-like, with apodization, etc.) with excellent properties, including gradient optical metamaterials [1] for devices based on transformation optics, have been produced.

The experiments showed the gradient and nanogradient refraction index profiles provide wide-band or narrow-band and wide-angle working spectral characteristics (antireflective and others) in the visible and near IR field of the full-dielectric low-loss coatings and their stability against high-power laser radiation, thermal, mechanical and space environmental factors. Thus, the perspectives of pulse magnetron sputtering technology of gradient optical structures for space photonics are confirmed.

ACKNOWLEDGMENT

The work was financially supported by the Ministry of Education and Science of the Russian Federation (Agreement with Fotron-Auto, Ltd. No. 14.579.21.0066) and the Far Eastern Federal University (project No. 14-08-2/3-20_u).

REFERENCES

1. Volpian, J. D. and A. I. Kuzmichev, "Negative refraction of waves. Introduction into physics and technology of electromagnetic metamaterials," *Avers*, Kiev, 2012 (in Russian).

Session 2P6a
SC3: Semiconductor Nanowires: Novel Optical and Electrical Properties Enabling Energy Harvesting and Sensing Applications

Harnessing the Nano-optics of Silicon and Germanium Nanowires for Color and Multispectral Imaging

Kenneth B. Crozier
The University of Melbourne, Australia

Abstract— Given the considerable interest that has existed for nanowires lately, it is surprising how little attention has been generally paid to dramatic influence that waveguide and resonance phenomena can have upon their optical properties. The presentation reviewer recent work by the author and his research group on the optical properties of silicon and germanium nanowires, and there use for imaging applications. We demonstrate that vertical silicon nanowires take on a surprising variety if colors covering the entire visible spectrum, in marked contrast to the gray color of bulk silicon [1]. We demonstrate that embedding silicon nanowires into polydimethylsiloxane (PDMS) presents a means for adding color, i.e., provides filtering at visible and near-infrared wavelengths [2]. We report the demonstration of a compact multispectral imaging system that uses vertical silicon nanowires to realize a filter array [3]. We fabricate pixels consisting of vertical silicon nanowires with integrated photodetectors, demonstrate that their spectral sensitives are governed by nanowire radius, and perform color imaging [4]. We demonstrate the fabrication of arrays of vertical Ge nanowires with different diameters [5]. Measured reflection spectra show dip features for which electromagnetic simulations predict enhanced absorption.

REFERENCES

1. Seo, K., M. Wober, P. Steinvurzel, E. Schonbrun, Y. Dan, T. Ellenbogen, and K. B. Crozier, "Multicolored vertical silicon nanowires," *Nano Letters*, Vol. 11, 1851–1856, 2011.
2. Park, H., K. Seo, and K. B. Crozier, "Adding colors to polydimethysioxane by embedding vertical silicon nanowires," *Appl. Phys. Lett.*, Vol. 101, 193104–193107, 2012.
3. Park, H. and K. B. Crozier, "Multispectral imaging with vertical silicon nanowires," *Sci. Rep.*, Vol. 3, 2460, 2013.
4. Park, H., Y. Dna, K. Seo, Y. J. Yu, M. Wober, and K. B. Crozier, "Filter-free image sensor pixels comprising silicon nanowires with selective color absorption," *Nano Letters*, Vol. 14, 1804–1809, 2014.
5. Solanki, A. and K. B. Crozier, "Vertical germanium nanowires as spectrally-selective absorbers across the visible-to-infrared," *Appl. Phys. Lett.*, Vol. 105, 191115, 2014.

Semiconductor Nanowires: New Opportunities for Light Trapping and Surface Enhanced Raman Scattering

I. Alessandri
INSTM and Chemistry for Technologies Laboratory, Mechanical and Industrial Engineering Department
University of Brescia, via Branze, 38, Brescia 25123, Italy

Abstract— Raman microspectroscopy gives access to key information for detection and analysis of several chemical species, including environmental pollutants, explosives, drugs and biomolecules. However, the very low Raman cross-section of most of the analytes asks for a strong intensification of the local electromagnetic field (Surface Enhanced Raman Scattering, SERS) to improve sensitivity and detection capabilities. This goal is typically achieved by exploiting surface plasmon resonances of coinage metals (Au, Ag, Cu and, more recently, Al) in form of nanoparticles or nanostructures. However, in most of the cases, this approach is affected by low reproducibility, owing to the strong perturbation of the local environment of the systems under analysis.

On the other hand, SERS in semiconductor-based nanostructures is an attractive alternative to conventional, metal-assisted SERS active materials [1, 2]. In particular, semiconductor nanowires (NWs) allow for efficient light trapping and stimulation of morphology-dependent optical resonances. Thanks to these optical resonances, surface evanescent fields can be exploited to achieve enhanced Raman sensitivity with low invasiveness [3, 4].

This talk will be organized in two parts. First,we will discuss the Raman response of chemically-etched Si NWs, which are usually investigated as antireflective substrates for solar cells or artificial leaves. The influence of morphology on light trapping and, as a consequence, Raman scattering, will be evaluated over both the substrate itself (self-diagnostics) and detection of molecular species (organic molecules) and thin films (TiO_2). In the case of thin films, the formation of Si/TiO_2 core/shell heterostructures allows for a direct experimental evaluation of the spatial extension of the local near-field, suggesting the intriguing possibility to probe analytes over a long range [5].

In the second part we will give some examples of recyclable Raman substrates based on semiconductor nanorods and nanowires. Here the photocatalytic activity of the semiconductors is exploited to remove the analytes after each measurement, allowing reuse of the same chip for multiple cycles. The coupling with plamonic nanoparticles will be also discussed [6].

REFERENCES

1. Alessandri, I., "Enhancing Raman scattering without plasmons: Unprecedented sensitivity achieved by TiO_2 shell-based resonators," *J. Amer. Chem. Soc.*, Vol. 135, 5541–5544, 2013.
2. Alessandri, I. and L. E. Depero, "All-oxide Raman-active traps for light and matter: Probing redox homeostasis model reactions in aqueous environment," *Small*, Vol. 10, 1294–1298, 2014.
3. Cao, L., B. Nabet, and J. E. Spanier, "Enhanced Raman scattering from individual semiconductor nanocones and nanowires," *Phys. Rev. Lett.*, Vol. 96, 157402, 2006.
4. Khorasaninejad, M., J. Dhindsa, J. Walia, S. Patchett, and S. S. Saini, "Highly enhanced Raman scattering form coupled vertical silicon nanowire arrays," *Appl. Phys. Lett.*, Vol. 101, 173114, 2012.
5. Bontempi, N., M. Salmistraro, M. Ferroni, L. E. Depero, and I. Alessandri, "Probing the spatial extension of light trapping-induced enhanced Raman scattering in high-density Si nanowire arrays," *Nanotechnology*, Vol. 25, 465705, 2014.
6. Sinha, G., L. E. Depero, and I. Alessandri, "Recyclable SERS substrates based on Au-coated nanorods," *ACS-Applied Materials and Interfaces*, Vol. 3, 2557–2563, 2011.

Nanophotonics in III-V Nanowire Arrays

Nicklas Anttu
Division of Solid State Physics and the Nanometer Structure Consortium (nmC@LU)
Lund University, Box 118, Lund S-22100, Sweden

Abstract— We have studied how light interacts with arrays of vertical nanowires made of the optoelectronically important III-V materials. Our combined theoretical and experimental investigations [1–7] have yielded guidelines for efficient light-management in these arrays. With proper tuning of the nanowire geometry, the absorption per volume semiconductor material can be 20 times higher than in a planar geometry [1]. At the same time, the arrays show low reflection losses, thus combining anti-reflection properties with light-trapping to enhance the absorption. Based on these guidelines, we have fabricated solar cells of InP nanowires [2]. These arrays show an efficiency of 13.8% under the AM1.5 solar spectrum illumination and convert more than 70% of above-bandgap photons into electric current, despite covering only 12% of the surface. Finally, we have shown through electromagnetic modelling that the Shockley-Queisser efficiency limit for an optimized nanowire array solar cell is higher than for a conventional, planar solar cell [8].

REFERENCES

1. Anttu, N., "Geometrical optics, electrostatics, and nanophotonic resonances in absorbing nanowire arrays," *Opt. Lett.*, Vol. 38, 730–732, 2013.
2. Wallentin, J., N. Anttu, D. Asoli, M. Huffman, I. Åberg, M. H. Magnusson, G. Siefer, P. Fuss-Kailuweit, F. Dimroth, B. Witzigmann, H. Q. Xu, L. Samuelson, K. Deppert, and M. T. Borgström, "InP nanowire array solar cells achieving 13.8% efficiency by exceeding the ray optics limit," *Science*, Vol. 339, 1057–1060, 2013.
3. Anttu, N. and H. Q. Xu, "Coupling of light into nanowire arrays and subsequent absorption," *J. Nanosci. Nanotechnol.*, Vol. 10, 7183–7187, 2010.
4. Wu, P. M., N. Anttu, H. Q. Xu, L. Samuelson, and M.-E. Pistol, "Colorful InAs nanowire arrays: From strong to weak absorption with geometrical tuning," *Nano Lett.*, Vol. 12, 1990–1995, 2012.
5. Anttu, N., K. Namazi, P. Wu, P. Yang, H. Xu, H. Q. Xu, and U. Håkanson, "Drastically increased absorption in vertical semiconductor nanowire arrays: A non-absorbing dielectric shell makes the difference," *Nano Res.*, Vol. 5, 863–874, 2012.
6. Anttu, N., A. Abrand, D. Asoli, M. Heurlin, I. Åberg, L. Samuelson, and M. Borgström, "Absorption of light in InP nanowire arrays," *Nano Res.*, Vol. 7, 816–823, 2014.
7. Anttu, N., S. Lehmann, K. Storm, K. A. Dick, L. Samuelson, P. M. Wu, and M.-E. Pistol, "Crystal phase-dependent nanophotonic resonances in InAs nanowire arrays," *Nano Lett.*, Vol. 14, 5650–5655, 2014.
8. Anttu, N., "Shockley-Queisser detailed balance efficiency limit for nanowire solar cells," *ACS Photonics ASAP*, 2015.

Strain Engineering in GaN Nanowires and Applications in Photonics

Chu-Hsiang Teng[1], **Lei Zhang**[2], **Brandon Demory**[1], **Tyler Hill**[2], **Hui Deng**[2], **and P. C. Ku**[1]

[1]Department of Electrical Engineering and Computer Science
University of Michigan, Ann Arbor, Michigan 48109, USA
[2]Department of Physics, University of Michigan, Ann Arbor, Michigan 48109, USA

Abstract— Gallium nitride (GaN) and its related alloys are technologically important for applications in short-wavelength LEDs, lasers, photodetectors, and power electronics. GaN is a piezoelectric material. As a result, when it is strained, a strong built-in electric field is generated which has profound impacts on its applications in LEDs and lasers. In these devices, strained InGaN heterostructures are routinely employed as the light-emitting active region. The strain induced built-in electric field can significantly lower the emitter efficiency, cause efficiency droop and undesirable wavelength drift. Nanowires can effectively relax the strain and nanowire LEDs have attracted substantial interests in recent years. In this work, we showed that by controlling and engineering the strain in GaN nanowires via a top-down fabrication scheme, not only can one realize benefits arised from strain relaxation, new degrees of control can be obtained which have potential applications for display, communication, and sensing. In this talk, I will discuss two of these applications: (1) on-demand single photon sources with highly pure and programmable polarization states; (2) monolithically integrated multi-color light emitter chips.

From Subband Structure to Single Electron Devices in Semiconductor Nanowires

Jonathan Baugh and Gregory Holloway
University of Waterloo, ON, Canada

Abstract— Controlling the electronic transport properties of semiconductor nanowires can benefit technologies ranging from optoelectronic sensors to spin-based quantum information processing. We investigate the subband structure of InAs nanowires due to radial confinement, exploiting the coupling of orbital angular momentum to an axial magnetic field. The magnetoconductance is shown to contain signatures that allow precise identification of subbands, and also reveals the nature of the radial potential [1]. We show that these effects are indeed manifested experimentally in InAs FET devices studied at low temperatures. Next, we turn to a study of the superconducting proximity effect by considering a Nb-InAs-Nb nanowire junction. These experiments reveal rich Andreev physics and span two distinct regimes: the S-N-S junction regime in which a supercurrent is realized and is modulated with field and gate voltage [2], and the S-dot-S regime in which Andreev transport competes with the dot charging energy. Finally, we discuss the controlled realization of quantum dots, tunable down to single electrons, for confining and manipulating electron spin qubits for future quantum information processors.

REFERENCES

1. Holloway, G. W., D. Shiri, C. M. Haapamaki, K. Willick, G. Watson, R. R. La Pierre, and J. Baugh, *Phys. Rev. B*, Vol. 91, 045422, 2015.
2. Gharavi, K., G. W. Holloway, C. M. Haapamaki, M. Ansari, M. Muhammad, R. R. La Pierre, and J. Baugh, arxiv: 1405.7455, 2014.

Session 2P6b
Translational and Clinical Research towards Microwave Medical Imaging (MiMed)

Dielectric Parameters Estimation Using Global Optimization Techniques

Ilja Merunka, **Ondrej Fiser**, **and Jan Vrba**
Department of Electromagnetic Field, Czech Technical University in Prague, Czech Republic

Abstract—

Introduction: In this contribution we present a method for dielectric parameters estimation of human breast tissue phantom. There are many papers focused on this topic and a lot of methods are presented [1]. We focused on a method based on global optimization techniques, more specifically genetic algorithm [2–4].

Material and Methods: Numerical model was prepared in COMSOL Multiphysics (Burlington, MA 01803, United States) simulation platform. The model is only two dimensional and consists of circle (cross section of simplified human breast) and eight ports placed equally in distance of 2 cm from human breast phantom (Fig. 1). The ports with diameter of 2 mm excite electromagnetic field in direction of z axis (i.e., perpendicular to the plane of the model) and also record the scattered field. Thus, the scattering matrix can be simply computed and exported after simulation. Built in frequency solver was used to simulate electromagnetic field. Circle representing the cross section of human breast phantom was firstly virtually filled by only one material (arithmetic mean of dielectric parameters of human breast fat and gland). Secondly, numerical phantom of tumour represented by circle of diameter 2 cm were added into the region on the specific position and again only dielectric parameters of these two materials were estimated. We used the simple euclidean distance as the cost function to evaluate the overall correspondence between s-parameters virtually measured and s-parameters extracted from results of simulations of the model with updated parameters. Genetic algorithm was employed in the optimization procedure. The process is implemented in MATLAB 2013a (The MathWorks, Inc., Natick, Massachusetts, United States) where the global optimization toolbox is used.

Results: Dielectric parameters of the tissues were estimated. However, the total computational time is very long. It is primarily caused by the relative long computational time of the forward solution (2 s per one port, 16 s per all ports). The regularization term will be included in the cost function in our next work.

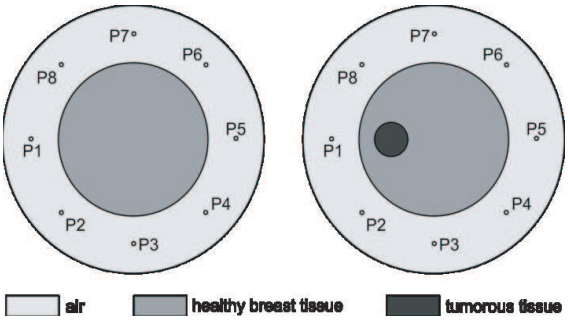

Figure 1: Configuration of numerical model with and without tumorous tissue.

REFERENCES

1. Meaney, P. M., "Microwave imaging and emerging applications," *Int. J. Biomed Imaging*, Vol. 2012, 2012.
2. Sabouni, A., S. Noghanian, and S. Pistorius, "A global optimization technique for microwave imaging of the inhomogeneous and dispersive breast," *Canadian Journal of Electrical and Computer Engineering*, Vol. 35, No. 1, 15–24, 2010.
3. Pastorino, M., S. Caorsi, and A. Massa, "A global optimization technique for microwave nondestructive evaluation," *IEEE Transactions on Instrumentation and Measurement*, Vol. 51, No. 4, 666–673, Aug. 2002.
4. Caorsi, S., A. Costa, and M. Pastorino, "Microwave imaging within the second-order Born approximation: Stochastic optimization by a genetic algorithm," *IEEE Transactions on Antennas and Propagation*, Vol. 49, No. 1, 22–31, Jan. 2001.

Analysis and Evaluation of Waveguide Methods to Measure the Dielectric Properties of Biological Materials

L. Farrugia[1], **P. Schembri Wismayer**[2], **L. Zammit Mangion**[1], **and C. V. Sammut**[1]

[1]Department of Physics, University of Malta, Msida, Malta
[2]Department of Anatomy, University of Malta, Msida, Malta

Abstract— Accurate knowledge of the dielectric properties of biological tissues is of crucial importance for both numerical and dosimetric studies. There are many ways to accurately measure the dielectric properties of a material, and the choice of method is highly dependent on the type of material under test (MUT). Nowadays, the coaxial probe technique is very often used for broadband measurements of the dielectric properties of biological tissues. The latter is very difficult to use with solid or semi-solid materials such as bone because of poor measurement repeatability. In this study we analyse the use of an alternative broadband method to perform dielectric measurements using a waveguide structure. Both reflection and transmission waveguide measurement methods are reviewed and the various methods to convert from the S-parameters to the complex permittivity are presented. Both reflection and transmission methods were studied numerically for materials with known dielectric properties and the values obtained were in very good agreement with both published and measured data obtained by coaxial probes. Furthermore, we carried out a detailed and systematic investigation of the minimum sample size required for accurate determination of the reflection coefficient with the rectangular waveguide method, and present an alternative numerical method to calculate the complex permittivity which compares well with the analytical solution of the waveguide structure.

Easy-to-produce Stable-in-time 3D-printed Breast Phantoms for Microwave Imaging

N. Joachimowicz[1], **O. Meyer**[1], **C. Conessa**[1], **B. Duchêne**[2], **O. Dubrunfaut**[1], **and M. Police**[1]

[1]Laboratoire Génie Electrique et Electronique de Paris, GeePs, UMR 8507 CNRS
Centrale Supelec, UPMC et UPSud, France
[2]Laboratoire des Signaux et Systèmes, L2S, UMR 8506 CNRS
Centrale Supelec, UPSud, France

Abstract— In recent years, quantitative microwave imaging systems have been investigated as a future alternative mammography technique. At the present time, there are several dozen-research teams around the world working on this topic [1]. The major potentials of using microwaves are, first, the significant contrast in dielectric properties between cancerous and normal healthy breast tissues [2] and, secondly, the non-ionizing nature of microwaves, which reduces the risk linked to frequent diagnoses during a screening program. The validation of inversion algorithms, used to build up images of the breast in microwave imaging systems, needs measurements of experimental data in controlled configurations, on realistic and stable-in-time reference breast phantoms. Oil-in-gelatin phantoms have been intensively investigated [3] since their dielectric properties are close to that of various breast tissues over a wide frequency range. However, if not properly sealed from the environment, such phantoms are not stable over time. On the other hand, we have already shown that liquid mixtures based upon Triton X-100 and salted water solutions are also able to mimic the various breast tissues and tumors in the 0.5–6 GHz frequency band [4]. These mixtures are easy to produce and their electromagnetic parameters are stable over time. Furthermore, their permittivity can be predicted as a function of Triton X-100 and salt concentrations, by means of a binary fluid mixture model that uses one pole Debye models. Thus, an adjustment of Triton X-100 and salt quantities can be obtained by fitting the Debye models corresponding to the different healthy or cancerous breast tissue types. In this work, such liquids are used to fill up 3D printed complex structures. This process allows us to produce realistic phantoms stable and adjustable in time, since liquids can easily be replaced or modified. Figure 1 displays two 3D models, used for printing phantoms dedicated to the test of 3D (a) and 2D (b) inversion algorithms, respectively. The 3D interior structure is very similar to realistic distributions of fibro-glandular (G_2) and adipose (G_3) tissues, surrounded by skin (G_1). The STL format file corresponding to the 3D phantom is produced from the one developed in [5], which is available at: https://uwcem.ece.wisc.edu/phantomRepository.html. The next step will be the dielectric characterization of these phantoms and, then, their test with microwave breast imaging systems.

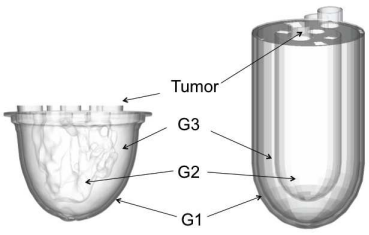

Figure 1: 3D printed phantoms to be filled up with Triton X-100-salted water mixtures dedicated to the test of (a) 2D and (b) 3D inversion algorithms.

REFERENCES

1. COST Action TD1301 MiMed: http://cost-action-td1301.org.
2. Lazebnik, M., et al., *Phys. Med. Biol.*, Vol. 52, 2637–2656, 2007.
3. Lazebnik, M., et al., *Phys. Med. Biol.*, Vol. 50, No. 18, 4245, 2005.
4. Joachimowicz, N., et al., *IEEE Antennas Wireless Propag. Lett*, Vol. 13, 1333–1336, 2014.
5. Burfeindt, M. J., et al., *IEEE Antennas Wireless Propag. Lett.*, Vol. 11, 1610–1613, 2012.

3-D Microwave Scanner for Biomedical Applications: A Preliminary Prototype

A. Cuccaro[1], **A. Brancaccio**[1], **B. Basile**[2], **M. J. Ammann**[3], **R. Solimene**[1], **and G. Ruvio**[3]

[1]Seconda Università di Napoli, Via Roma 29, Aversa, CE 81031, Italy
[2]B. & B. Sas, Strada Fienile 1, Casalnuovo di Napoli, NA 80013, Italy
[3]Dublin Institute of Technology, Kevin Street, Dublin 8, Ireland

Abstract— This paper introduces the prototype of a scanning system operating in the microwave range 0.5–4 GHz with strong potential in biomedical applications such as breast cancer detection or to assess shape-discontuinity in bones. Based on the research outcomes in [1], a fully automated scanner was designed to reduce mechanical uncertainties and data acquisition time. Accurate positioning and synchronization with data acquisition enables a rigorous proof-of-concept for the microwave imaging procedure.

The system can remotely control two printed antipodal Vivaldi antennas that scan a phantom across a set of positions arranged in cylindrical coordinates. For antenna miniaturization and improved coupling, the antennas, interface and phantom are immersed in a coupling medium that offers electric properties similar to adipose tissue. The antenna positioning, data acquisition and post-processing are automated. In the current version the reflection coefficients are measured by a Vector Network Analyzer (VNA). The integration of dedicated electronics attached to each antenna will replace the VNA to speed up data acquisition. Without any difficult *a priori* antenna characterization, the system is capable of detecting distinctive dielectric contrast in the phantom enclosed regions. By processing measured reflection coefficients with an interferometric version of the Multiple Signal Classification (MUSIC) algorithm [1], the detection of inserted targets in three-dimensional reconstructions is successful. The achievable performance obtained by I-MUSIC is then compared with two other methods in the literature: the non-coherent migration [2] which is a particular version of beamforming, and the standard wideband MUSIC technique [3]. From experimental results carried out on a multi-layer phantom made of glass and pork fat, a metallic bar of diameter equal to 8 mm was used as a target for a preliminary characterization of the scanning system.

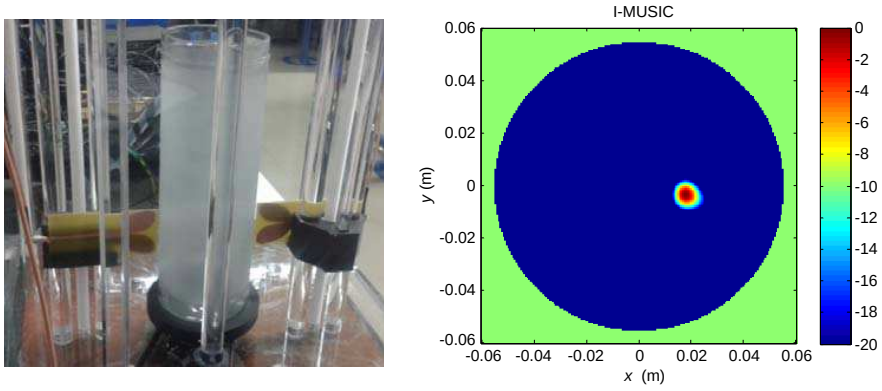

(a) (b)

Figure 1: (a) Detail of the scanner; (b) I-MUSIC detection of a 8-mm metal bar immersed in pork fat.

REFERENCES

1. Ruvio, G., R. Solimene, A. Cuccaro, D. Gaetano, J. E. Browne, and M. J. Ammann, "Breast cancer detection using interferometric MUSIC: Experimental and numerical assessment," *Medical Physics*, Vol. 41, No. 10, 103101/1–11, 2014.
2. Ahmad, F. and M. G. Amin, "Non-coherent approach to through-the-wall radar localization," *IEEE Trans. Aerosp. Electron. Syst.*, Vol. 42, No. 4, 1405–1419, 2006.
3. Yavuz, M. E. and F. L. Teixeira, "On the sensitivity of time-reversal imaging techniques to model perturbations," *IEEE Trans. Antennas Propag.*, Vol. 56, 834–843, 2008.

UWB Waveguide Breast Tumor Detection System Based on Delay and Sum Reconstruction Algorithm

Ondrej Fiser, **Ilja Merunka**, **and Jan Vrba**
Department of Electromagnetic Field, Faculty of Electrical Engineering
Czech Technical University in Prague, Czech Republic

Abstract— The main objective of this contribution is the breast tumor detection using four double ridged horn antennas system. Signals are obtained in time domain and "delay-and-sum" method is used.

Antenna, antenna configuration and breast phantom: For imaging purposes the UWB double-ridged horn antenna intended for medical imaging was adopted from [1]. Total four antennas are placed equidistantly around a breast model (see Fig. 1). The whole antenna system is immersed in canola oil. A simple homogeneous breast phantom with a thin skin layer was used. This used breast phantom is based on a phantom published in [2]. In this phantom spherical phantom of diameter 30 mm at various positions was inserted. The values of relative permittivity and conductivity of fat, skin and malignant tumor tissue has been taken from [3].

Simulation and image reconstruction: The reconstruction algorithm for delay and sum was implemented. The transmitting antenna sends a RF pulse through the breast model. Transmitted signal is Gaussian pulse with the central frequency 4.5 GHz and bandwidth 8 GHz. The place of the change in dielectric parameters of material (canola oil X skin X fat X tumor) scatters the incident wave. The scattered wave can be received in all antennas which are placed around the breast. The method consists of two phases. In the first phase scan of scattered field of breast without the tumor is performed. In the second phase (e.g., after 1 year in next medical examination) second scan is made. For all signals Hilbert transformation is applied and prepared signals with/without tumor are subtracted from each other. Obtained differential signals are reflections from changes which have occurred (e.g., tumor). From the knowledge of the average velocity wave propagation in the breast from measured time difference peak of the transmitted signal (from transmitting antenna) and received signal peak the distance of the reflections from each antenna is found (assumed tumor position). Position of the wave diffuser is on the circle with the center in the antenna power probe. For tumor localization must be measured distance even from other antennas. Then it is possible to calculate intersections of the circles defining the distance of the tumor from each antenna. For high accuracy it is good to use all antennas as transmitters sequentially. In the case of uncertain tumor position (in case that in signal sometimes appears more than one peak) we can rotate the whole antenna system by 30 degrees and thus increases the localization accuracy. Used method seems to be very promising for breast tumor detection. Its disadvantage is the need to have signals from the breast at a time when the tumor did not occur.

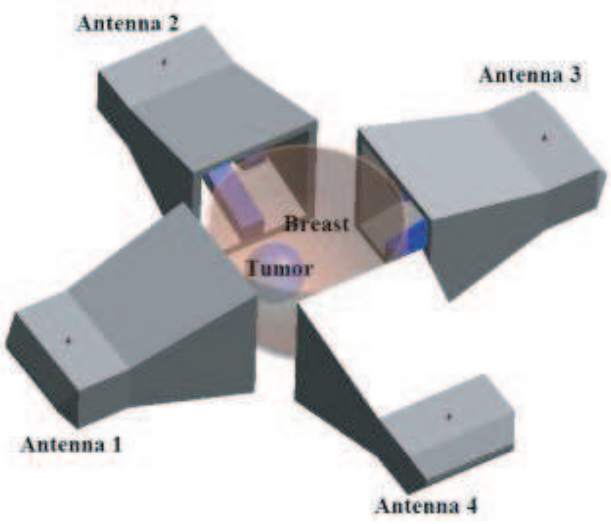

Figure 1: Antenna configuration with homogenous breast and spherical tumor.

REFERENCES

1. Latif, S., S. Pistorius, and L. Shafai, "A double-ridged horn antenna design in canola oil for medical imaging," *2013 International Conference on Advances in Electrical Engineering (ICAEE)*, 421–424, 2013.
2. Davis, S., H. Tandradinata, S. Hagness, and B. Van Veen, "Ultrawideband microwave breast cancer detection: A detection-theoretic approach using the generalized likelihood ratio test," *IEEE Transactions on Biomedical*, 2005.
3. Li, X. and S. Hagness, "A confocal microwave imaging algorithm for breast cancer detection," *IEEE Microwave and Wireless Components*, 2001.

Angular Separation Constraints in Cylindrical Multistatic UWB Radar Imaging

Daniel Flores Tapia[1], **Diego Rodriguez Herrera**[1], **and Stephen Pistorius**[1, 2, 3]

[1]Department of Physics and Astronomy, University of Manitoba, Canada
[2]Department of Radiology, University of Manitoba, Canada
[3]CancerCare Manitoba, Winnipeg, Canada

Abstract— In the last ten years, Ultra Wide Band (UWB) radar has been proposed as a complimentary imaging modality for breast cancer detection [1]. This technology is based in the significant dielectric contrast between healthy and malignant breast tissues (at least 2 to 1 according to the latest in vivo studies) [2]. UWB radar has a number of features that can be quite desirable from a clinical perspective, such as the use of low power non ionizing radiation and the lack of compression during the imaging procedure.

An area of particular interest in the last couple of years is the use of cylindrical or hemispherical multistatic scan geometries for UWB radar. Multistatic scan protocols exhibit an increased detection rate when compared to monostatic scan procedures [3]. Nevertheless, multistatic images may present artifacts for some transmission-reception scan location positions [3]. In this paper, the source of these artifacts will determined by performing a frequency domain analysis in the multistatic signal model. Let consider the multistatic signal spectral coverage band for a cylindrical scan geometry:

$$\Omega_q = \frac{k \cdot R \cdot r_q \cdot \sin(\phi_q - \theta)}{\sqrt{R^2 + r_q^2 - 2 \cdot R \cdot r_q \cdot \cos(\phi_q - \theta)}} + \frac{k \cdot R \cdot r_q \cdot \sin(\phi_q - \varphi)}{\sqrt{R^2 + r_q^2 - 2 \cdot R \cdot r_q \cdot \cos(\phi_q - \varphi)}}\Big|_{(\phi_q - \theta) = \pi/2} \quad (1)$$

where Ω_q is the spectral support band of the qth target in the scan region, k is the wavenumber, R is the radius of the scan geometry, (r_q, ϕ_q) are the polar coordinates of the qth target, and θ, φ are the angular locations of the transmitter and receiver respectively.

In the full paper, the complete procedure to derive (1) was will be given. Notice how the spectral coverage band reduces as the separation between the receiver and transmitter antenna increases. This result on the formation of a larger point spread function in the spatial domain. This will result in a possible loss of spatial resolution in the reconstructed image, which would limit the abilities to resolve individual targets. To validate this hypothesis, a set of two reflectors were created using the radar simulator described by the authors in [4] and their corresponding images were formed using the reconstruction approach presented in [5]. A representative example of this

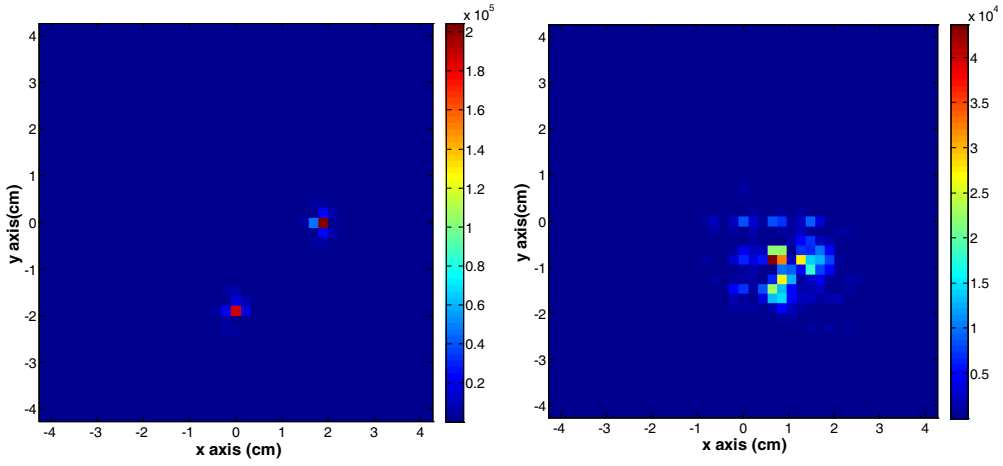

(a) (b)

Figure 1: (a) Reconstructed multistatic image from a dataset where the transmitter and receiver separation is 45 degrees, (b) reconstructed multistatic image from a dataset where the transmitter and receiver separation is 135 degrees.

effect is shown in Figure 1. Figure 1(a) shows the reconstructed image of the two target reflectors when the antenna separation between transmitter and receiver is 45 degrees. Figure 1(b) shows the reconstructed image of the two target reflectors when the antenna separation between the transmitter and receiver locations is 135 degrees.

Notice how the targets can be resolved in 1(a) while in Figure 1(b) the signatures of both targets are fused due to the larger point spread function. In conclusion, these preliminary results show the effect of the angular separation between the transmitter and recording location on the point spread function of the targets in multistatic UWB radar images acquired along cylindrical scan geometry. The complete paper will explain the mathematical model in full and will also provide additional examples and a full quantitative analysis to describe the relationship between the transmitter-receiver locations and the point spread function of the targets in the reconstructed image.

REFERENCES

1. Klemm, M., I. J. Craddock, J. A. Leendertz, A. Preece D. R. Gibbins, M. Shere, and R. Benjamin, "Clinical trials of a UWB imaging radar for breast cancer," *2010 Proceedings of the Fourth European Conference on Antennas and Propagation*, Vol. 1, 1–4, 2010.
2. Halter, R. J., T. Zhou, P. M. Meaney, A. Hartov, R. Barth, K. Rosenkranz, W. Wells, C. Kogel, A. Borsic, E. Rizzo, and K. D. Paulsen, "The correlation of in vivo and ex vivo tissue dielectric properties to validate electromagnetic breast imaging: Initial clinical experience," *Physiological Measurement*, Vol. 30, 121–136, 2009.
3. O'Halloran, M., M. Glavin, and E. Jones, "Performance and robustness of a multistatic mist beamforming algorithm for breast cancer detection," *Progress In Electrogmanetic Research*, Vol. 105, 403–424, 2010.
4. Flores-Tapia, D., G. Thomas, A. Sabouni, S. Noghanian, and S. Pistorius, "Breast tumor microwave simulator based on a radar signal model," *2006 IEEE International Symposium on Signal Processing and Information Technology,* Vol. 1, 17–22, 2006.
5. Flores-Tapia, D., O. Maizlish, C. M. Alabaster, and S. Pistorius, "A holographic reconstruction method for circular multistatic subsurface radar," *International Waveform Diversity and Design Conference 2012*, Vol. 1, 142–145, 2012.

Microwave Imaging of the Breast: Investigating Tumour Response with Classification

R. C. Conceição[1, 2], D. Byrne[3], J. A. Noble[1], and I. Craddock[3]

[1]Institute of Biomedical Engineering, University of Oxford, Headington, Oxford OX3 7DQ, UK
[2]Instituto de Biofísica e Engenharia Biomédica, Faculdade de Ciências, Universidade de Lisboa, Portugal
[3]Department of Electrical & Electronic Engineering, University of Bristol, UK

Abstract— In this study we evaluate the feasibility of using machine learning algorithms to investigate the scattering of breast tumours using ultra wideband radar microwave imaging. In particular, we aim to aid in differentiating between normal breast tissue (a "miss") or tumour tissue (a "hit") within data obtained from a radar scan of the breast. A machine learning algorithm (e.g., Support Vector Machines) will be trained with a database of series of measurements of both "hits" and "misses" in realistic breast phantoms, which have been performed with the microwave imaging prototype at the University of Bristol.

Introduction: Microwave Imaging of the breast has been thoroughly studied in the past years, with some recent studies addressing the use of classification algorithms (such as Linear Discriminant Analysis, Quadratic Discriminant Analysis, Support Vector Machines [1], Spiking Neural Networks [2] and Self-Organising Maps [3]) with the aim of estimating the size and shape of benign and malignant tumour phantoms.

In this study we further extend the use of classification algorithms to investigate the scatterings recorded in microwave radar breast imaging. We will estimate the likelihood of tumour occurrence at each synthetic focal point in resulting energy profiles of the breast.

Methodology: The measurement data used in this study are captured with the microwave imaging prototype at the University of Bristol. This comprises a Rohde-Shwarz ZVT 8 port VNA (frequency bandwidth: 3–8 GHz) and a conformal array of 60 wide-slot antennas [4].

Several breast phantoms are developed, some of which contain multiple targets. For all breast phantoms, the chest-wall is accounted for by maintaining a liquid to air interface at the base of the breast phantom. Synthetic focal points of 36 different phantoms are considered. The database considered for this study consists of a total of 1,925,455 measurements of "hits" and "misses" from 779 synthetic focal points corresponding to "hits", and 779 synthetic focal points corresponding to "misses".

A number of features are extracted from the measured data related to "hits" and "misses". The data is then divided into a training, a testing and a validation set in order to test the performance of classification algorithms. Performance is evaluated by metrics, including sensitivity, specificity, positive predictive value, negative predictive value and accuracy. The Receiving Operating Curve (ROC) for each classification algorithm is calculated.

Conclusions: The features extracted from the measured data and the performance of the classification algorithms will be discussed.

ACKNOWLEDGMENT

This paper is supported by EPSRC: EP/J00717X/1 and EP/J007293/1, and FP7: MC-IEF-301269. This paper has been developed in the framework of COST Action TD1301, MiMed.

REFERENCES

1. Conceição, R. C., M. O'Halloran, M. Glavin, and E. Jones, "Numerical modelling for ultra wideband radar breast cancer detection and classification," *Progress In Electromagnetics Research B*, Vol. 34, 145–171, 2011.
2. O'Halloran, M., B. McGinley, R. C. Conceicao, F. Morgan, E. Jones, and M. Glavin, "Spiking neural networks for breast cancer classification in a dielectrically heterogeneous breast," *Progress In Electromagnetics Research*, Vol. 113, 413–428, 2011.
3. Jones, M., et al., "Self-organising maps for breast cancer detection using ultra-wideband radar," *Self-organising Maps for Breast Cancer Detection Using Ultra-wideband Radar*, 46–51, Seville, Spain, 2013.
4. Henriksson, T., et al., "Clinical trials of a multistatic UWB radar for breast imaging," *Clinical Trials of a Multistatic UWB Radar for Breast Imaging*, 1–4, Loughborough, UK, 2011.

Session 2P7
SC1: Novel Mathematical Methods in Electromagnetics

Axiomatics of the Blondel-Park Transformation

G. F. Crosta[1] and G. Chen[2]

[1]University of Milan Bicocca, Italy
[2]Texas A & M University, USA

Abstract— The doubly-fed induction generator (*DFIG*) is a key constituent of energy conversion plants. The control of a *DFIG* is a challenge, whenever the primary energy supply (e.g., the wind velocity field) is characterised by intermittency. The mathematical model and control of a *DFIG* rely on the Blondel-Park transformation, which is known to simplify the governing equations. The distinctive feature of this contribution consists of showing how the Blondel-Park transformation derives from a set of conditions to be met by a group. Such a group is shown to exist and to continuously depend on one parameter. The uniqueness of its infinitesimal generator is also shown. As an application, the well-known electric torque theorem is proved in a simple way, which relies on a "product of matrices" formula. The latter, in turn, is a by-product of the axiomatic deduction of the Blondel-Park transformation.

Nonlinear Goubau Line: Numerical Study of TE-polarized Waves

E. Yu. Smol'kin[1] **and Yu. V. Shestopalov**[2]

[1]Penza State University, Russia
[2]University of Gävle, Sweden

Abstract— A conducting cylinder covered by a concentric dielectric layer called the Goubau Line (GL) is the simplest type of open metal-dielectric waveguides. A complete mathematical investigation of the spectrum of symmetric surface modes in a GL is performed in [1]. Papers [2, 3] develop the theory of wave propagation in layered nonlinear dielectric waveguides. However, there are very few results concerning the analysis of wave propagation in a GL with an external concentric layer having variable, nonlinear, or variable and nonlinear permittivity. We aim this study to fill this gap and consider the problem of electromagnetic TE (transverse-electric) wave propagation in a GL with nonlinear permittivity $\varepsilon = \varepsilon(\rho) + f(|\mathbf{E}|^2)$ of the dielectric medium filling the GL layer (here $\varepsilon(\rho)$ is a function of inhomogeneity which depends on the radius of the waveguide, f is a function that models nonlinearity, and $\mathbf{E}$ is the complex amplitude of the electric field). We consider only the intensity-dependent permittivity. The determination of TE waves is reduced to a nonlinear transmission eigenvalue problem for Maxwell's equations, which is then reduced to a system of nonlinear ordinary differential equations. Numerical experiments are carried out for two types of nonlinearities:

- $\varepsilon = \varepsilon(\rho) + \alpha u^2$ (Kerr law) and
- $\varepsilon = \varepsilon(\rho) + \alpha(1 - e^{-\beta u^2})$ (nonlinearity with saturation),

where $\varepsilon(\rho) = \frac{1}{\rho}$, const, or ρ. Comparison with linear homogeneous (inhomogeneous) and nonlinear homogeneous (inhomogeneous) cases are performed. Calculations are carried out for various frequency and parameter ranges.

REFERENCES

1. Shestopalov, Y., E. Kuzmina, and A. Samokhin, "On a mathematical theory of open metal-dielectric waveguides," *FERMAT*, Vol. 5, 1–9, 2014.
2. Valovik, D. V., Y. G. Smirnov, and E. Yu. Smol'kin, "Nonlinear transmission eigenvalue problem describing TE wave propagation in two-layered cylindrical dielectric waveguides," *Computational Mathematics and Mathematical Physics*, Vol. 53, 1150–1161, 2013.
3. Valovik, D. V. and E. Yu. Smol'kin, "Calculation of the propagation constants of inhomogeneous nonlinear double-layer circular cylindrical waveguide by means of the Cauchy problem method," *Journal of Communications Technology and Electronics*, Vol. 58, 759–767, 2013.

Numerical Path-integration Computation of the Capacity and Electric Polarizability Tensor of Complex-shaped Particles

Jack F. Douglas
Materials Science and Engineering Laboratory, NIST, Gaithersburg, MD 20879, USA

Abstract— Many boundary value problems arising in materials science modeling involve complicated boundary shapes and boundary data, making analytic solution based on conventional partial differential equation methods difficult. In particular, it is important to develop effective computational methods for calculating the electromagnetic and transport properties of nanoparticles for understanding their interaction with electromagnetic radiation to allow their manipulation with optical traps and separation with fields. These properties are also basic to characterizing particle and polymer geometry and interparticle interaction through solution property measurements. This class of problems is made challenging by the fact that large ensembles of objects having rather complex shape must be considered an ensemble averaged properties must be determined. As illustrative examples, we discuss specific systems such as carbon nanotubes and graphene, proteins, DNA and Au nanoparticles with grafted with DNA. These problems are daunting since there is still no accurate analytic theory for calculating basic transport properties (e.g., diffusion coefficient and intrinsic viscosity) and electromagnetic properties (capacity and polarizability) of even simple objects like a cube or stochastically defined objects such as random walk polymer chains modeling polymers in solution. In many cases, finite elements are also found to be intractable when the geometry shape becomes highly complex. As a step towards attacking this broad class of problems, we focus on the problem of calculating the self-capacity and electric polarizability tensor of conductive particles having essentially arbitrary geometry based a novel computational method involving path-integration. The basic concepts behind the method are described and the method validated in cases where exact analytic, or at least highly accurate numerical estimates, are known for comparison. Some applications of the program are then given for some non-trivial situations, such as the nanoparticle and polymer systems mentioned before. The path-integration method is evidently a powerful tool for computing basic electromagnetic and transport properties of complex-shaped polymers and should find wide application in polymer science, engineering, nanotechnological applications and medical and biological applications.

Unified Description of Chirped Gaussian Pulse Propagation of Arbitrary Initial Width in a Multiple Resonance Lorentz Medium

Constantinos M. Balictsis
Hellenic Telecommunications and Post Commission
60 Kifissias Avenue, Maroussi, Athens 15125, Greece

Abstract— Research interest regarding the reproducible generation, compression and characterization of ultrashort, pulse-modulated signals whose duration is comparable to the carrier oscillation cycle, is on the rise and spans various frequency domains [1–3]. Increased emphasis is placed on their dynamical evolution as they propagate through, and interact with, various material media due to the diverse and important applications, among others, in optical communications, radar systems and pulse compression. Pertinent theoretical efforts commonly invoke the slowly varying envelope approximation (SVEA) and are inapplicable in the sub-cycle pulse regime [1, 3]. A different stream of rigorous theoretical efforts to pulse propagation problems employs asymptotic techniques. These efforts have elucidated the dynamical evolution of the propagated field due to rapid rise and/or fall time or exponentially varying input pulses and their accuracy has been validated upon comparison with purely numerical results [1].

Recently, modern asymptotic techniques have been utilized in order to obtain an accurate uniformly valid description of Gaussian pulse propagation in a single-resonance causally dispersive, absorptive [4] or amplifying [5], Lorentz medium. Here, the unified asymptotic approach is applied to the important case of an input Gaussian pulse envelope modulated chirped harmonic wave whose envelope has a fixed but otherwise arbitrary initial full width $2T$ centered around $t_0 > 0$, and it modulates a harmonic wave of applied carrier frequency ω_c that is linearly chirped with a constant chirp parameter C. This input chirped Gaussian wave propagates in the source-free half-space $z \geq 0$ filled with a linear, homogeneous, isotropic temporally dispersive, non-hysteretic medium whose refractive index is described by the more realistic [1] multiple (m) resonance Lorentz model. The unified approach, which relies on an asymptotic analysis of the unified, exact integral representation of the propagated field, is shown to be valid from the SVEA to the theoretically and experimentally important sub-cycle pulse regimes, and its accuracy is confirmed upon comparison with the respective depicted results of an independent numerical experiment. Moreover, it generalizes previous findings on the appearance and dynamical evolution of the precursor fields associated with ultrashort and/or ultrawideband pulse propagation [1, 3–5]. According to the obtained unified asymptotic description, the propagated field $A(z,t)$ is comprised of pulse components $A_{Ul}(z,t)$ each being due to the asymptotic contribution of a respective relevant saddle point $\omega_{SP_{Ul}}(\theta)$ of the unified phase function $\Phi_U(\omega,\theta)$. This asymptotic description directly relates the propagation characteristics (including, the locus and propagation velocity of the stationary point(s) of the envelope, and the instantaneous angular oscillation frequency) of each $A_{Ul}(z,t)$ with the dynamics of the respective relevant saddle point $\omega_{SP_{Ul}}(\theta)$. Under certain conditions, such a stationary point of a pulse component's envelope occurs when the respective saddle point trajectory intersects the real frequency axis, and it travels with the group velocity at this frequency crossing value; superluminal velocity may then be observed.

The accuracy and insight of the unified asymptotic description may prove useful in applications involving chirped pulses, overcoming the limitations of other theoretical approaches especially in the extremely ultrashort pulse regime.

REFERENCES

1. Oughstun, K. E., *Electromagnetic and Optical Pulse Propagation 2: Temporal Pulse Dynamics in Dispersive, Attenuative Media*, Springer, New York, 2009.
2. Agrawal, G. P., *Fiber Optic Communication Systems,* Chapter 2, John Wiley & Sons Inc., New York, 1992.
3. Akhmanov, S. A., V. A. Vysloukh, and A. S. Chirkin, *Optics of Femtosecond Laser Pulses,* Chapter 1, American Institute of Physics, New York, 1992.
4. Balictsis, C. M. and K. E. Oughstun, "Generalized asymptotic description of the propagated field dynamics in Gaussian pulse propagation in a linear, causally dispersive medium," *Phys. Rev. E*, Vol. 55, 1910–1921, 1997.
5. Balictsis, C. M., "Unified asymptotic description of Gaussian pulse propagation of arbitrary initial pulse width in a Lorentz-type gain medium," *Phys. Rev. E*, Vol. 87, 013304, 2013.

Block LU Preconditioner for the Electric Field Integral Equation

S. L. Stavtsev
INM RAS, Russian Federation

Abstract— Boundary element discretizations are applied in many scientific and engineering areas, for example, to solve the problem of electromagnetics scattering with electric field integral equation (EFIE). To solve EFIE on the surfaces of arbitrary shape, RWG functions are traditionally used. The matrices, arising from the discretization of integral equations can be approximated well with low-rank matrices using mosaic-skeleton method. But to solver scattered problem with large wave size of object we have to solve large system $n \sim 10^5$–10^6. System of linear equation with matrixes of such order is solved by iterative method (GMRES). For large wave size matrix is ill-condition and we have to use preconditioner. In this paper to decrease a number iteration of GMRES method the block LU preconditioner is built. In the numerical experiments it is showed that the preconditioner permit to solve the problem of electromagnetic scattering on objects with lager wave size.

Permittivity Reconstruction of a Diaphragm in a Rectangular Waveguide: Unique Solvability of Benchmark Inverse Problems

Y. Shestopalov[2], **Y. Smirnov**[1], **and E. Derevyanchuk**[1]

[1]Penza State University, Russia
[2]University of Gävle, Sweden

Abstract— Determination of electromagnetic characteristics of dielectric bodies is an urgent problem for artificial materials: nanomaterials, metamaterials, and nanocomposite materials. As a rule, electromagnetic parameters of modern materials cannot be measured. Therefore for solving this problem, methods of mathematical modeling must be applied. In this work, we consider the inverse problem of permittivity reconstruction of diaphragms loaded in a rectangular waveguide and present theoretical and numerical results. This work is a continuation of the series of papers [1–3] devoted to the investigation of permittivity reconstruction of layered materials in the form of diaphragms (sections) in a single-mode waveguide of rectangular cross section from the transmission coefficient measured at different frequencies. The aim is the development of the mathematical technique for the analysis of the inverse problem for the case of a one- and multi-sectional diaphragms in a rectangular waveguide. We suppose that the diaphragm is made of material with real electromagnetic parameters. For this case, we obtain analytical solution of the inverse problem. Based on the analytical solution we study more complicated mathematical models, consider different cases of filling the diaphragm sections, and present results of numerical simulation. We perform comparison of experimental and numerical results that validate the efficiency of the proposed technique. The obtained solutions can be implemented in practical measurements for the investigation of new artificial materials and media and can be applied in optics, nanotechnology, and design of microwave devices.

REFERENCES

1. Smirnov, Yu. G., Yu. V. Shestopalov, and E. D. Derevyanchuk, "Permittivity reconstruction of layered dielectrics in a rectangular waveguide from the transmission coefficient at different frequencies," *Inverse Problems and Large-Scale Computations, Series: Springer Proceedings in Mathematics and Statistics*, Vol. 52, No. 12, 169–181, 2013.
2. Smirnov, Yu. G., Yu. V. Shestopalov, and E. D. Derevyanchuk, "Solution to the inverse problem of reconstructing permittivity of an n-sectional diaphragm in a rectangular waveguide," *Algebra, Geometry and Mathematical Physics, Springer Proceedings in Mathematics and Statistics*, Vol. 85, Ser. 10533-2014, 555–567, 2014.
3. Smirnov, Yu. G., Yu. V. Shestopalov, and E. D. Derevyanchuk, "Permittivity determination of multi-sectional diaphragm with metamaterial layers in rectangular waveguide," *PIERS Proceedings*, 135–139, Taipei, Mar. 25–28, 2013.

The Application of Non-linear Dynamics Methods for Radar Target Identification

F. J. Rachford and T. L. Carroll
US Naval Research Laboratory, USA

Abstract— Currently radar target identification is effected by finding the downrange distribution of scatterers on a platform using high definition radar and referencing this distribution to a look-up table of measured radar returns. This method is difficult due to the rapid scintillation of the radar signal of a flying target at short wavelengths. We investigate a method of target identification in the low definition, relatively long wavelength, limit using techniques derived from the field of non-linear dynamics. In this limit the radar reflection is much less sensitive to the orientation of the target to the radar and scintillation is greatly reduced. Modern detection advances allows the digitization and processing of raw real time non-pulse compressed waveforms. We simulate the raw radar returns from several very similar small (4 to 5 wavelength) objects (i.e., cylinder, cone-cylinder, cone-ogive and double ogive) illuminated with chaotic or random modulated waveforms using a commercial finite difference time domain code. In this aggressive limit we embed the return in two dimensions using the method of delays to form an attractor. The geometric properties of the attractors are analyzed to distinguish between these similar target objects in the low definition limit. One method selects points on a reference attractor (or strands of points) with many Euclidean nearest neighbors and compares these with the nearest neighbor density of points (or strands) with the same time index on an attractor from an "unknown" target. Comparing the density of nearest neighbors at these points on two attractors allows us to calculate probabilities of correct identification. (Is the unknown signal from the reference target or from one of the other targets?) The robustness of our method is probed by the addition of white noise and/or simulated clutter to the signals.

Verification of Computational Model of Transmission Coefficients of Waveguide Filters

P. Tomasek[1] and Y. V. Shestopalov[2]

[1]Tomas Bata University in Zlin, Czech Republic
[2]University of Gävle, Gävle, Sweden

Abstract— Owing to the recent research [1–3] the way of estimating transmission coefficients for a waveguide of rectangular cross-section loaded with multi-layered parallel-plane dielectrics is found. Consequently, the analysis of the transmitted and reflected fields in terms of the scattering matrix formalism can be performed explicitly. These results can be efficiently applied to modeling of waveguide filters. This article is mainly based on the previous research presented in [1], it enhances the theory and contains comparisons between real measured and computed transmission coefficients of a waveguide filter using a technique based on the method set forth in [2, 3]. The computation employs analysis of closed-form solutions and numerical multi-parameter optimization [4, 5]. The presented waveguide filter is formed by multi-sectional diaphragms placed in a waveguide of rectangular cross-section. The filter consists of a specific combination of diaphragms of FR4, plexi and RO4003 with defined permittivities and thicknesses. The resulting permittivity profile that provides significant range of the parameter and output variations has a characteristic almost-periodic stepwise structure which can be improved using the closed-form solution and numerical optimization. Comparison of the computed and measured transmission coefficients demonstrates that the difference is very low, rather marginal and thus the output of the work is considerably promising. The results prove the ideas, approach and the final implementation of the mathematical background used for computation of the transmission coefficients of a waveguide filter.

REFERENCES

1. Tomášek, P. and Y. Shestopalov, "Parameter optimization of waveguide filters employing analysis of closed-form solution," *PIERS Proceedings*, 296–299, Stockholm, August 12–15, 2013.
2. Shestopalov, Y. and Y. Smirnov, "Inverse scattering in guides," *J. Phys.: Conf. Ser.*, Vol. 346, 012019, 2012.
3. Shestopalov, Y., Y. Smirnov, and E. Derevyanchuk, "Permittivity determination of multisectional diaphragm with metamaterial layers in rectangular waveguide," *PIERS Proceedings*, 135–139, Taipei, March 25–28, 2013.
4. Chan, R., R. Mittra, and T. Cwik. Techniques for analyzing frequency selective surfaces — A review," *IEEE*, Vol. 76/12, 1593–1615, 1988.
5. Antoniou, A. and W. S. Lu, *Practical Optimization: Algorithms and Engineering Applications*, Springer, Pvt. Limited, India, 2009.

Computations Related to Nanoparticle Characterization and Nanocomposite Property Estimation

Fernando Vargas-Lara and Jack F. Douglas
Materials Science and Engineering Laboratory, NIST, Gaithersburg, MD 20879, USA

Abstract— Recently, there has been great interest in enhancing the electrical and thermal conductivity and mechanical properties of polymeric materials with carbon nanotube (CNTs) additives. Large changes in properties have been achieved with these additives and applications, especially in relation to enhanced electrical conductivity, have been realized. However, controlling and understanding these property changes has been a difficulty. It is well known that the resulting nanocomposite properties depend strongly on the geometrical properties of the CNTs such as length, diameter, and shape, as well as the dispersion of the CNT. Commercial forms of these fillers, as opposed to the rod-like structures that are the focus of many academic studies, are typically composed of roughly spherical multi-walled CNT domains having a highly ramified internal structure and a size on the order of a micron. Clearly, such structures, which we term "tumbleweeds" because their resemblance to these natural forms, cannot reasonably be modeled as "rods", and we address the properties of these composite materials through a combination of molecular dynamics simulations and path-integral calculations. As a specific illustration of this computational path, we first calculate electromagnetic properties of the tumbleweeds, such as the self-capacitance, electric polarizabilty tensor, and the intrinsic conductivity. Knowing these basic particle properties, one then can estimate electromagnetic properties of nanocomposites made with these complex- shaped "particles", i.e., conductivity, by incorporating this information in a generalized effective medium theory. Based on this model, we find that the conductivity percolation threshold of the tumbleweeds can be quite low, despite their quasi-spherical average shape.

Exponential Regularization of EM Dyadic Green's Functions via Green's Function-induced Dirac δ-functions

A. R. Baghai-Wadji
University of Cape Town, South Africa

Abstract— In a series of recently published contributions it was shown that dyadic Green's functions arising in computational electromagnetics can be utilized to construct problem-specific integral representations of the Dirac delta function. It was also shown that the constructed Dirac delta functions can be employed to regularize originating Green's functions associated with Poisson equation in isotropic and anisotropic dielectrics. This contribution extends previous efforts as follows: (i) The constructed Dirac delta functions are employed to regularize dyadic Green's functions associated with Maxwell's equations in isotropic media. Thereby, all formulae arising in the discussion are expressed in closed-form in spectral domain, a fact which allows intriguing insights into the dynamics of the proposed regularization method itself. (ii) Complex media do not allow the Green's functions to be constructed in closed form. Consequently, the integral representations for the Dirac delta functions cannot be expressed in closed-form either. An algorithm is presented for the numerical construction of Dirac delta functions. It is claimed that the latter result presents a genuine contribution to the computational physics. (iii) The soundness of the derivations are supported by several Lemmas. (iv) Applications in which near field phenomena play a decisive role, e.g., nanoscopic and plasmonic devices will benefit from the results.

Regularization problems arising in theoretical and computational field theory are fascinating and challenging at the same time; numerically, however, they are most undesirable and may lead to catastrophically ill-conditioned results. Singular field problems, requiring regularization, have characteristic footprints in spectral domain. Singularities in static fields are defined by a $1/|k|$ pole-like behavior in the infrared wavenumber region. The same $1/|k|$ functional behavior in the ultraviolet region leads to slow convergent or divergent Fourier-type integrals. In real domain, the infrared $1/|k|$ pole-like singularity is associated with the properties of the fields in the far-field, whereas, the ultraviolet slow-decay, divergent singularity is related to the near-field. Singularities in dynamic fields manifest themselves in poles and branch points in intermediate regions in spectral domain. It can shown that pole- and branch point singularities can be treated fairly conventionally, with one exception, which arises when constructing universal functions (addressed in an accompanying paper). Thus the prime focus becomes regularization of slow decay property of Green's functions in spectral domain (near-field region). To this end the present author has proposed algebraic as well exponential regularization techniques. This paper focuses on the exponential regularization which is facilitated by Dirac delta functions constructed from the Green's functions themselves.

ACKNOWLEDGMENT

This work is based on the research supported in part by the National Research Foundation (UID: 93114).

REFERENCES

1. Baghai-Wadji, A. R., "Self-consistent physics-based δ_η-regularized Green's function for 2D Poissons equation in anisotropic dielectric media," *Proceedings of the Applied Computational Electromagnetics Society*, Jacksonville, Florida, USA, 2014.
2. Baghai-Wadji, A. R., "Self-consistent physics-based δ_η-regularized Green's function for 3D Poissons equation in anisotropic dielectric media," *Proceedings of the Applied Computational Electromagnetics Society*, Jacksonville, Florida, USA, 2014.
3. Baghai-Wadji, A. R., "3D electrostatic charge distribution on finitely-thick bus-bars in micro-acoustic devices: Combined regularization in the near-and far-field," *IEEE Transactions on Ultrasonics, Ferroelectrics, and Frequency Control*, Special Issue, 2014 (Invited).

Superresolution Based on the Methods of Extrapolation

B. A. Lagovsky[1], **A. B. Samokhin**[1], **and Y. V. Shestopalov**[2]

[1]Department of Applied Mathematics
Moscow State Technical University of Radio Engineering, Electronics and Automatics, Russia
[2]University of Gävle, Sweden

Abstract— One of the most important ways to improve the radar systems based on smart antennas is to improve the accuracy of angle measurements and to increase the angular resolution. In this regard, the problem to be solved is restoring the image of the object with superresolution. This inverse problem is reduced to a Fredholm integral equation

$$U(\alpha) = \int_{\Omega} F(\alpha - \phi, \varphi) I(\phi, \varphi) d\phi d\varphi, \tag{1}$$

where $U(\alpha)$ is the signal received by the scanning, Ω angular region of location of the signal source, $I(\alpha, \varphi)$ desired angular distribution of the reflected signal amplitude, and $F(\alpha, \varphi)$ radiation pattern. The central problem based on the intelligent analysis and digital signal $U(\alpha)$ is to restore the image of the source using superresolution. In contrast to conventional phased array, the signals received by each element of the smart antennas can be recorded digitally. The new signal processing method is based on the extrapolation of the signals received by each element of the smart antennas beyond the aperture and yields synthesized smart antennas with a greater number of emitters and an aperture increased by the same factor. As a result, the accuracy of angular measurements and angular resolution increases. The best results were obtained using the extrapolation with the Berg linear prediction method. The algorithm predicts the values of the signals for the aperture array ten times higher than the original one with a negligible error. Numerical studies have shown that the Rayleigh criterion in this problem is exceeded by 6–7 times. An important characteristic of solutions is a minimal signal/noise ratio (SNR) with which a super-resolution image reconstruction is still possible. Stability of solutions and quality of image reconstruction were examined using a mathematical model. The results of numerical studies show that the angular resolution is increased 4–10 times under SNR 12–13 dB, which is much lower than that achieved by the known methods.

The proposed new method of signal processing based on digital aperture synthesis significantly improves the accuracy of angle measurements and provides a stable restoration of detailed images of the objects with superresolution in the presence of small distortions. The corresponding algorithm can be implemented in the real-time mode.

Analysis of Quasi-circular Polarization in Near Field of Smart Shelf RFID Antenna Radiation

A. S. Andrenko
SYSU-CMU Shunde International Joint Research Institute
No. 9 Eastern Nanguo Road, Shunde, Guangdong 528300, China

Abstract— This paper presents the EM simulation and accurate analysis of quasi-circular polarization (CP) of the so-called smart shelf antenna designed for the UHF RFID retail and item-tagging applications. The smart shelf antenna utilizes the near field communication in a range close to a wavelength between the planar reader/writer antenna and several tagged items being placed on the shelf. To provide reliable detection of the multiple tags which can generally be distributed within a wide interrogation volume over the shelf surface, uniform and strong near E-field radiated be the smart shelf antenna is required.

The design of the proposed antenna is based on the EM coupling between the open-ended or shorted-to-the ground meander microstrip line utilizing the standing wave current-voltage distribution and periodic metal strips printed on the top surface of a dielectric substrate. The required uniform near E-field has been provided by optimizing the layout of the periodic strips forming the smart shelf antenna layout. Series of full-wave EM simulations have been carried out to analyze the E-field distribution calculated at the different distances from the antenna surface, in a range from 5 cm to 40 cm. It has been confirmed that the proposed antenna creates strong near field within the entire volume where multiple RFID tags are placed. Two types of the smart shelf antenna have been designed and optimized. The first is the antenna where the periodic EM coupled elements are straight strips of approximately one wavelength so that the smart shelf antenna radiates predominantly linearly polarized E-field. The second one has been designed for the apparel tagging applications where tagged items are arbitrary oriented in the plane parallel to the antenna surface. Therefore, EM near field of this antenna has to be quasi-CP with quasi here meaning that the E-field is also having z-component (normal to antenna surface). What is the most important in such an application is that the E-field has to have a well balanced x- and y-components at the different distances from antenna and within an entire interrogation volume. The required quasi-CP near field has been numerically optimized in the series of EM simulations by utilizing the three-section layout of the periodic metal strips and changing the angles of strip sections so that it results in both E_x- and E_y-components being produced. Time-domain calculation of 3D E-field vector distribution has also demonstrated how a simple change of the meander line layout produces both quasi-RHCP and LHCP radiation in the near field.

The prototypes with different layouts of the proposed antenna have been produced and their performance in the UHF RFID system has been verified. 100% detection rate and measured read range for the large number of tagged items have confirmed the simulated near field distribution as well as an excellent performance of the proposed smart shelf antenna.

CICT: A Novel Framework for Biomedical and Bioengineering Application

R. A. Fiorini
Department of Electronics, Information and Bioengineering (DEIB)
Politecnico di Milano University, Italy

Abstract— In 2004, University of Michigan physicist Mark Newman, along with biologist Michael Lachmann and computer scientist Cristopher Moore, showed that if electromagnetic radiation is used as a transmission medium, the most information-efficient format for a given 1-D signal is indistinguishable from blackbody radiation. Since many natural and biological processes maximize the Gibbs-Boltzmann entropy, they should give rise to spectra indistinguishable from optimally efficient transmission. In 2013, Politecnico di Milano academic scientist R. A. Fiorini confirmed Newman, Lachmann and Moore's result, generating analogous example for 2-D signal (image), as an application of CICT (computational information conservation theory) to show that even the current, most sophisticated instrumentation system is completely unable to reliably discriminate so called "random noise" (RN) from any combinatorially optimized encoded message, which CICT called "deterministic noise" (DN). For observing and determining single molecule transport characteristics or for detecting a minute change in resistance or capacitance at biostrucuture nanoscale, we need stronger research and computational tools able to overcome the above operative limitation. To grasp a more reliable representation of experimental reality and to get stronger physical and biological system correlates, researchers and scientists need two intelligently articulated hands: both stochastic and combinatorial approaches synergically articulated by natural coupling. CICT approach brings classical and quantum information theory together in a single framework, by considering information not only on the statistical manifold of model states but also from empirical measures of low-level multiplicative noise source generators, related to experimental high-level overall perturbation. This approach is recommended to design reliable experiment and advanced instrumentation system. In various applications to physical problems, a function can be decomposed into physically meaningful eigenfunctions of a differential operator (typically the Laplace operator): this forms the foundation for the spectral study of functions, in reference to the spectrum of the differential operator. A concrete physical application involves the problem of hearing the shape of a drum: given the fundamental modes of vibration that a drumhead is capable of producing, can one infer the shape of the drum itself? The mathematical formulation of this question involves the Dirichlet eigenvalues of the Laplace equation in the plane, that represent the fundamental modes of vibration in direct analogy with the integers that represent the fundamental modes of vibration of the violin string. Spectral theory also underlies certain aspects of the Fourier transform of a function. Whereas Fourier analysis decomposes a function defined on a compact set into the discrete spectrum of the Laplacian (which corresponds to the vibrations of a violin string or drum), the Fourier transform of a function is the decomposition of a function defined on all of Euclidean space into its components in the continuous spectrum of the Laplacian. The Fourier transformation is also geometrical, in a sense made precise by the Plancherel theorem, that asserts that it is an isometry of one Hilbert space (the time domain) with another (the frequency domain). This isometry property of the Fourier transformation is a recurring theme in abstract harmonic analysis, as evidenced for instance by the Plancherel theorem for spherical functions occurring in noncommutative harmonic analysis. For discrete data, the Discrete Fourier Transform (DFT) is used. As an example, CICT number theoretic transform (NTT) is presented to envisage the development of competitive application devoted to automatic tailoring noise compensation countermeasure to real dynamic device characteristics and performance, even in real-time. That feature can get us closer to ideal self-registering and self-linearizing instrumentation able to generate virtually homogeneous and uniform device experimental probing domain, during its whole designed service life-cycle, offering superior reliable final result at least cost. Its adoption becomes a must either to real High Reliability Organization (HRO) or to mission critical project for low technological risk and crisis management system.

Multichannel Filter Banks and Their Implementation Using Computers with a Parallel Structure

D. I. Kaplun, D. M. Klionskiy, A. S. Voznesenskiy, and V. V. Gulvanskiy
Computer Science Department
Saint Petersburg Electrotechnical University "LETI", Saint Petersburg, Russian Federation

Abstract— The paper is devoted to the development and software-hardware implementation of the *weighted overlap-add algorithm* (WOLA-algorithm) for processing *vector signals* in wideband monitoring tasks. The algorithm is intended for functioning together with instruments that are responsible for airwave control in real time. We have performed the comparison of the suggested algorithm with the polyphase implementation of a multichannel digital filter bank. We have also considered the software-hardware implementation of multichannel processing and we have shown the advantages of applying the CUDA (Compute Unified Device Architecture) technology based on computations using graphical processors.

The WOLA-algorithm for processing vector signals can be considered as a generalization of the corresponding algorithm for processing one-dimensional signals. The suggested modification will make it possible to process a vector signal and also to perform software-hardware implementation using high-performance software and hardware tools.

When we have found signals in each channel it is necessary to perform their *sub-band processing* (each channel signal has its own frequency band) including spectral analysis, time-frequency analysis, statistical analysis in the time domain, demodulation, etc..

Digital filter banks perform parallel processing of an input signal and therefore to improve the hardware implementation efficiency it is most reasonable to employ computers with a parallel structure. Such computers include FPGA (field-programmable gate arrays) and processing devices with the use of CUDA.

CUDA is based on using a set of parallel graphical processors (Graphics Processing Unit — GPU) for handling non-graphical tasks. GPU is a specialized device, which is a co-processor to the Central Processing Unit (CPU), has its own memory and can execute a large number of separate data flows (data flows are parts of one program that run in a parallel way). The advantages of CUDA are cross-platform operation, the existence of complete libraries, use of the extended version of C with additional tools for parallel programming and development of multiflow applications. Furthermore, CUDA does not require application of a graphical interface (API), which has a number of restrictions on multiflow computation arrangements.

Hardware resources for digital filter bank implementation are not boundless (the most critical aspect is the total number of multipliers for FPGA). For this reason we need to design computationally efficient FIR-filters (filters with finite impulse response) that will allow us to reduce hardware-software costs and accelerate signal analysis. Such an approach will make it possible to reduce the total number of devices (including the number of FPGA multipliers) and increase the number of processing devices on a chip.

We suggest performing filter bank implementation using FPGA and the distributed arithmetic. The main difference between this approach and direct implementation with MAC-cores (multiply and accumulate cores) is the fact that the distributed arithmetic does not use any multipliers. Thus we can achieve a more efficient digital filter bank implementation.

Regularization of Ill-conditioned Numerical Scheme of an Analytical Formulation: Scattering by Circularly Layered Cylinders

Emrah Sever[1], **Fatih Dikmen**[1], **Farhad Mazlumi**[2], **and Yury A. Tuchkin**[1]

[1]Electronics Engineering Department, Gebze Technical University, Kocaeli, Turkey
[2]Aviation Electronics Department, Civil Aviation Technology College, Tehran, Iran

Abstract— The new regularization of the well-known analytical formulation of the monochromatic electromagnetic wave scattering by a few eccentrically multilayered homogenous circular dielectric [1] and impedance [2] cylinders will be demonstrated. The polarization of the fields are parallel to the longitudinal axes of the cylinders, thus a two dimensional problem for each both polarizations are under consideration. The ways to simulate such a physical or an engineering process are quite various, owing to the present techniques of using the capabilities of modern hardware and software. Therefore nowadays, the numerical stability of an analytically rigorous formulation of an electromagnetic scattering problem may be taken for granted unintentionally by the user of a powerful computer with modern hardware and software. We can meet the concerns about the numerically stable simulation of an analytical model, starting at least five decades ago [3, 4]. The formulation and its regularization in [3] were suggested for two neighboring perfectly conducting circular cylinders. We present herein the novel extension of the approach in [3] to the considered scattering problem. The integral formulation defined in [4], also having met in [5] gives the strong mathematical background of the analysis here. The main theoretical result herein is the mathematically equivalent reducing of the diffraction problem for the eccentrically multilayered dielectric circular cylinders to a linear algebraic equation system of the second kind in the functional space l_2. The numerical results to be presented will forewarn those who trust in the various numerical methods (even the classical ones) without a careful mathematical and numerical investigation of the methods validity.

REFERENCES

1. Dikmen, F., E. Sever, S. Vatansever, and Y. A. Tuchkin, "Well-conditioned algorithm for scattering by a few eccentrically multilayered dielectric circular cylinders," *Radio Science*, accepted, DOI: 10.1002/2014RS005501, 2015.
2. Sever, E., F. Dikmen, O. A. Suvorova, and Y. A. Tuchkin, "An analytical formulation with ill-conditioned numerical scheme and its remedy: Scattering by two circular impedance cylinders," *Turk. J. Elec. Eng. & Comp. Sci.*, accepted, DOI:10.3906/elk-1312-262, 2014.
3. Ivanov, E. A., *Diffraction of Waves from Two Bodies*, Nauka i Tekhnika, Minsk, 1968 (in Russian and Translated to English as NASA TT F-597).
4. Bates, R. H. T., "Analytic constraints on electromagnetic field computations," *IEEE Trans. Microwave Theo. Tech.*, Vol. 23, 605–623, 1975.
5. Ioannidou, M. P., K. D. Kapsalas, and D. P. Chrissouludis, "Electromagnetic-wave scattering by an eccentrically stratified, dielectric cylinder with multiple, eccentrically stratified, cylindrical, dielectric inclusions," *Journal of Electromagnetic Waves and Applications*, Vol. 18, No. 4, 495–516, 2004.

Session 2P8a
Luminescent Materials and Devices

Colloidal Quantum Dots and Semiconductor Heteronanocrystals: New Luminescent Materials with Tailored Optical Properties

Celso de Mello Donega
Debye Institute for Nanomaterials Science, Utrecht University, The Netherlands

Abstract— Colloidal semiconductor nanocrystals (NCs) are a versatile class of nanomaterials, whose properties are determined by their composition, size, and shape, thus allowing nanoscale excitons to be confined to zero- (quantum dots, QDs), one- (quantum rods, QRs), or two-dimensions. Semiconductor NCs comprising two (or more) different materials joined together by heterointerfaces, i.e., heteronanocrystals (HNCs), offer even more exciting possibilities regarding property control [1]. The spatial localization of charge carriers in HNCs can be manipulated by controlling the offsets between the energy levels of the materials that are combined at the heterointerface [1]. In Type-I HNCs both carriers are confined in the same material. In contrast, in Type-II HNCs a spatially indirect exciton is formed. In Type-I [1, 2] (or *quasi*-Type-II) HNCs one carrier is delocalized over the HNC, while the other is localized in one of the segments. This allows the electron-hole spatial overlap to be tailored, and gives semiconductor HNCs fascinating and unique properties, which are determined by the size, shape, and composition of each segment. Understanding the properties of nanoscale excitons in colloidal NCs and HNCs is of great scientific interest, from both fundamental and applied viewpoints, since these materials are promising for a variety of technologies (LEDs, solar cells, biomedical imaging, luminescent solar concentrators). In our group, we have applied a multistage preparation strategy that allows the combination of a variety of synthesis techniques (hot-injection, seeded growth, cation exchange, oriented attachment) in a sequential manner in order to achieve the targeted synthesis of colloidal NCs and HNCs. This has allowed us to systematically investigate the optical properties of a number of NC (e.g., CdSe, CdTe, PbSe, ZnO QDs) and HNC compositions (e.g., PbSe/CdSe, CdSe/(Cd,Zn)S/ZnS, CdTe/CdSe, ZnSe/CdSe core/shell QDs, CdSe/CdS core/rod shell nanorods, ultranarrow (Zn,Cd)Te/CdSe heteronanowires) [2-8]. In recent years, we also developed methods to synthesize Cd- and Pb-free HNCs, such as ultrathin $Cu_{2-x}S$ nanosheets [9] and $CuInS_2$ QDs [10]. In this contribution, I will discuss a selection of examples, chosen in order to illustrate specific synthesis strategies and combinations thereof, as well as to show that compositional, size, and shape control can be used to tailor nanoscale excitons, and consequently the optical properties of colloidal HNCs.

REFERENCES

1. Donega, C. D. M., *Chem. Soc. Rev.*, Vol. 40, 1512–1546, 2011.
2. Donega, C. D. M., *Phys. Rev. B*, Vol. 81, 165303, 2010.
3. Groeneveld, E. and C. D. M. Donega, *J. Phys. Chem. C*, Vol. 116, 16240–16250, 2012.
4. Groeneveld, E., et al., *Nano Lett.*, Vol. 12, 749–757, 2012.
5. Groeneveld, E., et al., *ACS Nano*, Vol. 7, 7913–7930, 2013.
6. Krumer, Z., et al., *Solar En. Mater. Solar Cells*, Vol. 111, 57–65, 2013.
7. Granados del Aguila, A., et al., *ACS Nano*, Vol. 8, 5921–5931, 2014.
8. Eilers, J., et al., *J. Phys. Chem. C*, Vol. 118, 23313–23319, 2014.
9. Van Der Stam, W., et al., *Chem. Mater.*, Vol. 27, 621–628, 2015.
10. Van Der Stam, W., et al., *Chem. Mater.*, Vol. 27, 283–291, 2015.

On the Route to Metal-free Phosphors

Adrian Kremer[1], **Barbara Ventura**[2], **Nicola Armaroli**[2], **Andrea Barbieri**[2], **and Davide Bonifazi**[1]

[1]Department of Chemistry, University of Namur (UNamur)
Rue de Bruxelles 61, Namur 5000, Belgium
[2]Istituto per la Sintesi Organica e la Fotoreattività (ISOF)
Consiglio Nazionaledelle Ricerche (CNR), Via Gobetti 101, Bologna 40129, Italy

Abstract— Phosphorescence is a key phenomenon on which are based devices for solid-state lighting such as Organic Light Emitting Diodes (OLEDs) [1]. Despite an increasing demand for phosphorescent materials, purely organic (i.e., metal-free) compounds have been very rarely explored as emitters in phosphor applications [2]. Indeed, only a few organic molecules are known to exhibit efficient phosphorescence emission at room temperature, as their long-living triplet excited state are extremely sensitive to collisional quenching by O_2 and other impurities. The main advantage of organic phosphorescent materials vs the inorganic analogues stems from the possibility to fabricate flexible devices and large-area displays by low-cost wet processing techniques (e.g., roll-to-roll printing), taking advantage of the fact that organic materials are typically soluble in a variety of common solvents.

To defy the paradigm that organic materials are not suitable as phosphors, we describe here novel design principles to prepare purely organic phosphorescent molecular materials by incorporating calchogenic atoms into their structure [3]. The synthesis, X-Ray crystal structures, ground and excited state UV-V is absorption spectra and luminescence properties of two series of chalcogen-containing organic emitters equipped on both extremities with benzoxa-, benzothia-, benzoselena- and benzotellurazoles moieties are reported. The insertion of four different chalcogen atoms within the same molecular skeleton enables the investigation of the sole internal heavy-atom effect on the photophysical properties of the organic compounds. A progressive quenching of the fluorescence and concomitant onset of phosphorescence features with gradually shorter lifetimes are detected as the atomic number of the chalcogen heteroatom increases, with the Te derivatives exhibiting only phosphorescence emission. Notably, the phosphorescence spectra of the Se and the Te compounds can be recorded even at room temperature in dilute de-aerated solution, a very rare finding for organic emitters.

These results open the route to the systematic exploitation of the internal heavy atom effect in the design of phosphorescent organic emitters, a rapidly expanding area of vast technological interest. This is a highly desirable goal in light of the difficulties still encountered in the preparation of cheap and stable triplet emitters based on transition metal complexes, particularly in the blue spectral region.

REFERENCES

1. Baldo, M. A., M. E. Thompson, and S. R. Forrest, *Nature*, Vol. 403, 750–753, 2000.
2. Bolton, O., K. Lee, H.-J. Kim, K. Y. Lin, and J. Kim, *Nature Chem.*, Vol. 3, 205–210, 2011.
3. Kremer, A., C. Aurisicchio, F. De Leo, B. Ventura, J. Wouters, N. Armaroli, A. Barbieri, and D. Bonifazi, *Chem. Sci.*, submitted.

Change of Mode Separation for Two-mode Laser with Semiconductor Quantum Dots

Kouichi Akahane, **Naokatsu Yamamoto**,
Atsushi Kanno, **Toshimasa Umezawa**, **and Tetsuya Kawanishi**
National Institute of Information and Communications Technology
4-2-1, Nukui-Kitamachi, Koganei, Tokyo 184-8795, Japan

Abstract— A two-wavelength emission laser (two-mode laser) can be used to generate millimeter and terahertz waves by irradiating high-speed photodiodes or nonlinear crystals. In recent times, electromagnetic waves at such frequencies have become important for use in high-speed wireless communication and accurate sensing. We have developed an InAs quantum dot (QD) wavelength tunable two-wavelength emission laser with a narrow linewidth and stable emission wavelength. In this study, we investigate the change of mode separation for a two-mode laser consisting of an InP based laser diode chip with InAs QDs as the gain medium and external cavity. The laser structure with InAs QDs was grown on InP(311)B substrates by solid-source molecular-beam epitaxy. After the growth of the QD laser wafer, the ridge waveguide was fabricated. In addition, an external cavity laser system was constructed using the QD gain chip, an optical band-pass filter, and an etalon filter. The single-mode laser emission is obtained in a conventional configuration in which the peak position of transmission by the band-pass filter is set to that of the etalon filter. The emission wavelength range is 1535 nm. Further, the configuration for a two-wavelength emission laser was modified from the conventional one. We observed two-mode lasing with a frequency separation of 90 GHz, 300 GHz, and 1 THz by changing etalon filter with different free spectral range as shown in Fig. 1. Clear beat signal was observed in the interference measurement for each mode separation. Therefore, two-mode lasing can be considered to have occurred simultaneously. Mode hopping and competition were largely suppressed by using QDs as the gain medium because the QDs have a delta-function-like density of states. Therefore, each of them contributed to the laser emission individually, stabilizing the laser emission wavelength.

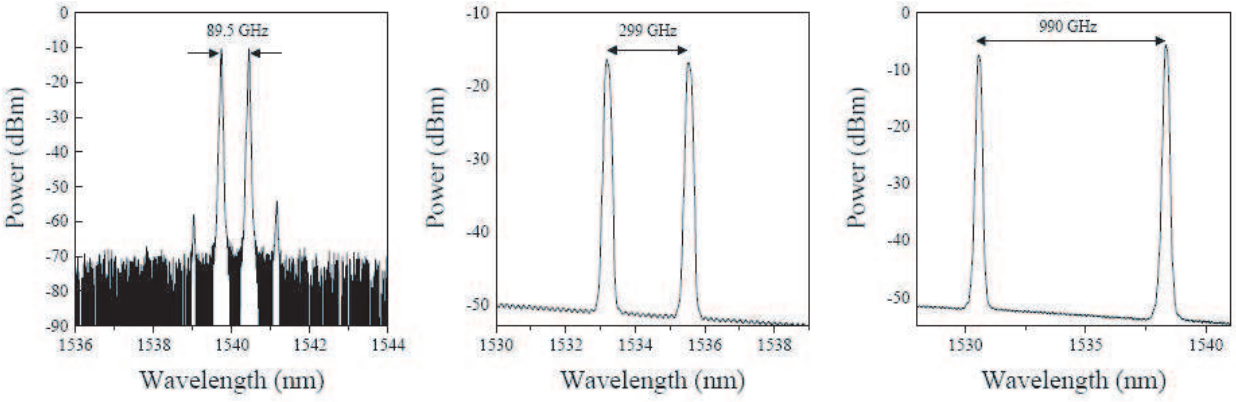

Figure 1: Two-mode lasing spectrum using QD optical gain chip with a frequency separation of (a) 90 GHz, (b) 300 GHz, and (c) 1 THz.

Energy Transfer Processes and Scintillation Performance of Ce^{3+}-doped Multicomponent Garnets

V. Babin[1], **K. Bartosiewicz**[1, 2], **K. Kamada**[3], **A. Yoshikawa**[3, 4], **and M. Nikl**[1]

[1]Institute of Physics AS CR, Cukrovarnicka 10, Prague 16253, Czech Republic
[2]Faculty of Nuclear Sciences and Physical Engineering
Czech Technical University in Prague, Brehova 7, Prague 11519, Czech Republic
[3]NICHe, Tohoku University, 6-6-10 Aoba, Aramaki, Aoba-ku, Sendai 980-8579, Japan
[4]Institute for Materials Research (IMR), Tohoku University, Sendai 980-8577, Japan

Abstract— Ce^{3+}-doped $Lu_3Al_5O_{12}$ (LuAG) and $Y_3Al_5O_{12}$ (YAG) single crystals are efficient scintillators due to their high density, short decay time and high light yield. However, their scintillating efficiency is degraded by the presence of the electron traps hampering the energy transfer to the dopant ion thus resulting in the appearance of the slow decay component and consequently, decrease of the light yield. Multicomponent garnet single crystals with general formula $(Gd,Lu,Y)_3(Ga,Al)_5O_{12}$ doped with Ce^{3+} recently became very promising candidates due to their greatly improved scintillation characteristics. In the case of optimized Gd^{3+}-Ga^{3+} composition [1, 2], the suppression of shallow electron traps and acceleration of the energy transfer towards Ce^{3+} ions results in a very significant light yield increase and strong reduction of the slow processes in the luminescence decay, see review in [3]. A further understanding of the scintillation mechanism and fine aspects of the energy transfer are of great interest for the ultimate materials optimization. Most recently, positive role of the stable Ce^{4+} centers in scintillation mechanism of Mg^{2+}-codoped garnet scintillators has also been evidenced [4].

In present contribution, the luminescent properties of undoped and Ce^{3+}-doped $(Y_{3-x}Gd_x)Al_{5-y}Ga_yO_{12}$ set of crystals with varying contents of Gd^{3+} and Ga^{3+} are investigated in wide temperature range. In undoped crystals, the Gd^{3+} emission intensity as well as decay time related to ^6P_x-^8S 4f-4f transition is dependent on the Gd^{3+} concentration. A Gd^{3+}-Gd^{3+} nonradiative energy migration was evidenced at room temperature and concentration quenching of Gd^{3+} emission takes place by energy migration to lattice defects. In Ce^{3+}-doped samples, a complex nonradiative Gd^{3+}-Ce^{3+} energy transfer is revealed, influencing the appearance of slow decay processes.

Another set of single crystal samples, Ce^{3+}-doped $(Y_{3-x}Gd_x)Al_5O_{12}$ is used to monitor the role of Gd^{3+}. The dependence of the onset of thermal quenching of Ce^{3+} luminescence on Gd^{3+} content are determined by the temperature dependence of Ce^{3+} decay times related to its 5d-4f emission transition. With the increase of Gd^{3+} content, the maxima of Ce^{3+}-related emission bands are shifted towards lower energy due to the increase in the crystal field splitting of the 5d levels, and as a consequence the onset of thermal quenching moves towards lower temperatures. Further characteristics, e.g., scintillation decay and light yield are also carefully studied.

Finally, for LuAG : Ce and GGAG : Ce samples the effect of Ce^{4+} presence is shown consisting mainly in the acceleration of scintillation response and, in the former case, in the increase of light yield.

REFERENCES

1. Kamada, K., T. Yanagida, T. Endo, K. Tsutumi, Y. Fujimoto, A. Fukabori, A. Yoshikawa, J. Pejchal, and M. Nikl, *Crystal Growth & Design*, Vol. 11, 4484–4490, 2011.
2. Kamada, K., T. Yanagida, J. Pejchal, M. Nikl, T. Endo, K. Tsutumi, Y. Fujimoto, A. Fukabori, and A. Yoshikawa, *J. Phys. D: Appl. Phys.*, Vol. 44, 505104, 2011.
3. Nikl, M., A. Yoshikawa, K. Kamada, K. Nejezchleb, C. R. Stanek, J. A. Mares, and K. Blazek, *Progr. Cryst. Growth Charact. Materials*, Vol. 59, 47–72, 2013.
4. Nikl, M., K. Kamada, V. Babin, J. Pejchal, K. Pilarova, E. Mihokova, A. Beitlerova, K. Bartosiewicz, S. Kurosawa, and A. Yoshikawa, *Crystal Growth Design*, Vol. 14, 4827–4833, 2014.

Challenges in Materials for Medical Imaging

Cees Ronda[1], **Vashilii Khanin**[1, 2], **Herfried Wieczoreka**[1], **and Piotr Rodnyi**[2]

[1]Philips Group Innovation Research, High Tech Campus 4, 5656 AE Eindhoven, The Netherlands
[2]St. Petersburg State Polytechnic University, Polytekhnicheskaya 29, 195251 St. Petersburg, Russia

Abstract— Current medical imaging equipment relies heavily on optical materials. These materials convert the high energy of γ-rays or X-rays into electron-hole pairs across the band gap. In scintillators, these electron-hole pairs excite luminescent centers (ions or molecular ion groups), leading to the generation of light in a process called scintillation. The light generated is subsequently detected using photo detectors. Alternatively to the scintillation process, the photoconductivity due to free electrons or holes can be measured. The latter scheme is called direct conversion.

The diagnostic value of clinical images is limited by many factors, among others the optical properties of the materials used. After having reviewed the state of the art of scintillating materials, the resulting challenges will be identified. On the basis of the theoretical estimations and experimental data, the optimal conditions for maximum light output, short decay time and low afterglow will be determined.

Correlation of Luminescence Decay and Thermoluminescence of Zinc Oxide Ceramics

K. A. Chernenko[1], **L. Grigorjeva**[2], **A. Zolotarjovs**[2], **E. I. Gorokhova**[3], **and P. A. Rodnyi**[1]

[1]Saint-Petersburg State Polytechnic University
Polytechnicheskaya 29, St. Petersburg 195251, Russia
[2]Institute of Solid State Physics, University of Latvia
8 Kengaraga, LV-1063 Riga, Latvia
[3]Research and Technological Institute of Optical Materials All-Russia Scientific Center
"S.I.Vavilov State Optical Institute", Babushkina 36, St. Petersburg 192171, Russia

Abstract— Bulk scintillating ceramics based on zinc oxide (ZnO) are very promising materials for many applications due to their ultrafast excitonic luminescence. Nowadays there are a lot attempts to create such a scintillator, but slow luminescence decay component that usually appears in ZnO hinders these efforts. Exact origin of slow decay component is still controversial as both excitation and emission mechanisms demonstrate complex properties.

This work is focused on peculiarities of kinetic characteristics of the slow luminescence with the aim to elucidate energy and charge transfer processes which are responsible for the emission.

In this report, temperature evolution of luminescence decay, luminescence spectra, thermoluminescence (TL) glow curves and spectra and in range of 15–300 K of nominally undoped ZnO ceramics are presented and discussed.

The ZnO ceramics were manufactured by the uniaxial hot pressing method in a high vacuum furnace in the form of discs with a diameter of 24 mm.

At room temperature, photoluminescence (PL) spectra of the ceramics consisted of two bands: excitonic luminescence (at 377 nm) and so-called green luminescence (at 495 nm). Green luminescence had a wide band (FWHM 392 meV at 15 K). Additional unresolved emission band arises at low energy side of green luminescence under X-ray excitation.

TL emission spectra with different maximum positions were observed. The spectrum of the most intensive TL peak located at 34 K was centered at 615 nm. In temperature range of 60–160 K, TL had nearly constant intensity without any resolvable peaks. Peaks of TL with relatively small intensity were also observed at 231 K and 291 K. TL in range of 60–160 K and peaks at 231 K and 291 K had the same emission maximum as green luminescence in PL spectra. TL emission peak centered at 720 nm appears at temperature of $\sim$ 170 K. Emission at 720 nm was not detected in emission spectra under X-ray or photoexcitation and appears only in TL.

At temperatures below 20 K, complex green luminescence decay process which includes kinetics of tunneling recombination, exponential component and first order hyperbola was observed. At the temperatures above the most intensive TL peak temperature the exponential component of decay disappears. With rising temperature in range 60–160 K where TL intensity is constant, absolute intensity of hyperbolical component of decay increases. With further rising of temperature, quenching of hyperbolic decay was observed and decay shape evolved into stretched exponential decay.

Processes responsible for the luminescence decay kinetic and defect spectroscopy of the studied ZnO ceramics are presented and discussed.

Enormously Long-wavelength Luminescence of SrS:Ce

Dagmara Kulesza[1], **Karolina Fiączyk**[1], **Aneta Wiatrowska**[2], **and Eugeniusz Zych**[1, 3]

[1]Faculty of Chemistry, University of Wrocław, 14F. Joliot Curie Street, 50-383 Wrocław, Poland
[2]Philips Research, Materials Technology Department, High Tech Campus 04
5656 AE Eindhoven, The Netherlands
[3]Wroclaw Research Centre EIT+, 147 Stablowicka Street, 54-066 Wroclaw, Poland

Abstract— The presentation will show a possibility to generate a new, red Ce^{3+} luminescence in SrS:Ce both in high- and low-concentration compositions. A comprehensive spectral characteristics of the long-wavelength emission will be given together with its relationship to the regular bluish green luminescence.

SrS:Ce is a known luminescent material with an efficient emission appearing in the 450–600 nm region and peaking around 480 nm. Occasionally, a red-shifted emission in SrS:Ce was reported. Yet, its appearance was always connected with high Ce concentrations and consequently with luminescence of Ce^{3+}-Ce^{3+} pairs rather than isolated dopantions.

In this presentation we shall prove that an extremely long-wavelength, abnormal luminescence of SrS:Ce may be generated even in a lightly doped material (0.05%). We shall show that at room temperature its intensity may harmonize with the intensity of the regular emission even if the excitation ($\sim$ 425 nm) goes only to the regular center. Compared to the regular emitting Ce^{3+} ions, the new emitting center has much different excitation spectrum and altogether both luminescent centers absorb the whole UV part of radiation as seen in Fig. 1. We shall also show that the abnormal luminescence has all the characteristics of Ce^{3+} emission its decay time is about 35 ns, while the regular center decays with the time of 27 ns. The long-wavelength luminescence is composed of two components separated by $\sim 2200\,cm^{-1}$, which is the characteristic value of the spin orbit splitting of the $4f^1$ configuration of Ce^{3+}. Spectroscopic data in the 25–450 K range of temperatures will be presented and discussed.

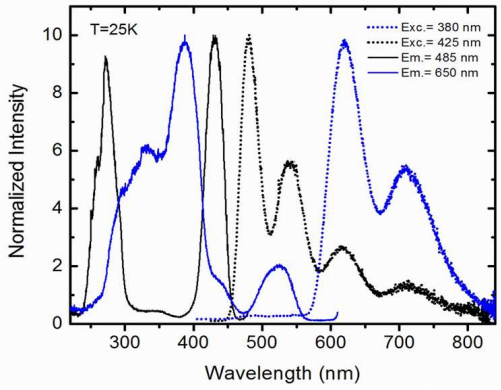

Figure 1: Emission and excitation spectra revealing existence of two different Ce^{3+} luminescence centers in SrS:Ce after a specifically designed processing.

ACKNOWLEDGMENT

This work was supported by POIG.01.01.02-02-006/09 project co-funded by European Regional Development Fund within the Innovative Economy Program. Priority I, Activity 1.1. Sub-activity 1.1.2, which is gratefully acknowledged.

Session 2P8b
FocusSession.SC3&4: Microwave Photonics for Wireless Spectrum Management 1

Integrated Spectral Shapers in Silicon Photonics for Generating Chirped Microwave Pulses Based on Optical Spectral Shaping and Wavelength-to-time Mapping

Lawrence R. Chen
Department of Electrical and Computer Engineering
McGill University, Montreal, QC H3A 0E9, Canada

Abstract— Chirped microwave pulses (CMPs) have been used widely in various applications, including spread spectrum communications, microwave remote sensing, and microwave computed tomography. While such waveforms can be generated in the electronic domain, their bandwidths, chirp rate, and central frequencies are limited by the sampling rate of digital electronics. On the other hand, photonic generation of CMPs offer the possibility of achieving central frequencies of tens to hundreds of GHz as well as significant chirp rates, thereby supporting tens of GHz of bandwidth. Photonic approaches also provide increased flexibility, particularly with regards to reconfigurabilty and tunability. The typical system implementation involves some form of optical pulse shaping to synthesize the desired temporal waveform followed by photodetection. To this end, a number of techniques have been employed, such as those based on direct space-to-time pulse shaping, temporal pulse shaping, and optical spectral shaping followed by wavelength-to-time mapping. The latter is straightforward to implement and involves a broadband source, e.g., from a mode-locked fiber laser, a spectral shaper, and a dispersive medium. The spectral shaper modifies the spectrum of the pulsed source, typically in amplitude only, and the shaped spectrum then propagates through the dispersive medium where a wavelength-to-time mapping process takes place, i.e., the shape of the spectrum is mapped to the time domain. The resulting temporal signal corresponds to the microwave waveform which is detected by a photodetector. The key component is the spectral shaper and in this presentation, we review recent progress on developing integrated spectral shapers in silicon photonics. In particular, we describe devices based on cascaded ring resonators as well as those incorporating Bragg grating structures.

Engineered Optical Parametric Processes for Wideband RF Analyzer and Pulse Generation

Camille-Sophie Brès
Ecole Polytechnique Fédérale de Lausanne, Photonic Systems Laboratory (PHOSL), STI-IEL
Station 11, CH-1015 Lausanne, Switzerland

Abstract— Optical parametric processes based on the $\chi^{(3)}$ nonlinear tensor of a waveguide medium have been used successfully for the complex manipulation of optical signals. The advantages of such processes are numerous and noteworthy are the instantaneous response, the efficiency or the large bandwidth. The versatile nature of parametric devices has been exploited for the advent of phase sensitive amplifiers and wideband amplifiers, for the generation of light in distant spectral windows but also for the development of unique processing devices capable of wavelength conversion, multicasting or sampling.

Recently, the development of dispersion engineered parametric fiber links has led to new possibilities in terms of wideband multicasting, analog signal processing and pulse shaping. For example photonic assisted architectures for instantaneous frequency measurements have attracted significant interest, mainly driven by the increasing physical bandwidth used in radar systems. Architectures based on high quality copying of microwave signals by wavelength multicasting in self-seeded mixers and subsequent filtering, trade frequency non-degeneracy of the newly generated copies for ease of filtering. Such scheme also enables compensation for filter fabrication tolerance and dynamic bandwidth/channel spacing reconfiguration by controlled adjustments of copy positioning. Recently filterless wideband channelizer have also been realized based on the similar principle. Another interesting aspect of engineered parametric processes lies in their potential for the generation and shaping of short optical pulses. Indeed it has been shown that the generated pulse shape and pulse duration depend on the signal frequency relative to the pump frequency such that bounding of the phase matching in two-pump parametric amplifiers enables the precise control of the generation process.

In this paper, we review the principle behind parametric wavelength conversion and distortion free wideband multicasting in engineered fiber based devices for applications to parametric channelizers and pulse generators.

The Path towards 100 Gbit/s Wireless Communications

J. Leuthold, **R. Bonjour**, **S. A. Gebrewold**, **S. Dash**, **W. Heni**, **C. Hoessbacher**, **C. Haffner**, **Y. Salamin**, **B. Bäuerle**, **A. Josten**, **P. Ma**, **P. Leuchtmann**, **Y. Fedoryshyn**, **D. Hillerkuss**, **and Christian Hafner**
Institute of Electromagnetic Fields (IEF), ETH Zurich, Zurich 8092, Switzerland

Abstract— Successful operation of wireless communication links with capacities above 100-Gbit/s require sub-THz carrier frequencies, pencil beams, usage of novel modulation techniques and novel photonic-electronic devices. We review a recent 100 Gbit/s wireless link demonstrations and discuss steps to make such systems more viable.

Introduction: Wireless transmission is forecast to grow by a 61% annual compound growth for the next five years [2]. Such growth is only sustainable if fundamental changes in the design of future wireless networks are adopted soon.

A possible path to vastly extend the capacity is to shift the RF carrier to the millimeter waves with frequencies above 100 GHz [3]. As an example, the frequency range between 200 GHz and 300 GHz is characterized by low atmospheric losses where wireless links can be operated even under averse weather conditions [4].

Moving towards higher frequencies will also make it necessary to increase the antenna gain significantly to offset the increased link losses. Thus, narrower beams, or pencil beams will be needed. In return, ultra-fast, continuously tunable true-time delays (TTDs) will be necessary as building blocks in phased array feeder networks to keep such systems flexible and to distribute the information spatially [5].

Additionally, multiple-input multiple-output (MIMO) will become more attractive as it offers another degree for scaling. It will ultimately be needed in order to enhance the capacity of base stations. Fortunately, with an increase in frequency, the constraints due to limited space for the number of antennas that goes along with MIMO will relax. This is particularly important on the user side C where space is scarce [3].

MmWave systems also have to overcome distinct hardware constraints [3]. Major constraints come from the high power consumption of mixed signal components, chiefly the analog-to-digital converters (ADCs) and digital-to-analog converters (DACs). In a conventional approach each antenna would be connected to a single high-rate ADC/DAC system. Equipping every antenna would not only lead to an immense surge in cost but also require large computation powers together with a huge power consumption. MmWave communications is thus unlikely to happen unless there is a huge leap forward in semiconductor technology. However, such constraints can be overcome by a clever hybrid approach based on photonics and microwave communications. Key microwave-photonic elements include true-time delay elements, high-speed photo detectors that can directly translate an optical signal into a microwave signal and microwave-to-photonic receivers.

In this talk we will review some recent approaches on wireless communication links with data rates up to 100 Gbit/s [1]. We will review some of the photonic-electronic hardware implementations.

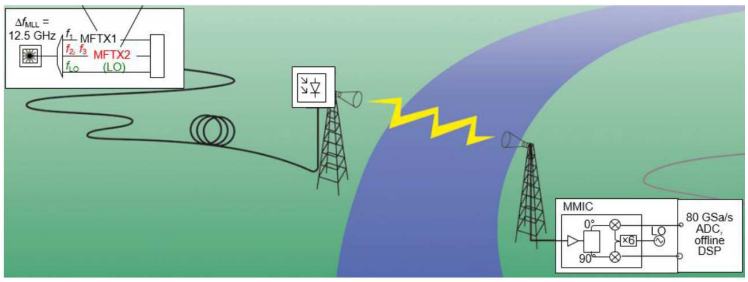

Figure 1: 100 Gbit/s Radio-over-Fiber Communications link [1].

REFERENCES

1. Koenig, S., D. L. Diaz, J. Antes, F. Boes, R. Henneberger, A. Leuther, A. Tessmann, R. Schmogrow, D. Hillerkuss, R. Palmer, T. Zwick, C. Koos, W. Freude, O. Ambacher, J. Leuthold, and I. Kallfass, "Wireless sub-THz communication system with high data rate," *Nature Photonics*, Vol. 7, 977–981, 2013.
2. Systems, C., "Cisco visual networking index: global mobile data traffic forecast update, 2013–2018," Cisco, San Jose, Singapore, The Netherlands, 2014.
3. Boccardi, F., R. W. Heath, A. Lozano, T. L. Marzetta, and P. Popovski, "Five disruptive technology directions for 5G," *Communications Magazine, IEEE*, Vol. 52, 74–80, 2014.
4. Su, K., L. Moeller, R. B. Barat, and J. F. Federici, "Experimental comparison of performance degradation from terahertz and infrared wireless links in fog," *J. Opt. Soc. Am. A*, Vol. 29, 179–184, 2012.
5. Bonjour, R., S. A. Gebrewold, D. Hillerkuss, C. Hafner, and J. Leuthold, "Continuously tunable true-time delays with ultra-low settling time," *Optics Express*, Vol. 23, 6952–6964, 2015.

Broadband Microwave Signal Acquisition by Photonics-assisted Compressive Sampling

Hongwei Chen[1, 2], **Qiang Guo**[1, 2], **Minghua Chen**[1, 2], **and Shizhong Xie**[1, 2]

[1]Tsinghua National Laboratory for Information Science and Technology (TNList), China
[2]Department of Electronic Engineering, Tsinghua University, Beijing, China

Abstract— Microwave signal acquisition plays a key role in radar, electric warfare, communication and other applications. The bandwidth of signal acquisition becomes larger and larger. As the signal bandwidth is beyond to ten GigaHertz, traditional Nyquist Sampling needs ultrafast ADCs used for signal acquisition. Meanwhile, there is a problem of big data but with high redundancy for that signals occupies only several sub bands in so large bandwidth. This means that many data are useless. How to reduce the sampling rate and the redundancy of data attracts researcher's attention. Photonic-assisted compressive sampling supplies a potential candidate to solve this problem. Our work focuses on breaking the limit of photonic CS's bandwidth from PRBS pulse rate and increasing the bandwidth up to tens of GHz. We propose to adopt nonlinear time-delayed PRBS pulses for spectrum compression, which can construct PRBS pulse with higher repetition rate and meanwhile guarantee stable signal recovery in broad band. Based on this, large-bandwidth compressive sampling scheme is proposed, and compressive sampling with 20-GHz bandwidth is successfully realized with four delayed PRBS pulses with 10.16-GHz pulse rate. Also, for the first time, a photonic-assisted CS system is proposed to acquire radar pulse steams. An IQ modulator and a photodetector are utilized to perform the spectral compression of the test pulses. A sliding window-based recovery algorithm is proposed to guarantee the signal sparsity within a time window and realize a continuous signal reconstruction. In the experiment, about 100 radar pulses ranging from 500 MHz to 5 GHz are acquired within 100 μs and exactly recovered with a 520-MHz ADC, experimentally demonstrating the feasibility of the proposed system in spectral estimation for radar pulses.

ACKNOWLEDGMENT

This work was supported by the National Program on Key Basic Research Project (973) under Contract 2012CB315703; NSFC under Contracts 61322113, 61271134, 61120106001; The authors also thank the young top-notch talent program sponsored by Ministry of Organization, China.

Recent Advances in On-chip Stimulated Brillouin Scattering Based Microwave Photonic Signal Processing

Ravi Pant[1], **David Marpaung**[2], **and Benjamin J. Eggleton**[2]

[1]School of Physics, Indian Institute of Science Education and Research (IISER) Trivandrum
Kerala 695016, India
[2]Centre for Ultrahigh Bandwidth Devices for Optical Systems (CUDOS)
The Institute for Photonics and Optical Sciences (IPOS), School of Physics
University of Sydney, NSW 2006, Australia

Abstract— On-chip Stimulated Brillouin scattering (SBS) has recently been exploited for realizing microwave photonic sources and signal processing. On-chip slow-light with a tunable delay of 23 ns and microwave photonic notch filter with ultrahigh selectivity (3 dB bandwidth $\sim$ 30 MHz) and wide frequency (0–30 GHz) and bandwidth tunability ($\sim$ 30–90 MHz) were demonstrated.In this talk, we present recent advances in microwave photonic signal processing exploiting SBS in photonic circuits.

Introduction: Stimulated Brillouin scattering is the strongest optical nonlinearity that results from three-wave interaction among two optical waves and an acoustic wave. Counter-propagating optical waves with frequencies ω_p (pump) and $\omega_s = \omega_p - \Omega_B$, where Ω_B is the frequency of the acoustic wave in the medium, create the acoustic wave (Ω_B) that in turn induces a coupling between the pump and Stokes signal (ω_s) generating a gain resonance at the Stokes frequency. The amplitude and phase response associated with the gain resonance is the key to realize slow-light, dynamic gratings, microwave signal processing and Brillouin lasers [1–3].

On-chip SBS Microwave Photonics: Realization of on-chip SBS requires careful choice of material and device design. A device designed to tightly confineboth optical and acoustic modes(see Fig. 1) and made from a material with large refractive index and elasto-optic coefficient is the key for on-chip SBS [4]. Recently on-chip SBS was realized in a 7 cm long photonic chip and was exploited for slow-light induced tunable delay(see Fig. 1) [5] and realizing a ultra-high selectivity microwave photonic notch filter (~ -55 dB) with wide frequency (0–30 GHz) and bandwidth ($\sim$ 30–90 MHz) tunability using low power of 8 mW (gain $\sim$ 0.8 dB) (see Fig. 2)) [6]. For the SBS slow-light tunable delay of $\sim$ 23 ns was achieved with a gain of 23 dB, which can be used in microwave signal processing tasks such as filters and phased array antenna.

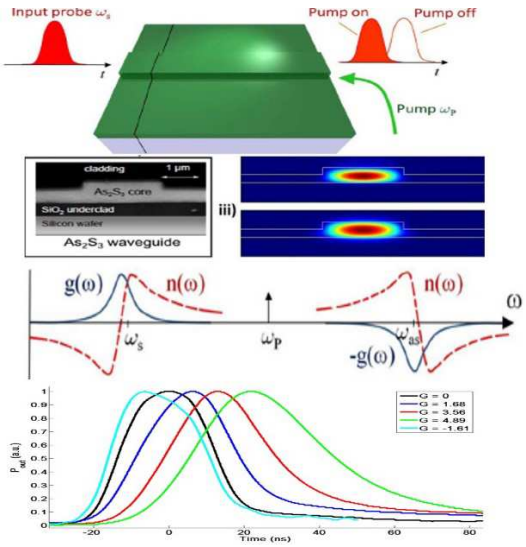

Figure 1: SBS slow-light in a Chalcogenide photonic chip demonstrating fractional delay of nearly one pulse width for a 25 ns long input Gaussian pulse [5].

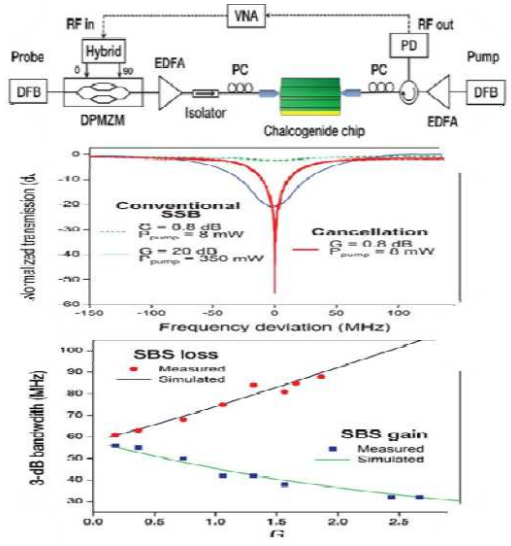

Figure 2: Photonic chip based microwave photonic notch filter with ultrahigh selection and wide tunability using low pump power of 8 mW [6].

REFERENCES

1. Pant, R., et al., "On-chip stimulated Brillouin scattering for microwave signal processing and generation," *Laser & Photonics Reviews*, 2014.
2. Li, J., H. Lee, and K. J. Vahala, "Microwave synthesizer using an on-chip Brillouin oscillator," *Nat. Commun.*, Vol. 4, 2013.
3. Li, J., H. Lee, and K. J. Vahala, "Low-noise Brillouin laser on a chip at 1064 nm," *Optics Letters*, Vol. 39, No. 2, 287–290, 2014.
4. Eggleton, B. J., C. G. Poulton, and R. Pant, "Inducing and harnessing stimulated Brillouin scattering in photonic integrated circuits," *Advances in Optics and Photonics*, Vol. 5, No. 4, 536–587, 2013.
5. Pant, R., et al., "Photonic-chip-based tunable slow and fast light via stimulated Brillouin scattering," *Optics Letters*, Vol. 37, No. 5, 969–971, 2012.
6. Marpaung, D., et al., "Low-power, chip-based stimulated Brillouin scattering microwave photonic filter with ultrahigh selectivity," *Optica*, Vol. 2, No. 2, 76–83, 2015.

On-chip Microwave Signal Processing Platforms Based on Silicon Photonics Technologies

M. Burla and J. Azaña
Institut National de la Recherche Scientifique, Énergie, Matériaux et Télécommunications (INRS-EMT)
800, de la Gauchetière Ouest, Montréal, Québec, H5A 1K6, Canada

Abstract— Microwave photonics (MWP) signal processing by means of photonic integrated circuits has attracted a large amount of attention in recent years, as an enabling technology for a number of functions not attainable by a purely electronic approach. In particular, waveguide Bragg grating (WBG) devices on silicon constitute a particularly attractive solution, thanks to their high compactness and flexibility in producing arbitrarily defined amplitude and phase responses. In this talk a brief overview of recent advances in the field of integrated WBGs applied to microwave photonics will be given, with emphasis on a number of recent demonstrations by our group of the use of WBGs for microwave and ultrafast optical signal processing. Application examples include broadband tunable RF filters, true-time-delay lines and phase shifters with large instantaneous bandwidth, optical pulse shapers operating in the THz regime, and instantaneous frequency measurement systems on-a-chip. A perspective on the exciting possibilities offered by the silicon photonics platform in the field of MWP will be given, potentially enabling integration of highly-complex active and passive functionalities with high yield on a single chip.

Microwave Photonics Techniques Supporting Flexible Wireless Communications Links

Simon Rommel[1], **Lucas Cavalcante**[1],
Juan Jose Vegas Olmos[1], **and Idelfonso Tafur Monroy**[1, 2]

[1]Department of Photonics Engineering, Technical University of Denmark, Kgs. Lygnby, Denmark
[2]ITMO University, St Petersburg, Russia

Abstract— Wireless data communication links supporting the next generation 5G and beyond mobile networking face a set of engineering challenges related to the mandatory operation at mmw and higher frequency bands, provide capacities above 10 Gb/s, satisfy latency, robustness, flexibility and low complexity constrains. Microwave photonic techniques support a number of key functionalities required to satisfy above-mentioned demands. We will review, in particular, experimental realizations of a number of functionalities such as mmw generation, detection, optical fiber transport and multi-Gigabit data transmission implementation exploiting photonic techniques.

ACKNOWLEDGMENT

This work was partly financially supported by the Government of the Russian Federation (Grant 074-U01) through ITMO Visiting Professorship scheme.

Instantaneous Microwave Frequency Measurement System Using On-chip Nonlinear Optics

David Marpaung
CUDOS, School of Physics, University of Sydney, NSW 2006, Australia

Abstract— Instantaneous frequency measurement (IFM) systems are essential in various defense, electronic warfare, and countermeasure applications. IFM systems are required to rapidly determine a received signal frequency with low error, without actually measuring the frequency. Most of IFM systems code the frequency information to another measureable quantity like power through a function known as amplitude comparison function (ACF). Recently, a number of photonic-assisted IFM systems have been proposed, taking advantage of the wide bandwidth and reconfigurability of photonic system. However, most techniques were based on long and bulky optical fibers. Not only this approach is not attractive in terms of size and weight, but long optical fibers also ad latency to the IFM system. It is thus imperative to integrated IFM systems in compact photonic chips to reduce latency and to achieve advantages in size, weight and power consumption.

In this work, we consider IFM systems that exploit optical nonlinearities in a photonic chip. The use of optical nonlinearities added values such as ultra-low estimation error and simplification of the IFM system. In one demonstration we harness stimulated Brillouin scattering (SBS) in a 7-cm chalcogenide photonic chip to achieve a hybrid IFM system that combines the characteristics of a scanning receiver and an ACF to estimate a wide range of RF frequencies from 7–35 GHz with ultra-low error below 1 MHz. In another demonstration, we report an IFM system based on four-wave mixing (FWM) in a 33 cm thick silicon waveguide. The use of this platform allows us to access higher signal to noise ratio beyond that of a previous demonstration in a length of highly nonlinear fiber. Over 40 GHz frequency range we achieved lower error in the long silicon waveguide compared to that of the fiber system.

Session 2P9
SC1: Time and Frequency Domain Modeling Techniques for Waveguides and Cables

Modeling of Coaxial Feed Topologies

Guy A. E. Vandenbosch[1], **Xuezhi Zheng**[1], **and Victor V. Moshchalkov**[2]

[1]Department of Electrical Engineering (ESAT-TELEMIC), KU Leuven, Belgium
[2]Institute for Nanoscale Physics and Chemistry (INPAC), KU Leuven, Belgium

Abstract— In this talk, the basic coaxial feed is revisited. The case under study is a coaxial feed exciting a grounded planar structure of arbitrary layers. This type of feeding structure occurs in a large number of practical microwave devices and antennas. A highly accurate model is given for this widely used topology. The core of the model is to make use of the eigenmodes of a conducting parallel plate system which can be derived analytically to reconstruct the field in the actual configuration. This is based on the physical observation that the differences between the modal fields found in the parallel plate system [1–3] and the ones of the actual configuration are negligible. As a result, we can build a highly accurate equivalent circuit model for the coaxial feed in a general multilayer structure. This circuit model is specifically simplified for two most commonly seen cases: one layer and two-layer structure. Since the model introduces only one unknown for the entire coaxial feeding topology, its numerical complexity is reduced to the same as for the simplest possible model, i.e., the imposed constant probe current model. The way of working opens possibilities for developing full time-domain methods to analyze the susceptibility of microwave electronic circuits based on the natural modes of a multilayer structure to pulsed-field electromagnetic (EM) disturbances [4].

REFERENCES

1. Vandenbosch, G. A. E. and A. R. van de Capelle, "Mixed-potential integral expression formulation of the electric field in a stratified dielectric medium — Application to the case of a probe current source," *IEEE Trans. Antennas Propagat.*, Vol. 40, 806–817, Jul. 1992.
2. Vandenbosch, G. A. E. and A. R. van de Capelle, "Reduction of coaxial feed between two parallel conductors into finite number of voltage sources," *Electron. Lett.*, Vol. 27, No. 25, 2387–2389, Dec. 1991.
3. Vandenbosch, G. A. E. and A. R. van de Capelle, "Admittance of coaxial feed between two finite parallel conductors," *Electron. Lett.*, Vol. 28, No. 19, 1780–1781, Sep. 1992.
4. De Hoop, A. T., H. Blok, I. E. Lager, M. Stumpf, and G. A. E. Vandenbosch, "Pulsed-field EMI susceptiblity analysis of microelectronic circuits — A full time-domain methodology," *Proceedings of the 42nd European Microwave Conference*, 337–339, 2012.

Pulsed EM Field Propagation in Cylindrically Layered Structures

Martin Štumpf[1] and Sven Nordebo[2]

[1]SIX Research Centre, Brno University of Technology
Technická 3082/12, Brno 616 00, The Czech Republic
[2]Department of Physics and Electrical Engineering, Linnnæus University
Hus D 1152, Växjö 351 95, Sweden

Abstract— Power-cable fault localization using time-domain reflectometry requires an efficient computational technique for the evaluation of pulsed electromagnetic fields in cylindrically layered structures. A robust way to handle the problem is to perform a contour complex integration at a number of frequency points and carry out an inverse fast Fourier transformation with respect to time [1]. Alternatively, one may employ a slowness representation along the cable axial direction in combination with a one-sided Laplace time transformation and obtain time-domain results more or less directly. This is exactly the main subject of the present contribution in which it is shown that the pulsed electromagnetic response of a cylindrically layered cable can be constructed with the aid of Cagniard-DeHoop (CdH) technique [2] and a numerical Laplace-transform inversion method in the intermediate step. Specifically, the pulsed electromagnetic wave field in N-layered medium can be then composed of generalized-ray time-domain constituents whose generic slowness-domain representation has the following form

$$\hat{K}(r,z,s) = \frac{s}{2\pi i}\int_{p=-i\infty}^{i\infty} \exp\left\{-s\left[pz + \sum_{K\in\Gamma}\gamma_K(p), \varrho K\right]\right\}\tilde{Q}\,(r,p,s)\,dp \tag{1}$$

where $\Gamma = \{1,\ldots,N\}$, z and r are the axial and radial spatial coordinates, respectively, $\{s \in \mathbb{R};\, s > 0\}$ is the (time) Laplace-transformation parameter, ϱK denotes the radial propagation path traversed in K-th cylindrical shell and $\gamma_K(p)$ is the corresponding propagation coefficient given as $\gamma_K(p) = (1/c_K^2 - p^2)^{1/2}$ with $\mathrm{Re}(\cdot)^{1/2} \geq 0$. It is worth noting that the factor $\tilde{Q}(r,p,s)$ is s-dependent and consists of a combination of the propagation coefficients and the scaled modified Bessel functions. Thanks to this property, the standard CdH procedure has to be supplemented with numerical Laplace transform inversion. As the latter is inherently an ill-conditioned procedure [4, Section 2.1], its evaluation requires a special attention. Finally, once the inversion of (1) is carried out, the resulting wave motion is composed from the corresponding body- and head-wave time-domain constituents that are propagating, reflecting and refracting upon interfaces between cylindrical layers. Sample numerical experiments concerning canonical configurations will be presented at the 36th PIERS.

REFERENCES

1. Nordebo, S., B. Nilsson, S. Gustafsson, T. Biro, G. Cinar, M. Gustafsson, A. Karlsson, and M. Sjöberg, "Low-frequency dispersion characteristics of a multilayered coaxial cable," *J. Eng. Math.*, Vol. 83, 169–184, 2013.
2. De Hoop, A. T., "A modification of Cagniard's method for solving seismic pulse problems," *Appl. Sci. Res.*, Vol. B8, No. 1, 349–356, 1960.
3. Cohen, A. M., *Numerical Methods for Laplace Transform Inversion,* Springer, New York, 2007.

Wiener-Hopf Analysis of TM Wave Reflection by a Step Discontinuity on the Junction of Two Coaxial Waveguides with Perfectly Conducting and Impedance Walls

G. Çınar[1], S. Akşimşek[2], B. Nilsson[3], S. Nordebo[3], and Ö. Yanaz Çınar[1]

[1]Eskişehir Osmangazi University, Turkey
[2]İstanbul Kültür University, Turkey
[3]Linnæus University, Sweden

Abstract— In this study, the reflection of TM waves by a junction of a perfectly conducting coaxial waveguide with a step discontinuity on its inner wall and an impedance coaxial waveguide is analyzed rigorously by Wiener-Hopf technique (see Fig. 1(a)). The problem represents two main scattering mechanisms which occur in the measurement setup for the experiments performed on a 80 km long High Voltage Direct Current (HVDC) power cable in a factory and on the 250 km long Baltic HVDC power cable [1]. The effect of the step discontinuity alone on the scattered fields has been studied by the authors recently in [2, 3].

In order to determine the reflection coefficient for this problem, one first needs to analyze TM wave propagation along the waveguide junctions shown in Fig. 1(b) and Fig. 1(c). The scattering coefficients obtained by solving these two problems can then be taken into account to apply the generalized scattering matrix method which eventually provide the reflection coefficient related to the original problem.

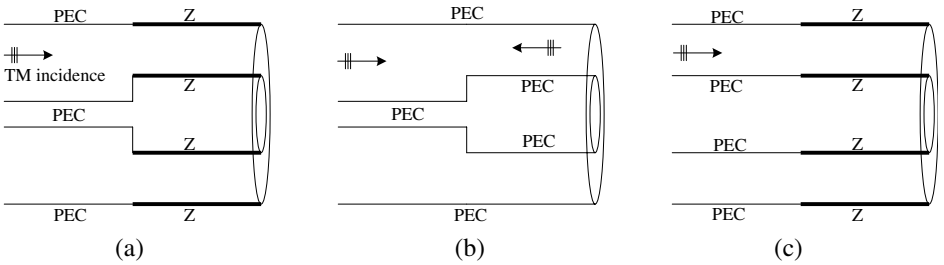

Figure 1.

The scattering coefficients for the problems given in Fig. 1(b) and Fig. 1(c) are obtained simply by extending the formulations described in [3] and [4] (which are done for only TEM modes) to the cases of TM wave incidences. In addition to these, the problem in Fig. 1(b) is also solved when the TM wave is incident from the opposite direction. With the help of these scattering coefficients and the generalized scattering matrix method, the reflection coefficient for the original problem is determined. The numerical results are compared to the ones obtained by applying mode-matching technique directly to the problem shown in Fig. 1(a).

REFERENCES

1. Nilsson, B., G. Çınar, S. Nordebo, and Ö. Yanaz Çınar, "Asymptotic methods for long distance monitoring of power cables," *The Sixth International Conference Inverse Problems: Modeling and Simulation*, Antalya, Turkey, May 2012.
2. Akşimşek, S., G. Çınar, B. Nilsson, and S. Nordebo, "TEM wave scattering by a step discontinuity on the outer wall of a coaxial waveguide," *IEEE Transactions on Microwave Theory and Techniques*, Vol. 61, No. 8, 2783–2791, 2013.
3. Çınar, G., S. Akşimşek, B. Nilsson, S. Nordebo, and Ö. Yanaz Çınar, "Reflection of TEM waves by a step discontinuity on the inner wall of a coaxial waveguide," *Progress In Electromagnetics Research Symposium Abstracts*, 771, Stockholm, Sweden, Aug. 12–15, 2013.
4. Hacıvelioğlu, F. and A. Büyükaksoy, "Scattering of the TEM mode at the junction of perfectly conducting and impedance coaxial waveguides," *Electrical Engineering*, Vol. 92, No. 4–5, 165–171, 2010.

Determination of Normalized Electric Eigenfields in Microwave Cavities with Corners

J. Helsing[1] and A. Karlsson[2]

[1]Centre for Mathematical Sciences, Lund University, Box 118, Lund 221 00, Sweden
[2]Department of Electrical and Information Technology
Lund University, Box 118, Lund 221 00, Sweden

Abstract— We show that high-order convergent Fourier-Nyström schemes for the MFIE can be efficiently implemented when applied to cavities with non-smooth PEC surfaces. Our explicit kernel-split panel-based Fourier-Nyström scheme relies on an underlying 16-point Gauss-Legendre quadrature and a technique called recursively compressed inverse preconditioner (RCIP). It gives a convergence of 16th order and a nearly optimal accuracy that is reached at very few discretization points per wavelength along the generating curve of the cavity. The scheme determines surface current densities and surface charge densities that, via a post-processor, are carried over to normalized electric and magnetic eigenfields at all positions inside the cavity, also close to surfaces where integral equation techniques usually encounter difficulties. At corners with opening angles larger than 180 degrees there are always components of the electric or magnetic fields that are singular. The RCIP technique manages to accurately resolve such singularities down to any desired spatial scale. The post-processor takes advantage of a new surface integral expression for the normalization.

In our collaboration with scientists at the synchrotron light source MAX IV and the European Spallation Source (ESS), both under construction in Lund, Sweden, we have seen a need for improved numerical tools for accurate wakefield evaluations in particle accelerators. This is the motivation for our project. Today, all high energy particle accelerators use microwave cavities for particle acceleration by means of eigenfields, excited by external sources. The cavities consist of one, or several, axially symmetric cells, where in each cell the excited eigenfield corresponds to the TM_{010} mode in a cylindrical cavity. In addition to the eigenfields excited by the external sources, the beam of particles excite wakefields that consist of a large number of higher-order modes (HOM). These wakefields affect the trajectories of the particles and, by that, the quality of the beam. To prevent that harmful wakefields are excited in the accelerator, numerical simulations are used both in its design process and during operation. These simulations need to cover a frequency band up to at least 10 times the frequency of the external source. Our method has been developed in several steps [1–3], to cover more and more applications. It is now at the stage where it can evaluate wakefields in linear accelerators and storage rings with high accuracy and by that become a tool in the design of accelerators.

ACKNOWLEDGMENT

This work was supported by the Swedish Research Council under contract 621-2011-5516.

REFERENCES

1. Helsing, J. and A. Karlsson, "An accurate boundary value problem solver applied to scattering from cylinders with corners," *IEEE Trans. Antennas Propag.*, Vol. 61, 3693–3700, 2013.
2. Helsing, J. and A. Karlsson, "An explicit kernel-split panel-based Nyström scheme for integral equations on axially symmetric surfaces," *J. Comput. Phys.*, Vol. 272, 686–703, 2014.
3. Helsing, J. and A. Karlsson, "Determination of normalized magnetic eigenfields in microwave cavities," *Computational Physics*, arXiv: 1410.0848v1, 2014.

Analysis of Multipactor Effect in Parallel-plate and Rectangular Waveguides

A. Berenguer[1], **A. Coves**[1], **E. Bronchalo**[1], **B. Gimeno**[2], **and V. E. Boria**[3]

[1]Departamento de Ingeniería de Comunicaciones. Universidad Miguel Hernández de Elche, Spain
[2]Departamento de Física Aplicada y Electromagnetismo, Instituto de Ciencia de Materiales Universidad de Valencia, Spain
[3]Departamento de Comunicaciones, Universidad Politécnica de Valencia, Spain

Abstract— The multipactor effect is an electron discharge that may appear in particle accelerators and microwave devices such as waveguides in satellite on-board equipment under vacuum conditions. This effect has been widely studied, and many investigations have been focused on the prediction of multipactor breakdown in a wide variety of microwave passive components for signals of different frequency and power levels, in order to prevent their damage. Many works [1, 2] take advantage of available susceptibility charts in empty parallel-plate waveguides obtained with analytical models [3], and they are directly used to predict multipactor breakdown in the component under study, which is going to happen in the point of highest field intensity. Thus, they are aimed to determine such highest field intensity region, which is generally the smallest device gap. However, such susceptibility diagrams do not take into account important effects such as the dependence of these diagrams on elastic and inelastic electrons, as well as the 3D character of the motion of the electrons inside the waveguide, or the non-uniform nature of the electromagnetic fields in some particular cases.

In the last years, the authors have developed a 1D model for studying the multipactor effect in partially dielectric-loaded rectangular waveguides [4–6].

In this work it is investigated, in the parallel-plate waveguide case, how the 1D, 2D or 3D motion of the electrons inside the waveguide can affect the generalized susceptibility diagrams, by means of a developed model capable of tracking the exact trajectory of multiple effective electrons which includes effects such as the spreading of the secondary electron departure kinetic energies or the dependence on elastic and inelastic electrons. On the other hand, a comparative study of the susceptibility charts in a parallel-plate and in its equivalent rectangular waveguide with the same height is performed, showing how the inhomogeneity of the electric field inside the waveguide modifies the multipactor region with respect to that predicted by the parallel-plate waveguide case.

The results of this study are going to be extended to a partially dielectric-loaded rectangular waveguide, which is a problem of great interest in the space industry that has not yet been rigorously investigated in the literature.

ACKNOWLEDGMENT

This work was supported by the Ministerio de Economía y Competitividad, Spanish Government, under the coordinated project TEC2013-47037-C5-4-R.

REFERENCES

1. Esteban, H., J. V. Morro, V. E. Boria, C. Bachiller, A. San Blas, and J. Gil, "Multipaction modelling of low-cost H-plane filters using an electromagnetic field analysis tool," *IEEE Antennas and Propagation Society International Symposium*, 2155–2158, San Antonio, TX, USA, Jun. 2004.
2. Quesada, F., V. E. Boria, B. Gimeno, D. Cañete, J. Pascual, A. Álvarez, J. Hueso, D. Schmitt, D. Raboso, C. Ernst, and I. Hidalgo, "Investigation of multipactor phenomena in inductively coupled passive waveguide components for space applications," *IEEE MTT-S Digest*, 246–249, San Francisco, CA, 2006.
3. Hatch, A. J. and H. B. Williams, "The secondary electron resonance mechanism of low-pressure high-frequency gas breakdown," *J. Appl. Phys.*, Vol. 25, No. 4, 417–423, Apr. 1954.
4. Torregrosa, G., A. Coves, C. P. Vicente, A. M. Pérez, B. Gimeno, and V. E. Boria, "Time evolution of an electron discharge in a parallel-plate dielectric-loaded waveguide," *IEEE Electron Device Lett.*, Vol. 27, No. 7, 629–631, Jul. 2006.

5. Coves, A., G. Torregrosa-Penalva, C. P. Vicente, A. M. Pérez, B. Gimeno, and V. E. Boria, "Multipactor discharges in parallel plate dielectric-loaded waveguides including space-charge effects," *IEEE Trans. Electron Devices*, Vol. 55, No. 9, 2505–2511, Sep. 2008.
6. Torregrosa-Penalva, G., A. Coves, B. Gimeno, I. Montero, C. P. Vicente, and V. E. Boria, "Multipactor susceptibility charts of a parallel-plate dielectric-loaded waveguide," *IEEE Trans. Electron Devices*, Vol. 57, No. 5, 1160–1166, May 2010.

Power Line Noise Measurements and Statistical Modelling in the Time Domain

A. M. Nyete, **T. J. O. Afullo**, **and I. E. Davidson**
Discipline of Electrical, Electronic and Computer Engineering
University of KwaZulu-Natal, Durban, South Africa

Abstract— The power grid provides a readily available medium for communication purposes. This means that the power grid is the cheapest communication medium since no new cabling is required. However, the power grid was design for the delivery of power and not for communication applications. As such no considerations have been made in the design of power networks to accommodate communication services. However, with the application of current digital signal processing techniques, the power network can be adapted to support communication services. This adaptation requires a full understanding of the power network characteristics, which are noise, distortion and channel effects. These power network characteristics are studied through measurements, modelling and characterization. The results obtained through such studies are then utilized in the redesign of conventional receiver structures and modulation schemes so as to adequately suit them for powerline communication applications. In this paper, we present time domain power line noise measurement results, and then apply a statistical technique for the characterization and modelling of the time domain noise amplitudes in typical indoor power networks. The results obtained are validated through error analysis. The models developed are vital in the optimization of communication applications through the power network.

Analytical Study of Large-scale Current Commutation Processes in Multiply-connected Transmission-line Networks

Dierk Bormann
ABB Corporate Research Väteräs, Sweden

Abstract— In a transmission line network which is multiply connected, like for instance a future DC cable grid, low-frequency or DC currents may temporarily circulate in large loops. Such loop currents can for instance be generated by the intentional disconnection of a current carrying link in the network, or by the unintentional occurrence of a ground fault. If the system has more than one grounding point, or in the case of a ground fault, part of the loop current path may pass through ground. The classical references on the impedance seen by such "ground return currents" are papers by Carson [1] and Pollaczek [2].

Commutation processes between globally different current paths in the system are then expected to be controlled by the effective resistances and inductances seen by corresponding loop currents, the loop inductances being substantially larger than typical differential-mode line inductances. The effects of these loop inductances cannot be accounted for by common system transients simulation programs which receive as input information about the topology of the network only (and not about its geometry).

In this talk, I will study the loop currents by analytical methods. Due to the skin effect in a conducting ground, the loop-current inductances are frequency dependent even at very low frequencies, which leads to surprisingly complex behavior of the current commutation processes. I will present an analytical solution of a slightly idealized model which however captures the essential features of the commutation process. The physical meaning of this solution will be discussed by comparing it with different approximations.

REFERENCES

1. Carson, J. R., "Wave propagation in overhead lines with ground return," *Bell System Technical Journal*, Vol. 5, 539–554, 1926.
2. Pollaczek, V. F., "Uber das Feld einer unendlich langen wechselstromdurchflossenen Einfachleitung," *Elektrische Nachrichtentechnik*, Vol. 9, No. 3, 339–360, Jul. 1926.

Estimation of Electromagnetic Parameters of Cable Steel

Y. Ivanenko and S. Nordebo
Department of Physics and Electrical Engineering, Linnæus University, Sweden

Abstract— Power losses related to the skin-effect, induced eddy currents and hysteresis losses, are all very important electromagnetic phenomena to consider in the design of high-voltage AC power cables [3]. Due to the complicated structure of these cables, which consist of a variety of material constituents and multiply twisted conductor bundles, it is a non-trivial task to accurately predict the effect of these loss mechanisms. Presently, it is for this purpose that analytical techniques [4] as well as numerical techniques based on Finite Element Modeling [1, 2] and the Method of Moments [5] are being developed.

In this presentation, we will address the problem of accurately estimating the conductivity as well as the magnetic hysteresis of the cable steel armour, as an important input parameter in the above mentioned modeling quest. In particular, we will address the problem of estimating the electromagnetic parameters of the armour with proper account taken to the dimensionality of the test object. A test transformer is built on a single straight wire of magnetic armour steel and wound with very thin copper wires. The transformer is modeled based on the conductivity of the steel and a linearization of the magnetic hysteresis by using a complex valued permeability. The parameters are then determined as an inverse problem based on measurement data and a localy convex optimization. Future work is aiming to validate the accuracy of the estimation based on a numerical simulation of the non-linear hysteresis phenomena.

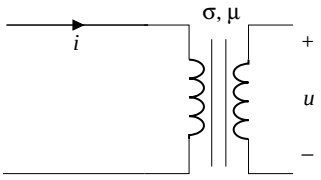

Figure 1: Test transformer based on the conductivity and the permeability of the steel.

REFERENCES

1. Gustavsen, B., A. Bruaset, J. J. Bremnes, and A. Hassel, "A finite-element approach for calculating electrical parameters of umbilical cables," *IEEE Trans. Power Del.*, Vol. 24, No. 4, 2375–2384, 2009.
2. Habib, S. and B. Kordi, "Calculation of multiconductor underground cables high-frequency per-unit-length parameters using electromagnetic modal analysi," *IEEE Trans. Power Del.*, Vol. 28, No. 1, 276–284, 2013.
3. Moutassem, W., "Configuration optimization of underground cables inside large magnetic steel casing for best ampacity," Ph.D. Thesis, Department of Electrical and Computer Engineering, University of Toronto, Toronto, Canada, 2010.
4. Nordebo, S., M. Gustafsson, G. Kristensson, B. Nilsson, A. Nosich, and D. Sjöberg, "On the natural modes of helical structures," *Classical Physics*, arXiv: 1502.00496, 2015.
5. Patel, U. R., B. Gustavsen, and P. Triverio, "An equivalent surface current approach for the computation of the series impedance of power cables with inclusion of skin and proximity effects," *IEEE Trans. Power Del.*, Vol. 28, No. 4, 2474–2482, 2013.

Periodic Green's Dyadics for Helical Current Distributions

S. Nordebo and Y. Ivanenko
Department of Physics and Electrical Engineering, Linnæus University, Sweden

Abstract— Power losses related to the skin-effect, induced eddy currents and hysteresis losses are all very important electromagnetic phenomena to consider in the design of high-voltage AC power cables [6]. Due to the complicated structure of these cables, which consist of a variety of material constituents and multiply twisted conductor bundles, it is a non-trivial task to accurately predict the effect of these loss mechanisms. Presently, it is for this purpose that analytical techniques [7] as well as numerical techniques based on Finite Element Modeling [2, 3] and the Method of Moments [8, 10] are being developed.

Helical waveguide structures have been treated previously such as, e.g., with helical sheaths [1, 4], and approximations for wire helices [5, 9]. However, to our knowledge there has not been any general presentation regarding the analytical modeling of the electromagnetic fields generated by a helical current distribution. The purpose of this presentation is to provide explicit formulas for the periodic electric and magnetic Green's dyadics [7], and to explain how they can be used to calculate the fields generated by an arbitrary helical current distribution. As an application example, the method is used in an approximate calculation of the induced currents in the metal sheaths and armour of a three-phase power cable.

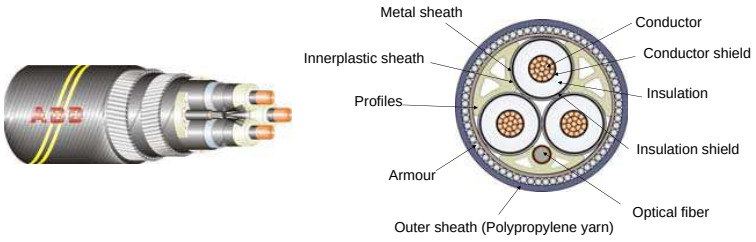

Figure 1: Geometry of a typical three-phase high-voltage AC cable.

REFERENCES

1. Collin, R. E., *Field Theory of Guided Waves*, 2nd Edition, IEEE Press, New York, 1991.
2. Gustavsen, B., A. Bruaset, J. J. Bremnes, and A. Hassel, "A finite-element approach for calculating electrical parameters of umbilical cables," *IEEE Trans. Power Del.*, Vol. 24, No. 4, 2375–2384, 2009.
3. Habib, S. and B. Kordi, "Calculation of multiconductor underground cables high-frequency per-unit-length parameters using electromagnetic modal analysis," *IEEE Trans. Power Del.*, Vol. 28, No. 1, 276–284, 2013.
4. Morgan, S. P. and J. A. Young, "Helix waveguide," *The Bell System Technical Journal*, 1347–1384, November 1956.
5. Moser, J. R. and R. F. Spencer, "Predicting the magnetic fields from a twisted-pair cable," *IEEE Transactions on Electromagnetic Compatibility*, Vol. 10, No. 3, 324–329, September 1968.
6. Moutassem, W., "Configuration optimization of underground cables inside large magnetic steel casing for best ampacity," Ph.D. Thesis, Department of Electrical and Computer Engineering, University of Toronto, Toronto, Canada, 2010.
7. Nordebo, S., M. Gustafsson, G. Kristensson, B. Nilsson, A. Nosich, and D. Sjöberg, "On the natural modes of helical structures," *Classical Physics*, arXiv: 1502.00496, 2015.
8. Patel, U. R., B. Gustavsen, and P. Triverio, "An equivalent surface current approach for the computation of the series impedance of power cables with inclusion of skin and proximity effects," *IEEE Trans. Power Del.*, Vol. 28, No. 4, 2474–2482, 2013.
9. Sensiper, S., "Electromagnetic wave propagation on helical structures," *Proceedings of the IRE*, 149–161, February 1955.
10. Zutter, D. D. and L. Knockaert, "Skin effect modeling based on a differential surface admittance operator," *IEEE Trans. Microwave Theory Tech.*, Vol. 53, No. 8, 2526–2538, 2005.

On Shape Reconstruction in Waveguide Like Structures

M. Norgren and M. Frid Dalarsson
KTH Royal Institute of Technology, Sweden

Abstract— The inverse problem of shape, or boundary, reconstruction has several applications. A potential application may be diagnosing the interior of electrotechnical components, like the winding structure inside a power transformer. For this kind of problem, we will discuss a couple of approaches based on waveguide modelling and theory. The first approach amounts to a full wave modelling of the winding structure, where the interspacing between the conductors is envisaged as a waveguide network. Using propagators and mode-matching, the scattering parameters can be determined and related to the locations of the individual winding conductors, which can be reconstructed by using optimization. This approach, we have verified in principle on generic parallel plate and cylinder geometries. However, a conclusion is that in realistic cases the modelling becomes exceedingly massive and the reconstruction procedure too slow, computationally. The second approach amounts to simplify the model, by in the first step to replace a sheet of winding conductors with an equivalent surface, modelled by a suitable boundary condition. The second step is motivated by that in a power transformer only small deformations of the windings are tolerable, since otherwise the transformer will fail. Hence, we focus on small deformations, which to some extent can be handled by linearizing the problem by means of perturbation theory. This amounts to replace the deformation with equivalent surface currents that radiate the scattered field into the unperturbed waveguide. We will present results for windings modelled as PEC surfaces, inside parallel plate, rectangular and coaxial waveguides, where the deformation varies along the direction of propagation. Our results so far are promising in that the linearized theory can be used for reconstructing unexpectedly large surface deformations, beyond what would be tolerable in a power transformer winding. Ongoing work on reconstructing surfaces deformed in two directions will also be discussed.

An Improved Form of Bessel Functions for Accurately Simulating Higher Order Modes in a Cylindrical Waveguide

M. C. Lin
Department of Electrical and Biomedical Engineering
Hanyang University, Seoul 133-791, Korea

Abstract— A cylindrical waveguide is widely used in electromagnetic (EM) applications for EM wave energy transportation or coupling inside or between systems. To study the wave transport in a cylindrical waveguide, the analytic waveguide theory based on Maxwell's equations is employed in those cases retaining homogeneity and cylindrical symmetry and Bessel functions are obtained for characterizing the guiding modes excited. In general, we use a numerical method such as finite element analysis or finite-difference method to study those non-homogeneous or non-symmetric waveguide systems. We could study a waveguide system either in the frequency domain or in the time domain. The former is good for characterizing stationary behavior and the latter is better for studying transient or time dependent phenomena. For higher order mode excitation in a cylindrical waveguide, a higher order Bessel function is required and numerically an expansion of this function in terms of a series is mostly used. However, the accuracy of mode pattern excited is getting worse when one pushes it to higher and higher order mode with a limited number of expansion series. This inaccuracy usually introduces unwanted or unphysical spurious modes and causes numerical errors in the simulation results. In order to excite a clean higher order mode, we have developed a delicate wave launcher using an improved form of Bessel functions. Since the excitation is located either in the ends (ports) or a cross section somewhere along the waveguide, for a TE or TM mode, the longitudinal magnetic or electric field component respectively is used only for the wave launching source according to the waveguide theory, i.e., all six components of electric and magnetic fields are not independent and all the transverse components can be expressed in terms of the two longitudinal components. This technique has been demonstrated successfully in our finite difference time domain simulations. An introduction of this approach and detailed results will be presented.

ACKNOWLEDGMENT

This work was supported by the U.S. Department of Energy under Grant No. DE-SC0004436, the research fund of Hanyang University (HY-201400000002393), and the Humboldt Research Fellowship for Experienced Researchers awarded by Alexander von Humboldt Foundation.

REFERENCES

1. Lin, M. C., D. N. Smithe, E. Choi, K. R. Chu, W. C. Guss, and R. J. Temkin, *Proc. 15th Int. IEEE Vac. Electron. Conf. (IVEC)*, 423–424, 2014.
2. Sawant, A., S. G. Kim, M. C. Lin, J. H. Kim, Y. Hong, J. So, and E. Choi, *IEEE Trans. Plasma Sci.*, Vol. 42, No. 12, 3989–3995, 2014.

The Novel Mixed Spectral Element Method for Waveguide Problems

Na Liu[1] and Qing Huo Liu[2]

[1]Institute of Electromagnetics and Acoustics, Xiamen University, China
[2]Department of Electrical and Computer Engineering, Duke University, USA

Abstract— The increasing complexity of microwave and optical waveguide structures requires highly accurate and efficient simulation methods to calculate waveguide modes and to optimize geometrical and material parameters for waveguide engineering, and so far the most successful one is the finite element method (FEM). By discretizing the waveguide cross section into a number of triangular or quadrilateral elements and applying the variational formulations, the FEM can be used to perform eigenmode analysis of waveguiding structures for their mode dispersion curves and cut-off frequencies. It has been proved by previous researchers that by using the tangential-vector finite element method (TVFEM), the propagation modes in a waveguide can be obtained without the occurrence of nonzero spurious solutions. However, there are still spurious modes confined to the subspace of zero eigenvalues. These spurious modes make it difficult to determine which modes are physical. Furthermore, at a given frequency, these spurious modes will slow down the convergence of desirable modes and cause additional computational complications. In order to suppress the spurious modes with zero eigenvalue, the divergence free condition (i.e., Gauss' law) must be enforced.

In this paper, a novel high-order mixed spectral element method is proposed for the analysis of anisotropic, lossy, and open waveguides. The new variational formulation incorporating Gauss' law into the vectorial wave equation is completely free of spurious modes. It utilizes the edge-based curl-conforming Gauss-Lobatto-Legendre (GLL) polynomials to approximate the tangential vector of the electric field and the nodal-based scalar GLL basis functions to discretize its longitudinal component to obtain the highly accurate simulations. By employing the mass-lumping technique only a smaller generalized eigenvalue problem needs to be solved. The new contributions of this work includes: (a) For the first time the mixed SEM is made free of all spurious modes in a waveguide problem, and the smaller eigenvalue equation speeds up the computation. (b) Both lossy and anisotropic media are made possible in the mixed SEM for a waveguide problem. (c) The perfectly matched layer (PML) has been demonstrated in the mixed SEM for open waveguides. Furthermore, several numerical examples are given to verify that the higher-order spectral element method is free of any spurious eigenmodes and has spectral accuracy with the propagation constant.

Session 2P10a
Wireless Power Transmission and Harvesting

A High Efficiency WPT System Using Helix Antennas

B. Dubovski and M. Haridim
HIT — Holon Institute Technology, Israel

Abstract— The field of wireless power transmission (WPT) has been growing rapidly in the last few years. WPT allows to remove the need for a wired connection in both short range and long range applications, ranging from laymen, which use it to charge their personal devices or medical devices, to large companies, which take advantage of the technology where they cannot use wired connectivity, furthermore, the use of WPT can help the environment, each year more than 15,000,000,000 non-rechargeable batteries are being thrown away, by using WPT we can reduce these numbers substantially. The gain of the transmitting and receiving antennas is a key measure for achieving a high overall RF-to-DC conversion efficiency.

In this paper, we present a high efficiency WPT system operating at 400 MHz for small to moderate distances. The proposed system is based on incorporating helix antennas in the transmitter and receiver. Use of helix antennas allows to achieve high directivity and high efficiency with a fairly compact antenna size. Various configurations were considered and analyzed with emphasis on compact transmitting and receiving modules. As shown in this paper, the proposed helix antenna can be easily manipulated to obtain small size with good radiation performance. It is shown that the proposed helix antennas operating at 400 MHz, with relatively small dimensions (length of 3.5 cm, and diameter 25 cm) can provide a high gain exceeding 5 dB, with low VSWR. Experimented results are in good agreement with those obtained by numerical electromagnetic simulations using the HFSS tools.

Wireless Transmission of Electromagnetic Energy Based on a Time Reversal Approach for Indoor Applications

R. Ibrahim[1, 2], **B. Allard**[1], **A. Breard**[1], **J. Huillery**[1], **C. Vollaire**[1], **D. Voyer**[1], **and Y. Zaatar**[2]

[1]Université de Lyon, Ampere (CNRS UMR 5005, École Centrale de Lyon, INSA-Lyon, UCBL)
Écully Cedex F-69134, France
[2]LPA, Lebanese University Faculty of Sciences 2, Campus Fanar, Jdeidet BP 90656, Lebanon

Abstract— An original approach based on a time reversal technique is proposed in order to realize a wireless transmission of electromagnetic energy for indoor applications. Experiments made in a low-Q cavity of human size with a frequency carrier of 2.45 GHz show that the energy efficiency is greater than for a wireless transmission based on a continuous wave.

Introduction: Most of the recent developments in wireless transmission of electromagnetic energy are concentrated on systems designed to harvest the exceed of electromagnetic energy lost by common wireless systems such as Wi-Fi network. However, the intermittent and unpredictable nature of these ambient sources makes energy harvesting critical for some applications [1]. In scenarii where the energy is transmitted intentionally, systems using continuous waves are not necessary the most efficient. We investigated an alternative approach based on time reversal that is found to be promising for indoor applications. Time reversal with electromagnetic waves was first proved to be feasable in [2]. The implementation needs two stages. In a first step called *learning stage*, a low energy pulse is transmitted through an antenna; at another place in the room, the received antenna records a signal constituted by a succession of many delayed pulses, less or more attenuated, and related to the reflections in the medium. In a second step called *time reversal stage*, a high energy signal built from the time reversal of the recorded signal is transmitted through one of the antennas; it follows that the time reversed waves focus spatially and temporally on the received antenna. These properties are particularly attractive for an energy recovery; moreover, the energy efficiency increases when the medium becomes more and more complex which makes this approach espescially suitable for indoor applications.

Experimental Setup and Results: Two antennas are placed inside a low-Q cavity of human size with two obstacles positionned between them in order to avoid the direct path. In the learning stage, a nanosecond pulse of 2.45 GHz frequency carrier and 5 V amplitude is transmitted; in reception, a complex microsecond signal with a maximum amplitude of 50 mV is recorded using a numerical oscilloscope. The time reversal as well as some filtering operations are made in a Matlab code. Then the reversed signal is transmitted using a wave form generator with a sample frequency of 12 GHz and an amplifier such that the maximum amplitude for the time reversed signal is 5 V ; in reception, one recovers a nanosecond pulse with an amplitude about 10 times a many as during the learning stage. Moreover, the energy efficiency in the reversal stage is about 30 times as many as the efficiency for a transmission of a continuous wave around 2.45 GHz. Note that in this later case, there is a sensivity with respect to the carrier frequency because of the cavity modes; on the contrary, the time reversal technique takes advantage of the complexity of the cavity.

REFERENCES

1. Krikidis, I., S. Timotheou, S. Nikolaou, G. Zheng, D. Derrick Wing Kwan Ng, and R. Schober, "Simultaneous wireless information and power transfer in modern communication systems," *IEEE Communications Magazine, Green Communications and Computing Networks Series*, Vol. 52, No. 11, 104–110, 2014.
2. Lerosey, G., J. De Rosny, A. Tourin, A. Derode, G. Montaldo, and M. Fink, "Time reversal of electromagnetic waves," *Physical Review Letters*, Vol. 92, No. 19, 193904, 2004.

High Efficiency RF Energy Harvesting from Electromagnetic Waves of Digital Terrestrial Television

Jiro Ida, Masanari Mabuchi, Yuta Kunori, Hiroshi Miyagoshi, Keisuke Noguchi, and Kenji Itoh
Division of Electrical Engineering, Kanazawa Institute of Technology
7-1 Ohgigaoka, Nonoichi, Ishikawa 921-8501, Japan

Abstract— Our target of the RF energy harvesting is harvesting from the electromagnetic wave of the Digital Terrestrial Television (DTTV) which frequency is around 470–770 MHz. It is because its covered area and its expected power will become large, compared with others, e.g., the Wi-Fi and the cellular phone. Although the DTTV was chosen, the expected received power is around and below the micro Watts range when the covered area is intended to be enlarged. Therefore, the most important issue of the RF energy harvester is the high efficiency of the rectification on the ultralow input power level.

For this issue, we have proposed the rectenna which is composed of the high impedance antenna and the optimized gate controlled diode (Fig. 1). Although based on the simulations, we have confirmed the efficiency around 40% at the input power level of −15 dBm, and around 10% at −30 dBm, which is the best ever reported value [1].

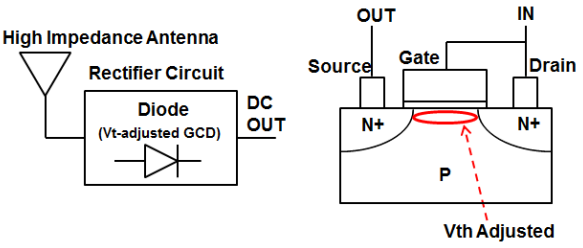

Figure 1: Our concept of the high efficiency RF energy harvesting and the structure of the gate controlled diode.

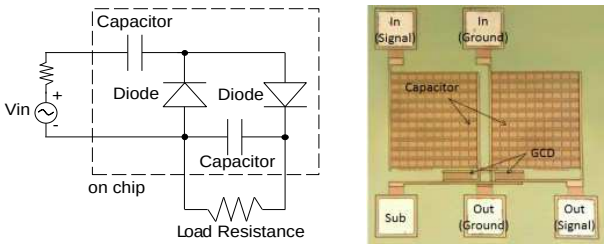

Figure 2: Rectifier circuit and its photograph on the chip.

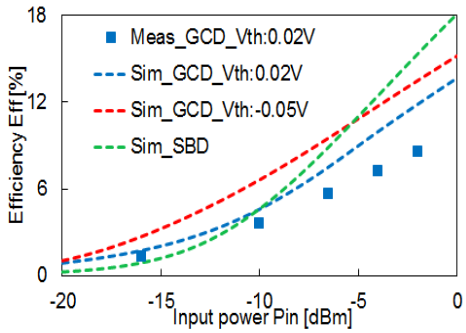

Figure 3: Measured and simulated efficiency of the rectifier on 500 MHz.

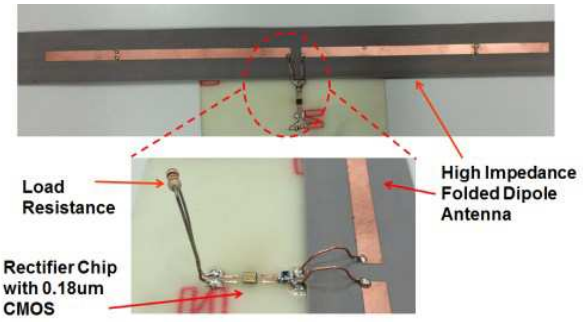

Figure 4: Fabricated rectenna with the high impedance antenna and GCD.

We introduce the status of our study, here. First, we show the results of evaluation on the gate controlled diodes (GCD) and the rectifier circuits fabricated with 0.18 µm CMOS (Fig. 2). It was confirmed that the efficiency of the rectifier with the GCD which has the optimum transistor threshold voltage (V_{th}) overcomes the rectifier using the best Schottky barrier diode for the small signal applications (Fig. 3) [2]. We have already developed the folded dipole antenna with the high impedance of 2 K ohm [3], which is also summarized here. Next, we show the methodology of the optimization with the combination of the high impedance antenna and the optimized GCD for the high efficiency rectification on the ultralow input power level. We have founded out that

the optimum V_{th} shits to the slightly high value and the optimum gate width shifts to the small value with increase of the antenna impedance.

Finally, we will show the fabrication result of the rectenna with the high impedance antenna and the optimized GCD (Fig. 4).

REFERENCES

1. Mabuchi, M., J. Ida, K. Noguchi, and K. Itoh, "Optimization of rectenna with gate controlled diode for high efficiency RF energy harvesting," Submitted to *IEEE NEWCAS*, 2015.
2. Umesao, R., J. Ida, M. Mabuchi, T. Kunori, S. Tashino, T. Mori, H. Miyakoshi, K. Noguchi, and K. Itoh, "High efficiency RF energy harvesting with threshold-voltage-adjusted gate control diode," *IEEE FTFC*, Session 4–5, 1–4, 2014.
3. Miyagoshi, H., K. Noguchi, K. Itoh, and J. Ida, "A high-impedance and wideband folded dipole antenna for energy harvesting applications," *Int'l Symp. on Antennas and Propagation, ISAP*, Session FR4B-01, 2014.

Use Case Analysis of Wiegand-based Energy Harvester in Mechanical Sensing Devices

Ralf Zentgraf and Ulrich Bochtler
Lab for Circuit Design, Aschaffenburg UAS, Germany

Abstract—

Summary: Conventional energy harvester approaches using magnetic-inductive technologies are often realized as mass-spring systems. Due to the small resonance-bandwidth of such systems, bistable magnetic wires can be a sound solution for slow and sporadic movements. On this issue, a pressure sensor system is adapted with a so-called Wiegand-harvester to implement self-sufficient electrical feature functionalities.

The Wiegand-harvester consists of an inductor coil mounted on an amorphous Vicalloy-Core (CoFeV). The large characteristic Barkhausen jump of the alloy is used to generate voltage peaks in the pickup coil in a slow changing magnetic field. Contrary to mass-spring systems or periodical induction, only the value of the coercivity field (ΔH_{ce}) is relevant for generating an energetic voltage pulse to power an electrical circuit.

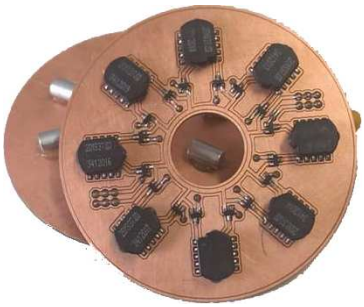

Figure 1: Magnetic harvesting PCB.

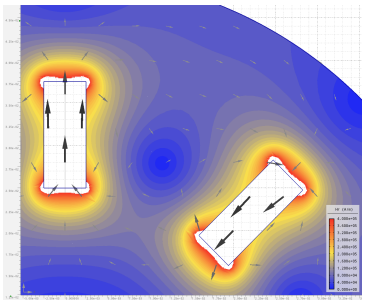

Figure 2: FEM simulation of the neodymium magnets.

This technology can be used in high transient as well as in nearly static environments. A use case analysis for a pressure gauge shows the benefit of Wiegand-based Systems. The powermodule is realized by placing eight harvesters circular on a PCB. Thereby a single rotation of a spindle (360°) is quantized in eight steps. A second disk equipped with eight neodymium permanent magnets is mounted parallel to the PCB. So a twist of 45° delivers a multiplied pulse each of the eight inductor coils [Fig. 1]. A electrical energy output of approx. 13.5 µWs and the twist-hysteresis of $0°2'$ could be achieved and verified using a magnetic FEM simulation [Fig. 2].

Optimal Operating Frequency for Wirelessly Powered Implanted Systems

V. Talla[1], **B. H. Waters**[1], **and J. R. Smith**[1, 2]

[1]Department of Electrical Engineering, University of Washington, USA
[2]Department of Computer Science Engineering, University of Washington, USA

Abstract— Wireless power transfer (WPT) using magnetically coupled resonators is a popular technique to charge/recharge and operate a range of devices such as electric vehicles, consumer electronics and implanted biomedical devices. As a result, numerous WPT systems and multiple standards such as Rezence by A4WP and Qi by WPC operate at different frequency bands (200 KHz, 6.76 MHz, 13.56 MHz to name a few) have been developed in recent years [2–4]. However, there isn't a clear choice of an optimal operating frequency since the system design and behavior is dependent on a variety of factors such as application scenario, size limitations, operating distance and desired power level. In this work, we will focus on choosing an optimal operating frequency for wirelessly powered implanted biomedical devices, while taking account these various system requirements.

One of the key challenges associated with developing WPT systems is to comply with existing regulatory and safety standards. We will focus on two specific applications, which cover the two extremes of the power spectrum of implanted devices. Firstly, we will discuss WPT for left ventricular assist device (LVAD) which require about 10 Ws of power and has a receiver size restrictions of about 10 cm in diameter [1]. Secondly, we will design a WPT for an implanted neural recording device which requires about 100 mWs and the receiver is restricted to 2 cm in diameter and 2 mm in thickness. We will ascertain the optimal operating frequencies for the two applications under the above-mentioned constraints and design the system to satisfy the safety and legal standards and regulations set worth by the Federal Communication Commission (FCC).

The primary goal of a WPT system is to deliver the desired power to the load at maximum efficiency and operating range [6]. An additional, but equally important requirement is to stay within the electromagnetic exposure limits. The electromagnetic exposure limits are set out to ensure that adverse effects associated with electro-stimulation (at lower frequencies 3 KHz–5 MHz) and tissue heating (at higher frequencies 100 KHz–300 GHz) is minimized. As a result there are basic restrictions (BRs) and maximum permission exposure (MPEs) limits, which place an upper bound on, induced fields, induced currents, temperature rise and specific absorption rate (SAR).

Recent work has investigated the choice of optimal frequency for consumer electronic charging applications [8]. Although it assesses RF exposure, it does account for the effect of human hand/body in proximity with the charging system. Herein, we will focus on implanted biomedical systems wherein the receiver will be encapsulated in the biomedical tissue and is of greater risk of electro-stimulation and tissue heating. For our analysis and design of the system, we will undertake the following approach:

- Since the Q-factor of the coils, the power dissipated (i.e., heating) and the WPT effifficiency are all dependent on operating frequency for a given coil size, we will optimize the MCRs for the two applications for different operating frequency bands [7].
- Given this design, we will evaluate the impact of the tissue and biological medium encapsulating the receiver on the efficiency and field distribution for the WPT system [5]. If required, the system will be redesigned to improve efficiency and power delivery.
- Next, we will evaluate and quantify the induced field strengths, induced current and SAR values for different operating frequencies.

Based on the analysis of the systems optimized for different frequency bands, we will ascertain the optimal operating frequency for various wirelessly powered implanted medical devices applications.

REFERENCES

1. Waters, B. H., A. P. Sample, P. Bonde, and J. R. Smith, "Powering a ventricular assist device (VAD) with the free-range resonant electrical energy delivery (FREE-D) system," *Proceedings of the IEEE*, Vol. 100, No. 1, 138–149, Jan. 2012.

2. Sample, A. P., D. Meyer, and J. R. Smith, "Analysis, experimental results, and range adaptation of magnetically coupled resonators for wireless power transfer," *IEEE Transactions on Industrial Electronics*, Vol. 58, No. 2, 544–554, Feb. 2011.
3. Van Wageningen, D. and T. Staring, "The Qi wireless power standard," *14th International Power Electronics and Motion Control Conference (EPE/PEMC)*, 2010.
4. Lu, X., D. Niyato, P. Wang, D. I. Kim, and Z. Han, "Wireless charger networking for mobile devices: Fundamentals, standards, and applications," arXiv preprint arXiv:1410.8635, 2014.
5. Talla, V., B. H. Waters, and J. R. Smith, "A study of detuning effects and losses in implantable coils for biomedical wireless power transfer," Session 4A4 SC4: Wireless Energy Transmission and Harvesting, Chicago, 2013.
6. Talla, V. and J. R. Smith, "An experimental technique for design of practical wireless power transfer systems," *IEEE International Symposium on Circuits and Systems (ISCAS)*, 2041–2044, Chicago, 2014.
7. Waters, B. H., B. J. Mahoney, G. Lee, and J. R. Smith, "Optimal coil size ratios for wireless power transfer applications," *IEEE International Symposium on Circuits and Systems (ISCAS)*, 2045–2048, 2014.
8. Nadakuduti, J., L. Lu, and P. Guckian, "Operating frequency selection for loosely coupled wireless power transfer systems with respect to RF emissions and RF exposure requirements," *IEEE Wireless Power Transfer (WPT)*, 234–237, 2013.

Wireless Power Transmission by Enlarging the Near Field Calculation of the Transition from Far to Near Field

Konstantin Meyl
Faculty of Computer and Electrical Engineering, Furtwangen University
1.TZS, Erikaweg 32, D-78048 Villingen-Schwenningen, Germany

Abstract— Continuing the contribution about "wireless power transmission by scalar waves", presented in Moscow 2012, this paper goes deeper, explaining the different types and properties of waves described by the wave equation.

Starting with the wave description of Maxwell an extended version of the Laplace equation is derived, expanding the standard derivations of the near field, showing how to influence the zone, where the longitudinal wave parts occur.

We come to the conclusion that the near field zone is enlarging, if the longitudinal parts of a wave or the antenna voltage are accelerated. This relationship is essential for the wireless transmission of energy. In addition this exciting new result could be tested experimentally.

The simple experiment will be demonstrated at PIERS 2013 in Stockholm. Only by changing the antenna design, it will be shown how both, the speed of propagation and the near field are enlarging proportional to each other.

In all practical applications as discussed in PIERS Proceedings 2012 (pp.664–668), the extended near field is the key of success.

Session 2P10b
SC4: Electromagnetic Energy

Causal Natural Modes, Retro-causal Natural Modes and Minimum Radiation Modes

Guy A. E. Vandenbosch[1], **Xuezhi Zheng**[1], **and Victor V. Moshchalkov**[2]

[1]Department of Electrical Engineering (ESAT-TELEMIC), KU Leuven, Belgium
[2]Institute for Nanoscale Physics and Chemistry (INPAC), KU Leuven, Belgium

Abstract— In this talk, we discuss three kinds of modes that are crucial to the understanding of a time domain electromagnetic (EM) response. The first targeted mode is called "causal" natural mode. This mode and its corresponding "causal" natural frequency are widely used in the analysis of the transient response of a radiating structure, for example, in the Singularity Expansion Method [1]. They are solutions to the non-standard eigenvalue problem of, e.g., for a microwave antenna, a surface integral equation. In this case, the integral equation only involves the retarded scalar and vector potentials and as a result the electric field at a given time instant t is solely due to an oscillating current in the past. Moreover, since the EM field equations are invariant under time-reversal symmetry, we can reverse the time axis and construct a retro-causal problem for the conventional integral equation. Then, similar to the "causal" natural mode, retro-causal natural modes can be defined when the integral equation is set free of driving force. Last but not the least, we can combine the causal and retro-causal cases to build a new "radiation field" operator. It will be proven that this operator is closely related to the concept of radiated energy [2, 3], and its modes may be defined as "minimum radiation" modes, i.e., where radiated energy and absorbed energy perfectly cancel each other.

REFERENCES

1. Baum, C. E., "The singularity expansion method," *Transient Electromagnetic Fields*," 129–179, Springer, Berlin, Heidelberg, 1976.
2. Vandenbosch, G. A. E., "Radiators in time domain, part I: Electric, magnetic, and radiated energies," *IEEE Trans. Antennas and Propagat.*, Vol. 61, 3995–4003, Aug. 2013.
3. Vandenbosch, G. A. E., "Radiators in time domain, part II: Finite pulses, sinusoidal regime, and Q factor," *IEEE Trans. Antennas and Propagat.*, Vol. 61, 4004–4012, Aug. 2013.

Stored Electromagnetic Energy in Bi-isotropic Media

Casimir Ehrenborg and Mats Gustafsson
Department Electrical and Information Technology, Lund University, Box 118, Lund SE-221 00, Sweden

Abstract— Characterizing stored electromagnetic energy is essential in antenna Q calculation [1]. Understanding stored electromagnetic energy as a physical quantity is thus instrumental in characterizing antenna limitations. There exists several expressions for stored electromagnetic energy. In general these expressions give physical results in loss less isotropic media. However, in more complex background materials, such as dispersive or lossy media, these expressions break down, predicting negative energies [2].

This contribution investigates the results of existing stored energy expressions when applied to bi-isotropic media. This is done by implementing the bi-isotropic greens function [3] in the electrical field integral equation in a method of moments code. Stored energy in different types of small antennas will be examined and compared to the stored energy in their equivalent circuit models. The circuit models are generated by Brune synthesis.

ACKNOWLEDGMENT

The support of the Swedish foundation for strategic research is gratefully acknowledged.

REFERENCES

1. Gustafsson, M. and B. L. G. Jonsson, "Stored electromagnetic energy and antenna Q," Technical Report LUTEDX/(TEAT-7222)/1-25/(2012), Department of Electrical and Information Technology, Lund University, P. O. Box 118, Lund S-221 00, Sweden, 2012, http://www.eit.lth.se.
2. Gustafsson, M., D. Tayli, and M. Cismasu, "Q factors for antennas in dispersive media," Technical Report LUTEDX/(TEAT-7232)/1-24/(2014), Department of Electrical and Information Technology, Lund University, P. O. Box 118, Lund S-221 00, Sweden, 2014, http://www.eit.lth.se.
3. Lindell, I. V., A. H. Sihvola, S. A. Tretyakov, and A. J. Viitanen. *Electromagnetic Waves in Chiral and Bi-isotropic Media,* Artech House, Boston, London, 1994.

On the Properties of Stored Electromagnetic Energy

Miloslav Capek and Lukas Jelinek
Department of Electromagnetic Field, Czech Technical University in Prague, Prague, Czech Republic

Abstract— A consistent definition of stored electromagnetic energy for non-stationary fields is one of the last fundamental and still unsolved problems of classical electrodynamics. One of the key issues is the potentially infinite total energy within a time-harmonic steady state [1]. There is an ill-defined separation of the total energy into radiated energy and stored energy, where it is assumed that the bearer of the infinity is the radiation [2].

The radiation energy is commonly subtracted separately in the region exterior and interior to the radiator, the boundary being defined by the smallest circumscribing sphere. Many methods are known for determining the radiated (stored) energy outside the circumscribing sphere. All these methods yield qualitatively similar results, although quantitative differences can be found. The situation is more severe in the interior region, since only a few methods are able to take effectively into account the actual shape of the radiator [3, 4]. The differences between the predictions of these methods are moreover qualitative [5].

Besides subtraction of the radiated energy, there are also other techniques for estimating the stored energy, the vast majority of which are inspired by circuit theory [6–8]. However, no matter what concept is used, several fundamental principles should always be kept in mind: e.g., the energy must be positively semi-definite, must be coordinate-independent, must be gauge invariant, and it should be possible to define it locally. Clearly, all the concepts of the stored energy for a dynamic field must also be coherent with those for a static field.

In our talk, we will review all the available concepts that have attempted to determine stored energy. It will be pointed out that all these concepts fail in at least one of the "must have" properties mentioned above. Finally, it will be concluded that no fully consistent definition of stored electromagnetic energy is yet known. This of course raises the question whether the very idea of stored (and radiated) energy is well-posed [9].

ACKNOWLEDGMENT

This work was supported by the Czech Science Foundation under project 15-10280Y.

REFERENCES

1. Jackson, J. D., *Classical Electrodynamics,* John Wiley, 1998.
2. Collin, R. E. and S. Rothschild, "Evaluation of antenna Q," *IEEE Trans. Antennas Propag.*, Vol. 12, No. 1, 23–27, Jan. 1964.
3. Vandenbosch, G. A. E., "Reactive energies, impedance, and Q factor of radiating structures," *IEEE Trans. Antennas Propag.*, Vol. 58, No. 4, 1112–1127, Apr. 2010.
4. Gustafsson, M. and L. Jonsson, "Stored electromagnetic energy and antenna Q," *Progress In Electromagnetics Research*, Vol. 150, 13–27, 2015.
5. Capek, M. and L. Jelinek, "Various interpretations of the stored and the radiated energy density," *IEEE Trans. Antennas Propag.*, arXiv: 1503.06752, submitted.
6. Grimes, C. A., G. Liu, F. Tefiku, and D. M. Grimes, "Time-domain measurement of antenna Q," *Microwave and Optical Technology Letters*, Vol. 25, No. 2, 95–100, Apr. 2000.
7. Yaghjian, A. D. and S. R. Best, "Impedance, bandwidth and Q of antennas," *IEEE Trans. Antennas Propag.*, Vol. 53, No. 4, 1298–1324, Apr. 2005.
8. Capek, M., L. Jelinek, P. Hazdra, and J. Eichler, "The measurable Q factor and observable energies of radiating structures," *IEEE Trans. Antennas Propag.*, Vol. 62, No. 1, 311–318, Jan. 2014.
9. Mikki, S. M. and Y. Antar, "A theory of antenna electromagnetic near field— Part I," *IEEE Trans. Antennas Propag.*, Vol. 59, No. 12, 4691–4705, Dec. 2011.

A Surface Integral Expression for the Electromagnetic Energy in a Microwave Cavity

J. Helsing[1] and A. Karlsson[2]

[1]Centre for Mathematical Sciences, Lund University, Box 118, Lund 221 00, Sweden
[2]Electrical and Information Technology, Lund University, Box 118, Lund 221 00, Sweden

Abstract— Today, all high energy particle accelerators use microwave cavities for particle acceleration by means of eigenfields, excited by external sources. In the design process of such cavities it is important to evaluate these eigenfields and the corresponding resonance frequencies. Numerical accuracy is crucial since even small errors in the evaluations may cause a deterioration of the performance of the accelerator. It is convenient, and sometimes necessary, to use normalized electric eigenfields $\mathbf{E}_n(\mathbf{r})$ such that

$$\int_V |\mathbf{E}_n(\mathbf{r})|^2 \, \mathrm{d}V = 1 \tag{1}$$

In [1] we developed a high-order convergent Fourier-Nyström scheme for the magnetic field integral equation (MFIE) that can determine the eigenfields and their resonance frequencies with very high accuracy. Since MFIE is a surface integral equation it is very costly to evaluate the volume integral in (1). For this reason we derived a surface integral expression for the normalization integral that is less expensive to evaluate. The integral is expressed in terms of the magnetic vector potential and the scalar electric potential. In this contribution we present an efficient numerical method for the numerical evaluation of the expression for some different types of cavities. We also apply the surface integral expression to the exterior problems of radiation from antennas and scattering of waves from perfectly conducting objects and give an interpretation of the energy it then corresponds to.

ACKNOWLEDGMENT

This work was supported by the Swedish Research Council under contract 621-2011-5516.

REFERENCES

1. Helsing, J. and A. Karlsson, "Determination of normalized magnetic eigenfields in microwave cavities," *IEEE Trans. Microwave Theory Tech.*, 2015 (in press).

Estimating Antenna Q-factor from the MoM Impedance Matrix

Doruk Tayli and Mats Gustafsson
Department of Electrical and Information Technology, Lund University, Lund, Sweden

Abstract— The antenna Q-factor is a useful figure of merit that estimates the antennas bandwidth [1, 2]. One difficult part of determining the antenna Q-factor is to calculate the stored energy of an antenna. A method that can be applied to any small antenna is presented in [3–6]. Where the Q-factor is computed using an in-house solver based on a custom method of moments (MoM) implementation. As this requires writing custom code, it is practical to take advantage of the widely available commercial electromagnetic software that have already implemented the MoM and have additional variety of post-processing capabilities.

In this paper the antenna Q-factor is computed from the numerical frequency derivative of the MoM impedance matrix. The impedance matrix is obtained from the commercial software FEKO [7]. Different Q-factor formulations are presented and used to estimate the Q-factor of antennas. These are then compared with the Q-factor calculated from the derivative of the input impedance [8], and the stored energies.

REFERENCES

1. Harrington, R. F., *Field Computation by Moment Methods,* Macmillan, New York, 1968.
2. Volakis, J., C. C. Chen, and K. Fujimoto, *Small Antennas: Miniaturization Techniques & Applications,* McGraw-Hill, New York, 2010.
3. Gustafsson, M., C. Sohl, and G. Kristensson, "Physical limitations on antennas of arbitrary shape," *Proc. R. Soc. A*, Vol. 463, 2589–2607, 2007.
4. Gustafsson, M. and S. Nordebo, "Optimal antenna currents for Q, superdirectivity, and radiation patterns using convex optimization," *IEEE Trans. Antennas Propagat.*, Vol. 61, No. 3, 1109–1118, 2013.
5. Gustafsson, M. and B. Jonsson, "Antenna Q and stored energy expressed in the fields, currents, and input impedance," *IEEE Trans. Antennas Propagat.*, Vol. 63, No. 1, 240–249, Jan. 2015.
6. Vandenbosch, G. A. E., "Reactive energies, impedance, and Q factor of radiating structures," *IEEE Trans. Antennas Propagat.*, Vol. 58, No. 4, 1112–1127, 2010.
7. Altair, S. A., "FEKO, field computations involving bodies of arbitrary shape, Suite 7.0," Development S. A. (Pty) Ltd., Stellenbosch, 2014, https://www.feko.info/, Retrieved: Nov. 24, 2014.
8. Yaghjian, A. D. and S. R. Best, "Impedance, bandwidth, and Q of antennas," *IEEE Trans. Antennas Propagat.*, Vol. 53, No. 4, 1298–1324, 2005.

Session 2P11
FocusSession.SC1: Casimir Effect and Heat Transfer 4

Three-body Momentum and Energy Transfer out of Thermal Equilibrium

Riccardo Messina and Mauro Antezza
Laboratoire Charles Coulomb (L2C), UMR 5221 CNRS and Université Montpellier 2, Montpellier, France

Abstract— A striking consequence of quantum electrodynamics is the existence of an electromagnetic force between any couple of neutral polarizable bodies even in the vacuum state of the electromagnetic field. This effect, known as Casimir effect, was first theoretically predicted in 1948. In 2005 it was shown that the absence of thermal equilibrium deeply modifies this effect, producing quantitative and qualitative differences, such as the appearance of new asymptotic behaviors and the possibility of a repulsive force. The out-of-equilibrium scenario brings to the attention a different closely related effect, the radiative heat transfer.

My talk addresses the combination of the absence of thermal equilibrium with three-body interactions. To this aim I discuss a recently developed general theory describing Casimir force and radiative heat transfer in a system consisting of three arbitrary bodies held at three independent temperatures and immersed in a thermal environment. As an application, I consider the force acting on an atom inside a planar cavity. I show that, differently from the equilibrium configuration, the absence of thermal equilibrium admits one or more positions of minima for the atomic potential, paving the way to a possible trapping scheme for Rydberg atoms.

REFERENCES

1. Messina, R. and M. Antezza, *Phys. Rev. A*, Vol. 89, 052104, 2014.

Near Field Heat Transfer Mediated by External Magnetic Fields

R. Esquivel-Sirvent
Instituto de Fisica, UNAM, Mexico D.F., Mexico

Abstract— We consider two bodies described by a local dielectric function at different temperatures. Tuning of the near field heat transfer (NFHT) at the nanoscale can be achieved by changing the dielectric function. However this means either changing the material or changing the concentration of carriers in the case of semiconductors. Another possibility is using composite materials that combined different materials with specific dielectric function, for example nested nanoparticles.

In this work we given the materials the heat transfer can be modulated by applying external magnetic fields. As a case study we consider the NFHT between a SiO_2 substrate and a plate of a III-V semiconductor such as InSb. When an external magnetic field is applied, the excitation of magneto plasmons introduces an optical anisotropy that will change the reflection coefficients of the InSb plate. This will change the radiative heat flux, depending on the magnitude and direction of the external magnetic field. From a practical point of view, using graphene to control the heat transfer is a better choice since low magnetic fields are needed.

Combining composites and external magnetic fields will provide for more flexibility on the tuning of the heat transfer. The case of a SIO_2 substrate and a superlattice with metal-semiconductor unit cells will also be discussed.

ACKNOWLEDGMENT

Support from DGAPA-UNAM IN111214.

Mesoscopic Transport of Heat in Trapped-ion Crystals

M. Bruderer[1], **A. Bermudez**[2], **and M. B. Plenio**[1]

[1]Institut für Theoretische Physik, Albert-Einstein-Allee 11, Universität Ulm, Ulm 89069, Germany
[2]Instituto de Física Fundamental, IFF-CSIC, Calle Serrano 113b, Madrid E-28006, Spain

Abstract— Measuring and controlling heat flow on the nanoscale poses formidable practical difficulties as elementary devices such as switches and 'ampere meters' for thermal currents are not available. We propose to overcome this problem by realizing heat transport through a chain of trapped ions, where currents of local vibrations (vibrons) are induced by chain edges kept at different temperatures. We show how to efficiently control and measure these currents by coupling vibrons to internal ion states, which in turn can be easily manipulated in experiments. Trapped-ion crystals therefore provide a promising platform for studying heat transport, e.g., through thermal analogues of quantum wires and quantum dots. Specifically, elusive phenomena such as the onset of Fourier's law or bosonic fluctuations of heat currents may be observable in trapped-ion systems.

REFERENCES

1. Bermudez, A., M. Bruderer, and M. B. Plenio, "Controlling and measuring quantum transport of heat in trapped-ion crystals," *Phys. Rev. Lett.*, Vol. 111, 040601, 2013.

Controllable van der Waals Interaction in a 1D Waveguide Geometry

Stefan Scheel[1] **and Harald Haakh**[2]

[1]Institute of Physics, University of Rostock
Universitätsplatz 3, D-18055 Rostock, Germany
[2]Max Planck Institute for the Science of Light
Günther-Scharowski-Straße 1/24, D-91058 Erlangen, Germany

Abstract— Dispersion forces such as Casimir, Casimir–Polder and van der Waals forces arise due to fluctuations of the quantised electromagnetic field. Any alteration of the environment in which the (virtual) photons propagate leads invariably to a modification of the respective interaction. Waveguide structures in particular are known to resonantly enhance Casimir-Polder interactions [1]. Here we will focus on the van der Waals interaction between two isolated atoms inside a cylindrical waveguide. Assuming an ideal, perfectly conducting waveguide, we will show how the far-field van der Waals interaction between atoms located on the cylinder axis shows an exponential distance dependence [2, 3], while the near-field potential scales polynomially as in free space. Using dyadic Green function techniques as the basis of phenomenological field quantisation, we are able to go beyond the ideal situation and treat arbitrary dielectric surface materials. In that way, we gain an understanding of the underlying mechanisms and limiting factors for the exponential suppression of the van der Waals interaction in the far field in waveguide structures [3]. The existence of a fundamental mode without cut-off [2] implies a far-field contribution to van der Waals interaction between excited atoms, thereby making it possible to observe the yet elusive retarded dispersion potential between two emitters.

REFERENCES

1. Ellingsen, S. A., S. Y. Buhmann, and S. Scheel, *Phys. Rev. A*, Vol. 82, 032516, 2010.
2. Shahmoon, E. and G. Kurizki, *Phys. Rev. A*, Vol. 87, 062105, 2013.
3. Haakh, H. and S. Scheel, in Preparation.

Aspects of Nonlinear Response in Fluctuational Electrodynamics

Matthias Krüger
University of Stuttgart & Max Planck Institute for Intelligent Systems, Stuttgart, Germany

Abstract— We discuss developments of theoretical description of electromagnetic fluctuations in out-of-equilibrium situations, as, e.g., radiative near field heat transfer and Casimir forces [1–4], including interpretation of recent experimental measurements. Specifically, we will present insights from statistical physics far from equilibrium applied to fluctuational electrodynamics.

REFERENCES

1. Krüger, M., T. Emig, and M. Kardar, "Non-equilibrium electromagnetic fluctuations: Heat transfer and interactions," *Phys. Rev. Lett.*, Vol. 106, 210404, 2011.
2. Krüger, M., G. Bimonte, T. Emig, and M. Kardar, "Trace formulas for nonequilibrium Casimir interactions, heat radiation and heat transfer for arbitrary objects," *Phys Rev. B*, Vol. 86, 115423, 2012.
3. Golyk, V. A., M. Krüger, and M. Kardar, "Linear response relations in fluctuational electrodynamics," *Phys. Rev. B*, Vol. 88, 155117, 2013.
4. Incardone, R., T. Emig, and M. Krüger, "Heat transfer between anisotropic nanoparticles: Enhancement and switching," *Europhys. Lett.*, Vol. 106, 41001, 2014.

Casimir-Polder Potential of Spheres and Discs and Its Impact on the Poisson Spot

J. Hemmerich, **M. Könne**, **and S. Y. Buhmann**
University of Freiburg, Germany

Abstract— The Casimir-Polder interaction of a ground-state atom or molecule with a dielectric body may be interpreted as a consequence of the vacuum fluctuations of the electromagnetic field. We study this interaction for spheres and discs on the basis of macroscopic QED [1], where it can be given in terms of the atomic polarisability and the Green's tensor of the electromagnetic field. The latter is known for a sphere, while we resort to a Hamaker approach for a disc. We calculate the potentials numerically and give analytical asymptotes for small and large distances and object sizes.

The Casimir-Polder potential plays are crucial role in the interpretation of matter-wave experiments. In particular, scattering at compact objects is known to lead to a bright spot — the Poisson spot — in the classical shadow region due to constructive interference [2]. The Casimir-Polder potential experienced by an atomic matter wave upon passing the scattering object imprints an additional phase and hence alters the Poisson-spot signal. We show how a comparison between theory and experiment can lead to direct evidence for Casimir-Polder interactions from matter-wave scattering.

REFERENCES

1. Buhmann, S. Y., *Dispersion Forces I — Macroscopic Quantum Electrodynamics and Ground-state Casimir, Casimir-Polder and van der Waals Forces*, Springer, Heidelberg, 2012.
2. Reisinger, T., et al., *Phys. Rev. A*, Vol. 79, 053823, 2009.

Tunable Casimir-like Interactions in Bosonic Ultracold Atoms

E. Compagno[1], **G. De Chiara**[2], **D. G. Angelakis**[3, 4], **and G. M. Palma**[5]

[1]Department of Physics and Astronomy, University College London, UK
[2]Centre for Theoretical Atomic, Molecular and Optical Physics, Queen's University Belfast BT7 1NN, United Kingdom
[3]School of Electronic and Computer Engineering, Technical University of Crete Chania, Crete 73100, Greece
[4]Centre for Quantum Technologies, National University of Singapore, Singapore
[5]NEST-INFM (CNR) and Dipartimento di Fisica e Chimica, Università degli Studi di Palermo, Italy

Abstract— A toolbox for the quantum simulation of attractive and repulsive polarons in ultracold atoms is presented. Motivated by impressing experimental advances in the area of ultracold atomic mixtures, we theoretically study the problem of ultracold atomic impurities immersed in a Bose-Einstein condensate (BEC). The impurity-BEC interaction gives rise to the formation of polarons whose interaction can be effectively tuned using an external laser in a quasi-resonant Raman scheme. Our scheme allows one to change the effective interactions between polarons from positive to negative. This is achieved by simply changing the intensity and the frequency of the two lasers. Such arrangement opens new avenues for the study of strongly correlated condensed matter models in ultracold gases.

Casimir Momentum in Complex Media

B. A. van Tiggelen[1], **G. L. J. A. Rikken**[2], **and M. Donaire**[1, 2, 3]

[1]Laboratoire de Physique et Modélisation des Milieux Condensés
UMR 5493, Université Grenoble 1/CNRS, B.P. 166, Grenoble 38042, France
[2]Laboratoire National des Champs Magnétiques Intenses, UPR 3228
CNRS/INSA/UJF Grenoble 1/UPS, Toulouse & Grenoble, France
[3]Laboratoire Kastler-Brossel, CNRS, ENS and UPMC, Case 74, Paris F-75252, France

Abstract— Casimir energy refers to the electromagnetic energy that quantum mechanics imposes to exist even in a fully empty space at temperature zero. In the presence of polarizable matter it gives rise to many fundamental phenomena in physics such as Lamb shift and Van de Waals forces, and maybe even the cosmological constant. In the conventional picture — either with or without matter — the expectation value of the electromagnetic momentum, $\langle \mathbf{E} \times \mathbf{B} \rangle$, called Casimir momentum vanishes. This may be physically obvious in "simple media", when $\langle \mathbf{E} \times \mathbf{B} \rangle$ is directly proportional to the energy flow $\langle \mathbf{E} \times \mathbf{H} \rangle$ which arguably vanishes unconditionally in thermodynamic equilibrium, but as soon as symmetries are broken (P, and T in particular) the question whether Casimir momentum can exist appears and turns out nontrivial.

The momentum of classical electromagnetic waves has been the subject of a longstanding controversy. In the presence of both an external electric $\mathbf{E}_0$ and magnetic field $\mathbf{B}_0$ the so-called Nelson version (our favorite) predicts a momentum $\alpha(0)\mathbf{E}_0 \times \mathbf{B}_0$ which results in the "Abraham force" $\mathbf{F} = \alpha(0)d/dt(\mathbf{E}_0 \times \mathbf{B}_0)$. We have measured this very tiny force in atomic gases and also searched — in vain — for possible deviations from the (Nelson version of) classical theory. In the QED picture in fact three momenta appear that are all different: kinetic momentum (related to force and thus observable), canonical momentum (conjugate to position operator and subject to gauge fields), and pseudo-momentum (which commutes with Hamiltonian and is thus conserved). We have developed a nonrelativistic QED theory for the electromagnetic momentum for simple objects coupled to the quantum vacuum. It produces the Abraham force *with* a QED correction. For the hydrogen atom the relative correction is equal to $-0.12\alpha^2$, nonzero, yet very small. We speculate that for other (hydrogen-type) atoms the correction scales as $(Z\alpha)^2$. Important to note is that the classical theory diverges in the infrared, and with some cut-off much higher QED corrections are proposed, that would have been within our experimental reach. In the full QED theory, this divergence disappears after mass renormalization.

Does Casimir momentum exist with only a magnetic field? If the matter is optically active, with $\beta(0)$ the static rotatory factor, a momentum $\beta(0)/\alpha(0)e\mathbf{B}_0$ could exist in view of its correct PCT symmetry and its correct dimension. However, such a momentum does not emerge from classical electrodynamics. We have developed a QED theory for a chiral, anisotropic, harmonic oscillator subject to a magnetic field. This theory, free of divergence, predicts a Casimir momentum proportional to $-(\alpha/4\pi)\beta(0)/\alpha(0)e\mathbf{B}_0$. Observation of this momentum is a next challenge. For atypical chiral compound $C_8H_{18}O$ we predict velocities $P/M = 0.5\,\mathrm{nm/sec}$ at 10 Teslas.

ACKNOWLEDGMENT

Supported by ANR PHOTONIMPLUS.

Vacuum Field Energy Densities and Casimir-Polder Forces near a Fluctuating Boundary

F. Armata[1], S. Butera[2], and R. Passante[3]

[1]QOLS, Blackett Laboratory, Imperial College London, London SW7 2BW, United Kingdom
[2]SUPA, Institute of Photonics and Quantum Sciences, Heriot-Watt University, Edinburgh, United Kingdom
[3]Dipartimento di Fisica e Chimica, Università degli Studi di Palermo and CNISM
Via Archirafi 36, Palermo I-90123, Italy

Abstract— We consider a quantum field inside a one- or a three-dimensional cavity with a wall which is allowed to move. We assume that the mobile wall is subjected to a harmonic potential, and its mechanical degrees of freedom are treated quantum-mechanically; it is also subjected to the radiation pressure. The wall's position has thus quantum fluctuations around the equilibrium position. The possible motion of the wall makes the cavity length variable, and this gives rise to a wall-field interaction and an effective interaction between the modes of the cavity [1]. Although this system has some analogy with the dynamical Casimir effect, in our case the motion of the wall is not prescribed by an external action but follows the system's internal dynamics.

We consider three different cases: a scalar field in a one-dimensional cavity, the electromagnetic field in a one-dimensional cavity and a scalar field in a three-dimensional cavity. For all these cases we consider the ground state of the interacting wall-field system at zero temperature. We show that the true ground state of the system contains admixtures with states containing excitations in the field and in the mechanical degrees of freedom of the moving wall. We evaluate the consequent change of the field energy densities and field fluctuations inside the cavity with respect to the fixed-wall case [2, 3]. We find that these vacuum energy-density changes are particularly relevant in the proximity of the mobile wall and discuss their dependence from the cutoff frequency, related to the plasma frequency of the conducting wall. The results obtained in the three cases considered (1D scalar, 1D electromagnetic and 3D scalar) are compared with each other. Observability of the new effects obtained through the Casimir-Polder interaction on a polarizable body such as an atom placed inside the cavity is also discussed, and we show that they should be measurable with actual optomechanical techniques. The dependence of the energy-density change and the atom-wall Casimir-Polder interaction on the relevant parameters of the mobile wall, such as its plasma frequency, mass and frequency of the harmonic potential, is discussed in detail.

REFERENCES

1. Law, C. K., "Interaction between a moving mirror and radiation pressure: A Hamiltonian formulation," *Phys. Rev. A*, Vol. 51, 2537, 1995.
2. Butera, S. and R. Passante, "Field fluctuations in a one-dimensional cavity with a mobile wall," *Phys. Rev. Lett.*, Vol. 111, 060403, 2013.
3. Armata, F. and R. Passante, "Vacuum energy densities of a field in a cavity with a mobile wall," *Phys. Rev. D*, Vol. 91, 025012, 2015.

Resonant and Dispersion Interactions between Uniformly Accelerated Atoms

M. Lattuca[1], **J. Marino**[2], **A. Noto**[1,3], **R. Passante**[1], **L. Rizzuto**[1], **and S. Spagnolo**[1]

[1]Dipartimento di Fisica e Chimica, Università degli Studi di Palermo and CNISM
Via Archirafi 36, I-90123 Palermo, Italy
[2]Institute of Theoretical Physics, TU Dresden, D-01062 Dresden, Germany
[3]Laboratoire Charles Coulomb UMR 5221 CNRS-UM2, Département Physique Théorique
Université Montpellier 2, F-34095, Montpellier Cedex 5, France

Abstract— We investigate the effect of a uniform acceleration on resonance interactions and dispersion Casimir-Polder interactions between uniformly accelerated atoms in vacuum. We first consider the Casimir-Polder interaction between two neutral ground-state atoms uniformly accelerated in the same direction and separated by a constant distance, orthogonal to their trajectories. The atoms interact with the electromagnetic field in the vacuum state. We obtain the dispersion energy between the two accelerating atoms as the interaction between the instantaneous atomic dipole moments, which are induced and correlated by the zero-point field fluctuations. We find that the interaction energy is time-dependent; we also find that the dependence of the interatomic Casimir-Polder interaction from the distance is different with respect to the case of atoms at rest. We discuss the physical meaning of these results [1] and their relation with the Unruh effect [2].

We then derive the interatomic scalar Casimir-Polder interaction energy using a different approach; specifically we calculate the interaction between the two atoms separating at the fourth order in perturbation theory the contributions of vacuum fluctuations and radiation reaction. We show that the Casimir-Polder force between the two uniformly accelerated atoms exhibits a transition from the short distance thermal-like behavior predicted by the Unruh effect, to a long distance non-thermal behavior. We identify the characteristic length scale for this crossover with the inverse of the proper acceleration of the two atoms [3].

Finally, we consider the resonance interaction between two uniformly accelerated atoms, one excited and the other in the ground state, and interacting with the quantum electromagnetic field in the vacuum state. We assume the two identical atoms prepared in a maximally entangled state. Separating the contributions of vacuum fluctuations and radiation reaction to the evolution of atomic observables, we show that Unruh thermal fluctuations do not affect the resonant interatomic interaction, which is exclusively modified by radiation reaction corrections. Beyond a characteristic length associated to the breakdown of a local inertial description of our two-particle system, non-thermal effects in the radiation reaction corrections change qualitatively the distance-dependence of the resonance interaction.

REFERENCES

1. Noto, A. and R. Passante, "Van der Waals interaction energy between two atoms moving with uniform acceleration," *Phys. Rev. D* , Vol. 88, 025041, 2013.
2. Crispino, L. C. B., A. Higuchi, and G. E. A. Matsas, "The Unruh effect and its applications," *Rev. Mod. Phys.*, Vol. 80, 787, 2008.
3. Marino, J., A. Noto, and R. Passante, "Thermal and nonthermal signatures of the unruh effect in Casimir-Polder forces," *Phys. Rev. Lett*, Vol. 113, 020403, 2014.

Small Self-contained Quantum Thermal Machines

Jonatan Bohr Brask
Département de Physique Théorique, Université de Genève, Switzerland

Abstract— Small autonomous quantum thermal machines function without any external source of coherence or control, but using only incoherent interactions with thermal baths. We discuss the generation of steady-state entanglement in a simple autonomous machine, with possible implementations in superconducting qubits and quantum dots, and we also look into the transient behaviour of a three-qubit quantum referigerator.

Thermodynamics of the Quantum Measurement Process

Philipp Kammerlander[1] **and Janet Anders**[2]

[1]Institute for Theoretical Physics, ETH Zürich, Switzerland
[2]Department for Physics and Astronomy, University of Exeter, UK

Abstract— Thermodynamics is a highly successful macroscopic theory widely used across the natural sciences and for the construction of everyday devices, from car engines and fridges to power plants and solar cells. With thermodynamics predating quantum theory, research now aims to uncover the thermodynamic laws that govern finite size systems which may in addition host quantum effects. Recent theoretical breakthroughs include the characterisation of the efficiency of quantum thermal engines [1–3] and the extension of widely used classical non-equilibrium fluctuation theorems to the quantum regime [4–7]. A new thermodynamic resource theory [8, 9] has led to the discovery of a set of second laws that replaces the standard macroscopic second law for finite size systems [10]. These results have substantially advanced our understanding of nanoscale thermodynamics, however putting a finger on what is genuinely "quantum" in quantum thermodynamics has remained a challenge.

We lay out consequences of seeing measurement, one of the central pillars of quantum theory, not merely as a mathematical projection but as a thermodynamic process. We uncover that measurement, a component of any experimental realisation, is accompanied by work and heat contributions and that these are distinct in classical and quantum thermodynamics. Implications are far-reaching, giving a thermodynamic interpretation to quantum coherence, extending the link between thermodynamics and information theory, and providing key input for the construction of a future quantum thermodynamic framework. Repercussions for existing quantum thermodynamic relations that omitted the role of measurement are discussed, including quantum work fluctuation relations and single-shot approaches.

ArXiv reference: arXiv:1502.02673.

REFERENCES

1. Scully, M. O., M. S. Zubairy, G. S. Agarwal, and H. Walther, *Science*, Vol. 299, 863, 2003.
2. Kosloff R. and A. Levy, *Annu. Rev. Phys. Chem.*, Vol. 65, 365, 2014.
3. Roßnagel, J., O. Abah, F. Schmidt-Kaler, K. Singer, and E. Lutz, *Phys. Rev. Lett.*, Vol. 112, 030602, 2014.
4. Morikuni, Y. and H. Tasaki, *J. Stat. Phys.*, Vol. 143, 1, 2011.
5. Batalhão, T., et al., *Phys. Rev. Lett.*, Vol. 113, 140601, 2014.
6. Mukamel, S., *Phys. Rev. Lett.*, Vol. 90, 170604, 2003.
7. Talkner, P., E. Lutz, and P. Hänggi, *Phys. Rev. E*, Vol. 75, 050102 (R), 2007.
8. Åberg, J., *Nat. Commun.*, Vol. 4, 1925, 2013.
9. Horodecki, M. and J. Oppenheim, *Nat. Commun.*, Vol. 4, 2059, 2013.
10. Brandão, F., M. Horodecki, N. Ng, J. Oppenheim, and S. Wehner, *PNAS*, 2015, doi:10.1073/pnas.1411728112.

Information Thermodynamics in a Hybrid Opto-mechanical System

Cyril Elouard, Maxime Richard, and Alexia Auffèves
Institut Néel, CNRS, France

Abstract— Information thermodynamics is a recent field that investigates the links between information and energy. Its most famous "Gedankenexperiments" are Landauer's erasure and Szilard's engine, that allow for the reversible conversion of a single bit of information into an elementary amount of work between a small system and a battery. In the twenty-first century, the validity of such a conversion has been extended to information of quantum nature, i.e., encoded into one or several quantum bits. Along this line, coherence and entanglement have also been shown to have energetical counterparts, leading to stimulating theoretical results about the efficiency of non-local thermal engines, the operational signification of Von Neumann entropy, or the energetical value of entanglement.

In this field, most theoretical proposals rely on the ability to reversibly convert information into energy, namely to experimentally realize Landauer's erasure and Szilard's engine. However so far, direct evidences of such reversible work exchanges have remained elusive: if Landauer's bound has been measured, Szilard's engines protocols are still perturbed by irreversible mechanisms, leading to best information-to-energy conversion rates of typically 30 percents.

In this talk, we investigate potential playgrounds for information thermodynamics. In particular, we show that a hybrid opto-mechanical transducer is a proper platform to monitor these conversions. Such devices consist in an optically active quantum emitter, playing the role of the bit, coupled to a mechanical resonator, playing the role of the battery. Heat is exchanged with the electromagnetic reservoir. Within a mechanical oscillation, we connect the entropy variations of the quantum emitter with the mechanical energy variations, that are identified with work exchanges. These results pave the road towards experimental investigation of quantum information thermodynamics.

Casimir Force within an Inhomogeneous Medium

Fanglin Bao[1, 2] **and Sailing He**[2, 3]

[1]Department of Physics, Zhejiang University, Hangzhou 310058, China
[2]Centre for Optical and Electromagnetic Research, Zhejiang University, Hangzhou 310058, China
[3]Department of Electromagnetic Engineering, Royal Institute of Technology, Stockholm 10044, Sweden

Abstract— As is well-known, the diverging part of Casimir energy can usually be regularized and expressed with the Heat-Kernel coefficients $\tilde{E} \propto V\xi^{-4} + S\xi^{-3} + \ldots + C + X\log\xi$, where $\xi \to 0$ is a cutoff parameter $E = \frac{1}{2}\sum_n \omega_n = \lim_{\xi\to 0} \frac{1}{2}\sum_n \omega_n e^{-\xi\omega_n}$. Coefficients V, S are geometric characteristics, i.e., the Volume and the Surface area of the space where field exists, while prefactor X is unknown of its physical meaning. Many Casimir problems have shown the existence of the logarithmically diverging term, and it is still unresolved how to remove such a logarithmic divergence.

On the other hand, considering Casimir energy or Casimir stress within inhomogeneous media, it is reported that the regular subtraction of the bulk contribution, leaving only the scattering part of the green function which comprises the interaction between molecules, is insufficient to obtain finite results. Additional regularizations must be introduced, however, no one has succeeded.

Here in our paper, we have connected the above two problems. We have shown that the remained infinity in the Casimir stress within inhomogeneous media, contains a logarithmically diverging term and a quadratically diverging term. These two terms, just like the worst diverging term $V\xi^{-4}$, can be compensated by introducing an adjoined cavity. That is, they become constant if we adopt the Casimir piston model rather than the half-space model, then they vanish in the Casimir force. We have also shown that, based on the piston model, for any continuous inhomogeneity we always have cutoff-independent (finite) Casimir force. To illustrate, we have given an explicit example, which should be the benchmark analytical solution for the Casimir force within inhomogeneous media. As for the physical meaning of the logarithmic divergence, we still need further study.

Singular Evanescent Waves in Moving Media

Yu Guo and Zubin Jacob
Department of Electrical and Computer Engineering
University of Alberta, Edmonton AB T6G 2V4, Canada

Abstract— Resonators fold the path of light by reflections leading to a phase balance and thus constructive addition of propagating waves. However, amplitude decrease of these waves due to incomplete reflection or material absorption leads to a finite quality factor of all resonances. Here we report on our discovery that evanescent waves can lead to a perfect phase and amplitude balance causing an ideal Fabry-Perot resonance condition in spite of material absorption and non-ideal reflectivities. This counterintuitive resonance occurs if and only if the metallic Fabry-Perot plates are in relative motion to each other separated by a critical distance. We show that the energy needed to approach the resonance arises from the conversion of the mechanical energy of motion to electromagnetic energy. The phenomenon is similar to lasing where the losses in the cavity resonance are exactly compensated by optical gain media instead of mechanical motion. Nonlinearities and non-localities in material response will inevitably curtail any singularities however we show the giant enhancement in non-equilibrium phenomena due to such resonances in moving media.

The canonical example of a resonator is the Fabry-Perot (FP) system consisting of two reflecting plates separated by a vacuum gap [1, 2]. Light bouncing between them serves as a textbook introduction to the concept of a resonance and is the basis of practical devices from the laser to the interferometer [1, 2]. A simple argument suffices to understand this resonance. The reflection coefficient of propagating waves with frequency ω from the first mirror ($r_1(\omega)$) times that of the second mirror ($r_2(\omega)$) along with the propagation phase accumulated over a round trip ($e^{2ik_z d}$) should reconstruct the wave, capturing it inside, leading to a resonant build-up of intensity. Here, d is the vacuum gap between the mirrors and k_z is the propagation constant perpendicular to the mirrors. We arrive at the Fabry-Perot resonance condition

$$r_1(\omega)r_2(\omega)e^{2ik_z d} = 1, \tag{1}$$

which also follows from a plane wave multiple scattering approach.

It is well known that this above equation cannot be fulfilled by any passive media. Note that the reflection coefficients are complex signifying the change in phase and amplitude of the propagating wave at the mirrors. A closer look reveals that an optimum choice of the gap can possibly lead to a net phase balance ($\arg(r_1(\omega)r_2(\omega)e^{2ik_z d}) = 2n\pi$) for a resonance, but material absorption and non-ideal reflections necessarily require $|r_1(\omega)r_2(\omega)| < 1$. A gain medium is needed to compensate for this loss in amplitude as in a laser. The arguments presented above can be generalized to arbitrary passive structures showing that the bound resonances are signified by the poles of the scattering matrix which always lie in the lower half ($\mathrm{Im}(\omega_{res}) < 0$) of the complex frequency plane [3]. This condition ensures that all resonances decay in time leading to a finite quality factor.

In this paper, we show that the conventional Fabry-Perot condition has fundamental differences in the case of moving media. We explain that evanescent waves bouncing between moving plates can lead to a counterintuitive resonance with perfect amplitude and phase balance. We introduce the concept of a negative Poynting vector flow arising from Doppler shifted negative frequency modes in moving media. The spontaneous emission of negative frequency modes from the moving plate forms the subtle reason for the existence of such a resonance, which in essence is similar to the concept of a laser. The gain is provided by the conversion of the mechanical energy of motion into electromagnetic energy through the negative frequency modes. Finally we show that this resonance can dominate the non-equilibrium heat transfer leading to a singularity for a critical velocity of the moving plate. The singularities will inevitably be curtailed by nonlinearities and non-localities close to the resonance and we discuss in detail the effect of hydrodynamic non-locality on our predicted resonance.

Nanolevitation Phenomena in Real Plane-parallel Systems Mediated by Gravity and Casimir Forces at Thermal Equilibrium

S. Carretero-Palacios, V. Esteso, and H. Míguez
Instituto de Ciencia de Materiales de Sevilla, Consejo Superior de Investigaciones Científicas
Universidad de Sevilla, Sevilla 41092, Spain

Abstract— One of the most exceptional predictions of the generalized Lifshitz's theory is the appearance of repulsive Casimir forces [1–11] when real materials are considered. Additionally, when two interacting objects are under the influence of both Casimir and gravity forces, nanolevitation may take place if the Casimir force equals the gravity force at a certain (equilibrium) distance. Here, we report on the theoretical analysis of equilibrium distances in real plane-parallel systems under the influence of Casimir and gravity forces at thermal equilibrium. Due to the balance between these forces, thin films of teflon, silica (SiO_2), or polystyrene (PS) in a single layer configuration and immersed in glycerol, stand over a silicon substrate at certain stable or unstable positions depending on the material and the slab thickness [12]. Hybrid systems containing SiO_2 and PS, materials which display Casimir forces and equilibrium distances of opposite nature when considered individually, are analyzed in either bilayer arrangements or as composite systems made of a homogeneous matrix with small inclusions inside. We show that the equilibrium distances are modified through the variation of the slab thickness in the single layer configuration, the thickness of the individual components in the bilayer configuration, and the filling fraction of inclusions in the nanocomposites, parameters which have a strong effect in both Casimir and gravity forces. Our results pave the way for novel suspension and nonadhesive strategies at the nanoscale.

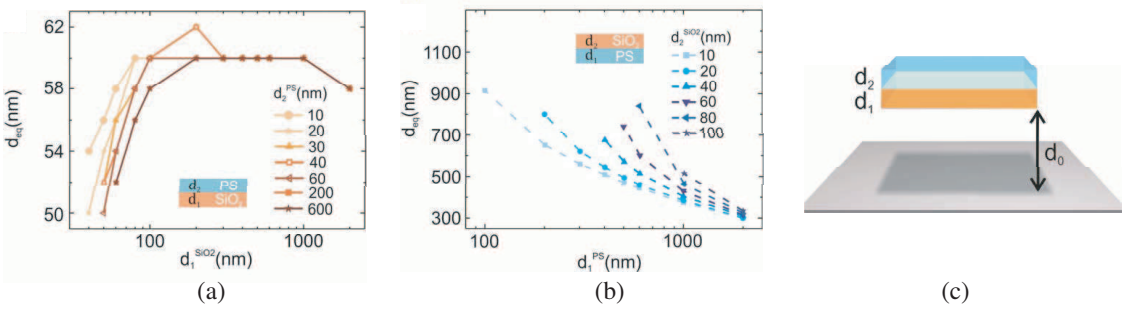

Figure 1: (a), (b) Equilibrium distance (d_{eq}) in a bilayer configuration (containing SiO_2 and PS), immersed in glycerol over a Si substrate, as a function of the slab thickness of the bottom layer (d_1), for different thicknesses of the top layer (d_2), for the configurations represented with the schematics in each panel. (c) Schematics of a bilayer system considered in our studies.

REFERENCES

1. Dzyaloshinskii, I. E., E. M. Lifshitz, and L. P. Pitaevskii, *Adv. Phys.*, Vol. 34, 10, 165–209, 1961.
2. Chan, H. B., V. A. Aksyuk, R. N. Kleiman, D. J. Bishop, and F. Capasso, *Science*, Vol. 291, No. 1941, 2001.
3. Milton, A. K., *J. Phys. A*, Vol. 37, No. R209, 2004.
4. Munday, J. N., F. Capasso, and V. A. Parsegian, *Nature*, Vol. 457, 170–173, 2009.
5. Hoye, J. S., I. Brevik, J. B. Aarseth, and K. A. Milton, *J. Phys. A*, Vol. 39, 6031–6038, 2006.
6. Lamoreaux, S. K., *Rep. Prog. Phys.*, Vol. 68, No. 201, 2005.
7. Bostrom, M. and B. E. Sernelius, *Phys. Rev. Lett.*, Vol. 84, 4757, 2000.
8. Bordag, M., B. Geyer, G. L. Klimchitskaya, and V. M. Mostepanenko, *Phys. Rev. Lett.*, Vol. 85, 503, 2000.
9. Bentsen, V. S., R. Herikstad, S. Skriudalen, I. Brevik, and J. S. Hoye, *J. Phys. A*, Vol. 38, 9575, 2005.

10. Yampol'skii, V. A., S. Savel'ev, Z. A. Mayselis, S. S. Apostolov, and F. Nori, *Phys. Rev. Lett.*, Vol. 101, 096803, 2008.
11. Obrecht, J. M., R. J. Wild, M. Antezza, L. P. Pitaevskii, S. Stringari, and E. A. Cornell, *Phys. Rev. Lett.*, Vol. 98, 063201, 2007.
12. Esteso, V., S. Carretero-Palacios, and H. Miguez, *J. Phys. Chem. C*, DOI: 10.1021/jp511851z.

Session 2P12
Small Antenna Design, Analysis and Miniaturization Techniques

Tunable and Reconfigurable Frequency Rejection Circular Slot Antenna for UWB Communication Applications

Yingsong Li[1] and Raj Mittra[2]

[1]College of Information and Communications Engineering, Harbin Engineering University, Harbin, China
[2]Electromagnetic Communication Lab, Penn State and Central Florida Universities, USA

Abstract— In this paper, a tunable and reconfigurable circular slot antenna with frequency rejection characteristics is proposed for UWB communication applications. The proposed antenna can provide triple-band-notch characteristics by using various stubs for filtering out unwanted narrowband signals shoes frequencies overlapped with those of the UWB band. Center frequencies of these notch bands are tunable, and are realized by adjusting the dimensions of the proposed stubs. Also, the proposed antenna has a reconfigurable frequency rejection function to render the designed antenna suitable for UWB, band-notched UWB, dual band-notched UWB, tri-band-notched UWB or multi-band communication applications. The experimental results show that the proposed can also provide wide tunability, excellent reconfigurable frequency rejection characteristics and good omnidirectional radiation patterns, which make it attractive for indoor UWB communication applications.

A Triple Band-notched UWB Antenna by Using an Arc-shaped Slot and a U-shaped Resonator Techniques

Yuanyuan Kong, Yingsong Li, and Wenhua Yu
College of Information and Communications Engineering
Harbin Engineering University, Harbin 150001, China

Abstract— In this paper, an ultra-wideband (UWB) antenna with triple notch bands is proposed and well designed by etching double arc-shaped slots (DASS) on the fan-shaped radiating parch and integrating a U-shaped resonator (USR) alongside the microstrip feed signal line. The proposed antenna consists of a microstrip feed structure, a trapezoidal ground plane, a fan-shaped radiating patch, which are printed on a substrate with its dielectric constant of 2.65. The three band-notched characteristics are successfully realized by the use of the DASS and USR techniques, while the center frequencies of these notch bands are tunable by adjusting the dimensions of the proposed DASS and USR. By using these techniques, the proposed antenna can filter out unwanted narrowband signals from WiMAX, WLAN and RFID band. The proposed antenna is well designed and extensively investigated. The experimental results are given to verity that the proposed antenna with a wide bandwidth, three designated band-notched functions and good omnidirectional radiation patterns, which is suitable for modern high rate UWB communication applications.

Design of a High Isolation Dual-band MIMO Antenna for WLAN and WIMAX Applications

Lanchao Zhang, Tao Jiang, and Yingsong Li
College of Information and Communications Engineering
Harbin Engineering University, Harbin 150001, China

Abstract— A high isolation dual-band multiple-input multiple-output (MIMO) antenna of two elements is presented for wireless local area networks (WLAN) and worldwide interoperability for microwave access (WIMAX) applications. The MIMO antenna is printed on a FR4-epoxy substrate with the dielectric constant of 4.3 and an overall size of $46 \times 40 \times 1.6\,\mathrm{mm}^3$. Each element consists of two monopole antennas which locate at the top and bottom sides of the substrate respectively. The top one is fed by a $50\,\Omega$ microstrip line directly, and operates in 2.45 GHz band. The bottom is fed by the coupling current and operates in 3.55 GHz band. The two elements are placed perpendicularly to reduce mutual coupling. The neutralization line and the narrow slot are fabricated to improve the isolation characteristic in the high frequency band. The minimum distance between elements is 10.15 mm and superior isolation performance (higher than 20 dB) is achieved in two operation bands (2.4–2.484 and 3.4–3.69 GHz). In addition, good return loss is achieved, above 20 dB in the low frequency band and 14.5 dB in the high frequency band respectively. It is shown that the MIMO antenna presented in this paper is suitable for WLAN and WIMAX applications.

A Compact Dual Band-notched UWB Band-pass Filter by Using a Stub and a Folded Stepped Impedance Resonator

Yanyan Wang, Tao Jiang, and Yingsong Li
College of Information and Communication Engineering
Harbin Engineering University, Harbin 150001, China

Abstract— Mobile communication systems must support multiple users achieving at same time privacy of users contents. Security common solutions are based on encrypted algorithms from higher layers, such as private and public encrypted keys. Other possibility is to implement physical layer security schemes. One advantage of physical layer security relies on their ability to be combined with other security schemes from higher layers.

MIMO (Multiple-input multiple-output) systems can increase throughput in modern wireless networks and reduce interference. Other advantage of MIMO systems is the reduction of the transmitted power. On the other hand, to achieve high spectral efficiency multilevel modulations with high peak-to-average power ratios should be used, which may affect efficiency of power amplification. This problem can be avoided with a transmission scheme, where the constellations are decomposed on several uncorrelated BPSK (Bi Phase Shift Keying), QPSK (Quadri Phase Shift Keying) or OQPSK (Offset QPSK) components, being each component amplified and transmitted independently by an antenna. Combination losses are also avoided since the several signal components are combined at channel level. On the other hand due to the broadcast nature of MIMO systems, security is another critical issue in such systems. However, the constellation shaping on the desired direction introduced by these new transmitters means that we have directivity at the transmitted constellation that can be employed to assure security at physical layer. Privacy is achieved since each user must know the set of coefficients associated to each BPSK component as well as the array configuration, otherwise receives useless data. Therefore, the inherent security lies on the constellation directivity, i.e., the direction in which the constellation is optimized, which can be improved by changes on coefficients' phases or using constellations that are decomposed with a higher number of BPSK components. The several cases analyzed here show effectiveness of the proposed approach to implement a security scheme at physical layer level.

A Compact Ultra-wideband Band-pass Filter Integrated with Dual Tunable Notch Bands

Shumiao Hao, **Tao Jiang**, **Lanchao Zhang**, **and Yingsong Li**
College of Information and Communications Engineering
Harbin Engineering University, Harbin 150001, China

Abstract— A novel ultra-wideband filter integrated with dual tunable notch bands is proposed on the basis of the source-load cross coupling and an L-shaped slot. The dual notch bands are realized by using L-shaped slot and coupled-line sections, which act as inverter circuits in this design. High-low impedance lines are used to form the basic resonators. A folded cross-coupled feeding structure is used to mimic the size and three open stubs are employed to enhance the performance of the band-notched function. The experimental results show that the proposed filter can provide a wide pass-band bandwidth, two designated notch bands and high selectivity, making it promising for UWB applications.

Miniaturized Tag Antennas with Artificial Magnetic Conductor for UHF RFID On-body Applications

Chien-Wen Chiu and Cheng-Yan Yang
Department of Electronic Engineering, National Ilan University, Ilan 260, Taiwan

Abstract— UHF RFID technique is popular in the logistics, inventory management or bioengineering. The performance of an UHF RFID tag antenna is seriously degraded as it is placed close to a human body. The input impedance, radiation pattern, and realized gain of the tag antenna are influenced due to the body-proximity and absorption effects. Recent study finds that reading range of a UHF RFID tag is limited to 3 m [1]. Therefore, the body-proximity effects must be considered when a tag is held or put on the body. Some literatures recommended using artificial magnetic conductors (AMCs) to insulate the effect of the human body for wearable devices.

In this presentation, a two-dimensional square metal patch is initially applied as the unit cell of an artificial magnetic conductor (AMC). The unit cell size of the AMC is $55 \times 55\,\text{mm}^2$ and the gap separation between each unit cell is 1 mm. To miniaturize the AMC size and lower the first resonant frequency, four T-type slots are symmetrically inserted into each side of the metal patch. Each slot is designed with $Lp = 40\,\text{mm}$ and $Wp = 3\,\text{mm}$ so that the operating frequency is reduced to 915 MHz. The periodic square patches are built on a grounded FR4 substrate with height = 3.2 mm, $\varepsilon r = 4.4$ and loss tangent = 0.02. In order to achieve maximum benefit and minimum size, 3×3 T-slot patch-typed AMC unit cells were studied. A miniaturized dipole with T-matching structure was discussed in this presentation. It is placed on the above plane of the AMC in to insulate the influence from the human body. The tag on the AMC substrate is then placed close to a four-layer stratified elliptical cylinder human model to study the performance of the designed tags. Another kind of miniaturized AMC will be presented and discussed in the reference.

The power transmission coefficient and realized gain for the tags with and without AMC were simulated by HFSS. The study finds that the influence due to the body effect is small for the tag with AMC. The maximum realized gain of the designed T-matching dipole without AMC is about 1.9 dBi in the free space. The designed dipole on the T-slot patch-typed AMC raises realized gain up to 3.5 dBi since the AMC has 0^0 reflection phase and it would not cause destructive interference between the direct and reflected waves. When the tag is placed near the human model, the realized gain of the dipole on the AMC is about 2.7 dBi but the realized gain of the tag antenna without AMC is only −10 dBi. The maximum radiation efficiency is up to 38 % for the tag with AMC but only 10% for the tag without AMC. The practical structures were also constructed to measure the input impedance and reading ranges. The measured reading range is about 11 m for the tag with AMC in the free space as the UHF RFID reader has 4W EIRP output power. Considering real body-proximity effects on the tag, the reading range can achieve 9 meters for the tag with AMC but only 2 m for the tag without AMC. However, the size of the AMC is still too large for on-body applications. The design for the miniaturized AMC and tags will be presented in the conference.

REFERENCES

1. Tsai, M.-C., C.-W. Chiu, H.-C. Wang, and T.-F. Wu, "Inductively coupled loop antenna design for UHF RFID on-body applications," *Progress In Electromagnetics Research*, Vol. 143, 315–330, 2013.

A Compact VHF Antenna for Smart Meters

Paul Record and Komsan Kanjanasit
School of Engineering & Physical Sciences, Institute of Sensors, Signals and Systems
Heriot Watt University, Mountbatten Building, Riccarton, Edinburgh EH14 4AS, UK

Abstract— To ease data collection and enable variable energy tariffs the energy companies have demanded two way communications between the consumer energy meter and the company. There are serval bands in use from GSM to short range terminals working at 315, 434 and 868 MHz. In hilly terrains and meters located in basements this frequencies do not propagate well, however frequencies below 200 MHz are much better. This work describes a narrow band antenna derived from a patch antenna with perturbations, working at 169 MHz. Its largest dimension is only 0.06λ at the resonant frequency and it has $ka = 0.18$. A gain of -1.2 dBi and an SII of -20 dB was achieved. The antenna was designed to fit directly to the smart meter so its radiation pattern was optimised to radiate broadside. It incorporates a novel matching element to allow ease of manufacture. From near field studies it can be described as parasitic resonator driven by a single driven electrode matching 50 Ohms. The main method of tuning was by altering the separation of the top fin structures. The antenna was tuned to the require resonant frequency when enclosed a ABS plastic housing.

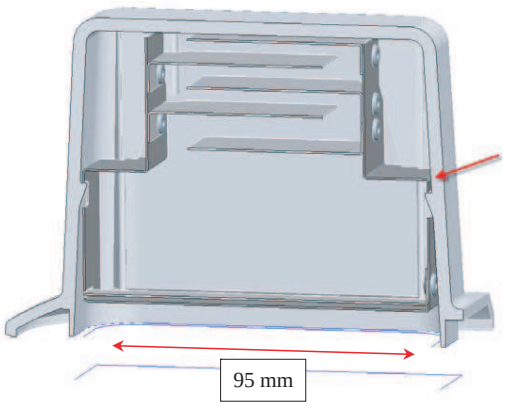

Figure 1: Antenna section within smart meter housing. Arrow indicates method of attachment.

The Performance Improvement of Printed Inverted-F Antennas Using the Slot Mesh on Ground Plane

Yao-Chiang Kan
Department of Communications Engineering, Yuan Ze University, Taoyuan City 320, Taiwan

Abstract— Most wearable or Band-Aid like sensors employed in mobile health (m-Health) applications is required to integrate a microcontroller, a RF chip, a sensor chip, and a printed antenna onto a small substrate. For the off-body communication, the radiative RF channel is responsible for node-to-gateway data transmission. The performance of the printed antenna is not only affected by the human body, but also the size of the area reserved for the radiator. As shown in Fig. 1, the area reserved for printed antenna is about 20 mm × 5 mm and a mender line monopole or an inverted-F antenna are good candidates for the application. However, the size of the ground plane is significantly sufficient with respect to the frequency at 2.4 GHz, the target frequency of this m-Health application. A slot mesh on the ground plane, located at the second layer in Fig. 2, is employed to improve the antenna performance in this study. The ground plane is first partitioned into a $2^m \times 10$ rectangle mesh. Each element of the mesh could be filled with a rectangle metal or air, the latter is named a slot. The arrangement of the slots in the mesh is decided by the particle swarm optimization (PSO) with the target functions derived from the required antenna parameters. The simulation is implemented using the distributed binary PSO (DBPSO) and run on four computers with HFSS and Matlab installed. A printed IFA with $2^4 \times 10$ slot mesh on the ground plane is found to have bandwidth from 2.4 to 2.5 GHz with efficiency above 80%. Note that the length of radiator, L_r in Fig. 2, is half of that calculated by the empirical formula of printed IFA if the slot mesh is employed. In DBPSO computation, the slot mesh can be replaced by any EBG or AMC element and more general computation algorithm can be developed.

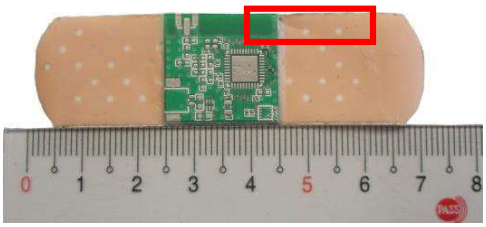

Figure 1: An on-body band-aid sensor.

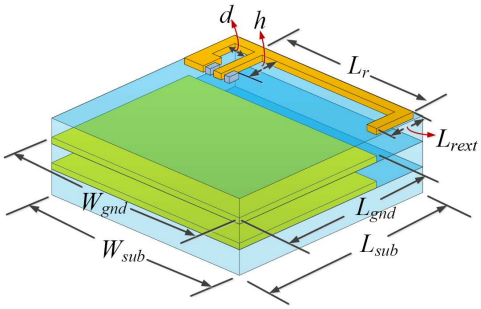

Figure 2: The structure of the printed IFA.

Sierpinski Fractal Monopole Antenna for Wireless Applications

Zachariah C. Alex and K. Shambavi
School of Electronics Engineering, VIT University , Vellore-14, Tamiladu, India

Abstract— Recently the Ultra Wide Band Technology has experienced a rapid growth in wireless communication applications, since federal communication commission (FCC) declared the frequency band (3.1–10.6 GHz) as unlicensed band. The UWB technology is very attractive because of its high data rate transmission and low power consumption, simple hardware configuration and excellent immunity to multipath interference when compared with existing wireless communication systems. Planar antennas reported in literature forUWB systems are large in size compared to our proposed antenna ($19.5 \times 19.5 \times 1\,\mathrm{mm}^3$) that incorporates fractal techniques and multiresonance effect. Fractal planar antennas generally contribute narrow bandwidth, but when realized in monopole configuration it exhibits wideband width and improved radiation efficiency

In this paper we propose Sierpinski fractal monopole antennas for wireless applications. We used Sierpinski fractals to realize antennas for wireless applications. Sierpinski fractal antenna in monopole configuration operates in WLAN/WiMAX frequency range (3.86 GHz to 5.7 GHz), whereas Sierpinski fractal monopole antenna inside a ring structure operates in UWB range (4.24 to 10.25 GHz). The wide bandwidth is due to multiresonance effect of ring and fractal structures. The proposed antennas are designed on FR4 substrate with $\epsilon_{\mathbf{r}} = 4.4$ and thickness 1 mm. Its parametric analysis was carried out using High Frequency Structure Simulator (HFSS v 13). Radiation pattern is omnidirectional in azimuth plane and it is like figure of eight in the elevation plane. Consistent radiation characteristics is observed in both the planes. Since the size of the proposed antenna is very small ($19.5 \times 19.5 \times 1\,\mathrm{mm}^3$) compared to other existing fractal antennas it is well suited for integration with portable UWB devices

It can be observed from the analysis that when the number of iterations of Sierpinski fractal increases, the bandwidth and return loss characteristics are improved with stable radiation pattern. Hence further enhancement in bandwidth and efficiency can be achieved by incorporating more fractal techniques.

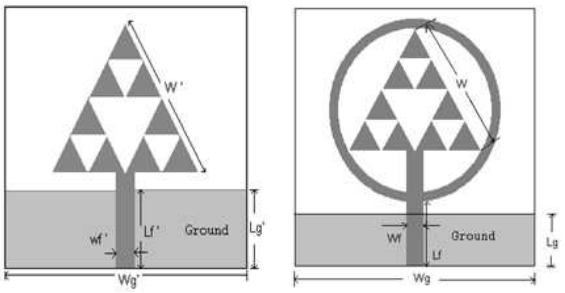

Figure 1: Geometry of (a) WLAN antenna, (b) UWB antenna.

A Miniaturized Metamaterial Inspired Hexaband Antenna for GSM, GPS-L1, WLAN and WiMAX Applications

Bharath Raj, **G. S. Kartikeya**, **K. Ullas**,
Sanjji N. Manjunath, **and C. Vindhya**
Antenna Research Laboratory, Department of Electronics and Communication
B.M.S. Institute of Technology and Management, Bengaluru, India

Abstract— This paper illustrates the application of metamaterial inspired unit cells in the patch as well as the ground plane to obtain a compact hexaband antenna. The patch consists of three split ring resonators separated by a distance of 0.5 mm. In addition, each ring has a thickness of 0.5 mm. The splits in the ring helps in reducing the size of the antenna by shifting the resonant frequency towards the lower frequency region. These rings exhibit definite inductive and capacitive characteristics. In addition to the split rings other metamaterial structures like a circular middle portion with interlocking pattern is also utilized. Besides the patch, the ground plane is in the shape of a square spiral, which is also a type of metamaterial structure. FR4 epoxy of thickness 1.6 mm is used as the substrate in the design. The excitation was provided by normal 50 Ohm linefeed. Distinct bands were obtained at various frequencies for LTE (900 MHz), GPS-L1 (1.575 GHz), GSM (1800/1900 GHz), UMTS (B2/B1), WLAN (2.4 and 5.5 GHz) and WiMAX (2.5 and 3.5 GHz). The radiation pattern obtained for the specified frequencies displays an Omni-directional pattern. Furthermore, the radiation pattern also possesses a wide beam width. These two properties are very useful when the purpose of the antenna is wireless communication. These results were obtained while maintaining the antenna dimensions to be limited to $30 \times 30\,\text{mm}^2$.

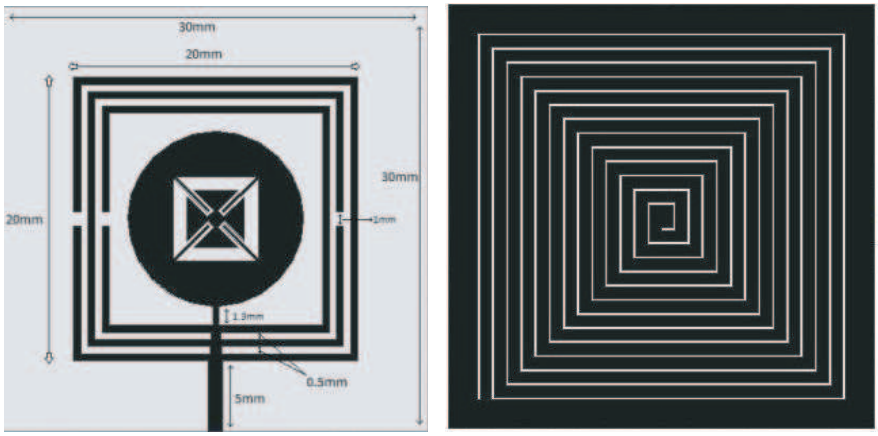

Figure 1: The proposed antenna.

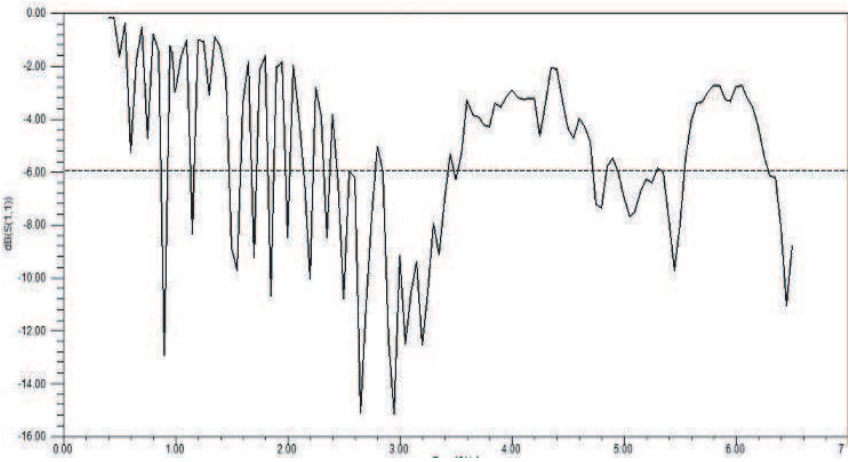

Figure 2: S_{11} of the proposed antenna.

The size of the patch for resonating at 900 MHz is theoretically calculated to be $79.4 \times 79.4\,\mathrm{mm}^2$. It was concluded that the proposed antenna has decreased the size of the antenna resulting in a miniaturization of over 62% and increased the number of bands at which it is resonating. Therefore, by utilizing metamaterial structures the size is reduced by a factor of $0.09\lambda_0$ and the number of bands covered by the antenna were improved.

Antenna Design: The unit cell consists of three split rings in addition to the central circular pattern with the interlocking design. The split rings have a thickness of 0.5 mm and is separated from each other by the same amount. The circular pattern has a radius of 6.2 mm. The complete unit cell occupies an area of $20 \times 20\,\mathrm{mm}^2$ and is positioned on top of the FR4 substrate of dimensions $30 \times 30 \times 1.6\,\mathrm{mm}^3$. The ground plane has the shape of a square spiral etched out.

Results and Discussion: The S_{11} of the proposed antenna is given in Fig. 2.

The S_{11} of the antenna shows resonance at several frequencies in the range from 900 MHz to 6.5 GHz. Among these the widely used ones are LTE (900 MHz), GPS-L1 (1.575 GHz), GSM (1800/1900 GHz), UMTS (B11/B1), WLAN (2.4 and 5.5 GHz). The overall dimension of the antenna is $30 \times 30\,\mathrm{mm}^2$. This accounts for a reduction of over 62% in the size of the antenna. In addition, the radiation patterns of the antenna at these frequencies were Omni-directional and has a wide beam width. Both of these properties are significant in portable wireless communication devices such as smart phones and tablets which are widely popular.

Quad Band Split Koch Snowflake Antenna for LTE/WLAN/WiMAX Applications

K. Ullas, G. S. Karthikeya, Bharath Raj, Sanjji N. Manjunath, and C. Vindhya
Antenna Research Laboratory, BMS Institute of Technology, India

Abstract— Quad Band Split Koch Snowflake antenna is investigated as radiating element. Resonant bands of 0.77–0.82 GHz, 2.3–2.42 GHz, 3.6–3.7 GHz and 5.3–6 GHz with center frequency of 0.8 GHz, 2.35 GHz, 3.65 GHz and 5.5 GHz.These bands very well cover the LTE/WLAN/WiMAX spectrum which are widely used to provide wireless service. The antenna was realized on a FR4 epoxy substrate with dimension $0.08\lambda_o \times 0.08\lambda_o \times 0.0042\lambda_o$ ($30\,\text{mm} \times 30\,\text{mm} \times 1.6\,\text{mm}$). The proposed antenna design is inspired from Koch snowflake fractal of first iteration and split element found in Split Ring Resonator (SRR) which is a metamaterial unit cell. The width of the transmission line in the proposed antenna is tapered gradually for impedance matching. The antenna was excited using a normal line feed technique. For the simulation of the proposed antenna a Finite Element Method solver was used. Antenna was analyzed with normal ground plane and the proposed ground plane, and the results were compared. The contribution of the split element in the Koch snowflake fractal of the proposed antenna was also studied by simulating the proposed antenna with and without the split element and the results were compared. Parametric analysis were carried out on the dimension of various elements of antenna. The radiation pattern of the proposed antenna was obtained at resonant frequencies in both E-plane and H-plane. After an extensive study of the proposed antenna it was found that the multiple Koch snowflake fractal

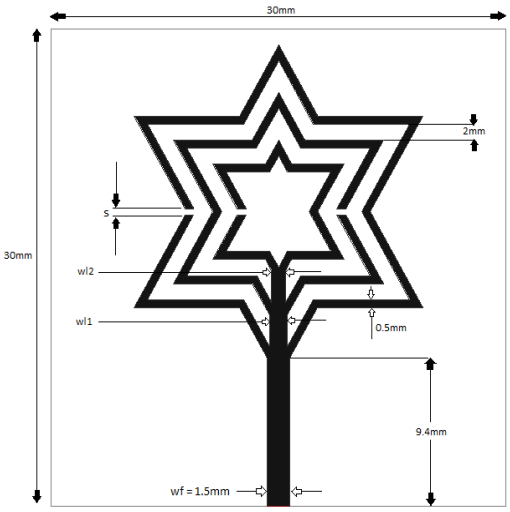

Figure 1: Proposed antenna design.

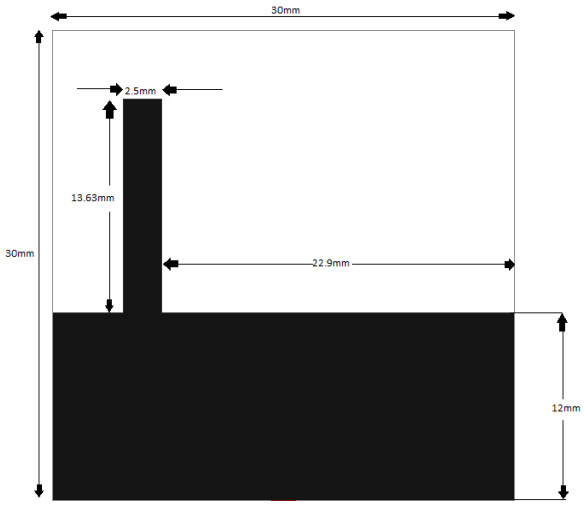

Figure 2: Ground plane of the proposed antenna.

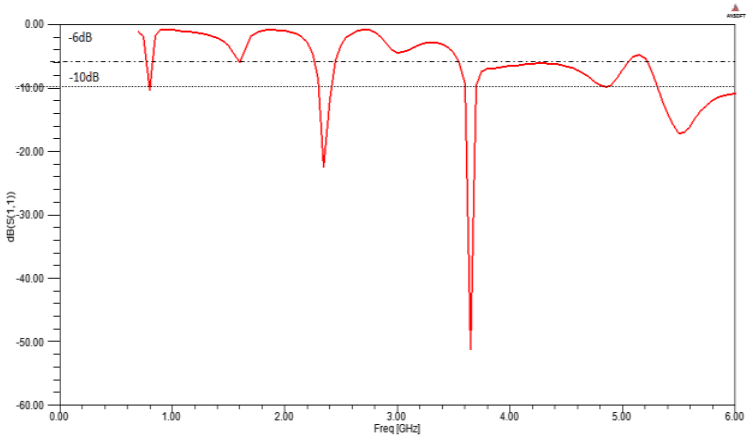

Figure 3: S_{11} of the proposed antenna.

structure was responsible for multiband resonance. The ground plane consisting of a protruding structure was responsible for the antenna to resonate at 5.3 to 6 GHz .The split element in the Koch snowflake fractal enhanced the antenna's ability to resonate at lower frequency of 0.8 GHz.

Miniaturized Multiband Antenna with Modified Split-ring Resonator for WLAN/WiMAX Applications

C. Vindhya, G. S. Karthikeya, Sanjji N. Manjunath, K. Ullas, and Bharath Raj
Antenna Research Laboratory, Department of Electronics and Communication
B.M.S. Institute of Technology and Management, Bengaluru, India

Abstract— In this letter, we propose a novel compact and planar triple band antenna designed using a metamaterial-inspired structure that consists of a slightly modified split-ring resonator (SRR). The ground plane has dielectric slots embedded in it. The proposed design measures $0.156\lambda_0 \times 0.156\lambda_0 \times 0.012\lambda_0$. It resonates at 2.351, 3.635 and 5.121 GHz respectively covering LTE2300, WiMAX and WLAN bands. Radiation pattern along H plane shifts by 90° between 3.8–4 GHz providing beam steering suitable for MIMO LTE (4G) and WiMAX. As a consequence of rapid development in wireless communication, compact multi-band antennas attracted research interest. It is desirable to have a single antenna operating at multiple bands. This enhances compactness which reduces VLSI real estate, cost and volume required in the casing of the device. The proposed design has multiple frequency bands at 2.351, 3.490–3.770 and 5.041–5.256 GHz with reflection co-efficient greater than −6, −10 and −10 dB respectively. It covers LTE2300 (2300–2400 MHz), WiMAX at 3.5 GHz and WLAN at 5.2 GHz. An attempt has been made to improvise on a conventional SRR to scale-down the dimensions while retaining multifrequency functionality. The radiating face of the antenna consists of a remodeled SRR. Resonant frequencies are created by fine tuning the gaps and embedding dielectric slots in the ground plane whose size and position were both realized through a parametric study. In addition to triple band operation, the antenna exhibits frequency beam-scanning ability inherent in a leaky wave antenna. Beam steering up to 90° can be achieved between 3.8–4 GHz. One of the LTE bands is centered

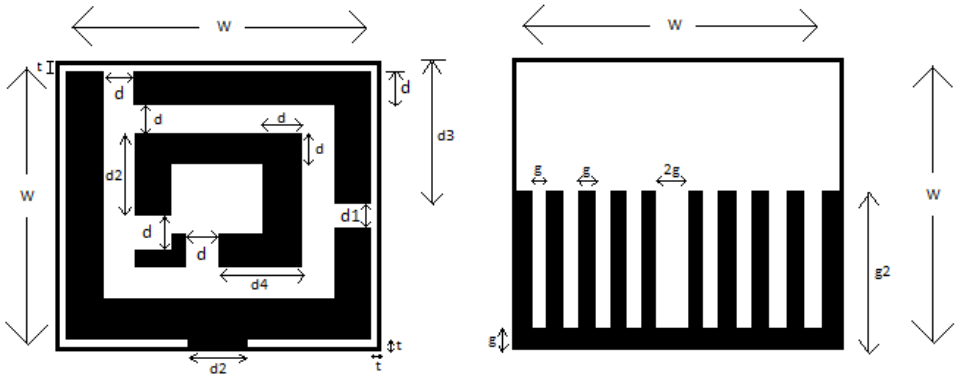

(a) (b)

Figure 1: (a) Radiating surface. (b) Ground plane.

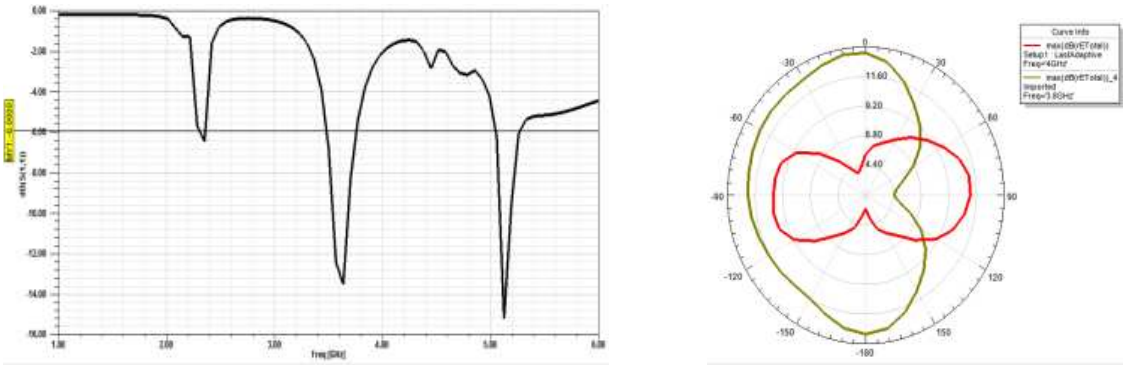

(a) (b)

Figure 2: (a) Simulated S_{11} for antenna 1, antenna 2, antenna 3 and antenna 4 and (b) radiation pattern shift.

at 3.5 GHz which is also applicable for WiMAX. This feature is similar to the property of a smart antenna used in MIMO system. The geometry of the proposed antenna is shown in Fig. 1. It is fabricated on FR4 epoxy substrate of dimension 20 mm × 20 mm × 1.6 mm with dielectric constant 4.4 and loss tangent of 0.02. The patch consists of a metamaterial structure comprising a rectangular split-ring configuration with two non-opposite slits in each ring which are repositioned. Out of a total of four gaps/splits, three have a width equal to the thickness of the ring and the fourth is slightly smaller. The design uses a novel ground plane configuration. The size of ground plane is half the overall size, i.e., 20 mm × 10 mm. It is slotted with a wide gap at the centre and narrower gap on either side. Gap between slots on either sides of the centre remains constant. It is fed by a microstrip line which can be connected by an SMA. Ansys HFSS software is used to evaluate the antenna performance. The other optimal parameters are $W = 20$ mm, $d = 2$ mm, $d1 = 1.5$ mm, $d2 = 7$ mm, $d3 = 9.75$ mm, $t = 1$ mm, $g = 1$ mm, $g2 = 10$ mm. Frequency bands at 2.351, 3.635 and 5.121 GHz with reflection co-efficient −6.467, −13.494, −15.201 dB respectively are presented in Fig. 2(a). Bandwidths for resonances with S_{11} better than −10 dB at 3.635 GHz is 140 MHz and at 5.121 GHz is 96 MHz. Addition of a new set of gaps/split resulted in multiple bizarre resonances. The position and width of each gap/split were tweaked to get the final result through parametric analysis. It can also be observed that the radiation pattern changes with frequency variation in the range 3.5–4 GHz which is a characteristic of leaky-wave antennas. A change from 3.8–4 GHz returns a 90° shift in radiation along H plane. This is depicted in Fig. 2(b).

Research on Dual Bandpass of Wide Stopband Filter with Tunable Center Frequency

Zhao-Qing Sun, **Yong-Sheng Zhao**, **Han-Lin Duan**, **and Tao Jiang**
College of Information and Communication Engineering
Harbin Engineering University, Harbin 150001, China

Abstract— A dual passband of wide stopband varactor tuned filter using stepped impedance resonators (SIRs) is proposed in this paper. A varactor is loaded on the middle of the E-shaped resonators, through changing the value of the bias voltage across the varactor, the center frequency of the second passband can be tuned from 1.56 GHz to 2.25 GHz, however, the center frequency of the first passband is fixed and maintained at 1.02 GHz. In fact, it is fixed during the whole process. The relative bandwidth of the first passband is 14.7%, the return loss of is 19 dB and the insertion loss is 0.2 dB. The second passband can tuning from 1.56 GHz to 2.25 GHz with the tuning range of 36.2%. The relative bandwidth almost keep unchanged. The return loss change from 16 dB to 30 dB and the insertion loss change from 0.2 dB to 0.8 dB. This filter proposed in this paper has a great characteristic of harmonic suppression, −20 dB up to 3.5 GHz. There are two advantages of the optimization process. The first is that a filter network is added in the input and output coupling line to depress stopband. The second is that spurlines are added at the input and output coupling line which can add zero between the two passbands, which improved the performance for filter. It is good to improve the selectivity of the filter. The filter proposed in this paper can achieve a compact size, lower insertion loss and wider rang harmonic suppression. Simulations show that the filter proposed is valid and has a good performance.

A Very Small Triangular Shaped Printed Monopole Antenna for Bluetooth/WLAN and UWB Applications

Praveen V. Naidu and Akshay Malhotra
Centre for Radio Science Studies, Symbiosis International University (DU), Pune 412115, India

Abstract— In this paper, a compact ($12 \times 20\,\mathrm{mm}^2$) triangular shaped microstrip antenna with dual band characteristics is presented for Bluetooth/WLAN and ultrawideband (UWB) applications. The proposed structure consist of a simple triangular shaped radiating patch for achieving UWB characteristics and quarter wavelength inverted L shaped strip for achieving 2.45 GHz Bluetooth applications. The first operating band characteristics can be controlled by changing the electrical length of the strip along with coupling gap between the patch and strip. To enhance the impedance bandwidth of second operating band, an equilateral triangular shaped cut has been introduced in the patch. The results demonstrates that the proposed antenna exhibit dual frequency operation from 2.4 to 2.52 GHz and from 3.6 to 10.6 GHz. The antenna has omnidirectional radiation patterns in H-plane, bidirectional patterns in E-plane and acceptable peak gains and radiation efficiencies.

Effect of Slow Wave Structures on Scan Angles in Microstrip Leaky-wave Antennas

Saeid Mohammadpour Jaghargh, **Pejman Rezaei**, **and Javad Soleiman Meiguni**
Faculty of Electrical and Computer Engineering, Semnan University, Semnan, Iran

Abstract— This paper presents two miniaturized slow wave structures in microstrip leaky-wave antennas (MLWAs) which operate about 8 GHz. The effects of these structures on the scan angles have been compared in the paper. The designed interdigital capacitors and folded-back line have been investigated with ADS Momentum software. It has been shown that the interdigital capacitors (IDCs) yield to a broad scan angles from +53 to −74 degree, while the folded-back line inductor scans only the positive angles.

Session 2P13a
SC3: Near-field Optics: Light-matter Interaction Inside a Wavelength Volume 2

Red-shift between Near- and Far-field Electric Intensity Peaks

Alex J. Yuffa and Gorden Videen
Computational & Information Science Directorate, Army Research Laboratory, Adelphi, MD 20783, USA

Abstract— In classical wave scattering by small particles problems, the quantities of general interest are the far-field quantities such as the scattering cross-section. Recent technological advances have made it possible to control the light at the nanoscale by using nanoparticles and nanostructures. At this scale the quantities of interest are related to the near-field and not the far-field as in the classical scenario. A particular quantity of interest in plasmonics is the near-field electric intensity. It has been recently observed that the resonances in the near-field electric intensity are red-shifted with respect to the far-field electric intensity resonances. With the help of a damped harmonic oscillator model, one can demonstrate that the red-shift is caused by the contribution of the evanescent waves to the near-field electric intensity. This model definitely provides valuable physical insight into the problem but it does not provide a value for the red-shift. Clearly an ability to predict the near-field resonances based on the far-field data would be of great practical value to the community. However, to the best of our knowledge, no such formula has appeared in the literature. In fact, currently one computes the red-shift by first numerically computing for the far-field and the near-field resonances and then, taking their difference, which is clearly very time consuming and cumbersome.

In this presentation, we will derive a simple analytical expression for the red-shift between the near- and the far-field electric intensity resonances. This formula will be derived for a cylinder as well as a sphere by using only the Lorenz-Mie theory. We will also demonstrate that our simple formula computes the red-shift within a relative error of one percent. Furthermore, we will discuss possible generalization of our red-shift formula to other particle shapes.

ACKNOWLEDGMENT

This research was supported in part by an appointment to the U.S. Army Research Laboratory Postdoctoral Fellowship Program administered by the Oak Ridge Associated Universities through a cooperative agreement with the U.S. Army Research Laboratory.

Scanning Near-field Optical Spectroscopy of Semipolar InGaN/GaN Single Quantum Wells

Mounir Mensi, **Ruslan Ivanov**, **and Saulius Marcinkevičius**
Department of Materials and Nanophysics
KTH Royal Institute of Technology, Stockholm, Sweden

Abstract— Group III-nitride ternary alloy light emitting devices present outstanding electroluminescence efficiency. However, they typically exhibit band potential fluctuations related to spatial variations of the alloy composition, strains, extended defects, and cation clustering. Such fluctuations may have different consequences on nitride device performance. In some cases, e.g., polar InGaN quantum wells (QWs), localization separates carriers from dislocations reducing the rate of the nonradiative recombination [1]. In addition, for emitters of polarized light based on non- and semipolar QWs, carrier localization may reduce degree of the linear polarization [2]. Detailed understanding of potential fluctuations and their relation to properties of material growth and defects is important for the development of efficient light emitting devices. Since fluctuations occur on the nanoscale, near-field optical techniques, allowing a resolution beyond the diffraction limit should be used.

This presentation will focus on near-field scanning optical spectroscopy of semipolar $(20\bar{2}1)$ plane $In_xGa_{1-x}N/GaN$ single QWs [3–6] for $0.11 \leq x \leq 0.36$. During the near-field scans, the photoluminescence spectra were measured at every point, which allowed performing correlations and statistical analysis of these maps. Results include spatial variations of emission spectra, peak emission wavelength, intensity, spectral width, and polarization ratio of the photoluminescence emission. The nanoscale data revealed by the subwavelength near-field measurement not only provide a deeper understanding of phenomena behind the band potential fluctuations, but also pinpoint directions towards improvement of device efficiency and stability.

REFERENCES

1. Hitzel, F., G. Klewer, S. Lahmann, U. Rossow, and A. Hangleiter, *Phys. Rev. B*, Vol. 72, 081309R, 2005.
2. Liuolia, V., S. Marcinkevičius, Y. D. Lin, H. Ohta, S. P. DenBaars, and S. Nakamura, *J. Appl. Phys.*, Vol. 108, 023101, 2010.
3. Liuolia, V., A. Pinos, S. Marcinkevičius, Y. D. Lin, H. Ohta, S. P. DenBaars, and S. Nakamura, *Appl. Phys. Lett.*, Vol. 97, 151106, 2010.
4. Marcinkevičius, S., K. M. Kelchner, S. Nakamura, S. P. DenBaars, and J. S. Speck, *Appl. Phys. Lett.*, Vol. 102, 101102, 2013.
5. Marcinkevičius, S., Y. Zhao, K. M. Kelchner, S. Nakamura, S. P. DenBaars, and J. S. Speck, *Appl. Phys. Lett.*, Vol. 103, 131116, 2013.
6. Gelžinytė, K., R. Ivanov, S. Marcinkevičius, Y. Zhao, D. L. Becerra, S. Nakamura, S. P. DenBaars, and J. S. Speck, *J. Appl. Phys.*, Vol. 117, 023111, 2015.

Generation of 1D High-frequency Interference Patterns of Evanescent Waves Using All-dielectric Photonic Crystals

E. A. Bezus[1, 2], **E. A. Kadomina**[1, 2], **and L. L. Doskolovich**[1, 2]

[1]Image Processing Systems Institute of the Russian Academy of Sciences, Samara 443001, Russia
[2]Technical Cybernetics Department, Samara State Aerospace University, Samara 443001, Russia

Abstract— During the last decade, many works dedicated to the generation of high-frequency interference patterns of evanescent electromagnetic waves were published due to both fundamental interest and potential applications in nanolithography and optical trapping and manipulation systems. Most of the research was centered on plasmonic structures [1, 2]. In a recent paper, the generation of such patterns in multilayer metal-dielectric structures was explained in terms of the excitation of volume plasmonic modes in hyperbolic metamaterials [3].

In the present work, we study theoretically and numerically the generation of high-frequency interference patterns of evanescent electromagnetic waves with essentially subwavelength period using all-dielectric structures containing a diffraction grating and a one-dimensional photonic crystal. It is shown that high-quality interference patterns with subwavelength hot-spots can be obtained due to resonant enhancement of the evanescent diffraction orders associated with one of the two possible mechanisms: the excitation of Bloch surface waves or the Fabry-Perot resonance of a high-k volume Bloch mode of the photonic crystal. Contrast of the generated patterns is close to unity, while the period is by an order-of-magnitude (10–20 times) smaller than the period of the used diffraction grating. The presented approach can be used in photolithography systems for the fabrication of periodic structures with nanoscale features.

ACKNOWLEDGMENT

This work was financially supported by RSF grant No. 14-19-00796, RFBR grants Nos. 13-07-00464 and 15-07-00548, RF Presidential scholarship No. SP-4554.2013.5.

REFERENCES

1. Liu, Z., Q.-H. Wei, and X. Zhang, "Surface plasmon interference nanolithography," *Nano Lett.*, Vol. 5, 957–961, 2005.
2. Bezus, E. A., D. A. Bykov, L. L. Doskolovich, and I. I. Kadomin, "Diffraction gratings for generating varying-period interference patterns of surface plasmons," *J. Opt. A: Pure Appl. Opt.*, Vol. 10, 095204-5, 2008.
3. Ishii, S., A. V. Kildishev, E. Narimanov, V. M. Shalaev, and V. P. Drachev, "Subwavelength interference pattern from volume plasmon polaritons in a hyperbolic medium," *Laser & Photon. Rev.*, Vol. 7, 265–271, 2013.

Polarisation Imaging Reveals Near-field Properties of Materials

P. Török, C. A. Macías-Romero, and M. R. Foreman
Department of Physics, Imperial College London, Prince Consort Rd, London SW7 2BW, UK

Abstract—

Introduction: Imaging systems have provided the means to gather information about the physical world throughout history. Recent years have witnessed the development of numerous super-resolution imaging schemes. These techniques however forego the greater information content afforded by polarisation, rather than irradiance, measurements. In this talk we confirm both experimentally and theoretically that far-field polarization imaging allows for continuous nanometric spatial variations in the polarization to be resolved. We present optical measurements of nanostructures resolving spatial polarization changes on the scale of tenths of nanometers. In optical data storage, polarization encoding via nanometric pits is furthermore shown to allow a sevenfold capacity increase.

Optical System: The optical system of a Müller matrix polarimeter microscope is shown in the figure below. The light of the laser is passed through a polarisation state generator that is capable of producing an arbitrary state of polarisation. The rest of the optical path is identical to that of a reciprocal confocal microscope. In the return path light passing through the pinhole is recollimated and split by a non-polarising beam splitter (NPBS). The polarisation state of the light emerging from the NPBS is then analyser by a Stokes polarimeter. By imparting at least four different states of polarisation on the incident light by the polarisation state generator, each one of these producing four intensity measurements in the Stoke polarimeter, it is possible to determine the Müller matrix of a given sample. The possession of this information in turns permits one to determine a wealth of information pertaining to the sample, such as polarisance, diattenuation, etc..

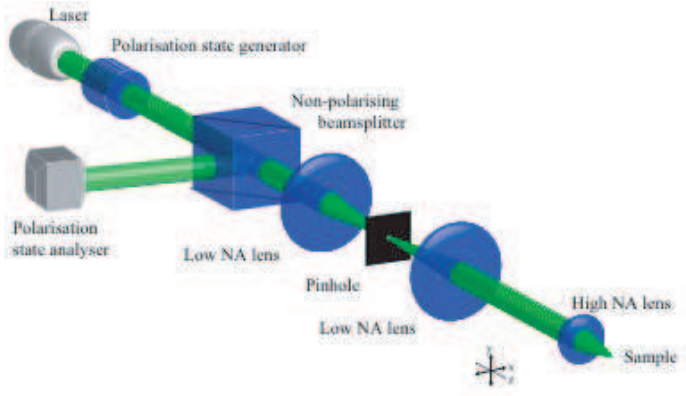

Discussion: It is possible to show using first principle arguments and more conventional optical system analysis that the determination of polarisation state in the far-field is not limited by Abbe's diffraction limit, even though it is emphasised that "breaking the diffraction limit" is not claimed by the present authors. The talk will present experimental images revealing that certain structures can be distinguished by a Müller matrix polarimeter microscope even when their spatial separation does not exceed 50 nm.

Structure-mediated Nano-biophotonics

Jesper Glückstad, Mark Villangca, Andrew Bañas, and Darwin Palima
DTU Fotonik, Department of Photonics Engineering
Technical University of Denmark, DK-2800 Kgs. Lyngby, Denmark

Abstract— The latest Nobel Prize in chemistry on Nanoscopy has cemented that optics is a key enabling technology for getting a grasp of the micro- and nano-world. By creatively combining a host of complementary approaches one can today realize advanced optical modalities that integrate an increasing number of functionalities and augment not just passive observation but also active access and control over the nanoworld [1, 2]. Using a merger of light and matter sculpting, we have 2PP-fabricated free-floating waveguides that can be optically trapped and "remote-controlled" in a volume; hence coined Wave-guided Optical Waveguides (WOWs). Combining micro-fabrication with optical trapping and manipulation allows us to exploit these WOWs in versatile and dynamically reconfigurable architectures [3]. A plurality of counter-propagating beam-traps relayed to the trapping volume by low-NA microscope objectives on our Biophotonics Worskstation (BWS) [4] control the WOW-structures demonstrating the possibility for a structure-mediated paradigm where micron-sized tools are used to achieve optical near-field tip-size access. However, realizing the full potential of this new structure-mediated approach in challenging microscopic geometries requires a versatile 3D light coupling that can dynamically track a plurality of WOWs to ensure continuous optimal light coupling on the fly.

To maintain high light throughput for the WOWs, we have integrated computer generated holography that can dynamically control the 3D focus position of the coupling beams. Our results show that we can simultaneously maneuver the WOWs in 3D space while dynamically coupling light through them (see Figs. 1(a) and 1(b)) [5]. This structure-mediated approach enables a host of new microscopic functionalities. WOWs with metal-coated tips can exploit plasmonic effects to achieve extreme confinement for localized light excitation and acquisition.

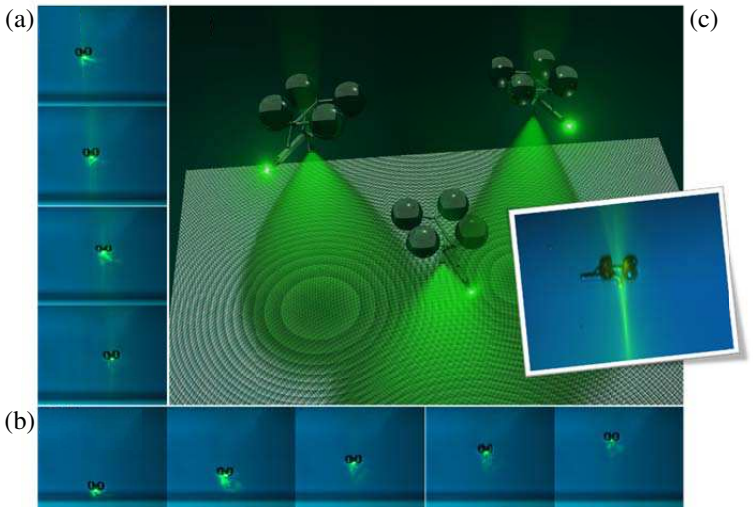

Figure 1: Dynamic coupling of light to 3D-manipulated Wave-guided Optical Waveguides (WOWs). The coupling beams are positioned holographically at the input facets of each WOW making targeted light-delivery at the sub-micron level possible at the WOW-tips. Experimental results show (a) lateral and (b) axial tracking of the coupling beams. (c) A concept art showing the holographically coupled WOWs and snapshot from the experiment.

Nanowires that exhibit particular optical properites can be attached to the WOWs to obtain tunable and fully maneuverable "nano-torches". Another potential application is for advanced Tip-Enhanced Raman Spectroscopy in a full 3D-manuevarable configuration. The micro-to-nano light coupling and the possibility of integrating material transport in the WOW-structures can be a new gate-way for life sciences at the sub-cellular level. The design possibilities offered by 2PP-fabricated WOWs, the augmented holographic light coupling combined with the advanced 3D micromanipulation opens the possibility for performing exciting precision engineered light-matter interaction where it is needed.

REFERENCES

1. Palima, D. and J. Glückstad, *Laser Photon. Rev.*, Vol. 7, 478–494, 2013.
2. Glückstad, J., *Nat. Photonics*, Vol. 5, 7–8, 2011.
3. Palima, D., et al., *Opt. Express*, Vol. 20, 2004–2014, 2012.
4. Ulriksen, H.-U., et al., *J. Eur. Opt. Soc. Rapid Publ.*, Vol. 3, 08034, 2008.
5. Villangca, M.,et al., *Opt. Express*, Vol. 22, 17880–17889, 2014.

Cascaded Field Enhancement in a Multi-scale Nanoparticle-in-cavity Plasmonic Nanoantenna Array Boosted by Fano Resonance

Benfeng Bai and Zhendong Zhu
State Key Laboratory of Precision Measurement Technology and Instruments
Department of Precision Instrument, Tsinghua University, Beijing 100084, China

Abstract— Strong optical near field (i.e., field "hot spots") can be generated in properly designed metallic nanostructures via the coupling and hybridization of localized surface plasmon modes [1], which can greatly enhance the light-matter interaction in the vicinity of the structures. In this work, we propose and realize a nanoparticle-in-cavity (PIC) plasmonic nanoantenna array, in which a 20 nm gold nanoparticle is located at the bottom of a 120 nm truncated gold void in each nanoantenna (see Fig. 1(a)). In this multi-scale system, cascaded field enhancement (CFE) [2] can be realized so that extremely strong and highly confined field hot spots can be generated in nanoscale volumes (Fig. 1(c)). Furthermore, by utilizing and tuning the mode hybridization between the plasmonic dark mode of the gold nanoparticle and a high-order cavity bright mode of the nanovoid, strong Fano resonance can be generated at a target wavelength of 720 nm (Fig. 1(b)), which can significantly boost the CFE. The maximum enhancement factor of the localized field amplitude can reach 10^3. We have developed a cost-effective, efficient and reliable nanofabrication method based on room-temperature nanoimprinting and anisotropic reactive ion etching to fabricate the PIC array (Fig. 1(d)). With this technique, only one gold nanoparticle is guaranteed in each nanovoid and the nanoparticle size can be finely controlled, which are crucial for realizing the CFE effect. To demonstrate the performance of the PIC array, the fabricated PIC samples are employed as active SERS substrates for detecting 4-ATP molecules. The experimentally obtained SERS enhancement factor is as high as 2×10^7, verifying the field enhancement and the potential application of this device.

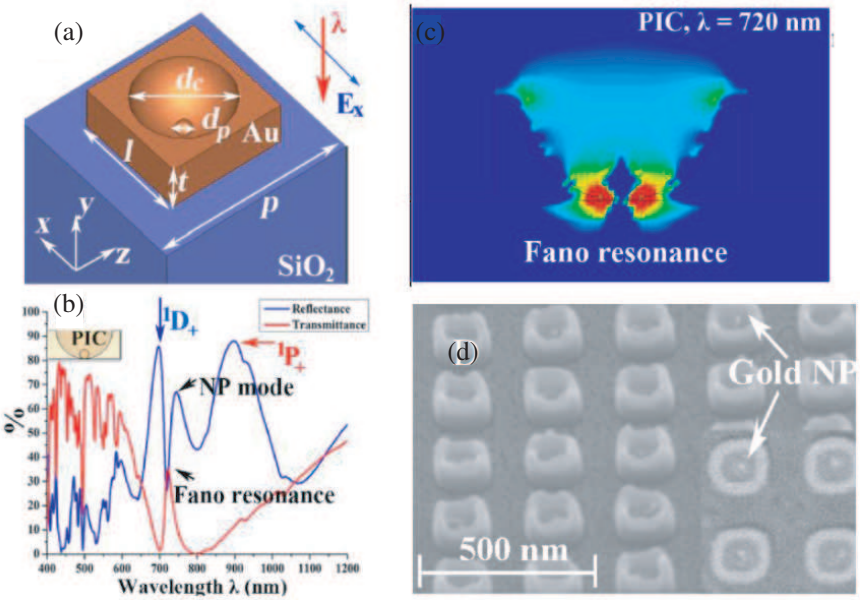

Figure 1: (a) Schematic of the PIC array; (b) Far-field and (c) near-field responses of the PIC array; (d) A fabricated PIC sample.

REFERENCES

1. Halas, N. J., et al., *Chem. Rev.*, Vol. 111, 3913, 2011.
2. Kravets, V. G., et al., *Phys. Rev. Lett.*, Vol. 105, 246806, 2010.

Demonstration of Unusual Nanoantenna Array Modes through Direct Reconstruction of the Near-field Signal

I. S. Sinev[1], **P. M. Voroshilov**[1, 2], **I. S. Mukhin**[1, 3], **A. I. Denisyuk**[1], **M. E. Guzhva**[1, 4], **A. K. Samusev**[1], **P. A. Belov**[1], **and C. R. Simovski**[1, 2]

[1]ITMO University, St. Petersburg 197101, Russia
[2]School of Electric and Electronic Engineers, Aalto University, Aalto 00076, Finland
[3]St. Petersburg Academic University, St. Petersburg 194021, Russia
[4]St. Petersburg State Polytechnical University, St. Petersburg 195251, Russia

Abstract— We perform complex investigation of the distribution of electromagnetic fields in the vicinity of an array of silver nanoantennas, which can operate as an efficient light trapping structure in the visible spectral range. In theory, this array should support unusual collective modes (referred to as domino-modes [1]) that possess an advantageous distribution of local electric fields, ensuring both strong field localization beneath nanoantennas and a low level of optical losses inside the metal. To study the distribution of the electromagnetic field near the array we use an aperture-type near-field scanning optical microscope (NSOM) with oblique excitation of the sample. We obtain near-field patterns that show excellent agreement with the NSOM signal which we directly reconstruct from rigorous numerical simulations using an approach based on the electromagnetic reciprocity theorem [2, 3]. This model relates the fields picked up by the near-field probe to the fields that this probe emits when excited by a point (dipole) source placed at the position of the detector. The approach allows us to account both for the non-locality of the NSOM detection process and the shape of the near-field probe. The agreement between theory and experiment allows us to claim the first-time experimental verification of the existence of domino-modes in an array of silver nanoantennas in the visible range.

We also demonstrate that the model of the near-field probe sensitivity based on the reciprocity theorem is very powerful and can be successfully used for the interpretation of the observed NSOM patterns, even in the case of complex geometry with oblique excitation and for structures made of high-index materials, where the probe-sample interaction can be significant. This encourages us to use this model for interpretation of the NSOM signal obtained from the most complex of structures.

REFERENCES

1. Simovski, C., D. Morits, P. Voroshilov, M. Guzhva, P. Belov, and Y. Kivshar, "Enhanced efficiency of light-trapping nanoantenna arrays for thin-film solar cells," *Opt. Express*, Vol. 21, A714–A725, 2013.
2. Porto, J. A., R. Carminati, and J.-J. Greffet, "Theory of electromagnetic field imaging and spectroscopy in scanning near-field optical microscopy," *J. Appl. Phys.*, Vol. 88, No. 8, 4845–4850, 2000.
3. Sinev, I. S., P. M. Voroshilov, I. S. Mukhin, A. I. Denisyuk, M. E. Guzhva, A. K. Samusev, P. A. Belov, and C. R. Simovski, "Demonstration of unusual nanoantenna array modes through direct reconstruction of the near-field signal," *Nanoscale*, Vol. 7, 765–770, 2015.

On the Effective Volume of Mie Resonators

X. Zambrana-Puyalto and N. Bonod
CNRS, Centrale Marseille, Institut Fresnel UMR 7249, Aix-Marseille Université, Marseille 13013, France

Abstract— We show that the effective volume of spherical resonators depends on ten parameters. We relate each of these parameters to meaningful classical parameters such as the orientation and position of the emitting dipole who gives rise to the effective volumes; Mie-like coefficients; and multipolar decomposition coefficients. As a consequence, we find that given a multipolar order j, the average electric effective volume (for an electric dipolar emitter) is always smaller than the magnetic one. This fact is reversed when a magnetic dipole is coupled to the same resonator.

Introduction: In his seminal letter, Purcell showed that the spontaneous emission of a radio-frequency dipolar emitter in contact with a resonator is enhanced by a factor F [1]. He defined it as $F = 6\pi c^3 Q/\omega^3 V$ where ω is the emission frequency of the dipolar emitter, Q the quality factor of the resonator, and V the effective volume of the resonator. Since then, the Purcell factor has been used in different domains, e.g., optics. It has been known for many years that the Purcell factor gives a good estimation of the enhancement of the decay rates when i) the resonator only supports one mode, ii) when the dipole is oriented along the polarization direction of the mode of the cavity, and iii) when the dipole is located at the modes' maximum [2]. Then, the effective volume is defined as $V = \int_V \epsilon(r)\|\mathbf{E}\|^2 dV$. However, it was seen that F cannot be directly applied in nanophotonics to obtain the enhancement of spontaneous decay rates. In order to do that, very recent works have been done to modify the definition of F [2–4]. The definition of effective volume has been changed to $V_\mu = 1/(\mathbf{p}\cdot\mathbf{E})^2$ where $\mathbf{u_p}$ is the dipolar moment of the emitter, and $\mathbf{E}_\mu$ is a cavity normal mode [3, 4].

Results: Here, we use Mie resonators to give a classical meaning to the effective volume defined by the expression above [5]. It is seen that the effective volume expresses the partial coupling between a dipolar emitter and the normal mode in consideration. Because of that, its expression can be given as a function of the translation-addition coefficients of multipolar theory [5]. As a result, its value can be predicted for some symmetric cases without doing any calculation [5]. Then, using these facts, we compute the average effective volume of an ensemble of uniformly distributed and randomly oriented dipoles for different normal modes of a Si-based resonator. It is observed that the average effective volume is always smaller than the magnetic one [5]. Our calculations can also be applied for magnetic dipoles.

REFERENCES

1. Purcell, E. M., "Spontaneous emission probabilities at radio frequencies," *Phys. Rev.*, Vol. 69, 681, 1946.
2. Kristensen, P. T. and S. Hughes, "Modes and mode volumes of leaky optical cavities and plasmonic nanoresonators," *ACS Phot.*, Vol. 1, No. 1, 2–10, 2013.
3. Sauvan, C., J.-P. Hugonin, I. S. Maksymov, and P. Lalanne, "Theory of the spontaneous optical emission of nanosize photonic and plasmon resonators," *Phys. Rev. Lett.*, Vol. 110, No. 23, 237401, 2013.
4. Muljarov, E. A., M. B. Doost, and W. Langbein, "Exact mode volume and Purcell factor of open optical systems," arXiv:1409.6877, 2014.
5. Zambrana-Puyalto, X. and N. Bonod, "Purcell factor of Mie resonators featuring electric and magnetic modes," arXiv:1501.07452, 2015.

Session 2P13b
FocusSession.SC3: Technologies for On-chip Optical Networking

Imaging with Multimode Fibers

Demetri Psaltis
Ecole Polytechnique Federale de Lausanne (EPFL), Switzerland

Abstract— Holography and phase conjugation were proposed in the middle 1960's for correcting the distortions in imaging systems due to aberrating or scattering media. These early methods have been revisited in recent years and successful experimental demonstrations have been reported with digital holographic methods in which the recording and reconstruction of the hologram is done with the help of a digital computer. The digital holographic methods offer a lot more flexibility and control compared to the all-optical methods of the past making holographic imaging much more practical. In addition, adaptive wavefront shaping techniques have been recently developed providing a set of related and synergistic methods for imaging in complex media. In this presentation we will focus primarily on the application of the modern tools of holography to the control of light transmission through multi-mode fibers. The modal dispersion that severely scrambles images propagating through multi-mode fibers can be compensated allowing us to exploit the many degrees of freedom available in the multi-mode fiber for imaging and sensing.

Fiber Lasers and Electro-optic Polymer/Si Waveguide Modulators and Their Applications

N. Peyghambarian
University of Arizona, College of Optical Sciences, USA

Abstract— This talk will be focused on (1) fiber lasers and their bio-medical applications and (2) electro-optic polymer modulators for telecom applications. Phosphate, telluride, and fluoride glasses allow new fiber laser frequencies. Some nonlinear effects including optical parametric oscillators (OPO), SRS and SBS extend the operating wavelengths while others like SBS prevent high power operation. Our recent advances in fiber lasers will be summarized including demonstration of a synchronously pumped fiber optical parametric oscillator (FOPO) operating in the normal dispersion regime. The second part of the talk will focus on the use of EO polymers with r_{33} of = 200–300 pm/V (r_{33} of $LiNbO_3$ = 30 pm/V) in polymer/Si nanowire modulators. Centimeter-length modulators will also be described. Polymers low dielectric constant and low capacitance make them suitable for > 100 G telecom applications.

Spectral Engineering with Tunable Photonic Molecules

Mario C. M. M. Souza[1], **Luis A. M. Barea**[2], **and Newton C. Frateschi**[1]

[1]Device Research Laboratory, Applied Physics Department, IFGW, UNICAMP, Campinas, Brazil
[2]Electrical Engineering Department, Federal University of São Carlos, São Carlos, Brazil

Abstract— The ability to control the spectral features of compact photonic devices is a key capability for photonic integration. Diligent device design and active control allow flexible spectral responses that can be tailored to deliver complex optical signal processing functionalities with low power consumption in a reduced footprint.

We present our recent advances using passive and actively controlled silicon photonic molecules for enhanced optical signal processing [1–3]. Based on arrangements of multiple coupled microresonators, these devices overcome the intrinsic interdependence between photonic lifetime, resonance spacing and footprint for single microresonators, introducing a new degree of freedom to perform spectral engineering. Carrier recycling [2], potential for modulation beyond resonance line-width limit, and low-power wavelength multicasting using multiple-split resonances that overcome the trade-off between the cavity free spectral range (FSR) and optical field enhancement [3] are demonstrated in micrometer-scale devices. Using active control, we will demonstrate reconfigurable and continuously tunable mode-splitting in a multi-GHz range with very low resonance shift using an embedded coupled microring device to control the excitation of counter-travelling modes (Figs. 1(a)–(b)). The change in phase response of tunable mode-split resonances is also shown to transit between distinct dispersion regimes, allowing for controllable optical pulse delay/advancement (Fig. 1(c)). These features will be shown to provide great flexibility in designing devices for optical signal processing using very compact structures based on silicon-on-insulator technology.

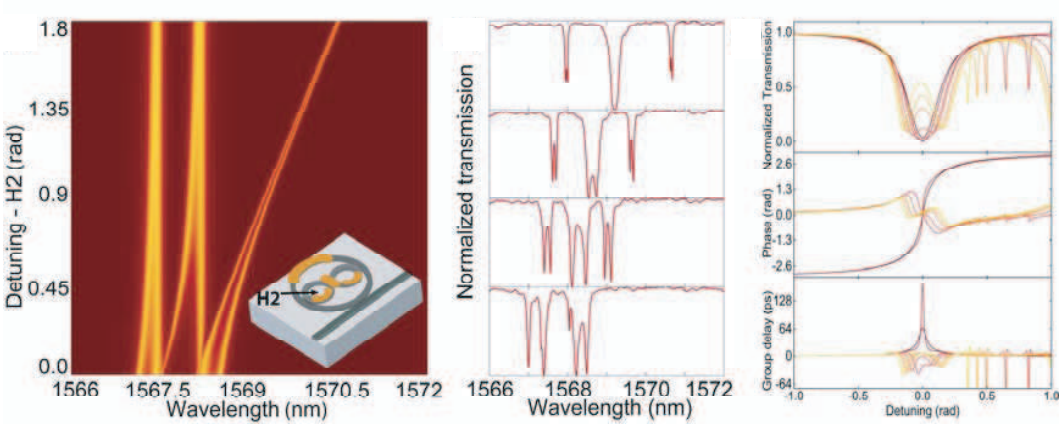

Figure 1: (a), (b) Tunable mode-splitting using embedded coupled microcavities when cavity H2 is detuned. (c) The dispersion regime is changed from normal to anomalous as mode-splitting increases in the central resonance, associated with the outer ring, leading to continuous tuning from light delay to advancement.

REFERENCES

1. Barea, L. A. M., F. Vallini, G. F. M. de Rezende, and N. C. Frateschi, "Spectral engineering with CMOS compatible SOI photonic molecules," *IEEE Photonics J.*, Vol. 5, 2202717, 2013.
2. Barea, L. A. M., F. Vallini, P. F. Jarschel, and N. C. Frateschi, "Silicon technology compatible photonic molecules for compact optical signal processing," *Appl. Phys. Lett.*, Vol. 103, 201102, 2013.
3. Souza, M. C. M. M., L. A. M. Barea, F. Vallini, G. F. M. Rezende, G. S. Wiederhecker, and N. C. Frateschi, "Embedded coupled microrings with high-finesse and close-spaced resonances for optical signal processing," *Opt. Express*, Vol. 22, 10430–10438, 2014.

Si Photonics for Exascale Computing

Paul S. Davids
Sandia National Laboratories, Albuquerque, NM 87185, USA

Abstract— Optical interconnects have been proposed for more than 25 years as the solution to distance and bandwidth limitations of electrical interconnects. They are currently used in long distance and metro-distance telecommunications and are making extensive inroads in data-center and high performance computing applications. Chip-scale optical interconnects based on Si photonics leverages advanced CMOS process technology but is constrained by the material systems used in standard CMOS processing. Recent advances in low power, small capacitance Si photonic modulators and detectors allows for the realization of compact low power chip-scale transceivers that can provide high bandwidth optical IO for advanced computing applications. In order to achieve the promise of Si photonics in exascale computing, heterogeneous integration of new materials and devices, such as III-V laser sources, and flip chip bonding of high performance electronics with Si photonics are needed to extend the functionality and provides new capability within the Si photonics platform.

In this talk, we will examine advances in the integration and new device architectures that enable low power, high bandwidth communications for exascale computing and also examine extension to quantum Si photonics that could lead to advanced communication networks that promise both algorithmic and physical security.

Photonics as a More-than-Moore Device Technology within Sub-100 nm SOI CMOS

M. A. Popović[1], M. T. Wade[1], J. S. Orcutt[2, 4], J. M. Shainline[1, 5], C. Sun[3], M. Georgas[2], B. Moss[2], F. Pavanello[1], J. Notaros[1], L. Alloatti[2], R. Kumar[1], Yu-Hsin Chen[3], A. Atabaki[2], J. Leu[2], V. Stojanović[2, 3], and R. J. Ram[2]

[1]University of Colorado Boulder, USA
[2]Massachusetts Institute of Technology, USA
[3]University of California Berkeley, USA
[4]IBM T.J. Watson Research Center, USA
[5]National Institute of Standards and Technology, USA

Abstract— I review recent progress of a collaborative effort (by Stojanović, Ram and Popović research groups) to enable the design of photonic devices, and complete on-chip electronic-photonic systems and interfaces, directly in standard microelectronics complementary-metal-oxide-semiconductor (CMOS) processes in a microprocessor foundry, with no in-foundry process modifications. This approach, "zero-change CMOS photonics", allows tight and large-scale mono-lithic integration of silicon photonics with state-of-the-art (sub-100 nm-node) microelectronics, here a 45 nm silicon-on-insulator (SOI) CMOS process. Very large scale integration is enabled by the same manufacturability design methodology that has enabled CMOS microelectronics to yield billions of working transistors on a chip. It enables natural scale-up to manufacturing, and rapid advances in device design due to process repeatability. Our initial driver application is to address the processor-to-memory communication energy bottleneck. In this talk, I will highlight the challenges, and unique opportunities, for photonic device design within an advanced-node scaled CMOS process, using a couple of examples, and their impact through demonstrations of mono-lithically integrated electronic-photonic subsystems on chip. First, I will describe energy-efficient modulators based on an interleaved junction that take advantage of the high resolution of the sub-100 nm (immersion lithography) CMOS process dopant implant masks. They enabled mono-lithically integrated electronic-photonic transmitters on chip (modulator + driver) with record 20 fJ/bit wall plug energy/bit. Second, I will describe array nanoantenna grating couplers that allow efficient and ultra-wideband unidirectional light emission and Gaussian beam forming in unmodified CMOS, and enable 1 dB or better optical coupling from fiber to a 45 nm-node CMOS chip. Last, I will briefly review other unique device technologies that provide a complete photonics platform, and will show results demonstrating the same photonics infrastructure smoothly transitioned one node down in the same CMOS technology strand, into the 32 nm node. These are encouraging developments for the prospects of monolithic electronics-photonics integration. Beyond processor-to-memory interconnects, approaching photonics as a "More-than-Moore" technology inside advanced CMOS promises to enable VLSI electronic-photonic chip platforms tailored to a vast array of emerging applications, from optical and acoustic sensing, high-speed signal processing, RF and optical metrology and clocks, through to analog computation and quantum technology.

Developing a Poly Silicon Photonic Platform on Bulk CMOS

Amir H. Atabaki[1], **C. Sun**[1], **M. Georgas**[1], **J. S. Orcutt**[1], **F. Pavanello**[2], **L. Alloatti**[1], **B. R. Moss**[1], **Y.-H. Chen**[1], **J. Shainline**[2], **M. Wade**[2], **K. Mehta**[1], **K. Nammari**[2], **E. Timurdogan**[1], **D. Miller**[3], **O. Tehar-Zahav**[3], **Z. Sternberg**[3], **J. C. Leu**[1], **J. Chong**[1], **R. Bafrali**[3], **G. Sandhu**[3], **M. Watts**[1], **R. Meade**[3], **M. A. Popović**[3], **V. Stojanović**[1, 4], **and R. J. Ram**[1]

[1]Department of Electrical Engineering and Computer Science
Massachusetts Institute of Technology, 77 Massachusetts Ave, Cambridge, Massachusetts 02139, USA
[2]Department of Electrical, Computer and Energy Engineering
University of Colorado at Boulder, Boulder, Colorado 80309, USA
[3]Micron Technology, USA
[4]Department of Electrical Engineering and Computer Sciences
University of California, Berkeley, CA, USA

Abstract— Bulk CMOS processes make up for the majority of manufactured electronics for applications as diverse as microprocessors, FPGAs, foundry ASICs and DRAM. Integration of photonics in bulk CMOS has the potential to provide low-power, low-latency interconnects for all of these applications. The main challenge for achieving this goal has been the focus on thick silicon-on-insulator substrates for photonics whereas the majority of CMOS transistors are fabricated directly on bulk Silicon. This fact has driven two-chip hybrid solutions that are not able to leverage the savings in energy, packaging, and manufacturing costs enabled by monolithic electronics and photonics.

In this work, we present a photonics platform in the same polysilicon that is used as the transistor gate in bulk CMOS processes. Through materials and process optimization low-loss polysilicon waveguides using the gate polysilicon have been demonstrated. Waveguides formed from high temperature columnar deposited polysilicon with chemical mechanical polishing (CMP) for improving the top surface roughness; and low temperature amorphous-deposited polysilicon with high temperature anneals without the need for CMP have been demonstrated. These waveguides can be embedded with appropriately doped diode junctions to realize both depletion modulators [1] and all-silicon photodetectors [2] at 1280–1550 nm. The process modules required to realize integrated photonics are inserted without requiring any modification to the performance of electronics.

Recently, passive and active photonic devices have been monolithically integrated with CMOS electronics used for driver and control electric circuits to implement monolithic optical receivers and transmitters that have enabled the successful demonstration of 5 Gbps optical links between two transceiver chips [3]. This demonstration shows the capabilities of the developed polysilicon material platform for electronic photonic integration for a wide range of applications [4].

REFERENCES

1. Shainline, J., et al., "Depletion-mode polysilicon optical modulators in a bulk complementary metal-oxide semiconductor process," *Opt. Lett.*, Vol. 38, 2729–2731, 2013.
2. Mehta, K. K., et al., "High-Q CMOS-integrated photonic crystal microcavity devices," *Scientific Reports*, Vol. 4, 2014.
3. Sun, C., et al., "A monolithically-integrated chip-to-chip optical link in bulk CMOS," *Symposium on VLSI Circuits Digest of Technical Papers*, Vol. 1, No. 2, 10–13, 2014.
4. Meade, R., et al., "Integration of silicon photonics in a bulk CMOS memory flow," *IEEE Optical Interconnects Conference*, 114–115, 2013.

Polarized Metal/Semiconductor Sources Based on Confined Tamm Plasmons

C. Symonds[1], **G. Lheureux**[1], **S. Azzini**[1], **A. Lemaitre**[2], **P. Senellart**[2], **J. J. Greffet**[3], **C. Sauvan**[3], **and J. Bellessa**[1]

[1]Institut Lumière Matière, Université de Lyon
UMR5306 Université Lyon 1-CNRS, Villeurbanne 69622, France
[2]Laboratoire de Photonique et de Nanostructures, CNRS UPR20
Route de Nozay, Marcoussis F-91460, France
[3]Laboratoire Charles Fabry, Institut d'Optique, CNRS
University Paris-Sud, 2 avenue Fresnel, Palaiseau cedex 91127, France

Abstract— Hybrid metal/dielectric structures are very promising for the fabrication of compact and efficient optical sources. Beside the development of micro- and nano-lasers based on surface plasmons, other surface modes presenting less damping than conventional plasmons can be used such as Tamm plasmons. These surface modes appear at the boundary between a distributed Bragg reflector (DBR) and a metallic layer [1], and present both the advantages of surface plasmons and of microcavities photonic modes. In particular, the losses are reduced compared to a conventional plasmon. We will describe some features of semiconductor quantum wells coupled to extended Tamm modes, like strong coupling with the excitons and lasing [2, 3].

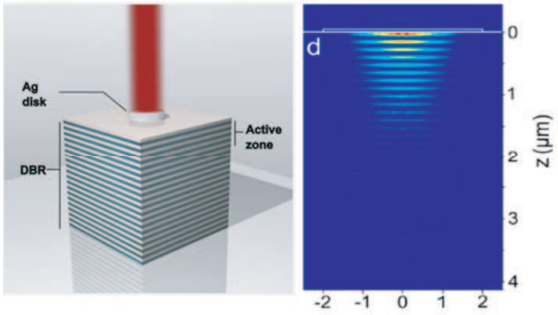

Figure 1: (a) Confined Tamm structure and (b) electric field associated with the Tamm mode.

The main advantage of the Tamm modes lies in the easy confinement of the mode which can be obtained by structuring the metallic part of the structure [4]. The reduction of the mode volume leads to an efficient control of the spontaneous emission (increased beta factor), making Tamm confined structures well suited for single photon emitters and lasers. We will show that confined Tamm plasmon modes can be advantageously exploited for the realization of new kind of metal/semiconductor lasers. Laser emission is studied for Tamm structures with various diameters of the metallic disks which provide the confinement. A reduction of the threshold with the size is observed.

The easy control of the mode properties offered by the patterning of the metallic layer can be applied to the control of the polarization of the emission. Polarization effects in asymmetrical Tamm structures will be discussed. Laser emission with a degree of linear polarization of more than 90% is demonstrated. The polarization can be controlled by tuning the gain of the quantum wells with the Tamm resonance.

REFERENCES

1. Kaliteevski, M., I. Iorsh, S. Brand, R. A. Abram, J. M. Chamberlain, A. V. Kavokin, and I. A. Shelykh, *Physical Review B*, Vol. 76, 165415, 2007.
2. Symonds, C., A. Lemaître, E. Homeyer, J. C. Plenet, and J. Bellessa, *Applied Physics Letters*, Vol. 95, 151114, 2009.
3. Symonds, C., A. Lemaître, P. Senellart, M. H. Jomaa, S. A. Guebrou, E. Homeyer, G. Brucoli, and J. Bellessa, *Applied Physics Letters*, Vol. 100, 121122, 2012.

4. Gazzano, O., S. M. de Vasconcellos, K. Gauthron, C. Symonds, J. Bloch, P. Voisin, J. Bellessa, A. Lemaitre, and P. Senellart, *Physical Review Letters*, Vol. 107, 247402, 2011.

Metal-coated Patch Nanolaser Resonators Coupled with a Waveguide

Qian Ding, **Amit Mizrahi**, **Yehaiahu Fainman**, **and Vitaliy Lomakin**
University of California, San Diego, USA

Abstract— An important component to enable miniaturized and integrated photonic circuits is small lasers, which can be required to be smaller than the wavelength of light. In this work, we present electromagnetic design and modeling of nanoscale laser resonators that are smaller than the wavelength of light in all dimensions, including the modal volume extent. The resonators are based on using a low-index dielectric shield layers surrounding a high index core, both placed between two metallic patches. The combination of the high- and low-index dielectric material as well as the metal patches allows significantly reducing both metal and radiation losses. The presented structures are suitable for both optical and electrical pumping, and are smaller than the vacuum wavelength in all three dimensions. The are shown to have a low threshold gain for lasing at room-temperature. Further, it is shown that shifting the gain (high-index) core enables controlled coupling of the resonator electromagnetic modes into a waveguide, opening opportunities for chip-scale integration. It also provides control of the radiation pattern of the resonator. The work includes a analytical analysis of the resonant frequencies and estimates of the threshold gain of the standalone resonators and numerical modeling supporting the analytical findings. The work also includes the analysis of the resonator radiation patterns as well as the resonator coupling to the guided modes of a dielectric waveguide.

Nanoscale Engineering Optical Nonlinearities and Nanoemitters

Y. Fainman
Department of Electrical and Computer Engineering, University of California, San Diego
9500 Gilman Drive, La Jolla, California 92093-0407, USA

Abstract— This paper discusses nanoscale engineered second order nonlinearities in silicon and a 3-D confined metal-dielectric-semiconductor resonant gain geometries used to create a new type of nanolasers for chip-scale integration of photonic information systems. The integration of a photonic information system onto a single chip requires great research effort toward miniaturization of the optical components, similar to the effort that has led to the extensive miniaturization of electronic components. For applications involving a photonics layer between different components on the same chip, the photonic components must be comparable in size to the electronic components, and minimally interfer with each other when densely packed. Such future systems, further require the discovery of new technologies that can operate not only at ultrafast rates ($< 1\,\mathrm{ps}$), but also at extremely low energies, and with low levels of insertion loss. Additionally, future technologies will need to be highly compact, as well as resilient to temperature change. Moreover, the device designs should provide scalability with respect to the operating wavelength, and the optical carrier should be allowed to range in a broad spectral range to support the necessary aggregate information bandwidth. Our most recent work emphasizes the construction of optical subsystems directly on-chip, with the same lithographic tools as the surrounding electronics.

As specific example of our most recent work towards these goals, we present nanoscale engineered second order nonlinearities in silicon. Strained silicon's nonlinear properties were demonstrated, but despite recent accomplishments, the physical mechanisms behind strained silicon's characteristics remain poorly understood. Therefore, the calculations of scaling coefficients which relate the nonlinearity to the local strain gradient are critical to the design of future devices implementing strained silicon. We theoretically analyzed the breaking of symmetry which occurs in silicon as a result of asymmetric strain. We also established phenomenological relationships between two of strained silicons nonlinear components, $\chi^{(2)}_{xxy}$ and $\chi^{(2)}_{yyy}$, and the local strain gradient. To verify our prediction of these nonzero tensor components, we fabricated Fabry-Perot resonators from silicon on insulator (SOI) waveguides strained by silicon nitride. By applying a positive and negative voltage of 25 volts vertically across the waveguides, we induced and measured shifts in the resonances exhibited by the transmission spectra. These shifts correspond to nonlinearities of $\chi^{(2)}_{xxy,eff} = 29.6\,\mathrm{pm/V}$ and $\chi^{(2)}_{yyy,eff} = 44.5\,\mathrm{pm/V}$. By combining our experimentally obtained optical nonlinearities with finite element model simulations, we defined and calculated two scaling coefficients which linearly translated the local strain gradient to the local nonlinearity. We obtained $C_{xxy} = \chi^{(2)}_{xxy}/(de_{xx}/dy) = 2.34(10^{-15})\,\mathrm{m^2/V}$ and $C_{xxy} = \chi^{(2)}_{yyy}/(de_{xx}/dy) = 7.23(10^{-15})\,\mathrm{m^2/V}$. Using these values, we were able to map local nonlinearities exhibited by our waveguides.

For construction of compact nanolasers and light emitters we incorporate metals to reduce the size of the resonator in all 3-D. The modes in such 3-D cavities can be grouped into two main categories: (i) surface bound (that is, surface plasmon polariton (SPP)) resonant modes and (ii) conventional resonant modes within the metal cavity. Although highly confined, the plasmonic modes are lossy and the lasing gain threshold for such cavities can be very large. However, the negative permittivity of metals enables them to act as efficient mirrors, leading to the second class of metallo-dielectric cavity modes, which can be viewed as lossy approximations of the modes in a perfectly conducting metal resonator. In this type of cavity it is possible to achieve higher Q factors and lower lasing gain thresholds, albeit at the expense of reduced mode confinement. Specifically, we describe two types of metal-dielectric 3-D resonators: (a) a composite metal-dielectric-semiconductor cavity where the low index dielectric acts as a shield to reduce the loss into the metal and (b) a coaxial resonator that supports a TEM-like mode which has no cut-off and the physical size of the cavity can be infinitely scaled down in lateral dimensions.

Session 2P14
SC3: Optical Microcavities and Waveguides 1

Real Time Single Nano-particle Detection and Sizing thru Whispering Gallery Micro-global Positioning

David Keng[1, 2] **and Stephen Arnold**[1]

[1]MicroParticlePhotoPhysics Lab
NYU Polytechnic School of Engineering, Brooklyn, NY 11201, USA
[2]MP3Laser, Inc., USA

Abstract— Over the past decade, Whispering Gallery Mode (WGM) based optical sensors have demonstrated the ultimate goal of real-time single nano-particle sensing in an aqueous environment; and this achievement has led to the detection of individual virions and single protein molecules from WGM frequency shifts that are proportional both to the volume of the particle and relative intensity at the biding location. However, stochastic random walk of nano-particles in aqueous environment leads to random binding locations on the WGM's sensor surface, causing large variations in the WGM frequency shift, and thereby making real-time sizing problematic. This has made researchers rely on a statistical sizing approach in which the largest signal from an ensemble is associated with equatorial binding, where particle size is extracted from the frequency shift signal. Here we have devised a simple method for determining the size of a nanoparticle in just one binding event by locating its latitudinal position using the shifts of two polar modes of a slightly eccentric WGM spheroidal resonator [1].

Due to the eccentricity of almost all fiber taper driven "micro-spherical" resonators, the $2l + 1$ degeneracy of WGM modes ($-l < m < l$) is lifted and the modes having different m values for a given l are individually accessible. The equatorial mode ($l - |m| = 0$) is concentrated near the equator and has the highest sensitivity. In contrast, the higher latitude modes ($l - |m| > 0$) cover a wider sensing surface area but have lower sensitivity. The ratio of WGM shifts of the equatorial mode to the next higher latitude mode ($l - |m| = 1$) locates the absolute latitude angle at which a nano-particle binds. This ratio has only binding latitude location dependency and is unaffected by the intrinsic properties of the nano-particle (i.e., size, refractive index). Using this binding location, the size of the nanoparticle is calculated using the *Reactive Sensing Principle*. In addition to single particle size and location determination, this sensing scheme also enlarges the effective sensor surface since non-equatorial higher latitude modes also convey the same particle size information. We have experimentally demonstrated this sensing scheme by detecting particle sizes of a colloidal bimodal mixture.

Although our latitude-only micro-global positioning scheme is applied to nanoparticle sizing using slightly eccentric spheroids in aqueous solution, this approach can also be applied to WGM micro-resonators having a variety of shapes and in non-aqueous surroundings (i.e., air, vacuum) as well.

ACKNOWLEDGMENT

We thank the National Science Foundation for support (Grant EECS 1303499).

REFERENCES

1. Keng, D., X. Tan, and S. Arnold, "Whispering gallery micro-global positioning system for nanoparticle sizing in real time," *Appl. Phys. Lett.*, Vol. 105, 071105, 2014.

Spectral Correlation in Coupled Random Lasers

Antonio Consoli and Cefe López
Instituto de Ciencia de Materiales de Madrid-ICMM (CSIC)
Sor Juana Inés de la Cruz 3, Madrid 28049, Spain

Abstract— Two coupled random lasers show spectral emissions with strong correlation, with the same mode frequencies activated in both resonators. Experimental evidence of strong mode coupling between adjacent resonators is reported.

In random lasers (RLs), the feedback is given by multiple scattering. A typical feature of RL is an emission with narrow peaks, where the spectral position of the modes arises from the randomness of the cavity. So far, experiments and theoretical work have been oriented to the study of a single random resonator where the cavity is defined either by the pump extension, in large sample, or by the confined region where scatterers are distributed, in micron sized samples. Indirect pumping has been demonstrated as a way of tailoring RL emission [1]. The transverse beam of the pump is properly shaped with the aim of changing the pumping conditions on the considered random resonator. This experimental configuration is particularly interesting for studying interactions between adjacent resonators. We designed our samples in order to have large (hundreds of μm to few millimetres) scatterers aggregates placed at distances of few millimetres (TiO_2 in a bath of dye). We performed experi-ments on a single resonator, by pumping a small region (150 μm) of the TiO_2 with stripe shaped beams of varying length. Selecting two adjacent clusters, placed at 4.0 mm separation, simultaneous pumping with a stripe shaped beam activates the same frequencies in both clusters. Experiments, varying the geometry of the shaped beam show mode competition and strong coupling [2]. These results open the way to a new field of application as networks of mutually coupled RLs.

REFERENCES

1. Leonetti, M., C. Conti, and C. López, "The mode-locking transition of random lasers," *Nature Photonics*, Vol. 5, No. 10, 615–617, 2011.
2. Consoli, A. and C. López, to be published.

Exceptional Points and Loss-induced Lasing in Coupled Micro-disk Lasers

S. Rotter[1], **M. Liertzer**[1], **M. Brandstetter**[1], **C. Deutsch**[1], **G. Strasser**[1], **K. Unterrainer**[1], **B. Peng**[2], **S. K. Özdemir**[2], **H. Yilmaz**[2], **F. Monifi**[2], **C. M. Bender**[2], **F. Nori**[3, 4], **and L. Yang**[2]

[1]Vienna University of Technology (TU Wien), Vienna A-1040, Austria
[2]Washington University, St. Louis, MO 63130, USA
[3]RIKEN, Wako-shi, Saitama 351-0198, Japan
[4]University of Michigan, Ann Arbor, Michigan 48109, USA

Abstract— When two resonant modes in a system with gain or loss coalesce in both their resonance position and their width, a so-called exceptional point occurs, which acts as a source of non- trivial physics in a diverse range of systems [1]. Lasers provide a natural setting to study such non-Hermitian degeneracies, as they feature resonant modes and a gain material as their basic constituents. In my talk I will demonstrate that exceptional points can be conveniently induced in a photonic molecule laser by a suitable variation of the applied pump [2] — a concept that was meanwhile also successfully implemented experimentally. In a first realization [3] we used a pair of coupled microdisk quantum cascade lasers, which were shown to produce a characteristic reversal of their pump dependence in the vicinity of these exceptional points. A particularly counter-intuitive aspect we demonstrated here explicitly was a strongly decreasing intensity of the emitted laser light for increasing pump power. In a second realization [4] based on two coupled silica micro-resonators, this phenomenon could directly be linked to the movement of resonance eigenvalues in the complex plane, which follow an avoided eigenvalue crossing near the position of the exceptional point. One of the curious results of this non-trivial behavior is that close to an exceptional point, lasing is inducible solely by adding loss to a resonator. Through this demonstration of "loss-induced lasing" we provide a counter-intuitive extension of the conventional rule that loss needs to be avoided for the laser to reach its lasing threshold.

REFERENCES

1. Berry, M. V., "Physics of nonhermitian degeneracies," *Czechoslov. J. Phys.*, Vol. 54, 1039–1047, 2004.
2. Liertzer, M., L. Ge, A. Cerjan, A. D. Stone, H. Tureci, and S. Rotter, "Pump-induced exceptional points in lasers," *Phys. Rev. Lett.*, Vol. 108, 173901, 2012.
3. Brandstetter, M., M. Liertzer, C. Deutsch, P. Klang, J. Schoberl, H. E. Tureci, G. Strasser, K. Unterrainer, and S. Rotter, "Reversing the pump-dependence of a laser at an exceptional point," *Nature Commun.*, Vol. 5, 4034, 2014.
4. Peng, B., S. K. Ozdemir, S. Rotter, H. Yilmaz, M. Liertzer, F. Monifi, C. M. Bender, F. Nori, and L. Yang, "Loss-induced suppression and revival of lasing," *Science*, Vol. 346, 328, 2014.

Silicon Microresonators: How to Give a New Twist to Silicon Photonics

Martino Bernard[1, 2], **Massimo Borghi**[2], **Davide Gandolfi**[2], **Mher Ghulinyan**[1], **Romain Guider**[2], **Mattia Mancinelli**[2], **Georg Pucker**[1], **Fernando Ramiro Manzano**[2], **Alyna Samusenko**[1, 2], **Fabio Turri**[2], **and Lorenzo Pavesi**[2]

[1]Centre for Materials and Microsystems, Fondazione Bruno Kessler
via Sommarive 18, I-38123 Povo, Trento, Italy
[2]Nanoscience Laboratory, Department of Physics, University of Trento
via Sommarive 14, I-38123 Povo, Trento, Italy

Abstract— Internet boom can be slowed down by power hungry data centers. Silicon photonics is the technology to face this. A new twist to silicon photonics is provided by microresonators which enable complex functions and devices. The large refractive index difference between silicon and silicon oxide allows a tight confinement in silicon waveguides with small bend radius. Therefore, very small silicon microrings with high quality factors are possible. Microrings show different properties that can be integrated into functional silicon photonic devices. Single, coupled or cascaded microring geometries can be used to achieve complex functions. Still many aspects of the physics of photon confinement in small optical cavities have to be investigated. Therefore silicon microresonators are ideal devices for looking at new phenomena and new physics. Here we review and summarize few of these.

Fiberized Novel Wavelength-scale Planar Waveguides

Xian Feng, **Jindan Shi**, **Peter Horak**, **and Francesco Poletti**
Optoelectronics Research Centre, University of Southampton, Southampton SO17 1BJ, UK

Abstract— The modern glass optical fiber, starting from the simplest circularly symmetric waveguide geometry, has been widely inspired by the geometrical structure and functionalities of glass or non-glass based planar channel waveguides. For instance, the currently well-developed microstructured optical fiber [1] has been inspired by works on planar photonic crystal waveguides [2]. On the other hand, planar channel waveguides, such as slab waveguides, ridge waveguides and slot waveguides, are typically fabricated by various processing approaches, e.g., deposition, sputtering, etching, lithography and so on, at relatively low temperatures. Compact microstructured planar waveguide devices play important roles in various technical areas including telecoms application, sensing, and biomedical diagnostics and imaging. In comparison with planar waveguides, optical fibers have numerous advantages, e.g., long length, low cost per unit length due to high yield and low propagation loss. Fiberization of planar waveguides is a simple and neat idea to combine the advantages of both planar and fiber waveguides for realizing economic and compact photonic devices.

In this work we presented our first fiberized ridge waveguide. A long, narrow raised strip waveguide was constructed on top of a thin, flat substrate, which has a refractive index lower than the ridge. The ridge waveguide with the supporting substrate was built inside a glass jacket, similar to the format of holey fiber. The fiber was fabricated using a sheet-stacking method [3]. Three types of commercial glasses were employed in constructing the fiber. The outer jacket glass has significant lower viscosity than the core glass during the fiber drawing. Because of this large thermal mismatch between the cladding glass and the core glass, the ridge geometry was maintained with acceptable distortion, even when the dimension of the ridge waveguide was reduced to 1 μm. The loss of was measured to be 0.039 dB/cm at 1.55 μm in the fiberized ridge waveguide with ~ 1 μm dimensions, showing a low loss comparable with reported low-loss planar waveguides. A high birefringence of 9.5×10^{-3} was measured in a fabricated fiber ridge waveguide at 1.55 μm. This is close to the highest reported birefringence (1.1×10^{-2}) in optical fibers. Because the ridge waveguide is surrounded by air on three sides, this kind of geometry allows a strong overlap of the optical evanescent field with the surrounding medium. Hence, it provides a highly sensitive structure for chemical sensing. In addition, the ridged geometry also provides a convenient platform for adding heterostructures composed of other materials such as polymer, glass, metal, and semiconductor onto the top of the ridge. Extra optical functionalities can thus be added onto the waveguides. Therefore, we believe that this fiberized waveguide can be a powerful platform to complement the lab-on-fiber technique for chemical sensing.

In addition, the fabrication and characterization of other types of fiberized planar waveguides, e.g., of a slot waveguide [4] which consists of two parallel rails of a high-index glass separated by a subwavelength (~ 100 nm) air-slot, are currently ongoing.

ACKNOWLEDGMENT

This work was supported by the UK Engineering and Physical Sciences Research Council (EPSRC), under grants of CIMP, Hyperhighway, and Continuously tunable optical buffer.

REFERENCES

1. Knight, J. C., et al., *Science*, Vol. 282, 1476, 1998.
2. Yablonovitch, E., et al., *Phys. Rev. Lett.*, Vol. 67, 2295, 1991.
3. Shi, J., et al., *Opt. Fiber Technology*, Vol. 20, 395, 2014.
4. Barrios, C. A., et al., *Opt. Lett.*, Vol. 32, 3080–3082, 2007.

Coupling between Photonic Microcavity and Plasmonic Nanocavity

Keiji Sasaki
Research Institute for Electronic Science
Hokkaido University, Sapporo 001-0020, Japan

Abstract— We present highly efficient coupling between whispering-gallery-mode photonic microcavity and multipolar-mode plasmonic nanocavity. The first topic concerns complete coupling between propagating light (PL) and a single localized-surface-plasmon (LSP) nanostructure. We proposed a tapered-fiber-coupled microspherical cavity system combining an Au-coated probe tip [1]. This system possesses the unique characteristic of precise adjustability for the fiber-cavity coupling rate and the cavity-plasmon coupling rate, which is indispensable for achieving the critical coupling conditions. We successfully demonstrated the 93% PL coupling into the LSP antenna with an effective area of 58-nm circle, exceeding the diffraction limit. In other words, the cross-section of a single plasmonic nanostructure can be effectively enlarged to a size comparable to a mode area of a waveguide, thereby bridging the three-order-of-magnitude difference in size. The well-designed combination of the microcavity enhancement and the LSP localization can realize light focusing into a single-nanometer area with perfect efficiency. The second topic is related to plasmonic nanovortex field. The Laguerre-Gaussian (LG) beam, called as the optical vortex, that possesses helical wave-front and doughnut beam profile has recently attracted significant attention because of the unique characteristics of carrying the orbital angular momentum [2–4]. We proposed a novel approach to forming the single-nanometer-scale localized fields of optical vortex, which works as optical nanocavity. We theoretically demonstrated that a tailored plasmonic multimer surrounding a nano-sized gap makes it possible to localize the LG-mode field into the gap space with conserving the high-order orbital and spin angular momenta. This plasmonic nanovortex field can be expected to fit with the shape of the molecular electron orbital and spin having the corresponding angular momenta. In the presentation, the relation between the degrees of freedom in the metal multimer structure and the transferable angular momenta is also discussed.

REFERENCES

1. Takashima, H., K. Kitajima, Y. Tanaka, H. Fujiwara, and K. Sasaki, "Efficient optical coupling into a single plasmonic nanostructure using a fiber-coupled microspherical cavity," *Phys. Rev.*, Vol. 89, 021801, 2014.
2. Tanaka, Y., A. Sanada, and K. Sasaki, "Nanoscale interference patterns of gap-mode multipolar plasmonic fields," *Sci. Rep.*, Vol. 2, 764, 2012.
3. Tanaka, Y., S. Kaneda, and K. Sasaki, "Nanostructured potential of optical trapping using a plasmonic nanoblock pair," *Nano Lett.*, Vol. 13, 2146, 2013.
4. Sakai, K., K. Nomura, T. Yamamoto, and K. Sasaki, "Excitation of multipole plasmons by optical vortex beams," *Sci. Rep.*, in press.

Bioinspired Soft Photonics

Melik Demirel
212 EES Bldg, Pennsylvania State University, University Park, PA 16802, USA

Abstract— This talk will focus on soft photonic devices with non-linear optical properties that are manufactured as fibers, waveguides, and resonators. Specifically, we will talk about soft photonic devices that have unique mechanical and optical properties. A broad body of literature has been published in the last decade on optical and photonics biomimetic structures. Recent developments in optical technologies have revealed the strong need for developing soft photonic devices and photonic structures with novel functionalities that cannot be attained with current optical materials. This, in turn, requires utilizing unconventional materials with physical properties different or superior to those presently implemented. Moreover, greener photonics products with less chemical processing and energy consumption are in high demand due to growing environmental concerns. The interplay between the molecular architecture, morphology, and composition of biological photonic systems can provide inspiration for bioinspired soft photonics. Particularly, soft photonics provide molecular level programmability that provides tunability to enable novel functionalities such as Raman enhanced lasing.

Optofluidic Lasers Based on Biological Gain Media Suspended in Liquid Droplet Microcavities

Alexandr Jonáš[1], **Mehdi Aas**[2], **Yasin Karadağ**[2], **Selen Manioğlu**[3], **Suman Anand**[2, 4], **David McGloin**[4], **Halil Bayraktar**[3], **and Alper Kiraz**[2]

[1]Department of Physics, Istanbul Technical University
Maslak, Istanbul 34469, Turkey
[2]Department of Physics, Koç University
Rumelifeneri Yolu, Sariyer, Istanbul 34450, Turkey
[3]Department of Chemistry, Koç University
Rumelifeneri Yolu, Sariyer, Istanbul 34450, Turkey
[4]School of Engineering, Physics & Mathematics
University of Dundee, Nethergate, Dundee DD1 4HN, UK

Abstract— Surface tension shapes liquid droplets of sub-millimeter size into virtually perfect spheres with atomically smooth surfaces. Such spherical droplets represent spontaneously formed optical microcavities capable of sustaining high-quality whispering gallery modes (WGMs). Strong spatial confinement of the WGM resonant light circulating near the droplet internal surface then results in very high optical intensity that can couple strongly to the molecules or small particles contained within the droplet liquid. Consequently, lasing emission from a suitable gain medium suspended in the droplets can be observed with pump thresholds that are significantly lower than those required for bulk liquid samples.

Naturally produced fluorescent proteins and their genetically engineered variants with adjustable spectral properties have become a tool of choice for quantitative, selective visualization of localization and mutual interactions of molecular constituents of live cells. In a typical experiment, the intensity of spontaneous light emission from optically pumped fluorescent proteins is detected and evaluated. However, the resulting optical signal is often too low to collect a sufficient number of photons before the chromophore photobleaches. In addition, detection of weak fluorescence signals is frequently hampered by the presence of non-specific background. Incorporation of fluorescent proteins into an optical cavity can lead to the significant increase of fluorescence signal levels due to stimulated emission and light amplification in the cavity, effectively forming a laser with biological active medium. Lasing emission from fluorescent biological molecules can then greatly enhance the performance of fluorescence-based biosensors benefiting from the high sensitivity of non-linear lasing processes to small perturbations in the cavity and the active medium.

We report on experimental characterization of miniature optofluidic biolasers utilizing liquid optical microcavities formed by aqueous droplets deposited on superhydrophobic surfaces. We exploit purified yellow fluorescent protein or a suspension of live *E. coli* bacterial cells expressing the fluorescent protein as the active medium of the studied optofluidic lasers. We characterize the dynamics of lasing emission from these biological materials and show that a single fluorescent bacterial cell of micrometer size confined in a droplet-based cavity is sufficient to serve as a laser gain medium. The lasing bacteria suspended in an aqueous droplet can be provided with all nutrients required for unimpeded growth, which may allow for extension of the operation time of this biologically controlled source of laser light by active regeneration of the gain medium. Using bacterial strains expressing two different fluorescent proteins that form a Förster resonance energy transfer (FRET) donor-acceptor pair, a non-radiative energy-transfer mechanism can be used for laser pumping which would further improve lasing efficiency and open up the possibility for emission wavelength tuning. Furthermore, FRET lasing in connection with self-recognition and self-assembly of biological molecules attached to the fluorescent proteins can be exploited to program and modulate the laser characteristics, thus paving the way to new routes of live-cell bio-sensing.

Whispering-gallery Mode Resonators Based on Liquid Droplets

Gianluca Gagliardi
Consiglio Nazionale delle Ricerche, Istituto Nazionale di Ottica (INO)
Comprensorio A. Olivetti, via Campi Flegrei 34, Pozzuoli, NA 80078, Italy

Abstract— Over the last decade, optical whispering-gallery modes (WGMs) have been observed in solid micro-cavities of various geometries. WGMs supported by dielectric microspheres and toroids exhibit and optical field that is confined near to the surface. Using highly-transparent glasses, light that is coupled into a WGM can circulate around the resonator for a long time before being scattered or absorbed. Q factors $> 10^9$ can be achieved using silica material. Silica resonators proved ultra-sensitive bio-chemical probes but were also studied as miniature systems to observe coupling and interaction phenomena between light and matter. The peculiarity of WGMs is that light travels along closed paths at the interface between the surface of the resonator and the surrounding environment. Unfortunately, most of the light circulates inside the resonator and only the evanescent wave tail may interact with the external medium, i.e., only a small fraction of light is actually used for sensing, thereby reducing the effective cavity enhancement. Here, we propose to use liquid droplets as micro-resonators for sensing applications. The droplet itself serves as the sensor and the sample at the same time, where the internal optical field is directly used to probe dissolved analytes or particles. We demonstrate free-space excitation and laser frequency locking on whispering-gallery modes in vertically-suspended mm-size liquid droplets. Photon lifetime measurements are performed by cavity ring-down techniques recording Q-factors ranging from $5 \cdot 10^5$ to 10^7 in the near-infrared and visible spectral regions. Lifetime changes are measured in mixtures made from different liquids as a proof-of-concept of chemical sensing. Effects of metallic nanoparticles dissolved in the droplets were studied in view of possible plasmon-assisted detection of rare analytes. Appealing applications for spectroscopy, biosensing, material characterization and non-linear optics are envisaged.

Design, Fabrication, and Evaluation of a Polymer Mach-Zehnder Electro-optic Modulator

Xinjie Song, **Rainer Leonhardt**, **and Stuart Gerald Murdoch**
Department of Physics, The University of Auckland, New Zealand

Abstract— We have designed and fabricated a novel polymer M-Z EO modulator for the use at the 1550 nm telecommunication wavelength. Our waveguide structures are cut with µm-resolution by laser ablation. The core layer of the device is made of Polycarbonate/Disperse Red1 (PC/DR1) polymer system. For proper operation, the waveguides of the modulator have to be single mode. A numerical simulation program MODE has been used and shows that typical configuration for a single mode ridge waveguide is $7 \times 4 \times 2.5$ µm (width × height × slab thickness). To achieve the necessary µm-resolution for our waveguides, a 248 nm KrF excimer laser machining system (running at 500 Hz with 5 ns pulse duration) is used to ablate the waveguide structures. Ablation rates for PC at different laser fluences have been characterized, and used for the waveguide machining. ESEM pictures have shown very good surface quality (Fig. 1). In order to measure the propagation loss, we proposed a new method, where waveguides of different lengths are fabricated on one substrate so that the attenuation can be characterized by plotting the output power of these waveguides as a function of length. For our waveguides, the loss was measured to be ∼2 dB/cm. MCL (a moisture-curing polyurethane coating product), UV15 (an epoxy based UV curable coating system) are our choice for the cladding materials, taking into consideration laser machining performance, curing process, refractive indices, resistivity, solubility, glass transition temperature and other properties. An Au-electrode is precisely deposited to cover one arm of the M-Z structure with a metal evaporator. The poling process takes place at 105°C with an applied field of 140 V/µm. A sinusoidal electrical signal (1 kHz) is applied to test the set-up, and the modulated output intensity is measured to determine the effective r_{33} EO coefficient (Fig. 2). Up-to-now, values of 2.5 pm/V have been achieved for r_{33}.

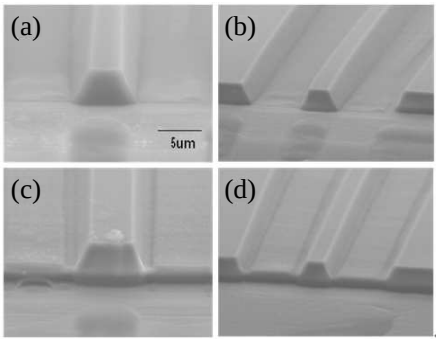

Figure 1: ESEM pictures for single-mode PC waveguides on glass substrate: (a), (b) rectangular waveguides (with material totally removed on both sides); (c), (d) ridge waveguides (with material partially removed on both sides).

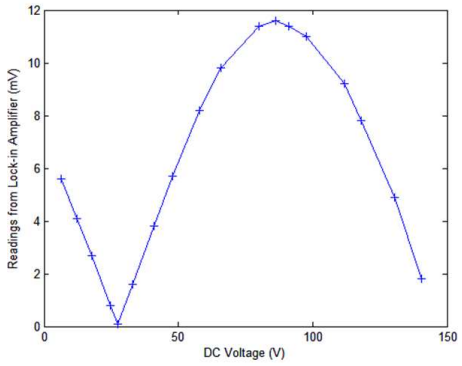

Figure 2: Modulated output amplitude as a function of the DC voltage for a polymer M-Z modulator. The corresponding r_{33} value was estimated to be ∼2.5 pm/V.

Simple Waveguide-QED-based Photonic Quantum Gates

Yuuki Tokunaga[1] and Kazuki Koshino[2]

[1]NTT Secure Platform Laboratories, 3-9-11, Midoricho, Musashinoshi, Tokyo 180-8585, Japan
[2]College of Liberal Arts and Sciences
Tokyo Medical and Dental University, 2-8-30 Konodai, Ichikawa 272-0827, Japan

Abstract— Photonic systems are promising for realizing quantum information processing because of their long coherence times. However, due to the weak interaction between photons, implementation of photon-photon gates has been difficult. One way to overcome this problem is to exchange the photonic and atomic qubits and to enhance the interaction using the cavity-QED or waveguide-QED systems [1–3], where the spatial modes of the input photon and the radiation from the atom match in a one-dimensional field and strongly interfere with each other. Recently, Zheng, et al. proposed a waveguide-QED based photon-photon gate [3], which has advantages compared to Ref. [1] such that it has a cavity-free setting and that single-qubit rotation of the atom is unnecessary. However, in their scheme, three atomic systems are required: a four-level atom is used for the interactions and also two five-level atoms are used for assisting the interaction. Those three atomic systems should be located separately and be kept coherent, which is highly demanding in practice.

In this work, we propose a simple scheme for a waveguide-QED based photonic quantum gate, using only a single six-level atom coupled to a waveguide. The M-shape five levels in the atom are used as a quantum memory like as Refs. [4, 5] for trapping the first incoming photon. The rest one level in the atom is used for performing the controlled-phase gate between the trapped photon and the second incoming photon. The second photon is reflected by the atom or the end of the waveguide without being trapped by the atom. After that, the first photon is retrieved by sending an ancillary photon. The scheme retains the advantages of Ref. [3] such as cavity-free setting and no single-qubit rotation on the atom. This system would be a simple building block for on-chip quantum computation using such as superconducting circuits or photonic crystal waveguides, which recently have dramatic progress [6–9].

REFERENCES

1. Duan, L.-M. and J. Kimble, "Scalable photonic quantum computation through cavity-assisted interactions," *Phys. Rev. Lett.*, Vol. 92, 127902, 2004.
2. Waks, E. and J. Vuckovic, "Dispersive properties and large Kerr nonlinearities using dipole-induced transparency in a single-sided cavity," *Phys. Rev. A*, Vol. 73, 041803(R), 2006.
3. Zheng, H., D. Gauthier, and H. Baranger, "Waveguide-QED-based photonic quantum computation," *Phys. Rev. Lett.*, Vol. 111, 090502, 2013.
4. Ritter, S., et al., "An elementary quantum network of single atoms in optical cavities," *Nature*, Vol. 484, 195, 2012.
5. Stute, A., et al., "Quantum-state transfer from an ion to a photon," *Nat. Photon.* Vol. 7, 219, 2013.
6. Wenner, J., et al., "Catching time-reversed microwave coherent state photons with 99.4% absorption efficiency," *Phys. Rev. Lett.*, Vol. 112, 210501, 2014.
7. Inomata, K., et al., "Microwave down-conversion with an impedance-matched Λ system in driven circuit QED," *Phys. Rev. Lett.*, Vol. 113, 063064, 2014.
8. Tiecke, T. G., et al., "Nanophotonic quantum phase switch with a single atom," *Nature*, Vol. 508, 241, 2014.
9. Goban, A., et al., "Atom-light interactions in photonic crystals," *Nat. Comm.*, Vol. 5, 3808, 2014.

Directional Emission from Chaotic Microdisk Lasers and the Role of Boundary Imperfections

J. Kreismann[1], **K. Kubo**[1,2], **P. Stockschläder**[1], **and M. Hentschel**[1]

[1]Institute for Physics, Technische Universität Ilmenau
Weimarer Str. 25, Ilmenau D-98693, Germany
[2]MPIPKS Dresden, Nöthnitzer Str. 38, Dresden D-01187, Germany

Abstract— Optical microdisk laser provide a promising alternative to the well-known Fabry-Perot lasers as well as to VCSELs as the size of optical devices is further reduced to the scale of few micrometers. Whereas high Q-modes are available through whispering-gallery (and similar) resonances that are trapped by total internal reflection inside the resonator, it remains a challenge to achieve directional emission by suitably breaking the rotational symmetry of the devices. In a previous work [1] we have shown that the so-called Limaçon-shape is provides a robust possibility to combine directional far-field emission with high Q-factors. In detail, the far-field characteristic is determined by the unstable manifold of the cavity, a quantity well-known in the field of dynamical systems and quantum chaos. It implies that ray-based calculations, wave-simulations and experiments yield practically the same result. In particular, the easy-to-implement ray-optics methods are an appropriate tool to predict the far-field of microdisk lasers.

We complement our results by discussing various other resonator geometries and alternative schemes to achieve directional light output from microoptics devices. Furthermore, we discuss how boundary imperfections may affect the far-field pattern. To this end we study the effect of sharp and rounded cusps reaching into the resonator or to the outside on the reflection of an incoming test ray.

Finally, we will briefly discuss the polarizations dependence of the emission characteristics as well as semiclassical corrections to the ray picture that occur in the form of beam-shift effects that may become important in the far-field pattern prediction of very small optical microdisk lasers.

REFERENCES

1. Wiersig, J. and M. Hentschel, *PRL*, Vol. 100, 033901, 2008.

Spherical Microresonators Coated with a High Refractive Index Coating for Different Applications

D. Ristić[1, 2], **A. Chiappini**[3], **H. Gebavi**[1, 2], **V. Đerek**[1, 2], **A. Lukowiak**[4], **R. R. Gonçalves**[5], **S. Pelli**[6], **G. Nunzi Conti**[6], **M. Ivanda**[1, 2], **G. C. Righini**[7], **G. Cibiel**[8], **and M. Ferrari**[3]

[1]Laboratory for Molecular Physics, Division of Materials Physics, Ruđera Bošković Institute
Bijenička cesta 54, Zagreb 10000, Croatia
[2]Center of Excellence for Advanced Materials and Sensing Devices
Research Unit New Functional Materials, Bijenička cesta 54, 10000 Zagreb, Croatia
[3]IFN-CNR CSMFO Lab, Via alla Cascata 56/C Povo, Trento 38123, Italy
[4]Institute of Low Temperature and Structure Research, PAS, ul. Okolna 2, Wroclaw 50-950, Poland
[5]Departamento de Química, Faculdade de Filosofia, Ciências e Letras de Ribeirão Preto
Universidade de São Paulo, Av. Bandeirantes, 3900, CEP 14040-901, Ribeirão Preto/SP, Brazil
[6]IFAC-CNR, MiP Lab, Sesto Fiorentino 50019, Italy
[7]Enrico Fermi Centre, Piazza del Viminale 1, Roma 00184, Italy
[8]Centre National d'Etudes Spatiales (CNES), 31401 Toulouse Cedex 9, France

Abstract— We will discuss several applications of the coating of silica microspheres. Silica microspheres fall in the group of so called whispering gallery mode (WGM) resonators. They are known to have a very high Q-factor and a low modal volume. Therefore they are suitable for a number of different applications such as lasing, frequency comb generation or sensing. In this paper we will discuss three different applications. Firstly we will discuss the sensing properties of the coated microsphere. We have found that a high refractive index coating can greatly improve the sensing properties of a silica microresonator, improving the theoretical sensing sensitivity from 5 nm/RIU for a blank silica sphere to a maximum of 145 nm/RIU for an amorphous silicon coating. We will also discuss some experimental results dealing with the coating of silica microspheres with a LPCVD a:Si coating. Second application which we will discuss is lasing and optical amplification. By coating the microsphere using an optically active material, microsized lasers can be produced. We have coated a silica microsphere using an erbium doped glass ($70SiO_2$-$30HfO_2$) and have shown that such a system exhibits both lasing and wavelength selective amplification. Finally we will discuss the possibility to tailor the modal dispersion of the resonator by applying a high refractive index coating on top of the microsphere. This can be a crucial step for improving the applicability of the microsphere in non-linear optics applications, such as for four-wave mixing. We used erbium doped silica hafnia glass as a probe to study the influence of the coating on the modal dispersion inside the microresonator and have found that the coating can be used to tailor the modal dispersion in a very wide range in both the normal and anomalous regime.

Wave-inspired Corrections for an Efficient Ray-optical Description of Micro-optics Devices

P. Stockschläder, J. Kreismann, and M. Hentschel
Institute for Physics, Technische Universität Ilmenau, Ilmenau, Germany

Abstract— Ray optics is a versatile tool to describe microscale optical systems like microlasers and their far-field emission. It is successful even in the regime where a wave-dynamical description would be expected to be appropriate. Indeed, when considering structures at length scales of a few light wavelengths, wave-inspired adjustments have to be taken into account to ensure the accuracy of ray-based predictions. These corrections to ray optics are known as the Goos-Hänchen shift, a lateral shift along the interface, and the Fresnel filtering effect, an angular shift, violating Snell's law and the principle of ray-path reversibility.

In a previous work, we have shown that these beam shifts at curved interfaces, characteristic of optical microcavities and microlasers, deviate strongly from the results anticipated for planar interfaces [1]. Especially, the Fresnel filtering effect grows considerably with increasing curvature. This is crucial for the precise prediction of far-field emission characteristics. In this contribution, we study in detail the influences of different factors on the exact size of the corrections paying special attention to the interplay between beam parameters and interface geometry. We obtain our results from analytical calculations using an expectation value approach to the beam shifts. These findings are supported by FDTD simulations.

Knowing the influences of the different parameters, we are able to incorporate well adjusted correction terms in the ray-optical calculations for a large class of micro-optics devices with curved and planar boundaries. Thus, we can make predictions for these devices exploiting the simplicity and efficiency of geometrical optics while keeping the accuracy of wave calculations.

REFERENCES

1. Stockschläder, P., et al., *EPL*, Vol. 107, 64001, 2014.

Modulation of Nanolaser Output for Information Encoding

T. Wang[1, 2], **G. P. Puccioni**[3], **and G. L. Lippi**[1, 2]

[1]Institut Non Linéaire de Nice, Université de Nice Sophia Antipolis, France
[2]CNRS, UMR 7335, 1361 Route des Lucioles, Valbonne 06560, France
[4]Istituto Sistemi Complessi, CNR, Via Madonna del Piano 10, Sesto Fiorentino 50019, Italy

Abstract— Nanolasers are currently at the focus of much research due to their potential as highly integrable, low-consumption and sub-microscopic footprint devices. Given the ultrahigh modulation speed which are projected for some of the most promising devices, modeling is being actively pursued to predict the modulation bandwidth achievable with these devices.

Sophisticated modeling has been conducted up until now on the basis of greatly enhanced rate equations which take into account the physical characteristics of the semiconducting structure both for nanolasers [1, 2] and for nanoLEDs [2]. However, the device's sensitivity to the intrinsic noise cannot be easily tested with these numerical approaches.

Using a recently developed alternative modeling technique [3], based on a Stochastic Simulator (SS) which reproduces the physical processes taking place in a laser, we investigate the potentials for direct modulation (and therefore bandwith response) of nanolasers. Since the SS intrinsically reproduces the stochastic nature of the events which take place in the pumping and in the emission processes, we focus our attention on the effect of noise on the fidelity with which a modulation signal can be transferred onto the optical carrier. Different regimes are considered, from the point of view of biasing, modulation amplitude and cavity quality factor.

REFERENCES

1. Suhr, T., N. Gregersen, K. Yvind, and J. Mork, "Modulation response of nanoLEDs and nanolasers exploiting Purcell enhanced spontaneous emission," *Optics Express*, Vol. 18, No. 11, 11230, 2010.
2. Ni, C.-Y. A. and S. L. Chuang, "Theory of high-speed nanolasers and nanoLEDs," *Optics Express*, Vol. 20, No. 15, 16450, 2012.
3. Puccioni, G. P. and G. L. Lippi, "Stochastic simulator for modeling the transition to lasing," *Optics Express*, Vol. 23, No. 3, 2369–2374, 2015.

Fano Resonances of a Silicon Microsphere on a Silica Optical Fiber

Ulaş Sabahattin Gökay[1], **Muhammad Zakwan**[1], **Abdullah Demir**[2], **and Ali Serpenguzel**[1]

[1]Microphotonics Research Laboratory, Department of Physics
Koç University, Rumelifeneri Yolu, Sarıyer, Istanbul 34450, Turkey
[2]JDSU Corporation, 80 Rose Orchard Way, San Jose, California 95134, USA

Abstract— Previously, Lorentzian lineshape optical resonances have been observed in silicon spherical optical microcavities. Here, we present Fano lineshape whispering gallery mode (WGM) resonances in the 90° elastic scattering obtained from a silicon microsphere. The Fano lineshape optical resonances arise from the constructive interference between a coherent DC background and the WGM resonances, where the Fano lineshape depend on the relative phase between the DC background and the WGM resonances. For the experimental part, an optical fiber half coupler (OFHC) is used to excite the WGMs of the silicon microsphere. A distributed feedback (DFB) laser is used as a tunable light source. The analysis of the experimental spectra shows that the polar angular mode spacing of 0.23 nm correlates well with the calculated mode spacing of the WGM resonances. The measured effective quality factor (Q) of the Fano resonance is on the order of 10^5, which can be further improved with an appropriate choice of experimental setup parameters.

Session 2P0
Poster Session 4

Study on Magnetic Shielding Effect versus Metal Thickness and Aperture Size of Metal Case

S. Yahagi, **R. Suga**, **T. Uwano**, **and O. Hashimoto**
Aoyama Gakuin University, Japan

Abstract— A power control unit for electric and hybrid electric vehicles contains inverter circuits and their switching noise interferes with AM radio. A shielding technique using metal case is widely used for avoiding the interferences, and lightweight case is desirable considering the fuel consumption of the vehicles. Usually, the case has apertures to connect wire cables and exhaust heat and the interferences due to the switching noise through the apertures are concerned. In this paper, the magnetic shielding effect versus metal thickness and aperture size of copper case is discussed.

Figure 1 shows a measurement system of the magnetic shielding effect of a copper case. The shielding effect versus metal thickness t of the case is measured using the system. A 10-turn loop coil with a diameter of 100 mm is located at the center of the case as a virtual noise source. Figure 2 shows the simulation model where W shows a square aperture size of the case. The simulated results with W of 0 mm are compared with measured ones. Here, the shielding effect is evaluated on the basis of the received power with W of 300 mm. Figure 3 shows the measured and simulated results of shielding effect versus t with W of 0 mm. The measured results agree well with the simulated ones and the usability of the simulation is shown. Figure 4 shows simulated results of the shielding effect versus W with t of 105 µm. The shielding effect more than 30 dB is obtained with W of 50 mm. It is shown that the shielding effect is constant by the aperture size below 30 mm.

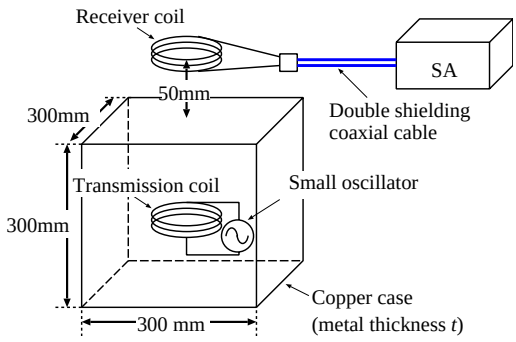

Figure 1: Measurement system of shielding effect.

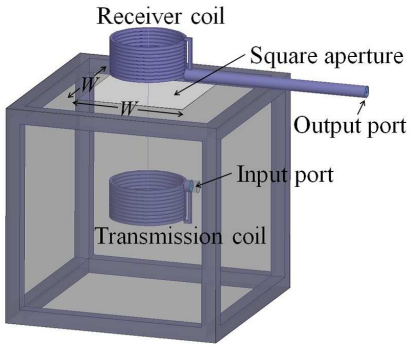

Figure 2: Simulation model of shielding effect.

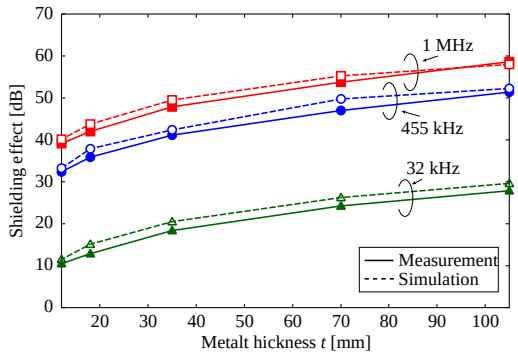

Figure 3: Shielding effect versus the metal thickness ($W = 0$ mm).

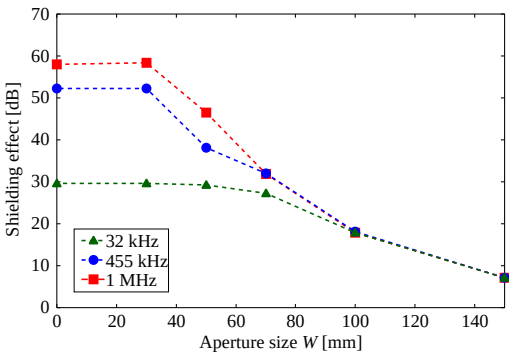

Figure 4: Simulated shielding effect versus aperture size ($t = 105$ µm).

Development of Radar Sensor for Intelligent Building Energy Systems

Tae-Yun Lee, **Vladimir Skvortsov**, **Junghwan Han**, **and Min-Ho Ka**
School of Integrated Technology, Yonsei Institute Convergence Technology
Yonsei University, Seoul, Korea

Abstract— Energy consuming has recently become an important research topic in the world. Buildings are one of the fastest growing energy consuming sectors. The identification of major factors of building energy consumption, together with a thorough understanding of the impacts of the identified on energy consumption patterns, could assist in achieving the goal of improving building energy efficiency and reducing greenhouse gas emissions due to the building energy consumption. One of main building energy consumption factors is Heating, Ventilation and Air-Conditioning (HVAC) energy efficiency. HVAC energy efficiency is closely related to sensors installed in building. Sensors determine that HVAC systems turn on/off. And those control temperature as well as a Wind direction and wind speed. IR-based sensors are one of main sensors that are currently used in building. IR-based sensors have a good performance to detect human. However, those performance are limited to just detection. Microwave-based sensors can to detect human as well as to estimate humans location. Location is an important factor in intelligent building energy systems because that has a strong in uence on HVAC energy efficiency. Radar is extensively used for disaster application. There are some areas in the disaster application field that use radar for detecting human and estimating humans location. This paper analyses the development of radar sensor for intelligent building energy systems. The paper focuses on a technique to detect human and to estimate a location of occupants. In the end, the experimental results show that the proposed radar sensor and algorithm is simple and feasible.

ACKNOWLEDGMENT

This research was supported by the MSIP (Ministry of Science, ICT and Future Planning), Korea, under the IT Consilience Creative Program (NIPA-2014-H0201-14-1002) supervised by the NIPA (National IT Industry Promotion Agency).

REFERENCES

1. Yu, Z., B. C. M. Fung, F. Haghighat, H. Yoshiono, and E. Morogcky, "A systematic procedure to study the in uence of occupant behavior on building energy consumption," *Energy and Buildings*, Vol. 43, 1409–1417, 2011.
2. Kim, H. H., K. N. Ha, S. Lee, and K. C. Lee, "Resident location-recognition algorithm using a Bayesian classifier in the PIR sensor-based indoor location-aware system," *IEEE Transactions on Systems, Man, and Cybernetics, Part C: Applications and Reviews*, Vol. 39, No. 2, 240–245, 2009.
3. Klein, T., M. Faassen, and A. Lauer, "Radar-based surveillance of persons from an elevated, tilted position using a two channel 24 GHz FMCW radar system," *Radar Symposium (IRS)*, 2011.
4. Morinaga, M., T. Nagasaku, H. Shinoda, and H. Kondoh, "24 GHz intruder detection radar with beam-switched area coverage," *Microwave Symposium*, 2007.

Improvement of Standard EM Fields Distribution in 4-port TEM Cell with Slit-structured Septum

Sung Woong Choi, **Sang Bong Jeon**, **and Heung Mook Kim**
Broadcasting & Telecommunications Media Research Lab.
Electronics and Telecommunications Research Institute
161 Gajeong-ro, Yuseong-gu, Daejeon 305-700, Republic of Korea

Abstract— In recent years, as many kinds of electronic devices are present, EM (electromagnetic) fields generated from these electronic devices may not only cause problems in the human body, but also affect the electronic devices to induce a malfunction and failure. Therefore, the EMC (electromagnetic compatibility) studies are actively ongoing so that radiation of undesired EM fields can be suppressed below a regulation value and a normal operation can be done in an EM field environment with a constant regulation value.

Standard EM field generators such as transverse electromagnetic (TEM) cell and Gigahertz Transverse Electromagnetic (GTEM) cell are widely used in these EMC field, but have a difficulty in reducing unwanted field components. That is, because the unwanted field components may occur highly in a direction corresponding to the traveling direction of the EM field, there is a problem when generating a near field mode as well as the TEM mode.

In this paper, we proposes a method of reducing the unwanted EM field component in the 4-port TEM cell with two internal septa, which is used for EMC test. Adopting slit structure in the internal septa, 4-port TEM cell provide the improved standard EM field distribution inside the usable test volume.

REFERENCES

1. Crawford, M. L., "Generation of standard EM fields using TEM transmission cells," *IEEE Trans. Electromagn. Compat.*, Vol. 16, No. 4, 189–195, Nov. 1974.
2. Hansen, D., P. Wilson, D. Konigstein, and H. Schaer, "A broadband alternative EMC test chamber based on a TEM-cell anechoic-chamber hybrid concept," *Proceedings of the 1989 International Symposium on Electronic Compatibility*, 133–137, Sep. 1989.
3. Yun, J. H., H. J. Lee, and H. J. Hwang, "Straight coupled transmission-line cell for generating standard electromagnetic fields," *IEEE Trans. Electromagn. Compat.*, Vol. 44, No. 4, 515–521, Nov. 2002.
4. Jeon, S. B., J. H. Yun, and S. K. Park, "On the new design of a 4-port TEM waveguide with a higher cutoff-frequency and wider test volume," *ETRI Journal*, Feb. 2012.

Measurement of Electromagnetic Radiated Field for Magnetic Resonance Wireless Power Transmission System

Sangbong Jeon, **Jong-Hwa Kwon**, **In-Kui Cho**, **Jung-Ick Moon**, **Seong-Min Kim**, **and Sung-Woong Choi**
Electronics and Telecommunications Research Institute, Korea

Abstract— Magnetic resonance wireless power transmission (WPT) have been used as charging systems without power cables such as mobile phones, laptop, etc. [1–3]. However, using WPT systems, unintentional high power interference in a near-field region gradually has become an important issue in practical fields of EMC test [4]. Recently, CISPR published unintentional radiation less than 30 MHz in this point [5]. In this paper, we measured of electromagnetic emission for WPT system as shown in Figure 1. The measurement is carried out in a semi-anechoic chamber using implemented E-bicycle wireless charging system and the measurement distance between the center of the antenna and the EUT (WPT system) is 3 m. In addition, we also analyzed noise source of WPT system.

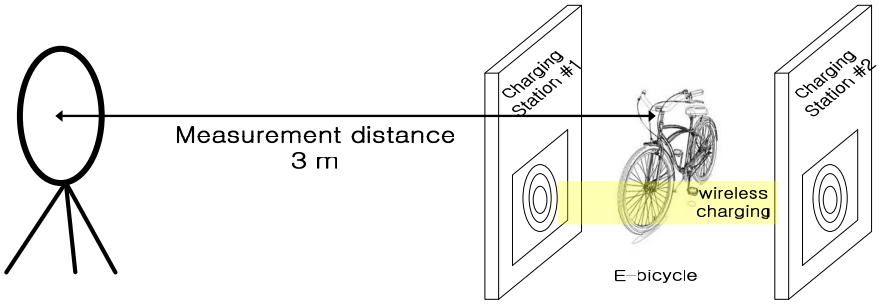

Figure 1: Measurement setup of EM radiated fields for wireless power transmission.

ACKNOWLEDGMENT

This research was funded by the IT R&D Program of MISP/ETRI, Korea in 2015.

REFERENCES

1. Kurs, A., et al., "Wireless power transfer via strongly coupled magnetic resonances," *Science*, Vol. 317, 83–86, Jul. 2007.
2. Lee, K. S. and D. H. Cho, "Simultaneous information and power transmission using magnetic resonance," *ETRI J.*, Vol. 36, No. 5, 808–818, Oct. 2014.
3. Kim, S. M., J. I. Moon, I. K. Cho, J. H. Yoon, W. J. Byun, and H. C. Choi, "Advanced power control scheme in wireless power transmission for human protection from EM field," *IEEE Trans. on MTT*, Vol. 63, No. 3, 847–856, Mar. 2015.
4. Jeon, S. B., S. K. Park, J. H. Kwon, and D. H. Kim, "Analysis of electromagnetic interference under different types of near-field environments," *IET Electronics letters*, Vol. 50, No. 9, 652–654, Apr. 2014.
5. "Methods of measurement and limits for radiated disturbances from plasma display panel TVs in the frequency range 150 kHz to 30 MHz," IEC/PAS 62825, Mar. 2013.

Study on Evaluation of Composite Electromagnetic Wave Absorber Made of Sendust Particles Dispersed in Polystyrene Resin

Takumi Kubota[1], **Kenji Sakai**[2], **Yuuki Sato**[1], **and Shinzo Yoshikado**[1]

[1]Doshisha University, Japan
[2]Okayama University, Japan

Abstract— Development of an electromagnetic wave absorber suitable for frequencies above 10 GHz is required because of the increasing use of wireless telecommunication systems. For example, it has been proposed to utilize electromagnetic wave of approximately 76 GHz and 90 GHz to the Intelligent Transport System (ITS). In the previous study, Composite electromagnetic wave absorber made of sendust dispersed in resin is low-cost and contains no rare metal. The frequency dependences of the relative complex permeability μ_r^*, the relative complex permittivity ε_r^* and the absorption characteristics for composite electromagnetic wave absorbers made of sendust particles dispersed in polystyrene resin were investigated in the frequency range from 100 MHz to 20 GHz. The composite made of spherical sendust particles with 5 μm were dispersed in polystyrene resin containing 20.0 vol% have approximately 27% normalized −20 dB bandwidth. In this study, to clarify the absorption characteristic in the high frequency range, which has not been evaluated in previous studies, the composites made of sendust particle dispersed in polystyrene resin with the volume ratio of 12.7–28.0 vol% were evaluated return loss in the frequency range of 12.4–110 GHz by free space method. Moreover, it was compared between the measurement values of the absorption characteristics and calculated values of the absorption characteristics obtained from the value of relative complex permeability μ_r^* and relative complex permittivity ε_r^*. As a result, the composites made of sendust particle dispersed in polystyrene resin ware obtain 1.4–3.0% normalized −20 dB bandwidth at frequency range of 12.4–110 GHz.

Thus, the composites made of sendust particle dispersed in polystyrene resin can be used as an electromagnetic wave absorber up to 90 GHz.

Nonlinear Plasmonic Converters for Solar Cell Applications

Musa Kurtulus Abak[1, 2], Bilge Can Yildiz Karakul[2, 3, 4], Yusuf Kasap[2, 3], Ildar Salakhutdinov[2], and Alpan Bek[2, 3]

[1]Micro and Nanotechnology Program, Middle East Technical University, Ankara, Turkey
[2]The Center for Solar Energy Research and Applications (GÜNAM)
Middle East Technical University, Ankara, Turkey
[3]Physics Department, Middle East Technical University, Ankara, Turkey
[4]Atilim University, Ankara, Turkey

Abstract— Development of alternative sources of energy is extremely important. Solar energy is one the most promising source of alternative energy and plasmonics can be an important tool to obtain a highly effective solar cells.

Most common material used to produce a solar cell is Silicon because of its availability and low price However, one of a serious limitation of the silicon based solar cells is related with the fact that Silicon does not absorb energies less than 1 eV significantly and there is a substantial amount of solar energy in this region [1]. Optical up-conversion properties of plasmonic structures can be used to efficiently convert unused portion of energy into the useful range. The main focus of our study is to investigate the nonlinear optical up-conversion properties of the plasmonic structures.

Two types of plasmonic interaction appear to be promising and will be investigated in this manner: (a) Localized surface plasmons (LSP) observed on metal nanoparticles. In order to obtain strong nonlinear responses we will decorate dielectric surfaces with periodic or random nano-patterned asymmetric structures which serve as optical antennae leading to strong interaction of solar radiation with LSP at these structures. This kind of design can couple the signal from individual LSP into combined nonlinear response. (b) Lang range surface plasmon-polaritons (LRSPP) observed on multilayer metal-dielectric structures. When the long range surface plasmon polaritons obtain required phase matching condition; effective conversion to higher harmonics is possible [2, 3]. We will create controllable metal-dielectric periodic modulations with holography to generate LRSPPs.

REFERENCES

1. Tedje, T., E. Yablonovitch, G. D. Cody, and B. G. Brooks, "Limiting effect of silicon solar cells," *IEEE Trans. on Electron. Dev.*, Vol. 31, No. 5, 711–716, 1984.
2. Kauranen, M. and A. V. Zayats, "Nonlinear plasmonics," *Nature Photon.*, Vol. 6, 737–748, 2012.
3. Salakhutdinov, I. F., V. A. Sychugov, A. V. Tishchenko, B. A. Usievich, F. A. Pudonin, and O. Parriaux, *IEEE J. of Quantum Electronics*, Vol. 34, 1054, 1984.

Simulations of Metamaterial Structures for Enhancement of Radiation Absorption in Long Infrared

Mihai Kusko[1], **Cristian Kusko**[1], **and Costin Onofrei**[2]

[1]National Institute for Research and Development in Microtechnologies IMT-Bucharest, Romania
[2] "Politehnica" University from Bucharest, Romania

Abstract— A promising option for the enhancement of radiation absorption for thermal detectors as YBCO based superconducting Transition Edge Sensors is the use of configured layers which manifest resonant absorption. Essentially, a resonant system surrounded by a medium with a small extinction coefficient may present high losses due the thermal dissipation appearing at resonance. The most used resonant system is the split ring resonator (SRR) which is an RLC oscillator having its resonance frequency determined by its geometrical parameters. The SRR is considered to be composed of a YBCO/YSZ/Au thin layer systems on YSZ substrate with the gold and YSZ upper layers to be patterned.

The absorption induced by SRR configurations has been evaluated with simulations performed with OptiFDTD software based on the Finite Difference Time Domain method — FDTD. The dependence with wavelength of power transmission and reflection has been calculated with a Gaussian Pulse which propagates through two observation planes situated after structure and before the radiation input plane, respectively. The obtained results have been used to evaluate the absorption dependence with wavelength. Since the entire system would function at transition temperature from the superconduction to normal state, the YBCO optical complex conductivity was described by using a two fluid model.

From numerical analysis a very sharp peak of absorption has been observed around 8 microns for a SRR with 1.6 micron ring radius. The maximum absorption value is 0.75. The absorption maximum position varies with the SRR ring value so it is possible to design detectors with great absorption at certain wavelengths which opens a way for more efficient thermal detectors.

From numerical analysis a very sharp peak of absorption has been observed around 8 microns. for a SRR with 1.6 micron ring radius. The maximum absorption value is 0.75. The absorption maximum position varies with the SRR ring value so it is possible to design detectors with great absorption at certain wavelengths which opens a way for more efficient thermal detectors.

ACKNOWLEDGMENT

This work has was supported by a grant of the Romanian National Authority for Scientific Research, Programe for research — Space Technology and Advanced Research — STAR, project number 34/19.11.2012.

A Short Note on the Optimization of Halbach Arrays Used as Magnetic Springs

D. Månsson
Royal Institute of Technology KTH, Sweden

Abstract— Neodymium magnets are today widely used for a wide variety of purposes and some commercial types have an adhesive capability of approximately 100 kg even though the dimensions are only $5 * 5 * 2.5$ cm. Therefore the idea of using permanent magnets as springs or bearings isn't uncommon. The simplest form of a linear magnetic spring constitutes of two permanent magnets, with opposing individual magnetizations (e.g., $\bar{M} = \pm M_0 \hat{z}$), this however is not the best choice.

If several small individual magnets are used according to a specific magnetization scheme often described as a "Halbach array" [1], i.e., $\bar{M} = M_0$ $(\hat{x} \sin kx \pm \hat{y} \cos kx)$, a structure that (ideally) have a one sided flux is formed [2]. I.e., the magnetic field is concentrated to the "enhancing side" and the field strength is (ideally) zero on the opposing, "cancellation side" of the structure. (This constitutes however not a magnetic monopole.) If two such Halbach arrays, with opposing magnetization schemes, are employed opposite each other, the total magnetic field is primarily concentrated in the gap between the two structures and an improved, linear, magnetic spring is formed.

Here, both analytical methods using Maxwell's stress tensor (MST) and numerical simulations using *FEMM* [3] are applied to calculate the vertical force on the lower structure (if this is considered to be fixed in space). The characteristics of the vertical force between the two Halbach arrays are very dependent upon the dimensions and the wavelength of the magnetization in the material (through $k = 2\pi/\lambda$). Thus, it should be clear (see Fig. 1) that varying λ will greatly affect the characteristics of the magnetic spring and different applications will require different dimensions and magnetization wavelengths.

In addition, increasing the discretization of the individual elements that are used to form a Halbach array quickly improves the formed magnetic field towards that which is created by a continuous magnetization. Thus, instead of looking at the number of elements per wavelength, the actual wavelength is a more important variable for optimization.

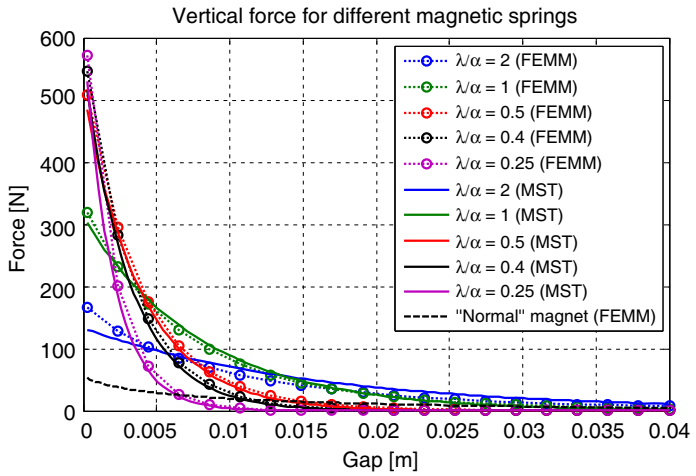

Figure 1: The vertical force created in different magnetic springs using two opposing Halbach arrays with different wavelengths, λ (in relation to the width, α, of the Halbach array). The dimensions here ($\alpha = 5$ cm, $\beta = 1$ cm, $\gamma = 1$ cm) are in the ($\hat{\mathbf{x}}$, $\hat{\mathbf{y}}$, $\hat{\mathbf{z}}$) direction respectively. The results are acquired both using numerical simulations (FEMM) and Maxwell's stress tensor (MST). Both methods agree very well. Notice the much lower force (i.e., at most a factor of 10) created between two "normal" magnets of the same dimensions and maximum magnetization (M_0). The small differences, between the MST and FEMM results, in some cases are due to approximations made in order to acquire a simple analytical expression. (In the case where $\lambda/\alpha = 2$, the magnetic structure can't really be considered a Halbach array anymore.).

Also, important aspects such as internal stresses, horizontal forces and spring stiffness are discussed.

REFERENCES

1. Halbach, K., "Physical and optical properties of rare earth cobalt magnets," *Nuclear Instruments and Methods in Physics Research*, Vol. 187, 109–117, August 1981.
2. Mallinson, J. C., "One-sided fluxes a magnetic curiosity?," *IEEE Trans. Magnetics*, Vol. 9, 678–682, 1973.
3. "Finite element method magnetics," available: http://www.femm.info/.

Integral Formulation of Rectangular Chirowaveguides Based on Green's Equations

M. J. Núñez-Trigueros[1], **G. J. Molina-Cuberos**[1], **J. Margineda**[1], **J. Muñoz**[1], **A. J. García-Collado**[2], **O. Fernandez**[3], **and A. Gómez**[3]

[1]Department Electromagnetismo y Electrónica, University de Murcia, Murcia, Spain
[2]Department Ciencias Politécnicas, University Católica San Antonio, Murcia, Spain
[3]Department Ingeniería de Comunicaciones, University Cantabria, Santander, Spain

Abstract— The boundary value problem in chirowaveguides with translational symmetry is formulated in this paper and used to study the rectangular case. By applying the Green's second identity to a metallic guide filled with chiral material and using the propagation modes in unbound chiral media, i.e., right (RCP) and left (LCP) circularly polarized waves, the electromagnetic field components in the waveguide can be retrieved. To do that, the boundary conditions were formulated in terms of the propagation modes and the integral equations discretized into a matrix equations. The application of the compatibility condition to the system of linear equations provides the propagation constant and, therefore, the dispersion diagram.

The model has been applied to study several chiral materials. The diagram dispersions and transversal cross secton of the propagation modes will be presented for a wide range of the chirality parameter, including a comparison with the achiral guide.

As an example the figure shows the transversal cross section of the longitudinal component of the RCP field for the first propagation mode as a function of the relative chirality parameter: $\kappa_r = 0.1$ (a), $\kappa_r = 0.3$ (b), and $\kappa_r = 0.5$ (c). It can be observed that the reflection symmetry of the typical TE_{10} mode for dielectric waveguide is broken and the fields still keep a rotacion symmetry.

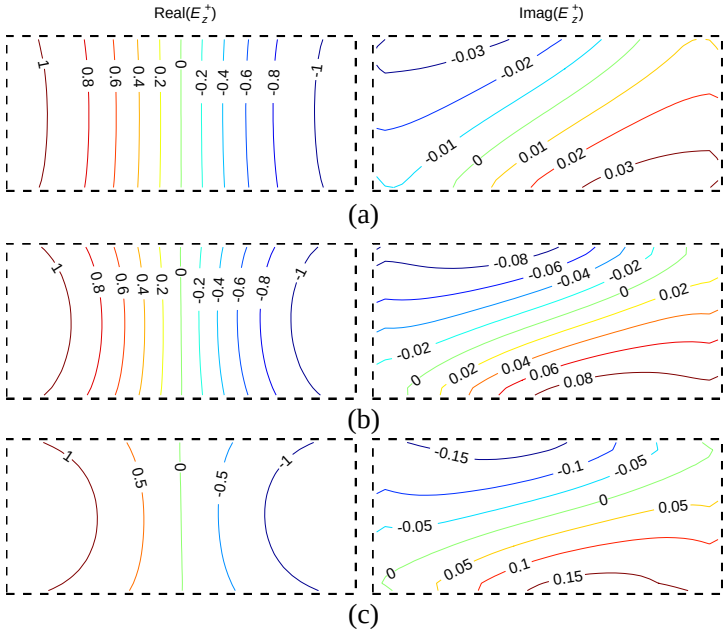

ACKNOWLEDGMENT

This work has been supported by the Spanish Government MINECO through the Research Projects TEC2014-55463-C3-1-P, TEC2014-55463-C3-3-P and by the European Commission (ERDF).

Propagation of EM Fields through a Rotating Circular Hollow Dielectric Cylinder: Numerical Simulation in 2Ds

Mingtsu Ho, **Hui-Hung Lin**, **and Tsaoan Chang**
Graduate School of Opto-Mechatronics and Materials, WuFeng University, Taiwan

Abstract— The propagation of electromagnetic (EM) fields through a rotating circular hollow lossless dielectric cylinder has been numerically simulated in two dimensions using the method of characteristics (MOC) and the numerical results were presented in this paper. The passing center swing back grids (PCSBG) technique was devised and introduced in collaboration of MOC in a modified O-type grid system to resolve the distortion of grid cell caused by the rotational movement. There are two cylinders under the illumination of EM pulse, made of dielectric and impedance matching materials, were used in this work. The computational results, presented in a side-by-side manner for clear comparisons, include the EM field distribution over the whole numerical domain and the EM fields sampled at the center of cylinder.

A Computational Model of Heat Spreader Sheet for Electromagnetic Shielding and Heat Spread

Jin-Sup Kim and Jong-Kyu Kim
Convergence Communication Components Research Center
Korea Electronics Technology Institute, Republic of Korea

Abstract— In this paper, we have designed a computational model of heat spreader sheet using smart device. Modeling heat transfer in a thin graphite sheet, this paper simulates how to use the heat transfer interface's out-of-plane heat transfer feature. Because the spreader sheet thickness is only 35 µm, it is appropriate to simulate the process using a 2-D approximation where the temperature is assumed to be constant along the thickness. Comparison of the temperature from both the 2-D and 3-D model. The simulation graphs coincide to a very high degree, making it difficult to tell them apart. In this paper, we used carbon sheet. The thermal conductivity is 1350 W/m·K (x-y axis) and electrical conductivity is 15000 S/cm. Fig. 1 shows the temperature profile in the 3-D case.

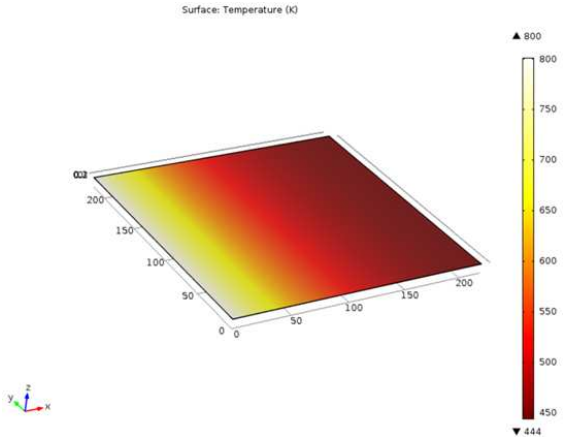

Figure 1: Heat Spreader Sheet Model for 3-D Thermal simulation.

ACKNOWLEDGMENT

This work was supported in part by the Ministry of Trade, Industry and Energy (MOTIE) grant funded by the Korean government (No. 10048605).

Rapid High-accuracy Modeling Simulation Method for Full Trajectory of the Ballistic Missile

Jianhua Wu, **Gang Li**, **Jian Chen**, **Shiyou Xu**, **and Zengping Chen**
Science and Technology on Automatic Target Recognition Laboratory
National University of Defense Technology, Changsha, China

Abstract— Ballistic missile trajectory modeling is one of the key technologies in the missile echo simulation and recognition system. However, to the best of our knowledge, all the existing modeling methods simply ignore the characteristics of different flight phase, the effect of the earth's rotation and the low speed of the ballistic generation. In order to overcome these problems, a simulation modeling method with six degree of freedom for the full ballistic trajectory is proposed. The method needs the latitude and the longitude of ballistic missile's launch point and impact point to be known. The first procedure of this method employs an improved inverse solution of Bessel's geodetic algorithm to calculate the trajectory's flight range and azimuth angles of missile's launch point and impact point. The main advantage of this improved algorithm is that it could be suitable for missiles with different trajectory ranges and obtain the results with higher accuracy. Then, based on the ellipse trajectory theory and the minimal energy trajectory theory, we put forward an optimized ballistic iterative method,during which performance parameters (including velocity, optimum ballistic angle and coordinates at the missile burnout point) were estimated. It turns out that the method can markedly decrease the iterations, speed up ballistic generation and improve the accuracy of the result. Moreover, the error of the missile's impact point also can be constrained in a permissible range. We have applied the modeling method into a system of target echo simulation and recognition; the results have shown that the modeling method is rather effective.

Electromagnetic Forces in the Complex-octonion Curved Space

Zi-Hua Weng
School of Physics and Mechanical & Electrical Engineering
Xiamen University, Xiamen 361005, China

Abstract— J. C. Maxwell was the first to research the electromagnetic field with the algebra of quaternions. This method encourages scholars to study the electromagnetic and gravitational theories with the complex quaternion and octonion. In the paper, the complex octonion can be separated into the complex quaternion and S-quaternion. And the curved complex octonion space is separated into two subspaces, the curved complex quaternion and S-quaternion spaces.

The curved complex quaternion space can be used to depict the gravitational field, while the curved complex S-quaternion space is able to describe the electromagnetic field. From the integrating function of field potential, the paper is able to study the field potential, field strength, and field source, in the curved complex octonion space. From the field source, it is capable of researching the linear momentum, angular momentum, torque, force and so forth in the curved complex octonion space.

The paper discusses the influence of curved complex octonion space on the motion of object in the electromagnetic and gravitational fields. It reveals that the field source and curved octonion space both will impact the object's motion in the two fields. By means of the coefficient and curvature in the curved complex octonion space, the field potential (or angular momentum, or the integrating function of field potential) has an extra influence on the field source (or force, or field strength).

ACKNOWLEDGMENT

The authors are grateful for the financial support from the National Natural Science Foundation of China under grant number 60677039.

Electromagnetic Force on Charged Objects with the Angular Velocity

Zi-Hua Weng
School of Physics and Mechanical & Electrical Engineering
Xiamen University, Xiamen 361005, China

Abstract— The quaternion was first used to study the electromagnetic theory by J. C. Maxwell. Nowadays the complex quaternion is applied to describe the electromagnetic and gravitational theories. Further the complex octonion is capable of studying the electromagnetic and gravitational fields simultaneously, including the field potential, field strength, field source, linear momentum, angular momentum, torque, force and so forth.

The complex octonion radius vector can be combined with the integrating function of complex octonion field potential to become one compounding radius vector, in the compounding complex octonion space. Meanwhile the compounding complex octonion space is able to be separated into two components, the compounding complex quaternion space, and the compounding complex S-quaternion space.

The compounding complex quaternion space is fit for describing the object's movement with the angular velocity in the gravitational field. While the compounding complex S-quaternion space is suitable to depict the charged object's movement with the angular velocity in the electromagnetic field. In other words, in the compounding complex octonion space, it is able to investigate the force in the presence of the velocity curl, acceleration, jerk, and jounce.

The compounding force includes the gravity, inertial force, and Lorentz force and so on. When the compounding force and torque are equal to zero respectively, it is able to deduce some equilibrium states. When the field source does not equal zero, the compounding force and torque may deviate from zero. That is, the rotating charged object will not stay on the equilibrium state. It causes the field to exchange the angular momentum and so on with the rotating charged object.

ACKNOWLEDGMENT

The author is grateful for the financial support from the National Natural Science Foundation of China under grant number 60677039.

Power Spectrum Method for the Processing of the DNA in the Genome Sequencing

M. Valla, **E. Gescheidtova**, **and P. Fiala**
Department of Theoretical and Experimental Electrical Engineering, DTEEE, FEKT
Brno University of Technology, Brno, Czech Republic

Abstract— The fractal systems are broadly found throughout the nature, generally in any scale. For each dimension (1D, 2D...) in any structures and in any mathematical algorithms or in any object (sequence, line, square) its dimension can be calculated. These dimensions are specific parameters for description of the DNA sequence characters ACGT strings. Generally a first step consists in the converting of a one-dimensional sequence into the image. In the second step, the method for calculating the dimensions for all scales is selected. For the calculations of the above mentioned dimensions the Power Spectrum (PS) method has been proposed and examined. The Power Spectrum method provides universal calculation of dimension and it allows to obtain the resulting multifractal coefficient. The multifractal coefficient represents the means rate of approximation to ideal power spectrum. It has to be emphasized that the multifractal coefficient is independent of any scale to be chosen. Moreover, the multifractal coefficient serves as an advanced parameter for mathematical description of analyzed specific sequence of the deoxyribonucleic acid (DNA) or the whole genome. The conversion of the sequence into the image as the first step of the pre-processing can be used also for the alternative imaging and the description of sequence and it is possible to choose another method for the processing and analysing a fractal image (for example Box Counting method).

In the paper, the method for the processing of the DNA in the genome sequencing, the Power Spectrum method, will be introduced. The results of the Power Spectrum methods will be presented also.

Electrically Tunable Spin Polarization in Silicene

Son-Hsien Chen
Department of Applied Physics and Chemistry, University of Taipei, Taiwan

Abstract— It was shown recently that charge currents can be highly spin-polarized during transport through silicene in the phase of marginal valley-polarized metal (MVPM). In this paper, by employing the spin-density matrix formalism capable of dealing with spin-flip processes such as in the case of Rashba spin-orbit (SO) interaction, we show that the spin polarization can be tuned via amenable electrical means. Considering the setup consisting of metallic source (injector) and drain (detector) in contract of a MVPM silicene nanoribbon (SN), where two opposite out-of-plane electric fields are applied to the left and right portions, respectively, we find that the outgoing polarization can be adjusted by varying the position of the internal boundary of the two electric fields for injected spins that are in x direction, in y direction, or unpolarized. In the case of two opposite fields applied to top and bottom portions, the polarization oscillates rapidly with the position of the internal boundary. This suggests that the polarization is more controllable by left-right than top-bottom internal boundary. The polarization grows linearly with the Fermi energy in the linear band regime near zero energy. As the length of the SN becomes larger, polarization first oscillates, and starts to increase when the ribbon length is comparable to the width. For incoming spins polarized in arbitrary directions, the out-going polarizations all approach one-hundred percent in the limit of long SN (length much greater than width), which even holds when injecting currents are unpolarized. In the case of weak Rashba SO interaction (weaker than intrinsic SO coupling), if the injected spins are in z direction, then the detected spins are almost fully polarized because z direction is approximately the spin quantization axis. In fact, irrespective of the injected spin directions, the presence of the Rashba SO interaction suppresses polarization because of the entanglement of the spin and orbit degrees of freedom. Contrarily, the disorder effectively closes conducting channels and thus reduces the entanglement, giving larger polarization. The enhancement of the polarization due to similar diminishing of the entanglement is also found by increasing the applied electric field uniformly applied to the SN so that the SN reaches the phase of band insulator in which field-dependent bulking potential is greater than some value characterized by the intrinsic SO interaction. This again implies that the spin polarizations are electrically tunable.

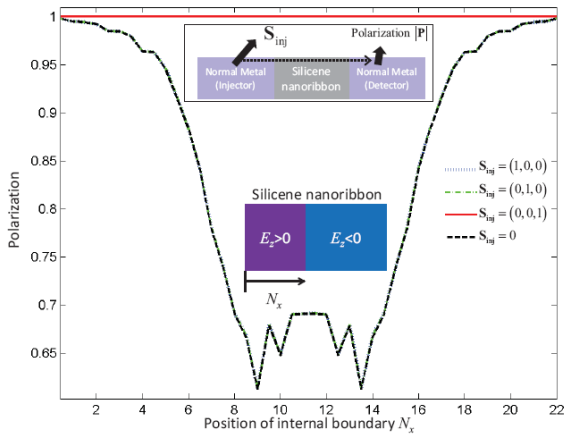

Figure 1: Detected outgoing spin polarization as a function of position of the internal boundary N_x with different directions S_{inj} of injecting spins. Here $S_{inj} = 0$ denotes the case of injecting unpolarized currents. The inset shows the studied setup, while the schematics indicates the direction of the applied electric fields E_z.

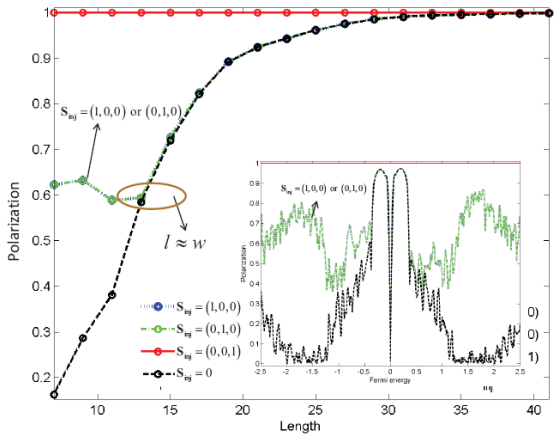

Figure 2: Detected outgoing spin polarization as a function of the length of silicene nanoribbon. The inset shows polarization as a function of Fermi energy.

Lorentz-like Transformations for the Velocity and Acceleration

Zi-Hua Weng
School of Physics and Mechanical & Electrical Engineering
Xiamen University, Xiamen 361005, China

Abstract— Analyzing the existing studies relevant to the Lorentz transformation reveals that all of these existing theories started off with some invariants (space-time interval, or speed of light), to deduce the Lorentz transformation and so forth. However the paper is able to direct deduce some invariants and the Lorentz transformation and so forth in the complex quaternion coordinate system, without the help of introducing the basic postulate.

In the complex quaternion space, when the coordinate system transforms orthogonally from one to the other, the scalar part or norm of one complex quaternion physical quantity remains invariable. The coordinate transformation between two threedimensional coordinate systems with the time, in the presence of relative movement, is equivalent to the orthogonal transformation between two complex quaternion coordinate systems.

Obviously it is able to direct deduce the invariants and Lorentz transformation and so forth, for the three-dimensional coordinate systems in the presence of relative movement, from the orthogonal transformation of complex quaternion coordinate systems. Especially it is not necessary to introduce additionally the invariant or basic postulate into the complex quaternion space, to deduce the coordinate transformations in the Special Theory of Relativity.

Furthermore, making use of the orthogonal transformation in the complex quaternion coordinate system relevant to the radius vector and velocity, it is able to deduce directly the invariants and some other coordinate transformations, besides the Galilean and Lorentz transformations. Similarly one can derive the Galilean-like and Lorentz-like transformations for the velocity and acceleration and so forth, from the above equivalency and invariants.

ACKNOWLEDGMENT

The authors are grateful for the financial support from the National Natural Science Foundation of China under grant number 60677039.

Realization of a Compact High Speed Mass Storage System

Haishan Tian, **Wenge Chang**, **and Xiangyang Li**
College of Electronic Science and Engineering
National University of Defense Technology, Deya Street 109, Changsha 410073, China

Abstract— The ongoing effort of the miniaturization of the airborne synthetic aperture radar (SAR) systems demands for the compact SAR storage components, particularly in the application where the data rate of the SAR is very high. Conventional on-board storage systems are often weighty, large and power consuming, which can't meet the requirement of the miniature carrier platform.

A new data storage system, integrated with SAR signal processor on one board, is presented in this paper. It uses compact flash (CF) card as storage medium and the FPGA as the host of the CF card. However, there are two obstacles for the high speed data storage. The first one is the internal overhead that the operation of the content erasing of the sectors is needed before the write operation of the CF card. Another obstacle is the frequently cluster switching involving the retrieving and updating of the cluster connection information in the file allocation table (FAT) and file information in the file directory table (FDT). The write response time due to above two obstacles is relatively long and can't be predicted precisely.

Two methods are presented in this paper to solve the problems. The first one is that the DDR3 flashes connecting with the DSP are used as the buffer of the SAR data in the irregular write response time. When the CF card start to store the data, the SAR data in the buffer is transferred to the DSP and then to the FPGA through the high speed interface:the SRIO. The flashes with the capacity of 1 GB are large enough as the buffer of the SAR data. In addition, the speeds of the SRIO and DDR3 interface are all so high that it wouldn't influence the speed of the storage. Another method is that all the available clusters are pre-allocated at once when the files are created. Thus the file can be written without further cluster allocation which requires the updating and retrieving in the FAT and FDT. When the data storage ends, the unused clusters and files are released. According to the two methods and the data flow of the signal processor, the hardware circuit and the software design of the data storage are presented respectively. The block diagram of the implementation is shown in Fig. 1, which consists of the data channel, containing data transfer and CF card read/write unit, and their control channel which controls the work of data channel.

To verify our proposal, the prototype data storage system is implemented on a signal processing board and a CF card with the capacity of 128 GB, as shown in Fig. 2. Yellow marked parts are the key devices of data storage system: CF card, FPGA, DDR3 flashes and DSP. The added size for the data storage is about 60 mm × 41 mm × 2 mm and the added weight is no more than 70 grams. Moreover, the data writing rate is over 100 MB/s and the added power consumption is no more than 1.2 W. As a consequence, the system achieves our goal successfully in that the storage system of the miniature SAR is compact, high speed and large capacity.

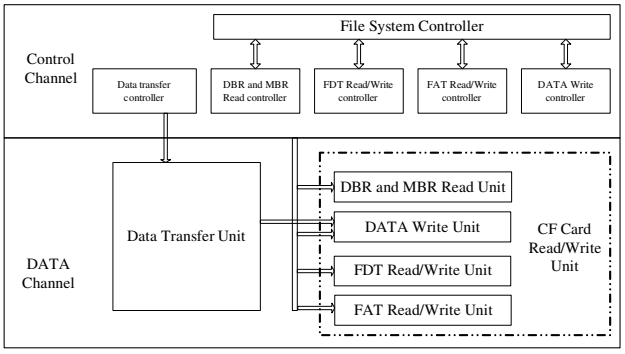

Figure 1: The block diagram of implementation of data storage.

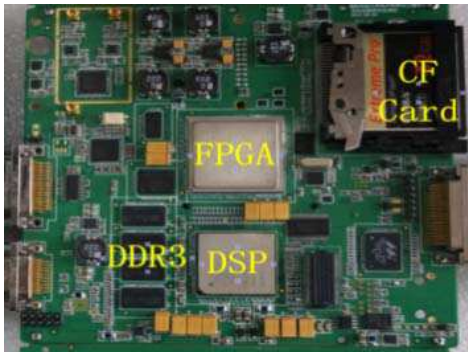

Figure 2: Hardware platform of data storage system.

Development of Intelligent Electronic Fence System

Jin-Sup Kim
Convergence Communication Components Research Center
Korea Electronics Technology Institute, Korea

Abstract— Radar sensors for monitoring the movements have been continuously evolved from the radar sensor module to the integrated circuit form. Such integrated circuits include RF front-end, analog block, and voltage regulator. Intelligent Electronic Fence (IEF) system is one of the important system for avoiding critical accidents in industrial area. In this paper, IEF system based on radar for avoiding accidents is proposed and implemented using 0.13 µm CMOS technology. The block diagram of the proposed one is shown in Figure 1. In this work, we design and fabricate the IEF system with Bi-CMOS transceiver for low power consumption. The detecting range is about 25 m. The output power is 10 dBm at 24.15 GHz. The frequency tuning range is from 24.05 to 24.25 GHz. The supply voltage is 12-V.

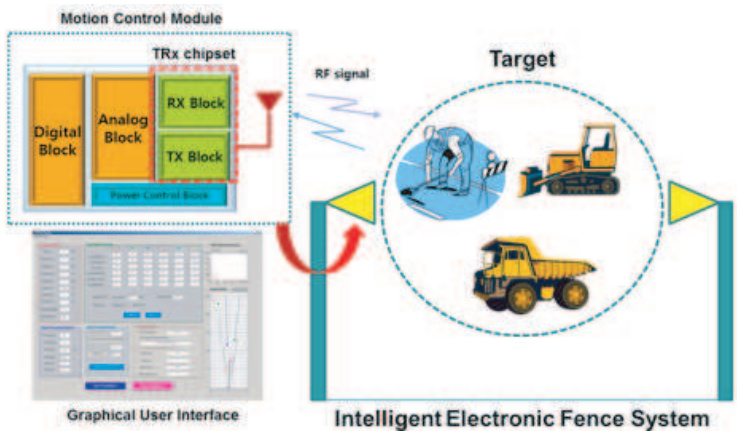

Figure 1: Block diagram of the proposed IEF system.

ACKNOWLEDGMENT

This work was supported in part by the Ministry of Trade, Industry and Energy (MOTIE) grant funded by the Korean government (No. 10050527).

Analyzing Five-layer Planar Optical Waveguides with Kerr-type Nonlinear Metamaterial Guiding Films

Yaw-Dong Wu, Ming-Hsiung Cheng, and Tien-Tsorng Shih
Department of Electronic Engineering
National Kaohsiung University of Applied Sciences, Kaohsiung, Taiwan

Abstract— In this paper, we proposed a method to analyze the electric field distributions of the five-layer planar optical waveguide structure with nonlinear metamaterial guiding films. The proposed nonlinear metamaterial planar optical waveguide is composed of two different kinds of media. One is the Kerr-type nonlinear metamaterial in the guiding films, and the other is the linear double-positive medium (DPS) in the interaction layer, the cladding and the substrate. We have derived the transcendental equations of the proposed five-layer planar optical nonlinear metamaterial waveguide structure. The propagation characteristics of the transverse electric (TE) waves were investigated analytically and numerically in the this structure. The analytical and numerical results show excellent agreement. The simulation results are helpful to figure out the propagation situation of the TE polarized waves in the five-layer nonlinear metamaterial waveguide structure. The transverse magnetic (TM) polarized waves can also be predicted by the similar process. It can also be very useful for designing a planar nonlinear metamaterial waveguide devices.

Z-scan Determination of the Nonlinear Optical Properties of Assembled Gold-nanoparticle Films

Tsong-Ru Tsai[1], **Ming-Chan Shieh**[1], **I-Chi Ni**[2], **and Shien-Der Tzeng**[2]

[1]Institute of Optoelectronic sciences, National Taiwan Ocean University, Keelung 20224, Taiwan
[2]Department of Physics, National Dong Hwa University, Hualien 974, Taiwan

Abstract— The nonlinear optical properties that were obtained by femtosecond pulsed Z-scan measurements in assembled gold-nanoparticle films were investigated at 720 nm. Very large value of the nonlinear optical absorption coefficient β was estimated to be 10^{-3} cm/W. And the imaginary part of susceptibility $\mathrm{Im}\chi^{(3)} \sim 10^{-7}$ esu was obtained. These experimental results suggest that the assembled gold-nanoparticle films are promising materials for applications in nonlinear optical devices.

Plasmons Generation at a Lossy Interface with Induced Anisotropy

Jaromír Pištora[1], **Tibor Fördös**[1], **Michal Lesňák**[2], **and Marek Kolenčík**[1]

[1]Nanotechnology Centre, VŠB — Technical University of Ostrava
17. listopadu 15, 708 33 Ostrava-Poruba, Czech Republic
[2]Institute of Physics, VŠB — Technical University of Ostrava
17. listopadu 15, 708 33 Ostrava-Poruba, Czech Republic

Abstract— The paper is devoted to the analysis of a plasmon field at a metal-dielectric boundary. The model approach based on matrix algebra is used to describe plasmon polariton solutions at a lossy interface with magnetic ordering. The attention has been focused on specification of exact expressions for normal and longitudinal wave vector components on metal-dielectric boundary with induced anisotropy. The influence of permittivity and wavelength on wave vector components is discussed in detail.

The matrix formalism is an extremely useful form of describing the steady-state solution to Maxwell's equations subject to the boundary conditions imposed by isotropic and anisotropic multilayer stacks. The effects of magnetization on the relative permittivity tensor components are usually small and they can be expanded into series:

$$\varepsilon_{ij} = \varepsilon_{0,ij} + K_{ijk}M_k + G_{ijkl}M_kM_l + \ldots = \varepsilon_{0,ij} + \varepsilon_{1,ij} + \varepsilon_{2,ij} + \ldots$$

where $\varepsilon_{0,ij}$ are the permittivity components without magnetization in the crystal ($M = 0$), K_{ijk} are components of the third rank linear magneto-optical tensor describing linear dependence on the magnetization and G_{ijkl} are components of a fourth rank quadratic magneto-optical tensor characterizing quadratic dependence on the magnetization. Since the quadratic contribution to the relative permittivity is generally small, the modeling has been focused on linear magneto-optical properties. The chosen Cartesian system has the xy plane parallel to the planar system (x-axis is normal to the incidence plane); z-axis is normal to the structure. For an anisotropic case in the transverse geometry, the relatively single elements of characteristic matrices provide a valuable insight into the magnetic and optical behavior of the system. In this special arrangement, the mode conversion is not observed and waves are traveling through the structure without polarization conversion. The analytical formulae for real and imaginary parts of longitudinal (parallel to interface and plane of incidence) and normal wave vector components have been determined as function of tensor permittivity elements. The realized model and analytical results including induced anisotropy have been tested by using Bi:YIG off-diagonal tensor permittivity values. The distribution of real part and imaginary one of normalized (k_y/k_0) tangential component of wave vector (longitudinal orientation) as permittivity function of anisotropic medium has been specified. The graphical results have been completed by the dependence of real k_y/k_0 component in 3D image on permittivity and wavelength. Bottom curves characterize induced anisotropy influence. The modulation of mentioned dependences created by induced anisotropy has been observed. This effect explains on the one hand some incorrections when the approximate results are employed for the analysis of a plasmon field at a metal-dielectric boundary, on the other hand brings new ideas for SPR applications.

Permittivity of Thin Quantum Dot Film with Local Field Effects

M. N. Anokhin, **A. A. Tishchenko**, **and M. N. Strikhanov**
National Research Nuclear University "MEPhI", Moscow, Russia

Abstract— It is known that electronic properties of a quantum dot (QD) depend on its size and shape. Spectrum of emission light of a QD is changed by tuning their core diameter. For example, the cadmium selenite (CdSe) QDs emit blue light when the diameter of the core is 2 nm and emit red light when it is 7 nm [1]. Because of it QDs have a good potential for using in different light emitting devices including organic light emitting diodes (OLEDs). For example, QDs gives a good opportunity for design white OLEDs etc..

In this work we study a natural variation of dielectric properties of a very thin film consisting of QDs, with thickness in some QD diameters. For such thin film usually used macroelectrodinamical approach does not work, which needs improving of existing techniques. We manage to obtain the generalized Clausius-Mossotti relation for dielectric permittivity of thin film from the first principles with help of the local field theory [2–4]. The distinctive feature of the local field theory is that it permits to take into account interaction between the QDs, and to express the results through the properties of single QD and radial function of distribution, characterizing their mutual disposition. In article [4] such method was developed for an amorphous substance occupying a half-space. Here we develop this technique for the case of very thin layer using dipole approximation assuming that a QD diameter is considerably smaller than the wave-length of light. We obtain the conditions when resonance lines for system of interacting QDs are shifted in comparison with the resonance lines of a single QD, which is defined by local field effects.

REFERENCES

1. Uddin, A. and C. C. Teo, "Fabrication of high efficient organic/CdSe quantum dots hybrid OLEDs by spin-coating method," *Proc. SPIE 8622, Organic Photonic Materials and Devices XV*, 86220X, Mar. 6, 2013.
2. Ryazanov, M. I., "The effect of the natural variation in the polarization of a near-surface layer onelectromagnetic surface waves," *JETP*, Vol. 83, 529, 1996.
3. Ryazanov, M. I. and A. A. Tishchenko, "Clausius-Mossotti-type relation for planar monolayers," *JETP*, Vol. 103, 539, 2006.
4. Anokhin, M. N., A. A. Tishchenko, M. I. Ryazanov, and M. N. Strikhanov, "Permittivity of anisotropic dielectric near surface with local field effects," *J. Phys.: Conf. Ser.*, Vol. 541, 012023, 2014.

Dielectric Properties and Solvothermal Synthesis of Nanocrystalline TiO_2 in Toluene with Surfactant

Jong-Ho Park
Department of Science Education, Chinju National University of Education, Jinju 660-756, Korea

Abstract— Nowadays as the concerns with global environmental issue increase, the application of TiO_2 to the treatment of polluted air and wastewater has become more and more widespread because of its promising photocatalytic performance. Solvothermal treatment is useful because it can control the grain size, the particle morphology, the crystalline phases, and the surface chemistry by regulating the sol composition, the reaction temperature, pressures, solvents, additives, and aging time. In this article, we report the synthesis of TiO_2 nanoparticles with a solvothermal method and their characteristics in anhydrous toluene solutions. Since toluene has a relatively lower vapor pressure than other organic solvents, the synthesis of TiO_2 nanoparticles can be achieved safely at a relatively high temperature in a shorter time than usual with a relatively simple process. Therefore, we could control the shapes of the TiO_2 nanoparticles by using the solvothermal method.

Synthesis of narrow-dispersed nanocrystalline TiO_2 was investigated by surfactant-aided solvothermal synthetic method in toluene solutions. Titanium isopropoxide, $Ti[OCH(CH_3)_2]_4$ (TIP) was used as precursor, which was decomposed at high temperature in the surfactant-dissolved solution. After the solution was thermally treated at 250 °C for 20 h in an autoclave, low-dispersed TiO_2 nanocrystalline particles with average size of < 6 nm were synthesized. When a sufficient amount of TIP, was added to the solution, the shapes of TiO_2 nanoparticles changed from spheres to long dumbbell rods.

The aggregated microstructures of the nano-sized TiO_2 in systems of spheres, long dumbbell rods were studied using X-ray, TEM, dielectric spectroscopy. From X-ray experiment, when sufficient amount of TIP or surfactant was added in the solution, long dumbbell-shaped nano-rods were formed, which may be due to the oriented growth of particles along [0 0 1] axis.

The dielectric property in spheres and rod-nano TiO_2 were measured over a temperature range of 30–500 °C at several frequencies. we carried out a data analysis in the frequency space. The rod TiO_2 nano particles present the variation of the imaginary dielectric (e") vs. frequency using a double logarithmic scale for several temperatures. The relaxational peak frequency of e" moves to a high-frequency region with increasing temperatures. In the low-frequency region, the other relaxational peak frequency of e" in rod nano TiO_2 particle appeared from room temperature and rose with the increase in temperature. These two different tendencies in temperature dependence suggest that two dispersion mechanisms may be involved.

Optical Properties of Poly-3-hexylthiophene Crystalline Nanofibers Oriented by the Electric Poling Procedure

Gleb Lobov, **Yichen Zhao**, **Alexandrs Marinins**, **Sergei Popov**, **and Muhammet Toprak**
KTH, Sweden

Abstract— Non-linear optics (NLO) had recently made a great contribution to the integration of various photonic devices to the circuit and even chip scale. Organic chromophores with the donor-bridge-acceptor structure are known as good candidates to replace the well-studied non-organic materials. However the area of search for more efficient NLO materials extends beyond the boundaries of azo dyes.

It was recently shown that the conjugated polymer poly-3-hexylthiophene (P3HT) which lacks the classical donor-acceptor structure shows the third-order susceptibility higher than that of Disperse Red 1 [1]. The third-order susceptibility for a 0.1–0.2% wt solution of P3HT was measured to be 1.55×10^{-8} esu, while the maximum value for a 1% wt solution of Disperse red 1 was shown to be 10^{-7} esu [2]. Moreover, it was discovered that the $\chi^{(3)}$ of P3HT is strongly enhanced by the lamellar stacking through a π-orbital overlap [3]. This stacking results in having P3HT in a conformation of separated fibers of controlled thickness and length with a random orientation (Figure 1).

Further on our task was to show that it is possible to achieve other unique optical properties by breaking the centro-symmetry through introducing the spatial ordering of the fibers. The alignment of the fibers was achieved under application of a quasi-static electric field between specially designed electrodes. The results were verified by SEM analysis after poling a very diluted sample at $\approx 1.8\,\mathrm{V/\mu m}$ and are shown on Figure 2.

As seen on the Figure 2, fibers react to electric field and align perpendicular to the gold electrodes. Such induced anisotropy of crystalline polymer conformation is absolutely novel and unstudied in terms of spectroscopic measurements and electro-optical properties. Anisotropic ordering of the fibers also allows 2nd order non-linear effects which had not been studied in this material ever before.

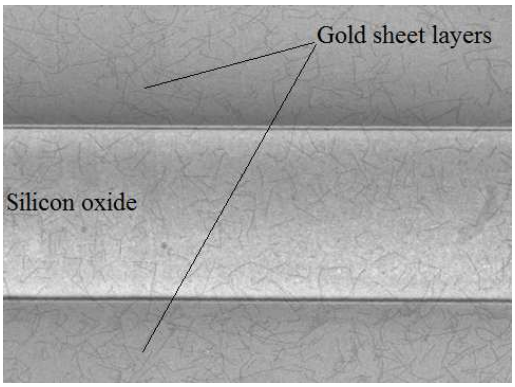

Figure 1: SEM image of unordered P3HT nanofibers.

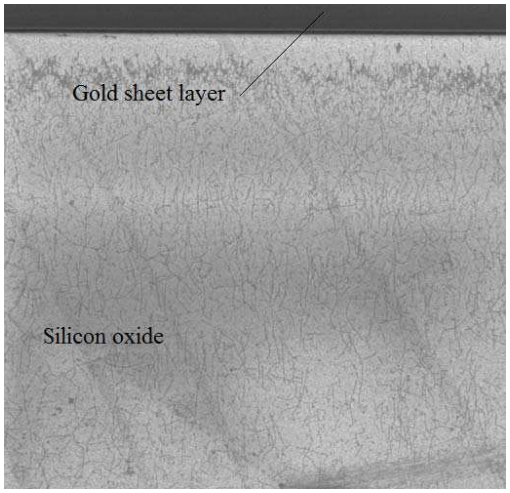

Figure 2: SEM analysis of the ordered P3HT nanofibers.

REFERENCES

1. Sethuraman, K., et al., *Jpn. J. Appl. Phys.*, Vol. 47, 450, 2008, Doi: 10.1143/JJAP.47.450.
2. Muto, S., T. Kubo, Y. Kurokawa, and K. Suzuki, *Thin Solid Films*, Vol. 322, Nos. 1–2, 233–237, 1998, Doi: 10.1016/S0040-6090(97)00953-X.
3. Sirringhaus, H., P. J. Brown, and R. H. Friend, *Nature*, Vol. 401, No. 6754, 685–688, 1999, Doi: 10.1038/44359.

New Design of All-optical Flip-flop Device Based on Multimode Interference Photonic Crystal Waveguides

Yaw-Dong Wu, Jui-Hong Hsu, Hsiu-Chuan Huang, and Tien-Tsorng Shih
Department of Electronic Engineering
National Kaohsiung University of Applied Sciences, Kaohsiung, Taiwan

Abstract— In this paper, we proposed an all-optical flip-flop device based on the multimode interference (MMI) with photonic crystal (PC) waveguides. The proposed all-optical logic gate was numerically studied by the finite-difference time-domain method (FDTD). In recent years, the photonic crystal is a very popular topic due to photonic band gaps (PBGs) which were known to exist in the periodically modulated dielectric materials. We try to combine the MMI principle and photonic crystal waveguide to design a whole new all-optical RS flip-flop device based on the MMI PC waveguide structures. By introducing a point defect rod both in the control ports, we can make outgoing field propagating in the output waveguide or not. The intensity profiles show snapshots optioned at different times. This numerical results show that the proposed PC waveguide structure could really function as an all-optical RS flip-flop logic gate. Note that if we have an RS flip-flop, we can realize various much complex logic processing based on it.

Ultrashort Pulse Generation in Tapered Photonic Crystal Fiber at 400 nm

A. Manimegalai[1, 5], E. Gunasundari[1], Abdosllam M. Abobaker[2], K. Senthilnathan[1], S. Sivabalan[3], K. Nakkeeran[4], and P. Ramesh Babu[1]

[1]Photonics, Nuclear and Medical Physics Division, School of Advanced Sciences
VIT University, Vellore 632 014, India
[2]Department of Communications Engineering, College of Electronic Technology, Bani Walid, Libya
[3]School of Electrical Engineering, VIT University, Vellore 632 014, India
[4]School of Engineering, University of Aberdeen, Aberdeen AB24 3UE, UK
[5]Department of Electronics and Communication Engineering, GTEC, Vellore 632 102, India

Abstract— The generation of ultrashort pulses at shorter wavelength near 450 nm is especially preferred in satellite sensors, ophthalmology in optical coherence tomography system, optical imaging, etc.. However, it is difficult to produce such a shortest pulse at near visible wavelength even from the best available laser sources. Of late, the generation of desired pulse width of ultrashort pulses is quite possible through pulse compression technique with the advent of photonic crystal fiber (PCF) where the anomalous dispersion can also be obtained at visible regime. Achieving single mode and high dispersion near the visible wavelength are considered to be challenging tasks in the generation of ultrashort pulses in PCF. In general, there are two proven ways to enhance the nonlinearity and dispersion values in PCFs. First, one can modify the design of PCF with large air hole size leading to high nonlinearity and large dispersion. However, the single mode tends to vanish for larger values of air hole size. Second, the nonsilica technology such as SF6, TF10, CS2, nitrobenzene, and so on, enhances the nonlinearity and eventually the required input energy of the pulse can be minimized considerably. Even in the non-silica technology, obtaining a single mode as well as anomalous dispersion at visible regime is very difficult in PCF for large air hole diameter.

In general, the tapering is done by reducing the pitch and diameter. Fiber tapering provides a convenient way to reduce the mode-field diameter of fibers, thereby allowing for a better pulse compression. We, thus, emphasize that the tapered PCFs (TPCFs) are very much suitable for effective pulse compression when compared to conventional PCFs. In this paper, we design hexagonal and octagonal TPCFs wherein dispersion and nonlinearity vary exponentially in line at 400 nm wavelength according to the self-similar analysis. By exploiting these optical properties, we demonstrate the effective pulse compression schemes at 400 nm wavelength.

Geometrical structure and variations of group velocity dispersion (GVD) and nonlinearity along the propagation direction for both hexagonal and octagonal TPCFs at 400 nm wavelength are given by:

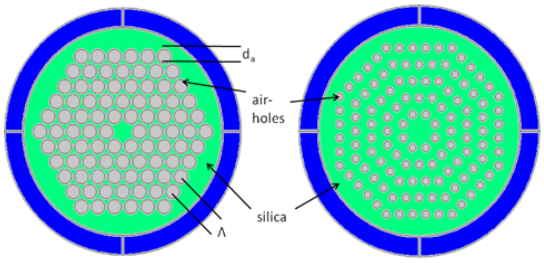

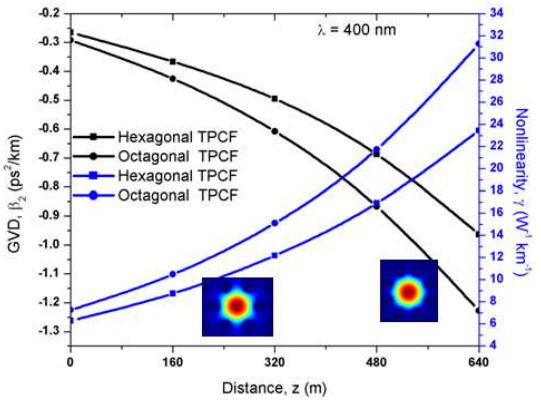

Electrical Field Energy Oscillation near the Photonic Structure Faces

Vyacheslav A. Trofimov, Elena S. Komarova, Alexey S. Barykin, and Mikhail V. Fedotov
Lomonosov Moscow State University, Leninskie Gory, Moscow 119992, Russia

Abstract— Using on the 1D Maxwell's equations, we analyze a femtosecond laser pulse interaction with transparent layered structure (1D photonic crystal — PhC). As it is well-known, such structure is wide used in photonics.

Laser pulse falls on a PhC and propagates inthe structure. Because of multi-layers the laser pulse reflects many times from boundaries between the PhC. As a consequence of this, part of a laser pulse localizes in the PhC during certain time interval. Analyzing this process we found out new effect: oscillation of laser pulse energy near the PhC faces but outsides the PhC. More precisely, part of laser pulse, leaving the photonic crystal through its faces, changes its motion direction and returns into the structure. A reason of such electric field energy evolution is wave vector direction change. Therefore, the corresponding part of wave packet moves more towards to the PhC and comes back into the structure.

Amplitude of electric field energy oscillation depends on dielectric permittivity of PhC layers and their lengths. We investigate in details the laser pulse duration influence on the electric field energy oscillation as well as the PhC characteristic influence on this regime of laser radiation interaction with PhC.

Accuracy of Waveguide Mode Solver Based on Boundary Integral Equations

J. Vincent[1,2], **A. Calvez**[3], **R. Perrussel**[1], **and J.-R. Poirier**[1]

[1]LAPLACE, Université de Toulouse, Toulouse, France
[2]LAAS — Optoelectronics for Embedded Systems, Toulouse, France
[3]IRMAR — Université de Rennes 1, Rennes, France

Abstract— In this paper, we investigate the accuracy of a waveguide mode solver based on boundary integral equations. The propagation of light in several Photonic Crystal Fibers with different geometries of their cross section is analyzed. The obtained results are compared with those given by the Finite-Element Method.

Introduction: To design Photonic Crystal Fibers (PCF) for various applications, fast and accurate numerical simulations are needed. Recent studies [1, 2] shows the efficiency of a high order waveguide mode solver based on the Boundary Integral Equations (BIE). The aim of this paper is to use this solver with different PCF geometries and to evaluate the accuracy of the results with those given by the Finite-Element Method (FEM) computed with the commercial software COMSOL.

Formulation and Solution of the Problem: The cross section of a PCF consists of a finite number of homogeneous inclusions with refraction index n_i, embedded in a homogeneous background material with refraction index n_e. The problem is to determine the total effective refraction index n_{eff} of the structure. Writing Maxwell equations and the interface conditions on the electromagnetic field, one obtains a system of equations. The use of the single and double layer potentials on all the hole boundaries in the previous system gives rise to a nonlinear eigenvalue problem

$$A(n_{\text{eff}})x = 0, \tag{1}$$

where the vector x gathers the unknown values and the matrix A is an analytic function of n_{eff}. The main advantage of using BIE instead of the FEM is that only the boundary holes are discretized. This matrix problem can be turned into a complex root finding process for the function $f(n_{\text{eff}})$ with two fixed random vectors y and z

$$f(n_{\text{eff}}) = \frac{1}{(y^T A^{-1}(n_{\text{eff}})z)} = 0, \tag{2}$$

where $A^{-1}z$ is computed by solving the system $Ab = z$. Since the operator in the matrix A are hypersingular and the interfaces between the holes and the cladding of the PCFs are smooth, kernel-splitting techniques developed by Kress [3] are used. As in [1, 2], we solve $n_{\text{eff}} \in [n_e; n_i]$ from (2) using Müller's method.

Conclusion: This study shows the accuracy of a waveguide mode solver based on boundary integral equations for different PCFs. The results are compared with those given by the FEM computed with COMSOL.

REFERENCES

1. Lu, W. and Y. Y. Lu, "Efficient high order waveguide mode solvers based on boundary integral equations," *Journal of Computational Physics*, Vol. 272, 507–525, September 1, 2014.
2. Lu, W. and Y. Y. Lu, "Efficient boundary integral equation method for photonic crystal fibers," *Journal of Lightwave Technology*, Vol. 30, No. 11, 1610–1616, June 1, 2012.
3. Kress, R., "On the numerical solution of a hypersingular integral equation in scattering theory," *Journal of Computational and Applied Mathematics*, Vol. 61, 345–360, August 1995.

A Method of ISAR Sequences Quality Assessment for Aerospace Target

Gang Li, **Qingkai Hou**, **Shiyou Xu**, **and Zengping Chen**
Science and Technology on Automatic Target Recognition Laboratory
National University of Defense Technology, Changsha, China

Abstract— Inverse synthetic aperture radar (ISAR) can generate 2D image for a non-cooperative moving target and be used for military and civilian purpose. In practice, however, the effect of ISAR imaging is affected by many factors, some quality problem is existed in the ISAR image, such as blur, deformation, tailing, ghost copy etc.. So it is necessary to evaluate the image quality by some corresponding parameters. In addition, the research on that how to choose the high quality image from the mass result, has important significance to realize image interpretation and obtain the target information. The techniques for SAR image quality assessment have been developed in recent years, and already formed a commercial product, but the research on ISAR image is still poor.

In the traditional method, image entropy and contrast is adopted to evaluate the image quality, however, this method is only suitable for comparing the image quality from the same measurement data in different processing algorithm. It still has no viable standard on that how to evaluate the ISAR images in different measurement periods.

In this paper, the traditional ISAR image quality evaluation standard and its limitation is analyzed. An ISAR quality evaluation method of aerospace targets is presented, combining with ISAR imaging mechanism and the structural characteristics of aerospace targets, referencing the standard of optical image quality evaluation. Beyond some current commonly used indications, a new indication based on the power spectrum is adopted in this method. The simulation data and real data shows the validity of the algorithm.

Compensation for System Distortion Using Low Signal-to-noise-ratio Echo from Spherical Satellite

Jianzhi Lin, **Weixing Li**, **Weihua Wang**, **Gang Li**, **and Zengping Chen**
Science and Technology on Automatic Target Recognition Laboratory
National University of Defense Technology, Changsha 410073, China

Abstract— Compensation for amplitude and phase distortion in inverse synthetic aperture radar (ISAR) system is important for the system performance. There are two types of techniques to measure the amplitude and phase distortions in the system: closed loop and the employment of an external test target. The former excludes the antenna and propagation medium, leading to limited results. The latter uses the complete system and is better. The type of the test target may be a corner reflector, a metallic ball towed by a balloon, an active radar calibrator (ARC) on a tower, or a spherical satellite. However, the corner reflector may suffer from high level of clutter. The metallic ball towed by a balloon will be difficult to carry out daily in practice and is costly. The current approach is to use the ARC. But the ARC includes optic transceivers, fibre-optic delay line, and amplifiers, which induces additional distortion. Although it is best to take the spherical satellite as the test target, it is unpractical because the signal-to-noise-ratio (SNR) is too low.

In this paper, we analyze the reason why the low SNR signal received from the spherical satellite fails to compensate for the distortion. Then we utilize pulse compression technique based on matched filtering to find the target region and then take inverse matched filtering on the region to get high SNR signal. Thus we can achieve the distortion coefficients and compensate for the system distortion. Experiments based on real radar data show that the results are better than that by the ARC.

Enhanced Efficiency of Second Harmonic Generation with Twelve-fold Photonic Quasi-crystal Fiber in Telecommunication Band

Ritapa Bhattacharjee[1], **Abdosllam M. Abobaker**[2], **K. Senthilnathan**[1], **S. Sivabalan**[3], **K. Nakkeeran**[4], **and P. Ramesh Babu**[1]

[1]Photonics, Nuclear and Medical Physics Division
School of Advanced Sciences, VIT University, Vellore, Tamil Nadu 63214, India
[2]Department of Communications Engineering, College of Electronic Technology, Bani Walid, Libya
[3]School of Electrical Engineering, VIT University, Vellore, Tamil Nadu 63214, India
[4]University of Aberdeen, Fraser Noble Building, Aberdeen AB24 3UE, UK

Abstract— We design an index guided silica core photonic quasi-crystal fiber of twelve-fold symmetry for enhancing the efficiency of second harmonic generation by using the fundamental input wavelength of 1.55 μm in the telecommunication band. We find the quasi periodic arrangement of holes in the cladding does highly influence the modal confinement as well as the intensity distribution of both the fundamental and second harmonic fields inside the core. As a result, the two most important aspects of second harmonic generation, namely, phase mismatch factor and overlap area related to the efficiency of second harmonic generation get highly affected. Moreover, these two quantities must be as minimum as possible for enhancing the efficiency of second harmonic generation. Hence, in this study, we emphasize on minimizing these two factors with proper choice of geometrical parameters of the photonic quasi-crystal fiber. In this analysis, we consider the pitch range of 1–15 μm and relative hole diameter of 0.5. We find that the overlap area increases with increase in pitch but the phase-mismatch factor decreases. Also here we consider the first order quasi phase matching technique for phase matching. In quasi phase matching, the phase mismatch factor is taken care by the quasi phase matching period. Hence, in quasi phase matching, the overlap area takes much significant role in determining the efficiency of second harmonic generation. But a lower value of phase mismatch factor always supports ease of poling by increasing the quasi phase matching period. With the available poling technology, we optimize the pitch of the photonic quasi-crystal fiber at 7 μm and report a relative efficiency of second harmonic generation as 38.22% $W^{-1}cm^{-2}$, when the overlap area is 2.74 μm^2 and phase-mismatch factor is 0.102 μm^{-1}. This value is much higher than that of already reported relative efficiency of second harmonic generation with photonic crystal fiber. This work can be extended for higher harmonic generation and atto-second pulse generation.

Few-cycle Pulse Generation Using Solid-core Photonic Quasi-crystal Fiber

K. Senthilnathan[1], **M. S. Aruna Gandhi**[1], **S. Sivabalan**[2], **P. Ramesh Babu**[1], **Abdosllam M. Abobaker**[3], **and K. Nakkeeran**[4]

[1]Photonics, Nuclear and Medical Physics Division, School of Advanced Sciences
VIT University, Vellore 632 014, India
[2]School of Electrical Engineering, VIT University, Vellore 632 014, India
[3]Department of Communications Engineering, College of Electronic Technology, Bani Walid, Libya
[4]School of Engineering, Fraser Noble Building, University of Aberdeen, Aberdeen AB24 3UE, UK

Abstract— In recent years, the generation of few cycle pulses has been of great scientific and technological interest. In this line, the microstructured optical fibers have been playing a vital role since the desired optical properties can easily be engineered by adjusting the geometrical parameters. The recent results reveal that the quasicrystals exhibit several interesting photonic properties over periodic crystals. A solid core photonic quasi-crystal fiber (SC-PQF) is a novel microstructured fiber with quasi periodicity in structure and has a long range order with aperiodic arrangement in its cladding region. The structure of the cladding region consists of air holes of diameter d and pitch, Λ, with five rings of air holes. In the central region, the air hole is removed and the resulting solid silica core acts as a defect and gives rise to the propagation of guided modes.The photonic quasi-crystal fiber provides a very large nonlinearity and sufficiently lowdispersion that could be exploited for generating single cycle pulses.We look for the hitherto mentioned optical properties in the proposed SC-PQF by carefully optimizing the geometrical parameters namely, core diameter and the pitch. Eventually, with the proposed fiber, we study both dispersion and nonlinearity for a range of wavelengths from 300 to 2000 nm and demonstrate sufficiently low dispersion ($-1.9478\,\mathrm{ps}^2/\mathrm{m}$) with zero confinement loss and enhanced nonlinearity ($\gamma = 578\,\mathrm{W}^{-1}\mathrm{m}^{-1}$) for a wavelength of 850 nm. The higher-order soliton effect compression of the femtosecond pulses in the proposed SC-PQF at 850 nm wavelength is numerically studied. An input pulse of 15 fs widthis compressed down to 5 fs nearly 1.8 cycles of pulse generation.Besides, we also calculate the power (211 W) and energy (0.9 pJ) of the compressed few-cycle pulse at 850 nm wavelength.

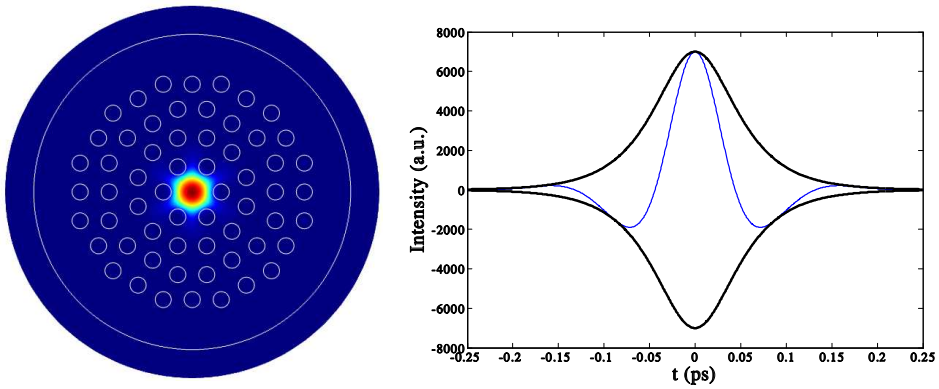

Figure 1: (a) Geometric structure of the proposed fiber with the fundamental mode field distribution and (b) output pulses with number of oscillations at 850 nm wavelength.

Overcoming Bandwidth Limitation of LED by Using Multilevel Differential PAM in VLC

S. H. Yang, D. H. Kwon, and S. K. Han
Department of Electrical and Electronic Engineering, Yonsei University
50 Yonsei-ro, Seodaemun-Gu, Seoul, Korea

Abstract— Narrow modulation bandwidth of commercial white LED is limitation of optical wireless visible light communication system. Thus, several studies have been researched to overcome the bandwidth limitation of white LED. First, for the white lighting, most devices use a blue LED which illuminates a layer of yellow phosphor. However, modulation bandwidth is typically lower than several MHz by slow time constant of the yellow phosphor, thus optical blue filtering techniques have been researched to improve the modulation bandwidth. Secondly, to enlarge modulation bandwidth and compensate the channel response, electrical equalizer is adopted. Thirdly, to secure the additional optical channel, WDM based on RGB LED with optical filter at receiver and PDM based on polarizer are researched. Last, high-speed wireless connectivity is implemented using adaptive modulation: QAM with OFDM or DMT. The transmission capacity can be increased significantly, because spectral efficiency is maximized. However, these modulation methods need additional digital signal processing such as FFT and IFFT, thus hardware and computational complexity of transmitter and receiver is increasing. In addition, modulated signals have a high PAPR, thus the linear devices to have large dynamic range is required. As a result, nonlinear characteristics of RF and optical devices are cause of undesired distortions.

In this paper, we propose a novel modulation and de-modulation format to reduce the complexity of transmitter and receiver which is named multilevel differential pulse amplitude modulation (MD-PAM). The proposed modulation scheme transmits different PAM signals with same amplitude and unit time delay using multiple LED chips, respectively. Optical signals from every LED chips are linearly accumulated during through the optical wireless channel and directly detected at the single optical receiver. Received signal is demodulated using received signal power difference which is changed by light intensity. As a result, we experimentally confirmed that 100-Mbit/s transmission was possible using LED which has 25 MHz modulation bandwidth.

Photo-induced Electrical Instability in Transparent Electronics

Jun-Young Jeon and Tae-Jun Ha
Department of Electronic Materials Engineering, Kwangwoon University, Seoul 139-701, Korea

Abstract— Transparent conducting oxides (TCOs) are based on post-transition of metal combined oxides with an outer major quantum number of > 4. Since the s orbital possesses a large spatial size and forms hybridization, oxide can be a good electrical dopant securing high density and stability. Most TCOs exhibit visible-light insensitivity and difficulty attaining charges by light absorption due to the wide band gap. High performance transparent electronics consisting of metal-oxide semiconductors such as zinc-oxide (ZnO), indium-zinc-oxide (IZO) and indium-gallium-zinc-oxide (IGZO) have been extensively investigated to realize the unit pixels for next-generation displays. However, unexpected instability caused by photo-induced electrical bias in amorphous metal-oxide based thin film transistors (oxide-TFTs) retards the development of transparent electronics.

We will present the origin of photo-induced electrical instability in oxide-TFTs based on transparent electronics by applying the photo irradiation with a wave length of $400 \sim 800$ nm by using a monochromator. The combination of photo irradiation and prolonged gate bias stress enhanced the electrical instability in transparent devices. Such results stem from the extended trapped charges possessing the energy absorbed from light-wave at the localized defect states related to oxygen vacancy. We will also demonstrate the chemically clean interface in oxide-TFTs by employing oxygen annealing which reduces the density of trap states, thereby resulting in improved photo-induced stability.

We believe that this study provides significant information on the device physics of optoelectronics, which commonly exhibit photo-induced instability and charge transport, as a results of prolonged exposure to photo irradiation.

Split-step Time-domain Analysis of Optical Code Division Multiple Access En/Decoder Composed of Ring Resonator Waveguides

Youngchul Chung
Department of Communications and Electronics Engineering, Kwangwoon University
20, Gwangun-ro, Nowon-gu, Seoul 139-701, Korea

Abstract— By applying CDMA (Code Division Multiple Access) to optical communication systems, it is possible to use wide bandwidth of optical fiber, to provide passive code decryption, and to protect the optical physical layer. Two-dimensional (2-D) OCDMA (Optical CDMA) en/decoders can be realized in the form of compact photonic integrated circuits by cascading ring resonator waveguide filters as shown in Fig. 1. The 2-D optical en/decoder based on micro-ring resonators can provide wavelength hopping and spectral phase coding patterns which can be simultaneously reconfigured. In this paper, a split-step time-domain modeling (SS-TDM) is adopted to analyze the reconfigurable 2-D OCDMA en/decoders. The SS-TDM is implemented in two-steps. First the optical wave propagation through every divided section of the bus and ring waveguides is calculated with appropriate boundary conditions. Using the calculated electric field values, the bus-ring and ring-ring coupling calculations are performed. In the calculation the stepping time interval should be equal to the section length divided by the group velocity. With this algorithm the pulse propagation characteristics through the ring resonator filters can be efficiently analyzed, thus the encoded and decoded waveform can be readily obtained to assess the applicability of the designed en/decoder devices. The 2-D en/decoder with two wavelengths and two phases are simulated for a demonstration and the results are shown in Fig. 2. The encoded waveform is shown in Fig. 2 and the decoded waveforms are shown in Fig. 3. When the conjugate code is used for decoding, the original optical pulse is found to be recovered.

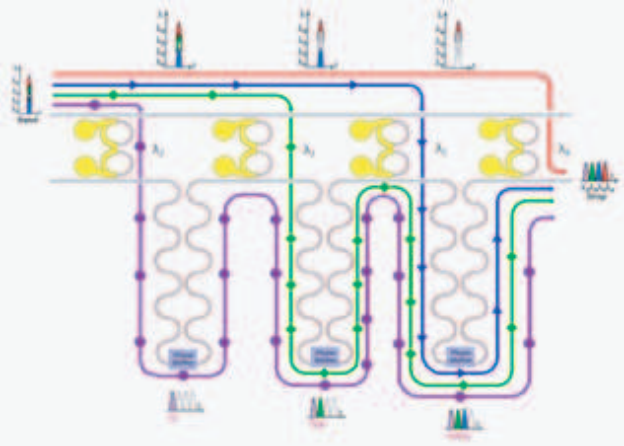

Figure 1: A configuration of a 2-D OCDMA en/decoder composed of four cascaded double-ring add/drop filters.

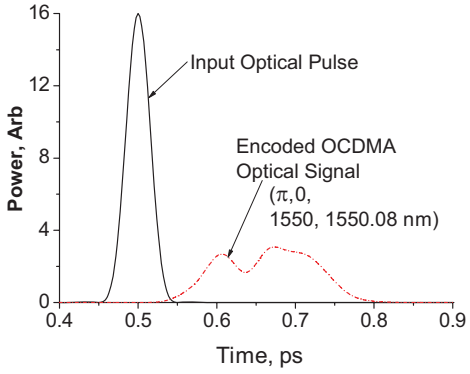

Figure 2: An encoded waveform.

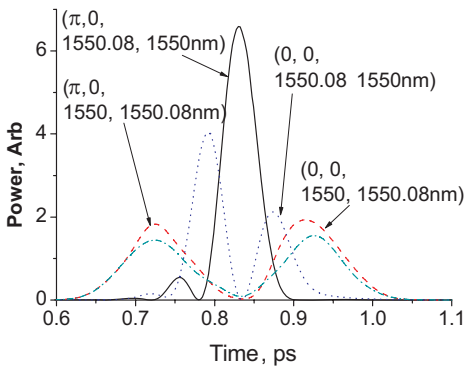

Figure 3: Decoded waveforms with various codes.

ACKNOWLEDGMENT

This work was supported by Basic Science Research Program through the National Research Foundation of Korea funded by the Ministry of Science, ICT and Future Planning in 2013 (NRF-2013R1A1A2007276).

Dependence of Radio Frequency Magnetron Sputter-deposited ZnO-SnO_2 Thin Films on Substrate Temperature

Ik-Jae Lee, Hoju Kang, and Nark-Eon Sung
Pohang Accelerator Laboratory (PAL), Pohang University of Science and Technology
Pohang 790-784, South Korea

Abstract— ZnO-SnO_2 (ZTO) thin films were deposited by radio frequency sputtering on quartz substrates at various substrate temperatures T_S, and characterized using x-ray diffraction (XRD), selected-area electron diffraction, atomic force microscopy (AFM) and spectrophotometer, four-point probe method and Hall measurement. XRD analysis indicates that the ZTO films can be either amorphous ($T_S \leq 350°C$) or crystalline ($T_S \geq 450°C$). AFM studies of the ZTO films indicate that the surfaces are fairly smooth with root-mean-squared surface roughness of 1.04 to 3.55 nm. The average optical transmittance of the ZTO films was $\geq 85\%$. The optical bandgap, estimated using a Tauc plot, increased as T_S increased. Blue shift was observed in the absorption edge and was attributed to decrease in the oxygen vacancies and dangling bonds. The lowest resistivity was on the order of $10^{-2}\,\Omega$·cm for films deposited at $T_S \geq 650°C$: films deposited at $T_S \leq 450°C$ were weakly conducting. The conductivity of films increased as T_S increased. These results can guide modifications of ZTO for applications that incorporate electrically-conducting, optically-transparent thin films.

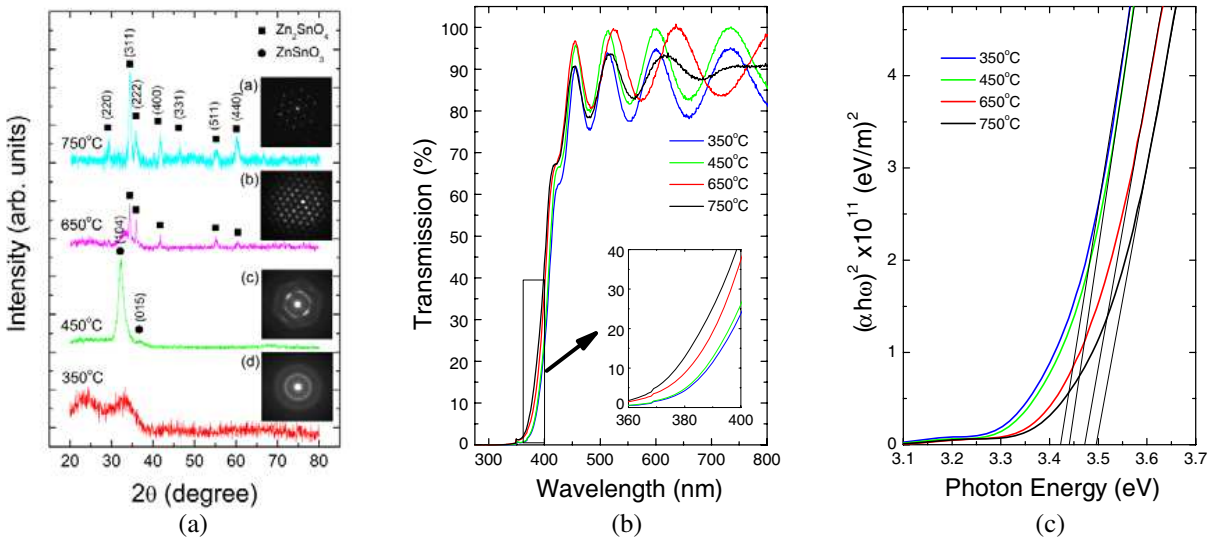

Figure 1: (a) XRD patterns of ZTO thin films deposited on quartz substrates by RF magnetron sputtering at various substrate temperatures. (b) Optical transmittance as function of wavelength for ZTO thin films deposited at various substrate temperatures (350–750°C). Inset: enlarged view of transmission spectra from 360 to 400 nm. (c) Relationship between $(\alpha h\omega)^2$ and $h\omega$ for ZTO thin films at various substrate temperatures.

Design Procedure for 2D Slotted Waveguide Antenna with Inclined Coupling Slots for Sidelobe Level Control

H. M. El Misilmani[1], **M. Al-Husseini**[2], **and K. Y. Kabalan**[1]

[1]American University of Beirut, Beirut 1107 2020, Lebanon
[2]Lebanese Center for Studies and Research, Beirut 2030 8303, Lebanon

Abstract— Slotted Waveguide Antennas (SWAs) radiate energy through slots cut in a broad or narrow wall of a rectangular waveguide. They offer clear advantages in terms of their design, weight, volume, power handling, directivity, and efficiency. SWAs can be resonant (standing wave) or non-resonant (traveling wave). Resonant SWAs outperform the non-resonant SWAs in terms of efficiency due to its termination with a short circuit, compared to matching load in the case of the latter, but with a narrower bandwidth. For broad-wall SWAs, the slot displacements from the wall centerline determine the antenna's sidelobe level (SLL). In addition, the rotation angle of the coupling slot in a 2D system array of SWAs determines the power fed by each slot into each branchline SWA.

This paper presents an inventive simple procedure for the design of a two-dimensional (2D) SWA array system with desired sidelobe level (SLL). The system consists of multiple branchline waveguides with broadwall radiating shunt slots. A main waveguide is used to feed the branch waveguides through a series of inclined coupling slots with well-defined rotation angles for low SLLs. For a specified number of identical longitudinal slots, the described procedure finds the slots length, width, locations along the length of the waveguide, and displacements from the centerline, for each branch waveguide. Furthermore, for a specified number of branch waveguides, the method finds the rotation angle of each of the coupling slots.

To explain the controllable-sidelobe 2D SWA design procedure, an SWA with 8×8 elliptical slots, designed for an SLL lower than -20 dB, is taken as an example. An 8-element 1D SWA with a desired SLL is designed first. Eight identical such SWAs are then attached side by side. The proper design of the 1D SWAs ensures having the desired SLL in one principal plane. To enforce the same SLL over the whole 3D pattern, special care should be given to the design of the feed SWA, whose slots should power the radiating SWAs according to a correct distribution. For the taken example, the feed SWA should have 8 slots, separated consecutively by a distance related to the radiating SWA aperture width and wall thickness. The power fed by each slot in the feeder and fed to the branchline waveguide is controlled by the inclination angle of the coupling slot.

Figures 1(b) and 1(c) show a comparison of the gain patterns for the following 2 cases: Case 1 where the radiating slots have a uniform displacement and the coupling slots have a uniform rotation angle; and Case 2 where the radiating slots have non-uniform displacements and the coupling slots have non-uniform rotation angles as per the design procedure. As inspected, the SLL decreased from -12.1 dB in case of uniform displacements and rotation angles to less than -20 dB with the non-uniform displacements and inclinations calculated using the presented simple design procedure.

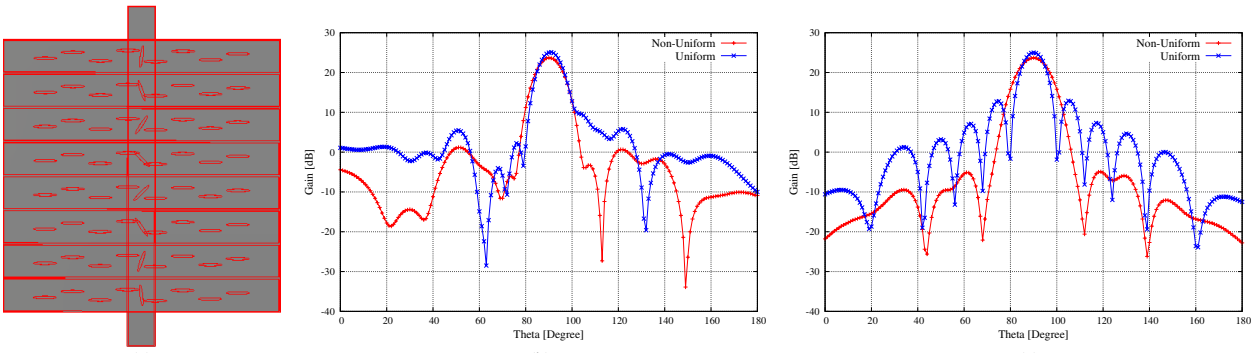

(a) (b) (c)

Figure 1: (a) 2D System, Compared gain pattern results of the uniform and non-uniform displacements and rotation angles design cases: (b) E-plane, (c) H-plane.

Tripolarization Antenna for DSRC Applications

Sumin Yun and Sangwook Nam
INMC, School of Engineering and Computer Science, Seoul National University, Korea

Abstract— With a development of wireless communications, a DSRC (Dedicated Short Range Communication) applications are proposed for various applications like collision avoidance, traffic control, autonomous driving. Therefore, the reliability of DSRC is essential because the vehicle safety is directly affected by the communication reliability. In this paper, the MIMO (Multiple Input Multiple Output) antenna is proposed for the DSRC applications.

A patch antennas, which has many favorable characteristics like low-profile, planar structure, are widely used in various applications. A patch antenna also can be used in MIMO systems [1], because it has degenerate modes. A horizontal polarization can be easily generated by the patch antenna. However, it is hard to generate perpendicular polarization in same frequency. The monopole like characteristic mode, which generates the vertical polarization, has lower resonance frequency compared to that of the resonant modes generating the horizontal polarization.

In this paper, the parallel plate is placed between a patch and a ground for the monopole mode. By using the parallel plate, the resonance frequency of monopole mode has increased to the resonance frequency of patch modes. Along with the two degenerate patch modes, the excited monopole mode generate tripolarization. As the three ports excite orthogonal characteristic mode, higher than 30 dB isolation is achieved. The simulated result shows that the proposed antenna has −10 dB impedance bandwidth from 5.8 to 6 GHz. The proposed antenna has a dimension of $24 \times 24 \times 3.14\,\text{mm}^3$, which is a size of a conventional patch antenna. The proposed achieved tripolarization without increasing the conventional size of the patch antenna.

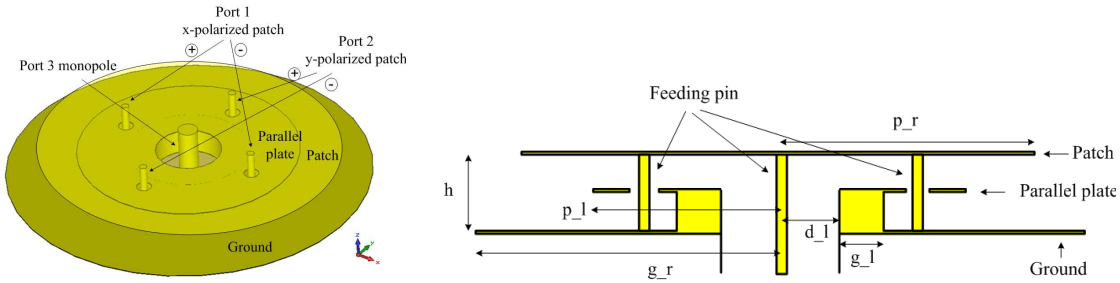

Figure 1: Geometry of the proposed tripolarization antenna (dimensions of the simulated antenna, $h = 3.14$, $p_l = 7.2$, $p_r = 9.4$, $g_r = 12$, $d_l = 2.18$, $g_l = 1.4$, all in the unit of mm.).

REFERENCES

1. Sarrazin, J., Y. Mahe, S. Avirillon, and S. Toutain, "A new multimode antenna for MIMO system using a mode frequency convergence concept," *IEEE Transactions on Antennas and Propagation*, Vol. 59, No. 12, 4481–4489, Dec. 2011.

Wide Bandwidth Compact Size Meander Antenna for the 800 MHz LTE Band

Sanghoon Park, **Ki-Jin Kim**, **Kwangho Ahn**, **Koon-Tae Kim**, **and Sehwan Choi**
Convergence Communication Components Research Center
Korea Electronics Technology Institute, South Korea (R.O.K.)

Abstract— The machine-to-machine (M2M) connection is the key technology nowadays. Lots of sensors and devices have acquired the communication ability. Then, more and more devices become connected and will constitute a huge network in the future. However, current communication modules or chipsets are mainly focusing on the higher data rate. In order to facilitate the machine connection, an exclusive small and cheap communication module which supports long-term evolution (LTE) is highly desired. One of the most important factors to build the M2M exclusive LTE module is to minimize the antenna size. We chose the meandering with the CPW feeding method for this purpose. The antenna is optimized to use the adaptive particle swam optimization with the ten particles and six design parameters. The FR-4 type PCB showing the permittivity constant of 4.4 has the size of $30 \times 35\,\text{mm}^2$ with height of 1 mm. The measured resonant frequency band ranges from 810 to 915 MHz which is 10 MHz wider than the simulation results, as shown in Fig. 1.

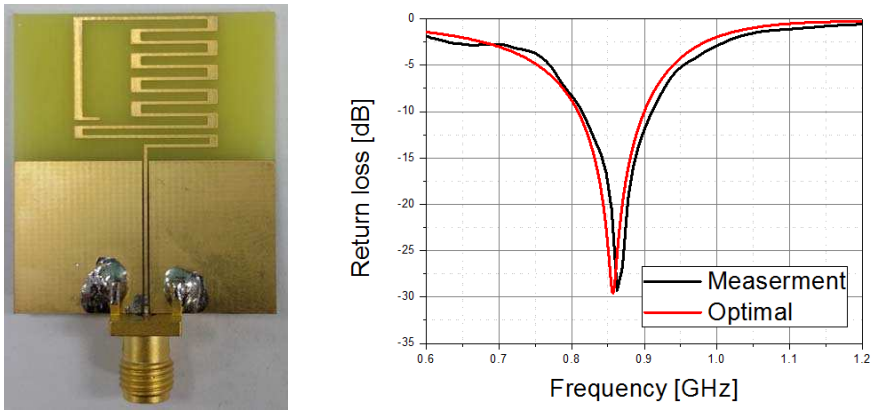

Figure 1: Compact size meander antenna for the 800 MHz LTE band.

Cavity-backed and Shorted Microstrip Patch Antenna for On-body Systems

Sehwan Choi and Hojun Lee
Korea Electronics Technology Institute, Seongnam-si, Gyeonggi-do 463-816, Korea

Abstract— After the introduction of wireless wearable devices, the interest to applications utilizing this technology has increased. These devices have been applied in sports, military and medical area such as monitoring of heart rate and blood pressure. But it has been an obstacle to use them because of the inconvenience caused to be attached to the human body. Antennas must have the characteristics of low profile, small size and high efficiency in order to reduce the inconvenience. Various antennas such as textile and UWB have been researched actively and electro-magnetic band-gap materials are also researched to reduce phenomena such as frequency shift and efficiency decline appears when they are closer to the human body.

This paper proposes the cavity-backed and shorted microstrip patch antenna for antenna miniaturization and insensitivity for surrounding environment. The proposed antenna is fabricated by bonding two substrates that are Rogers RT5880 31 mil. In order to know the changes depending on environment, placing the antenna on air, arm, breast and pig skin, the frequency responses were measured by network analyzer. And the radiation efficiency is measured in anechoic chamber. As a result of the measurement, frequency responses are hardly changed and radiation efficiency reduces from 73.2% in the air to 32.5% on the pig skin.

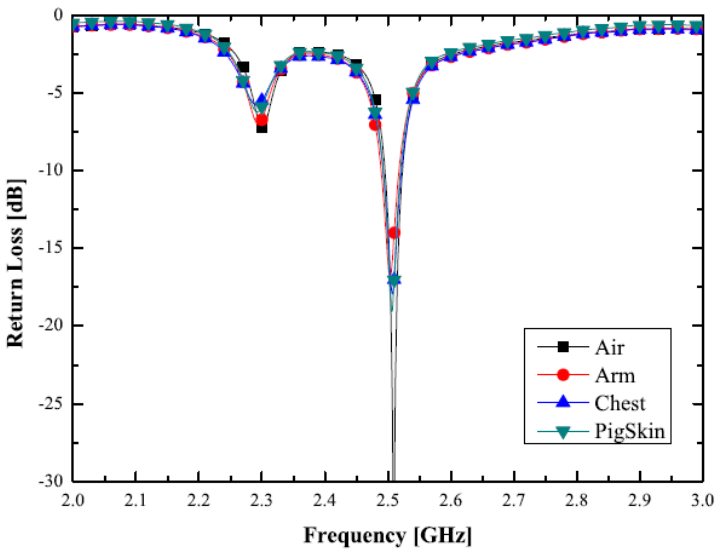

Figure 1: Measured return loss of the proposed antenna.

Frequency Invariant Beamforming under Bandpass Sampling Based on Convex Optimization

Lijie Fan, **Bian Tian**, **Shiyou Xu**, **and Zengping Chen**
Science and Technology on Automatic Target Recognition Laboratory
National University of Defense Technology, Changsha, Hunan 410073, China

Abstract— Beamforming is a spatial filtering technique for receiving signals illuminating an array of sensors from some specific directions, whilst attenuating signals from other directions. As higher frequency and lager bandwidth has been utilized in many real platforms especially in the field of radar and electronic reconnaissance systems, wideband beamforming has been studied extensively in the past decade. For wideband signals, there exists phase difference between sensor outputs cause wideband signals consist different frequency components and usually this phenomenon is called "the array dispersion". For a fixed aperture, the spatial resolution of a beamformer is proportional to frequency. Our purpose is to obtain the nearly identical beam response for wideband signals getting through the array of sensors. Such beamformers are independent of frequency, they are often called frequency independent beamformers or frequency invariant beamformers (FIBs). Many literatures have considered and promoted various methods to solve this problem. Among these methods, the class of optimization method is the main stream. Wideband beamformer is implemented by a group of FIR filters after each sensor and the coefficients of FIR filters are obtained through the optimization process.

A common assumption is made that these algorithms handle the receiving signals by Nyquist sampling, but we are acquainted with that signals are often bandpass sampled getting through the sensors and transformed to the base band through the digital down conversion (DDC) processing in many practical systems. After the DDC processing, the signals are passed to the FIR beamformer. The bandpass sampling and DDC alter the signal expression and make the objective function different compared with signals under Nyquist sampling. The main difference induced by bandpass sampling and DDC is the implementation resource consumption under the identical desired beam pattern, in detail the FIR beamformer cost more taps to achieve the same beam pattern under bandpass sampling. In this paper, the effect caused by bandpass sampling and DDC is addressed and analyzed in detail; through convex optimization toolbox a strategy to deal with this circumstance is proposed; the formulation of such convex optimization problem is presented.

A comparison has been made between two kinds of sampling procession to achieve FIB beamforming. The effect caused by bandpass sampling and DDC is addressed and analyzed in detail for wideband beamforming. Simulation results show that the method proposed in this paper is effective in dealing with FIB problem under bandpass sampling.

A Novel InP Based Planar PIN Diode

Hao Sun, **Lingyun Li**, **Qilian Zhang**, **Huifeng Ding**,
Likun Ai, **Rui Tong**, **Rong Qian**, **and Xiao-Wei Sun**
Shanghai Institute of Microsystem and Information Technology, Chinese academy of Sciences, China

Abstract— A InP based novel planar PIN diode was fabricated for high frequency and high speed circuits applications. This novel structure diode provided new ideas for fabrication high speed and frequency switch circuits.

PIN diode heterostructures were grown on a 2″ SI-InP substrate by V90 GSMBE system using AsH_3 and PH_3 as group V sources and CBr_4 as p-type doping source. The epitaxial layers include a thick (∼3 µm) un-doped $In_{0.53}Ga_{0.47}As$ buffer layer. Followed a 300 nm thick heavily silicon doped $In_{0.53}Ga_{0.47}As$ N layer, a 1 µm thick un-doped $In_{0.53}Ga_{0.47}As$ as I layer and a 200 nm thick heavily carbon doped $In_{0.53}Ga_{0.47}As$ (3×10^{19} cm^{-3}) P layer.

A novel planar air-bridge structure was utilized to form good connection with the anode and cathode of the PIN diode, of which structure can simplify the processing compared to the traditional one. The air-bridges were fabricated using phosphoric acid base wet lateral etching technologies. Etching velocities as well as morphology of the etched $In_{0.53}Ga_{0.47}As$ materials were studied for different rations of phosphoric acid base etchant solutions by the profiler, and scanning electron microscopy (SEM) respectively.

InGaAs/InP PIN diodes with an anode of 4 µm radius were fabricated. The planar air-bridge was of 4 µm wide, 30 µm wide and 4 µm high. A turn on voltage of 0.43 V and breakdown voltage of larger than 7 V were obtained by DC measurement. The equivalent turn-on resistance of 9 ohm and shut-off capacitance of 18 fF can be obtained from the S-parameters measurement. This novel structure diode provided new ideas for fabrication high speed and frequency switch circuits.

Layer	Dopant	Doping (cm^{-3})	Thickness (nm)
P+ InGaAs	C	3×10^{19}	200
I InGaAs	-	-	1000
N+ InGaAs	Si	3×10^{19}	300
I InGaAs	-	-	3000
InP S.I. Substrate			

Table 1: InGaAs/InP PIN diode epitaxy heterostructure.

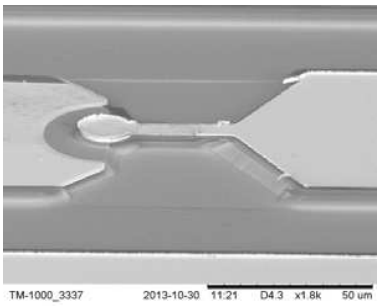

Figure 1: SEM image of PIN diode with planar air-bridge.

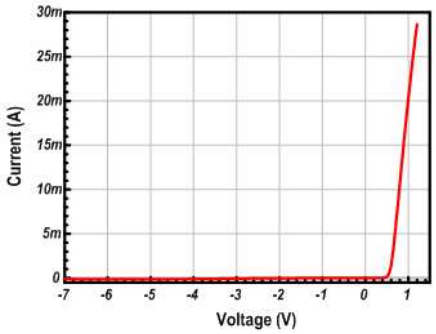

Figure 2: DC I-V curve of the PIN diode.

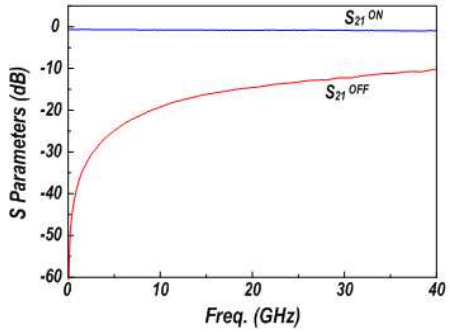

Figure 3: S parameters of the PIN diode.

Switched Phase Shifter for Load Modulation of QPSK Signal

Sehwan Choi, **Jin-Sup Kim**, **and Jae-Young Lee**
Korea Electronics Technology Institute, Republic of Korea

Abstract— For the demand for high-speed wireless communications, MIMO (Multiple-Input and Multiple-Output) has become mandatory in many modern wireless communication systems. This MIMO technology provides significantly us with a spectral efficiency but increases the number of antennas and RF front-end modules. This finally causes an increasement of current consumption and overall size of the system. In order to solve these problems, researches utilizing a single RF system based on ESPAR (Electronically Steerable Parasitic Antenna Radiators) and LMA (Load Modulated Array) have been actively conducted.

In the case of ESPAR, various orthogonal radiation patterns are generated by impedance loading circuits. Digital signals are modulated by mapping digital signals onto radiation patterns. So, these systems requires many orthogonal radiation patterns and ultra-high speed switches with a few nanoseconds. LMA systems are operated independently by multiple antennas with high isolation. Because each antenna sends the separate stream, these systems have the advantage of improving the system implementation and data-rate. In order to implement LMA system, phase shifter was developed by using high speed switches in this paper. It was successfully sent 4-stream QPSK signal of 2.5 MHz chip-rate at 2.38 GHz using this board.

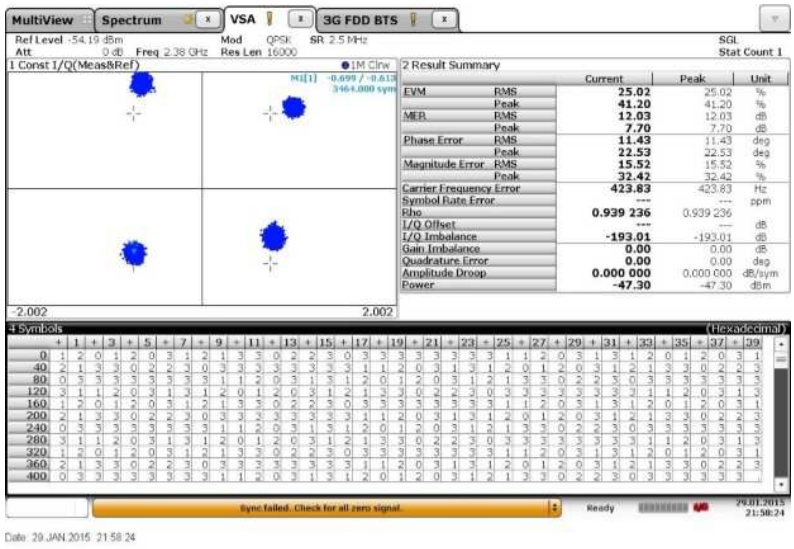

Figure 1: Constellation using the proposed switched phase shifter.

ACKNOWLEDGMENT

This work was supported by ICT R&D program of MSIP/IITP. [1482304001, Development of small basestation supporting multiple streams based on LTE-A systems].

Compact Waveguide Load with Thin Film Resistor

Manseok Uhm, **Hongyeal Lee**, **Changsoo Kwak**, **Sohyeun Yun**, **and Inbok Yom**
Satellite & Wireless RF Technology Section, Electronics and Telecommunications Research Institute, Korea

Abstract— Due to excellent electrical performance such as low insertion loss, high return loss and high power handling capacity, waveguide components are widely adopted for microwave communication systems in spite of a relatively larger volume than microstrip or coaxial components. Waveguide loads are needed for directional couplers used for test set-up and hybrid waveguide couplers for obtaining high output power from parallel power amplifiers. Especially, a compact waveguide load is required to develop compact SSPA using hybrid couplers (branch coupler or magic-tee combiner) with matched loads.

Since absorbing material in the waveguide attenuates input RF signal, the shape and the place of absorber depend on electrical performances of loads. In general, gradual increase of absorber makes good impedance matching over a wide bandwidth. The absorber is located at the highest electric field intensity.

We proposed a compact rectangular waveguide load using a thin film resistor as an absorber. It works by placing a resistor in the center of the waveguide where the electric field intensity is the greatest. An increase in step width of the resistor will lead to good return loss. The thin film resistor with good temperature coefficient and stable performances is produced on an alumina substrate that shows suitable accuracy of dimension. We designed a compact waveguide load with TaN thin film resistor for Ka band applications. The resistivity is 100 Ω/sq and the height of substrate is 5 mil. The proposed matching termination can be easily attached at an end wall of a waveguide. Thus it can be easily connected to the waveguide flange of a component.

Several samples for WR 28 standard waveguide were fabricated and measured to confirm the reproducibility. The actual size of the alumina substrate is 3.5 mm × 9.0 mm. We confirmed that all the results agreed excellently. The measured results have proved the design results, as shown in Figure 1. Return loss above 20.0 dB has been obtained over 4.0 GHz of bandwidth in the Ka band.

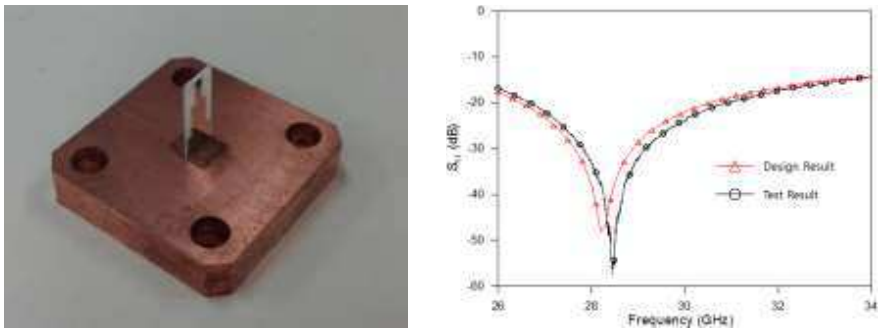

(a) (b)

Figure 1: Design and test results of the fabricated waveguide load composed of thin film resistor. (a) Photo of the fabricated waveguide load. (b) Results.

Channel Equilibration in Wideband Digital Array Radar Test-bed

Weixing Li, **Jianzhi Lin**, **Weihua Wang**, **Biao Tian**, **and Zengping Chen**
Science and Technology on Automatic Target Recognition Laboratory
National University of Defense Technology, Changsha, China

Abstract— Digital array radar (DAR) is remarkable for the characteristics of large instantaneous dynamic range, flexible control, multi-beams simultaneously and superior ability of anti-interference. Most array processing algorithms are based on ideal assumption of both the signals and channels. For actual systems, amplitude and phase errors caused by antennas, amplifiers and ADCs will lead to substantial performance degradation of digital processing such as digital beam-forming (DBF) and direction of arrival (DOA).

Based on a wideband DAR test-bed operating at 0.6∼3.0 GHz with the instantaneous bandwidth of 500 MHz, this paper presents the design and implement of channel equilibration module. In the first part, a wideband waveform generator based on DAC + FPGA architecture is designed with the purpose of generating various analog waveforms for channel equilibration. The waveform generator is a FPGA Mezzanine Card integrated with a 12 bits, 3 Gsps DAC. It is capable of generate desired waveforms from 0 GHz to 6.0 GHz flexibly by direct digital synthesize technology. In order to calibrate the reconstruction errors, a pre-distortion filter is designed to compensate the waveforms generated by DAC. In the second part, a practical algorithm is proposed for wideband channel equilibration in jamming environment. The operating bandwidth of DAR is divided in to two parts: the frequency band without interferences and with interferences. In the first frequency band, the channel responses can be obtained by coupling high quality wideband signals into the receive channels. As for the frequencies that exist in unknown interferences, this paper takes the interferences as calibration signals to evaluate the amplitude and phase errors. After the distortion characteristics of the whole bandwidth are obtained, an improved frequency-domain equilibration algorithm based on overlap-save is studied and realized in FPGA to eliminate the discontinuity of phase. Finally, experiments are carried out using the DAR test-bed. The processing results of measured data demonstrate the feasibility and effectiveness of the channel equilibration module.

An Ultra Low-power and Low-noise VCO Using Transformer Coupled Dual LC Tanks Topology

Tzu-Yun Chou, **Kuan-Hsiu Chien**, **and Hwann-Kaeo Chiou**
Department of Electrical Engineering, National Central University, Jhongli City, Taoyuan, Taiwan

Abstract— A K-band low power voltage-controlled oscillator (VCO) using transformer coupled dual LC tanks is implemented in a tsmc^{TM} commercial 90-nm CMOS process. The use of transformer provides tight coupling factor between two identical LC tanks that improves the phase noise performance by increasing the output signal swing and waveform symmetry of the VCO. The cross-coupled transistors provide an effective negative resistance for the VCO core to compensate the resistive loss in the primary and secondary LC-tanks. The secondary LC tank is DC isolated from the primary one, thus it does not consume DC power from the primary LC tank. Accordingly, compared to the conventional topology, this core power consumption can be significantly reduced. The drain voltage could swing above the supply voltage by using the proposed transformer. Effectively, the oscillation amplitude is enhanced, and the supply voltage can be reduced for the same phase noise with lower power consumption or for better phase noise with the same power consumption. By taking advantage of the tight-coupling transformer, the inductor layout is properly designed to obtain a high Q-factor and a die area comparable to single-inductor VCO. The VCO core dissipates very small DC power of 1.61 mW from a 0.7-V supply due to the benefit of tight-coupled transformer. The measured phase noise is −97.61 dBc/Hz at 1-MHz offset frequency from the oscillation frequency of 24 GHz. The proposed VCO has an excellent FOM of −183.14 dBc/Hz. This novel VCO topology will find wide applications in 24 GHz low power wireless sensor networks.

ACKNOWLEDGMENT

This work was supported in part by the Ministry of Science and Technology, Taiwan, R.O.C. under Contract MOST 101-2221-E-008-073-MY3. National Chip Implementation Center (CIC) of National Applied Research Laboratories, Taiwan, R.O.C., is also acknowledged for chip fabrication.

A Reconfigurable Bandpass to Bandstop Filter Using PIN Diodes Based on the Square Ring Resonator

Salman Arain, **Muhammad Ali Babar Abbassi**, **Symeon Nikolaou**, **and Photos Vryonides**
Department of Electrical Engineering, Frederick University, Cyprus

Abstract— Microwave filters are of primitive importance when dealing with RF communication systems. Modern day development in this technology has led to the requirement of a compact, multipurpose and efficient design. In this context electronically switchable filters are gaining wide interest of both researchers and developers. Microwave filters are designed keeping in mind the compactness and ease in switching ability among different operational modes. Using commercially available PIN diodes, filters can be engineered to switch between different resonating frequencies hence making the structure reconfigurable.

This paper presents a reconfigurable bandpass to bandstop switchable filter based on square ring resonator with two tuning stubs controlling bandpass response. In this work, switching between the bandpass and bandstop filter has been achieved by strategically placing PIN diodes in locations which do not affect the resonating response of the overall design. Skyworks SMP1345-079LF RF PIN diodes are used to switch from bandpass to bandstop filter. Central frequency of the filter is 2.4 GHz. The −3 dB bandwidth for the bandpass filter is from 1.9 GHz to 3.2 GHz with an insertion loss of 0.8 dB. For the bandstop filter loss is 0.3 dB and −10 dB rejection bandwidth is from 2.3 GHz to 2.6 GHz. DC bias lines of $\lambda/4$ lengths are integrated with radial stubs to ensure compact physical length of circuit. The key advantage of this type of filter is efficient switchability between two frequency responses. The filter is simulated on commercially available cost effective substrate. The proposed filter can be a good candidate date for communication in strong interference environments, for reconfigurable radios, or for alternating transmission and reception schemes, in the highly congested, 2.4 GHz frequency band.

Metallic Grating-dielectric-metal Microcavities for Far-infrared Narrowband Absorption

Pei-Kang Chung and Shun-Tung Yen
Department of Electronics Engineering and Institute of Electronics
National Chiao Tung University, Hsinchu 30010, Taiwan

Abstract— We study absorption properties of metallic grating-dielectric-metal microcavities for resonant absorbers in the far infrared. The microcavities are composed of a subwavelength silicon dioxide (SiO_2) film sandwiched between a flat bottom metal and a top metallic film perforated with a two-dimensional square hole array. We investigate the microcavities by measuring absorbance spectra and observing their variations with the size and the period of the holes. The experimental data agree well with theoretical ones calculated with the model expansion method. The absorbance spectra reveal two characteristic resonant modes which are strongly influenced in both the resonant frequencies and the absorbance magnitude by the hole size and array periodicity. The resonant frequencies correspond to emergence of the two lowest diffraction orders and hence depend on the grating period. The resonant absorption is therefore ascribable to the excitation of surface electromagnetic waves around the interfaces between the SiO_2 film and the top metallic film. Interestingly, as the hole size increases, the two resonant frequencies blue–shift slightly; the lower resonant frequency shifts less than the higher one. The two resonances are accompanied by strong localized fields around the edges of the holes and the lower-frequency resonance has a higher quality factor. The resonant absorption strength depends on the hole size and a maximal absorption occurs at a specific hole size for each of the resonant modes. Absorption depends also on the thickness and the material of the dielectric film. This study indicates that the proposed microcavity structure can act as a good reflective resonant absorber at a desired frequency by proper design of the structure.

Analysis of Substrate-defected Coplanar Waveguide of EBG

Lingyun Li, Tianyu Pen, Hao Sun, Qilian Zhang, Huifeng Ding, and Xiaowei Sun
Shanghai Institute of Micro-system and Information Technology, CAS, China

Abstract— The Electromagnetic Band-Gap (EBG) structures deduced from Photonic Band-Gap (PBG) have attracted much attention, and many works focused on the pattern of signal trace metal and Defected Ground Structure (DGS). However, along with the research progress, the patterns of the trace metal or defected ground become more and more complicated and result in difficulty in design and fabrication. In this paper, based on the concept of photonic crystal, a Substrate-Defected Coplanar Waveguide (SD-CPW) is presented, whose substrate is wet-etched to periodic pits, while the 50 Ohm metal trace and ground remaining intact. After the fabrication and measurement, a wide frequency band gap is observed and the EBG characteristic is proved.

The process of wet-etching was used, because it is more economical than Deep Reactive Ion Etching (DRIE). And by the wet-etching process, there is lateral erosion under the metal. So the actual pits' width is wider than the CPW gap, which is included in the simulation model too. Actually it is found that the cavity under metal layer can improve the stop band characteristic. The different percentages of etching length along the CPW line were analyzed. The depth of the stop band gap is altered with the etching ratio ($u = L1/T$), and it shows that 57.5% of the substrate's loss will provide the best stop band performance. And the central frequency of the band gap depends on the period length of the etched pits. If the length is increased while the etching ratio is fixed, the frequency of the stop band will be shifted toward lower band consequently. So the frequency response of the band gap can be controlled. A SD-CPW was

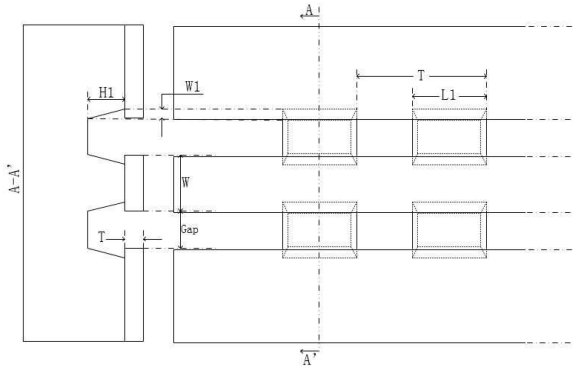

Figure 1: Structure chart of the substrate-defected coplanar waveguide.

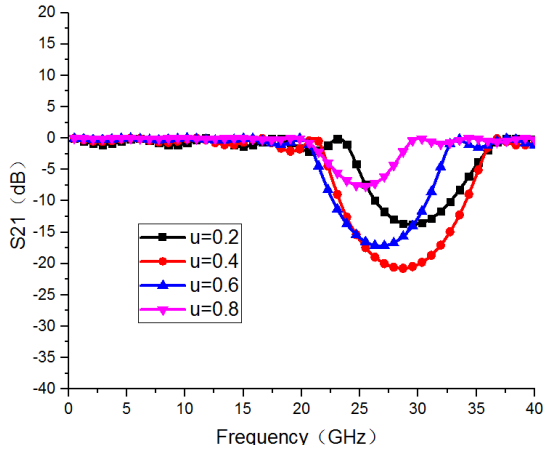

Figure 2: Band-gaps of different etching ratios.

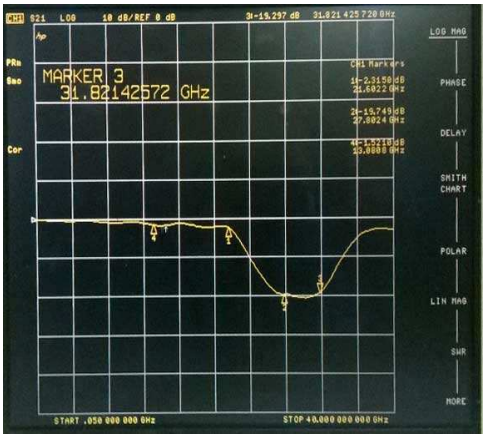

Figure 3: Measured S_{21} of the SD-CPW.

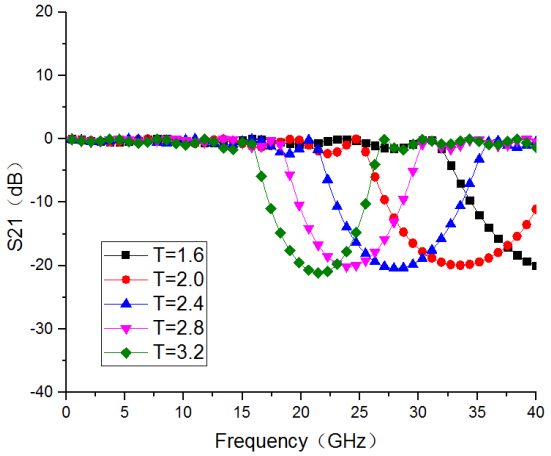

Figure 4: Band-gaps of different period length.

fabricated, whose etching length was 1.38 mm, period is 2.4 mm and 5 cycles repeated. The measurement shown there was a deeper than −20 dB band gap between 28–32 GHz, which was more than 4GHz bandwidth.

Power Electronics for an Energy Harvesting Concept Applied to Magnetic Resonance Tomography

L. Middelstaedt[1], **S. Foerster**[2], **R. Doebbelin**[1], **and A. Lindemann**[1]

[1]Otto-von-Guericke-University Magdeburg, Germany
[2]formerly Otto-von-Guericke-University Magdeburg, Germany

Abstract— Within Magnetic Resonance Tomography (MRT) applications magnetic fields of different orientations, magnitudes and frequencies are generated in order to produce images of different body tissues. Three main magnetic fields need to be distinguished:

- the strong static uniform magnetic field B_0 in z-axes,
- the high frequency excitation field B_1 ($\approx$ 123 MHz) rotating in the x-y-plane and having the highest amplitude in the isocenter,
- and the gradient field B_G, that changes properties along the z-axes.

In order to supply small power electronic applications for devices used in the interventional medical field, e.g., for the wireless power supply of small sensors and electronics in catheters, this paper investigates the approach of energy harvesting inside the MRI scanner. The magnetic fields of the scanner are transformed into electric energy supplying a device under test (DUT) using the method of induction. Considering the present magnetic fields and according to Faraday's Law, the B_1 and B_G fields can be utilized for this approach.

For designing and building a suitable energy harvesting device different aspects need to be taken into account. The effective area of the inductor needs to be orthogonal to the varying field and should be appropriately large. With excitation frequencies of 123 MHz the layout of the inductor should be chosen in a way, that the first resonant frequency is above the excitation frequency. Contrary, the small amplitudes of B_1 and B_G theoretically ask for a high number of turns in order to get sufficiently large induced voltages. However, the resulting large inductance and its parasitic inter-winding capacitances result in small resonant frequencies. The power electronic circuit needs to be built of small, non-magnetic elements with a minimum on-state voltage drop, to achieve significant maximum output voltage. Overall, the imaging process of the MRT should not be affected. In this study relevant magnetic fields are modeled with Empire XCcel^{TM} providing the basic environment for simulating induced voltages for different inductor geometries. Inductors with different resonant frequencies have been designed and tested in terms of induced open circuit voltage. Positioning the inductor inside or outside of the isocenter leads to different induced voltages. In the isocenter the B_1-induced voltage dominates, outside the B_1-influence decreases but B_G induces considerable voltages. Finally, a power electronic circuit has been designed and realized that fulfills the most important requirements of an MRI application for interventional medical applications, i.e., small size and the use of non-magnetic materials. Placing the device in the investigated MRI scanner lets the power supply operate and the LED luminate (see Figure 1(b)). The block diagram of the designed power electronic circuit and the test setup with the designed inductor is shown in Figure 1.

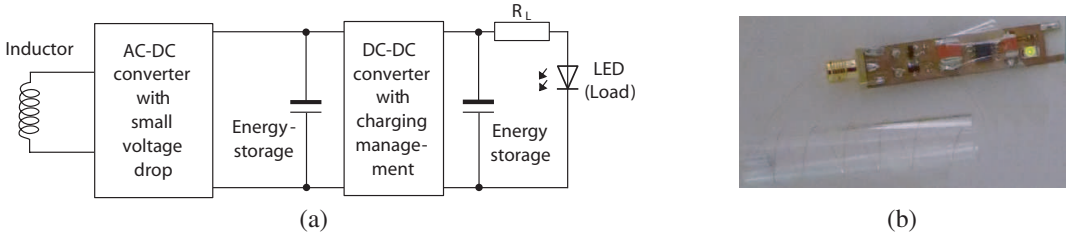

Figure 1: Developed power electronic circuit with an inductor as source and LED as load for energy harvesting in MRI-application. (a) Block diagram of power electronic circuit [1]. (b) Wireless power supply of an LED within an MRI [1].

REFERENCES

1. Middelstaedt, L., S. Foerster, and A. Lindemann, "Energy harvesting im MRT," *IGIC, Conference on Image-guided Interventions*, Magdeburg, 2014.

Fast Time-domain Imaging for One-stationary Bistatic Forward-looking SAR

Hongtu Xie, Daoxiang An, Xiaotao Huang, and Zhimin Zhou
College of Electronic Science and Engineering
National University of Defense Technology, Changsha, Hunan 410073, China

Abstract— One-stationary bistatic forward-looking SAR (OSBFSAR) is a special bistatic SAR (BSAR) with a stationary radar, working in forward-looking mode. It has advantages of reducing military vulnerability and improving target detectability, and implements imaging in forward direction. However, its larger bistatic angle and synthetic aperture may induce the complicated range-azimuth coupling of echoes and increases the difficulty of the precise imaging by frequency-domain methods. So, such imaging usually relies on the time-domain backprojection algorithm (BPA), but it requires a high computational load. Fast BPA (FBPA) has been implemented for the strip-map BSAR imaging, but has not been mentioned for the OSBFSAR imaging in earlier publications. In this paper, a FBPA is presented to process the OSBFSAR echoes. It can keep the accuracy of the BPA but with a reduced computational load.

The key content of the proposed FBPA is organized as follows.

1. Definition of the polar subimage grid (See Fig. 1). First, the origin of the polar grid is defined as the central point of the subaperture center and stationary radar. Then, ρ_n is the range from the origin of a polar grid to the sample $\mathbf{r}$, and θ_n is the angle from the major axis a_n to the range ρ_n. Thus

$$\begin{cases} \rho_n = \sqrt{[x_S/2 - x]^2 + [y_M(\eta_n)/2 - y]^2 + [(z_S + z_M)/2]^2} \\ \theta_n = \arccos\left(\left(c_n^2 + \rho_n^2 - ((x_S - x)^2 + y^2 + z_S^2)\right) / 2\rho_n c_n \right), \ \theta_n \in [0, \pi] \end{cases} . \quad (1)$$

2. Sampling requirements of the polar subimage grid (See Fig. 2). The sampling requirements of the polar subimage grid are derived from the bandwidth angle, which is given by

$$\Delta\rho_n \le c_0 \sqrt{1 + \delta_n^2} \Big/ (2(f_{\max} - f_{\min})); \quad \Delta\theta_n \le c_0 \sqrt{1 + \delta_n^2} \Big/ (f_{\max} d_{Mn}). \quad (2)$$

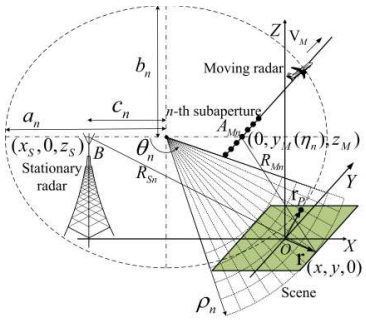

Figure 1: Imaging geometry of the OSBFSAR.

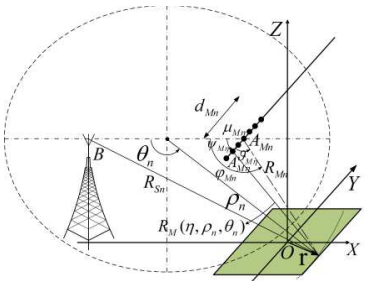

Figure 2: Bistatic range calculation for the sampling requirements derivation.

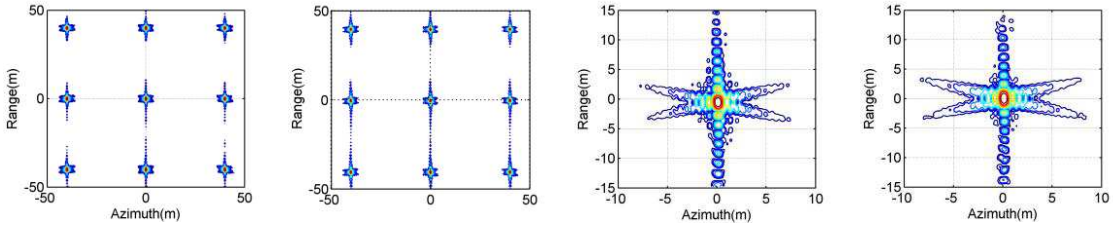

Figure 3: Imaging results obtained by different algorithms. (a) BPA; (b) FBPA; (c) Imaging result of the central target extracted from Fig. 3(a); Imaging result of the central target extracted from Fig. 3(b).

c_0 is the speed of light, δ_n is the ratio of c_n to ρ_n. d_{Mn} is the subaperture length of the moving radar. $f_{\max}$ and $f_{\min}$ are the maximum and minimum signal frequency.

To prove the validity of the proposed FBPA, the simulation is carried out to compare the performances of the proposed FBPA and BPA (See Fig. 3). From Figs. 3(a)–(b), it is seen that all the targets are focused well. Figs. 3(c)–(d) are shown that the focusing performance of the central target by the FBPA is very similar to that by the BPA. The processing time of the BPA and FBPA is 128.1 s and 11.2 s, respectively.

Rapid Echo Simulation for One-stationary Bistatic SAR Based on FFT and Subaperture Processing

Hongtu Xie, **Daoxiang An**, **Xiaotao Huang**, **and Zhimin Zhou**
College of Electronic Science and Engineering, National University of Defense Technology
Changsha, Hunan 410073, China

Abstract— One-stationary bistatic SAR (OSBSAR) is a special bistatic SAR (BSAR) with a stationary radar fixed on a tower. It has advantage of reducing military vulnerability and getting additional information. Echo simulation is important in the SAR research, such as the system design, algorithms test and so on. Echo simulation contains the scene simulation and rapid echo generation; we only focus on the rapid echo generation of the OS-BSAR in this paper. Echo simulation method main include the time-domain target by target (TBT) method, two dimensional fast Fourier transform (2DFFT) method and imaging inverse processing (IMIP) method. TBT method has high precision but with high computational load, while 2DFFT and IMIP methods has high efficiency but with some approximate processing. In this paper, a rapid simulation approach (RSA) based on the FFT and subaperture processing is presented to generate the OSBSAR echo. It can keep the accuracy of the TBT method but with a reduced computational load.

Imaging geometry of the OSBSAR in elliptical polar coordinate and subaperture processing in the echo simulation are shown in Fig. 1 and Fig. 2. Implementation of the proposed RSA is depicted as follow:

(1) Set the simulation parameters and scene scattering coefficients; (2) Generate the transmitted signal and compute its FFT; (3) Divide the moving radar synthetic aperture into subapertures; (4) Start subaperture processing, separate the scene into several equidistant elliptical ring domain and elliptical subscenes; (5) Calculate the equivalent scattering coefficients of elliptical subscenes at the subaperture central pulse. Based on the elliptical subscene scattering coefficients, calculate the equidistant elliptical rings' scattering coefficients for all the subaperture pulses using the FFT; (6) Calculate the system's impulse response function and its FFT for all subaperture pulses; (7) Multiply the results of (2) and (6), and then transform their product into time domain using

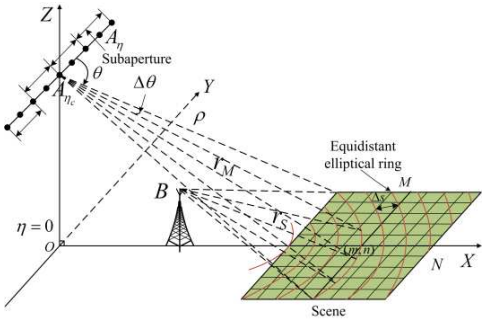

Figure 1: Imaging geometry in elliptical polar coordinate.

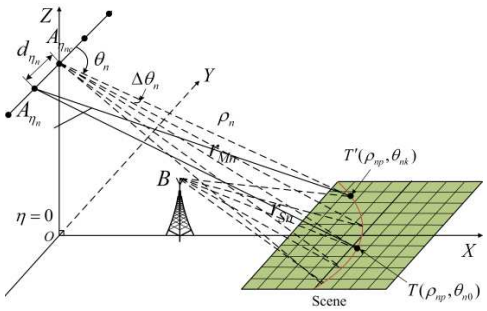

Figure 2: Subaperture processing in the echo simulation.

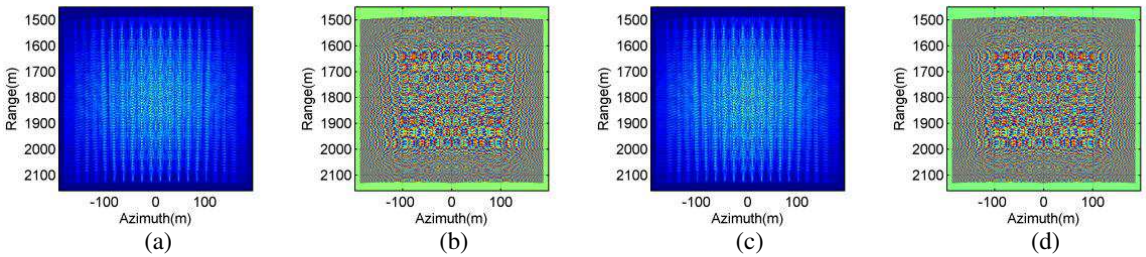

Figure 3: Scene echoes including 81 discrete point targets. (a) (b) Amplitude and phase of the scene echo simulated by the TBT method; (c) (d) Amplitude and phase of the scene echo simulated by the proposed RSA.

the IFFT and obtain the subaperture pulse echo; (8) In terms of the subaperture order, repeat (4)–(7), and then the scene echo can be simulated.

To prove the validity of the proposed RSA, the simulation is carried out to compare the performances of the proposed RSA and TBT method (See Fig. 3). It is seen that the scene echoes simulated by the two methods are almost identical. From Fig. 4, it is found that all the scattering targets are focused well, and the focusing performance of the central target in Fig. 4(d) is very similar to that in Fig. 4(c). Simulation time of the proposed RSA and TBT method is 1042.2 s and 21086.1 s, respectively.

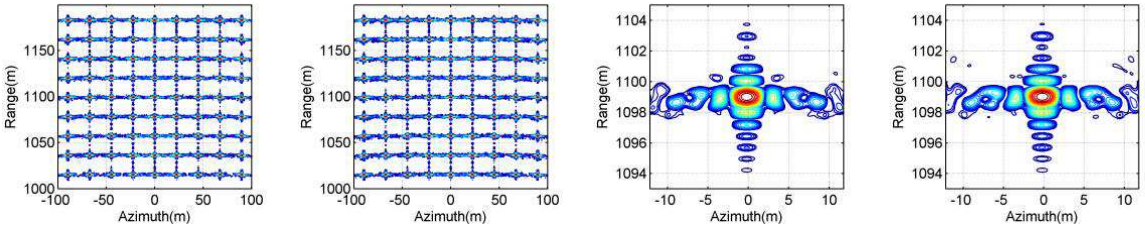

Figure 4: Imaging results. (a) Imaging result of the echo simulated by the TBT method; (b) Imaging result of the echo simulated by the RSA; (c) Imaging result of the central target in (a); (d) Imaging result of the central target in (b).

NDT Imaging Method for Detection of Surface and inside Defect Using Secondary Harmonic Signal of TMR Sensor

Keiji Tsukada, **Keisyu Shiga**, **Yuya Tsukamoto**, **Takuya Yasugi**, **Kenji Sakai**, **and Toshihiko Kiwa**
Graduate School of Natural Science and Technology, Okayama University
3-1-1 Tsushima-naka, Kita-ku, Okayama-Shi, Okayama Prefecture, 700-8530, Japan

Abstract— Eddy current test using a search coil detecting high frequency as magnetic nondestructive test (NDT) is widely used. When a defect inside or back side of the metal exists, the detection is very difficult because of shallow skin depth of the exposed high frequency magnetic field. To detect a deep defect, high sensitive magnetic sensor operable with wide range from extreme low to high frequency is necessary. In this study, we applied high sensitive magnetic sensor with nanogranular type tunnel magnetoresistive (TMR) thin film operable from DC to high frequency for NDT. TMR has an even functional characteristic to magnetic field. Therefore, DC magnetic field bias or additional circuit is necessary to obtain linear magnetic response. We developed a new second harmonic detection method without linearization. Moreover, eddy current distribution can be imaged by the detection of tangential magnetic field component from the sample. Using a pair of TMR sensor detecting x- and y-magnetic field components parallel to the metal surface. The sensor probe consists of the exposure coil and MR sensors. Each of the magnetic field vectors was calculated from two parameters of signal amplitude and phase obtained by a lock-in amplifier. Using these magnetic field vector, the eddy current in the subject was reconstructed. By the imaging of the disturbance of the eddy current distribution caused by the defect, defect imaging at not only surface but also deep inside the subject was enabled. Especially, the depth information of the defect was obtained by the changing frequency.

Iterative K-means Clustering Based Fast Hybrid Segmentation Method for Biomedical Optical Images

Seungbae Ji, Seung-Beom Yu, and Jae-Ho Han
Department of Brain and Cognitive Engineering, Korea University
145 Anam Rd., Seoul 02841, Republic of Korea

Abstract— Optical coherence tomography (OCT) is a well-established biomedical optical imaging technique that non-invasively provides high-resolution images for cross-sectional view of retinal structures [1, 2]. Retinal layers are observed in the acquired morphology depending on the optical properties of neurosensory tissues. Even though most of the functional layers present the changes of pixel intensities, it is not sufficient to find the precise retinal boundaries through simple edge acquisition. Instead, in order to accurately investigate them, graph-cut segmentation method has been widely employed [3, 4], which usually necessitates a high-time complexity for fully realizing this algorithm. In this work, we propose a fast method for layer segmentation with a high-accuracy with less time complexity than the conventional graph-cut method, which is based on a hybrid method employing iterative k-means clustering in conjunction with edge recognition. In our method, the former extracts the details at the interfaces of a similar pixel group and the latter handles a drastic change of pixel intensity which appears as thick lines. This introduced method can be expanded for other various image segmentation fields such as delicate brain and vascular images as well as the fundography images for diagnostic purposes.

ACKNOWLEDGMENT

This work was partly supported by the ICT R&D program of MSIP/IITP [14-824-09-014, Basic Software Research in Human-level Lifelong Machine Learning (Machine Learning Center)] and was supported in part by the Basic Science Research Program through the National Research Foundation of Korea (2013R1A1A2062448). Correspondence and requests for materials should be addressed to Prof. Jae-Ho Han.

REFERENCES

1. Mishra, A., A. Wong, K. Bizheva, and D. A. Clausi, "Intra-retinal layer segmentation in optical coherence tomography images," *Opt. Express*, Vol. 17, No. 26, 23719–23728, 2009.
2. Cha, Y.-M. and J.-H. Han, "High-accuracy retinal layer segmentation for optical coherence tomography using tracking kernels based on Gaussian mixture model," *IEEE J. Sel. Top. Quantum Electron.*, Vol. 20, No. 2, 6801010, 2014.
3. Chiu, S. J., X. T. Li, P. Nichols, C. A. Toth, J. A. Izatt, and S. Farsiu, "Automatic segmentation of seven retinal layers in SDOCT images congruent with expert manual segmentation," *Opt. Express*, Vol. 18, No. 18, 19413–19428, 2010.
4. Srinivasan, P. P., S. J. Heflin, J. A. Izatt, V. Y. Arshavsky, and S. Farsiu, "Automatic segmentation of up to ten layer boundaries on SD-OCT images of the mouse retina with and without missing layers due to pathology," *Biomed. Opt. Express*, Vol. 5, No. 2, 348–365, 2014.

Static Magnetic Fields Improve Proliferation of Osteoblast-like Cells Cultured on the Poly-L-lactide Discs

Wei-Fang Lee[1], **Ya-Hui Chan**[2], **Chun-Chen Lai**[2], **and Sheng-Wei Feng**[2]

[1]School of Dental Technology, College of Oral Medicine
Taipei Medical University, Taipei, Taiwan
[2]School of Dentistry, College of Oral Medicine
Taipei Medical University, Taipei, Taiwan

Abstract—

Objective: Biodegradable polymer [Poly(L-lactide), PLLA] scaffolds have been popular used in the reconstruction of craniomaxillofacial defects because of their good biocompatibility and low toxicity after degradation in vivo. However, lower cell proliferation rate and poor cell attachment were reported when culturing osteoblst on the PLLA discs. The purpose of this study was to evaluate the biological effects of static magnetic fields from Nd-Fe-B magnets on the morphology and growth behavior of osteoblast-like cells cultured on the surface of a PLLA discs.

Material and Methods: PLLA discs (14-mm in diameter and 1-mm in thickness) were fabricated with an injection molding technique at an injection temperature of 185°C. MC3T3-E1osteoblast-like cells were cultured on the surface of a poly-L-lactide disc. These cells were continuously exposed to a 4000 Gauss-SMF for 5 days. Sham-exposed cells were served as controls. The morphologic changes of osteoblast-like cells were observed by scanning electron microscopy. The proliferation effects of the SMF were measured by MTT assay. In addition, the effects of the SMF on alkaline phosphatase activity levels were compared between exposed and unexposed cells.

Result: Scanning electron microscopy images revealed that SMF promote MC3T3-E1 cells express extracellular matrix on the Poly-L-lactide discs. The SMF exposed MC3T3-E1 cells exhibited increased MTT values at 3 and 4 days of culture. The SMF exposed MC3T3-E1 cells express the lower alkaline phosphatase-specific activity than that of the unexposed cells at 3 and 4 days of culture ($p < 0.05$).

Conclusion: These results demonstrated SMF can improve MC3T3-E1 cells growth on the Poly-L-lactide discs.

Effects of Static Magnetic Fields on the Growth of Dental Pulp Stem Cells

Yu-Chi Chang, **Wei-Zhen Lew**, **Kuo-Ning Ho**, **and Sheng-Wei Feng**
School of Dentistry, College of Oral Medicine, Taipei Medical University, Taipei, Taiwan

Abstract— Dental pulp stem cells (DPSCs) have multiple superior growth capacities when compared to bone marrow stem cells. Therefore, it could be as a potential resource for clinical cell therapy and tissue engineering. However, large amount of time are needed to generate sufficient number of cells for tissue defects repairing. Therefore, the aim of this study was to evaluate whether 0.4-Tesla static magnetic fields (SMF) can enhance the proliferation of dental pulp cells (DPCs) and DPSCs in vitro.

Cells extirpated from dental pulp tissue were identified by surface markers expression and differentiation stimuli. Our results showed that these cells can express the same characteristics as the mesenchymal stem cells. Positive expressions of CD70, CD90, CD105, CD146, STRO-1 and negative expression of CD14, CD34 were demonstrated from these dental pulp cells. Moreover, calcium deposition, intracellular lipid droplets formation and GAG matrix deposition were found after different kinds of stimulation. Therefore, we can confirm that these cells are DPSCs. After that, the isolated DPSCs were cultured with 0.4 T SMF exposure and exhibited a higher proliferation rate when comparing to control group. Stem cells identification assays as mentioned above were performed to exposure cells to characterize its stem cells properties. We found that either exposure cells or sham cells have similar results. DPSCs cultured in SMF environment have no adverse effects on the CD marker expression and their differential potential.

Thus, we suggest that in vitro 0.4 T SMF stimulation is positive for the proliferation rate of DPSCs without adverse effect on its characteristic and differential potential.

Impact of Static Magnetic Fields on the Microscopic Changes of Dental Pulp Stem Cells

Pei-Yu Tsai[1], **Ching-Hua Su**[2], **Chia-Chen Hsu**[3], **and Sheng-Wei Feng**[1]

[1]School of Dentistry, College of Oral Medicine, Taipei Medical University, Taipei, Taiwan
[2]Division of Microbiology and Immunology, Graduate Institute of Medical Sciences
College of Medicine, Taipei Medical University, Taipei, Taiwan
[3]Department of Dentistry, Taipei Medical University-Shuang Ho Hospital, Taipei, Taiwan

Abstract— 0.4 T static magnetic fields (SMFs) can enhance the proliferation of dental pulp stem cells (DPSCs) in vitro. However, the microscopic subcellular changes of the exposed cells are still unknown. Therefore, the aim of this study was to investigate the actual mechanism activated by the stimulus of SMFs.

Because cell membrane is the biosensor of external applied SMFs, anisotropy of lipid bilayers was examined by fluorescence polarization-depolarization assay. TMA-DPH labeled results showed that exposed cells had higher anisotropy value, indicating that SMFs changed the order of lipid bilayers. Because the actin cytoskeleton is link to cell membrane by a complex protein structure, the change of cell membrane may affect the actin cytoskeleton. For this reason, we labeled the cytoskeleton of exposure and sham cells by phalloidine fluorescence. Confocal microscope images estimated that exposed cells had more order and thicker actin cytoskeletal structure,while the actin cytoskeleton of sham cells was randomly oriented. Then, we focused on the MAPK pathways to find out the possibility signaling cascade which induce the proliferation of 0.4 T SMFs exposure cells. ERK inhibitor PD98059, JNK inhibitor SP was supplied to cultured medium respectively. MTT results showed that p38 signaling pathway may be the possibility signaling cascade activated by 0.4 T SMFs.

According to our results, we suggest that 0.4 T SMFs will affect the cell membrane and reorganized of the cytoskeleton. Besides, p38 signaling pathway also will be activated to increase DPSCs proliferation.

7 Tesla Magnetic Resonance Imaging Does Not Induce DNA Double-strand Breaks in Isolated Human Lymphocytes

Mahsa Fatahi[1], **Annika Reddig**[2], **Björn Friebe**[3], **Karina Guttek**[2], **Roland Hartig**[2], **Frank Godenschweger**[1], **Dirk Roggenbuck**[4], **Jens Ricke**[3], **Dirk Reinhold**[2], **and Oliver Speck**[1, 5, 6]

[1]Department of Biomedical Magnetic Resonance
Otto-von-Guericke-University Magdeburg, Magdeburg, Germany
[2]Institute of Molecular and Clinical Immunology
Otto-von-Guericke-University Magdeburg, Magdeburg, Germany
[3]Department of Radiology and Nuclear Medicine
Otto-von-Guericke-University Magdeburg, Magdeburg, Germany
[4]Medipan GmbH, Dahlewitz/Berlin, Germany
[5]Center for Behavioral Brain Sciences, Magdeburg, Germany
[6]German Center for Neurodegenerative Disease, Site Magdeburg, Germany

Abstract—

Purpose and Introduction: Magnetic resonance imaging (MRI) is a powerful, non-invasive diagnostic medical imaging technique which has experienced increasing demand over the past decades to also be used in the research with higher strength of magnetic fields (mainly 7T). Although ultra-high field MRI has shown a very good safety record for 10 years, the scientific basis for safe use in broader clinical applications is weak. Despite a fair number of studies in this field, overall, the published data about the potential effect of UHF MR on inducing genetic damage is not sufficiently conclusive. Most of the available literature reported no genetic effects; however a few studies, including a recent study reported DNA damage detected after cardiac MRI and suggested similar restrictions as for ionizing techniques [1].

In this *in vitro* study, we aimed to investigate the genotoxic and cytotoxic potential of 7T MRI on isolated human peripheral blood mononuclear cells (PBMCs). Hence, unstimulated PBMCs were exposed to 7T static magnetic field alone or in combination with maximum permissible gradient fields and radio frequency pulses as well as ionizing radiation.

Methods: Peripheral venous blood was drawn from 16 healthy volunteers (8 male; 8 female; age 25–58 years, mean 36 years). To detect and validate the MR-related effects, particular care was taken in choosing ideal conditions for negative and positive control groups. Isolated PBMCs suspension of each donor was divided into five sample tubes; unexposed, 7T static magnetic field, echo-planar imaging (EPI), CT and γ-radiation. The echo-planar imaging sequence was employed on a 7T whole-body MR scanner (Siemens AG, Healthcare Sector, Erlangen, Germany) and tailored to the maximum switched gradient as well as 100% permissible specific absorption rate (SAR) in 1 hour scanning. We used immunofluorescence staining of phosphorylated serine 139 in the core histone variant H2AX (γH2AX) which forms a distinct focus at each break site in DNA strands [2]. Automated fluorescence microscopy (AKLIDES system, Medipan GmbH, Germany) and flow cytometric analysis were used to quantify the γH2AX foci intensity immediately (0 hour) as well as 1 h and 20 h after the exposure.

Results: Exposure of unstimulated PBMCs to 7T static magnetic field alone or combined with gradient magnetic fields and pulsed radiofrequency fields did not induce DSB, whereas irradiation with X- and γ-ray led to a dose-dependent induction of γH2AX foci. Further, there was no evidence for altered proliferation responses after cells were exposed to 7T MRI.

Conclusions: In this study, we evaluated the impact of 7T MR-generated electromagnetic fields on the induction of DNA DSBs in human PBMC. We examined and compared the extent of damage with that observed in un-exposed and irradiated cells. Our results showed no significant increase in DSBs level, in all individuals, immediately (0 hour), 1 h and 20 h after UHF MRI exposure, compared to the unexposed group. Further, in *vitro, in vivo* and large scale epidemiological studies with sufficient statistical power which include several genotoxic endpoints, such as, chromosomal aberrations (CA) and micronuclei (MN) may further enrich the findings of the present study. Data from such comprehensive studies are useful to pave the way for transferring ultra-high field MRI to clinical adoption.

ACKNOWLEDGMENT

This study is supported by the Initial Training Network, HiMR, funded by the FP7 Marie Curie Actions of the European Commission (FP7-PEOPLE-2012-ITN-316716).

REFERENCES

1. Fiechter, M., et al., "Impact of cardiac magnetic resonance imaging on human lymphocytes DNA integrity," *Eur. Heart J.*, Vol. 34, 2340–2345, 2013.
2. Kuo, L. J., et al., "Gamma-H2AX — A novel bio-marker for DNA double-strand breaks," *In Vivo*, Vol. 22, No. 3, 305-9, 2008.

Shielding and Mitigations of the Magnetic Fields Generated by the Underground Power Cables

N. İl, S. Ozen, M. Çakir, and H. F. Carlak
Electrical & Electronics Engineering, Akdeniz University, Antalya 07058, Turkey

Abstract— In urban areas, especially in city centers, underground power cable usage in power distribution lines has been increasing dramatically. Increasing energy demand results in more loading in the power transmission lines and correspondingly more magnetic field occur around transmission lines. These excessive magnetic fields can cause harmful effects on human health. These fields can also cause deteriorating effects on the sensitive electronic equipment due to the electromagnetic interference. Therefore, the investigation of the magnetic field that occurs around the underground cable lines used in the energy distribution network become an important research topic. There are number of design options that would mitigate the magnetic field. However, magnetic field management can be basically classified into two main categories; which are shielding the subject and shielding the source. In this study, shielding the source and shielding the underground power cable raceway are investigated. In order to mitigate the magnetic field caused by underground power cables, two different shield topologies, the flat plate and reverse-U shape shielding screens, are examined theoretically and practically on currently used cable raceways. The most appropriate shielding type was investigated.

The analysis of different shielding configurations with flat plate material denoted that, the efficiency of the shielding strongly depends on the employed material. In case of reverse-U shield configuration, higher shielding efficiency is obtained as shown in Figure 1.

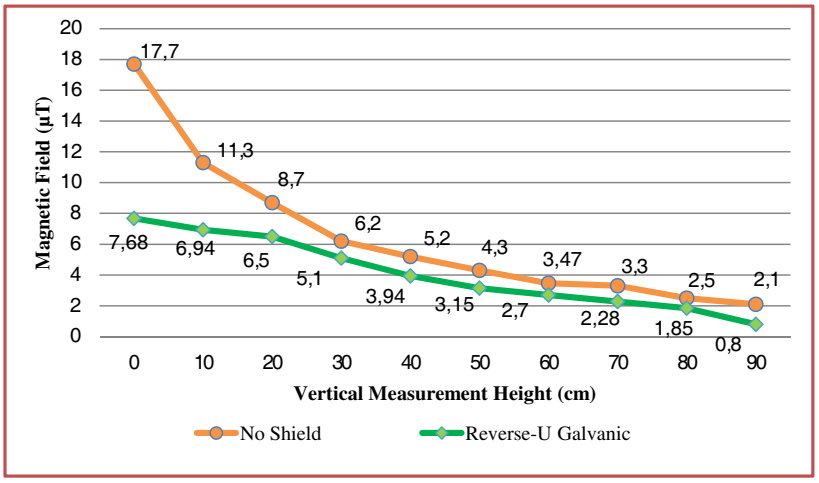

Figure 1: Shielding efficiency of reverse-U shield.

It is concluded that, better shielding efficiency is achieved when closed shields are used. On the other hand, in case of the flat plate shield usage, the efficiency depends on the electrical features and the thickness of the material.

Occupational Exposure Assessment of Power Frequency Magnetic Field in 154/31.5 kV Electric Power Substation in Turkey

S. Ozen, **S. Helhel**, **and H. F. Carlak**
Electrical & Electronics Engineering Department, Akdeniz University, Antalya 07058, Turkey

Abstract— The effects from exposure to power frequency electromagnetic fields are of interest to the public. These 50-Hz field exposures raise the question of what effects these may have on human health. Power subsystems are expected to produce very high magnetic field, since they are driving very high electric current density that results in an accumulating exposure to electric, magnetic and electromagnetic fields that cause some health problems if systems are designed without obeying the standards. Some epidemiological studies have found weak associations between exposure to power-frequency EMFs and some forms of cancer, such as leukemia; while other studies have failed to find such associations.

In this study has been proposed the survey of magnetic field measurements taken in a 154/31.5 kV substation in the City of Antalya for occupational exposure assessment. The magnetic field measurements carried out from substation equipment, including all transformers, circuit breakers, feeders and buses, under the in-coming and out-going power lines and operator tables surrounding the substation. Operator desk at read a lowest magnetic field of 0.46 μT at minimum loaded season and reached up to 1.34 μT at maximum loaded season that means operators exposed to a magnetic field of 0.3 μT and more by eight hours a day. In switchgear regions, maximum magnetic field reading is 20 μT at minimum loaded season and reached up to 65 μT. Outdoor magnetic field measurement at circuit breaker region goes up to 45 μT with respect to operator heights.

Table 1: Maximum induced electric fields and current densities for different locations in the substation.

Measurement Locations	**Magnetic field (μT)**	$\boldsymbol{J}$ **(μA/m²)**
Operator desktop	0.35	1.517
In front of 31.5 kV Command panel for main bar	40	173.416
31.5 kV side of TR-A	4.7	20.376
31.5 kV side of TR-B (2 m from TR-B)	7.4	32.082
In front of the circuit breaker (SF6)	8.8	38.15
Under the 154 kV busbar for TR-B input	3.95	17.124
Under the 154 kV busbar for TR-A	**6.5**	**28.18**

Effect of Renewable Energy Sources to the Stability of the Low Voltage Distribution Networks

Z. Szabo[1,3], **F. Zezulka**[2,3], **Z. Roubal**[1,3], **P. Marcon**[1,3], **O. Sajdl**[2,3], **and I. Vesely**[2,3]

[1]FEEC, Department of Theoretical and Experimental Electrical Engineering
Brno University of Technology, Technicka 12, Brno, Czech Republic
[2]FEEC, Department of Control and Instrumentation
Brno University of Technology, Technicka 12, Brno, Czech Republic
[3]FEEC, Centre for Research and Utilization of Renewable Energy
Brno University of Technology, Technicka 12, Brno, Czech Republic

Abstract— The paper describes the recent development in the area of renewable energy sources (RES). Shows the situations in countries supporting a great growth of RES, particularly in photovoltaic energy what leads to the big problems. The modelling of situation shows that in a very near future there will be a big overflow of electrical energy production in the low voltage networks (LVN). It would evoke necessity to transfer energy into higher voltage networks. However it's not possible, because of the protection systems of high voltage networks (HVN) are developed for the opposite flow of energy. The traditional power engineering industry assumes centralized energy sources (power plants), and delivers electrical energy into consumers via very high voltage networks (transition networks VHN), high voltage networks (HVN) into LVN. In the low voltage networks the energy is totally consumed. Because of the existing protection systems in the HVN, and the recent energy distributors and producers correspond with this traditional conception, is necessary to consume all energy from RES in the low voltage networks where it was produced. Our contribution deals with this phenomenon and offers some part solution of the problem.

Sensor Design and Data Transfer in a Smart Grid

Z. Roubal[1, 3], **P. Marcon**[1, 3], **Z. Szabo**[1, 3],
O. Saidl[2, 3], **I. Vesely**[2, 3], **and F. Zezulka**[2, 3]

[1]Department of Theoretical and Experimental Electrical Engineering, Brno University of Technology
Technicka 12, Brno 612 00, Czech Republic
[2]Department of Control and Instrumentation, Brno University of Technology
Technicka 12, Brno 612 00, Czech Republic
[3]Centre for Research and Utilization of Renewable Energy
Technicka 12, Brno 612 00, Czech Republic

Abstract— It this paper is showed design sensors physical variables, which is using for modelling power in smart grid. In the next step is showed transfer data using GPRS and modelling power provided renewable energy sources. In our distant sources we measure depend between physical variables as lighting and photovoltaic power plants, the water level and hydroelectric power plants. The power wind power plat is measure directly using wattmeter between plat and battery. For transfer data is used datalogger DA4, which used GPRS and data represented physical variables is storage in SQL database. In our 24 V smart gird is modelled power using power source. In the hydroelectric power plants was problem with non-harmonic voltage and current generated turbine. The design module includes analog multiplier for accurate measure power, necessary for give depend power to the water level. This module and datalogger DA4 is powered small photovoltaic panel. The module measure lighting between photovoltaic power plants is directly connection cable to the Compact Rio. The last renewable energy sources power wind power plat is powered battery and charged power give power wind power.

ACKNOWLEDGMENT

This research work has been carried out in the Centre for Research and Utilization of Renewable Energy (CVVOZE). Authors gratefully acknowledge financial support from the Ministry of Education, Youth and Sports of the Czech Republic under NPU I programme (project No. LO1210).

A Novel Design of the Wearable Antenna

Cheng-Nan Hu, **Jhih-Neng Yang**, **Siam-Chen Huang**, **and Ju-Chun Lin**
Communication Research Center, Oriental Institute of Technology, Taiwan

Abstract— Utilization of wearable textiles in the antenna segment is on demands for the blooming development of the body-centric communication systems. A wearable antenna is meant to be a part of the clothing used for communication purposes, which includes tracking and navigation, mobile computing and public safety. In this study, a proof-of-concept dual-band (2.4/5.7 GHz) wearable antenna design is realized using a multiple inverted-L antenna printed on a circular FR4 substrate above a ground plane with shape of button, termed as a button antenna. Due to its shape (like button) and compact volume (12 mm in diameter and 5 mm in height), the antenna can be easily implemented onto the wearable textiles for body PANs applications. Numerical and experimental study are presented herein.

Low-complexity Design of an 8×8 Modulation Configurable K-best MIMO Detector

Muh-Tian Shiue and Syu-Siang Long
Department of Electrical Engineering, National Central University, Zhongli 32001, Taiwan

Abstract— With growth of high throughput requirement in advanced communication standards such as IEEE 802.11ac, multiple-input multiple-output (MIMO) spatial multiplexing is an important technique to increase data throughput in a limited bandwidth. In this paper, a high power-efficiency 8×8 MIMO detector which supports multiple modulation schemes is presented. According to the tree-type decoding process, a pipelined circuit architecture suitable for high throughput is proposed for breadth-first type algorithm. To further reduce the circuit complexity, a shift-multiplier is proposed to avoid a conventional multiplier in our design. Multiple data modulation is also supported by flexibly extending the enumeration signal range. The circuit implementation has proved that our design has high power efficiency comparing with other works.

In algorithmic aspect, a breadth-first type algorithm can achieve near-ML performance and a fixed throughput, an algorithm modified from conventional K-best which is named distributed K-best (DKB) is applied in our design. Comparing with the conventional K-best algorithm, DKB can reduce the number of visiting nodes to 23.8% at each searching layer under 8×8, 64-QAM and $K = 10$ condition, i.e., prevents unnecessary power consumption. The MIMO system model in our design is converted into a real-numbered one, and we modify the enumeration scheme to further reduce computing power. Therefore, a shift-multiplier can be applied with only bit-shifting and addition operations. Furthermore, multiple data modulation schemes are supported by 1-D SE-enumeration without increasing algorithmic complexity.

In hardware aspect, our design applies multistage pipelined architecture to achieve high throughput requirement. Each stage processes one tree-searching layer with DKB algorithm, a single DKB block contains a first-child (FC) and a next-child (NC) functional block. The FC and NC operate exclusively to find best K candidates within only K clock cycles. Thanks to DKB algorithm, the sorting circuit in conventional K-best algorithm is avoided in our hardware architecture. The center calculation in order to find a FC is achieved by shift-multiplier which only contains a few adders and MUXs. Since the proposed hardware architecture is very regular, it has flexibility extending to other antenna configurations.

The proposed 8×8 MIMO detector has been implemented in a 90-nm CMOS technology with core area of $0.99 \times 0.99\,\mathrm{mm}^2$. The maximum throughput achieves 710 Mbps at operating frequency 74 MHz. At this condition, the power consumption is 17.2 mW at 1 V supply voltage. The normalized power is 24 pJ/bit, comparing with other works in the literatures, our proposed design delivers very high power efficiency.

Analysis and Construction of Static Inverter with Multi-windings Transformer for High Power Voltage Source

J. M. Grochowalski and Z. Frąckiewicz
Faculty of Electrical Engineering, West Pomeranian University of Technology, Szczecin, Poland

Abstract— High power static voltage inverters found their application in a power conversion for isolated power grids, especially in the shipbuilding and the maritime industry. When there is a need for interconnecting ship with an external electric power source for technical (i.e., a vessel is under a maintenance is shipyard, and it cannot use its own onboard power generator) or economical (a ship is being unloaded in a harbor) reasons there are a few options. One of them is to supply electrical energy from a static power inverter, which converts energy from a public grid to the appropriate frequency and voltage needed on board.

Most of the problems related to the design of such inverters are that very often nominal power of such devices is comparable to nominal power of its load. In case of a ship the major part of the load are cranes, pumps, fans and so on, all driven by electrical machines (most frequently induction machines). Starting current of the induction electrical machine is about $6 \div 7$ times nominal current. And this starting current must be withstood by a static power inverter, which place great demands on its design.

The voltage source presented in this paper consist of two main elements: a static inverter and a multi-windings transformer. To meet the requirements of ship electrical network, namely frequency (60 Hz), voltage (440 V, 690 V) and high overload current it is proposed to use thyristors as switching devices. The downside of this approach is that operating frequency of the inverter cannot be as high as in a case of IGBT or other transistors, so a total harmonics distortion in output voltage is high. To counter this effect and lower the THD to required by law or other regulations a specially designed and connected multi-windings transformer is used. It also adjust the output voltage level to the required one.

In this contribution a design of proposed voltage source, its computer simulations and experimental results are shown.

Modelling and Analysis of an Electro-optical System with an Off-quadrature Biased Modulator

D. M. S. Morais[1], **J. Panasiewicz**[1, 2], **and G. M. Pacheco**[1]

[1]Aeronautics Technical Institute, Brazil
[2]National Institute for Space Research, Brazil

Abstract— This paper describes the behavior of a microwave external modulation link composed of: optical and radio frequency sources, Mach-Zehnder modulator (MZ), optical fiber and photodetector. The electro-optical circuit modulates the RF signals and transmits them to the detector through the optical fiber. The main contribution of this paper lies on the different approach to the system analysis; we consider an off-quadrature biased MZM.

By extending the mathematical model found in the literature for the case of different bias voltages, we compute a few performance parameters of the system like Gain and SFDR. For computing those parameters we use a custom made program written in the MATLAB environment.

In addition to the system's characterization and insights on its off-quadrature operation, another contribution of this article is the model validation. We assembled the electro-optical circuit and measured some performance parameters for different values of bias voltages. By comparing the experimental results with the theoretical ones, we validated the model. Finally, we also consider the applications for microwave signals distribution by optical fiber links.

Studies on the Photoluminescence of a Novel Europium (III) Complex in Solution

Meng Shi[1], **Xinxin Meng**[1], **Fufang Su**[1], **Zongbao Li**[4], **and Xiaobo Xing**[2, 3]

[1]Shandong Provincial Key Laboratory of Laser Polarization and Information Technology
Qufu 273165, China
[2]Centre for Optical and Electromagnetic Research
South China Normal University, Guangzhou 510006, China
[3]Education Ministry's Key Laboratory of Laser Life Science & Institute of Laser Life Science
College of Biophotonics, South China Normal University, Guangzhou 510631, China
[4]Department of Physics and Electronic Science, Tongren University, Guizhou 554300, China

Abstract— The novel ternary europium (III) complex is synthesized. The photophysical sensitization process involves an energy transfer from functional hemicyanine (aminostyrylpyridinium) cation. The sensitization mechanism follows the F?rster, which is significantly different from the Dexter, the most commonly used energy transfer mechanism from ligand. When the complex is dissolved in a variety of solvents (acetone, dimethylformamide, ethanol and acetonitrile), a remarkable solvent effect is observed. The emission intensity of europium (III) complex in acetonitrile is much stronger than that in other solvents. The solvent effect on the photophysical properties is studied. The result indicates that the solvent influences the emission intensity by aid of many factors not only polarity.

Numerical Study of Electrically-induced Physiotherapy: Influence of Working Frequency and Electrode Type on Temperature Distribution

J. Vrba[1], **D. Vrba**[1], **and M. Lorenc**[2]

[1]Faculty of Biomedical Engineering, Czech Technical University in Prague, Czech Republic
[2]Faculty of Electrical Engineering, Czech Technical University in Prague, Czech Republic

Abstract— Temperature increase has a proved positive effect on pain relief, inflammation and muscle spasms treatment. It is therefore utilized in physiotherapy as well as in other biomedical applications. Temperature increase of the treated biological tissues is often performed by a well-controlled exposure of the tissues to time-harmonic electric fields. To obtain only localized and safe heating active electrode and return pad electrode differ by their size and shape. In this paper, a numerical study of influence of working frequency and electrode type on power loss and corresponding temperature distribution in exposed biological tissues was performed and some results are presented and discussed.

A simplified 2D numerical model in the well-proven numerical simulation tool COMSOL Multiphysics was created. The human body was represented by an elliptical layered model consisting of skin and an inner region modeled as a muscle tissue. In the presented numerical study, thermal material properties as well as frequency-dependent dielectric properties of the biological tissues were considered. Within this study three working frequencies $f = 0.5$, 1 and 1.5 MHz and following two types of electrodes are included. Resistive electrodes are in a direct contact with treated biological tissues and capacitive electrodes which are equipped with a thin nonconductive coating. Active electrode is circular with 15.9 cm^2 area. Grounding pad is of rectangular shape and approximately 7.5 times larger.

Main outcome of the performed numerical simulations is a prediction of spatial distribution of power losses induced in the treated tissues. Corresponding temperature distribution obtained by solving the Pennes' bioheat equation is displayed graphically and further discussed.

The Bone Regeneration Effect of 3D Printed Ferromagnetic Magnetite-based Polylactide Composite Bone Screw

Haw-Ming Huang[1], **Jy-Jiunn Tzeng**[1], **Ya-Hui Chan**[1, 2], **and Chien-Fang Tseng**[3]

[1]Graduate Institute of Biomedical Materials and Engineering, Taipei Medical University, Taipei, Taiwan
[2]Dental Department, En-Chu-Kong Hospital, Taipei, Taiwan
[3]School of Dentistry, Taipei Medical University, Taipei, Taiwan

Abstract— Polylactic acid (PLA)-based composites were used as bone/tissue regeneration materials for many years. Recently, how to modify the physical, chemical and biological properties of the PLA-based materials for improving its medical application has become an issue for biomaterial sciences. It has been reported that iron oxide magnetic nanoparticles exhibit not only biocompatibility, but also bioactive effect on the osteoblastic proliferation. Accordingly, the aim of this study was to develop a novel nano-magnetic bioresorbable bone screw by using both injection molding and 3D printing techniques. For methodology, nanoscale magnetite was incorporated into the PLA matrix with various nano-Fe_3O_4/PLA mixing ratios. Pure PLA samples were carried out as a control. Thermodynamic, mechanical, and biocompatibility of the materials were tested to confirm the performance of this composite. Then nano-Fe_3O_4/PLA bone screws were fabricated by injection molding and 3D printing techniques. The mechanical properties of these bone screw were tested by simulated model in vitro. In addition, animal studies were performed to test the healing status between nano-Fe_3O_4/PLA screw and bone tissue. In the strength tests, our results showed that the screws produced by 3D-printer are weaker than the screws made by injection molding. In animal study, we found the implant side with screws that contain ferromagnetic particles showed more regenerated bone volume and induce less inflammation and tissue mass. The CT imaging enhancement of the nano-Fe_3O_4/PLA bone screw was proved. With these results, we concluded that this novel magnetic bioresorbable screw can be applied in future orthopaedic treatment.

The Gene Expression of Dental Pulp Stem Cells Due to 0.4 T SMF Treatment

Yen-Lan Chang[1], **Wei-Zhen Lew**[1], **Yuh-Yuan Shiau**[2], **and Haw-Ming Huang**[3]

[1]School of Dentistry, College of Oral Medicine, Taipei Medical University, Taipei, Taiwan
[2]School of Dentistry, National Taiwan University, Taipei Taiwan
[3]Graduate Institute of Biomedical Materials and Tissue Engineering
Taipei Medical University, Taipei, Taiwan

Abstract—

Objective: Human dental pulp stem cells (DPSCs) have become an alternative source for tissue engineering. Accordingly, how to increase viability of human DPSCs is vitro has become an important issue in medical applications. Several studies showed that static magnetic field (SMF) has positive biological effect on stem cells. However, the real signal transduction mechanisms are still unknown. In this study, we focus our aim test the effect of SMF on human DPSCs. The possible gene expression of DPSCs after exposure to SMF was explored.

Materials and methods: In this study, human DPSCs were isolated using magnetic activating cell sorting technique. The test cells were treated with 0.4 T SMF exposure. A neodymium disc was used to provide the magnetic field. For control group, the cells were exposed to a non-magnetized neodymium disc. The cell proliferation rate and gene expression profiles were performed by MTT assay and RNA microarray, respectively.

Results: Our results showed that the proliferation rate of SMF-treated human DPSCs significantly increased. A total of 216 genes changed with a 2-fold or more ratio was found in SMF-treated human DPSCs. In addition, Slightly increase of TGFB-2 and Col III genes were noted after 24-hour exposure. Moreover, FGF2 gene increased after 48-hour exposure.

Conclusion: According to these results, we conclude that 0.4 T SMF significantly improve the proliferation and gene expression of human DPSCs.

Increases Cryopreservation Efficiency of Stem Cells Using Static Magnetic Field

Kan-Shin Fan[1], **Chun-Yen Lin**[2], **Haw-Ming Huang**[3], **and Jen-Chang Yang**[4]

[1]Dental Department, En-Chu-Kong Hospital, Taipei, Taiwan
[2]School of Dentistry, Taipei Medical University, Taipei, Taiwan
[3]Graduate Institute of Biomedical Materials and Engineering
Taipei Medical University, Taipei, Taiwan
[4]School of Dental Technology, Taipei Medical University, Taipei, Taiwan

Abstract— How to successful cryopreservation of stem cells is a key issue for application of regenerative medicine. Recently, magnetic cryopreservation has been reported to be an efficient method for cell banking and cryopreservation. The purpose of this study was to test whether static magnetic fields can improve cryoprotective effects of stem cells during cryopreservation process. In methodology, human dental pulp stem cells were frozen with a 0.8-T SMF and then stored at −196°C for 24 hr. During freezing, the cells were suspended in freezing media containing with 0%, 3%, or 10% DMSO. After thawing, the survival rate of the stem cells were tested and compared to the control cells which were frozen without SMF. In addition, physical property of the cellular membrane was determined to understand the possible cryoprotective mechanisms of the SMF. The results indicated, the positive cryoprotective effect of SMF can be observed when the freezing medium was DMSO-free. The survival rates of the thawed stem cells increased up to 2.5-fold when the cells were exposed to a 0.8-T SMFs, respectively ($p < 0.01$). Meanwhile, our results showed that the major mechanism of SMF-induced cryopreservation is due to the membrane distortion due to magnetic force applied. These results suggested that SMF exposure improved stem cell cryopreservation at DMSO-free environment. This phenomenon can be a useful reference for future tissue engineering application.

Metamaterial Terahertz Bandpass Filters: A Comparison between Metallic and Graphene-based Structures

M. Bana Kermani[1], **M. Khodaee**[1], **A. Nasiri**[2], **and H. Baghban**[1]

[1]School of Engineering-Emerging Technologies, University of Tabriz
Tabriz 51666-14761, Iran
[2]Department of Engineering, University College of Nabi Akram, Tabriz 51385-1488, Iran

Abstract— Metamaterial-based optoelectronic devices including Terahertz filters play a definitive role in advancement of THz technology. In this article we present a design procedure to obtain voltage-dependent carrier density control in a GaN-based hetero structure with a Schottky gate configuration which serves as the substrate for a THz bandpass filter (BPF). The introduced structure consists of a cross shaped metallic layer on the AlGaN/GaN hetero structures as presented in Figure 1(a). Then, we investigate tuning of transmission properties and the tunability of the filter. Figure 1(b) illustrates the transmission properties of the designed structure at different bias voltages. An overall tunability of about 103 GHz in the resonance frequency was obtained by varying the applied voltage from −8 V to 2 V. Also, a plasmonic metamaterial based on the graphene cross-shaped structure is studied and a comparison has been performed between the optical properties of graphene-based cross-shaped structure and the original structure. It is noteworthy to mention that graphene-based THz filters are more flexible to achieving tunability, and the continuous forms of graphene can be transferred to a flat substrate and the carrier concentration of each layer in a graphene-based multi-layer filter can be dynamically tuned.

The surface conductivity of graphene that contains the effect of interband and intraband transitions has been calculated through the local limit of random-phase approximation (RPA). The surface conductivity depends on the temperature, the intrinsic carrier relaxation time, τ, and the Fermi level (which depends on the external bias voltage). Obtained results show considerable resonance strength and dynamically controllable feature. Both of the presented structures can be promising for developing electrically tunable THz BPFs.

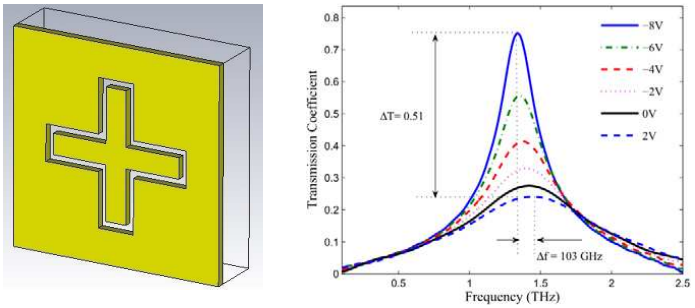

Figure 1: Cross-shaped THz BPF (a) and the obtained transmission characteristics as a function of applied bias voltage.

REFERENCES

1. Wang, J., W. Lu, X. Li, X. Gu, and Z. Dong, "Plasmonic metamaterial based on the complementary split ring resonators using graphene," *J. Phy. D: Appl. Phys.*, Vol. 47, 325102, 2014.
2. Chiang, Y. J., C. S. Yang, Y. H. Yang, C.Pan, and T. J. Yen, "An ultrabroad terahertz bandpass filter based on multiple-resonance excitation of a composite metamaterial," *Applied Physics Letters*, Vol. 99, 191909, 2011.
3. Rostami, A., H. Rasooli, H. Baghban, *Terahertz Technology, Fundamentals and Applications*, Springer, 2010.

Continuous Wireless Monitoring and Wireless Power Transfer for Leadless Pacemaker Systems

Rupam Kumar Das[1], **Dong Sik Woo**[2], **and Hyoungsuk Yoo**[1]

[1]University of Ulsan, Ulsan, South Korea
[2]Kyungpook National University, South Korea

Abstract— Pacemakers provide electrical stimuli to cause cardiac contractions when intrinsic cardiac activity is inappropriately slow or absent. Traditional cardiac pacing or pacemaker systems comprise an implantable pulse generator and lead system. A conventional pulse generator has an interface for connection to and disconnection from the electrode leads that carry signals to and from the heart. The complex connection between connectors and leads provides multiple opportunities for malfunction. Moreover, the pacemaker lead may also interact with magnetic resonance imaging (MRI) systems, which can cause tissue damage. Recently, an MRI-compatible capsule-type leadless pacemaker was introduced to resolve these problems. A leadless pacemaker has several advantages, such as being less invasive (no surgery, more cosmetically pleasing for the patient, i.e., invisible), improved efficiency (no system connections, more readily MRI-compatible), and cost-effectiveness (reduced length of hospital stay, less infection or erosion). However, the potential disadvantages or technical challenges of the leadless pacemaker cannot be neglected. These challenges include multiple chamber pacing, novel delivery systems, battery longevity, telemetry and long-term efficacy.

The leadless pacemaker's telemetry might facilitate a development that would allow healthcare professionals to control the device and monitor patients using a standard programmer via smart phones, thereby providing individual treatment to patients in the most rural of areas. Moreover, the leadless pacemaker must remain in place even after the batteries are exhausted. If a noninvasive method of recharging the batteries or powering the leadless pacemaker could be found then this would cease to be a problem and could even be considered an advantage. The implantable antenna allows for wireless monitoring and device control in patients, and the inclusion of wireless power transfer allows for continuous monitoring beyond normal battery lifetimes.

Here, we introduce an implantable antenna which can be incorporated into a capsule-type leadless pacemaker for telemetry. This antenna was designed at Medical Implanted Communication Service (MICS) band ($\sim 400\,\mathrm{MHz}$). We also utilize the recently published midfield energy transfer technique to check the likeliness of wireless powering of the leadless pacemaker and for removal of batteries. A midfield transmitter antenna was designed for this purpose at 1.5 GHz. Finally, we simulated and measured the performance of both antennas, and we also checked any significant coupling between these two schemes.

Some Effects of Specific Interest on the Brain of Children with Autism Spectrum Disorder (ASD): A Functional Near-infrared Spectroscopy Study

Huilin Zhu[1*], **Yuebo Fan**[3], **Xinge Li**[1,2], **Dan Huang**[3], **Huan Guo**[2], **and Sailing He**[1,4]

[1]Centre for Optical and Electromagnetic Research, South China Academy of Advanced Optoelectronics South China Normal University (SCNU), Guangzhou 510006, China
[2]School of Psychology, South China Normal University (SCNU), Guangzhou 510631, China
[3]Guangzhou Rehabilitation and Research Center for Children with ASD, Guangzhou 510540, China
[4]Department of Electromagnetic Engineering, Royal Institute of Technology, Stockholm 10044, Sweden

Abstract— Autism spectrum disorder (ASD) is a neuro-developmental disorder, characterized by two major domains: impairments in the social cognition and communication as well as restricted, repetitive, stereotyped interests and behaviors. In this study, functional near-infrared spectroscopy (fNIRS) was applied to investigate the atypical activation pattern of language areas (bilateral inferior frontal gyrus and bilateral temporal cortex) and uncover the impact of a specific interest on the brain function of children with ASD. We employed a listening comprehension task to stimulate the language areas of 2 ASD boys (A1 and A2) who had strong interests in the experiment material ("Lightning McQueen") and another 2 ASD boys (A3 and A4) who were matched with A1 and A2 respectively by age, intelligence quotient, language ability and the severity of symptoms. Our results showed that, during the task, the picture of "Lightning McQueen", but not the words of "The little red car", elicited stronger activation in the bilateral inferior frontal gyrus and temporal cortex of A1 and A2 than A3 and A4. These results could facilitate our understanding of language development of ASD and reconsider the role of specific interests (especially visual stimuli) played in the brain functional development of ASD.

*Corresponding author: Huilin Zhu (huilin.zhu@coer-scnu.org).

Broadband Cross Polarization Converter Formed by Twisted F-shaped Chiral Metamaterial

D. K. Sharma and S. K. Pathak
Microwave and ECE Diagnostic Division, Institute for Plasma Research, India

Abstract— A broadband cross polarization convertor (CPC) formed from Twisted-F Shaped Chiral Metamaterial (TFSCM) having high optical activity is reported in this work. The proposed structure supports high polarization conversion efficiency which has been demonstrated numerically. The achieved optical activity in the structure is due to the presence of cross coupling phenomena between electric and magnetic fields. The coupling mechanism is explained on the basis of surface current distribution in between top and bottom metallic plates of TFSCM. The TFSCM is a bilayered structure having F-shaped metallic inclusions on both sides having twist in opposite direction and separated by FR-4 dielectric spacer. In direction of EM wave propagation, structure lacks mirror symmetry which provides structure the property to have strong optical activity in order to realize cross polarization conversion [1].

In Figure 1(a) numerical results of co- and cross polarization transmission coefficients of the TFSCM are presented. At frequency of 25.8 GHz the observed maximum cross polarization efficiency (CPC) is very high. At that frequency the distribution of surface current is as shown in Figure 2. It observed that incident electric field in y-direction excites symmetric current in front and back metal strips. Due to this a dominant electric dipole coupling is observed at resonance frequency [2]. The proposed broadband TFSCM cross polarization convertor is anticipated to have applications in microwave and photonics in the fields of communication, polarization spectroscopy, imaging microscopy etc..

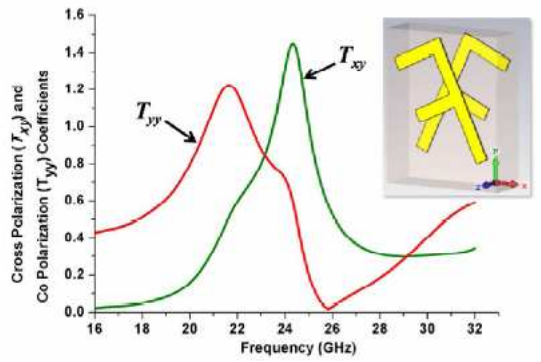

Figure 1: Cross and Co polarization coefficients of TFSCM structure.

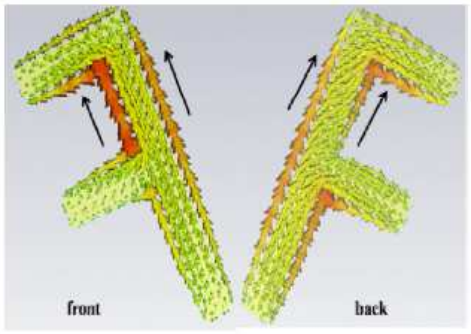

Figure 2: Surface current distribution of front and back metallic plate of TFSCM structure at frequency of 25.8 GHz.

REFERENCES

1. Rajkumar, R., N. Yogesh, and V. Subramanian, *J. Appl. Phys.*, Vol. 114, 224506, 2013.
2. Li, Z., R. Zhao, T. Koschny, M. Kafesaki, K. B. Alici, E. Colak, H. Caglayan, E. Ozbay, and C. M. Soukoulis, *Appl. Phys. Lett.*, Vol. 97, 081901, 2010.
3. Kenanakis, G., R. Zhao, A. Stavrinidis, G. Konstantinidis, N. Katsarakis, M. Kafesaki, C. M. Soukoulis, and E. N. Economou, *Optical Material Express*, Vol. 2, 1702, 2012.

Effect of Frequent Degree of Deceiving on the Prefrontal Cortical Response to Deception: A Functional Near-infrared Spectroscopy (fNIRS) Study

Fang Li[1,2], **Huilin Zhu**[1*], **Shijing Wu**[1], **Qianqian Gao**[1,2], **Ziqiang Hu**[1,2], **Jie Xu**[1], **Guixiong Xu**[1], **and Sailing He**[1,3]

[1]Centre for Optical and Electromagnetic Research
South China Academy of Advanced Optoelectronics South China Normal University (SCNU)
Guangzhou 510006, China
[2]School of Psychology, South China Normal University (SCNU), Guangzhou 510631, China
[3]Department of Electromagnetic Engineering, Royal Institute of Technology, Stockholm 10044, Sweden

Abstract— Functional near-infrared spectroscopy (fNIRS) is an emerging brain-imaging technique which has been used to various areas. Previous studies have indicated that frequent deceiving would make deceiving easier. In this study, fNIRS was used to explore the effect of frequent degree of deceiving on the prefrontal cortical response to deception. Self-related questions were used in the experiment. The results showed different patterns of neural activation between non-frequent deceiving and frequent deceiving. In Channel 11 (in the left prefrontal cortex), non-frequent deceiving led to a greater neural activation than telling the truth, while this pattern did not appear in frequent deceiving. Our finding suggested that fNIRS has ability to detect deception under different situations.

*Corresponding author: Huilin Zhu (huilin.zhu@coer-scnu.org).

Session 3A1
SC2: Thermal and Acoustic Metamaterials

Phononic Metamaterials: Past, Present and Future Challenges

Johan Christensen
DTU Fotonik, 2800 Kgs. Lyngby, Denmark

Abstract— The boost experienced by acoustic and elastic (phononic) metamaterial research during the past years has been driven by the ability to sculpture the flow of sound waves at will. Motivated by the desire to engineer artificial structures in the form of metamaterials and the quest to map quantum mechanical phenomena onto classical waves such as sound has led to vast possibilities in material designs for control of wave motion and the potential for engineering applications. Some striking material properties have shown in the past to be able to leave an objective acoustically concealed, hence they are cloaks of "unhearability". Also, fascinating materials have been designed to be able to bend a ray of sound the "wrong" way when, for example, a loudspeaker turned on irradiates such artificial structure with a negative refraction index. In this talk, I like to review some of the key achievements made in this field and wish to address some of the unanswered questions that might lead to a breakthrough in the future.

Elastic Wave Propagation in Soft Matter Materials

Stephan Rudykh
Department of Aerospace Engineering, Technion-Israel Institute of Technology, Israel

Abstract— We study elastic wave propagation in finitely deformed soft materials [1]. First, we derive explicit dispersion relations for homogeneous materials undergoing large deformations [2]. We show that large deformations significantly affect elastic wave propagation in soft materials. Next, we analyze a class of periodically structured phonon crystals with layered microstructures. These structures are known to develop elastic instability-induced wrinkling of interfacial layers [3]. The onset of a wrinkling instability in initially straight interfacial layers occurs when a critical compressive strain or stress is achieved. Further compression beyond the critical strain leads to an increase in the wrinkle amplitude of the interfacial layer. This, in turn, gives rise to the formation of a system of periodic scatterers, which reflect and interfere with wave propagation. We demonstrate that the topology of wrinkling interfacial layers can be controlled by deformation and used to produce band-gaps in wave propagation and, hence, to selectively filter frequencies [1]. Remarkably, the mechanism of frequency filtering is effective even for composites with similar or identical densities, such as polymer-polymer composites. Since the microstructure change is reversible, the mechanism can be used for tuning and controlling wave propagation by deformation.

REFERENCES

1. Rudykh, S. and M. C. Boyce, "Transforming wave propagation in layered media via instability-induced interfacial wrinkling," *Phys. Rev. Lett.*, Vol. 112, 034301, 2014.
2. Galich, P. and S. Rudykh, "Explicit dispersion relations for elastic waves in extremely deformed soft matter with application to nearly incompressible and auxetic materials," http://arxiv.org/abs/1501.00134, 2014.
3. Li, Y., N. Kaynia, S. Rudykh, and M. C. Boyce, "Wrinkling of interfacial layers in stratified composites," *Advanced Engineering Materials*, Vol. 15, No. 10, 921–926, 2013.

Single Negative Metamaterials Take on Negative Indices Owing to Multiple Scattering: Demonstration with an Acoustic Super-lens

N. Kaina, **F. Lemoult**, **M. Fink**, **and G. Lerosey**
Institut Langevin, ESPCI ParisTech, France

Abstract— We evidence that single negative metamaterials can turn into double negative ones, hence leading to a negative band solely by breaking the symmetry. We explain this phenomenon from multiple scattering effects and give an analogy with the phonon optical branch. We experimentally demonstrate a negative index acoustic super-lens using a soda can hexagonal array with $\lambda_0/15$ spot.

Media presenting negative indices of refraction were first considered theoretically by Veselago in the 60's [1]. They have recently become a very attractive field of research since they theoretically offer the compelling possibility of designing flat super-lenses that can beat the diffraction limit, as suggested by Pendry [2]. This negative refraction can be achieved using metamaterials presenting simultaneously two negative effective properties (permittivity and permeability in electromagnetics or modulus and mass density in acoustics). From a practical point of view, this requires to combine two single negative locally resonant meta-atoms, each bringing one of the negative properties. On the other hand, it was highlighted that the negative refraction may also occur from the superposition of a monopolar and a dipolar resonance of a single acoustic Mie scatterer [3]. In this work, we show analytically and numerically, that, contrarily to previous ideas, double negative media can be created from a single negative metamaterial, that is a metamaterial having a single resonant atom. We chose to work with an acoustic metamaterial made out of soda cans as Helmholtz resonators. We start from a periodic one dimensional medium, for which the elementary cell, of deeply subwavelength dimension, is composed of a single acoustic resonator and whose dispersion relation is polaritonic (Fig. 1(a)). By slightly breaking this medium's symmetry, thus creating a bi-periodic medium (Fig. 1(b)), we evidence the creation of a negative band in the bandgap of the original medium. We prove that this can be explained only by considering the multiple scattering within the unit cell, which allows the rise of a dipolar mode otherwise inexistent. An analogy with the phonon optical branch will be provided. We then experimentally demonstrate a negative index acoustic super-lens for a frequency within the negative band of an hexagonal array of soda cans, that focus sound on a $\lambda_0/15$ focal spot behind the lens, in the vicinity of the output surface.

This new approach of a double negative medium from symmetry broken metamaterials stresses the importance of multiple scattering at subwavelength scales that is generally considered unimportant, as metamaterials are considered as effective media. We believe this work simplifies the design of negative index materials and paves the way to the design of new and exotic metamaterials.

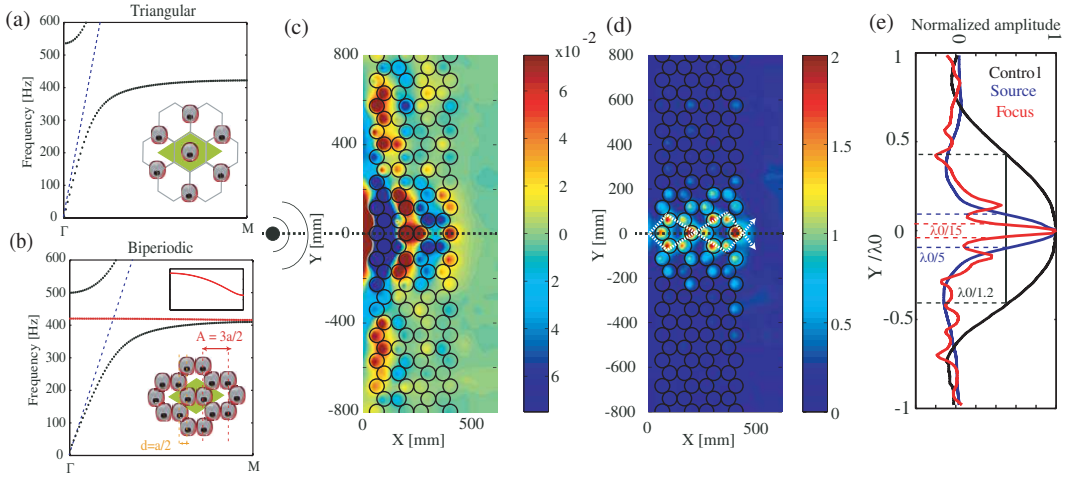

Figure 1: (a), (b) Simulated dispersion relation of a periodic triangular (resp. biperiodic hexagonal) array of soda cans in the Γ-M direction and schematic of the simulated medium. (c), (d), (e) Experimental results of super-lensing.

REFERENCES

1. Veselago, V. C., *Sov. Phys. Usp.*, Vol. 10, 509, 1968.
2. Pendry, J. B., *Phys. Rev. Lett.*, Vol. 85, 3966, 2000.
3. Li, J. and C. T. Chan, *Phys. Rev. E*, Vol. 70, 055602(R), 2004.

Sound Absorption by a Structure with Straight Rectangular Pores Loaded by Periodically Distributed Detuned Resonators

J.-P. Groby[1], **R. Pommier**[2], **and Yves Aurégan**[1]

[1]Laboratoire d'Acoustique de l'Université du Maine (LAUM), UMR-6613 CNRS
Av. O. Messiaen, Le Mans 72085, France
[2]LUNAM Université, Université du Maine, Av. O. Messiaen, Le Mans 72085, France

Abstract— We demonstrate that the phenomenon of slow sound propagation associated with its inherent dissipation (dispersion + attenuation) arising from visco-thermal losses can be efficiently used to design broadband sound absorbing materials. The propagation in straight pores of rectangular cross-section loaded with tuned or detuned resonators is first analyzed. Below the bandgap associated with the resonance, the sound speed is slow down inside the pores and depends on the dimensions of both the pores and the resonators. Between the two resonances, a transparency band is open also associated with a speed of sound much smaller than the one in the air. We show that this speed is necessarily dispersive within the transparency band, while it possesses a plateau at low frequency.

The absorption coefficient of a periodic arrangement of one straight pore loaded with detuned resonators is then analyzed to obtained a perfect absorption condition, via an analysis in the complex frequency domain. Perfect absorption is obtained for a wavelength in the air much larger than four times the thickness of the structure, whose efficiency largely overcome the absorption properties of usual air saturated porous materials. It is shown that this perfect absorption arises from a critical coupling condition, the radiation loss being exactly compensated by the visothermal ones for specific dimensions of the structure.

The absorption of a metamaterial consisting of a periodic arrangement of pores with different lengths and cross-sections loaded with tuned or detuned resonators is finally shown to be unity or close to unity over a broad frequency range due to a correct frequency distribution of the resonances.

These conclusions are supported by experimental results.

Boundary Layer Effects on Acoustic Transmission through Narrow Slit-cavities

G. P. Ward[1], **R. K. Lovelock**[1], **A. R. J. Murray**[1], **A. P. Hibbins**[1], **J. R. Sambles**[1], **and J. D. Smith**[2]

[1]Electromagnetic and Acoustic Materials Group, Department of Physics and Astronomy
University of Exeter, Stocker Road, Devon, EX4 4QL, United Kingdom
[2]DSTL, Porton Down, Salisbury, Wiltshire, SP4 0JQ, United Kingdom

Abstract— We explore the slit-width dependence of resonant transmission of sound in air through both a slit-array formed of aluminium slats, and a single open-ended slit-cavity (not shown in this abstract) in an aluminium plate. By studying Fabry-Perot-like cavity resonances, we find significant attenuation of the transmitted signal, and a reduction of the effective speed of sound through the slits by as much as 18%, for slit sizes narrowed below 2% of the free space wavelength. Our experimental results agree with numerical modelling and with theory which stems from Lord Rayleigh [1], concerning how viscous and thermal boundary layers at the slit walls effect the acoustic wave across the whole slit-cavity.

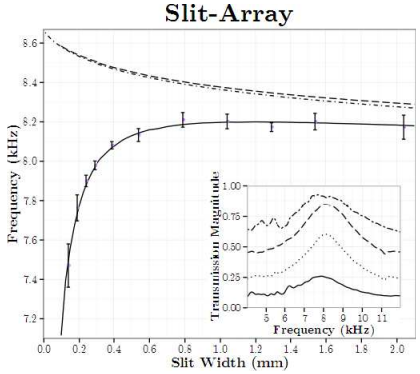

Figure 1: Dependence of the frequency of the fundamental Fabry-Perot resonance on slit width for the slit-array with slats of length $L = 19.80 \pm 0.12$ mm. The data was taken under different temperature, pressure and humidity, and then normalised to 293.15 K, with the other variables having negligible effect. The long dashed line represents a lossless FEM numerical prediction, the solid line a numerical prediction that includes the viscous and thermal properties of the system, and the circles the experimental results. Also shown as a dot-dash line is the prediction of the lossless model-matching model proposed by Christensen [1]. (Inset) Examples of the experimentally measured transmitted frequency spectra for the slit-array sample. Four different slit widths 2.0 mm, 1.0 mm, 0.5 mm and 0.2 mm, are represented by the dot-dashed, long-dashed, dotted and solid lines respectively.

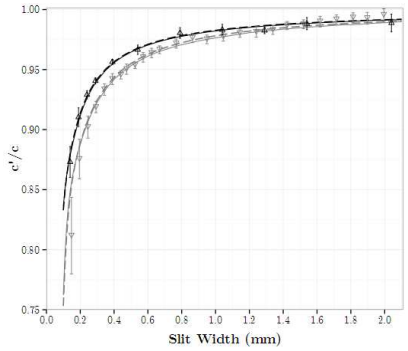

Figure 2: Ratio of the effective speed of sound c' to bulk speed c in each slit-cavity. Black represents the array sample, and grey the single slit sample. The solid lines show the result extracted from the finite element method model, the dashed lines are Stinson's [2] simplified analytic theory. Points are experimental data.

REFERENCES

1. Rayleigh, L., *Philos. Mag.*, Vol. 1, 301, 1901.
2. Christensen, J., L. Martin-Moreno, and F. J. Garcia-Vidal, *Phys. Rev. Lett.*, Vol. 101, 014301, 2008.
3. Stinson, M. R., *J. Acou. Soc. Am.*, Vol. 89, 550, 1990.

Fick's Second Law Transformed for Cloaking in Mass Diffusion

T. M. Puvirajesinghe[1, 2, 3] **and S. Guenneau**[3, 4]

[1]CRCM, Inserm, U1068, Marseille F-13009, France
[2]Institut Paoli-Calmettes, Marseille F-13009, France
[3]Aix-Marseille Université, Marseille F-13284, France
[4]Institut Fresnel, UMR CNRS 7249, Marseille, France

Abstract— We have adapted the concept of transformational thermodynamics, whereby the flux of temperature is controlled via anisotropic heterogeneous diffusivity, for the diffusion and transport of mass concentration. The n-dimensional, time-dependent, anisotropic heterogeneous Fick's equation is considered, which is a parabolic partial differential equation also applicable to heat diffusion, when convection occurs, for example, in fluids. We initially used finite-element computations to model liposome particles surrounded by a cylindrical multi-layered cloak in a water-based environment, and for a spherical multi-layered cloak consisting of layers of fluid with an isotropic homogeneous diffusivity, deduced from an effective medium approach [1]. Independent research groups have applied our model to applications implicating the protection of steel by protecting concrete against chloride ions penetration [2] as well as for the design of water-based invisibility cloaks [3]. We now investigate the utility of the biocloak for vectorization of drugs [4].

REFERENCES

1. Guenneau, S. and T. M. Puvirajesinghe, "Fick's second law transformed: One path to cloaking in mass diffusion," *J. R. Soc. Interface*, Vol. 10, No. 83, 20130106, 2013.
2. Zeng, L. and R. Song, "Controlling chloride ions diffusion in concrete," *Sci. Rep.*, Vol. 3, 3359, 2013.
3. Schittny, R., et al., "Metamaterials. Invisibility cloaking in a diffusive light scattering medium," *Science*, Vol. 345, No. 6195, 427–429. 2014.
4. Zhao, Y., et al., "A preloaded amorphous calcium carbonate/doxorubicin@silica nanoreactor for pH-responsive delivery of an anticancer drug," *Angew. Chem. Int. Ed. Engl.*, Vol. 54, No. 3, 919–922, 2015.

Topological Acoustics

Zhaoju Yang[1] **and Baile Zhang**[1, 2]

[1]Division of Physics and Applied Physics, School of Physical and Mathematical Sciences
Nanyang Technological University, Singapore 637371, Singapore
[2]Centre for Disruptive Photonic Technologies
Nanyang Technological University, Singapore 637371, Singapore

Abstract— The concept of topologically nontrivial bandstructures, which originally arose in the study of the quantum Hall effect and topological insulator materials, has recently led to the emergence of the field of "topological photonics". Here, we further extend the concept to acoustics by designing a phononic crystal which maps theoretically onto the integer quantum Hall effect. Time-reversal symmetry is broken by a circulating fluid flow in each unit cell, which corresponds to nonzero periodic effective magnetic flux density. We derive the bandstructure, and show the existence of topologically nontrivial bands possessing nonzero Chern numbers. Numerical simulations reveal the existence of unidirectional acoustic modes at the boundaries of the phononic crystal, which are topologically protected against backscattering from disorder. Such topological phononic crystals may have novel applications in acoustics.

Phonon Tunneling Times of Semiconductor Heterostructures with Different Tunneling Channels

Diosdado Villegas[1], **J. Arriaga**[1], **Fernando de León-Pérez**[2], **and Rolando Pérez-Álvarez**[3]

[1]Instituto de Física, Benemérita Universidad Autónoma de Puebla
Apartado Postal J-48, Puebla 72570, México
[2]Centro Universitario de la Defensa de Zaragoza, Ctra. de Huesca s/n, E-50090, Zaragoza, Spain
[3]Universidad Autónoma del Estado de Morelos, Av. Universidad 1001, Cuernavaca 62209, México

Abstract— Theoretical and experimental studies of periodic structures that exhibit the so-called phononic band gaps have received great interest in recent years due to their potential applications. Recently, a long-wavelength continuum phenomenological model [1, 2] has been employed to study the phonon tunneling time at normal incidence in semiconductor heterostructures [3].

In this work, we study the phonon tunneling times at oblique incidence in asemiconductor heterostructure. Using the continuity equation for the vibrational energy density inside the system, we deduce ageneral analytical formula containing the different tunneling times. In particular, we demonstrate that this relation is reduced to the equation for the tunneling time at normal incidence, corresponding to uncoupled modes. We present analytical expressions for the transmission, reflexion, interference, and dwell times, for both, longitudinal and transversal modes. We show that the interference time is a dwell time associated with the interference effect in front or behind the barrier. As an additional complement, analysis for the vibrational energy and for the energy density flux of the system is considered. We carried out numerical calculations based on the transfer-matrix method. This study is easily extrapolated to other systems, and our results could be useful for the design of acoustic devices.

REFERENCES

1. De León-Pérez, F. and R. Pérez-Álvarez, *Phys. Rev. B*, Vol. 63, 245304, 2001.
2. De León-Pérez, F. and R. Pérez-Álvarez, *Phys. Rev. B*, Vol. 61, 4820, 2000.
3. Villegas, D., F. de León-Pérezand R. Pérez-Álvarez, *Phys. Rev. B*, Vol. 71, 035322, 2005.

Fabrication of Large Area Metamaterials for Acoustic Attenuation

Sung Ho Lee[1], **Ji Hoon Lee**[1], **Jeong Hyeon Lee**[1], **Hoon Eui Jeong**[2], **Jun-Ho Choi**[3], **and Moon Kyu Kwak**[1]

[1]School of Mechanical Engineering
Kyungpook National University, 1370 Sankyuk-dong, Buk-gu, Deagu 702-701, South Korea
[2]Department of Mechanical Engineering
Ulsan National Instititue of Science and Technology, Ulsan 689-798, South Korea
[3]Department of Fire Protection Engineering
Pukyong National University, Busan 608-737, South Korea

Abstract— We report the development of film type acoustic metamaterials by utilizing micro scale resonators. In detail, we show the establishment of fabrication techniques for micro resonator by using photolithography and replication processes. Throughout the research, we have verified geometrical, material properties of metamaterials and target sound properties for better optimizing acoustic attenuation. We observed micro-structured resonator has acoustic attenuation at specific frequency range and absorbing resonant frequency can be adjust as change the resonator's geometrical values. Also, we developed mass production system by overcoming traditional wafer scale fabrication system by using visually tolerable tiling method and roll to roll imprint system. Ultimately, we hope to apply these acoustic metamaterials to various applications such as national defence area and medical field.

Airborne Acoustic Transmission through Compound Arrays of Subwavelength Slits

G. P. Ward, A. P. Hibbins, and J. R. Sambles
Electromagnetic and Acoustic Materials Group, Department of Physics and Astronomy
University of Exeter, Stocker Road, Devon, EX4 4QL, UK

Abstract— The angular dependence of the transmission of sound in air through four different arrays of 2D slit-cavities formed from aluminium slats is explored, both experimentally and numerically. For a simple array of geometrically identical and equally spaced slits, it is well known that Fabry-Perot-like wave-guide resonances, supported by the slit-cavities, result in 'Enhanced Acoustic Transmission' at frequencies determined by the length, width and separation of each slit-cavity [1, 2]. We demonstrate that altering the spacing or width of some of the slits (i.e., the structure factor) to form a compound array results in sharp dips in the transmission spectra, that may have a strong angular dependence. These features correspond to 'phase resonances', which have been studied extensively in the electromagnetic case [3, 4]. The introduction of structure factor to each array period allows additional near-field configurations, whereby the field in adjacent cavities can be out-of-phase. Useful insight is gained by employing a surface-wave band-folding picture to describe the phenomena as 'Spoof Acoustic-Surface-Waves' (SASWs) propagating along a very deep grating structure, that arise from the strong coupling of Fabry-Perot cavity resonances between adjacent slits. One of the structures investigated is optimised to minimise the effect of boundary-layer loss mechanisms present in each slit cavity, thereby achieving broad and deep transmission minima.

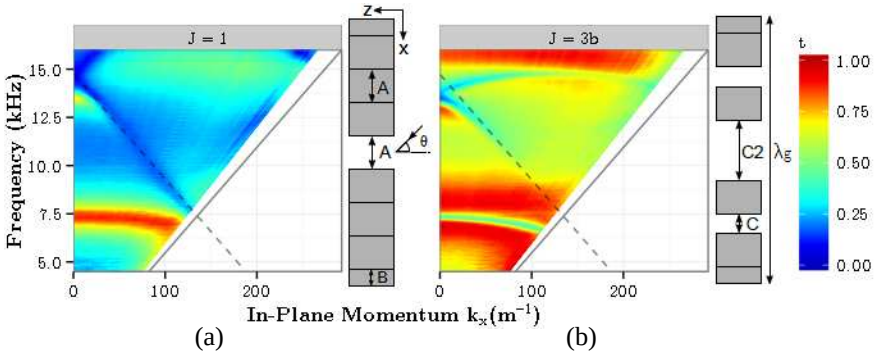

Figure 1: (Schematics) Periodic unit cells for a (a) simple and (b) compound array structure. The grey blocks represent the aluminium slats that form the sample walls. Labelled dimensions are $B = A/2$, $A = 2.9\,\text{mm}$, $L = 19.8\,\text{mm}$, $C2 = 5.9\,\text{mm}$, $C = 1.5\,\text{mm}$ and $\lambda_g = 23.3\,\text{mm}$. (Colour Plots) The corresponding experimentally recorded transmission of sound (colour scale) through each sample, plotted as a function of frequency vs in-plane momentum ($k_x = k_0 \sin(\theta)$). For reference, a solid line representing grazing incidence k_0 is included on each plot. The first order diffracted sound line k_g calculated from the unit cell periodicity is represented by the black dashed line.

REFERENCES

1. Christensen, J., L. Martin-Moreno, and F. J. Garcia-Vidal, "Theory of resonant acoustic transmission through subwavelength apertures," *Phys. Rev. Lett.*, Vol. 101, No. 1, 014301, 2008.
2. Lu, M. H., X. K. Liu, L. Feng, J. Li, C. P. Huang, Y. F. Chen, Y. Y. Zhu, S. N. Zhu, and N. B. Ming, "Extraordinary acoustic transmission through a 1D grating with very narrow apertures," *Phys. Rev. Lett.*, Vol. 99, No. 17, 174301, 2007.
3. Hibbins, A. P., I. R. Hooper, M. J. Lockyear, and J. R. Sambles, "Transmission resonances of metallic compound gratings with subwavelength slits," *Phys. Rev. Lett.*, Vol. 96, No. 25, 257402, 2006.
4. Skigin, D. C. and R. A. Depine, "Transmission resonances of metallic compound gratings with subwavelength slits," *Phys. Rev. Lett.*, Vol. 95, No. 21, 217402, 2005.

Session 3A2
SC2&3: Manipulating and Control of Light-matter Interactions with 2D Materials and Meta-Materials

Graphene Plasmonics and Beyond

Tony Low
University of Minnesota, USA

Abstract— I will review our recent work on graphene plasmonics and nanophotonics based on other 2D materials, such as black phosphorus, transition metal dichalcogenides, boron nitrides and their heterostructures.

Strong Absorption in a 2D Materials-based Spiral Nanocavity

Mohammad H. Tahersima and Volker J. Sorger
Department of Electrical and Computer Engineering, The George Washington University
Washington, D.C. 20052, USA

Abstract— Recent investigations of semiconducting two-dimensional (2D) transition metal dichalcogenides have provided evidence for strong light absorption relative to its thickness attributed to high density of states. Stacking a combination of metallic, insulating, and semiconducting 2D materials enables functional devices with atomic thicknesses. While photovoltaic cells based on 2D materials have been demonstrated, the reported absorption is still just a few percent of the incident light due to their sub-wavelength thickness leading to low cell efficiencies. Here we show that taking advantage of the mechanical flexibility of 2D materials by rolling a molybdenum disulfide (MoS_2)/graphene (Gr)/hexagonal Boron Nitride (hBN) stack to a spiral solar cell allows for solar absorption up to 90%. The optical absorption of a 1 m long hetero-material spiral cell consisting of MoS_2, graphene and hBN is about 50% stronger compared to a planar MoS_2 cell of the same thickness; although the ration of the absorbing material, here Gr and MoS_2, relative to the cell volume is only 6%. We anticipate these results to provide guidance for photonic structures that take advantage of the unique properties of 2D materials in solar energy conversion applications.

Hyperbolic Media

Zubin Jacob
Department of Electrical and Computer Engineering
University of Alberta, Edmonton, AB T6G 2V4, Canada

Abstract— We review the recent progress in the field of hyperbolic media and in particular the exciting developments of hyperbolic modes in graphene multilayers and hexagonal boron nitride.

Polaritons, collective excitations of light and matter are uniquely poised to usher a generation of applications beyond the reach of conventional electronics and photonics. From exciton-polaritons combining semiconductor electron-hole pairs with light for low threshold lasing [1] to plasmon-polaritons which mix metallic free electrons and photons for nanoconfinement [2], unique applications exist for each polariton. Recent discovery of strongly confined phonon-polaritonic modes in hexagonal boron nitride (hBN) can usher in new imaging, thermal and quantum applications in the mid-infrared wavelength region [3–5].

Phonon-polaritons are collective oscillations of phonons (lattice vibrations) and light in polar dielectrics such as silicon carbide (SiC), silicon oxide (SiO_2) and strontium titanate ($SrTiO_3$). The characteristic frequencies at which these modes occur are related to the ionic mass ($\omega \propto 1/\sqrt{M_{ion}}$) and fall in the mid-infrared wavelength range for most materials. The dielectric permittivities take on unique forms at phonon-polaritonic resonances either passing through a zero ($\varepsilon \approx 0$) or being enhanced to large values at a pole ($\varepsilon \gg 1$). In between the epsilon-near-zero (ω_{LO}) and epsilon-near-pole (ω_{TO}) frequencies, these naturally occurring media behave like a simple conventional metal and strongly reflect incident radiation. This range of frequencies is called the "Reststrahelen band" which is forbidden for propagating rays of light.

However recent work has shed light on fundamentally interesting phenomena precisely within this forbidden band of a unique phonon-polaritonic medium: hBN. The weak Van der Waals bonded nature makes this medium optically anisotropic due to different effective masses of phonons along the crystal axes. An unusual anisotropy leads to dielectric responses of opposite signs in perpendicular directions ($\varepsilon_{\parallel}\varepsilon_{\perp} < 0$). This gives rise to hyperbolic polaritons within the bulk medium allowing electromagnetic modes to propagate in the forbidden band which is not possible for conventional polar dielectrics. The word hyperbolic derives from the topology of the isofrequency surface which is a hyperboloid in contrast to a closed sphere as in conventional dielectric media [6, 7].

I will discuss many of the above properties and multiple new directions for the field.

REFERENCES

1. Bhattacharya, P., et al., "Room temperature electrically injected polariton laser," *Phys. Rev. Lett.*, Vol. 112, 236802, 2014.
2. Nikolajsen, T., K. Leosson, and S. I. Bozhevolnyi, "Surface plasmon polariton based modulators and switches operating at telecom wavelengths," *Appl. Phys. Lett.*, Vol. 85, 5833–5835, 2004.
3. Caldwell, J. D., et al., "Sub-diffractional volume-confined polaritons in the natural hyperbolic material hexagonal boron nitride," *Nat. Commun.*, Vol. 5, 2014.
4. Dai, S., et al., "Tunable phonon polaritons in atomically thin Van der Waals crystals of boron nitride," *Science*, Vol. 343, 1125–1129, 2014.
5. Xu, X. G., et al., "One-dimensional surface phonon polaritons in boron nitride nanotubes," *Nat. Commun.*, Vol. 5, 2014.
6. Smith, D. R., P. Kolinko, and D. Schurig, "Negative refraction in indefinite media," *J. Opt. Soc. Am. B*, Vol. 21, 1032–1043, 2004.
7. Podolskiy, V. A. and E. E. Narimanov, "Strongly anisotropic waveguide as a nonmagnetic left-handed system," *Phys. Rev. B*, Vol. 71, 201101, 2005.

Metamaterials for Solar Energy Conversion and Chiral Sensors

Vivian Ferry
Department of Chemical Engineering and Materials Science
University of Minnesota, 421 Washington Ave SE, Minneapolis, MN 55455, USA

Abstract— The combination of plasmonics and metamaterials with tunable materials offers new possibilities to manipulate optical and device properties. This talk will discuss the integration of plasmonics into two application areas: solar energy conversion, and chiral nanoscale structural sensors.

The first part will focus on combining photonic structures with semiconductors to enhance solar energy conversion, and particularly on the design, fabrication, and characterization of luminescent solar concentrators. In a standard LSC, light is absorbed by a dye and re-emitted at a longer wavelength which is guided by total internal reflection to an adjacent solar cell. LSCs offer many benefits compared to traditional concentrator designs, including the ability to operate under both direct and diffuse incident sunlight, but are limited by parasitic losses. I will discuss recent efforts to improve the concentration ratio of LSCs by combining narrow emission band light emitters with wavelength-selective photonic structures.

The second portion of the talk will focus on tunable chiral metamaterials. Using DNA as a scaffold, we self-assemble nanoparticles into chiral geometries where the circular dichroism response arises from the spatial arrangement of nanoparticles rather than the DNA. These structures can be made tunable by targeting interactions to specific DNA sequences, thereby changing the distances between nanoparticles in the chiral assembly. These assemblies can be used as nanoscale distance sensors, as the wavelength, intensity, and sign of the CD spectra all encode information about the nanoscale distances that are present. Through small structural modifications, these assemblies can be made to flip handedness. In this geometry, CD spectra also arise from interactions between nonresonant nanoparticles, and we show how different combinations of materials produce spectroscopic signatures.

Exact Solution for the Reflectivity of Grapheme at Nonzero Temperature over the Wide-band Frequency Range

Victor Petrov[1], **Michael Bordag**[2], **Galina Klimchitskaya**[3], **and Vladimir Mostepanenko**[3]

[1] Institute of Physics, Nanotechnology and Telecommunications
St.-Petersburg Politechnical University, Russia
[2]Institute for Theoretical Physics, Leipzig University, Germany
[3]Central Astronomical Observatory at Pulkovo of the Russian Academy of Sciences, Institute of Physics Nanotechnology and Telecommunications, St.-Petersburg Politechnical University, Russia

Abstract— The quantum field theoretical consideration for the reflectivity of graphene will be presented. This consideration exploits the polarization tensor of graphene at nonzero temperature in (2+1)-dimensional space-time. The obtained form of polarization tensor possesses the required analytic properties over the entire plane of complex frequencies. At zero temperature obtained tensor coincides with that obtained in [1]. At nonzero temperature it takes the same values as the one obtained in [2] at all Matsubara frequencies. This justifies all numerous applications of the polarization tensor [1, 2] used for calculation of the Casimir interaction for graphene and graphene-coated substrates [2–4]. However, as will be shown in our report, the polarization tensor [2] is an oscillating function along the imaginary frequency axis, and this precludes the use of its analytic continuation to real frequency axis for further theoretical description. In our case, the obtained form of the polarization tensor is a monotonously decreasing function of the imaginary frequencies and admits the analytic continuation to real frequency axis satisfying all physical requirements.

The analytic expressions for the reflection coefficients and reflectivities of graphene for two independent polarizations for high and low frequencies were obtained by us using the derived form of the polarization tensor at nonzero temperature. Finally, we have performed numerical computations of the TM and TE reflectivities of graphene over the wide frequency range.

REFERENCES

1. Bordag, M., I. V. Fialkovsky, D. M. Gitman, and D. V. Vassilevich, "Casimir interaction between a perfect conductor and graphene described by the dirac model," *Phys. Rev. B*, Vol. 80, 245406, 2009.
2. Fialkovsky, I. V., V. N. Marachevsky, and D. V. Vassilevich, "Finite-temperature casimir effect for graphene," *Phys. Rev. B*, Vol. 84, 035446, 2011.
3. Klimchitskaya, G. L. and V. M. Mostepanenko, "Observability of thermal effects in the casimir interaction from graphene-coated substrates," *Phys. Rev. A*, Vol. 89, 052512, 2014.
4. Klimchitskaya, G. L., V. M. Mostepanenko, and V. M. Petrov, "Reflectivity properties of graphene and graphene-coated substrates," *Internet of Things, Smart Spaces, and Next Generation Networks and Systems*, Eds.: Balandin S., Andreev S., Koucheravy Y., 451–458, Springer, Cham, 2014.

Active 2D Material-based Nanophotonic Devices for Optical Interconnects

Ren-Jye Shiue[1], **Yuanda Gao**[2], **Cheng Peng**[1],
Dmitri Efetov[1], **James Hone**[2], **and Dirk Englund**[1]

[1]Research Laboratory of Electronics, Massachusetts Institute of Technology, Cambridge, MA, USA
[2]Columbia University, New York, NY, USA

Abstract— The past decades have seen concerted efforts to combine optical and electrical components into optoelectronic integrated circuits for a range of applications, including optical interconnects, sensing, and signal processing. The leading architectures for electro-optic integration today are based on bulk semiconductor materials — for example, for detectors, predominantly bulk Ge, InP, and InGaAs. However, the integration of bulk semiconductor-based detectors has faced important challenges, including for instance the need for frontend changes in complementary metal-oxide-semiconductor (CMOS) processing, fixed spectral response due to material's bandgap, and an intrinsic speed limited by material's carrier mobility. In addition, optical nonlinearities are typically low in bulk semiconductor materials. Recently, the family of twodimensional (2D) materials has been shown to offer new functionalities for optoelectronic applications, including onchip electro-optic modulation, ultrafast broadband photodetection, light emission, and non-parametric and parametric nonlinearities. Moreover, it has been shown that different types of 2D materials can be assembled nearly defect-free into entirely new types of 2D heterostructures, producing optoelectronic properties and device concepts that were not feasible or very difficult using bulk semiconductors.

Here, we describe recent work on 2D materials and 2D heterostructures for on-chip photodetectors, modulators, and light emitters in photonic integrated circuits, see Figure 1. First, we discuss a new type of waveguide-integrated photodetector consisting of a single-layer graphene (SLG) encapsulated by hexagonal boron nitride (hBN) that enables both high-responsivity photodetection and ultrafast pulse measurements in a compact and efficient waveguide-integrated design [1, 2]. Second, we discuss a high-speed graphene electro-optic modulator design based on a SLG-hBN heterostructure integrated with a silicon photonic crystal nanocavity. Strongly enhanced light-matter interaction of graphene in this sub-wavelength cavity enables efficient electrical tuning of the cavity reflection with a modulation depth of 3.2 dB and a cut-off frequency in excess of 1 GHz [3]. Finally, we describe how nanophotonic device concepts for slow-light and modification of radiative rates via the nanocavity Purcell effect can be used to enhance light emission from 2D materials [4].

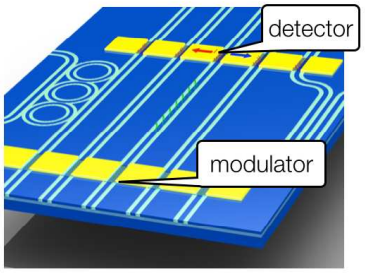

Figure 1: 2D materials-based active electrooptic components on a photonic integrated circuit.

REFERENCES

1. Shiue, R.-J., et al., "High-responsivity graphene photodetector and autocorrelator on a CMOS compatible photonic integrated circuit," 2015, to be submitted.
2. Gan, X., et al., "Chip-integrated ultrafast graphene photodetector with high responsivity," *Nature Photonics*, 2013.
3. Gao, Y., et al., "High-speed electro-optic modulator integrated with graphene-boron nitride heterostructure and photonic crystal nanocavity," *Nano Letters ASAP*, 2015.

4. Gan, X., et al., "Controlling the spontaneous emission rate of monolayer MoS_2 in a photonic crystal nanocavity," *Applied Physics Letters*, Vol. 103, No. 18, 2013.

A Numerically Stable Model of Eccentrically Metamaterial Coated Wire Antenna

Emrah Sever[1], **Fatih Dikmen**[1], **and Cumali Sabah**[2]

[1]Electronics Engineering Department, Gebze Technical University, Kocaeli, Turkey
[2]Electrical and Electronics Engineering Department
Middle East Technical University, Northern Cyprus Campus
Kalkanli, Guzelyurt, 99738, TRNC/Mersin 10, Turkey

Abstract— Nowadays, there is an increase in the interest of the metamaterials (MTMs) and their applications and this development has already altered the direction of the electromagnetic wave scattering including cylindrical media. This is an important development in the field since these types of structures can open a new way to design and characterize novel devices based on MTMs. In this manner, a frequency dispersive MTM scatterer [1], the case of a metallic cylinder coated by MTM [2], the fields in a multilayered cylinder containing MTMs, multiple scattering by MTM cylinders, and scattering by two MTM cylinders have been already investigated by different researchers. In [3] it is shown that the proper posing of the scattering problem necessitates originating the standing and travelling wave Rayleigh modes in the circular cylindrical regions from the Green's integral formulae. The truncation of the obtained linear algebraic equations via such approach requires physical check of the boundary conditions to obtain a reasonable solution. But via regularization, this requirement is alleviated and the solution becomes immune to the round-off errors [4, 5]. In this study, this new numerically stable version of modal scattering formulation of circularly cylindrical boundaries is applied to the problem of scattering by an eccentrically metamaterial coated wire antenna where wire is assumed perfectly conducting. Here, all formulations will be for the TM mode since the main focus does not differ from the corresponding TE mode formulations. The stability of the algorithm which is free from checking of the boundary conditions [1] and special considerations on geometry to ensure convergence [2], under various metamaterial parameters and different geometries and a wide frequency range will be demonstrated.

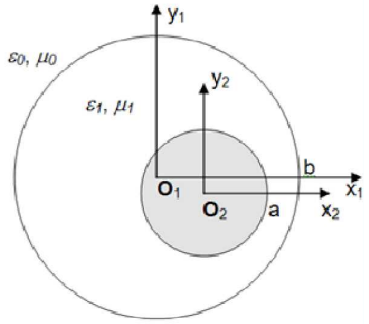

Figure 1: MTM covered ($\varepsilon_1,\ \mu_1$) PEC wire (grey circle) in free space ($\varepsilon_0,\ \mu_0$).

REFERENCES

1. Valagiannopoulos, C. A., "Electromagnetic scattering from two eccentric metamaterial cylinders with frequency-dependent permittivities differing slightly each other," *Progress In Electromagnetics Research B*, Vol. 3, 23–34, 2008.
2. Mushref, M. A., "Closed solution to electromagnetic scattering of a plane wave by an eccentric cylinder coated with metamaterials," *Optics Communications*, Vol. 270, 441–446, 2007.
3. Ioannidou, M. P., K. D. Kapsalas, and D. P. Chrissouludis, "Electromagnetic-wave scattering by an eccentrically stratified, dielectric cylinder with multiple, eccentrically stratified, cylindrical, dielectric inclusions," *Journal of Electromagnetic Waves and Applications*, Vol. 18, No. 4, 495–516, 2004.
4. Dikmen, F., E. Sever, S. Vatansever, and Y. A. Tuchkin, "Well-conditioned algorithm for scattering by a few eccentrically multilayered dielectric circular cylinders," *Radio Science*, accepted, DOI: 10.1002/2014RS005501, 2015.

5. Sever, E., F. Dikmen, O. A. Suvorova, Y. A. Tuchkin, "An analytical formulation with ill-conditioned numerical scheme and its remedy: Scattering by two circular impedance cylinders," *Turk. J. Elec. Eng. & Comp. Sci.*, 2014, accepted, DOI:10.3906/elk-1312-262.

Probing Graphene-nanoparticle Interactions via Hot Carrier Dynamics

Adam Gilbertson, Yan Francescato, Viktoryia Shautsova, Vincenzo Giannini, Stefan A. Maier, Lesley F. Cohen, and Rupert F. Oulton
Blackett Laboratory, Imperial College London, Prince Consort Rd, SW7 2BZ, UK

Abstract— Hybrid graphene-metal plasmonic systems exploit the near-field coupling between graphene carriers and surface plasmon (SP) excitations supported in the metal, and are emerging as a class of optical metamaterials that facilitate strong light-matter interactions and are of potential importance for hot carrier graphene-based light harvesting [1] and active plasmonic applications [2, 3]. Central to the physics of such systems are plasmon-induced hot carriers, generated directly in the graphene via the intense near-fields and in the metal nanoparticle (NP) via absorption (plasmon decay). However, a complete understanding of the near-field interaction between graphene and nearby plasmonic nanoparticles is lacking.

In this talk, we report the plasmon-induced hot carrier dynamics of a hybrid metal-graphene system consisting of a gold plasmonic nanodisk resonators coupled to a graphene overlayer. Nanodiscs are an ideal test structure due to their ease of fabrication that allows close packing and readily tunable dipole resonance that couples strongly to the far-field. By selectively probing the photocarrier dynamics in the graphene layer, following excitation at the SP band of the NP array, we gain direct access to the influence of graphene-NP interactions on the transient hot carrier population in the graphene. In order to distinguish between plasmon-induced hot carrier generation processes we compare samples where graphene is in direct contact with the metal NP (sample A) to those in which a hexagonal boron nitride (BN) monolayer has been introduced at the graphene-metal interface (sample B), shown schematically in Fig. 1a. The BN spacer layer serves as an effective barrier to charge transfer, while being just angstroms thick it has little effect on the plasmon-mediated electromagnetic field intensity at the graphene (verified by numerical simulations). We demonstrate that direct near-field photo-excitation is the dominant process for plasmon-induced hot carrier generation in the graphene and gives rise to a strong optical anisotropy in the hybrid samples, absent in bare graphene and NP control samples, as revealed by polarisation-resolved measurements. Intrinsic optical anisotropy, driven by the preferential occupation of specific states in k-space through to the carrier-field interaction, is known to occur in various semiconductors including graphene, but is generally short lived due to fast carrier-phonon scattering (~ 100 fs) that redistributes the photo-carrier momentum. Here we show that the strong optical near-field coupling of graphene to plasmonic NPs underpins a long lived extrinsic optical anisotropy. The effect arises from the action of highly localised hot carriers in the graphene on the sub-resonant NP polarisability, and persists for several 100 fs, determined by the diffusion of hot carriers away from hot-spots. Our observations highlight the rich physics associated with the graphene-NP interaction, and the potential to exploit plasmonic metal-graphene nanostructures in photo-thermoelectric applications.

REFERENCES

1. Koppens, F. H. L., T. Mueller, P. Avouris, A. C. Ferrari, and M. S. Vitiello, *Nature Nanotechnology*, Vol. 9, No. 10, 780–793, 2014.
2. Brongersma, M. L., N. J. Halas, and P. Nordlander, *Nature Nanotechnology*, Vol. 10, No. 1, 25–34, 2015.
3. Yao, Y., M. A. Kats, R. Shankar, Y. Song, J. Kong, M. Loncar, and F. Capasso, *Nano Letters*, Vol. 14, No. 1, 214–219, 2014.

Faraday Rotation in Periodic Graphene Structures

L. Martin-Moreno[1], **T. M. Slipchenko**[1], **and A. Yu. Nikitin**[2]

[1]Instituto de Ciencia de Materiales de Aragon, Zaragoza, Spain
[2]CIC nanoGUNE Consolider, Donostia, San Sebastian, Spain

Abstract— It is known that a graphene sheet, under the action of a perpendicular static magnetic field, provides a Faraday rotation that, per atomic layer, is much larger than that of any other known material [1]. The Faraday rotation in continuous graphene originates from the cyclotron resonance of massless carriers, which in turn depends on the carrier concentration. This property allows for dynamical tuning of the Faraday angle through either external electrostatic or magneto-static setting. Furthermore, the rotation direction can be controlled by changing the sign of the carriers in graphene, which can be done by means of an external electric field.

However, large Faraday rotation in the THz regime still requires large magnetic fields. In a previous work [2], we demonstrated that the needed magnetic field can be reduced in arrays of graphene microribbons (alternatively the working frequency can be larger for a given applied magnetic field) through the excitation of the magnetoplasmons of individual ribbons. This 1D geometry is just one of the many possibilities which can lead to useful Graphene-based non-reciprocal devices, for which the fundamental limits set by physical constrains [3] do not severely limit useful applications. For instance, recently, it has been shown that strong Faraday rotation can be achieved in lattices of graphene meta-atoms [4].

In this talk we consider the general situation of a 2D periodic metamaterial, and relate the Faraday rotation resonances to the excitation of the different magnetoplasmon modes that can be excited in the system.

ACKNOWLEDGMENT

We acknowledge support by the Spanish Ministerio de Economia y Competitividad within Project No. MAT2011-28581-C02 and the EC under Graphene Flagship (Contract No. CNECT-ICT-604391).

REFERENCES

1. Crassee, I., J. Levallois, A. L. Walter, M. Ostler, A. Bostwick, E. Rotenberg, T. Seyller, D. van der Marel, and A. B. Kuzmenko, "Giant faraday rotation in single- and multilayer graphene," *Nat. Phys.*, Vol. 7, 48–51, 2010.
2. Tymchenko, M., A. Y. Nikitin, and L. Martin-Moreno, "Faraday rotation due to excitation of magnetoplasmons in graphene microribbons," *ACS Nano*, Vol. 11, 9780–9787, 2013.
3. Tamagnone, M., A. Fallahi, J. R. Mosig, and J. Perruisseau-Carrier, "Fundamental limits and near-optimal design of graphene modulators and non-reciprocal devices," *Nat. Photonics*, 1–13, 2014.
4. Hadad, Y., A. R. Davoyan, N. Engheta, and B. Z. Steinberg, "Extreme and quantized magneto-optics with graphene meta-atoms and metasurfaces," *ACS Photonics*, Vol. 1, 1068–1073, 2014.

Perfect Extinction of Terahertz Waves in Monolayer Graphene over 2-nm-wide Coaxial Apertures

Hyeong-Ryeol Park[1], **Seon Namgung**[1], **Xiaoshu Chen**[1], **Nathan C. Lindquist**[2], **Vincenzo Giannini**[3], **Yan Francescato**[3], **Stefan A. Maier**[3], **and Sang-Hyun Oh**[1]

[1]Department of Electrical and Computer Engineering, University of Minnesota, Minneapolis, United States
[2]Physics Department, Bethel University, Saint Paul, United States
[3]Department of Physics, Imperial College London, London, United Kingdom

Abstract— Two-dimensional (2D) materials such as graphene possess unique electrical and optical properties that are not present in bulk materials. Due to their atomic-scale thickness, however, 2D materials usually interact only weakly with electromagnetic waves, presenting challenges for realizing high-performance optoelectronic devices. This work demonstrates that by confining light into ultra-small metallic gaps, it is possible to dramatically boost this interaction with graphene. As an extreme case, terahertz (THz) waves are squeezed into gaps about 10^5 times smaller, allowing them to interact with 99% efficiency with a 0.3 nm-thick graphene layer.

To realize this experiment, we used atomic layer lithography to define 2-nm-wide gaps in a thin gold film. While the resulting gaps cover only 0.002% of the sufrace, 25% of incident THz energy passes through the metal film. Surprisingly, placing a monolayer graphene at the exit side of these gaps without an Al_2O_3 spacer allows 99% THz extinction leading to a reduction by another 2 orders of magnitude at the resonance, while the graphene on the bare substrate shows a typical extinction of $\sim$ 20% over a broad THz frequency range. This huge extinciton is mostly caused by strong absorption near the nanogaps.

As an application of this strong absorption, we also demonstrate high-contrast modulation of THz transmission using monolayer graphene. We constructed an electrically controllable hybrid material platform, consisting of the 2-nm-wide annular gaps, monolayer graphene, and an ionic gel layer. The enhanced intraband absorption in the graphene leads to a very large modulation depth of 80% with an operational voltage as low as 1.5 V. In addition to graphene, such ultra-strong light-matter interactions mediated by nanogap structures could benefit a wide range of applications involving 2D materials.

REFERENCES

1. Park, H.-R., S. Namgung, X. Chen, N. C. Lindquist, V. Giannini, Y. Francescato, S. A. Maier, and S.-H. Oh, "Perfect extinction of terahertz waves in monolayer graphene over 2-nm-wide metallic apertures," *Adv. Opt. Mater.*, DOI: 10.1002/adom.201400546, 2015.
2. Chen, X., H.-R. Park, M. Pelton, X. Piao, N. C. Lindquist, H. Im, Y. J. Kim, J. S. Ahn, K. J. Ahn, N. Park, D.-S. Kim, and S.-H. Oh, "Atomic layer lithography of wafer-scale nanogap arrays for extreme confinement of electromagnetic waves," *Nature Communications*, Vol. 4, 2361, 2013.

Photothermal Microbubbles-assisted Optofluidic Control

Jiapeng Zheng[1], **Kezhang Shi**[1], **Jianxin Yang**[1], **Xijun Li**[1], **Meng Shi**[2], **Sailing He**[1], **and Xiaobo Xing**[1, 3]

[1]Centre for Optical and Electromagnetic Research
South China Normal University, Guangzhou 510006, China
[2]Shandong Provincial Key Laboratory of Laser Polarization and Information Technology
Laser Institute, Qufu Normal University, Qufu 273165, China
[3]Education Ministry's Key Laboratory of Laser Life Science & Institute of Laser Life Science
College of Biophotonics, South China Normal University, Guangzhou 510631, China

Abstract— Optofluidics, the science and technology of integrating optical systems with fluids, have been demonstrated a wide range of applications in areas including analytical chemistry, biotechnology sensing, nanofluidic concentration, DNA manipulation, and virus detection. Optofluidic systems can synthesize the advantages of hydrodynamics and optics such as reduced sample consumption, improved sensitivity and detection time, representing a new evolution of microfabrication techniques. Over the past decade, optofluidic systems can be categorized into three major groups: (1) A fluids-in-solids system by introducing fluids with specific optical properties into the porous solid to elicit changeable optical effects. (2) A fluids-in-fluids system by mixing fluids in other fluids with relevant optical properties to enhance the controllability and flexibility of the resulting system. (3) A solids-in-fluids system by manipulating solid particles in a fluid to enable large changes in the optical properties of the resulting system. And its development requires more novel devices to outreach the other application fields and deepen the fundamental research. This we present and demonstrate a simple optofluidic device served by assembling graphene oxide (GO) into micro/nanofibers (MNFs). By integrating the excellent absorption and scattering properties of GO with attractive waveguide dispersions of MNFs, it is possible to elicit the extraordinary photothermal effect from GO under light illumination. The controllable vapor microbubbles can be generated from the excited GO. Theoretical and experimental studies show that thermocapillary convection can be initiated by the microbubbles to manipulate particles.

ACKNOWLEDGMENT

This work is partially supported by the National Natural Science Foundation of China (Nos. 61177077, 1104162, 21476052, 91233208, 61178062), the Guangdong Natural Science Foundation (2013B090500123, 2014A030313432), the Guangdong Innovative Research Team Program (Grant 201001D0104799318), the National High Technology Research and Development Program (863 Program) of China (No. 2012AA012201), Swedish VR grant (# 621-2011-4620) and AOARD.

Modified Periodic Method of Moments for the Analysis and Design of Metasurfaces Consisting of 2D Materials

Arya Fallahi
DESY-Center for Free-Electron Laser Science, Notkestrasse 85, Hamburg D-22607, Germany

Abstract— A full-vector semi-analytical numerical technique for the analysis of metasurfaces made out of 2D materials is presented. The method is based on the periodic method of moment for the analysis of general frequency selective surfaces. The required modifications to consider the anisotropic conductivity model as well as the spatial dispersion are described. The paper is intended to serve as a general and complete reference for modeling planar metamaterials containing 2D materials. Therefore, the various computational aspects of the method, such as effect of basis functions type and combination with transmission line model for studying periodically inhomogeneous substrates, are also investigated. As the choice for the 2D materials, we mainly focus on graphene and black phosphorous. Through the analysis of some examples, the properties of a periodic structure containing the aforementioned 2D materials are investigated.

Nano-resolving the Optical and Electronic Properties of Graphene Encapsulated in Boron Nitride

M. B. Lundeberg
The Institute of Photonic Sciences (ICFO), Spain

Abstract— Since a couple of years, a new dry transfer method has been producing clean heterostructures of graphene encapsulated in hexagonal boron nitride (BN). The graphene in these devices shows exceptional electronic quality, with carrier mobilities no longer limited by disorder.

Besides the improvement in DC electrical properties seen in these heterostructures, improvement is likewise expected for the optical, or AC, response. In particular, graphene's propagating plasmons were observed to damp out quickly in traditional graphene devices, a consequence of the high electronic resistance. We show with scanning near field optical microscopy (SNOM) that the plasmons in BN-graphene heterostructures show a dramatic improvement in propagation time, approaching the intrinsic limits at room temperature [1, 2]. The measurements also demonstrate the extreme size confinement for plasmons, enhanced by the high permittivity environment offered by BN.

Time permitting, other practical aspects of encapsulated graphene devices will be discussed: conductivity inhomogoneities, and induced photocurrents.

REFERENCES

1. Woessner, A., et al., "Highly confined low-loss plasmons in graphene–boron nitride heterostructures," *Nature Materials*, Vol. 14, 421, 2014, Doi: 10.1038/nmat4169.
2. Principi, A., et al., "Plasmon losses due to electron-phonon scattering: The case of graphene encapsulated in hexagonal boron nitride," *Phys. Rev. B*, Vol. 90, 165408, 2014, Doi: 10.1103/PhysRevB.90.165408.

Session 3A3
SC3: Silicon Photonics — Novel Materials, Hybrid Integration, Sensors and Nonlinear Devices

Experimental Measurement of Nonlinear Phenomenain Silicon Waveguides

S. Serna[1,2], **W. Zhang**[1], **X. Le Roux**[1], **L. Vivien**[1], **N. Dubreuil**[2], **and E. Cassan**[1]

[1]Institut d'Electronique Fondamentale, CNRS UMR 8622, Université Paris-Sud 11
Bat. 220, 91405 Orsay Cedex, France
[2]Laboratoire Charles Fabry, Institut d'Optique, CNRS, Université Paris-Sud 11
2 Avenue Augustin Fresnel, 91127 Palaiseau Cedex, France

Abstract— The main drawback of silicon for nonlinear application is its absence of second order nonlinear effects ($\chi^{(2)}$) and the strong free-carrier phenomena (Free Carrier Dispersion: FCR, Free Carrier Absorption: FCA) accompanying the Kerr effect when using $\chi^{(3)}$-processes.To overcome this problem, the design and fabrication of Silicon guiding structures under different geometries is reported with particular emphasis in Slot Photonic Crystal Waveguides [1, 2]. The latest offers a natural potential for nonlinear $\chi^{(3)}$ optical applications, due to the strong enhancement of the electric field in the slot region and further more in the slow light regime.Chosen according to its second and third order non-linear susceptibilities $\chi^{(2)}$ and $\chi^{(3)}$, the low index material that fills the slot and the holes can dramatically enhance the non-linear effects in the photonic crystal waveguides. $\chi^{(2)}$ electro-optic modulation in slotted photonic crystals and $\chi^{(3)}$ Four-Wave Mixing in slot waveguides have been for instance, successfully demonstrated [2, 3].

The samples under analysis consist of SOI wafers (Soitec) with a 260 nm-thick silicon film over 2 µm of buried oxide. Patternsare defined in ZEP-520A resist (Zeon Chemical Co.) by 80 kV electron beam lithography (Nanobeam nb4 system) and then etched by Inductive Coupling Plasma Reactive Ion Etching process using SF6 gas. The facets of the sample were finally cleaved after removal of the resist.The surface of the samples is covered by a refractive liquid (Cargille) with an index of 1.46 infiltrating both the holes and the slot. The total length of the sample is 4.5 mm, which includes 3 µm-wide access waveguides intended for end-fire coupling. These waveguides are tapered down along 300 µm to match the 400 nm-wide wire waveguides, which are then connected to the SPCW through a three-stage converter [4]. A SEM image of the structure is shown with a respective zoom in Fig. 1(a), the optical linear transmission for different length SPCW in a wavelength range of 100 nm, starting from 1510 nm until 1610 nm is shown in Fig. 1(b), the transmission of a strip waveguide is added as a reference, allowing to distinguish clearly the light cone effect, the fast and slow light regimes and the bandgap, higher than 20 dB in less than 5 nm.

The nonlinear response of SPCW has been measured under a pulsed excitation of 7 nm bandwidth and duration time of 2 ps varying the input average powers until 15 mW as shown in Fig. 1(c), which given the duty-cycle of the laser correspond to maximum peak powers of around 5 W coupled into the waveguide. Emphasis is put on the slow light properties and the bandgap effect of the investigated waveguide. For instance the asymmetric output spectra, unexpected due to the normally symmetric broadening given by the Kerr effect could be explained by the inhibition due to the forbidden band of the photonic crystal From this analysis the TPA saturation curve could be extracted and compared with the reference strip. These experimental measurements

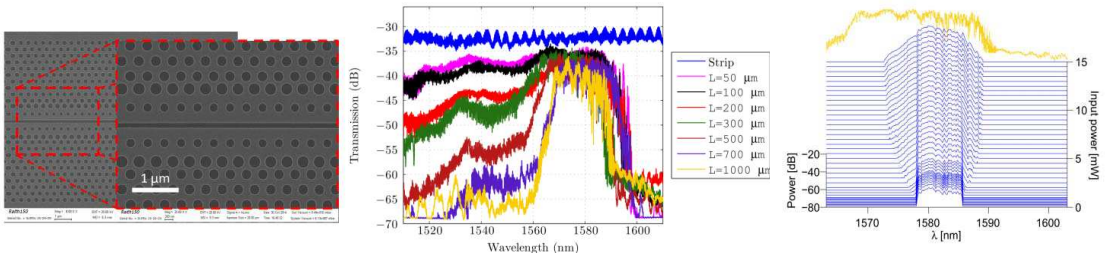

(a) (b) (c)

Figure 1: (a) SEM view of the engineered slot photonic crystal waveguide (SPCW), (b) transmission spectra of different length SPCW with a strip as a reference level and (c) measured output spectra after 1 mm length of light propagation for various input average power levels, in yellow the linear transmission spectrum of the waveguide.

open an interesting discussion about the slow light regime (close to the band edge) that will be detailed during the conference.

REFERENCES

1. Xu, Q., V. R. Almeida, R. Panepucci, and M. Lipson, "Experimental demonstration of guiding and confining light in nanometer-size low-refractive-index material," *Opt. Lett.*, Vol. 29, No. 14, 1626–1628, 2004.
2. Lin, C.-Y., X. Wang, S. Chakravarty, B. S. Lee, W. Lai, J. Luo, A. K.-Y. Jen, and R. T. Chen, "Electro-optic polymer infiltrated silicon photonic crystal slot waveguide modulator with 23 dB slow light enhancement," *Appl. Phys. Lett.*, Vol. 97, 093304-1–3, 2010.
3. Koos, C., P. Vorreau, T. Vallaitis, P. Dumon, W. Bogaerts, R. Baets, B. Esembeson, I. Biaggio, T. Michinobu, F. Diederich, W. Freude, and J. Leuthold, "All-optical high-speed signal processing with silicon-organic hybrid slot waveguides," *Nat. Photon.*, Vol. 3, 216–219, 2009.
4. Caer, C., X. Le Roux, L. Vivien, and E. Cassan, "Dispersion engineered slot photonic crystal waveguides for slow light operation," *Appl. Phys. A*, Vol. 109, 895–899, 2012.

Nonlinear Optimization of Slot Si Waveguides: Effective Mode Area vs FOM_{TPA}

Weiwei Zhang[1], **Samuel Serna**[1,2], **Nicolas Dubreuil**[2], **and Eric Cassan**[1]

[1]Institut d'Electronique Fondamentale, Université Paris-Sud
CNRS UMR 8622, Bat. 220, 91405 Orsay, France
[2]Laboratoire Charles Fabry, Institut d'Optique, CNRS, Université Paris-Sud
2 Avenue Augustin Fresnel, 91127 Palaiseau Cedex, France

Abstract— In the context of the planar silicon photonics technology, optical nonlinear ($\chi^{(3)}$) Kerr effects are every easily obtained by using submicron silicon wires in the telecommunication wavelength window due to a dramatic reduction of the needed power compared with fibres Unfortunately, the third order effects ($\chi^{(3)}$) are partially spoiled due to the strong strength of the two-photon absorption (TPA) effect, which in turn generates free-carriers and induces additional absorption and refractive index changes. The relative competition between the optical Kerr and TPA effects is usually quantified by the use of the figure of merit $FOM_{TPA} = n_2/\alpha_2\lambda$, with n_2 the nonlinear refractive index and α_2 the TPA coefficient.

One of the key solutions to minimize the detrimental effects of free carriers in silicon while still benefiting from the high index core/cladding contrast of silicon on insulator (SOI) waveguides relies on the use of hollow core silicon guiding structures, the so-called slot waveguides [1], filled by highly nonlinear materials, for instance polymers. Under such a guiding geometry, the light power confinement in the silicon rails can be reduced, leading to the reduction of the TPA effect. This approach has received a considerable interest in the last years, showing demultiplexing capabilities of 170 Gbits $\cdot$ s^{-1} data, 100 Gbits $\cdot$ s^{-1}/1 V electro-optical modulation and the demonstration of slot waveguides with FOM_{TPA} up to the record value of 2.19 [2], i.e., far above the intrinsic silicon FOM_{TPA} material value, which is around 0.38 [3].

In this context, we will firstly present results obtained by the conventional optimization method based on minimizing the waveguide mode effective areas A_{eff} (Fig. 1(b)) in order to maximize the nonlinear Kerr coefficient $\gamma = n_2\omega/cA_{eff}$ in the assumption that the introduced nonlinear material dominates the nonlinear behavior of the slotted waveguide and that strong light confinement in the slot allows neglecting TPA process in the silicon rails [4, 5]. On contrary, we will come up in a second step with a semi-analytical approach fully accounted all nonlinear contributions from the different materials on the whole mode profile area in order to investigate the FOM_{TPA} evolution. We will show that FOM_{TPA} can vary from 1.8 to 4.25 in the case that nonlinear cladding material has a bulk FOM_{TPA} of 5. This strategy of nonlinear slot waveguide's design for on-chip all-optical signal processing will be thoroughly discussed at the conference.

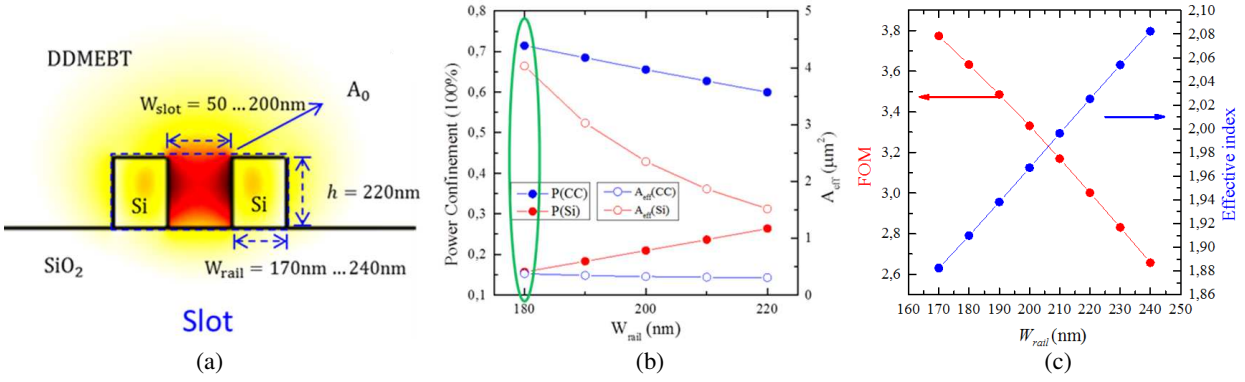

Figure 1: (a) Scheme of SOI slot waveguide geometry configurations, (b) Calculated Power confinement factor (P) and effective mode area (A_{eff}) of cover cladding and Silicon, (c) Calculated effective mode index (n_{eff}) and FOM of slot the waveguides, in case of $W_{slot} = 100$ nm.

REFERENCES

1. Almeida, V. R., Q. Xu, C. A. Barrios, and M. Lipson, *Opt. Lett.*, Vol. 29, 1209, 2004.
2. Vallaitis, T., S. Bogatscher, L. Alloatti, P. Dumon, R. Baets, M. Scimeca, I. Biaggio, F. Diederich, C. Koos, W. Freude, and J. Leuthold, *Opt. Express*, Vol. 17, 17357, 2009.
3. Dinu, M., F. Quochi, and H. Garcia, *Appl. Phys. Lett.*, Vol. 82, 2954, 2003.
4. Koos, C., L. Jacome, C. Poulton, J. Leuthold, and W. Freude, *Opt. Express*, Vol. 15, 5976, 2007.
5. Muellner, P., M. Wellenzohn, and R. Hainberger, *Opt. Express*, Vol. 17, 9282, 2009.

Challenges for Silicon Photonics Based Mid Board Modules to Achieve High Data Rate Transmissions

B. Blampey, **S. Bernabé**, **K. Rida**, **O. Castany**, **A. Myko**, **and C. Kopp**
University Grenoble Alpes, CEA, LETI, MINATEC Campus
17 rue des Martyrs, Grenoble F-38054, France

Abstract— Silicon-based integrated photonics nowadays generates a huge interest mainly for optical data transmission and increasingly also for sensing. The developments of elementary passive and active components have to reach high performance level in terms of sensitivity; modulation efficiency and power consumption to be commercialized. To get such performances, active silicon photonics modules need to be carefully studied, designed and optimized, from the electro-optical integration into the chip up to the packaging. This is especially the case for the modulator used in transmitter modules.

From the Si Electro-optical Modulator . . .: In this paper, we will first focus on RF design challenges for electro-optical Mach-Zehnder modulator (MZM) using the PN junction carrier depletion, to achieve high data rate transmission over 40 Gb/s. We will for example show how the shield coplanar waveguide can increase the RF bandwidth and also the electro-optical performances compared to the conventional coplanar one [1]. We will discuss new RF electrode architectures [2]. Parasitic effects to be minimized to design MZM in travelling wave configuration or by distributed electrodes will be pointed out.

. . . **towards the hybrid silicon photonics module:** In a second part, we will talk about integration of transmitter photonic chips in modules, with several different architectures. Each one has its figures of merits and can fulfill a specific application (e.g., rack to rack, board to board or intra-board link). Depending on the targeted application, the packaging strategy will differ, and various interconnection methods can be used, from legacy wire-bonding technology to advanced micro-bump interconnections and Through Silicon Vias (TSV) technologies, or direct Cu bonding technologies [3]. These interconnection technologies are used to connect the Photonic Integrated Circuit (PIC) to the related control electronics (EIC), and also in some advanced architecture to the host chip (switch, microprocessor, FPGA). In some cases the host chip can be co-packaged with the Photonic transceiver in the same package. Each interconnection technology has its own figure of merit in term of density, parasitic effects, data rate and manufacturing throughput. We will consider it in three particular cases:

- Standalone module: the photonic transmitter in apart from the host chip module, on the same motherboard.
- System In Package approach, the photonic transmitter and the host chip share the same BGA package.
- Photonics Interposer: the Photonic chips acts as a 2.5D interposer, the host chip and EIC are flip-chipped on the top of the PIC.

REFERENCES

1. Xu, H., et al., "Demonstration and characterization of high-speed silicon depletion-mode Mach-Zehnder modulators," *IEEE J. Sel. Topics Quantum Electron.*, Vol. 20, No. 4, 2014.
2. Ferrotti, T., et al., "Power-efficient carrier-depletion SOI Mach-Zehnder modulators for 4 × 25 Gbit/s operation in the O-band," *Photonics West 2015*, San Francisco (CA), USA, February 7–12, 2015, to be Published.
3. Fedeli, J.-M., et al., "Photonic-electronic integration with Cu bonding," *IEEE J. Sel. Topics Quantum Electron.*, Vol. 20, No. 4, 2014.

Impact of Nonlinear Loss on Stimulated Brillouin Scattering in Silicon Waveguides

C. Wolff[1, 2], **M. J. Steel**[1, 3], **B. J. Eggleton**[1, 4], **and C. G. Poulton**[1, 2]

[1]Centre for Ultrahigh Bandwidth Devices for Optical Systems (CUDOS), Australia
[2]School of Mathematical Sciences, University of Technology
Sydney (UTS), NSW 2007, Australia
[3]MQ Photonics Research Centre, Department of Physics and Astronomy
Macquarie University Sydney, NSW 2109, Australia
[4]Institute of Photonics and Optical Science (IPOS), School of Physics
University of Sydney, NSW 2006, Australia

Abstract— Stimulated Brillouin Scattering (SBS) is a highly resonant acousto-optic interaction that leads to the formation of a hypersonic wave, which in turn acts as a traveling grating that converts the incident pump wave into a red-shifted Stokes wave. This can be effectively described as a third order optical nonlinearity. In this work, we investigate the impact of two-photon absorption (TPA) and the resulting free carrier absorption (FCA) on the SBS gain especially of silicon waveguides, which are one of the best candidates for the on-chip integration of SBS-based functional devices such as amplifiers and oscillators.

To this end, we formulate a set of nonlinear steady state coupled mode equations that involve effective TPA- and FCA-coefficients, which we derive as overlap integrals of the nonlinear material parameters and higher order powers of the eigenmodes' electric field distributions. As a further approximation, we assume that the Stokes wave is weak. The resulting equations are solved analytically. We find that two-photon absorption — being a third order process like SBS itself — leads to a algebraic yet monotonic evolution of the Stokes signal as a function of both the waveguide length and the pump power. The exponent is determined by the ratio of the SBS gain and the effective TPA-coefficient. In contrast, free carrier absorption results in a Stokes profile with an extremum as the pump power is varied; excessive pump powers in fact lead to net loss in the Stokes wave. From this we obtain an expression for the optimal pump power as a function of the material parameters and the waveguide length. Finally, we find that nonlinear loss has exactly the same impact on forward SBS as on backward SBS within the weak Stokes approximation.

Silicon Photonics Integrated Devices for Low Cost End-user Bidirectional Transmission in Passive Optical Networks: The FABULOUS European Project

Guido Giuliani
University of Pavia, Pavia, Italy

Abstract— We present the Silicon Photonics technologies developed within the European project "FABULOUS" aimed at the demonstration of a low cost integrated end-user device (Optical Network Unit, ONU) to be deployed in Passive Optical Networks (PON) for bidirectional downstream and upstream optical communication.

The Si-Photonics chip integrates several sub-components, namely: i) fiber-to-device polarization-splitting coupler with record coupling efficiency based on 2D-grating photonic crystal technology; ii) ring-shaped waveguide pass-band filters; iii) Semiconductor Optical Amplifier (SOA) realized by hybrid integration of III-V gain material on Si; iv) bidirectional Mach-Zehnder Modulator (MZM) to be driven by different electrical signals travelling in the two opposite directions; v) photodetectors; vi) electronic driver for the MZM integrated on the Si chip.

The combination of the above sub-components allows the ONU to communicate bidirectionally with a central node (Optical Line Terminal, OLT). The ONU is capable to receive a downstream optical signal and, simultaneously, to impress an upstream modulation to a selected un-modulated blank wavelength generated by the OLT. This scheme is compatible with the PON philosophy, where the optical fiber connecting the OLT and the ONU is passive, and with the Wavelength Division Multiplexing (WDM) configuration, where multiple wavelengths are used to enhance the transmission capacity. The filter selects a specific blank wavelength, onto which the bidirectional MZM impresses a signal modulation using the so-called Frequency Division Multiplexed Access (FDMA) format, that has a high spectral efficiency thanks to the 16-QAM code used. The bidirectional MZM, in conjunction with the polarization-splitting coupler, realizes a sort of Faraday mirror, thus making the coherent detection of the upstream signal easier. The integrated SOAs provide an optical gain that compensates for optical fiber propagation losses and instrinsic device losses.

Predictions, based on experimental results obtained from the integrated device and its hybrid version, show that a total upstream transmission capacity of 32 Gb/s per single wavelength is feasible over fiber networks with 31 dB optical loss.

ACKNOWLEDGMENT

This work was supported by the EU through FP7-ICT-2011 contract No. 318704 "FABULOUS".

Advanced Building Blocks in Thick Silicon on Insulator Technology: Echelle Grating Multiplexers and Reflective Multimode Interference Couplers

P. Muñoz[1, 2], **J. D. Doménech**[2], **J. S. Fandiño**[1], **R. Baños**[1], **and B. Gargallo**[1]

[1]Universitat Politécnica de Valéncia, Spain
[2]VLC Photonics S.L., Spain

Abstract— In this paper we present the design, fabrication and experimental demonstration of advanced building blocks in a thick Silicon generic photonic integration platform. The platform provides a fabrication process with waveguides of different contrast ratio, through different etch levels, and the possibility of metalization in selected areas. Combining waveguiding and metals we report on Echelle Gratings (EG) multiplexers and re ective Multimode Interference (R-MMI) couplers. Several devices were designed in the same reticle and several dies were supplied by the fabrication platform. The experimental results for the individual devices are reported, as well as a die to die comparison and statistical analysis.

Silicon Optical Routers for Photonic Networks-on-Chip

Lin Yang, Yuhao Xia, Hao Jia, Qiaoshan Chen, and Fanfan Zhang
State Key Laboratory on Integrated Optoelectronics
Institute of Semiconductors, Chinese Academy of Sciences, Beijing 100083, China

Abstract— The performance of chip multiprocessor (CMP) is determined not only by the number of the processor cores integrated on a chip, but also by the communication efficiency among them. With CMP continuously requiring more communication bandwidths, metallic-based electrical networks-on-chip (NoC) gradually becomes the bottleneck for improving the performance of CMP due to its high power consumption, limited bandwidth and long latency. Photonic NoC is considered as a potential solution to overcome the limitations of its electrical counterpart. Optical router is an essential component for photonic NoC, which is responsible for switching data from one optical link to another one.

In this paper, we will review the status of the optical routers for photonic NoC and introduce our efforts on this topic. Firstly, we will introduce several demonstrated optical routers based on microring or Mach-Zehnder optical switches. Then, we will introduce a universal method for constructing an N-port non-blocking optical router for photonic NoC. The optical router constructed by this method has minimum optical switches, in which the number of the optical switches is reduced about 50% compared to the reported optical routers based on microring optical switches and about 30% compared to the reported optical routers based on Mach-Zehnder optical switches, and therefore is more compact in footprint and more power-efficient. Finally, we will introduce the fabricated 4- and 5-port optical routers constructed by this method.

Optical Properties of 2D Materials on Silicon and Silicon Nitride Waveguides

H. K. Tsang, Z. Cheng, L. H. Liu, J. Wang, K. Xu, X. Wan, B. Q. Zhu, C. Shu, and J. B. Xu
Department of Electronic Engineering, The Chinese University of Hong Kong, Hong Kong, China

Abstract— The unique optical and electronic properties of two-dimensional (2D) materials (such as graphene, MoS_2) have attracted much research interest. The integration of 2D materials on photonic integrated circuits (PICs) can offer dramatically increased interaction length with light propagating along the plane of the 2D sheet, and can offer potential applications in nonlinear devices and photodetectors [1]. In this talk, we will review our recent study of the optical properties of 2D materials integrated silicon/silicon nitride (Si_3N_4) PICs.

Monolayer chemical vapor deposition (CVD) grown graphene can be placed on top of silicon or Si_3N_4 waveguides by wet transfer and give rise to enhanced optical absorption. The absorption is strongly polarization dependent. In a waveguide formed by 340 nm thick silicon-on-insulator (SOI), graphene introduced 7.7 dB higher losses for transverse-magnetic mode in a 150 μm long waveguide [2]. The graphene also improved the 1 dB grating bandwidth which was increased from $\sim$ 60 nm to $\sim$ 72 nm because of the reduction of grating dispersion [3]. The free carrier absorption and spectral hole burning of graphene-on-silicon waveguide were observed by using a pump-probe measurement over microsecond timescales [4]. The graphene-on-Si_3N_4 microring structure was optimized to enhance its effective absorption from 25 dB/mm to 174 dB/mm. Q factors of graphene-on-Si_3N_4 microring resonator, was measured between $\sim$ 28200 to $\sim$ 3800 depending on the graphene length, in agreement with theoretical calculations [5].

Another interesting 2D material is MoS_2. We transferred a flake of MoS_2 onto silicon waveguide. The high refractive index (RI) of MoS_2 [6] induced a significant red shift in the grating's coupling center wavelength, with which the effective RI of the material was extract to be $\sim$ 4.5. Self-phase modulation of chirped picosecond pulses were observed. The MoS_2-on-silicon (MOS) structure exhibited larger spectral broadening of the $\sim$ 60 ps gain switched pulses than the silicon waveguides. This magnitude of the Kerr coefficient of MoS_2 was estimated to about two orders of larger than that of silicon in order to account for the enhanced spectral broadening.

ACKNOWLEDGMENT

This work is supported by Research Grants Council of Hong Kong, via GRF CUHK 416913. We thank Prof. J.-B. Xu for useful discussions and Dr. X. Wang and Mr. Z. Chen for preparing graphene samples.

REFERENCES

1. Wang, J., Z. Cheng, Z. Chen, J. Xu, H. K. Tsang, and C. Shu, "Graphene photodetector integrated on silicon nitride waveguide," *Journal of Applied Physics*, accepted.
2. Cheng, Z., H. K. Tsang, X. Wang, X. Chen, K. Xu, and J. Xu, "Polarization dependent loss of graphene-on-silicon waveguides," *IEEE Photonics Conference, Bellevue Washington*, USA, 460–461, 2013.
3. Cheng, Z., Z. Li, K. Xu, and H. K. Tsang, "Increase of the grating coupler bandwidth with a graphene overlay," *Applied Physics Letters*, Vol. 104, 111109, 2014.
4. Cheng, Z., H. K. Tsang, X. Wang, K. Xu, and J. Xu, "In-plane optical absorption and free carrier absorption in graphene-on-silicon waveguides," *IEEE Journal of Selected Topics in Quantum Electronics*, Vol. 20, No. 1, 4400106, 2014.
5. Wang, J., Z. Cheng, C. Shu, and H. K. Tsang, "Optical absorption in graphene-on-silicon nitride microring resonator," Submit to *IEEE Photonics Technology Letters*.
6. Shen, C. C., Y. T. Hsu, L. J. Li, and H. L. Liu, "Charge dynamics and electronic structures of monolayer MoS_2 films grown by chemical vapor deposition," *Applied Physics Express*, Vol. 6, No. 12, 125801, 2013.

Femtosecond Modulations Based on Periodic Patterns of Excited Free-carriers in Semiconductors

Y. Sivan[1], **G. Ctistis**[2], **and A. P. Mosk**[2]

[1]Unit of Electro-optics Engineering, Ben-Gurion University, Israel
[2]Complex Photonic Systems (COPS) Group, Mesa+ Institute for Nanotechnology
University of Twente, Enschede, The Netherlands

Abstract— We demonstrate femtosecond-scale switching and modulations of ultrashort optical pulses using transient Bragg gratings of free-carriers in a semiconductor waveguide. This is enabled by employing the fast carrier diffusion or a double (non-uniform) pump schemes. The demonstrated efficiencies are unusually high for the interaction durations employed.

Ultrafast switching is considered as one of the oldest and most important applications of nonlinear optics. Traditionally, ultrafast switching is based either on Kerr nonlinearity, which is instantaneous, but weak, or on free carrier nonlinearity, which could be much stronger, but comes at the cost of a substantially slower turn-off time [1].

Here, we demonstrate a simple scheme that enables to enjoy the best of the two worlds — to have an utrafast and strong switching, based on free-carrier generation in a semiconductor. Specifically, we describe a novel switching scheme operating on femtosecond time scales, which is based on the generation of a periodic pattern of free-carriers (FCs) which serves as a transient Bragg grating. In the first realization, we rely on diffusion to erase the initial FC pattern, hence, to remove the reflectivity of the system. In the second realization, we erase the FC pattern by launching a second pump pulse at a controlled delay. We discuss the advantages and limitations of the proposed approach and demonstrate it for modulating and switching ultrashort pulses propagating in silicon waveguides. We show reflection efficiencies of up to 50% for 100 fs pump pulses (see Fig. 1), which is an unusually high level of efficiency for such a short interaction time, a result of the use of the strong FC nonlinearity. Due to limitations of saturation and pattern effects, the scheme can be employed for switching applications requiring femtosecond features but standard repetition rates. Such applications include switching and modulations of ultrashort pulses, femtosecond spectroscopy (gating) and time-reversal of short pulses for abberation compensation [2].

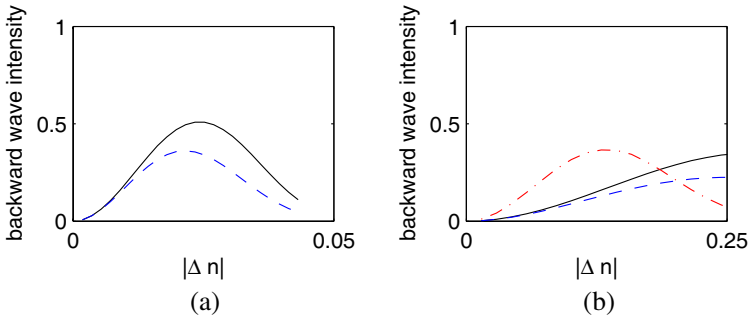

Figure 1: (a) Intensity of the backward wave for the diffusive switching scheme for $T_{rise} = 50$ fs, $T_f = 1000$ fs, $T_{mod} = 600$ fs for various lengths of switching regions. (b) The same for the write-erase technique with $T_{mod} = 50$ fs and $T_{mod} = 150$ fs.

REFERENCES

1. Harding, P. J., H. J. Bakker, A. Hartsuiker, J. Claudon, A. P. Mosk, J.-M. Gérard, and W. L. Vos, "Observation of a stronger-than-adiabatic change of light trapped in an ultrafast switched GaAs-AlAs microcavity," *J. Opt. Soc. Am. B*, Vol. 29, A1–A5, 2012.
2. Sivan, Y. and J. B. Pendry, "Broadband time-reversal of optical pulses using a switchable photonic-crystal mirror," *Optics Express*, Vol. 19, 14502, 2011.

Session 3A4
FocusSession.SC3: Numerical Modeling of Ultrashort Laser Pulse Propagation in Transparent Materials: Micro/nanomodification, Part 2

Laser-induced Thermomechanical Processes around Metal Nanoparticles in a Transparent Medium

Alexey N. Volkov
Department of Mechanical Engineering, University of Alabama
7th Avenue, Tuscaloosa, AL 35487, USA

Abstract— Utilization of metal nanoparticles (NPs) for selective laser treatment of biological tissues is a promising approach in medicine and, in particular, in cancer treatment. The therapeutic effect is achieved by delivering NPs to cancer cells and irradiating the tissue by a laser at a wavelength which can be efficiently absorbed by NPs only. Laser heating of NPs results in the formation of thermal and pressure waves that propagate through the surrounding medium and kill cancer cells. The practical use of this methodology, however, requires a detailed understanding of thermomechanical processes induced in the surrounding medium by laser heating of NPs.

In the present work, the thermal and mechanical processes around gold NPs in water are studied numerically in the broad range of laser fluences and pulse durations. Water is assumed to be transparent to the laser radiation, so that all processes in the medium surrounding a NP are induced by the heat transfer at metal-liquid interface and thermal expansion of metal nanoparticles. Heating and thermal expansion of NPs are described by the balance equations based on the one-temperature or two-temperature thermo-elastic models. The two-temperature thermal model takes into account non-equilibrium energy exchange between the electrons and phonons in metals irradiated by ultrashort, pico- and femtosecond, laser pulses. Heat conduction as well as propagation and attenuation of the pressure waves in water are described by onedimensional Navier-Stokes equations. Compressibility of water and water vapor is taken into account, and the pressure and internal energy of water are calculated based on the semi-empirical multiphase equation of state. Thermal boundary resistance and surface tension at metal-water interface are taken into account, and the model of thermal boundary conductance is parameterized based on results of molecular dynamics simulations. Both volume and surface mechanisms of vaporization of overheated water are taken into account.

The calculations performed for the pulse duration varied from tens of femtosecond to microseconds. The limiting case of continuous wave laser heating is also considered. Transient distributions of temperature and pressure in the surrounding liquid are obtained and analyzed. Threshold values of the laser fluence which correspond to the onsets of boiling and spinodal decomposition in the liquid adjacent to the gold particle are determined as a function of particle radius and pulse duration. The effects of the finite thermal boundary resistance and surface tension at metal-liquid interface are shown to be significant in the broad range of irradiation conditions. The size of region around the absorbing particle, where the biological cells can be killed due to high pressure or high temperature, is estimated for various irradiation conditions. Selected simulation results are compared with experimental data.

Effect of Laser Field Enhancement on Collision Frequencies and Absorption during Ultra-short Laser Interactions with Dielectric Materials

T. E. Itina, **A. Rudenko**, **J.-Ph. Colombier**, **and N. S. Shcheblanov**
Laboratoire Hubert Curien, UMR CNRS 5516, Lyon University
18 rue de Prof. Benoit Lauras, Bat. F, Saint-Etienne 42000, France

Abstract— Laser-induced electronic excitation, absorption and relaxation are the key issues in ultra-short laser interactions with dielectric materials. To numerically analyze these processes, a detailed non-equilibrium model is developed [1] based on the kinetic Boltzmann equations without any appeal to the classical Drude model. The calculations are performed including all possible collisional processes. As a result, electron energy distributions are obtained allowing a better analysis of ultra-short laser interactions. The results reveal a remarkable effect of the laser-field on collision frequencies resulting in smaller free-carriers absorption than the one predicted by commonly used rate-equation models. In addition, our calculations clearly demonstrate laser intensity limits for the applicability of Keldysh's equation for the photoionization process [2]. Both electron-electron and electron-phonon relaxation are then examined, and the mean energy density of the electron sub-system is investigated as a function of laser fluence and pulse duration. Because efficient bond breaking requires energy, these calculations provide the required thresholds.

The dependency of the calculated fluence threshold on laser pulse duration is compared with the available experimental data. The obtained results also explain several recent pump-probe experiments. The developed model is useful for many laser applications including high precision in laser treatment, laser-assisted atomic probe analysis, and for the development of new powerful laser systems.

Furthermore, a finite-difference time-domain (FDTD) solution of Maxwell's equations is numerically coupled with time-dependent electron carrier density equation for dielectric material (fused silica) with a small inclusion. The process of plasma generation near the inclusion is studied and local field distribution is obtained. The generated plasma is studied and the roles of the electron collisional frequency and the irradiated wavelength are demonstrated.

REFERENCES

1. Shcheblanov, N. S. and T. E. Itina, *Appl. Phys. A*, 2012, DOI: 10.1007/s00339-012-7130-0.
2. Shcheblanov, N. S. and T. E. Itina, *New J. Phys.*, submitted.

Femtosecond Laser Irradiation of Fused Silica with a Nanometric Inhomogeneity

Anton Rudenko, Jean-Philippe Colombier, and Tatiana E. Itina
Laboratoire Hubert Curien, UMR CNRS 5516, Lyon University
Bât F, 18 rue du Prof. Benoît Lauras, Saint-Etienne 42000, France

Abstract— Small nanometric defects, such as color centers or impurity sites, located in dielectrics, irradiated by focused ultrashort laser pulses, can reinforce field localization and lead to inhomogeneous distribution of multiphoton nonlinear ionization and formation of nanoplasmas.

A finite-difference time-domain (FDTD) method based on Maxwell's equations coupled with time-dependent electron carrier density's equation is proposed to investigate numerically femtosecond laser irradiation of dielectrics with a small inhomogeneity. The process of plasma generation due to multiphoton absorption near small defect in fused silica is studied in details and local field distribution around the void inhomogeneity is first explained by using the Rayleigh scattering theory. Further investigation of the laser-matter interaction has shown that the generated plasma properties do not significantly depend on the size of the inhomogeneity as long as it remains considerably smaller than the irradiation wavelength. The calculation results show, however, that there are several parameters, which are crucial. Among such parameters, for instance, is collision frequency,which affects strongly both the created electron density and laser propagation. In addition, the characteristics of the generated plasma are studied as a function of the irradiated wavelength and the changes in the refractive index are explained by the Lorentz-Drudemodel with time-dependent carrier density. The differences between the results obtained by considering Keldysh theory for multiphoton ionization and by taking into account only six-photon ionization are discussed. Finally, temporal changes in behavior of scattering due to generated nanoplasma are observed and analyzed by using Mie scattering theory, which is more complete than Rayleigh one.

Femtosecond Laser Material Alteration by Means of Micro- and Nano-particles

N. Bityurin, A. Pikulin, and A. A. Smirnov
Institute of Applied Physics RAS, Nizhniy Novgorod, Russia

Abstract— We consider laser nanostructuring of a material surface by means of a colloidal particle lens array deposited on the surface. Here, the monolayer of dielectric micro- or nanospheres placed right on the surface acts as an array of near-field lenses that focus the laser radiation into the multitude of distinct spots, allowing the formation of many structures in a single stage. We consider optical properties of such layer taking into account that within this layer spherical particles do not act as independent microlenses. Due to the coupling of the spherical modes, the field near the clusters of spherical microparticles cannot be calculated by means of the superposition of Mie solutions for individual spheres. We consider opportunities offering by combing femtosecond pulses of the fundamental frequency and of the second harmonic.

We analyze the opportunities provided by the plasmonic nanoparticles inserted into the bulk of a transparent medium to modify the material by laser light irradiation. This study is provoked by the advent of photo-induced nano-composites consisting of a typical polymer matrix and metal nanoparticles located in the light-irradiated domains of the initially homogeneous material. The subsequent irradiation of these domains by femtosecond laser pulses promotes a further alteration of the material properties. We separately consider two different mechanisms of material alteration. First, we analyze a photochemical reaction initiated by the two-photon absorption of light near the plasmonic nanoparticle within the matrix. We show that the spatial distribution of the products of such a reaction changes the symmetry of the material, resulting in the appearance of anisotropy in the initially isotropic material or even in the loss of the center of symmetry. Second, we analyze the efficiency of a thermally-activated chemical reaction at the surface of a plasmonic particle and the distribution of the product of such a reaction just near the metal nanoparticle irradiated by an ultrashort laser pulse.

REFERENCES

1. Pikulin, A., A. Afanasiev, A. P. Alexandrov, N. Agareva, V. Bredikhin, and N. Bityurin, "Effects of spherical mode coupling on near-field focusing by clusters of dielectric microspheres," *Optics Express*, Vol. 20, No. 8, 9052–9057, 2012.
2. Bityurin, N., A. Afanasiev, V. Bredikhin, A. Alexandrov, N. Agareva, A. Pikulin, I. Ilyakov, B. Shishkin, and R. Akhmedzhanov, "Colloidal particle lens arrays-assisted nano-patterning by harmonics of a femtosecond laser," *Optics Express*, Vol. 21, No. 18, 21485–21490, 2013.
3. Smirnov, A. A., A. Pikulin, N. Sapogova, and N. Bityurin, "Femtosecond laser irradiation of plasmonic nanoparticles in polymer matrix: Implications for photothermal and photochemical material alteration," *Micromachines*, Vol. 5, 1202–1218, 2014, Doi: 10.3390/mi5041202.

Advantages of Contact Arrays of Spheroidal Particles for Femtosecond-laser Micro- and Nanoprocessing of Materials

A. Pikulin, **N. Mitin**, **and N. Bityurin**
Institute of Applied Physics RAS, Nizhniy Novgorod, Russia

Abstract— Monolayers of dielectric spherical microparticles have become a convenient tool for laser alteration of material surface [1–3]. Under the irradiation by a wide laser beam, such particles act as focusing microlenses. When placed right on the surface, the arrays of microparticles provide the multitude of distinct field enhancement spots within the material, allowing for the large-area single-step material nanomodification. The ultra-short laser pulse also provides simultaneous withdrawal of the spheres from the surface.

The close-packed monolayers of spherical microlenses can be conveniently deposited onto the surface, e.g., by means of drying of the colloidal solution droplet. However, the spherical shape is not optimal for the beam focusing due to strong aberrations [4, 5]. In the case of silica or polymeric microspheres with refractive index of about 1.5, the field maximum is situated close to the surface of the sphere thus resulting in a small aspect ratio of the obtained nanostructures. In the case of the higher refractive index, the maximum is placed inside the sphere, thus rendering such particles inapplicable for the surface nanostructuring.

In this work, we study the possibility to employ spheroidal microparticles instead of the spherical ones in order to reduce the aberrations. With self-made FDTD code, we calculate the laser field intensities provided by monolayers of spheroidal particles and analyze the advantages and disadvantages of such focusing systems for surface nanomodification. In particular, we demonstrate the possibility to improve the aspect ratio of the nanostructures and increase the density of the modification spots.

REFERENCES

1. Chong, T. C., M. H. Hong, and L. P. Shi, "Laser precision engineering: From microfabrication to nanoprocessing," *Laser Photon. Rev.*, Vol. 4, 123–143, 2010.
2. Pikulin, A., A. Afanasiev, N. Agareva, A. P. Alexandrov, V. Bredikhin, and N. Bityurin, "Effects of spherical mode coupling on near-field focusing by clusters of dielectric microspheres," *Opt. Express*, Vol. 20, 9052, 2012.
3. Bityurin, N., A. Afanasiev, V. Bredikhin, A. Alexandrov, N. Agareva, A. Pikulin, I. Ilyakov, B. Shishkin, and R. Akhmedzhanov, "Colloidal particle lens arrays-assisted nano-patterning by harmonics of a femtosecond laser," *Opt. Express*, Vol. 21, 21485–21490, 2013.
4. Kofler, J. and N. Arnold, "Axially symmetric focusing as a cuspoid diffraction catastrophe: Scalar and vector cases and comparison with the theory of Mie," *Phys. Rev. B*, Vol. 73, 235401, 2006.
5. Arnold, N., "Influence of the substrate, metal overlayer and lattice neighbors on the focusing properties of colloidal microspheres," *Appl. Phys. A*, Vol. 92, 1005–1012, 2008.

Comparison of Kinetic and Continuum Models for Simulations of Laser-induced Plasma Plumes

A. N. Volkov, **G. Silverstein**, **and O. Ranjbar**
Department of Mechanical Engineering, University of Alabama
H. M. Comer Hall, 7th Avenue, Tuscaloosa, AL 35487, USA

Abstract— Plasma effects in laser-induced plume flows are known to be important for processing of various materials by high-power nanosecond pulsed lasers. In particular, the plasma plumes can efficiently absorb the incident laser radiation, thus substantially decreasing the amount of energy absorbed directly by the target, reducing the target temperature, and, finally, decreasing the amount of ablated material. Along with this major "shielding effect," the plasma plume induces a number of secondary effects like the heating and etching of the target by adjacent high-temperature plasma. These plasma-related effects substantially limit the overall efficiency of industrial laser systems and reduce the accuracy of laser machining.

The present work is aimed at the numerical modeling of laser-induced plasma plume expansion. Although a number of diverse models of plasma flow in laser plumes were proposed in the literature, these models were not compared in a unified framework. The major goal of the present work is to accurately compare the results of laser-induced plume expansions obtained with continuum and kinetic models. The continuum model solves the one-dimensional gas dynamics equations of the multi-component plume flow and incorporates both equilibrium, based on Saha-Langmuir equations, and non-equilibrium, based on kinetic rates of ionization and recombination, models of plasma. Boundary conditions at the irradiated target take into account the formation of the Knudsen layer. The kinetic model of multi-component plume flow is based on the Direct Simulation Monte Carlo (DSMC) method. This kinetic model is capable of taking into account the same plasma models as the gas-dynamic model. Both the gas-dynamic and the kinetic models are coupled with the same thermal model of the target. Boundary conditions at the target surface account for the evaporation and condensation, thermionic emission, and back heating of the target by the high-temperature plume. These models are applied to study the one-dimensional plume expansion from a copper target irradiated by nanosecond and shorter laser pulses. The gas dynamic and kinetic models are found to result in substantially different flow structures in broad ranges of laser fluence and background gas pressure.

Computer Modeling of Material Modification by Short Laser Pulses and Optically-induced Surface Acoustic Waves

Leonid V. Zhigilei[1], **Chengping Wu**[1], **Maxim V. Shugaev**[1], **and Vladimir Yu. Zaitsev**[1, 2]

[1]Department of Materials Science and Engineering, University of Virginia
395 McCormick Road, Charlottesville, VA 22904-4745, USA
[2]Institute of Applied Physics, Russian Academy of Sciences
Uljanova St. 46, Nizhny Novgorod, 603950, Russia

Abstract— Short pulse laser irradiation can trigger a cascade of structural and phase transformations in the region of direct laser energy deposition and can also generate strong acoustic pulses (bulk and surface waves) capable of affecting key processes responsible for material modification at a substantial distance from the absorption region. Large-scale atomistic simulations are used in this work to investigate both the direct femtosecond laser material modification and the acoustically-induced surface processes. In the case of the direct laser modification of metal targets, the processes responsible for the formation of a sub-surface porous region covered by a nanocrystalline surface layer with random crystallographic orientation of nanograins and a high density of stacking faults, twins, and nanoscale twinned structural elements with five-fold symmetry will be discussed and related to the experimental observation of surface swelling and incubation effect in multi-pulse laser ablation. For the acoustic activation of surface processes, the conditions leading to the maximum enhancement of surface diffusion are analyzed and explained by nonlinear wave profile sharpening leading to efficient generation of high-frequency harmonics that directly couple to the vibrational modes of surface species. The implications of the computational predictions for the design of new techniques where the acoustic energy serves as an effective substitution for thermal activation of surface processes are discussed.

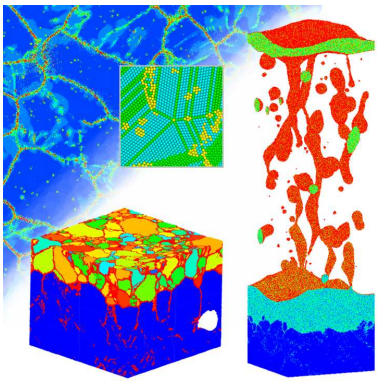

Figure 1: Illustration of some of the results of large-scale atomistic simulations of laser-induced structural modification of Ag targets irradiated by 200 fs laser pulses. The simulations predict the generation of sub-surface voids and nanocrystalline surface layer and explain the experimental observation of surface swelling at laser fluences close to the ablation threshold.

REFERENCES

1. Wu, C., M. S. Christensen, J.-M. Savolainen, P. Balling, and L. V. Zhigilei, *Phys. Rev. B*, Vol. 91, 035413, 2015.

Nonlinear Absorption of Femtosecond Pulses in Fused Silica and Inscription of Refractive Index Periodic Structures in Silica Fibers

A. V. Dostovalov[1], **A. A. Wolf**[1], **V. K. Mezentsev**[2], **A. G. Okhrimchuk**[3], **and S. A. Babin**[1, 4]

[1]Institute of Automation and Electroetry SB, RAS, Russia
[2]Photonics Research Group, Aston University, UK
[3]Fiber Optics Research Center, RAS, Russia
[4]Novosibirsk State University, Russia

Abstract— Results of numerical and experimental studies are presented for the absorption of near-IR and visible femtosecond laser pulses focused in the bulk of fused silica and the application of the method for the creation of fiber Bragg and long-period gratings in different types of silica fibers.

Introduction: Femtosecond (fs) laser technologies making it possible to produce high-energy ultrashort pulses are increasingly used in laser processing of materials. In comparison with other well-developed methods of laser processing (cutting, ablation etc.), the key advantage of fs pulses is the possibility of local change in the refractive index of nonphotosensitive transparent materials, which allows one to create elements of integrated optics [1]. We report the results of numerical and experimental studies of nonlinear absorption of fs laser pulses focused in the bulk of fused silica and the application of the method for the creation of fiber Bragg (FBG) and long-period gratings (LPG) in different types of silica fibers.

Modelling and experiments: Laser wavelength is one of the most important characteristics that determine the process of material modification because it defines the order of multiphoton absorption. In our work, the numerical and experimental investigations of fs laser pulses absorption were carried out for the fundamental ($\lambda = 1026\,\text{nm}$) and the second ($\lambda = 513\,\text{nm}$) harmonics of Yb-doped laser. Numerical model adopted in this work comprises a nonlinear evolution equation for the envelope amplitude of the laser beam in a form of extended nonlinear Schrödinger equation (NLSE) coupled to the balance equation for the concentration electrons-hole plasma [2]. It was found that second harmonic is more efficient in terms of amount of absorbed energy which leads to lower inscription threshold, but localization of the absorbed energy is higher for IR pulses due to higher order of multiphoton process.

Inscription of LGPs was carried out in different types of single-mode fibers including standard telecom Corning SMF-28e+, Nufern 1060-XP and polarization maintaining "Panda" type Nufern FUD-3561. The applied slit beam shaping technique allowed us to enlarge the cross-section of created modification area in the core and thereby to increase the mode coupling coefficients. Relatively low level of out-of-band losses (down to 0.3 dB) and high resonant dip amplitude ($> 12\,\text{dB}$) allows one to use such gratings in filtering applications. The first- and the second-order FBGs, with the periods of 0.535 and 1.07 μm respectively, were inscribed in Corning SMF-28e+ fiber through the acrylate coating as well as in specialty fibers through the polyimide coating: high-temperature tolerant Fibercore SM1500(9/125)P fiber and pure-silica core hydrogen tolerant SM1500SC(9/125)P. Characterization of the FBGs was performed using differential interference contrast microscopy and the measurement of refractive index modulation by means of quantitative phase microscopy.

REFERENCES

1. Gattass, R. R. and E. Mazur, "Femtosecond laser micromachining in transparent materials," *Nat. Photonics*, Vol. 2, No. 4, 219–225, 2008.
2. Bergé, L., S. Skupin, R. Nuter, J. Kasparian, and J.-P. Wolf, "Ultrashort filaments of light in weakly ionized, optically transparent media," *Reports Prog. Phys.*, Vol. 70, No. 10, 1633–1713, 2007.

Investigation of Instabilities in Femtosecond Laser Irradiated Semiconductors Using Numerical Modeling and Dispersion Relations

Thibault J.-Y. Derrien
HiLASE Centre, Institute of Physics, Academy of Science of the Czech Republic
Za Radnicí 828/5, Dolní Břežany 25241, Czech Republic

Abstract— Illumination of semiconducting and transparent materials by a femtosecond laser pulse leads to transient excitation of electrons from the valence band to the conduction band during the laser pulse action [1]. As the front part of the pulse locally excites carriers and transiently modifies the properties of matter, the tail of the laser pulse interacts with an inhomogeneously excited plasma [2, 3]. As a result, modulation effects can be stimulated, leading to the development of instabilities in the laser-excited region of the solid [4–6]. This study presents preliminary theoretical works aiming at understanding the excitation of possible electrodynamic instabilities in this context. To reach this aim, two complementary approaches are proposed.

First approach is a 2D time-dependent numerical modeling of the processes induced by a femtosecond laser pulse focused on the silicon surface which was developed based on a finite element method. The core of the modeling is a two-temperature model [3] taking into account the transient excitation of the electron-hole pairs by laser irradiation which is solved together with the wave equation for the electromagnetic field of the laser pulse of a Gaussian temporal and spatial shape. It has been found that, when reaching the critical density of the electron-hole plasma, a spatial modulation is generated in the excitation region, where the gradients of electron density and energy are large.

To understand the origin of the modulation of the electron-hole plasma density arising as a result of highly non-linear interaction, a perturbative study is performed for the case of a laser-irradiated system. The results reveal two oscillatory modes of the electron-hole plasma. While the first mode exhibits a near-wavelength spatial modulation, the second mode is found to be linked to the electron-hole plasma temperature, exhibiting a spatial period of ∼200 nm. Both modes are found to be highly dependent on the laser wavelength and the band structure of the material.

REFERENCES

1. Sokolowski-Tinten, K. and D. von der Linde, *Phys. Rev. B*, Vol. 61, 2643, 2000.
2. Derrien, T. J.-Y., Ph.D. Thesis, Aix-Marseille Université, France, 2012.
3. Derrien, T. J.-Y., T. E. Itina, R. Torres, T. Sarnet, and M. Sentis, *J. Appl. Phys.*, Vol. 114, 083104, 2013.
4. Bulgakova, N. M., V. P. Zhukov, and Y. P. Meshcheryakov, *Appl. Phys. B*, Vol. 113, 437, 2013.
5. Bulgakova, N. M., V. Zhukov, Y. P. Meshcheryakov, L. Gemini, J. Brajer, D. Rostohar, and T. Mocek, *J. Opt. Soc. America B*, Vol. 11, C8–C14, 2014.
6. Buschlinger, R., S. Nolte, and U. Peschel, *Phys. Rev. B*, Vol. 89, 18, 2014.

Temperature Relaxation after Modulated Absorption of Femtosecond Laser Pulses in Dielectrics: Possible Impact on LIPSS Formation

Yoann Levy[1], **Nadezhda M. Bulgakova**[1, 2], **Evgeny Gurevich**[3], **and Tomas Mocek**[1]

[1]HiLASE Centre, Institute of Physics ASCR, v.v.i, Dolní Břežany, Czech Republic
[2]Institute of Thermophysics SB RAS, Novosibirsk, Russia
[3]Applied Laser Technology, Ruhr-University Bochum, Bochum 44801, Germany

Abstract— In this work a simplified 2D model has been developed to analyze the temperature relaxation of dielectric materials after excitation by femtosecond laser pulses at 800 nm wavelength in the regimes of formation of laser-induced periodic surface structures (LIPSS). The model assumes that laser absorption is modulated upon laser action as a result of partial scattering of the incident electromagnetic wave by surface roughness. The model is based on the rate equation for free electron generation dynamics and the heat flow equations for electron and lattice subsystems. Modeling has been performed for fused silica as an example. Peculiarities of modulated temperature profile evolution are analyzed. The effects of nanoscaled melting/softening and heat and defect accumulation are discussed.

Session 3A5
Electromagnetic Models and Applications in Remote Sensing

Study of Orientational Effects in Magnetic Induction Tomography (MIT) Using a Weakly Coupled Finite Elements (FE) Solver

Wuliang Yin and Anthony Peyton
School of Electrical and Electronic Engineering, University of Manchester
Sackville Street Building, Manchester M13 9PL, United Kingdom

Abstract— Non symmetrical objects show strong orientational effect in a MIT Sensor. In this paper, we developed a fast magnetic induction FEM solver in the thick skin regime. This solver delivers higher accuracy with reduced computation load. Using this solver, we investigated the rotational effects of an object in MIT. A potential use of MIT for object recognition, which exploits the new solver, is also investigated.

A Formulation for Predicting the Asymptotical Magnetic Polarization Tensors for Complex-shaped Samples Using the Boundary Element Method

M. Y. Lu, W. Yin, and A. J. Peyton
School of Electrical and Electronic Engineering, University of Manchester, Manchester M13 9PL, UK

Abstract— The magnetic polarization tensor is a frequency-dependent, rotation-invariant and object-specific property of a metallic object. This paper presents an approach to compute the magnetic polarization tensor of a metallic object based on the Boundary Element Method (BEM) which treats the object as a perfect electrical conductor (PEC) and therefore is able to predict the limiting cases where very high frequency and/or high conductivity is assumed. A uniform magnetic field is applied to an object and the scattered field at a certain distance is obtained in the simulations. The magnetic tensor can then be deduced from the scattered field. The simulated results agree well with an analytical solution for spheres and with measured results for a number of cylinders at limiting cases. An explicit formulation is deduced for the magnetic polarization tensor.

Retrieval of Land Surface Temperature from Landsat 8 Thermal Infrared Sensor in Heihe River Basin

Xiaoying Ouyang
State Key Laboratory of Remote Sensing Science
Institute of Remote Sensing and Digital Earth, Chinese Academy of Sciences, Beijing 100101, China

Abstract— One of the important land surface products derived from Landsat is the land surface temperature (LST). The Thermal Infrared Sensor (TIRS) onboard Landsat 8 collects two thermal bands with appropriate response spectral distribution in the atmospheric window between 10–12 µm (833–1000 cm^{-1}) at a spatial resolution of 100 m: B10, 10.6–11.2 µm (890–945 cm^{-1}) and B11, 11.5–12.5 µm (800–870 cm^{-1}). This advance sensor could give the LST data for global change analysis due to its highly technical advancements in both spectral and spatial resolution in thermal infrared regions.

A split-window (SW) algorithm to obtain satellite-derived LST of semi-arid areas from freely available and easily accessible data of the latest Landsat 8/TIRS is first developed. So far, great efforts have been made in estimating LST using SW method from either geostationary or polar-orbiting thermal infrared data. The SW method estimates LST by correcting for atmospheric effects based on the different absorption in two adjacent infrared bands [1–4]. Wan and Dozier (1996) proposed a generalized split-window (GSW) method and applied to top-of-atmospheric (TOA) radiance observed by AVHRR and MODIS SW channels respectively to retrieve LST. The retrieval parameters can be given by interpolation on a set of multi-dimensional look-up tables (LUT) [1]. The accuracy in atmospheric water vapor content is vital for obtaining suitable coefficients in Wan and Dozier's SW method in different ranges of atmospheric humidity condition. Method using radiance observations in thermal infrared bands, say the Split-Window Covariance-Variance Ratio (SWCVR) method [5, 6] is adapted to the Landsat 8/TIRS sensor for water vapor content retrieval in this study. In situ LST data for the period from mid-June to mid-September 2012 were acquired from automatic meteorological stations (AMS) that are part of Heihe Watershed Allied Telemetry Experimental Research (HiWATER) project. TIRS-based LSTs are compared with in situ measurements at 16 AMS sites with land cover types of vegetable, maize and orchards. The standard deviation (STD), root mean square error (RMSE), and correlation coefficient (R) of TIRS/LST vs. the in situ measurements are 2.45 K, 2.78 K, and 0.67, respectively, whereas those for the MODIS 1 km LST product vs. the in situ measurements are 4.07 K, 2.98 K, and 0.79, respectively. The spatial pattern of the TIRS/LST over the study area in the Heihe River Basin generally agreed well with the MODIS 1 km LST product and contained more detailed spatial textures.

REFERENCES

1. Wan and Dozier, 1996.
2. Becker and Li, 1990.
3. Li and Becker, 1993.
4. Sobrino and Romaguera, 2004.
5. Sobrino, et al., 1994.
6. Li, et al., 2004.

Model Initialization and Inversion for Geophysical Retrieval Based on Time Series Optimization of AMSR-E X-band Data

Steven Chan, Eni Njoku, and Mariko Bürgin
Jet Propulsion Laboratory, California Institute of Technology, Pasadena, CA 91109, USA

Abstract— The zeroth-order radiative transfer model, also known as the *tau-omega* model, has been used extensively for decades in passive remote sensing of soil moisture. In order to apply the model successfully to obtain soil moisture estimates, the model must first be initialized with known model coefficients, along with other ancillary data inputs. Although the values of these coefficients are generally available at smaller spatial scales applicable to studies at point or field scale, their values and geographical variability are usually not known at larger spatial scales applicable to many recent satellite missions (AMSR2, SMOS, Aquarius, and SMAP) whose objectives include frequent global mapping of soil moisture for hydroclimatological and hydrometerological applications.

In this presentation, a time series optimization (TSO) approach will be proposed to address the ambiguity associated with the initialization of these model coefficients, and the subsequent uncertainty in geophysical retrieval. In this approach, satellite-based brightness temperature (TB) measurements at a given geolocation from successive overpasses are used as observations to construct the cost function $\varphi(\mathbf{x})$ to be optimized, where $\mathbf{x}$ is a multi-dimensional vector that contains model coefficients as well as geophysical parameters. By iterative optimization on $\varphi(\cdot)$ formed from successive TB observations accumulated over a certain period, it is possible to obtain an optimal $\mathbf{x_o}$ that minimizes $\varphi(\cdot)$ in a least-squares sense. As this procedure repeats, the TSO results in two-dimensional mapping of model coefficients and geophysical parameters. Because the same computation can be repeated for the next time window, this approach also sheds insights into the seasonality of model coefficients and geophysical retrieval.

An annual record of the X-band TB data acquired by the Advanced Scanning Microwave Radiometer EOS (AMSR-E) onboard the NASA Aqua satellite will be used to illustrate the principles and results of this approach. The TSO-based soil moisture estimate will be discussed. In addition, estimates using other common soil moisture retrieval techniques will be presented as a comparison to highlight the differences in spatial pattern among these methods. Finally, the prospect of extending this approach to other satellites and hence the creation of a long-term consistent soil moisture record will be discussed.

Effect of the Rock/Water/Air Interaction on the Complex Dielectric Permittivity and Electromagnetic Waves Attenuation in Water-saturated Sandstones

P. P. Bobrov, A. S. Lapina, and A. V. Repin
Omsk State Pedagogical University, Omsk, Russia

Abstract— We have described how the complex relative permittivity (CRP) of water-saturated rocks depends on textural and interfacial effects. We used an experimental wideband frequency domain method for the CRP measurements of a porous medium at the frequency 10 kHz–1 GHz [1].

In the literature, for example in [2], the properties of elastic waves in the water-saturated sandstones, particularly the dispersion and attenuation, were described in details, but the properties of electromagnetic waves were described insufficiently. It is known that the real part of CRP of completely saturated sandstones depends on the porosity and it remains almost constant in the frequency range of 1 MHz to 1 GHz. At frequencies below 1 MHz observed abrupt increase due to the relaxation of the double layer at the rock-water interface.

It is usually assumed that reduction of water content in the rock reduces the real part of CRP. We measured CRP water-saturated powders of the quartz granules and hard sandstones with a porosity from 7% to 40%, and showed that at the frequencies 0.1–10 MHz the real part of CRP increases with decreasing of water content to 60–90% of the total porosity. In this case the conductivity drops sharply. The CRP frequency dependence is similar to the dielectric relaxation, described by the models of Debye or Cole-Cole.

A possible reason for this phenomenon is the interlayer polarization of the air-water boundary. Relaxation time weakly depends on the overall porosity, but greatly increases with the increasing of the pore size. In this case, the relaxation domain shifts down at frequency. In connection with an increase of the real part of CRP and conductivity decrease, the attenuation of the electromagnetic wave in relaxation domain decreases. The thickness of the skin layer at water-saturation of 70–80% in 1.5–2 times higher than at the water-saturation of 50%.

REFERENCES

1. Bobrov, P. P., A. V. Repin, and O. V. Rodionova, "Wideband frequency domain method of soil dielectric properties measurements," *IEEE Trans. Geosci. Remote Sens.*, Vol. 53, No. 5, 2366–2372, May 2015.
2. David, E. C., J. Fortin, A. Schubnel, Y. Guéguen, and R. W. Zimmerman, "Laboratory measurements of low- and high-frequency elastic moduli in Fontainebleau sandstone," *Geophysics*, Vol. 78, No. 5, D369–D379, 2013.

The Electrical Characteristics of the Rocks with Different Texture

P. P. Bobrov, A. S. Yashchenko, O. V. Rodionova, A. V. Repin, and A. S. Lapina
Omsk State Pedagogical University, Russia

Abstract— In the methods using ultra wideband electromagnetic pulses, as well as for dielectric logging data interpretation while oil searching the complex relative permittivity (CRP) over a wide frequency range are required [1].

The species CRP measurement indicates that the dielectric properties are the complex functions of particle size, clay content, saturating the fluid and its components.

To determine the influence of these parameters we have measured the frequency characteristics of the CRP of artificial mixtures that have different textures and saturating fluid. The mixtures consisted of spherical quartz grains of various sizes, river sand, bentonite of 3 types or kaolin clay in different proportions. They were saturated with liquid: distilled water, oil or saline. The measurements were made using a vector network analyzer in the frequency range from 10 MHz to 8.5 GHz. Samples were placed in a cell that can be connected as a coaxial line segment and a cylindrical capacitor. The surface area was calculated for each sample.

For the analysis of the spectra of CRP the relaxation time was chosen. It was determined by the model of Cole-Cole. It is shown that the relaxation time increases with a decrease in the specific surface area of granule mix with all types of bentonite. The same relationship is observed in mixtures of kaolin and bentonite with sand at low water content.

In the samples having the same specific surface area and the same fluid saturant but containing different concentrations dissolved the relaxation time decreases with the increasing of the salt content.

The CRP spectra of the mixtures with the same surface area emulsion saturated with diesel fuel — water were also investigated. Simulations have shown that as the proportion of oil in the emulsion decreases the relaxation time decreases too.

REFERENCES

1. Epov, M. I., V. L. Mironov, K. V. Muzalevskiy, and I. N. Yeltsov, "UWB borehole logging tool to explore the electrical and structural properties of near-wellbore fluid-filled areas," *PIERS Online*, Vol. 7, No. 6, 559–562, 2011.

Modeling of Microwave Backscattering from Rice Crops Based on Radiative Transfer Theory and Antenna Array Concept

Yu Liu[1], **Kun-Shan Chen**[1, 2, 3], **and Zhao-Liang Li**[2]

[1]Institute of Remote Sensing and Digital Earth, Chinese Academy of Sciences, Beijing 100101, China
[2]Key Laboratory of Agri-informatics
Ministry of Agriculture/Institute of Agricultural Resources and Regional Planning
Chinese Academy of Agricultural Sciences, Beijing 100101, China
[3]Department of Electrical Engineering, The University of Texas at Arlington, Arlington, TX 76019, USA

Abstract— Typically, the three growth phases of a rice plant are vegetative, reproductive, and ripening. The growth duration is determined by changes in the length of the vegetative phase. Accordingly, radar response at different stages that present different scattering mechanisms, either single mechanism or mixture, is of vital interest. In terms of scattering mechanisms, seedling and tillering in vegetative phase present surface scattering, and often water body or wet ground, while in stem elongation stage, vegetation crown appears, scattering may be from volume together with surface depending on the radar probing wavelength. In reproductive phase, the rice plant approaches to full-grown. From heading to flowering, the scattered signal levels may change. Finally, in ripening phase, from gain milking to mature, the wetness of the ground underneath changes as the rice filed undergoes practice of inundation and drainage. The rice plant height, leave area index, and stem density, among other parameters, vary from reproductive to ripening phases, although the land-cover may just look like a vegetation canopy as whole. All possible scattering mechanisms may present but weight in differently to total returns. After harvest, the bare soil presence prompts the surface scattering as the dominant scatterers.

In all, it can be seen that the complex process of rice growth makes an electromagnetic wave modeling of it difficult, if not possible. In this paper, a three layer scattering model based on radiative transfer theory by Karam and Fung [1], originally proposed to characterize backscattering from vegetation canopy, is modified for rice plant and their growth phases. A rice plant is electromagnetically modeled as cluster of rice plant components, a bunch. In particular, antenna array concept is adopted into the three-layer scattering model to account for the intra-clusters interactions between quasi-periodic bunches subtended by the antenna footprint. The performance of the proposed method is validated by comparison with continuous ground-based measurements for a complete cycle of rice growth [2], in which in-situ ground truths were collected as well and used as the model inputs. Result shows that excellent agreement of backscattering coefficients for various growth phases between model predictions and measured data is obtained. Dependence and sensitivity of radar scattering on various radiometric and geometric parameters, including water content, leaf size, curvature, and stem height and so on, will be discussed and reported.

REFERENCES

1. Karam, M. A., A. K. Fung, R. H. Lang, and N. S. Chauhan, "A microwave scattering model for layered vegetation," *IEEE Transactions on Geoscience and Remote Sensing*, Vol. 30, No. 4, 767–784, July 1992.
2. Jia, M. Q., L.Tong, and Y. Chen, "Multifrequency and multitemporal ground-based scatterometers measurements on rice fields," *32nd IEEE Int. Geoscience and Remote Sensing Symposium (IGARSS)*, 642–645, Institute of Electrical and Electronics Engineers, Munich, Germany, 2012.

An Inverse Model for Sea Ice Thickness Retrieval Using Simulated Annealing

Y. J. Lee, **K. C. Yeong**, **and H. T. Ewe**
Universiti Tunku Abdul Rahman, Malaysia

Abstract— An inverse model named the Radiative Transfer Inverse Scattering Model (RTISM) for the retrieval of sea ice thickness using Radiative Transfer Theory (RTT) had previously been developed by the authors. The model incorporates the use of the Dense Medium Phase and Amplitude Correction Theory (DMPACT) for better accuracy in the radar backscatter calculations and the application of the Levenberg-Marquardt Algorithm (LMA) to predict the sea ice thickness from the radar backscatter data. While the model has been successful in its attempts to predict the sea ice thickness from radar backscatter data, it has limitations in extending its applications to other sea ice parameters. In this paper, the study of using Simulated Annealing (SA) as an alternative solution for the LMA in the RTISM is presented. SA is appealing as a viable option to replace the LMA due to several reasons. It is a global optimizer and reduces the likelihood of being trapped in a local extremum, thus improving convergence. In addition, SA eliminates the cumbersome recalculation of the Jacobian matrices of the problem function for different applications, as required by LMA. Thus, the use of SA generalizes the inverse model and allows for more room to extend its applications. A comparison between the performances of both optimizers implemented in the RTISM shall be explored in terms of the execution time and accuracy in predicting the sea ice thickness.

Adaptive Boundary Approach for EMF Exposure Assessment in Broadband Measurements

Dragan Kljajic, **Nikola Djuric**, **Karolina Kasas-Lazetic**, **and Danka Antic**
Faculty of Technical Sciences, University of Novi Sad
Trg D. Obradovica 6, Novi Sad 21000, Serbia

Abstract— Recently proposed boundary approach for exposure assessment of humans to electromagnetic field (EMF), regarding continuous broadband monitoring, offers determination of daily upper and lower exposure boundaries. This means that the range with potential exposure of the general population, as well as occupational one, can be located in real time. As an advancement of this method, our paper presents a new approach based on adaptation of exposure boundaries in order to reduce the difference between them and this will increase the precision of the assessment. Frequency spectrum analysis has been applied, determining the appropriate reference levels, at particular in-situ location, for the boundary approach improvement. The results of performed in-situ test measurement of high-frequency electric field strength show attainment in reduction of boundaries difference of 36.25%, consequently resulting with increased precision of the daily exposure assessment for the broadband EMF monitoring.

Introduction: The two most commonly applied approaches for the insitu measurements of EMF level are frequency selective and broadband approaches. For requirements of the longterm continuous EMF level monitoring in the environment and obtaining of real-time EMF level fluctuations, the broadband measuring approach seems to be a more appropriate solution, because it results with single value of the overall and cumulative EMF strength, unlike frequency selective approach, which simultaneously offers results for each separate frequency in particular frequency range.

Unfortunately, due to the lack of information on EMF sources operating frequencies, the utilization of the broadband measuring approach leads to the difficulties in performing exposure assessment, since it is not known which of reference levels has to be applied for a comparison.

The Boundary Exposure Assessment Approach: The proposed boundary approach suggests comparison of the obtained measured values with the lowest and highest reference levels in the field probe frequency range. Applying such an approach, the upper and lower boundaries of exposure have been determined. In the case of high-frequency electric field measurements, the boundaries are calculated via following expressions:

$$\mathrm{GER}_{\mathrm{low}} = \left(\frac{E_m}{E_{ref\,\max}}\right)^2 \quad \text{and} \quad \mathrm{GER}_{\mathrm{up}} = \left(\frac{E_m}{E_{ref\,\min}}\right)^2, \tag{1}$$

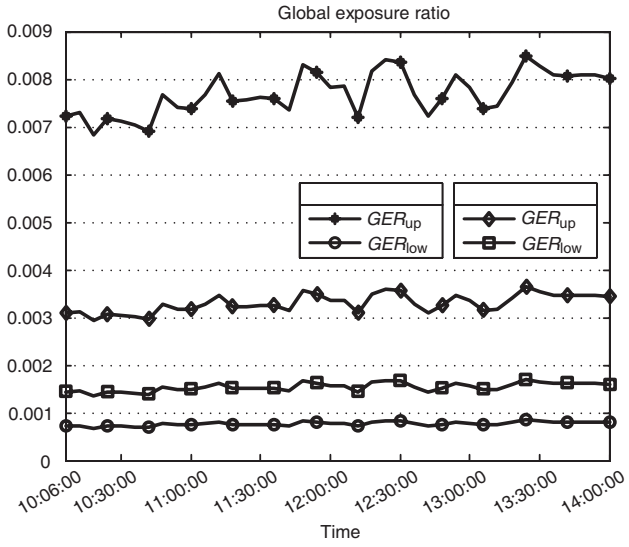

Figure 1: Adaptation of exposure boundaries.

where E_m is the measured electric field strength, while the $E_{ref\,\min}$ and $E_{ref\,\max}$ are minimum and maximum electric field reference levels, defined by corresponding legislation acts.

Combining this approach and the results of continuous in-situ EMF broadband monitoring, the daily boundaries can be obtained, showing fluctuation of the potential exposure over a long period of time.

The Adaptive Boundary Approach: Calculation of exposure boundaries results with certain difference between them. Therefore, this paper focuses on reduction of that difference through the appropriate adaptation of exposure boundaries. The main idea is based on the utilization of frequency selective in-situ measurement combined with broadband EMF monitoring.

The frequency spectrum scanning is applied to determine the frequencies on which EMF sources emits over particular in-situ location. Consequently, it is possible to narrow the frequency range over which the new minimum and maximum reference level should be selected for the exposure boundaries. The performed test measurement brings the reduction of the difference between exposure boundaries, as presented in Fig. 1.

The results show that, involving a frequency selective measurement, a reduction in boundaries difference of 36.25% is attained, resulting with much clearer insight of the human exposure to EMFs at particular in-situ location.

Conclusion: The performed analysis shows that having information on frequency spectrum and EMF sources in the vicinity of in-situ location, it is possible to adapt proposed exposure boundaries and reduce the difference between them.

It can be concluded that such adaptive boundary approach could offer clearer overview of exposure of human population to EMF and increase the precision of the daily exposure assessment on the chosen in-situ location.

Topographic Effect on the Canopy Reflectance

Weiliang Fan[1, 2], **Qinhuo Liu**[1, 2], **Jing Li**[1, 2],
Gaofei Yin[1, 2], **Yelu Zeng**[1, 2], **and Baodong Xu**[1, 2]
[1]State Key Laboratory of Remote Sensing Science, Institute of Remote Sensing and Digital Earth
Chinese Academy of Sciences, Beijing 100101, China
[2]Joint Center for Global Change Studies (JCGCS), Beijing 100875, China

Abstract— Many researches indicate that the topographic factors have strong influence on forest canopy reflectance. However, the quantatively effects of canopy reflectance by topographic is difficulty to be evaluated. For this purpose, the topographic effects on sloping forest reflectance are quantitatively evaluated based on GOST model and the observed remotely-sensed images. The following objectives are addressed: 1) the topographical effects on the sloping canopy reflectance; 2) the topographical effects on the multi-angle view canopy reflectance; and 3) the topographical effects on the reflectance with different canopy structures. The major findings are summarized as follows: First, the topographic factors (slope and aspect) have great impacts on sloping canopy reflectance. A case study shows that the modeled topographic index for reflectance ([bidirectional reflectance distribution of a sloping forest-bidirectional reflectance distribution of a flat forest]/bidirectional reflectance distribution of a flat forest), which is the relative error in modeled canopy reflectance by ignoring the topographic effects, can reach up to 138%, while the maximum observed topographic index for reflectance from a Landsat image is 99%. Therefore, the forest reflectance models considering the topographic factors are recommended for canopy reflectance simulation and canopy parameters retrieval. Second, model simulations show that topography has differents effects on the sloping canopy reflectance in different view directions. These effects should be considered in analyzing multi-angle images. Third, topographic factors have different impacts on sloping canopy reflectance of different canopy structures. Canopy structure should also be considered in topographic correction on reflectance images because topographic factors alone is insufficient for correcting all variations of reflectance with slope and view angle.

A Study of Scattering of Scatterers Using Equivalence Principle Algorithm

Chan-Fai Lum[1], **Fu Xin**[2], **Hong-Tat Ewe**[1], **and Li-Jun Jiang**[2]

[1]Universiti Tunku Abdul Rahman, Malaysia
[2]University of Hong Kong, China

Abstract— For theoretical models used in microwave remote sensing of earth terrain, it is quite common to represent the medium as a random discrete medium where the medium can be modelled as layers of scatterers of basic shapes embedded in the host medium and bounded by upper and lower rough surfaces. By solving the wave propagation and scattering in the medium through Radiative Transfer (RT) theory, the scattering returns from the medium can be obtained. Traditionally, analytical expression of scattering from these scatterers of basic shapes is derived and computed with simplification based on basic assumptions. However, it is generally found from ground truth measurement that the actual shapes of those scatterers are much more complex and irregular. Although it is difficult to simulate the scattering from this wide range of scatterers of different sizes, orientation and shapes, it is possible to model the medium better by representing the scatterers with the major types of scatterers of particular shapes, though the shapes may not be of basic geometrical shapes like spheres. In this study, it is proposed to use the Equivalence Principle Algorithm (EPA) method under the approach of computational electromagnetics to perform the calculation of scattering from these scatterers and incorporate this for the simulation of radar scattering returns from Radiative Transfer (RT) formulation. With this approach, the theoretical model developed can be extended to cover scattering from scatterers which are not easily represented by basic geometrical shapes. Comparison of the simulation based on Mie scattering and EPA will be presented with theoretical analysis for better application of this method in medium such as snow or sea ice. The model prediction is also compared with satellite SAR data with physical parameters input from ground truth measurement conducted in Antarctica.

Session 3A6
SC3: Fiber Optic Sensors

Ultra-sensitive Near-infrared Fiber-optic CO_2 Sensors

Xinyuan Chong[1], **Ki-Joong Kim**[2], **Paul R. Ohodnicki**[3], **Chih-Hung Chang**[2], **and Alan X. Wang**[1]

[1]School of Electrical Engineering and Computer Science
Oregon State University, Corvallis, OR 97331, USA
[2]School of Chemical, Biological & Environmental Engineering
Oregon State University, Corvallis, OR 97331, USA
[3]National Energy Technology Lab
United States Department of Energy, Pittsburgh, PA 15236, USA

Abstract— IR absorption spectroscopy is widely used as a simple and reliable technique for both detection and identification of hazardous and greenhouse gases. Various mid-IR (2.5–10 μm wavelength) methods that work at the highly sensitive fundamental vibration bands, such as Fourier transform IR (FT-IR) spectroscopy that detect gases through spectroscopic signatures, are available commercially. However, most commercial mid-IR spectrometers are large, expensive, and heavy tabletop instruments. On the other hand, near-infrared (NIR $\sim$ 0.6–2.5 μm wavelength) optoelectronic devices are miniaturized, low cost, and highly reliable. The biggest challenge is that most gases do not have fundamental vibration bands at NIR regions, and hence it has relatively low detection sensitivity.

To resolve this challenge, we develop an ultra-short NIR fiber-optic gas sensor by depositing a thin layer of metal-organic framework (MOF) on the core of multimode fibers. MOF is a new class of highly porous crystalline material consisting of metal ions and bridging organic ligands linked together by coordination bonds. Due to its high surface area, chemical and physical tailorability and tunable nanostructured cavities, it can be used for gas sensing by effectively concentrating various gases from the ambient environment. The fiber-optic gas sensor was fabricated by growing nanoporous MOF materials on the core surface of an etched optical fiber. First, standard buffered oxide etchant was used to etch away the cladding of a fluorine-doped silica cladded/silica core multimode fiber (MMF) (Thorlabs AFS 105/125Y). The etched length is about 8 cm. To increase the interaction between the evanescent field and the surrounding gas molecules, the core of the fiber was etched to approximately 75 μm. Second, the etched MMF was cleaned thoroughly, followed by O_2 plasma treatment (50 w) for 20 minutes. Finally, a 100 nm thick MOF was grown on the surface of the etched core by stepwise layer-by-layer (LBL) method. The fiber-optic sensor was then placed inside a gas cell connecting with CO_2 flowing system. Gas sensing experiment was performed by scanning the wavelength from 1571.5 nm to 1573.5 nm. The detection limit is 500 ppm with overall real-time response of only 40 s. Such ultra-short fiber-optic gas sensors with rapid response time can be used for greenhouse gas detection and environmental protection.

Development of a Six-dof Fiber Bragg Grating Force-torque Sensor for Minimally Invasive Robotic Surgery

Cheol Kim, Chan-Hee Lee, and Seong-Min Yun
Department of Mechanical Engineering, Kyungpook National University
80 Daehak-Ro, Book-Gu, Daegu 702-701, South Korea

Abstract— Minimally invasive robotic surgery is recently attracting much attention, because it can alleviate patients' pain, bleeding, and long-term recovery, etc.. If the robotic surgery end has a haptic device equipped with a 6-dof force sensor, surgeons can easily control their operating grasping forces. In an effort to develop a 6-dof optical sensing device with a FBG (Fiber Bragg Grating) sensor which is applicable to detect forces acting on the end-effectors of a minimally invasive surgical robot, a new design analysis method has been developed. The sensing device attached to an end-effector consists of a cylindrical frame structure (Fig. 1) and a FBG optical fiber surrounding the frame diagonally. As the frame deforms subjected to forces and moments, the attached FBG fiber with 2000 micro-strain of pretension also elongates or contracts. Deformations of the frame was calculated by the finite element method subjected to x-, y-, and z-direction forces and three moments about x, y, and z axes, respectively. Displacements of the FBG fiber regarding to six load-types could be then extracted from frame deformation data and converted to changes in wavelength on the basis of an equation of optical fiber reflected wavelength and FBG strain. Using the developed method, various wave lengths were calculated as three forces changed from 0 to 10 N and three moments varied 0 N-mm to 500 N-mm. To validate accuracy of the analytic design method, a system of the 6-dof FBG sensor with a frame was fabricated and tested under the loads used for analyses. The changes in wavelength were measured by an optical spectrum analyzer in the experiment. Analytical and experimental results showed a good correlation with 4% error. The sensitivities of the theoretical and analytical models were very similar.

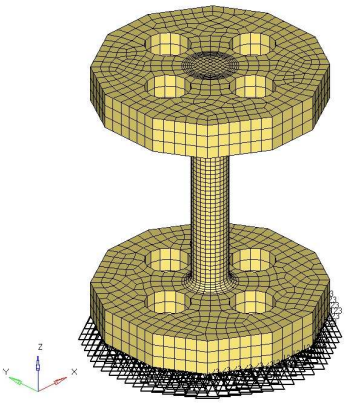

Figure 1: An 6-dof sensing device with a frame and FBG a fiber.

In-line Fiber Filters Using Tapered Flat-clad Fiber

Jian-Wei Zheng[1], **Shih-Hsin Lo**[1], **and Nan-Kuang Chen**[2]

[1]Department of Electro-Optical Engineering
National United University, Miaoli 360, Taiwan
[2]Optoelectronics Research Center
National United University, Miaoli 360, Taiwan

Abstract— Making optical fiber sensor components technology have chemical-etching, fused-tapering, laser ablation etc., Most of used the hydrogen flame to made the tapered fiber. In this experiment, is used the hydrogen flame to made the taper fiber at the flat-clad fiber, shown in Fig. 1. The diameter is around 20 µm, then the fiber was connected to superluminescent diodes and optical spectrum analyzer, Fig. 2 is the experimental set-up, we found the taper flat-clad fiber has interference, shown in Fig. 3, and further explore.

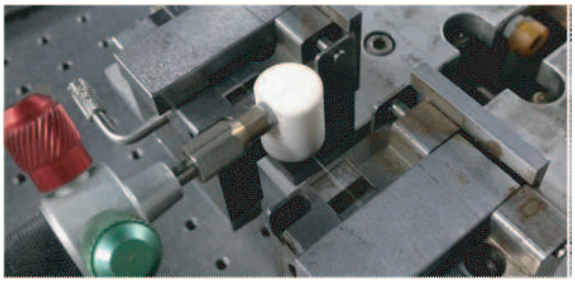

Figure 1: The hydrogen flame-brushing technique.

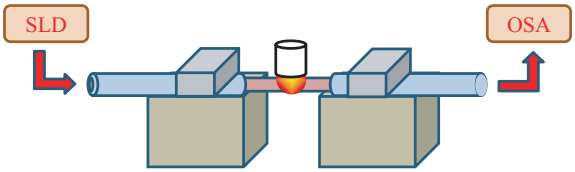

Figure 2: Experimental set-up.

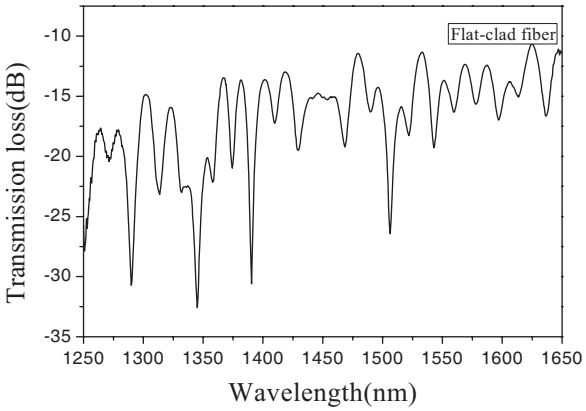

Figure 3: Spectrum of the taper flat-clad fiber.

REFERENCES

1. Li, C., A. H. Feng, X. J. Gu, and D. L. Chen, "Localized cyclic strain measurements of friction stir welded aluminum alloy using flat-clad optical fiber sensor array," *IEEE Sens. J.*, Vol. 10, 888–892, 2010.
2. Feng, A., et al., "Flat-cladding fiber Bragg grating sensors for large strain amplitude fatigue tests," *Sensors*, Vol. 10, No. 8, 7674–7680, 2010.

High Sensitivity Index Sensor Based on Core-cladding Modes Interferences in Hollow Core Fiber

Shih-Hsin Lo[1], **Jian-Wei Zheng**[1], **and Nan-Kuang Chen**[1, 2]

[1]Department of Electro-Optical Engineering, National United University, Miaoli 360, Taiwan
[2]Optoelectronics Research Center, National United University, Miaoli 360, Taiwan

Abstract— In this work, we demonstrate using a single mode fiber (SMF-28) end-spliced with a hollow optical fiber (HOF) composition broadband high sensitivity micro fiber Michelson interferometers (FMI) possess a fiber spherical lens can test outside refraction index (RI). The output end of the HOF is fused by arc to form a spherical lens, shown in Fig. 1, for efficiently collecting reflection lights from external moving materials under test. This broadband high sensitivity micro-FMI with extinction ratio of 25 dB over 1250–1650 nm wavelength and the reflected cladding modes can rise to beat signals, shown in Fig. 2. The transmission spectra of using this experimental set-up (Fig. 3) to test different external environment RI, the Fig. 4 shows the transmission spectra in the difference RI of 1.456, 1.54 and 1.6. When refraction index increase the extinction ratio will gradually decreased. Therefore, sensing external environment refractive index for using this micro fiber Michelson interferometers is feasible.

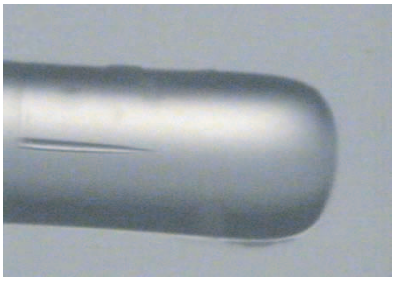

Figure 1: FMI with a lensed HOF.

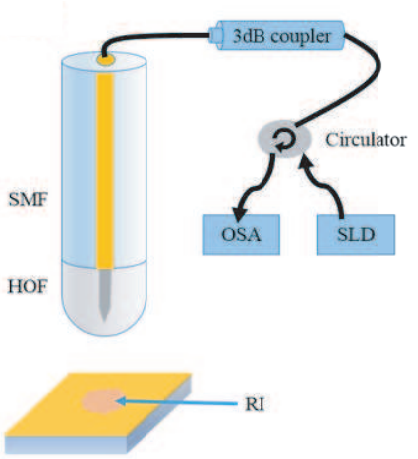

Figure 2: The experimental set-up for FMI.

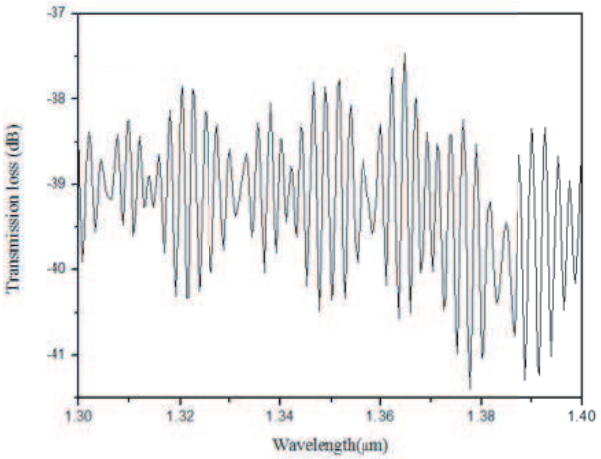

Figure 3: Transmission spectra of the FMI with an end-sphered HOF.

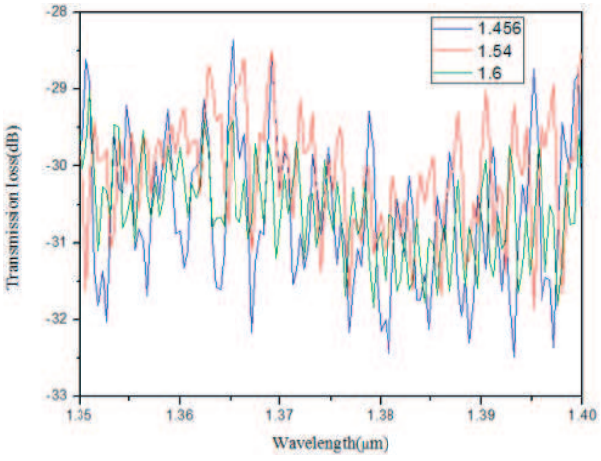

Figure 4: The transmission spectra in the difference RI.

REFERENCES

1. Chen, N.-K., K.-Y. Lu, and C. Lin, "High-sensitivity broadband micro-Michelson-interferometer based on an end-sphered hollow-core fiber," *National Fiber Optic Engineers Conference, Optical Society of America*, 2011.
2. Chen, N.-K., K.-Y. Lu, and C. Lin, "Asymmetric fiber Michelson interferometer with a spatial mode beating arm for moving direction determination," *CLEO: Science and Innovations, Optical Society of America*, 2012.
3. Rong, Q., et al., "In-fiber quasi-Michelson interferometer with a core-cladding-mode fiber end-face mirror," *Applied Optics*, Vol. 52, No. 7, 1441–1447, 2013.
4. Du, Y., et al., "Polarization-dependent in-line quasi-Michelson interferometer based on PM-PCF reflection," *Applied Optics*, Vol. 52, No. 15, 3591–3596, 2013.

Surface Plasmon Resonance Excitation in Metal-clad Single-mode Optical Fiber through the Tunneling of Fundamental Mode Across the Fiber Cladding

Yuri N. Kulchin[1], **Oleg B. Vitrik**[1,2], **and Anton V. Dyshlyuk**[1,2]

[1]Institute of Automation and Control Processes, FEB, RAS, Russia
[2]Far Eastern Federal University, Russia

Abstract— We present a novel approach to the excitation of surface plasmon resonance (SPR) in a single mode optical fiber with metal-coated optical cladding for precision refractometery and biosensing applications. As a rule fiber-optic SPR-refractometers built around single-mode fibers require removal of a part of optical cladding so that the metal layer could be deposited in close proximity of the fiber core to make it possible for the fundamental mode to couple to surface plasmons [1, 2]. The proposed method uses a bent fiber with a reduced normalized frequency to enable the fundamental mode to tunnel across the cladding and excite surface plasmons in the metal film applied to the outer surface of the cladding. Such an approach eliminates the need for mechanical or chemical modification of the fiber thus simplifying the fabrication procedure and increasing the robustness and longevity of the sensitive element.

The schematic of the waveguide under study is shown in Fig. 1(a). It consists of straight input and output sections and a bent metal-clad central section. We used numerical modeling based on eigenmode expansion method to simulate the propagation of light through the studied waveguide. It was shown that by choosing a proper combination of normalized frequency, bend radius, and metal film thickness one can achieve strong coupling between the fundamental mode guided by the fiber core, and symmetric surface plasmon mode supported by the metal layer applied to the fiber cladding. This brings about a narrow dip in the transmission spectrum of the waveguide whose resonant wavelength has a strong and nearly linear dependence on the refractive index of the surrounding medium n_3, which enables precision refractometric measurements with spectral sensitivity and resolution estimated at 70 µm/refractive index unit and $3 \cdot 10^{-7}$, respectively.

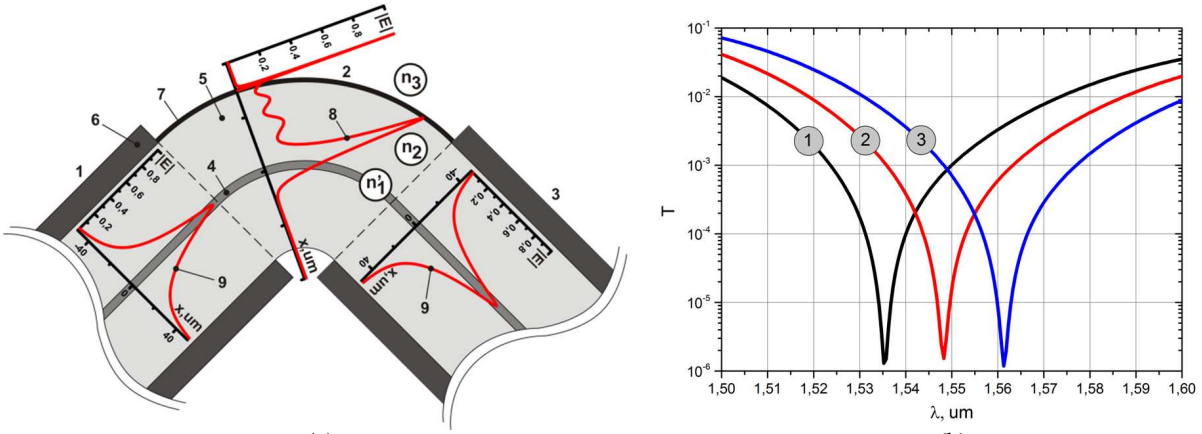

(a) (b)

Figure 1: (a) The schematic of the waveguide under study: 1 — straight input section, 2 — bent metal-coated sensing section, 3 — straight output section, 4 — waveguide core, 5 — waveguide cladding, 6 — polymer jacket, 7 — silver layer, 8 — amplitude profile of one of the two modes responsible for the transfer of the core mode power to surface plasmons, 9 — amplitude profile of the fundamental mode of sections 1 and 3. (b) Calculated transmission spectra for three values of the surrounding medium refractive index: $n_3 = 1.4312$ (1), 1.4314 (2), 1.4316 (3).

REFERENCES

1. Xiao, G. and W. J. Bock, eds., *Photonic Sensing: Principles and Applications for Safety and Security Monitoring*, Wiley, 2012.
2. Verma, R. K. and B. D. Gupta, *J. Phys. D: Appl. Phys.*, Vol. 41, 095–106, 2008.

High Sensitivity Vibration Sensor Using Monolithic Micro Michelson Fiber Interferometer

Chia-Lung Tsai, Jhih-He Jhang, and Nan-Kuang Chen
Lienda, Miaoli 36063, Taiwan

Abstract— We demonstrate high sensitivity monolithic micro Michelson fiber interferometer with high order spatial modes beating using a hundreds-of-micrometer-long hollow core fiber, with a lensed fiber end, splicing to a singlemode fiber for vibration sensing applications. In device fabrication and experiment set-up we use single mode fiber (SMF-28) welding hollow-core fiber (HOF) the sample HOF length is 151.13 µm, HOF core diameter is 5 µm then end spherical we measurement sample Maximum power of 13.59 µm then we use super luminescent diodes (SLDs), 3 dB coupler and optical spectrum analyzer (OSA) spectrum measurement (Figure 1) Measurements use SLDs and OSA from this (Figure 2) use SLDs and OSA from this sample then put mirror to end in this (Figure 3) use tunable laser and OSA from this (Figure 4) use tunable laser and oscilloscope (OSC) from this sample no vibration straight 17 mv peak to peak (Figure 5) use tunable laser and OSC from this vibration mirror peak-to-peak dynamic 118 mV (Figure 6).

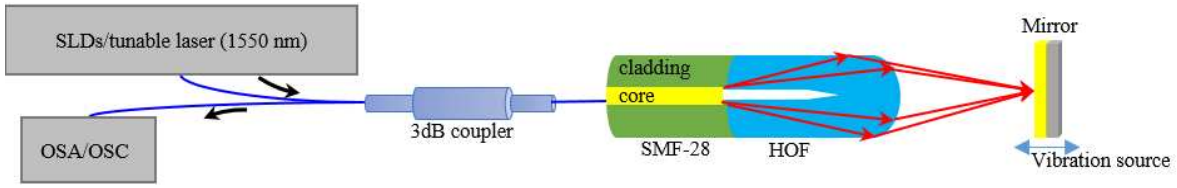

Figure 1: We use super luminescent diodes(SLDs), 3 dB coupler and optical spectrum analyzer (OSA) spectrum measurement.

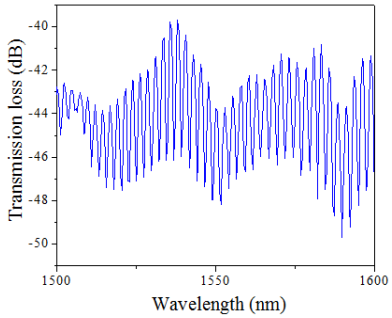

Figure 2: SLDs and OSA measurements.

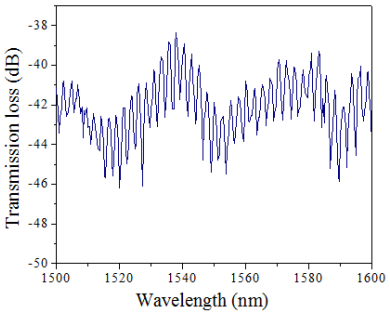

Figure 3: Use SLDs and OSA this sample then put mirror to end.

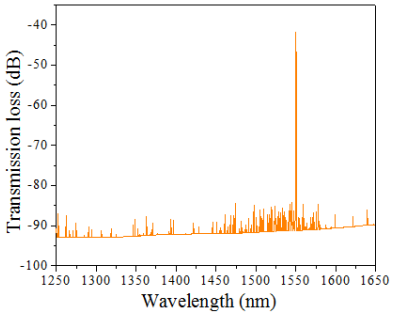

Figure 4: Tunable laser and OSA.

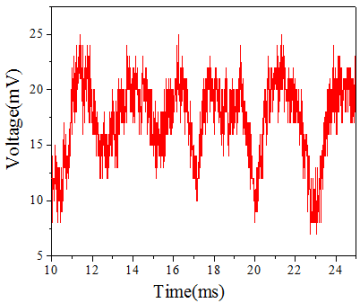

Figure 5: Use tunable laser and OSC from this sample no vibration.

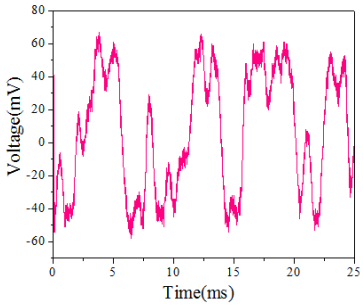

Figure 6: Use tunable laser and OSC from this vibration mirror.

REFERENCES

1. Rong, Q., X. Qiao, T. Guo, W. Bao, D. Su, and H. Yang, "Orientation-dependent fiber-optic accelerometer based on grating inscription over fiber cladding," *Optics Letters*, Vol. 39, No. 23, December 1, 2014.

Flow Rate Sensing Based on Monolithic Fiber Michelson Interferometer

Kuan-Yu Lou[1], **Shih-Hsin Lo**[1], **and Nan-Kuang Chen**[1, 2]

[1]Department of Electro-Optical Engineering, National United University, Miaoli 360, Taiwan
[2]Optoelectronics Research Center, National United University, Miaoli 360, Taiwan

Abstract— The fiber sensor had been widely used, such as strain, temperature, and in different liquid. In this work, we demonstrate the micro-Michelson interferometer (MMI) flow speed sensor. The micro-Michelson is made by single mode fiber end-flat and then fusion with hollow core fiber (HOF), the end-flat of the HOF is the sphere. HOF core diameter is 5 μm and the length is 152 μm. We measurement the water flowing when the bobble past throw the sensor. Fig. 1 shows the device structure and the experimental set up, the MMI is connect to the tunable laser and the oscilloscope. The distance of MMI to the pipes is 6 μm. Fig. 2(a) shows non-flow speed in the pipes. When the bubbles pass through the sensor it with the different speed it will have different effect it shown in Figs. 2(b), (c).

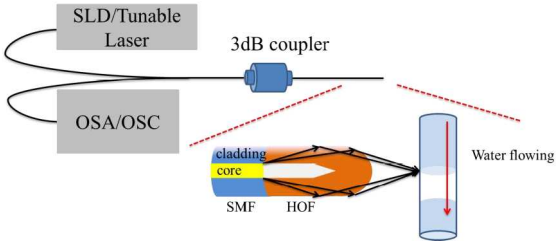

Figure 1: Device structure and the experimental set up.

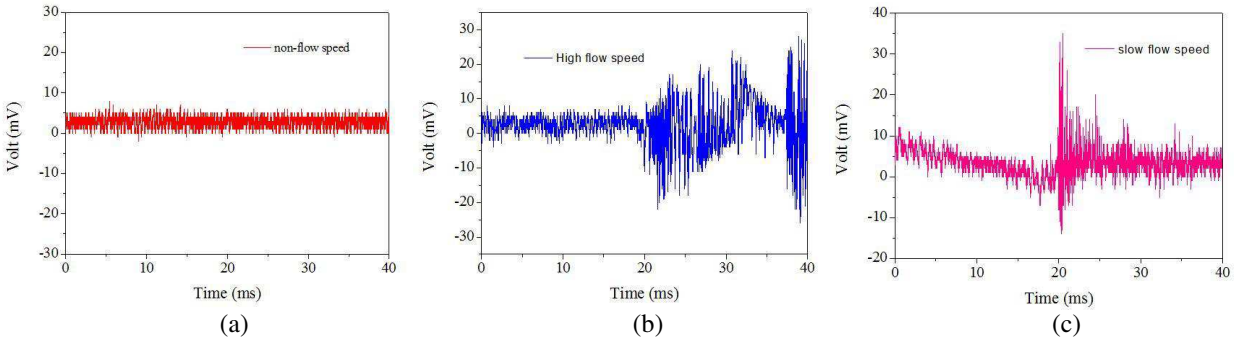

Figure 2: (a) Non-flow speed pass through sensor, (b) high-flow speed pass through sensor, (c) slow-flow speed pass through sensor.

REFERENCES

1. Chen, N.-K., et al., "Ultracompact monolithic broadband in-line micro interferometric sensor based on multi-beam interference," *CLEO: Science and Innovations*, Optical Society of America, 2011.
2. Chen, N.-K., K.-Y. Lu, and C. Lin, "High-sensitivity broadband micro-Michelson-interferometer based on an end-sphered hollow-core fiber," *Optical Fiber Communication Conference and Exposition and the National Fiber Optic Engineers Conference*, 2011.
3. Feng, X., et al., "Characterization of liquid flow in the spinning cloth disc reactor: Residence time distribution, visual study and modeling," *Chemical Engineering Journal*, Vol. 235, 356–367, 2014.
4. Lorenz, U. J. and A. H. Zewail, "Observing liquid flow in nanotubes by 4D electron microscopy," *Science*, Vol. 344, No. 6191, 1496–1500, 2014.

Micro Non-contact Profilometer Using Integrated Fiber Michelson Interferometer

Jhih-He Jhang[1], **Yu-Lin Tseng**[1], **and Nan-Kuang Chen**[1, 2]

[1]Department of Electro-Optical Engineering, National United University, Miaoli, Taiwan
[2]Optoelectronics Research Center, National United University, Miaoli, Taiwan

Abstract— Fiber sensors had been widely used in many different places, the traditional fiber Michelson interferometer is non-integrated. In this work, we demonstrate a high-sensitivity micro-Michelson interferometer (MMI) using a single mode fiber end-spliced with a short hollow-core fiber end-fused by arc to measure a tiny variation of topography. The experimental set-up as shows in Fig. 1, the topography using a gold tape and a silver tape to made topography. Thickness of gold tape and silver tape are 70 μm and 37 μm, respectively. The depth on the gold tape is equivalent to the lower topography. Non-cleaved place on the gold tape is equivalent to the higher topography. Fig. 2 shown the spectrum respond of the MMI is correspondence to the high and low topography.

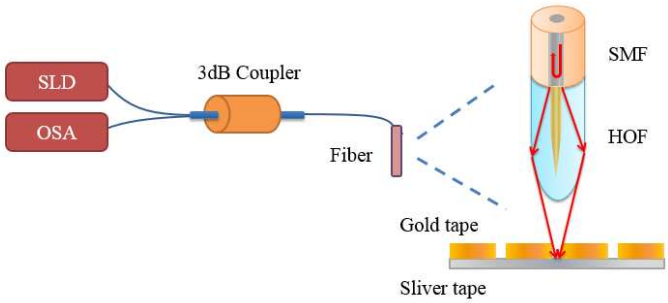

Figure 1.

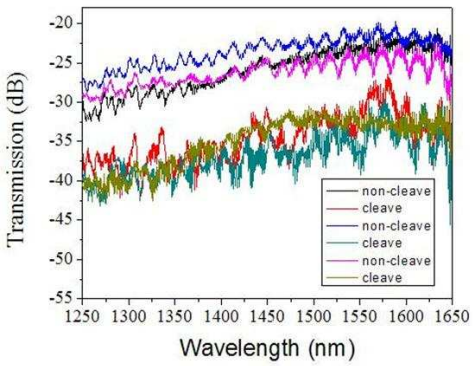

Figure 2.

REFERENCES

1. Chen, N.-K., et al., "Ultracompact monolithic broadband in-line micro interferometric sensor based on multi-beam interference," *CLEO: Science and Innovations*, Optical Society of America, 2011.
2. Chen, N.-K., K.-Y. Lu, and C. Lin, "High-sensitivity broadband micro-Michelson-interferometer based on an end-sphered hollow-core fiber," *Optical Fiber Communication Conference and Exposition and the National Fiber Optic Engineers Conference*, 2011.
3. Takeda, M., H. Ina, and S. Kobayashi, "Fourier-transform method of fringe-pattern analysis for computer-based topography and interferometry," *J. Opt. Soc. Am.*, Vol. 72, No. 1, 156–160, 1982.

Micro Fiber Accelerometer Based on Multibeam Michelson Interferometer

Yu-Lin Tseng[1], **Jhih-He Jhang**[1], **and Nan-Kuang Chen**[1, 2]

[1]Department of Electro-Optical Engineering, National United University, Miaoli, Taiwan
[2]Optoelectronics Research Center, National United University, Miaoli, Taiwan

Abstract— We use a High-sensitivity broadband micro-Michelson-interferometer to measure acceleration. Use a single mode fiber (SMF) end-spliced with a short hollow-core fiber (HOF) end- fused by arc to measure a sway of spring piece. Tunable laser is launched into the optical fiber and fixed spring piece on the fixture. The distance of optical fiber to spring piece is around 16.14 nm. Then, make the optical fiber and spring piece together become a devise, shown in Fig. 1. Push the devise going quickly and make it stop suddenly. At this time, we can see spring piece sway violently to weakly and then stop, shown in Fig. 2. When light passes through an optical fiber to the spring piece, the light will be reflected back from the surface of spring piece and get spectrum from Oscilloscope. By calculating, we can get acceleration from sway of spring piece.

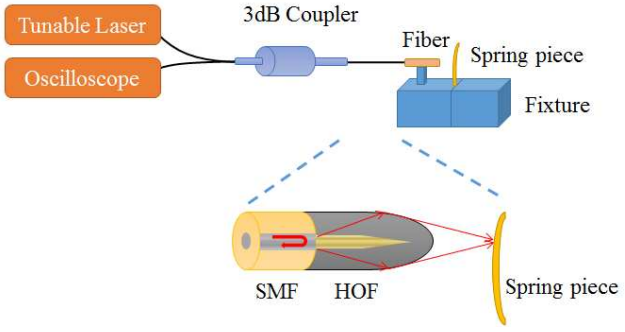

Figure 1.

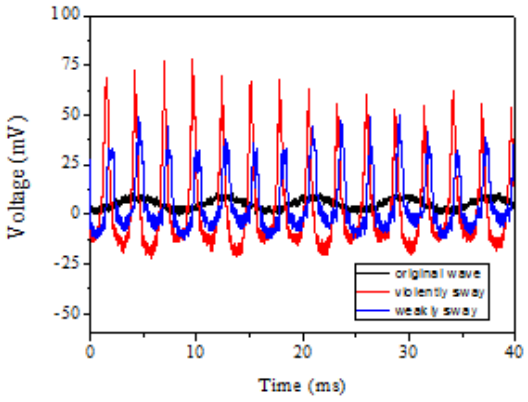

Figure 2.

REFERENCES

1. Peng, F., et al., "In-fiber integrated accelerometer," *Optics Letters*, Vol. 36, No. 11, 2056–2058, 2011.
2. Peng, F., et al., "Compact fiber optic accelerometer," *Chinese Optics Letters*, Vol. 10, No. 1, 2012. 011201.
3. Chen, C., et al., "Broadband Michelson fiber-optic accelerometer," *Applied Optics*, Vol. 38, No. 4, 628–630, 1999.

Session 3A7a
SC3: Non-reciprocal and Topological Features in Photonic Systems

Generating Non-reciprocal Phases in Photonic Systems

Benjamin J. Eggleton[1] and Enbang Li[2]

[1]CUDOS, University of Sydney, NSW, Australia
[2]University of Wollongong, NSW, Australia

Abstract— Photonic topological insulators support unidirectional protected modes and enable light to flow around imperfections with perfect transmission. Generating non-reciprocal phases in photonic systems is vital in realizing photonic topological insulation. In this talk, methodologies and techniques for experimentally generating non-reciprocal phases will be discussed.

Topological Photonics Quasicrystals

Miguel A. Bandres[1], **Mikael C. Rechtsman**[1], **and Mordechai Segev**[2]

[1]Physics Department and Solid State Institute, Technion, Haifa 32000, Israel
[2]Department of Physics, The Pennsylvania State University, University Park, PA 16802, USA

Abstract— Topological insulators are materials that insulate in their bulk, but allow extremely robust flow of current on their surfaces [1]. In two dimensions, they possess one-way edge currents that that are immune to scattering and imperfections. Recently, the ongoing theoretical effort to realize topological insulation and protection in optics [2–8] culminated in the first experimental observation of photonic topological insulators in optics [9], as demonstrated in an honeycomb array of evanescently coupled helical waveguides. This effect was also demonstrated in a silicon-chip platform using a lattice of coupled ring resonators [10]. Introducing topological protection into photonics not only brings technology closer to employing the unique properties of topological phases in real applications but also provides an entirely new platform for probing and understanding topological protection.

Quasicrystals are unique structures with long-range order but no periodicity [11]. They constitute an intermediate phase between crystals and disordered media. Quasicrystal transport is extremely rich, this is evidenced by the surprising regime of disorder-enhanced transport in a photonics quasicrystal [12], and the direct connection between 1D quasi-crystalline band structures and topological physics [13].

Here we show that it is possible to have a topological phase in two-dimensional quasicrystals without zero magnetic field. This topological quasicrystal exhibits gapless one-way edge states that scale with the systems perimeter, contrary to the general states of a quasycristal system which are critical, characterized by a power law decay. We show that the spectrum exhibits a rich structure of topological minigaps whose gapless edge states only form by increasing the system size due to their long penetration depths into the bulk. This is a new phenomenon in which the quasicrystal topological structure emerges as a function of the system size, in contrary to periodic systems where the topological phase can be completely characterized using its unit cell. We demonstrate the existence of this topological phase both by using a topological index (Bott index) and also by studying the dynamics (unidirectional transport) of the gapless edge states. Our specific model is a Penrose lattice of helical optical waveguides, a photonic quasicrystal; however we expect this new topological quasicrystal phase to be universal.

ACKNOWLEDGMENT

The research leading to these results has received funding from the European Union's — Seventh Framework Programme (FP7/2007-2013) under grant agreement No. 629114 MC. Structured Light.

REFERENCES

1. Kane, C. and E. Mele, *Phys. Rev. Lett.*, Vol. 95, 226,801, 2005.
2. Wang, Z., Y. Chong, M. Soljacic, and J. D. Joannopoulos, *Nature*, Vol. 461, 772–775, 2009.
3. Khanikaev, A. B., et al., *Nature Materials*, 2012.
4. Fang, K., Z. Yu, and S. Fan, *Nature Photonics*, Vol. 6, 782–787, 2012.
5. Hafezi, M., E. A. Demler, M. D. Lukin, and J. M. Taylor, *Nature Physics*, Vol. 7, 907–912, 2011.
6. Khanikaev, A. B., S. H. Mousavi, W.-K. Tse, M. Kargarian, A. H. MacDonald, and G. Shvets, *Nature Materials*, Vol. 12, 233–239, 2013.
7. Umucalılar, R. O. and I. Carusotto, *Phys. Rev. A*, Vol. 84, 043,804, 2011.
8. Haldane, F. D. M. and S. Raghu, *Phys. Rev. Lett.*, Vol. 100, 013,904, 2008.
9. Rechtsman, M. C., et al., *Nature*, Vol. 496, 196–200, 2013.
10. Hafezi, M., et al., *Nature Photonics*, 2013.
11. Shechtman, D., I. Blech, D. Gratias, and J. W. Cahn, *Phys. Rev. Lett.*, Vol. 53, 1951–1953, 1984.
12. Levi, L., M. Rechtsman, B. Freedman, T. Schwartz, O. Manela, and M. Segev, *Science*, Vol. 332, 1541–1544, 2011.
13. Kraus, Y. E., Y. Lahini, Z. Ringel, M. Verbin, and O. Zilberberg, *Phys. Rev. Lett.*, Vol. 109, 106,402, 2012.

Measuring Topological Invariants in Photonic Systems

Sunil Mittal[1, 2], **Sriram Ganeshan**[1, 3], **Jingyun Fan**[1],
Abolhassan Vaezi[4], **and Mohammad Hafezi**[1, 2]

[1]Joint Quantum Institute, NIST/University of Maryland, College Park, MD 20742, USA
[2]Department of Electrical Engineering and Institute for Research in Electronics and Applied Physics
University of Maryland, College Park, MD 20742, USA
[3]Condensed Matter Theory Center, University of Maryland, College Park, MD 20742, USA
[4]Laboratory of Atomic and Solid State Physics, Cornell University, Ithaca, NY 14853, USA

Abstract— Recently, there has been a surge of interest in investigating topological edge states, with synthetic gauge fields, in various photonic systems. In particular, topological robustness of photonic transport was quantitatively confirmed both in the microwave [1] and telecom domains [2], using synthetic 2D structures. Moreover, topological photonic edge states have been imaged in two concurrent experiments [3, 4]. Edge states are char- acterized by a topologically invariant integer, the winding number. However, measurements of the winding number have so far remained elusive in photonic systems. Here, we report first measurement of the winding number of photonic edge states. We implement the integer quantum Hall model in a photonic system: a two dimensional square lattice of ring resonators with a uniform synthetic magnetic field in the bulk and a tunable gauge field coupled only to the lattice edge. By selectively tuning the gauge flux coupled to the edge, we show that the edge states resonances in the transmission spectra of the device undergo a spectral ow. In particular, for a gauge ux of 2π, the edge state resonances move by their winding number. This experiment provides a new approach for direct measurement of topological invariants, independent of the microscopic details, and thus could be extended to probe topological orders in other photonic and atomic systems.

REFERENCES

1. Wang, Z., et al., "Observation of unidirectional backscattering-immune topological electromagnetic states," *Nature*, Vol. 461, 772–775, 2009.
2. Mittal, S., et al., "Topologically robust transport of photons in a synthetic gauge field," *Phys. Rev. Lett.*, Vol. 113, 087403, 2014.
3. Hafezi, M., et al., "Imaging topological edge states in silicon photonics," *Nat. Photonics*, Vol. 7, 1001–1005, 2013.
4. Rechtsman, M. C., et al., "Photonic floquet topological insulators," *Nature*, Vol. 496, 196–200, 2013.

Realizing One-way Negative Refraction in Magneto-optical Photonic Crystal by Both Parity and Time-reversal Symmetry Breaking

Yan-Feng Chen[1], **Cheng He**[1], **Yin Poo**[2], **and Rui-Xin Wu**[2]

[1]National Laboratory of Solid State Microstructures and Department of Materials Science and Engineering College of Engineering and Applied Science, Collaborative Innovation Center of Advanced Microstructures Nanjing University, Nanjing 210093, China

[2]School of Electronic Science and Engineering, Nanjing University, Nanjing 210093, China

Abstract— One-way propagation of optical wave is highly desired due to its applications as photonic devices, whereas negative refraction have attracted much attention since it companies such novel effects as super-lensing and subwavelength resolution potential. With recent studies on one-way optical propagation, how to realize one-way negative refraction or even one-way cloaking attracts much attention, which has particular importance in security and military applications. Up to now all realized negative refraction are reciprocal. Very recently some theoretical studies predict the nonreciprocal refraction can exist in PCs with symmetry breaking however, they need further experimental verification. In this work, we theoretically and experimentally demonstrate one-way negative/positive refraction based on a two-dimensional composite magneto-optical photonic crystal (MPC), which is fabricated by alumina and ferrite square rods. Biased by magnetic field, the ferrite element breaks the time-reversal (T) symmetry. In the meantime, the heterostructure of the MPC makes the parity (P) symmetry broken. The two broken symmetries induce the MPC has distinguished refractions under a pair of counter-incidence angles (+ and −). The EM wave can transport through the MPC at one incidence angle but be forbidden totally at the opposite angle, forming a one-way refraction. In addition, such one-way refraction could be either positive or negative, which depends on the incidence angle and operating frequency. Further, corresponding experimental demonstrations are given and the results are in good agreement with theoretical predictions. These interesting properties would offer promising applications in optoelectronic devices such as optical isolator, and provide a practical way toward one-way focusing and one-way cloak.

Chiral Interaction of Light and Matter in Confined Geometries

A. Rauschenbeutel
Vienna Center for Quantum Science and Technology, Institute of Atomic and Subatomic Physics
Vienna University of Technology, Wien, Austria

Abstract— When light is strongly transversally confined, significant local polarization components that point in the direction of propagation arise. In contrast to paraxial light fields, the corresponding intrinsic angular momentum of the light field is position-dependent — an effect referred to as spin-orbit interaction of light. Remarkably, the light's spin can even be perpendicular to the propagation direction. The interaction of emitters with such light fields leads to new and surprising effects. For example, when coupling gold nanoparticles or atoms to the evanescent field surrounding a silica nanophotonic waveguide, the intrinsic mirror symmetry of the particles' emission is broken. This allowed us to realize chiral nanophotonic interfaces in which the emission direction of light into the waveguide is controlled by the polarization of the excitation light [1] or by the internal state of the atoms [2], respectively. Moreover, we employ this chiral interaction to demonstrate nonreciprocal transmission of light at the single-photon level through a silica nanofiber [3].

REFERENCES

1. Petersen, J., et al., *Science*, Vol. 346, 67, 2014.
2. Mitsch, R., et al., *Nature Commun.*, Vol. 5, 5713, 2014.
3. Sayrin, C., et al., arXiv: arXiv:1502.01549, 2015.

Non-Hermitian Topological Photonics

S. Weimann[1], **J. Zeuner**[1], **M. Kremer**[1], **M. Rechtsman**[2], **K. G. Makris**[3, 4], **Y. Plotnik**[5], **Y. Lumer**[5], **M. S. Rudner**[6], **M. Segev**[5], **and A. Szameit**[1]

[1]Abbe School of Photonics, Institut für Angewandte Physik
Friedrich-Schiller-Universität Jena, Max-Wien Platz 1, Jena 07743, Germany
[2]Department of Physics, The Pennsylvania State University, University Park, PA 16801, USA
[3]Institute for Theoretical Physics, Vienna University of Technology, Vienna, EU A-1040, Austria
[4]Department of Electrical Engineering, Princeton University, Princeton, NJ 08544, USA
[5]Department of Physics, Technion — Israel Institute of Technology, Haifa 32000, Israel
[6]The Niels Bohr International Academy, Niels Bohr Institute, Copenhagen 2100, Denmark

Abstract— The recent development of topological insulator states for photons [1–3] has led to an exciting new field of "topological photonics," which has as a central goal the development of extremely robust photonic devices [4]. Topological insulator physics has been studied extensively in condensed matter [5] and cold atoms [6], but photonics facilitates introducing non-Hermitian effects through the engineering of optical gain and loss. In this talk, we will present two results demonstrating non-Hermitian topological systems for the first time, as described below. Our systems are realized in an array of laser-written waveguides. Losses in the waveguides are engineered by oscillating waveguide trajectories (Fig. 1(b)). Although in the experiment there are only passive components, this maps directly onto the problem with gain and loss (modulo an overall exponential decay).

(1) The first experiment concerns a one-dimensional dimer model (lattice part S in Fig. 1(b)) in which the non-Hermitian character of the system can be used to extract topological information purely from the bulk dynamics of the system [7]. Since the diffraction of light through the waveguides maps to the Schrödinger equation, its topological character carries over into the optical domain. We show that, as predicted in [7], the 'mean displacement' $\langle \Delta m \rangle$ of the optical wavepacket on the Bsites undergoes a transition as a function of the 'dimerization' $[d_1 - d_1]/2$ of the lattice (Fig. 1(a)). This transition measures the 'winding number' of the lattice, a topological number that must be either zero or one in our case.

(2) The second is the proposal of the first non-Hermitian, PT-symmetric topological system, and its experimental realization in the 'passive-PT' framework. It had been previously thought that PT-symmetric topological states were impossible [8]. Here we provide an example of such a state. The model comprises a topological defect state in a one-dimensional system (shown in Fig. 1(b)). Due to the global PT symmetry, both the bulk and defect states have real eigenvalues. The defect state is observed in Fig. 1(c).

In conclusion, these two experiments constitute the first realization of non-Hermitian topological states in any system in nature.

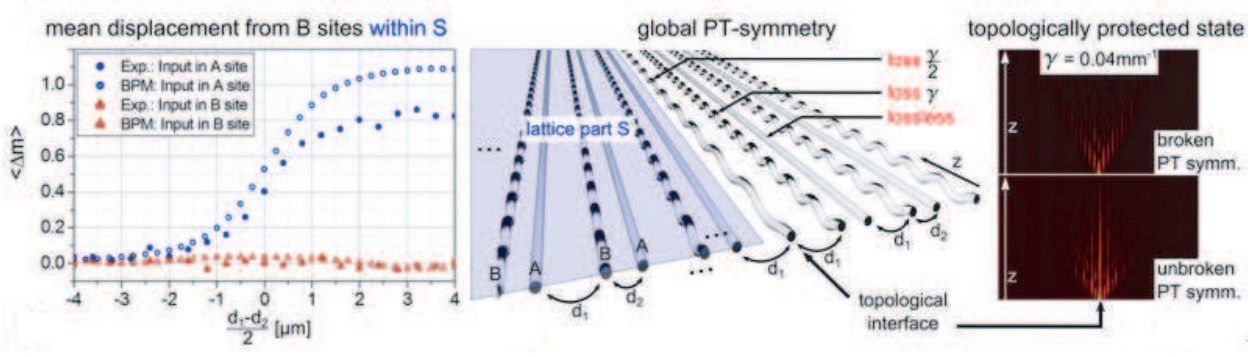

Figure 1: (a) Simulation and experiment showing the topological transition in the non-Hermitian dimer model; (b) schematic showing the experimental setup with global PT symmetry; (c) experiment showing no topological state (above), and with topological state (below).

REFERENCES

1. Haldane, F. D. M. and S. Raghu, *Phys. Rev. Lett.*, Vol. 100, 013904, 2008.
2. Wang, Z., et al., *Nature*, Vol. 461, 772–775, 2009.
3. Rechtsman, M. C., et al., *Nature*, Vol. 496, 196–200, 2013.
4. Hafezi, et al., *Nature Physics*, Vol. 7, 907–912, 2011.
5. Hasan, M. Z. and C. L. Kane, *Rev. Mod. Phys.*, Vol. 82, 3045–3067, 2010.
6. Jotzu, G., et al., *Nature*, Vol. 515, 237–240, 2014.
7. Rudner, M. S. and L. S. Levitov, *Phys. Rev. Lett.*, Vol. 102, 065703, 2009.
8. Hu, Y. C. and T. L. Hughes, *Phys. Rev. B*, Vol. 84, 153101, 2011.

Unidirectional Spontaneous Emission in Waveguides with Tailored Photonic Spin-orbit Coupling

Søren Stobbe and Peter Lodahl
Niels Bohr Institute, University of Copenhagen, Blegdamsvej 17, DK-2100 Copenhagen, Denmark

Abstract— We review the recent experimental progress on using the spin-orbit interaction of light to construct deterministic light-matter interfaces. We show that photonic-crystal waveguides with particular symmetries exhibit a pronounced photonic spin-orbit coupling, and quantum emitters placed inside such media exhibit highly directional emission. The direction depends on the orientation of the dipole moment of the emitters and we experimentally demonstrate a directionality of 90% of single photons emitted from a quantum dot into a single propagating mode.

When an excited quantum emitter decays by spontaneous emission, light is normally emitted in all directions. By embedding the emitter in photonic nanostructures, the emission can be funnelled into specific optical modes [1]. Using photonic-crystal waveguides, nearly all spontaneous emission is emitted in the propagating modes (propagating in opposite directions) of the waveguide and so far a coupling efficiency of 98.4% has been demonstrated experimentally [2]. Photonic-crystal waveguides are therefore amongst the most promising platforms for deterministic quantum gates with optical photons.

Photonic-crystal waveguides offer an exceptional exility in their design and fabrication, and novel functionalities may be implemented by imposing a particular glide-plane symmetry of the crystal. Here we are concerned with structures optimized for creating large regions with a local circular polarization. In this case the internal quantum state of an embedded emitter is directly mapped onto a single propagation direction due to the photonic spin-orbit interaction [3]. This interaction is inherent to Maxwell's equations but has only been studied rather recently because it vanishes in the paraxial approximation, which is often a good approximation for laser beams but breaks down in photonic nanostructures due to the strong transverse mode confinement. The link between polarization and direction constitutes a deterministic chiral light-matter interface, which may be probed by embedding quantum dots with circularly polarized excitonic states [4, 5].

REFERENCES

1. Lodahl, P., S. Mahmoodian, and S. Stobbe, "Interfacing single photons and single quantum dots with photonic nanostructures," arXiv:1312.1079, to appear in *Rev. Mod. Phys.*, 2015.
2. Arcari, M., I. Söllner, A. Javadi, S. L. Hansen, S. Mahmoodian, J. Liu, H. Thyrrestrup, E. H. Lee, J. D. Song, S. Stobbe, and P. Lodahl, "Near-unity coupling efficiency of a quantum emitter to a photonic-crystal waveguide," *Phys. Rev. Lett.*, Vol. 113, 093603, 2014.
3. Petersen, J., J. Volz, and A. Rauschenbeutel, "Chiral nanophotonic waveguide interface based on spin-orbit interaction of light," *Science*, Vol. 346, 67, 2014.
4. Luxmoore, I. J., N. A. Wasley, A. J. Ramsay, A. C. T. Thijssen, R. Oulton, M. Hugues, S. Kasture, V. G. Achanta, A. M. Fox, and M. S. Skolnick, *Phys. Rev. Lett.*, Vol. 110, 037402, 2013.
5. Söllner, I., S. Mahmoodian, S. L. Hansen, L. Midolo, A. Javadi, G. Kirsanske, T. Pregnolato, H. El-Ella, E. H. Lee, J. D. Song, S. Stobbe, and P. Lodahl, "Deterministic photon-emitter coupling in chiral photonic circuits," arXiv: 1406.4295.

Surface Impedance and Bulk Zak Phase Correspondence in Two Dimensional Photonic Crystals

Meng Xiao[1], **Xueqin Huang**[1], **Zhihong Hang**[2], **Z. Q. Zhang**[1], **and C. T. Chan**[1]

[1]Department of Physics and Institute for Advanced Study
The Hong Kong University of Science and Technology, Clear Water Bay, Hong Kong, China
[2]Department of Physics, Soochow University, 1 Shizi Street, Suzhou 215006, China

Abstract— Surface impedance is an important concept in classical wave systems. It tells how a wave reacts when encountering an interface, say between the vacuum and a dielectric photonic crystal (PC). We find that the surface impedance of a truncated PC is related to the geometric property (Zak phase) of the bulk band of this PC. This surface bulk correspondence plays a crucial role in understanding the formation of interface states between PCs. While the existence of interface states can be obtained with the surface impedance, this correspondence uncovers the underlying physics which explains the robustness of the interface state through the Zak phases of reduced 1D bulk bands. We give two examples to illustrate the significance of this surface bulk correspondence.

The first example is about interface states between two PCs consisting of square array of dielectric cylinders in the vacuum. The low frequency response of the PC can be described with the monopole and dipole excitations of the dielectric cylinder. When the parameters of the cylinders are carefully chosen, there exists an accidental degeneracy point between the monopole mode and the dipole mode at the Brillouin zone center. We show that if the parameters of two PCs are both near this accidental degeneracy point, we can always find at least one interface state at the boundary. This peculiar feature can be explained with the surface bulk correspondence.

The other example is about the interface state between two PCs with mutually inverted structure sharing a common gap above the lowest band. We show that the interface state exists as long as the PCs possess a mirror symmetry on average along the direction of the interface. The robustness of the interface state stems from the difference of the Zak phases of the lowest bulk bands across the boundary. Zak phase is related to the distribution of the Wannier function and that of the lowest band tends to concentrate on the high dielectric component of the PC. Hence the Zak phases of the lowest bulk bands are different for PCs with inverted structure. According to the surface bulk correspondence, the surface impedance of the gaps above the lowest band are also different and thus interface state exists in the common gap region above the lowest band.

Session 3A7b
SC3: Strong Light-matter Coupling and Strongly Interacting Photons 1

Single Molecules Coherently Coupled to a Dielectric Nanoguide

V. Sandoghdar
Max Planck Institute for the Science of Light (MPL) and Friedrich Alexander University
Erlangen-Nürnberg, Erlangen 91058, Germany

Abstract— An efficient interface between photons and a controlled number of individual quantum emitters would allow one to study fundamental many-body effects relying on cooperative phenomena and polaritonic excitations. Several years ago, we demonstrated the first long-distance coupling of two individual molecules via tight focusing [1]. In this talk I will report on a new experimental system that allows the coupling of a mesoscopic ensemble of molecules. The core of our setup consists of a glass capillary with a subwavelength and high refractive index core that is doped with dye molecules. The highly confined mode of such a nanoguide can allow coupling efficiencies up to 18%. By combining high-resolution microscopy with extinction, fluorescence excitation and resonance fluorescence spectroscopy, we demonstrate the versatility of this geometry for reaching high optical densities while maintaining a low background and addressability of each single emitter. I will present our published experimental results [2], the prospects of our approach, as well as the ongoing efforts for achieving higher coupling efficiencies in a chip-compatible geometry. Furthermore, I show how efficient coupling of propagating photons to a single molecule can make it possible to observe four-wave mixing of continuous-wave laser beams via a single molecule [3].

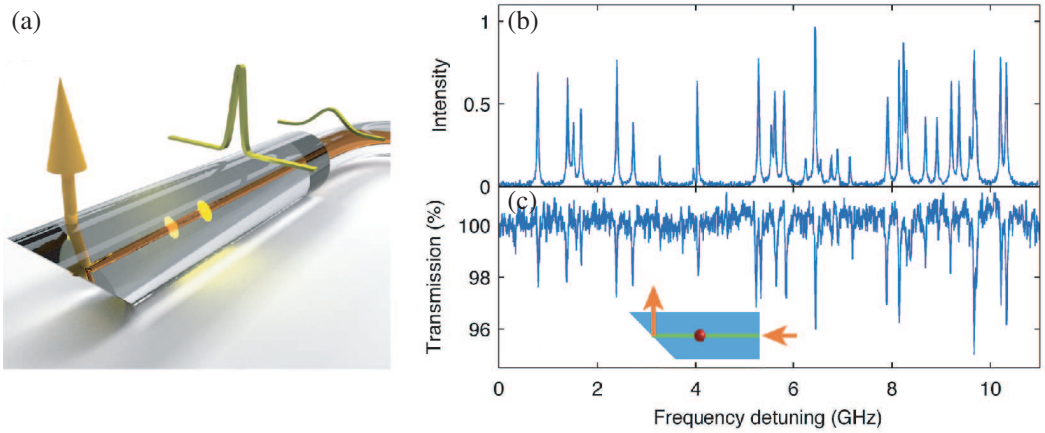

Figure 1: (a) Visualization of the sample geometry including the nano-capillary butt-coupled to a conventional single mode fiber. (b) Transmission spectra of the nanofiber showing the stokes-shifted fluorescence and (c) the extinction of the resonant light.

REFERENCES

1. Rezus, Y., S. Walt, R. Lettow, G. Zumofen, A. Renn, S. Götzinger, and V. Sandoghdar, "Single photon spectroscopy of a single molecule," *Phys. Rev. Lett.*, Vol. 108, 093601, 2012.
2. Faez, S., P. Türschmann, H. R. Haakh, S. Götzinger, and V. Sandoghdar, "Coherent interaction of light and single molecules in a dieletric waveguide," *Phys. Rev. Lett.*, Vol. 113, 213601, 2014.
3. Maser, A., B. Gmeiner, T. Utikal, S. Götzinger, and V. Sandoghdar, "Continuous-wave four-wave mixing at a single molecule," in preparation, 2015.

Using Dressed-state Resonance Fluorescence from a Single (In,Ga)As/GaAs Quantum Dot for Alkali Atomic Vapor Spectroscopy

S. M. Ulrich[1], **R. Löw**[2], **and P. Michler**[1]

[1]Institut für Halbleiteroptik und Funktionelle Grenzflächen
Universität Stuttgart, Allmandring 3, Stuttgart 70569, Germany
[2]5. Physikalisches Institut, Universität Stuttgart, Pfaffenwaldring 57, Stuttgart 70569, Germany

Abstract— Hybrid quantum systems combining semiconductor quantum dots (QDs) and atomic vapors promise interesting applications in quantum information technology. Recent research in this field has explored the resonant coupling between single GaAs QDs and Rubidium gas to generate, e.g., frequency-stabilized non-classical emission ($\sim$ 780 nm) as well as slow light for qubit storage/retrieval operations [1, 2].

As an alternative hybrid approach, we use a cw laser-driven single (In,Ga)As/GaAs QD (4 K) in the "dressed state" resonance fluorescence (RF) regime to address the $D1$ transitions of atomic Caesium (Cs) vapor (300 K) [3]. QD-atom resonance is achieved by tuning the frequency of the dressing laser close to the QD ground state $v \sim 335.116$ THz (894.592 nm) and shifting the narrow-band center and side channels of the QD Mollow triplet. Using this laser frequency controlled QD probe light for absorption measurements allows to precisely identify all four Cs hyperfine-split transitions. Therefore, narrow-band (In,Ga)As/GaAs QD RF is demonstrated as suitable to optically address individual channels of the $D1$ quadruplet without magnetic field or electric field tuning. Further ongoing experiments will be discussed in the talk.

REFERENCES

1. Akopian, N., L. Wang, A. Rastelli, O. G. Schmidt, and V. Zwiller, *Nat. Phot.*, Vol. 5, 230, 2011.
2. Akopian, N., R. Trotta, E. Zallo, S. Kumar, P. Atkinson, A. Rastelli, O. G. Schmidt, and V. Zwiller, arXiv:1302.2005.
3. Ulrich, S. M., S. Weiler, M. Oster, M. Jetter, A. Urvoy, R. Löw, and P. Michler, *Phys. Rev. B*, Vol. 90, 125310, 2014.

Nonlinear Optics with Coupled Polariton Modes

S. R. K. Rodriguez, **A. Amo**, **I. Sagnes**, **E. Galopin**, **A. Lemaître**, **and J. Bloch**
Laboratoire de Photonique et de Nanostructures, LPN/CNRS
Route de Nozay, Marcoussis 91460, France

Abstract— Extreme optical nonlinearities emerge when photons are spatially confined and rendered mutually interacting. Semiconductor optical microcavities are promising solid-state systems wherein these two conditions can be simultaneously fulfilled. Photons in a microcavity can couple strongly to excitons in semiconductor quantum wells, giving rise to composite light-matter quasi-particles known as polaritons. The excitonic constituent confers polaritons giant interaction strengths, while the photonic constituent enables micron-scale confinement of polaritons followed by photon emission. Hence, polaritons constitute an excellent system for studying light-matter interactions under the influence of tunable coupling, driving, nonlinearity, and dissipation. In addition to single-mode nonlinearities, coupled polariton modes exhibit rich nonlinear dynamics and steady-states due to the interplay between nonlinear interactions and linear coupling. Here, we will present recent experimental results on coupled semiconductor micropillars exhibiting such strongly nonlinear optical dynamics and steady-states.

Our group has demonstrated several hallmark features of nonlinear Josephson oscillations in a photonic system [1]. The system studied consists of two tunnel-coupled semiconductor micropillars. The dynamics was characterized by measuring the population imbalance and phase difference between polaritons in adjacent pillars under pulsed excitation. In the linear regime (low pump power), polaritons oscillate between the two pillars — Rabi oscillations. For increased pumping, the oscillations become nonlinear. For even higher pumping, polaritons are trapped by the intensity-induced nonlinearity in the pumped pillar. This fascinating phenomenon, known as macroscopic self-trapping, was observed for the first time in a photonic system in Ref. [1].

Recently, we have studied the steady-states of coupled polariton modes under resonant excitation [2]. In particular, we have observed how the symmetries of the hybrid modes formed by the tunnel coupling between the two cavities can be broken, and restored, as the pump power increases. Distinct nonlinear thresholds enable us to abruptly increase the emitted intensity by one of the two coupled cavities or both. As we will show, these effects are associated with optical multistability and a pronounced hysteresis spanning several orders of magnitude in pump power. These results illustrate new ways to achieve all-optical nonlinear switching, and offer intriguing prospects for accessing the quantum regime with polaritons. In particular, non-classical states of light seem within reach with state-of-the-art polariton systems. Such extremely nonlinear optical cavities hold great promise for the realization of polariton blockade, photon fermionization, and quantum phase transitions beyond the Bose-Hubbard model.

REFERENCES

1. Abbarchi, M., et al., "Macroscopic quantum self-trapping and Josephson oscillations of exciton polaritons," *Nature Phys.*, Vol. 9, 275–279, 2013.
2. Rodriguez, S. R. K., et al., "Manuscript," under preparation, 2015.

Single Photon Generation and Non-linearity with a Semiconductor Quantum Dot

Valérian Giesz[1], **Niccolo Somaschi**[1], **Lorenzo De Santis**[1], **Simone Luca Portalupi**[1], **Justin Demory**[1], **Christophe Arnold**[1], **Olivier Gazzano**[1], **Anna Nowak**[1], **Aristide Lemaitre**[1], **Isabelle Sagnes**[1], **Loic Lanco**[1, 2], **and Pascale Senellart**[1, 3]

[1]Laboratoire de Photonique et de Nanostructures, CNRS
UPR20, Route de Nozay, Marcoussis 91460, France
[2]Département de Physique, Université Paris Diderot
4 rue Elsa Morante, Paris 75013, France
[3]Département de Physique, Ecole Polytechnique, F-91128 Palaiseau, France

Abstract— In a semiconductor quantum dots, the coulomb interaction between carriers results in a strong anharmonicity of the energy levels. This non-linearity is widely used to generate single photons on demand. It has also been recently explored to implement single photon routers. Both these applications requires to implement a highly efficient single photon-single quantum dot interface, so as to collect every photon emitted by the quantum dot or, symmetrically, so that every photon sent on the device interacts with the quantum dot. In this talk, we will present our recent progresses along this research line.

By deterministically coupling a single quantum dot to the optical mode of a micropillar cavity, we implement a highly efficient single quantum dot-single photon interface. We demonstrate the fabrication of ultrabright sources of indistinguishable single photons with a record brightness of 79% collected photon per pulse [1]. Under non-resonant excitation, we demonstrate indistinguishability of successively emitted photons in the 70- to 90% range. With electrically controlled structures [2], strictly resonant excitation can also be achieved. Under a p-pulse excitation, a near unity indistinguishability is observed. The quantum interference of photons emitted by two remote devices is finally shown to be greatly enhanced by the acceleration of spontaneous emission [3].

Symmetrically, we show that such devices can be used to demonstrate optical non-linearities at the level of only few incident photons [4]. When a single spin is inserted in the quantum dot, the polarization of a photon sent on the device can be rotated by $\pm 6^\circ$ depending on the single spin state [5].

REFERENCES

1. Gazzano, O., et al., *Nature Communications*, Vol. 4, 1425, 2013.
2. Nowak, A., et al., *Nature Communications*, Vol. 5, 3240, 2014.
3. Giesz, V., et al., 2015, submitted.
4. Loo, V., et al., *Phys. Rev. Lett.*, Vol. 109, 166806, 2012.
5. Arnold, C., et al., *Nature Communications*, Vol. 6, 6236, 2015.

Session 3A8a
Medical Electromagnetics, Biological Effects, Bioimaging

Nanoparticle-assisted Stimulated Emission Depletion (STED) Microscopy, Theory and Experimental Demonstration

Y. Sivan[1], **Y. Sonnefraud**[2], **H. Sinclair**[3], **M. Foreman**[4], **C. Dunsby**[3], **M. Neil**[3], **P. French**[3], **and S. A. Maier**[3]

[1]Ben-Gurion University, Israel
[2]Institut Neél, France
[3]Imperial College London, UK
[4]Max Planck Institute for the Science of Light, Germany

Abstract— We show experimentally a 4-fold reduction of the intensity required to achieve sub-diffraction resolution in a stimulated-emission-depletion microscope, in good agreement with theory. This shows that the theoretical prediction of a 100-fold intensity-reduction is achievable.

The limit that diffraction puts on imaging was considered as the most fundamental problem in wave physics. This limit was broken in the early 2000s in the context of fluorescence microscopy, eventually resulting in the awarding of the Nobel Prize in Chemistry, 2014. One of the prominent super-resolution technique is stimulated-emission-depletion (STED) nanoscopy, which offers superb resolution along with fast acquisition times. The STED nanoscope, however, suffers from the need for high intensities required for efficient depletion. Here, we show that using metal nanoparticles (NPs) improves the performance of STED nanoscopes [1]. Compared with a standard STED nanoscope, we show theoretically a resolution improvement by more than an order of magnitude, or equivalently, depletion intensity reductions by more than 2 orders of magnitude; these come along with a strong photostabilization due reduction of photobleaching. We show that such performance improvement can be attained without excessive heating, making it useful for live-cell studies.

We demonstrate the technique experimentally by comparing the resolution attained by imaging dye-doped silica nanoparticles with or without a thin shell of gold [2]. We observe that an optimum resolution, limited by the particle sizes, can be reached for the NPs for a power of the STED beam 4 times smaller than for the bare cores, see Figure below, in good agreement with the theoretical calculations. We show that the experimental obstacles encountered all have very satisfactory solutions. Accordingly, we expect to reach the theoretical predictions once the measurements will be repeated with particles of optimal geometries. Our experimental demonstration opens the way to improvement of existing STED nanoscopes and assisting the development of low-power, low-cost nanoscopes. This has the potential to increase the availability of STED nanoscopes and lead to an expansion of our understanding of nanoscale biological phenomena.

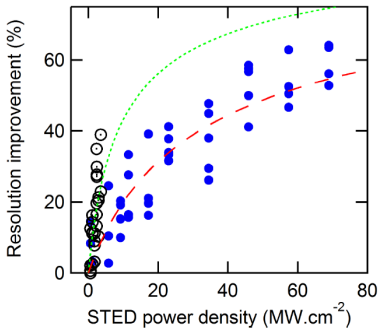

Figure 1: Resolution improvement using coreshell NPs vs. the STED depletion power density. Blue disks: bare doped silica cores only. Black dotted circles: coreshell nanoparticles. The red dashed (respectively green dotted) line is a least-square fit of the bare silica (respectively coreshell).

REFERENCES

1. Sivan, Y., et al., "Nanoparticle-assisted stimulated emission depletion nanoscopy," *ACS Nano*, Vol. 6, 5291, 2012.
2. Sonnefraud, Y., et al., "Experimental proof of concept of nanoparticle-assisted STED," *Nano Letters*, Vol. 14, 4449, 2014.

The Wedding of Bioelectromagnetic and Biochemistry: Bridging a Molecule and Its Own Electromagnetic Information

Alberto Foletti[1, 2], **Mario Ledda**[1], **Settimio Grimaldi**[1], **and Antonella Lisi**[1]

[1]Institute of Translational Pharmacology, National Research Council-CNR, Rome, Italy
[2]Clinical Biophysics Research Group, Lugano, Switzerland

Abstract— Previously we showed an interesting effectiveness of the electromagnetic information delivery of a specific source molecule in mimicking its specific biological effect [1, 2]. Nevertheless the effect was quite lower than the original positive control. Therefore we decide to assess a possible synergism between a reduced dose of a molecule and its own electromagnetic information in order to increase the efficacy of this procedure trying to disclose new possible avenues in translational pharmacology [3] following suggestion from other works reporting synergistic effect between molecules and extremely low frequency electromagnetic fields [4, 5]. A reduced dose of retinoic acid, corresponding to a tenth of the usual, was delivered together with its own electromagnetic information to LAN-5 neuroblatoma cells. The signals from retinoic acid molecules was transferred to the cell culture medium employing as for our previous reports a commercial available electro medical device (Vegaselect 719). The effect on cell differentiation was significantly higher, and statistically significant, than the one obtained by the electromagnetic information delivery procedure when performed alone. A positive and effective synergism between a reduced drug dose and its own electromagnetic information seems to emerge as a promising and useful perspective in translational pharmacology outlining future applications in new drug delivery protocols allowing to reduce the amount of drug's doses especially in the elderly and in the increasing number of patients with multiple comorbidities. Bioelectromagnetic and biochemistry should, therefore, be considered on the way of a promising wedding instead of a permanently independent life. Future researches should either optimize the protocols of preparation of these potentially new drugs, either assess the lifespan of their biological effect in order to translate them into effective clinical application at the bedside through Biolectromagnetic medicine [6].

REFERENCES

1. Foletti, A., M. Ledda, E. D'Emilia, S. Grimaldi, and A. Lisi, "Differentiation of human LAN-5 neuroblastoma cells induced by extremely low frequency electronically transmitted retinoic acid," *J. Altern. Complement. Med.*, Vol. 17, 701–704 2011.
2. Foletti, A., M. Ledda, E. D'Emilia, S. Grimaldi, and A. Lisi, "Experimental finding on the electromagnetic information transfer of specific molecular signals mediated through the aqueous system on two human cellular models," *J. Altern. Complement. Med.*, Vol. 18, 258–261, 2012.
3. Foletti, A., M. Ledda, S. Piccirillo, S. Grimaldi, and A. Lisi, "Electromagnetic information delivery as a new tool in translational medicine," *Int. J. Clin. Exp. Med.*, Vol. 7, No. 9, 2550–2556, 2014.
4. Marcantonio, P., B. Del Re, A. Franceschini, M. Capri, S. Lukas, F. Bersani, and G. Giorgi, "Synergic effect of retinoic acid and extremely low frequency magnetic field exposure on human neuroblastoma cell line BE(2)C," *Bioelectromagnetics*, Vol. 31, No. 6, 425–33, 2010.
5. Whissell, P. D. and M. A. Persinger, "Persinger emerging synergisms between drugs and physiologically-patterned weak magnetic fields: Implications for neuropharmacology and the human population in the twenty-first century," *Curr. Neuropharmacol.*, Vol. 5, No. 4, 278–88, 2007.
6. Foletti, A., S. Grimaldi, A. Lisi, M. Ledda, and A. R. Liboff, "Bioelectromagnetic medicine: The role of resonance signaling," *Electromagn. Biol. Med.*, Vol. 32, No. 4, 484–499 2013.

Oversensing and Undersensing of Implantable Cardiac Medical Devices Exposed to EMI

I. L. Spano, **A. Serpi**, **M. Tomasi**, **I. Marongiu**, **and G. Gatto**
Department of Electrical and Electronic Engineering, University of Cagliari, Italy

Abstract— In the last decade, the development of new technologies and the increased use of Radio Frequency (RF) sources make Electromagnetic Interference (EMI) a growing issue. In fact, when an electronic device is exposed to RF signals, they may prevent it to operate correctly, causing malfunctions. EMI issues are particularly critical for Implantable Cardiac Medical Device (ICMDs), which are generally employed for people whose spontaneous heartbeat is not good enough to ensure normal living conditions. Nowadays, ICMDs are implanted even from a very young age, thus it is no longer unusual for people wearing an ICMD to be highly exposed to EMI, such as in factories.

In this context, EMI immunity of ICMDs against RF signals is a growing issue, particularly electromagnetic interactions between ICMDs and intentional and unintentional RF sources (e.g., cell phones, safety systems, magnetic resonance, radiation, X-rays, etc.) may impair ICMD sensing performances. Consequently, the device may interpret spurious signals as threatening arrhythmias, starting unsuitable pacing activities or providing an improper defibrillation shock. Despite the use of appropriate filtering systems and/or recognition algorithms, misunderstandings can still occur, leading to undersensing or oversensing, as shown in Fig. 1. Particularly, undersensing prevents ICMD to detect the heartbeat, whereas oversensing makes ICMD sensitive to spurious signals.

In this paper, the problems of oversensing and undersensing due to EMI are addressed referring to two different types of ICMDs, i.e., a pacemaker (PMK) and an Implantable Cardioverter Defibrillator (ICD). This is done by means of a novel experimental testing procedure, which is developed in order to reveal EMC susceptibility of the device under test. Experiments have been carried out within an RF anechoic chamber, which guarantees a proper EMI injection, shielding against external EMI sources at the same time. In particular, an equivalent EMI source is employed, i.e. a Bilog antenna generates an RF signal (80% AM modulation), the frequency of which has been chosen in accordance with ANSI/AAMI ISO 14117: standard 2012. In fact, this last provides specific frequency ranges for EMC testing of ICMDs. As a result, different ICMD behaviours have been revealed in absence/presence of EMI, as highlighted in Fig. 1. Much more results will be enclosed in the final version of the paper, as well as a detailed description of the proposed procedure.

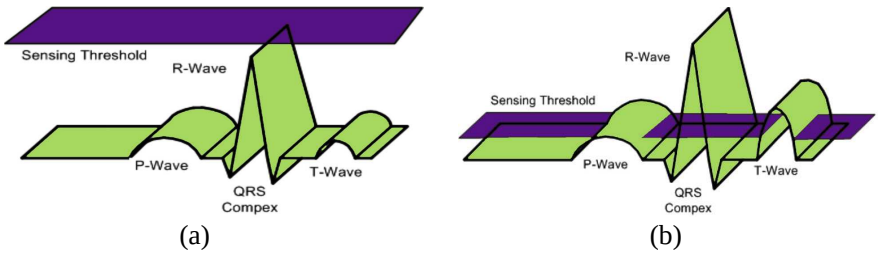

Figure 1: (a) Undersensing and (b) oversensing: heartbeat (green waves) and sensing thresholds (purple).

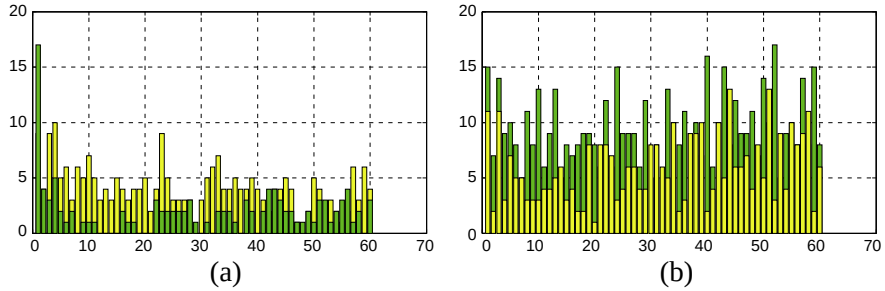

Figure 2: Pacing occurrences for (a) PMK and (b) ICD over about fifty one-minute tests, with and without EMI (yellow and green respectively).

Biomagnetic Fields of Propagating Electric Activity in Functional Syncytia Measured Using Amorphous Metal Magnetic Sensor

Shinsuke Nakayama[1] **and Tsuyoshi Uchiyama**[2]

[1]Graduate School of Medicine, Nagoya University, Japan
[2]Graduate School of Engineering, Nagoya University, Japan

Abstract— Electric current propagates in excitable cellular organizations so as to achieve their functions. In the heart, pacemaker potentials are amplified and forwarded from the atrium to ventricle muscle, thus synchronizing heart beats. Also, in the gut, coordinated motions, such as peristalsis and segmentations, require electric activities to organize smooth muscle segments. Magnetic detection would provide a non-invasive and aseptic estimate of their functional states.

In this study, we performed real-time measurements of biomagnetic fields in the musculatures of functional syncytium, using a gradio-type magneto sensor. Smooth muscles were isolated from gastrointestinal and urinary systems of guinea-pigs. Also, right ventricular muscle along with the right atrium was isolated from the heart of mice. In the gradio-magneto sensor, the performance of differentiation was improved by using a single amorphous metal wire with a pair of transducer coils, which produced well-balanced induction potentials. The distance between the sample and the wire was $\sim 1\,\mathrm{mm}$.

When musculature samples were incubated in a physiological extracellular solution at 32–35°C, spontaneous magnetic waves of up to several nT were observed. The frequency and the time course of biomagnetic waves reflected the cellular tissue-dependent excitability. For instance, in stomach samples only several magnetic waves occurred in a minute, while in cardiac samples magnetic transients occurred at 1–2 cycles/s at the beginning of recording. Since the thickness of ventricular musculature was $< 1\,\mathrm{mm}$ in mice, it is considered that our sensor would be able to measure magnetic activity in cardiac muscle sheets of regenerative medicine, if available.

Performance Evaluation of Dipole versus Modified Bow-Tie in Annular Phased Array Applicators

P. Takook, **H. D. Trefná**, **A. Fhager**, **and M. Persson**
Chalmers University of Technology, Sweden

Abstract— The main goal of the hyperthermia treatment is to heat up tumors to temperatures above 42°C while keeping healthy tissues at normal temperatures. To reach this goal, accurate hyperthermia treatment planning is necessary. This demands finding the optimal excitation amplitudes and phases of the antenna applicator to heat the tumor.

In this paper we utilized the 3D time reversal focusing method for hyperthermia treatment planning application [1]. The method which is based on the constructive wave interference at the tumor site, is implemented. The implementation used the finite-difference time-domain (FDTD) to solve Maxwell's equations. In a previous study conducted by the authors, the effect of different parameters as the input settings of 3D method for optimal heating of tumor models was shown in a head-and-neck phantom [2]. Among those, the antenna model is one the most influential parameters.

This paper aims to study the effect of a simplified antenna model in hyperthermia treatment of different tumor types and positions. The antenna used in this study is a modified version of wide-band Bow-Tie antenna [3]. To simplify the architecture of the 3D model, the Bow-Tie antenna models were replaced by half-wave dipole antennas. To evaluate the performance of the simplified model, treatment planning outcome of Bow-Tie antenna applicator were compared with that of the half-wave dipole antenna applicator. The efficacy of these two antennas in heating the tumors were then evaluated in terms of average power absorption ratio (aPA), remaining tissue maximum index (RTMi) [1] and target coverage$_{25\%}$ [4].

Two spherical tumors were positioned in the center and the side of a homogeneous phantom with radius 80 mm. The performance measures were then computed for each simulation. An irregular shaped tumor in a non-homogeneous head-and-neck phantom of similar size was studied afterwards.

The results of the simulations for the spherical tumors, demonstrated that for a centrally located tumor with radius of 10 mm (where distance of tumor center to the phantom surface is $d = 80$), array of Bow-Tie antennas presented 3.3% higher aPA, 1% higher $TC_{25\%}$ and 3.9% lower RTMi compared to array of dipoles. When tumor was located closer to the phantom surface, $d = 60$, all quality indicators were approximately the same for Bow-Tie and dipole. For the irregular shaped tumor in the laryngeal region which was even closer to the phantom surface, $d = 50$, dipole antennas showed considerably higher aPA and $TC_{25\%}$ and lower RTMi values compared to the Bow-Tie. The aPA = 47, $TC_{25\%} = 84\%$ and RTMi = 0.3 for dipole and aPA =25, $TC_{25\%} = 78\%$ and RTMi = 0.64 for Bow-Tie respectively. This confirmed authors previous study, in which for the same laryngeal tumor the treatment outcome from dipole antennas modeled in 3D code was better than Bow-Tie in CST [2]. Figure 1 shows the power absorption distribution radiated by Bow-Ties and dipoles in a 10-antenna applicator along the transverse plane of the laryngeal tumor.

Hyperthermia treatment quality indicators are correlated with the size of tumor and its relative position to other non-homogeneities. However, the results demonstrated that only based on the

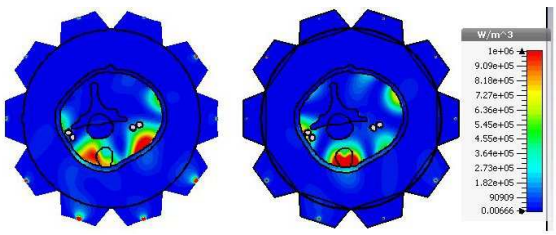

Figure 1: (a) Power absorption distribution radiated by Bow-Tie and (b) dipole in a laryngeal tumor, shown along the transverse plane.

relative distance between center of the tumor and the phantom surface, it can decided which antenna type leads to a better treatment outcome. For example, more tumor coverage can be achieved by Bow-Tie antennas for a tumor in tongue region, centrally located in a head-and-neck phantom.

Further studies are necessary to reach higher treatment quality for all tumor positions, e.g., by combination of different treatment plannings and hot-spot reduction techniques.

REFERENCES

1. Dobšíček Trefná, H., J. Vrba, and M. Persson, "Time-reversal focusing in microwave hyperthermia for deep-seated tumors," *Phys. Med. Biol.*, Vol. 55, No. 8, Apr. 2010; Vol. 26, 185–197, 2010.
2. Takook, P., H. Dobšíček Trefná, A. Fhager, and M. Persson, "Evaluation of the 3D time reversal method for hyperthermia treatment planning in head and neck tumors," *9th European Conference on Antennas and Propagation*, Apr. 2015.
3. Takook, P., H. Dobšíček Trefná, and M. Persson, "A compact wideband antenna for microwave hyperthermia system over 0.4–0.9 GHz," *ESHO 2013*, Munich, 2013.
4. Rijnen, Z., J. F. Bakker, R. A. M. Canters, P. Togni, G. M. Verduijn, P. C. Levendag, G. C. Van Rhoon, and M. M. Paulides, "Clinical integration of software tool VEDO for adaptive and quantitative application of phased array hyperthermia in the head and neck," *Int. J. Hyperthermia*, Vol. 29, No. 3, 181–193, May 2013.

Session 3A8b
FocusSession.SC3&4: Microwave Photonics for Wireless Spectrum Management 2

RF-photonic 2D/3D Integrated Circuits for Arbitrary Waveform Generation and Detection in Temporal, Spectral, and Spatial Domains

S. J. Ben Yoo
Department of Electrical and Computer Engineering, University of California, Davis, USA

Abstract— We will discuss 2D and 3D photonic integrated systems designed for coherent synthesis, processing, and detection of optical waves in time, space, and frequency domains. In particular, we will discuss a new class of RF-photonic devices based on 3D ultrafast laser inscription methods. The talk will be in three parts addressing applications in future communication, computing, and imaging systems including chip-scale LIDAR, satellite communication, and data systems. The 3D photonic integrated circuit (PIC) platform exploits direct inscribing of arbitrarily shaped waveguides using femtosecond lasers. In one example, such a 3D PIC allows arbitrary beam forming for spatial division multiplexing using orbital angular momentum states. We will further discuss 2D integrated photonic technologies based on InP, silicon, and silica material platforms. Examples at UC Davis include > THz coherent optical transmitters and receivers on a monolithically integrated InP platform, silicon photonic RF-photonic lattice filters, and orbital-angular-momentum (OAM) MUX/DEMUXes. Dynamic optical arbitrary waveform generation and measurement (OAWG and OAWM) technologies enable > THz scale coherent optical transmission systems with arbitrary modulation formats and bandwidth. Integrated 3D OAM devices can realize arbitrary spatial beam forming. Finally, we will address future prospects of the new 2D/3D RF-photonic integration circuits towards realizing future communication, computing, and imaging systems.

Software-defined Integrated Microwave Photonics for Radio Access Networks

Daniel Pérez, Ivana Gasulla, and José Capmany
ITEAM Research Institute, Universitat Politecnica de Valencia, Spain

Abstract— Microwave Photonic (MWP) systems are usually at the heart of analog signal processing engines that are placed in between the signal acquisition devices and front-end digital signal processors (DSPs) to accommodate the signal formats to the constraints imposed by the DSP limited sampling rates. This entails the realization of a wide variety of functionalities. Typical space, weight and power (SWAP) figures for commercial MWP systems are around 0.04–0.2 m^2 in size, 1.5–10 kg in weight and 15–20 W in power consumption, making them unsuitable for mass production and widespread use required by the next generation and emerging applications. Integrated photonics has the potential to change the power scaling laws of high bandwidth systems through proper architectural choices that combine photonics with electronics to optimize performance, power, footprint, and cost. In particular, analog photonics has a qualitatively different behavior compared to digital electronics since the energy per analog task is dominated by the steady-state bias power and does not increase significantly as the bandwidth increases.

Integrated Microwave Photonics (IMWP) [xx] that aims at the incorporation of MWP components/subsystems in monolithic or hybrid photonic circuits is instrumental to achieve the aforementioned evolution objectives. The activity in IMWP has been almost exclusively focused towards the so-called Application Specific Photonic Integrated Circuits (ASPICs) where a particular circuit and chip configuration is designed to optimally perform a particular MWP functionality. As a result, there are almost as many technologies as applications and, due to this considerable fragmentation, the market for many of these application-specific technologies is too small to justify their further development into low-cost industrial mass-volume manufacturing processes.A radically different approach that we propose in this paper is to design a software defined universal MWP signal processor architecture that can be integrated on a chip and is capable of performing all the main functionalities by suitable programming of its control signals. This is inspired by the flexibility of software-radio [16] and digital signal processors, where a common hardware is shared by multiple functionalities through a software-defined approach (or programmability), leading to significant cost reduction in the hardware fabrication. In the paper we propose a general configuration of this processor, discuss its application as a reconfigurable front-end subsystem in centralized radio access networks (CRANs) and its possible implementation in the different available material platforms.

REFERENCES

1. Capmany, J. and D. Novak, "Microwave photonics combines two worlds," *Nature Photonics*, Vol. 1, 316–330, 2007.
2. Marpaung, D., C. Roeloffzen, R. Heideman, A. Leinse, S. Sales, and J. Capmany, "Integrated microwave photonics," *Lasers Photon. Rev.*, Vol. 7, 506, 2013.
3. Pizzinat, A., et al., "Infrastructure convergence for fixed and mobile access networks", OFC 2009, Workshop "Migration scenarios toward future access networks I", San Diego, March 22nd, 2009.

Application of Multicore Fibers to Microwave Photonics

Ivana Gasulla and Sergi Garcia
ITEAM Research Institute, Universitat Politecnica de Valencia, Spain

Abstract— The exploitation of the last available degree of freedom for optical multiplexing -space- has been recently touted as a solution to the upcoming capacity bottleneck in Digital Communications [1]. The future optical network can benefit from Space-Division Multiplexing (SDM) by establishing independent light paths in a single optical fiber via multicore fibers or few-mode fibers. This paper presents the novel extension of this concept to the areas of analogue photonics and radio-over-fiber in order to create a new paradigm in the field of Microwave Photonics (MWP).

Microwave photonics is currently being used in many information and communication scenarios, including satellite communications, converged fiber-wireless communication networks, distributed antenna sensing systems, signal processing, medical imaging systems and optical coherence tomography [2]. Most of the MWP solutions applied to these scenarios rely on a core optical component, *the true time delay line*, which is typically implemented using discrete optoelectronic or fiber-based devices, including switched and dispersive single-core fibers, photonic crystal structures and active semiconductor waveguides.

We propose to exploit the inherent parallelism of SDM to implement a sampled true time delay line featuring, not only a reduction of size, weight and power consumption, but also unique processing capabilities beyond the current state of the art in terms of system stability, flexibility, versatility and record bandwidth. More specifically, we envision the application of heterogeneous multicore fibers, which are composed of a set of non-identical cores, to provide in a single optical fiber a broadband true time delay line featuring 2 dimensional tunability thanks to the simultaneous use of space and optical wavelength diversities. While keeping comparable propagation characteristics in all the cores of heterogeneous multicore fibers is important in digital communications, tunable true time delay lines for MWP require to design each single core so that it presents a different group delay and a different chromatic dispersion behavior.

We will also show how this SDM-based true time delay line can be applied to different MWP applications, such as tunable microwave signal filtering, optical beamforming networks for phased-array antennas, arbitrary waveform generation, optoelectronic oscillators and radio-over-fiber distribution in converged fiber-wireless access networks.

REFERENCES

1. Richardson, D. J., J. M. Fini, and L. E. Nelson, "Space-division multiplexing in optical fibres," *Nature Photonics*, Vol. 7, 354–362, 2013.
2. Capmany, J., J. Mora, I. Gasulla, J. Sancho, J. Lloret, and S. Sales, "Microwave photonic signal processing," *J. of Lightwave Technology*, Vol. 31, 571–586, 2013.

Electro-optic Dual-comb Interferometry

Vicente Duran[1], **Santiago Tainta**[2], **and Victor Torres-Company**[1]

[1]Department of Microtechnology and Nanoscience
Chalmers University of Technology, 41296 Gothenburg, Sweden
[2]Department of Electrical Engineering, Universidad Pública de Navarra, 31006 Pamplona, Spain

Abstract— Dual-comb interferometry is a multiheterodyne technique based on two phase-locked frequency comb sources. This technique permits to measure the complex spectral response of a sample under test at ultrafast speeds because it avoids using any mechanically moving parts. Dual-comb interferometry has impacted a wide range of fields, including spectroscopy, ranging or Raman microscopy.

In this contribution, we present our results on dual-comb interferometry implemented with electro-optic combs. These coherent light sources operate at repetition rates $> 10\,\mathrm{GHz}$, which allows for realizing dual-comb interferometry at speeds in the $\sim$MHz range. The fundamental tradeoffs between number of lines, detection speed and number of bits are exemplified with pulse shaping experiments.

Ultrahigh-speed Photonically-enabled Compressive Microwave Spectrum Sensing

Mark A. Foster
Department of Electrical and Computer Engineering
Johns Hopkins University, Baltimore, Maryland 21218, USA

Abstract— With its multitude of uses in communications and sensing, the radio spectrum is a highly regulated and finite resource. At present the radio spectrum is tightly and statically allocated This static allocation model is necessary to ensure that primary users have unimpeded access free of interference from other users. However, the modern proliferation of wireless electronics is placing pressure on this 100 year old model. Modern electronic devices will increasingly rely on high-bandwidth wireless communications for internet connectivity as well as inter-device communications. Furthermore, while the radio spectrum is tightly allocated, recent investigations indicate that usage at any spatiotemporal location is generally sparse with a limited number of active channels, scattered across an extremely broad bandwidth. This observation indicates that a cognitive radio system that can efficiently and rapidly sense spectral usage could adapt to exploit these temporary spectral opportunities and thus make more efficient use of the finite radio spectrum resource. However, efficiently detecting spectrum usage across an extremely wide bandwidth remains a primary challenge for any such system. Here we will discuss our recent work on a microwave photonic compressive sampling system for extremely wideband microwave spectrum sensing. Our approach employs chirp processing of ultrafast laser pulses to achieve all-optical high-rate compressed sensing measurement. Pseudorandom binary sequence (PRBS) patterns are modulated onto time-stretched optical pulses, encoding them onto the optical spectra at a rate of one unique pattern per laser pulse. The pulses are then partially-compressed, increasing the system's effective sampling rate well beyond the electronic limits. The partially-compressed patterned pulses are then modulated again with the microwave signal under test and fully compressed to perform optical integration of the PRBS to microwave signal inner product before output photodetection and digitization. Using this approach, we have successfully acquired multi-tone sparse microwave spectra with instantaneous bandwidths beyond 15 GHz utilizing both an electronic sampling rate two-orders of magnitude lower than the Nyquist rate and also less than 1% of the measurements traditionally required for Nyquist sampling. Thus this approach allows for a significant reduction in the hardware resources needed for wideband spectrum sensing while maintaining rapid and continuous spectral awareness.

Session 3A9
Density Functional Theory and Its Applications to Nanomaterials

Thermally-assisted-occupation Density Functional Theory (TAO-DFT)

Jeng-Da Chai
Department of Physics, National Taiwan University, Taipei 10617, Taiwan

Abstract— In this talk, I will briefly describe the formulation of our recently proposed thermally-assisted-occupation density functional theory (TAO-DFT) [1] and the density functional approximations to TAO-DFT [2]. In contrast to Kohn-Sham DFT, TAO-DFT is a DFT with fractional orbital occupations given by the Fermi-Dirac distribution (controlled by a fictitious temperature), for the study of large ground-state systems with strong static correlation effects. Relative to TAO-LDA (i.e., the local density approximation to TAO-DFT), TAO-GGAs (i.e., the generalized-gradient approximations to TAO-DFT) are significantly superior for a wide range of applications, such as thermochemistry, kinetics, and reaction energies. For noncovalent interactions, TAO-GGAs with empirical dispersion corrections are shown to yield excellent performance. Due to their computational efficiency for systems with strong static correlation effects, TAO-LDA and TAO-GGAs are applied to study the electronic properties of acenes with different number of linearly fused benzene rings (up to 100), which is very challenging for conventional electronic structure methods. Some interesting results will be presented in this talk.

REFERENCES

1. Chai, J.-D., "Density functional theory with fractional orbital occupations," *J. Chem. Phys.*, Vol. 136, No. 15, 154104, 2012.
2. Chai, J.-D., "Thermally-assisted-occupation density functional theory with generalized-gradient approximations," *J. Chem. Phys.*, Vol. 140, No. 18, 18A521, 2014.

Ensemble Formalism of the Orbital-free Density Functional Theory

Á. Nagy
Department of Theoretical Physics, University of Debrecen, Debrecen, Hungary

Abstract— There are two ways to perform density functional calculations: solving the Kohn-Sham equations or the Euler equation. Nowadays mainly the Kohn-Sham equations are utilized. This scheme has the disadvantage that there are several equations for systems with a lot of electrons. The Euler equation, on the other hand, is a single equation, independently on the number of electrons of the system under study. Naturally, the solution of a single equation instead of several Kohn-Sham equations leads to a huge simplification. That explains the growing interest in orbital-free methods. The reason for the fact that the orbital-free scheme is not so popular lies in the lack of accurate approximation for the kinetic energy functional. Here, a way avoiding the kinetic energy functional problem is presented.

Ensembles are constructed in the ground-state non-interacting density functional theory [1–4]. Ensemble Euler equation is derived from the ground-state non-interacting Euler equation. It can be formulated as a one-particle Sccrödinger-like equation for the square root of the ensemble density. The potential in this equation is the sum of the original Kohn-Sham potential plus the ensemble Pauli potential. The latter satisfies a first-order differential equation. The true electron density can be easily obtained from the ensemble electron density. The properties of the ensemble electron density will be presented.

REFERENCES

1. Nagy, Á., *Chem. Phys. Lett.*, Vol. 460, 343, 2008.
2. Nagy, Á., *Int. J. Quant. Chem.*, Vol. 110, 2117, 2010.
3. Nagy, Á., *J. Chem. Phys.*, Vol. 135, 044106, 2011.
4. Nagy, Á., *Recent Advances in Orbital-free Density Functional Theory*, Y. A. Wang and T. A. Wesolowski, eds., World Scientific, Singapore, 2013.

Plasmon Excitations in Na Nanoparticles and Graphene Studied by Time-dependent Density Functional Calculations

Guang-Yu Guo
Department of Physics, National Taiwan University, Taipei 10617, Taiwan

Abstract— Plasmon, a collective type of electronic excitations generally featured by metallic systems, has been an old topic in physics. However, the prominent outlook of plasmonics for various applications in nanotechnology has stimulated its intense studies in recent years. Previous theoretical and experimental investigations on plasmons in metal nanostructures have mainly been focused on the Mie surface plasmons, as opposed to volume plasmons which cannot be optically excited in extended bulk metals. However, volume plasmons in small metal nanoclusters and graphene nanoflakes have been theoretically and experimentally shown to be significant. Furthermore, in nanoscale size regime, quantum plasmons could have distinct behaviors that are different from classical plasmons.

In this talk, I will report our recent quantum mechanical calculations of plasmon excitations in quantum-sized neutral Na clusters [1] and also in graphene [2]. Our theoretical calculations are based on linear-response time-dependent density functional theory. In particular, the optical absorption spectrum, density response function and static polarizability of the Na clusters are evaluated [1]. The π- and $\pi + \sigma$-plasmon dispersions in graphene are calculated and compared with electron energy loss spectroscopy [2].

REFERENCES

1. Li, J.-H., M. Hayashi, and G. Y. Guo, *Phys. Rev. B*, Vol. 88, 155437, 2013.
2. Liou, S. C., C.-S. Shie, C. H. Chen, R. Breitwieser, W. W. Pai, G. Y. Guo, and M. W. Chu, *Phys. Rev. B*, Vol. 91, 045418, 2015.

First-principles Simulation of Real-time Electronic Dynamics on Surfaces of Materials

Rulin Wang[1, 2], **Dong Hou**[1], **and Xiao Zheng**[1]

[1]Hefei National Laboratory for Physical Sciences at the Microscale
University of Science and Technology of China, Hefei, Anhui 230026, China
[2]Beijing Computational Science Research Center, No. 3 He-Qing Road, Beijing 100084, China

Abstract— Understanding the electronic dynamics on material surfaces or at interfaces of adsorbate-surface systems is crucially important to a variety of applications in physics and chemistry, such as photovoltaic conversion, heterogeneous catalysis, and scanning tunneling microscopy. However, theoretically it is very challenging to simulate the electronic dynamics at material surfaces/interfaces at atomic level. One major difficulty is that the conventional first-principles methods, particularly those based on the time-dependent density-functional theory (TDDFT), were developed mainly for isolated or periodic systems, while the surface of bulk material has an open boundary and is thus beyond the realm of conventional TDDFT methods [1, 2].

To overcome the above difficulty, we develop a practical TDDFT approach for systems with open boundaries [3]. Our novel TDDFT approach is based on a combined Padé and Lorentzian decomposition scheme for resolving the energetic structure and memory content of bulk material environment. A hierarchy of equations of motion is constructed, which accurately characterizes the real-time electronic response to local potential perturbations at material surfaces/interfaces. The new practical approach for open systems thus greatly extends the applicability of TDDFT.

The accuracy and practicality of our novel TDDFT approach is exemplified by simulations on two prototypical systems: (1) the dynamic relaxation of an excess electron on the two-dimensional surface of a graphene monolayer, and (2) the real-time electron transfer at the interface of a molecule-graphene complex. Both the transient and long-time asymptotic dynamics are examined. The numerical results clearly affirm the correctness and usefulness of our open-system TDDFT approach. The simulations also provide important insights into the characteristic features of temporal electron evolution and dissipation on surfaces of bulk materials.

REFERENCES

1. Zheng, X., F. Wang, C. Y. Yam, Y. Mo, and G. H. Chen, "Time-dependent density-functional theory for open systems," *Phys. Rev. B*, Vol. 75, 195127, 2007.
2. Zheng, X., G. H. Chen, Y. Mo, S. Koo, H. Tian, C. Y. Yam, and Y. J. Yan, "Time-dependent density-functional theory for quantum transport," *J. Chem. Phys.*, Vol. 133, 114101, 2010.
3. Wang, R., D. Hou, and X. Zheng, "Time-dependent density-functional theory for real-time electronic dynamics on material surfaces," *Phys. Rev. B*, Vol. 88, 205126, 2013.

Application of Density Functional Theory Combined with Lippmann-Schwinger Equation to Thermoelectric Properties in Atomic/Molecular Junctions from First Principles

Yu-Chang Chen[1, 2]

[1]Department of Electrophysic, National Chiao Tung University, Hsinchu, Taiwan
[2]National Center of Theoretical Science, National Chiao Tung University, Hsinch, Taiwan

Abstract— Thermoelectric nanojunctions for use in the development of new forms of energy-conversion devices at the nanoscale have attracted rapidly growing attention. Thermoelectric nanojunctions consist of a nano-structured object sandwiched between source-drain electrodes. As the Seebeck coefficients are relevant not only to the magnitude but also to the slope of density of states (DOSs), it is of key importance to investigate the details of electronic structures in thermoelectric nanojunctions. Electronic structures offered by sized reduction thereby provide new opportunities and challenges for exploring new forms of nanoscale renewable energy system. Due to the relatively small sizes of junctions, the nature of electron transport are characterized by coherent wave functions. To calculate the wave functions in atomic/molecular junctions, density-functional theory (DFT) combined with Lippmann-Schwinger equation (LS) is applied to investigate non-equilibrium electron transport and thermoelectric properties. Firstly, we will briefly present an introduction for DFT+LS theory for nanoscale junctions formed by atoms/molecules sandwiched between bimetallic electrodes. We then focus on how we apply LS+DFT to investigate the Seebeck coefficients in atomic/molecular junctions from first-principles approaches. To gain further insight into the quantum transport of electrons and energy under nonequilibrium conditions, we investigate effects of electron-vibration interactions on the Seebeck coefficient and the figure of merit ZT. We also propose several atomic-scale thermoelectric devices, such as nano-refrigerators, power generators, and self-powered atomistic transistor.

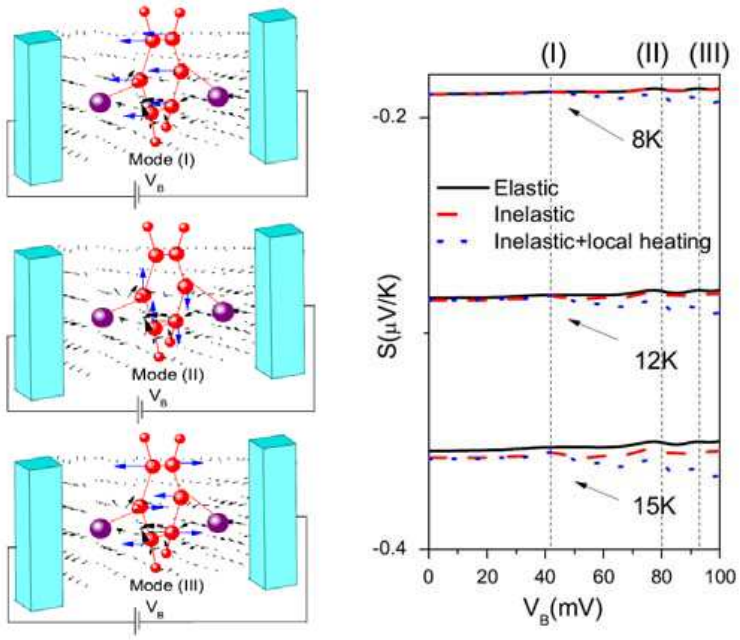

Figure 1: Inelastic Seebeck coefficients due to electron-vibration interactions.

Exchange-correlation Functionals from the Strongly-interacting Limit of DFT

Francesc Malet Giralt[1], **A. Mirtschink**[1], **C. B. Mendl**[2], **J. Cremon**[3], **S. M. Reimann**[3], **and P. Gori-Giorgi**[1]

[1]Department of Theoretical Chemistry and Amsterdam Center for Multiscale Modeling, FEW Vrije Universiteit Amsterdam, The Netherlands
[2]Mathematics Department, Technische Universitat Munchen, Germany
[3]Mathematical Physics, Lund University, Sweden

Abstract— The strongly-interacting limit of the Hohenberg-Kohn functional is represented by a reference system that is the opposite counterpart of the non-interacting Kohn-Sham one. The properties of this strictly-correlated-electrons system can be used to build an exchange-correlation potential that is able to describe strongly-correlated effects without introducing any artificial symmetry breaking. We show applications of this method on semiconductor 1D quantum wires and 2D quantum dots.

Spin-polarized Transport through Single-molecule Magnetic Junctions

Chao-Cheng Kaun
Acad Sinica, Res. Ctr. Appl. Sci., Taipei 11529, Taiwan

Abstract— We investigate spin-polarized (SP) electronic transport properties and hybrid states of a single manganese phthalocyanine (MnPc) molecule adsorbed on a Co nanoisland, with the SP scanning tunneling microscopy measurements and the first-principles calculations. Our analyses show that the MnPc molecule can pin the Co surface state to the Fermi level, forming hybrid stationary spin resonance states which, with an antiparallel-magnetization tip, give a resonant SP conductance peak. Our calculations further reveal that as the tip approaches the molecule, electronic and magnetic couplings in the junction are tuned as the Zener indirect exchange coupling becomes prominent, which switches the conduction carriers from s to d electrons and leads to the tailored magnetic moments and magnetoresistance.

Theoretical Investigations on Band Gaps of Extended Systems

T. Tsuneda
Fuel Cell Nanomaterials Center, University of Yamanashi, Japan

Abstract— The difference between fundamental and optical band gaps is presented by comparing the excitation energies and corresponding orbital energy gaps of extended systems. In solid state physics, optical band gaps are significant to investigate the electric conductivity of semiconductors. These have often been evaluated as HOMO-LUMO gaps in band structure calculations by neglecting excitonic effects, which are electron-hole interactions through Coulomb-exchange-correlation integral kernels called Landau interactions. To figure out the excitonic effects, we compared the time-dependent Kohn-Sham (TDKS) excitation energies and corresponding orbital energy gaps of extended systems: all-trans polyacetylenes, linear oligoacenes, symmetric graphenes, and fullerenes. Calculated results showed that the difference is significant when long-range exchange interactions are properly involved, though long-range exchange interactions should be incorporated to obtain accurate charge transfer excitation energies [1, 2]. We also performed spin-flip (SF) TDKS calculations [3] to make clear the effects of double excitations. As a result, we found that double excitations become significant especially in long oligoacenes and large fullerenes, though the SF-TDKS method is found to considerably underestimate the excitation energies for the excitations from HOMO.

REFERENCES

1. Tsuneda, T., *Density Functional Theory in Quantum Chemistry*, Springer, Tokyo, 2014.
2. Tawada, Y., T. Tsuneda, S. Yanagisawa, T. Yanai, and K. Hirao, "A long-range-corrected time-dependent density functional theory," *J. Chem. Phys.*, Vol. 120, No. 18, 8425–8433, 2004.
3. Shao, Y., M. Head-Gordon, and A. I. Krylov, "The spin-flip approach within time-dependent density functional theory: Theory and applications to diradicals," *J. Chem. Phys.*, Vol. 118, No. 11, 4807–4818, 2003.

The Effect of Nitrogen-doping and Mechanical Strain on the Enhanced Visible Light Absorption of Anatase TiO_2

Chin-Lung Kuo
Department of Materials Science and Engineering
National Taiwan University, Taipei, Taiwan

Abstract— Atomic-level control and determination of the electronic band gaps of the semiconductor-based photocatalysts such as TiO_2 is of great importance for their applications in the challenging photo-electrochemical water splitting reactions using sunlight. Due to the relatively large band gap of TiO_2, only a small portion of the solar spectrum in the UV light region can be absorbed to excite electrons from the valence band top region to the conduction band edge of TiO_2 to generate photocurrents for use in photocatalytic reactions. Therefore, many research efforts have been made to extend the absorption edge of TiO_2 to the visible light part of the solar spectrum to increase its photocatalytic efficiency under sunlight. Currently, one main strategy to achieve this goal is to dope TiO_2 with various transition metals or non-metal elements to effectively narrow down the electronic band gap of TiO_2. In particular, N-doped TiO_2 has recently become one of the most popular and widely investigated systems in the field of photocatalysis since Asahi et al.'s experiment in 2001. Nevertheless, the physical origins of the enhanced visible-light absorption of the N-doped TiO_2 remain unclear to date and many critical issues are still under intensive debate.

In the first part of my talk, I will briefly introduce our recent work on studying the effect of nitrogen doping on the enhanced visible-light absorption of anatase TiO_2. Regarding this aspect, we have performed first principles calculations in conjunction with our newly developed method to investigate the long-term controversy regarding the effect of nitrogen doping on the electronic and optical properties of TiO_2. Our main focus here is to reveal whether the enhanced optical property is primarily attributed to the band gap narrowing of TiO_2 or that is simply induced by the excitation of the localized states within the electronic band gap. Moreover, we are also interested in finding out if there is any other possible origin for the redshift-like behavior of the light absorption edge, such as the O vacancy and H impurities in the TiO_2 bond network. In the second part of this talk, I will present our previous work on modulating the electronic properties of anatase TiO_2 via imposing a uniaxial/biaxial strain. Based on first principles calculations, we have explored the effects of mechanical strains on the electronic band gaps, VBM/CBM positions, and the effective masses of holes and electrons in anatase TiO_2. Our calculations showed that the effective masses of charge carriers and the band gap of TiO_2 can be effectively modulated by imposing mechanical strains along certain directions. This result also suggests that epitaxial growth of TiO_2 on some selected substrates/processing conditions could be a promising route toward enhancing the charge carrier mobility and the visible light absorption in anatase TiO_2.

Simulating Nuclear Quantum Effects on the Fly with DFT

Jian Liu
Institute of Theoretical and Computational Chemistry
College of Chemistry and Molecular Engineering, Peking University, Beijing 100871, China

Abstract— The norm-mode analysis is useful for near-harmonic systems but does a poor job when nuclear quantum effects become significant for anharmonic molecular systems. We have recently combined quantum dynamics and thermodynamics methods (path integral Liouville dynamics and path integral molecular dynamics) on the fly with DFT and TD-DFT to study several types of spectra (such as IR, Raman, electronic absorption, fluorescence spectra) of molecules in gas phase and in solution. The traditional approaches — employing the norm-mode analysis around the optical structure and/or *ab initio* molecular dynamics are often inadequate for describing these spectra in a consistent way. Comparison to experimental data reveals that nuclear quantum effects can sometimes be important in these spectra.

Application of Graphene Dopants to Anodes of Dye-sensitized Solar Cells

Yu-Chao Wang and Chun-Pei Cho
Department of Applied Materials and Optoelectronic Engineering, National Chi Nan University, Taiwan

Abstract— Graphene oxide could be successfully reduced to graphene using autoclave, and this has been demonstrated by the results of Raman, XRD and XPS analyses. Graphene was doped into TiO_2 electrode, which was applied to DSSC to improve device performance. It has been discovered that appropriate graphene doping could enhance dye adsorption and absorption of visible light. The optimum ratio of graphene doping in TiO_2 was $0.005:1$. Furthermore, it was demonstrated that three-layer graphene-doped TiO_2 covered on FTO conductive substrates would be better than two- or one-layer graphene-doped TiO_2 and could achieve an optimum DSSC performance. Graphene was favorable for dispersion of TiO_2 nanoparticles and reduction of electrolyte by the dye, leading to improved electron transfer at the interface and decreased probability of electron-hole recombination. The path and time of electron transport were thereby reduced. Nevertheless, excessive graphene doping resulted in non-uniform dispersion of TiO_2 nanoparticles and reduced specific surface area and amount of dye adsorption. This could cause lower photocurrent density and DSSC performance. In this study, the most optimized ratio of graphene doping in TiO_2 has been ascertained.

Session 3A10
SC5: Inverse Scattering Methods and Applications for NDE

Microwave Tomography Technique for Concrete Diagnosis

Z. Meng
Fukuoka Univercity, Japan

Abstract— Concrete is a very fantastic construction material and concrete buildings occupy over than 30% of whole buildings of office, hotel, and facilities for education and employee welfare. However, concrete can be damaged by fire, aggregate expansion, sea water effects, bacterial corrosion, calcium leaching, physical and chemical damage, and many incidents, such as falling concrete, happen all over the world. Because some of the degradation could also occur unseen in concrete, techniques for concrete diagnosis are needed in construction industry. Radiography is one of well-known non-destructive inspection techniques with very high precision, but human health risk is involved and applicable location is limited. On the other hand, Reinforced Concrete Radar is developed for concrete diagnosis. The device radiates electromagnetic waves to a target and receives the waves scattered by surface of the target as well as reinforcing steel bars, cavities, or other objects in the target body. However, in practice it is difficult to comprehend and interpret the scattering waveforms shown on screen of the device directly.

Microwave tomography is a hopeful technique for concrete diagnosis. The distributions of permittivity ε, magnetic permeability μ and conductivity σ of a concrete body are computer-reconstructed by making use of measured data of scattering waves. For example, a cost-function

$$Cost(\varepsilon,\mu,\sigma)=\frac{\|\mathbf{E}_{\text{measured}}-\mathbf{E}_{\text{estimated}}(\varepsilon,\mu,\sigma)\|}{\|\mathbf{E}_{\text{measured}}\|}$$

is introduced, where the $\mathbf{E}_{\text{measured}}$ is measured scattering wave by a receiver, and $\mathbf{E}_{\text{estimated}}(\varepsilon,\mu,\sigma)$ is the scattering wave estimated by using wave scattering analysis technique, such as FDTD method, and then ε, μ and σ are estimated by minimizing the $Cost$. Unlike common case of inverse scattering problems, usually a target of concrete diagnosis cannot be separated from concrete structure body and taken into a radio wave dark room for measurement. This is why it is so important in microwave tomography technique for concrete diagnosis how to determine the area of scattering analysis and use measured data of scattering wave effectively.

In this paper, "Successive Estimation Technique" is introduced for concrete diagnosis, which is an iteration method reconstructs the target part by part automaticly. Intuitive tomography images of concrete targets are shown in numerical experiments.

DC Impedance Tomography in Anisotropic Media

Stewart Greenhalgh[1], **Tim Wiese**[2], **Bing Zhou**[3], **Mark Greenhalgh**[4], **and Laurent Marescot**[5]

[1]Institute of Geophysics, ETH Zürich, Sonneggstrasse 5, Zürich 8092, Switzerland
[2]Santos Ltd., 60 Flinders Street, Adelaide 5000, Australia
[3]Department of Petroleum Geoscience, The Petroleum Institute
P. O. Box 2533, Abu Dhabi, United Arab Emirates
[4]Thumping Geophysics, Great Eastern Highway, Rivervale, Western Australia 6103, Australia
[5]Risk Management Solutions, Stampfenbachstrasse, Zürich 8021, Switzerland

Abstract— Many rocks and layered/fractured sequences have a clearly expressed electrical anisotropy although it is rare in practice to incorporate anisotropy into low frequency impedance tomography to reconstruct the resistivity structure of the subsurface. Most DC electric inversions are based on the assumption of medium isotropy. In this study we develop a 2.5D anisotropic impedance tomography algorithm using a novel Gaussian quadrature grid forward modeling approach, valid for arbitrary surface topography and the most general class of medium anisotropy. We perform a series of 2.5D synthetic inversion experiments for various electrode configurations and 2D models (tilted transversely isotropic solids) to recover the spatial variations of the longitudinal and transverse resistivities as well as the tilt angles of the local the plane of isotropy. We examine and compare the image reconstructions obtained using the correct anisotropic inversion code to those obtained using the false but widely used isotropic assumption. Superior reconstruction in terms of reduced data misfit, true anomaly shape and position, and anisotropic parameters were obtained when the correct anisotropic assumption was employed for medium to high coefficients of anisotropy. However, for low anisotropy coefficient values the isotropic assumption produced slightly better-quality results because the problem is better determined with fewer unknown parameters to recover. When an incorrect isotropic inversion is performed on medium to high level anisotropic data the images are dominated by patterns of banded artefacts and high data misfits. Various pole-pole, pole-dipole and dipole-dipole data sets were investigated and the inversion images compared against the true model. Eigen spectra analysis of the pseudo Hessian matrix was performed along with computation of the model relative resolution matrix to determine and contrast in a quantitative sense the information content and goodness of the results. We also present a data selection strategy based on high sensitivity measurements which drastically reduces the number of data to be inverted but still produces comparable results to that of the comprehensive data set. Inversion was carried out using transversely isotropic model parameters described in two different co-ordinate frames for the resistivity tensor viz. Cartesian versus natural or eigen frame. The Cartesian frame provided a more stable inversion product. This can be simply explained from inspection of the differing sensitivities for the two model descriptions.

Non-contact Measurements of Power-line Currents Using the External Magnetic Field

F. Ghasemifard, M. Johansson, and M. Norgren
KTH Royal Institute of Technology, Sweden

Abstract— With the on-going development into more complex and controllable power grids, monitoring of voltages and currents at different locations in the grids becomes of increasing importance. In a non-contact measurement setup the voltages and currents are determined indirectly by measuring the extraneous electric and magnetic fields. This study concerns the inverse source problem of determining the currents in a parallel conductor structure, e.g., a power line or a bus bar, from the magnetic field, measured in a finite number of points. The method we have developed is capable of handling disturbance field from external sources, by modelling the external field as an expansion into spherical harmonics. Hence, the field in the different measurement points becomes a linear combination of the expansion coefficients and the currents to be determined. For situations with a finitely conducting ground below the currents, a model of the conductivity in the ground can also be included into the method. For a given level of Gaussian measurement noise, the theoretically attainable standard deviation in the reconstructed currents is quantified using the Cramer-Rao bounds (CRB). It turns out that a direct inversion of the linear system yields results exceeding the CRB with about two orders of magnitude; a consequence of the illposedness of the problem. To remedy this, we have employed Tikhonov regularization, where the regularization parameter is determined using the L-curve criterion, which results in reconstructions about one order above the CRB. Our numerical results show that with a signal to noise ratio of 30 dB, the currents can be reconstructed with accuracy better than five percent. Interestingly, when applying regularization, the incorporation of the model of the ground does not significantly improve the results, which indicate that the spherical harmonic expansion is in practice sufficient; in practice one does not need to know the ground conductivity.

Auto-focused Imaging of a Moving Target Using an Ultra-wideband Array Radar

T. Sakamoto[1], **T. Sato**[2], **P. Aubry**[3], **and A. Yarovoy**[3]

[1]University of Hyogo, Japan
[2]Kyoto University, Japan
[3]Delft University of Technology, The Netherlands

Abstract— Recent terrorist threats necessitate the development of new measures for the prevention of future attacks, especially in public places such as airports. One such measure is the adoption of ultra-wideband radar body scanners. Many commercial body scanners employ a mechanical scanning antenna array, and passengers are asked to remain stationary for a period of seconds during measurement. For a moving target, however, the resultant image is blurred, which prevents quick and convenient passenger screening.

To prevent such blurriness, the motion of the target must be compensated for. However, it is not an easy task to estimate this motion because the antenna scans while the target is moving at an unknown speed. In addition, the target shape is unknown, which makes the reflection point sweeping on the target surface unpredictable. The conventional Doppler-based speed estimation is thus not valid in such a case.

This paper demonstrates the imaging of moving targets using a scanning one-dimensional array ultra-wideband radar system. We apply a fast radar imaging algorithm, referred to as revised range point migration, to quickly obtain multiple images for various target speeds assumed. We then select one of the images according to a certain criterion. The size of the image focus cannot be adopted for the criterion because the image of a finite-sized target such as a human body does not necessarily focus on a small area. Therefore, we exploit prior knowledge about human bodies to estimate the target speed accurately, and realize auto-focused radar imaging of a moving target. A measurement using a mannequin on a moving platform is conducted to demonstrate the effectiveness of the proposed approach.

Gradient-based Inverse Scattering Approach Using Only Total Electric Field Data

Toshifumi Moriyama, **Toshiyuki Tanaka**, **and Takashi Takenaka**
Graduate School of Engineering, Nagasaki University
1-14 Bunkyo-machi, Nagasaki 852-8521, Japan

Abstract— We consider image reconstruction of an object imbedded in a homogeneous medium. The object is successively illuminated by fields generated from several primary sources. The data of the total field as the sum of incident and scattered fields is collected on an observation surface for each illumination. By using these total field data, inverse scattering reconstructs the image of the object. Most inverse scattering methods assume a priori information on incident field generated by a transmitting antenna. In near-field measurement situations, incorporation of antenna modeling into numerical simulation of scattering by the object is preferable to take account of incident field accurately. In our previous work [1], we have proposed an inverse scattering approach which uses only total electric field data on an observation surface and does not assume the incident field information. This results in reduction of the calculation complexity. We set up an interior boundary value problem in which the solution is the same as that of the original scattering problem in the region Ω interior to the observation surface S enclosing the object. The boundary value is given by the tangential components of total electric field of the original scattering problem on the surface S. The data of the total electric field on S is collected till the time $t = T$ when the electromagnetic fields disappear almost entirely in the interior region Ω. Then, the electromagnetic field $\mathbf{u}(\mathbf{r}, t)$ of the equivalent boundary value problem is also null after $t = T$. If the material in the interior region is different from that of the original problem, the field $\mathbf{u}(\mathbf{r}, t)$ of the boundary value problem does not become null at $t = T$. Therefore, the value of $\mathbf{u}(\mathbf{r}, t)$ at $t = T$ can be used as an indicator of misfit between an estimated and the original objects. The inverse scattering problem considered here is cast as an optimization problem where the cost functional consisting of the stored energy in the interior region Ω at $t = T$.

It was demonstrated that the proposed method can estimate the locations and sizes of homogeneous scatterers in the region of interest by using a genetic algorithm (GA) as an optimization tool to minimize the cost functional [1]. Since GA cannot deal with many unknowns, it is difficult to reconstruct the electrical parameter's distributions of inhomogeneous object. In this paper, we apply a gradient-based optimization method to the proposed inversion method instead of GA and examine a reconstruction of inhomogeneous object. Numerical examples show the effectiveness of the method.

REFERENCES

1. Takenaka, T. and T. Moriyama, "Image reconstruction from total electric field data with no knowledge of incident field," *Progress In Electromagnetics Research Symposium Abstracts*, 1266, Guangzhou, China, August 25–28, 2014.

The Hollow Detection in the Concrete Wall Using 2D-FBTS Method from Real Data

Toshiyuki Tanaka, **Yuki Tanaka**, **Toshifumi Moriyama**, **and Takashi Takenaka**
Department of Electrical and Electronic Engineering, Graduate School of Engineering
Nagasaki University, Nagasaki 852-8521, Japan

Abstract— Concrete radar is used the detection of a rebar or a hollow in concrete structure. The existence of a rebar or a hollow is found easily using concrete radar. But we don't estimate the size, the position and the electric constant of the object. To estimate these values inverse scattering analysis is required. One of them is Forward-Backward-Time-Stepping Method (FBTS method). According to FBTS method, the distributions of the electric parameter of unknown objects are clarified.

In this paper, the imaging of concrete wall from real data is discussed. The reconstruction of concrete wall is performed by comparison between measured data and estimated field calculated by FDTD. Three-dimensional analysis is necessary to reproduce observation data by numerical analysis exactly. However, 2D-FDTD is used approximately to make computation time short. A transmitter and a receiver are arranged at both side of concrete wall respectively. Dielectric loading Vivaldi antennas are used for a transmitter and a receiver. In 2D-FDTD, as the shape of antenna can be not incorporated, it is incorporated in program as directivity function. Also, the directivity function is decided by the amplitude of electric field that was observed with a homogeneous concrete wall. Furthermore, the incident current source is decided so that the observation wave shape propagating the homogeneous concrete wall becomes the third derivative shape of Gaussian function with center frequency 2 GHz. The thickness of the concrete wall to explore is 10 cm, and a cylindrical hollow of 5 cm in diameter exists in the concrete wall. As the number of transmitting point and receiving point is 5 respectively, the number of the total data is 25. It is shown to have succeeded in the reconstruction of a cylindrical hollow from measured data by using 2D-FBTS method which incorporated antenna's directivity.

Exploiting a Sparsity Enhanced Microwave Imaging Approach for Non-destructive Evaluation

M. Bevacqua[1], **L. Crocco**[2], **L. Di Donato**[3], **and T. Isernia**[1]

[1]DIIES, University 'Mediterranea' of Reggio Calabria, Italy
[2]IREA, CNR, Naples, Italy
[3]DIEEI, University of Catania, Catania, Italy

Abstract— Compressive Sensing [1, 2] (CS) has recently become a relevant paradigm in the signal processing and recovery community, due to the possibility of overcoming the Nyquist criterion or to achieve "superresolution" in a number of recovery (and imaging) problems. CS theory is based on the concept of "sparsity" of the unknown function, i.e., on the possibility of representing the unknown by means of a limited number of nonzero coefficients with respect to a given basis. Then, CS theory guarantees an accurate reconstruction of the unknown, even if the number of data is much lower than the overall number of coefficients.

In inverse scattering problem the number of available data is limited, but in many applications it is possible to assume that the unknown function is sparse. As such, the CS theory could improve the accuracy of inversion techniques and/or drive the design of simpler and cheaper measurement set-ups. In this respect, non-destructive evaluation (NDE) via microwave imaging is a particularly relevant case, since localized anomalies are sought for in the imaging problem and the reduction of the complexity of the hardware is an important goal. Unfortunately, a fundamental difficulty exists, since CS theory is well developed for the case of linear problems, while inverse scattering is generally cast through a non-linear (ill-posed) problem. Again this is especially true in NDE, where often the target is an air gap (hosted in an electrically dense medium) and possibly more damages may occur and have to be revealed.

In this contribution we present a new inversion approach [3–5], which allows an effective application of CS theory for microwave imaging without neglecting the underlying no-linear nature of the problem.

REFERENCES

1. Donoho, D., "Compressed sensing," *IEEE Transactions on Information Theory*, Vol. 52, No. 4, 1289–1306, 2006.
2. Candès, E. J., J. K. Romberg, and T. Tao, "Robust uncertainty principles: Exact signal reconstruction from highly incomplete frequency information," *IEEE Transactions on Information Theory*, Vol. 52, No. 2, 489–509, 2006.
3. Bevacqua, M., L. Crocco, L. Di Donato, and T. Isernia, "Microwave imaging of non-weak targets via compressive sensing and virtual experiments," *IEEE Antennas and Wireless Propagation Letters*, Vol. 13, No. 1, Dec. 2014.
4. Crocco, L., I. Catapano, L. Di Donato, and T. Isernia, "The linear sampling method as a way for quantitative inverse scattering," *IEEE Trans. Antennas Propag.*, Vol. 4, No. 60, 1844–1853, 2012.
5. Bevacqua, M., T. Isernia, L. Crocco, and L. Di Donato, "A $(CS)^2$ approach to inverse scattering," *2014 IEEE Conference on Antennas Measurements & Applications (CAMA)*, 1–3, Nov. 16–19, 2014.

Near-subsurface Imaging with a Single Frequency Scanner

C. Eyraud[1], **A. Litman**[1], **H. Tortel**[1], **M. Sobrero**[1], **and F. Daout**[2]

[1]Aix-Marseille Université, CNRS, Centrale Marseille, Institut Fresnel UMR 7249, Marseille 13013, France
[2]IUT/UFR SITEC Ville d'Avray, 50 rue de Svre, Ville d'Avray 92410, France

Abstract— Probing the near-subsurface is a very challenging problem. The usual methods consist in prob- ing the soil with temporal techniques, i.e., directly with a temporal pulse or with a synthetic pulse using a step-frequency acquisition. These techniques are widely exploited since several years, but they may present some limitations. Indeed, the main advantage of these approaches — the possibility to remove the contribution of the interface — fails for near-surface probing when the target echo is in the temporal ambiguity with the interface echo. Moreover natural soil consists of heterogeneous media having different types of dispersion relationships with respect to the frequency.

Within that framework, we thus propose an original approach, where we analyze the capabilities of a mono-frequency/multistatic setup for imaging shallowly buried targets. We have shown the possibility to perform such an imaging in a previous study working with equivalent media — composed by foams charged with carbon particles. Our study is now conducted with a realistic embedding medium composed of silica sand. In the present contribution, we moreover focus on the available information which can be acquired in such configuration and propose some strategies to gather the maximum amount of it. The measured fields are post-processed with an efficient method which takes benefit from the spectral bandwidth properties of the scattered field. The calculated fields are performed with a home-made Finite Element Method software. Efforts are put to precisely modelize the real configuration. In particular, an accurate method for modeling the antennas behavior using a balanced set of elementary sources has been developed. Imaging results of the near-subsurface from numerical and experimental fields are then fulfill with the E-DORT method — an extension of the DORT method to elongated targets. This qualitative and fast imaging procedure, which exploits the spectral properties of the multistatic scattering matrix, has been adapted to the present stratified configuration. The resulting images will be presented at the conference.

Microwave Imaging of Dispersive Scatterers Using Vectorial Lagrange Multipliers

T. G. Papadopoulos[1], **T. I. Kosmanis**[2], **and I. T. Rekanos**[1]

[1]School of Electrical and Computer Engineering, Aristotle University of Thessaloniki, Greece
[2]Department of Automotive Engineering
Alexander Technological Educational Institute of Thessaloniki, Greece

Abstract— A time-domain microwave imaging method is proposed for the reconstruction of the spatial distribution of the electromagnetic properties of dispersive scatterers. The method is based on the minimization of a cost function, which describes the discrepancy between measured and estimated scattered field data. The Maxwell's curl equations satisfied by the electromagnetic field are introduced in the augmented cost function, as equality constraints, via vectorial Lagrange multipliers. By means of the calculus of variations and the stationarity condition, it is shown that the vectorial Lagrange multipliers are the solution of the adjoint scattering problem subjected to the Sommerfeld's radiation condition. Moreover, the Fréchet derivatives of the cost function with respect to the distributions of the scatterer properties are derived analytically. It should be mentioned that their evaluation involves the solution of the adjoint scattering problem. As a result, the Fréchet derivatives obtained can be utilized by any gradient-based optimization technique that updates the estimated scatterer properties iteratively. Also, it is possible to apply any time-domain computational electromagnetics method to compute the estimated scattered field data (direct scattering problem solution) as well as the vectorial Lagrange multipliers (adjoint scattering problem solution). In this study, two cases of dispersive scatterers have been investigated. The first case concerns Debye scatterers where the spatial distributions of the electromagnetic properties of the medium, namely the relaxation time, the static and the optical permittivity, are reconstructed simultaneously. In the second case, the method is applied to the reconstruction of the resonant frequency, the damping factor, the static and the optical permittivity of Lorentz dispersive media. The implementation of the proposed microwave imaging method has been based on the finite-difference time-domain method and the Polak-Ribière conjugate gradient optimization algorithm.

ACKNOWLEDGMENT

This research has been co-financed by the European Union (European Social Fund-ESF) and Greek national funds through the Operational Program "Education and Lifelong Learning" of the National Strategic Reference Framework (NSRF)-Research Funding Program: ARCHIMEDES III. Investing in knowledge society through the European Social Fund.

Session 3A11
SC1: Computational Techniques in Electromagnetics and Applications 1

Analysis of Radiation from X-band Slotted-waveguide Antenna Arrays Using the Parallel DDA-FE-BI-MLFMA

Xu-Min Sun, **Ming-Lin Yang**, **and Xin-Qing Sheng**
Center for Electromagnetic Simulation, School of Information Science and Technology
Beijing Institute of Technology, Beijing 100081, China

Abstract— The slotted-waveguide array antennas are widely used in real-life applications because of their small size, light weight, compact structure, high efficiency, and low side lobe characteristics. Due to their importance, various methods have been developed to compute the radiation from slotted waveguide antennas, such as the variational approach in terms of equivalent network, the method of moments (MoM), the finite-difference time-domain (FDTD) method, the finite element method (FEM) and the hybrid finite element-boundary integral (FE-BI) method. However, previous researches only study on radiation by a single slot in a waveguide, 1-D slotted-waveguide arrays or small 2-D slotted-waveguide arrays in a planar surface. Full-wave analysis for radiation from a 3-D X-band slotted-waveguide antenna array still faces great challenges due to the electrically large size, large amounts of tiny slots in the narrow wall of each waveguide and mutual coupling between two close slotted-waveguides through the inner interior the exterior free space of the waveguide.

We adopted in this paper, the finite element-boundary integral-multilevel fast multipole algorithm (FE-BI-MLFMA) for fast and accurate computation of radiation from large slotted-waveguide antenna arrays. To simplify the calculation, for each single slotted-waveguide, a short and infinitesimally thin current probe is used as the front-end excitation. A perfectly matched layer (PML) is used to terminate end of the waveguide port and absorb the reflected wave from the antenna without any spurious reflection to make each slotted-waveguide antenna work in the travelling wave mode. In a slotted-waveguide antenna array, each slotted-waveguide antenna can be generally considered as a single sub-domain. Hence the domain decomposition algorithm (DDA) can be applied to reduce computation resource and achieve a higher efficiency. To validate the presented method for characteristic study of radiation from slotted-waveguide antenna arrays, numerical results of radiation patterns for a slotted-waveguide array antenna are presented together with the results from the commercial software CST. Good agreement can be observed between the computed results by our DDA-FE-BI-MLFMA and the CST. To show capability of the proposed parallel DDA-FE-BI-MLFMA, a large X-banded slotted-waveguide antenna array contains eighteen waveguides with Taylor amplitude and inverse phase excitation is designed and its radiation patterns are studied with the DDA-FE-BI-MLFMA.

ACKNOWLEDGMENT

This work is partially supported by the National Basic Research Program (973) under Grant No. 2012CB720702 and No. 61320602 and the 111 Project of China under the grant B14010.

Scattering of a Gaussian Beam by an Ellipsoidal Particle with Vectorial Complex Ray Model

K. F. Ren
CORIA — UMR 6614, Normandie Université, CNRS, Université et INSA de Rouen
675 Av. de l'Université, BP 12, 76801 Saint Etienne du Rouvray, France

Abstract— The numerical prediction of the scattering properties of electromagnetic waves or light by objects of complex shape and of size much larger than the wave length has being always a great challenge in both the filed of electromagnetic computation or light interaction with particles. Among a large number of theories, models and algorithms the methods based on the ray models seem the the most appropriate. But their precision is not often satisfactory because the wave properties (phase, divergence/convergence...) are not or not properly taken into account.

In the model developed by the author — Vectorial Complex Rays Model (VCRM) [1, 2], the aforementioned wave properties are counted correctly by introducing the wave front curvature as a generic property of rays. So VCRM improves considerably the precision of ray models. It has been validated by comparison with two rigorous methods: Lorenz-Mie theory for spherical particle and the Multilevel Fast Multipole Algorithm (MLFMA) [3] for the ellipsoidal particles. It is already used to the prediction of the scattering diagrams of the plane wave by large ellipsoidal particles [4] and the elliptical infinite cylinders [5]. It has also been applied to the scattering of a two dimensional Gaussian beam by an elliptical infinite cylinder at normal incidence. In this communication, the VCRM will be further extended to the scattering of a Gaussian beam by an ellipsoidal particle.

The amplitude, the phase and the wave front curvature of the incident Gaussian beam are considered in the model, but the diffraction has not yet taken into account. The developed code has been compared with the rigorous Generalized Lorenz-Mie Theory (GLMT) and we found that the agreement is perfect when the particle is on or near an incident Gaussian beam of waist radius smaller the particle radius accept in a very narrow forward direction angle. This is due to the diffraction effect to be considered in VCRM. Typical scattering diagrams will be exemplified in the presentation to show the new phenomena of scattering when an ellipsoidal particles is illuminated by a beam.

ACKNOWLEDGMENT

This work has been partially supported by the French National Agency under the grant number ANR-13-BS09-0008-01 (AMOCOPS).

REFERENCES

1. Ren, K. F., F. Onofri, C. Roz, and T. Girasole, "Vectorial extended geometrical optics for scattering of a spheroid," *Progress In Electromagnetics Research Symposium Abstracts*, 145, Cambridge, MA, USA, Jul. 5–8, 2010.
2. Ren, K. F., F. Onofri, C. Rozé, and T. Girasole, "Vectorial complex ray model and application to two-dimensional scattering of plane wave by a spheroidal particle," *Opt. Lett.*, Vol. 36, No. 3, 370–372, 2011.
3. Yang, M., Y. Wu, X. Sheng, and K. F. Ren, "Comparison of scattering diagrams of large nonspherical particles calculated by VCRM and MLFMA," *J. Quant. Spect. Rad. Trans.*, 2015 in Press.
4. Ren, K. F., C. Rozé, and T. Girasole, "Scattering and transversal divergence of an ellipsoidal particle by using vectorial complex raymodel," *J. Quant. Spectrosc. Radiat. Transfer*, Vol. 113, 2419–2423, 2012.
5. Jiang, K., X. Han, and K. F. Ren, "Scattering from an elliptical cylinder by using the vectorial complex ray model," *Appl. Opt.*, Vol. 51, No. 34, 8159–8168, 2012.

Sesquicentennial Year of Maxwell's Equations and Computational Electromagnetics

W. C. Chew
Department of Electrical and Computer Engineering
University of Illinois, Urbana-Champaign, USA

Abstract— This year is the sesquicentennial year of Maxwell's equations. Electromagnetics and Maxwell's equations have been instrumental in the conception of many electrical engineering and optical technologies. It the beginning, it was telegraphy, and rotating machineries. Over the years, Maxwell's equations have given rise to wireless communications, antennas, radar, masers, optics, and photonics.

An amazing feature of Maxwell's equations is that they are valid from subatomic length scale to galactic length scale. Therefore, they are valid over a vast frequency range where the wavelength could be very long as well as being very short. Furthermore, they are also valid in classical electromagnetics as well as in quantum electromagnetics. The validity of electromagnetic theory has been tested at many different length scales. It has been tested to a few parts in a billion. As a result, electromagnetic theory has impacted a whole sleuth of technologies in electrical engineering, optics, photonics, as well as in material science.

Because of the highly predictive value of Maxwell's equations, there is always a quest for their accurate solutions. Various methods to solve Maxwell's equations have been developed since the dawn of their discovery. With the advent of computers, the need for more accurate and robust solutions does not diminish, but indeed increases.

In this presentation, we will present the history of different solution methods in electromagnetic theory, ranging from analytic methods, to approximate methods, to numerical methods, namely, the computational electromagnetics methods. We will discuss some issues associated with computational electromagnetics in solving Maxwell's equations and their enduring legacy. We will also discuss future directions in this area.

Scattering of a Cylindrical Wave by the End-face of an Ordered Waveguide System

Akira Komiyama
Osaka Electro-Communication University, Hatsu-cho Neyagawa-shi 572-8530, Japan

Abstract— A periodic grating scatters an incident plane wave only in discrete directions and the scattered wave is expressed as a sum of diffracted plane waves. At low grazing angle limit of incidence high order diffracted waves disappear and only the zero order diffracted wave with a diffraction amplitude of -1 remains. Nakayama has pointed out that the zero order diffracted wave cancels the incident wave and a dark shadow takes place [1]. On the basis of a shadow hypothesis a diffraction theory has been proposed by Nakayama [2]. In there the scattering factor has been introduced as an essential quantity and an integral representation of Green's function in terms of the scattering factor has been presented. So far, however, the execution of the integration is not reported.

An image fiber is composed of a large number of cores embedded in a single cladding, which is used to transmit directly an optical image. By illuminating the end-face of an image fiber with a laser beam a diffraction pattern reflecting the arrangement of cores can be simply observed. We can see experimentally that the diffraction pattern does not almost depend on the polarization of the laser beam. From a theoretical interest in the problem the scattering of a plane wave by the end-face of a waveguide system composed of a large number of cores has been analytically treated by the perturbation method [3]. The method is applicable to an infinite waveguide system.

In this paper the scattering of a cylindrical wave by the end-face of a two-dimensional ordered waveguide system composed of an infinite number of cores is analytically treated by the perturbation method and the behaviour of the scattered wave near the end-face is clarified.

REFERENCES

1. Nakayama, J., K. Hattori, Y. Tamura, "Diffraction amplitudes from periodic Neumann surface: Low grazing limit of incidence (III)," *IEICE Trans. Electron.*, Vol. E90-C, 536–538, 2007.
2. Nakayama, J., "Shadow theory of diffraction grating," *IEICE Trans. Electron.*, Vol. E92-C, 17–24, 2009.
3. Taki, A. and A. Komiyama, "Scattering of plane wave from the end-face of a threedimensional waveguide system," *IECE Trans. Electron.*, Vol. E94-C, No. 1, 63–67, 2011.

Computation of Spheroidal Micro-organisms Cross Sections Using the Aperiodic Fourier Modal Method

M. Abboud[1,2], **G. Granet**[1,2], **K. Edee**[1,2], **J. F. Cornet**[1,2], **and J. Dauchet**[1,2]

[1]Clermont Université, Université Blaise Pascal, BP 10488, F-63000 Clermont Ferrand, France
[2]CNRS, UMR 6602, IP, Aubière F-63177, France

Abstract— It is well known that our society is facing numerous ecological challenges. Cultivation of photosynthetic micro-organisms within controlled environments such as photobioreactor processes is recognized today as a serious alternative to contribute to the CO_2 capture and to produce bio-diesel and bio-hydrogen.

In order to optimize convertion of light energy into chemical energy within the process of photosynthesis, we have to predict the light scattering properties, such as the absorption, scattering and extinction cross sections as well as the scattering diagrams [5].

Based on the rigorous solution of Maxwell's equations, Mie [4] has studied the scattering properties of the spherical particles when it is illuminated by a plane wave.

However, most micro-organisms are not spherical and differ by their size and shape parameters. Their scattering properties are significantly different from those of spherical scatterers. A better approximation of micro-organisms is to consider them as spheroidal particles. In order to deal with general shapes, the true geometry is replaced by a staircase approximation which allows to solve the corresponding scattering problem with the Fourier Modal Method (FMM) [6].

In this communication, we investigate light scattering properties of spheroidal particles with various sizes and complex refractive indexes. Our results are successfully compared with those obtained by Asano [1–3].

REFERENCES

1. Asano, S. "Light scattering properties of spheroidal particles," *Appl. Opt.*, Vol. 18, 712–723, 1979.
2. Asano S. and M. Sato, "Light scattering by randomly oriented spheroidal particles," *Appl. Opt.*, Vol. 19, 962–974, 1980.
3. Asano, S. and G. Yamamoto, "Light scattering by spheroidal particles," *Appl. Opt.*, Vol. 14, 29–49, 1975.
4. Bohren, C. F. and D. R. Huffman, *Absorption and Scattering of Light by Small Particles*, New York, Wiley-Interscience, 1983.
5. Cornet, J. F., "Calculation of optimal design and ideal productivities of volumetricallylightened photobioreactors using the constructal approach," *Chemical Engineering Science*, Vol. 65, 985–998, 2010.
6. Li, L., "Use of fourier series in the analysis of discontinuous periodic structures," *JOSA A*, Vol. 13, 1870–1876, 1996.

A Couple of Topics in Numerical Analysis of Diffraction by a Metal Grating Using Yasuura's Method of Modal Expansion

T. Matsuda[1], **X. Xu**[2], **and Y. Okuno**[3]

[1]Department of Information, Communication and Electronic Engineering
Kumamoto National College of Technology, Koshi, Kumamoto 861-1102, Japan
[2]Department of Electrical Engineering and Information Technology
School of Engineering, Kyushu Sangyo University, Fukuoka 813-8503, Japan
[3]Centre for Optical and Electromagnetic Research, South China Academy of Advanced Optoelectronics
South China Normal University, Guangzhou 510006, China

Abstract— In solving the problem of scattering or diffraction on a computer, we often encounter small issues. Assuming a numerical solution process of grating problems by Yasuura's method of modal expansion [1–7], we pick up a few of such issues or topics that require us to take some action. The issues taken up here are:

(1) Choice of modal functions: In the method we define an approximate solution in terms of a finite linear-combination of modal functions. We state our opinion on the choice of the set of modal functions because the effectiveness of the method depends strongly on the choice.
(2) Modification of the functions in approximation process: We fit the approximate solution to the boundary condition in the sense of least-squares. Because the grating problems are pseudo-periodic, we need to modify each function that appears to be periodic.
(3) Behavior of the Jacobian matrix: We employ the orthogonal decomposition of the Jacobian in solving the least-squares problem and the behavior of the matrix is important. We observe the behavior and add some comments.
(4) Refractive index of a metal: The index of a metal is of a great interest in application to plasmonics. Here we show a couple of examples of plasmon resonance absorption predicted by our computer program using four different values of gold index.

Although most of the topics taken here might have been discussed elsewhere, we should consider these old topics together with many similar subjects again now to make good use of them. This is because such matters, sometimes, are inadequately forgotten in today's progressed computer environment.

REFERENCES

1. Yasuura, K. and T. Itakura, "Approximation method for wave functions (I)," *Kyushu Univ. Tech. Rep.*, Vol. 38, No. 1, 72–77, 1965 (in Japanese).
2. Yasuura, K. and T. Itakura, "Approximation method for wave functions (II)," Vol. 38, No. 4, 378–385, 1966 (in Japanese).
3. Yasuura, K. and T. Itakura, "Approximation method for wave functions (III)," Vol. 39, No. 1, 51–56, 1966 (in Japanese).
4. Ikuno, H. and K. Yasuura, "Improved point-matching method with application to scattering from a periodic surface," *IEEE Trans. Antennas Propagat.*, Vol. 21, 657–662, 1973.
5. Petit, R., et al., *Electromagnetic Theory of Gratings*, Chapters 1, (R. Petit) and Vol. 2, (M. Cadilhac), R. Petit, ed., Springer-Verlag, 1980.
6. Okuno, Y., "The mode-matching method," *Analysis Methods for Electromagnetic Wave Problems*, E. Yamashita, ed., 107–138, Artech-House, Boston, 1990.
7. Okuno, Y. and H. Ikuno, "Yasuura's method, its relation to the fictitious source methods, and its advancements in solving 2-D problems," *Generalized Multipole Techniques for Electromagnetic and Light Scattering*, 111–141, T. Wriedt, ed., Elsevier, Amsterdam, 1999.

Dispersion Characteristic Analysis of Open Cylindrical Waveguide and Its Metalic Closed Model

P. Kelebekler[1] and N. Yener[2]

[1]Technical Education Faculty, Kocaeli University, Turkey
[2]Biomedical Engineering Department, Technology Faculty, Kocaeli University, Turkey

Abstract— In the study, complex dispersion characteristics of cylindrical plasma column open waveguide are obtained from method of moment by modeling the open waveguide with cylindrical plasma column loaded closed waveguide. The complex dispersion curves obtained from the exact solution and the MoM are presented correspondingly in the same figure.

Plasma called fourth state of matter is an ionized state of matter, which exists in universe and can be obtained artificially in the earth. Plasma medium is an anisotropic medium. But it is typically tackled under special conditions which transform anisotropic medium into isotropic medium. Thus supplies simplification in solutions. One of these simplifications is that the radian electron cyclotron frequency (ω_c) is taken zero, which is called plasma column with zero magnetic field in the literature. In our study, isotropic plasma medium with frequency depended permittivity, $\tilde{\varepsilon} = \varepsilon_0(1 - \frac{\omega_p^2}{\omega^2}) = \varepsilon_0\varepsilon_p$ is investigated by using the simplification. Where, ω is the angular frequency, ω_p is the radian electron plasma frequency and ε_0 is free space permittivity. The parametric values of the structure used for numerical computations are that plasma column radius (a) is 10 mm, azimuthal variation (m) is one and normalized plasma frequency (ω_p a/c) is 0.25.

In the study, the MoM based on the generalized telegraphist's equations is fundamental method. For the sake of analysis, cylindrical plasma column is enclosed with a metallic cylindrical frame, because the method gives in the most general solution cluster of closed waveguide structures. The method was used especially to obtain propagating modes for dielectric open waveguides in the literature.

The propagation constant of complex modes has real and imaginary part at the same time. Complex Dispersion curves generally indicate wide spectrum of dispersion characteristics involving forward waves, backward waves, damped waves and complex waves. The complex dispersion characteristics were presented in different studies for different structures as cylindrical dielectric rod loaded closed waveguide or two-lawyer circular shielding waveguide. In these studies, the common feature for complex modes is that they rise at frequency point in which the dispersion curve changes direction. In the view of this feature, the complex modes for the structure are investigated numerically in the neighborhood of these points from exact solution by using fsolve function in MATLAB. Besides, the studies which report the complex modes and complex dispersion curves of open waveguides are rather restricted in the literature. Consequently, major contribution of our study is that the complex dispersion curves of cylindrical plasma column open waveguide obtained from exact solution and also its closed waveguide model using the MoM are presented. Additionally, it is indicated by computing with different ratio of plasma column and metallic frame, that radius of waveguide metallic frame is getting wider, solutions obtained from the method is approaching the exact solutions in different figures.

Rigorous Coupled-wave Analysis of Plane-wave Scattering from Defected Lamellar Grating in Conical Mounting

Koki Watanabe
Fukuoka Institute of Technology, Japan

Abstract— Lamellar gratings are widely used for spectrographs, monochromators, laser tuning, integrated optics etc.. However, the fabrication of lamellar grating with nanometer scale has the potential to cause various defects, and the specification of defects influence on the diffraction efficiency is very important. On the other hand, the defects are artificially generated to change the physical properties of periodic structures. The principle of defects implementation is used in photonics crystals.

This paper proposes a spectral-domain approach to the electromagnetic scattering problem of defected lamellar grating in conical mounting. The fields in imperfectly periodic structures have continuous spectra in the wavenumber space, and the main problem of the spectral-domain approach is wavenumber sampling. The present approach introduces the pseudo-periodic Fourier transform (PPFT) [1]. The PPFT makes it possible to consider the scheme only inside the Brillouin zone because the transformed fields have a periodic property in terms of the transform parameter related to the wavenumber. Also, the transformed fields are pseudo-periodic in terms of the spatial parameters, and the conventional approaches to the periodic structures become possible to be applied for the scattering problem of imperfectly periodic structures. The present formulation is based on the rigorous coupled-wave analysis [2, 3] with the help of pseudo-periodic Fourier transform.

REFERENCES

1. Watanabe, K. and K. Yasumoto, "Two-dimensional electromagnetic scattering of non-plane incident waves by periodic structures," *Progress In Electromagnetics Research*, Vol. 74, 241–271, 2007.
2. Knop, K., "Rigorous diffraction theory for transmission phase gratings with deep rectangular grooves," *J. Opt. Soc. Am.*, Vol. 68, 1206–1210, 1978.
3. Moharam, M. G. and T. K. Gaylord, "Diffraction analysis of dielectric surface-relief gratings," *J. Opt. Soc. Am.*, Vol. 72, 1385–1392, 1982.

Three Dimensional Electromagnetic Simulations of Complex Scenes with FDTD Based Hybridization Method

J. Vincent[1], **P. Borderies**[2], **V. Gobin**[2], **and J.-R. Poirier**[1]

[1]Research Group in Electromagnetism, LAPLACE, Toulouse, France
[2]Electromagnetism and Radar Department, ONERA, Toulouse, France

Abstract— In this paper, we investigate the effects of multiple natural environments located in the far-field of a vertical electric current element at low frequencies. A three dimensional Finite-Difference in Time-Domaine based hybridization technique is used to compute the electromagnetic field around complex kind of environments remotely located from the radiating source.

Introduction: A recent study [1] shows the effects of natural environments in the near-field of low frequency antennas. The Finite-Difference in Time-Domain (FDTD) method was used to carry out these investigations. However FDTD is difficult to apply in large 3D areas because of the huge amounts of computational resources. A FDTD based hybridization technique was created in order to avoid these numerical problems and validated in [2]. The aim of this paper is to show the effects of natural environments on the surface wave propagation using the hybridization technique.

Computation of Natural Environments with 3D FDTD: Among the main existing natural environments, five scenes are proposed: a forest, a hill, a valley, a lake and a groundwater. Theses elements are created taking into account the cartesian grid used by the FDTD.

It has been shown that a forest can be represented by a dielectric slab for a frequency up to 100 MHz [3]. The values of the relative permittivity ε_r is 1.065 and the conductivity σ is $10^{-3}\,\mathrm{S{\cdot}m^{-1}}$. Dielectric blocs are stacked on each other in order to create a hill with an average slop and its dielectric constants are the same as the ground. The groundwater and the lake are freshwater reserves, the value of the relative permittivity ε_r is 80 and the conductivity σ is $5 \cdot 10^{-2}\,\mathrm{S{\cdot}m^{-1}}$.

Effects of Natural Environments in the Far-field: The current element emits at the frequency $f_0 = 100\,\mathrm{kHz}$ and the natural elements are located at 24 km $(8 \cdot \lambda_0)$ from the source. The hybridization technique provides 3D electromagnetic field mapping with and without the environment. Both are compared in order to determine the positive and negative effects on surface wave propagation.

Conclusion: This study shows the effects of multiple environments on the propagation of eletric field using a FDTD based hybridization technique. The effects of a lossy earth, including obstacles such as hills and forested areas are observed.

REFERENCES

1. Vincent, J., P. Borderies, J. R. Poirier, and V. Gobin, "Simulations and effects of natural environments on low frequency antennas with three-dimensional FDTD Method," *Progress In Electromagnetics Research M*, Vol. 38, 45–52, 2014.
2. Vincent, J., P. Borderies, V. Gobin, and J. R. Poirier, "Modelling the effects of realistic environments in the near-field and far-field of low frequency antennas with 3D FDTD method," *2014 International Conference on IEEE-NEMO*, 1–4, May 2014.
3. Tewari, R. K, S. Swarup, and M. N. Roy, "Evaluation of relative permittivity and conductivity of forest slab from experimentally measured data on lateral wave attenuation constant," *International Journal of Electronics*, Vol. 61, 597–605, Nov. 1996.

An Efficient Sinc-Collocation Domain Decomposition Method for Optical Waveguides Analysis

A. A. El-Mohsen[1], **A. M. Heikal**[1,2], **and S. S. A. Obayya**[1]

[1]Centre for Photonics and Smart Materials, Zewail City of Science and Technology Sheikh Zayed District
6th of October City, Giza, Egypt
[2]Department of Electronics and Communication Engineering
Mansoura University, Mansoura 35516, Egypt

Abstract— Since their development to solve differential equations boundary value problems [1], sinc numerical methods have attracted much attention. This is due to their incredible exponential rate of convergence $O(e^{-\gamma\sqrt{n}})$, γ is a positive constant. Along with domain decomposition methods, sinc numerical schemes can be developed to deal with problems which have discontinuous refractive index profiles. In this paper, a novel numerical scheme based on the sinc-collocation method is proposed for waveguides analysis. The domain of interest is decomposed into inner finite domains and outer semi-infinite domains. Patching domain decomposition is applied where the physical boundary conditions are matched at interfaces.For the finite domains, a much more convergence rate is achieved by using a double exponential transformation [2].

Mathematical Formulations: The wave equations used in each subdomain for H_x or H_y are as follows:

$$\nabla^2 H_\tau + k_0^2\left(n^2 - n_{eff}^2\right) H_\tau = 0, \quad \tau = x, y, \tag{1}$$

where $n_{eff} = \beta/k_0$ is the mode effective index, and β is the propagation constant. The field components H_x and H_y are expanded in each subdomain k as follows:

$$H_\tau^{(k)} = \sum_{i=-M}^{N}\sum_{j=-M}^{N} c_{ij}^{(\tau)} S_i^{(k)} S_i^{(k)}, \tag{2}$$

$$S_i^{(k)}(\tau) = \frac{\sin\left[(\pi/h_\tau)\left(\phi_\tau^{(k)} - jh_\tau\right)\right]}{(\pi/h_\tau)\left(\phi_\tau^{(k)} - jh_\tau\right)} \tag{3}$$

where $\phi_\tau^{(k)}$ is a suitable conformal map for each subdomain k.

Numerical Results: A standard rib waveguide structure whose cross section is shown in Fig. 1 will be analyzed. The rib width, W, is 2.0 µm, the rib height, $H = 1.1$ µm, and the outer slab depth, $D = 0.2$ m, and the operating wavelength is 1.55 µm. The refractive indices of the guiding, n_c, and substrate, n_s, regions are 3.44 and 3.34, respectively. The values of the effective index for fundamental quasi-TE and quasi-TM modes are 3.38876 and 3.8756 which accord well with the multi-domain spectral collocation method [3].

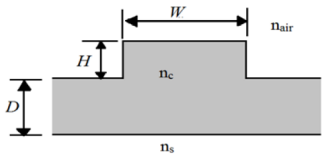

Figure 1: Schematic diagram of the rib waveguide structure.

REFERENCES

1. Stenger, F., "A sinc-galerkin method of solution of boundary value problems," *Math. Comput.*, Vol. 33, No. 145, 85–109, 1979.
2. Sugihara, M. and T. Matsuo, "Recent developments of the Sinc numerical methods," *J. Comput. Appl. Math.*, Vol. 164, 673–689, 2004.
3. Alharbi, F. and J. C. Scott, "Multi-domain spectral method for modal analysis of optical waveguide," *Opt. Quant. Electron.*, Vol. 41, No. 8, 583–597, 2009.

Session 3A12
SC4: Antenna-Channel Interactions and Wireless Propagation Channels

Research on Ka Rough Ocean Surface Channel Modeling Based on Stochastic Processes

Xiaodong Cao[1], **Xiaojun Wang**[1, 2], **and Tao Jiang**[1]

[1]College of Information and Communication Engineering, Harbin Engineering University, China
[2] Electrical and Computer Engineering Department, National University of Singapore, Singapore

Abstract— It is presented in this paper that a channel modeling technique based on GTD and stochastic bridge, which may boost the usage of low elevation angle Ka or higher frequency satellite down-link radio propagation prediction and estimation. First, it is introduced a random rough ocean surface modeling method under typical ocean states which is the foundation and the first step for electromagnetic simulation of telecommunication channel. Second, a huge data ocean surface reflection, scattering and diffraction based on GTD algorithm are calculated by high performance computer to provide a large number of samples for channel modeling. Third, a multipath channel model is set up to describe the statistical properties of received signal waveform which is modified by rough ocean surface. Last, all the steps are summed up and discussed to show the benefits of the presented modeling technique.

WLAN Based Indoor Locating Systems Enhanced by Ultrasonic Sensors; Hybrid Indoor Locater Systems (HILoS)

Selcuk Helhel, **Atalay Kocakusak**, **Yalcın Albayrak**, **and Sukru Özen**
Department of Electrical and Electronics Engineering, Engineering Faculty
Akdeniz University, Antalya 07058, Turkey

Abstract— In building location system requirements are growing very rapidly, since location information is a critical knowledge, for marketing and rehabilitation campuses as well as security applications. Instead GPS systems yield the highest location precision at outdoors; they are not available in indoor environments. Cellular based indoor location system is another possibility [1], and they proposed a method that uses accelerometer instead of mobile phone itself, but this solution is operator dependent and very expensive. Studies [2–4] present in the literature using Wi-Fi systems are examples of those indoor locating studies. Campos et al. [2] presented a system for multi-floor indoor positioning considering architectural aspects. They proposed a Data Correlation Method combined with neural network applications on them. They compared measured RSS levels by applying natural data clustering method and data correlation method.

Experimental results and literature tell us that While WiFi based systems get weak in case of close distance to transmitters, ultrasonic sensors respond much better in acceptable precise then the WiFi systems in that region. Similar way, they get worse by increasing distance. By the way, this paper focuses on enhanced indoor locating systems by ultrasonic sensors that offered system is called as Hybrid Indoor Locator.

ACKNOWLEDGMENT

This project was granted by TÜBİTAK 2209-A (PN:1919B011303278) and Akdeniz University, Scientific Research Projects Supporting Unit (BAP).

REFERENCES

1. Yaoa, D., C. Yu, A. K. Dey, C. Koehler, G. Minc, L. T. Yanga, and H. Jin, "Energy efficient indoor tracking on smartphones," *Future Generation Computer Systems*, Vol. 39, 44–54, 2014.
2. Campos, R. S., L. Lovisolo, and M. L. R. de Campos, "Wi-Fi multi-floor indoor positioning considering architectural aspects and controlled computational complexity," *Expert Systems with Applications*, Vol. 41, 6211–6223, 2014.
3. Helhel, S. and A. Kocakuşak, "Yol kaybı indeks hesabı ve wifi tabanlı kontrolsüz gezginlerden arındırılmış bina içi konum tespit sistemi," *VII. URSI-Türkiye Bilimsel Kongresi*, Cilt. 1, No. 1, ss. 1–4, KAYSERİ TÜRKIYE, August 28–30, 2014.
4. Helhel, S. and A.Kocakuşak, "Algorithms for indoor localization on wlan networks applications," *PIERS Proceedings*, 2174–2177, Guangzhou, China, August 25–28, 2014.
5. Zhao, Y., M. Li, and F. Shi, "Indoor radio propagation model based on dominant path," *Int. J. Communications, Network and System Sciences*, Vol. 3, 330–337, 2010, doi:10.4236/ijcns.2010.33042 blished Online March 2010.
6. Çelik, S., O. Kurnaz, Y. Albayrak, M. Bitirgan, İ. B. Basyigit, and S. Helhel, "An idoor to outdoor propagation model aT GSM900 GSM1800 and CDMA2100," *International Journal of Engineering & Applied Sciences (IJEAS)*, Vol. 5, No. 2, 9–17, 2013.
7. Taichung, Y. S. L., R. C. Chen, and Y. C. Lin, "An indoor location identification system based on neural network and genetic algorithm," *3rd International Conference on Awareness Science and Technelogy (iCAST)*, September 27–30, 2011.

New Intuitive Metrics for Diversity Performance Evaluation of Multi-element Antenna Systems

Vasileios C. Papamichael[1] and Petros Karadimas[2]

[1]Department of Electrical Engineering, Technological Educational Institute of Western Greece and Wireless Systems Performance (WiSPer), Patras 26441, Greece
[2]Department of Computer Science and Technology, University of Bedfordshire, Luton LU1 3JU, UK

Abstract— The mitigation of multipath fading is an issue of primary importance in wireless communications systems. Multi-element antenna (MEA) systems combat fading through diversity combining which potentially increases the received power. The performance evaluation of MEA system is quantified by the diversity gain (DG).

Until now, there have been proposed different metrics for the DG with the most important being the diversity antenna gain (DAG) [1], the effective diversity gain (EDG) [2] and the actual diversity gain (ADG) [3]. They are derived by comparing the cumulative distribution function (CDF) of the received signal-to-noise ratio (SNR) of the MEA and a reference antenna at a specific outage probability level (usually 1% outage probability level). Their only difference lies on the choice of that reference antenna. The DAG is based on comparing the MEA with an isotropic, dual polarized reference antenna and is thus a metric of universal applicability when deriving DG. The EDG arises by comparing the MEA with one of its single elements having 100% efficiency and the ADG by comparing the MEA with an arbitrarily selected antenna.

As the CDF just presents probabilities of specific SNR levels, DAG, EDG and ADG do not account for DG provided by a MEA system when only deep fades take place in one or more of the diversity branches. DG in such cases would be a better indicator of how effectively the MEA system combats fading. Thus, in this paper, three new intuitive metrics focusing on deep fade cases are proposed. The first is called *fading mitigation gain (FMG)* and accounts for the DAG when at least one of the diversity branches of the MEA system has *20 dB* less SNR with respect to the average received by the reference antenna SNR. It is thus a random variable. The second is called *reliability percentage (RP)* and accounts for the percentage of the cases when the MEA system has greater received SNR compared with that of the reference antenna. The third is called generalized *diversity antenna gain (GDAG)* and arises after weighting the two DAGs, i.e., the DAG (weighted by *RP*) when the MEA received SNR is greater than that of the reference antenna and the DAG (weighted by *1-RP*) when is lower. The MEA systems and propagation environments are jointly modeled by using the stochastic approach presented in [4].

REFERENCES

1. Ogawa, K. and J. Takada, "An analysis of the effective performance of a handset diversity antenna influenced by head, hand, and shoulder effects-A proposal for a diversity antenna gain based on a signal bit error rate and analytical results for the PDC system," *Electronics and Communications in Japan*, Part 2, Vol. 84, No. 6, 852–865, 2001.
2. Kildal, P., K. Rosengren, J. Byun, and J. Lee, "Definition of effective diversity gain and how to measure it in a reverberation chamber," *Microwave Optical Technology Letters*, Vol. 34, No. 1, 56–59, 2002.
3. Plicanic, V., B.-K. Lau, A. Derneryd, and Z. Ying, "Actual diversity performance of a multi-band diversity antenna with hand and head effects," *IEEE Transactions on Antennas and Propagation*, Vol. 57, No. 5, 1547–1556, May 2009.
4. Papamichael, V. and C. Soras, "Generalised selection combining diversity performance of multi-element antenna systems via a stochastic electromagnetic-circuit methodology," *IET Microwaves, Antennas and Propagation*, Vol. 4, No. 7, 837–846, July 2010.

A Practical Approach to Measuring Propagation Channel in the Spherical Vector Wave Domain

Y. Miao[1], **A. A. Glazunov**[2], **K. Haneda**[3], **and J. Takada**[1]

[1]Tokyo Institute of Technology, Japan
[2]Chalmers University of Technology, Sweden
[3]Aalto University, Finland

Abstract— This paper proposes a practical approach to measuring the propagation channel in the spherical vector wave domain. By using the spherical vector wave expansion, the propagation channel can be modeled as a mode-to-mode mapping matrix or **M**-matrix. This matrix provides a compact representation of the spatial and polarimetric properties of the propagation environment without influences of the transmit or receive antennas at link ends. In addition, this mode-to-mode mapping matrix can be used in conjunction with other antennas to estimate their performances in the same propagation environment. Hence, the importance of achieving an accurate estimation of the mode-to-mode mapping matrix **M**.

In the proposed approach of estimating the mapping matrix, a virtual spherical array realized by the rotated and translated Dielectric Resonant Antenna (DRA) is used. The array size, the element spacing and location are chosen so that all the dominant spherical vector waves within the spatial bandwidth of the antenna's minimum circumscribing sphere are excited to provide a well-conditioned matrix pseudo-inverse. With the virtual spherical DRA array at both ends in a propagation environment, the radio channel transfer function denoted as $\mathbf{H}_{\mathrm{sph}}$ can be simulated or measured. From the $\mathbf{H}_{\mathrm{sph}}$, and the excitation and weighting coefficients of the virtual spherical DRA array, an estimation of the mode-to-mode mapping matrix **M** of the propagation channel can be obtained directly.

The proposed approach is evaluated by both simulations and measurements. The measurements, were conduced i) in an anechoic chamber scenario with a single line-of-sight path, ii) in a multi-path indoor scenario (a relatively empty office). For all the measurement scenarios, a reference measurement was also performed with a patch antenna located at the center of the virtual spherical array. The channel transfer function of the reference measurement is used to evaluated the synthesized channel transfer function by recombining the estimated **M** with the patch antenna.

Challenges of Radio Propagation Measurements for 5G Systems

S. Salous
School of Engineering and Computing Sciences, Durham University, UK

Abstract— Future wireless communication systems are expected to operate in the higher frequency bands due to the availability of high contiguous spectrum on the order of GHz. This provides the required bandwidths for transmission of high data rates commensurate with real time applications such as high definition TV and immersive user experiences. However, the higher frequency bands between 30–90 GHz have a number of propagation issues such as high path loss, depolarisation, and scattering; hence to be to be limited to line of sight applications to ranges on the order of 200–300 m. Essential to the design of 5G systems is the characterisation of the wireless channel in these bands. In this paper an overview of the challenges of designing and conducting radio propagation measurements in the mm wave band are outlined and the architecture of a multi-band channel sounder that covers several bands between 30–90 GHz is presented. The sounder has been used in the 60 GHz band to carry out dual antenna measurements indoor and outdoor. Results of measurements in the 60 GHz band are presented in terms of rms delay spread and path loss.

Double Broadband Balun Structure Using CRLH TL for Differential Excitation of Dual-polarized Self-grounded Bow-tie Antenna

Sadegh Mansouri[1], **John Kvarnstrand**[2], **Andrés Alayon Glazunov**[1], **Jian Yang**[1], **and Per-Simon Kildal**[1]

[1]Department of Signals and Systems, Chalmers University of Technology, Gothenburg, Sweden
[2]Bluetest AB, Gothenburg, Sweden

Abstract— Using multiple port antennas at both the transmitter and the receiver sides of a communications link has been shown to improve the wireless communication system performance in terms of capacity and also reliability for given fixed system bandwidth and transmitted power [1]. These so-called Multiple Input Multiple Output (MIMO) systems are at the core of 4G, 5G and beyond wireless standards. In that respect, communication over orthogonally polarized wireless channels will be essential to achieve the anticipated performance. The antenna design for base stations is therefore of paramount significance. Besides, multi-port dual polarized wideband antennas can be used in many other applications. For example, in the Over-The-Air (OTA) testing of autonomous cars in a Random-Line- Of-Sight (RLOS) testing environment, a dual polarized uniform linear array antenna has been proposed [2].

One promising candidate for the array antenna element in such applications is the 4-port self-grounded bow-tie antenna shown in Fig. 1(a) [3]. However, in order to achieve the dual polarized performance by differentially exciting two ports of the bowtie antenna, we need to incorporate two baluns together with the antenna design. These baluns should satisfy the required bandwidth constraint (1.6–3 GHz) and they also should have a compact structure in order to maintain a low profile. Despite the wideband characteristics of microstrip baluns they do not meet our compactness requirement.

Therefore, in this paper we propose a broadband compact lumped element balun that meets the above requirements of bandwidth and compactness. As the starting point for our design we employ the fractal shaped CRLH TL balun presented in [4] modified to the frequency band of interest. This balun comprises one +90 branch and three −90 branches to provide the 180 degree phase difference at the output. The simulated results show an amplitude imbalance less than 1 dB and phase imbalance less than 10 degrees over the bandwidth of 1.6–3 GHz. Then to validate the performance, the two designed baluns are integrated with the bow-tie antenna in such a way that could totally fit at the back of the antenna as shown in Fig. 1(b). The performance of the whole structure is also evaluated. Return loss remains below −10 dB for the whole structure. And at last, the farfield pattern of the antenna in ideal differential excitation is compared to the case with using baluns. The results shows good agreement and gain degradation only about 0.5 dB in worst case.

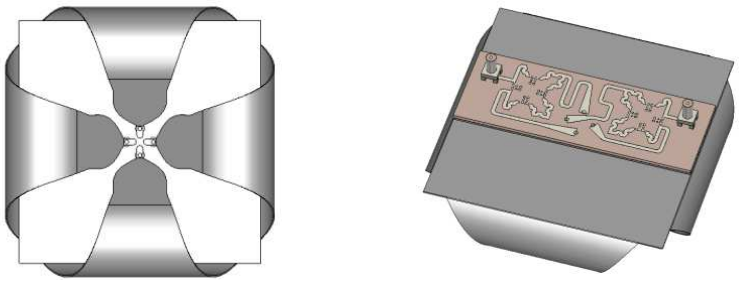

(a) (b)

Figure 1: (a) the self-grounded bow-tie antenna. (b) Balun integration with the bow-tie antenna.

REFERENCES

1. Molisch, A. F., *Wireless Communications*, 2nd Edition, John Wiley, New York, ISBN: 978-0-470-74186-3, 2010.

2. Kildal, P.-S., A. A. Glazunov, J. Carlsson, and A. Majidzadeh, "Cost-effective measurement setups for testing wireless communication to vehicles in reverberation chambers and anechoic chambers," *IEEE Conference on Antenna Measurements & Applications (CAMA)*, 1, 4, Nov. 16–19, 2014, doi: 10.1109/CAMA.2014.7003428.
3. Raza, H., A. Hussain, J. Yang, and P.-S. Kildal, "Wideband compact 4-port dual polarized self-grounded bowtie antenna," *IEEE Trans. Antennas Propag.*, Vol. 62, No. 9, 4468–4473, Sep. 2014.
4. Xu, H.-X., G.-M. Wang, X. Chen, and T.-P. Li, "Broadband balun using fully artificial fractal-shaped composite right/left-handed transmission line," *IEEE Microwave and Wireless Components Letters*, Vol. 22, No. 1, 16–18, 2012.

Capacity Analysis for On-body Communications in an Indoor Environment

C. Oliveira and L. M. Correia
Instituto Superior Técnico/INOV-INESC University of Lisbon, Lisbon, Portugal

Abstract— Body Area Networks (BANs) [1] will be strategic actors of the next generation of wireless systems beyond the fourth generation, supporting the world of everything for connected devices and objects. This work focuses on on-body communications, i.e., both transmitter and receiver antennas are attached to or located very near the body of a BAN user, most of the channel being on its surface. Potential scenarios include monitoring of biological signals in healthcare care units, as well as elderly people monitoring in home environments. The data collected by the wearable sensors can be used either in the network itself or forwarded to any appropriated external one (e.g., emergency service). A novel model is proposed using a smart and cooperative configuration of the wearable nodes, i.e., using clusters of nodes and combining multiple independent paths to behave like multi-antennas systems (i.e., Virtual MIMO). The aim is to enhance the reliability of communications and to overcome the effects of deep fading, which can be critical for some applications (e.g., life support decisions). Different metrics are proposed for the selection of the best wearable nodes, namely, the relative MIMO capacity gain (ratio between the MIMO capacity and the maximum throughput from the SISO branches), and the configuration score (relative capacity of a selected 2×2 configuration in relation to the maximum theoretical capacity of a particular BAN). This approach is supported by a channel model that considers the received signal composed of an on-body component (obtained from full wave simulations [2]) and of several multipath components present in the environment (obtained from a geometrically based statistical channel model adapted to BANs [3]). The model includes realistic body dynamics (taken from motion capture analysis), as described in [4]. Results are presented for the possible usage scenario of a female walking in an indoor complex propagation environment, and wearing a network of nine on-body sensors, organised in a 2×2 configuration (e.g., 2 data sensors transmitting hearing information to a sink composed by 2 nearby nodes). The case studies of the data sensors on the head (front and back), on the ears or on the arms, while the sink is on the front of the body (e.g., belt) are analysed. In case of the head-belt connection the signals are balanced, but, being highly correlated due to the short distances and similar propagation conditions and relative MIMO gains are small (1.57). If the data sensors are moved to the ears, higher relative MIMO gains are achieved (1.81). The trend of the average capacity over time when the sensors are on the arms exhibits higher fluctuations when compared to the placements on the head/ears, corresponding to the arms swinging, leading to an average gain of 1.73. Nevertheless, the performance of the selected virtual MIMO case studies (with relative MIMO capacity gains ranging in [1.57, 1.81]) is always enhanced when compared to the best SISO scenario, even for line-of-sight branches. The selection of the optimum placements should be done according to the specific system under study. The best performance for the analysed case studies corresponds to the sensors on the ears, reaching a configuration score of 0.76.

REFERENCES

1. Hall, P. and Y. Hao, *Antennas and Propagation for Body-centric Wireless Communications*, Artech House, Norwood, MA, USA, 2006.
2. Mackowiak, M., C. Oliveira, and L. M. Correia, "Radiation pattern of wearable antennas: A statistical analysis of the influence of the human body," *International Journal of Wireless Information Networks*, Vol. 19, No. 3, 209–218, Sep. 2012.
3. Oliveira, C., M. Mackowiak, and L. M. Correia, "Modelling on- and off-body channels in body area networks," *Proc. of IMOC 2013 — International Microwave and Optoelectronics Conference*, Rio de Janeiro, Brazil, Aug. 2013.
4. Oliveira, C. and L. M. Correia, "Perspectives for the use of MIMO in dynamic body area networks," *Proc. of EuCPAP 2013 — European Conference on Antennas and Propagation*, Gothenburg, Sweden, Apr. 2013.

Spatial Probability of Detection Distribution as a Performance Measure of ZF Massive MIMO

A. Alayon Glazunov and Per-Simon Kildal
Department of Signals and Systems, Chalmers University of Technology, Sweden

Abstract— In this paper we investigate the impact of the spatial user distribution on the down-link Zero-Forcing (ZF) algorithm applied to the output signals from a dual-polarized Massive MIMO antenna array with Na antenna elements. Each element of the array antenna consists of four elementary Huygens sources that are differentially excited to form two orthogonally polarized beams. It is assumed that the Massive MIMO antenna array operates in Random Line-Of-Sight (RLOS). RLOS, here means that (i) there is a single LOS path connecting the user equipment with the base station and that (ii) the orientation of the user equipment antenna is assumed to be random. The antenna array is assumed to be wall-mounted on the facade of a building. A uniform distribution of Nu users on a circular sector in front of the array antenna is considered in order to emulate users at various distances to the base station as well as various angular separations. We present simulation results in terms of the spatial coverage given by the Probability of Detection [1] corresponding to the resulting polarisation and beamforming gain of 2-bitstream per user throughput and the corresponding coverage 2D radiation pattern of the $2N_a \times 2N_u$ multiuser Massive MIMO scenario. We also investigate wether there is an optimal antenna arrangement and size that maximize the multiplexing gain over a given coverage area based on the distribution of the Probability of Detection.

REFERENCES

1. Kildal, P.-S., X. Chen, M. Gustafsson, and Z. Shen, "MIMO characterization on system level of 5G microbase stations subject to randomness in LOS," *IEEE*, Vol. 2, 1064–1077, 2014, doi: 10.1109/ACCESS.2014.2358937.

Research on Random Wireless Channel of Radio Indicator for Mariners

Tao Jiang[1], **Xiaodong Cao**[1], **Xiaojun Wang**[1, 2]

[1]College of Information and Communication Engineering, Harbin Engineering University, China
[2]Electrical and Computer Engineering Department, National University of Singapore, Singapore

Abstract— It is presented a random wireless channel model of marine emergence radio indicator in this paper, which describe the performance of telecommunications in difference typical ocean states. First, it is introduced a random rough ocean surface modeling method under typical ocean states which is the foundation for simulation of LOS and NLOS telecommunication channel. Second, massive data is calculated by running simulation code which is necessary for statistical analysis of linking properties. Last, the telecommunication performance is predicted by signal to noise ratio vs bit rate error in situation of typical ocean states and elevation angles which may provide key information for the design of next generation of marine indicators.

Feasibility Study of Emulating Extended Spatial Channel Models in a Multi-probe MIMO OTA Antenna Test Setup

Md Suzan Miah, **Afroza Khatun**, **and Katsuyuki Haneda**
Department of Radio Science and Engineering, School of Electrical Engineering
Aalto University, P. O. Box 13000, Aalto FI-00076, Finland

Abstract— Multiple input multiple output (MIMO) techniques, which use multiple antennas in both sides of the radio communication system, have been a promising method to support the increased demand for higher data rate transmission. However, the performance of MIMO systems depends not only on the antenna performance but also on the propagation environment. Hence, for accurate MIMO performance testing of terminal devices, it needs to consider both the multiple terminal antennas as well as the propagation environment. Over-the-air (OTA) testing is widely used for single-input single-output (SISO) performance testing, and its extension to the MIMO device testing has been actively investigated.

Standardization works for MIMO OTA testing have been intensively coordinated by CTIA and 3GPP, where several different MIMO OTA test methods have been proposed [1]. One mandatory requirement of any MIMO OTA test methods is to emulate an electromagnetic environment, which resembles the scenario where the terminal operates. Geometry-based channel models such as the Spatial Channel Model (SCM), its extension (SCME), WINNER II or IMT-Advance constitute a good means to describe the propagation environment, which is translated into the electromagnetic environment in the OTA testing. The use of such well-defined channel model in MIMO OTA testing makes the test methods well justified.

One of the proposed techniques in the standardization of the OTA testing is a multi-probe anechoic chamber based MIMO OTA testing, which can emulate the electromagnetic environment defined by a channel model in a controllable manner. To emulate the spatial and temporal characteristics of the channel, two channel emulation techniques have been reported in the literature [2]; one is the plane wave synthesis (PWS) and another is prefading signal technique (PFS). In this paper, we address the PWS technique based on the spherical wave theory in order to prove its consistency with other MIMO OTA testing techniques such as the PFS.

The purpose of the paper is to validate the PWS technique for emulating the electromagnetic environment in a multi-probe based MIMO OTA test system. We use the SCME as the reference channel model, for which the validation of the PWS technique has not been reported. The validation of the channel emulation is performed in terms of power delay profile, temporal correlation, spatial correlation, cross-polarization and channel capacity. Our results facilitate analyzing consistency of the performance of the PWS technique with other MIMO OTA techniques such as the PFS. The validation results are to be presented in the manuscript.

REFERENCES

1. "Verification of radiated multi-antenna reception performance of user equipment," 3GPP, TR 37.977 V12.1.0, March 2014.
2. Kyösti, P., T. Jämsä, and J. Nuutinen, "Channel modelling for multiprobe over-the-air MIMO testing," *International Journal of Antennas and Propagation*, 2012.

Session 3A13
FocusSession.SC3&2: Disordered Photonics 1

Random Optical Media for Third Generation Photovoltaics

Hernán Míguez
Institute of Materials Science of Seville, Spanish National Research Council, University of Seville
C/Américo Vespucio 49, Sevilla 41092, Spain

Abstract— In this keynote, different light trapping strategies based on the use of optical materials to enhance the light harvesting efficiency of third generation photovoltaic devices, such as dye sensitized and perovskite solar cells, will be discussed. Focus will be put on methods based on the inclusion of diffuse scattering particles randomly arranged, and a comparison to approaches based on ordered nanostructures, such as photonic crystals or surface texturing, will be provided. Near optical field effects in metal particles embedded in the photoanode will also be reported. Our work provides a theoretical framework in which the response of solar cells containing optical materials by design can be rationalized. The different synthetic routes to implement them in actual devices will be shown and their effect on the photovoltaic performance will be discussed, as well as the interplay with the tuneable semitransparency or color of the device, of interest for building-integrated photovoltaic devices.

REFERENCES

1. Zhang, W., M. Anaya, G. Lozano, M. E. Calvo, M. B. Johnston, H. Míguez, and H. J. Snaith, "Highly efficient perovskite solar cells with tunable structural color," *Nano Lett.*, 2015, DOI: 10.1021/nl504349z.
2. Anaya, M., G. Lozano, M. E. Calvo, W. Zhang, M. B. Johnston, H. J. Snaith, and H. Míguez, "Optical description of mesostructured organic-inorganic halide perovskite solar cells," *The Journal of Physical Chemistry Letters*, Vol. 6, 48–53, 2015.
3. Gálvez, F. E., P. R. Barnes, J. Halme, and H. Míguez, "Dye sensitized solar cells as optically random photovoltaic media," *Energy & Environ. Sci.*, Vol. 7, 689, 2014.
4. Gálvez, F. E., E. Kemppainen, H. Míguez, and J. Halme, "Effect of diffuse light scattering designs on the efficiency of dye solar cells: An integral optical and electrical description," *J. Phys. Chem.*, Vol. 116, 11426, 2012.
5. Colodrero, S., A. Forneli, C. López-López, L. Pellejà, H. Míguez, and E. Palomares, "Efficient transparent thin dye solar cells based on highly porous 1D photonic crystals," *Adv. Funct. Mater.*, Vol. 22, 1303, 2012.
6. Colonna, D., S. Colodrero, H. Lindström, A. Di Carlo, and H. Míguez, "Introducing structural colour in DSCs by using photonic crystals: Interplay between conversion efficiency and optical properties," *Energy & Environ. Sci.*, Vol. 5, 8238, 2012.

Innovative Materials and Methods for Disorder Photonics

Álvaro Blanco and Cefe López
Instituto de Ciencia de Materiales de Madrid-ICMM (CSIC)
Sor Juana Inés de la Cruz 3, Madri 28049d, Spain

Abstract— Understanding the interaction of light with active and passive photonic structures creates challenges for new materials and preparation methods. In a self-assembly approach this concerns both structures and guest components. We prepare disordered templates by new dry methods and synthesise emitting materials both from semiconductor and dyes. The latter are efficient sources that can enter multifunctional systems and in pairs permit to engineer emission by exploiting FRET processes.

Creating structured materials from the bottom up is a widely used method owing to the easy and inexpensive techniques it involves. Self-assembly entails allowing or inducing small particles to arrange themselves into photonic structures like photonic crystals and photonic glasses. Non-spherical particles are less prone to control but still offer great possibilities always related to disorder.

Novel techniques dispensing with the liquid are nowadays being explored [1]. In this way we demonstrate monodisperse disordered structures in minutes and without the hassle associated with colloidal sedimentation.

Templating is used to infiltrate materials into the preformed structures. A good example is ZnO that permits to build both Bloch-mode and random lasers. Organic dyes have been mostly used impregnating preassembled colloidal structures. In such cases the use of FRET coupling between dyes can expand their potential as laser sources. An interesting case is when both dyes are contained inside the beads [2]. This requires a careful selection of the dyes paying attention to both their emission properties and their chemistry for a good match of their energy transfer properties.

Finally an example of multifunctional [3] material is exemplified in the preparation of elastomeric materials where a scattering medium is dispersed along with a gain material so as a shape memory functionality is accompanied by control over lasing.

REFERENCES

1. Montesdeoca, D., et al., to be published.
2. Muñoz, A., et al., to be publihsed.
3. Espinha, A., M. C. Serrano, Á. Blanco, and C. López, "Thermoresponsive shape-memory photonic nanostructures," *Advanced Optical Materials*, Vol. 2, No. 6, 516–521, 2014.

Adaptive and Nonlinear Optics in the Transverse Localization Regime

Marco Leonetti[1], **Salman Karbasi**[2], **Arash Mafi**[3], **and Claudio Conti**[4]

[1]Center for Life Nano Science@Sapienza, Istituto Italiano di Tecnologia
Viale Regina Elena, Roma 291 00161, Italia
[2]Department of Electrical and Computer Engineering
University of California, San Diego, La Jolla, California 92093, USA
[3]Department of Physics and Astronomy and Center for High Technology Materials
University of New Mexico, Albuquerque, New Mexico 87131, USA
[4]ISC-CNR and Department of Physics, University Sapienza, P.le Aldo Moro 5, I-00185, Roma, Italy

Abstract— Transverse Anderson localization (TAL) is the trapping of waves due a disordered potential which is invariant along propagation direction, cancelling the effects of diffraction. We recently demonstrate that it is possible to exploit optical nonlinearity and adaptive optics to tailor light inside disordered optical fibers supporting TAL.

Recent experimental results stimulated a large body of theoretical work dealing with the role of self- focusing and defocusing in the evolution of the disorder induced localizations [1]. There is a relevant debate about the fact that nonlinearity may enhance, or hamper, this linear trapping mechanism, and there are many open research directions, as for example, considering quadratic nonlinearities. Indeed, the interplay between disorder and a nonlinear response is expected to alter the commonly accepted scenario about the absence of diffusion and transport in the Anderson regime, when all of the states are exponentially localized. Particularly intriguing is the role of spatial nonlocality. Indeed, if disorder induces exponential localizations and reduces the interactions of distant modes, nonlocality (i.e., a nonlinear perturbation that extends far beyond the region of interaction) is expected to create some action at a distance dependent on power. In recent papers, we demonstrate the effects of nonlinearity in disordered optical fibers supporting TAL [2, 3]. We notice two different striking phenomena: disorder induced self focusing [4] and mode migration [5] (see Fig. 1). In a nutshell exploiting nonlinearity and nonlocality it is possible to control light modes by tuning intensity in distant control beams that modify the refractive index landscape.

Moreover we performed adaptive focusing experiments [6] in disordered optical fibers. in the transverse Anderson localization regime [7]. By wavefront shaping and optimization, we observe the generation of a propagation-invariant beam, where light is trapped transversally by disorder,

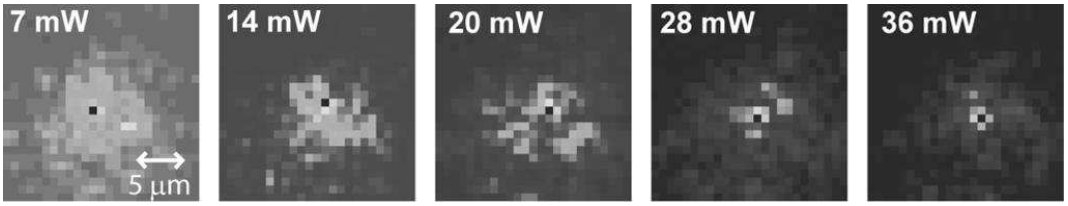

Figure 1: Visualized mode self focusing. The images represent of a localized state whose extension shrinks by increasing light intensity (value of the intensity indicated in the figures).

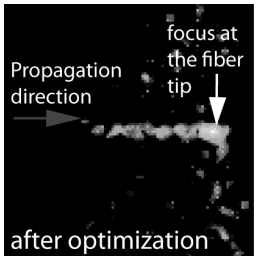

Figure 2: Side view of the fiber tip. The focus at the fiber tip shows a tail on the left, which is a signature of the localized states cooperating the adaptive focusing.

and show that localized states can be excited by extended speckled beams. We demonstrate that disordered fibers allow a more efficient focusing action with respect to standard fibers. This enhancement is due both to the cooperative action of localized states with adaptive focusing, and to the effects of localization which inhibits light paths far from the target (see Fig. 2).

REFERENCES

1. De Raedt, H., A. Lagendijk, and P. de Vries, "Transverse localization of light," *Phys. Rev. Lett.*, Vol. 62, 47, 1989.
2. Karbasi, S., C. R. Mirr, P. Gandomkar Yarandi, R. J. Frazier, K. W. Koch, and A. Mafi, "Observation of transverse Anderson localization in an optical fiber," *Opt. Lett.*, Vol. 37, 2304, 2012.
3. Karbasi, S., T. Hawkins, J. Ballato, K. W. Koch, and A. Mafi, "Transverse Anderson localization in a disordered glass optical fiber," *Opt. Mater. Expr.*, 2012.
4. Leonetti, M., S. Karbasi, A. Mafi, and C. Conti, "Experimental observation of disorder induced self-focusing in optical fibers," *Appl. Phys. Lett.*, Vol. 105, 171102, 2014.
5. Leonetti, M., S. Karbasi, A. Mafi, and C. Conti, "Observation of migrating transverse anderson localizations of light in nonlocal media," *Phys. Rev. Lett.*, Vol. 112, 193902, 2014.
6. Vellekoopl, I. M., A. Lagendijk, and A. P. Mosk, "Exploiting disorder for perfect focusing," *Nat. Phot.*, Vol. 4, 320, 2010.
7. Leonetti, M., S. Karbasi, A. Mafi, and C. Conti, "Light focusing in the anderson regime," *Nat. Commun.*, Vol. 5, 4534, 2014.

Disorder in Nature: Optimisation of Light Scattering in Beetles

Matteo Burresi[1], **Lorenzo Cortese**[1], **Diederik S. Wiersma**[1], **and Silvia Vignolini**[2]

[1]European Laboratory for Non-linear Spectroscopy (LENS), Sesto Fiorentino (FI), Italy
[2]Department of Chemistry, University of Cambridge, Cambridge, UK

Abstract— In nature, an amazing range of optical strategies exists that is optimised by at least 500 million years of evolution. Animal displays are often assembled of mainly two basic materials, chitin/keratin and melanin, in various parts of animal bodies that often result in intriguing optical effects ranging from matte to iridescent colours, and from black to extremely white. These structural colours arise from complex nanostructures such as ordered and quasi-ordered photonic crystals and random assemblies.

While the most dazzling displays are due to ordered photonic structures with a strong selective reflection of single colours, whiteness arises from diffuse and broadband reflection of light and is less explored. Whiteness is typically achieved through optical scattering in randomly structured media. A white surface appearance generally requires a relatively thick system comprising randomly positioned high refractive-index scattering centres, in strong contrast to structural colour where the colour is due to coherent scattering.

Here we demonstrate how the exceptionally bright white appearance of *Cyphochilus* and *Lepidiota stigma* beetles is provided by a remarkably optimised polydispersity and anisotropy of the intra-scale chitin networks, which act as scattering elements [1]. Using time-resolved measurements, we show that light propagating in the scales of the beetles undergoes strong multiple scattering that is associated with the lowest transport mean free path and diffusion constants reported to date for low-refractive-index systems. The high-brightness white appearance from a small layer thickness and density that extends from near ultra-violet to the near infrared.

These findings are complemented by advanced finite-difference time-domain modelling on three-dimensional networks with controlled anisotropy ratios to understand the important parameters in the design of efficient scattering media. The systems extracted optical parameters infer new designs for efficient strongly-scattering 3D bio-inspired photonic structures.

Figure 1: Picture of the two white beetles.

REFERENCES

1. Burresi, M., L. Cortese, L. Pattelli, M. Kolle, P. Vukusic, D. S. Wiersma, U. Steiner, and S. Vignolini, "Bright-white beetle scales optimise multiple scattering of light," *Sci. Rep.*, Vol. 4, 6075, 2014.

Hyperuniform Disordered Photonic Structures

Marian Florescu
Advanced Technology Institute, Faculty of Engineering and Physical Sciences, University of Surrey
Guildford, Surrey, GU2 7XH, UK

Abstract— Hyperuniform disordered solids (HUDS) are a new class of materials [1] that harness structural disorder and control light transport, emission and absorption in unique ways, beyond the constraints imposed by conventional photonic architectures [2–8]. HUDS materials are statistically isotropic and possess a constrained randomness such that density fluctuations on large scales behave more like those of ordered solids, crystals or quasicrystals, rather than those of conventional amorphous materials [9].

We present new design strategies for light flow and confinement on HUDS platforms, which exploit the interplay between disorder, topological correlations and hyperuniformity. In an otherwise unperturbed HD structure, we demonstrate that it is possible to create localized states of the electromagnetic field by reducing or enhancing the dielectric constant at a certain points in the sample. Due to the presence of the defect, a number of localized cavity modes are created within the photonic band gap at specific frequencies. Despite the statistical isotropy of the network structure surrounding the cavity, the modes display well defined (approximate) symmetries and our simulations show that 2D quality factor of the confined modes is higher than 10^9. We also demonstrate waveguides ("linear" defect mode created by filling of network cells along a connected path), which exploit the statistical isotropy of the photonic band gap. The physical properties of the localized modes in HUDS materials are determined by PBG formation mechanisms in these materials and the elimination of the constraints imposed by long-range order has a major influence on the properties of the localized modes.

In conclusion, we have employed their unique properties to introduce novel architectures for optical cavities that achieve an ultimate isotropic confinement of radiation, and waveguides with arbitrary bending angles. Our results demonstrate low-loss waveguiding and high-Q cavities in hyperuniform structures and open the way for the realization of highly flexible, disorder-insensitive optical micro-circuit platforms.

REFERENCES

1. Florescu, M., S. Torquato, and P. Steinhardt, *Proceedings of the National Academy of Sciences*, Vol. 106, 20658, 2009.
2. Florescu, M., S. Torquato, P. and Steinhardt, *Phys. Rev. B*, Vol. 87, 165116, 2013.
3. Man, W., M. Florescu, E. P. Williamson, Y. He, S. R. Hashemizad, B. Y. Leung, D. R. Liner, S. Torquato, P. Chaikin, and P. Steinhardt, *Proceedings of the National Academy of Sciences*, Vol. 110, 15886, 2013.
4. Man, W., M. Florescu, K. Matsuyama, P. Yadak, G. Nahal, S. Hashemizad, E. Williamson, P. Steinhardt, S. Torquato, and P. Chaikin, *Opt. Express*, Vol. 21, 19972, 2013.
5. Florescu, M., S. Torquato, and P. J. Steinhardt, *Appl. Phys. Lett.*, Vol. 97, 201103, 2010.
6. Florescu, M., S. Torquato, and P. Steinhardt, *Phys. Rev. B*, Vol. 80, 155112, 2009.
7. Amoah, T. and M. Florescu, *Phys. Rev. B*, Vol. 91, 020201(R), 2015.
8. Florescu, M., S. Torquato, and P. Steinhardt, *Phys. Rev. B*, Vol. 87, 165116, 2013.
9. Torquato, S. and F. H. Stillinger, *Phys. Rev. E*, Vol. 68, 041113, 1–25, 2003.

Direct and Inverse Ceramic Photonic Glasses

Pavel N. Dyachenko[1], **Elisabeth W. Leib**[3], **Jefferson J. do Rosario**[2], **Alexander Yu. Petrov**[1,4], **Roman Kubrin**[2], **Gerold Schneider**[2], **Horst Weller**[3], **Tobias Vossmeyer**[3], **and Manfred Eich**[1]

[1]Institute for Optical and Electronic Materials, Hamburg University of Technology
Eissendorfer Straße 38, Hamburg 21073, Germany
[2]Institute of Advanced Ceramics, Hamburg University of Technology
Denickestrasse 15, Hamburg 21073, Germany
[3]Institute of Physical Chemistry, University of Hamburg, Grindelallee 117, Hamburg 20146, Germany
[4]ITMO University, 49 Kronverskii Ave., St. Petersburg 197101, Russia

Abstract— Multiple scattering of light in a random media is a subject of great interest in fundamental and applied photonics research [1]. García et al. [2] presented a new three-dimensional system called "photonic glass" that is composed of monodisperse polymer spheres arranged in a completely disordered way. Due to the resonant behavior of the spheres discrete light states exist so that every sphere acts as a meta-atom for light. Applications such as random lasing [3] and structural coloration [4] have been suggested. However, strong scattering of light in the disordered structure and resulting high diffuse reflectance over a broad wavelength range make photonic glass also attractive for other fields of science and technology. Here we report on high-temperature stable ceramic photonic glasses which benefit from the high refractive index and high temperature stability of refractory ceramics.

Direct and inverse ceramic glasses were studied. A direct photonic glass was obtained by sedimentation of monodisperse zirconia microparticles [5]. For fabrication of inverse photonic glass from yttrium-stabilised zirconia (YSZ), a single-step deposition method was developed [6]. These novel materials can be used for a wide range of applications, such as thermal radiation barrier coatings, high-temperature stable structural coloration, broadband reflectors, resonant random lasers, and photonic Anderson localization. We show that disordered arrays of ceramic microparticles or shells can efficiently reflect visible and infrared electromagnetic radiation in a broad wavelength range. The hemispherical diffuse reflection from the disordered structure has broadband characteristics with a cut off defined by the sphere size. A reflectivity up to 93% in the visible range was achieved for 40 µm film thickness.

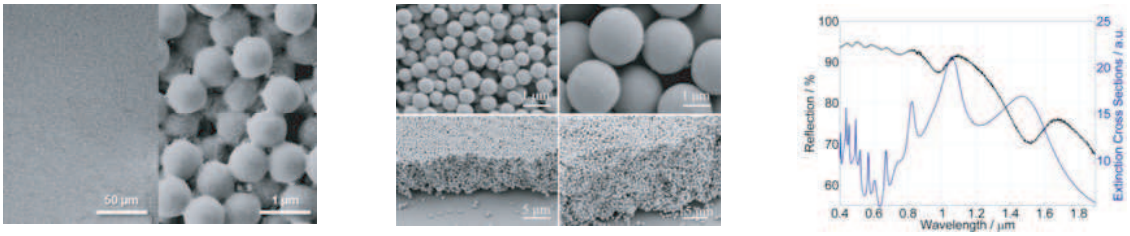

(a) (b) (c)

Figure 1: (a) SEM images of YSZ based inverse photonic glass with pore diameter 0.756 µm. (b) SEM images of zirconia based direct photonic glass. (c) Experimental hemispherical diffuse reflection from direct ceramic photonic glass with sphere diameter $D = 0.67$ µmm ($L = 40$ µmm) and extinction cross section for single sphere of the same diameter.

ACKNOWLEDGMENT

We gratefully acknowledge financial support from the German Research Foundation (DFG) via SFB 986 "M3" projects C2, C4, C6. The authors acknowledge the support from CST, Darmstadt, Germany with their Microwave Studio software.

REFERENCES

1. Wiersma, D. S., *Nat. Photonics*, Vol. 7, 188, 2013.
2. García, P. D., R. Sapienza, A. Blanco, and C. López, *Adv. Mater.*, Vol. 19, 2597, 2007.

3. Gottardo, S., R. Sapienza, P. D. García, A. Blanco, D. S. Wiersma, and C. López, *Nat. Photonics*, Vol. 2, 429, 2008.
4. Takeoka, Y., *J. Mater. Chem. C*, Vol. 1, 6059, 2013.
5. Dyachenko, P. N., J. J. do Rosário, E. W. Leib, A. Yu. Petrov, R. Kubrin, G. A. Schneider, H. Weller, T. Vossmeyer, and M. Eich, *ACS Photonics*, Vol. 1, 1127, 2014.
6. Do Rosário, J. J., P. N. Dyachenko, R. Kubrin, R. M. Pasquarelli, A. Yu. Petrov, M. Eich, and G. A. Schneider, *ACS Appl. Mater. Interfaces*, Vol. 6, 12335, 2014.

Statistical Physics of Multimode Ordered and Disordered Lasers

F. Antenucci[1,2], **A. Crisanti**[1,3], **M. Ibáñez Berganza**[1,4], **and L. Leuzzi**[1,2]

[1]Dipartimento di Fisica, Università di Roma Sapienza, Piazzale A. Moro 2, Rome I-00185, Italy
[2]NANOTEC-CNR, Soft and Living Matter Lab, Piazzale A. Moro 2, Rome I-00185, Italy
[3]ISC-CNR, UOS Sapienza, Piazzale A. Moro 2, Rome I-00185, Italy
[4]INFN, Gruppo Collegato di Parma, via G.P. Usberti, Parma 7/A-43124, Italy

Abstract— The adoption of a statistical mechanics framework in optics provides realistic models for multimode laser systems in random media whose experimental implications are presented and critically analyzed. The approach is based on the hypothesis of effective equilibrium. Lasers are manifestly off-equilibrium and energy is pumped into the system but as the system power is kept constant, though, the resulting stationary regime can be described as if at equilibrium with an effective "thermal bath" whose "temperature" is related to the pumping rate and to the true environment temperature. The analytic solution of a mean field model for multimode laser in open and irregular cavities will be first addressed. The model is exact for a narrow bandwidth and extended modes and includes the mode intensity dynamics as well as the presence of a linear coupling between the modes, due, e.g., to leakages from the open cavity. The complete phase diagram, in terms of disorder strength, source pumping and non-linearity, consists of four different optical regimes: incoherent fluorescence, standard mode locking, random lasing and the novel spontaneous phase locking. A replica symmetry breaking transition is predicted at the random lasing threshold. In this situation, identical copies of the system show different amplitude equilibrium configurations, as the ergodicity is broken in many distinct states. For a high enough strength of non-linearity, a whole region with nonvanishing complexity anticipates the transition and the light modes in the disordered medium display typical discontinuous glassy behavior, i.e., the photonic glass has an exponential number of metastable states that corresponds to different mode-locking processes in random lasers. Symmetry breaking in the intensity fluctuation overlap is shown to be equivalent to the one occurring in the complex amplitude overlap, providing an easily verifiable test in typical experimental setups. The relevance of this order parameter is considered in describing the laser transition in random media and in explaining its glassy nature in terms of emission spectra data. The theoretical analysis is compared to recent measurements. Further on, the mode-locking lasers can be modeled and analyzed beyond the mean field approximation, accounting, e.g., for the presence of many well-resolved frequencies of the lasing modes. By means of optimized, parallel Monte Carlo simulations, system properties are studied varying interaction random dilution, gain profile and number of modes. The inhomogeneous structure in the nonlinear "mode-locked" interaction network is shown to yield short pulses and phase waves with nontrivial slopes, corresponding to a phase delay of the pulsed laser signal.

Invariance Property of Wave Scattering through Disordered Media

R. Pierrat[1], **P. Ambichl**[2], **S. Gigan**[3], **A. Haber**[2], **R. Carminati**[1], **and S. Rotter**[2]

[1]Institut Langevin, ESPCI, Paris, France
[2]Vienna University of Technology (TU Wien), Vienna, Austria
[3]Laboratoire Kastler Brossel, Ecole Normale Supérieure, Paris, France

Abstract— The diffusion of particles and waves through disordered media encompasses a large variety of phenomena, from the motion of insects to the scattering of electrons or light in complex environments. A fundamental insight in the theory of diffusive random walks is that the mean length of trajectories traversing a finite open system is independent of the details of the diffusion process [1]. Instead, the mean trajectory length depends only on the system's boundary geometry and is thus unaffected by the value of the mean free path. This result is particularly counter-intuitive when considering that many other quantities in disordered transport do depend on the mean free path, like the transmission and the reflection through a disordered system as well as the associated times. In my talk I will demonstrate that this invariance property follows from the so-called Weyl law for the average density of states in a system and is thus rooted on a much deeper level than that of a random walk. As a result, we can extend the reach of this universal invariance property beyond the diffusion approximation [2]. Specifically, we demonstrate that an equivalent invariance relation also holds for the scattering of waves in resonant structures as well as in ballistic, chaotic or in Anderson localized systems. Our work unifies a number of specific observations made in quite diverse fields of science. Potential experimental realizations using light fields in disordered media are discussed and analyzed in terms of their promise for practical applications.

REFERENCES

1. Blanco, S. and D. Fournier, "An invariance property of diffusive random walks," *Europhys. Lett.*, Vol. 61, 168, 2003.
2. Pierrat, R., P. Ambichl, S. Gigan, A. Haber, R. Carminati, and S. Rotter, "Invariance property of wave scattering through disordered media," *PNAS — Proc. Natl. Acad. Sci.*, Vol. 111, 17765, USA, 2014.

Wavelength-scale Localization with Heavy Photons

R. Faggiani[1], **A. Baron**[2], **X. Zang**[1], **L. Lalouat**[3], **S. A. Schulz**[4,5], **K. Vynck**[1], **B. O'Regan**[4,6], **B. Cluzel**[3], **F. de Fornel**[3], **T. F. Krauss**[4,6], **and P. Lalanne**[1]

[1]Laboratoire Photonique Numérique et Nanosciences (LP2N), UMR 5298
CNRS-IOGS-Univ. Bordeaux, Institut d'Optique Aquitaine, Talence 33400, France
[2]Centre de Recherche Paul Pascal (CRPP), UPR 8641, CNRS-Univ. Bordeayx, Pessac 33600, France
[3]Laboratoire Interdisciplinaire Carnot de Bourgogne (ICB)
UMR 6303, CNRS-Univ. Bourgogne, Dijon 21078, France
[4]SUPA, School of Physics & Astronomy, University of St Andrews, St Andrews, KY16 9SS, UK
[5]Department of Physics, University of Ottawa, Ottawa, Ontario K1N 6N5, Canada
[6]Department of Physics, University of York, York YO10 5DD, UK

Abstract— We investigate the formation of localized modes in 1D randomly-perturbed optical periodic media near the photonic band-edge. While the group index is generally considered to be the key quantity in this process, we demonstrate that the relation between the disorder level and the spatial extent of individual localized modes is driven instead by the effective photon mass. Near-field measurements on photonic crystal waveguides and statistical numerical calculations on various structures reveal that periodic media exhibiting flat dispersion bands can support surprisingly small localized modes at almost imperceptible disorder levels ($\sigma < \lambda/1000$). A scaling law that relates the disorder level to the modes spatial extent is proposed and is found to agree well with the numerical and experimental results.

Introduction: Random imperfections can have a profound impact on light propagation in periodic media, the most striking phenomenon being undoubtedly the formation of localized modes in the vicinity of photonic band-gaps. Localization in photonic crystal waveguides (PhCWs) has garnered special attention due to the important limitations it imposes on the realization of slow-light photonic devices, but also for the opportunities it offers for strong light-matter interaction in quantum electrodynamics experiments. It is widely accepted that Anderson localization is enhanced with decreasing group velocity, i.e., when approaching the band-edge [1], and that tiny perturbations are sufficient to create defect modes forming the decaying Lifshitz tail in band-gaps [2]. These behaviors are generally described via ensemble-averaged quantities, namely the localization length [3, 4] and the density of states [2]. Conversely, very little is known on the properties of individual localized modes. In this work we are showing that, surprisingly, disorder level of the order of $\lambda/1000$ allows to form modes with spatial extents comparable to those achieved with engineered nanocavities. In contrast with the widely-held view that the key quantity impacting localization near photonic band-edges is the group index, we argue that the relation between the disorder level and the mode spatial extent is driven by the effective photon mass, i.e., the second-derivative of the dispersion band.

Results: We have performed near-field measurements of a PhCW in the slow light regime where the disorder is only due to fabrication imperfections (of the order of 1–2 nm). A localized mode with a spatial extent of 6 µm was observed in the scanning area. To complete this observation, extensive numerical calculations have been performed on PhCWs and Bragg stacks, two 1D periodic media, with different disorder levels and effective masses. Results are showing a threshold-like behavior, defining a minimal spatial extent of the modes $L_{\min}$. To explain this phenomenon, a simple model has been made that link $L_{\min}$ to the disorder level and the effective mass m. The relation $L_{\min}\alpha(m\Delta\omega)^{-1/2}$, where $\Delta\omega$ is a frequency shift of the mode induced by the disorder, is in good agreement with the numerical results.

Conclusion: To summarize, we have provided new understanding into the physical mechanism underlying the formation of localized modes at band-edges of periodic media, showing that the relation between the disorder level and the spatial extent of individual localized modes is driven to a large part by the effective photon mass. In particular we have investigated the possibility to form wavelength-scale localized modes at vanishingly-small disorder levels, revealing that such modes naturally form up in PhCWs at intrinsic disorder levels due to the flatness of the dispersion curve.

REFERENCES

1. John, S., *Phys. Rev. Lett.*, Vol. 58, 2486, 1987.

2. Huisman, S. R., G. Ctistis, S. Stobbe, A. P. Mosk, J. L. Herek, A. Lagendijk, P. Lodahl, W. L. Vos, and P. W. H. Pinkse, *Phys. Rev. B*, Vol. 86, 155154, 2012.
3. Mazoyer, S., J. P. Hugonin, and P. Lalanne, *Phys. Rev. Lett.*, Vol. 103, 063903, 2009.
4. Izrailev, F. M. and N. M. Makarov, *Phys. Rev. Lett.*, Vol. 102, 203901, 2009.

Polaritonic Behavior of Quantum Scatterers in a Nanoguide

H. R. Haakh[1], **S. Faez**[2], **and V. Sandoghdar**[1]

[1]Max-Planck-Institute for the Science of Light, Erlangen, Germany
[2]Institute of Physics, University of Leiden, Leiden, Netherlands

Abstract— Recent demonstrations of efficient coherent coupling between quantum scatterers and guided modes of a subwavelength optical fiber (nanoguide) [1] or photonic crystal waveguides [2, 3] have introduced a novel platform for studying polariton formation and optical transport in reduced dimensions (Fig. 1). We present a theoretical characterization of the polariton modes arising from ensembles of quantum emitters coupled via a waveguide, that yields a full phase diagram, indicating the presence of several phases dominated by either localized or extended states. A rigorous theoretical treatment based on many-body Green's functions [6] allows for a careful analysis of the interplay of nonradiative near-field coupling [6], density, and disorder. We link the different phases to the optical transport properties and the spectral response of the waveguide. The results can be immediately transferred to various emitters such as NV centers in diamond structures [4], quantum dots in silicon waveguides [2, 3, 5], or molecules in nanoguides [1].

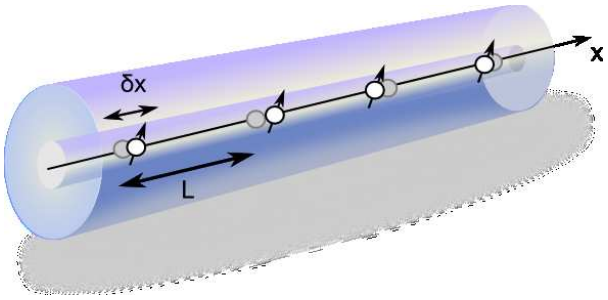

Figure 1: Nanoguide containing an ensemble of disordered quantum scatterers.

REFERENCES

1. Faez, S., P. Türschmann, H. R. Haakh, S. Götzinger, and V. Sandoghdar, *Phys. Rev. Lett.*, Vol. 113, 213601, 2014.
2. Sapienza, L., H. Thyrrestrup, S. Stobbe, P. D. Garcia, S. Smolka, and P. Lodahl, *Science*, Vol. 327, 1352, 2010.
3. Thyrrestrup, H., S. Smolka, L. Sapienza, and P. Lodahl, *Phys. Rev. Lett.*, Vol. 108, 113901, 2012.
4. Babinec, T., B. Hausmann, M. Khan, Y. Zhang, J. Maze, P. Hemmer, and M. Loncar, *Nature Nanotech.*, Vol. 5, 195, 2010.
5. Claudon, J., J. Bleuse, N. N. Malik, M. Bazin, P. Jaffrennou, N. Gregersen, C. Sauvan, P. Lalanne, Philippe, and J.-M. Gard, *Nature Phot.*, Vol. 4, 174, 2010.
6. Rusek, M., J. Mostowski, and A. Orłowski, *Phys. Rev. A*, Vol. 61, 022704, 2000.

Impact of Anderson Localization on the Light-matter Interaction in Low-dimensional Photonic Nanostructures

Søren Stobbe
Niels Bohr Institute, University of Copenhagen, Blegdamsvej 17, Copenhagen DK-2100, Denmark

Abstract— Photonic nanostructures enable confining light to subwavelength dimensions as well as controlling its propagation and enhancing its interaction with matter. This unprecedented control over light opens new opportunities ranging from fundamental studies of quantum electrodynamics to applications in optical interconnects. However, enhancement the electromagnetic field strength leads to an increased sensitivity to random structural disorder. In some cases this is a nuisance but it may be an advantage that unlocks new regimes of the statistical physics of cavity quantum electrodynamics, spatial correlations, and random lasing in the Anderson-localization regime.

Any fabrication method has a finite precision, which careful engineering can improve but not completely diminish. Structural disorder is therefore a fundamental phenomenon prevalent in all structures and devices and while it plays a rather trivial role in many situations, sufficiently pronounced disorder leads to Anderson localization. Low-dimensional photonic systems may greatly enhance the local density of optical states [1], which increases the interaction between light and matter but also enhances the influence of structural disorder. Anderson localization plays an important role when the light-matter coupling is increased.

We have studied the effect of structural disorder on photonic-crystal structures with embedded light emitters. In photonic-crystal waveguides in the slow-light regime, Anderson localization gives rise to localized photonic modes. The Anderson-localized modes give rise to pronounced cavity quantum electrodynamic effects, which can be probed by embedded quantum dots [2].

Using quantum dots as internal light sources enable probing the local density of optical states. Interestingly, the variance of the fluctuations in the local density of optical states contain information about non-universal spatial correlations intensity correlations in the far-field emission [3].

The Anderson-localized modes may also be employed for studying random lasing in the Anderson-localized regime. This study reveals a complex interplay between gain, dispersion-controlled slow light, and disorder [4].

REFERENCES

1. Lodahl, P., S. Mahmoodian, and S. Stobbe, "Interfacing single photons and single quantum dots with photonic nanostructures," to Appear in *Rev. Mod. Phys.*, arXiv: 1312.1079, 2015.
2. Sapienza, L., H. Thyrrestrup, S. Stobbe, P. D. Garcia, S. Smolka, and P. Lodahl, "Cavity quantum electrodynamics with Anderson-localized modes," *Science*, Vol. 327, 1352, 2010.
3. García, P. D., S. Stobbe, I. Söllner, and P. Lodahl, "Nonuniversal intensity correlations in two-dimensional Anderson-localizing random medium," *Phys. Rev. Lett.*, Vol. 109, 253902, 2012.
4. Liu, J., P. D. Garcia, S. Ek, N. Gregersen, T. Suhr, M. Schubert, J. Mørk, S. Stobbe, and P. Lodahl, "Random nanolasing in the Anderson localized regime," *Nature Nanotech.*, Vol. 9, 285, 2014.

Lasing in Plasmonic Periodic, Aperiodic, and Disordered Systems

Hinke Schokker, C. I. Osorio, and Femius Koenderink
Center for Nanophotonics, FOM Institute AMOLF, Amsterdam, The Netherlands

Abstract— Motivated by seminal proposals for surface plasmon amplification by stimulated emission, we conduct experiments on 2D plasmonic particle arrays in waveguiding layers that provide gain. We find that purely periodic plasmonic particle systems provide lasing characteristics similar to DFB lasers, yet on basis of a quite different underlying band structure. Using a newly developed spectrally-resolved Fourier microscope [1] we perform "high-NA band structure microscopy" and find that the strong and resonant scattering by plasmon particles markedly modify stop gap widths and band anti-crossing topology. Since stop gap size is inversely related to the number of unit cells required to generate the stop gap, our large stop gap system is very suitable to study the fundamental question: how much can we perturb our system? We find that these plasmon lasers are exceptionally robust against disorder: lasing persists even when removing as many as 98% of particles from a square lattice and shifting them by as much as a quarter of the periodicity. We quantify the transition from DFB to random lasing by analyzing laser output in terms of intensity statistics and real-space autocorrelations using tools borrowed from speckle analysis. Plasmon particle systems in waveguiding layers are an ideal platform to study lasing in purely periodic systems, completely disordered systems and systems with correlated disorder. As point in case, our latest result map lasing as function of spatial correlation order parameter in a suite of quasiperiodic, aperiodic and random systems, ranging from Fibonacci to Thue-Morse and Rudin-Shapiro lattices.

REFERENCES

1. Schokker, A. H. and A. F. Koenderink, *Phys. Rev. B*, Vol. 90, 155452, 2014.

Session 3A14
SC3: Optical Microcavities and Waveguides 2

New Directions for High-Q Optical Micro Cavities

Kerry Vahala
California Institute of Technology, Pasadena, California, USA

Abstract— Over the last ten years there has been remarkable progress in boosting the storage time (Q-factor) in micro and millimeter-scale optical resonators (1). Chip-based devices have attained Q factors of nearly 1 billion (2) and micro-machined crystalline devices have provided Q_s exceeding 100 billion (3). The resulting long, energy-storage times combined with small form factors have made it possible to access a wide range of nonlinear phenomena and to create laser devices that operate with remarkably low turn-on powers. Also, new science has resulted from radiationpressure coupling of optical and mechanical degrees-of-freedom in the resonators themselves (4).

After a brief review of nonlinear physics in high-Q micro cavity systems, this talk will focus on recent progress in generation of high-coherence light and application of optical frequency division for stable microwave synthesis. For the former, Brillouin lasers on a silicon chip are described (2, 5). These devices leverage both the small form factor and high optical Q of silicon-chip-based disk resonators (see Figure 1) to achieve high efficiency (less than 100 microWatt turn-on power) and high coherence (short-term, optical line width near 0.1 Hertz). It is also shown how the process of Brillouin cascade can be used to generate stable X and K-band microwave signals through direct detection (6). Finally, a new form of optical frequency division (OFD) is described (7). Similar to frequency comb based OFD methods (8) the technique allows coherent frequency division of very high (non-detectable) rate optical signals down to radio-frequency rates. It is applied to the Brillouin laser system to show that many orders of additional frequency stability can be extracted from these devices to generate high-performance microwave signals.

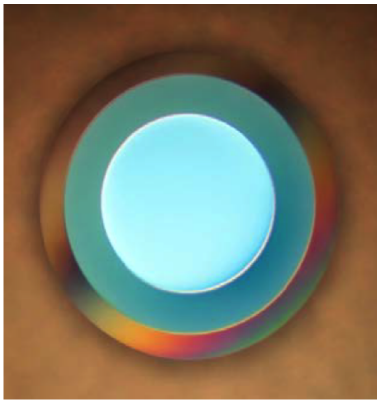

Figure 1: Optical micrograph showing a silica-onsilicon disk resonator having a Q-factor of nearly 1 billion (2).

REFERENCES

1. Vahala, K. J., "Optical microcavities," *Nature*, Vol. 424, 839–846, 2003.
2. Lee, H., T. Chen, J. Li, O. Painter, and K. Vahala, "Chemically etched ultrahigh-Q wedge-resonator on a silicon chip," *Nature Photonics*, Vol. 6, 369, 2012.
3. Grudinin, I. S., V. S. Ilchenko, and L. Maleki, "Ultrahigh optical Q factors of crystalline resonators in the linear regime," *Phys. Rev. A*, Vol. 74, 063806, 2006.
4. Kippenberg, T. J. and K. J. Vahala, "Cavity optomechanics: Back-action at the mesoscale," *Science*, Vol. 321, 1172–1176, 2008.
5. Li, J., H. Lee, T. Chen, and K. Vahala, "Characterization of a high coherence, Brillouin microcavity laser on silicon," *Opt. Express*, Vol. 20, 20170, 2012.
6. Li, J., H. Lee, and K. Vahala, "Microwave synthesizer using an on-chip Brillouin oscillator," *Nat. Commun.*, Vol. 4, 2097, 2013, Doi: 10.1038/ncomms3097.
7. Li, J., Y. Xu, H. Lee, S. A. Diddams, and K. Vahala, "Electro-optical frequency division and stable microwave synthesis," *Science*, Vol. 345, 309–313, 2014.

8. Fortier, T., et al., "Generation of ultra stable microwaves via optical frequency division," *Nat. Photon*, Vol. 5, 425, 2011.

Applications of Second Order Microring Resonators

C. Vázquez
Department Tecnología Electrónica, Universidad Carlos III Madrid
Av. Universidad 30, Leganés, Madrid 28911, Spain

Abstract— single microring resonator may not perform properly in those applications were a high number of channels with minimal crosstalk within a free spectral range (FSR) is required. In those cases, filterbanks consisting of second-or higher-order microring [1, 2] can be used. But in some cases, the control of the resonant frequency of each ring requires dimensional precision in the order of tens of picometer [3], so more thermal tunning is required to overcome the frequency mismatch between the two rings of a channel and each channel location mismatch. Some novel configurations of second order microring resonators more robust to fabrication tolerances [4], based on previous designs [5, 6] will be discussed along with potential application. Special emphasis will be given to the properties provided by designs on high index contrast waveguides.

REFERENCES

1. Popović, M. A., et al., "Tunable, fourth-order silicon microring-resonator add-drop filters," *33rd European conference and Exhibition on Optical Communication*, Berlin, Germany, 2007.
2. Xiao, S., M. H. Khan, H. Shen, and M. Qi, "Multiple-channel silicon micro-resonator based filters for WDM applications," *Optics Express*, Vol. 15, No. 12, 7489–7498, 2007.
3. Dahlem, M. S., C. W. Holzwarth, A. Khilo, F. X. Kartner, H. I. Smith, and E. P. Ippen, "Reconfigurable multichannel second-order silicon microring-resonator filterbanks for on-chip WDM systems," *Opt. Exp.*, Vol. 19, No. 1, 306–316, 2011.
4. Vázquez, C., P. Contreras, and S. Vargas "Low power consumption silicon photonics tuning filters based on compound microring resonators," *Proceedings OPTO Conference*, Vol. 8629, 50, Photonics West, 2013.
5. Vázquez, C., S. Vargas, and J. M. S. Pena, "Sagnac loop in ring resonators for tunable optical filters," *Journal of Lightwave Tech.*, Vol. 23, No. 8, 2005.
6. Vargas, S. and C. Vázquez "Synthesis of optical filters using microring resonators with ultra-large FSR," *Opt. Express*, Vol. 18, 25936–25949, 2010.

Coupling-tuned Silicon Ring Resonators for Optical Modulation and Microwave Phase Shift

Linjie Zhou, Rui Yang, Haike Zhu, Yanyang Zhou, and Jianping Chen
State Key Laboratory of Advanced Optical Communication Systems and Networks
Department of Electronic Engineering, Shanghai Jiao Tong University, Shanghai 200240, China

Abstract— Optical ring resonators are fundamental building blocks in integrated photonics. A variety of passive and active, linear and nonlinear devices can be built using ring resonators as the core components. Usually, rings are coupled with single or double waveguides in a photonic integrated circuit with tuning performed either on the ring cavity or the coupling region. These two tuning methods have different effects on the resonances: cavity tuning shifts the resonances wavelength while coupling tuning adjusts the resonance extinction ratio. Here we report our recent process on coupling tuned silicon ring resonators to generate high-speed optical modulation and microwave phase shift. The coupling of the ring resonator is enabled by a Mach-Zehnder interferometer integrated with single-drive push-pull electrodes. With two DC biases applied to the electrodes, the phase shift of the two arms can be separated controlled and thus the coupling can be freely tuned while resonance wavelength is fixed. It is advantageous to separate the coupling tuning from the resonance shift.

We first characterize the high speed modulation performances of this device. Silicon modulators are key components in photonic integrated circuits for both optical communications and interconnects. The coupling modulation can eliminate the cavity lifetime limited speed bottleneck as accounted in resonance modulation. The on-chip insertion loss of the device is ~ 3 dB. Critical coupling is obtained with the resonance extinction ratio exceeding 35 dB at the wavelength of 1544.3 nm. Near critical coupling, the transmission is very sensitive to the drive voltage, allowing for low voltage modulation. On-off-keying (OOK) eye diagrams are measured with a modulation depth of 7 dB at a date rate of 25 Gbps and RF drive voltage of $V_{pp} = 1$ V. The modulation depth reduces to 3 dB at 32 Gbps. Binary-phase-shift-keying (BPSK) modulation is also achieved at 28 Gbps by setting the resonance at critical coupling. The eye diagram shows a Q-factor of 6.3 dB and the constellation diagram reveals an error vector magnitude (EVM) of 23.3%.

The transmission phase of the ring resonator sees rapid change around resonances. At the under-coupling regime the phase change is less than π, while at the over-coupling regime the phase change can be a full 2π. Therefore, the resonance phase can be tuned by coupling. Utilizing this feature, we can generate microwave phase shift by setting one of the frequency tones of a microwave modulated optical signal to the resonance wavelength. By tuning the coupling, the microwave phase shift can be varied with a large and continuous tuning range.

Silicon Nitride Waveguides for Plasmon Optical Trapping and Sensing Applications

Ozdal Boyraz[1], **Qiancheng Zhao**[1], **Caner Guclu**[1], **Filippo Capolino**[1], **and Regina Ragan**[2]

[1]Department of Electrical Engineering and Computer Science
University of California-Irvine, Irvine, California 92697, USA
[2]Department of Chemistry
University of California-Irvine, Irvine, California 92697, USA

Abstract— Optical force has long been investigated and proved by moving micro-scale particles, membranes and optical micro cavities. On one hand, the use of strong field confinement at the apex of a sharp metallic tip enables optical trapping of low-contrast Rayleigh objects or metal nanoparticles. Extensive studies on prism platform using noble metal antenna and objective lens for optical tweezing have been put forward. However the system is composed of discrete components, making it bulky and sensitive to environment vibration. One the other hand, microfluidic channels proved to be successful platforms for sorting and manipulating particles by optical force. Nevertheless, lacking of on-chip launch light fails to make the system compact. Therefore, it is desired to integrate waveguides, antennas, and microfluidic channels in a planar structure, which can minimize the structure volume and make it more robust. Here we present the optimum waveguide geometries that can be utilized for optical sensing and particle applications. In particular, submicron silicon nitride waveguide geometries based on conventional optical lithography will be presented for plasmonic sensing and nonlinear optics applications.

Surface plasmons coupled with optical waveguides due to metallic colloidal particles demonstrate higher optical nonlinearities that can be used for two photon fluorescence, optical frequency mixing, spectral broadening and optical switching. Here we will discuss deposition of colloidal nano particles to enhance the optical nonlinearity of waveguides. Same deposition techniques can be tailored to fabricate plasmonic nanoantennas that convert evanescent modes into radiation. Here we present recent developments in plasmonic antennas in particle sensing and trapping applications. In particular, we discuss the optical trapping capability of silicon nitride planar waveguide geometries with plasmonic antennas, such as bowtie antennas. We show that the bowtie antennas can lead to 60-fold enhancement of electric field in the antenna gap. With the help of scattering by the antenna, the optical trapping force on a nanoparticle is boosted by three orders of magnitude. A strong tendency shows the nanoparticle is likely to move to the high field strength region, exhibiting the trapping capability of the antenna. Effect of trapping on spectroscopic measurements will be discussed.

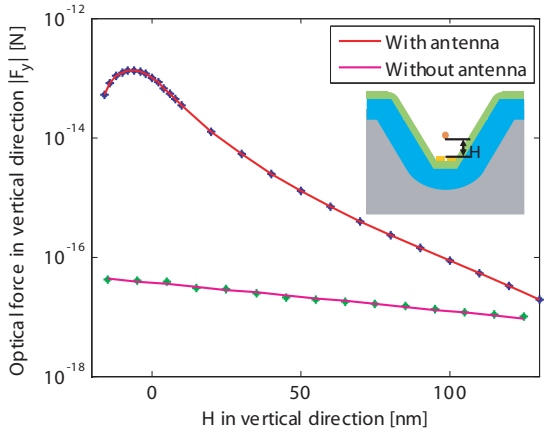

Figure 1: Optical trapping force in vertical direction (y axis) vs. vertical distance from the particle bottom surface to the antenna top surface. The force is enhanced by bowtie antenna compared to non-antenna case.

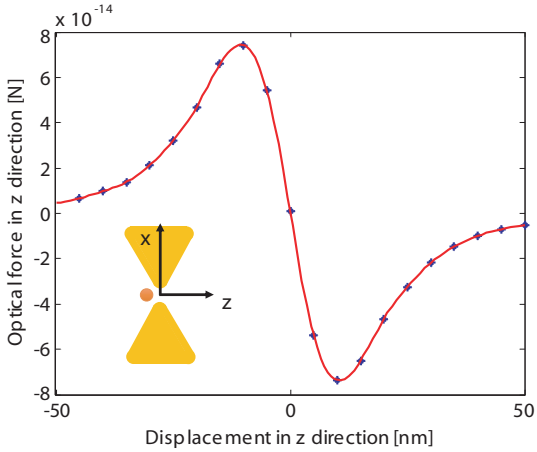

Figure 2: Optical trapping force in longitudinal direction (z axis) vs. displacement from the antenna center. The particle bottom surface is 4 nm below the antenna top surface.

Whispering Gallery Mode Biosensing: An Approach to Simultaneous Multiplexed Detection

Stephen Holler and John Murray
Department of Physics & Engineering Physics, Fordham University
441 East Fordham Road Bronx, NY 10458, USA

Abstract— The whispering gallery mode (WGM) biosensor has emerged as a robust tool for the sensitive detection of biological micro- and nano-particles, including bacteria, virus and protein. Relying on the specific biochemical interactions, perturbations to the cavity mode induced by the binding of such particles to the microcavity surface result in a quantifiable shift in the resonance mode frequency. The amount by which the resonance frequency shifts is directly proportional to the quantity of adsorbed material and the location at which it binds. Additives, such as plasmonic nanoparticles, can serve to enhance reactive effect and thus the degree to which the resonance frequency shifts, and have been shown to lower the detection limit of WGM devices to single protein level.

These optical microcavities may take on a myriad of shapes (e.g., spheres, spheroids, toroids, rings, disks, etc.) and, consequently, WGMs are also known as morphology dependent resonances (MDRs). Our work will focuses on the use of a spherical geometry because such microcavities offer low-cost ease of manufacture and accessible analytic models. Despite these advantages, spherical cavities offer challenges for multiplexed detection and monitoring of analytes. We will review the physics behind whispering gallery biosensing and introduce a detection/monitoring approach, which employs a sensing geometry that offers the prospect for robust and simultaneous multi-sphere monitoring. This multi-cavity approach allows for reference channels to account for common mode and environmental factors, and/or channels for additional target analytes.

Results will be presented for adsorption of biological nanoparticles. In particular we will demonstrate the approach using the human papillomavirus (HPV), the causative agent of cervical and head & neck cancers. Projections will be made for detection limits and maximum allowable resonators.

Optical Kerr Switching and COMB Generation in a Silica Whispering Gallery Mode Microcavity

Takasumi Tanabe
Department of Electronics and Electrical Engineering, Keio University, Japan

Abstract— Ultrahigh-Q whispering gallery mode microcavities exhibit optical nonlinearities at a very low input power. The efficiency of the nonlinearity often scales with Q/V, where Q is the quality factor and V the mode volume of the cavity.

First I will report on the demonstration of a Kerr switch at a record low power of a few tens of microwatts, achieved with a whispering gallery mode microcavity made of silica [1]. Comparisons between switches made with photonic crystal nanocavity and silica whispering-gallery mode microcavity are discussed in terms of speed, power, and different nonlinearities. Although the required energy is much lower for carrier based photonic crystal nanocavity switches [2, 3], the insertion loss of the whispering galley mode cavity system is much lower due to the higher Q of the cavity and low-loss of the tapered fiber. In addition, we can use Kerr nonlinearity when the cavity is made of silica, which is attractive for the use of various quantum applications.

Next, I will discuss about the generation of optical Kerr comb which is demonstrated by using a high-Q silica whispering gallery mode microcavity. It allows us to obtain ultrahigh repetition rate optical pulses (at a repetition rate $> 800\,\mathrm{GHz}$) when we pump the cavity with continues wave input. We numerically and experimentally studied the condition required to generate the comb, in respect to the pumping power and waveguide coupling. We found that the history of the input power variation is the key to obtain mode-locked comb, which is due to the hysteresis behavior of the nonlinear cavity. Particularly, we found that a stable comb is obtained only when we reduce the input power after hard pumping, whereas the cavity exhibit modulation instability when we increase the input [4].

REFERENCES

1. Yoshiki, W. and T. Tanabe, "All-optical switching using Kerr effect in a silica toroid microcavity," *Opt. Express*, Vol. 22, No. 20, 24332–24341, 2014.
2. Tanabe, T., M. Notomi, A. Shinya, S. Mitsugi, and E. Kuramochi, "All-optical switches on a silicon chip realized using photonic crystal nanocavities," *Appl. Phys. Lett.*, Vol. 87, 151112, 2005.
3. Nozaki, K., T. Tanabe, A. Shinya, S. Matsuo, T. Sato, H. Taniyama, and M. Notomi, "Sub-femtojoule all-optical switching using a photonic crystal nanocavity," *Nature Photon.*, Vol. 4, 477–483, 2010.
4. Kato, T., T. Kobatake, R. Suzuki, Z. Chen, and T. Tanabe, "Harmonic mode locking in a high-Q whispering gallery mode microcavity," arXiv: 1408.1204.

Whispering Gallery Mode Microbubble Resonators

S. Nic Chormaic
Light-Matter Interactions Unit
Okinawa Institute of Science and Technology Graduate University
Onna, Okinawa 904-0495, Japan

Abstract— Whispering gallery mode microbubble resonators are a relative recent addition to the whispering gallery resonator family and have demonstrable applications across several areas of research, including pressure sensing, frequency comb generation and other nonlinear optics phenomena, and in the field of optomechanics. These resonators behave very similar to microsphere resonators, with the distinct advantage that their hollow core can be filled with fluids, thereby rendering them more functional for many sensing scenarios. In this paper, we will first introduce the concept of microbubble resonators and discuss how they can be fabricated in a controlled manner in order to ensure their design is optimised for high resolution sensing by operating in the quasi-droplet regime. Next, we will discuss some recent achievements in relation to fabricating high quality factor microbubbles from a variety of different materials. As a first example, we have fabricated PDMS-filled, silica glass microbubbles with very thin walls, thereby ensuring that they operate in the quasi-droplet regime whereby the optical mode penetrates deep within the core material allowing us to study temperature shifting on the optical resonances. As a further example, we have fabricated microbubbles using lead silicate glass, a material with high nonlinearities suitable for exploring a range of nonlinear optics effects such as Raman scattering and four-wave mixing at low optical powers. Finally, we will show examples of coupled-mode induced transparency that was achieved by internal pressure tuning of the whispering gallery modes in a silica glass microbubble. Overall, this paper aims to highlight the versatility of microbubble resonators across a variety of research topics and we will provide a number of examples of areas where their properties can be exploited in future work.

Femtosecond Laser Inscription of 3D Optical Waveguides in Glasses, Polymers and Crystals

Shane M. Eaton[1], **Vibhav Bharadwaj**[2], **and Roberta Ramponi**[1]

[1]Dipartimento di Fisica, Istituto di Fotonica e Nanotecnologie (IFN), CNR
Politecnico di Milano, Milano, Italy
[2]Center for Nano Science and Technology, Istituto Italiano di Tecnologia, Milano, Italy

Abstract— Focused femtosecond laser pulses drive nonlinear absorption in a wide variety of transparent materials including glasses, crystals and polymers. This nonlinear interaction enables a micrometer-sized modification confined to the focus, which allows one to pattern micro-photonic devices with novel three-dimensional geometries.

In glasses and crystals, the ultrashort laser pulse interaction leads to a permanent alteration of the refractive index, enabling the formation of 3D photonic circuits. In polymers, the laser-induced modification tends to decay with time, an effect which is unsuitable for the fabrication of photonic devices [1]. Among the many parameters used to tailor the modification in transparent materials, the pulse delivery rate (repetition rate) is perhaps the most significant. At suitably high repetition rates, typically greater than 100 kHz, the time between pulses is shorter than time for heat from the absorbed laser pulses to diffuse out of the focal volume. This leads to an accumulation of heat at the focus and if the pulse energy is sufficiently high, the material at the focus is melted. As further pulses arrive, the size of the melted zone expands outwards. After the final incident pulse, therapidly cools into a permanent modification with refractive index greater than the pristine bulk. In this way, the dwell time in static exposures or scan speed in scanned exposures can be used to tailor the final waveguide size for a specific application [2].

Here we will describe how high repetition rate fabrication can be exploited to form high performance and novel photonic devices in transparent materials for the burgeoning fields of quantum information, sensing and lab on a chip.

REFERENCES

1. Eaton, S. M., R. Martinez-Vazquez, R. Ramponi, G. Cerullo, and R. Osellame, "Femtosecond laser microstructuring for polymeric lab-on-chips," *J. Biophotonics*, Vol. 5, 687–702, 2012.
2. Eaton, S. M., H. Zhang, M. L. Ng, J. Li, W. Chen, S. Ho, and P. R. Herman, "Transition from thermal diffusion to heat accumulation in high repetition rate femtosecond laser writing of buried optical waveguides," *Opt. Express*, Vol. 16, 9443–9458, 2008.

Lasing and Applications of Flexible Optical Micro-resonators

Handong Sun[1, 2]

[1]Division of Physics and Applied Physics, School of Physical and Mathematical Sciences
Nanyang Technological University, 637371, Singapore
[2]Centre for Disruptive Photonic Technologies (CDPT)
Nanyang Technological University, 637371, Singapore

Abstract— Optical microresonators have attracted intensive attention due to their importance in practical applications as well as of fundamental physics interest in light-matter interaction. The optical confinement provided by a microresonator greatly enhances the coupling between optical spatial mode and the matter inside. Conventional fabrication of micro-cavities adopting semiconductor processing technology through either top-down or bottom-up approaches still faces some challenges. In this talk, we demonstrate the feasibility of constructing solid state micro-cavities with various configurations like spheres, hemispheres and fibres in a flexible way. We realize optically pumped lasing with high quality factor from these structures after loading gain materials (organic dyes or quantum dots). The optical modes are well defined by WGM lasing. We have demonstrated single-frequency operation in both spheres and fibres with reduced sizes. We are also able to tune the lasing by deforming the shape of micro-spheres, which represents the convenient manipulation of light matter interaction. Refractive index sensing with high sensitivity can be readily realized from these structures enabled by the existence of evanescent waves.

Meandering Waveguide Distributed Feedback Lightwave Elements: Phasor Diagram Analysis

C. B. Dağ[1], **M. A. Anıl**[1], **and A. Serpengüzel**[2]

[1]Department of Electronics and Telecommunications Engineering
Istanbul Technical University, Maslak, Istanbul 34469, Turkey
[2]Microphotonics Research Laboratory, Department of Physics
Koç University, Rumelifeneri Yolu, Sarıyer, Istanbul 34450, Turkey

Abstract— Meandering waveguide distributed feedback (DFB) structures are introduced as novel photonic lightwave circuits elements and their amplitude and phase response are studied in frequency and phasor domain. A preliminary transfer matrix method analysis is applied for taking the coupling purely directional and with constant coefficient on geometrically symmetric and anti-symmetric elements. The meandering loop mirror is the building block of all meandering waveguide based lightwave circuit elements. The simplest uncoupled meandering DFB structure exhibits Rabi splitting in the transmittance spectrum. The symmetric and antisymmetric coupled meandering DFB geometries can be utilized as band-pass, Fano, or Lorentzian filters or Rabi splitters. Meandering waveguide DFB elements with a variety of spectral responses can be designed for a variety of lightwave circuit element functions and can be implemented with generality due to the analytic approach taken. Meandering waveguide distributed feedback structures with a variety of spectral responses can be designed for a variety of lightwave circuit element functions.

Novel Fiber Array Scheme for Light Guiding and Trapping in Ultra-thin Solar Devices

Jordi Martorell[1, 2], **Marina Mariano**[1], **G. Kozyreff**[3], **G. Gerling**[2], **J. Puigdollers**[2], **P. Romero-Gomez**[1], **and J. Bravo-Abad**[4]

[1]ICFO-Institut de Ciencies Fotoniques, Castelldefels, Barcelona 08860, Spain
[2]Universitat Politècnica de Catalaunya, Barcelona, Spain
[3]Université libre de Bruxelles (U.L.B.), Campus de la Plaine
CP 231, Bld du Triomphe, Bruxelles B-1050, Belgium
[4]Departamento de Física Teórica de la Materia Condensada and Condensed Matter Physics Center (IFIMAC), Universidad Autónoma de Madrid, Madrid 28049, Spain

Abstract— To obtain the maximum possible efficiency, in thin film light harvesting or light emitting devices, light incidence or extraction must be achieved simultaneously to light trapping in an orthogonal direction. This is the case, for instance, in many thin film solar cells where the most effective sunlight harvesting would require a bending of the incident light propagation path followed by a trapping within the active material layer. To some extent, the opposite behavior is needed in the light guiding plate from edge-lit electronic devices to achieve a homogeneous illumination of the LCD.

In here, we will consider configurations to effectively reach such, to some extend contradictory, behavior for the light propagation. We will pay special attention to light harvesting and photovoltaic performance of thin film solar cells deposited on the back side of an array of parallel fibers. In such periodically ordered system an ergodic light propagation resulting from a chaotic photon trajectory is achieved when the adjacent fibers are intercalated. The light intensity distribution brakes into a largely disordered pattern, but with a clearly identifiable larger light intensity on the caustic. This allows coupling to a whispering gallery mode (WGM) on the top interface of the array. In other words, the window opening in between fibers allows for an effective trapping of the light that was incident orthogonal to the plane of the array.

We fabricated a fiber array with a solar cell coated on the side opposite to the light entering side. The photovoltaic performance of such solar cell was measured and we showed that the efficiency in photon to charge collection can be increased by more than 30% on average and up to 50% at certain wavelengths. The performance for such fiber array solar cell will be evaluated against other light management configurations in thin film cells.

Session 3A0
Poster Session 5

FDTD Simulation of a Cylindrical Waveguide Using Longitudinal Current Distribution as an Excitation Scheme

D. V. Peponis, G. P. Latsas, Z. C. Ioannidis, and I. G. Tigelis
Faculty of Physics, National and Kapodistrian University of Athens
University Campus, Athens 157 84, Greece

Abstract— In the study of high-power and high-frequency microwave structures several semi-analytical and numerical approaches are employed. In this work, we use the FDTD method to study the propagation characteristics in cylindrical waveguide structures with a longitudinal current distribution as an excitation scheme. Maxwell equations are formulated in cylindrical coordinates and a cylindrical mesh is used to obtain conformity to the geometry and avoid the staircase error that would arise by using Cartesian coordinates. The longitudinal current excitation distribution is selected, since it can probably model the excitation by an electron beam (in the small signal regime), or the excitation of the waveguide using an electric probe. The waveguide is terminated at both sides by Complex Frequency Shifted-Perfect Matched Layers (CFS-PML) in order to absorb both the travelling and the evanescent waves. In order to verify the method and benchmark the corresponding numerical code, the simple case of a smooth cylindrical waveguide is examined, excited by a current distribution with a Gaussian modulated sinusoidal time dependence. The current distribution is modeled as a longitudinal thin wire (placed on the axis of the waveguide), conducted by a constant spatial current density. Due to the location of the wire and the proper choice of the frequency range of the excitation, only TM_{01} mode can be excited. The radial distribution of the electric field components as well as the 2D (ρ-φ plane) contour plot are presented and compared with the theoretically expected ones, showing good agreement between them. Moreover, the presence of the CFS-PML layer is examined as well as how it affects the propagation characteristics. It is shown that by fine-tuning of its characteristics, satisfactory absorption rate can be achieved and thus infinitely long and open-ended waveguides can be properly studied. Finally, possible applications of the numerical code are presented as well as how this excitation scheme can model more realistic structures.

ACKNOWLEDGMENT

This work has been carried out within the framework of the EUROfusion Consortium and has received funding from the Euratom research and training programme 2014–2018 under grant agreement No. 633053 (WPEDU). The views and opinions expressed herein do not necessarily reflect those of the European Commission.

High Precision Range Measurement Processor Design with Low Complexity for FMCW Radar Systems

E. Hyun[1] **and J. H. Lee**
ART (Advanced Radar Technology) Lab
DGIST (Daegu Gyeongbuk Institute of Science & Technology), Korea

Abstract— FMCW (Frequency Modulation Continuous Wave) radar systems have been widely used for the measurement of range in a variety of industrial applications: automotive safety, traffic monitors, level gauges, security, defense seekers. Especially, level measurement is popular in almost every modern industrial plant for the measurement of bulk materials. That is, digital level measurement based on FMCW radar is a trend because the digital approach is more flexible and program updates are very easy.

In FMCW radar, when a continuous frequency modulated microwave signal is transmitted, the receive echo signal is down-converted into the baseband by the transmit frequency. The difference in frequency between the transmit and the receive signals is called the beat-frequency. The beat-frequency is typically obtained using FFT (Fast Fourier Transform) processing; range measurement is calculated using the detected beat-frequency. Thus, for exact level measurement in FMCW radar, it is very important to obtain a high precision beat-frequency. That can be realized using enough sample data and many FFT points. However, in a high precision FFT processor, many hardware resources and long processing time are required due to the increased computational complexity.

In this paper, we propose a low complexity frequency measurement processor. First, using the low precision FFT processor, the coarse ROI (Range Of Interest) is detected. Then, in the ROI, the fine frequency spectrum is analyzed using a frequency spectrum estimator consisting of a complex multiplier-accumulator. Compared with traditional FFT processors, even though the performance of the proposed processor is the same, the utilized hardware resources and the processing time can be decreased.

[1]Corresponding author: E. Hyun (braham@dgist.ac.kr).

Schur Complement Based Method of Moments Solution for 2D Scattering Problem from Mixed Dielectric-conductor Targets

Mehmet Nuri Akıncı and M. Çayören
Department of Electronics and Communication Engineering, Istanbul Technical University, Turkey

Abstract— In this paper, we deal with the two dimensional scattering problem from mixed dielectric-conductor targets. In particular, we analyze a Schur-complement based Method of Moments technique as the solution procedure. In fact, different solutions to the mixed dielectric-conductor scatterer problem [1–3] and several works on Schur preconditioners can be found in the literature [4, 5]. Here, what we propose is simply that the currents on different kinds of scatterer must be appended in different vectors. For this purpose, we use a rectangular mesh to discretize the dielectric scatterers. Pulse functions are used as basis functions and the integral of the Green's function on the discretized rectangles is analytically calculated by using the well-known circle approximation [6]. For the conductor objects the surface is discretized into points and the integrals of Green's function is numerically calculated on the lines which connect the discretized points. Finally, dirac-delta functions are used as weighting functions and an equation system for the currents on the scatterers are obtained. As stressed above, the currents on the different kind of materials (dielectric-conductor) are casted into two different vectors. Then the inversion of "the object equation" are done by means of the Schur complement. By doing so, the inversion of the large Green matrix turns into the inversion of two subblocks of this matrix. The accuracy of this Schur complement based Method of Moments solution is tested against the analytical solution of the scattering from a dielectric coated conductor. Moreover, an error rate analysis is made by comparing the theoretical expressions with the simulated fields. Obtained results show that the Schur complement based inversion of object equation increases the validity range of the solution obtained from Method of Moments.

ACKNOWLEDGMENT

This work was supported by Turkish Scientific and Research Council (TUBITAK) under the project number 113E977.

REFERENCES

1. Donepudi, K. C., J.-M. Jin, and W. C. Chew, "A higher order multilevel fast multipole algorithm for scattering from mixed conducting/dielectric bodies," *IEEE Transactions on Antennas and Propagation*, Vol. 51, No. 10, 2814–2821, 2003.
2. Djordjevic, M., and B. M. Notaros, "Double higher order method of moments for surface integral equation modeling of metallic and dielectric antennas and scatterers," *IEEE Transactions on Antennas and Propagation*, Vol. 52, No. 8, 2118–2129, 2004.
3. Ewe, W.-B., L.-W. Li, and M.-S. Leong, "Fast solution of mixed dielectric/conducting scattering problem using volume-surface adaptive integral method," *IEEE Transactions on Antennas and Propagation*, Vol. 52, No. 11, 3071–3077, 2004.
4. Ergul, O., T. Malas, and L, Gurel, "Analysis of dielectric photonic-crystal problems with MLFMA and schur-complement preconditioners," *Journal of Lightwave Technology*, Vol. 29, No. 6, 888–897, 2011.
5. Wu, Y.-Q., M.-J. Gou, and X.-Q. Sheng, "On the preconditioners of higher order method of moments for scattering by homogeneous dielectric objects," *Journal of Electromagnetic Waves and Applications*, Vol. 26, No. 14–15, 1809–1819, 2012.
6. Richmond, J., "Scattering by a dielectric cylinder of arbitrary cross section shape," *IEEE Transactions on Antennas and Propagation*, Vol. 13, No. 3, 334–341, 1965.

Dynamic Speckle Laser Technique for the Characterization of Electrotechnical-porcelain

F. J. Salguero[1], **G. Bertolini**[2], **C. I. Cabello**[2, 3], **E. Grumel**[3, 4], **M. Trivi**[3, 4], **and G. Barbera**[5]

[1]Facultad de Ingeniería, UNLP
[2]CINDECA, (CCT CONICET La Plata-UNLP), Facultad de Ingeniería, UNLP
Calle 47 No. 257, La Plata 1900, Argentina
[3]CIC PBA, Argentina
[4]Centro de Investigaciones Ópticas (CCT CONICET La Plata CIC) and UID Optimo
Facultad de Ingeniería, UNLP, Casilla de Correo 3, Gonnet, La Plata 1897, Argentina
[5]IITREE, (Instituto de Investigaciones Tecnológicas para Redes y Equipos Eléctricos)
Facultad de Ingeniería, UNLP, Calle 48 No. 116 (B1900AMF), La Plata, Argentina

Abstract— Dynamic speckle is a scattering phenomenon occurring when coherent laser light illuminates an active surface. Scattered waves are Doppler shifted by movements of the scattering centres or other dynamic changes, such as refractive index time variations. These random coherent electromagnetic waves beat on the detector thus producing low-frequency intensity variations. As a result, the surface appears to be covered by tiny bright dots that fluctuate in a seemingly random way similar to boiling liquid.

The study of the temporary evolution of the speckle patterns may provide an interesting tool to characterize the parameters involved in the sample dynamic processes. It has been used for several applications in biology, medicine and industry.

In this paper, we use this technique to analyze the hygroscopic properties of different types of porcelain for electrotechnical purposes. Experimental speckle results showed different behavior depending on both physicochemical and textural properties of the samples.

The typical porcelain consists of a mixture of three aluminum-silicates in a ratio: 50% kaolin 25% quartz and 25% feldspar. This porcelain has basic electrical, mechanical, thermal and porosity properties which naturally vary according to the composition of the mixture.

These materials are commonly used due to their insulating quality (e.g., insulation resistance) which basically depends on its porosity and hygroscopicity.

This work analyzes four types of commercial electrotechnical-porcelain using both textural and physical-chemical methods and their water adsorption capacity by the Dynamic Speckle Laser technique.

Experimental results showed the evolution of the speckle patterns during hydro-adsorption process, permitting to discriminate different behavior for each material. It was determined that it is possible to correlate changes in the speckle patterns with the porosity and composition of materials.

Random Electromagnetic Interferometry Method Applied to Aluminosilicates Analysis

R. D. Mojica-Sepúlveda[1, 2], **L. J. Mendoza-Herrera**[3], **E. Grumel**[3], **D. B. Soria**[1], **C. I. Cabello**[2], **and M. Trivi**[3]

[1]CEQUINOR, (CONICET La Plata-UNLP), calle 47 y 115 (1900) La Plata, Argentina
[2]CINDECA, (CONICET La Plata-UNLP), calle 47 No. 257 (1900) La Plata, Argentina
[3]Centro de Investigaciones Ópticas (CCT CONICET La Plata CIC) and UID Optimo Facultad de Ingeniería, UNLP, Casilla de Correo 3, (1897) Gonnet, La Plata, Argentina

Abstract— The minerals based on aluminosilicates such as clays (kaolinite, montmorillonite) and zeolites (clinoptilolite) are abundant and inexpensive. These are used as adsorbents for the removal of bacteria and pollutants. It has been proven that the presence of hydrogen bonding interactions, and electrostatic forces of attraction on the surface of zeolites modified with anionic and/or cationic species have a significant effect on the process of microorganisms elimination. The treatment of the zeolite surface with concentrated acids or bases also modifies their hygroscopic properties.

This paper presents advances in the Dynamic Speckle Laser hydroadsorption analysis of materials based on a rich mineral "clinoptilolite" and their acidic and basic forms, which served as support for the incorporation of a binary complex sulfadiazine cobalt, promising in antibacterial drug design, fungicides, anti-inflammatory, etc..

To determine the water adsorption capacity of these materials as a function of time, the traditional method consists of introducing a sample in water and plotting the time dependent weight change in order to determine the amount of water adsorbed.

In this work we use a technologically advanced and methodologically more accurate method for determining the speed of hydroadsorption of a zeolite (clinoptilolite) based on the optical random interferometric phenomenon named "speckle", produced when a laser light illuminates a rough surface of zeolite. The data derived from the latter methodology is fitted using a numerical model that yields a better fitting as compared with several physicochemical (or physical) methods well established in the literature.

Modeling of Electromagnetic Scattering from Simplified Leaf Structures by Using Spherical Wave Expansion

Paul Jason Co and Jun-Ichi Takada
Department of International Development Engineering, Tokyo Institute of Technology, Tokyo, Japan

Abstract— Leaf scatterers are a type of obstacle that is abundant in rural propagation environments. These leaf scatterers interact with propagating radio waves which may affect the performance of wireless systems operating in such environments. Modelling the effects of these leaf scatterers in the propagation medium is necessary to ensure the performance of wireless systems in the presence of such obstacles. In this paper, deciduous leaf scatterers are modelled as thin dielectric disks. The electromagnetic scattering from these disks are modelled using the generalized Rayleigh-Gans (GRG) approximation as well as numerically using a commercial method of moments solver, and is evaluated at a frequency of 2 GHz. For the single scatterer case, results show good agreement between the GRG approximation and the numerical results, with the GRG approximation generally underestimating the scattered fields, as well as significant errors appearing in the null regions of the scattering. To evaluate the difference between the GRG approximation and the numerical results, spherical wave expansion is performed on the scattered fields from both the GRG approximation and the method of moments solution. The spherical modes of the scattered fields from both solutions are compared, and the number of spherical modes needed to represent the scattered fields from the single disk from both solutions are evaluated.

An approximation of the scattered fields for the multiple scatterer scenario is applied by performing a superposition of the GRG scattered fields from each of the individual disk scatterers. The scattering from multiple realizations of 30 disk scatterers randomly oriented and positioned within a 1 cubic meter volume is evaluated. First order scattering results which only consider the fields directly scattered from the incident wave show that the scattering pattern from the superposition approximation is similar to the scattering pattern from the full wave numerical solution, but under estimates the magnitude of the scattered fields by approximately 4 dB. Second order scattering is evaluated, where the scattered fields from the GRG approximation is used as secondary incident waves to other disks in the region. Results from the second order approximation showed an improvement in the accuracy of the scattered field magnitudes in the backscatter region to within 1dB of the numerical results, with minimal improvement in the forward scattering region. To isolate the error in the multiple scatterer approximation due to the errors in the GRG approximation, a hybrid superposition of the numerical results is proposed. The scattering from the individual disk scatterers are represented as a spherical wave expansion of the numerical results. Applying the superposition approximation to these spherical wave expansion of individual scatterers eliminates the errors from the GRG approximation.

REFERENCES

1. Karam, M. A. and A. K. Fung, "Leaf shap effects in electromagnetic wave scattering from vegetation," *IEEE Transactions on Geoscience and Remote Sensing*, Vol. 27, No. 6, 687–697, 1989.
2. Hansen, J. E., *Spherical Near-Field Antenna Measurement, IEE Electromagnetic Wave Series*, Vol. 26, London, 1988.

Behaviour of Conformal Conical Frequency Selective Surfaces

Giovanni Leone[1], **Francesco Mattiello**[1], **Giuseppe Ruvio**[1, 2], **and Rocco Pierri**[1]

[1]Dipartimento di Ingegneria Industriale e dell'Informazione, Seconda Università di Napoli
Via Roma 29, Aversa, CE 81031, Italy
[2]Antenna & High Frequency Research Centre
Dublin Institute of Technology, Kevin Street, Dublin 8, Ireland

Abstract— Planar Frequency selective surfaces (FSS) have attracted large attention during the last five decades because of their mechanical and electrical flexibility. They behave as spatial filters that are largely employed in applications like hybrid radomes for radars and antennas where high performance is necessary. The FSS have evolved from simple canonical forms to the complex geometries. For these structures, we must consider both the effects related to the periodicity that those related to the size of the individual elements. While periodicity impacts firstly on the general reflecting properties of the surface, the shape and the size of the individual element affects both spatial and frequency filtering behaviour. In particular the frequency response is dictated mainly by the scattering of the incident plane wave by the individual element and attains its maximum at resonance conditions. Accordingly, we mean to investigate whether the same occurs also for non planar surfaces and curved elements, and in particular conical surfaces. The analysis is performed in two steps. As scattering by a passive single element depends also on the radiating behavior of the same element when fed as an antenna, first the frequency behaviour of its input impedence is numerically computed by a commercial code. Of course this computation is performed assuming the single active element emebedded within a number of similar ones to take into account partly mutual interactions within the FSS. In the paper, as scattering elements, both radial and circumferencial strips conforming a conical shape are considered. Subsequently the frequency behiavour of the conical surface is fully analysed by a numerical code solving the Electric Field Integral Equation for a FSS of finite size made of thin elements conforming a curved surface.

Time Domain Transient Analysis for Ellipsoidal and Hyperbolic Reflector Antennas

Shih-Chung Tuan[1] and Hsi-Tseng Chou[2]

[1]Department of Communication Engineering, Oriental Institute of Technology, Pan-Chiao, Taiwan
[2]Department of Communication Engineering, Yuan Ze University, Chung-Li, Taiwan

Abstract— In this paper we present an early-time transient analysis of electromagnetic (EM) fields scattered from a perfectly conducting ellipsoidal and hyperbolic reflector when it is illuminated by a spherical wave of a feed's radiation with a cosine-tapered pattern and transient time response. This work is motivated by the needs of transient EM analysis in the booming applications of ultra-wide-band or short-pulse antenna systems for target identification and remote sensing such as in the design of impulse-radiating antennas (IRA). A transient-step response of the feed's radiation is considered because it will produce an impulsive response near the second focus of the ellipsoidal reflector, which is very interested in the applications of impulse-radiating antennas (IRA). Furthermore, an ellipsoidal reflector may reduce to a either spherical or parabolic reflector and hyperbolic with a proper parameter assignment. Thus, the developed solution has an advantage of exhibiting field phenomena when the surface changes to hyperbolic or from a spherical to a parabolic reflector.

A Time Domain Analytic Solution to Predict the Transient Radiation for Phased Periodic Array

Shih-Chung Tuan[1] **and Hsi-Tseng Chou**[2]

[1]Department of Communication Engineering, Oriental Institute of Technology, Pan-Chiao, Taiwan
[2]Department of Communication Engineering, Yuan Ze University, Chung-Li, Taiwan

Abstract— Most recently the applications have been extended to treat the problems arising in the near zone of electrically large antennas such as the vital life-detection systems and noncontact microwave detection systems, where the objects under detection may locate in the near zone of antenna. A TD analytic solution to predict the transient radiation from a phased periodic array of elemental antennas is thus developed. The TD phenomena are investigated in this paper. The TD phenomena of Floquet modes in the quantity of field potentials with a transient impulse excitation in the current moments were examined. In this generalized analysis, one first considers a two dimensional finite array of current moments with phases impressed to radiate fields focused in the near zone of array aperture, where the focal field point can be arbitrarily selected.

Analytical Study on Transmission Characteristics of MSL with Dielectric Adhesive-backed NSS

Y. Tomizuka, G. Ichihara, M. Setsu,
T. Ohno, K. Tanii, and M. Uehara
National Institute of Technology, Kisarazu College, Japan

Abstract— In this paper, transmission characteristics affected by a dielectric adhesive between a noise suppression sheet (NSS) and a transmission line are examined. A microstrip line (MSL) based on IEC standard (IEC62333-2) is fabricated, and a transmission characteristic of the MSL attached with a dielectric adhesive-backed NSS is simulated and measured.

Figure 1 shows the measurement system of the MSL attached with an NSS. The substrate shown in Fig. 1 is fabricated on ARLON DiClad522 ($\varepsilon_r = 2.55$, $\tan\delta = 0.0022$). Fig. 2 shows the FDTD simulation model based on the measurement system above. The thickness of the adhesive is defined as d [mm].

Figure 3 shows the simulated and measured transmission characteristics in the case of $d = 0.0$ [mm] or $d = 0.1$ [mm]. The maximum difference of transmitted electric power between simulated and measured results is 2.8% in $d = 0.0$ [mm], and is 3.1% in $d = 0.1$ [mm], respectively. Therefore, the simulation model shown in Fig. 2 is available from the above results.

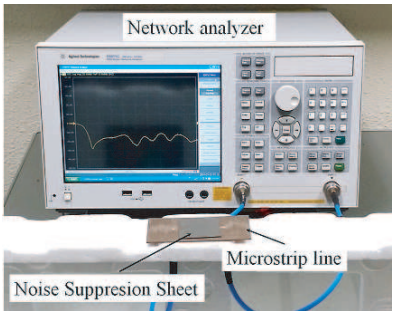

Figure 1: Measurement system of transmission characteristics on a microstrip line.

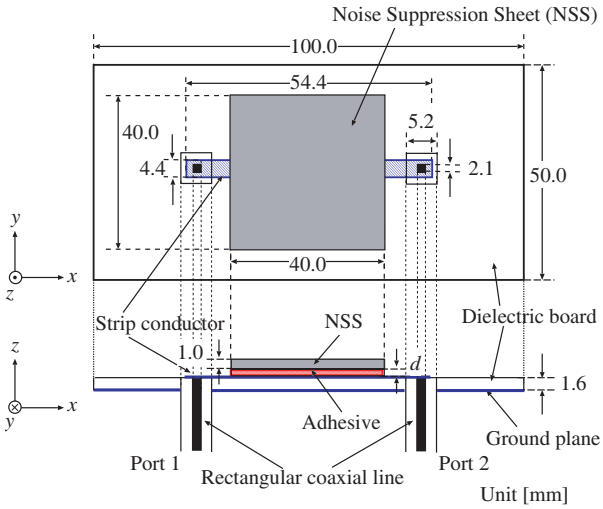

Figure 2: Simulation model of the MSL with NSS.

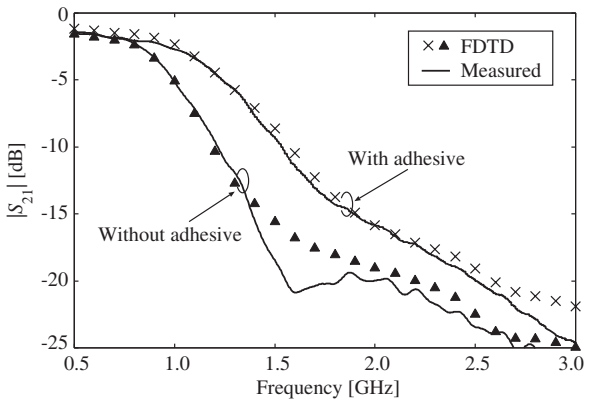

Figure 3: Simulated and measured results of Fig. 1.

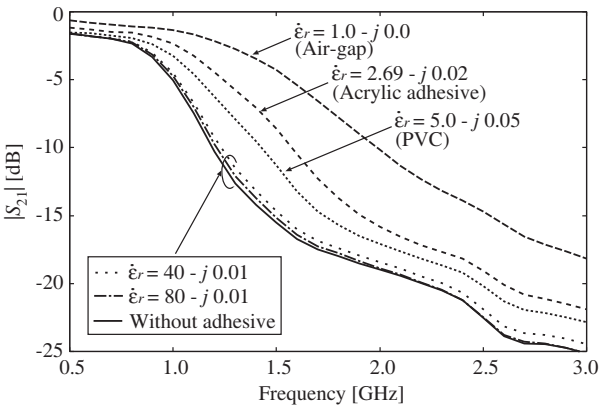

Figure 4: Simulation results of NSS with different adhesive.

Figure 4 shows the transmission characteristics of the MSL attached with the NSS using different dielectric adhesive. From Fig. 4, the cutoff frequency in the case of without adhesive is 0.87 GHz. The cutoff frequency is shifted to 1.33 GHz when the adhesive shown Fig. 2 is replaced by air-gap. Moreover, the effect to transmission characteristic is clearly decreased when adhesive is used compared to the air-gap. When the real part of permittivity of adhesive is increased to 40 or 80, these transmission characteristics are similar to the characteristic in the case of without adhesive. As a result, it is important to consider the complex relative permittivity in the adhesive between an NSS and a transmission line.

Ferroelectrics in RF and MW Adaptive (Electronically Tuned) Matching Circuits

R. A. Platonov[1], **I. V. Kotelnikov**[1], **V. N. Osadchy**[1], **D. M. Kosmin**[1], **A. D. Kanareykin**[2], **E. A. Nenasheva**[3], **and A. B. Kozyrev**[1]

[1]Saint Petersburg Electrotechnical University "LETI"
5 Professor Popov St., St. Petersburg 197376, Russian Federation
[2]Euclid TechLabs, LLC, 5900 Harper Road Suite 102 Solon, Ohio 44139, USA
[3]Ceramics Co. Ltd., 10 Kurchatov St., St. Petersburg 194223, Russian Federation

Abstract— The creation of effective adaptive (electronically tuned) matching circuits is one of the key problems for development of modern RF and MW electronics. Traditional adaptive matching circuits are tuned by using semiconductor, ferromagnetic or MEMS elements. Ferromagnetic tuning consumes a large amount of power and rather slow tuning time (μsec scale); besides of slow tuning time (μsec scale) the MEMS elements have a limitedRF and MW operating power. Semiconductor elements in spite of their fast switching time (ns scale) have a limited power handling capability in point of a parasitic intermodulation product. The use of ferroelectric (FE) materials in paraelecrtic state makes it possible to suppress the negative featuresmentioned above.

Ferroelectric materials such as barium strontium titanate ($Ba_xSr_{1-x}TiO_3$ (BSTO)) in paraelecrtic state and strontium titanate ($SrTiO_3$ (STO)) are the most perspective compositions for RF and MW applications especially at high operation power. These materials have no frequency dispersion of dielectric constant (ε) up to 100 GHz and the suitable tunability ($k = \frac{\varepsilon(E=0)}{\varepsilon(E\neq 0)} \geq 3$) with time of tuning of 10 ps scaleunder electrical control voltages. Dielectric losses in a ferroelectric elements are comparable to the losses in semiconductor ones. In present work the properties of tunable RF and MW elements on the base of thin ($\leq$1 μm) films and bulk ceramics (thickness of $(0.15 \div 1.00)$ mm) of STO and BSTO compositions are analyzed. The parameters of theFE materials and elements on their base were obtained in a broad frequency range using a set of measurement procedures elaborated by authors.

It can be concluded that the main barrier for application of ferroelectrics on microwave is the residual polarization phenomena leading to the decrease of tunability of microwave devices and the degradation of the speed of tuning. Nature of residual polarization phenomena is considered and methods of their suppression are presented.

Modeling and testing the new multilayer FE capacitance construction which provides the operation under high RF power with low level of parasitic harmonics were done. Adaptive matching circuits on the base of the tunable FE capacitors were elaborated andtested and conclusions about their application inindustrial systems (drying chambers, food defrozen chamber etc.), systems of wireless device charging and front antenna end of communication system were done.

Local Field Effects for Left-handed Planar Metamaterials

O. V. Porvatkina, **A. A. Tishchenko**, **and M. N. Strikhanov**
National Research Nuclear University "MEPhI", Moscow, Russia

Abstract— Metamaterials are artificially designed materials that have effective properties, such as anomalous refraction or reflection. Particularly, planar metamaterials have unusual properties such as manipulation of the polarization states of light diffracted from the surface. These structures also demonstrate extremely high confinement of electromagnetic fields and thus strong variations of field intensities, which can significantly enhance near-field optical forces [1]. In addition the planar nature of these structures means they could be incorporated into thin-film coatings for numerous optical components [2].

We consider dielectric and magnetic properties of left-handed planar metamaterials with negative permittivity and permeability. In our work we investigate planar metamaterials consist of anisotropic particles. We obtain dependence of permittivity on dielectric polarizability and permeability on magnetic polarizability of the particles. Local field effects are taken into account in calculations. These effects are caused by interaction between single particles. The analogue of such theory for 3D metamaterials was developed in our recent article [2]. We also obtain the generalized Clausius-Mossotti relations for planar metamaterials made of anisotropic particles in the long wave approximation. We calculate a response function to an external electromagnetic field in case of planar metamaterial. This function describes connection between external electromagnetic field and the local field. On the one hand, such connection allows us to analyze structure of electromagnetic field in the near-field regime [3]. On the other hand,the relationship between the field interacting with particles in the planar metamaterials and the external field is of key importance for calculations of characteristics of the electromagnetic radiation generated by charged particles or particle beams passing through or near the planar structures [4].

REFERENCES

1. Zhang, J., K. F. MacDonald, and N. I. Zheludev, "Giant optical forces in planar dielectricphotonic metamaterials," *Optics Letters*, Vol. 39, 4883, 2014.
2. Zhang, W., A., D. M. Potts, and J. Bagnal, "Giant optical activity in dielectric planar metamaterials with two- dimensional chirality," *Opt. A: Pure Appl. Opt.*, Vol. 8, 878, 2006.
3. Porvatkina, O. V., A. A. Tishchenko, M. I. Ryazanov, and M. N. Strikhanov, "Local field effects in anisotropic metamaterials," *IOP Conference Series*, Vol. 541, 012024, 2014.
4. Ryazanov, M. I. and A. A. Tishchenko, "Clausius-Mossotti-type relation for planar monolayers," *Journal of Experimental and Theoretical Physics*, Vol. 103, 539, 2006.
5. Ryazanov, M. I., M. N. Strikhanov, and A. A. Tishchenko, "Local field effect in diffraction radiation from a periodical system of dielectric spheres," *Nucl. Instr. and Meth. B*, Vol. 266, 3811, 2008.

Total Internal Reflection as a Technique for Study of Surface Optical Characteristics of Left-handed Materials

A. M. Feshchenko, **A. A. Tishchenko**, **and M. N. Strikhanov**
National Research Nuclear University "MEPhI", Moscow, Russia

Abstract— Real material surface is known to differ from ideal plane surface because of the presence of nonuniform near-surface layer. The properties of the layer may influence considerably on various processes of macroscopic electrodynamics, such as reflection and refraction of light, propagation of surface waves, radiation from fast charged particle beams [1–3]. As the thickness of the layer is much smaller than the light wavelength, all inhomogeneities caused by natural surface anisotropy, impurity atom adsorption, surface relaxation and reconstruction, fluctuations in surface electronic states, — all these can be taken into account via introduction of surface polarization current into boundary conditions [3]. This surface polarization current is linearly dependent on the electrical field, and proportionality factor is the phenomenological characteristic of dielectric and magnetic surface features.

In this work we consider an effect of surface inhomogeneities of left-handed materials on light reflection and refraction. It is shown that total internal reflection could be useful for investigation of surface optical characteristics of metamaterial. Scattering of refracted wave in the near-surface layer leads to existence of radiation propagating from the boundary to the point of observation. It is convenient to describe this radiation as a result of excitation of the surface current. Note, this radiation does not arise in the absence of the inhomogeneities in case of total internal reflection. The angular distribution of the resulting radiation is derived and the opportunity of getting information about the properties of metamaterial surface with help of this method is discussed. Information about surface properties can be of great use for developing of metamaterial optics, for example, multilayered structures and waveguides [4], perfect lens [5], terahertz optics [6], cloaking and so on.

REFERENCES

1. Ryazanov, M. I., M. N. Strikhanov, and A. A. Tishchenko, "Diffraction radiation from an inhomogeneous dielectric film on the surface of a perfect conductor," *JETP*, Vol. 99, 311, 2004.
2. Koshelev, I. V. and M. I. Ryazanov, "On transition emission on an inhomogeneous interface," *Laser Physics*, Vol. 14, 897, 2004.
3. Ryazanov, M. I., "Phenomenological description of the dielectric-properties of a surface-surface waves," *JETP*, Vol. 66, 725, 1987.
4. Canto, J. R., C. R. Paiva, and A. M. Barbosa, "Dispersion and losses in surface waveguides containing double negative or chiral metamaterials," *Progress In Electromagnetics Research*, Vol. 116, 409–423, 2011.
5. Ambati, M., N. Fang, C. Sun, and X. Zhang, "Surface resonant states and superlensing in acoustic metamaterials," *Physical Review B*, Vol. 75, 195447, 2007.
6. Acuna, G., S. F. Heucke, F. Kuchler, H. T. Chen, A. J. Taylor, and R. Kersting, "Surface plasmons in terahertz metamaterials," *Optics Express*, Vol. 16, 18745, 2008.

Evaluation of a Buckypaper's Electromagnetic Shielding Efficiency in X Band

N. Curreli, **C. Puddu**, **G. Muntoni**, **M. Simone**, **and A. Fanti**
Department of Electrical and Electronic Engineering, University of Cagliari, Italy

Abstract— Carbon nanotubes (CNTs) properties and applications are one of the most innovative and interesting research areas in physics and engineering. The electromagnetic behaviour of CNTs composites and plastic material such as PE and PMMA has been analized in several works. Recent works have highlighted how CNTs can be effectively applied in electromagnetic interference (EMI) as high shielding material. Basically, this is due to their high aspect ratio and their tunable conductivity, which allows the electrical percolation (with a little number of CNTs). It is crucial to understand and control the electromagnetic properties of these materials to apply them to devices' design in several research fields. A buckypaper is a shield made only with CNTs, it is used mainly to protect electronic devices from electromagnetic interferences inside the plains to prevent equipment damaging and unintended setting modification. At the same time, CNT shields could be applied to avoid radar detection of militar aircrafts. Moreover, in the next years these structures could have a wide application in nano- and bio-science: Potential application in the electromagnetical shielding concern nanoelectronis devices, nano-biomedical imaging and sensing or, in the near future, the protect medical equipments from high-frequency radiations.

This paper studies the shielding efficiency of an buckypaper interposed between a multifrequency source and a electromagnetic waved detector. Our analysis has considered a frequency spectrum from the microwave (1 GHz) to the UV band (10^7 GHz).

Waveform Measurement of Ultra-high Repetition Mode-locked Pulses Generated from a Silica Toroid Microcavity

Zhelun Chen, Takuma Nagano, Yusuke Okabe, Tomoya Kobatake, and Takasumi Tanabe
Department of Electronics and Electrical Engineering, Faculty of Science and Technology
Keio University, 3-14-1 Hiyoshi, Kohoku-ku, Yokohama, Kanagawa 223-8522, Japan

Abstract— An optical frequency comb exhibits a pulse train when we observe it in the time domain. The repetition rate of the pulse train is determined by the frequency interval of the comb space. Since the spacing of a frequency comb generated from a microcavity is extremely large, it exhibits an ultrahigh repetition rate and the phases of the modes are locked. In this study, we demonstrated and measured the arbitrary generation of ultrahigh repetition rate pulses ranging from 0.8 to 8 THz by utilizing a silica toroid microcavity. The Kerr comb interval is controlled by changing the input laser power, wavelength and wavelength scan speed. The experimental results are shown in Fig. 1, where the pulses were measured with an SHG autocorrelator. We clearly observed that the generated comb exhibited mode-locking and also pulse trains at an ultrahigh repetition rate. It should be noted that such pulses are generated by continuous wave laser pumping. This demonstration of the generation of ultrahigh repetition rate pulses at an arbitrary frequency opens the possibility for future application of the Kerr comb as a high-speed signal-processing source.

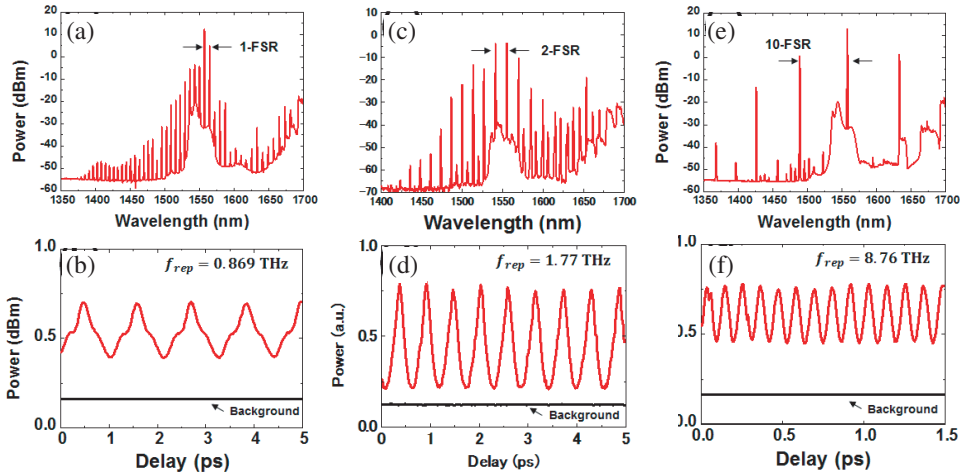

Figure 1: Experimental results for generated Kerr combs and their SHG autocorrelation traces. We used a toroid microcavity with a Q factor of 2×10^6 and a free spectral range (FSR) of 0.875 THz. The input wavelength and power are (a) (b) 1557.1 nm and 0.49 W, (c) (d) 1540.56 nm and 0.55 W, and (e) (f) 1557.1 nm and 0.49 W, respectively.

Fundamental Mode Cutoff Filter for Highly Sensitive Fiber Strain Sensing Applications

Yu-Cheng Li[1], **Wen-Chuang Lin**[1], **Kuan-Yu Lou**[1], **Jhih-He Jhang**[1], **Yu-Lin Tseng**[1], **and Nan-Kuang Chen**[1, 2]

[1]Department of Electro-Optical Engineering, National United University, Miaoli 360, Taiwan
[2]Optoelectronics Research Center, National United University, Miaoli 360, Taiwan

Abstract— Short-pass filter has been widely in S band erbium-doped fiber amplifiers wavelength tunable by erbium-doped fiber Laser B femtosecond pulse stretching [1–4] this is because the short-pass filter have a high cutoff effect. In this work we using the short-pass filter to become the strain sensor. In Figure 1 shows the device structure and L is the length of the fiber. Figures 2, 3 show the spectral of the different diameter, when diameter about 21 µm the cutoff point is about 1.35 µm. When the diameter about 27 µm the cutoff point is about 1.30 µm. When the diameter about 21 µm the sensitivity is about 1.44 µm/mε.

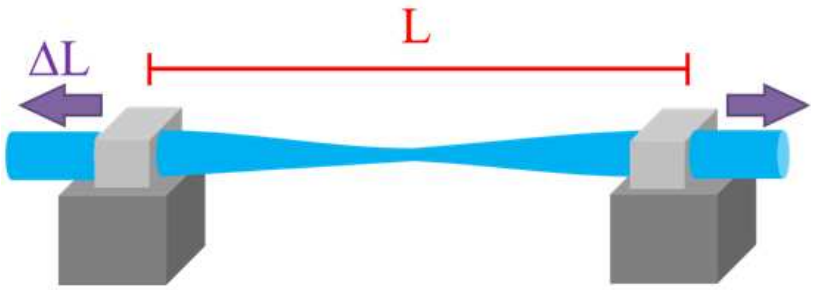

Figure 1: Show the device structure and the L is the length of the fiber.

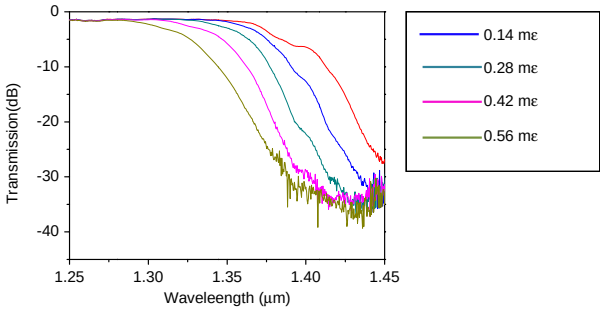

Figure 2: Show the diameter is about 21 µm and the index is 1.456.

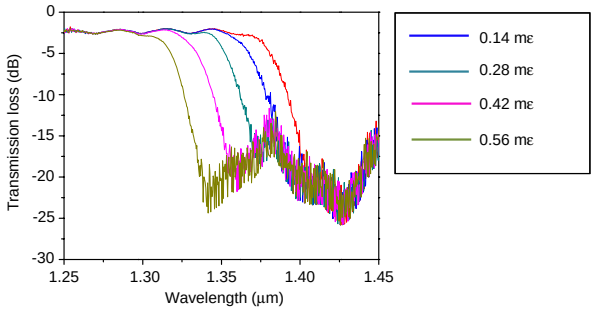

Figure 3: Show the diameter is about 27 µm and the index is 1.456.

REFERENCES

1. Chen, N. K., K. C. Hsu, S. K. Liaw, Y. Lai, and S. Chi, "Influence of depressed-index outer ring on evanescent tunneling loss in tapered double-cladding fibers," *Opt. Lett.*, Vol. 33, 1666–1668, 2008.
2. Xu, X., et al., "Colorless grating couplers realized by interleaving dispersion engineered subwavelength structures," *Opt. Lett.*, Vol. 38, No. 18, 3588–3591, 2013.
3. Chen, N. K., K. C. Hsu, S. Chi, and Y. Lai, "Tunable Er^{3+}-doped fiber amplifiers covering S and C+L bands over 1490–1610 nm based on discrete fundamental-mode cutoff filters," *Opt. Lett.*, Vol. 31, 2842–2844, 2006.
4. Chen, S., et al., "Dynamics of short-pulse generation via spectral filtering from intensely excited gain-switched 1.55-µm distributed-feedback laser diodes," *Optics Express*, Vol. 21, No. 9, 10597–10605, 2013.

Photon-Avalanche-Like Nonlinear Excitation and Optical Low-Energy Ultrafast Switching in Solids

E. Yu. Perlin and A. V. Ivanov
ITMO University, 14 Birzhevaya liniya, St. Petersburg 199034, Russia

Abstract— A new mechanism of photoexcitation of transparent crystals is studied. The mechanism exhibits an exceptionally high degree of optical nonlinearity and shows itself even at moderate laser radiation intensities $j \sim 10^5\,\mathrm{W/cm^2}$. A three-band model of a crystal is treated. It is assumed that the photon energy of laser radiation $\hbar\omega$ is such that $\hbar\omega < E_g < 2\hbar\omega$, where E_g is the energy gap between the top of the valence band v and the bottom of the lower conduction band c_1. At the same time, it is assumed that, near the bottom of the band c_1, the energy $\hbar\omega$ is equal to the energy gap between the band c_1 and the upper conduction band c_2. At low excitation intensities j, no photo-induced transitions occur in the material, since in accordance with the above assumption, there are no free electrons in the band c_1 and there is no one-photon resonance between the bands v and c_1. At high intensities j, the situation is quite different. Due to two-photon transitions between the bands v and c_1, a certain number of free electrons appear in the band c_1. An electron generated in the band c_1 absorbs a photon and transits to the band c_2, in which it quickly falls (within a time of $\sim (2\text{–}7)\cdot 10^{-13}\,\mathrm{s}$) into the region of states close to the bottom of the band (e.g., because of emission of optical phonons). Then, due to "standard" radiative or nonradiative relaxation processes, however, in a longer time, the electron can transit to the conduction band c_1. In this case, the photon-involving Auger process $c_2 + \hbar\omega \to c_1 c_1 v$ is possible as well. In such process, in one elementary event, a photon is absorbed, and the electron from the band c_2 transits to the band c_1, liberating energy for the creation of an electron-hole pair consisting of a hole in the band v and an electron in the band c_1. As a result, there are now two electrons in the band c_1. In turn, these electrons, when transiting to the upper conduction band c_2, participate in the same process $c_2 + \hbar\omega \to c_1 c_1 v$, etc.. In this case, the concentration of nonequilibrium electrons in both of the conduction bands increases in an avalanche-like manner. The increase in the number of electrons in the lower conduction band yields a very sharp increase in absorption of light through one-photon transitions between the conduction bands.

The above-considered effect is in essence one of the modifications of the photon avalanche effect (see, e.g., [1–3]).

In this study, the probabilities of one- and two-photon interband transitions and the probability of the photon-involving Auger process are calculated. These probabilities enter into the system of differential balance equations for populations of free charge carriers in the bands v, c_1, and c_2. Numerical solutions of this system are obtained for a number of sets of typical band-structure parameters and relaxation times.

It is shown that, at the light intensities $j < 10^5\,\mathrm{W/cm^2}$, the crystal switches from state I, in which free electrons and holes are practically lacking and there is no noticeable absorption of light, to state II, in which the concentration of free charge carriers is as high as 10^{19}–$10^{20}\,\mathrm{cm^{-3}}$ and the absorption coefficient reaches 10^3–$10^4\,\mathrm{cm^{-1}}$. The switching time is 1–10 ns [4, 5].

A number of crystals, whose electron band structure allows the above-described photon-avalanche mechanism of photoexcitation and optical switching, are considered in detail.

REFERENCES

1. Guy, S., M.-F. Joubert, and B. Jacquier, *Phys. Rev. B*, Vol. 55, 8240, 1997.
2. Perlin, E. Yu., A. V. Ivanov, and R. S. Levitskii, *JETP*, Vol. 96, 543, 2003.
3. Perlin, E. Yu., A. V. Ivanov, and R. S. Levitskii, *JETP*, Vol. 101, 357, 2005.
4. Perlin, E. Yu., A. V. Ivanov, and A. A. Popov, *Opt. Spectrosc*, Vol. 113, I:376; II: 383, 2012.
5. Perlin, E. Yu., A. V. Ivanov, and A. A. Popov, *Opt. Spectrosc*, Vol. 115, 739, 2013.

Secondary Instabilities of Steady Stationary Solution in Wide-aperture Lasers with Negative Detuning

D. A. Anchikov[1], **A. V. Pakhomov**[1, 2], **A. A. Krents**[1, 2], **and N. E. Molevich**[1, 2]

[1]Department of Physics, Samara State Aerospace University, Samara 443086, Russia
[2]Theoretical Sector, Lebedev Physical Institute, Samara 443011, Russia

Abstract— Pattern formation and the evolution of complexity in spatially extended dynamical systems has been the subject of many investigations in widely diverse branches of science. In nonlinear optics, such studies have been motivated by the goal of developing a general understanding to describe the emergence of periodic and quasiperiodic patterns, vortices or spatial solitons using various nonlinear systems as well as gas, solid-state and semiconductor lasers. These systems are very complex devices having a rich spatiotemporal dynamics. The control parameter that determines the mechanism, which give rise to the transverse structure formation, is the Fresnel number.

In this work, we report on numerical and analytical investigations of the wave instability occurring for negative detuning (cavities tuned above resonance) in lasers class B. In that case, relations amongthe decay rate of polarization ,the decay rate of population difference and the cavity rate were $\gamma_\perp \gg \gamma_\parallel \gg \kappa$. We use the Maxwell-Bloch equations to describe the dynamics of transverse patterns in single longitudinal mode lasers, where the active medium is composed of two level atoms inside a cavity with flat mirrors. An important parameter for determining the behavior of the system is the cavity detuning of field frequency from the atomic resonance transition frequency.

With increase of the pump level the homogeneous solution becomes unstable against spatiotemporal perturbations with a finite wavelength. We have numerically simulated the dynamics of laser field above the second laser threshold in one- and two-dimensional cases. In the result of stability loss of steady solution, the regime that evolves in the system consists of a sequence of switches between traveling wave solutions with different wave numbers. The laser intensity presents the areas of nearly constant values which interrupted by bursts of large amplitude oscillations. The sequence of wave numbers can be predicted as perturbation with highest growth rate.

We use analytical and numerical approaches to perform the linear stability analysis. We found that the regime of dynamical switches is the result of secondary instabilities. By both methods, the evolution may be predicted with a relatively good precision.

Radiofrequency Impedance Spectroscopy of Active Optical Fiber Heating under Laser Generation and Amplification Conditions

R. I. Shaidullin[1, 2], **I. A. Zaytsev**[2], **and O. A. Ryabushkin**[1, 2]

[1]Moscow Institute of Physics and Technology
Institutskiy per. 9, Dolgoprudny, Moscow Region 141700, Russia
[2]Kotelnikov IRE of RAS, Vvedensky Sq. 1, Fryazino, Moscow Region 141190, Russia

Abstract— In active fibers, doped with rare-earth elements, in process of lasing some part of optical pump power is converted into heat. Main mechanisms responsible for fiber heating are optical quantum defect (difference between pump and emitting photon energies) and nonradiative relaxation of excited rare-earth ions. High CW power levels of modern fiber lasers (up to 20 kW in single-mode and 100 kW in multimode regimes) lead to the strong heating of active fiber, changing its absorption and photoluminescence optical spectra. Recently, we have proposed novel method based on radiofrequency impedance spectroscopy for temperature measurement of optical fibers [1]. Block scheme of the experimental setup applied for fiber temperature measurement (Fig. 1(a)) includes dielectric tube with copper wire reeled on it, forming connected in series induction coil and single-turn double-wire capacitor with placed inside active fiber segment and filled by additional polymer of the same type as cladding one. This configuration represents an oscillating LC-circuit. The resonant frequency of this circuit depends on temperature T, since the capacitance value $C(T)$ is specified by temperature dependent permittivity of the polymer. Equivalent temperature of the fiber amplifier segment in the operating mode (Fig. 1(b)) was measured using calibration dependence of resonant frequency measured in uniform heating experiment.

General theoretical model of fiber heating, based on solution of heat conduction equation with the heat source conditioned only by quantum defect inside active core [2], cannot explain experimental results. In order to find correspondence between measured equivalent temperature and actual temperature distribution inside fiber we developed coaxial model of fiber heating. Fig. 1(c) shows a cross-section of two-wire capacitor and mathematically simulated distribution of thermal field. Also additional verifying experiment was conducted, where optical fiber was replaced by the polymer coated copper wire, heated by the electric current. Simultaneous measurements of copper wire temperature basing on its resistance change and equivalent temperature of the polymer cladding showed that maximum equivalent temperature change of the polymer −41 K (measured at 120 W pump and 90 W lasing power) corresponds to 63 K of copper wire temperature change. In order to calculate true temperature distribution of the system we conducted one more experiment aimed at heat transfer coefficient determination by measuring kinetics of fiber cooling. This coefficient was found to be $60 \pm 5\ \mathrm{W/m^2{*}K}$. Using these data temperature distribution of the system was calculated. Average temperatures are: active core −57.6 K, silica cladding −52.6 K, polymer cladding −38.4 K. Developed theoretical model allowed us to find correspondence between experimentally measured equivalent temperature and actual temperature distribution inside active fiber.

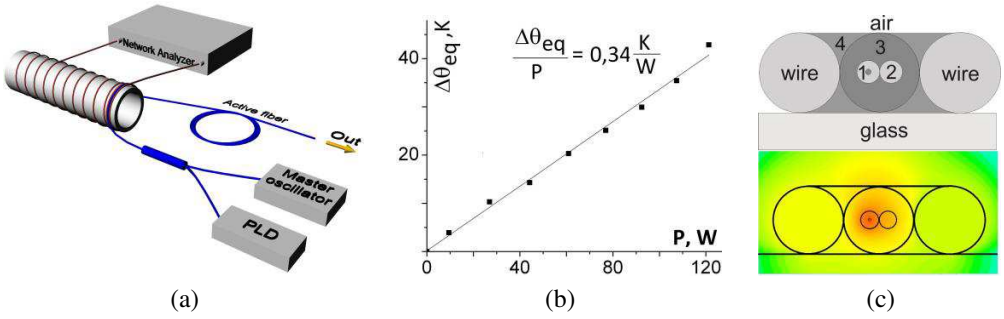

Figure 1: (a) Simplified block scheme of experimental setup. (b) Dependence of equivalent heating temperature of active fiber on pump power. (c) Cross-section of two-wire capacitor (1 — SM core, 2 — MM core, 3 — polymer cladding, 4 — additional polymer) (top) and its temperature distribution (bottom).

REFERENCES

1. Ryabushkin, O. A., R. I. Shaidullin, and I. A. Zaytsev, "Radiofrequency impedance spectroscopy of laser fiber heating," *6th EPS-QEOD Europhoton Conference*, ThP-T2-P-07, Neuchatel, Switzerland, August 24–29, 2014.
2. Davis, M. K., et al., "Thermal effects in doped fibers," *J. Lighwave Techn.*, Vol. 16, 1013–1023, 1998.

Cerenkov Radiation in Presence of Squeezed Electromagnetic Vacuum

Peter A. Meleshenko[1, 2], Hang T. T. Nguyen[3], Vladimir A. Gorlov[1], Mikhail E. Semenov[1, 2, 4], and Alexander F. Klinskikh[2]

[1]Zhukovsky-Gagarin Air Force Academy, Russia
[2]Voronezh State University, Russia
[3]Institute of Technology, Vietnam National University — Ho Chi Minh City, Vietnam
[4]Voronezh State University of Architecture and Civil Engineering, Russia

Abstract— Cerenkov effect [1] have a long history but it remains relevant in relation to the different areas of application of such a phenomena (the wide list of publication on this subject takes place, see, e.g., [2–4] and related references). The expression for the radiated power was obtained by solving the equations of classical electrodynamics in the medium. A large number of studies have been devoted to other aspects of the Cerenkov effect. They concern the extension to the case of magnetic media, a detailed analysis of radiation in crystals, the role of boundaries, etc.. The classical theory of spontaneous Cerenkov effect is fairly accurate, however the quantum analysis gives a more complete understanding of the phenomenon. Moreover, the quantum approach is most useful when considering the motion of a charged particle in a dielectric medium in the external electromagnetic wave. The radiation in this case has an induced nature and quantum approach gives a better understanding of the physical nature of phenomena.

Creation of powerful sources of electromagnetic radiation initiated extensive research in the area of particle-field interaction. The squeezed states of light [5] play an important role in such researches. These states generalize the well-known class of coherent states and are characterized by the fact that the uncertainty of one of the canonical variables of the electromagnetic field is less than in a conventional coherent state. The squeezed states are important in such areas as optical communication, interferometry, nonlinear optics, the detection of gravitational waves, etc.. It should also be noted that the squeezed states are objects of purely quantum nature. So the description of the motion of a charged particle on a background of the squeezed vacuum can be performed using the quantum field theory only. This problem is of great practical interest (new sources of electromagnetic radiation such as free-electron lasers and Cerenkov lasers).

In this work we investigate the Cerenkov radiation in the case of motion of a charged particle on a background of the squeezed electromagnetic vacuum. Using the quantum approach (time dependent perturbation theory) we obtain the following expression for the Cerenkov radiated power:

$$P = \left(1+|\nu|^2\right)\frac{e^2 v_e}{c^2}\int\limits_0^\infty \omega\left[1-\left(\frac{\hbar n(\omega)\omega}{2m_e c v_e}+\frac{c}{n(\omega)v_e}\right)^2\right]\Theta\left(1-\left|\frac{\hbar n(\omega)\omega}{2m_e c v_e}+\frac{c}{n(\omega)v_e}\right|\right)d\omega$$
$$+|\nu|^2\frac{e^2 v_e}{c^2}\int\limits_0^\infty \omega\left[1-\left(\frac{\hbar n(\omega)\omega}{2m_e c v_e}-\frac{c}{n(\omega)v_e}\right)^2\right]\Theta\left(1-\left|\frac{\hbar n(\omega)\omega}{2m_e c v_e}-\frac{c}{n(\omega)v_e}\right|\right)d\omega,$$

where ν is the squeezing parameter, $\Theta(z)$ is the Heaviside step-function. This expression contains two terms. First term corresponds to radiation power, while the second one corresponds to absorption power.

REFERENCES

1. Cherenkov, P. A., "Visible radiation produced by electrons moving in a medium with velocities exceeding that of light," *Physical Review*, Vol. 52, 378–379, 1937.
2. Altschul, B., "Cerenkov radiation in a Lorentz-violating and birefringent vacuum," *Phys. Rev. D*, Vol. 75, 105003(1–9), 2007.
3. Gal'tsov, D. V., E. Yu. Melkumova, and K. Salehi, "Cerenkov radiation from moving straight strings," *Phys. Rev. D*, Vol. 75, 105013(1–22), 2007.
4. Altschul, B., "Absence of long-wavelength Cerenkov radiation with isotropic Lorentz and CPT violation," *Phys. Rev. D*, Vol. 90, 021701(1–5), 2014.
5. Scully, M. O. and M. S. Zubairy, *Quantum Optics*, Cambridge University Press, 1997.

Frequency Characterization of Planar Resonators by THz Josephson Spectroscopy

A. V. Snezhko[1, 2], **O. Y. Volkov**[1], **V. N. Gubankov**[1], **I. I. Gundareva**[1, 3], **Y. Y. Divin**[1, 3], **V. V. Pavlovskiy**[1], **and V. I. Pokalyakin**[1]

[1]Kotelnikov Institute of Radio Engineering and Electronics of RAS, Russian Federation
[2]Moscow Institute of Physics and Technology, Russian Federation
[3]Peter Grunberg Institute, Forschungszentrum Julich, Germany

Abstract— Broadband electromagnetic measurement at frequencies above 100 GHz is still challenging problem because of limited frequency ranges of oscillators, complicated matching networks and ambiguous deembedding procedures. It is known that Josephson junction (JJ) is very sensitive to electromagnetic environment. When JJ interacts with external electromagnetic structure, characteristics of the structure in frequency domain are mapped into the modification of dc characteristics of JJ in voltage domain. Recently a new spectral technique based on nonstationary Josephson effect was proposed for frequency analysis of electromagnetic resonant structures, which were integrated with JJ. Here we extend this method to perform spectral characterization of planar resonators on separate substrates. We have studied resonator characteristics at frequencies from 50 GHz to 500 GHz, using $YBa_2Cu_3O_{7-x}$ high-T_c bicrystal grain boundary junctions on $NdGaO_3$ and MgO substrates. Differential resistance vs. voltage curves $R_d(V)$ modified by the interaction between JJ and resonator have been analyzed. Resonators were formed by from cooper thin films on Al_2O_3 separate substrates by UV photolithography. The planar resonator has been presented as RLC-circuit. Parameters of equivalent circuit have been obtained by fitting simulated $R_d(V)$ curves to experimental data. Set of resonance frequencies have been obtained for split ring resonators from 50 GHz to 500 GHz and quality factors have been estimated. An excitation of fundamental resonance mode in the planar resonator by Josephson oscillations was demonstrated. The technique developed might be used for frequency characterization of THz photonic elements and structures.

ACKNOWLEDGMENT

This work was partly supported by the grant Russian Fund for Basic Research (No. 14-07-3132-3 MOJI_a).

Stronger Nanoscale EM and BEM Solutions by CICT Phased Generators

R. A. Fiorini
Department of Electronics, Information and Bioengineering (DEIB)
Politecnico di Milano University, Italy

Abstract— There is no doubt that the IC (Infinitesimal Calculus) has played in the past and will play in future a major role in the mathematical treatment of EM (electromagnetic) and BEM (bioelectromagnetic) modeling problems, but we must be aware that its addiction hides some important features of the phenomenon being described, such as the geometrical and topological features. The addiction is such that, since the digital computer requires an algebraic formulation of physical laws, it is preferred to discretize the differential equations, rather than considering other more convenient tools for problem mathematical description like, for instance, FDC (Finite Differences Calculus) or more sophisticated algebraic methods. Hence, to apply the numerical methods we are forced to return to a discrete formulation using one of the many methods of discretization, starting from classic FEM, BEM, FVM, FDM, etc., to arrive to specialized algorithms to achieve fast operational compromises in specific application areas. Nevertheless, traditional FDC and even more sophisticated and advanced algebraic approaches are unable to conserve overall system information. In fact, misplaced precision leads to information opacity, fuzzyness, irreversibility, chaos, complexity and confusion. To find innovative solution and to open the door to more reliable scientific problem description and solution ("Science 2.0" approach), we just need to remember the Relativity's father inspiration quote: "We cannot solve our problems with the same thinking we used when we created them." Eventually, our overview suggests us that to grasp a more reliable representation of experimental reality and to get stronger physical and biological system correlates, researchers and scientists need two intelligently articulated hands: both stochastic and combinatorial approaches synergically articulated by natural coupling. The former, applied to all branches of human knowledge under the "continuum hypothesis" assumption, has reached highly sophistication level, and a worldwide audience. Many "Science 1.0" researchers and scientists up to scientific journals assume it is the ultimate language of science. The latter, less developed under the "discrete hypothesis" assumption in specific scientific disciplines, has been considered in peculiar application areas only. It has been further slowly developed by a few specialists and less understood by a wider audience. The computational information conservation theory (CICT) approach brings classical and quantum information theory together in a single framework, by considering information not only on the statistical manifold of model states but also from empirical measures of low-level multiplicative noise source generators, related to experimental high-level overall perturbation. According to CICT Infocentric Wordview, traditional elementary arithmetic long division remainder sequences can be interpreted as combinatorially optimized exponential cyclic sequences (OECS) encoding hyperbolic geometric structured information, as points on a discrete Riemannian manifold, under HG metric, indistinguishable from traditional random noise sources by classical Shannon entropy, and current most advanced instrumentation approach. In other words, if we want to achieve overall system information representation conservation and to get stronger solution to advanced problems, like resonant nanoparticle, nanophotonic, opti uidics structure modeling, etc., we have to look for convenient arbitrary scaling BU (bottom-up) point-of-view (POV) (from discrete to continuum view $\equiv$ BU POV) to start from first, and NOT the other way around! Then, a top-down (TD) POV can be applied for overall final model validation and endorsement, if needed. CICT formulation has the great merit of maintaining close contact between the mathematical description and the physical phenomenon described, showing how to obtain a purely algebraic formulation of information and physical laws relating directly elementary information generators to experimental measurements. A few examples are presented and discussed.

Dynamical Model of Elastic-plastic Hysteresis in Fullerens Film

Boris M. Darinsky[1], **Mikhail E. Semenov**[1, 2, 3],
Andrey M. Semenov[1], **and Peter A. Meleshenko**[1, 2]

[1]Voronezh State University, Voronezh, Russia
[2]Zhukovsky-Gagarin Air Force Academy, Voronezh, Russia
[3]Voronezh State University of Architecture and Civil Engineering, Voronezh, Russia

Abstract— The hysteretic effects take place in various areas of material science (both in macro and micro levels). Depending on the purposes of investigation both the phenomenological and constructive models can be used and there are many literature sources on this subject (see, e.g., [1] and related references). As a rule in the constructive models which are described by the relations "input-state" "state-output" [2, 3] the dynamical properties of the hysteresis carrier have no taken into account. It is a well-known fact that the mechanical properties almost all the materials (these properties the elastic-plastic hysteresis) remain unchanched (hysteretic dependence of elastic-plastic materials does not depend on the speed of mechanical affection). However, the results of experiments with the fulleren nanofilms [4] show that the hysteretic curve in the coordinates "force-displacement" depends on the speed of force application.

In this work we propose the dynamical probability model of hysteresis for description of elastic-plastic properties of nanoscale fulleren film taking into account the electromagnetic nature of fulleren clusters binding. This model is based on the fact that the decay law for fulleren super-cluster $[C_{60}]_n$ (especially for $n = 2$) depends on the external conditions (temperature, pressure, etc.) as well as has a probability nature. The description of the decay law in the macroscopic level can be made using the theory of random processes (Kolmogorov-Chapman equation). The results of numerical simulations are in good agreement with the known experimental data.

REFERENCES

1. Ikhouane, F. and T. Rodellar, *Systems with Hysteresis: Analysis, Identification and Control Using the Bouc-Wen Model*, Willey, 2007.
2. Semenov, M. E., D. V. Shevlyakova, and P. A. Meleshenko, "Inverted pendulum under hysteretic control: stability zones and periodic solutions," *Nonlinear Dynam.*, Vol. 75, 247–256, 2014.
3. Semenov, M. E., D. V. Grachikov, A. G. Rukavitsyn, and P. A. Meleshenko, "On the state feedback control of inverted pendulum with hysteretic nonlinearity," *MATEC Web of Conferences*, Vol. 16, 05009(1–5), 2014.
4. Penkov, O. V., V. E. Pukha, A. Yu. Devizenko, et al., "Self-healing phenomenon and dynamic hardness of C_{60}-based nanocomposite coatings," *Nano Lett.*, Vol. 14, 2536–2540, 2014.

Binary Collision with Energetic Ions of Carbon Nanotubes

D. Bajalan
St. Pölten, Austria

Abstract— Carbon nanotubes (CNTs) are very interesing technological branch. Due to their low dimensionality, nanometer size and remarkable electronic, mechanic and magnetic properties, nanotubes are promising structures for many purposes in several fields of physics, materials science or biomedicine [1]. Channeling of energetic ions through solids is a phenomenon which should be accounted for in the present day semiconductor technology, as it gives rise to deeper implantation and less lattice disorder. The channeling effects are particularly important for materials with high crystallization and anisotropic atomic structure [2]. Experiments on the irradiation of carbon nanotubes with energetic particles poses many interesting properties. These effects may potentially be used in various practical applications, such as nanoelectronicdevices.

REFERENCES

1. Uribe, J. D., C. Celedon, A. Cortes, and J. E. Valdes, Laboratorio de Colisiones Atomicas, Depto de Fsica, Universidad Tecnica Federico Santa Mara, 2005.
2. Krasheninnikov, A. V. and K. Nordlund, *Nuclear Instruments and Methods Physics Research B*, Vol. 228, 2005.

Applications of Carbon Nanotubs and Other Nanomagnetic Nanowires

D. Bajalan
St. Pölten, Austria

Abstract— MWNTs are widely used in lithium ion batteries for notebook computers and mobile phones, marking a major commercial success [1].

Carbon nanotubes (CNTs) are hollow cylindrical molecules consisting of single or many sheets of graphite wrapped into cylinders with diameters of from less than 1 nm up to hundreds of nm. CNTs have extraordinarymechani cal and electrical properties. For example, their densitynormalized Youngs modulus and strength are estimated bo be, respectively, about 19 and 56 times that of steel. Depending on the wayof how the graphite sheets are rolled up, CNTs can be either metals or narrow-band semiconductors, which, along with their inherent nm-size, makes [2].

Carbon Nanotubes 1 atom thick, with diameters of only 1 to 2 nm, seems to be one of the perfect candidates to take us right to the end of Moores Law curve by 2019. We possibly cannot go beyond that. carbon Nanotubes is of importance for future nanodevice applications.

REFERENCES

1. De Volder, M. F. L., S. H. Tawfick, R. H. Baughman, and A. J. Hart, *Science*, Vol. 339, 2013.
2. Krasheninnikov, K. N., *Nuclear Instruments and Methods in Physics Research B*, Vol. 216, 2004.

In-line Fiber Anemometer Based on Strain Sensing in Stretched Abrupt-tapered Fiber

Yu-Cheng Li[1], **Jheng-Jyun Wang**[2], **Wen-Chuang Lin**[1], **and Nan-Kung Chen**[1, 2]

[1]Department of Electro-Optical Engineering, National United University, Miaoli 360, Taiwan
[2]Optoelectronics Research Center, National United University, Miaoli 360, Taiwan

Abstract— Optical fiber strain sensors have been widely used in precision optical sensing application. The traditional fiber strain sensors can be made based on Michelson [1] and Mach-Zehnder interferometers [2, 3]. In this work, we show the air velocity sensor in fiber strain sensor made by single mode fiber. This sensor is constructed based on the stretched abrupt-tapered micro-fiber (SAT-MF). The single mode fiber will become to the tapered fiber with a diameter of around a few microns. So we used this structure to become the air velocity sensor.

Since the light program go through the abrupt tapered the fundamental mode will be converted and transferred into high order cladding modes and generate interference. We definition the taper diameter is D, first taper point to second taper point is L, as shown in Fig. 1(a). Fig. 1(b) shows experimental set-up of the air velocity sensor.

The thermal expansion coefficient of silica is as low as on the order of 10^{-7}, thus we can reduce the effect of temperature variations on strain sensitivity. The sensing area is a SAT-MF it can be easier to change the air velocity sensitivity.

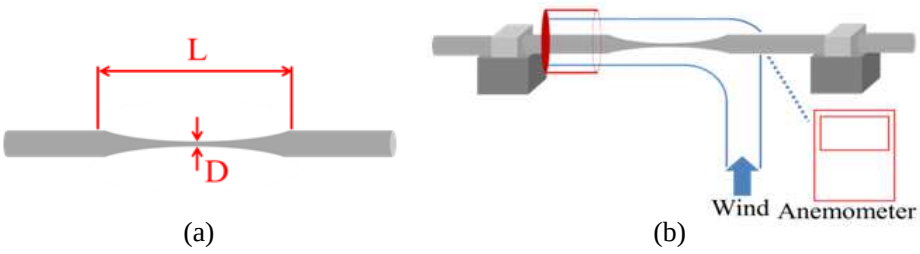

Figure 1.

REFERENCES

1. Gatti, D., G. Galzerano, D. Janner, S. Longhi, and P. Laporta, *Opt. Express* Vol. 16, 1945–1950, 2008.
2. Beverini, N., E. Maccioni, M. Morganti, F. Stefani, R. Falciai, and C. Trono, *J. Opt. A: Pure Appl. Opt.*, Vol. 9, 958–962, 2007.
3. Chen, N.-K., et al., "Investigation of temperature independence in highly sensitive fiber strain sensor based on microfiber interferometer," *Asia Communications and Photonics Conference*, Optical Society of America, 2014.

Conception of Radiofrequency-optical Fiber-scanning Modulation Spectroscopy

O. A. Ryabushkin[1, 2] **and D. V. Protasenya**[1, 2]

[1]Moscow Institute of Physics and Technology (State University)
Dolgoprydnyi, Moscow region 141700, Russia
[2]NTO "IRE-Polus", Russia

Abstract— There are various methods applied for investigation of semiconductors electrical and optical properties. Some of them are based on excitation of charge carriers and measurement of light reflection from semiconductor surface. Changes in optical properties of semiconductors occur due to spatial redistribution of hot electrons, so that reflection spectra in the vicinity of fundamental absorption edge change considerably. In photoreflectance method, optical pump with quanta energy higher than semiconductor bandgap is used for excitation [1]. In microwave modulation reflectance method conduction electrons are heated by external high frequency electric field [2].

Investigation method that we propose is based on microwave modulation reflectance method. The main idea suggests localization of exciting field and probe light within microscopic area and spatial scanning in millimeter region. For this purpose probe made of optical fiber with two metallic electrodes inside cladding is used (see Figs. 1(a), (b)). Optical fiber is tapered in order to decrease both mode field diameter and distance between electrodes. Modern technology enables to fabricate such fibers with mode field diameters of several micrometers [3]. External surface of fiber is covered with metal and grounded in order to increase strength of localized electric field.

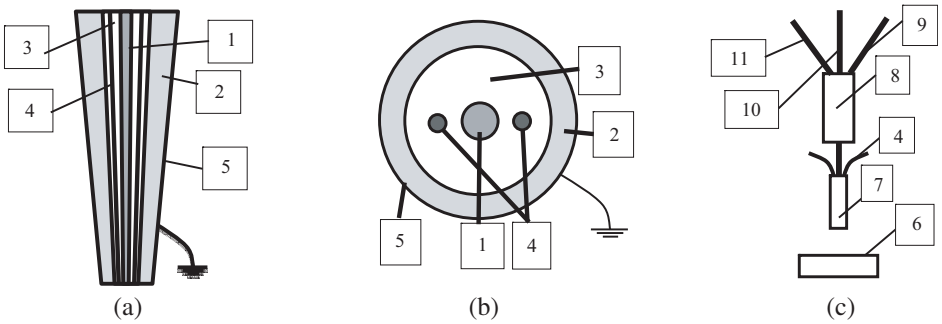

Figure 1: Structure of fiber with two electrodes inside cladding ((a) Side view and (b) cross section view) and scheme of the probe. Designations: 1-core, 2-outer cladding, 3-inner cladding, 4-electrodes, 5-metal cladding, 6-sample, 7-fiber structure, 8-3-to-1 optical coupler, 9-probe light channel, 10-reflected light channel, 11-pump light channel (optional).

Probe scheme is shown in Fig. 1(c). Probe is placed above the semiconductor structure and can be moved along the surface by positioning system. Radiofrequency field is created by application of alternating voltage to electrodes. 3-to-1 optical coupler is used for transmission of probe and reflected signals, it can also provide optical pumping of semiconductor. Reflected light is analyzed by spectrometer and its spectral changes are detected via lock-in detection at modulation frequency of radiofrequency electric field.

Calculations of radiofrequency electric field distribution and electrical capacity of the probe were performed. Capacity dependence on distance between probe tip and substrate surface can be measured experimentally.

Thus, principal possibility of conductive samples investigation by microstructured fiber with electrodes inside was demonstrated. Proposed combination of microscopy and radiofrequency-optical spectroscopy enables to study samples at a submicrometer level and to obtain useful information about field and current distributions.

REFERENCES

1. Cardona, M., "Modulation spectroscopy of semiconductors," *Advances in Solid State Physics*, Vol. 10, 125–173, 1970.

2. Ryabushkin, O. A. and V. A. Sablikov, "Radio-frequency modulation of the reflection of light in semiconductor heterostructures," *Journal of Experimental and Theoretical Physics Letters*, Vol. 67, No. 3, 233–238, 1998.
3. Myrén, N., "Poled fiber devices," Department of Physics and Quantum Optics, Royal Institute of Technology, Stockholm, 2005.

Radiofrequency Calorimetry of High-power Laser Radiation

O. A. Ryabushkin[1, 2] **and A. V. Konyashkin**[1, 2]

[1]NTO "IRE-Polus", 141190 Vvedensky Sq. 1, Fryazino Moscow Region, Russia
[2]Moscow Institute of Physics and Technology
141700, Institutskiy per. 9, Dolgoprudniy Moscow Region, Russia

Abstract— Output powers of modern CW laser sources, applied in laser industry for material processing, exceed 20 kW in single-mode and 100 kW in multimode regimes. Measurement of such high-power levels during laser operation is a great challenge. Most commercial CW high-power meters employ total conversion of laser radiation energy into heat and subsequent measurement of temperature distribution inside sensing element. This approach inevitably results in radiation beam quality impairment and does not allow online power control. Besides, it offers relatively low measurement precision especially for high laser powers.

We introduce novel principle for precise laser power measurement independent on beam quality. It is based on measurement of the definite small part (0.01–0.1%) of the overall radiation power transmitted through the piezoelectric resonator made of nonlinear-optical crystal. Absorbed part of laser power is determined by measuring calibrated piezoelectric resonance (PR) frequency shift. It is well known that PR can be observed in nonlinear-optical crystal response to the applied electric field when its frequency corresponds to one of the crystal internal vibration modes. PR frequencies Rf are highly sensitive to crystal temperature change. We demonstrated that thermodynamic temperature of the crystal heated by laser radiation can be replaced by its equivalent temperature that is directly determined by measuring temperature calibrated Rf shift with power [1]. Crystal heating depends on optical absorption $\alpha(\lambda)$ at the given wavelength λ and heat transfer coefficient h^T with ambient. It was demonstrated that both coefficients can be measured using equivalent temperature concept [2]. Block-scheme of experimental setup for laser power measurement is shown in Fig. 1. Cylindrical piezoelectric resonator made of low-absorption quartz crystal is placed inside electrical capacitor connected in series with radiofrequency (RF) generator and load resistor R_L, which is used for measurement of electrical current via lock-in detection.

In order to minimize capacitor heating induced by scattered radiation its electrodes are made of two sets of thin metallic wires. For optical power measuring it is necessary to know values of the PR frequency $Rf(T)$ at any crystal uniform temperature T. Calibration measurements of Rf dependence on T give linear function: $Rf(T) = Rf(0)+K^{\mathrm{prt}}T$. Dependence of Rf on laser power P is also linear: $Rf(P) = Rf(0) + K^{\mathrm{pro}}P$. Unknown power P_x is then directly obtained from measured frequency shift $\Delta Rf(P_x)$ and coefficient K^{pro} : $P_x = [Rf(P_x) - Rf(0)]/K^{\mathrm{pro}}$ using extrapolation of $Rf(P)$ power calibration. In measurement process the irrelevant frequency shift caused by the ambient temperature change is excluded using $Rf(T)$ temperature calibration.

Introduced technique allows direct measurement and control of high average laser powers in wide dynamic and spectral ranges independently on radiation beam quality because any suitable nonlinear-optical crystal with appropriate absorption properties can be used as piezoelectric resonator.

Figure 1: Block-scheme of experimental setup.

REFERENCES

1. Ryabushkin, O. A., et al., "Equivalent temperature of nonlinear-optical crystals interacting with laser radiation," *J. of European Optical Society — Rapid Publications*, Vol. 6, 11032, 2011.
2. Ryabushkin, O. A., et al., "Piezoelectric resonance calorimetry of nonlinear-optical crystals under laser irradiation," *Proc. of SPIE*, Vol. 8847, 88470Q, 2013.

Separating the Field Radiated by Two Rectilinear Sources

A. Natale, **M. A. Maisto**, **R. Solimene**, **G. Leone**, **and R. Pierri**
Dipartimento di Ingegneria Industriale e dell'Informazione, Seconda Universita' di Napoli
via Roma 29, Aversa 81031, Italy

Abstract— When dealing with electromagnetic field measurements for antenna diagnostics or even in inverse scattering problems one collects the radiated field (resp. the scattered field) over a domain and from such measurements the features of the antenna (resp. scatterer) under test have to be inferred.

It often happens that beside the field due to the structure under test (SUT), the fields produced by further sources (generally unwanted) are collected as well. This give rises to clutter signals from which the useful field signals (i.e., those one due to the SUT) must be singled out.

In this contribution we tackle a related problem for a canonical configuration. More in detail, two electric current sources are considered radiating in free-space. They are assumed to be supported over two parallel strips whose positions are a priori known. Their radiated fields are collected over a single domain located in far-zone (with respect the whole radiating system). Invariance is assumed along the direction orthogonal to the strips, which coincides with the currents' directions as well. Hence, a two-dimensional scalar framework is set.

The problem of concern is to distinguish between the two contributions. To this end, the problem is addressed by a two-step procedure. First, the currents are reconstructed by the radiated field measurements. This entails dealing with an inverse source problem that is tackled by comparing three different strategies of inversion. The first strategy consists in inverting the radiating operator, which rigorously describe the radiation by both the sources. In the second one, the radiated field data is inverted by considering each source as being radiating alone. Of course, in the latter case we have an approximate modeling but a less expensive computational procedure. Finally, the third method is a modification of the second one. Now, having reconstructed one of the two sources the corresponding radiated field is synthetically computed and subtracted from the data. Then the second source is reconstructed. The second step of the overall procedure then consists of computing the radiated field due to each source once they have been estimated according to the previous step.

Numerical examples are provided in order to compare the different strategies from the achievable performance and numerical complexity point of views.

REFERENCES

1. Solimene, R. and R. Pierri, "Number of degrees of freedom of the radiated field over multiple bounded domains," *Optics Letters*, Vol. 32, No. 21, 3113–3115, 2007.

A Bowtie Antenna Using a Broadband Microstrip to CPS Transition Balun

H. S. Ro and Y. S. Choi
Electronics and Telecommunications Research Institute, Korea

Abstract— A dipole patch antenna is widely used to obtain the performance of wideband and omnidirectional radiation pattern in wireless communication. Especially, a patch element of a bowtie shape offers good performances in the bandwidth and radiation pattern. By the way, this bowtie patch has to be fed by a suitable feeding network to satisfy the requirement.

A microstrip to coplanar stripline(CPS) transition balun has been used commonly used as feeding networks in this kind of antenna design. Various structures of microstrip to CPS transitions have been reported before. However, the previous structures have the difficulty in fabrication, or require large surface area for sufficient coupling.

In this paper, a bowtie antenna using a broadband microstrip to CPS transition balun is proposed. This antenna with a new transition structure has several advantages such as small size, wide bandwidth, and good impedance matching. In the balun of this antenna, the electric field distribution of the microstriop line as unbalanced transmission line is transformed to one of CPS as a balance one by using a via-hole and a tapered ground line on the bottom plane. In addition, the low impedance of the mircrostrip lines is gradually changed to the high impedance of the CPS. We had achieved an electrical contact between two different layers by only one via-hole in this transition.

The proposed antenna was optimally simulated for bandwidth from 2.2 GHz to 6 GHz. The antenna was fabricated on Teflon substrate with a dielectric constant of 3.5 and measured. The measured insertion loss is less than 10 dB from 2.1 GHz to 6.5 GHz. The measured gain is from −4.7 dBi to 2.4 dBi.

Both the measured and simulated results for return loss are in good agreement. The result of gain also shows a good performance.

Therefore, the proposed broadband antenna is very useful in various wireless application areas due to small size and simple structure.

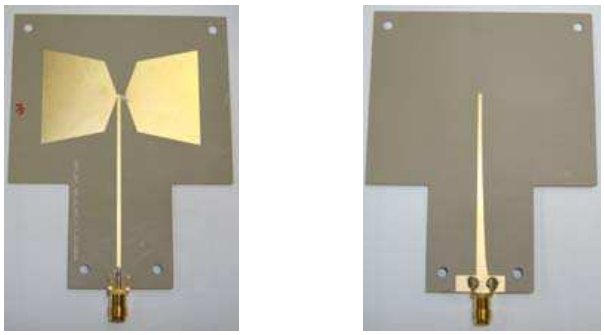

(a) (b)

Figure 1: Fabricated antenna with the proposed balun. (a) Top view. (b) Bottom view.

Two Elements MIMO Antenna for a WLAN System

Hui Liu[1, 2], **Cheng Liu**[2], **Binjie Wang**[2], **Qibin Deng**[2], **and Youhuan Guo**[1]

[1]Computer Science and Engineering Department, Guangdong Peizheng College, Guangzhou, China
[2]Centre for Optical and Electromagnetic Research, Academy of Advanced Optoelectronics
South China Normal University, Guangzhou, China

Abstract— Many printed elements of antenna for MIMO system have the same structure element in literature recently. Because of the asymmetric structure of MIMO system in the actual engineering application, the same structure elements may not be suitable for MIMO system. For example, the S_{11} and S_{22} will be different if the two elements have the same dimensions in a real MIMO system, hence the design of elements should be consisted of different structures to improve good performance of the MIMO antenna.

A MIMO antenna with two elements, operating on 2.45 GHz ISM band frequency, for a asymmetric structure WLAN system was designed in this paper. One of the antenna element's dimensions was changed to make both of the antenna elements meet the same 2.45 GHz band frequency. The printed inverted-F and meander line structures were used for the antenna element. The parameters of S_{11}, S_{22}, isolation and envelop correlation coefficient (ECC) are discussed. It is shown that good results can be achieved with different dimensions of antenna elements.

A Printed Inverted-F MIMO Antenna for WiFi Applications

Cheng Liu[1], **Hui Liu**[1], **Binjie Wang**[1], **Zhibin He**[1], **and Sailing He**[1, 2]

[1]Centre for Optical and Electromagnetic Research, Academy of Advanced Optoelectronics
South China Normal University, Guangzhou, China
[2]The Royal Institute of Technology, Stockholm, Sweden

Abstract— Some Antennas with printed Inverted-F structure have been proposed in literature recently few antennas were discussed the antenna test with mounted ICs in the practical engineering applications. Because the mounted ICs have affects, the size of simulated antenna may not directly be used in some WiFi Applications.

A printed MIMO antenna system designed with compact size is presented. The proposed MIMO antenna, consists two Inverted-F antenna elements, is designed on a two-layer FR-4 printed circuit board (PCB). The MIMO antenna provides adequate bandwidth coverage for WiFi (2.45 GHz). The antenna simulation and test with mounted ICs results are discussed and compared. The MIMO antenna with and without mounted ICs show that working frequency is shifting. Therefore the sizes of simulation antenna should be changed to decrease the shifting frequency.

Design and Analysis of a Phased-MIMIO Array Antenna with Frequency Diversity

Nour El-Din Ismail, **Sherif Hanafy Mahmoud**, **Ahmed Hamed, and Alaa Hafez**
Faculty of Engineering, Alexandria University, Alexandria, Egypt

Abstract— Phased-Multiple-Input Multiple-Output (phased-MIMO) radar has been thoroughly investigated in the literature. This approach divides the transmit antenna array into multiple subarrays that are allowed to overlap. Each subarray coherently transmits a distinct waveform, which is orthogonal to the waveforms transmitted by other subarrays. While phased array radar enjoys the advantage of high coherence gain with no diversity gain, MIMO radar enjoys high diversity gain — whether waveform or spatial diversity gain — with no coherence gain. Phased-MIMO radar enjoys both advantages of coherence gain and diversity gain which enhance the main-to-side lobe levels but unfortunately decrease the antenna directivity.

Frequency diversity can improve antenna directivity by applying a small frequency increment between two successive elements but consequently increases average side lobes level. In this paper, we propose a new Phased-MIMO radar with frequency diversity which offers a tradeoff between main-to-side lobe levels and antenna directivity. This technique can exploit frequency diversity which is applied between subarray adjacent elements and between adjacent subarrays. The total beam pattern is an optimum case of the lowest side lobes level as phased-MIMO radar but with higher directivity.

A Simple Monopole Slot Antenna with High Band-notch Characteristics for Ultra-wideband Communication Applications

Yingsong Li[1], **Zhuqun Zhai**[2], **Wenxing Li**[1], **and Si Li**[1]

[1]College of Information and Communications Engineering
Harbin Engineering University, Harbin 150001, China
[2]Institute of Systems, Beijing 100161, China

Abstract— In this paper, a simple ultra-wideband antenna with flexible and tunable band-notch characteristics is proposed on the basis of a polygon slot structure. The notch band is realized by the use of an inverted V-shaped stub inserted into inside of the polygon slot. The flexible and tunable band-notch characteristics are achieved by adjusting the dimensions of the inverted V-shaped stub. The experimental results show that the proposed antenna can provide a wide bandwidth, a flexible and tunable band-notch characteristic and good omnidirectional radiation patterns, making it suitable for various UWB communication applications.

Dual-band Microstrip Antenna with Defected Ground Structure for WLAN Application

Wen-Chung Liu, **Ya-Yun Shih**, **and Chao-Ming Wu**
Department of Aeronautical Engineering
National Formosa University, Yunlin 632, Taiwan

Abstract— In recent years, more and more attention is paid in antenna design with multi-band operation for modern wireless communication systems. Therefore, in this paper, we present a novel compact printed antenna with dual strips and a defected ground structure (DGS), as shown in Figure 1, for dual-band operation. By folding and loading the twin strips, and defecting the ground plane of the antenna, multi-mode resonance with dual broad bandwidths can be excited. To verify the simulation results obtained from the CST electromagnetic simulator, the prototype of the proposed antenna was constructed and experimentally investigated. As shown in Figure 2, the measured bandwidths are 500 MHz (2.28–2.78 GHz) and 1.37 GHz (5.14–6.35 GHz) for the lower and upper bands, respectively, which agree well with the simulation. The experimentally obtained average gains across the two operating bands are 1.5 and 2 dBi, respectively, with typical monopole-like radiation patterns. The proposed antenna with a compact size of only $25 \times 25\,\text{mm}^2$ sufficiently covers performance requirement of the 2.4/5.2/5.8 GHz WLAN operation system. The proposed antenna with properties of simple and planar structure, dual and wide bandwidth, and easy fabrication can be effectively used in the upcoming generation of wireless communication systems.

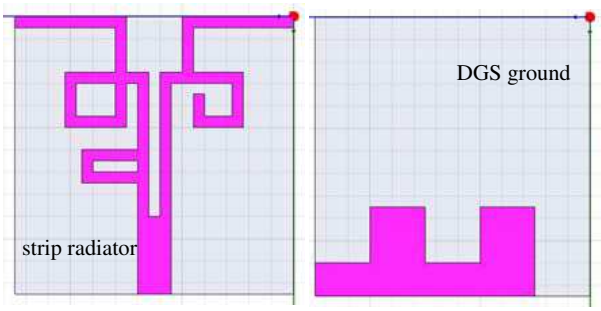

Figure 1: Configuration of proposed dual-band planar strip antenna for WLAN operation.

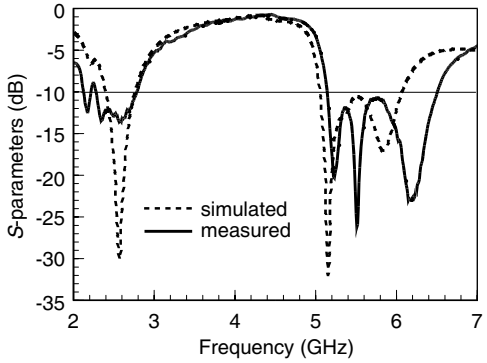

Figure 2: Measured S values for the proposed dual-band planar strip antenna.

ACKNOWLEDGMENT

This work was supported by the Ministry of Science and Technology, Taiwan, under Grant MOST 103-2221-E-150-045.

Implementation of an Inverted-F Antenna with Improved Bandwidth

Jong-In Ryu, **Dongsu Kim**, **Jun Chul Kim**, **and Jong Chul Park**
Package Research Center, Korea Electronics Technology Institute, South Korea

Abstract— In this paper, an InvertedF Antenna (IFA) with improved bandwidth is designed and implemented in printed-circuit-board (PCB). Design objective is to apply an IFA with improved bandwidth in a Wi-Fi module. A normal IFA and a proposed IFA are designed and implemented. The performance is measured and compared.

A normal IFA and a proposed antenna are designed in 4 layers PCB [1]. The dielectric constant and loss of PCB are 4 and 0.03. A normal IFA is composed of short pin (L_{m1}, L_{m2}) and main radiation part (L_r). A proposed antenna has a sector shape with radius (L_r) as shown in Fig. 1. The proposed antenna is optimized through a simulation for verifying the difference in performance according to changes in the factors such as total length ($L_{m2} + L_r$) of antenna, width (W), and L_{m1}. As results, L_{m1}, L_{m2}, L_r and W, are 4.6 mm, 3.8 mm, 12.3 mm, and 1 mm. The size of the antenna is designed 48 mm × 12 mm × 1.4 mm.

In order to measure and compare the performance of a normal IFA and a proposed IFA, two kinds of antennas are implemented in PCB as shown in Fig. 2. The total size of implemented PCB in each antenna is 48 mm × 35 mm × 1.4 mm.

As can be seen from the measurement results of two kinds of picture antenna as depicted in Fig. 3, resonant frequency simulation both with about 150 MHz degree difference can be seen.

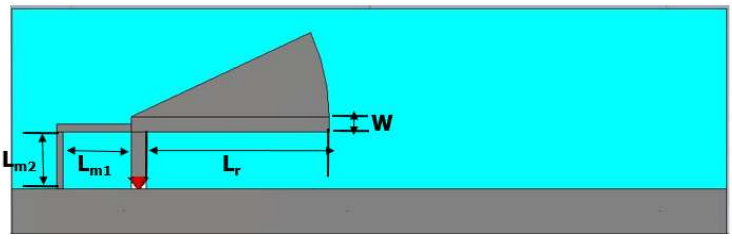

Figure 1: A proposed inverted-F antenna.

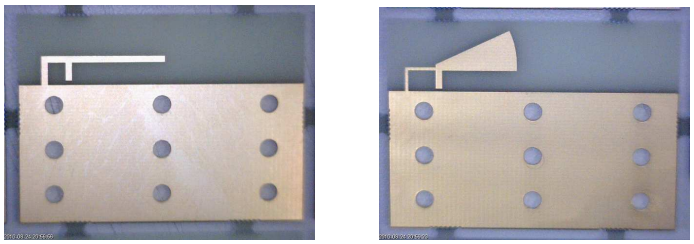

Figure 2: The implemented antennas for (a) a normal IFA and (b) a proposed IFA.

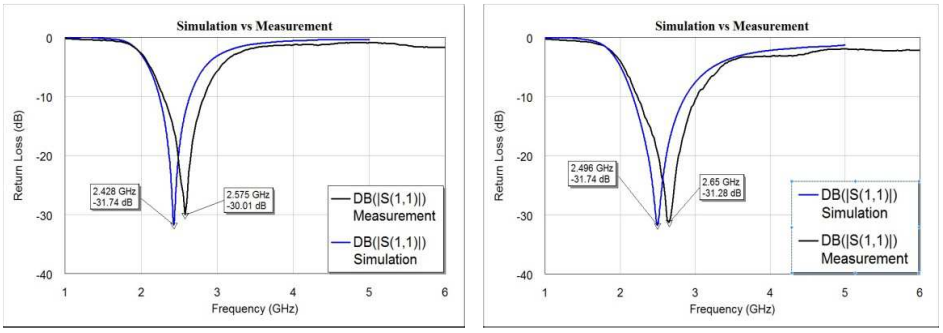

Figure 3: Simulation and Measurement for (a) a normal IFA and (b) a proposed IFA.

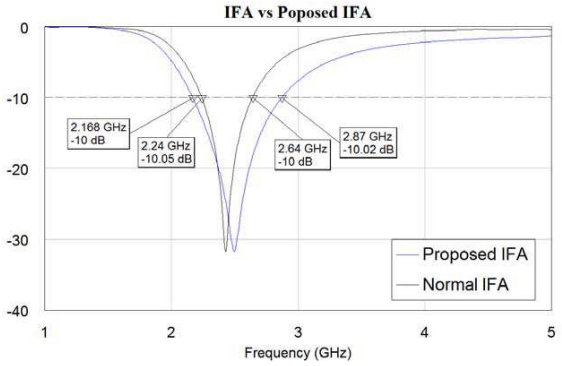

Figure 4: The compared results for antennas.

However, measured 30 dB return loss of resonant frequency and measured bandwidth did not differ significantly from the simulation results. And 10 dB bandwidth of the normal antenna and a proposed antenna is almost 400 MHz and 700 MHz as shown in Fig. 4. The proposed antenna has the increased bandwidth of almost 300 MHz. As a result, the resonant frequency was slightly different between simulation and measurement in each antenna, but results has good agreement with simulation for two antennas.

In this paper, a proposed IFA that improves bandwidth by modifying the shape of the IFA was designed and implemented. To obtain compared data, a normal IFA and proposed antenna were designed and measured. The bandwidth of almost 300 MHz was improved and total bandwidth was 700 MHz.

REFERENCES

1. Pazin, L., N. Telzhensky, and Y. Leviatan, "Wideband flat-plate inverted-F laptop antenna for Wi-Fi/WiMAX operation," *IET Microwaves, Antennas & Propagation*, Received on January 20, 2008, Revised on March 6, 2008.

Isolation Improvement for Two Planar Dual-band Antenna Elements Placed Perpendicularly

Yu-Feng Shih and Ching-Lieh Li
Department of Electrical Engineering, Tamkang University, Tamsui, New Taipei City, 25137, Taiwan

Abstract— This paper investigated the MIMO dual-band antenna design for the isolation improvement with two planar antenna elements perpendicularly placed in a small device. The MIMO antenna consists of two antenna elements, of which each element consists of two antenna components: One is a narrow slit antenna, which is responsible for the radiation at low band (2.4 GHz), the other is a dipole antenna, which serves as the load of the previous narrow slit antenna and is responsible for the high-band (5 $\sim$ 6 GHz). These two antenna elements are perpendicularly placed in order to achieve the polarization diversity for the high band, such that the coupling between the antenna elements can be reduced. On the other hand, additional slot cut on the common ground plane is introduced to further enhance the isolation for the low band.

Simulated results show that the isolation for the low band and high band is about -30 dB, and -27 dB, respectively, while experimental results of the prototype show that the isolation for the low band and high band is about -22 dB, and -27 dB. As comparison, a MIMO dual-band antenna design is simulated with the same planar antenna elements parallel placed and without the slot cut on the common ground plane; and the simulated results show that the isolation for the low band and high band is about -6.31 dB ~ -9.03 dB, and -16.09 dB ~ -22 dB, respectively (with the separation varying from 20 mm $\sim$ 100 mm).

It is thus confirmed that the combined techniques can effectively inhibit the coupling to avoid mutual coupling of the MIMO dual-band antenna elements. This design techniques can keep the required FR4 board size small, and don't need additional lumped components. In general, the antenna design is able to meet the demands $|S_{11}| < -10$ dB and $|S_{12}| < -20$ dB for S parameters, and its scope of application covers IEEE (802.11a/b/g/n/ac) WLAN bands.

Design of a Compact Planar Spiral Antenna for Sensor Network

Ju-Derk Park and Byeong-Cheol Choi
IoT Convergence Technology Research Department
Electronics and Telecommunications Research Institute, 218 Gajeong-ro, Daejeon, Republic of Korea

Abstract— With the development of wireless sensor network systems and application devices, needs for various types of antennas are increasing. A compact planar spiral antenna composed with monopole is designed for sensor network, operating in the center frequency 420 MHz, is introduced in this paper. Doubled side spiral lines on the circular PCB (FR-4, lossy materials) are connected with via-hole electrically and central monopole element is driven by RF signal source. Length of the antenna is 45 mm, radius of the PCB is 15 mm. This size of the antenna is enough small to mount on sensor network devices. The variable parameters for simulation (radius variation of the spiral line, spiral line width, number of turns of spirals, position of via hall, so on) are chosen to correct center frequency, bandwidth, beam width (vertical radiation angle) and antenna gain. As the simulation results, the antenna is fabricated with case and then, tested. Test result shows that elevation beam width is about 90°, frequency band width is about 65 MHz (387 MHz–452 MHz), gain is about 1.7 dBi. This performances, especially wide beam width and wide frequency band width compared to characteristics of conventional monopole antenna, support several benefits for sensor network system operating in harsh environments such as landslide monitoring region.

(a) (b)

Figure 1: Fabricated antenna. (a) Parts of the antenna. (b) Shape of assembled antenna.

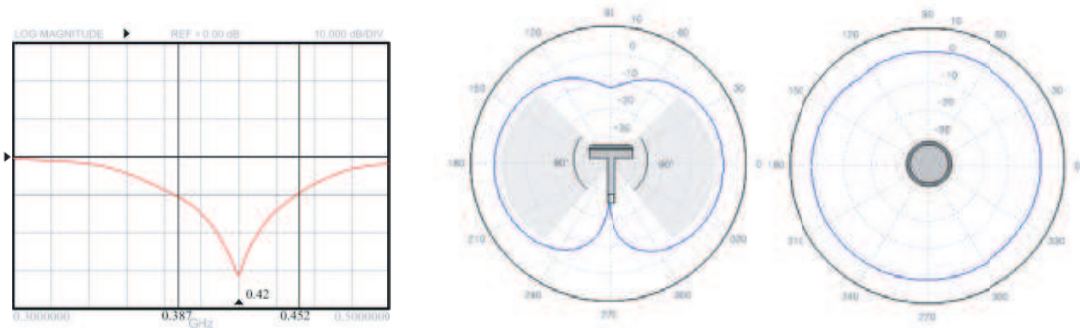

(a) (b)

Figure 2: Test results. (a) Reflection coefficient (S_{11}). (b) Radiation patterns.

ACKNOWLEDGMENT

This study was supported by the Basic Research Project (Technology development of landslide rapid detection based on a real-time monitoring, 15-3413) of the Korea Institute of Geoscience and Mineral Resources (KIGAM) funded by the Ministry of Knowledge Economy of Korea.

REFERENCES

1. Chiu, C.-N. and W.-H. Chuang, "A novel dual-band spiral antenna for a satellite and terrestrial communication system," *IEEE Antennas and Wireless Propagation Letters*, Vol. 8, 624–626, 2009.

2. Barton, R. J., P. J. Collins, P. E. Crittenden, M. J. Havrilla, and A. J. Terzuoli, "Analytical development of the far-zone radiation integral for an arbitrary planar spiral antenna," *IEEE Antennas and Wireless Propagation Letters*, Vol. 52, 19–30, 2010.

Design of Wideband Multi-way Power Divider with the Modified Impedance Transformer

C. W. Tang and W. M. Chuang
Center for Telecommunication Research, Advanced Institute of Manufacturing with High-Tech Innovations
Department of Cmmunications Engineering, National Chung Cheng University, Taiwan

Abstract— In current wireless communication, the need for wide bandwidth is growing rapidly. Moreover, the compact size, low-power consumption, and low noise are also essential for the design of receivers and transmitters in a microwave communication system. Power dividers are important components in microwave applications. In addition, the multi-way power divider is a key component for phase-array antennas, power amplifiers, and multi-port circuits. Wilkinson power dividers are generally adopted for two-way power division. Consequently, the multi-way power divider can be realized by interconnecting two-way Wilkinson power dividers. The general method of designing the multi-way power divider is utilizing the binominal response on the multi-stage transmission lines. However, the available bandwidth of the multi-way power divider remains limited. A calculated method of designing the multi-way power divider with the interconnection between two-way power dividers had been published. Unfortunately, the interconnection between two-way power dividers may restrict the optimal design.

In this paper, the novel planar wideband power divider with compact size has been proposed. In order to obtain a wideband multi-way power divider, the corrected coefficients K_n are adopted for the modified impedance transformer. With the assistance the modified impedance transformer, the design of power dividers with required input reflection level can be simplified. Moreover, the even- and odd-mode analyses are provided to obtain the optimal isolation resistor values. Furthermore, a prototype of the wideband four-way power divider is designed, fabricated, and measured. With the proposed structure, performance of return loss at input port can be predicated in advance. Well-matched results of simulation and measurement validate the proposed approach.

Design for Ultra Wideband Filter Using Open- and Short-ended Stepped Impedance Resonators and Coupled Lines by Genetic Algorithm

M. Setsu, **G. Ichihara**, **Y. Tomizuka**, **T. Ohno**, **K. Tanii**, **and M. Uehara**
National Institute of Technology, Kisarazu College, Japan

Abstract— This paper describes a design for ultra wideband (UWB) filter by genetic algorithm (GA). The circuit structure consists of open- and short-ended stepped impedance resonators (SIRs) and coupled lines. The transmission characteristic of the UWB filter is simulated and measured.

Figure 1 shows a schematic circuit of a UWB filter using open- and short-ended SIRs and coupled lines. As shown in Fig. 1, l and Z are length and characteristic impedance of a transmission line and a SIR, and l_c, w and s are length, width and gap of a coupled line. Fig. 2 shows the simulated transmission characteristic of the UWB filter designed by GA. As shown in Fig. 2, the UWB filter obtains the bandwidth from 3.13 to 10.58 GHz, and almost fulfills the FCC (Federal Communications Commission) indoor limit in both low and high frequency. The pass band is obtained by the attenuation poles generated at 2.64 and 10.70 GHz by the open-ended SIR. The characteristics in both low and high frequency are attenuated by the short-ended SIRs. Therefore, the above result shows that using both open- and short-ended SIRs is effective for designing UWB filter.

Figure 3 shows a photograph of the fabricated UWB filter. Fig. 4 shows the measured transmission characteristic of the UWB filter. As shown in Fig. 4, the UWB filter obtains the bandwidth

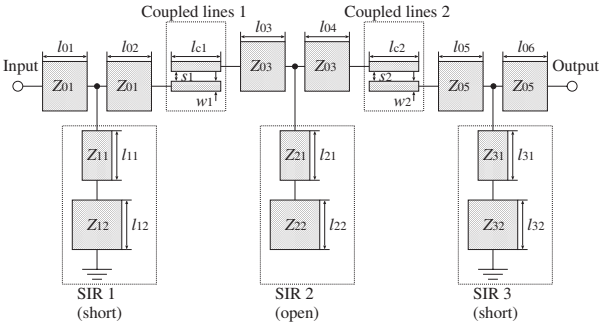

Figure 1: Schematic circuit of UWB filter using open- and short-ended SIRs and coupled lines.

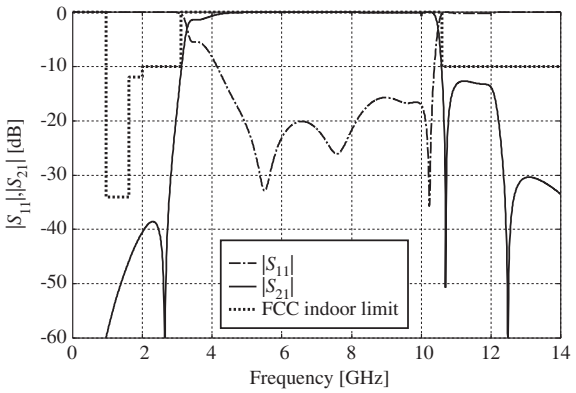

Figure 2: Simulated results of UWB filter shown in Fig. 1.

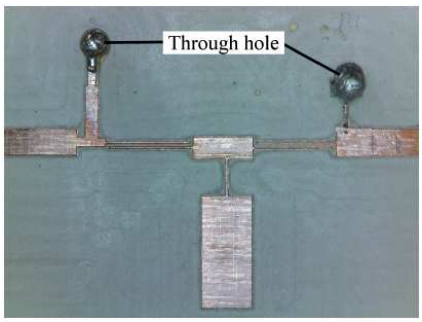

Figure 3: Photograph of UWB filter using open- and short-ended SIRs and coupled lines.

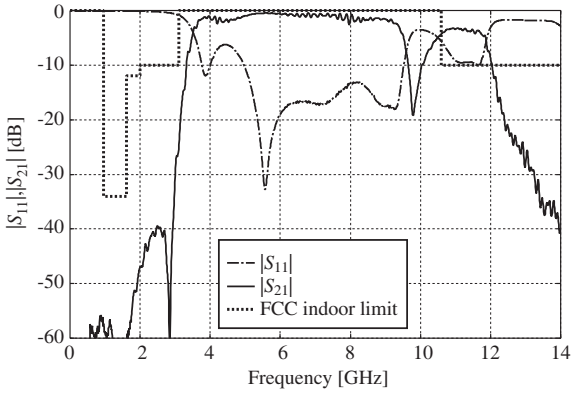

Figure 4: Measured results of UWB filter shown in Fig. 3.

from 3.33 to 9.65 GHz, and the result indicates similar transmission characteristic with the simulated result in Fig. 2. However, the characteristic in high frequency is not attenuated than the simulated result. It is assumed that electrical length of the through holes cause the narrower bandwidth and insufficient attenuation near 11 GHz. Therefore, a better transmission characteristic will be obtained by adding electrical length of through holes to GA calculation.

Novel Module Including a Waveguide for 40 GHz High-gain Amplifier Applications

Young Chul Lee[1], **Amran Bin Hj Naemat**[2], **and Zulkifli Bin Ambak**[2]

[1]Department of Electronics Engineering, Mokpo National Maritime University (MMU), Korea
[2]Telecom Malaysia Research & Development (TMR&D), Malaysia

Abstract— In this work, a 40 dB high-gain amplifier module has been presented for millimeter wave applications. Two amplifiers are integrated into the single module case by inserting a WR22 waveguide between them in the module case, in order to suppress oscillation. The high-gain amplifier module consists of two amplifiers and four WR22-to-microstrip line transitions which were fabricated on 5 mil thick RT5880 substrate. The transition loss of −0.44 dB per a transition was achieved from 35 to 50 GHz. The module showed the higher gain than 39.7 dB from 38 to 41 GHz. At 38.7 GHz, the maximum gain of 44.25 dB was obtained.

A Wideband Microstrip Line-to-waveguide Transition on LCP for 70 and 80 GHz-band Applications

Young Chul Lee
Department of Electronics Engineering, Mokpo National Maritime University (MMU), Korea

Abstract— In this work, a broadband microstrip line (MSL)-to-waveguide transition has been presented for E-band module applications. For improvement of a bandwidth, the extended GND and triple patches around the MSL probe are utilized on the low-loss liquid crystal polymer (LCP) substrate. Considering the loss contribution of the cable adapter and waveguide transition, the proposed transition loss can be analyzed as −1.45 and −1.59 dB per a transition at 70 and 80 GHz, respectively. The bandwidth of the proposed transition for reflection at −10 dB is 26 GHz at all test frequencies from 67 to 95 GHz.

Coaxial-line Structured SMT Pad for LTCC SiP Applications

Young Chul Lee
Department of Electronics Engineering
Mokpo National Maritime University (MMU), Korea

Abstract— In this work, a surface-mount type (SMT) pad using a coaxial-line structure is presented for low temperature co-fired ceramic (LTCC) SiP (system-in-package) applications. The vertical via transition is devised in type of the coaxial line. An overlap part between its outer conductor and a transmission line on the main board is cut off in order to eliminate their interaction. A cap on the top layer of the vertical via transition is designed in order to reduce radiation due to discontinuity. The designed SMT pad was fabricated using the standard LTCC process. The measured S_{11} and S_{21} are -14 and 0.9 dB, respectively at 15 GHz.

Reduction of Uncertainties of Resonant Properties for Permittivity Measurements by Considering Incompleteness of TRL Calibration Kit

Y. Kato and M. Horibe
National Institute of Advanced Industrial Science and Technology, Japan

Abstract— We have developed a new algorithm of the Monte Carlo calculations for the uncertainty evaluation of resonant properties, which directly relates to the incompleteness of the calibration standard used on a vector network analyzer (VNA). Resonant properties are derived from the resonant trace of S_{21} measured at discrete frequency points. In the previous study, the uncertainty propagations of S_{21} to the uncertainties of resonant properties are considered by using the Monte-Carlo method in which S_{21} at each frequency point is randomized independently. However, S_{21} at different frequency points have correlations with each other, because we measure S_{21} at all frequency points after performing a calibration on a VNA by using the same calibration kits. In this study, this correlation is rigorously taken into account by evaluating the S_{21} uncertainty from the incompleteness of calibration standards. Because the resonant properties are derived from the frequency dependence of S_{21}, this correlation is essential for the determination of resonant properties. Correlations between amplitudes and phases of S_{21} are also taken into account by performing the uncertainty analysis of S_{21} without resolving its amplitude from its phase. By considering these two correlations, the developed algorithm is expected to provide more rigorous analysis and reduce uncertainties of resonant properties compared to the conventional algorithm.

For the case when the through-reflect-line (TRL) calibration is used on a VNA, we confirmed that the uncertainties of resonant properties resulted from the propagation of S_{21} uncertainties were significantly reduced, and became negligibly small by using the developed algorithm. By applying this algorithm to permittivity measurements using resonant methods, the uncertainty of the permittivity can be reduced, and evaluated in a more rigorous manner.

Plasma Density Measurement Using Mutual Impedance Technique on the Jupiter Mission JUICE: The MIME Instrument

J. L. Rauch, P. Henri, J. P. Lebretoun, O. Le Duff, F. Colin, and D. Lagoutte
LPC2E, 3A av. de la Recherche Scientifique, 45071 Orléans Cedex 2, France

Abstract— Mutual Impedance Measurements, MIME, instrument is a part of the Radio Wave Plasma Investigation, RPWI, consortium which has been selected by European Space Agency, ESA, on the nest planetary mission JUICE. JUpiter ICy moons Exploer aims to launch in 2022 to explore Jupiter and its potentially habitable icy moons and study its plasma environment.

Impedance probes, which are well known in geophysical prospection, in particular for ground permittivity investigations, have been successfully transposed to space plasmas. Transmitting and receiving electrodes are used for measuring on open circuit the dynamic impedance of the system at several fixed frequencies over a range that includes characteristic frequencies of the ambient plasma. The measurements are then interpreted using a suitable theory and the values of plasma parameters, such as the electron density, temperature, and possibly the relative velocity of the plasma and the spacecraft, can be deduced. To show how powerful this technique is, results obtained in the Earth's plasmasphere by the mutual impedance probe onboard ROSETTA are presented as example. The MIME Mutual Impedance Measurements proposal is then described and its ability to make valuable measurements in the Jupiter space environment, and in particular round Callisto and Ganymede is investigated.

InISAR Imaging of Dechirp Data under Squint Model

Biao Tian, Gang Li, Shiyou Xu, and Zengping Chen
Science and Technology on Automatic Target Recognition Laboratory
National University of Defense Technology, Changsha, China

Abstract— The interferometric ISAR (InISAR) technology has been proposed to enhance the probability of target identification. Through interferometric processing of each scattering point in two ISAR images, the corresponding coordinate of them on the target can be obtained. In previous InISAR research papers, targets are usually assumed to closely locate at the axis of antenna for convenience. In real situation, however, targets are usually far away from it. They are called as "normal mode" and "squint mode", respectively.

Aiming at InISAR imaging of dechirp data under squint model, this paper proposes a new 3D InISAR imaging algorithm based on joint squint iteration optimization and image distortion correction. The influence of squint model mainly includes two aspects, namely accessional phase and image distortion. The 3D imaging results degrade seriously as the squint angle increases. Then, through squint iteration optimization, the accessional phase can be compensated. While the image distortion can be corrected by the coordinate transform. In this way, the 3D reconstruction performance and imaging quality are improved. Simulation results demonstrate that the algorithm is effective under squint model, achieving high quality 3D InISAR images consequently.

The steps of squint iteration optimization and distortion correction can be summarized as follows:

1) Calculate the interferometric phase of antenna A and B, achieving $\Delta\varphi_{AB}$ and $\Delta\varphi_{AC}$.
2) Obtain the initial coordinate of scattering point P, where x_P and y_P are from $\Delta\varphi_{AB}$ and $\Delta\varphi_{AC}$, while z_p is from scaling of ISAR image.
3) Get the distance values of each scattering point to each antenna.
4) Update the coordinates x_P and y_P using the iteration equations.
5) Update the coordinate z_P using coordinate transform equation.
6) Repeat steps 3–5 until the convergence condition is achieved.

Using the method, all the 3D spatial coordinates of each scattering point on the target are obtained, and the high precision 3D InISAR image is obtained. According to the analysis, the proposed imaging algorithm is shown in the following figure.

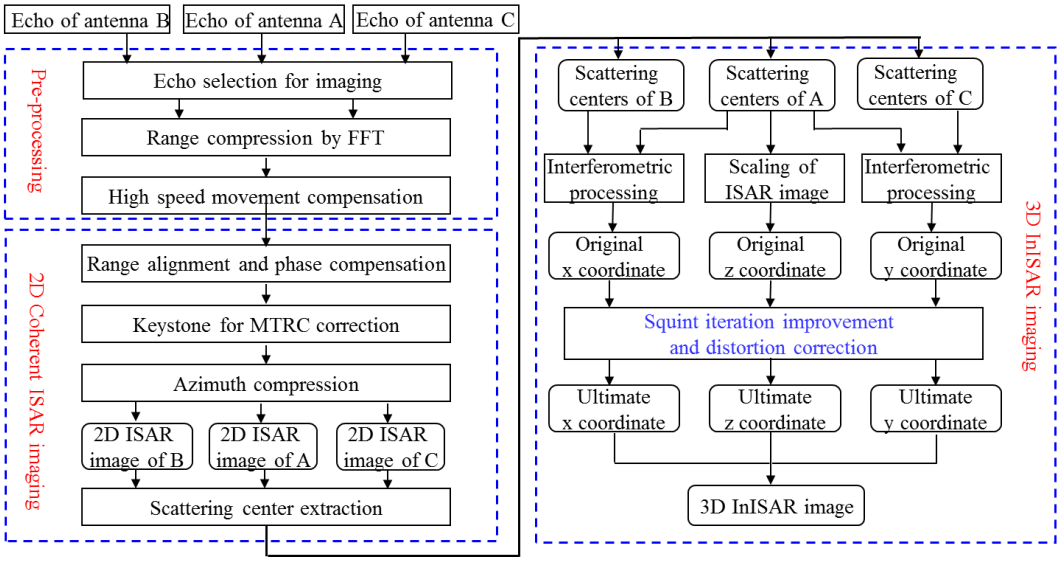

Figure 1: Block scheme of 3D InISAR imaging system.

Moving Radar Target Detection Using an Improved OFDM Chirp Waveform Scheme

Jiahua Zhu, **Pengzheng Lei**, **Chongyi Fan**, **Xiaotao Huang**, **and Zhimin Zhou**
College of Electronic Science and Engineering
National University of Defense Technology, Changsha, Hunan 410073, China

Abstract— Waveform diversity for moving target detection is always a challenging problem in radar field. Recently, a waveform design scheme — the orthogonal frequency division multiplexing (OFDM) chirp waveform, which combines the OFDM principle with the linear frequency modulation (LFM) waveform, was proposed with almost constant modulus, large time-bandwidth and good performance on correlation. However, the previous researches mainly discuss the processing techniques of multiple-input multiple-output (MIMO) synthetic aperture radar (SAR) systems with limited number of orthogonal subcarriers. Few achievement about target detection based on OFDM chirp waveform was published before. In this paper, the OFDM chirp waveform generation model is extended to arbitrary numbers of orthogonal signals in theory. Moreover, the OFDM chirp waveform is proved to have good target detection performance, which is better than the traditional OFDM and chirp waveforms.

First use an LFM signal spectrum as the input of each OFDM modulator, which could be given as

$$S[\bar{p}] = \mathcal{F}\{s[n]\} = \mathcal{F}\left\{\exp\left[j\pi k\left(nT_s\right)^2\right]\right\} \tag{1}$$

where $s[n]$ is the N-point discrete time samples of a complex LFM signal, k denotes the chirp rate, T_s means the sampling interval and $\mathcal{F}\{\cdot\}$ is the Fourier transform operator. Then, we can generate M input data sequence with zeros interleaved as follows using $S[\bar{p}]$.

$$\mathbf{S}_1[p] = [S[0], 0, 0, \ldots, 0, 0, S[1], 0, 0, \ldots, 0, 0, \ldots, S[N-1], 0, 0, \ldots, 0, 0] \tag{2}$$

$$\mathbf{S}_2[p] = [0, S[0], 0, 0, \ldots, 0, 0, S[1], 0, 0, \ldots, 0, \ldots, 0, S[N-1], 0, 0, \ldots, 0] \tag{3}$$

$$\ldots$$

$$\mathbf{S}_M[p] = [0, 0, \ldots, 0, 0, S[0], 0, 0, \ldots, 0, 0, S[1], \ldots, 0, 0, \ldots, 0, 0, S[N-1]] \tag{4}$$

where $p = 0, 1, \ldots, MN-1$.

Next, based on the binary hypothesis problem, we use two detectors: (1) MFD, which is the optimal detector when no clutter is presented in the scene; (2) ED, which is the generalized likelihood ratio test (GLRT) for conventional detection to analyze the detection performance under the ideal scenario with only target and noise. The simulation results prove that the OFDM chirp waveform performs better than the traditional OFDM and LFM waveforms on moving target detection, and the MFD shows a significant performance gain over the ED when clutter is not exist.

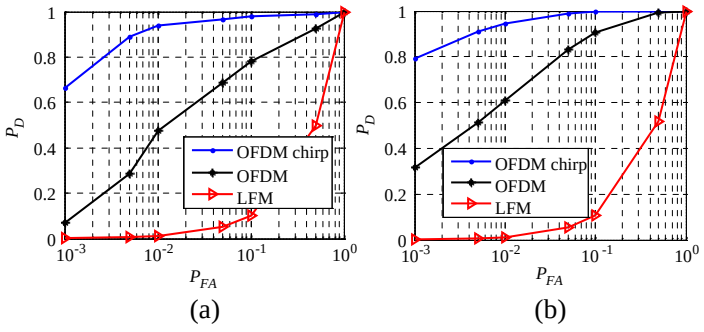

Figure 1: ROC curves of the OFDM chirp, OFDM and LFM waveforms using (a) ED; (b) MFD.

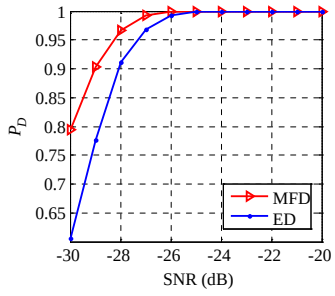

Figure 2: Detection probability versus SNR for the OFDM chirp waveform using two detectors.

Methods and Experiments for the Sensing and Evaluation of Ionosphere Changes and Their Impact on the Human Organism

M. Hanzelka[1], **J. Dan**[2], **P. Fiala**[1], **M. Friedl**[1], **and Vladan Holcner**[3]

[1]Department of Theoretical and Experimental Electrical Engineering
Brno University of Technology, Technická 3082/12, Brno 616 00, Czech Republic
[2]Rector's Office, Personnel Management Office
Masaryk University, Žerotínovo nám. 9, Brno 601 77, Czech Republic
[3]Faculty of Economics and Management
University of Defence, Kounicova 65, Brno 662 10, Czech Republic

Abstract— The impact of the environment upon living organisms constitutes a crucial problem examined by today's science. In this context, research institutes worldwide have analysed diverse positive and negative factors affecting the biological system of the human body. One such factor consists in the influence of the surrounding electromagnetic field. This paper presents the results of an investigation focused on ionosphere parameter changes and their impact on the basic function of the nervous system. It is a well-known fact that the frequency of the alpha waves of brain activity [1] ranges within 6–8 Hz. Changes in the electromagnetic and chemical structure of the Earth's surface may cause variation of signals in the above-defined frequency region of 6–8 Hz. Detailed examination of the overall impact of environmental factors upon the human organism is performed within a large number of medical disciplines. The research presented in this paper is concentrated on the sensing and detection of changes in the region of very low frequencies of the electromagnetic field; the authors use both theoretical and experimental procedures to define the effects that influence brain activity. It was tested in laboratory on a homogenous groups of people.

REFERENCES

1. Ferris, J., "The brain generates an electric field that influences its own activity," *Scientific American Mind*, Vol. 21, 10, 2010. Published Online: October 28, 2010, Doi: 10.1038/scientificamericanmind1110-10a
2. Tuchly, M. S., 2000.

The Parameters of a Special High Voltage Function Generator

P. Marcon, **P. Fiala**, **M. Steinbauer**, **and P. Drexler**
Department of Theoretical and Experimental Electrical Engineering
Brno University of Technology, Technicka 12, Brno 616 00, Czech Republic

Abstract— The paper describes design, realize and test of a special high voltage function generator. This generator was designed for special use. A purpose of the generator is to generate a variable electrical field. In course of design of the generator the properties of the output electrode voltage was the key element.

The high voltage function generator is designed as a switched flyback high voltage source. Voltage of the output electrode of the realized generator is possible to regulate in range 0 kV to 20 kV. Shape of the output voltage is possible to choose as sine, square or ramp. Frequency capabilities of this voltage source start on 0 Hz and reach 300 Hz. Frequencies close to 300 Hz are affected by the parasitic capacitance. For special use, the high output impedance was required. Generator use PWM modulated signal from control unit for regulating primary coil current of the high voltage transformer.

This article discusses the parameters of special high voltage function generator and also presents special application of this generator.

Measurement of Tissue Cultures of Early Somatic Embryos of Norway spruce

E. Vlachova Hutova[1], **R. Korinek**[2], **K. Bartusek**[2], **L. Havel**[1], **and P. Drexler**[1]

[1]Department of Theoretical and Experimental Electrical Engineering
Faculty of Electrical Engineering and Comunication, Brno University of Technology
Technicka 12, Brno 616 00, Czech Republic
[2]ASCR, Institute of Scientific Instruments, Kralovopolska 147, Brno 612 64, Czech Republic

Abstract— The objective of this study was to determine the effects of static magnetic fields to growth of plant tissue cultures (callus). Following the previously performed and described experiments that failed to clearly confirm nor deny the positive effect of static magnetic fields on the development and changes in growth of ESEs (early somatic embryos). The experiment was performed using of the static magnetic field, which is formed by the action of 4.7 T MR.

In this experiment we used a Petri dishes with a diameter of 60 mm, into which was inserted always one cluster ESEs of Norway spruce. The dishes were divided into two groups, and after the initial determination of the size ESEs were successively exposed to the influence of the stationary magnetic field with predefined parameters. The experiment time was set at an interval of three days and the duration of the experiment at 14 days. At this time, was given a Petri dish with ESE exposed always to the same kind of configuration stationary magnetic field. The growth of the ESEs was regularly documented, evaluation was carried out using MATLAB programs. To evaluate changes of the parameters inside the tissue was used Marevisi program, in which were analyzed changes in the examined tissue and other parameters.

This article evaluates the used parameters and sequences and their effect on the growth and development of the ESEs and the possibility of further use of MRI for this type of experiments.

Comparison Study of Layered Homogeneous Models with Detailed Human Tissue Models for Through-body Communications

Muhammad Ali Babar Abbasi, **Dimitris Philippou**, **and Symeon Nikolaou**
Department of Electrical Engineering, Frederick University, Nicosia, Cyprus

Abstract— Any wireless communication between an implanted antenna and an external, on-body antenna suffers from significant link degradation due to the lossy nature of the human body. Before an implantable system is proposed, it is usually thoroughly simulated, using numerical methods in order to study the electromagnetic propagation loss inside human body. A number of 3D models, deduced from MRI scans of living subjects, depicting indirectly measured electrical properties of human tissues, are widely used, for case to case based, implantable device design problems. These models generally have frequency dependent electric properties, and they are similar in shape to realistic human body parts and thus geometrically complex. Alternatively another simpler approach is widely used, where dense material blocks or homogeneous layers with constant electric properties similar to those of predominant human tissues are built and used in EM simulations for implantable devices problems. These mainly homogeneous blocks consist of simple geometric shapes which result in low mesh complexity, during modeling in 3D CAD tools, and are therefore far less resources hungry when simulated using full wave EM solvers. The main problem limiting the use of layered homogeneous models, is related to their accuracy and consequently their reliability. This study aims to assess the reliability of such simpler models in comparison with the more complex, and realistic structures of body-mimicking models. To study this comparison, an implantable antenna, placed inside a human stomach model, is set to communicate with an off-body antenna at Medical Implant Communication Service (MICS) band. Keeping the distance between implantable antenna and off-body antenna constant, the realistic human body phantom is then replaced by two types of layered body phantoms with different complexity. It was observed that when a realistic phantom was replaced by widely used simpler phantom models, significant detuning of the resonant frequency of the implantable antenna occurred. Due to the narrow bandwidth of MICS band, this detuning will be vital for any such implantable simulation setups. Results in the form of calculated s-parameters and phantom complexity matric are further investigated to conclude the study.

Analysis on SAR Values of Commercial Mobile Phones

Ae-Kyoung Lee, Seon-Eui Hong, and Jong-Hwa Kwon
Radio Technology Research Department
Electronics and Telecommunications Research Institute, Daejeon, Korea

Abstract— The SAR of mobile phones has been regulated since 2002 and more than 1200 models have been tested for SAR compliance in Korea. The limits of spatial peak SAR in the head referred to IEEE Std 95.1. A mobile phone model should be compatible with spatial peak SAR, i.e., 1.6 W/kg for 1 g of mass based on the measurement procedure of IEC 62209-1.

For epidemiological studies investigating the potential association between mobile phone use and the risk of brain diseases, more than 1400 SAR test reports from 2002 to June 2013 have been collected. We organized a large amount of data including a manufacturer, a frequency band, outer shape, antenna type (internal/external), a maximum output power, body dimensions, and spatial peak 1-g SAR values in the four test positions of cheek/left, cheek/right, tilt/left and tilt/right at the center frequency for all the models. SAR distribution of 70 mobile phones was measured in the flat phantom.

Eleven representative phone models were numerically implemented based on the SAR distributions and spatial peak 1-g SAR values from the SAR test reports [1]. The numerical phone models produce the mean SAR distribution for each corresponding phone type. However, radiation levels from commercial phones are in wide range even though they are the same type of models, as shown in Figure 1. As a part of the exposure assessment, spatial peak 1-g SAR values in the four test positions are statistically analyzed to include SAR characteristics of a specific phone model in the SAR calculation result for a representative phone model.

From scatter plots about SAR data of commercial models, the correlation between SAR values on the left and right sides was good (0.6–0.9) and the difference between SAR values under the cheek and tilt positions was clear. Therefore, the SAR optimizing factor for the test position is proposed.

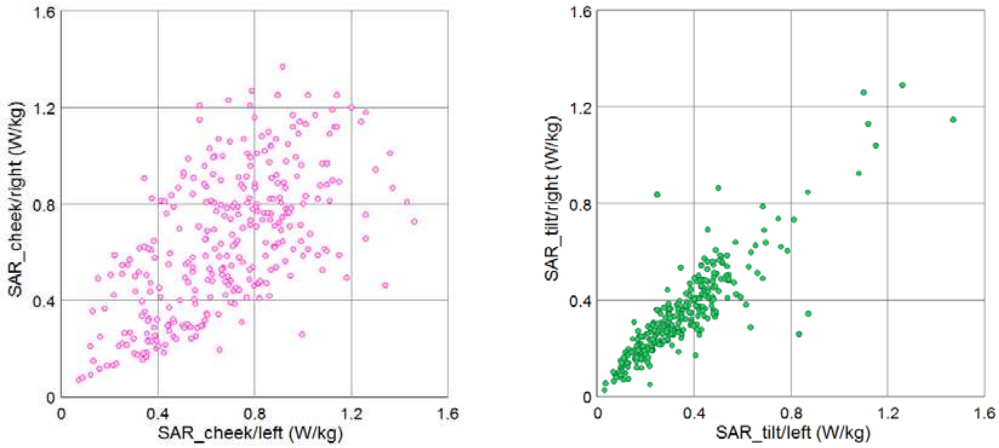

Figure 1: Scatter plot between SAR values measured at the right and left sides of the SAM phantom for the bar type of commercial phone models. (a) Cheek position. (b) Tilt position.

REFERENCES

1. Lee, A.-K., et al., "Design of representative mobile phone models for epidemiological studies," Submitted to *ETRI Journal*.

Fabrication of a Nano-magnetic Biodegradable Composite for Medical Applications

Che-Tong Lin[1], **Ting-Lin Wu**[2], **Horng-Mo Lee**[3], **and Haw-Ming Huang**[2]

[1]Division of Prosthodontics, Department of Dentistry
Taipei Medical University Hospital, Taipei, Taiwan
[2]Graduate Institute of Biomedical Materials and Tissue Engineering
Taipei Medical University, Taipei, Taiwan
[3]Graduate Institute of Pharmaceutical Science and Technology, Collage of Health Sciences
Central Taiwan University of Science and Technology, Taiwan

Abstract—

Objective: Polylactic acid (PLA)-based composite has been used as tissue engineering (GBR/GTR) materials for many years. Several substances, including nano-hydroxyapatite, were added to the composite to modify their material properties.

The aim of this study is to fabricate a magnetic biodegradable PLA-based composite using iron oxide magnetic nanoparticle as fillers for tissue engineering applications.

Material and methods: Nanoscale magnetite was incorporated into the PLA matrix with proportions of 0, 5, 10, and 20% (w/w). Standard samples were fabricated by means of injection molding method. After that, the physical properties of these samples were tested using Differential scanning calorimetry (DSC) analysis and contact angle (CA) assess.

Result: Our results demonstrated that PLA incorporated with nanoscale magnetite significantly increase the intensity of the PLA composite. In addition, addition of magnetite has negative effect on the crystallization temperature of the polymer. The measured contact angle of the nano-magnetite/PLA was 69.3 degree which was significantly lower than the pure PLA (77.3 degree).

Conclusion: In this study, we found that addition of nanoscale magnetite significantly increase hydrophilic property compared to the pure PLA material. This results suggests that the nano-magnetic composite has a potential to be a biomaterial in tissue engineering.

Parameter Identification of PMSM Nonlinear Part

I. Vesely[1, 2]

[1]Department of Control and Instrumentation, FEEC
Brno University of Technology, Technicka 12, Brno, Czech Republic
[2]Centre for Research and Utilization of Renewable Energy, FEEC
Brno University of Technology, Technicka 12, Brno, Czech Republic

Abstract— The following paper describes the identification of quadrature inductances of permanent magnet synchronous motor. The identification is based on the principle of Hammerstein model.

The electrical diagram of permanent magnet synchronous motor could be divided into two parts. First one is a static nonlinearity and second one is a linear dynamics. The identification of quadrature inductance from nonlinear part is in this paper. Only inputs and outputs can be read, when the Hammerstein model is used. The others variables are computed or estimated. Because only nonlinear part is used, the outputs of this part must be calculated from system outputs.

The identification is carried out on the non-linear part by Newton method. One specific feature of this identification is that it identifies during constant current and it has a large error if the current is not constant. The ratio of the measured current and noise level affects the accuracy of the method. The effect of noise is partially removed by changing the calculation of the non-linear output. It uses the fact that the method works only at constant current. Further improvement is achieved by identifying the inductance as a polynomial function of the current, where one element is already known. This is the value of inductance at low currents. The identification can be replaced by this value of inductance if the current is small enough and could be too much affected by noise. This method could be used as auxiliary method for other methods which do not identify during the constant conditions.

Simulation of Circulation Module

F. Solc[1, 2], **I. Vesely**[1, 2], **and F. Zezulka**[1, 2]

[1]Department of Control and Instrumentation, FEEC
Brno University of Technology, Technicka 12, Brno, Czech Republic
[2]Centre for Research and Utilization of Renewable Energy, FEEC
Brno University of Technology, Technicka 12, Brno, Czech Republic

Abstract— Paper describes a model for lung nutrient circuit and its control. This circuit is currently developed and it is the part of a project dealing with the transport of the lungs. Lung tissue is very sensitive and it loses its quality during a few hours without nutrition. If such lungs is transported the transportation time must be as short or nutrition system must be used.

As mentioned above, the lung is very sensitive and some conditions must be complied. The first one of these conditions is the maintenance of required temperature and the second one of these conditions is the maintenance of required pressure. The whole system was expressed by equations and modeled in Matlab Simulink for the better control design of real model.

The controlled system consists of several parts. The most important of them is the tank where the nutrient fluid is stored and its temperature is checked. The pump, which is controlled by the user, ensures the fluid flow. The pressure and flow sensors are deployed throughout the circuit and they are used for automatic control of these variables. The article discusses the equations, which is used for creation of model, the creation model and various verification tests on this model are carried out. The proposed controller performs temperature control in specific limits.

Design of Dual Band Monopole Antenna with Considering Human Body Effect for Wearable Device Applications

Ho-Jun Lee[1] **and Jin-Myung Kim**[2]

[1]Convergence Communication Components Research Center
Korea Electronics Technology Institute, R. O. Korea
[2]ACE Technologies Co., Ltd., R. O. Korea

Abstract— In this paper, a dual band monopole antenna with considering human body effect is proposed. The proposed antenna is designed to operate at 2.4 and 5.8 GHz. The lower-frequency band (2.4 GHz) can be obtained by using the folded monopole, and the upper-frequency band (5.8 GHz) is operated by using a U-shaped microstrip line. Whether the antenna which is placed on the human body phantom or in free space, the performance of the proposed antenna including dual bandwidth (2.4, 5.8 GHz ISM band) is good enough to be used for wearable device applications.

The proposed antenna configuration is shown in Figure 1. Antennas in this paper are simulated by using the CST Microwave Studio (CST MWS). A prototype of this antenna was fabricated on FR-4 substrate with thickness $h = 1$ mm and dielectric constant $\varepsilon_r = 4.4$. The measurements of electrical characteristics such as radiation patterns, VSWR, and return loss of the implemented antenna were conducted in an anechoic chamber equipped with network analyzer and far field measurement system. Figure 2 shows a photograph of the fabricated antenna and return loss (S_{11}) characteristics. We manufactured the antenna based on the results of optimized simulation results and measured characteristics of the suggested antenna in the anechoic chamber. Details of the proposed antenna designs are described, and typical experimental results are presented and discussed.

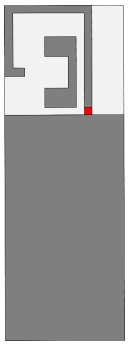

Figure 1: Proposed antenna.

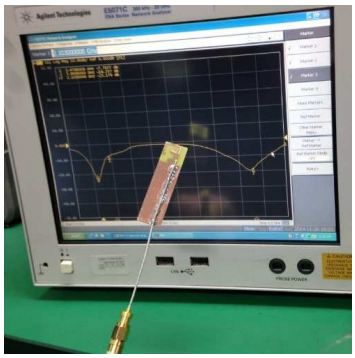

Figure 2: Photograph of the fabricated antenna measured return loss.

REFERENCES

1. Hall, P. S. and H. Yang, *Antennas and Propagation for Body-centric Wireless Communications*, Artech House, 2006.

High Gain and Low Noise Brain-Machine-Interface (BMI) SoC and Module for Dry Contact Electrode

Sanghoon Park, Ki-Jin Kim, Kwangho Ahn, and Jin-Sup Kim
Convergence Communication Components Research Center
Korea Electronics Technology Institute, South Korea

Abstract— A medical device to monitor the human's electroencephalography (EEG) has gained lots of interests more and more. Its application varies from the traditional medical to fast changing IT fields. However, the traditional way to investigate one's EEG signal is very inconvenient and time-consuming. We designed a high gain and low noise BMI module to extract one's EEG signal under more human friendly condition. A specially designed dry electrode, as shown in Fig. 1(a), has lower tension and a round head, and so most of the user can feel comfortable when the dry electrodes contact their scalp. The EEG signal sensed by the dry electrode is processed by the following SoC. The SoC divided into two parts. First, the front-end analog blocks process the incoming EEG signal. It consists of two stages of instrumental amplifiers and the 4th order Bessel filter. The 1st stage instrumental amplifier is designed to focus on increasing noise performance and the 2nd stage instrumental amplifier is for the variable gains. The 4th order Bessel filter is basically has programmable cut-off frequency and removes all the high frequency due to the chopping technique. The amplified and filtered EEG signal is digitized by the following analog-to-digital converter (ADC). The successive approximation register (SAR) ADC is designed to minimize the power consumption and increase the efficiency. The digitized EEG signal will be post-processed by the DSP module.

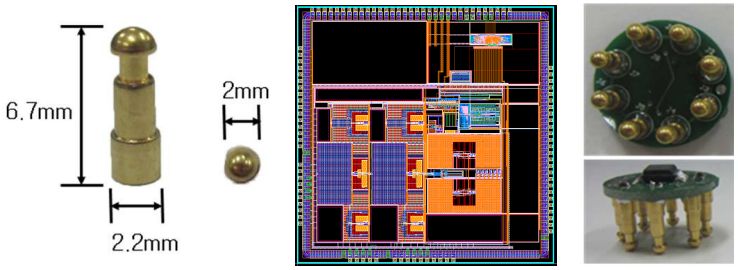

(a) Dry Electrode (b) SoC Layout (c) BMI Module

Figure 1: The BMI module and measured frequency response.

Analysis of Light Absorbance on the Effects of Low Frequency Magnetic Fields on Cell Proliferation

M. Sosa[1], **T. Cordova-Fraga**[1], **A. Martinez-Longoria**[1], **A. Horta-Rangel**[2], **J. C. Villagomez**[3], **M. Sabanero**[3], **R. Monroy-Torres**[4], **and N. Padilla-Raygoza**[5]

[1]Department of Physical Engineering, University of Guanajuato, Campus Leon, Mexico
[2]Engineering Division, University of Guanajuato, Campus Guanajuato, Mexico
[3]Department of Biology, University of Guanajuato, Campus Guanajuato, Mexico
[4]Department of Medicine and Nutrition, University of Guanajuato, Campus Leon, Mexico
[5]Department of Nursing and Obstetrics, University of Guanajuato, Campus Celaya-Salvatierra, Mexico

Abstract— An experiment to measure the effects of low frequency magnetic fields on cell proliferation was performed. Magnetic fields of low amplitudes, ranging from 1 to 4 mT, at frequencies of 60, 100, 800, 1500 and 2450 Hz were used to stimulate cell cultures of yeast Saccharomyces cerevisiae. The stimulation was carried out during 5 minutes, with intervals of 5 minutes rest, for 8 hours. A control and an experimental sample were measured two times for each frequency at the beginning of the experiment and at 2, 4, 6 and 8 hours later. In each measurement series a new cell culture was prepared for both non-stimulated and stimulated samples. The cells were grown in a liquid medium composed by 0.3 g yeast extract, 1.0 g gelatin peptone and 2.0 g dextrose for 100 ml solution of growth medium, with pH adjusted to 4.5 with NaOH. Measurements of cell proliferation were based on light absorbance using a spectrophotometer BECK-MAN DU 650 at 600 nm wavelength. A comparison of growth rate increasing of cell proliferation in stimulated cells larger than the non-stimulated ones, with differences from 8% to 16% after 8 hours of exposure, for most of the frequencies employed, except at 60 and 800 Hz, where the control sample showed an increasing larger than the stimulated cultures, particularly at the final of the experiment. For the first hours of the experiments the results are variable, coming to present a clear trend only after 4 hours. In conclusion, the results of this experiment show an influence of magnetic fields on cell evolution, which is a function of both the exposure time and the stimulation frequency.

IMA for a Mobile Phone Using the Coupling Method

Ho-Jun Lee[1] **and Jin-Myung Kim**[2]

[1]Korea Electronics Technology Institute, Korea
[2]ACE Technologies Co., Ltd, Korea

Abstract— Antenna, since the transmitting and receiving performance is increased in proportion to the size and volume, downsizing is difficult, occupies a considerable part in the interior of the mobile phone. Antenna, acted as a major obstacle to the trend of mobile phone slimmer. Recently, a manufacturing method for the IM (In-mold) antenna of another new concept appeared the conventional antenna. IM antenna (IMA), since integrated with the cellular phone case is possible, can be further streamlining the mobile phone that does not require a separate space which has been existing accounts.

In this paper, we proposed a novel design of in-mold antenna integrated into the case of a mobile phone. The proposed antenna configuration is shown in Figure 1. The proposed antenna operating at 2.4/5.8 GHz dual band by mutual coupling in the rear case of the thickness of 1 mm (Case permittivity = 3). Figure 2 shows the design result reflection loss (S_{11}) of the proposed antenna.

We manufactured the antenna based on the results of optimized simulation results and measured characteristics of the suggested antenna in the anechoic chamber. Details of the proposed antenna designs are described, and typical experimental results are presented and discussed.

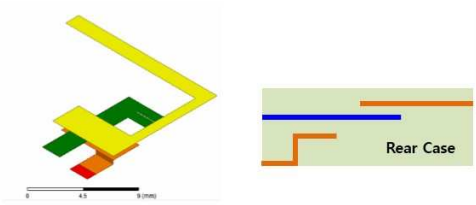

Figure 1: Proposed antenna.

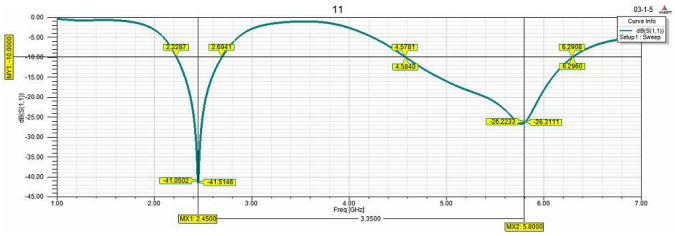

Figure 2: Design result (S_{11}).

REFERENCES

1. Stutzman, W. L. and G. A. Thiele, *Antenna Theory and Design*, 2nd, Hohn Wiley & Sons, New York, 1998.
2. Harrington, R. F., "Effect of antenna size on gain, bandwidth and efficiency," *J. Res. Nat. Bur. Stand.*, Vol. 64, 1–12, Jan./Feb. 1960.
3. Wong, K. L., Y. C. Lin, and B. Chen, "Internal patch antenna with a thin air-layer substrate for GSM/DCS operation in a PDA phone," *IEEE Trans. Antennas Propagat.*, Vol. 55, 1165–1172, Apr. 2007.

An Efficiency of Broadcast Mechanisms Based on Cluster Heads in Dependence on Clustering Algorithm Type

Wojciech Bednarczyk, **Jerzy Dołowski**, **and Jarosław Michalak**
Faculty of Electronics, Military University of Technology
Gen. S. Kaliskiego 2 Str., Warsaw 00-908, Poland

Abstract— It is well known that broadcast communication is a very popular type of transmission used in military systems for route discovering, topology dissemination, alarm notification, location update, multicast tree building etc..

Technical solution is dependent on a scenario and a network topology. Effectiveness of BC can be measured (assessed) by:

- Time of information delivery (or maximum delay),
- energy used by network and/or particular radios,
- probability of information delivery,

where energy used by a system has a special importance not only from energy consumption point of view (especially in battery supplied devices) but from interference level introduced by the system which has essential impact on a capacity of system and its ability to simultaneous working among others wireless links.

Efficiency of broadcast transmission based on Cluster Heads in clusterized wireless network in dependence on Clustering Algorithm type will be assessed in this paper.

The proposed clustering algorithms are based on Modified Lowest ID (own modification), Highest Degree and our own based on weighted parameters.

The main differences between mentioned above algorithms are:

- A position of CH in cluster in relation to other cluster members.
- Number of clusters in the network at the end of clustering process.
- Time of clusterization process.
- Energy used by the network in clusterization process.
- Stability of the network organized in clusters.

BC algorithms use MPR (Multi Point Relay) method based on Cluster Heads (CH-MPR-BC) compared with classical solution which uses Gateway nodes at the edge of clusters as retransmitters.

Simulations will be done for static network assuming Free Space Path Loss propagation model with chosen reliability of information delivery in a radio link.

Advantages of Weighted Nodes Parameters algorithm will be presented using numbers and graphs including energy analysis and its impact on interference level.

Restoration of Antenna Patterns Using Iterative Method

Jinhwan Koh and Fan Fan
Department of Electrical and Electronic Engineering, ERI
Gyeong Sang National University, Jinju, Korea

Abstract— A new approach to reconstructing antenna far-field patterns from the missing part of the pattern is presented in this paper. The antenna far-field pattern can be reconstructed by utilizing the iterative Hilbert transform, which is based on the relationship between the real and imaginary part of the Hilbert transform. A moving average filter is used to reduce the errors in the restored signal as well as the computation load. Under the constraint of the causality of the current source in space, we could successfully reconstruct the data. Several examples dealing with line source antennas and antenna arrays are simulated to illustrate the applicability of this approach.

Wave Packet Propagation of Guided Optical Modes in a Thin Left-handed Film near a Frequency of Zero Power Flux

Dmitry A. Konkin, Rudol'ph V. Litvinov, and Alexander A. Shibelgut
Tomsk State University of Control Systems and Radioelectronics
40 Lenina Prospect, Tomsk 634050, Russia

Abstract— Dependences of the propagation constants β of guided optical modes of a thin left-handed film with an air coating medium and a dielectric substrate on a frequency ω are considered. It has been showed that the power flux of guided mode (group velocity of the mode) vanishes at a definite frequency ω_0. Two branches of the dispersion dependence $\beta(\omega)$ of one mode converge at the point ω_0. The branches are determined by conditions $\beta(\omega) < \beta(\omega_0)$ and $\beta(\omega) > \beta(\omega_0)$. Phase and group velocities of the mode on the first (second) branch have the same (the opposite) directions. The dependences $\beta(\omega)$ in the vicinity of the point ω_0 can't be approximated by a truncated series in integral powers of a frequency deviation $\Delta\omega = \omega_0 - \omega$. In the case under consideration the dependences can be presented as a series in powers of the square root $\Delta\omega^{1/2}$.

A propagation analysis of narrowband intramode packets with frequencies of modes in the vicinity of the frequency ω_0 is performed. In the general case, two different pairs of the intramode packets correspond to this vicinity. The modes of these pairs of the intramode packets have the opposite directions of phase velocities. At the same time the modes of one of the packet of each pair have the same directions of phase and group velocities. The modes of other packet of the pair have the opposite directions of these velocities. Analytical relations for case of a constant spectral density of the modes in a mode packet and in a first approximation by parameter $\Delta\omega^{1/2}$ have been found. The relations describe a space-time transformation of the power flux of an intramode pulse. Contributions of the dispersion of propagation constants and the dispersion of a spatial distribution shape of electromagnetic field of the mode to this transformation are distinguished. It has been demonstrated that the propagation of the intramode pulse into the film is accompanied by a vigorous broadening because of the strong dispersion of the left-handed material. At that the velocity of maximum propagation of this pulse depends on the spectral width of mode packet and can be considerably lower than the group velocity of the optical pulse in a volume left-handed material. This effect can be used for a light deceleration in devices of the optical information processing.

Unconventional Relaxation in Metal-dielectric Iron Boron Nitride Nanoceramics in the Readiofrequency Range

Karen Oganisian[1], **Pawel Gluchowski**[1], **Andrzej Vogt**[2], **and Wieslaw Strel**[1]

[1]Institute of Low Temperature and Structure Research, PAS, Okolna 2, Wroclaw 50-422, Poland
[2]Faculty of Chemistry, Wroclaw University, F. Joliot-Curie 14, Wroclaw 50-383, Poland

Abstract— Metal-dielectric composition is one of the most intriguing system due to the possibility to unify incompatibility properties of the materials which could not to be found in nature, such as magnetic dielectric or transparent conductor. Within investigations of electromagnetic properties of magnetic dielectric composite of iron boron nitride (Fe:BN) it was found that even few percent of BN may drastically change not only conductivity but it also strongly modify the electromagnetic properties of this compound.

Here we report an observation of unconventional relaxation in metal-dielectric system of iron boron nitride nanoceramic in the radio frequency range. The samples of Fe:BN of 95:5, 94:6 and 93:7 mass ratio were studied by x-ray diffraction, scanning electron microscopy and by the measurements of capacitance as a function of frequency in the 1–1000 MHz range.

Structural studies revealed well separated core-shell structure of micro and nanoparticles of iron thoroughly covered by a thin layer of boron nitride. Such a structure characterized by reduced conductivity but high saturation of magnetic induction which is very important for high frequency applications.

Frequency dependence of permittivity showed unexpected relaxation for the samples of 94:6 and 93:7 mass ratio. The FeBN94:6 manifested electric resonance near 550 MHz, probably, related with grain boundary relaxation. But permittivity of the FeBN93:7 sample is continuously decreasing accompanying with wide absorption from 100 to 800 MHz. This anomaly can be easily detected from the frequency dependence of conductivity (see Fig. 1). As can be seen, FeBN95:5 showed conventional dependence of conductivity; FeBN94:6 revealed similar to FeBN95:5 behavior of conductivity with relaxation near 550 MHz. However, the FeBN93:7 revealed completely different semicircle-like dependence of conductivity with wide maximum between 100 and 800 MHz. It is clear, influence of BN on this complex system results unconventional behavior accompanied with wide relaxation in the radio frequency range suggesting on the Drude relaxations in the iron grains.

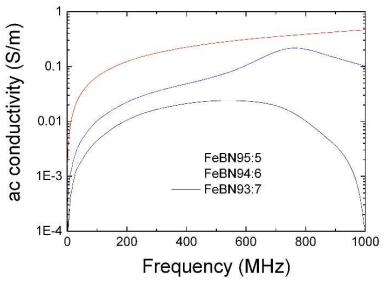

Figure 1: Ac conductivity of FeBN95:5, FeBN94:6 and FeBN93:7 as a function of frequency.

Lasing Emission by Side-pumped Emulsion Droplets in Pendant Positions

M. Boni[1, 2], **I. R. Andrei**[1], **V. Nastasa**[1, 2], **A. Staicu**[1], **and M. L. Pascu**[1, 2]

[1]National Institute for Laser, Plasma and Radiation Physics, Magurele, Romania
[2]Faculty of Physics, University of Bucharest, Magurele, Romania

Abstract— This paper presents the resonant interaction between laser beams and individual pendant dye-doped oily emulsion droplets. When the laser beam is partially or fully absorbed by the droplet's components the interaction is called resonant. Following absorption, laser induced fluorescence (and even lasing) effects are produced and are investigated through fluorescence spectra analysis. In the reported experiments it was studied the resonant interaction, a single droplet behaving as an optical spherical cavity in which the optical signal is amplified, as in the well-known whispering gallery modes (WGMs) case. By varying the dye concentration and pumping energy, we obtained typical fluorescence broad band and a narrow peak assigned to lasing effect.

The excitation is made with the second harmonic generated beam emitted by a pulsed Nd:YAG laser system at 532 nm. The pumping energies domain was chosen in such way to obtain resonant effects and at the same time to avoid mechanical effects (vibrations, liquid expulsion) specific to unresonant interaction.

The pendant microdroplets containing emulsions exhibit an enhanced emission signal. This effect can be explained as being due to the scattering of light by the sub-micrometric drops of oil in emulsion coupled with the spherical geometry of the pendant droplet. The droplet acts as an optical resonator amplifying the fluorescence signal with the possibility of producing a lasing effect. Here, we also investigate how Rhodamine 6G concentration, pumping laser beam energies and number of pumping laser pulses influence the fluorescence behavior. The results can be useful in optical imaging, since they can lead to the use of smaller quantities of fluorescent dyes to obtain the same quality of results.

ACKNOWLEDGMENT

This work was supported by the Romanian ANCS/CNDI-UEFISCDI program, projects PN-II-ID-PCE-2011-3-0922 and NUCLEU program, project LAPLAS 3-PN09 39. COST MP1205 contribution is also acknowledged. Viorel Nastasa was supported by the strategic grant POSDRU/159/1.5/S-/137750, "Project Doctoral and Postdoctoral programs support for increased competitiveness in Exact Sciences research" co-financed by the European Social Found within the Sectorial Operational Program Human Resources Development 2007–2013.

The Time Approach to Analysis of the Probing Radiation and Electromagnetic Fields, Scattered by Rough Objects

V. I. Mandrosov
Moscow Institute of Physics and Technology, Russia

Abstract— It is proposed application of the time approach to analysis of the probing radiation and electromagnetic fields, scattered by rough objects, based on the use of the time correlation function $B_u(\tau) = \langle u(t)u*(t+\tau)\rangle_t$, where $u(t)$ is the modulation function of the probing radiation, and brackets $\langle\rangle_t$ mean operation of averaging over a time $T > 10\tau_c$, where τ_c is the coherence time of the probing radiation. This approach allow us to determine a clear boundary between a narrow-band and a wide-band of the probing radiation, and also to establish a clear boundaries between monochromatic, quasi-monochromatic and poly-chromatic probing radiations. These boundaries substantially depend on surface forms of scattered objects and dimensions of scattered fields monitoring area determine differences between coherent, partially coherent and incoherent scattered fields.

With the help of the time approach it is shown that there is the minimal coherence length L_{cm} of probing radiation. This length is estimated by means of analyzing the interference structure in the intensity distribution of fields scattered by rough surfaces or point-like objects, averaged over a time $T > 10\tau_c$, where τ_c is the coherence time of the probing radiation, under the condition that $\tau_c > 3/\omega_0$, ω_0 being the central frequency of the radiation spectrum. It is shown that the minimal coherence length L_{cm} of the probing radiation at which it is still possible to observe a interference structure of the scattered field is equal to $8\lambda_0$, where $\lambda_0 = 2\pi/\omega_0$ is the central wavelength of probing radiation.

It is discussed application of the time approach in low-coherence tomography on opposite reference and objects beams in optical and terahertz wave ranges. This tomography is provides the best layered resolution, equaled to $L_{\text{cm}}/4 = 2\lambda_0$. It is discussed also two methods of forming with the help of the time approach 3D-image of remote rough objects on the speckle-structure of their coherent image and on the picture of interference of two beams, propagated with a different pairs of various plots of these images. The latter method also allows us to define rotation angular velocities of remote rough objects.

Correlated-electron Emission in Nonsequential Double Ionization of Ar Atoms by Intense Laser Fields

Jingtao Zhang
Department of Physics, Shanghai Normal University, No. 100 Guilin Rd., Shanghai, China

Abstract— Electron correlation is the core of attoscience and molecular tomography. Nonsequential double ionization (NSDI) provides a process to study and control the electron correlation, in which the electron recollision plays a key role. Longitudinal momentum distribution of the correlated electrons is the principal tool to reveal electron correlation in NSDI and is frequently studied. It has been observed that the longitudinal momentum distribution exhibits an anticorrelation feature at lower laser intensities, but a correlation feature when the laser intensity is higher than the recollision threshold. Seeking for the physical origin of the transition provides a deep insight into the electron correlation in intense laser fields.

We use a classical ensemble method to study the NSDI of Ar atoms in a linearly polarized laser pulse of different intensities, and trajectory back analysis is performed. We classify the NSDI electrons by the interval between the ionization time of the second electron and the recollision time. The RII denotes the second electron was ionized shortly after the recollision, while the RESI denotes the recollision-excited electron was ionized by the laser field. We show that as the laser intensity increases, the RESI electrons always exhibit an uniform distribution in four quadrants of the momentum distribution diagram, while the RII electrons change their emission priority from anticorrelation to correlation. By following the instantaneous momentum distribution of the RII electrons, we find that the Coulomb repulsion between the two RII electrons contributes mainly to the anticorrelation feature, and that the drift momentum is responsible for the correlation feature in the longitudinal momentum distributions. The transition in the electron emission reveals a strong electron-electron correlation in intense laser pulses.

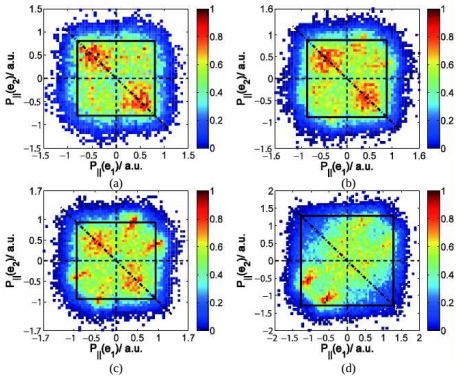

Figure 1: The correlated momentum distributions of the two electrons of Ar atoms by laser pulses of 800 nm wavelength and intensity: (a) 0.75, (b) 0.9, (c) 1.0, and (d) 2.0×10^{14} W/cm^2, respectively; The 2nd and the 4th quadrants in (a) but the 1st and 3rd quadrants in (d) are highlighted , denoting the transition from anticorrelated to correlated distributions of the correlated electrons.

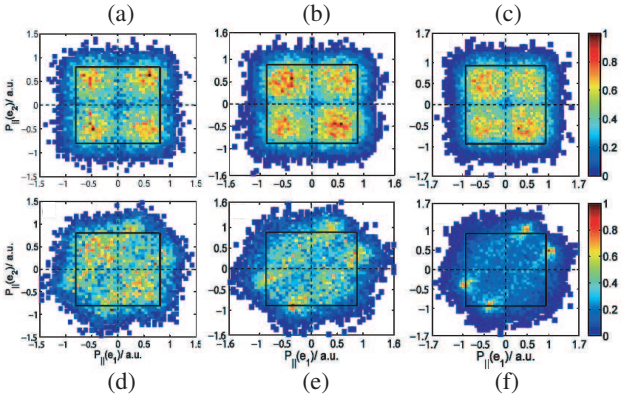

Figure 2: The correlated momentum distributions of the RESI (top) and the RII (bottom) electrons by laser pulses of intensity (a) (d) 0.7, (b) (e) 0.9, and (c) (f) 1.0×10^{14} W/cm^2, respectively.

Mutual Coupling between Parasitic Elements of Split Ring Resonator on Antenna

Dang-Oh Kim and Uooyeol Yoon
Wireless Power Transfer Research Center
Korea Advanced Institute of Science and Technology, South Korea

Abstract— The parasitic elements on antenna have become an important issue in improving the antenna performance in various wireless devices. These elements are mostly used as radiator and resonator in antenna. However, an investigation of the mutual coupling between parasitic elements is rare to be found in metamaterial resonator antenna studies. From this unusual approach, this paper presents the new mutual coupling structure of parasitic elements with the split ring resonator (SRR) on antenna. The suggested antenna consists of two rectangular SRRs and conventional monopole antenna. These resonators play the role of the parasitic element in antenna. In order to operate these SRRs, linear monopole antenna is used as an active antenna which can provide the time-varying magnetic field with normal direction. In metamaterial technology, a negative effective permeability can be generated at resonant frequency via periodic arrangement of these SRRs which are electrically small LC resonant elements with a high quality factor. Fundamentally, mutual coupling phenomenon has been observed between adjacent resonators, so that the antenna with two resonators has the same effect on parasitic elements, too. In this study, the coupling coefficient between two parasitic element resonators on antenna is obtained from scattering parameter simulation results. On the basis of the electromagnetic field characteristics and the result of antenna parameter, this study will be exquisite from the previous studies of antennas that utilize the SRR.

Near-field Imagery with Bow-tie Antenna Probes at 60 GHz

Laurent Chusseau, Rachid Omarouayache, Pierre Payet, and Jérémy Raoult
IES l'Institut d'Électronique, Université de Montpellier, 860 rue de Saint Priest, Montpellier 34097, France

Abstract— Near-field scanning microwave microscopy (NFSMM) is a well-established technique to characterize material properties such as conductivity, dielectric permittivity or magnetic permeability. Owing to very small probe sizes as compared to wavelength, high spatial resolutions at the micron scale can be achieved. So far, very few NFSMM experiments have been proposed at mm-waves.

In view of material and circuit inspection, we chose to develop a new NFSMM operating at 60 GHz. The experimental setup involves a Gunn source diode feeding a directional coupler connected to the near-field probe and we collect the reflectometry signal via a Schottky detector. Since we are interested in samples for which the imaging result may depends of the electromagnetic field (E or H) and polarization, we manufacture our own probes on the basis of nano antennas attached to the waveguide. Probe realization is done by bonding two equilateral triangles fabricated by femtosecond laser cutting at the end of a WR15 waveguide. Final assembly is done manually and the air gap g between tips can be adjusted at the end of the process. Two such probes with gap sizes of $g = 18\,\mu\text{m}$ and $g = 50\,\mu\text{m}$ were fabricated for the present study.

The first probe was used to acquire near-field profiles at constant distance above a cleaved semiconductor substrate figuring out a topological edge. The spatial resolution is estimated to $\approx 35\,\mu\text{m}$ ($\lambda/150$) at a $h \approx 25\,\mu\text{m}$ height above the sample. However if the distance h is further reduced, near-field profiles become much more complicated and depict polarization-dependent features with a strongly varying oscillatory signal when crossing the sample edge. This feature is identified as the near-field intensity of a point dipole which is known to produce a response that varies depending of the s or p polarisation and h-distance. Our results are in perfect agreement with these predictions, and clearly illustrate the nontrivial nature of topological near-field imaging in the mm-wave range.

The second probe was used to investigate NFSMM as an efficient technique for material characterization. Near-field profiles at constant distance were acquired above three metallic lines deposited on Si substrate and using three different metals: Al, Au and Cu. We clearly observed a sudden increase of the detected signal above the line for all three deposited metals but with intensities that is directly related to their conductivity. Worth to be related is that signal intensity is within a few % identical to the local conductivities deduced from DC measurements and physical characteristics of the lines.

We have built a new NFSMM operating at 60 GHz with a special effort in the design and fabrication of the bow-tie antenna probes. Near-field intensity profiles in extreme near-field conditions show the dipolar nature of the probe that may induce difficulties in image interpretation. We have also shown that this NFSMM is not only a topological instrument and that measurements can be quantitatively related to the conductivity in the near-field.

ACKNOWLEDGMENT

Authors kindly acknowledge the french Agence Nationale de la Recherche for funding this research under the E-MATA HARI contract No. ANR-12-INSE-0005.

An Formation Algorithm of the Synthetic Aperture in an Automotive Radar with Use of the MUSIC Algorithm

Zhargal T. Erdyneev, Gleb O. Manokhin, Elena P. Velikanova, Eugeniy V. Rogozhnikov, Andrey A. Geltser, and Alexander A. Shibelgut
Tomsk State University of Control Systems and Radioelectronics
40 Lenina Prospect, Tomsk 634050, Russia

Abstract— An algorithm of a resolution increase of an automotive frequency-modulated continuous-wave (FMCW) radar with the synthetic aperture (SAR) using the multiple signal classification (MUSIC) algorithm is considered. The radar operates in the side-looking mode. It has been showed that in contrast to the classical case the automotive radar can't be considered as stationary during the repetition period of the FMCW signal. Furthermore, an approximation "stop-and-go" doesn't operate in that case.

To obtain a radar image, it is necessary to compensate the Doppler shift in a spectrum of beat signals and an video phase error. The video phase error appears in mixer by multiplication of a reference signal and an received signal. By moving car a range migration will be changed because of small values of slant distances within a scanned area in comparison with airborne SAR. It appreciably increases the complexity of compensation algorithm of this effect.

Analytical expressions which describe a contribution of the considered errors in the useful signal and expressions for elimination of the errors have been derived. Particularly to solve the problems of the range migration is proposed to use the Stolz interpolation. A mathematical model that takes into consideration the listed effects and an algorithm that eliminates the effects are realized.

After elimination of the described problems the image processing using the MUSIC algorithm is performed. As a first approximation an assumption is accepted. The assumption requires that the number of targets within a specified window on the radar image is a priori known. In the future this problem can be solved by AIC, BIC, WIC methods. A result of post-processing is an increase the range and azimuth resolution which allows to separate the targets within a magnitude of a resolution cell. The radar images for the classical and proposed algorithms of the signal processing are obtained by simulation. The images have a difference over the resolution by the example of two closely-spaced point targets. Simulation parameters are taken into account with the equipment available for the experimental verification of the considered algorithms.

Bioradar in Study of Low-power Radio Frequency Radiation Influence on Sleep of Laboratory Animals

L. N. Anishchenko, E. S. Gaysina, and I. L. Alborova
Remote Sensing Laboratory, Bauman Moscow State Technical University, Russia

Abstract— At present an influence of low-power RF on physiological parameters of biological objects is of high interest because the number of RF sources, which surrounds us in everyday life, is increasing. Studies concerning these effects have been carried out all over the world, however the results of them are controversial.

To investigate the influence of low-power RF on biological objects we used a specially designed complex, which allows generating RF in frequency range from 1 to 20 GHz with different types of modulation and RF output lower than 3 mW. Control of the biological objects vital signs during the experiments with and without additional RF exposure was done remotely by mean of bioradar BioRASCAN-14 designed at Remote Sensing Laboratory of the Bauman Moscow State Technical University. Two rats (female, 4 month old each) were used as biological objects in the experiments. The complex for RF exposure and bioradar were located at the distance of 0.5–1.0 m from a plastic box with a sleeping rat inside. For each rat, 30 records of received bioradar signals were collected for each of simulated experimental conditions (with and without additional modulated or non-modulated RF exposure).

Experimental data were analyzed. For each bioradar record mean value of respiration frequency and total duration of movements artifacts were used for comparison of the data in different experimental conditions (with and without RF exposure). The results of the experimental data analysis showed that respiration frequency increased in RF exposure conditions compared with non-exposure conditions (62 ± 2 and 71 ± 3 acts per minute increase, respectively; $P < 0.05$, t-test).

Several study groups made an assumption that biologically informative modulation should impose on vital signs of the examinee. In our future work it is planned to study this hypothesis by using respiration pattern of a sleeping animal as modulation signal.

Specific Absorption Rates in Women of Three Different Body Types Exposed to EM Waves from 30 MHz to 6 GHz

Tomoaki Nagaoka and Soichi Watanabe
National Institute of Information and Communications Technology, Japan

Abstract— The continuing spread of radio-frequency (RF) devices has led to the increased presence of electromagnetic (EM) waves at various locations. Thus, concerns regarding the safety of humans exposed to RF electromagnetic fields (EMFs) have been increasing. Computational human models with fine resolution have been developed by some research groups and have also been used as models for EMF dosimetry. However, most of the models constructed in previous works are of humans of average size. Physical features, such as height, weight, body type, and body fat percentage, vary between individuals even if the individuals are of the same age. Therefore, we require various models for studying EMF dosimetry. In this study, we developed computational human models of different body types by using a volume deformation framework to generate computational human models as target persons from existing human models. We used the magnetic resonance imaging (MRI) data of adult female models as target data and also developed three target models of different body types (slim, mildly obese, and severely obese) by deforming a Japanese female model. The target models were composed of $2 \times 2 \times 2\,\mathrm{mm}^3$ voxels. By the finite-difference time-domain (FDTD) method, we calculated the whole-body-averaged specific absorption rates (WBA-SARs) in the three female models exposed to vertically and horizontally polarized EM waves ranging from 30 MHz to 6 GHz. In the calculation, the human models were assumed to be in free space. The incident wave propagation was from the front of the body to the back. The cell sizes of the calculation domain including the human model were 2 mm from 30 MHz to 1 GHz and 1 mm from 2 to 6 GHz. The maximum WBA-SARs for each model were observed at 80 MHz. This frequency corresponds to the whole-body resonant frequency of each model. For vertical polarization, the WBA-SARs of the models tend to increase with decreasing weight. The maximum difference in the WBA-SARs between the models is 2.2 dB. This result indicates that the WBA-SAR is slightly affected by differences in body type, height, and weight.

Resonant Micro-strip Lines Analog to Electromagnetically Induced Transparency

Ben Yi Wang[1], **Teh-Chau Liau**[1, 2], **Jian Qi Shen**[3], **and Shun-Feng Su**[2]

[1]Department of Electronic Engineering
Zhejiang Industry & Trade Vocational College, Wenzhou, Zhejiang 325003, China
[2]Department of Electrical Engineering
National Taiwan University of Science and Technology, Taipei 10607, Taiwan
[3]Centre for Optical and Electromagnetic Research, East Building No. 5
Zijingang Campus, Zhejiang University, Hangzhou 310058, China

Abstract— Electromagnetically induced transparency (EIT) observed in three-level atomic vapor media is a coherent quantum process whose optical response to a laser beam is modified by a second beam with a well-determined detuning. In references, some classical analogs to EIT have been presented. We propose a microstrip transmission line structure to mimic the optical behavior of a three-level Lambda type EIT phenomenon. This research may enable us to understand how the quantum coherence works in real atomic vapor experiments.

Measurement of Complex Permittivity of Warping Thick Film Using Cylindrical Cavity Resonator

G. Ichihara, **Y. Tomizuka**, **M. Setsu**, **T. Ohno**, **K. Tanii**, **and M. Uehara**
National Institute of Technology, Kisarazu College, Japan

Abstract— This paper discusses the relationship between warping thick film and complex permittivity using cavity resonator method.

Figures 1(a), (b), and (c) show the measurement system using 2.45 GHz cavity resonator, a sample (Polyimide $\dot{\varepsilon}_r$: $3.600 - j0.027$), and a sample holder (Polystyrene). The distance d shown in Figure 1(b) is defined as warpage of the sample. The complex permittivity of the sample with/without the holder is calculated by perturbation formula using measured result of a resonance frequency and Q factor.

Figure 2 shows the measured result of real part of complex permittivity of the sample without the holder. In Figure 2, the difference between the measured result and reference value is increased in accordance with increasing d. Figure 3 shows measured results in the case of using the holder to reduce the warping of the sample. As shown in Figure 3, the similar results to the reference value are obtained. Threfore, it has confirmed that the use of the holder is effective for determining the complex permittivity of the thick film which has warpage.

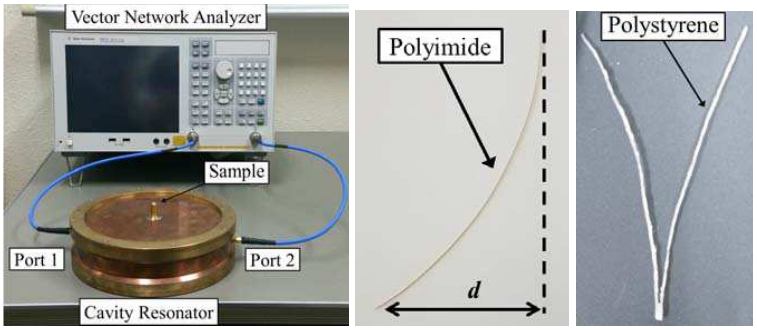

Figure 1: System of cavity resonator method using cylindrical cavity resonator and sample. (a) Measurement system. (b) Sample. (c) Holder.

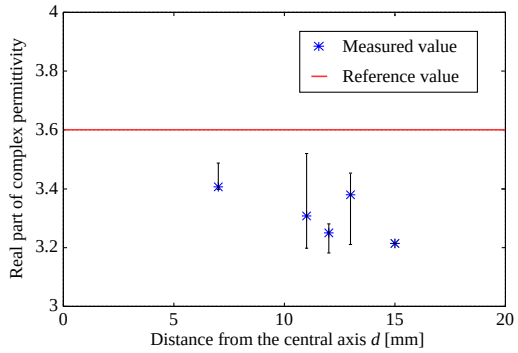

Figure 2: Measurement of real part of complex permittivity of the sample.

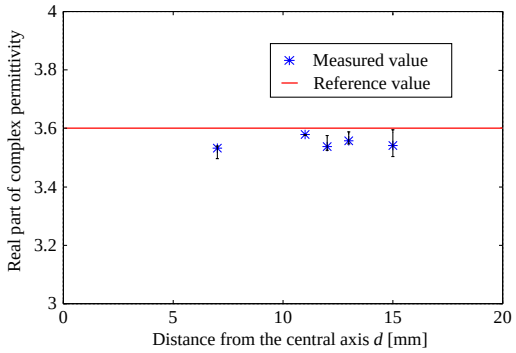

Figure 3: Measurement of real part of complex permittivity of the sample using the holder.

Improved Concept of Numerical Modeling of Dielectric Properties of Emulsions: Error Reduction Caused by Droplets Close to or Crossing Boundaries of Constant Electric Potential

J. Vrba, Jr. and D. Vrba
Faculty of Biomedical Engineering, Czech Technical University in Prague, Czech Republic

Abstract— The existing 3D model was analuzed and following main source of higher variance of the predicted values of complex permittivity was identified. It corresponds to the effect when the droplets are close to or crosses the boundaries of defined time-harmonic electric and ground potential (sources of electric field in the unity cell). This effect can be reduced by a strategy developed here. Implementation of the strategy can be described by following steps.

A unity cell with randomly placement of droplets is generated. The geometry of the unit cell is generated as periodic in two directions, all droplets' parts exceeding a side wall(s) of the unit cell have to appear on the opposite wall(s) too (see Fig. 1).

A quasi-static numerical simulation of electric potential distribution within the unity cell is performed. Stored electrical energy as well as lost power between two contours of different two electrical potentials between ground and the maximal one are recorded.

A new unit cell is generated, which geometry corresponds to side walls from original geometry and upper and lower walls are of the same shape as of the contours of the above mentioned two potentials. Implementation of this strategy is not trivial and therefore the strategy is tested on 2D cases only.

In iterative manner quasi-static numerical simulations are performed while changing both parts of permittivity and conductivity and comparing the stored energy and lost power with the values recorded above. This was implemented as optimization problem. The presented strategy was implemented and the results are shown for test scenario of droplet in different positions within a unit cell.

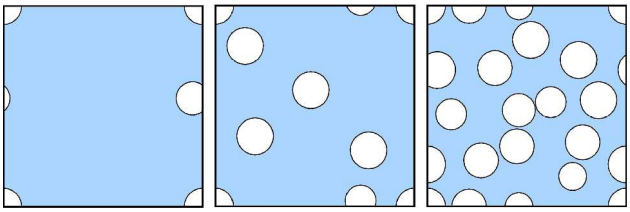

Figure 1: Representative top view of unit cells with different volume fractions ϕ. From left to right $\phi = 1\%$, 10% and 30%. A monodisperse emulsion is considered with droplet radius $r_{\text{droplet}} = 3.5\,\mu\text{m}$

ACKNOWLEDGMENT

This research has been supported by the research program of the Czech Science Foundation (GACR) of the Czech Republic, Project No. 14-00386P Study of Thermal and Nonthermal Effects of High-Power EM Field Structure of Matter.

Numerical Modeling of Dielectric Properties of Blood-glucose Solutions

J. Vrba, Jr., **P. Spurny**, **and D. Vrba**
Faculty of Biomedical Engineering
Czech Technical University in Prague, Czech Republic

Abstract— In 2014, 382 million people (8.3% of the overall population) have diabetes and it is expected that up to year 2035 the number of people with diabetes will rise to 592 millions. More than 11% of worldwide healthcare spending amount diabetes-treatment cost [1]. Current techniques for blood glucose monitoring are all invasive associated with number of obvious inconveniences. Regular blood glucose monitoring by diabetes patients would both significantly improve their quality of life as well as decrease the diabetes-treatment cost. Therefore, there is a clear demand for an inexpensive non-invasive blood glucose monitoring technique. There are already number of research groups and companies developing non-invasive blood glucose monitoring systems [2–5]. A company MediWiSe announced start pre-orders for their microwave device in late 2016. With respect of development of an electromagnetic non-invasive glucose monitoring system some authors reports dielectric properties of physiological saline-glucose [6] and of blood plasma-glucose solutions [7, 8]. In [9, 10], it has been shown that glucose influence dielectric properties of blood significantly, but an analytical model has not been published there. To authors best knowledge the only paper publishing empirical model of dielectric properties of blood-glucose solutions is [11]. In [12], the authors measured dielectric properties of blood-glucose solutions but mathematical model has not been published. In previous paper [Vrba et al. IJAP 2015] it was shown, both by numerical simulation results as well as by measurement results, that there are significant differences between dielectric properties of physiological saline-glucose and blood-glucose solutions. Correspondingly, the physiological saline-glucose solutions are, at least in the considered frequency range from 1 to 8 GHz, not suitable models of blood-glucose solutions for experimental design/evaluation of blood glucose level monitoring systems.

Furthermore, it was concluded that the empirical model of dielectric properties of blood-glucose solutions [11] should be, according to our observations, revised.

In this paper, an existing 3D numerical concept for estimation of effective dielectric properties of oil and water emulsions with random droplet distribution was adapted for estimation of effective dielectric properties of blood-glucose solutions. Geometries of different blood cells were used in generation of the numerical models. The adapted concept uses a numerical model in COMSOL Multiphysics controlled with MATLAB scripts. In this study dielectric properties of blood cells as well as of blood plasma-glucose and physiological saline-glucose solutions were considered. The results of the numerical simulations were compared to data estimated by the existing empirical model and differences were discussed.

ACKNOWLEDGMENT

This research has been supported by the research program of the Czech Science Foundation (GACR) of the Czech Republic, Project No. 14-00386P Study of Thermal and Nonthermal Effects of High-Power EM Field on Structure of Matter.

REFERENCES

1. International Diabetes Federeation, "IDF DIABETES ATLAS," 6th Edition, ISBN 2-930229-85-3, online, www.idf.org/diabetesatlas, 2013.
2. So, C.-F., K.-S. Choi, T. K. Wong, and J. W. Chung, "Recent advances in noninvasive glucose monitoring," *Medical Devices*, Vol. 5, 45–52, Auckland, N.Z., Jun. 2012.
3. Jean, B., E. Green, and M. McClung, "A microwave frequency sensor for non-invasive blood-glucose measurement," *IEEE Sensors Applications Symposium, SAS 2008*, 4–7, 2008.
4. Green, E. C., "Design of a microwave sensor for non-invasive determination of blood-glucose concentration," Thesis, 53–56, 2005, includes bibliographical references.
5. Freer, B. and J. Venkataraman, "Feasibility study for non-invasive blood glucose monitoring," *2010 IEEE Antennas and Propagation Society International Symposium (APSURSI)*, 1–4, Jul. 2010.

6. Smulders, P. F. M., M. G. Buysse, and M. D. Huang, "Dielectric properties of glucose solutions in the 0.5–67 GHz range," *Microwave and Optical Technology Letters*, Vol. 55, 1916–1917, Aug. 2013.
7. Topsakal, E., T. Karacolak, and E. Moreland, "Glucose-dependent dielectric properties of blood plasma," *2011 XXXth URSI General Assembly and Scientific Symposium*, 1–4, Aug. 2011.
8. Karacolak, T., E. C. Moreland, and E. Topsakal, "Cole-cole model for glucose dependent dielectric properties of blood plasma for continuous glucose monitoring," *Microwave and Optical Technology Letters*, Vol. 55, 1160–1164, May 2013.
9. Hayashi, Y., L. Livshits, A. Caduff, and Y. Feldman, "Dielectric spectroscopy study of specific glucose influence on human erythrocyte membranes," *Journal of Physics D: Applied Physics*, Vol. 36, 369–374, Feb. 2003.
10. Livshits, L., A. Caduff, M. S. Talary, and Y. Feldman, "Dielectric response of biconcave erythrocyte membranes to d- and l-glucose," *Journal of Physics D: Applied Physics*, Vol. 40, 15–19, Jan. 2007.
11. Venkataraman, J. and B. Freer, "Feasibility of non-invasive blood glucose monitoring: In-vitro measurements and phantom models," *2011 IEEE International Symposium on Antennas and Propagation (APSURSI)*, 603–606, Jul. 2011.
12. Hofmann, M., G. Fischer, R. Weigel, and D. Kissinger, "Microwave-based noninvasive concentration measurements for biomedical applications," *IEEE Transactions on Microwave Theory and Techniques*, Vol. 61, 2195–2204, May 2013.

Design and Fabrication of a Low-profile mmWave Antenna Solution for the 5G Cellular Handsets

Byung-Su Kang[1], **Hyen-Kook Kwon**[1], **and Dong-Ho Kim**[2]

[1]Communications and Internet Research Lab
Electronics and Telecommunications Research Institute(ETRI), Republic of Korea
[2]Sejong University, Republic of Korea

Abstract— In this paper, a high-gain and low-profile mmWave Antenna solution for the 5G cellular user terminal is presented. A 28 GHz antenna solution for the upcoming 5G cellular communication is presented in detail. The proposed Antenna solution is for the handsets using switching beamforming structure. Extensive simulations and fabrication/measurement results ascertain the presented Antenna solution to be a simple and effective for cellular handsets operating in mmWave environments.

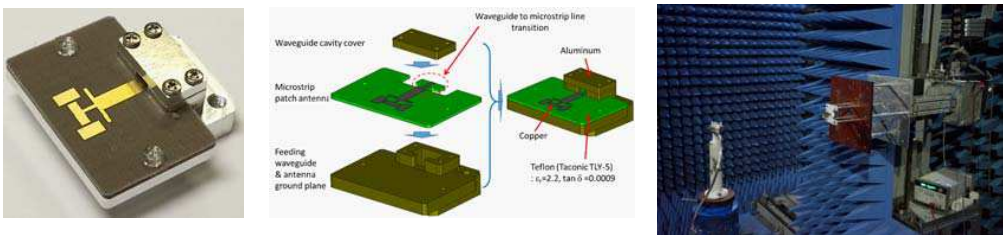

Figure 1: Fabricated antenna and chamber measurement environment.

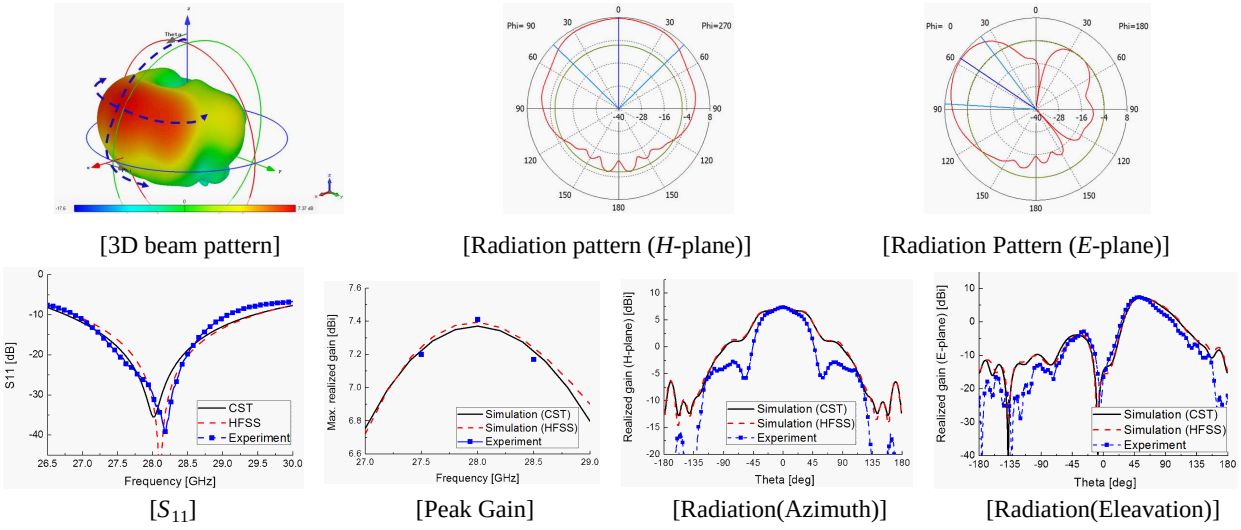

Figure 2: Simulation and measurement results.

ACKNOWLEDGMENT

This research was supported by 'The Cross-Ministry Giga KOREA Project' of The Ministry of Science, ICT and Future Planning, Korea. [GK14N0100, 5G mobile communication system development based on mmWave].

Broadband Slotted Bow-tie Antennas for Terahertz Resonant Tunnelling Diode Based Oscillators

Khalid Hamed Alharbi, Afesomeh Ofiare, Jue Wang, Monageng Kgwadi, Ata Khalid, and Edward Wasige
High Frequency Electronics Group, School of Engineering, University of Glasgow
Oakfield Avenue, G12 8LP Glasgow, Scotland, UK

Abstract— Terahertz (THz) radiation, whose frequency range lies between millimetrewaves and infrared light in the electromagnetic spectrum has many potential applications in different scientific fields such as medical diagnostics, security imaging, and wireless communication. Resonant tunnelling diode (RTD) based THz oscillators in integrated circuit (IC) form have recently been shown to be the technology in which many of these applications could be implemented. They operate at room temperature and have the potential to produce output power of around 1 mW at these frequencies. In this paper, a broadband bow-tie slot antenna for THz applications will be presented. The coplanar waveguide (CPW) fed bow-tie antenna is fabricated on an InP substrate for same chip integration with the promising resonant tunnelling diode terahertz oscillator. The antenna exhibits a very wide bandwidth (return loss $S_{11} < -10$ dB) around the design frequency (300 GHz). However, most of the radiation in the initial design is directed into the substrate because of the large dielectric constant ($\varepsilon_r = 12.56$) of the InP substrate. A technique to overcome this problem employing a reflector ground plane underneath a thin substrate of low dielectric constant is presented. The substrate used is benzocyclobutene (BCB) with dielectric constant $\epsilon_r = 2.6$. This substrate is realised by spinning it on a carrier substrate such as InP substrate with a coating of metallisation to act as the ground plane (and isolate the high permittivity InP substrate from the high frequency radiation). Initial simulation results (at 300 GHz) of this technique are reported and experimental validation at lower frequency (17 GHz) shows the feasibility of the concept.

On-wafer 2D Characterization Technique for Quasi-Yagi Antenna for G-band Applications

Khalid Hamed Alharbi, Afesomeh Ofiare, Jue Wang, Ata Khalid, David Cumming, and Edward Wasige
High Frequency Electronics Group, Division of Electronics and Nanoscale Engineering
School of Engineering, University of Glasgow, Oakfield Avenue, G12 8LP Glasgow, Scotland, UK

Abstract— The G-band of the electromagnetic spectrum (140–220) GHz is of great interest for different applications such as detection of concealed weapons and explosives, aircraft navigation in adverse low visibility weather conditions, and automotive collision-avoidance radar. Planar and directive antennas integrated in monolithic microwave/millimeter-wave integrated circuits (MMIC) could offer many advantages for such applications. High directivity will ensure that most of the RF power is radiated into a specific direction and, as a consequence, offer larger coverage distance and improve the communication link in the adverse weather conditions. This paper presents a G-band quasi-Yagi antenna and an associated on wafer setup for the characterization of its radiation pattern using a vector network analyser (VNA). The designed antenna shows a wide bandwidth (return loss < -10 dB) across the entire G-band. The proposed radiation pattern setup consists of identical one receiver and multi-transmitter antennas distributed angularly around the receiver antenna. All these antennas are fabricated on the same InP substrate that makes the angular positioning precise using lithography. Apart from the transmitting antenna directly opposite the receiving antenna, the antenna under test (AUT), all other transmitting antennas were realized with longer and curved lengths of coplanar waveguide (CPW) feed lines to ensure that these antennas always faced the AUT and that they could be probed Figure 1 shows the fabricated planar quasi-Yagi antennas for on-wafer radiation pattern characterization. The antenna exhibits an end-fire radiation pattern at frequencies around 200 GHz. The setup allows for E-plane radiation pattern to be measured and there is good agreement between measured and simulated results.

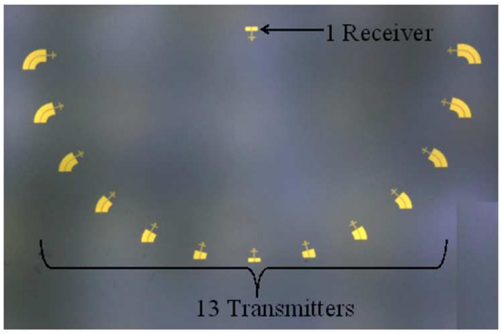

Figure 1: Fabricated planar quasi-Yagi antennas for on-wafer radiation pattern characterization. The extended CPW feed lines to facilitate probing and ensure the antennas face the AUT are clear to see.

Spontaneous Hemodynamic Activity in Prefrontal Cortex of Depression Patients Assessed with Functional Near-infrared Spectroscopy

Jiangxue Li[1], **Huilin Zhu**[2,*], **Xinge Li**[2,4], **Hongjun Peng**[3], **Jie Xu**[2], **Tingting Cai**[2], **and Sailing He**[2]

[1]The Research Center of Psychological Counseling
South China Normal University (SCNU), 510006, China
[2]Centre for Optical and Electromagnetic Research, South China Academy of Advanced Optoelectronics
South China Normal University (SCNU), Guangzhou 510006, China
[3]The Department of Clinical Psychology, Guangzhou Brain Hospital
(Guangzhou Huiai Hospital, The Affiliated Brain Hospital of Guangzhou Medical School), China
[4]School of Psychology, South China Normal University (SCNU), Guangzhou 510631, China

Abstract— Patients with major depressive disorder (MDD) typically suffered from pervasive depressed mood or anhedonia, accompanied by several cognitive and physical symptoms. In this study, functional near-infrared spectroscopy (fNIRS) was applied to investigate the spontaneous activity of hemodynamic in the prefrontal cortex (PFC) of the brain. 21 patients with MDD (including 12 with antidepressant and 9 without medication) participated in 8-min resting state measurement. By analyzing the interhemispheric correlation and the correlation maps of the PFC, our results indicated that patients with MDD showed significantly reduced interhemispheric correlation in the PFC and disrupted cortical organizations in the PFC. This study showed that fNIRS could be an effect and convenient way to assess neural features of depression.

*Corresponding author: Huilin Zhu (huilin.zhu@coer-scnu.org).

Session 3P1
FocusSession.SC2: Transformation Optics

Metamaterials and Transformation Optics for Single-photon Emitters

V. M. Shalaev[1], **M. Y. Shalaginov**[1], **N. Kinsey**[1], **P. R. West**[1], **M. Ferrera**[1, 2], **A. V. Kildishev**[1], **and A. Boltasseva**[1]

[1]School of Electrical and Computer Engineering & Birck Nanotechnology Center
Purdue University, West Lafayette, IN 47907, USA
[2]School of Engineering and Physical Sciences
Heriot-Watt University, Edinburgh, Scotland EH14 4AS, UK

Abstract— We have experimentally demonstrated the broadband enhancement of single-photon emission from nanodiamond NV centers coupled to planar multilayer metamaterial with hyperbolic dispersion. A tapered metamaterial waveguide for efficient outcoupling of high-k metamaterial modes has been numerically studied and fabricated.

Introduction: The major thrust of research in quantum photonics is to build quantum computing and networking technologies [1]. The simplest and most fundamental quantum photonic states to be employed are single photons. Many techniques based on nonlinear phenomena and atom-like systems have been demonstrated to generate single photons. Nitrogen vacancy (NV) color centers in diamond have attracted widespread attention due to their stable, broadband, and anti-bunched emission at room temperature [2], however, the efficiency of such emission is naturally low. Massive research efforts to solve this problem have utilized resonant based structures, which are typically narrowband and have a relatively slow response.

Enhancement of Single-photon Emission by Hyperbolic Metamaterials: An unorthodox approach is to use metamaterials with hyperbolic dispersion (HMM) [3], which enables one to implement highly efficient, broadband, and fast single-photon sources. In our recent work, we have experimentally studied the broadband enhancement of single-photon emission from nanodiamond NV centers coupled to a planar multilayer metamaterials with hyperbolic dispersion [4]. The metamaterial is fabricated as an epitaxial metal/dielectric superlattice consisting of CMOS-compatible ceramics: titanium nitride (TiN) and aluminum scandium nitride ($Al_xSc_{1-x}N$). It has been demonstrated that employing the metamaterial results in significant enhancement of collected single-photon emission and reduction of the excited-state lifetime.

Tapered HMM as an Efficient Method for Outcoupling High-k Modes: The emission enhancement mechanism is based on the HMM ability to support extra radiative channels. These channels are surface and bulk high-k metamaterials modes. Hence, the emission rate of NV center coupled to HMM can be further increased by proper outcoupling of these high-k HMM modes into free-space modes. As a next step, we suggest a modification of both the HMM structure and the detection scheme to enable more efficient photon collection. In this new approach, adiabatically tapered HMM waveguides which transition from high filling fraction for maximal emitter enhancement to a lower filling fraction for optimal outcoupling were designed and fabricated using shadowed angle deposition technique. The total outcoupling efficiency of the high-k modes in the in-plane direction is expected to be two to three orders of magnitude better than standard out-of-plane outcoupling methods.

ACKNOWLEDGMENT

This work was supported by AFOSR-MURI grant (FA9550-10-1-0264), AFOSR grant (FA9550-12-1-0024), NSF-MRSEC grant (DMR-1120923), and ARO Grant 56154-PH-MUR.

REFERENCES

1. Monroe, C., *Nature*, Vol. 416, No. 6877, 238, 2002.
2. Gruber, A., et al., *Science*, Vol. 276, No. 5321, 2012, 1997.
3. Jacob, Z., et al., *Appl. Phys. B*, Vol. 100, 215, 2010.
4. Shalaginov, M. Y., et al., *Laser Photon. Rev.*, Vol. 9, No. 1, 120, 2015.
5. P. R. West, et al., *Nano. Lett.*, Vol. 15, No. 1, 498, 2015.

Omnidirectional Light Concentrators-absorbers — How to Make Their Core Flat?

Alexander V. Kildishev[1] **and Ludmila J. Prokopeva**[1, 2, 3]

[1]Birck Nanotechnology Center, West Lafayette, USA
[2]Novosibirsk State University, Novosibirsk, Russia
[3]Institute of Computational Technologies, Novosibirsk, Russia

Abstract— We review our previous and most recent progress in designing omnidirectional optical concentrators that can be used to trap almost all light with no dependence on the incident angle. The classical design is arranged of a spherical (circular cylinder) shell encapsulating a concentric absorbing core of the same shape. Omnidirectionality is an important feature for non-imaging applications, including efficient photovoltaic cells for mobile and drop-and-forget systems, as well as multicolor IR sensing, which is known to have problems with oblique incidence of light. An important desired feature is a thin and flat design of the absorbing semiconductor element which is integrated into the omnidirectional lens device. Our most recent results show that flattening the absorbing element is possible by using the oblate spheroidal (elliptic cylinder) shell as the trapping lens so that a disk (strip) absorber could be fabricated.

Previous studies [1, 2] have shown that almost total omnidirectional absorption of light can be achieved with a gradient radial distribution of the refractive index $n(r) = n_0(r_0/r)^p$ ($p \geq 1$, r is the radial coordinate, and n_0 is the refractive index of the ambient media) [1, 2]. Theoretical analysis was performed in terms of geometric optics and full wave propagation. Moreover, an estimation of the absorbing efficiency was obtained depending on the device parameters. Further, this design was successfully tested with microwave metamaterials [3], and most recently, a nanostructured device performance was validated in experiments for visible light [4].

We flatten the absorbing core [5] by mapping the radial distribution $n(r) = n_0(r_0/r)^p$ onto an elliptic distribution $n(u) = n_0(\sinh u_0/\sinh u)^p$ where u is either the elliptic cylinder or spheroidal coordinate. In contrast to the previous case where the Hamiltonian equations for ray traces can be integrated explicitly, here the system of equations is more complex. We have developed accurate numerical solutions of the Hamilton equations that agree well with our simulations in the Ray Optics module of COMSOL Multiphysics. The results confirm the trapping performance for two geometrical variations — elliptic cylinder and oblate spheroid. Further we add an absorbing core to our designs and full-wave simulations with a Gaussian beam are done to finally prove the trapping and absorbing capability of the proposed designs.

Equipped with flat absorbing cores, which are easily fabricated, microlenses with omnidirectional absorption open up unparalleled possibilities for designing efficient sensing devices and photovoltaic low-power sources for mobile and unattended applications.

REFERENCES

1. Narimanov, E. E. and A. V. Kildishev, "Optical black hole: Broadband omnidirectional light absorber," *Appl. Phys. Lett.*, Vol. 95, 041106, 2009.
2. Kildishev, A. V., L. J. Prokopeva, and E. E. Narimanov, "Cylinder light concentrator and absorber: Theoretical description," *Opt. Express*, Vol. 18, 16646–16662, 2010.
3. Cheng, Q., et al., "An omnidirectional electromagnetic absorber made of metamaterials," *New J. of Phys.*, Vol. 12, 063006, 2010.
4. Sheng, C., et al., "Trapping light by mimicking gravitational lensing," *Nat. Photonics*, Vol. 7, 902–906, 2013.
5. Prokopeva, L. J. and A. V. Kildishev, "Elliptic light absorber: Trapping light between two foci," *Frontiers in Optics 2014, OSA Technical Digest*, online, paper FTu2G.2, 2014, http://www.-opticsinfobase.org/abstract.cfm?URI=FiO-2014-FTu2G.2.

Farfield Sub-wavelength Imaging with Compact Dielectric Lens

Jingjing Zhang
Department of Photonics Engineering, Technical University of Denmark
DTU Fotonik, DK-2800 Kgs. Lyngby, Denmark

Abstract— For decades researchers have made various attempts to beat the diffraction limit and realize subwavelength imaging. Here I present the approach to design modified solid immersion lenses that deliver the subwavelength information of objects into the far field, yielding magnified images. The lens is designed by combining a transformation optics forward design with an inverse design scheme, where an evolutionary optimization procedure is applied to find the material parameters for the matching layers. Compared to previous approaches based on the simple discretized approximation of a coordinate transformation design, my method allows for much more precise recovery of the information of objects, especially for those with asymmetric shapes. The lens can be realized by an isotropic dielectric core and anisotropic or isotropic dielectric matching layers. The total radius of the lens is only 2.5 wavelengths and the resolution can reach up to $\lambda/6$. It allows for the far-field subwavelength imaging at optical frequencies with compact dielectric devices.

A Wide-angle Broadband Polarizer Based on a Field Transformation Approach

Junming Zhao[1, 2], **Yang Hao**[2], **and Yijun Feng**[1]

[1]School of Electronic Science and Engineering
Nanjing University, Nanjing 210093, China
[2]School of Electronic Engineering and Computer Science
Queen Mary University of London, London E1 4NS, United Kingdom

Abstract— Controlling polarization states is one of the most important topics in electromagnetic (EM) wave manipulation. Up to now, various polarizer designs have been proposed for both transmission and reflection achieving polarization conversions between TE (transverse electric) and TM (transverse magnetic), LCP (left-handed circular polarization) and RCP (right-handed circular polarization), linear and circular polarizations. However, most conventional designs are only adapted to normal incidence with fundamental physical limitations in the product of bandwidth and incident angle. Transformation optics offers a geometrical approach in designing optical components, which can automatically work for arbitrary excitations. Such a transformation technique has been extended to the polarization domain based on a recently proposed field transformation (FT) method [1]. By employing a reduced-parameter approximation in constructing FT media with purely dielectric composites, we design and demonstrate a FT-based polarizer in converting between TE and TM and between LCP and RCP with both wide-angle and broadband operation. Such a polarizer can also be easily extended to different operation modes for both transmitted and reflected waves by adjusting its thickness and adding an optional metallic ground plane. We prove that the proposed technique has its potential to overcome the fundamental limit of current polarizers and can be applied to a broad range of applications from microwave to optics.

ACKNOWLEDGMENT

This work is partially supported by the National Nature Science Foundation of China (61301017, 61371034, 61101011), the Key Grant Project of Ministry of Education of China (313029), the Ph.D. Programs Foundation of Ministry of Education of China (20120091110032), and partially supported by Jiangsu Key Laboratory of Advanced Techniques for Manipulating Electromagnetic Waves.

REFERENCES

1. Liu, F., Z. Liang, and J. Li, "Manipulating polarization and impedance signature: A reciprocal field transformation approach," *Phys. Rev. Lett.*, Vol. 111, 033901, 2013.

Design Metasurface from Transformation Optics

Yadong Xu, Yangyang Fu, and Huanyang Chen
College of Physics, Optoelectronics and Energy, Soochow University, Suzhou 215006, China

Abstract— In this talk, we will show that transformation optics could be used to design metasurface in steering beams. Such a metasurface or slab could be realized by a sub-wavelength grating with dielectrics and metal. The generalized laws of reflection and refraction should be modified in such a structure. We also realized a related acoustic metasurface based on this similar idea.

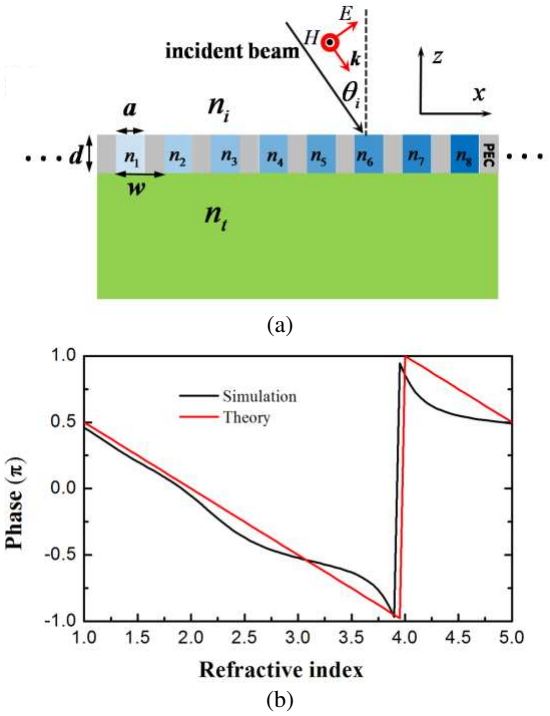

Figure 1: (a) The schematic plot of a sub-wavelength grating based on transformation optics. (b) The phase delay at different positions of the structure.

REFERENCES

1. Xu, Y., Y. Fu, and H. Chen, "Steering light by a sub-wavelength grating based on transformation optics," *Scientific Reports*, under review, 2015.
2. Xie, Y., W. Wang, H. Chen, A. Konneker, B.-I. Popa, and S. A. Cummer, "Wavefront modulation and subwavelength diffractive acoustics with an acoustic metasurface," *Nature Communications*, Vol. 5, 5553, DOI: 10.1038/ncomms6553, 2014.

Transformation Optics and EELS in Plasmonics

Matthias Kraft[1], **Yu Luo**[2], **and John B. Pendry**[1]

[1]Blackett Laboratory, Imperial College London, SW7 2AZ, UK
[2]School of Electrical and Electronic Engineering, Nanyang Technological University, Singapore

Abstract— Transformation optics is a relatively new subfield in electromagnetic research. Yet, it has been at the heart of many of the most promising advancements in electromagnetism in recent years. Originally developed to aid numerical simulations in cylindrical geometries, it has since been applied as a design tool for such exotic devices as invisibility cloaks or negative refractive index lenses. Within the last 5 years, Transformation optics has entered the field of plasmonics. It has proved valuable as a design tool for devices such as beam shifters, surface cloaks or light harvesters. Moreover, it has also proven itself as an analytical tool in the study of interacting plasmonic nano-particles or van der Waals forces. In this talk we would like to add an entry to the already long list of fields where Transformation optics can make a difference. The study of electron energy loss spectroscopy of plasmonic nano-particles.

Passive and Active Devices for Spoof Surface Plasmon Polaritons in the Microwave Frequency

Tie Jun Cui
State Key Laboratory of Millimeter Waves, Southeast University, Nanjing 210096, China

Abstract— We propose planar plasmonic metamaterial on thin metal films with nearly zero thickness to support spoof surface plasmon polaritons (SPPs) in microwave and terahertz frequencies. From the theoretical simulations and experiments, we show that spoof SPPs can propagate along an ultrathin metallic film by corrugating its edge with periodic array of grooves. Such a planar plasmonic metamaterial can sustain highly localized SPPs along two orthogonal directions in broadband by keeping good modal shape and propagating long distance with low bending loss. The ability to bend spoof SPPs freely on ultrathin film makes the planar plasmonic metamaterial more practical to produce passive plasmonic devices, such as the SPP bends, splitters, filters, polarizers, and resonators. Experiments validate the feasibility of planar plasmonic metamaterial. Based on the above idea, we present the concept of conformal surface plasmons (CSPs), i.e., the surface plasmon waves that can propagate on ultrathin and flexible films to long distances. The flexible ultrathin films can be bent, folded, and even twisted to mould the flow of CSPs.

We also propose and experimentally demonstrate spoof localized surface plasmons (LSPs) on a planar textured metallic disk at the microwave and terahertz frequencies. We design and realize the plasmonic metamaterial using ultrathin metal film printed on a thin dielectric substrate and observe the multipolar plasmonic resonances in both numerical simulations and experiments, including the dipole, quadrupole, hexapole, octopole, decapole, dodeca-pole, and quattuordecpole modes. The simulation and experiment results have very good agreements. We show that the spoof LSP resonances are sensitive to the disk's geometry and local dielectric environments, and hence the ultrathin textured metallic disk has potential applications as plasmonic sensor in the microwave and terahertz frequencies.

Finally, we present active SPP devices using the subwavelength-scale amplifier chips in the microwave frequency, including the significant amplification of SPP waves and higher-order harmonic generations of SPPs, which result in SPP amplifier and SPP mixer. We also propose an efficient conversion between the conventional spatial waves and the SPP modes. Based on the conversion and passive and active SPP and LSP devices, we propose integrated spoof SPP/LSP circuits to realize a series of functionalities, and give experimental demonstrations.

Transformation Optics with Spatially Dispersive Electromagnetic Media

Jie Luo, **Yu Ting Yang**, **Zhi Hong Hang**, **C. T. Chan**, **and Yun Lai**
Optoelectronics and Energy & Collaborative Innovation Center of Suzhou Nano Science and Technology
College of Physics, Soochow University, Suzhou 215006, China

Abstract— Metamaterials and transformation optics have enormously enriched human's ability to control electromagnetic waves and light, leading to novel applications such as cloaking, exotic lens, illusion optics, etc..

In previous designs of transformation optics devices, local media with special parameters and anisotropy have been widely used. However, the realization of these parameters is really difficult. For example, in most of previous experimental realization of cloaking, reduced parameters have been applied, which would lead to reflection and therefore compromised cloaking effect.

In fact, we demonstrate that ultra-transparent materials with wide-angle and even omnidirectional non-reflection and total transmission can be realized with spatially dispersive electromagnetic media, whose parameters are k-dependent.

We theoretically and experimentally demonstrate realization of ultra-transparent spatially dispersive media. We also demonstrate novel transformation optics devices beyond traditional theory based on local media [1].

Our work shows the possibility of spatially dispersive media in controlling electromagnetic waves and light in unprecedented ways.

REFERENCES

1. Luo, J., Y. T. Yang, Z. H. Hang, C. T. Chan, and Y. Lai, to be Submitted.

Manipulating Microwaves Using Metamaterials and Metasurfaces

A. P. Hibbins, **R. Mitchell-Thomas**, **J. A. Dockrey**, **L. Parke**,
S. A. Horsley, **I. R. Hooper**, **B. Woods**, **and J. R. Sambles**
Electromagnetic and Acoustic Materials Group, Department of Physics and Astronomy
University of Exeter, Stocker Road, Exeter EX4 4QL, United Kingdom

Abstract— The latest experimental results undertaken as part of Exeter's metamaterials research theme are presented, and will include narrow (subwavelength) beaming of surface waves, reflection-less metamaterials and other transformation-optics devices.

This presentation showcases some of the most recent experimental work being undertaken in the field of microwave metamaterials and metasurfaces at Exeter as part of the EPSRC programme grant, "the Quest for Ultimate Electromagnetics using Spatial Transformations (QUEST)". This 5-year grant is shared with electrical engineers at the Queen Mary University of London, and material engineers at University of Oxford.

The patterning of surfaces with small, closely spaced elements is well known to influence their interaction with electromagnetic radiation. As long ago as the 1940s [1], radar engineers were considering how the addition of a sub-wavelength corrugation to a metal can modify its electromagnetic boundary condition so that surface waves become tightly bound to the interface. Our experimental research has demonstrated how metasurfaces and metafilms can be utilised to spatially engineer artificial boundary conditions and modify the mode-index of the waves supported [2]. We have very recently shown that a dumb-bell array (essentially a double-ended mushroom) can support surface waves with negative mode index, i.e., surface eigenstates that have antiparallel momentum and power vectors. The FFT of a 2D field scan from such a surface allows us to visualise the complete band structure of the modes of the system. Using this

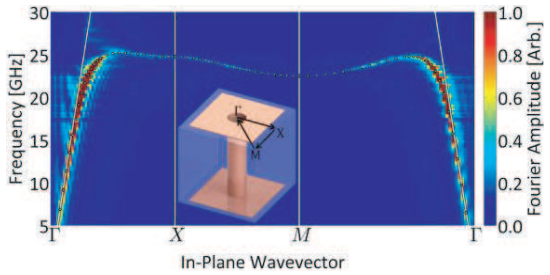

Figure 1: Experimentally determined band structure of surface waves on array of dumb-bells, illustrating the regions of negative mode index.

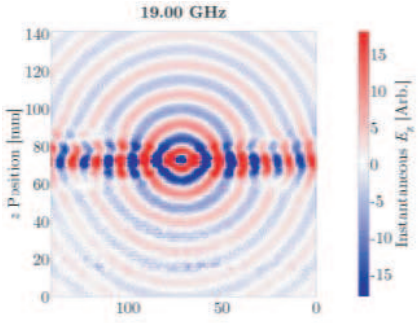

Figure 2: The electric field associated with beaming of surface waves measured above an array of complimentary double SRRs. Excitation is via a dipole antenna.

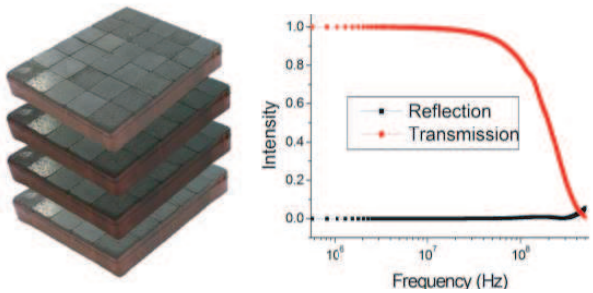

Figure 3: Anisotropic array of ferrite-composite cubes, and its anti-reflection response. (Layer spacing in photograph is not to scale).

Figure 4: Modelled radiation pattern from patch antenna, and the enhanced directivity achieved via the use of a lens designed via quasi-conformal mapping.

technique we also demonstrate surface geometries that can support channelling of surface energy into beams that have a subwavelength width, and which do not spread.

Other research themes being explored include the design and testing of broadband, reflection-less materials. Some of the advances that we have made in this theme have been brought about by the realisation that the particle size in a ferrite-composite (e.g., with PTFE as the matrix) yields an additional degree of freedom in the design of bespoke material properties. Impedance matching has been demonstrated via the careful design of composites alone, or using structuring of the composites [3]. Whereas the use of ferrites for this purpose is often limited to frequencies below 1 GHz, a new and exciting approach, based on a Kramers-Kronig-like relation in space rather than frequency, is now being explored experimentally.

More conventional incarnations of spatial transformation techniques are also being explored. These include changing the radiation of simple antennas, using bespoke dielectric lenses designed using quasi-conformal mapping. We have also designed and tested a curved Luneburg lens and surface wave cloak for 2D geometries by utilising a combination of variation of guide curvature and thickness to provide the required mode index.

REFERENCES

1. Cutler, C. C., "Bell telephone labs," *Report*, Vol. 10, 44–160, 1944.
2. Dockrey, J. A., et al., *Phys. Rev. B*, Vol. 87, 125137, 2013.
3. Parke, L., et al., *Applied Physics Letters*, Vol. 104, 221905, 2014.

Realization of Invisible Cloaking for Multiphysics

Yichao Liu, **Jianfei Zhu**, **We Jiang**, **and Yungui Ma**
State Key Lab of Modern Optical Instrumentation, Centre for Optical and Electromagnetic Research
Zhejiang University, Hangzhou 310058, China

Abstract— Invisible cloaks have attracted great attentions for their magic application on electromagnetic waves [1, 2]. Recently this concept has been vastly extended to other fields and phenomena controlled by different equations. Previously we have successfully applied the coordinate transformation to thermal conduction equations by showing a transient heat cloak [3] and also a thin thermal plate that could provide a homogeneous heating surface with a tiny source [4]. In this talk, we will report our recent work on the first realization of a multiphysics cloaking experiment that showed a desired dual thermal-electric cloaking behavior [5]. In the end, we will also introduce our new experiment results on AC magnetic cloaks using combined nature materials that allows a promising application in hiding metallic objects.

REFERENCES

1. Pendry, J., D. Schurig, and D. R. Smith, "Controlling electromagnetic fields," *Science*, Vol. 312, 1780–1781, 2006.
2. Leonhardt, U., "Optical conformal mapping," *Science*, Vol. 312, 1779–1780, 2006.
3. Ma, Y. G., L. Lan, W. Jiang, F. Sun, and S. L. He, "A transient thermal cloak experimentally realized through a rescaled diffusion equation with anisotropic thermal diffusivity," *NPG Asia Mater.*, Vol. 5, e75, 2013.
4. Liu, Y. C., W. Jiang, S. L. He, and Y. G. Ma, "An efficient plate heater with uniform surface temperature engineered with effective thermal materials," *Opt. Express*, Vol. 22, 170006, 2014.
5. Ma, Y. G., Y. C. Liu, M. Raza, Y. Wang, and S. L. He, "Experimental demonstration of a multiphysics cloak: Manipulating heat flux and electric current simultaneously," *Phys. Rev. Lett.*, Vol. 113, 205501, 2014.

Transformation Cloaks for Surface Electromagnetic Waves

Hongyi Xu[1], **Xu Su**[2, 3, 4], **Handong Sun**[1, 5], **Hongsheng Chen**[2, 3, 4], **and Baile Zhang**[1, 5]

[1]Division of Physics and Applied Physics, School of Physical and Mathematical Sciences
Nanyang Technological University, Singapore 637371, Singapore
[2]State Key Laboratory of Modern Optical Instrumentation
Zhejiang University, Hangzhou 310027, China
[3]The Electromagnetics Academy at Zhejiang University
Zhejiang University, Hangzhou 310027, China
[4]Department of Information Science & Electronic Engineering
Zhejiang University, Hangzhou 310027, China
[5]Centre for Disruptive Photonic Technologies
Nanyang Technological University, Singapore 637371, Singapore

Abstract— Surface wave such as surface plasmon polaritons in optical wavelength has become one of the most promising signal carriers for future information technologies with virtue of high energy confinement in a subwavelength volume. However, before it can be further applied in practical electromagnetic and optoelectronic applications, there remain several major obstacles that need to be addressed. One of the long-existing problems is that the propagation of surface wave is subject to high scattering loss on rough surface. Here we propose some cloaking devices that can realize near-perfect suppression of surface wave scattering at rough surface.

Generalized Refractive Index for Transformation Optics and beyond

M. McCall, **P. Kinsler**, **and D. Topf**
Department of Physics, Imperial College London, Prince Consort Road, London SW72AS, UK

Abstract— The refractive index $n(\mathbf{r})$, of an inhomogeneous electromagnetic medium is a familiar, but derived electromagnetic quantity, that not only governs the rate of phase advance of electromagnetic waves in a medium, but also determines the trajectory of optical rays according to the ray equation

$$\frac{d}{ds}\left[n(\mathbf{r})\frac{d\mathbf{r}}{ds}\right] = \nabla n. \tag{1}$$

This equation also results from the conformal transformation space according to $g \to n^2 g$, where g is the metric of the initial (e.g., Euclidean) space. In discussing transformation optics, and its possible extensions beyond electromagnetics, it would be useful to have available an analogous quantity $n(\mathbf{r})$ that generalizes to arbitrary, non-conformal transformations. The direction at a given point $\mathcal{P}$ on a ray is characterized by its tangent vector $\mathbf{v}$. If the ray is deformed via the (diffeo)-morphism φ: $\mathbb{R}^3 \to \mathbb{R}^3$, then we find that a generalized index is given by

$$n_{\varphi(\mathcal{P})} = \left[\frac{g_{\mathcal{P}}(\mathbf{v},\mathbf{v})}{g_{\varphi(\mathcal{P})}(\varphi_*\mathbf{v},\varphi_*\mathbf{v})}\right]^{1/2},$$

where $\varphi_*\mathbf{v}$ is the so-called *push forward of* $\mathbf{v}$. Although the generalized index is a scalar quantity, it carries an angular dependance through the choice of the direction of the vector $\mathbf{v}$.

The concept of the generalized index seems to lie at the heart of all ray-based transformation theories (e.g., transformation optics, transformation acoustics, etc.). In transformation optics, for example, the morphism φ defines an electromagnetic medium for which

$$\epsilon = \mu\frac{\mathbf{J}\mathbf{J}^T}{|\det(\mathbf{J})|} = \kappa \quad \text{say},$$

where $\mathbf{J}$ is the Jacobian associated with the morphism φ. In this case we find that the generalized refractive index is given by

$$n(\theta,\phi,\mathbf{r}) = \left[\det\left(\kappa^{-1}\right)_{\perp}\right]^{1/2},$$

where $\perp$ indicates a projection perpendicular to the direction defined by the angular variables θ and ϕ. In fact we find that $n(\theta,\phi,\mathbf{r})$ defines an ellipsoid at each point $\mathbf{r}$.

Turning the argument around, *given* some $n(\theta,\phi,\mathbf{r})$, say the generalized index distribution for an optical cloak, we can *derive* the principal coefficients of the associated electromagnetic medium via

$$\kappa_1 = \frac{n_2 n_3}{n_1}, \quad \kappa_2 = \frac{n_3 n_1}{n_2}, \quad \kappa_3 = \frac{n_1 n_2}{n_3},$$

where $n_{1,2,3}$ are the principal indices associated with $n(\theta,\phi,\mathbf{r})$.

Moving to acoustics we find the relationship between generalized index and the acoustic medium parameters is given by

$$n(\mathbf{r}) = \left[\frac{(B/\rho)_{ij}s^i s^j}{B_0/\rho_0}\right]^{1/2},$$

where

$$(B/\rho)_{ij} = \left(\frac{B_0}{\rho_0}\right)(\phi_*)_i^m\,(\phi_*)_i^n\,g_{mn}$$

We will present our numerical evidence to support the correctness of these ideas.

A Revisit to Transformation Optics: A Precise Or Approximated Method?

Jin Hu
School of Information and Electronics, Beijing Institute of Technology, Beijing 100081, China

Abstract— Transformation optics is one of the most important design tools in the field of artificial electromagnetic materials or metamaterials. It is well accepted that the transformation optics can precisely control the electromagnetic fields. In this talk, we revisit this method and find in general it is in fact an approximate one in controlling the fields amplitudes if the transformation is started from isotropic and homogeneous materials. The transformation optics is usually established based on the Maxwell's equations without the Gauss's laws, and then it can be noted that there are no derivations of materials parameters, the physical model is thus a piece-wise homogeneous one that the variations of the materials round any point are ignored, the equations have same form whether $\boldsymbol{\varepsilon}$ or $\boldsymbol{\mu}$ is constant or variable of the positions, the locally affine based transformation relations can be applied in such a model. However, if the Gauss's laws are included into consideration, the derivations of the materials parameters appear which means the variations of the materials round any point cannot be ignored, the whole system will have different forms depending on the character of $\boldsymbol{\varepsilon}$ or $\boldsymbol{\mu}$, thus the physical model is not a piece-wise homogeneous but higher order one. The local affine feature of the transformation relations makes it is impossible to transform a piece-wise homogeneous element to a higher order one, and vice versa. That is to say, in general the system loses the form-invariance through the given transformation relation. The approximation is verified by an example of isotropic lens for electromagnetic wave control. The application scope of transformation optics thus is clarified. The conclusions here are important to the applications that utilizing the transformation field amplitudes and the study is also helpful to develop the framework of transformation optics.

Analogue Transformations and Their Application to Optics

Carlos García-Meca[1, 2]

[1]Nanophotonics Technology Center, Universitat Politècnica de València, Spain
[2]Instituto de Astrofísica de Andalucía (CSIC), Granada, Spain

Abstract— During the last few years, transformation acoustics has emerged as a powerful tool for designing devices able to control sound waves in an unprecedented manner. This technique takes advantage of the form invariance of the acoustic equations under spatial transformations to obtain the material parameters that deform acoustic space in a prescribed way, e.g., for cloaking acoustic waves [1].

However, this approach has been undermined by the Galilean character of fluid mechanics, which reduces the power of the traditional transformational method when applied to acoustics. Specifically, classical acoustic equations are not form invariant under transformations that mix space and time [2, 3]. As a consequence, the method cannot be applied to design devices based on this kind of transformation, contrarily to what has been done in optics.

Recently, the problem of transformation acoustics was approached from another angle [2, 3]. Instead of using directly the symmetries of the acoustic equations to bridge between different solutions for the propagation of acoustic waves, the symmetries of an analogue abstract space-time (described by relativistic form-invariant equations) are exploited. In this method, each couple of solutions connected by a general coordinate transformation in the analogue space-time can be mapped to acoustic space. This way, it is possible to find the relation between the acoustic material parameters associated with each of these transformation-connected solutions. The result is an alternative version of transformation acoustics as powerful as its optical counterpart.

On the other hand, with their underlying relativistic geometry, Maxwell's equations are invariant under any space-time transformation. In this sense, the use of an optical analogue transformation technique is, in principle, not required in any case.

Nevertheless, in this talk we show that the concept of analogue transformations can be applied to the field of optics in order to achieve a variety of effects different from those obtained with the standard transformation technique. We illustrate the potential of this new approach with some practical examples.

ACKNOWLEDGMENT

The author acknowledges support from Generalitat Valenciana through the VALI+D postdoctoral program (exp. APOSTD/2014/044).

REFERENCES

1. Chen, H. and C. T. Chan, "Acoustic cloaking and transformation acoustics," *J. Phys. D: Appl. Phys.*, Vol. 43, 113001, 2010.
2. García-Meca, C., S. Carloni, C. Barceló, G. Jannes, J. Sánchez-Dehesa, and A. Martínez, "Analogue transformations in physics and their application to acoustics," *Sci. Rep.*, Vol. 3, 2009, 2013.
3. García-Meca, C., S. Carloni, C. Barceló, G. Jannes, J. Sánchez-Dehesa, and A. Martínez, "Space-time transformation acoustics," *Wave Motion*, Vol. 51, 78–797, 2014.

Toroidal Dipole Induced Scattering Transparency of Nanoparticles

Wei Liu[1, 2]

[1]College of Optoelectronic Science and Engineering
National University of Defense Technology, Changsha, China
[2]Nonlinear Physics Centre, Research School of Physics and Engineering
Australian National University, Australia

Abstract— We show that toroidal dipoles can be excited within high-permittivity dielectric nanoparticles and significantly influence the scattering profile in the optical regime. We further reveal that the scattering transparencies of core-shell plasmonic nanoparticles can be classified into two categories: i) the *trivial* transparency with no effective multipole excitations within the particle, and ii) the *non-trivial* one induced by the destructive interferences of induced electric and toroidal multipoles.

The almost identical descriptions of multipole expansions for radiation sources in many textbooks (including the classical one by J. D. Jackson [1]) lead to a dogma that the decomposition into electric and magnetic multipoles are sufficient. Consequently, though the scattering of individual nanoparticles plays a profound role in the flourishing fields of plasmonics and metamaterials, scattering related interpretations are still based on electric and magnetic resonances only, where the toroidal components are overlooked [2]. This unfortunately results in inaccurate explanations for some fundamental scattering properties, and thus may hinder further breakthroughs in both scattering related basic researches and applications.

We revisit the seminal problem of spherical nanoparticle scattering based on the multipole expansion method with toroidal components included [2–5]. In Fig. 1(a) the configuration of the scattering problem is shown and in Fig. 1(b) we show the schematic illustration of the magnetic field and current distribution of the toroidal dipole (TD) excited. As is shown, the TD can be interpreted as a series of magnetic dipoles aligned along a circle [2], which actually also represents the field-lines of **H**. Then we study a dielectric (refractive index $n = 3.5$) sphere of radius $R = 100\,\mathrm{nm}$ and show the near-field distributions at the TD (can be effectively excited within the sphere) resonant position in Fig. 1(c), which agree well with the results shown in Fig. 1(b). We further study the hybrid metaldielectric core-shell nanoparticles (results not shown), and identify two different mechanisms of the scattering transparencies of those particles: i) the *trivial* transparency without effective multipole excitation inside and ii) the *non-trivial* one caused by scattering cancellation of electric and toroidal dipoles excited simultaneously. We note here that though there have already been extensive studies on the transparency phenomena in core-shell nanoparticles (e.g., see Ref. [6]), the crucial roles that could be played by toroidal multipoles have not been clearly identified as we have done here.

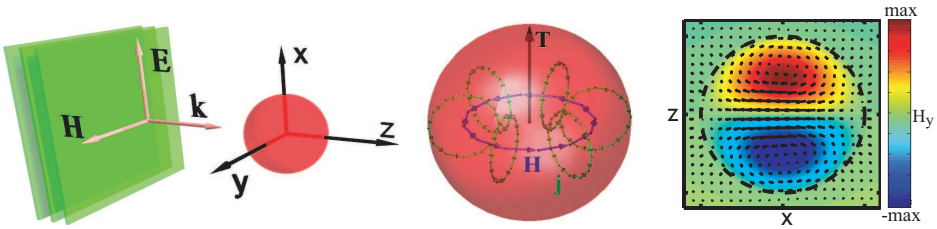

Figure 1: (a) The scattering of a spherical particle with an incident plane wave. (b) Schematic illustration of the toroidal dipole excited within the particle. Both the current **j** and magnetic field **H** distributions have been shown. (c) Near-fields of the TD resonance on the x-z plane (color-plot: $\mathbf{H}_y$; vector-plots: electric fields on plane).

The introduction of toroidal multipoles into scattering particles sheds new light to many related studies and can possibly expand significantly the applications of scattering particles. Moreover, investigations into light-matter interactions involving toroidal multipoles can possibly merge with the fields of topological and low-dimensional photonics, and thus help to establish new platforms for the study of many exotic optical effects.

REFERENCES

1. Jackson, J. D., *Classical Electrodynamics*, Wiley, New York, 1962.
2. Kaelberer, T., et al., *Science*, Vol. 330, 1510, 2010.
3. Miroshnichenko, A. E., et al., arXiv:1412.0299, 2014.
4. Liu, W., et al., arXiv:1412.4931, 2014.
5. Liu, W., et al., arXiv:1502.02205, 2015.
6. Alu, A. and N. Engheta, *Phys. Rev. E*, Vol. 72, 016623, 2005.

Using Complex Coordinates to Understand Reflection

S. A. R. Horsley
University of Exeter, Stocker Road, Exeter, UK

Abstract— In this talk I will explain that to understand the propagation of waves it can be useful to treat the space-time coordinates as complex numbers. For instance, our results demonstrate that there is a simple way to control reflection from an inhomogeneous medium in terms of the properties of the permittivity in the complex position plane. This technique is distinct from existing work that makes use of complex coordinates in transformation optics [1, 2]. Rather than *transform* the propagation axis from the real line into the complex plane, here we solve the wave equation in the entire complex plane and relate properties of the wave at complex positions to the propagation on the real axis.

To illustrate how complex coordinates can be useful, we'll take simple example. Consider wave propagating in one dimension according to the equation

$$\left[\frac{d^2}{dz^2} + k_0^2\epsilon(z)\right]\varphi(z) = 0 \tag{1}$$

where φ could be single component of the electric field, or some scalar field such as sound, and z is complex number representing position. In this case take the following permittivity profile

$$\epsilon(z) = 1 + \frac{1}{(z/a + i)^2}. \tag{2}$$

which has single second order pole at the point $z = -ia$. Figure 1 shows plot of the permittivity (2), and wave propagation both along the real line, and in the entire complex position plane.

There are several things to notice about Figure 1. Firstly, this is PT-symmetric permittivity profile with zero reflection for wave incident from the left (such behaviour of PT-symmetric structures is already known [4]). In the complex position plane the profile has single pole at $z = -ia$, and from this pole runs branch cut in the value of the field φ. In fact, we have found that when there is pole in the permittivity in the complex position plane then there is nearly

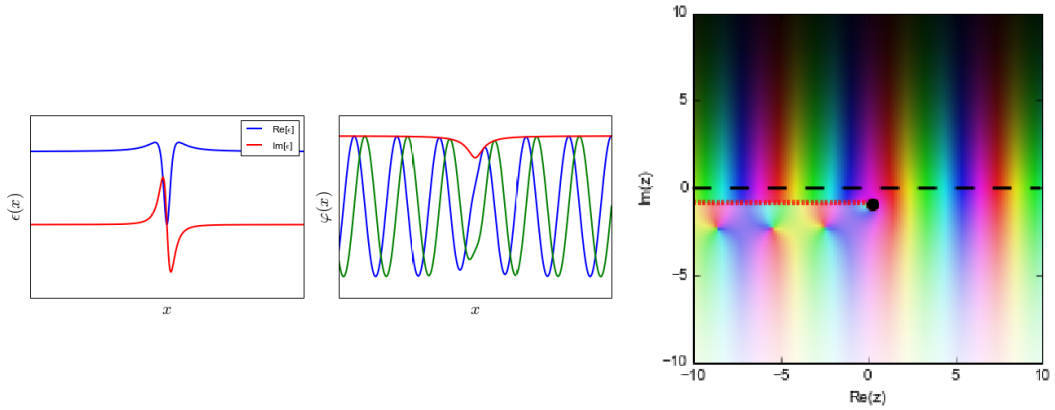

(a) (b) (c)

Figure 1: (a) Shows a plot of the permittivity profile (2), and (b) shows wave propagating to the right within this profile (the real part of the wave is green, the imaginary part is blue, and the absolute value is red). Evidently this particular profile exhibits PT-symmetry, and the lack of oscillations in the absolute value of the field means that there is zero reflection from the profile. (c) Shows plot of the value of the field φ in the complex position plane where brightness indicates the magnitude, and colour the phase (zero phase is red, π phase is light blue). The real axis is shown as black dashed line, and the pole in (2) is the black circle. The red dotted line runs from the pole to infinity, and indicates branch cut in the field in the complex position plane. The position of this branch cut determines whether the profile reflects radiation.

always branch cut in the field. The position of the branch cuts is important. We have found that whenever all the branch cuts in φ can be placed *below* the real axis then the profile will not reflect radiation from the left, and whenever they can be placed *above* the real axis then the profile will not reflect any radiation from the right. Figure 2 shows the effect of moving the pole in $\epsilon(z)$ from $z = -ia$ to $z = ia$. Notice that the branch cut in φ now occurs above the real axis, and there is large reflection for incidence from the left.

The phenomenon shown in Figures 1–2, can be generally stated as follows: poles in the permittivity at complex positions lead to branch cuts in the field. When these branch cuts are all below the real axis then there is no reflection for incidence from the left, and when the branch cuts are all above the real axis then there is no reflection for incidence from the right. This means that if we have any permittivity profile where all the poles occur in the lower half position plane, then all such profiles will not reflect any radiation incident from the left (and vice versa for all the poles in the upper half plane).

In turn this means that to guarantee zero reflection for incidence from the left we can use the Kramers-Kronig relations *in space* to determine the real and imaginary parts of the permittivity,

$$\mathrm{Re}[\epsilon(x)] - 1 = \frac{1}{\pi} \int_{\infty}^{\infty} \frac{\mathrm{Im}[\delta\epsilon(y)]}{x - y} dy \tag{3}$$

Figure 3 illustrates an example of an index profile that obeys (3), showing that there is indeed zero reflection, which we have found to be true for the full angular range of emission, and both polarizations.

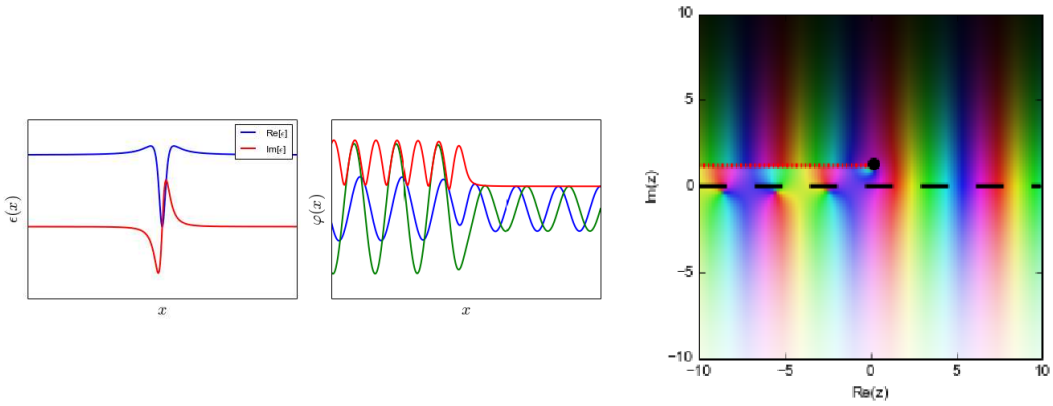

(a) (b) (c)

Figure 2: Identical to Figure 1, but the pole in $\epsilon(z)$ has been moved from $z = -ia$ to $z = ia$. Notice that now there is large reflection.

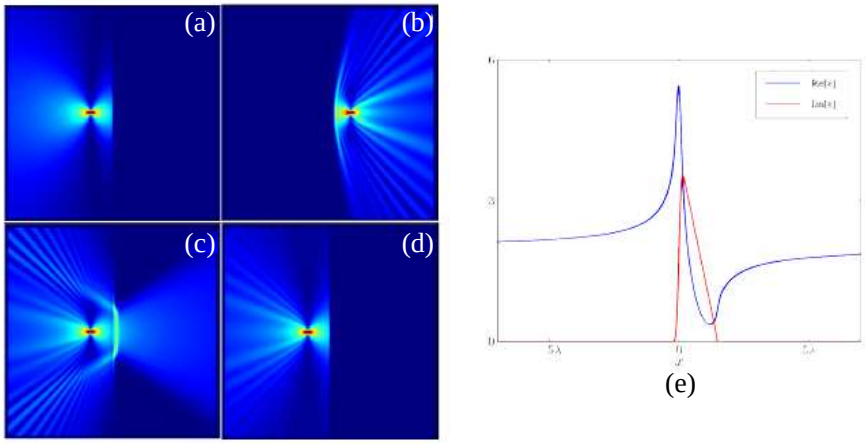

Figure 3: (a) Shows the results of a numerical calculation of the absolute value of the field of dipole emitter placed in front of the permittivity profile shown in panel (e) which satisfied the Kramers-Kronig relations in space. In (b) the dipole is place to the right of the profile, and panels (c) and (d) show the field in the case when only the real or imaginary parts of the permittivity are included, respectively.

REFERENCES

1. Popa, B.-I. and S. A. Cummer, *Complex Coordinates in Transformation Optics*, 063837, 2011.
2. Castaldi, G., S. Savoia, V. Galdi, A. Alù, and N. Engheta, *Phys. Rev. Lett.*, 173901, 2013.
3. Nguyen, V. C., L. Chen, and K. Halterman, *Phys. Rev. Lett.*, Vol. 105, 233908, 2010.
4. Lin, Z., H. Ramezani, T. Eichelkraut, T. Kottos, H. Cao, and D. N. Chrisodoulides, *Phys. Rev. Lett.*, Vol. 106, 213901, 2011.

Session 3P2
FocusSession.SC3: Optical Properties of Resonant Dielectric and Plasmonic Nanostructures 2

All-dielectric Huygens' Metasurfaces and Their Applications in Wave-shaping

Manuel Decker[1], **Isabelle Staude**[1], **Matthias Falkner**[2], **Jason Dominguez**[3], **Dragomir N. Neshev**[1], **Igal Brener**[3], **Thomas Pertsch**[2], **and Yuri S. Kivshar**[1]

[1]Nonlinear Physics Centre, Research School of Physics & Engineering
Australian National University, Australia
[2]Institute of Applied Physics, Abbe Center of Photonics
Friedrich-Schiller-Universität Jena, 07743 Jena, Germany
[3]Sandia National Laboratories, Center for Integrated Nanotechnologies
Albuquerque, New Mexico 87185, USA

Abstract— Optical metasurfaces have developed as a breakthrough concept for advanced wavefront. Key to these "designer metasurfaces" [1] is that they provide full 2π phase coverage and that their local phase can be precisely controlled. The local control of phase, amplitude and polarization of an optically thin plane will lead to a new class of flat optical components in the areas of integrated optics, flat displays, energy harvesting and mid-infrared photonics, with increased performance and functionality. However, reflection and/or absorption losses as well as low polarisation-conversion efficiencies pose a fundamental obstacle for achieving high transmission efficiencies that are required for practical applications.

A promising way to overcome these limitations is the use of metamaterial Huygens' surfaces [2–4], i.e., reflectionless surfaces that can also provide full 2π phase coverage in transmission. Plasmonic implementations of Huygens' metasurfaces for microwave [2] and mid-infrared spectral range [3], where the intrinsic losses of the metals are negligible, have been suggested for efficient beam steering [2, 3], beam shaping [2], and focusing [3]. However, these designs cannot be transferred to near-infrared or even visible frequencies because of the high dissipative losses of plasmonic structures at optical frequencies.

Here we introduce highly efficient Huygens' metasurfaces for near-infrared frequencies with high-permittivity all-dielectric nanoparticles with tailored Mie-type resonances as Huygens' meta-atoms [4]. Our low-loss Huygens' surface is realized by two-dimensional subwavelength arrays of loss-less silicon nanodisks with both electric and magnetic dipole resonances [4, 5]. By controlling the intrinsic properties of both resonances, i.e., their relative electric and magnetic polarizabilities and their quality factors in addition to their spectral position, we can design silicon nanodisks to behave as near-ideal Huygens' sources. This allows us to realize effective all-dielectric Huygens' metasurfaces that lack dissipative losses and also suppress unwanted reflections. At the same time they provide full 2π coverage for the phase shift imposed onto a transmitted light wave without relying on cross-polarization schemes and, thus, without suffering from polarization-conversion losses as most of the plasmonic counterparts. As a result, silicon-nanodisk Huygens' metasurfaces in principle allow for light-wave manipulation with ideally 100% transmission efficiency and also provide almost arbitrary spatial distributions of phase discontinuities depending on the design of the meta-atoms at each position. We provide a comprehensive analytical analysis and numerical modeling of the properties of this Huygens' metasurface and we experimentally demonstrate a Huygens' metasurface in the near-infrared spectral range which results in complete 360 degrees phase coverage of the transmitted light in combination with high transmittance values. We show that that near-unity transmission efficiency can be achieved for an optimized design and we discuss several applications including efficient wavefront-shaping, dispersion-control devices, and optical holograms where the unique properties of all-dielectric Huygens' surfaces play a key role for the realization of highly efficient metadevices.

REFERENCES

1. Yu, et al., *Nat. Mater.*, Vol. 13, 139, 2014.
2. Pfeiffer, C., et al., *Phys. Rev. Lett.*, Vol. 110, 197401, 2013.
3. Monticone, F., et al., *Phys. Rev. Lett.*, Vol. 110, 203903, 2013.
4. Decker, M., et al., *Adv. Opt. Mater.*, 2015, DOI: 10.1002/adom.201400584.
5. Staude, I., et al., *ACS Nano*, Vol. 7, 7824, 2013.

Electrodynamics of Cylinders with Radial Anisotropy

H. Kettunen[1], **H. Wallén**[2], **and A. Sihvola**[2]

[1]Department of Mathematics and Statistics
University of Helsinki, Finland
[2]Department of Radio Science and Engineering
School of Electrical Engineering, Aalto University, Finland

Abstract— In this presentation, we suggest an effective material configuration based on a lattice of dielectric radially anisotropic (RA) cylinders. Such all-dielectric metamaterials that are based on Mie resonances of high-permittivity objects are currently under much interest, as they could largely overcome the detrimental effect of materials losses that are characteristic to plasmonic metals. Dielectrics are also much less vulnerable to frequency dispersion enabling tunability in broader bandwidths.

To be more specific, we study scattering of a TE_z polarized plane wave from a circular infinitely long dielectric radially anisotropic (RA) cylinder, whose axis is parallel to the z-axis. The permittivity dyadic of an RA cylinder is given in polar coordinates as $\bar{\bar{\varepsilon}} = \varepsilon_0(\varepsilon_\rho \mathbf{u}_\rho \mathbf{u}_\rho + \varepsilon_\varphi \mathbf{u}_\varphi \mathbf{u}_\varphi)$, where ε_ρ and ε_φ are the radial and the tangential permittivity components of the cylinder, respectively. As shown in [1], in the long-wavelength limit, the external response of an RA cylinder resembles the one of an isotropic cylinder with effective permittivity $\varepsilon_{eff} = \sqrt{\varepsilon_\rho \varepsilon_\varphi}$. However, in the actual dynamic case, we need to apply the Mie scattering theory for radially anisotropic cylinders [2].

By solving the coefficients a_n of the expansion of the scattered wave, we are able to locate the resonances of the cylinder. We are especially interested in the magnetic and electric dipolar resonances, that are given by the maxima of the two first coefficients a_0 and a_1, respectively. By changing the values of the permittivity components ε_ρ and ε_φ, we also shift the occurrence of the resonances in frequency. We have earlier showed that by choosing ε_φ very large, the cylinders give rise to artificial magnetism enabling even negative effective permeability values [3].

Our objective for this presentation is to adjust the magnetic and electric resonances to appear simultaneously, which could be a way to construct an all-dielectric double negative material with negative index of refraction. We will also discuss photonic crystals consisting of RA cylinders.

REFERENCES

1. Kettunen, H., H. Wallén, and A. Sihvola, "Cloaking and magnifying using radial anisotropy," *J. App. Phys.*, Vol. 114, No. 4, 044110, 2013.
2. Ni, Y., L. Gao, and C.-W. Qiu, "Achieving invisibility of homogeneous cylindrically anisotropic cylinders," *Plasmonics*, Vol. 5, No. 3, 251–258, 2010.
3. Kettunen, H., H. Wallén, and A. Sihvola, "Magnetic response from electrically invisible anisotropic dielectric cylinders," *Proceedings of META'14, the 5th International Conference on Metamaterials, Photonic Crystals and Plasmonics*, 1440–1442, Singapore, May 2014.

Optimum Forward Light Scattering with High Refractive Index Nanoparticles

Boris S. Luk'yanchuk[1, 2], **Nikolai V. Voshchinnikov**[3], **Ramón Paniagua-Domínguez**[1], **and Arseniy I. Kuznetsov**[1]

[1]Data Storage Institute, Agency for Science, Technology and Research
5 Engineering Drive 1, 117608, Singapore
[2]School of Electrical and Electronic Engineering
Nanyang Technological University, 639798, Singapore
[3]Sobolev Astronomical Institute, St Petersburg University, 198504, Russia

Abstract— High-refractive index dielectric nanoparticles may exhibit strong directional forward light scattering at visible and near-infrared wavelengths due to interference of simultaneously excited electric and magnetic dipole resonances. For a spherical high-index dielectric, the so-called first Kerker's condition can be realized, at which the backward scattering practically vanishes for some combination of refractive index and particle size. However, Kerker's condition for spherical particles is only possible at the tail of the scattering resonances, when the particle scatters light weakly. Here we demonstrate that significantly higher forward scattering can be realized if spheroidal particles are considered instead. For each value of refractive index n exists an optimum shape of the particle, which produces minimum backscattering efficiency together with maximum forward scattering. This effect is achieved due to the overlapping of magnetic and electric dipole resonances of the spheroidal particle at the resonance frequency. It permits the design of very efficient, low-loss optical nanoantennas. We found that the results for spheroidal particles accurately describe the response of a wide range of shapes with the same aspect ratio.

Optical Magnetism and Active Devices from All Dielectric Metasurfaces

Igal Brener
Center for Integrated Nanotechnologies, Sandia National Laboratories
Albuquerque, New Mexico 87185, USA

Abstract— Magnetic mirrors or high impedance surfaces were first demonstrated at microwave frequencies to improve antennas radiation efficiency. Magnetic mirrors exhibit unusual electromagnetic boundary conditions. In contrast to a normal mirror that exhibits a 180-degree phase shift of the reflected electric field, a magnetic mirror does not reverse the phase of the reflected electric field but reverts the phase of the reflected magnetic field. Therefore, while the emission from a transverse electric dipole placed close to a normal mirror will be largely canceled by its image, a transverse electric dipole emitter placed close to a magnetic mirror can radiate efficiently. Conversely, transverse dipole absorbers placed close to a magnetic mirror will be located at an anti-node of the total electric field and can absorb efficiently. These exceptional properties of magnetic mirror will lead to potential applications in the areas of sensors, photodetectors, and spectroscopy [1].

We used a special phase-locked time-domain system operating in the mid IR and directly observed that the electric field reflected from our dielectric optical magnetic mirror is in-phase with the incident wave, which directly demonstrates the magnetic mirror behavior [2]. This behavior is further confirmed by observing ~ 180 degree phase difference between the electric and magnetic resonances. I will also discuss the radiative rate enhancement of a dipole close to our optical magnetic mirror. This is in contrast to the behavior for regular metallic surfaces where dipole emission is strongly quenched. Finally, if time permits, I will present preliminary results on dielectric metasurfaces patterned on different semiconductors or with more complex fabrication steps, that can lead to the realization of active all dielectric metasurfaces.

ACKNOWLEDGMENT

This work was performed, in part, at the Center for Integrated Nanotechnologies, a U.S. Department of Energy, Office of Basic Energy Sciences user facility. Sandia National Laboratories is a multiprogram laboratory managed and operated by Sandia Corporation, a wholly owned subsidiary of Lockheed Martin Corporation, for the U.S. Department of Energy's National Nuclear Security Administration under contract DE-AC04-94AL85000.

REFERENCES

1. Ginn, J. C., I. Brener, D. W. Peters, J. R. Wendt, J. O. Stevens, P. F. Hines, L. I. Basilio, L. K. Warne, J. F. Ihlefeld, and P. G. Clem, *Physical Review Letters*, Vol. 108, No. 9, 097402, 2012.
2. Liu, S., M. B. Sinclair, T. S. Mahony, Y. C. Jun, S. Campione, J. Ginn, D. A. Bender, J. R. Wendt, J. F. Ihlefeld, P. G. Clem, J. B. Wright, and I. Brener, *Optica*, Vol. 1, No. 4, 250–256, 2014.

Probing Magnetic and Electric Optical Responses of Silicon Nanoparticles

D. Permyakov[1], **I. Sinev**[1], **D. Markovich**[1], **P. Ginzburg**[1, 2], **A. Samusev**[1]
P. Belov[1], **V. Valuckas**[3, 4], **A. I. Kuznetsov**[3], **B. Luk'yanchuk**[3], **A. Miroshnichenko**[5],
D. Neshev[5], **and Y. Kivshar**[1, 5]

[1]ITMO University, St. Petersburg 197101, Russia
[2]School of Electrical Engineering, Tel Aviv University, Ramat Aviv, Tel Aviv 69978, Israel
[3]Data Storage Institute, A*STAR (Agency for Science Technology and Research), 117608, Singapore
[4]Department of Electrical and Computer Engineering, National University of Singapore, 117576, Singapore
[5]Nonlinear Physics Centre, Australian National University, Canberra, ACT 0200, Australia

Abstract— We study experimentally both magnetic and electric optically-induced resonances of silicon nanoparticles fabricated by femtosecond laser ablation [1] by combining polarization-resolved dark-field spectroscopy and near-field scanning optical microscopy (NSOM) measurements. First, to study the scattering properties of Si nanoparticles as a function of wavelength and polarization of the incident beam, we use a home-made polarization-resolved dark-field microscope with independent excitation and collection optical channels. The obtained spectra allow to determine spectral positions of optical magnetic and electric scattering resonances and demonstrate excellent agreement with the scattering spectra of a silicon sphere on a glass substrate calculated using analytical solution [2]. Comparing *s*- and *p*-polarized spectra we observe different polarization-dependent behaviour of the spectral features corresponding to electric and magnetic dipole resonances.

To gain even better data allowing to distinguish magnetic and electric dipole contributions, we complement our dark-field measurements with NSOM experiments performed at electric and magnetic dipole resonant wavelengths determined from the dark-field spectroscopy measurements. We show that the magnetic dipole response of the nanoparticle can be directly identified through the characteristic asymmetry in NSOM patterns obtained using an aperture-type probe operating as an effective magnetic field analyzer [3]. We also compare the experimental patterns to the near-field signal maps reconstructed from rigorous finite-difference time-domain (FDTD) simulations using an approach based on the reciprocity theorem of electromagnetism [4, 5]. The presented results confirm that the proposed experimental approach allows for discrimination of the dipole optical responses of both magnetic and electric nature. Importantly, this can be done directly from the experimental data without employing complementary numerical simulations.

REFERENCES

1. Fu, Y. H., A. I. Kuznetsov, A. E. Miroshnichenko, Y. F. Yu, and B. Lukyanchuk, "Directional visible light scattering by silicon nanoparticles," *Nature Communications*, Vol. 4, 1527, 2013.
2. Bobbert, P. and J. Vlieger, "Light scattering by a sphere on a substrate," *Physica A: Statistical Mechanics and Its Applications*, Vol. 137, No. 1, 209–242, 1986.
3. Bakker R. M., D. Permyakov, Y. F. Yu, D. Markovich, R. Paniagua-Domínguez, L. Gonzaga, A. Samusev, Y. S. Kivshar, B. Lukyanchuk, and A. I. Kuznetsov, "Magnetic and electric hotspots with silicon nanodimers," *Nano Letters*, 2015, doi:10.1021/acs.nanolett.5b00128.
4. Porto, J. A., R. Carminati, and J.-J. Greffet, "Theory of electromagnetic field imaging and spectroscopy in scanning near-field optical microscopy," *J. Appl. Phys.*, Vol. 88, No. 8, 4845–4850, 2000.
5. Sinev, I. S., P. M. Voroshilov, I. S. Mukhin, A. I. Denisyuk, M. E. Guzhva, A. K. Samusev, P. A. Belov, and C. R. Simovski, "Demonstration of unusual nanoantenna array modes through direct reconstruction of the near-field signal," *Nanoscale*, Vol. 7, 765–770, 2015.

Nonlinear Optics of Dielectric Nanoparticles and Metasurfaces Assisted by Magnetic Mie-type Resonances

M. R. Shcherbakov[1], **D. N. Neshev**[2], **B. Hopkins**[2], **A. S. Shorokhov**[1], **I. Staude**[2], **E. V. Melik-Gaykazyan**[1], **M. Decker**[2], **A. A. Ezhov**[1], **A. E. Miroshnichenko**[2], **I. Brener**[3], **A. A. Fedyanin**[1], **and Yu. S. Kivshar**[2]

[1]Faculty of Physics, Lomonosov Moscow State University, Moscow 119991, Russia
[2]Nonlinear Physics Centre, Research School of Physics and Engineering
The Australian National University, Canberra, Australian Capital Territory 0200, Australia
[3]Center for Integrated Nanotechnologies, Sandia National Laboratories
Albuquerque, New Mexico 87185, United States

Abstract— Over the past decade, extensive efforts have been dedicated to finding effective nonlinear optical media on the nanoscale [1]. The main strategy to enhance the efficiency of the nonlinear optical processes lies in utilizing localized modes, e.g., in plasmonic nanostuctures. In particular, a pronounced modification of the second- and third-order nonlinear response has been observed in various nano- and metamaterials [1–3]. In contrast, the effect of *magnetic resonances* on the nonlinear properties of nanostructures is much less studied and limited to conventional geometries such as split-ring resonators [4] or fishnet metasurfaces [5]. However, the nonlinear frequency generation in plasmonic nanostructures suffers from strong losses of metals at optical frequencies, losses which are further enhanced near the resonances.

To overcome this problem, in this work we study the third-harmonic generation (THG) from silicon-nanoparticle-based oligomers and metasurfaces. High-permittivity, dielectric nanoparticles are emerging as a promising alternative to metallic nanostructures for a wide range of nanophotonics applications; such nanoparticles exhibit both electric and magnetic multipolar resonances in the visible an near-IR spectral ranges [6]. In combination with their very low Ohmic losses, these nanoparticles and their composites offer many unique opportunities for tailoring their nonlinear optical response.

In single silicon nanodisks fabricated out of a silicon-on-insulator substrate, we report on a significant enhancement of the third-harmonic radiation intensity when the incoming femtosecond laser pulses excite the magnetic dipole resonance of the disk. Originating from the strong light confinement to a mode volume of $\sim \lambda^3/60$, the observed THG is shown to be approximately an order of magnitude larger that that of the bulk silicon slab [7]. Bringing the silicon nanodisks to the oligomer (trimer) arrangement provides an additional degree of freedom in tuning the spectral position of the magnetic resonance to a partial overlap with the electric resonance. We observe a pronounced reshaping of the third-harmonic spectra due to interference of the nonlinearly generated waves and an interplay between the electric and magnetic dipolar resonances. Packing the nanodisks to the metasurface arrangement provides a two order of magnitude THG enhancement over the THG from the bulk silicon; the THG is visible by the naked eye under the table-lamp illumination conditions [7]. Finally, the silicon nanodisk samples are shown not to suffer from the powerful laser radiation used in the experiment, as opposed to the widely used metallic nanostructures. To conclude, we demonstrate a novel platform that paves the way for nonlinear nanophotonics and silicon photonics devices enabled by resonant subwavelength low-loss all-dielectric nanoparticles.

REFERENCES

1. Kauranen, M. and A. V. Zayats "Nonlinear plasmonics," *Nature Photon.*, Vol. 6, 737–748, 2012.
2. Van Nieuwstadt, J. A. H., M. Sandtke, R. H. Harmsen, F. B. Segerink, J. C. Prangsma, S. Enoch, and L. Kuipers, "Strong modification of the nonlinear optical response of metallic subwavelength hole arrays," *Phys. Rev. Lett.*, Vol. 97, 146102, 2006.
3. Metzger, B., M. Hentschel, T. Schumacher, M. Lippitz, C. B. Murray, B. Knabe, K. Buse, and H. Giessen, "Doubling the efficiency of third harmonic generation by positioning ITO nanocrystals into the hot-spot of plasmonic gap-antennas," *Nano Lett.*, Vol. 14, 2867–2872, 2014.
4. Klein, M. W., C. Enkrich, M. Wegener, and S. Linden, "Second-harmonic generation from magnetic metamaterials," *Science*, Vol. 313, 502–504, 2006.

5. Reinhold, J., M. R. Shcherbakov, A. Chipouline, V. I. Panov, C. Helgert, T. Paul, C. Rockstuhl, F. Lederer, E.-B. Kley, A. Tünnermann, A. A. Fedyanin, and T. Pertsch, "Contribution of the magnetic resonance to the third harmonic generation from a fishnet metamaterial," *Phys. Rev. B*, Vol. 86, 115401, 2012.
6. Kuznetsov, A. I., A. E. Miroshnichenko, Y. H. Fu, J. Zhang, and B. Luk'yanchuk, "Magnetic light," *Sci. Rep.*, Vol. 2, 492, 2012.
7. Shcherbakov, M. R., D. N. Neshev, B. Hopkins, A. S. Shorokhov, I. Staude, E. V. Melik-Gaykazyan, M. Decker, A. A. Ezhov, A. E. Miroshnichenko, I. Brener, A. A. Fedyanin, and Y. S. Kivshar, "Enhanced third-harmonic generation in silicon nanoparticles driven by magnetic response," *Nano Lett.*, Vol. 12, 6488–6492, 2014.

Resonant Lithium Niobate Nanostructures for Nonlinear Frequency Conversion

Frank Setzpfandt, **Reinhard Geiss**, **Severine Diziain**,
Sina Saravi, **and Thomas Pertsch**
Abbe Center of Photonics, Institute of Applied Physics
Friedrich-Schiller-Universität Jena, Max-Wien-Platz 1, Jena 07743, Germany

Abstract— Lithium niobate is an excellent material for nonlinear optics due to its high nonlinear coefficients and large transparency window. These favorable properties have been extensively used for classical integrated optics. However, nanostructures, which allow for a much broader range of achievable optical properties, are much harder to fabricate in lithium niobate due to the complicated properties of this material. In recent years, we developed the technique of ion-beam enhanced etching. This electron-beam lithography based approach uses spatially structured irradiation with swift heavy ions, which locally destroy the crystal structure, to control the wet etching processes used to define nanostructures. With this fabrication technique we are able to manufacture different types of resonant nanostructures for nonlinear optical frequency conversion. In our talk we will summarize our recent experimental and theoretical result concerning the design and experimental characterization of such nanostructures for different applications.

In rectangular nano-waveguides, resonances in two spatial dimensions form transversely localized modes which propagate along the waveguide. Such waveguides achieve strong field localization and have low losses, thus enabling efficient second-harmonic generation and also the generation of photon pairs for quantum optical applications, which we demonstrate experimentally.

To further enhance the efficiency, the dispersion of the waveguide has to be controlled to achieve slow-light modes with a very low group velocity. This we achieve in Photonic Crystal waveguides. Here, waveguiding and dispersion control are enabled by resonant interaction of the light in the waveguide with the surrounding periodic structure of the photonic crystal. We will present systematic design guidelines and experimental realizations of such Photonic Crystal waveguides for efficient second-harmonic generation.

Finally, we will consider resonators, where the light is confined in all three dimensions. In comparison to the structures mentioned before, resonators enable much higher quality factors and thus higher nonlinear efficiencies. We experimentally characterized the linear and nonlinear responses of both disc-resonators and resonators in Photonic Crystals and measured strong second-harmonic signals.

Summarizing, we believe that lithium niobate is an ideal material platform for nonlinear optics. The results we will present in this talk will be an important step towards the practical implementation of lithium niobate's capabilities in integrated nanophotonics.

Integrated Nanophotonic Components Enabled by Alternative Materials

N. Kinsey[1], **M. Ferrera**[1, 2], **C. DeVault**[3], **J. Kim**[1],
A. V. Kildishev[1], **V. M. Shalaev**[1], **and A. Boltasseva**[1]

[1]School of Electrical & Computer Engineering and Birck Nanotechnology Center
Purdue University, 1205 West State St., West Lafayette, IN 47907, USA
[2]School of Engineering and Physical Sciences, Heriot-Watt University
David Brewster Building, Edinburgh, Scotland EH14 4AS, UK
[3]Department of Physics, Purdue University, 512 Northwestern Ave, West Lafayette, IN 47907, USA

Abstract— Recent advances in alternative nanophotonic materials, specifically CMOS-compatible compounds, have propelled a unique class of integrated devices to achieve high performance with realistic materials.

Integrated optical technologies are critical for many fundamental applications such as telecommunications, chemistry, quantum science, and medicine [1]. However, for these devices to be realized in a large scale, they should be CMOS-compatible — a problem for plasmonic devices which have generally relied on noble metals [2]. Recently, there has been a flurry of research in the field of alternative plasmonic materials, but for telecommunication applications, CMOS-compatible materials titanium nitride and transparent conducting oxides (such as doped zinc oxide) are among the most promising materials currently available [3].

TiN is a gold-like ceramic material with a permittivity cross-over near 500 nm. In addition, TiN can attain ultra-thin, ultra-smooth epitaxial films on substrates such as c-sapphire, MgO, and silicon. Partnering TiN with CMOS-compatible silicon nitride enables a fully solid-state waveguide which is able to achieve a propagation length greater than 1 cm for a $\sim$8 µm mode size at 1.55 µm. In fact, similar designs using TiN have outperformed gold waveguides due in large part to the reduced scattering loss of epitaxial quality films [4].

Utilizing highly doped zinc oxide films as a dynamic photonic material, high performance modulators can also be realized due to the low-loss achieved by the TiN/Si_3N_4 waveguide. Simply by placing a thin layer of aluminum doped zinc oxide (AZO) on top of the waveguide structure, a modulator with very low insertion loss is achieved. However, to determine the performance of the device, the ability to which the AZO can be tuned must be understood. Our recent work has investigated optical tuning of AZO films by the pump-probe method, demonstrating a change in the refractive index of $-0.17 + 0.25i$ at 1.3 µm with an ultrafast response of 1 ps. Assuming this change in the refractive index for the AZO film, a modulation of $\sim$0.7 dB/µm is possible in the structure with $\sim$0.5 dB insertion loss and an operational speed of 1 THz. Further optimization of the design is expected to lead to an increased modulation depth without sacrificing insertion loss or speed.

Together, these alternative materials form the base of a fully integrated nanophotonic system, capable of exceptional performance with speeds greater than 1 THz, in large part due to the development of alternative materials. Consequently, nanophotonic technologies are reaching a critical point where many applications including telecom, medicine, and quantum science can see practical systems which provide new functionalities.

ACKNOWLEDGMENT

This work was supported by AFOSR Grant FA9550-14-1-0138DEF and ONR Grant 555991.

REFERENCES

1. Kinsey, N., et al., *JOSA B*, Vol. 32, No. 1, 121–142, 2015.
2. Boltasseva, A. and H. Atwater, *Science*, Vol. 331, No. 6015, 290–291, 2011.
3. Naik, G., et al., *Adv. Materials*, Vol. 25, No. 24, 3264–3294, 2013.
4. Kinsey, N., et al., *Opt. Express*, Vol. 22, No. 10, 12238–12247, 2014.

Plasmon-exciton Coupling in Stacked 2D Perovskite Semiconductors

D. Leipold[1], **W. Niu**[2], **L. A. Ibbotson**[2], **G. V. Prakash**[3], **J. J. Baumberg**[2], **and E. Runge**[1]

[1]Institut für Physik and Institut für Mikro-und Nanotechnologien
Technische Universität Ilmenau, Germany
[2]NanoPhotonics Centre, Cavendish Laboratory, University of Cambridge, CB3 0HE, UK
[3]Nanophotonics Lab, Department of Physics
Indian Institute of Technology Delhi, New Delhi 110016, India

Abstract— The coupling of plasmons and non-linear materials is most likely a vital part in the development of future plasmonic devices. Strong coupling and the formation of new plasmon-exciton quasiparticles called excimons or plexcitons was previously observed in metal-semiconductor hybrid systems and organic dye-coated metal-gratings [1, 2]. The system presented here combines the stability and room-temperature operation of inorganic semiconductors with the potential of cost-effective large-scale production that is typical for organic dyes. Both aspects are preconditions for a commercial breakthrough of ultrafast-nanooptical devices.

Here, we study cyclohexenyl-ethyl-ammonium lead-iodide (CHPI), which is well known from solar-energy research, as a candidate material for active plasmonic devices. Due to the huge organic ion in the R position between the PbI_6 octahedra of the general R-PbI_3 perovskite structure, semiconducting sheets of lead-iodide octahedra are formed. These are separated by layers of the organic ions. CHPI shows strong excitonic response and high stability even at room temperature. It can easily be processed from solution and forms regular stacks.

In order to study the interaction of CHPI with plasmons, CHPI was grown on a silver grating by drying from a solution in a thermal process [3]. We present experimental angle-resolved reflectivity spectra in the visible range and compare to theoretical calculations. These spectra reveal the formation of collective plasmon-exciton modes that are coupled with a huge Rabi energy of 125–150 meV, see Fig. 1. We also observe a red-shift of the excitonic absorption. This shift is attributed to the formation of an image-biexciton: a quasiparticle made up by the excitonic dipole coupled to its own image dipole in the metal [4, 5].

In addition, we present theoretical calculations with the finite-element method (FEM). The calculations solve the full vectorial Maxwell equations taking the inherent anisotropy of the stacked material CHPI into account. The frequency-dependent response of the CHPI and the metal is taken into account by multi-Lorentzian and Drude-Lorentz fits, respectively, to experimental reference data. These calculations reproduce the important aspects of the far-field experiments and describe the experimentally inaccessible near-field distributions in the groves.

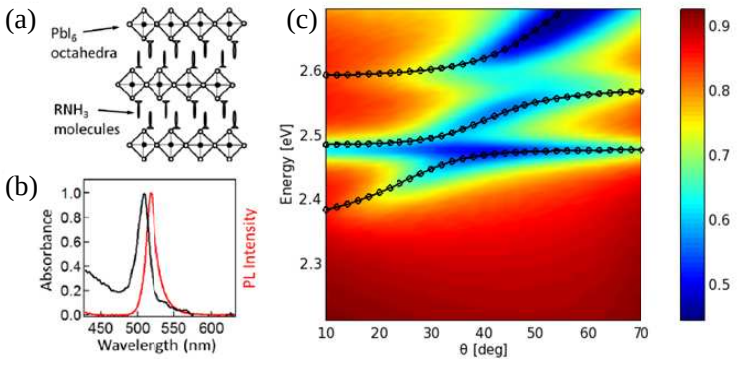

Figure 1: (a) Sketch of the perovskite semiconductor CHPI: PbI semiconductor monolayers alternate with layers of organic spacer molecules. (b) Absorption and photoluminescence spectra of a thin CHPI film on glass substrate at room temperature. (c) Calculated angle-resolved reflectivity spectrum (color code) of a thin CHPI film on a metal grating. Black lines show a fit using a 3×3 coupled-modes model.

REFERENCES

1. Vasa, P., E. Runge, et al., *PRL*, Vol. 101, 116801, 2008.
2. Vasa, P., D. Leipold, E. Runge, et al., *ACS Nano*, Vol. 4, 7559, 2010.
3. Pradeesh, K., J. J. Baumberg, et al., *Optics Express*, Vol. 17, 22171, 2009.
4. Baumberg, J. J., et al., *Appl. Phys. Lett.*, Vol. 104, 191105, 2014.
5. Niu, W., et al., Submitted to *Phys. Rev. B*.

Forward-backward Light Emission Symmetry Breaking with Localized and Collective Magnetoelectric Resonances in Arrays of Pyramid-shaped Aluminum Nanoantennas

S. R. K. Rodriguez[1, 4], **F. Bernal Arango**[1], **T. P. Steinbusch**[1], **M. A. Verschuuren**[2], **A. F. Koenderink**[1], **and J. Gómez Rivas**[1, 3]

[1]Center for Nanophotonics, FOM Institute AMOLF, c/o Philips Research Laboratories, The Netherlands
[2]Philips Research Laboratories, Eindhoven, The Netherlands
[3]COBRA Research Institute, Eindhoven University of Technology, Eindhoven, The Netherlands
[4]Laboratoire de Photonique et de Nanostructures, LPN/CNRS, France

Abstract— Periodic arrays of metallic nanoantennas constitute a versatile system for enhancing light emission. Nanoantenna arrays sustain single-particle localized surface plasmon resonances (LSPRs), and hybrid plasmonic-photonic resonances due to the coupling between LSPRs and diffracted or guided modes. Recently, the mutual coupling strength between these modes was shown to transition from weak to strong [1]. Hybrid plasmonic-photonic resonances can lead to unconventional effects such as large fluorescence enhancements at frequencies and wave vectors of far-field induced transparency [2]. Here, we present recent results on an array of pyramid-shape nanoantennas and its interaction with fluorescent molecules [3]. Diffractive coupling of LSPRs in the array leads to a collective resonance known as surface lattice resonance (SLR) [4]. We designed an array wherein fluorescent molecules drived both LSPRs and SLRs. Interestingly, we observed an unbalanced forward-backward light emission spectrum which breaks the conventional forward-backward symmetry of planar structures. Through rigorous electrodynamic calculations we show that the pyramid shape of the nanoantennas enhances their magnetoelectric response, i.e., the excitation of magnetic moments by electric fields and viceversa. The enhanced magneto-electric response enables electric and magnetic dipole moments of similar magnitude to interfere distinctly in the forward and backward direction. In turn, different colors of light are beamed forward or backward. Our observations resemble the Kerker condition for light scattering of dielectric particles, but here realized in the context of fluorescence enhancement with metallic nanoantennas. In addition, we demonstrate that localized and delocalized magnetic surface waves with an excitation strength depending on the plane wave direction are linked to these effects. We discuss applications to the field of solid-state lighting [5], and to the potential realization of a quantum condensed plasmonic state [6].

REFERENCES

1. Rodriguez, S. R. K., Y. T. Chen, T. P. Steinbusch, M. A. Verschuuren, A. F. Koenderink, and J. Gómez Rivas, "From weak to strong coupling of localized surface plasmons to guided modes in a luminescent slab," *Phys. Rev. B*, Vol. 90, 235406, 2014.
2. Rodriguez, S. R. K., S. Murai, M. A. Verschuuren, and J. Gómez Rivas, "Light-emitting waveguide-plasmon polaritons," *Phys. Rev. Lett.*, Vol. 109, 166803, 2012.
3. Rodriguez, S. R. K., F. Bernal Arango, T. P. Steinbusch, M. A. Verschuuren, A. F. Koenderink, and J. Gómez Rivas, "Breaking the symmetry of forward-backward light emission with localized and collective magnetoelectric resonances in arrays of pyramid-shaped aluminum nanoparticles," *Phys. Rev. Lett.*, Vol. 113, 247401, 2014.
4. Rodriguez, S. R. K., A. Abass, B. Maes, O. T. A. Janssen, G. Vecchi, and J. Gómez Rivas, "Light-emitting waveguide-plasmon polaritons," *Phys. Rev. Lett.*, Vol. 1, 021019, 2011.
5. Lozano, G., D. J. Louwers, S. R. K. Rodriguez, S. Murai, O. T. A. Jansen, M. A. Verschuuren, and J. Gómez Rivas, "Plasmonics for solid-state lighting: Enhanced excitation and directional emission of highly efficient light sources," *Light. Sci. Appl.*, Vol. 2, e66, 2013.
6. Rodriguez, S. R. K., J. Feist, M. A. Verschuuren, F. J. Garcia Vidal, and J. Gómez Rivas, "Thermalization and cooling of plasmon-exciton polaritons: Towards quantum condensation," *Phys. Rev. Lett.*, Vol. 111, 166802, 2013.

Plasmonic Fano-like Resonances and Their Near-field Properties in Finite Arrays of Metal Particles

S. Bakhti, N. Destouches, and A. V. Tishchenko
Laboratoire Hubert Curien, Université Jean-Monnet, Université de Lyon
CNRS, UMR 5516, 18 rue Pr. Lauras, Saint-Etienne F-42000, France

Abstract— Localized Surface Plasmon resonances attract for many years a considerable attention due to their unique ability to concentrate electromagnetic energy at nano-scale. Fano resonances [1] emerge in finite structures from a strong coupling between individual or group of particles. This kind of resonance is characterized by a highly asymmetric line profile in the scattering or extinction spectrum of the structure, and provides a promising platform for sensing applications.

In this work, we characterize Fano resonances in finite silver particle arrays through the use of the coupled mode model [2]. This model is applied to the complex valued partial extinction of each particle (having the same phase behavior than their dipolar moment oscillation) on which a pole searching algorithm is used to retrieve all phenomenological parameters. By this way, the asymmetric line profile of Fano resonances appears as resulting from the combination of super-radiant and sub-radiant hybrid modes in the coupled system. In the case of a simple quadrumer (Fig. 1(a)), two coupling regimes appear depending on the inter-particle distance. The weak coupling regime is characterized by broad super-radiant and sharp sub-radiant modes, whereas the strong coupling regime shows a broader sub-radiant mode and a larger Fano dip in the extinction spectrum. In the case of a two dimensional array of particles (Fig. 1(b)), corresponding to a strong coupling regime, the Fano resonance exhibit an interesting near-field behavior. Depending on the excitation wavelength relative to the Fano dip, the hot spot can be localized on different lines of the arrays. This unique ability opens new opportunities to spectrally control the near-field enhancement location in a finite structure.

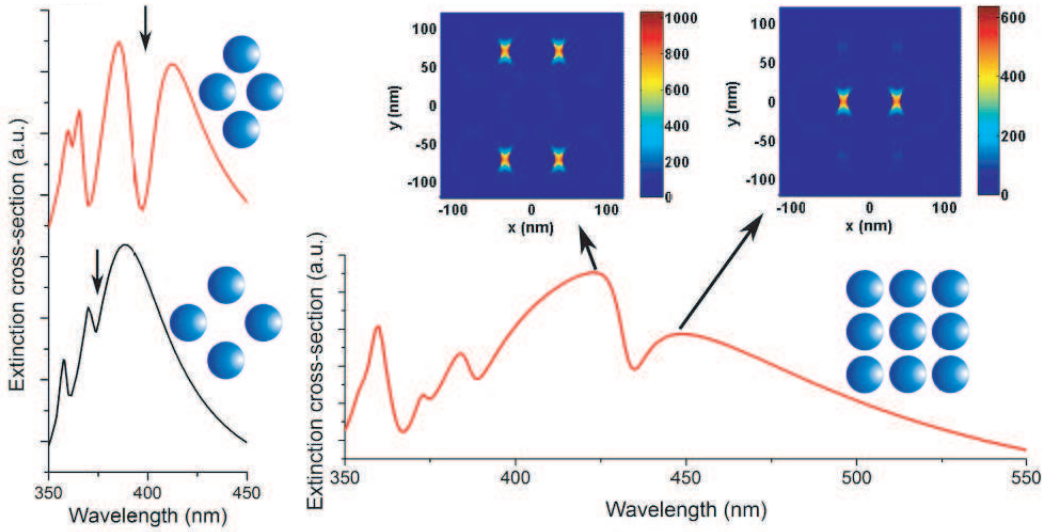

Figure 1: (a) Fano resonance (located by an arrow) in the extinction spectrum of a quadrumer in the strong and weak coupling regimes. (b) Extinction spectrum of a 3×3 array of particles with a mapping of near-field intensities on both sides of the Fano dip. All particles are silver spheres of 30 nm in radius and the structures are excited with a horizontally polarized incident plane wave.

REFERENCES

1. Luk'yanchuk, B., et al., *Nat. Mater.*, Vol. 9, 707–715, 2010.
2. Haus, H. A., *Waves and Fields in Optoelectronics*, Prentice Hall, Incorporated, 1984.

Nanoscale Form Dictates Mesoscale Function in Plasmonic DNA-nanoparticle Superlattices

Michael B. Ross[1], **Jessie C. Ku**[2], **Victoria M. Vaccarezza**[2], **Chad A. Mirkin**[1, 2], **and George C. Schatz**[1]

[1]Department of Chemistry, Northwestern University
2145 Sheridan Rd., Evanston, IL 60208, USA
[2]Department of Materials Science, Northwestern University
2220 Campus Drive, Evanston, IL 60208, USA

Abstract— The manipulation of matter on the nanoscale provides a means to achieving material properties that are difficult or impossible to achieve in the bulk state. Progress toward nanoscale architectures with tangible utility requires (1) the development of methods to controllably and precisely locate nanoscale objects in multiple dimensions and (2) the formation of rigorous structure-function relationships across multiple size regimes. We use DNA as a programmable ligand to arrange gold nanoparticles into two- and three-dimensional crystalline superlattices. By controlling the spacing between gold nanoparticle building blocks, the superlattices can be transitioned from exhibiting the properties of the constituent plasmonic nanoparticles to adopting the photonic properties dictated by the mesoscale crystal habit (here a rhombic dodecahedron). In particular, thin films with dimensions smaller than the wavelength primarily resemble the absorption of the free nanoparticle. Comparatively, rhombic dodecahedron superlattices on the order of $\sim$1 micron exhibit distinct photonic red-shifted resonances far to the red of the free particle resonance. To rigorously quantify these seemingly disparate optical effects, we implement anomalous diffraction theory, a geometric optics approximation designed for low index materials. Using this generally applicable theoretical framework, we illustrate that crystal habit is a powerful design consideration for controlling far-field extinction and light confinement in plasmonic metamaterial superlattices. The precise control over nanoscale spacing, in combination with control over five distinct mesoscale crystal habits, gives rise to unprecedented control over far-field light manipulation in bottom-up optical materials. We envision that this work will impact the development of and progress towards functional nanoscale assemblies in energy harvesting, metamaterials, photovoltaics, and sensing.

Nonlinear Traffic Control Across Waveguides

Mikhail Lapine[1], **Alexey P. Slobozhanyuk**[2], **Ilya V. Shadrivov**[2], **David A. Powell**[2], **Ross C. McPhedran**[3], **and Yuri S. Kivshar**[2]

[1]School of Mathematical Sciences, University of Technology Sydney, NSW 2007, Australia
[2]Nonlinear Physics Centre, Australian National University, Canberra, ACT 2601, Australia
[2]School of Physics, University of Sydney, NSW 2006, Australia

Abstract— We implement an independent additional interaction channel between microwave waveguides, which otherwise would have no interaction with each other, mediated by an optical link. For this purpose, we employ nonlinear optical coupling [1] in a pair of split-ring resonators, equipping one SRR with varactors biased by a photo-diode (PD), and the other one with a light-emitting diode (LED), Fig. 1. We place the photo-coupled meta-atom at the intersection of the two magneto-inductive waveguides (Fig. 2), adjusted so as to maintain integrity in each of the waveguides. Due to the symmetry of the configuration, the waveguides have no explicit magnetic coupling and at low power, signal propagation in them is not mutually affected. However, when the power in the waveguide passing through the LED-SRR (shown red in Fig. 2) increases, the LED shines light onto the PD of the orthogonal SRR, which imposes additional voltage on the varactors and shifts the effective capacitance of the PD-SRR. This leads to the shift of the resonance in the element at the intersection, and affects signal propagation through the other waveguide (shown black in Fig. 2). Consequence is the "traffic light" effect, when the increasing intensity in one waveguide suppresses propagation in the other. Moreover, the dynamics of this effect is different at different frequencies, so the system actually supports power-dependent propagation control across multiple channels (see the two curves in Fig. 3). We will present alternative designs as well as experimental results, demonstrating that our approach enables efficient control of the transmission over one channel depending on the power supplied over the other, providing a "traffic light" for the signals.

Figure 1: Experimental prototype of the optically coupled meta-atom: one of the broadside-coupled split-ring resonators is loaded with photo-diodes (PD); the other one, orthogonally positioned, is equipped with a light-emitting diode (LED).

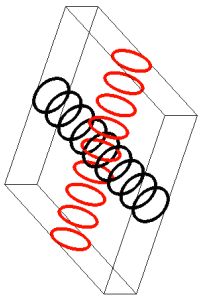

Figure 2: Conceptual schematic of the two perpendicular magnetoinductive waveguides with the opticallycoupled meta-atom at the intersection (black ring for the PD-SRR, red ring for the LED-SRR).

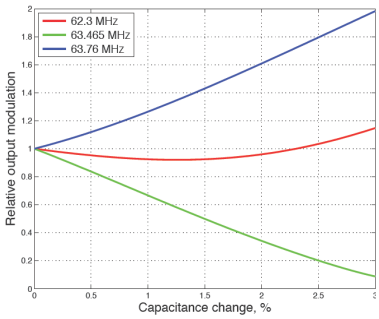

Figure 3: Relative change in the transmission coefficient (here, the ratio between the output and input current) over the PD-waveguide (black in Fig. 2) depending on the capacitance change in the PD-SRR, imposed by the increasing power over the LED-waveguide (red in Fig. 2); a 2% change in the capacitance corresponds to 1 W power increase. The results are shown for three frequency channels, demonstrating traffic suppression, enhancement or little variation, depending on frequency.

REFERENCES

1. Slobozhanyuk, A. P., et al., "Nonlinear interaction of meta-atoms through optical coupling," *Appl. Phys. Lett.*, Vol. 104, 014104, 2014.

Retrieving the Polarizability Tensor of Wire Media

J. Ben Yakar[1], **P. Chen**[2], **Y. Sivan**[2], **and D. J. Bergman**[2]

[1]School of Physics and Astronomy, Raymond and Beverly Sackler Faculty of Exact Sciences
Tel Aviv University, Tel Aviv 69978, Israel
[2]Unit of Electro-optics Engineering, Ben-Gurion University, Israel

Abstract— Metamaterials consisting of long, circular, cylinders are very popular. It is a fundamental challenge to characterize the effective electromagnetic response of such composites. In this framework, the radius of cylinder is assumed to be considerably smaller than the external wave length, thus the dominant scattered EM fields can be approximately replaced by dipole fields. Previous works dealt mainly with two dimensional (2D) scenarios, i.e., characterizing the effective electromagnetic response for light propagation perpendicular to the cylinder axis.

In this work, we generalize this treatment to three dimensions (3D), i.e., we characterize the effective electromagnetic response for light propagation at any angle, and find that the resulting electromagnetic response is non-local, i.e., it depends on the wavevector component parallel to the cylinder axis. We retrieve analytically, the full polarizability tensor and show that it has different contributions for different polarized incoming EM waves (transverse electric and transverse magnetic with respect to the cylindrical axis), i.e.,

$$\begin{pmatrix} \mathbf{p} \\ \mathbf{m} \end{pmatrix} = \overleftrightarrow{\alpha}^{TM} \begin{pmatrix} \mathbf{E}_{TM} \\ \mathbf{H}_{TM} \end{pmatrix} + \overleftrightarrow{\alpha}^{TE} \begin{pmatrix} \mathbf{E}_{TE} \\ \mathbf{H}_{TE} \end{pmatrix}. \tag{1}$$

It is also diagonal, i.e., it contains no magneto-electric coupling, showing that claims in previous studies were incorrect. Having closed form expressions for polarizability allows us to use effective medium approximation methods, and tailor the spectral response for both electric and magnetic dipolar contributions. It is important to emphasize that for the first time, this gives a fully systematic way to characterize the magnetism (for example, see Fig. 1) of wire media.

Our analysis holds for additional structures based on cylindrical geometry, such as hole arrays, all-dielectric metamaterials, and multi-layer cylinders. It can be used to explain the electromagnetic response of wire media attributed with a negative refractive index, effective magnetism and hyperbolic dispersion relations. In addition, this approach can be applied to more complex unit cells e.g., consisting of clusters of parallel cylinders.

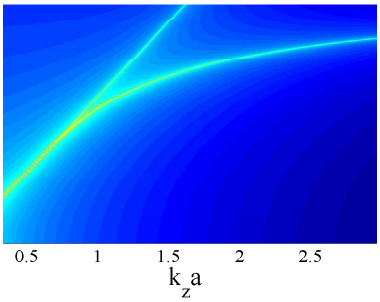

Figure 1: Intensity in log-scale, of the normalized transverse TE magnetic polarizability of a single, metallic cylinder placed in vacuum. The permittivity inside the cylinder is modeled using the dispersive Drude model, i.e., $\varepsilon_1 = 1 - \frac{\omega_p^2}{\omega^2+\gamma^2} + i\frac{\gamma\omega_p^2}{\omega^3+\omega\gamma^2}$, where $\omega_p = 13.7 \times 10^{15}$ Hz, and $\gamma = 32 \times 10^{12}$ Hz. The intensity shown in the figure, resonates near the (straight) light-line and the dispersion relation of surface modes along the cylinder surface. Additional important parameters: the cylinder radius $a = 50$ nm; the surface plasmon frequency $\omega_s = \omega_p/\sqrt{2}$, and k_z the wavevector component parallel to the cylinder axis.

Session 3P3a
SC1: Computational Techniques in Electromagnetics and Applications 2

An Intelligent Platform for Effective Management of Time-consuming Electromagnetic Simulation Problems

Andreas P. Kapsalis[1], **Panagiotis K. Gkonis**[1], **Constantinos L. Zekios**[2], **Dimitra I. Kaklamani**[1], **Iakovos S. Venieris**[1], **and George A. Kyriakou**[2]

[1]Intelligent Communications and Broadband Networks Laboratory
School of Electrical and Computer Engineering, National Technical University of Athens
9 Heroon Polytechneioy Str., Zografou, Athens, Greece
[2]Microwaves Lab, Department of Electrical and Computer Engineering
Democritus University of Thrace, Xanthi, Greece

Abstract— Modern simulation applications that carry out large scale iterative processes, such as Monte-Carlo simulations, or manipulate large data structures, tend to be extremely time-consuming due to the shortage of computational resources or the inherent nature of the simulation itself. Typical simulations can take up to several days to complete on conventional systems, while high-end supercomputers can be cost-prohibitive. Therefore, the need for effective parallelization of software execution and resource management is more imperative.

The goal of thus paper is to present a fully-distributed platform that enables software simulations to be executed within user-acceptable time periods, by predicting the resource requirements of each simulation. In this context, the platform analyzes user-defined simulation parameters as well as files that contain historical data about past executions of the particular simulation. Processor and memory utilization, overall execution time, level of parallelization and distributed execution are some of the information collected and used by an efficient training algorithm, in order to determine the optimal amount of resources to be allocated in a particular simulation. The training algorithm applies several machine-learning techniques such as multi-feature linear regression in order to efficiently predict the resource vector that will satisfy the user requirements.

The proposed architecture has been thoroughly tested for a variety of computationally and time intensive software applications, such as the eigenanalysis of electromagnetic structures using a series of numerical techniques (FEM, FDFD, MoM) as well as Monte-Carlo simulations for capacity calculations in 3G networks employing multiple antennas at both transmission ends. Moreover, parallelization techniques such as shared-memory parallel frameworks (OpenMP) as well as distributed-memory models have been utilized as well, that allow distributed execution (MPI) of the studied problems. Finally, for effective resource management, the described platform has been deployed on a medium-scale Cloud Infrastructure that is capable of spanning multiple Virtual Machines (VMs), which in turn will host the simulation software.

Two-dimensional Spatial Frequency Technique for Calculating Electromagnetic Scattering from Large Objects

Dayalan Kasilingam and Anthony Fascia
Department of Electrical & Computer Engineering, University of Massachusetts Dartmouth, USA

Abstract— In computational electromagnetics, there is a need for fast and accurate methods for calculating electromagnetic scattering from large objects and surfaces. Typically, in scattering problems an integral equation (IE) is defined and solved for calculating the fields or the currents on a scattering structure. In numerical solution methods such as the method of moments (MoM), the IE is discretized and solved by the inversion of a matrix. However, since the matrices in the MoM method are generally dense, for large scattering objects, matrix inversion is not computationally efficient. More efficient iterative methods such as the conjugate gradient method have since been developed to handle the numerical complexity of inverting large matrices. These iterative methods have significantly reduced the computational demands of solving the IE for scattering and radiation problems.

Another important technique which has shown great potential for reducing the computational demands of large matrix inversion problems, is the use of the spatial frequency technique. In the spatial frequency technique, the matrix equation is transformed into the spatial frequency domain by the use of the computationally efficient, FFT algorithm. Generally, the IE represents a set of boundary conditions which are the result of a convolution of a Green's function and surface currents or fields. Using the property of the Fourier transform, a convolution in space is converted to a product in the spatial frequency domain. The dense matrix multiplication in the spatial domain representation of the IE is thereby transformed into a multiplication by a diagonal matrix.

In addition, another significant advantage of the spatial frequency method is that it converts derivatives of fields or currents into simple multiplication by the appropriate spatial frequency component. In many scattering or radiation problems, the effective Green's function is derived by taking the derivatives of an original Green's function. In all of these cases, the modified Green's functions for different polarizations can be derived easily from one original Green's function by utilizing this property of the spatial frequency method.

Most of the previous work using the spatial frequency approach for analyzing scattering has focused on one-dimensional surfaces. In this study, the spatial frequency method is extended to scattering from two-dimensional, conducting objects, such as metallic cylinders of arbitrary cross-sections. In discrete processing, only Green's functions represented by circulant Toeplitz matrices can be converted to diagonal matrices in the spatial frequency domain. However, in practice, the Green's function matrices are generally Toeplitz matrices and not circulant Toeplitz matrices. A method for converting the Toeplitz matrix to a circulant Toeplitz matrix without altering the problem and increasing the computer storage requirements is developed and used in this technique. An expression for the induced currents are obtained in terms of a diagonal Green's function matrix in the spatial domain and the spatial frequency transform of the incident fields. A Taylor series expansion is used to avoid the need for matrix inversion. By truncating the Taylor series, one is able to generate results with different degrees of accuracy. Simulation results for scattering from cylinders of different sizes and cross-sections are generated and compared with other fast algorithms such as the conjugate gradient method for speed and accuracy. In addition to the analysis of electromagnetic scattering, this technique also lends itself well to the synthesis of scattering patterns. Several examples of how the spatial frequency technique is applied to the synthesis of two-dimensional targets with prescribed scattering patterns are also given.

A Conformal FDTD Model for Anisotropic Dielectric Interfaces in the GPU-accelerated PIC Code Neptune

S. J. Cooke[1], **G. M. Stantchev**[1], **and T. M. Antonsen, Jr.**[2]

[1]US Naval Research Laboratory, Washington, DC, USA
[2]Leidos Inc., Herndon, VA, USA

Abstract— The 3D Electromagnetic FDTD algorithm provides a practical and powerful technique to solve Maxwell's equations based on known device geometry and material properties. To obtain accurate simulations with this technique it is necessary to discretize the problem geometry onto the Cartesian FDTD grid using conformal (cut-cell) techniques. For metal boundaries these account for geometry at the sub-cell level to improve the order of accuracy of the field boundary conditions, and for smooth conducting geometries may provide 2nd-order convergence of electromagnetic eigenmode frequencies with respect to the grid cell size. For dielectric interfaces, sub-cell schemes have been demonstrated to obtain convergence initially 2nd-order, but for high resolution grids or high permittivity ratios it is observed that lower-order error terms dominate, and convergence revert to 1st-order [1].

In this paper we present a novel sub-cell averaging scheme to discretize material parameters on a Cartesian 3D FDTD grid for cells at the interfaces between regions of isotropic or anisotropic dielectric material. For cells intercepted by a dielectric interface we obtained a tensor expression for the average dielectric permittivity tensor in the cell, as a function of the two local permittivity tensors and the interface normal vector, assumed to be constant in the cell. For the particular case of two isotropic material tensors the resulting effective tensor is anisotropic due to the in fluence of the normal vector. In all cases, the method explicitly preserves the tensor symmetry and therefore is expected to provide stable evolution for time domain simulations.

We have implmented the new scheme in the electromagnetic model of the *Neptune* code [2], a FDTD particle-in-cell (PIC) code developed at the US Naval Research Laboratory since 2010 to model electromagnetic interactions with charged-particle beams. *Neptune* has an accurate conformal representation for metal surfaces, including loss [3], and is optimized for both multicore CPU and NVIDIA GPU hardware.

To illustrate the new scheme we solved for the lowest 97 eigenmodes of an isotropic dielectric sphere ($r = 0.5$) inside a concentric, spherical, perfectly conducting metal cavity ($r = 1.0$) using the new discretization model. The computed eigenmode frequencies were observed to converge to analytical solutions according to the 2nd-order relation,

$$\frac{\Delta f}{f} < \left(\frac{h}{\lambda_0}\right)^2 \varepsilon_r \tag{1}$$

where h is the grid cell size, and $\lambda_0 = c/f$ is the free-space wavelength. This was verified for $\varepsilon_r = 8$, 30 and 100, with cell sizes as low as $h \approx \lambda_0 = 100$.

ACKNOWLEDGMENT

Work supported by the US Office of Naval Research.

REFERENCES

1. Werner, G. R., C. A. Bauer, and J. R. Cary, "A more accurate, stable, FDTD algorithm for electromagnetics in anisotropic dielectrics," *J. Comput. Phys.*, Vol. 255, 436–455, 2013.
2. Cooke, S. J., et al., "GPU-accelerated 3D large-signal device simulation using the particle-in-cell code Neptune," *13th International Vacuum Electronics Conference*, 21–22, Monterey, CA, USA, Apr. 2012.
3. Cooke, S. J. and G. M. Stantchev, "Conformal time-domain particle-in-cell simulation of vacuum electronic devices with accurate surface loss," *14th International Vacuum Electronics Conference*, Paris, France, May 2013.

Energy Distribution of Waveguides with Air-hole Dielectric Cylinder Outside of the Defect Layers

Ryosuke Ozaki and Tsuneki Yamasaki
Department of Electrical Engineering, College of Science and Technology
Nihon University, Japan

Abstract— Guiding and scattering problems of electromagnetic waves with periodic structures are very interesting in many areas of physics and engineering such as metamaterials or photonic crystal. Metamaterials are well known as technology which can be controlled mutual coupling of antennas with EBG (Electromagnetic Band Gap) structures and noise of circuit substrate. Also, EBG is the periodic array structure which consists of dielectric and perfect conductor. On the other hand, photonic crystals such as optical nanostructures with periodically permittivity distribution are known as technology which can be controlled the light in the periodic structure by interaction of both the wave nature of light and periodicity. Therefore, in the design of photonic crystals or metamaterials with periodic array or as much as optical wavelength, it is very important to investigate the stop band region or photonic band gaps. Though it is not analyzed the stop band area in Bragg region in detailed, several numerical results are shown only fields distribution by utilizing the FDTD method, FEM method based on variational method, and another numerical techniques.

In recent papers [1–3], we have proposed the periodic dielectric waveguide composed of dielectric circular cylinder and air-hole circular cylinder array, and investigated the influence of energy distribution in the defect area and complex propagation constants at the first stop band region by utilizing the combination of improved Fourier series expansion method and multilayer method for TE mode.

In this paper, we have analyzed the energy distribution of waveguide with air-hole dielectric cylinder outside of the defects layer as shown in Fig. 1. Consequently, the aim of this paper is to obtain optimum dielectric waveguide structure to concentrate the energy into the defect area for TE and TM mode. Numerical results indicate for the complex propagation constants at the first stop band region and the energy distribution for TE mode compared with TM mode.

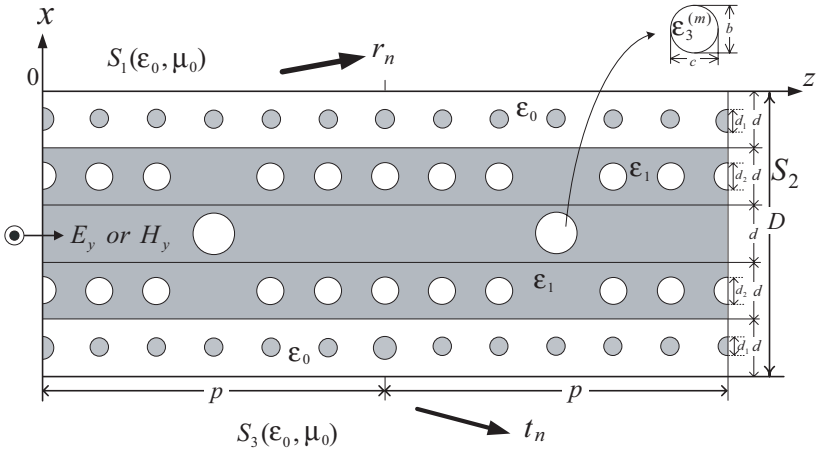

Figure 1: Structure and coordinate system of dielectric waveguides with air-hole dielectric cylinder outside of the defects layer.

REFERENCES

1. Ozaki, R. and T. Yamasaki, "Distribution of energy flow by dielectric waveguide with defects composed of air-hole type circular cylinder array," *Progress In Electromagnetics Research Symposium Abstracts*, 589, Taipei, Mar. 25–28, 2013.
2. Ozaki, R. and T. Yamasaki, "Distribution of energy flow by dielectric waveguide composed of dielectric circular cylinders and air-hole type circular cylinders array," *Progress In Electromagnetics Research Symposium Abstracts*, 823, Stockholm, Sweden, Aug. 12–15, 2013.

3. Ozaki, R. and T. Yamasaki, "Energy distribution of dielectric waveguide by various circular cylinder array with defect layers," *Progress In Electromagnetics Research Symposium Abstracts*, 890, Guangzhou, China, Aug. 25–28, 2014.

Development of ADI-FDTD Methods with Dispersion-Relation-Preserving Features

T. T. Zygiridis[1], **N. V. Kantartzis**[2], **and T. D. Tsiboukis**[2]

[1]Department of Informatics & Telecommunications Engineering, University of Western Macedonia, Greece
[2]Department of Electrical & Computer Engineering, Aristotle University of Thessaloniki, Greece

Abstract— The incorporation of dispersion-optimized finite-difference expressions, instead of standard Taylor-based approximations, has been proposed in various publications for the construction of explicit finite-difference time-domain methodologies with upgraded reliability [1]. On the other hand, this practice has not been pursued extensively in the case of unconditionally-stable FDTD methods, with the most common one being the alternating-direction-implicit (ADI) FDTD scheme [2]. A rather popular approach that targets the accuracy improvement of such methods is the direct incorporation of high-order derivative approximations [3]. Although these may ensure milder anisotropy and smaller spatial errors, they do not constitute the most suitable choice for performance enhancement. This becomes clear, if one takes into account the nature and the practical applications of unconditionally-stable methods: the latter are deemed appropriate discretization strategies mainly in cases of densely-sampled spaces, where explicit FDTD schemes require excessive number of iterations, due to their restricted stability range. Furthermore, if we consider the fact that time-steps larger than the common stability limits are selected in the context of unconditionally-stable methods (hence, significant temporal errors emerge), we naturally conclude that a proper error amendment calls for the efficient treatment of the combined space-time errors, rather than the spatial ones only.

The ADI-FDTD method is a perturbation of the Crank-Nicolson scheme and is realized as a two-stage process with implicit update equations:

$$\left(\mathbf{I}-\frac{\Delta t}{2}\mathbf{A}\right)\mathbf{u}^{n+1/2}=\left(\mathbf{I}+\frac{\Delta t}{2}\mathbf{B}\right)\mathbf{u}^{n},\quad \left(\mathbf{I}-\frac{\Delta t}{2}\mathbf{B}\right)\mathbf{u}^{n+1}=\left(\mathbf{I}+\frac{\Delta t}{2}\mathbf{A}\right)\mathbf{u}^{n+1/2} \tag{1}$$

where $\mathbf{A}$, $\mathbf{B}$ are derivative matrices, $\mathbf{I}$ is the identity matrix, and u is the vector of all field components. Our goal is to modify only the derivative matrices, yet derive an algorithm with lowered space-time errors. As in most FDTD methods, pursuing the correction of accuracy on a single-frequency basis is usually simpler than performing wideband amendments. In our case, we first introduce three-cell spatial operators,

$$D_u f|_i=\frac{1}{\Delta u}\left[C_1\left(f|_{i+\frac{1}{2}}-f|_{i-\frac{1}{2}}\right)+C_2\left(f|_{i+\frac{3}{2}}-f|_{i-\frac{3}{2}}\right)\right] \tag{2}$$

which are designed to minimize the corresponding spatial flaws at a selected frequency point. This is accomplished by treating plane-wave expressions as trial functions, and defining suitable error estimators, whose minimization leads to optimized values of the C_1, C_2 coefficients. Then, the algorithm's overall performance is further controlled by proceeding with an artificial modification of the speed of light, which is equivalent to altering the properties of the background medium. This approach rectifies the error pertinent to the numerical phase velocity (which is calculated from the corresponding dispersion relation), by ensuring a vanishing mean value.

Apart from the aforementioned methodology, we also discuss the possibility of exploiting the scheme's dispersion relation for the construction of optimized ADI-FDTD techniques, when different orders of space and time discretizations are considered. A power-series based approximation of the dispersion relation and the matching of terms with equal order can produce new spatial operators with attractive error-balancing properties. Therefore, this paper accomplishes the construction of more reliable unconditionally-stable computational models, by exploiting alternative ways for the definition of improved spatial approximations.

REFERENCES

1. Finkelstein, B. and R. Kastner, "Finite difference time domain dispersion reduction schemes," *J. Comp. Phys.*, Vol. 221, No. 1, 422–438, Jan. 2007.
2. Namiki, T., "3-D ADI-FDTD method — Unconditionally stable time-domain algorithm for solving full vector Maxwell's equations," *IEEE Trans. Microw. Theory Techn.*, Vol. 48, No. 10, 1743–1748, Oct. 2000.
3. Fu, W. and E. L. Tan, "A compact higher-order ADI-FDTD method," *Microw. Opt. Technol. Lett.*, Vol. 44, No. 3, 273–275, Feb. 2005.

Polarimetric and Phased Array Weather Radar Observations Using Optimized Pulse Compression Waveforms

James M. Kurdzo, **Robert D. Palmer**, **and Boon Leng Cheong**
Advanced Radar Research Center, University of Oklahoma, Norman, OK, USA

Abstract— The meteorological community has traditionally utilized single-frequency pulsed Doppler radar observations for the detection, surveillance, and forecasting of severe convective thunderstorms, flash floods, winter storms, and other potentially life-threatening weather events. Despite the widespread use of pulse compression waveforms in other radar disciplines, meteorological radars have yet to embrace this technology. With numerous studies exploring the potential for both phased array and low-power/low-cost dish platforms for weather observations, the necessity for extremely high-sensitivity waveforms has become a major issue for the weather radar community. Recently, the Advanced Radar Research Center (ARRC) at the University of Oklahoma has been developing pulse compression waveform optimization, design, and real-world system implementation techniques, and has been using these waveforms on a series of weather radar platforms. The use of pulse compression has provided good sensitivity while significantly lowering the cost of complex systems, and provides the potential for spatial resolutions nearly an order of magnitude higher than typically seen in operational weather radar. This paper presents a series of comparative weather observations using pulse compression waveforms on the ARRC's PX-1000 100 W, X-band, transportable solid-state radar, as well as the ARRC's Atmospheric Imaging Radar (AIR), a 3.5 kW, X-band, mobile digital beamforming tornado radar. PX-1000 case examples including the 20 May 2013 Moore, Oklahoma EF5 tornado will be shown, with a focus on multi-lag processing for high quality polarimetric estimates that captured unique debris ejection signatures. AIR case examples including the 19 May 2013 Shawnee, Oklahoma EF4 tornado, the 31 May 2013 El Reno, Oklahoma EF3 tornado, and the 21 May 2014 Denver, Colorado tornadoes will be presented. The AIR cases focus on a combination of extremely high spatial and temporal resolution, with native range resolutions as high as $1^\circ \times 1^\circ \times 37.5$ meters, and $90^\circ \times 20^\circ$ volumetric updates as fast as 5 seconds. Examples of unique meteorological phenomena only observable with the combination of extremely high temporal resolution and pulse compression waveforms are presented, including simultaneous volumetric vortex tilt structures, horizontal hook echo convective lines, and 3-dimensional debris trajectories.

Transparent Cathode Virtual Cathode Oscillator

Seyed Morad Ali Hashemi[1], **Erfan Zabeh**[2], **and Ali Pirmoradi**[2]

[1]Electromagnetics Research Laboratory, Sharif University of Technology, Tehran, Iran
[2]Department of Electrical Engineering, Sharif University of Technology, Tehran, Iran

Abstract— This paper reports structural considerations on virtual cathode oscillator (VCO) resulting in a new cathode structure that increase final efficiency while decreasing system chaotic behavior. Nonlinear phenomena are the most important sources of the complexity of the electron beam dynamics and microwave generation process in VCO. Chaos, maybe the most important nonlinear phenomenon appearing in VCO considered as a dynamical system is studied. Small changes in the oscillator parameters, such as input voltage or structural parameters values, could make undesirable variations in output parameters, meaning potential instability, causing difficulties getting enough close to the forbidden limits of those parameters. At these conditions final efficiency will be reduced considerably.

A novel structural optimization is introduced by the authors that controlling chaotic behavior of the system, allows the input voltage to increase without any notable distractive effects on the microwave beam. We found that if we divide-cathode to several separate concentric annular parts located apart from each other on a plane surface with designed distances, chaotic behavior of the system will decrease considerably in large anode-cathode distances. The novel cathode, called transparent cathode, was simulated with PIC-code method to study the chaotic behavior of the new structure. It was shown that increasing input voltages pushes the system towards the chaos, as is usual in the VCOs but with some considerable differences regarding those with conventional cathodes: in the novel design, the chaotic behavior appears at much higher input voltages letting higher microwave powers and higher efficiencies to be achieved.

Session 3P3b
Computational Electromagnetics, Hybrid Methods

Optimization of General Microwave Passive Circuits Based on Zero-pole Technique

N. Leszczynska, **A. Lamecki**, **and M. Mrozowski**
Gdansk University of Technology, Poland

Abstract— Passive circuits such as directional couplers and power dividers are key building blocks in various microwave and millimeter-wave systems, since they are used in almost every high frequency component including power amplifiers, mixers, multipliers and antenna feeding networks. General techniques for designing of those circuits are well known in the literature, but at a final design stage, electromagnetic solvers are commonly used to perform the final verification and numerical optimization. Usually large computational resources are involved at this stage. As a result, the full-wave design-by optimization is usually very time consuming.

In this submission a novel approach for numerical tuning of the design is shown. In this approach, the circuits are optimized using cost function involving zeros and poles of the rational function approximating scattering parameters. Such a formulation of a cost function has been utilized to design microwave filters, and it was found that this function yields very rapid convergence. The extension of the zero-pole technique to other types of passive circuit is non-obvious since reference (target) zeros and poles have to be known. In the case of filters the reference zeros and poles are known form the circuit synthesis. For other types of circuits, the synthesis procedure does not directly lead to a rational function so the reference zeros and poles are not known. To overcome this limitation, in this submission the reference zeros and poles for arbitrary structures are extracted from simulated response of a low-fidelity model. Since the low-fidelity model should be easy to compute, a good choice for this purpose is a device's equivalent circuit or a simplified low resolution numerical model.

Such a model can be easily tuned and optimized to meet the design requirements. Then the zeros and poles extracted from optimized response are used as a reference to perform a numerical tuning of original, complex design. The effectiveness and robustness of the proposed technique is presented in illustrative examples.

ACKNOWLEDGMENT

This work was supported by the Polish National Science Centre under contract UMO-2012/07 /B/ST7/01241.

Large Scale Characteristic Mode Analysis with Multilevel Fast Multipole Algorithm

Q. I. Dai, H. Gan, and W. C. Chew
University of Illinois at Urbana-Champaign, USA

Abstract— After a humble beginning in the early 1970s, theory of characteristic mode (TCM) has gained a recent resurgence of interest in the field of antenna design and optimization. Although use of characteristic mode (CM) analysis shows success in systematic antenna designs, relatively little effort has been devoted to the numerical computation of such modes. Conventional TCM based on the electric field integral equation (EFIE) can only deal with small scale problems where the matrix pair in a dense generalized eigenvalue problem (GEP) is explicitly generated. However, such a scheme fails in applications where in multimode excitation, a large platform such as the entire vehicle chassis works as an antenna, or in multi-scale modeling, the object contains fine structures which lead to a dense mesh and a large number of unknowns.

Large scale characteristic mode computation poses challenges in computational electromagnetics (CEM) as it calls for efficient solutions of large dense GEPs. Multilevel fast multipole algorithm (MLFMA) can greatly reduce the computational complexity and memory cost for matrix-vector multiplications (MVMs), which is powerful in iteratively solving large scattering problems. In this work, we demonstrate that MLFMA can be easily incorporated into the implicit restarted Arnoldi method for CM computation after simple modifications. For the large platform application, we propose a combined integral equation (CFIE) based TCM, where the mid-frequency MLFMA is employed to speed up the required MVMs. A radiating characteristic mode of a NASA almond which has a length of 15 wavelengths is obtained with the proposed scheme and demonstrated in Fig. 1, where around 54,000 unknowns are involved. For the multi-scale modeling, we propose an augmented electric field integral equation (AEFIE) based TCM, where the mixed-form MLFMA is adopted to accelerate the required MVMs.

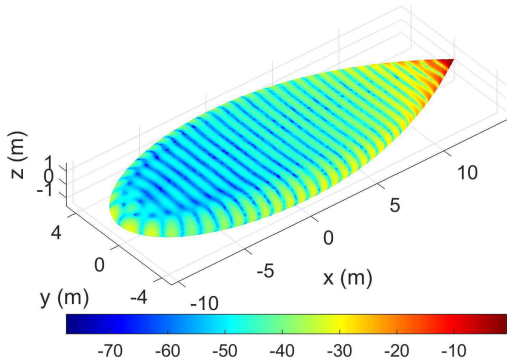

Figure 1: A radiating characteristic mode of a NASA almond computed with CFIE based TCM and MLFMA.

Efficient Calculating the High Frequency Scattered Fields from the Fock Currents of 3-D Convex Scatterers with the Incremental Length Diffraction Coefficients Technique

Y. M. Wu[1], W. C. Chew[2], Y. Q. Jin[1], T. J. Cui[3], and L. J. Jiang[4]

[1]Key Laboratory for Information Science of Electromagnetic Waves (MoE)
School of Information Science and Technology, Fudan University, Shanghai, China
[2]Department of Electrical and Computer Engineering
University of Illinois at Urbana-Champaign, Urbana, USA (Visiting professor of HKU)
[3]The State Key Laboratory of Millimeter Waves, Southeast University, Nanjing, China
[4]Department of Electrical and Electronic Engineering, The University of Hong Kong, Hong Kong, China

Abstract— In this work, the efficient algorithms for the high frequency scattered fields from 3-D convex scatterers are studied in detail. We propose the Fock current and the incremental length diffraction coefficient (ILDC) technique to efficiently calculate the high frequency scattered fields.

As is known, the physical optics (PO) current makes use of the local tangential plane approximation technique and usually loses accuracy, especially when the observation point lies around the transition regions and in the deep shadow regions. In order to remedy this limitation, we comprehensively study and adopt the Fock currents from the convex scatterers. Next, to capture the high frequency wave physics phenomenon from convex scatters, the Fock current is separated into the classical physical optics (PO) current and the non-uniform (NU)-Fock current along the shadow boundary and in the deep shadow region. Due to the highly oscillatory nature of the Fock currents, we propose the numerical contour deformation technique to efficiently evaluate the Fock currents. On invoking the ILDC technique, the high frequency scattered fields are clearly formulated in the lit, shadow and transition regions of the 3-D convex scatterers. Compared to the PO scattered fields from the 3-D convex sphere, numerical results demonstrate the significant accuracy enhancement of the scattered field in terms of the Fock current, especially for the large bistatic angle case. Finally, the work offers the high frequency wave physics picture from the 3-D convex scatterers, including the Fock current behaviors around the transition regions and the creeping wave fields.

A Variational Method to Solve Maxwell's Equations in Singular Axisymmetric Domains with Arbitrary Data

F. Assous[1] **and I. Raichik**[2]

[1]Ariel University, Israel
[2]Bar-Ilan University, Israel

Abstract— We propose a new variational method to compute 3D Maxwell's equations in an axisymmetric singular 3D domain, generated by the rotation of a singular polygon around one of its sides, namely containing reentrant corner or edges. We consider the equations written in $(r,\ \theta,\ z)$ and use a Fourier transform in θ to reduce 3D Maxwell's equations to a series of 2D Maxwell's equations, depending on the Fourier variable k. The principle is to compute the 3D solution by solving several 2D problems, each one depending on k.

Let us denote by $(\mathbf{E}_k,\ \mathbf{B}_k)$ the electromagnetic field for each mode k. Following [1, 2], it can be proved that this solution can be decomposed into a regular and a singular part. The regular part can be computed with a classical finite element method. The singular part is more difficult to compute: it belongs to a finite-dimensional subspace. Its dimension is equal to the number of reentrant corners and edges of the 2D polygon that generates the 3D domain. We will propose a new variational approach, based on a decomposition of the computational domain into subdomains, and we will derive an ad hoc variational formulation, in which the interface conditions are imposed with a method deduced from a Nitsche approach.

We will first consider the case $k = 0$, corresponding to the full axisymmetric case. We will show how to compute $\mathbf{w}_0^s$, the singular part of the electric field solution $\mathbf{B}_0$. We will then derive the non stationary variational formulation to compute the total part of the solution. After, we will consider the computation of the case $k \neq 0$. Following [2], this will require first to derive the system of equations solved by the singular parts for each k. Then to derive and solve the time-dependent variational formulation depending on k, for each mode. Finally to reconstruct the approximate 3D electromagnetic fields from each mode k.

REFERENCES

1. Assous, F., P. Ciarlet, Jr., S. Labrunie, and J. Segré, "Numerical solution to the time-dependent Maxwell equations in axisymmetric singular domains: The singular complement method," *J. Comput. Phys.*, Vol. 191, 147–176, 2003.
2. Ciarlet, Jr., P. and S. Labrunie, "Numerical solution of Maxwell's equations in axisymmetric domains with the Fourier singular complement method," *Differential Equations and Applications*, Vol. 3, No. 1, 113–155, 2011.

Semi-analytical Modeling of Single Loop Inductive RF Sensors Used to Sense and Locate Inclusions in Dielectric Media

M. Wang[1, 2], P.-Y. Joubert[1], S. Serfaty[2], T. Bore[2], and D. Placko[2]

[1]Université Paris Sud, IEF, CNRS, Bat. 220, 94 230 Orsay Cedex, France
[2]SATIE, CNRS, ENS Cachan, 61 Avenue du Président Wilson, 94 230 Cachan, France

Abstract— The electromagnetic characterization of dielectric media is a major issue in many industrial fields such as civil engineering, oil, food or agriculture industries as well as medicine. The radiofrequency (RF) inductive techniques are non-contact and therefore well suited for the non-invasive evaluation and monitoring of dielectric media [1], so they appear to be quite promising compared with the capacitive techniques. In order to foresee the sensitivity of such inductive RF sensors as well as to carry out quantitative evaluation of dielectric media, a versatile and computationally efficient modeling tool is required. To do so, analytical models have been developed [2] but they are limited to simple configurations. Numerical modeling techniques such as finite element computations are more versatile but they require heavy computational resources when three dimensional computations of complex configurations are required. In this paper, we investigated the relevance of a mesh-free semi-analytical modeling technique, so-called distributed point source method (DPSM) [3] to model the interactions of a RF sensor with a dielectric media. The basic principle of DPSM is based on the use of i) active equivalent source densities (ESD) used to model the actives sources in the workspace (here the current flowing in the RF antenna) and ii) virtual ESD used to take account of the boundaries between the different material included within the workspace. The distributed ESD radiate as Green's functions in the considered media so the variables of interest at any point of the workspace (e.g., magnetic field...) can then be determined as the sum of the contribution of all radiating ESD. The main advantage of the DPSM is that it is a "mesh-free" method. It just discretizes the active sources and the boundary, so the objects of any geometry may be modeled with no theoretical limitations on the shape and on the number of objects. As a result, the DPSM can be considered as a computationally efficient and versatile 3D modeling tool. In this paper, the configuration of a single RF loop interacting with a dielectric media including a buried object (e.g., a tumor in a biological tissue) is considered. The DPSM modeling is implemented and a parametric study of the sensitivity of the RF antenna to the changes of material conductivity is studied according to sensor position and used frequency. The computation results are validated by experiments involving a 2 cm diameter single loop RF sensor operated in the 1–100 MHz bandwidth. In addition, a simple system of two RF single loop antennas is also considered to locate the position of the inclusion. The first computation results show that it is possible to locate a buried dielectric inclusion thanks to the variations of the ratio of current intensities feeding the two antennas. The obtained results enable the DPSM to be considered in further works for the modeling of complex inductive sensors, such as transmission-line resonators [5], or for antennas arrays dedicated to dielectric imaging.

REFERENCES

1. Sosa-Morales, M. E., L. Valerio-Junco, A. López-Malo, and H. S. García, "Dielectric properties of foods: Reported data in the 21st Century and their potential applications," *LWT — Food Sci. Technol.*, Vol. 43, No. 8, 1169–1179, Oct. 2010.
2. Kraichman, M. B., "Impedance of a circular loop in an infinite conducting medium," *J. Res. Nat. Bureau of Standards, D. Radio Propagation*, Vol. 66, No. 4, 499–503, 1962.
3. Placko, D., T. Bore, and T. Kundu, "Distributed point source method for imaging in electrostatic and electromagnetic problems," *Ultrasonic and Electromagnetic NDE for Structure and Material Characterization: Engineering and Biomedical Applications*, 249–295, CRC Press, 2012.
4. Masilamany, G., P.-Y. Joubert, S. Serfaty, B. Roucaries, and Y. Le Diraison, "Radiofrequency inductive probe for non-contact dielectric characterisations of organic medium," *Electronics Letters*, Vol. 50, No. 7, 496, 497, Mar. 27, 2014.
5. Serfaty, S., et al., "Multi-turn split-conductor transmission-line resonators," *Magnetic Resonance in Medicine*, Vol. 38, No. 4, 687–689, 1997.

Quasi-modes in Segmented Waveguides

G. Demésy, A. Nicolet, and F. Zolla
Institut Fresnel, Aix-Marseille Université, CNRS, ECM, France

Abstract— In the present paper, we show that it is possible to use a periodic structure of disconnected elements to guide electromagnetic waves. To study such structures, we use the concept of quasi-modes associated to complex frequencies (also named quasi-normal modes or leaky modes).

In the present paper, we show that it is possible to use a periodic structure of disconnected elements (segmented waveguides [1]) to guide electromagnetic waves, **in the direction of the periodicity**, on significant distances with very limited losses. To study such structures, we use the concept of quasi-modes associated to complex frequencies [2]. The numerical determination of quasi-modes is based on a finite element formulation completed with Perfectly Matched Layers (PMLs) [3]. These PMLs lead to non Hermitian matrices whose complex eigenvalues correspond to quasi-mode frequencies. Using Floquet-Bloch theory [4], a numerical model is set up that allows the spectral study of structures that are both open and periodic. With this model, we explain how light can be guided on significant distances and with very limited losses through disconnected elements.

Figure 1 shows the real part of the electric field in the xy plane for a finite chain of finite length cylinders with a dipole source at 750 nm.

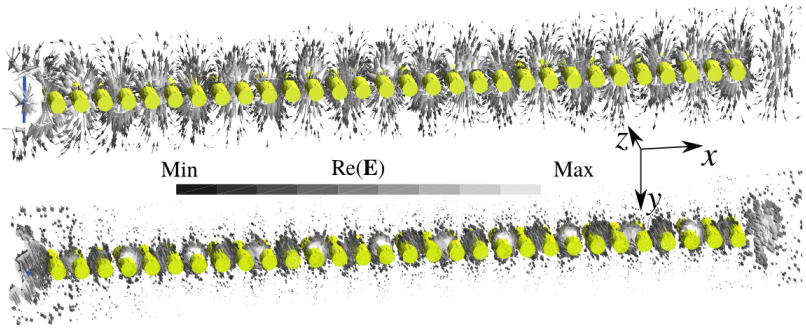

Figure 1: Finite chain of 30 cylinders of finite length $l = 6r$, with $d = 300\,\text{nm}$, $r = 125\,\text{nm}$ and $\epsilon_c = 2.25$ enlighten by a dipole antenna at 750 nm. Real part of the electric field in the xz plane. Two possible orientations — along (a) y or (b) z — of the dipole antenna leads to the excitation of one of the two quasi-modes with $\text{Re}\{w\} = 2.5 \times 10^{15}\,\text{rad/s}$.

REFERENCES

1. Němec, H., P. Kužel, J.-L. Coutaz, and J. Čtyrokỳ, "Transmission properties and band structure of a segmented dielectric waveguide for the terahertz range," *Optics Communications*, Vol. 273, 99–104, 2007.
2. Vial, B., F. Zolla, A. Nicolet, and M. Commandré, "Quasimodal expansion of electromagnetic fields in open two-dimensional structures," *Phys. Rev. A*, Vol. 89, 023829, 2014.
3. Ould Agha, Y., F. Zolla, A. Nicolet, and S. Guenneau, "On the use of PML for the computation of leaky modes — An application to microstructured optical fibres," *COMPEL*, Vol. 27, No. 1, 95–109, 2008.
4. Nicolet, A., S. Guenneau, C. Geuzaine, and F. Zolla, "Modelling of electromagnetic waves in periodic media with finite elements," *Journal of Computational and Applied Mathematics*, Vol. 168, No. 1, 321–329, 2004.

Chaos Control in Virtual Cathode Oscillator by Cathode Structural Optimization

Seyed Morad Ali Hashemi[1], **Ali Pirmoradi**[2], **and Erfan Zabeh**[2]

[1]Electromagnetics Research Laboratory, Sharif University of Technology, Tehran, Iran
[2]Department of Electrical Engineering, Sharif University of Technology, Tehran, Iran

Abstract— Virtual cathode oscillator (VCO), as one of the simplest vacuum tube microwave generators considering its geometrical and constructional simplicity, has one of the most complex dynamical behaviors.

Nonlinear phenomena, present in the microwave-plasma interaction in the active region of the VCO, are the most important sources of the complexity of the electron beam dynamics and microwave generation process in the device.

Chaos, as one of the most important phenomena appearing in the nonlinear dynamical systems, has been studied in the VCO performance. The microwave generation process, considered as the overall dynamical operation of a complicated system of nonlinear partial differential equations (PDE) with boundary values as given by the geometry, materials and other structural properties of the tube and initial conditions defined by the input driving pulses, is an appropriate start point for the chaos to appear.

It has been shown that input anode-cathode voltage is one of the most important parameters in the formation of the chaotic solutions of the considered system of nonlinear boundary value PDEs. PIC-code simulation of the system has been widely used to study the various aspects of the chaotic behavior of the designed VCO. It has been shown that increasing input voltage pushes the system towards the appearance of more and more periodic oscillations with different periods leading finally to a completely chaotic performance. Bifurcation diagram showing this procedure has been derived via numerical processing of the PIC-code results and has confirmed the results of the time and frequency domain diagrams showing the deeply chaotic behavior of the system.

The same has been done applying the PIC-code simulation of VCO for studying the effects of the cathode radius on the chaotic behavior of the system and it has been shown that this parameter deeply affects the chaotic performance of the designed system. Increasing cathode radius results in increased disorder in the output microwave parameters. Bifurcation diagram has been extracted considering the variations of the system output via changing cathode radius. This diagram elegantly shows the chaos formation process through the cathode radius variations.

Analyzing the simulation results, authors suggest design optimization of the cathode structure to improve the system performance and control the undesirable chaotic behavior of the system. It has been shown that the new cathode structure is capable of delivering higher current flows and beam powers to the interaction region of the vacuum tube avoiding the chaos occurrence compared to the conventional cathodes used in the similar systems.

Rigorous Optimizations of Three-dimensional Antenna Arrays Using Full-wave Simulations

C. Önol[1, 2], Ö. Gökçe[1], H. Boyacı[1], and Ö. Ergül[1]

[1]Department of Electrical and Electronics Engineering, Middle East Technical University, Ankara, Turkey
[2]ASELSAN Inc., Ankara, Turkey

Abstract— Optimizations of antenna arrays for required values of the directive gain, side-lobe level, beamwidth, and in general, for the characterization of the overall radiation pattern, are popular problems in antenna design and engineering [1–3]. Given an array of antennas, the aim is to find the optimal set of excitations of its elements for desired radiation characteristics. For rapid optimizations, simple approaches based on the array factor are very suitable, leading to very efficient designs of excitations. Unfortunately, using these approaches, mutual couplings between antennas are neglected or simplified, leading to significant deviations of the optimization results from real-life measurements when the antennas are strongly coupled [4, 5]. For realistic optimizations, antennas need to be modeled accurately, and if possible, via full-wave solvers; but, using highly accurate solutions for the purpose of optimizations may not be trivial [6].

In this work, we consider rigorous optimizations of antenna arrays using heuristic algorithms, such as the genetic algorithms and particle swarm optimization methods, which are employed on simulation results obtained with the multilevel fast multipole algorithm (MLFMA). MLFMA allows for accurate simulations of antenna arrays, without any periodicity, infinity, and similarity assumptions, and by taking into account all mutual couplings between the antennas. For the optimizations of an M-element array at a single frequency, the number of full-wave simulations is only M, since complex current densities and radiation patterns can be combined via superposition without omitting mutual couplings. For a given array of static elements, these simulations also have common computations, which can be used to accelerate the overall solution phase. The results of M full-wave simulations are used by the heuristic algorithms in order to perform the optimizations, e.g., for increasing the directive gain at desired directions, minimizing radiations at given locations, and shaping the main beam by controlling the excitations.

The proposed mechanism that is based on MLFMA and heuristic algorithms is very flexible and applicable to arrays of nonidentical elements with arbitrary positions and orientations. In addition to arrays with fully excited elements, for which phase optimizations is more critical, we consider arrays with parasitic elements, especially when large antennas are used as reflectors. As an important advantage, the developed optimization environment allows for multi-band optimizations, where radiation characteristics at multiple frequencies are considered and optimized simultaneously for multi-band applications.

REFERENCES

1. Orchard, H. J., R. S. Elliot, and G. J. Stern, "Optimising the synthesis of shaped beam antenna patterns," *IEE Proceedings H*, Vol. 132, No. 1, 63–68, 1985.
2. Ergül, Ö. and L. Gürel, "Modeling and synthesis of circular-sectoral arrays of log-periodic antennas using multilevel fast multipole algorithm and genetic algorithms," *Radio Sci.*, Vol. 42, No. 3018, 2007.
3. Yang, K., Z. Zhao, Z. Nie, J. Ouyang, and Q. H. Liu, "Synthesis of conformal phased arrays with embedded element pattern decomposition," *IEEE Trans. Antennas Propag.*, Vol. 59, No. 8, 2882–2888, 2011.
4. Gupta, I. J. and A. A. Ksienski, "Effect of mutual coupling on the performance of adaptive arrays," *IEEE Trans. Antennas Propag.*, Vol. 31, No. 5, 785–791, 1983.
5. Shavit, R. and E. Rivkin, "An efficient and practical decoupling feeding network for antenna phased arrays," *IEEE Antennas Wireless Propag. Lett.*, Vol. 9, 966–969, 2010.
6. Yan, K.-K. and Y. Lu, "Sidelobe reduction in array-pattern synthesis using genetic algorithm," *IEEE Trans. Antennas Propag.*, Vol. 45, No. 7, 1117–1122, 1997.
7. Ergül, Ö. and L. Gürel, *The Multilevel Fast Multipole Algorithm (MLFMA) for Solving Large-scale Computational Electromagnetics Problems*, Wiley-IEEE, 2014.

On the Electric-current-driven Microstructural Evolution

R. S. Qin
Department of Engineering and Innovation, The Open University, UK

Abstract— Application of an electric field to the conductive heterogeneous media causes the non-uniform current distribution. The magnetic energy associated to the current distribution can be calculated using a numerical method [1]. Different microstructural configurations of the heterogeneous media cause different current distributions, and hence associate to the different magnetic energies of the electrically discontinuous media. The magnetic energy is a type of free energy.

The irreversible thermodynamic law predicts the system evolution trajectory. This indicates the heterogeneous media to evolve toward an optimum configuration with least magnetic free energy. The evolution is driven by the irreversible thermodynamics. An equivalent electromagnetic force can be constructed to drive the electrical neutral suspension particles to propagate [2]. This provides kinetic understanding of electromagnetic-driven microstructure evolution.

We present in this report our systematic calculation of the microstructure evolution driven by the applied electric potential and the associate magnetic field. Some new results on the have been revealed for the conductive media containing multiple, deformable and splitable inclusions. This provides some theoretical understandings to the experimental observation on the electropulse-induced nanostructured materials synthesis [3]. The phase with low electric conductivity can change from a laminar plate to many small particles by the applied electric current. The electrical neutral particles in a conductive media can be manipulated to move toward desirable directions by the electric field.

ACKNOWLEDGMENT

The work was financially supported by the Engineering and Physical Sciences Research Council at UK (No. EP/J011460/1).

REFERENCES

1. Qin, R. S. and A. Bhowmik, "Computational thermodynamics in electric current metallurgy," *Mater. Sci. Technol.*, 2015, DOI: 10.1179/1743284714Y.0000000746.
2. Zhang, X. F. and R. S. Qin, "Electric current-driven migration of electrically neutral particles in liquids," *App. Phys. Lett.*, Vol. 104, No. 11, 114106, 2014.
3. Qin, R. S., E. I. Samuel, and A. Bhowmik, "Electropulse-induced cementite nanoparticle formation in deformed pearlitic steels," *J. Mater. Sci.*, Vol. 46, No. 9, 2838–2842, 2011.

Session 3P4
Analysis and Simulation of Waves in Complex Media

Light Enpolarization and Depolarization: Bulk and Surface Scattering

G. Soriano[1], **M. Zerrad**[1], **X. Orlik**[2], **A. Ghabbach**[1], **S. Liukaityte**[1], **J. Dupont**[2], **and C. Amra**[1]

[1]CNRS, Centrale Marseille, Institut Fresnel, UMR 7249
Aix-Marseille Université, Marseille 13013, France
[2]Theoretical and Applied Optics Department, ONERA, Toulouse 31055, France

Abstract— Several procedures for the accurate polarimetric characterization of the speckle pattern of light scattered from disordered media were recently proposed [1, 2]. Those characterizations were driven at an angular scale much smaller than the speckle grain size in order to avoid spurious spatial coherence effects. Inhomogeneous bulks and rough surfaces were analysed, with both polarized and unpolarized laser sources [3]. With the degree of polarization (DoP) histogram accurately estimated from data, enpolarization and depolarization phenomena were evidenced. For unpolarized illumination, the speckle pattern shows partial polarization, with a DoP rising up to an average of 0.75 for the most strongly scattering media. The opposite behaviour appears for polarized illumination, where the speckle pattern can present a DoP distributed around values significantly smaller than unity.

The enpolarization effect was first successfully and quantitatively predicted for bulk scattering of unpolarized light using the sum of random phasors model for fully developed speckle. Note that the scattering medium is here considered as disordered but deterministic rather than random: for simulation purpose, the medium is described by a single realization of a random process. This simple theory however fails to modelize depolarization in the case of polarized illumination. The model was thus extended in [4] to take into account the scattering coefficients dependency to frequency. This dependency is generally neglected according to the quasi-monochromatic assumption. This spectrally extended model now outputs the complete speckle DoP histogram for two inputs: the incident light DoP and the ratio of the incident light bandwidth to the characteristic scale of scattering coefficients frequency variation.

In this talk, we present comparisons between measured [1–3] and simulated speckle DoP histograms for non-absorbing bulks. Rough surfaces and absorbing bulks speckle patterns experimentally present lower levels of enpolarization/depolarization. We discuss how the spectral model can be extended anew to modelize this class of intermediate scatterers.

REFERENCES

1. Ghabbach, A., M. Zerrad, G. Soriano, and C. Amra, "Accurate metrology of polarization curves measured at the speckle size of visible light scattering," *Optics Express*, Vol. 22, No. 12, 14594–14609, 2014.
2. Dupont, J., X. Orlik, A. Ghabbach, M. Zerrad, G. Soriano, and C. Amra, "Polarization analysis of speckle field below its transverse correlation width: Application to surface and bulk scattering," *Optics Express*, Vol. 22, No. 20, 24133–24141, 2014.
3. Ghabbach, A., M. Zerrad, G. Soriano, S. Liukaityte, and C. Amra, "Depolarization and enpolarization dop histograms measured for surface and bulk speckle patterns," *Optics Express*, Vol. 22, No. 18, 21427–21440, 2014.
4. Soriano, G., M. Zerrad, and C. Amra, "Enpolarization and depolarization of light scattered from chromatic complex media," *Optics Express*, Vol. 22, No. 10, 12603–12613, 2014.

Surface Integral Equation for Plasmonic Media: Near-field, Scattering and Forces

T. V. Raziman[1], **Eric C. Le Ru**[2], **and Olivier J. F. Martin**[1]

[1]Nanophotonics and Metrology Laboratory (NAM)
Swiss Federal Institute of Technology Lausanne (EPFL), Lausanne 1015, Switzerland
[2]The MacDiarmid Institute for Advanced Materials and Nanotechnology
School of Chemical and Physical Sciences, Victoria University of Wellington
P. O. Box 600, Wellington 6140, New Zealand

Abstract— Advances in plasmonics research and its ever-increasing practical applications have necessitated the development of accurate and efficient computational tools for simulating the electromagnetic response of plasmonic nanostructures. To this end, various numerical methods have been developed which are suitable for simulating different structures, and have their own advantages and limitations.

Surface integral equation (SIE) formulation is an integral method to simulate the optical response of nanostructures in the frequency domain. This method is based on the Green's tensor formalism, and can be used to simulate nanostructures in homogeneous as well as periodic backgrounds. The SIE requirement of having to discretise only the surfaces of the scatterers reduces the computational costs and avoids complications such as the requirement of truncating the background medium artificially. Also, the triangular meshing used in this scheme can approximate irregular particle surfaces very well, allowing the simulation of realistic plasmonic structures. Surface electric and magnetic currents which are the natural output of SIE simulations also enable direct and efficient computation of physically relevant quantities.

Here, we utilise SIE to compute the optical response of complex and realistic systems encountered in plasmonics. Various near-field properties such as intensity enhancement, lifetime modification and surface charges, as well as far-field quantities such as optical cross sections and second harmonic scattering are analysed. In addition, we also demonstrate the extension of SIE to compute the resultant optical forces and torques.

Furthermore, we discuss how the implementation and use of SIE can be optimised. We present a tailored recipe for the computation of SIE matrix integrals which improves the calculation accuracy without a significant overhead in computational costs. The use of this recipe permits the SIE simulation of more complicated geometries requiring less surface discretisation in the process. We also talk about the constraints to adhere to while building meshes to describe the simulation geometry. Besides choosing the correct size for the mesh elements, we show how it is necessary to enforce the correct symmetry on the meshes for accurate computation of quantities such as second harmonic scattering.

Numerical Modeling of Light/Matter Interaction at the Nanoscale with a High Order Finite Element Type Time-domain Solver

S. Lanteri[1], **C. Scheid**[1,2], **and J. Viquerat**[1]

[1]Inria Sophia Antipolis-Méditerranée Research Center, France
[2]University of Nice-Sophia Antipolis, France

Abstract— The numerical modeling of light interaction with metallic nanostructures requires to solve the system of time-domain Maxwell equations coupled to appropriate models of physical dispersion in the metal such as the Drude and Drude-Lorentz models. In the computational nanophotonics literature, a large number of studies are devoted to Finite Difference Time-Domain (FDTD) type discretization methods based on Yee's scheme [1]. As a matter of fact, the FDTD [2] method is a widely used approach for solving the systems of partial differential equations modeling nanophotonic applications. In this method, the whole computational domain is discretized using a structured (cartesian) grid. However, in spite of its exibility and second-order accuracy in a homogeneous medium, the Yee scheme suffers from serious accuracy degradation when used to model curved objects or when treating material interfaces.

During the last twenty years, numerical methods formulated on unstructured meshes have drawn a lot of attention in computational electromagnetics with the aim of dealing with irregularly shaped structures and heterogeneous media. In this talk, we will report on our recent efforts aiming at the development of a family of high order finite element type time-domain solvers for the numerical treatment of nanophotonics/plasmonics applications in the linear regime. The basic ingredient is a discretization method which relies on a compact stencil high order interpolation of the electromagnetic field components within each cell of an unstructured tetrahedral mesh. This piecewise polynomial numerical approximation is allowed to be discontinuous from one mesh cell to another, and the consistency of the global approximation is obtained thanks to the definition of appropriate numerical traces of the fields on a face shared by two neighboring cells. Time integration is achieved using an explicit scheme and no global mass matrix inversion is required to advance the solution at each time step. Moreover, the resulting time-domain solver is particularly well adapted to parallel computing. The proposed method is an extension of the so-called DGTD (Discontinuous Galerkin Time-Domain) method that we initially proposed in [3] for the simulation of electromagnetic wave propagation in non-dispersive heterogeneous media at microwave frequencies. For the numerical treatment of dispersion models in metals, we have adopted an Auxiliary Differential Equation (ADE) technique that has already proven its effectiveness in the FDTD framework. From the mathematical point of view, this amounts to solve the time-domain Maxwell equations coupled to a system of *ordinary differential equations*. The resulting ADE-based DGTD method is detailed in [4] and is part of a larger initiative aiming at the development of a software suite dedicated to nanophotonics/nanoplasmonics.

REFERENCES

1. Yee, K. S., "Numerical solution of initial boundary value problems involving Maxwell's equations in isotropic media," *IEEE Trans. Antennas and Propag.*, Vol. 14, No. 3, 302–307, 1966.
2. Taflove, A. and S. C. Hagness, *Computational Electrodynamics: The Finite-difference Time-domain Method*, 3rd Edition, Artech House Publishers, 2005.
3. Fezoui, L., S. Lanteri, S. Lohrengel, and S. Piperno, "Convergence and stability of a discontinuous Galerkin time-domain method for the 3D heterogeneous Maxwell equations on unstructured meshes," *ESAIM: Math. Model. Numer. Anal.*, Vol. 39, No. 6, 1149–1176, 2005.
4. Viquerat, J., S. Lanteri, and C. Scheid, "Theoretical and numerical analysis of local dispersion models coupled to a discontinuous galerkin time-domain method for Maxwell's equations," *Technical Report RR-8298*, Inria, 2013.

Homogenization of Periodic Electromagnetic Structures: An Uncertainty Principle

Igor Tsukerman[1] and Vadim A. Markel[2]

[1]Department of Electrical and Computer Engineering, The University of Akron, USA
[2]Departments of Radiology and Bioengineering and the Graduate Group in Applied Mathematics and Computational Science, University of Pennsylvania, USA

Abstract— The analytical and numerical results of the paper show that effective magnetic response of periodic intrinsically nonmagnetic structures has limitations: strong response is unavoidably accompanied by a commensurate loss of accuracy in the effective medium representation of the material. This can be viewed as an uncertainty principle for homogenization of electromagnetic metamaterials.

One of the most intriguing features of periodic structures composed of intrinsically nonmagnetic constituents is their nontrivial magnetic response, which can be particularly strong under electromagnetic resonance conditions. It is often tacitly assumed that this response is limited only by the characteristics of the constituent materials (most notably, their losses). However, we demonstrate that this artificial magnetism has a more fundamental limitation: the stronger the magnetic response, the less accurate ("certain") predictions of the effective medium theory are. We view this as an uncertainty principle for homogenization of electromagnetic metamaterials.

Our analysis is based on the recently developed non-asymptotic homogenization theory [1] and on the comparison of fields around a metamaterial slab and an (approximately) equivalent homogeneous slab. In addition to analytical derivation, we consider, as an instructive example, a triangular lattice of cylindrical air holes in a dielectric host [2]. Despite the high level of isotropy around the Γ-point in the second photonic band, the uncertainty principle holds. First, isotropy with respect to the Bloch wavenumber is not accompanied by isotropy of the Bloch impedance; second, surface waves [3, 4] play a significant role at shorter wavelengths.

ACKNOWLEDGMENT

This research was supported by the US National Science Foundation under grant DMS-1216970.

REFERENCES

1. Tsukerman, I. and V. A. Markel, "A nonasymptotic homogenization theory for periodic electromagnetic structures," *Proc. Royal Society A*, Vol. 470, 2014–0245, 2014.
2. Pei, T.-H. and Y.-T. Huang, "Effective refractive index of the photonic crystal deduced from the oscillation model of the membrane," *J. Opt. Soc. Am. B*, Vol. 29, No. 9, 2334–2338, 2012.
3. Xiong, X. Y. Z., L. J. Jiang, V. A. Markel, and I. Tsukerman, "Surface waves in three-dimensional electromagnetic composites and their effect on homogenization," *Optics Express*, Vol. 21, No. 9, 10412–10421, 2013.
4. Markel, V. A. and J. C. Schotland, "Homogenization of Maxwell's equations in periodic composites: Boundary effects and dispersion relations," *Phys. Rev. E*, Vol. 85, No. 6, 066603, 2012.

High-order Trefftz Absorbing Conditions for Wave Problems

Igor Tsukerman[1] **and Ralf Hiptmair**[2]

[1]Department of Electrical and Computer Engineering
The University of Akron, USA
[2]Seminar of Applied Mathematics
ETHZ, CH-8092, Zürich, Switzerland

Abstract— For scalar frequency-domain wave equations in 2D or 3D, we propose a "Trefftz generator" of local nonreflecting conditions — a critical part of finite difference (FD) and finite element solution of wave problems in unbounded domains. Trefftz approximations are, by definition, provided by functions that satisfy the wave equation exactly. At the exterior boundary, these are outgoing plane/cylindrical/spherical waves or some of their derivatives. The second component of the Trefftz generator is a set of degrees of freedom — linear functionals such as the value of the solution and some of its derivatives at boundary points. We show that the proposed generator reproduces classical nonreflecting conditions (Engquist-Majda and Bayliss-Turkel) and generates a variety of new high-order conditions.

This paper is a substantial further development of finite difference (FD)-Trefftz absorbing conditions [1–4]. For scalar frequency-domain wave equations in 2D or 3D, we propose a "Trefftz generator" of such conditions. Two key ingredients of this generator are (i) a set of local Trefftz functions [1–6] — outgoing waves satisfying the wave equation and approximating the solution near a given point on the exterior boundary, and (ii) a set of degrees of freedom — linear functionals such as the value of the solution and some of its derivatives at boundary points. The ultimate result is a sparse linear FD system.

Our Trefftz machine reproduces classical Engquist-Majda [7] and Bayliss-Turkel [8] conditions and generates a variety of new conditions. For canonical problems of scattering from dielectric or perfectly conducting cylinders, convergence of order six on 9-point stencils is demonstrated, with the relative solution error $\sim 10^{-5}$–10^{-8} with 10–20 grid points per wavelength. We are not aware of alternative methods yielding a similar level of accuracy on comparable grids. Extensions to 3D and vectorial problems are possible.

ACKNOWLEDGMENT

The research of IT was supported by the US National Science Foundation under grant DMS-1216970 and by U.S. Army Research Office under grant W911NF1110384.

REFERENCES

1. Tsukerman, I., "A class of difference schemes with exible local approximation," *J. Comput. Phys.*, Vol. 211, No. 2, 659–699, 2006.
2. Tsukerman, I., "Electromagnetic applications of a new finite-difference calculus," *IEEE Trans. Magn.*, Vol. 41, No. 7, 2206–2225, 2005.
3. Tsukerman, I., *Computational Methods for Nanoscale Applications: Particles, Plasmons and Waves*, Springer, 2007.
4. Tsukerman, I., "A "Trefftz machine" for absorbing boundary conditions," http://arxiv.org/abs/1406.0224, 2014.
5. Hiptmair, R., A. Moiola, and I. Perugia, "Plane wave discontinuous Galerkin methods for the 2D Helmholtz equation: Analysis of the p-version," *SIAM J. Numer. Analysis*, Vol. 49, No. 1, 264–284, 2011.
6. Moiola, A., R. Hiptmair, and I. Perugia, "Plane wave approximation of homogeneous Helmholtz solutions," *Z. Angew. Math. Phys.*, Vol. 62, No. 5, 809–837, 2011.
7. Engquist, B. and A. Majda, "Absorbing boundary conditions for the numerical simulation of waves," *Math. Comp.*, Vol. 31, 629–651, 1977.
8. Bayliss, A. and E. Turkel, "Radiation boundary-conditions for wave-like equations," *Comm. on Pure and Appl. Math.*, Vol. 33, No. 6, 707–725, 1980.

Modeling of a Slab Photonic Crystal with a One-dimensional Multilayer Mirror with Given Dispersive and Spectral Characteristics

Mikhail Libman[1, 2] **and Nikita Kondratiev**[2]

[1]Moscow State University, Moscow 119991, Russia
[2]Russian Quantum Center, Moscow 143025, Russia

Abstract— Many photonics applications need devices with special spectral and dispersive properties. Generating optical signals of a given form such as ultra-short laser pulses or supercontinuum are among those tasks. Photonic crystals which spectral and dispersive properties are set by their design can be employed for that purpose. A simple model of such one-dimensional photonic crystal is a Bragg mirror, consisting of alternating dielectric layers with high and low refractive indices. This simple model enables us to understand the way of engineering optical properties. It is possible to achieve required dispersion law and to extend the bandwidth of the mirror at the same time by chirping width of the layers. The same method should be applicable for the photonic crystal.

In our work we justify the applicability of a dielectric mirror model to the description of a real photonic crystal. A slab waveguide with periodically changing width is considered and it is shown that this width change can be recalculated to the effective refraction index modulation. The applicability of transfer-matrix method of transmission properties calculation was demonstrated. Two methods of deriving of the expressions for the photonic bandgap were considered and proved to be consistent, while emphasizing different aspects of the propagation process. The position and width of the bandgap as a function of waveguide's width was investigated. Finally, modeling of one-dimensional chirped Bragg mirror was performed with respect to the material and waveguide dispersion. Numerical optimization method and analytical method were realized to calculate the chirp law for the desired dispersive characteristics.

Nonlinear Standing Waves on a Periodic Array of Circular Cylinders

Lijun Yuan[1] and Ya Yan Lu[2]

[1]College of Mathematics and Statistics, Chongqing Technology and Business University, China
[2]Department of Mathematics, City University of Hong Kong, Hong Kong, China

Abstract— For periodic array of circular dielectric cylinders surrounded by air, where the cylinders are made of linear medium, it is well known that standing waves that are periodic along the array and decay exponentially away from the array could exist at discrete set of frequencies [1], corresponding to the non-uniqueness of related diffraction problem. In this paper, we consider periodic array of nonlinear cylinders with Kerr nonlinearity, and show numerically that standing waves exist continuously with the frequency. These standing waves are periodic along the array and decay exponentially away from the array. Their amplitudes depend on the frequency. As the frequency decreases, their amplitudes increases. It appears that there are infinite number of nonlinear standing waves at each frequency.

To compute the nonlinear standing waves, we solve the nonlinear Helmholtz equation as an eigenvalue problem with frequency as the eigenvalue. Assuming that the period of the array is L and the radius of the cylinders is $a < L/2$. In the Cartesian coordinate system (x, y, z), we assume the cylinders are parallel to the z axis and their centers (in the xy plane) are located on the y axis at $y = mL$ for integers m. Due to the periodicity of the array and the solution, the problem can be considered in unit cell $S = \{(x, y) : |x| < L/2, |y| < L/2\}$ containing one cylinder, with periodic boundary condition in the y direction and transparent boundary conditions at $x = \pm L/2$. In the domain Ω outside the cylinder and inside the unit cell, the Helmholtz equation is linear and its solution can be expanded in cylindrical waves. This allows us to find the Dirichlet-to-Neumann (DtN) map (which depends on frequency) for the Hemlholtz equation on Ω. Combining these conditions, we can find boundary condition on the boundary of disk D given for $r < a$. With this condition, it is only necessary to solve the nonlinear Helmholtz equation on D. In earlier works, similar techniques have been used to analyze optical bistability [2] and symmetry breaking [3] in structures with nonlinear circular cylinders. To solve this problem, we discretize the nonlinear Hemlholtz equation by mixed Fourier-Chebyshev pseudospectral method [4], with Fourier and Chebyshev methods for θ and r respectively, where is the polar angle, and use an iterative method.

REFERENCES

1. Bonnet-Bendhia, A.-S. and F. Starling, "Guided waves by electromagnetic gratings and nonuniqueness examples for the diffraction problem," *Math. Methods Appl. Sci.*, Vol. 17, 305–338, 1994.
2. Yuan, L. and Y. Y. Lu, "Efficient numerical method for analyzing optical bistability in photonic crystal microcavities," *Optics Express*, Vol. 21, 11952–11964, 2013.
3. Yuan, L. and Y. Y. Lu, "Bilateral symmetry breaking in nonlinear circular cylinders," *Optics Express*, Vol. 22, 30128–30136, 2014.
4. Trefethen, L. N., *Spectral Methods in MATLAB,* Society for Industrial and Applied Mathematics, 2000.

A Space-time Discontinuous Galerkin Trefftz Method

F. Kretzschmar[1,2], **S. M. Schnepp**[3], **H. Egger**[1], **I. Tsukerman**[4], **and T. Weiland**[1,2]

[1]Graduate School of Computational Engineering, TU Darmstadt, Germany
[2]Institut fuer Theorie Elektromagnetischer Felder, TU Darmstadt, Germany
[3]Institute of Geophysics, Department of Earth Sciences, ETH Zurich, Switzerland
[4]Department of Electrical & Computer Engineering, The University of Akron, USA

Abstract— We present a space-time discontinuous Galerkin method for time-domain Maxwell's equations that employs polynomial Trefftz basis functions [1], i.e., polynomials that solve Maxwell's equations exactly in an element-wise fashion. This reduces the number of degrees of freedom from $\mathcal{O}(p^4)$ in the method with all polynomials of order p to $\leq \mathcal{O}(p^3)$, while preserving the approximation accuracy. The new method retains the exibility of the discontinuous Galerkin framework [2] while improving the dispersion behavior. New features such as inhomogeneous media and optimized transparent boundary conditions can be applied.

Maxwell's Equations: We consider propagations of electromagnetic waves in the absence of sources; For problems of this kind time-dependent Maxwell's equations

$$\nabla \times \mathbf{E} = -\mu \frac{\partial \mathbf{H}}{\partial t} \quad \text{and} \quad \nabla \times \mathbf{H} = \mu \frac{\partial \mathbf{E}}{\partial t} \tag{1}$$

form the set of governing equations. Here, $\mathbf{E} = (E_x, E_y, E_z)^{\mathbf{T}}$ denotes the electric field, $\mathbf{H} = (H_x, H_y, H_z)^{\mathbf{T}}$ is the magnetic field whereas ϵ and μ are the permittivity and the permeability, respectively. We assume the fields to be divergence free $\nabla \cdot \mathbf{E}_0 = 0$ and $\nabla \cdot \mathbf{H}_0 = 0$.

Polynomial Trefftz Functions: The considered system of Maxwell's Equation (1) can be solved by 6-dimensional Trefftz functions of the form $\mathbf{F} = (\mathbf{E}, \mathbf{H})^{\mathbf{T}}$. One particular choice of Trefftz basis functions are polynomial Trefftz functions of order p which are a desired choice for numerical integrations. General properties such as dimension and stability as well as different construction procedures are described in [4]. Following [3, 4], a polynomial Trefftz basis can for instance be composed of Transport polynomials

$$\mathbf{F}_i^p = \begin{pmatrix} \mathbf{E}_i \\ Z^{-1}\mathbf{H}_i \end{pmatrix} \cdot (\mathbf{d}_i \cdot \mathbf{r} - \mathrm{v}t)^p, \tag{2}$$

with $\mathrm{v} = 1/\sqrt{\epsilon\mu}$ being the local speed of light and $Z^{-1} = \sqrt{\mu/\epsilon}$ the intrinsic impedance, that describe a plane wave traveling in direction $\mathbf{d}_i$.

Conclusion: We have outlined a discontinuous Galerkin Trefftz method for Maxwell's equations. Our numerical results demonstrate the spectral convergence of the method; Consequently, small sets of basis functions can result in a very high accuracy. Excellent dispersion behavior has been obtained. In addition a transparent boundary conditions of arbitrary order can be (easily) implemented.

REFERENCES

1. Trefftz, E, "Ein Gegenstück zum Ritzschen Verfahren," *Internationaler Kongress fuer Technische Mechanik*, No. 2, 131–137, 1926.
2. Griesmair, T. and P. Monk, "Discretization of the wave equation using continuous elements in time and a hybridizable discontinuous Galerkin method in space," *J. Sci. Comput.*, Vol. 58, 472–498, 2014.
3. Kretzschmar, F., S. M. Schnepp, I. Tsukerman, and T. Weiland, "Discontinuous Galerkin methods with Trefftz approximations," *J. Comput. Appl. Math.*, Vol. 279, 211–222, 2014.
4. Egger, H., F. Kretzschmar, S. Schnepp, and T. Weiland, "A space-time discontinuous galerkin trefftz method for time dependent Maxwell's equations," Preprint under arxiv:1412.2637, 2014.

The Sommerfeld Halfspace Problem Redux: Alternative Field Representations, Role of Zenneck and Surface Plasmon Waves

K. A. Michalski[1] and J. R. Mosig[2]

[1]Department of Electrical and Computer Engineering
Texas A&M University, College Station, Texas 77843-3128, USA
[2]Laboratory of Electromagnetics and Acoustics
École Polytechnique Fédérale de Lausanne, Lausanne CH-1015, Switzerland

Abstract— The problem of a vertical Hertzian dipole (time-harmonic current element of infinitesimal length) radiating in the presence of a lossy conducting halfspace was first rigorously solved by Sommerfeld in 1909 and other dipole configurations were treated in his later works. Sommerfeld's solution was expressed in terms of improper integrals with Bessel function kernels, which cannot be evaluated in closed form. A major finding of the original Sommerfeld paper was that the integrands exhibit a pole, whose residue he identified as a cylindrical form of the surface wave postulated earlier by Zenneck. Sommerfeld's work was motivated by the desire to explain the radio wave propagation along the surface of the earth, before it was realized that re ections from the ionosphere were in fact the decisive factor, making the still recurring discussions of the importance of the Zenneck wave rather immaterial. However, since the end of the last century, there has been a resurgence of interest in the Sommerfeld halfspace problem and the Sommerfeld surface wave in particular, in the context of THz applications, near-field optics, plasmonics and nanophotonics. The Zenneck wave becomes a surface plasmon polariton in the case of noble metals at optical wavelengths. In this paper, a complete *ab initio* solution is presented for the problem of an arbitrarily oriented Hertzian dipole radiating in the presence of a material halfspace. The solution method combines a vector potential approach with a transmission line analogue of the medium, which is a convenient means of scalarizing the Maxwell equations and it facilitates the inclusion of any number of layers in the analysis. Following Sommerfeld, the solution is first expressed in terms of Fourier-Bessel transforms, also known as Sommerfeld integrals. The analytical properties of the integrands in the complex plane are investigated. In particular, a proof of the existence of the Sommerfeld-Zenneck pole on the proper Riemann sheet is given and the relation of the Zenenck wave and the surface plasmon polariton is confirmed. Alternative integral representations of the vector potential Green functions are derived by contour deformation and analytic continuation of the integrands into the complex plane. Closed-form asymptotic expressions for the fields at the interface are also derived and the role of the Zenneck wave and the surface plasmon is discussed.

Propagation of Electromagnetic Wave Packet in a Dispersive Anisotropic Metamaterial

Jie-Luen Wu[1] and Pi-Gang Luan[2]

[1]System Development Center, National Chung-Shan Institute of Science and Technology
Longtan Township, Taoyuan County 325, Taiwan
[2]Department of Optics and Photonics, National Central University
Jhongli City, Taoyuan County 320, Taiwan

Abstract— A metamaterial consisting of subwavelength dielectric and metallic layers can be treated as a homogeneous anisotropic medium having indefinite permittivity tensor and hyperbolic dispersion relation in some frequency ranges. Recently, interests have been raised about the issues concerning the propagation of wave energy in dispersive media, and contradicted results about the possibility of superluminal propagation of electromagnetic wave packets in hyperbolic metamaterials were claimed by different authors [1, 2]. Since special relativity puts absolute speed limitation on any kind of signal or energy propagation, and this is related to the notion of causality, we thus believe to clarify this issue as clear as possible is very important.

In this work, we study the propagation behaviors of a wave packet in a dispersive anisotropic medium. The medium is assumed to be the effective medium corresponding to the structure consisting of dielectric and metallic layers. The two principal values of the permittivity tensor thus have the Drude and Lorentz type dispersions if the dielectric and metallic layers are assumed to be having constant and Drude type permittivity, respectively. We derive the energy density for this medium and show that for a propagating mode the energy velocity is equal to the group velocity, and examine the propagating behaviors of a wave packet, assuming all the plane waves composing this packet have frequencies far from the absorption band.

Many plane waves having proper frequencies and wave vectors satisfying the dispersion relation of the medium were chosen so as to compose the wave packet [3]. In order to trace the motion of the wave packet, the idea like 'center of mass distribution' is used. The center position of a Gaussian-wave packet is defined by evaluating the 'weighted sum' of the position vectors, using the energy density as the weight function. The packet velocity can be calculated numerically by tracing the packet center position at every time step. We compare the predicted group velocities of single-frequency propagating modes with the wave packet velocities for different frequency widths and angular widths for the k-vectors, and find they fit very well if the frequency and angular widths were chosen appropriately. Most importantly, according to our results we find that neither the energy velocity for a propagating mode nor the packet velocity for a wave packet can exceed the speed of light in vacuum if the dispersion of the medium were carefully taken into account. We also discuss the possible origins of the contradicted predictions made by previous researches.

REFERENCES

1. Luo, H., W. Hu, W. Shu, F. Li, and Z. Ren, *Europhys. Lett.*, Vol. 76, 1081, 2006.
2. Welters, A., Y. Avniel, and S. G. Johnson, *Phys. Rev. A*, Vol. 90, 023847, 2014.
3. Lu, W. T., J. B. Sokoloff, and S. Sridhar, *Phys. Rev. E*, Vol. 69, 026604, 2004.

Electromagnetic Field Distributions in Stratified Structures

Huai-Yu Wang[1] and Chao Li[2]

[1]Department of Physics, Tsinghua University, Beijing 100084, China
[2]School of Physics and Engineering, Sun Yat-sen University, Guangzhou 510275, China

Abstract— In studying dipole radiation, the near field and far field should be treated separately. In a vacuum background, it has been well known that the near field/far field (NFFF) boundary L is about the light wavelength λ_0, $L \sim \lambda_0$. Stratified structures are often encountered in practice. A typical situation is the air-sea-earth trilayer structure. The NFFF boundary in such backgrounds has not been well studied yet. In this work, we carefully study how to determine the NFFF boundaries in stratified structures.

The general model is depicted in Fig. 1. There can be Q layers and $Q-1$ interfaces between them. The region between the top and bottom layers are called intermediate region. A vertical electric dipole (VED) is located on the origin of the cylindrical coordinates (ρ, z, φ). The VED can be in either the top layer or the intermediate region. Each layer has its own refraction index (RI). In each RI configuration, the largest and smallest RI's are denoted as $n_{\max}$ and $n_{\min}$, respectively.

We carefully evaluated the field distribution in bilayer, trilayer and multilayer structures with various possible RI configurations. Two kinds of far-field expression of the electric field were derived. It was proved that the approximation methods obeyed reciprocal theorem. The results of far-field approximations were compared to those of precise numerical calculation to determine the NFFF boundaries.

In stratified structures, two factors severely influenced the field distribution. One was that if $Q \geq 3$ in Fig. 1, multi-reflection happened in the intermediate region wherever the VED is. The other was that the lateral waves moved along the interfaces which mainly existed in the layer with higher RI and exponential decayed in the lower RI layer. These two factors complicated the field distribution in space and made the NFFF boundary much farther than that in vacuum background.

Through the detailed investigation, the NFFF boundary was proposed to be

$$L \sim 1000 \max\{D, 0.1\lambda_0\} n_{\max}/n_{\min}.$$

This expression is valid for any stratified structure with any RI configuration. In a bilayer structure, $D \sim |d_1|$, while in a structure with more layers, D is the thickness of the intermediate region, $D \sim d_1 - d_{Q-1}$. The structural parameters reasonably entered the expression of the boundary.

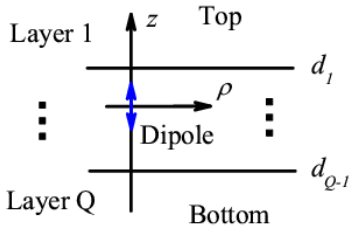

Figure 1: Stratified structure model.

ACKNOWLEDGMENT

National Natural Science Foundation of China (No. 61275028).

Transmission of EM Waves through Very Dry Reinforced Concrete

Thierry Gilles and Ghilkrist Afomasse
Ecole Royale Militaire, Laboratoire d'Electromagnétisme Appliqué (LEMA)
Avenue de la Renaissance 30, Bruxelles 1000, Belgium

Abstract— Considering realistic frequency and moisture content dependant electromagnetic characteristics of concrete [1] simulations with FEKO in the frequency domain show that at some frequencies and at normal incidence, reinforced concrete exhibits a very high transmission loss at some frequencies. This phenomenon is very weak for lossy concrete but ranges 10 to 20 dB for very dry concrete, indicating that the transmission loss is not due to absorption in the concrete but results from destructive interactions.

To better understand the origin of this transmission loss, reflection and diffraction ray tracing theory could be called for, but there are numerous combinations of reflections and diffractions inside reinforced concrete. To figure out which of those are the main contributors to the high transmission loss, one can resort to time domain simulations with CST. The very short time duration of the pulses must be set to allow discrimination of the individual pulses following the various reflection and diffraction paths.

CST also allows to derive by FFT the transmission loss caused by the pulses received at a given location past the structure. Without time gating, retaining all pulses occurring after arrival of the first one, a transmission loss pattern similar to the one obtained with FEKO through an inifinite slab is obtained. Using timegating to retain less and less of those pulses, CST allows to identify how many among the first pulses are necessary to generate the resonant high transmission losses.

Very few reflection and/or transmission measurements through reinforced concrete have been published [2, 3], and none of them exhibits a resonant high transmission loss. To perform measurements reproducing the behavior of an infinite slab, special care must be taken to efficiently eliminate unwanted reflections and diffractions, either by using appropriate absorbing material everywhere needed or with a time gating technique. For time gating technique it is important to properly dimension the reinforced concrete slab sample in conjunction with the transmit and receive antenna positions to make sure that all pulses contributing significantly to the transmission loss will be retained before the appearance of the first unwanted pulse due to edge diffraction on the sample edges.

Combining various simulations and measurements, it has been possible to explain the high transmission losses observed at specific frequencies through dry reinforced concrete.

REFERENCES

1. Haddad, R. H. and I. L. Al-Qadi, "Characterization of portland cement concrete using electromagnetic waves over the microwave frequencies," *Cem. Concr. Res.*, Vol. 28, No. 10, 1379, 1998.
2. Richalot, E., M. Bonilla, and M.-F. Wong, "Electromagnetic propagation into reinforced-concrete walls," *IEEE Transactions on Microwave Theory and Techniques*, Vol. 48, No. 3, March 2000.
3. "Electromagnetic signal attenuation in construction materials," NIST Construction Automation Program Report No. 3, October 1997.

A Dynamic Transmission Line, Temporal Photonic Crystals, and Wave Vector Gaps

J. R. Reyes-Ayona and P. Halevi
Instituto Nacional de Astrofísica, Óptica y Electrónica, Tonantzintla, Puebla 72840, México

Abstract— Frequency or energy gaps are ubiquitous in physics and electronic engineering. On the other hand, wave vector- or k-gaps are hard to come by, if at all. Here we report what is likely the first measurement of a genuine k-gap. This has been achieved by propagating microwaves in a specially modulated transmission line (TL). The measurements have been confirmed by a calculation based on realistic modeling.

In our low-pass TL of eight cells the capacitors have been replaced by varactors that — unlike the situation in traveling wave amplifiers — are modulated externally at some frequency $\Omega/2\pi$ by the same time-periodic voltage. The dispersion relation $\omega = \omega(k)$ has been determined by a method similar to the differential phase-shift method of fiber optics engineering. This resulted in a photonic band structure of two k-bands separated by a k-gap, corresponding to forbidden values of the wave vector for any ω. This gap Δk is determined at the waist of the two k-bands, that occurs at the frequency $\Omega/2$. We get a very good fit between the experimental points and the realistic calculation, which shows that the gap Δk increases with the strength of modulation m of the voltage.

It is well known that a static low-pass TL can be represented by an effective medium in the long wavelength limit $ka \ll 1$, where a is the period or size of the unit L-C cell. We have generalized this equivalence to the dynamic case: at every instant of time the permittivity and permeability must satisfy the relations $\varepsilon(t) = C(t)/a$ and $\mu(t) = L(t)/a$. We find that, as long as $ka \ll 1$, the mean-field theory also fits well the experimental and theoretical results for the TL.

In general, the effective medium is characterized by time-periodic $\varepsilon(t)$ and $\mu(t)$, namely, it is a *temporal* photonic crystal [1]. We expect that the periodically modulated transmission line described above will exhibit all the features predicted by our group for the temporal photonic crystals: frequency comb in the reflectivity and transmittivity [1], parametric resonances that depend on a geometric condition [2], and faster-than-light transmission of the peaks of some harmonics of pulses that are traversing a slab [3]. Much higher frequencies should be feasible if the capacitances and inductances are replaced by split-ring resonators.

So, transmission lines and temporal photonic crystals — here's "Where Microwave and Lightwave Communities Meet", as the PIERS *motto* goes!

REFERENCES

1. Zurita-Sánchez, J. R., P. Halevi, and J. C. Cervantes-González, *Phys. Rev. A*, Vol. 79, 053821, 2009.
2. Zurita-Sánchez, J. R. and P. Halevi, *Phys. Rev. A*, Vol. 81, 053834, 2010.
3. Zurita-Sánchez, J. R., J. H. Abundis-Patiño, and P. Halevi, *Opt. Exp.*, Vol. 20, 5586, 2012.

Sub-band Gap Light Harvesting in Random Porous Materials

Paolo Bettotti[1] **and Fabrizio Sgrignuoli**[2]

[1]Nanoscience Laboratory, Department of Physics, University of Trento
via Sommarive 14, Povo, Trento 38123, Italy
[2]Department of Physics, University of Florence
via Nello Carrara 1, Sesto Fiorentino, Firenze 50019, Italy

Abstract— Recent advances in light harvesting using micro- and nano-structured materials have demonstrated the possibility to achieve striking increase of the efficiency of photovoltaics systems [1, 2]. Several proposed strategies achieved really interesting results but their implementation in photovoltaic market is questionable due to the high technological fabrication steps required that sensibly increase the fabrication costs.

Light harvesting photovoltaics are often based on porous materials because they give the possibility to carefully tune optical properties by reducing the reflectivity, while maximizing the absorption of light across large portions of the visible spectra [3–5].

Despite the majority of the studies on light harvesting were focused on the visible part of the spectra, the near infrared region contains a substantial amount of the energy density (about 25% in the range 1 to 3 µm).

Here we proposed a strategy to exploit the long photon lifetime, achievable in random structure, to enhance optical absorption in the sub bandgap spectral region.

We model a 2D random system composed by anisotropic pores elongated along a preferential axis and we analyse the role played by the rough-surface in the enhancement of the absorption through multiple scattering processes. The roughness is modelled by decomposing the pore onto short section with different radii.

The results show that rough-pores induce a large enhancement in the near-IR absorption compared to flat-pores, yet the backscattering from the top interface increases considerably also the reflection.

We show that reflection can be kept at low value if a bilayer structure is employed: the first layer (the one that face the incoming radiation) is made of flat pores, while the underlying one has a large roughness. In this case, simulations show that the integrated absorption increases by 50% compared to bulk silicon and of about 20% compared to flat pores. Interestingly the enhancement shows a flat response over the entire near-IR regime.

Our study suggests a scheme to realize photovoltaics systems with optimized absorption response for the near-IR range. The proposed structure can be implemented as back reflector in 3rd generation PV to increase cell's performances exploiting the sub-bandgap incident radiation. Finally the structure is compatible with silicon technologies and does not necessitate of complex nanofabrication techniques.

ACKNOWLEDGMENT

The work was partially supported by the Italian Ministry of University and Research through the "Futuro in Ricerca" project RBFR12OO1G-NEMATIC.

REFERENCES

1. Yu, Z., A. Raman, and S. Fan, *PNAS*, Vol. 107, 17491–17496, 2010.
2. John, S., *Nat. Mater.*, Vol. 11, 997–999, 2012.
3. Callahan, D. M., J. N. Munday, and H. A. Atwater, *Nano Lett.*, Vol. 12, 214–218, 2012.
4. Basu Mallick, S., M. Agrawal, and P. Peumans, *Opt. Express*, Vol. 18, 5691–5706, 2010.
5. Chutinan, A. and S. John, *Phys. Rev. A*, Vol. 78, 023825, 2008.

Session 3P5
SC3&4: Photonic-Electronic Integration for Miilimeter and Terahertz Wave Generation, Detection and Applications

Effect of Material Properties on Transmission through Metallic Hole Arrays at Terahertz Frequencies

Renu Bhadresha, **Nisha Sarwade**, **Arnab Pattanayak**, **and S. P. Duttagupta**
Veermata Jijabai Technological Institute, India

Abstract— Ebbesen demonstrated enhanced transmission through subwavelength hole arrays for a metal dielectric interface at optical frequencies in [1]. This was in contrast to the previous studies [2] that associated subwavelength arrays with weak transmission. While there is no consensus about the exact transmission mechanism, it is most widely accepted that this enhancement at optical frequencies is due to the generation of surface plasmon polaritons due to the complex dielectric constant exhibited by metals exhibited by metals with value $|\epsilon_r/\epsilon_i| > 1$ (where ϵ_r is the real part and ϵ_i is the imaginary part of the compex dielectric constant). At terahertz, the large conductivity of metals is usually considered a hindrance in the generation of SPPs. However it was shown that bulk plasma frequencies are can propagate along the interface for a range of frequencies from $\omega = 0$ to $\omega = \omega_p/2$, where ω_p [3] is the bulk plasmon frequency. In this paper, the material properties were modeled using these plasma frequencies for Au, Ag and Al.

As seen by Krishnan et al. [4], for maximum enhancement in transmission, the two materials on both sides of the metal should have the same dielectric constant. Keeping this in mind, a free-standing structure is designed where the material properties of the metal become the deciding factor in the transmission characteristics. The advantage of a free-standing design is that there is drastic reduction in fabrication steps because modern micro-fabrication techniques such as micro-machining can be used for design. Another advantage is that the dielectric is essentially taken as air and this simplifies the theoretical transmission calculations. In this paper, for the design, the plasma frequency for each metal is calculated from experimental values. These values were taken from [5] and the plasma and collision frequencies were calculated using the Drude Model equations. The design of the array is for operation in the 0.5 to 2.5 Thz range.

The geometric parameters were kept constant and the effect of variation of material for the same design was studied. The array was designed as a periodic array with a hole dimension d and a periodicity of a and a normal incidence. The design was analysed using CST Microwave Studio and each array was designed as a unit cell and simulated as a periodic array of these unit cells. The transmission characteristics show that there is a distinct peak related to the enhanced transmission due to generation of SPPs.

The results show that the enhanced transmission is due to the generation of surface plasmons. The thickness variation also affects each metal differently which is also analysed. This work gives a comparative study that can be used for efficient material and design parameter selection for different applications such as THz imaging, short distance indoor communication, etc..

REFERENCES

1. Ebbesen, T. W., H. J. Lezec, H. F. Ghaemi, T. Thio, and P. A. Wolff, "Extraordinary optical transmission through sub-wavelength hole arrays," *Nature*, Vol. 391, 667–669, 1998.
2. Bethe, H. A., "Theory of diffraction by small holes," *Phys. Rev.*, Vol. 66, 163–182, 1944.
3. Ritchie, R. H., "Plasma losses by fast electrons in thin films," *Phys. Rev.*, Vol. 106, 874–881, 1957.
4. Krishnan, A., T. Thio, T. J. Kim, H. J. Lezec, T. W. Ebbesen, P. A. Wolff, J. Pendry, L. Martin-Moreno, and F. J. Garcia-Vidal, "Evanescently coupled resonance in surface plasmon enhanced transmission," *Opt. Commun.*, Vol. 200, 1–7, 2001.
5. Ordal, M. A., L. L. Long, R. J. Bell, S. E. Bell, R. R. Bell, R. W. Alexander, Jr., and C. A. Ward, "Optical properties of the metals Al, Co, Cu, Au, Fe, Pb, Ni, Pd, Pt, Ag, Ti, and W in the infrared and far infrared," *Applied Optics*, Vol. 22, No. 7, 1099–1120, 1983.

Terahertz Generation from DAST Depending on Chirp of Pump Pulses Amplified by Double-clad Yb-doped Fiber Amplifier

Junichi Hamazaki, Norihiko Sekine, Akifumi Kasamatsu, and Iwao Hosako
National Institute of Information and Communications Technology, Japan

Abstract— High-power broadband terahertz (THz) generation has attracted much attention for various THz applications such as THz spectroscopy. To generate highpower broadband THz pulse, optical rectification effect is generally used, by using an ultra-short high-power pump pulse and a nonlinear crystal. Regarding pump pulse, pulse is characterized by wavelength, pulse energy, pulse width but also its chirp. It is known that dechirped pump pulse is the most suitable condition for THz generation. However, this is the case when a crystal is thin enough When a crystal is thick, it is non-trivial owing to material dispersion Effects of the pump pulse chirp in THz generation have not been well investigated.

To obtain chirp-controlled high-power femtosecond pump pulses, we used double-clad Yb-doped fiber (DC-YDF) amplifier. Since YDF has large gain and broad gain spectrum (1.0–1.1 μm). Furthermore, DC-YDF has extremely larger gain than usual YDF. Output power over 1 W is easily expected by using DC-YDF. Thus, DC-YDF amplifier is suitable for high-power ultra-short pulse generation. From the amplifier, average output power > 3.1 W with a pulse width of 110 fs at high repetition ration of 100 MHz is obtained. Chirp is controlled by varying distance of grating pair for pulse compression.

In this paper, we report the effects of the pump pulse chirp in THz generation. We generated THz pulse using DAST crystal and chirp-controlled femtosecond high-power pump pulses amplified by DC-YDF amplifier. By using THz time domain spectroscopy technique, we investigated THz spectra as a function of the chirp parameter. We found positive-chirp pump pulse can generate higher power and broader-band THz pulse, compared with dechirped pulse.

Photonic-based Millimeter Wave Wireless Link

Sungil Kim[1, 2]

[1]Future Technology Research Department, Creative Future Research Laboratory
Electronics and Telecommunications Research Institute
138 Gajeong-ro, Yuseong-gu, Daejeon 305-700, Republic of Korea
[2]Department of Advanced Device Technology
Korea University of Science & Technology (UST), Republic of Korea

Abstract— Nowadays, millimeter (mm)-wave frequency bands have become important as a candidate frequency band for wireless links of 5 G networks. This is because wide bandwidths to increase data rates up to several Gbps can be gotten in the mm-wave frequency bands with minimizing interference to allocation frequency bands. In order to check out a feasibility of a high-speed wireless link using the mm-waves, we have presented various photonic-based continuous wave (CW) generation schemes in mm-wave frequency bands. Using a generated mm-wave, a wireless link has demonstrated. Generally, photonic-based mm-wave generation schemes make a CW in the mm-wave frequency bands by beating two optical signals with wavelength differences. A conventional double sideband suppressed carrier (DSB-SC) scheme is very popular scheme to get two correlated optical signals with wavelength differences. We modified the DSB-SC scheme to increase frequency tunability, to overcome electronic dependency, and to reduce evaluation cost. Some achievements are listed in this paper. Especially, based on our results, we have accomplished a CW in the mm-wave frequency bands using a local oscillator with one-sixth frequency of a wanted mm-wave frequency. Using the DSB-SC scheme and some electronics, a high-speed wireless link operating up to 10 Gbps is successfully demonstrated and verified. Consequently, our results can be useful for developing mm-wave wireless link up to several tens Gbps.

50-Gbit/s Wireless Transmission over 20 Meters at 300 GHz

T. Nagatsuma[1], **K. Oogimoto**[1], **Y. Minamikata**[1], **and J. L. Hesler**[2]

[1]Graduate School of Engineering Science, Osaka University, 1-3 Machikaneyama, Toyonaka 560-8531, Japan
[2]Virginia Diodes, Inc., Charlottesville, VA 22902-6172, USA

Abstract— There has been a growing interest in the application of terahertz (THz) waves, whose frequencies range from 100 GHz to 1 THz, to ultra-broadband wireless communications. Photonic techniques have been efficiently employed to generate and modulate THz carrier signals. Real-time and error-free transmission experiments have so far been demonstrated at bit rates of 40 Gbit/s using a photonics-based transmitter with an on-off keying (OOK) modulation and a direct detection receiver at 300 GHz [1]. Such a simple configuration offers low-cost, small-size and energy-efficient transceiver modules by future electronic and photonic integration technologies [2].

In this paper, we present our recent results on the increase of bandwidth of the 300-GHz band transmitter and receiver, enabling real-time 50-Gbit/s transmission over the link distance of 20 m.

ACKNOWLEDGMENT

This work was supported in part by the 2014/2015 Strategic Information and Communications R&D Promotion Programme (SCOPE: 135010103), from the Ministry of Internal Affairs and Communications, Japan.

REFERENCES

1. Nagatsuma, T., et al., "Terahertz communications based on photonics technologies," *Optics Express*, Vol. 21, No. 20, 23736–23747, 2013.
2. Carpintero, G., et al., "Microwave photonic integrated circuits for millimeter-wave wireless communications," *IEEE Journal of Lightwave Tech.*, Vol. 32, No. 20, 3495–3501, 2014.

Photonic Integrated Circuits for mmW Systems

J. J. Vegas Olmos[1], **M. J. R. Heck**[2], **and I. Tafur Monroy**[1]

[1]Department of Photonics Engineering, Technical University of Denmark
Ørsted Plads, Building 343, Kg. Lyngby 2800, Denmark
[2]Department of Engineering, Photonics, Aarhus University
Finlandsgade 22, 8200, Denmark

Abstract— The bandwidth of wireless networks needs to grow exponentially over the next decade, due to an increasingly interconnected and smart environment. By 2020 there will be 50 billion devices connected to the internet. Low-cost, compact and broadband wireless transceivers will be required. The current WiFi frequency bands do not have enough capacity and wireless communication needs to move to the millimeter-wavelength or sub-terahertz range. The use of all-electronic solutions becomes increasingly prohibitive, though, at these higher frequencies. Microwave photonic technology offers the bandwidth and carrier frequencies required for high-capacity wireless networks and remote sensing applications. In this paper, we will introduce our efforts to leverage the advantages of microwave photonics and photonic integrated circuits to develop low-cost and ubiquitous wireless technology enabled by silicon photonics based transceivers.

ACKNOWLEDGMENT

This research has been funded by the DFF FTP mmW-SPRAWL and the Marie Curie FIWIN5G (grant agreement No. 642355).

Millimeter and Terahertz Wave Generation with a Photonic Integrated Source Using an on-chip Colliding Pulse Mode Locked Laser Diode and Arrayed Waveguide Grating Optical Filter

Carlos Gordon Gallegos[1], **Robinson Guzman**[1],
Xaveer Leijtens[2], **and Guillermo Carpintero del Barrio**[1]

[1]Universidad Carlos III de Madrid, Madrid 28911, Spain
[2]COBRA Research Institute, Eindhoven University of Technology
Den Dolech 2, Eindhoven 5612AZ, the Netherlands

Abstract— We present a novel Photonic Integrated Dual Wavelength Source with increased functionality and performance for Millimeter and Terahertz wave generation using an on-chip Colliding Pulse Mode Locked Laser Diode (OC-CPMLLD) and Arrayed Waveguide Grating (AWG) optical filter. The on-chip Colliding Pulse Mode Locked Laser Diode is a versatile pulsed source which includes multimode interference reflectors which are on-chip mirrors structures that allows defining the length of the cavity with lithographic precision so the repetition rate can be precise defined. Then the optical frequency comb generated by the pure colliding pulse mode locked condition is addressed to an Arrayed Waveguide Grating (AWG) optical filter which allows selecting two optical modes separated at the desired frequency within the Millimeter and terahertz frequency ranges. The key issue has been to design the pulse repetition rate at a sub-harmonic of the AWG channel spacing so in the dual wavelength source the colliding pulse mode locked repetition rate is 30 GHz and the Channel spacing of the AWG is 90 GHz. if we have the second harmonic repetition rate of 30 GHz provided by the on-chip Colliding Pulse Mode Locked Laser Diode, we can add an AWG filter with a channel spacing setting at a harmonic of the repetition rate within the millimeter and terahertz range like 60 GHz, 90 GHz, 120 GHz, 150 GHz, 180 GHz, etc.. As a result, we are able to design a dual wavelength source that allows choosing the frequency you want within the millimeter and terahertz frequency range based on lithographic precision.

Photonic Integration Solutions Enabling Coherent Millimeter Wave and THz Systems

Cyril C. Renaud
Department of Electronic and Electrical Engineering, University College London, London, UK

Abstract— Photonic technologies are seen as a potential key technology to the development of efficient sources in the millimetre-wave and THz range [1, 2]. This is mostly due to their relatively high power, coherence and tuneability. However, despite offering high-speed modulation and tuneabilty, it is clear that for many application and the development of THz technology a smaller footprint and lower power consumption will also be essential. While photonic solutions using discrete components have shown promising results [3], it remains essential to solve these remaining problems. To do so will require integrated photonic solutions as it will naturally offer smaller footprint while some of the losses within a discrete element system could be better managed thus enabling lower power consumption.

This contribution will concentrate on heterodyne photonic sources. Such sources have achieved emission across the THz range with linewidth lower than 10 Hz when used with locking systems [4]. Furthermore, being based on optical telecommunication technologies, these systems enable fast modulation.

The typical heterodyne coherent system we are envisaging may include an optical frequency comb generator (OFCG) used to lock the heterodyne source on a microwave reference. It is then composed of a dual tuneable laser source that provides the two optical oscillations spaced by the frequency of interest and a photomixer with antenna to generate the millimetre-wave or THz signal. The discussion will thus concentrate on the integration of these different components.

We will first present solutions for the OFCG and present results on three different configurations; mode-locked Fabry-Perot laser, FM-laser and amplified recirculating loop. We then will describe different set of dual laser heterodyne sources including potential locking techniques to enable highly coherent systems. A discussion on the different locking performances will show that linewidth of less than 10 Hz are achievable for frequencies in the THz range. Finally a fully integrated millimetre wave source including the photomixer will be presented including results on locking techniques.

ACKNOWLEDGMENT

This work was supported by Engineering and Physical Sciences Research Council grants for coherent terahertz system (COTS) (EP/J017671/1), and by the European Commission through the European project iPHOS (grant agreement No.: 257539).

REFERENCES

1. Seeds, A. J. and K. J. Williams, "Microwave photonics," *Journal of Lightwave Technology*, Vol. 24, 4628–4641, Dec. 2006.
2. Marpaung, D. and C. Roeloffzen, "Integrated microwave photonics for phase modulated systems," *IEEE Photonics Conference (IPC)*, 84–85, 2012.
3. Seeds, A. J., M. J. Fice, K. Balakier, M. Natrella, O. Mitrofanov, M. Lamponi, et al., "Coherent terahertz photonics," *Optics Express*, Vol. 21, 22988–23000, Sep. 23, 2013.
4. Seeds, A. J., M. J. Fice, F. Pozzi, L. Ponnampalam, C. C. Renaud, C. P. Liu, et al., "Photonic-enabled microwave and terahertz communication systems," *OFC: 2009 Conference on Optical Fiber Communication*, Vols. 1-5, 2032–2034, 2009.

Photonic Integrated Circuits for Generation and Detection of Coherent CW THz Radiation

Thorsten Göbel, Michael Theurer, Dennis Stanze, Francisco Soares, and Martin Schell
Fraunhofer Heinrich-Hertz-Institute, Germany

Abstract— Within the last years, THz technologies became mature and ready for everyday use. Many applications have been demonstrated, but the industrial breakthrough has yet to come, though. In order to make THz technologies available for large scale applications, compact and low cost solutions need to be developed. Photonic THz systems at the optical telecommunication wavelength of 1.5 µm are most suitable to fulfill industry's demand for reliable and reasonable priced systems. Here, cw THz systems profit most from telecom technologies, since all required optical components are available off-the-shelf in high quality and at low price. But even the latest generation of cw THz photomixing systems is based on discrete components and therefore limited in size, flexibility and cost.

In this paper, we present the next evolutionary step for cw THz photomixing systems: The transition from discrete components to Photonic Integrated Circuits (PICs). The Terahertz-PICs are fabricated with an InGaAsP/InP material system and operate in the optical wavelength range of 1550 nm. They comprise DFB-lasers, optical phase modulators and integrated optical waveguides for on-chip signal distribution. A unique bidirectional operation technique allows for driving the THz emitter and the THz detector at the same time and enables full control of the THz signal (amplitude, frequency and phase) via standard electronics, whereas the tuning of the laser wavelength is enabled by integrated heaters.

The performance of different THz-PIC implementations will be discussed on the basis of experimental results. Further, the paper will give an outlook for future PIC implementations and discuss how and where THz-PICs can enable the breakthrough for THz technology from lab applications to real life applications.

Plasmonic Terahertz Emitters and Detectors for Sensing and Wireless Communications

T. Otsuji[1], **A. Satou**[1], **S. Boubanga Tombet**[1], **T. Watanabe**[1], **G. Ducournau**[2], **Y. M. Meziani**[3], **W. Knap**[4], **and V. V. Popov**[5]

[1]Research Institute of Electrical Communication, Tohoku University, Sendai, Japan
[2]Institut d'Electronique, de Micro electronique et de Nanotechnologie
Universite de Lille, France
[3]Department de Fisca Aplicada, Universidad de Salamanca, Salamanca, Spain
[4]Laboratory Charles Coulomb & TERALAB
Université Montpellier 2 & CNRS, Montpellier, France
[5]Kotelnikov Institute of Radio Engineering and Electronics (Saratov Branch)
RAS, and Saratov State University, Saratov, Russia

Abstract— This paper reviews recent advances in emission and detection of terahertz radiation using two dimensional (2D) plasmons in semiconductor heterostructure integrated devices and their applications to sensing and high-speed wireless communication systems. The nonlinear dynamics of the 2D plasmons including the plasmon instability and rectification effects is first presented as the operation principle to demonstrate its potentiality of broadband intense emission and sensitive detection of terahertz radiation. The Doppler-shift effect of the plasma wave velocity under an asymmetric plasmon cavity boundary and/or the spatial modulation of electron transit time in a sub-micrometer scaled 2D plasmon system with a non-uniform 2D electron density distribution can promote the plasmon instability, resulting in self-oscillation of plasmons in the terahertz regime. The hydrodynamic nonlinearity of 2D plasmons can rectify the incoming electromagnetic radiation, resulting in photovoltaic detection of terahertz radiation under an asymmetric 2D plasmon cavity boundary. Second, the device structure that can provide practical emission and detection performances are addressed, which is based on a high-electron mobility transistor and incorporates the authors' original asymmetrically interdigitated dual-grating gates (DGGs). Numerical analysis reveals that in comparison with conventional symmetric DGG structure the asymmetric DGG can substantially improve the detection sensitivity as well as the instability (emissivity) by three to four orders of magnitude. Third, excellent terahertz emission and detection performances including coherent, monochromatic emission beyond 1-THz range at relatively low temperatures and the record detection responsivity of 22.7 kV/W (2.2 kV/W) at 200 GHz (1 THz) at 300 K with low noise equivalent power of 0.48 pW/Hz$^{0.5}$ (15 pW/Hz$^{0.5}$) are experimentally demonstrated by using InAlAs/InGaAs/InP heterostructure material systems. The frequency dependence of the responsivity is in good agreement with the theory deduced from the plasmonic drag and ratchet effects. Their arrayed monolithic integration and module assembly/packaging issues are also discussed. Finally their applications to terahertz-imaging-based sensing as well as high-speed wireless communications are demonstrated.

Terahertz-wave Integrated Circuits Based on Photonic Crystals

Kazuisao Tsuruda[1, 2], **Masayuki Fujita**[1], **Asako Suminokura**[1], **Masahiro Yata**[1], **Toshikazu Mukai**[2], **and Tadao Nagatsuma**[1]

[1]Graduate School of Engineering Science, Osaka University
1-3 Machikaneyama, Toyonaka, Osaka 560-8531, Japan
[2]Sensor Business Strategy Optical Device Research and Development Div.
ROHM Co., Ltd. 21, Saiin Mizosaki-cho, Ukyo-ku, Kyoto 615-8585, Japan

Abstract— Recently, the frequency band of terahertz electromagnetic waves (from 0.1 to 10 THz) has attracted much attention owing to its unique application possibilities such as in spectroscopic sensing, non-destructive imaging, and ultra-broadband wireless communication [1]. However, building terahertz-wave application systems and devices requires the use of bulky and discrete components, including sources, detectors, waveguides, and lenses. Size reduction of the active devices and development of integration platform are required to build a terahertz-wave integrated circuit.

Resonant tunneling diodes (RTDs) are promising as compact terahertz-wave source [2] and detector [3] because they can operate at room temperature in the terahertz-wave bands. Error-free wireless transmissions have been successfully demonstrated in the 0.3-THz band at bit rates of 2.5 Gbit/s [4] and 10 Gbit/s [5] using an RTD transmitter and a receiver, respectively. As a terahertz integration platform, metal-based structures such as metallic transmission lines and electromagnetic metamaterials are being extensively studied. However, the intrinsic absorption loss of metals in the terahertz-wave frequency region is high and uncontrollable. We have proposed a photonic-crystal slab consisting of a two-dimensional lattice of air holes formed on silicon as an alternative platform (Fig. 1) for terahertz-wave manipulation [6]. In addition, ultralow propagation loss (< 0.2 dB/cm) using terahertz photonic-crystal waveguides have been successfully demonstrated in the 0.3-THz band [7]. We have also achieved 1.5-Gbit/s error-free THz-wave communications and high-definition video transmission in a photonic-crystal waveguide of as long as 47 cm with bends of 28 times [7], a waveguide with a grating coupler [8], and a diplexer [9].

The most critical issue currently is how terahertz waves confined in the dielectric photonic-crystal waveguide can be efficiently coupled to an RTD, which is a tiny electronic device with a small metallic electrode. We have proposed the integration of a photonic-crystal waveguide and RTD chips by hybrid bonding [10]. In this paper, we first theoretically discuss an efficient integration scheme for the photonic-crystal waveguide and RTDs. Then we describe the experiments on the frequency characteristics of an integrated receiver using an RTD detector. Finally, we demonstrate an error-free gigabit transmission using the integrated device at the 0.3-THz band.

ACKNOWLEDGMENT

This work was supported in part by the Strategic Information and Communications R&D Promotion Programme (SCOPE) from the Ministry of Internal Affairs and Communications of Japan, by the Grant-in-Aid for Scientific Research from the Ministry of Education, Culture, Sports, Science and Technology of Japan, and by the TEPCO Memorial Foundation.

REFERENCES

1. Nagatsuma, T., *IEICE Electron. Exp.*, Vol. 8, 1127, 2011.
2. Asada, M., S. Suzuki, and N. Kishimoto, *Jpn. J. Appl. Phys.*, Vol. 47, 4375, 2008.
3. Shiode, T., T. Mukai, M. Kawamura, and T. Nagatsuma, *Asia-Pacific Microw. Conf. (APMC2011)*, 1122, 2011.
4. Shiode, T., M. Kawamura, T. Mukai, and T. Nagatsuma, *Asia-Pacific Microw. Photon. (APMP2012)*, WC-1, 2012.
5. Tsuruda, K., A. Kaku, T. Shiode, T. Mukai, M. Fujita, and T. Nagatsuma, *7th Global Symposium on Millimeter Wave 2014 (GSMM2014)*, T1B-3, 2014.
6. Kakimi, R., M. Fujita, M. Nagai, M. Ashida, and T. Nagatsuma, *Nature Photon.*, Vol. 8, 657, 2014.
7. Tsuruda, K., T. Ishigaki, A. Suminokura, R. Kakimi, M. Fujita, and T. Nagatsuma, *IEEE Int. Top. Meet. on Microw. Photon. (MWP2013)*, 9, 2013.

8. Suminokura, A., T. Ishigaki, M. Fujita, and T. Nagatsuma, *Asia-Pacific Radio Sci. Conf.*, DJ2b-3, 2013.
9. Yata, M., M. Fujita, and T. Nagatsuma, *Int. Top. Meet. Microw. Photon./Asia-Pacific Microw. Photon. Conf. (MWP/APMP2014)*, 40, 2014.
10. Suminokura, A., K. Tsuruda, T. Mukai, M. Fujita, and T. Nagatsuma, *Int. Top. Meet. Microw. Photon./Asia-Pacific Microw. Photon. Conf. (MWP/APMP2014)*, 419, 2014.

Stable and High Dynamic Range CW Terahertz Spectroscopy System

Ho-Jin Song[1], **Jae-Young Kim**[1], **Hidetaka Hishi**[1], **Hiroshi Fukuda**[2], **and Katsuhiro Ajito**[1]

[1]NTT Device Technology Laboratories, NTT Corporation
3-1 Morinosato-Wakamiya Atsugi, Kanagawa 243-0198, Japan
[2]NTT Device Innovation Center, NTT Corporation
3-1 Morinosato-Wakamiya Atsugi, Kanagawa 243-0198, Japan

Abstract— Terahertz (THz) waves have several interesting features, including strong THz fingerprints, the capability of penetrating those dielectric materials, and no radioactive contamination. Because of those features, THz waves are being investigated for various potential applications in, for instance, quality control, remote gas sensing, and security imaging [1]. In last a couple of decades, the time-domain spectroscopy (TDS) system with a femtosecond pulsed laser have been mainly used. The other approach is to use continuous waves (CW) THz signal, commonly based on commercially available fiber-optic components originally developed for telecommunications in the 1550-nm wavelength region. Recent CW THz spectroscopy systems have exhibited compact feature with fair performance in dynamic range and fast measurement [2, 3]. Moreover, a homodyne detection scheme dramatically improved the signal-to-noise ratio (SNR) of the system [4]. We have reported 100 and 75 dB-Hz maximum dynamic range of the intensity measurement at 300 GHz and 1 THz, respectively [5] with the fiber-optic components. In theory, the homodyne detection scheme enables us to measure phase information, such as relative dielectric constant, of a sample under the test. However, a few meter long pit-tailed fibers work as thermo-optic modulators and therefore we were unable to reconstruct a physically comprehensible dielectric constant or relative permittivity of samples under test from the measured phase information.

In this report, we describe the design of the silicon photonic integrated circuit for the THz homodyne spectroscopy system [6] and present spectroscopic measurements of several materials. To improve the reliability of the measurement, particularly in phase, silicon photonics technologies have been adapted in the homodyne CW THz spectroscopy system. Phase modulators, optical couplers and waveguides were fully integrated in a 2-mm^2 area on silicon-on-insulator substrate and the probe and reference signals was generated form the tiny single chip. With a high speed UTC-PD, PCA, and the silicon photonic circuit, we experimentally demonstrated the homodyne measurement of the complex dielectric property, absorption coefficient, and relative permittivity at a given sample thickness at up to 2 THz with excellent phase stability.

REFERENCES

1. Tonouchi, M., "Cutting-edge terahertz technology," *Nature Photonics*, Vol. 1, No. 2, 97–105, 2007.
2. Kim, N., S.-P. Han, H. Ko, Y. A. Leem, H.-C. Ryu, C. W. Lee, D. Lee, M. Y. Jeon, S. K. Noh, and K. H. Park, "Tunable continuous-wave terahertz generation/detection with compact 1.55 µm detuned dual-mode laser diodeand InGaAs based photomixer," *Opt. Express*, Vol. 19, 15397–15403, 2011.
3. Göbel, T., D. Stanze, U. Troppenz, J. Kreissl, B. Sartorius, and M. Schell, "Integrated continuous-wave THz control unit with 1 THz tuning range," *Proceeding of 37th Int. Conf. on Infrared, Millimeter and Terahertz Waves*, 1–3, Wollongong, Australia, 2012.
4. Kim, J.-Y., H.-J. Song, K. Ajito, M. Yaita, and N. Kukutsu, "Continuous-wave THz Homodyne spectroscopyand imaging system with electro-optical phase modulation for high dynamic range," *IEEE Trans. THz, Sci. Tech.* Vol. 3, 158–164, 2013.
5. Kim, J.-Y., H.-J. Song, M. Yaita, A. Hirata, and K. Ajito, "CW-THz vector spectroscopy and imaging systembased on 1.55-µm fiber-optics," *Opt. Express*, Vol. 22, 1735–1741, 2014.
6. Kim, J.-Y., H. Nishi, H.-J. Song, H. Fukuda, M. Yaita, A. Hirata, and K. Ajito, "Compact and stable THz vector spectroscopy using silicon photonics technlogy," *Opt. Express*, Vol. 22, 7178–7185, 2014.

Implementation of Photonics in High-performance, Zero-change SOI CMOS: From Design to Back-end Integration

Amir H. Atabaki[1], C. Sun[1], M. Georgas[1], J. S. Orcutt[1], F. Pavanello[2], L. Alloatti[1], B. R. Moss[1], Y.-H. Chen[1], J. Shainline[2], M. Wade[2], K. Mehta[1], K. Nammari[2], E. Timurdogan[1], D. Miller[3], O. Tehar-Zahav[3], Z. Sternberg[3], J. C. Leu[1], J. Chong[1], R. Bafrali[3], G. Sandhu[3], M. Watts[1], R. Meade[3], M. A. Popović[3], V. Stojanović[1, 4], and R. J. Ram[1]

[1]Department of Electrical Engineering and Computer Science
Massachusetts Institute of Technology, 77 Massachusetts Ave, Cambridge, Massachusetts 02139, USA
[2]Department of Electrical, Computer and Energy Engineering
University of Colorado at Boulder, Boulder, Colorado 80309, USA
[3]Micron Technology, USA
[4]Department of Electrical Engineering and Computer Sciences
University of California, Berkeley, CA, USA

Abstract— In the past decade, integrated photonics on silicon on insulator (SOI) platform has been shown to be promising for many applications of photonics from interconnects to sensing. While the knowledge of mature fabrication processes in CMOS has helped to achieve high optical quality passive and high bandwidth active optoelectronic devices in silicon, the current state of silicon photonics does not exploit the state of the art CMOS infrastructure for low-cost, high-yield manufacturing and fast prototyping in the same fashion that analog and digital electronics do. As a result, the fabrication of silicon photonic devices and systems for research and development or even in some cases for low to medium volume manufacturing is done either in-house or in small-scale foundries customized for specific applications. In this work, we have shown that it is possible to integrate photonic components in IBM's 45 nm SOI CMOS process, which is an open-foundry native electronics CMOS process [1]. There are three components to this effort: 1) understanding the materials and processes in the CMOS process, 2) understanding the design guide rules and proper layout generation techniques, and 3) careful optimization of backend post-processing for substrate release/transfer.

In using a native CMOS process to lay out photonics there are two main issues to tackle; first, there is no direct access to all of the mask layers (some layers are automatically generated from other layers) and considering that the process is mainly designed for MOSFETs this could potentially be problematic (e.g., getting unwanted doping in the device layer) and requires careful understanding of the process design kit (PDK) and devising methods to get around it; and second, there are design guide rules (e.g., minimum gap or width, minimum and maximum density rules) that can potentially constrain our freedom for designing photonic devices. We have shown that for our process of choice (IBM 45 nm SOI CMOS) it is possible to utilize all of the design capabilities to tackle these challenges and to develop parameterized cells for complex photonic devices such as microring modulators and detectors with sufficient flexibility over the design space.

The other major challenge for using electronics SOI platforms for the integration of photonics is that the insulator under the device layer is optically too thin to prevent the leakage of light into the substrate (thickness it kept small for good heat sinking). We have optimized a Xenon Difluoride etching process that enables us to remove the underlying silicon substrate (either selectively under the photonic devices or over the entire die) with excellent optical quality. Using this technique, we have demonstrated optical losses as low as 4 dB/cm and resonator intrinsic quality factors above 100,000 at 1550 nm.

In summary, we have demonstrated that despite numerous material, process and design constraints in a native electronics CMOS process, it is still possible to build photonic components that can approach the performance of their counterparts with custom substrates and processes. We have previously shown high speed optical receivers [2] and transmitters [3] in this platform.

REFERENCES

1. Orcutt, J. S., et al., "Open foundry platform for high-performance electronic-photonic integration," *Opt. Express*, Vol. 20, No. 11, 12222–12232, 2012.
2. Georgas, M., J. Orcutt, R. J. Ram, and V. Stojanovic, "A monolithically-integrated optical receiver in standard 45-nm SOI," *IEEE J. Solid St. Circuits*, Vol. 47, 2012.

3. Wade, M. T., et al., "Energy-efficient active photonics in a zero-change, state-of-the-art CMOS process," *Optical Fiber Communication Conference*, San Francisco, CA, paper Tu2E.7, Mar. 11, 2014.

Session 3P6a
SC3: Novel Electromagnetic Simulation, Components, and Design for the THz Region

Computation and Analysis of Terahertz Wire Grid Polarizer Self-resonance Using Transmission Line Theory

J. S. Cetnar[1] and E. R. Brown[2]

[1]Air Force Research Laboratory, Sensors Directorate, Wright Patterson AFB, Ohio 45433, USA
[2]Departments of Physics and Electrical Engineering
Wright State University, Dayton, Ohio 45435, USA

Abstract— A terahertz metal wire-grid polarizer on a low-loss dielectric (crystalline quartz) substrate was simulated using High Frequency Structure Simulator (HFSS) and modeled with equivalent-circuit theory. The transmittance of the polarizer was calculated for electromagnetic radiation at normal incidence from 100 to 1000 GHz for both s-polarization (perpendicular to the grid) and p-polarization (parallel to the grid). The phase difference in S_{21} between the HFSS input and output ports was calculated and plotted versus frequency and versus fill-factors of 0.3, 0.5, 0.7, 0.9, and 0.95 for both polarizations. Analysis of the s-polarized S_{21} shows that the phase-angle differences are all negative. This is interpreted as the phase of the current in the wire grid leading the phase of the voltage across the gaps, and thus the electric field across the gaps. This behavior was seen for all fill-factors. Therefore, a capacitive effect is exhibited by the wire-grid polarizer for s-polarization. Analysis of the p-polarization results show the phase angle differences are positive for fill-factors less than or equal to 0.9 and negative at the fill-factor of 0.95. Thus, the wire-grid current lags the gap voltage for p-polarization at fill-factors ≤ 0.90 (an inductive effect) while wire current leads the gap voltage at fill-factor $= 0.95$ (a capacitive effect). This behavior is the spatial analog of a parallel LC circuit.

The self-resonance of the wire-grid polarizer was then modeled using the lumped circuit parameters of specific sheet inductance and specific gap capacitance for the wire grid, and transmission line theory for the substrate, for various fill-factors. Specific sheet inductance, specific gap capacitance, and self-resonant frequency versus fill-factor were calculated and plotted. The results show a monotonic increase in both specific sheet inductance and specific gap capacitance with increasing fill-factor. Meanwhile, the self-resonant frequency decreases monotonically with increasing fill-factor and asymptotically approaches a constant of approximately 125 GHz at very high fill factors.

Analysis for Improving the Radiation Behavior for THz Devices

L. E. García-Muñoz[1], **A. Rivera-Lavado**[1], **S. Llorente-Romano**[1], **M. Salazar-Palma**[1], **G. Carpintero-del Barrio**[2], **and D. Segovia Vargas**[1]

[1]Signal Theory and Communications Department, Carlos III University of Madrid, Madrid 28911, Spain
[2]Electrical Engineering Department, Carlos III University of Madrid, Madrid 28911, Spain

Abstract—

Introduction: One of the main issues in THz technology (both emitters and receivers) is radiating the energy effectively. It can be split the issue into two topics: on one hand, the well-known concept of matching impedance. The current state of the art for THz devices, typically gives a high input impedance (few kohm) with a strong capacitance behavior [1]. On the other hand, the second issue is having a broadband radiator for covering the ultra wideband capabilities of THz generators devices [2]. Both requirements, as one can imagine, are extremely difficult to accomplish.

In this paper, a theoretical approach will be done, showing a new approach for getting a broadband behavior with high input impedance, based on loading periodically a transmission line conveniently tapered for getting a suitable backfire radiation behavior. These kind of structures are a generalization of the well-known classical topologies log-per or log-spiral antennas. By means of the proposed structure, those classical geometries will improve both their radiation behavior together with a better matching with the THz device. An explanation of such structures based on the Brillouin plot will be firstly exposed. Some examples as potential solutions for covering the THz issues will be treated. Comparisons with array topologies and single elements state of the art topologies will be done.

REFERENCES

1. Montero-de-Paz, J., E. Ugarte-Muñoz, L. E. García-Muñoz, I. Camara Mayorga, and D. Segovia-Vargas, "Meander dipole antenna to increase CW THz photomixing emitted power," *IEEE Transactions on Antennas and Propagation*, Vol. 62, No. 9, 4868–4872, Sep. 2014
2. Rivera-Lavado, A., S. Preu, L. E. García-Muñoz, A. Generalov, J. Montero-de-Paz, G. Döhler, D. Lioubtchenko, M. Méndez-Aller, F. Sedlmeir, Martin Schneidereit, Harald G. L. Schwefel, Stefan Malzer, D. Segovia-Vargas, and A. V. Räisänen, "Dielectric rod waveguide antenna as THz emitter for photomixing devices," *IEEE Transactions on Antennas and Propagation*, accepted, 2015.

Full System Model for Terahertz Generation by Optical Rectification

Koustuban Ravi[1], **Damian N. Schimpf** [2, 3], **Wenqian R. Huang**[1], **Sergio Carbajo**[2, 4, 3], **Emilio A. Nanni**[1], **and Franz X. Kärtner**[1, 2, 3, 4]

[1]Massachusetts Institute of Technology, USA
[2]Center for Free-Electron Laser Science, DESY, Germany
[3]The Hamburg Center for Ultrafast Imaging, Germany
[4]Department of Physics, University of Hamburg, Hamburg 22761, Germany

Abstract— Experiments of high-field terahertz (THz) generation by intra-pulse difference frequency generation (or optical rectification) deviate significantly from predictions by existing models. We address this problem via a model which considers the spatial and temporal shaping of the optical pump pulse, the coupled nonlinear interaction between THz and optical radiation as well as crystal geometry for the first time.

Existing models either (i) neglect the depletion of the optical pump [1] which drastically overestimates conversion efficiency or (ii) consider only one spatial dimension [2] which cannot account for crystal geometry or terahertz (THz) beam properties. We solve for both THz and optical electric fields via an infinite set of coupled nonlinear wave equations in two spatial dimensions [3]

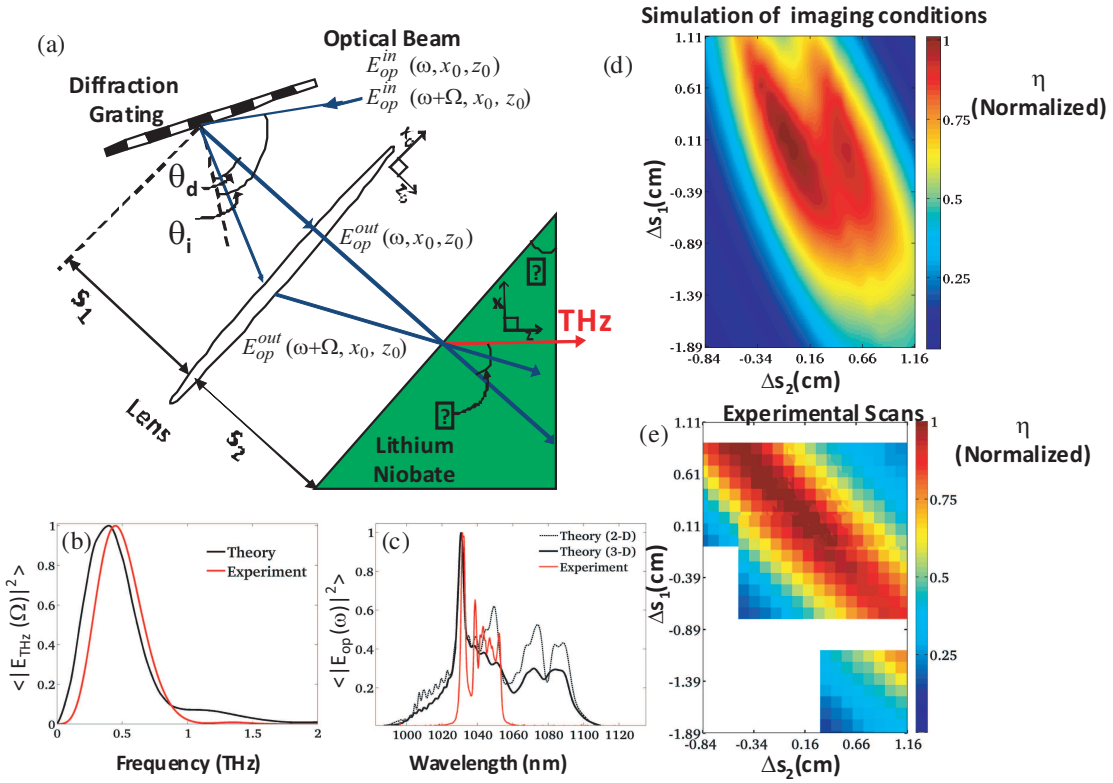

Figure 1: The effects of an arbitrary optical setup such as a tilted-pulse-front setup and prism like crystal geometry can be considered. The simulated (b) THz and (c) optical spectra are in good agreement with experiments. The input Gaussian optical spectrum centered at 1030 nm is predicted to be drastically modified by the THz radiation. (d)–(e) The model provides a one-to-one correspondence between experimental conditions and THz properties as seen in the plots of conversion efficiency Vs imaging distances (s_1, s_2).

as depicted in Eq. (1).

$$\nabla^2 E_{THz}(\Omega,x,z) + k^2(\Omega)E_{THz}(\Omega,x,z) = \frac{-\Omega^2\chi^{(2)}_{eff}(x,z)}{c^2}\int_0^\infty E_{op}(\omega+\Omega,x,z)E_{op}*(\omega,x,z)d\omega$$

$$\nabla^2 E_{op}(\omega,x,z) + k^2(\omega)E_{op}(\omega,x,z) = \frac{-\omega^2\chi^{(2)}_{eff}(x,z)}{c^2}\left[\int_0^\infty E_{op}(\omega+\Omega,x,z)E_{THz}*(\Omega,x,z)d\Omega + \int_0^\infty E_{op}(\omega-\Omega,x,z)E_{THz}(\Omega,x,z)d\Omega\right] \quad (1)$$

A solution for the case of THz generation using tilted-pulse-fronts in lithium niobate is presented. The schematic of the system is depicted in Fig. 1(a). The model accounts for spatio-temporal variations such as angular dispersion, spatial and temporal chirp of the optical pump pulse imparted by the optical setup and geometry of the crystal. The predicted THz and and optical spectra in Figs. 1(b)–(c) are in good agreement with experiments. In Fig. 1(c), the incident Gaussian optical spectrum is drastically reshaped as a consequence of THz generation. In Figs. 1(d)–(e), the conversion efficiency as a function of perturbations to distances s_1, s_2 is plotted. This illustrates the ability of the model to describe effects of system perturbations on various THz properties.

The presented model is thus a highly versatile simulator for understanding the spectral, spatial properties of the generated THz radiation and is an advancement towards optimizing a variety of terahertz generation systems.

REFERENCES

1. Bakunov, M. I., S. B. Bodrov, and E. A. Maskovich, "Terahertz generation with titled-front laser pulses: Dynamic theory for low absorbing crystals," *J. Opt. Soc. Am. B*, Vol. 28, No. 7, 1724–1734, 2011.
2. Jewariya, M., M. Nagai, and K. Tanaka, "Enhancement of terahertz wave generation by cascaded chi_2 processes," *J. Opt. Soc. Am. B*, Vol. 26, No. 9, A101–A106, 2009.
3. Ravi, K., W. R. Huang, S. Carbajo, E. A. Nanni, D. N. Schimpf, and F. X. Kärtner, "Theory of terahertz generation by optical rectification using tilted-pulse-fronts," arXiv:1410.8120, 2014.

Design Challenges for Electro-optic Tuning of Amplitude and Phase in THz Region

Robert Lindquist[1, 2], **Abubaker Tareki**[1], **Daniele Lo Forti**[1], **Wonkyu Kim**[1], **and Junpeng Guo**[1, 2]

[1]Department of Electrical and Computer Engineering, University of Alabama in Huntsville
Huntsville, Alabama 35899, USA
[2]Center for Applied Optics, University of Alabama in Huntsville, Huntsville, Alabama 35899, USA

Abstract— Electro-optic (EO) modulation of the amplitude and phase of an electromagnetic waves in the optical and infrared regions is commonplace and has led to commercially available components used in spectral filtering, polarization management, beam steering, transmitters, displays, etc.. However, electro-optic techniques have had limited success in the THz region due to several practical design challenges. The first barrier for components is the long interaction lengths required to modulate a THz wave. Since the EO modulation depth is directly proportional to the multiplication of the change of permittivity and the ratio of interaction length over wavelength, THz systems with wavelengths ranging from 150 µm to 1 mm pose a challenge. Even a basic tunable half-wave plate using a highly birefringent liquid crystal (LC)with a birefringence of $\Delta n \cong 0.33$ requires an effective film thickness ranging from 225 µm to 1.5 mm. More complicated structures could require interaction lengths of several millimeters. Thick EO films are typically unreliable, require unreasonably large voltages, and tend to be very slow. The second challenge is the selection and design of the electrodes. The material properties of a conductive material in the THz region are significantly different than the infrared and optical region leading to large impedance mismatch at dielectric/electrode interfaces. For instance, the indium tin oxide (ITO) electrodes used in common LC display are practically opaque to the THz wave.

In this paper, the basic EO modulation configuration engineered and fabricated using longitudinal or transverse stratified sub-wavelength structures will presented. By using sub-wavelength layered structures, the thickness limitation of an electro-optic tuning films such as liquid crystals (LC) can be overcome. Consistent with electro-optic modulation convention, the transverse structure will have the applied field and structure periodicity perpendicular to the THz beam propagation. The longitudinal configuration will have the applied field and structure periodicity parallel to the THz beam propagation. Since the transverse configuration allows for long interaction lengths with small apertures and the longitudinal configuration allows for large aperture and short interaction length, the transverse configuration is used primarily in communications application with single beams or within a waveguide while the longitudinal configuration is used in imaging or display applications. The transverse configuration can be designed to provide several practical high transmission, distortion-less, flat top channel filters. Both a novel tunable narrowband notch filter and a tunable transmission filter will be presented. The focus on the longitudinal configuration will be related to the high transmission, polarization independent electrodes. The electrode design is a Frequency Selective Surface consisting of subwavelength periodic structures patterned in continuous gold on a transparent dielectric. The maximum feature size of the structure holes is maintained below a fraction of the thickness of the electro-optic film to allow fringing field to uniformly excite the entire electrode area. Initial experiments have shown polarization independence and transmission peaks that reach as high as 93% in measurements.

Simulation and Design of a Heterogeneously Integrated III-V/Silicon Dual-wavelength Laser

Yingchen Wu and Jian-Jun He
State Key Laboratory of Modern Optical Instrumentation, Centre for Integrated Optoelectronics
Department of Optical Engineering, Zhejiang University, Hangzhou 310027, China

Abstract— THz wireless communication is considered as an excellent candidate to meet the rapidly increasing demand for broadband wireless network, due to its inherently higher bandwidth compared to microwave solutions. Mode-beating dual-wavelength lasers, which can be used for continuous wave (CW) THz carrier signal generation and all-optical clock recovery, have attracted much attention. Monolithically integrated dual-wavelength lasers are more compact, cost-effective than the free-running laser pair as an optical beat source. The dual-wavelength lasers which experience similar environmental fluctuations with the two discrete free-running laser have more stable frequency leading to a smaller drift of the THz signal. Some published multi-section dual-wavelength lasers show potential for tunability. However, these structures need multiple current injections, which lead to a more complicated controlling system and increasing the instability of the generated THz signal. In this paper, we present the design and simulation results of a novel dual-wavelength laser based on III-V/silicon heterogeneously integrated platform. A single-mode symmetric splitting is achieved by embedding shoulder gratings inside a micro-ring resonator. By adjusting the coupling coefficient between the ring and straight waveguide, we can obtain a large SMSR between the two splitting modes and the side mode. The gap between the splitting peaks can vary from 0 to 1 nm by varying the reflection coefficient of the gratings.

Terahertz Metasurface Antireflection Coatings

Hou-Tong Chen[1] and Li Huang[2]

[1]Los Alamos National Laboratory, USA
[2]Harbin Institute of Technology, China

Abstract— Conventional single- or multi-layer antireflection coatings to suppressing the undesirable interface reflection and enhance the transmission have strict requirements in the refractive index and film thickness of the materials being coated. Alternative approaches have been developed, for example, using surface relief structures. However, they pose difficulties and severe restrictions in device fabrication and integration. Taking advantage of the tailored reflection/transmission and their dispersion, metasurfaces consisting of subwavelength planar metallic structures and combining with a dielectric spacer enable ultrathin antireflection coatings without much requirement in the refractive index of the spacer material.

We have developed this concept particularly in the terahertz (THz) frequency range [1, 2]. In our first metamaterial antireflection coating structure, we selectively etch down silicon surface forming an array of silicon cylinders by photolithographic methods and reactive ion etching, which is followed by directional metal (gold) deposition. Eventually we obtain a metal-dielectric-metal structure consisting of metal resonators on top, a hole array at the bottom, and air/silicon cylinders in between as the dielectric spacer. We further find that excellent antireflection performance can be accomplished using much simpler metal-dielectric structures — a combination of a single-layer metallic metasurface and an ultrathin dielectric film, achieving a bandwidth comparable to quarter-wave antireflection. This can be realized by spin-coating of a low refractive index polymer film on top of a high refractive index substrate, and then fabricating an array of metallic resonators. This antireflection approach was also accomplished at mid-infrared wavelengths [3]. In another design we fabricate a metallic mesh on top of the substrate, and then laminating an ultrathin silicon wafer. All of these metamaterial/metasurface antireflection coatings with appropriate design parameters can completely eliminate the reflection at specific frequencies, with a bandwidth approaching quarter-wave antireflection coatings. We emphasize that the metamaterial/metasurface antireflection coatings do not require refractive index matching of the materials being used, and the overall thickness is much less than the traditional quarter-wave antireflection coatings. Further improvement of the bandwidth or achieving multi-band antireflection is possible by using more complex unit cells of the metasurfaces [4]. We will present our numerical and experimental results, together with analytical calculations to elucidate the underlying principles [5].

REFERENCES

1. Chen, H.-T., et al., "Antireflection coating using metamaterials and identification of its mechanism," *Phys. Rev. Lett.*, Vol. 105, 073901, 2010.
2. Chen, H.-T., et al., "A numerical investigation of metamaterial antireflection coatings," *THz Sci. Technol.*, Vol. 3, 66–73, 2010.
3. Zhang, B. Y., J. Hendrickson, N. Nader, H. T. Chen, and J. P. Guo, "Metasurface optical antireflection coating," *Appl. Phys. Lett.*, Vol. 105, 241113, 2014.
4. Grady, N. K., et al., "Terahertz metamaterials for linear polarization conversion and anomalous refraction," *Science*, Vol. 340, 1304–1307, 2013.
5. Chen, H.-T., "Interference theory of metamaterial perfect absorbers," *Opt. Express*, Vol. 20, 7165–7172, 2012.

The Optimisation and Analysis of Multi-moded Feed Horn Structures at Terahertz Frequencies

D. McCarthy, N. Trappe, J. A. Murphy, M. Gradziel, C. O'Sullivan, and S. Doherty
Department of Experimental Physics, Maynooth University, Ireland

Abstract— Carrying out astronomical observations at far-infrared wavelengths is critical in enabling further progress in the fields of cosmology and astrophysics. Such observations will allow additional insight into the birth and evolution of the Universe. To allow progress in these areas, it is necessary to improve the sensitivity and resolution of the instrumentation that is used to carry out these observations.

At the high frequencies in question (terahertz), the instruments typically make use of horn antenna fed detector systems. To achieve the required performance, the horn designs must be highly optimised. Full electromagnetic solvers (CST, HFSS, COMSOL etc.) struggle to predict the performance of horn antennas at such high frequencies in a timely manner due to the large electrical size of the structures. It is therefore very challenging to perform the optimisation using such solvers particularly for multi-mode systems where each mode would have to be considered individually.

In this paper we outline an alternative technique for modelling multi-mode (partially coherent) horn antennas based on the mode-matching technique, which allows electrically large structures to be modelled in a highly efficient manner. This technique returns a set of scattering matrices which gives a full vector definition of the transmission and re ection characteristics of the resulting design at a given frequency. We demonstrate how this can be used to extract field patterns and other figures of merit that are important for evaluating the electromagnetic performance of a horn design.

An efficient genetic algorithm based optimisation technique (using mode-matching) is also presented. The optimisation process is based on a piecewise conical profile horn design and produces a geometry that is optimised with respect to some figure of merit that is of critical importance for the application in question. This allows the instrument to realise the high levels of optical performance that are required for astronomical applications.

Simultaneous Generation of Terahertz and X-ray Radiation with Ultrashort Femtosecond Laser Pulses in Nano-cluster Medium

A. V. Balakin[1], **A. V. Borodin**[1, 2], **M. S. Dzhidzhoev**[3], **M. G. Evdokimov**[1], **M. N. Esaulkov**[2], **I. A. Zhvaniya**[1], **N. A. Kuzechkin**[2], **A. Yu. Sidorov**[1], **P. M. Solyankin**[1], **and A. P. Shkurinov**[1, 2]

[1]Faculty of Physics, M. V. Lomonosov Moscow State University
Leninskie Gory, Moscow 119991, Russia
[2]Institute on Laser and Information Technologies of the Russian Academy of Sciences
1 Svyatoozerskaya Str., Shatura Moscow Region 140700, Russia
[3]International Laser Center
M. V. Lomonosov Moscow State University, Leninskie Gory, Moscow 119991, Russia

Abstract— We have studied for the first time the simultaneous generation of terahertz and X-ray radiation from noble gas based nano-cluster supersonic jet under "one-" and "two-color" (fundamental and its second harmonic) excitation with high-power femtosecond laser pulses. It was shown that optimal conditions for effective generation of terahertz and X-ray radiation are different, that makes possible efficient control by ratio between values of terahertz and X-ray signals generated simultaneously from gas based nano-cluster jet by means varying of time delay between laser pulse and cluster jet formation and by varying of laser pulse's chirp.

It has been shown that efficiency of THz generation from cluster jet could be efficiently controlled by varying the ratio between clustered and buffer gases gas mixture; angular distribution of terahertz beam generated near by optical axis under "two-color" laser excitation conditions has been measured as well.

Session 3P6b
Microwave Photonics, THz Technology

Electromagnetic Properties of Ultrathin Quadrifilar Spirals and Their Complementary Structures

Nina Meinzer, **Alastair P. Hibbins**, **and J. Roy Sambles**
Electromagnetic and Acoustic Materials Group
School of Physics and Astronomy, University of Exeter, United Kingdom

Abstract— Metallic spiral structures have been employed as subwavelength antenna elements in the microwave regime for some time. Recently they also been shown to support localised magnetic spoof plasmons similar to corrugated surfaces or cylinders [1]. Following on from these results we, in this paper, study the electromagnetic properties of ultrathin quadrifilar copper spirals and of their complementary structures, spiral-shaped apertures in an extended copper film. The samples are fabricated by a wet-etching technique using a mask printed onto a thin copper film on top of a mylar substrate. We experimentally map the near-fields of the samples. We further perform numerical finite-element modelling for comparison with our experimental data and to provide further information to aid our understanding of the system.

We start from single spiral elements and compare the electro-magnetic response of a direct copper spiral with that of its complementary (spiral aperture in a copper sheet) structure. From this starting point we move on to an investigation of combinations of small numbers of such spiral elements, both in the direct and inverse case, which exhibit the mode coupling one expects from a system of closely spaced or connected antennas. Depending on the excitation geometry or the arrangement of elements specific eigenstates of the coupled systems can be selectively addressed or suppressed, which adds an additional degree of control over the resonant behavior of these ensembles of a few spiral (spiral aperture) antennas. This latter part of our work is related to previous studies on the channeling of electromagnetic waves.

REFERENCES

1. Huidobro, P. A., et al., *Phys. Rev. X*, Vol. 4, 021003, 2014.

Optical Frequency-interleaving Full-duplex Technique for Fiber-optic Transmission of Millimeter-wave-band Frequency-modulated Continuous-wave Downlink Signal and 10-Gb/s On-off-keying Uplink Signal

T. Kuri[1], **A. Kanno**[1], **and T. Kawanishi**[2, 1]

[1]National Institute of Information and Communications Technology, Japan
[2]Waseda University, Japan

Abstract— An optical frequency-interleaving full-duplex technique for fiber-optic transmission of millimeter-wave-band frequency-modulated continuous-wave downlink signal and 10-Gb/s on-off-keying uplink signals is newly proposed. The proposed full-duplexing technique with a flexible wavelength channel selector is experimentally demonstrated.

High-precision imaging technology has been in strong demand for safety and security at important facilities. For example, for runway monitoring, several-inch class debris should be detected and removed to ensure safe takeoff and landing [1]. To achieve such high-precision imaging by radio, millimeter-wave (mm-wave) is a promising candidate because of its broad transmission bandwidth. To overcome the large propagation loss and atmospheric attenuation in the mm-wave bands, the introduction of a distributed antenna system (DAS) concept is necessary for large-area surveillance. In the DAS, radio-over-fiber (RoF) technology aids in realizing easy radio signal distribution with a low-loss optical fiber. We have demonstrated the optical generation for highly accurate frequency-modulated continuous-wave (FM-CW) signal, which has high affinity with the RoF technology [2]. We have also demonstrated the distribution of FM-CW signals with three different frequency band in a wavelength division multiplexing (WDM) RoF system [3, 4]. In the demonstrations, although the downlink transmission of FM-CW signals has been verified, an uplink transmission for sending sensed data back to a central control station (CCS) has never been considered.

In this paper, we investigate an optical frequency-interleaving full-duplex technique for fiber-optic transmission of mm-wave-band FM-CW downlink signal and 10-Gb/s on-off-keying (OOK) uplink signals. Their optical duplexing is experimentally demonstrated with a flexible wavelength channel selector for two cases of downlink mm-wave-band, that is, 96-GHz-band and 48-GHz-band. In the demonstration, we show that no serious degradation for both the downlink and the uplink transmission is observed even if our proposed full-duplex technique is introduced in the fiber-optic full-duplex link.

ACKNOWLEDGMENT

This research was conducted as a part of "Research and Development to Expand Radio Frequency Resources," supported by the Ministry of Internal Affairs and Communications (MIC), Japan.

REFERENCES

1. Federal Aviation Administration, AC150/5220-24, US Department of Transportation, 2009.
2. Umezawa, T., A. Kanno, K. Inagaki, T. Kawanishi, A. Kohmura, S. Futatsumori, N. Yonemoto, and N. Shibagaki, "EO-OE converting technologies for 90 GHz radio over fiber systems," *Third ENRI Int'l Workshop on ATM/CNS Tech. Dig.*, EN-006, Feb. 2013.
3. Kanno, A. and T. Kawanishi, "Broadband frequency-modulated continuous-wave signal generation by optical modulation technique," *IEEE J. Lightwave Technol.*, Vol. 32, No. 20, 3566–3572, 2014.
4. Kuri, T., A. Kanno, and T. Kawanishi, "De-multiplexer of wavelength division multiplexed radio-over-fiber signal for application of W-band frequency-modulated continuous-wave radar systems," *Proc. OECC/ACOFT2014*, MO2F2, Jul. 2014.

2D and 3D Modeling of Electro-optic Effect in Whispering Gallery Mode Optical Microresonators

N. G. Pavlov[1, 3], **N. M. Kondratyev**[1], **and M. L. Gorodetsky**[1, 2]

[1]Russian Quantum Center, Russia
[2]Moscow State University, Russia
[3]Moscow Institution of Physics and Technology, Russia

Abstract— Microwave systems, cellular networks and other various personal communications systems require devices that are capable of receiving, converting and processing signals in the millimeter and centimeter wave ranges. A broad palette of devices was developed recently for transferring radio frequency and microwave signals directly to optics. This presents all advantages of optical communication channels, allowing to transmit data securely with high rates, low loss, low power consumption. Electro-optic modulators based on interaction of optical and microwave waves in high-Q nonlinear optical resonators with whispering gallery modes provide a promising platform of that kind.

In our work we present analysis of electro-optic interaction of a fundamental whispering gallery optical mode in a dielectric microdisc and a radio frequency mode of a half-wave microstrip line placed on the disc circumference. 2D and 3D numerical models of the system are developed. Both optical and radio frequency modes are simulated using finite element method with Comsol Multiphysics software. The comparison between the models is presented, and a theory of modulation in the multi-mode system is discussed. The magnitude of electro-optic effect is calculated depending on optical and radio frequency mode numbers. The cases of different polarizations of signal and pump optical field for standing and travelling waves are also considered. It is shown that the modulation in the system exists only for particular sets of mode numbers determined by selection rules. The magnitude of the effect in such system is shown to have an extremal dependence on the microstrip length for a given set of mode numbers.

Optical FM-CW Signal Generation for a Terahertz Radar System by Higher-order Optical Modulation

Atsushi Kanno[1], **Norihiko Sekine**[1], **Yoshinori Uzawa**[1], **Iwao Hosako**[1], **and Tetsuya Kawanishi**[1, 2]

[1]National Institute of Information and Communications Technology, Japan
[2]Waseda University, Japan

Abstract— To realize high precision imaging system based on radar technology, high-frequency carrier radio is promising owing to its broadness of available bandwidth. Actually, some radar system for detection of debris with a size of several centimeters on airport runways are being developed for enhancement of civil security using millimeter-wave band such as 77 GHz and 90-GHz bands. However, available bandwidth of the millimeter-wave is limited owing to radio regulations. Therefore, possible range resolution will be several centimeters. Terahertz wave at a frequency greater than 300 GHz is another candidate for high-precision radar system due to its broad available bandwidth. On the other hand, the precise signal generation technology is required for precise ranging. An optical modulation technology can meet the demands by using frequency multiplication configuration in optical domain. Actually, an optical frequency quadrupling based on an optical intensity modulation can provides a frequency-chirp bandwidth of 30 GHz at a carrier frequency of 100 GHz. To expand the frequency with a large number of multiplication factor of the optical multiplier, an optical frequency comb generation technique is indispensable.

We demonstrate an optical frequency-chirped signal generation using higher-order optical modulation technique. An optical frequency comb generator by using optical modulation is utilized as a frequency multiplier with a multiplication factor of 12 to generate 300-GHz-band terahertz radar system. Input signal at a center frequency of 25 GHz with a chirp bandwidth of 1 GHz and 2 GHz provides 6-GHz and 12-GHz-bandwidth optical signals in 6th-order harmonics. Finally, a frequency separation of +6th- and −6th-order components would be 300 GHz with a chirp bandwidth of 12 GHz and 24 GHz. The technique is capable for high-precision imaging system.

ACKNOWLEDGMENT

The authors would like to thank the Ministry of Internal Affairs and Communications, Japan, for the financial support through the project entitled "Research and development of high-precision imaging technology using 90 GHz band linear cells," and "Research and development on amplifier technology in 300 GHz band, in a part of research and development program on key technology in terahertz frequency bands", funded by the "Research and Development to Expand Radio Frequency Resources".

Long-life Microwave Lighting

Vladimir Danilychev
Quantum Technologies, Irvine, CA 92612, USA

Abstract— Technology of Multi-Lamp Large Area Lighting Systems, based on Microwave Excitation of new Electrodeless Long-Life Lamps is discussed. Critical parameters of Multi-Mode microwave cavities for uniform excitation of many electrodeless lamps are presented. Limitations on output Intensity, available emission Spectra, applications for Visible Lighting, Surface Treatment and UV Curing, related with use of Large Area Multi-Lamp Sources are analized. Experimental results are presented. Technical characteristics and design of Large Area Long-Life Lighting Systems and Electrodeless Microwave Lamps are shown. Pictures of operating Quantum Multi-Lamp microwave Lighting Systems and Electrodeless Microwave Lamps are presented.

Session 3P7
SC3: Strong Light-matter Coupling and Strongly Interacting Photons 2

Quantum Engineering of Light with an Intracavity Rydberg Gas

Erwan Bimbard[1], **Rajiv Boddeda**[1], **Andrey Grankin**[1], **Nicolas Vitrant**[1], **Florence Nogrette**[1], **Valentina Parigi**[1], **Imam Usmani**[1], **Jovica Stanojevic**[1], **Philippe Grangier**[1], **Armand Delavalle**[2], **Quentin Lavigne**[2], **Kilian Müller**[2], **and Alexei Ourjoumtsev**[2]

[1]Laboratoire Charles Fabry, Institut d'Optique, CNRS
Universite Paris-Sud, 2 av. Augustin Fresnel, Palaiseau cedex 91127, France
[2]Jeunes Équipes de l'Institut de Physique du Collège de France
CNRS, 11 place Marcelin Berthelot, 75231 Paris Cedex 05, France

Abstract— Coupling single quantum objects (atoms, ions, quantum dots...) to high-finesse optical resonators is a well-explored route towards strong deterministic photon-photon interactions. Very successful in the microwave regime, this approach is more difficult to implement at optical wavelengths, in particular due to optical losses and to difficulties in obtaining a strong, constant and reproducible light-matter coupling. It has been recently realized that many of these constraints could be lifted by replacing single atoms with strongly interacting atomic ensembles behaving as collective "superatoms" and showing strongly enhanced optical properties. In practice, photons injected in the intracavity atomic gas are converted to atomic polarization waves involving highly excited, strongly polarizable Rydberg atomic states. Their interactions lead to a blockade effect, making atoms located within a $\sim 10\,\mu$m range behave as a single "superatom" which can contain only a single Rydberg excitation but which presents a collectively enhanced coupling to light, allowing to strongly relax the constraints on the cavity geometry and finesse. In this talk I will review the progress accomplished along this line in the last few years in our experiment in Institut d'Optique in Palaiseau. I will then present new research directions we are planning to explore in a new project starting in Collège de France in Paris, which will use specific features of these collective "superatoms", in particular their relatively large spatial extension.

Few-body Physics of Strongly Interacting Photons in a Rydberg Medium

Michael J. Gullans[1], **Mohammad F. Maghrebi**[1], **A. V. Gorshkov**[1], **P. Bienias**[2], **H. P. Büchler**[2], **S. Choi**[3], **O. Firstenberg**[3], **M. D. Lukin**[3], **and I. Martin**[4]

[1]Joint Quantum Institute and Joint Center for Quantum Information and Computer Science NIST/University of Maryland, College Park, Maryland 20742, USA
[2]Institute for Theoretical Physics III, University of Stuttgart, Germany
[3]Physics Department, Harvard University, Cambridge, Massachusetts 02138, USA
[4]Materials Science Division, Argonne National Laboratory, Argonne, Illinois 60439, USA

Abstract— Free space photons can be made to strongly interact by dressing the photons with atomic Rydberg states under conditions of electromagnetically induced transparency. Recently a two-photon bound state was experimentally observed in such systems [1]. Here we develop the full scattering theory for two dark state polaritons and explore the various classes of bound states and scattering states that emerge. We identify previously unexplored parameter regimes where polariton-polariton interactions are repulsive. Furthermore, in the regime of attractive interactions, we identify multiple two-polariton bound states, calculate their dispersion, and study the resulting scattering resonances.

We then focus on the regime where the photonic bound states overlap with the continuum of purely atomic two-body bound states. In this continuum, we find the photonic bound states survive as metastable states whose energy spectrum is governed by the Coulomb problem, thus obtaining a photonic analogue of the hydrogen atom. These states eventually decay into bound pairs of Rydberg atoms, but are long-lived, in analogy to the quantum tunneling of a particle trapped by two potential barriers. Furthermore, we find that these states propagate with a negative group velocity. We demonstrate the metastability and backward propagation of these Coulomb bound states with full numerical simulations and discuss the prospects for experimental preparation and observation of these states.

Finally we discuss the experimental implications of this work and explore the possibility of extending these results to the many-body problem.

REFERENCES

1. Firstenberg, O., et al., *Nature*, Vol. 502, 71, 2013.

Strongly Interacting Rydberg Atoms in Hot Vapours

R. Löw
Universität Stuttgart, Germany

Abstract— Strongly interacting Rydberg atoms have proven to serve as an efficient nonlinear medium, even on the single photon level. The drawback is, that most experiments so far have to rely on ultracold atoms in room filling setups. For a better applicability in terms of size, integratability, power consumption and bandwidth we try to adopt the concepts developed for ultracold atoms for atomic vapours at room temperature in microscopic vapour cells. Our approach is twofold: First we have to understand how the interaction mechanisms among Rydberg states influence the optical properties of the gas at room temperature. Here we have already approved that the van-der-Waals interaction, mandatory for any Rydberg blockade, is flawless up to a excitation bandwidth of 1 GHz for a gas of Rubidium atoms. For Cesium the situation is quite different and a large bandwidth excitation results in a rapid aggregation dynamics of Rydberg states, which we also probe optically. The second line of research is dedicated to the miniaturization and furnishing of vapour cells with various functionalities for optimal coupling to the excitation and probing light fields as well for a direct read out of the Rydberg population by an ionization current. Finally I will report on our recent experiments on atom filled hollow core fibres including electrical contacts.

Spontaneous Phase Coherence of a Statistically Flickering Bose-Einstein Condensate of Light

Julian Schmitt[1], **Tobias Damm**[1], **David Dung**[1], **Christian Wahl**[1], **Frank Vewinger**[1], **Jan Klaers**[1, 2], **and Martin Weitz**[1]

[1]Institut für Angewandte Physik, Universität Bonn, Wegelerstr. 8, Bonn 53115, Germany
[2]Institut für Quantenelektronik, ETH Zurich
Auguste-Picard-Hof 1, Zurich 8093, Switzerland

Abstract— Phase transitions are ubiquitous phenomena in nature, which are most often accompanied by a spontaneous breaking of a system's underlying symmetry, as for example a broken rotational invariance in ferromagnets below the Curie temperature due to global spin alignment. For Bose-Einstein condensates, a spontaneously broken $U(1)$ gauge symmetry causes the selection of an arbitrary, yet extensively coherent phase for the ground-state wave function. Interference experiments present valuable tools for the study of spontaneous symmetry breaking and the first-order coherence of such systems. Here we report a time-resolved study of the heterodyne interference of a Bose-Einstein condensate of photons with a narrowband laser source acting as a phase reference. To prepare the optical Bose-Einstein condensate, we trap photons in an optical microcavity filled with a liquid dye solution, where repeated absorption and re-emission processes lead to a thermal equilibration of the transverse motional degrees of freedom of the photon gas. The reservoir of dye molecular excitations serves as both heat bath and particle reservoir, which allows us to realize a regime with large "grand-canonical" number fluctuations of order of the total photon number. Correspondingly, no second-order coherence emerges, as in a thermal (lamp-type) source. The intensity fluctuations lead to phase jumps in the observed interference signal, with a rate reducing for increasing condensate sizes. Further, by engineering different-sized reservoirs, we can relate first to second-order coherence properties, which are determined by the grand-canonical nature of the photon condensate. Our data, when extrapolated to the thermodynamic limit, demonstrates the emergence of persistent phase coherence, while no second-order coherence emerges in the macroscopically populated, fluctuating photon condensate. This outlines the photon Bose-Einstein condensate under grand-canonical statistical conditions as a novel brilliant light source, distinct from both spectrally filtered thermal light and laser sources, which holds prospects for optical imaging techniques.

REFERENCES

1. Klaers, J., F. Vewinger, and M. Weitz, *Nature Phys.*, Vol. 6, 512, 2010.
2. Klaers, J., J. Schmitt, F. Vewinger, and M. Weitz, *Nature*, Vol. 468, 545, 2010.
3. Schmitt, J., T. Damm, D. Dung, F. Vewinger, J. Klaers, and M. Weitz, *Phys. Rev. Lett.*, Vol. 112, 030401, 2014.
4. Schmitt, J., T. Damm, D. Dung, F. Vewinger, J. Klaers, and M. Weitz, arXiv:1410.5713, 2014.

Strongly Interacting Rydberg Slow Light Polaritons

H. P. Büchler
Institute for Theoretical Physics III, University of Stuttgart, Germany

Abstract— Weak interactions of photons with each other are the basis for many applications of light signals in areas such as optical communication. However, many other applications in classical and quantum communication, computation, and metrology would greatly benefit from tunable photon-photon interactions. Moreover, photon-photon interactions at the level of individual quanta could pave the way to the realization of exotic strongly correlated photonic states. A typical approach to achieve strong two-photon interactions relies on confining photons to high-finesse cavities. An alternative approach towards this goal has recently emerged using Rydberg slow-light polaritons. The key idea is to combine electromagnetically induced transparency (EIT) with the strong interaction between Rydberg atoms. Both phenomena have been well-studied in the past: it has been demonstrated that photons can be slowed down and stored in atomic gases using EIT, while recent experiments on Rydberg atoms have demonstrated the strong interaction and the associated blockade of Rydberg excitations. In the Rydberg-EIT system, a photon entering the atomic gas is converted into a slow-light polariton with a substantial admixture of the Rydberg state. It is the latter admixture that maps the Rydberg-Rydberg interaction onto an effective interaction between slow Rydberg polaritons. Within this approach, a single-photon source and switch was realized, the photon blockade and the formation of bound states of Rydberg polaritons has been demonstrated, and atom-photon entanglement was observed.

Here, we derive the scattering properties and bound-state structure of Rydberg polaritons in one dimension. Our analysis provides a rigorous theoretical framework for analyzing a variety of problems in Rydberg-polariton systems. This framework allows us to analytically derive the effective interaction potential between two Rydberg polaritons and to identify a regime with a purely repulsive interaction. We derive the low-energy scattering length and find the appearance of resonances; we expect the corresponding tunability of the scattering length to play the role that Feshbach resonances play in ultra-cold atomic gases. Moreover, we identify multiple two-polariton bound states for attractive interactions and determine their dispersion relation. In addition, we demonstrate the possibility to design a high fidelity quantum gate between photons, and analytically derive all leading terms reducing the fidelity. A detailed discussion for its experimental realization is provided.

Probing Nanofiber-trapped Atomic Ensembles at the Quantum Level

J. Appel, J.-B. Béguin, H. L. Sørensen, S. L. Christensen, E. Bookjans, K. Kluge, I. Iakoupov, A. Sørensen, J. H. Müller, and E. Polzik
Niels Bohr Institute, University of Copenhagen, Denmark

Abstract— We prepare a mesoscopic ensemble containing a few thousand atoms, trapped in a one-dimensional atomic lattice in the evanescent field of a nanofiber. A dual-color homodyne interferometry method with a pW-power shot noise limited probe is used to measure the atom number. Strong coupling of the evanescent probe guided by the nanofiber allows for a real-time measurement with a precision of 8 atoms on an ensemble of some 10^3 atoms in the one-dimensional trap, we thus demonstrate preparation and detection of an atom number distribution in a one-dimensional atomic lattice with the variance $-14\,\mathrm{dB}$ below the Poissonian noise level. This method is very well suited for generating collective atomic entangled or spin-squeezed states via a quantum non-demolition measurement as well as for tomography of exotic atomic states in a one-dimensional lattice.

We will also present our investigation of reflection off a spatially structured 1-dimensional ensemble: Cesium atoms trapped along the nanofiber are pumped from the $F = 4$ into $F = 3$ hyperfine level by a standing-wave laser pulse, thus generating a Bragg-grating of atoms in different spin states. We coherently probe the reflected field and find coherent reflection from a mirror consisting of only about 100 atoms, well exceeding the incoherent backscattering of a many times bigger ensemble. Using a dual-color Raman field for coherent dark-state preparation of the spatial spin structure, the influence of motional effects can be mitigated.

Cold Atoms Coupled to Photonic Crystals: A Platform for Non-local Non-linear Optics

J. S. Douglas, **T. Caneva**, **and D. E. Chang**
ICFO-Institut de Ciencies Fotoniques, Castelldefels 08860, Spain

Abstract— At optical frequencies photons do not interact with one another in free space. While this facilitates faithful information transfer using photons, it also restricts the possible physics and applications that can be realized using photons alone. To overcome this limitation various systems have been realized where the photons are coupled to atoms, using for example cavities [1] or atomic ensembles [2]. Effective interactions can then be achieved between photons as a result of the particular properties of the atoms. One particularly successful method to induce photonic interactions is to use atomic media that support electromagnetically induced transparency (EIT). In these systems the photonic degrees of freedom can be mapped to atomic ones which may then interact with each other. The photonic interaction is then constrained by the type of interaction that can be achieved between the atoms.

Experiments utilizing EIT media have focused on achieving the required atomic interaction via Rydberg excitation of atoms [2–4]. However, Rydberg interactions typically yield step-like potentials where the strength is coupled to the interaction length scale, limiting the range of phenomena that can be produced. Instead we propose to use the new platform of atoms trapped near photonic crystal waveguides that has been developed in recent experiments [5, 6]. In these systems the presence of an atom near the photonic crystal can induce a cavity mode around the atomic position, and when multiple atoms are trapped the atoms can interact dynamically via these induced cavities. In particular the interactions between the atoms are highly tunable and can be coherent over length scales of the order of one hundred optical wavelengths [7]. Using these systems interactions can then be actively designed between photons allowing, for example, molecular-like bound states of photons.

REFERENCES

1. Birnbaum, K. M., et al., "Photon blockade in an optical cavity with one trapped atom," *Nature*, Vol. 436, 87–90, 2005.
2. Pritchard, J. D., et al., "Cooperative atom-light interaction in a blockaded rydberg ensemble," *Phys. Rev. Lett.*, Vol. 105, 193603, 2010.
3. Peyronel, T., et al., "Quantum nonlinear optics with single photons enabled by strongly interacting atoms," *Nature*, Vol. 488, 57–60, 2012.
4. Firstenberg, O., et al., "Attractive photons in a quantum nonlinear medium," *Nature*, Vol. 502, 71–75, 2013.
5. Goban, A., et al., "Atom-light interactions in photonic crystals," *Nat. Commun.*, Vol. 5, 3808, 2014.
6. Yu, S.-P., et al., "Nanowire photonic crystal waveguides for single-atom trapping and strong light-matter interactions," *Applied Physics Letters*, Vol. 104, 111103, 2014.
7. Douglas, J. S., et al., "Quantum many-body models with cold atoms coupled to photonic crystals," ArXiv e-prints, 1312.2435, 2013.

Single Molecules as Bright & Narrow-band Single Photon Sources

Mohammad Rezai[1], **Wilhelm Kiefer**[1], **Jörg Wrachtrup**[1, 2], **and Ilja Gerhardt**[1, 2]

[1]3. Physics Institute, University of Stuttgart, Pfaffenwaldring 57, Stuttgart 70569, Germany
[2]Max Planck Institute for Solid State Research, Heisenbergstr. 1, Stuttgart 70569, Germany

Abstract— Single photon sources based on single molecules under cryogenic conditions can be extremely bright and narrow-band. We introduce a single photon source based in dibenzanthanthrene which is spectrally matched to atomic sodium.

Introduction: Single organic dye molecules allow to serve as high-brightness single photon sources [1]. Among other candidates, dibenzanthahthrene [2] (DBATT) emits in the yellow/red part of the visible spectrum and shows its optimal properties under cryogenic conditions below $T = 2\,\mathrm{K}$. Under these conditions, the molecules do not bleach or blink and the molecules can be used for an indefinite time. The organic host matrix in conjunction with a solid immersion lens (SIL) allows for an efficient extraction of the photons [3]. Commonly more than 1.000.000 clicks on a normal silicon based avalanche photo diode can be detected.

Not only that a high fraction of the emitted photons can be collected — the emission can also be spectrally narrow-band and corresponds to the lifetime limited value. With the molecule dibenzanthanthrene, we observe spectral linewidths down to 12.5 MHz [2, 4]. Commonly, below 20 MHz emission is detected. The presented single photon source represents a very high spectral brightness, and we detect up to 100.000 clicks per second and Megahertz. We are not aware of other sources which exhibit comparable spectral flux.

Since the center of the molecular inhomogeneous band coincides nicely with the D-lines of atomic sodium ($\approx 589\,\mathrm{nm}$), we are able to spectrally select a single molecule to match with atomic sodium. Experiments with slow single photons in atomic vapor have been performed [5]. If a molecule is bright and well-behaved, but slightly shifted against the sodium transitions, we are able to apply an electric field [6] and detune the emitter by several GHz. This allows to "fine-tune" a molecule to match exactly to a desired sodium transition.

To suppress background emission from the host matrix and other emitters, we are able to filter the photons from the molecule with an atomic filter. These Faraday anomalous dispersion optical filters [7] (FADOFs) allow to discriminate the wanted single photon emission from the background and guarantee that the emission matches the atomic transition. We will outline our current efforts to use Faraday filters in conjunction with single photon sources [8].

We will discuss prospects how to generate higher order Fock-states and triggered photons on demand from our source.

REFERENCES

1. Lounis, B. and M. Orrit, "Single-photon sources," Reports on Progress in Physics, Vol. 68, 1129, 2005.
2. Boiron, A.-M., et al., "Single molecules of dibenzanthanthrene in n-hexadecane," *The Journal of Chemical Physics*, Vol. 105, 3969–3974, AIP, 1996.
3. Lee, K., et al., "A planar dielectric antenna for directional single-photon emission and near-unity collection efficiency," *Nature Photonics*, Vol. 5, 166–169, Nature Publishing Group, 2011.
4. Lettow, R., et al., "Realization of two fourier-limited solid-state single-photon sources," *Opt. Express*, Vol. 15, 15842–15847, OSA, 2007.
5. Siyushev, P., et al., "Molecular photons interfaced with alkali atoms," *Nature*, Vol. 509, 66–70, Nature Publishing Group, a division of Macmillan Publishers Limited, All Rights Reserved, 2014.
6. Orrit, M., et al., "Stark effect on single molecules in a polymer matrix," *Chemical Physics Letters*, Vol. 196, 595–600, 1992.
7. Dick, D. J. and T. M. Shay, "Ultrahigh-noise rejection optical filter," *Opt. Lett.*, Vol. 16, 867–869, OSA, 1991.
8. Kiefer, W., et al., "The Na-Faraday filter: The optimum point," Scientific Reports, 2014.

Exciton-polariton Interactions in 0D Confinement

Thomas Fink[1], **Christian Schneider**[2], **Sven Höfling**[1], **and Ataç Imamoğlu**[1]

[1]Institute of Quantum Electronics, ETH Zürich, CH-8093 Zürich, Switzerland
[2]Technische Physik, Universität Würzburg, D-97074 Würzburg, Germany

Abstract— Exciton-polaritons not only exhibit fascinating physical properties such as nonlinearities, superfluidity, and Bose-Einstein condensation at elevated temperatures, but also offer ease of tailoring their potential landscape, which makes them promising candidates for quantum simulation applications. However, all experiments to date can be described using a mean-field approach. Consequently, it has been a long-standing goal to demonstrate single-particle nonlinearities in these systems through the observation of polariton blockade [1].

To do so, one requires long polariton lifetimes τ (i.e., spectrally narrow quantum well excitons and a high-Q cavity), and strong lateral confinement of the photonic mode to achieve a sizable exciton-exciton interaction E_{nl}. For $1/\tau \sim E_{nl}$, one then expects to see a reduction of the probability to find two photons at a time in the cavity, which is heralded by light leaking out of the cavity exhibiting photon antibunching. Introducing high-quality quantum well samples and the latest generation of home-made fibers into our semi-integrated fiber cavity approach [2], we measure photon correlations. The tunability of our semi-integrated system also allows us to investigate biexciton Feshbach resonance [3] which may be used to enhance polariton interactions.

REFERENCES

1. Verger, A., C. Ciuti, and I. Carusotto, *Phys. Rev. B*, Vol. 73, 193306, 2006.
2. Besga, B., et al., *Phys. Rev. Applied*, Vol. 3, 014008, 2015.
3. Takemura, N., et al., *Phys. Rev. B*, Vol. 90, 195307, 2014.

Single-photon Routing in Strongly Interacting Ensembles

Callum Murray
Max Planck Institute for the Physics of Complex Systems, Dresden, Germany

Abstract— The coherent coupling of photons to strongly interacting Rydberg states, via electromagnetically induced transparency, has recently emerged as a promising approach to photon-photon interactions acting on the level of single light quanta. The central idea is to enhance and mediate optical nonlinearities via the long ranged interactions of the matter system. The tuneability in interaction characteristics of this setting in turn renders it pertinent to a broad range of applications in quantum information processing, from realizing quantum phase gates to all-optical transistors. However, the optical nonlinearities typically are reliant on the ability to break EIT conditions, rendering the emergent photonic interactions intrinsically dissipative and imposing substantial limitations on the fidelity of quantum operations.

In this talk, I will describe a new approach to photonic quantum logic based on an interaction induced reflection of light to serve as a quantum router. Our scheme leverages on the modification of EIT conditions, rather than breaking them, to yield a nonlinearity that is well suited to performing high fidelity gate operations or coherent optical switching in strongly interacting atomic ensembles.

Photonic Quantum Gates via Rydberg States of Atoms in Microwave Resonators and Waveguides

David Petrosyan
Institute of Electronic Structure & Laser
Foundation for Research and Technology — Hellas, Heraklion, Crete GR-71110, Greece

Abstract— I will describe several techniques employing electromagnetically induced transparency in cold atomic media and long-range interactions between the highly-excited Rydberg states of atoms to achieve strong interactions and high-fidelity quantum gates between single photon qubits.

Electromagnetically induced transparency [1] is a quantum interference effect in which an application of a coherent control field to a resonant atomic medium dramatically reduces the absorption of a weak probe pulse accompanied by a steep dispersion. The probe pulse, upon entering the medium, is transformed into the so-called dark-state polariton — a superposition of light and matter degrees of freedom — which propagates with greatly reduced group velocity. With the ladder configurations of atomic levels, whereby the control field couples near-resonantly the intermediate excited state of atoms to the Rydberg state, such polaritons contain a large admixture of the Rydberg states. These Rydberg states can exhibit long-range, dipole-dipole interactions [2] which translate into strong absorptive or dispersive interactions between the polaritons.

In this talk, I will describe two schemes realizing dispersive interactions between the Rydberg states of atoms. In the first scheme [3], a pair of quantum fields counter-propagating in a hollow-core waveguide filled with the atoms, undergo a conditional phase shift corresponding to the action of the dipole-dipole interaction between the Rydberg components of the two colliding polaritons.

In the second scheme [4], two or more atomic ensembles are trapped above the surface of a coplanar waveguide resonator whose microwave modes near-resonant with the transitions between the neighboring Rydberg states of atoms can mediate effective ultra-long range resonant (Förster) or non-resonantly (van der Waals) dipole-dipole interactions between any pair of atoms within the resonator mode. The Forster, or blockade, regime can be used to create single photonic excitations within one or more atomic ensemble, while the van der Waals regime can be employed to induce a conditional phase shift upon a pair of single-photon pulses each propagating or stored in a different atomic ensemble.

By properly choosing the group velocities of the polaritons and thereby their interaction time, the conditional phase shift can be made spatially uniform and equal to pi, corresponding to a high-fidelity CPHASE gate between the single-photon qubits.

REFERENCES

1. Fleischhauer, M., A. Imamoglu, and J. P. Marangos, *Rev. Mod. Phys.*, Vol. 77, 633, 2005.
2. Saffman, M., T. G. Walker, and K. Mølmer, *Rev. Mod. Phys.*, Vol. 82, 2313, 2010.
3. Shahmoon, E., G. Kurizki, M. Fleischhauer, and D. Petrosyan, *Phys. Rev. A*, Vol. 83, 033806, 2011.
4. Petrosyan, D. and M. Fleischhauer, *Phys. Rev. Lett.*, Vol. 100, 170501, 2008.

Bistability in a Strongly Driven Rydberg Gas

N. Šibalić[1], C. G. Wade[1], T. Pohl[2], C. S. Adams[1], and K. J. Weatherill[1]

[1]Joint Quantum Centre (JQC) Durham-Newcastle, Department of Physics
Durham University, Durham DH1 3LE, UK
[2]Max Planck Institute for the Physics of Complex Systems, Nöthnitzer Strasse 38, Dresden 01187, Germany

Abstract— Nonlinear optical processes involving highly-excited Rydberg gases have become a topic of great interest in recent years [1]. Recently, we experimentally demonstrated a nonequilibrium phase transition in a dilute thermal Cs atomic gas [2]. The system was driven strongly with a resonant three-photon excitation scheme [3]. The observed phase transition, between states of low and high Rydberg occupancy, is induced by resonant dipole-dipole interactions between Rydberg atoms and can be observed in both transmission and fluorescence measurements. In the frequency domain, we observe a shift of the Rydberg state which results in intrinsic optical bistability above a critical Rydberg number density. In the time domain, we observe critical slowing down where the recovery time to system perturbations diverges with critical exponent $\alpha = -0.53 \pm 0.10$. The atomic emission spectrum of the phase with high Rydberg occupancy provides evidence for a superradiant cascade.

We create a toy model of the system by investigating the dynamics of a driven-dissipative ensemble of interacting two-level systems with random spatial distribution. Using rate-equation Monte Carlo modelling, we observe the emergence of metastable states, producing a bistable response, as the spatial extent of the long-range pair-wise interactions is increased. The importance of the range of interactions is explored through disappearance of bistability in the 3D to 2D crossover. Mixing within the system, due to atomic motion, stabilises the excited state, increasing overall hysteresis. We explain these observations in terms of long-range insensitivity to shot-noise, corresponding to the mean field used in simplified models. We believe that these results are consistent with other recent Rydberg experiments on cold atoms where bimodal behaviour is observed [4, 5].

REFERENCES

1. Pritchard, J. D., et al., "Nonlinear optics using cold Rydberg atoms," *Ann. Rev. Cold. Atm. Mol.*, Vol. 1, 301, 2013.
2. Carr, C., et al.. "Three-photon electromagnetically induced transparency using Rydberg states," *Opt. Lett.*, Vol. 118, 3858, 2012.
3. Carr, C., et al., "Nonequilibrium phase transition in a dilute Rydberg ensemble," *Phys. Rev. Lett.*, Vol. 111, 113901, 2013.
4. Malossi, N., et al., "Full counting statistics and phase diagram of a dissipative Rydberg gas," *Phys. Rev. Lett.*, Vol. 113, 023006, 2014.
5. Schempp, H., et al., "Full counting statistics of laser excited Rydberg aggregates in a one-dimensional geometry," *Phys. Rev. Lett.*, Vol. 112, 013002, 2014.

Achieving Single-shoton Nonlinearities with an Intracavity Rydberg Medium

I. Usmani[1], **R. Bodedda**[1], **E. Bimbard**[1], **A. Grankin**[1], **E. Brion**[2], **A. Ourjoumtsev**[1], **and P. Grangier**[1]

[1]Laboratoire Charles Fabry, Institut d'Optique, CNRS/Universite Paris-Sud, Palaiseau, France
[2]Laboratoire Aimé-Cotton, CNRS/Universite Paris-Sud/ENS-Cachan, Palaiseau, France

Abstract— The realization of a strong and deterministic photon-photon interaction is a challenging task, but could enable the implementation of a two-photon phase gate or the generation of non-classical states of light. The standard nonlinearities in conventional optical media are however too weak to induce such effects. One approach to create single-photon nonlinearities is to temporally convert the photons into dark-state polaritons involving Rydberg atoms [1]. The principle is that a single Rydberg excitation may modify strongly the susceptibility of a small region, thanks to Rydberg blockade [2].

Recent experiments, implemented in an ultracold cloud of ^{87}Rb atoms held in an optical dipole trap, demonstrated nonlinearities at the quantum level, such as it creates a medium transparent for single-photons, but is absorptive for photon pairs [3, 4]. This effect was used to create an attractive potential between photons [5] and single-photon switches [6, 7].

Here, our atomic cloud is placed into a one-ended low finesse optical cavity which amplifies the nonlinear effects [8]. We are also able to perform second-order correlation measurements and homodyne detections of the outgoing field [9].

We will present our current efforts to observe nonlinear effects at the single-photon level. This includes the implementation of a dipole trap to increase the atomic density, or increasing the cavity finesse and its concentricity. We aim at observing bunching or anti-bunching of light and phase jumps induced by Rybderg excitations in our intracavity cloud.

REFERENCES

1. Pritchard, J. D., et al., *Annu. Rev. of Cold Atoms and Molecules*, 301–350, 2013.
2. Lukin, M. D., et al., *Phys. Rev. Lett.*, Vol. 87, 037901, 2001.
3. Peyronel, T., et al., *Nature*, Vol. 488, 57, 2012.
4. Dudin, Y. O., et al., *Science*, Vol. 336, 887, 2012.
5. Firstenberg, O., et al., *Nature*, Vol. 502, 71, 2013.
6. Tiarks, D., et al., *Phys. Rev. Lett.*, Vol. 113, 053602, 2014.
7. Gorniaczyk, H., et al., *Phys. Rev. Lett.*, Vol. 113, 053601, 2014.
8. Parigi, V., et al., *Phys. Rev. Lett.*, Vol. 109, 233602, 2012.
9. Bimbard, E., et al., *Phys. Rev. Lett.*, Vol. 112, 033601, 2014.

Strongly Interacting Rydberg Polaritons in Optical Cavities

Ariel Sommer, **Nathan Schine**, **Ningyuan Jia**,
Albert Ryou, **Alex Georgakopoulos**, **and Jonathan Simon**
University of Chicago, USA

Abstract— Quantum materials of strongly-interacting photons will allow novel quantum simulation studies of many-body systems. In particular, photonic materials are well suited to studying long range interactions, strong gauge fields, and driven open quantum systems. We describe a novel platform for realizing a photonic many-body system using Rydberg polaritons in degenerate optical cavities.

Degenerate optical cavities provide a flexible platform to engineer photon dynamics, while electromagnetically induced transparency (EIT) using a Rydberg level induces strong interactions between polaritons. We show that photons in nearly-degenerate optical cavities can be described as massive particles in two dimensions subject to an applied potential. When a Rydberg EIT medium is included in the cavity, the dark polariton modes inherit the properties of the underlying cavity modes, but with an increased effective mass and a reduced effective trapping frequency, analogous to the reduced group velocity in free space EIT. The strong interaction between Rydberg atoms induces a strong interaction between the dark polaritons. At large distances, the polariton-polariton interaction retains the form of the Rydberg-Rydberg interaction, while at short distances the interaction saturates due to detuning from the EIT condition. The long range of the interaction gives access to a quantum phase transition to a crystal, allowing novel studies of quantum crystallization in an open system.

We describe progress on realizing Rydberg EIT and single photon nonlinearity in a high-finesse optical cavity. Additionally, we demonstrate an optical cavity that induces an effective magnetic field for photons and is compatible with the proposed Rydberg EIT setup. Strongly-interacting Rydberg polaritons subject to an effective magnetic field give access to fractional quantum Hall states, which are of great interest for quantum simulation.

Cavity Design and Mode Analysis in Woodpile Based Three-dimensional Photonic Crystals

X. Zheng, Y.-L. D. Ho, L. Chen, M. P. C. Taverne, and J. G. Rarity
Merchant Ventures Building, Department of Electrical and Electronics Engineering
University of Bristol, UK

Abstract— In a three dimensional (3D) photonic crystal (PhC) structure with an embedded defect cavity, the cavity mode is strongly associated with the surrounding environment which results in a variety of mode field distributions [1–3]. Inspired by comparing the woodpile lattice with the diamond lattice, here we present a cavity design which supports well confined Gaussian-like cavity modes in a woodpile based 3D PhC structure. By carefully choosing the position of the defect, we can create a cavity with high symmetry and tune the cavity mode with desired order and frequency by adjusting its size. Defects at this position show clearly defined mode orders simplifying analysis.

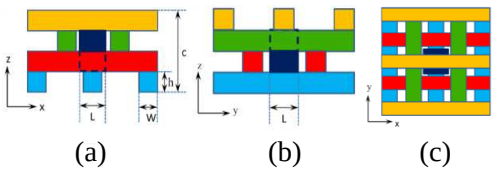

Figure 1: The location of the cavity in one vertical period (four stacking layers in z axis). (a) View of x-z plane, (b) view of y-z plane, and (c) view of the x-y plane (from the top).

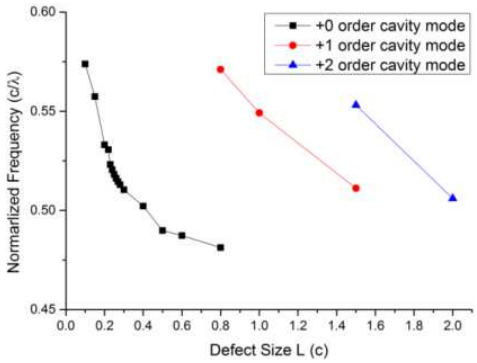

Figure 2: Normalized resonant frequency as a function of cavity size L/c.

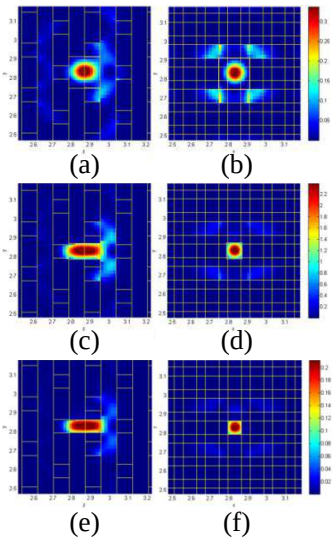

Figure 3: 3. Energy distribution of cavity modes when cavity size (a), (b) $L = 0.5c$, (c), (d) $L = 0.25c$, (e), (f) $L = 0.2c$. (a), (c), (e) View of y-z plane, (b), (d), (f) view of x-y plane. Due to the symmetry of x-z plane and y-z plane, only views of y-z plane and x-y plane are shown.

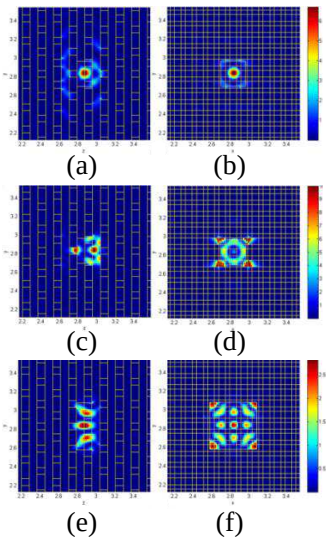

Figure 4: Energy distribution of cavity modes. Resonant mode at (a), (b) normalized frequency 0.48 when $L = 0.8c$; (c), (d) normalized frequency 0.57 when $L = 0.8c$; (e), (f) normalized frequency 0.55 when $L = 1.5c$. (a), (c), (e) View of y-z plane, (b), (d), (f) view of x-y plane

The cavity is formed by introducing a cube defect between two adjacent layers (2nd and 3rd) in one vertical period c (Fig. 1). L is the size of the cavity in x-y plane while the height of cavity is $2h$ (two rod heights) to make it connect with rods in 1st layer and 4th layer. In both 2nd layer and the 3rd layer, the centre of the cavity is also between two adjacent rods in plane. The position of the defect shown in this paper is thus located at the centre of the FCC lattice, the most symmetrical position. The refractive indices of woodpile and cavity are $n = 3.3$, and background material is air.

The calculated cavity modes with resonant frequencies are obtained by using our in house finite-difference time-domain (FDTD) software. When changing the size of the cavity L from $0.1c$–$2c$ (Fig. 2) the resonant frequency traverse the bandgap region. Variation of Q-factor and mode volume will be presented at the conference. The energy distribution in cavity modes can be seen in (Fig. 3) showing Gaussian like modes. Finer confinement and smaller mode volume can be achieved on reducing L from $0.5c$ to $0.2c$. Two resonant modes coexist in the cavity when $L = 0.8c$ and $L = 1.5c$. Energy distributions of each cavity mode are shown (Fig. 4). Due to the symmetry of x-z plane and y-z plane, only views of y-z plane and x-y plane are shown. The corresponding mode numbers 0, 1, 2 can be distinguished.

We will also present preliminary fabrication results towards woodpile photonic crystals with embedded cavities using our direct laser writing (DLW) system [4] and preliminary progress on simulation and fabrication method for introducing emitter inside low-refractive index cavities.

REFERENCES

1. Woldering, L. A., et al., "Design of a three-diamensional photonic band gap cavity in a diamondlike inverse woodpile photonic crystal," *Physics Review B*, Vol. 90, 115140, 2014.
2. Ho, Y.-L. D., et al., "FDTD simulation of inverse three-dimensional face-centered cubic photonic crystal cavities," *IEEE J. Quantum Electron.*, Vol. 47, 1480–1492, 2011.
3. Taverne, M. P. C., et al., "Investigation of defect cavities formed in three-dimensional photonic crystals," *J. Opt. Soc. Am. B*, Vol. 32, arXiv: 1409.4209, Quant.-Ph., 2015, in Press.
4. Chen, L.-F., et al., "First evidence of near-infrared partial photonic bandgap in polymeric rod-connected diamond structure," *Physics Optics*, arXiv: 1501.03741, 2015.

Session 3P8a
SC2: Active, Tunable and Nonlinear Metamaterials 1

Dynamic Digital Metamaterials for Single Pixel Imaging Systems

Willie J Padilla
Department of Electrical and Computer Engineering, Duke University, Durham, NC, USA

Abstract— Focal plane arrays form the foundation for the vast majority of imaging systems. However, at wavelengths of 10 μm and longer, it becomes difficult, expensive, and/or impractical to form focal plane arrays for imaging. Single pixel cameras are an alternative method for imaging where cost, size or efficiency rule out use of focal plane arrays. A common implementation of the single pixel camera uses a spatial light modulator (SLM) to multiplex various portions of the image. The multiplexed image is sent to a detector and the measurement is repeated a number of times — usually equal to the desired resolution. Commercially available SLMs are based on either liquid crystals or digital mirror devices. Thus these devices may be modulated only to a few kHz and provide little control of the type of modulation available, i.e., usually only phase and amplitude modulation are offered.

Metamaterial spatial light modulators provide advanced functionality compared to commercially available devices. Here we present metamaterial based spatial light modulators which provide the ability to digitally encode images thus permitting high speed high fidelity images. Images are encoded as the coefficients of the Hadamard matrix which provides the best possible signal to noise single pixel imaging system possible. We also explore the related S-matrix for single pixel imaging and additionally utilizes compressive sensing techniques to increase imaging frame rate. Lastly we highlight the ability of metamaterials to realize hyperspectral, polarimetric, and phase sensitive imaging.

Unlocking the Potential of Liquid Crystals as a Functional Component of Active Metamaterials

V. A. Fedotov[1], **O. Buchnev**[1], **J. Wallauer**[2], **N. Podoliak**[1], **M. Kaczmarek**[3], **M. Walther**[2], **and N. I. Zheludev**[1, 4]

[1]Optoelectronics Research Centre, University of Southampton, SO17 1BJ, UK
[2]Department of Molecular and Optical Physics, University of Freiburg, D-79104, Germany
[3]School of Physics and Astronomy, University of Southampton, SO17 1BJ, UK
[4]Centre for Disruptive Photonic Technologies, Nanyang Technological University, 637371, Singapore

Abstract— Metamaterials have rapidly advanced over the past decade and are now expected to have major impact across the entire range of technologies where electromagnetic radiation is used. The current effort in the field is being focused on implementing the idea of active and tuneable metamaterials, a generation of artificial photonic media with dynamically controlled optical properties. The latter should enable to dramatically expand the range of the potential applications of the metamaterials making them the fundamental base of future photonic devices.

The control in such metamaterials is commonly achieved by hybridising their fabric with naturally available functional (e.g., nonlinear, phase change or gain) materials. Among such materials, liquid crystals (LCs) possess arguably the strongest and most broadband optical nonlinearity and birefringence, which can be externally controlled by temperature, light, and electric or magnetic fields. That has made liquid crystals one of the first and most popular ingredients of active metamaterial designs.

Although the refractive index changes characteristic to liquid crystals are extraordinarily large, the expected tuneability of the hybrid metamaterial response is still too modest for some of real-world applications, while in practice the efficiency of the tuning is further reduced due to strong surface anchoring of LC-molecules. The latter, in particular, presents a serious challenge for engineering nano-structured LC-loaded metamaterials operating in the visible and near-IR spectral ranges. In this talk we will discuss various strategies that may help to realize the full potential of electrically-controlled liquid crystals, and will illustrate their practical implementation in active metamaterial hybrids.

Voltage-tunable Hybrid Plasmonic Nanostructures

M. V. Gorkunov, S. P. Palto, M. I. Barnik,
V. V. Artemov, N. M. Shtykov, A. R. Geivandov, and S. G. Yudin
A. V. Shubnikov Institute of Crystallography, Russian Academy of Sciences, Moscow 119333, Russia

Abstract— We demonstrate the electro-optical switching of hybrid plasmonic-liquid crystal structures consisting of subwavelength interdigitated aluminum slit gratings covered with a layer of nematic liquid crystal. We report the switching times of 10 ms and switching voltages of 4–8 volts and discuss the possibilities of further functionality improvements.

Optical properties of subwavelength arrays of metal particles, holes and slits are determined by an interplay of various resonant phenomena: surface plasmon resonances (localized and traveling) [1], Fabry-Perot guided mode resonances [2], Rayleigh and Wood anomalies, etc.. Combining plasmonic metal nanostructures with liquid crystals (LC) and semiconductors one can exploit the high sensitivity of the resonances to adjacent environment and create hybrid materials tunable by temperature, irradiation, fields and voltage [3].

We report the results of fabrication and electro-optical characterization of hybrid plasmonic-LC structures consisting of aluminum subwavelength slit gratings (see Fig. 1(a)) used as interdigitated electrodes that reorient the nematic LC upon voltage applied. Gratings with a period of 330 nm and slit widths of 130 nm (G_1) and 165 nm (G_2) were prepared by focused ion beam (FIB) milling of 80 nm thick aluminum layers thermally sputtered on glass substrates. We report the characteristic switching times of the order of 10 ms and demonstrate that voltages of 4–8 V are sufficient for the electro-optical switching (see Figs. 1(b) and 1(c)), which is in line with our theoretical estimates [3]. We discuss the prospects of employing solid state ingredients (e.g., transparent semiconductors) to speed up the switching and improve the performance.

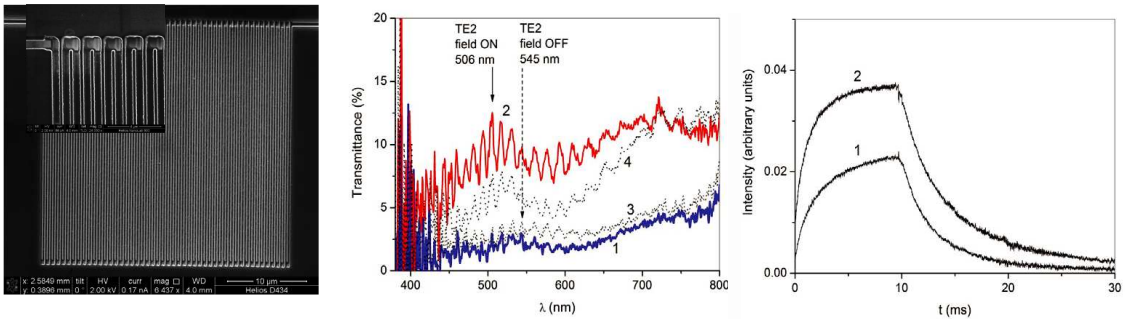

Figure 1: (a) SEM images of interdigitated grating G_2 milled by FIB in Al film; (b) TE transmission spectra of the gratings G_1 (1, 2) and G_2 (3, 4) in nematic LC cell between crossed polarizers in the field-OFF (lines 1, 3) and field-ON (lines 2, 4; $U = 8$ V) states; (c) Time-resolved transmission of the hybrid cell between crossed polarizers for the voltages of 4 V (1) and 8 V (2) applied from 0 to 10 ms.

ACKNOWLEDGMENT

The work was supported by the Russian Foundation for Basic Research (project 13-02-12151 ofi_m). We are grateful to IC RAS Shared Research Center supported by the Russian Ministry of Education and Science (project RFMEFI62114X0005) for the equipment provided.

REFERENCES

1. Genet, C. and T. W. Ebbesen, "Light in tiny holes," *Nature*, Vol. 445, 39–46, 2007.
2. Sturman, B., E. Podivilov, and M. Gorkunov, "Theory of extraordinary light transmission through arrays of subwavelength slits," *Phys. Rev. B*, Vol. 77, 075106-1–075106-12, 2008.
3. Gorkunov, M. V., A. E. Miroshnichenko, and Yu. S. Kivshar, "Metamaterials tunable with liquid crystals," *Nonlinear, Tunable and Active Metamaterials*, Vol. 200, 237–253, I. V. Shadrivov, et al., ed., Springer Series in Materials Science, Springer Int. Pub., 2015.

Multi-stablility and Switching in Superconducting Metamaterials

P. Jung[1], **S. Butz**[1], **and A. V. Ustinov**[1, 2]

[1]Physikalisches Institut, Karlsruhe Institute of Technology, Karlsruhe D-76128, Germany
[2]National University of Science and Technology MISIS, Leninsky prosp. 4, Moscow 119049, Russia

Abstract— We will review our recent experimental studies on ultra-low loss electromagnetic medium comprised of networks of compact superconducting resonators employing SQUIDs as nonlinear tunable meta-atoms.

The design flexibility of superconducting thin-film resonators and circuits allows for utilizing small structures down to the nanoscale while maintaining low loss properties, very strong and well-controlled nonlinearity, and frequency tunability in the microwave and mm-wave frequency range [1]. This approach opens up an opportunity to develop superconducting metamaterials with non-trivially tailored electromagnetic properties, which can be functionalized as ultra-compact resonant magnetic dipole arrays [2, 3], which resonance frequency is widely tunable by varying external dc magnetic field.

Superconducting QUantum Interference Devices (SQUIDs) are implemented as superconducting loops interrupted by Josephson junctions. Recently, we discovered very peculiar multi-stability of SQUIDs in relatively strong ac magnetic fields [4]. In this regime, nonlinear SQUID metamaterials operate as optically switchable microwave propagation media. The nonlinear effects occur in the circuits containing SQUIDs at the high level of the RF-induced current, comparable to the critical current of Josephson junctions. We studied nonlinear properties of SQUIDs integrated into a coplanar waveguide. High microwave currents in the waveguide result in the inductance of the critical current becoming dependent on the instantaneous value of the signal current in the ring. Furthermore, strong microwave driving of a Josephson junction leads to a bifurcation on the lower side of its intrinsic resonance (Josephson plasma resonance). Using a single junction this dynamic bifurcation has been employed to implement a Josephson bifurcation amplifier. The strongly driven Josephson junction enters the bi-stable regime with two stable non-dissipative dynamical states, which differ by both amplitude and phase. The low-amplitude state oscillates nearly in phase with the driving signal, while the high-amplitude state is characterized by the phase shifted approximately by π.

A SQUID-based metamaterial can be operated in a similar multi-stable manner, for which the in-phase response corresponds to positive magnetic permeability χ and the out-of-phase response translates into having χ negative. For properly chosen driving frequency and power, these states are stable and switching between them achieved by changing the driving power or frequency. As these two states with $\chi > 0$ and $\chi < 0$ are both locally stable for a given set of driving signal parameters, they may coexist in a way that some part of meta-atoms oscillate at phase close to π and another part at phase close to 0. Having these groups of meta-atoms mixed together and randomly distributed in the metamaterial should produce kind of birefringence for waves incident on such a metamaterial. Once the two parts are separated by design parameters, they will form an interface between two metamaterials, one with positive and another with negative permeability.

ACKNOWLEDGMENT

This work was supported by the Ministry for Education and Science of Russian Federation under contract No. 11.G34.31.0062 and in the framework of Increase Competitiveness Program of the National University of Science and Technology MISIS under contract No. K2-2014-025.

REFERENCES

1. Jung, P., A. V. Ustinov, and S. M. Anlage, *Supercond. Sci. Techn.*, Vol. 27, 073001, 2014.
2. Jung, P., S. Butz, S. V. Shitov, and A. V. Ustinov, *Appl. Phys. Lett.*, Vol. 102, 062601, 2013.
3. Butz, S., P. Jung, L. V. Filippenko, V. P. Koshelets, and A. V. Ustinov, *Opt. Express*, Vol. 21, 22540, 2013.
4. Jung, P., S. Butz, M. Marthaler, M. V. Fistul, J. Leppaekangas, V. P. Koshelets, and A. V. Ustinov, *Nature Communs.*, Vol. 5, 3730, 2014.

A Tunable Flat Lens via Meta-fluidic-materials

Ai-Qun Liu[1], **Din Ping Tsai**[2], **Nikolay Zheludev**[3], **and Federico Capasso**[4]

[1]School of Electrical & Electronic Engineering
Nanyang Technological University, Singapore
[2]Department of Physics, National Taiwan University, Taiwan
[3]Optoelectronics Research Centre
University of Southampton, Highfield, Southampton, UK
[4]School of Engineering and Applied Sciences
Harvard University, Cambridge, Massachusetts 02138, USA

Abstract— Meta-fluidic-materials aim at manipulating light and metal-liquid flow in the microchannel and exploiting their interaction to create highly versatile devices have received significant scientific interests in many areas. The novelties of the integrated meta-fluidic-material are two-fold. First, metal-fluids can be used to carry substances for analysis in highly sensitive optical micro-devices. Second, metal-fluids can also be exploited to control light, making them tunable, reconfigurable and adaptive. In this paper, the state-of-the-art of meta-fluidic-material research is reviewed with breakthrough innovations in optical and photonic devices, including the high potential applications of meta-fluidic-material in biophysical, biochemistry and biomedical studies [1–3].

Meta-fluidic-materials represents a new paradigm for designing light-manipulating devices, such as cloaks, transformation optics and field concentrators, through the engineering of electromagnetic space using materials with spatially variable parameters. Here we report for the first time a proof-of-principle demonstration of a planar metamaterial where resonant properties of every individual metamolecule can be continuously controlled at will. This work provides new insight into the unique optical properties of meta-fluidic devices and their potential applications [4–6].

Meta-fluidic-material is not only to change the material properties through tuning or reconfiguring the unit element structure size or shapes, which is changed by the metal-liquid flow in the microchannel. It is significant breakthrough research for the meta-fluidic-material to demonstrate new materials with new physics phenomena that are never been observed before. In the paper, the different types of meta-fluidic-material will be presented with some future industry applications.

REFERENCES

1. Liu, A. Q., H. J. Huang, L. K. Chin, Y. F. Yu, and X. C. Li, "Label-free detection with micro-opto-fluidic systems (MOFS): A review," *Anal. Bioanal. Chem.*, Vol. 391, 2443–2452, 2008.
2. Yang, Y., A. Q. Liu, L. Lei, L. K. Chin, C. D. Ohl, Q. J. Wang, and H. S. Yoon, "A tunable 3D optofluidic waveguide dye laser via two centrifugal Dean flow streams," *Lab on a Chip*, Vol. 11, 3182–3187, 2011.
3. Yang, Y., A. Q. Liu, L. K. Chin, X. M. Zhang, D. P. Tsai, C. L. Lin, C. Lu, G. P. Wang, and N. I. Zheludev, "Optofluidic waveguide as a transformation optics device for lightwave bending and manipulation," *Nature Communications*, Vol. 3, 651, 2012.
4. Zhu, W. M., A. Q. Liu, X. M. Zhang, D. P. Tsai, T. Bourouina, J. H. Teng, X. H. Zhang, H. C. Guo, H. Tanoto, T. Mei, G. Q. Lo, and D. L. Kwong, "Switchable magnetic metamaterials using micromachining processes," *Advanced Materials*, Vol. 23, No. 15, 2011.
5. Fu, Y. H., A. Q. Liu, W. M. Zhu, X. M. Zhang, D. P. Tsai, J. B. Zhang, T. Mei, J. F. Tao, H. C. Guo, X. H. Zhang, J. H. Teng, N. I. Zheludev, G. Q. Lo, and D. L. Kwong, "A micromachined reconfigurable metamaterials via reconfiguration of asymmetric split-ring resonators," *Advanced Functional Materials*, Vol. 21, No. 18, 2011.
6. Zhu, W. M., A. Q. Liu, T. Bourouina, D. P. Tsai, J. H. Teng, X. H. Zhang, G. Q. Lo, D. L. Kwong, and N. I. Zheludev, "Microelectromechanical maltese-cross metamaterial with tunable terahertz anisotropy," *Nature Communications*, Vol. 3, 1274, 2012.

Optical Tuning of Ultra-thin, Flexible Terahertz Metamaterials with Embedded Silicon

M. A. Hoeh, J. Neu, K. M. Schmitt, and M. Rahm
Department of Electrical and Computer Engineering and Research Center OPTIMAS
University of Kaiserslautern, Erwin-Schroedinger-Str., Kaiserslautern 67663, Germany

Abstract— We present a fabrication technique for the implementation of ultra-thin, flexible metamaterial membranes with embedded crystalline silicon. The electromagnetic properties of the metamaterial can be optically tuned by an external stimulus. For example, we fabricated a 25 µm thick terahertz bandpass filter whose amplitude transmission could be tuned with a maximal modulation depth of 98% at an operating frequency of 0.67 THz in accordance with the transmission maximum of the bandpass filter. The demonstrated fabrication technique can be universally applied for implementation of more general metamaterial structures and is budget-priced due to the usage of standard silicon.

Introduction: In the last few years metamaterials have gained increasing importance for the implementation of novel adaptive optics in the microwave, terahertz and infrared spectral range. Among various schemes, tuning of the electromagnetic properties of metamaterials by electronic or optical means seem to be the most promising approaches [1, 2]. With respect to optical tuning, the basic methodology relies on the fabrication of plasmonic metamaterial structures on top of thick semiconductor substrates. The drawback of this technique lies in the strong terahertz signal modulation due to etalon effects in the thick substrate and the introduction of artifacts in the measured terahertz spectra. In contrast, ultrathin, optically tunable metamaterials can overcome these limitations due to increased transparency and due to a significantly larger free spectral range that shifts the resonance peaks outside the spectral bandwidth of interest.

Results: Here, we present a methodology for the fabrication of ultrathin adaptively tunable THz metamaterials for the example of an optically tunable bandpass filter. The thickness of the bandpass filter was less than 25 µm and thus sub-wavelength with respect to an operating frequency of 0.67 THz. We obtained a maximal modulation depth of 98% for the amplitude transmission of the filter at the center frequency of 0.67 THz. The maximum amplitude transmission of the filter without photo-excitation was 85%. The fabrication method includes three basic procedures: wet and dry etching of a standard silicon wafer, bonding to a benzocyclobutene polymer and processing and embedding of the metamaterial structure. In the talk, the method will be explained in detail and investigations of the carrier dynamics in a silicon wafer will be presented.

Conclusion: We demonstrate a method for fabrication of ultrathin, sub-wavelength thick metamaterials with embedded silicon as a semiconductor. In general, the presented approach can be applied to a great variety of different metamaterial structures.

ACKNOWLEDGMENT

We acknowledge financial support from the Federal Ministry of Education and Research under contract number 13N11905 (Project MetaTune).

REFERENCES

1. Chen, H.-T., W. J. Padilla, J. M. O. Zide, A. C. Gossard, A. J. Taylor, and R. D. Averitt, "Active terahertz metamaterial devices," *Nature*, Vol. 444, 597–600, 2006.
2. Chen, H.-T., J. F. O'Hara, A. K.Azad, A. J. Taylor, R. D. Averitt, D. B. Shrekenhamer, and W. J. Padilla, "Experimental demonstration of frequency-agile terahertz metamaterials," *Nature Photonics*, Vol. 2, 295–298, 2008.

Reconfigurable Optical Metamaterial Composed of Nanoparticles with Magnetic Inclusions

O. Zhuromskyy[1], R. Klupp Taylor[2], W. Lobaz[3], W. Peukert[2], and U. Peschel[4]

[1]Institute of Optics, Information and Photonics
Friedrich-Alexander University of Erlangen-Nürnberg
Haberstrasse 9a, Erlangen 91058, Germany
[2]Institute of Particle Technology
Friedrich-Alexander University of Erlangen-Nürnberg
Cauerstrasse 4, Erlangen 91058, Germany
[3]Institute of Macromolecular Chemistry
Heyrovského nám. 2, CZ-162 06 Praha 6, Czech Republic
[4]Institute of Solid State Theory and Optics
University of Jena, Max-Wien-Platz 1, Jena 07743, Germany

Abstract— Extraordinary electromagnetic properties of metamaterials result from the resonant response of constituent elements [1]. At radio frequencies electric and magnetic responses are usually provided by two different types of elements, loop like elements provide for interaction with magnetic field [2] whereas rod like elements govern "dielectric" properties of metamaterials [3]. Lack of suitable materials and fabrication techniques with sufficient precision make radio and microwave metamaterial concepts hardly applicable for optical frequencies. Resent advances in the synthesis of nano-structured particles provide alternative building blocks for optical metamaterials [4]. The desired response can be obtained from the electric and magnetic Mie resonances of nanoparticles. In principle both electric and magnetic resonances can be obtained from a single structure, this being achieved by adjusting the geometry of composite particles to equalize the responses and shift them to the desired frequency. In our contribution we will present an optical metamaterial composed of complex multilayer plasmonic particles with magnetic inclusions. The outer metal-dielectric part of the particle provides for the electromagnetic properties while the magnetic inclusion is introduced to manipulate the particle position in suspensions. In such suspensions particles with intrinsic magnetic moments can arrange into chains under influence of external magnetic field. This property can be used to change the optical response of the suspension by changing the direction of the external magnetic field. For different orientations of the chain axis relative to the light propagation direction and polarization, different structural resonances are excited resulting in different extinction spectra. Optical properties of such magnetically ordered suspensions can be simulated with the help of the superposition T-matrix method [5].

ACKNOWLEDGMENT

The authors gratefully acknowledge the German Research Council (DFG), which, within the framework of its 'Excellence Initiative' supports the Cluster of Excellence 'Engineering of Advanced Materials' and the Graduate School in Advanced Optical Technologies at the University of Erlangen-Nuremberg.

REFERENCES

1. Pendry, J. B., "Negative refraction makes a perfect lens," *Phys. Rev. Lett.*, Vol. 85, 3966, 2000.
2. Pendry, J. B., A. J. Holden, D. J. Robbins, and W. J. Stewart, "Magnetism from conductors and enhanced nonlinear phenomena," *IEEE Trans. Microw. Theory Tech.*, Vol. 47, 2075–2084, 1999.
3. Pendry, J. B., A. J. Holden, W. J. Stewart, and I. Youngs, "Extremely low frequency plasmons in metallic MESO structures," *Phys. Ref. Lett.*, Vol. 76, 4773–4776, 1996.
4. Klupp Taylor, R. N., F. Seifrt, O. Zhuromskyy, U. Peschel, G. Leugering, and W. Peukert, "Painting by numbers: Nanoparticle-based colorants in the post-empirical age," *Adv. Mater.*, Vol. 23, 2554–2570, 2011.
5. Peterson, B. and S. Ström, "T matirx for electromagnetic scattering from an arbitrary number of scatterers and representations of $E(3)$," *Phys. Rev. D*, Vol. 8, 3661–3678, 1973.

Session 3P8b
SC3: Nano-photonic Devices for Optical Interconnects and Optical Sensing

SOI Slot Photonic Crystal Cavities on SiO_2 from $\lambda = 1.3\,\mu m$ to $1.6\,\mu m$ with Q/V Factors Beyond 800000

T.-H.-C. Hoang[1], **W. Zhang**[1], **S. Serna**[1], **C. Caer**[1, 2, 3], **X. Le Roux**[1], **L. Vivien**[1], **and E. Cassan**[1]

[1]Institut d'Electronique Fondamentale, Université Paris-Sud, CNRS, UMR 8622
Bat. 220, Orsay, Orsay 91405, France
[2]Laboratoire Charles Fabry, Institut d'Optique, CNRS, Université Paris-Sud
2 Avenue Augustin Fresnel, Palaiseau Cedex 91127, France
[3]IBM Research — Zurich Laboratory, Säumerstrasse 4, Rüschlikon 8803, Switzerland

Abstract— Silicon photonics has been of interest for its versatile properties. The silicon bandgap is such that the material is transparent to wavelength commonly used in optical communications (1.28 µm–1.6 µm) and micro-nano-fabrication of structures can rely on large silicon on insulator (SOI) wafers and mature CMOS processes. In order to emphasize the light-matter interactions in this integrated platform, hollow core resonators are needed as well as low interaction volumes, thus meaning large Q/V ratio and small footprint dielectric resonators. Slot photonic crystal cavities are a way to achieve this purpose [1]. Among many candidates, photonic crystal cavities bring a good chance for enhancing photoluminescence of nanomaterials due to their small mode volumes and high quality factors.

We present here the design and fabrication of heterostructure photonic crystal (PhC) cavities on SOI infiltrated by a liquid and with mode volumes of around $0.03(\lambda/n)^3$ [2]. The heterostructure PhC cavities have been reported for achieving very large Q-factors among photonic crystal resonators [3]. We have thus chosen this kind of geometry and have fabricated a series of cavities in order to demonstrate high-Q resonances in a large wavelength window ($1.28\,\mu m \leq \lambda \leq 1.6\,\mu m$). The cavities' design is based on a chirp of the lattice constant in the propagation of light. Fig. 1(a) shows typical scanning electron microscope (SEM) views of the fabricated sample.

Figures 1(b) and 1(c) depict the two cavities in our series of cavities within the resonant wavelength window ranging from 1.3 µm to 1.6 µm. The first cavity is designed with a basic lattic constant $a_0 = 330\,nm$ and presents a resonant wavelength peak at 1284 nm with a Q factor of 10467, and the other one was designed with $a_0 = 400\,nm$ and presents a resonant peak at $\lambda = 1605\,nm$ with a Q factor of 23187. Other fabricated cavities have also proved to have Q factors of around several tens of thousand and (Q/V) values of approximately 800000. The low insertion losses of these devices also prove the quality of the fabrication steps.

We stress that these cavities have been fabricated on silica, i.e., the buried oxide layer of SOI wafers was not removed. In order to properly characterize the samples, we first drop cast an optical liquid on top of the structures ($n_{clad} = 1.46$). Owing to the non free-standing membrane approach explored in this work, these works efficiently demonstrate the potentials of slot photonic crystal cavities relying on a mechanically robust approach to enhance light-matter interactions for silicon photonics nonlinear signal processing and on-chip biosensing.

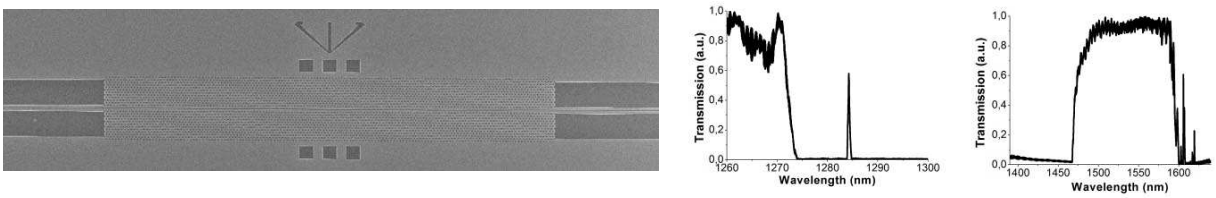

(a) (b) (c)

Figure 1: (a) SEM picture of a typical fabricated slot hetereostructure PhC cavity, (b) transmission spectrum of the slot heterostructure cavity using a basic lattice constant $a_0 = 330\,nm$ and presenting a resonant peak at 1284 nm with a Q factor of 10467, (c) transmission spectrum of another slot heterostructure cavity using $a_0 = 400\,nm$: resonant peak at $\lambda = 1605\,nm$ with a Q factor of 23187.

REFERENCES

1. Gao, J., J. F. McMillan, and S. Assesfa, "Demonstrations of an air-slot photonic mode-gap confined photonic crystal slab nanocavity with ultrasmall mode volumes," *Appl. Phys. Lett.*, Vol. 96, 051123, 2010.
2. Caer, C., X. L. Roux, and E. Cassan, "High-Q silicon-on-insulator slot photonic crystal cavity infiltrated by a liquid," *Appl. Phys. Lett.*, Vol. 103, 221106, 2013.
3. Taguchi, Y., Y. Takahashi, Y. Sato, T. Asano, and S. Noda, "Statistical studies of photonic heterostructure nanocavities with an average Q factor of three millions," *Opt. Express*, Vol. 19, 11916, 2011.

Compact 60 GHz Hybrid Integrated Photoreceiver Module with 1.5-μm InAs Quantum Dot SOA

T. Umezawa, K. Akahane, N. Yamamoto, A. Kanno, and T. Kawanishi
National Institute of Information and Communication Technology (NICT)
4-2-1, Nukui-Kitamachi, Koganei, Tokyo 184-8795, Japan

Abstract— With the data traffic carried over optical-fiber communication systems increasing every year, advanced modulation formats such as QPSK, 16QAM, and advanced parallel transmission technology such as space-division multiplexing are now implemented at baud rates of 25–30 Gbps. Higher-baud-rate optical transmission is very attractive to improve the data rate capacity in long-reach to short-reach communications. Opto-electronic devices are a bottleneck for achieving high-frequency-response performance. For example, in photoreceivers using a transimpedance amplifier (TIA), the 3-dB bandwidth is limited by the TIA's bandwidth of 30 GHz. Using an optical amplifier in place of an electric amplifier (TIA) makes high-baud-rate communication possible because of its wide frequency bandwidth. Very few compact photoreceiver modules operating at high baud rates have been reported. In this report, we present a compact photoreceiver module integrated with a PIN photodiode (PD) and 1.5-μm quantum dot (QD)-based semiconductor optical amplifier (SOA).

We have a developed 60-GHz hybrid integrated photoreceiver, which consists of a 1.5-μm QD-SOA and a high-speed PIN-PD. A maximum responsivity of 25 A/W at a QD-SOA driving current of 400 mA and a 3-dB bandwidth of 62 GHz was achieved. A high sensitivity of −20.5 dBm was obtained through a BER test at 10 Gbps, and a clear eye diagram at 50 Gbps was also obtained. We believe that this design is well suited for high-baud-rate optical-fiber communications. A monolithic integrated device combining the QD-SOA and QD-PD will show higher responsivity. Further, the photoreciever can be used for optical fiber communications including Radio over Fiber communications.

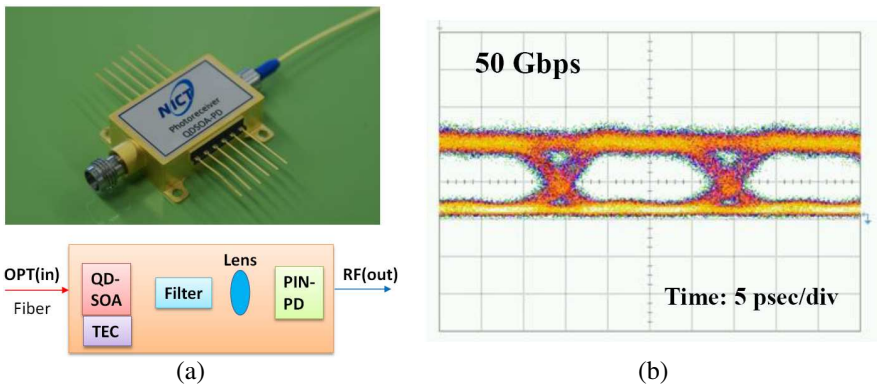

Figure 1: (a) 60-GHz hybrid integrated photoreceiver with a QD-SOA and its schematic diagram, and (b) eye diagram at 50 Gbps, optical input power of −10 dBm, SOA driving current of 290 mA.

Review of Electro-Optic Polymer Nano-Photonic Devices for On-chip Optical Interconnects

Alan X. Wang[1], **Ray T. Chen**[2], **and Alex K.-Y. Jen**[3]

[1]School of Electrical Engineering and Computer Science
Oregon State University, Corvallis, OR 97331, USA
[2]Department of Electrical and Computer Engineering
University of Texas at Austin, Austin, TX 78758, USA
[3]Department of Materials Science and Engineering
University of Washington, Seattle, WA 98195, USA

Abstract— In the field of optical communication, organic materials and devices are highly complementary to their inorganic counter parts such as silica fibers and semiconductor lasers and detectors. Particularly, organic materials offer large, ultra-fast nonlinear optical (NLO) responses, and broad spectral tunability, and they can be solution processed at low cost onto large-area substrates. NLO organic materials demonstrate superior performance over inorganic NLO materials such as $LiNbO^3$ and silicon. Electro-optic (E-O) polymer materials are second-order nonlinear ($\chi^{(2)}$) organic materials. The refractive indices of E-O polymers can be dynamically changed by an applied electric field, which is known as Pockels Effect. Compared to inorganic E-O crystals, E-O polymers offer intrinsic advantages:

- Large Pockels coefficient with r_{33} values greater than 300 pm/V.
- Ultrafast E-O response time of less than 10 femtoseconds.
- Relatively low dielectric constant ($3 \sim 4$) with small dispersion up to 250 GHz, and very low dielectric loss tangent (10^{-4}).
- Compatibility with virtually any substrate.
- Intrinsic radiation hardness and wide operation temperatures for space communication applications.

During the past 15 years, the E-O coefficient, thermal stability, optical loss, and power handling capability of E-O polymers have been significantly improved by push-pull chromophores, typically consisting of a π-conjugated bridge end-capped with strong electron-donating and accepting groups. E-O polymers have been successfully used for ultra-high-speed E-O modulators, high linearity and high bandwidth RF modulators, hybrid silicon-organic slot waveguide modulators, E-O polymer filled photonic crystal waveguide (PCW) modulators, organic-plasmonic modulators, and polymer ring resonators. This presentation will review the most recent research progress of E-O polymer nano-photonic devices and discuss the applications for on-chip optical interconnects.

Intracellular Molecular Detection by Light Localization Using Graded Plasmonic Nanoapertures

Wonju Lee[1], **Taehwang Son**[1], **Donghyun Kim**[1], **and Eunji Sim**[2]

[1]School of Electrical and Electronic Engineering, Yonsei University, Republic of Korea
[2]Department of Chemistry, Yonsei University, Republic of Korea

Abstract— In this study, we explore feasibility of super-resolved axial imaging based on extraordinary light transmission by metallic nanoaperture arrays. Incident light can transmit over several orders of magnitude through subwavelength nanoaperture arrays fabricated at thick metal film due to plasmonic coupling, which is well known as extraordinary transmission (EOT). Many studies based on EOT have generally concentrated on several applications for enhanced sensing techniques. Otherwise, relatively little has been attempted for the resolution enhancement of biomedical imaging based on EOT. For live cell imaging, it is required to observe an axial distance deeper than what is typically done under total internal reflection. Since EOT can be induced to have a much longer penetration depth with a transmission range of a few hundreds of nanometers from surface, sub-diffraction-limited axial sectioning for cellular imaging can be performed. Here, we measured axial information of live cells using subwavelength nanoaperture arrays based on EOT. For axial sectioning of live cells, a linear nanoaperture array was designed to induce a differential penetration depth of EOT formed at apertures of different size. Fluorescent targets were excited up to a different preset distance in the axial direction. Axial distribution of FITC-conjugated ganglioside in mouse macrophage-like cells was analyzed with subdiffraction-limited resolution, 20 nm in the best case, after reconstruction based on signal differences extracted from neighboring nanoapertures. The feasibility of super-resolved axial sampling was extended into gliding bacteria on nanoapertures.

Enhancement of SPR-sensor Sensitivity in Magnetophotonic Plasmonic Heterostructures

D. O. Ignatyeva[1, 2], **S. K. Sekatskii**[3], **A. N. Kalish**[1, 2], **and V. I. Belotelov**[1, 2]

[1]Faculty of Physics, Lomonosov Moscow State University, Moscow, Russi
[2]Russian Quantum Center, Moscow, Russia
[3]Ecole Polytechnique Federale de Lausanne, Institute of the Physics of Biological Systems Lausanne, Switzerland

Abstract— We present a novel type of the surface plasmon resonance (SPR) sensor based on the magnetophotonic plasmonic heterostructure and show that utilization of specially designed 1D photonic crystals (PC) along with the magnetic layers (ML) significantly enhances the quality factor and magnitude of the optical and magnetooptical resonances and therefore allows for a several orders of magnitude increase of the SPR-sensor sensitivity.

The sensing heterostructure consists of a plasmonic layer which can be perforated or smooth film of a noble metal (e.g., gold) covered with a dielectric (e.g., bismuth-substituted iron garnet) or metal ML (e.g., cobalt) and coated with 1D PC. ML increases the sensitivity of the SPR-sensor since the magneto-plasmonic resonances are sharper than the plasmonic ones. At the same time 1D PC support ultralong-range propagating modes that enhances the magnitude and sharpens the magneto-plasmonic resonances even more. Although the surface plasmon polaritons (SPPs) can be excited in a magnetic metal directly our analysis shows that the structure where this layer is combined with a film of a noble metal has significantly higher quality factor and is preferable.

We performed the design of the magnetophotonic plasmonic heterostructures and tuned the parameters of the structure in order to enhance the magneto-optical response of the structure via excitation of the ultalong-range propagating SPP mode. The numerical simulations predict extremely narrow plasmonic and magneto-optical resonances and sensitivity enhancement up to 10^{-8} RIU.

Both types of the structures, with dielectric and metal ML were fabricated. The sensing process was performed by two different experimental schemes. Extremely sharp magneto-optical resonance (with a width of about 0.1 degrees) allowed us to detect with a good precision the shift of the magneto-plasmonic resonance position with the variations of the sensor environment. The fabricated spectral sensor sensitivity is 45 deg/RIU (2300 nm/RIU). On the other hand the transverse magneto-optical Kerr effect (TMOKE) is enhanced up to 15% magnitude. Therefore the environment variation can be tracked via the measurement of the absolute value variation of the TMOKE for the fixed wavelength and angle. The sensor magneto-optical response to the refractive index change is 10%/RIU.

ACKNOWLEDGMENT

The work is supported by Russian Science Foundation (grant No. 14-32-00010).

Super-period Nanograting Surface Plasmon Resonance Spectrometer Biosensor

Junpeng Guo, **Hong Guo**, **and Xueli Tian**
Department of Electrical and Computer Engineering
University of Alabama in Huntsville, Huntsville, AL 35899, USA

Abstract— Surface plasmon resonance in various metal nanostructures has been extensively investigated for biochemical sensing which detect bonding of biomolecules on metal nanostructure surfaces. Measurement of surface plasmon resonance typically relies on an optical spectrometer that measures the spectrum of transmission, reflection, or scattering light from metallic nanostructures. Here we report a new surface plasmon resonance sensor platform that eliminates the use of optical spectrometers for measuring the surface plasmon resonance. With diffraction grating patterned metal nanostructures, surface plasmon resonance can be measured with a linear photodetector such as a CCD imager in one of the diffraction orders. That way, an optical spectrometer is not needed for measuring the surface plasmon resonance and the shift of resonance due to the bonding of target biochemical. We have demonstrated this new biosensor platform with super-period gold nano-disks, super-period nanoholes, and super-period hybrid metal-dielectric photonics crystal gratings. Our integrated nanophotonics spectrometer biosensor can measure the bonding of bovine serum albumin (BSA) proteins of several nanometers on nanostructure surface. Surface plasmon resonance which cannot be measured in the traditional transmission and reflection modes, can be measured in the diffraction mode with our super-period nano-plasmonics gratings.

Bio-enabled SERS Sensors for Ultra-sensitive Immuno-assay Detection

Jing Yang[1], **Le Zheng**[2], **Fanghui Ren**[1], **Gregory L. Rorrer**[2], **and Alan X. Wang**[1]

[1]School of Electrical Engineering and Computer Science
Oregon State University, Corvallis, OR, 97331, USA
[2]School of Chemical, Biological & Environmental Engineering
Oregon State University, Corvallis, OR, 97331, USA

Abstract— Immunoassay based on specific recognition between an antigen and a complementary antibody has become an essential and reliable tool for clinical diagnoses and diseases detection in recent years. Surface-enhanced Raman scattering (SERS) detection has attracted significant attention due to its narrow spectral bandwidth, immune to photo-bleaching, and fingerprint information of various molecules. Typically, SERS-based immunoassays are implemented on flat glass slides coated with colloidal nanoparticles. These substrates are inexpensive and easy to be functionalized, but the sensitivity is relatively low. Diatoms are photosynthetic microorganisms that create their own skeletal shells of hydrated amorphous silica, called frustules, which naturally possess hierarchical micro- & nano-scale features that are extremely cumbersome and expensive to duplicate by top-down fabrication techniques. In this paper, we present the design, fabrication, and characterization of diatom-based SERS immunoassay by integrating Ag NPs into diatom frustules. The immunoassay was designed according to a standard sandwich protocol of enzyme-linked immunosorbent assay (ELISA). The model antibody, goat-anti-mouse immunoglobulin G (IgG) was first attached to the surface of Ag NPs. The antigen, mouse IgG was then immobilized onto the antibody-functionalized diatom frustules for the specific recognition. To evaluate the specific recognition between the antibody and the antigen, we challenged the immunoassay with a negative control IgG, human IgG. Afterward, the immunoassay was incubated with antibody-functionalized Au NPs, which were initially labeled with Raman reporter, 5,5′-Dithiobis-(2-Nitrobenzoic Acid) (DTNB). We achieved 10 pg/mL detection limit, which is 100× better than conventional colloidal SERS sensors in the comparison group.

Session 3P9a
Applied Electromagnetics for Smart Cities

Wireless Friendly and Energy Efficient Buildings (WiFEEB)

J. M. Rigelsford[1], K. L. Ford[1], T. Yu[3], Z. Lai[3], R. Shiram[1], P. Valtr[2], J. Weng[3], Y. Wang[3], A. Vallecchi[1], H. Altan[1], H. Song[3], J. Zhang[1], J. Wu[3], M. Cerveny[2], W. Zhao[3], L. Subrt[2], Y. Alharbi[1], C. J. Davenport[1], P. Pechac[2], and R. J. Langley[1]

[1]Department of Electronic & Electrical Engineering
The University of Sheffield, Mappin Street, Sheffield S1 3JD, United Kingdom
[2]Department of Electromagnetic Field, Czech Technical University
Technická 2, Praha 166 27, Czech Republic
[3]Ranplan Wireless Network Design Ltd., Hart Business Centre
Kimpton Road, Luton LU2 0SX, United Kingdom

Abstract— The design and construction of buildings has historically been driven by structural, functional, and aesthetic considerations. However, the working and home environment is driven increasingly by energy efficiency and electronic communications whether it be the internet, smart energy metering (to be implemented by 2020), telephone, computer data or multimedia exchange and in future by remote patient monitoring (Telecare) and Assisted Living. The wireless performance of building design is not understood and the construction industries do not consider wireless system performance in their designs or specifications despite the rapid employment of metal skins and windows and facades containing metallised layers for energy conservation, both of which are a significant problem for wireless signal propagation. Hence there is a significant need to understand the performance of buildings and construction materials for efficient energy consumption and for the efficient propagation of radio waves.

Security in buildings is also a very important issue. The emergency services require pervasive communications at 400 MHz throughout the built environment. In addition City Managers and built environmental professionals will monitor a range of different aspects of the environment, including factors such as air and water quality, noise and lighting levels as well as human and vehicular movement and behaviour. Most of these services are wireless and they will significantly increase in number and importance in the future. Wireless control is also used in buildings for lighting, heating and energy control systems. The growth of use of these systems into new and demanding applications requires greater efficiency in use of the electromagnetic spectrum and control of wireless interference both within and between adjacent buildings and in the environment itself. Hence, modern buildings must be designed to be wireless radio-friendly and energy efficient whether they are hospitals, schools, offices, prisons or the home.

This paper presents the key findings resulting from the WiFEEB project and addresses how buildings and the built environment can be both energy efficient and wireless friendly. Our objectives have been to develop and verify the new concept of the wireless friendly, energy efficient building. The wireless propagation properties of building and insulation materials have be assessed and are presented. The same properties must be measured for building structures such as walls (internal and external), floors, facades and window systems. These properties have been evaluated from 400 MHz to 20 GHz to include both current and future wireless networks and systems. Results are given resulting from the bespoke optimisation of CAD tools that combine wireless propagation models with energy efficiency models producing a complete model for the built environment. New innovative construction materials such as glass and steel fibre reinforcement are studied and new architectural designs investigated to improve wireless signal propagation while maintaining energy efficiency. Techniques are presented to control wireless propagation within buildings, namely frequency selective surfaces (FSS), smart wall units, adaptive antennas and scattering surfaces. Finally, results of several case studies will be given.

ACKNOWLEDGMENT

This work is a deliverable of WiFEEB — Wireless Friendly and Energy Efficient Buildings, a Marie Curie Industry-Academia Partnerships and Pathways (IAPP) project grant agreement 286333.

Recycling Radio Waves with Smart Walls

M. Dupré, N. Kaïna, G. Lerosey, and M. Fink
Institut Langevin, ESPCI Paris Tech & CNRS, France

Abstract— We propose to use electronically reconfigurable ultrathin metasurfaces as smart walls to reflect more intelligently the waves in indoor environments. We experimentally prove at 2.47 GHz that it is possible to use these as spatial microwave modulators, using a simple energy feedback. In particular, we show that we can enhance the transmission between two antennas by orders of magnitude or locally conceal a volume from the penetration of waves in a typical office room.

An increasing amount of data is nowadays conveyed wirelessly by radio waves in dense environments such as cities or buildings [1]. While propagating, the electromagnetic waves carrying the information are reflected several times off obstacles such as walls and furnitures, thus causing a spread of the associated electromagnetic energy throughout those complex and reverberating media. This raises health issues and wastes energy. Here we show that part of this seemingly lost energy can be recycled by reflecting more intelligently these multiply scattered waves using smart walls rather than bare ones. To do so we propose to use ultrathin metasurfaces [2] that we design to be electronically reconfigurable in real time as spatial microwave modulators [3]. We show that they can be utilized to cover part of the walls of a typical office room, hence transforming these dumb surfaces into smart ones. We demonstrate that, akin to the spatial light modulators which can focus light through complex media [4, 5], those spatial microwave modulators can passively turn a random electromagnetic field resulting from reverberated and multiply scattered waves into a shaped one using a simple energy feedback and simple optimization algorithms [6]. Specifically, we prove that such smart walls can, in real time, increase by orders of magnitude the energy of a wireless signal received by any antenna or locally conceal a volume from penetration of microwaves [7]. We will present simulation and experimental results as well as a quantitative estimation of the benefits brought by the approach, by introducing and modeling the notion of wavefront shaping in reverberating media.

Our smart walls have applications in green wireless communications and electromagnetic protection. Indeed this approach could be used alongside others [8, 9] to develop energy efficient wireless communication systems. They are also amazing tools for fundamental physics related to the propagation of waves in complex, highly scattering or reverberating media.

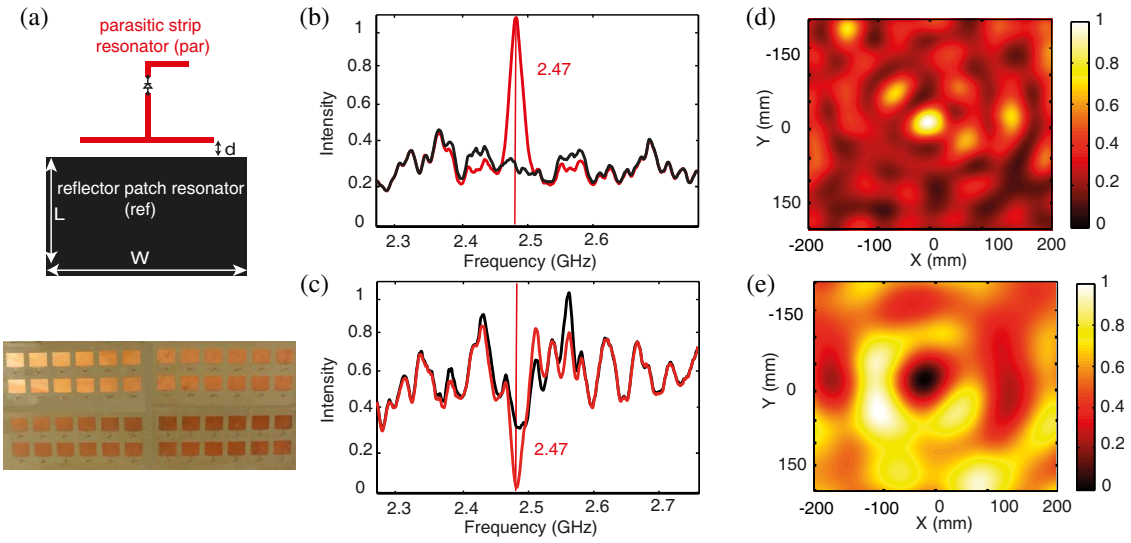

Figure 1: (a) Scheme of the unit cell (up) and picture of the metasurface. (b) Average transmission spectra for a field maximization and (c) field minimization. (d) Average maps of the field after maximization and (e) minimization.

REFERENCES

1. Paulraj, A., R. Nabar, and D. Gore, *Introduction to Space-time Wireless Communications*, Cambridge University Press, London, 2003.
2. Kildishev, A. V., A. Boltasseva, and V. M. Shalaev, *Science*, Vol. 339, 1232009–1232009, 2013.
3. Kaïna, N., M. Dupré, M. Fink, and G. Lerosey, *Optics Express*, Vol. 22, No. 16, 18881–18888, 2014.
4. Mosk, A. P., A. Lagendijk, G. Lerosey, and M. Fink, *Nat. Photon.*, Vol. 6, 283–292, 2012.
5. Aulbach, J., B. Gjonaj, P. M. Johnson, A. P. Mosk, and A. Lagendijk, *Phys. Rev. Lett.*, Vol. 106, 103901, 2010.
6. Vellekoop, I. M. and A. P. Mosk, *Opt. Lett.*, Vol. 32, 2309–2311, 2007.
7. Dupré, M., N. Kaïna, M. Fink, and G. Lerosey, Scientific Reports, Vol. 4, 6693, 2014.
8. Subrt, L. and P. Pechac, *IEEE 6th Eur. Conf. Antennas Propag.*, 1–5, 2012.
9. Subrt, L. and P. Pechac, *ET Commun.*, Vol. 6, 1004, 2012.

An Inductive Frequency Selective Surface for Use in Secure Facilities

Michal Cerveny[1] **and Jonathan M. Rigelsford**[2]

[1]Department of Electromagnetic Field, Czech Technical University
Technická 2, Praha 166 27, Czech Republic
[2]Department of Electronic & Electrical Engineering, The University of Sheffield
Mappin Street, Sheffield S1 3JD, United Kingdom

Abstract— The use of contraband mobile phones within prisons is an increasing global phenomenon. It enables criminals to continue unlawful activity, including organizing drug deals, assassinations and witness harassment [1, 2]. According to official statistics, 7301 mobile phones or SIM cards were found in UK prisons during 2012 [3]. TETRA (Terrestrial Trunked Radio) is the communications protocol used by emergency services in over 100 countries worldwide and operates between 380 MHz and 420 MHz. It is widely used by Police forces, paramedics, fire brigades, and special response units (including riot police), as well as other government agencies. Historically, cellular mobile phone networks have operated on clearly defined frequency bands. For example, AMPS and D-AMPs was used on systems operating between 806–880 MHz; GSM 900 operates between 880–960 MHz; GSM1800 operates between 1710–1880 MHz; and UMTS 1900–2170 MHz. With the adoption and roll out of LTE and 4G systems cellular network operators have over 40 designated frequency bands which can be used across the existing spectrum allocation and with the addition of newer bands including Band 38 which covers 2570–2620 MHz [4, 5]. Wi-Fi operates in the 2.4 GHz and 5.8 GHz ISM bands and can be used for peer to peer communication on mobile devices.

There are four major issues to consider when designing a system to limit the usability of mobile cellular networks for secure facilities such as prisons. Firstly, mobile phones are capable of sending and receiving messages even when signal strength is low, due to the high sensitivity of the receivers which is typically in the range −110 to −130 dBm. Secondly, the high number of mobile base stations means coverage is vast, so it is probably that many prisons in the UK have good quality signal [7]. Thirdly, to block signals of varying frequencies, a large band stop filter response must be utilised by the FSS, whilst allowing 400 MHz to transmit through. Finally, if the solution such as an FSS, is to be installed into a window frame, optical transparency is essential.

This paper therefore presents an inductive frequency selective surface (FSS) which can be applied to prison cell windows to prevent the transmission of unwanted signals from mobile phones but allows TETRA based systems to operate correctly (as shown in Fig. 1). The performance of the FSS is presented in Fig. 2. In this work it is assumed that the walls of the prison are assumed perfectly isolating and can be achieved using metalized construction materials including

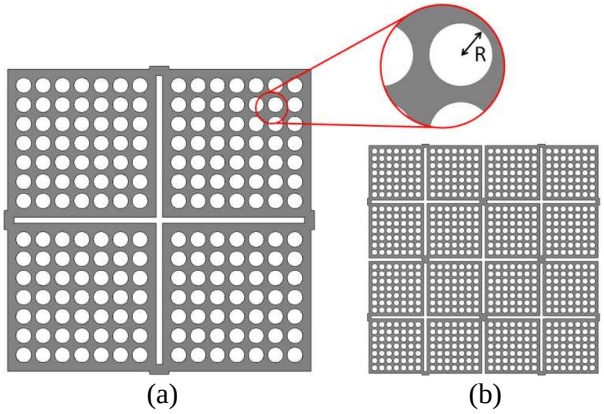

Figure 1: Illustrations of (a) simple inductive cross FSS with better optical transparency by the introduction of an array of holes between the cross arms and (b) an array of 4 unit cells providing 5 interleaved cross elements.

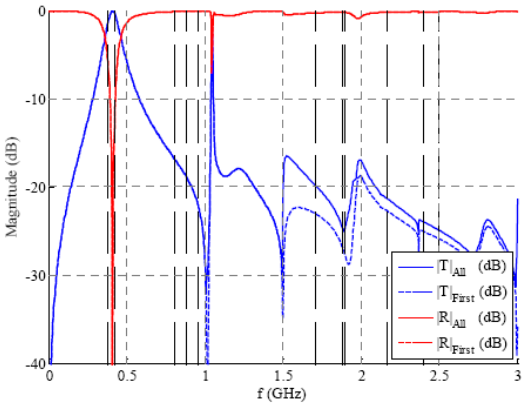

Figure 2: Illustrations of (a) simple inductive cross FSS with better optical transparency by the introduction of an array of holes between the cross arms and (b) an array of 4 unit cells providing 5 interleaved cross elements.

Celotex [8] or Kingspan [9]. Beyond its potential for optical transparency, advantages of the proposed solution over other technologies such as jamming devices or active capacitive FSS [6], are that an inductive FSS is cheap to manufacture as it can be self-supporting and manufactured from a single metallic sheet. Furthermore, it requires no external power supply to correctly run, reducing operating and maintenance costs and is in line with current legislative requirements (i.e., restrictions on jamming overspill for public access areas).

The full paper will provide a detailed description of the FSS design and its performance as well as an assessment of its optical opacity for window applications.

ACKNOWLEDGMENT

This work is a deliverable of WiFEEB — Wireless Friendly and Energy Efficient Buildings, a Marie Curie Industry-Academia Partnerships and Pathways (IAPP) project grant agreement 286333.

REFERENCES

1. Blakey, D., "Disrupting the supply of illicit drugs into prisons — A report for the director general of national offender management service," Feb. 2, 2015, Online Available: http://www.drugscope.org.uk/Resources/Drugscope/Documents/PDF/Good%20Practice/blakeyreport.pdf.
2. "Mobile phones in prisons — The demand and use of illicit mobile phones," Feb. 2, 2015, Online Available: http://www.government-online.net/research-brief-use-illicit-mobile-phones-prison/.
3. "Recording of incidents related to mobile phones and SIM cards," Feb. 2, 2015, Online Available: https://www.gov.uk/government/uploads/system/uploads/attachment_data/file/32925-5/recording-incidents-mobile-phones.doc.
4. Geßner, C., "Long term evolution — A concise introduction to LTE and its measurement requirements," Rohde&Schwarz GmbH & Co. KG, 2011.
5. 3GPP TS 36.101, "User Equipment (UE) radio transmission and reception (Release 9)," Version 9.3.0, Mar. 2010.
6. Ford, K. L., J. Roberts, S. Zhou, G. Fong, and J. Rigelsford, "Reconfigurable frequency selective surface for use in secure electromagnetic buildings," *Electronics Letters*, Vol. 49, No. 14, 861–863, Jul. 4, 2013.
7. Roberts, J., J. M. Rigelsford, and K. L. Ford, "Diffraction from frequency selective surfaces for secure building applications," *2012 6th European Conference on Antennas and Propagation (EUCAP)*, 2388–2391, 2012.
8. Celotex, Feb. 2, 2015, Online Available: http://www.celotex.co.uk/.
9. Kingspan, Feb. 2, 2015, Online Available: http://www.kingspan.cz/.

A Simulation Based Distributed MIMO Network Optimisation Using Channel Map

J. Weng, J. M. Rigelsford, and J. Zhang
The University of Sheffield, UK

Abstract— Channel map is an essential tool in network planning and optimisation. In this work, we present an example of MIMO channel map for distributed MIMO network optimisation. Based on the simulation of MIMO channel map, we optimise the MIMO channel capacity and the bit error rate. The results demonstrate that the effectiveness of the MIMO channel map in network optimisation.

An Introduction to Physical-layer Security for Wireless Smart Cities

Matthew A. Bourke, Kenneth L. Ford, Mohammed Benaissa, and Jonathan M. Rigelsford
Department of Electronic & Electrical Engineering, The University of Sheffield
Mappin Street, Sheffield S1 3JD, United Kingdom

Abstract— An overview of physical-layer security theory for wireless communication is presented, along with a discussion of the potential feasibility to smart cities and potential future research directions. For a long time security at the physical-layer has been neglected in favour of computational methods implemented at the upper-layers of the protocol stack. Upper-layer cryptography techniques use encryption with a shared-key to achieve secrecy. This security is invariably achieved using cryptographic methods. Current encryption methods are deemed to be secure because the level of computational power required to crack the keys is not attainable using current technology. Nonetheless, the rise of more powerful technologies such as quantum computing may soon challenge this assumption. The computational complexities required to implement public key encryption prevents low-resource devices from using them. This can have a significant impact on wireless systems for Smart Cities which might be limited in terms of available power or computational overhead.

Cryptography at the physical-layer can be used to complement current upper-layer encryption, or act as an independent security mechanism. This is beneficial for many reasons. It can facilitate upper-layer key exchanges by providing a secure channel and allow independent security mechanisms to be implemented on low-resource devices. The nature of physical-layer cryptography also means that adaptive security measures can be put in place depending on application and classification of the threat. Common types of attacks on wireless systems include:

- **Passive Eavesdropping** — eavesdropping on messages passed between two legitimate parties without actively engaging in any return communications.
- **Denial-of-Service (DoS)** — deny access to legitimate users by exhausting system resources or signal jamming.
- **Spoofing** — masquerading as a legitimate user or system to gain access to privileged resources.
- **Man-in-the-Middle** — relaying messages between two legitimate communication nodes, without knowledge from either user, in an attempt to gain valid authentication.

These attacks can have a big impact on both civilian and military systems. For massively interconnected smart cities these attacks could cause disruptions or damage to smart meters, remote healthcare, transport, and other public services. From a theoretical point of view, information-theoretical secrecy can be achieved at the physical-layer if the signal-to-noise ratio (SNR) of the eavesdropper channel is worse than that of the legitimate receiver; however, problems occur when the eavesdroppers channel is better, or equal to the legitimate receiver. This paper presents a review of current physical-layer security systems and their potential benefits to wireless smart cities.

Selected Aspects of RF Signal Propagation in Buildings

Pavel Valtr[1], **Pavel Pechac**[1], **Ondrej Moravek**[1], **Milan Prihoda**[1], **Lee Ford**[2], **Jonathan M. Rigelsford**[2], **and Richard J. Langley**[2]

[1]Department of Electromagnetic Field, Faculty of Electrical Engineering
Czech Technical University in Prague, Technicka 2, Prague 166 27, Czech Republic
[2]Department of Electronic & Electrical Engineering, The University of Sheffield
Mappin Street, Sheffield S1 3JD, United Kingdom

Abstract— Co-existence of various communication services within buildings requires detailed knowledge of behavior of electromagnetic wave propagation in such environment. One of the aspects related to indoor communication is the outdoor-to-indoor penetration. Indoor navigation, for instance, is heavily dependent on indoor signal level due to wall attenuation. Another issue is interference mitigation. This paper addresses several topics related to wave propagation into and within buildings.

The focal point of understanding penetration loss into buildings is the knowledge of electrical properties of building materials. Table 1 shows measured values of relative permittivity and loss tangent of selected building materials. The measurements were done in the frequency range of 5 GHz to 70 GHz and the numbers represent the mean value over the frequency range.

Table 1: Electrical properties of building materials.

Material	Rel. Permittivity	Loss tangent
Plaster board — base	2.14	0.005
Plaster board — wall	2.26	0.005
Plaster board — sound shield	2.78	0.006
Chip board	2.17	0.06
Glass	6.4	0.02

Excess penetration loss due to window blinds and window blind-like structures are usually not taken into account in signal coverage planning. On top of wall attenuation and window attenuation, however, window blinds can impose additional loss which can further downgrade the signal quality from a source located outside the building. Experimental results of window blind insertion loss are presented for frequency range of 5 GHz to 50 GHz, see Fig. 1. The insertion loss is studied depending on frequency, polarization and inclination of the window blind's lamellas. Detailed knowledge of the effects of window blinds on electromagnetic wave propagation can improve existing prediction models.

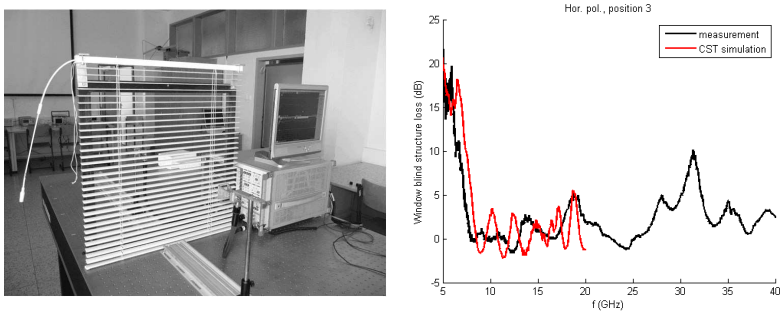

(a) (b)

Figure 1: (a) Window blind insertion loss measurement setup; (b) Measurement result of insertion loss compared with numerical simulation.

ACKNOWLEDGMENT

This work was supported by WiFEEB — Wireless Friendly and Energy Efficient Buildings, a Marie Curie Industry-Academia Partnerships and Pathways (IAPP) project grant agreement 286333.

Realization of a Flexible Technological Demonstrator for HF Sky-wave Data Links

A. L. Saverino[1], **A. Capria**[1], **and F. Berizzi**[1, 2]

[1]Radar and Surveillance Systems (RaSS) National Laboratory, CNIT, Italy
[2]Department of Information Engineering, University of Pisa, Italy

Abstract— Radio frequency range between 3–30 MHz is called high frequency or shortwave radio. For a long time, the high frequency band has been considered as the most important means for communications over long distance. The advent of new technologies, such as satellite and terrestrial communications, made the high frequency systems obsolete. Despite that, a new interest for these systems is growing due to the need of having a relatively cheap and simple system for data and voice exchange, which could be a real alternative to existing system in case of their failure. This paper aims to present an effective and flexible HF digital transceiver demonstrator based on the software defined radio paradigma. The purpose of this demonstrator is to maintain the "essential" information among the authorities in case of the failure of both satellite and Internet communications for critical scenarios (e.g., terroristic attacks, natural disasters).

Session 3P9b
SC1: Electromagnetic Modelling Methods for EMC Problems

Reciprocity-based Applications of the Time-domain Contour Integral Method

Martin Štumpf
SIX Research Centre, Brno University of Technology, Technická 3082/12, Brno 616 00, The Czech Republic

Abstract— The reciprocity theorem of the time-convolution type is not only the starting point for constructing the time-domain contour integral method (TD-CIM) itself [1], but also it is an efficient means for describing closely related EMC aspects of power-ground structures. This may include, space-time electromagnetic mutual coupling between two power-ground structures [2], pulsed electromagnetic- field radiation characteristics [3], their pulsed radiated susceptibility or even remote sensing of power-ground structure's constitutive parameters, for instance.

In the present contribution it is shown that through the application of the reciprocity theorem with a suitable choice of the 'testing' field state, complex (time-domain) EMC modeling of a power-ground structure is feasible and computationally very efficient. In this analysis, the 'testing' field is found either via the TD-CIM (for arbitrarily-shaped circuits) or using the time-domain 'ray-type' expansion (for rectangular circuits) (see [4], for example).

Systematic applications of the reciprocity theorem related to time-domain modeling of power-ground structures supplemented with the corresponding sample numerical examples will be presented at the 36th PIERS.

REFERENCES

1. Štumpf, M., "Time-domain contour integral method — An approach to the analysis of double-plane circuits," *IEEE Trans. Electromagn. Compat.*, Vol. 56, No. 2, 367–374, 2014.
2. Štumpf, M., "Time-domain mutual coupling between power-ground structures," *Proceedings of the 2014 IEEE International Symposium on EMC*, 240–243, Raleigh, NC, USA, August 2014, 2014.
3. Štumpf, M., "Pulsed EM field radiation, mutual coupling, and reciprocity of thin planar antennas," *IEEE Trans. Antennas Propag.*, Vol. 62, No. 8, 3943–3950, 2014.
4. Štumpf, M., "Time-domain analysis of rectangular power-ground structures with relaxation," *IEEE Trans. Electromagn. Compat.*, Vol. 56, No. 5, 1095–1102, 2014.

Numerical Modeling of Reverberation Chambers: The Cavity Green's Function Boundary Element Method in Comparison to Other State-of-the-art Algorithms

M. E. Gruber and T. F. Eibert
Lehrstuhl für Hochfrequenztechnik, Technische Universität München, Munich, Germany

Abstract— Different cavity Green's function boundary element methods are discussed and compared with other state-of-the-art methods for the numerical modeling of reverberation chambers. The algorithms are compared in terms of accuracy, computing speed and memory requirements. Different scenarios from a reverberation chamber with a single plate stirrer to a chamber with multiple stirrers are considered.

Without acceleration techniques, the use of the cavity Green's function (CGF) boundary element method (BEM) is limited to cavities which contain small, one-dimensional objects [1]. The quadratic complexity in filling the system matrix together with the numerically expensive integral kernel (i.e., the Green's function of the rectangular cavity) impede the modeling of mid- and large-sized objects. To model large objects, different acceleration techniques have been proposed in recent years [2–4]. In 2014, the CGF BEM was accelerated by [2] using the Ewald summation technique together with the adaptive integral method (AIM), where only the near-zone part of the system matrix is computed directly. Far interactions are calculated on-the-fly using AIM during the iterative solution of the matrix-vector equation. In [3], Gruber et al. evaluated the CGF based on the Ewald method. It was observed that the Ewald summation technique can be accelerated with the fast Fourier transform when the Green's function is sampled on an equispaced grid. To calculate values in between the grid, Lagrange interpolation was employed. In [4], the CGF was evaluated with a hybrid approach. The hybrid approach employs the Ewald representation in the near range of the source and a two-dimensional spectral representation in the far range, thereby combining the advantages of both representations. To address the quadratic complexity of the system matrix, a fast group spectral domain approach (FGSDA) was proposed: the system matrix is evaluated in the reciprocal instead of the real-space domain. Although the FGSDA does not reduce the complexity of the system matrix, the constant factor is drastically reduced (over three orders of magnitude) as the integration over test and source domain is not needed in the reciprocal domain.

Besides the CGF BEMs, a hybrid discrete singular convolution (DSC)-method of moments (MoM) was presented in [5]. The electrically large, rectangular cavity is considered in the DSC method while the geometrically more complex objects within the reverberation chamber are modeled with the more flexible MoM. Last bot not least, the specialized methods are also compared to a standard method, namely a multilevel fast multipole method (MLFMM) accelerated free-space Green's function BEM [6].

To analyze the strengths and shortcomings of the different approaches, various scenarios from a reverberation chamber with a single object to a chamber with multiple objects are considered at different frequencies. The algorithms from [3, 4] are, in particular, advantageous when few objects are within the cavity. The AIM accelerated CGF BEM and the standard BEM are favorable when reverberation chambers with many objects are considered.

REFERENCES

1. Gronwald, F., "Calculation of mutual antenna coupling within rectangular enclosures," *IEEE Transactions on Electromagnetic Compatibility*, Vol. 47, No. 4, 1021–1025, 2005.
2. Yang, K. and A. E. Yilmaz, "An FFT-accelerated integral-equation solver for analyzing scattering in rectangular cavities," *IEEE Transactions on Microwave Theory and Techniques*, Vol. 62, No. 9, 1930–1942, 2014.
3. Gruber, M. E., C. Koenen, and T. F. Eibert, "An inverse fast Fourier transform accelerated Ewald method for the computation of the rectangular cavity Green's function," *Journal of Computational Physics*, 2014.
4. Gruber, M. E. and T. F. Eibert, "A hybrid Ewald-Spectral cavity Green's function boundary element method with spectral domain acceleration for modeling of over-moded cavities," *IEEE Transactions on Antennas and Propagation*, 2014, accepted with minor revisions.

5. Zhao, H. and Z. Shen, "Efficient modeling of three-dimensional reverberation chambers using hybrid discrete singular convolution-method of moments," *IEEE Transactions on Antennas and Propagation*, Vol. 59, No. 8, 2943–2953, 2011.
6. Eibert, T., "A diagonalized multilevel fast multipole method with spherical harmonics expansion of the k-space integrals," *IEEE Transactions on Antennas and Propagation*, Vol. 53, No. 2, 814–817, 2005.

A Hybrid Computational-statistical Approach to Calculating Electromagnetic Coupling in Complex Environments

T. M. Antonsen, Jr.[1], **G. Gradoni**[2], **E. Ott**[1], **and S. Anlage**[1]

[1]IREAP, University of Maryland, College Park, MD, USA
[2]Nottingham University, University Park, Nottingham NG7 2RD, UK

Abstract— The coupling of electromagnetic radiation into enclosures or cavities through apertures and by circuit elements both electrically small and large has attracted the interest of electromagnetic community for many years. Full solutions of this problem are particularly complicated because of the mathematical complexity in the solution of the boundary-value problem and because of the sensitivity of the solution to details of the enclosure's dimensions, content, and the frequency spectrum of the excitation. These difficulties have motivated the formulation of a statistical description (known as the random coupling model, RCM [1, 2]) of the excitation of cavities, in particular the linear relation between voltages and currents at ports in the cavity, when the ports are treated as electrically small antennas. The RCM has also recently been extended to the case of apertures [3] of arbitrary size. The issue addressed here is the methodology needed to take the results of computational electromagnetic solutions for manageable parts of the system; such as an aperture, an antenna, or a configuration of conducting wires, and integrate these results with astatistical model for the interaction of these parts. The approach will be based on our previous work with rectangular apertures in conducting planes [3]. The key element will be the identification of an appropriate set of fields, far from the system part under consideration, for which an admittance or impedance matrix can be defined and computed. Once this matrix is determined it can be modified according to the RCM prescription to describe the behavior of the part in an enclosing electromagnetic environment.

REFERENCES

1. Zheng, X., T. M. Antonsen, and E. Ott, "Statistics of impedance and scattering matrices in chaotic microwave cavities: Single channel case," *Electromagnetics*, Vol. 26, 3, 2006.
2. Zheng, X., T. M. Antonsen, and E. Ott, "Statistics of impedance and scattering matrices of chaotic microwave cavities with multiple ports," *Electromagnetics*, Vol. 26, 33, 2006.
3. Gradoni, G., T. M. Antonsen, E. Ott, and S. Anlage, *IEEE Trans EMC*, to be published.

GPU-accelerated Stochastic-FDTD Study of Lightning-induced EM Fields over Non-deterministic Terrains

G. G. Pyrialakos[1], **T. T. Zygiridis**[2], **N. V. Kantartzis**[1], **and T. D. Tsiboukis**[1]

[1]Department of Electrical & Computer Engineering, Aristotle University of Thessaloniki, Greece
[2]Department of Informatics & Telecommunications Engineering, University of Western Macedonia, Greece

Abstract— A non-trivial number of engineering problems are pertinent, either directly or implicitly, to the electromagnetic (EM) fields produced by lightning strike. This fact has motivated the development of several methodologies, analytical as well as computational, aiming at the precise and efficient prediction of lightning-induced EM pulses. Unfortunately, existing solutions commonly make simplified assumptions regarding the geometric and/or electromagnetic properties of the problems under study, thus rendering the handling of realistic setups rather questionable.

In this paper, we develop a computational framework based on the finite-difference time-domain (FDTD) method that takes into account the uncertainty inherent in certain aspects of lightning-related problems. Specifically, we investigate the effects that the terrain has on the lightning-induced fields, when its geometry is considered non-flat (i.e., its altitude varies with respect to the horizontal x-y plane). The realistic geometric features are realized with the aid of a random rough surface algorithm, where a length-correlation parameter is introduced as an indicator of the terrain roughness. In order to statistically resolve the problem, we first employ the Monte-Carlo method via repeated simulations, as a means to extract the two basic statistical parameters of the EM fields (their expected value and variance). A representative result in the case of the subsequent lightning stroke is displayed in Fig. 1. We next compare our results with a geometric adaptation of the Stochastic FDTD method, based on a covariant-contravariant formulation, where the statistical variation of suitable curvilinear parameters is considered. An attempt is also made to associate the length correlation with the corresponding correlation parameter inherent to the S-FDTD. In the cases examined herein, an almost linear relationship is found to exist.

To accelerate computations and exploit the capabilities of modern multiprocessor GPUs, the full 3D FDTD codes are developed on the CUDA 6.0 programming platform. This decision is favored from the parallelization potential of the FDTD method, the exploitation of which can ensure substantial reduction of simulation times. To guarantee optimal implementation, various parameters (e.g., the block-grid structure) are optimized, and several programming techniques are adopted, including the use of streams for out-of-kernel parallelization, and atomics for avoiding parallelization errors. Our results indicate up to 50 times decrease in execution time for the S-FDTD method and Monte-Carlo approach.

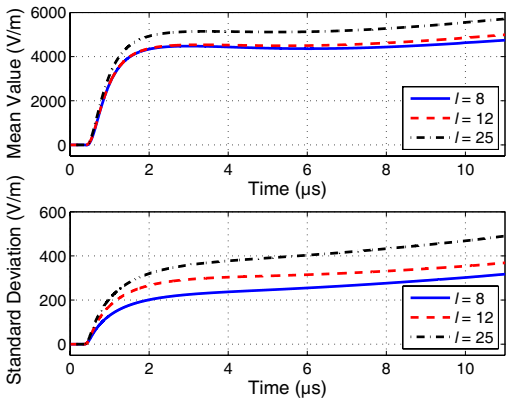

Figure 1: Statistical parameters of the radial electric field, obtained with Monte-Carlo simulations, at position $(r, z) = (100\,\text{m}, 10\,\text{m})$, in the case of non- at terrain. Cases where the correlation length l is set to different values are displayed.

Embedding Anisotropic Carbon Fibre Composite Thin Layers in TLM Simulations

Xuesong Meng, **Phillip Sewell**, **Ana Vukovic**, **and Trevor M. Benson**
The University of Nottingham, UK

Abstract— Carbon fibre composites (CFCs) are widely used in the aerospace and car industries and their electromagnetic properties have been intensively investigated using various experimental and numerical simulation techniques. However, their small thickness and anisotropic properties are still two challenging issues for numerical modelling. We have previously reported a computationally efficient thin layer model [1] for modelling embedded thin isotropic CFC panels with the Transmission Line Modelling (TLM) method. In this contribution, the embedded thin layer model is now extended to the practically important case of anisotropic CFC materials and its role within simulations of more complex 3D geometries are demonstrated.

By definition, the electric and magnetic properties of anisotropic materials vary in different directions. In this paper, CFC thin panels are modelled as anisotropic with respect to the two in plane coordinates (x and y) with the principal directions of the anisotropy assumed orthogonal and aligning with the x and y directions for clarity of presentation. This means that the response of a flat CFC panel to an incident plane wave whose electric field is polarised along one of the coordinate directions can be locally independently modelled using one of two different one-dimensional (1D) thin layer TLM models. In the case of an arbitrary polarisation, $\vec{E}^i = E_x\hat{\mathbf{x}} + E_y\hat{\mathbf{y}} = |E^i|\cos\varphi\cdot\hat{\mathbf{x}} + |E^i|\sin\varphi\cdot\hat{\mathbf{y}}$, where φ is the angle between the electric field $\vec{E}^i$ and the x axis, and $\hat{\mathbf{x}}$ and $\hat{\mathbf{y}}$ are the in plane unit vectors, the incident field is first decomposed into components aligning with the anisotropic principal axes. Each of these components excites a different thin layer model and the net reflection and transmission can be determined by combining the two responses.

As a simple illustration, Fig. 2 shows the comparison of the TLM and theoretical result for (a) reflection and (b) transmission coefficients of an anisotropic CFC thin panel as a function

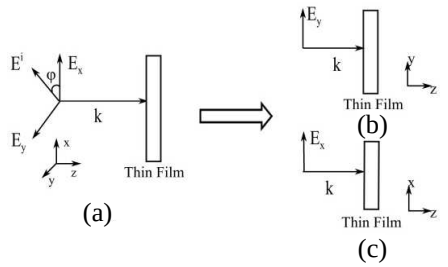

Figure 1: (a) The electric field E^i incident upon an anisotropic thin film can be decomposed into x and y field components. (b) E_y field component incident on a thin film. (c) E_x field component incident on a thin film.

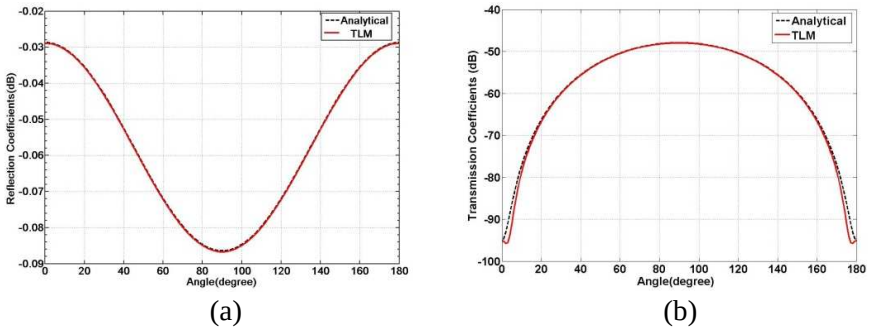

Figure 2: (a) Reflection coefficients and (b) transmission coefficients of an anisotropic CFC thin layer against the angle between the incident field with x axis at 1 GHz. The CFC thin film has the parameters in the x direction $\varepsilon_r = 2$ and $\sigma_e = 10,000\,\mathrm{S/m}$ from [2] and in the y direction assumed $\varepsilon_r = 3$ and $\sigma_e = 1,000\,\mathrm{S/m}$. The thickness of the film is 1 mm.

of the angle between the electric field and the x axis at 1 GHz. It can be seen that excellent agreement between the numerical and the TLM results is obtained. In the presentation, the anisotropic multilayer CFC thin layer model embedded into the three-dimensional examples will also be discussed and more practical examples will be presented.

REFERENCES

1. Meng, X., P. Sewell, A. Vukovic, H. G. Dantanarayana, and T. M. Benson, "Efficient broadband simulations for thin optical structures," *Optical and Quantum Electronics*, Vol. 45, No. 4, 343–348, Oct. 2012.
2. Sarto, M. S., "A new model for the FDTD analysis of the shielding performances of thin composite structures," *IEEE Transactions on EMC*, Vol. 41, No. 4, 298–306, Nov. 1999.

On the Limits of Numerical Modelling of Electromagnetic Field Coupling through Small Apertures

Gazmend Mavraj and Frank Gronwald
Institute of Electromagnetic Theory, Hamburg University of Technology, Germany

Abstract— The modelling of electromagnetic field coupling through apertures is a classic problem of Electromagnetic Compatibility (EMC). In particular for the case of electrically small apertures a variety of analytic modelling schemes exists [1–4]. In view of numerical modelling it is tempting to apply standard numerical techniques, such as the Finite Integration Technique (FIT) or the Method of Moments (MoM), to this problem as well. However, as a matter of experience, it turns out that a direct application of these standard methods can lead to inaccuracies due to the difficulty of properly discretizing the apertures, see [5, 6] and references therein. In this contribution we want to establish criteria and limits that can be used to estimate whether a standard numerical technique still can be applied to a specific aperture problem. To this end a number of canonical aperture coupling problems is numerically investigated by means of the FIT and MoM and compared to analytical solutions. It is seen that with decreasing aperture size or increasing numbers of apertures the numerical effort becomes impractical and refined hybrid numerical methods are required.

REFERENCES

1. Bethe, H. A., "Theory of diffraction by small holes," *Phys. Rev.*, Vol. 66, Nos. 7–8, 163–182, Oct. 1944.
2. Butler, C. M., Y. Rahmat-Samii, and R. Mittra, "Electromagnetic penetration through apertures in conducting surfaces," *IEEE Trans. Antennas Propagat.*, Vol. 26, No. 1, 82–93, Jan. 1978.
3. Tesche, F. M., M. V. Ianoz, and T. Karlsson, *EMC Analysis Methods and Computational Models*, Wiley, New York, 1997.
4. Celozzi, S., R. Araneo, and G. Lovat, *Electromagnetic Shielding*, Wiley, Hoboken, 2008.
5. Araneo, R. and G. Lovat, "An efficient MoM formulation for the evaluation of the shielding effectiveness of rectangular enclosures with thin and thick apertures," *IEEE Trans. on Electromagnetic Compatibility*, Vol. 50, No. 2, 294–304, May 2008.
6. Siah, E. S., K. Sertel, J. L. Volakis, V. V. Liepa, and R. Wiese, "Coupling studies and shielding techniques for electromagnetic penetration through apertures on complex cavities and vehicular platforms," *IEEE Trans. on Electromagnetic Compatibility*, Vol. 45, No. 2, 245–257, May 2003.

Electromagnetic Near Field Injection Model on Integrated Circuit

R. Omarouayache[1], **J. Raoult**[1], **P. Payet**[1], **L. Chusseau**[1], **B. Vrignon**[2], **A. Doridant**[2], **and A. Boyer**[3]

[1]IES, Université Montpellier
860 rue de Saint Priest, Montpellier 34097, France
[2]Freescale Semiconductor, Toulouse 31023, France
[3]LAAS-CNRS, 7 Avenue du Colonel Roche, Toulouse 31077, France

Abstract— The electromagnetic (EM) injection is a technique which has already proved its efficiency for the studies of susceptibility of integrated circuits (IC). Recently, its application in IC cryptographic allowed the generation of significant faults in crypto-system. Near field probes are used to inject EM fault into the circuit. Nevertheless, an understanding of coupling phenomena in term of optimization and efficiency is still lacking. In the context of EM fault injection, probes must be optimized to deliver an intense and localized magnetic field.

Taking into account these optimization criteria, a magnetic loop probe was fabricated and characterized. To concentrate the magnetic field loops are wired around a ferrite-core with a conical cut. The ferrite material is Nickel-Zinc. The diameter of the cylindrical ferrite is about 2 mm, and the ferrite tip ends with a 20 µm diameter size. An electrical model of the probe was established owing to S-parameters measurements. The next step was to understand the EM interaction between the probe and the IC in order to perform an electrical model of the magnetic coupling.

A test chip has been designed by Freescale® in 0.25 µm SMARTMOS 8 technology with 4 metal layers. It allows to study the near-field injection on basic interconnect structures. Voltage sensors was integrated within the chip to measure the local voltage fluctuations induced by EM injection. We conducted this study on 50 Ω micro-strip lines of 1.75 µm × 1 mm deposited on the third layer of metallization. The lines have a 50 Ω termination and are connected to a voltage sensor. The major interest of these sensors is to deliver an accurate measurement of in situ voltage induced by EM injection.

The probe-line coupling is evaluated from measurements results. The basic and intuitive idea of the proposed model is that the system probe-line can be viewed as a transformer. The probe, primary winding, transfers energy to the electrical line, secondary winding, through electromagnetic induction. An equivalent electrical model with lumped elements is proposed. The main advantage is the relative ease of his implementation in SPICE-like electrical simulation software. The most important element to determine is the mutual inductance of the system. We have extracted its using measurements of the voltage coupled under sinusoidal excitation. A good prediction of the interaction between the probe and the IC was obtained on a large frequency range [100 kHz–1 GHz]. Our method has been validated against experiments with a pulse excitation applied to the probe since this kind of excitation signal is frequently used to inject EM faults in IC. Excitation signal is a square at 10 MHz repetition and 10 V peak to peak. Rise and fall times are 10 ns with a pulsewidth of 50 ns. Measurements and calculated results using our model are shown in excellent agreement, thereby validating the model. This procedure will thus be an interesting and useful tool to predict the disruptive effect induced by magnetic probes on secure ICs.

ACKNOWLEDGMENT

Authors kindly acknowledge the french Agence Nationale de la Recherche for funding this research under the E-MATA HARI contract No. ANR-12-INSE-0005.

Session 3P10a
Scattering, Diffraction, and Inverse Scattering

Bound States in the Continuum: Interference Way to Trap Electromagnetic Waves in Open Resonators

Almas F. Sadreev
L. V. Kirensky Institute of Physics, Krasnoyarsk 660036, Russia

Abstract— In 1929, von Neumann and Wigner [1] predicted the existence of discrete solutions of the single-particle Schrödinger equation embedded in the continuum of positive energy states, bound states in the continuum (BSC). Their analysis long time was regarded as mathematical curiosity because of certain spatially oscillating central symmetric potentials. Situation cardinally has changed after Friedrich and Wintgen [2] in framework of two-level Fan-Anderson model formulated the BSC as a resonant state whose width tends to zero as at least one physical parameter varies continuously. Physically a localization of one of resonant states of open system, i.e., the BSC can be interpreted as destructive interference of two resonance states which occurs for crossing of eigen levels of the closed system. That accomplished by avoiding crossing of the resonant states one of which transforms into the trapped state with vanishing width for crossing of the eigen levels of closed system [2]). This simple phenomenon has the same significance as the Aharonov-Bohm effect or the Anderson localization because all of them are manifestation of quantum interference effects.

We propose two layouts for experimental observation of trapping of microwaves inside the open resonator. The first one is the rectangular plane resonator with variable width with two attached waveguides which support propagating TM electromagnetic modes in the first channel [3]. For variation of the resonator's width an accidental degeneracy of two eigenmodes with the same symmetry might occur. A variation of the shape can be achieved by moving well of the resonator or by squeezing of the waveguides. We show that for this process the nearest resonances undergo avoiding crossing during of which one of the resonance widths becomes zero. That is the bound state in the continuum accomplished by intersection of transmission zero with the transmission maximum. That phenomenon was observed by Lepetit et al. [4, 5] in metallic waveguide with dielectric resonator in the THz range. The BSC is trapped mostly inside the open resonator.

The second layout consists of two identical resonators connected by waveguide [6]. Resonators are opened by attaching of waveguide resulting transmission through double resonator's system. Each resonator has multiple transmission zeros at some frequencies and therefore serves as a mirror. Whole system can be interpreted as the Fabry-Perot resonator at these frequencies which supports respectively the bound states [7] for definite quantized distances between the resonators. The double-bent waveguide presents the type of waveguides in which both types of the bound states occur. Each corner is capable to trap electromagnetic waves below the continuum [8, 9]. For definite lengths of bridge between the corners bound states in the continuum occur [10].

We show numerically that the bound states in continuum can be excited for transmission of wave packet if a width of resonator dot is varied linearly in time and reaches those selected values of the width when the BSC arises. Moreover we consider numerically a decay process of different eigen-states in the closed resonator to show that some of them trap in the BSC after the QD is opened [11].

REFERENCES

1. Von Neumann, J. and E. Wigner, *Phys. Z.*, Vol. 30, 465, 1929.
2. Friedrich, H. and D. Wintgen, *Phys. Rev. A*, Vol. 32, 3231, 1985.
3. Sadreev, A. F., E. N. Bulgakov, and I. Rotter, *Phys. Rev. B*, Vol. 73, 235342, 2006.
4. Lepetit, T., E. Akmansoy, J.-P. Ganne, and J.-M. Lourtioz, *Phys. Rev. B*, Vol. 82, 195307, 2010.
5. Lepetit, T. and B. Kanté, *Phys. Rev. B*, Vol. 90, 241103, 2014.
6. Rotter, I. and A. F. Sadreev, *Phys. Rev. E*, Vol. 71, 046204, 2005.
7. Sadreev, A. F., E. N. Bulgakov, and I. Rotter, *J. Phys. A: Math. Gen.*, Vol. 38, 10647, 2005.
8. Exner, P. and P. Ŝeba, *J. Math. Phys.*, Vol. 30, 2574, 1989.
9. Carini, J. P., J. T. Londergan, D. P. Murdock, D. Trinkle, and C. S. Yung, *Phys. Rev. B*, Vol. 55, 9842, 1997.
10. Sadreev, A. F., D. N. Maksimov, and A. S. Pilipchuk, ArXiv:1501.020337v1, 2015.
11. Bulgakov, E. and A. Sadreev, *Phys. Rev. B*, Vol. 83, 235321, 2011.

Mode-matching Analysis of TEM Wave Reflection by a Junction of Perfectly Conducting and Impedance Coaxial Waveguides

Ö. Yanaz Çınar[1], **G. Çınar**[1], **and S. Akşimşek**[2]

[1]Eskişehir Osmangazi University, Turkey
[2]İstanbul Kültür University, Turkey

Abstract— In this paper, the reflection of TEM waves by a step discontinuity on the junction of perfectly conducting and impedance coaxial waveguides is analyzed rigorously by applying modematching technique. Such problems may occur on certain microwave measurement systems where the cable on test is coated with a dielectric material. The formulation of the problem is achieved by defining field components at each side of the junction seperately and matching them at the junction by the use of continuity relations (see Fig. 1(a)) as described in [1, 2]. Leontovich boundary conditions are assumed on the coated walls of the cable on test. Finally, the coatings on the inner and outer walls are assumed to be different as shown in Fig. 1(b) and the formulation is repeated accordingly. At the end of the analysis, the effects of the cross-sectional areas of the waveguides and the coatings on the walls of the cable on test are illustrated numerically.

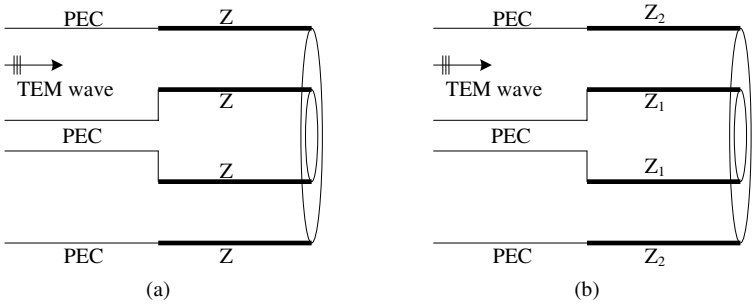

Figure 1.

REFERENCES

1. Eleftheriades, G. V., A. S. Omar, L. P. B. Katehi, and G. M. Rebeiz, "Some important properties of waveguide junction generalized scattering matrices in the context of the mode matching technique," *IEEE Transactions on Microwave Theory and Techniques*, Vol. 42, No. 10, 1896–1903, 1994.
2. Akşimşek, S., G. Çınar, B. Nilsson, and S. Nordebo, "TEM wave scattering by a step discontinuity on the outer wall of a coaxial waveguide," *IEEE Transactions on Microwave Theory and Techniques*, Vol. 61, No. 8, 2783–2791, 2013.

On the Type of Wave-incidence in Multiple-cylinder Diffraction Analysis at 60 and 100 GHz

José-Víctor Rodríguez, **Juan Pascual-García**, **Maria-Teresa Martinez-Ingles**, **Jose-Maria Molina-Garcia-Pardo**, **and Leandro Juan-Llácer**
Universidad Politécnica de Cartagena, Cartagena, Murcia, Spain

Abstract— The analysis of radiowave multiple-diffraction has been carried out through a large number of formulations which, usually, consider a plane-wave incidence over the array of diffracting obstacles. However, when it comes to a transmitter located at a small distance from the series of elements, a spherical-wave incidence assumption could be more appropriate in order to obtain more accurate and realistic results. In this work, a comparison of plane against spherical-wave incidence consideration in multiple-cylinder diffraction analysis is performed, both at 60 and 100 GHz, in order to clarify the margin in which both incidences differ. In this sense, the scheme of the propagation environment considered can be observed in Fig. 1. Moreover, the attenuation due to multiple-cylinder diffraction obtained with the uniform theory of diffraction-physical optics (UTD-PO) formulation proposed in [1], when assuming both plane and spherical-wave incidences, is depicted — as a function of d (distance between the transmitter and the first cylinder) — in Fig. 2, for n =10, $\alpha = 1°$ (with H properly varying with d in the spherical case), $w = 0.232$ m, $r = 0.04$ m, frequencies of 60 and 100 GHz, and *soft* and *hard* polarizations. The relative error between the two solutions ([*Att. Spherical* — *Att. Plane*]/*Att. Plane*) is shown in Fig. 3.

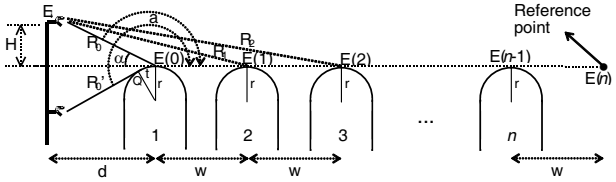

Figure 1: Scheme of the propagation environment under study.

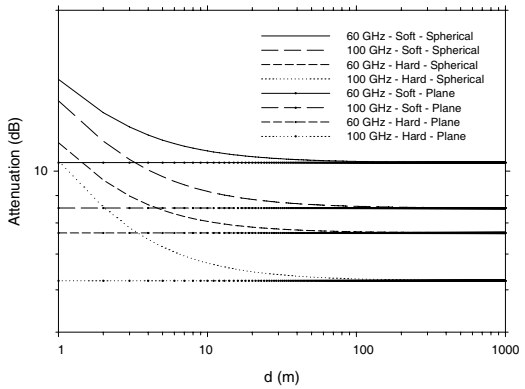

Figure 2: Comparison between both incidences.

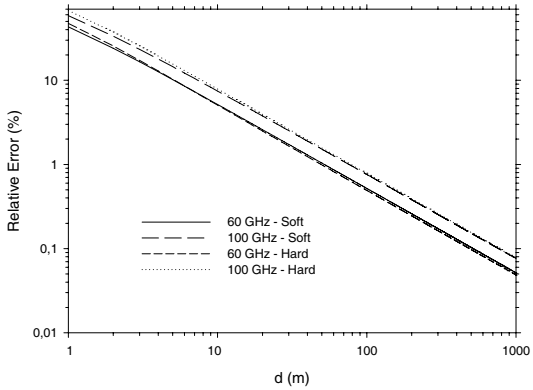

Figure 3: Relative error between both incidences.

As can be observed, it is not until $d = 105$ m that the relative error between the two types of wave incidence is less than 0.5%, for 60 GHz, and 0.75%, for 100 GHz.

ACKNOWLEDGMENT

This work was supported by the Ministerio de Economía y Competitividad, Spain (TEC2013-47360-C3).

REFERENCES

1. Rodríguez, J.-V., J.-M. Molina-García-Pardo, and L. Juan-Llácer, "A hybrid UTD-PO solution for multiple-cylinder diffraction analysis assuming spherical-wave incidence," *IEEE Trans. Antennas Propag.*, Vol. 56, No. 9, 3078–3081, 2008.

On the Importance of Double Bounce Diffuse Scattering in Indoor Wireless Channels

Juan Pascual-García, **José María Molina-García-Pardo**, **José Víctor Rodríguez**, **María Teresa Martínez-Inglés**, **and Leandro Juan-Llácer**
Universidad Politécnica de Cartagena (UPCT), Cartagena, Murcia, Spain

Abstract— The diffuse scattering propagation mechanism accounts for a significant percentage of the received energy, even at high frequencies. One of the most accurate diffuse scattering models is the Lambertian model which is based on the Effective Roughness approach [1]. This model allows the incorporation of diffuse scattering in ray tracing tools and the development of propagation prediction tools based exclusively on diffuse scattering. However, only single bounce diffuse scattering components have been considered so far. Double bounce diffuse scattering must be considered in order to increase the accuracy of the channel analysis. In this work, double bounce diffuse scattering components are considered in a ray tracing (RT) tool allowing a more accurate wireless channel simulation at 60 GHz in an indoor environment. The Lambertian model was selected for both single and double bounce scattering components; both formulations are shown in [1]. The frequency response in the range [57–66 GHz] was simulated and measured in the position depicted in Fig. 1. Subsequently, the complex impulse time response (CIR) was obtained by applying the inverse Fourier transform. As seen in Fig. 2, the double-bounce scattering allows a better agreement between simulations and measurements since single bounce components travel a maximum of 10 meters.

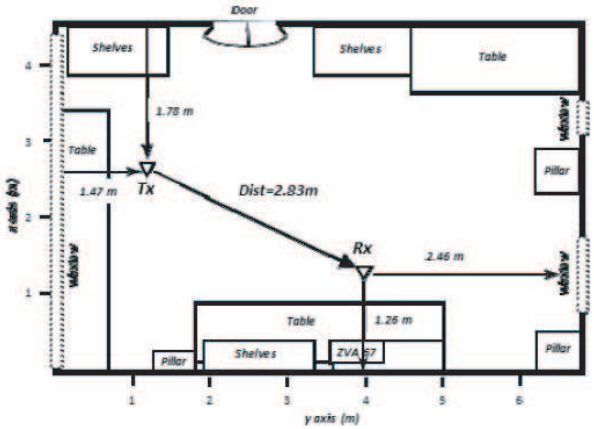

Figure 1: Indoor scenario.

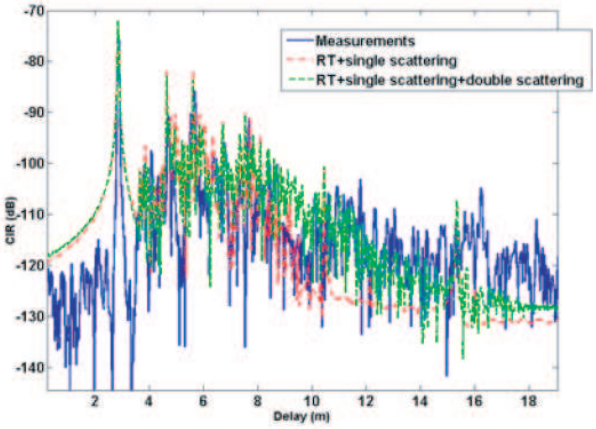

Figure 2: Complex impulse response comparison.

ACKNOWLEDGMENT

This work was supported by the Ministerio de Economía y Competitividad (MINECO), Spain (TEC2013-47360-C3-2) and by the European FEDER funds.

REFERENCES

1. Tian, L., V. Degli-Esposti, E. M. Vitucci, X. Yin, F. Main, and X. S. Lu, "Deterministic modeling of diffuse scattering component based on propagation graph theory," *European Cooperation in the Field of Scientific and Technical Research EURO-COST*, Ferrara, Italy, February 2007.

Determination of Optimal Pairs of Radii of Dielectric Samples for Complex Permittivity Measurement of Dispersive Materials

R. Kushnin, **J. Semenjako**, **and T. Solovjova**
Riga Technical University, Latvia

Abstract— The goal of this work is to find the optimum pair of values of radii of two full height cylindrical samples with the same constitutive properties centrally located in a rectangular waveguide for measurements of the complex dielectric constant. A pair of values of radii of samples is called optimal if the value of measurement uncertainty for that pair is smaller than for other pairs of values. One of the problems of this kind was first considered by Paez et al. in [1], where the optimal value of a circular cylindrical post in a cylindrical resonant cavity was found by using the well-known Monte Carlo method. A similar problem was considered in [2], where the optimum value of the radius of a circular dielectric post in a rectangular waveguide was found.

Notwithstanding the advent of powerful computers, the uncertainty analysis still remains a very time consuming task, because the Monte Carlo method requires a very large number of iterations in order for estimation of the measurement uncertainty to be reliable and because in each of these iterations the inverse scattering problem needs to be solved that, in turn, is very time consuming task. Since the computational effort required to solve the inverse scattering problem depends directly on the computational time required by the method for the direct scattering problem one needs to find the fastest approach for solving the direct scattering problem. From many approaches that have been proposed over the last several decades, we have chosen that proposed by Sahalos et al. [3] as it provides reasonably accurate results and at the same time shows very rapid convergence.

Also, in [2] the further reduction in the computation time have been achieved by using piecewise linear interpolation of the reflection and transmission coefficients, but unfortunately this type of interpolation is quite inaccurate in vicinity of resonances. We found that it is more efficient to interpolate the sum and difference of the reflection and transmission coefficients, since for a symmetric obstacle both these quantities have absolute value equal to unity for all real values of the relative dielectric constant that, in turn, means that each pole of this function have the corresponding root such that they are mutually complex conjugate values. Also, these two functions are analytic with respect to the relative complex dielectric constant. Both these properties enable us to use rational approximation involving the roots and poles of theses functions. These pairs can be found successively from the derivative of the phase of the functions. Also, we found that it is more convenient to work with normalized system parameters instead of actual ones, as in the case of a dielectric obstacle two of three parameters take values in limited intervals, since the waveguide is intended to be operated in the single-mode regime. In this study we use the following three normalized quantities, namely, the relative wavelength, relative radius and relative dielectric constant. Numerical studies show that it is sufficient to find only first twenty root-pole pairs. However, for lossy materials such approximation is not accurate, since more poles and roots are required, because the number of root-pole pairs to be taken into account increases as the imaginary part of the complex dielectric constant increases. Fortunately, this issue can be overcome by using asymptotes for root-pole pairs, namely, it is found that for large values of the dielectric constant root-pole pairs can be divided into several groups such that for each of theses groups asymptotic approximation can be found.

REFERENCES

1. Paez, E., M. A. Azpurua, C. Tremola, and R. Callarotti, "Uncertainty minimization in permittivity measurements in shielded dielectric resonators," *Progress In Electromagnetics Research M*, Vol. 26, 127–141, 2012.
2. Kushnin, R. and J. Semenjako, "Determination of the optimal value of the radius of a circular cylindrical post in a rectangular waveguide for measurement of the dielectric permittivity," *Progress In Electromagnetics Research B*, Vol. 34, 125–144, 2013.
3. Sahalos, J. N. and E. Vafiadis, "On the narrow-band microwave filter design using dielectric rod,' *IEEE Trans. Microwave Theory Tech.*, Vol. 33, No. 11, 1165–1171, 1985.

Method of Measuring the Dielectric Constant of Grain in Granaries Using Electromagnetic Antennas

Leidong Yang, **Bingfang Wu**, **and Fangming Wu**
Institute of Remote Sensing and Digital Earth, China Academy of Science, China

Abstract— A method is proposed in this paper to calculate the dielectric constant of grain in granaries by measure the speed of electromagnetic wave transforming in the grain.

In granaries, the quantity of the grain is calculated by its volume and density. The grain's standard density can be measured by specific device but cannot be used to calculate the quantity directly. In order to measure grain's storage density, the dielectric constant is used as a middle parameter in this paper. With the same grain sample, the dielectric constant varies with its density which is changed by vibrating [1]. In electromagnetic theory, when electromagnetic wave transfers in medium, its speed depends on the medium's dielectric constant. As to measure the dielectric constant of grain, the transforming speed of electromagnetic wave in it is measured. An experimental device based on electromagnetic wave antenna is designed. The antennas will be input into grains in parallel, and electromagnetic wave will translate between the antennas. The speed of the electromagnetic wave will be measured and the dielectric constant of grain can be calculated.

The largest transmission distance of electromagnetic wave in medium depends on its frequency. The frequency of electromagnetic wave used in these experiments ranged from 10 MHz to 16 MHz. The speed of electromagnetic wave is so fast that some high precision chips were used to measure the tiny difference of phase in the experimental device. Several experiments were done in granaries which have wheat stored in them and the result will be analyzed in the paper.

REFERENCES

1. Kraszewski, A. W., S. Trabelsi, and S. O. Nelson, "Temperature-compensated and density-independent moisture content determination in shelled maize by microwave measurements," *Journal of Agricultural Engineering Research*, Vol. 72, No. 1, 27–35, Jan. 1999.

Session 3P10b
Inverse Scattering, Imaging and Applications

On the Possibility of Water Detection under Asphalt Layer Using Microwave Radar System

A. V. Brovko
Yuri Gagarin State Technical University of Saratov, Russia

Abstract— Detection of water between asphalt and concrete layers is important part of monitoring and maintenance of road quality. For the sake of non-destructive evaluation of the road state, different NDE/NDT technologies can be used. In his paper, possibility of application of microwave radar system for detection of water layer under asphalt is explored.

Two types of radar system is considered: the system with a single antenna (Fig. 1(a)), and the system with two horn antennas (Fig. 1(b)). The performance of the system was estimated numerically with FDTD modeling of wave diffraction on the layers of road.

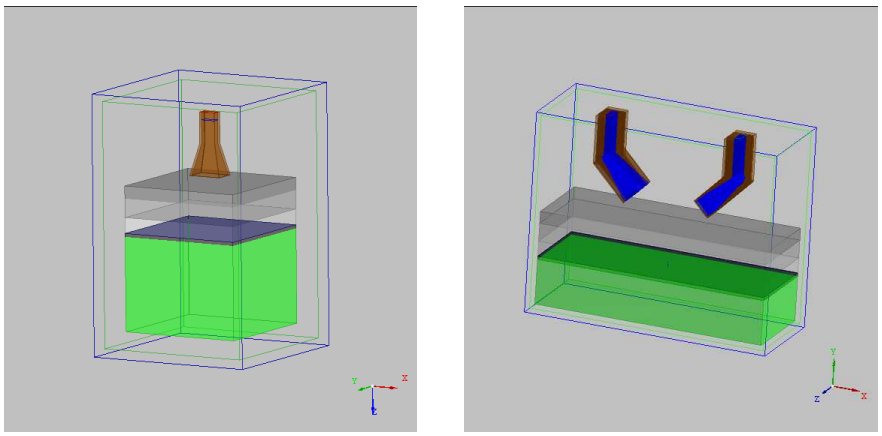

(a) (b)

Figure 1: Numerical model of (a) single antenna and (b) multiple antennas radar systems for detection of water under asphalt layer.

Numerical analysis allows making the following conclusions:

- Detection of water layer under asphalt with the use of microwave energy is possible.
- System with two horn antennas is more sensitive to the water layer in terms of transmission coefficient S_{21}.
- System with TE polarization of electromagnetic wave is less sensitive to the water layer in terms of transmission coefficient S_{21}, than the system with TM polarization.
- With increasing of water layer thickness from 0 to 1 mm the difference in S_{21} parameter is increasing gradually, but after 1 mm the difference in S_{21} is small.
- Dissipated power in water layer is of the same values as in the first asphalt layer dispite of smaller values in the intermediate layers; this provides potential way of elimination of water from asphalt layer by microwave heating.

Detection of Discontinuities in the Samples of Changing Sizes with ANN-based Technique

A. V. Brovko
Yuri Gagarin State Technical University of Saratov, Russia

Abstract— Detection of discontinuities in dielectric samples using microwave imaging is an important part of non-destructive evaluation and testing technology. Recently, the technique of detection of a spherical inclusion in homogeneous dielectric sample has been proposed [1]. The technique is based on application of artificial neural network (ANN) as numerical inverter, which is trained with numerical modeling data, and after training the ANN may be applied for reconstruction of the inclusion parameters using physical measurement results. Advantages of the approach described in [1] include simple measurement technique and possibility to work with closed measurement waveguide system. However, the technique is limited to the case of constant sizes of dielectric sample. Variations of sizes may destroy completely the procedure and corrupt the results. Moreover, the technique described in [1] requires changing of the positions of sample inside measurement system in the course of measurement, which is not convenient for practical implementation.

In this paper, the attempt to overcome the limitations of technique, described in [1], is undertaken. The sizes of sample are included into a set of parameters which are reconstructed using ANN. In order to provide more input information for ANN to reconstruct the extended set of parameters, different multiport measurement systems are investigated in this paper, namely, turnstile waveguide junction, and junctions of four and five rectangular waveguides.

Numerical experiments with spherical inclusion of changing radius, position, and dielectric permittivity, and changing sizes of rectangular sample of constant homogeneous material show that turnstile junction measurement system permits to reach relative errors 1.5%–3.5% in determination of position of the inclusion, 3%–4% in determination of radius of the sphere, 7%–15% in determination of permittivity. Application of five-port rectangular waveguide junction leads to increasing the relative errors to the following values: 6%–10% in determination of position of the inclusion, 4%–7% in determination of radius of the sphere, 8%–16% in determination of permittivity. Application of four-port waveguide junction seems to be not practical because of too large relative errors in determination of the parameters of inclusion.

REFERENCES

1. Brovko, A. V., E. K. Murphy, M. Rother, H. P. Schuchmann, and V. V. Yakovlev, "Waveguide microwave imaging: Spherical inclusion in a dielectric sample," *IEEE Microwave & Wireless Components Lett.*, Vol. 18, No. 9, 1234–1237, 2008.

Explicit Discretization Schemes for Linear Sampling and Factorization Methods

M. N. Akıncı and M. Çayören
Department of Electronics and Communication Engineering, Istanbul Technical University, Turkey

Abstract— Qualitative inverse scattering consists of various inverse scattering techniques, which aim to recover only the shape of the target rather than the frequency dependent dielectric parameters of the scatterers [1]. These methods have certain advantages over quantitative approaches. Simplicity of implementation and requirement of less computational resources are just two examples of these advantages. Contradictory to this circumstance, such methods are not widely used in engineering applications like subsurface sensing [2, 3], medical imaging [4] and etc.. In particular, finding a mathematical treatment for the derivation of the explicit discretization schemes of such methods is a problematic issue, especially in the near field region [3, 5]. In this context, this work presents a mathematical derivation of the explicit discretization schemes for two famous qualitative inverse scattering methods, which are the linear sampling method (LSM) and the factorization method (FM), for certain near field measurement scenarios. Explicitly, we mathematically derive the discretizations of the well-known "near-field equations" for three different case: measurements taken on a planar surface, measurements taken on a cylindrical surface, measurements taken on a spherical surface. Apart from giving the discretization of the near-field equations for different measurement configurations, we also mention how the discretized equations related with the physical interpretations of LSM [6, 7]. It is important to note that after understanding the mathematical and physical principles which motivate the LSM and the FM, it is straightforward to extend this analysis to another measurement configurations. Lastly, we also give several experimental reconstructions, which are obtained from Fresnel data [8, 9], to prove the accuracy the derived discretization schemes.

ACKNOWLEDGMENT

This work was supported by Turkish Scientic and Research Council (TUBITAK) under the project number 113E977.

REFERENCES

1. Potthast, R., "A survey on sampling and probe methods for inverse problems," *Inverse Problems*, Vol. 22, No. 2, R1, 2006.
2. Akinci, M. N. and M. ayren, "Microwave subsurface imaging of buried objects under a rough airsoil interface," *Remote Sensing Letters*, Vol. 5, No. 8, 703–712, 2014.
3. Catapano, I., L. Crocco, and T. Isernia, "Improved sampling methods for shape reconstruction of 3-D buried targets," *IEEE Transactions on Geoscience and Remote Sensing*, Vol. 46, No. 10, 3265–3273, 2008.
4. Bozza, G., M. Brignone, and M. Pastorino, "Application of the no-sampling linear sampling method to breast cancer detection," *IEEE Transactions on Biomedical Engineering*, Vol. 57, No. 10, 2525–2534, 2010.
5. Aramini, R., "Computational inverse scattering via qualitative methods," Ph.D. Dissertation, University of Trento, 2011.
6. Catapano, I., L. Crocco, and T. Isernia, "On simple methods for shape reconstruction of unknown scatterers," *IEEE Transactions on Antennas and Propagation*, Vol. 55, No. 5, 1431–1436, 2007.
7. Catapano, I. and L. Crocco, "An imaging method for concealed targets," *IEEE Transactions on Geoscience and Remote Sensing*, Vol. 47, No. 5, 1301–1309, 2009.
8. Belkebir, K. and M. Saillard, "Special section: Testing inversion algorithms against experimental data," *Inverse Problems*, Vol. 17, No. 6, 1565–1571, 2001.
9. Geffrin, J. M. and P. Sabouroux, "Continuing with the Fresnel database: Experimental setup and improvements in 3D scattering measurements," *Inverse Problems*, Vol. 25, No. 2, 024001, 2009.

The Scaled Gradient Projection Method: An Application to Nonconvex Optimization

M. Prato[1], **A. La Camera**[2], **S. Bonettini**[3], **and M. Bertero**[2]

[1]Dipartimento di Scienze Fisiche, Informatiche e Matematiche
Università di Modena e Reggio Emilia, Via Campi 213/b, Modena 41125, Italy
[2]Dipartimento di Informatica, Bioingegneria, Robotica e Ingegneria dei Sistemi
Università di Genova, Via Dodecaneso 35, Genova 16145, Italy
[3]Dipartimento di Matematica e Informatica
Università di Ferrara, Via Saragat 1, Ferrara 44122, Italy

Abstract— The scaled gradient projection (SGP) method [1] is a variable metric forward-backward algorithm designed for constrained differentiable optimization problems, as those obtained by reformulating several signal and image processing problems according to standard statistical approaches. The main SGP features are a variable scaling matrix multiplying the gradient direction at each iteration and an adaptive steplength parameter chosen by generalizing the well-known Barzilai-Borwein rules.

An interesting result recently shown by Bonettini [2] is that SGP can be exploited within an alternating minimization approach in order to address optimization problems in which the unknown can be splitted in several blocks, each with a given convex and closed feasible set. Classical examples of applications belonging to this class are the non-negative matrix factorization [3] and the blind deconvolution [4] problems.

In this work we applied this method to the blind deconvolution of multiple images of the same target obtained with different PSFs. In particular, for our experiments we consider the NASA funded Fizeau interferometer LBTI of the Large Binocular Telescope [5], which is already operating on Mount Graham and has provided the first Fizeau images, demonstrating the possibility of reaching the resolution of a 22.8 m telescope. Due to the Poisson nature of the noise affecting the measured images, the resulting optimization problem consists in the minimization of the sum of several Kullback-Leibler divergences, constrained in suitable feasible sets accounting for the different features to be preserved in the object and the PSFs.

REFERENCES

1. Bailey, V. P., P. M. Hinz, A. T. Puglisi, et al., "Large binocular telescope interferometer adaptive optics: On-sky performance and lessons learned," *Proc. SPIE*, Vol. 9148, 914803, 2014.
2. Bonettini, S., "Inexact block coordinate descent methods with application to the nonnegative matrix factorization," *IMA J. Numer. Anal.*, Vol. 31, No. 4, 1431–1452, 2011.
3. Bonettini, S., R. Zanella, and L. Zanni, "A scaled gradient projection method for constrained image deblurring," *Inverse Probl.*, Vol. 25, No. 1, 015002, 2009.
4. Lee, D. D. and H. S. Seung, "Learning the part of objects from non-negative matrix factorization," *Nature*, Vol. 401, No. 6755, 788–791, 1999.
5. Levin, A., Y. Weiss, F. Durand, and W. T. Freeman, "Understanding and evaluating blind deconvolution algorithms," *IEEE Conference on Computer Vision and Pattern Recognition, 2009, CVPR 2009*, 1964–1971, Paris, France, Jun. 2009.

Inverse Source in a Multipath Environment

A. Cuccaro, R. Solimene, and R. Pierri
Dipartimento di Ingegneria Industriale e dell' Informazione
Seconda Unviersita' degli Studi di Napoli, via Roma 29, Aversa 81031, Italy

Abstract— Generally, the problem of detecting and localizing small targets can be tackled by adopting a number of different methods. Migration algorithm, time reversal and strategy based on compressive sensing (when the scene under investigation is sparsely populated) are only a few of examples of them. In all inversion techniques, from the scattered field (radiated field if the target is a source) collected over domain, the position of target have to be inferred. However, it often happens that apart from the field due to the target, the fields produced by further object (generally unwanted) are collected as well. This degrades the performance achievable and the detection can be fail.

In this contribution we measure ourselves with this problem, or rather we addressed the detection of point-like sources in multipath environments. This entails dealing with an inverse source problem. More in detail, the scenario of interest includes an ensemble of point-like passive elements (infinitely long PEC cylinders) positioned between investigation domain (containing only the source) and measurement line. A two dimensional scalar framework is set.

From physical point of view, extra in-homogeneities in the environment originates multipath. Multiple scattered waves are often treated as a disturb to be rejected as they give rise to spurious artifacts in the reconstructed images. However, if the in-homogeneous background is someway characterized (i.e., because it is artificially created) these waves can be exploited positively.

In particular, using effectively this spatial diversity and not a priori discard it, we compare two different linear inversion schemes. The first strategy consists in inverting the radiating operator, which rigorously describe the radiation and interaction between the source and passive elements. In the second one, the inversion is achieved by back-projection, which is one of the methods most commonly used in imaging.

We will show how the performance achievable change with the passive structure compared to the free-space, and how the detection system depend on the positions of these extra-scatterers. Finally, we establish which of two different strategies exploits the best the multipath introduced artificially.

Quantitative Imaging in an Aspect-limited/transmission Configuration: Incorporation of Antennas Radiation Pattern

C. Eyraud, **A. Litman**, **S. Nounouh**, **and H. Tortel**
Aix-Marseille Université, CNRS, Centrale Marseille, Institut Fresnel UMR 7249, Marseille 13013, France

Abstract— Electromagnetic wave probing is an interesting tool to obtain the physical features of unknown targets (position, shape, size, complex permittivity). Indeed, these characteristics can be retrieved from scattered fields measurements thanks to the resolution of a non-linear inverse problem. A key point when dealing with quantitative imaging and experimental data is the calibration procedure.

In spherical/circular configurations, when the antennas are sufficiently far away from the target, the calibration can be performed with a single complex coefficient calculated using a reference target. When the antennas are moving closer to the target, even in full-aperture configurations, the impact of the antenna radiation pattern must be investigated, and more complicated calibration procedures might be required. For example, full coefficient matrices can compensate from the fact that, in antenna arrays, the illumination may differ from one antenna to the other. As well, in aspect-limited configurations, the radiation pattern of each antenna greatly influences the target illumination as well as the scattered field collection.

In this work, we consider a transmission configuration, with antennas moving on open-line. This complicated situation forces us to take into account the effective behaviour of the emitters and the receivers. We thus propose to properly model the radiation pattern of the involved antennas by means of a linear combination of electric dipoles and to incorporate it in inversion algorithms. The forward model as well the computation of the various gradients which are involved in the inversion procedure will be affected by such a model. In this talk, we will analyse the influence of these information thanks to reconstructions obtained from measurements performed in an anechoic chamber.

Frequency and Polarization Diversity in through-the-wall Breath Detection

A. Narbudowicz[1], **M. J. Ammann**[2], **G. Ruvio**[2], **A. Dell'Aversano**[3], **and R. Solimene**[3]

[1]IHF — Institute of High Frequency Technology, RWTH Aachen University, Germany
[2]Dublin Institute of Technology, Ireland
[3]Dipartimento di Ingegneria Industriale e dell'Informazione, Seconda Università di Napoli, Italy

Abstract— In this paper a novel through-the-wall (TTW) breath detection system is studied in terms of different operating frequencies and signal polarization diversity for improved accuracy. The measurement set-up is organized as in Figure 1(a) and includes two sets of circularly-polarized patch antennas (Figure 1(b)) fed by a Vector Network Analyzer (VNA) placed one meter away from a conventional 12-cm thick wall. A subject breathing normally is positioned at a distance of one meter from the other side of the wall with the chest oriented in the direction of maximum radiation of the antenna (1.5 meter from the ground). The return loss of the antenna is acquired at the frequencies 1,575 and 2.575 GHz for vertical, horizontal and Circular-Polarization (CP) of the antenna system, respectively. This large dataset allows a deep investigation on the effects of frequency- and polarization-diversity on the accuracy of the vital sign detection. In particular, measurements taken for different polarizations allow an understanding of the effects of ground bouncing and signal rotation.

The antennas used for the study are CP patches, which offer high gain at minimum complexity. Measurement at 1.575 GHz were conducted using two antennas, located next to each other: one rightand one left-hand circularly polarized. For 2.575 GHz measurement, where the spacing between antennas is more critical due to shorter wavelengths, a dual circularly polarized antenna [1] was used. This allowed to achieve perfect colocation of both polarizations.

As for the breath detection methods, different algorithms are evaluated. In particular, a classical Fourier based method is compared with a novel version of the MUltiple Signal Classification (MUSIC) algorithm.

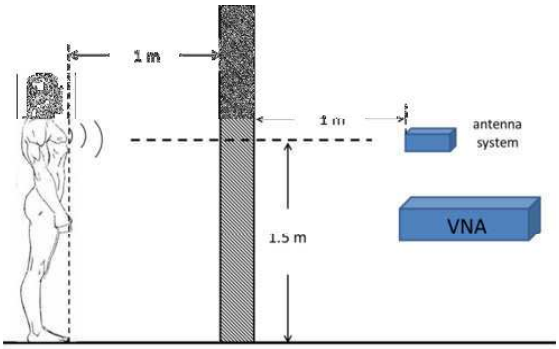

Figure 1: Detail of the measurement set-up.

REFERENCES

1. Narbudowicz, A., X. Bao, and M. J. Ammann, "Dual circularly-polarized patch antenna using even and odd feed-line mode," *IEEE Transactions on Antennas and Propagation*, Vol. 61, No. 9, 4828–4831, 2013.
2. Ascione, M., A. Buonanno, M. D'Urso, L. Angrisani, and R. Schiano Lo Moriello, "A new measurement method based on music algorithm for through-the-wall detection of life signs," *IEEE Transactions on Instrumentation and Measurement*, Vol. 62, No. 1, 13–26, 2013.

Waveforms for SAR Imaging in Dispersive Material

N. A. Cartwright
State University of New York at New Paltz, USA

Abstract— Precursor waveforms are derived from the asymptotic analysis of plane waves scattered from an isotropic point scatterer. These waveforms are then used as the transmit waveform for synthetic-aperture radar imaging through dispersive material. Numerical simulations are used to compare these waveforms with "optimal waveforms".

Motivation: As an electromagnetic wave propagates through a dispersive material, those frequencies that lie below the absorption band experience the least amount of attenuation and hence become the dominant contribution to the field for large propagation distances. Asymptotic analysis has shown that in dielectrics, this low-frequency contribution, the so-called Brillouin precursor, has a peak amplitude point that decays algebraically with propagation distance z, as $z^{-1/2}$ [1]. It has been suggested that near-optimal pulse penetration is possible by using the Brillouin precursor as the transmit pulse, which may then have applicability to radar imaging [2].

The question as to which transmit pulse produces an optimal image in synthetic-aperture radar imaging through dispersive media was addressed in [3, 4]. For large signal-to-noise ratios, the optimal waveform "closely resembles the precursor which is generated from a one-cycle sinusoid. This suggests that under certain conditions, precursors may indeed be useful as transmit waveforms in SAR imaging" [4].

Method of Analysis: Here, we derive the low-frequency transmit precursor waveform for imaging isotropic point scatterers embedded in a Debye-type dielectric material indicative of foliage. This "scattering precursor" is obtained by asymptotic analysis of the integral equation for the scattered field using the Born approximation; it is given in terms saddle point locations and modified Weber functions. In comparison to the Brillouin precursor (or the nonscattered precursor), the scattering precursor pulse consists of higher frequencies but it too has a peak amplitude that decays algebraically with propagation distance, now as $z^{-3/2}$.

Numerical Simulations: We compare the propagation characteristics and imaging results obtained for each transmit pulse (both the nonscattered and scattered precursor waveforms, and the optimal waveform given in [4]). Comparison of the bandwidth of each received pulse gives the spatial resolution of each transmit pulse. It is clear from the results that which waveform is "optimal" depends upon the propagation distance from transmitter to scatterer and back, as well as the dispersive properties of the material.

ACKNOWLEDGMENT

This research has been supported, in part, by the Air Force Office of Scientific Research under grant # FA9500-13-1-0013, and the Department of Mathematics at Colorado State University.

REFERENCES

1. Oughstun, K. E. and G. C. Sherman, "Propagation of electromagnetic pulses in a linear dispersive medium with absorption (the Lorentz medium)," *J. Opt. Soc. Amer. B*, Vol. 5, No. 4, 817–849, 1988.
2. Oughstun, K. E., "Dynamical evolution of the brillouin precursor in rocard-powles-debye model dielectrics," *IEEE Trans. Ant. Prop.*, Vol. 53, No. 5, 1582–1590, 2005.
3. Varslot, T., J. H. Morales, and M. Cheney,"Synthetic-aperture radar imaging through dispersive media," *Inverse Problems*, Vol. 26, 025008, 27 pages, 2010.
4. Varslot, T., J. H. Morales, and M. Cheney,"Waveform design for synthetic-aperture radar imaging through dispersive media," *SIAM J. Appl. Math.*, Vol. 71, No. 5, 1780–1800, 2011.

Session 3P11
SC2&3: Optoelectronics and Photonics of Graphene and Two-dimensional Materials

Graphene Photonics and Optoelectronics

Andrea C. Ferrari
Cambridge Graphene Centre, University of Cambridge, CB3 OFA, UK

Abstract— Graphene has great potential in photonics and optoelectronics, where the combination of its unique optical and electronic properties can be fully exploited, the absence of a bandgap can be beneficial, and the linear dispersion of the Dirac electrons enables ultra-wideband tunability [1–3]. Despite being a single atom thick, graphene can be optically visualized [4]. The linear dispersion of the Dirac electrons enables broadband applications. Saturable absorption is observed as a consequence of Pauli blocking [5–7] and can be exploited for mode-locking and Q switching of a variety of ultrafast and broadband lasers [1, 5–8]. Chemical and physical treatments enable luminescence [1, 8]. Graphene and other two-dimensional materials are also ideal as photodetection platforms [1–3]. The versatility of these material systems enables their application in areas including ultrafast and ultrasensitive detection of light in the ultraviolet, visible, infrared and terahertz frequency ranges [1–3, 10–13]. These detectors can be integrated with other photonic components based on the same material, as well as with silicon photonic and electronic technologies. By combining graphene with plasmonic nanostructures, the efficiency of graphene-based photodetectors can be increased, because of efficient field concentration in the area of a p-n junction [10]. Light-graphene interaction can be tailored by using microcavities [11].

REFERENCES

1. Ferrari, A. C., et al., *Nanoscale*, Vol. 7, 4598, 2015.
2. Bonaccorso, F., et al., *Nature Photon.*, Vol. 4, 611, 2010.
3. Koppens, F. H. L., et al., *Nature Nano*, Vol. 9, 780, 2014.
4. Casiraghi, C., et al., *Nano Lett.*, Vol. 7, 2711, 2007.
5. Hasan, T., et al., *Adv. Mat.*, Vol. 21, 3874, 2009.
6. Sun, Z., et al., *ACS Nano*, Vol. 4, 803, 2010.
7. Sun, Z., et al., *Nano Research*, Vol. 3, 653, 2010.
8. Zaugg, C. A., et al., *Optics Exp.*, Vol. 21, 31548, 2013.
9. Gokus, T., et al., *ACS Nano*, Vol. 3, 3963, 2009.
10. Echtermeyer, T. J., et al., *Nature Commun.*, Vol. 2, 458, 2011.
11. Engel, M., et al., *Nature Commun.*, Vol. 3, 306, 2012.
12. Vicarelli, L., et al., *Nature Materials*, Vol. 11, 865, 2012.
13. Echtermeyer, T. J., et al., *Nano Lett.*, Vol. 14, 3733, 2014.

Graphene Based Optical Modulators

Vito Sorianello[1], **Michele Midrio**[2], **and Marco Romagnoli**[1]

[1]Laboratory of Photonic Networks, CNIT, Via Moruzzi 1, Pisa 56124, Italy
[2]CNIT, Università degli Studi di Udine, Udine 33100, Italy

Abstract— Graphene is shown to allow for the design of an SOI phase modulator with negligible residual amplitude modulation, low insertion loss and record figures of merit with respect to any other technology used so far. In fact graphene based optoelectronics is attracting increasing interest because graphene electro-optical properties can be tuned with a proper gate, as well as because graphene is technologically compatible with other materials, and substantially wavelength independent.

Graphene-assisted electro-absorption modulators, photoconductors and other photodiodes have been demonstrated recently [1, 2]. However, for telecom applications, notably when complex modulation formats are employed to increase the spectral efficiency, availability of phase modulators is of paramount importance too. In this work we show that graphene may allow to realize such a component, with better performance than existing technologies.

A Graphene-Insulator-Graphene capacitor on top of a Si waveguide is used to induce a proper shift of the Fermi potential in graphene. With large enough carrier concentration on the graphene layers, graphene becomes an almost transparent material due to Pauli's blocking principle. Any further change of the carrier concentration only impacts on the graphene dielectric constant. This way, biasing the capacitor and subsequently modulating the applied voltage, phase modulation is achieved [3]. A voltage-length product as low as $V_\pi L = 0.1\,\mathrm{Vcm}$ can be obtained, with an insertion loss of 12 dB/cm. This yields the overall record FOM of 1.2 VdB in a device with driving voltage, footprint and energy per bit consumption in the range of 1 V, $0.5 \div 1$ mm and 0.25–0.01 pJ/bit at 50 Gb/s, depending on the modulator configuration. These figures show that graphene outperforms any other technology used so far for phase modulation. As a matter of fact, modulators based on the plasma-dispersion effect suffer of both residual amplitude modulation and large insertion loss due to the accumulation of carriers. Whereas the footprint of a $LiNbO_3$ modulator is almost an order of magnitude larger than its graphene counterpart.

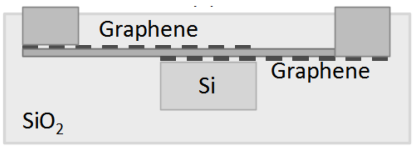

Figure 1: Schematic cross-section of a phase modulator with two layers of graphene on top of a silicon waveguide.

ACKNOWLEDGMENT

The authors acknowledge funding from the EU Graphene Flagship (contract No. 604391).

REFERENCES

1. Liu, M., X. Yin, E. Ulin-Avila, B. Geng, T. Zentgraf, L. Ju, F. Wang, and X. Zhang, "A Graphene-based broadband optical modulator," *Nature*, Vol. 474, 64–67, 2011.
2. Koppens, F. H., T. Muller, Ph. Avouris, A. C. Ferrari, M. S. Vitiello, and M. Polini, "Photodetectors based on graphene, other two-dimensional materials and hybrid systems," *Nature Nanotech.*, Vol. 9, 780–793, 2014.
3. Sorianello, V., M. Midrio, and M. Romagnoli, "Design optimization of single and double layer Graphene phase modulators in SOI," *Optics Express*, Vol. 23, No. 5, 6478–6490, 2015.

Valley and Spin Dynamics in Monolayer MoS_2

S. Dal Conte[1, 2], F. Bottegoni[2], E. A. A. Pogna[2], S. Ambrogio[3], D. De Fazio[4], A. Lombardo[4], M. Bruna[4], I. Bargigia[5], C. D'Andrea[5], A. C. Ferrari[4], F. Ciccacci[2], G. Cerullo[2], and M. Finazzi[2]

[1]IFN-CNR, Piazza L. da Vinci 32, I-20133 Milano, Italy
[2]Dipartimento di Fisica, Politecnico di Milano, Piazza L. da Vinci 32, I-20133 Milano, Italy
[3]Dipartimento di Elettronica, Politecnico di Milano, IU.NET, I-20133 Milano, Italy
[4]Cambridge Graphene Centre, University of Cambridge, 9 JJ Thomson Avenue, Cambridge CB30FA, UK
[5]Center for Nano Science and Technology at PoliMi
Istituto Italiano di Tecnologia, Via Giovanni Pascoli, 70/3Milan, Italy

Abstract— The ability to control the valley degrees of freedom is the foundation of the emerging field of valleytronics [1]. Atomically thin Transition Metal Dichalcogenides (TMDs) are a promising platform for the implementation of new devices exploiting the valley and spin degrees of freedom [2]. Here we measure separately the spin and valley relaxation dynamics of both electrons and holes in the prototypical TMD MoS_2. We disentangle the different processes by the combination of ultrafast optical spectroscopy techniques, i.e., Time Resolved Circular Dichroism (TRCD) and Time Resolved Faraday Rotation (TRFR). TRCD experiments are performed by exciting the sample with an ultrashort circularly polarized pulse, resonant with the optical gap, and measuring the difference between the transient absorption response probed by co- and counter-circularly polarized pulses. The transient absorption is measured on a broad energy range including the A ($\lambda = 650\,\mathrm{nm}$) and B ($\lambda = 605\,\mathrm{nm}$) excitonic transitions at K and K'. These measurements reveal an extremely fast intravalley relaxation of the spin of the photoexcited electrons at the bottom of the conduction band. Furthermore, our data demonstrate that the two non-equivalent valleys K and K' are strongly coupled and the valley polarization is strongly quenched after few ps [3]. In TRFR experiments the pump pulse creates a spin polarized population of electrons/holes in the conduction/valence band, while the rotation angle of the linearly polarized probe pulse is measured by a balanced photodiode bridge technique. We use a two-color TRFR configuration, in which the energy of the probe pulse is tuned well below the absorption gap. In these conditions, the TRFR signal is only sensitive to the helicity-dependent light scattering of the photoexcited electron and hole populations. Since the probe pulse couples with the carrier orbital degree of freedom, the Faraday rotation signal is related to an unbalanced distribution of the photoexcited carrier orbital degrees of freedom. The orbital momentum in MoS_2 single layer is locked with the valley index. Thus, the two color TRFR measurements probe exclusively the intervalley dynamics of electrons and holes. The combination of TRFR and TRCD allows us to disentangle intervalley and intravalley dynamics. Both TRCD and TRFR experiments are quantitatively explained by a set of rate equations which take into account intervalley and intravalley relaxation channels.

REFERENCES

1. Nebel, C. E., "Valleytronics: electrons dance in diamond," *Nature Materials*, Vol. 12, 690–691, 2013.
2. Bahnia, K., "Condensed matter physics: Polarized light boosts valleytronics," *Nature Nanotech.*, Vol. 7, 488–489, 2012.
3. Mai, C., et al., "Many-body effects in valleytronics: Direct measurement of valley lifetimes in single-layer MoS_2," *Nano Lett.*, Vol. 14, 202, 2014.

Charge Photogeneration in Few-layer MoS_2

T. Borzda[1, 2], C. Gadermaier[1, 2], P. Topolovsek[1, 2], M. Borovsak[1, 3], T. Mertelj[1], N. Vujicic[1, 4], G. Cerullo[5], D. Viola[5], C. Manzoni[5], E. A. A. Pogna[5], D. Brida[6], M. R. Antognazza[7], G. Lanzani[5, 7], F. Scotognella[5, 7, 1], and D. Mihailovic[1, 2, 8]

[1]Department of Complex Matter, Jozef Stefan Institute, Jamova 39, Ljubljana 1000, Slovenia
[2]Jozef Stefan International Postgraduate School, Jamova 39, Ljubljana 1000, Slovenia
[3]Faculty of Mathematics and Physics, University of Ljubljana, Jadranska 19, Ljubljana 1000, Slovenia
[4]Institute of Physics, Bijenicka 46, Zagreb 10000, Croatia
[5]IFN-CNR, Department of Physics, Politecnico di Milano, P. Leonardo da Vinci 32, Milan 20133, Italy
[6]Department of Physics and Center of Applied Photonics
University of Konstanz, D-78457 Konstanz, Germany
[7]Center for Nano Science and Technology, Italian Institute of Technology
Via Pascoli 70/3, Milano 20133, Italy
[8]Center of Excellence in Nanoscience and Nanotechnology
Jamova 39, Ljubljana 1000, Slovenia

Abstract— Recent progress in the exfoliation of layered materials and the nanofabrication of functional structures has revived the interest in two-dimensional materials with properties complementary to graphene, in particular transition metal dichalcogenides such as MoS_2. Their potential for electronics has become evident by the realization of a field effect transistor and a logic circuit device based on a single flake of monolayer MoS_2. Despite its high exciton binding energy, monolayer MoS_2 shows a strong photovoltaic effect and potential for high sensitivity photodetectors. Both these functionalities require efficient charge carrier photogeneration, either via direct excitation of mobile carriers or via exciton dissociation.

Here we use continuous wave photomodulation and femtosecond pump-probe spectroscopy to identify the spectral features of photogenerated charges in an ensemble of few-layer MoS_2 dispersed in a transparent polymer and trace their dynamics, starting with their generation either by direct impulsive excitation into the charge continuum or via exciton dissociation. We find that the primary photoexcitations are excitons which dissociate efficiently with a characteristic time of 700 fs. Thus few-layer MoS_2 displays a behavior which is intermediate between conventional semiconductors on the one hand, and high exciton binding energy materials, such as organic semiconductors, carbon nanotubes, and presumably single-layer MoS_2 on the other. High efficiency photodetectors and photovoltaic elements based on monolayer MoS_2 require additional measures to achieve efficient exciton dissociation, such as a strong built-in field using appropriate electrode materials, engineering a p-n junction, or a heterojunction device. According to our findings, in few-layers, which have the added benefit of absorbing a larger fraction of the incident light, such measures should not be necessary and simpler, more scalable device structures could be used.

Negative Dynamic Conductivity in Pumped Graphene Layers "Decorated" with Quantum Dots

M. Ryzhii[1], **D. Svintsov**[2], **T. Otsuji**[3], **V. Ryzhii**[3], **and V. Mitin**[4]

[1]Department of Computer Science and Engineering
University of Aizu, Aizu-Wakamatsu 965-8580, Japan
[2]Laboratory of Nanooptics and Plasmonics
Moscow Institute of Physics and Technology, Dolgoprudny 141700, Russia
[3]Research Institute of Electrical Communication
Tohoku University, Sendai 980-8577, Japan
[4]Department of Electrical Engineering
University at Buffalo, SUNY, Buffalo, NY 1460-1920, USA

Abstract— The gapless energy spectra of graphene layers, bilayers, and non-Bernal-stacked multilayers enables their applications in different terahertz (THz) devices, in particular, THz lasers with the interband population inversion created by optical pumping or injection [1, 2]. The intraband indirect radiative processes lead to significant THz radiation losses due to the Drude absorption. These processes complicate the realization of the graphene-based THz lasers.

Recently, it was shown that the contribution of the indirect interband transitions to the graphene layer dynamic THz conductivity can compensate or even dominate over that of the intraband radiative transitions, provided that the carrier scattering is primarily associated with long-range scattering potentials (natural or artificial) [3]. The total suppression of the Drude absorption in pumped graphene layers is possible if the size of the scattering clusters is sufficiently large (50–100 nm).

In this work, we evaluated of the role of the indirect interband transitions in pumped hybrid graphene-quantum-dot heterostructures (or graphene layers "decorated" with quantum dots [4, 5]). In these structures, the charged quantum dots (or domes) placed near the graphene layer plane form the spatially fluctuating potential relief providing the carrier scattering with relatively small variations of the electron and hole momenta. We demonstrated that despite a fairly small density of states near the graphene layer band edges, the indirect interband generation of photons can surpass their intraband (Drude) absorption, resulting in rather large absolute values of the negative dynamic conductivity in a wide range of THz frequencies at elevated (room) temperatures. The considered graphene-quantum-dot heterostructures can be perspective for graphene-layer-based THz lasers.

REFERENCES

1. Ryzhii, V., M. Ryzhii, and T. Otsuji, *J. Appl. Phys.*, Vol. 101, 083114, 2007.
2. Ryzhii, M. and V. Ryzhii, *Jpn. J. Appl. Phys.*, Vol. 46, L151, 2007.
3. Svintsov, D., V. Ryzhii, and T. Otsuji, *Appl. Phys. Express*, Vol. 7, 115101, 2014.
4. Konstantatos, G., M. Badioli, L. Gaudreau, J. Osmond, M. Bernechea, F. P. Garcia de Arquer, F. Gatti, and F. H. L. Koppens, *Nature Nanotechnol.*, Vol. 7, 363, 2012.
5. Stauber, T., G. Gomez-Santos, and F. Javier Garcia de Abajo, arXiv:1310.6187.

Graphene Nanophotonics

F. Javier García de Abajo[1, 2]

[1]ICFO Institut de Ciències Fotòniques
Mediterranean Technology Park, Castelldefels (Barcelona) 08860, Spain
[2]ICREA-Institució Catalana de Recerca i Estudis Avançats
Passeig Lluís Companys 23, Barcelona 08010, Spain

Abstract— Recent experimental and theoretical advances in the study of graphene plasmons have triggered the search for similar phenomena in other materials that are structured down to the atomic-scale, and in particular, alternative 2D crystals, noble-metal monolayers, and polycyclic aromatic hydrocarbons, which can be regarded as molecular versions of graphene. The number of valence electrons that are engaged in the plasmon excitations of these materials is small compared with those of conventional 3D metallic nanostructures, and consequently, the addition or removal of a comparatively small number of electrons produces sizeable changes in their frequencies and near-field distributions. Graphene in particular has been shown to exhibit a large degree of electrical modulation due to its peculiar electronic band structure, which is characterized by a linear dispersion relation and vanishing of the electron density of states at the Fermi level; few electrons are needed to considerably change the Fermi energy. However, plasmons in graphene have only been observed at mid-infrared and lower frequencies, and therefore, small molecular structures and atomically thin metals constitute attractive alternatives to achieve fast electro-optical modulation in the visible and near-infrared (vis-NIR) parts of the spectrum. In this presentation, were view different strategies and recent advances in the achievement of strong optical tunability in the vis-NIR using plasmons of atomic-scale materials, as well as their potential application for quantum optics, light manipulation, and sensing.

Third Harmonic Generation and Saturable Absorption in Graphene

S. A. Mikhailov and N. A. Savostianova
Institute of Physics, University of Augsburg, D-86135 Augsburg, Germany

Abstract— It was theoretically predicted [1] that the linear energy dispersion of graphene electrons leads to a strongly nonlinear electrodynamic response of this material. This fact has been confirmed in a number of experiments, both at microwave [2] and optical [3] frequencies: the nonlinear parameters of graphene were found to be many orders of magnitude larger than those of many other nonlinear materials.

The results of the theory [1] have been obtained within the quasi-classical Boltzmann kinetic theory which is valid at low (microwave/terahertz) frequencies $\hbar\omega \ll 2E_F$; here E_F is the Fermi energy of graphene electrons. In addition, the nonlinear response of graphene was analyzed in [1] in the collisionless approximation $\tau \to \infty$, where τ is the effective scattering time. In this work we will report on the full quantum theory of the third-harmonic response of graphene [4, 5] valid at arbitrary values of the parameter $\hbar\omega/2E_F$. We show that the dependence of the third-harmonic intensity on the frequency ω of the incident wave should demonstrate a huge resonance at the frequency $\omega = 2E_F/\hbar$. corresponding to the inter-band absorption edge in graphene. The third harmonic intensity is calculated both for the case of an isolated graphene sheet and for graphene layer lying on a dielectric substrate like, e.g., SiO_2/Si.

In addition, we will report on results of the quasi-classical theory of the nonlinear response of graphene at arbitrary values of the external ac electric field and arbitrary values of the scattering parameter $\omega\tau$. Such a non-perturbative solution demonstrates, for example, strong absorption saturation at microwave/terahertz frequencies in the ac electric fields of order of 1 kV/cm.

REFERENCES

1. Mikhailov, S. A., *Europhys. Lett.*, Vol. 79, 27002, 2007.
2. Dragoman, M., D. Neculoiu, G. Deligeorgis, G. Konstantinidis, D. Dragoman, A. Cismaru, A. A. Muller, and R. Plana, *Appl. Phys. Lett.*, Vol. 97, 093101, 2010.
3. Hendry, E., P. J. Hale, J. J. Moger, A. K. Savchenko, and S. A. Mikhailov, *Phys. Rev. Lett.*, Vol. 105, 097401, 2010.
4. Mikhailov, S. A., *Phys. Rev. B*, Vol. 90, 241301(R), 2014.
5. Mikhailov, S. A., *Phys. Rev. B*, Vol. 91, 039904(E), 2015.

Design and Analysis of Tunable Photonic Devices Based on the Co-integration of Graphene and Dielectric Waveguides

A. Locatelli and C. De Angelis
Dipartimento di Ingegneria dell'Informazione, Università degli Studi di Brescia, Brescia, Italy

Abstract— The peculiar properties of graphene have been attracting the ever increasing interest of the scientific community since the 2010 Nobel Prize in Physics, which was awarded to Novoselov and Geim for their groundbreaking studies. Scientists have already envisaged a plethora of innovative applications in electronics and photonics which exploit the unique characteristics stemming directly from the Dirac dispersion relation of electrons in graphene [1]. In particular, the ultrafast tunability of the electromagnetic parameters of this two-dimensional material can be a key feature for the realization of novel photonic devices. In this context, well-established analytical models are available nowadays to describe both the linear and the nonlinear optical properties of graphene in terms of its 2D complex surface conductivity σ_{2D} [2].

The interaction length between light and graphene is limited by the atomic thickness of the material therefore, following the idea proposed by Liu et al. in a seminal paper [3], several structures based on the co-integration of conventional dielectric waveguides and graphene have been reported, with the goal of perturbing the propagation of a guided mode by means of localized variations of the electromagnetic parameters. This concept allowed to propose, for instance, optical amplitude [3, 4] and phase modulators [5], tunable directional couplers [6, 7] and highly nonlinear waveguides [8]. Most of these structures have been characterized by resorting to full-wave simulations where graphene was modeled as a 3D brick with atomic thickness Δ, and volume conductivity $\sigma_{3D} = \sigma_{2D}/\Delta$. This approach is straightforward but it is characterized by a huge (and often unacceptable) computational burden, thus modeling techniques based on surface current boundary conditions [7, 8] and/or perturbation theory [5, 7, 9] have also been proposed.

In this work we will first review the state-of-the-art of modeling of photonic devices based on the co-integration of conventional dielectric waveguides and graphene. Then, we will systematically study the possibility of applying computationally efficient techniques, such as perturbation theory [9], for the analysis and the design of linear and nonlinear devices for optical processing. We will demonstrate that the effects induced by the tunability of the conductivity of graphene, which can be due to an electrical bias and/or to the Kerr effect, can be accurately predicted by exploiting the "concentrated" nature of the perturbation introduced by the graphene layers.

REFERENCES

1. Focus Issue on "Graphene applications," *Nature Nanotech.*, Vol. 9, No. 10, 2014.
2. Mikhailov, S. A., "Quantum theory of third-harmonic generation in graphene," *Phys. Rev. B*, Vol. 474, No. 21, 241301(1–4), 2014.
3. Liu, M, X. Yin, E. Ulin-Avila, B. Geng, T. Zentgraf, L. Ju, F. Wang, and X. Zhang, "A graphene-based broadband optical modulator," *Nature*, Vol. 90, No. 21, 64–67, 2011.
4. Midrio, M., S. Boscolo, M. Moresco, M. Romagnoli, C. De Angelis, A. Locatelli, and A. D. Capobianco, "Graphene-assisted critically-coupled optical ring modulator," *Opt. Express*, Vol. 20, No. 21, 23144–23155, 2012.
5. Midrio, M., P. Galli, M. Romagnoli, L. C. Kimerling, and J. Michel, "Graphene-based optical phase modulation of waveguide transverse electric modes," *Photon. Res.*, Vol. 2, No. 3, A34–A40, 2014.
6. Locatelli, A., A. D. Capobianco, M. Midrio, S. Boscolo, and C. De Angelis, "Graphene-assisted control of coupling between optical waveguides," *Opt. Express*, Vol. 20, No. 27, 28479–28484, 2012.
7. Locatelli, A., A. D. Capobianco, G. F. Nalesso, S. Boscolo, M. Midrio, and C. De Angelis, "Graphene-based electro-optical control of the beat length of dielectric couplers," *Opt. Commun.*, Vol. 318, 175–179, 2014.
8. Auditore, A., C. De Angelis, A. Locatelli, S. Boscolo, M. Midrio, M. Romagnoli, A. D. Capobianco, and G. F. Nalesso, "Graphene sustained nonlinear modes in dielectric waveguides," *Opt. Lett.*, Vol. 38, No. 5, 631–633, 2013.
9. Kogelnik, H., "Theory of dielectric waveguides," *Integrated Optics*, Springer-Verlag, 1985.

Enhanced Nonlinear Interactions in Graphene-based Photonic Structures

D. de Ceglia[1], **M. A. Vincenti**[1], **M. Grande**[2], **A. D'Orazio**[2], **and M. Scalora**[3]

[1]Charles M. Bowden Research Laboratory, National Research Council — AMRDEC
Redstone Arsenal, AL 35898, USA
[2]Dipartimento di Ingegneria Elettrica e dell'Informazione (DEI)
Politecnico di Bari, Via Re David 200, Bari 70126, Italy
[3]Charles M. Bowden Research Laboratory, AMRDEC
US Army RDECOM, Redstone Arsenal, AL 35898, USA

Abstract— Third-order nonlinear response of monolayer graphene may be significantly magnified by inserting it in properly designed photonic structures, such as defective periodic structures and resonant gratings. Placing graphene within the defect layer of an asymmetric, one-dimensional photonic crystal induces near-perfect absorption in the narrow frequency band associated with the defect mode of the structure. In particular, the enhanced field localization within the defect state amplifies third-harmonic generation efficiency by nearly five orders of magnitude compared with bare monolayer graphene. The role of the structure's asymmetry, the angular and polarization dependence of the linear and nonlinear response will be discussed. The effects of saturation of the third-order susceptibility will be investigated at both the fundamental and third-harmonic frequencies. Finally, we will show the possibility to achieve controllable saturable absorption for the pump signal.

Modeling Graphene Based Couplers and Arrays

Alejandro B. Aceves
Department of Mathematics, Southern Methodist University, Dallas, TX 75275, USA

Abstract— Exploiting the nonlinear properties of graphene layers, we study multi-layer systems for which each layer can be independently modulated. We have shown proof of principle in a 2-layer nonlinear coupler, where small variations of the chemical potential gives wide variations in the beating length, idea for a graphene-based fast switch. Here we will present studies in multi-layer graphene-based systems including nonlinear arrays and the dynamics and properties that can exhibit such systems.

Discrete Solitons in Graphene-based Metamaterials

Yu. V. Bludov[1], **D. A. Smirnova**[2], **Yu. S. Kivshar**[2], **N. M. R. Peres**[1], **and M. V. Vasilevskiy**[1]

[1]Centro de Física and Departamento de Física, Universidade do Minho
Campus de Gualtar, Braga 4710-057, Portugal
[2]Nonlinear Physics Center, Research School of Physics and Engineering
Australian National University, Canberra ACT 0200, Australia

Abstract— One of the remarkable properties of nonlinear systems is the ability to sustain a localized wavepackets-solitons, which can propagate over long distance without loosing its shape. In the area of plasmonics discrete solitons can be observed in the metal-dielectric multilayers [2]; periodical arrays of nanowires [3] or nanoparticles [4]. Recently it was shown, that a 2D material graphene is strongly nonlinear material [5]. In order to increase the effective nonlinearity of photonic structures with graphene, a natural idea is to use graphene multilayers which, depending on different wavelength regimes, may possess the basic properties of photonic crystals and metamaterials.

In this article, we study nonlinear properties of multilayer metamaterials. created by graphene sheets separated by dielectric layers. We show that this type of metamaterial is essentially nonlinear, and the origin of nonlinearity is the Dirac-cone shape of the charge-carriers spectrum in the graphene. The expression for the graphene's nonlinear conductivity [6] is obtained using the Boltzmann kinetic equation formalism. We demonstrate that such a multilayer structures are described exactly by the stationary discrete nonlinear Schrödinger equation, and, as a result, can support spatially localized nonlinear modes in the form of discrete solitons. We show the existence of two types of solitons. The plasmonic soliton (example is shown in Fig. 1) bifurcates from the low-frequency boundary of the first band (black domain in left panel of Fig. 1), exists in the semi-infinite gap, and is characterized by the evanescent waves in the dielectric between the graphene layers. In the vicinity of the band edge the soliton is delocalized — its electric field is distributed over a large number of graphene layers [panel A]. When frequency is detuned from the band edge, the soliton becomes more localized [panel B]. The *photonic soliton* exist in the upper (finite) gaps of the spectrum, and is characterized by propagating waves in the dielectric between graphene layers.

We also analyze the nonlinear surface modes in truncated graphene metamaterials being a nonlinear analog of surface Tamm states.

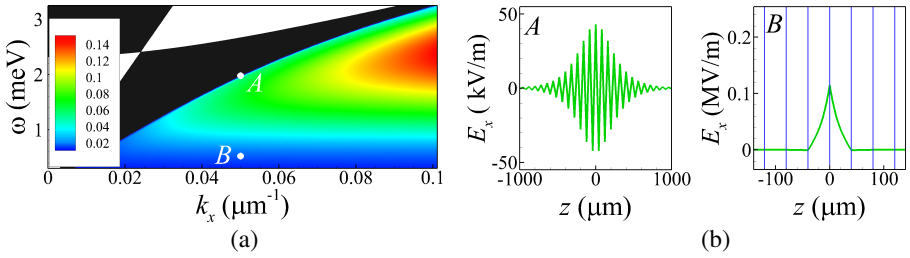

Figure 1: (a) Dependence of soliton norm P (in MV^2/m^2) upon frequency ω and wave vector k_x for the Fermi energy of graphene $E_F = 0.157\,\text{eV}$, interlayer distance $d = 40\,\mu\text{m}$, and dielectic layer permeability $\varepsilon = 3.9$; (b) Soliton spatial profiles for $k_x = 0.05\,\mu\text{m}^{-1}$ and $\omega = 1.98\,\text{meV}$ [panel A], or $\omega = 0.52\,\text{meV}$ [panel B].

REFERENCES

1. Kou, Y., F. Ye, and X. Chen, *Opt. Lett.*, Vol. 38, 1271, 2013.
2. Ye, F., D. Mihalache, B. Hu, and N. C. Panoiu, *Phys. Rev. Lett.*, Vol. 104, 106802, 2010.
3. Noskov, R. E., P. A. Belov, and Y. S. Kivshar, *Phys. Rev. Lett.*, Vol. 108, 093901, 2012.
4. Mikhailov, S. A. and K. Ziegler, *J. Phys.: Condens. Matter*, Vol. 20, 384204, 2008.
5. Bludov, Y. V., D. A. Smirnova, Y. S. Kivshar, N. M. R. Peres, and M. V. Vasilevskiy, *Phys. Rev. B*, Vol. 91, 045424, 2015.

Dyakonov-like Plasmonic Localized Waves on Graphene Metasurfaces

I. V. Iorsh[1], **I. Trushkov**[1], **O. Yermakov**[1,2], **A. Ovcharenko**[1,2], **A. A. Bogdanov**[1,3], **P. A. Belov**[1], **and Yu. S. Kivshar**[1,4]

[1]ITMO University, Russia
[2]V. N. Karazin Kharkiv National University, Ukraine
[3]Ioffe Institute, Russia
[4]Australian National University, Australia

Abstract— We study electromagnetic properties of a metasurface formed by array of coupled graphene nanoribbons. We show that surface conductivity tensor has principal components of different sign and the system supports Dyakonov-like plasmonic surface modes.

Introduction: Graphene, two-dimensional lattice of carbon atoms, exhibits a wide range of unique electronic and optical properties [1]. Graphene plasmonics [2] became a rapidly growing research field, both because plasmons in graphene exist in widely demanded THz field and because they can be effectively tuned with an external gate voltage. In [3] it has been shown that a wide range of metasurfaces can be construced based on graphene sheets. In our work we show that nanostructuring the graphene sheet we can tailor the electronic properties directly and as consequence control the conductivity of these metasurfaces.

Conductivity and localized surface waves of the metasurface: We study the system shown in Fig. 1: We calculate the electronic band structure and eigenfunctions for the array of tunnel coupled armchair and zigzag nanoribbons. We show that the coupled edge states of zigzag nanoribbons form the additional electronic band characterizing by the hyperbolic Fermi surface and the band structure of coupled armchair ribbons is characterized by the overlap of electron and hole bands which results in the Fermi surfaces which simultaneously possess electron and hole pockets. Then, using the Kubo formula we calculate the AC conductivity tensors of these structures. We show that for the case of armchair nanoribbons (see Fig. 1) the system can be described by an uniaxial conductivity tensor with principal components of different sign and low loss. We obtain the dispersion equation for the Dyakonov-like surface modes at the anisotropic metasurface. We also study the polarization properties of the localized waves: these modes are linear combination of TM and TE surface plasmon modes appearing in 2 dimensional graphene. Directivity of these plane waves can be controlled with the external voltage which can be used for the creation of graphene-based photonic integrated circuits.

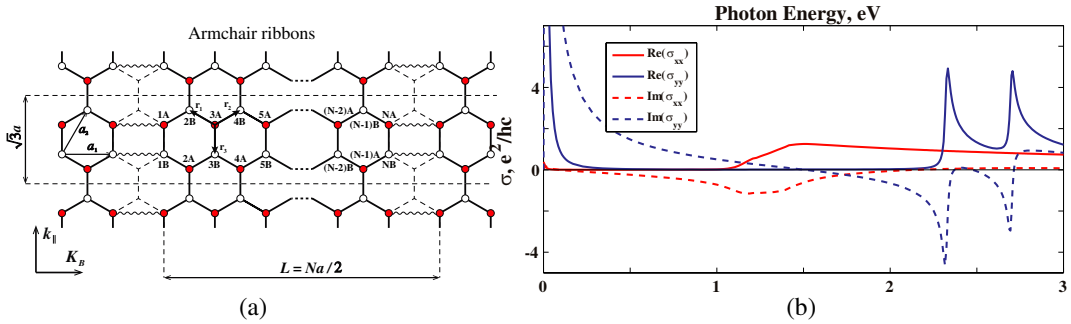

Figure 1: (a) Atomic structure and (b) conductivity of the array of armchair nanoribbons.

REFERENCES

1. Nair, R. R., P. Blake, A. N. Grigorenko, K. S. Novoselov, T. S. Booth, T. Stauber, N. M. R. Peres, and A. K. Geim, "Fine structure constant defines visual transparency of graphene," *Science*, Vol. 320, 1308, 2008.
2. Grigorenko, A. N., M. Polini, and K. S. Novoselov, "Graphene plasmonics," *Nature Photonics*, Vol. 6, 749, 2012.
3. Vakil, A. and N. Engheta, "Transformation optics using graphene," *Science*, Vol. 332, 1291, 2011.

Analysis of Graphene Plasmonic Waveguides and Switching Components via a Finite Element Formulation with Surface Conductivity

I. Demirtzioglou and T. V. Yioultsis
Department of Electrical and Computer Engineering, Aristotle University of Thessaloniki
Thessaloniki 54124, Greece

Abstract— We present an efficient finite element formulation for the eigenmode analysis of graphene-based plasmonic waveguides with switching functionalities. The formulation is full-vectorial and addresses graphene as a surface conductivity, as opposed to a bulky material considerations, thus eliminating the need for fine discretizations inside thin graphene models.

Introduction: Graphene is a ground-breaking material, with a multitude of significant properties and effects, including the ability to support surface plasmon propagating modes and switching functionalities [1]. Optical conductivity of graphene has been shown to consist of a Drude intraband term and an interband contribution. These properties may result in either plasmonic modes in THz [2] or enhanced switching in photonic waveguides for the optical communications regime [3].

Finite Element Formulation: The proposed finite element eigenmode formulation starts from a general framework that has been proposed in [4], where the electric field is used as a working variable, with vector finite elements in the transverse plane and a scalar axial component. The quadratic eigenvalue problem is of the form,

$$\left\{ \begin{bmatrix} \mathbf{S}^t - k_0^2 \mathbf{T}^t & 0 \\ 0 & -\mathbf{S}^{z,m} + k_0^2 \mathbf{T}^z \end{bmatrix} + n_{eff} \begin{bmatrix} 0 & -jk_0 \mathbf{P} \\ -jk_0 \mathbf{Q} & 0 \end{bmatrix} + n_{eff}^2 \begin{bmatrix} k_0^2 \mathbf{T}^{t,m} & 0 \\ 0 & 0 \end{bmatrix} \right\} \begin{bmatrix} \mathbf{E}_t \\ \mathbf{E}_z \end{bmatrix} = 0 \quad (1)$$

where the corresponding finite element matrices may involve transverse or axial basis functions or a combination of both. Mass matrices in (1) involve also line integral terms coming from the surface treatment of graphene structures. Perfectly matched layers are used as domain terminating conditions, while linearization of (1) results in positive semidefinite matrices, suitable for sparse eigensolvers.

Plasmonic and Switching Components: The proposed formulation is able to analyze both plasmon graphene ribbon waveguides in the THz regime (Fig. 1(a)) and a switching-capable waveguide structure for telecom applications, based on the CGS waveguide [5], which is properly enhanced by graphene (Fig. 1(b)). Based on the analysis, we have been able to propose a graphene-enhanced plasmonic CGS waveguide with an extinction ratio of 8.6 dB and a 2.15 dB insertion loss for a 10 μm length, which is highly promising for further study.

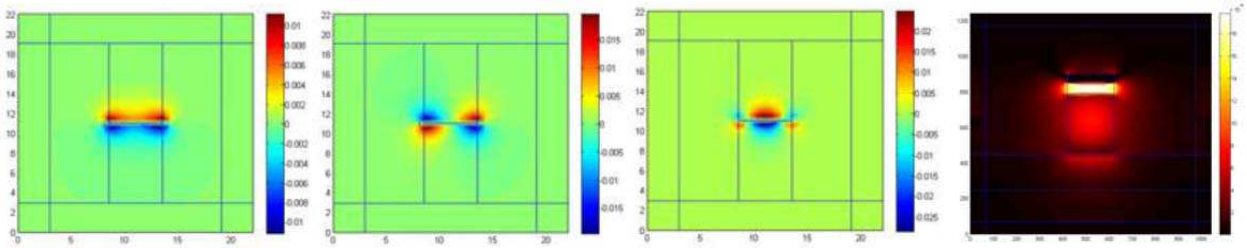

(a) (b)

Figure 1: Mode profiles (a) for three modes of a 5 μm graphere ribbon waveguide, (b) for a graphene-enhanced CGS waveguide.

REFERENCES

1. Bludov, Y. V., A. Ferreira, N. M. R. Peres, and M. I. Vasilevskiy, "A primer on surface plasmon-polaritons in graphene," *Int. J. Mod. Phys. B*, Vol. 27, 1341001, 2013.
2. Nikitin, A. Y., F. Guinea, and F. J. García-Vidal, "Edge and waveguide terahertz surface plasmon modes in graphene microribbon," *Phys. Rev. B*, Vol. 84, 161407(R), 2011.

3. Sun, Y., Z. Zheng, J. Cheng, and J. Liu, "Graphene surface plasmon waveguides incorporating high-index dielectric ridges for single mode transmission," *Optics Communications*, Vol. 328, 124–128, 2014.
4. Selleri, S., L. Vincetti, A. Cucinotta, and M. Zoboli, "Complex FEM modal solver of optical waveguides with PML boundary conditions," *Optical and Quantum Eletronics*, Vol. 33, Nos. 4–5, 359–371, 2001.
5. Wu, M., Z. Han, and V. Van, "Conductor-gap-silicon plasmonic waveguides and passive components at subwavelength scale," *Optics Express*, Vol. 18, No. 11, 11728–11736, 2010.

Propagation of Quasi-TEM Waves in a Graphene Parallel Plate Waveguide Involving Discontinuities

S. Akşimşek
Istanbul Kültür University, Turkey

Abstract— In this paper, propagation of quasi-TEM waves in a 2-D graphene parallel plate waveguide (GPPWG) involving discontinuities [1] is investigated. The purposed waveguide structure involves some certain geometrical and physical discontinuities as illustrated in Figure 1, and the mentioned discontinuity (scattering) mechanisms are: 1) a junction region of thickness b stemming from the latitudinal sudden change between the plates, and 2) different dielectric substrates on each side of the junction region and on this region as well, respectively. The surface of the plates are represented by an anisotropic model of an infinitesimally thin graphene sheet which has a dispersive conductivity term derived from Kubo formula [2].

The Mode-Matching technique, which is the well-known rigorous frequency domain method, is applied to the geometry by determining the guided field terms at the junction region and both sides of this region, and matching them at the junction's boundaries by employing the continuity relations following a similar procedure in [3]. At the end of the analysis the obtained infinite sets of equations are truncated by a truncation number such N. After numerical evaluation of these equations, the scattering coefficients are obtained and solved computationally [4]. The graphical results of the scattering coefficients show the effect of the discontinuities on the propagation of quasi-TEM waves along the purposed waveguide modal, and these results construct a solid knowledge for future applications of nanophotonic devices at sub-THz frequency range.

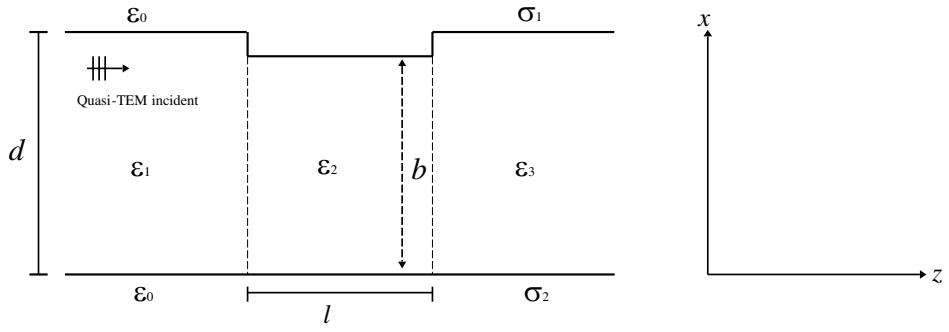

Figure 1: The geometry of 2-D graphene parallel plate waveguide involving discontinuities.

REFERENCES

1. Hanson, G. W., "Quasi-transverse electromagnetic modes supported by a graphene parallelplate waveguide," *Journal of Applied Physics*, Vol. 104, No. 8, 084314–084314-5, 2008.
2. Lovat, G., P. Burghignoli, and R. Araneo, "Low-frequency dominant-mode propagation in spatially dispersive graphene nanowaveguides," *IEEE Transactions on Electromagnetic Compatibility*, Vol. 55, No. 2, 328–333, 2013.
3. Akşimşek, S., G. Çınar, B. Nilsonn, and S. Nordebo, "TEM wave scattering by a step discontinuity on the outer wall of a coaxial waveguide," *IEEE Transaction on Microwave Theory and Techniques*, Vol. 61, No. 8, 2783–2791, 2013.
4. Wartak, M. S., *Computational Photonics: An Introduction with MATLAB*, Cambridge University Press, New York, 2013.

Session 3P12
Antennas and RF Devices Based on Superconductors and Other Advanced Materials

Reconfigurable Antenna Design

Yahya S. H. Khraisat and Ahmad H. N. Qubaia
Electrical and Electronics Department, Al-Balqa' Applied University/Al-Huson University College
P. O. Box 1375, Irbed 21110, Jordan

Abstract— A compact of a reconfigurable rectangular microstrip slot patch antenna of operating frequencies in the range of (2–6) GHz is proposed for Wireless Local Area Network (WLAN) applications. It has one port excited with microstrip line feed mechanism. The proposed antenna consists of a single layer patch antenna with two parallel slots designed that can be controlled via two switches. Two parallel slots are incorporated to perturb the surface current path, introducing local inductive effect that is responsible for the excitation of the second resonant mode. By adjusting the status of the switches state either *on* or *off* mode in simultaneously, the resonance frequencies can be varied, thus achieving frequency reconfigurable.

I represent a fully information and design for reconfigurable antenna to use it in a new hybrid device known Cognitive Radio CR. A cognitive radio CR is a wireless transponder that can sense the environment in which it wishes to operate and can adapt itself to optimize its operation. Sensing the environment may involve the measurement of the communications traffic and interference across a large part of the electromagnetic spectrum. The radio will also have knowledge of the intentions of its user, to enable it to match its searches to the needs of the user. In simple words the operations consist of Sensing and Reconfigurability called a Cognitive Radio CR.

A Utility Maximization Approach to MAC Layer Channel Access and Forwarding

Sunil Kumar[1, 2], **Priya Ranjan**[1], **and Malay Ranjan Tripathy**[1]

[1]Amity School of Engineering and Technology
Amity University Uttar Pradesh, Noida, Uttar Pradesh, India
[2]ABES Engineering College, Ghaziabad, Uttar Pradesh, India

Abstract— The directional antenna technology in wireless mesh network is used to improve the spatial reuse of the wireless channel, where nodes communicate simultaneously without interference of each other. Compare to omnidirectional antenna, directional antenna establish links between nodes far away from each other, and reduce the number of routing hops.

Innovative technology is required to meet customer demands and improve the performance in WLAN 802.11. Large number of access point cannot be implemented due to infrastructure limitation like wiring from access point to router or modem. Wireless is a scalable, reliable and cost effective technology which can be used to propose a utility maximization approach to MAC layer channel access and forwarding.

In this paper a nonlinear utility optimization based approach is proposed to share bandwidth channel resources among interfering interfaces both in presence of balanced and unbalanced traffic. We propose a new algorithm to provide channel access information in dynamic network scenario. This work implements nonlinear utility maximization based on data rate and tested indoor IEEE WLAN 802.11n+s. It will hopefully bridge the gap between economic perspective of resource allocation and technological efficiency of WLAN. This can lead to a programmable interface for management and control of physical layer resources in an optimal fashion.

REFERENCES

1. Sana, G., M. G. Sonia, and K. Farouk, *Comparison of Proposed Path Selection Protocols for IEEE 802.11s WLAN Mesh Networks*, 17–28, Springer, Boston, 2010.
2. Chakraborty, S., S. Sharma, and S. Nandi, "Performance optimization in single channel directional multi-interface IEEE 802.11s EDCA using beam prioritization," *Proceedings of the IEEE International Conference on Communication*, Jun. 2012.
3. "IEEE standard for information technology-telecommunications and information exchange between systems local and metropolitan area networks specific requirements part 11: Wireless LAN medium access control (MAC) and physical layer (PHY) specifications," *IEEE Std 802.11-2012 (Revision of IEEE Std 802.11-2007)*, 1–2793, Mar. 2012.
4. Kapnadak, V., M. Senel, and E. J. Coyle, "Distributed iterative quantization for interference characterization in wireless net-works," *Digit. Signal Process.*, Vol. 22, No. 1, 96–105, Jan. 2012.

Superconducting Receive-only 7 Tesla Antennas for High Resolution Magnetic Resonance Imaging

Jarek Wosik[1, 2], **Krzysztof Nesteruk**[3], **Kuang Qin**[1, 2], **Tan I-Chih**[4], **Kurt Bockhorst**[5], **and Ponnada A. Narayana**[5]

[1]1Electrical and Computer Engineering, University of Houston, Houston, Texas, United States
[2]Texas Center for Superconductivity, United States
[3]Institute of Physics of Polish Academy of Sciences, Warsaw, Poland
[4]The Brown Foundation Institute of Molecular Medicine
The University of Texas Health Science Center, Houston, Texas 77030, United States
[5]Department of Radiology, University of Texas Health Science Center, Houston, Texas, United States

Abstract— The noise in magnetic resonance imaging (MRI) systems is primarily thermal noise generated in the receiver Faraday coil (rf resonator) and in the imaged body. There are two regimes for the thermal noise induced conductive losses in the MRI systems. In the first one, the overall rf loss is body loss dominated, so the SNR is governed by the body loss, in the second instance, loss occurs predominantly in the coil. Therefore in the latter case, reducing the coil resistance or/and temperature can result in significant thermal noise reduction. This can be realized by coils made out of high-temperature superconducting (HTS) materials known for their very low rf surface resistance R_s. Furthermore, relatively high critical temperature of HTS materials allows for cryostat design simplifications, which enables short range distance between the HTS coil and the body.

We report on the design, construction, and validation of receive-only MRI cryo-probe operating at 7 T based on HTS coil integrated with tuning/matching to 50 Ω and de-coupling circuitry. The coil is designed as a double-sided structure, consisting of two split rings, the gaps in each quasiring rotated 180 from each other (Fig. 1). Such structures have been referred to as twin horse-shoe (H-S) resonator and its double-sided configuration introduces not only distributed capacitance, but also reduces capacitive loss by concentrating the electric field within low-loss substrate. HFSS software package (Ansoft) was used to design both copper and HTS coils with dimensions according to the resonant frequency and field-of-view requirements.

The Cu coil and electronic circuit layout was patterned using LPKF PhotoMat C100. Double-sided Cu high frequency laminate ($\varepsilon = 2.2$ and thickness of 0.38 mm) was used for the coil fabrication. Superconducting coils were made of epitaxially grown 0.5 μm thick YBCO superconducting films, which were patterned using optical lithography and wet etching. Two split quasi rings were fabricated on both sides of a 0.33 mm thick Al_2O_3 ($\varepsilon = 10.4$) wafer to create a 300 MHz resonator. A closed cycle pulsed tube cryogenic system (CryoMech HTP10) was used to cool the probe.

Our main interest in this work was the identification of all losses, such as rf coil ($\sim 1/Q_{coil}$), body ($\sim 1/Q_{body}$), cryostat ($\sim 1/Q_{cryostat}$) and tuning/maching/decoupling electronics ($\sim 1/Q_{electronics}$) losses, and assessment of the probe SNR limits. We have measured all loss components of the system. In addition, the influence of magnetic flux (7 T) on the HTS coil was also investigated. YBCO thin film is in the mixed superconducting state at 7 T, which can result in higher losses. The electronic loss ($\sim 1/Q_{electronics}$) increased in 7 T from 1/1600 to $\sim$ 1/900. Most likely such increase is due to magneto-resistive effects in varactors diodes used in the electronic circuit.

From Q measurements (Qcoil, Q_{body}, $Q_{cryostat}$ and $Q_{electronics}$) it was found that for *in-vivo* rat imaging the SNR gain of the system is limited by rf body losses. In such a case, the SNR gain can be adjusted by changing the coil size. For small samples, such as those used for *in-vitro* microscopy imaging, electronics losses turned out to be limiting factors. Further increase of the SNR gain for microscopy will require use of a cryogenic preamplifier and also further reduction of the tuning/matching circuit losses.

SNR gains, tested on phantom and rats at 300 MHz in a few cryogenic configurations, were measured as $\sim$ 6 dB and $\sim$ 8 dB for cooled Cu and HTS coils over room temperature copper, respectively.

Long Range Induction between Josephson Junction Arrays via Microwave Photon Emission and Absorption

Wei-Chen Chien[1], **Cheng-An Jiang**[2], **Jia-Yu Hong**[2], **Yung-Fu Chen**[3], **Cen-Shawn Wu**[2], **Hiroshi Shimada**[4], **and Watson Kuo**[1]

[1]Department of Physics, National Chung Hsing University, Taichung 402, Taiwan
[2]Department of Physics, National Chang-Hua University of Education, Chang Hua 500, Taiwan
[3]Department of Physics, National Central University, Chung-Li, Taiwan
[4]Department of Engineering Science, University of Electro-Communications, Tokyo, Japan

Abstract— Strong induction between one-dimensional arrays of Josephson junctions separated with tens of micrometers were observed and analyzed. Arrays have a structure of superconducting quantum interference device (SQUID) connected in series, allowing one to tune Josephson coupling energy by changing the flux threading a SQUID loop. Constituent Josephson junctions were made of $Al/AlO_x/Al$ with a typical size of 100 nm, giving a charging energy of about 50 μeV. A dc current biased in one array may increase the conductance of nearby isolated arrays. Because of large inter-array distance, this mutual induction cannot be explained by capacitive coupling between two arrays [1]. It turns out that the conductance change can be understood under a picture of phase diffusion introduced by microwave excitation [2]. A detail analysis reveals that excitation microwave power is proportional to bias current in the emitter. The induction strength is largest when charging energy is dominant over Josephson coupling energy, a similar trend that an array responds to microwave excitations [3]. In short range, induction strength is inversely proportional to inter-array distance, suggesting a microwave power emission. This induction provides an application of long-range and fast signal coupler.

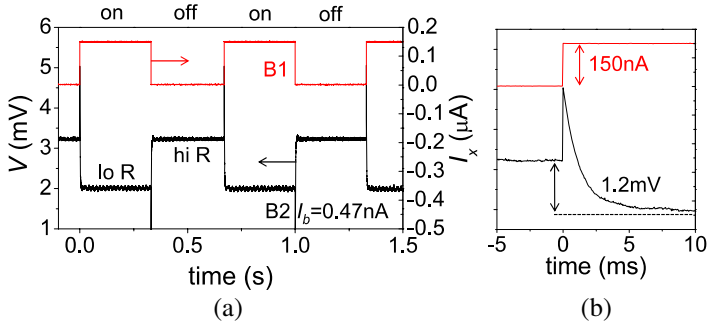

Figure 1: Demonstration of long-range digital signal coupler. (a) Time scan of the output voltage of receiving array under a bias current of 0.47 nA when the emitting array is cyclically switched on and off. When emitter current is switched on, the voltage drops due to a rapid change from high resistance (hi R) state to a low resistance state (lo R). (b) The receiving array responses with a characteristic time smaller than 5 ms, which is limited by our wiring and voltage pre-amplifier.

REFERENCES

1. Shimada, H., C. Ishida, and Y. Mizugaki, *Phys. Rev. Lett.*, Vol. 109, 196801, 2012.
2. Liou, S., W. Kuo, Y. W. Suen, C. S. Wu, and C. D. Chen, *New Journal of Physics*, Vol. 10, 073025, 2008.
3. Liou, S., C. C. Chang, and W. Kuo, *EPL (Europhysics Letters)*, Vol. 108, 67003, 2014.

Multi Band Metamaterial Based Bowtie Antenna for Wireless Applications

Rajesh Kumar[1, 2], **M. R. Tripathy**[1], **and Daniel Rönnow**[3]

[1]Department of Electronics and Communication Engineering, ASET, Amity University, Noida, India
[2]Department of Electronics and Communication Engineering, BSAITM, Faridabad, Haryana, India
[3]Department of Electronics, Mathematics and Natural Sciences, University of Gavle, Gavle, Sweden

Abstract— In this paper a new design of meta-fractal antenna is proposed. The dimension of the patch is $40 * 40\,\mathrm{mm}^2$ and the FR4 substrate is used for this. The patch antenna with metamaterial ground plane is shown in Fig. 1(a). The first iterated fractal antenna with the meta-material is shown in Fig. 1(b). The 2nd and 3rd iterated fractal antennas with metamaterial ground plane are shown in Fig. 1(c) and Fig. 1(d).

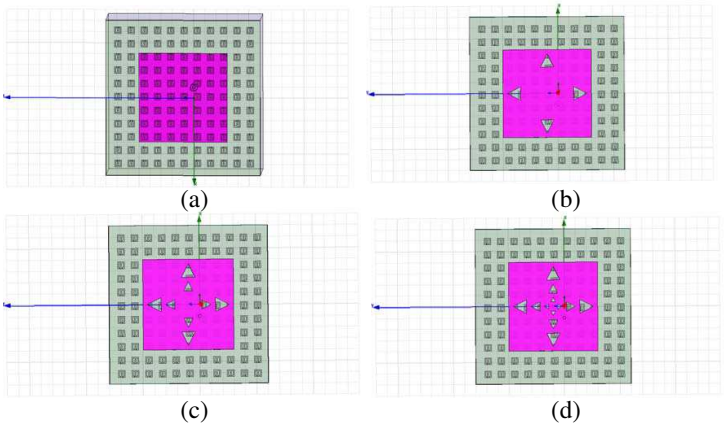

Figure 1: (a) Patch antenna with metamaterial ground plane. (b) 1st iterated meta-fractal antenna. (c) 2nd iterated meta-fractal antenna. (d) 3rd iterated meta-fractal antenna.

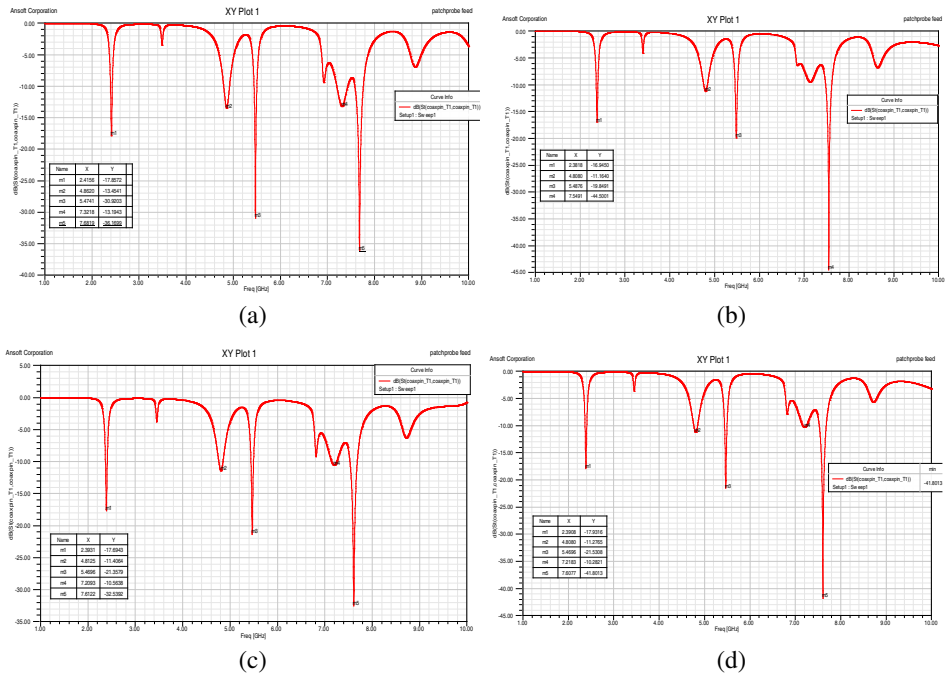

Figure 2: (a) Patch antenna with metamaterial. (b) 1st iterated meta-fractal antenna. (c) 2nd iterated meta-fractal antenna. (d) 3rd iterated meta-fractal antenna.

The results are shown in Figs. 2(a)–(d). As we increase the iterations, different results are seen. The band width used to increase for higher iterations. The return loss results shows better in some of frequency bands for higher iterations and it get degraded for other frequency bands. All these results are analyzed and discussed in detail in the paper.

REFERENCES

1. Smith, D., D. Vier, T. Koschny, and C. Soukoulis, "Electromagnetic parameter retrieval from inhomogeneous metamaterials," *Physical Review E*, Vol. 71, 036617, 1–11, 2005.
2. Chen, J., W. Chen, J. Yen, L. Chen, and C. Wang, "Comparative analysis of split-ring resonators for tunable negative permeability metamaterial based on anisotropic dielectric substrates," *Progress In Electromagnetics Research M*, Vol. 10, 25–38, 2009.
3. Ye, J., Q. Cao, and W. Tam, "Design and analysis of a miniature metamaterial microstrip patch antenna," *IEEE Trans. on Anatenna and Wave Propagation*, 290–293, 2011.

Effect on Lefthandedness from SRR Rotational Disorder

D. Rönnow[1], M. Shahbazali[1], W. Baki[1], and M. R. Tripathy[2]

[1]Department of Electronics, Mathematics and Natural Sciences
University of Gavle, Gavle SE-801 76, Sweden
[2]Department of Electronics and Communication Engineering
Amity School of Engineering and Technology, Amity University Campus
Sector-125, Noida (U.P.)-201303, India

Abstract— The split ring resonator (SRR) is the key element to obtain left handedness at microwave frequencies [1]. The orientation of the SRR relative to the electromagnetic field is decisive for achieving left handedness (refractive index $n < 0$). It has been suggested that left handedness is sensitive to disorder and that breakdown of left handedness may occur [2]. That would be important for many applications, where manufacturing will cause imperfections, in particular in low cost applications and at high frequencies. We investigate by simulations how the left handedness is affected by rotational disorder of the SRR. The studied structure is shown in Fig. 1.

The structure was designed for left handness in the X-band. The inner, ϕ_1, and outer rings, ϕ_2, rings were rotated, but the position was not changed. The rod position was not changed. In Fig. 2 the refractive index vs. frequency is shown for the case with $\phi = \phi_1 = \phi_2$. ϕ was independent for all SRR and was uniformly distributed between $\pm 0°$, $\pm 15°$, $\pm 45°$, $\pm 90°$. The left handedness ($n < 0$) changes in frequency range and amplitude, but no breakdown of left handedness from orientation disorder is seen. The highest negative refractive index is actually achieved for ϕ between $\pm 45°$. Varying ϕ_1 only had negligible effect and ϕ_2 only similar to the case with $\phi = \phi_1 = \phi_2$.

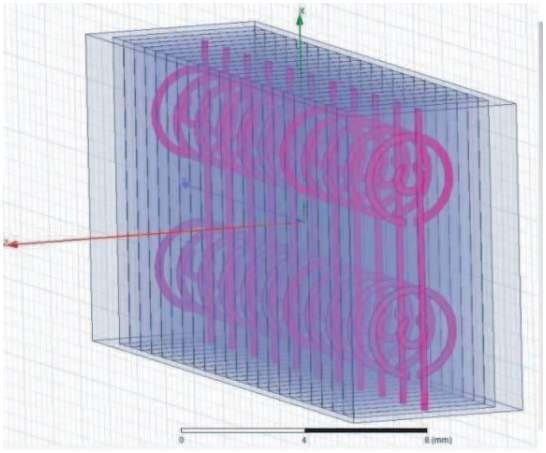

Figure 1: The investigated structure.

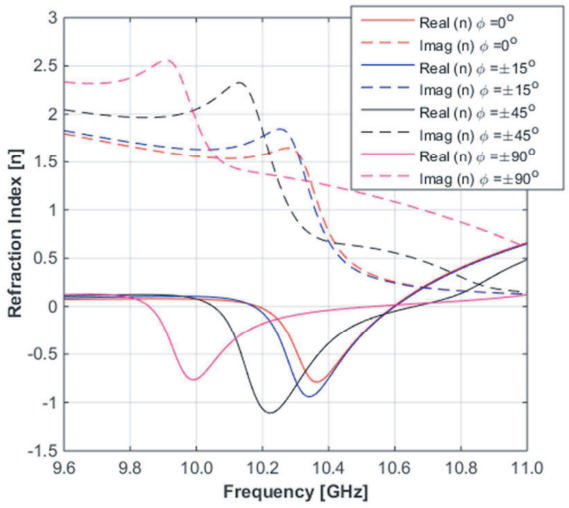

Figure 2: The effect of random SRR rotation ($\phi = \phi_1 = \phi_2$).

REFERENCES

1. Marques, R., F. Martin, and M. Sorolla, *Metamaterials with Negative Parameters*, Wiley, 2008.
2. Zharov, A. A., I. V. Shadrivov, and Y. S. Kivshar, "Suppression of left-handed properties in disordered metamaterials," *J. Appl. Phys.*, Vol. 97, 113906, 2005.

Bandpass-to-allstop Switchable Filter with Broadband Harmonics Suppression

Phirun Kim[1], **Junhyung Jeong**[1], **Girdhari Chaudhary**[1], **Yongchae Jeong**[1], **and Jongsik Lim**[2]

[1]Chonbuk National University, Republic of Korea
[2]Soonchunhyang University, Republic of Korea

Abstract— A microwave switchable filter is one of key circuits in wireless communication systems. A challenging bandpass filter design are tunable, good selectivity characteristics, low insertion loss, and compact size. In this paper, a switchable bandpass to all stopped filter with broad stopband is proposed (Fig. 1). The bandpass filter consists of a hairpin resonator and three capacitors at the ends of resonator with capacitive coupling feed lines. As shown in Fig. 1, two upper capacitances, C_1, are fixed and lower capacitance C_2 is varied The main function of C_1 is used to attenuate the stopband The capacitor C_2 is used to tune the bandpass to all stopped filter by changing DC voltage The proposed filter provides a good selectivity and compact sized. For experimental validation of proposed structure, the bandpass to all stop filter is proposed at an operating frequency of 2.6 GHz The filter is designed on a substrate with a thickness (h) of 31 mil and dielectric constant (ε_r) of 2.2. The fabricated circuit is shown in Fig. 2. The circuit size is $8 \times 25\,\text{mm}^2$ The SMV1233-040LF varactor diode is used for the capacitance variation. The passband is occurred when bias voltage 1.7 V ($C_2 = 3$ pF) From experiment, the passband is shifted to lower frequency compare to EM simulation that is because of the effect of parasitic of the varactor diode and the fabrication error (Figs. 3 and 4). In the simulation, the ideal capacitor C_1 and C_2 are used. The insertion loss in the passband is 1.4 dB and the return loss is better than 15 dB at 2.42 GHz Since transmission zeros near to the passband are obtained at 1.85 GHz and 2.84 GHz it provides a good selectivity characteristic. The 3 dB fractional bandwidth is 6.3%. The upper stopband is suppressed higher than 17 dB from 2.67 GHz to 9 GHz. The lower transmission zero is moved to the passband when bias voltage 3.7 V ($C_2 = 1.55$ pF) providing all attenuated as shown in Fig. 4.

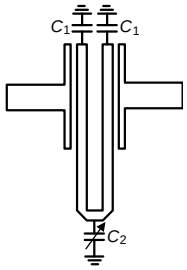

Figure 1.

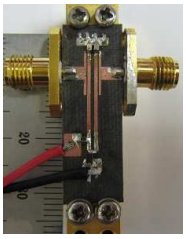

Figure 2.

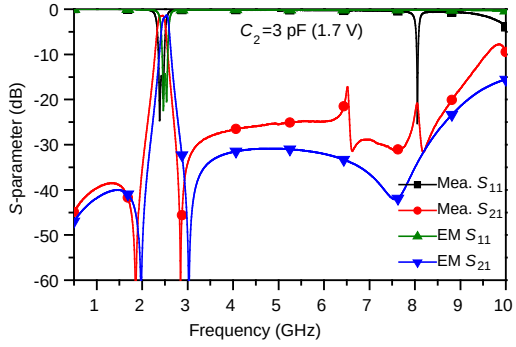

Figure 3.

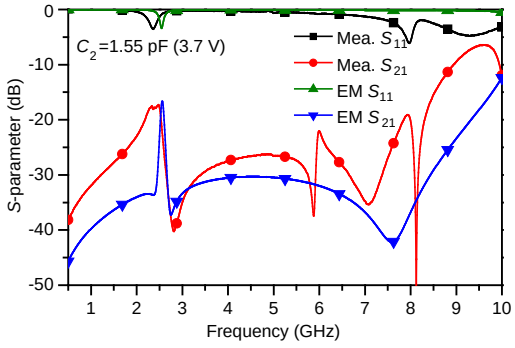

Figure 4.

Design and Analysis of Metafractal Antenna for Wireless Applications

Malay Ranjan Tripathy[1], **Rajesh Kumar**[1, 2], **and Daniel Rönnow**[3]

[1]Department of Electronics and Communication Engineering, ASET, Amity University, Noida, India
[2]Department of Electronics and Communication Engineering, BSAITM, Faridabad, Haryana, India
[3]Department of Electronics, Mathematics and Natural Sciences, University of Gavle, Gavle, Sweden

Abstract— In this paper a new design of meta-fractal antenna is proposed. The dimension of the patch is $40 * 40\,\mathrm{mm}^2$ and the FR4 substrate is used for this. The patch antenna with metamaterial ground plane is shown in Fig. 1(a). The first iterated fractal antenna with the meta-material is shown in Fig. 1(b). The 2nd and 3rd iterated fractal antennas with metamaterial ground plane are shown in Fig. 1(c) and Fig. 1(d).

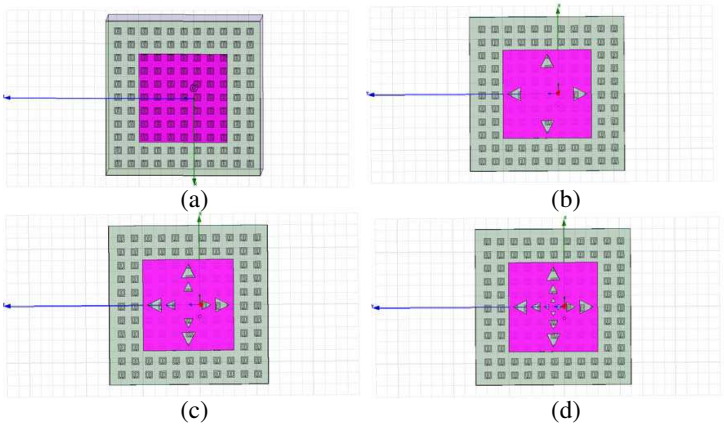

Figure 1: (a) Patch antenna with metamaterial ground plane. (b) 1st iterated meta-fractal antenna. (c) 2nd iterated meta-fractal antenna. (d) 3rd iterated meta-fractal antenna.

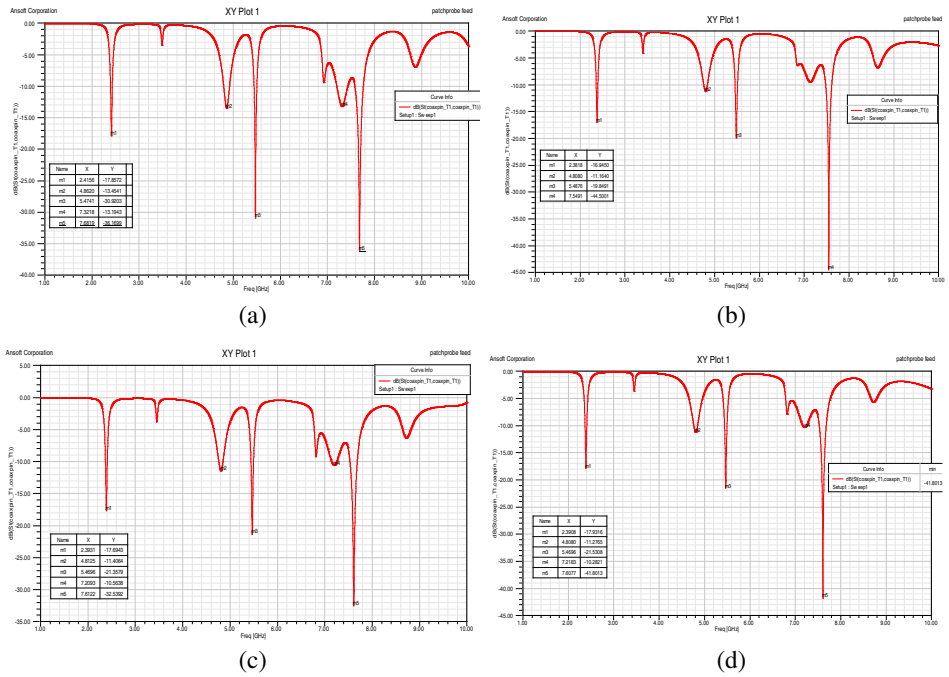

Figure 2: (a) Patch antenna with metamaterial. (b) 1st iterated meta-fractal antenna. (c) 2nd iterated meta-fractal antenna. (d) 3rd iterated meta-fractal antenna.

The results are shown in Figs. 2(a)–(d). As we increase the iterations, different results are seen. The band width used to increase for higher iterations. The return loss results shows better in some of frequency bands for higher iterations and it get degraded for other frequency bands. All these results are analyzed and discussed in detail in the paper.

REFERENCES

1. Smith, D., D. Vier, T. Koschny, and C. Soukoulis, "Electromagnetic parameter retrieval from inhomogeneous metamaterials," *Physical Review E*, Vol. 71, 036617, 1–11, 2005.
2. Chen, J., W. Chen, J. Yen, L. Chen, and C. Wang, "Comparative analysis of split-ring resonators for tunable negative permeability metamaterial based on anisotropic dielectric substrates," *Progress In Electromagnetics Research M*, Vol. 10, 25–38, 2009.
3. Ye, J., Q. Cao, and W. Tam, "Design and analysis of a miniature metamaterial microstrip patch antenna," *IEEE Trans. on Anatenna and Wave Propagation*, 290–293, 2011.

Low Power WSN and Cloud Infrastructure for Remote Lake Water Quality Monitoring

S. Singh[1], **P. Ranjan**[2], **R. Jha**[1], **and M. R. Tripathy**[2]

[1]Yuktix Technologies Pvt. Ltd., India
[2]Amity School of Engineering and Technology, Amity University, Uttar Pradesh, Noida, India

Abstract— Bangalore is state capital of karnataka, India and also know as IT capital of India. In 1975, total number of lakes in Bangalore was 51 which had reduced down to 17 now because of pollution growth, land encrochment and water pollution. Earlier they were a good source of daily use water for Bangalore but now due to extensive pollution, it cannot be used. We in this paper propose a project based on Low power WSN clubbed with cloud infrastructure to monitor water quality in the lakes in real time during different seasons in a year and see the variation of water quality in different region, i.e., close to human infra, in middle of lake, during rainy season etc.. We want to conduct this experiment simultaneously across the 17 lakes in Bangalore. With the data collected, suitable measures can be suggested to government to take effective actions in order to save the exiting bio-diversity across the lakes. Cloud infrastructure can be useful to see and analyze real time data from anywhere and even archive data which can be further downloaded to see variation in last few year. Similar approach can be implemented to measure real time air quality in Bangalore and some of other major polluted cities like Delhi.

Microwave Characterization of Normal and Superconducting States of Superconducting Flexible Tapes on Metal Substrate; Dielectric Resonator Technique

Jarek Wosik[1, 2], **Jerzy Krupka**[3], **Kuang Qin**[1, 2], **Eduard Galstyan**[2, 4], **and Venkat Selvamanickam**[2, 4]

[1]Electrical and Computer Engineering Department
University of Houston, Houston, Texas 77204-5002, USA
[2]Texas Center for Superconductivity, University of Houston, Houston, Texas 77204-5002, USA
[3]Institute of Microelectronics and Optoelectronics, Warsaw University of Technology, Warsaw, Poland
[4]Mechanical Engineering Department, University of Houston, Houston, Texas 77204, USA

Abstract— Recent developments in the manufacturing of second-generation (2G) high temperature superconductor (HTS), deposited on buffered flexible metal substrates, have opened more possibilities for application in electric power grid and superconducting magnets. In the current manufacturing process, HTS tapes such as $YBa_2Cu_3O_{7-x}$ on Hastelloy substrate (YBCO/Hastelloy) often have in-situ quality control of surface morphology using high-speed cameras that can detect and flag defects and X-ray diffractometers to access and regulate the tape texture. However, these tools do not provide direct information on the expected critical current performance of the superconductor tape. Since, kilometers long 2G tapes are manufactured by the MOCVD process, an ideal solution would encompass a non-contact and non-destructive technique capable of providing real time information about both the buffer and superconducting layers at each point of the manufacturing process.

We report on development of such method with the aim to use it as a potential room temperature quality control for fabrication of YBCO tapes. The tapes were deposited at different temperatures, what resulted in their different quality, on Hastelloy-supported oxide buffer layers using the MOCVD technique. T_c was about 89.3 K for all three (GdY)BCO tapes and I_c values in zero magnetic field were 165 A, 270 A and 339 A for tapes with measured thickness of 0.84 μm, 1.02 μm and 1.06 μm, respectively. The buffer stack consisted of aluminum oxide (Al_2O_3), yttrium oxide (Y_2O_3), and textured IBAD-MgO and $LaMnO_3$ layers.

Two configurations of dielectric resonators (DR), the single post (SPDR) consisting of highpermittivity barium zirconium titanate (BZT) ceramic operating at 9.4 GHz in quasi $TE_{01\delta}$ and the rod (RDR) consisting of rutile operating at 13 GHz in TE_{011} mode were designed to measure the complex conductivity (σ) of the tapes (12 mm wide) at the normal and superconducting states, respectively. In order to extract complex conductivity (σ) from experimental data of Q-factor and resonant frequency shift, a commercial electromagnetic simulator HFSS, based on finite elements analysis, was used to calculate resonator EM fields. The theoretical Q-factor and resonant frequency shift curves obtained from numerical simulations were matched with the experimental data to determine conductivity of the YBCO tapes in both normal and superconducting states. Three different tapes were fully characterized and correlation between superconducting and normal state properties was investigated.

Discussion of feasibility and limits of using the microwave dielectric resonator technique for measurements of σ on temperature slope in normal YBCO state will be presented.

Coplanar Waveguide Fed Coplanar Patch Antenna for Nanorectifiers at 2.45 GHz

Arun K. Singh[1, 2], **Shahrir R. Kasjoo**[2, 3], **and A. M. Song**[2]

[1]PEC University of Technology, Sector-12, Chandigarh, India
[2]School of Electrical & Electronic Engineering, University of Manchester, Manchester, UK
[3]School of Microelectronic Engineering, Universiti Malaysia, Perlis, Perlis 02600, Malaysia

Abstract— The recent developments in semiconductor industry have demonstrated the pervasive use of digital broadband communication handling a huge data to be processed and transmitted at the faster speed. In order to increase the operating speed, the device dimensions have been scaled down following the Moore's Law and reached at the verge of saturation [1]. Therefore, researchers have proposed a wide variety of novel nanoelectronic devices such as Self-Switching Device (SSD) [2] and Ballistic rectifier [3] which can be fabricated in two-dimension electron gas (2-DEG) heterostructures by using standard nanolithography followed by wet chemical or dry etching. Both the devices can be used a rectifier to convert microwave signals into DC signal, however, they don't require any *pn* and/or Schottky barrier when compared to conventional multi-layered rectifiers. Due to their planar device architecture, they have shown very small internal capacitance meaning that their frequency response doesn't have RC charging time limitations as convention electronic devices and can be used for various applications starting from radio frequency (RF) to terahertz (THz) frequencies [2, 3]. Such devices can easily be integrated to outside macroscopic world using coplanar transmission lines and planar antennas which demonstrate very low parasitic capacitances.

Here, we report the design and fabrication of coplanar waveguide (CPW) fed coplanar patch antenna (CPA) to integrate with SSD and ballistic rectifier at Unlicensed Industrial, Scientific and Medical (ISM) band frequency of 2.45 GHz for radio frequency identification (RFID) systems. The custom-built antenna has a similar configuration as loop slot antenna [4] consisting of a patch surrounded by closely spaced ground conductor and a CPW feed line of 50 Ω as shown in Figs. 1(a) and (b). The 1.2 mm thick glass epoxy (FR4) substrate with dielectric constant (ε_r) and loss tangent ($\tan\delta$) of 4.4 and 0.0002, respectively, is used for the fabrication of antenna. The antenna has demonstrated a gain of 3.82 dB and its measured return loss of about 37.24 dB is in reasonable accordance with the simulated values of 47.4 dB as depicted in Fig. 2.

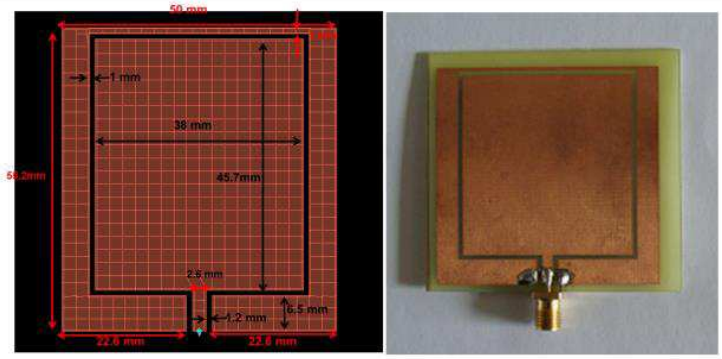

(a) (b)

Figure 1: (a) CPW fed coplanar Patch Antenna with optimized dimensions. (b) Fabricated antenna with a SMA connector.

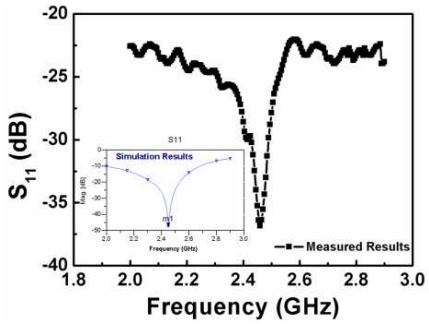

Figure 2: The return loss of 37.24 dB was measured using Agilent's network analyser (model: E 5061B ENA Series) which is in well accordance with the simulated results obtained using ADS software as shown in the inset.

REFERENCES

1. Russer, P. and N. Fichtner, "Nanoelectronics in radio-frequency technology," *IEEE Microwave Mag.*, Vol. 11, No. 3, 119–135, 2010.

2. Song, A. M., M. Missous, P. Omling, A. R. Peaker, L. Samuelson, and W. Seifert, "Unidirectional electron flow in a nanometer-scale semiconductor channel: A self-switching device," *Appl. Phys. Lett.*, Vol. 83, 1881–1883, 2003.
3. Song, A. M., A. Lorke, A. Kriele, J. P. Kotthaus, W. Wegscheider, and M. Bichler, "Nonlinear electron transport in an asymmetric microjunction: A ballistic rectifier," *Phys. Rev. Lett.*, Vol. 80, 381–3834, 1998.
4. Chen, H. D. and H. T. Chen, "A CPW-fed dual-frequency monopole antenna," *IEEE Trans. Antennas Propag.*, Vol 52, No. 4, 978–982, 2004.

UWB Antenna with Optically Controlled Notches

Nagwa S. Abd El-Hamed[1], **Moataza A. Hindy**[2], **and Hesham F. A. Hamed**[1]

[1]Faculty of Engineering, Menia University, Menia, Egypt
[2]Electronics Research Institute, Cairo, Egypt

Abstract— This paper presents an UWB antenna with optically controlled frequency notches. Behavior of the photoconductive optical switches under light illumination and in the dark are modeled. The optical signal in turn alters the radiation properties of the antenna structure and consequently changes the notched frequency bands. The photoconductive switches are activated by laser light that is coupled through an optical fiber which extends from the ground plane to just underneath the silicon element (silicon filled gap) placed on the radiating face of the antenna structure. Such a construction allows for easy integration of such antenna designs into conformal packaging for wireless devices [1, 2]. Photoconductive switches are used because of their superior performance as compared to MEMS, p-i-n diodes, and lumped elements. The photoconductive approach does not require the use of bias lines, which typically lie in the plane of the antenna and can interfere with the electromagnetic performance of the antenna. Also, photoconductive switches exhibit extremely fast switching speeds on the order of nanoseconds [2, 3]. The antenna structure is shown in Fig. 1. The four switches S_1, S_2, S_3 and S_4 are controlled using optical signal via optical fiber. Fig. 2 shows the performance of the antenna (return loss S_{11}) for different cases of the optical switches which are either OFF (opened) or ON (closed). Experimentally measured RF performance of the antenna is in good agreement with the numerical simulations.

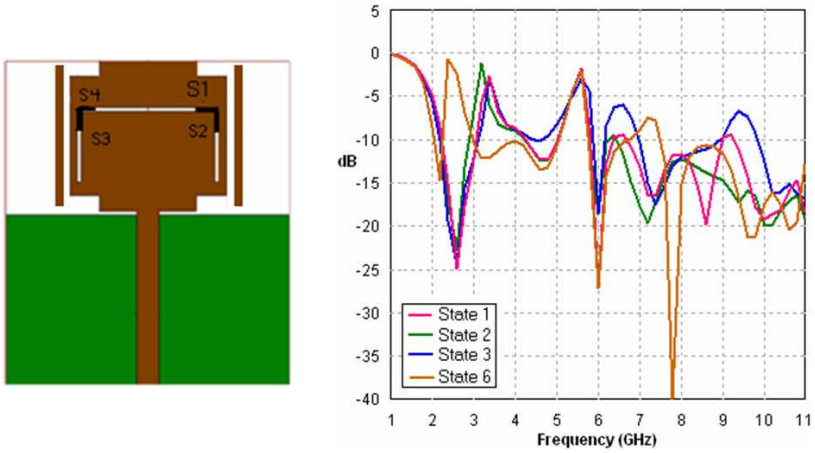

(a) (b)

Figure 1: (a) Microstrip antenna with partial ground and four optical switches, and (b) return loss of the antenna with switches at different states.

REFERENCES

1. Majid, H. A., M. K. Abdul Rahim, M. R. Hamid, N. A. Murad, and M. F. Ismail, "Frequency-reconfigurable microstrip patch-slot antenna," *IEEE Antennas and Wireless Propagation Letters*, Vol. 12, 218–220, 2013.
2. Su, H., I. Shoaib, X. Chen, and T. Kreouzis, "Optically tuned polarization reconfigurable antenna," *IEEE Asia-Pacific Conference on Antennas and Propagation*, 27–29, Singapore, August 2012.

Session 3P13a
FocusSession.SC3&2: Disordered Photonics 2

Realization of a Topological Anderson Insulator

S. Stützer[1], **M. C. Rechtsman**[2], **Y. Plotnik**[2], **Y. Lumer**[2],
J. M. Zeuner[1], **S. Nolte**[1], **M. Segev**[2], **and A. Szameit**[1]

[1]Abbe Center of Photonics, Institute of Applied Physics
Friedrich-Schiller-University, Jena 07743, Germany
[2]Department of Physics, Technion — Israel Institute of Technology, Haifa 32000, Israel

Abstract— Topological states have emanated a fascination in condensed matter physics and the discovery of topological insulators [1] was one of big successes of recent years. Our team experimentally demonstrated a photonic topological insulator [4] using the so-called Floquet topological insulators (FTI) [2, 3]. This is a 2D lattice where evanescently coupled waveguides are arranged in a honeycomb (graphene-like) geometry and and waveguide is twisted around its axis in a helical fashion.

We now consequentially challenge, how disorder would impact the FTI. In 1958, it was shown that disordered systems exhibit Anderson localization: the suppression of wave transport [5]. In fact, in two-dimensional disordered systems, all eigenstates are localized even for an infinitesimal amount of randomness, without any observable threshold [6, 7]. In contrast, topological systems exhibit a radically different nature which allows them to retain extended states even under the influence of disorder in two dimensions. However, it was still extremely intriguing when the so-called Topological Anderson Insulator was proposed [8]: a system with topological properties — displaying extended edge modes — due to the presence of disorder.

For the first time, we present an experimental demonstration of a Topological Anderson Insulator in any physical system in nature. Our photonic system is similar to that in previous work [4]. In addition, we employ a staggered mass potential, that is, the two sublattices of the honeycomb structure exhibit different refractive indices n_a and n_b (see Fig. 1(a)). When $n_a = n_b$ our system is identical to the FTI in [4] and, hence, exhibits topologically protected edge states (Fig. 1(b)). However, when breaking the inversion symmetry in the transverse plane by detuning the sublattices ($n_a \neq n_b$) a topologically trivial bandgap opens and topological insulation vanishes. In the presence of disorder (helically synchronized with the lattice) this trivial bandgap closes and acquires a nonzero topological invariant when it finally reopens. This is proofed by the formation of a one-way edge state, as shown in Fig. 1(c).

The basic idea of a TAI is as follows. In the periodically driven system with a staggered potential, the drive (the helicity manifested in the gauge $A(z)$) and staggering act as two opponents. While staggering produces a trivial gap with positive effective mass at both Dirac cones, the drive causes a topological gap with opposite masses. When the staggering dominates over the drive, the system has trivial topology. This is where disorder comes in: it effectively reduces the effect of the staggering and, at sufficiently large disorder it closes the trivial gap and the topological phase is restored.

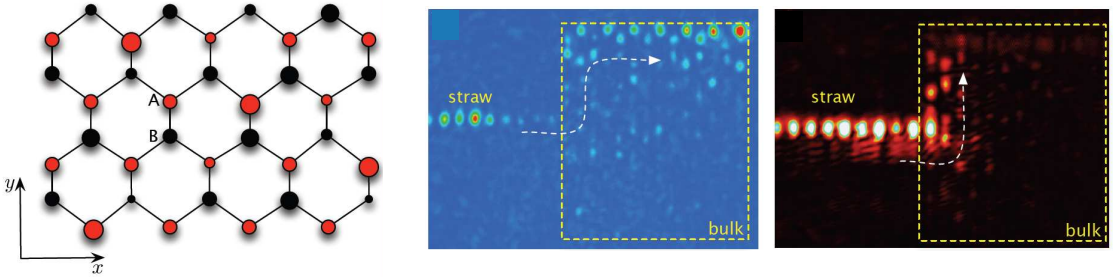

(a) (b) (c)

Figure 1: (a) Schematic representation of the honeycomb lattice with a staggered mass potential composed of two sublattices A (red) and B (black). The uniformly disordered onsite energy is indicated by variable radius of the lattice sites. (b) For $A = B$ and no disorder the wave function at the output clearly travelled along the edge without any scattering. (c) For $A \neq B$ the edge state can be recovered in a disorderd system.

REFERENCES

1. Kane, C. L. and E. J. Mele, *Phys. Rev. Lett.*, Vol. 95, 226801, 2005.
2. Lindner, N. H., et al., *Nature Physics*, Vol. 7, 490–495, 2011.
3. Kitagawa, T., et al., *Phys. Rev. B*, Vol. 82, 235114, 2010.
4. Rechtsman, M., et al., *Nature*, Vol. 496, 196–200, 2013.
5. Anderson, P. W., *Phys. Rev.*, Vol. 109, 1492–1505, 1958.
6. Schwartz, T., et al., *Nature*, Vol. 446, 52–55, 2007.
7. Lahini, Y., et al., *Phys. Rev. Lett.*, Vol. 100, 2008.
8. Li, J., et al., *Phys. Rev. Lett.*, Vol. 102, 136806, 2009.

The Beetle's White Album: How White Beetles Optimize Multiple Scattering of Light

L. Cortese[1, 2], **L. Pattelli**[1, 2], **F. Utel**[1, 2], **S. Vignolini**[3], **M. Burresi**[1, 4], **M. Kolle**[5], **P. Vukusic**[6], **U. Steiner**[7], **and D. Wiersma**[1, 2, 4]

[1]LENS, European Laboratory for Non-Linear Spectroscopy, University of Florence, Italy
[2]Department of Physics, University of Florence, Italy
[3]Department of Chemistry, University of Cambridge, UK
[4]Istituto Nazionale di Ottica (INO-CNR), Italy
[5]Department of Mechanical Engineering, Massachussets Institute of Technology, USA
[6]School of Physics, University of Exeter, UK
[7]Adolphe Merkle Institute, University of Freiburg, Switzerland

Abstract— The colors shown by several insects often arise from light scattering by very complex photonic structures rather than selective absorption by pigments. Such structures are the result of optical strategies developed during millions of years of evolution. The bright and iridescent colors shown by certain butterflies and beetles, for example, arise from coherent effects which requires ultrathin periodic layers of material [1]. In contrast, a *bright white* coloration is more complicated to achieve, since all colors has to be scattered with the same high efficiency. In this case the wave nature of light is not involved in the appearance of the object, and a bright white is achieved only in presence of multiple scattering, for which thicker, high refractive index contrast systems are usually required. Nevertheless, the extremely brilliant whiteness shown by the *Cyphochilus* beetle is generated by multiple scattering of light inside the *ultra-thin* scales that cover its body. The intra scale structure is characterized by a dense, nanostructured network of chitin filaments, which seems to be optimized (during million of years of evolution) to increase the total reflectance, and thus the bright appearance of the beetle, employing as less material as possible [2, 3].

In this work we analyzed light transport inside the beetle's scales, showing that multiple scattering of light occurs, in spite of its thinness (5–9 µm). We proved, with static and time resolved experiments, that white beetle's scales show the lowest transport mean free path and diffusion coefficient for low-refractive-index systems ($n = 1.5$) reported until now. We found that the crucial aspect of the optimization of light scattering is the structural anisotropy of the chitin network. We indeed demonstrated that light transport inside the scales is anisotropic, and it is engineered to increment the scattering strength in the direction orthogonal to the scale surface, at expense of the in plane scattering, which is not relevant for the total reflectance. With such morphology and geometry of the intra scale structure the beetle succeed achieving a bright white reflectance with a thin, anisotropic, lightweight structure.

Such kind of discoveries can have immediate impact in developing new highly scattering optical systems with applications ranging from thin coatings to LEDs illumination.

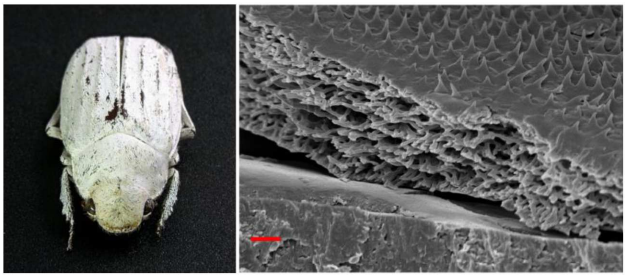

Figure 1: Image of Cyphochilus white beetle and SEM micrograph of a dissected scale (scale bar 2 µm).

REFERENCES

1. Kinoshita, S., *Structural Colors in the Realm of Nature*, World Scientific Publishing Co., Singapore, 2008.

2. Vukusic, P., B. Hallam, and J. Noyes, *Science*, Vol. 315, 348, 2007.
3. Burresi, M., L. Cortese, L. Pattelli, M. Kolle, P. Vukusic, D. Wiersma, U. Steiner, and S. Vignolini, *Sci. Rep.*, Vol. 4, 6075, 2014.

Coupling between Disorderd Photonic Structure and DBT Molecules: Possible Chain of Hybrid Modes

Fabrizio Sgrignuoli[1], **Giacomo Mazzamuto**[1, 2, 3], **and Costanza Toninelli**[2, 3, 4]

[1]Department of Physics, University of Florence
Via Sansone 1, Sesto Fiorentino, Firenze I-50019 , Italy
[2]European Laboratory for Non-Linear Spectroscopy (LENS)
Via Nello Carrrara 1, Sesto Fiorentino, Firenze I-50019, Italy
[3]Istituto Nazionale di Ottica (INO), Largo Fermi 6, Firenze I-50125, Italy
[4]QSTAR, Largo Enrico Fermi 2, Firenze I-50125, Italy

Abstract— Recent advances in the engineering of light confinement have demonstrated the ability to fully control the spectral properties of an individual photonic mode in two-dimensional disordered photonic structures paving the way for the creation of open transmission channels in strongly scattering media. The optical confinement and the coupling between modes open new perspectives over the control of the light flow in random media, as well as the possibility to build architectures tuned for efficient light-matter interaction.

Here we propose a novel geometry to achieve coupling between single quantum emitters (Dibenzoterrylene (DBT) molecules, embedded in a thin anthracene crystals), and disordered photonic structures. We investigate the quasi-modes of a disordered pattern to create a chain of hybridized localized modes extended from one end of the sample to the other. Such topology has the advantage of bringing distant molecules to exchange energy, thanks to the shared photonic mode.

In particular the structures that we study are suspended Si_3N_4 membranes in which a triangular lattice of holes is fabricated. The disorder is introduced by shifting the holes by a small normally distributed displacement relative to the position in the perfect periodic lattice. In this way, adding disorder on top of an initial ordered structure, we tune the appearance of Anderson localized modes at the proper frequency, for coupling with DBT molecules FDTD simulations are performed in which several dipoles, that simulate the DBT molecules, are used to excite the photonic structures. In order to detect the appearance of localized or hybridized modes, we have developed a "simulation tool" based on Fourier analysis, phase rigidity, complexity factor, spreading factor, spatial correlation and cross correlation integrals.

A simple case-study platform has been performed as a test bed for the analysis in the disordered case. In particular, two coupled D2 cavities have been analysed. Such system provides an easy model for coupled modes since the modes of the single cavity are well characterized. Considering two adjacent D2 cavities, the coupling strength can be tuned by adjusting the tunnelling rate acting on the radius of the holes shared by the two cavities, while a detuning between the two cavities can be introduced by acting on the non-shared holes. It is therefore relatively easy to study all combinations of coupling and detuning. Combining information about the phase distribution, the field spatial and spectral profile, we anticipate level crossing and anticrossing between modes. The results provide new understanding of the hybridmode nature and define a fingerprint to spot necklace states in two dimensions.

Photonic Band Gaps in Disordered Materials: Stealthy Hyperuniformity Versus Local Ordering

Luis S. Froufe-Pérez[1], **Pablo F. Damasceno**[2], **Michael Engel**[3], **Nicolas Muller**[1], **Jakub Haberko**[4], **Sharon C. Glotzer**[2, 3, 5], **and Frank Scheffold**[6]

[1]Physics Department, University of Fribourg, Chemin du Musée 3, Fribourg 1700, Switzerland
[2]Applied Physics Program, University of Michigan, Ann Arbor, Michigan 48109, USA
[3]Department of Chemical Engineering, University of Michigan, Ann Arbor, Michigan 48109, USA
[4]Faculty of Physics and Applied Computer Science
AGH University of Science and Technology, al. Mickiewicza 30, Krakow 30-059, Poland
[5]Department of Materials Science and Engineering
University of Michigan, Ann Arbor, Michigan 48109, USA
[6]Physics Department, Fribourg Center for Nanomaterials, University of Fribourg
Chemin du Musée 3, Fribourg 1700, Switzerland

Abstract— Photonic Crystals (PCs) have represented a major driving force for the optical materials community for the last three decades. In analogy with solid-state physics, the goal of photonic crystal science and technology is to understand, engineer and fabricate materials with specific light transport and emission properties. Photonic band engineering is at the heart of virtually any application of PCs. In the early stages of the development of the technological capacities to fabricate photonic bandgap structures, it was realized that fabrication defects inhibit the formation of a gap and thus spoil to a large extent the performance of any practical photonic device, up to a point where commercial applications might be practically precluded.

Recently however the picture of considering disorder as the limiting factor for the fabrication of photonic band gap materials has changed dramatically. Several groups realized that, indeed, certain types of correlated disorder may be beneficial for the creation of a photonic bandgap. Moreover such amorphous bandgap materials would feature a spatially isotropic gap difficult to attain in a truely crystalline structure.

In the pioneering work of M. Florescu and coworkers [1], it was shown that the so called stealthy hyperuniform (HU) disorder can lead the buildup of isotropic photonic bandgaps in two and three [2, 3] dimensions. In contrast with the structures studied in [4], it was suggested that crystalline order is not required to obtain a full band gap but local ordering, uniform topology and, importantly, stealth hyperuniformity.

Stealth HU is a structural property related to the structure factor $S(q)$ of the disordered system: HU patterns present a vanishing $S(q)$ as q tends to zero, while stealthy HU imposes a much more restrictive constrain to $S(q)$: it exhibits vanishing values over a finite range of values from $q = 0$ up to a critical value q_c. Stealthy HU materials can be regarded, to some extent, as the reciprocal space counterpart of the constrains imposed by the hard-sphere (hard-disc in 2D) model in the real space.

In the present paper, we study a system where uniform topology is not relevant as the system is composed of isolated two-dimensional scattering units (circular cylinders). We compare non-polycrystalline disordered samples with different degrees of correlation, showing both stealthy hyperuniformity or only short range ordering due to random packing in real space. We show that an isotropic bandgap emerges in both cases and that the short-range correlated system can present even wider isotropic bandgaps as compared to stealthy hyperunform structures with similar constraints on the degrees of freedom (in q-space or real space respectively). We show how the interplay between different characteristic scattering lengths in the system, namely transport mean free path, correlation distance and pseudo-Bragg length play a role in these systems. We conclude that any constrain imposed in the accessible degree of freedom leads to peaks (at appropriate positions) in the radial distribution function or the structure factor and in promotes the emergence of a photonic bandgap provided the scattering strength of the individual building blocks is sufficiently strong.

REFERENCES

1. Florescu, M., S. Torquato, and P. J. Steinhardt, "Designer disordered materials with large, complete photonic band gaps," *PNAS*, Vol. 106, 20658–20663, 2009.

2. Liew, S. F., J.-K. Yang, H. Noh, C. F. Schreck, E. R. Dufresne, C. S. O'Hern, and H. Cao, "Photonic band gaps in three-dimensional network structures with short-range order," *Phys. Rev. A*, Vol. 84, 063818, 2011.
3. Muller, N., J. Haberko, C. Marichy, and F. Scheffold, "Silicon hyperuniform disordered photonic materials with a pronounced gap in the shortwave infrared," *Adv. Opt. Mat.*, Vol. 2, 115–119, 2014.
4. Yang, J.-K., C. Schreck, H. Noh, S. F. Liew, M. I. Guy, C. S. O'Hern, and H. Cao, "Photonic-band-gap effects in two-dimensional polycrystalline and amorphous structures," *Phys. Rev. A*, Vol. 82, 053838, 2010.

Dynamics of Strong and Weak Localization of Light in a Correlated 2D Photonic Disorder

Julien Armijo[1], **Raphaël Allio**[1], **and Laurent Sanchez-Palencia**[2]

[1]Departamento de Fisica, MSI-Nucleus on Advanced Optics
and Center for Optics and Photonics (CEFOP), Facultad de Ciencias
Universidad de Chile, Santiago, Chile
[2]Laboratoire Charles Fabry, Institut d'Optique
CNRS, University Paris Sud 11, Palaiseau cedex F-91127, France

Abstract— We study the dynamics of light waves propagation in correlated 2D disordered landscapes. A non-diffracting disorder with adjustable strength V_R and correlation length σ_R is generated in a photorefactive crystal using spatial light modulators (SLM) [1], and tailored wavepackets prepared also using SLM are launched in those photonic disorders. Our disorder, as also in previous similar studies [2], has a well-defined spectral edge $k_{\max,} = 1/\sigma_R$ that causes peculiar propagation patterns. In particular, we observe in real space distributions, a ballistic front of exponential Anderson Localization defined by the ballistic position of waves with $k = k_{\max}$ (Fig. 1(a)), that reminds Bragg plane effects in regular lattices [3]. We compare our observations to simulations using a novel calibration technique for the refractive index [4].

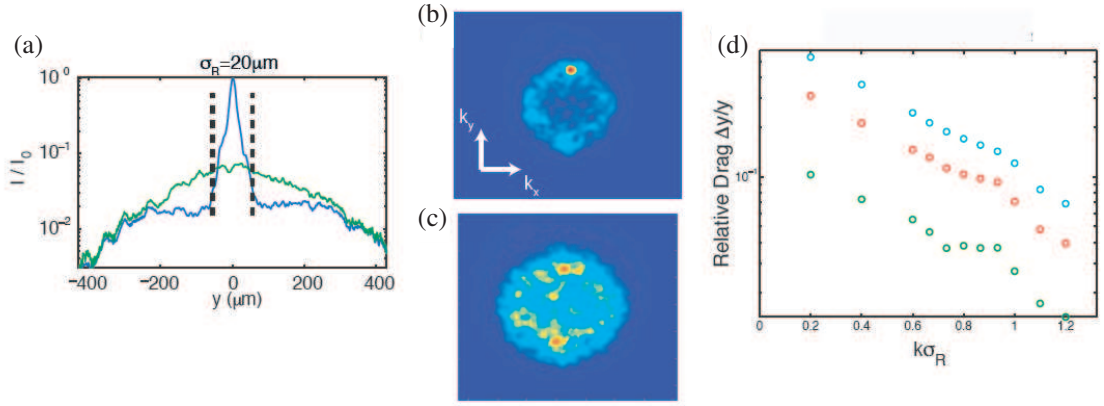

Figure 1: (a) Light intensity at crystal output face for a Gaussian probe beam without (green) and with disorder (blue). Vertical dashed lines show the ballistic positions of components of momentum $k_{\max}$. (c), (d) Fourier space pictures for a plane wave with momentum k with weak (b) and stronger disorder (c). (d) Relative drag (transverse transport reduction) measured at crystal output for plane waves of different transverse momenta k, for 3 disorder strengths.

We also observe intriguing effects in Fourier space. For plane waves with a well-defined transverse momentum k, we observe the formation of elastic diffusion rings (Fig. 1(b)) and a peak of coherent back-scattering (CBS), with contrast close to the ideal maximum of 2 (Fig. 2(c)), which proves the coherence of transport [5]. We study the dynamics of the CBS peak formation by varying V_R: after an increase of the asymmetry in the momentum distribution, we observe a decrease that may be related to the onset on strong localization. Further, measuring the relative stopping ("drag force") of plane waves with different momenta k at the crystal output face, we note a non-monotonous dependence and a maximum close to $k = k_{\max}$ (Fig. 1(d)) that strongly resembles the behaviour predicted for the localization length in a disorder with similar correlation properties [6].

Our work provides a detailed study of light propagation in our correlated disorder, and shows the potential of using wave shaping techniques for the momentum-resolved studies of light propagation in disordered media.

REFERENCES

1. Boguslawski, M., S. Brake, J. Armijo, F. Diebel, P. Rose, and C. Denz, "Analysis of transverse Anderson localization in refractive index structures with customized random potential," *Opt. Express*, Vol. 21, 31,713–31,724, 2013.

2. Schwartz, T., G. Bartal, S. Fishman, and M. Segev, "Transport and Anderson localization in disordered two-dimensional photonic lattices," *Nature*, Vol. 446, 52–55, 2007.
3. Allio, R., D. Guzman-Silva, C. Cantillano, L. Morales-Inostroza, D. Lopez-Gonzalez, S. Etcheverry, R. A. Vicencio, and J. Armijo, "Photorefractive writing and probing of anisotropic linear and nonlinear lattices," *J. Opt.*, Vol. 17, 025,101, 2015.
4. Armijo, J., R. Allio, and C. Mejía-Cortés, "Absolute calibration of the refractive index in photo-induced photonic lattices," *Opt. Express*, Vol. 22, 20,574–20,587, 2014.
5. Skipetrov, S. E., "Disorder makes a robust matter-wave interferometer," *Physics Online Journal*, Vol. 5, 123, 2012.
6. Piraud, M., A. Aspect, and L. Sanchez-Palencia, "Anderson localization of matter waves in tailored disordered potentials," *Physical Review A*, Vol. 85, 063,611, 2012.

Uni-directional Photonic Modes Due to Strong Random Scattering

Klaus Ziegler
Institut fuer Physik, University of Augsburg, Germany

Abstract— In a photonic medium with a spectral degeneracy, where two orthogonal modes appear with the same wave number, Anderson localization can be avoided in the case of strong random scattering by the formation of uni-directionally propagating modes. This phenomenon was observed previously for strong random scattering of electrons in graphene [1], where electronic states avoid Anderson localization by creating two uni-directionally propagating modes. The reason for this phenomenon are nodes in the spectrum, where the electronic modes have a degeneracy and backscattering is suppressed.

Here we discuss this effect in photonic systems with strong random scattering. The spectral degeneracies can be generated by a randomly deformed photonic crystal. Several examples will be discussed for different structures and different types of random scattering. It will be shown that for weak random scattering we obtain diffusion, whereas for strong random scattering a finite length scale appears which is proportional to the inverse scattering rate. This scale, however, is not the conventional localization length but describes the spatial decay of the photonic mode away from a semi-infinite line. Along this line the electric field is constant. These uni-directional modes are reminiscent of the edge states in quantum Hall systems, where a spectral gap exists rather than a spectral degeneracy. The described effect provides a method for angular localization of a spherical wave by strong random scattering. We derive our results within a convergent perturbation theory and discuss potential applications for focusing light from an isotropic source.

REFERENCES

1. Ziegler, K., *J. Phys. A: Math. Theor.*, Vol. 48, 055102, 2015.

Biocompatible Random Lasing

S. Caixeiro[1], **M. Gaio**[1], **M. Peruzzo**[1], **M. Castro-Lopez**[1],
B. Marelli[2], **F. Omenetto**[2, 3], **and R. Sapienza**[1]

[1]Department of Physics, King's College London, Strand, London WC2R 2LS, United Kingdom
[2]Department of Biomedical Engineering
Tufts University, 4 Colby Street, Medford, Massachusetts 02155, USA
[3]Department of Physics, Tufts University, 4 Colby Street, Medford, Massachusetts 02155, USA

Abstract— Biolasers are laser sources made out of biopolymers and powered by nanophotonic interactions. We will report on biocompatible self-assembled random lasers, made entirely of doped silk, showing clear threshold behaviour and spectral narrowing [1]. We will show that with a simple self-assembly process the porous silk matrix can be incorporated with different dyes and casted in a free-standing inverse photonic glass with designed collective scattering Mie resonances. A diffusive model in which we have included also material dispersion accounts well for the observed lasing curve [2]. The combination of a natural biopolymer and random lasing — a lasing system that uses highly disordered materials to obtain laser action without the need for carefully aligned mirrors — offers the opportunity for integration of a laser within living tissue, opening a new path at the interface between nanophotonic and medicine.

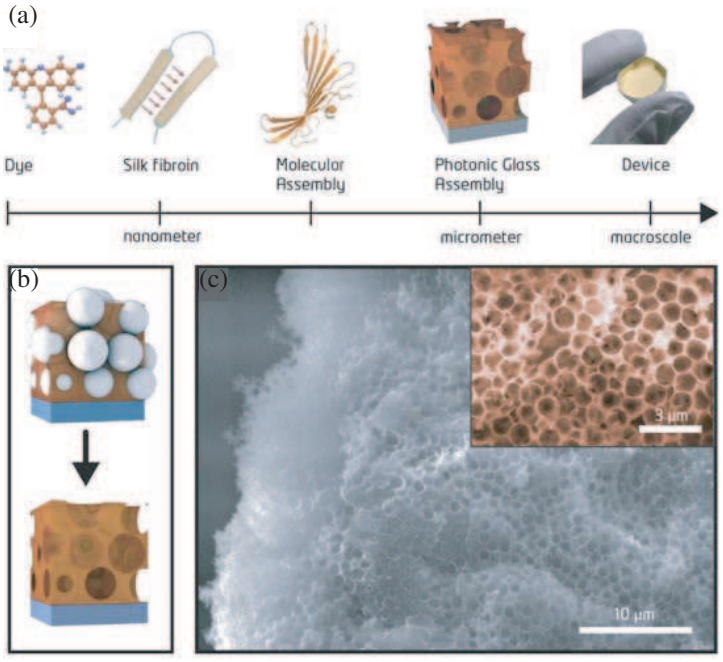

Figure 1: Fabrication process of the inverse silk photonic glass.

REFERENCES

1. Caixeiro, S., M. Gaio, B. Marelli, F. G. Omenetto, and R. Sapienza, "Silk-based biocompatible random lasing," in preparation.
2. Gaio, M., M. Peruzzo, and R. Sapienza, "Tuning random lasing in photonic glasses," *Optics Letters*, Doc. ID 233577, 2015.

Session 3P13b
Laser Nanofabrication, Characterization and Physical Properties 1

Interpulse and Inrapulse Optical Feedback during Femtosecond Laser Surface Nanostructuring: Experimental Study and Numerical Modeling

S. V. Makarov[1], **A. A. Ionin**[2], **and S. I. Kudryashov**[2, 3]

[1]ITMO University, Kronverkskiy pr. 49, Saint-Petersburg, Russia
[2]P. N. Lebedev Physical Institute of the Russian Academy of Sciences
Leninskiy pr. 53., Moscow, Russia
[3]NRNU "MEPhI", Kashirskoe sh. 31, Moscow, Russia

Abstract— Nonlinear cumulative dynamics of femtosecond laser-induced surface ripples was experimentally studied on silicon and aluminum surfaces, reflecting ultrafast nonlinear dynamics of corresponding optical interference surface patterns. Such dynamics was revealed by detailed electrodynamic modeling to be directly driven by related instantaneous surface optical patterns, which are sensitive not only to cumulative ripples deepening (interpulse feedback), but also to laser-induced instantaneous variation of surface dielectric function (intrapulse feedback), providing either positive, or negative fluence-dependent optical feedbacks. Aluminum and silicon are two typical materials, which represent low and high, respectively, sensitivity of their dielectric function on laser fluence. Therefore we carried out numerical modeling of interpulse feedback for aluminum, and intrapulse feedback modeling for silicon.

The interpulse feedback numerical modeling provides information about the fastest growing relief period at given ripples amplitude. As a result of direct comparison of our experimental data on multishot ripples evolution with corresponding numerical modeling of femtosecond laser energy deposition into growing relief on aluminum, we found out that optical feedback has a maximum value when the ratio $\Lambda/\lambda \sim 0.7$, where Λ is the ripples period and λ is laser wavelength. We show that similar trend should be observed for all materials with high value of imaginary part of dielectric function ($\mathrm{Im}\varepsilon \gg 1$) or high negative value of ε real part ($\mathrm{Re}\varepsilon \ll -1$) [1].

Analysis of the intrapulse optical feedback, basing on modeling of both prompt dielectric function and laser energy deposition into ripples, reveals multiple switching of optical feedback sign during femtosecond laser induced dielectric-to-metal transition. Such behavior of optical feedback causes ripples both degradation and revival during multishot laser irradiation observed in corresponding experiments with silicon [2].

ACKNOWLEDGMENT

This work was partly financially supported by the Government of the Russian Federation (Grant 074-U01) through ITMO Post-Doctoral Fellowship for S. V. Makarov.

REFERENCES

1. Ionin, A. A., S. I. Kudryashov, S. V. Makarov, A. A. Rudenko, L. V. Seleznev, D. V. Sinitsyn, T. P. Kaminskaya, and V. V. Popov, "Nonlinear evolution of surface relief on aluminum under multiples femtosecond laser irradiation," *JETP Letters*, Vol. 101, No. 5, 2015, accepted.
2. Ionin, A. A., S. I. Kudryashov, S. V. Makarov, A. A. Rudenko, L. V. Seleznev, D. V. Sinitsyn, and V. I. Emel'yanov, "Nonlinear optical dynamics during femtosecond laser nanostructuring of silicon surface," *Laser Physics Letters*, Vol. 12, No. 2, 025902, 2015.

Classical Theory of Surface Plasmon Polaritons at the Interface between Two Absorbing Materials

Thibault J.-Y. Derrien[1], **Nadezhda M. Bulgakova**[1, 2], **Jörg Krüger**[3], **and Jörn Bonse**[3]

[1]HiLASE Centre, Institute of Physics, Academy of Science of the Czech Republic
Za Radnicí 828/5, Dolní Břežany 25241, Czech Republic
[2]Institute of Thermophysics SB RAS, 1 Lavrentyev Ave., Novosibirsk 630090, Russia
[3]BAM Federal Institute for Materials Research and Testing
Unter den Eichen 87, Berlin D-12205, Germany

Abstract— At the interface between two media, the properties of Surface Plasmon Polaritons (SPPs) strongly depend on the optical properties of the involved materials. So far, plasmonic effects in noble metals are well described by the widely accepted formulas [1, 2] which are based on the assumption that the imaginary part of the dielectric permittivity is negligible. However, for many materials/systems such an approximation is not valid. This includes interfaces between doped or transiently excited semiconductors and dielectrics with plasmon-active transition metals (such as titanium or platinum), or with organic compounds. An accurate description of such systems requires a refinement of the SPP theory beyond the "perfect metal — perfect dielectric interface" approximation, hence taking into account the neglected imaginary parts [2–5]. In this context, the excitation conditions and properties of SPPs such as the spatial period of the field modulation, the lifetime of the SPP, the SPP decay length and depth strongly deviate from predictions based on the accepted theory.

In this paper, rigorous analytical calculations taking into account the imaginary parts of the dielectric permittivities have been performed which involve the dielectric function terms mostly neglected so far. These refined calculations are presented for various interfacial material combinations. SPPs are found to be excitable on a much wider class of interfaces than just 'noble metal — perfect dielectric' ones. This suggests a possibility to develop plasmon-active photovoltaic cells and new photonic applications based on alternative materials while allowing a wider range of SPP excitation. A list of plasmon-active interfaces is given and supported by near-field modeling using the numerical Finite-Difference Time Domain (FDTD) method. Consequences are detailed for the SPPs in the excitation regimes where the classical approximation is not valid.

REFERENCES

1. Raether, H., *Surface Plasmons on Smooth and Rough Surfaces and on Gratings*, Springer-Verlag, 1986.
2. Novotny, L. and B. Hecht, *Principles of Nano-Optics*, Cambridge University Press, 2006.
3. Bell, R. J., R. W. Alexander, W. F. Parks, and G. Kovener, *Optics Communications*, Vol. 8, 147, 1973.
4. Norrman, A., T. Setälä, and A. T. Fridberg, *Opt. Letters*, Vol. 38, 7, 2013.
5. Norrman, A., T. Setälä, and A. T. Friberg, *Opt. Express*, Vol. 22, 4628, 2014.

Nanostructure Formation by Quasi-1D Plasmon Excitation

Christian Patzek and Ruediger Grunwald
Max-Born-Institute for Nonlinear Optics and Short-Pulse Spectroscopy, Germany

Abstract— Sub-100-nm laser-induced periodic surface structures (LIPSS) can be generated by irradiating materials with intense femtosecond laser pulses. The basic mechanisms of LIPSS are not completely understood because of their high complexity. Compared to lithographic methods which require multistep procedures and cleanroom technologies, the LIPSS approach is easier and cost-effective. By exploiting nonlinear channels for the excitation of surface plasmon-polaritons (SPPs), LIPSS can even be obtained in large-bandgap dielectric materials. The field of applications, however, is limited by the particular tolerance against the residual degree of randomness. For example, random structures can serve as functional surfaces for photocatalysis, anti-icing layers, hydrophobic surfaces or substrates for surface enhanced Raman spectroscopy. Other applications like optical diffraction gratings demand a significantly higher degree of order and require a better control of the laser-material interaction. Important parameters which influence the randomness are the homogeneity of the intensity profile, size and density of defects, the number of laser pulses, the pointing stability of the laser, the polarization orientation and the differential transversal elongation of the translation stage over the path of the substrate. Large areas of material can be structured by scanning methods where the substrate or the laser spot is moved at an optimized speed. Recently we proposed a scanning geometry based on a line focus and a moving substrate. In such a geometry, random defects are statistically changing their relative position along the line focus. Here we report on experimental studies on the formation conditions of coherently linked ripple structures with such a quasi-1D plasmon excitation geometry. The role of nanoscale optical and plasmonic feedback mechanisms is discussed.

Normal and Abnormal Nanoripples Produced on Materials Surfaces by Ultrashort Laser Pulses

Sergey I. Kudryashov[1], **Andrey A. Ionin**[1], **Sergey V. Makarov**[2], **and Wolfgang Husinsky**[3]

[1]P. N. Lebedev Physical Institute, Russian Academy of Sciences, Russia
[2]ITMO University, Russia
[3]Institut für Angewandte Physik, Technische Universität Wien, Austria

Abstract— Ultimate (sub-100-nanometer) nanoripples fabricated on different materials surfaces via multi-shot femtosecond (fs) laser exposure are analyzed according to their polarization (ridge orientation) in respect to the laser one — normal (ridges across the laser polarization) or abnormal (ridges along the laser polarization). This polarization aspect is considered in terms of different diffracted EM components on fs-laser photo-excited materials surfaces at photoexcitation conditions, corresponding to their transient optical characteristics, which support excitation of their corresponding surface plasmon resonances. The experimental observation of such normal and abnormal nanoripples is enlightened, invoking the transient optics of fs-laser photo-excited materials experimentally studied by optical pump/probe reflection method, and profound plasmonic description, including plasmon-plasmon interactions, to calculate transient "energy frequency-spatial wavenumber" dispersion relationships for surface plasmon-polaritons in these photoexcited materials.

Waveguiding Metallic Photonic Crystals Produced by Plasmon-driven Self-organization

Nathalie Destouches[1], **Zeming Liu**[1], **Guy Vitrant**[2], **Yaya Lefkir**[1], **and Stéphanie Reynaud**[1]

[1]Laboratoire Hubert Curien, Université Jean-Monnet, Université de Lyon
CNRS, UMR 5516, 18 rue Pr. Lauras, Saint-Etienne F-42000, France
[2]IMEP-LAHC, Minatec, Grenoble-INP, CNRS-UMR 5130
3 Parvis Louis Néel-CS 50257, Grenoble F-38016, France

Abstract— Metallic photonic crystals combined with waveguides are interesting structures that provide a strong interaction between the electronic resonance of a plasmon and the optical resonance of a quasi-guided mode; they can give rise to waveguide-particle-plasmon polaritons with a Rabi splitting. We show here that such structures can result from a plasmon-driven self-organization process [1]. 2D arrays of silver nanoparticles are generated upon laser exposure in a TiO_2 film (Figs. 1(a)–(b)). They exhibit tunable optical properties (Fig. 1(c)) thanks to the control of their size, periodicity, orientation and degree of organization. The physico-chemical mechanisms leading to such a self-organization process are also investigated. Both radiative and non-radiative decays of the localized surface plasmon resonance of silver nanoparticles appear to play an important role in the mechanisms. The non-radiative excitation of hot electrons leads either to charge transfers from metallic nanoparticles to the semiconductor TiO_2 matrix, through the Schottky junction, or to the material heating. These two processes result in two opposite effects that are the shrinkage or the growth of silver nanoparticles through oxidation or reduction reactions, respectively (Fig. 1(d)). Their competition is put to the fore through theoretical and experimental approaches and is shown to control the onset of self-organization [2]. The parameters of the self-organized photonic crystals are however driven through scattering by plasmonic nanoparticles, i.e., through the radiative decay of the plasmon. The latter excites a guided mode of the TiO_2 film, whose interference with the incident field is shown to directly influence the period and the orientation of nanostructures. This novel fabrication method is compatible with large area processing at a realistic cost for technological implementation.

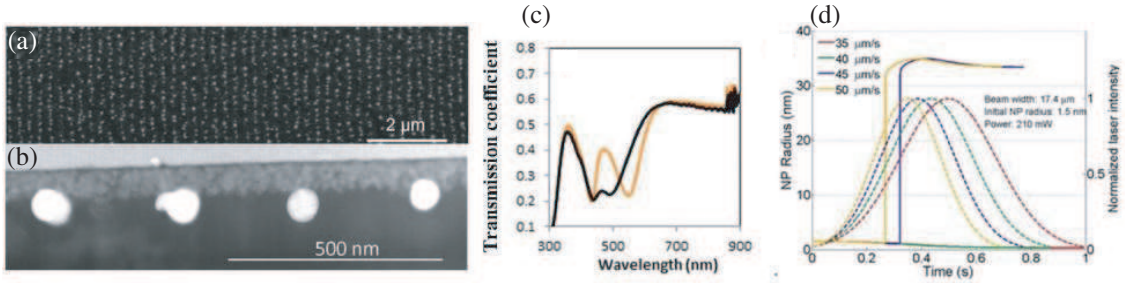

Figure 1: (a) SEM top view and (b) cross-section of a self-organized waveguiding metallic photonic crystal. (c) Transmission coefficient for cross-polarizations. (d) Simulated changes in the nanoparticle size during laser scanning for various scanning speeds.

REFERENCES

1. Destouches, N., N. Crespo-Monteiro, G. Vitrant, Y. Lefkir, S. Reynaud, T. Epicier, Y. Liu, F. Vocanson, and F. Pigeon, *J. Mater. Chem. C*, Vol. 2, 6256, 2014.
2. Liu, Z., N. Destouches, G. Vitrant, Y. Lefkir, T. Epicier, F. Vocanson, S. Bakhti, Y. Fang, B. Bandyopadhyay, and M. Ahmed, in preparation.

Femtosecond LIPSS Formation on Complex Multilayer Target

Olga Varlamova, **Markus Ratzke**, **and Juergen Reif**
Brandenburg University of Technology, BTU, Cottbus-Senftenberg
Platz der Deutschen Einheit 1, Cottbus 03046, Germany

Abstract— We report on femtosecond LIPSS formation on multilayer targets consisting of a glass substrate, a 100-nm film of a ferromagnetic metallic alloy, covered by a 5-nm protective polymer film. Irradiation with 1 up to 5,000 laser pulses (duration 100 fs, wavelength 800 nm, intensity 2.60 TW/cm^2) results in a peculiar overall ablation pattern, consisting of a system of sharp-edged, flat concentric ring-like terraces, despite the Gaussian beam profile. On each of these terraces, a peculiar LIPSS pattern is developed, with, generally, increasing wavelength towards the spot center. Further, for the inner terraces the LIPSS orientation is parallel with a wavelength of about 700 nm, whereas further out it is perpendicular to the laser polarization. In the latter case, the LIPSS wavelength increases towards the spot center from 100 to 250 nm, despite the flatness of the terrace. This indicates that structure formation is more dependent on local intensity than overall ablation.

Already with the first pulse, the protecting layer is fully removed over the whole spot. After a sufficient irradiation dose, the complete layers are removed at the spot center, and the bare substrate is visible, which does not exhibit LIPSS. So, all structure formation appears to occur in the ferromagnetic alloy film.

Interestingly, the laser-target coupling strongly depends on the laser polarization with respect to the target orientation. This might be an effect of the ferromagnetic film properties.

100-nm-periodic Surface Structures upon Femtosecond Laser Irradiation of Silicon in Water: Experiment and Theory

T. J.-Y. Derrien[1, 3], R. Koter[1], J. Krüger[1], S. Höhm[2], A. Rosenfeld[2], and J. Bonse[1]

[1]BAM Bundesanstalt für Materialforschung und-prüfung
Unter den Eichen 87, Berlin D-12205, Germany
[2]Max-Born-Institut für Nichtlineare Optik und Kurzzeitspektroskopie (MBI)
Max-Born-Straße 2A, Berlin D-12489, Germany
[3]HiLASE Centre, Institute of Physics, Academy of Science of the Czech Republic
Za Radnicí 828/5, Dolní Břežany 25241, Czech Republic

Abstract— Laser-induced periodic surface structures (LIPSS) are a universal phenomenon upon irradiation of solids with linearly polarized laser radiation [1]. During the last decade remarkable efforts have been made for controlling the LIPSS and for studying their formation dynamics by using ultrashort laser pulses [2–6]. It is generally accepted now that the excitation of surface electromagnetic waves is involved in the formation of near-wavelength sized LIPSS. This may include the excitation of Surface Plasmon Polaritons (SPPs) at the sample surface [7, 8]. For laser processing in air environment, in most cases, both the LIPSS periods and orientations can be successfully explained by taking into consideration transient changes of the optical properties of the laser-excited materials [7]. For laser processing in liquids, usually the LIPSS periods are significantly reduced by up to one order of magnitude. However, only a few studies provide complementing experimental and theoretical analyses of LIPSS formation in different environments [9–11].

In this work, we experimentally study the formation of laser-induced periodic surface structures (LIPSS) upon irradiation of silicon by multiple linearly polarized 30-fs laser pulses (wavelength of $\lambda = 790\,\mathrm{nm}$) in air and water environment. The LIPSS surface morphologies are characterized by scanning electron microscopy and their spatial periods are quantified by two-dimensional Fourier analyses. It is demonstrated that the irradiation environment significantly influences the periodicity of the LIPSS. In air, low-spatial frequency LIPSS (LSFL) were found with periods somewhat smaller than the laser wavelength ($\Lambda \sim 570\,\mathrm{nm} \sim 0.7\lambda$) and an orientation perpendicular to the laser polarization. In contrast, for laser processing in water, a reduced ablation threshold and LIPSS with approximately five times smaller periods ($\Lambda \sim 100\,\mathrm{nm} \sim 0.15\lambda$) were observed in the same direction as in air.

These experiments are complemented by a theoretical modeling of the excitation of Surface Plasmon Polaritons (SPP) in a thin-film surrounded by two semi-infinitely extended media. Three configurations were considered. (i) While, in air, a thin layer of silicon is transiently excited by the femtosecond laser irradiation, it is found that the period of the SPP-laser interference in the excited layer can reach 100 nm at very high intensities. (ii) In water, such a small period can be also reached at very high intensities. However, these two scenarios are not consistent with the experimentally induced carrier densities. Hence, a third scenario is proposed here: (iii) By taking into account the transient excitation of water and the presence of an oxide layer at the laser-excited silicon sample surface, the excitation of SPP in the oxide layer allowed to explain the 100-nm-period at reasonable carrier densities. Such a thin-film SPP model successfully describes the tremendously reduced LIPSS periods in water, and the orientation perpendicular to the laser polarization.

REFERENCES

1. Van Driel, H. M., J. E. Sipe, and J. F. Young, *Phys. Rev. Lett.*, Vol. 49, 1955, 1982.
2. Bonse, J., J. Krüger, S. Höhm, and A. Rosenfeld, *J. Laser Appl.*, Vol. 24, 042006, 2012.
3. Sokolowski-Tinten, K., et al., *AIP Conf. Proc.*, Vol. 1278, 373, 2010.
4. Höhm, S., A. Rosenfeld, and J. Krüger, *J. Bonse, Appl. Surf. Sci.*, Vol. 278, 7, 2013.
5. Derrien, T. J.-Y., J. Krüger, T. E. Itina, S. Höhm, A. Rosenfeld, and J. Bonse, *Opt. Express*, 29643, 2013.
6. Derrien, T. J.-Y., J. Krüger, T. E. Itina, S. Höhm, A. Rosenfeld, and J. Bonse, *Appl. Phys. A*, Vol. 117, 77, 2014.
7. Bonse, J., A. Rosenfeld, and J. Krüger, *J. Appl. Phys.*, Vol. 106, 104910, 2009.

8. Derrien, T. J.-Y., T. E. Itina, R. Torres, T. Sarnet, and M. Sentis, *J. Appl. Phys.*, Vol. 114, 083104, 2013.
9. Miyaji, G., K. Miyazaki, K. Zhang, T. Yoshifuji, and J. Fujita, *Opt. Express*, Vol. 20, 14848, 2012.
10. Kudryashov, S. I., E. V. Golosov, A. A. Ionin, Y. R. Kolobov, A. E. Ligachev, L. V. Seleznev, D. V. Sinitsyn, and A. R. Sharipov, *AIP Conf. Proc.*, Vol. 1278, 156, 2010.
11. Derrien, T. J.-Y., R. Koter, J. Krüger, S. Höhm, A. Rosenfeld, and J. Bonse, *J. Appl. Phys.*, Vol. 116, 074902, 2014.

Ablation Threshold and Nanostructuring of Laser Irradiated Diamond

B. Obreshkov[1], **T. Apostolova**[1], **A. A. Ionin**[2],
S. I. Kudryashov[2], **S. V. Makarov**[2], **and D. A. Zayarny**[2]

[1]Institute for Nuclear Research and Nuclear Energy, Sofia 1784, Bulgaria
[2]Lebedev Physical Institute, Moscow 119991, Russia

Abstract— We investigate the ablation threshold and nanostructuring of polished natural diamond exposed to 515 nm intense 200 femtosecond laser pulse. The dynamics of the photo-excited electrons inside the bulk is modelled with time-dependent Schrodinger equation. We find that electron dynamics depends sensitively on the characteristics of the substrate band structure, the intensity and polarization of the radiation field. We show that 8 photons are required to surpass the diamond bandgaps for relatively weak field strength. We scrutiny the intensity dependence of the electron density, that is helpful in the interpretation of the experimental data.

On-chip Laser-written Photonic Circuits for Quantum Applications

Armando Perez-Leija, Markus Gräfe, René Heilmann, and Alexander Szameit
Institute of Applied Physics, Abbe Center of Photonics
Friedrich-Schiller-Universität Jena, Max-Wien-Platz 1, Jena 07743, Germany

Abstract— Quantum computation and information science is a new and rapidly developing interdisciplinary research field. In this context, one of the most ambitious goals is to realize scalable quantum information processing and computing based on only linear optical configurations and photon-counting devices [1, 2]. In that vein, a promising approach for miniaturizing and scaling optical quantum circuits is to use on-chip laser written waveguides, which promises strong improvements in performance due to high stability, low noise and therefore almost negligible decoherence. In addition, this particular fabrication method allows creating complex three-dimensional waveguide architectures with multiple degrees of freedom, such as diffraction control and birefringence.

In this talk, we report on our recent progress in integrating laser-written photonic quantum circuits. The presentation will be twofold: in the first part we give a brief overview of the physics and fabrication of integrated multiport waveguide configurations. In the second part we provide a closer look at several particular examples regarding the experimental realization of quantum circuits to achieve particular tasks: On-chip generation of high-order single-photon W-states [3], implementation of Fractional Fourier transforms of classical and quantum wave functions [4], an integrated single-photon counter device [5], and a perfect state transfer protocol [6].

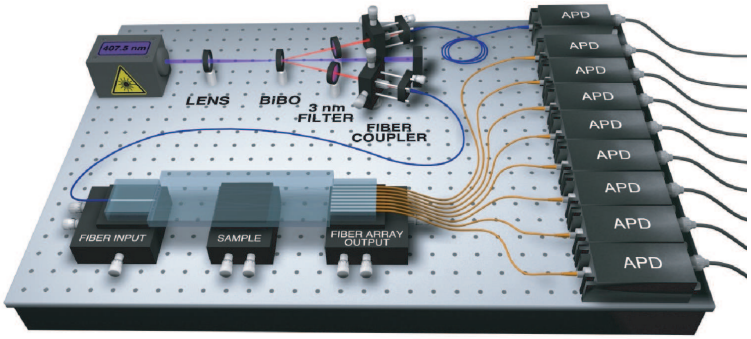

Figure 1: Characterizing quantum waveguide networks on chip. Except photon source and detection devices, all optical components such as beam splitters or wave plates are integrated on chip.

REFERENCES

1. Kok, P., et al., *Rev. Mod. Phys.*, Vol. 79, 135, 2007.
2. Knill, E., et al., *Nature*, Vol. 409, 46–52, 2000.
3. Gräfe, M., et al., *Nature Photonics*, Vol. 8, 791–795, 2014.
4. Weimann, S., et al., "Implementation of quantum and classical fractional fourier transforms using the heisenberg XY model in waveguide arrays," to be published.
5. Heilmann, R., et al., "Divide-and-conquer: An integrated photon-counting scheme," ArXiv e-prints, 2015.

Session 3P14
SC3: Optical Microcavities and Waveguides 3

Coupling Single Molecules to a Fabry-Perot Cavity with Ultrasmall Mode Volume

V. Sandoghdar
Max Planck Institute for the Science of Light (MPL) and
Friedrich Alexander University Erlangen-Nürnberg, Erlangen 91058, Germany

Abstract— Cavity Quantum Electrodynamics has offered a powerful approach for manipulating and enhancing light-matter interaction. Two central parameters in this type of study are the quality factors (Q) and cavity mode volume (V). Ideally, one aims to maximize the former while minimizing the latter, but this combination is often very challenging, especially if one insists on facile tenability of the cavity resonance. Indeed, most spectacular results of the last two decades were obtained by increasing Q while V was left at hundreds or thousands of λ^3. Working in this regime means that one deals with very narrow resonances with two undesirable consequences. First, one can only couple to one atomic transition at a time, Second, one has to tune the cavity precisely and work hard to keep its resonance frequency against thermal and mechanical instabilities in the laboratory.

In this work, I will report on the realization of a tunable and scannable microcavity with an ultralow mode volume of the order of $0.5\lambda^3$. The cavity is made of a curved micromirror fabricated using focused ion beam milling and coated with gold placed in front of a planar distributed Bragg reflector (see Fig. 1). Using a very highly curved mirror at the end of an AFM tip, we also achieve a high numerical aperture of 0.4, which offers a large collection angle and compatibility with tightly focused laser beams. A further important feature of our design is maintaining a low Q of about 150, corresponding to a cavity linewidth of 5 nm. The ultrasmall mode volume of such a cavity yields a Purcell enhancement factor of more than 25.

We present our results on the investigation of the effect of a single gold nanoparticle on the cavity resonance and Q. Furthermore, we discuss ongoing work on the coupling of single organic molecules to the microcavity at cryogenic temperatures, where a modest Purcell factor of 25 is expected to have a substantial influence on the emission branching ratio of the excited state. Finally, we will discuss the potential of our experimental arrangements for novel studies of nonlinear quantum optical effects and for optomechanics.

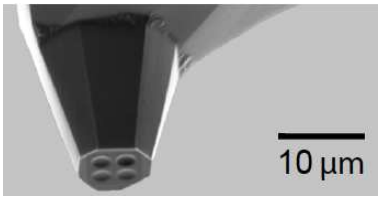

Figure 1: An electronmicroscope image of an AFM tip with four microfabricated curved mirrors.

REFERENCES

1. Kelkar, H., D. Wang, D. Martin-Cano, B. Hoffmann, S. Christiansen, S. Götzinger, and V. Sandoghdar, "A sub-λ^3-volume cantilever-based fabry-perot cavity," submitted, arXiv: 1502.02736v1.

Crystalline WGM Resonators on the Road from R&D to Photonics Products

Vladimir Ilchenko, Andrey Matsko, and Lute Maleki
OEwaves Inc., 165 N Halstead St., Se. 140, Pasadena, CA 91107, USA

Abstract— Crystalline optical resonators with whispering gallery modes (WGM) with their uniquely high value of quality factors 10^8–10^{10} and beyond can serve as core elements in photonic filters, modulators, receivers, narrow-linewidth lasers and low phase noise microwave oscillators. We will review the development status of WGM resonators of different crystalline materials, coupling and tuning methods, high speed modulation techniques utilized in functional photonic devices, as well as discuss performance parameters of crystalline WGM resonator-based microwave and millimeter-wave optoelectronic and Kerr comb oscillators. Architectures and properties of agile photonic receivers and filters will be outlined. Latest results on frequency stability and noise in injection-locked semiconductor lasers with optical feedback from crystalline WGM resonators will be presented in context of their utility for traditional and emerging applications ranging from spectroscopy and remote sensing, to data transmission, metrology and navigation. Prospects and challenges of novel WGM resonator materials and devices for expanded spectral range, from visible to mid-infrared, will be discussed.

Small Refractive Index, High Performance: Magnesium Fluoride Whispering Gallery Mode Sensors

F. Sedlmeir[1, 2, 3], **R. Zeltner**[1], **G. Leuchs**[1, 2], **and Harald G. L. Schwefel**[1, 2, 4]

[1]Max Planck Institute for the Science of Light, Erlangen 91058, Germany
[2]Institute for Optics, Information and Photonics
Friedrich-Alexander University of Erlangen-Nürnberg, Erlangen 91058, Germany
[3]SAOT, School of Advanced Optical Technologies
Friedrich-Alexander University of Erlangen-Nürnberg, Erlangen 91052, Germany
[4]Department of Physics, University of Otago, 730 Cumberland Street, Dunedin, New Zealand

Abstract— Whispering gallery mode (WGM) resonators have been used for sensing for more than a decade [1, 2]. The most common implementation are resonators based on silica microspheres [3] and toroids. Although their performance is good [4] we propose a novel class of materials for WGM resonator sensors namely single crystalline materials [5]. Such resonators can feature higher quality factors $Q > 10^{10}$, expand the range of refractive indicies as well as provide birefringent materials as resonators. Such birefingent WGM resonators can show circular and elliptic polarization behaviors if the angle of the optic axis with respect to the rotational symmetry axis is chosen properly [6]. We will show that especially low index materials as well as birefingent materials are ideally suited for sensors such as refractometric aqueous environment sensors [7]. In particular WGM resonators made out of magnesium uoride (MgF_2) have a refractive index very close to that of water $\Delta n \approx 0.05$ and therefore feature significantly enhanced evanescent fields length compared to silica microresonators [7]. Their birefingence and especially the thermorefractive coefficients of MgF_2 allow furthermore to stabilize the temperature of the mode volume down to a few nano Kelvin [8].

REFERENCES

1. Vollmer, F. and H. G. L. Schwefel, "Taking detection to the limit with optical microcavities: Recent advances presented at the 560. WE Heraeus Seminar," *The European Physical Journal Special Topics*, Vol. 223, 1907–1916, Sep. 2014.
2. Vollmer, F. and L. Yang, "Review label-free detection with high-Q microcavities: A review of biosensing mechanisms for integrated devices," *Nanophotonics*, Vol. 1, No. 3–4, 267–291, 2012.
3. Braginsky, V., M. Gorodetsky, and V. Ilchenko, "Quality-factor and nonlinear properties of optical whispering-gallery modes," *Physics Letters A*, Vol. 137, 393–397, May 1989.
4. Baaske, M. D., M. R. Foreman, and F. Vollmer, "Single-molecule nucleic acid interactions monitored on a label-free microcavity biosensor platform," *Nature Nanotechnology*, Vol. 9, 933–939, Nov. 2014.
5. Grudinin, I. S., V. S. Ilchenko, and L. Maleki, "Ultrahigh optical Q factors of crystalline resonators in the linear regime," *Physical Review A*, Vol. 74, 063806–9, Dec. 2006.
6. Sedlmeir, F., M. Hauer, J. U. Fürst, G. Leuchs, and H. G. L. Schwefel, "Experimental characterization of an uniaxial angle cut whispering gallery mode resonator," *Optics Express*, Vol. 21, 23942–23949, Oct. 2013.
7. Sedlmeir, F., R. Zeltner, G. Leuchs, and H. G. Schwefel, "High-Q MgF_2 whispering gallery mode resonators for refractometric sensing in aqueous environment," *Optics Express*, Vol. 22, 30934–30942, Dec. 2014.
8. Strekalov, D. V., R. J. Thompson, L. M. Baumgartel, I. S. Grudinin, and N. Yu, "Temperature measurement and stabilization in a birefringent whispering gallery mode resonator," *Optics Express*, Vol. 19, 14495–14501, Jul. 2011.

Oscillatory Lateral Coupling in a Waveguide-microdisk-resonator System

Fang Bo[1,2], **Sahin Kaya Ozdemir**[2], **Faraz Monifi**[2], **Guoquan Zhang**[1], **Jingjun Xu**[1], **and Lan Yang**[2]

[1]The MOE Key Laboratory of Weak Light Nonlinear Photonics
TEDA Applied Physics Institute and School of Physics, Nankai University, Tianjin 300457, China
[2]Department of Electrical and Systems Engineering
Washington University in St. Louis, St. Louis, Missouri 63130, USA

Abstract— A notch filter consisting of a resonator and a waveguide plays an important role in both fundamental and applied research such as optomechanics quantum information processing, low-threshold lasing and high-performance sensing. It is always desirable to maintain efficient resonator waveguide coupling (RWC) of the notch filter for the success of all these studies In general, we consider the case in which the waveguide is placed outside the rim of the resonator. In this case, the field exchange between the resonator and the waveguide takes place through their evanescent fields in a region where their spatial modes overlap. As the waveguide approaches the resonator, the RWC goes from under coupling, through critical coupling, to over coupling due to the increase of the spatial overlap between the light leaking out from the resonator and that from the fiber taper.

Here, we investigate a new RWC configuration in which the waveguide is placed between the center and edge of the resonator in a plane parallel to the surface of the resonator. In this case, the RWC takes place at two different regions where the spatial modes of the resonator and waveguide have spatial overlap. We show that with this new configuration, one can obtain as efficient RWC as nearly critical coupling even when the waveguide is moved far from the rim of the resonator toward its center. This is attributed to the destructive interference between the light fields coupled out from the resonator at two different regions and the light propagating through the waveguide directly. As the horizontal position of the waveguide with respect to the center of the resonator is scanned laterally, RWC experiences periodic oscillation when the waveguide is fixed at a constant height above the resonator. A theoretical model based on coupled-mode theory and two-point coupling successfully explains the experimental observations. Similar horizontal oscillatory coupling behavior is also observed in two vertically coupled microdisk resonators.

Ring Resonator Based Silicon Photonic Devices

D. J. Thomson[1], **B. Troia**[2], **M. Nedeljkovic**[1], **F. Y. Gardes**[1], **J. Soler Penades**[1], **A. Z. Khokhar**[1], **J.-M. Fedeli**[3], **V. M. N. Passaro**[2], **G. Z. Mashanovich**[1] **and G. T. Reed**[1]

[1]Optoelectronics Research Centre, University of Southampton
Highfield, Southampton, Hampshire. SO17 1BJ, United Kingdom
[2]Department of Electrical and Information Engineering, Politecnico di Bari
Via E. Orabona 4, Bari 70125, Italy
[3]CEA, LETI, Minatec, 17 rue des Martyrs, Grenoble 38054, France

Abstract— Silicon as a material for forming photonic devices is attractive for several reasons. Devices can be fabricated in CMOS like facilities in large volumes and with high yield and as a result costs are low. Another attraction is compactness. In most cases silicon photonic devices are built on silicon-on-insulator substrates. Sub-micrometer single-mode strip and rib waveguides based in this high index contrast system are highly confining and low loss bends can be produced with a radius of just a few micro meters. This feature allows ring resonators which occupy extremely small footprints to be produced. In this work an overview of some of our recent work in the area of ring resonators will be given.

Our recent results about cascade-coupled ring and racetrack resonators based on the Vernier effect for filtering and sensing applications and operating in the near-infrared wavelength range are reported. In particular, Vernier spectra with overall free spectral ranges as long as $\sim 36\,\text{nm}$, Vernier gains up to 30, extinction ratio of 30 dB and overall insertion loss as low as 2 dB have been achieved experimentally around 1.55 μm in excellent agreement with the theoretical predictions

Optical modulators are key components in photonic systems for data transmission. In silicon the use of the plasma dispersion effect to achieve optical modulation in a carrier depletion structure has been the preferred approach for many working in the field due to their ease of fabrication, attainable performance and CMOS compatibility. There are two main approaches for converting the phase modulation produced by such a device into intensity modulation. The first involves incorporating the phase modulator into a Mach-Zehnder interferometer (MZI) and the second into a ring resonator. In this work we present experimental results from both approaches demonstrating a ring resonator based optical modulator operating up to 40 Gbit/s.

The Midinfrared wavelength range is become an increasingly vibrant research area in silicon photonics for many application areas. In particular, ring resonator based structures are particularly suitable for sensing and filtering applications to be performed in the mid-infrared; although integrated microcavities based on suspended and membrane waveguides on silicon-on-sapphire technology platform, As_2Se_3 chalcogenide glass, and $Ge_{23}Sb_7S_{70}/Zr_{0.6}Ti_{0.4}O_2$ material systems have been demonstrated to operate up to $\sim 5\,\mu\text{m}$, to date there have been very few demonstrations of silicon ring resonators based on non-exotic waveguide architectures, operating in this wavelength range. In this work we also present our work on single and cascade-coupled ring and racetrack resonators based on standard rib and strip silicon waveguides operating in the 3.7–3.8 μm wavelength range. Our devices can exhibit insertion loss lower than 1 dB, extinction ratios up to 30 dB, quality factor up to $\sim 10,000$ and free spectral ranges even shorter than 5 nm.

Spatial and Temporal Control of Cavities

E. Yüce[1], J. Lian[1], S. Sokolov[1], H. Thyrrestrup[1], G. Ctistis[1], E. Peinke[2], J. Claudon[2], S. Combrié[3], A. De Rossi[3], J.-M. Gérard[2], A. P. Mosk[1], and W. L. Vos[1]

[1]Complex Photonic Systems (COPS), MESA+ Institute for Nanotechnology
University of Twente, AE Enschede 7500, The Netherlands
[2]Nanophysics and Semiconductor Laboratory, CEA/INAC/SP2M, 38054 Grenoble, France
[3]Thales Research and Technology, Route Départementale 128, Palaiseau 91767, France

Abstract— Semiconductor microcavities have proven to be essential for light confinement in space and also for storage in time, which enables manipulating light matter interactions [1]. The control of the cavity refractive index spatially and temporally will allow for complete control over the light stored in a cavity; in real space, wavevector space, frequency space, and in time domain. The control of the refractive index at ultrafast time scales enables to convert the frequency of light stored in a cavity [2]. The spatial control will allow for controlling the coupling of the cavity to the environment and enable to shape the mode profile.

The generation of light with a controllable frequency is a long standing challenge. Literature has it that the physics of frequency conversion in a cavity differs from traditional non-linear optics, regarding the rate of phase change and output spectrum [2, 3]. Here, we unify these disparate views. We have reversibly switched the resonance of GaAs-AlAs microcavities in the near-infrared ($\lambda = 1280\,\mathrm{nm}$) within 300 fs by the electronic Kerr effect [4]. Fig. 1(a) shows spectra measured at several pump-probe delays Δt. We observe a significant red- and blue-shift of light trapped in the cavity, controlled by the pulse-timing. Blue-shift occurs at $\Delta t = -100\,\mathrm{fs}$ when the phase decreases, and red-shift light at $\Delta t = -500\,\mathrm{fs}$ where the phase increases, in seeming agreement with usual non-linear optics [4]. Fig. 1(b) shows that the integrated blue-converted reflectivity increases remarkably with inverse quality factor. We identify $(1/Q)$ as a measure of the density of optical states (DOS) that leak into any cavity at frequencies off-resonance. We conclude that frequency conversion in a cavity is controlled by the density of vacuum states and the non-linear polarization [4]. Our new insights provide a unified framework for seemingly disparate results in traditional nonlinear optics and nanophotonics, and offer a complete control of on-chip frequency conversion.

Arrays of coupled high-Q nanocavities, collectively provide a superior system than a single cavity that can be used to observe light localization [5, 6]. A challenge remains; namely to fabricate an array of cavities at the same resonance frequency to observe localization. Due to technical limitations, fabrication of many high-Q cavities at the same resonance frequency is not simply achievable. Here, we control the resonance frequency of each cavity individually by locally changing the refractive index in an InGaP photonic crystal cavity array. We use wavefront shaping to shape the pump beam and we address individual cavities [7]. As a result, we spatially control the refractive index and manage to manipulate the coupling of the cavities. We show that we can counteract the unintentional shift of the cavity resonance frequency and we can bring multiple cavities to a collective resonance.

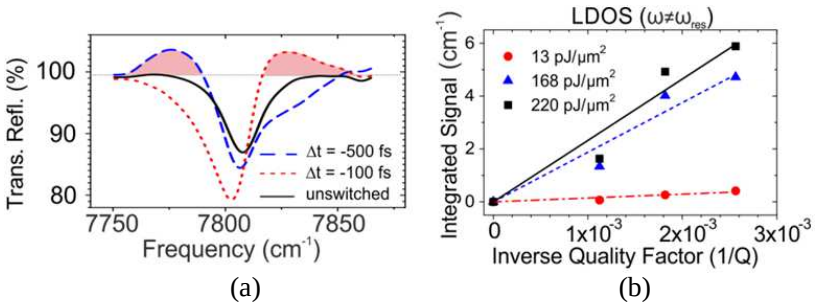

Figure 1: The measured transient reflectivity versus frequency at several time delays. Filled regions show newly generated frequencies. In the absence of color conversion the transient reflectivity is 100%. Cavity has $Q = 390$. (b) Integrated signal versus inverse quality factor $(1/Q)$, a measure of the density of states, for different pump intensity. Top abscissa: LDOS. Lines are guides to the eye.

REFERENCES

1. Vahala, K. J., *Nature*, Vol. 424, 2003.
2. Notomi, M. and S. Mitsugi, *Phys. Rev. A*, Vol. 73, 051803(R), 2006.
3. Boyd, R., *Nonlinear Optics*, Academic Press, 2008.
4. Yüce, E., G. Ctistis, J. Claudon, J. M. Gérard, and W. L. Vos, *Phusics Optics*, arXiv: 1406.3586, 2014.
5. Yariv, A., Y. Xu, R. K. Lee, and A. Scherer, *Opt. Lett.*, Vol. 24, 711, 1999.
6. Notomi, M. E. Kuramochi, and T. Tanabe, *Nature Photon.*, Vol. 2, 741, 2008.
7. Mosk, A. P., A. Lagendijk, G. Lerosey, and M. Fink, *Nature Photon.*, Vol. 6, 283–292, 2012.

Whispering Gallery Mode Microresonators for Sensing

S. Pelli[1, 2], **A. Barucci**[1], **F. Baldini**[1], **S. Berneschi**[1], **F. Cosi**[1], **A. Cosci**[1, 2], **D. Farnesi**[1, 2], **A. Giannetti**[1], **G. Nunzi Conti**[1, 2], **S. Soria**[1], **S. Tombelli**[1], **C. Trono**[1], **M. Ferrari**[2, 3], **D. Ristić**[4], **and G. C. Righini**[1, 2]

[1]Istituto di Fisica Applicata "Nello Carrara", C.N.R.
Via Madonna del Piano 10, Sesto Fiorentino (Firenze) 50019, Italy
[2]Museo Storico della Fisica e Centro Studi e Ricerche "Enrico Fermi"
Piazza del Viminale 1, Roma 00184, Italy
[3]IFN-CNR CSMFO Lab., Via alla Cascata 56/C Povo, Trento 38123, Italy
[4]Center of Excellence for Advanced Materials and Sensing Devices
Institut Ruđer Bošković, Bijenička, cesta 54, Zagreb 10000, Croatia

Abstract— Optical sensors can offer many advantages in terms of increased sensitivity or compatibility with environments where electronic devices are not suitable.

Whispering gallery modes microresonators (WGMRs) exhibit high quality factor ($> 10^7$) optical resonances. These are very sensitive to changes to the structure of the resonator and their wavelength position shifts when molecules bind to its chemically functionalised surface.

This effect can be exploited to build very sensitive sensors and can be utilised to develop point of care equipment or environmental sensors, among the most relevant applications.

In this presentation, after a short recall of the working principles of these structures and a review of the highlights of the advances in this field, the presentation will describe our activity in the development of optical sensors based on WGMRs.

The presentation will focus in particular on our activity in the development of microbubble resonators.

We have been working on the interdependent aspects such as modelling, fabrication, localised chemical functionalization for selective response, structural and modal characterisation, coupling, which are all challenging tasks in order to obtain optimised devices. The presentation will give an account of our efforts to harness all these factors and the related results we obtained.

Coupling, Controlling, and Processing Non-transversal Photons with a Single Atom

A. Rauschenbeutel
Vienna Center for Quantum Science and Technology, Institute of Atomic and Subatomic Physics
Vienna University of Technology, Wien, Austria

Abstract— I will report on recent experimental investigations of the interaction between single rubidium atoms and light that is confined by continuous total internal reflection in a whispering-gallery-mode (WGM) bottle microresonator. We discovered that the non-transversal polarization of WGMs fundamentally alters the physics of light-matter interaction [1]. Taking advantage of this effect, we recently demonstrated switching of signals between two distinct optical fibers controlled by a single atom [2]. Owing to the excellent optical properties of our bottle microresonator, the scheme yields high switching fidelities and low losses. Furthermore, we made use of the strong nonlinear response of the atom-resonator system and experimentally realized an optical Kerr nonlinearity at the level of single photon [3]. Analyzing the transmitted light, we observe a nonlinear phase shift of π between the cases of one and of two photons passing the resonator. This phase shift leads to entanglement between previously independent fiber-guided photons, which we verify by performing a full quantum state tomography of the transmitted two-photon state. And finally, via the WGM microresonator, we coupled a single atom to a nanophotonic silica waveguide and demonstrate nonreciprocal transmission of light at the single-photon level through the system [4]. The resulting optical diode is the first example of a new class of nonreciprocal nanophotonic devices which exploit the chiral interaction between quantum emitters and transversally confined photons.

REFERENCES

1. Junge, C., et al., *Phys. Rev. Lett.*, Vol. 110, 213604, 2013.
2. O'Shea, D., et al., *Phys. Rev. Lett.*, Vol. 111, 193601, 2013.
3. Volz, J., et al., *Nat. Photon.*, Vol. 8, 965, 2014.
4. Sayrin, C., et al., arXiv: arXiv:1502.01549, 2015.

Micro-optical Wall Shear Stress Sensor for Fluid Mechanics Applications

Ulas K. Ayaz[1], **Tindaro Ioppolo**[2], **and Volkan Otugen**[2]

[1]Mechatronics Department, German University in Cairo, Berlin, Germany
[2]Mechanical Engineering Department, Southern Methodist University, Dallas, TX, USA

Abstract— In recent years, several micro-sensors have been proposed based on the excitation of optical modes of dielectric micro-resonators. These optical resonators could come in spherical, cylindrical or torroidal geometries and vary in size from a few microns to several hundreds of microns. The optical modes of these resonators are called whispering gallery modes (WGM), and have been exploited in a number of applications in spectroscopy, micro-lasers, optical communications as well as sensor technologies. The WGM based optical sensors in the literature include biosensors, trace gas detection, impurity detection in liquids, structural health monitoring of composite materials, detection of electric and magnetic fields, as well as mechanical sensing such as force, pressure, shear stress and acceleration. In this talk, some of these optical sensors in mechanical sensing, with the focus given on the wall shear stress sensor for fluid mechanics applications, will be presented.

Quantum Operations Based on Waveguide Nonlinear Optical Materials

Takashi Yamamoto
Graduate School of Engineering Science, Osaka University, Toyonaka, Osaka 560-8531, Japan

Abstract— Photonic frequency conversions based on nonlinear optical phenomena have attracted much interest in the context of the manipulation of the quantum states recently. One of the immediate applications is the frequency conversion of a single photon without destroying its quantum states. Such a quantum frequency converter is useful for linking diverse matter based quantum systems through the quantum states of light. Especially, when we look at the long distance quantum communication, entangling the distantly located matter quantum memories via photons is considered to be an elemental building block for the quantum repeaters. Here we report on such a single photon frequency converter from visible to telecommunication wavelength with a second order nonlinear optical phenomena based on a waveguide PPLN, which aims at linking Rb atom quantum memories with a long distance optical fiber communication. The single photon frequency converter with a adjusted conversion efficiency is also useful for the manipulation of quantum states encoded in the frequency degree of freedom. Along this direction, we also present an interference of a photon in two different frequency modes and also Hong-Ou-Mandel (HOM) interference of two photons in two different frequency modes. The enhancement of the conversion efficiency with microcavities is also an important issue for the future applications. We also present our recent activity on slow and fast light observation based on high-quality-factor whispering gallery mode (WGM) resonators in the form of microtoroids and bottle microresonators with high quality factors.

Silicon Optical Matrix Processor for Parallel Computing

Lin Yang, Lei Zhang, Hao Jia, and Jianfeng Ding
State Key Laboratory on Integrated Optoelectronics
Institute of Semiconductors, Chinese Academy of Sciences, Beijing 100083, China

Abstract— Matrix-vector multiplication is a fundamental operation in modern digital signal processing fields. Inspired by the intrinsic spatial parallelism of optics, much effort has been made to develop optical apparatuses that can perform such a parallelizable operation. The Stanford multiplier is one of the most notable demonstrations, which is composed of light source array, optical lens, spatial light modulator matrix and photodetector array. Almost all implementations are large in volume and high in power consumption. Moreover, many removable elements adopted make them extremely sensitive to the environmental vibration. To overcome these limitations, we propose an on-chip optical matrix processor (MVM), which is composed of laser-modulator array, multiplexer, splitter, microring modulator matrix and photodetector array. The fan-out and fan-in with optical lenses in the traditional optical MVMs are replaced by the power splitting and wavelength multiplexing with waveguide devices in the proposed optical MVM, which greatly reduces the complexity and size of the system. The discrete components in the traditional optical MVMs are replaced by the integrated ones in the proposed optical MVM, which improves the stability and power efficiency of the system. 1.6×10^9 multiplications and accumulations per second is implemented by a demo system with a 4×4 microring modulator matrix.

Efficient Optical Fiber Coupling to Whispering Gallery Modes of Optically Manipulated Emulsion Microdroplets

S. Anand[1], **M. Eryürek**[1], **Y. Karadag**[2], **A. Serpengüzel** [1], **and A. Kiraz**[1]

[1]Department of Physics, Koç University, Rumelifeneri Yolu, Sarıyer, İstanbul 34450, Turkey
[2]Department of Physics, Marmara University, Göztepe, İstanbul 34722, Turkey

Abstract— We demonstrate efficient coupling to the optical whispering gallery modes of a spherical resonator consisting of a liquid droplet embedded in another liquid medium. Whispering gallery mode particle sensing experiment is commonly performed with solid resonators, whereby the sensing volume is limited to the weak evanescent tail of the mode near the resonator surface. In this work, we demonstrate efficient coupling to the optical whispering gallery modes by introducing a portable, all liquid emulsion microdroplet resonator held in a single beam optical trap. We have observed coupling to the fundamental whispering gallery modes of 10 to 60 µm diameter emulsion droplets at 1550 nm. The experimental challenges towards making, stabilizing and coupling to the droplet resonators are also addressed in this paper.

Optical Resonances in Quantum Plasmonics

M. S. Tame
University of KwaZulu-Natal, South Africa

Abstract— Quantum plasmonics is a rapidly growing field of research that involves the study of the quantum properties of light and its interaction with matter at the nanoscale. Here, surface plasmons — electromagnetic excitations coupled to electron charge density waves on metal-dielectric interfaces or localized on metallic nanostructures — enable the confinement of light to scales far below that of conventional optics. We review recent progress in the experimental and theoretical investigation of resonant optical phenomena in quantum plasmonic systems, including the role of surface plasmons in controlling light-matter interactions at the quantum level and potential applications, such as entanglement generation and the distillation of entanglement.

REFERENCES

1. Tame, M. S., et al., "Quantum plasmonics," *Nature Physics*, Vol. 9, 329–340, 2013.
2. Lee, C., et al., "Robust-to-loss entanglement generation using a quantum plasmonic nanoparticle array," *New J. Phys.*, Vol. 15, 083017, 2013.
3. Asano, M., et al., "Distillation of photon entanglement using a plasmonic metamaterial," Submitted, 2015.

Sapphire Microspheres as Photonic Biosensors

M. S. Murib[1], W. S. Yeap[1], D. Martens[2], L. Michiels[3], M. J. Schöning[4], W. De Ceuninck[1], K. Haenen[1,5], P. Bienstman[2], A. Serpengüzel[6], and P. Wagner[1,5]

[1]Institute for Materials Research, IMO, Hasselt University
Wetenschapspark 1, B-3590 Diepenbeek, Belgium
[2]Department of Information Technology, INTEC, Gent University
Sint-Pietersnieuwstraat 41, B-9000 Gent, Belgium
[3]Biomedical Research Institute, Hasselt University
Agoralaan, B-3590 Diepenbeek, Belgium
[4]Institute of Nano- and Biotechnologies, Aachen University of Applied Sciences
Heinrich-Muβmann-Straβe 1, D-52428 Jülich, Germany
[5]Division IMOMEC, IMEC vzw, Wetenschapspark 1, B-3590 Diepenbeek, Belgium
[6]Microphotonics Research Laboratory, Department of Physics, Koç University
Rumelifeneri Yolu, Sarıyer, Istanbul 34450 Turkey

Abstract— Circular cavities [1] such as microspheres [2], microdisks [3], and microtoroids [4] with high quality factor whispering gallery modes (WGMs) continue to open up new perspectives in sensing [5–8]. In this paper, an optical setup for a DNA optical biosensor based on sapphire microsphere was built. Transmitted and elastic scattering intensity at 1510 nm were analyzed from a sapphire microsphere on an optical fiber half coupler for the first time. The 0.43 nm angular mode spacing of the WGMs correlated well with the optical size of the sapphire microsphere. The spectral linewidths of the WGMs were on the order of 0.01 nm, which corresponded to quality factors on the order of 10^4. As a proof for principle, a polydopamine (PDA) layer has been used as a functionalizing agent on sapphire microspheres in view of the implementation of biosensors. The various PDA layer thicknesses on the sapphire microsphere were characterized as a function of the WGMs wavelength shift. It was shown that the polymeric functionalization does not affect the high quality factor ($Q \approx 10^4$) of the WGMs. This functionalizing process of the microsphere constitutes a promising step towards the achievement of an ultrasensitive biosensor. Afterwards, the sapphire microsphere was modified with DNA and an optical biosensor is demonstrated for the first time using an insulating implant material such as sapphire. A probe DNA, consisting of a 36-mer fragment was covalently immobilized on sapphire microsphere and hybridized with a 29-mer target DNA. WGMs were monitored before the sapphire was being functionalized with DNA and after it was functionalized with single stranded DNA (ssDNA) and double stranded DNA (dsDNA). The shift in WGMs due to the surface modification with DNA was measured and correlated well with the estimated add-on DNA layer. It was shown that ssDNA are more uniformly oriented on the sapphire surface than the dsDNA. In addition, it was shown that the functionalization of the sapphire microsphere's surface with DNA does not affect the high quality factor ($Q \approx 10^4$) of the WGMs. All in all, we have taken the first step towards utilizing a structural, electrically insulating implant material as an optical microcavity based biosensor platform paving the way for future in vivo biosensing devices [9, 10].

REFERENCES

1. Serpengüzel, A. and A. W. Poon, Eds., *Optical Processes in Microparticles and Nanostructures: A Festschrift Dedicated to Richard Kounai Chang on His Retirement from Yale University*, World Scientific, 2011.
2. Bilici, T., S. Işçi, A. Kurt, and A. Serpengüzel, "Microsphere-based channel dropping filter with an integrated photodetector," *IEEE Photon. Technol. Lett.*, Vol. 16, 476–478, 2004.
3. Lu, X., J. Y. Lee, P. X.-L. Feng, and Q. Lin, "Silicon carbide microdisk resonator," *Opt. Lett.*, Vol. 38, 1304–1306, 2013.
4. Zhu, J., S. K. Ozdemir, Y.-F. Xiao, L. Li, L. He, D.-R. Chen, and L. Yang, "On-chip single nanoparticle detection and sizing by mode splitting in an ultrahigh-Q microresonator," *Nature Photon.*, Vol. 4, 46–49, 2009.
5. Arnold, S., R. Ramjit, D. Keng, V. Kolchenko, and I. Teraoka, "Micro particle photophysics illuminates viral bio-sensing," *Faraday Discussions*, Vol. 137, 65–83, 2008.
6. Vollmer, F., S. Arnold, and D. Keng, "Single virus detection from the reactive shift of a whispering-gallery mode," *PNAS*, Vol. 105, 20701–20704, 2008.

7. Arnold, S., M. Khoshsima, I. Teraoka, S. Holler, and F. Vollmer, "Shift of whispering gallery modes in microspheres by protein adsorption," *Opt. Lett.*, Vol. 28, 272–274, 2003.
8. Vollmer, F., D. Braun, A. Libchaber, M. Khoshsima, I. Teraoka, and S. Arnold, "Protein detection by optical shift of a resonant microcavity," *Appl. Phys. Lett.*, Vol. 80, 4057, 2002.
9. Murib, M. S., W. S. Yeap, D. Martens, X. J. Liu, P. Bienstman, M. Fahlman, W. De Ceuninck, M. J. Schöning, L. Michiels, K. Haenen, M. Ameloot, A. Serpengüzel, and P. Wagner, "Photonic studies on polymer-coated sapphire-spheres: A model system for biological ligands," *Sens. Actuator A — Phys.*, Vol. 222, 212–219, 2015.
10. Murib, M. S., W. S. Yeap, D. Martens, P. Bienstman, W. De Ceuninck, M. J. Schöning, L. Michiels, K. Haenen, M. Ameloot, A. Serpengüzel, and P. Wagner, "Photonic detection and characterization of DNA using sapphire spheres," *J. Biomedical Opt.*, Vol. 19, 097006, 2014.

Sensitivity Enhancement of FRET-based Biosensors Using Amplified Stimulated Emission

M. Aas[1], **Q. Chen**[2], **A. Jonáš**[3], **A. Kiraz**[1, 2], **and X. Fan**[2]

[1]Department of Physics, Koç University, Rumelifeneri Yolu, 34450 Sariyer, Istanbul, Turkey
[2]Department of Biomedical Engineering, University of Michigan, Ann Arbor, MI 48109, USA
[3]Department of Physics, Istanbul Technical University, 34469 Maslak, Istanbul, Turkey

Abstract— Non-radiative Forster Resonance Energy Transfer (FRET) between a pair of donor and acceptor chromophores can serve as a precise ruler to measure the distance between the two chromophores in the nanometer range with atomic-scale resolution. The strong dependence of the Energy Transfer (ET) rate in FRET on the donor/acceptor distance has already been used to detect conformational changes in large biomolecules such as proteins and nucleic acids or to quantify interactions between different biomolecules and molecular complexes in live cells. Commonly, the change in the intensity of the donor or acceptor fluorescence is used to determine the change in the ET rate. To increase the sensitivity of fluorescence measurements, the ET can be coupled to a suitable optical cavity, forming a laser with FRET-based active medium. This approach takes advantage of the strongly non-linear dependence of the amplified stimulated emission on minute changes of the overall laser gain.

Using rate equations describing FRET coupled to a Fabry-Perrot optical resonator, we study theoretically the dependence of the output lasing energy from a simple donor/acceptor dye pair placed in the cavity on the distance between the two chromophores. Subsequently, we compare these results with the sensitivity of the output fluorescence intensity when there is no lasing or feedback mechanism present. Our analysis shows that for an example dye pair of Rhodamine 6G as a donor and Acid Blue 7 as an acceptor with 6.1 nm Forster distance, the sensitivity of the fluorescence intensity to the changes in the donor-acceptor separation in the FRET-lasing case increases at least by a factor of 10 relative to the non-lasing case with identical dye concentrations in the 1 to 10 micro-molar range. The presented theoretical analysis supports our recent experimental works on optofluidic FRET lasers and suggests a direct strategy for optimizing the performance of FRET-based molecular sensors.

Operating Speed Extension of SOA External Modulator Using Microring Resonator

Zoe V. Rizou, Kyriakos E. Zoiros, and Thanassis Houbavlis
Lightwave Communications Research Group, Department of Electrical and Computer Engineering
Democritus University of Thrace, Xanthi 67 100, Greece

Abstract— Semiconductor optical amplifiers (SOAs) have recently been receiving intense research interest for use as external modulators. The main technical challenge faced in this effort is the SOAs modulation bandwidth, which is limited below 1 GHz due to the SOAs finite differential carrier lifetime [1]. In order to overcome this difficulty, a widely adopted option exploits optical filtering to manipulate the spectral components of the signal at the SOA output [1]. For this purpose various technologies have been employed [1, and References [11–14] therein]. In this paper we propose to apply a passive single microring resonator (MRR) as notch filter [2] for extending the modulation speed of directly modulated SOAs. This scheme features several attractive operating and practical characteristics [2], which render it an alternative solution for allowing conventional SOAs to be used as external modulators at enhanced data rates.

Figure 1 depicts the block diagram of the directly modulated SOA followed by the MRR of radius R, notch (resonance) detuning, $\Delta\lambda$, to the longer sideband of the data carrier position, and field transmission coefficient r that meets the necessary requirement of critical coupling [2]. We simulated the operation of this setup by calculating first the temporal response of the SOA [2] when the latter is driven under the same input signal and bias conditions as in [1]. Afterwards we transferred this function into the frequency domain by means of Fast Fourier Transform (FFT) in Matlab software and convolved it with the MRR spectral response. This response is described by a compact mathematical form [2] and has the periodic comb-like profile shown inside the MRR box in Fig. 1. Finally, we converted the convolution product back into the time domain using Inverse FFT. By following this procedure we investigated the impact of the MRR radius and detuning on the quality of the encoded optical signal. Provided that the MRR is properly designed against these parameters, which is practically feasible, then it can efficiently suppress the SOA pattern-dependent distortion. Thus the MRR-based notch filter can help improve the performance of SOAs as externally modulators at data rates several times faster than those enabled by their electrical bandwidth.

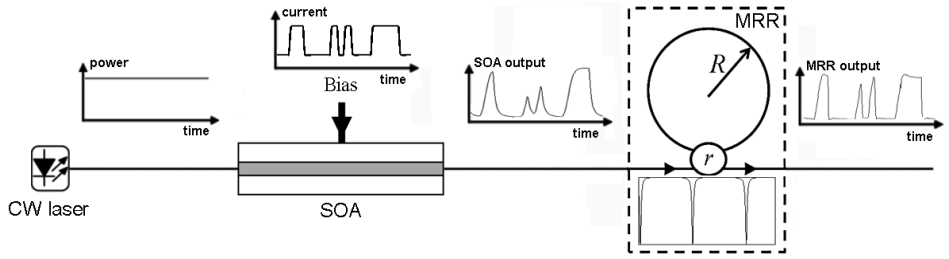

Figure 1: Configuration of directly modulated SOA and MRR-based notch filter.

REFERENCES

1. Zoiros, K. E. and P. Morel, "Enhanced performance of semiconductor optical amplifier at high direct modulation speed with birefringent fiber loop," *AIP Advances*, Vol. 4, No. 7, 077107/1–7, 2014.
2. Rizou, Z. V., K. E. Zoiros, and A. Hatziefremidis, "Semiconductor optical amplifier pattern effect suppression with passive single microring resonator-based notch filter," *Opt. Commun.*, Vol. 329, 206–213, 2014.

Developing Microwave Photonic Temperature Sensors

Arec Jamgochian[1], **John Quintavalle**[2], **Alejandra Torres-Diaz**[1], **James Filla**[2], **Gregory F. Strouse**[1], **and Zeeshan Ahmed**[1]

[1]Thermodynamic Metrology Group, Sensor Science Division, Physical Measurement Laboratory
National Institute of Standards and Technology, Gaithersburg, MD 20899, USA
[2]Innovations and Solutions Division
National Institute of Standards and Technology, Gaithersburg, MD 20899, USA

Abstract— In recent years there has been considerable interest in exploiting temperature dependence of sapphire whispering gallery mode resonator's (WGMR) frequency to develop a mechanical stable temperature sensor that could provide measurement capabilities on par with a Platinum resistance thermometer (PRT). While PRTs can routinely measure temperatures with uncertainties of 10 mK, they are sensitive to mechanical shock which causes the sensor resistance to drift over time requiring frequent off-line, expensive, and time consuming calibrations. Disk-resonator-based devices have been demonstrated to measure temperature with accuracies of 10 mK or better in the temperature range of 273 K to 373 K. We are utilizing automated data acquisition and processing to rapidly evaluate a mechanically-stabilized sapphire whispering gallery mode resonators based on a hollow cylindrical configuration. Our results preliminary results indicate the metal support structure contributes to increased loses of the resonator which results in significant reduction in resonator mode's quality factors.

Session 3P0
Poster Session 6

Magnetic Storms at High Latitudes and Slips in GPS Operating

V. I. Zakharov[1, 2], **Yu. V. Yasyukevich**[2], **and M. A. Titova**[3]

[1]Lomonosov Moscow State University, Moscow, Russia
[2]Institute of Solar-Terrestrial Physics of Siberian Branch of Russian Academy of Sciences
Irkutsk, Russia
[3]IZMIRAN, Moscow, Russia

Abstract— Variability of space weather and its impact on the near-Earth environment is a natural norm. These phenomena can not be avoided, but should be studied and taken into account for the successful functioning of modern communication and GNSS systems. Moreover, the rapid development of technology in the last 20–30 years has meant that the potential accuracy of the use of modern communication and navigation systems are limited to the influence of media in which information signals are distributed. It is particularly sensitive the malfunctions of high-orbit GNSS due to the impact of the physical conditions (space weather) prevailing in the near-Earth space.

The considered "slips" or "failures" are the two possible events in the GPS operation. First of all, it is impossible to determine as the phase or pseudo accompanying signal. These phenomena have a direct impact on the positioning accuracy. Secondly, the failure may also be considered short-term variations of the recorded total electron content (TEC), the values of which can not bear the physical sense and explains the process in the ionosphere and magnetosphere.

In our work we analyzed the dynamics of manifestation of GPS slips and failure in some significant time periods around the date of the studied powerful geomagnetic disturbances 2010–2014. Discussed magnetic storms have the amplitude more 1500 nT. In consideration GPS data on more than 100 stations in the modern global and regional networks (IGS and CHAIN) are used. The used stations are located north of the inclination of the system GPS. Consideration of the chains of power plants mainly in a northerly direction on the territory of Alaska, Canada, northern Europe has allowed for the first time to study the dynamics of the growing influence of the high-latitude ionosphere to the received satellite signal.

The data on the occurrence of slips compared to the behavior of the high-latitude geomagnetic indices AE and AL. We found that failures in determining pseudorange occur much less frequently than in phase measurements. The probability of slips for the phase L2 frequency even in calm conditions receive are several times more than the frequency code capture L1. These relations are preserved and for the pseudorange faults. The presence of geomagnetic storms (or disturbances) leads to an increase of this magnitude in a few dozen times for the considered magnetic events.

Slips rate in determining the TEC significantly — 100 times — more than the phase losses and also during the growing geo-solar magnetic disturbances of different nature. The analysis shows that a possible solution to reduce the impact of failures on the navigation GPS system is to increase the mask on the elevation angle of the satellite 20° .

ACKNOWLEDGMENT

This work was financially supported by a grant of the Russian Science Foundation (Project No. 14-37-00027).

Characteristics of HF Radio Waves Propagation along Subauroral and Mid-latitude Paths over Eastern Siberia during Magnetoactive Period in February 2014

V. I. Kurkin, **N. M. Polekh**, **S. N. Ponomarchuk**, **A. V. Podlesny**, **N. A. Zolotukhina**, **and E. B. Romanova**
Institute of Solar-Terrestrial Physics SB RAS, Irkutsk, Russia

Abstract— Based on vertical and oblique-incidence sounding data we carried out an analysis of HF propagation characteristics during magnetoactive period in February 2014. The oblique-incidence data were obtained along subauroral and midlatitude paths: from Magadan to Irkutsk, from Khabarovsk to Irkutsk, from Khabarosk to Norilsk The period under consideration was characterized by series of solar flares accompanied by X-ray flares, intensification of proton fluxes and coronal mass ejections (CME). These processes caused two magnetic storms of different intensity. The former storm developed on February 18–26. It was characterized by minimum Dst $= -112$ nT at 08 UT on February 19 and prolonged recovery phase. The latter one with minimum Dst $= -99$ nT at 23 UT on February 27 happened on February 27–March 3. Increase of X-ray radiation on February 25 (X4.9/2B) led to a growth in the lowest observed frequencies at the oblique and vertical sounding ionograms and weakening of a signal near the maximum observed frequencies (MOF). During the main and recovery phases of the storms the MOF along the path from Magadan to Irkutsk sharply fell by 3–5 MHz. Intervals of low MOF values alternated with those of absence of reflected signals at the ionograms. It specifies that boundaries of the main ionospheric trough could be displaced to the latitude of this path average point. Similar absence of reflected signals at the ionograms was registered along Khabarosk-Norilsk path. Besides, during these two storms at the oblique sounding ionograms the additional signals with large temporary delays were observed over paths from Magadan to Irkutsk and from Khabarovsk to Irkutsk in the evening and nocturnal hours. The amplitude relief of abnormal signals was characterized by strong diffusion and frequencies exceeded MOF of standard propagation modes. Since the ionosphere is not perfectly horizontally stratified during magnetic storms the signal associated with propagation mode may arrive at received point over a wide range of azimuth angles.

ACKNOWLEDGMENT

This study was supported by the Grant of the Russian Scientific Foundation (Project No. 14-37-00027).

Comparative Analysis of Geomagnetic Field and GPS-TEC Variations for Middle-latitude and Arctic Regions

Ilya K. Edemskiy[1], **Nataly P. Perevalova**[1], **Anna S. Polyakova**[1], **Olga V. Timofeeva**[1, 2], **and Darya D. Katashevtseva**[1, 2]

[1]ISTP SB RAS, Russia
[2]Irkutsk State University, Russia

Abstract— We present the results of comparative analysis of geomagnetic field and total electron content (TEC) variations. The analysis is based on the long series of data from the Siberian GPS network of the Institute of solar-terrestrial physics (ISTP) of Siberian Brunch of Russian Academy of Science (SB RAS) and Norilsk GPS station operated by the Geophysics Service of RAS (GS RAS.) ISTP SB RAS Siberian network make continuous TEC measurements since 2012 and provide TEC-variation data with time resolution of 1 sec. The calculation of TEC is based on two-frequency phase measurements of GPS receivers. We analyzed TEC variations in two period ranges (0–10 min and 10–40 min), which are correspond to different modes of ionospheric disturbances. Magnetic intensity data were obtained from ISTP SB RAS observatories and INTERMAGNET sites. The common level of TEC disturbance is estimated by the index W_{tec} of the TEC-variation intensity. The index is calculated for all available GPS satellites, with the data of highest elevation angle at every moment. This method allow to investigate continuous changes of TEC variation intensity. The Wtec calculated for all the GPS data 2013. The W_{tec} dynamics features is revealed for different times of day, seasons and levels of geomagnetic activity for middle-latitude and Arctic regions. The response of the W_{tec} to sudden storm commencements (SSC) was also investigated.

ACKNOWLEDGMENT

The authors thank the Geophysics Service of RAS and INTERMAGNET for the data they provide. This work was supported by the Grant of the Russian Scientific Foundation (Project No. 14-37-00027.).

TEC Response to Geomagnetic Storms and Solar Flares as Observed with SBAS L1/L5 Signals

G. A. Kurbatov[1], **V. E. Kunitsyn**[1], **A. M. Padokhin**[1], **and Yu. V. Yasyukevich**[2]

[1]Faculty of Physics, Lomonosov Moscow State University, Russia
[2]Institute of Solar-Terrestrial Physics SB RAS, Russia

Abstract— The development of Satellite Based Augmentation Systems (SBAS) provides the possibility to retrieve ionospheric Total Electron Content (TEC) from the dual frequency L1/L5 observations from a number of geostationary satellites using the same approach as for dual frequency GPS/GLONASS observations.

In this work we study L1/L5 signals of Indian GAGAN and American WAAS geostationary satellites observed with geodetic GNSS receivers at several stations at mid- and low-latitudes and estimate corresponding geostationary TEC variations and errors of such estimations. We discuss the quality of these data showing that SBAS TEC RMS could reach up to 1.5 TECU with typical values of 0.25–0.5 TECU which is up to one order greater than for common GPS/GLONASS observations. We present the evidence that such large values of SBAS TEC RMS are satellite dependent and are not of ionospheric origin, so they could be easily filtered out without losing significant ionospheric information providing continous TEC datasets for selected satellite-receiver pairs instead of short 2–6 hours records as in GPS/GLONASS case.

We present geostationary SBAS TEC response to increasing solar X-Ray and EUV ionizing radiation during several recent X-class flares. Good correlation was found between TEC and EUV flux for the stations at the sunlit hemisphere. We also present SBAS TEC response to geomagnetic field variations during strong and moderate geomagnetic storms showing examples of both positive and negative TEC anomalies of order of tens of TECU during main storm phase.

Our results show the capability of SBAS L1/L5 observations for continuous monitoring of ionospheric TEC. Intensively growing networks of receivers capable to work with L1/L5 SBAS signals (for example MGEX network) and increasing number of dual-frequency satellites in SBAS constellation potentially make it a powerful instrument for TEC climatology.

Acoustic-gravity Waves in Space Generated by Near-ground and Volume Sources

Elena S. Andreeva[1], **Viacheslav E. Kunitsyn**[1,2], **Ivan A. Nesterov**[1], **and Artem M. Vorontsov**[1]

[1]M.V. Lomonosov Moscow State University, Moscow, Russia
[2]Institute of Physics of the Earth, Russian Academy of Sciences, Moscow, Russia

Abstract— Numerical analysis of acoustic-gravity waves (AGW) generation and propagation in the Earth's atmosphere is performed based on computer model of stratified atmosphere with dissipation.Atmospheric and ionospheric wavelike disturbances generated by near-ground or volume sources such as oscillations of the Earth's or oceanic surface, earthquakes, explosions, seiches, tsunami waves and temperature heating are studied. These wavelike phenomena in the atmosphere and ionosphere appear as the alternating areas of enhanced and depleted density (in the atmosphere) or electron concentration (in the ionosphere).

Observation and investigation of various ionospheric perturbations under assumption of their correct physical interpreting and understanding of their hydrodynamic generation mechanisms commonly allows obtaining current or predictive configuration of near-ground or volume sources of disturbances. The least studied problem here is a question about acoustic energy transferring from the ground sources into near-Earth space that primarily is related with incompleteness of AGW propagation theory in the real atmosphere. Moreover, complete analysis of the observed ionospheric perturbations should be performed using conventional characteristics of ionospheric waves such as amplitude, phase, period, velocities of corresponding wave packets and angular characteristics of the wave vector. Notice, that for most near-ground or volume sources in geophysical bibliography there is a significant variance regarding values of basic AGW parameters as well as absence of unified point of view on AGW generation mechanisms. As the examples of mentioned mechanisms different authors provide infrasound wave generation, internal gravity waves generation, eddying motion of the neutral component generated by an acoustic pulses, the generation of shock-acoustic waves, etc..

The numerical simulation of upper atmosphere responses to various near-ground or volume sources can provide estimations of basic AGW characteristics and to clarify AGW generation mechanisms. The major results of the paper consist in determining of common as well as unique tendencies in AGW behavior for a wide class of sources, analysis of these tendencies and estimation of AGW wave packets' parameters. Numerical simulation studies of wavelike AGW disturbances generation by particle precipitation are presented. The ionospheric footprints of atmospheric disturbances are given. These two sentences should be removed.

Testing NmF2 Data from UV SSUSI Measurements with Global Ionospheric Maps and Satellite Radio Tomography at Mid and High Latitudes

G. A. Kurbatov, **E. S. Andreeva**, **S. A. Kalashnikova**, **V. E. Kunitsyn**, **I. A. Nesterov**, **A. M. Padokhin**, **and Yu. S. Tumanova**
Lomonosov Moscow State University, Russia

Abstract— Development of the Defense Meteorological Satellites Program (DMSP) and its new instruments such as Global Ultraviolet Imager (GUVI) and Special Sensor Ultraviolet Spectrographic Imager (SSUSI) provides the opportunity to get ionospheric F2-layer peak density (NmF2) as the product of the measurements of the natural nighttime emissions of O+ ions, generated by its reaction of radiative recombination. This dataset is distributed via http://ssusi.jhuapl.edu/ by Johns Hopkins University Aplied Physics Laboratory.

The aim of the present work is to compare this new NmF2 product with broadly used Global Ionospheric Maps (GIM) and data obtained using such well-developed method as GNSS radiotomography (with both low- and high-orbiting navigational satellites) for various geomagnetic conditions during last two solar cycles.

The results of such comparison along radio tomography system in Russia (covers mid and high latitudes) during the periods of various geomagnetic conditions showed that large structures reaching the size of about 10° are distinctly reconstructed in both RT and UV data and are in good agreement within the accuracy of both methods, while the same structures are typically smoothed in GIM data due to poor spatial and time resolution.

Having poorer SNR values compared to radio measurements, UV data can give important information about the ionosphere, especially over the regions where application of radio tomography methods is limited. The possibility of incorporating UV measurements into radiotomography routines should be further investigated and modeled.

ACKNOWLEDGMENT

The authors acknowledge Johns Hopkins University Aplied Physics Laboratory and Larry Paxton, SSUSI Principle Investigator, for SSUSI data used in this work.

Adaptation of IRI-2012 Model for Estimation of IAR Harmonic Structure

A. S. Potapov[1], **T. N. Polyushkina**[1], **A. V. Oinats**[1], **T. Raita**[2], **and B. Tsegmed**[1, 3]

[1]Institute of Solar-Terrestrial Physics SB RAS, Irkutsk, Russia
[2]Sodankylä Geophysical Observatory, Finland
[3]Institute of Astronomy and Geophysics MAS, Ulaanbaatar, Mongolia

Abstract— The ionospheric Alfvén resonator (IAR) is a structural formation in the ionosphere between two peaks of Alfvén speed in its altitude profile. The IAR can amplify and accumulate ultra low frequency (ULF) wave energy in the upper ionosphere. As a result of the IAR occurrence the multiband spectral resonance structure (SRS) appears in the ULF observations, both ground-based and satellite. Frequency of discrete spectral bands and spacing between them are determined by the geometry of the resonator and the Alfvén speed in its cavity; the change in band frequency during the day with a minimum around noon and a maximum after midnight or in the early morning hours is due to diurnal variation of ionospheric parameters. Close connection of SRS mode and features with state of the ionosphere motivates many authors to study the details of this connection, and make suggestions about how to use observations of the spectral structure of the electromagnetic background in the range of 0.5–10 Hz for sounding ionospheric parameters and clarifying ionospheric models.

In this paper we propose a new approach to analysis of emission of ionospheric Alfvén resonator (IAR). We apply the IRI-2012 version of International Reference Ionosphere model to calculate difference between frequencies of adjacent harmonics (frequency scale) of IAR emission. The calculated values are compared with the frequency scale data obtained from search-coil magnetometer observations made at two different stations, the mid-latitude observatory Mondy (Eastern Sayan, Russia) and the high-latitude Sodankylä Geophysical Observatory (Finland). For measurements made at medium latitudes, it appears that to reach satisfactory results it is necessary to modify IRI-2012 model replacing the vertical profile of ionospheric parameters adopted in the standard model with the profile elongated along the magnetic field lines. For polar latitudes, where the field lines deviate from the vertical insignificantly, such a procedure is not so important. On the other hand, irregular behavior of the polar ionosphere results in the diffusive character of the SRS. That is why the spectral bands of the SRS at SGO spectrograms are blurred which cumbers precise measurements of frequency values. To improve the estimates of the frequency scale we corrected the model using local f0F2 measurements. Finally, our results showed strong correlation between the estimated and measured values of the frequency scale.

ACKNOWLEDGMENT

The part of work made by A. S. P. and A. V. O. (development of the IAR spectrum formation model and ionosphere data analysis) was supported by the Russian Science Foundation, grant 14-37-00027; the part of work made by T. N. P and B. V. D. (observations and morphological studies) was supported by the Russian Foundation for Basic Research, grant 13-05-00529.

Comparison of Polar, Sub-polar and Mid-latitude Ionospheric Variability Using Ionosonde and SuperDARN Data

K. G. Ratovsky[1], **A. V. Oinats**[1], **and N. Nishitani**[2]

[1]Institute of Solar-Terrestrial Physics SB RAS, Russia
[2]Solar-Terrestrial Environment Laboratory, Nagoya University, Japan

Abstract— We study ionospheric variability using HF radio facilities within three latitudinal regions: polar (Norilsk vertical sounder; 69.4N, 88.1E), sub-polar (Ekaterinburg SuperDARN radar; 56.4N, 58.5E) and mid-latitude (Hokkaido East SuperDARN radar; 43.53N, 143.61E). As characteristics we select the peak electron density (NmF2) and peak height (hmF2) measured with the ionosonde and the ground backscatter range corresponding to the skip distance (Rsd) from HF radar measurements. The disturbances of characteristics are the deviations of characteristics from their 27-day running median values. We assume that 27-day running medians are associated with climatological specifics of the diurnal, seasonal, and long-term solar activity variations. The variability is considered as the root mean square of disturbances. For different tasks we used different types of averaging. Annual averaging was used for studying year-to-year changes in the variability (solar cycle variations). To study the difference between the day- and nighttime variability we made separate averaging for the day- and nighttime using ground terminator as a day-night boundary. To obtain the diurnal-seasonal pattern of the variability we performed averaging over years for each local time and day of year. In the paper we discuss similarities and differences between the selected characteristics and between the polar, sub-polar and mid-latitude ionospheric variability.

ACKNOWLEDGMENT

The work was supported by Russian Scientific Foundation (project 14-37-00027). We grateful Nagoya University and ISTP SB RAS for the provided experimental data.

Geomagnetic Effects on GNSS Measurements

I. V. Bezler[1, 2], **A. B. Ishin**[1], **E. V. Konetskaya**[1, 2], **A. V. Kulizhsky**[1, 2], **M. V. Tinin**[1, 2], **and S. V. Voeykov**[1, 2]

[1]Institute of Solar-Terrestrial Physics, SB RAS, P. O. Box 4026, Irkutsk 664033, Russia
[2]Irkutsk State University, 20 Gagarin Blvd, Irkutsk 664003, Russia

Abstract— In this paper, the analysis of geomagnetic effects on measurements, made by Global Navigation Satellite Systems (GNSS), relies on both the contribution of the geomagnetic field to the refractive index of ionospheric plasma and the presence of random irregularities aligned along the magnetic field lines. In the geometrical optics approximation at high GNSS frequencies, the refractive index, phase and code distances can be expanded in a rapidly decreasing series in inverse powers of frequency. This allows us to eliminate ionospheric effects from multifrequency measurements. In dual-frequency measurements, the ionosphere-free combination is used to remove most of the ionospheric error — first-order error proportional to electron density. Improvement in accuracy of dual-frequency GNSS measurements is associated with elimination of the second-order error caused by geomagnetic effects on the refractive index of magnetoactive ionospheric plasma. The paper reports results of exploration of the possibility for simultaneous removal of first- and second-order errors by modifying the ionosphere-free combination of dual-frequency measurements. The geomagnetic field affects not only the refractive index but also the structure of ionospheric irregularities. Afraimovich et al. [1] based on the dependence of the GNSS phase slips on the angle between the satellite-receiver line of sight (LOS) and the magnetic field line, have revealed the anisotropy effect of ionospheric irregularities. To analyze the role of this effect on GNSS measurements, we used numerical simulation for studying anisotropy effects of ionospheric irregularities on the probability of occurrence of slips in phase measurements. When examining GNSS signal phase fluctuations, we determined the relation between the probability of slips in GNSS system operation and the degree of elongation of field-aligned irregularities. The simulation results allow us to study and account for the factors which mask effects of this anisotropy. In the future, we are going to exploit this method of estimating the degree of elongation of irregularities to monitor parameters of ionospheric irregularities in the Arctic region.

ACKNOWLEDGMENT

This study was supported by the Grant of the Russian Scientific Foundation (Project No. 14-37-00027).

REFERENCES

1. Afraimovich, et al., *Advances in Space Research*, Vol. 47, 1674–1680, 2011.

Diffraction Effects in Electromagnetic Probing of Atmosphere and Ionosphere

A.V. Kulizhsky[1, 2] **and M. V. Tinin**[1, 2]

[1]Institute of Solar-Terrestrial Physics, SD, RAS, P. O. Box 4026, Irkutsk 664033, Russia
[2]Irkutsk State University, 20 Gagarin Blvd, Irkutsk 664003, Russia

Abstract— At present, remote sensing methods relying observations of signals from global navigation satellite systems (GNSS) are finding ever-widening application in environmental research. These methods allow remote diagnostics of wide sectors of overground space, which makes them attractive for use especially in the Arctic region. However, the spatially and temporally variable ionosphere significantly affects the accuracy and reliability of GNSS remote sensing, hence the need to study inhomogeneous ionosphere effects on GNSS measurements, and to explore possibilities of their elimination. In the geometrical optics approximation, the ionospheric part of error in measuring phase and code delays of the satellite signal may be represented as a rapidly decreasing series in inverse power of frequency. Such simple frequency dependence allows us to use multi-frequency measurements for eliminating the error in multi-frequency GNSS. However, the elimination of errors is handicapped by diffraction effects during signal propagation through turbulent ionospheric plasma. In this study, the elimination of diffraction effects from the measurement error via Fresnel inversion and then the elimination of this error via multi-frequency combination are analyzed. We demonstrate the possibility of reducing residual ionospheric errors in ionosphere-free combination by Fresnel inversion. The inversion parameter — the distance to the virtual screen — may be selected from the minimum of amplitude fluctuations. This suggests the possibility of improving the accuracy of GNSS remote sensing in meteorology. In investigations into ionospheric disturbances through geometry-free combinations, the Fresnel inversion eliminates only the third-order correction. To eliminate the random TEC component which, like the measured average TEC, is the first-order correction, we should use temporal filtering. However, measurements of this random TEC component allow us to examine the fine structure of ionospheric plasma via GNSS. The Fresnel spatial processing requires constructing a phase GNSS array of sufficiently large sizes. Despite the difficulty in constructing this array, it seems necessary to develop the array, taking into account feasibility of using it in many fields of research on the troposphere, ionosphere, earthquakes, and volcanic activity.

ACKNOWLEDGMENT

This study was supported by the Grant of the Russian Scientific Foundation (Project No. 14-37-00027).

High-resolution Wave Field Processing for Diagnostics of Inhomogeneous Media

S. I. Knizhin, **M. V. Tinin**, **and A. V. Kulizhsky**
Institute of Solar-Terrestrial Physics, SB, RAS
Lermontov st. 126a, P. O. Box 291, Irkutsk 664033, Russia

Abstract— For the analysis of transparent inhomogeneous, it is appropriate to use phase tomography, which is based on measuring the phase of the wave transmitted from the transmitter to receiver. Finding the physical characteristics of inhomogeneous media by these methods carried out in several stages. At the first stage the receiving system consisting of antennas registers the phase of wave scattered by the inhomogeneity. Then, depending on the type of tomographic measurements the optimal method of computer tomography is selected. The final step is finding the required physical parameter of the inhomogeneous medium. In particular the diagnosis of the inhomogeneous plasma by standard methods ray and diffraction tomography is not always possible to find the parameters of the medium. For more accurate diagnostic results of the inhomogeneous medium we can use additional processing phase measurements. Earlier in the papers was obtained spatial processing phase measurements based on the method of double weighted Fourier transform (DWFT). This process allows to diagnose small-scale plasma under conditions of strong and weak phase fluctuations. However, the use of DWFT for direct and inverse problems of wave propagation in inhomogeneous media is often hampered by the necessity to integrate in two planes. In particular, in tropospheric and ionospheric investigations we can integrate measurement data in coordinates of only one plane, say a receiving plane.

Here we will consider the DWFT method modifications permitting the use of it both without possibility of integrating over two planes and under wave reflection from an inhomogeneous medium (plasma).

ACKNOWLEDGMENT

This study was supported by the Grant of the Russian Scientific Foundation (Project No. 14-37-00027).

Investigation of Nanoantennas Using Surface Integral Equations and the Multilevel Fast Multipole Algorithm

B. Karaosmanoğlu, U. M. Gür, and Ö. Ergül
Department of Electrical and Electronics Engineering, Middle East Technical University, Ankara, Turkey

Abstract— Nanoantennas, i.e., antennas designed for optical frequencies, have attracted the interest of many researchers [1–4]. Although the idea of using nanoscale antennas operating at visible lights, e.g., for harvesting solar energy, was purposed decades ago, realization of nanoantennas had to wait for the developments in nanotechnology. Recently, various nanoantennas have been designed, manufactured, and tested for diverse applications, including energy harvesting [1], optical sensing [2], and imaging. Along this direction, computational simulations of nanoantennas have become essential for designing and investigating these structures in alternative scenarios before their actual realizations [4].

Computational analysis of nanoantennas using the conventional solvers is not trivial. While nanoantennas are commonly made of highly conducting materials, such as silver and gold, scaled solvers with perfectly conducting assumptions fail to provide realistic and accurate modeling of nanoantennas [4]. This is mostly due to different behaviors metals at optical frequencies, namely plasmonic effects [5], which become dominating factors especially for nanoscale objects. Incorporating plasmonic effects in the existing solvers is also a challenging task, especially for full-wave solvers. This challenge can partially be solved by resorting to Drude or Lorentz-Drude models that allow for macroscopic analysis via electromagnetic parameters. Specially, changing the electrical permittivity to a complex value with a negative real part based on these models leads to a direct analysis of a plasmonic structure using existing solvers developed for penetrable objects.

In this study, we investigate nanoantennas using surface integral equations and a powerful method, namely, the multilevel fast multipole algorithm (MLFMA) [6]. Among alternative formulations, we prefer the electric and magnetic current combined-field integral equation (JMCFIE) for accurate and fast iterative solutions using MLFMA. JMCFIE is modified carefully by considering complex permittivity values with negative real parts. MLFMA is also updated for stability in handling complex wavenumbers with large imaginary parts, leading to rapidly decaying interactions. In this paper, after demonstrating the effectiveness of the developed solver on canonical problems, we present numerical simulations of bowtie nanoantennas at optical frequencies. Different material properties and frequencies are considered for single bowtie nanoantennas. Electromagnetic interactions between pairs of nanoantennas and their effects in the power enhancement abilities are also investigated. Numerical results show that MLFMA is a strong alternative to space-discretization solvers for accurate and efficient full-wave analysis of nanoantennas.

REFERENCES

1. Muhlschlegel, P., H.-J. Eisler, O. J. F. Martin, B. Hecht, and D. W. Pohl, "Resonant optical antennas," *Science*, Vol. 308, 1607–1609, 2005.
2. Kinkhabwala, A., Z. Yu, S. Fan, Y. Avlasevich, K. Mullen, and W. E. Moerner, "Large single-molecule fluorescence enhancements produced by a bowtie nanoantenna," *Nat. Photonics*, Vol. 3, 654–657, 2009.
3. Kosako, T., Y. Kadoya, and H. F. Hofmann, "Directional control of light by a nanooptical Yagi-Uda antenna," *Nat. Photonics*, Vol. 4, 312–315, 2010.
4. Solis, D. M., J. M. Taboada, F. Obelleiro, and L. Landesa, "Optimization of an optical wireless nanolink using directive nanoantennas," *Opt. Exp.*, Vol. 21, No. 2, 2369–2377, 2013.
5. Johnson, P. B. and R. W. Christy, "Optical constants of the noble metals," *Phys. Rev. B*, Vol. 6, No. 12, 4370–4379, 1972.
6. Ergül, Ö. and L. Gürel, *The Multilevel Fast Multipole Algorithm (MLFMA) for Solving Large-scale Computational Electromagnetics Problems*, Wiley-IEEE, 2014.

Weigert-effect in the Recording Media on the Base of the Polarization-sensitive Compositions

Valentina Shaverdova, Svetlana Petrova, Lado Tarasashvili, Anna Purtseladze, and Nino Obolasvili
Laboratory of Holographic Recording and Processing of Information, Institute of Cybernetics
Georgian Technical University, Sandro Euli Str. 5, Tbilisi 0186, Georgia

Abstract— The paper discusses the polarization properties of the compositions of the light-sensitive media. The compositions include a polymer matrix, fluorescent tags: the dyes-phosphors which have been used, including specially synthesized, and the fluorescent polymer. The activators of photo anisotropy based on the organic dyes, chiral dopants, dendrimer. As the matrix polymer were used: polycarbonate, polystyrene, polymethyl methacrylate. Were created the optical schemes, allowing us to investigate the polarized luminescence, and conduct the ellipsometric measurements of the photo-anisotropic parameters obtained compositions. For polarized radiation were used the standard lasers with lengths of waves: 405 nm, 441.6 nm, 532 nm. For the quantitative measuring of the polarized luminescence the parameter-coefficient of anisotropic radiation was used. The created compositions had had few maximums of the polarized luminescence, what determined by the structure of making elements. Data are presented as tables and spectral curves of coefficient of anisotropic radiation. Were developed compositions with initial optical activity, thanks to the introduction of specific chiral additives. We investigated the change in the optical activity of the resulting compositions by the irradiation with circularly polarized radiation. Conducted ellipsometric measurements allowed us to estimate both the magnitude and the direction of rotation of the polarization plane of the media. We investigated the change in the optical activity of the resulting compositions by the irradiation with circularly polarized radiation. Were obtained curves of the exposition induced anisotropy of the investigated circular media for the purpose of comparing the gradient sensitivity, depending on the chemical structure of the used dopants. Were revealed the dependence arised anisotropy and gyrotropy in the samples under investigation on the chemical activity of the used dopants. The done work allows to make conclusions about the mutual influence of elements of the composition on the magnitude and specificity of the induced Weigert effect, which demonstrates the enormous scope for the developers of polarization-sensitive media.

Investigation of the Free-space Propagation Operator Eigenfunctions in the Near-field Diffraction

Mikhail S. Kirilenko[1], **Valery V. Pribylov**[1], **and Svetlana N. Khonina**[1, 2]

[1]Samara State Aerospace University Named After Academician S.P. Korolyov, Samara, Russia
[2]Image Processing Systems Institute of the RAS, Samara, Russia

Abstract— In recent years, there have been many attempts to overcome diffraction limit. It could provide the visualization of features that are smaller than half a wavelength. In this work we demonstrate possibilities of creating monochromatic light distribution with details comparable with the wavelength. The investigations are based on the scalar diffraction theory. We consider one-dimensional case of a beam expansion by plane waves in analogy with [1]. We take into account finite aperture size and spectrum width (for example, evanescent waves are not examined if the spectrum is limited to the range of minus one to one).

The plane of optical signal formation is located at a distance of several wavelengths from the input plane. The observed domain width is equal to the aperture size D, so we get two equivalent areas on the input and output of the optical system.

We use integral transformation based on the method of plane wave expansion for laser beam modeling. After sampling considered transformation we get a square matrix with eigenvalues and eigenfunctions that we should find. These functions represent a system of orthogonal modes propagating from the input plane to the output without changes except the scale factor.

Previously, we study eigenfunctions for the limited system of two lenses where Fourier transform (or Hankel transform in case of radial symmetry) plays the role of propagation operator [2, 3]. The eigenfunctions are spheroidal functions if the optical system is Cartesian [2]. The difference of this work consists in free-space propagation in the near-field diffraction rather than through the lenses, therefore, modeling can be done at a small distance from the input plane.

The beam propagation distance is a parameter of the operator and it significantly changes the set of eigenvalues and eigenfunctions. The eigenvalues modules define corresponding "survival" eigenfunction at a given distance. Thus, calculations allow to find out the number of degrees of freedom in dependence of the distance. In addition, it is determined the maximum number $N_{\max}$ of "survived" eigenfunction at the distance. Hence, the minimum size of details, reproduced on the propagation distance, is approximately equals $d \approx D/N_{\max}$. Thereby, we get the answer to the question, what resolution is achievable at a given distance.

REFERENCES

1. Huang, F. M. and N. I. Zheludev, "Super-resolution without evanescent waves," *Nano Lett.*, Vol. 9, No. 3, 1249–1254, 2009.
2. Kirilenko, M. S. and S. N. Khonina, "Coding of an optical signal by a superposition of spheroidal functions for undistorted transmission of information in the lens system," *Proc. SPIE 9156, Optical Technologies for Telecommunications 2013*, 91560J, Apr. 4, 2014, Doi: 10.1117/12.2054214.
3. Kirilenko, M. S. and S. N. Khonina, "Calculation of the eigenfunctions of two lens imaging system," *Proc. SPIE 9450, Photonics, Devices, and Systems VI*, 945012, Jan. 6, 2015, Doi: 10.1117/12.2070371.

Shielding Effectiveness in Coaxial Cable Connectors in Ultra High Frequency — UHF — 1 GHz to 3 GHz

Kenedy Marconi Geraldo dos Santos[1,2], **Marcela Silva Novo**[2], **Glauco Fontgalland**[3], **Marcelo Bender Perotoni**[4], **and Caio Luminatti Andrade**[5]

[1]UFBA — Federal University of Bahia, Brazil
[2]IFBA — Federal Institute of Bahia, Brazil
[3]UFCG — Federal University of Campina Grande, Brazil
[4]UFABC — Federal University of ABC, Brazil
[5]SENAI — CIMATEC, Brazil

Abstract— The Shielding Effectiveness parameter of the transmission lines and coaxial cables/connectors is an important item to ensure the correct operation of electro-electronic devices. Eventual problems in this shielding could generate unintentional electromagnetic disturbs. Fundamentally, an Electromagnetic Compatibility (EMC) problem can be divided into three parts: noise source, coupling and receptor (victim) [1, 2]. In this paper, the coupling will be investigated in order to mitigate the radiated or induced electromagnetic interferences. Cable and connectors shielding is one of the most used techniques to minimize this kind of disturbs [1, 2]. The Shielding Effectiveness (SE) can be defined by [3, 4]

$$\mathrm{SE_{dB}} = 20\log\frac{V\ \text{(without shielding)}}{V\ \text{(with shielding)}} \quad \mathrm{SE_{dB}} = 20\log\frac{E\ \text{(electric al field without shielding)}}{E\ \text{(electric al field with shielding)}} \tag{1}$$

In order to determine the SE factor of a coaxial cable connector, this paper proposes a methodology based on a physical model, using the R&S ® EMC32 Measurement Software. Figs. 1(a) and 1(b) illustrate the measurement software and the measurement setup, respectively.

The measurement setup consist of an electric field probe, the coaxial cable and connectors. Both the electric field and the voltage standing wave ratio (VSWR) will be measured. The main objective of this paper is to investigate shielding effectiveness of coaxial cable connectors, in order to ensure the best performance in Ultra High Frequency (UHF) and also to reduce electromagnetic radiation. By using the EMC32 integration software that controls both injected signals and measured parameters, a constant power is injected into the cable and the electric field is measured. To reduce the irradiated and inducted electromagnetic interferences in the transmission line, a coaxial cable with solid outer conductor will be used. It should be noted that there are still many challenges to determine the transfer impedance, as well as the shielding effectiveness of coaxial cables in the microwave range [5].

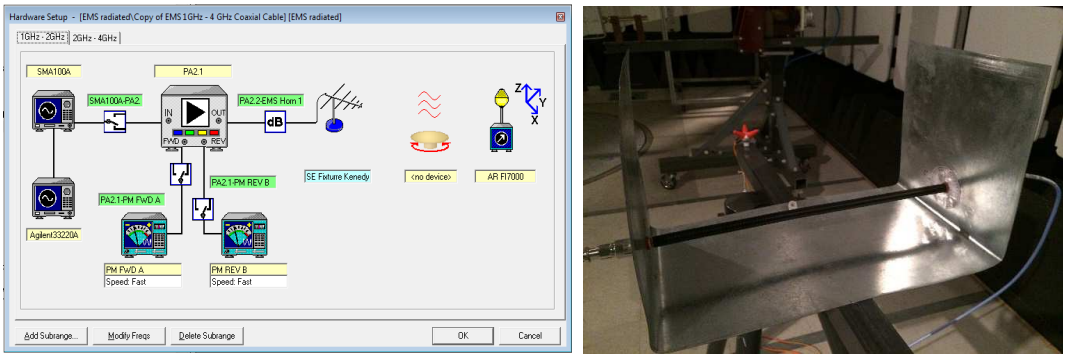

(a) (b)

Figure 1: (a) Measurement Software EMC32. (b) Measurement setup.

REFERENCES

1. Donald, R. J. and M. Mardiguian, *Electromagnetic Shielding,* Vol. 3, Interference Control Technologies, Inc., Gainesville, Virginia, 1988.

2. Santos, K. M. G., et al., "Measure of the shielding effectiveness in coaxial cables," *XIV International Symposium on Electromagnetic Fields in Mechatronics Electrical and Electronic Engineering*, Arras, France, 2009.
3. Santos, K. M. G., et al., *Measure of the Shielding Effectiveness in Coaxial Cables,* Vol. 1, 540–548, IOS Press, Amsterdam, 2010, ISSN: 1383-728.
4. Taghivand, M., "Correlation between shielding effectiveness and transfer impedance of shielded cable," *2004 International Symposium on Electromagnetic Compatibility, EMC 2004*, California Institute of Technology MC 136-93, 1200 E. California blvd., Pasadena, CA 91 125, 2014.
5. Démoulin, B. and L. Koné, "Shielded cable transfer impedance measurements in the microwave range of 1 GHz to 10 GHz," *IEEE-EMC*, 52–61, Newsletter, 2011.

On The Anti-correlation between Degree of Entanglement and Polarization for Biphoton States

Hang T. T. Nguyen[1], **Peter A. Meleshenko**[2, 3], **Vladimir A. Gorlov**[2], **Mikhail E. Semenov**[2, 3, 4], **and Alexander F. Klinskikh**[3]

[1]Institute of Technology, Vietnam National University — Ho Chi Minh City, Vietnam
[2]Zhukovsky-Gagarin Air Force Academy, Russia
[3]Voronezh State University, Russia
[4]Voronezh State University of Architecture and Civil Engineering, Russia

Abstract— There are various parameters of quantum system which play important role in quantum computing. However the most interesting and perspective parameters are entanglement and polarization. In particular, entanglement has many applications in quantum information theory. Namely, the best-known applications of entanglement are superdense coding and quantum teleportation [1]. Also the entanglement is used in some protocols of quantum cryptography [2]. In quantum interferometry, entanglement is necessary for surpassing the standard quantum limit and achieving the Heisenberg limit [3].

In this work we consider the biphoton states formed in the process of degenerate spontaneous parametric down-conversion. The purely polarization biphoton states (the so-called qutrits) are described by a superposition [4, 5]:

$$|\psi\rangle = c_1|\psi_{HH}\rangle + c_2|\psi_{HV}\rangle + c_3|\psi_{VV}\rangle$$

of photons in modes with horizontal (H) and vertical (V) polarizations. The degree of entanglement can be derived from the Wootters' parameter (the so-called Wootters' concurrence):

$$C = |2c_1c_3 - c_2^2|.$$

The degree of biphoton polarization [4, 6]

$$P = |\mathrm{Tr}\,(\rho_r\vec{\sigma})| = |\mathrm{Tr}\,[\vec{\sigma}\mathrm{Tr}_2\,(|\psi\rangle\langle\psi|)]|\,,$$

where ρ_r is the reduced density matrix, $\vec{\sigma}$ are the standard Pauli matrices, can be compared with the Wootters' concurrence and the result is [4]:

$$C^2 + P^2 = 1.$$

This expression (first derived in [4]) shows the anti-correlation between the entanglement and polarization.

In this work we also discuss in details the von Neumann entropy of the qutrit, namely

$$S_r = -\mathrm{Tr}\,(\rho_r \log_2 \rho_r)\,.$$

Moreover, we consider the time evolution of parameters P (polarization) and C (Wootters' concurrence) using the solution of equation for density matrix (von Neumann equation) taking into account the various initial states of the biphoton system.

REFERENCES

1. Bouwmeester, D., J.-W. Pan, K. Mattle, et al., "Experimental quantum teleportation," *Nature*, Vol. 390, 575–579, 1997.
2. Ekert, A. K., "Quantum cryptography based on Bell's theorem," *Phys. Rev. Lett.*, Vol. 67, 661–663, 1991.
3. Pezzé, L. and A. Smerzi, "Entanglement, nonlinear dynamics, and the heisenberg limit," *Phys. Rev. Lett.*, Vol. 102, 100401(1–4), 2009.
4. Fedorov, M. V., P. A. Volkov, J. M. Mikhailova, et al., "Entanglement of biphoton states: qutrits and ququarts," *New J. Phys.*, Vol. 13, 083004(1–32), 2011.
5. Fedorov, M. V., P. A. Volkov, and J. M. Mikhailova, "Qutrits and ququarts in spontaneous parametric down-conversion, correlations and entanglement," *JETP*, Vol. 115, 15–35, 2012.
6. Burlakov, A. V. and D. N. Klyshko, "Polarized biphotons as 'optical quarks'," *JETP Lett.*, Vol. 69, 839–843, 1999.

T-matrix Formulation of the Linear Sampling Method

Gregory Samelsohn and Kobi Aflalo
Center for Advanced Imaging Systems, Department of Electrical and Electronics Engineering
Shamoon College of Engineering, Ashdod 77245, Israel

Abstract— The linear sampling method (LSM) aimed at the reconstruction of target shape and based on the so-called far field equation [1] is reformulated in terms of the transition (T) matrix. The latter reflects only the intrinsic properties of the scatterer and does not depend on locations and radiation patterns of the antennas constituting the transmitting and receiving arrays [2]. The information on the antenna arrays is contained in the corresponding sampling matrices $\mathbf{A}_t$ and $\mathbf{A}_r$ transforming $\mathbf{T}$ matrix into the response matrix, $\mathbf{H} = \mathbf{A}_r\mathbf{T}\mathbf{A}_t^{\dagger}$, measured in experiments. For simplicity, a scalar 2D version is considered, however the proposed approach can be generalized to both scalar or vector 3D problems.

LSM is reduced to solving the linear problem $\mathbf{Ta}(\mathbf{r}) = \mathbf{b}(\mathbf{r})$ for all points $\mathbf{r} = (r, \phi)$ of the sampled domain, providing the transition matrix $\mathbf{T}$ is estimated at the previous step. The unknown vector $\mathbf{a}(\mathbf{r})$ is the incident field causing, after interaction with the target, a scattered field $\mathbf{b}(\mathbf{r})$, a cylindrical wave emanating from sampling point $\mathbf{r}$, i.e., the elements of $\mathbf{b}(\mathbf{r})$ are given by $b_m(\mathbf{r}) = J_m(kr)\exp(-im\phi)$. The behavior of $\|\mathbf{a}(\mathbf{r})\|$ serves as an indication of the scattering object support. This formulation of LSM is more flexible than the original far field version [1].

Usually, we would like to recover a large T-matrix using as few as possible measure-ments (a small response matrix $\mathbf{H}$). This is a classical under-determined problem. Also, the data includes noise. To improve the situation, the inversion is supplemented with a number of physical constraints the transition matrix should satisfy. In particular, conservation of energy leads to the passivity of the related scattering matrix, $\mathbf{S} = \mathbf{I} + 2\mathbf{T}$, the eigenvalues of which have to lie inside the unit circle in the complex plane. Another constraint is the reciprocity of the T matrix; this means that only (roughly) one half of its elements should be found, the others may be restored by using the symmetry relation: $T_{mn} = (-1)^{m+n}T_{-n,-m}$.

The quality of the object recovery may be controlled by the normalized Frobenius norm $\varepsilon_F = \|\mathbf{T} - \hat{\mathbf{T}}\|/\|\mathbf{T}\|$, and can be seen directly in the LSM-based images, see Fig. 1. Upper row corresponds to unconstrained inversion ($\varepsilon_F = 0.41$ and $\varepsilon_F = 0.71$, respectively, for SNR values equal to 5 and 0 dB), lower row presents constrained results ($\varepsilon_F = 0.23$ and $\varepsilon_F = 0.38$, respectively).

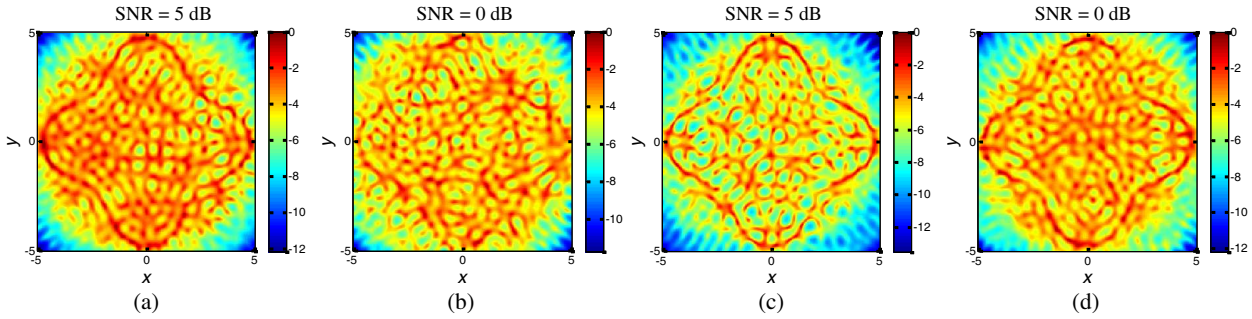

Figure 1: Results of the LSM reconstruction.

REFERENCES

1. Colton, D. and A. Kirsch, *Inverse Problems*, Vol. 12, 383, 1996.
2. Ishimaru, A., *Electromagnetic Wave Propagation, Radiation, and Scattering*, Englewood Cliffs, NJ, Prentice Hall, 1991.

Radon Tomography of Forward-scattering Objects

Gregory Samelsohn and Eliya Ben-Avraham
Center for Advanced Imaging Systems, Department of Electrical and Electronics Engineering
Shamoon College of Engineering, Ashdod 77245, Israel

Abstract— In classical X-ray tomography it is assumed that the radiation propagates along straight lines [1]. The log-intensity measured in the observation plane is then a Radon transform of the attenuation coefficient α. Since the Radon transform is invertible, it is possible to reconstruct uniquely the distribution of α, providing the measurements are performed for all possible projections. In optical or microwave tomography the propagation is no longer along straight lines, because the refraction and diffraction effects can play an essential role. In this situation the use of the same Radon-based algorithms leads to low resolution and strong artefacts in the image, or even makes the reconstruction impossible. In this paper we analyze a new reconstruction algorithm based on approximate propagators describing the high-frequency radiation scattered by (lossy) dielectric objects [2, 3].

We assume that the wave propagation is governed by a standard parabolic wave equation [4] relating the wavefield measured in point $(\mathbf{r}, z)$ to a point source located in $(\mathbf{r}_0, z_0)$. Since the parabolic equation coincides with the Schrödinger equation of quantum mechanics, we apply the path integral formalism to obtain a required solution. The main motivation of using the path integral technique here is to reduce the (infinite-dimensional) path integral to an approximate finite-dimensional quadrature provided the solution is able to reproduce the relevant diffraction effects [3, 5]. Introducing mixed input/output coordinates, $\mathbf{r}_1 = \mathbf{r} + \mathbf{r}_0/2$ and $\mathbf{r}_2 = \mathbf{r} - \mathbf{r}_0/2$, we show that an approximate solution for the normalized wave field $h(\mathbf{r}_1, \mathbf{r}_2)$ can be presented in the form $\Phi_1 \Phi_2^{-1}\{h_0(\mathbf{s}_1, \mathbf{s}_2)\}$. This operator consists of two independent ordinary Fresnel transforms (the first one is direct and the second is inverse), coupled only by the object "hologram" h_0. Function $h_0(\mathbf{s}_1, \mathbf{s}_2)$ is the exponential of the permittivity integrated along a *straight line* connecting the points $\mathbf{s}_1$ and $\mathbf{s}_2$, which are defined in the same mixed space. Hence, in order to perform the inversion, the transmit/receive arrays should cover a sufficiently large area of the hyperplane $(\mathbf{r}_1, \mathbf{r}_2)$.

Having at hand the reconstructed hologram h_0, we can calculate its logarithm (a phase unwrapping can be required at this stage), and then apply the usual Radon transform. Note that in a possible tomographic experiment the scanning is not restricted to the fan (cone) beam geometry. In particular, using only a cross-section of the reconstructed hologram, which in the mixed coordinates satisfies the condition $\mathbf{s}_2 = \mathbf{s}_1/3$ (this corresponds to $\mathbf{s} = \mathbf{s}_0$ in the original space), the parallel scanning geometry may be realized. The results of simulations show a rather good resolution of reconstructed images well beyond the weak scattering regime. In contrast to many known lensless imaging techniques suitable for reconstructing only thin samples [6], our method allows for imaging extended objects.

REFERENCES

1. Natterer, F. and F. Wübbeling, *Mathematical Methods in Image Reconstruction*, SIAM, Philadelphia, 2001.
2. Kravtsov, Y. A. and M. V. Tinin, *Radio Sci.*, Vol. 35, 1315–1322, 2000.
3. Samelsohn, G., *IEEE Trans. Antennas Propagat.*, Vol. 61, 5637–5648, 2013.
4. Ishimaru, A., *Wave Propagation and Scattering in Random Media*, Academic, New York, 1978.
5. Mazar, R., L. Kodner, and G. Samelsohn, *J. Opt. Soc. Am. A*, Vol. 14, 2809–2819, 1997.
6. Williams, G. J., H. M. Quiney, A. G. Peele, and K. A. Nugent, *New J. Phys.*, Vol. 12, 035020, 2010.

Focusing Properties of Walsh Zone Plates: Experimental Implementation with a Liquid-crystal Display

W. D. Furlan[1], **V. Ferrando**[1, 2], **F. Giménez**[3], **and J. A. Monsoriu**[2]

[1]Departamento de Óptica, Universitat de València, Burjassot 46100, Spain
[2]Centro de Tecnologías Físicas, Universitat Politècnica de València, Valencia 46022, Spain
[3]I.U. Matemática Pura y Aplicada, Universitat Politècnica de València, Valencia 46022, Spain

Abstract— Walsh functions are a complete set of normal orthogonal functions that, except at a finite number of points of discontinuity, take on values 1 or -1 over a given finite interval. The number of zero crossings within the specified domain determines the order of the Walsh functions. As is well known, a Fresnel zone plate consists of alternately transparent and opaque zones whose radii are proportional to the square root of the natural numbers. Thus, it can be generated starting from a 1D compact-supported periodic function $q(x)$, followed by a change of coordinates $x = r^2$ (r is the radial coordinate) and then by a rotation of the transformed function around one of its extremes. In a similar way a Walsh zone plate can be constructed by replacing the periodic function $q(x)$ by a given Walsh function. Walsh zone plates (WZPs) of various orders are designed from corresponding Walsh functions by realizing values of 1 or -1 with 0 or π phase, respectively. To evaluate the focusing properties of the WZPs we have computed the irradiance along the optical axis (z coordinate) provided by these lenses illuminated by a plane wave of wavelength λ, using the Fresnel approximation. Fig. 1(a) shows axial irradiances provided by the WZPs of several orders along the normalized reduced axial coordinate: $u' = ka^2/2\lambda z$, being a the radius of the WZP, and k is a constant for each order. It can be observed that in general a WZP has several foci depending on the order of the Walsh function. Self-similarity can also be observed in the axial intensity distributions. We have experimentally tested the focusing properties of the WZPs by implementing them on a liquid-crystal display. Fig. 1(b)) shows the transverse irradiance of the order $k = 22$ (red arrow in Fig. 1(a)). A profile of the experimental axial irradiance is represented in the same figure together with the analytical axial irradiance for comparison.

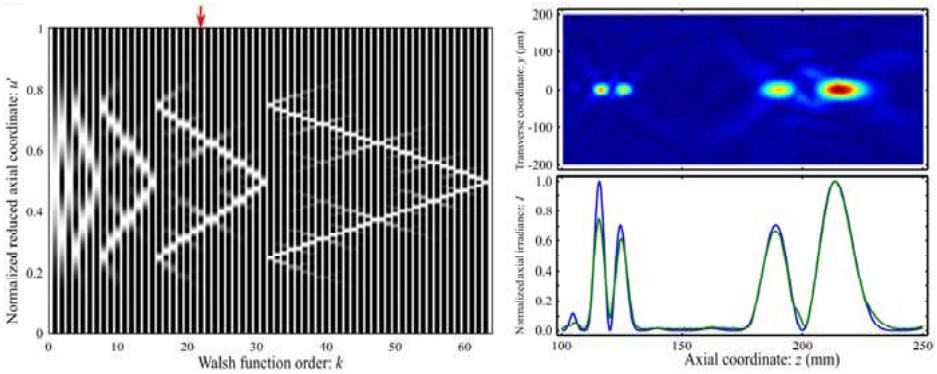

(a) (b)

Figure 1: (a) Axial irradiances provided by the WZPs of several orders. (b) Experimental transverse irradiance of the WZP with order $k = 22$ (blue line) and the corresponding analytical axial irradiance (green line).

Experimental Study on Low-profile of Multi-layer Noise Suppression Sheet Using Periodic Metal Film

K. Otsuka[1], **T. Ohno**[2], **and K. Tanii**[2]

[1]The University of Electro-Communications, Japan
[2]National Institute of Technology, Kisarazu College, Japan

Abstract— This paper examines a method to reduce the thickness of a Noise suppression sheet (NSS) by using a periodic metal film. NSS with the periodic metal film is placed on the microstrip line, and the transmission characteristics are measured.

Figure 1 shows the setup to measure the attenuation of conducting current noise along a transmission line, including a microstrip line (MSL) based on the IEC (International Electrotechnical Commission) standard. A network analyzer is connected to the MSL by coaxial lines, the transmission characteristics $|S_{21}|$ of the MSL shown in Figure 2 is measured. The MSL is fabricated by dielectric substrate (manufactured by ARLON, DiClad522, $\varepsilon_r = 2.55$, $\tan\delta = 0.0022$). The NSS ($\dot{\varepsilon}_r = 169.15 - j15.31$, $\dot{\mu}_r = 8.40 - j5.22$ @ 1 GHz) is placed on 4.4 mm wide strip conductor. Then NSS with and without the periodic metal film (Aluminum, $\sigma = 37.4 \times 10^6$ [S/m]) are measured. Figure 3 shows the multi-layer NSS with periodic metal film. The sheet consists of the metal film sandwitched by NSS to prevent from radiated noise. Figure 4 shows the result of measured transmission characteristics of the MSL with the multi-layer NSS and with the NSS not to use the metal film. In Figure 4, when the thickness of NSS decreases from 0.834 to 0.204 mm, f_c is shifted from 0.98 to 1.92 GHz. It is also noticeable that f_c of the NSS with periodic metal film is 0.99 GHz, which is approximately equal to fc in the case of the NSS thickness of 0.834 mm. Moreover, the low-pass characteristic of the multi-layer NSS is similar to the NSS which has 0.834 mm thick. As a result, the thickness of NSS can be reduced up to 40.9% by attaching the periodic metal film. As further investigation, re ection and absorpition of radiated noise by the multi-layer NSS should be examined.

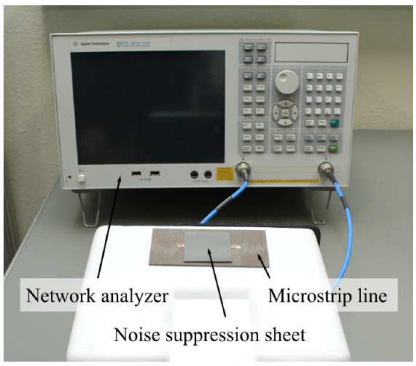

Figure 1: Measurement system of transmission characteristics on a microstrip line.

Figure 2: Schematic diagram of the microstrip line.

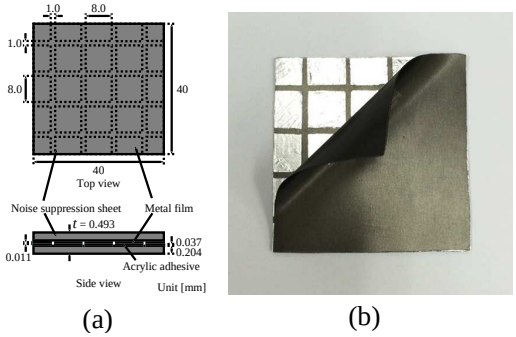

Figure 3: The multi-layer NSS with periodic metal film. (a) Structure. (b) Manufactured NSS

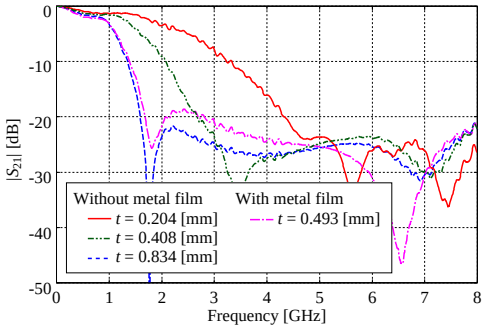

Figure 4: Measured transmission characteristics of microstrip line with the NSS shown in Figure 3.

Losses Reduction in Composite Chiral Metamaterials

Oscar Fernández[1], **Álvaro Gómez**[1], **Angel Vegas**[1],
G. J. Molina-Cuberos[2], **and Angel J. García-Collado**[3]

[1]Dpto. de Ingeniería de Comunicaciones, Universidad de Cantabria, Santander, Spain
[2]Dpto. de Electromagnetismo y Electrónica, Universidad de Murcia, Murcia, Spain
[3]Dpto. de Ciencias Politécnicas, Universidad Católica San Antonio, Murcia, Spain

Abstract— It is known that, due to the high optical activity, some chiral metamaterial structures implemented in printed circuit board (PCB), such as those based on mutual rotation between faces [1, 2] and on conjugated faces [3, 4], exhibit negative values of the refractive index ($n_{\pm}$) for the right handed (+) or left handed (−) circularly polarized waves. Unfortunately, in these structures the negative refractive index is related to high losses because of the high value of the refractive index imaginary parts. Only in a narrow frequency range the structure presents negative refractive index and low losses simultaneously. However, in this case the figure of merit of the negative refractive index (defined as $FoM_{\pm} = n'_{\pm}/n''_{\pm}$), is small. Consequently, these facts prevent the use of the aforementioned CMM structures for developing applications that take advantage of the negative refraction.

In order to decrease the losses and the FoM, Zhaofeng in [5] proposes a composite chiral metamaterial (CCMM) constituted by the combination of a conjugated rosettes CMM structure with a fishnet structure that presents continuous metallic wires at the edges and in the center of the unit cell (see Fig. 1 of [5]). With the addition of the continuous metallic wires the maximum FoM values enlarges from 8.4 for the original conjugated rosettes structure to 50 for the CCMM.

In this work a new CCMM composed by a conjugated gammadion CMM structure [4] and a cross-shaped fishnet structure without metallic wires at the edges is analyzed numerically with the aid of Keysight EMPro 3D electromagnetic simulator. For that purpose the aforementioned structures are individually characterized using the EMPro Finite Differences Time Domain engine. The obtained results show that the CCMM enlarges in more than 20° the moduli of the polarization plane rotation angle than the original CMM does. Regarding to the refractive index, the CCMM displays a wider frequency band with negative index, lower losses and higher FoM values (See Fig. 2).

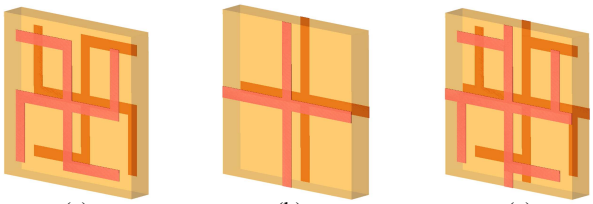

(a) (b) (c)

Figure 1: (a) Conjugated gammadion CMM. (b) Fishnet structure. (c) Conjugated gammadion structure combined with fishnet structure (CCMM).

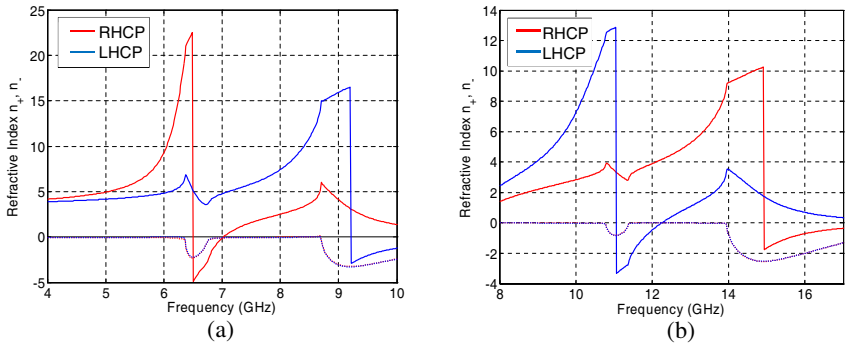

(a) (b)

Figure 2: Real (solid) and imaginary (dotted) parts of the RHCP and LHCP refractive index: (a) CMM and (b) CCMM.

ACKNOWLEDGMENT

This work has been supported by the Spanish Government MINECO through the Research Projects TEC2014-55463-C3-1-P, TEC2014-55463-C3-3-P and by the European Commission (ERDF).

REFERENCES

1. Plum, E., J. Zhou, J. Dong, V. A. Fedotov, T. Koschny, C. M. Soukoulis, and N. I. Zheludev, "Metamaterial with negative index due to chirality," *Phys. Rev. B*, Vol. 79, 035407, 2009.
2. Zhou, J., J. Dong, B. Wang, T. Koschny, M. Kafesaki, and C. M. Soukoulis, "Negative refractive index due to chirality," *Phys. Rev. B*, Vol. 79, 121104, 2009.
3. Li, J., F. Q. Yang, and J. F. Dong, "Design and simulation of l-shaped chiral negative refractive index structure," *Progress In Electromagnetics Research*, Vol. 116, 395–508, 2012.
4. Zhao, R., L. Zhang, J. Zhou, T. Koschny, and C. M. Soukoulis, "Conjugated gammadion chiral metamaterial with uniaxial optical activity and negative refractive index," *Phys. Rev. B*, Vol. 83, 035105, 2011.
5. Li, Z. F., K. B. Alici, H. Caglayan, M. Kafesaki, C. M. Soukoulis, and E. Ozbay, "Composite chiral metamaterials with negative refractive index and high values of the figure of merit," *Opt. Express*, Vol. 20, 6146–6156, 2012.

Diffraction by a Nano-hole in a Two-dimensional Plasmonic Layer

Norman J. M. Horing[1], **Désiré Miessein**[1, 2], **and Godfrey Gumbs**[1, 2]

[1]Department of Physics and Engineering Physics
Stevens Institute of Technology, Hoboken, New Jersey 07030, USA
[2]Department of Physics and Astronomy
Hunter College of the City University of New York, 695 Park Avenue, New York, NY 10065, USA

Abstract— A method of successive integral equations is developed to describe electromagnetic wave transmission through a subwavelength nano-hole in a thin plasmonic sheet in terms of the dyadic Green's function for the associated Helmholtz problem. No assumptions about boundary conditions are needed as they are implicitly embodied in the integral equations. This approach has facilitated relatively simple numerical computation, and it is not in any way restricted to a metallic screen. Taking the subwavelength radius of the nano-hole to be the smallest length of the system, we have obtained an exact solution of the integral equations for the dyadic Green's function analytically and in closed form. This dyadic Green's function is then employed in the numerical analysis of electromagnetic wave transmission through the nano-hole for normal incidence of the incoming wave train. The electromagnetic transmission involves two distinct contributions, one emanating from the nano-hole and the other is directly transmitted through the thin plasmonic layer itself (which would not occur in the case of a perfect metal screen). The transmitted radiation exhibits diffraction interference fringes in the vicinity of the nano-hole, and they tend to atten as a function of increasing lateral separation from the hole, reaching the uniform value of transmission through the sheet alone at large separations. The calculated results also exhibit a positional broadening of the central electromagnetic transmission maximum as the height above the hole increases from the near to the far zones. This is to be expected as a simple geometric spreading of the radiation emanating from the nano-hole itself, but, as indicated above, the transmitted radiation is further supported by electromagnetic transmission *directly* through the plasmonic sheet. Furthermore, our results incorporate the role of the 2D plasmon of the thin layer, which is smeared by its lateral wavenumber dependence.

Photodynamic Properties of a C_{60} Organosol

I. M. Kislyakov[1, 2], **I. M. Belousova**[1, 2], **A. V. Volkova**[3], **N. G. Gogoleva**[2], **V. M. Kiselev**[2], **and T. K. Krisko**[2]

[1]ITMO University, St. Petersburg, Russia
[2]S. I. Vavilov State Optical Institute, St. Petersburg, Russia
[3]St. Petersburg State University, St. Petersburg, Russia

Abstract— The fullerene C_{60} is a wonderful molecule becoming more common in photonics due to high optical nonlinearities and singlet oxygen quantum yields ($\varphi = 0.96$) [1, 2]. The both properties are determined by high probable singlet-triplet intersystem crossing in fullerene molecule populating a metastable triplet state ($T1$) with appropriate characteristics. In practice, large polarizabilities lead to the aggregation of the C_{60} molecules owing to strong dispersion forces, the process causing formation of various supramolecular structures depending on physicochemical properties of media.

The strongest aggregation of fullerenes is observed in polar solvents, in which long-living or stable colloidal sols can be formed on the grounds of solely repulsive electrostatic interactions between the aggregates [3]. It is well known that aggregated fullerenes have rather poor $T1$ quantum yield and pretty short life-times, these factors decrease photodynamic ability of materials [4]. This is the most important issue regarding singlet oxygen photosensibilization in such potential applications as photodynamic therapy and oxygen-iodine lasing [2]. In the present communication we show that under certain circumstances C_{60} aggregation is not so dramatically detrimental with respect to its photodynamic properties in some media.

C_{60} solution in CCl_4 was mixed with acetone in different proportion provided fullerene concentration constant. Absorption spectra changes, representative the begging of cluster formation in the liquid, appeared in the mixtures with values of its dielectric constant ε over 14. At ε about 19 we found a stable suspension on the time scale of two days. The dynamic light scattering study shows a narrow size distribution about 220 nm with polydispersity index 0.005.

Singlet oxygen ($^1\Delta_g$ state) IR luminescence ($\lambda = 1268$ nm) was measured both in the C_{60}/CCl_4 and the C_{60}/CCl_4&Acetone-D_6 systems at the excitation by LED light of different wavelengths ($\lambda_{ex} = 370$ nm, 405 nm, 465 nm, 525 nm, 625 nm) under the same experimental conditions. The singlet oxygen quantum yield φ of C_{60} in the sol form was found to be only 3 times less than the one of C_{60} in solution.

A theoretical model of quasi-two-level scheme for fullerene and three-level scheme for oxygen employed to describe the generation process involving fullerene light absorption, singlet-triplet intercrossing, photosensibilization and quenching of $^1\Sigma_g$ oxygen state by $T1$, $^1\Sigma_g$–$^1\Delta_g$ oxygen transition and $^1\Delta_g$ quenching by the solvent molecules. The solution of the set of kinetic equations using kinetic constants of the levels as parameters established a dependence of generated singlet oxygen concentration vs. $T1$ lifetime. This dependence explains why although the $T1$ lifetime value is dramatically decreased by two orders of magnitude following the aggregation, the singlet oxygen photosensibilization efficiency still remains high.

The results obtained show up rather perspective regarding working out fullerene-aggregates-based singlet oxygen generators, which are expectedly germane to practical applications.

REFERENCES

1. Belousov, V. P., I. M. Belousova, V. P. Budtov, et al., "Fullerenes: Structural, physicochemical, and nonlinear-optical properties," *J. Opt. Technol.*, Vol. 64, No. 12, 1081–1109, 1997.
2. Belousova, I. M., O. B. Danilov, V. M. Kiselev, et al., "Solid-phase fullerene-like nanostructures as singlet oxygen photosensitizers in liquid media," *Proc. of SPIE*, Vol. 6613, 66130C, 2007.
3. Alargova, R. G., S. Deguchi, and K. Tsujii, "Stable colloidal dispersions of fullerenes in polar organic solvents," *J. Am. Chem. Soc.*, Vol. 123, 10460–10467, 2001.
4. Ishibashi, Y., M. Arinishi, T. Katayama, H. Miyasaka, and T. Asahi, "Excited-state dynamics of fullerene nanoparticles dispersed in pure water," *Chem. Lett.*, Vol. 41, 1104–1106, 2012.

Non-linear Optical and Luminescent Properties of PbS Materials Stabilized by High-molecular Polyvinylpyrrolidone

I. M. Belousova[1, 2], **S. K. Evstropiev**[1, 2], **I. M. Kislyakov**[1, 2], **A. S. Panfutova**[1], **and A. A. Ryzhov**[1, 2]

[1]S. I. Vavilov State Optical Institute, Saint-Petersburg, Kadetskaya line, 5/2, Russia
[2]ITMO University, Saint-Petersburg, Kronverksky pr., 49, Russia

Abstract— It is well-known that semiconductor nanocrystals (NCs) have high non-linear optical properties. But the interaction between these NCs and with surrounding matter can have strong influence on their non-linear light absorption and scattering [1].

In this work we present the results of the preparation of the suspension and coatings containing PbS QDs stabilized by high-molecular (M_s =1300000) polyvinylpyrrolidone (PVP). PbS suspensions were prepared from mixed water — propanol-2 solution of Na_2S and $Pb(NO_3)_2$ at the presence of PVP. Composite PbS/PVP coatings were deposited on glass surface by dip method at room temperature.

The spectra of prepared suspensions demonstrated the absence of absorption bands in visible spectral range. Experiments show that PbS suspensions and coatings demonstrate strong luminescence in NIR spectral range (1100–1200 nm) at the excitation of visible light with different wavelengths. Luminescent properties of our suspensions non-linearly depend on the power of exciting irradiation and, also, they are changing during storage at room temperature.

The measurements of non-linear transmittance of PbS suspensions were made on special setup using Nd:YAG laser ($\lambda = 0.532\,\mu$m). Experiments show that prepared suspensions can effectively limit powerful laser irradiation at $\lambda = 1.06\,\mu$m with the limiting threshold $2 \cdot 10^{-4}$ J.

Non-linear refractive index γ and two-photon absorption coefficient β were measured at $\lambda =$ 1540 nm by Z-scan method with open and closed apertures. These measurements gave values $\beta = 4.2 \cdot 10^{-9}$ cm/W and $\gamma = -3.4 \cdot 10^{-13}$ cm^2/W for the suspension containing 8.6 10^{-4} mol/l PbS.

The registered effects are seen to be explained through dependencies between luminescent and non-linear optical properties of PbS aggregates, and their structure in the polymer environment. The use of the polymer composites studied makes appearance as promising in fixing issues of photo-voltaics and non-linear optical limiters. The observed regularities would enhance efficacy of such solutions.

REFERENCES

1. Bolotin, L., D. J. Asunskis, A. M. Jawaid, Yaoming Liu, P. T. Snee, and L. Hanley, "Effects of surface chemistry and shape on nolinear absorption, scattering and refraction of PbSe nanocrystals," *SPIE Proceedings*, Vol. 7935, Organic Photonic Materials and Devices XIII, February 21, 2011.

Semipolar InN Growth on $LaAlO_3$(112) Substrate by Metal Organic Molecular Beam Epitaxy

Fang-I Lai[1] and Shou-Yi Kuo[2]

[1]Department of Photonic Engineering, Yuan Ze University, Taoyuan, Taiwan
[2]Department of Electronic Engineering, Chang Gung University, Taiwan

Abstract— Most of the III-nitride semiconductor hetero-structures are grown along the *c*-axis on Si (111), GaAS (111), SiC and sapphire (0001) with wurtzite structure which the basal plane (0001) is a slide plane. The basal plane dislocation slip brought about the majority of dislocation in the III-nitride semiconductor layers. The spontaneous and piezoelectric electrical polarizations produce the electric fields along the ⟨0001⟩ direction to separate the spatially electrons and holes and to reduce the recombination probability result in the poor performance in optoelectronic device devices.

Indium nitride (InN) is one of the members in III-nitrides semiconductors, and has attracted intensive interest because of the narrow band gap $\sim 0.7\,\mathrm{eV}$ and high electron mobility approximately $4400\,\mathrm{cm}^2/\mathrm{V\text{-}S}$ among III-nitrides semiconductors. However the Fermi level pinning above the conduction band in InN accompanied with donor-like surface states leading to an ultrahigh-density of surface electron accumulation layer on the InN surface. Most InN reported recently are degenerate *n*-type materials with an electron concentration of approximately $1 \times 10^{18}\,\mathrm{cm}^3$ or higher, and these problems result in the difficulties in the fabrication of InN-based devices practically. Hence, the semi- and non-polar III-nitride semiconductors including InN have been attracted considerable attention in recent years because of the reduction of the polarization-induced electric fields and the improvement of the efficiency of optoelectronic devices. Moreover, the problems of the Fermi-level pinning and the surface electron accumulation were predicted that would be mitigated by distract from the growth in polar orientation.

In this paper, we present the structural and optical properties of metal organic molecular beam epitaxy grown semi-polar InN with (10–13) surface orientations on $LaAlO_3$ (112). The (10–13) crystal spacing of InN films is very close to the bulk InN revealed the almost stress-free in the InN (10–13) axis direction confirming by XRD. The result of XRD in-plane □-scan indicates there a two domains InN epitaxy on $LaAlO_3$ substrate. The PL spectrum display the near-band-edge and free-to-bound recombination with localization effect due to the urbach band tails located at both conduction and valence band edge. The surface electron accumulation is mitigated by the growth of InN (10–13). In contract to *c*-plane InN, the polarization-depended PL reveals strong optical anisotropic polarization in semi-polar InN due to the valence band structure could be modified by anisotropic in-plane strain in semi-polar InN.

Optical Method for Investigation of the Parameters of the Thin Film

M. Bolshakov[1, 2], **N. Kundikova**[1, 2], **and I. Popkov**[1, 2]
[1]The Institute of Electrophysics of the Ural Division of the Russian Academy of Sciences (IEP UD RAS) Russia
[2]"South Ural State University" (National Research University), Russia

Abstract— The Snell law and Fresnel formulas for plane monochromatic waves were successfully used during generations, but they are not correct for light beams. Any light beam can be represented as a superposition of plane waves propagating at different angles and each plane wave has its own amplitude and phase. The dependence of the reflection and refraction on the angle of incidence and refraction index leads to the violation of the Snell law for light beams. For the first time the Snell law violation was predicted and observed by Goos and Hanchen in 1947. The longitudinal shift of the linear polarized beam center of gravity was observed under the total internal reflection. The shift was about a wavelength. The transverse shift of a circular polarized light beam was predicted by Fedorov in 1955 and was experimentally observed by Imbert in 1978. The shift direction depended on the circularity sign and the shift value was about a wavelength. The longitudinal shift can be increased by the beam reflection from layered medium.

We present our results of computer simulation and experimental observation of the Gauss beam reflection from a thin film (an one-dimension photonic crystal). The beam splitting and the beam center of gravity shift were observed after the beam reflection. The shifts were different for s and p-polarization and depended on the angle of incidence, the film thickness and the refractive indices of the film and the substrate. The value of the shifts was a few micrometers. The beam intensity distribution after reflection is shown in Fig. 1.

We have demonstrated coincidence between of the experimental results and the results of computer simulation. The results can be used for the thin film parameters determination.

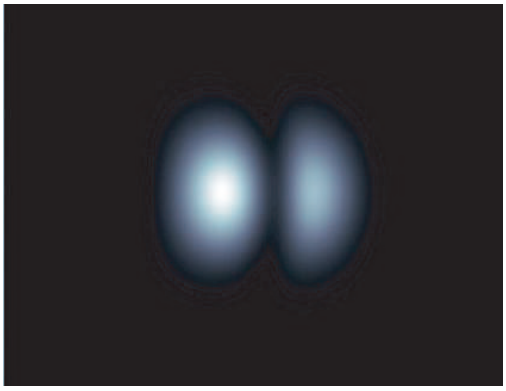

Figure 1: The intensity distribution of the Gauss beam after reflection from the film-substrate system.

ACKNOWLEDGMENT

This work was performed under the partial support of the government program 0389-2014-0004.

Luminescence Evolution of Co-evaporated $Cu(In,Ga)Se_2$ Films

Fang-I. Lai[1] and Shou-Yi Kuo[2]

[1]Department of Photonic Engineering, Yuan Ze University, Taoyuan, Taiwan
[2]Department of Electronic Engineering, Chang Gung University, Taiwan

Abstract— $Cu(In,Ga)Se_2$ (CIGS) thin films and related materials are promising absorbers for use in solar cells. They have attracted considerable research interest because of their wide gap, $E_g > 1.3\,\mathrm{eV}$ ($x = \mathrm{Ga}/(\mathrm{In}+\mathrm{Ga}) > 0.5$), large absorption coefficient of greater than $10^5\,\mathrm{cm}^{-1}$ close to the band gap, and the cheapness of the large-scale deposition of polycrystalline CIGS. Low-cost and high-efficiency CIGS-based solar cells have recently been fabricated with a high recording conversion efficiency over 21%. The improvement of the film quality and reducing defects in CIGS absorber layer were significant issues for high-performance of CIGS solar cell. However, the characteristics of defects in CIGS films are not clearly understood because of the fluctuation in its complex device structures, and multinary composition.

In this study, the $Cu(In,Ga)Se_2$ absorption layers were prepared on an Mo-coated soda-lime glass (SLG) by three-stage co-evaporation. The mean alloy composition had [Cu]/[In]+[Ga] and [Ga]/([In]+[Ga]) (GGI) ratios of approximately 0.67 and 0.28 respectively. The as-deposited CIGS thin film was utilized to fabricate a CIGS solar cell with a ZnO:Al (AZO)/ZnO/CdS/CIGS-/Mo/SLG structure with an efficiency of 10–12%. Optical properties of $Cu(In,Ga)Se_2$(CIGS) films were investigated by taking temperature-dependent (TD), power-dependent (PD) and time-resolved photoluminescence (TRPL) measurements. The TDPL results revealed that various carrier dynamics and recombination processes in CIGS thin films, and obvious near-infrared emission peaks were observed. Two dominant emission peaks were associated with the donor-acceptor pair (DAP) transitions in a CIGS absorber layer with an inhomogeneous structure and composition. The PDPL measurement demonstrated anomalous evolution of emission spectra as the excitation power is increased. We conclude that this phenomenon is attributed to the competition between two DAP emissions, which are correlated to indium vacancies (V_{In}), copper vacancies (V_{Cu}) and isolated oxygen substituted selenium (O_{Se}) atoms in CIGS thin films. The nature of defects in CIGS films significantly influenced the luminescence performance and current density-voltage characteristics of photovoltaic devices as well.

Patterned Nano Magneticstructures

D. Bajalan
St. Pölten, Austria

Abstract— Patterned magnetic nanowires are extremely well suited for data storage and logic devices. They offer non-volatile storage, fast switching times, efficient operation and a bistable magnetic configuration that are convenient for representing digital information. Key to this is the high level of control that is possible over the position and behaviour of domain walls (DWs) in magnetic nanowires. Magnetic random access memory based on the propagation of DWs in nanowires has been released commercially, while more dynamic shift register memory and logic circuits have been demonstrated. Here, we discuss the present standing of this technology as well as reviewing some of the basic DWeffects that have been observed and the underlying physics of DWmotion. We also discuss the future direction of magnetic nanowire technology to look at possible developments, hurdles to overcome and what nanowire devices may appear in the future, both in classical information technology and beyond into quantum computation and biology [1].

REFERENCES

1. Hrkac, G., J. Dean, and D. A. Allwood, *Phil. Trans. R. Soc. A*, 2011.

Design of Double Cladding Photonic Crystal Fibers with Low-loss and Broad Dispersion

Na Wang, **Shanglin Hou**, **Yanjun Liu**, **Jingli Lei**, **Suoping Li**, **and Wenyu Zhang**
School of Science, Lanzhou University of Technology, Lanzhou, Gansu 730050, China

Abstract— Photonic crystal fiber (PCF) is a new type of optical fiber with periodic arrangement of air hole on certain substate materials. Due to the periodic cladding structures PCF can be changed flexibly, double cladding structure photonic crystal fiber (double-cladding photonic crystal fiber, DC-PCF) is designed and its transmission characteristics are much more easily tailored. In recent years researchers were interested in reducing the loss of PCF because the high loss restricts the further development of some applications. The method to control the loss by tailoring the structure of PCF is studied and optimizing design of PCF can obtain low loss and broad dispersion. This paper demonstrates a new type DC-PCF with hexagonal air hole configuration. This kind of PCF is composed of double-cladding made by different air holes, the double-cladding structure not only makes the coupling reduced difficultly but also has a unique dispersion characteristics. In order to investigate the influences of this structure on its dispersion and loss, the effects of the inner cladding diameters, outer cladding diameters and air-hole pitches on dispersion and loss are all numerically simulated.

When the cladding structure of DC-PCF is similar as the conventional PCF, the similar dispersion characteristics can be obtained for that the dispersion characteristics of DC-PCF is mainly determined by the inner core and the surrounding air hole structure. And the loss can be reduced by optimizing the out-layer structure that affects the limited loss. In the paper, the dispersion characteristics of PCF is tailored by changing the diameters of inner and outer cladding air holes, and the effective index of which is lower than that of the fiver core so that the total internal reflection theorem is satisfied. The results indicate that values of its dispersion varies from $-23\,\mathrm{ps/(nm \cdot km)}$ to $-10\,\mathrm{ps/(nm \cdot km)}$ in the band of 1.30–1.8 μm, which has broadband dispersion compensation characteristics. By changing these structure parameters carefully, the loss can reach $7.39 \cdot 10^{-6}\,\mathrm{dB/km}$ at the wavelength of 1.55 μm, which is the smallest value that has ever been reported. The results of this DC-PCF provide a reference for designing some devices based on PCF with dispersion compensation, and also provides a theoretical basis for practical applications for the low loss characteristics which can increase the transmission efficiency of PCF.

Investigation on Reflection of Brillouin Dynamic Grating in Single Mode Optical Fibers

Junfeng Li, **Shanglin Hou**, **Wenyu Zhang**, **Yanjun Liu**, **Jingli Lei**, **and Suoping Li**
School of Science, Lanzhou University of Technology, Lanzhou, Gansu 730050, China

Abstract— Stimulated Brillouin scattering (SBS) is a nonlinear process that can occur in optical fibers, which can be described classically as a nonlinear interaction between the pump and Stokes fields through an acoustic wave. The pump field generates an acoustic wave through the process of electrostriction. The acoustic wave in turn modulates the refractive index of the medium. This pump-induced index grating scatters the pump light through Bragg diffraction. Scattered light is downshifted in frequency because of the Doppler shift associated with a grating moving at the acoustic velocity v_a.

Optical fiber gratings is manufactured by the photosensitive characteristic of fiber, the refractive index of fiber core is modulated periodicity, where will occurred coherence reflection when the frequency have coincidence with phase-matching condition during incident light. With this special property and the advantage of optical fiber such as low losses, anti electromagnetism etc.. It have developed into a mature technology with a wide range of applications in various areas, including physical sensing for temperature, strain, acoustic waves and pressure.

In this letter, the theory of static fiber Bragg grating was used to investigate the phenomenon that the perturbation of the refractive index modulated during the process of SBS which named as Brillouin dynamic gratings in optical fibres. Then the reflection of Brillouin dynamic gratings are studied and simulated by the coupled-mode theory in single-mode optical fibers. It is shown that the reflectivity becomes larger and the FWHM becomes narrower with the length of Brillouin dynamic grating increasing. However, with the increasing of refractive index modulation, the reflectivity becomes larger and the FWHM becomes broad. Additionally, the maximum reflectance red-shifts with the increase of core index. Finally, the maximum reflectivity is 0.9329 when the length of Brillouin dynamic grating is 100 meters and the refractive index modulation is 1×10^{-8}.

Enhanced Femtosecond Optical Pulses Compression in Highly Nonlinear Photonic Crystal Fibers at 850 nm

Qiling Wu, **Shanglin Hou**, **Yanjun Liu**, **Jingli Lei**, **Suoping Li**, **and Wenyu Zhang**
School of Science, Lanzhou University of Technology, Lanzhou, Gansu 730050, China

Abstract— Ultrashort optical pulse have potential applications in ultrafast optical communication, optical signal processing, optical machining, sensing technology and other fields. Fiber-based pulse compression technology is one of effective ways for obtaining ultrashort optical pulse. However, the conventional fiber has been restricted by its geometric parameters and it's not easy to get a good pulse compression effect. Photonic crystal fibers effectively overcome the deficiency of conventional fiber, and greatly improve the efficiency of pulse compression. Thus, the photonic crystal fiber-based pulse compression technology has become a hotspot in the research of pulse compression technologies.

Highly nonlinear photonic crystal fiber has important applications in various areas such as ultrashort laser pulse frequency conversion, spectrum broadening, pulse compression, wave breaking and so on. The effect of high nonlinearity can be achieved by minishing the area of core, increasing the air filling fraction or using the background material with large nonlinear refractive index. The development of optical communication system has experienced the process from the short wavelength (850 nm) to the long wavelength (1310 nm and 1550 nm), considering the communicating cost of the short wavelength of 850 nm is lower than the long wavelength, we numerically investigate the compression of femtosecond optical pulses in HN-PCF at 850 nm.

In this letter, we numerically investigate the soliton-effect compression of femtosecond optical pulses in highly nonlinear silica-core photonic crystal fiber at near-infrared region of the spectrum (specially at 850 nm) using full-vector finite element method and split-step Fourier method. We propose a novel photonic crystal fiber structure featuring a anomalous group velocity dispersion ($\beta_2 = -50.698\,\mathrm{ps}^2/\mathrm{km}$), small higher-order dispersions and enhanced nonlinearity ($\gamma = 268.4191\,\mathrm{w}^{-1}/\mathrm{km}$) for efficient soliton-effect compression of femtosecond optical pulses. We numerically investigate the effect of the high-order soliton compression of chirped Gaussian pulses in HN-PCF. It shows that high-quality ultrashort optical pulses with little pedestal energy can be obtained. The parameters, such as the fiber length, chirp parameter or the soliton order, have significant influence on the pulse compression properties, such as compression ratio and peak power.

A Universal Optical Network Unit for Hybrid TDM-PON and WDM-PON Transport Systems

Ching-Hung Chang, **Liang-Shuo Tu**, **and Meng-Chun Tseng**
Department of Electrical Engineering, National Chiayi University, Taiwan

Abstract— Fiber to the Home (FTTH) transport systems have attracted plentiful attentions to provide triple-play multimedia services for residential and business clients due to their low loss and high capacity characteristics. Time-division multiplexing (TDM)-passive optical networks (PONs) are therefore developed to share the extended bandwidth for clients. Nevertheless, if the bandwidth requirement is increased with the extended multimedia service environment, the network capacity of an optical network unit (ONU) in such TDM-PON structure is difficult to be upgraded. Converting the TDM-PON structure to wavelength-division multiplexing (WDM)-PON structure will be a suitable solution to upgrade the ONUs' capacity. A WDM-PON with logical point-to-point connection for each ONU will be able to extend the available downstream bandwidth from 100 Mbps in TDM-PONs to 1 Gbps or larger bandwidth for a client. There are two main methods to achieve this objective. One is to insert an optical wavelength selector, such as tunable optical bandpass filter (TOBPF), in front of an TDM-ONU to select a dedicated optical wavelength and reject other inserted optical wavelengths, and another one is to replace the optical passive splitter deployed in the remote node of a TDM-PON by an optical wavelength de-multiplexer, such as arrayed waveguide grating (AWG), to direct various downstream optical carriers into dedicated directions. Utilizing a TOBPF to select the inserted optical carriers in an ONU is convenient and the entire TDM-PON can be gradually migrated to WDM-PON according to consumers' requirements. However, the expensive TOBPF makes this solution inacceptable. On the other hand, the TDM-ONU is still able to be utilized in WDM-PON architecture if the optical splitter of a TDM-PON is replaced by an AWG. This can save a lot of cost but the entire network will need to be upgrade from TDM-PON to WDM-PON simultaneously. In addition, the type and amount of the employed optical wavelengths in such WDM-PON are fixed by the employed AWG. The internet service provider will not able to gradually achieve the migration according to consumers' requirements and the scale of the WDM-PON is fixed. It is clear from the discussion that utilizing a TOBPF to achieve the TDM-PON to WDM-PON migration is much more flexible than employing an AWG, if there is a method to provide economic wavelength selector for a TDM-ONU. To achieve this target, a novel wavelength selector is proposed and developed to compose a universal optical network unit (ONU) for both TDM- and WDM-PON architecture. Unlike the published TDM-PON to WDM-PON migration architectures which utilizing expensive TOBPF or complicated optical routing schemes to select proper optical wavelengths, the proposed universal ONU can utilize an economic vertical-cavity surface-emitting laser (VCSEL) as a TOBPF to select a specific lightwave from multiple injected optical carriers. Besides, the VCSEL-composed wavelength selector with electrically adjustable characteristic will be able to assist the universal ONU with an ability to switch its receiver functionality for either economic TDM-PONs application or high-capacity WDM-PONs structure. Experimental results proof that by modifying the driving current of the VCSEL-based wavelength selector, both TDM-PON signal and WDM-PON signal can be received individually. This proposal provides an economic and flexible method for clients to migrate between TMD-PON and WDM-PON architecture.

Sub-micron Particle Detection Using a Spatial Light Modulator Based on Fluorescent Imaging

Serap Altay Arpali[1] and Çağlar Arpali[2]

[1]Department of Electronic and Communication Engineering, Çankaya University, Ankara, Turkey
[2]Department of Mecatronic Engineering, Çankaya University, Ankara, Turkey

Abstract— Because of the high modulation efficiency and programmability, Spatial Light Modulator (SLM) is widely used in many fields of optical imaging. In this study, we implement the multiple and scanning type Gaussian beams using SLM with amplitude modulation to detect fluorescent sub-micron particles in the specimen. With this new on-chip fluorescent imaging modality, fluorescent samples onto an opto-electronic sensor-array (e.g., a CCD chip) are scanned by multiple Gaussian spots. Using multiple Gaussian excitations we can detect the sub-micron fluorescent beads which are not apparent with classical illumination schemas such as plane wave illumination. In this experiment, blue laser is collimated and directed to the SLM. The whole active area of the SLM was used to produce Gaussian spots with amplitude modulation. To create the each Gaussian spot, one pixel is used from the SLM screen (1024×768 pixels, $19\,\mu$m pixel size). And then amplitude modulated light is reflected to the cascaded lens system to provide demagnification at opto-electronic sensor-array. Higher diffraction orders were eliminated by a filter at back focal plane of the lens system. Using the $21\times$ demagnification rate, $0.9\,\mu$m spot size that is half beam with of each Gaussian spot was obtained onto an opto-electronic sensor-array. In this on-chip fluorescent imaging platform, specimen which is smeared on top of the faceplate (that is a planar optical component) to increase the efficiency of fluorescent emission is positioned onto an opto-electronic sensor array. Since we use vertical illumination, the rejection rate of the filter that is onto an opto-electronic sensor array is very important. So we used the only coated faceplate as a filter to increase the efficiency of fluorescent emission. Based on this on-chip fluorescent imaging technology, $1\,\mu$m particles were detected nearly within $1\,\text{mm}^2$ area. This system might be useful for detection of viruses in scatter media such as whole blood.

Analogy between the Ising Model and the Polarization Switching of Vertical-cavity Surface-emitting Lasers

Tsu-Chiang Yen, **Yueh-Chen Li**, **and Yu-Heng Wu**
Department of Physics, National Sun Yat-sen University
No. 70, Lienhai Rd., Kaohsiung 80424, Taiwan

Abstract— Conventional vertical-cavity surface-emitting lasers (VCSELs) have a cylindrical laser cavity, which provides an intrinsic two-degree of freedom to the polarization direction of the emitted light. This isotropic symmetry of polarization is usually broken by the anisotropy of the physical structure of VCSELs; for example, the anisotropy of the lattice structure, residual stress, or thermal distribution. In some VCSELs, the broken polarization symmetry conducts a polarization switching (PS) phenomenon. During this process, the VCSEL remains in a phase of emitting linearly polarized light around the laser's threshold, and then switches to another phase of emitting orthogonally polarized light when the laser's current surpasses a switching current. The VCSEL's PS (VPS) can help to build some components for the high speed optical computing. Accordingly, the characteristic of VPS is an important research pursuit.

Recently, VPS was reported to be a second-order phase transition (SOPT). That discovery was based on the criticalities observed in the experiments, which are the unique characteristics of SOPTs. This research attempts to explore the connection between VPS and the conventional Ising model. The said model employs the spin-up and spin-down spins to study the transition of magnetic materials from the ferromagnetic state to the paramagnetic state and identifies that transition as an SOPT. Therefore, both of the phase transitions of VPS and Ising model are SOPTs between two orthogonal states. Typical Ising model employs a two dimensional spin lattice to simulate the magnetic material. In this work, a Gaussian-distributed interaction was introduced into the center of the spin lattice to simulate the laser's beam profile and the spatial coherence. The investigation focused on the examination of the relaxation time required to transit from the ferromagnetic state to the paramagnetic state. The simulation results present an exponent of the relaxation time of about 2.23. This result approximates the experimental result of 2.3 well, revealing a success of this model. Some other results will also be reported.

Electromagnetic Modeling of Antenna Array Based on Circular Carbon Nanotubes Bundle

M. Aidi and T. Aguili
SysCom Laboratory, National Engineering School of Tunis, BP 37 Le Belvedere 1002, Tunis, Tunisia

Abstract— A novel antenna array structure, formed by carbon nanotube bundle is proposed. The geometric structure and radiation characteristics have been investigated using a proposed integral equations system. This equations system is numerically solved using the moments method. The dependence of the radiation performance, upon geometrical parameters, e.g., nanotube length and number and the coupling distance is accurately discussed. Some illustrative numerical results have been presented to discuss the radiation performance of carbon nanotube antenna array for different coupling distances.

Radiative Heat Transfer in the Extreme Near-field

V. Fernández Hurtado[1], K. Kim[2], B. Song[2], W. Lee[2], W. Jeong[2], J. Feist[1], F. J. Garcia-Vidal[1], J. C. Cuevas[1], E. Meyhofer[2], and P. Reddy[2]

[1]Departamento de Física Teórica de la Materia Condensada and Condensed Matter Physics Center (IFIMAC), Universidad Autónoma de Madrid, Madrid 28049, Spain
[2]Department of Mechanical Engineering
University of Michigan, Ann Arbor 48109, USA

Abstract— One of the central open problems in nanoscience is the study of the heat transport in nanoscale devices, which has remained largely unexplored due to experimental challenges. In this context, a key issue is the understanding of the heat transfer via thermal radiation between systems separated by nanometer-size gaps. In this extreme regime, the electromagnetic near-field is expected to give rise to a dramatic enhancement of the radiative heat transfer, something that has only be quantitatively verified for gaps on the order of 20–30 nm [1]. In this work, we present a combined experimental and theoretical study of the radiative heat transfer in the extreme near-field regime (gaps of 1–10 nm). From the experimental side, we performed systematic studies using AFM-based scanning probes with integrated nanoscale thermocouples [2], which were coated with dielectrics (SiO_2 or SiN_x). Our experiments of heat transport between the scanning probes and a flat substrate coated with dielectrics, performed in an ultra-high vacuum environment, confirm that heat transport is dramatically enhanced in the near-field. To understand our experimental results, we investigated these near-field enhancements within the framework of the theory of fluctuational electrodynamics [3]. To be precise, we performed extensive numerical simulations making use of a combination of a fluctuating-surface-current formulation of radiative heat transfer with the boundary element method [4, 5]. Such a combination allows us describing realistic geometries for our tip-sample setups. Our theoretical results are in good agreement with the measured heat flows between both dielectric and metallic surfaces, which establishes the validity of fluctuational electrodynamics in modeling near-field heat transport all the way to nanometer-size separations.

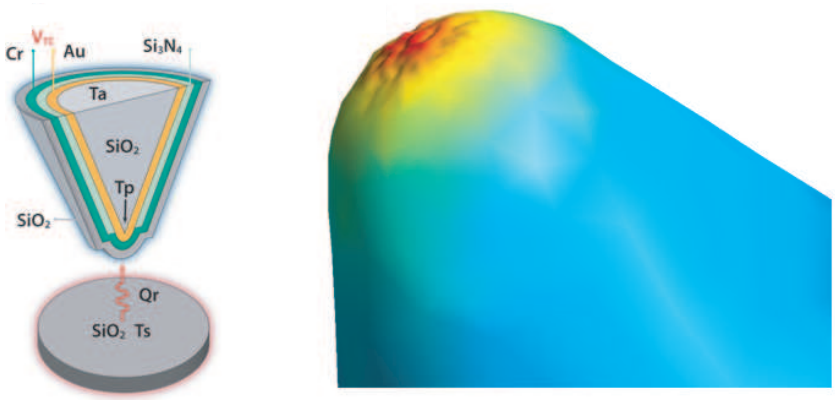

(a) (b)

Figure 1: (a) Schematic diagram of the experimental setup. The AFM probes incorporate a thermocouple, made by a spherical Au/Cr junction with a diameter of 200 nm. (b) Numerical simulation of the spatially resolved heat transfer between a tip and a plate made of silica and separated by a distance of 1 nm. The radius of the tip is 225 nm. The color scale is logarithmic, showing the radiative heat transfer enhancement in the extreme near-field.

REFERENCES

1. Basu, S., Z. M. Zhang, and C. J. Fu, *Int. J. Energy Res.*, Vol. 33, 1203, 2009.
2. Lee, W., K. Kim, W. Jeong, L. A. Zotti, F. Pauly, J. C. Cuevas, and P. Reddy, *Nature*, Vol. 498, 209, 2013.

3. Joulain, K., J. P. Mullet, F. Marquier, R. Carminati, and J. J. Greffet, *Surf. Sci. Rep.*, Vol. 57, 59, 2005.
4. Rodriguez, A. W., M. T. H. Reid, and S. G. Johnson, *Phys. Rev. B*, Vol. 86, 220302(R), 2012.
5. Rodriguez, A. W., M. T. H. Reid, and S. G. Johnson, *Phys. Rev. B*, Vol. 88, 054305, 2013.

A Compact Printed Spiral FM Antenna

Abraham Loutridis[1, 2], **Kansheng Yang**[1, 2], **Matthias John**[2], **and Max Ammann**[1]

[1]Antenna & HF Research Centre, Dublin Institute of Technology, Dublin 8, Ireland
[2]CTVR — The Telecommunications Research Centre, Trinity College Dublin, Dublin 2, Ireland

Abstract— Electrically Small Antennas (ESAs) are desired and essential for many applications and especially at lower frequencies like HF and VHF band. Nowadays, compact antennas have become standard equipment for radio receivers on vehicles and mobile terminals which lead to new requirements for small, efficient and low cost designs. The good performance of a radio receiver is heavily depended on the antenna performance. A variety of FM antenna types have been reported for automotive and portable applications including, the active [1] and short meander line monopoles [2], fractal Hilbert curve antenna [3], chip antennas [4], window-printed active antennas [5] and the shark type antennas [6].

In this work, a compact printed FM antenna is reported and operates over the frequency range of 87.5–108 MHz. The antenna was designed and printed on a 100 mm × 50 mm double sided FR-4 substrate ($\varepsilon_r = 4.3$, $\tan\delta = 0.025$, thickness = 1.5 mm) with copper metallization thickness of 0.035 mm. The antenna is fed by a microstrip line which is connected to a SMA connector. The miniaturization is based on its spiral structure occupying a 50 mm ($0.023\lambda_0$) × 50 mm ($0.023\lambda_0$) area on the PCB board. In order to improve the antenna bandwidth, a network matching circuit is added so that the impedance bandwidth of antenna can be wider, covering the frequency range of 20 MHz bandwidth at VSWR 6 : 1. The antenna was also measured and simulated on 900 mm × 900 mm ground plane which is representative of a vehicle roof.

REFERENCES

1. Negut, A., L. Reiter, J. Hopf, and S. Lindenmeier, "Performance of a 20 cm short active AM/FM monopole antenna for automotive application," *IEEE European Conference on Antennas and Propagation (EuCAP)*, 2009.
2. Perri, E. B. and S. Forcellini, "Very short meander monopole antennas," *IEEE Antennas and Propagation Society International Symposium AP-S*, 2008.
3. Borja, C., J. Anguera, C. Puente, and J. Vergés, "How much can be reduced the internal FM antenna of mobiles phones," *IEEE European Conference on Antennas and Propagation (EuCAP)*, 2010.
4. Song, S.-M., L. Jin, Y. Zheng, and G.-Q. Yang, "A miniaturized FM chip antennas for handset devices," *International Workshop on Microwave and Millimeter Wave Circuits and System Technology (MMWCST)*, 2012.
5. Schaffner, J. H., H. J. Song, A. Bekaryan, H.-P. Hsu, M. Wisnewski, and J. Graham, "The impact of vehicle structural components on radiation patterns of a window glass embedded FM antenna," *IEEE Transactions on Antennas and Propagation*, Vol. 60, No. 10, 4979, 2012.
6. Chang, D.-C., F.-Y. Lin, B.-H. Zeng, and J. Chen, "Compact size antenna for car FM radio," *PIERS Proceedings*, 223–224, Taipei, Mar. 25–28, 2013.

A Wideband Matching Technique for Polarization Versatile Applications

A. G. Koutinos, G. A. Ioannopoulos, M. T. Chryssomallis, and G. A. Kyriacou
Microwaves Lab, Department of Electrical and Computer Engineering
Democritus University of Thrace, Xanthi 67100, Greece

Abstract— A novel patch feeding technique is proposed, in order to achieve wideband matching for linear (horizontal or vertical) and circular polarization around the WiFi band of 2.4 GHz, which is allocated for computer-to-computer communications and Internet access. In addition, patch antennas fulfill many requirements regarding portable communication systems, combined with ease of fabrication at low cost and therefore are a fair solution.

As stated in [1], polarization diversity can be achieved by imposing a 90° phase difference between two adjacent linear resonances TM_{10} and TM_{01}, exploiting shorting posts. Each resonance (one regarding vertical and one horizontal polarization) can be slightly moved higher than the other by small differences in a square patch dimensions, so that the input impedance of, e.g., the vertical mode is inductive, while the input impedance of the horizontal mode is capacitive. Thus, the patch can effectively radiate in vertical mode or horizontal mode, while when operating in an intermediate frequency (thus giving rise to both resonances), circular polarization is achieved.

Furthermore, wideband linear resonances can be achieved using a technique proposed in our previous work [2]. The shorting posts which play a crucial role in [1] are replaced with feeding points, each symmetrical pair of them giving rise to either vertical or horizontal polarization. The point is that, regarding a single mode, we can enhance its bandwidth by introducing a feeding path inequality between its symmetrical feeding points. The novelty in the proposed configuration is that wideband operation for linear resonances is managed, while there is still the possibility for circular polarization mode by appropriately adjusting the frequency of operation between the two resonances.

As shown in Fig. 1, the feeding points centered on the x-axis are fed via holes in the substrate, while the path inequality regarding their distance to the common source (source 1) enables wideband matching for the horizontal mode around a frequency f_{R1}. The same approach is adopted for the feeding points located on the y-axis (source 2, for vertical polarization), this time around a frequency $f_{R2} \neq f_{R1}$. Introducing now 90° phase difference between sources 1 and 2, circular polarization is achieved at an intermediate frequency, between f_{R1} and f_{R2}. The designed patch antenna dimensions are 33.5 mm long and 34 mm wide, which printed on a $50 \times 50 \times 1.524$ mm Rogers dielectric substrate with $\varepsilon_r = 3.4$ and $\tan\delta = 0.002$.

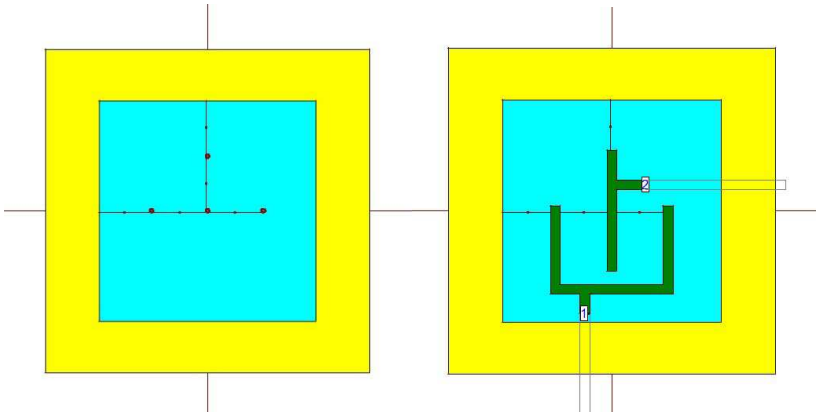

Figure 1: (a) Downwards and (b) backwards aspects of the proposed configuration.

REFERENCES

1. Schaubert, D. H., F. G. Farrar, A. Sindoris, and S. T. Hayes, "Microstrip antennas with frequency agility and polarization diversity," *IEEE Transactions on Antennas and Propagation*, Vol. 29, No. 1, January 1981.
2. Koutinos, A. G., G. A. Ioannopoulos, M. T. Chryssomallis, and G. A. Kyriacou, "A dual-feed rectangular patch antenna for bandwidth enhancement," *2014 Loughborough Antennas and Propagation Conference*, Loughborough, UK, November 2014.

Design and Implementation of a Planar Slot Antenna for SSR

Maziar Hedayati, Gholamreza Askari, Parisa Moslemi, and Hamid Mirmohammad Sadeghi
Information and Communication Technology Institute (ICTI)
Isfahan University of Technology (IUT), Isfahan 84156, Iran

Abstract— Secondary surveillance radar (SSR) mechanism is based on sending a pair of signals at the frequency of 1030 MHz for interrogation and receiving a pair of signals as an answer at 1090 GHz [1]. SSR radars are built in the form of planar or cylindrical array antenna [2]. Reflector and multi layer antennas are the most common SSR antennas in the literatures that have some disadvantages like complexity and being bulky [3, 4]. One layer microstrip array antenna which is proposed in this work is useful in mass production because of its advantages like easily printed, light weight and low cost which makes it suitable for radar applications. However it has some disadvantages like narrow bandwidth and high side lob level which is solved in this paper. To enhance the bandwidth, many attempts have been done in microstrip technolpgy. [5] using stacked elements for increasing the bandwidth of microstrip antenna and [6] proposed an stacked patch array of 1×8 elements with 14 dBi gain and the SLL of -14 dB, which is not enough to satisfy the Side Lobe Suppression (SLS) for the SSR [1]. In addition using stacked element increase the complexity of the system.

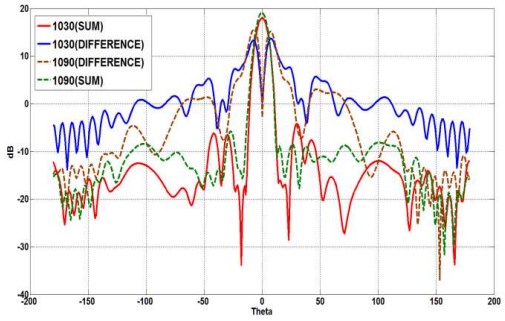

Figure 1.

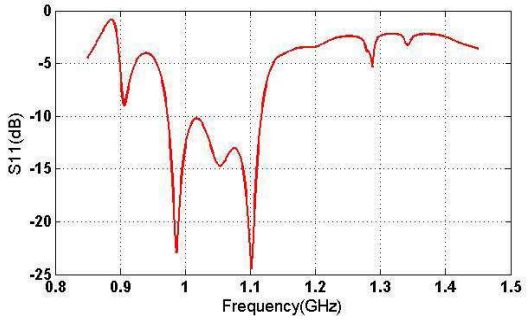

Figure 2. Simulated S_{11} of the 2×8 SSR antenna.

Table 1. Total characteristics of the proposed antenna.

Features	Unit	Value
#Channels	-	2 (Sum/Difference)
Frequency Range	MHz	1030 ± 5, 1090 ± 5
Polarization	-	Vertical
Sum Gain	dB	18.5
Sum Azimuth SLL	dB	-23
Sum Azimuth BLL	dB	-28
Difference Nu	dB	19
Difference Coverage	dB	> 4
Sum Azimuth B.W	Degree	9.5
Sum Elevation B.W	Degree	52
Size	cm^3	$200 \times 10 \times 60$
Gain at Elevation Angle ($-20°$, $-40°$)+5 dB > maximum Gain		
Gain at Elevation Angle (± 60) + 12 dB < maximum Gain		
Gain at Elevation Angle (± 90) + 18 dB < maximum Gain		
Gain at Elevation Angle (± 145) + 28 dB < maximum Gain		
Back lobe + 30 dB < maximum Gain		

In this paper a useful, low cost, low complexity, and one layer microstrip slot antenna for secondary surveillance Radar (SSR) application is presented. The feed network of antenna is a rat-race divider to create sum and difference ports and sixteen unequaled power dividers to satisfy the Chebyshev distribution with −30 dB SLL. The feed network has a special structure that creates constant group delay in all output ports and wide frequency bandwidth. The antenna gain for the sum pattern is 18.5 dB and 19 dB at 1030 MHz and 1090 MHz respectively (Fig. 1), with a 3 dB beam width of 52° in elevation and 9.5° in azimuth. The difference has a −19 dB null at the peak of the sum pattern and an acceptable pattern against the sum pattern for SSR applications. Furthermore, the antenna pattern has no need the back fill antenna to satisfy the back lobe conditions, which is critical for SSR applications. The total characteristics of the proposed antenna are shown in Table 1. A 2 : 1 VSWR bandwidth of 9.4% is achieved with the presented geometry in simulation to cover the 1030 ± 10 MHz transmit and the 1090 ± 10 MHz receive frequency band (Fig. 2).

REFERENCES

1. Vladimir, S., et al., "Secondary surveillance radar antenna antenna Designer's notebook," *IEEE Antennas and Propagation Magazine*, IEEE 55.2, 2013.
2. Stevens, M. C., *Secondary Survillance Radar*, Artech House, 1936.
3. Silver, A., *Microwave Antenna Theory and Design*, Sec. 5.7, Mcgraw-Hill, New York, 1949.
4. Stutzman, W. L. and W. A. Davis, *Antenna Theory*, John Wiley & Sons, Inc., 1998.
5. Lee, R. Q., K. F. Lee, and J. Bobinjak, "Characteristic of a two layer electromagnetically coupled rectangular patch antenna," *Electron Lett.*, Vol. 23, No. 20, 1070–1072, Sep. 1987.
6. Kumar Sharma, A., C. K. Kumar, and A. Mittal, "EM coupled L-band antenna array for secondary surveillance Radar," *European Microwave Conference 2009. EuMC 2009*, 1465, 1467, Sep. 29–Oct. 1, 2009.

Design And Analysis of Uniplanar Compact Electromagnetic Bandgap Structures

Shivam Gautam[1], **Komalbir Kaur**[1], **N. S. Raghava**[1], **and Asok De**[2]

[1]Delhi Technological University, India
[2]NIT Patna, India

Abstract— A uniplanar compact electromagnetic bandgap (UCEBG) antenna and its performance analysis is presented in this paper. The EBG structure in the antenna presented improves the antenna's efficiency and increases its compactness, enabling it to perform better at a lower frequency.

The antenna is composed of a ground plane, an EBG plane, a dielectric substrate and a radiating patch. Figure 1 depicts the top view of the antenna. The length of each side of the ground plane is L which is equal to 191.2 mm. The antenna consists of a 17×17 matrix of unit UCEBG structure. The substrate between the UCEBG layer and the radiating patch is of 0.7 mm thickness and a dielectric constant of 1.96. The air gap between the ground plane and the UCEBG layer is 9 mm. The radiating patch element is of dimension 70 mm $\times$ 54 mm.

CST Microwave Studio is used for the design and analysis of the UCEBG antenna. The results obtained from the simulation show that the central frequency of operation of the antenna is 1.271 GHz. The antenna has a reflection coefficient bandwidth (< -10 dB) of 17 MHz and covers the frequency range from 1.263 GHz to 1.28 GHz. The graphical representation of reflection coefficients are shown in Figure 2. The radiation pattern of the antenna is shown in Figure 3.

The antenna has a gain of 8.08 dB at $\theta = 0°$, $\phi = 0°$.

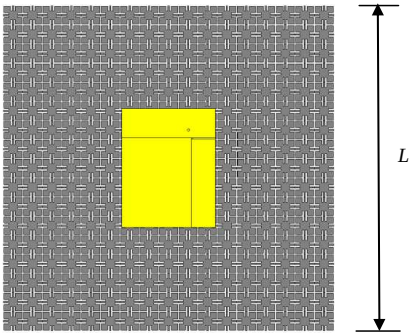

Figure 1: Top view of UCEBG antenna.

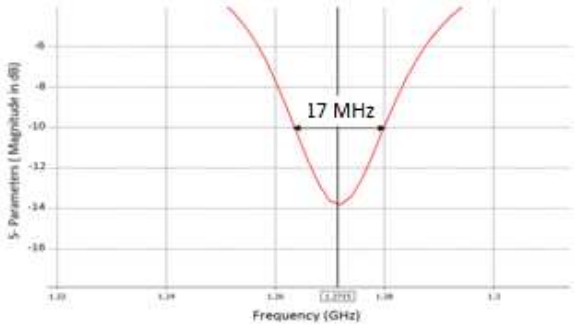

Figure 2: Reflection coefficient vs frequency.

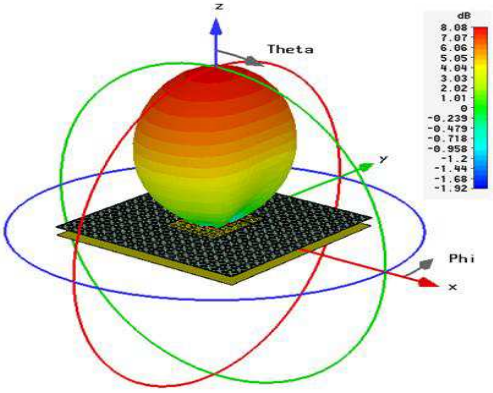

Figure 3: Radiation pattern.

Novel Wideband Quadrature Hybrid Coupler with Tunable Power Dividing Ratio

Hong-Tao Li[1, 2], **Hong-Lin Zhang**[1], **Bin-Jie Hu**[1], **Xiao-Dong Wei**[1], **and Wei-Sen Zeng**[2]

[1]School of Electronic and Information Engineering
South China University of Technology, Guangzhou, China
[2]Department of Physics and Optoelectronic Technology
Guangdong University of Technology, Guangzhou 510006, China

Abstract— Hybrid coupler is an essential component in modern wireless communication systems. It has been widely used in a variety of applications, such as the feeding network of an antenna array, power dividing/combining networks and balanced-mixers. Recently, electric tunable quadrature hybrid coupler has gained much attention, because of its reconfigurable performance. In this paper, we propose a novel wideband quadrature hybrid with tunable power dividing ratio. It is consist of a modified structure of hybrid and two varactor diodes (Cp), as shown in Fig. 1. By verifying the biasing voltage, the power dividing ratios between the two output ports (i.e., port 3 and port 4) of the hybrid can be easily controlled. Analytical design equations are derived using the even-odd mode method. To verify the design concepts, a miniaturized tunable power dividing ratio hybrid working at 1.85 GHz is designed. The parameters of the proposed antenna are as follows: $L_0 = 14.2$ mm, $L_1 = 16$ mm, $L_2 = 9$ mm, $W_0 = 1.5$ mm, $W_1 = 2.8$ mm, $W_2 =$1mm, $W_3 = 0.25$ mm, $W_4 = 1.2$ mm. When verifying the capacitance of the varactor diodes from 0.9 to 3.3 pF, the power dividing ratios between the two output ports of the hybrid can be controlled from 0 to 6 dB within a wide bandwidth for (1.75–1.95 GHz). Moreover, the size of the quadrature hybrid is much small ($60.4 \times 26.8\,\text{mm}^2$). The measured results agree well with the simulated ones.

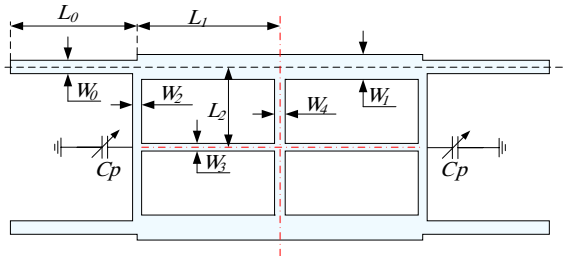

Figure 1: The structure of the proposed tunable power dividing ratio wideband quadrature hybrid coupler.

A Wide Stopband Filter with Source-load Coupling Technique

Kwok-Keung Chon[1], **Ching-Jui Wu**[1], **Feng-Lin Jenq**[2], **Hong-Yu Jhuang**[1], **and Shih-Fong Chao**[1]

[1]Department of Microelectronics Engineering, National Kaohsiung Marine University, Taiwan
[2]Department of Electronic Engineering, Far East University, Taiwan

Abstract— In this paper, a wide stopband bandpass filter with source-load coupling technique is proposed. Multiple transmission zeros are generated at the stopband to suppress the harmonic responses of the bandpass filter. With the gap-coupling structure, transmission zeros can be controlled by adjusting the input/ouput tapped position. Moreover, additional transmission zeros can be obtained by using the source-load coupling technique. By controlling the value of the gap capacitance, the locations transmission zeros can be controlled. The stepped-impedance resonator (SIR) is utilized to minimize the overall circuit size. The impedance and length ratios of the SIR are determined to move its first harmonic to a higher frequency. The center frequency of the filter is 2.45 GHz, and the stopband rejection is higher than 30 dB from 2.9 GHz to 13.36 GHz. The circuit is fabricated on a Rogers RO4003C substrate with $\epsilon_r = 3.6$, $h = 32$ mil, and $\tan\delta = 0.0027$. The total circuit size is $0.15\lambda_g \times 0.23\lambda_g$.

Analysis and Implementation of a Dual Mode Cavity Band Pass Filter

Zohre Pourgholamhossein, **Fattah Talaei**,
Gholamreza Askari, **and Hamid Mirmohammad Sadeghi**
Microwave and Antenna Group, Information and Communication Technology Institute (ICTI)
Isfahan University of Technology (IUT), Isfahan 84156, Iran

Abstract— Microwave filters play an important role in almost every RF-microwave communications system. In communication system, narrowband filters are essential components to reject the interference signals. Therefore it is necessary to utilize high Q resonant circuits to achieve a narrow bandwidth in the pass band at high frequency. Microwave band pass filters have been typically implemented using waveguide technology or cavity due to low loss, high quality factors, narrow bandwidth and high power handling capabilities [1]. On the other hand, waveguide filters are massive and heavy. A solution has been done to reduce the size and weight of filters involves using dual mode cavities that support two degenerate resonances. Therefore, to reduce the number of physical cavities, dual mode or triple mode resonators are often employed. The advantages of these filters are the fewer number of cavities and improved performance. The first working multi-mode cavity microwave filter has been introduced by Li [2]. Elliptic dual mode filters for space applications were introduced by Atia and Williams [3]. Designs in other methods were reported by many authors [4, 5]. In addition, the transmission line must be coupled together. In the coaxial case, the probe excitation is carried out in the cavity resonator by introducing the probe inside the cavity.

This paper presents a structure of the dual mode rectangular cavity filter using coaxial probes for excitation. By using cross coupling technique with perturbation theory, transmission zeros in the stop band are realized, so the shape factor can be improved. Also, by this technique, bandwidth of pass band can be optimized. On the one hand, cross coupled filters are difficult to tune, due to coupling effects in the filter. This dual mode cavity design is used for the implementation of second order filters with two TE_{101} and TE_{011} modes. The two independent modes can be coupled so that, energy is transferred from the first modes into the second. Actually, the probe is inserted from the broad dimension of the cavity and it should be kept at the place inside the cavity where electric field is maximum, which is discussed completely. Considering the topology of two orders band pass, is designed to meet the center frequency of 9050 MHz, 3-dB bandwidth of 60 MHz, insertion loss less than 0.5 dB, and 20 dB return loss in the pass band. In this design cavity is perturbed by a small deformation of its boundary as shown in Figure 1(a). This perturbation causes disturbing in the electrical field and so direct coupling between them is occurred. Also this cause cross coupling that is discussed completely. It is obvious that the bandwidth of the filter can be altered to desired values by changing the dimension of perturbation Furthermore, to indicate the effect of perturbation on the bandwidth, circuit analysis is done. The proposed cavity filter is structurally compact size and requires only one tuning screw. This tuning mechanism is presented to adjust the resonant frequency without causing any coupling of the degenerate cavity modes. Finally, EM simulation is done for the filter. Full wave analysis of the filter confirms the designed filter and performance of the full wave simulation of the complete structure. In order to validate the performance of the filter design, the filter was fabricated and measured. Figure 1

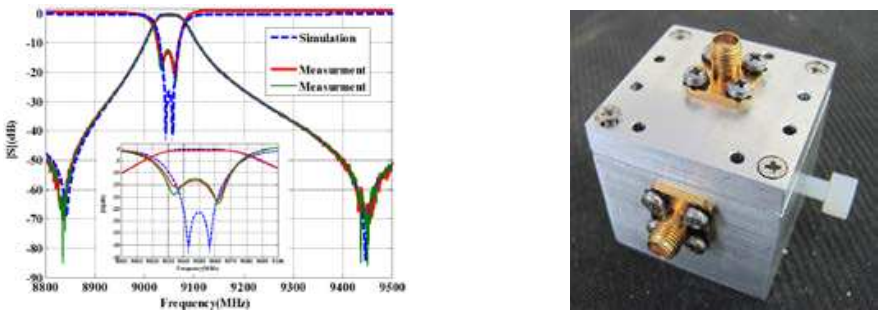

Figure 1: EM Simulated and measured results of the proposed band pass rectangular dual mode cavity filter and its photo.

shows the comparison between the measured response as the solid curves and simulated response (dashed lines) and its photo. The 3 dB bandwidth of the simulated filter is 63 MHz centered at 9050 MHz, insertion loss is about 0.28 dB, and return loss is better than 26.4 dB in over the pass band. The measured results are the return loss of better than 12.5 dB in the pass band and the insertion loss of better than 0.5 dB.

REFERENCES

1. Rizzi, P. A., *Microwave Engineering: Passive Circuits*, 1987.
2. Lin, W., "Microwave filters employing a single cavity excited in more than one mode," *J. Applied Physics*, Vol. 22, 989–1001, Aug. 1951.
3. Atia, A. E. and A. E. Williams, "Narrow bandpass waveguide filters," *IEEE Transactions on Microwave Theory and Techniques*, Vol. 20, 258–265, Apr. 1972.
4. Amari, S., U. Rosenberg, and J. Bornemann, "A novel approach to dual and triple-mode pseudo-elliptic filter design," *34th European Microwave Conference, 2004*, Vol. 2, 993–996, Oct. 12–14, 2004.
5. Shang, X., W. Xia, and M. J. Lancaster, "The design of waveguide filters based oncross-coupled resonators," *Microw. Opt. Technol. Lett.*, Vol. 56, No. 1, Jan. 2014.
6. Pozar, D., *Microwave Engineering*, 3rd Edition, Wiley, 2005.
7. Williams, A. E. and A. E. Atia, "Dual-mode canonical waveguide filters," *IEEE Transactions on Microwave Theory and Techniques*, Vol. 25, 1021–1026, Dec. 1977.
8. Fiedziuszko, S. J., "Dual-mode dielectric resonator loaded cavity filters," *IEEE Transactions on Microwave Theory and Techniques*, Vol. 30, 1311–1316, Sep. 1982.
9. Wang, C., K. A. Zaki, and A. E. Atia, "Dual-mode conductor-loaded cavity filters," *IEEE Transactions on Microwave Theory and Techniques*, Vol. 45, 1240–1246, Aug. 1997.
10. Hong, J.-S. and M. J. Lancaster, *Microstrip Filters for RF-microwave Applications*, 2001.
11. Liang, J.-F., H.-C. Chang, and K. A. Zaki, "Coaxial probe modeling in waveguides and cavities," *IEEE Transactions on Microwave Theory and Techniques*, Vol. 40, No. 12, 2172–2180, Dec. 1992.
12. Matthaei, G. L., L. Young, and E. M. T. Jones, *Microwave Filters, Impedance-matching Networks, and Coupling Structures*, McGraw-Hill, New York, 1985.

Propagation of Electromagnetic Waves in Cylindrical Three-layers Waveguide with Metamaterial Layer

V. A. Meshcheryakov and V. A. Zhuravlev
Tomsk State University, Tomsk 634050, Russian Federation

Abstract— Results of computer modeling of the coefficients of waveguide mode propagation in a tree-layered circular screened waveguide are presented. The waveguide center is filled with the medium having a negative refractive index. The results presented here suggest that frequency transparency windows, complex waves, waves with anomalous dispersion, and waves with significant retardation of the phase velocity exist in such waveguides.

In the course of computer modeling, different variants of relationship between the thickness of the internal dielectric core made from the left-handed material and the layer of the right-handed material have been studied. The qualitative pattern of the behavior of the parameter propagation differed significantly from that in the waveguide with two right-handed media. Thus, we can indicate the following special features of electromagnetic wave propagation in the examined waveguide:

1. In the tree-layered screened waveguide whose the second layer has negative refractive index and external layer represents an air layer, both the wave process and the cutoff regime of waveguide mode propagation can be observed for definite internal layer radii.

2. The layer of the left-handed medium leads to the occurrence of modes with large retardation coefficient.

3. Regions of complex waves (without losses in the filling media) are observed.

4. There are waves with anomalous behavior of the propagation parameter.

5. The presence of the central LHM layer leads to the occurrence of the frequency transparency windows. The waveguide represents a bandpass filter.

Thus, this suggests the possibility of designing bandpass filters, retardation lines, and devices operating based on retarding systems from segments of such waveguides.

A Broad-band End Launch Double Ridge Waveguide to Coaxial Transition Using LPDA

Maziar Hedayati, Mohsen Abdolahi, Hamid Mirmohammad Sadeghi, Parisa Moslemi, and Gholamreza Askari
Information and Communication Technology Institute (ICTI)
Isfahan University of Technology (IUT), Isfahan 84156, Iran

Abstract— Waveguide to Coaxial transition, as an important passive component has wide application in antennas, radars and microwave systems. Nowadays, broad band transitions are necessary for feeding wideband antenna in developing of the microwave systems. Most of designs like aperture-coupled slot [1] or aperture coupled patch element [2] have been expanded in the literature to introduce a useful transition from waveguide to microstrip. Although aperture-coupled structures are compact, but their fractional bandwidth is compact. Besides, the waveguide to microstrip transition based on the coupled probe at the E-plane [3] has been presented which is small but its bandwidth is limited ($\sim$ 22% for less than 15-dB return loss). To modify the bandwidth, [4] has proposed transition using the stepped waveguides and [5] has presented the short-circuited tapered finline to widen the band width. However, the circuit size is also large. To decrease the size of the circuit, some researchers use the aperture slot coupling [6], and patch element [7] as a transition. The circuit size of these transitions can be reduced but in cost of narrow bandwidth. To enhance the bandwidth, waveguide to microstrip transitions using the open-circuited probe [8] and tapered coplanar strip (CPS) probe [9] were presented. But there is an additional slotline to microstrip transition in their designs. Furthermore, although [10] has presented a compact and broadband waveguide to microstrip transition using the anti-symmetric tapered probes, but there is an imbalance problem while transitioning from the ML to the rectangular waveguide. All of those transitions have been designed for simple rectangular waveguides, but for wideband application the ridge waveguides are more useful than rectangular waveguides which is not commonly presented any transition for them in the literatures.

In this paper, a wideband end launch ridge waveguide to coaxial transition is proposed, which operates in 8 $\sim$ 14 GHz. The microwave characteristics of double-ridge waveguide to coaxial transition are analyzed and simulated by full-wave analysis. Quarter wavelength Chebyshev impedance matching method used to design the middle part of the transition. Dimensions of the first part of transition have been calculated by time domain solver of Ansoft Designer based on finite element method (FEM). The compact LPDA is designed on microstrip to receive signal from the waveguide. This antenna is placed in the E-plane of the ridge waveguide to stimulate the TE_{10} dominant mode which is shown in Fig. 1. Higher modes propagation can disturb the performance of the wide band transition. Also in this paper a C shape part is used to increase the cut off frequency of higher modes. Furthermore; power analysis is done to investigate arcing across the transition for 100 Watt input power. The simulation results show that the S_{11} of the transition is below -10 dB in 8–14 GHZ that is shown in Fig. 2.

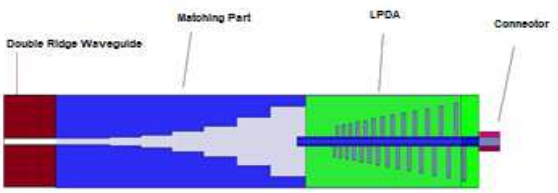

Figure 1: The layout of the proposed coaxial-to-waveguide transition.

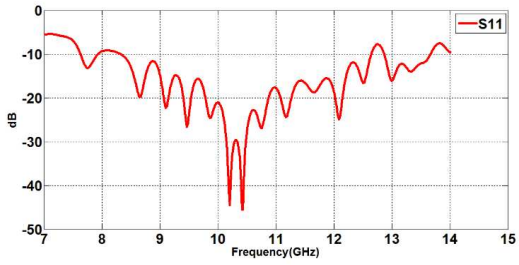

Figure 2: The return loss of final transition.

REFERENCES

1. Das, B. N., K. V. S. V. R. Prasad, and K. V. Seshagiri Rao, "Excitation of waveguide by stripline- and microstrip-line-fed slots," *IEEE Trans. Microw. Theory Tech.*, Vol. 34, No. 3, 321–327, Mar. 1986.

2. Grabherr, W. and W. Menzel, "A new transition from microstrip line to rectangular waveguide," *Proc. 22nd Eur. Microw. Conf.*, 1170–1175, Sep. 1992.
3. Lou, Y., C. H. Chan, and Q. Xue, "An in-line waveguide-to-microstrip transition using radial-shaped probe," *IEEE Microw. Wireless Compon. Lett.*, Vol. 18, No. 5, 311–313, May 2008.
4. Yao, H.-W., A. Abdelmonem, J.-F. Liang, and K. A. Zaki, "Analysis and design of microstrip-to-waveguide transitions," *IEEE Trans. Microw. Theory Tech.*, Vol. 42, No. 12, 2371–2380, Dec. 1994.
5. Van Heuven, J. H. C., "A new integrated waveguide-microstrip transition," *IEEE Trans. Microw. Theory Tech.*, Vol. 24, No. 3, 144–147, 1976.
6. Herrero, P. and J. Schoebel, "A WR-6 rectangular waveguide tomicrostrip transition and patch antenna at 140 GHz using low-costSolutions," *Proc. IEEE Radio and Wireless Symp.*, 355–358, Orlando, FL, USA, 2008.
7. Wu, P., Z. Wang, Y. Zhang, S. Sun, and R. Xu, "Wideband waveguide-to-microstrip probe transition with LTCC technology," *Electron. Lett.*, Vol. 47, No. 1, 43–44, 2011.
8. Lou, Y., C. H. Chan, and Q. Xue, "An in-line waveguide-to-microstriptransition using radial-shaped probe," *IEEE Microw. Wirel. Compon. Lett.*, Vol. 18, No. 5, 311–313, 2008.
9. Lin, T.-H. and R.-B. Wu, "A broadband microstrip-to-waveguidetransition with tapered CPS probe," *Proc. 32nd Eur. Microwave Conf.*, 1–4, Milan, Italy, 2002.
10. Chuang, J.-K., R.-Y. Fang, and C.-L. Wang, "Compact and broadband microstrip-to-waveguide transition using antisymmetric tapered probes," *Electron. Lett.* Vol. 48, No. 6, 332–333, Mar. 2012.

3D ISAR Imaging of Realistic Target Model Based on General Purpose EM Simulators

Seok Kim[1, 2], **Konstantin Nikitin**[1], **Inchan Paek**[2], **and Min-Ho Ka**[1]

[1]School of Integrated Technology, Yonsei University, Seoul, South Korea
[2]R&D Center, Samsung Thales, Inc., Yongin, South Korea

Abstract— Recent progress in computation performance and computational electrodynamics allows various analyses on many problems related to electro-magnetic (EM) waves using general purpose EM simulators. In this paper, we describe and demonstrate 3D ISAR image generation of a realistic target using FEKO, which is one of the representative general purpose EM simulators on the commercial market. This method can benefit us many advantages like building the database of many targets for target recognition with cost-and-time effective way and designing a radar and evaluating its performance under more realistic situations.

ACKNOWLEDGMENT

"This research was supported by the MKE (The Ministry of Knowledge Economy), Korea, under the "IT Consilience Creative Program" support program supervised by the NIPA (National IT Industry Promotion Agency)" (NIPA-2014-H0201-14-1002); "Civil Military Technology Cooperation (13-DU-EE-11), Development of LTCC Transceiver Module for Small SAR"; "The authors gratefully acknowledge the support from Electronic Warfare Research Center at Gwangju Institute of Science and Technology (GIST), originally funded by Defense Acquisition Program Administration (DAPA) and Agency for Defense Development (ADD)."

REFERENCES

1. Wehner, D. R., *High-Resolution Radar,* 2nd Edition, Artech House, 1995.
2. Mensa, D., *High Resolution Radar Cross Section Imaging,* Artech House, 1991.
3. Ozdemir, C., *Inverse Synthetic Aperture Radar Imaging with MATLAB Algorithms,* Wiley, 2012.
4. Xu, X. J. and R. M. Narayanan, "Three-dimensional interferometric ISAR imaging for target scattering diagnosis and modeling," *IEEE Transactions on Imaging Processing*, Vol. 10, No. 7, 1094–1102, Jul. 2001.
5. Wang, G. Y., X. G. Xia, and V. C. Chen, "Three-dimensional ISAR imaging of maneuvering targets using three receivers," *IEEE Transactions on Imaging Processing*, Vol. 10, No. 3, 436–447, Mar. 2001.
6. Cao, X. H., F. L. Su, H. D. Sun, et al., "Three-dimensional In-ISAR imaging via the emulated bistatic radar," *Processing of ICIEA*, 2826–2830, 2007.
7. *FEKO User's Manual,* EM Software & Systems, S. A. (Pty) Ltd., 2014.

A Comparison of SAR Imaging Performance between Matching Filter and Compressed Sensing

Gang Wang, Ze Yu, and Peng Xiao
School of Electronics and Information Engineering, Beihang University, Beijing 100191, China

Abstract— Compressed sensing (CS) is a newly developed technology for sparse or compressible signal which can be applied to synthetic aperture radar (SAR) imaging to achieve high-resolution images. As the SAR image is the spatial distribution map of target reflectivity function, it can be sparse or compressible in some transform domain such as wavelet domain or Fourier domain. This character is just exactly meet the requirement of CS theory, and provides the theoretical support for application of CS in SAR imaging. Generally, SAR utilizes matching filter (MF) technique to improve resolution, but due to the superiority of CS, the need for MF technique has been doubted. In recent years, some scholars have discussed CS in SAR imaging and published some related articles. Based on the above, this paper analyzed the principle of both methods, and compared CS with MF during processing SAR images in several aspects such as resolution and SNR, which aims to expatiate the differences between them. Furthermore, several new indicators are proposed in this paper during the comparison between these two methods, such as microscopic and macroscopic resolution and group spread function (GSF), to evaluate imaging performance due to new features caused by CS processing. The comparison results are given and verified by theory derivation and data simulation. Several experiments are carried out and simulation results are presented to illustrate imaging performance based on MF and CS theory. Firstly, we present reconstruction result obtained when range is greater than and less than microscopic resolution and macroscopic resolution in CS imaging. Next, we introduced GSF comparison between MF and CS. After that we explained statistical results on SNR when changing input SNR and the value of M/N in CS imaging, and finally demonstrated SNR comparison between MF and CS. According to the simulation results, the resolution can be improved considerably by using CS when the sampling rate is greater than corresponding bandwidth, but ambiguity phenomenon will appear as the distance increases which does not occur when using MF. Besides macroscopic and microscopic resolution, GSF is also an important indicator to measure resolution, and it is proved that two methods' GSF are almost the same when sampling rate is close to bandwidth. In addition, output SNR for CS imaging varies with the number of rows and columns in sparse dictionary when input SNR is given, and its anti-noise ability is weaker than that when using MF which is designed to produce the maximum achievable SNR. Each method has its own strength and weakness, and CS can't replace MF even if it has so many advantages because CS still has some characteristics not so good as that of MF, such as SNR. So we must select appropriate imaging method based on the specific situation. Moreover, besides this two methods mentioned in this paper, there are still many other effective SAR imaging processing methods for consideration, and we have also listed the advantages and disadvantages between them.

Micro-motion Target Detection Based on Wall Envelope Alignment in Through-the-wall Ultra-wideband Radar

Lei Qiu, **Tian Jin**, **Biying Lu**, **and Zhimin Zhou**
College of Electronic Science and Engineering, National University of Defense Technology
Changsha, Hunan 410073, China

Abstract— The detection of human targets behind obstacle has become a keen research topic in recent years and is highly desired in military and civil applications particularly in urban battle, anti-terrorism, disaster rescue, and medical application. Change Detection techniques are used to detect moving targets and mitigate the heavy clutter caused by strong reflections from stationary targets in through-the-wall ultra-wideband radar. However, the radar antenna platform jitter caused by working engine wobble or environmental factors such as wind blowing, results in stationary targets position change in different data frames. Although the change is tiny, the residual energy of stationary targets after change detection is much greater than that of moving targets, particularly of micro-motion human targets due to the low reflectivity of human and high signal attenuation of wall. This paper proposes an antenna platform jitter compensation method based on wall envelope alignment, aiming to detect micro-motion targets behind wall. Firstly, the antenna platform jitter model is established. The stationary position is assumed unchanged during a frame time, and the motion compensation is only performed between different frames. Then wall envelope alignment method is applied to compensate antenna jitter in range direction. There exists a strong plane reflection of the wall, the jitter can be compensated by the front surface of the wall who has the maximum amplitude in every frame data. Finally, the jitter effect in cross direction is evaluated. Simulation and experimental results demonstrate that the proposed approach can compensate antenna platform jitter, eliminate the stationary clutter and detect micro-motion targets correctly and effectively.

Analysis of a Polycarbonate RFID Tag for Blood Chain Tracking

G. Boi, **R. Secci**, **S. Casu**, **A. Fanti**, **and G. Mazzarella**
Department of Electrical and Electronic Engineering
University of Cagliari, Italy

Abstract— In this paper we describe an antenna especially designed used for a RFiD passive tag working at UHF (987 MHz), for healthcare applications, in particular for the transfusion medicine and the blood supply chain. The tag has to be able to work placed on the top of a blood sack, while the bag is full of blood, and the antenna has been designed with this goal in mind. Therefore we require an antenna able to work close to a (relatively large amount of) lossy medium with high permittivity. Moreover, the bag shape is curved but cannot be predicted exactly, so that the antenna worst retain its behavior for a large set of different environments. In order to comply with all those requirements, a printed slot antenna built with a flexible substrate has been selected, so that the whole tag can be flexible too. The first step was the optimization of the working parameters of the antenna while placed in a perfect planar surface (i.e., assuming the blood bag to be a parallelepiped). Since the actual bag shape is not known, this choice allows to take into account the lossy material, but using a simple geometry. The antenna has been optimized to get the maximum reading distance. Then we consider the effects of a real blood bags (i.e., a curved one), filled with blood, on the antenna behavior. We consider a bag with a transverse section bounded by two arc of circles (with a radius quite a larger than the bag size). Since we found a reasonable agreement with the planar antenna we can assume that the antenna behavior is quite insensitive to the bag shape. Finally, we evaluated the SAR into the blood and compare it with the compatibility parameters. A robustness analysis, respect to the bag curvature radius, has been performed, too, to assess the antenna use in real environments.

EM Level Evaluation in Hospital Indoor Environment

G. Boi[1], **S. Casu**[1], **A. Fanti**[1], **G. Gatto**[1], **G. Mazzarella**[1], **S. Pisu**[1], **P. F. Orrù**[2], **I. Spano**[1], **E. Tanzi**[1], **and F. Zedda**[2]

[1]Department of Electrical and Electronic Engineering
University of Cagliari, Piazza d'Armi, Cagliari 09123, Italy
[2]Department of Mechanical, Chemical and Materials Engineering
University of Cagliari, Piazza d'Armi, Cagliari 09123, Italy

Abstract— During the last decades, the level of the EM field in urban areas has increased at a fast rate, due to the increase of radio services using RF electromagnetic waves, mainly in the VHF and UHF bonds. Among those services, we can quote cellular phone systems, broadcasting, public utility services and, more recently, wireless internet networks.

This shady increase of EM field level in urban areas is the reason for an equal increase of the public concern about the (possibly hazardous) effect of EM field on the human body. And, as a consequence, both the number of researchers in this field and the (more or less cogent) regulations have been boosted.

A completely different problem is the prediction of indoor EM field. As a matter of fact the co-existence of a significant number of RF sources in an almost of environment makes the monitoring of EM field level inside a building a difficult task. The starting point for the monitoring of the electromagnetic field inside a building can be represented by the study of the propagation of electromagnetic waves' in indoor environments. The indoor propagation characteristic is a fundamental point in the design of wireless LAN, cordless phones networks and every other type of indoor system based on radiofrequency communication. It is easy to understand that indoor environments are very complex and it is clear that the level of electromagnetic fields usually depends on many, different, factors. As a matter of fact, it is well known that is sometime sufficient to move a device just a couple of centimeters to significantly, odify the service level of that device. The scope of this work is to evaluate how long the standard antenna knowledge (gain and radiation pattern) help to product the EM level in an hospital indoor environment.

Comparison of Optimization Methods for Background Rejection in High Resolution UWB ISAR Imaging

Se-Yeon Jeon, **Sumin Kim**, **Tae-Yun Lee**, **Jiwoong Yu**, **and Min-Ho Ka**
School of Integrated Technology, Yonsei Institute of Convergence Technology
Yonsei University, Republic of Korea

Abstract— Inverse synthetic aperture radar (ISAR) is an imaging technique that provides images of the targets by observing the targets in rotational movements using stationary radar sensor system. By using impulse ultra wideband (UWB) radar, high resolution ISAR images can be acquired. Since radar signals are non-destructive to human body, the high resolution UWB ISAR imaging is a promising technology for biomedical, security, through wall observation, and military applications. To achieve better quality ISAR images of a wanted target only, a process for removing background signals is necessary. To remove the background signal, the UWB radar system measures the background only signal and the background with target signal. In most cases, the background only signal is simply subtracted from the background with target signal to acquire the target only signal. Unfortunately, this method is not effective because of the phase error between the background only signal and the background with target signal due to the pulse drift UWB radar equipment. One way to solve this problem is to calibrate the pulse drift by measuring the transmitting signals directly from the transmitter. However, this method requires additional receiving channel. This research provides an effective pulse drift correction method for background rejection in UWB ISAR imaging. The proposed background rejection method does not require any additional receiving channels or additional measurement for calibration. The pulse drift correction is optimized by finding the amount of pulse shift that has minimum mean absolute error (MAE), mean squared error (MSE) or total energy between the background only signal and the background with target signal. This study shows the results of optimized background rejection in UWB ISAR images and compares the performances of the optimization methods.

ACKNOWLEDGMENT

This research was supported by the MSIP (Ministry of Science, ICT and Future Planning), Korea, under the "IT Consilience Creative Program" (NIPA-2014-H0201-14-1002) supervised by the NIPA (National IT Industry Promotion Agency).

REFERENCES

1. Levitas, B. and J. Matuzas, "UWB radar high resolution ISAR imaging," *Second International Workshop Ultrawideband and Ultrashort Impulse Signals*, 2004.
2. Khor, W. C., et al., "An ultra wideband microwave imaging system for breast cancer detection," *IEICE Transactions on Communications*, Vol. 90, No. 9, 2376–2381, 2007.
3. Li, J., et al., "Through-wall detection of human being's movement by UWB radar," *Geoscience and Remote Sensing Letters, IEEE*, Vol. 9, No. 6, 1079–1083, 2012.
4. Sullivan, R. J., *Microwave Radar: Imaging and Advanced Concepts*, Artech House, Inc., Norwood, MA, 2000.

Response of Oscillator Model of Cardiac Conduction System on Modulated Electromagnetic Radiation

E. Ryzhii and M. Ryzhii
Complex Systems Modeling Laboratory, University of Aizu, Japan

Abstract— Various model approaches utilizing systems of ordinary differential equations have been applied to study cardiac rhythm dynamics. Different modifications of Van der Pol oscillator equations are the most popular in such studies as they allow adoption of intrinsic pacemaker frequency to the driving signal with minimal change in its amplitude.

Recently, we proposed a mathematical model of cardiac conduction system based on set of heterogeneous oscillators including main pacemakers and heart muscles [1, 2]. Sinoatrial node, atrioventricular node and His-Purkinje system are represented by modified Van der Pol type oscillators connected with time-delay coupling. For description of atrial and ventricular muscles, the depolarization and repolarization processes are considered as separate waves described by modified FitzHugh-Nagumo equations.

The model allows generating physiologically correct electrical signals of action potentials of all three major natural pacemakers (sinoatrial node, atrioventricular node, and His-Purkinje system) as well as atrial and ventricular muscle response. Resulting dynamic response of the oscillator system is obtained in the form of the synthetic electrocardiogram (ECG) which is one of the most important clinically comparable characteristic of human heart electrical activity. The model allows reproducing a number of various normal and pathological situations including arrhythmias.

We consider the behavior of the heterogeneous oscillator model of cardiac conduction system under periodic electrical stimulation caused by applied modulated electromagnetic radiation. We investigate initiation and termination of different arrhythmias, in particular, conduction blocks, atrial and ventricular fibrillations.

REFERENCES

1. Ryzhii, E. and M. Ryzhii, "Modeling of heartbeat dynamics with a system of coupled nonlinear oscillators," *Commun. Comput. Inform. Sci.*, Vol. 0404, 157–165, 2013.
2. Ryzhii, E. and M. Ryzhii, "A heterogeneous coupled oscillator model for simulation of ECG signals," *Comput. Methods Prog. Biomed.*, Vol. 113, 55–68, 2014.

Measurement of Electromagnetic Activity of Living Cells

Jiří Pokorný[1], **Jan Pokorný**[2], **Jan Vrba**[3], **and Jan Vrba, Jr.**[4]

[1]Institute of Photonics and Electronics, Czech Academy of Sciences, Czech Republic
[2]Institute of Physics, Czech Academy of Sciences, Czech Republic
[3]Faculty of Electrical Engineering, Czech Technical University in Prague, Czech Republic
[4]Faculty of Biomedical Engineering, Czech Technical University in Kladno, Czech Republic

Abstract— Continuous energy supply to a biological system creates a state far from thermodynamic equilibrium. Excitation of coherent electromagnetic field is considered to be a crucial condition for life. [1] formulated a hypothesis of excitation of electric polar vibration and energy condensation in a single vibration mode forming a coherent state with essential biological function. Fröhlich's hypothesis is supported at acoustical frequencies by a) measurement of mechanical vibration in yeast cells *Saccharomyces cerevisiae*-dead cells do not exhibit any vibrations [2], b) comparison of measured mechanical vibrations and electric oscillations [3], c) analysis of nanoscale vibrations of different cellular systems as an expression of metabolic activity and signature of life [4]. The majority of biological macromolecules and structures are electric polar systems and vibrations generate electromagnetic field which was measured by dielectrophoretic attraction of small dielectric particles with a high permittivity by cells [5, 6] and the greatest electromagnetic activity in the M phase was confirmed by [7] in the frequency range 8–9 MHz. Microtubules represent the oscillating structure in eukaryotic cells [8]. [9] measured resonant frequencies of isolated microtubules in the frequency range 10–30 MHz, 100–200 MHz, in the far infrared region (at about 500 and 700 cm^{-1}), and the UV absorption spectrum at about 270 nm. The frequency spectrum from 1 to 100 GHz should be analysed to.

The frequency spectra below 1 GHz and in the far infrared region measured by [9] and Vedruccio and [10] should be verified. The power supply to the electric polar vibrations in a cell is assumed to be of the order of magnitude 0.1 pW (10^{-13} W). If the number of microtubules in a cell is about 400 then the power supply to a single microtubule is of about 0.1 fW (10^{-16} W). For quality factor of about 80 the power of electric polar vibrations in one microtubule is about 10 times greater (i.e., of 1 fW). The electromagnetic component of oscillations may be smaller than 1 fW. The measurement system should consist of a sensor (metal contacts of linear dimension 50 nm or smaller) integrated with preamplifier with extremely low noise followed by further amplifiers. Impedance matching of the preamplifier is a special problem. The sensor measures the potential difference of the near field excited by electric polar vibrations in microtubules between two points at the membrane. The input impedance of the preamplifier should correspond to the impedance of the plasma membrane in the region of the sensor. Nevertheless, reaction of the living cell to power losses caused by preamplifier consumption is an unknown factor. The whole measurement system should be in a doubly screened box. The coherent signal evaluation should be performed by a real time spectrum analyser controlled by a computer. Measurement in the far infrared region may be performed by Surface Enhanced Raman Spectroscopy (SERS) using a substrate with convenient metallic space pattern and infrared excitation. Synchronized, non synchronized, and control group of yeast cells (*Saccharomyces cerevisiae*) might be investigated at the beginning to assess properties of the measurement system.

REFERENCES

1. Fröhlich, H., *Adv. Electronis Electron. Phys.*, Vol. 53, 85, 1980.
2. Pelling, A. E., et al., *Science*, Vol. 305, 1147, 2004.
3. Jelínek, F., et al., *Electromag. Biol. Med.*, Vol. 28, 233, 2009.
4. Kasas, S., et al., *PNAS*, Early Ed., 2015.
5. Pohl H. A., et al., *J. Biol. Phys.*, Vol. 9, 133, 1981.
6. Hölzel, R., *Electro-Magnetobiol.*, Vol. 20, 1, 2001.
7. Pokorný, J., et al., *Electro-Magnetobiol.*, Vol. 20, 371, 2001.
8. Pokorný, J., et al., *Integr. Biol.*, 2013, DOI: 10.1039/c3ib40166a.
9. Sahu, S., et al., *Biosensors Biooelectron.*, Vol. 47, 141, 2013.
10. Vedruccio, C. and A. Meessen, *Proc. PIERS*, Pisa, 2004.

28 GHz Delay Spread Measurement Using a Broadband Channel Sounder in Small Urban City

Young Keun Yoon, **Jong Ho Kim**, **Myoung Don Kim**,
Young Jun Chong, **and Myoung Sun Song**
ETRI (Electronics and Telecommunications Research Institute), Republic of Korea

Abstract— This paper describes the relations between the R.M.S delay spread and TX-RX separation distance for Daejeon City measurements at 28 GHz frequency with 500 MHz channel bandwidth. R.M.S delay spread is caused by multipath due to a large number of reflective characteristics none line of sight environments in small urban city.

Introduction: Recently, the fifth generation (5G) mobile communication to satisfy the needs of high data rates in the small cell environment has attracted the attention. Millimeter frequency bands for 5G services are the lands of new frontier being able to support broadband bandwidth from 0.5 up to 2.0 GHz. We know that feasibility research at millimeter bands is carried out currently. Yet, there is still the lack of the collected field data and statistical models based on measurement. Therefore, we performed measurement in small urban city of Korea to find specific R.M.S delay spread characteristics.

Hardware & Measurement Campaign: Millimeter wave Band Exploration and Channel Sounder (mBECS) developed by ETRI was used in the outdoor R.M.S delay spread measurement campaign. Using a 500 Mcps broadband channel sounder with 2.0 ns multipath resolution, we conducted R.M.S delay spread measurements at 28 GHz in Daejeon City, Korea. A 4095 chips pseudo-random noise (PN) sequence sliding correlator was utilized, which was modulated to a 5.2 GHz intermediate frequency (IF) and upconverted 28 GHz. The maximum transmitter (TX) power was 29 dBm, fed to a 30° beamwidth 15.4 dBi horn antenna that was mechanically rotated or tilted. The receiver (RX) used the 10° beamwidth 24.4 dBi horn antenna and the same type of enable mechanically rotating or tilting structure as the transmitter.

The measurement campaign was taken during daytime. During measurement, TX location was fixed, and RX put none line of sight (NLOS) locations. We choose one TX at a height of 4 m and 15 RX measurement locations. The distance between the TX and RX ranged from 120 to 400 m. At RX at a height of 1.5 m, a 360° azimuth sweep at each RX position was automatically performed in steps of 10° because of using 24.4 dBi horn antenna with the 10° half power beamwidth. Extensive measurements were conducted for the thirty six different RX azimuth angles ranged from 0 to 350°, and for the three different RX elevation angles of −10°, 0°, and +10° creating one hundred eight possible antenna pointing steps. For each of one hundred eight steps, measurement data were recorded. Finally, R.M.S delay measurements were done at the RX locations in Daejeon, Republic of Korea.

Results: We note that the maximum value of R.M.S delay spread appears to be up to 400 m TX-RX separation distance at 28 GHz frequency, and then decreases for relative large TX-RX separation distance. In NLOS case, the TX and RX antennas were indirectly pointed at each other, and large multipath existed. But, when the separation distance between a TX and Rx is too large (exceeding 400 m), the path loss is so great that the power of the transmitted signal declines to zero before reaching the RX, resulting in fewer or no received multipath. For the relations between the R.M.S delay spread and TX-RX separation distance as well as the cumulative distribution function (CDF) of the R.M.S delay spread at 28 GHz. The maximum value of measured multipath components in our research using wide band channel sounder with 2.0 ns multipath time resolution has R.M.S delay spreads below 125 ns, the average has below 58 ns to NLOS environments in small commercial urban environment, Daejeon, Republic of Korea.

Conclusion: We found that the measured values from the light urban environment of Daejeon City in Korea have substantial differences in comparison with the dense urban environment in R.M.S delay spread in [1]. To find adequate R.M.S delay spread components, we believe that the results through extensive measurement in various urban environments should be more discussed.

ACKNOWLEDGMENT

REFERENCES

1. Rappaport, T., S. Sun, R. Mayzus, H. Zhao, Y. Azar, K. Wang, J. Schulz, M. Samimi, and F. Gutierrez, "Millimeter wave mobile communications for 5G celluar: It will work!," *IEEE Access*, Vol. 1, 335–349, May 2013.

Minimum Sum Algorithm Decoder for LDPC Nonregular Parity Check Matrix in BPSK System

Yi Hua Chen, **Jue Hsuan Hsiao**, **Zong Yi Saio**, **and Hua Ting Syu**
Oriental Institute of Technology
Institute of Information and Communication Engineering, New Taipei, Taiwan

Abstract— Referring to the approximate lower triangular low-density parity-check code check matrix of the IEEE P802.11n™/D1.04 (Part 11: Wireless Local Area Network Medium Access Control and Physical Layer specifications), this study established a decoder based on LabVIEW program language on a single program architecture that can adjust the transmission end to generate diverse codeword patterns, including three subblock sizes (27, 54, and 81 bit) and four code rates (1/2, 2/3, 3/4, and 5/6). Combined with the minimum sum algorithm (MSA), the decoder completed decoding tasks by changing the check node and variable node structures on the basis of the selected subblock size and code rate In addition to providing an introduction on the decoding mechanism of the MSA and completing decoding program optimization and analysis of bit error rate (BER) performance curves, this study applied the LabVIEW program to simulate the BER of the ratio of energy per bit to the spectral noise density (Eb/No) at each point from 0 to 10 dB, when subblock sizes (27, 54, and 81 bit) were combined with code rates (1/2, 2/3, and 5/6) operating in an additive white Gaussian noise channel environment. The error rate performance curve diagrams of two studies were referenced (regular weight (3,6) and 802.11n irregular subblock size 27 bit combined with code rate 5/6) and compared with the simulation outcome yielded in this study. The result showed that the subblock size did not affect the error rate, but the code rates substantially affected the error rates. When the code rate was set to 1/2, the error correction performance of the irregular check matrix was considerably higher than that of the regular check matrix.

Asymptotic Analysis of Scattering from Transmitarray for Near Field Focused

Shih-Chung Tuan[1] **and Hsi-Tseng Chou**[2]

[1]Department of Communication Engineering, Oriental Institute of Technology, Pan-Chiao, Taiwan
[2]Department of Communication Engineering, Yuan Ze University, Chung-Li, Taiwan

Abstract— This paper presents the asymptotic formulation of ray fields in the decomposition of electromagnetic (EM) scattering mechanisms from a one-dimensional, semi-infinite and periodic array when it is illuminated by a line source. This technique can be applied to analyze the passive FSS (frequency selective surface) type periodic structure with identical elements, the transmitarray type antennas that are phased to radiate EM fields focused in the near zone of the array aperture. The solutions are built up based on the Floquet mode expansion of the scattering fields, and are obtained by asymptotically evaluating the resulted integrals to express the fields in terms of transmitted and edge diffracted fields as previously addressed in the framework of uniform geometrical theory of diffraction (UTD).

Didactic Simulations in Electromagnetics

Khalid Salmi[1], **João Luiz Afonso**[2], **Hamid Magrez**[3], **and Abdelhak Ziyyat**[1]

[1] Electronics and Systems Laboratory (LES), Faculty of Sciences
University Mohamed Premier, Oujda, Morocco
[2]ALGORITMI Research Centre, University of Minho, Guimarães, Portugal
[3]CRMEF, Oujda, Morocco

Abstract— Electromagnetic theory forms the basis of all electrical engineering from electrostatics to optics. However, the teaching of the basic area of electromagnetics has been considered, for a long time, to be a challenge and a matter of concern due to low student motivation and underperformance in electromagnetic courses. This was attributed to the mathematical complexity and abstract nature of the topic. Moreover, EM field phenomena are normally expressed in 3D vector notation, which are physically invisible and students, at the beginning, have difficulty in relating mathematical models to good mental images. Simulations and computer graphics are strongly suggested to overcome many of the conceptual difficulties. In this direction, we present in this paper some virtual didactic simulations developed as a supplementary tool for teaching electromagnetic field. In the following, we describe some sample simulations which have been developed for some simple electronics components such as capacitors and inductors. The magnetic and electric field lines and distribution can be displayed in real time which makes the application ideal for use in interactive undergraduate and high diploma teaching. In this kind of simulation the student will be able to manipulate variables such as electric and magnetic field strength, field lines and have an idea on the relationship between the value of these electronic components, their geometry and the medium properties. Furthermore, in order for our simulation to comply with the new trends of distance learning and e-learning, the simulation where made using Action-Script to take full advantage of Adobe Flash technology as deemed by its power in the areas of multimedia and the Internet.

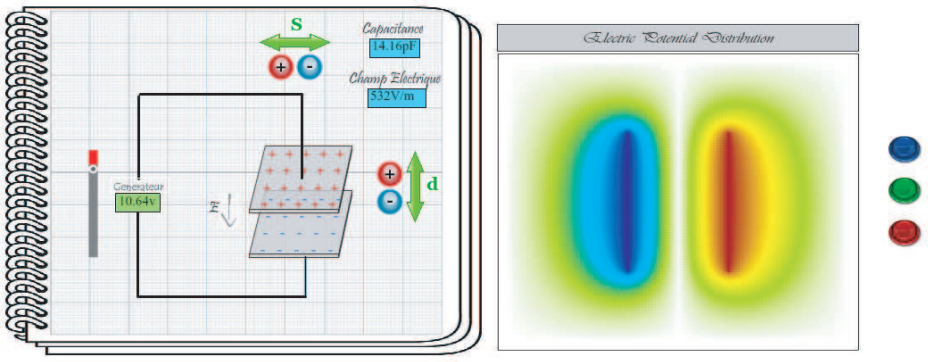

Figure 1: A screenshot of the parallel plate capacitor simulation.

Perfect Light Absorption in Ultra-thin Silicon Films on Aluminum and Optical Color Filters

Seyed Sadreddin Mirshafieyan and Junpeng Guo
Department of Electrical and Computer Engineering, University of Alabama in Huntsville
301 Sparkman Dr, Huntsville, Alabama 35899, USA

Abstract— We have demonstrated wavelength selective perfect light absorption in ultra-thin single layer silicon films deposited on aluminum metal surface in the visible and near infra-red spectral range. The perfect light absorption is due to the critical coupling of the incident light to the second-order Fabry-Perot resonance mode of the nano-optical cavity formed by the silicon film on aluminum surface. Perfect light absorption wavelength varies with the thickness of the silicon film. Spectral selective perfect absorption results in different optical colors corresponding to different silicon film thicknesses. The colors of fabricated devices do not change with the increase of viewing angle up to 70 degree with respect to the surface normal. The demonstrated silicon absorption filter technology is intrinsically low cost and compatible with silicon processing platform, and can be used for many applications such as optical displays and wavelength selective photo detectors.

Investigation on Rudimentary Geometries of Dielectric Resonator Antenna

Jitendra Kumar and Navneet Gupta
Department of Electrical and Electronics Engineering
Birla Institute of Technology and Science (BITS), Pilani, Rajasthan 333031, India

Abstract— Due to the variety of basic geometries available to antenna designers such as rectangular, cylindrical, hemispherical etc., a proper practice to select the best geometry for Dielectric Resonator Antenna (DRA) is required. In this paper, various rudimentary geometries of DRA excited by a coaxial probe fed is designed and investigated for selecting the preeminent geometry of antenna. The rudimentary geometries of DRA are rectangular, cylindrical and hemispherical, which are used for investigation of DRA performance as shown in Fig. 1. The dielectric material used for rudimentary geometries is TMM10i, a ceramic thermoset polymer composite material of Rogers high-frequency laminates. The dielectric constant (ε_r) of the material is 9.8, the dissipation factor ($\tan\delta$) is 0.002, and the density is 2.8 gm/cm^3. The DRA is designed to operate around 3.2 GHz. However, the resonant frequency may alter due to different rudimentary geometries. CST Microwave Studio transient solver is used to design and simulate the different rudimentary geometries of DRA. Table 1 summarizes the numerical results for different geometries of DRA. It can be seen that the impedance bandwidth (for return loss below −10 dB) of the DRA is 56%, 46% and 50% for rectangular, hemispherical and cylindrical respectively. These rudimentary geometries of DRA give a better understanding of design parameters of an antenna and their effect on return losses, impedance bandwidth, VSWR, gain, efficiency and resonant frequency.

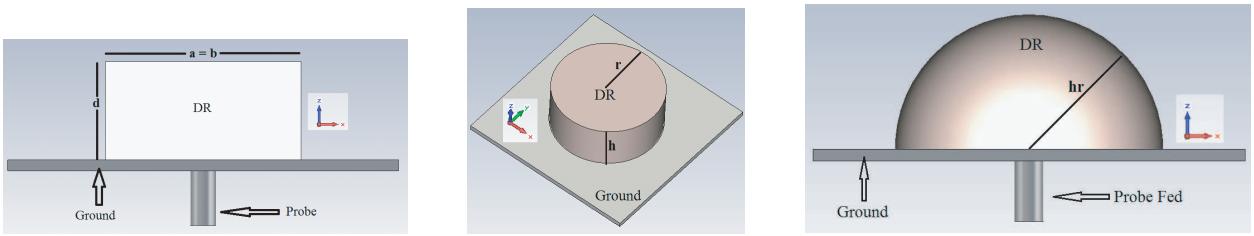

(a) (b) (c)

Figure 1: Configuration of rudimentary geometries of DRA: (a) Rectangular, (b) cylindrical, (c) hemispherical.

Table 1: Comparisons between different rudimentary geometries of DRA.

Rudimentary Geometries	***Rectangular***	***Cylindrical***	***Hemispherical***
Dimensions (mm)	$a = b = 30$, $d = 15$	$r = 18$, $h = 15$	$hr = 18.61$
Resonant Frequency	3.2 GHz	3.2 GHz	3.3 GHz
Bandwidth Range	2.9–4.7 GHz	2.9–4.75 GHz	3–4.5 GHz
Bandwidth ($S_{11} < -10$ dB)	56%	50%	46%
Total Peak Gain	1.56 dBi	1.50 dBi	1.54 dBi

Features Processing Lidar Signals in the GHz Frequency Range

A. S. Grishkanich, **S. V. Kascheev**, **V. V. Elizarov**, **and A. P. Zhevlakov**
National Research University of Informational Technologies, Mechanics and Optics
Saint-Petersburg, Russia

Abstract— Laser sensing — a highly effective method of remote operational environmental monitoring on land and over the surface of water bodies. As required substances can be used various substances Indicator hydrocarbon leaks from pipelines and processing plants, toxic agents necessary for chemical plants, smoke from fires, etc.

However, for high-speed sensing, speed of processing information received and ease of operation lidar units necessary to use appropriate hardware and software systems used to solve the problems of collecting, processing, storage, ordering large volumes of data.

The structure of a lidar system includes components that must communicate with each other by exchanging data and control signals. Each component performs a specific function and has a specific set of commands and control signals, as well as send or receive data.

In lidar system uses the method of spontaneous Raman scattering. This physical process is very short-lived, in some cases, no more than a few nanoseconds, so you need to work in the gigahertz frequency range for detecting signals with nanosecond.

Each component of the lidar system must respond a set of requirements due to work in the gigahertz frequency range. Therefore it is necessary to choose both hardware and software solutions that will deliver high-speed data exchange between parts of the system and high-speed processing of the data and system parameters.

The hardware is realized using modules and components with a high speed, as well as interfaces that allow you to exchange data with a high frequency that would exclude the loss of data due to time delays.

Software modules used for controlling, processing and organization of database systems should have adequate algorithms to perform real-time processing of information.

Are known to Raman scattering cross-section is very small (10^{-25}–10^{-27}), so in some cases back radiation captured by the objective can be several tens of photons. For registration of such weak signals and reliable conversion is preferred to use a photomultiplier operating in the photon counting mode. The PMT uses a high-speed electronic circuit that allows measurement with a pulse-pair resolution up to 10 ns. Interface USB 2.0 High-speed provides data exchange rate up to 480 Mbit/s. Information processing using software developed in Labview. To debug and validate the algorithm calculations instead of the photomultiplier used PXI system. This approach allows you to simulate operation of the system in real conditions, using a laboratory bench.

A laser beam scanning system has been developed. It comprises a mirror which oscillates with a frequency of 20 Hz, and the angle of rotation of 20 degrees. For precise positioning of mirrors used stepper motor with controller and specialized control software. For developing of this software was used C#. Control signals are transmitted using RS-232 interface.

In lidar system provides navigation and mapping. Mapping system is organized using a compatible GPS devices and software. The device is connected to the USB port of a PC. All data transmitted over the NMEA 0183 protocol. The obtained coordinates attached to the card, as well as recorded in a database simultaneously with the measurement results.

All information collected from the system components processed by the application developed using C#. The objectives of this application is to monitor uptime and connection of components, management report of possible errors and entering information about them in the database.

As a result of the scheme established inter-component communication hardware lidar complex and selected options that allow you to achieve the required measurement accuracy and high speed data exchange between components. Just developed the software needed to process volumes of information obtained from multiple system components.

Oil and Gas Prospecting by High Resolution Raman Lidar

A. S. Grishkanich[1], **S. V. Kascheev**[1], **V. V. Elizarov**[1], **I. S. Sidorov**[2], **A. A. Il'inskiy**[3], **and A. P. Zhevlakov**[1]

[1]National Research University of Informational Technologies, Mechanics and Optics Saint-Petersburg, Russia
[2]University of Eastern Finland, Kuopio, Finland
[3]All Russia Petroleum Research Exploration Institute, Saint-Petersburg, Russia

Abstract— Remote laser spectroscopy availability for airborne search of the oil-and-gas deposits has been examined. The migration of oil and gas (H_2S, CO, CO_2, H_2, He) leads to a change of the physical properties of the rocks above the deposit and the formation of halos of methane, propane, and other hydrocarbons in the surface sediments and the atmospheric boundary layer. Experiments were carried out under the CARS and SRS circuit. Minimal concentrations of 200 ppb of heavy hydrocarbon gas have been remotely measured in laboratory tests. We have developed airborn lidar system to detect pipeline leakage and explore oil and gas deposits. Tests were carried out on the gas pipeline Urengoy-Novopskov. Field tests (50 to 500 m helicopter flight altitudes) demonstrate that the lidar allows detection of methane with a sensitivity up to 6 ppm for methane and 3 ppm for hydrogen sulfide.

GeoChemical surveys of hydrocarbon deposits based on detection of the oil and gas migration as well as the other molecules such as C_yH_x, H_2S, CO, CO_2. The migration leads to a change of the physical properties of the rocks above the hydrocarbon (methane, propane) deposit and anomalous concentrations of hydrocarbon gases in an atmospheric boundary layer.

Laser sensing is a highly effective method for the deposit exploration. We present a Raman lidar with ultraspectral resolution for airborne oil&gas exploration and pipeline leakage detection. Tests were carried out on the gas pipeline Urengoy-Novopskov. The experiments were carried out to detect leaks on the working section of pipeline with an internal pressure of 60–70 bar. Test flights show the level of sensitivity about 6 ppm (methane) and 3 ppm (hydrogen sulfide) with the measurements at 50 to 500 m flight altitudes.

The probing is done by a compact pulsed diode pumped Nd:YLF laser (50 mJ, 6 ns, 100 Hz) with KTP ISHG (50% conversion efficiency) and BBO frequency shifting (261.7 nm, 6–10 mJ).

Ultraspectral resolution of the double polychromator (3600 mm^{-1}, $d\lambda/dl = 0.224$ nm/mm) reliably differentiates methane (283.31 and 284.42 nm), nitrogen (278.69 nm), and hydrogen sulfide (280.89 nm) what ensures reliable 80% HHG detection for the integration of seismic prospecting and laser remote sensing.

Unlike Raman spectroscopy, CARS employs multiple photons to address the molecular vibrations, and produces a signal in which the emitted waves are coherent with one another. As a result, CARS signal is much stronger than spontaneous Raman emission.

A chamber filled by a mixture of HHG gases and air served as a simulator of hydrocarbon halo. It was irradiated by femtosecond and nanosecond laser pulses. A pump beam (at the frequency referenced ωp) from Ti:Sapphire laser (800 nm, 30 fs, 0.2 mJ, 50 Hz) and a probe beam (at the frequency referenced ωpr) from Nd:YAG laser (1064 nm, 8 ns, 60 mJ, 50 Hz) were focused at the chamber. These beams interact with the sample mixture of gases and generate a coherent optical signal at the anti-Stokes frequency ($\omega pr + \omega p - \omega S$) (Fig. 1). The anti-Stokes signals ($\lambda = 656$ nm for CH4 and $\lambda = 658$ nm for C3H8) are resonantly enhanced when the frequency difference between the pump and Stokes beams (ωp-ωS) coincides with the frequency of Raman resonance due to the intrinsic vibrational contrast mechanism.

In order to anayse back scattering anti-Stocks spectral component, we use HR4000+ compact optical fiber spectrometer (Ocean Optics) with further numerical processing. Pressure of methane and propane chosen as an indicator of hydrocarbon deposits was ~ 0.01 Torr in 0.2 m-length chamber that corresponds to 10 m-thickness of the real halo with concentration at level of $5 \cdot E12$ cm^{-3}, i.e., 200 ppb, for each of these gases (Fig. 2). Since Ti:Sapphire laser has a wide spectrum, the coherent anti-Stock scattering of radiation occurs from corresponding Fourier-components of the pump ($\lambda = 800$ nm) and Stocks signals ($\lambda = 1064$ nm), removed on Stocks shift size of researched gases. Therefore, it was possible to observe an occurrence of the various new components around 650 nm for different heavy hydrocarbon gases (HHG), in the anti-Stock scattering spectrum.

Method CARS allows detection at the level of 3–10 molecules and determines hydrocarbons in the natural atmosphere under the presence of impurities.

Two-sided Inverted F Antenna with LTE, GSM, WLAN, WiMax Frequency Bands for Mobile Phones

Churng-Jou Tsai and Bing-Yan Sie
Department of Computer and Communication
Kun Shan University, Tainan, Taiwan

Abstract— This work presents an internal mobile phone antenna occupying a small board space of 520 mm^2 on the system circuit board and providing three wide operating bands of at least 746–796, 860–1000, 1760–1880, 2390–2499, 3480–3708 and 5120–5957, for the long term evolution (LTE)/wideband local area network (WLAN)/Worldwide Interoperability for Microwave Access (WiMax) operations. These 8 bands includes one LTE bands of LTE700, one bands of GSM900/1800, three bands of WLAN 2.4/5.2/5.8, and two WIMAX 3.5/5.5 GHz bands. The antenna is a modified PIFA with coupled-strip and shows a height of 13 mm and a width of 40 mm only, when mounted at the top edge of the display panel in mobile phone. The ground plane size is 87×40 mm^2.

The antenna architecture is shown in Figure 1. This is a two-sided inverted F antenna structure with a side ground point at left side. The more detail structure is shown in Figure 2. The simulated return losses is shown in Figure 3. These simulated return losses covers the 700 MHz LTE, 900/1800 MHz GSM, 2.4/5.2/5.8 GHz WLAN, 3.5/5.5 GHz WiMax band. The detail operations bands can be divided two parts: the low-frequency bandwidth operation in (746–796 MHz) (860–1000 MHz) (1760–1880 MHz), while operating at high frequency bandwidth (2390–2499 MHz) (3480–3708 MHz) (5120–5957 MHz), in line with the basic LTE, GSM, WLAN and WiMax operating bandwidth.

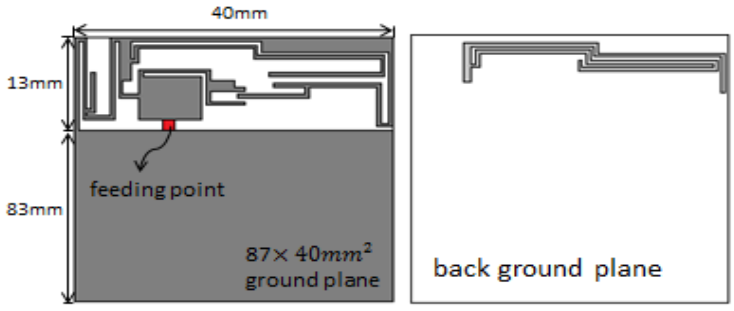

Figure 1: Architecture of the proposed antenna.

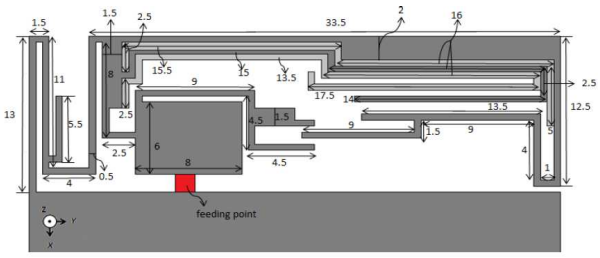

Figure 2: Detail architecture of the proposed antenna.

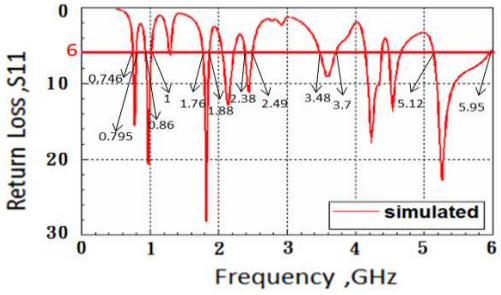

Figure 3: Return losses of the proposed antenna.

Analysis of the Imaging Realization of Frequency Modulated Continuous Wave Circular SAR

Gaowei Jia, **Wenge Chang**, **and Ruibin Tu**
College of Electronic Science and Engineering
National University of Defense Technology, Changsha, Hunan 410073, China

Abstract— Frequency modulated continuous wave (FMCW) synthetic aperture radar (SAR) is a compact, lightweight, and low-cost imaging system with high resolution. There has been increasing interest in FMCW SAR in the last years, which has led to the construction of several experimental systems. On the other hand, circular synthetic aperture radar (CSAR) has lately become of the hotspot in the field of SAR due to its characteristics like all-aspect observation, super-high two-dimensional (2-D) resolution, and potential three-dimensional imaging possibility. In order to combine the advantages of both FMCW radar and CSAR, it is suggested to change the acquisition geometry of FMCW SAR from a straight line to a circular trajectory. Thus we could get a novel imaging model FMCW CSAR.

As for the imaging processing of linear trajectory FMCW SAR, it is well known that the intra-pulse movement would introduce new range migration and affect the range cell migration correction (RCMC). Similarly, and it is found that the intra-pulse movement also leads to new range migration in the case of FMCW CSAR and further distorts the imaging results. Correspondingly, we have proposed a modified back projection algorithm (BPA) in a former paper, in which the new range migration has been taken into account. However, the modified BPA and its potential improvements encounter huge computation. To improve the imaging efficiency, the modified Fourier-based imaging procedures of FMCW CSAR is investigated in this paper.

In this paper, we focus on the two dimensional (2-D) imaging of X-band FMCW CSAR in the frequency domain and it is assumed that the targets are located in the flat ground-plane. The main contributions contain:

1. The exact signal spectrum of FMCW CSAR is presented firstly.

2. The influence of the intra-pulse movement on the Fourier-based imaging processing of FMCW CSAR is analyzed in detail and the corresponding correction method is proposed.

To verify the feasibility of the proposed correction method, numerical simulation test is carried out. Specifically, The FMCW CSAR system operates at 10 GHz, and the bandwidth of the transmitted linear frequency modulation (LFM) pulse is 600 MHz. During the simulation test, the modified BPA which is available for FMCW CSAR is used for comparison. The results of simulation test denote that the proposed correction method is feasible to remove the influence of the intra-pulse movement exactly in the frequency domain and figure out well-focused FMCW CSAR image eventually.

A New Sidelobe Reduction Method for Circular SAR

Gaowei Jia, **Wenge Chang**, **and Ruibin Tu**
College of Electronic Science and Engineering
National University of Defense Technology, Changsha, Hunan 410073, China

Abstract— Due to its advantages of all-aspect observation, super high-resolution, the potential three-dimensinal (3-D) imaging, circular synthetic aperture radar (CSAR) has become of particular interest to the SAR community. For isotropic targets, the spectrum of which is ring-shaped so that the corresponding point spread function (PSF) is related to Bassel function, not the sinc function. Correspondingly, the sidelobe level according to isotropic targets is higher than that of linear-trajectroy SAR, which drastically limits the quality of CSAR images. More importantly, the traditional window-function technique is not valid any more and yields even worse results for CSAR. Therefore it is essential to investigate new methods to reduce the sidelobe level for CSAR.

This paper focuses on the sidelobe reduction of two-dimensional (2D) CSAR image, according to isotropic targets. The fundamental motivation of the proposed sidelobe reduction method is to extract the sidelobe-image firstly and then to deduct it. During the sidelobe reduction strategy, the method of extracting the sidelobe image is essential. Specially, a method of dividing the CSAR spectrum is proposed, based on which the sub-images are obtained firstly and then the sidelobe image is produced afterwards. Subtracting the sidelobe image from the former CSAR image yields the sidelobe-reduced CSAR image.

Simulation Result: In order to have a better insight into the performance of the proposed method, a numerical simulation is carried out. The CSAR system operates at 10 GHz, and the bandwidth of the transmitted linear frequency modulation (LFM) pulse is 600 MHz. The radii of the circular trajectory and the observed area are 1000 m and 40 m, respectively. The height of airplane is assumed to be 500 m. Fig. 1(a) shows the pseudo-3D PSF of a marginal point target.

With the proposed sidelobe-image extraction-strategy, we obtains the sidelobe image, as shown in Fig. 1(b). The corresponding pseudo-3D view of the sidelobe image is shown in Fig. 1(c).

Substrating the sidelobe image (in Fig. 1(c)) from the former image (in Fig. 1(a)) yields the sidelobe-reduced CSAR image, as shown in Fig. 1(d). Figs. 1(e) and (f) denote the comparison of profiles of PSF in x and y direction, respectively. Directions x and y are arbitrary orthorhombic axes. In Figs. 1(e) and (f), the dotted and solid profiles denote the result without and with

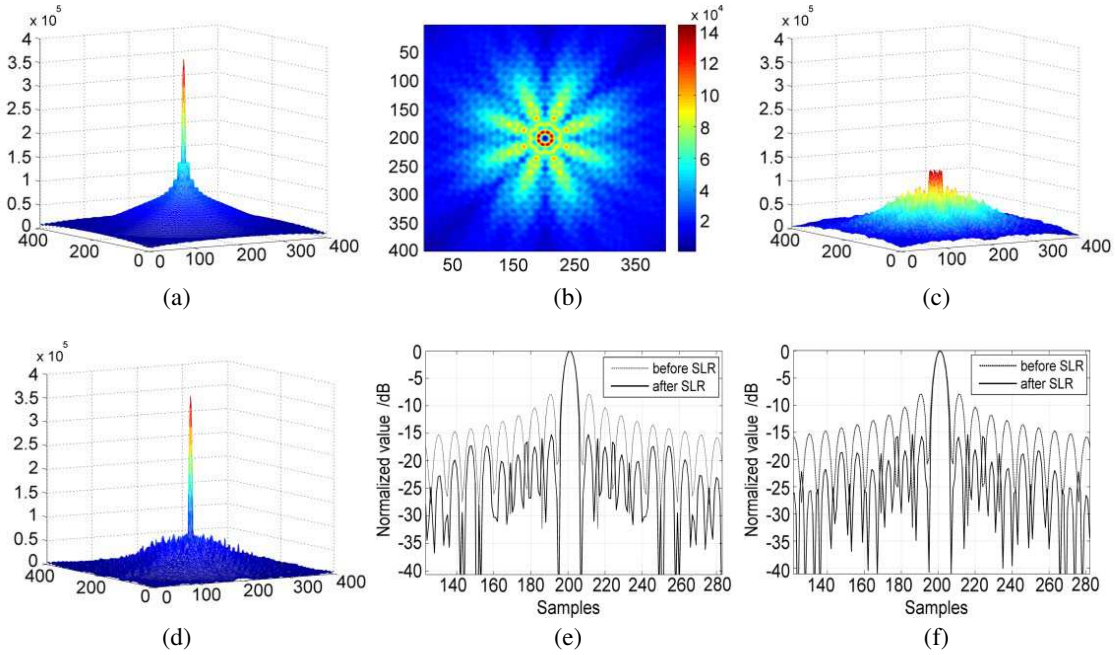

Figure 1: Result of sidelobe reduction.

sidelobe reduction (SLR), respectively. It is learnt that after the sidelobe reduction, the mainlobe of the PSF is preserved, but the peak-to-sidelobe ratio (PSLR) reduces from $-7.95\,\mathrm{dB}$ to $-16\,\mathrm{dB}$, and the 2D integrated sidelobe ratio (ISLR) reduces from $10.62\,\mathrm{dB}$ to $4.27\,\mathrm{dB}$.

Terabit WSDM Optical Access Network Using Multicore Fibers and Advanced Modulation Formats

Z. Feng[1], B. Li[1], R. Wang[1], R. Lin[1,2], M. Tang[1], Z. Xu[1], S. Fu[1], W. Tong[3], S. Liu[1], and P. P. Shum[4]

[1]Next Generation Internet Access National Engineering Lab (NGIA)
School of Optical and Electronic Information, Huazhong University of Sci&Tech (HUST), Wuhan, China
[2]School of ICT, The Royal Institute of Technology (KTH), Kista, Sweden
[3]State Key Laboratory of Optical Fiber and Cable Manufacture Technology
Yangtze Optical Fibre and Cable Company Ltd. (YOFC), Wuhan, China
[4]School of EEE, Nanyang Technological University, Singapore

Abstract— Next generation optical access network are envisioned to evolve into a converged, high-speed and heterogeneous-service platform supporting large capacity transmission to enormous number of users covering a wider area. To satisfy these requirements, we proposed a hybrid wavelength-space division multiplexing (WSDM) optical access network architecture utilizing multicore fibers with advanced modulation formats, as shown in Fig. 1(a). As a proof of concept, we experimentally demonstrated a WSDM optical access network with duplex transmission using our developed and fabricated multicore (7-core) fibers and fan-in/fan-out device with 58.7 km distance. To increase the access data rate in the cost-sensitive access network, the IM/DD optical 16QAM-OFDM signal and RSOA based adaptive DMT signal have been adopted for downstream (DS) and upstream (US) transmission, respectively. As a universal platform for wired/wireless data access, our proposed architecture provides additional dimension for high speed mobile signal transmission and we hence demonstrated an upstream delivery of PDM-QPSK modulated signal using the inner core of MCF emulating a mobile backhaul (MB) service. Fig. 1(b) illustrates the experimental setup. For DS transmission, 20 wavelengths with 25 GHz channel spacing from an optical comb generator are employed and each wavelength is loaded with 10 Gb/s baseband

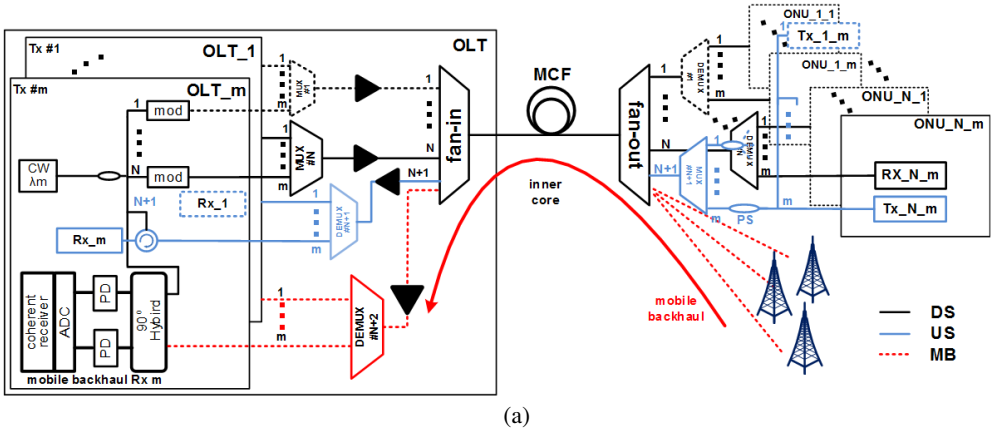

(a)

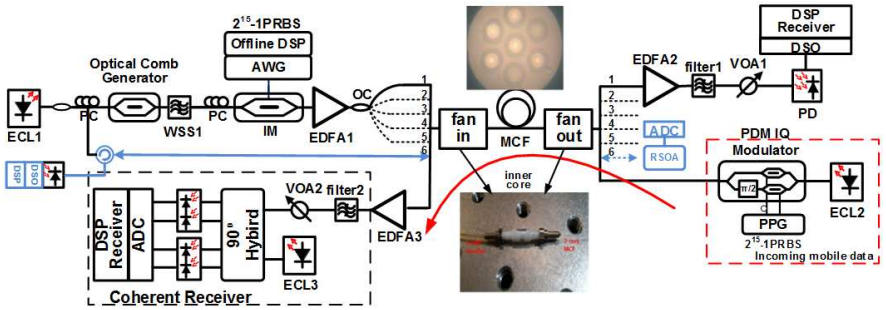

(b)

Figure 1: Proposed architecture of converged WSDM optical access network: (a) schematic, (b) experimental setup.

16QAM-OFDM signal generated off-line by Matlab, where the IFFT/FFT size is 128 and 63 effective subcarriers are used to convey data information. Boosted by EDFA, 20-wavelength DS signal are power splitted and simutaneously launched into five of the six outer cores of the MCF through the fan-in device, thus the aggregation downstream capacity reaches 1 Tb/s. About -11 dBm sensitivity has been achieved for 3.8×10^{-3} bit error ratio (BER) with 7% Forward Error Correction (FEC) limit for all wavelengths in every core. For US transmission, wavelengths seeded from DS using the 6th outer core are modulated with DMT signal adapted with the channel conditions and then reflected back to the OLT. ONUs served by the same DS wavelength can share a US wavelength within different time slots through TDMA. As an emulation of high speed MB transmission, IQ modulated PDM-QPSK signal with 50 Gb/s per wavelength is transmitted in the inner core of MCF and coherently detected in the OLT side. -19 dBm sensitivity has been achieved under the FEC limit and more than 18 dB power budget is guaranteed. Both DS and US optical signal exhibit acceptable performance with sufficient power budget.

Progress in Developing Fabrics Coated with Nano-particles as Radar Absorbing Materials

A. Teber[1], **H. Kavas**[2], **A. Baykal**[3], **B.Aktas**[4], **I. Unver**[4], **and R. Bansal**[1]

[1]University of Connecticut, USA
[2]Medeniyet University, Turkey
[3]University of Fatih, Turkey
[4]Gebze Technical University, Turkey

Abstract— There exists a long-standing interest in the development of thin, lightweight, and flexible radar absorbing materials (RAM) for various civilian and military applications. One promising research direction [1, 2] has been the use of conducting polymeric textiles incorporating a coating of magnetic metal nano-particles either at the yarn-stage or after weaving the fabric. This paper reports on an experimental investigation that uses a knitted *Polyacrylonitrile* (PAN) fabric (thickness = 2 mm with a yarn diameter of 20 μm) as the host matrix for the composite RAM. The fabric is coated with nano-particles of Ni and Co via an electroless metal deposition method using Sodium borohydride ($NaBH_4$) as a reducing agent. The relative concentrations of Ni and Co as well as the coating time are varied with a view to tailoring the EM absorption characteristics of the resulting material for the intended application. The morphology of the clusters of the Ni-Co alloy incorporated into the fabric volume is established through a microstructure investigation. It is found that the metallic structures grow in a wide range of sizes, from nano- to micrometer, which are believed to contribute to *broadband* microwave absorption.The microwave absorption measurements are carried out in the X, K_u, and K Bands using a vector network analyzer in conjunction with a waveguide system incorporating samples of the coated fabric. Electromagnetic constitutive parameters for the coated sample are calculated from the measured *s*-parameters using the Nicolson-Ross-Weir technique In addition, the return loss (RL) of the samples for RAM applications is estimated from the measured complex permittivity and permeability values.As a potential application, the use of these materials in the design of microwave Fresnel Zone Plate (FZP) lenses is discussed.

REFERENCES

1. Akman, O., H. Kavas, A. Baykal, M. S. Toprak, A. Coruh, and B. Aktas, "Magnetic metal nanoparticles coated polyacrylonitrile textiles as microwave absorber," *Journal of Magnetism Magnetic Materials*, Vol. 327, 151–158, 2013.
2. Bogush, V., "Application of electroless metal deposition for advanced composite shielding materials," *Journal of Optoelectronics and Advanced Materials*, Vol. 7, No. 3, 1635–1642, June 2005.

Numerical Simulation on the Self-assembled Structures of Colloidal Particles through Magnetic Dipole-dipole Interactions

Chunwei Liu[1], **Zhi Sun**[2], **Shuigen Huang**[1], **Bart Blanpain**[1], **and Muxing Guo**[1]

[1]Department of Materials Engineering, KU Leuven, Leuven 3000, Belgium
[2]Department of Materials Science and Engineering, TU Delft, CD Delft 2628, The Netherlands

Abstract— Functional materials with desired crystal morphologies have demonstrated a vast range of applications because of their advanced properties, such as the ability to achieve thermal, optical and acoustic rectification. Novel fabrication techniques based on magnetic self-assembly, as an attractive method for positioning particles, are currently drawing extensive research interests. Due to the difficulties in manipulating micro- and nanoparticles, however, it remains a considerable challenge to perform accurate experiments in practice. In this study a two-dimension numerical model is developed to provide a fundamental understanding as well as visualization of the magnetic assembly process. In the simulation, dipole-dipole interaction among the particles and hydrodynamic drag between particles and matrix fluid are taken into consideration, and the former is believed to be the dominant force of forming various crystalline morphologies. Three factors, i.e., magnetic field intensity (H), global particle concentration (ϕ), and relative particle concentration (φ) are investigated for the colloidal particle systems on scales ranging from micrometer to millimeter. Additionally, both binary and ternary colloidal systems are evaluated and in particular, the systems composed of different sized particles are investigated systematically. Finally, the evolution of typical assembled structures is observed in-situ, offering a straightforward manner to understand the magnetic self-assembly. The simulation results agree well with the experimental results, which could validate the accuracy of the model. The effect of magnetic field intensity (H), global particle concentration (ϕ), and relative particle concentration (φ) on the assembled structures is revealed. Consequently, desired assembled structures can be expected through varying H, ϕ and φ. A two-dimension numerical model is used to investigate the magnetic self-assembly, enabling a low-cost method for artificial crystalline materials preparation.

Ultra Weak Photon Emission from Yeast Cells Can Be Modulated by Antioxidants

Kateřina Červinková[1, 2], **Michaela Nerudová**[1, 2], **Jiří Hašek**[3], **and Michal Cifra**[1]

[1]Institute of Photonics and Electronics, Academy of Sciences of the Czech Republic
Prague, Czech Republic
[2]Faculty of Electrical Engineering, Czech Technical University in Prague
Prague, Czech Republic
[3]Institute of Microbiology, Academy of Sciences of the Czech Republic, Czech Republic

Abstract— The majority of living organisms exhibit a very low but measurable level of electromagnetic radiation in the visible range of the spectrum. This phenomenon is common to metabolically active cells and is referred as the ultra weak photon emission (UPE). Its intensity is usually less than 1000 photons $cm^{-2}s^{-1}$. Origin of UPE is biologically endogenous and is attributed to reactions of reactive oxygen species (ROS) with biomolecules which give rise to electron excited states. In other words, the energy comes solely from chemical reactions, therefore the UPE is also known as weak chemiluminescence. Reasons why organisms exhibit UPE have not been satisfactorily elucidated yet. It is assumed that it may play role in regulatory processes of cells; however it could be simply a byproduct of oxidative metabolism.

The goal of our research is to delineate the origin of UPE from a model organism; yeast cells *Saccharomyces cerevisiae*. UPE from the yeast cells arises spontaneously during the growth of the culture. UPE signal from organism is highly dependent on external factors such as temperature, pH, biotic agents, molecular oxygen consumption or composition of the environment.

Damaging effects of ROS formed during the metabolism can be partly suppressed either by natural antioxidant defense system or by scavengers artificially supplied into the environment or directly into the organism. In this work, the experiments are focused on the description of effects caused by antioxidants. Several kinds of antioxidants were used and we studied the temporal development and changes in intensities of ultra weak photon emission from the culture. Study of antioxidants scavenging effects on UPE signal is crucial in order to understand UPE generating processes.

RF Dynamics of Mode-locked Intracavity Frequency Doubled Laser

A. V. Kovalev and V. M. Polyakov
ITMO University, Birzhevaya Liniya, 14, St Petersburg 199034, Russia

Abstract— Mode-locked lasers are of a great interest in fundamental and applied sciences. Their capability to generate ultrashort pulse trains and equidistant optical spectra has already revolutionized such fields as spectroscopy, data networks, optical clocking and biomedicine.

We report on radiofrequency (RF) dynamics of Nd:YVO_4 laser with intracavity frequency doubling in a KTP crystal. Experimentally, the laser cavity was 109 mm long and consisted of $1 * 3 * 3\,\mathrm{mm}^3$ 1% at. doped a-cut Nd:YVO_4 active element and $5 * 3 * 3\,\mathrm{mm}^3$ KTP crystal. An output coupler was mounted on fast and slow PZTs for cavity length modulation and the output coupler position attenuation.

A narrow longitudinal modes beat signal (less than 300 Hz FWHM) which is an evidence of mode-locking regime was observed for both fundamental and second harmonic radiation. For a certain power and temperature range (the KTP temperature $28 \pm 0.2^{\circ}$C, 420 mW pump power) and a proper placing of the output coupler against the KTP crystal, a regime of the second harmonic amplitude weak modulation was obtained. The fundamental radiation remained not modulated. The modulation manifests itself in the RF spectrum as two sidebands of the central beat note frequency and a low-frequency (order of 50–100 MHz) difference signal. We implemented the cavity length modulation via the PZT with the frequency of several kilohertz which led to occurrence of weak sidebands for the central beat note of the second and fundamental harmonics and a Lorentzian shaped spectrum of equidistant frequencies for the low-frequency signal and the sidebands of the second harmonics beat note. The distance between the spectral components was equal to the modulation frequency.

We propose that the appearance of the second harmonic modulation regime results from bounded phase variations of the laser field. The transition between states with and without the modulation occurred continuously. The stability of the phase bounded mode-locked operation was limited by the cavity elements alignment and stable operation in the regime lasted longer than 300 s. The weak modulation frequency dependence on the central beat note frequency is well fitted by a parabola confirming that the output is that of a stable mode-locked laser with bounded phase.

This newly obtained regime of the phase bounded mode-locked operation can be utilized for synthesis of low-noise microwave frequencies, and can be used for iodine-stabilized schemes of laser frequency standards without additional modulators.

Self-similar Dynamics in Free Space Optics

Nan Gao and Changqing Xie
Key Laboratory of Nano-Fabrication and Novel Devices Integrated Technology
Institute of Microelectronics of Chinese Academy of Sciences, Beijing 100029, China

Abstract— Self-similar dynamics is common in nonlinearity optics. It is well-known that the light spot would collapse self-similarly while keeping the Townes profile, if self-focusing dominates over diffraction [1]. Self-similar optical pulses can also happen with the coexistence of dispersion, gain and nonlinearity, which can be useful in fiber amplifiers and lasers [2]. However, it is difficult to directly extrapolate these solutions to the linear cases by making the nonlinear coefficient to approach toward zero. For example, using variable scaling, the $(2+1)$D nonlinear Schrödinger equation $2ik\partial_z U + (\partial_x^2 + \partial_y^2)U + q|U|^2U = 0$ has solutions in the from of $U_q(x,y,z) = U_{q=1}(\alpha x, \alpha y, \alpha^2 z)/\beta$, where $\alpha = \beta q^{1/2}$. If q approaches zero, which is the case of free space, the solution must tend to a constant value, which is a trivial plane wave.

Here we study self-similar dynamics in linear systems systematically, by finding the exact solution of paraxial wave equation in scaled coordinates. The allowed solutions include:

1) Paraxial Bessel beams [3]: $J_m(\sqrt{d}r)\exp[i(-dz/2k + m\theta + kz)]$,

2) Linear scaling beams: $J_m(\sqrt{d}r/s_0 z)\exp[i(kr^2/2z + d/2ks_0^2 z + m\theta + kz)]/z$,

3) Gaussian-type beams: $M_{dz_R/4ks_0^2,\pm m/2}[kr^2 z_R/(z_R^2+z^2)]\exp\{i[\frac{kr^2 z}{2(z_R^2+z^2)} - \frac{dz_R \arctan(z/z_R)}{2ks_0^2} + m\theta + kz]\}/r$,

4) Elliptic-hyperbolic scaling beams: $\psi_{EHS}(r,\theta,z) = J_{\pm m/2}[kr^2/2z_R(1-z^2/z_R^2)]\cdot\exp\{i[kr^2/2z(1-z_R^2/z^2) + m\theta + kz]\}/\sqrt{1-z^2/z_R^2}$,

and 5) Parabolic scaling beams [4]: $J_{\pm m/2}(kr^2/4z)\exp[i(kr^2/4z + m\theta + kz)]/\sqrt{z}$.

We will show their self-similar propagation dynamics in free space, and Gaussian apodization will also be considered for practical realization. The linearity of free space eliminates the annoying stability problems, and we can construct these beams easily utilizing linear superposition. As shown in Fig. 1, we use diffractive optical elements (Figs. 1(a) and (b)) to experimentally realize the non-trivial self-similar beams (Figs. 1(c)∼(e)).

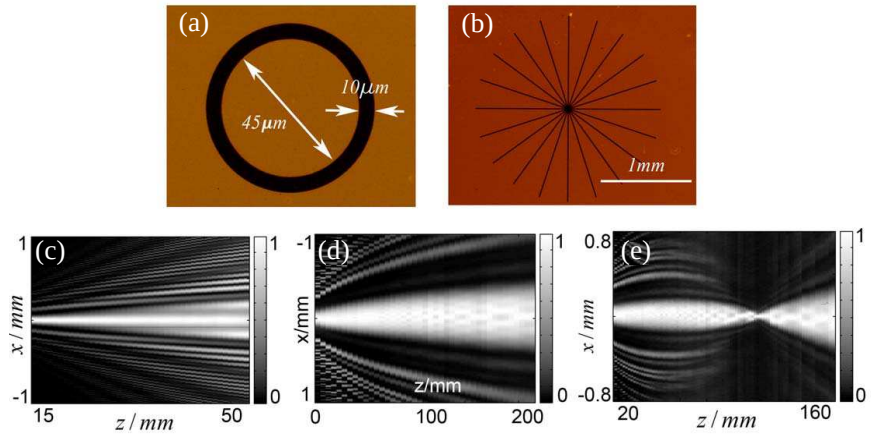

Figure 1.

REFERENCES

1. Moll, K. D., A. L. Gaeta, and G. Fibich, *Phys. Rev. Lett.*, Vol. 90, 203902, 2003.
2. Dudley, J. M., C. Finot, D. J. Richardson, and G. Millot, *Nat. Phys.*, Vol. 3, 597, 2007.
3. Durnin, J., J. J. Miceli, Jr., and J. H. Eberly, *Phys. Rev. Lett.*, Vol. 58, 1499, 1987.
4. Gao, N. and C. Xie, *Opt. Lett.*, Vol. 39, 3619, 2014.

Size Reduction of Magnetic Resonance Coils for Wide Wireless Power Transfer Applications

In-Kui Cho, **Jung-Ick Moon**, **Seong-Min Kim**, **Jae-Hun Yun**, **and Woo-Jin Byun**
Radio Technology Research Department
Electronics and Telecommunications Research Institute(ETRI), Korea

Abstract— Many researchers have developed the wireless charging system using the magnetic coupling or magnetic resonance [1]. In this paper, we extend previous studies of coupled magnetic resonance into reducing size of the coils for wide wireless power transfer applications.

As shown in Fig. 1, the diameter of TRx magnetic resonance coils is not same. The diameter of Rx coil is even smaller than that of Tx coil by using the impedance matching technology (C-C matching). The resonance frequency is 1.78 MHz. Diameters of TRx' spiral coil are 30 cm and 7 cm. Fig 1(c) shows the measurement result of fabricated TRx coils. The transfer efficiency η is shown with transfer distance and radius distance(misalignment). The proposed coil structure is expected to be applied for energy transfer technology of various home electrical devices as well as portable devices.

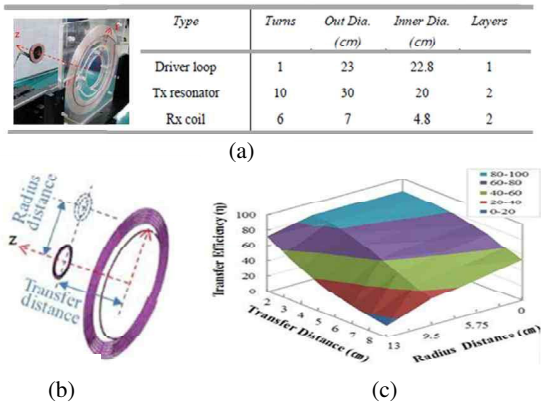

Figure 1: TRx coil's transfer efficiency η with normal transfer distance and radius distance (misalignment).

ACKNOWLEDGMENT

This research was funded by the MSIP (Ministry of Science, ICT & Future Planning), Korea.

REFERENCES

1. Cheon, S., et al., "Wireless energy transfer system with multiple coils via coupled magnetic resonances," *ETRI Journal*, Vol. 34, 2012.

Near-field Analysis in Wireless Power Transfer Using Magnetic Dipole

Jung-Ick Moon, **In-Kui Cho**, **Seong-Min Kim**, **Jae-Hun Yun**, **and Woo-Jin Byun**
Radio Technology Research Department
Electronics and Telecommunications Research Institute (ETRI), Korea

Abstract— This paper presents the intuitive and simplified analysis of near-magnetic field using magnetic dipole and image theory in wireless power transfer. In modeling of magnetic resonator, it is practice to ignore the volume of the resonator in comparison with the wavelength and consider it into the magnetic dipole on the ground plane. And the analysis presented here leads to reasonable modeling and analyzed results compare well with full-wave simulation. The utility of this approach is useful for the case when the human safety with respect to electromagnetic fields (EMFs) and interference problems should be considered in the design of wireless power transfer system.

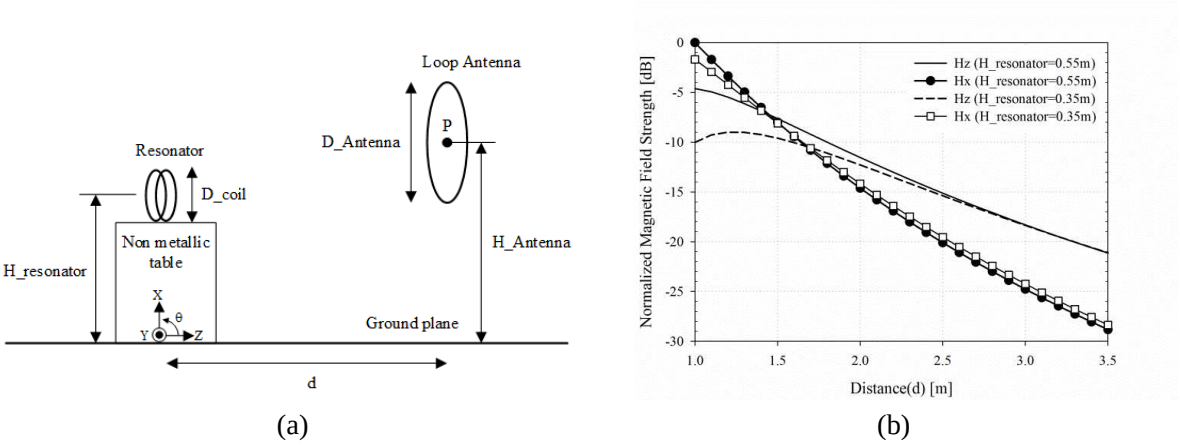

Figure 1: The near-field test environment and characteristics of wireless charging system.

ACKNOWLEDGMENT

This research was funded by the ICT R&D Program of MSIP/ETRI, Korea in 2015.

REFERENCES

1. Lee, K. S. and D. H. Cho, "Simultaneous information and power transfer using magnetic resonance," *ETRI Journal*, Vol. 36, No. 5, 808–818, Oct. 2014.
2. Kim, S. M., I. K. Cho, J. I. Moon, J. H. Yoon, W. J. Byun, and H. D. Choi, "System level power control algorithm in wireless power transmission for reducing EMF," *IEEE Wireless Power Transfer Conference (WPTC)*, 193–196, 2014.

Design of 60 W Charging Circuit for Wireless Charging System Using Magnetic Resonance Method

Seong-Min Kim, Jung-Ick Moon, In-Kui Cho, Jae-Hun Yun, and Woo-Jin Byun
Radio Technology Research Department
Electronics and Telecommunications Research Institute (ETRI), Korea

Abstract— In this paper, 60 W power charging circuit for the wireless charging system using the magnetic resonance method is presented. The proposed charging circuit is composed of a constant current signal converter and a controller. The constant current signal converter is designed to convert the dc signal which its voltage range is variable from the rectifier in the wireless charging system. The output current value can be changed from 0.1 A to 1.7 A with 0.1 A step according to the control of the controller. This changing is used for the protection of the human body from the EM field around the system. The controller is designed to control the charging circuit in accordance with the communication results with the transmitter and the final load. Two communication schemes, a 424 MHz FSK and a RS-232C, are adopted in the controller to communicate with the transmitter and the final load. The wireless charging system is implemented to charge a 24 V battery. The system consists of a 100 W power transmitter, two magnetic resonators having 30 cm diameter, a 100 W rectifier, a 24 V battery, a personal computer, and the proposed 60 W charging circuit. The personal computer is used for the user interface of the system. The transmission frequency is 1.8 MHz band. By the test results, the transmission efficiency is about 50% at 30 cm distance between two resonators.

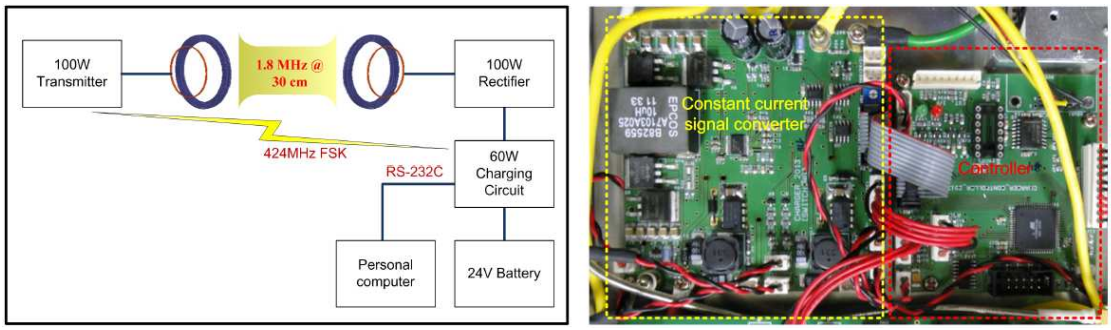

Figure 1: System configuration and the implemented charging circuit.

ACKNOWLEDGMENT

This research was funded by the ICT R&D Program of MSIP/ETRI, Korea in 2015.

REFERENCES

1. Kim, S. M., I. K. Cho, J. I. Moon, J. H. Yoon, W. J. Byun, and H. D. Choi, "System level power control algorithm in wireless power transmission for reducing EMF," *IEEE Wireless Power Transfer Conference (WPTC)*, 193–196, 2014.
2. Lee, K. S. and D. H. Cho, "Simultaneous information and power transfer using magnetic resonance," *ETRI Journal*, Vol. 36, No. 5, 808–818, Oct. 2014.

Photonic Integrated Circuits for Electro-optic Microwave Frequency Multiplication and Frequency Translation: Spurious Harmonics Suppression by Design

Ramón Maldonado-Basilio and Trevor J. Hall
Photonic Technology Laboratory, University of Ottawa
800 King Edward Avenue, K1N 6N5, ON, Canada

Abstract— In the past two decades or so there has been a plethora of publications in the field of microwave photonics that have described essentially the same generalized Mach-Zehnder interferometer (GMZI) circuit architecture: a $1 \times N$ splitter directly interconnected to a $N \times 1$ combiner via an array of N electro-optic $LiNbO_3$-based phase modulators; each GMZI adapted to particular design goals. The applications have generally been to single-side-band modulation or electro-optic microwave signal frequency multiplication [1–3]. The difference between the circuits proposed have largely concerned variations of the static optical and electrical phase shifts required or the implementation of an equivalent circuit using standard Mach-Zehnder modulators (MZM) rather than individual phase-modulators as the basic building brick. After our latest investigations [4, 5], in this paper a methodology is presented that specifies the architecture required to meet specified design objectives such as the suppression of unwanted products (Fig. 1). Moreover, it is shown how to use the intrinsic phase relations between the ports of splitters and combiners and specifically multi-mode interference couplers to implement the static optical phase shifts required by these circuits, thereby avoiding the need to apply static DC bias to the electro-optic modulators and the associated drift issues that otherwise require complex stabilization circuitry. Circuits capable of single-side-band suppressed-carrier modulation and frequency octo-tupling show a simulation performance equal to or better than results reported in the literature

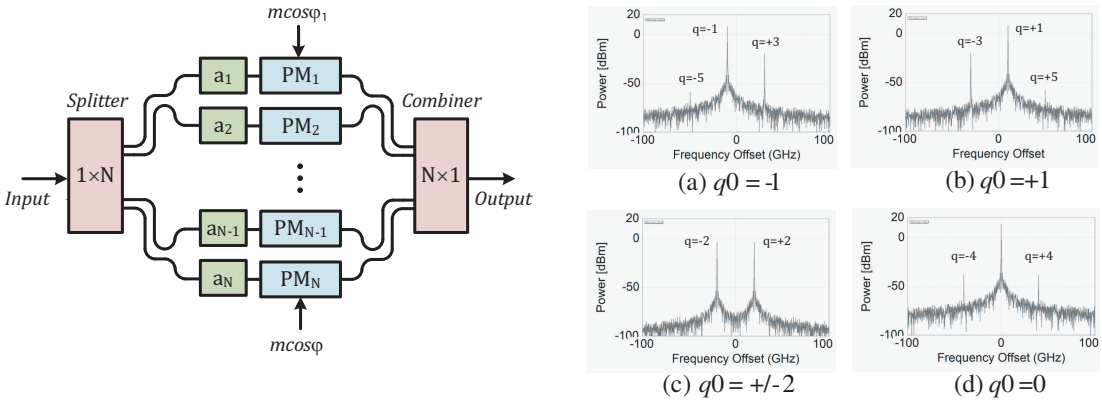

Figure 1: Schematic diagram of a GMZI and the output for various design conditions in a 4-modulator array.

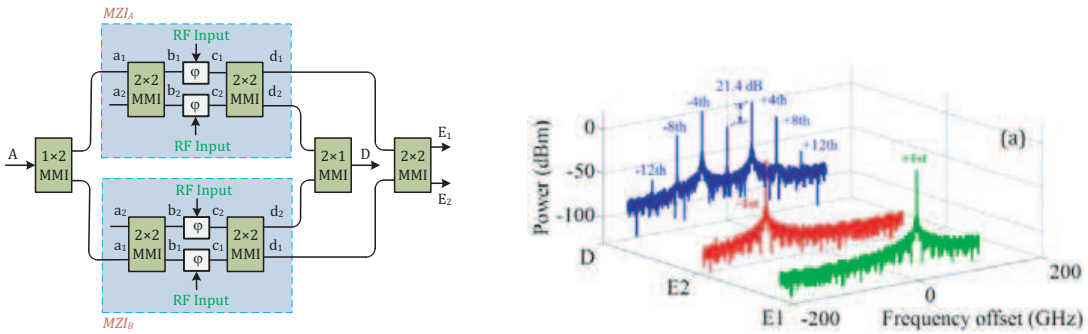

Figure 2: Schematic of a dual-function photonic circuit and output for frequency octo-tupling and single-side-band modulator.

(Fig. 2). In particular, a new cascade architecture implementation is reported that offers 50% lower optical insertion loss and 50% reduced RF power drive requirement compared to previously known circuits. While $LiNbO_3$ technology offers a mature solution to the small scale integration of MZM structures, this work anticipates photonic integrated circuits based on Si and/or InP material integration platforms emerging as the preferred choice. In this context the continuous advances made in improved speed, linearity, footprint, and energy consumption of electro-optic phase modulator devices in both material platforms augurs well for the future.

REFERENCES

1. Qi, G., J. Yao, J. Seregelyi, S. Paquet, and C. Bélisle, *Trans. Microw. Theo. Techn.*, Vol. 53, No. 10, 3090–3097, 2005.
2. Li, W. and J. Yao, *Photon. Technol. Lett.*, Vol. 22, No. 1, 24–26, 2010.
3. Zhu, Z., S. Zhao, Y. Li, X. Chu, X. Wang, and G. Zhao, *Quantum Electronics Letters*, Vol. 49, No. 11, 919–922, 2013.
4. Hasan, M., R. Guemri, R. Maldonado-Basilio, F. Lucarz, J.-L. de Bougrenet, and T. J. Hall, *Opt. Lett.*, Vol. 39, No. 24, 6950–6953, 2014.
5. Hasan, M., R. Maldonado-Basilio, and T. J. Hall, " Short communication," *J. Modern Optics*, 2015, in-print.

Design of a Printed Antenna for Mobile Terminals

Hui Liu[1, 2], **Youhuan Guo**[2], **Ping Yu**[2], **and Xueman Wu**[2]

[1]Centre for Optical and Electromagnetic Research, Academy of Advanced Optoelectronics
South China Normal University, Guangzhou, China
[2]Computer Science and Engineering Department, Guangdong Peizheng College, Guangzhou, China

Abstract— A printed mobile terminals antenna with multi operating bands for the 2G/3G/4G LTE (long term evolution) is presented. The antenna has three operating bands covering low band of 900 MHz, middle band 1900 MHz and high band 2600 MHz for GSM 900 MHz, UMTS 1900 MHz and LTE 2600 MHz. The antenna occupies a ground clearance of 54 mm × 19 mm and has a thin of 1 mm. The antenna comprises radiating branches to generate multi operating bands. Dimensions and working principle of the antenna are discussed.

A Wideband Circularly Polarized Antenna with Wilkinson Feed Network for Worldwide UHF Band RFID Reader

Bingjie Wang, **Zhibin He**, **Hui Liu**, **Yoichi Okuno**, **and Sailing He**
Centre for Optical and Electromagnetic Research, Academy of Advanced Optoelectronics
South China Normal University, Guangzhou 510006, China

Abstract— A radio frequency identification (RFID) reader antenna with circular polarization (CP) radiation is proposed to operate at worldwide UHF band which covers 840–960 MHz. The size of the antenna is $0.555\lambda_0 \times 0.553\lambda_0 \times 0.099\lambda_0$. A micro-strip patch with truncated corners as the main radiation patch is placed between the wilkinson feed network layer and the parasitic patch layer. The ground plate is placed on the top of the feed network layer. The feed network is connected with the main radiation patch via two metal cylindrical probes which produce two orthogonal signals of equal amplitude and 90 degree phase difference. The proposed antenna has wideband circularly-polarization characteristics. The truncated corners on the main radiation patch can increase 3 dB axial ratio (AR) bandwidth while improving the best axial ratio. And the parasitic patch can adjust the radiation direction of the antenna while increasing its gain. The simulation results show that the proposed circularly polarized UHF reader antenna has an input impedance matching bandwidth ($S_{11} \leq -10$ dB) of 456 MHz (675–1131 MHz), the band of reflection coefficient $S_{11} \leq -20$ dB covering 842–955 MHz, 3-dB axial ratio bandwidth of 296 MHz (741–1037 MHz), minimum axis ratio reaching 0.33 dB, and the highest gain reaching 3.53 dBi in the operating frequency band. Both the impedance bandwidth and the axial ratio band cover the entire UHF band of RFID systems.

A Small Printed Antenna for Bluetooth Wireless Communication

Liu Hui[1], **Bingjie Wang**[1], **Cheng Liu**[1], **Zhibin He**[1], **and Sailing He**[1, 2]

[1]Centre for Optical and Electromagnetic Research, Academy of Advanced Optoelectronics
South China Normal University, Guangzhou, China
[2]Department of Electromagnetic Engineering, Royal Institute of Technology, Stockholm S-100 44, Sweden

Abstract— A small printed inverted-F antenna, operating at 2.44 GHz, for Bluetooth system is designed in this paper. The RF system diagram and PCB layout are drawn by Cadence Allegro. The small printed antenna, integrated in the PCB, is modeled by HFSS and both the simulation and experimental results verify of its suitability for the Bluetooth wireless communication.

Measurement of the Dielectric Properties of Micaceous Minerals Using Scattering Parameters

I. F. Dos Anjos[1] and S. E. Barbin[2]

[1]UFPB-Federal University of Paraiba, João Pessoa, Brazil
[2]USP-University of São Paulo, São Paulo, Brazil

Abstract— The determination of the dielectric properties of materials is very important in the development of microwave heating systems. In this case, the dielectric properties of the materials to be processed are the key point in order to achieve a good efficiency of the system. In the present study it is presented the determination of the complex permittivity of vermiculite that is a hydrated phyllosilicate. In a previous work the dielectric constant of vermiculite has been determined using a TDR based probe. In this study dielectric constant has been determined through the measurement of the volumetric water content and the refractive index. Although the method has demonstrated a good accuracy, it was not possible to determine the complex permittivity of the mineral due to the characteristics of the equipment used. So, in order to determine the complex permittivity using an accurate and non-destructive method, the scattering parameters has been chosen. The method is based on the usage of a microstrip line and through the measurement of the S-parameters by a VNA the data has been processed in MATLAB® code. The results were very close to the ones obtained with the TDR probe, but now with the determination of the complex permittivity and loss tangent. The dataobtained with the present studyshow that the determination of the dielectric properties of materials such as vermiculite using S-parameters is a good accurate and non-destructive method.

Session 4A1
SC2: Active, Tunable and Nonlinear Metamaterials 2

Active Tuning of Silicon Nanodisk Metasurfaces

Jürgen Sautter[1], **Isabelle Staude**[1], **Manuel Decker**[1], **Evgenia Rusak**[1], **Dragomir N. Neshev**[1], **Igal Brener**[2], **and Yuri S. Kivshar**[1]

[1]Nonlinear Physics Centre, Research School of Physics & Engineering
Australian National University, Australia
[2]Center for Integrated Nanotechnologies, Sandia National Laboratories
Albuquerque, New Mexico 87185, USA

Abstract— As optical metasurfaces become useful for practical applications, the possibility of dynamically controlling their optical properties becomes increasingly important. For plasmonic metasurfaces, considerable efforts have concentrated on tuning and switching their optical properties using liquid crystals (LCs) [1–3] utilizing either the strong temperature dependence of the LC optical anisotropy or their realignment in an external electric field. However, plasmonic metasurfaces suffer from strong dissipative losses of metals at optical frequencies. A solution to this problem is provided by all-dielectric metasurfaces consisting of two-dimensional arrangements of high-permittivity dielectric nanoparticles with tailored optical properties, which allow for controlling a wavefront at the nanoscale with near-unity efficiency [4]. However, to date dynamic control of all-dielectric metasurfaces remains an open challenge and experimental realizations are still missing.

In our work we use a silicon nanodisk metasurface featuring two pronounced resonances in the spectral range of interest — an electric and a magnetic dipole resonance. The metasurface is integrated into a 170 µm-thick LC-cell. The samples are fabricated via electron-beam lithography and reactive-ion etching on silicon-on-insulator wafers. We use the 'Licristal E7' LC from Merck that features a strong optical anisotropy along the axis of the LC molecules in its nematic phase. In order to demonstrate dynamic resonance tuning originating from the temperature-dependent refractive-index change of the LC and symmetry switching of the optical response, we measure the sample's transmittance when increasing the LC temperature from $T = 20°\mathrm{C}$ (nematic phase) above its phase transition point at $T \geq 58°\mathrm{C}$ (isotropic phase). The maximum spectral tuning range realized in our experiment is approximately 40 nm with a maximum relative transmittance change of up to a factor of 5. Importantly, for temperatures above $T = 58°\mathrm{C}$ the optical anisotropy of the metasurface is removed and the high symmetry, i.e., the isotropy of the sample's optical response is restored. Our experimental observations are in excellent agreement with numerical simulations. We believe that this first demonstration of tuning of dielectric metasurfaces will open the way for a new generation of efficient and tunable ultra-thin devices based on optical metasurfaces. Specifically, we will discuss three application examples of dielectric metasurfaces from our recent work, namely wavefront manipulation, shaping of photoluminescence spectra of quantum dots, and nonlinear frequency generation.

ACKNOWLEDGMENT

This work was performed, in part, at the Center for Integrated Nanotechnologies, an Office of Science User Facility operated for the US Department of Energy (DOE) Office of Science. Sandia National Laboratories is a multi-program laboratory managed and operated by Sandia Corporation, a wholly owned subsidiary of Lockheed Martin Corporation, for the US Department of Energy's National Nuclear Security Administration under contract DE-AC04-94AL85000.

REFERENCES

1. Khoo, I. C., A. Diaz, M. V. Stinger, J. Huang, and Y. Ma, "Liquid crystal tunable optical metamaterials," *IEEE J. Sel. Top. Quantum Electron*, Vol. 16, 410, 2010.
2. Minovich, A., J. Farnell, D. N. Neshev, I. McKerracher, F. Karouta, J. Tian, D. A. Powell, I. V. Shadrivov, H. H. Tan, C. Jagadish, and Y. S. Kivshar, "Liquid crystal based nonlinear fishnet metamaterials," *Appl. Phys. Lett.*, Vol. 100, 121113, 2012.
3. Decker, M., C. Kremers, A. Minovich, I. Staude, A. E. Miroshnichenko, D. Chigrin, D. N. Neshev, C. Jagadish, and Y. S. Kivshar, "Electro-optical switching by liquid-crystal controlled metasurfaces," *Opt. Exp.*, Vol. 21, 8879, 2013.
4. Decker, M., I. Staude, M. Falkner, J. Dominguez, D. N. Neshev, I. Brener, T. Pertsch, and Y. S. Kivshar, "High-efficiency dielectric Huygens' surfaces," *Adv. Opt. Mater.*, Early View, 2015, Doi: 10.1002/adom.201400584.

Tunable Multilayer Graphene Metamaterials for Terahertz/Infrared Waveguide Modulators

Irina Khromova[1], **Andrei Andryieuski**[2], **and Andrei V. Lavrinenko**[2]

[1]University Colledge London, UK
[2]Technical University of Denmark, Oersteds pl. 343, KongensLyngby, DK-2800, Denmark

Abstract— Active development of terahertz (THz)/infrared (IR) science and technology has created a growing demand for new electronic and quasi-optical devices. In particular, the promising opportunities for broadband high-speed terahertz communication require new techniques for real-time manipulation of radiation. Various approaches have been proposed for THz/IR amplitude, phase, spatial and temporal profile modulation, including the employment of metamaterials [1] and, recently, one-atom-thick graphene [2].

Most of the proposed modulators, including graphene-based ones, are developed for free-space propagation configurations. However, high-speed THz/IRcommunication channels will unlikely be based on such architectures — atmospheric absorption peaks and small wavelengths (from submillimeter to tens of micrometers) imply strong free-space attenuation. It is therefore preferential to apply waveguide-based modulation platform similar to those used in telecom photonics. Due to specific properties constrains it is natural to consider metamaterial (structured) approach to satisfy simultaneous demands for low losses and high tunability in the waveguide configuration.

We study and classify the electromagnetic regimes of multilayer graphene-dielectric artificial metamaterials. The interplay between interband and intraband transitions in graphene allows converting the structure into a transparent and/or electromagnetically dense artificial medium. The gate voltage can be used to electrically control the concentration of carriers in the graphene sheets and, thus, efficiently change the dispersion of the whole structure. Placed inside a hollow waveguide, a multilayer graphene/dielectric metamaterial provides high-speed modulation and tunable bandpass filtering. The absence of scattered radiation enables dense integration of such THz waveguides and modulators without influencing their neighboring elements.

We exemplify the employment of graphene-dielectric metamaterial for waveguide-integrated modulators with three examples of tunable devices. The first one is a modulator with excellent ON-state transmission and very high modulation depth: $> 38\,\mathrm{dB}$ with only $70\,\mathrm{meV}$ graphene electrochemical potential change. The second one is a modulator with extreme sensitivity towards graphene Fermi energy. The third one is a tunable waveguide-based passband filter. The narrow-band cut-off conditions around the ON-state allow the latter to shift its central frequency by $1:25\%$ perevery meV graphene Fermi energy change.

We believe that graphene-dielectric multilayer metamaterials will constitute the functional platform for THz-IR waveguide-integrated devices.

REFERENCES

1. Rahm, M., J. S. Li, and W. Padilla, *J. Infrared Millim. Terahertz Waves*, Vol. 34, 1–27, 2013.
2. Liu, M., X. Yin, E. Ulin-Avila, B. Geng, T. Zentgraf, L. Ju, F. Wang, and X. Zhang, *Nature*, Vol. 474, 64–67, 2011.

Stimulated Brillouin Scattering: Limitations and Possibilities in Integrated Optical Waveguides

C. Wolff[1,2], **M. J. Steel**[1,3], **B. J. Eggleton**[3], **and C. G. Poulton**[1,2]

[1]Centre for Ultrahigh Bandwidth Devices for Optical Systems (CUDOS), Australia
[2]School of Mathematical Sciences, University of Technology Sydney, Australia
[3]Department of Physics and Astronomy, Macquarie University, Australia
[4]School of Physics, University of Sydney, Australia

Abstract— We investigate Stimulated Brillouin Scattering (SBS) in the context of integrated optics. We examine the necessary conditions on material properties, waveguide symmetry, and waveguide dimensions that are required to obtain technologically useful SBS gain, as well as potential limitations on the amount of gain achievable. We discuss the technological possibilities for the harnessing of SBS for optomechanical applications.

Introduction: Stimulated Brillouin Scattering (SBS) is a coherent interaction between the electromagnetic and acoustic waves that occurs in optical waveguides [1]. Although traditionally associated with optical fibres, there has been a recent surge of interest in applying SBS in the context of integrated optics; thus far a broad range of capabilities have been demonstrated, from on-chip slow and fast light to high-frequency pulse generation [2]. These on-chip SBS experiments open the door to the exploitation of SBS in fully integrated photonic environments [2–4].

SBS in Integrated Waveguides: The basic physical processes of SBS can be derived from thermodynamics: this gives a connection between scattering processes (including the photoelastic effect and scattering from boundaries) and force-like processes, which include electrostriction and radiation pressure. These processes lead to necessary conditions on material properties for acoustic and optical guidance, symmetry, as well as dielectric contrast that must be met in order to achieve sufficient gain. We outline the possibilities for achieving SBS in various material platforms at different wavelengths, from communications frequencies to the mid-IR (see Fig. 1). We also explore the effects of both optical and acoustic loss, and see how fabrication imperfections such as waveguide roughness can lead to a reduction in gain in the same regimes that the effects of radiation pressure cause SBS enhancement. Finally, we examine the effect of finite lengths on achieving desired levels of gain in realistic SBS structures.

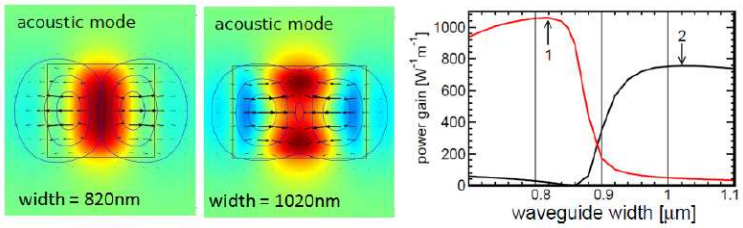

Figure 1: SBS acoustic mode and gain computations for a mid-IR waveguide [5].

ACKNOWLEDGMENT

This work was supported by the Australian Research Council (ARC) through grants DP130100832, CE110001018, and FL120100029.

REFERENCES

1. Boyd, R. W., *Nonlinear Optics*, 3rd Edition, Academic Press, 2003.
2. Eggleton, B. J., et al., *Adv. in Opt. and Photon.*, Vol. 5, 536, 2013.
3. Grudinin, I. S., et al., *Physical Review Letters*, Vol. 104, 083901, 2010.
4. Shin, H., et al., *Nat. Comm.*, Vol. 4, 1944, 2013.
5. Wolff, C., et al., *Optics Express*, Vol. 22, 30735, 2014.

Femtosecond Magneto-optic Kerr Effect in Magnetoplasmonic Crystals

M. R. Shcherbakov, **P. P. Vabishchevich**, **A. Yu. Frolov**,
T. V. Dolgova, **and A. A. Fedyanin**
Faculty of Physics, Lomonosov Moscow State University, Moscow 119991, Russia

Abstract— We have studied ultrafast effects in magnetoplasmonics by observing nontrivial evolution of transversemagneto-optical Kerr effect within 45-fs pulses reflected from an iron-based magnetoplasmonic crystal. The effect takes place for resonant excitation of surface plasmon-polaritons (SPPs), has opposite signs of time derivative for different slopes of the resonance, and is addressed to magnetization-dependent dispersion relation of SPPs.

One of the most prominent opportunities of using SPP nanostructures is to shape femtosecond laser pulses. The mean lifetime of SPPs in nanostructures varies from several femtoseconds to several hundreds of femtoseconds. A femtosecond laser pulse interacting with such a short-living excitation gets coherently modified as indicated in many preceding works. Recently, temporal shaping of femtosecond laser pulses by plasmonic nanostructures was observed both for the intensity and polarization state. it was shown that external quasistatic magnetic field can be used to control dispersion of SPP in magnetic media [1]; despite immense number of works on magnetoplasmonics emerged during the last years, magnetoplasmonic effects have been considered static so far. In this work, we experimentally demonstrate manifestations of time-dependent transverse magneto-optical Kerr effect (TMOKE) within ultrashort femtosecond laser pulses reflected from a one-dimensional iron-based magnetoplasmonic crystal. The sample of one-dimensional magnetoplasmonic crystal based on a commercially available digital versatile disk polycarbonate template having periodic corrugation with the depth of approximately 50 nm and the period of 750 nm. The dielectric template was covered by a 100 nm layer of polycrystalline iron deposited by magnetron sputtering and protected by a 20 nm-thick silica layer from the top. To obtain information about time-resolved TMOKE, the correlation function measurement setup was used. A train of 45-fs laser pulses from a Coherent Micra Ti:sapphire oscillator was precompressed at a chirped-mirror assembly to account for dispersive optics in the setup. The pulses were split into two beams, where one was the signal beam that contained the sample and the other was a gate beam with a 3-fs step delay line. Two electrically serial electromagnets placed around the sample were used to apply a quasistatic magnetic field in the TMOKE configuration, i.e., in the plane of the sample perpendicular to the plane of incidence. The magnets were driven by an ac source at a frequency of 117 Hz and provided approximately 30 mT of magnetic flux density,which was sufficient to saturate the magnetization of the iron in the sample. Manifestations of time-dependent transverse magneto-optical Kerr effect are experimentally demonstrated in fs-laser pulses reflected from a iron-based magnetoplasmonic crystal. Kerr effect evolution is shown to have either positive or negative time derivative depending on the position of the incident pulse carrier wavelength with respect to the SPP resonance. Proper grounds are given for this effect within the Lorentzian spectral line shape approach. Being a subwavelength-thickness tailorable nanostructure, the iron-based plasmonic crystal under study is a promising tool for manipulating femtosecond laser pulses with the external magnetic field that is to find applications in the novel active plasmon-based telecom devices [2, 3].

ACKNOWLEDGMENT

Partial support from the Russian Foundation for Basic Research and the Russian Ministry of Education and Science (contract RFMEFI61314X0029) is acknowledged.

REFERENCES

1. Grunin, A. A., A. G. Zhdanov, A. A. Ezhov, E. A. Ganshina, and A. A. Fedyanin, *Appl. Phys. Lett.*, Vol. 97, 261908, 2010.
2. Vabishchevich, P. P., A. Y. Frolov, M. R. Shcherbakov, A. A. Grunin, T. V. Dolgova, and A. A. Fedyanin, *J. Appl. Phys.*, Vol. 113, 17A947, 2013.
3. Shcherbakov, M. R., P. P. Vabishchevich, A. Y. Frolov, T. V. Dolgova, and A. A. Fedyanin, *Phys. Rev. B*, Vol. 90, 201405(R), 2014.

Three-wave Frequency Mixing in Stacks of Binary Nonlinear Dielectric and Semiconductor Layers

A. Schuchinsky
Queen's University Belfast, ECIT, Queen's Road, Queen's Island, Belfast, BT3 9DT, UK

Abstract— Nonlinear metamaterials have been a subject of increasing interest over the last few years. Owing to their capability of independent control of both the nonlinear properties and the linear characteristics, such as dispersion and phasing, they are attractive for a variety of diverse applications. Majority of the studies performed to date have been concerned with the metamaterials intended to improve the efficiency of harmonic generation. Combinatorial frequency generation (CFG) has been another direction where the purposely tailored metamaterials can be particularly instrumental for shaping and localising fields and controlling the phase coherence in distributed wave interactions rendering the three- and four-wave processes of mixing two or more pump tones. Uncovering the fundamental mechanisms of CFG in metamaterials proved to be of the special significance for the opposite aim — highly linear response of the medium and mitigation of spurious intermodulation effects.

Majority of metamaterials and metasurfaces are nowadays manufactured by layer-by-layer deposition or growth. To identify the main mechanisms of CFG in such kind of structures, it is instructive to examine first the nonlinear wave interactions in the canonical planar arrangements with the basic constitutive elements comprised of stacked binary dielectric and/or semiconductor layers. Both periodic and quasi-periodic (Fibonacci and Thue-Morse) structures have been analysed in this work to assess the qualitative effects of the lattice disorder on CFG in the finite stacks illuminated by a pair of plane waves of frequencies ω_1 and ω_2, incident at different angles. Stacks of semiconductor layers have been modelled in the self-consistent problem formulation taking into account the nonlinear dynamics of mobile carriers. A unified methodological framework based upon the modified transfer matrix method has been developed and applied to the CFG analysis in the finite stacks of binary layers. It has been demonstrated that the quasi-periodic stacks of Fibonacci and Thue-Morse types can be treated as the perturbed periodic stacks with the defects located in the positions determined by the respective quasi-periodic sequences. The results of numerical simulations have provided important qualitative insight in the mechanisms responsible for the performance of the stratified metamaterial structures and a means for controlling frequency mixing and CFG.

The main features of CFG in periodic and quasi-periodic stacks will be discussed and illustrated by examples of the simulation results for combinatorial frequencies $\omega_3 = \omega_1 + \omega_2$ generated in the three-wave mixing process. The effects of the stack linear reflectance, and the constituent layer anisotropy and losses on the CFG efficiency will be addressed in the talk.

Characterization of Chiral Nanostructured Plasmonic Surfaces with Second Harmonic Generation

Ventsislav K. Valev
MultiPhoton NanoPhotonics, Department of Physics, University of Bath, United Kingdom

Abstract— Because of its high surface and interface sensitivity, the nonlinear optical technique of second harmonic generation (SHG) appears as a designated method for investigating nanostructured metal surfaces. Indeed, the latter present a high surface-to-volume ratio, but, even more importantly, they can exhibit strong near-field enhancements, or "hotspots". Hotspots often appear as a result of geometric features at the nanoscale or of surface plasmon resonances, which are collective electron oscillations at the surface that, on the nanoscale, can readily be excited by light. In addition, SHG is a symmetry-sensitive technique and, due to the recent development of nanofabrication techniques, it has become possible to endow nanostructured metal surfaces with virtually any possible symmetry. As a consequence, SHG based techniques have gained popularity at both the microscopic and the macroscopic level [1]. One particular symmetry related property that has benefited a lot from the developments in nanofabrication is chirality.

Because of its high surface and interface sensitivity, the nonlinear optical technique of second harmonic generation (SHG) appears as a designated method for investigating nanostructured metal surfaces. Indeed, the latter present a high surface-to-volume ratio, but, even more importantly, they can exhibit strong near-field enhancements, or "hotspots". Hotspots often appear as a result of geometric features at the nanoscale or of surface plasmon resonances, which are collective electron oscillations at the surface that, on the nanoscale, can readily be excited by light. In addition, SHG is a symmetry-sensitive technique and, due to the recent development of nanofabrication techniques, it has become possible to endow nanostructured metal surfaces with virtually any possible symmetry. As a consequence, SHG based techniques have gained popularity at both the microscopic and the macroscopic level [1]. One particular symmetry related property that has benefited a lot from the developments in nanofabrication is chirality.

Chirality, the handedness of nature, constitutes a fundamental concept throughout the universe. Entire galaxies can be chiral, just as well as the smallest amino acids. Chiral plasmonic nanostructures are emerging as a very promising branch of nanophotonics, with numerous potential applications [2]. Recently, so called "superchiral" electromagnetic configurations have been demonstrated, whereby the pitch of the electric field of light is shorter than that of circularly polarized light. These configurations have lead to enhanced chiroptical interactions with matter. In addition, it has also been reported that negative refractive index can be achieved in chiral metamaterials. Furthermore, due to the favorable power-law scaling of near-field enhancements, new nonlinear optical properties, for instance in SHG, are emerging in chiral nanomaterials as well.

Chiroptical (chiral-optical) effects in SHG are usually three orders of magnitude larger than their linear optical counterparts. Therefore, upon using superchiral excitation, nonlinear nanomaterials are anticipated to achieve record-high chiroptical values compared to those of natural materials and consequently to serve as highly sensitive probes for exploring chiral molecular chemistry. At the moment though, little has been done towards fulfilling these high expectations. Basic understanding of the nonlinear chiroptical properties of nanosurfaces is also lacking; for instance, it is not clear how the chiroptical effects of nanosurfaces would be affected upon expanding to more pronounced 3D geometries.

Among other developments, a surprising direct relationship between superchiral light and SHG has been reported [3]. By varying the dimensions of nanostructures, superchiral light can be tuned to optimize material dimensions for enhanced nonlinear chiroptical response. The use of superchiral elements as building blocks opens very interesting possibilities in both 2D and 3D nanomaterials.

REFERENCES

1. Valev, V. K., *Characterization of Nanostructured Plasmonic Surfaces with Second Harmonic Generation*, Vol. 28, 15454–15471, Langmuir, 2012.
2. Valev, V. K., J. J. Baumberg, C. Sibilia, and T. Verbiest, "Chirality and chiroptical effects in plasmonic nanostructures: Fundamentals, recent progress and outlook," *Adv. Mater.*, Vol. 25, 2508–2628, 2013.

3. Valev, V. K., J. J. Baumberg, B. De Clercq, N. Braz, X. Zheng, E. J. Osley, S. Vandendriessche, M. Hojeij, C. Blejean, J. Mertens, C. G. Biris, V. Volskiy, M. Ameloot, Y. Ekinci, G. A. E. Vandenbosch, P. A. Warburton, V. V. Moshchalkov, N. C. Panoiu, and T. Verbiest, "Nonlinear superchiral meta-surfaces: Tuning chirality and disentangling non-reciprocity at the nanoscale," *Adv. Mater.*, Vol. 26, 4074–4081, 2014.

Ultrafast Kerr Nonlinearities in Multimodal Plasmonic Metamaterials: Elliptic, Hyperbolic and Epsilon-near-zero Regimes

S. Peruch, **A. Neira**, **G. A. Wurtz**, **and A. V. Zayats**
Department of Physics, King's College London, Strand, London WC2R 2LS, United Kingdom

Abstract— The ability to actively manipulate optical signals at the nanoscale represents an essential tool in modern and future nanophotonics. This can be achieved all-optically exploiting optical nonlinearities in metals, which are some of the fastest available. Plasmonic metamaterials represent an ideal platform to implement active functionalities, given their capability to support complex field distributions, which are geometry-controlled and impact the metamaterials ultrafast nonlinear response. Thus, enhanced optical nonlinearity can be engineered at the required wavelengths.

Previous work [1] has shown a strong, ultrafast response from metamaterials based on plasmonic nanorod assemblies, with sub-ps transient change in transmission reaching 80%. This exceptionally strong and fast response was assigned to the nonlocal behaviour of the metamaterial in the vicinity of the epsilon near zero (ENZ) frequency, where the real part of the effective permittivity vanishes and its wavevector-dependent contribution may become strong [2–4].

Here we present a full-vectorial microscopic model to study the Kerr-type, ultrafast nonlinear response of a plasmonic metamaterial consisting of an array of vertically aligned gold nanorods, with the plasmonic (Au) components of the metamaterial considered as the source of the optical nonlinearity.

We have performed a numerical study of the transient nonlinear response of the metamaterial taking into account the effects of both control illumination conditions and induced non-equilibrium electron temperature distribution in the Au nanorods forming the metamaterial. The nonlinear response of the Au nanorods is governed by a polarization-induced electron temperature change driven by the femtosecond optical excitation. We describe the evolution of the position-dependent electron temperature in the metal via the two temperature model (TTM) [5], keeping the phonons temperature effectively constant. The nonlinear absorption is then modelled via the temperature dependent Au permittivity [1].

We found that the nonlinear response of the system is stronger when exciting in the vicinity of the ENZ frequency. We also show that the enhancement of the nonlinear response depends on the spatial distribution of the electromagnetic energy density induced by the pump pulse . Considering these effects, the magnitude and time response of the metamaterial is further studied, in different dispersion regimes of the metamaterial.

REFERENCES

1. Wurtz, G. A., R. Pollard, W. Hendren, G. P. Wiederrecht, D. J. Gosztola, V. A. Podolskyi, and A. V. Zayats, "Designed ultrafast optical nonlinearity in a plasomonic nanorod metamaterial enhanced by nonlocality," *Nat. Nanotachnol.*, Vol. 6, 106, 2011.
2. Pollard, R. J., A. Murphy, W. R. Hendren, P. R. Evans, R. Atkinson, G. A Wurtz, A. V. Zayats, and V. A. Podolskiy, "Optical nonlocalities and additional waves in epsilon near zero metamaterials," *Phys. Rev. Lett.*, Vol. 102, 127405, 2009.
3. Wells, B., A. V. Zayats, and V. A. Podolskiy, "Nonlocal optics of plasmonic nanowire metamaterials," *Phys. Rev.*, Vol. B 89, 035111, 2014.
4. Tsai, K.-T., G. A. Wurtz, J.-Y. Chu, T.-Y. Cheng, H.-H. Wang, A. V. Krasavin, J.-H. He, B. M. Wells, V. A. Podolskiy, J.-K. Wang, Y.-L. Wang, and A. V. Zayats, "Looking into meta-atoms of plasmonic nanowire metamaterial," *Nano Lett.*, Vol. 14, 4971, 2014.
5. Chen, J. K., D. Y. Tzou, and J. E. Beraun, "A semiclassical two-temperature model for ultrafast laser heating," *Int. J. Heat Mass. Tran.*, Vol. 49, 307, 2006.

Wavefront Shaping in Cavities: Waves Trapped in a Box with Tailored Boundaries

M. Dupré, M. P. Del Hougne, M. Fink, F. Lemoult, and G. Lerosey
Institut Langevin, ESPCI Paris Tech & CNRS, France

Abstract— Usually cavities of a given shape and dimensions support definite eigen frequencies and modes. They are used in a vast number of fields of research and frequency ranges, from microwave ovens to masers, from QED to electromagnetic compatibility. The eigenmodes of a cavity are always modified and tuned through mechanical parts, like mode stirrers in reverberation chambers in electromagnetic compatibility or screws in masers and quantum electrodynamices. Nevertheless, thanks to integral theorems, tailoring the boundaries of a cavity permits to design at will its eigenmodes and therefore the fields inside it. Here we show that this is possible to do so by using electronically tunable metasurfaces that litteraly modify locally the boundaries of cavities, switching them from electric to magnetic conductors. We prove that it permits, contrary to intuition, to focus waves at desired locations inside cavities. Using a binary tunable metasurface as a spatial microwave modulator (SMM) [1, 2], we show that we can control those eigenmodes up to some point which depends on one hand of the number of modes inside the cavity N given by the losses and the mean level spacing, and on the other hand on the number of degrees of freedom p which is also the number of elements of our SMM. We show experimentally, with the set-up shown on Figure 1(a), and theoretically that different behaviours of the cavity with a SMM inside can be expected. We explain the physical mechanism underlying the concept, which allows us to give a criteria that ensures that a cavity can be turned into a completely different one as in Figure 1(b) and contrary to Figure 1(d), by modifying parts of its boundaries. We finally show that this can even permit, in a cavity of given shape, to position at will the eigenfrequencies and corresponding eigenmodes as shown on Figure 1(d).

We believe those results will have application in fields requiring mode stirrers, optimizing transmission or frequency filters such as EMC, microwave ovens, or telecommunications.

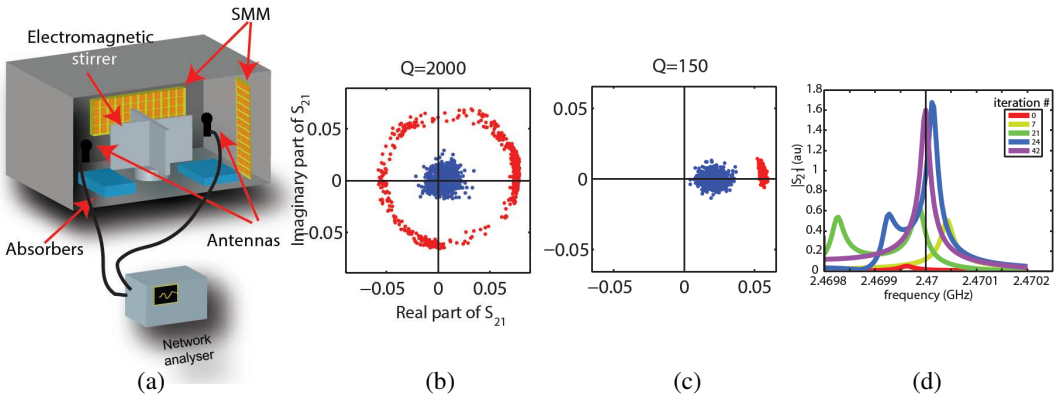

Figure 1: (a) Experimental set-up. (b), (c) Two different behaviours of the transmission between two antennas in a cavity for different Q factors when the configuration of the SMM is changed. Blue points correspond to initial measured transmission and red points correspond to optimized transmission points. (d) Spectra obtained numerically of the transmission between two antennas in the cavity, for different steps of the optimization procedure.

REFERENCES

1. Kaïna, N., M. Dupré, M. Fink, and G. Lerosey, *Optics Express*, Vol. 22, No. 16, 18881–18888, 2014.
2. Dupré, M., N. Kaïna, M. Fink, and G. Lerosey, Scientific Reports, Vol. 4, 6693, 2014.

Magnetic Field Controlled Microwave Hybrid Oscillations in Composite Resonator Dielectric-weak Ferromagnet

M. A. Popov[1], **I. V. Zavislyak**[1], **M. B. Strugatsky**[2], **S. V. Yagupov**[2], **and G. Srinivasan**[3]

[1]Department of Radiophysics, Electronics and Computer Systems
Taras Shevchenko National University of Kyiv, Kyiv 01601, Ukraine
[2]Department of Physics, Taurida National University, Simferopol 295007, Russia
[3]Physics Department, Oakland University, Rochester, MI 48309, USA

Abstract— Dielectric resonator based UHF filters, which are the key elements of the modern transceiver equipment [1], have one major drawback — they lack dynamical tuning of their characteristics. Since utilization of resonators with electronically tunable electrodynamic characteristics can greatly increase the functionality of microwave devices (for instance, in reconfigurable matched filters), in this paper we present a new concept for magnetic field tunable device, based on the electrodynamically coupled dielectric and weak ferromagnet resonators.

Weak ferromagnets are of special interest, since their typical quasi-feromagnetic resonance (FMR) frequencies can easily reach Ku- and K-bands for extremely small bias fields H_0 of few hundreds Oe [2], due to the presence of Dzialoshinskii-Moriya effective field H_{DM}, whereas quasi-antiferromagnetic excitations lays on the borderline between mm and sub-mm wavebands.

Here we investigated a $2.1 \times 2.3 \times 0.1\,\mathrm{mm}^3$ high-quality sample of iron borate ($FeBO_3$), a well-known weak ferromagnet [2]. It was grown by us from solution in melt. As a first step, a sample was characterized, by placing it atop of coplanar transmission line and measuring FMR frequency for in-plane bias magnetic field, in range from 10 to 400 Oe. After fitting resulting curve with model equation [2]

$$\omega_F^2 = \gamma^2 \left(H_0 \left(H_0 + H_{DM} \right) + H_\Delta^2 \right)$$

magnetic parameters of $FeBO_3$ were successfully determined (see Fig. 1(a)). Next, this sample was epoxy bonded to the disk dielectric resonator (commercially grade microwave ceramics) and put inside the rectangular metallic $23 \times 10\,\mathrm{mm}^2$ waveguide. Composite resonator was positioned at the middle of the wide wall, with $FeBO_3$ in direct contact with metal. Dielectric resonator was excited on $HE_{11\delta}^{(\pm)}$ modes (due to the lack of cylindrical symmetry of waveguide section, the frequency degeneracy was removed) and FMR oscillation in iron borate acted as a perturbation. Results on transmission characteristics modification with external in-plane bias magnetic field are shown on Figs. 1(b), (c). The strongest effect is observed when magnetic field tunable FMR frequency coincides with that of either of $HE_{11\delta}^{(\pm)}$ modes.

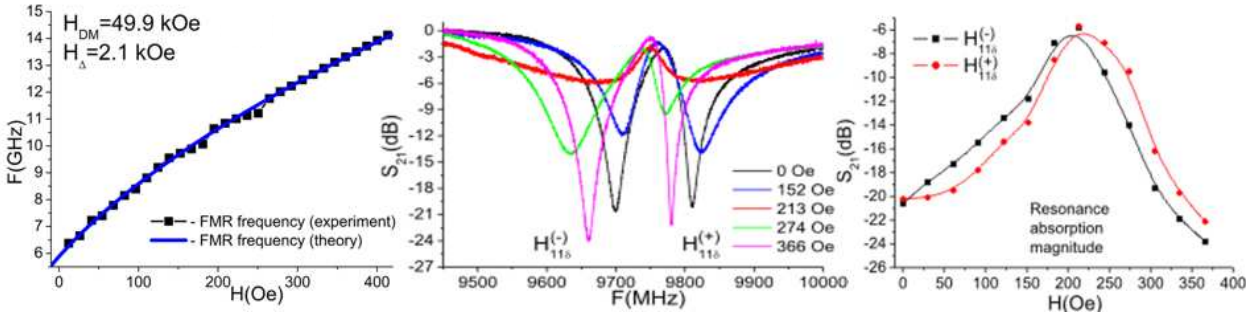

(a) (b) (c)

Thus, we have shown that inclusion of weak ferromagnet constituent leads to possibility of electronic control over a composite resonator amplitude and phase transmission characteristics, and have potential for both K-band and (in perspective) sub-mm wave device applications.

REFERENCES

1. Wang, C. and K. A. Zaki, "Dielectric resonators and filters," *IEEE Microwave Magazine*, Vol. 8, No. 5, 115–127, 2007.
2. Jantz, W. and W. Wettling, "Spin wave dispersion of $FeBO_3$ at small wavevectors," *Appl. Phys.*, Vol. 15, No. 4, 399–407, 1978.

Imaging Coherent Response of a Superconducting Metasurface

A. S. Averkin[1], **A. Zhuravel**[2], **P. Jung**[3], **N. Maleeva**[1], **V. P. Koshelets**[4], **L. V. Filippenko**[4], **A. Karpov**[1], **and A. V. Ustinov**[1, 3, 5]

[1]National University of Science and Technology (MISIS), Leninskiy prosp. 4, Moscow 119049, Russia
[2]B. Verkin Institute for Low Temp. Physics and Engineering, NAS of Ukraine, Kharkov 61103, Ukraine
[5]Physikalisches Institut, Karlsruhe Institute of Technology (KIT), Karlsruhe 76131, Germany
[4]Kotel'nikov Institute of Radio Engineering and Electronics, Moscow 125009, Russia
[5]Russian Quantum Center (RQC), 100 Novaya St., Skolkovo, Moscow Region 143025, Russia

Abstract— We study microwave response of the individual meta-atoms of a superconducting metasurface formed by a two-dimensional array of Superconducting QUantum Interference Devices (SQUIDs). In our experiment, RF currents in the metasurface are directly imaged by using Laser Scanning Microscopy (LSM) technique. We tested a sample with 21×21 SQUID array in a waveguide cavity designed to achieve a uniform microwave distribution over the entire array. The demonstrated tunability of 2D SQUID metasurface resonance frequency by external magnetic field is about 56%, covering 8–12.5 GHz range. The obtained LSM images of the RF current distributions over the SQUID array confirm a high degree of coherence of the entire metasurface.

Introduction: A two-dimensional array of SQUIDs is an example of a tunable superconducting metasurface [1]. Here the SQUIDs are playing a role of magnetically coupled meta-atoms, tunable with external magnetic field [2]. Recently the microwave response of SQUID arrays has been studied theoretically [3, 4] and also experimentally [5, 6]. In published experiment it is difficult to estimate the actual number of the SQUIDs involved in synchronized RF response. We are using a cryogenic LSM [7] in order to observe the responses of the individual SQUIDs in the array, and to characterize the spatial distribution of the coherent response of the array to microwave signal.

Experiment and Results: In the test setup, the probing microwave signal should be uniform and have magnetic field component directed orthogonal to the plane of the SQUID array. To achieve this, we place the SQUID array sample in the plane of symmetry of a rectangular waveguide, where the magnetic field of the fundamental TE_{10} mode is perpendicular to the sample plane. The designed waveguide test section has two coaxial adapters for the broadband connection to the network analyzer. The LSM access is made via a small hole in the waveguide wall, with the size much smaller than the cutoff wavelength for RF. The test sample is an array of 21×21 SQUIDs, where each SQUID is a Nb thin-film rectangular loop, with outer dimensions of $70 \times 50\,\mu m^2$, interrupted by a single Nb/AlO_x/Nb Josephson junction.

In transmission experiment with the SQUID array, the array collective response is visible as a resonance peak tunable over 56% band (8.5–12 GHz). The resonance peak is narrow, about 20 MHz wide, and resembles a response of a single resonator. We used LSM to visualize the RF currents in the individual SQUIDs at the resonance frequency of the array. The LSM imaging shows that about 50% of the SQUIDs in the array are resonating coherently.

Conclusion: Our experimental study of superconducting metasurface with 21×21 SQUID array indicates a nearly synchronized resonant response of the array and a broad frequency tuning range of the metasurface. The LSM imaging of the currents in the individual SQUIDs shows a partial uniformity, where about 50% of the SQUIDs participate in the coherent response. The spatial structure of the SQUID array response will be discussed. SQUID-based metasurface has low losses and a good frequency tunability, and can be useful for designing compact cryogenic RF systems.

ACKNOWLEDGMENT

This work was supported by the Ministry of Education and Science of the Russian Federation Grant 11.G34.31.0062.

REFERENCES

1. Jung, P., A. V. Ustinov, and S. M. Anlage, "Progress in superconducting metamaterials," *Supercond. Sci. Technol.*, Vol. 27, 073001, 2014.
2. Silver, A. H., et al., "Quantum states and transitions in weakly connected superconducting rings," *Phys. Rev.*, Vol. 157, 317, 1967.

3. Maimistov, A. I., et al., "Nonlinear response of a thin metamaterial film containing Josephson junctions," *Opt. Commun.*, Vol. 283, 2010.
4. Lazarides, N., et al., "Multistability and selforganization in disordered SQUID metamaterials," *Supercond. Sci. Technol.*, Vol. 26, 084006, 2013.
5. Butz, S., et al., "A one-dimensional tunable magnetic metamaterial," *Optics Express*, Vol. 21, 22540, 2013.
6. Trepanier, M., et al., "Realization and modeling of metamaterials made of RF SQUIDs," *Phys. Rev. X*, Vol. 3, 041029, 2013.
7. Zhuravel, A. P., S. M. Anlage, and A. V. Ustinov, *IEEE Trans. Appl. Supercond.*, Vol. 17, 902, 2007.

Session 4A2
Laser Nanofabrication, Characterization and Physical Properties 2

Hydrodynamic Instabilities of Thin Au and Ag Films Induced by Tightly Focused Femtosecond and Nanosecond Laser Pulses

Aleksandr Kuchmizhak[1], **O. B. Vitrik**[1, 2], **Yu. N. Kulchin**[1, 2], **S. I. Kudryashov**[3], **and S. V. Makarov**[4]

[1]Institute of Automation and Control Processes, Far Eastern Branch
Russian Academy of Science, Vladivostok 690041, Russia
[2]Far Eastern Federal University, Vladivostok 690041, Russia
[3]P. N. Lebedev Physical Institute
Russian Academy of Science, Moscow 119991, Russia
[4]ITMO University, St. Petersburg 197101, Russia

Abstract— Functional plasmonic nanostructures made of noble metals owing to their unique optical and spectral properties are currently of great scientific interest. A number of promising applications in such areas as plasmonics, nanophotonics, biosensing, etc. were theoretically predicted and experimentally demonstrated. For these applications it is often necessary to fabricate both single element at a given point and sufficiently large ordered arrays of nanostructures, which can be realized by a number of relatively expensive or time-consuming techniques. Laser material processing potentially provides the easiest and cheapest way to fabricate single and large ordered arrays of different functional metallic nanostructures through initiating various hydrodynamic instabilities excited on the metal film surface under nano- and femtosecond pulse irradiation.

In present paper we report on rigorous experimental study of various nanoscale surface hydrodynamic instabilities on the thin Au and Ag films induced by tightly focused single femtosecond and nanosecond pulses. Each type of laser-induced hydrodynamic instabilities results in the formation of corresponding resolidified surface relief nanostructure: nanojets, nanocrowns, self-organized nanoparticle's chains or hybrid structures (a nanojet surrounded by a nanocrown). The hybrid structures as well as the nanoparticle chains are reported for the first time. The thickness of the metal film, pulse energy and duration were found to be the key parameters determining the type as well as the geometrical shape of the resulted surface nanostructure. Underlying physical mechanisms responsible for the formation of all these laser-induced nanostructures are also discussed in this paper. Possible implementation of the fabricated nanojets, nanocrowns, nanoparticle's chains and hybrid structures as promising plasmonic elements for SERS signal enhancement in molecular sensors, hot electron generation in solar cells and light localization at nanoscale are also discussed in this paper.

Three Dimensional Ablation Flow Produced by Ultrashort Laser Pulse from Perfectly Flat Target

N. A. Inogamov[1] V. V. Zhakhovsky[2], and V. A. Khokhlov[1]

[1]L. D. Landau Institute for Theoretical Physics of Russian Academy of Sciences, Russian Federation
[2]Joint Institute for High Temperatures of Russian Academy of Sciences, Russian Federation

Abstract— We consider laser peeling and structure formation of thin and thick films on substrate. Let us present shortly a general picture of laser structuring. It is known, that the structuring of materials by short laser pulses with duration in the range of 10 fs–1 ps has many important technological applications. But underlying physics is not well understood. On our view, the corresponding processes are interplay of plasmon enhanced absorption from one side and a thermomechanical triplet from the another side, where the triplet is: (i) spallation, (ii) capillary deceleration in tandem with (iii) diffusion limited freezing. Particular morphology of structures depends on absorbed fluence and number of pulses. Formation of the structures is usually attributed to plasmon activity, which leads to the LIPSS (laser induced periodic surface structures, ripples). On our opinion, plasmons only dominate in the interplay if absorbed fluences are small and the multiple repetition regime is used. Indeed, the chaotic (not ripples) structures are produced by X-ray pulse where plasmon excitation is not possible. Therefore the wavelength should be added into the list of parameters governing the final morphology of an irradiated surface. It was shown that for the small number of pulses, either large fluences or short wavelength the chaotic structures different from ripples are formed. Another important governing parameters are connected with geometrical limitations. They are a radius of a focal spot on an irradiated surface and thickness of a film. Indeed, surface structures have the finite lateral sizes (submicron scales). Therefore for tightly focused optical light pulses, when diameter of a focal spot is smaller than lateral spatial scales, definitely will influences the surface structures. Those problems are analyzed in the report.

ACKNOWLEDGMENT

Work was supported by Russian Science Foundation (project No. 14-19-01599).

Evaporative Effects during Nanoscale Laser Ablation of Materials Surfaces Driven by Ultrashort Laser Pulses

Sergey I. Kudryashov[1], **Andrey A. Ionin**[1], **Sergey V. Makarov**[2], **Sergey A. Uryupin**[1], **Stanislav G. Bezhanov**[1], **Andrey Kanavin**[1], **and Vladimir I. Emelyanov**[3]

[1]P. N. Lebedev Physical Institute, Russian Academy of Sciences, Russia
[2]ITMO University, Russia
[3]Moscow State University, Russia

Abstract— Nanofabrication of single and multiple near- and sub-100-nanometer surface nanofeatures — nanoholes [1, 2], nanospikes (solidified nanojets) [2, 3], as well as intermediate submicron bumps [2–5] — by tighly focused nanosecond and femtosecond laser pulses appears to be driven interfacial or sub-surface boiling in thin films, or thick films and bulk materials, respectively. The necessary prerequisites for such buried evaporative phenomena is strong picosecond evaporative cooling of the fs-laser heated surfaces [6] and heat conduction laterally or to the bulk [1–5], which both leave the transient temperature maximum at the corresponding transient heat conduction length. Furthermore, when the peak subsurface temperature exceeds the boiling temperature of the laser-heated material [7], spontaneous nanoscale elementary single-bubble boiling, formation of sub-micron buried vapor cavity, or nanoscale melt expulsion occur, yielding in sub-100-nanometer nanoholes, bumps and nanospikes, respectively.

REFERENCES

1. Kulchin, Yu. N., et al., "Through nanohole formation in thin metallic film by single nanosecond laser pulses using optical dielectric apertureless probe," *Opt. Lett.*, Vol. 38, 1452, 2013.
2. Danilov, P. A., et al., "Single-shot front-side nanoscale femtosecond laser ablation of a thin silver film," *Appl. Phys. A*, Vol. 117, 981, 2014.
3. Emelyanov, V. I., et al., "Nanoscale hydrodynamic instability in a molten thin gold film induced by femtosecond laser ablation," *JETP Lett.*, Vol. 99, 518, 2014.
4. Danilov, P. A., et al., "Mechanisms of formation of sub- and micro-metre-scale holes in thin metal films by single nano- and femtosecond laser pulses," *Quant. Electron.*, Vol. 44, 540, 2014.
5. Kulchin, Yu. N., et al., "Formation of nanobumps and nanoholes in thin metal films by sharply focused nanosecond laser pulses," *JETP*, Vol. 119, 15, 2014.
6. Artyukov, I. A., et al., "Relaxation phenomena in electronic and lattice subsystems on iron surface during its ablation by ultrashort laser pulses," *JETP Lett.*, Vol. 99, 51, 2014.
7. Zayarny, D. A., et al., "Nanoscale boiling processes during single-shot femtosecond laser ablation of gold films," *JETP Lett.*, Vol. 101, 2015, accepted.

On Different Regimes of Condensed Matter Ablation Depending on Intensity and Duration of Absorbed Electromagnetic Pulses

V. I. Mazhukin[1], **A. A. Samokhin**[2], **A. V. Shapranov**[1], **M. M. Demin**[1], **and P. A. Pivovarov**[2, 3]

[1]M. V. Keldysh Institute of Applied Mathematics, RAS, Myusskaia sq. 4, Moscow 125047, Russia
[2]A. M. Prokhorov General Physics Institute, RAS, Vavilov str. 38, Moscow 119990, Russia
[3]National Research Nuclear University MEPhI, Kashirskoye sh. 31, Moscow 115409, Russia

Abstract— Absorption of intense electromagnetic pulses gives rise to various non equilibrium processes in condensed matter resulted in ablation of irradiated materials. Here the ablation processes are analyzed in the framework of molecular dynamic simulations combined with continual description of electron subsystem in metals. At nanosecond pulse duration in metal (Al) film targets with 48 and 430 nm thickness which in liquid states with temperature 6400 K four different ablation regimes are observed depending on electromagnetic pulses intensities: surface evaporation, explosive (volume) boiling, spinodal decomposition and supercritical fluid expansion [1–3]. At shorter (picosecond) pulses spallation effect (see, e.g., [4, 5]) due to negative pressure values generated in the thin film is also observed. Appearance of explosive (volume) boiling in metals irradiated with intense electromagnetic pulses is not evident beforehand because of high values of thermal conductivity and small radiation penetration length. Nevertheless, the explosive boiling process at absorbed radiation intensity $I = 44\,\mathrm{MWt/cm^2}$ is clearly visible in Fig. 1(a) which shows several flying away target fragments formed after explosions at earlier moments 1.16 ns, 1.5 ns and 1.79 ns. The fragments with initially well defined boundaries then become thinner and disintegrate due to surface evaporation process. Remnants of the first fragment which was formed due to the first explosion at 0.71 ns are not visible here. Fig. 1(b) shows spinodal decomposition regime where density fluctuations have no such distinct boundaries as in the explosive boiling case. Initial thickness of the explosive boiling fragment is of the order radiation penetration length (about 10 nm). This result means, in particular, that in theoretical description of the explosive boiling process in irradiated metals [6] it is necessary to take properly into account finite value radiation penetration length.

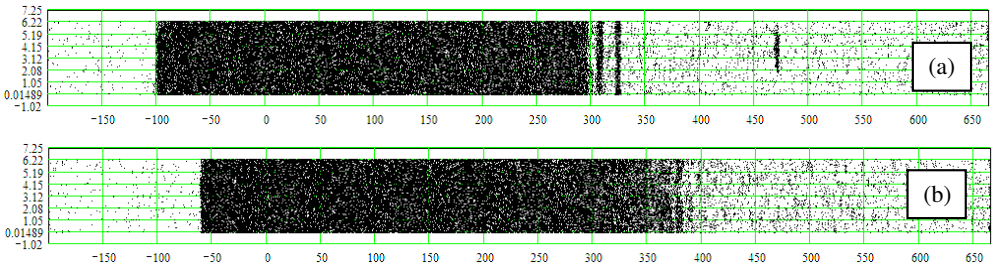

Figure 1: Snapshots of irradiated (from the right) metal film at $t = 1.82$ ns after the radiation pulse with constant intensity $I = 44\,\mathrm{MWt/cm^2}$ is switched on (a), and (b) at $t = 0.73$ ns with $I = 88\,\mathrm{MWt/cm^2}$.

REFERENCES

1. Mazhukin, V. I., A. A. Samokhin, M. M. Demin, and A. V. Shapranov, "Explosive boiling of metals upon irradiation by a nanosecond laser pulse," *Quantum Electronics*, Vol. 44, No. 4, 283–285, 2014.
2. Mazhukin, V. I., A. A. Samokhin, M. M. Demin, and A. V. Shapranov, "Modeling of nanosecond laser vaporization and explosive boiling of metals," *Mathem. Montisnigri.*, Vol. 29, 68–90, 2014.
3. Mazhukin, V. I., A. A. Samokhin, A. V. Shapranov, and M. M. Demin, "Modeling of thin film explosive boiling — Surface evaporation and electron thermal conductivity effect," *Mater. Res. Express*, Vol. 2, No. 1, 016402 (1–9), 2015.
4. Wu, C. and L. V. Zhigilei, "Microscopic mechanisms of laser spallation and ablation of metal targets from large-scale molecular dynamics simulations," *Appl. Phys. A*, Vol. 114, 11–32, 2014.

5. Ionin, A. A., S. I. Kudryashov, and L. V. Seleznev, "Thermal melting and ablation of silicon by femtosecond laser radiation," *J. Exp. Theor. Phys.*, Vol. 116, No. 3, 347–362, 2013.
6. Jiang, M. Q., Y. P. Wei, G. Wilde, and L. H. Dai, "Explosive boiling of a metallic glass superheated by nanosecond pulse laser ablation," *Appl. Phys. Let.*, Vol. 106, 021904 (1–6), 2015.

Femtosecond Laser Ablation of Thin Films on Substrate

N. A. Inogamov[1], **V. A. Khokhlov**[1], **V. V. Zhakhovsky**[2], **Yu. V. Petrov**[1,3], **K. V. Khishchenko**[2], **and S. I. Anisimov**[1]

[1]L.D. Landau Institute for Theoretical Physics of Russian Academy of Sciences, Russian Federation
[2]Joint Institute for High Temperatures of Russian Academy of Sciences, Russian Federation
[3]Moscow Institute of Physics and Technology, Russian Federation

Abstract— In many applications an ultrashort laser pulse irradiates films deposited onto a dielectric substrate. E.g., microbumping phenomena caused by blistering of the irradiated film are important for laser bio-printing and LIFT technology [1–3], for formation of arrays of nanoholes [4], and for nanophotonics (creation of nanoantennas [5]). The case with a film on substrate is interesting. Indeed, a system with a thin film between a substrate from the one side and vacuum from the other side is very different from a case of bulk targets and from a case of a freestanding film. In the report the systems "film on substrate" are considered in details. Modern model of two-temperature (2T) physics is used [6, 7]. We show that for 40–100 nm thick thin films the conductive leveling of electron temperature across film thickness takes few picoseconds in gold, copper, and silver. The duration of the leveling is small in comparison with the electron-ion temperature equalization time t_{eq} [6, 7] and is small in comparison with acoustic time t_s defined by thickness of film and speed of sound. At the same time values t_{eq} and t_s are comparable. Thus electron-ion coupling coefficient and 2T equation of state [6, 7] are important ingredients of 2T physics since they define a rate of electron cooling and dynamic significance of electron pressure. Interplay of rarefaction waves in a film and dynamic interaction between the film and the substrate control a process of film separation from substrate. Finite size of a heated spot on a film surface is included into consideration. Velocity of a film after its separation from substrate has a maximum at the axis of a beam in case of Gaussian distribution of pulse intensity across a cross-section of a laser beam [1–4]. That's why the film after separation from the substrate expands having a shape of cupola. An area of surface of a target under the cupola is defined by a radius of a laser beam. Absorbed fluence is above a melting threshold in our applications. Therefore the shell of the cupola is made from molten metal. Surface tension plays the decisive role in a stopping of expansion of cupola. Tension focuses mass ow inside a shell in direction to the axial region forming a jet and droplets. Mutual action of capillary effects and cooling/freezing process define a final shape of a cupola.

ACKNOWLEDGMENT

Authors acknowledge Russian Science Foundation, grant 14-19-01599.

REFERENCES

1. Ivanov, et al., *Appl. Phys. A*, Vol. 111, 675, 2013.
2. Emelyanov, et al., *JETP Lett.*, Vol. 99, 518, 2014.
3. Inogamov, et al., *JETP*, Vol. 120, 15, 2015.
4. Nakata, et al., *Appl. Surf. Sci.*, Vol. 253, 6555, 2007.
5. Gubko, et al., *Laser Phys. Lett.*, Vol. 11, 065301, 2014.
6. Petrov, et al., *Appl. Phys. B*, DOI: 10.1007/s00340-015-6048-6, 2015.
7. Petrov, et al., *JETP Lett.*, Vol. 97, 20, 2013.

All-laser Fabrication of Metallic Nanoantenna with Planar Lens for Surface Plasmon Polaritons

S. V. Makarov[1, 2], **A. A. Ionin**[2], **S. I. Kudryashov**[2, 3], **and A. A. Kuchmizhak**[4]

[1]ITMO University, Kronverkskiy pr. 49, Saint-Petersburg, Russia
[2]P. N. Lebedev Physical Institute of the Russian Academy of Sciences
Leninskiy pr. 53, Moscow, Russia
[3]NRNU "MEPhI", Kashirskoe sh. 31, Moscow, Russia
[4]Institute of Automation and Control Processes
Far Eastern Branch, Russian Academy of Science, Vladivostok 690041, Russia

Abstract— We demonstrate new simple methods of all-laser fabrication of nanoantenna (nanojet) with an additional elements for coupling/focusing of surface plasmon-polaritons (SPPs).

The first method is realized by using an aluminum plasmonic lens irradiated by linear polarized femtosecond laser pulses at fluences higher than the ablation threshold of aluminum. These plasmonic lenses are surface rings with tunable mean diameter in the range of 1.0–2.5 μm, which are easily fabricated by a single fs-laser pulse over the whole laser spot via self-organization processes. Following the first fs pulse, the next one irradiates these plasmonic lenses and initially excites quite intense SPPs which are focused in their center. The remaining part of the pulse interferes with the focused SPPs, resulting in field enhancement in the very center of the lenses and causing strong local (nanoscale) heating. The resulting plasmonic lenses contain single nanojets in their centers owing to melt expulsion in the locally heated area [1]. Such surface structure resembles a parabolic antenna, which has a receiver and focusing reflector.

The second method is based on double-shot femtosecond laser nanoablation of thin supported metallic (Au) film. The first fs-laser pulse produces nanojet, standing on bump of microscale diameter. Irradiation by spatially shifted (on several microns) second laser pulse results in the bump removing, transition of nanojet into nanosphere and formation of concentric periodical semi-rings. Resulted surface structure represents nanoantenna (gold nanospere), surrounded by plasmonic lens, delivering more incident energy to the nanoantenna [2].

The proposed new principle of all-laser nanoantenna fabrication is very simple and high-productive technology to be applied in nanophotonics soon. For instance, we showed almost 30-fold enhancement of fs-laser induced ultrafast electron emission from such nanoantennas, which is promising for time-resolved electron microscopy [1].

ACKNOWLEDGMENT

This work was partly financially supported by the Government of the Russian Federation (Grant 074-U01) through ITMO Post-Doctoral Fellowship for S. V. Makarov.

REFERENCES

1. Gubko, M. A., W. Husinsky, A. A. Ionin, S. I. Kudryashov, S. V. Makarov, C. R. Nathala, et al., "Enhancement of ultrafast electron photoemission from metallic nanoantennas excited by a femtosecond laser pulse," *Laser Physics Letters*, Vol. 11, No. 6, 065301, 2014.
2. Ionin, A. A., S. I. Kudryashov, S. V. Makarov, A. A. Rudenko, Yu. N. Kulchin, O. B. Vitrik, T. V. Efimov, and A. A. Kuchmizhak, "Flash-imprinting of intense femtosecond surface plasmons for advanced nanoantenna fabrication," *Optics Letters*, (submitted).

Characterisation of Polymeric Rod-connected Diamond Photonic Crystal Templates at Near-infrared Range

L. Chen[1], **M. P. C. Taverne**[1], **X. Zheng**[1], **C. C. Huang**[2], **M. L. Garcia**[1], **Y.-L. D. Ho**[1], **D. W. Hewak**[2], **and J. G. Rarity**[1]

[1]Merchant Ventures Building, Department of Electrical and Electronics Engineering
University of Bristol, United Kingdom
[2]Optoelectronics Research Centre, University of Southampton
Southampton, SO17 1BJ, United Kingdom

Abstract— We present a low-index polymeric three-dimensional photonic crystal, rod-connected diamond structure, created via direct laser writing, showing a partial photonic band gap at near-infrared wavelengths in both P and S polarization, measured by angular resolved Fourier image spectroscopy. We show initial tests of backfilling with high refractive index material aimed at achieving a full photonic bandgap in the near-infrared.

Rod connected diamond (RCD) [1], which is known to exhibit the largest full PBGs among all photonic crystal designs with the same index contrast [2], has been investigated but remains a significant challenge to create [3]. Here we use the direct laser writing method to fabricate a polymeric ($n = 1.52$) RCD template and characterize its band structure via angular-resolved spectroscopy. We first calculate the RCD bandstructure using MPB software around wavelengths of interest using the results to optimize lattice parameters (Fig. 1(a)). We then fabricated a structure and measured transmission (reflection) at normal incidence along the X' symmetry direction where we see a clear 20% dip (peak) in transmission (reflection) with center wavelength around 1500 nm (Fig. 1(b)). We then measure reflection spectra mapped as function of angle (Fig. 1(c)) showing good agreement with the bandstructure features seen in Fig. 1(a).

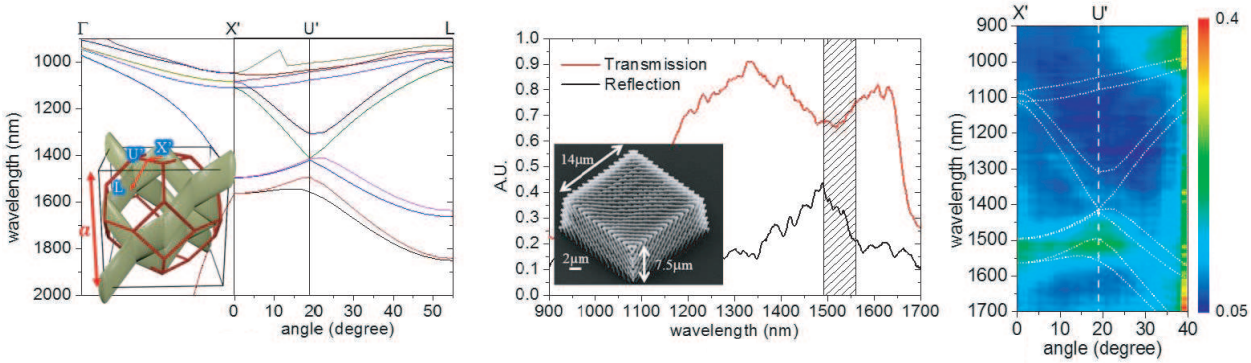

(a) (b) (c)

Figure 1: (a) MIT photonic-bands (MPB) calculation of RCD band structure at our measurement range, the insert defines the Brillouin zone of RCD and the principle directions (X', U', L), (b) transmission and reflection measurements at normal incidence, the insert show dimensions of structure, (c) measurement of reflection spectra against collection angle, incident with S polarized light.

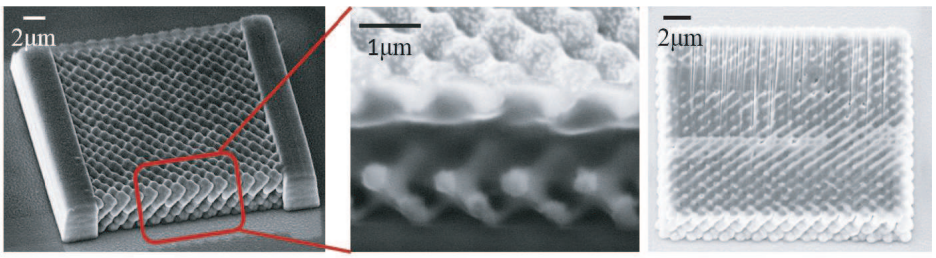

(a) (b) (c)

Figure 2: (a) Overview of a backfilled RCD structure, (b) cross section and (c) top peel showing good back fill quality, bright parts are chalcogenide material and dark parts are polymer templates.

Having successfully made polymeric RCD, we can then backfill this template with high refractive index ($n = 2.4$) chalcogenide material [4] to form high refractive index contrast (2.4:1) photonic crystal with full photonic bandgap. Our preliminary backfilled sample is shown in Figs. 2(a)–(c). By removing the polymer templates in a further process we can achieve high refractive index contrast. In the conference we will show our latest measurement results for these full photonic band gap RCD structures.

REFERENCES

1. Chan, C., S. Datta, K. Ho, and C. Soukoulis, "A7 structure: A family of photonic crystals," *Phys. Rev. B*, Vol. 50, No. 3, 1988–1991, 1994.
2. Men, H., K. Y. K. Lee, R. M. Freund, J. Peraire, and S. G. Johnson, "Robust topology optimization of three-dimensional photonic-crystal band-gap structures," *Optics Express*, Vol. 224, No. 2000, 17, May 2014.
3. Aoki, K., "Practical approach for a rod-connected diamond photonic crystal operating at optical wavelengths," *Appl. Phys. Lett.*, Vol. 95, No. 19, 191910, 2009.
4. Huang, C. C., C. C. Wu, K. Knight, and D. W. Hewak, "Optical properties of CVD grown amorphous Ge-Sb-S thin films," *J. Non. Cryst. Solids*, Vol. 356, No. 4–5, 281–285, Feb. 2010.

Simulation of Intense Laser Irradiation of Silicon and Diamond

T. Apostolova and B. Obreshkov
Institute for Nuclear Research and Nuclear Energy, Sofia 1784, Bulgaria

Abstract— The processes of photo excitation of band gap materials by intense pulsed laser radiation taking place on a femtosecond time scale is modeled by time dependent Schrodinger equation. The subsequent time evolution of the dynamical system near the end and after the termination of the pulse due to impact ionization, auger recombination, exciton formation and electronphonon scattering are modeled by quantum-kinetic Boltzmann type equation.

We apply our theoretical approach to investigate ripple formation and graphitization in laser irradiated silicon [1] and diamond [2] crystals.

REFERENCES

1. Ionin, A. A., et al., *Laser Phys. Lett.*, Vol. 12, 025902, 2015.
2. Lagomarsino, S., et al., *Diamond and Related Materials*, Vol. 43, 23, 2014.

Formation and Properties of 3D Metamaterial Composites Fabricated Using Nanometer Scale Laser Lithography

S. M. Prokes[1], **F. K. Perkins**[1], **O. J. Glembocki**[1], **and T. Larrabee**[2]

[1]US Naval Research Lab, USA
[2]NRC post doctoral Fellow, USA

Abstract— Metamaterials are engineered composite materials containing subwavelength arrangements, which often exhibit properties not available in nature or traditional synthetic materials. The field of metamaterials has brought about novel designs, since researchers have been able to overcome the constraints associated with conventional materials and explore entirely new concepts with a much larger range of material parameters available through structured media.

The key aspect of these materials is that they are artificially engineered, and although some of these structures can be formed by the use of appropriate deposition or growth techniques, most must be formed by patterning. To design a metamaterial in the terahertz or longer wavelengths, the patterning does not require much effort, since current optical lithography or pattern transfer techniques suffice. For metamaterials designed for the visible or near IR wavelengths, however, the patterning is much more of a challenge. To achieve this, techniques such as e-beam lithography are used, but it is slow, extremely difficult and can only produce 2D structures. An alternative technique to produce 2D and 3D structures involves laser fabrication using the Nanoscribe 3D laser lithography system. This is a direct laser writing technique which can form arbitrary 3D nanostructures and is based on multi-photon polymerization. The laser light is tightly focused in an ultra short pulse, so that the photoresist within the focused area is exposed by multi-photon absorption.

We are creating 2D and 3D metamaterials via this technique using a Nanoscribe proprietary acrylic-based negative-tone resist, and subsequently conformally coating them using Atomic Layer Deposition of oxides and Ag. The resolution of our Nanoscribe system is 80 nm, measured by writing a 2D grating structure. We also recently developed a novel plasmonic material, based on Plasma Enhanced Atomic Layer Deposition (PEALD) of Ag [1], which results in strong plasmonic properties of flat Ag films. We have modeled the ALD-Ag film using FDTD and FEM full wave E-M simulations, representing the film as a ring shaped air gap in Ag. The results show a very strong confinement of optical fields in the air gaps with an enhancement $> 10x$. When PEALD Ag is combined with an active plasmonic material, such as dielectric core nanowires, the additional field enhancement over the plasmonic material can be $> 100x$. This behavior is due to these air gaps, which are an inherent property of the PEALD growth of Ag. This unusual plasmonic behavior is very similar to what would be expected in hybrid spoof plasmonics and suggests that PEALD Ag is a metamaterial. Thus, we are now able to form a composite metamaterial by conformally coating an engineered 3D structure fabricated by laser lithography with a 2D naturally forming Ag metamaterial deposited by PEALD. An SEM image of such a 3D composite and its SERS

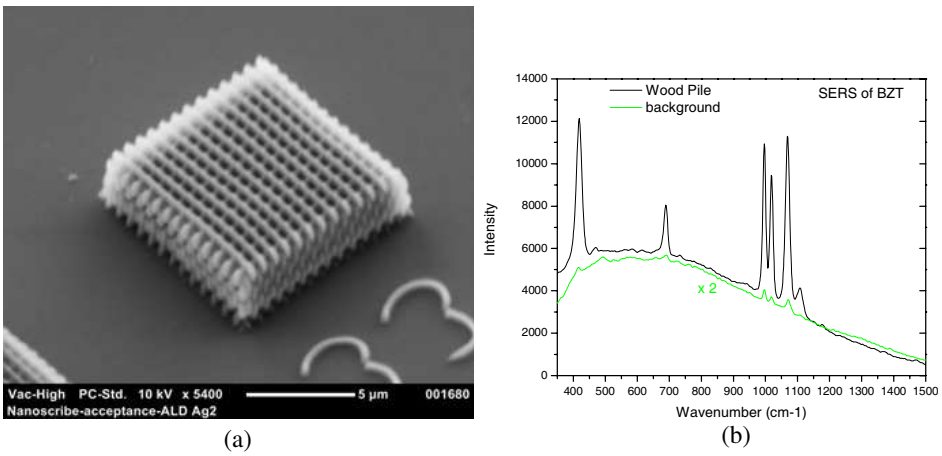

(a) (b)

Figure 1: (a) 3D composite "wood pile" structure formed in photoresist/ALD Ag and (b) SERS of BZT showing $30x$ enhancement.

response are shown above. Note that the SERS is $30x$ stronger than the ALD Ag background. We will discuss the optical properties of these novel composite structures and their potential for dual resonant metamaterials.

REFERENCES

1. Prokes, S. M., O. J. Glembocki, E. Cleveland, J. Caldwell, E. Foos, J. Niinistö, and M. Ritala, *Applied Physics Letters*, Vol. 100, 053106, 2012.

Two-temperature Heat Conductivity of Gold

Yu. V. Petrov[1], **N. A. Inogamov**[1], **and K. P. Migdal**[2]

[1]L.D. Landau Institute for Theoretical Physics RAS, Russia
[2]All-Russia Research Institute of Automatics, Russia

Abstract— Data on thermal conductivity in states with hot electrons are necessary for the simulations of ultrashort laser pulse-metal interaction. We develop a new analytical approach describing a coefficient of heat conductivity within a broad range of two-temperature phase diagram including the melting curve. This is a region in the three dimensional space defined by electron temperature, ion temperature, and density. Coefficient of thermal conductivity is an order of magnitude larger than the room temperature value of this coefficient if electrons are hot — electron temperature is one — few eV. This large increase in the heat conductance is due to a sharp increase of a heat capacity of carriers (electrons) when they are significantly heated because electrons partially lose their degeneracy. The developed model is based on a solutions of the kinetic equations. The model also is based on experimental data and on calculations of the electronic spectrum. Electronic spectrum was calculated using the density functional theory (DFT). The model works well also at low electron and ion temperatures. This is significant since for applications it is necessary to describe the cooling process of molten metal down to melting temperature and below the melting temperature.

ACKNOWLEDGMENT

Authors acknowledge partial support from Russian Foundation for Basic Research (RFBR, grant 13-02-01078-a).

Mode Analysis and Far Field Characteristics of Metallic Coated Circular Subwavelength Laser

Chucai Guo[1], **Zhihong Zhu**[1, 2], **Ken Liu**[1], **and Xiaodong Yuan**[1]

[1]College of Optoelectronic Science and Engineering
National University of Defense Technology, Changsha 410073, China
[2]State Key Laboratory of High Performance Computing
National University of Defense Technology, Changsha 410073, China

Abstract— Semiconductor nanolasers with subwavelength sizes are greatly demanded for their potential applications in photonic integrated circuits, optical interconnection, data storage and imaging [1–4]. Here we demonstrate an aluminum/silica coated InAlGaAs/InP circular subwavelength laser, which is bonded on a silicon wafer using a benzocyclobutene (BCB) layer. Room temperature lasing operation is observed for the nanolaser with the semiconductor core height of 800 nm and the radius of 740 nm. Resonant modes in the subwavelength laser are analyzed by 3D finite-difference time-domain (FDTD) simulation, and the simulated spectrum agrees well with the observed lasing spectrum. Meanwhile, the far-filed characteristics of the resonant modes in the subwavelength laser are also investigated by 3D FDTD method.

Figure 1(a) shows the schematic figure of our fabricated subwavelength laser, which consists of a circular cross-section semiconductor core coated by silica/aluminum on the bottom and sidewall. Eight pairs of compressively strained InAlGaAs multiple quantum wells (MQWs) are used as the gain material of the laser. The height and radius of the semiconductor core are about 800 nm and 740 nm, respectively. The fabricated laser was tested at room temperature by a micro-photoluminescence setup with a pumping source of a 976 nm pulsed laser. A 40× objective lens was used to focus the pump laser beam on the laser sample and collect the emitting light of the laser at the same time. Fig. 1(b) shows the typical above-threshold spectrum of the fabricated laser. As shown in Fig. 1(b), a lasing mode with peak wavelength of 1436 nm and some other resonant modes of the laser were observed. The mode spectrum of the fabricated laser was simulated by 3D FDTD technique and compared with the observed spectrum. In addition, the far-field characteristics of the resonant modes in the laser were also investigated by 3D FDTD technique. Fig. 1(c) shows the calculated far-field pattern of the mode $TE_{1,4,1}$ (the three indices represent the azimuthal, the radial, and the longitudinal mode numbers) in the laser.

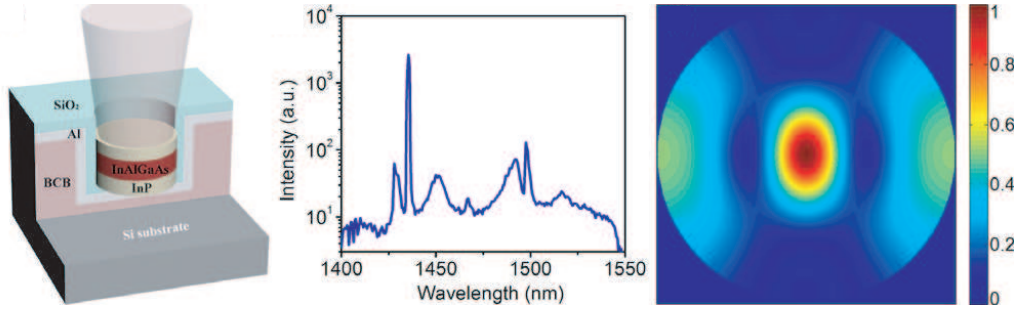

(a) (b) (c)

Figure 1: (a) Scheme of the fabricated subwavelength laser. A circular semiconductor core is coated by silica/aluminium layers, and then bonded on a silicon substrate by using a BCB layer. (b) Measured lasing spectrum of the fabricated laser at room temperature. (c) Calculated far-field pattern of the mode $TE_{1,4,1}$ in the laser.

We demonstrated a metallic confined InAlGaAs/InP circular subwavelength laser. Single lasing mode with peak wavelength of 1436 nm and linewidth of 1 nm was observed. The mode spectrum of the laser and the far-field patterns of the resonant modes were investigated by 3D FDTD method.

REFERENCES

1. Smit, M., J. van der Tol, and M. Hill, "Moore's law in photonics," *Laser Photonics Rev.*, Vol. 6, 1–13, 2012.

2. Miller, D. A. B., "Device requirements for optical interconnects to silicon chips," *Proc. IEEE*, Vol. 97, 1166–1185, 2009.
3. Ning, C. Z., "Semiconductor nanolasers," *Physica Status Solidi B — Basic Solid State Physics*, Vol. 247, 774–788, 2010.
4. Nezhad, M. P., A. Simic, O. Bondarenko, B. Slutsky, A. Mizrahi, L. A. Feng, V. Lomakin, and Y. Fainman, "Room-temperature subwavelength metallo-dielectric lasers," *Nature Photonics*, Vol. 4, 395–399, 2010.

Session 4A3
Extended/Unconventional Electromagnetic Theory, EHD(Electro-hydrodynamics)/EMHD(Electro-magneto-hydrodynamics), and Electro-biology

Calculations Concerning the Variable Size of Protons and Other Nuclei

Konstantin Meyl
Faculty of Computer and Electrical Engineering
First Transfer Center of Scalar Wave Technology (1.TZS)
Furtwangen University, Germany

Abstract— 30 years ago already, the then nuclear research center in Karlsruhe publicized experimentally determined dimensions and shapes of various nuclei. Apart from the obvious spherical shape, cylindrical and elliptical nuclei had also been found. Such experimental results have to be compared with calculations. Not only the number of p^+ and n° involved, but also spin, direction of rotation, and nuclear cohesion through magnetic moment need to fit together. The mathematical basis can already be found in the work from 1755 by the founder of the modern field theory, Prof. Roger Joseph Boscovich. According to his assumption is calculated, as an example, that the radius of a particle is dependent on the field and, ultimately, on the mass of all particles involved in the measurement. Thus the radius of the proton is reduced by muons about 5% in contrast to electrons. The factor, widely confirmed by recent measurements, is calculated. This should also apply to other atoms measured by the help of muons, when for this purpose the corresponding particle mass is influencing the calculation. At the end of the paper mathematically justified predictions are given.

Dissipative Magnetorotational Instability: Wavelength Asymptotic Saturation

F. E. M. Silveira
Centro de Ciências Naturais e Humanas, Universidade Federal do ABC, Santo André, Brazil

Abstract— When a plasma, which rotates differentially about a fixed center, is subjected to a magnetic field, perpendicular to the plane of rotation of the fluid, the coupling of the current with the field (the Lorentz force density) may be disruptive if the angular velocity of the gas decreases with the increase of the radial coordinate. This phenomenon is commonly referred to as the magnetorotational instability (MRI). For a perfectly conducting, inviscid plasma (ideal approximation), the problem can be treated analytically. Such an approach is particularly useful for the description of the dynamical evolution of accretion disks, astrophysical structures consisting of ionized gases which rotate about compact objects (black holes, neutron stars). In this case, the flow is assumed to exhibit a Keplerian profile, thereby leading to a dispersion relation which is biquadratic in the growth rate of the MRI. However, the associated instability condition implies the perturbative wavelength increases with the increase of the radial coordinate [1]. This means that, as the radial coordinate decreases, the perturbative frequency increases with no limit. Recently, there has been some progress towards an analytical formulation of the MRI by including dissipative effects for the rotating plasma [2, 3]. In this work, by introducing both finite resistivity and viscosity for a Keplerian accretion disk, it is found that the growth rate of the instability may satisfy a quadratic equation and become suppressed by a term which depends on the magnetic Prandtl number. It is also shown that, when resistive effects dominate, the perturbative wavelength saturates asymptotically to a minimum value which does not depend on the radial coordinate.

REFERENCES

1. Balbus, S. A. and J. F. Hawley, "Powerful local shear instability in weakly magnetized disks I — Linear analysis," *Astrophys. J.*, Vol. 376, 214, 1991.
2. Silveira, F. E. M. and R. M. O. Galvão, "Magnetorotational instability, current relaxation, and current-vortex sheet," *Phys. Plasmas*, Vol. 20, 082126, 2013.
3. Silveira, F. E. M., "Asymptotic saturation of mode frequency for the magnetorotational instability in resistive plasmas," *J. Phys.: Conf. Ser.*, Vol. 574, 012071, 2015.

The Efficiency of a Hydrogen Circuit in a Smart Grid

P. Marcon[1], **Z. Szabo**[1], **Z. Roubal**[1], **F. Zezulka**[2], **and I. Vesely**[2]

[1]FEEC, Department of Theoretical and Experimental Electrical Engineering
Brno University of Technology, Technicka 12, Brno, Czech Republic
[2]FEEC, Department of Control and Instrumentation
Brno University of Technology, Technicka 12, Brno, Czech Republic

Abstract— The paper describes the connection of a hydrogen circuit to a 24 V experimental smart grid. The principle of the proposed design consists in improving the stability of the current grid and enabling maximum exploitation of the electric energy produced by renewable sources (micro-hydropower plant, photovoltaics, and wind power plants). In this respect, the authors present a very important module to save the energy and show an efficiency calculation of the hydrogen circuit.

Our hydrogen circuit consists of an electrolyzer (hydrogen generator) with a purifier; the second part is a hydrogen storage, in our case the storage presents a metal hydride canister with a valve system to switch between a charge operation and consumption, and the third one is a fuel cell. A hydrogen generator is based on an innovative alkaline membrane technology and produces 100 sl of hydrogen per hour. The generator produces hydrogen on demand from water, directly compressed, dry and pure using a patented electrolytic process. It contains 5 l water tank.

OvonicTM Solid Hydrogen Storage Canisters are used to store pure gaseous hydrogen in a solid form and under a low pressure level. The stored hydrogen can be used by a fuel cell system or by other hydrogen consuming systems.

Fuel cells with a polymer electrolyte membrane are characterized by a high current density, which allows the construction of a low weight and small dimensions. The solid electrolyte membrane simplifies sealing in a chemical process, reduces corrosion and increases the life of the cell.

Advanced Methods of UHF EM Diagnostic of Discharge Activity in High Voltage Transformers Dielectric

P. Drexler[1], **M. Cap**[1], **P. Fiala**[1], **M. Steinbauer**[1], **M. Kaska**[2], **and L. Kocis**[3]

[1]Department of Theoretical and Experimental Electrical Engineering
Brno University of Technology, Brno, Czech Republic
[2]TES, Trebic, Czech Republic
[3]EGU HV Laboratory, Praha, Czech Republic

Abstract— The reliable and economical production and distribution of electrical energy and safety impacts of these processes are crucial aspects of sustainable development in industry and generally the human society. The energy production and distribution chain comprises of various blocks with specific functions and the safety and reliability of each of the blocks are under intensive monitoring. The key component of the chain is the block transformer in the power plant. It is carrying high electrical power under very high voltage conditions. Therefore, the condition of its oil dielectric is carefully watched in order to prevent the development of partial discharges (PD). PD in oil represents an electrical discharge activity at the microscopic nonhomogeneities — e.g., released microbubbles of dissolved gasses. The oil degeneration due to PD activity rapidly deteriorates its insulating properties which can lead to subsequent intensive arc and catastrophic transformer failure.

Various methods have been developed over time. Currently the most advancing is the ultra-high frequency (UHF) method which is based on the real-time detection of electromagnetic radiation generated by PD. Moreover, this approach allows also the time-difference-of-arrival (TDOA) localization of PD source. We have previously reported the development of PD diagnostic system based on the UHF method, including TDOA localization and we have presented results of real field measurement on the nuclear power plant's transformers. Despite of the common view of the UHF method, which assumes excellent sensitivity due to transformer's vessel shielding properties against outer interference, we have noted low-level signal detection difficulties. They are caused by the influence of discharge activity in the encapsulated feeding lines which connect the transformers with turbo-generator system. We have developed a new method for weak PD signal detection which utilizes discrimination of disturbed signal acquisitions. The method was verified by field measurement of very weak injected artificial pulse signal. The results indicate that the sensitivity down to tens picocoulombs can be achieved.

In the proposed article we would like to report the results obtained be the new detection method application. The steps of procedure of method application will be described also. Further advances of the method represents the discharge radiated signal filtration with the goal of separation of the frequency band which are typical for rapid PD and the suppression of frequency bands occupied by components of different electrical discharge types. This advancement further enhances the sensitivity and reliability of the UHF method with discrimination of disturbed signal acquisitions approach.

Numerical Model and Analysis of a Graphene Periodic Structure

P. Drexler, **P. Fiala**, **D. Nešpor**, **M. Steinbauer**, **T. Kříž**, **and M. Friedl**
FEEC BUT, UTEE, Technická 12, Brno 616 00, Czech Republic

Abstract— The aim of this paper is to present the particulars of new research in special numerical models of structures used for nanoapplications. These models can be advantageously used in the evaluation of electromagnetic parameters, thus helping researchers and designers to solve problems related to nanoelements and nanotechnology. The first numerical model of large peridodic structure is designed to test electromagnetic wave propagation in a graphene composite structure. According to the interpretation of the results, the basic design will be prepared for experimental fabrication of the functional sample. There are the results of a numerical analysis of simple nano-electric line.

Introduction: It is obvious from the research presented in papers [1, 3] that the periodic structure of graphene should exhibit certain interesting electrical and electromagnetic properties regarding the propagation of an electromagnetic wave. Thus, new horizons could be opened for the use of graphene in electrical engineering (EMG) and electronics. The referenced articles nevertheless do not provide a clear conclusion that would facilitate prospective application of periodic structures with extreme properties in the field of electromagnetic wave propagation; these structures can be based on either natural or artificial materials.

The authors of this paper have developed the idea to set up a simple numerical model and to propose an experiment suitable for the related verification. Fig. 1 shows the known concepts of carbon nanostructures [2, 3] and layered polymer. The numerical model enables us to evaluate the propagation of an electromagnetic wave along the surface consisting of a periodic structure (such as graphene or metamaterial) and the surrounding dielectric environment The aim of the model is to evaluate the components of both the EMG wave and the power flux density in the time domain; thus, based on our knowledge of today's manufacturing technologies, it would be easily possible to define the applicability of the periodic structure for specific purposes in electrical engineering and electronics. Examples of periodic structure arrangements can be found in several studies, for instance in the referenced paper [2], Fig. 1.

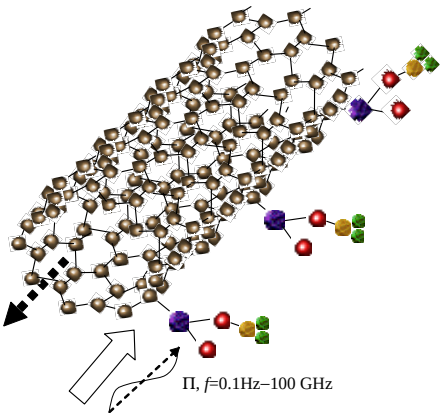

Figure 1: Geometrical structure of the numerical analysis of surface wave propagation.

REFERENCES

1. Castro Neto, A. H., F. Guinea, K. S. Novoselov, and A. K. Geim, "The electronic properties of graphene," *Reviews of Modern Physics*, Vol. 81, The American Physical Society, Jan.–Mar. 2009.
2. Yan, C., K.-S. Kim, S.-K. Lee, S.-H. Bae, B. H. Hong, J.-H. Kim, H.-J. Lee, and J.-H. Ahn, "Mechanical and environmental stability of polymer thin-film-coated graphene," *ACS Nano*, Vol. 6., No. 3, 2096–2103, 2012.
3. Singh, K., A. Ohlan, and S. K. Dhawan, "Polymer-graphene nanocomposites: Preparation, characterization, properties, and applications," Intech©, http://dx.doi.org/10.5772/50408, 2012.

Magnetic Field Shaping with Quasi-Periodic Resonators

D. Nespor and P. Drexler
Department of Theoretical and Experimental Electrical Engineering
Brno University of Technology, Technická 3082/12, Brno 616 00, Czech Republic

Abstract— Metamaterials are composite structures which have electrical and magnetic parameters (permittivity and permeability) which don't exist in the nature. Metamaterials are composed of small segments. For example, they compose of long parallel conductors or planar coils. In fact, metamaterials aren't homogenous. But if we use an electromagnetic wave with wavelength much larger than the size of metamaterial segment, we can consider the metamaterial as homogenous. Generally, metamaterials with negative parameters represent the media which has negative value effective permittivity ε_{ef} or permeability μ_{ef}. These materials are known since 1960s but only theoretically.

It is possible to manipulate electromagnetic field by means of dielectric materials. Electromagnetic field will be affected due to values of dielectric constant ε_r and permeability μ_r. Viktor Veselago has defined theoretically the usage of material with negative parameters (metamaterial) as an electromagnetic lens. If we put metamaterial between transceiver and receiver, we can see an increase in detected energy. It appears that the metamaterial behaves like an electromagnetic lens.

Negative permeability can increase magnetic coil range. It means that metamaterial with negative permeability behave as an electromagnetic lens. Negative effective permeability can be created by Split Ring Resonators (SRR). The resonator is constructed as a concentric metal ring with interspaces. These rings are deposited as regular matrix on dielectric substrate. For better homogenous of magnetic the field it is possible to designed Kvasi-Periodic Resonators (KPR). KPR are composed from SSR. The subject of this work is design and measuring of KPR.

ACKNOWLEDGMENT

Research described in this paper was financed by the National Sustainability Program under grant LO1401, by the Czech Science Foundation under grant No. GA15-08803S, a project of the BUT science fund, No. FEKT-S-14-2545, and a project from the Education for Competitiveness Operative Programme, No. CZ.1.07.2.3.00.20.0175 (Electro-researcher). For the research, infrastructure of the SIX Center was used.

Control of Breath Simulator

I. Vesely[1, 2], **F. Solc**[1, 2], **and F. Zezulka**[1, 2]

[1]Department of Control and Instrumentation, FEEC
Brno University of Technology, Technicka 12, Brno, Czech Republic
[2]Centre for Research and Utilization of Renewable Energy, FEEC
Brno University of Technology, Technicka 12, Brno, Czech Republic

Abstract— The paper discusses the control of a specific LUNG simulator. This model was created for education and it is used for the simulation of required respiration wave. These simulations may be used on either rubber substitute lung or real lungs. The simulator can simulate breathing during various diseases or detect different lung properties (e.g., stiffness, puncture).

The simulator consists of several parts. They are piston, lung and box, where is connection for lung. The whole process in simulator was described by equations and created a simulation model in Matlab for the suitable design of controller. In this model are taken into account various distractions such as leak of box.

Control of simulator is programmed in LabVIEW and implemented in the real-time platform CompactRio. The simulator program has several modes. User can choose one mode and set parameters of this mode. They are the generating of required speed and feedback control. The CompactRio is used for reading the sensor values and control the pump and the piston movement. The values which are read from input can be divided into two parts: safety sensors and sensors for control. Values from the pressure sensor and the limit motion sensor are safety sensors and values of flow sensors are used to control. These values are processed in the CompactRio and the he PWS signal is sent to output for the control of bellow speed. Safety sensors are used for switching the vacuum pump and checking of the bellow position. The result is a simulator that realizes the required course of respiration curve.

Session 4A4
Advanced Photonic Systems for Datacommunications

Future Ultra-low Latency Flexible and Programmable All-optical Interconnect Architectures for High-capacity Datacentre Networking

Emilio Hugues-Salas
University of Bristol, UK

Abstract— Increasing number of Internet applications are migrating to the Cloud. In addition, High-Performance Computing (HPC) applications, big data storage/processing along with multi-tenancy, impose new requirements that challenge current data centre networks (DCN) infrastructure with warehouse-scale datacentres (DCs) being deployed in order to support these DC new services. To overcome these challenges, optical-based components are foreseen as promising DC technologies since such devices inherently offer high-bandwidth, low-latency and flexible intra-DCN interconnections. In this invited talk, recent research progress on datacentre interconnect architectures is reviewed in terms of the advanced optical fibres and components used, beyond the state-of-the-art all-optical equipment, programmable flexible high-speed electronics and various multiplexing techniques for datacentre connectivity. On one hand, spatial-division-multiplexing (SDM) transmission is proposed to provide a large quantity of optical links between top-of-the-racks (ToRs) and the function programmable cluster switch. Multicore or multi-element fibres (MEFs) are SDM fibre alternatives to achieve these functionalities. On the other hand, Hollow-Core Photonic Band-Gap Fiber (HC-PBGF) is suggested as another kind of interconnection fibre link to offer significant propagation delay reduction. With regards to equipment, the use of high-port count fibre switches and reconfigurable spectrum selective switches provide important flexibility and adaptability to the DCN architecture to combat the unpredictable DCN applications and services. With respect to DCN interfaces for chip-level access, high-speed electronics based on field-programmable gate arrays (FPGAs) ameliorate the bottleneck whenever optical-to-electronic (O/E) conversion occurs. Finally, different multiplexing techniques, such as Time Division Multiplexing (TDM) and Wavelength Division Multiplexing (WDM), together with SDM, are discussed as ways to achieve high scalability and connectivity amongst systems and subsystems of the DCN as well as in between DCNs.

Golomb Ruler Sequences Optimization for FWM Crosstalk Reduction: Multi-population Hybrid Flower Pollination Algorithm

Prince Jain, **Shonak Bansal**, **Arun Kumar Singh**, **and Neena Gupta**
PEC University of Technology, Sector-12, Chandigarh, India

Abstract— The adverse nonlinear effects degrade the performance of optical wave length division multiplexing (WDM) systems. One of the performance degradation effects is four wave mixing (FWM) crosstalk, a serious problem for WDM systems and can be reduced by unequal channel spacing [1]. Here, we present an unequal channel allocation scheme based on the optimal Golomb ruler (OGR) sequences [2]. It allows the reduction of FWM crosstalk signals preserving the effectiveness of optical channel bandwidth. Recently, the Golomb ruler, a class of non-deterministic polynomial (NP)-complete problems, has been solved by multi-objective, nature-inspired based optimization algorithm [3].

An improved version of Multi-Objective Flower Pollination Algorithm (MOFPA) [4] is proposed to solve the OGR sequences. The modified algorithm called MHMOFPA divides the entire population into several sub-populations/multi-populations at each iteration. All the sub-populations exchange the best solutions by applying the differential mutation strategy. This enhances the ability of original MOFPA algorithm and attains the balance between exploration and exploitation abilities in the search space preserving the solutions diversity in the population.

The proposed algorithms are executed 20 times until optimal sequences are found. The experimental results demonstrate better and efficient generation of OGRs in a reasonable computational time compared to its original forms. Figures 1(a) and (b) show the reduction in the ruler length computation time and total channel bandwidth occupied, respectively.

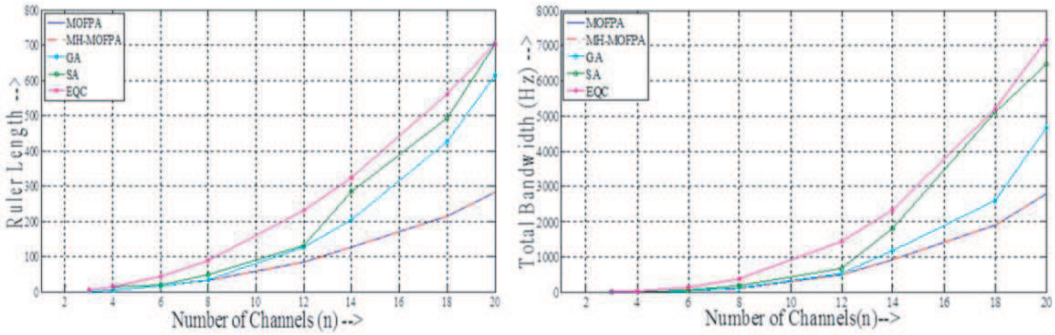

Figure 1: The proposed algorithm demonstrates the significant reduction in (a) ruler length and (b) total channel bandwidth in comparison to the existing algorithms.

REFERENCES

1. Kwong, W. C. and G. C. Yang, "An algebraic approach to the unequal-spaced channel-allocation problem in WDM lightwave systems," *IEEE Trans. on Commun.*, Vol. 45, No. 3, 352–359, 1997.
2. Bloom, G. S. and S. W. Golomb, "Applications of numbered undirected graphs," *Proceedings of the IEEE*, Vol. 65, No. 4, 562–570, 1977.
3. Bansal, S. "Optimal golomb ruler sequence generation for FWM crosstalk elimination: Soft computing versus conventional approaches," *Applied Soft Computing*, Vol. 22, 443–457, 2014.
4. Yang, X.-S., M. Karamanoglu, and X. S. He., "Flower pollination algorithm: A novel approach for multiobjective optimization," *Engineering Optimization*, Vol. 46, No. 9, 1222–1237, 2014.

Photonic Microwave Amplification for Radio-over-Fiber Links Utilizing Semiconductor Lasers at Stable Locking Dynamics

Kun-Lin Hsieh[1] and Sheng-Kwang Hwang[2]

[1]Department of Photonics, National Cheng Kung University, Tainan, Taiwan
[2]Advanced Optoelectronic Technology Center, National Cheng Kung University, Tainan, Taiwan

Abstract— The radio-over-fiber technology has attracted considerable attention in the last two decades since it enables the distribution of microwaves over long distances through optical fibers. The simplest scheme to superimpose microwaves on optical carriers is direct or external modulation of semiconductor lasers. However, due to their low modulation efficiency, especially at high frequencies, low optical modulation depth is typically generated. This leads to low microwave power after photodetection at a remote base station and therefore limits the distance of microwave radiation. The most straightforward approach to enhance the microwave power is to increase the optical power received by the photodetector, which however may induce unnecessary fiber nonlinearity and may also result in severe detector damage. To overcome these problems, a variety of different approaches based on, for example, optical filtering, fiber Bragg grating, and Brillouin scattering have been proposed for microwave power amplification under a fixed optical power received by the photodetector through improving the modulation depth of a microwave-modulated optical signal. These approaches rely on considerable power suppression of the optical carrier and therefore require optical amplifiers to compensate for the optical power loss. In this study, the stable locking dynamics of semiconductor lasers are applied to achieve modulation depth enhancement through sideband enhancement, instead of carrier suppression, without significant power dissipation. Under proper continuous-wave optical injection, while the optical oscillation of a semiconductor laser is stably frequency-locked to the injection, the lower sideband of its relaxation resonance becomes resonantly enhanced due to the red-shift of the cavity resonance. By taking advantage of such a resonant enhancement characteristic, the modulation depth of a microwave-modulated optical signal can be considerably enhanced by sending it into the laser under the same operating conditions. As a result, the power of the photodetected microwave is amplified by more than 17 dB under the same received optical power. Accordingly, the sensitivity of the phtodetection is significantly improved by more than 8 dB. The phase quality, such as linewidth and phase noise, of the microwave is preserved after amplification. The amplification system can operate for microwave frequency ranging from less than 12 GHz to more than 60 GHz by properly controlling the operating conditions or by choosing proper lasers.

ACKNOWLEDGMENT

S. K. Hwang's work is supported by the Ministry of Science and Technology of Taiwan under Contract MOST103-2112-M-006-013-MY3.

100-Gb/s Point-to-point Solutions for Long-reach Passive Optical Networks in Sparse Rural and Urban Areas

Elias Giacoumidis[1,2], **Giuseppe Talli**[3], **Naoise Mac Suibhne**[1], **Son T. Le**[1], **Nick J. Doran**[1], **and David B. Payne**[1,4]

[1]Aston Institute of Photonic Technologies (AIPT), Aston University, Birmingham B4 7ET, UK
[2]Centre for Ultrahigh Bandwidth Devices for Optical Systems (CUDOS), School of Physics University of Sydney, NSW 2006, Australia
[3]Tyndall National Institute, University College Cork (UCC), Cork, Ireland
[4]Trinity College Dublin, Dublin, Ireland

Abstract— Long reach-passive optical networks (LR-PON) are being proposed as a means of enabling ubiquitous fiber-to-the-home (FTTH) by massive sharing of network resources and therefore reducing per customer costs to affordable levels. To be ubiquitous the solutions must be suitable for sparse rural areas and also must cater for very high capacity links (∼100-Gb/s) for large business customers. The difficulty for conventional PON designs in sparse rural areas is connecting a sufficient number of customers to the PON system in order to get adequate sharing of the physical infrastructure and therefore achieve a low cost per customer. A further problem is the longer distances between splitter nodes and customers, which requires longer cable lengths with higher fiber count which also increases cost per customer. Also the size of small rural communities can be much less than the total LR-PON split which would mean that the conventional "lollipop" design, with long feeder and large split within a relatively small fiber reach < 10 km, can be underutilized which directly increases the cost per customer. In this paper, we consider the use of "chained" cable and amplifier solutions to improve LR-PON utilization in rural areas. The amplifier nodes for a single LR-PON are presented in a chain configuration with 4 fibers required between the amplifier nodes for each LR-PON chain, while only 2 fibers are required from the primary and secondary metro-nodes to the closest respective amplifier nodes. This solution shares one optical line terminal (OLT) working and one protection OLT for all the amplifier nodes in the chain, it maintains full wavelength availability at all amplifier nodes and also works for single wavelength entry solutions. We analyze the chain solutions at 100-Gb/s point-to-point transmission using dual polarization-quaternary phase shift-keying (DP-QPSK) modulation. The numerical analysis shows that with appropriate finite impulse response (FIR) filter designs, 100-Gb/s transmission can be achieved with at least 512 way split and up to 160 km total distance which is sufficient for many of the optical paths in a practical situation (e.g., private circuits across large metropolitan area) for a point-to-point link from one LR-PON to another LR-PON through the optical switch at the metro nodes and across a core light path through the core network without regeneration.

Photonic Microwave Generation and Stabilization Using Semiconductor Lasers at Period-one Dynamics

Kai-Hung Lo[1] **and Sheng-Kwang Hwang**[1, 2]

[1]Department of Photonics, National Cheng Kung University, Tainan, Taiwan
[2]Advanced Optoelectronic Technology Center
National Cheng Kung University, Tainan, Taiwan

Abstract— Photonic microwave generation using optically injected semiconductor lasers at period-one dynamics has attracted great research attention owing to its promising broadband frequency tunability and all-optical approach. However, due to the intrinsic laser noise, the 3 dB linewidth of such generated microwaves is typically of the order of megahertz, which is disadvantageous for many application purposes. Therefore, several linewidth reduction schemes have been proposed, including direct modulation, optoelectronic feedback, and optical feedback. The last scheme is particularly attractive since no electrical microwave source is necessary, making the scheme all-optical and therefore bypassing severe electronic limitation and parasitics for high frequency microwave generation. In this study, research work is conducted to study how the microwave linewidth varies as a function of the feedback level and time, which shall provide important guidelines in operating the system for better linewidth reduction. If the feedback level is high except for extremely short feedback delay times, the optical feedback can actually suppress the period-one dynamics and excite other more complex dynamics. However, within the range of the period-one dynamics, the optical feedback can stabilize the period-one dynamics in such a manner that significant reduction of microwave linewidth and phase noise is achieved, up to more than two orders of magnitude. A high feedback level and/or a long feedback delay time are generally preferred for such microwave stabilization. However, considerably enhanced microwave linewidth and phase noise happen periodically at certain feedback delay times, which is strongly related to the behavior of locking between the period-one microwave oscillation and the feedback loop modes. The extent of these enhancements reduces if the feedback level is high.

IMDD Formats for High-speed Data Center Interconnect Applications up to 80 km

H. Griesser[1], **A. Dochhan**[2], **N. Eiselt**[2], **J. L. Wei**[2], **and J.-P. Elbers**[1]

[1]ADVA Optical Networking SE, Campus Martinsried
Fraunhoferstraße 9a, Martinsried, Munich 82152, Germany
[2]ADVA Optical Networking SE, Märzenquelle 1-3, Meiningen, Germany

Abstract— Services like cloud storage, video streaming, and on-demand computing moves big data centers into the focal point of the internet. A large part of internet traffic is just between data centers and not to the end user. Regionally close data centers with massive interconnections form a single distributed data center, driving the need for many cheap 100 GbE and 400 GbE connections over a single fiber up to 80 km distance. This application is not covered by the IEEE P802.3bs 400 GbE Task Force which defines objectives for multimode fiber (MMF) and for single mode fiber (SMF) including 500 m, 2 km and 10 km length of SMF.

While coherent DP-16QAM with two wavelengths could be used to transport 400 GbE over 80 km such a solution most likely will not meet the stringent requirements on cost, power and footprint for these short distances. DP-64QAM on a single wavelength would be more appealing, but currently the performance is dominated by the low resolution of the converters and the limited bandwidth of the electrical components. Therefore, intensity-modulated and directly-detected (IMDD) formats might be an interesting alternative to potential coherent solutions. In the paper we present an overview on interesting modulation formats currently considered for WDM transport of 400 GbE signals over metro distances promising lower costs compared to long-haul implementations. DP-64QAM with coherent reception is compared to the IMDD formats PAM4 and DMT, with regard to reach, form factor, and energy consumption. Although an IMDD format most probably requires eight wavelengths for the application under consideration it might benefit significantly from the ecosystem and the economy of scale of the 400 GbE client interface.

Numerical Analysis of Artificial Neural Network and Volterra-based Nonlinear Equalizers for Coherent Optical OFDM

Elias Giacoumidis[1,2], **Jinlong Wei**[3], **Mutsam A. Jarajreh**[4], **Son T. Le**[1], **Paul A. Haigh**[5], **Jan Bohata**[6], **Andreas Perentos**[1], **Sofien Mhatli**[7], **Mohammad Ghanbarisabagh**[8], **Ivan Aldaya**[9], **and Nick J. Doran**[1]

[1]Aston Institute of Photonic Technologies (AIPT), Aston University, Birmingham B4 7ET, UK
[2]Centre for Ultrahigh bandwidth Devices for Optical Systems (CUDOS)
School of Physics, University of Sydney, NSW 2006, Australia
[3]ADVA Optical Networking SE, Campus Martinsried
Fraunhoferstrasse 9a, Martinsried/Munich 82152, Germany
[4]Engineering Department, School of Computing
Fahad Bin Sultan University, Tabuk, Kingdom of Saudi Arabia
[5]High Performance Networking (HPN) Group
Faculty of Engineering, University of Bristol, Bristol BS8 1UB, UK
[6]Faculty of Electrical Engineering, Czech Technical University in Prague, Czech Republic
[7]SERCOM-Lab, EPT Université de Carthage, La Marsa, Tunis 2078, Tunisia
[8]Faculty of Engineering, Islamic Azad University North Tehran Branch, Tehran, Iran
[9]Department of Electrical and Computational Engineering
Instituto Tecnológico y de Estudios Superiores de Monterrey, 64800, Mexico

Abstract— Coherent optical orthogonal frequency-division multiplexing (CO-OFDM) is a high spectral-efficient modulation technique able to virtually eliminate inter-symbol interference caused by chromatic dispersion and polarization-mode dispersion. One major drawback of CO-OFDM that remains unsolved is its vulnerability to nonlinear fiber effects due to its high peak-to-average power ratio. Several digital signal processing (DSP) techniques have been investigated for the compensation of fiber nonlinearities, such as the traditional digital back propagation (DBP), nonlinear pre- and post-compensation and nonlinear equalizers (NLEs) based on the inverse Volterra-series transfer function (IVSTF). The main disadvantage of DBP is the extensive use of the fast Fourier transform, which results in high DSP computational load. Pre- and post-compensation algorithms are complex to implement and present a marginal performance enhancement (< 0.5 dB in Q-factor). IVSTF-based equalization has been considered as an effective method for combating fiber nonlinearities. Alternatively, nonlinearities can be mitigated using nonlinear decision classifiers such as artificial neural networks (ANNs) based on a multilayer perceptron (MLP). MLP-ANNs form a complex map with nonlinear decision boundaries between its input and output spaces, which helps in inverting the effects of nonlinear distortions. ANNs have shown promising results in wireless communications applications to reduce the effect of the nonlinear distortion of amplifiers in OFDM signals. In this paper, a novel reduced-complexity ANN-NLE for 16QAM CO-OFDM is analyzed. The capability of the proposed approach to compensate the fiber nonlinearities is numerically demonstrated for up to 100-Gb/s and over 1000 km and compared to the benchmark IVSTF-NLE. Results show that in terms of Q-factor, for 100-Gb/s at 1000 km of transmission, ANN-NLE outperforms linear equalization and IVSTF-NLE by 3.2 dB and 1 dB, respectively. Additionally, it is shown that both ANN and IVSTF NLEs offer $\sim$50% reduced computational complexity compared to the single-step/span DBP.

Quantum-dot Semiconductor Optical Amplifiers: Novel Technique for Gain Management and Noise Suppression

Hamed Baghban and Amir Hashemloo
School of Engineering-Emerging Technologies
University of Tabriz, Tabriz 51666-14761, Iran

Abstract— The saturation behavior of a quantum-dot semiconductor optical amplifier (QD-SOA) is governed by a complex combination of ground state and excited state replenishment in saturation condition. Also, due to inhomogeneously broadened gain of a QD-SOA, various spectral regions are coupled via the common quantum dot (QD) reservoir, i.e., wetting layer, and the barrier layer. Hence, a frequency domain model has been developed to effectively exhibit the saturation properties of a QD-SOA in this article. Based on performed experimental tests, and also, developed model we exploit gain dynamic, gain saturation characteristics and noise suppression capability at different SOA operation conditions. The effect of an external beam on different characteristics of QD-SOAs has been investigated experimentally when the applied beam is in the gain or transparency region of the amplifiers. Also, based on different external beam power levels, the performance of the discussed method is characterized in terms of signal-to-noise ratio at the input of the QD-SOA, and output quality factor, which directly quantifies the level of intensity noise. A comprehensive comparison is performed between the quality factor of noisy input bit stream and the output data which contains the pattern effect at higher bit rates. Finally, noise suppression specification of the device at different bias currents is discussed.

Figure 1 (left panel) illustrates the experimental setup utilized for gain characteristics measurement at the presence of the external holding beam (HB). Also, the noise suppression features at different bit rates in terms of the input and the output Q-factors along with the Q-factor-bit rate competition have been presented in the middle and right panel of Figure 1.

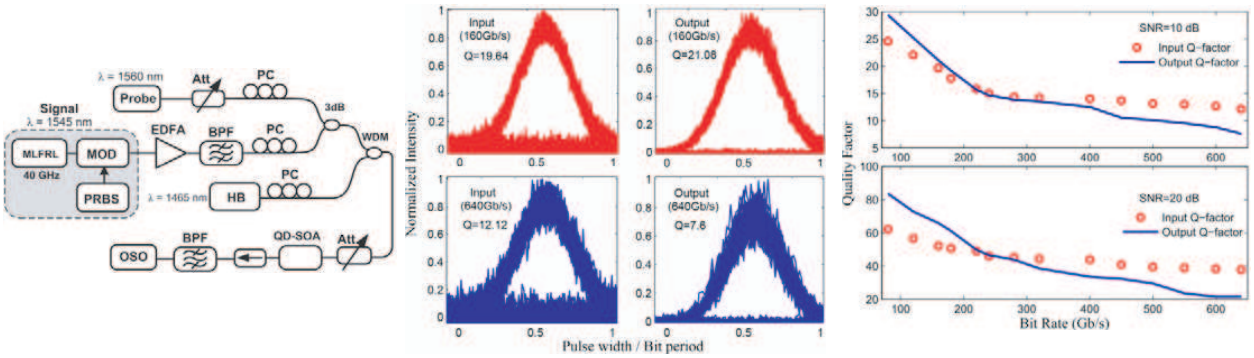

Figure 1: Experimental setup used for investigation of the effect of an external beam on QD-SOA gain and noise features as well as the noise characteristics obtained from the developed model.

REFERENCES

1. Baghban, H. and F. Alimohammadi, "Noise suppression in quantum-dot semiconductor optical amplifiers: A bit rate-SNR analysis," *IEEE Transactions on Electron Devices*, 2015 (under publication).
2. Alavizadeh, S., H. Baghban, and A. Rostami, "Quantum-dot semiconductor optical amplifier performance management under optical injection," *J. Modern Optics*, Vol. 60, 509–514, 2013.
3. Rostami, A., H. Baghban, and R. Maram, *Nanostructure Semiconductor Optical Amplifiers: Building Blocks for All-optical Processing*, Springer-Verlag, 2010.

Session 4A5
Power Electronics 1

Parameters Identification of Controlled Systems with Electrical Drives Using Genetic Algorithms

P. Brandstetter, J. Hajovsky, and M. Kuchar
Department of Electronics, VSB-Technical University of Ostrava, Czech Republic

Abstract— There are a lot of new approaches and principles which are based on a relatively new scientific discipline which is called soft computing. The main feature of soft computing is a departure from traditional modelling based on Boolean logic, analytical models, sharp classification and deterministic search. Among the main representative of soft computing we can include fuzzy logic, neural networks and genetic algorithms. Genetic algorithms solve optimization problems in different fields of the industry. In the field of electrical drives, the genetic algorithms can be used to identify the parameters of the controlled system, optimization of the controller parameters settings and optimization of the parameters adjustment of adaptive controllers.

The electrical controlled drives usually work with controlled systems that contain one or two large time constants and several small time constants, whose influence is replaced by approximately sum time constant. The large time constants is then compensated by a serial correction using a controller, while the sum time constant remains uncompensated. The quality of the control is assessed according to the response of the control loop to step change of input variable.

In the paper, there is used the genetic algorithm to identify the unknown time constants of the controlled system with electrical drive from the step response characteristics.

The most important part of the genetic algorithm is the fitness function — An equation describing searched problem. The first population is generated randomly from specified range of values. According to the results of the individual in the fitness function for each individual is assigned a fitness value that reflects how strong this individual is. The strongest individuals continue in the algorithm and the weaker die.

Next is applied operations of mutation and crossover of most powerful individuals. During the crossing parents remain and the population grows by the new offspring resulting from accidental crossing of chromosomes randomly selected individuals — parents. The newly formed individual may be stronger than parents or weaker and dies in the next generation. The next step is the implementation of a mutation. This creates new individuals by mutation of individuals randomly selected from the population. In the developed algorithm is mutation implemented by multiplication chromosomes and random value close to one. In the next step of the algorithm are randomly generated new individuals. If not to create new random individuals, the space would be poorly scanned and the algorithm would get stuck in a local extreme of fitness function. Add new randomly generated individuals ensures a random search of the entire area, allowing the algorithm to jump out of the field of local extreme. The population was thus extended by new individuals resulting from the crossing and mutation of new individuals, but also randomly generated individuals. The whole population progresses to the next generation, where the process is repeated again — determining of fitness values — selection — crossover — mutation — the emergence of new randomly generated individuals. This process is repeated continuously till not reached the desired number of generations or until the individual is sufficiently mature — high enough fitness value.

The measured points and the function which describe the controlled system are loaded to the application. Chromosomes of the individual are function parameters and function values are calculated in measured points. Differences between measured and calculated values are calculated and summed. Total sum of the deviations then indicates how the individual is strong. The lower sum of differences means that the individual is stronger. The aim therefore is to find the parameters of the function to function as close as possible to the measurement points.

Summation of differences has the consequence that in this case the behaviour of the function exactly intersects some points and some points are disproportionately away. Sum of differences is the lowest in this case. Even during the fitting function all points can provide the sum of squared differences. The sum of squared deviations is smaller number than the large square of one difference.

The sum of the differences is exactly interleaves the most points and ignores points outside the course of function. The sum of the deviations quadrates create graphs of functions uniformly interleaved all points.

All measurements generally are flawed and because of this error sometimes it is not possible to achieve sufficient results by substituting into the equation, or by inserting of the measured points in to the system of equations and solve the equation parameters. In case of an inaccurate measurement should be measured points evenly interspersed by curve.

Model of Voltage Source Inverter for Estimation Methods with Observers

P. Brandstetter, **J. Hajovsky**, **O. Petrtyl**, **and R. Sulak**
Department of Electronics, VSB — Technical University of Ostrava, Czech Republic

Abstract— AC motors are often preferred choice in variable-speed drive applications. For high performance, it is possible to use vector control or direct torque control of the AC motor. The pulse-width modulation (PWM) inverters are most commonly applied in such AC drives. The PWM voltage source inverter, based upon IGBTs, has gained a dominant position in the AC drives market due to its ease of application, good power factor and potential to provide good dynamic performance.

At present, the importance of the so-called sensorless control of AC drives is growing. More common sensorless methods are methods working with the mathematical model of machines. Mathematical models of the AC motor that are used in sensorless control methods with different types of observers and estimators require knowledge of stator currents and voltages.

The essence of the model based methods is the use of a particular algorithm for calculation of the speed and rotor position from known or measured variables such as stator currents and voltages. The values of stator currents and voltages can be obtained by direct measurement using current and voltage sensors at the terminals of the AC motor.

For the measurement of the phase stator currents, the situation is simpler because we can measure directly the value that we need. The stator voltage generated by the PWM voltage inverter causes a ripple of the phase currents. For the control, there is not necessary to know the current waveform during switching period. It is necessary to determine the mean value of the stator currents per PWM period, not per period of the stator current. The mean value can be easily obtained using the PWM module synchronization with the AD converter. The stator currents should be scanned at the same time. From the viewpoint of the current control, there is appropriate to measure stator currents just before entry into the current control loop algorithm. Then we have actual data at disposal.

The stator voltages can be estimated direct or indirect. The direct measurement requires high quality voltage sensors. At indirect method, there is used simpler voltage sensor that is connected to DC link. This voltage sensor measures DC voltage with a low frequency voltage ripple. The stator voltages are calculated using the DC link voltage and actual switching combination of the voltage source inverter. It is known that the voltage source inverter represents generally non-linear system. A relationship between the control voltage and the output supply voltage of the voltage source inverter is not linear. The non-linearities are caused mainly by the dead-time and real properties of the power switching devices, for example a voltage drop on the power switching device. By neglecting these non-linearities, it is obvious that the calculated stator voltages are not correct at indirect method. However, the observers need correct terminal voltage of the AC motor.

The mathematical model of the machine and the entire control structure of the AC drive neglect non-linearities, or replace these non-linearities by linearized dynamic members. Then the observer or estimator which is composed of these blocks will be linear. When we use the distorted stator voltage at the input of the linear observer, we will not obtain on its outputs correct estimated values of quantities. After closing feedback control loops, behaviour of the AC drive can be very unstable. The easiest way is the mentioned non-linear effects to compensate.

The paper deals with the possibility of the compensation non-linear effects such as dead-time and the voltage drop on a power switching device.

Model of Power Electronics Used for Electric Vehicles Contactless Charging

M. Košík, **R. Fajtl**, **K. Buhr**, **and J. Lettl**
Department of Electric Drives and Traction, Faculty of Electrical Engineering
Czech Technical University in Prague, Technická 2, 166 27 Prague 6, Czech Republic

Abstract— This paper deals with modeling of adverse effects of Contactless power transfer (CPT) system to its surroundings and supply AC line. The CPT system is used for electric vehicle charging.

The first chapter of the article mentions basic equations which describe parameters of CPT. The CPT transformer is the main component of CPT and most of the equations describes its operation principle.

To increase CPT transmission efficiency, CPT has to operate at high frequency. But high operational frequency means also high value of reactance power. The second chapter of the paper lists four basic electric circuits used to compensate reactance power and thus increase the CPT transmission efficiency. This part also expands the CPT basic equations of compensation influence and adds equations for calculation of transfer efficiency, optimal operational frequency, compensation capacitor values, etc..

The third chapter of the article describes power electronics used in CPT for creating desired waveforms of current and voltage. Power electronics must meet specific requirements given by operation at frequencies about 100 kHz and with transferred active power in order of kW.

In the fourth chapter is described CPT model used for electric vehicle charging. Main focus of the model is to simulate power electronics operation. The CPT power electronics has to be able to transform waveform of electric energy distributed by AC line to high frequency waveform which is transferred by CPT transformer and then to waveform needed for electric vehicle batteries charging. Simulation shows current and voltage waveforms at every CPT component. This chapter also discuss how CPT affects AC line and other electric devices in CPT surroundings. Without magnetic core CPT transformer has low no-load losses (magnetization losses occurs only in coil conductors). As shown in simulation, due to low no-load losses the high current values are taken by CPT during device turn-on process. This phenomenon causes increased electromagnetic noise during device turn-on. The simulation shall be used for outlining of increased noise elimination method.

In conclusion, this article reminds basic principles of contactless power transfer used for electric vehicles charging. The main part of the paper focuses on simulation of power electronics, its operational functions and CPT operation effects on AC line.

Elimination of Undesirable Transients in Direct Torque Control of Induction Motor

P. Brandstetter, M. Kuchar, and J. Hajovsky, and T. Verner
Department of Electronics, VSB — Technical University of Ostrava, Czech Republic

Abstract— For a direct torque control (DTC) of induction motors, several methods were developed in the past. Among the oldest known, Depenbrock's method (D-DTC) and Takahashi?s method (T-DTC) are included. In an effort to improve or simplify these methods of the direct torque control, there was also developed several other methods, for example modified Takahashi?s method (M-DTC), a twelve-sector method (TS-DTC), a method with direct calculation of the voltage vector (DVC-DTC). In some applications, it is advantageous to achieve a constant switching frequency of a voltage inverter which basic principles of the direct torque control do not allow. For these applications, a pulse-width modular has to be integrated into the control structure of the direct torque control (PWM-DTC).

In case of the direct torque control, undesirable transients can easily occur in the process of the induction motor excitation and torque reversation. To eliminate or to reduce the undesirable transients, different ways are utilized. In the paper, there are some methods for the elimination of these undesirable transients described and experimentally verified on a laboratory stand with the induction motor drive.

An induction motor start by simply running the DTC algorithm is problematic. In general we can say that all described DTC methods allow the start of the induction motor. This start process is not in any way optimal.

The DTC algorithms require a special subroutine for the motor excitation. By running DTC methods without the special subroutine for the induction motor excitation, it is possible to describe two different transients during the motor excitation:

In the case of D-DTC and M-DTC, there is a linear increase of a stator flux in the direction of the switched active voltage vector. The time constant of the stator flux increase is greater than the time constant of the stator current. Therefore, when the stator flux modulus becomes its reference value, the stator current reaches already relatively large value. This transient is prohibited and may lead to a reaction of the voltage inverter protection, or even it can damage it. The methods T-DTC, TS-DTC, DVC-DTC and PWM-DTC have a helical increase of the stator flux. This is also accompanied by an unacceptable increase of the stator currents, but the maximum value is smaller than in the previous case.

The best way that ensures the reliable excitation of the induction motor and limits the stator currents is an application of the pulse-width modulation. The motor start is practically performed so that the subroutine is executed before starting the DTC algorithm that switches between the selected active voltage vector and one of the zero vectors. The average value of the stator current during the induction motor excitation can be set by selecting the switching ratio of the active and zero voltage vectors.

A direction change of the motor rotation is achieved by changing the sign of the desired torque. The induction motor speed begins to decrease with the steepness according to the desired torque and then the induction motor is running in the opposite direction. Some mentioned DTC methods are able to perform this reversation without any undesirable transient, for example T-DTC, M-DTC, TS-DTC and PWM-DTC. This means that there are not the over currents even a torque overshoot. Their switching table (or algorithm for the calculation of the voltage vector in the case of PWM-DTC) is not depend on the direction of the induction motor rotation, i.e., these methods are able to maintain the motor torque at the desired value even when the rotation direction disagrees with the sign of the desired torque.

For methods with the switching table (or algorithm for the calculation of the voltage vector in the case of DVC-DTC), which depend on the direction of the motor rotation, it is necessary to use a special reversal subroutine. If the sign change of the desired torque and the replacement of the switching table are at the same time, then an uncontrolled torque overshoot occurs during the torque reversation. This overshoot increases with the speed value at the reversation time. Therefore it is necessary to insert to these DTC methods the subroutine that ensures the correct time course of the motor torque during the torque reversation.

Compensation of Disturbed Load Currents Using Active Power Filter and Generalized Non-active Power Theory

Jiří Lettl[1], **Petr Šimek**[2], **and Viktor Valouch**[1]

[1]Department of Electric Drives and Traction
Faculty of Electrical Engineering, CTU Prague, Czech Republic
[2]Institute of Thermomechanics, Academy of Sciences of the Czech Republic Prague, Czech Republic

Abstract— Today, the compensation of subharmonic, non-periodic, and stochastic disturbances in the electric power systems has emerged as a very serious problem to be solved. Diversity of the features of these disturbances makes their compensation quite difficult. The compensation devices based on power electronics converters must work in the real time, so the time domain approach to control algorithms for the compensation of non-periodic disturbances seems to be promising.

The original Fryze's theory of the non-active current may be extended using a general averaging time interval T_C that can be chosen either one-half fundamental cycle, one full fundamental cycle T, that is the same as that in Fryze's theory, or multiple fundamental cycles, depending on the character of the load current, compensation objectives and the energy storage capacity of a power electronics-based compensator.

If the current $\mathbf{i}(t)$ is the current of an unbalanced load, which may contain, in general, harmonic and also non-periodic or stochastic components, and the active current $\mathbf{i}_a(t)$ is the demanded source current, then $\mathbf{i}_n(t) = \mathbf{i}(t) - \mathbf{i}_a(t)$ is the non-active current that should be injected by a parallel compensator connected to the PCC (Point of Common Coupling).

By choosing $T_C \to 0$, the GNP (Generalized Non-active Power) theory gives the same results as those obtained by using the well-known IRP (Instantaneous Reactive Power) theory. If $T_C \to \infty$, the non-active component in the non-periodic load current is completely eliminated, so the source current is only active.

A principal and analysis of usage of this GNP theory for the parallel compensation of periodic and non-periodic disturbances is presented in the paper. A non-linear unbalanced load generating periodic as well as non-periodic stochastic currents connected to an unsymmetrical non-sinusoidal voltage source is considered.

The impact of the value of T_C on the magnitude rate I_{La}/I_L for different frequencies has been studied in the frequency domain (I_{La} is a residuum of the load current magnitude I_L remaining in the active current after applying GNP strategy). It was found that especially the interharmonic current components above 100 Hz are sufficiently suppressed for $T_C = (5-10)T$. As for subharmonics, the lower their frequency is, the higher the value of T_C should be used for a sufficient compensation. On the other hand, the compensation dynamics in case of transient processes is becoming worse for T_C increasing.

The effectiveness of the generalized non-active power theory to mitigate non-periodic current disturbances is demonstrated by simulations in the time domain on an example of a reactive, unbalanced load current with several harmonic and interharmonic components, additionally modulated either by the subharmonic component or the white noise signal.

Combined Magnetic Bearing

J. Vitner, J. Pavelka, and J. Lettl
Department of Electric Drives and Traction, Faculty of Electrical Engineering
Czech Technical University in Prague, Technicka 2, 166 27 Prague 6, Czech Republic

Abstract— Magnetic bearings are becoming more and more the object of interests to designers and producers of rotating machines. Their advantages, as ability to work in vacuum, in weightlessness, in chemical aggressive environment and alike, are demonstrable. Next advantage is the possibility to change their stiffness and damping and thereby to change the rotating system oscillation frequency.

From technical point of view magnetic bearings can be divided into passive bearings and active bearings. Passive magnetic bearings exploit repelling resp. attracting permanent magnets to create a force between their stator and rotor. It is known that it is not possible to obtain a stable equilibrium by using passive magnetic bearings only and therefore at least one direction has to be stabilized by means of a mechanical bearing or an active magnetic bearing. Passive magnetic bearings operate without consummation of electric energy but low stiffness and low damping are their disadvantages. Active magnetic bearings exploit attractive force of magnetic flux in an air gap between their stator and rotor. This force, that can be controlled by the stator winding exciting current, has only attractive character and therefore two electromagnets located on opposite sides must be used for one axis. The resulting force is determined as difference of the both forces.

The paper deals with sorting active magnetic bearings according to their principle of function. Their abilities, advantages and disadvantages, as well as functional principles are discussed. Further the detailed design, development and rotor stabilization process of the combined magnetic bearing placed in the laboratory of the Department of Electric Drives and Traction FEE CTU in Prague are demonstrated. During the development applied mathematical proposal of the combined magnetic bearing, calculation of the magnetic circuit parameters, as well as calculation of the 3-phase winding and determination of the force effects of the passive and active magnetic field are explained. Last part of the paper deals with control methods of the active magnetic field, the task of them is to stabilize the rotor. Measurement results of behaviour of the stabilization process and of the individual control components are presented, too.

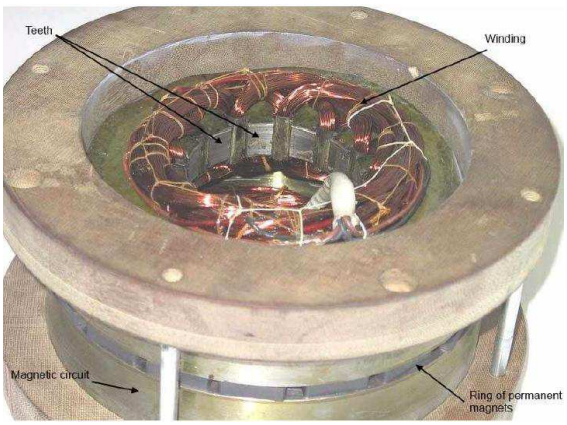

Figure 1: Stator of the realized combined magnetic bearing.

Induction Motor Drive Predictive Control Method Analysis and Comparison with Fundamental Direct Torque Control Method

J. Lettl and P. Karlovsky
Department of Electric Drives and Traction, Faculty of Electrical Engineering
Czech Technical University in Prague, Technicka 2, 166 27 Prague 6, Czech Republic

Abstract— Thanks to their simplicity, low price and high reliability, induction motor drives are one of the most common in many applications nowadays. Many ways of their control strategies have been developed since launching of mass production of the modern semiconductor devices of high power at high switching frequency. These methods include not only standard frequency control but also modern techniques of field oriented control or direct torque control.

The fundamental direct torque control method of induction motor drive, using two hysteresis controllers to maintain the asked stator flux amplitude and generated torque values, is simple and efficient, however, in some applications relatively high torque ripple can be seen as its disadvantage. That is why various modifications of the method, such as direct torque control with space vector modulation, multilevel inverter application or some forms of predictive algorithms have been performed reduce the torque ripple.

The paper presents suggested predictive direct torque control method of induction motor drive based on predicting the most suitable inverter output voltage vector for the next control step. The prediction calculation is proceeding from torque and stator flux reference values, motor parameters, and actual values estimated from voltage and current measurements. In the paper theoretical analysis of the method is performed, mathematical description of the system is created and the functionality of the proposed control algorithm is verified both by simulation in MatLab/Simulink environment and by measurement on the real induction motor drive. Comparison of the designed predictive control method with the fundamental direct torque control method developed by Takahashi is presented, too.

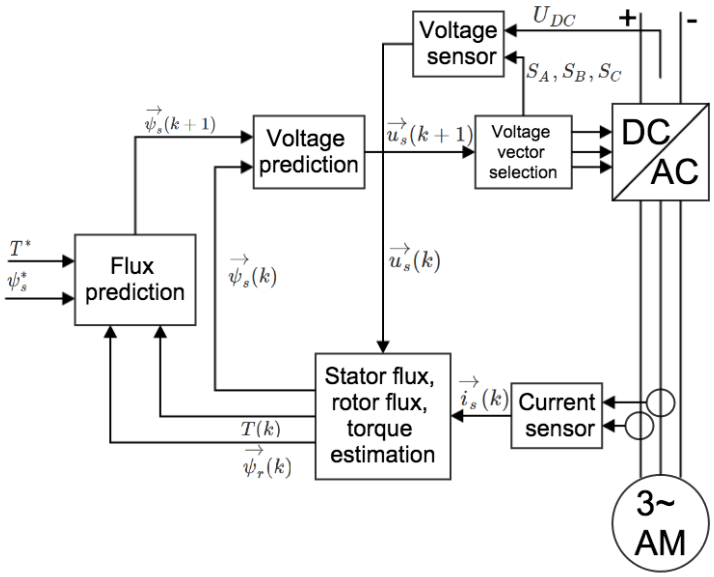

Figure 1: Block diagram of the proposed predictive direct torque control method.

Electric Vehicle Control Based on GPS and GSM Path Parameters

T. Haubert, P. Mindl, Z. Čeřovský, P. Mňuk, and J. Lettl
Department of Electric Drives and Traction, Faculty of Electrical Engineering
Czech Technical University in Prague, Technicka 2, 166 27 Prague 6, Czech Republic

Abstract— Minimizing of energy consumption is important task which is solved at all vehicles. In the case of electric vehicles (EV), energy stored on board in chemical accumulators must be used very effectively. For this purposes mathematical model of EV and real journey data used for energy consumption calculation must be used. On the basis of journey regime optimization lower energy consumption will be achieved.

Optimal journey regime is calculated by means of known road data, obtained by means of GPS and GSM navigation system. From the road horizontal and vertical data basic route elements are calculated. Basic route elements are compared with needed torque, generated by driver's pedal. All this information is processed, optimized, and needed mechanical torque is transmitted to the control unit of electric drive.

For model implementation the dSPACE DS1103 has been employed. The DS1103 dSPACE platform is used as a simulator of the electric vehicle in laboratory and it is used for HIL (Hardware In the Loop) tests. The DS1103 device is covered in the AutoBox with Ethernet communication interface and Autoboot option enabling usage of Compact Flash card. The complete EV mathematical model is loaded in DS1103 device.

For laboratory verification special testing bench has been built. Testing bench consists of permanent magnet synchronous motor, power inverter and power sources. The load is substituted by the dynamometer. Both machines are controlled by master controller. Hardware structure of the laboratory stand is depicted below.

In the first step of journey simulation, the required torque of EV drive in the single path elements has been calculated. Real path data obtained within the journey were generated by means of GPS and GSM mobil-phone and stored in the memory.

Stored data were used as EV simulation model input data. Then values ofr needed driving torque, actual power and consumed energy are calculated. With respect to the obtained results optimized path elements strategy calculation has been developed.

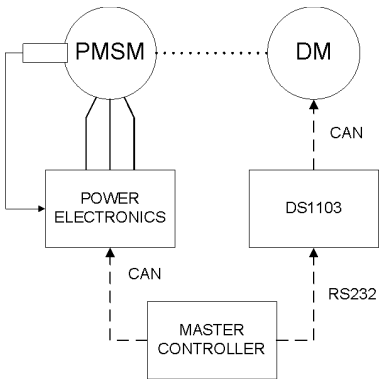

Figure 1: Hardware structure of the laboratory stand.

Railway Traction Vehicle Longitudinal Velocity Estimation by Kalman Filter

P. Pichlik, **O. Zoubek**, **J. Zdenek**, **and J. Lettl**
Department of Electric Drives and Traction, Faculty of Electrical Engineering
Czech Technical University in Prague, Technicka 2, 166 27 Prague 6, Czech Republic

Abstract— Important task of railway traction vehicles is to achieve maximal tractive effort in any conditions. For this purpose the vehicles have slip controllers. Some types of the controllers need the vehicle longitudinal velocity as input. The vehicle longitudinal velocity is typically derived from the wheel velocity or measured by Doppler radar in modern vehicles. It is difficult to measure the vehicle longitudinal velocity directly because the vehicle longitudinal velocity could not be directly determined from the wheel velocity. Wheel velocity is higher than vehicle longitudinal velocity when the wheel is driven because of the slip phenomenon. In the case of braking the wheel the wheel velocity is lower than vehicle velocity because of the skid phenomenon. In some cases the vehicle has some non-driven wheels that enable to measure the vehicle longitudinal velocity, but the measurement has higher level of noise. In any case the wheel velocity is influenced by vehicle dynamic motion that can change the measured actual velocity accuracy.

Railway traction vehicle wheel velocity is measured by incremental encoders that are mounted on wheelsets or on motor shaft. The locomotives with DC motors have the incremental encoders mounted on wheelsets. Locomotives with induction motors have the incremental encoders mounted on induction motor shaft. The encoder position was chosen due to the vector control of the traction induction motor. The used incremental encoders are typically of magnetic types with low number of pulses per revolution to be robust and reliable. The encoders are exposed to high mechanical stress and electromagnetic interference that have influence to the velocity measurement accuracy.

When the longitudinal velocity is determined from driven wheel velocity the actual longitudinal velocity cannot be calculated because the driven wheel velocity is higher than the longitudinal velocity. Therefore only approximate velocity could be determined. This is why methods for vehicle longitudinal velocity determination have to be designed. Methods are typically based on evaluation of the slowest wheelset velocity. The paper proposes railway traction vehicle longitudinal velocity estimation based on Kalman filter. The filter contains the vehicle model in state-space form and enables to estimate the velocity and an adhesion force that is difficult measurable value and that is needed for the slip controller, too. The proposed method has been verified using the actual data gathered from actual vehicle with a heavy train. The paper presents results obtained by processing this actual data with designed Kalman filter.

Analysis of the Electromagnetic Field of Electric Machines Based on Object-oriented Design Principles

V. Pliugin[1], **L. Shilkova**[1], **J. Lettl**[2], **K. Buhr**[2], **and R. Fajtl**[2]

[1]Department of Electric Machines, Faculty of Power Engineering
National Technical University "Kharkiv Polytechnic Institute", Frunze 2, Kharkiv 61002, Ukraine
[2]Department of Electric Drives and Traction, Faculty of Electrical Engineering
Czech Technical University in Prague, Technicka 2, 166 27 Prague 6, Czech Republic

Abstract— Object-oriented design — an approach to solve problems using models based on the concepts of the real world. Fundamental element is an object that combines the data structure with its behaviour.

One-sided approach to the problem of study and research of electric machines, characterized by a great variety of species and structural-functional classes, led to corresponding negative consequences. As in fact was permanently closed a way of using structural and systemic approaches to their study and setting goals of higher level of its generalization.

Regarding the numerous objects of Electromechanics, the problem is most clearly manifested in the way of explaining the principles of their structural construction, which determines the diversity of spatial forms of electrical machines, so that they can be considered as a basis for the development of generalized structural models. The present level of ideas in this area is based on the idea of forming a single improvement framework that would get all the other varieties of structures of electric machines using certain group of transformations.

Considering the theory of object-oriented design, assumes a basic (abstract or virtual) class of generalized electric machine, where its descendants are well-known types of electrical machines. By inheritance or added clipped of some characteristics that can lead to the synthesis of the specific model of the electric machine.

Maxwell's equations underlying the description of the processes occurring in electric machines can be formulated for all types of electrical machines with arbitrary geometric design.

In presented paper problem of finding common principles of synthesis of electromagnetic field models for the main types of electrical machines is solved. The main objective is to create field models of electric machines by inheritance of their characters from the original Maxwell's equations.

This will show the application of the object-oriented design principles in modelling of electric machines and its inextricable link with the basic principles of the theory of the electromagnetic field. An inverse problem — the synthesis of electric machines electromagnetic field equations using object-oriented design is solved, too.

Locomotive Wheel Speed Measurement under Wheel Slip Conditions

O. Zoubek, P. Pichlik, J. Zděnek, and J. Lettl
Department of Electric Drives and Traction, Faculty of Electrical Engineering
Czech Technical University in Prague, Technická 2, 166 27 Prague 6, Czech Republic

Abstract— Wheel speed of heavy freight train locomotive under non-ideal traction conditions was measured with very high resolution and fine precision. Many authors published papers in this area over a past century, but only recent advance in information technology enabled measurement in such extent and resolution at the same time.

Most modern locomotives have the speed sensor coupled with the traction motor. Unlike many other authors doing research in area of wheel-slip, in the presented case the wheel speed was measured directly on the wheel, not indirectly on the traction motor. This approach made it possible to observe the wheel speed directly, without the requirement to implement motor — wheel model, which can carry inaccuracies.

Thanks to an independent method of determining train speed using sensitive GPS receiver, wheel slip speeds were identified accurately regardless of synchronous slip phenomenon.

Despite the adhesion theory, three types of operation mode were identified: stable traction with negligible slip without oscillations, semi-stable traction with evident slip and oscillations and prominent wheel slip. As the wheel speed was measured directly on the wheel, much larger oscillations than ever published were revealed. The source of the oscillations is discussed in the paper.

A simple MatLab model of rotational masses was constructed and tuned to match the measurements. Eigenvalues and eigenvectors of the model are discussed, too. The model of rotational masses is completed with adhesion model to perform simulation. The simulation results are presented and compared to the results of measurement.

Session 4A6
Electromagnetic Probing of Atmosphere and Ionosphere in Arctic Region 1

Ionosphere Response to Stratospheric Circulation in High-midlatitudes

Boris G. Shpynev[1], **Vladimir I. Kurkin**[1], **Konstantin G. Ratovsky**[1], **Marina A. Chernigovskaya**[1], **Anastasiya Yu. Belinskaya**[2], **Svetlana A. Grigorieva**[3], **Alexander E. Stepanov**[4], **Vasily V. Bychkov**[5], **Valery A. Panchenko**[6], **Nina A. Korenkova**[7], **and Vladimir S. Leschenko**[7]

[1]Institute of Solar-Terrestrial Physics SB RAS, Irkutsk, Russia
[2]Altay-Sayan Department, Geophysical Survey SB RAS, Novosibirsk, Russia
[3]Institute of Geophysics UB RAS, Yekaterinburg, Russia
[4]Institute of Cosmophysical Research and Aeronomy SB RAS, Yakutsk, Russia
[5]Institute of Cosmophysical Researches and Radio Wave Propagation EB RAS, Paratunka, Russia
[6]Pushkov Institute of Terrestrial Magnetizm Ionosphere and Radio Wave Propagation, Moscow, Russia
[7]West Department of Pushkov Institute of Terrestrial Magnetism
Ionosphere and Radio wave Propagation RAS, Kaliningrad, Russia

Abstract— In the study we investigate the impact of polar neutral atmosphere dynamics on the high-midlatitude ionosphere during sudden stratospheric warming (SSW) events. For this purpose the reanalysis data from ECMWF Era Interim and data from high-midlatitude chain of Russian ionosonde stations are used. The results show that the ionospheric response to the SSW events at high-midlatitudes depends on the position of the ionosonde stations relatively to the stratospheric circulation pattern. Two well pronounced effects were found in the study. First effect, observed in January 2009, is a negative effect in the critical frequency (f_oF2) and a positive effect in F2 layer maximum (h_mF2) above the border of stratospheric cyclone and anticyclone with northward flow direction. During six days the ionosphere had sharply inhomogeneous longitudinal structure when ionosondes, displaced on ~ 20 degrees longitude, showed differences ~ 1 MHz in f_oF2 and more than 50 km in h_mF2. Second feature, which was clearly observed in January 2013, implied a positive effect in f_oF2 (up to ~ 2.5 MHz) and a negative effect in h_mF2 (~ 10 km) above the centre of stratospheric cyclone. We suppose that for the first case the effect is caused by upward transport of molecular gas to the lower thermosphere above the region of interaction between two stratospheric jet-streams. In the second case we suggest effect is due to a pull-down forcing of molecular species above the low pressure zone inside the stratospheric cyclone. Changing of O^+/N_2 ratio in the lower thermosphere produced changing of O^+ recombination rate and corresponding variations of ionosphere parameters.

ACKNOWLEDGMENT

This work was supported by the Grant of the Russian Scientific Foundation (Project No. 14-37-00027).

The Possibility for Full Profile Incoherent Scatter Data Processing on the Base of the Simplex-processor Algorithm

Boris G. Shpynev, Gely A. Zherebtsov, Alexander L. Voronov, and Denis S. Khabituev
Institute of Solar Terrestrial Physics, SB RAS
Irkutsk p/o box 291, Lermontov st., 126a, 664033, Russia

Abstract— The experimental data of Irkutsk Incoherent Scatter Radar (IISR) pose the non linear inverse problem where the ionospheric parameters (such as electron density, electron and ion temperature, as well as drift velocity and ion composition) can be derived from the experimental autocorrelation functions or energy spectrums. Due to the presence of non linear core in integro-differential equation of IISR data processing this problem can be solved only by the least-square fitting or by statistical methods such as Monte-Carlo algorithms. In our recent research we suggest a new method for solving of multi-dimensional inverse problem for processes that are continuous in time and which have a pre-history of solutions. The typical IISR measurements have as a result the set of lag-products (or spectrums) which can be used for derivation of ionospheric parameters from the solution of a repeatable nonlinear inverse problem respectively to lag-product properties. When this problem is solving for full profiles of parameter, such as attitude profiles of electron density, electron and ion temperatures etc., we have a multidimensional problem which requires from $2N$ to N^2 calculations of objective function per dimension. This requires large computational resources and can be realized practically only on super computers.

In the present study we suggest a new approach to IISR data processing on the base of recently developed algorithm which solves the nonlinear inverse problem in the special projection space where any motion between the projection space noodles can be done along the multi-dimensional simplex grid. This kind of gradient conjugate algorithm has no a significant limitations on problem dimension, it require only $(N+1)$ calculations of objective function per dimension and it can be realized on any usual personal computer systems. The method called simplex-processor is realized on IISR for simultaneous fitting of few tens of spline coefficients that gives approximations for all parameters profiles mentioned above. The simplex-processor method can be implemented to variety of linear and nonlinear inverse problems in many experimental geophysical applications.

ACKNOWLEDGMENT

This study was supported by RF President Grant of Public Support for RF Leading Scientific Schools (NSh-2942.2014.5), by the Earth Sciences Department RAS (program IV.11, project "Cyclone") and Russian Foundation for Basic Research (RFBR Grant No. 15-05-05387).

Analysis of Speed and Acceleration of GPS/GLONASS Phase in the Polar Ionosphere

V. V. Demyanov[1], **Yu. V. Yasyukevich**[2], **and T. V. Kashkina**[1]

[1]Irkutsk State Railway University, Irkutsk, Russia
[2]Institute of Solar-Terrestrial Physics, Irkutsk, Russia

Abstract— Currently polar ionosphere is of great interest. This is connected with creation of global model of ionospheric storms and providing stable navigation in polar region. Currently dual- and multi-frequency GNSS phase measurements have been utilized widely and these measurements combination yields us current TEC-values along all SV's line-of-sights in view. One of the main parameters is stability of phase measurements and their noise level.

We carry out the GNSS signal monitoring campaign under the polar ionosphere condition (in Taimyr cape, Russia) in 2013. JAVAD Delta-G3T receiver was used. We observed amount of the rapid and sharp phase acceleration variations. The absolute value of these variations were as much as 30–40% up to 2–2.5 times higher in comparison the background level for both GPS and GLONASS signals. In some cases we found a strong positive correlation between the phase acceleration variations and TEC variations in the variation frequency band of 0.08–1 Hz. It is well known that this frequency band relates to the 1-st Fresnel zone sized ionospheric irregularities. On the other hand we found some cases when there was no an obvious correlation between the 0.08–1 Hz TEC-variations and the phase acceleration variations. In these cases the phase acceleration variations could be inspired by the SV's reference oscillator frequency drift.

In order to separate all the observed phase acceleration variations according to they physical origin we arranged a new measurement campaign of both GPS and GLONASS signals in Norilsk (69°N, 88°E) and Irkutsk (52°N, 104°E). Additionally we used Moscow (55°N, 37°E) data. This report is devoted to discussion of the main results of the campaign data treatment.

ACKNOWLEDGMENT

This study was supported by the Grant of the Russian Scientific Foundation (Project No. 14-37-00027).

Estimation of GPS/GLONASS Differential Code Biases and Their Long-time Variations

Yury V. Yasyukevich[1, 2], **Anna A. Mylnikova**[1],
Vyacheslav E. Kunitsyn[1, 3], **and Artem M. Padokhin**[1, 3]

[1]Institute of Solar-Terrestrial Physics, Siberian Branch of Russian Academy of Sciences, Irkutsk, Russia
[2]Irkutsk State University, Irkutsk, Russia
[3]Lomonosov Moscow State University, Moscow, Russia

Abstract— Along with precision positioning and timing applications, Global Navigation Satellite Systems (GNSS) are widely used nowadays for remote sensing of ionosphere in equatorial, mid-latitude and arctic regions. While estimating absolute total electron content (TEC) using the combination of dual frequency code and phase measurements, a satellite and receiver dependent systematic error occurs. This error is associated with differential code biases (DCB) — the different, frequency dependent processing times of L1 and L2 signals in radio frequency paths, both for satellites and receivers. For example, a 1-ns DCB causes a $\sim$ 3 TECU error in TEC estimation. Due to these DCBs, TEC, in some cases, can obtain even non-physical negative values.

We analyze DCBs dynamics and errors in TEC estimations associated with satellites and receivers DCBs for 2000–2014. For such estimates, we used the CODE laboratory data [ftp://ftp.unibe.ch/aiub/CODE/] as well as the results of our own technique of DCB estimation based on single station data. The systematic variability of the TEC estimation errors associated with DCBs according to our results is about $\sim$ 1 TECU/year for GPS and three times greater ($\sim$ 3 TECU/year) for the GLONASS satellites. There are significant variations in TEC errors for GLONASS with amplitude up to $\sim$ 5 TECU compared to rather small variations for GPS.

Systematic DCBs change both for GLONASS and GPS frequency channels is observed significantly varying depending on the receiving station. For GLONASS and GPS frequency channels, seasonal variations in estimated TEC errors (up to $\sim$ 20 TECU) associated with DCBs are observed. We show that such strong variations could be associated with variations in the receiver environment, especially meteoparameters, such as temperature and humidity.

ACKNOWLEDGMENT

This study was supported by the Grant of the Russian Scientific Foundation (Project No. 14-37-00027).

Variations of O+/H+ Transition Height over East Siberia from Joint Analysis of Irkutsk Incoherent Scatter Data and GPS Total Electron Content

Denis S. Khabituev and Boris G. Shpynev
Institute of Solar-Terrestrial Physics SB RAS, Irkutsk, Russia

Abstract— In the study we compare data on O+/H+ transition height (TH) derived on the base of Irkutsk Incoherent Scatter Radar (IISR) data and GPS Total Electron Content (TEC) with other topside ionosphere models. IISR-GPS technique of TH derivation based on the calculating of difference between TEC and ionospheric electron content derived from IISR Faraday rotation measurements. IISR and TEC data are assimilated in topside ionosphere model based on the modified Chapmen layer with assumption of different scale height for each ion components. Also, the model uses special transition scale height which describes the exponential changing of O+ and H+ ions concentrations.

According to this model we calculate the dynamics of O+/H+ transition height for Eastern Siberia region and compare our results with theoretical models and actual empirical models developed on the base of topside sounding ionosphere data. The comparison shows that practically all topside models have no satisfied agreement between each other especially for daytime conditions. Theoretical models usually overestimate O+/H+ transition height. IISR-GPS technique well agrees with topside sounding data models, but there are sufficiently differences between our results and theoretical models. Direct IISR measurements of transition height that available only below $\sim$ 700 km show that in night time IISR-GPS technique gives more realistic results then theoretical models. We suppose that TH overestimating in theoretical models results from incorrect account for meridional neutral wind effects and plasma flux between ionosphere and plasmasphere. In turn, the underestimation of daytime TH in IISR-GPS technique can be result of assumption that plasmasphere scale height is constant in altitude range above TH and below GPS satellites orbit.

The Study of the Ionospheric Dynamics during Strong Sudden Stratospheric Warmings in the Russia's Arctic Region

A. S. Polyakova, **M. A. Chernigovskaya**, **and A. A. Mylnikova**
Institute of Solar-Terrestrial Physics of Siberian Branch of the Russian Academy of Sciences
Irkutsk, Russia

Abstract— A sudden stratospheric warming (SSW) is a global phenomenon occurring in the winter stratosphere and covering a large area of hemisphere up to the polar latitudes. As a result of this phenomenon an essential breaking of the circumpolar vortex, determining largely the behavior of the lower and middle neutral polar atmosphere in winter, is occurred. Because the state of the high-latitude ionosphere during the winter period is partly determined by neutral processes, it is natural to expect that such global phenomenon as SSW may have an impact on it.

The behavior of the ionosphere in the Russia's Arctic region during periods of strong sudden stratospheric warmings was investigated using the data of the international network of phase dual-frequency GPS receivers, global ionospheric maps (GIM) of the total electron content (TEC) and vertical sounding data. Eight events of major stratospheric warmings that occurred in the Northern hemisphere in the last decade were considered. For identifying the possible response of the high-latitude ionosphere on SSW events the analysis of the total electron content and F2-layer critical frequency deviation from background level was done. Spatial and temporal distributions of the amplitude of diurnal variations of TEC were also studied. It is revealed that diurnal dynamics of high-latitude ionosphere at the points located near the SSW zone during periods of a warming differs significantly from regular. It is also identified that the events of strong SSW are usually accompanied by a decrease of the amplitude of diurnal variations of TEC during the SSW development stage and by an increase of the amplitude, which may be observed up to $\sim 75°$N latitude after the SSW peak.

ACKNOWLEDGMENT

The work is performed under support of the RF President Grant of Public Support for RF Leading Scientific Schools (NSh-2942.2014.5) and the RFBR grant No. 15-05-05227_a.

The Stratosphere Jet Stream Effects in High-latitude Ionosphere according to Vertical Radio Sounding Data

M. A. Chernigovskaya[1], **B. G. Shpynev**[1], **K. G. Ratovsky**[1], **and A. E. Stepanov**[2]

[1]Institute of Solar-Terrestrial Physics SB RAS, Irkutsk, Russia
[2]Institute of Cosmophysical Research and Aeronomy SB RAS, Yakutsk, Russia

Abstract— This study deals with ionospheric disturbances caused by the wave-like processes in the lower and middle atmosphere. The ionospheric data were obtained from continuous measurements made at the vertical sounding ionosondes in the high-latitude region of Eastern Siberia, Russia, in 2008–2010. We studied the seasonal variations of the high-frequency part of the $F2$ peak density variability caused by traveling ionospheric disturbances associated with gravity waves (GWs) propagation from the lower and middle atmosphere. The ionospheric disturbances referred to deviations of the maximum electron density N_mF2 from the median values, i.e., deviation of the observed value from a regular behavior.

We identified periods of large-scale wave-like motions in the stratosphere between November and February 2008–2010 based on the ECMWF ERA-Interim reanalysis data. These wave motions were associated with the jet streams at heights of the stratosphere, localized mainly at latitudes 50–80 °N. The waves propagated eastward, generally in latitudinal direction; however, sometimes meridional direction of the wave propagation was observed. It was shown these wave-like disturbances propagate upward from the stratosphere to the mesosphere, with the increase in the amplitude. Propagating up to the atmosphere the waves cause changes in the structure and internal dynamics of the lower thermosphere and ionosphere as travelling atmospheric and ionospheric disturbances.

A noticeable increase in the GWs activity was found at heights of $F2$ layer during the periods of stratospheric wave activity over analyzed region. Satellite temperature measurements MLS Aura confirmed the existence of variations in parameters of the stratosphere and mesosphere, which accompanied by increases in wave disturbances of the $F2$ layer.

ACKNOWLEDGMENT

This study was supported by the Grant of the Russian Scientific Foundation (Project No. 14-37-00027) and by the Russian Foundation for Basic Research, project No. 15-05-05227.

Simulation of HF Ground Backscatter Measured by the Ekaterinburg SuperDARN Radar. Comparison with Observations

A. V. Oinats, **K. A. Kutelev**, **and V. I. Kurkin**
Institute of Solar-Terrestrial Physics SB RAS, Russia

Abstract— The Ekaterinburg SuperDARN radar (Ekb; 56.4N, 58.5E) operates in the high frequency band (HF) and can measures the echoes from the ranges of about 180 km to 3500 km. The Ekb antenna system represents a phased array which allows to form a narrow radiation pattern (azimuthal width of $\sim 3.24°$), called "beam", in the 16th azimuthal directions. The width of the radar field-of-view is about 50°. Radar scans sequentially all 16 beams in the standard operation mode. Duration of the whole scan is about 2 min. There are two types of the echoes in radar data: ionospheric scatter and ground backscatter. Ionospheric scatter is typically irregular, because it is caused by HF wave scattering by geomagnetic field-aligned plasma inhomogeneities of decameter scale. Ground backscatter is caused by HF wave scattering by ground surface roughness. Due to ground backscatter is mostly determined by regular change (diurnal and seasonal) of the ionosphere, its behavior is more predictable.

In the paper we study diurnal-seasonal pattern of the ground backscatter characteristics such as minimum slant range, corresponding elevation angle and skip distance. Also we study a behavior of true reflection height, slant range and ground distance to the ionospheric reflection region. Taking into account the Ekb technical parameters, simulation of the mentioned ground backscatter characteristics is carried out in the framework of waveguide approach as well as using ray tracing technique. Global international reference ionosphere model (IRI) is used as a propagation media. We compare simulation results obtained using different calculation techniques with observational Ekb data recorded during 2013–2014. Current study could be used for further correct interpretation of the Ekb data, and also it might be useful for improvement of IRI model predictions.

Correction of the Ekaterinburg SuperDARN Data Mapping Using Ionospheric Vertical Sounding

A. V. Oinats, **K. A. Kutelev**, **O. I. Berngardt**, **and V. I. Kurkin**
Institute of Solar-Terrestrial Physics SB RAS, Russia

Abstract— One of the effective tools to investigate the ionosphere dynamics are SuperDARN radars which operate in the high frequency band of 8–20 MHz. High temporal resolution and wide azimuthal field-of-view of SuperDARN radar allow us to perform effective monitoring of the ionosphere in large spatial region. However HF waves, propagating in the Earth's ionosphere, are strongly affected by refraction. Excluding the refraction leads to significant errors in the SuperDARN data mapping. The errors could reach the magnitude of tens or even hundreds kilometers with regard to the true reflection position. Such accuracy is insufficient for ionospheric dynamics investigations at the present level especially at high-latitudes (auroral and subauroral) where ionosphere is characterized by high degree of variability in both time and space.

In the current paper we study possibilities for the Ekaterinburg SuperDARN (Ekb; 56.4N, 58.5E) data mapping improvement in both quiet and disturbed geomagnetic conditions. To take into account refraction, we apply the simulation of the HF wave propagation using the techniques based on waveguide approach as well as ray tracing. Global international reference ionosphere model (IRI) is used as a propagation media. In order to overcome IRI shortcomings of high-latitude ionosphere representation, we adjust IRI prediction using ionospheric vertical sounding data recorded by a number of high- and mid-latitude stations (Arti, Norilsk, Amderma, Salekhard, Dikson). Different IRI adjustment and Ekb SuperDARN mapping techniques are compared and discussed.

Space Weather Variations and Corpuscular Ionization

E. S. Andreeva[1], **V. E. Kunitsyn**[1], **E. D. Tereshchenko**[2], **M. A. Kozharin**[1], **and M. O. Nazarenko**[1]

[1]Faculty of Physics, M. Lomonosov Moscow State University, Russia
[2]Polar Geophysical Institute RAS, Murmansk, Russia

Abstract— The ionospheric manifestations of space weather in the northwest Russia and Alaska are analyzed from the ionospheric images reconstructed by the satellite radio tomography (RT). The methods of ionospheric radio tomography based on the low-orbiting navigational satellite systems (LORT) are capable of reconstructing the two-dimensional (2D) distributions of electron density in the vertical plane (height-latitude) above the chain of ground receivers in a wide spatial sector covering a few thousand km. The ionospheric snapshots provided by LORT show the structure of the ionospheric plasma distribution in the studied spatial sector over an interval of 10–15 min. LORT spatial resolution is 20–30 km horizontally and 30–40 km along the vertical.

The geomagnetic storms belong to the most striking phenomena impacting the space weather. A series of the complex ionospheric patterns resulting from various space weather factors were revealed by the RT methods during the geomagnetic storms. We discuss the series of RT images for strongly disturbed geomagnetic conditions during the 23rd and 24th solar cycles. The RT reconstructions demonstrate a number of the features both inherent in all or most of the considered events and specific to the local spatiotemporal conditions. The first group includes complex patterns of the ionospheric plasma distributions with numerous extrema, rapid rearrangement of the ionospheric structure, variations in the position and shape of the main ionization trough, wave and wavelike disturbances, increased ionization in the night-time ionosphere compared to the quiet periods, etc.. The second group comprises rapidly emerging and dissipating isolated irregularities with different shapes and spatiotemporal scales, the ionospheric manifestations of particle precipitation, etc..

We present and discuss the examples of qualitative comparison between the RT cross sections of the ionosphere and the data on the ionizing particle fluxes measured by the DMSP satellites. Based on the comparison of the RT data with DMSP observations, we analyze the effects of corpuscular ionization of the ionosphere. During the periods of the strong geomagnetic storms, the spatial scales of the fluxes of corpuscular injections widely vary from a few to ten degrees along the latitude. The RT images for these periods demonstrate highly structured ionization patterns with numerous extrema and wavelike structures on the scales ranging from a few tens to a few hundred km. Our studies show that the spatial structure of the additional corpuscular ionization, which is observed in the RT ionospheric cross sections, qualitatively agrees with the latitudinal distributions of the fluxes of precipitating particles.

Arctic Ionosphere Imaging and GNSS Tomography

V. E. Kunitsyn[1, 2], **E. S. Andreeva**[1, 2], **I. A. Mazaeva**[1], **M. O. Nazarenko**[1, 2], **I. A. Nesterov**[1, 2], **and Yu. S. Tumanova**[1, 2]

[1]M. Lomonosov Moscow State University, Faculty of Physics, Russia
[2]Institute of Solar-Terrestrial Physics RAS, Irkutsk, Russia

Abstract— For better understanding the nature and mechanisms of the physical processes that occur in the Arctic atmosphere and ionosphere it is vital to have the adequate experimental input for the research. Global Navigation Satellite Systems (GNSS) can be used as one of the sources of these data, whose processing and analysis enables the structure and dynamics of the ionosphere to be explored by different methods including the ionospheric radio tomography. At present, GNSS include the first-generation and second-generation satellite systems. The low-orbiting (LO) Transit and Parus systems belong to the first-generation GNSS. The second-generation systems comprise high-orbiting (HO) satellite constellations such as GPS and GLONASS systems, which are currently in operation; the European Galileo system, which is currently under development; the Chinese BeiDou, and Japanese QZSS satellite systems. The GNSS space segments together with the corresponding ground-based receiving networks make it possible to carry out sounding of the ionosphere along a system of the intersecting fan-shaped ray families and to apply radio tomographic (RT) approaches.

We show and discuss a series of the examples of RT reconstructions to illustrate a variety of the ionospheric patterns observed in different latitudes. For reconstructing these images, we applied the methods of the low-orbiting (LO) and high-orbiting (HO) RT. By combining the advantages of these approaches (the high spatial resolution of LORT together with the extensive spatial coverage and rather high time resolution of HORT), we identified and studied the structure and dynamics of the equatorial anomaly, ionospheric troughs, blobs, fingerlike irregularities and spotty plasma distributions with numerous local enhancements and depletions, patches, wavelike structures, travelling ionospheric disturbances (TIDs), ionospheric displays of the manmade impacts such as rocket launches, explosions, and artificial modifications of the ionosphere by high-power high-frequency radiation or, etc. We analyze the spatiotemporal ionospheric responses in relation to solar activity, natural geophysical impacts (e.g., earthquakes), and seasonal conditions. We present the examples of comparing the RT images with the measurements by the ionosondes.

Emphasis in our presentation is placed on discussing the results of the ionospheric radio tomography above the Arctic. These RT images illustrate various structures, events, and processes associated with the convection and other phenomena. We observed the characteristic ring-shaped irregularities encircling the North Pole, the tongues of ionization, antisunward drift of the ionization patches from the dayside to the night-side ionosphere, etc..

Recently, the input data for the ionospheric studies were expanded by the widely used 2D global ionospheric maps (GIMs) of the total electron content (TEC), which are generated from the IGS data with a thin sheet approximation. We present and discuss the results of comparison between GIMs and RT reconstructions.

Session 4A7
Applications of EM Field in Biomedical Technique

Identification of Abnormal Blood Cells Using Scattering of a Focused Laser Beam by a Cluster

Hany. L. S. Ibrahim[1], **Elsayed Esam M. Khaled**[2], **and Ahmed Elsayed Esam M. Khaled**[2]

[1]Telecom Egypt Company, Qina, Egypt
[2]Electrical Engineering Department, Faculty of Engineering, Assiut University, Assiut, Egypt

Abstract—

Introduction: Normal mature red blood cells (RBCs) are shaped as biconcave oblate discs. These shapes can be deformed by several inherited disorders, e.g., spherical, crescent, oval, or any other abnormal shapes [1]. Therefore these deviations are sensitive remarks for various blood disorders and diseases, e.g., malaria and anemia, ... etc. [2]. For this reason, finding such shape deviations is an important research issue and has been studied considerably. In this paper analysis of the modified cluster T-matrix method, as introduced in a previous work [3], is used to calculate the angular scattering intensity of a cluster consists of healthy and abnormal cells illuminated with a focused Gaussian beam. This angular scattering can give good identification of the abnormal cells in the cluster. The technique combines the cluster T-matrix method with the plane wave spectrum method to model the incident beam. We think that this technique is a powerful one to define the diseased RBCs for more accurate diagnostics purposes.

Analysis and Results: Here the technique is applied to real life applications such as clusters of normal and abnormal RBCs. The computed angular scattering of a cluster composed from different cells as shown in Fig. 1(b) is compared with those of a cluster of normal biconcave RBCs shown in Fig. 1(a). Each biconcave particle is of size parameter $x = 10$, refractive index $m = 1.4$ and deformation parameter $\xi = 0.2$. Each abnormal cell presented in Fig. 1(b) (crescent shape) is formulated by a coated spherical cell of an offset core $l = 0.3\,\mu$m, coating parameter $R = a_c/a_s = 0.7$ (where a_c and a_s are the radius of the core and the shell respectively) and refractive indices for the shell and the core are $m_s = 1.4$, $m_c = 1.0$ respectively. The size parameter of the cell is $x = 2\pi a_s/\lambda = 10$. Both clusters of the normal and abnormal cells are illuminated with a Gaussian beam of wavelength $\lambda = 0.6328\,\mu$m and waist $w_0 = 2\,\mu$m. The computed angular scattering is illustrated in Fig. 2 for different cases of clusters.

The first case is for the cluster consisting of five normal biconcave cells. Then the cells are replaced in steps by abnormal cells. The second case is for a cluster consists of four normal (biconcave) cells and one abnormal cell at the edge of the cluster, and so on to sixth case is

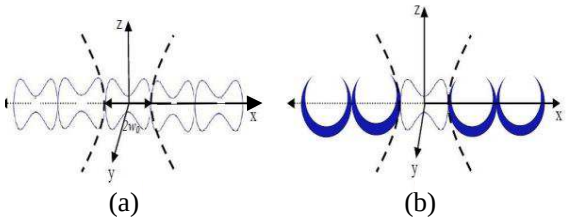

Figure 1: A cluster of different cells centered at the origin of a Cartesian coordinate system (x, y, z). The cells are illuminated with a focused beam of a spot size w_0, and propagating in the z-direction. The considered clusters consist of (a) a linear chain of five identical biconcave cells, (b) a linear chain of four identical abnormal cells, and one centered biconcave cell.

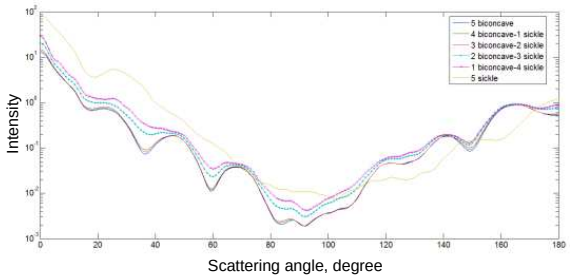

Figure 2: Angular scattering intensities as a function of the angle θ measured from the $+z$-axis for a cluster consists of a linear chain of (a): Case 1, five biconcave cells as illustrated in Fig. 1(a) (blue curve). Case 2, one abnormal cell in one side beside four biconcave cells (green curve). Case 3, two abnormal cells in one side beside three biconcave particles (red curve). Case 4, three abnormal cells in one side beside two biconcave cells (aqua curve). Case 5, two abnormal cells in both side of a centered biconcave cell as illustrated in Fig. 1(b) (purple curve). Case 6, five abnormal cells (yellow curve).

for a cluster of five abnormal cells. The results in Fig. 2 illustrate that the angular scattering intensity of a cluster contains more than 50% of abnormal cells (for example cases 5 and 6) deviate from the intensity distributions of the cluster contains normal cells (case 1). As the number of abnormal cells increases in the cluster of the sample compared with the normal RBCs the angular scattering distributions get more deviation from those of the sample of normal cells and the ripples get smaller. For the cluster of five abnormal cells, the angular scattering intensity has greater front scattering amplitudes compared with those for a cluster of normal RBCs as shown in Fig. 2 (yellow curve).

REFERENCES

1. Kinnunen, M., A. Kauppila, A. Karmenyan, and R. Myllyla, "Effect of the size and shape of a red blood cell on elastic light scattering properties at the single-cell level," *Biomedical Optics Express*, Vol. 2, No. 7, 1803–1814, Jul. 2011.
2. Pan, W., O. Galkin, L. Filobelo, R. L. Nagel, and P. G. Vekiloy, "Metastable mesoscopic clusters in solutions of sickle-cell hemoglobin," *Biophysical Journal*, Vol. 92, 267–277, Jan. 2007.
3. Ibrahim, H. L. S. and E. E. M. Khaled, "Light scattering from a cluster consists of layered axisymmetric objects," *Int. J. Curr. Eng. Technol.*, Vol. 3, 1299–306, 2013.

Emergence of a Traveling Wave Regime on an Unmodified Clinical 3T MRI

Alexey A. Tonyushkin[1], **Norman B. Konyer**[2], **Michael D. Noseworthy**[2, 3], **and Andrew J. M. Kiruluta**[1]

[1]Radiology Department, Massachusetts General Hospital
Harvard Medical School, Boston, MA, United States
[2]Imaging Research Centre, St. Joseph's Healthcare, Hamilton, Ontario, Canada
[3]Electrical and Computer Engineering Department, McMaster University, Hamilton, Ontario, Canada

Abstract—

Introduction: Traveling wave (TW) MRI holds both promise and challenges to tackling B_1 field inhomogeneity at ultra-high MRI fields [1], which are well above the clinically relevant field strength. At conventional clinical field strength ($< 4\,\mathrm{T}$), TW concept is not easily applied due to the relatively small bore diameter to wavelength ratio (< 0.5). A few earlier demonstrations at 3T includedthe use of coaxial [2], metal plates [3] waveguides, and high dielectric inserts in quasi-static regime [4]. Here, we demonstrate an emergence of TW regime in a large cylindrical phantom at 3T using a simple loop-coil as transmit-receive probe. Using this approach, we generated MR images of a phantom with a large field of view (FOV) and with an SNR comparable to traditional near-field approach. Compared to quasi-static regime, we demonstrate that there is no longitudinal decay of B_1 field over the maximum achievable FOV as limited by the linearity of the gradient coil. The TW concept at clinical fields offers the potential to adapt far-field ideas into clinical applications such as larger FOV imaging, accessing deep region of interest, and mode manipulations via multi-channel TW excitations for B_1 field shaping and homogeneity.

Methods and Materials: Our experimental setup consists of unmodified bore based on a standard unmodified GEMR750 (Waukesha, Wisconsin) 3T scanner with an RF shield that serves asa waveguide ($D = 64\,\mathrm{cm}$), a cylindrical acrylic tube filled with distilled water ($D = 20\,\mathrm{cm}$, $L = 1\,\mathrm{m}$), and a 15 cm-diameter Tx/Rx loop-coil as a probe for mode coupling into/from the guide system (Fig. 1). Such a partially filled cylindrical waveguide allows propagating hybrid EH modes inside a dielectric phantom, or pure axially symmetric TE (TM) modes [5]. In addition to a simple loop coil, we used a modified circular polarized (CP) probe that consists of two loop-coils ($D = 15\,\mathrm{cm}$) placed orthogonal to each other so that each B_1 field is also orthogonal to B_0 [6]. The loop-coils are mounted on an acrylic frame to ensure that they remain orthogonal, hence ensuring that they are completely decoupled with isolation between the loops to measured as $-18\,\mathrm{dB}$. The loops are driven in quadrature using a quadrature hybrid splitter, which divides the transmit signal and recombines the MR signal, connected to the inputs of the coils. A balun is present at each coil input to minimize currents flowing on the cable shields. We obtained images of the phantom placed at is ocenter with a single loop-coil or quadrature coils placed 5 cm from the edge of the phantom and 55 cm away from isocenter. Data were acquired using a GRE pulse sequence, TR/TE = 100/6.8 ms, bandwidth = 15.6 kHz, FOV = 48 cm, 5 mm slice, skip 1.5 mm, 256×256, nex = 8, 7 slices, with a total imaging time of 3 : 28 min; an dB_1 MAP pulse sequence: 25 slices, TR/TE = 46/13.2, bandwidth = 15.6 kHz, FOV = 48 cm, 10 mm slice, skip 10 mm, 128×128, nex = 1, with scan time of 5 : 05 min; GE-EPI sequence: TR = 2 s, TE = 30 ms, bandwidth = 250 kHz, FOV = 30 cm, 10 mm slice, skip 10, 64×64, 8 nex, 0 : 16 min. To confirm the concept and predict the observed mode and B_1 field profile we carried out simulations using FEM eigenmode simulator (COMSOL Multiphysics, Burlington, MA).

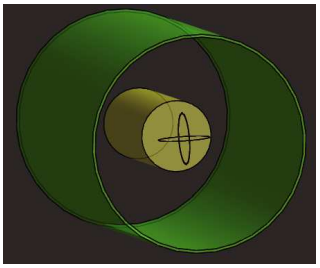

Figure 1: Experimental setup with two possible orientations of single coil, or quadrature coils.

Results and Discussions: Figure 2 shows the experimental and simulation results for our MRI experiment with a cylindrical phantom. For the MRI experiment, we utilized various probe setup geometries: single loop oriented in sagittal, coronal, and tilted by $\sim 20^\circ$ to coronal planes, as well as quadrature coil setup, in order to study how the B_1 field orientation affects the efficiency of RF coupling and the mode inside the cylinder. All the setups produced the same single axially symmetrical mode (TM_{01}) showed in Fig. 2(a) with its distinct feature of a null in the center, contrary to the regularly observed central brightening effects in dielectrics at high fields. The highest SNR of 220 corresponds to the single loop oriented at an angle of approximately 20 degrees to coronal plane and located 5 cm away from the edge of the phantom. All the axially symmetric loop-coil configurations including CP quad-coil, which could be thought as magnetic dipoles, are generally effective for TE mode excitation and less effective for the observed TM mode. The other feature of the observed field pattern is non-decaying propagation of the field along z-axis over the full FOV (48 cm), indicating TW regime. While the persistence of a single,but not the lowest,mode is somewhat surprising from the electrodynamics point of view, the clinical scanner setup is distinctive from the typical screened dielectric waveguides with variety of modes, where the metal screen is adjacent to the dielectrics. In our case, the relatively small diameter dielectric (20 cm) is less coupled to the metal screen, and the pure dielectric waveguide has larger effect on the modes. The B_1 field map shows (Fig. 2(b)) the mode structure with the center null pattern. Our 3D eigenmode simulations (Fig. 2(c)) producea B_1 field that supports the experimental results. The vector map of the field corresponds to TM_{01} mode with a small decaying constant of $\alpha = 1.7 \times 10^{-4}$ that is inherent to complex hybrid modes inside high dielectric materials [5]. We also show that our TW concept is capable of generating relatively high quality images with other clinical sequences such as GE-EPI as shown in Fig. 3.

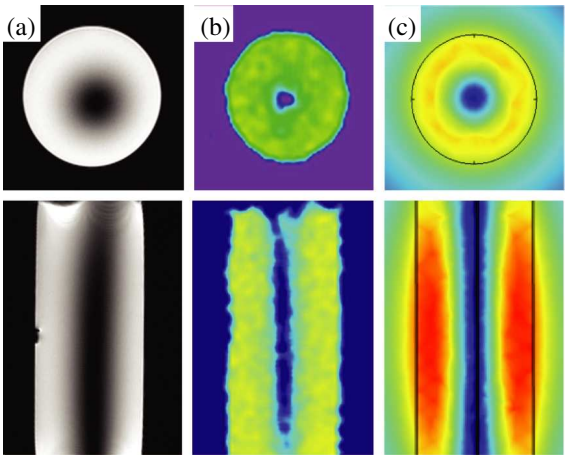

Figure 2: Images of TM_{01} mode in cylindrical phantom (FOV = 48 cm): (a) experimental MRI; (b) experimental B_1 field map; (c) simulations of B_1 field, axial — top row, sagittal — bottom row (arb units).

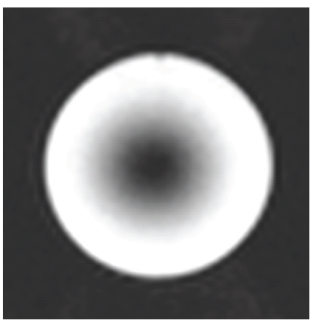

Figure 3: EPI axial TW-MRI image of cylindrical phantom.

Conclusion: We have demonstrated MR imaging with TW concept using an unmodified clinical 3T MRI scanner as an under-moded RF waveguide. The MRI images of a large cylinder are comparable to the ones obtained with TW imaging at ultra-high field strength (7T) [1] and with an SNR comparable to conventional near field coils. Our demonstration of TW in a dielectric

waveguide applicable to aclinical field strength (3T) may result in a more robust large FOV imaging acquired in relatively less time in a clinical setting, as well as new applications in deep tissue imaging of hard to access areas. The presented analysis is relevant to understanding high field artifacts in human torso observed with similar scanning conditions. Future directions include designing probes and guide structures for high efficiency excitation of TW in the bore, mode propagation in human body, and RF field profile control with meta-materials or artificial dielectrics.

REFERENCES

1. Brunner, D. O., N. De Zanche, J. Froehlich, J. Paska, and K. P. Pruessmann, *Nature*, Vol. 457, 994–998, 2009.
2. Alt, S., M. Müller, R. Umathum, A. Bolz, P. Bachert, W. Semmler, and M. Bock, *Magn. Reson. Med.*, Vol. 67, No. 4, 1173–1182, April 2012.
3. Vazquez, F., R. Martin, O. Marrufo, and A. O. Rodriguez, *J. Appl. Phys.*, Vol. 114, 064906, 2013.
4. Tonyushkin, A., N. Konyer, M. Noseworthy, and A. Kiruluta, *Proc. ISMRM*, Vol. 20, #3995, 2012.
5. Tonyushkin, A. and A. Kiruluta, *Proc. ISMRM*, Vol. 19, #1903, 2011.
6. Konyer, N., A. Tonyushkin, A. Kiruluta, and M. Noseworthy, *Proc. ISMRM*, Vol. 21, #5155, 2013.

Waveguide Hyperthermia Applicator with Circular Polarisation

I. Merunka, O. Fiser, L. Vojackova, and J. Vrba
Department of Electromagnetic Field, Czech Technical University in Prague, Czech Republic

Abstract—

Introduction: In this contribution we present a circular waveguide applicator with circularly polarized wave at its aperture. In our previous contributions, where we studied UWB antenna and its application to microwave hyperthermia [1], we observed polarization of dielectric on the interface between spherical phantom of tumour and phantom of human breast in numerical simulations. This phenomenon causes hotpots on the interface while the temperature inside of the tumour does not even reach the therapeutic level. Using of a circularly polarized hyperthermia applicator could at least partially solve this issue.

Materials and Methods: Circular waveguide was virtually filled by distilled water and designed to work perfectly on frequency 434 MHz [2]. In order to get circularly polarized wave at the aperture, polarization plate was inserted into it [3]. Waveguide hyperthermia applicator was facing to the water bolus ($\varepsilon_{\mathrm{rel}} = 80$, $\sigma = 0\,\mathrm{S/m}$) of thickness of 2 cm followed by human breast phantom with average dielectric parameters ($\varepsilon_{\mathrm{rel}} = 10$, $\sigma = 0.8\,\mathrm{S/m}$). Moreover, there is also spherical phantom of tumour ($\varepsilon_{\mathrm{rel}} = 49$, $\sigma = 0.79\,\mathrm{S/m}$) with radius of 1 cm placed 0.5 cm under the breast phantom surface. This configuration can be seen in Fig. 1. Numerical simulations of electromagnetic field were performed in SEMCAD X 14.8.6 Aletsch (Schmid & Partner Engineering AG, Zurich).

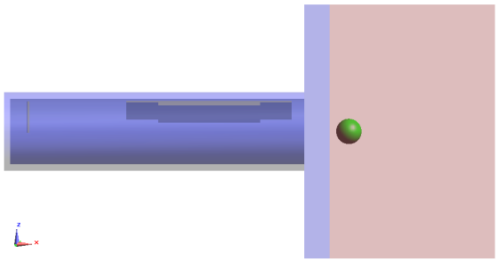

Figure 1: The applicator and configuration of numerical model.

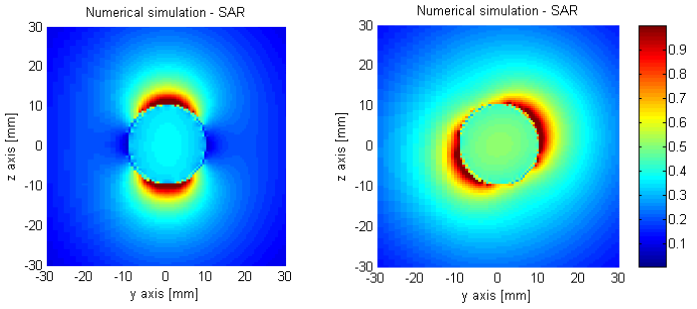

Figure 2: SAR [W/kg] in the cross section of the tumour phantom. (a) Without polarizer, (b) with polarizer.

Results: Specific absorption rate (SAR) in the cross section of the tumour is depicted in Fig. 2. There is a comparison between the SAR obtained by applicator with the polarizer and without the polarizer. Circularly polarized field helped to cover the tumour by SAR from all directions. On the other hand, the effective penetration depth decreased and the ability of focusing microwave power by using a multi-antenna array is also limited with this kind of hyperthermia applicator.

REFERENCES

1. Merunka, I., O. Fiser, L. Vojackova, J. Vrba, and D. Vrba, "Utilization potential of balanced antipodal Vivaldi antenna for microwave hyperthermia treatment of breast cancer," *2014 8th European Conference on Antennas and Propagation (EuCAP)*, 706–710, 2014.
2. Pozar, D. M., *Microwave Engineering*, 4 Edition, Wiley, Hoboken, NJ, 2011.
3. Montgomery, C. G., R. H. Dicke, and E. M. Purcell, Eds., *Principles of Microwave Circuits*, New Edition, The Institution of Engineering and Technology, London, U.K., 1986.

Study of Hot Spots by Oncological Patients with Metal Implants in Head and Neck Region

Ondrej Fiser, Ilja Merunka, Lucie Vojackova, and Jan Vrba
Department of Electromagnetic Field, Faculty of Electrical Engineering
Czech Technical University in Prague, Czech Republic

Abstract— The purpose of this contribution is to study the risk of unwanted hotspots around metallic implants in head and neck area of the new waveguide applicator system and thereby to increase the safety for patients with metallic implants. Metallic implants may interact with the EM field. The reaction rate depends on the implants dimensions [1]. The next objective is to find solution how to reduce hotspots around metallic implants.

Applicator System: We developed a new applicator system intended for microwave hyperthermia in head and neck area (see Figure 1). The applicator system is constructed from four equal waveguide applicators. They are water filled waveguide applicators with strip line horn aperture. The suitable working frequency for this type of applications is 434 MHz. By amplitude and phase combination of each applicator we are able to steer the field and cover the most of treated tissue.

Methods: Metal implants like wires, titan screws or stents are often considered as contraindication for microwave hyperthermia. We choose three different metal implants, which are commonly used in surgery.

- Stent in esophagus or in carotid artery;
- Screws in cervical vertebras;
- Cochlear implant.

In the numerical model the considered metal implants in different positions were inserted. An example model is shown in the Figure 2. For numerical simulations SEMCAD X Aletch 14.8 and human model part of the SEMCAD X models database [2]. For our purposes the human model Ella from Virtual Family 1.2 was utilized. All dielectric and thermal parameters of the model were taken from IT'IS foundation materials database [3]. For comparison and evaluation specific absorption rate [W/kg] and temperature [°C] analysis in human body are used.

Conclusion: In this contribution a study and reduced solution proposal of potential hot spots around metal implants of new type applicator system are performed.

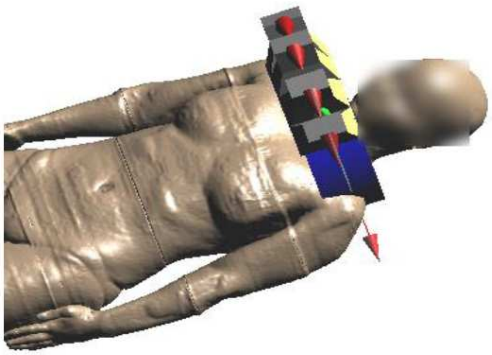

Figure 1: Applicators position.

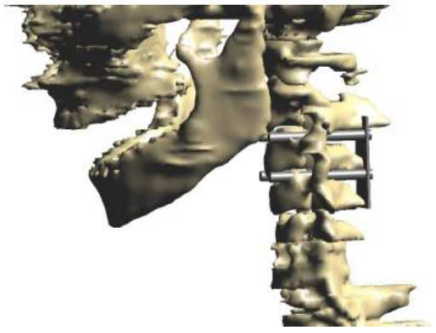

Figure 2: Example of used metallic implant (srews in cervical vertebras).

REFERENCES

1. De Bruijne, M., D. H. M. Wielheesen, J. van der Zee, N. Chavannes, and G. C. van Rhoon, "Benefits of superficial hyperthermia treatment planning: Five case studies," *International Journal of Hyperthermia*, Vol. 23, No. 5, 417–429, Aug. 2007.

2. Rascher, W., R. Janka, W. Bautz, J. Chen, B. Kiefer, P. Schmitt, H.-P. Hollenbach, J. Shen, M. Oberle, D. Szczerba, A. Kam, J. W. Guag, and N. Kuster, "The virtual family-development of surface-based anatomical models of two adults and two children for dosimetric simulations," *Physics in Medicine and Biology*, Vol. 55, N23–N38, Jan. 2010; online, Dec. 2009, http://dx.doi.org/10.1088/0031-9155/55/2/N01.
3. Hasgall, P., E. Neufeld, M. Gosselin, A. Klingenbök, and N. Kuster, "IT'IS database for thermal and electromagnetic parameters of biological tissues," 2011, www.itis.ethz.ch/database.

A Couple of Methods for Power Focusing of Vector Felds in Non-homogenous Media

D. A. M. Iero[1], **L. Crocco**[2], **and T. Isernia**[1, 2]

[1]DIIES-Università Mediterranea di Reggio Calabria
via Graziella, loc. Feo di Vito, Reggio Calabria 89100, Italy
[2]CNR-IREA, National Research Council of Italy
Institute for Electromagnetic Sensing of the Environment
via Diocleziano 328, Naples 80124, Italy

Abstract— Power focusing in non homogeneous media is a canonical problem relevant in many applications such as hyperthermia [1] and targeted drug delivery [2]. In these cases, the overall intensity of the electric field has to be focused in a given target point while possibly keeping the field intensity as low as possible elsewhere.

In this communication, we report about two different strategies we have developed to tackle the problem of focusing transverse electric vector fields, when the primary sources, fed by monochromatic signals, surround the 2D region under test. These approaches apply to generic vector fields so that they can be easily extended to tackling the electromagnetic focusing problem in 3D scenarios.

One of the developed focusing method relies on the well known Time Reversal (TR). TR is a spatial/temporal re-focusing technique, which was originally developed to focus ultrasonic (scalar) fields [3] and recently extended to electromagnetic (vector) fields [4, 5]. An overlooked aspect of electromagnetic TR is the influence of test source polarization, used during the sensing phase, on the overall focusing performance. The common choice of a linearly polarized test source (along the x or y axes) is, indeed, equivalent to focusing just one component of the field and, hence, it affects the focusing performances as the other component does not cooperate to the field focusing phenomenon. Therefore, using a suitable elliptically polarized test source is advisable as it corresponds to a proper combination of the two field components and can produce a better focused field. In this respect, we have developed a simple, general and efficient procedure aimed at optimizing the selection of the test source polarization according to the application requirements.

Although the above method outperforms the more usual TR version, it still cannot guarantee that the field intensity is below assigned (application induced) bounds in the regions outside the target area. To this end, we have developed an extension to vector fields of the focusing technique applied to scalar fields, presented in [6, 7]. It is interesting to note that the method can be interpreted as a (constrained) optimization of the field polarization in the target point. More details on the two methods and some comparisons will be shown at the conference.

REFERENCES

1. Trefna, H. D., J. Vrba, and M. Persson, "Time-reversal focusing in microwave hyperthermia for deep-seated tumors," *Phys. Med. Biol.*, Vol. 55, No. 8, 2167, 2011.
2. Lin, J. C., P. M. K. Yuan, and D. T. Jung, "Enhancement of anticancer drug delivery to the brain by microwave induced hyperthermia," *Bioelectrochemistry and Bioenergetics*, Vol. 47, 259–264, 1998.
3. Fink, M., "Time reversal of ultrasonic fields. Part I: Basic principles," *IEEE Trans. Ultrason. Ferroelectr. Freq. Control.*, Vol. 39, No. 5, 555–566, 1992.
4. De Rosny, J., G. Lerosey, and M. Fink, "Theory of electromagnetic time-reversal mirrors," *IEEE Trans. Antennas and Propagation*, Vol. 58, No. 10, 3139–3148, 2010.
5. Carminati, R., R. Pierrat, J. de Rosny, and M. Fink, "Theory of the time reversal cavity for electromagnetic fields," *Opt. Lett.*, Vol. 32, No. 21, 3107–3109, 2007.
6. Iero, D. A. M., L. Crocco, and T. Isernia, "Thermal and microwave constrained focusing for patient-specific breast cancer hyperthermia: A robustness assessment," *IEEE Trans. Antennas and Propagation*, Vol. 62, No. 2, 814–821, 2014.
7. Iero, D. A. M., T. Isernia, A. F. Morabito, I. Catapano, and L. Crocco, "Optimal constrained field focusing for hyperthermia cancer therapy: A feasibility assessment on realistic phantoms," *Progress In Electromagnetics Research*, Vol. 102, 125–141, 2010.

Biological Signals Transmitted by a Resonant L-C-oscillator; Transmission Controlled by Measuring the Growth of Plants

Konstantin Meyl[1] **and Heide Schnabl**[2]

[1]Faculty of Computer and Electrical Engineering
First Transfer Center of Scalar Wave Technology (1.TZS), Germany
[2]Institut für Molekulare Physiologie und Biotechnologie der Pflanzen (IMBIO)
Universität Bonn, Germany

Abstract— In the experiments presented the effects of transmitting information derived from the growth hormone gibberellic acid (GA) to peas over a distance of some meters have been measured. Transmission of the biochemical characteristics of GA was achieved through a carrier wave of approximately 6.78 MHz running along a copper wire comparable to a strip line from the gibberellic acid as the source of information to the exposed peas, which reacted by a statistically significant enhanced root growth. The measured averages of the germinating pea root lengths were compared to control values, i.e., values corresponding to untreated peas. While continuous GA transmission resulted in an average increase of root length by approximately 50–60%, a singular burst of 15 minutes could increase roots' length by an additional 42%, raising the increase relative to the control group by as much as 125% in total. Both values could be established with very high statistical significance. In a third experimental setup, the peas were treated instead of a GA-signal, with an apoptotic signal produced in *two* different ways: with a pulse carrying the information of peas (a) either stored anaerobically (48–100 hours) or (b) peas macerized and therefore decomparmented. The almost total inhibition of root growth showed, again with high statistical significance, that an information transmission must have occurred remotely. The molecule hypothesized should be *cytochrome c*, released by the stress occurring during the apoptotical process. Some hypotheses in technical as well as in biological respect are being discussed.

Novel Microwave Applicators Inspired by Metamaterials for Hyperthermia Treatment of Cancer

D. Vrba and J. Vrba, Jr.
Faculty of Biomedical Engineering, Czech Technical University in Prague, Czech Republic

Abstract— In this paper, three novel microwave applicator prototypes based on zero-order mode resonators are proposed for use in hyperthermia treatment of cancer. The ability of all three applicators to homogenously irradiate muscle tissue-equivalent phantoms is demonstrated with results of numerical simulations, and relative performance of the applicators is compared.

Based on previous research [1], it can be stated that metamaterial (MTM) Zeroth-Order mode resonators (ZOR) can provide improved thermotherapy for cancer in several ways, by improving the homogeneity of electromagnetic (EM) power absorption, the depth of EM wave penetration, and offering the possibility of either homogeneous treatment of very large areas or conversely focusing EM power into well-defined small areas [2].

New capabilities include, among others, the creation of electrically small applicators that can work without water filling. This could facilitate the delivery of microwave hyperthermia treatment simultaneous with 3D monitoring of temperature distribution in the patient with Magnetic Resonance (MR) thermal imaging.

Another advantage of MTM technology is that this phenomenon enables the creation of a special kind of resonator whose physical length is completely independent of the classical resonance condition (wavelength). This allows us to design the applicator with dimensions matching the clinical need and as a result of the spatial arrangement of MTM resonators we are able to radiate an almost perfect electromagnetic plane wave into the treated area. This improvement in wave propagation produces the advantage of optimizing homogeneity of power deposition within the target tissue region resulting in an improved temperature distribution throughout the treated area.

All three applicators are designed for use at 434 MHz and have similar working principle. Thanks to the excitation of zero-order mode, vectors of surface current density in all inductive parts of the proposed applicators show approximately the same magnitude and phase. The radiated contributions from the all inductive parts of the applicator are in good superposition as they exit the front aperture of the applicator and combine in phase in tissue. This allows the Huygens principle to be applied to describe the resulting EM field distribution in tissue.

ACKNOWLEDGMENT

This research has been supported by the research program of the Czech Science Foundation (GACR) of the Czech Republic, Project No. 13-29857P Human Body Interactions with EM Field Radiated by Metamaterial Structures.

REFERENCES

1. Vrba, D. and J. Vrba, "Novel applicators for local microwave hyperthermia based on zeroth-order mode resonator metamaterial," *International Journal of Antennas and Propagation*, Vol. 2014, Apr. 2014.
2. Tao, Y. and G. Wang, "Conformal hyperthermia of superficial tumor with left-handed metamaterial lens applicator," *IEEE Trans. Biomed. Eng.*, Vol. 59, No. 12, 3525–3530, Dec. 2012.

Phased Arrays Pre-treatment Evaluation in Antitumoral Hyperthermia

Piero Tognolatti[1] and Fernando Bardati[2]

[1]Department of Industrial and Information Engineering and Economics, University of L'Aquila, Italy
[2]Department of Civil Engineering and Computer Science, University of "Tor Vergata", Rome, Italy

Abstract— There is general consensus that quality of hyperthermia treatment is a key factor for clinical effectiveness. A correlation between clinical outcome and thermal dose parameters has been shown. The optimal treatment is defined by efficient tumor heating without patient discomfort by hot spots. To improve hyperthermia treatment quality, optimization of SAR or temperature distribution in the tumor by hyperthermia treatment planning (HTP) is considered before or during treatment. HTP procedures start with tissue map acquisition, then various heating modalities are explored and compared by solving the appropriate electromagnetic (or ultrasound) problem, depending on the equipment in use. Finally the temperature distribution is found for treatment pre-evaluation. However, due to the more complex thermal characterization of vascularised tissues and organs, temperature increase modeling is generally omitted and the optimum problem is formulated in terms of SAR. As the robustness of electromagnetic solvers has increased importantly over recent years, the presently available systems provide excellent opportunities to perform SAR characterization as a start point for SAR optimization. Radiating systems that are currently used to heat deep seated tumors include phased arrays of elementary radiators (dipole, waveguide or microstrip antennas) for which SAR-optimization based HTP is pursued by amplitude and phase setting.

Objective functions have been proposed for SAR optimization according to various quality indicators. They include maximum absolute SAR and SAR homogeneity in the target both to be optimized as well as hot spots to be minimized. The power deposited in the tumor as a fraction of the generators power and of that delivered to the patients body are further indicators. For given array, patient and lesion to be heated, evaluating whether or not the array is able to heat the lesion in accordance with prescribed quality indicators is a somehow different problem a solution of which logically precedes HTP. Only in case of positive answer the search for optimal feed settings will be meaningful. The purpose of this paper is to propose means to exploit in this pre-evaluation. Since the electromagnetic solvers decompose the whole body exposed to radiation (both tumor and healthy tissues) into elementary cells, it is natural to treat each cell as a target and to evaluate the maximum SAR deliverable by the array to that cell. At this stage it is sufficient to know that a feed setting exists that is able to deliver such a maximum SAR to that cell. Repeating this for all cells of the body provides maps of *heatability* that can be used to investigate maximum SAR and SAR uniformity, if the cells belong to a tumor, or to delineate hot spots. Since power deposition is limited by the largest available power from amplifiers referred to as *nominal power*, the latter will be included in the optimization problem.

The paper is organized as follows. Two optimization methods with the constraint on amplifier nominal power are presented. Quality parameters related to systemic heating, tumor heating uniformity and hot spot are introduced. Then a voxel-based numerical analysis is performed for 8 dipoles on two rings, positioned around a head/neck volume within a distilled-water bolus

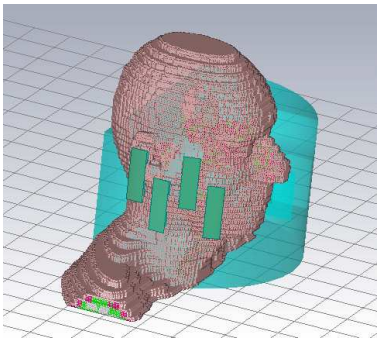

Figure 1: Array of 8 dipoles on 2 rings around a head/neck phantom.

(Fig. 1). Then an extended target, i.e., a 60 ml sphere in central position (oropharynx), is considered. Amplitude and phase settings that are obtained by optimizations are compared on the basis of the maximal absolute power delivered to the target and the other quality parameters that have been previously defined.

Some generators are kept off during a treatment due to unavailability or maintenance of amplifiers or even to awareness that a subset of the available radiators suffices to heat a target. In conclusion, heatability will be discussed in presence of such array thinning.

Complex Permittivity Measurement in Hyperthermia Treatment Planning

Jaroslav Vorlíček[1], **Ladislav Oppl**[2], **and Jan Vrba**[2]
[1]Faculty of Biomedical Engineering, Department of Biomedical Technology
Czech Technical University in Prague, Technicka 2, Prague, Czech Republic
[2]Faculty of Electrical Engineering, Department of Electromagnetic Field
Czech Technical University in Prague, Technicka 2, Prague, Czech Republic

Abstract— The goal of hyperthermia cancer treatment is to raise the temperature of the targeted tissue area. Thus, temperature can be maintained above 43°C for up to one hour. To evaluate the expositions of microwave radiation from thermo-therapeutical microwave applicators, we need to know the dielectric properties of the tissues. This can be performed using measure of the complex permittivity of the tissues in the desired area of the treatment. For this purpose, we constructed a sensor based on the coaxial transmission line for measuring the complex permittivity. Measurement method on an open-ended coaxial line is based on the reality that the reflection coefficient of an open-ended coaxial line depends on dielectric parameters of material which is attached to the coaxial line. For calculation of biological tissue dielectric parameters from the measured reflection coefficient, it is necessary to use an equivalent circuit of an open-ended coaxial line. The values of elements in the equivalent circuit depend on the dielectric properties of the material attached to the end of coaxial line.

To determine the values of elements in an equivalent circuit, we use calibration by means of material with known dielectric properties. Open-ended coaxial probe has a capability of broadband measurements and simple sample preparation. Also, its nondestructive nature and capability for in-vivo measurements provide open-ended coaxial probes with a significant advantage over other techniques for biological applications. There have been many techniques to correlate the measured input admittance to the complex permittivity of the sample material, which resulted in significant improvement in the extraction process. Accurate measurements of the complex permittivity of biological tissues gain great importance in both basic and applied research.

The performance of this system was evaluated by measuring of the deionized water. The measured data were compared with the value calculated by Debye's model. The relative errors between the measurement and the calculation were less than ±4%. The reliability of this method was confirmed by the measurement of deionized water in wide frequency range.

Feasibility Study of Microwave Interstitial Applicator Array for Treatment Pancreatic Cancer

Lucie Vojackova, Jan Vrba, Ondrej Fiser, Ilja Merunka, and Katerina Cervinkova
Department of Electromagnetic Field, Faculty of Electrical Engineering
Czech Technical University in Prague, Czech Republic

Abstract— The aim of this paper is to check a possibility of usage of interstitial helix applicators for a treatment pancreatic cancer by microwave hyperthermia. The typical characteristics of pancreatic cancer are little chance for a complete cure, high mortality and in the majority cases a tumor is considered inoperable due to local spread or presence of metastatic disease. The finding a new possible alternatives to a classical approach is highly important. Thus, this work is focused on the simulation of the hyperthermia treatment.

The simulation for three different frequencies 434, 915 and 2450 MHz were performed in the simulation program of electromagnetic field SEMCAD X [1]. As the applicators were considered interstitial, the first requirement for helix applicators design was made them thin as much as possible. For the later possible realization thin enough coaxial cable was chosen. Simultaneously the coaxial should be sufficiently "thin" to allow wind the turns of helix antenna on the dielectric coaxial cable without necessity to use a special winding technique.

A diameter of helix was clearly established by the choice of coaxial cable. For the individual frequencies only a length of helix and number of turns were changed. The second step, after selecting the suitable coaxial cable was the impedance matching of helix applicator for the aforementioned frequencies. First, the only one helix was placed in a simple homogeneous phantom with dielectric parameters of pancreatic tissue. The checked characteristic was the impedance matching respectively SWR (Standing Wave Ratio). For achieving the best SWR the length of helix and number of turns were changed gradually for single frequencies. It means, every frequency had its helix with specific dimensions after the optimization.

In the next step were done the simulations of SAR (Specific Absorption Rate), already by using the matrix of helix for frequency 434, 915 and 2450 MHz. The first SAR simulations were performed in a simple homogeneous phantom with dielectric parameters of the pancreas as well as by detecting the SWR. After obtaining satisfactory results for so called simple homogeneous model, another simulation of SAR was done for anatomical model. For simulation procedure was used "High-Resolution Human Models for Simulations: Virtual Population" which, together with the dielectric parameters, comes from the pages IT'IS Foundation [2]. In our case it is a virtual family member "Duke" — 34 year old man. For the simulations were considered only bodies in the immediate vicinity of the pancreas, as the proposal for frequencies assumed location 4 applicators around the pancreas. Using SAR values allows us to calculate very precisely extent of the exposure of biological tissue. By different frequencies respectively the lengths of helixes it was possible to affect approximately the size of the area and its volume, which would achieve the highest temperatures respectively the greatest heat.

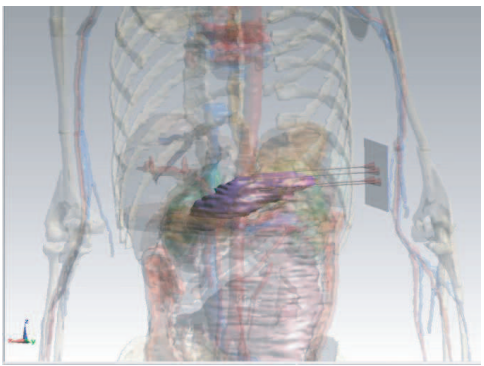

Figure 1: An anatomical model with the highlighted pancreas (violet) and the applicators.

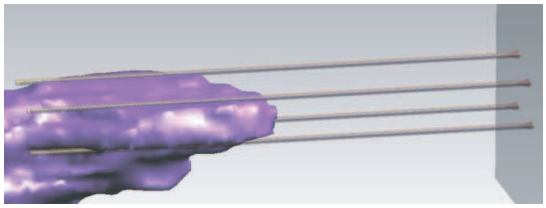

Figure 2: Detail of placing the helix applicators around the pancreas.

REFERENCES

1. http://www.speag.com/products/semcad/intro/.
2. http://www.itis.ethz.ch/itis-for-health/virtual-population/human-models/.

Session 4A8
Microstrip Antennas and Defected Ground Structure (DGS) Filters

A Microstrip Line with Additional Capacitive and Inductive Effects Loaded

Jongsik Lim[1], **Kyunghoon Kwon**[1], **Seungwook Lee**[2], **Seok-Jae Lee**[1], **Sang-Min Han**[1], **Dal Ahn**[1], **and Yongchae Jeong**[2]

[1]Soonchunhyang University, Republic of Korea
[2]Chonbuk National University, Republic of Korea

Abstract— Microstrip line depicted in Fig. 1 is one of representative transmission lines, and its characteristic impedance (Z_o) is proportional to the ratio of the equivalent inductance (L) to capacitance (C) per unit length with the mathematical expression of ($Z_o = \sqrt{L/C}$). If a perturbation structure is added to the normal microstrip line, the additional parasitic inductance and capacitance arise and make the characteristic impedance change from the normal value. The changed characteristic impedance depends on the property of the added perturbation structure, so Z_o would increases or decreases depending whether the perturbation is an inductive or capacitive structure, respectively. Fig. 2 shows SIAD (substrate integrated artificial dielectric) structure proposed by Coulombe et al. in 2007. This structure has a lot of metalized via-holes through the second dielectric substrate. One of major effects of SIAD falls on the increased equivalent capacitance. The realizable limitation of the characteristic impedance goes down further to the lower side if SIAD is added. This means when a specified characteristic impedance of microstrip line is required after SIAD has been combined, the line width maybe much thinner than normal one, so sometimes it is necessary to compensate the line width. Fig. 3 is a defected microstrip structure (DMS), which has the additional equivalent inductance per unit length. If a DMS pattern is inserted alone on the microstrip line, characteristic impedance increases. It means one need to enlarge the line width to keep the same specific characteristic impedance. When SIAD and DMS structures are combined to a normal microstrip line as illustrated in Fig. 4, the characteristic impedance and line width are preserved similarly to the normal ones while the advantages of adding perturbation structure such as the increased slow-wave effect and enlarged electrical length. These advantages are fruitful in reducing the physical length of a fixed specific electrical length. Fig. 5 shows dimensions of DMS as example in this work. One can compare the physical lengths of four microstrip lines for the same frequency (1 GHz) and fixed electrical length ($\lambda/4$) in Table 1.

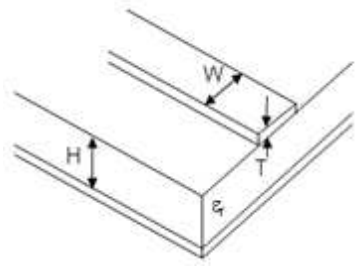

Figure 1.

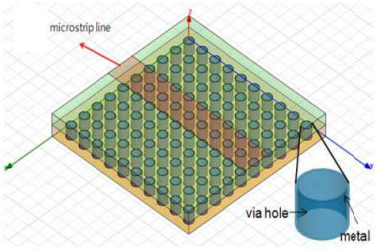

Figure 2.

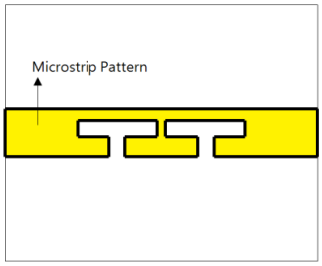

Figure 3.

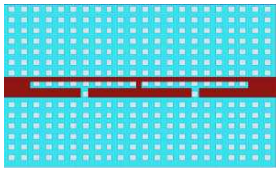

Figure 4.

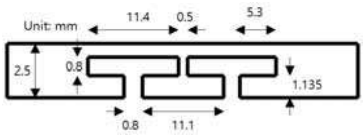

Figure 5.

	Normal	With SIAD	With DMS	With SIAD+DMS
W	2.37	1.28	3.4	2.5
λ/4@1GHz	53.71	41.92	43.21	29.11
Remarks	H=(31+5)mils, ε_r=2.2, T=0.018 Diameter of via-holes=0.8, pitch=1.3 Zo=50Ω, Unit: mm			

Table 1.

Applications of Artificial Magnetic Conductors to the Innovative Design of Various RFID Tag Antennas

D. Kim
Department of Electronic Engineering, Sejong University
209 Neungdong-ro, Gwangjin-gu, Seoul 143-747, Korea

Abstract— We propose a new and advanced design method of RFID tag antennas. The proposed approach is very simple and differentiated from conventional design ways that mostly need highly complicated geometry of tags in order to obtain good impedance matching between RFID chips and the tags.

In our method, we exploit distinctive phase behaviors of reflected waves from versatile artificial magnetic conductors (AMC). As is well known, one of the most attractive characteristics of the AMC is its readily controllable response of reflection phase. As a matter of fact, we can obtain any required phase values between $+180^\circ$ and -180° by changing dimensions of the AMC, which can be directly integrated into our tag design.

According to target applications, we categorize our design approaches into three types; low-profile tags, tags for long reading distances, and those for dual frequency bands.

For the low-profile applications, we install the tag with a RFID chip right on the AMC that is used as a ground plane. Therefore, the low-profile tag is inherently platform tolerant, which means the tag is directly attachable on the various target objects including metal and high-dielectrics with almost no degradation in its performance.

The other two tags are built in metallic cavities with an AMC ground, in which we use coupling effect among the tag, the cavity, and the AMC ground plane so that we can acquire good impedance matching. Consequently, we can avoid figurational complexity of tags. In addition, for the dual-band application, we use two symmetric phase values with respect to the zero phase, at which there is no difference from $+180^\circ$ or -180°, respectively.

All the tags show relatively good agreement between prediction and experiment, which proves that our proposal is practically useful in the design of RFID tag antennas.

Design of the Wide-tuning-range Notch Filter with Wide Constant Absolute Bandwidth

C. W. Tang and W. M. Chuang
Center for Telecommunication Research, Advanced Institute of Manufacturing with High-Tech Innovations
Department of Cmmunications Engineering, National Chung Cheng University, Taiwan

Abstract— Recently, due to the rapid development of wireless communication systems, there are growing demands for filters with good performance of filtering. Moreover, in order to track the operating frequency, frequency-tunable filters are often used for the multiband communication systems, wide-band radar systems, and measuring instruments. Compared with the conventional filters, tunable filters are more functional. Moreover, the same hardware can be utilized for various bands.

Bandstop filters can easily suppress spurious responses and distinguish weak signals from the interference. Moreover, with the tunable bandstop filter, the requirement for high selectivity of the bandpass filter can be diminished. Therefore, the tunable bandstop filters have gained a lot of attention. Because the channel bandwidth is usually fixed even with varying carrier frequencies, the constant absolute bandwidth is crucial for the filter design. The bandstop filters with multi-staged T-shaped cell have been studied. It is found that the more the LC resonator pairs there are, the wider the stopband bandwidth there is. However, when tuning the central frequency, a constant absolute bandwidth cannot be sustained with the T-shaped structure adopted for the bandstop filter. On the contrary, a wide and constant absolute bandwidth is obtained in this paper because the π-shaped circuit is employed for the design of the bandstop filter. This tunable filter is composed of two varactor-tuned resonators, shunted at input/output ports separately, and one quarter-wavelength transmission line connecting two varactor-tuned resonators. These two varactor-tuned resonators are arranged symmetrically, and realized by a varactor and an inductor with series connection. Moreover, the varactor is introduced to control the central frequency within the stopband. Significantly, we provide easy methods to increase the absolute bandwidth of the stopband by enlarging impedance of the transmission line section and adopting larger values of the ripple in this study. Moreover, the higher the order of the bandstop filter is, the sharper the roll-off stopband will be.

A Simple Tunable Filter Antenna Design with No Bias Lines

M. Al-Husseini[1, 2], K. Y. Kabalan[2], and A. El-Hajj[2]

[1]Beirut Research & Innovation Center, Lebanese Center for Studies & Research, Lebanon
[2]Electrical & Computer Engineering Department, American University of Beirut, Lebanon

Abstract— Existing tunable antenna designs are complex and many of them use a large number of switching elements. Even the less complicated ones still require external DC bias lines to control the employed RF switches or varactors. The design of these bias lines is a daunting task since their presence affect the antenna properties.

In this work, a simple design of a tunable filter antenna is presented. The design uses a single varactor and does not require any external DC bias lines. The design is based on a basic ultra-wide-band antenna with a microstrip line feed, a partial ground plane, and a rectangular patch with rounded corners. A rectangular ring slot is etched in the ground plane beneath the feed line. One varactor is mounted over the ring slot, transforming it into a single-ring complementary split-ring resonator (CSRR). In this configuration, the CSRR causes a tunable band notch whose frequency depends on the varactor's capacitance value. A narrow cut is then made to the feed line, which acts as a capacitor and transforms the band stop caused by the CSRR into a band pass. A shorting is made, through the substrate, to connect the section of the feed before the cut and the inside of the CSRR in the ground plane. This shorting serves to improve the band-pass behavior and to relay the DC voltage to the CSRR's varactor. A DC voltage is applied at the antenna's feed, mixed with the RF input using a DC bias tee. Due to the shorting, the inside of the CSRR is at this same DC voltage level, putting the varactor between two different DC voltage regions. The capacitance value of the varactor is thus controlled by changing the DC voltage at the bias tee input. The cut in the feed prevents the DC current from flowing into the patch.

A prototype antenna is fabricated and tested. Its geometry is shown in Fig. 1 and the measured reflection coefficient is given in Fig. 2 for several reverse DC voltage values. Clear frequency tunability is achieved, in this case over a 1 GHz band. The antenna has good gain values and omnidirectional patterns. The detailed configuration and results will be presented in the full paper.

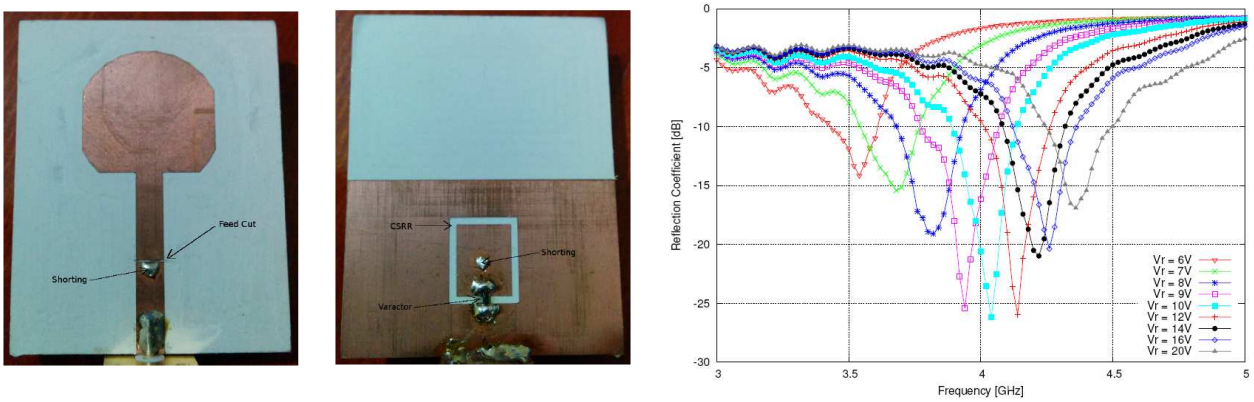

(a) (b) (c)

Figure 1: (a) Prototype photo top view, (b) bottom view, (c) measured S_{11}.

The Golden Spiral Antenna

Bhaskar Harsha, **G. S. Kartikeya**, **Praveenkumar Patil Kedar**, **and Gowda N. G. Monish**
Antenna Research Laboratory, BMS Institute of Technology, India

Abstract— In this paper the possibility of a golden spiral antenna which is derived from the Fibonacci series is applied to a patch antenna and is investigated. It was found that for the substrate dimensions of 14.4 cm × 8.9 cm (144 being the 11th successive number of the Fibonacci series) 13 resonating bands in the range of 1 GHz to 8 GHz without the application of the EBG structure was found. The return loss graph for six different iterations of different substrate dimensions based on the successive numbers of the Fibonacci series is investigated. For the substrate dimensions of 14.4 cm × 8.9 cm mentioned above, Electromagnetic Band Gap (EBG) structures are positioned in the ground plane of the golden spiral antenna. Slotted EBG structures are used to enhance the gain at a particular frequency. As a consequence of this it was found that gain of the Golden Spiral antenna from 1.09 GHz to 2.5 GHz and 6.0535 to 6.25 GHz was increased by the addition of the EBG structures. A peak gain of 15 db and 9.2 db was found at 1.98 GHz and 6.18 GHz respectively.

Antenna Design:

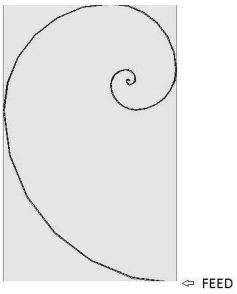

Figure 1: The radiating surface of the golden spiral antenna. The black coloring is the metal surface.

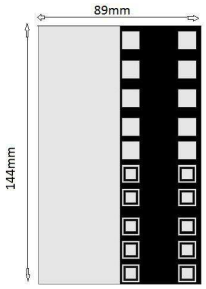

Figure 2: The ground plane of the golden spiral antenna. The black coloring is the metal surface.

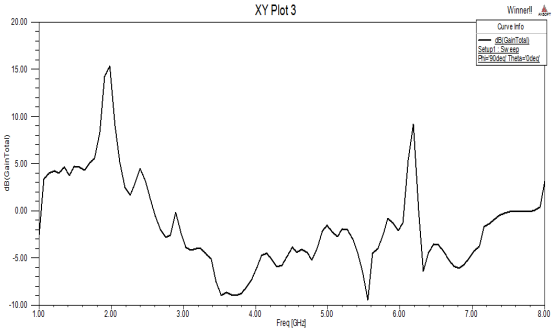

Figure 3: The gain vs frequency from 1 GHz to 8 GHz.

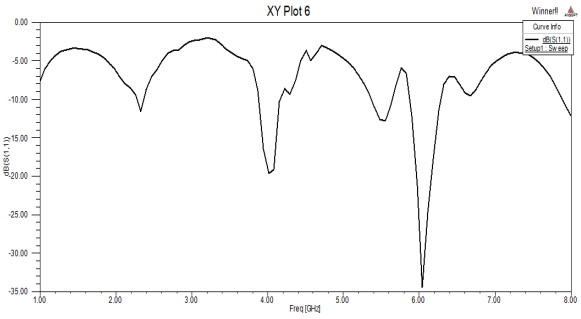

Figure 4: The S_{11} curve from 1 GHz to 8 GHz.

Sierpinski Gasket Fractals Implemented as Electromagnetic Band Gap (EBG) Structures on a Multiband Antenna for WLAN/WiMAX Applications

Praveenkumar Patil Kedar, **G. S. Karthikeya**, **Gowda N. G. Monish**, **and Bhaskar Harsha**
Antenna Research Laboratory, Department of Electronics and Communication Engineering
B.M.S. Institute of Technology & Management, Vishweshwaraya Technological University, India

Abstract— Electromagnetic Band-Gap (EBG) Structure is an area of study in which researchers are growing interested and are investigating. Loading EBG to antennas imparts, to the antennas, many properties including surface wave suppression, band rejection or increased gain. But there has not been much research on fractals loaded as EBG. The amalgamation of these two areas of research is yet to be explored. Implementation of Sierpinski Gasket Fractals as Electromagnetic Band-Gap (EBG) Structures on a multiband planar patch antenna, for WLAN/WiMAX applications, is investigated in this paper. An L Slot Patch Antenna is selected as the test antenna for the fractals to be loaded as EBG. This antenna has a FR4 epoxy substrate of thickness 1.6 mm with a dielectric constant 4.4 and loss tangent of 0.02. The overall dimension of the patch antenna is 35 mm × 30 mm × 1.6 mm. Fig. 1 shows the top and bottom view of the antenna along with the point of excitation represented by X in the figure. Initially, the gain of the patch antenna over the frequency range of 2 GHz to 5 GHz is measured for reference and comparison. Before introducing the EBG structures, the gain of the patch antenna is measured to be 2.38 dB. Later, different iterations of the fractals are loaded as EBG onto the antenna in different configurations. The results obtained, with and without EBG structures, are compared and studied. A peak gain of 2.51 dB is obtained after introducing the fractal structures in the antenna, in one of the various proposed designs which is shown in Fig. 2. The results obtained are depicted in Fig. 3. Thus, this paper illustrates a novel approach of Sierpinski Gasket Fractals to be loaded as EBG.

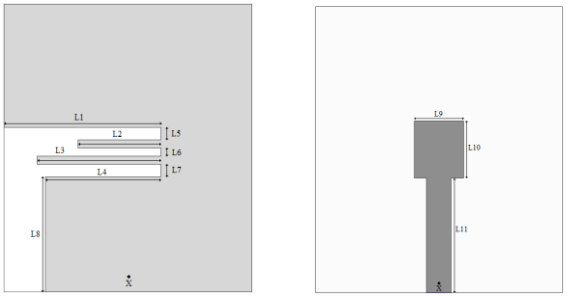

(a) Top View (b) Bottom View

Figure 1: $L1 = 19$ mm, $L2 = 10$ mm, $L3 = 15$ mm, $L4 = L8 = L11 = 14$ mm, $L5 = L7 = 1.5$ mm, $L6 = 1$ mm, $L9 = 6$ mm, $L10 = 7$ mm.

Antenna Design:

Fractals loaded as EBG around the patch: Fractals were arranged around the patch on the bottom plane of the substrate. Parametric analysis is done and the side length of the fractals is varied from 3 mm to 4.5 mm, the gap between the fractals is varied from 7 mm to 11 mm and the orientation of the fractals is changed from 0° to 180°. The design is shown in Fig. 2.

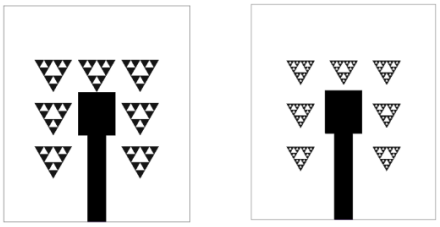

Figure 2: Fractals loaded, around the patch, on the bottom of the antenna.

Results and Discussion:

Fractals loaded as EBG around the patch: The third iteration of the fractal structures are analyzed in this design. After the parametric analysis, it is found that the peak gain of the third iteration fractal loaded design is 2.51 dB.

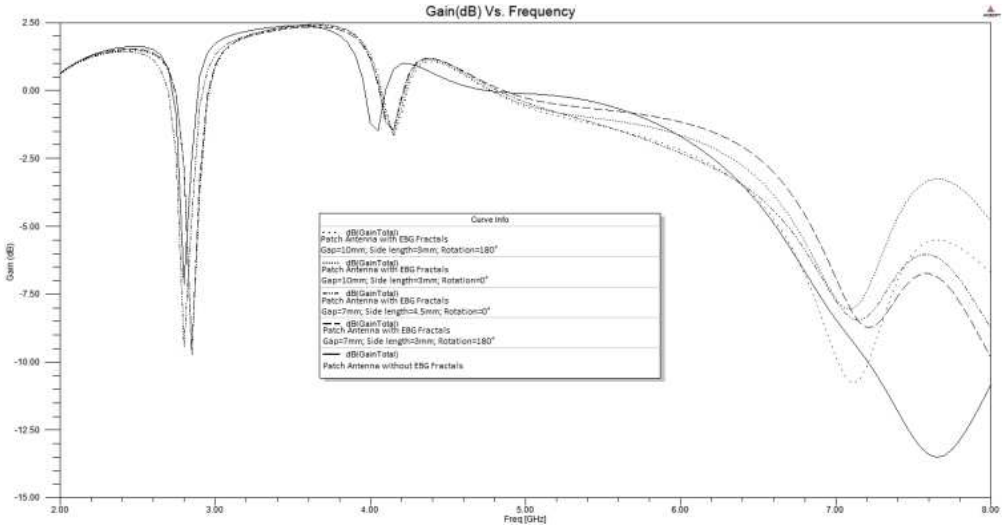

Figure 3: Gain (dB) vs. Frequency graph of third iteration fractals loaded as EBG around the patch compared with the antenna without EBG.

Improvement in Planar Array Antenna Performance by Using Center-fed Coaxial-to-SIW Transition and UC-EBG Structure for 60 GHz Wireless Communication

Ehsan Ghahramani, Ramazan Ali Sadeghzadeh, Mahmood Karami, and Behzad Boroomandisorkhabi
Faculty of Electrical and Computer Engineering, K. N. Toosi University of Technology, Tehran, Iran

Abstract— Microstrip patch antennas (MPA) are widely used in modern communication systems, because of low profile, conformability to planar or curved surface, low cost and light weight. Therefore, they are a good candidates for low cost Microstrip millimeter wave (MMW) applications. But these antennas have low efficiency and low gain because of having small size and high conductive losses. To overcome this problem, the waveguide resonance slot antennas are employed. These antennas have high gain, high cross-polarization and low side lobe levels. But there are some disadvantages with these antennas. Heavy weight and high price are two of these disadvantages. By using substrate integrated waveguide (SIW), these problems can be solved. In this paper, the performance of a conventional two-layer 2×2 SIW-fed MMW MPA array is improved using new center-fed coaxial-to-SIW transition and UC-EBG structure. In recent years, Electromagnetic band-gap structures have become more interesting because of having desirable properties. Suppressing undesired surface waves on the antenna, increasing the antenna gain and reducing mutual coupling between antenna radiation elements are some of these properties. In this paper, first, process of substrate integrated waveguide (SIW) transition line designing is discussed and then a novel coaxial to SIW transition structure introduced since employing microstrip line for feeding millimeter wave antenna in commercial use is not appropriate because of internal losses. Finally, the gain and side lobe level of proposed antenna are improved by using surface wave suppression properties of EBG structure in antenna. If antenna center frequency has been in the UC-EBG band-gap areas, mutual coupling, antenna gain and side lob level will be improved effectively. Presented antenna model is offering good impedance bandwidth (900 MHz) and boresight Gain (> 11.7 dB). The proposed configuration is simulated using CST Microwave Studio.

S-band Proximity Coupled Patch Antenna Based on TiN/Ag Multilayer Material

M. Yarlequé[1], R. Cerna[1], J. L. Ampuero[2], A. Talledo[2], and K. Paucar[3]

[1]Departamento de Ingeniería, Pontificia Univerisdad Católica del Perú, PUCP, Lima, Peru
[2]Laboratorio de Sputtering, Facultad de Ciencias, Universidad Nacional de Ingeniería, Lima, Peru
[3]Gabinete de Corrosión, Facultad de Ingenieria Química y Textil
Universidad Nacional de Ingeniería, Lima, Peru

Abstract— One of the challenges in the development of antennas is their resistance to the environment and corrosion, which is extreme on shore or cost region due to humidity and corrosion agent such as chlorine and sulphides. On the other hand, there is a trend and increase use of planar antennas due to their low profile, integration capability and size for high frequency and wideband applications. The conventional structures for these antennas consist of a dielectric substrate and two separate conducting layers. The latter are implemented with copper and a resin protection cover. However, this structure is not always convenient to endure the stringent conditions of a costal city. For this purpose, it is well known that Titanium nitride (TiN) has important properties as high hardness and high corrosion resistance. Nevertheless, its electrical resistance is high and not convenient for antenna use. Due to this, a multilayer material consists of TiN and silver was grown on Alumina substrate by using DC magnetron sputtering, resulting in a conductive material with corrosion-resistance properties.

In this paper, a first antenna design with this TiN/Ag multilayer material is demonstrated. Since the patterning of this material by photolithography is not simple, neither it cannot be soldered to coaxial connectors nor bonding wires easily, a proximity electromagnetic coupling method is employed for this design. To this purpose Keysight EMPro program was used for the simulation of this antenna, which structure is shown in Fig. 1. This antenna comprises an Alumina substrate (with the grown TiN/Ag layers) on top of a baquelite substrate, where the microstrip feeding line is patterned. This antenna was measured showing a central frequency of 3.3 GHz with 100 MHz of bandwidth, and a gain of 5.6 dBi.

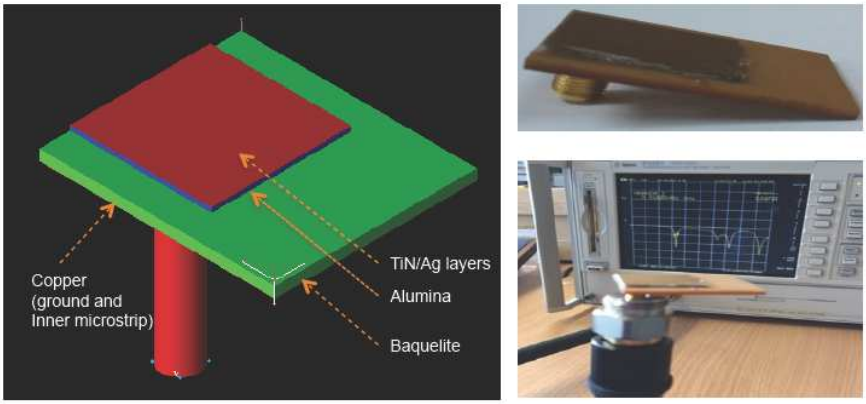

Figure 1: Proximity coupled patch antenna, model and measurements.

Analysis of High Gain Dual Beam Pentagonal Patch Antenna Array

R. Anand[1], **Jesmi Alphonsa Jose**[1], **and Sreedevi K. Menon**[2]

[1]Amrita Center for Wireless Networks and Applications, Amrita School of Engineering, Amritapuri, India
[2]Electronics and Communication Engineering, Amrita School of Engineering, Amritapuri, India

Abstract— In this paper, a high gain pentagonal patch antenna array with dual beam is presented. The pentagonal geometry is inspired from a rectangle patch antenna and a triangle patch antenna. The architecture of the antenna resembles an irregular pentagon comprised of a triangle placed on top of a rectangle. FEM is used to analyze the antenna design.

We used the characteristics of an inset feed rectangular patch antenna and an inset feed triangular patch antenna, with resonant frequency at 2.45 GHz, as a reference. The reference antennas had a directional radiation pattern with a gain of 6.88 dBi and 5.33 dBi, respectively. The geometry of the single element pentagonal antenna was designed by placing the triangle on top of a rectangle shape. The pentagonal antenna gave good reflection and radiation characteristics with a 2 : 1 VSWR bandwidth of 8.1% at resonant frequency. As we combined the geometry of a rectangle and a triangle for the pentagonal design, the single pentagon patch antenna radiated two directional beams with a peak gain of 6.1 dBi at resonant frequency. In the entire operating bandwidth, the gain was better than 5.8 dBi with HPBW of 40°/30° (for the two directional beams) in the azimuth plane and 70° in the elevation plane. Even though the pentagon patch had slightly less gain than the rectangular patch, it had an additional advantage since it radiated in two directions. The proposed pentagonal antenna architecture can be used in applications where there is a need to produce a dual beam without the need of any additional circuits for switching.

To enhance the gain of the pentagonal patch, we designed a 2×1 linear array with pentagonal elements. The spacing between the array elements and the feeding mechanism were optimized to achieve maximum gain. The array elements were spaced at a distance of 0.5λ. The pentagon array was fed by a $50\,\Omega$ impedance line. The line was split into two $100\,\Omega$ impedance lines for each of the elements of the pentagon. The 2×1 linear pentagon array produced dual beams with a peak gain of 9.27 dBi. In comparison, the rectangle 2×1 linear array and the triangle 2×1 linear array produced a single beam with a peak gain of 9.86 dBi and 7.03 dBi, respectively Thus, the 2×1 linear pentagon array with dual beams achieved a similar gain as the 2×1 linear rectangular array with a single beam.

We further enhanced the gain of the antenna system by constructing a 4×1 linear pentagon array, which produced a dual beam with a gain of 10 dBi The gain of the antenna was similar when compared to a 4×1 single beam rectangle array and a 4×1 single beam triangle array, whose gains were 11.24 dBi and 8.39 dBi, respectively. The simulated results obtained for the pentagonal antennas were validated by the network analyzer. Therefore, the proposed pentagonal antennas with dual beams can be applied in areas such as object detection, RF ablation, MIMO among others.

Bandpass Filters with Mixed Hairpin and Patch Resonators

Yi Wang, Eugene Ogbodo, and Predrag Rapajic
Department of Electronic, Electrical and Computer Engineering
University of Greenwich, Kent, ME4 4TB, UK

Abstract— Conventional planar bandpass filters are usually formed of coupled-resonators of the same type for the ease of modelling and implementation. Increasingly more sophisticated filters composed of a mixture of different types of resonators are proposed for various purposes. Some are intended to use non-uniform Q-factors across the resonators to better control the passband flatness in lossy filters [1]. Others use specific resonators for dual purpose such as in the case of integrated filter antennas, where the resonant antenna element serves as the radiator as well as one resonant pole in a filter [2, 3]. The antenna element there is usually of a completely different structure and characteristics from the other resonators.

This work explores the combination of single-mode and dual-mode resonators. A mixture of two hairpins and one patch resonator are used to produce a three-pole filter with one transmission zero. The three resonators are in-line coupled without any cascaded quadruplet or triplet structures. The patch is used for its dual modes. One is coupled to the hairpins forming the transmission path, whereas the other orthogonal mode generates the transmission zero. Such a configuration is simple but significantly increases the selectivity of the filter. The metred corner and the size of the patch are the main parameters used to optimise the coupling between the modes and to adjust the position of the transmission zero.

As shown in Figure 1, a 2.5 GHz filter with a bandwidth of 8% and a transmission zero at 2.4 GHz is designed. A return loss of 16 dB is achieved. The substrate has a dielectric constant of 11.2, a loss tangent of 0.0023 and a thickness of 1.27 mm. To minimise the radiation loss and preserve the high Q-factor of the patch, the filter is housed in a metal box. Such a filter configuration with mixed types of resonators has the flexibility and potential in implementing other novel and multiple-functional components and circuits. This will be discussed in more details in the full paper.

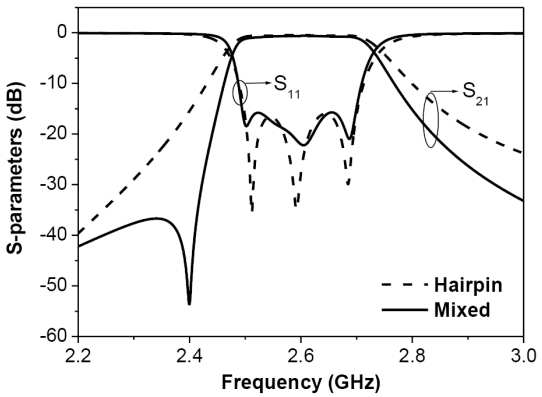

Figure 1: Comparison between a conventional hairpin filter and a mixed hairpin-patch-resonator filter of the same order.

REFERENCES

1. Meng, M. and I. Hunter, "The design of parallel connected filter networks with non-uniform Q resonators," *IEEE MTT-S Int. Microw. Symp. Dig.*, June 17–22, 2012.
2. Yusuf, Y. and X. Gong, "Compact low-loss integration of high-3-D filters with highly efficient antennas," *IEEE Trans. Microw. Theo. Techn.*, Vol. 59, No. 4, 857–865, April 2011.
3. Mao, C. X., S. Gao, Z. P. Wang, Y. Wang, F. Qin, B. Sanz-Izquierdo, and Q. X. Chu, "Integrated filtering-antenna with controllable frequency bandwidth," *The 9th Europ. Conf. on Antennas and Propagation (EuCAP)*, April 12–17, 2015.

Effect of Complementary Split-ring Resonators on Beam Scanning in the CRLH-leaky Wave Antennas Based on Split-ring Resonators and Slotline

Saeid Mohammadpour Jaghargh, **Pejman Rezaei**, **and Javad Soleiman Meiguni**
Faculty of Electrical and Computer Engineering, Semnan University, Semnan, Iran

Abstract— In this paper, a new leaky wave antenna (LWA) based on complementary split-ring resonators (CSRRs) and slot line are proposed. Effects of CSRRs on beam scanning in a composite right/left handed (CRLH) LWA based on split-ring resonators (SRRs) are investigated. Actually, the effects of these structures on the scan angles have been compared. The commercial Ansoft HFSS software is adopted for the simulations. The proposed LWA is analyzed in S and C band frequency, and the results reveal that the CSRR improves the gain in backward leaky wave radiation. The CSRR-LWA just scans the negative angles. Furthermore, the simulation results demonstrate the potential of the SRR-LWA to radiate from backward to forward scanning angles. As a result this miniaturized CSRR-LWA main beam can scan the space for C-band from -115 to -170 degree in phi $= 0$ (deg) plane. In the other word, the CSRR-LWA only scans in the negative ranges of theta, but SRR-LWA scans the space from $+94^\circ$ to $+156^\circ$ in positive ranges and -133° to -177° in negative ranges of theta.

Session 4A9a
Casimir and Other Quantum Effects

The Near-field Radiative Heat Transfer for Doped Si-Ge Multi-layered Metamaterials Supporting Surface Plasmon Polaritons

Yang Bai[1] **and Yongyuan Jiang**[1, 2]

[1]Department of Physics, Harbin Institute of Technology, Harbin 150001, China
[2]Key Lab of Micro-Optics and Photonic Technology of Heilongjiang Province, Harbin 150001, China

Abstract— The near-field radiative heat transfer between doped silicon (Si)-germanium (Ge) multi-layered metamaterials is studied by fluctuation electrodynamics. By considering the contribution of surface plasmon polaritons (SPPs) supported by doped Si layer in the infrared, we have investigated the spectral heat transfer coefficient, the energy transmission factor and the total heat transfer coefficient versus separation distance between the doped-Si multilayered metamaterial with a filling factor of 0.4, where the doped Si layer is 40 nm and the Ge layer is 60 nm. Results show that the heat transfer coefficient between doped Si-Ge multi-layered metamaterials is attributed to the surface plasmon polaritons (SPPs) excited at the interface of the doped-Si and vacuum, the Bloch modes supported by the multi-layered structure and the intrinsic loss of the doped-Si. On the other hand, the contribution of SPPs can be obviously suppressed when choosing Ge as the topmost layer, and the energy transmission factor is comparable with the calculated results using the parameter obtained by effective medium theory. Moreover, the total heat transfer coefficient between the multi-layered structures is weaker than that of bulk doped-Si when the separation distance is smaller than 100 nm, but strong in large separation distance. This is due to the fact that the contribution of Bloch mode is restricted at large distance by the strong intrinsic loss of the dope-Si. Whereas the heat transfer coefficient between multi-layered structures composed of material with low loss, such as silicon carbide (SiC), is stronger than that of bulk medium. This study should facilitate the application of nanostructures in more efficient noncontact thermal management, near-field thermophotovoltaics and thermal imaging.

Contribution of Non-local Effects to the Casimir Forces

Y. Francescato and V. Giannini
The Blackett Laboratory, Imperial College London, London SW7 2BZ, UK

Abstract— Dispersion forces, that is Casimir and Van der Waals forces, impregnate our everyday life through physical processes as common as cohesion, friction and attraction. Yet their origin is deeply rooted in quantum mechanics and can be solved for only the most simple geometries. In the late 1940s, Casimir together with Polder predicted the attraction phenomenon taking place between two conducting plates, known as Casimir forces. Since the extension of the theory by Lifshitz in 1956 to the case of dissipative materials, the study of these effects has resulted in a large body of literature arising from both experimental and theoretical investigations [1].

Here we show that in addition to dissipation and dispersion [1, 2], a full description of the Casimir forces must take into account the effect of non-locality, or in other words the dependency of a medium response to the wavevector of the field. Indeed, we demonstrate that the Casimir forces arising from this representation is in stark contrast to the usual-local-optical properties assigned generally to materials. This is illustrated in Fig. 1 where the integrand of the Casimir force [3] is compared between the local and non-local cases. As one can see, the modes contributing to the force are largely unequivalent at high k-vectors. We will discuss typical cases where non-locality plays a crucial role in dispersion forces and draw conclusion on its observation in realistic epxeriments.

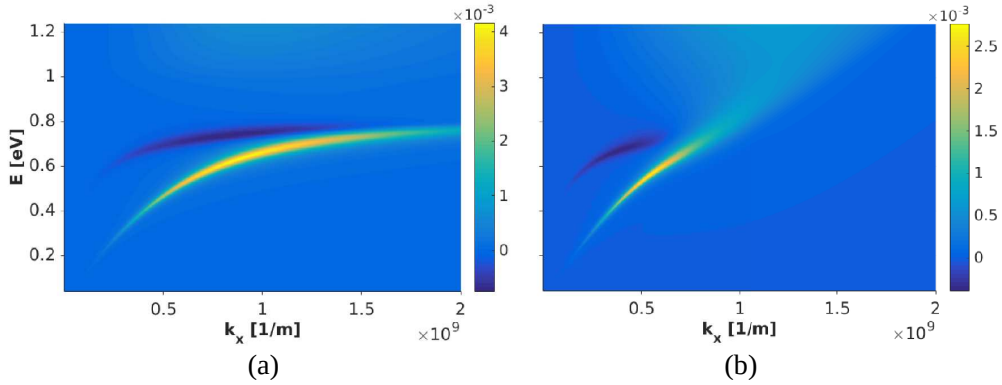

Figure 1: Force spectrum for two graphene sheets separated by 1 nm in the (a) local and (b) non-local picture.

REFERENCES

1. Klimchitskaya, G. L., U. Mohideen, and V. M. Mostepanenko, "The Casimir force between real materials: Experiment and theory," *Rev. Mod. Phys.*, Vol. 81, 1827–1885, 2009.
2. Pirozhenko, I. and A. Lambrecht, "Repulsive Casimir forces and the role of surface modes," *Phys. Rev. A*, Vol. 80, 042510, 2009.
3. Henkel, C., K. Joulain, J.-P. Mulet, and J.-J. Greffet, "Coupled surface polaritons and the Casimir force," *Pys. Rev. A*, Vol. 69, 023808, 2004.

Radiative Heat Transfer through Nanometer-size Gaps

V. Fernández Hurtado[1], K. Kim[2], B. Song[2], W. Lee[2], W. Jeong[2], J. Feist[1], F. J. Garcia-Vidal[1], J. C. Cuevas[1], E. Meyhofer[2], and P. Reddy[2]

[1]Departamento de Física Teórica de la Materia Condensada and Condensed Matter Physics Center (IFIMAC), Universidad Autónoma de Madrid, Madrid 28049, Spain
[2]Department of Mechanical Engineering, University of Michigan, Ann Arbor 48109, USA

Abstract— One of the central open problems in nanoscience is the study of the heat transport in nanoscale devices, which has remained largely unexplored due to experimental challenges. In this context, a key issue is the understanding of the heat transfer via thermal radiation between systems separated by nanometer-size gaps. In this extreme regime, the electromagnetic near-field is expected to give rise to a dramatic enhancement of the radiative heat transfer, something that has only be quantitatively verified for gaps on the order of 20–30 nm [1]. In this work, we present a combined experimental and theoretical study of the radiative heat transfer in the extreme near-field regime (gaps of 1–10 nm). From the experimental side, we performed systematic studies using AFM-based scanning probes with integrated nanoscale thermocouples [2], which were coated with dielectrics (SiO_2 or SiN_x). Our experiments of heat transport between the scanning probes and a flat substrate coated with dielectrics, performed in an ultra-high vacuum environment, confirm that heat transport is dramatically enhanced in the near-field. To understand our experimental results, we investigated these near-field enhancements within the framework of the theory of fluctuational electrodynamics [3]. To be precise, we performed extensive numerical simulations making use of a combination of a fluctuating-surface-current formulation of radiative heat transfer with the boundary element method [4, 5]. Such a combination allows us describing realistic geometries for our tip-sample setups. Our theoretical results are in good agreement with the measured heat flows between both dielectric and metallic surfaces, which establishes the validity of fluctuational electrodynamics in modeling near-field heat transport all the way to nanometer-size separations.

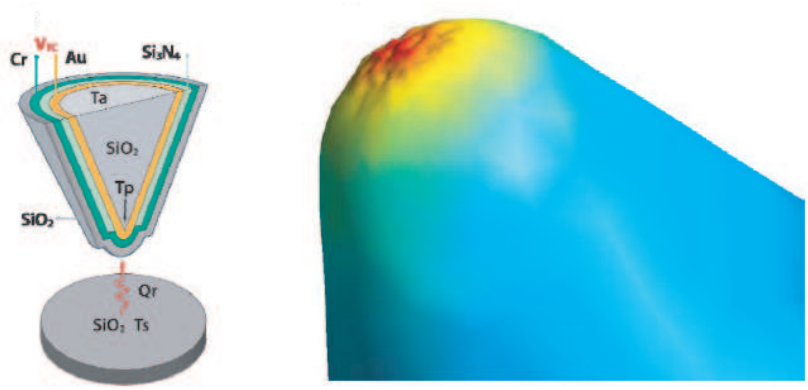

(a) (b)

Figure 1: (a) Schematic diagram of the experimental setup. The AFM probes incorporate a thermocouple, made by a spherical Au/Cr junction with a diameter of 200 nm. (b) Numerical simulation of the spatially resolved heat transfer between a tip and a plate made of silica and separated by a distance of 1 nm. The radius of the tip is 225 nm. The color scale is logarithmic, showing the radiative heat transfer enhancement in the extreme near-field.

REFERENCES

1. Basu, S., Z. M. Zhang, and C. J. Fu, *Int. J. Energy Res.*, Vol. 33, 1203, 2009.
2. Lee, W., K. Kim, W. Jeong, L. A. Zotti, F. Pauly, J. C. Cuevas, and P. Reddy, *Nature*, Vol. 498, 209, 2013.
3. Joulain, K., J. P. Mullet, F. Marquier, R. Carminati, and J. J. Greffet, *Surf. Sci. Rep.*, Vol. 57, 59, 2005.
4. Rodriguez, A. W., M. T. H. Reid, and S. G. Johnson, *Phys. Rev. B*, Vol. 86, 220302(R), 2012.
5. Rodriguez, A. W., M. T. H. Reid, and S. G. Johnson, *Phys. Rev. B*, Vol. 88, 054305, 2013.

Casimir Interaction between Atoms in Motion: From Unruh Effect to Ginzburg Radiation

J. Marino[1], **A. Noto**[2], **R. Passante**[2], **A. Recati**[3, 4], **and I. Carusotto**[3]

[1]Institute of Theoretical Physics, TU Dresden, Dresden D-01062, Germany
[2]Dipartimento di Fisica e Chimica, Università degli Studi di Palermo and CNISM
Via Archirafi 36, Palermo I-90123, Italy
[3]INO-CNR BEC Center and Dipartimento di Fisica, Università di Trento, Povo 38123, Italy
[4]Technische Universit ät München, James-Franck-Strasse 1, Garching 85748, Germany

Abstract— In this talk, I plan to show how Casimir interactions can be used as successful tools to probe quantum effects beyond the domain of quantum electrodynamics.

The first part of the talk concerns the field of Casimir forces subject to an external driving, through a model at the interface between quantum optics and general relativity.

The Unruh effect predicts that a single relativistically accelerated detector associates to quantum vacuum fluctuations a thermal power spectrum. Although many single-particle physics studies confirm this scenario, I will explicitly show that, when a couple of uniformly accelerated atoms is considered, also non-thermal effects can manifest and they can be highlighted through the Casimir-Polder interaction among the two particles [1].

The second part of the talk deals with the domain of ultra-cold gases, and I will show how the Casimir force felt by an impurity moving in a Bose-Einstein condensate, can exhibit different scaling behaviours with distance, depending on the velocity of the impurity itself.

I will, in particular, discuss a concrete experimental implementation of this setup, where novel physics of potential impact for optical measurements of Casimir forces can be highlighted [2].

REFERENCES

1. Marino, J., A. Noto, and R. Passante, *Phys. Rev. Lett.*, Vol. 113, 020403, 2014.
2. Marino, J., A. Recati, and I. Carusotto, in Preparation, 2015.

Casimir-Polder Interaction between Rydberg Atoms and a Photonic Crystal Fibre

Wijnand Broer and Stefan Scheel
Institut für Physik, Universität Rostock, Rostock, Germany

Abstract— The Casimir-Polder (CP) force is an electromagnetic dispersion interaction between an atom and a neutral surface without permanent dipoles. This force arises from quantum mechanical (and thermal) fluctuations of the electromagnetic field. The CP interaction can become very strong for a Rydberg atom, which by definition has a large principal quantum number n. As the size of its wavefunction increases as $\propto n^2$, so does its transition dipole moment. The CP interactions thus affect the spectra of the atoms in the presence of macroscopic geometries. Hence, these interactions are of interest for proposals to build atomic lattice clocks in hollow-core fibres. Another example of a potential application is the development of single photon sources using Rydberg atoms in microcells. Both of these applications require a detailed understanding of the atomic structure near macroscopic surfaces.

Here we theoretically study the CP potential between cesium atoms in a Rydberg state and a hollow core photonic crystal fibre made of silica. Our analysis includes the following effects: 1) that of the Rydberg states of the atoms, 2) that of the material properties of the fibre (for example α-, β-quartz or amorphous silica), 3) that of its dimensionality (i.e., its shape and size), and 4) that of temperature. This system is typically out of thermal equilibrium because of the highly excited state of the atoms. This gives rise to an additional narrowband contribution to the Casimir-Polder potential, which can hence become considerably larger than in the case of thermal equilibrium.

Session 4A10
Resonators, Filters, Transmission Lines

Simultaneous Approximation Method of Attenuation and Group Delay Characteristics for Coupled Resonators Filter

Toshiki Matsubara[1], **Toshikazu Sekine**[2], **and Yasuhiro Takahashi**[2]

[1]Graduate School of Engineering, Gifu University, 1-1 Yanagido, Gifu-shi 501-1193, Japan
[2]Department of Electrical and Electronic Engineering, Gifu University
1-1 Yanagido, Gifu-shi 501-1193, Japan

Abstract— In the pulse transmission system, both the attenuation and the group delay characteristic can be given as a specification in the filter. However, synthesis method of simultaneous characteristic approximation for these properties is still unresolved. It is derived by formulating the optimization problem. In this paper, Vector Fitting [1] can be applied to the approximation of characteristics of the minimum phase filter is considered. We have obtained these simultaneous characteristics approximatation by adding the complex transmission zeros to the filter with real transmission zeros. Advantages of our method is that the number of resonators is not increased, since the complex transmission zeros can be obtained by couplings of resonators. Effectiveness of our method is confirmed by numerical examples. As a result, we conclude that the Vector Fitting can be applied to approximation of the filter characteristics.

Using polynomial $f(\omega')$; $g(\omega')$ and $h(\omega')$ of the normarized actual frequency ω', $\mathbf{S}$ matrix of lossless reciprocal circuit is expressed by the following expression.

$$\mathbf{S} = \begin{bmatrix} S_{11}(\omega') & S_{11}(\omega') \\ S_{21}(\omega') & S_{22}(\omega') \end{bmatrix} = \frac{1}{g(\omega')} \begin{bmatrix} h(\omega') & f(\omega') \\ f(\omega') & \frac{f(\omega')}{f^*(\omega')} h^*(\omega') \end{bmatrix}, \tag{1}$$
$$g(\omega')g^*(\omega') = h(\omega')h^*(\omega') + f(\omega')f^*(\omega')$$

where, $g^*(\omega') = \overline{g(\omega')}$ and leading coefficient of $f(\omega')$ is one. When the equivalent circuit of filter include the imaginary resistances (frequency independent reactances), $g(\omega')$ is a Hurwitz polynomial in a broad sense. Following two functions $|S_{21}(\omega')|^2$ and normarized group delay $\tau_n(\omega')$ are applied to the Vecter Fitting.

$$\begin{aligned} |S_{21}(\omega')| &= \sum_{i=1}^{N_g} \left(\frac{c_i' + jc_i''}{\omega' - (a_i' + ja_i'')} + \frac{c_i' - jc_i''}{\omega' - (a_i' - ja_i'')} \right), \\ \tau(\omega') &= \frac{j}{2} \sum_{i=1}^{N_g} \left(\frac{1}{\omega' - (a_i' - ja_i'')} - \frac{1}{\omega' - (a_i' + ja_i'')} \right) \end{aligned} \tag{2}$$

We note that the poles of both expressions are common. First, we derived initial values of S-parameters from filter design methods [2, 3]. Next, improveed poles and residues are obtained by using Vector Fitting. Figure 1 shows that the results of numerical example of rational function approximation. There are good approximations of Chebyshev type both attenuation and group delay.

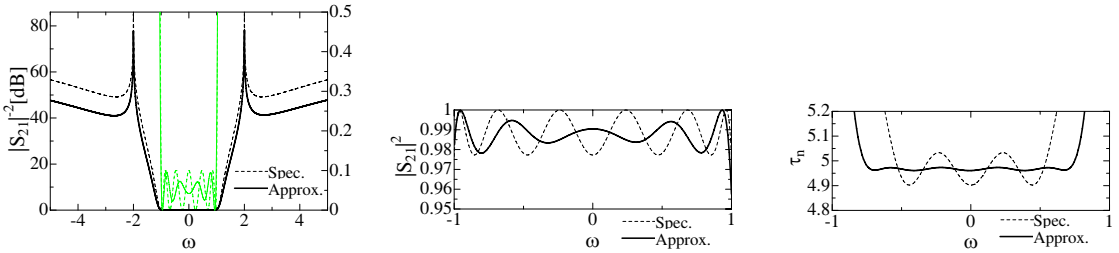

Figure 1: Numerical example, (a) attenuation, (b) attenuation of passband, (c) group delay of passband.

REFERENCES

1. Gustavsen B. and A. Semlyen, "Rational approximation of frequency domain responses by vector fitting," *IEEE Trans. Power Del.*, Vol. 14, No. 3, 1052–1061, July 1999.
2. Bell, Jr., H. C., "Transformed-variable synthesis of narrow-bandpass filters," *IEEE Trans. on Circuits and Systems*, Vol. 26, No. 6, 389–394, June 1979.
3. Murasawa, K., T. Sekine, and Y. Takahashi, "Investigation of the methods of improving group delay characteristic using complex transmission zeros for coupled resonators filter," *Proc. IEEE APMC 2012*, 670–672, Kaohsiung, Taiwan, December 2012.

A Compact Band Pass Filter with Wide Stop-band in LGA Package by Low-temperature Co-fired Ceramic

Lisa Li-Ju Chen and Ken-Huang Lin
Department of Electrical Engineering, National Sun Yat-Sen University, Kaohsiung, Taiwan

Abstract— A compact band pass filter with wide stop-band in LGA (Land Gird Array) package was proposed in this paper. The proposed filter was designed to operate at 5.15 GHz–5.85 GHz for 802.11ac applications and implemented in low-temperature co-fired ceramic (LTCC) substrate. The proposed schematic introduces transmission zeros at the lower band to reject the unwanted frequency and provides wide stop-band at high side with 30 dB rejection level. The proposed circuit is composed of three coupled line (TL1 ∼ TL2), three capacitors (C12/C23/C13), two capacitor to ground (C10/C20/C30), four small inductor (L1/L2/L10/L20) and two shunt open stub-lines (TL1/TL2).

This filter was realized in multilayer structure with LGA package which only need smaller footprint on print circuit board. All the components of filter were embedded into the LTCC multilayer substrate with a relative constant of 33, loss tangent of 0.001. The each foil had a thickness of 23 μm and the used conductor was silver with 10 μm thickness at each layer. The minimum line width and space between the lines were 100 μm and 150 μm, respectively. The inductor elements and coupling line can be implemented by via and it can make the filter to have compact size. The 3D design for the proposed filter is to arrange the shielding ground on the top layer and it avoids the performance of filter to be effected by external environment, especially on SiP module application due to height limitation. The 3D structure of proposed filter was shown in Fig. 1.

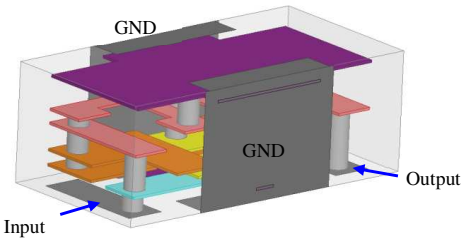

Figure 1: The 3D construction in HFSS.

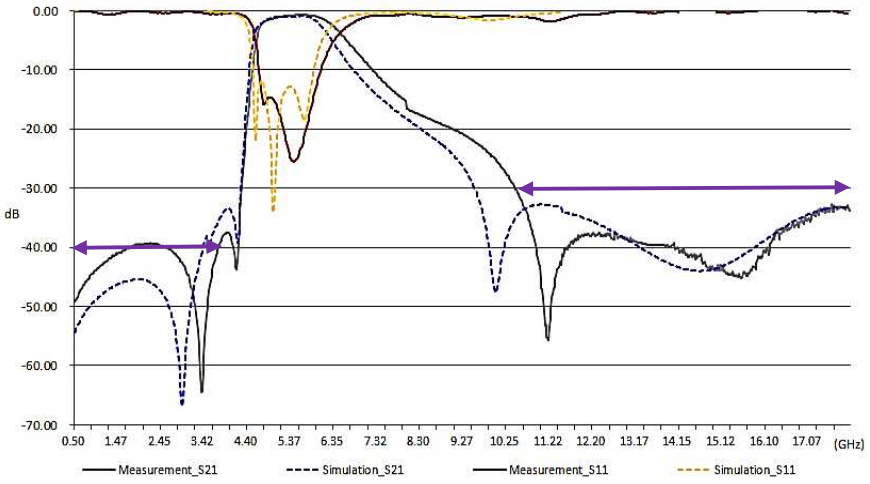

Figure 2: The simulation and measurement result.

The overall size of band pass filter are 1.6 mm (L) × 0.8 mm (W) × 0.6 mm (H) which has small size. The simulated response was shown in Fig. 2. The simulation insertion losses at 5.15 GHz and 5.85 GHz are 1.1 dB and 1.2 dB, respectively. The rejection band with 30 dB attenuation covers from 9.5 GHz to 18 GHz to have good ability to filter out the harmonic noise. The proposed filter also has good attenuation at 500 MHz–4 GHz to reject the unwanted frequency band at low side. Finally, simulated and measured results are presented in Fig. 2 as well.

Heuristic Circuit Transformation Based on Left-handed Filter and Right-handed Filter

Kosei Tanii[1], **Koji Wada**[2], **and Takanobu Ohno**[1]

[1]National Institute of Technology, Kisarazu College, Japan
[2]The University of Electro-Communications, Japan

Abstract— Passive filters such as bandpass filter (BPF) or bandstop filter (BSF) are fundamental components for wireless communication equipment, and planar filters are preferred since they can easily be fabricated at low cost and suited to the various frequency channels. Meanwhile, composite right/left-handed (CRLH) circuits based on the metamaterial technology have recently been researched [1, 2]. Metamaterials are man-made artificial structures that show unnatural electromagnetic phenomena by negative permeability and permittivity, which means that the phase velocity is negative but the group velocity is positive.

In this study, we firstly present a compact BPF on a printed circuit board (PCB) assuming the use of the microstrip line structure. Duroid 6010 (relative permittivity: $\epsilon_r = 3.6$, loss tangent: $\tan\delta = 0.0023$, thickness of the substrate: $h = 0.635\,\mathrm{mm}$, thickness of the conductor: $t = 18\,\mu\mathrm{m}$) is considered for the dielectric substrate. The BPF is composed of a coupled line and transmission lines with inductive elements, and it produces a dual-mode resonance and transmission zeros. Their conditions are easily solved by using the even-/odd-mode analysis. Since the conditions can be provided as the left-handed (LH) operation, the BSF can also be composed by using the transformation from LH transmission line to right-handed (RH) transmission line. The interdigital coupled line is changed to two open-circuited stubs in order to reduce the series capacitance and the inductive element is eliminated in order to remove the shunt inductance. As a result, the BPF shown in Fig. 1(a) is transformed to the BSF shown in Fig. 1(b).

Both types of filters can be realized in the almost same and very compact size at the same frequency range of 2–3 GHz. Their performances are confirmed by the electromagnetic simulation and measurement.

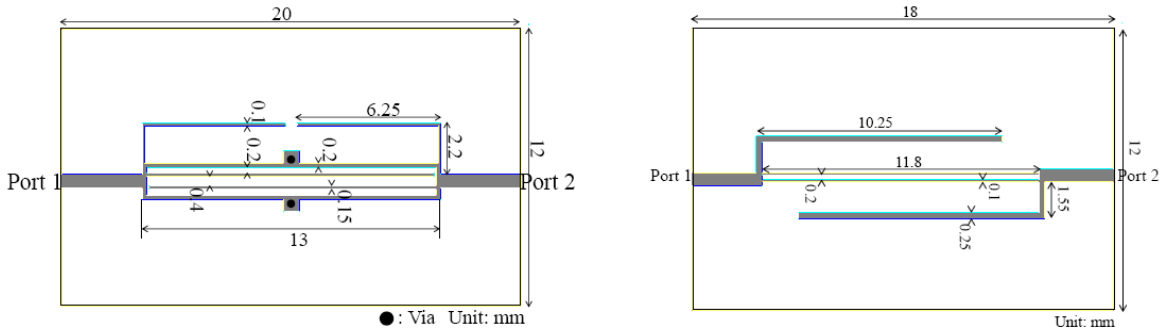

Figure 1: Circuit patterns of the filters: (a) LH-BPF, (b) RH-BSF.

REFERENCES

1. Horii, Y., C. Caloz, and T. Itoh, "Super-compact multilayered left-handed transmission line and diplexer application," *IEEE Trans. Microw. Theory Tech.*, Vol. 53, No. 4, 1527–1534, Apr. 2005.
2. Mao, S.-G., M.-S. Wu, Y.-Z. Chueh, and C.-H. Chen, "Modeling of symmetric composite right/left-handed coplanar waveguides with applications to compact bandpass filters," *IEEE Trans. Microw. Theory Tech.*, Vol. 53, No. 11, 3460–3466, Nov. 2005.

A Compact Tunable Dual-band Bandpass Filter Using Varactor-loaded Step-impedance Resonators

Xiang Zhang, Chang Chen, Mingkang Li, Lingyun Zhou, and Bin Liu
Key Laboratory of Electromagnetic Space Information
Chinese Academy of Sciences, University of Science and Technology of China, Hefei, Anhui 230026, China

Abstract— This paper presents a novel design of a compact tunable dual-band bandpass filter (BPF) using varactor-loaded step-impedance resonators (SIRs). The proposed varactor-loaded SIR is shown in Fig. 1(a). Since the structure is symmetrical, the even- and odd-mode analysis method can be applied to obtain the resonant frequencies. By theoretical analysis, the odd-mode resonant frequency fully depends on the capacitance of the varactor diode connected at the ends of the resonator and the even-mode resonant frequency depends on the capacitances of all the three varactor diodes. This characteristic of the proposed resonator can be utilized to design a tunable dual-band BPF with two controllable passbands. Compared to uniform impedance resonator (UIR), the SIR has more excellent performance such as compact size, and adjustable harmonic resonance frequency etc.. The harmonic resonance frequency of SIR is determined by the length of SIR and the ratio of the two characteristic impedances. By choosing proper ratio of the two characteristic impedances, the length of SIR can be shorter than UIR while keeping the resonance frequency constant. So the proposed filter using varactor-loaded SIRs shown in Fig. 1(b) can be compact.

A tunable dual-band BPF using varactor-loaded SIRs is designed, simulated and measured, as shown in Fig. 1(c). The ratio of the two characteristic impedances of SIR is 0.6. Fig. 2 shows the simulation and measurement results. The designed first tuning passband is from 0.72 GHz

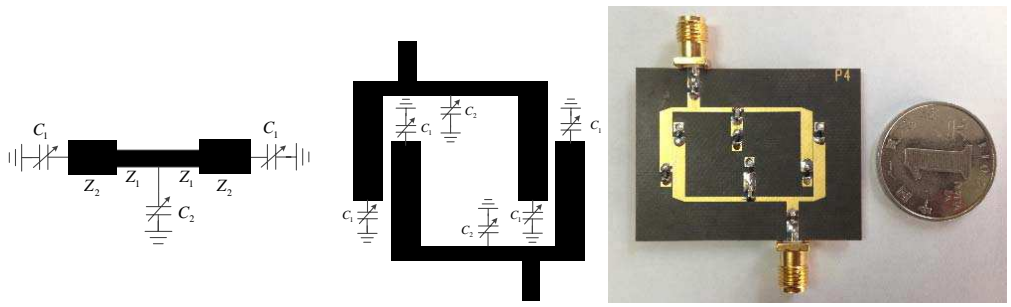

(a) (b) (c)

Figure 1: (a) Basic structure of the proposed resonator. (b) Schematic of the proposed tunable dual-band filter. (c) Photograph of fabricated tunable dual-band filter.

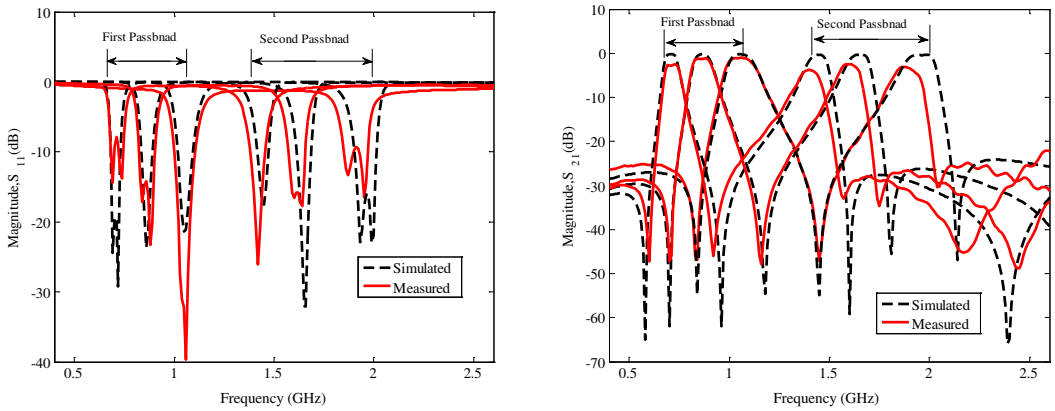

(a) (b)

Figure 2: Simulation and measurement results. (a) S_{11}-magnitude. (b) S_{21}-magnitude.

to 1.06 GHz, and the designed second tuning passband is from 1.45 GHz to 2 GHz. The first passband center frequency tunable range measured is from 0.73 GHz to 1.07 GHz and the second passband center frequency tunable range measured is from 1.4 GHz to 1.9 GHz. The designed second passband center frequency is higher than the measured results because of the capacitance error and fabrication error. The whole size of the tunable dual-band filter using SIRs decrease 22% compared to the tunable dual-band filter using UIRs in [1].

REFERENCES

1. Chaudhary, G., Y. Jeong, and J. Lim, "Harmonic suppressed dual-band bandpass filter with tunable passbands," *IEEE Trans. Microw. Theory Tech.*, Vol. 60, No. 7, 2115–2123, Jul. 2012.

Concentric Open End Rings Resonator Filter

Mahmood Karami, **Ramezan Ali Sadeghzadeh**, **and Mahdi Oliaei**
Electrical & Computer Engineering Department, K. N. Toosi University of Technology, Iran

Abstract— In this paper, a single open ring resonator (ORR) filter with three resonants within its equivalent circuit has been investigated. This filter has a good response at ISM band from 3.13 GHz to 5.56 GHz. According to this filter, a concentric double open end ring resonator filter with an ultra wide band (UWB) behavior has been approached. The frequency response of this one is very appropriate up to 15 GHz. The loop of the filter constitutes both periodic self and mutual inductive-capacitive property between two rings which provides many resonants in these frequencies. The interconnections between these tanks are an important factor of its UWB behavior and they have overlap on each other impressively.

Conductor Loss Evaluation of Thin Microstrip Line with Various Copper Roughnesses

R. Suga[1], **T. Suzuki**[1], **T. Uwano**[1], **Y. Akatsuka**[2], **K. Ishii**[2], **and O. Hashimoto**[1]

[1]Aoyama Gakuin University, Japan
[2]Nippon Kayaku Co. Ltd., Japan

Abstract— The surfaces of the copper foils on a dielectric substrate are generally rougnened to obtain a sufficient adhesion strength as depicted in Figure 1, and the lower effective conductivity due to the roughness brings characteristic degradations of microwave and millimeter-wave circuits. This paper presents an experimental study on an impact of conductor surface roughness on thin microstrip line (MSL). Three types of copper foils were used for the fabricated 50 Ohm MSLs using a same dielectric substrate with thickness of 100 µm and the roughness of the foils are listed in Table 1. R_a is a evaluation figure of the surface roughness. The dielectric constants and dielectric loss tangents of the substrates are the same as 2.17 and 1.53×10^{-3} at 17 GHz. Figure 2 shows the measured attenuation constants of the fabricated MSLs with various surface roughness of the copper foils. The loss with the non roughened foil was measured to be less than half the loss of the MSL using the standard roughened foil. The dielectric losses of three MSLs are the same shown as simulated dielecric loss in the figure, and the difference between measured ones are due to the difference of the effective conductivities of the foils. The effective relative conductivities of the foils were estimated from the measured attenuation constants. Figure 3 indicates the estimated relative conductivities. Here, the conductivity is relative to the conductivity of copper (5.8×107 S/m). The non roughened foil has the at effective conductivity around 1 up to 50 GHz. However, the effective conductivity of the other foils decrease drastically with the frequency increase, because their skin depths move toward the surface roughness.

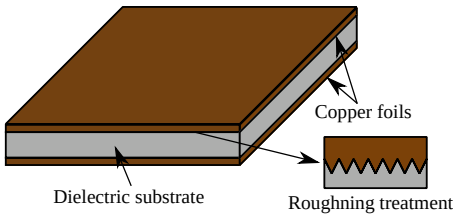

Figure 1: Surface roughness of copper foil on dielectric substrate.

Roughness	R_a [µm]
Non	0.09
Low	0.39
Standard	0.53

Table 1: Measured surface roughness R_a of copper foils.

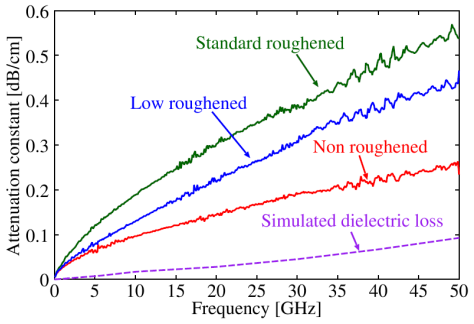

Figure 2: Measured attenuation constants of MSLs with various surface roughness of copper foils.

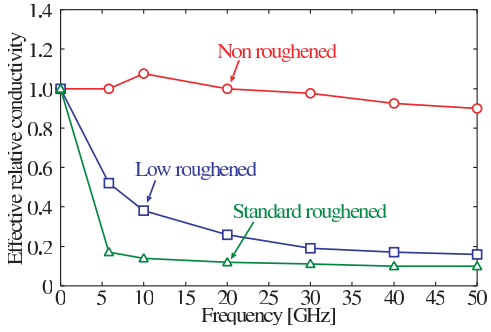

Figure 3: Estimated effective relative conductivities of copper foils.

Composite Right-/left-handed Transmission Line Stub Resonator with Improved Out-of-band Rejection Characteristics

K. Saito and S. Tanaka
Shibaura Institute of Technology, Japan

Abstract— Previously, we reported composite right-/left-handed (CRLH) transmission line stub resonators that are compact and can enhance the unloaded-Q beyond the limit of microstrip line resonator [1]. The mechanism of the enhanced unloaded-Q ($Q_u = \omega/2av_g$) can be explained by the near zero group velocity ($v_g \approx 0$) of the CRLH TL used as stub line, which is realized by engineering the dispersion of the CRLH TL in the left-handed (LH) region. The novel BPF type resonator, however, suffered from spurious responses at both sides of the center resonant frequency, limiting the applicability of the resonator. In this work, we present an alternative type of CRLH stub resonator with improved out-of-band rejection characteristics.

Figure 1 compares the circuit schematics and the $|S_{21}|$ frequency responses for the CRLH stub resonators of two different types. The basic idea of the present type of the resonator is to place the shunt inductors in the unit-cells before the series capacitors (looking from the main signal line), whereas they were placed the other way around in the conventional type [1]. This modification affects the order of the transmission zeros (TZs) and reflection zeros (RZs) that appear in the LH frequency region. Figure 2 shows how the out-of-band rejection can be improved using the parameters such as C_2 and L_1. Since the resonant modes in the LH frequency region can be controlled easily by tuning the reactive components of the unit cells, RZ^+ can be pushed away from RZ^- which is the center frequency of the resonator. One design challenge of the proposed resonator is to achieve very low inductance for L_1, which is necessary to increase loaded-Q as well improve overall rejection level. To accomplish this, we used two or more short-ended stubs connected in parallel, as shown in Figure 3.

The proposed CRLH stub resonator, with compact size, enhanced unloaded-Q and good out-of-band rejection characteristics, should prove useful for microwave planar circuit such as low phase-noise oscillators.

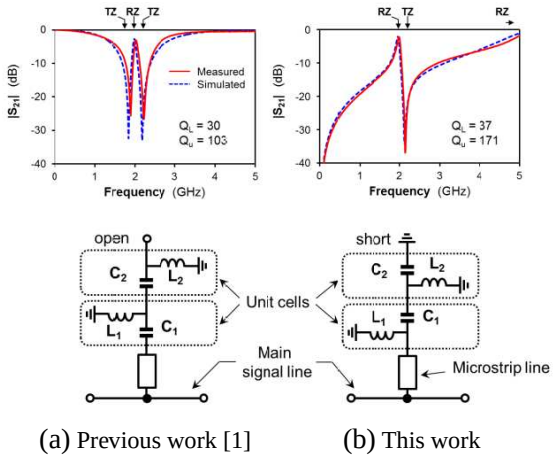

Figure 1: Comparison of the two types of CRLH stub resonators.

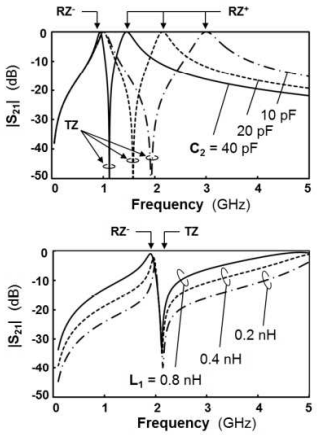

Figure 2: Design optimization to improve the out-of-band rejection.

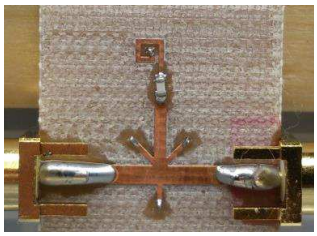

Figure 3: Picture of the fabricated 2-GHz CRLH stub resonator.

REFERENCES

1. Tanaka, S., et al., "High-Q CRLH transmission line stub resonator utilizing negative order resonance modes," *European Microwave Conference (EuMC), Digest*, 585–588, 2013.

Effect of Bending on RF Performance of Ink-jet Printed Microstrip Line on Flexible Substrate

Yeonsu Lee[1], **Sung-Min Sim**[1], **Kwon-Yong Shin**[2], **Sang-Ho Lee**[2], **and Jung-Mu Kim**[1]

[1]Department of Electronics and Information Engineering
Chonbuk National University, Korea
[2]Korea Institute of Industrial Technology, Korea

Abstract— Ink-jet printing techniques are good alternative to conventional photolithography for the fabrication of electronic devices [1]. This printing technology is mostly applied to flexible electronics devices. The most common substrate for flexible electronics devices is polyimide due to its outstanding electrical properties, good mechanical strength [2]. Effect of bending on RF performance of ink-jet printed device should be investigated because of the flexible electronics devices are operated in the bending state. In this paper, microstrip line was fabricated on 200 µm thick polyimide substrate by ink-jet printing method. Length, height and width of fabricated microstrip line is 14.2 cm, 3 µm and 500 µm, respectively. To measure the RF performance of the fabricated microstrip line with SMA connector (0.8 T) using network analyzer, copper-plated 600 µm thick FR-4 substrates are attached to both ends of the fabricated microstrip line. RF performance of the fabricated microstrip line is simulated using EM simulator and measured at the bending states using VNA (Agilent technology, E5061B). Insertion loss of the fabricated microstrip line is measured according to the varied end-to-end distance from 14.2 cm to 10 cm at intervals of 1 cm. Measured insertion loss is 6.26 dB @ 14.2 cm, 6.23 dB @ 13 cm, 6.20 dB @ 12 cm, 6.13 dB @ 11 cm, 6.10 dB @ 10 cm, respectively at 1 GHz. Return loss is measured to over 10 dB in the frequency range 300 kHz to 3 GHz.

Figure 1: Photograph of microstrip line.

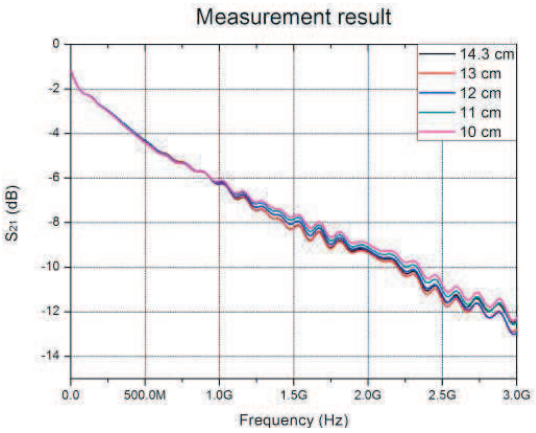

Figure 2: Insertion loss of microstrip line.

REFERENCES

1. Azucena, O., J. Kubby, D. Scarbrough, and C. Goldsmith, "Inkjet printing of passive microwave circuitry," *Microwave Symposium Digest*, Vol. 10399312, 1075–1078, 2008.
2. Halonen, E., A. Halme, T. Karinsalo, P. Iso-Ketola, M. Mantysalo, and R. Makinen, "Dynamic bending test analysis of inkjet-printed conductors on flexible substrates," *ECTC*, Vol. 12906899, 80–85, 2012.

Fabrication of Silver Ink-jet Printed Microstrip Line on Polyimide Substrate

Sung-Min Sim[1], **Yeonsu Lee**[1], **Kwon-Yong Shin**[2], **Sang-Ho Lee**[2], **and Jung-Mu Kim**[1]

[1]Department of Electronics and Information Engineering, Chonbuk National University, Korea
[2]Korea Institute of Industrial Technology, Korea

Abstract— The flexible electronics device called next generation electronic devices is actively studied in recent years [1]. The flexible electronics device is fabricated by printed electronics technology such as Roll-to-Roll printing, ink-jet and screen printing. Most of all, ink-jet printing has advantages such as no waste of ink, non-contact patterning and simple fabrication process [2]. In this paper, microstrip line was fabricated on the FC (fluorocarbon) coated PI (polyimide) substrate (thickness 200 μm) by ink-jet printing method. In order to remove solvent in conductive ink, the fabricated microstrip line is sintered by the heated nitrogen gas-beam. Length, height and width of fabricated microstrip line is 30 mm, 3 μm and 500 μm. To measure the RF performance of the fabricated microstrip line with SMA connector (0.8 T) using network analyzer, copper-plated FR-4 substrate (thickness 600 μm) is attached to PI substrate. RF performance of the fabricated microstrip line is simulated using HFSS (High Frequency Structural Simulator) EM simulator and measured using VNA (Agilent technology, E5061B). Transmission loss of the fabricated microstrip line is measured to be −0.55 dB/cm@1 GHz, −0.76 dB/cm@2 GHz, −1 dB/cm@3 GHz, respectively. Return loss is measured to over 15 dB, where the length of the silver signal line is 30 mm.

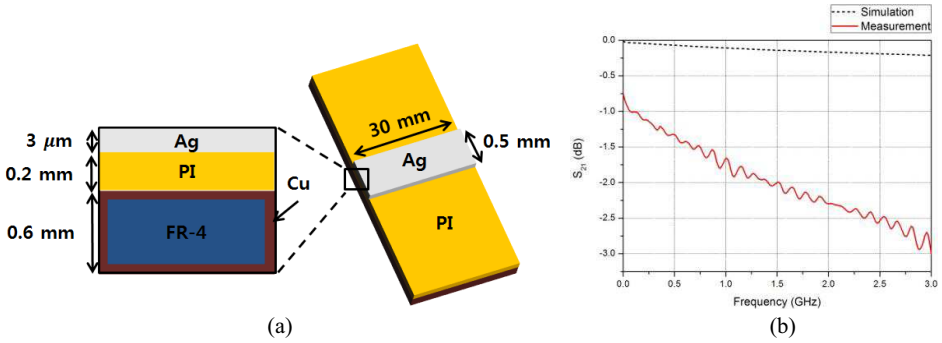

Figure 1: (a) Schematic view of microstrip line. (b) Insertion loss of fabricated microstrip line.

REFERENCES

1. Ko, S. H., "Status of research on selective laser sintering of nanomaterials for flexible electronics fabrication," *KSME-B*, Vol. 35, 533–538, 2011.
2. Perelaer, J., B.-J. de Gans, and U. S. Schubert, "Ink-jet Printing and microwave sintering of conductive silver tracks," *Adv. Mater. 2006*, Vol. 18, 2101–2104, 2006.

Coupled Line Power Divider with Multiple-pole Negative Group Delay Characteristics

Girdhari Chaudhary, **Seungho Jeong**, **Phirun Kim**, **and Yongchae Jeong**
Chonbuk National University, Republic of Korea

Abstract— Power dividers are essential blocks in microwave and millimeter systems and have been applied for power combining and splitting in various applications such as antenna feeding networks, high power amplifiers (PAs), linearization of PAs, mixers, test setups, and measurement circuits. The conventional power dividers provide the positive group delay. Moreover, the group delay matching between different paths is essential in various circuits and systems such as supply modulated PAs and feedforward linearization technique. For these circuits and systems, the power divider with negative group delay (NGD) characteristics will be beneficial to compensate positive group delay. Therefore, two-way power NGD divider is proposed in this paper. The schematic of the proposed NGD power divider is shown in Fig. 1, which consists of serial coupled line and shunt connected short-circuited coupled lines with open-circuited isolation port. The center frequencies of shunt coupled lines are slightly different in order to get wideband multiple-pole NGD characteristics. For experimental validation, the NGD power divider with equal-power dividing ratio operating at center frequency of 2.14 GHz was designed, fabricated, and measured. From the measurements, the transmission parameters are determined as $S_{21} = -9.01$ dB and $S_{31} = -8.96$ dB at $f_0 = 2.15$ GHz, which is shown in Fig. 2. Similarly, the measured group delay between different paths are determined as $\tau_{21} = -0.338 \pm 0.07$ ns and $\tau_{31} = -0.341 \pm 0.09$ ns over bandwidth of 170 MHz, which is shown in Fig. 3. The measured amplitude and phase differences between the two output ports are shown in Fig. 4. It can be seen that the maximum amplitude imbalance of ± 0.6 dB and the phase imbalance of $\pm 2.2°$ are observed over the 10 dB return loss bandwidth.

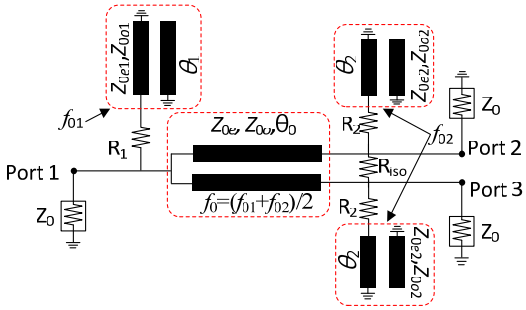

Figure 1.

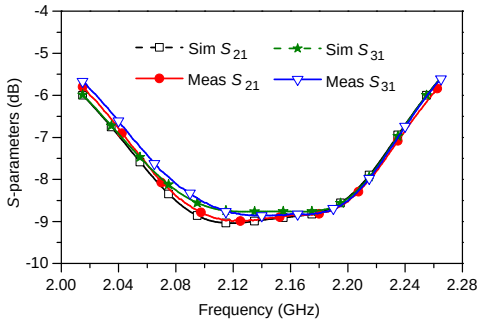

Figure 2.

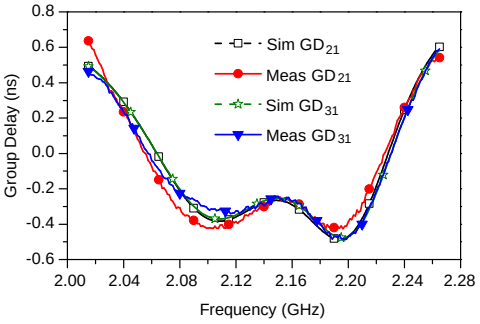

Figure 3.

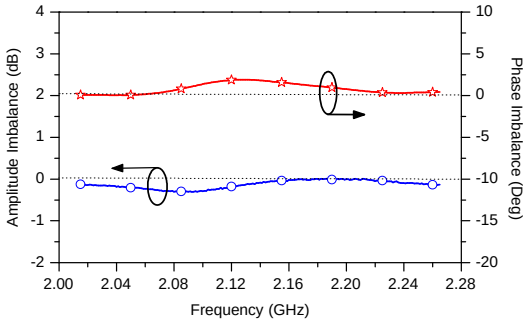

Figure 4.

ACKNOWLEDGMENT

This research was supported by the Basic Science Research Program through the National Research Foundation of Korea (NRF) funded by the Ministry of Education (2014R1A1A2007779).

An Estimation Method for 2-port *S*-parameters Using Cable or Jig with Leakage Couplings

Shinji Ohno[1], **Toshikazu Sekine**[2], **and Yasuhiro Takahashi**[2]

[1]Graduate School of Engineering, Gifu University, Japan
[2]Department of Electrical and Electronic Engineering, Gifu University, Japan

Abstract— An estimation method for **S**-parameters of 2-port circuit by using cable or jig with leakage couplings is presented. In our method, two ports of 4-port cable or jig are terminated with 2-port circuit or known loads. And the **S**-parameters between remaining two ports are measured. Advantages of our method is that the **S**-parameters of 2-port circuit are to be estimated only by solving the linear least squares problem. Our method can be applied to determine the **S**-parameters of the circuit with a difficult port to connect the probe of the instrument as the IC package and to determine the **S**-parameters of the circuit ground is not common.

Some estimation methods for the **S**-parameters of the multi port circuit having the port which cannot connect the probe of the measuring instrument to directly are considered [1, 2]. The reason why we cannot connect probes to directly are two mainly. The first reason is in the case of a circuit having the ports which are hard to connect a measuring instrument like IC tips in the package. The other reason is in the case of a circuit having the ports without common ground. In this case, some circuit properties are change if we connect the probes of measuring instrument with common ground.

A models of reciprocal 4-port cable or jig is shown in Figs. 1(a), (b) which has 2 ports that are hard to access with measurement probes. Figs. 1(c), (d) are examples of Figs. 1(a), (b). Port 1 and port 2 can be connected by measuring probes directory, and port 3 and port 4 cannot be connected directory. Using incident wave $\mathbf{a}_a$; $\mathbf{a}_u$ and reflection wave $\mathbf{b}_a$; $\mathbf{b}_u$, **T** matrix **T** of this 4-port is expressed as

$$\begin{bmatrix}\mathbf{a}_a\\ \mathbf{b}_a\end{bmatrix} = \begin{bmatrix}\mathbf{T}_1 & \mathbf{T}_2\\ \mathbf{T}_3 & \mathbf{T}_4\end{bmatrix}\begin{bmatrix}\mathbf{b}_u\\ \mathbf{a}_u\end{bmatrix}, \quad \left(\mathbf{b}_a = \hat{\mathbf{S}}_C\mathbf{a}_a,\ \mathbf{a}_u = \mathbf{S}_C\mathbf{b}_u\right) \text{ or } \left(\mathbf{b}_a = \hat{\mathbf{S}}_L\mathbf{a}_a,\ \mathbf{a}_u = \mathbf{S}_L\mathbf{b}_u\right) \tag{1}$$

$\mathbf{S}_C$ is the estimated **S**-matrix of the unknown 2-port circuit and $\hat{\mathbf{S}}_C$ is the measured **S**-matrix. Here, the known loads $\mathbf{S}_L$ are connected instead of 2-port circuit in Fig. 1(b). So, the following estimation equation is derived from Eq. (1).

$$\mathbf{S}_C = -\left(\mathbf{T}_4 - \hat{\mathbf{S}}_C\mathbf{T}_2\right)^{-1}\left(\mathbf{T}_3 - \hat{\mathbf{S}}_C\mathbf{T}_1\right), \quad \mathbf{T}_3 + \mathbf{T}_4\mathbf{S}_L - \hat{\mathbf{S}}_L\mathbf{T}_1 - \hat{\mathbf{S}}_L\mathbf{T}_2\mathbf{S}_L = 0 \tag{2}$$

Equation (2) is solved by the least squares method. As a result **T**-parameters of the 4-port and unknown **S**-parameters of the 2-port are found. The validity of the method is shown in the numerical and measured examples.

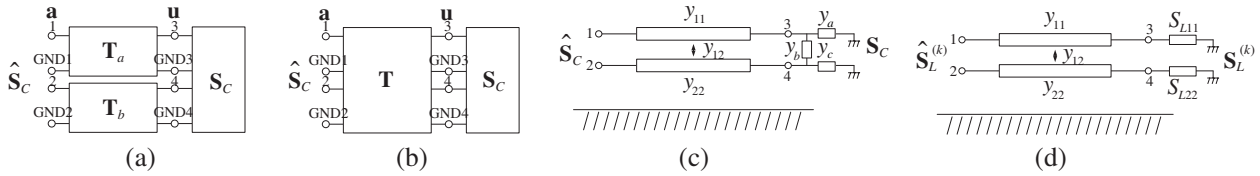

Figure 1: **S**-parameters measurement system with jig. (a) Non-leakage couplings. (b) Leakage couplings. (c) Coupled transmission line with 2-port circuit. (d) Coupled transmission line with known loads.

REFERENCES

1. Maeda, N., S. Fukui, K. Ichikawa, Y. Sakurai, T. Sekine, and Y. Takahashi, "An estimation method for the n port S parameters with $n-1$ port measurements," *EMC Europe 2013*, 348–353, Sep. 2013.
2. Maeda, N., S. Fukui, T. Sekine, and Y. Takahashi, "An estimation method for the 3 port S-parameters with 1 port measurements," *21st European Conference on Circuit Theory and Design*, Sep. 2013.

Session 4P1
Metamaterials and Plasmonics

Spheres and Circles with Radial Anisotropy: Unexpected Scattering Properties

A. Sihvola[1], **H. Kettunen**[2], **and H. Wallén**[1]

[1]Department of Radio Science and Engineering
Aalto University School of Electrical Engineering, Espoo, Finland
[2]Department of Mathematics and Statistics, University of Helsinki, Finland

Abstract— Even if the first studies on radially anisotropic (RA) spheres appeared decades ago [1], it seems that their peculiar properties have only lately attracted the particular attention they deserve. Cloaking properties of scatterers can be substantially boosted by resorting to anisotropy compared with layered isotropic structures [2, 3]. In addition, the astonishing phenomenon of anomalous absorption in spheres with indefinite (hyperbolic) radial anisotropy has been analyzed carefully only very recently [4].

In this presentation, we will focus on certain particular characteristics of scattering efficiencies of radially anisotropic spheres and circular cylinders. There are surprising qualitative differences of the scattering behavior in three and two dimensions, which will be paid special attention, e.g., existence of cloaking and resonating conditions in the hyperbolic regime for 3D case which does not take place for the 2D constellation. This means that for three-dimensional RA spheres, the scatterer can become (in the quasistatic limit) invisible even if there is a strong variation in the internal field pattern. Likewise, there are two types of internal field distributions that appear along with a plasmon resonance behavior.

Furthermore, the non-Rayleigh character of small-particle scattering that has been observed for plasmonic scatterers [5, 6] will be given attention. Ordinary Rayleigh scattering follows the fourth-power (third-power) dependence on the size parameter of the particle for spheres (circles). The deviations of this this quartic (cubic) dependence will be studied systematically and extended into all cloaking and resonant singularity cases for radially anisotropic scatterers in two and three dimensions.

REFERENCES

1. Roth, J. and M. J. Dignam, "Scattering and extinction sections for a spherical particle coated with an oriented molecular layer," *Journal of the Optical Society of America*, Vol. 63, No. 3, 308–311, 1973.
2. Qiu, C.-W., A. Novitsky, H. Ma, and S. Qu, "Electromagnetic interaction of arbitrary radial-dependent anisotropic spheres and improved invisibility for nonlinear-transformation-based cloaks," *Physical Review E*, Vol. 80, No. 1, 016604, 2009.
3. Kettunen, H., H. Wallén, and A. Sihvola, "Cloaking and magnifying using radial anisotropy," *Journal of Applied Physics*, Vol. 114, No. 4, 044110, 2013.
4. Wallén, H., H. Kettunen, and A. Sihvola, "Anomalous absorption, plasmonic resonances, and invisibility of radially anisotropic spheres," *Radio Science*, 2015, doi:10.1002/2014RS005534.
5. Tribelsky, M. and B. S. Luk'yanchuk, "Anomalous light scattering by small particles," *Physical Review Letters*, Vol. 97, No. 26, 263902, 2006.
6. Ni, Y. X., L. Gao, A. E. Miroshnichenko, and C. W. Qiu, "Non-Rayleigh scattering behavior for anisotropic Rayleigh particles," *Optics Letters*, Vol. 17, No. 16, 3390–3392, 2012.

Ultra Thin Metamaterial Absorbers for Short Millimeter Wave Bolometers: Multiparametric Optimization and Practical Implementation

S. A. Kuznetsov[1, 2, 3], **A. G. Paulish**[3], **and A. V. Arzhannikov**[1, 2]

[1]Novosibirsk State University, Pirogova St. 2, Novosibirsk 630090, Russia
[2]Budker Institute of Nuclear Physics SB RAS, Lavrentiev Ave. 11, Novosibirsk 630090, Russia
[3]Institute of Semiconductor Physics SB RAS, Novosibirsk Branch "TDIAM"
Lavrentiev Ave. 2/1, Novosibirsk 630090, Russia

Abstract— The range of short millimeter waves (SMMW) remains highly attractive for a number of important practical applications, such as security and nondestructive material quality inspection, due to its opportunity to combine the options of relativity high penetrability through atmosphere and different non-metallic objects versus terahertz, infrared and optical radiation, as well as attainability of spatial resolution of the order of several millimeters acceptable for imagining of concealed targets.

Among different methods for detecting SMMW, we may highlight a method of bolometric sensing using ultra thin metamaterial films. Such films, typically configured as a single layer metasurface laying over a grounded dielectric slab, are capable of resonantly absorbing the incoming electromagnetic waves with 100% efficiency and have the thickness d much smaller than the resonant wavelength λ. Minimization of d is essential for decreasing the absorber's heat capacity and, therefore, for achieving high sensitivity and low response time of the bolometric detector.

According to fundamental limitations, the condition $d/\lambda \ll 1$ inevitably leads to narrowing the absorption bandwidth that is used to be considered as a key drawback of the metamaterial absorbers. On the contrary, in our work this condition is turned to the advantage and is exploited to implement high-performance multi-channel SMMW bolometers with high spectral and polarization discrimination. Such detectors are demanded in spectro-polarimetric imaging and measurements schemes with broad-band SMMW sources. Also, such detectors are well suitable for sensing applications with active illumination from a monochromatic SMMW oscillator.

In our contribution we summarize the results of extensive investigations focused on developing metamaterial-based SMMW bolometric detectors operating in the frequency range of 0.09–0.4 THz. In the first part of this work, the multiparametric electromagnetic analysis and optimization of the absorbers' design is presented and the route to maximize the λ/d ratio at the minimal absorption bandwidth and high out-of-band spectral purity is discussed. In the second part, we demonstrate the results of experimental testing for high-performance metamaterial absorbers, whose λ/d ratios reach the value of 200 at the relative bandwidth of around several percent. These absorbers are integrated with bolometric sensors implemented in different schemes, including SMMW-to-IR conversion and pyro-electric detection, and the operational characteristics for each scheme are analyzed.

ACKNOWLEDGMENT

This work is supported by the Ministry of Education and Science of the Russian Federation under the State Assignment Contract #3002 (technological implementation and experimental testing) and the Russian Science Foundation under the Project 14-12-01037 (full-wave electromagnetic simulations).

Left-handed Transmission Lines Equivalent Circuit Model Based on *ABCD* Matrices

U. Martinez-Iranzo, **B. Moradi**, **and J. Garcia-Garcia**
Grupo de Aplicaciones Electromagnéticas Industriales — GAEMI
Engineering Electronic Department, Universidad Autónoma de Barcelona, Cerdanyola del Vallès, Spain

Abstract— Simultaneous negative permittivity and permeability media was first considered by Veselago in the late 1960s. In these media, the sign reversal for both permittivity and permeability results in a negative refractive index, referred to as metamaterial. Since then, these concepts have been used in microwaves for numerous applications due to the unusual properties that exhibit such as inverted Snell's law, Doppler shift, and Cherenkov radiation, in addition to unusual focusing properties. From the theoretical point of view, metamaterials have been described with an equivalent circuit model formed by a capacitor C and a RLC resonator, and in shunt with an inductor L. This description with lumped elements only works in the nearby of resonant frequency. In this work, it is proposed a metamaterial theoretical description using transmission matrices, instead of lumped elements. This study provides two key advantages compared to lumped elements analysis. First, it allows wide frequency range description and establishes clear relations between physical dimensions and the metamaterial transmission characteristics. On the other hand, it provides the possibility to obtain analytically a wide frequency spectrum range provides useful information about the resonances modes and enables the particle studies as can be obtained analytically parameters as group delay or group velocity. In the study and design of metamaterial particles, the direct association of physical dimensions implies the possibility to control design parameters. To verify the theoretical predictions, has been designed a metamaterial structure that has been analytically studied, it has been calculated its $ABCD$ matrix, fabricated and measured, showing a good agreement between measured and analytical results.

Unusual Percolation Threshold of Electromagnetic Waves

Jie Luo, **Zhihong Hang**, **C. T. Chan**, **and Yun Lai**
Optoelectronics and Energy & Collaborative Innovation Center of Suzhou Nano Science and Technology
College of Physics, Soochow University, Suzhou 215006, China

Abstract— We demonstrate an unusual percolation threshold of electromagnetic waves in index-near-zero media embedded with random inclusions. Such a critical behavior is induced by the long-range connectivity of the "non-conducting" component instead of the "conducting" component. Therefore, such a percolation threshold shows a very different nature from previous percolation like fluids in porous media or conductivity of metal-dielectric composites. It is induced by the vector wave nature of electromagnetic waves.

REFERENCES

1. Luo, J., Z. H. Hang, C. T. Chan, and Y. Lai, to be Submitted.

Chiral Localized Plasmon Resonances Leading to Extreme Optical Chirality

A. V. Kondratov and M. V. Gorkunov
A.V. Shubnikov Institute of Crystallography, Russian Academy of Sciences, 119333, Russia

Abstract— We present an analysis of FDTD simulations of light transmission trough arrays of chiral nanoholes in metal. We report that extreme optical activity and circular dichroism are related with excitation of chiral localized plasmon resonances.

Chirality is a point of great interest in physics, chemistry and biology. Due to the fact that chiral nanostructures can interact with biomolecules and organic objects, chirality on the nanoscale is potentially very useful for biosensing and pharmacy [1]. Subwavelength arrays of chiral holes (Fig. 1(a)) exhibit extremely strong optical activity (OA) and circular dichroism (CD) [2]. Theoretical analysis in terms of the causality principle shows that OA and CD obey generalized Kramers-Kronig relations, but the nature of the phenomenon still remains unrevealed [3]. Another question is why structures with very similar shapes of the nanoholes yield qualitatively different spectral characteristics of OA and CD.

To answer these questions and clarify the effect of the shape of holes we performed simulations for different types of conical and chiral holes. We developed a data processing pipeline consisting of the correction and averaging of the raw atomic force microscopy (AFM) data, creation of the unit cell 3D-model and subsequent FDTD simulations. The results of simulations (Fig. 1(b)) show a good agreement with experimental frequency dependence of OA and CD and strong electric field localization at the output of the chiral nanohole at the peak of CD (Fig. 1(c)). On the other hand, the field distribution far from the peak of CD is significantly different (Fig. 1(d)). Thus, we conclude that the chiral localized plasmon resonance is responsible for the extreme values of OA and CD in such structures.

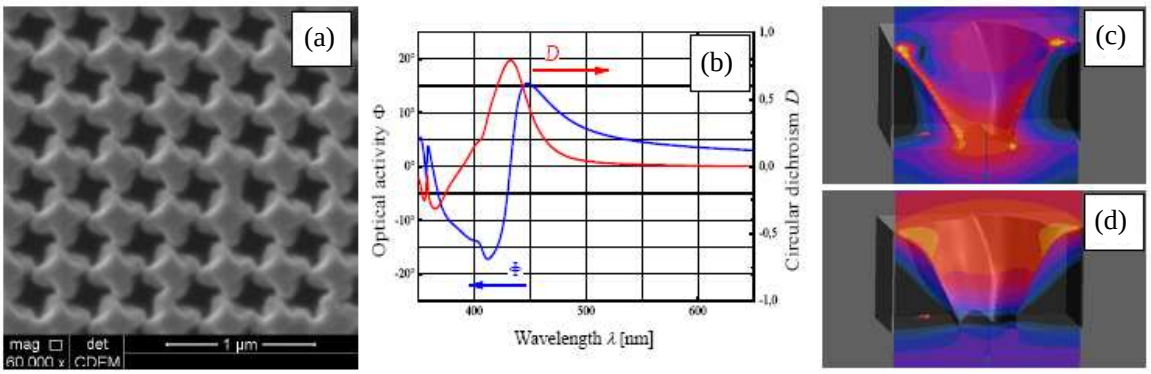

Figure 1: (a) SEM image of a fragment of the chiral nanoholes array milled in a 380 nm thick silver foil; (b) calculated values of OA and CD for a hole shape obtained by reconstructing and averaging AFM scans data; distribution of electric field absolute value inside the chiral nanohole: (c) at the peak of CD and (d) far from the peak of CD.

ACKNOWLEDGMENT

The work was supported by the Russian Science Foundation (project 14-12-00416).

REFERENCES

1. Wang, Y., et al., "Emerging chirality in nanoscience," *Chem. Soc. Rev.*, Vol. 42, 2930, 2013.
2. Gorkunov, M. V., A. A. Ezhov, et al., "Extreme optical activity and circular dichroism of chiral metal hole arrays," *Applied Physics Letters*, Vol. 104, 221102, 2014.
3. Gorkunov, M. V., V. E. Dmitrienko, et al., "Causality relations for materials with strong artificial optical chirality," *Physics Optics*, arXiv: 1408.4977, 2014.

Magneto-optical Effects Optimal for Observation of the in-plane Magnetization of the Magnetoplasmonic Crystals

A. N. Kalish[1, 2], **V. I. Belotelov**[1, 2], **and A. K. Zvezdin**[1, 3, 4]

[1]Russian Quantum Center
Novaya Street, Skolkovo Village, Odintsovo District, Moscow Area 143025, Russia
[2]Faculty of Physics, Lomonosov Moscow State University
Leninskie Gory, Moscow 119991, Russia
[3]Prokhorov General Physics Institute of Russian Academy of Sciences
Vavilova Street, Moscow 119991, Russia
[4]Moscow Institute of Physics and Technology
Institutskiy per., Dolgoprudny, Moscow Region 141700, Russia

Abstract— Magneto-optical effects have become the subject of active research due to the possibility of ultrafast and effective control of light properties such as polarization and intensity. Recently it has been demonstrated that these effects can be enhanced in specially tailored nanostructures, in particular, in plasmonic structures [1]. The giant values of magneto-optical effects lead to huge variety of applications such as optical telecommunication devices or highly sensitive magnetic field sensors. With the goal of the latter application here we study those effects that are related to the in-plane magnetization in magneto-plasmonic crystals and find the conditions for achievement of their high values.

The structures under considerations are one-dimensional plasmonic crystals consisting of a noble-metallic grating and a smooth magnetic dielectric film. Four magneto-optical effects take place in such configuration.

Firstly, the transverse Kerr effect (the TMOKE) is present. It allows direct visualization of magnetization component parallel to the grating slits. The light should be TM polarized and the incidence should be oblique. At the excitation of the structure's TM modes the TMOKE is resonantly enhanced. The value of the TMOKE can be several percent that is by three orders higher than for the smooth film without plasmon covering [2].

Secondly, there is the longitudinal Kerr effect (the LMOKE). It is resonantly enhanced at the excitation of modes of any type. The most favorable condition for the LMOKE enhancement is the intersection of dispersion curves for TE and TM modes. The values of the effect are about several degrees that is 10 times higher than for the non-plasmonic structure.

The most important feature of the considered structure is the emergence of the effect of the third kind, that is the longitudinal intensity effect (the LMPIE) [3]. This effect is prohibited in smooth magnetic media. The effect is of resonant nature because it is related to the excitation of the structure's eigenmodes. The LMPIE takes place even at the normal incidence. Usually this effect is quadratic in magnetization. It was found both theoretically and experimentally that this effect can be as high as several tens of percent. The highest value of the LMPIE happens at the simultaneous excitation of both TE and TM modes. This effect is likely to be the most effective way of visualization of longitudinal magnetization.

Finally, the whole class of the phase effects can be considered. Optical resonances that are sensitive to magnetization lead to changes in phases of reflected and transmitted light. These changes can be observed in any magnetization configuration and they are either even or odd in magnetization depending on the light incidence configuration. The magnetization-induced phase change in longitudinal configuration can achieve 7 degrees while for the transversal configuration it is weaker.

The described effects provide efficient modulation of transmitted and reflected light intensity, polarization and phase.

ACKNOWLEDGMENT

The work is supported by the Russian Science Foundation (project No. 14-32-00010).

REFERENCES

1. Inoue, M., M. Levy, and A. Baryshev, Eds., *Magnetophotonics: From Theory to Applications,* Springer Verlag, Berlin Heidelberg, 2013.

2. Belotelov, V. I., et al., *Nature Nanotechnology*, Vol. 6, 370, 2011.
3. Belotelov, V. I., et al., *Nature Communications*, Vol. 4, 2128, 2013.

The Role of Mechanisms Responsible for the Extraordinary Transmission through Sub-wavelength Periodic Arrays

J. Fiala and I. Richter
Faculty of Nuclear Sciences and Physical Engineering, Czech Technical University in Prague
Břehová 7, CZ-11519 Prague, Czech Republic

Abstract— This contribution is focused on the investigation of the enhanced optical transmission (EOT) phenomenon through both 1-D and 2-D sub-wavelength periodic arrays perforated in metallic films. In order to gain the basic physical insight into the transmission mechanisms and to reveal the basic resonant processes in interaction of a plane wave with 1-D array of sub-wavelength slits, we have derived two approximate analytical models. Two relevant simplifications were incorporated within the derivation procedure of the first model — (i) surface-impedance boundary conditions were imposed on the metallic boundaries, except on the vertical walls of the slits which are treated as a perfectly conducting metal, and (ii) only the fundamental eigenmode is assumed inside the slits. As for the second model, in order to highlight the surface plasmon-polariton (SPP) excitation based on the scattering of the plane wave or the slit mode into the SPP, a combined model comprising the SPP as an explicit bound mode was further derived.

Using the rigorous numerical modelling, the total transmitted energy maps of various 1-D array of slits are calculated as a function of both the structure geometrical and wave parameters, and, there, the dispersion curves of the existing modes are clearly identified together with the cut-off frequencies of the respective modes and the positions of resonances in these maps [1]. Apart from the cavity resonances of the fundamental slit-guided mode (CM), playing a significant role, the SPP bound modes and CM-SPP hybrid modes are also analysed in the case of 1-D structures.

For the case of 2-D structures, map of modes possessing the lowest attenuation constant inside the hole is calculated, and, furthermore, plasmon-polariton modes of the metallic film are identified. Finally, the prediction capabilities of the approximate models were put under comparison with the rigorously computed data.

Additionally, the attention is also devoted to the much disputed question about the role of SPP and the Rayleigh anomaly (RA) [2, 3]. It is found that the RA does not play such crucial role in contrast to the SPPs that drastically alter the dispersion relations of the Fabry-Perot conditions of the CMs inside the slit, and which mutual interaction subsequently results in the Fano resonances with the pronounced maxima and minima in the spectra — the grating Wood's anomalies. A formalism for describing such Fano resonances is subsequently proposed.

ACKNOWLEDGMENT

This work was financially supported by the Czech Science Foundation (project No. P205/12/G118) and the Czech Technical University in Prague (grant No. SGS13/221/OHK4/3T/14).

REFERENCES

1. Fiala, J. and I. Richter, "Explanation of extraordinary transmission on 1-D and 2-D metallic gratings," *Proceedings SPIE 9450, Photonics, Devices, and Systems VI*, 94501T-1–9, 2015.
2. Cao, Q. and P. Lalanne, "Negative role of surface plasmons in the transmission of metallic gratings with very narrow slits," *Phys. Rev. Lett.*, Vol. 88, 057403-1–4, 2002.
3. Yoon, J. W., J. H. Lee, S. H. Song, and R. Magnusson, "Unified theory of surface-plasmonic enhancement and extinction of light transmission through metallic nanoslit arrays," *Sci. Rep.*, Vol. 4, 5683-1–7, 2014.

On the Characteristics of Spoof Surface Plasmons (SSP) in the High Frequency Limit

Sayak Bhattacharya and Kushal Shah
Department of Electrical Engineering, Indian Institute of Technology Delhi, India

Abstract— In the low frequency limit (i.e., when operating wavelength is very large compared to the feature-size and periodicity), the field of spoof surface plasmon (SSP) is characterized by a single evanescent order and the corresponding dispersion relation is described by an expression analogous to the dispersion relation of surface plamon polaritons (SPP). However, in the high-frequency limit, the analogy between SSP and SPP breaks down [1, 2]. As the feature-size becomes comparable to the wavelength, the low frequency dispersion relation starts deviating from the dispersion calculated numerically [3].

In this paper, we show that diffraction from the subwavelength features at the surface of a perfect electric conductor (PEC) plays a very important role in determining the near-field characteristics and dispersion of spoof surface plasmon (SSP) in the high-frequency limit. Since the holes on the PEC surface are of subwavelength dimension, the diffracted field from these features would be evanescent in the direction perpendicular to the interface (z-direction). Also, the scattered field will have maximum intensity near to the holes and decay rapidly as the distance along the plane of the interface increases. The decay length (α) and the spatial frequencies (f_x, f_y) of the surface wave are related by: $\alpha^2 + k^2 = 4\pi^2(f_x^2 + f_y^2)$. Here, k is the wavenumber in the dielectric above the interface. This leaves us with two choices: either α would have a unique value (if this is the case, the near-filed would be exactly analogous to SPP and the propagation would be isotropic since, $(f_x^2 + f_y^2)$ would be constant at a fixed frequency) or, α would have multiple values for a fixed frequency (in this case, the near field would be described by multiple evanescent orders in contrast to a single evanescent order for SPP and low-frequency SSP. Also, the propagation would be anisotropic). However, the boundary conditions suggest that the transition of the field across the interface should be smooth if there is no change in the dielectric constant below and above the interface. For single exponential decay, the transition of the field profile across the interface would not be smooth. However, superposition of multiple evanescent orders can make the transition smooth (for example, this phenomenon is found in fluorescence from a bulk material, where stretched exponential decay is used to describe the emission decay curves). In addition, the aperture of the hole occupies most part of the unit cell and constitutes a considerable fraction of the operating wavelength. So, in the high frequency limit, one expects the field profile of SSP to be described by superposition of multiple evanescent orders. We have determined the decay constants of these evanescent orders using angular spectrum representation and have verified the multi-exponential nature of the field profile against data obtained from full vectorial 3-D finite difference time domain (FDTD) simulation. In essence, we have shown that enforcement of the boundary conditions makes the propagation of SSP inherently anisotropic. Anisotropy of SSP propagation is very important in realization of several applications like self-collimation, beam-splitting etc..

In order to further understand the properties of SSP in the high frequency limit, we note that the scattered field from each of the holes can interact with its neighboring holes in a manner analogous to the electron orbitals of different atoms in a crystal. We show that a tight binding model which takes into account next nearest neighbor interactions leads to a closed form expression for the SSP dispersion relation and an analytic prediction for the self-collimation frequency with reasonable accuracy. We also give numerical results in support of our theoretical expressions.

REFERENCES

1. Stone, E. K. and E. Hendry, "Dispersion of spoof surface plasmons in open-ended metallic hole arrays," *Phys. Rev. B.*, Vol. 84, 035418, 2011.
2. Bhattacharya, S. and K. Shah, "Multimodal propagation of the electromagnetic wave on a structured perfect electric conductor (PEC) surface," *Optics Comm.*, Vol. 328, 102–108, 2014.
3. Qiu, M., "Photonic band structures for surface waves on structured metal surfaces," *Opt. Express*, Vol. 13, No. 19, 7583–7588, 2005.

Design of a Low Loss Silicon Based Hybrid Dielectric-loaded Plasmonic Waveguide and a Compact, High Performance Optical Resonator

Cheng-Hung Hsieh, **Chien-Ming Kuo**, **Min-Jyun Huang**, **Yu-Ting Chu**, **and Keh-Chyang Leou**
Department of Engineering and System Science, National Tsing Hua University, Hsinchu 300, Taiwan

Abstract— Here we report the design of a top metal silicon (Si) hybrid dielectric-loaded plasmonic waveguide (TM-SiHDLW) and a compact, high performance TM-SiHDLW-based optical disk resonator. For the TM-SiHDLW, a propagation length of 0.35 mm and a mode area of $\sim$ 0.029 μm^2 were demonstrated by numerical simulation analysis based on finite element method. The waveguide adopted a top metal stripe structure for easier process integration with conventional micro fabrications and a thick (200 nm) metal stripe was found to yield optimal performance due to reduced Ohmic loss in conductor around the stripe edge/corner. Moreover, a relatively thick (150 nm) dielectric spacer between the Si ridge and the metal stripe was employed to achieve both long propagation length and good field confinement. Based on the same consideration, a waveguide width of 200 nm was chosen so that the mode area could be still less than 0.030 μm^2. The effect of a thin silicon nitride (SiN_x) layer covering the waveguide for minimizing uncertainties on optical properties of TM-SiHDLW resulting from high density of dangling bonds on Si surface, has also been investigated. For a SiNx layer thickness less than 10 nm, no significant degradation on the performance of the TM-SiHDLW was found, as revealed by simulation analysis.The disk resonator based on TM-SiHDLW employs a metal enclosure to significantly reduce the radiation loss while minimizing the overall size of the resonator. From the simulation results, a quality factor up to 2000, more than twice the results in previous studies, can be obtained with an acceptable resonator dimension. Therefore, the TM-SiHDLW is a particularly promising candidate for compact plasmonic devices in photonic integrated circuits.

ACKNOWLEDGMENT

Work supported by the Ministry of Science and Technology or R.O.C.. The authors also thank the "National Center for High-Performance Computing" of R.O.C. for providing simulation code.

Plasmonic Optical Tweezers Based on Random Metallic Nano-islands

Zhiwen Kang, **Jiajie Chen**, **Haixi Zhang**, **and Ho-Pui Ho**
Department of Electronic Engineering
The Chinese University of Hong Kong, Shatin, N.T., Hong Kong SAR, China

Abstract— We report a highly versatile optical trapping device substrate based on random metallic nano-islands deposited on glass surface. The plasmonic absorption peak of the nano-islands, which is within the visible and near-infrared region, can be tuned by controlling their size and separation using a low temperature anneal process. Optical trapping of polystyrene beads suspended in an aqueous medium at low power density of $\sim 10^2$ W/cm^2 has been recorded. This value is at least 3 orders of magnitudes lower than the threshold power density required by conventional optical tweezers. We have analyzed the force components acting on the beads, which are associated with optical gradient under plasmonic enhancement, convection of fluid above the laser-heated spot and thermophoretic effects caused by the temperature gradient in the hot zone. Our results suggest that thermophoresis plays a significant role in the observed trapping phenomenon. Its dependence on the ion concentration of the aqueous medium is discussed. Optical trapping on the cleaved end of a single-mode optical fiber that has been coated with nano-islands is also possible. The device can be used for trapping life cells such as *E. Coli*. Further incorporation of the nano-island substrate to a microfluidic system readily leads to the demonstration of practical optofluidic applications including guided flow control, light-activated valves and fluidic mixing based on plasmonic local heating in the nano-islands. The reported work provides a simple platform for on-chip optical manipulation of nano- and micro-sized objects, and may offer a wide range of application possibilities in physical and life sciences.

UV Plasmonic Performance of Ga, Mg and Al. Influence of Growing Oxide Shell

D. Ortiz, J. M. Sanz, J. M. Saiz, F. Gonzalez, and F. Moreno
Group of Optics, Department of Applied Physics, University of Cantabria, Spain

Abstract— Resonant response of nanoparticles as a reaction to external electromagnetic fields make them attractive for a wide range of applications, such as real-time sensors, surface enhanced Raman spectroscopy (SERS), light energy guiding, nanosensing or electromagnetically induced transparency, among others [1]. The demands to detect, recognize, and/or destroy biological toxins, to enhance biological imaging, and to characterize semiconductor devices at the nanometer scale has increased the interest in UV plasmonics [2–4]. Previous studies have shown the good plasmonic performance of various metals as Aluminum, Gallium and Magnesium in the UV part of the spectrum [5]. However, taking into account that oxides naturally form on most of the metals, it is important to understand the effect of oxidation on their plasmonic response [6, 7].

In this research, the effect of the growing oxide shell on the plasmonic performance is numerically analyzed using the Discrete Dipole Approximation (DDA) method [8]. To perform the calculations, a hemispherical nanoparticle, radius of 40 nm, located on a dielectric substrate (sapphire, $n = 1.78$), is considered to mimic typical experimental conditions [9]. The nanoparticle consists of a core/shell metal/native oxide structure, in which the core radius changes from 20 to 38 nm. The system has been excited by a monochromatic, linearly polarized plane wave at normal incidence. For each of the metals considered, the spectral dependence of the following two parameters has been calculated and analyzed: 1) the absorption efficiency of the particle system, and 2) the intensity of the electric field enhancement averaged over the surface.

From the results, it can be concluded that the addition of an oxide shell on the nanoparticle surface produces a decrease of both the amplitude of the electric field and the absorption efficiency for all cases. Besides, the resonance could be either red or blue shifted depending on the material and the thickness of the shell. These results may help explaining the behavior of metals nanoparticles. They also show the importance of controlling the oxide contamination and open a way to tune resonances in nano-antenna design.

REFERENCES

1. Prasad, P., *Nanophotonics*, John Wiley & Sons, Inc., Hoboken, New Jersey, 2004.
2. Anker, J. N., W. P. Hall, O. Lyandres, et al., *Nature Mater.*, Vol. 7, 442, 2008.
3. Chowdhury, M. H., K. Ray, S. K. Gray, et al., *Anal. Chem.*, Vol. 81, 1397, 2009.
4. Taguchi, A., N. Hayazawa, K. Furusawa, et al., *J. Raman Spectrosc*, Vol. 40, 1324, 2010.
5. Sanz, J. M., D. Ortiz, R. Alcaraz de la Osa, et al., *J. Phys. Chem. C*, Vol. 117, 19606, 2013.
6. Kuzma, A., M. Weis, S. Flickyngerova, J. Jakabovic, A. Satka, et al., *J. Appl. Phys.*, Vol. 112, 103531, 2012.
7. Knight, M. W., N. S. King, L. Liu, H. Everitt, P. Nordlander, and N. J. Halas, *ACS Nano*, Vol. 8, No. 1, 834, 2014.
8. Draine, B. T. and P. J. Flatau, http://arXiv.org/abs/1202.3424, 2012.
9. Yang, Y., N. Akozbek, T. H. Kim, J. M. Sanz, F. Moreno, M. Losurdo, A. S. Brown, and H. O. Everitt, *ACS Photonics*, Vol. 1, No. 7, 582, 2014.

Effective Medium Theory for Metamaterials beyond the Long-wavelength Limit

Shiwei Tang, Baocheng Zhu, Qiong He, Shulin Sun, Yongfeng Mei, and Lei Zhou
State Key Laboratory of Surface Physics
Key Laboratory of Micro and Nano Photonic Structures (Ministry of Education)
Physics Department, Fudan University, Shanghai 200433, China

Abstract— Metamaterials are electromagnetic composites constructed by subwavelength-sized microstructures, and thus can exhibit tailored *effective* permittivity ε and permeability μ. Metamaterials have attracted much attention recently due to their strong abilities to manipulate electromagnetic waves, leading to many fascinating physical effects unattainable in naturally existing materials. In this research field, effective-medium theory (EMT) plays a crucial role since it serves as a bridge to link theories, which are frequently conducted on model hypothetical systems, and experiments which are always performed on realistic metamaterial systems with complex microstructures. Therefore, a good EMT, which can better guide people to design appropriate metamaterials to realize the predicted phenomena, is always highly desired. In the past years, many versions of EMTs were successfully developed, but many of them suffer different limitations in different aspects [1].

Here, we proposed a new version of EMT, which is particularly suitable for determining the effective parameters of a periodic structure involving *dispersive* metallic structures. Based on the mode-expansion theory under a single-mode approximation, we can derive the analytical expressions for the reflection/transmission coefficients at the interface between air and the target metamaterial. Mapping such a complex structure to a homogeneous system, we then obtain the effective-medium parameters of the metamaterial by requesting the two systems to exhibit the same reflection/transmission coefficients. We first employ our EMT to study the effective-medium properties a multilayered structure (Fig. 1(a)) composed by two different slabs with arbitrary constitutional and geometrical parameters [2]. Our EMT not only recovers those previously derived formulas valid only at certain limiting conditions [3, 4], but works well far beyond these limitations to nearly cover the whole parameter spaces as long as the subwavelength condition is satisfied. Finite-difference-time-domain (FDTD) simulations and microwave experiments are performed on realistic structures to justify our theory. We next generalize our theory to a more complex situation which consists of a two-dimensional periodic array of metallic structures with arbitrary cross sections (Fig. 1(b)). More applications of our theory will be described in the conference [5, 6].

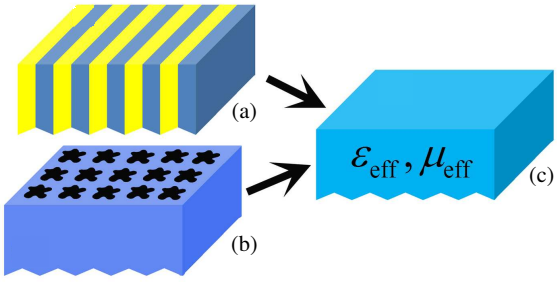

Figure 1: Meta-materials under study and their effective medium models.

REFERENCES

1. Choy, T. C., *Effective Medium Theory: Principles and Applications*, Clarendon Press, Oxford, 1999.
2. Tang, S., et al., *Phys. Rev. B*, submitted.
3. Rytov, S. M., *Soviet Physics JETP*, Vol. 2, 466, 1956.
4. Garcia-Vidal, F. J., L. Martín-Moreno, and J. B. Pendry, *J. Opt. A: Pure Appl. Opt.*, Vol. 7, S97, 2005.
5. Zhu, B., S. Xiao, and L. Zhou, *Phys. Rev. B*, Vol. 90, 045110, 2014.
6. He, Q., S. Xiao, X. Li, and L. Zhou, *Opt. Express*, Vol. 21, 28948, 2013.

Ultrathin Metasurfaces with Ultrahigh Cross-polarization Conversion Efficiency

Cheng-Wei Qiu[1], **Xumin Ding**[1, 2], **Kuang Zhang**[2], **Lei Zhang**[1], **Qun Wu**[2], **and Fei Qin**[1]

[1]Department of Electrical and Computer Engineering, National University of Singapore, 117583, Singapore
[2]Department of Microwave Engineering, Harbin Institute of Technology, Harbin 150001, China

Abstract— Recent years have witnessed a great surge of interest in metasurfaces providing phase-discontinuities, which find novel applications in flat lenses, spin-orbit manipulation, wavefront engineering, holography, etc.. Compared to conventional lenses or imaging devices, metasurfaces provide an alternative approach to wave manipulation, thickness reduction, pixel refinement, and transverse resolution. However, ultrathin metasurfaces operating in transmission face the challenge of extremely low efficiency, as only a few percent of the total power of incident light gets processed by the metasurface, preventing the widespread use of these devices. Here, we experimentally demonstrate two types of ultrathin metasurface with manipulation efficiency one order higher than previous works in visible and microwave frequencies.

On one hand, without sacrificing the ultrathin flatness (with finite — yet small — thickness), we proposed a complementary bilayer metasurface operating at visible range by incorporating stacking a V-shaped metasurface atop its Babinet inverted version with a gap of 70 nm in between, which demonstrated a remarkably high conversion efficiency of 29% and extinction ratio of 12.7 dB simultaneously within a broadband. For the first time, positive extinction ratio is achieved, indicating an anomalous light dominated transmission.

On the other hand, based on Pancharatnam-Berry phase elements, we design and verify a planar ultrathin metalens ($\sim \lambda/1000$ in thickness) demonstrating anomalous cross-polarization transmission efficiency reaching $\sim 24.7\%$ in our proof-of-concept experiment, which is almost at the theoretically predicted upper limit 25% for ultrathin metasurfaces. By controlling the handedness of the incident wave, in fact, converging and diverging functions are interchangeable using the same flat lens. Our finding presents a significant leap for the transmission type metasurface, beneficial to put metasurface into practical application.

New Applications for Zero-index Metamaterials

Yangyang Fu, Aichen Chen, Yadong Xu, and Huanyang Chen
College of Physics, Optoelectronics and Energy, Soochow University, Suzhou 215006, China

Abstract— In this talk, we will firstly introduce an interesting property of epsilon-near-zero (ENZ) metamaterials — The Goos-Hanchen effect. After that we will show that electromagnetic wave transmission could be manipulated in a zero-index-metamaterials (ZIM) waveguide structure which consists of a narrow dielectric slit. Finally, we will design a light emitter based on another interesting property of ZIM.

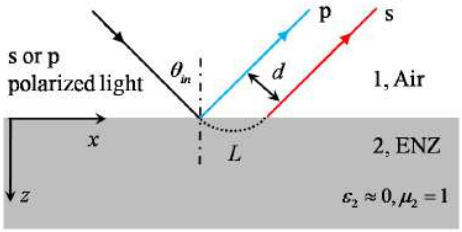

Figure 1: The schematic plot for the Goos-Hanchen effect in ENZ metamaterials.

REFERENCES

1. Xu, Y., C. T. Chan, and H. Chen, "Goos-Hanchen effect in epsilon-near-zero metamaterials," *Scientific Reports*, in press, 2015.
2. Chen, A., Y. Fu, Y. Xu, and H. Chen, "Total transmission through a sub-wavelength slit based on zero-index-metamaterials," *Applied Physics Letters*, under review, 2015.

Effective Surface Conductivity and Absorption Enhancement of Graphene Meta-surface

Yuancheng Fan and Fuli Zhang
Key Laboratory of Space Applied Physics and Chemistry
Ministry of Education, Department of Applied Physics, School of Science
Northwestern Polytechnical University, Xi'an 710072, China

Abstract— A kind of single-layer metamaterials, namely meta-surface [1, 2], has drawn enormous attention in recent years for various possibilities to manipulate light with ultra-thin structured surfaces. Plasmonic resonance of graphene micro/nano-structure is promising for atomically thin and tunable meta-surface [3–5]. We employed a recently proposed sheet retrieval method [6], which is quite suitable for the two-dimensional materials, to get the effective surface conductivity of graphene meta-surface [5]. The effective surface conductivity is helpful in understanding the optical response of graphene meta-surface, we will present our recent studies on graphene meta-surface based tunable absorption enhancements [7–9].

ACKNOWLEDGMENT

The authors would like to acknowledge financial support from the NSFC (Grants No. 11372248 and 61101044), the Fundamental Research Funds for the Central Universities (Grant No. 3102015ZY079), and the National 863 Program of China (Grant No. 2012AA030403).

REFERENCES

1. Kildishev, A. V., A. Boltasseva, and V. M. Shalaev, "Planar photonics with metasurfaces," *Science*, Vol. 339, No. 6125, 1232009, 2013.
2. Yu, N. and F. Capasso, "Flat optics with designer metasurfaces," *Nat. Mater.*, Vol. 13, No. 2, 139–150, 2014.
3. García de Abajo, F. J., "Graphene plasmonics: Challenges and opportunities," *ACS Photonics*, Vol. 1, No. 3, 135–152, 2014.
4. Low, T. and P. Avouris,, "Graphene plasmonics for terahertz to mid-infrared applications," *ACS Nano*, Vol. 8, No. 2, 1086–1101, 2014.
5. Fan, Y., N.-H. Shen, T. Koschny, and C. M. Soukoulis, "Tunable terahertz meta-surface with graphene cut-wires," *ACS Photonics*, Vol. 2, No. 1, 151–156, 2015.
6. Tassin, P., T. Koschny, and C. M. Soukoulis, "Effective material parameter retrieval for thin sheets: Theory and application to graphene, thin silver films, and single-layer metamaterials," *Physica B*, Vol. 407, No. 20, 4062–4065, 2012.
7. Fan, Y., Z. Wei, Z. Zhang, and H. Li, "Enhancing infrared extinction and absorption in a monolayer graphene sheet by harvesting the electric dipolar mode of split ring resonators," *Opt. Lett.*, Vol. 38, No. 24, 5410–5413, 2013.
8. Fan, Y., F. Zhang, Q. Zhao, Z. Wei, and H. Li, "Tunable terahertz coherent perfect absorption in a monolayer graphene," *Opt. Lett.*, Vol. 39, No. 21, 6269-6272, 2014.
9. Fan, Y., Z. Liu, F. Zhang, Q. Zhao, Z. Wei, Q. Fu, J. Li, C. Gu, and H. Li, "Tunable mid-infrared coherent perfect absorption in a graphene meta-surface," *arXiv*:1502.07435, 2015.

Session 4P2a
Coherent Optics, Laser Beam, Beam Propagation

Nonclassical Light Propagation through Atmospheric Turbulence

Jeffrey H. Shapiro
Research Laboratory of Electronics, Massachusetts Institute of Technology
Cambridge, MA 02139-4307, USA

Abstract— Free-space optical (FSO) communication, by which is meant line-of-sight laser communication of classical information through the earth's atmosphere, has received enormous attention, starting from soon after the invention of the laser. It is long been understood that reliable, high data-rate (say Gbps) FSO communications will be precluded by the presence of clouds or fog in the line of sight, limiting such links to operation in clear weather conditions, in which the principal propagation impairments — at wavelengths outside of atmospheric absorption lines — are those due to refractive-index turbulence. The extended Huygens-Fresnel principle — augmented to include atmospheric extinction loss — provides a powerful tool for analyzing and optimizing FSO optical communication in clear-weather conditions. Because turbulence is non-depolarizing, and has sub-psec multipath spread plus msec or longer coherence times, the extended Huygens-Fresnel principle takes the following form

$$E_L(\rho', t) = \int_{\mathscr{A}_0} d\rho E_0(\rho, t - L/c) h(\rho', \rho), \quad \text{for} \quad \rho' \in \mathscr{A}_L. \tag{1}$$

Here, $E_0(\rho, t)$ and $E_L(\rho', t)$ are the scalar complex envelopes of the $\sqrt{\text{W/m}^2}$sec-units laser fields for the transmitted and received light, respectively, as functions of the transverse coordinate vectors $\rho = (x, y)$ and $\rho' = (x', y')$ in the transmitter's exit pupil ($\mathscr{A}_0$ in the $z = 0$ plane) and the receiver's entrance pupil ($\mathscr{A}_L$ in the $z = L$ plane) and time t. Equation (1) assumes that the transmitted field's bandwidth is less than the atmosphere's coherence bandwidth (reciprocal of its multipath spread), and that this field's time duration is shorter than the atmosphere's coherence time. As a result, the temporal behavior of the extended Huygens-Fresnel principle is reduced to the line-of-sight time delay, L/c, where c is light speed. More importantly, Equation (1) is a spatial-superposition integral — a consequence of propagation through turbulence being a linear, albeit stochastic, process — whose Green's function is often written as

$$h(\rho', \rho) = e^{-\alpha L/2} \frac{e^{ikL + ik|\rho' - \rho|^2/2L}}{i\lambda L} e^{\chi(\rho', \rho) + i\phi(\rho', \rho)}. \tag{2}$$

From left to right, the terms on the right-hand side represent: atmospheric extinction loss with path-average extinction coefficient α; paraxial propagation through vacuum at the laser's center wavelength λ (center wave-number $k = 2\pi/\lambda$); and the turbulence-induced logamplitude $[\chi(\rho', \rho)]$ and phase $[\phi(\rho', \rho)]$ fluctuations imposed on the field received at $\rho' \in \mathscr{A}_L$ from a point-source emission from $\rho \in \mathscr{A}_0$ during the coherence time in question. Within the weak-perturbation regime, complete statistics for the turbulence fluctuations have been developed from the Rytov approximation. For many purposes, however, the mutual coherence function of the $\exp[\chi(\rho', \rho) + i\phi(\rho', \rho)]$ suffices, and this function is known — from the local method of smooth perturbations or the small-angle approximation to the linear transport equation — well into the regime of saturated scintillation.

With the rise of interest in quantum information processing, the use of nonclassical light beams, e.g., photonnumber states, squeezed states, and entangled states, for transmission of classical and/or quantum information over atmospheric paths has likewise garnered increasing attention. In this paper we will start from the quantum form of the Huygens-Fresnel principle for propagation through vacuum [1, 2] and develop the corresponding quantum form of the extended Huygens-Fresnel principle. We will also present some illustrative results obtained therefrom.

REFERENCES

1. Yuen, H. P. and J. H. Shapiro, "Optical communication with two-photon coherent states — Part I: Quantum state propagation and quantum noise reduction," *IEEE Trans. Inform. Theory*, Vol. 24, 657–668, 1978.
2. Shapiro, J. H., "The quantum theory of optical communications," *IEEE J. Sel. Top. Quantum Electron.*, Vol. 15, 1547–1569, 2009.

High Harmonic Generation in the Undulators for Free Electron Lasers

K. Zhukovsky
Department of Theoretical Physics, Physical Faculty
M. V. Lomonosov Moscow State University, Moscow 119992, Russia

Abstract— Undulator radiation (UR) was discovered by Motz in the middle of the 20th century. It represents a form of a synchrotron radiation (SR) and is due to the photon emission by accelerated relativistic electrons, executing oscillatory trajectories in a periodic magnetic field. Free electron lasers (FEL) require UR sources with special properties, calibrated for the user's needs. In particular, high UR harmonics are used to advance towards X-ray range. Modern UR designs include precision made many period undulators with, sometimes, double period magnetic field. High quality of the UR harmonic is of paramount importance. UR line is unavoidably subjected to broadening, originated from various sources, such as the electron energy spread, the beam divergency, the transport losses and the non-periodic magnetic components. Analytical expressions for the UR spectrum and for the intensity are obtained in the case of high-energy electrons with account for major sources of the spectral line broadening. The compensation of the divergency by the constant magnetic component is demonstrated in the analytical form. High harmonic generation is studied with account for all relevant sources of homogeneous and inhomogeneous broadening. In long undulators with $N > 150$ and $k > 1$, instead of the expected gain for the high harmonics a significant line broadening may occur, being a negative factor for high gain SASE FEL. The X-FEL source electron beam with $E = 17.5\,\mathrm{GeV}$ ($\gamma = 35000$), the energy spread $\sqrt{\sigma_e} = 10^{-4}$ and the initial deflection $\theta_0 = 2 \cdot 10^{-3}\,\mathrm{mrad}$ is considered. The shapes and the normalized intensities of the generated UR harmonics are shown. Good usability of wide range of the harmonics with the small deviation $|\Delta\nu_{n=9}| \approx 3$ of the frequencies from the ideal spectrum is confirmed. The radiation of a FEL with a double frequency undulator is evaluated with account for losses. Even for a highly monoenergetic beam with $\sqrt{\sigma_e} = 10^{-4}$ and with the divergency $\gamma\psi_{\max} = 0.1$ we obtain for a SASE FEL a significant reduction of the high harmonic saturated power, almost down to the level of the FEL performance with a common planar undulator. When the third harmonic is suppressed by the field H_2 of the proper sign, the fifth harmonic dominates, but its intensity decreases by one order due to the homogeneous and the inhomogeneous losses, as compared with the evaluations for an ideal undulator.

Coherent Synchrotron Radiation and Self Amplified Spontaneous Emission Free Electron Lasers (SASE-FEL)

K. Zhukovsky
Department of Theoretical Physics, Physical Faculty
M. V. Lomonosov Moscow State University, Moscow 119992, Russia

Abstract— New type of X-ray radiation source — X-ray free-electron laser (XFEL) should give the potential of providing the sub-picosecond pulse length of a conventional laser at the X-ray wavelength of a synchrotron radiation source.

In FEL electrons enter the undulator with initially random phases, so that mostly incoherent undulator radiation (UR) is emitted at the resonant UR wavelength. Because the electrons interact collectively with the radiation they emit, small coherent fluctuations in the radiation field grow and simultaneously begin to bunch the electrons at the resonant wavelength. This collective process continues until the electrons are strongly bunched at the end of the undulator, where the process saturates and the electrons begin to de-bunch.

In between undulators and SASE FEL oscillators are positioned. They employ mirrors, which limit the high frequency range — common mirrors do not reflect well $< 100\,\mu$m but allow easy mode locking mechanism. Inside the gain bandwidth, longitudinal modes of the laser will constructively periodically interfere with each other when in phase, producing an intense burst of light. Only phase-matched wavelengths will constructively interfere and form the modes of the radiation field to create a comb of equally spaced modes in the output frequency spectrum. Mode locking modifies the temporal envelope of the output field from a continuous wave to a series of short, periodically spaced pulses.

Laser macropulse of microsecond duration consist of a train of short micropulses, which are picoseconds in length. Used for ultrafast spectroscopy and femto-chemistry. The macropulses repeat at a repetition ratio limited by the accelerator usually 10–100 of Hz. The micropulse repetition rate can be from several MHz to even THz. Electrons move some slower than photons and as the wave in the undulator travels over a distance $\lambda/2$ in a time $\lambda/(2c)$, the electron travels over a smaller distance $\lambda_u/(2c)$, so that wave slip on half undulator period becomes $\lambda_u/2$.

Why is it more difficult to build free-electron lasers for X-rays than for larger wavelengths? For small wavelengths we need high-energy electrons, but high electron energy also increases the gain length LG $\sim \gamma$. We must keep the gain length short, as required for an X-FEL. The undulator field H_0 and period λ_u must be maximized, but λ_u must remain short for short wavelength $\lambda{\sim}\lambda_u/\gamma^2$. The electron beam current i must be high and its transverse cross section σ small. However, the γ-factor cannot be freely decreased if we want to obtain X-ray wavelengths. In the X-ray there are almost no good mirrors to form an oscillator cavity. The FEL functions as a single-pass amplifier, generating peak powers of the order of 10^{10} W in pulses, lasting tens of femtoseconds.

The high-gain FEL interaction is a positive feedback process — the electrons emit radiation, which affects their position (phase) and thus causes them to emit with greater coherence. SASE FEL process arises from noise. First waves emitted by the electrons trigger formation of microbunches. Contrary to non-micro-bunched electrons (c), the emission in micro-bunches of electrons (d), separated from each other by one wavelength, is correlated! This causes an exponential intensity increase with the distance that continues until saturation is reached. If an initial coherent laser seed wave is superimposed over the random electron phase, this seed is amplified along the undulator and yields bunching at seed wavelength until saturation. In this regime, the energy oscillates between the wave and the electrons rather than continuing to increase exponentially for the wave.

High gain harmonic generation (HGHG) schemes exploit Seed laser + harmonic generation section + amplifier. The first, short undulator is tuned to the frequency of the coherent seed laser whose interaction with the electron beam introduces a small longitudinal energy modulation. The magnetic dispersion section converts this energy modulation into a density modulation. The second undulator, called the radiator, is tuned to the n-th harmonic of the seed frequency. When the modulated electron beam passes the radiator, the radiation produced by the n-th harmonic component is amplified to saturation pulses with < 20 fs duration.

To make pulses shorter a SASE FEL design with chicane mode-locking is introduced. The magnetic chicanes give an extra slippage of the radiation with respect to the electron bunch.

Only those radiation wavelengths that have an integer number fit into the relative — radiation to electron bunch — slippage in one module will remain phase-matched to constructively interfere over many modules. Such constructively interfering wavelengths form the modes of the radiation field to create a comb of equally spaced modes in the output frequency spectrum.

Alternatively, self-seed FEL scheme forms short pulses. Its advantage: independent of any external radiation source (which must be very stable, precisely matched to the electron beam in space and time). Same frequency in two undulators! First undulator, a short SASE FEL, operates in the linear gain regime, produces radiation pulses with the characteristic features of SASE at a power level approximately three orders of magnitude below saturation. The electron beam is then sent through a magnetic chicane, which destroys the density modulation introduced in the first undulator and delays the electron beam by the same amount as the radiation pulse. The radiation pulse is spectrally filtered by a narrow-band grating monochromator, which stretches the pulse and provides a coherence length longer than the electron bunch length. This radiation is the seed for the second undulator, which amplifies it to saturation. The output radiation exhibits a narrow spectral line with only a small background of spontaneous radiation. Spectral brightness increases in this way by almost two orders of magnitude!

Main factors degrading the FEL emission are electron energy spread, angular divergence, transverse electron beam size, diffraction of the wave. As the electrons transfer energy to the wave, their own energy decreases. The wave emission is not the same from all electrons, so that different electrons have different energies, with an increasing energy spread. At a certain point, the energy spread is so large that there is no gain anymore.

Much before the electrons loose a substantial portion of their energy they slow down by emitting electro-magnetic energy, change their phase with respect to the wave and start taking energy rather than giving it!

Future developments of X-FELs include improved temporal coherence of X-ray SASE and the development of relatively high-reflectivity diamond crystal mirrors in the X-ray regime makes them feasible. Reducing X-ray pulse durations to the attosecond regime will provide spatiotemporal resolution of atomic processes below 100 as.

Investigation the Possibility of Obtaining Spiral Light Beams with Adjustable Parameters

N. Kundikova[1, 2], **Yu. Miklyaev**[1, 2], **I. Popkov**[1, 2], **and A. Popkova**[1, 2]

[1]The Institute of Electrophysics of the Ural Division of the Russian Academy of Sciences (IEP UD RAS) Russia

[2]"South Ural State University" (National Research University), Russia

Abstract— Light beams with controllable parameters are widely used in science and industry. Beams with non-uniform distribution of intensity, phase and polarization are used in laser tweezers, for microscopic objects manipulation, objects non-destructive testing, surface treatment, laser welding and drilling, studying the surface properties and the new materials creation.

Here we show how it is possible to generate a light beam in a form of spiral with the controllable pitch, length and radius. Beams with wavefront dislocations have a spiral phase distribution in the direction of propagation. The maximum intensity of the interference pattern of a Gauss beam and a co-propagating beam with a wavefront dislocation forms a spiral curve in the space. Selecting the appropriate parameters of the light beams it is possible to obtain the desired intensity distribution in the direction of propagation.

In order to calculate the intensity distribution of the interference pattern the scalar wave equation was solved using MATLAB software. The beam waists of the beams under consideration were supposed to be coincident.

The numerical simulations have shown that the spiral pitch decreases with the Bessel beam of the first order divergence increasing, the stable length of the spiral decreases with the Gauss beam divergence decreasing.

We present a method of generation of beams with the spiral intensity distribution in the direction of propagation. The pitch of spiral distribution is determined by the numerical aperture of the Bessel beam and the stable length of the spiral distribution is determined by the numerical aperture of the Gauss beam. The proposed method was tested experimentally.

ACKNOWLEDGMENT

This work has been performed in the framework of Basic Research Program of Ministry of Education and Science of the Russian Federation (888/2014 102-GZ).

Structured Laser Radiation in Optical Inhomogeneous Media Refractography

B. S. Rinkevichyus, I. L. Raskovskaya, A. V. Tolkachev, and A. V. Vedyashkina
V. A. Fabrikant Physics Department, National Research University "Moscow Power Engineering Institute"
Moscow 11250, Russia

Abstract— The report devoted to analysis of the properties of structured laser radiation (SLR) produced from Gaussian beam passing through a refractive (ROE) or diffraction (DOE) optical elements and its applications in the modern method of optically inhomogeneous media investigation — laser refractography [1]. Fig. 1 shows example of schematic diagram of laser refractographic setup. SLR passes through transparent optically inhomogeneous medium with temperature stratification (4), recorded by digital camera 6, processed by personal computer 7 and then we can obtain characterization of optically inhomogeneous medium (temperature graph 8).

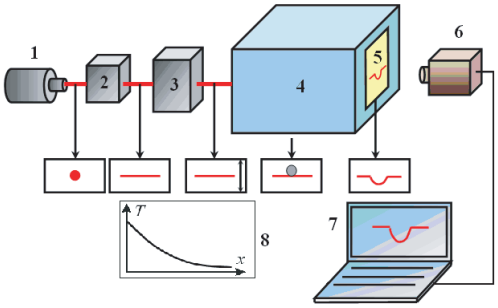

Figure 1: Schematic diagram of the experimental setup: 1 — laser, 2 — DOE, 3 — scanning system, 4 — medium under study, 5 — diffuse screen, 6 — CCD camera, 7 — PC, 8 — refractogram processing.

The setup uses semiconductor laser 1 emitting radiation in the red or the green wavelength region. The radiation power amounts to 5–25 mW. The laser beam passes through DOE 2 that transforms the initial narrow laser beam into a structured laser radiation differing in shape, for example, plane, conical, or cross-shaped laser beams. To position these beams with respect to the object under study, use is made of scanning system 3 that allows these beams to be moved in two orthogonal planes. Temperature and concentration boundary layers in the vicinity of heated or cooled bodies, as well as diffusion layers, are investigated in glass cell 4. Two-dimensional refractograms are observed on diffuse screen 5 from the cell and recorded with digital camera 6 whose output is entered into personal computer 7. The computer processing of the refractograms by means of a special program yields information 8 about the parameters of the near-wall and boundary layers. The bottom row of images in the above Figure 1 illustrates the stages of transformation of the narrow laser beam into structured radiation and then into a 2D refractogram.

The experimental technique for studying various boundary temperature layers near heated or cooled bodies was described in detail in the monograph [1].

REFERENCES

1. Rinkevichyus, B. S., O. A. Evtikhieva, and I. L. Raskovskaya, *Laser Refractography*, 187, Springer, New York, 2010.

Controlling the Lasing Threshold in Two-dimensional Photonic Crystals with Gain

Sotiris Droulias[1], **Peng Zhang**[2], **Thomas Koschny**[2], **and Costas M. Soukoulis**[1, 2]

[1]Institute of Electronic Structure and Laser, FORTH, Heraklion 71110, Crete, Greece
[2]Ames Laboratory and Department of Physics and Astronomy, Iowa State University
Ames, Iowa 50011, USA

Abstract— The need for lasers with dimensions as small as possible leaves little space for the gain material, which can push the lasing threshold to extremely high levels. In order to overcome this, light must interact with the gain material as long as possible. This can be achieved when the group velocity is very low and the fact that photonic crystals offer this feature at their band edges makes them an excellent candidate.

Based on this idea, we investigate the lasing threshold in microstructured systems containing a four level gain medium and show how it can be modified as a result of the interplay between the group velocity and interface reflectivity of the lasing mode. To this end, we establish a simple theoretical model that decomposes the contributions of these features to the Q factor. In order to demonstrate them in realistic structures we choose a 2D PC of a finite amount of layers. The Maxwell equations are coupled with the semi-classical 4-level rate equations and are self-consistently solved under a finite-difference time-domain (FDTD) scheme [1]. Our simulations show that operation near the band edge can lead to strong reduction of the lasing threshold with respect to a uniform gain slab of the same dimensions, in spite of the lower gain density, even for as few as 10 layers [2]. Moreover, with a slight structural modification, the PC is surprisingly demonstrated to exhibit lower lasing threshold at steeper band edges. Our self-consistent FDTD calculations are explained in a straightforward manner by the theoretical model, which may also predict other counter-intuitive behaviors, such as lower lasing threshold inside a band, rather than the band edge.

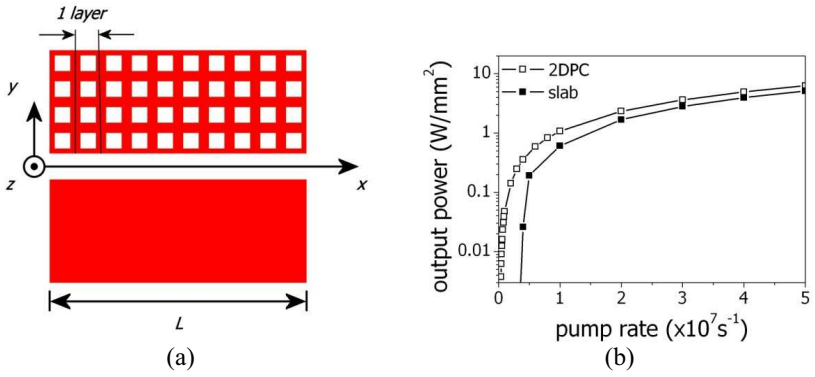

Figure 1: (a) Schematic of the 2DPC consisting of 10 layers (top) and the respective slab of uniform gain and same length (bottom). The red areas denote the host dielectric which is homogeneously embedded with the four-level gain material. Both systems are infinite in the yz plane and confined in the x direction, along which the emitted wave propagates. (b) Lasing power in log scale of the 2DPC (open squares) and gain slab (filled squares) as depicted in Figure 1(a) for different pump rates. Both systems operate at the frequency which corresponds to the bottom of the 2nd band of the 2DPC. The lasing threshold of the photonic crystal is 1 order of magnitude lower than that of the gain slab.

REFERENCES

1. Fang, A., T. Koschny, and C. M. Soukoulis, *J. Opt.*, Vol. 12, 024013, 2010.
2. Droulias, S., C. Fietz, P. Zhang, T. Koschny, and C. M. Soukoulis, *Opt. Expr.*, Vol. 22, 19242, 2014.

Investigation of Kinetic Processes of a Diode-pumped Alkali Laser

Guofei An, You Wang, Juhong Han, He Cai, Wei Zhang, Liangping Xue, Hongyuan Wang, Zhigang Jiang, Jie Zhou, and Ming Gao
Southwest Institute of Technical Physics, Chengdu, Sichuan 610041, China

Abstract— A diode-pumped alkali laser (DPAL) provides the significant promise for high-powered performances. For a high-powered DPAL, both the absorption and the lasing distribution crucially affect the output physical features. In this report, a mathematical model is introduced for examining the kinetic processes of the gas-state media by using a segmental approach. The energy transmission inside the oscillator has been theoretically analyzed for construction of a reciprocating regime which is based on the self-consistency principle. Basically, the conclusion can be extended to any end-pumped laser configurations.

Session 4P2b
Optical Fiber, Sensing, Optical Devices

Radiofrequency Impedance Spectroscopy for Measurement of Optical Power of Scattered Radiation in Nonlinear Crystal

O. A. Ryabushkin[1, 2], **A. V. Konyashkin**[1, 2], **and A. S. Demkin**[1, 2]

[1]NTO "IRE-Polus", 141190 Vvedensky Sq. 1, Fryazino Moscow region, Russia
[2]Moscow Institute of Physics and Technology
141700, Institutskiy per. 9, Dolgoprudniy Moscow Region, Russia

Abstract— Frequency conversion efficiency of IR laser radiation in nonlinear-optical crystals extremely depends on both absorption and scattering properties of the crystal. Recently, piezoelectric resonance laser calorimetry was introduced for the precise measurement of optical absorption coefficients of crystals [1].

In present paper novel method is proposed for measurement of scattered radiation power of nonlinear-optical crystals. Like piezoelectric resonance laser calorimetry it is based on the concept of equivalent temperature of crystal heated by laser radiation [2]. Equivalent temperature of nonlinear-optical crystal is determined directly by measuring frequency shift of the temperature calibrated piezoelectric resonance. Piezoelectric resonance can be observed when the external electric field frequency corresponds to one of the crystal internal vibration mode frequencies. At first approximation piezoelectric resonances frequencies linearly dependent on temperature during uniform heating of the crystal $Rf_i(T) = Rf_i(T_0) + K_i^{\mathrm{prt}}(T - T_0)$. It was demonstrated that thermodynamic temperature of the crystal, nonuniformly heated by laser radiation of P power, can be replaced by its equivalent temperature: $\Theta_{\mathrm{eq}}(P) = T_0 + (Rf_i(P) - Rf_i(T_0))/K_i^{\mathrm{prt}}$, where T_0 is crystal temperature at zero power. Power of radiation scattered by nonlinear-optical crystal, can be determined by measuring equivalent temperatures of two additional resonators that are made of the identical crystal material and are placed at fixed equal distances from the main nonlinear-optical crystal that interacts with laser radiation. Difference between two additional resonators is that first one is transparent to the scattered radiation and the second one is absolutely opaque ("black body") and completely absorbs radiation in wide spectral range. Temperature change of additional resonators is primarily conditioned by the ambient air heating. Still additional heating of the second resonator is caused by absorption of both scattered radiation and thermal radiation of the main crystal. In the experiment $KTiOPO_4$ (KTP) crystal with dimensions $3 \times 3 \times 30\,\mathrm{mm}^3$ was used as the main crystal and additional resonators were made of thin ($0,\ 2 \times 3 \times 30\,\mathrm{mm}^3$) $LiNbO_3$ crystals. Transmission of 7 W laser radiation at 1064 nm wavelength through KTP of resulted in 1 K difference between equivalent temperatures of non-transparent and transparent $LiNbO_3$ crystals. Theoretical estimation gives several mW of total power scattered in KTP that corresponds to the 0.1% scattering coefficient. It should be noted that KTP optical absorption coefficient has the same order.

REFERENCES

1. Ryabushkin, O. A., et al., "Piezoelectric resonance calorimetry of nonlinear-optical crystals under laser irradiation," *Proc. of SPIE*, Vol. 8847, 88470Q, 2013.
2. Ryabushkin, O. A., et al., "Equivalent temperature of nonlinear-optical crystals interacting with laser radiation," *J. of European Optical Society — Rapid Publications*, Vol. 6, 11032, 2011.

The Effect of Iron Nano-inclusions in Multilayered Integrated Optical Waveguides

Isabelle G. de Moraes[1], **Anderson O. Silva**[1],
Maria Aparecida G. Martinez[1], **and Maria Thereza M. R. Giraldi**[2]

[1]Photonics Laboratory, Centro Federal de Educação Tecnológica Celso Suckow da Fonseca, Brazil
[2]Photonics Laboratory, Instituto Militar de Engenharia — IME, Brazil

Abstract— In the last years, research on new materials and technologies together with established modal coupling theories has featured the construction of directional couplers, power dividers, polarizers and isolators [1]. Most of these devices are based on the control of the electrical field properties, as the propagation modes, polarization and others. In this work, we investigate the impact of ferromagnetic composite nano-inclusion in the coupling of multilayered optical waveguides structure based on alternating InGaAsP and InP layers, operating at 1550 nm. The complex refractive index of the mixture (the host and inclusion materials) is obtained from iron experimental optical properties data and Maxwell Garnett models [2]. The beating length and power transfer within the multilayer structure are determined by the use of the nonorthogonal Coupled Mode Theory [3, 4] for an identical and a non-identical cases. In the identical case, the guiding layers are incrusted identically with the same filling factors in the structure and otherwise in the non-identical case. The motivation is to use nano-inclusions to improve the coupler efficiency increasing the modal confinement, and decreasing the beating length. This effect occurs because increasing the concentration of these nano-inclusions enhances the difference between the refractive index in the waveguide layers. On the other hand, ferromagnetic composite adds loss to the system, creating a trade-off between decreasing beating length and output power. Overall, for the identical case, the beating length decreases with the increase of the nano-particles filling factor, for the cladding thickness ranging from 0.3 µm up to 1 µm. The reduction rate is more sensitive to the filling factor for a cladding thickness greater than 0.6 µm. For a filling factor of 0.2%, the beating length reduces from 107.2 µm to 34.5 µm, a 70% reduction with respect to the lossless case, for a cladding thickness of about 0.8 µm. The total power decreases with the enhancement of the filling factor values and cladding thickness. For a 0.2% filling factor, losses in the structure vary from 3 dB up to 8dB for the cladding thickness ranging from 0.3 µm up to 1 µm. For the non-identical case, the structure beating length reduces with the nano-inclusion filling factor. For a 0.2% filling factor, the beating length reduces from 107.2 µm to 60 µm, about 56% of reduction with respect to the lossless case for a cladding thickness of 0.8 µm. The structure total losses reduce substantially when compared to the identical case, reaching a maximum of 2 dB loss for a 0.2% filling factor. The total loss reduction in the non-identical case strongly depends on cladding thickness. As the cladding thickness increases, the coupling waveguide slightly decouples, and light remains mainly in the lossless waveguide, reducing the overall loss. We demonstrate that suitably controlling the nano-inclusion filling factor and cladding thickness, particularly for the fundamental TE modes, a more efficient multilayer coupling structure, with reduced beating length and reasonably losses can be designed.

REFERENCES

1. Dai, D., J. Bauters, and J. E. Bowers, "Passive technologies for future large-scale photonic integrated circuits on silicon: Polarization handling, light non-reciprocity and loss reduction," *Light: Science & Applications*, 1–12, 2012.
2. Sihvola, A., "Homogenization of a dielectric mixture with anisotropic spheres in anisotropic background," *Electromagnetics*, Vol. 17, No. 3, 269–286, 1997.
3. Chuang, S.-L., "A coupled mode formulation by reciprocity and a variational principle," *Journal of Lightwave Technology*, Vol. 5, 5–15, 1987.
4. Hardy, A. and W. Streifer, "Coupled mode theory of parallel waveguides," *Journal of Lightwave Tecnology*, Vol. 3, 1135–1146, 1985.

Radiation-resistant Temperature Sensor Based on Fiber Bragg Grating Inscribed Specialty Optical Fiber

Seongmin Ju[1], **Youngwoong Kim**[1], **Seongmook Jeong**[1], **Jong-Yeol Kim**[2], **Nam-Ho Lee**[2], **Hyun-Kyu Jung**[2], **and Won-Taek Han**[1]

[1]School of Information and Communications/Department of Physics and Photon Science
Gwangju Institute of Science and Technology
123 Cheomdan-gwagiro, Buk-Gu, Gwangju 500-712, Republic of Korea
[2]Nuclear Convergence Technology Development Department
Korea Atomic Energy Research Institute
Daedeok-daero, Yuseong-gu, Daejeon 989-111, Republic of Korea

Abstract— Temperature sensor based on the FBG inscribed radiation-resistant specialty optical fiber under γ-ray irradiation was demonstrated. The measured temperature sensitivity at dose-rate of 35.33 Gy/min from 30°C to 100°C was about 7.2 pm/°C.

Recently, we have developed a radiation-resistant germano-silicate fiber with two inner cladding layers of a pure silica buffer and a boron-doped silica, to enhance photosensitivity for inscribing FBG in the fiber core without decreasing the radiation resistance [1]. We demonstrate a novel temperature sensor based on the FBG inscribed radiation-resistant fiber within a temperature range from 30°C to 100°C under γ-ray irradiation with a ^{60}Co γ-ray (MSD Nordion, pencil type/C-188 sealed) at dose-rate of 35.33 Gy/min (total dose of 10,458 Gy). A 10 mm length of FBG was inscribed onto the 200 mm fiber by using a phase mask (QPS Photronics Inc.) with a KrF excimer laser at 248 nm. The temperature dependent Bragg reflection wavelength of the FBG was measured under γ-ray irradiation by using the optical spectrum analyzer (OSA, Ando AQ 6317B) together with the white light source (WLS, Ando AQ 4305) operating around 1310 nm as an input light source.

The peak power of the Bragg reflection band at 1310.09 nm and the full width at half maximum (FWHM) bandwidth of the fabricated FBG were about 15.62 dB and 0.24 nm, respectively. With the increase of temperature from 30°C to 100 °C under the γ-ray irradiation from 0 to 6,642 Gy for 188 minutes, the power and the wavelength of the Bragg reflection peak were found to decrease to 15.28 dB and shift toward longer wavelength of 1310.81 nm, respectively. But the FWHM bandwidth remained practically unchanged during the γ-ray irradiation, regardless temperature. The measured temperature sensitivity of the fabricated FBG at dose-rate of 35.33 Gy/min was about 7.2 pm/°C.

ACKNOWLEDGMENT

This work was partially supported by Basic Science Research Program through the National Research Foundation of Korea (NRF) funded by the Ministry of Education (No. 2013R1A1A2063250), the New Growth Engine Industry Project of the Ministry of Trade, Industry and Energy, the Brain Korea-21 Plus Information Technology Project through a grant provided by the Gwangju Institute of Science and Technology, Korea.

REFERENCES

1. Ju, S., Y. Kim, S. Jeong, J.-Y. Kim, N.-H. Lee, H.-K. Jung, and W.-T. Han, "Gamma-ray dose-rate dependence of fiber Bragg grating inscribed germano-silicate glass optical fiber with boron-doped inner cladding" *Proceedings of the 2nd International Conference on Photonics, Optics and Laser Technology*, 107, 2014.

Effect of Gamma-ray Pre-irradiation on Radiation Response of Photonic Crystal Fiber with Fluorine Doped Silica Core

Youngwoong Kim, Seongmin Ju, Seongmook Jeong, Youngmin Kim, Seung Ho Lee, Dong Hoon Son, and Won-Taek Han
Department of Physics and Photon Science/School of Information and Communications
Gwangju Institute of Science and Technology
123 Cheomdan-gwagiro, Buk-Gu, Gwangju, Republic of Korea

Abstract— Formation of point defects in optical fibers by intense ionizing radiation causes radiation-induced attenuation (RIA) that can seriously degrade the capabilities of most fiber-based devices such as fiber lasers, high-speed communication systems, nonlinear optical devices, and fiber sensors, etc.. Radiation-hardening against the RIA is therefore indispensable for the fiber-based applications in radiation-harsh environments.

By modifying the fiber geometry or glass composition, one can simply obtain desirable optical properties. Photonic crystal fiber (PCF) has a cladding region comprised of arrays of air holes that run along the fiber length surrounding the central core. Investigations concerning the radiation response of the PCF have been performed to evaluate the feasibility of the PCF based applications in radiation-harsh environments, which seems to be promising due their radiation resistance [1].

In this study, we have fabricated a PCF with fluorine (F) doped silica glass core which is known to be the most radiation resistant composition under steady-state gamma-ray irradiation conditions [2]. The PCF was fabricated by the stack-and-draw technique using fused silica capillary tubes and a F-doped silica glass rod with F concentration of $\sim 1,000$ ppm (Shin-Etsu Quartz Products Co., Ltd.). The core size, the hole diameter, and the pitch of the PCF were around 1.9 μm, 1.2 μm, and 2.4 μm, respectively. A 1 meter length of the PCF was intermittently pre-irradiated by gamma-ray from ^{60}Co source. The RIA characteristics of the PCF was investigated under different irradiation conditions (dose rates, accumulated dose, and irradiation interval). After the pre-irradiation, the RIA level at 1310 nm of the fiber was found to greatly decrease and became rapidly saturated. The measured rapid and large extent recovery of the RIA after the end of the irradiation was thought to be worthy of notice.

ACKNOWLEDGMENT

This work was partially supported by the Advanced Technology Radiation Laboratory of the Korea Atomic Energy Research Institute, the New Growth Engine Industry Project of the Ministry of Trade, Industry and Energy, the Basic Science Research Program through the National Research Foundation of Korea (NRF) funded by the Ministry of Education (No. 2013R1A1A2063250), the Brain Korea-21 Plus Information Technology Project through a grant provided by the Gwangju Institute of Science and Technology, South Korea.

REFERENCES

1. Girard, S., Y. Ouerdane, M. Bouazaoui, C. Marcandella, A. Boukenter, L. Bigot, and A. Kudlinski, "Transient radiation-induced effects on solid core microstructured optical fibers," *Opt. Express*, Vol. 19, No. 22, 21760–21767, 2011.
2. Francesca, D. D., S. Agnello, S. Girard, C. Marcandella, P. Paille, A. Boukenter, Y. Ouerdane, and F. M. Gelardi, "Influence of O_2-loading pretreatment on the radiation response of pure and fluorine-doped silica-based optical fibers," *IEEE Trans. Nucl. Sci.*, Vol. 61, No. 6, 3302–3308, 2014.

Various Microbubbles Generation by Light Excited Graphene Oxide Heater

Jiapeng Zheng[1], **Kezhang Shi**[1], **Jianxin Yang**[1], **Xijun Li**[1], **Meng Shi**[3]
Xiang Cai[4], **Sailing He**[1], **and Xiaobo Xing**[1, 2]

[1]Centre for Optical and Electromagnetic Research
South China Normal University, Guangzhou 510006, China
[2]Education Ministry's Key Laboratory of Laser Life Science & Institute of Laser Life Science
College of Biophotonics, South China Normal University, Guangzhou 510631, China
[3]Shandong Provincial Key Laboratory of Laser Polarization and Information Technology
Laser Institute, Qufu Normal University, Qufu 273165, China
[4]Department of Light Chemical Engineering Guangdong Polytechnic, Foshan 528041, China

Abstract— Microbubble has stimulated broad attention for the highly-efficient contrast agents in biomedicine and drug delivery, and microfluidic control. There is still a challenge to generate different kinds of microbubbles by numerous techniques including flow-focusing devices and ultrasound-induced cavitation. The complex focused laser controlled systems can produce for microbubbles based on photothermal effect, but has large loss. In view of cost and operability, assembling photothermal materials onto microwire exhibiting strong evanescent field should be more desirable to produce microbubbles. Herein, we present a representative photothermal device by depositing graphene oxide (GO) onto a microwire. Excited by the near-infrared light, GO-deposition can act as a heater for creating a variety of microbubbles. Three kinds of microbubble were successfully generated by the GO-heater. Firstly, when the GO-microheater was immersed in N,N-dimethylformamide (DMF) and superheat limit of the liquid was reached, a lot of spherical microbubbles with diameters from tens to hundreds of micrometers were generated directly on the microheater based on nucleate boiling. Secondly, when the GO-microheater was located at the DMF/air interface and its neighboring microwire was immersed in GO-DMF suspension, ellipsoid microbubbles were indirectly generated on the smooth microwire based on heterogeneous nucleation and continuously grew in the thermal gradient field governed by GO-microheater. Finally, massive cavitating microbubbles can be generated near a GO microcavity and ejected away at the high excitation power. This technique has prospective applications in microfluidics, optofluidic control, and other biochip techniques.

ACKNOWLEDGMENT

This work is partially supported by the National Natural Science Foundation of China (Nos. 61177077, 1104162, 21476052, 91233208, 61178062), the Guangdong Natural Science Foundation (2013B090500123, 2014A030313432), the Guangdong Innovative Research Team Program (Grant 201001D0104799318), the National High Technology Research and Development Program (863 Program) of China (No. 2012AA012201), Swedish VR grant (# 621-2011-4620) and AOARD.

A High Survivability Mesh Topology FBG Based Optical Sensing System with SDN Controlling

Jhih-Heng Yan[1], **Wei-Cheng Chen**[2], **You-Wei Chen**[1], **Kai-Ming Feng**[1, 2], **and Chung-Yu Wu**[3]

[1]Institute of Photonics Technologies, National Tsing Hua University, Hsinchu, Taiwan
[2]Institute of Communications Engineering, National Tsing Hua University, Hsinchu, Taiwan
[3]National Chung-Shan Institute of Science and Technology, Taoyuan, Taiwan

Abstract— Optical sensing technique has been studied and developed for decades, where fiber Bragg grating (FBG) based optical sensing systems are one of the most attractive research topics. Due to the light weight, electromagnetic interference immunity, and high sensing accuracy properties, optical sensing system with FBG sensors have been applied to various sensing environments, not only large-scale infrastructures but also industrial equipment and personal wearing devices. However, due to the weak structure nature of fibers, FBG as well as their connection fibers usually suffer from environmental and human damages. Many conventional optical sensing systems will be partially or totally out of work even one link/node failure occurs.

To enhance the system survivability, we have proposed a FBG sensing system with a novel mesh network topology in our previous works. In the design of our proposed FBG based optical sensing system, each sensor set integrates multiple FBG segments referred to different Bragg wavelengths. The wavelength arrangement not only follows an interleaved manner among the designed four sensor sets, but also corresponds to the applied arrayed waveguide grating (AWG) channels. With such design, the sensing resolution can be optimized based on different sensing environments by manipulating the FBG segment combination in each sensor set. Furthermore, almost all sensor sets can act as the light-paths while they are not the sensing target during the sensing procedure period, which greatly enhances the sensing network survivability.

Based on our previous achievement, in this paper ready for PIERS submission, we introduce *software-defined network* (SDN) technique to our sensing system. Also, although SDN technique is recently popular in wireless sensing networks, to authors' best knowledge, this is the first time that SDN technique is employed in an optical sensing system. The manual operation is basically out of the network control procedure, which is exactly one of the design principles of SDN technique. To further reduce the system controlling complexity, we design a multiple-region sensing network with multiple SDN controllers. With the interconnection specification of SDN controllers, this multiple sensing-region can be effectively realized, where the most noteworthy features are listed below.

- *The power and the round-trip time of sensing signal are reduced.* The whole sensing network is reorganized as multiple smaller regions, where each of them is supervised by a SDN controller. Since the distance between central office and every FBG sensor set decreases, the power and the round-trip time of sensing signal are thus largely reduced.
- *The complexity of the remote node controlling is relieved.* The remote node controlling has been used to be a complicated issue. With the employment of multiple-region sensing network as well as SDN controlling, the quantity of supervising remote node is reduced, and therefore the controlling complexity is relieved.
- *The survivability of sensing network is further strengthened.* While a link/node failure occurs, its SDN controller will inform this network state to other controllers. Therefore, all the SDN controllers in the sensing network may take over the alternative sensing paths recalculated by *Dijkstra's algorithm*. The network survivability is consequently increased.
- *The flexibility of sensing network configuration is enlarged.* To upscale the sensing network has become an easy work with the design of sensing network building blocks. Moreover, when the sensing network is upscaling, the controlling complexity can be remained at the same level as that of a small sensing region.

In this paper, the demonstrations are arranged for two steps, the experimental step and the simulation step. In experimental step, we build a 2-by-2 single SDN-controlled central office including a fiber ring laser based transmitter and an AWG based receiver. The link failures can be easily located with the analysis of received sensing signal power by the SDN controller. Two alternative light-paths are then calculated by SDN controller after failures are reported. In the simulation step, we build the multiple central office sensing systems with various network scales. The relationship between link failures and system survivability is verified. As a result, in the

sensing system with a 6-by-6 network scale, the results indicate that the sensing system is still survived for up to seven link failures.

Direct Writing of Fiber Bragg Gratings through Polyimide Coating by Femtosecond Laser Pulses at the Wavelength of 1026 nm

A. V. Dostovalov[1], **A. A. Wolf**[1], **and S. A. Babin**[1, 2]

[1]Institute of Automation and Electroetry, SB, RAS, Russia
[2]Novosibirsk State University, Russia

Abstract— Experimental results are presented on direct point-by-point writing of the first- and the second-order fiber Bragg gratings through polyimide protective coating by femtosecond laser pulses at the wavelength of 1026 nm. Writing was carried out in specialty optical fibers: high-temperature tolerant Fibercore SM1500(9/125)P and pure-silica core hydrogen tolerant SM1500SC(9/125)P.

Introduction: Fiber Bragg gratings (FBG) are widely used optical components in different areas: from spectral filtering in lasers to sensing applications. The main advantages of femtosecond laser writing in comparison with conventional UV modification of refractive index consist in possibility to modify non-photosensitive fibers through plastic coating and to obtain gratings with higher resistance to thermal decay. We present the results of direct point-by-point FBGs writing in specialty polyimidecoated fibers by high-energy femtosecond laser pulses.

Experiment: The first- and the second-order FBGs were inscribed using direct point-by-point writing technique in high-temperature tolerant Fibercore SM1500(9/125)P fiber (Fig. 1) and pure-silica core hydrogen tolerant SM1500SC(9/125)P fiber, through 10 µm polyimide protective coating in both cases. The results of the FBGs testing at high temperatures (up to 350°C) showed that for a given exposure time (6 hours) there is no degradation of grating strength which is typical for FBGs written by the UV radiation. At the same time, after temperature exposure, the protective polyimide coating of the fibers remained undamaged, which gives an advantage over acrylate coating which is resistant only for temperatures up to 150°C.

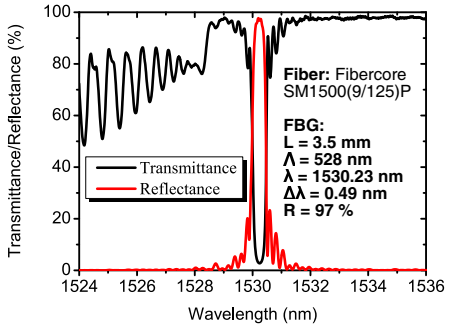

Figure 1: Transmittance and re ectance spectra of the first-order FBG written in polyimide coated fiber using point-by-point technique.

Conclusion: The FBGs written in specialty fibers by point-by-point direct writing technique through protective polyimide coating may serve as robust in-fiber laser mirrors and temperature/strain sensors.

A Novel Demodulation Scheme for Fiber Sensor Based on Chaotic Fiber Laser

Lingzhen Yang[1, 2] **and Jun Zhang**[1, 2]

[1]College of Physics and Optoelectronics
Taiyuan University of Technology, Shanxi, Taiyuan 030024, China
[2]Lab of Advanced Transducers and Intelligent Control System, Ministry of Education
Taiyuan University of Technology, Shanxi, Taiyuan 030024, China

Abstract— Fiber Bragg grating (FBG) is attracting considerable interest in sensing elements. A novel demodulation system for a concatenation of identical FBGs based on tunable fiber chaotic laser is proposed. The chaotic fiber laser is the ultra-long ring cavity structure. The tunable fiber grating (TFBG) in the cavity as a narrow-band filter has the tuning range from 1540.26 nm to 1571.86 nm. A sensor network consists of five identical weak fiber gratings separated by a short length of single mode fiber. The chaotic correlation that can allow every Bragg grating of the sensor addressed simultaneously. The correlation peaks of the cross-correlation between the reflected light from FBG sensor and reference light from chaotic fiber laser has been studied for the demodulation of FBG sensors network in strain measurement. Simulation and experimental results on the capability of strain measurement are presented and discussed. The cross-correlation peaks depend on the voltage strength between the reference chaos and reflected signals from the identical weak fiber Bragg grating sensor. The experimental observations confirm that the demodulation results are in excellent agreement with the acquired by the theoretical analysis. This method is not only simple and low cost, but also achieves the multi-point synchronous measurement.

Session 4P3
Plasmas, Composite Media, Waves and Media

A Relativistic Self-consistent Model for Studying Enhancement of Child-Langmuir Limit Due to Counter-streaming Ions

M. C. Lin[1] and J. P. Verboncoeur[2]

[1]Department of Electrical and Biomedical Engineering
Hanyang University, Seoul 133-791, Korea
[2]Department of Electrical and Computer Engineering
Michigan State University, East Lansing, Michigan 48824, USA

Abstract— A maximum electron current transmitted through a planar diode gap is limited by space charge of electrons dwelling across the gap region, the so called Child-Langmuir (CL) law. By introducing a counter-streaming ion flow to neutralize the electron charge density, the CL limit can be dramatically raised, so electron current transmission gets enhanced. In this work, we have developed a relativistic self-consistent model for studying the enhancement of maximum transmission by a counter-streaming ion current. The maximum enhancement is found when the ion effect is saturated, as shown analytically. The solutions in non-relativistic, intermediate, and ultra-relativistic regimes are obtained and verified with 1-D particle-in-cell simulations. This self-consistent model is general and can also serve as a comparison for verification of simulation codes, as well as extension to higher dimensions.

ACKNOWLEDGMENT

This work was supported by the research fund of Hanyang University (HY-201400000002393) and a Michigan State University Strategic Partnership Grant.

REFERENCES

1. Child, C. D., *Phys. Rev. (Ser. I)*, Vol. 32, 492, 1911.
2. Langmuir, I., *Phys. Rev.*, Vol. 2, 450, 1913.
3. Jory, H. R. and A. W. Trivelpiece, *J. Appl. Phys.*, Vol. 40, 3924, 1969.
4. Goldstein, S. A. and R. Lee, *Phys. Rev. Lett.*, Vol. 35, 1079, 1975.
5. Choi, E. H., H. M. Shin, and D. I. Choi, *J. Appl. Phys.*, Vol. 61, 2160, 1987.
6. Lin, M. C., P. S. Lu, P. C. Chang, B. Ragan-Kelley, and J. P. Verboncoeur, *Phys. Plasmas*, Vol. 21, 023118, 2014.

Octuplet of Direction Indicators with Distinct Spatio-temporal Symmetries

Jiri Hlinka
Department of Dielectrics, Institute of Physics, Czech Academy of Scinces, Prague, Czech Republic

Abstract— Physical quantities defined by a magnitude and an oriented axis in 3D space are often represented by three-component Euclidean vectors. Frequently, axial and polar vectors are distinguished, depending on whether they do flip their sense or not, respectively, upon the action of the spatial inversion (parity symmetry operator). For classification of temporal processes or the properties of magnetically ordered materials, the action of the time-inversion operator ($1'$) can be used. For example, magnetization M and magnetic field vector H are "time-odd axial" vectors, the electric polarization P or electric field E are "time-even polar" vectors. At the same time, other quantities like velocity or toroidal moment are "time-odd polar" vectors. The two inversion operations generate an Abelian (commutative) group of 4 elements with 4 one-dimensional irreducible representations; the symmetry operations this group allow to classify these vectors into 4 categories [1–4].

We emphasize [1] that there are another four types of directional quantities, which are also defined by a magnitude, an axis and a geometrical sign, and which are also often associated with the three-component Euclidean vectors, but which show a different spatiotemporal symmetry than the above mentioned examples. These extra families can be exemplified as follows: two kinds of chiral "bidirectors" (associated with the so-called true and false chirality, resp.) and two achiral "bidirectors", transforming as the nematic liquid crystal order parameter and as the antiferromagnetic order parameter of the hematite crystal α-Fe_2O_3, respectively [1].

The aim of this contribution is to discuss applications of this concept and the notation proposal to the properties of magnetoelectric crystals and to the electromagnetic phenomena related to them.

REFERENCES

1. Hlinka, J., *Phys. Rev. Lett.*, Vol. 113, 2014.
2. Birss, R. R., *Symmetry and Magnetism*, North-Holland, Amsterdam, 1964.
3. Grimmer, H., *Ferroelectrics*, Vol. 161, 181, 1994.
4. Ascher, E., *Int. J. Magnetism*, Vol. 5, 287, 1974.

Full Graphitization of Amorphous Carbon by Microwave Heating with Catalyst

Taewon Kim, Jaegeun Lee, and Kun-Hong Lee
Department of Chemical Engineering
Pohang University of Science and Technology (POSTECH), South Korea

Abstract— Metallic properties (high electric and thermal conductivities) and nonmetallic properties (high thermal resistance, inertness, and lubricity) of graphite make it as an essential material for refractories, automobiles, lithium-ion batteries, fuel cells, solar cells, nuclear reactors, and graphene production. Owing to the limited reserve of natural graphite and the ever-increasing demand in energy applications, graphite has been designated as a "supply risk material" by the British Geological Survey. (Graphite is ranked 9th in terms of supply risk, higher than the platinum group elements). Synthetic graphite can fill the gap between supply and demand, but there has been not much research on the process of making synthetic graphite. The common manufacturing process used to synthesize graphite, known as Acheson process, relies on thermal heating of amorphous carbon to 3000°C. (Typical processing time is 2 weeks). Although the energy requirements are enormous, the Acheson process remains the major industrial process since its invention in the 1960s. Therefore, a novel and energy-efficient graphitization process is highly desirable.

Here, we report a novel method of graphitization using microwave heating with catalyst. Although microwave heating has been reported previously, full graphitization of amorphous carbon powders is achieved for the first time by adding catalyst precursors to the amorphous carbon powders. Interlayer spacing and I_G/I_D ratio of amorphous carbon powders became almost identical to those of the reference graphite powders after microwave heating in 5 minutes.

Present work implies that microwave graphitization can be an alternative process for synthetic graphite production. Furthermore, it can also be applied to the production of other graphitic materials like highly crystalline graphene or carbon nanotubes and their derivatives.

Determination of the Parameters of Composites with Magnetic Particles from the Study of the Spectra of Ferromagnetic Resonance in the Microwave Frequency Range

V. A. Zhuravlev, **V. A. Meshcheryakov**, **and E. P. Lilenko**
Tomsk State University, Tomsk 634050, Russian Federation

Abstract— Active exploration of the microwave frequency range sharpened the need for magnetic materials absorbing electromagnetic radiation. Such materials are required to reduce harmful influence on biological objects, to provide electromagnetic compatibility of units and blocks of high-frequency devices, to build anechoic chambers and to protect information. Composite radar absorbing coating (RAC) which consists of a matrix of high-molecular polymer compounds and filler particles of ferromagnetic or ferrimagnetic materials are widely used. Such materials are most effectively used as electromagnetic waves absorbers located on the metal surfaces.

It is necessary to know the material parameters of the filler particles of the composite material for targeted development and production of RAC in a given frequency range and level of reflectance in the operating band. These parameters are the values of the magnetocrystalline anisotropy fields (H_{ai}), the gyromagnetic ratio (γ) and saturation magnetization (M_0).

The study of the spectra of ferromagnetic resonance (FMR) in the microwave frequency range is one of the few methods to determine the required material parameters such inhomogeneous and macroscopically isotropic materials, including materials with nanosized and nanostructured particles.

The development and testing based on the study of FMR methods of determining the characteristics of the anisotropic powder and composite materials is the aim of this work.

To do this, we calculated the permeability tensor of the composite material containing randomly oriented particles uniaxial magnetic material. We proposed based on the analysis of FMR spectra in the microwave frequency range two-stage method of determining the anisotropic characteristics of such composite materials.

In the first stage the frequency dependences of the maxima and the derivatives of the resonance curves are analyzed. It gives us the estimation for the gyromagnetic ratio γ and anisotropy fields H_{ai}. In the second stage by a detailed comparison the shape of experimental and theoretical resonance curves we obtain more accurate values of the anisotropy field.

The paper presents the results of applying this method to determine the anisotropic characteristics of polycrystalline samples of hexaferrites and composite materials containing nano-sized ferrimagnetic particles.

Microwave Absorption Properties of Foam Glass Material Modified by Adding Ilmenite Concentrate

O. V. Kazmina[1], **V. I. Suslyaev**[2], **M. A. Dushkina**[1], **V. A. Zhuravlev**[2], **and K. V. Dorozhkin**[2]

[1]Tomsk Polytechnic University, Tomsk 634050, Russian Federation
[2]Tomsk State University, Tomsk 634050, Russian Federation

Abstract— Currently, due to the increasing background microwaves the development of radar absorbing materials (RAM) for various purposes are particularly relevant. RAM are used to solve problems of electromagnetic compatibility of radio electronic devices, protection of biological objects from electromagnetic radiation, as well as to reduce the radar signature objects of military and civil purposes. The materials that combine several useful consumer properties are of particular interest.

The unique combination of properties that do not have any of the known heat insulator has foam glass material. This material is environmentally safe and has a low thermal conductivity and density with relatively high strength. The purpose of this work — study microwave transmission and reflection coefficients in the frequency range 26–260 GHz of foam glass, modified by titanium concentrates and the establishment of the possibility of its use as a radar absorbing material.

We studied the radar absorption and mechanical properties of foamed glass, made from industrial cullet glass tube with the addition of ilmenite concentrate. Concentrate composition in wt.% was follow: TiO_2 — 61.85; Fe_20_3 — 27.90; $Si0_2$ — 2.00; $A1_20_3$ — 2.00; Cao — 0.15; MgO — 0.40. Additive concentration was varied from 0.5 to 1.5 wt.%. Previously, we have found that with small additions of ilmenite concentrate the foam glass becomes more durable. Adding to of the foaming mixture the ilmenite concentrate in an amount of 0.5 wt.% increases the compressive strength of the foam glass twice.

Measuring the transmission and reflection coefficients produced by the "free space methods" on the vector network analyzer Agilent Technologies E8363B in the frequency range of 26–36 GHz and terahertz spectrometer type STD-21 in the frequency range 60–260 GHz.

For study of the electromagnetic response we used flat samples $30 \times 30\,\mathrm{mm}^2$. Thickness of the samples was 2.2–2.4 cm. The measurements showed that the microwave reflection coefficients for all of the samples are small. This is due to the microwave properties of material and diffuse scattering from surface of foamed glass.

The experiments showed that small additions of ilmenite concentrate to foam glass can not only improve the mechanical properties of material, but also to expand the scope of its application. Material is actively cooperating with electromagnetic radiation and can be used as an absorber to create: protective shields that reduce the harmful effects of microwaves on biological objects, anechoic chambers and rooms with low levels of electromagnetic fields.

Maximum radar-absorbing properties have a foam glass samples with addition of ilmenite concentrate with a particle size of 3 microns and amount of 0.5 wt.%. The value of the transmission coefficient at a frequency 26 GHz was about -10.5 dB/cm and -15.2 dB/cm at a frequency 260 GHz.

Significantly Improved Absorption Properties at Microwave Bands for Multi-layer Hexaferrite Thick Film Composites

Z. W. Li and Z. H. Yang
Temasek Laboratories, National University of Singapore, 5A Engineering Drive 1, 117411, Singapore

Abstract— With the developments of electronic, telecommunication and radar technologies, the absorption and shielding of electromagnetic (EM) radiation has attracted much attention. When EM waves are irradiated into magnetic materials, a natural resonance (ferromagnetic resonance without an applied magnetic field) occurs, thus achieving the attenuation of EM waves.

The absorption EM materials generally consist of magnetic fillers and silicone, as known the EM composites. The fillers play an important role in determining the absorption properties of composites. In this work, three hexaferrite fillers, namely often used particles, flakes and thick films, are prepared and their absorption properties are compared. It is found that composites filled with the thick films have excellent high-frequency magnetic properties and absorption properties, as compared to other two fillers.

First, for often used magnetic fillers, such as hexaferrite or carbonyl iron particles, the permeability is rather small; real and imaginary permeability are only about 3–4 and 1–2, respectively, for composites with volume concentration of 50%. For the hexaferrite film composites, the real and imaginary permeability significantly increase to 7 and 4.3, respectively. The increase is attributed to an in-plane arrangement of the films in composites.

More important, due to significantly enhanced permeability and almost the same permittivity, the hexaferrite film composites show excellent EM absorption properties: the thickness is only 3 mm, absorption bands cover from 2.1 to 14.5 GHz for return loss $RL < -10$ dB, and the percentage bandwidth is 150%, which achieves 3/4 of theoretically maximum bandwidth 200%.

Final, the mechanism of enhanced broad bandwidth is discussed. EM absorption comes from two different mechanisms: quarter-wavelength resonator and magnetic resonance. The former is determined by the ratio of permeability to permittivity and the latter is associated with the magnetic loss. For the film composites, two absorptions with $RL < -10$ dB can exist on the same thickness, thus significantly expanding the absorption bandwidth.

In conclusion, the hexaferrite film composites are potential candidates for use as EM absorption materials with small thickness, low return loss and broad bandwidth at microwave S, C, X and Ku bands.

Low-frequency Electromagnetic Bands in Metallic Lattices

K. Wang
Laboratoire de Physique des Solides
UMR CNRS/Université Paris-Sud, Orsay 91405, France

Abstract— We present a complete study on the low-frequency electromagnetic band structures in various metallic lattices in air background, using both numerical and tight-binding approaches. The band structures and evolutions are comparatively investigated with respect to local resonances and their variations following the sizes, shapes and the symmetries of the structure unities. We show that the lowest-frequency bands are formed by s-like resonance modes sustained by the local structure unities, of which the contributions vary following structure modulations, and, under certain conditions, the second bands (above the first band gaps) are formed by p-like modes sustained by the same structure unities. The s and p bands can both be described in the frame work of a tight-binding model, allowing band structure analyses in terms of relations between local resonance modes and their mutual correlations. This work demonstrates that the origin of the low-frequency electromagnetic bands and gaps in general metallic structures can be explicitly analyzed from the perspective of local structure arrangements, that determine both the local resonance conditions and their mutual coupling. The plasma gaps and the first band gaps arise naturally from specific local structure patterns.

Heat Transfer between Anisotropic Nanoparticles

Roberta Incardone[1, 2] **and Matthias Krüger**[1, 2]

[1]Max-Planck-Institut für Intelligente Systeme
Heisenbergstr, 3, Stuttgart D-70569, Germany
[2]Institut für Theoretische Physik IV, Universität Stuttgart
Pfaffenwaldring 57, Stuttgart D-70569, Germany

Abstract— We study radiative (near field) heat transfer between objects in vacuum at different temperatures. By use of classical scattering theory [1], we derive closed expressions for this transfer for objects of arbitrary shape and material, from which general properties of the transfer can be analyzed. We present several examples including spheres, cylinders and ellipsoidal particles [2], thereby demonstrating the size and shape dependence of radiative heat transfer.

REFERENCES

1. Krüger, M., G. Bimonte, T. Emig, and M. Kardar, *Phys. Rev. B*, Vol. 86, 115423, 2012.
2. Incardone, R., T. Emig, and M. Krüger, *EPL*, Vol. 106, 41001, 2014.

Nonlinear Optical Phenomena in Iron Oxide Containing Magnetic Nanocolloids

A. V. Prokofiev[1, 2], **V.M. Petrov**[1], **I. V. Pleshakov**[1, 2], **and A. V. Shamray**[1, 2, 3]

[1]St.-Petersburg Polytechnic University, St.-Petersburg, Russia
[2]Ioffe Institute, St.-Petersburg, Russia
[3]ITMO University, St.-Petersburg, Russia

Abstract— The report is concerned with optical properties of magnetic nanocolloids (ferrofluids), i.e., materials of a special type which are solutions of magnetic particles suspended in a carrier fluid. These materials exhibit specific physical properties [1]. Ferrofluids have been studied since the 1960s but still remain an important research object because new physical phenomena are constantly revealed in them. Ferrofluids find different applications, for example, they are considered to be promising for biomedical purposes [2]. Of considerable interest are also optical devices in which ferrofluids are used as active elements. Their operation is based on the magneto-optic effects which have pronounced specific features in nanocolloidal solutions of magnetic particles. There are optoelectronic devices in which the interaction of light with the material occurs at large lengths. These are fiber-optic systems with a ferrofluid-filled microstructure [3–5]. It can be expected that under certain conditions nonlinear properties of ferrofluids will manifest themselves in them, which is important from not only practical but also fundamental point of view.

We studied optical nonlinearity in kerosene and water solutions of magnetite (Fe_3O_4) prepared by using the technology which gives nanoparticles with an average size of about 10 nm. To provide an optical transparency, the samples were diluted from the initial concentration (several percent) to 0.2 Vol. % of the solid phase content.

The experimental technique was chosen to be z-scanning [6] involving displacement of the material studied along a focused laser beam. The setup included a compact electromagnet which produced a magnetic field of 0–500 Oe applied to the sample. It was perpendicular to the light beam. The light polarization could be either parallel or perpendicular to the field. The electromagnet could move together with the sample along the beam, thus passing through the region with the maximum optical energy concentration. As a radiation source, a Nd:YAG-laser was used (the second harmonic, $\lambda = 532$ nm).

As the experiment showed, at high optical power levels the ferrofluids exhibited a strong nonlinearity detected from the dependences typical of the z-scanning technique [6]. It was found that the magnetic field exerted a strong influence on the nonlinear characteristics, which can be attributed to formation of agglomerates of nanoparticles in the fluid. The effects related to the light scattering which depended on the field and radiation power were also observed.

Possible mechanisms of the observed phenomena one of which is thermal diffusion of nanoparticles in the field gradient created by the focused laser radiation are discussed.

REFERENCES

1. Scherer, C. and A. M. Figueiredo Neto, *Braz. J. Phys.*, Vol. 35, 718, 2005.
2. Neuberger, T., B. Schopf, H. Hofmann, M. Hofmann, and B. Rechenberg, *JMMM*, Vol. 293, 483, 2005.
3. Candiani, A., M. Konstantaki, W. Margulis, and S. Pissadakis, *Optics Letters*, Vol. 37, 4467, 2012.
4. Chan, C. C., P. Zu, W. S. Lewet, et al., *Optics Letters*, Vol. 37, 398, 2012.
5. Agruzov, P. M., I. V. Pleshakov, E. E. Bibik, and A. V. Shamray, *Appl. Phys. Lett.*, Vol. 104, 071108, 2014.
6. Chapple, P. B., J. Staromlynska, J. A. Hermann, and T. J. McKay, *Journal of Nonlinear Optical Physics and Materials*, Vol. 6, 251, 1997.

Session 4P4
Remote Sensing, Radar, Imaging

Effects of Target Reflectivity on the Reflected Laser Pulse for Range Estimation

Sing Yee Chua[1], **Xin Wang**[1], **Ningqun Guo**[1],
Ching Seong Tan[2], **and Tong Yuen Chai**[3]

[1]School of Engineering, Monash University Malaysia
Jalan Lagoon Selatan, Bandar Sunway, Selangor 47500, Malaysia
[2]Faculty of Engineering, Multimedia University
Jalan Multimedia, Cyberjaya, Selangor 63000, Malaysia
[3]Universiti Tunku Abdul Rahman, Setapak, Kuala Lumpur 53300, Malaysia

Abstract— The development of laser ranging technology benefits remote sensing, machine vision and three-dimensional (3D) imaging. Accuracy of these systems strongly relies on the characteristics of laser and detector response. In this paper, reected laser pulse profile is investigated and analysed based on different target reflectivity. Results show that reflected laser pulse appears to deviate from ideal Gaussian model that is commonly assumed. The reflected laser pulse demonstrates asymmetric Gaussian-shape temporal associates with a time delay. It is observed that target reflectivity that is influenced by the material types and roughness has direct impact to the sensitivity of detection and intensity variations but does not change the distribution characteristic. These show direct connection to deviation in range estimation and should be further evaluated for correction to improve the accuracy in a range gated system.

From Markovian Jump Processes to Ionospheric Waves Disturbances

R. Talhi
CNRS/LPC2E and University of Tours
3A, Avenue de la Recherche Scientifique, 45071 Orleans Cedex 2, France

Abstract— The objective of this paper is to provide an overview of Markovian Jump Processes (with continuous time and discrete state space) applied to the modelling of some ionospheric wave disturbances. Markovian Jump Processes (MJPs) are fundamental stochastic processes that are used to model some unpredictable observable phenomena related to disordered and inhomogeneous environments, and can be readily implemented in numerical algorithms. Hence, these stochastic processes play an important role in many fields of science and technology, ranging from computational finance (in credit risk modelling [1]), and wireless communication networks (in random traffic performance [2]), to physics (in electron transport inside disordered organic semiconductors [3]), chemistry and biology (in stochastic kinetic models [4]), among others. MJPs aim to aid our understanding of the previous unpredictable phenomena by providing a consistent probabilistic framework to predict their future behaviour.

More precisely, the main purpose of this work is to focus on this probabilistic technique applied to study the asymptotic behaviour of some wave disturbances propagating in a typical random medium such as the ionosphere which is characterized by spatial and temporal chaotic fluctuations, and therefore unknown in detail, ill-defined, and poorly understood. In this context, the basic methodology is as follows: the radiative transfer theory, which governs the propagation and scattering of electromagnetic waves in the general case of random media, is used. More specifically, the radiative transfer equation, which describes the electromagnetic wave-energy propagation, under its vector (or matrix) form including energies and polarization parameters (in Stokes representation), is considered. This equation which has no analytical solution, is solved by means of numerical methods or simulation based techniques. One has to consider the energy propagation at a certain time (t), at a certain position (X), in a certain angular direction (K), and with a certain polarization (P), where $K(t)$ and $P(t)$ jump at scattering times, while $X(t)$ is continuous in space. Hence, the previous equation admits a probabilistic interpretation represented by a Markovian Jump Process (or stochastic process with minimal memory, i.e., given the present state of the process, the future is independent of the past states) for the position $X(t)$, direction $K(t)$, and polarization $P(t)$ of each photon (in quantum representation) undergoing scattering by random ionospheric inhomogeneities. In the simulation of MJPs trajectories, it is important to notice that steps are considered independent and identically distributed; moreover, the computation of any next scattering time is done according to the Poisson (or exponential) distribution. Then, we consider the forward Kolmogorov equation associated with the previous MJP (i.e., equation of the time-evolution of the MJP probability density function), that we solve numerically by a Monte-Carlo estimation procedure (based on the large numbers law, and on the central limit theorem). Finally, we get an approximate solution of the vector RTE, by averaging over the first order moments of the previous discrete probability densities with respect to the polarization parameters matrix.

Our methodology is illustrated with some applications to attempt to analyse the impact of turbulence strength and electron density fluctuations on radio-waves scattering in HF-frequency band (∼5 to 20 MHz). To this end, we assumed a typical ionospheric parameters, turbulence spectrum (power law form), and electron density profile (Chapman profile). Then, we focused firstly on the prediction of the 3D-angular power distribution and the rate of polarization of HF-waves altered by multiple scattering, and secondly on the important role of the 3D-anisotropic irregularities encountered in many scattering problems. Obtained results, which seem rather good when compared to published ones, will be presented and discussed.

As concerns the above mentioned methodology, we have to point out some open questions or subjects of controversy [5, 6]. Since we use the wave-particle duality, are stochastic processes related to quantum mechanics? Furthermore, is a Markov process equivalent to a quantum process? In other words, how to formulate a Markov process (with its crucial Markov property) into the framework of quantum mechanics?

REFERENCES

1. Jarrow, R. A., et al., "A Markov model for the term structure of credit risk spreads," *The RFS*, Vol. 10, No. 2, 1997.

2. Adas, A., "Traffic models in broadband networks," *IEEE Communications Magazine*, Vol. 35, 1997.
3. Brereton, T. J., et al., "Efficient simulation of charge transport in deep-trap media," *Proc. of WSC*, Berlin, 2012.
4. Golightly, A., et al., "Bayesian parameter inference for stochastic biochemical network models using particle Markov chain Monte Carlo," *Interface Focus*, Vol. 1, No. 6, 807–820, Dec. 2011.
5. Gillespie, D. T., "Why quantum mechanics cannot be formulated as a Markov process," *Phys. Rev. A*, Vol. 49, 1994.
6. Belavkin, V. P., "Quantum quasi-Markov processes in eventum mechanics dynamics, observation, filtering and control," *Journal of Quantum Information Processing*, Vol. 12, No. 3, 1539–1626, 2013.

Spatio-temporal Visual Saliency for Adaptive Weather Sensing

D. Schvartzman[1, 2], **T.-Y. Yu**[1, 2], **and S. M. Torres**[1, 3]

[1]Advanced Radar Research Center, University of Oklahoma, Norman, OK, USA
[2]School of Electrical and Computer Engineering, University of Oklahoma, Norman, OK, USA
[3]Cooperative Institute for Mesoscale Meteorological Studies, University of Oklahoma
and NOAA/OAR/National Severe Storms Laboratory, Norman, Oklahoma, USA

Abstract— In this paper we address the problem of performing adaptive weather sensing with a phased array radar by exploiting information-theory-based methods with the goal of adaptively defining scanning strategies for weather observations. Through their unique beam agility, phased array radars can instantaneously change the pointing direction and acquisition parameters of the scanning beam. This capability can be exploited to dynamically and adaptively define scanning strategies that achieve an optimum compromise between update time, spatial sampling and sampling, and data quality, which can potentially lead to improved warnings and forecasts. Using information theoretic methods, scanning strategies can be tailored so that the information extracted from the atmosphere is maximized. The distinguishing attribute of the information measures is that they provide a single metric able to automatically capture the complex tradeoffs involved in the design of scanning strategies for weather observation. In this paper we present an algorithm that tailors the scanning strategies for different regions based on their information content. We demonstrate the advantages of this algorithm over conventional scanning by mimicking phased array observations using high temporal and spatial resolution data collected with the University of Oklahoma Advanced Radar Research Center's PX-1000 radar.

Impacts of a Gap-filling Radar in a Mountainous Area: Case of Lobo Overlook, Colorado

B. L. Cheong[1, 2], **P. E. Kirstetter**[1, 3], **T.-Y. Yu**[1, 2], **J. Busto**[4], **T. Speeze**[4], **and J. Dennis**[5]

[1]Advanced Radar Research Center, University of Oklahoma, Norman, USA
[2]School of Electrical and Computer Engineering, University of Oklahoma, Norman, USA
[3]National Severe Storms Laboratory, National Oceanic and Atmospheric Administration, Norman, USA
[4]Rio Grande Watershed Emergency Action Coordination Team
Colorado Water Conservation Board, Colorado, USA
[5]Rio Grande County Emergency Management, Colorado, USA

Abstract— The Weather Surveillance Radar — 1988 Doppler (WSR-88D) of the United States is presently the operational radar system for forecasters to monitor the weather. While the radar network has been upgraded to provide polarimetric and Super-Resolution (0.5 degree) coverage out to 300 km, there are many regions, particularly in the Rocky Mountains, that the WSR-88D radars do not provide sufficient coverage due to the complexity of terrain and planetary curvature of the Earth. Forecasters often rely on the scans from high elevations to infer what is happening near the surface. Under circumstances where no other means are available, the upper scans are the only source of measurements. In order to produce qualitative precipitation estimate (QPE), however, these upper scans do not provide the critical measurements needed for numerical models to produce accurate predictions. The Mineral County of the State of Colorado is one of the many regions within the Rocky Mountains that suffers poor radar coverage due to the surrounding mountain ridges, which are in the line-of-sight of the closest three WSR-88D radars, blocking radar beams from reaching this area. The limitations impede the ability of forecasters and local emergency managers to make accurate predictions and issuing weather warnings. In Fall 2014, a transportable polarimetric X-band radar was deployed at the Lobo Overlook of the Mineral County for a 45-day experimental campaign to assess the value of a permanent radar setup in this area. Large systems like the WSR-88D radars are costly, a compact radar, such as the PX-1000, however, costs tremendously less and could be sufficient for short-range (60 km) weather surveillance. This was the case for the Mineral County and several counties adjacent to it. The experiment was successfully conducted and several case studies have shown added values of deploying a polarimetric radar in this area, supplementing the current radar coverage of the WSR-88D network. Three selected cases are provided in this presentation for illustration.

A Novel Approach to Counter the Low Observable Characteristic of Stealthy Targets by Analyzing the Radar Cross Section

Faran Awais Butt[1], **Ijaz Haider Naqvi**[2], **and Ali Imram Najam**[3]

[1]University of Management and Technology (UMT), Lahore, Pakistan
[2]Lahore University of Management Sciences (LUMS), Lahore, Pakistan
[3]National Engineering and Scientific Commission (NESCOM), Islamabad, Pakistan

Abstract— Stealth technology has brought up a revolution in the field of electronic counter measure and has exposed the ineffectiveness of the mono-static radars. The stealth aircrafts diffract and/or scatter very low power electromagnetic radiations owning to its special geometry and highly absorbent material. However, if an electromagnetic wave is incident at 'good' angles, stealth aircraft though low observable cannot be called as invisible. In this paper, the results of the extensive simulations on a model stealth aircraft have been presented. Simulations are performed on an aircraft model to prove the effectiveness of the proposed model. By energizing the aircraft at 'good' angle(s) of incidence, significant scattering can be observed over a range of aspect angles. Thereafter, a multi-static approach is proposed making a polygon arrangement of radar transceivers in order to guarantee the detection of a stealth aircraft.

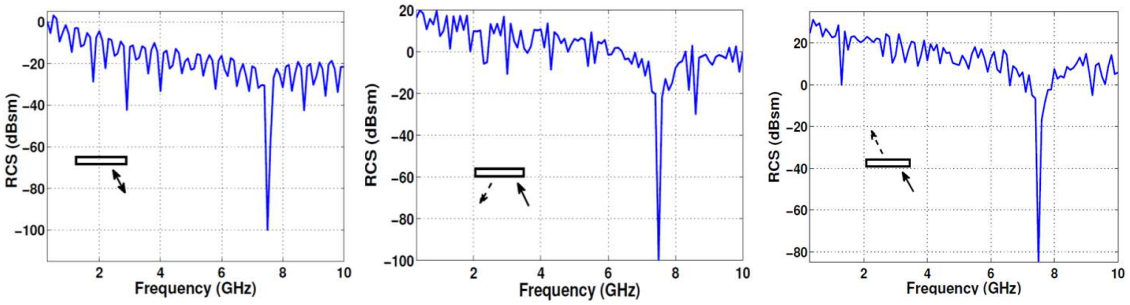

Figure 1: RCS vs. frequency for various angle of incidence and reflection.

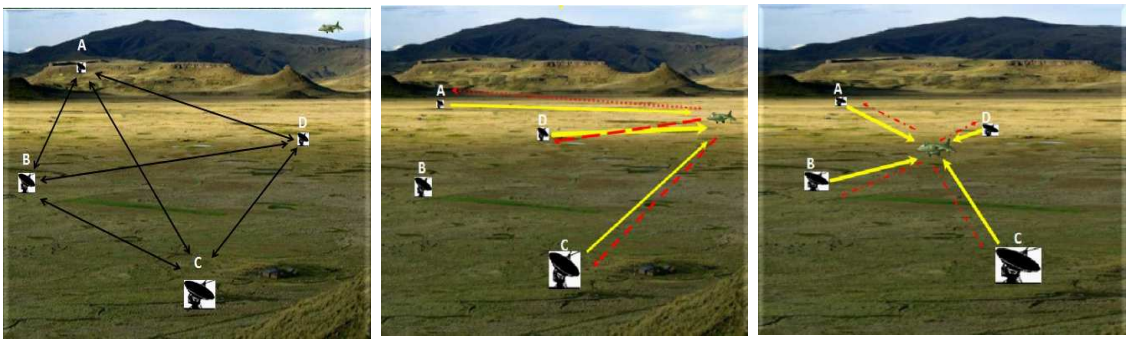

Figure 2: Our proposed solution of using 4 radar transceivers arranged in a polygon.

The bi-static and multi-static radar must use data in fusion in the process of information collection. The concealment feature of bi-static radar is not complete as the transmitter station is still electromagnetically exposed and can be easily attacked. Our configuration overcomes the negative effects of such a situation since there are four radars working with each other. Our proposed configuration can be used for low frequency radar since the radars are acting as transceivers for each other and by using correlation and proper filtering, clutters can be avoided and at the same time our proposed system can easily be upgraded with any desirable feature like changing of polarity, operating frequency or miscellaneous features.

From the observations we saw that there was a maximum positive RCS for greater range of frequencies at the shadowed side of stealth aircraft, so if there is a receiver there, it can make use of these scatterings to detect the target threat.

Ultra Short and High Voltage Pulse Shaping for Atom Probe Tomography Improvement

L. Zhao[1], **A. Normand**[1],
F. Delaroche[1], **B. Ravelo**[1], **and F. Vurpillot**[2]

[1]Groupe de Physique des Matériaux, UMR 6634 CNRS
Université de Rouen, Saint-Etienne-du-Rouvray, France
[2]IRSEEM, EA 4353, Graduate School of Engineering ESIGELEC, France

Abstract— Improvement of atom probe tomography technique requires the use of high voltage rectangular pulses on a sample inside an ultra-high vacuum chamber. In this paper, a design for ultra-short (∼ps) rise time and less than one nanosecond rectangular pulses, based on a photo-conductive switch, is described. The performances of the device are compared to theoretical predictions.

An Amplitude Based on Vital Sign Monitoring Using Impulse-radio UWB Radar

J. Yu[1], **J. Matuzas**[2], **T.-Y. Lee**[1], **and M.-H. Ka**[1]

[1]School of Integrated Technology, Yonsei Institute of Convergence Technology
Yonsei University, Republic of Korea
[2]Center for Physical Science and Technology at Vilnius, Geozondas JSC, Lithuania

Abstract— In this paper, a method for vital signs which are breathing rate and heart beat rate using impulse radio UWB radar is proposed. The method of calculating breathing and heart beat based on an amplitude variation of received short pulse signal. When an impulse UWB radar is measure the vital signs, rates are usually measured by a movement of peak position of received signal. To obtain high accuracy frequency, a receiver requires a high speed sampling rate. The fast sampling rate has problems of cost and a large size of H/W. The suggested method is unnecessary the high speed sampling rate receiver. It is used a variation of an amplitude of cross correlation of each received signal. The fourier transform of the variation is represented vital signs. In addition, an uneven sampling rate is used. The rates are estimated by least square spectral method instead of the fourier transform. In spite of low sampling rate, these methods have a better signal to noise ratio than method for detecting movement of peaks.

ACKNOWLEDGMENT

This research was supported by the MSIP (Ministry of Science, ICT and Future Planning), Korea, under the "IT Consilience Creative Program" (NIPA-2014-H0201-14-1002) supervised by the NIPA (National IT Industry Promotion Agency).

Analysis of Micro-Doppler Characteristics of Human Activity Using Hilbert-Huang Transform Analysis

Ram M. Narayanan
Department of Electrical Engineering, 202 Electrical Engineering East
The Pennsylvania State University, University Park, PA 16802, USA

Abstract— Various parts of the human body have different movements when a person is performing different physical activities, thereby resulting in unique micro-Doppler signatures. The conventional time-frequency analyses of human activity (usually including the short time Fourier transform (STFT), Wigner-Ville distribution (WVD), and wavelet analysis) are not adaptive to nonlinear and nonstationary signals. If one can decompose the noisy human Doppler information and extract only the human-induced Doppler from it, the identification of various human activities becomes easier. We have applied the Hilbert-Huang transform (HHT) technique to analyze micro-Doppler signals arising from human activities, since this approach is adaptive to such nonlinear and nonstationary signals. The Hilbert-Huang Transform (HHT) is a novel signal analysis technique based on the combination of the empirical mode decomposition (EMD) and the Hilbert spectral analysis approaches. This method implements the 'empirical mode decomposition' using which a dataset can be decomposed into a finite and often small number of 'intrinsic mode functions' that possess well-behaved Hilbert transforms. Since this decomposition is adaptive, it is very efficient. The decomposition is based on the local characteristic time scale of the data and is applicable to both nonlinear and nonstationary processes. The EMD identifies intrinsic oscillatory modes by their characteristic time scales in the data empirically. It separates the intrinsic mode functions (IMFs) from the original signal one by one, until the residue is monotonic. The original signal is thus decomposed into a finite and a small number of IMFs, where an IMF is any function with the same number of extrema and zero crossings, with symmetric envelopes. This method was applied to radar data resulting from human activities. The HHT based signal processing can effectively improve pattern recognition and reject unwanted uncorrelated noise. The Hilbert Transform presents results in the form of an energy-frequency-time distribution, designated as the Hilbert spectrum, which can provide sharp identifications of embedded structures. In the HHT approach, the IMFs based on local signal properties define an instantaneous frequency. The introduction of the instantaneous frequencies for complicated datasets eliminates the need for spurious harmonics to represent nonlinear and nonstationary signals. This method when applied to radar data resulting from human activities shows significant differences in the IMF spectrum for various human activities, which can be used for activity classification and recognition using radar micro-Doppler.

Measurements and Analysis of the Doppler Signatures of Rotating Targets by the Hilbert Huang Transform

Mickael Bruno[1], **Alessio Balleri**[1], **and Clayton Stewart**[2]

[1]Centre for Electronic Warfare, Cranfield University, Defence Academy of the UK, UK
[2]Department of Electronic and Electrical Engineering, University College London, London, UK

Abstract— Radar echoes from moving targets present a shift in frequency due to the well-known Doppler effect. Typical radar targets are often composed of several moving components which, with their own micro motions, induce a frequency modulation around the principal Doppler shift. These modulations are called the target micro-Doppler signature and contain specific information on the target that can be used for target classification.

In recent years, micro-Doppler signatures for target classification have attracted considerable research interest and they have been used to classify many different types of targets, including cars, tracked vehicles, humans and animals. Considerable research efforts have been dedicated to characterising the micro-Doppler signatures of rotating target components in order to allow and improve classification of aircraft, helicopters, UAVs and to study the clutter returns from wind turbines.

A significant proportion of the previous work on classification of rotating targets by micro-Doppler is based on the use of time-frequency methods, such as the Short Time Fourier Transform (STFT), which impose a trade-off between time and frequency resolution; the longer the dwell time the better the frequency resolution and the poorer the time resolution and vice versa.

The Empirical Mode Decomposition (EMD) is a recent method which has been developed to decompose signals into a series of functions, called Intrinsic Mode Functions (IMFs), which admit a regular Hilbert transform. The EMD, together with the Hilbert Huang Transform (HUT) is a method for the analysis of nonlinear and non-stationary time series and may potentially offer significant advantages for the task of target classification as it does not suffer from the trade-off between frequency and time resolution.

Very little work has been published in the literature on the EMD and the HUT for target classification by micro-Doppler. Most of the previous work on micro-Doppler of rotating targets based on the EMD has been carried out on simulated data and there is very little in the literature presenting experimental results. Previous algorithms have largely been tested on noise-free simulations and often, when experimental data was used, very little information on the radar parameters and the target echo signal characteristics was provided. This has made it difficult to draw conclusions on the performance of this technique and its robustness against the radar carrier frequency and the data Signal to Noise Ratio. To the best of our knowledge, in the existing literature, there have been very little attempts, if any, to carry out a thorough analysis of the information contained in the IMFs of real rotating targets.

In this paper we measure the signature of a rotating propeller at X-band and we study the properties of the IMFs of the target and their corresponding HUTs. Results are analysed as a function of the target aspect angle, the target rotation speed and the target number of blades. Results show that the it is possible to extract the information on the rotating speed of the propeller and on the number of blades over a large number of IMFs and at all aspect angles, including those where the Doppler shift induced by the blades is low.

Waveform Diversity for Ultra-wideband Ground Penetrating Radar Imaging

Delphine H. N. Marpaung and Yilong Lu
School of Electrical and Electronic Engineering, Nanyang Technological University
50 Nanyang Avenue, Singapore 639798, Singapore

Abstract— Waveform diversity has been one of the intensive research areas in ultra-wideband (UWB) wireless systems, including wireless communication systems and radar systems. For radar applications, waveform diversity may enhance the performance of the narrow-band radar. In this paper, we explore the potential benefits of waveform diversity for 3-dimensional (3D) UWB ground penetrating radar (GPR) imaging. One of the important issues in the 3D GPR imaging is the interpretation of objects that present in the GPR data/images. Therefore, our focus is on utilizing the waveform diversity for better detection and characterization of an object in GPR imaging.

We propose a novel waveform diversity approach for 3D UWB GPR imaging, where a set of a few UWB waveforms are used for transmitting and collecting respective echo data/images, sequentially. In this paper, we use the first 4 orders of Hermitian waveforms, which are widely used in the waveform diversity in UWB communications. We perform simulation to generate GPR echo data on the following target shape: sphere, plate, and corner re ector, and the following target electromagnetic properties: dielectric, normal conductor, and good conductor.

We then process the simulation data from each waveform independently and extract several features that can be used to distinguish the shape and the material of the target. These features are then utilized to derive the colour assignment of the target. Such colour provides better representation on the shape and the electromagnetic properties of the target.

The result shows that the waveform diversity can be used for distinguishing the shape and the material of the target. These properties are very useful for better detection and interpretation of objects in 3-dimensional ultra-wideband ground penetrating radar imaging.

On the Coneigenvalue Decomposition of Sinclair Matrices

T. Dallmann and D. Heberling
Institute of High Frequency Technology, RWTH Aachen University, Germany

Abstract— The Sinclair matrix is a 2×2 matrix which can be used to describe the polarimetric backscattering of radar targets. By decomposing this matrix into the so-called Huynen-Euler parameters various scattering mechanisms occuring at the target can be identified [1]. One of these mechanisms is the single reflection, which is typically caused by flat or slightly bended surfaces. A second mechanism is the double reflection which usually occurs between two surfaces which are oriented orthogonal to each other. A third mechanism is dipole scattering, which can be caused by wire-like structures. The Huynen-Euler parameters allow to distinguish between these scattering events and provide even more information like the orientation of the target. Since the aforementioned mechanisms not only influence the polarization of the scattered wave but also indicate at which angles and frequencies the radar cross-section (RCS) of a target increases, this set of parameters is of special interest for radar cross-section analysis. Therefore this decomposition is used in some recent publications about the measurement and analysis of RCS signatures and radar images [2, 3].

Unfortunately one of the Huynen-Euler parameters causes problems: There are conflicting opinions regarding the question if the skip angle ν which allows the distinction between single and double reflections can be determined from the Sinclair matrix. The extraction of the Huynen-Euler parameters requires a coneigenvalue decomposition of the Sinclair matrix S which can be described with [5]

$$Sx^* = \lambda x. \tag{1}$$

For coneigenvalues it can be shown that if λ is a valid coneigenvalue of a matrix S, then all $\lambda e^{j\theta}$, $\theta \in \mathbb{R}$ are also valid coneigenvalues [5]. On the first sight this indeterminacy prevents that the skip angle can be determined properly and led Lüneburg to the following conclusion:

> "The phase indeterminacy of the coneigenvalue is an essential feature of the anti-linear time-reversal operation in backscattering. Its interpretation and significance for target characterization and classification purposes (Huynen's skip angle) is at present not fully understood." [4].

In contrast to this a technique was developed by Baird which allows to extract Huynen's skip angle from the Sinclair matrix [3]. To the knowledge of the authors this discrepancy is still an unresolved problem.

To resolve the aforementioned contradiction a physical interpretation of the coneigenvalues of the Sinclair matrix will be given in this paper. Moreover, the connection between coneigenvalues and coneigenvectors will be explained. Finally an alternative approach for the calculation of the Huynen-Euler parameters from a Sinclair matrix will be presented. The explanations and approaches discussed in this paper therefore contribute to the effort of placing radar polarimetry on a solid mathematical foundation.

REFERENCES

1. Lee, J. and E. Pottier, *Polarimetric Radar Imaging: From Basics to Applications*, CRC Press, Boca Raton, 2009.
2. Dallmann, T. and D. Heberling, "Discrimination of scattering mechanisms via polarimetric rcs imaging [measurements corner]," *IEEE Antennas and Propagation Magazine*, Vol. 56, No. 3, 154–165, 2014.
3. Baird, C. S., "Design and analysis of an Euler transformation algorithm applied to full-polarimetric ISAR imagery," Ph.D. Dissertation, University of Massachusetts Lowell, Massachusetts, 2007.
4. Lüneburg, E., "Aspects of radar polarimetry," *Turk J. Elec. Engin.*, Vol. 10, No. 2, 219–243, 2002.
5. Horn, R. A. and C. R. Johnson, *Matrix Analysis*, Cambridge University Press, Cambridge, 2013.

3D Polarimetric Imaging of Complicated Surfaces

Alex J. Yuffa, Kristan P. Gurton, and Gorden Videen
Computational & Information Science Directorate
Army Research Laboratory, Adelphi, MD 20783, USA

Abstract— Approximately ninety percent of all radiation naturally emitted by humans lies in the long-wavelength infrared (LWIR) part of the electromagnetic spectrum. This emitted radiation is partially polarized by the human skin [1] and thus, it contains information about the surface normal. In this presentation, we will demonstrate how the polarization state of the emitted radiation can be used to obtain a three-dimensional (3D) image reconstruction of a human face [2]. This technique only requires a single view of the subject and is completely passive. This is an important advantage as it is usually difficult to have precise control over illumination sources.

To construct the 3D image, we first record the Stokes parameters of the emitted radiation with a polarimetric camera equipped with a Stirling-cooled mercury cadmium telluride focal-plane array of 640×480 pixels. The camera uses a Fourier modulation technique to obtain the Stokes parameters on a pixel-by-pixel basis. By combining these pixel-by-pixel Stokes parameters with Fresnel relations, we obtain the orientation of the surface normal at each pixel. These surface normals are not unique as the Stokes parameters are invariant under a rotation of π radians. This ambiguity is resolved by introducing an additional constraint that requires surface normals on the occluding boundary to point away from the subject's head. This constraint is enough to resolve the surface normal ambiguity for almost all pixels in the image and thus, we finally obtain unambiguous surface normal for each pixel. Lastly, by integrating these surface normals we obtain a 3D facial image as shown in figure below.

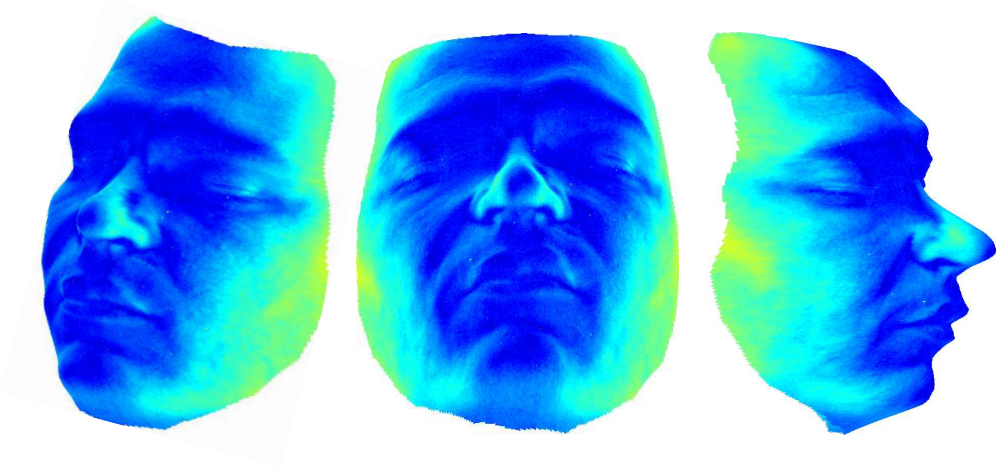

ACKNOWLEDGMENT

This research was supported in part by an appointment to the U.S. Army Research Laboratory Postdoctoral Fellowship Program administered by the Oak Ridge Associated Universities through a cooperative agreement with the U.S. Army Research Laboratory.

REFERENCES

1. Gurton, K. P., A. J. Yuffa, and G. Videen, "Enhanced facial recognition for thermal imagery using polarimetric imaging," *Optics Letters*, Vol. 39, No. 13, 3857–3859, 2014.
2. Yuffa, A. J., K. P. Gurton, and G. Videen, "Three-dimensional facial recognition using passive LWIR polarimetric imaging," *Applied Optics*, Vol. 53, No. 36, 8514–8521, 2014.

Session 4P5a
Power Electronics 2

Current Control of the Matrix Converter Fed Induction Motor Drive

J. Lettl, **J. Bauer**, **and S. Fligl**
Faculty of Electrical Engineering, Department of Electric Drives and Traction
Czech Technical University in Prague, Czech Republic

Abstract— The area of the controlled AC drives is very wide and most of them are based on the induction motors (IM) fed by frequency converters. Compared to the indirect frequency converter consisting of input rectifier, DC link and output inverter, matrix converter lacks need of bulky passive accumulation element and that is why it shows several advantages. Because the output voltage is produced by the means of direct switching of the proper input voltage to the output terminals the dynamics of the output voltage control is higher and also the output frequency can be changed very fast. Concurrently the main disadvantage of the converter is the limitation of the output voltage amplitude, provided that the sinusoidal currents on the input are demanded.

Advantages of the induction machine as the electro-mechanical converter in modern drive can't be questioned, however its control is more complicated and requires control algorithms based on separate control of the flux and torque. Field oriented control strategies are well known for this purpose. The input voltage is used as a controlled quantity. However, current feeding of the IM is also possible.

Problem of current source inverters (CSI) is that compared to voltage source inverters (VSI), CSI has to be designed for exact motor. That is why also methods how to replace CSI by VSI with current control were developed. The inverter then requires closed loop control with feedback directly from output AC currents. The currents have to have therefore wide bandwidth from nearly zero frequency up to carrier frequency. Usually two current sensors are enough, because without connected neutral point the third IM current has to add to zero. Moreover, this solution avoids zero sequence component errors. The output of the converter then differs from the CSI output. Its waveform follows a shape of the reference current with a superimposed PWM ripple. Form this point of view such current controller has several differences:

- it requires reference signals in actual time domain,
- the harmonic content can be reduced with PWM frequencyincrease,
- current controllers have to operate with AC signals instead of DC ones,
- the precision is higher because the controllers havenot to work in dynamic operation,
- the higher accuracy of the field orientation is reached.

In this paper a method of realization of rotor flux oriented control of the induction machine fed by matrix converter with current control is described. Simulation results are compared with results of measurement on the realised prototype of the matrix converter drive.

Physical Meaning of an Induction Machine Dynamic Model

S. Fligl, **J. Bauer**, **and J. Lettl**
Czech Technical University in Prague, Czech Republic

Abstract— The presented paper summarizes the approaches to dynamic description of an induction machine and presents them from the view point of the modern theory of dynamic systems. Great impact has the selection of the particular state variables. It decides about the mutual dependency of calculated values. Despite of the fact that it is still a correct description of the same system, it influences the design of control structures. Only the matrix form underlines clearly the particular differences.

The dynamic model of an induction machine is well known, but still it covers its secrets. Depending on the author, a different decision are made, what state variables will be used. However, this happens often without any justification, just according the trained technical experience or feeling. Thus, let us investigate here, how the set of equation changes in accordance with the selected particular set of variables.

Since the T-shaped model as well as the Gamma–shaped model is designed to describe the same physical object, we can find many similarities. However, the gamma shaped two phase model simplifies significantly the description and thus will be used throughout this article. The selection of the state variables can be defined as a combination, i.e., in particular selecting two members from a grouping of four (stator and rotor current, stator and rotor flux), such that the order of selection does not matter. The number of $4!/(2! \times (4\text{-}2)!)$ combinations is existing. From these six combinations, only three enable to decouple one half of the model from the supplying system and thus realize a truly hierarchical control system. This results also into significantly different time constants. This paper presents all necessary derivations for any particular equitation and provides guidance what variable set to use based on the target application.

Control Strategy of Grid Connected Converter under Unbalanced Conditions

Jiří Lettl[1], **Martin Bejvl**[2], **and Viktor Valouch**[1]

[1]Department of Electric Drives and Traction, Faculty of Electrical Engineering
CTU, Prague, Czech Republic
[2]Institute of Thermomechanics, Academy of Sciences of the Czech Republic
Prague, Czech Republic

Abstract— In ideal situation, the three-phase grid voltage is harmonic, phase to phase shifted by 120°; voltage and current are in phase. The track of the space vector of the three-phase voltage transformed to $\alpha\beta$ coordinates has a form of the circle.

In real situation, the three-phase grid voltage is distorted by high-order harmonics and by a negative sequence component, producing ripples in the voltage on the capacitors in the intermediate circuit and in active and reactive power, too. The three-phase AC current is disturbed as well.

Thus, there is a demand to develop such a control strategy of the converter that can cope with grid voltage disturbances, among them high-order harmonics and the negative sequence component mainly belong.

The object of the work is an analysis of the control of the positive and negative sequence of the AC current of the converter in order to eliminate reactive power, high-order harmonics of the grid current and ripples of the voltage in the DC intermediate circuit.

Both sequences of the grid current are controlled separately and simultaneously. The positive sequence of the current is controlled in the positive coordinates, which looks like DC control. The negative sequence of the current is controlled in the negative coordinates, which looks like DC control, too. Both the controls are realized by separate PI controllers working simultaneously.

A lot of effort has been made to analyse and compare many published control schemes that aspire to compensate the input voltage unbalance reliably. A new simple dual current control algorithm was developed and tested in the MatLab/Simulink environment and verified by measurement in laboratory with good results.

The developed method of the reference converter current calculation for the dual current controller is based on the measured and control variables and does need neither the solution of the set of nonlinear equations nor using previous patterns of the calculated reference current. To avoid a solution of a system of non-linear equations we can respect the losses produced in the line inductor by modifying the value that is produced as the output of the DC voltage controller. The losses calculated iteratively from the currents in the previous instant provide us with such a correcting term that may be added to the output of the voltage controller.

Different grid voltage conditions were considered, including the positive symmetrical component, negative symmetrical component, harmonic as well as the subharmonic signals with low frequencies.

Windowing Effect on Electromagnetic Interference and Efficiency at Using Pulse Width Modulation Techniques

T. Lelek, V. Lenoch, J. Lettl, O. Sadilek, V. Schejbal, and P. Sykora
Department of Electrical and Electronic Engineering and Signaling in Transport
Jan Perner Transport Faculty, University of Pardubice, Czech Republic

Abstract— In power semiconductor voltage converters, semiconductor elements are used mainly in switching mode because of decreasing power losses. Pulse-frequency and pulse-width modulation are two basic operation modes mainly used today. In both of them switching voltage with very sharp edges causes higher harmonic frequencies as a result. Traction drives of high power nowadays typically contain induction motors or permanent magnet synchronous motors fed by voltage inverters nowadays. Because it is not possible to use another operation mode of semiconductor elements it is necessary to be engaged in research of those devices in terms of electromagnetic compatibility and from the point of view of decreasing electronic distortion.

It is well known that windowing is one of the earliest techniques for designing the finite-impulse response (FIR) filters. The filter coefficients can be obtained in closed form without the need to solve complex optimization problems as in some other sophisticated FIR design techniques. Therefore, the design time is very short and the technique remains to be an attractive tool for FIR filter design.

For a rectangular window, the maximum sidelobe amplitude is equal to approximately $-13\,\mathrm{dB}$ relative to the maximum value, i.e., the sharp transition in the ideal response is converted into a gradual transition. To reduce the oscillations, i.e., higher harmonics, other window functions having spectra exhibiting smaller sidelobes should be used. The sidelobes of the rectangular window represent the high-frequency components and due to the sharp transitions from one to zero are placed at the edges of the window. Therefore, the amplitudes of these sidelobes can be reduced by replacing the sharp transitions by more gradual ones.

The design of various low-pass FIR filters has been done using several windows. The rectangular (with $-13\,\mathrm{dB}$ sidelobes), Bartlett (with $-25\,\mathrm{dB}$), Hanning (with $-31\,\mathrm{dB}$), Hamming (with $-41\,\mathrm{dB}$) and Blackman (with $-57\,\mathrm{dB}$) windows have been used. This allows decreasing the electromagnetic interference substantially.

In the paper, the pulse-width modulation (PWM) techniques are analysed and electromagnetic interferences and efficiencies are examined using numerical simulation.

Analysis of Multi-resonant Circuitin Overloading States

J. Koscelnik, B. Dobrucky, M. Frivaldsky, and M. Prazenica
Faculty of Electrical Engineering, Department of Mechatronics and Electronics
University of Zilina, Univerzitna 1, Zilina 010 26, Slovakia

Abstract— The paper deals with the analysis of multi-resonant circuit during overload states. Investigated topology is multi-resonant non-isolated LCL2C2 converter. The main focus is given on its transient properties and ability to withstand short circuit. Simulation analysis was verified by experimental measurements.

Standard categorization of resonant tanks is series or parallel combinations. The proposed LC2L2C2 belongs to the category of non-isolated multi-resonant converters. Resonant circuit is composed of two serial LC branches between which, two parallel LC filters are connected.

The shape of output voltage has to be pure sinusoidal waveform, due to fact, that L-C filters at the output are tuned on first order harmonic. Switching frequency is equal to resonant frequency of R-L components. Regulation of magnitudes can be done using pulse frequency modulation (PFM) or asymmetric pulse width modulation control (APWM). Simple modification of main circuit with the implementation of high frequency transformer forms the isolated version of LCL2C2 converter. In this way, due to transformer ratio, a higher regulation range of output voltage can be achieved.

Nevertheless, the determination of proper operation area is necessary in order to investigate how to achieve suitable operation regions. Based on input impedance frequency characteristic, it is possible to choose two load-invariant input impedance operational points for determination of switching frequency. At this point of input impedance characteristic, its value is not dependent on the load of the converter.

Based on the computed values of LCL2C2 elements, the gain characteristic of proposed converter was made using Matlab simulation tool. Dependency of the gain curves on the load change will be graphically presented. Based on this characteristic it would be possible to determine the proper operation regions of converter. It is generally know that the optimal value of switching frequency for nominal operation equals to resonant frequency of LC element. Anyway, it is more suitable to set the switching frequency in the range from $f_{\min}$ up to $f_{\max}$ under overload (e.g., 200–800%), or short-circuit operation. In this way it won't be able to overcome nominal value of the input current and/or output voltage, respectively. Of course, it can be combined with the asymmetrical control of input voltage of the inverter.

The short circuit occurs hen the value of output current rises. It causes the saturation of magnetic elements and changes the induktance values. Therefore, it changes the ratio between switching and resonant frequency. These has also effect on the output voltage gain. These phenomena can be considered by the method of self-regulation due to own internal feedback. In case of short circuit the output current is limited by the converter self-regulation. Also, the regulation causes the current shape distortion and its THD increases by approximately 3–5%. THD final values are about 6–9%. All these "negatives" are the tax on self-regulating feedback. Under these conditions, it is necessary to consider the regulation by asymmetric change of duty-cycle or changing the ratio of f_{sw} and f_{res}. Also, it is possible to consider over-dimensioned the accumulation elements. Theoretical aspects, simulation experiments and experimental verification will be given in full paper.

Mutual Inductance of Two Helical Coils — Theory, Calculation, Verification

Michal Frivaldsky, **Pavol Spanik**, **Marek Piri**, **and Viliam Jaros**
Department of Mechatronics and Electronics, Faculty of Electrical Engineering
University of Zilina, Slovak Republic

Abstract— One of the important parameter for wireless power transmission is the mutual inductance that tells us about how much is the electromagnetic coupling between two cylindrical coils strong, when an air is positioned between them, and when are without coaxial and angular deflection.

Proposed paper will deal about the verification of calculation processes of a mutual inductance between two helical coils. Nowadays, there are many procedures how to compute mutual inductance between two coils. The main approach of proposed paper is exact specification of the formula, which may be used for the determination of the mutual inductance.

The first step before mathematical calculation is verified, the development of source code in Matlab was done. This code shall serve for computation of self-inductance, and mutual inductances. The code is divided into three parts. First part is part, where we define main parameters of both coils, e.g., radius or height of coil. Main parameters of coils can be taken over from existing system for wireless energy transfer. Second part is calculation of self-inductance. At first, the program calculates module the elliptic integrals and then next subsystem calculates self-inductance. Third part is similar as second, but this part is for calculation of the mutual inductance of two wire coils.

As was already mentioned, the main parameters of the coils can be taken over from existing system for wireless energy transfer. The transmitting and receiving coils were designed with helical geometry. For the investigation of mutual inductance between transmitter and receiver, it was necessary to measure input current of transmitting coil I_{Lp} and voltage on the load U_Z. This is due to fact, that mutual inductance cannot be measured directly.

Next figure shows final comparison between computation and measurement of mutual inductance. Proposed paper will also describe the theoretical procedure that is necessary for computation of mutual inductances as well as for design of computation algorithm. The extension of this algorithm will be further done in order to investigate voltages and currents of transmitting and receiving coil. For this purpose, determination of parasitic components of wireless power transfer system is very important.

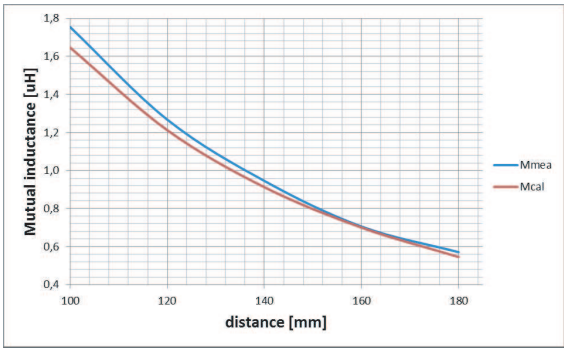

Figure 1: Graphical interpretation of the measured and calculated mutual inductance in dependency on distance between transmitter and reciever.

Session 4P5b
EM Field Based Industrial Technologies

Application of Meta-materials in the Ports of Conveyor Belt Microwave Heating Systems

A. V. Brovko
Yuri Gagarin State Technical University of Saratov, Russia

Abstract— Meta-materials can be considered as a promising resource of improvement of the existing technologies, as well as a key element of novel technologies due to unusual interaction with electromagnetic waves. In particular, negative values of effective permittivity and/or permeability of these materials allow obtaining such technically interesting electromagnetic effects as negative refraction, band gaps, magneto-electric coupling, etc..

In this paper meta-materials are investigated with the purpose of improvement of existing conveyor-belt microwave heating systems. One of the actual tasks for these systems is construction of input/output ports for the conveyor belt, which do not allow electromagnetic energy to escape from the microwave processing volume. Existing methods do not provide attenuation of microwave energy in the case of large aperture of the ports, or suffers from arcing effect due to high power of microwaves. To this end the idea of application of meta-materials at the ports arises.

Results of numerical analysis show possibility of construction of meta-material walls of waveguide ports with cross section up to 200×500 mm, which significantly reduce leakage of microwave energy from conveyor-belt heating chamber. Meta-material considered in this paper consists of printed circuit boards with metallization as a set of split-ring resonators. Estimation of effective permittivity and permeability of the meta-material was performed by FDTD analysis of the microstructure following Nicolson-Ross-Wier approach. Numerical results show that both effective permittivity and permeability may have negative values at the frequency 2.45 GHz, and these values provide negative (left-handed) refraction, which can be used for preventing escape of microwave energy from processing chamber through conveyor belt port.

Reflection of the eigenmodes in meta-material wall waveguide was estimated by FDTD analysis on macro-level. In this approach the meta-material is considered as continuous media, which permittivity and permeability are governed by Drude dispersion model. Parameters of the model provide negative values of the permittivity and permeability on the frequency 2.45 GHz.

Numerical estimation of the performance is presents in this paper, and aspects of practical implementation are discussed.

Detection of Wood Decay by Microwaves

H. Dobšíček Trefná, **Y. Yu**, **T. McKelvey**, **and M. Persson**
Chalmers University of Technology, Sweden

Abstract—

Introduction: In Sweden, approximately 20% of harvestable trees are affected by rot. Furthermore, there are many trees with hidden damage caused by eg. mooses or machines. During harvesting, this leads to the downgrading of wood from sawlog to pulpwood. Today, the first three meters of damaged log are directly graded as pulpwood, while the rest is subjected to a new inspection. This leads to unnecessary waste, which is roughly valued at 600 million/year. In this paper we present a microwave system which can quickly differentiate the rotten timber from the healthy.

Methods and Results: Our method is based on analysis of the differences in behaviour of electromagnetic signals propagating through healthy and damaged wood. We developed a measurement system consists of a circular antenna array and two-port vector network analyser integrated with computer controlled switch matrix module. The whole system can be mounted on the harvester head in the way the log is placed approximately in the center of antenna array. The signals that are transmitted through the cross-section of the log are then analysed by a so-called subspace distance based classification algorithm. We have performed proof of concept testing the prototype system on freshly-cut healthy and decayed trees. In total 16 wooden logs were measured of which 10 were healthy and 6 contained white rot fungi.

The detector identifed 82% of rotten and healthy samples. The success rate increased above 90% for subgroup of samples with smaller diameter which contained clearly defined rot.

Conclusion: We demonstrated the capability of the designed system to detect decayed wood. Due to the relative simplicity and size of microwave based system accompained with the high acquisition speed make them a potent candidates to be transfered to industrial environment.

ACKNOWLEDGMENT

The authors acknowledge Hákan Torén the company SP Maskiner AB in Ljungby for supporting the measurements and providing us with a harvester head and the company spaces.

Enhance the Protection Capability of Intentional Electromagnetic Interference with Inductive Gas Discharge Tube

Chien-Fu Shih[1], **Liann-Be Chang**[1], **Tung-Wuu Huang**[1], **Jhang-Hsing Hsieh**[3], **Ping-Yu Kuei**[2], **and Chu-Yeh Tien**[2]

[1]Department of Electronic Engineering, Chang Gung University, Kueisan-Taoyuan, Taiwan
[2]Chung Cheng Institute of Technology, National Defence University, Tashi-Taoyuan, Taiwan
[3]Research Center of Thin Film Technology, Ming Chi University, Taisan-Taoyuan, Taiwan

Abstract— A proposed inductive gas discharge tube (IGDT) including two electrodes and one hollow insulator ring is studied. The insulating ring of a GDT has spinal metal outside with inductive characteristics. In comparison to the conventional design, the proposed IGDT can provide early triggering capability during fast IEMI introduced and results a smaller residual surge current.

Numerical Simulation of Droplet Motion Induced by High Power Electromagnetic Field: Estimation of Errors Induced by Using Phase Field and Level Set Methods

J. Vrba, Jr. and D. Vrba
Faculty of Biomedical Engineering, Czech Technical University in Prague, Czech Republic

Abstract— Phase Field and Level Set methods are often used for tracking interface between two immiscible liquids in Computational Fluid Dynamics (CFD). There were several works dealing with simulations of emulsion coalescence using electric field (electrocoalescence) of Water in Oil emulsions using coupled electric and fluid dynamic simulations employing these two methods. The methods use a transition region of the Phase Field and Level Set function on the interface between the two phases (Level Set function is depicted in Fig. 2). In this region all material properties change smoothly between the values of material properties of the two phases. This artificial layer of the smoothly changing dielectric properties changes electric field distribution and correspondingly the dielectrophoretic force density which governs the droplet motions. Since the thickness of this transition region decreases with increasing mesh density the problem is dependent on the mesh density used in the simulation. In this paper, influence of the mesh density as well as of the distance between droplets on accuracy of the dielectrophoretic force density is investigated. For this purpose two 2D axial symmetric models (depicted in Fig. 1) which track the both phases of the emulsion in time domain was done using in COMSOL Multiphysics implemented Phase Field and Level Set methods. Parallel to this model a simple electrostatic (single-physic) 2D axial symmetric model, without considering the LS and PF methods was created and the dielectrophoretic forces are computed with it. The results of the three models are compared and the error is evaluated and discussed.

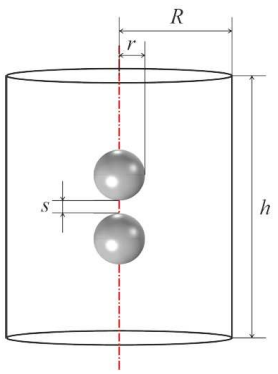

Figure 1: Two droplets placed in a homogeneous time-harmonic electric foeld $\vec{E}_0$. Parameters s, r, R and h stands for the distance between the droplets, radus of the droplets, radius and height of the computational domain, respectively. The oscillation direction of the electric field $\vec{E}_0$ is parallel to the connection line between the droplet centers.

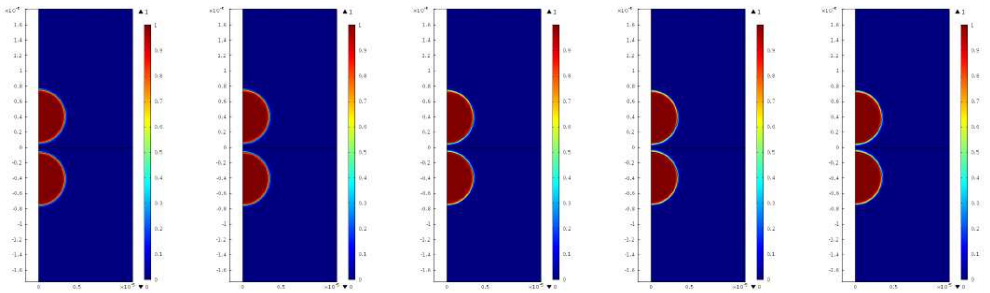

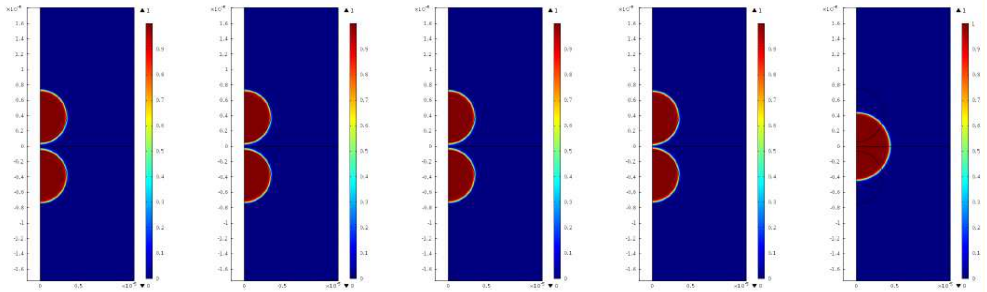

Figure 2: Droplets' positions at different time instances for the case of W/O emulsions predicted with the 2D axially symmetric numerical model.

ACKNOWLEDGMENT

This research has been supported by the research program of the Czech Science Foundation (GACR) of the Czech Republic, Project No. 14-00386P Study of Thermal and Nonthermal Effects of High-Power EM Field on Structure of Matter.

Visualization of Exposure in Industrial and Medical Applications

Jan Vrba[1], **Ladislav Oppl**[1], **Jan Vrba, Jr.**[2], **and David Vrba**[2]

[1]Department of EM Field, Czech Technical University, Technicka 2, Prague 6, Czech Republic
[2]Department of Biomedical Technique, Czech Technical University, Nám. Sítná, Kladno, Czech Republic

Abstract—

Background: As the importance of usage of microwave technologies in many applications (e.g., industrial, medical, biological, scientific etc.) is rising it is necessary to develop simple to use, reproducible and exact methods of evaluation of microwave primary (i.e., thermal) effects on various materials. In medical application we aim not to hurt the patient and we try to enhance efficiency of the treatment to minimize the adverse impact on the healthy tissue. On the other hand in industrial use we need the processing to be economical and energy efficient.

It is very difficult to monitor effects of electromagnetic field on exposed material in real time but it can be crucial for deeper understanding of processes that take place during procedures using microwave energy (i.e., microwave processing of various materials, microwave thermotherapy, microwave heating and drying etc.). Using conventional methods of evaluation of temperature, volume and other properties usually effects the distribution of electromagnetic field and interferes with it. It is possible to stop the process at any time and evaluate effects of this partial exposure but it is not very sophisticated approach and for example temperature measurements will be affected by this methodology as well. In this paper we are aiming to put contactless and noninvasive methods of measurement of temperature and volume into practical use and we propose methodology and present design of microwave system for visualization.

Methods: Design of the applicator used in the visualization system had to be altered from standard design approach used in conventional applications (i.e., microwave drying, hyperthermia applications etc.). We aimed to design open resonator type applicator which could be used safely and would allow sufficient insight for the visualization equipment.

In this paper we chose to visualize microwave processing of cornstarch beads and evaluate obtained results by processing several separate frames of produced film. Standard camera (i.e., recording in visible part of spectrum) and infrared camera served as the visualization equipment.

For processing of obtained images (from the film) we used Matlab and we were able to determine how volume of layer of cornstarch beads and its average surface temperature are changing. We propose that this method is suitable for many other applications (i.e., evaluation of applicators for medical procedures etc.).

Results: Results of the visualization of the microwave processing and results of evaluation of various single frames in Matlab are presented. We propose that we developed suitable and simple to use method for evaluation of processes in microwave applications. In this paper we also designed microwave system for visualization which enables homogenous exposure of various materials to electromagnetic field.

ACKNOWLEDGMENT

This research is supported by Grant Agency of the Czech Republic, project: "Non-standard application of physical fields — analogy, modeling, verification and simulation" (102/08/H081)".

Demonstration of Multi-beam Microwave Heating Based on the Wave Confinement of Hexagonal Photonic Crystal Multilayered Cavity

N. Yogesh, **Quanqiang Yu**, **and Zhengbiao Ouyang**
Solid State Photonics Laboratory, THz Technical Research Center
Shenzhen Key Laboratory of Micro-nano Photonic Information Technology
Key Laboratory of Optoelectronic Device and Systems of Ministry of Education and Guangdong Province
College of Electronic Science and Technology
Shenzhen University, Shenzhen 518060, China

Abstract— Multi-beam microwave heating based on the wave confinement of hexagonal photonic crystal multilayered cavity is reported. The proposed hexagonal cavity is formed by alternative layers of alumina (Al_2O_3) and air with the thickness of $0.3a$ and $0.7a$ respectively, where 'a' is the lattice constant. The 17 layer cavity is normally excited with six microwave beams with the peak strength of 1000 V/m. The center of the cavity is loaded with a low loss dielectric and electromagnetic thermal co-simulations are carried out to study the heat transfer due to multi-beam confinement. It is found that characteristic modes of the proposed cavity show the temperature raising rate of 0.77°C/s, 190.26°C/s and 29.52°C/s at 13.855 GHz, 14.54164 GHz, and 14.78175 GHz respectively. This feature is highly useful for arriving the higher temperatures and the creation of plasmas. Particularly, it is anticipated that the proper scaling of the proposed cavity at laser length-scales provide an excellent source of laser beam heating in industrial welding and green photonic solutions.

Session 4P6
RF and Wireless Communication

Design and Implementation of a Reliable Wireless Real-time Home Automation System Based on Arduino Uno Single-board Microcontroller

Iman I. M. Abu Sulayman[1], **Sami H. A. Almalki**[1], **and Mohamed S. Soliman**[1, 2]

[1]Department of Electrical Engineering, Faculty of Engineering
Taif University, Taif, Kingdom of Saudi Arabia
[2]Department of Electrical Engineering
Faculty of Energy Engineering, Aswan University, Aswan, Egypt

Abstract— Recently, man's work and life are increasingly tight with the rapid growth in communications and information technology. The informationized society has changed human being's way of life as well as challenged the traditional residence. Followed by the rapid economic expansion, living standard keeps raising up day by day that people have a higher requirement for dwelling functions. The intellectualized society brings diversified information where safe, economic, comfortable and convenient life has become the ideal for every modern family.

This paper presents design and implementation concepts for a wireless real-time home automation system based on Arduino microcontroller as central controllers. The proposed system has two operational modes. The first one is denoted as a cellular telephone mode in which the user can monitor and control the home appliances from anywhere over the world using the cellular phone through Wi-Fi communication technology. The second one is referred to a self-automated mode that makes the controllers to be capable of monitoring and controlling different appliances in the home automatically in response to the signals comes from the related sensors. To support the usefulness of the proposed technique, a hardware implementation with Matlab-GUI for the proposed system is carried out and the reliability of the system is introduced. The proposed system is shown to be a simple, cost effective and flexible that making it a suitable and a good candidate for the smart home future.

Correlation Characteristics for an Event/Sports Center at 3.2 GHz

Alejandro Aragón-Zavala[1], **Vladan Jevremovic**[2], **and Ali Jemmali**[3]

[1]Electronics Department, Tecnológico de Monterrey, Campus Querétaro, Querétaro, Mexico
[2]R&D Department, iBwave Solutions Inc., Houston, TX, USA
[3]R&D Department, iBwave Solutions Inc., Montreal, Canada

Abstract— The key to reliable and fast mobile digital data connections is signal to noise + interference ratio (SINR). The degree of signal cross-correlation between the serving and interfering signal(s) has a significant impact on SINR. Shadowing (slow fading) cross-correlation must be quantified in order to properly calculate SINR. For significant shadowing cross-correlation to occur, the LOS requirement is essential, and as macro mobile networks have almost exclusively Non-Line of Sight (NLOS) coverage, the impact of signal cross-correlation is low. However, as distances between small cells in indoor networks are much smaller, the LOS requirement is mostly satisfied in those types of networks. While many authors have investigated shadow fading for indoor networks, very few have reported results for sports venues, such as stadiums, in which sector handover can become critical and where handover mismanagement could lead to excessive network resource usage.

In systems that relay in a tight power control like CDMA2000 and WCDMA, shadowing autocorrelation and de-correlation distance are important as they allow a good estimate of mobile transmit power fluctuation around its mean value. While there are numerous studies that measure shadowing autocorrelation and calculate shadowing correlation distance in macro networks, there are very few such studies done for in-building networks.

As mobile data consumption has been dramatically increased, various national spectrum governing bodies started to look into ways to allocate more spectrum bands to mobile networks outside those frequencies. An example is the Federal Communications Commission (FCC), the US Spectrum governing body, which proposed a new Citizen Broadband Radio Service in the 3.5 GHz band, specifically to allow small cells deployment on shared basis with incumbent federal and non-federal users of the band. While the rulemaking has not been made yet, the proposal is a part of greater strategy to free up 500 MHz of spectrum for commercial use by 2020. Therefore, it is of interest to investigate cross correlation and auto-correlation properties of stadium networks at frequencies near 3.5 GHz. Likewise, 3.5 GHz spectrum is authorized for mobile use in European countries, and Japan plans to make the 3400–3600 MHz band available for mobile broadband.

This paper presents radio measurement results that were conducted at a university sports/event center at 3.2 GHz. Radio measurements undertaken at this frequency show that signals from two base stations have correlation in the 0.04–0.43 range for small angles (below 30°), showing a positive correlation coefficient, in agreement with our previous work. De-correlation distances are in the range of 1.2 to 14.4 meters, which are strongly dependent on the presence of metallic structures in the vicinity of the tested antennas as well as on the antenna height. Autocorrelation shows an exponentially decay behavior, as previously reported. These measurements were used to establish suitable auto and cross correlation models and de-correlation distances at the venue at the frequency that is reasonably close to the proposed Citizen Broadband Radio Service band. From these findings, recommendations for modelling auto-correlation and cross-correlation in sporting venues at these frequencies could be made, which then can be used to extend out study to similar venues at higher and lower frequencies.

Hidden Markov Models Based Channel Status Prediction for Cognitive Radio Networks

Wojciech Bednarczyk and Piotr Gajewski
Faculty of Electronics, Military University of Technology
Gen. S. Kaliskiego 2 Str., Warsaw 00-908, Poland

Abstract— Cognitive radio (CR) networks can be designed to manage the radio spectrum more efficiently by utilizing of temporarily not used channels in primary users' licensed frequency bands. Here, the spectrum utilization can be improved significantly by spectrum sharing between primary and secondary users (who are not being served by the primary system). In this paper, we propose to use so called Hidden Markov Models (HMM) to predict the spectrum occupancy of sharing radio bands.

The proposed technique can dynamically select different licensed bands for secondary user with significantly less interference from and to the licensed users. This can be solved by predicting of the time duration of primary users non-active state in selected band. Using the HMM to build the channel prediction algorithm, for dynamic spectrum allocation in cognitive radio networks, the CR can utilize them more efficiently because it should leaving the currently occupied band, before the primary user starts of his transmission in that band.

In this paper, we discuss the theoretical aspects of statistical modeling by HMM and show how HMM can be applied to dynamic spectrum management. At the beginning, we will shortly describe the theory of HMM using simple examples. Then we will focus our attention on the three fundamental problems for HMM design. Firstly we show the evaluation of the probability of an observations sequence by using a specific HMM. The second question will be discussed is how to determine a best sequence of model states. And finally the adjustment of model parameters so as to best account for the observed signal will be discussed. We will show that once these three fundamental problems are solved, the HMM can be applied to dynamic spectrum management in cognitive radio networks. The details of simulation will be described. The results obtained using HMM are very promising and they show that HMM offer a new paradigm for predicting channel behavior in cognitive radio.

Modified Lowest ID Algorithm for Practical Wireless Clustered Network

Wojciech Bednarczyk, **Jerzy Dołowski**, **and Jarosław Michalak**
Faculty of Electronics, Military University of Technology
Gen. S. Kaliskiego 2 Str., Warsaw 00-908, Poland

Abstract— Clustering is a promising approach for building hierarchies and simplifying the routing process in mobile Ad-hoc network environments. The main objective of clustering is to identify suitable node representatives, i.e., Cluster Heads (CHs), to store routing and topology information and maximize clusters stability. Traditional clustering algorithms suggest CH election exclusively based on node IDs or location information and involve frequent broadcasting of control packets, even when network topology remains unchanged.

Several heuristics have been proposed to address Ad-hoc networks clustering problem. One of the most popular ones is Lowest-ID (LID), wherein each node is assigned a unique ID. Periodically, nodes broadcast their IDs through a *Hello* control message, within a period time *Hello* period. The lowest-ID node in a neighborhood is then elected as the CH; nodes which can hear two or more CHs become gateways.

The main asset of LID method is its implementation simplicity. It is also quick clustering method, as it only takes two *Hello* periods to decide upon cluster structure and also provides a more stable cluster formation.

We proposed a modified clustering algorithm, the Lowest Node ID (LNID). This algorithm has the following crucial features:

- a state machine with semi-stable states,
- ability to change the state during work,
- additional control messages (as development of original OMNET messages),
- MAC address as ID of nodes,
- stabilizing procedures

It is well known that energy used by a system has a special importance not only from energy consumption point of view (especially in battery supplied devices) but from interference level introduced by the system which has essential impact on a capacity of system and its ability to simultaneous working among others wireless links.

Efficiency of LNID algorithm in practical constraints were assessed in dependence on special network stabilizing algorithms from point of view:

- Time of clusterization process,
- Energy used by the network in clusterization process,
- Clusterization correctness,
- Structure stability of clusterized network.

Simulations will be done for static network assuming Free Space Path Loss propagation model with chosen reliability of information delivery in a radio link.

Application of DRTM to Aircraft Landing System

Junichi Honda
Surveillance and Communications Department, Electronic Navigation Research Institute
Chofu, Tokyo 182-0012 Japan

Abstract— This paper describes a numerical simulation of multipath interferences caused by buildings for aircraft landing system. Focusing on the LOC (Localizer) among ILS (Instrument Landing System), we discuss on the effect of multipath interferences. The LOC consists of carrier and sideband signals. The landing aircraft move along the ILS course whose signal phase variable becomes almost zero. However, the reflected and diffracted waves from buildings cannot be ignored because unexpected waves result in disturbances of the normal landing course. Therefore, we need to simulate electromagnetic field in advance in order to prevent the signal errors, especially for the relocation of building and LOC. In this paper, we numerically compute multipath interferences caused by buildings. In the numerical simulation, we use the DRTM (Discrete Ray Tracing Method) which were proposed by Prof. Uchida. The DRTM based on the ray tracing method is able to reduce ray searching time. We compute ray distribution between a source and a receiver by using a simple airport model, and we analyze electromagnetic field and the current of electricity at the receiver side. We discuss the multipath interferences in airport. We show that the DRTM is one of suitable numerical technique for aircraft landing system.

Using Antenna Diversity to Improve Wake-up Range and Probability

T. Kumberg, R. Tannhaeuser, and L. M. Reindl
IMTEK Laboratory for Electrical Instrumentation, Department of Microsystems Engineering
University of Freiburg, Georges-Koehler-Allee 106, Freiburg 79110, Germany

Abstract— Wireless sensor networks (WSN) can be used to monitor critical infrastructure such as bridges. WSNs often consist of small sensor nodes which have only limited power supply and are installed at places that are hard to reach [1]. But, due to the goal of long term monitoring, which usually is in the range of more than ten years, long lifetimes of WSNs should be realized [2]. Therefore, energy consumption of WSNs needs to be minimized for example by using low-power wake-up receivers. They reside in a low-power stand-by state until they receive a wake-up signal. After receiving this signal, or a trigger from a sensor, they wake-up to full functionality [2, 3].

With the development of wake-up receivers, a paradigm shift can be observed in wireless sensor networks communication protocols [4]. Now, communication and as such, sending of messages is only necessary if a sensor node has data available that needs to be sent or if the sensor node was asked to send data. In other words, idle listening and sending of synchronization messages is no longer required.

But low-power wake-up receivers introduce also new challenges as their sensitivity is much lower than the sensitivity of communication radios, as depicted in Figure 1 where nodes A and B are in wake-up range of the Sender and nodes C, D and E are also in communication range. Due to this, several wake-up messages may be necessary to reach a sensor node that is in communication range but not in wake-up range. Another challenge is that sending of a wake-up message may be as expensive as sending of a communication message [4].

The low-power wake-up sensor node presented by [3] uses the AS3932 low-power wake-up receiver that listens permanently to a 125 kHz signal that is modulated on an 868 MHz carrier frequency and demodulated by the use of a rectifier and a low-pass filter. Changing between communication and low-power wake-up listening is realized with the antenna switch (ADG918).

In this paper we present a wake-up node, which is based on the node presented by [3]. Figure 2 shows the modified design that uses antenna diversity in the wake-up path. Due to this, the node shows an improved wake-up range in free-space propagation and improved wake-up probability in a multipath propagation environment. We show that no additional active parts are needed, which would increase power consumption. The general design and its performance are tested by using simulations. A test setup is used to verify the simulation results and to show the behavior of the new design.

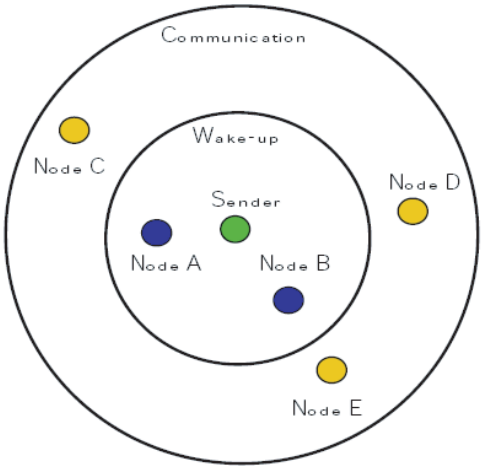

Figure 1: The nodes A and B which are in wake-up range of the Sender. Nodes C, D and E are also in communication range of the Sender.

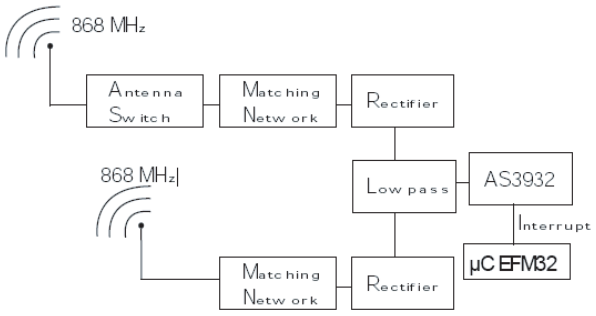

Figure 2: Schematic of a sensor node using antenna diversity in the wake-up path to improve wake-up range or wake-up probability.

REFERENCES

1. Chang, P. C., A. Flatau, and S. Liu, "Review paper: Health monitoring of civil infrastructure," *Structural Health Monitoring*, Vol. 2, No. 3, 257–267, 2003.
2. Kumberg, T., R. Tannhaeuser, G. Gamm, and L. Reindl, "Energy improved wake-up strategy for wireless sensor networks," *Proceedings of ITG/GMA Symposium Sensors and Measuring Systems 2014*, Vol. 17, 1–6, Jun. 2014.
3. Gamm, G., M. Kostic, M. Sippel, and L. M. Reindl, "Low-power sensor node with addressable wake-up on-demand capability," *International Journal of Sensor Networks*, Vol. 11, No. 1, 48–56, 2012.
4. Bannoura, A., C. Ortolf, L. Reindl, and C. Schindelhauer, "The wake up dominating set problem," *Theoretical Computer Science*, 2015.

Interference Aware Iterative Receiver Performance for the Uplink of LTE-A

Carlos Reis, **Nuno Souto**, **Américo Correia**, **and Mário M. da Silva**
ISCTE-University Institute of Lisbon and Instituto de Telecomunicações, Portugal

Abstract— In this paper we study the performance of an interference aware iterative block decision feedback equalizer (IBDFE) for the uplink of LTE-Advanced with single carrier (SC) transmissions. The receiver makes use of the correlation between the interference in the receiving antennas and minimizes the mean squared error (MMSE) of the detected symbols. Link level simulation results show that the proposed receiver clearly outperforms the conventional IBDFE and the linear interference rejection combining (IRC) detector. System level simulation results show that the use of the new iterative receiver achieves additional throughput gains. However, the gains obtained depend on the schedulers employed and on the number of receiving antennas.

ACKNOWLEDGMENT

This work was partially supported by the FCT — Fundação para a Ciência e Tecnologia (project PEst-OE/EEI/LA0008/2013).

Physical Layer Security Scheme Based on Power Efficient Multi-antenna Transmitter

Paulo Montezuma[1, 2, 3], **Rui Dinis**[1, 2], **and Mario Marques da Silva**[2, 4]

[1]CTS, Uninova, Dep.^{o} de Eng.^{a} Electrotécnica, Faculdade de Ciências e Tecnologia, FCT Universidade Nova de Lisboa, Caparica 2829-516, Portugal
[2]IT, Instituto de Telecomunicações, Av. Rovisco Pais, Lisboa, Portugal
[3]Uninova, Instituto de Desenvolvimento de Novas Tecnologias, Quinta da Torre, Caparica, Portugal
[4]Universidade Autonoma de Lisboa, Portugal

Abstract— Mobile communication systems must support multiple users achieving at same time privacy of users contents. Security common solutions are based on encrypted algorithms from higher layers, such as private and public encrypted keys. Other possibility is to implement physical layer security schemes. One advantage of physical layer security relies on their ability to be combined with other security schemes from higher layers.

MIMO (Multiple-input multiple-output) systems can increase throughput in modern wireless networks and reduce interference. Other advantage of MIMO systems is the reduction of the transmitted power. On the other hand, to achieve high spectral efficiency multilevel modulations with high peak-to-average power ratios should be used, which may affect efficiency of power amplification. This problem can be avoided with a transmission scheme, where the constellations are decomposed on several uncorrelated BPSK (Bi Phase Shift Keying), QPSK (Quadri Phase Shift Keying) or OQPSK (Offset QPSK) components, being each component amplified and transmitted independently by an antenna. Combination losses are also avoided since the several signal components are combined at channel level. On the other hand due to the broadcast nature of MIMO systems, security is another critical issue in such systems. However, the constellation shaping on the desired direction introduced by these new transmitters means that we have directivity at the transmitted constellation that can be employed to assure security at physical layer. Privacy is achieved since each user must know the set of coefficients associated to each BPSK component as well as the array configuration, otherwise receives useless data. Therefore, the inherent security lies on the constellation directivity, i.e., the direction in which the constellation is optimized, which can be improved by changes on coefficients' phases or using constellations that are decomposed with a higher number of BPSK components. The several cases analyzed here show effectiveness of the proposed approach to implement a security scheme at physical layer level.

Experimental Characterization of In Vivo Radio Channel at MICS and ISM Bands

Aya F. Abdelaziz[1, 2], **Qammer H. Abbasi**[1], **A. Fatih Demir**[3], **Khalid Qaraqe**[1], **Erchin Serpedin**[4], **and Huseyin Arslan**[3, 5]

[1]Electrical and Computer Engineering Department, Texas A&M University, Qatar
[2]Department of Electronics and Communication Engineering, Cairo University, Egypt
[3]Department of Electrical Engineering, University of South Florida, USA
[4]Department of ECEN, Texas A&M University, College Station, USA
[5]Medipol University, Turkey

Abstract— Wireless communication and channel modeling for implantable biomedical devices have received more attention in recent years for diagnosis and therapy. Mutual communication between the implantable medical devices and the ex-vivo devices is commonly performed in the medical implant communications service (MICS) band (402–405 MHz) as it represents reasonable signal propagation characteristics in human body [1]. MICS has wide range of applications such as stimulatory devices including pacemakers and implantable cardioverter/defibrillator. It is crucial to analyze the signal attenuation in the lossy human tissues and the propagation around the human body. Experimental measurements used to confirm the validity of the simulation results done using human body models are usually performed inside phantoms. Phantoms are relatively easy to be analyzed and implemented; however, real time in vivo measurements of implantable devices are essential to verify the performance in a real environment that has many and different tissue layers. These multitissues have different electrical properties such as conductivity and signal attenuation depending on the used frequency as well as age, size, sex, etc.. A comparison between a single equivalent layer of a body model and a three layer structure was presented showing the advantages and limitations of each one [2]. Numerical electromagnetic analysis was applied to model in/on body radio propagation channels which clarified the importance of digital phantom accuracy [3].

In this study, numerical versus experimental analysis of implantable antennas for biomedical telemetry in the MICS is presented. In addition to simulation studies, measurements are performed on adult cadaver. For both simulation and measurement studies, an antenna is placed at different organs inside the body (keeping in view the most promising implantable applications) i.e., heart, stomach and intestine. The ex-vivo antenna is initially placed on the surface of body and then at 5 different locations outside the body with spacing of 20 mm upto 100 mm with steps of 20 mm from the surface of body. In addition different depths of implant antenna is considered as well. Path loss is calculated for all scenarios and compared with the simulation results. A reasonably good agreement is obtained among the simulation and measurement results. The study enables better understanding of losses inside the body for different organs, which will help in developing better implantable devices.

REFERENCES

1. Bradley, P. D., "An ultra low power, high performance medical implant communication system (MICS) transceiver for implantable devices," *Biomedical Circuits and Systems Conference, IEEE BioCAS*, 158–161, Nov. 2006.
2. Gemio, J., J. Parron, and J. Soler, "Human body effects on implantable antennas for ISM bands applications: Models comparison and propagation losses study," *Progress In Electromagnetic Research*, Vol. 110, 437–452, 2010.
3. Alomainy, A. and Y. Hao, "Modeling and characterization of biotelemetric radio channel from ingested implants considering organ contents," *IEEE Transactions on Antennas and Propagation*, Vol. 57, 999–1005, 2009.

Performance of Ultra-wideband Body-centric Wireless Networks

Zied Bouida[1], **Marwa Qaraqe**[2], **Qammer Abbasi**[1],
Mohamed Abdallah[1], **and Erchin Serpedin**[2]

[1]Department of Electrical and Computer Engineering, Texas A&M University at Qatar, Doha, Qatar
[2]ECE Department, Texas A&M University, College Station, TX, USA

Abstract— The main idea behind body-centric wireless communications is to connect multiple devices that are located on the human body. In this context, several research topics have covered the study of body-centric communications especially with the scope of personal area networks and body-area networks. Indeed, the urgent need for wireless personal communication systems (PCS) is a normal result of the highly-increasing demand for technological advances required to satisfy humans' rapid-paced life-style changes. Many innovative PCS have been proposed, particularly in the area of body-worn devices. These body-worn devices initiated the concept of body-centric communication systems (BCCS) offering a huge number of applications in healthcare systems.

Both narrow-band and wide-band frequencies can be used for body centric wireless communications. However, ultra-wideband (UWB) is a promising wireless communications technology that is characterized by low energy and large bandwidth and can be used for short-range, high-data-rate communications. UWBs low-power requirements makes it an ideal candidate for BCCS [1]. Moreover, the use of such higher frequencies reduces the propagation of waves into the human body. As the demand for higher data rate increases, new techniques that aim at achieving these data rates are evolving. Among the most popular is the combination of the UWB technology with multiple-input-multiple-output (MIMO) systems, i.e., multiple-antennas-based transceivers [2].

In this submission, we study the performance of ultra-wideband body-centric wireless networks (BCWN). In this context, we evaluate the capacity of UWB MIMO on-body channels. In order to study the effect of on-body antenna positions, we consider four different transmit-receive antenna location scenarios where the transmit antenna is fixed on the Waist and the receive antenna is placed in different positions. More specifically, the four considered scenarios are the Chest-Waist, Wrist-Waist, Ankle-Waist, and the Back-Waist settings as shown in Figure 1. Based on field-measurements, the obtained results reflect the impact of different antenna positions on the performance of on-body networks. For each of these scenarios, we evaluate the channel capacities depending on the amount of channel state information (CSI) available to the transmitter. More specifically, we evaluate the equal-power capacity and the water-filling capacity for the cases where no CSI and full CSI is available to the transmitter. We also provide a mathematical framework for the computation of the capacity of UWB MIMO systems.

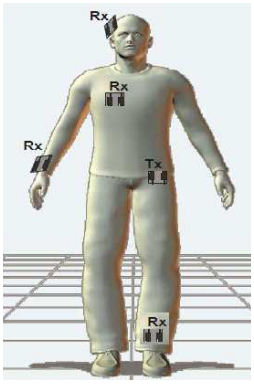

Figure 1: MIMO antenna positions.

REFERENCES

1. Hall, P. S. and Y. Hao, *Antennas and Propagation for Body-centric Wireless Communications*, 2nd Edition, Artech House, Norwood, MA, USA, 2012.
2. Kaiser, T. and F. Zheng, *Ultra Wideband Systems with MIMO*, 1st Edition, John Wiley & Sons, New York, 2010.

Measurements and Simulations of Electric Fields Emitted from LTE Femtocells inside a Building Office

Hsing-Yi Chen and Shu-Huan Wen
Department of Communications Engineering, Yuan Ze University
135, Yuan-Tung Road, Nei-Li, Chung-Li, Taoyuan Shian 32003, Taiwan

Abstract— In the near future, long term evolution (LTE) femtocells will play a key role in enterprise and metro deployment areas for indoor wireless communications. With the increasing use of indoor wireless networks, there is a challenge to provide a better coverage, higher cell capacity, and higher data rates for mobile applications in the initial design and planning. Therefore, EM field distribution and variability of LTE femtocells in indoor-environments should be well studied in order to ensure an adequate coverage and good performance for indoor wireless communications. In this study, the FDTD method was used to calculate electric fields emitted from a LTE femtocell placed at the left-hand-side of an empty office at frequencies of 700, 860, 1990, and 2600 MHz. The validity of the simulation results of the electric fields is further checked by measurement data. After validating the accuracy of the FDTD method, the FDTD method was used to calculate electric field distributions inside the office, with and without the presence of 20 people and furniture for the LTE femtocell placed near the center of a horizontal plane with a distance of 1.0 m from the upper slab and transmitting a power of 10 dBm. Simulated electric fields at most of the locations on the horizontal plane with a height of 1.0 m above the bottom slab for the office with and without the presence of 20 people and furniture are found in the range of -10 to -30 dBV/m which means a good signal will be picked up in the office. The maximum power density emitted from the LTE femtocell is 1.326×10^{-4} W/m^2 which is far below the ANSI/IEEE safety standard of 4.6–17.3 W/m^2 for public exposure at frequencies of 700–2600 MHz.

Session 4P7a
Microwave and Millimeter Wave Circuits and Devices, CAD

Meshing Noise in Parametric Analysis of Passive Components with 3D FEM

A. Lamecki, L. Balewski, and M. Mrozowski
Faculty of Electronics, Telecommunications and Informatics
Gdansk University of Technology, Poland

Abstract— Design of passive components for modern RF and microwave systems requires the application of high accuracy software for electromagnetic simulation. Amongst a variety of numerical techniques that can be utilized to compute device's response, the finite element method (FEM) has emerged as an industry standard due to flexibility to handle complex, arbitrary shaped 3D devices.

A typical design cycle uses some kind of an iterative tuning method (based on optimization) which requires a device to be simulated multiple times in order to fit the response to required design specifications. During the tuning procedure, the design parameters are modified at each step and the simulation of the updated design is performed. This procedure is repeated until the specification is met. In the case of a FEM solver, the geometry of a modelled structure is represented in a discretized form as a mesh (usually tetrahedral or quadrilateral). At each tuning iteration the mesh is generated and built from scratch. As it will be shown in this submission, the major difficulty with such design procedure is the lack of continuity of design response vs. the change of design parameters (geometric variables). This effect can be observed in the simulated device's response as a meshing noise and it is most disadvantageous when optimization is performed and may ultimately prevent convergence.

In order to reduce the influence of the meshing noise on the convergence of the tuning procedure, a different strategy has to be applied in order to eliminate remeshing at every tuning step. This can be achieved by the application of mesh deformation techniques, as proposed in in [1]. It can be proven that such strategy allows for the elimination of the remeshing noise from the parametric sweep. Preliminary results of application of mesh deformation techniques obtained within InventSim — a novel 3D FEM Simulation and Optimization Framework [2, 3] confirm the advantages of the proposed approach.

ACKNOWLEDGMENT

This work was supported by Polish National Science Centre under agreement UMO-2013/09/B/ST7/04202.

REFERENCES

1. Sieger, D., S. Manzel, and M. Botsch, "High quality mesh morphing using triharmonic radial basis functions," *Proceedings of the 21st International Meshing Roundtable*, 1–15, 2013.
2. Lamecki, A., L. Balewski, and M. Mrozowski, "An efficient framework for fast computer aided design of microwave circuits based on the higher-order 3D finite-element method," *Radioengineering*, Vol. 23, No. 4, 970–978, 2014.
3. www.eminvent.com.

280 GHz Signal Sensor Design Using Subharmoinc Mixing in 40 nm CMOS Technology

Tzu-Chao Yan[1], **Chun-Hsing Li**[2], **and Chien-Nan Kuo**[1]

[1]National Chiao-Tung University, Hsinchu 30010, Taiwan
[2]Natioanl Central University, Jhongli, Taiwan

Abstract— THz imaging sensing has become an emerging wireless application beyond communications in the past few years, especially for CMOS technology [1]. An imaging detector makes use of the plasma wave theory and operates in the frequency range higher than the cutoff frequency in FET devices [2]. The construction of an image relies on raster scanning of the received power from each pixel. Consequently, power detection is a fast method to obtain a 2D image. It would be more valuable to construct a 3D image, which requires phase detection. To carry out phase detection, frequency mixing turns out to be a simple way. The detected signal phase is determined and referred to a local reference signal (LO).

In this summary, we present the circuit design forsignal phase detection at 280 GHz, using subharmoinc frequency mixing based on the plasma wave theory [2]. Previous works of frequency mixing typically apply a Schottky mixer as in [3]. In [4], the theory and circuit configuration using FETs are discussed in details. Nevertheless the LO signal is combined with the RF signal in the free space as one single input before the antenna. In this work, an on-chip LO is generated. The LO signal frequency is chosen in a half of the RF signal frequency around 140 GHz. An external signal at 23.3 GHz is input to generate the LO signal through an on-chip frequency multiplier chain. The single-ended input passes through bonding wires with careful design to minimize the insertion loss. The multiplier chain includes a frequency tripler, an amplifier, and a frequency doubler. It still requires some other passive components, such as March and balun and Wilkison divider circuits designed using transmission lines, to obtain quadrature RF signals. MOSFETs perform frequency down conversion with LO and RF at the gate and source port, respectively. The output IF signal frequency is set around 10 MHz. It is necessary to add an IF amplifier of 57 dB gain to boost up the level for measurement. The simulated result shows that the output voltage of 117 mV is obtained, given the received RF power of −60 dBm. The gain level of the IF amplifier is so high that dc offset cancellation is required. A feedback network with low-pass filtering works for the cancellation purpose. According to the IF output of quadrature phases, we can make post processing to retrieve the RF signal phase.

REFERENCES

1. Hadi, R. A., et al., "A 1 k-pixel video camera for 0.7–1.1 terahertz imaging applications in 65-nm CMOS," *IEEE J. Solid-State Circuits*, Vol. 47, No. 12, 2999-3012, Dec. 2012.
2. Dyakonov, M. and M. Shur, "Detection, mixing, and frequency multiplication of terahertz radiation by two-dimensional electronic fluid," *IEEE Trans. Electron Devices*, Vol. 43, No. 3, 38-0-387, Mar. 1996.
3. Schlecht, E., et al., "A unique 520–590 GHz biased subharmonically-pumped Schottky mixer," *IEEE Micro. Wireless Compon. Lett.*, Vol. 17, No. 12, 879–881, Dec. 2007.
4. Lisauskas, A., et al., "Subharmonic mixing with field-effect transistors: Theory and experiment at 639 GHz high above ft," *IEEE Sensors J.*, Vol. 13, No. 1, 124–132, Jan. 2013.

On-Wafer Calibration Technique with Fixed Probe Positions for Production Tests of Radio Frequency Integrated Circuits

Chien-Chang Huang and Wei-Che Lin
Department of Communication Engineering, Yuan Ze University
135, Yuan-Tung Rd., Chung-Li, Taoyuan 32003, Taiwan

Abstract— Scattering parameter (S-parameter) calibration of vector network analyzer is essential and important for device/circuit measurements in high frequency applications. For production tests of radio frequency integrated circuits (RFICs), the on-wafer probes in fixed positions to fit the dimension of the device-under-test (DUT) is usually preferred, and the associated calibration standards in the same dimension can further save the testing time since the probes need not to be moved during calibrations and measurements. Though some commercial impedance-standard substrates (ISSs) have the same probing position for their calibration standards, the probing position may not meet the DUT dimensions. In this paper, a calibration technique with three on-chip standards including a transmission line, a series resistor with offset line segment, and a shunt resistor with offset line segment, in the fixed probing constraint suited for RFIC production test is presented, where the on-chip standards need not to be characterized in advance. The self-calibration feature of the proposed technique relaxes the accuracy requirements of the on-chip standards, and becomes attractive for production test applications. To show the robustness of the proposed calibration technique, some simulation studies with noise effects are conducted in GaAs substrates with the on-wafer measurement verifications up to 110 GHz.

A High-Q Linear CMOS Digitally Controlled Accumulation-mode Varactor Array for Multiband RF Circuits

Sanggil Kim and Donggu Im
Division of Electronics Engineering
Chonbuk National University, Jollabuk-do 561-756, Korea

Abstract— Electronically tunable capacitors are key elements for tunable and reconfigurable RF circuits. The most popular tunable capacitor topologies in CMOS are the analog varactor and digitally controlled switched capacitor array (SCA). The conventional analog varactor shows a high quality factor (Q-factor) in both the minimum capacitance ($C_{\min}$) and the maximum capacitance ($C_{\max}$) states with a wide tuning range, but it has a poor linearity performance due to the voltage dependent nonlinear capacitance. In case of the digitally controlled SCA, while it shows a very good linearity, its Q-factor in $C_{\min}$ state is strongly dependent on the substrate loss by the parasitic junction capacitances between P-well, deep N-well, and P-substrate and the parasitic junction resistance. Especially, if the SCA is implemented in a standard digital CMOS process without deep N-well, it suffers from severe Q-factor degradation in $C_{\min}$ state at higher frequencies. In order to overcome the aforementioned drawbacks of the analog varactor and the digitally controlled SCA, the digitally controlled binary-weighted accumulation-mode varactor array (AVA) is proposed. Contrast to the conventional analog varactor tuned by continuous analog voltage, the proposed AVA uses only two states of $C_{\min}$ and $C_{\max}$ of the analog varactor by digitally on/off control. Instead of a zero voltage reference, the negative voltage ($-VDD$) is applied to the gate of the analog varactor in $C_{\min}$ state in order to maximize the tuning range, power handling capability, and linearity. The total capacitance varies by turning on ($+VDD$) or off ($-VDD$) each branch of the proposed AVA The proposed AVA keeps a high Q-factor in all states even if it is implemented in a standard digital CMOS process without deep N-well, while showing comparable linearity performance in comparison with the conventional SCA. In simulation, the Q-factor at 2.4 GHz is greater than 70 over all states and the tuning range is about 3.1. The simulated third-order input-referred intercept point (IIP3) at the same frequency is greater than +35 dBm over all states.

A V-band Balanced MMIC Power Amplifier

S. Ismail, S. Karimian, and R. Sloan
School of Electrical and Electronic Engineering
The University of Manchester, Manchester, M60 1QD, UK

Abstract— A highly stable V-band balanced power amplifier has been proposed based on MMIC using the pseudomorphic High Electron Mobility Transistor (pHEMT). The amplifier consists of two stages with device length of $8 \times 25\,\mu m$ and $2 \times 25\,\mu m$ gate widths. The design kit of PP10 WIN Semiconductor Corp. has been used. The simulation results show power and gain levels of 18 dBm and 12.5 dB, respectively, with a tolerance of ± 0.8 dB over the broadband range of 40–80 GHz. Microstrip Lange couplers are used as 3 dB quadrature power splitters and combiners. The amplifier has an acceptable performance with low input and output VSWRs, high stability, fairly flat gain and constant power over the whole bandwidth; and so it can be a good candidate for broadband millimetre-wave front end transceivers systems, and also, as an instrumentation amplifier in measurement systems. The MMIC amplifier is being sent for fabrication and will be tested when received.

Session 4P8
Antenna Theory and Radiation 2

Optimal Focusing by Means of Convex Programming: A Review

T. Isernia, D. A. M. Iero, and A. F. Morabito
DIIES, University 'Mediterranea' of Reggio Calabria, Italy

Abstract— Two decades ago, two different research groups [1–3] showed how the problem of focusing a field in a given direction subject to arbitrary sidelobe bounds elsewhere, and where excitations are the unknowns of the problem, can be formulated as a Convex Programming problem. Later, the same result was re-discovered by Balanis and Bevelacquain [4]. Notably, the approach in [3] already allowed to take into account near field constraints.

The basic approach has then evolved in a number of different directions, including the case where you cannot define an array factor [5], the extension to the optimal synthesis of delta patterns [6], and the exploitation of these results and procedures to the case when both excitations and locations were to be determined [7].

More recent results include the extension of the basic result to the synthesis of continuous sources (under given sidelobe constraints) for both cases wherein one wants to maximize directivity, or to maximize separation amongst the main beam and peak sidelobes [8], as well as the optimal synthesis of sum-delta reconfigurable beams by means of phase only control [9]. Extension to spatial (rather than angular) focusing has also been provided in [10]. A very recent further extension tackles the optimal spatial focusing of the power associated to a vector field [11].

Contribution will briefly discuss basics, relevance (per se as well as for creating reference solutions for more cumbersome synthesis problems), and possible extensions of the results above.

REFERENCES

1. Isernia, T., "On the optimal focusing of scalar fields," *Atti Rinione Nazionale di Elettromagnetismo*, Firenze, 1996 (in Italian).
2. Lebret, H. and S. Boyd, "Array antenna pattern synthesis via convex optimization," *IEEE Trans. on Signal Processing*, 1997.
3. Isernia, T. and G. Panariello, "Optimal focusing of scalar fields subject to arbitrary sidelobe bounds," *Electronic Letters*, 1998.
4. Bevelacqua, P. J. and C. A. Balanis, "Minimum sidelobe levels for linear arrays," *IEEE Trans. on Antennas and Propagation*, 2007.
5. Caccavale, L., F. Soldovieri, and T. Isernia, "Methods for the optimal focusing of microstrip array antennas including mutual coupling," *IEE Proc. on Microwaves, Antennas and Propagation*, 2000.
6. Bucci, O. M., M. D'Urso, and T. Isernia, "Optimal synthesis of difference patterns subject to arbitrary sidelobe bounds by using arbitrary array antennas," *IEE Proc. on Microwaves, Antennas and Propagation*, 2005.
7. D'Urso, M. and T. Isernia, "Solving some array synthesis problems by means of an effective hybrid approach," *IEEE Trans. on Antennas and Propagation*, 2007.
8. Bucci, O. M., T. Isernia, and A. F. Morabito, "Optimal synthesis of directivity constrained pencil beams by means of circularly symmetric pencil beams," *IEEE Trans. on Antennas and Propagation*, 2009.
9. Morabito, A. F. and P. Rocca, "Optimal synthesis of sum and difference patterns with arbitrary sidelobes subject to common excitation constraints," *IEEE Antennas and Wireless Propagation Letters*, 2010.
10. Iero, D. A. M., T. Isernia, A. F. Morabito, I. Catapano, and L. Crocco, "Optimal constrained field focusing for hyperthermia cancer therapy: A feasibility assessment on realistic phantoms," *Progress In Electromagnetic Research*, Vol. 102, 125–141, 2010.
11. Iero, D. A. M., L. Crocco, and T. Isernia, "Optimal spatial focusing of the power associated to vector fields," 2015, submitted.

F/S Ratio Improvement of Directional Bow-tie Antenna with Parasitic Elements

K. Kanai[1], **M. Nagasawa**[1], **R. Suga**[1], **T. Yasuzumi**[2], **T. Uwano**[1], **O. Hashimoto**[1], **and Y. Hasegawa**[2]

[1]Aoyama Gakuin University, Japan
[2]Toshiba Corporation, Japan

Abstract— Electromagnetic interference (EMI) levels of appliances should meet the electromagnetic compatibility standard. A large wide-band antenna is used for the radiation EMI measurements. The finding of noise sources is highly important to suppress the radiation EMI efficiently. Thus a small wide-band directional antenna with high front to side (F/S) ratio is expected for the measurement. A bow-tie antenna is known as a compact and broadband antenna, however it has omnidirectional radiation characteristics and its sidelobe levels increase at higher frequencies due to the higher order modes. In this paper, a directional bow-tie antenna suitable for specifying the noise sources is proposed.

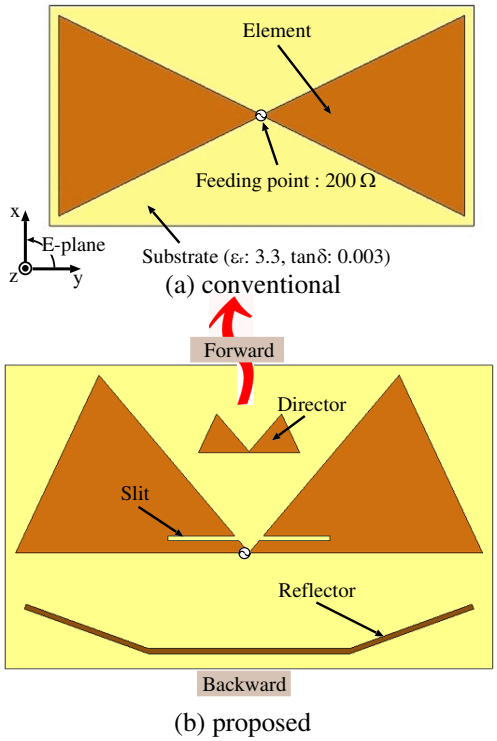

Figure 1: Simulated reflection characteristics.

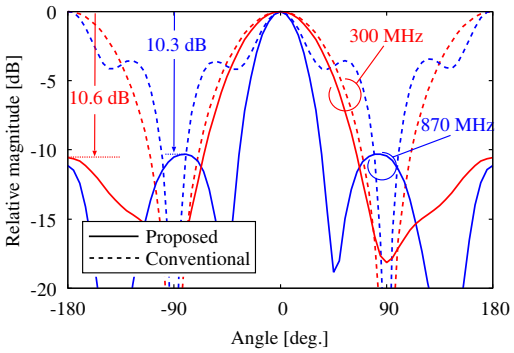

Figure 2: Simulated radiation patterns in the *E*-plane.

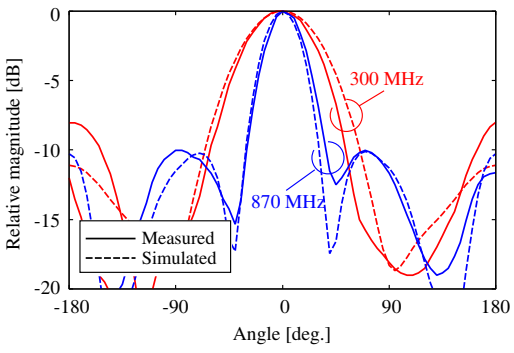

Figure 3: Measured radiation patterns of the fabricated bow-tie antenna.

Figure 1 illustrates (a) conventional and (b) proposed printed bow-tie antenna. A broadband 1 : 4 balun is used for the antennas to obtain 50 Ω input impedance. The target frequency band is assumed between 300 and 870 MHz considering EMI measurement application and the balun characteristics. For obtaining the directionality, two backward edges of each half element are on the straight-line, and two slits are placed on the elements to suppress the sidelobe level at 870 MHz. The director and reflector are placed to improve F/S ratio in the high and low frequency.

Figure 2 shows the simulated radiation patterns in the E-plane. The F/S ratio of the proposed antenna at 300 and 870 MHz is improved to be 11.1 dB and 10.1 dB, respectively. Figure 3 shows the measured radiation pattern in the E-plane. As the results, the measured results agree well with the simulated ones.

Ultra-wideband Butler Matrix Fed MIMO Antennas

F. E. Fakoukakis[1], **Tz. Empliouk**[1], **Ch. I. Kolitsidas**[2], **G. Ioannopoulos**[1], **and G. A. Kyriacou**[1]

[1]Department of Electrical and Computer Engineering, Democritus University of Thrace
Xanthi, Greece
[2]Department of Electromagnetic Engineering, KTH Royal Institute of Technology
Stockholm SE-100 44, Sweden

Abstract— Modern wireless systems, such as communications and Radar, are in the need for wide operational bandwidths, in order to satisfy the increased demands of their operation. This characteristic has become even more essential in the latest Long Term Evolution (LTE) communications systems, where there is the need for high and robust data rate transmission. Moreover, modern multifunctional phased array Radars demand for wide operational bandwidths, which they enable different operational modes, such as simultaneous air and weather surveillance.

As a result, significant work is taking place on the design and development of wideband antenna systems and RF front-ends. A critical part of the research deals with the design of the antenna array and its feeding network. One of the mostly used wideband antenna elements is the so-called Vivaldi slot antenna, which can offer an operational bandwidth extending to multiple octaves. Regarding the feeding networks, various approaches have been followed, mainly focusing on the design of wideband circuits and subsystems.

In this paper, we make an effort to extend the results of our previous work [1] on the design and development of ultra-wideband (UWB) antenna array systems for communications and Radar applications. The emphasis is given on the implementation of a MIMO beamforming scheme enabling high data rates, interference and noise suppression and suitable for use under different wireless applications scenarios. Specifically, the proposed system consists of a Vivaldi antenna array fed by an UWB Butler matrix type network. It could be used in modern multifunctional Radar systems with analog beamforming, as well as in future LTE communications applications. The Butler matrix is designed using UWB couplers and phase shifters [2, 3], being able to support the wideband Vivaldi array operation up to several octaves. The system design is presented, along with the beamforming procedure and the resulting array radiation patterns. Different MIMO beamforming scenarios are applied to maximize system performance, with particular emphasis on a 4×4 and 8×8 configurations. The possibilities of achieving low sidelobe levels and radiation pattern null steering are investigated, in order to suppress and minimize noise and interference. Conclusions and some aspects for future work are adduced in the last part of the paper.

REFERENCES

1. Kolitsidas, C. I., C. S. Lavranos, and G. A. Kyriacou, "Design of wideband RF front-end based on multilayer technology," *PIERS Proceedings*, 733–737, Moscow, Russia, Aug. 19–23, 2012.
2. Abbosh, A. M. and M. E. Bialkowski, "Design of compact directional couplers for UWB applications," *IEEE Trans. on Microw. Theory & Techniques,* Vol. 55, No. 2, Feb. 2007.
3. Abbosh, A. M., "Ultra-wideband phase shifters," *IEEE Trans. on Microw. Theory & Techniques*, Vol. 55, No. 9, Sep. 2007.

CRLH Waveguide Based Ka-band Beam-steering Leaky-wave Antenna for Radar Application

Qingshan Yang[1, 2], **Xiaowen Zhao**[1, 2, 3], **and Yunhua Zhang**[1, 2]

[1]Key Laboratory of Microwave Remote Sensing, Chinese Academy of Sciences (CAS), China
[2]Center for Space Science and Applied Research, CAS, Beijing 100190, China
[3]University of Chinese Academy of Sciences (UCAS), Beijing 100049, China

Abstract— Beam-steering capability is highly desired for many radars, especially for tracking radars. Frequency scanning and phase scanning are two general approaches for beam-steering. Traditional frequency scanning array antennas is hard to achieve continuous beam scanning from backward to forward directions because of their forward-wave propagation nature. While phased arrays have been applied widely due to their continuous beam scanning capability from backfire to endfire, however, the feed networks are often bulky and very complicated. In the past decades, composite right/left-handed (CRLH) metamaterials have been investigated extensively due to their unique properties such as backward wave and infinite wavelength propagation, which can be applied to leaky-wave antennas (LWAs) to realize continuous beam-steering from backfire to endfire.

In this work, we exploit the CRLH waveguide with double ridge corrugations to realize a Ka-band LWA with continuous beam-steering capability from backward to forward quadrants. The CRLH waveguide is composed of a traditional rectangular waveguide with one of its broadwalls periodically loaded with short-circuited double ridge corrugations [1]. This CRLH structure is air-filled to avoid dielectric loss. An offset straight long slot is made on the other broadwall of the rectangular waveguide acting as the radiating aperture to realize a LWA (see Figure 1). The LWA is composed of 100 CRLH radiating unit cells. Stepped transitions are included in the two ends of the LWA for connecting the structure to standard WR-28 waveguides.

The continuous beam-steering capability is validated by simulation, which shows that the main-lobe can scan continuously from $-32°$ to $+29°$ as the frequency changes from 32.4 GHz to 40 GHz, and correspondingly the realized gains changes from 15 dBi to 20 dBi. Compared with planar CRLH LWAs, the waveguide LWA proposed in this work has the advantages of high power capacity, low loss and consistent high gains and high radiation efficiency, which is very suitable for actual radar systems.

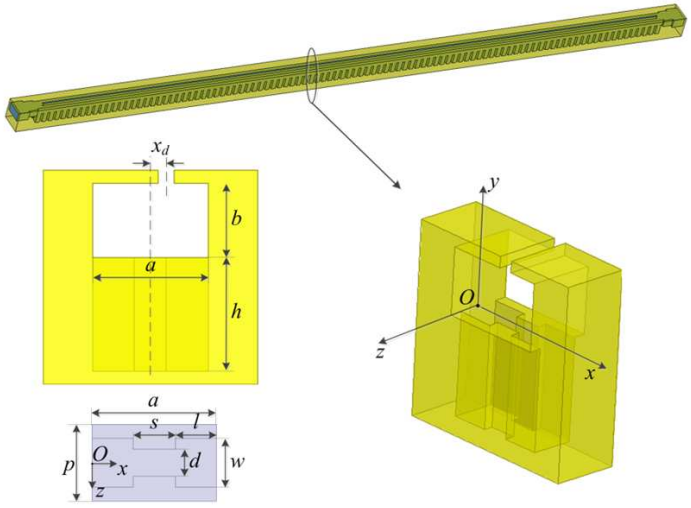

Figure 1: Configurations of the proposed CRLH waveguide LWA and its unit cell.

REFERENCES

1. Eldeen, A. M. N. and I. A. Eshrah, "CRLH waveguide with air-filled double-ridge corrugations," *IEEE International Symposium on Antennas and Propagation (APSURSI)*, 2965–2968, 2011.

Performance Analysis of Directive UWB Antennas as Reflector Feeds

Hazel Kara and Nurhan T. Tokan
Department of Electronics and Communications Engineering
Yıldız Technical University, Istanbul, Esenler 34220, Turkey

Abstract— In reflector applications, it is desirable to have a single feed that covers the entire frequency band of operation with a symmetric, directive pattern, dual-linear polarization, and frequency invariant phase centre and radiation pattern. To obtain a highly directive antenna, the size of the feed antenna should be enlarged which results with more phase centre movement with the change in the frequency. Long antenna elements exhibit high phase-center instability, which is very undesirable characteristic when the antenna is used to illuminate a reflector. A trade-off is necessary between directivity and phase errors. In order to avoid phase-center instability, short elements can be used but then higher losses for spillover are obtained.

When a wideband antenna is to be used as a reflector feed, the phase center variation with frequency introduces an error on the phase of the primary field impinging on the reflector surface. This is because the antenna phase center will be coincident with the focus only at one particular frequency and displacement at other frequencies will result as the phase error losses due to axial defocusing (Fig. 1). Tapered slot antennas are the most utilized antennas in Ultra Wide Band (UWB) high-performance applications. In this work, performance of the UWB Vivaldi antennas (exponentially tapered slot antennas) in reflector feed applications is investigated. A long Vivaldi is designed, manufactured (Fig. 2) and its phase center movement with frequency is measured. The correspondent phase error loss is estimated. Besides, spilover, amplitude taper and crosspol losses are calculated.

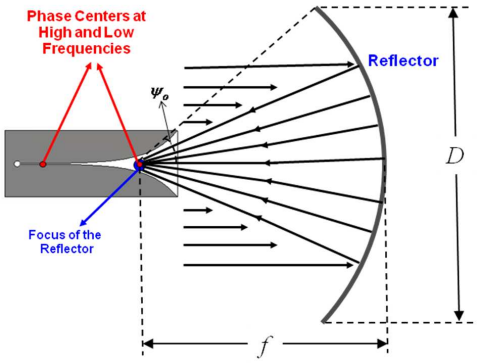

Figure 1: Phase centre positions of the Vivaldi antenna at high and low frequencies.

Figure 2: Vivaldi antenna in measurement setup.

Comparative Study on Stability of Total Gain and Input Impedance of Side Fed Bifilar Helix Antenna for Large Fixed Size Ground Plane

Muhammad Ahmad, **Muhammad Amin**, **and Asim Ali Khan**
COMSATS Institute of Information Technology, Lahore, Pakistan

Abstract— This research presents comparative study of input impedance and total gain of Side Fed Bifilar Helix Antenna (SFBHA) against the variation in height (in terms of wavelength) from large fixed size Perfect Electric Conducting ground plane (PEC). The simulations show that metallic ground plane of size $10\lambda \times 10\lambda$ approximate the infinite PEC ground plane with reasonable accuracy. The variations in input impedance and Voltage Standing Wave Ratio (VSWR) are noticed between the heights of 0.05λ to 0.35λ both in simulations and measurements. Above the height of 0.35λ, fewer variations are observed that are negligible. Measurement results of input impedance and VSWR are reasonably matched with simulations. The total gain pattern of SFBHA remains stable in simulations and measurements as height of SFBHA varies above PEC. The performance of SFBHA is compared with Horizontal Dipole antenna (HD), Vertical rectangular Loop antenna (VL) and with another orientation of rectangular loop antenna that is Horizontal and Perpendicular Loop (H&PL). Comparatively, the electromagnetic performance of SFBHA is better and affect of the ground plane above 0.35λ on total gain pattern, input impedance and VSWR is negligible.

Aperture Coupled Microstrip Antenna with Three Resonants

Mohsen Jafari Chashmi[1], **Ramezan Ali Sadeghzadeh**[2], **Hadi Ghobadi**[2], **Mahdi Oliaei**[2], **and Esfandiar Mehrshahi**[1]

[1]Electrical & Computer Engineering Department, Shahid Beheshti University, Iran
[2]Electrical & Computer Engineering Department, K. N. Toosi University of Technology, Iran

Abstract— This paper presents improved aperture coupled microstrip antenna with three resonants which its bandwidth has been enhanced due to vary the current distributions. There is a compromise between radiation characteristics and the bandwidth. Radiation patterns indicate the appropriate propagation pattern of antenna is between 1.3 GHz to 2.3 GHz frequency band which clarifies a bandwidth more than 53%. There is bandwidth enhancement up to this limit by utilization of multiple radiating elements. The antenna operates in both linear and circular polarization (1.64 GHz to 1.76 GHz for less than 3 dB Axial Ratio). The simulated results done by two methods, i.e., Finite Element Method (FEM) and Finite Difference Time Domain (FDTD) collaborated by two full-wave softwares ANSYS HFSS and CST MWS have good agreements with the measurement ones.

Planar Dielectric Lens Antennas as Reflector Feeds

Fikret Tokan
Department of Electronics and Communication Engineering
Yıldız Technical University, İstanbul, Turkey

Abstract— In recent years, high dielectric lens antennas are widely used in millimeter-wave applications. The most important reason of that is these antennas have high directivity and high efficiency thanks to the high permittivity materials used as the lens core.

In this application, the focusing problems will be probably faced when planar lens antennas are used as the feeding of the reflector antennas and solution suggestions are deeply investigated.

The planar lateral wave antenna is selected as the reflector feed [1]. The lateral wave antenna is unique for ultra wide band applications (1 : 3) with its planar structure. The geometrical configuration of the antenna is given in Fig. 1(a).

Some problems will be faced when the planar dielectric antenna is used as the reflector feed can be summarized as follows:

- Phase center of the ultra-wide band antennas is not stable and strongly vary with frequency. In such a situation, it is almost impossible to place the feeding antenna to the focus of the reflector in the whole frequency range.
- The far-field radiation pattern of the antenna has different half-power beam width characteristics in E-($\pm 4°$) and H-($\pm 45°$) planes, thus to design a reflector having appropriate f/D value for both planes is the second problem.
- The phase center of the antenna in E-plane locates at the antenna aperture, while the phase center in H-plane is located behind the feeding point as sketched in Fig. 1(b). Accordingly, the antenna is characterized by astigmatism, being the phase center in different points for the E-and H-planes.

Consequently, the reflector antenna should be designed by considering these details. Such a design is completed and the radiation pattern given in Fig. 2 is obtained.

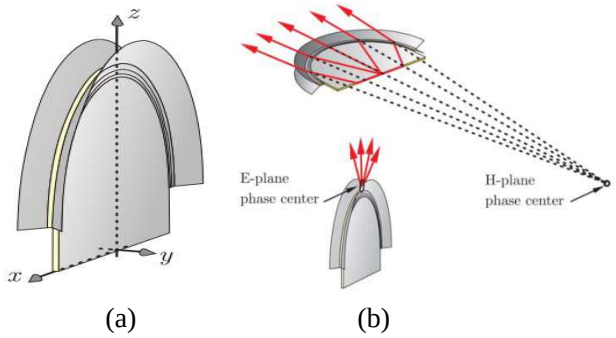

Figure 1: Feeding antenna (a) geometrical structure; (b) phase centers in both planes.

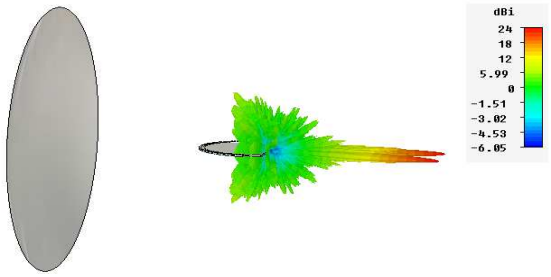

Figure 2: The radiation pattern of a reflector fed by planar dielectric lens antenna.

REFERENCES

1. Tokan, F., N. T. Tokan, A. Neto, and D. Cavallo, "The lateral wave antenna," *IEEE Transactions on Antennas and Propagation*, Vol. 62, No. 6, 134–141, June 2014.

Design, Simulation, and Fabrication of Low-cost Inkjet Antennas

C. Önol[1,2], T. Çiftçi[1], S. Küçük[1], B. Karaosmanoğlu[1], and Ö. Ergül[1]

[1]Department of Electrical and Electronics Engineering, Middle East Technical University, Ankara, Turkey
[2]ASELSAN Inc., Ankara, Turkey

Abstract— Inkjet antennas that are fabricated by metal printing on paper or similar substrates have recently become popular as they are relatively inexpensive, flexible, and environmentally friendly [1]. In addition to special material printers designed for this purpose [2–4], one can use silver-based toners in standard inkjet printers to manufacture this type of antennas with reduced costs. Different types of inkjet antennas, including dipole antennas, meander antennas [1], bowtie antennas [2], Vivaldi antennas [3], and arrays [4] have been proposed, fabricated, and analyzed in the literature, while less attention has been paid to more detailed antenna structures [5], even though inkjet printers can offer quite high resolutions. In this study, we present fractal antennas with Koch snowflake shapes that are produced by fully exploiting the advantages of the inkjet printing technology.

As depicted in Figure 1, we print antennas on photograph papers using silver toner in a standard commercial printer. Before manufacturing, antennas are designed and simulated using a fast solver based on the multilevel fast multipole algorithm [6]. For a high-quality fabrication, many factors are considered and optimized, including the printer parameters and style, paper and toner types, curing duration and temperature, and post processing. As also shown in Figure 1, measurements are compared with simulation results to confirm the multi-band characteristics of the produced antennas. The constructed and optimized manufacturing process is efficient and inexpensive, enabling fast fabrications of the designed antennas with small details.

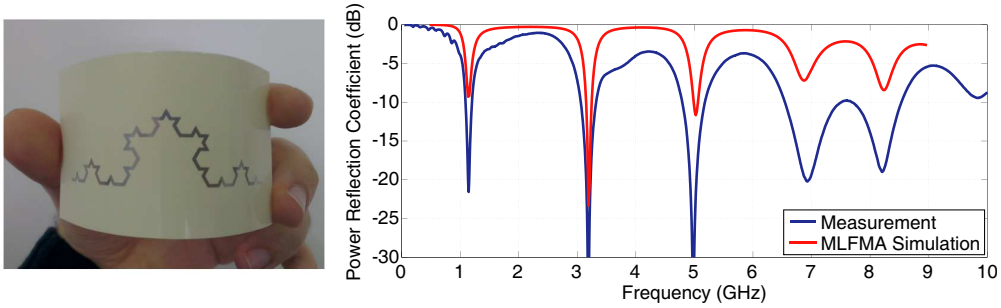

Figure 1: A Koch snowflake antenna produced by inkjet printing on a photograph paper and power reflection coefficient values when the antenna is matched to 50 Ω.

REFERENCES

1. Nikitin, P. V., S. Lam, and K. V. S. Rao, "Low cost silver ink RFID tag antennas," *Proceedings of IEEE Antennas and Propagation Soc. Int. Symp.*, 353–356, Washington DC, USA, Jul. 2005.
2. Rida, A., L. Yang, R. Vyas, and M. M. Tentzeris, "Conductive inkjet printed antennas on flexible low-cost paper-based substrates for RFID and WSN applications," *IEEE Antennas Propag. Mag.*, Vol. 51, No. 3, 13–23, Jun. 2009.
3. Cook, B. S. and A. Shamim, "Inkjet printing of novel wideband and high gain antennas on lowcost paper substrate," *IEEE Trans. Antennas Propag.*, Vol. 60, No. 9, 4148–4156, Sep. 2012.
4. Subbaraman, H., D. T. Pham, X. Xu, M. Y. Chen, A. Hosseini, X. Lu, and R. T. Chen, "Inkjet-printed two-dimensional phased-array antenna on a flexible substrate," *IEEE Antennas Wireless Propag. Lett.*, Vol. 12, 170–173, 2013.
5. Maza, A. R., B. Cook, G. Jabbour, and A. Shamim, "Paper-based inkjet-printed ultra-wideband fractal antennas," *Microwaves, Antennas & Propagation, IET*, Vol. 6, No. 12, 1366–1373, Sep. 2012.
6. Ergül, Ö. and L. Gürel, *The Multilevel Fast Multipole Algorithm (MLFMA) for Solving Large-Scale Computational Electromagnetics Problems*, Wiley-IEEE, 2014.

Design of Integrated Triple Band Notched for Ultra-wide Band Microstrip Antenna

Yahya S. H. Khraisat
Electrical and Electronics Department, Al-Balqa' Applied University/Al-Huson University College
P. O. Box 1375, Irbid, Irbed 21110, Jordan

Abstract— This paper demonstrates the design of integrated triple band notched for ultra-wide band Microstrip antenna. We used UWB (ultra-wide band) short range systems which require low power and these are built using inexpensive digital components. Microstrip antenna is used for implementing UWB systems as it shows good broadband characteristics.

We proposed a compact triple band notched CPW (Co-planar Waveguide) fed MSA (Micro strip Antenna) for UWB (Ultra-Wide Band) applications.

This band-notched antenna has rejection characteristics at 3.2 GHz (for Wi-MAX band 3.16 to 3.32 GHz), at 5.5 GHz (for WLAN 2 band-5.3 to 5.72 GHz) and at 7.9 GHz (for ITU band 7.72 GHz to 8.13 GHz).

First a Primitive antenna is taken. This antenna consists of a beveled rectangular radiating patch and a CPW (co-planar waveguide) type feed structure. The essence of this design strategy is that three notching elements are embedded onto the primitive patch antenna to produce band-stop filtering function at those above mentioned frequencies. Notch elements are meticulously selected and embedded onto the antenna.

Pattern Reconfigurable Antenna Using Non-uniform Serpentine Flexure Based RF-MEMS Switches

Ashish Kumar Sharma[1] **and Navneet Gupta**[2]

[1]Department of Electronics & Telecommunication Engineering
Veer Surendra Sai University of Technology Burla, Odisha, India
[2]Department of Electrical & Electronics Engineering
Birla Institute of Technology and Science, Pilani, Rajasthan, India

Abstract— This paper presents the design and analysis of reconfigurable antenna using two circular microstrip patch antenna array with non-uniform RF-MEMS switches in L and S band. It consists of a pair of circular patch antenna with CPW on the same side of Si substrate. This reconfigurable antenna design consists of two RF-MEMS switches, to achieve pattern reconfigurability. Figure below represents the schematic view of reconfigurable antenna with RF-MEMS switch. The total width (W_{tot}) and length (L_{tot}) of this antenna are 94 mm and 67 mm, respectively. A CPW feed line with central conductor width $W = 4$ mm and ground signal gap $S = 0.45$ mm is used, resulting in a characteristic impedance (Z_0) of 50 Ω. Two RF-MEMS switches are used to electrically connect and disconnect the two circular radiating patches. These switches are positioned at 6 mm from the circular patch along x axis.

The analysis of reconfigurable antenna using RF-MEMS switch is done using the simulation performed on Ansys HFSS electromagnetic simulator for the frequency range of 1 to 10 GHz. The reconfigurability of the antenna is analyzed for L to S band (2 to 4 GHz) in terms of return loss and radiation pattern. The proposed antenna shows the pattern reconfigurability at 2.3 GHz and 3.4 GHz.

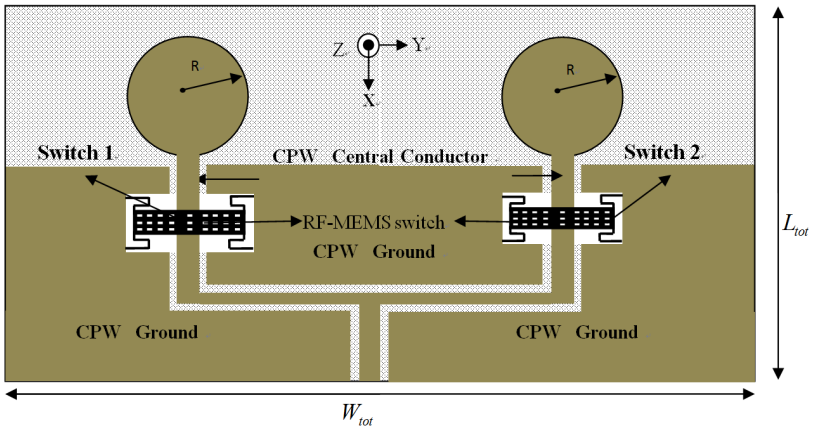

Figure 1: Schematic view of RF-MEMS switch based reconfigurable antenna.

Compact Band Notched UWB Filter Based on Open-load Stub

Xuemei Zheng[1, 2], **Yanyan Wang**[1], **and Tao Jiang**[1]

[1]College of Information and Communications Engineering
Harbin Engineering University, Harbin, China
[2]College of Information Engineering, Northeast Dianli University, Jilin, China

Abstract— In recent years, with the application and development of UWB (Ultra-Wide Band, UWB) technology in the communication field, the research of UWB filters and antennas has been one of the hot issues in the field. At present, the typical structure with the notched band performance is always aimed at the particular narrow-band interference sources, the research of UWB filters and antenna design which can adjust the number and width of notched stop-band is not systematic and deep enough. This paper reports on a new compact UWB band pass filter based on stepped impedance resonator (SIR) and open stub loaded resonator structure. The main advantage of the proposed filter is that the frequency of the notched band can be tuned easily in a wide frequency range. According to the odd/even resonant excitation conditions, the UWB filter characteristics are analyzed. The filter is simulated by 3D EM commercial software HFSS, The resulting indicates that the presented UWB BPF covers the UWB frequency range. The simulation results show that the proposed good UWB characteristics and the notch band can be changed optionally from 5 GHz to 10 GHz. The filters can efficiently enhance the interference immunity from undesired signals with certain application prospects.

Metamaterial Inspired Compact Antenna for UWB and GPS Applications

Sanjji N. Manjunath, **G. S. Karthikeya**, **Bharath Raj**,
K. Ullas, **and C. Vindhya**
Antenna Research Laboratory, Department of Electronics and Communication
B.M.S. Institute of Technology and Management, Bengaluru, India

Abstract— This paper proposes the design of a miniaturized antenna and is investigated for UWB and GPS applications. The main challenges faced in the design of UWB antennas are the miniaturization, improving the efficiency, uniform gain, larger operating range, optimized radiation pattern and polarization to provide wide coverage. It has been a greater challenge to accommodate both the UWB and the GPS band for a compact antenna and an effort is made in this paper such that these drawbacks are overcome.

One such effort to resolve the drawbacks is the implementation of metamaterial structures. Metamaterials are artificially engineered structures providing electromagnetic properties which are not

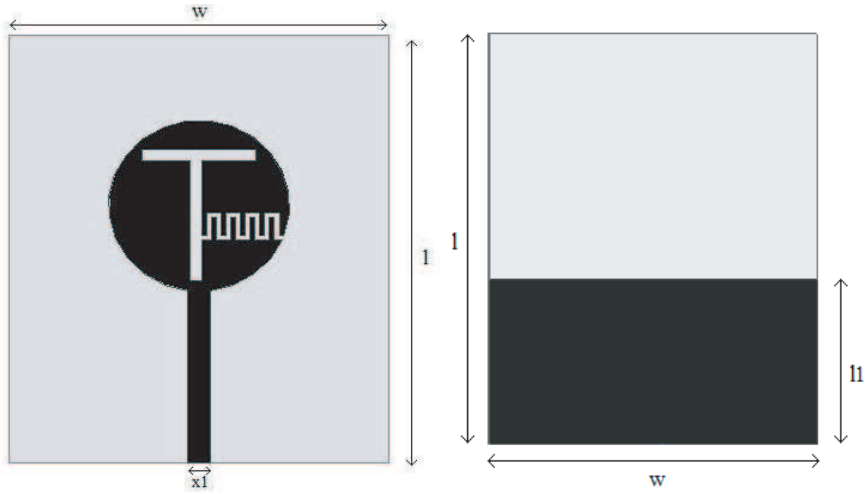

Figure 1: The proposed antenna.

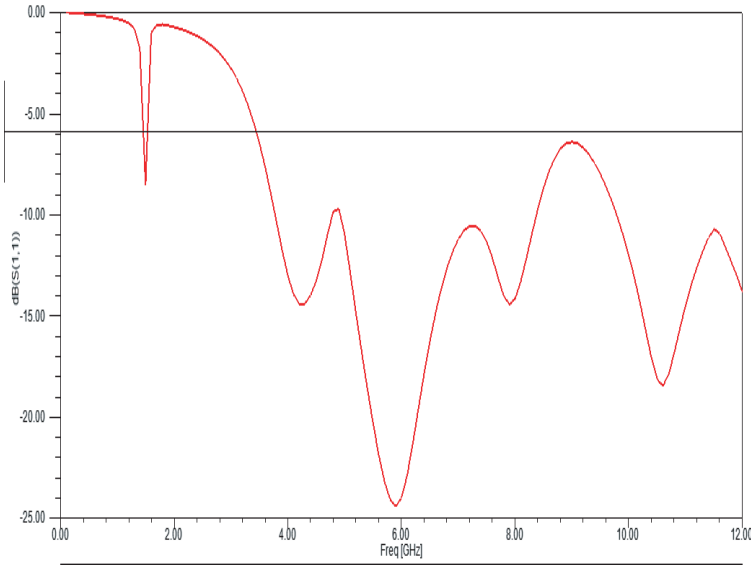

Figure 2: S_{11} graph of the proposed antenna.

encountered in nature. These materials simultaneously have negative permeability and permittivity which was first theoretically predicted by Veselago.

The proposed antenna consists of a planar circular monopole patch, ultrawideband antenna which is incorporated along with the GPS (1.5 GHz) band due to addition of four unit cells of Complimentary Meander-Line (CML) and a T-slot on the patch.

The antenna is designed on a low-cost FR4 substrate having dimensions $37.5 \times 31.5 \times 1.6\,\text{mm}^3$ and is excited by a 50 Ohms microstrip line of width 1.95 mm using line feed technique and fabricated on a 1.6-mm thick FR4 substrate. The relative permittivity and loss tangent of the substrate is 4.4 and 0.02 respectively.

The improvement in the performance and reduction of size in the antenna design is due to the t-slot made on the patch. This T-slot is a metamaterial inspired structure. Meander line cuts which are meta-structures are implemented in the proposed design such that a new resonant band is formed at a particular frequency.

The simulated S_{11} graph has a resonance at 1.5 GHz with a bandwidth of 100 MHz and an ultrawide band with a -10 dB return loss starting from a frequency of 3.7 GHz. It has fractional bandwidth of $> 100\%$ in the UWB spectrum.

It has a uniform gain in the S and C Bands and can be a used for GPS (1.5 GHz), WiMAX (3.45–3.8 GHz), WLAN (4.9–5.8 GHz) and other UWB (3.45–10.6 GHz) applications.

A Low-profile Wideband RFID Tag Antenna Attached to Metallic Surfaces

Y. J. Zhang, **G. C. Wan**, **J. Zhang**, **and M. S. Tong**
Department of Electronic Science and Technology, Tongji University
4800 Cao'an Road, Shanghai 201804, China

Abstract— The radio frequency identification (RFID) system in the ultra high frequency (UHF) band from 860 MHz to 960 MHz has become more popular in recent years and has been widely used in the labels of products and services. Compared to the RFID system working in the frequency band lower than the UHF, the system has several benefits such as the safer security mechanism, larger data storage, and better stability. Furthermore, it can read several tags simultaneously and rapidly, making it become the preferred choice in many applications. There are usually four important aspects that should be considered in the design of tag antenna, i.e., size, impedance matching, radiation pattern, and gain. Also, the RFID tags have to be attached to various materials in practical situations and the cancellation of electric current on the surface of antenna will significantly worsen the performance of tags if they are attached to metallic objects. Aiming to the problem, some solutions have been proposed, such as embedding a slotted via-patch in the middle of the dual layer RFID tag antenna, incorporating an artificial magnetic conductor (AMC) with a printed meander monopole tag antenna, and applying a proximity-coupled feed to a radiating patch.

In this work, we propose a different design for the UHF-RFID tag antenna which will be attached to metallic objects. The meandering technique, capacitive-tip loading structure, and T-matching network are wisely hybridized to improve the impedance matching of the RFID tag antenna. The simulated results show that the design can remarkably enhance the performance of tag antenna in both bandwidth and gain when it is attached to a metal sheet. We will show the details of design and testing results in the presentation.

A Long Range UHF RFID Tag for Metallic Objects

Manoel Vitório Barbin[1], **Michel Daoud Yacoub**[1], **and Silvio Ernesto Barbin**[2]

[1]Communications Department, Faculty of Electrical and Computing Engineering
University of Campinas, Brazil
[2]Telecommunication and Control Engineering Department, Polytechnic School of Engineering
University of São Paulo, Brazil

Abstract— The performance of passive UHF RFID tags, commonly available in the market, is significantly degraded when they are placed near a conducting surface. A possible solution to overcome this problem is to design tags based on PIFA (Planar Inverted F Antenna) the performance of which is less sensitive to the presence of objects in its surroundings. This ability is mainly due to the existence of a ground plane inherent to its structure. In this paper, a PIFA is utilized in the design of a passive tag that can be used to identify metallic objects with medium to large dimensions. A new type of antenna feeder is presented with a slot in the radiating element where the RFID IC is attached. The maximum range of utilization, covering all licensed RFID UHF bands (860 to 960 MHz), is in excess of 8 m, according to simulations using a MoM based software, verified by practical measurements. Further results from simulation and measurements show that the tag can also be used attached to other materials with good performance.

Author Index